1.01 Classification of Organotransition Metal Compounds

Gerard Parkin, Columbia University, New York, New York, USA

1.01.1 Introduction

The ability to evaluate whether a particular organotransition metal compound is likely to be inert or highly reactive is of considerable significance with respect to understanding, and predicting, the chemistry of a specific system. While experienced practitioners of organometallic chemistry may have a good sense as to what type of reactivity would be

expected for a specific organometallic compound, it is often difficult for non-specialists to assimilate this knowledge in an expeditious manner. In this regard, the only guide that is generally invoked is the "18-electron rule". Despite its name, however, the "18-electron rule" is *not* a rule, and many chemists are aware of examples that deviate from it. One of the purposes of this article, therefore, is to place the applicability of the "18-electron rule" in context by evaluating the distribution of organotransition metal compounds as a function of electron count. By necessity, this requires knowledge of the procedure and pitfalls pertaining to electron counting. In addition to evaluating organometallic compounds according to their electron count, the distribution of compounds is also analyzed according to Green's "Covalent Bond Classification (CBC) Method"[1] which provides a more useful means to evaluate the stability of a molecule than merely applying the "18-electron rule".

1.01.2 Electron Counting Procedures and Valence Shell Electron Count in Transition Metal Complexes

The stability (loosely defined as "ability to be isolated")[2] of an organotransition metal compound is dictated by a number of factors which include *(i)* the valence electron count, *(ii)* the coordination number, *(iii)* the d^n configuration and *(iv)* the valence (*cf* oxidation number) of the transition metal. Of these, the valence electron count (or, more simply, the "electron count") is often the first to be evaluated, in large part because of the so-called "18-electron rule".[3,4] While the applicability of the "18-electron rule" will be discussed later, the usefulness of the electron count is that it provides a first order evaluation as to whether the complex is likely to contain *(i)* empty metal based orbitals (<18 electrons) or *(ii)* occupied metal-ligand antibonding orbitals (>18 electrons). This notion is often rationalized by consideration of the molecular orbital diagram of simple octahedral complexes employing σ-only interactions, *e.g.* $Mo(PMe_3)_6$, as illustrated in Figure 1. In terms of a molecular orbital analysis, the electron count corresponds to the number of electrons that occupy metal based orbitals and consideration of Figure 1 indicates that an 18-electron count results in full occupation of all bonding and nonbonding orbitals, with no occupation of metal-ligand

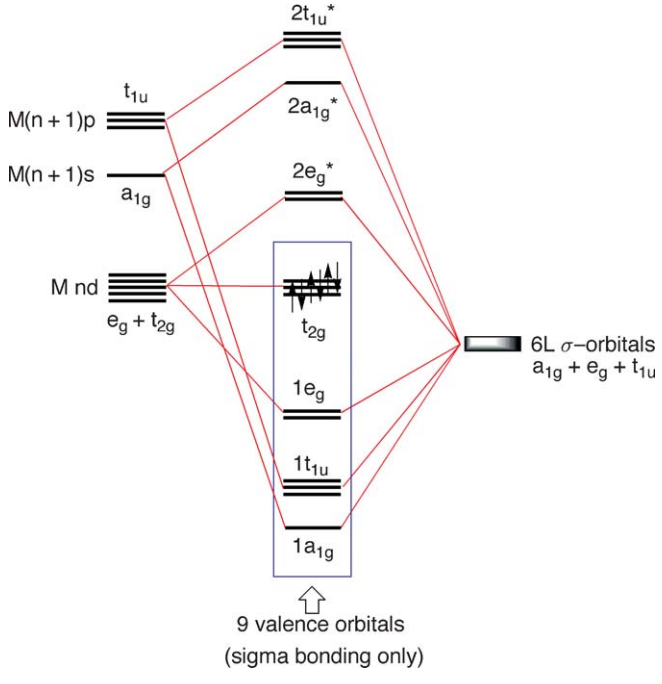

Figure 1 Molecular orbital diagram for an octahedral complex with σ-only interactions. Population of the molecular orbitals by 18-electrons results in occupation of six bonding and three nonbonding orbitals, with no occupation of antibonding orbitals. As such, it provides a simple rationalization for the concept of the 18-electron rule: a 20-electron complex with occupied antibonding orbitals would be expected to be unstable and dissociate a ligand to transform to an 18-electron complex, while a 16-electron complex would be able to bind an additional ligand and transform to an 18-electron complex. However, the nature of the molecular orbital diagram depends critically on the molecular structure (for example, see Figure 2) and so this explanation is necessarily over simplistic.

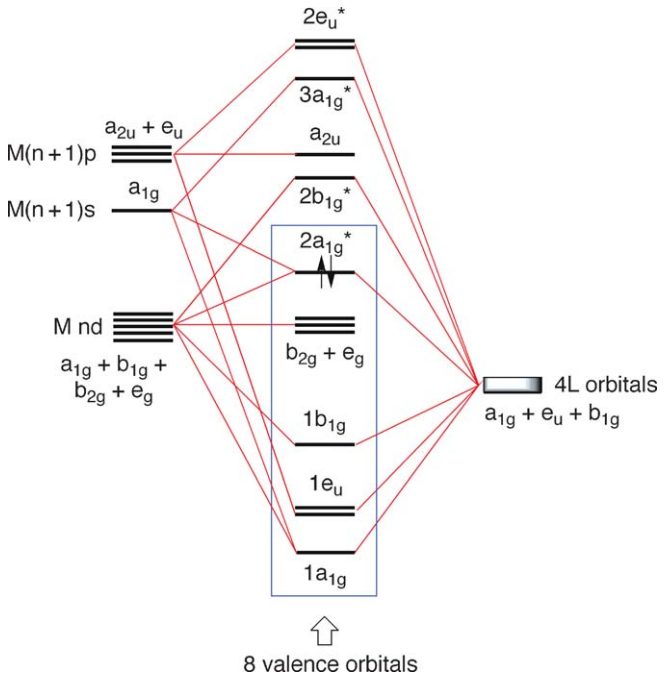

Figure 2 Molecular orbital diagram for a square planar complex with σ-only interactions. The MO diagram is closely related to that for an octahedral complex but with two important (and obvious) differences: (i) the ligand orbitals contribute only four bonding orbitals in the square planar structure, whereas six are contributed in the octahedral structure, and (ii) whereas the $d_{x^2-y^2}$ and d_{z^2} orbitals in an octahedral complex are degenerate and interact equally with the ligand orbitals, only the $d_{x^2-y^2}$ interacts strongly in a square planar geometry. Thus, only one of the d orbitals becomes strongly antibonding. An 18-electron configuration would require the occupation of the strongly antibonding orbital and, as such, a 16-electron configuration becomes favored for a square planar complex.

antibonding orbitals. The 18-electron count, in essence, may therefore be viewed to be a result of the transition metal using its nine valence orbitals, *i.e.* nd, (n + 1)s, and (n + 1)p,[5] in such a manner that only bonding and nonbonding orbitals are occupied; as such, it is a counterpart to the Lewis-Langmuir "octet rule".[6] However, the molecular orbital diagram for a transition metal complex is highly dependent on its structure (see, for example, Figures 2 and 3), a consequence of which is that simple electron counting cannot always be used to indicate whether antibonding orbitals are occupied, or nonbonding orbitals are unoccupied.

For example, the molecular orbital diagram for a square planar complex (Figure 2) indicates that an 18-electron configuration results in the occupation of *two* metal-ligand antibonding orbitals derived from the $d_{x^2-y^2}$ and d_{z^2} orbitals. Thus, rather than an 18-electron configuration, a 14-electron count is required to achieve the situation in which all bonding and nonbonding orbitals are occupied and all antibonding orbitals are unoccupied. However, while the metal based $d_{x^2-y^2}$ orbital becomes strongly antibonding because its lobes point directly at the ligands, the d_{z^2} orbital becomes only slightly antibonding because its taurus does not overlap significantly with the ligand orbitals. As such, occupation of the d_{z^2} antibonding orbital is not prohibitive and square planar organotransition metal compounds such as $(R_3P)_2PtR_2$ are commonly characterized by a 16-electron count. Thus, an 18-electron configuration should, by no means, be considered an essential requirement for the existence of a stable organotransition metal compound. As will be discussed in more detail in Section 1.01.4.6.1, different metals favor different electron counts and, for this reason, the determination of the electron count of the metal in an organotransition metal compound remains an important component of evaluating its stability, even though the "18-electron rule" is not universally valid. In view of the importance of the electron count, the procedures used to determine these values are described below.

1.01.2.1 Procedures for Determining the Electron Count

While the electron count for molecules such as $Mo(PMe_3)_6$ or $(R_3P)_2PtR_2$ is explicitly indicated by the respective molecular orbital diagrams (Figures 1 & 2), evaluation of the electron count for most molecules does not require one

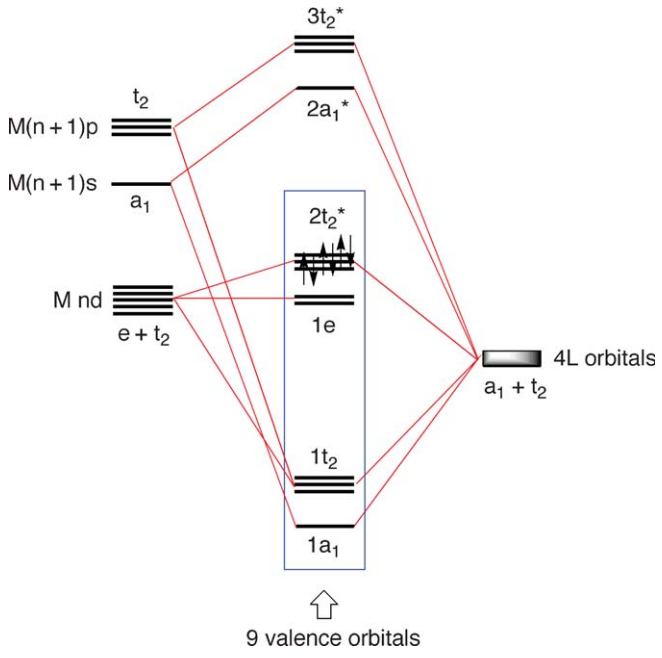

Figure 3 Molecular orbital diagram for a tetrahedral complex with σ-only interactions. The population of all bonding and nonbonding MO's of a tetrahedral complex results in a 12-electron, rather than 18-electron, configuration. An 18-electron configuration for a tetrahedral geometry requires the population of an antibonding t_2^* set. However, since the t_2^* set is only weakly antibonding because the d-orbitals do not point directly at the ligands, its occupation is not prohibitive and the 18-electron rule is applicable to many tetrahedral organometallic compounds.

to construct a molecular orbital diagram for the molecule of interest. Rather, the determination of the electron count of a metal in a compound merely requires knowledge of how many electrons the ligand array contributes to the valence shell of the metal.

There are two procedures for determining the electron count of an atom in a molecule which, *by necessity*, give the same value if applied correctly. The two electron counting procedures involve either (i) a neutral ligand formalism or (ii) an oxidation number formalism.[7,8] The essential difference between the two methods is that the neutral ligand formalism deconstructs the molecule such that *all* ligands are neutral, whereas the oxidation number formalism deconstructs the molecule such that the pair(s) of bonding electrons are transferred to one partner (typically, but not always, the most electronegative), with the exception of homonuclear element–element bonds which are cleaved homolytically.[7]

An essential component of establishing the electron count for a metal in a molecule is identifying the number of electrons that each ligand contributes to the bonding and the electron donor numbers for a selection of common ligands according to the two formalisms are summarized in Table 1.

1.01.2.1.1 Procedure for electron counting using the neutral ligand formalism

Employing the neutral ligand method, the electron count is the sum of (i) the number of valence electrons of the neutral metal (Table 2) and (ii) the number of electrons donated by all of the ligands in their neutral form; for cationic and anionic species, the sum is modified appropriately to take account of the charge on the molecule (Figure 4). The neutral form of some ligands may appear confusing at first glance, especially if it exists as a zwitterion. For example, consider the neutral form of the $[PhB(CH_2PR_2)_3]$ ligand in $\{[PhB(CH_2PR_2)_3]M\}$ derivatives (Figure 5). Since boron is attached to four groups it must bear a negative formal charge. To preserve electrical neutrality, one of the phosphorus atoms must bear a formal positive charge, with the result that the phosphorus can only contribute one electron to the metal (Figure 5). As such, $[PhB(CH_2PR_2)_3]$ corresponds to a five electron donor, with both neutral phosphorus atoms contributing two electrons each, and the positively charged phosphorus contributing one electron. It is evident that this results in the same electron count that would be obtained if $\{[PhB(CH_2PR_2)_3]M\}$ were to be viewed as an "ion-pair" with three phosphorus lone pairs of anionic $[PhB(CH_2PR_2)_3]^-$ being donated to a cationic metal center.

Table 1 Number of electrons provided by various ligands. Note that, for the oxidation number formalism, the sum of the number of electrons donated and the charge is equal to the number of electrons donated according to the neutral ligand formalism

Ligand	*Metal–Ligand interaction*	*No. of electrons donated (neutral ligand formalism)*	*No. of electrons donated & charge (closed-shell formalism)*
H		1	2 (−1)
R		1	2 (−1)
CR_2 (Schrock alkylidene)	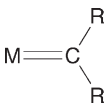	2	4 (−2)
CR(X) (Fischer carbene)	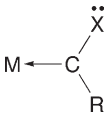	2	2 (0)
CR		3	6 (−3)
η^2–C_2H_4		2	2 (0)
η^3–C_3H_5	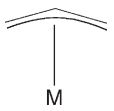	3	4 (−1)
η^3–C_4H_6	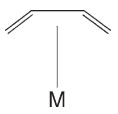	4	4
η^3–C_3H_3	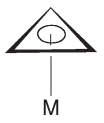	3	2 (+1)
η^4–C_4H_4	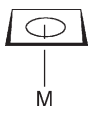	4	6 (−2)[a] 4 (0)[a]
η^5–C_5H_5	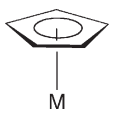	5	6 (−1)

(*Continued*)

Table 1 (Continued)

Ligand	*Metal–Ligand interaction*	*No. of electrons donated (neutral ligand formalism)*	*No. of electrons donated & charge (closed-shell formalism)*
η^6–C_6H_6	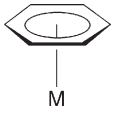	6	6 (0)
η^7–C_7H_7	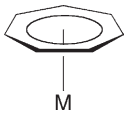	7	6 (+1)[b] 8 (−1)[b] 10 (−3)[b]
η^8–C_8H_8	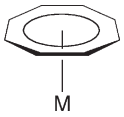	8	10 (−2)[c]
CO	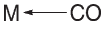	2	2 (0)
PR_3	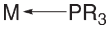	2	2 (0)
NO (bent)	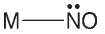	1	2 (−1)
NO (linear)	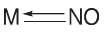	3	2 (+1)
PR_2 (pyramidal)	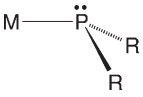	1	2 (−1)
PR_2 (planar)	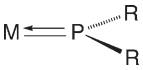	3	2 (+1)
N_2R (doubly bent)	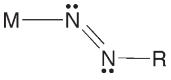	1	2 (−1)
N_2R (singly bent)	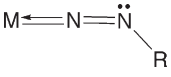	3	2 (+1)

[a]The closed shell form of square cyclobutadiene is a dianion. However, some articles assign a non–closed shell charge of zero to the cyclobutadiene ligand (see, for example: Collman, J. P.; Hegedus, L. S.; Norton, J. R.; Finke, R. G. *Principles and Applications of Organotransition Metal Chemistry*, University Science Books: Mill Valley, Californinia, 1987).
[b]The cycloheptatrienyl ligand has variously been assigned charges of +1, −1, and −3. See the text for a discussion of the merit of these values.
[c]The closed shell form of planar cyclooctatetrane is a dianion; the neutral form of cyclooctatetrane is not planar.

Table 2 Number of valence electrons associated with the neutral transition metal atoms (i.e. the group valence). Note that the number of valence electrons is independent of their distribution within the nd and (n + 1)s levels

Group 3 *Sc, Y, La*	*Group 4* *Ti, Zr, Hf*	*Group 5* *V, Nb, Ta*	*Group 6* *Cr, Mo, W*	*Group 7* *Mn, Tc, Re*	*Group 8* *Fe, Ru, Os*	*Group 9* *Co, Rh, Ir*	*Group 10* *Ni, Pd, Pt*
3	4	5	6	7	8	9	10

neutral ligand method

Electron count = no. of M electrons + no. of ligand electrons – charge

oxidation number method

Electron count = no. of M^{n+} electrons + no. of $(ligand)^{\pm q}$ electrons

Figure 4 Procedures for determining the electron count by the neutral ligand formalism and the oxidation number formalism.

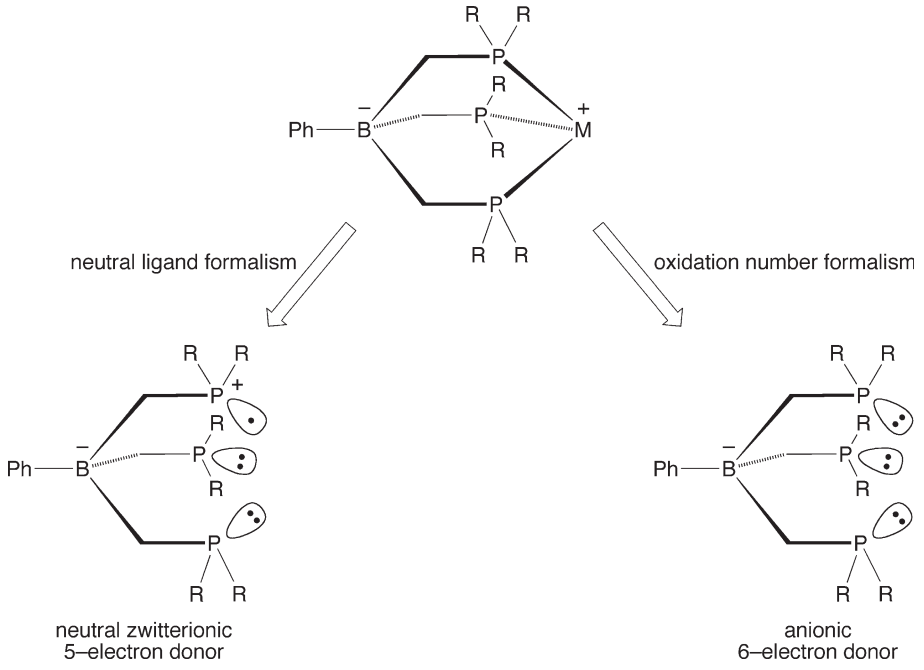

Figure 5 Electron count for the $[PhB(CH_2PR_2)_3]$ ligand according to the neutral ligand and oxidation number formalisms. The neutral form of the ligand is a zwitterion with a negative formal charge on boron and a positive formal charge on phosphorus. As a result of the positive charge, one of the phosphorus atoms is only a single electron donor, such that the neutral ligand is a 5-electron donor to M. With respect to the oxidation number formalism, the anionic form of the ligand serves as a 6-electron donor to cationic M^+.

1.01.2.1.2 Procedure for electron counting using the oxidation number formalism

Electron counting using the oxidation number formalism is often referred to as either the ionic method or the closed shell method.[9,10] However, it should be recognized that neither of these terms are particularly appropriate because *(i)* ligands such as CO are considered to be ***neutral*** in this formalism and *(ii)* certain ligands do not have a closed shell[11] with the assigned charge. Most notably, the bent nitrosyl ligand is assigned a charge of −1, but the species NO^- is *not* a closed shell molecule since it is isoelectronic with O_2 and has a triplet ground state.

Using the oxidation number formalism, the electron count is the sum of *(i)* the number of valence electrons corresponding to the metal in its M^{n+} oxidation state (for cationic and anionic species, the charge is included in the oxidation state of the metal) and *(ii)* the number of electrons donated by all of the ligands in their assigned form

($L^{\pm q}$), as summarized in Figure 4. A requisite for using this method of electron counting is, therefore, the determination of oxidation number.

The oxidation number of a transition metal is determined by consideration of the charges associated with each ligand. However, while this is normally a trivial exercise when dealing with coordination compounds, problems arise when evaluating certain classes of organometallic (and related) compounds because the charge assigned to a ligand may be ambiguous. The first problem that arises is concerned with the precise rule that should be used to assign the charge on a ligand. In this regard, there are two methods that are frequently used: (i) the charge on the ligand is derived by transferring each shared pair of electrons to the more electronegative atom,[7] and (ii) the ligand is removed in a closed shell configuration[8] (for both of these methods, bonds between the same element are broken homolytically so that each atom receives one electron). In many cases, the application of these results has the same outcome and there is no ambiguity. For example, consider a M–Cl bond. Chlorine is more electronegative than the transition metals and, as such, the chlorine would be removed as Cl^- following rule (i). Application of rule (ii) requires the chlorine to be removed in a closed shell form, *i.e.* Cl^-. Thus, rules (i) and (ii) have the same outcome in this case; however, for more complex situations of the type that are frequently encountered in organometallic chemistry, the outcomes are *not* necessarily the same.

A simple illustration of a situation for which the application of the two rules has different outcomes is provided by (η^5-C_5H_5)Ti(η^7-C_7H_7). Application of rule (i) would require both carbocyclic rings to be removed as anions because carbon is more electronegative than titanium, *i.e.* $[C_5H_5]^-$ and $[C_7H_7]^-$, and thus titanium would be assigned an oxidation number of +2. A totally different outcome, however, results if rule (ii) is applied because although $[C_5H_5]^-$ is a 6 π-electron aromatic closed shell species, the C_7-symmetric $[C_7H_7]^-$ anion is *not closed shell*. The most commonly encountered closed shell form of the cycloheptatrienyl ligand is the 6 π-electron aromatic tropylium cation $[C_7H_7]^+$ and, on this basis, titanium would be assigned an oxidation number of zero. However, there is an additional problem because there exists another closed shell form of the cycloheptatrienyl ligand, which is the 10 π-electron aromatic trianion, $[C_7H_7]^{3-}$. If one were to select this form of the cycloheptatrienyl ligand, titanium would be assigned an oxidation number of +4. Thus, depending upon whether one were to classify the cycloheptatrienyl ligand as either a cation $[C_7H_7]^+$ (closed shell aromatic 6 π-electron configuration),[12,13] a monoanion, $[C_7H_7]^-$ (open shell),[14] or a trianion $[C_7H_7]^{3-}$ (closed shell aromatic 10 π-electron configuration),[15] each of which have been presented in the literature, the oxidation number of titanium in (η^5-C_5H_5)Ti(η^7-C_7H_7) may be assigned values of either 0, +2 or +4! Since the actual bonding in the molecule is invariant to the oxidation number, the large variation of oxidation number indicates that, by comparison to simple coordination compounds, the oxidation number is of limited utility in organometallic compounds. Indeed, a recent IUPAC article entitled *Nomenclature of Organometallic Compounds of the Transition Metals* concludes that it is inappropriate to assign oxidation numbers with respect to the nomenclature of organometallic compounds, *viz*: "As oxidation numbers cannot be assigned unambigously to many organometallic compounds, no formal oxidation numbers will be attributed to the central atoms in the following section on organometallic nomenclature."[16]

Problems in the assignment of oxidation numbers are by no means restricted to the cycloheptatrienyl ligand. For example, the simple "hydride" ligand exists in two closed shell forms, *i.e.* H^+ and H^-, but it is invariably viewed as H^- for the purpose of assigning oxidation numbers in transition metal compounds - despite the fact that certain metals (*e.g.* Pt) have a greater Pauling electronegativity than that of hydrogen![17] A similar dichotomy is observed for Lewis acid ligands such as AlR_3, which may be treated as either neutral AlR_3 or as dianionic $[AlR_3]^{2-}$, depending upon whether the electron pair is transferred to the aluminum or to the transition metal. Aluminum has a Pauling electronegativity (1.61) that is in between the values for the transition metals (1.22–2.54),[17] and thus the charge formally assigned to an AlR_3 ligand (0 or −2) could, in principle, vary for two otherwise closely related compounds if the oxidation number were to be determined by rule (i).

A related problem also results if rule (ii) is used to determine the oxidation number of complexes that possess Lewis acid ligands for which two closed shell forms exist. Thus, the AlR_3 ligand may be considered to be either neutral AlR_3 with a closed shell sextet (note that the term closed shell does *not* require and octet configuration)[11] or dianionic $[AlR_3]^{2-}$ with a closed shell octet. In these cases, some consideration needs to be given to determine the most appropriate closed shell form of the ligand. Two different criteria have been suggested. Firstly, it has been proposed that the closed shell form of the donor atom should generally have an octet configuration.[18] When applied to an AlR_3 ligand, this rule would result in using $[AlR_3]^{2-}$ to determine oxidation numbers; the latter complex, however, is an unusual example of a species with aluminum in the +1 oxidation state and is unknown.[19] An alternative suggestion, which is in keeping with the notion that the oxidation number of an atom was originally derived by removing the ligand in the form that it is *commonly encountered* in an uncoordinated state (*e.g.* Cl^-, NH_3, and OH_2), is that, in ambiguous situations, the charge assigned to the ligand should correspond to its *stable* uncoordinated

form.[20] On this basis, it is more appropriate to assign the AlR_3 ligand a charge of zero, but this procedure is by no means adopted by all authors.

The above discussion emphasizes that one must be very careful to establish the criteria (which may by no means be explicitly stated) by which an author assigns oxidation numbers. The criterion generally employed in this article is that the ligand is assigned the charge which is associated with the ligand in its *stable* closed shell configuration, *e.g.* $[C_7H_7]^+$ rather than $[C_7H_7]^-$ or $[C_7H_7]^{3-}$, AlR_3 rather than $[AlR_3]^{2-}$, and C_2H_4 rather than $[C_2H_4]^{2-}$; in each case, the assigned charge corresponds to the species that is commonly encountered in the free state in chemical systems. The charges assigned to a variety of ligands are summarized in Table 1, from which it is evident that the oxidation number formalism treats ligands as negative (*e.g.* R^-), neutral (*e.g.* CO), or positive (*e.g.* η^7-$C_7H_7^+$), whereas they are always treated as neutral according to the neutral ligand formalism.

While the η^7-C_7H_7 ligand has been assigned different charges for the same coordination mode, several other ligands have been assigned different charges for different coordination modes. For example, with respect to the oxidation number formalism, the nitrosyl ligand is assigned a charge of +1 if the M–N–O bond is linear, and a charge of −1 if it is bent.[21] The NO^+/NO^- classification for metal nitrosyls has, however, been severely criticized.[22] For example, Enemark and Feltham have noted that "it is quite misleading to describe all linear complexes as derivatives of NO^+ and all bent complexes as derivatives of NO^-" and that "assignment of oxidation states to the metal atom and NO is undesirable".[23] Furthermore, Scheidt has succinctly stated that the NO^+/NO^- formalism leads to unusual oxidation assignments and that "this formalism has little or no heuristic value",[24] while Richter-Addo and Legzdins emphasize that "assigning oxidation states to M–NO links is undesirable, since the formal oxidation states in $Co(CO)_3NO$, $Fe(CO)_2(NO)_2$, $Mn(CO)(NO)_3$ and $Cr(NO)_4$ have the unrealistic values of −1, −2, −3 and −4, respectively!".[25] Finally, as noted above, another inconsistency with the assignment of oxidation numbers is that NO^- is *not* a closed shell species.

Two other ligands that are related to NO in the sense that the oxidation number formalism classifies them as either positive or negative depending upon the coordination geometry are the N_2R diazenido ligand[26] and the PR_2 phosphido ligand.[27] Thus, complexes with bent M–N–NR units are classified as derivatives of anionic $(N_2R)^-$ ligands, while those with linear M–N–NR units are classified as derivatives of cationic $(N_2R)^+$ ligands. Likewise, $[MPR_2]$ complexes that are pyramidal at phosphorus are classified as derivatives of anionic $(PR_2)^-$ ligands, while those that are planar at phosphorus are classified as derivatives of cationic $(PR_2)^+$ ligands.

As noted for the nitrosyl complexes, the classification of these ligands as cations renders some rather unusual oxidation number assignments. For example, the phosphido complexes $(Cp^R)_2M(PR_2)_2$ (M = Zr, Hf)[28] which possess both planar and pyramidal PR_2 ligands would be classified as a Zr(II) and Hf(II) derivatives using the above oxidation number formalisms. However, in view of the fact that the organometallic chemistry of Zr and Hf is dominated by the +4 oxidation state, as exemplified by Cp_2MX_2 (e.g. X = Cl, Me, NMe_2),[29] the notion that $(Cp^R)_2M(PR_2)_2$ should be classified as M(II) is most unusual. In this regard, the structurally characterized complex $(Cp^{SiMe_3})_2Zr(PPh_2)_2$ has been classified as possessing a Zr(IV) center,[28b,29] with the authors thereby viewing both planar and pyramidal PPh_2 ligands as anionic $(PPh_2)^-$. In support of this suggestion, the reduction potential of $(Cp^R)_2ZrCl_2$ (R = Me_3Si) (−1.59 V *vs* SCE) is similar to the quasi-reversible reduction potential for $(Cp^R)_2Zr(PPh_2)_2$ (−1.72 V *vs* SCE)[28b] and other Zr(IV) complexes.[30] It would, therefore, appear that the cationic $(PR_2)^+$ classification of planar phosphido ligands is of limited utility.

1.01.2.1.3 Examples of electron counting

While both electron counting methods give the same answer for a given complex, the neutral ligand formalism is inherently simpler to apply since it eliminates the unnecessary step of first assigning oxidation numbers. Furthermore, for the set of cyclic η^n-C_nH_n ligands, the number of electrons donated according to the neutral ligand method is equal to the number of carbon atoms (*i.e.* the value of *n*), whereas the number of electrons donated by the oxidation number method shows no direct relationship to the number of carbon atoms unless *n* is even. For example, the η^7-C_7H_7 cycloheptatrienyl ligand is considered to be a 7-electron donor using the neutral formalism but has been considered to be either a cationic 6-electron donor, a monoanionic 8-electron donor, or a trianionic 10-electron donor using the oxidation number formalisms. Likewise, regardless of the detailed nature of the bonding in carbene complexes {M[C(R)X]} (Section 1.01.4.3.2), the [C(R)X] ligand is always considered to contribute two electrons using the neutral ligand formalism, whereas it is viewed as a 4-electron dianionic ligand in Schrock alkylidenes and as a neutral 2-electron donor in Fischer carbenes. Thus, for the purpose of electron counting, the neutral ligand formalism provides the most direct method, as illustrated for some simple examples in Figure 6.

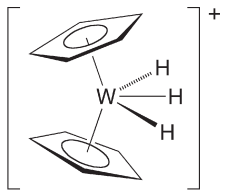

Neutral Ligand Method				Oxidation Number Method			
W	6	=	6	W^{VI}	$6-6^a$	=	0
$2(\eta^5\text{-}C_5H_5)$	2×5	=	10	$2(\eta^5\text{-}C_5H_5)^-$	2×6	=	12
3H	3×1	=	3	$3H^-$	3×2	=	6
(+) charge	–1	=	–1				18
			18				

(a) oxidation number = 1 – (–2 – 3) = 6

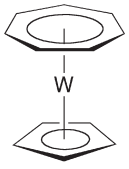

Neutral Ligand Method				Oxidation Number Method			
W	6	=	6	W^0	$6-0^a$	=	6
$(\eta^5\text{-}C_5H_5)$	1×5	=	5	$(\eta^5\text{-}C_5H_5)^-$	1×6	=	6
$(\eta^7\text{-}C_7H_7)$	1×7	=	7	$(\eta^7\text{-}C_7H_7)^+$	1×6	=	6
			18				18

(a) oxidation number = 0 – (1 – 1) = 0

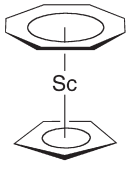

Neutral Ligand Method				Oxidation Number Method			
Sc	3	=	3	Sc^{III}	$3-3^a$	=	0
$(\eta^5\text{-}C_5H_5)$	1×5	=	5	$(\eta^5\text{-}C_5H_5)^-$	1×6	=	6
$(\eta^8\text{-}C_8H_8)$	1×8	=	8	$(\eta^8\text{-}C_8H_8)^{2-}$	1×10	=	10
			16				16

(a) oxidation number = 0 – (–1 – 2) = 3

Figure 6 Comparison of the two procedures for determining the valence electron count. The advantage of the neutral ligand method is that it eliminates the unnecessary step of first determining the oxidation number of the metal (charge on molecule – Σcharge on ligands). Also, note that the number of electrons donated by a (η^n–C_nH_n) ligand is simply equal to the value of *n* for the neutral ligand method, whereas this is not generally true for the oxidation number method.

In addition to its greater simplicity, other points to support the use of the neutral ligand formalism are that *(i)* it is the same method that is generally taught for determining the electron count in simple molecules such as CH_4, NH_3, and H_2O,[31] and *(ii)* historically, it is the same method that Sidgwick used in his discussion of the "effective atomic number" of an atom in a molecule.[32] On the other hand, proponents of the oxidation number formalism favor it because the charge assigned to a ligand often corresponds to that of its uncoordinated state in chemical systems. However, as will be discussed in detail later, the charge on the metal suggested by this approach bears no relationship to reality and it does *not* accurately reflect the nature of the ligand *in the molecule*. The neutral ligand formalism will, therefore, be used exclusively throughout the remainder of this article for the purpose of electron counting.

1.01.2.1.4 A caveat for electron counting

The significance of electron counting is that it provides a simple means to establish how many electrons reside in molecular orbitals associated with the metal in a complex. Coupled with the basic knowledge of how a molecular orbital diagram depends on molecular symmetry (see, for example, Figures 1–3), the electron count provides a means to establish the extent to which metal–ligand bonding orbitals, nonbonding metal orbitals, and metal–ligand antibonding orbitals are occupied. For, example, the electron count of 18 for $Mo(PMe_3)_6$ indicates that a total of 9 bonding/nonbonding/antibonding orbitals associated with the metal are occupied, whereas the electron count of 16 for $Pt(PR_3)_2R_2$ indicates that a total of 8 bonding/nonbonding/antibonding orbitals associated with the metal are occupied. Examination of the respective molecular orbital diagrams in Figures 1 and 2 confirms this prediction.

However, it is important to note that simple electron counting does not always correctly predict the number of occupied bonding/nonbonding/antibonding orbitals associated with the metal in a molecular orbital diagram. A particularly notable example is provided by $W(C_2R_2)_3CO$, for which simple electron counting procedures, invoking the acetylene ligand as a 4-electron donor and the carbonyl ligand as a 2-electron donor, would predict a 20-electron count for the tungsten center. However, a molecular orbital analysis of this molecule indicates that one of the six $[(C_2R_2)_3]$ combination orbitals does not have the appropriate symmetry to interact with the metal and thus the electron count is 18, with the additional pair of electrons residing in a $[(C_2R_2)_3]$ ligand based a_2 orbital with no symmetry match amongst the metal s, p and d orbitals (Figure 7).[33]

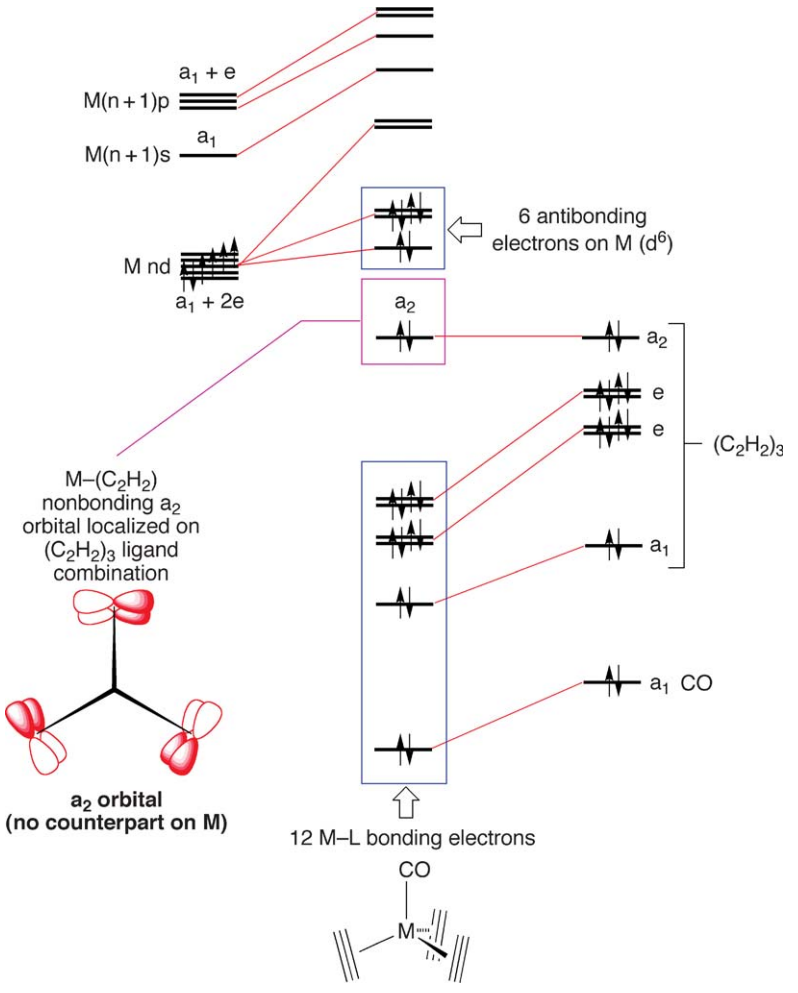

Figure 7 Molecular orbital diagram for $(\eta^2\text{–}C_2H_2)_3M(CO)$ with C_{3v} symmetry. Three C_2H_2 ligands may donate 12 electrons, but 2 electrons reside in a M–(C_2H_2) nonbonding orbital. Thus, the three C_2H_2 ligands donate only 10 electrons to the metal center, such that $(\eta^2\text{–}C_2H_2)_3M(CO)$ has an 18-electron configuration for M = W.

Analogous situations arise for Cp_3MX,[34] $Os(NAr)_3$,[35] $(RN)_3MoL$,[36] $M(BH_4)_4$[37] and [η^8-pentalene]$_2$M (M = Ti, Zr, Hf);[38,39] in each case, the electron count is reduced from 20 to 18 because a specific ligand orbital combination has no symmetry match with a metal based s, p or d orbital.[40] It is, therefore, evident that electron count can only be viewed as a *guide* – albeit a very useful guide – to indicate the nature of the occupied and unoccupied orbitals, and hence stability of a compound.

1.01.2.2 Ligands with Variable Electron Donor Number and Coordination Number

Many ligands have the ability to coordinate with variable hapticity and consequently variable electron donor number. For example, the cyclopentadienyl ligand commonly coordinates *via* η^5-, η^3- and η^1-modes,[41] for which the electron donor numbers are 5, 3, and 1, respectively (Figure 8).[42] Likewise, benzene may coordinate *via* η^6-, η^4- and η^2-modes, for which the electron donor numbers are 6, 4, and 2, respectively. Acyclic ligands that exhibit variable coordination modes are also known. For example, allyl coordinates in both η^3- and η^1-modes, serving as a 3-electron donor and a 1-electron donor ligand, respectively. Other examples of ligands that exhibit variable electron donor and coordination numbers are listed in Table 3.

1.01.2.3 Ligands with Variable Electron Donor Number without Change in Coordination Number

In addition to ligands such as cyclopentadienyl and benzene that donate variable numbers of electrons due to differences in hapticity, there are also ligands that may donate variable numbers of electrons while *maintaining the*

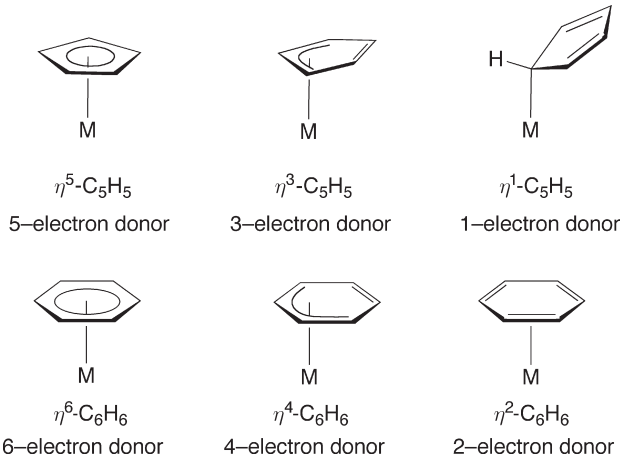

Figure 8 Variable electron donor numbers resulting from different coordination modes for cyclopentadienyl and benzene ligands.

Table 3 Examples of ligands that exhibit variable electron donor number associated with a change in coordination number

Ligand & coordination mode	*Electron donor number*
η^5–C_5H_5	5
η^3–C_5H_5	3
η^2–C_5H_5	3
η^1–C_5H_5	1
η^6–C_6H_6	6
η^4–C_6H_6	4
η^2–C_6H_6	2
η^3–C_3H_5	3
η^1–C_5H_5	1
κ^2–O_2CMe	3
κ^1–O_2CMe	1

Table 4 Examples of ligands that exhibit a variable electron donor number while maintaining the same coordination number

Ligand & coordination mode	*Electron donor number*
OR (bent)	1 or 3
OR (linear)	5
NO (bent)	1
NO (linear)	3
NR_2 (pyramidal)	1
NR_2 (planar)	3
NR (bent)	2
NR (linear)	4
C_2R_2	2 or 4
E (E = O, S, Se, Te)	0, 2, or 4

same coordination number to the metal (Table 4). In each case, the electron donor number of the ligand is dictated by the electronic requirements of the metal center. For example, an alkoxide (OR) ligand is a neutral 1-electron σ-donor but may also function as neutral 3-electron and 5-electron donor ligands (Figure 9). The nitrosyl (NO) ligand is closely related to the alkoxide ligand and coordinates to a metal center as either a neutral 1-electron donor and as a neutral 3-electron donor if the lone pair on nitrogen donates to the metal center. The 1-electron donor interaction is characterized by a bent M–N–O geometry, while the 3-electron donor interaction requires a linear geometry. The amide (NR_2) ligand also serves as a 1-electron and 3-electron donor ligand, corresponding to pyramidal and planar geometries, respectively, at nitrogen.

The imido ligand (NR) is an example of a multiply bonded group that may coordinate as either a neutral 2-electron donor and as a 4-electron donor. While nitrogen-to-metal lone pair donation and the formation of a $\bar{M}{\equiv}\overset{+}{N}R$ triple bond requires a linear M–N–R unit, it must be emphasized that the converse is not true. Thus, it is possible for steric interactions to enforce a linear geometry, in which case the lone pair resides in a p-orbital on the nitrogen.[43]

A subtle example of variable electron donor properties is provided by alkynes which may be either 2- or 4-electron donors, with negligible change in coordination properties (Figure 10).[44] Thus, in addition to the C–C π-bond in the $[MC_2]$ plane ($\pi_{\parallel}$) serving as a 2-electron σ-donor in a similar manner to that in metal–olefin complexes, the perpendicular π-bond of the alkyne ($\pi_{\perp}$) may also serve as donor, but in a π rather than σ sense. Thus, alkynes may be classified as 2-electron (σ) or 4-electron ($\sigma + \pi$) donors. To facilitate electron counting, these interactions may be represented with single and double arrows, respectively.

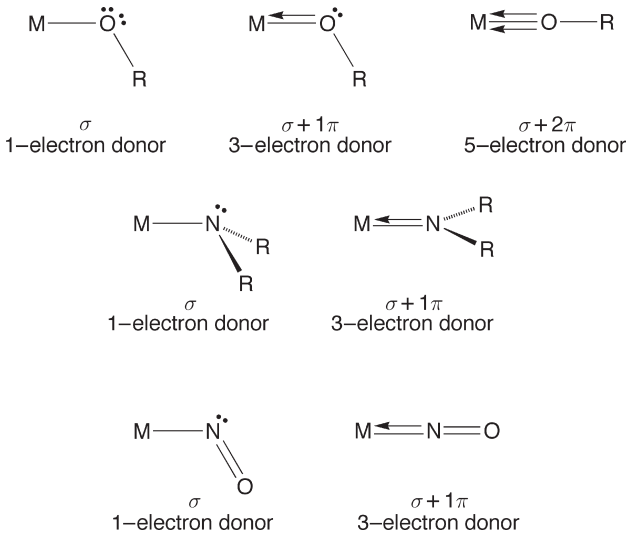

Figure 9 Variable electron donor numbers for ligands with the same coordination number (for clarity, the backbonding component is not illustrated for the nitrosyl ligand; see Section 1.01.4.3.2).

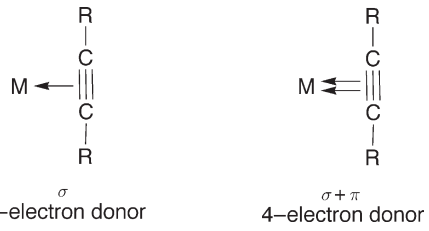

Figure 10 Variable electron donor numbers for ligands with the same coordination mode.

Chalcogenido ligands (O, S, Se and Te), and especially the most commonly encountered oxo and sulfido ligands, provide an even more subtle means to provide different electron donor properties with negligible variation in coordination properties.[45] Specifically, metal-chalcogenido interactions may be considered to be a composite of three resonance structures, with formal single [$\overset{+}{\text{M}}$–$\overset{-}{\text{E}}$], double [M═E], and triple $\overset{-}{\text{M}}\equiv\overset{+}{\text{E}}$ bonds, corresponding to 0-electron, 2-electron, and 4-electron donors, respectively.[45]

1.01.2.4 Bridging Ligands

An essential component of electron counting requires representing the molecule in a form that conveys the number of electrons a ligand donates to a metal center. However, certain bridging ligands cause problems with respect to determining the electron count in polynuclear organometallic compounds. Specifically, whereas the contribution of many bridging ligands to the electron count may be readily inferred by a simple valence bond description of the bonding, as illustrated by Cl, carbonyl, and alkylidene ligands, bridging hydride and alkyl ligands frequently cause problems because the 3-center-2-electron interaction is often not represented properly for electron counting purposes. In this regard, a large variety of bonding representations for bridging hydride ligands have been presented in the literature (Figure 11), but most of these are not particularly helpful from the perspective of electron counting. Thus, while a dashed line could be used to indicate the existence of a 3-center-2-electron interaction, it is not immediately obvious how this representation enables the electron count to be determined.

Bridging hydride and alkyl compounds bear a close analogy to other molecules that possess 3-center-2-electron bonds, such as transition metal dihydrogen complexes [M(η^2-H_2)] and alkane σ-complexes [M(η^2-RH)]. For the

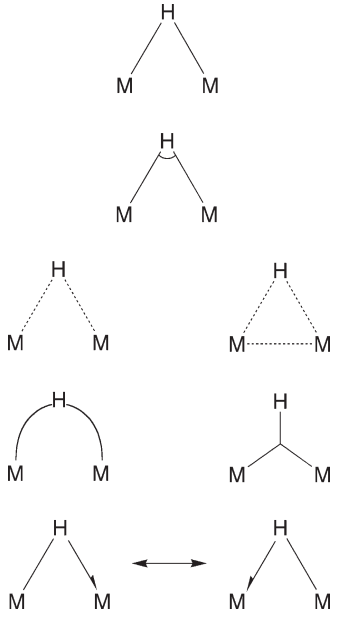

Figure 11 Representations of 3-center-2-electron M–H–M interactions presented in the literature.

purposes of electron counting, the 3-center-2-electron bond in a transition metal dihydrogen complex [M(η^2-H_2)] can be described as a sharing of the pair of electrons in the H–H σ-bond with the metal, and thus a dihydrogen ligand contributes a pair of electrons to the electron count of M. The situation is exactly the same with a bridging hydride complex [M(μ–H)M], as illustrated for simplicity by diborane, the archetype of 3-center-2-electron bonding. In essence, the two B–H–B interactions may be viewed as involving donation of the σ-bond electron density of the B–H bond of one BH_3 fragment into an empty orbital on boron of the other fragment (Figure 12). In this way, one clearly sees how the electronic unsaturation of the boron atom in BH_3 is removed and an octet configuration is attained.

Green has introduced a modified representation for the 3-center-2-electron bonding interaction in which a "half arrow" is drawn from the bridging hydrogen atom rather than a "full arrow" from the midpoint of the M–H bond (Figure 13);[1,46] note that the "straight half arrow" is not to be confused with the "curly half arrow" that is used in describing organic reaction mechanisms. Despite the different form of the representation, the "half arrow" notation is intended to convey exactly the same information as that involving an arrow from the center of the bond, and thus the representation M–H⇀M′ depicts that the pair of electrons associated with the M–H sigma bond is donated into a vacant orbital on M′. The principal advantage of the "half arrow" notation is that it is less cumbersome for molecules with multiple bridging groups. This notation is also very similar to that using a "full arrow" from an atom to represent interactions involving bridging ligands that possess a lone pair, such as chloride. The important distinction between the "half arrow" and "full arrow" representations is that the former implies donation of a *bond* pair into a vacant orbital (such that the bonding involves one 3-center-2-electron bond), while the latter implies that a *lone* pair is available for donation into a vacant orbital (such that the bonding may involve two 2-center-2-electron bonds).

The "half arrow" notation is not restricted to M–H–M interactions, but applies equally well to other complexes that exhibit 3-center-2-electron bonds, such as those involving coordination of *(i)* C–H and B–H bonds, *e.g.* agostic alkyl complexes[47] and borohydride derivatives,[48] and *(ii)* M–C bonds, *e.g.* symmetrically bridging methyl ligands.

In contrast to the above electron counting method for M–H–M and related 3-center-2-electron interactions, an alternative method merely apportions the electron associated with the hydride ligand equally to both metals,[49,50] and the bond order is determined by application of the formula $m = (18n - N)/2$ where m is the number of 2-center-2-electron M–M bonds, n is the number of M atoms, and N is the total electron count. Employing the neutral ligand electron counting procedure, this method has the outcome that a bridging hydrogen atom or alkyl radical contributes half of an electron to the electron count at each metal center of a dinuclear complex. An important consequence of the difference between these two electron counting procedures is that they result in different M–M bond orders in order to achieve a specific electron count, as illustrated by the selection of compounds in Figure 14. Computations on a variety of dinuclear [M(μ-H)M] complexes, however, indicate that the most appropriate description of the bonding is that obtained by application of the "half arrow" method rather than that assuming a bridging hydrogen atom contributes half of an electron to the electron count at each metal center. For example, a molecular orbital analysis of the bonding in [CpMo(μ-O_2CH)]$_2$(μ-PH_2)(μ-H) indicates that the direct Mo–Mo interaction is a single bond, in accord with that predicted using the "half arrow" method, whereas the "half electron" method would predict a Mo═Mo double bond.[51] The extent of metal-metal bonding in a complex may also be evaluated in terms of the Complementary Spherical Electron Density Model which seeks to minimize the number of "unavailable" orbitals.[4]

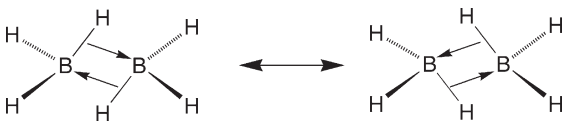

Figure 12 Representations of the 3-center-2-electron B–H–B interaction in diborane which emphasizes the octet configuration of boron.

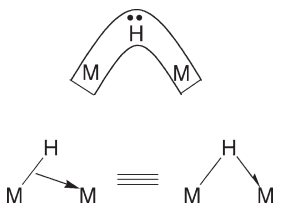

Figure 13 The "half-arrow" representation of a 3-center-2-electron M–H–M interaction, which may be viewed as donation of a pair of electrons associated of the M–H sigma bond into a vacant orbital on the other M.

Other examples which illustrate that the "half electron" method for counting bridging hydride and alkyl ligands is flawed are provided by $[Cp_2ZrH_2]_2$ and $[CpReH_3]_2$. Thus, for the zirconocene dimer, $[Cp_2Zr(H)]_2(\mu\text{-}H)_2$, the "half-electron" method predicts a Zr═Zr double bond whereas the "half-arrow" method indicates that each Zr center can attain an 18-electron configuration without forming two 2-center-2-electron Zr–Zr bonds (Figure 14). Since the Zr center of mononuclear Cp_2ZrH_2 is d^0, and therefore incapable of forming a 2-center-2-electron Zr–Zr bond, it is evident that the "half electron" description of the bonding results in an untenable description of the Zr–Zr interaction. With respect to $[CpReH_3]_2$, three isomers that differ according to whether there are *(i)* no bridging hydrogens, $[CpReH_3]_2$, *(ii)* two bridging hydrogens, $[CpReH_2]_2(\mu\text{-}H)_2$ and *(iii)* four bridging hydrogens, $[CpReH]_2(\mu\text{-}H)_4$ have been considered.[52] The "half-electron" method predicts the existence of a Re≡Re triple bond for each of these isomers, regardless of how many hydrogen atoms bridge the two metals. The notion that the Re–Re bond order would not vary with the number of bridging hydrogen atoms is counterintuitive and, indeed, calculations indicate that the Re–Re bond order is actually reduced as the hydride ligands bridge,[52] a result that is consistent with the "half-arrow" counting method.

With respect to the isomer with four bridging hydrogen atoms, $[CpReH]_2(\mu\text{-}H)_4$, it is important to note that situations arise where the "half-arrow" method does *not* predict an 18-electron configuration for both metals in a dinuclear complex. Thus, molecules such as $[CpReH]_2(\mu\text{-}H)_4$, $[Cp^*Re(CO)_2]_2(\mu\text{-}H)_2$, $\{[\{MeC(CH_2AsPh_2)_3\}Co]_2(\mu\text{-}H)_3\}^+$, $[Cp^*Ru]_2(\mu\text{-}H)_4$, and $[(Et_2PhP)_2Re(H)_2]_2(\mu\text{-}H)_4$ each possess a 20-electron configuration, which indicates that

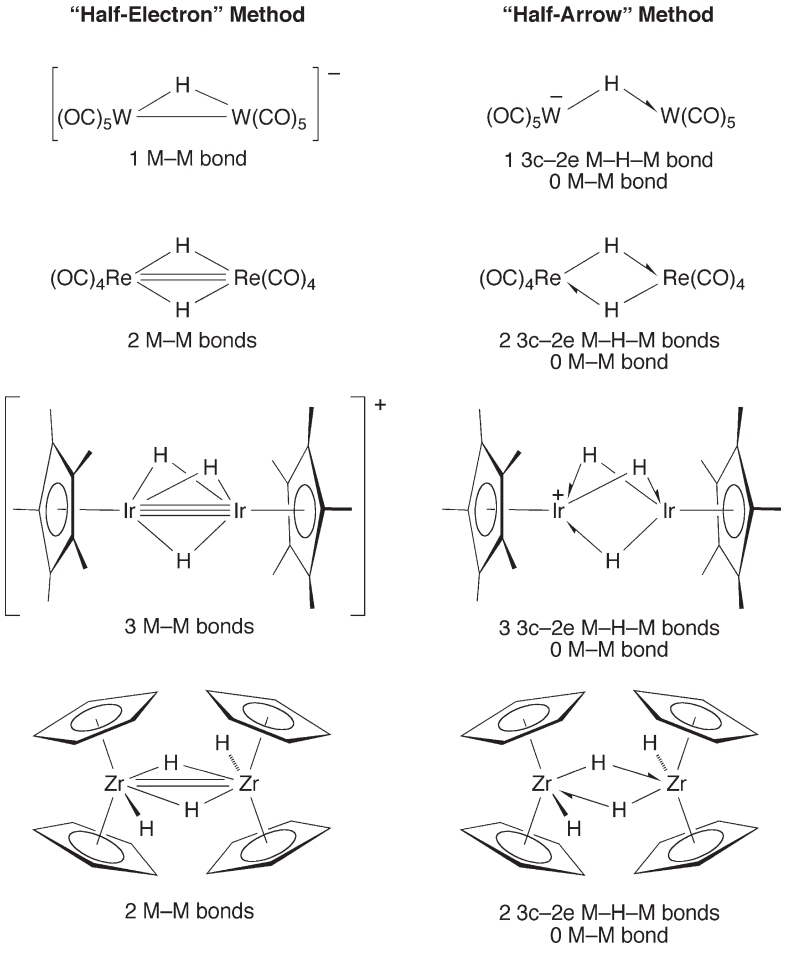

Figure 14 Different descriptions of the metal–metal bond orders in some dinuclear complexes with bridging hydride ligands according to the electron counting method. The ''half-electron'' method does not explicitly take into account the 3-center-2-electron nature of the M–H–M interaction and thus results in a greater M–M bond order than would be predicted theoretically. In contrast, the ''half-arrow'' method treats the 3-center-2-electron nature of the M–H–M interactions explicitly and thereby predicts a M–M bond order which is in accord with theory.

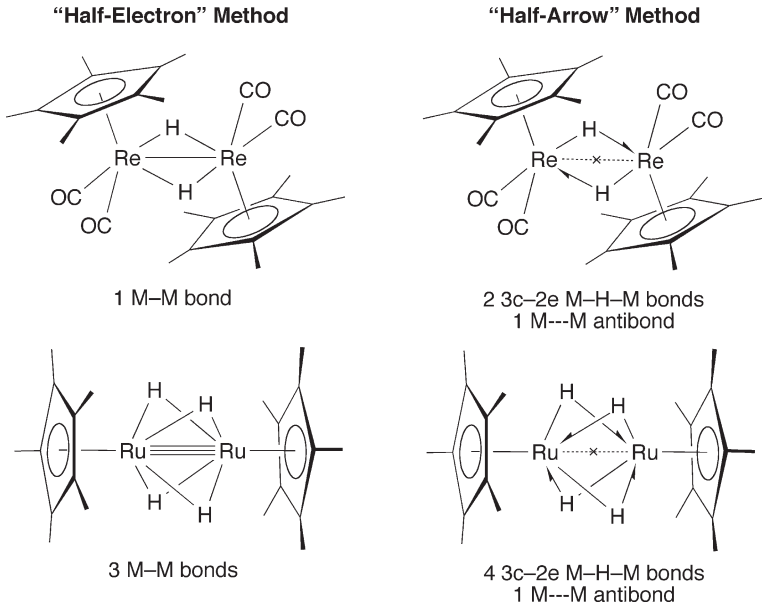

Figure 15 Examples of compounds that exhibit M···x···M antibonding interactions resulting from a 20-electron configuration that places a pair of electrons in a M–M antibonding orbital. In contrast, the formula employing the ''half-electron'' method defines each metal center as possessing an 18-electron configuration and so the true nature of the M–M interaction is not evident.

a metal-metal antibonding orbital is occupied and, as a result, the M–M bond order is reduced (Figure 15). Consider, for example, the hypothetical protonation of a dinuclear system in which there is no formal 2-center-2-electron M–M bond because both bonding and antibonding components are occupied (Figure 16). The hydrogen 1*s* orbital interacts specifically with the bonding component to form a 3-center-2-electron bond, thereby leaving a pair of electrons in a

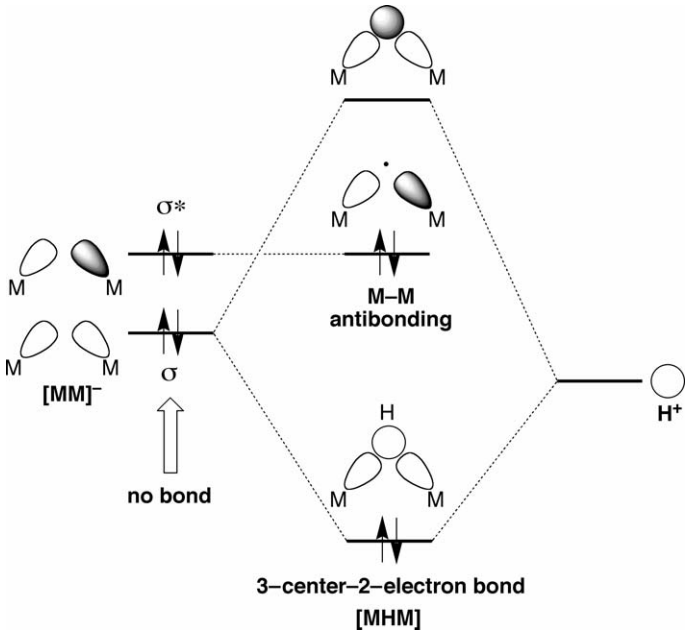

Figure 16 Molecular orbital description of a M···x···M antibonding interaction in a [MHM] species derived by interaction of $[M_2]^-$ and H^+ fragments in which each atom uses a single orbital. Protonation of the $[M_2]^-$ fragment results in the interaction of the H 1s orbital with the M–M bonding orbital, thereby forming a 3-center-2-electron M–H–M bonding orbital and leaving a pair of electrons in the M–M antibonding orbital. As such, the direct M–M interaction becomes repulsive, *i.e.* an *antibond*.

M–M antibonding orbital. The resulting interaction has been termed an "antibond",[53] and may be depicted by using a crossed-dashed M···×···M representation in which the cross is intended to emphasize that the direct interaction is *antibonding*.[51] Despite the presence of an "antibond", the overall interaction between the two metal centers is favorable because of the stabilization resulting from the formation of the 3-center-2-electron bond.[54]

1.01.3 Valence, Oxidation Numbers and Coordination Numbers in Organometallic Compounds

It is important to emphasize that assessing the viability of the existence of a molecule by only evaluating the electron count at a metal center has serious limitations. For example, although the hypothetical molecule "$W(PMe_3)_2(CH_3)_8$" may be regarded as an 18-electron molecule, it has little chance of existing because the tungsten requires eight valence electrons to coordinate the eight methyl groups in a 2-center-2-electron bonding scheme, but tungsten only possesses six valence electrons. The formulation "$W(PMe_3)_2(CH_3)_8$" is, therefore, clearly unreasonable unless 3-center-2-electron bonding is invoked. In addition to electronic considerations, steric considerations would suggest that the 10-coordinate tungsten complex "$W(PMe_3)_2(CH_3)_8$" could be unstable; indeed, since a transition metal has only nine valence orbitals available, a metal center that is coordinated to 10 monodentate ligands is unusual. It is, therefore, evident that, in addition to the electronic count of the metal center, other criteria are required to discern whether a molecule possesses a reasonable structure. In this regard, formal charge, oxidation number, and valence are often used to address electronic properties, while coordination number generally provides an indication of steric saturation.

1.01.3.1 Valence, Oxidation Number and d^n Configuration

As indicated above, the nonexistence of a molecule such as "$W(PMe_3)_2(CH_3)_8$" is implied by the fact that the valence of tungsten, *i.e.* the number of electrons that the atom uses in bonding, is greater than the group valence. At this point, it is pertinent to discuss explicitly this usage of the term "valence" because the concepts and definitions of valence have been refined considerably over the years. In this regard, the definition employed by Sidgwick remains the most useful for covalent molecules: the valence of an atom in a covalent molecule is simply the number of electrons that it has used in bonding.[55] In a molecular orbital sense, the valence corresponds to the number of electrons that a specific element contributes to molecular orbitals that have bonding character and is therefore equal to the difference between *(i)* the number of valence electrons in the free atom (*i.e.* the group valence) and *(ii)* the number of "nonbonding" electrons on the atom in the molecule.

$$\text{valence} = \text{no. electrons in valence shell of } \textbf{\textit{free}} \text{ atom} - \text{no. ''nonbonding'' electrons on atom in molecule} \quad (1)$$

Despite this simple and useful definition, it is unfortunate that valence has been taken to be synonymous with *(i)* oxidation number, *(ii)* number of bonds, and *(iii)* coordination number.[55,56] The origin of this confusion is that, for certain simple molecules, the valence is often coincidentally equal to either the oxidation number, number of bonds or coordination number. For example, for neutral AH_n hydrides (*e.g.* CH_4, NH_3, and OH_2) the valence, magnitude of the oxidation number, number of bonds and coordination number each have the same value, *n*. This relationship, however, breaks down in many cases, as illustrated by $[NH_4]^+$, for which the nitrogen atom has used all five of its valence electrons and is pentavalent, but its oxidation number is −3, the number of bonds is 4, and the coordination number is 4.

The most serious problems, however, arise when valence and oxidation number are confused. In many cases, the valence and oxidation number are identical, but there are many examples for which they deviate. For instance, the equivalence between valence and oxidation number breaks down when either *(i)* homonuclear element-element bonds are present, *(ii)* the ligands attached to the atom of interest are dissociated with opposite charges, *e.g.* H^+ and Cl^-, or *(iii)* the ligand is dissociated as a cation, *e.g.* H^+, NO^+ and $(C_7H_7)^+$. Illustrative examples of these breakdowns are provided by consideration of some simple molecules. Thus, with respect to the issue of the neglect of homonuclear element-element bonds in the determination of oxidation number, the valence of the central carbon in $\underline{C}Me_4$ is four, but the oxidation number is zero. Likewise, the valence of carbon in CH_2Cl_2 is also four, but the oxidation number is zero because, in terms of electronegativity differences, H is viewed as "H^+" and Cl is viewed as "Cl^-" when attached to carbon. Finally, as noted above, the valence of nitrogen in $[NH_4]^+$ is five, but its oxidation number is −3.

In transition metal chemistry, the most important ramification of confusing valence and oxidation number pertains to the determination of the d^n configuration of the metal in the complex. The d^n configuration describes the number of electrons of the transition metal atom that are *not* involved in the formation of the metal-ligand bonds,[57] and, in a molecular orbital sense refers to the number of electrons in nonbonding metal and slightly metal-ligand antibonding orbitals, as illustrated by the general molecular orbital diagram in Figure 17.[1,57,58] The d^n configuration is an important quantity since it *(i)* indicates whether or not a metal possesses sufficient electrons for further reactivity and *(ii)* influences the magnetic and spectroscopic properties of a molecule. In terms of the valence, the value of n in the d^n configuration is described by the relationship.

$$n = \text{number of valence electrons in neutral atom} - \text{valence} \quad (2)$$

A related expression based on oxidation numbers is also frequently used to determine the d^n configuration.[59]

$$n = \text{number of valence electrons in neutral atom} - \text{oxidation number} \quad (3)$$

However, while these two expressions are identical when the valence and oxidation number are coincidentally the same, different values of d^n result when the valence and oxidation number differ. For example, the manganese atoms of $(CO)_5Mn–Mn(CO)_5$ are monovalent but have a zero oxidation state. The zero oxidation state would imply that each manganese has a d^7 configuration (equation 3) with an odd number of electrons, whereas the monovalence implies that each manganese has a d^6 configuration (equation 2). Likewise, coordination of a Lewis acid such as R_3E (E = B, Ga, Al, In),[60,61] $HgCl_2$,[62,63] and ZnX_2 (X = Cl, Br),[63,64] to a transition metal does not change the oxidation number, but does have an impact on the valence. For example, consider the adduct $[CpFe(CO)_2(AlPh_3)]^-$ which is obtained *via* addition of Ph_3Al to $[CpFe(CO)_2]^-$.[60] Although the oxidation number of iron does not vary upon coordination of R_3Al (Section 1.01.2.1.2), its valence increases by two because the iron must provide both of the electrons used in forming the Fe–Al bond. Thus, while the oxidation number of iron in $[CpFe(CO)_2(AlPh_3)]^-$ is zero, its valence is two and the iron possesses a d^6 configuration. In this regard, consideration of the structure with a negative formal charge located on aluminum indicates how $[CpFe(CO)_2(AlPh_3)]^-$ belongs to the common class of $CpFe(CO)_2X$ derivatives that are widely regarded as possessing d^6 configurations (Figure 18). Calculations on $[\kappa^4\text{-}B(mim^{Bu^t})_3]Ir(PPh_3)Cl$ also indicate that the metal center possesses a d^6 configuration rather than the d^8 configuration derived assuming the borane ligand is a neutral ligand.[65]

In each case where the d^n value determined by consideration of valence and oxidation number differ, that determined by employing the valence shows a better correspondence to the molecular orbital diagram of the compound under consideration.

Another caveat concerned with oxidation numbers refers to the often perceived notion that they refer in some way to an "actual" charge on an atom in a molecule. However, the oxidation number is the charge that is derived by breaking all bonds (except homonuclear bonds) heterolytically such that the pair of electrons in the bond are

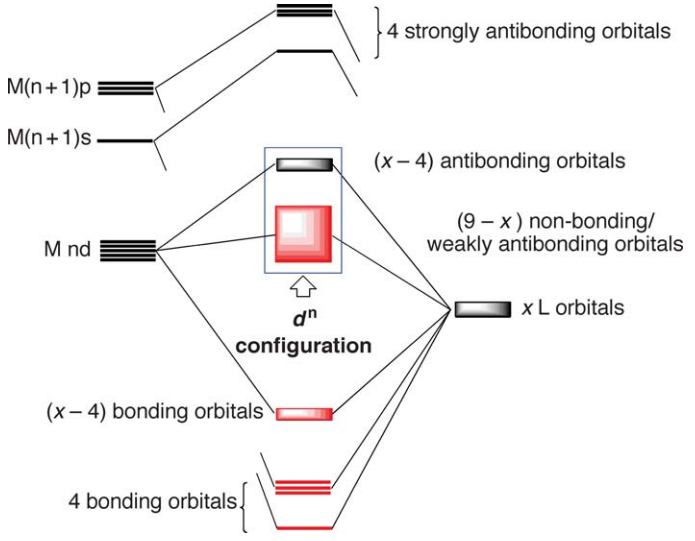

Figure 17 A simplified generalized MO diagram for a ML_x ($x \geq 4$) complex for σ-only interactions illustrating the d^n configuration which corresponds to occupancy of the nonbonding and the metal–ligand antibonding orbitals with d character.

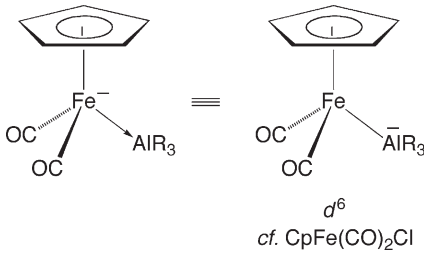

Figure 18 A representation of $[CpFe(CO)_2(AlPh_3)]^-$ which draws an analogy with $CpFe(CO)_2Cl$ to emphasize the d^6 configuration of the metal center.

transferred to a single atom; as such, the derived charge does *not* correspond to a charge on an atom *in a molecule*. Oxidation number is only one type of charge that may be assigned to atoms in molecules, with a second type of charge being the "formal charge" (FC). The formal charge of an atom in a given Lewis structure is the charge it would possess if all bonds are broken *homolytically*.[66]

$$\begin{aligned} \text{FC} = {} & \text{no. electrons in valence shell of } \textit{free} \text{ atom} \\ & - \text{no. electrons remaining on the atom in a molecule} \\ & \quad \text{when all bonds are broken } \textbf{\textit{homolytically}} \end{aligned} \qquad [4]$$

As a result of these definitions, which respectively exaggerate the ***ionic*** and ***covalent*** character of the bonding (Figure 19), the oxidation number and formal charge have very different values and neither one is necessarily related to the actual charge. Rather, the charge (as evaluated by calculations)[67] is usually intermediate between the extremes represented by the oxidation number and formal charge (Table 5). Unfortunately, the distinction between the actual charge and the hypothetical extremes of formal charge and oxidation number is not always properly recognized.[68] For example, the formal charges of a given resonance structure are often taken to be indicative of the charge distribution in a molecule, but this is not always the situation. As an illustration, the formal charge on nitrogen in $[NH_4]^+$ is positive, but the actual charge is negative.[69]

It is also pertinent to note that the charge on an atom is typically considered to be less than $|\pm 1|$, a concept referred to as the Pauling Electroneutrality Principle.[70] In this regard, Hoffmann discusses the oxidation number of iron in

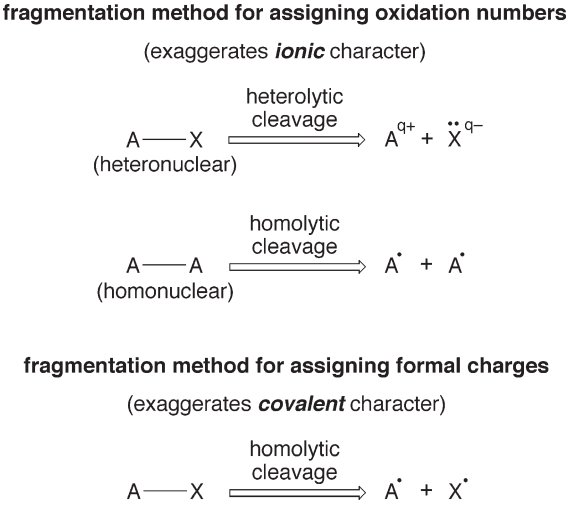

Figure 19 Fragmentation methods for assigning oxidation number and formal charge. The fragmentation method for assigning oxidation numbers involves the conceptual ***heterolytic cleavage*** of the A–X bond such that the pair of electrons is typically transferred to the more electronegative atom (an exception is for homonuclear bonds which are cleaved homolytically). In contrast, the fragmentation method for assigning formal charges involves the ***homolytic cleavage*** of the A–X bond such that each atom receives a single electron.

Table 5 Comparison of oxidation number, formal charge and calculated charge for some simple molecules (data taken from Parkin, G. *J. Chem. Educ*. **2006**, *83*, 791–797)

Molecule	*Oxidation Number*	*Calculated Charge*	*Formal Charge*
CH_4	−4	−0.82	0
$[CH_3]^+$	−2	0.35	+1
$[CH_3]^-$	−4	−1.36	−1
NH_3	−3	−1.05	0
NH_4^+	−3	−0.84	+1

$[FeO_4]^{2-}$ and $[Fe(CO)_4]^{2-}$ as follows: "Is there really a charge of +6 on the iron in the first compound, and a −2 charge in the carbonylate? Of course not, as Pauling told us in one of his many correct (among some incorrect) intuitions. Such large charge separation in a molecule is unnatural. Those ions aren't bare – the metal center is surrounded by more or less tightly bound 'ligands' of other simple ions (Cl^- for instance) or molecular groupings (CN^-, H_2O, PH_3, CO). The surrounding ligands act as sources or sinks of electrons, partly neutralizing the formal charge of the central metal atom. At the end, the net charge on a metal ion, regardless of its oxidation state, rarely lies outside the limits of +1 to −1."[71]

Although formal charges are very useful for electron bookkeeping purposes, inorganic chemists tend to focus more on the oxidation number as being of greater significance. The origin of this focus is that oxidation numbers were originally introduced for classical coordination compounds for which the oxidation number and valence are coincidentally equivalent. However, this equivalence breaks down for a significant number of organometallic compounds. Examples of such compounds include those with *(i)* metal-metal bonds and *(ii)* ligands that are treated as cations, *e.g.* NO^+ and $(\eta^7\text{-}C_7H_7)^+$. Thus, the chemical insight that is provided by the value of the oxidation number in classical coordination compounds cannot be universally transferred to organometallic compounds. Despite this problem, the notion of oxidation number is so deep-rooted in inorganic chemistry that it is still common for organometallic compounds to be assigned oxidation numbers and, in this regard, oxidation numbers could still have a value in terms of compound classification. Indeed, to quote from Seddon and Seddon: "···the oxidation state concept can be thought of as the Dewey Decimal Classification of inorganic chemistry – if the rules are applied, a number is obtained".[72] However, Seddon and Seddon continue: "Does oxidation state have a chemical significance? A number is always obtained – does it mean anything?" A more useful classification method is provided by the "Covalent Bond Classification Method", which is based on the concept of valence and therefore provides considerably more insight into the nature of a molecule, as discussed in detail in Section 1.01.4.

1.01.3.2 Coordination Number

Consideration of the coordination number of an element is a useful means of assessing the stability of molecule by judging whether it is coordinatively saturated or unsaturated. Surprisingly, however, the assignment of "coordination number" is not always trivial because the term is interpreted with more than one meaning in the literature. For example, what are the coordination numbers of chromium in $(\eta^5\text{-}C_5H_5)_2Cr$ and $(\eta^6\text{-}C_6H_6)_2Cr$? Common answers for $(\eta^5\text{-}C_5H_5)_2Cr$ range from 10 to 2, while for $(\eta^6\text{-}C_6H_6)_2Cr$ the answers range from 12 to 2![73] The reason for such a large discrepancy is due to the different notions that chemists have regarding the term "coordination number".

The traditional coordination number is simply defined as the number of atoms attached to the atom of interest in a molecule.[74] Using this definition, the coordination numbers of chromium in $(\eta^5\text{-}C_5H_5)_2Cr$ and $(\eta^6\text{-}C_6H_6)_2Cr$ are 10 and 12, respectively. However, this definition of coordination number was introduced at a time when inorganic molecules were "simple" and ligating atoms were not themselves directly bonded to each other. With the advent of more complex ligands, such as $(\eta^5\text{-}C_5H_5)$ and $(\eta^6\text{-}C_6H_6)$, the notion of "coordination number" has changed, with some viewing the "coordination number" to be the number of *ligands* coordinated to a metal center.[75] Using this definition, the coordination number of the chromium atoms in both $(\eta^5\text{-}C_5H_5)_2Cr$ and $(\eta^6\text{-}C_6H_6)_2Cr$ is 2.

Interestingly, organometallic chemists tend to use neither of these definitions for "coordination number". Instead, organometallic chemists assign a coordination number to a ligand based on the number of "coordination sites" they judge it to occupy. For example, a symmetrically bound ethylene ligand is viewed as occupying a single coordination site, even though it is attached *via* two carbon atoms and therefore has, in the strictest sense, a coordination number of *two*. Extending this approach, organometallic chemists classify the $(\eta^6\text{-}C_6H_6)$ ligand as occupying three coordination

sites, viewing the bonding to be composed of three metal olefin interactions. Likewise, the (η^5-C_5H_5) ligand is also considered to occupy three coordination sites, derived from one metal-alkyl and two metal-olefin interactions. Using this notion of "coordination number", the chromium atoms in both (η^5-C_5H_5)$_2$Cr and (η^6-C_6H_6)$_2$Cr are six coordinate.[73] While the latter classifications are pleasing to organometallic chemists, it is perhaps a little disconcerting that the chromium atoms in (η^5-C_5H_5)$_2$Cr and (η^6-C_6H_6)$_2$Cr would have the same coordination number when the structures clearly differ by two in the number of ligating atoms.

Finally, the coordination number is sometimes viewed to be the number of electron pairs donated by the ligand (with a charge corresponding to the oxidation number formalism).[16] Thus, using this definition, the coordination number of (η^6-C_6H_6)$_2$Cr is six because each benzene ligand donates three pairs of electrons. However, there are several obvious problems with this definition, for example, *(i)* coordination of a Lewis acid would not increase the coordination number, *(ii)* a terminal nitrido ligand would be classified as occupying three coordination sites, which is untenable for a single atom, and *(iii)* terminal chalcogenido ligands would be classified as occupying 0, 2 or 3 coordination sites depending upon whether the bonding interaction is best described as [$\overset{+}{M}$–$\overset{-}{E}$], [M═E], or [M$\equiv\overset{+}{\overset{-}{E}}$], respectively. It is, therefore, evident that these modified views of coordination number are inappropriate and that the original precise definition, as the number of atoms bonded, should be retained.

1.01.4 The $ML_lX_xZ_z$ Covalent Bond Classification of Organotransition Metal Compounds

1.01.4.1 The covalent Bond Classification Method

The problems associated with classifying molecules by oxidation number and coordination number stem from the application of a classification system to a set of molecules for which it is not appropriate. Thus, although oxidation number and coordination number (as defined by the number of ligating atoms) are most useful concepts in discussing classical coordination compounds, such as $Co(NH_3)_6^{3+}$ and $CoCl_6^{3-}$, they are not in general the best means of evaluating organometallic compounds. Nor should they be, since organometallic compounds possess types of ligands that were unknown at the time when the oxidation number concept was introduced and developed. Historically, however, rather than recognizing at the outset that organometallic compounds are not appropriately classified by the concepts used by coordination chemists, organometallic compounds were essentially forced into having attributes pertinent to classical coordination compounds. In essence, rationalizing the structures of organometallic compounds in terms of oxidation state and coordination number is akin to forcing a square peg into a round hole.

In order to surmount problems of the types described above, Green has introduced an innovative method for the formal classification of covalent compounds.[76,77] The principal advantage of the so-called "Covalent Bond Classification (CBC) Method" is that it was specifically designed for covalent molecules and so does not suffer from any limitations or problems resulting from the rules imposed on the definition of oxidation state.[78,79] In essence, the CBC method seeks to classify a molecule according to the nature of the ligands around the central element of interest. The method is based on the notion that there are three basic types of interaction by which a ligand may bond to a metal center and the ligand is classified according to the nature and number of these interactions. The three basic types of interaction are represented by the symbols L, X, and Z, which correspond respectively to 2-electron, 1-electron and 0-electron *neutral* ligands and are clearly differentiated according to a molecular orbital representation of the bonding (Figure 20).

An L-function ligand is one which interacts with a metal center *via* a dative covalent bond (*i.e.* a coordinate bond),[80] in which both electrons are donated by the L ligand. As such, an L-function ligand donates two electrons to a metal center. Since the metal uses no electrons in forming the M–L bond, an L-function ligand does not influence the valence of a metal center. Simple examples of L-type ligands include R_3P, R_2O, and CO, *i.e.* donor molecules that have lone pairs (Lewis bases).

An X-function ligand is one which interacts with a metal center *via* a normal 2-electron covalent bond, composed of 1 electron from the metal and 1 electron from the X ligand. As such, an X-function ligand donates one electron to a metal center. Since the metal uses one electron in forming the M–X bond, each X-function ligand raises the valence of the metal center by one unit. Simple examples of X-type ligands include H and CH_3, *i.e.* radicals.

A Z-function ligand also interacts with a metal center *via* a dative covalent bond, but differs from the L-function in that both electrons are donated by the metal rather than the ligand. As such, a Z-function ligand donates zero electrons to a metal center. Since the metal uses two electrons in forming the M–Z bond, a Z-function ligand raises

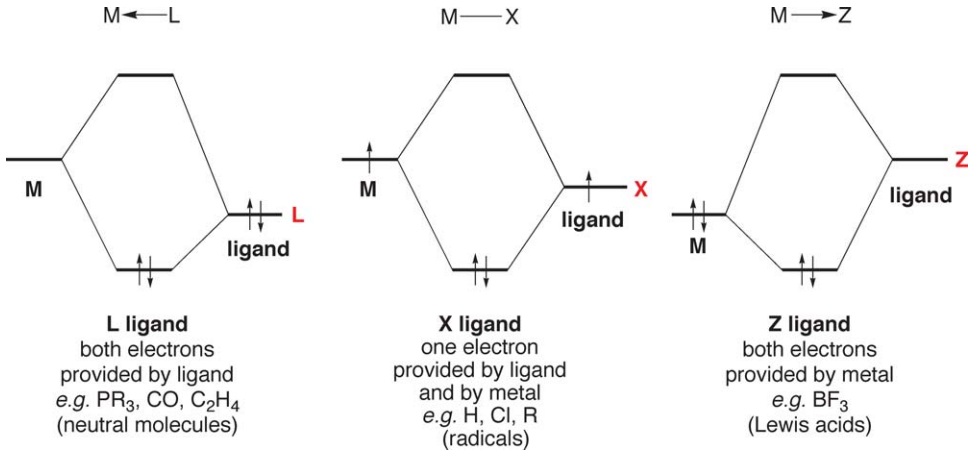

Figure 20 Molecular orbital representations of the three fundamental types of 2-center-2-electron interactions.

the valence of the metal center by two units. Simple examples of Z-type ligands include BF_3, BR_3 and AlR_3, *i.e.* molecules that have a vacant orbital (Lewis acids).

More important than merely referring to the *number* of electrons involved in the bonding is the fact that the types of interaction are differentiated according to the *nature* of the molecular orbital interaction (Figure 20). It is, therefore, apparent that the CBC method is of much more relevance to classifying and providing insight into the nature of *covalent* organometallic molecules than are methods based on *(i)* oxidation number (which merely hypothetically decomposes a molecule into its constituent ions) and *(ii)* electron count (that focuses only on the number of electrons, regardless of their origin).

A given ligand may have one or more of the above functions. As such, the ligand may be classified as $[L_lX_xZ_z]$, where l, x, and z are the respective number of L, X, and Z functionalities. For example, the η^6-benzene ligand is classified as $[L_3]$, with the three L functionalities corresponding to the three "olefinic" moieties (Figure 21). Likewise, the η^5-cyclopentadienyl ligand is classified as $[L_2X]$, with the two L functionalities corresponding to the two "olefinic" fragments while the X functionality corresponds to the CH "radical" portion of the resonance structure (Figure 21).

At a more fundamental level than merely relating to the number of electrons a ligand donates, however, the $[L_lX_xZ_z]$ classification refers to the nature of the frontier orbitals of the neutral ligand, as illustrated for the C_n-symmetric C_nH_n ligands in Figure 22. The three highest energy occupied orbitals of the C_5-symmetric C_5H_5 radical comprise a pair of doubly degenerate orbitals (HOMO) and a nondegenerate orbital (HOMO-1). The HOMO-1 orbital is fully occupied and corresponds to an L function, while the HOMO is occupied by three electrons and corresponds to an L and an X function. As such, C_5H_5 is classified as an $[L_2X]$ ligand. The three highest energy occupied orbitals of C_6H_6 also comprise a pair of doubly degenerate orbitals (HOMO) and a nondegenerate orbital (HOMO-1), but since these are all occupied, C_6H_6 is classified as an L_3 ligand. An interesting situation arises, however, with C_7-symmetric C_7H_7 because the HOMO is a singly occupied *doubly* degenerate orbital.[15b] As such, the

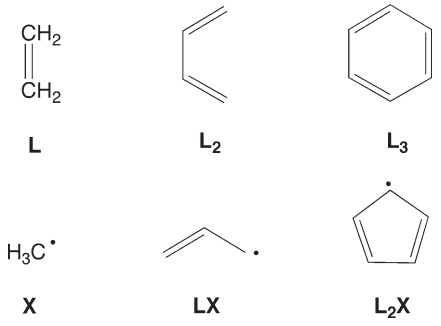

Figure 21 Simple examples of ligand classifications when exhibiting their maximum coordination modes.

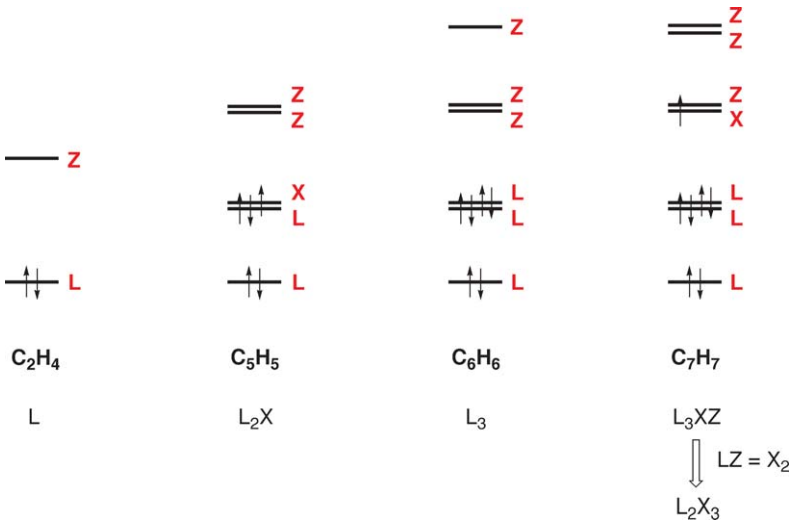

Figure 22 Frontier orbitals for a variety of ligands indicating the L, X, and Z character of each orbital according to whether it is doubly occupied, singly occupied, or empty, respectively.

HOMO is an XZ combination. Coupled with the L_2 nature of the fully occupied doubly degenerate HOMO-1 orbital, and the L nature of the HOMO-2 orbital, the C_7H_7 ligand is classified as L_3XZ; however, this classification reduces to L_2X_3 (Figure 22) because an LZ combination is equivalent to that of an X_2 combination. In essence, one may view the valence state of the C_7H_7 ligand to have three unpaired electrons, in much the same way that carbon has a sp^3 valence state with four unpaired electrons when it combines to form a tetrahedral compound.

The equivalence between an LZ and X_2 combination is derived from the fact that both require the involvement of two metal orbitals (Figure 23). Thus, an LZ combination requires an empty orbital and a fully occupied orbital on the metal, whereas an X_2 combination requires two singly occupied orbitals. It is, therefore, evident that the "triplet" state of the ligand becomes accessible if the Z orbital is of sufficiently low energy; this situation is well represented by the relationship between Fischer carbenes and Schrock alkylidenes (Section 1.01.4.3.2).[81] In this regard, it is important to note that C_5H_5 and C_6H_6 also possess Z orbitals (*i.e.* their LUMOs), but the situation is very different from that of C_7H_7 because their Z orbitals are much higher in energy than their HOMOs, whereas the Z function of C_7H_7 is necessarily of low energy because it is a component of the HOMO. Thus, the backbonding components for cyclopentadienyl and benzene ligands are not as significant as that in cycloheptatrienyl derivatives and, for this reason, the *primary* bonding interaction in cyclopentadienyl and benzene derivatives may be described as L_2X and L_3 rather than L_2XZ_2 or L_3Z_2.

Backbonding is of pivotal importance with respect to the metal-olefin interaction and the so-called "Dewar-Chatt-Duncanson model",[82,83] in which donation of electron density from the filled olefin π-orbital (an L function) is supplemented by backbonding into the empty π^*-orbital (a Z function). Depending upon the extent of backbonding, which depends critically on the nature of the metal center, the compound may be described as either a metal-olefin

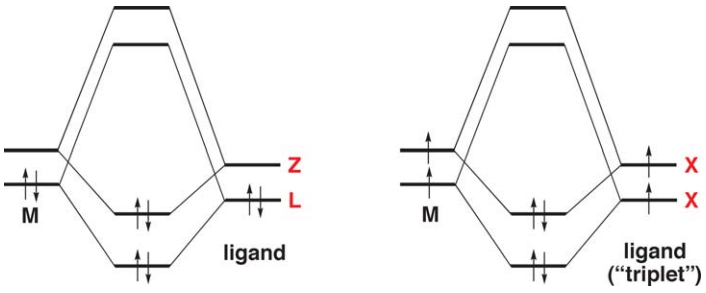

Figure 23 Conceptual illustration of how an L and Z combination becomes equivalent to an X_2 combination if backbonding is significant.

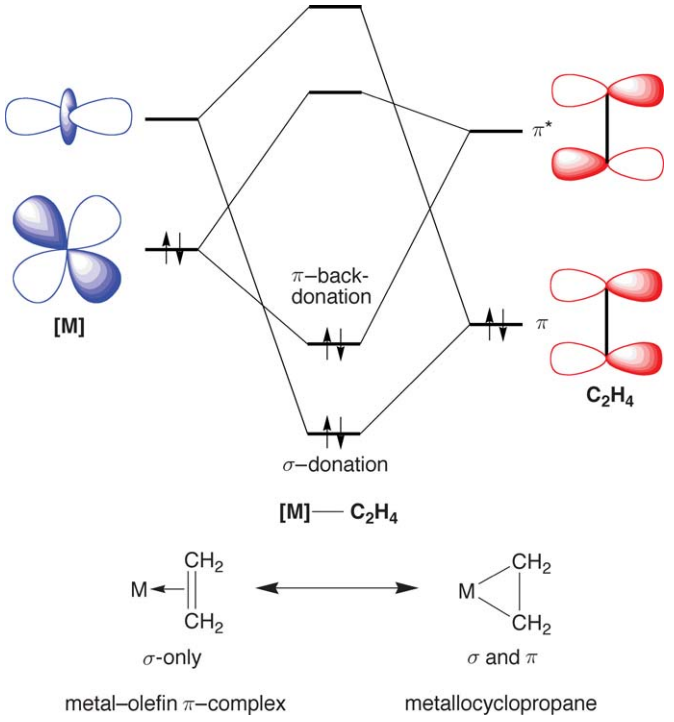

Figure 24 The "Dewar–Chatt–Duncanson model" for coordination of an olefin in which donation of electron density from the filled olefin π-orbital (an L function) is supplemented by backbonding into the empty π^*-orbital (a Z function). Depending upon the extent of backbonding, the compound may be described as either a metal–olefin adduct (little backbonding) or a metallacyclopropane derivative (extensive backbonding).

adduct (little backbonding) or a metallacyclopropane derivative (extensive backbonding), as illustrated in Figure 24. The latter extreme corresponds to the olefin serving as an LZ (*i.e.* an X_2) ligand, and is observed when the metal has a pair of electrons in a high energy orbital. The CBC method, therefore, successfully predicts and classifies the two types of metal-olefin complex. This result is significant in view of the fact that this distinction in bonding is not provided by consideration of oxidation numbers because, regardless of how an olefin is coordinated in the complex, it should be considered as a neutral ligand since that is its stable closed shell form (see Section 1.01.2.1.2).

An important feature of the CBC method is, therefore, that it is not prescriptive and does not require a ligand with a specific coordination mode to have single classification. In this way, it allows the nature of the metal center to have an impact on the overall bonding description. Although the CBC method provides a natural means to accommodate an olefin bonding as either an L or an X_2 ligand, it is not possible to state which alternative is preferred without further consideration of the compound, and spectroscopic or structural information are required to establish the preferred ligand classification. For this reason, it is useful to consider ligands such as C_2H_4 and CO with the designation LZ′, where Z′ refers to an unspecified degree of backbonding.

In contrast to C_2H_4 and CO where the acceptor orbital is not degenerate with the donor orbital, the acceptor orbitals of ligands such as NO and (η^7-C_7H_7) are degenerate with a donor orbital. For these ligands, it is, therefore appropriate to include fully the Z component in the $[ML_lX_xZ_z]$ classification.

A further simple example of the flexibility of the CBC method that is not afforded by consideration of oxidation numbers is provided by the chloride ligand which serves an X function when coordinated to a 17-electron fragment, *e.g.* $Mn(CO)_5Cl$, but may also act as an LX (or L_2X) ligand when coordinated to a $\leq$15-electron fragment and π-donation is significant, *e.g.* $W(PMe_3)_4Cl_2$.

The $[L_lX_xZ_z]$ classifications for a variety of other common ligands are summarized in Table 6. It is important to note that, in addition to complex ligands possessing more than one $[L_lX_xZ_z]$ classification, single atoms may also bind with different classifications, as illustrated in Table 6. For example, terminal oxo ligands may be classified as Z, $[\bar{X}_2]$, and $[L\bar{X}_2]$, according to whether the interaction is best described as having a single, double or triple bond (Figure 25). Illustrative examples of molecules that exhibit these characters are provided by $Cp^*_2Zr(O)(py)$, Cp^*_2WO, and

Table 6 Classifications of some common ligands

Ligand	*CBC Description*
H	X
R	X
CR_2	$\bar{X}_2$(Schrock alkylidene)
	LZ'[a] (Fischer carbene)
CR	$\bar{X}_3$
η^2–C_2H_4	LZ'[a]
η^3–C_3H_5	LX
η^3–C_4H_6	L_2Z'[a]
η^3–C_3H_3	X_3
η^4–C_4H_4	LX_2
η^5–C_5H_5	L_2X
η^6–C_6H_6	L_3Z'[a]
η^7–C_7H_7	L_2X_3
η^8–C_8H_8	L_3X_2
CO	LZ'[a]
PR_3	L
NO	XZ'[a] (bent)
	$\bar{X}_3$(linear)
BR_3	Z
AlR_3	Z
O	Z
	$\bar{X}_2$
	$L\bar{X}_2$
N	$\bar{X}_3$
C	$\bar{X}_2Z$
OR	X (bent)
	LX (bent)
	L_2X (linear)
NR	$\bar{X}_2$ (bent)
	$L\bar{X}_2$(linear)
NR_2	X (pyramidal)
	LX (planar)

[a]The Z′ backbonding component is undetermined. As such, it is neglected for the purpose of determining the $[ML_lX_xZ_z]$ classification used in the statistical survey which focuses on the *primary* bonding interactions (Section 1.01.4.7). However, its involvement should not be neglected when attempting to provide a detailed description of the compound. In this regard, it is important to note that certain ligands may have more than one Z′ acceptor orbital; for example, CO has two π–acceptor orbitals.

$Mo(PR_3)_3(O)Cl_2$, respectively.[45a] The $[\bar{X}_2]$ "bar" notation indicates that the two X-functions belong to a single atom (a so-called polyfunctional ligating atom) and the distinction is only of significance with respect to reducing an anion to its equivalent neutral class (see Section 1.01.4.2).

Finally, bridging ligands may be classified using a similar approach. For example, a bridging alkylidene is classified with the notation [X-μ-X], while a bridging chloride or acetate ligand would be represented by [X-μ-L] (Figure 26).[84]

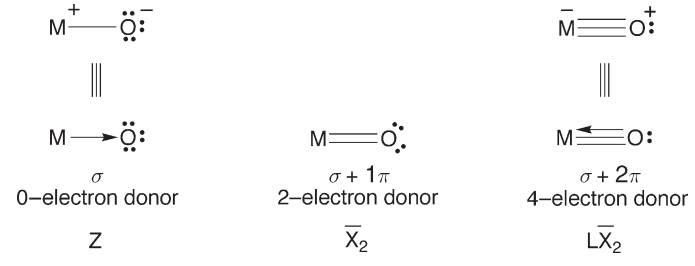

Figure 25 CBC description of terminal oxo ligands according to the number of bonds.

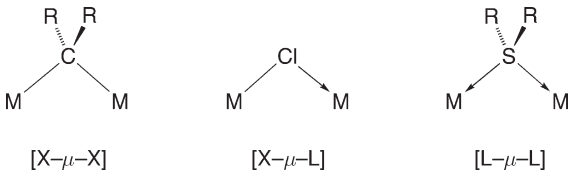

Figure 26 CBC description of some bridging ligands.

1.01.4.2 The Equivalent Neutral Class

Once all the ligands about a metal center have been classified as described above, the molecule itself is classified as $[MLX_xZ_z]^{Q\pm}$ by summing all the L-, X-, and Z- functionalities, as illustrated in Figure 27 for some tungsten complexes. For example, Cp_2WH_2 is classifed as $[ML_4X_4]$ since $Cp \equiv [L_2X]$ and $H \equiv [X]$. Correspondingly, $[Cp_2WH_3]^+$ would be classified as $[ML_4X_5]^+$. However, in order to allow for comparisons between molecules that have different charges, it is useful to reduce the $[MLX_xZ_z]^{Q\pm}$ assignment to its "equivalent neutral class", which is essentially the classification that would be obtained if the Q± charge were to be localized on the ligand and not on the metal center. Localization of the charge on the ligands changes the classification of the ligand functions and the various transformations are summarized in Figure 28.

For cations, the transformations are: (i) $L^+ \rightarrow X$, *i.e.* a cationic 2-electron donor is equivalent to a neutral 1-electron donor, and (ii) $X^+ \rightarrow Z$, *i.e.* a cationic 1-electron ligand is equivalent to a neutral 0-electron ligand. For anions, the most commonly encountered transformations are: (i) $X^- \rightarrow L$, *i.e.* an anionic 1-electron donor is equivalent to a neutral 2-electron donor and (ii) $L^- \rightarrow LX$, *i.e.* an anionic 2-electron donor is equivalent to a 3-electron donor. It is important to emphasize that the latter two transformations should be applied sequentially, *i.e.* a negative charge is only placed on an L-function if there is no X-function. The origin of this priority is that an X-function orbital is singly occupied and can

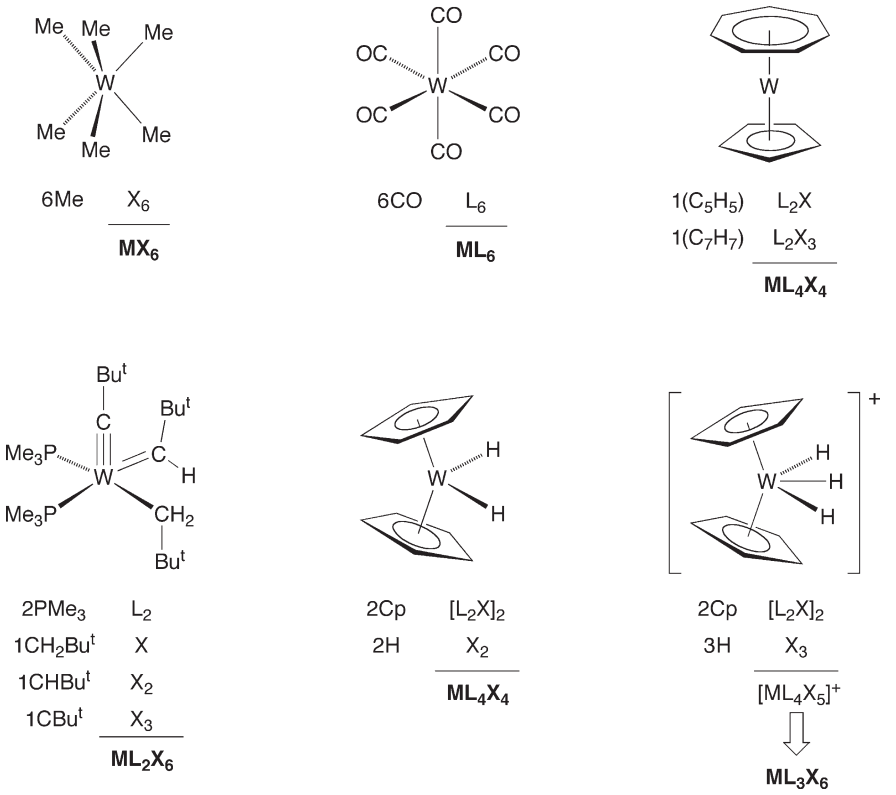

Figure 27 $[ML_lX_xZ_z]$ classifications of some simple tungsten compounds. Note that the initially derived $[ML_4X_5]^+$ classification of $[Cp_2WH_3]^+$ is transformed to the equivalent neutral class of ML_3X_6 upon applying the rule $L^+ \rightarrow X$.

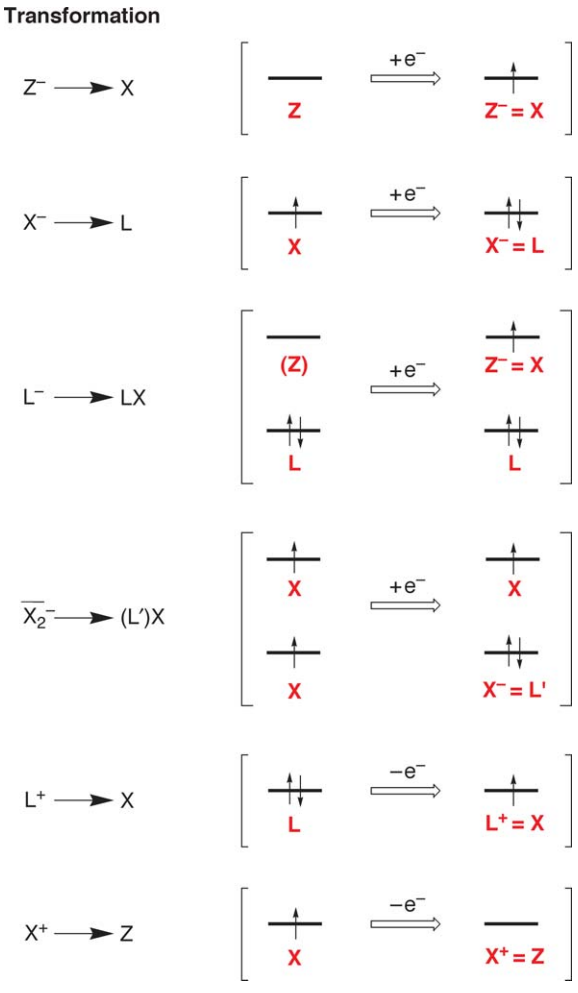

Figure 28 Orbital explanation for the rules used to transform $[ML_lX_xZ_z]^{Q\pm}$ to its equivalent neutral class. Note that the transformation $\bar{X}_2^- \rightarrow (L')X$ for a polyfunctional atom means that due consideration must be given to evaluate whether the L′ function remains involved in the bonding or whether it becomes a lone pair localized on the ligand.

accommodate an additional electron, whereas an L-function is fully occupied and cannot accept an electron. The added electron must, therefore be accommodated by a higher energy unoccupied orbital on the ligand (*i.e.* a nascent Z function), which thereby becomes an X-function. The fact that the electron needs to occupy an unoccupied orbital means that molecules of the type $[ML_n]^{x-}$ are only likely to be feasible if the ligand has an empty orbital of sufficiently low energy. For this reason, CO, which has low energy π-acceptor orbitals available (*i.e.* LZ′), is much more likely to afford anionic $[ML_n]^{x-}$ derivatives than would PMe_3. In support of this statement, $[Fe(CO)_4]^{2-}$ has been widely investigated, whereas $[Fe(PMe_3)_4]^{2-}$ is unknown, despite the fact that the neutral isoelectronic counterpart $Ni(PMe_3)_4$ has been synthesized. Applying the transformation $L^- \rightarrow LX$ (alternatively viewed as $(LZ^- \rightarrow LX)$ for $[Fe(CO)_4]^{2-}$, the latter molecule becomes classified as ML_4X_2, a very common class of organometallic iron compound (*vide infra*).

An important additional consideration must be given for reducing an anion that incorporates a polyfunctional $[\bar{X}_n]$ ligating atom, such as an oxo or nitrido ligand. The general rule for reducing the anionic form of this ligand is $[\bar{X}_n]^- \rightarrow [L'\bar{X}_{n-1}]$, and the distinction with the monofunctional counterpart, $X^- \rightarrow L$, is that for polyfunctional ligands it is necessary to consider whether the L′ component remains involved in the bonding or becomes a lone pair localized on the ligand. To answer this question, it is important to consider the nature of the atom to which the polyfunctional ligating atom is attached. For example, the $[CO_3]^{2-}$ anion is classified as $[C(\bar{X}_2)_3]^{2-} = [C(\bar{X}_2)(\bar{X}_2^-)_2] = [C(\bar{X}_2)(L'X)_2] = CL'_2X_4$, which reduces to CX_4 because the L′ functions become lone pairs localized on the oxygen atoms since there are no empty orbitals on the carbon with which to interact. In contrast, the L′ function may be retained for transition metal compounds if there are orbitals available.

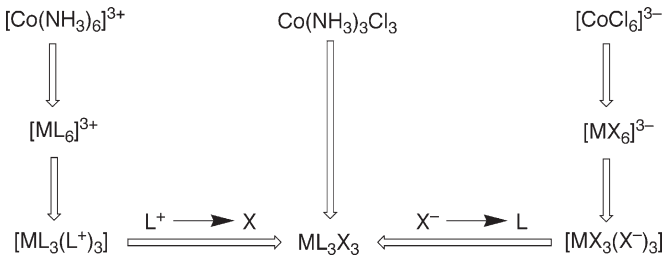

Figure 29 $[ML_lX_xZ_z]$ classifications of $[Co(NH_3)_6]^{3+}$, $[Co(NH_3)_3Cl_3]$, and $[CoCl_6]^{3-}$. Note that all three compounds belong to the same class, ML_3X_3.

Finally, if the derived classification after performing the above transformations contains both an L and a Z function, the classification is reduced further by using the transformation $LZ = X_2$, as described in Section 1.01.4.1. As a result of this final transformation, it becomes irrelevant as to whether priority is given to placing the positive charge for cations on either the L- or X-function, although the final classification may be obtained more directly by placing it initially on the L-function.

A consideration of some simple compounds serves to indicate the rationale for describing a molecule in terms of its equivalent neutral class. For example, the cationic, neutral, and anionic octahedral Co(III) species $[Co(NH_3)_6]^{3+}$, $[Co(NH_3)_3Cl_3]$, and $[CoCl_6]^{3-}$, which are related by the formal substitution of Cl^- by NH_3, each belong to the same fundamental molecular class, *i.e.* $[ML_3X_3]$ (Figure 29). Thus, even though the compounds have different charges, the CBC method indicates that the three molecules belong to the same class of compound.

It is pertinent to note that certain aspects of the CBC method have been described in textbooks[79] but the importance of reducing the classification to that of the equivalent neutral class, which is essential from a categorization perspective (Sections 1.01.4.4 and 1.01.4.5), has not been stressed. Finally, a "chemputer" to obtain the $[ML_lX_xZ_z]$ classification of molecules is presently available on the World Wide Web (http://www.shef.ac.uk/chemistry/chemputer/mlxz.html); however, in view of ambiguities that exist for certain ligands, it is recommended that caution be used in utilizing this program.

1.01.4.3 Caveats and Subtleties

1.01.4.3.1 π-Donation

The coordinating atoms of ligands are sometimes polyfunctional and may interact with a metal center by using more than one orbital interaction. A simple illustration is provided by NR_2 ligands which may coordinate to a metal center *via* either a σ-bond or *via* a σ and π-combination. The NR_2 ligand thus acts as either a 1-electron or 3-electron donor, with the two coordination modes being readily distinguished according to whether the geometry at nitrogen is pyramidal or planar, respectively. Not all ligands, however, have a simple stereochemical probe to identify the existence of π-donation, a notable example of which is provided by halide ligands. For such ligands, due consideration must be given to the nature of the molecule to evaluate the degree to which π-donation is feasible. For example, while a single halide ligand has two occupied p orbitals that may participate in a π-interaction with a transition metal center, *i.e.* the halide ligand may be classified as L_2X, a molecular orbital analysis of octahedral WCl_6 indicates that only three ligand combination orbitals (the t_{2g} set) are of appropriate symmetry to interact in a π-manner with the metal. Thus, WCl_6 would be classified as ML_3X_6 if π-donation is incorporated into the description. Since π-donation represents a secondary component to the bonding of halide ligands, it is neglected for the purpose of obtaining the $ML_lX_xZ_z$ classification of the molecule which focuses on the *primary* bonding interactions. However, it is important to emphasize that the interaction should not be neglected if one wishes to present a detailed description of the molecule.

1.01.4.3.2 π and δ-Backbonding

While ligands such as NH_3 are considered to be exclusively σ-donor ligands, and may be decisively identified as L ligands, many other ligands have a greater functionality and due consideration needs to be given to the classification of the ligand. In particular, the availability of low energy acceptor orbitals (*i.e.* Z functions) suitable for backbonding are of considerable importance because they have ability to change, in a fundamental manner, the description of the metal-ligand interaction, as exemplified by the Dewar-Chatt-Duncanson description of the bonding in metal olefin

complexes (section 1.01.4.1). Unfortunately, the precise contribution of π and δ-backbonding to the overall interaction is generally unknown. It is, therefore, pertinent to consider in a qualitative manner the backbonding capabilities of some of the more commonly encountered ligands.

Tertiary phosphine ligands (PR_3), while commonly regarded as strong σ-donor ligands, also possess some π-acceptor character. Originally, the π-acceptor orbitals were considered to be phosphorus 3d orbitals, but are now recognized to be P–X (X = H, F, R) σ^* antibonding orbitals.[85,86] For the purpose of determining the $ML_lX_xZ_z$ description, however, PR_3 ligands are classified as L ligands, which is consistent with the commonly encountered zerovalent description of $M(PR_3)_n$ complexes.

The carbonyl ligand is widely regarded to be a more efficient π-acceptor than are PR_3 ligands. For the purpose of determining the $ML_lX_xZ_z$ classification, however, the backbonding component is neglected and CO is considered to be an L ligand. As with PR_3 ligands, this description of the carbonyl ligand is in line with the traditional notion that coordination of CO does not change the d^n configuration of a metal center; it is also in accord with the fact that these ligands may coordinate to d^0 metal centers (albeit weakly) for which backbonding is not, to a first approximation, feasible. However, it must be emphasized that while this neglect of the unspecified Z′ backbonding component simplifies the classification of a molecule, it comes with a compromise which is that it is not prudent to use the derived CBC description of such molecules to construct elaborate arguments pertaining to the detailed nature of a molecule. For example, the neglect of the unspecified Z′ component means that it may be inappropriate to infer details of the structure and reactivity of a molecule in terms of the d^n configuration derived from the CBC method. For applications of this type, it is useful to retain the Z′ component to alert one to the possibility that effective backbonding may modify the nature of the molecule.

As a simple illustration, whereas $W(PMe_3)_6$ is classified as ML_6, $W(CO)_6$ could be better described as ML_6Z' where Z′ refers to an unspecified degree of backbonding. The extent of backbonding to a carbonyl ligand depends critically on the nature of the metal center, as demonstrated by calculations on octahedral $[M(CO)_6]^{Q\pm}$ complexes. Thus, the contribution of the t_{2g} orbital to the bonding in $[M(CO)_6]^{Q\pm}$ increases from 4.2% in $[Ir(CO)_6]^{3+}$ to 76.6% in $[Hf(CO)_6]^{3-}$,[87] a clear manifestation of the charge on the complex. It is, therefore, evident that the degree of backbonding, and hence the extent to which the metal orbital is removed from being a rigorously nonbonding orbital, depends specifically on the molecule in question.

Closely related to the interaction between CO and a metal center is the corresponding interaction of a carbene R_2C: ligand. In this regard, it has long been known that the complex obtained by interaction of R_2C: with a transition metal may be described as either a "Fischer carbene"[88] or a "Schrock alkylidene",[89] depending upon the extent of π-backbonding from the metal center. The bonding in a Fischer carbene may be described as involving a singlet carbene donating an sp^2 pair of electrons to an empty metal orbital, supplemented by backdonation from a filled metal orbital to the empty carbene p-orbital, while the bonding in a Schrock alkylidene may be described as a triplet carbene interacting with two singly occupied metal orbitals resulting in the formation of a M═C double bond akin to the C═C double bond in ethylene.[81,90] Fischer carbene complexes are typically characterized by the presence of heteroatom π-donor substituents which stabilize the singlet state, while Schrock alkylidene complexes are typically characterized by hydrogen or alkyl substituents. Schrock alkylidene complexes are therefore characterized by extensive backbonding and are best described as derivatives of $\bar{X}_2$ ligands, whereas the Fischer carbenes are best characterized as derivatives of L ligands for the purpose of obtaining the primary $ML_lX_xZ_z$ description. Note that this is very similar to the Dewar-Chatt-Duncanson description of the bonding for metal olefin complexes, which may be described as possessing either L or X_2 ligands. In a molecular orbital sense, the difference between Schrock alkylidenes and Fischer carbenes is dictated by the relative energies of the occupied d orbital and the empty carbene p orbital: a Schrock alkylidene ideally results from a situation in which the empty carbene p orbital is lower in energy than the occupied d orbital, while a Fischer carbene corresponds to the reverse situation.[91] π-Donation from the heteroatom has the effect of raising the energy of the acceptor orbital (since it is now the π^* component of the C–X bond) and thereby reduces the backbonding component, such that the complex takes on Fischer carbene character.

Another class of carbenes, which are emerging as popular ligands with interesting applications, are so-called *N*-heterocyclic carbenes (NHC).[92] *N*-heterocyclic carbenes differ from those in Fischer carbene complexes by virtue of the fact that the "carbene" carbon atom is stabilized by interaction with the lone pairs of *two* adjacent nitrogen atoms. As a consequence, metal-to-ligand π-backbonding for *N*-heterocyclic carbenes is typically considered to be less important than for R_2C: and R(X)C: ligands.[92,93,94] For this reason, *N*-heterocyclic carbenes are best considered as L ligands for their primary bonding interaction. Another interesting aspect pertaining to the metal–NHC bond is that the metal d orbital which interacts with the potential π-acceptor orbital of the NHC ligand is also of appropriate symmetry to interact with a *filled* π-orbital of the NHC ligand thereby modulating the

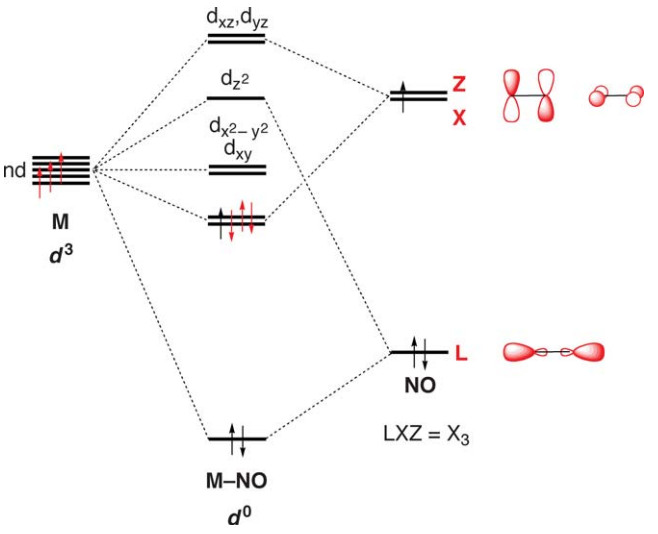

Figure 30 Qualitative molecular orbital diagram illustrating the bonding in a linear metal nitrosyl species focusing on interactions with the d orbitals. The HOMO of NO is a singly occupied doubly degenerate orbital and its involvement in the bonding requires the metal to contribute three electrons to the derived molecular orbitals. Thus, a d^n metal center becomes d^{n-3} upon coordination of NO, as illustrated for the case in which $n = 3$. The interaction may, therefore, be represented *via* the triply bonded resonance structure $M{\equiv}\overset{+}{N}{-}\bar{O}$.

overall π-acceptor character of the NHC ligand.[93,95] In this regard, it has been noted that the π-acceptor character of a NHC ligand is likely to be highly dependent on the system under consideration.[96]

While the Z′ component is neglected in determining the *primary* $ML_lX_xZ_z$ classification of a molecule that incorporates CO and C_2H_4 ligands, it is not neglected for ligands such as linear NO and η^7-C_7H_7 that require extensive backbonding to coordinate to a metal center. A simple illustration which emphasizes the importance of backbonding for coordination of these ligands is provided by the fact that the isolable cationic forms, NO^+ and $(C_7H_7)^+$, do not coordinate to d^0 metal centers. For this reason, NO and η^7-C_7H_7 retain the Z function in the CBC classification. Examination of the frontier orbitals of NO (Figure 30) indicates that it should be classified as an $LXZ{\equiv}\bar{X}_3$ ligand when coordinated in a linear manner, while η^7-C_7H_7 is classified as an $L_3XZ{\equiv}L_2X_3$ ligand (Figure 22). The essential features of the molecular orbital diagram for a terminal metal–nitrosyl interaction are illustrated in Figure 30, which demonstrates that the metal must contribute *three* electrons to the bonding.[97] In terms of a valence bond representation, this description corresponds to $M{\equiv}\overset{+}{N}{-}\bar{O}$, with a M≡N triple bond and a N–O single bond (Figure 31). While this bonding representation is quite different from the $\bar{M}{\leftarrow}N{\equiv}\overset{+}{O}$ description that is normally encountered in the literature, it is pertinent to note that the M≡N triply bonded description of the linear metal nitrosyl was offered in an early theoretical description of the bonding[97a] and has also been described in a review.[98]

The $M{\equiv}\overset{+}{N}{-}\bar{O}$ triply bonded representation of the bonding is also in accord with the fact that the M–NO bond length is typically very short and much closer to the values in related M≡N nitrido compounds than the bond lengths in $M{\leftarrow}NR_3$ complexes. For example, the Os–N bond length in *trans*-$[Os(tpy)Cl_2(NO)]^+$ (1.70 Å) is only marginally longer than the corresponding bond length in the nitrido complex *trans*-$[Os(tpy)Cl_2(N)]^+$ (1.66 Å), thereby providing

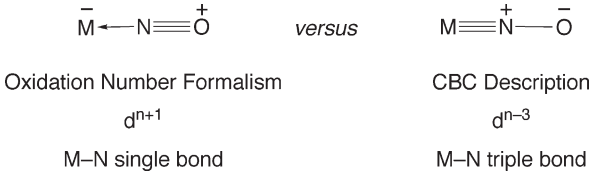

Figure 31 Different descriptions of the linear metal nitrosyl interaction. The oxidation number formalism implies that coordination of NO to a d^n metal center results in d^{n+1} configuration, whereas a d^{n-3} configuration is implied by the CBC description.

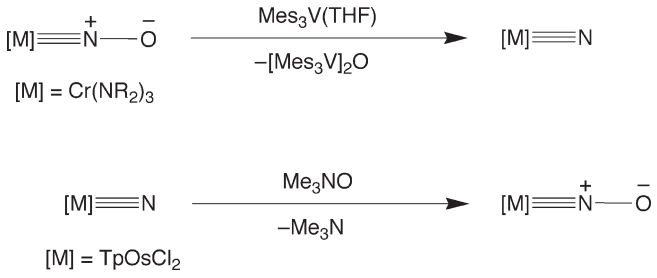

Figure 32 Interconversion of metal nitrosyl and metal nitrido compounds *via* oxo transfer reactions.

clear evidence of multiple bonding; for further comparison, the three dative Os–N bonds for the tpy ligand are considerably longer (2.02–2.07 Å).[99]

Chemical evidence that M≡N–O is a reasonable description of the bonding is provided by the observation that it is possible to deoxygenate linear nitrosyl compounds to generate the corresponding nitrido derivative,[100] and also perform the reverse and oxygenate a terminal nitrido ligand to give a nitrosyl ligand (Figure 32).[99,101]

Calculations also provide evidence which indicates that it is important not to neglect the π-backbonding interaction in linear nitrosyl derivatives. For example, calculations indicate that the W–NO bond length in $[W(CO)_5(NO)]^+$ (1.891 Å) is considerably shorter than the W–CO bond lengths (2.107 Å and 2.178 Å),[102] by a value that is much greater than the difference in covalent radii of carbon (0.77 Å) and nitrogen (0.73 Å).[103] In contrast, the W–N_2 bond length in $W(CO)_5(N_2)$ (2.126 Å) is longer than the W–CO bond lengths (2.057 Å and 2.013 Å).[102] These observations provide compelling evidence that backbonding to the NO ligand plays a more important role in the bonding than does backbonding to a carbonyl or dinitrogen ligand.

In view of the $\bar{X}_3$ nature of the linear nitrosyl ligand, the d^n configuration of a metal in a neutral [MNO] fragment is d^{n-3} (Figure 30), where n is the number of d electrons in the neutral atom (Table 2). This configuration is very different to the d^{n+1} configuration that is predicted by using the oxidation number formalism in which the linear nitrosyl ligand is classified as the cation, NO^+. Enemark and Feltham recognized the problems resulting from the oxidation number assignments associated with nitrosyl ligands (see Section 1.01.2.1.2) and therefore proposed that metal nitrosyl compounds should instead be defined in terms of a $\{M(NO)_x\}^n$ classification, where *n* is the total number of electrons associated with the metal d and NO π^*-orbitals.[23] As such, the classification makes no distinction as to whether the *n* electrons are located in metal–NO bonding orbitals, "nonbonding" metal-based orbitals, or NO-based orbitals (important for polynitrosyl compounds). It is also pertinent to note that because the value of *n* in the $\{M(NO)_x\}^n$ classification is equivalent to that of the d^n configuration derived by assuming the nitrosyl ligand is a cation, the latter "d^n configuration" does not correspond to the number of electrons in "nonbonding" metal based d orbitals. In contrast, however, the CBC method derives a d^n configuration for a metal-nitrosyl that does correspond to the number of electrons in "nonbonding" metal based d orbitals.

While the majority of backbonding interactions are of a π-nature, the acceptor orbitals of several ligands, such as benzene, are of δ-symmetry. Since δ-overlap is generally not as significant as π-overlap, δ-backbonding interactions are normally neglected in the primary classification of ligands using the CBC method.

1.01.4.3.3 Multicenter bonding

While the $[L_lX_xZ_z]$ description of a ligand accurately predicts the nature of the molecular orbital diagram pertaining to a single metal–ligand interaction, it is important to emphasize that subtleties sometimes arise when evaluating the molecule as a whole because the bonding may not be adequately described in terms of 2-center-2-electron interactions. For example, as noted above, $W(C_2R_2)_3(CO)$ appears to be a 20-electron ML_8 molecule if the acetylene ligand is considered to be a 4-electron L_2 donor, but a detailed molecular orbital analysis (Figure 7) indicates that of the six possible C_2R_2 ligand L-donor combinations, one does not have appropriate symmetry to interact with the metal center. As such, the molecule is more appropriately classified as ML_6 with an 18-electron configuration. Thus, on a per ligand basis, acetylene behaves as a $3\frac{1}{3}$ electron donor.

In addition to donor interactions, due consideration must be given to molecules that feature multiple π-acceptor ligands because it is possible that the metal may use the same orbital to backbond to more than one ligand. For example, consider a *trans*-$M(NO)_2$ moiety (Figure 33). Focusing on the π-backbonding interactions, both nitrosyl

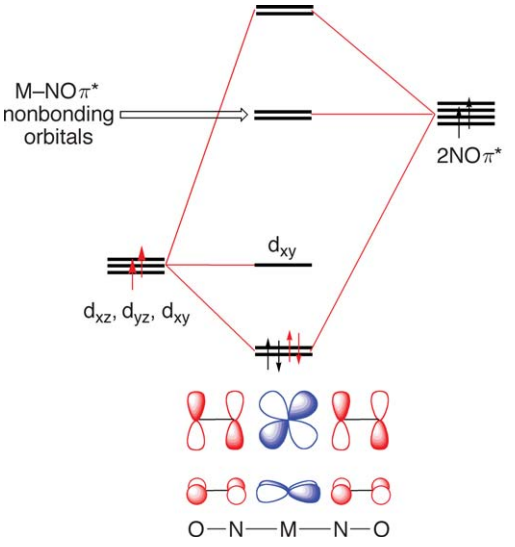

Figure 33 Partial MO diagram for a *trans* dinitrosyl compound focusing on the π-interactions. Since the two sets of NO π^* orbitals on each ligand interact with the same metal d orbitals, the metal is only required to contribute *two* electrons to the bonding. Coupled with the two ON→M dative covalent interactions (not shown), each nitrosly may be classified as an LX ligand.

ligands interact with the same pair of d orbitals, such that the metal is required to contribute only *two* electrons. The pair of NO ligands thereby acts as an $[L_2X_2]$ combination with the result that a single NO ligand behaves as an LX ligand, rather than the $\bar{X}_3$ classification for a single terminal nitrosyl ligand. This variability of bonding mode is by no means restricted to the NO ligand and a well known example is provided by the oxo ligand. Thus, while the bonding in many terminal metal oxo species may be described as a $\bar{M}\equiv\overset{+}{O}$ triple bond, the bonding within a *trans*-$M(O)_2$ moiety is better described as involving M═O double bonds because the two oxo ligands compete for the same d_π-orbitals.[45a] In contrast, a *cis* disposition of oxo ligands enables access to a third d_π-orbital and the bonding within a *cis*-$M(O)_2$ moiety is better described as possessing an average M∼O bond order of 2.5.

1.01.4.4 The $[ML_lX_xZ_z]$ Classification, Electron Number, Valence and Ligand Bond Number

Once the $[ML_lX_xZ_z]$ classification of a molecule is known, it is a simple matter to extract other useful information pertaining to the nature of a molecule, including the electron count, valence, and ligand bond number (Table 7).

Table 7 Definitions pertaining to the CBC method

Symbol	*Definition*
L	2–electron donor function
l	number of L functions
X	1–electron donor function
x	number of X functions
Z	0–electron donor function
z	number of Z functions
m	number of electrons on neutral metal
VN	valence number $VN = x + 2z$
LBN	ligand bond number $l + x + z$
EN	electron count $m + 2l + x$
d^n	number of electrons in "nonbonding" metal orbitals $n = m - x - 2z = m - VN$

For example, the electron number (EN) of the metal in $[ML_lX_xZ_z]$, *i.e.* the electron count, is given by $EN = m + 2l + x$, where m is the number of valence electrons on the neutral metal atom (Table 2).

The valence number (VN) of the metal center, *i.e.* the number of electrons that the metal uses in bonding, is $VN = x + 2z$. In most organotransition metal complexes, the number of Z ligands in the equivalent neutral class is zero. As such, the valence number is typically equal to x, *i.e.* the number of one-electron donor X-ligands. The value of the d^n configuration is given by $n = m - x - 2z = m - VN$.

Finally, the ligand bond number (LBN) represents the effective total number of ligand *functions* surrounding M, and is defined as $LBN = l + x + z$. While not defined as the coordination number, it is pertinent to note how the ligand bond number as defined by $l + x + z$ gives the value that organometallic chemists "want" the coordination number to be in many compounds. For example, both $(\eta^5\text{-}C_5H_5)_2Cr$ and $(\eta^6\text{-}C_6H_6)_2Cr$ (*i.e.* ML_4X_2 and ML_6, respectively) have a ligand bond number of six, even though the classical definition of coordination number gives values of 10 and 12, respectively. Furthermore, it is noteworthy that the ligand bond number reduces to the classical definition of coordination number when the ligands are "simple", *i.e.* monofunctional ligands that coordinate to the metal using a single orbital, *e.g.* H and CH_3.

1.01.4.5 MLX Plots

Since the $[ML_lX_xZ_z]$ classification contains information that relates to the electron count, the valence and ligand bond number, it provides a greater dimension for classifying compounds than methods based on either electron count or oxidation number. For example, while certain textbooks summarize the chemistry of elements in a single, rather complex table based on oxidation numbers, the CBC method spreads this into two dimensions by using a plot in which the $[ML_lX_xZ_z]$ classification is represented as a function of the electron count and valence of the metal. For isolated organometallic complexes of the transition metals, the value of z is almost invariably zero,[104] and so each box is occupied by a single $[ML_lX_x]$ class of molecules; as such, these diagrams are often simply referred to as "MLX plots". An illustration of an MLX plot is provided by the example for iron shown in Figure 34, which was constructed by using the compounds listed in the *Dictionary of Organometallic Compounds* as a database;[105,106] the corresponding plots for other elements are summarized in Section 1.01.4.5. Thus, while consideration of the electron count for iron compounds results in the conclusion that the organometallic chemistry of iron is dominated by 18-electron molecules, *i.e.* a single class of molecules, consideration of the MLX plot shows that this class of molecule can be further conveniently divided into additional classes. Specifically, 18-electron iron complexes belong to $[ML_5]$, $[ML_4X_2]$, and $[ML_3X_4]$ classes, representatives of which are $Fe(CO)_5$, Cp_2Fe, and $[CpFe(CO)(\mu\text{-}CO)]_2$.

MLX plots are a characteristic of each element and are provided in Section 1.01.4.5 for the transition metals of Groups 3–10. In general, each element favors one or several $[ML_lX_xZ_z]$ classes and the three most common for each element are summarized Table 8. By summarizing a vast quantity of factual information, the MLX plot reveals important characteristics of the chemistry of the element under consideration. It is important to emphasize, however, that the MLX plot does not, *per se*, explain *why* a particular class of compound is common – but, likewise, neither does the electron count nor oxidation number of an atom in a molecule *explain* why a molecule may be stable. Correspondingly, it should not be inferred that a molecule belonging to the most popular class in an MLX plot will be stable because the classification does not incorporate a sufficiently detailed view of the bonding. Some rationalization as to why certain compounds are unknown, even though they belong to a reasonable classification, is provided by Pauling's electroneutrality principle which postulates that the charge on an atom in a molecule is less than $|\pm 1|$.[70] For example, consider the series of molecules, MoL_6 ($L = NH_3$, PMe_3, CO): $Mo(NH_3)_6$ is unknown, $Mo(PMe_3)_6$ is an isolable, albeit highly reactive, molecule, and $Mo(CO)_6$ is a stable, comparatively unreactive molecule. The principal difference between NH_3, PMe_3, and CO is concerned with their σ-donor and π-acceptor properties. At one extreme, NH_3 is a strong σ-donor ligand with no π-acceptor character, while CO is a weak σ-donor but strong π-acceptor ligand. Strong σ-donor ligands transfer a substantial amount of electron density to the metal, thereby resulting in an excessive buildup of negative charge on the metal and an unstable structure. π-Acceptor functions, however, minimize this charge buildup and thus $Mo(CO)_6$ is more stable than $Mo(NH_3)_6$.

Molecules that have $[ML_lX_xZ_z]$ classifications that are remote from the highly populated areas in an MLX plot are necessarily of considerable interest because of their uniqueness. For example, with respect to scandium chemistry, while the majority of compounds possess a ML_lX_3 classification ($l = 2$–6), there are some very interesting examples of a zerovalent arene complexes $(\eta^6\text{-}ArH)_2Sc$ (*e.g.* $ArH = C_6H_3Bu^t_3$) which possess the ML_6 classification.[107] This corresponds to a most unusual valence state for scandium, and the ability to isolate

Fe		Electron Number								
		10	11	12	13	14	15	16	17	18
Valence	0	ML		ML_2		ML_3		ML_4 <1%		ML_5 20%
	1		MLX		ML_2X		ML_3X		ML_4X <1%	
	2	MX_2		MLX_2		ML_2X_2 <1%		ML_3X_2 <1%		ML_4X_2 71%
	3		MX_3		MLX_3		ML_2X_3		ML_3X_3 <1%	
	4	MX_2Z		MX_4 <1%		MLX_4		ML_2X_4		ML_3X_4 7%
	5		MX_3Z		MX_5		MLX_5		ML_2X_5	
	6	MX_2Z_2		MX_4Z		MX_6		MLX_6		ML_2X_6 <1%
	7		MX_3Z_2		MX_5Z		MX_7		MLX_7	
	8	MX_2Z_3		MX_4Z_2		MX_6Z		MX_8		MLX_8 <1%

Figure 34 MLX plot for organometallic iron compounds. While the majority of iron compounds are characterized by an 18-electron configuration, it is evident that these molecules belong to three molecular classes: ML_5 (20%), ML_4X_2 (71%) and ML_3X_4 (7%). Compounds which belong to MX_xZ_z classes (bottom left hand portion) are unknown.

Table 8 Commonly occurring classes of organotransition metal complexes

Group 3	Group 4	Group 5	Group 6	Group 7	Group 8	Group 9	Group 10
ScL_4X_3 (36%)	TiL_4X_4 (49%)	VL_6X (22%)	CrL_6 (48%)	MnL_5X (79%)	FeL_4X_2 (69%)	CoL_3X_3 (54%)	NiL_2X_2 (33%)
ScL_5X_3 (33%)	TiL_5X_3 (9%)	VL_4X_4 (16%)	CrL_5X_2 (24%)	MnL_4X_3 (12%)	FeL_5 (20%)	CoL_4X (34%)	NiL_3X_2 (26%)
ScL_3X_3 (10%)	TiL_2X_4 (7%)	VL_4X_3 (14%)	CrL_4X_4 (7%)	MnL_3X_5 (1%)	FeL_3X_4 (7%)	CoL_2X_5 (4%)	NiL_4 (16%)
YL_5X_3 (37%)	ZrL_4X_4 (55%)	NbL_5X_3 (32%)	MoL_5X_2 (40%)	TcL_5X (75%)	RuL_4X_2 (79%)	RhL_3X (41%)	PdL_2X_2 (81%)
YL_6X_3 (22%)	ZrL_5X_4 (25%)	NbL_6X (17%)	MoL_4X_4 (25%)	TcL_4X_3 (14%)	RuL_3X_4 (9%)	RhL_3X_3 (27%)	PdL_3X_2 (9%)
YL_4X_3 (19%)	ZrL_6X_2 (6%)	NbL_4X_5 (15%)	MoL_6 (19%)	TcL_3X_5 (2%)	RuL_5 (8%)	RhL_4X (22%)	PdL_3 (4%)
LaL_4X_3 (31%)	HfL_4X_4 (58%)	TaL_2X_5 (23%)	WL_5X_2 (34%)	ReL_5X (49%)	OsL_4X_2 (83%)	IrL_3X_3 (47%)	PtL_2X_2 (69%)
LaL_6X_3 (22%)	HfL_6X_2 (11%)	TaL_4X_5 (15%)	WL_4X_4 (27%)	ReL_4X_3 (29%)	OsL_5 (8%)	IrL_3X (26%)	PtL_2X_4 (11%)
LaL_3X_3 (17%)	HfL_5X_4 (8%)	TaL_5X_3 (14%)	WL_6 (15%)	ReL_3X_5 (4%)	OsL_3X_4 (7%)	IrL_4X (20%)	PtL_3 (9%)

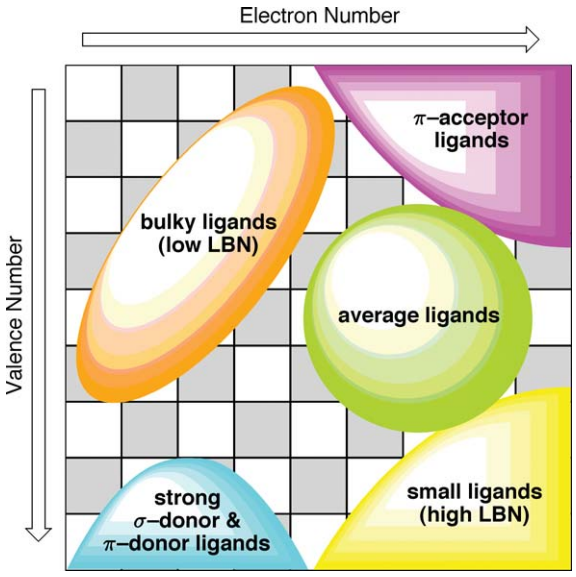

Figure 35 Domains favored by certain classes of ligands in a MLX plot.

these molecules may be attributed to the application of the novel preparative technique of metal vapor synthesis (see Chapter 1.08).

With respect to iron chemistry, the [*tris*(pyrazoly)hydroborato]iron carbonyl compound [PhTp$^{Bu^t}$]Fe(CO),[108] which is classified as ML_3X, represents a novel class of iron compound since the vast majority of iron compounds belong to the classes ML_5, ML_4X_2 and ML_3X_4 (see Table 8 and Figure 34). In this regard, it is evident that the $[ML_lX_xZ_z]$ classification provides a much better means of evaluating the nature of a molecule than does the oxidation number. For example, if one were to limit the description of [PhTp$^{Bu^t}$]Fe(CO) to its oxidation number (+1), one would conclude that the molecule is similar to well-known $[CpFe(CO)_2]_2$, which possesses iron with the same oxidation number. On this basis, [PhTp$^{Bu^t}$]Fe(CO) would be regarded as being unexceptional. However, the CBC method indicates that [PhTp$^{Bu^t}$]Fe(CO) and $[CpFe(CO)_2]_2$ possess *very* different classifications of ML_3X and ML_3X_4, respectively, and thereby clearly indicates that [PhTp$^{Bu^t}$]Fe(CO) belongs to a new and interesting class of monovalent iron compounds.

Examination of the MLX plots for all elements indicates that certain types of ligands may have a favored domain. For example, *(i)* π-acid ligands favor low valence numbers, *(ii)* small ligands favor high valence numbers and high ligand bond numbers, and *(iii)* bulky ligands favor low ligand bond numbers (Figure 35).

1.01.4.6 Trends Elucidated from MLX Plots

The information embodied in an MLX plot enables a variety of periodic trends to be established by comparing the distributions for the elements, as discussed in the following sections. Additional information pertaining to MLX distributions is available at http://www.columbia.edu/cu/chemistry/fac-bios/parkin/group/index.html.

1.01.4.6.1 Electron count

Since the electron count for a molecule of class $[ML_lX_xZ_z]$ is given by $EN = m + 2l + x$, it is a simple matter to use the $[ML_lX_xZ_z]$ classification to evaluate the distribution of molecules according to a specific electron count. Furthermore, given the prominence of the "18-electron rule" in the organometallic chemistry literature, it is pertinent to use these data to address the extent to which the "18-electron rule" can be considered a "rule".

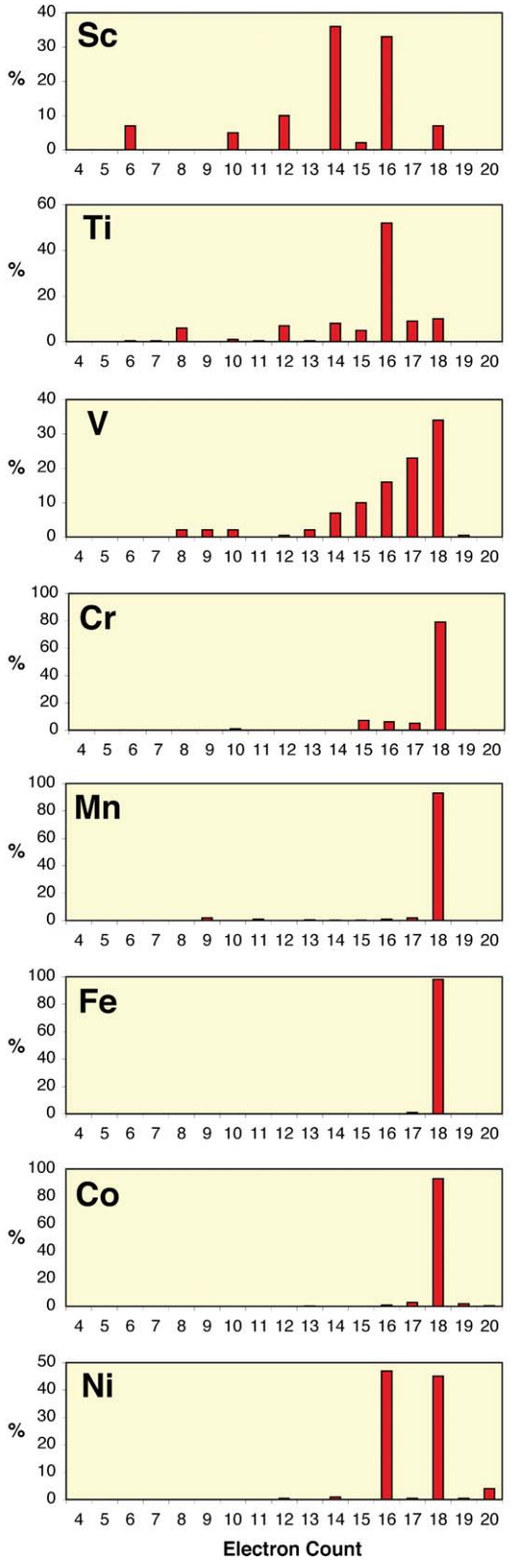

Figure 36 Variation of electron count for metals of the 1st transition series. An 18-electron configuration is most favored for the elements Cr to Co.

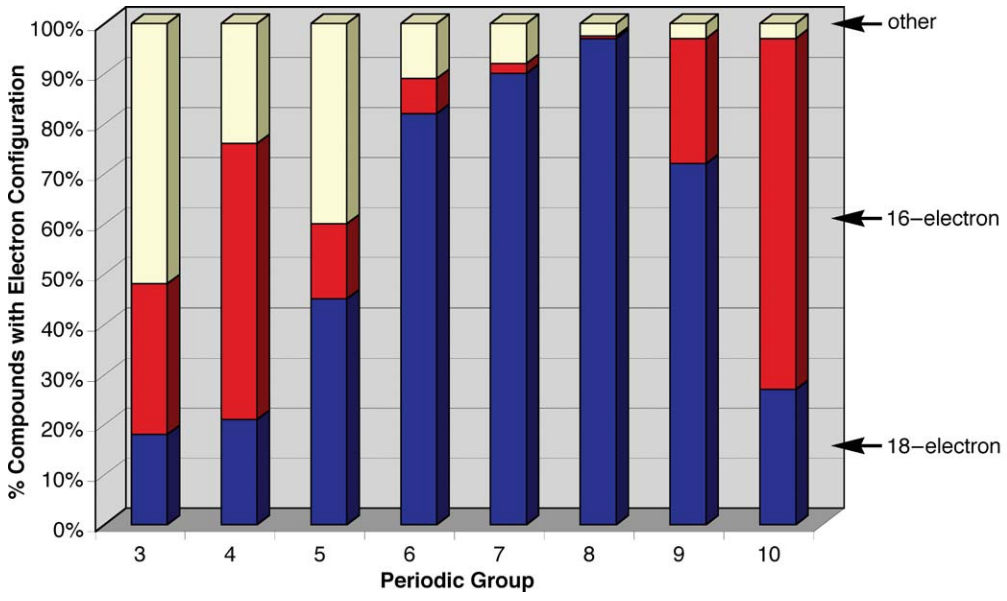

Figure 37 Distribution of compounds with 16- and 18-electron configurations as a function of periodic group. The 18-electron configuration is most common for the groups 6–8 transition metals.

For this reason, the electron counts for compounds of the 1st transition series are illustrated in Figure 36, from which it is evident that deviations from an 18-electron configuration are commonplace, with several elements (*e.g.* Sc, Ti, and V) having no strongly preferred electron count. The distribution of 18-electron compounds is illustrated as a function of periodic group in Figure 37, which indicates that the "18-electron rule" is most closely obeyed for the middle portion of the transition series (Groups 6–8). Both the earlier and later transition metals exhibit many deviations from this rule, as demonstrated by the distribution of 16-electron and 14-electron complexes (Figure 37). In fact, the preponderance of 16-electron and 14-electron complexes for the Groups 3 and 4 transition metals indicates that the "18-electron rule" provides a very poor description for the organometallic chemistry of these elements, and that their chemistry is much better described by a 14/16-electron rule.

For the earlier transition metals (*e.g.* Groups 3–5), the departure from the "18-electron rule" is commonly attributed to the fact that a large number of ligands are required to provide an 18-electron configuration because the neutral metal atoms have few valence electrons. For example, $V(CO)_6$ exists as a stable 17-electron molecule since it is sterically incapable of dimerizing to give the 18-electron species $(CO)_6V–V(CO)_6$. Such behavior is in marked contrast with respect to that of 17-electron $[Mn(CO)_5]$ which is coordinatively unsaturated and is unstable with respect to $(CO)_5Mn–Mn(CO)_5$. Likewise, $Cp^*_2ScCH_3$, albeit a 14-electron complex, is stable as a monomeric species due to the steric protection afforded by the bulky Cp^* ligands.

For the later transition metals (*e.g.* Groups 9 and 10), the departure from the "18-electron rule" is commonly associated with the fact that complexes of the later transition metals are typically associated with high d^n configurations (typically d^8 and d^{10}). The metal based d orbitals that house these electrons comprise a combination of 5 nonbonding and antibonding orbitals. The relative distribution of the nonbonding and antibonding orbitals is a sensitive function of the geometry and the favored geometries for high d^n counts are those that preserve the maximum number of nonbonding orbitals and result in fewer antibonding orbitals. This criterion is most readily achieved by low coordination numbers, a corollary of which is a low electron count. For example, an 18-electron d^8 trigonal bipyramidal geometry for NiL_3X_2 is unfavorable because it would require four electrons to occupy a pair of antibonding d orbitals, whereas the 16-electron square planar NiL_2X_2 counterpart requires only two electrons to occupy an antibonding orbital (Figure 38).

It is also worth noting that the occurrence of a $<$18-electron rule for the later transition metals is more pronounced for those of the 2nd and 3rd series (Figure 39). This trend is a consequence of larger radii of the 4d

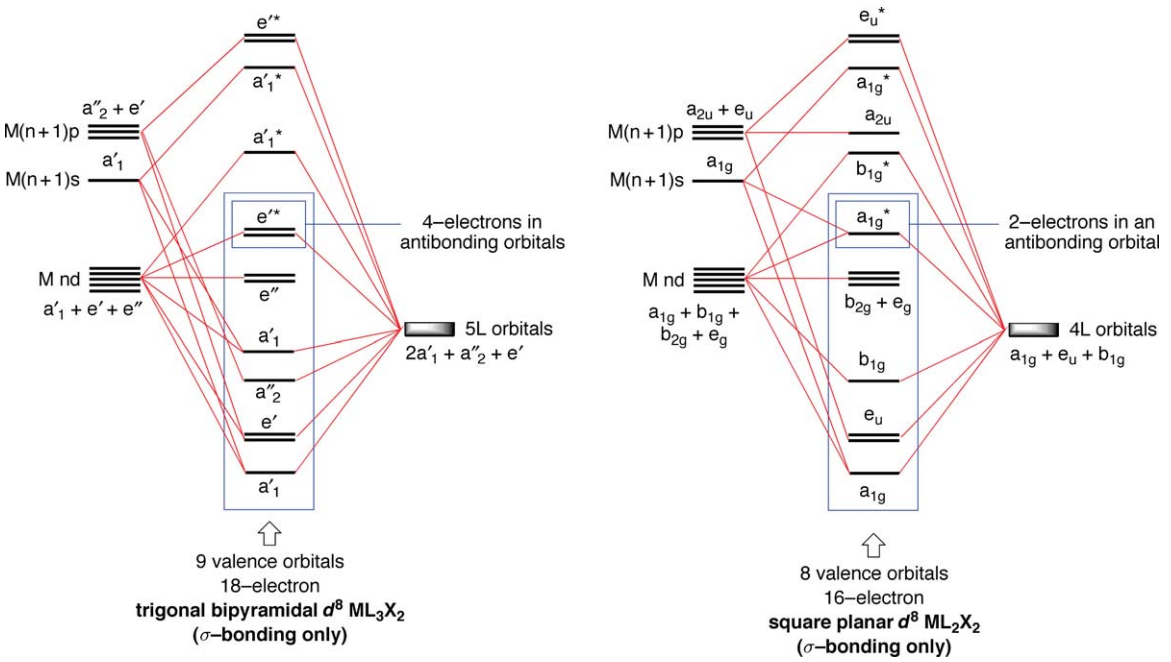

Figure 38 Comparison of the molecular orbital diagrams for trigonal planar and square planar geometries. Metals with high d^n configurations require electrons to occupy metal–ligand antibonding orbitals. An 18-electron d^8 ML_3X_2 complex requires four electrons to occupy antibonding orbitals, whereas a square planar 16-electron d^8 ML_2X_2 complex only requires two electrons to occupy antibonding orbitals. Thus, 16-electron configurations become common for the late transition metals.

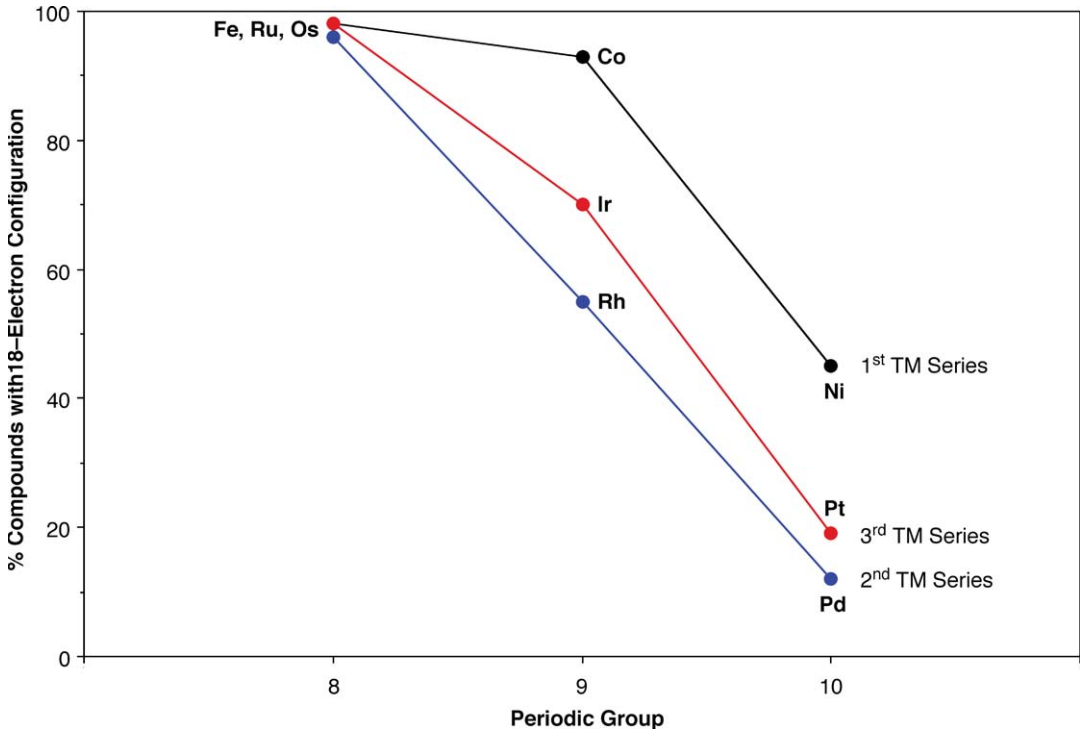

Figure 39 Occurrence of 18-electron molecules for the groups 8-10 transition metals. The proportion of non-18-electron compounds increases from group 8 to group 10, and is also greater for the metals of the 2nd and 3rd transition series than for the metals of the 1st transition series.

and 5d orbitals, which results in more effective overlap with the ligand orbitals, and thereby increases the ligand field splitting;[109] as such, the population of the metal-ligand antibonding orbitals is more unfavorable for the 2nd and 3rd transition series metals than for those of the 1st transition series. Correspondingly, the 2nd and 3rd transition series metals also form fewer compounds with >18-electron configurations. Classic examples of >18-electron compounds for the 1st transition series are provided by cobaltocene (Cp_2Co) and nickelocene (Cp_2Ni) which have 19- and 20-electron configurations, respectively.[110] The electron configurations of Cp_2Co and Cp_2Ni are such that the excess electrons are required to occupy antibonding orbitals, with the result that the M–Cp bond lengths increase with the electron count: Cp_2Fe (2.064 Å), Cp_2Co (2.119 Å), and Cp_2Ni (2.196 Å).[111]

1.01.4.6.2 Valence

Several observations can be made concerned with the periodic variation of the valence. Firstly, with respect to the distribution as a function of group, examination of Figure 40 demonstrates that the occurrence of the group valence is common up to Group 5, after which the two lowest valence states with an even d^n configuration become prevalent. The inability of the late transition metals to adopt their group valence states is a consequence of the fact that the availability of the d electrons for bonding diminishes dramatically across the transition series due to the increase in effective nuclear charge, as illustrated in Figure 41.[112,113] Furthermore, since the energy of the d-orbitals are very sensitive to the effective nuclear charge, their energy decreases significantly as the valence state of the metal increases with the addition of electronegative ligands. As a result of these two factors, the late transition metals rarely achieve their group valence in organometallic compounds.

A second observation is that the occurrence of higher valence states increases down a group, as illustrated for the Group 6 elements in Figure 42. Specifically, the proportion of zerovalent [ML_6] complexes decreases in the sequence Cr > Mo > W, while the proportion of hexavalent [ML_3X_6] complexes increases in the opposite sequence Cr < Mo < W.

The ability of the metals of the 2nd and 3rd transition series to form higher valent compounds than those of the 1st transition series may be attributed to the fact that the 3d orbitals are more sensitive than the 4d and 5d orbitals to the increase in effective nuclear charge because they penetrate the core more effectively. As a result of the greater sensitivity of the 3d orbitals, their availability for bonding diminishes rapidly as the partial positive charge on the metal increases upon coordination of electronegative substituents.[1]

It is also pertinent to note that that M–X bond strengths typically increase in progressing from the first to third transition series as illustrated by the M–H bond enthalpies of $CpM(CO)_3H$ (Cr, 61.7 kcal mol^{-1}; Mo, 67.4 kcal mol^{-1}; W, 81.0 kcal mol^{-1}).[114] The increase in M–H bond enthalpies is generally attributed to more favorable sd hybridization for the 2nd and 3rd transition series which results in a greater d component to the bonding (Figure 43).[115] Specifically, the transition metal orbitals that interact with the H 1s orbital are primarily the nd and (n + 1)s orbitals and the strength of the interaction depends upon the ability of these orbitals to hybridize. For the metals of the 1st transition series, the 3d and 4s orbitals have very different radial distributions, with the 4s orbitals being relatively diffuse, while the 3d orbitals are significantly contracted because they penetrate the core very effectively. Hybridization is particularly effective for the metals of the 3rd transition series because the 6s orbitals are contracted due to two factors (Figure 43). Firstly, the incorporation of the lanthanides results in a large increase in nuclear charge that is only partially screened by the filled 4f orbitals (the lanthanide contraction) and the impact of the increase in effective nuclear charge is greater for the 6s orbital than for the 5d orbitals because the latter have a zero coefficient at the nucleus. Secondly, relativistic effects also contract the 6s orbital which, as a consequence, minimizes contraction of the 5d orbital.[116] The overall result is that the 5d and 6s orbitals have more comparable radial distribution functions than the 3d/4s pair and thus are more prone to undergo hybridization.[117] In addition to more effective hybridization, the 5d orbital has a greater radial extent than those of the 4d and 3d orbitals (Figure 43) and thereby achieves greater overlap with the hydrogen 1s orbital.

Finally, the occurrence of valence states with an odd d^n configuration decreases upon going from the first to third transition series, as illustrated for V, Nb, and Ta (Figure 44), which shows that the number of d^1, d^3, and d^5 compounds is much greater for vanadium.

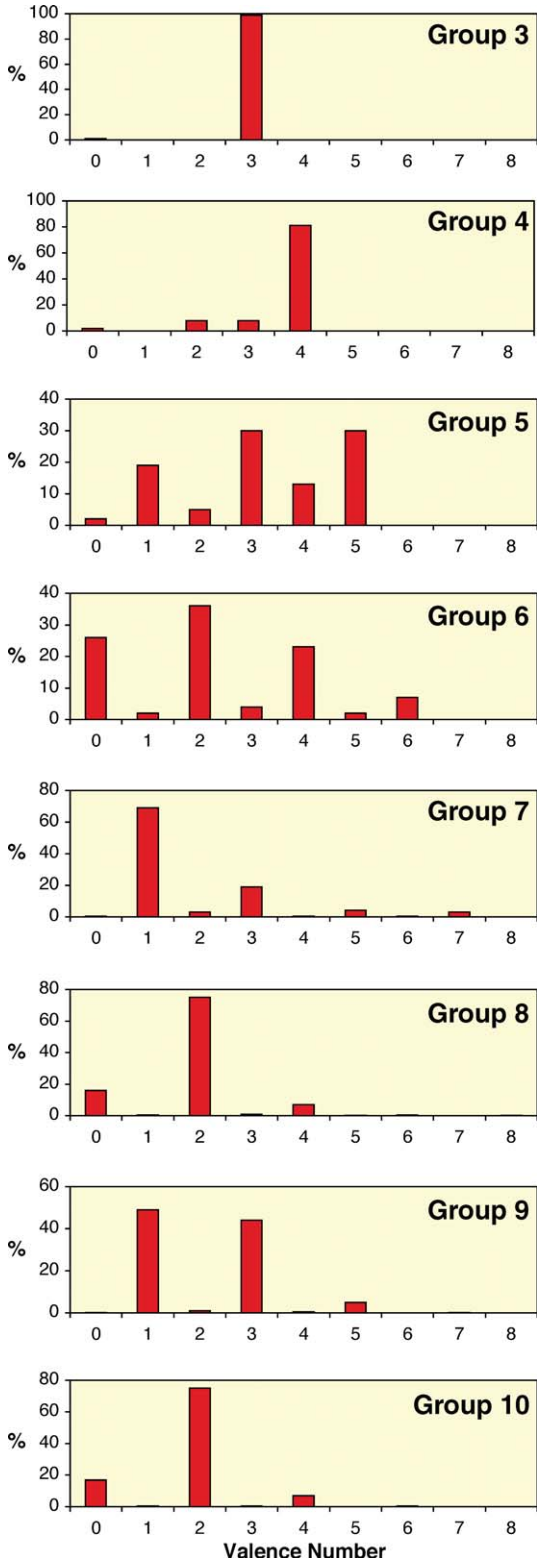

Figure 40 Variation of the valence of the transition metals as a function of periodic group.

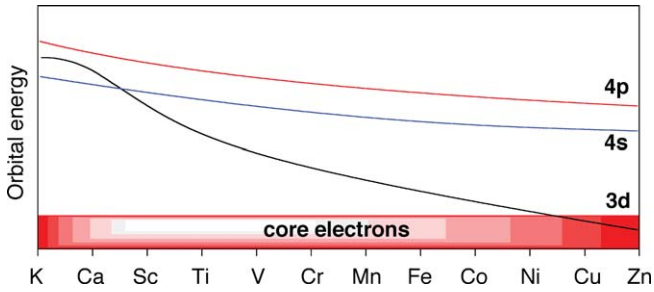

Figure 41 Schematic variation in the energies of the 3d, 4s and 4p orbitals across the 1st transition series. The 3d orbitals are stabilized rapidly upon progressing across the transition series because the d electrons do not shield each other effectively. Specifically, the d electrons have the same radial dependence such that the increase in nuclear charge across the transition series is not countered by the additional d electrons and so Z_{eff} for the 3d orbital increases rapidly. The 4s orbital also increases in stability across the transition series, but less rapidly than that for the 3d orbital. The lower sensitivity of 4s orbital energy is a consequence of the fact that the principal maximum of the 4s orbital lies beyond that of the 3d orbital. As a result, the 3d electrons effectively shield the 4s orbital from the increase in nuclear charge.

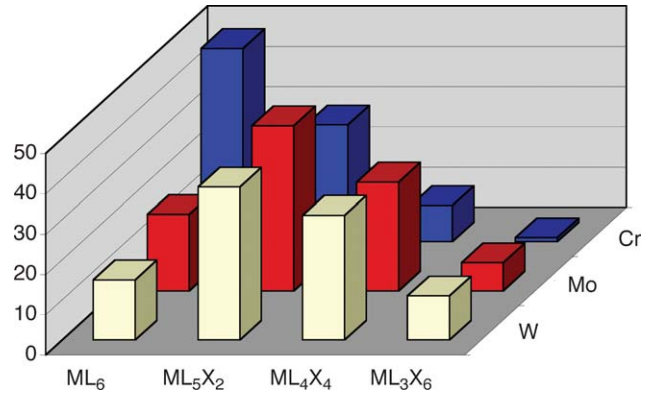

Figure 42 Comparison of the distribution of 18-electron complexes of Cr, Mo, and W according to their ML_lX_x classification. The number of zerovalent ML_6 complexes decreases in the sequence Cr > Mo > W, while the number of hexavalent ML_3X_6 complexes increases in the sequence Cr < Mo < W. Thus, high valence states are more common for the 3rd transition series.

1.01.4.6.3 Ligand bond number

The ligand bond number (*cf.* "coordination number") decreases smoothly upon passing from Group 3 to Group 10. Specifically, the most common ligand bond number decreases from 8 for Group 3 to a value of 4 for Group 10 (Figure 45). The greater ligand bond numbers for the early transition metals can be explained by consideration of two simple factors: *(i)* the early transition metals possess fewer valence electrons than the late transition metals and hence a greater number of ligand donor groups is required to remove the electron deficiency, and *(ii)* the early transition metals are larger than the late transition metals and can therefore accommodate more ligands.

1.01.4.6.4 Reactivity patterns

The MLX plot indicates classes of molecules that are particularly favored and those that are not favored. Although these are empirical observations, they provide an initial means of establishing whether or not a molecule is likely to be stable (isolable). The distribution also provides a guide for subsequent reactivity since it would be empirically expected that a molecule would undergo a transformation that would convert it to one with a more common class (Figure 46). All possible reactions of a compound may be described in terms of the variation of l and x in the ML_lX_x classification and may be represented accordingly in the MLX plot. For example, oxidative addition and reductive elimination are represented by transitions along a diagonal, while L-ligand addition and dissociation are represented by horizontal transitions (Figure 46).

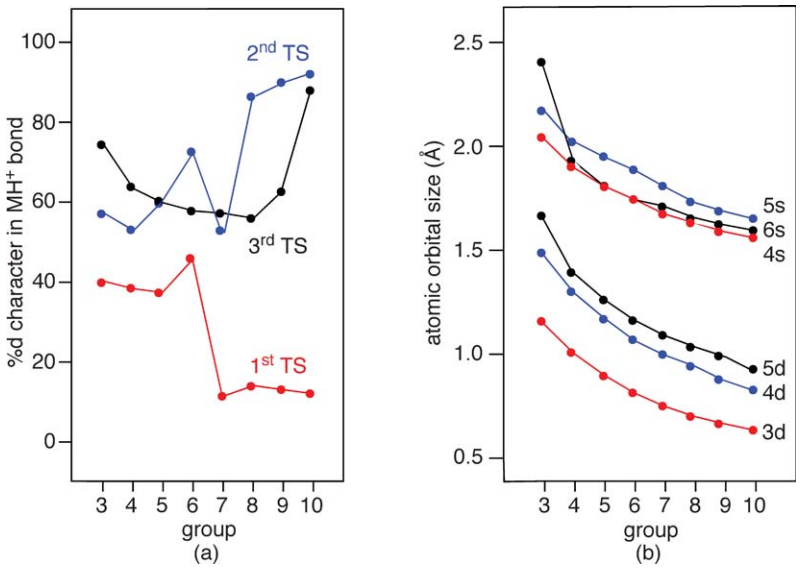

Figure 43 (a) Percent d orbital character in $[M–H]^+$ bond and (b) size of nd and (n + 1)s orbitals for the transition metals (data taken from: Ohanessian, G.; Goddard, W. A., III *Acc. Chem. Res.* **1990**, *23*, 386–392). (n + 1)s/nd hybridization is less effective for the metals of the 1st transition series because of the large difference in 4s and 3d orbital sizes.

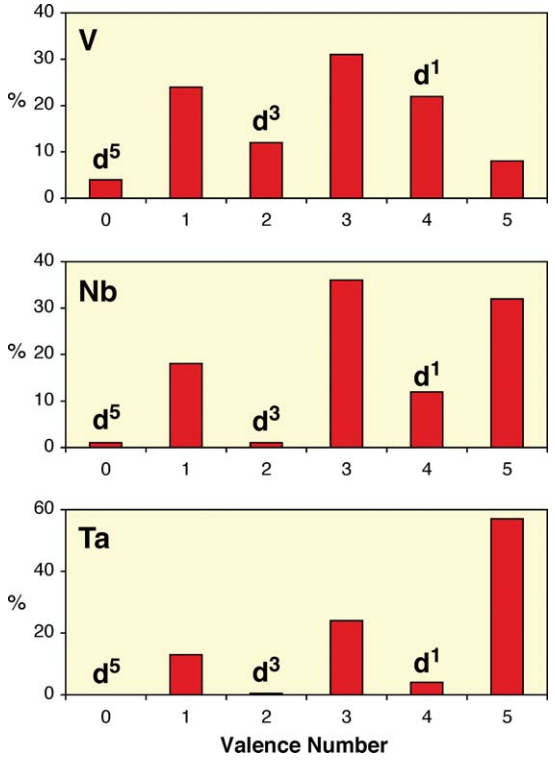

Figure 44 Comparison of the valence numbers of V, Nb, and Ta. In addition to the general increase in valence across the series V < Nb < Ta, there is a decrease in the occurrence of paramagnetic compounds with an odd d^n configuration.

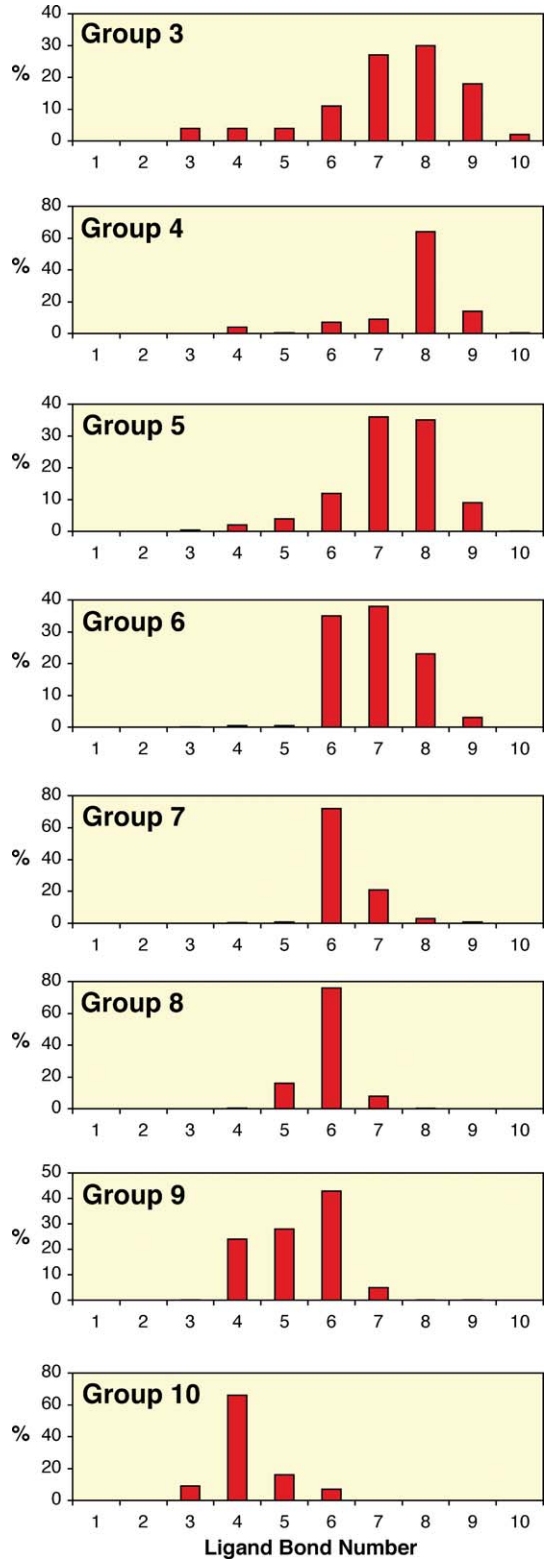

Figure 45 Variation of the ligand bond number of the transition metals in organometallic compounds as a function of periodic group. The most common value of the ligand bond number decreases progressively from a value of 8 for group 3 to a value of 4 for group 10.

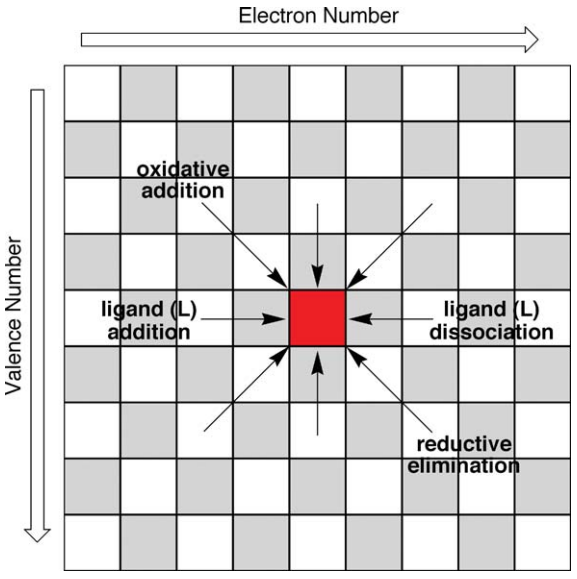

Figure 46 Reactivity guide implied by an MLX plot. Statistically, a molecule would be expected to undergo a reaction that would transform it from a class with low probability to one with high probability (highlighted in red). Each direction in a MLX plot corresponds to a specific type of reaction.

1.01.4.7 Distribution of Organotransition Metal Compounds According to their $ML_lX_xZ_z$ Classification

The MLX plots for the transition metals, constructed by using the compounds listed in the *Dictionary of Organometallic Compounds*,[105,106] are illustrated in Figures 47–54. These plots provide an immediate overview of the chemistry of a specific element. For example, the MLX plot for osmium indicates that this element shows a very strong tendency to form a single class of molecule, with the classification ML_4X_2 being 83% abundant. Representative examples of this class of compound include Cp_2Os and $Os(CO)_4(Me)H$. At the opposite extreme to osmium, some elements have no predilection to form a single class of compound. For example, examination of the MLX plot for vanadium indicates that the most popular class of organometallic vanadium compound, ML_6X (*e.g.* $V(CO)_6PbPh_3$, $[V(CO)_6]^-$, and $[V(dmpe)_2(CO)_2(MeCN)]^+$), is only 22% abundant.

1.01.5 Summary

In summary, the CBC method is based on an elementary molecular orbital analysis of metal-ligand bonding interactions and a molecule is described in terms of the representation $ML_lX_xZ_z$ where L_l, X_x and Z_z refer to the number of 2-electron, 1-electron, and 0-electron donor functions. By embodying the electron count $(m+2l+x)$, the valence of the metal $(x+2z)$, the ligand bond number $(l+x+z)$, and the d^n configuration $(n=m-x-2z)$, the $ML_lX_xZ_z$ classification affords much more information than that provided by the oxidation number. Furthermore, by identifying the different types of metal-ligand bonding interactions, the $ML_lX_xZ_z$ classification describes the nature of the metal *in the molecule* of interest, while the oxidation number merely describes the charge on the metal *after all ligands have been removed* (!). Finally, since there are several different methods used to assign oxidation numbers, there is often ambiguity in the derived values. These problems are exacerbated for organometallic compounds and, as such, the $ML_lX_xZ_z$ classification provides a much more useful method of classification for these molecules.

1.01.6 Dedication

This article is dedicated to Professor Malcolm L. H. Green, an incredible mentor whose concepts and insights provided the origin of this article, on the occasion of his 70th birthday.

Sc		Electron Number								
		10	11	12	13	14	15	16	17	18
Valence	0		ML_4		ML_5		ML_6 2%		ML_7	
	1	ML_3X		ML_4X		ML_5X		ML_6X		ML_7X
	2		ML_3X_2		ML_4X_2		ML_5X_2		ML_6X_2	
	3	ML_2X_3 5%		ML_3X_3 10%		ML_4X_3 36%		ML_5X_3 33%		ML_6X_3 7%

Y		Electron Number								
		10	11	12	13	14	15	16	17	18
Valence	0		ML_4		ML_5		ML_6		ML_7	
	1	ML_3X		ML_4X		ML_5X		ML_6X		ML_7X
	2		ML_3X_2		ML_4X_2		ML_5X_2		ML_6X_2	
	3	ML_2X_3 6%		ML_3X_3 17%		ML_4X_3 31%		ML_5X_3 11%		ML_6X_3 22%

La		Electron Number								
		10	11	12	13	14	15	16	17	18
Valence	0		ML_4		ML_5		ML_6 2%		ML_7	
	1	ML_3X		ML_4X		ML_5X		ML_6X		ML_7X
	2		ML_3X_2		ML_4X_2		ML_5X_2		ML_6X_2	
	3	ML_2X_3 5%		ML_3X_3 10%		ML_4X_3 36%		ML_5X_3 33%		ML_6X_3 7%

Figure 47 MLX plots for Sc, Y and La.

Ti

Valence \ Electron Number	8	9	10	11	12	13	14	15	16	17	18
0	ML_2		ML_3		ML_4		ML_5		ML_6 2%		ML_7 1%
1		ML_2X		ML_3X		ML_4X		ML_5X		ML_6X <1%	
2	MLX_2		ML_2X_2		ML_3X_2		ML_4X_2 1%		ML_5X_2 1%		ML_6X_2 4%
3		MLX_3		ML_2X_3 <1%		ML_3X_3 <1%		ML_4X_3 5%		ML_5X_3 9%	
4	MX_4 6%		MLX_4 1%		ML_2X_4 7%		ML_3X_4 6%		ML_4X_4 49%		ML_5X_4 4%

Zr

Valence \ Electron Number	8	9	10	11	12	13	14	15	16	17	18
0	ML_2		ML_3		ML_4		ML_5		ML_6 <1%		ML_7 <1%
1		ML_2X		ML_3X		ML_4X		ML_5X		ML_6X	
2	MLX_2		ML_2X_2		ML_3X_2 <1%		ML_4X_2		ML_5X_2 <1%		ML_6X_2 6%
3		MLX_3		ML_2X_3 <1%		ML_3X_3		ML_4X_3		ML_5X_3 2%	
4	MX_4 2%		MLX_4		ML_2X_4 3%		ML_3X_4 3%		ML_4X_4 55%		ML_5X_4 25%

Hf

Valence \ Electron Number	8	9	10	11	12	13	14	15	16	17	18
0	ML_2		ML_3		ML_4		ML_5		ML_6 <1%		ML_7 2%
1		ML_2X		ML_3X		ML_4X		ML_5X		ML_6X	
2	MLX_2		ML_2X_2		ML_3X_2		ML_4X_2		ML_5X_2 3%		ML_6X_2 11%
3		MLX_3		ML_2X_3 <1%		ML_3X_3		ML_4X_3 3%		ML_5X_3 9%	
4	MX_4 4%		MLX_4		ML_2X_4 7%		ML_3X_4 6%		ML_4X_4 58%		ML_5X_4 8%

Figure 48 MLX plots for Ti, Zr and Hf.

V

Valence \ Electron Number	10	11	12	13	14	15	16	17	18	19
0		ML_3		ML_4 <1%		ML_5		ML_6 3%		ML_7
1	ML_2X		ML_3X		ML_4X <1%		ML_5X 1%		ML_6X 22%	
2		ML_2X_2		ML_3X_2		ML_4X_2 8%		ML_5X_2 3%		ML_6X_2 <1%
3	MLX_3		ML_2X_3		ML_3X_3 3%		ML_4X_3 14%		ML_5X_3 11%	
4		MLX_4		ML_2X_4 1%		ML_3X_4 1%		ML_4X_4 16%		ML_5X_4
5	MX_5		MLX_5 <1%		ML_2X_5 4%		ML_3X_4 <1%		ML_4X_5 <1%	

Nb

Valence \ Electron Number	10	11	12	13	14	15	16	17	18	19
0		ML_3		ML_4		ML_5		ML_6 1%		ML_7
1	ML_2X		ML_3X		ML_4X		ML_5X 2%		ML_6X 17%	
2		ML_2X_2		ML_3X_2 <1%		ML_4X_2		ML_5X_2 <1%		ML_6X_2
3	MLX_3		ML_2X_3		ML_3X_3 2%		ML_4X_3 2%		ML_5X_3 32%	
4		MLX_4		ML_2X_4		ML_3X_4		ML_4X_4 12%		ML_5X_4
5	MX_5		MLX_5 2%		ML_2X_5 2%		ML_3X_4 10%		ML_4X_5 15%	

Ta

Valence \ Electron Number	10	11	12	13	14	15	16	17	18	19
0		ML_3		ML_4		ML_5		ML_6		ML_7
1	ML_2X		ML_3X		ML_4X		ML_5X <1%		ML_6X 13%	
2		ML_2X_2		ML_3X_2		ML_4X_2		ML_5X_2 <1%		ML_6X_2 <1%
3	MLX_3		ML_2X_3		ML_3X_3 6%		ML_4X_3 3%		ML_5X_3 14%	
4		MLX_4		ML_2X_4		ML_3X_4 1%		ML_4X_4 3%		ML_5X_4
5	MX_5		MLX_5 3%		ML_2X_5 23%		ML_3X_4 9%		ML_4X_5 15%	

Figure 49 MLX plots for V, Nb and Ta.

Cr

Valence	Electron Number 12	13	14	15	16	17	18
0	ML_3		ML_4		ML_5 <1%		ML_6 48%
1		ML_3X		ML_4X		ML_5X 3%	
2	ML_2X_2 <1%		ML_3X_2 <1%		ML_4X_2 5%		ML_5X_2 24%
3		ML_2X_3 <1%		ML_3X_3 7%		ML_4X_3 2%	
4	MLX_4		ML_2X_4		ML_3X_4 <1%		ML_4X_4 7%
5		MLX_5		ML_2X_5 <1%		ML_3X_5 <1%	
6	MX_6		MLX_6		ML_2X_6 <1%		ML_3X_6 <1%

Mo

Valence	Electron Number 12	13	14	15	16	17	18
0	ML_3		ML_4		ML_5 <1%		ML_6 19%
1		ML_3X		ML_4X		ML_5X 1%	
2	ML_2X_2		ML_3X_2		ML_4X_2 1%		ML_5X_2 40%
3		ML_2X_3 <1%		ML_3X_3 <1%		ML_4X_3 2%	
4	MLX_4		ML_2X_4 <1%		ML_3X_4 1%		ML_4X_4 25%
5		MLX_5		ML_2X_5 2%		ML_3X_5 <1%	
6	MX_6 <1%		MLX_6 <1%		ML_2X_6 3%		ML_3X_6 2%

W

Valence	Electron Number 12	13	14	15	16	17	18
0	ML_3		ML_4		ML_5 <1%		ML_6 15%
1		ML_3X		ML_4X		ML_5X 1%	
2	ML_2X_2		ML_3X_2		ML_4X_2 3%		ML_5X_2 34%
3		ML_2X_3		ML_3X_3 <1%		ML_4X_3 <1%	
4	MLX_4		ML_2X_4 <1%		ML_3X_4 3%		ML_4X_4 27%
5		MLX_5 <1%		ML_2X_5 <1%		ML_3X_5 <1%	
6	MX_6 3%		MLX_6 2%		ML_2X_6 3%		ML_3X_6 4%

Figure 50 MLX plots for Cr, Mo and W.

Mn

Valence	Electron Number 11	12	13	14	15	16	17	18	19
0	ML_2 <1%		ML_3		ML_4		ML_5 <1%		ML_6
1		ML_2X		ML_3X		ML_4X <1%		ML_5X 79%	
2	MLX_2 <1%		ML_2X_2 <1%		ML_3X_2		ML_4X_2 1%		ML_5X_2 <1%
3		MLX_3 <1%		ML_2X_3 <1%		ML_3X_3 <1%		ML_4X_3 12%	
4	MX_4 <1%		MLX_4		ML_2X_4 <1%		ML_3X_4		ML_4X_4
5		MX_5		MLX_5		ML_2X_5		ML_3X_5 1%	
6	MX_4Z		MX_6		MLX_6		ML_2X_6		ML_3X_6
7		MX_5Z		MX_7		MLX_7		ML_2X_7 <1%	

Tc

Valence	Electron Number 11	12	13	14	15	16	17	18	19
0	ML_2		ML_3		ML_4		ML_5		ML_6
1		ML_2X		ML_3X		ML_4X		ML_5X 75%	
2	MLX_2		ML_2X_2		ML_3X_2		ML_4X_2		ML_5X_2
3		MLX_3		ML_2X_3		ML_3X_3		ML_4X_3 14%	
4	MX_4		MLX_4		ML_2X_4 2%		ML_3X_4		ML_4X_4
5		MX_5		MLX_5		ML_2X_5		ML_3X_5 2%	
6	MX_4Z		MX_6		MLX_6		ML_2X_6		ML_3X_6
7		MX_5Z		MX_7 4%		MLX_7		ML_2X_7 2%	

Re

Valence	Electron Number 11	12	13	14	15	16	17	18	19
0	ML_2		ML_3		ML_4		ML_5		ML_6
1		ML_2X		ML_3X		ML_4X		ML_5X 49%	
2	MLX_2		ML_2X_2		ML_3X_2		ML_4X_2 1%		ML_5X_2
3		MLX_3		ML_2X_3		ML_3X_3 1%		ML_4X_3 29%	
4	MX_4 <1%		MLX_4 <1%		ML_2X_4		ML_3X_4 <1%		ML_4X_4
5		MX_5		MLX_5 1%		ML_2X_5 3%		ML_3X_5 4%	
6	MX_4Z		MX_6 <1%		MLX_6 <1%		ML_2X_6 <1%		ML_3X_6
7		MX_5Z		MX_7 3%		MLX_7 <1%		ML_2X_7 3%	

Figure 51 MLX plots for Mn, Tc and Re.

Fe

Valence \ Electron Number	10	11	12	13	14	15	16	17	18
0	ML		ML_2		ML_3		ML_4 <1%		ML_5 20%
1		MLX		ML_2X		ML_3X		ML_4X <1%	
2	MX_2		MLX_2		ML_2X_2 <1%		ML_3X_2 <1%		ML_4X_2 71%
3		MX_3		MLX_3		ML_2X_3		ML_3X_3 <1%	
4	MX_2Z		MX_4 <1%		MLX_4		ML_2X_4		ML_3X_4 7%
5		MX_3Z		MX_5		MLX_5		ML_2X_5	
6	MX_2Z_2		MX_4Z		MX_6		MLX_6		ML_2X_6 <1%
7		MX_3Z_2		MX_5Z		MX_7		MLX_7	
8	MX_2Z_3		MX_4Z_2		MX_6Z		MX_8		MLX_8 <1%

Ru

Valence \ Electron Number	10	11	12	13	14	15	16	17	18
0	ML		ML_2		ML_3		ML_4 <1%		ML_5 8%
1		MLX		ML_2X		ML_3X		ML_4X <1%	
2	MX_2		MLX_2		ML_2X_2 <1%		ML_3X_2 <1%		ML_4X_2 79%
3		MX_3		MLX_3 <1%		ML_2X_3		ML_3X_3 1%	
4	MX_2Z		MX_4 <1%		MLX_4 <1%		ML_2X_4 <1%		ML_3X_4 9%
5		MX_3Z		MX_5		MLX_5		ML_2X_5 <1%	
6	MX_2Z_2		MX_4Z		MX_6		MLX_6 <1%		ML_2X_6 <1%
7		MX_3Z_2		MX_5Z		MX_7		MLX_7	
8	MX_2Z_3		MX_4Z_2		MX_6Z		MX_8		MLX_8

Os

Valence \ Electron Number	10	11	12	13	14	15	16	17	18
0	ML		ML_2		ML_3 <1%		ML_4		ML_5 8%
1		MLX		ML_2X		ML_3X		ML_4X <1%	
2	MX_2		MLX_2		ML_2X_2		ML_3X_2		ML_4X_2 83%
3		MX_3		MLX_3		ML_2X_3		ML_3X_3 2%	
4	MX_2Z		MX_4 <1%		MLX_4		ML_2X_4		ML_3X_4 7%
5		MX_3Z		MX_5		MLX_5		ML_2X_5	
6	MX_2Z_2		MX_4Z		MX_6		MLX_6		ML_2X_6
7		MX_3Z_2		MX_5Z		MX_7		MLX_7	
8	MX_2Z_3		MX_4Z_2		MX_6Z		MX_8		MLX_8

Figure 52 MLX plots for Fe, Ru and Os.

Co

Valence \ Electron Number	11	12	13	14	15	16	17	18	19
0	ML		ML_2		ML_3		ML_4 <1%		ML_5
1		MLX		ML_2X		ML_3X <1%		ML_4X 34%	
2	MX_2		MLX_2 <1%		ML_2X_2		ML_3X_2 <1%		ML_4X_2 2%
3		MX_3		MLX_3 <1%		ML_2X_3 <1%		ML_3X_3 54%	
4	MX_2Z		MX_4 <1%		MLX_4		ML_2X_4 4%		ML_3X_4
5		MX_3Z		MX_5		MLX_5		ML_2X_5	
6	MX_2Z_2		MX_4Z		MX_6		MLX_6		ML_2X_6
7		MX_3Z_2		MX_5Z		MX_7		MLX_7 <1%	

Rh

Valence \ Electron Number	11	12	13	14	15	16	17	18	19
0	ML		ML_2		ML_3 <1%		ML_4		ML_5
1		MLX		ML_2X		ML_3X 41%		ML_4X 22%	
2	MX_2		MLX_2		ML_2X_2 <1%		ML_3X_2		ML_4X_2 <1%
3		MX_3		MLX_3 <1%		ML_2X_3 3%		ML_3X_3 27%	
4	MX_2Z		MX_4		MLX_4		ML_2X_4 4%		ML_3X_4
5		MX_3Z		MX_5		MLX_5		ML_2X_5 6%	
6	MX_2Z_2		MX_4Z		MX_6		MLX_6		ML_2X_6
7		MX_3Z_2		MX_5Z		MX_7		MLX_7 <1%	

Ir

Valence \ Electron Number	11	12	13	14	15	16	17	18	19
0	ML		ML_2		ML_3		ML_4		ML_5
1		MLX		ML_2X		ML_3X 26%		ML_4X 20%	
2	MX_2		MLX_2		ML_2X_2 <1%		ML_3X_2		ML_4X_2 <1%
3		MX_3 <1%		MLX_3		ML_2X_3 3%		ML_3X_3 47%	
4	MX_2Z		MX_4 <1%		MLX_4		ML_2X_4		ML_3X_4
5		MX_3Z		MX_5		MLX_5 <1%		ML_2X_5 4%	
6	MX_2Z_2		MX_4Z		MX_6		MLX_6		ML_2X_6
7		MX_3Z_2		MX_5Z		MX_7 <1%		MLX_7	

Figure 53 MLX plots for Co, Rh and Ir.

Ni

Valence \ Electron Number	12	13	14	15	16	17	18	19	20
0	ML <1%		ML_2 1%		ML_3 14%		ML_4 16%		ML_5 <1%
1		MLX		ML_2X		ML_3X <1%		ML_4X <1%	
2	MX_2 <1%		MLX_2 <1%		ML_2X_2 33%		ML_3X_2 26%		ML_4X_2 3%
3		MX_3		MLX_3		ML_2X_3 <1%		ML_3X_3 <1%	
4	MX_2Z		MX_4		MLX_4 <1%		ML_2X_4 4%		ML_3X_4 <1%
5		MX_3Z		MX_4		MLX_5		ML_2X_5	
6	MX_2Z_2		MX_4Z		MX_6 <1%		MLX_6		ML_2X_6

Pd

Valence \ Electron Number	12	13	14	15	16	17	18	19	20
0	ML		ML_2 <1%		ML_3 4%		ML_4 2%		ML_5
1		MLX		ML_2X		ML_3X		ML_4X <1%	
2	MX_2 <1%		MLX_2		ML_2X_2 81%		ML_3X_2 9%		ML_4X_2
3		MX_3		MLX_3 <1%		ML_2X_3		ML_3X_3	
4	MX_2Z		MX_4		MLX_4 <1%		ML_2X_4 2%		ML_3X_4
5		MX_3Z		MX_4		MLX_5		ML_2X_5	
6	MX_2Z_2		MX_4Z		MX_6 <1%		MLX_6		ML_2X_6

Pt

Valence \ Electron Number	12	13	14	15	16	17	18	19	20
0	ML		ML_2 <1%		ML_3 9%		ML_4 1%		ML_5
1		MLX		ML_2X		ML_3X		ML_4X	
2	MX_2		MLX_2		ML_2X_2 69%		ML_3X_2 7%		ML_4X_2
3		MX_3		MLX_3 <1%		ML_2X_3		ML_3X_3	
4	MX_2Z		MX_4 <1%		MLX_4 2%		ML_2X_4 11%		ML_3X_4
5		MX_3Z		MX_4		MLX_5		ML_2X_5	
6	MX_2Z_2		MX_4Z		MX_6 <1%		MLX_6		ML_2X_6

Figure 54 MLX plots for Ni, Pd and Pt.

References

1. Green, M. L. H. *J. Organomet. Chem.* **1995**, *500*, 127–148.
2. Although the words "stable" and "stability" are often used without qualification, it must be remembered that one must always consider kinetic and thermodynamic aspects of stability and it must also be specified to what transformation the stability refers.
3. The "18-electron rule" is variously referred to as "effective atomic number rule", "inert gas rule" and "rare gas rule" in the literature. For reviews of the 18-electron rule, see:

a. Mitchell, P. R.; Parish, R. V. *J. Chem. Educ.* **1969**, *46*, 811–814.
b. Craig, D. P.; Doggett, G. *J. Chem. Soc.* **1963**, 4189–4198.
c. Tolman, C. A. *Chem. Soc. Rev.* **1972**, *1*, 337–353.
d. Braterman, P. S. *Struct. Bond.* **1972**, *10*, 57–86.

4. For a discussion of the 18-electron rule in terms of the Complementary Spherical Electron Density Model, see:

a. Mingos, D. M. P. *J. Organomet. Chem.* **2004**, *689*, 4420–4436.
b. Mingos, D. M. P.; Hawes, J. C. *Struct. Bond.* **1985**, *63*, 1–63.

5. While the role of the nd and (n + 1)s orbitals in bonding is undisputed, the role of the (n + 1)p orbitals has been debated. Specifically, a suggestion has been made that the (n + 1)p orbitals are *not* used in the bonding description of transition metal alkyl and hydride complexes.[a–c] A consequence of this suggestion is that it implies a "12-electron rule". Molecules with >12-electron configurations would therefore be classified as hypervalent, which is an unusual concept since the vast majority of organotransition metal compounds fall into this category. The validity of the proposed non-participation of (n + 1)p orbitals has, however, subsequently been questioned, and the general consensus is that the (n + 1)p orbitals actually do play an important role in bonding.[d–f]

a. Landis, C. R.; Cleveland, T.; Firman, T. K. *J. Am. Chem. Soc.* **1995**, *117*, 1859–1860.
b. Landis, C. R.; Firman, T. K.; Root, D. M.; Cleveland, T. *J. Am. Chem. Soc.* **1998**, *120*, 1842–1854.
c. Landis, C. R.; Cleveland, T.; Firman, T. K. *J. Am. Chem. Soc.* **1998**, *120*, 2641–2649.
d. Bayse, C. A.; Hall, M. B. *J. Am. Chem. Soc.* **1999**, *121*, 1348–1358.
e. Diefenbach, A.; Bickelhaupt, F. M.; Frenking, G. *J. Am. Chem. Soc.* **2000**, *122*, 6449–6458.
f. Frenking, G.; Wichmann, K.; Fröhlich, N.; Loschen, C.; Lein, M.; Frunzke, J.; Rayón, V. M. *Coord. Chem. Rev.* **2003**, *238–239*, 55–82.

6. For a discussion of the history and origin of the "octet rule", see: Jensen, W. B. *J. Chem. Educ.* **1984**, *61*, 191–200.
7. For an early set of rules to determine oxidation numbers see: Pauling, L. *J. Chem. Soc.* **1948**, 1461–1467.
8. Lewis, J.; Nyholm, R. S. *Sci. Prog. (London)* **1964**, *52*, 557–580.
9. Jean, Y. In *Molecular Orbitals of Transition Metal Complexes*; Oxford University Press: New York, 2005, p 12.
10. Crabtree, R. H. In *The Organometallic Chemistry of the Transition Metals*, 4th edition; Wiley: New York, 2005, p 31.
11. The term "closed shell" refers to molecules for which all occupied orbitals are fully occupied, *i.e.* there are no unpaired electrons and there are no partially occupied degenerate orbitals. It is important to note that a closed shell configuration does *not* require an inert gas configuration. For example, BH_3 is a closed shell molecule. See:

a. Kutzelnigg, W.; Smith, V. H., Jr. *Int. J. Quantum Chem.* **1968**, *2*, 531–552.
b. Daudel, R.; Kozmutza, C.; Goddard, J. D.; Csizmadia, I. G. *J. Mol. Struct.* **1978**, *50*, 363–369.

12a. Elschenbroich, Ch.; Salzer, A. In *Organometallics*, 2nd edition; VCH: New York, 1992, p 309.
b. Spessard, G. O.; Miessler, G. L. In *Organometallic Chemistry*; Prentice-Hall: New Jersey, 1996, p 44.

13. For specific examples, see:

a. Andréa, R. R.; Terpstra, A.; Oskam, A.; Bruin, P.; Teuben, J. H. *J. Organomet. Chem.* **1986**, *307*, 307–317.
b. Gourier, D.; Samuel, E. *Inorg. Chem.* **1988**, *27*, 3018–3024.
c. Vogler, A.; Kunkely, H. *Coord. Chem. Rev.* **2004**, *248*, 273–278.

14a. Collman, J. P.; Hegedus, L. S.; Norton, J. R.; Finke, R. G. In *Principles and Applications of Organotransition Metal Chemistry*; University Science Books: Mill Valley, Califorinia, 1987, p 26.
b. Crabtree, R. H. In *The Organometallic Chemistry of the Transition Metals*, 4th edition; Wiley: New York, 2005, p 43.

15a. Janiak, C.; Klapötke, T. M.; Hans-Jürgen Meyer, H. J.; Reidel, E. *Moderne Anorganische Chemie*, 2003.
b. Green, M. L. H.; Ng, D. K. P. *Chem. Rev.* **1995**, *95*, 439–473.

16. Salzer, A. *Pure Appl. Chem.* **1999**, *71*, 1557–1585.

17a. Pauling, L. In *The Nature of The Chemical Bond*, 3rd ed.; Cornell University Press: Ithaca, NY, 1960, p 93.
b. Allred, A. L. *J. Inorg. Nucl. Chem.* **1961**, *17*, 215–221.
c. Porterfield, W. W. In *Inorganic Chemistry: A unified Approach*, 2nd Edn.; Academic Press: New York, 1993, p 46.

18. Jean, Y. In *Molecular Orbitals of Transition Metal Complexes*; Oxford University Press: New York, 2005, p 13.
19. Aluminum(I) compounds are known,[a] but typically possess Al–Al bonds.[b]

a. Haaland, A.; Martinsen, K.-J.; Shlykov, S. A.; Volden, H. V.; Dohmeier, C.; Schnöckel, H. *Organometallics* **1995**, *14*, 3116–3119.
b. Witt, M.; Roesky, H. W. *Curr. Sci.* **2000**, *78*, 410–430.

20. For example, as illustrated by the quote "··· assign the complexed ligand the same charge as in its most stable uncoordinated form. The formal oxidation state of the metal is then derived by balancing the charge." See: Elschenbroich, Ch.; Salzer, A. In *Organometallics*, 2nd edition; VCH: New York, 1992, p 309.
21. For recent reviews of metal nitrosyl compounds, see:

a. Hayton, T. W.; Legzdins, P.; Sharp, W. B. *Chem. Rev.* **2002**, *102*, 935–991.
b. McCleverty, J. A. *Chem. Rev.* **2004**, *104*, 403–418.
c. Machura, B. *Coord. Chem. Rev.* **2005**, *249*, 2277–2307.
d. Scheidt, W. R.; Ellison, M. K. *Acc. Chem. Res.* **1999**, *32*, 350–350.
e. Mingos, D. M. P.; Sherman, D. J. *Adv. Inorg. Chem.* **1989**, *34*, 293–377.

22. An additional problem with oxidation number assignments of nitrosyl compounds is the fact that the *International Union of Pure and Applied Chemistry* has recommended that NO should be viewed as a neutral ligand, analogous to CO! See: *International Union of Pure and Applied Chemistry*, *Nomenclature of Inorganic Chemistry*, Definitive Rules (2nd Edition); Section 7.323.

23a. Enemark, J. H.; Feltham, R. D. *Coord. Chem. Rev.* **1974**, *13*, 339–406, see especially page 348.

b. Feltham, R. D.; Enemark, J. H. In *Topics in Inorganic and Organic Stereochemistry*; Wiley: New York, **1981**; 12, pp 155–215, see especially page 158.
c. Westcott, B. L.; Enemark, J. H. In *Inorganic Electronic Structure and Spectroscopy*; Lever, A. B. P., Solomon, E. I., Eds.;*Inorganic Electronic Structure and Spectroscopy, Volume II: Applications and Case Studies*, Chapter 7, 1999; pp 403–450.
24. Scheidt, W. R.; Ellison, M. K. *Acc. Chem. Res.* **1999**, *32*, 350–359.
25. Richter-Addo, G. B.; Legzdins, G. B. *Metal Nitrosyls;* Oxford University Press: New York, 1992.
26a. Sutton, D. *Chem. Soc. Rev.* **1975**, *4*, 443–470.
b. Sutton, D. *Chem. Rev.* **1993**, *93*, 995–1022.
c. Collman, J. P.; Hegedus, L. S.; Norton, J. R.; Finke, R. G. In *Principles and Applications of Organotransition Metal Chemistry*; University Science Books: Mill Valley, Califorinia, 1987, p 29.
27. Collman, J. P.; Hegedus, L. S.; Norton, J. R.; Finke, R. G. In *Principles and Applications of Organotransition Metal Chemistry*; University Science Books: Mill Valley, Califorinia, 1987, p 75.
28a. Baker, R. T.; Whitney, J. F.; Wreford, S. S. *Organometallics* **1983**, *2*, 1049–1051.
b. Larsonneur, A.-M.; Choukroun, R.; Daran, J.-C.; Cuenca, T.; Flores, J. C.; Royo, P. *J. Organomet. Chem.* **1993**, *444*, 83–89.
29. Hey-Hawkins, E. *Chem. Rev.* **1994**, *94*, 1661–1717.
30. Zachmanoglou, C. E.; Docrat, A.; Bridgewater, B. M.; Parkin, G.; Brandow, C. G.; Bercaw, J. E.; Jardine, C. N.; Lyall, M.; Green, J. C.; Keister, J. B. *J. Am. Chem. Soc.* **2002**, *124*, 9525–9546.
31. Housecroft, C. E.; Sharpe, A. G. In *Inorganic Chemistry*; Prentice Hall: New York, 2001; p 35.
32. Sidgwick, N. V. In *The Electronic Theory of Valency*; The Clarendon Press: Oxford, 1927; p 216.
33a. Tate, D. P.; Augl, J. M.; Ritchey, W. M.; Ross, B. L.; Grasselli, J. G. *J. Am. Chem. Soc.* **1964**, *86*, 3261–3265.
b. King, R. B. *Inorg. Chem.* **1968**, 7, 1044–1046.
c. Laine, R. M.; Moriarty, R. E.; Bau, R. *J. Am. Chem. Soc.* **1972**, *94*, 1402–1403.
34a. Lauher, J. W.; Hoffmann, R. *J. Am. Chem. Soc.* **1976**, *98*, 1729–1742.
b. Jacobsen, H.; Berke, H.; Brackemeyer, T.; Eisenblätter, T.; Erker, G.; Fröhlich, R.; Meyer, O.; Bergander, K. *Helv. Chim. Acta* **1998**, *81*, 1692–1709.
c. Lukens, W. W., Jr.; Andersen, R. A. *Organometallics* **1995**, *14*, 3435–3439.
d. Palmer, E. J.; Bursten, B. E. *Polyhedron* **2005**, *25*, 575–584.
e. Strittmatter, R. J; Bursten, B. E. *J. Am. Chem. Soc.* **1991**, *113*, 552–559.
f. Bursten, B. E.; Rhodes, L. F.; Strittmatter, R. J. *J. Am. Chem. Soc.* **1989**, *111*, 2758–2766.
g. Bursten, B. E.; Strittmatter, R. J. *Angew. Chem., Int. Ed. Engl.* **1991**, *30*, 1069–1085.
35a. Schofield, M. H.; Kee, T. P.; Anhaus, J. T.; Schrock, R. R.; Johnson, K. H.; Davis, W. M. *Inorg. Chem.* **1991**, *30*, 3595–3604.
b. Anhaus, J. T.; Kee, T. P.; Schofield, M. H.; Schrock, R. R. *J. Am. Chem. Soc.* **1990**, *112*, 1642–1643.
c. Lin, Z.; Hall, M. B. *Coord. Chem. Rev.* **1993**, *123*, 149–167.
36. Morrison, D. L.; Wigley, D. E. *Inorg. Chem.* **1995**, *34*, 2610–2616.
37. Davison, A.; Wreford, S. S. *Inorg. Chem.* **1975**, *14*, 703.
38. Jonas, K.; Kolb, P.; Kollbach, G.; Gabor, B.; Mynott, R.; Angermund, K.; Heinemann, O.; Krüger, C. *Angew. Chem. Int. Ed. Engl.* **1997**, *36*, 1714–1718.
39a. Costuas, K.; Saillard, J.-Y. *Chem. Commun.* **1998**, 2047–2048.
b. King, R. B. *Appl. Organomet. Chem.* **2003**, *17*, 393–397.
c. Gleiter, R.; Bethke, S.; Okubo, J.; Jonas, M. *Organometallics* **2001**, *20*, 4274–4278.
40. Note, however, that there is an f orbital of appropriate symmetry to interact with this ligand combination orbital and this interaction is of importance to actinide derivatives.
41. η^2-coordination of the cyclopentadienyl ligand is also known, and a molecular orbital analysis suggests that it serves as a three electron donor. See:
a. Lucas, C. R.; Green, M.; Forder, R. A.; Prout, K. *J. Chem. Soc., Chem. Commun.* **1973**, 97–98.
b. Corradi, M. M.; Duncalf, D. J.; Lawless, G. A.; Waugh, M. P. *Chem. Commun.* **1997**, 203–204.
c. Diamond, G. M.; Chernaga, A. N.; Mountford, P.; Green, M. L. H. *J. Chem. Soc., Dalton Trans.* **1996**, 921–938.
d. Hansen, L. M.; Marynick, D. S. *Organometallics* **1989**, *8*, 2173–2179.
42. O'Connor, J. M.; Casey, C. P. *Chem. Rev.* **1987**, *87*, 307–318.
43a. Parkin, G.; van Asselt, A.; Leahy, D. J.; Whinnery, L.; Hua, N. G.; Quan, R. W.; Henling, L. M.; Schaefer, W. P.; Santarsiero, B. D.; Bercaw, J. E. *Inorg. Chem.* **1992**, *31*, 82–85.
b. Walsh, P. J.; Hollander, F. J.; Bergman, R. G. *J. Am. Chem. Soc.* **1988**, *110*, 8729–8731.
c. Schofield, M. H.; Kee, T. P.; Anhaus, J. T.; Schrock, R. R.; Johnson, K. H.; Davis, W. M. *Inorg. Chem.* **1991**, *30*, 3595–3604.
44a. Templeton, J. L. *Adv. Organomet. Chem.* **1989**, *29*, 1–100.
b. Templeton, J. L.; Ward, B. C. *J. Am. Chem. Soc.* **1980**, *102*, 3288–3299.
45a. Parkin, G. *Prog. Inorg. Chem.* **1998**, *47*, 1–165.
b. Trnka, T. M.; Parkin, G. *Polyhedron* **1997**, *16*, 1031–1045.
c. Nugent, W. A.; Mayer, J. M. *Metal-Ligand Multiple Bonds*; Wiley-Interscience: New York,1998.
46. Berry, M.; Cooper, N. J.; Green, M. L. H.; Simpson, S. J. *J. Chem. Soc., Dalton Trans.* **1980**, 29–41.
47a. Brookhart, M.; Green, M. L. H. *J. Organomet. Chem.* **1983**, *250*, 395–408.
b. Brookhart, M.; Green, M. L. H.; Wong, L. L. *Prog. Inorg. Chem.* **1988**, *36*, 1–124.
48. Xu, Z.; Lin, Z. *Coord. Chem. Rev.* **1996**, *156*, 139–162.
49a. Collman, J. P.; Hegedus, L. S.; Norton, J. R.; Finke, R. G. In *Principles and Applications of Organotransition Metal Chemistry*; University Science Books: Mill Valley, Califorinia, 1987, p 24 and 36.
b. Owen, S. M. *Polyhedron* **1988**, 7, 253–283.
c. Housecroft, C. E.; Sharpe, A. G. In *Inorganic Chemistry*; Prentice Hall: New York, 2001, p 591.
50. For a specific example, see: Bennett, M. J.; Graham, W. A. G.; Hoyano, J. K.; Hutcheon, W. L. *J. Am. Chem. Soc.* **1972**, *94*, 6232–6233.
51. Baik, M.-H.; Friesner, R. A.; Parkin, G. *Polyhedron* **2004**, *23*, 2879–2900.
52. Bursten, B. E.; Cayton, R. H. *Organometallics* **1988**, 7, 1349–1356.
53. Casey, C. P.; Sakaba, H.; Hazin, P. N.; Powell, D. R. *J. Am. Chem. Soc.* **1991**, *113*, 8165–8166.

54. Koga, N.; Morokuma, K. *J. Mol. Struct.* **1993**, *300*, 181–189.
55. For a brief review, see:Parkin, G. *J. Chem. Educ.* **2006**, *83*, 791–799.
56. Smith, D. W. *J. Chem. Educ.* **2005**, *82*, 1202–1204.
57. Jean, Y. In *Molecular Orbitals of Transition Metal Complexes*; Oxford University Press: New York, 2005, p 12 and 31.
58. Albright, T. A.; Burdett, J. K.; Whangbo, M. H. In *Orbital Interactions in Chemistry*; Wiley: New York, 1985, p 299 & 301.

59a. King, R. B., Ed. *Encyclopedia of Inorganic Chemistry* Wiley: New York, 1994; Vol. 2, 961.
b. Crabtree, R. H. In *The Organometallic Chemistry of the Transition Metals*, 4th edition; Wiley: New York, 2005, p 43.

60. Burlitch, J. M.; Leonowicz, M. E.; Petersen, R. B.; Hughes, R. E. *Inorg. Chem.* **1979**, *18*, 1097–1105.
61. Mayer, J. M.; Calabrese, J. C. *Organometallics* **1984**, *3*, 1292–1298.

62a. Nowell, I. N.; Russell, D. R. *Chem. Commun.* **1967**, 817.
b. Cook, D. J.; Daws, J. L.; Kemmitt, R. D. W. *J. Chem. Soc. (A)* **1967**, 1547–1551.
c. Nowell, I. N.; Russell, D. R. *J. Chem. Soc., Dalton Trans.* **1972**, 2393–2395.

63. Dey, K.; Werner, H. *J. Organomet. Chem.* **1977**, *137*, C28–C30.
64. Crotty, D. E.; Anderson, T. J.; Glick, M. D.; Oliver, J. P. *Inorg. Chem.* **1977**, *16*, 2346–2350.
65. Landry, V. K.; Melnick, J. G.; Buccella, D.; Pang, K.; Ulichny, J. C.; Parkin, G. *Inorg. Chem.* **2006**, *45*, 2588–2597.
66. In this regard, it is important to emphasize that, in contrast to oxidation number, the formal charge of an atom in a molecule depends on the resonance structure that is being considered. For example, the formal charge on osmium in OsO_4 is zero if the osmium-oxygen bond is represented as a Os═O double bond, but is +4 if the bond is represented as Os^{+}-O^{-}; in each case, however, the oxidation number is +8 because the oxygen is removed as a "−2" ligand regardless of the precise nature of the bonding interaction.
67. It is important to note that the calculated charges for atoms in molecules depends critically on the method used. For illustrative examples, see:
a. De Proft, F.; Van Alsenoy, C.; Peeters, A.; Langenaeker, W.; Geerlings, P. *J. Comput. Chem.* **2002**, *23*, 1198–1209.
b. Haaland, A.; Helgaker, T. U.; Ruud, K.; Shorokhov, D. J. *J. Chem. Ed.* **2000**, *77*, 1076–1080.
c. Bader, R. F. W.; Matta, C. F. *J. Phys. Chem. (A)* **2004**, *108*, 8385–8394.
68. See, for example, a discussion pertaining to $ArGaFe(CO)_4$:
a. Cotton, F. A.; Feng, X. *Organometallics* **1998**, *17*, 128–130.
b. Boehme, C.; Frenking, G. *Chem. Eur. J.* **1999**, *5*, 2184–2190.
69. See, for example:
a. Greenberg, A.; Winkler, R.; Smith, B. L.; Liebman, J. F. *J. Chem. Educ.* **1982**, *59*, 367–370.
b. Wurthwein, E. U.; Sen, K. D.; Pople, J. A.; Schleyer, P. V. *Inorg. Chem.* **1983**, *22*, 496–503.
c. Sorensen, J. B.; Lewin, A. H.; Bowen, J. P. *Theochem-J. Mol. Struct.* **2003**, *623*, 145–158.
70. Pauling originally expressed the charge range as |±0.5|. See: Pauling, L. *J. Chem. Soc.* **1948**, 1461–1467.
71. Hoffmann, R. *American Scientist* **2001**, *89*, 311–313.
72. Seddon, E. A.; Seddon, K. R. *The Chemistry of Ruthenium* Elsevier: New York, 1984, Chapter 4.
73. See, for example: Albright, T. A.; Burdett, J. K.; Whangbo, M. H. In *Orbital Interactions in Chemistry*; Wiley: New York, 1985; p 277.
74. The term "coordination number" was first introduced by Werner. See and: Sidgwick, N. V. In *The Electronic Theory of Valency*; The Clarendon Press: Oxford, 1927, p 109.
a. *International Union of Pure and Applied Chemistry, Nomenclature of Inorganic Chemistry*, Definitive Rules (2^{nd} Edition); Section 0.2.
b. Pauling, L. In *The Nature of The Chemical Bond*, 3rd ed.; Cornell University Press: Ithaca, NY, 1960, p 63.
75. For example, the cyclopentadienyl ligand has been considered as occupying a single coordination site in Cp_2ZrPh_2. See: Clegg, W.; Horsburgh, L.; Lindsay, D. M.; Mulvey, R. E. *Acta Cryst.* **1998**, *C54*, 315–317.

76a. Green, M. L. H. *J. Organomet. Chem.* **1995**, *500*, 127–148.
b. Green, M. L. H., Braithwaite, E. R., Haber, J., Eds.; In *Molybdenum: an Outline of its Chemistry and Uses,* Elsevier: Amsterdam 1994, Chapter 2.

77. For an early system to provide a formal organization of coordination compounds with monodentate ligands, see: King, R. B. *Adv. Chem. Ser.* **1967**, *62*, 203–220.
78. Seddon and Seddon have applied the CBC method to the chemistry of ruthenium and have critically discussed the concept of oxidation state. See:Seddon, E. A.; Seddon, K. R. *The Chemistry of Ruthenium*; Elsevier: New York, 1984, Chapter 2.
79. For textbooks that have adopted aspects of the CBC method, see
a. Crabtree, R. H. In *The Organometallic Chemistry of the Transition Metals*, 4th edition; Wiley: New York, 2005, p 32.
b. Spessard, G. O.; Miessler, G. L. In *Organometallic Chemistry*; Prentice-Hall: New Jersey, 1996, p 47.
c. Jean, Y. In *Molecular Orbitals of Transition Metal Complexes*; Oxford University Press: New York, 2005, p 4.
80. Haaland, A. *Angew. Chem. Int. Ed. Engl.* **1989**, *28*, 992–1007.
81. Taylor, T. E.; Hall, M. B. *J. Am. Chem. Soc.* **1984**, *106*, 1576–1584.
82. For an early reference which combines the two independent papers with the term "Dewar–Chatt–Duncanson model", see: Nelson, J. H.; Wheelock, K. S.; Jonassen, H. B. *Chem. Commun.* **1969**, 1019–1020.
83. For a historical perspective of the origin of the Dewar–Chatt–Duncanson model, see: Mingos, D. M. P. *J. Organomet. Chem.* **2001**, *635*, 1–8.
84. Note that the [X-μ-L] terminology is intended to imply that the bridging ligand behaves as an X ligand to one metal center and as a L ligand to the other. It is not intended to imply that it behaves as an [XL] ligand to both metals *at the same time*. However, in certain cases, the bonding could equally well be described by [L-μ-X], and thus the bonding is better described as a resonance hybrid of the two extremes.

85a. Lynn, P. D.; Mingos, D. M. P. *J. Organomet. Chem.* **1994**, *478*, 141–151.
b. Marynick, D. S. *J. Am. Chem. Soc.* **1984**, *106*, 4064–4065.
c. Dunne, B. J.; Morris, R. B.; Orpen, A. G. *J. Chem. Soc., Dalton Trans.* **1991**, 653–661.

86. In contrast, the N–H σ^{*} antibonding orbitals are of high energy and do not serve as good acceptor orbitals.
87. Frenking, G. *J. Organomet. Chem.* **2001**, *635*, 9–23.
88. Fischer, E. O. *Adv. Organomet. Chem.* **1976**, *14*, 1–32.

89a. Schrock, R. R. *Chem. Commun.* **2005**, 2773–2777.
b. Schrock, R. R. *Chem. Rev.* **2002**, *102*, 145–179.
c. Schrock, R. R. *J. Chem. Soc., Dalton Trans.* **2001**, 2541–2550.

90a. Frenking, G.; Fröhlich, N. *Chem. Rev.* **2000**, *100*, 717–774.
b. Frenking, G.; Sola, M.; Vyboishcikov, S. F. *J. Organomet. Chem.* **2005**, *690*, 6178–6204.

91. Jean, Y. In *Molecular Orbitals of Transition Metal Complexes*; Oxford University Press: New York, 2005, p 167.
92. Herrmann, W. A. *Angew. Chem. Int. Ed. Engl.* **2002**, *41*, 1290–1309.
93. Lee, M.-T.; Hu, C.-H. *Organometallics* **2004**, *23*, 976–983.
94. Green, J. C.; Herbert, B. J. *Dalton Trans.* **2005**, 1214–1220.
95. Cavallo, L.; Correa, A.; Costabile, C.; Jacobsen, H. *J. Organomet. Chem.* **2005**, *690*, 5407–5413.
96. Crabtree, R. H. *J. Organomet. Chem.* **2005**, *690*, 5451–5457.
97a. Manoharan, P. T.; Gray, H. B. *Inorg. Chem.* **1966**, *5*, 823–839.
b. Fenske, R. F.; DeKock, R. L. *Inorg. Chem.* **1972**, *11*, 437–444.
c. Hoffmann, R.; Chen, M. M. L.; Elian, M.; Rossi, A. R.; Mingos, D. M. P. *Inorg. Chem.* **1974**, *13*, 2666–2675.
d. Thomas, J. L. C.; Bauschlicher, C. W., Jr.; Hall, M. B. *J. Phys. Chem. (A)* **1997**, *101*, 8530–8539.
98. Note, however, that there is a typographical error with respect to the formal charges on the triply bonded structure (30). Mingos, D. M. P.; Sherman, D. J. *Adv. Inorg. Chem.* **1989**, *34*, 293–377.
99. Williams, D. S.; Meyer, T. J.; White, P. S. *J. Am. Chem. Soc.* **1995**, *117*, 823–824.
100a. Odom, A. L.; Cummins, C. C.; Protasiewicz, J. D. *J. Am. Chem. Soc.* **1995**, *117*, 6613–6614.
b. Veige, A. S.; Slaughter, L. M.; Lobkovsky, E. B.; Wolczanski, P. T.; Matsunaga, N.; Decker, S. A.; Cundari, T. R. *Inorg. Chem.* **2003**, *42*, 6204–6224.
101. Crevier, T. J.; Lovell, S.; Mayer, J. M.; Rheingold, A. L.; Guzei, I. A. *J. Am. Chem. Soc.* **1998**, *120*, 6607–6608.
102. Ehlers, A. W.; Dapprich, S.; Vyboishchikov, S. F.; Frenking, G. *Organometallics* **1996**, *15*, 105–117.
103. Batsanov, S. S. *Russ. Chem. Bull.* **1995**, *44*, 2245–2250.
104. The reason for *z* being 0 is a consequence of the fact that organotransition metal molecules that contain a Z function ligand invariably possess an L function ligand, with the result that the combined LZ function transforms to the X_2 description. Molecules that contain a Z function in the classification are, nevertheless known; for example, $[NH_4]^+$ is classified as $[NX_3Z]$ upon reducing the $[NX_4]^+$ classification to the equivalent neutral class using the rule that $X^+ = Z$.
105. *Dictionary of Organometallic Compounds*; Chapman and Hall: New york, **1984**.
106. The compounds were classified and compiled by Cary E. Zachmanoglou.
107. Cloke, F. G. N. *Chem. Soc. Rev.* **1993**, 17–24.
108. Kisko, J. L.; Hascall, T.; Parkin, G. *J. Am. Chem. Soc.* **1998**, *120*, 10561–10562.
109a. Mingos, D. M. P. In *Essential Trends in Inorganic Chemistry*; Oxford University Press: New York, 1998, p 330.
b. Gray, H. B.; DeKock, R. L. *Chemical Structure and Bonding;* Benjamin/Cummings: Menlo Park, California, **1980**.
110. In fact, Green has noted that the early discovery of metallocene complexes, Cp_2M (M = V, Cr, Mn, Fe, Co, Ni), with electron counts ranging from 15 to 20 actually undermined the confidence in the 18-electron rule for organometallic compounds which previously had found much success with carbonyl compounds. See: Green, M. L. H. *J. Chem. Soc., Dalton Trans.* **1991**, 575–577.
111. Haaland, A. *Acc. Chem. Res.* **1979**, *12*, 415–422.
112a. Wulfsberg, G. In *Inorganic Chemistry*; University Science Books: Sausalito, California, 2000, p 21.
b. Cotton, F. A.; Wilkinson, G. In *Advanced Inorganic Chemistry*, 5th Edn.; Wiley: New York, 1988 p 627.
c. Frenking, G.; Fröhlich, N. *Chem. Rev.* **2000**, *100*, 717–774.
113a. Vanquickenborne, L. G.; Pierloot, K.; Devoghel, D. *J. Chem. Educ.* **1994**, *71*, 469–471.
b. Melrose, M. P.; Scerri, E. R. *J. Chem. Educ.* **1996**, *73*, 498–503.
c. Melrose, M. P.; Scerri, E. *J. Chem. Educ.* **1997**, *74*, 616–616.
d. Bills, J. L. *J. Chem. Educ.* **1998**, *75*, 589–593.
e. Vanquickenborne, L. G.; Pierloot, K.; Devoghel, D. *Inorg. Chem.* **1989**, *28*, 1805–1813.
f. Pilar, F. L. *J. Chem. Educ.* **1978**, *55*, 2–6.
g. Meek, T. L.; Allen, L. C. *Chem. Phys. Lett.* **2002**, *362*, 362–364.
h. Bills, J. L.; Snow, R. L. *Inorg. Chim. Acta* **1995**, *229*, 171–178.
i. Autschbach, J.; Siekierski, S.; Seth, M.; Schwerdtfeger, P.; Schwarz, W. H. E. *J. Computational Chem.* **2002**, *23*, 804–813.
114. Martinho Simões, J. A.; Beauchamp, J. L. *Chem. Rev.* **1990**, *90*, 629–688.
115a. Ohanessian, G.; Goddard, W. A. III *Acc. Chem. Res.* **1990**, *23*, 386–392.
b. Landis, C. R.; Firman, T. K.; Root, D. M.; Cleveland, T. *J. Am. Chem. Soc.* **1998**, *120*, 1842–1854.
c. Bayse, C. A.; Hall, M. B. *J. Am. Chem. Soc.* **1999**, *121*, 1348–1358.
d. Frenking, G.; Fröhlich, N. *Chem. Rev.* **2000**, *100*, 717–774.
e. Niu, S.; Hall, M. B. *Chem. Rev.* **2000**, *100*, 353–405.
f. Maseras, F.; Lledos, A.; Clot, E.; Eisenstein, O. *Chem. Rev.* **2000**, *100*, 601–636.
116. Relativistic effects result in contraction of the radial size of ns orbitals because they penetrate the core to the nucleus very effectively. As such, electrons in ns orbitals obtain high instantaneous velocities in the vicinity of the nucleus and thereby result in a relativistic increase in mass $[m = m_0/(1 - (v/c))^{1/2}]$ and hence a decrease in Bohr radius $[a_0 = 4\pi\varepsilon_0\hbar^2/me^2]$. See:
a. Pyykkö, P. *Chem. Rev.* **1988**, *88*, 563–594.
b. Wezenbeek, E. M.; Baerends, E. J.; Ziegler, T. *Inorg. Chem.* **1995**, *34*, 238–246.
117. In this regard, it is pertinent to note an analogy with the main group elements. Specifically, the radial distribution functions of the 2s and 2p are more comparable than the ns/np pairs for higher principal quantum numbers and thus hybridization is a common feature of the 2nd row elements but not for those of the higher periods. The origin of the similar size of the 2s and 2p orbitals is that the 2p orbitals, being the first orbitals with p symmetry, are not subject to Pauli repulsion and therefore penetrate the core relatively more effectively than do 3p orbitals. See: Kutzelnigg, W. *Angew. Chem. Int. Ed. Engl.* **1984**, *23*, 272–295.

1.02
Ligands, Reagents, and Methods in Organometallic Synthesis

J Peters, Caltech Chemistry, Pasadena, CA, USA
J C Thomas, University of California – San Diego, La Jolla, CA, USA

1.02.1 Introduction

This chapter describes some recent trends in organometallic synthesis. We pay particular attention to the types of ligands, reagents, and methods that have become popular during the past decade, and contextualize them within the broad fields of organometallic and inorganic chemistry more generally. The chapter, which is necessarily limited in scope, discusses a range of varied topics including the use of steric bulk in small molecule activation, reversibly cyclometallated species, highly electrophilic organometallics and their corresponding non-coordinating anions, zwitterionic organometallic species, carbene ligands, secondary coordination sphere interactions, fluorous phases, and C atom transfer reagents in organometallic synthesis. Many of the reagents, ligands, and methods employed in these various areas of synthesis are described, and many relevant references are provided.

1.02.2 Steric Bulk

Perhaps no approach to transition metal-mediated organometallic chemistry has experienced as much growth over the past decade as the use of sterically demanding ligands. Many common ligand types have been retrofitted to provide newer, much bulkier varietals, and a large battery of ligands especially suited to the attachment of sterically encumbering substituents has been realized. The explosion in this area stems from several factors. First and foremost are the new and exciting reaction profiles that coordinatively unsaturated complexes can display. Consider, for example, the CO cleavage reaction exhibited by Wolczanski's $Ta(silox)_3$ system (silox = OSi^tBu_3),[1,2] and the N_2 cleavage reaction exhibited by Cummins' $Mo(NRAr)_3$ (NRAr = N(^{t}Bu)(3,5-Me_2Ph)).[3] It was only after the isolation of the low-coordinate metal ions (in these cases three coordinate),[2,4] enshrouded by very bulky ancillary ligands (see Figure 1), that such reaction profiles were realized. Second concerns the renaissance that has occurred in ligand design. No longer do the majority of organometallic chemists opt for commercially available ligands or ligands that are readily prepared from time-tested literature protocols (e.g., $[Cp]^-$, $[Tp]^-$, $[(N(SiMe_3)_2)]^-$). Instead, novel ligand design has itself become a fundamental part of most organometallic research programs. While the design of bulky ligands is by no means a new concept to the field (consider the introduction of Cp^* to organometallic chemistry more than three decades ago!), the surge of research activity toward this endeavor is growing exponentially. Armed with search engines like Sci-Finder Scholar (© 2003 American Chemical Society) and powerful molecular modeling packages, protein-like reaction cavities can be envisaged.[5] Finally, the amalgamation between the classical techniques of coordination chemistry with those familiar to organometallic chemistry has enabled the characterization of low-coordinate species that are often paramagnetic (e.g., pseudo-tetrahedral Mo(IV) and Fe(II)). Indeed, the intense interest in the organometallic chemistry of paramagnetic species closely parallels the growth in low-coordinate organometallics. Whereas in earlier days it was common that organometallic chemists would regard the presence of paramagnetic organometallics in solution as undesirable impurities, paramagnetic components are now often regarded as key species within organometallic reaction processes. Analytical techniques, such as electrochemistry, optical and EPR spectroscopies, SQUID magnetometry, and paramagnetic NMR spectroscopy have become common to many of the research groups that practice the synthesis and study of low-coordinate organometallic species. In some sense it has become increasingly difficult, perhaps even futile, to try to distinguish between organometallic and traditional inorganic chemistry.

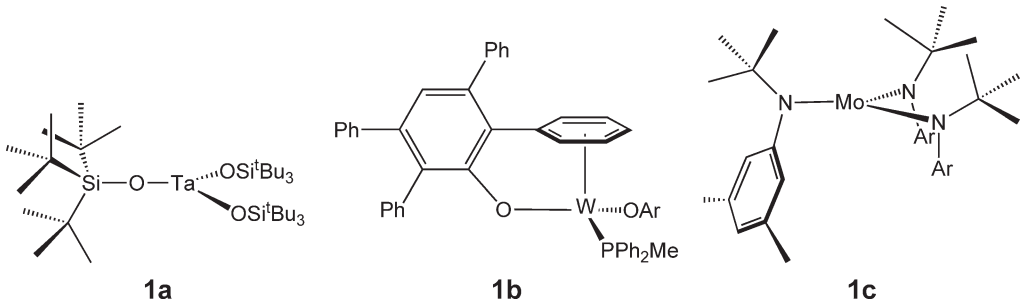

1a **1b** **1c**

Figure 1 Examples of sterically encumbering, monodentate hard ligands.

1.02.2.1 Sterically Encumbering Hard Ligands

There are a variety of encumbering ligands that present hard donor atoms to a coordinated metal center (e.g., C, N, O), many of which have been known for decades. Take, for example, diisopropylamide ($N^iPr_2^-$), commercially available as the free amine or its lithium species (LDA). The latter affords beautiful three-coordinate (e.g., $(^iPr_2N)_3Cr$)[6] or more commonly four-coordinate species (e.g., $\{(^iPr_2N)_3V\}_2(\mu\text{-}N_2)$)[7] via transmetallation reactions with metal halides (e.g., $CrCl_3$) or other precursors (e.g., metal alkoxides). Andersen and Wolczanski popularized the use of bulky monodentate amides and alkoxides during the late 1970s and 1980s, respectively, exploiting $[N(SiMe_3)_2]^-$ and $[OSi^tBu_3]^-$ (silox) to great effect to stabilize complexes such as $U\{N(SiMe_3)_2\}_3$,[8] $Ti(silox)_3$,[9,10] and $Ta(silox)_3$ **1a**.[1,2] Likewise, the Rothwell team utilized extremely bulky aryloxide ligands to provide access to nominally low-coordinate tungsten centers (e.g., $(W(OAr)_2(PPh_2Me)$, **1b**), thereby exposing fascinating four-electron oxidative cleavage reactions.[11] During the 1990s and up to the present time, a number of groups have taken monodentate bulky amide chemistry to another level. Most prominent concerns the work of Cummins and co-workers, who pioneered the use of a host of monoalkylaryl (NRAr) amides to stabilize three- and four-coordinate transition metal species **1c**.[12] A thorough review of these and other three-coordinate complexes supported by hard donor ligands, and their reactivity properties, was published in 1998.[13]

There are also many useful, bulky chelating ligands that feature hard donor atoms, a prototypical example being the tris(amido)amine (TREN) systems (e.g., $N(CH_2CH_2NAr)_3$) popularized by Schrock and Verkade (see Figure 2).[14–17] Amide ligands of these types serve to stabilize highly reduced early metals and generally enforce either four-coordinate trigonal-pyramidal or five-coordinate trigonal-bipyramidal geometries **2a**.[14] The apical *N*-donor ligand sometimes serves as a hemilabile group. Conceptually related to these ligands are the tris(aryloxide)TACN scaffolds,[18] which have been exploited by Meyer and co-workers in the context of molecular uranium chemistry.[19–21] By adding extremely bulky groups to the aryl substituents, trigonally coordinated uranium aryloxides can be obtained, in which the TACN group weakly binds and effectively blocks one hemisphere of the uranium ion, leaving the opposite face poised for transformations within a well-defined pocket **2b**.

Three other bulky, hard ligand chelates that now enjoy widespread utility in organometallic synthesis are the tris(pyrazolyl)borates [Tp],[22] the β-diketiminates (the so-called "nacnac" ligands, often abbreviated as $[R_2NN]$), and the α-diimines (see Figure 3). These ligands benefit from, for the most part, relative ease of preparation and modification. For the tris(pyrazolyl)borates **3a**, numerous bulky substituents have been used to decorate the 3- and 5-positions of the pyrazolyl rings, the isopropyl and *tert*-butyl substituents having been most commonly employed. While Tp ligands are often referred to as tetrahedral enforcers, the true geometries of four-coordinate complexes of these ligands are both geometrically and electronically distinct from their tetrahedral counterparts.[23–25] Bulky β-diketiminates most often give rise to four-coordinate first-row complexes, though recently groups such as those of Tolman, Holland, Warren, and others have realized three-coordinate derivatives.[26–29] In such cases, bulky aryl substituents that orient perpendicular to the β-diketiminate plane, thereby protecting the axial positions, have been employed **3b**. Theopold has exposed these ligands as useful tools for developing organochromium chemistry.[30] A related explosion in organometallic, bulky α-diimine chemistry followed the landmark discovery by Brookhart and co-workers that diimine-supported nickel and palladium complexes facilitate efficient late metal olefin polymerization reactions **3c**.[31]

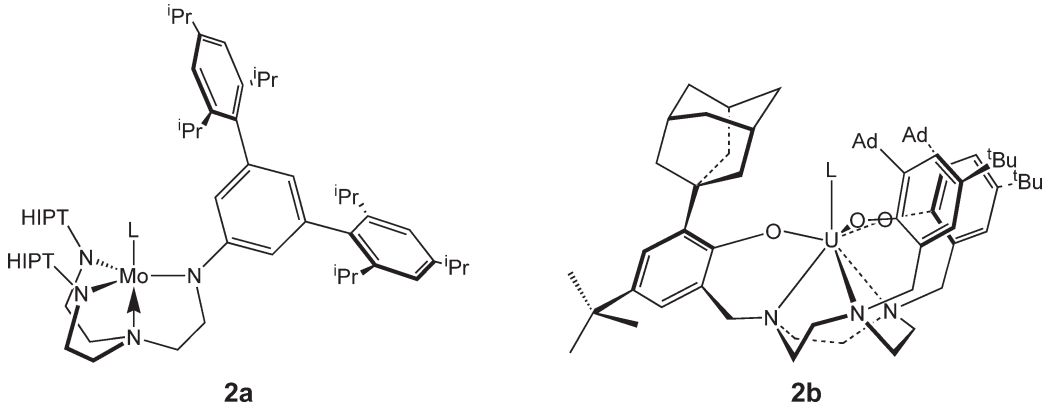

Figure 2 Examples of sterically encumbering, chelating hard amide and alkoxide ligands.

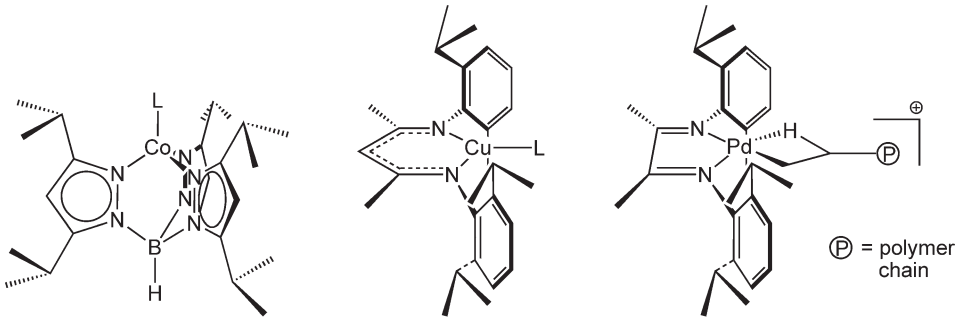

3a 3b 3c

Figure 3 Examples of sterically encumbering, chelating hard imine-type ligands.

While not yet as popular as the β-diketiminates, three sterically hindering, hard LX ligand types (see Figure 4), whose utility shows promise, include bulky carboxylates **4a**,[32] amidinates **4b**,[33–36] and the aminopyridinates **4c**.[37,38]

Bulky organometallic reagents can also be very useful with respect to the stabilization of low-coordinate species. There are commonly employed alkyl substituents, including neopentyl ($-CH_2CMe_3$), neophenyl ($-CH_2CMe_2Ph$), and 1-norbornyl, all of which lack problematic β-hydrogens that might undergo elimination. Bulky aryl ligands are also common (see Figure 5). One classic example concerns the mesityl substituent, which enabled the synthesis of $Ir(Mes)_3$ **5a** and its corresponding terminal oxo complex.[39] Power's group and others have championed the use of bulky aryl substituents, such as the increasingly popular terphenyl ligand, toward the stabilization of low-coordinate transition metal and main group species.[40–46] The one-coordinate indium(I) derivative illustrates this approach **5b**.[47]

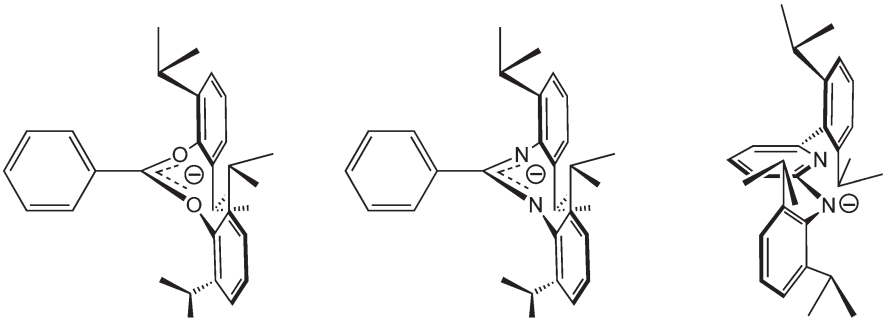

4a 4b 4c

Figure 4 Examples of sterically encumbering LX-type ligands.

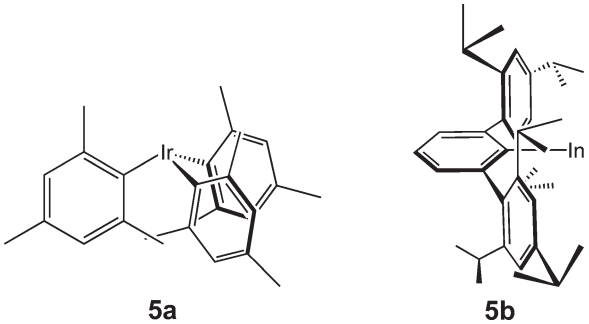

5a 5b

Figure 5 Examples of sterically encumbering alkyl and aryl ligands.

1.02.2.2 Sterically Encumbering Soft Ligands

One reason hard and bulky ligands like amides and alkoxides are so useful in early metal chemistry is due to the propensity of earlier metals to occupy their highest oxidation states. In contrast, trianionic donor sets afforded by tris(amide) and tris(alkoxide) auxiliaries are not as well suited to the stabilization of low oxidation state species (e.g., Fe(I), Ni(I), Co(I), and Cu(I)). For these instances, bulky ligands that are either neutral or possess a low net negative charge are more effective. The most popular hard donor auxiliaries for this purpose are the aforementioned tris(pyrazolyl)borate (e.g., $[Tp']Fe^{I}(CO)$[48] and $[Tp']Cu^{I}(CO)$[49,50]) and β-diketiminates ($(Me_2NN)Ni^{I}(L)$[51] and $(Me_2NN)Cu^{I}$(ethylene)[52]). It seems likely that bulky carboxylates, benzaminidates, and aminopyridinates will prove equally efficacious.

Soft, sterically hindering ligands, such as those featuring phosphine and thioether donor groups, are often better suited to the stabilization of later metals in their lower oxidation states. Monodentate phosphine ligands can be incredibly bulky, with cone angles that surpass 200°.[53] Common reagents of these types include $P^{i}Pr_3$, $P^{t}Bu_3$, and P(mesityl)$_3$, and later metals supported by more than one of these types of phosphines are often low coordinate, substitutionally labile, and therefore useful as additives in catalysis such as cross-coupling reactions. Good illustrations of this principle (see Figure 6) include (i) Hartwig's report of a nominally three-coordinate, T-shaped palladium(II) complex, stabilized by a bulky $^{t}Bu_2$P(1-adamantyl) phosphine that is coordinated via the *P*-donor and via a C–H agostic interaction from the adamantyl substituent;[54] (ii) Buchwald's synthesis and exploitation of a series of very bulky phosphines that are particularly effective as co-additives in Pd^0-catalyzed cross-coupling reactions **6a**;[55] (iii) Hillhouse's use of the bulky bis(phosphine) ligand di-*tert*-butylbis(phosphino)ethane to prepare a family of three-coordinate Ni(II) derivatives, stabilized by either an agostic interaction, as for the alkyl derivative shown **6b**,[56] or via lone pair donation from a heteroatom donor ligand such as an amide, imide,[57] phosphide, or phosphinidene;[58] and (iv) Tilley's three-coordinate platinum silylene complex, which is stabilized by dicyclohexylbis(phosphino)-ethane **6c**.[59]

A new and very useful family of bulky phosphine ligands that feature a borate anion embedded within the ligand framework has recently appeared (see Figure 7). Preparative strategies are available to assemble tris- **7a**,[60–63] bis- **7b**,[60,64] and monophosphine[65] **7c** derivatives of ligands of these types (respectively abbreviated as $[PhBP^{R}_3]^-$, $[Ph_2BP^{R}_2]^-$, and $[Ph_3BP^{R}]^-$ depending on the R substituent on the phosphine). The borate unit renders these phosphine donors appreciably more electron releasing than their neutral counterparts.[64,66] Ligands of these types are assembled by attack of a lithiated methylphosphine carbanion ($LiCH_2PR_2$) at a suitable borane electrophile. These phosphines can be prepared as tetra-*N*-butylammonium salts,[60] as lithio species,[60,62] and as thallium adducts,[60,61,63] the latter being particularly useful for clean metallation chemistry with late metal precursors, as they tend to avoid problematic reduction chemistry. Ligands of these types have been used to prepare organometallic zwitterions, as described later, and in certain cases to support unusual multi-electron redox reactions at mid-to-late first-row ions. One striking example of such a reaction is the oxidative N atom transfer process to a pseudo-tetrahedral iron center shown in Figure 7 **7d**.[67] In this reaction, a high energy amido intermediate expels anthracene[68] to deliver nitride to Fe(II), thereby producing an Fe(IV) nitride species. The latter, diamagnetic species is thermally unstable, and in solution eventually decays via bimolecular nitride coupling to produce a diiron(I)-bridged dinitrogen complex. The coupling reaction constitutes a bona fide six-electron redox process mediated by two iron centers.

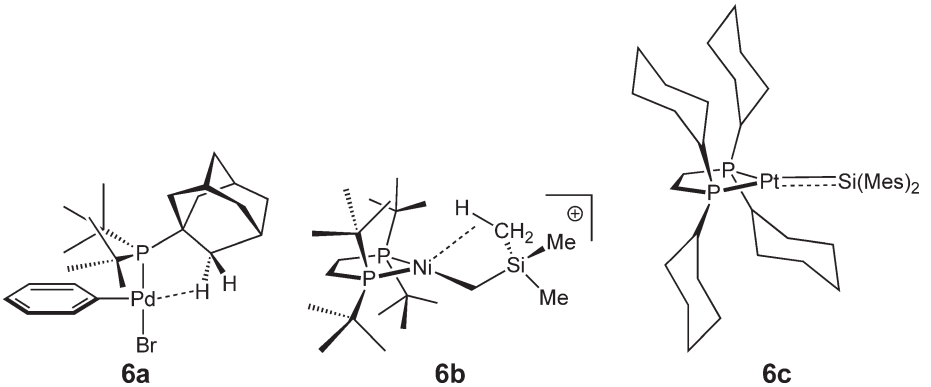

Figure 6 Examples of sterically encumbering, neutral phosphine ligands.

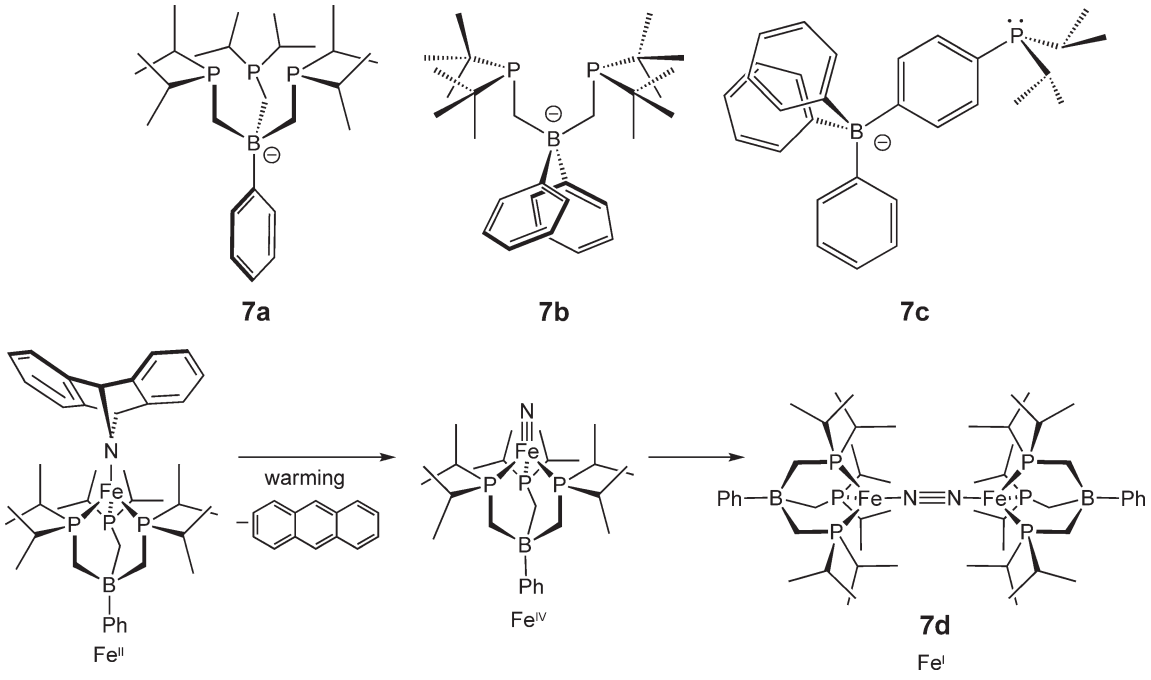

Figure 7 Examples of sterically encumbering, anionic phosphine ligands, and a representative transformation (see text).

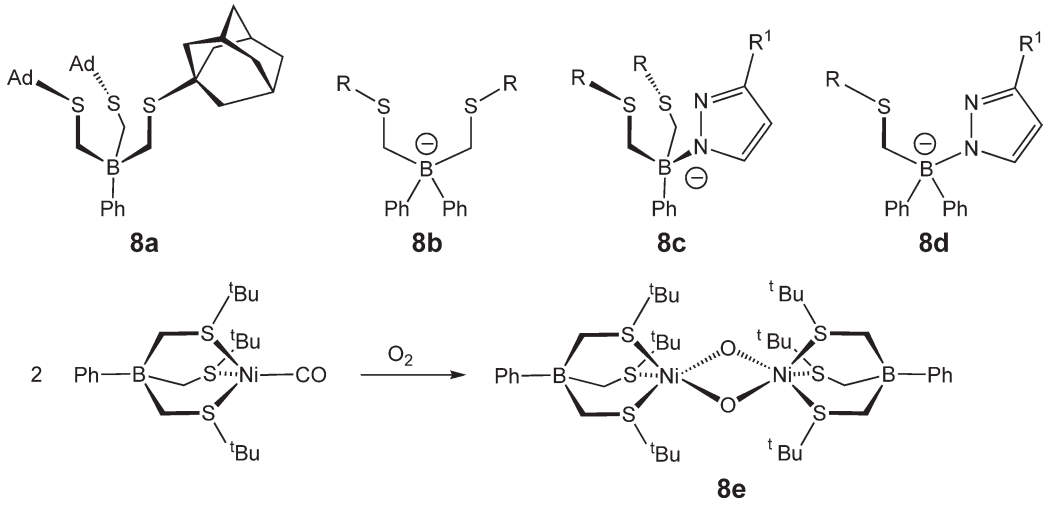

Figure 8 Examples of sterically encumbering, anionic thioether and thioether/pyrazolyl hybrid ligands, and a representative transformation (see text).

Bulky sulfur counterparts (see Figure 8) preceded the (phosphino)borates and are known for tri- **8a** and bidentate **8b** ligands.[69–73] These ligands are particularly noteworthy as thioether auxiliaries because neutral thioether donors commonly suffer from high ligand lability. Riordan's group has made use of these (thioether)borate derivatives, as well as pyrazolyl/thioether hybrid borates **8c** and **8d**, in the preparation of a suite of interesting late metal complexes.[70,74,75] Figure 8 provides another fascinating example of oxidative group transfer, in this case using a tris(thioether)borate-stabilized nickel(I) system that can be cleanly oxygenated to produce a bimetallic dinickel(III) μ-oxo bridge system.[74]

1.02.2.3 Amide Hybrid Ligands

It is common that hybrid donor ligands impart distinctive properties to transition metals. Among the more classic examples where such behavior has been suggested concerns Fryzuk's hard/soft ligands that feature anionic amido

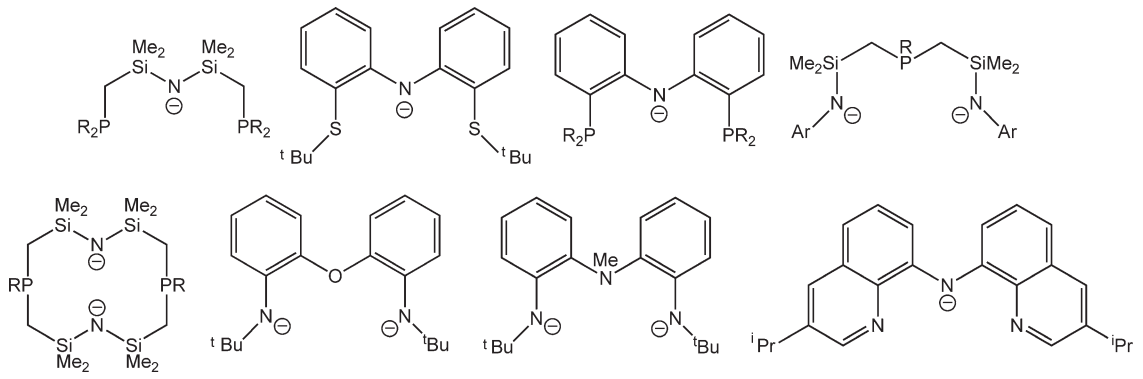

Figure 9 Examples of amide hybrid ligands.

(NR_2^-) and neutral phosphine donors within the same chelate framework.[76–82] Promising recent additions to this ligand class include [PNP] derivatives with aryl groups in the backbone,[83–85] as well as diarylamides with other soft donors such as thioethers.[86] Diamidoamine and ether ligands (NNN and NON) are fascinating chelates in their own right, and have been studied extensively in the context of living polymerization catalysis in recent years.[87–90] Related pincer-type, monanionic NNN amido ligands incorporating two 8-quinolinyl donor groups have also been exploited recently.[91,92] Figure 9 provides a few illustrative examples of these types of hybrid ligands.

1.02.3 Reversibly Cyclometallated Complexes

While the use of sterically encumbering ligands continues to be the most reliable method of access to coordinatively unsaturated and hence reactive metal complexes, alternative strategies exist to expose a metal coordination site. One particularly attractive option is to mask a reaction center with a reversibly cyclometallated metallocycle, often in the form of an alkyl hydride that can reductively eliminate prior to or upon coordination of a substrate. Such a scenario in effect exposes a reaction site that would otherwise be difficult to realize without employing excessively bulky ligands. Figure 10 illustrates several elegant examples whereby such a strategy has been rationally employed. In each case shown, an alkyl hydride moiety protects a coordination site and releases an alkyl (or alkane) upon reaction with a substrate. The first transformation **10a** demonstrates the synthesis of a terminal chalcogenido complex, $W(PMe_3)_4(Te)_2$, upon addition of elemental tellurium to the metallated trimethylphosphine adduct $W(PMe_3)_4(\eta^2\text{-}CH_2PMe_2)(H)$.[93] In a similar fashion, N atom transfer from elemental N_2 to a metallaziridine hydride molybdenum(V) complex occurs **10b**.[94] The latter transformation reductively transfers the hydride ligand back to the isopropylamide substituent such that the final product features two Mo centers, each supported by three equivalent isopropylarylamide ligands and a bridging nitride. The three-coordinate Mo(III) species is thus masked by the metallaziridine hydride functionality, thereby giving rise to a five-coordinate Mo(V) precursor. The chemistry of the low-coordinate Mo center becomes available upon exposure to substrate. In related transformations, metallated bis(cyclopentadienyl) zirconium complexes undergo reversible metallation, and thus become competent for H_2 and N_2 activation **10c** and **10d**.[95–97] This strategy is taken to the extreme in the doubly metallated permethylcyclopentadienyl tungsten(VI) dihydride monocation, which reacts with secondary silanes as a silylene acceptor, formally transferring dihydrogen from the silane back to the Cp^* ligand **10e**.[98,99] This type of strategy was first exploited in the synthesis of transition metal silylene derivatives using a tris(phosphino)borate iridium allyl hydride **10f**.[62] As shown, cyclooctene release accompanies silylene transfer to the iridium fragment, and the allyl hydride moiety thus acts as a protecting group for the "$[PhBP_3]Ir(I)$" fragment. In one last example, an octahedral Pt(IV) methyl dihydride complex exhibits intermolecular alkane C–H bond activation processes with alkane substrates via the reductive elimination of methane **10g**.[100–103] Whereas reactive Pt(II) precursors with an exposed coordination site are more typically targeted with respect to C–H bond activation studies,[104] this example reminds us that a higher coordinate, more oxidized species can also be efficacious so long as a reversible elimination process is available. In this instance, the protecting group is an alkyl hydride rather than a metallated metallacycle hydride.

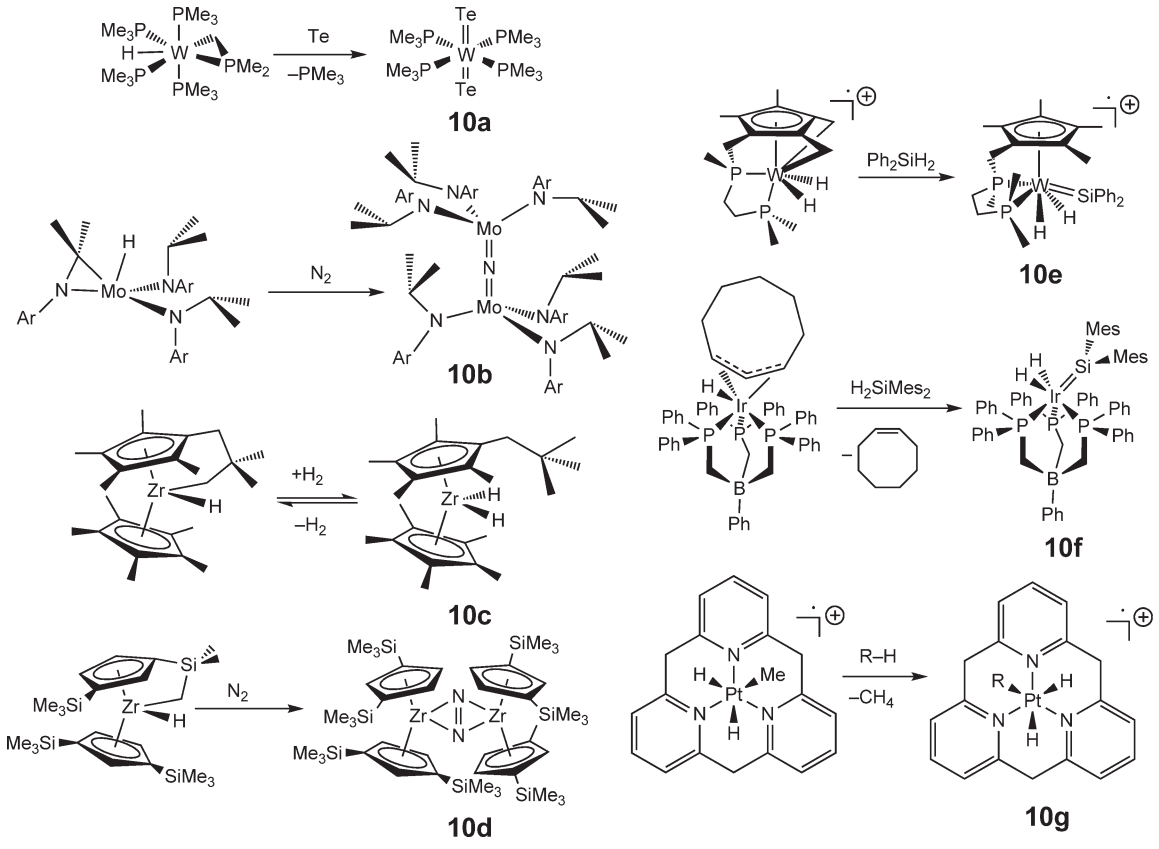

Figure 10 Examples of reversibly cyclometallated complexes.

1.02.4 Carbenes as Spectator Ligands

One of the most significant advances in ancillary ligand design in the last decade has been the steady development of heteroatom-stabilized carbenes for organometallic chemistry. Many reviews have been written on the subject, covering their formation, stability, diversity, their metal complexes, and applications.[105–130] The most common structure types for carbenes used as ligands are *N*-heterocyclic carbenes (NHCs). Saturated, unsaturated, triazole, and phenyl backbone versions are currently among the most popular derivatives (see Figure 11). Carbene ligands act as neutral two-electron donors to a metal center through strong σ- and relatively weak π-interactions. Despite the common view that NHC ligands are pure σ-donors, several experimental and computational studies support the idea that varying degrees of π-interactions can be important.[131–140] NHCs are particularly favored because they can exhibit air and moisture stability depending on their substitution pattern.[141] In some cases, the carbene stability is sufficient to undertake aqueous studies, such as the carbene formation and protonation work of Amyes *et al.*[142] Overall, the ligand properties of NHCs often result in their being described as an alternative or a complement to the more common tertiary phosphines. In this vein, Nolan and co-workers have studied NHC interactions with $Ni(CO)_4$[132] to provide an analogy to Tolman's classic studies of tertiary phosphines.[53,143,144]

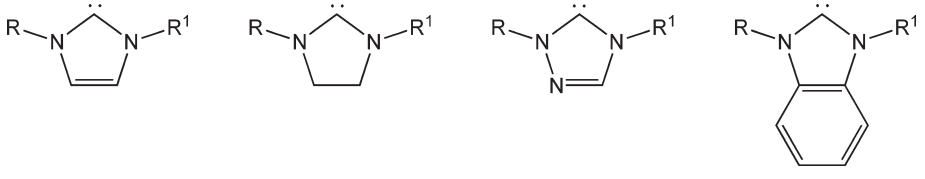

Figure 11 Examples of monodentate N-heterocyclic carbene structures.

1.02.4.1 Monodentate NHCs

The most prevalent carbene ligands for organometallic chemistry are monodentate carbenes. Most of the widely used forms of NHCs are either saturated or unsaturated five-membered heterocycles as shown in Figure 11. Many methods have been developed for the preparation of monodentate carbene ligands, and these methods have been covered in several recent reviews.[105,107,109–112,116,119,122–125,128] Importantly, the steric and electronic nature of the carbene ligand can be controlled through the *N*-substitution, degree of saturation, and ring size. With respect to *N*-substitution, both alkyl and aryl substituents are incorporated easily into an NHC, providing for a large degree of tunability. For example, Nolan and co-workers examined how steric changes in an aryl NHC effect the activity of a palladium-catalyzed aryl amination reaction.[145] Similarly, by changing from an unsaturated five-membered ring to a saturated five-membered ring, both the Grubbs and Herrmann groups showed that more active catalysts for metathesis could be formed.[146,147] The asymmetric substitution of carbenes also has been exploited. Furstner *et al.* have demonstrated the effectiveness of asymmteric NHC ligands containing a tether in ruthenium metathesis catalysts.[148] The variety of monodentate carbenes now available is virtually unlimited, and they can be tuned both sterically and electronically to suit the demands of the chemistry.

Installing an NHC onto a metal center can be accomplished by several methods. The original route for installation, which remains quite useful, takes advantage of a basic ligand on the metal to deprotonate the azolium salt.[149,150] Sometimes it is a more straightforward to generate the free carbene and then displace a neutral donor ligand from a transition metal. A wide range of neutral ligands can be displaced, including ethers, thioethers, amines, phosphines, and carbonyls.[105,107–112,114,119,121,123–125,127–129] Another popular route involves carbene transmetallation, most often using silver as the transfer metal, as was first described by Wang and Lin.[151] This method requires that the transmetallating agent be prepared, but it remains a valuable method, particularly for displacing halides.[121,129] Oxidative addition has also been explored as a direct stoichiometric installation route, and has been demonstrated to occur in imidazolium-based ionic liquids. Crudden and Allen have reviewed both of these topics recently.[114] While these various methods for installation are emphasized for monodentate carbenes, all of them have been exploited with respect to the multidentate derivatives described below.

1.02.4.2 Multidentate Chelating Ligands Containing NHCs

The many synthetic methods available for preparing NHCs have allowed for their ready incorporation into an increasingly diverse set of multidentate ligands. The topic of chelating ligands containing NHCs has been covered in several reviews.[105–109,111–114,123–125,127–129] Heteroleptic variations have included phosphines, amines, imines, pyridines, oxazolines, amides, alkoxides, aryloxides, thioethers, and other donors.

As an expansion of the NHC family, a few examples of tri- and tetradentate triscarbene ligands have been described (See Figure 12).[136,152–155] Homoleptic C_3 and heteroatom NC_3 ligands have been prepared and used to develop novel organometallic structures of the late transition metals. The general synthetic approach for these complexes has been the nucleophilic attack of an *N*-substituted imidazole on a framework containing primary alkyl halides. Both 1,3,5-tris(bromomethyl)benzene **12a** and 1,1,1-tris(bromomethyl)ethane **12b** have been used to prepare neutral tridentate carbenes in this manner.[153] These multidentate carbene ligands are L_3 donor ligands. By comparison, the NC_3 platform **12c** has been shown to be either an L_3 or an L_4 ligand, depending on the coordination

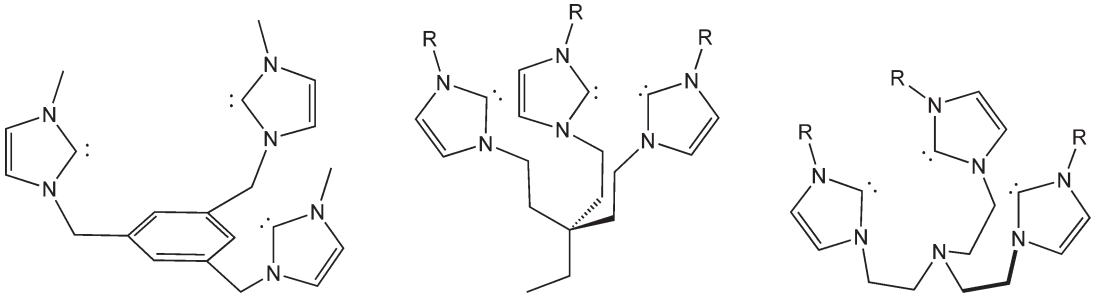

12a **12b** **12c**

Figure 12 Examples of multidentate N-heterocyclic carbene ligands.

of the central nitrogen atom.[152] These ligands are conceptually quite similar to the classic Sacconi-type tridentate and tetradentate phosphine systems, such as $MeC(CH_2PPh_2)_3$ and $N(CH_2CH_2PPh_2)_3$,[156–161] though their steric and electronic properties are distinct.

1.02.4.3 (NHC)borates

In contrast to the well-studied (pyrazolyl)borates, synthetic studies using the structurally related (NHC)borate family of ligands is in its infancy (see Figure 13).[162–166] These ligands combine the steric features of the highly successful tris(pyrazolyl)borate ligands with the electronic nature of carbene donors. Examples of both bis(NHC)borates[162] **13a** and tris(NHC)borates **13b** have been generated.[163–166] The bis(carbene)borates act as L_2 donors, but to take into account the formal charge on the metal are better considered as LX, three-electron donors for purposes of electron counting. Similarly, the tris(carbene)borates act as L_3 donors, but can be counted as L_2X, five-electron donors due to the presence of the borate anion in the backbone. The synthesis of bis- and tris-substituted derivatives has been achieved by either alkylating the corresponding (imidazole)borates followed by deprotonation with strong base,[162–165] or more recently by the reaction of *N*-alkyl imidazoles with $NH_3{\cdot}BHBr_2$ followed by deprotonation.[166] Two examples of potential tris(carbene)borate transmetallating agents have been presented in the literature: the dimeric lithium adduct of an ethyl-substituted tris(carbene)borate[164] and the magnesium bromide adduct of a *tert*-butyl-substituted tris(carbene)borate[166] have been isolated and characterized. To date, very little is known of the transition metal chemistry of these ligands.

1.02.4.4 Other Carbenes

Beyond NHCs, an additional class of carbenes are those incorporating non-cyclic or non-nitrogenous donors to stabilize the carbene.[109–111,116,130,167] Bertrand and co-workers, for example, have studied the formation and stability of phosphorus-substituted derivatives of carbenes, including their electronic structure and donor properties.[110,167–177] Similarly, various amino–alkyl and amino–silyl,[178–182] sulfur–amine,[183,184] and amine–oxygen[162,185,186] substituted carbenes have been prepared and studied.

1.02.5 Macrocyclic Ligands

For the organometallic chemist, macrocycles represent challenging but useful ligands for a wide variety of transformations. Most typically, macrocycles used in organometallics contain either three or four donor atoms and often rigidly confer either the *fac*- or *mer*-binding geometry. Macrocycles present synthetic challenges due to the difficulty in controlling condensation reactions that generate the product. Successful syntheses often find ways around random condensation methods, through templating or joining of discrete precursors. Several macrocycle families have been extensively reviewed recently in *Comprehensive Coordination Chemistry II*, including Schiff base macrocycles,[187] *N*-macrocyclic ligands,[188] phosphorus and arsine macrocyclic ligands,[189] calixarenes,[190] porphyrins,[191] and phthalocyanines.[192] These macrocycles can be classified within the MLX scheme as L_3, L_4, L_2X_2, LX_3, and X_4 systems, as dictated by the choice of donor types in conjunction with the framework. We present

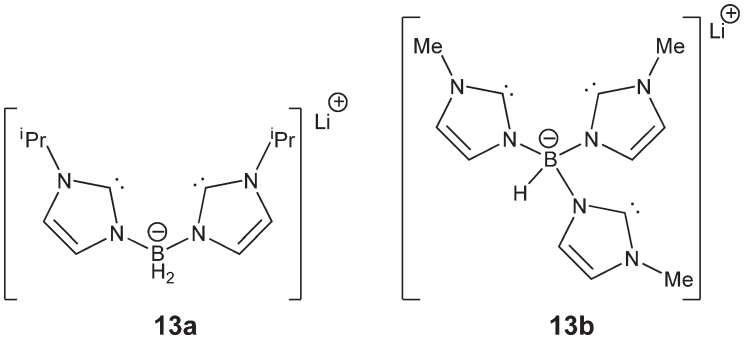

13a **13b**

Figure 13 Examples of multidentate (N-heterocyclic carbene)borate ligands.

here a small selection of specific macrocycles that have contributed to the synthetic methodology of macrocycle synthesis in addition to providing interesting examples of organometallic and inorganic chemistry.

1.02.5.1 Pyridinophane Macrocycles

An extended series of trispyridine-containing macrocycles (pyridinophanes) have recently been prepared by Vedernikov and co-workers (see Figure 14).[100–102,193–198] Pyridinophanes have been selectively designed to be neutral, facially capping ligands that can alternate between bidentate and tridentate chelating modes. Thus, these macrocycles are either L_3 or L_2 ligands depending on their coordination mode. Both twofold and threefold symmetric variants have been synthesized by altering the number of methylene spacers between the pyridine rings. Many of these macrocycles have been isolated in multigram quantities.[102,195] The synthetic approaches for generating pyridinophanes also allow for discrete control over the macrocycle size. Controlling the ring size can be key to the reactivity patterns of the coordinated metal center. For example, pyridinophanes have proven to be effective in exploring new avenues of hydrocarbon activation through oxidation state stabilization/destabilization at platinum.[100,101,194,197] The size of the macrocycle was tuned to accommodate the desired two-electron reaction chemistry. Additionally, new copper olefin aziridination catalysts have been described whose activity can be modified by the size of the macrocycle ring.[193,198]

1.02.5.2 P_2N_2 Dianionic Macrocycle

In contrast to the ubiquitous role that simple tertiary phosphines play in organometallic chemistry, macrocycles containing phosphines are uncommon.[189,199–203] The synthesis of phosphine-containing macrocycles has typically been hampered by the tendency to form configurational and/or diastereomeric isomers due to the high inversion barrier for phosphorus(III). Templated syntheses, however, have been employed to successfully produce useful quantities of desired macrocycles. In 1996, Fryzuk *et al.* described the preparation of a dianionic P_2N_2 macrocycle (see Figure 15).[204] This ligand is an L_2X_2 donor, comprised of two neutral phosphines and two anionic amides. Additionally, the P_2N_2 ligand can donate through the lone pairs of the amides to π-acidic metal centers (L_4X_2). This electronic flexibility lends itself well to the stabilization of a range of oxidation states. The synthesis of the P_2N_2 dianion proceeds through consecutive condensations, and is templated in the final step by the presence of lithium counterions **15a**.[204] The sensitivity of the final ligand stereochemistry to solvent has been noted.[204] The P_2N_2 ligand has been used in a variety of organometallic transformations with early transition metals, including dinitrogen reduction and functionalization reactions.[76,205–215] In one example, the P_2N_2 zirconium dichloride complex was reduced under a dinitrogen atmosphere to form the bridged dinitrogen complex **15b**. This complex went on to react with dihydrogen. Recently, Carmichael and Fryzuk have also reported the arsine As_2N_2 derivative of this ligand.[216] The simplicity and versatility of this macrocyclic scaffold, as well as its success in transition metal chemistry, provide a foundation for new directions in the chemistry of phosphine-containing macrocycles.

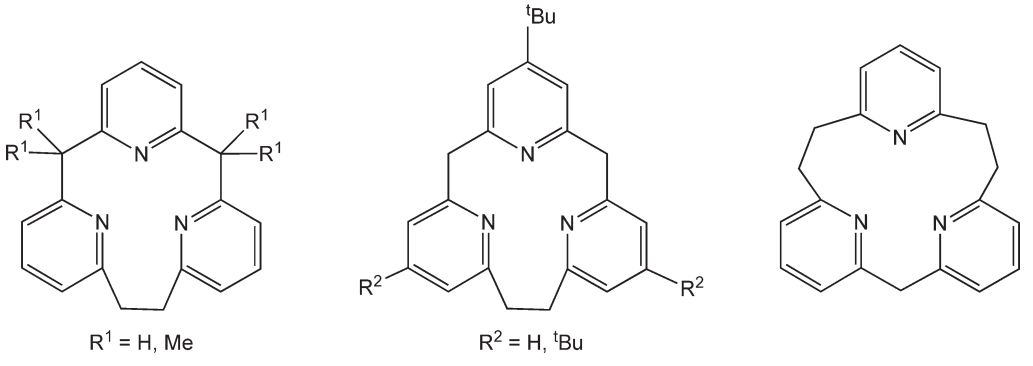

Figure 14 Examples of pyridinophane macrocyclic ligands.

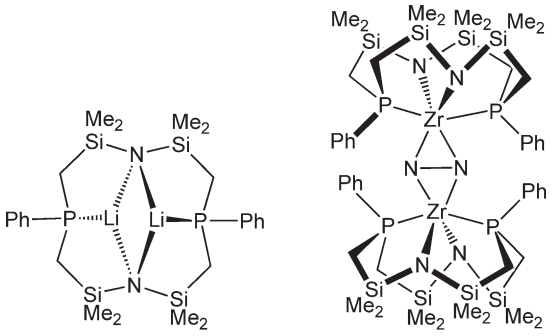

Figure 15 Representative P_2N_2 dianionic macrocyclic ligand, and a zirconium-dinitrogen complex supported by this P_2N_2 ligand.

1.02.5.3 Hexadentate *N*-substituted Triazacyclononane (TACN) Derivatives

Many substituted triazacyclononane (TACN) derivatives have been reported in the literature. Here, we highlight the chemistry of one particular hexadentate platform derived from the symmetric tri-*N*-alkylation of TACN with phenolate or thiolate derivatives. The first report of this class of L_3X_3 molecules was in 1989 by Moore *et al.*,[217] who prepared the 3,5-dimethyl-substituted aryloxide derivative. Subsequent work from Wieghardt's group explored the utility of various substituted hexadentate derivatives incorporating either N_3O_3[18,218–230] or N_3S_3[221,231–239] donor sets for encapsulating transition metals in an octahedral geometry. These species can be isolated directly as octahedral complexes or can be used as complex ligands to further coordinate additional metals. This secondary complexation provides a unique opportunity to modify the electronic properties of the ligand in conjunction with the incorporated metal ion via its redox properties and electronic interactions with the hexadentate platform. Because of the phenolate or phenothiolate donors, ligand-centered redox reactions can occur. Phenolate derivatives of these L_3X_3 ligands have been exploited most recently by Meyer and co-workers to coordinate the large uranium ion (see Structure **2b**).[19–21,240]

1.02.5.4 Corroles

Corroles, relatives of porphyrins, have become increasingly popular in recent years. The removal of a single bridging carbon from the porphyrin framework results in an LX_3 *mer*-macrocycle with a smaller binding pocket relative to porphyrins (see Figure 16). Corroles were first introduced in the literature in 1965 by Johnson and Kay.[241] Their use in organometallic chemistry had been restricted due to their low yielding syntheses and limited substitution patterns. In 1999, however, work from Gross *et al.*[242,243] and Paolesse *et al.*[244] provided highly improved syntheses of *meso*-substituted corroles. These syntheses exploit the condensation of aryl aldehydes with pyrroles to afford better product yields, often with extended substitutional scope relative to the original methods. These synthetic advances have been reviewed by Gryko.[245] In addition to single corrole frameworks, new methods have provided access to *pacman*-type multicorrole systems analogous to the *pacman*-porphyrins (*vide infra*). These improved preparatory methods have enabled the development of corrole-based transition metal chemistry. Not surprisingly, corroles tend

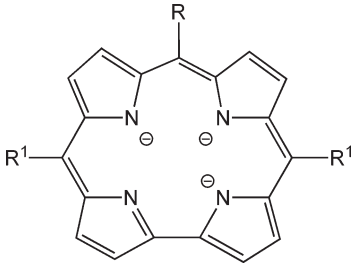

Figure 16 Structure of meso-substituted trianionic corrole macrocyclic ligand.

to favor metals in higher oxidation states because they are trianionic. Examples of such species include the isolation of high-valent, multiply bonded compounds such as chromium(V) and chromium(VI) nitrides,[246] a manganese(V) imide,[247] a manganese(V) oxo capable of olefin epoxidation,[248] and iron(IV) corroles that mediate olefin aziridination.[249]

1.02.5.5 New Bisporphyrin/Corrole Architectures

Porphyrins have been studied thoroughly in the context of inorganic, bioinorganic, and organometallic chemistry. Their preparation and uses are the subject of both ongoing journals and book series due to their incredible versatility. Porphyrin ligands[191] and their organometallic chemistry[250,251] have been covered in recent reviews. The L_2X_2 *mer*-architecture of porphyrins makes them particularly useful as ligands to support square-planar, square-pyramidal, and octahedral metal complexes. Due to the vast amount of recent research into pyrrole-based macrocycles, highlighted below are recent developments in the preparation of extended architectures of porphyrins and corroles—new syntheses of co-facial, or *pacman*, derivatives that provide controlled bimetallic environments.[252,253]

Co-facial bisporphyrin ligand scaffolds facilitate a number of very interesting transformations of small molecules, including N_2, O_2, and CH_4.[254–257] The first examples of rigidly co-facial bisporphyrins were published by Collman, Ogoshi, Chang, and Kagan in 1977.[258–261] A review of early bisporphyrin work appeared in 1994.[262] Although these metallobisporphyrins display unique reactivity patterns, work in this field has been somewhat limited with respect to the linking unit used to create the co-facial architecture. In the last 10 years, however, several groups have introduced new ligand architectures for bisporphyrins that incorporate novel links (see Figure 17). A significant advance in pillared bisporphyrin chemistry, for example, came from Nocera and co-workers, who have synthesized co-facial bisporphyrin systems containing xanthene[263–267] **17a** or dibenzofuran **17c** links.[264,267,268] These L_4X_4 bisporphyrins (L_2X_2 with respect to each metal center) complement the previously developed systems based on anthracene or biphenylene by providing enhanced flexibility within the link while maintaining the rigid co-facial arrangement. Additionally, the preparation of the xanthene and dibenzofuran linkers is somewhat less tedious than those used for previous bisporphyrins. Synthetic methods have also been reported for *meso*-substituted systems using Suzuki coupling chemistry, thus providing a useful route to the selective formation of functionalized co-facial bisporphyrins.[267]

Besides xanthene and dibenzofuran links, several other co-facial porphyrin assemblies have been developed based on different linking groups. An interesting methodology using Co-mediated cycloadditions of ethyne-elaborated porphyrin substrates to produce 5,6-indanyl linkers **17d** for the preparation of co-facial bisporphyrins has been pioneered by Fletcher and Therien.[269,270] Calixarene spacers have been introduced via palladium aryl–alkyne coupling routes or amide bonds.[271–273] Finally, Wayland's group has applied diether links such as *meta*-xylyl ethers **17e** to advance small molecule activation using Rh(II) bimetallic species.[254,274–278]

By analogy to co-facial bisporphyrins, co-facial biscorroles[279–285] and mixed porphyrin–corroles[283–287] linked by a rigid spacer have been pursued. Co-facial biscorroles containing anthracene or biphenylene links first appeared in 1998 from the work of Guilard.[279] These platforms have been extended to include xanthene **17a**, dibenzothiophene **17b**, and dibenzofuran **17c** links as well.[280–285] Subsequent work by Guilard and Kadish has been aimed at developing the syntheses and small molecule activation of these macrocyclic scaffolds.[280–285] As compared to the homo-bismacrocycles, mixed

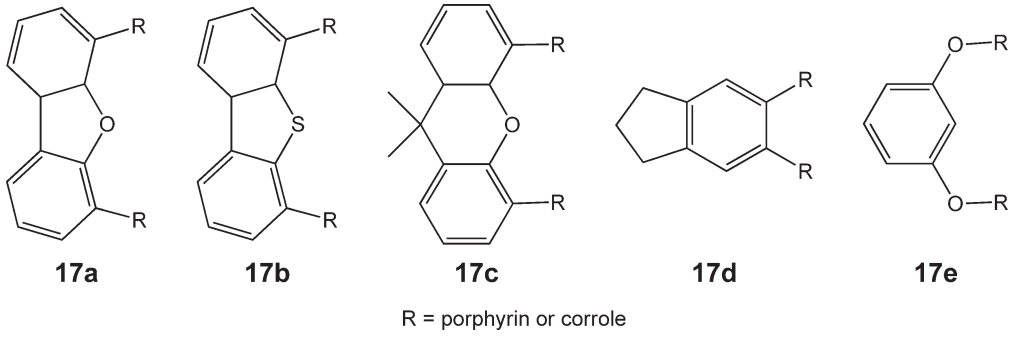

Figure 17 Representative scaffolds used in co-facial bis(porphyrins), bis(corroles), and hybrid porphyrin/corroles.

co-facial porphyrin–corroles require a stepwise approach, where first one macrocycle is attached to the linker molecule followed by the addition of the second macrocycle. The resultant co-facial bismacrocycle is structurally and electronically tunable by functionalization at either the porphyrin/corrole ring or at the linker. To date, the emphasis has been placed primarily on dioxygen activation studies, but these systems promise to expose a wide range of small molecule activation chemistry that complements the previous work with co-facial bisporphyrins.

1.02.6 Electrophilic Approaches

1.02.6.1 Weakly Coordinating Anions

Organometallic chemistry has greatly benefited from the use of highly electrophilic, most typically cationic, metal complexes that exhibit enhanced reactivity patterns. Typically, the more electrophilic a metal complex, the more likely are interactions between the metal ion and weakly binding secondary species, such as solvent molecules and counteranions. Here we discuss the use of weakly coordinating anions (WCAs) that preserve an open coordination site (or provide a readily displaced weak ligand) at highly electrophilic metal centers.[288,289] Several factors determine the effectiveness of a WCA: its donor properties (i.e., its ability to serve as a weak ligand), its degradation patterns, its solubility properties, and the relative ease with which it can be prepared. Many WCAs have highly delocalized structures with distributed anionic charge via the incorporation of electron-withdrawing aromatic groups. WCAs were thoroughly reviewed in 1993 by Strauss.[288] More recently, Krossing and Raabe have written an extensive review on newly developed WCAs, including discussions of their relative stabilities, their synthetic availability, and their methods of use.[289] Highlighted here are three specific examples of WCAs that are now common in organometallic chemistry: fluorinated aryl borates, carboranes, and polyfluorinated aluminum alkoxides.

1.02.6.1.1 Fluorinated aryl borates

Fluorinated aryl borates have emerged as versatile organometallic WCA reagents in the last decade. Their availability through reliable preparative procedures, or commercial sources, as well as their excellent solubility and stability properties, has made fluorinated aryl borates the anion of choice in many organometallic research programs. Two derivatives, in particular, are extremely common: tris(pentafluorophenyl)borane derivatives and tetrakis(3,5-trifluoromethylphenyl)borate (see Figure 18).

1.02.6.1.1.(i) Tris(pentafluorophenyl)borane derivatives

Tris(pentafluorophenyl)borane **18a** is commonly used as an alkyl abstraction agent. The chemistry of $B(C_6F_5)_3$ has been reviewed, particularly, with regard to the activation of metallocene complexes to initiate polymerization reactions in the presence of olefins.[290–293] Massey and Park first reported $B(C_6F_5)_3$ in 1964.[294] The first literature report describing the use of $B(C_6F_5)_3$ as an alkyl abstraction agent came from Marks and co-workers in 1991, when they described the generation of zirconocene polymerization catalysts using stoichiometric $B(C_6F_5)_3$.[295] Around the same time, Elder and Ewen patented the technology.[296] Typically, a methyl group is abstracted from a metallocene **18b**, and the resulting metal cation often forms a stable adduct with the methyl borate species. Mechanistic studies of homogeneous polymerization systems such as these benefit from the spectroscopic innocence of the fluorinated aryl

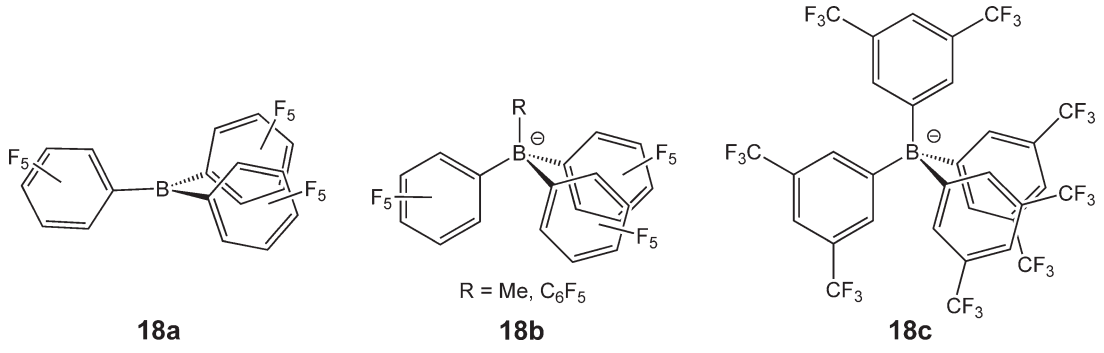

18a **18b** **18c**

Figure 18 Examples of polyfluorinated borane and borate derivatives.

borates due to the clean spectral window they provide in the ^{1}H NMR. NMR chemical shifts can also be informative with respect to the binding affinity of $[Me(BC_6F_5)_3]^-$ in a particular system.[297] $B(C_6F_5)_3$ is noteworthy as a stoichiometric abstraction agent, as it is in this regard distinct from, for example, aluminum species such as methylaluminumoxide (MAO) that are typically used in excess.

In addition to early metal polymerization catalysis, alkyl abstraction with $B(C_6F_5)_3$ has been used extensively with respect to late transition metal chemistry. This is evident in the area of platinum C–H activation chemistry.[298–300] Wick and Goldberg, for example, used $B(C_6F_5)_3$ to abstract a methyl group from a square-planar tris(pyrazolyl)borate platinum dimethyl complex. This step exposed an available coordination site that triggered a subsequent C–H activation step. The final isolated product was that of alkane oxidative addition.[298] An important feature of $B(C_6F_5)_3$ is its high hydrophilicity, as this feature can produce several strongly acidic species, even in the presence of trace water.[301–304] Since many metal alkyl species are susceptible to protonation as well as to alkyl abstraction, mechanistic ambiguities can arise with respect to which pathway is responsible for the cleavage of a metal–alkyl bond.

In addition to alkyl abstraction reactions, tris(pentafluorophenyl)borane also has been used to form stable adducts with many anions, generating a family of related WCAs.[290,293,305] The most popular of these anions is tetrakis-(pentafluorophenyl)borate **18b**, which is derived from the addition of a fourth perfluorophenyl anion to $B(C_6F_5)_3$. First described by Massey and Park as its lithium, potassium, and tetraethyl ammonium salts,[294] a host of other salts of the $[B(C_6F_5)_4]^-$ anion have since been prepared and applied in organometallic chemistry. Protic sources conjugated with this anion, such as $[PhMe_2NH]^+$[296,306–311] and $[H(OEt_2)_2]^+$,[312] have found particular value in the generation of coordinatively unsaturated metal centers. While $[B(C_6F_5)_4]^-$ is highly useful as an inert anion with good solubility properties, especially in hydrocarbon media, $[B(C_6F_5)_4]^-$ can be somewhat more troublesome with respect to the crystallization of organometallic ion pairs due to its high lipophilicity and its tendency to form clathrates/oils in aromatic solvents such as benzene.

1.02.6.1.1.(ii) Tetrakis(3,5-trifluoromethylphenyl)borate

Another fluorinated aryl borate anion that is now very popular is the trifluoromethyl-containing $[B(3,5\text{-}C_6H_3(CF_3)_2)_4]^-$ anion **18c**. This species was first reported by Kobayashi and co-workers in 1981 as a sodium salt.[313] Like $[B(C_6F_5)_4]^-$, the $[B(3,5\text{-}C_6H_3(CF_3)_2)_4]^-$ anion is resistant to decomposition and provides favorable solubility for cation–anion pairs in non-polar media. Additionally, it is rather straightforward to prepare. An improved synthesis of $[Na][B(3,5\text{-}C_6H_3(CF_3)_2)_4]$ was recently published.[314] The protic acid $[H(OEt_2)_x][B(3,5\text{-}C_6H_3(CF_3)_2)_4]$, first prepared by Brookhart and co-workers,[315] is now a typical reagent in organometallic chemistry due to its ready availability. Additionally, the alkali (Li(tetrahydrate),[316] Li(anhydrous),[317] Na,[313,318] K[319]) and other metal (Ag,[319,320] Tl,[321]) salts have proven to be useful for halide abstraction reactions that generate coordinatively unsaturated species.

1.02.6.1.2 Carboranes

Carboranes provide another interesting class of WCAs (see Figure 19).[322] The 12-vertex icosahedral carboranes are very weakly donating, stable, and quite soluble in non-polar media. They are perhaps the least coordinating anions known. Because of these properties, substituted carboranes have been used to prepare bona fide examples of such

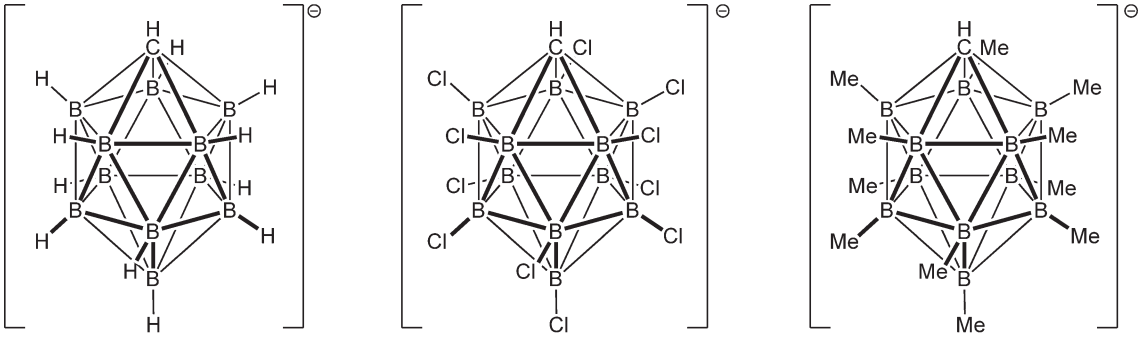

Figure 19 Examples of monoanionic carboranes used as weakly coordinating anions.

highly electrophilic species such as carbocations, protonated arenes, and silyl cations.[323–325] The first report of the simplest carborane, $[B_{11}CH_{12}]^-$ **19a**, came from Knoth in 1967.[326] Starting in 1986, Reed's group began exploring carboranes as exceptionally weakly coordinating anions.[327] Subsequently, several research groups extended the range of accessible functionalized carboranes through halogenation **19b** and alkylation **19c** routes.[324,328–337] In one case, the ostensibly desirable perfluoromethylated carborane was synthesized but found to be explosively unstable.[331] Both halogenation and alkylation of different vertices result in decreased nucleophilicity of the carborane anion to varying degrees. Despite their many beneficial attributes, carboranes have not yet been so widely used in organometallic chemistry, presumably because they are challenging to prepare, which is especially true of the more useful substituted derivatives.

1.02.6.1.3 Polyfluorinated aluminum alkoxides

Polyfluorinated alkoxide– and aryloxide–aluminate anions have emerged recently as a potential alternative to the boron-based anions (see Figure 20). Several fluorinated alkoxides have been used as ligands in these aluminate systems, including C_6F_5O–, $(CF_3)_2HCO$–, $(CF_3)_2(CH_3)CO$–, $(CF_3)_3CO$–, and $(CF_3)_2PhCO$–.[289,338–341] Synthesis of the lithium salts proceeds from $LiAlH_4$ and the desired fluorinated alcohol. Despite the relatively high cost of many fluorinated alcohols, the preparative simplicity and high yield of the aluminate anions make these polyfluorinated alkoxide– and aryloxide–aluminate species very attractive systems. Some of these aluminates display relatively strong donor properties compared to other WCAs, and are moreover susceptible to undesirable degradation pathways that are typically initiated by interaction of an oxygen atom with the Lewis-acidic countercation.[339,341–345] These problems can be avoided by resorting to sterically encumbered derivatives. Perhaps the most promising candidate is $[Al(OC(CF_3)_3)_4]^-$ **20a**.[289,340,346] Using perfluorinated *tert*-butoxide in conjugation with a Lewis-acidic or oxophilic metal provides a sterically protected, electronally delocalized anion. Several useful reagents of the $[Al(OC(CF_3)_3)_4]^-$ anion have been prepared, such as the Cs, Li, trityl, Ag, and $H(OEt_2)_2$ salts, and they in general exhibit good kinetic and thermal stability.[340,343,347] Krossing has observed the decomposition of $[Al(OC(CF_3)_3)_4]^-$ to the fluoride-bridged anion $[((CF_3)_3CO)_3Al–F–Al(OC(CF_3)_3)_3]^-$ **20b** in the presence of very strong electrophiles such as $P_2X_5^+$ (X = Br, I), demonstrating a potential weakness of the polyfluorinated alkoxide– and aryloxide–aluminate anions; however, the fluoride-bridged anion promises to be an excellent WCA itself, as it is the preferred end product of several decomposition reactions.[345]

1.02.6.2 Weakly Coordinating Neutral Donor Ligands–σ-adducts and Agostic Interactions

As noted above, highly electrophilic, coordinatively unsaturated metal centers tend to bind a variety of weakly coordinating ligands. These adducts are quite often labile and can include, for example, three-center two-electron interactions with a nearby C–E bond (E = H, Si), haloalkane adducts, and σ-adducts with dihydrogen, silanes, and even alkanes, though the latter tend not to result in long-lived species. Complexes containing such weakly coordinated ligands often display the properties expected of the truly unsaturated, cationic species. Therefore, the use of weakly coordinating ligands can provide stable and isolable, yet highly reactive, electrophilic organometallics. We highlight here several examples of such donor ligands and their complexes.

1.02.6.2.1 σ-Complexes

Sigma adducts are ligands that are bound to a metal center via a σ-bond pair (an L-type ligand). The σ-adduct can be a reaction intermediate that arises prior to an oxidative addition step or subsequent to a reductive elimination step. In this way, a σ-adduct is a midpoint between a free molecule or substrate and an activated molecule that then serves as

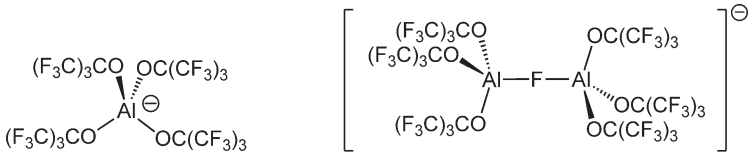

20a **20b**

Figure 20 Examples of monoanionic polyfluorinated weakly coordinating aluminum alkoxides.

two X-type ligands at the two-electron oxidized metal center. While the dominant interaction between the σ-bond pair and the metal center is primarily two-electron donation to the metal center, π-backbonding into the σ-antibonding orbital can also play a significant role, especially for dihydrogen and silane adducts. σ-Adducts and agostic interactions were extensively reviewed by Crabtree in 1993[348] and were summarized more recently by Kubas in a comprehensive fashion.[349]

1.02.6.2.1.(i) Dihydrogen adducts and silane adducts

Dihydrogen adducts have been studied extensively since their initial landmark discovery was made in 1984 by Kubas.[348–357] One of the most noteworthy features of dihydrogen ligands is the continuum of H–H distances that is observed for different complexes. These represent the entire range representing a pure dihydrogen molecule, only weakly coordinated to the metal center, to systems where the H–H bond is nearly broken due to substantial backbonding into the H–H σ-antibonding orbital. While the chemistry of dihydrogen complexes is at this stage a very mature subject, the field has experienced a renewed surge of interest due to the promise that certain organometallic complexes might be able to mediate efficient hydrogen evolution at positive potentials.[358–361] Dihydrogen adduct complexes are likely to be intermediates of hydrogen generation (or consumption), and such intermediate species have even been proposed within the active sites of various hydrogenase enzymes (e.g., Fe-only H_2ase and FeNi H_2ase).[362–365] Figure 21 depicts a hypothetical intermediate dihydrogen adduct structure within the cofactor of Fe-only H_2ase,[366] which could be formed by protonation of an iron-bound hydride precursor.

Silane adducts of transition metal complexes are related to dihydrogen species, and likewise display a wide range of structural variability. Due to the number of possible binding modes for silanes with more than one hydride substituent, such as SiH_4, $RSiH_3$, and R_2SiH_2, a great variety of structures have been observed, and it can be difficult to ascertain whether and how the hydrides are shared between the transition metal and the silicon center. Silane adduct complexes were first discovered by Graham and co-workers,[367–371] and the chemistry of these types of species has been reviewed recently.[349,372–376] One important distinction that can be drawn between silane adducts and their dihydrogen adduct cousins is that metal-to-ligand backbonding interactions can be substantially stronger for silanes, as has been discussed by Lin.[372] Like dihydrogen adducts, silanes can exhibit very facile and reversible Si–H bond cleavage processes that generate metal silyl hydride species. Also worth noting is that a structurally characterized germane σ-adduct complex was isolated only recently.[377]

1.02.6.2.1.(ii) Alkane adducts

Alkane complexes have received special attention within the organometallic community because of their potential intermediacy in alkane activation reactions.[378–380] Additionally, because alkanes are very poor ligands, associating only weakly to transition metals, they have become attractive synthetic targets. Hall and Perutz reviewed the literature of alkane complexes in 1996,[381] and Kubas presented a thorough discussion in 2004.[349] Several workers have obtained direct spectroscopic evidence for *bona fide* alkane adducts of transition metal complexes. The classic examples of such species came from Turner's group, where photolysis methods were employed in alkane matrices to examine by infrared spectroscopy the photoproducts resulting from CO dissociation.[382–384] Additional spectroscopic evidence has been presented for alkanes binding to transition metals using methods such as IR, UV-VIS, and NMR spectroscopies. Low-temperature approaches are often employed to obtain spectroscopic snapshots of these ephemeral species; however, examples of alkane adduct complexes have also been observed at higher temperatures (298 K).[385] Only two X-ray structures of complexes that can be possibly regarded as intermolecular alkane species have been reported to date, both within the last 10 years.[240,386] The first example was presented by Reed and co-workers in 1997.[386] They published the structure of a double A-frame iron porphyrin complex

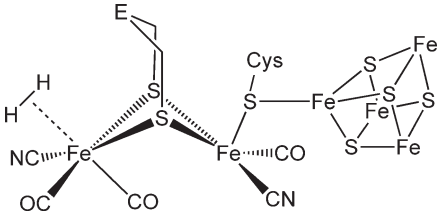

Figure 21 Hypothetical dihydrogen adduct structure at the active site of the Fe-only hydrogenase enzyme.

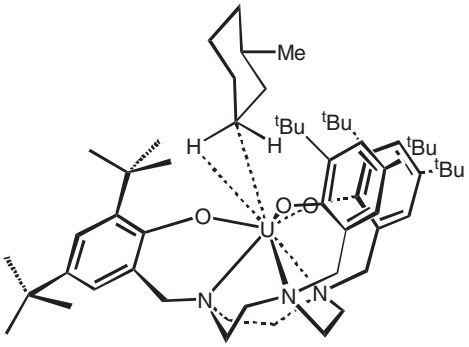

Figure 22 Example of a proposed uranium alkane adduct.

featuring a heptane molecule in close contact to the iron center. The double A-frame porphyrin provides a host–guest binding pocket which the authors attribute to aiding in stabilizing the heptane inclusion. However, disorder of the iron and the heptane molecule makes an exact assignment of the nature of the Fe–(heptane) interaction difficult, and a full paper resolving these problems is yet to appear. The second structural example of a metal–alkane interaction was presented in 2003 by Meyer and co-workers.[240] Using a uranium system supported by a trianionic hexadentate ligand (see Figure 22), the authors reported several crystal structures in which an alkane molecule, for example methylcyclohexane, resides in a position that places a C–H bond conspicuously close to the uranium center. The presence of short contacts between the alkane and the alkyl functionalities of the ligand framework again suggests that host–guest interactions help to stabilize the adduct species. This is moreover supported by the fact that only alkanes of a certain size and shape appear to crystallize in such a manner. However, the authors do suggest a direct orbital interaction between the C–H bond pair of the alkane and the uranium center, and cite U–C_{alkane} distances slightly shorter than 3.9 Å (the calculated van der Waals radius for a U–CH_2R or U–CH_3), as supporting experimental evidence.

1.02.6.2.2 Agostic interactions

Agostic interactions represent a special coordination mode between a ligand and a metal. These types of interactions are typically described by three-centered, two-electron "intramolecular" bonding between a C–H bond pair and a metal center.[387,388] Complexes containing agostic interactions were reviewed by Crabtree in 1993[348] and more recently for d^0-metal complexes by Scherer and McGrady.[389] Clot and Eisenstein have also reviewed computational aspects of agostic interactions recently.[390] Over the last 40 years, many examples of agostic interactions have been studied and characterized.[348,349,387,388] Extensive work on early transition metals, particularly that of metallocene mediated olefin polymerizations, has shown that the presence of a suitable agostic interaction can stabilize an active catalyst that would otherwise be deactivated by β-hydride elimination.[391,392] Indeed, agostic interactions can help to stabilize otherwise coordinatively unsaturated complexes for many transition metal systems. For example, Hartwig and co-workers have isolated and characterized a nominally three-coordinate palladium(II) complex, where a C–H agostic interaction occupies the fourth coordination site.[54] This complex is catalytically competent for cross-coupling reactions. Baratta *et al.* have characterized a related three-coordinate complex of platinum that is again stabilized by a fourth agostic ligand interaction.[393] A third example comes from Caulton's group, where a four-coordinate ruthenium species containing two agostic interactions was discovered.[394] The unusual "saw-horse" geometry of this system can likewise be viewed as a *cis*-divacant octahedral complex, where the two vacant sites are in fact occupied by agostic interactions. This ruthenium complex exhibits interesting reactivity with E–H bonds (E = B, C(sp)). It seems likely that the rational employment of weak agostic-type interactions within organometallic catalyst systems will continue to represent a fruitful research area in catalysis.

1.02.6.2.3 Halocarbon adducts

Although halocarbons are most typically described with regard to their ability to undergo oxidative reactions at transition metals,[395] they can also serve as weakly coordinating ligands through lone pair donation from the halide (see Figure 23).[396–399] Halocarbon coordination can be favored when either the metal center or the halocarbon is ill-suited to oxidative addition processes. For example, d^0-metals are unable to undergo oxidation, and instead sometimes bind halocarbons as L-type ligands to increase their electron count, as for a recent example featuring

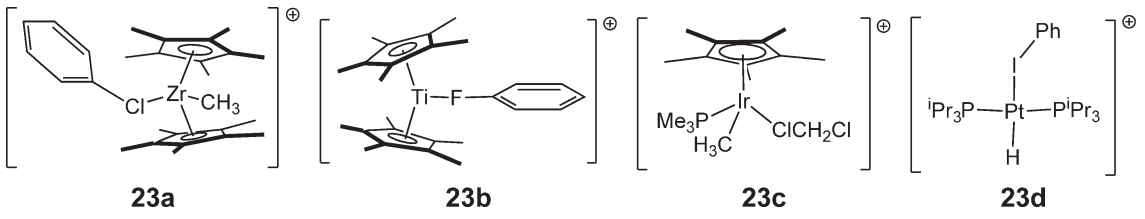

Figure 23 Examples of halocarbon adducts.

chlorobenzene coordinated to Zr(IV) **23a**.[400] Similarly, fluorocarbons, which are typically more resistant to oxidative addition than other halocarbons due to their strong F–C bonds, can weakly bind metal centers. Accordingly, Hessen and co-workers have structurally characterized an example of fluorobenzene coordinated to titanium **23b**.[401] Late metals can demonstrate halocarbon coordination as well, despite their propensity to participate in a great many oxidative addition reactions. Bergman's group has provided an example of a dichloromethane molecule that is weakly coordinated to iridium, thus providing a complex that displays reactivity with alkane C–H bonds **23c**.[402] Kubas and co-workers have shown that platinum(II) will also bind various haloalkanes without undergoing oxidative addition **23d**.[403] These examples demonstrate that halocarbons can act as weakly coordinating neutral ligands, and can thus serve as coordination site placeholders, no doubt a useful strategy for organometallic synthesis and catalysis.

1.02.7 Zwitterionic Organometallics

As discussed previously, reactive metal cations are ubiquitous to many areas of homogeneous catalysis,[404] and highly non-coordinating counteranions have emerged as the most generally effective way to expose and often preserve the reactivity of pseudo-unsaturated, highly electrophilic metal centers.[405] Reaction types where the use of non-coordinating anions have proved to be effective include catalytic C–C and other C–E bond-forming reactions (E = C, N, O, S, Si, H, etc.,),[406–416] olefin polymerization, and co-polymerization reactions,[31,34,417–421] and light alkane activation processes.[402,422–427]

An emerging alternative approach to reveal the reactivity patterns typical of reactive metal cations relates to the use of organometallic zwitterions. In these types of species, a formally anionic subunit is attached to a metal complex but does not interact with the metal center via a direct covalent bond. Efforts to systematically exploit organometallic zwitterions in homogeneous catalysis have been surprisingly limited in scope since their initial discovery.[428] Perhaps the most noteworthy exceptions concern (see Figure 24) (i) recent work involving Cp-supported early metal

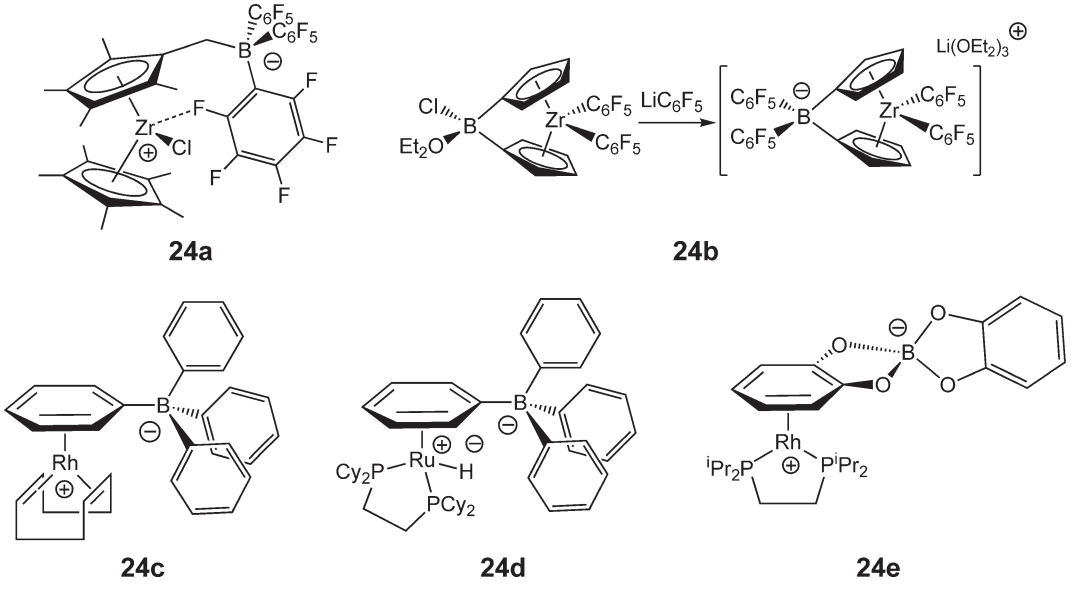

Figure 24 Examples of zwitterionic transition metal complexes.

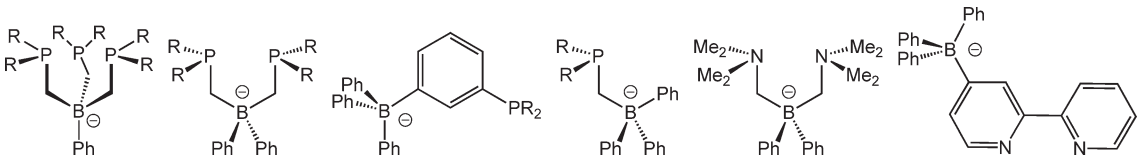

Figure 25 Examples of monoanionic phosphorus and nitrogen donor ligands that incorporate an anionic borate unit.

zwitterions that mediate Ziegler–Natta-type polymerization (**24a** and **b**),[429–431] (ii) tetraphenylborate adducts of $L_2Rh(I)^+$ **24c** and $L_2(H)Ru(II)^+$ **24d**,[432–435] and related zwitterionic rhodium hydroboration catalysts derived from catechol borane **24e**.[436–438] A remotely activated nickel polymerization system that can be described as an *in situ*-generated zwitterion has also been described.[439,440]

One particularly promising approach to zwitterionic catalyst design emphasizes readily isolable complexes featuring a partially insulated borate counteranion, locked at a remote (4–7 Å) distance from a coordinated transition metal center by phosphine, amine, or related neutral donor arms (see Figure 25).[64–66,441–444] While neutral metal complexes featuring borate-derived ligands of these general structure types have been known for decades (e.g., tris(pyrazolyl)borates),[22] emphasizing these types of borate frameworks in the context of zwitterion-mediated reaction chemistry has emerged only recently. A key advantage of this approach is that it generalizes synthetic methods for the construction of organometallic zwitterions. Moreover, these systems allow one to undertake systematic structure/function studies that can establish how formally zwitterionic and isostructural but cationic metal complexes compare with respect to their (i) degree of electrophilic character and (ii) their reactivity patterns.[66,441,442,444] Studies of these types should help to define under what conditions a zwitterionic approach to homogeneous catalysis might prove most efficacious.

Several practical considerations underscore the potential advantages of zwitterionic organometallic catalysts. Aside from the consequence of eliminating the need for an activating co-catalyst (e.g., to expose a coordination site by anion abstraction), reactivity differences between zwitterionic and traditionally cationic systems due to (i) differences in their relative electrophilicities, (ii) differences in their relative donor ligand labilities, and (iii) potentially reduced or completely eliminated ion-pairing effects in the zwitterionic systems by comparison to their cationic counterparts can be anticipated. Moreover, solvents that dissolve ionic compounds almost always have polar, hence coordinating, functional groups that can attenuate their reactivity. In principle, zwitterionic species can provide access to the chemistry of cationic metal centers in relatively non-polar hydrocarbon media. This in turn might increase overall catalytic activity. Because zwitterionic systems are likely to be less electrophilic than their corresponding conventional cations, they might also show increased tolerance to the presence of polar donor solvents or substrate functional groups.

Resonance contributors. The impetus to describe neutral complexes supported by (phosphino)borates (or related ligands) as zwitterionic derives from the lack of simple resonance contributors that can efficiently delocalize the anionic borate charge to the coordinated metal center.[64] From an electron-counting perspective, the zwitterionic formulation suggests that metal complexes supported by bis(phosphino)borates be regarded as cationic complexes chelated by an L_2, four-electron donor ligand. This electronic description is distinct from that which has been used for the related families of bis- and tris(pyrazolyl)borates.[22] In the (pyrazolyl)borates, the borate charge is presumed to be more uniformly distributed due to important resonance contributors that fully delocalize the borate charge. In the extreme, electron-counting schemes designate bis(pyrazolyl)borates as LX-type, three-electron donors, whereas bis(phosphino)borates can be classified as four-electron, L_2 donor ligands coordinated to a formal cation. Likewise, a tris(pyrazolyl)borate ligand can be described as an L_2X five-electron donor akin to Cp, whereas a tris(phosphino)-borate ligand is better described as an L_3-type ligand where a cationic charge is preserved at the metal.

Two final types of late metal zwitterions (see Figure 26) that have emerged very recently and appear to offer a good deal of promise as alternative catalysts are a *P*,*N*-substituted indenide system **26a** and **26b**,[445,446] and a chiral, boron-bridged bis(oxazoline) system **26c**.[447] Future studies with these and other organometallic zwitterionic systems should elucidate the role of the zwitterion in fundamental transformations.

1.02.8 Secondary Coordination Sphere Interactions

The incorporation of secondary coordination sphere interactions within ligand design has matured substantially in organometallic and inorganic chemistry during the last 10 years.[448–457] Secondary effects can imply influences beyond the initial coordination sphere of a metal, such as proximal hydrogen bond acceptors or donors and redox active ligands. In these systems, the ligand transcends beyond a simple electron-donating group with local steric

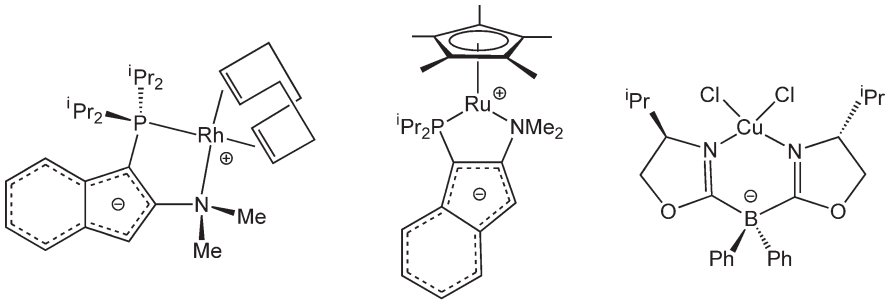

26a 26b 26c

Figure 26 Examples of indenide- and oxazoline-containing zwitterionic transition metal complexes.

effects and becomes integral to the reaction chemistry through accompanying functional groups outside the metal's immediate coordination sphere. These effects are distinct from reactive ligands that are expected to enter and leave the coordination sphere in a transformation. A review by Sawamura and Ito in 1992 highlights early contributions to this field, particularly with respect to the effects of pendant functional groups in enantioselective catalysis.[448] In many instances, the purpose of these secondary interactions is to engender a more facile or selective transformation through a more readily accessible transition state. For example, the field of asymmetric two-center catalysis frequently takes advantage of single catalysts containing both Lewis-acidic and Lewis-basic sites to promote conversions.[449,450,452–455,457] Alternatively, such secondary effects can help to stabilize an otherwise unfavorable transition state.[456] Here we highlight a few illustrative examples where secondary sphere interactions have been used successfully. One example concerns bifunctional ligand hydrogenation catalysts, and another example concerns hydrogen bonding effects to stabilize unusual structures that promote new reactivity pathways.

1.02.8.1 Bifunctional Ligand Hydrogenation Catalysts

One of the most successful areas of bifunctional ligand effects in the last decade is the development of highly successful ruthenium hydrogenation catalysts (see Figure 27).[455,457–460] Most notably, Noyori and his group have demonstrated the utility of bifunctional ligands through their work with ruthenium hydrogenation catalysts **27a**.[457,461–463] In these systems, the presence of a primary amine ligand is essential to the hydrogenation function. The coordinated amine transfers a proton to the substrate in a concerted fashion with the transfer of a metal-bound hydride to the substrate, thereby delivering H_2 in a heterolytic fashion.[461] This mechanistic pathway requires that the metal center be able to accommodate the resulting amide ligand that results from proton transfer from the amine, as well as the change in geometry that results from the loss of the hydride ligand. Morris and co-workers have reported on the mechanism of this type of transformation in detail.[450,464] One of the key features of the Noyori catalyst mechanism that distinguishes it from many other hydrogenation catalysts is the outer sphere nature of the hydrogen transfer: the substrate does not coordinate directly to the metal during the overall transformation.

A second, conceptually related system is the hydroxycyclopentadienyl ruthenium carbonyl systems first introduced by Shvo and co-workers **27b**.[458,465–467] Similar to the amine-ligated ruthenium systems of Noyori, the hydroxycyclopentadienyl ligand plays an active role in transferring a proton to the substrate.[468–470] Bäckvall's and Casey's groups have undertaken detailed studies of these ruthenium dimers for ketone and imine hydrogenation reactions,

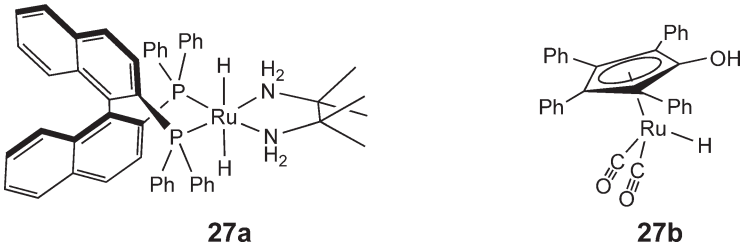

27a 27b

Figure 27 Examples of hydrogenation catalysts containing bifunctional ligands.

and also for the kinetic resolution of alcohols.[459,460,468–475] Again, the hydrogenation appears to occur without the substrate directly coordinating to the metal center.

1.02.8.2 Hydrogen Bonding Interactions

The presence of secondary coordination sphere hydrogen bond donors can help to stabilize what would otherwise be reactive functional groups at a metal center. Borovik's group has demonstrated this principle using elegant systems derived from a tetradentate trianionic platform.[456,476–486] By using urea groups as amide donors, several amide hydrogen bond donor groups are presented to the active coordination site. These amide hydrogens indeed participate in hydrogen bonding, and have been shown to attenuate the electron density of, and to stabilize, electron-rich ligands such as oxo and hydroxy groups.[477,478,482,484–486] An excellent example of this concept is an iron(III) complex containing an oxygen atom that is bound only to iron except for the secondary sphere hydrogen bond interactions with each of the three urea groups (see Figure 28).[484] The synthetic versatility of this ligand system also allows for incorporation of fewer hydrogen bond donors in the coordination sphere.[487] This feature should provide an opportunity to tune the reactivity of metal oxo and related ligands.

Pendant donors covalently linked to porphyrins, corroles, and more recently, salophens (see Figure 29) have also been used in the design of secondary sphere interactions.[488–490] All of these L_2X_2 (porphyrins and salophens) and LX_3 (corroles) ligands contain an additional supporting functionality in the form of hydrogen bond donor/acceptor groups that can stabilize potential reaction intermediates, and help to generate catalytic systems inspired by biological systems such as heme-type systems responsible for dioxygen activation and proton-coupled electron transfer (PCET).[490–494]

A classic example of a macrocyclic system with a pendant donor arm is the picket fence porphyrin system of Collman and co-workers.[495] This system features four potential donors around the porphyrin ring periphery. Collman and co-workers have used picket fence porphyrins to model heme–dioxygen interactions. In a refinement of this concept, porphyrins incorporating a single pendant hydrogen bond donor appended to a *meso*-position of the porphyrin ring were demonstrated by Chang and co-workers in 1986.[496] Using a substituted naphthalene covalently linked to a porphyrin, Chang *et al*. demonstrated that the presence of a hydrogen bond donor hanging over a cobalt center resulted in improved dioxygen binding. Subsequent studies from Chang's group expanded this idea.[497–499] More recently, Nocera and co-workers have adapted synthetic methods for *meso*-substitution of porphyrins[500,501] to introduce new *hangman*-porphyrin scaffolds **29a**.[488,502] By adapting new methods for the creation of fascinating co-facial porphyrin assemblies,[263,265,266,268] Nocera's group has incorporated xanthene and dibenzofuran pillars with pendant functional groups onto the porphyrin frame.[488,502] These new pendant donor porphyrins have substantially increased the range of platforms available for the incorporation of hydrogen bond interactions within small molecule activation systems.

The Collman group has more recently built on their early success with picket fence porphyrins[491,495] to develop a versatile platform for picket fence corroles.[489] This recent addition to macrocycles containing a pendant hydrogen bond donor group takes advantage of the improved methods for corrole synthesis[245] to incorporate arylamines in *meso*-positions. The arylamines can then be functionalized with acid chlorides to provide picket fence and other corrole structures. For example, reacting the triarylamine corrole with pivaloyl chloride results in a picket fence corrole containing hydrogen bond donors near to the metal center binding cavity **29b**.

A final class of ligands worthy of note where pendant hydrogen bond donors have been incorporated concerns the salophen family. Although not true macrocycles, salophens share many of the characteristics of porphyrin-type macrocycles as they are L_2X_2 ligands and adopt a *mer*-binding mode.[503,504] Nocera and co-workers have exploited their methods for the generation of pillared co-facial porphyrins to create *hangman*-salophens through selective

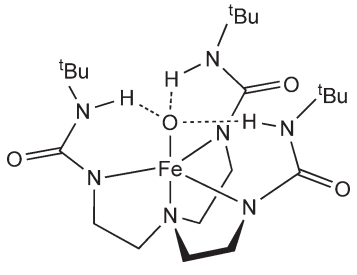

Figure 28 Example of a transition metal complex containing a hydrogen bond-stabilized terminal oxygen atom.

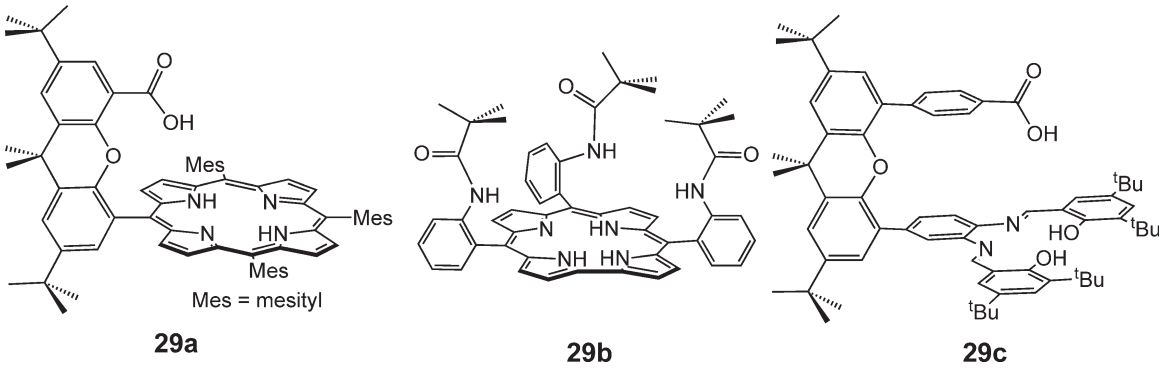

Figure 29 Examples of ligands capable of presenting a remote hydrogen bond interaction.

modification of a xanthene pillar **29c**.[490] Although this area of chemistry is very much in a developmental stage, the versatility of the salophen scaffold and its successful application to some areas of catalysis[503,504] suggest that the *hangman*-salophens will prove to be an exciting addition to the ligands available in organometallic and inorganic chemsitry.

1.02.9 Fluorinated Ligands for Alternative Solvents

1.02.9.1 Fluorous Soluble Ligands

Since its inception in 1991 by Vogt[505] and its public presentation by Horvath and Rabai in 1994,[506] the field of fluorous biphasic catalysis has matured rapidly[507] and has led to a flurry of new fluorous ligand syntheses for catalytic applications.[508–517] The premise of the fluorous-phase approach is that the generation of a biphasic system, which has historically been water and an aqueous immiscible phase, can also be prepared between fluorinated and hydrocarbon solvents. This method removes the aqueous layer, which is often a significant concern for organometallic chemists. At elevated temperatures, hydrocarbon and fluorous phases can combine into a single phase, creating a homogenous reaction mixture. Then, at lower temperatures where the two phases separate, the catalyst can be recovered and recycled through partitioning of the catalyst into the fluorous phase and away from the organic layer. The thrust of research in this area has been the synthesis of fluorous soluble ligands through addition of polyfluorinated groups to typical organometallic ligands (see Figure 30). Representative examples of ligands prepared with fluorinated functional groups and used in biphasic catalysis include phosphines **30a**,[506] Schiff base salen **30b**,[518] bis(oxazolines) **30c**,[519] and porphyrins.[520] Many other fluorinated ligands have also been studied in the context of fluorous catalysis, and the reader is referred to reviews addressing this topic for further examples.[510,516,517] Significant effort has been

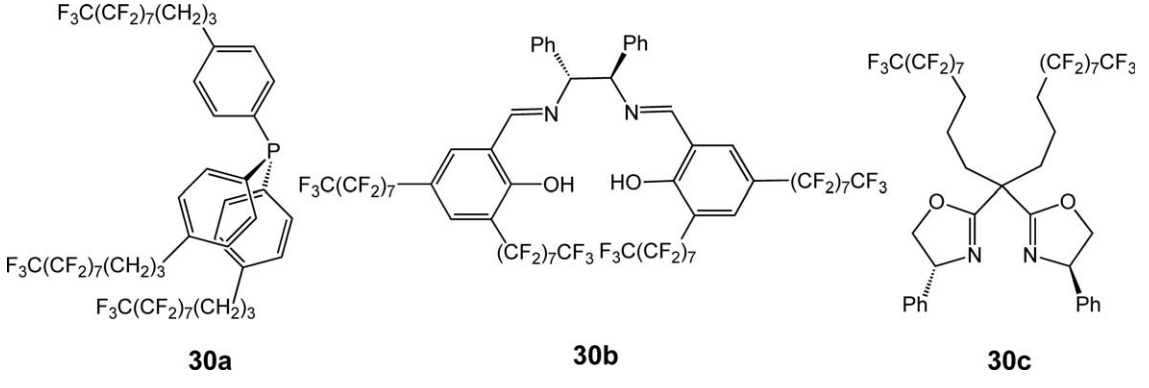

Figure 30 Examples of fluorous phase soluble ligands.

expended to understand the electronic effects of adding highly fluorinated groups to conventional ligand structures.[521–526] In general, the presence of a highly electron-withdrawing group alters a coordinated metal center's reactivity, if the metal center and fluorinated group are not sufficiently electronically insulated. Thus, inclusion of an electronic insulator in the form of alkyl linkages between the fluorous "ponytail" and the ligand donor atom has been adopted as one avenue for avoiding deactivation due to the presence of electron-withdrawing fluorides.[522,523] Several variations on the fluorous separation concept have been explored for catalyst recovery, including fluorous reverse-phase silica gel[527,528] and Teflon® tape.[529] The area of fluorous-phase chemistry is likely to continue to develop as an important field of organometallic catalysis because of the many available methods for isolating, recovering, and recycling flourous-tagged catalysts.

1.02.9.2 Supercritical CO_2-soluble Fluorous Ligands

In conjunction with the work being done on fluorous biphasic systems, the development of fluorinated ligands has also made an impact in the area of supercritical carbon dioxide ($scCO_2$) catalysis. Supercritical CO_2 has been heavily studied as a reaction medium for organometallic chemistry due to its unique properties.[530–536] Its advantages include being environmentally benign (as compared to most common organic solvents), its chemical inertness, the solubility of gaseous reagents such as O_2 and H_2 in $scCO_2$, and useful separation techniques for catalyst recovery. Dense phases of CO_2 exhibit a solubility preference for fluorine-containing metal complexes, whereas complexes containing phenyl-substituted ligands are poorly soluble.[536] Fluorous molecules are significantly more soluble in $scCO_2$, as exemplified by the polymerization of fluorinated polymers by DeSimone *et al.* in 1992.[537] In general, these solubility characteristics present a limitation for many traditional organometallic catalysts that often have aryl-containing ligands rather than highly fluorinated groups. Building on developments in fluorous-phase chemistry, Leitner and co-workers demonstrated the utility of polyfluorinated derivatives of well-known phosphine ligands in homogeneous organometallic catalysis in $scCO_2$ in 1997.[538] Subsequent studies from Leitner's group have demonstrated the potential for $scCO_2$ as a reaction medium for organometallic catalysis.[533]

1.02.10 Terminally Bonded Carbides

The chemistry of metal-to-carbon multiply bonded complexes continues to flourish. The critical role olefin metathesis chemistry now plays in so many areas of synthesis and materials science has provided important impetus for the continued discovery and study of such species.[539–543] While the scope of this contribution is far too narrow to even begin to touch upon this broad area of organometallic chemistry, the authors wish to highlight one new class of organometallic complexes that falls within this category, that of the terminally bonded carbides.

The first terminally bonded carbide complex was characterized by Peters, Odom, and Cummins in 1997 (see Figure 31).[544,545] Employing the bulky tris(*N-tert*-butylanilide)molybdenum system, a favorable reductive procedure was discovered to transfer the C atom from carbon monoxide after its initial conversion to a pivaloyl carbyne ligand. While reduction by sodium mirror resulted in ca. 75% net cleavage of the C–O bond, it proved to be synthetically most efficient to isolate the terminal methylidyne complex, formed in ca. 50% isolated yield by an acetonitrile workup procedure, and to subsequently effect its clean deprotonation to the terminal carbide species. Azacryptands and crown ethers were used to sequester the potassium countercation when benzylpotassium was used as the base, aiding the structural characterization of the terminally bound complex. The Templeton group has generated a Tp′-supported tungsten(VI) lithio carbide species by deprotonation of a terminally bound methylidyne complex (see Figure 32).[546] In this instance, the methylidyne species is first generated by hydride attack at a cationic phosphonium carbyne precursor. More recently, an elegant new method of C atom transfer to molybdenum was elucidated by the Cummins team that proceeds via benzene expulsion (see Figure 31) from an intermittent 1-norbornyl carbyne species. Chlorine atom abstraction by a tris(amido)titanium(III) species generates norbornyl radical, which is cleanly trapped in the presence of molybdenum(III) to produce the required high energy intermediate that then decays to the terminal methylidyne complex and benzene. This method of arene expulsion from a high energy intermediate species to generate a thermally robust metal-to-ligand multiple bond has also been employed in the context of terminal nitride syntheses.[67,68] Along similar lines, Heppert and co-workers have realized a surprisingly robust ruthenium carbide complex that is generated by olefin loss from an intermediate carbene species (see Figure 33). The carbene itself is the expected intermediate of an olefin metathesis reaction.

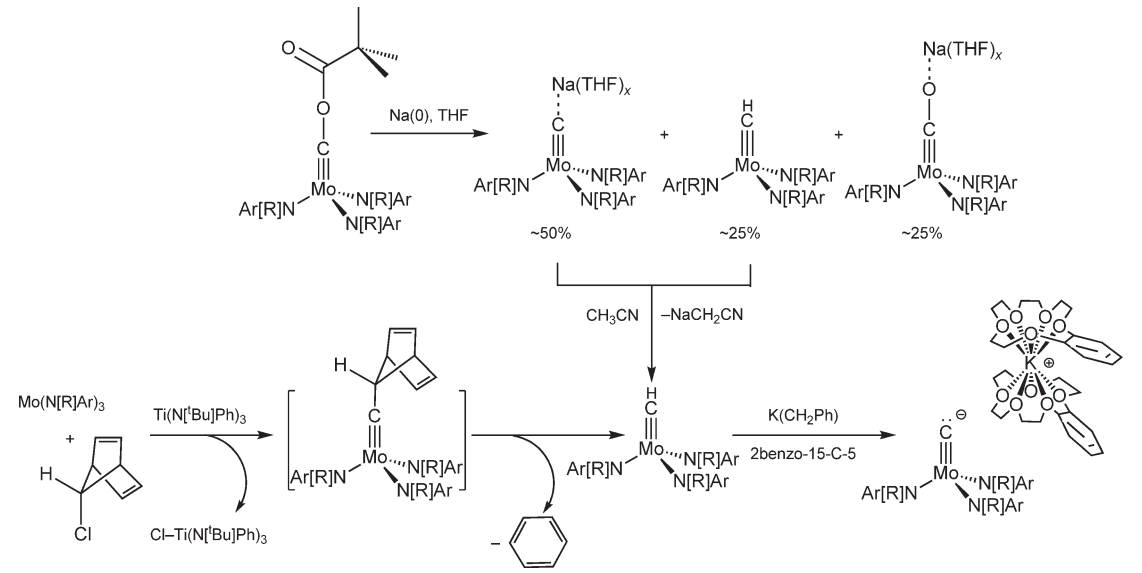

Figure 31 Reaction scheme for the generation of a molybdenum species containing a terminal carbide.

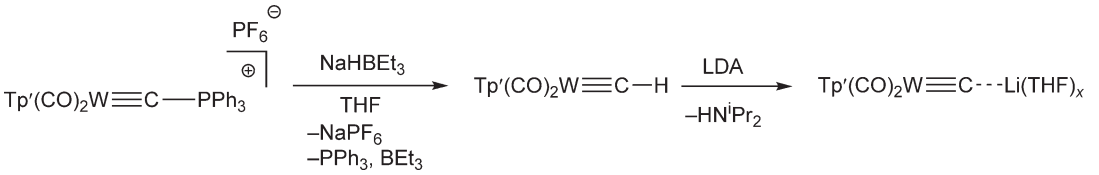

Figure 32 Reaction scheme for the generation of a tungsten species containing a terminal carbide.

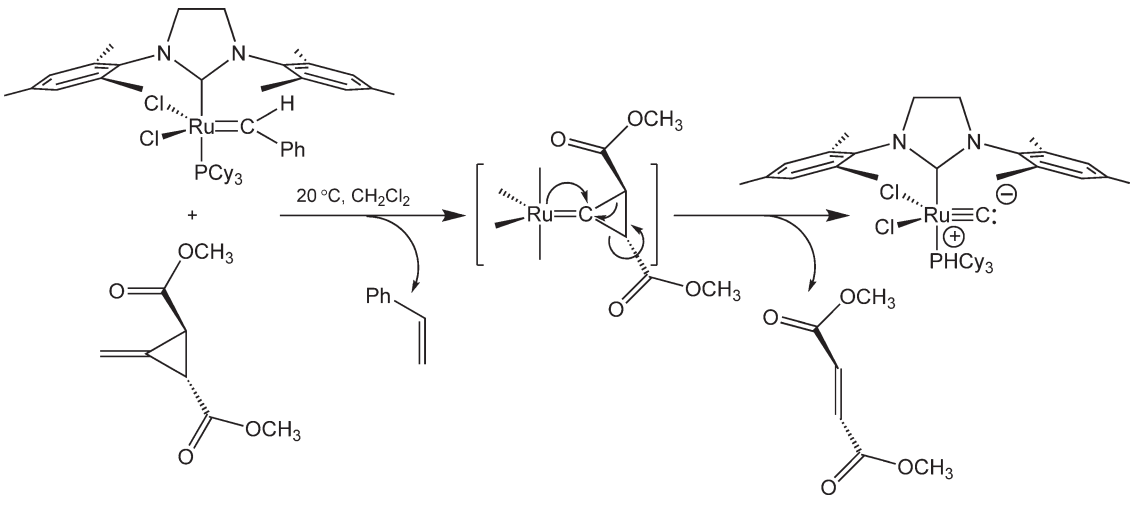

Figure 33 Reaction scheme for the generation of a ruthenium species containing a terminal carbide.

References

1. Neithamer, D. R.; Lapointe, R. E.; Wheeler, R. A.; Richeson, D. S.; Vanduyne, G. D.; Wolczanski, P. T. *J. Am. Chem. Soc.* **1989**, *111*, 9056–9072.
2. Lapointe, R. E.; Wolczanski, P. T.; Mitchell, J. F. *J. Am. Chem. Soc.* **1986**, *108*, 6382–6384.
3. Laplaza, C. E.; Johnson, M. J. A.; Peters, J. C.; Odom, A. L.; Kim, E.; Cummins, C. C.; George, G. N.; Pickering, I. J. *J. Am. Chem. Soc.* **1996**, *118*, 8623–8638.
4. Laplaza, C. E.; Odom, A. L.; Davis, W. M.; Cummins, C. C.; Protasiewicz, J. D. *J. Am. Chem. Soc.* **1995**, *117*, 4999–5000.
5. Yandulov, D. V.; Schrock, R. R. *J. Am. Chem. Soc.* **2002**, *124*, 6252–6253.
6. Alyea, E. C.; Basi, J. S.; Bradley, D. C.; Chisholm, M. H. *Chem. Commun.* **1968**, 495.
7. Song, J. I.; Berno, P.; Gambarotta, S. *J. Am. Chem. Soc.* **1994**, *116*, 6927–6928.
8. Andersen, R. A. *Inorg. Chem.* **1979**, *18*, 1507–1509.
9. Covert, K. J.; Wolczanski, P. T.; Hill, S. A.; Krusic, P. J. *Inorg. Chem.* **1992**, *31*, 66–78.
10. Covert, K. J.; Neithamer, D. R.; Zonnevylle, M. C.; Lapointe, R. E.; Schaller, C. P.; Wolczanski, P. T. *Inorg. Chem.* **1991**, *30*, 2494–2508.
11. Lockwood, M. A.; Fanwick, P. E.; Eisenstein, O.; Rothwell, I. P. *J. Am. Chem. Soc.* **1996**, *118*, 2762–2763.
12. Cummins, C. C. *Chem. Commun.* **1998**, 1777–1786.
13. Cummins, C. C. *Prog. Inorg. Chem.* **1998**, *47*, 685–836.
14. Schrock, R. R. *Acc. Chem. Res* **1997**, *30*, 9–16.
15. Verkade, J. G. *Coord. Chem. Rev.* **1994**, *137*, 233–295.
16. Verkade, J. G. *Acc. Chem. Res* **1993**, *26*, 483–489.
17. Cummins, C. C.; Lee, J.; Schrock, R. R.; Davis, W. D. *Angew. Chem., Int. Ed. Engl.* **1992**, *31*, 1501–1503.
18. Chaudhuri, P.; Wieghardt, K. *Prog. Inorg. Chem.* **2001**, *50*, 151–216.
19. Castro-Rodriguez, I.; Nakai, H.; Zakharov, L. N.; Rheingold, A. L.; Meyer, K. *Science* **2004**, *305*, 1757–1760.
20. Castro-Rodriguez, I.; Olsen, K.; Gantzel, P.; Meyer, K. *J. Am. Chem. Soc.* **2003**, *125*, 4565–4571.
21. Castro-Rodriguez, I.; Olsen, K.; Gantzel, P.; Meyer, K. *Chem. Commun.* **2002**, 2764–2765.
22. Trofimenko, S. *Chem. Rev.* **1993**, *93*, 943–980.
23. Detrich, J. L.; Konecny, R.; Vetter, W. M.; Doren, D.; Rheingold, A. L.; Theopold, K. H. *J. Am. Chem. Soc.* **1996**, *118*, 1703–1712.
24. Jenkins, D. M.; Peters, J. C. *J. Am. Chem. Soc.* **2005**, *127*, 7148–7165.
25. Jenkins, D. M.; Di Bilio, A. J.; Allen, M. J.; Betley, T. A.; Peters, J. C. *J. Am. Chem. Soc.* **2002**, *124*, 15336–15350.
26. Spencer, D. J. E.; Aboelella, N. W.; Reynolds, A. M.; Holland, P. L.; Tolman, W. B. *J. Am. Chem. Soc.* **2002**, *124*, 2108–2109.
27. Amisial, L. D.; Dai, X. L.; Kinney, R. A.; Krishnaswamy, A.; Warren, T. H. *Inorg. Chem.* **2004**, *43*, 6537–6539.
28. Spencer, D. J. E.; Reynolds, A. M.; Holland, P. L.; Jazdzewski, B. A.; Duboc-Toia, C.; Le Pape, L.; Yokota, S.; Tachi, Y.; Itoh, S.; Tolman, W. B. *Inorg. Chem.* **2002**, *41*, 6307–6321.
29. Holland, P. L.; Cundari, T. R.; Perez, L. L.; Eckert, N. A.; Lachicotte, R. J. *J. Am. Chem. Soc.* **2002**, *124*, 14416–14424.
30. MacAdams, L. A.; Kim, W. K.; Liable-Sands, L. M.; Guzei, I. A.; Rheingold, A. L.; Theopold, K. H. *Organometallics* **2002**, *21*, 952–960.
31. Ittel, S. D.; Johnson, L. K.; Brookhart, M. *Chem. Rev.* **2000**, *100*, 1169–1203.
32. Hagadorn, J. R.; Que, L.; Tolman, W. B. *J. Am. Chem. Soc.* **1998**, *120*, 13531–13532.
33. Schmidt, J. A. R.; Arnold, J. *J. Chem. Soc., Dalton Trans.* **2002**, 3454–3461.
34. Coles, M. P.; Jordan, R. F. *J. Am. Chem. Soc.* **1997**, *119*, 8125–8126.
35. Nijhuis, C. A.; Jellema, E.; Sciarone, T. J. J.; Meetsma, A.; Budzelaar, P. H. M.; Hessen, B. *Eur. J. Inorg. Chem.* **2005**, 2089–2099.
36. Bambirra, S.; van Leusen, D.; Meetsma, A.; Hessen, B.; Teuben, J. H. *Chem. Commun.* **2003**, 522–523.
37. Scott, N. M.; Kempe, R. *Eur. J. Inorg. Chem.* **2005**, 1319–1324.
38. Scott, N. M.; Schareina, T.; Tok, O.; Kempe, R. *Eur. J. Inorg. Chem.* **2004**, 3297–3304.
39. Haymotherwell, R. S.; Wilkinson, G.; Hussainbates, B.; Hursthouse, M. B. *Polyhedron* **1993**, *12*, 2009–2012.
40. Hino, S.; Brynda, M.; Phillips, A. D.; Power, P. P. *Angew. Chem., Int. Ed.* **2004**, *43*, 2655–2658.
41. Wright, R. J.; Phillips, A. D.; Allen, T. L.; Fink, W. H.; Power, P. P. *J. Am. Chem. Soc.* **2003**, *125*, 1694–1695.
42. Power, P. P. *Chem. Rev.* **1999**, *99*, 3463–3503.
43. Twamley, B.; Haubrich, S. T.; Power, P. P. *Adv. Organomet. Chem.* **1999**, *44*, 1–65.
44. Robinson, G. H. *Adv. Organomet. Chem.* **2001**, *47*, 283–294.
45. Robinson, G. H. *Acc. Chem. Res.* **1999**, *32*, 773–782.
46. Su, J. R.; Li, X. W.; Crittendon, R. C.; Robinson, G. H. *J. Am. Chem. Soc.* **1997**, *119*, 5471–5472.
47. Haubrich, S. T.; Power, P. P. *J. Am. Chem. Soc.* **1998**, *120*, 2202–2203.
48. Kisko, J. L.; Hascall, T.; Parkin, G. *J. Am. Chem. Soc.* **1998**, *120*, 10561–10562.
49. Caballero, A.; Diaz-Requejo, M. M.; Belderrain, T. R.; Nicasio, M. C.; Trofimenko, S.; Perez, P. J. *J. Am. Chem. Soc.* **2003**, *125*, 1446–1447.
50. Schneider, J. L.; Carrier, S. M.; Ruggiero, C. E.; Young, V. G.; Tolman, W. B. *J. Am. Chem. Soc.* **1998**, *120*, 11408–11418.
51. Puiu, S. C.; Warren, T. H. *Organometallics* **2003**, *22*, 3974–3976.
52. Dai, X. L.; Warren, T. H. *Chem. Commun.* **2001**, 1998–1999.
53. Tolman, C. A. *Chem. Rev.* **1977**, *77*, 313–348.
54. Stambuli, J. P.; Buhl, M.; Hartwig, J. F. *J. Am. Chem. Soc.* **2002**, *124*, 9346–9347.
55. Tomori, H.; Fox, J. M.; Buchwald, S. L. *J. Org. Chem.* **2000**, *65*, 5334–5341.
56. Kitiachvili, K. D.; Mindiola, D. J.; Hillhouse, G. L. *J. Am. Chem. Soc.* **2004**, *126*, 10554–10555.
57. Mindiola, D. J.; Hillhouse, G. L. *J. Am. Chem. Soc.* **2001**, *123*, 4623–4624.
58. Melenkivitz, R.; Mindiola, D. J.; Hillhouse, G. L. *J. Am. Chem. Soc.* **2002**, *124*, 3846–3847.
59. Feldman, J. D.; Mitchell, G. P.; Nolte, J. O.; Tilley, T. D. *J. Am. Chem. Soc.* **1998**, *120*, 11184–11185.
60. Thomas, J. C.; Peters, J. C. *Inorg. Synth.* **2004**, *34*, 8–14.
61. Shapiro, I. R.; Jenkins, D. M.; Thomas, J. C.; Day, M. W.; Peters, J. C. *Chem. Commun.* **2001**, 2152–2153.
62. Peters, J. C.; Feldman, J. D.; Tilley, T. D. *J. Am. Chem. Soc.* **1999**, *121*, 9871–9872.
63. Betley, T. A.; Peters, J. C. *Inorg. Chem.* **2003**, *42*, 5074–5084.
64. Thomas, J. C.; Peters, J. C. *Inorg. Chem.* **2003**, *42*, 5055–5073.

65. Thomas, C. M.; Peters, J. C. *Inorg. Chem.* **2004**, *43*, 8–10.
66. Thomas, J. C.; Peters, J. C. *J. Am. Chem. Soc.* **2003**, *125*, 8870–8888.
67. Betley, T. A.; Peters, J. C. *J. Am. Chem. Soc.* **2004**, *126*, 6252–6254.
68. Mindiola, D. J.; Cummins, C. C. *Angew. Chem., Int. Ed.* **1998**, *37*, 945–947.
69. Chiou, S. J.; Ge, P. H.; Riordan, C. G.; Liable-Sands, L. M.; Rheingold, A. L. *Chem. Commun.* **1999**, 159–160.
70. Schebler, P. J.; Riordan, C. G.; Guzei, I. A.; Rheingold, A. L. *Inorg. Chem.* **1998**, *37*, 4754–4755.
71. Ge, P. H.; Riordan, C. G.; Yap, G. P. A.; Rheingold, A. L. *Inorg. Chem.* **1996**, *35*, 5408–5409.
72. Ge, P. H.; Haggerty, B. S.; Rheingold, A. L.; Riordan, C. G. *J. Am. Chem. Soc.* **1994**, *116*, 8406–8407.
73. Ge, P. H.; Rheingold, A. L.; Riordan, C. G. *Inorg. Chem.* **2002**, *41*, 1383–1390.
74. Mandimutsira, B. S.; Yamarik, J. L.; Brunold, T. C.; Gu, W. W.; Cramer, S. P.; Riordan, C. G. *J. Am. Chem. Soc.* **2001**, *123*, 9194–9195.
75. Schebler, P. J.; Mandimutsira, B. S.; Riordan, C. G.; Liable-Sands, L. M.; Incarvito, C. D.; Rheingold, A. L. *J. Am. Chem. Soc.* **2001**, *123*, 331–332.
76. Fryzuk, M. D.; Love, J. B.; Rettig, S. J.; Young, V. G. *Science* **1997**, *275*, 1445–1447.
77. Fryzuk, M. D.; Love, J. B.; Rettig, S. J. *Chem. Commun.* **1996**, 2783–2784.
78. Fryzuk, M. D.; Gao, X. L.; Joshi, K.; Macneil, P. A.; Massey, R. L. *J. Am. Chem. Soc.* **1993**, *115*, 10581–10590.
79. Fryzuk, M. D.; Mao, S. S. H.; Zaworotko, M. J.; Macgillivray, L. R. *J. Am. Chem. Soc.* **1993**, *115*, 5336–5337.
80. Fryzuk, M. D. *Can. J. Chem.* **1992**, *70*, 2839–2845.
81. Ozerov, O. V.; Pink, M.; Watson, L. A.; Caulton, K. G. *J. Am. Chem. Soc.* **2004**, *126*, 2105–2113.
82. Watson, L. A.; Ozerov, O. V.; Pink, M.; Caulton, K. G. *J. Am. Chem. Soc.* **2003**, *125*, 8426–8427.
83. Harkins, S. B.; Peters, J. C. *J. Am. Chem. Soc.* **2005**, *127*, 2030–2031.
84. Ozerov, O. V.; Guo, C. Y.; Papkov, V. A.; Foxman, B. M. *J. Am. Chem. Soc.* **2004**, *126*, 4792–4793.
85. Liang, L. C.; Lee, W. Y.; Yin, C. C. *Organometallics* **2004**, *23*, 3538–3547.
86. Harkins, S. B.; Peters, J. C. *J. Am. Chem. Soc.* **2004**, *126*, 2885–2893.
87. Cochran, F. V.; Bonitatebus, P. J.; Schrock, R. R. *Organometallics* **2000**, *19*, 2414–2416.
88. Flores, M. A.; Manzoni, M. R.; Baumann, R.; Davis, W. M.; Schrock, R. R. *Organometallics* **1999**, *18*, 3220–3227.
89. Baumann, R.; Stumpf, R.; Davis, W. M.; Liang, L. C.; Schrock, R. R. *J. Am. Chem. Soc.* **1999**, *121*, 7822–7836.
90. Baumann, R.; Davis, W. M.; Schrock, R. R. *J. Am. Chem. Soc.* **1997**, *119*, 3830–3831.
91. Harkins, S. B.; Peters, J. C. *Organometallics* **2002**, *21*, 1753–1755.
92. Peters, J. C.; Harkins, S. B.; Brown, S. D.; Day, M. W. *Inorg. Chem.* **2001**, *40*, 5083–5091.
93. Rabinovich, D.; Parkin, G. *J. Am. Chem. Soc.* **1995**, *34*, 6341–6361.
94. Tsai, Y. C.; Johnson, M. J. A.; Mindiola, D. J.; Cummins, C. C.; Klooster, W. T.; Koetzle, T. F. *J. Am. Chem. Soc.* **1999**, *121*, 10426–10427.
95. Bercaw, J. E. *Adv. Chem. Ser.* **1978**, *167*, 136–148.
96. Bernskoetter, W. H.; Pool, J. A.; Lobkovsky, E.; Chirik, P. J. *J. Am. Chem. Soc.* **2005**, *127*, 7901–7911.
97. Pool, J. A.; Lobkovsky, E.; Chirik, P. J. *J. Am. Chem. Soc.* **2003**, *125*, 2241–2251.
98. Mork, B. V.; Tilley, T. D. *J. Am. Chem. Soc.* **2004**, *126*, 4375–4385.
99. Mork, B. V.; Tilley, T. D. *J. Am. Chem. Soc.* **2001**, *123*, 9702–9703.
100. Vedernikov, A. N.; Caulton, K. G. *Angew. Chem., Int. Ed.* **2002**, *41*, 4102–4104.
101. Vedernikov, A. N.; Caulton, K. G. *Chem. Commun.* **2003**, 358–359.
102. Vedernikov, A. N.; Huffman, J. C.; Caulton, K. G. *Inorg. Chem.* **2002**, *41*, 6867–6874.
103. Vedernikov, A. N.; Caulton, K. G. *Chem. Commun.* **2003**, 358–359.
104. Lersch, M.; Tilset, M. *Chem. Rev.* **2005**, *105*, 2471–2526.
105. Herrmann, W. A. *Angew. Chem., Int. Ed.* **2002**, *41*, 1290–1309.
106. Peris, E.; Crabtree, R. H. *Coord. Chem. Rev.* **2004**, *248*, 2239–2246.
107. Cesar, V.; Bellemin-Laponnaz, S.; Gade, L. H. *Chem. Soc. Rev.* **2004**, *33*, 619–636.
108. Crabtree, R. H. *Pure Appl. Chem.* **2003**, *75*, 435–443.
109. Herrmann, W. A.; Kocher, C. *Angew. Chem., Int. Ed. Engl.* **1997**, *36*, 2162–2187.
110. Canac, Y.; Soleilhavoup, M.; Conejero, S.; Bertrand, G. *J. Organomet. Chem.* **2004**, *689*, 3857–3865.
111. Bourissou, D.; Guerret, O.; Gabbaie, F. P.; Bertrand, G. *Chem. Rev.* **2000**, *100*, 39–91.
112. Perry, M. C.; Burgess, K. *Tetrahedron: Asymmetry* **2003**, *14*, 951–961.
113. Chianese, A. R.; Crabtree, R. H. *ACS Symp. Series* **2004**, *885*, 169–183.
114. Crudden, C. M.; Allen, D. P. *Coord. Chem. Rev.* **2004**, *248*, 2247–2273.
115. Grubbs, R. H.; Trnka, T. M.; Sanford, M. S. *Curr. Meth. Inorg. Chem.* **2003**, *3*, 187–231.
116. Kirmse, W. *Angew. Chem., Int. Ed.* **2004**, *43*, 1767–1769.
117. Yong, B. S.; Nolan, S. P. *Chemtracts* **2003**, *16*, 205–227.
118. Zinn, F. K.; Viciu, M. S.; Nolan, S. P. *Annu. Rep. Prog. Chem. B* **2004**, *100*, 231–249.
119. Jafarpour, L.; Nolan, S. P. *Adv. Organomet. Chem.* **2000**, *46*, 181–222.
120. Kissling, R. M.; Viciu, M. S.; Grasa, G. A.; Germaneau, R. F.; Gueveli, T.; Pasareanu, M.-C.; Navarro-Fernandez, O.; Nolan, S. P. *ACS Symp. Ser.* **2003**, *856*, 323–341.
121. Lin, I. J. B.; Vasam, C. S. *Comments Inorg. Chem.* **2004**, *25*, 75–129.
122. Arduengo, A. J., III. *Acc. Chem. Res.* **1999**, *32*, 913–921.
123. Herrmann, W. A.; Weskamp, T.; Bohm, V. P. W. *Adv. Organomet. Chem.* **2001**, *48*, 1–69.
124. Weskamp, T.; Bohm, V. P. W.; Herrmann, W. A. *J. Organomet. Chem.* **2000**, *600*, 12–22.
125. Regitz, M. *Angew. Chem., Int. Ed. Engl.* **1996**, *35*, 725–728.
126. Baba, E.; Cundari, T. R.; Firkin, I. *Inorg. Chim. Acta* **2005**, *358*, 2867–2875.
127. Scott, N. M.; Nolan, S. P. *Eur. J. Inorg. Chem.* **2005**, 1815–1828.
128. Viciu, M. S.; Nolan, S. P. *Top. Organomet. Chem.* **2005**, *14*, 241–278.
129. Arnold, P. L. *Heteroat. Chem.* **2002**, *13*, 534–539.
130. Cavell, R. G.; Kamalesh Babu, R. P.; Aparna, K. *J. Organomet. Chem.* **2001**, *617–618*, 158–169.
131. Huang, J.; Schanz, H.-J.; Stevens, E. D.; Nolan, S. P. *Organometallics* **1999**, *18*, 2370–2375.
132. Dorta, R.; Stevens, E. D.; Scott, N. M.; Costabile, C.; Cavallo, L.; Hoff, C. D.; Nolan, S. P. *J. Am. Chem. Soc.* **2005**, *127*, 2485–2495.

133. Lee, M.-T.; Hu, C.-H. *Organometallics* **2004**, *23*, 976–983.
134. Tafipolsky, M.; Scherer, W.; Oefele, K.; Artus, G.; Pedersen, B.; Herrmann, W. A.; McGrady, G. S. *J. Am. Chem. Soc.* **2002**, *124*, 5865–5880.
135. Boehme, C.; Frenking, G. *J. Am. Chem. Soc.* **1996**, *118*, 2039–2046.
136. Hu, X.; Castro-Rodriguez, I.; Olsen, K.; Meyer, K. *Organometallics* **2004**, *23*, 755–764.
137. Abernethy, C. D.; Codd, G. M.; Spicer, M. D.; Taylor, M. K. *J. Am. Chem. Soc.* **2003**, *125*, 1128–1129.
138. Boehme, C.; Frenking, G. *Organometallics* **1998**, *17*, 5801–5809.
139. Deubel, D. V. *Organometallics* **2002**, *21*, 4303–4305.
140. Termaten, A. T.; Schakel, M.; Ehlers, A. W.; Lutz, M.; Spek, A. L.; Lammertsma, K. *Chem. Eur. J.* **2003**, *9*, 3577–3582.
141. Denk, M. K.; Rodezno, J. M.; Gupta, S.; Lough, A. J. *J. Organomet. Chem.* **2001**, *617–618*, 242–253.
142. Amyes, T. L.; Diver, S. T.; Richard, J. P.; Rivas, F. M.; Toth, K. *J. Am. Chem. Soc.* **2004**, *126*, 4366–4374.
143. Tolman, C. A. *J. Am. Chem. Soc.* **1970**, *92*, 2956–2965.
144. Tolman, C. A. *J. Am. Chem. Soc.* **1970**, *92*, 2953–2956.
145. Huang, J.; Grasa, G.; Nolan, S. P. *Org. Lett.* **1999**, *1*, 1307–1309.
146. Scholl, M.; Ding, S.; Lee, C. W.; Grubbs, R. H. *Org. Lett.* **1999**, *1*, 953–956.
147. Herrmann, W. A.; Weskamp, T. *Book of Abstracts*; American Chemical Society, Washington, D.C., USA, 217th ACS National Meeting, Anaheim, CA, USA, March 21–25 1999, INOR-022.
148. Furstner, A.; Ackermann, L.; Gabor, B.; Goddard, R.; Lehmann, C. W.; Mynott, R.; Stelzer, F.; Thiel, O. R. *Chem. Eur. J.* **2001**, *7*, 3236–3253.
149. Wanzlick, H. W.; Schoenherr, H. J. *Angew. Chem., Int. Ed. Engl.* **1968**, *7*, 141–142.
150. Öfele, K. *J. Organomet. Chem.* **1968**, *12*, P42–P43.
151. Wang, H. M. J.; Lin, I. J. B. *Organometallics* **1998**, *17*, 972–975.
152. Hu, X.; Castro-Rodriguez, I.; Meyer, K. *J. Am. Chem. Soc.* **2003**, *125*, 12237–12245.
153. Hu, X.; Tang, Y.; Gantzel, P.; Meyer, K. *Organometallics* **2003**, *22*, 612–614.
154. Hu, X.; Castro-Rodriguez, I.; Meyer, K. *J. Am. Chem. Soc.* **2004**, *126*, 13464–13473.
155. Hu, X.; Meyer, K. *J. Am. Chem. Soc.* **2004**, *126*, 16322–16323.
156. Morassi, R.; Sacconi, L. *Inorg. Synth.* **1976**, *16*, 174–180.
157. Stoppioni, P.; Mani, F.; Sacconi, L. *Inorg. Chim. Acta* **1974**, *11*, 227–230.
158. Sacconi, L.; Di Vaira, M. *Inorg. Chem.* **1978**, *17*, 810–815.
159. Di Vaira, M.; Ghilardi, C. A.; Sacconi, L. *Inorg. Chem.* **1976**, *15*, 1555–1561.
160. Di Vaira, M.; Midollini, S.; Sacconi, L. *Inorg. Chem.* **1977**, *16*, 1518–1524.
161. Mani, F.; Sacconi, L. *Comments Inorg. Chem.* **1983**, *2*, 157–186.
162. Frankel, R.; Kniczek, J.; Ponikwar, W.; Noth, H.; Polborn, K.; Fehlhammer, W. P. *Inorg. Chim. Acta* **2001**, *312*, 23–39.
163. Kernbach, U.; Ramm, M.; Luger, P.; Fehlhammer, W. P. *Angew. Chem., Int. Ed. Engl.* **1996**, *35*, 310–312.
164. Frankel, R.; Birg, C.; Kernbach, U.; Habereder, T.; Noth, H.; Fehlhammer, W. P. *Angew. Chem., Int. Ed.* **2001**, *40*, 1907–1910.
165. Frankel, R.; Kernbach, U.; Bakola-Christianopoulou, M.; Plaia, U.; Suter, M.; Ponikwar, W.; Noth, H.; Moinet, C.; Fehlhammer, W. P. *J. Organomet. Chem.* **2001**, *617–618*, 530–545.
166. Nieto, I.; Cervantes-Lee, F.; Smith, J. M. *Chem. Commun.* **2005**, 3811–3813.
167. Bourissou, D.; Bertrand, G. *Adv. Organomet. Chem.* **1999**, *44*, 175–219.
168. Igau, A.; Grutzmacher, H.; Baceiredo, A.; Bertrand, G. *J. Am. Chem. Soc.* **1988**, *110*, 6463–6466.
169. Martin, D.; Illa, O.; Baceiredo, A.; Bertrand, G.; Ortuno, R. M.; Branchadell, V. *J. Org. Chem.* **2005**, *70*, 5671–5677.
170. Martin, D.; Baceiredo, A.; Gornitzka, H.; Schoeller, W. W.; Bertrand, G. *Angew. Chem., Int. Ed.* **2005**, *44*, 1700–1703.
171. Krysiak, J.; Lyon, C.; Baceiredo, A.; Gornitzka, H.; Mikolajczyk, M.; Bertrand, G. *Chem. Eur. J.* **2004**, *10*, 1982–1986.
172. Merceron-Saffon, N.; Gornitzka, H.; Baceiredo, A.; Bertrand, G. *J. Organomet. Chem.* **2004**, *689*, 1431–1435.
173. Despagnet-Ayoub, E.; Sole, S.; Gornitzka, H.; Rozhenko, A. B.; Schoeller, W. W.; Bourissou, D.; Bertrand, G. *J. Am. Chem. Soc.* **2003**, *125*, 124–130.
174. Despagnet, E.; Miqueu, K.; Gornitzka, H.; Dyer, P. W.; Bourissou, D.; Bertrand, G. *J. Am. Chem. Soc.* **2002**, *124*, 11834–11835.
175. Despagnet, E.; Gornitzka, H.; Rozhenko, A. B.; Schoeller, W. W.; Bourissou, D.; Bertrand, G. *Angew. Chem., Int. Ed.* **2002**, *41*, 2835–2837.
176. Merceron, N.; Miqueu, K.; Baceiredo, A.; Bertrand, G. *J. Am. Chem. Soc.* **2002**, *124*, 6806–6807.
177. Kato, T.; Gornitzka, H.; Baceiredo, A.; Savin, A.; Bertrand, G. *J. Am. Chem. Soc.* **2000**, *122*, 998–999.
178. Canac, Y.; Conejero, S.; Donnadieu, B.; Schoeller, W. W.; Bertrand, G. *J. Am. Chem. Soc.* **2005**, *127*, 7312–7313.
179. Lavallo, V.; Canac, Y.; Prasang, C.; Donnadieu, B.; Bertrand, G. *Angew. Chem., Int. Ed.* **2005**, *44*, 5705–5709.
180. Cattoeen, X.; Gornitzka, H.; Bourissou, D.; Bertrand, G. *J. Am. Chem. Soc.* **2004**, *126*, 1342–1343.
181. Lavallo, V.; Mafhouz, J.; Canac, Y.; Donnadieu, B.; Schoeller, W. W.; Bertrand, G. *J. Am. Chem. Soc.* **2004**, *126*, 8670–8671.
182. Solet, S.; Gornitzka, H.; Schoeller, W. W.; Bourissou, D.; Bertrand, G. *Science* **2001**, *292*, 1901–1903.
183. Calo, V.; Nacci, A.; Lopez, L.; Mannarini, N. *Tetrahedron Lett.* **2000**, *41*, 8973–8976.
184. Calo, V.; Del Sole, R.; Nacci, A.; Shingaro, E.; Scordari, F. *Eur. J. Org. Chem.* **2000**, 869–871.
185. Kernbach, U.; Lugger, T.; Hahn, F. E.; Fehlhammer, W. P. *J. Organomet. Chem.* **1997**, *541*, 51–55.
186. Tubaro, C.; Biffis, A.; Basato, M.; Benetollo, F.; Cavell, K. J.; Ooi, L.-L. *Organometallics* **2005**, *24*, 4153–4158.
187. Hernandez-Molina, R.; Mederos, A. Acyclic and macrocyclic Schiff base ligands. In *Comprehensive Coordination Chemistry II*; McCleverty, J. A., Meyer, T. J., Eds.; Elsevier: Oxford, 2004; Vol. 1, pp 411–446.
188. Curtis, N. F. N macrocyclic ligands. In *Comprehensive Coordination Chemistry II*; McCleverty, J. A., Meyer, T. J., Eds.; Elsevier: Oxford, 2004; Vol. 1, pp 447–474.
189. Levason, W.; Reid, G. Macrocyclic phosphine and arsine ligands. In *Comprehensive Coordination Chemistry II*; McCleverty, J. A., Meyer, T. J., Eds.; Elsevier: Oxford, 2004; Vol. 1, pp 475–484.
190. Roundhill, D. M. Calixarenes. In *Comprehensive Coordination Chemistry II*; McCleverty, J. A., Meyer, T. J., Eds.; Elsevier: Oxford, 2004; Vol. 1, pp 485–491.
191. Smith, K. M. Porphyrins. In *Comprehensive Coordination Chemistry II*; McCleverty, J. A., Meyer, T. J., Eds.; Elsevier: Oxford, 2004; Vol. 1, pp 493–506.
192. McKeown, N. B. Phthalocyanines. In *Comprehensive Coordination Chemistry II*; McCleverty, J. A., Meyer, T. J., Eds.; Elsevier: Oxford, 2004; Vol. 1, pp 507–514.
193. Vedernikov, A. N.; Caulton, K. G. *Org. Lett.* **2003**, *5*, 2591–2594.

194. Vedernikov, A. N.; Huffman, J. C.; Caulton, K. G. *New J. Chem.* **2003**, *27*, 665–667.
195. Vedernikov, A. N.; Pink, M.; Caulton, K. G. *J. Org. Chem.* **2003**, *68*, 4806–4814.
196. Vedernikov, A. N.; Pink, M.; Caulton, K. G. *Inorg. Chem.* **2004**, *43*, 4300–4305.
197. Vedernikov, A. N.; Pink, M.; Caulton, K. G. *Inorg. Chem.* **2004**, *43*, 3642–3646.
198. Vedernikov, A. N.; Caulton, K. G. *Chem. Commun.* **2004**, 162–163.
199. Bauer, I.; Habicher, W. D.; Antipin, I. S.; Sinyashin, O. G. *Russ. Chem. Bull.* **2004**, *53*, 1402–1416.
200. Bauer, I.; Habicher, W. D. *Phosphorus, Sulfur Silicon Relat. Elem.* **1997**, *130*, 89–105.
201. Weber, L. *Coord. Chem. Rev.* **1997**, *158*, 1–67.
202. Caminade, A.-M.; Majoral, J. P. *Chem. Rev.* **1994**, *94*, 1183–1213.
203. Belen′kii, L. I.; Kruchkovskaya, N. D.; Gramenitskaya, V. N. *Adv. Heterocycl. Chem.* **1999**, *73*, 295–395.
204. Fryzuk, M. D.; Love, J. B.; Rettig, S. J. *Chem. Commun.* **1996**, 2783–2784.
205. Fryzuk, M. D.; Kozak, C. M.; Bowdridge, M. R.; Patrick, B. O. *Organometallics* **2002**, *21*, 5047–5054.
206. Fryzuk, M. D.; Kozak, C. M.; Bowdridge, M. R.; Jin, W.; Tung, D.; Patrick, B. O.; Rettig, S. J. *Organometallics* **2001**, *20*, 3752–3761.
207. Fryzuk, M. D.; Johnson, S. A.; Rettig, S. J. *Organometallics* **2000**, *19*, 3931–3941.
208. Fryzuk, M. D.; Johnson, S. A.; Rettig, S. J. *Organometallics* **1999**, *18*, 4059–4067.
209. Fryzuk, M. D.; Love, J. B.; Rettig, S. J. *Organometallics* **1998**, *17*, 846–853.
210. Fryzuk, M. D.; Giesbrecht, G. R.; Rettig, S. J.; Yap, G. P. A. *J. Organomet. Chem.* **1999**, *591*, 63–70.
211. Fryzuk, M. D.; Kozak, C. M.; Patrick, B. O. *Inorg. Chim. Acta* **2003**, *345*, 53–62.
212. Fryzuk, M. D.; Corkin, J. R.; Patrick, B. O. *Can. J. Chem.* **2003**, *81*, 1376–1387.
213. Fryzuk, M. D.; Kozak, C. M.; Mehrkhodavandi, P.; Morello, L.; Patrick, B. O.; Rettig, S. J. *J. Am. Chem. Soc.* **2002**, *124*, 516–517.
214. Fryzuk, M. D.; Johnson, S. A.; Rettig, S. J. *J. Am. Chem. Soc.* **2001**, *123*, 1602–1612.
215. Fryzuk, M. D.; Kozak, C. M.; Bowdridge, M. R.; Patrick, B. O.; Rettig, S. J. *J. Am. Chem. Soc.* **2002**, *124*, 8389–8397.
216. Carmichael, C. D.; Fryzuk, M. D. *Dalton Trans.* **2005**, 452–459.
217. Moore, D. A.; Fanwick, P. E.; Welch, M. J. *Inorg. Chem.* **1989**, *28*, 1504–1506.
218. Auerbach, U.; Eckert, U.; Wieghardt, K.; Nuber, B.; Weiss, J. *Inorg. Chem.* **1990**, *29*, 938–944.
219. Auerbach, U.; Weyhermueller, T.; Wieghardt, K.; Nuber, B.; Bill, E.; Butzlaff, C.; Trautwein, A. X. *Inorg. Chem.* **1993**, *32*, 508–519.
220. Auerbach, U.; Stockheim, C.; Weyhermueller, T.; Wieghardt, K.; Nuber, B. *Angew. Chem., Int. Ed. Engl.* **1993**, *32*, 714–716.
221. Beissel, T.; Glaser, T.; Kesting, F.; Wieghardt, K.; Nuber, B. *Inorg. Chem.* **1996**, *35*, 3936–3947.
222. Sokolowski, A.; Bothe, E.; Bill, E.; Weyhermueller, T.; Wieghardt, K. *Chem. Commun.* **1996**, 1671–1672.
223. Sokolowski, A.; Leutbecher, H.; Weyhermuller, T.; Schnepf, R.; Bothe, E.; Bill, E.; Hildebrandt, P.; Wieghardt, K. *J. Biol. Inorg. Chem.* **1997**, *2*, 444–453.
224. Trautwein, A. X.; Wieghardt, K.; Mochizuki, K.; Kesting, F.; Weyhermuller, T.; Butzlaff, C.; Paulsen, H.; Ding, X.-Q.; Grodzicki, M.; Hartung, R. In *Bioinorganic Chemistry*; Trautwein, A. X., Ed.; Wiley: New york, 1997; pp 741–759.
225. Adam, B.; Bill, E.; Bothe, E.; Goerdt, B.; Haselhorst, G.; Hildenbrand, K.; Sokolowski, A.; Steenken, S.; Weyhermueller, T.; Wieghardt, K. *Chem. Eur. J.* **1997**, *3*, 308–319.
226. Sokolowski, A.; Mueller, J.; Weyhermueller, T.; Schnepf, R.; Hildebrandt, P.; Hildenbrand, K.; Bothe, E.; Wieghardt, K. *J. Am. Chem. Soc.* **1997**, *119*, 8889–8900.
227. Schnepf, R.; Sokolowski, A.; Mueller, J.; Bachler, V.; Wieghardt, K.; Hildebrandt, P. *J. Am. Chem. Soc.* **1998**, *120*, 2352–2364.
228. Burdinski, D.; Wieghardt, K.; Steenken, S. *J. Am. Chem. Soc.* **1999**, *121*, 10781–10787.
229. Snodin, M. D.; Ould-Moussa, L.; Wallmann, U.; Lecomte, S.; Bachler, V.; Bill, E.; Hummel, H.; Weyhermuller, T.; Hildebrandt, P.; Wieghardt, K. *Chem. Eur. J.* **1999**, *5*, 2554–2565.
230. Burdinski, D.; Bothe, E.; Wieghardt, K. *Inorg. Chem.* **2000**, *39*, 105–116.
231. Beissel, T.; Buerger, K. S.; Voigt, G.; Wieghardt, K.; Butzlaff, C.; Trautwein, A. X. *Inorg. Chem.* **1993**, *32*, 124–126.
232. Glaser, T.; Beissel, T.; Bill, E.; Weyhermueller, T.; Schuenemann, V.; Meyer-Klaucke, W.; Trautwein, A. X.; Wieghardt, K. *J. Am. Chem. Soc.* **1999**, *121*, 2193–2208.
233. Krebs, C.; Glaser, T.; Bill, E.; Weyhermuller, T.; Meyer-Klaucke, W.; Wieghardt, K. *Angew. Chem., Int. Ed.* **1999**, *38*, 359–361.
234. Glaser, T.; Kesting, F.; Beissel, T.; Bill, E.; Weyhermueller, T.; Meyer-Klaucke, W.; Wieghardt, K. *Inorg. Chem.* **1999**, *38*, 722–732.
235. Glaser, T.; Bill, E.; Weyhermueller, T.; Meyer-Klaucke, W.; Wieghardt, K. *Inorg. Chem.* **1999**, *38*, 2632–2642.
236. Albela, B.; Bothe, E.; Brosch, O.; Mochizuki, K.; Weyhermueller, T.; Wieghardt, K. *Inorg. Chem.* **1999**, *38*, 5131–5138.
237. Albela, B.; Bill, E.; Brosch, O.; Weyhermuller, T.; Wieghardt, K. *Eur. J. Inorg. Chem.* **2000**, 139–146.
238. Chibotaru, L. F.; Girerd, J.-J.; Blondin, G.; Glaser, T.; Wieghardt, K. *J. Am. Chem. Soc.* **2003**, *125*, 12615–12630.
239. Mochizuki, K.; Kesting, F.; Weyhermueller, T.; Wieghardt, K.; Butzlaff, C.; Trautwein, A. X. *J. Chem. Soc., Chem. Commun.* **1994**, 909–911.
240. Castro-Rodriguez, I.; Nakai, H.; Gantzel, P.; Zakharov, L. N.; Rheingold, A. L.; Meyer, K. *J. Am. Chem. Soc.* **2003**, *125*, 15734–15735.
241. Johnson, A. W.; Kay, I. T. *J. Chem. Soc.* **1965**, 1620–1629.
242. Gross, Z.; Galili, N.; Saltsman, I. *Angew. Chem., Int. Ed.* **1999**, *38*, 1427–1429.
243. Gross, Z.; Galili, N.; Simkhovich, L.; Saltsman, I.; Botoshansky, M.; Blaeser, D.; Boese, R.; Goldberg, I. *Org. Lett.* **1999**, *1*, 599–602.
244. Paolesse, R.; Sagone, F.; Macagnano, A.; Boschi, T.; Prodi, L.; Montalti, M.; Zaccheroni, N.; Bolletta, F.; Smith, K. M. *J. Porphyrins Phthalocyanines* **1999**, *3*, 364–370.
245. Gryko, D. T. *Eur. J. Org. Chem.* **2002**, 1735–1743.
246. Golubkov, G.; Gross, Z. *Angew. Chem., Int. Ed.* **2003**, *42*, 4507–4510.
247. Eikey, R. A.; Khan, S. I.; Abu-Omar, M. M. *Angew. Chem., Int. Ed.* **2002**, *41*, 3592–3595.
248. Gross, Z.; Golubkov, G.; Simkhovich, L. *Angew. Chem., Int. Ed.* **2000**, *39*, 4045–4047.
249. Simkhovich, L.; Gross, Z. *Tetrahedron Lett.* **2001**, *42*, 8089–8092.
250. Brothers, P. J. *Adv. Organomet. Chem.* **2000**, *46*, 223–321.
251. Brothers, P. J. *Adv. Organomet. Chem.* **2001**, *48*, 289–342.
252. Barbe, J.-M.; Stern, C.; Pacholska, E.; Espinosa, E.; Guilard, R. *J. Porphyrins Phthalocyanines* **2004**, *8*, 301–312.
253. Guilard, R.; Barbe, J.-M.; Stern, C.; Kadish, K. M. New Developments in Corrole Chemistry: Special Emphasis on Face-to-Face Bismacrocycles. In *Porphyrin Handbook*; Kadish, K. M., Smith, K. M., Guilard, R., Eds.; Academic Press: New York, 2003; Vol. 18, Chapter 116, pp 303–349.
254. Zhang, X.-X.; Wayland, B. B. *J. Am. Chem. Soc.* **1994**, *116*, 7897–7898.
255. Collman, J. P.; Denisevich, P.; Konai, Y.; Marrocco, M.; Koval, C.; Anson, F. C. *J. Am. Chem. Soc.* **1980**, *102*, 6027–6036.

256. Collman, J. P.; Marrocco, M.; Denisevich, P.; Koval, C.; Anson, F. C. *J. Electroanal. Chem.* **1979**, *101*, 117–122.
257. Collman, J. P.; Hutchison, J. E.; Lopez, M. A.; Guilard, R.; Reed, R. A. *J. Am. Chem. Soc.* **1991**, *113*, 2794–2796.
258. Collman, J. P.; Elliott, C. M.; Halbert, T. R.; Tovrog, B. S. *Proc. Nat. Acad. Sci.* **1977**, *74*, 18–22.
259. Kagan, N. E.; Mauzerall, D.; Merrifield, R. B. *J. Am. Chem. Soc.* **1977**, *99*, 5484–5486.
260. Chang, C. K.; Kuo, M.-S.; Wang, C.-B. *J. Heterocycl. Chem.* **1977**, *14*, 943–945.
261. Ogoshi, H.; Sugimoto, H.; Yoshida, Z. *Tetrahedron Lett.* **1977**, 169–172.
262. Collman, J. P.; Wagenknecht, P. S.; Hutchison, J. E. *Angew. Chem., Int. Ed. Engl.* **1994**, *33*, 1537–1554.
263. Chang, C. J.; Deng, Y.; Heyduk, A. F.; Chang, C. K.; Nocera, D. G. *Inorg. Chem.* **2000**, *39*, 959–966.
264. Chang, C. J.; Deng, Y.; Peng, S.-M.; Lee, G.-H.; Yeh, C.-Y.; Nocera, D. G. *Inorg. Chem.* **2002**, *41*, 3008–3016.
265. Chang, C. J.; Baker, E. A.; Pistorio, B. J.; Deng, Y.; Loh, Z.-H.; Miller, S. E.; Carpenter, S. D.; Nocera, D. G. *Inorg. Chem.* **2002**, *41*, 3102–3109.
266. Chang, C. J.; Yeh, C.-Y.; Nocera, D. G. *J. Org. Chem.* **2002**, *67*, 1403–1406.
267. Chng, L. L.; Chang, C. J.; Nocera, D. G. *J. Org. Chem.* **2003**, *68*, 4075–4078.
268. Deng, Y.; Chang, C. J.; Nocera, D. G. *J. Am. Chem. Soc.* **2000**, *122*, 410–411.
269. Fletcher, J. T.; Therien, M. J. *J. Am. Chem. Soc.* **2002**, *124*, 4298–4311.
270. Fletcher, J. T.; Therien, M. J. *J. Am. Chem. Soc.* **2000**, *122*, 12393–12394.
271. Jokic, D.; Asfari, Z.; Weiss, J. *Org. Lett.* **2002**, *4*, 2129–2132.
272. Jokic, D.; Boudon, C.; Pognon, G.; Bonin, M.; Schenk, K. J.; Gross, M.; Weiss, J. *Chem. Eur. J.* **2005**, *11*, 4199–4209.
273. Dudic, M.; Lhotak, P.; Petrickova, H.; Stibor, I.; Lang, K.; Sykora, J. *Tetrahedron* **2003**, *59*, 2409–2415.
274. Zhang, X. X.; Parks, G. F.; Wayland, B. B. *J. Am. Chem. Soc.* **1997**, *119*, 7938–7944.
275. Cui, W. H.; Zhang, X. P.; Wayland, B. B. *J. Am. Chem. Soc.* **2003**, *125*, 4994–4995.
276. Cui, W. H.; Wayland, B. B. *J. Am. Chem. Soc.* **2004**, *126*, 8266–8274.
277. Zhang, X. X.; Wayland, B. B. *Inorg. Chem.* **2000**, *39*, 5318–5325.
278. Cui, W.; Wayland, B. B. *J. Porphyrins Phthalocyanines* **2004**, *8*, 103–110.
279. Jerome, F.; Gros, C. P.; Tardieux, C.; Barbe, J.-M.; Guilard, R. *Chem. Commun.* **1998**, 2007–2008.
280. Pacholska, E.; Espinosa, E.; Guilard, R. *Dalton Trans.* **2004**, 3181–3183.
281. Jerome, F.; Barbe, J.-M.; Gros, C. P.; Guilard, R.; Fischer, J.; Weiss, R. *New J. Chem.* **2001**, *25*, 93–101.
282. Guilard, R.; Jerome, F.; Barbe, J.-M.; Gros, C. P.; Ou, Z.; Shao, J.; Fischer, J.; Weiss, R.; Kadish, K. M. *Inorg. Chem.* **2001**, *40*, 4856–4865.
283. Kadish, K. M.; Ou, Z.; Shao, J.; Gros, C. P.; Barbe, J.-M.; Jerome, F.; Bolze, F.; Burdet, F.; Guilard, R. *Inorg. Chem.* **2002**, *41*, 3990–4005.
284. Guilard, R.; Gros, C. P.; Barbe, J.-M.; Espinosa, E.; Jerome, F.; Tabard, A.; Latour, J.-M.; Shao, J.; Ou, Z.; Kadish, K. M. *Inorg. Chem.* **2004**, *43*, 7441–7455.
285. Kadish, K. M.; Fremond, L.; Ou, Z.; Shao, J.; Shi, C.; Anson, F. C.; Burdet, F.; Gros, C. P.; Barbe, J.-M.; Guilard, R. *J. Am. Chem. Soc.* **2005**, *127*, 5625–5631.
286. Jerome, F.; Gros, C. P.; Tardieux, C.; Barbe, J.-M.; Guilard, R. *New J. Chem.* **1998**, *22*, 1327–1329.
287. Guilard, R.; Jerome, F.; Gros, C. P.; Barbe, J.-M.; Ou, Z.; Shao, J.; Kadish, K. M. *C. R. Acad. Sci.* **2001**, *4*, 245–254.
288. Strauss, S. H. *Chem. Rev.* **1993**, *93*, 927–942.
289. Krossing, I.; Raabe, I. *Angew. Chem., Int. Ed.* **2004**, *43*, 2066–2090.
290. Bochmann, M.; Lancaster, S.; Hannant, M.; Rodriguez, A.; Schormann, M.; Walker, D.; Woodman, T. *Pure Appl. Chem.* **2003**, *75*, 1183–1195.
291. Brintzinger, H. H.; Fischer, D.; Muelhaupt, R.; Rieger, B.; Waymouth, R. M. *Angew. Chem., Int. Ed. Engl.* **1995**, *34*, 1143–1170.
292. Chen, E. Y.-X.; Marks, T. J. *Chem. Rev.* **2000**, *100*, 1391–1434.
293. Piers, W. E. *Adv. Organomet. Chem.* **2005**, *52*, 1–76.
294. Massey, A. G.; Park, A. J. *J. Organomet. Chem.* **1964**, *2*, 245–250.
295. Yang, X.; Stern, C. L.; Marks, T. J. *J. Am. Chem. Soc.* **1991**, *113*, 3623–3625.
296. Elder, M. J.; Ewen, J. A. CA2027145, April 11, 1991.
297. Deck, P. A.; Beswick, C. L.; Marks, T. J. *J. Am. Chem. Soc.* **1998**, *120*, 1772–1784.
298. Wick, D. D.; Goldberg, K. I. *J. Am. Chem. Soc.* **1997**, *119*, 10235–10236.
299. Hill, G. S.; Manojlovic-Muir, L.; Muir, K. W.; Puddephatt, R. J. *Organometallics* **1997**, *16*, 525–530.
300. Hill, G. S.; Rendina, L. M.; Puddephatt, R. J. *J. Chem. Soc., Dalton Trans.* **1996**, 1809–1813.
301. Danopoulos, A. A.; Galsworthy, J. R.; Green, M. L. H.; Doerrer, L. H.; Cafferkey, S.; Hursthouse, M. B. *Chem. Commun.* **1998**, 2529–2530.
302. Doerrer, L. H.; Green, M. L. H. *J. Chem. Soc., Dalton Trans.* **1999**, 4325–4329.
303. Bergquist, C.; Bridgewater, B. M.; Harlan, C. J.; Norton, J. R.; Friesner, R. A.; Parkin, G. *J. Am. Chem. Soc.* **2000**, *122*, 10581–10590.
304. Beringhelli, T.; Maggioni, D.; D'Alfonso, G. *Organometallics* **2001**, *20*, 4927–4938.
305. Bavarian, N.; Baird, M. C. *Dalton Trans.* **2004**, 4089–4091.
306. Pellecchia, C.; Proto, A.; Longo, P.; Zambelli, A. *Makromol. Chem.-Rap. Comm.* **1991**, *12*, 663–667.
307. Turner, H. W.; Hlatky, G. G. WO9112285, August 22, 1991.
308. Hlatky, G. G.; Upton, D. J.; Turner, H. W. WO9109882, July 11, 1991.
309. Hlatky, G. G.; Turner, H. W. WO9102012, February 21, 1991.
310. Hlatky, G. G.; Turner, H. W. WO9114713, October 3, 1991.
311. Canich, J. M.; Hlatky, G. G.; Turner, H. W. WO9200333, January 9, 1992.
312. Jutzi, P.; Mueller, C.; Stammler, A.; Stammler, H.-G. *Organometallics* **2000**, *19*, 1442–1444.
313. Kobayashi, H.; Sonoda, T.; Iwamoto, H.; Yoshimura, M. *Chem. Lett.* **1981**, 579–580.
314. Yakelis, N. A.; Bergman, R. G. *Organometallics* **2005**, *24*, 3579–3581.
315. Brookhart, M.; Grant, B.; Volpe, A. F., Jr. *Organometallics* **1992**, *11*, 3920–3922.
316. Golden, J. H.; Mutolo, P. F.; Lobkovsky, E. B.; DiSalvo, F. J. *Inorg. Chem.* **1994**, *33*, 5374–5375.
317. Fujiki, K.; Ikeda, S.-Y.; Kobayashi, H.; Mori, A.; Nagira, A.; Nie, J.; Sonoda, T.; Yagupolskii, Y. *Chem. Lett.* **2000**, 62–63.
318. Nishida, H.; Takada, N.; Yoshimura, M.; Sonoda, T.; Kobayashi, H. *Bull. Chem. Soc. Jpn.* **1984**, *57*, 2600–2604.
319. Buschmann, W. E.; Miller, J. S. *Chem. Eur. J.* **1998**, *4*, 1731–1737.
320. Hayashi, Y.; Rohde, J. J.; Corey, E. J. *J. Am. Chem. Soc.* **1996**, *118*, 5502–5503.
321. Hughes, R. P.; Lindner, D. C.; Rheingold, A. L.; Yap, G. P. A. *Inorg. Chem.* **1997**, *36*, 1726–1727.
322. Reed, C. A. *Acc. Chem. Res.* **1998**, *31*, 133–139.
323. Kato, T.; Reed, C. A. *Angew. Chem., Int. Ed.* **2004**, *43*, 2908–2911.

324. Ivanov, S. V.; Rockwell, J. J.; Polyakov, O. G.; Gaudinski, C. M.; Anderson, O. P.; Solntsev, K. A.; Strauss, S. H. *J. Am. Chem. Soc.* **1998**, *120*, 4224–4225.
325. Reed, C. A. *Chem. Commun.* **2005**, 1669–1677.
326. Knoth, W. H., Jr. *J. Am. Chem. Soc.* **1967**, *89*, 1274–1275.
327. Shelly, K.; Reed, C. A.; Lee, Y. J.; Scheidt, W. R. *J. Am. Chem. Soc.* **1986**, *108*, 3117–3118.
328. Tsang, C.-W.; Yang, Q.; Sze, E. T.-P.; Mak, T. C. W.; Chan, D. T. W.; Xie, Z. *Inorg. Chem.* **2000**, *39*, 5851–5858.
329. Tsang, C.-W.; Xie, Z. *Chem. Commun.* **2000**, 1839–1840.
330. Xie, Z.; Tsang, C.-W.; Sze, E. T.-P.; Yang, Q.; Chan, D. T. W.; Mak, T. C. W. *Inorg. Chem.* **1998**, *37*, 6444–6451.
331. King, B. T.; Michl, J. *J. Am. Chem. Soc.* **2000**, *122*, 10255–10256.
332. King, B. T.; Janousek, Z.; Gruener, B.; Trammell, M.; Noll, B. C.; Michl, J. *J. Am. Chem. Soc.* **1996**, *118*, 3313–3314.
333. Stasko, D.; Reed, C. A. *J. Am. Chem. Soc.* **2002**, *124*, 1148–1149.
334. Xie, Z.; Manning, J.; Reed, R. W.; Mathur, R.; Boyd, P. D. W.; Benesi, A.; Reed, C. A. *J. Am. Chem. Soc.* **1996**, *118*, 2922–2928.
335. Reed, C. A.; Xie, Z.; Bau, R.; Benesi, A. *Science* **1993**, *262*, 402–404.
336. Xie, Z.; Jelinek, T.; Bau, R.; Reed, C. A. *J. Am. Chem. Soc.* **1994**, *116*, 1907–1913.
337. Jelinek, T.; Baldwin, P.; Scheidt, W. R.; Reed, C. A. *Inorg. Chem.* **1993**, *32*, 1982–1990.
338. Sun, Y.; Metz, M. V.; Stern, C. L.; Marks, T. J. *Organometallics* **2000**, *19*, 1625–1627.
339. Ivanova, S. M.; Nolan, B. G.; Kobayashi, Y.; Miller, S. M.; Anderson, O. P.; Strauss, S. H. *Chem. Eur. J.* **2001**, *7*, 503–510.
340. Krossing, I. *Chem. Eur. J.* **2001**, *7*, 490–502.
341. Barbarich, T. J.; Handy, S. T.; Miller, S. M.; Anderson, O. P.; Grieco, P. A.; Strauss, S. H. *Organometallics* **1996**, *15*, 3776–3778.
342. Barbarich, T. J.; Miller, S. M.; Anderson, O. P.; Strauss, S. H. *J. Mol. Catal. A: Chem.* **1998**, *128*, 289–331.
343. Krossing, I.; Brands, H.; Feuerhake, R.; Koenig, S. *J. Fluorine Chem.* **2001**, *112*, 83–90.
344. Krossing, I.; Raabe, I. *Chem. Eur. J.* **2004**, *10*, 5017–5030.
345. Bihlmeier, A.; Gonsior, M.; Raabe, I.; Trapp, N.; Krossing, I. *Chem. Eur. J.* **2004**, *10*, 5041–5051.
346. Barbarich, T. J. Fluoroalkoxide Aluminates as Weakly Coordinating Anions: Significant O–H···F–C Hydrogen Bonding. Ph.D. Thesis, Colorado State University, Fort Collins, Colorado, USA, 1998.
347. Krossing, I.; Reisinger, A. *Eur. J. Inorg. Chem.* **2005**, 1979–1989.
348. Crabtree, R. H. *Angew. Chem., Int. Ed. Engl.* **1993**, *32*, 789–805.
349. Kubas, G. J. *Metal Dihydrogen and s-Bond Complexes: Structure, Theory and Reactivity*; Kluwer: New York, 2001.
350. Kubas, G. J.; Ryan, R. R.; Swanson, B. I.; Vergamini, P. J.; Wasserman, H. J. *J. Am. Chem. Soc.* **1984**, *106*, 451–452.
351. Heinekey, D. M.; Oldham, W. J. *Chem. Rev.* **1993**, *93*, 913–926.
352. Kubas, G. J. *Acc. Chem. Res.* **1988**, *21*, 120–128.
353. Jessop, P. G.; Morris, R. H. *Coord. Chem. Rev.* **1992**, *121*, 155–284.
354. Crabtree, R. H. *Acc. Chem. Res.* **1990**, *23*, 95–101.
355. Esteruelas, M. A.; Oro, L. A. *Chem. Rev.* **1998**, *98*, 577–588.
356. Crabtree, R. H.; Siegbahn, P. E. M.; Eisenstein, O.; Rheingold, A. L.; Koetzle, T. F. *Acc. Chem. Res.* **1996**, *29*, 348–354.
357. Maseras, F.; Lledos, A.; Clot, E.; Eisenstein, O. *Chem. Rev.* **2000**, *100*, 601–636.
358. Hu, X.; Cossairt, B. M.; Brunschwig, B. S.; Lewis, N. S.; Peters, J. C. *Chem. Commun.* **2005**, 4723–4725.
359. Razavet, M.; Artero, V.; Fontecave, M. *Inorg. Chem.* **2005**, *44*, 4786–4795.
360. Koelle, U. *New J. Chem.* **1992**, *16*, 157–169.
361. Appel, A. M.; DuBois, D. L.; DuBois, M. R. *J. Am. Chem. Soc.* **2005**, *127*, 12717–12726.
362. Darensbourg, M. Y.; Lyon, E. J.; Zhao, X.; Georgakaki, I. P. *Proc. Nat. Acad. Sci.* **2003**, *100*, 3683–3688.
363. Rauchfuss, T. B. *Inorg. Chem.* **2004**, *43*, 14–26.
364. Evans, D. J.; Pickett, C. J. *Chem. Soc. Rev.* **2003**, *32*, 268–275.
365. Tard, C.; Liu, X. M.; Ibrahim, S. K.; Bruschi, M.; De Gioia, L.; Davies, S. C.; Yang, X.; Wang, L. S.; Sawers, G.; Pickett, C. J. *Nature* **2005**, *433*, 610–613.
366. Peters, J. W.; Lanzilotta, W. N.; Lemon, B. J.; Seefeldt, L. C. *Science* **1998**, *282*, 1853–1858.
367. Graham, W. A. G. *J. Organomet. Chem.* **1986**, *300*, 81–91.
368. Hoyano, J.; Elder, M.; Graham, W. A. G. *J. Am. Chem. Soc.* **1969**, *91*, 4568–4569.
369. Graham, W. A. G.; Bennett, M. J. *Chem. Eng. News* **1970**, *48*, 75.
370. Bennett, M. J.; Simpson, K. A. *J. Am. Chem. Soc.* **1971**, *93*, 7156–7160.
371. Andrews, M. A.; Kirtley, S. W.; Kaesz, H. D. *Adv. Chem. Ser.* **1978**, *167*, 215–231.
372. Lin, Z. *Chem. Soc. Rev.* **2002**, *31*, 239–245.
373. Nikonov, G. I. *J. Organomet. Chem.* **2001**, *635*, 24–36.
374. Nikonov, G. I. *Angew. Chem., Int. Ed.* **2001**, *40*, 3353–3355.
375. Corey, J. Y.; Braddock-Wilking, J. *Chem. Rev.* **1999**, *99*, 175–292.
376. Schubert, U. *Adv. Organomet. Chem.* **1990**, *30*, 151–187.
377. Vincent, J. L.; Luo, S.; Scott, B. L.; Butcher, R.; Unkefer, C. J.; Burns, C. J.; Kubas, G. J.; Lledos, A.; Maseras, F.; Tomas, J. *Organometallics* **2003**, *22*, 5307–5323.
378. Schneider, J. J. *Angew. Chem., Int. Ed. Engl.* **1996**, *35*, 1068–1076.
379. Crabtree, R. H. *J. Chem. Soc., Dalton Trans.* **2001**, 2437–2450.
380. Crabtree, R. H. *J. Organomet. Chem.* **2004**, *689*, 4083–4091.
381. Hall, C.; Perutz, R. N. *Chem. Rev.* **1996**, *96*, 3125–3146.
382. Graham, M. A.; Perutz, R. N.; Poliakoff, M.; Turner, J. J. *J. Organomet. Chem.* **1972**, *34*, C34–C36.
383. Poliakoff, M.; Turner, J. J. *J. Chem. Soc., Dalton Trans.* **1974**, 2276–2285.
384. Perutz, R. N.; Turner, J. J. *J. Am. Chem. Soc.* **1975**, *97*, 4791–4800.
385. Sun, X.-Z.; Grills, D. C.; Nikiforov, S. M.; Poliakoff, M.; George, M. W. *J. Am. Chem. Soc.* **1997**, *119*, 7521–7525.
386. Evans, D. R.; Drovetskaya, T.; Bau, R.; Reed, C. A.; Boyd, P. D. W. *J. Am. Chem. Soc.* **1997**, *119*, 3633–3634.
387. Brookhart, M.; Green, M. L. H.; Wong, L. L. *Prog. Inorg. Chem.* **1988**, *36*, 1–124.
388. Brookhart, M.; Green, M. L. H. *J. Organomet. Chem.* **1983**, *250*, 395–408.
389. Scherer, W.; McGrady, G. S. *Angew. Chem., Int. Ed.* **2004**, *43*, 1782–1806.

390. Clot, E.; Eisenstein, O. *Struct. Bond.* **2004**, *113*, 1–36.
391. Mashima, K.; Nakamura, A. *J. Organomet. Chem.* **1992**, *428*, 49–58.
392. Grubbs, R. H.; Coates, G. W. *Acc. Chem. Res.* **1996**, *29*, 85–93.
393. Baratta, W.; Stoccoro, S.; Doppiu, A.; Herdtweck, E.; Zucca, A.; Rigo, P. *Angew. Chem., Int. Ed.* **2003**, *42*, 105–109.
394. Huang, D.; Streib, W. E.; Bollinger, J. C.; Caulton, K. G.; Winter, R. F.; Scheiring, T. *J. Am. Chem. Soc.* **1999**, *121*, 8087–8097.
395. Crabtree, R. H. *The Organometallic Chemistry of the Transition Elements*, 3rd ed.; Wiley: New York, 2001.
396. Kiplinger, J. L.; Richmond, T. G.; Osterberg, C. E. *Chem. Rev.* **1994**, *94*, 373–431.
397. Kulawiec, R. J.; Crabtree, R. H. *Coord. Chem. Rev.* **1990**, *99*, 89–115.
398. Plenio, H. *ChemBioChem* **2004**, *5*, 650–655.
399. Plenio, H. *Chem. Rev.* **1997**, *97*, 3363–3384.
400. Wu, F.; Dash, A. K.; Jordan, R. F. *J. Am. Chem. Soc.* **2004**, *126*, 15360–15361.
401. Bouwkamp, M. W.; de Wolf, J.; Morales, I. d. H.; Gercama, J.; Meetsma, A.; Troyanov, S. I.; Hessen, B.; Teuben, J. H. *J. Am. Chem. Soc.* **2002**, *124*, 12956–12957.
402. Arndtsen, B. A.; Bergman, R. G. *Science* **1995**, *270*, 1970–1973.
403. Butts, M. D.; Scott, B. L.; Kubas, G. J. *J. Am. Chem. Soc.* **1996**, *118*, 11831–11843.
404. Schrock, R. R.; Osborn, J. A. *J. Am. Chem. Soc.* **1971**, *93*, 3089–3091.
405. Chen, E. Y. X.; Marks, T. J. *Chem. Rev.* **2000**, *100*, 1391–1434.
406. Oi, S.; Terada, E.; Ohuchi, K.; Kato, T.; Tachibana, Y.; Inoue, Y. *J. Org. Chem.* **1999**, *64*, 8660–8667.
407. Ghosh, A. K.; Matsuda, H. *Org. Lett.* **1999**, *1*, 2157–2159.
408. Hagiwara, E.; Fujii, A.; Sodeoka, M. *J. Am. Chem. Soc.* **1998**, *120*, 2474–2475.
409. Furstner, A.; Voigtlander, D.; Schrader, W.; Giebel, D.; Reetz, M. T. *Org. Lett.* **2001**, *3*, 417–420.
410. Madine, J. W.; Wang, X.; Widenhoefer, R. A. *Org. Lett.* **2001**, *3*, 385–388.
411. LaPointe, A. M.; Rix, F. C.; Brookhart, M. *J. Am. Chem. Soc.* **1997**, *119*, 906–917.
412. Paik, S. J.; Son, S. U.; Chung, Y. K. *Org. Lett.* **1999**, *1*, 2045–2047.
413. Yasutake, M.; Gridnev, I. D.; Higashi, N.; Imamoto, T. *Org. Lett.* **2001**, *3*, 1701–1704.
414. Kawatsura, M.; Hartwig, J. F. *J. Am. Chem. Soc.* **2000**, *122*, 9546–9547.
415. Hartwig, J. F. *Acc. Chem. Res.* **1998**, *31*, 852–860.
416. Wolfe, J. P.; Tomori, H.; Sadighi, J. P.; Yin, J. J.; Buchwald, S. L. *J. Org. Chem.* **2000**, *65*, 1158–1174.
417. Jordan, R. F. *Adv. Organomet. Chem.* **1991**, *32*, 325–387.
418. Killian, C. M.; Johnson, L. K.; Brookhart, M. *Organometallics* **1997**, *16*, 2005–2007.
419. Younkin, T. R.; Conner, E. F.; Henderson, J. I.; Friedrich, S. K.; Grubbs, R. H.; Bansleben, D. A. *Science* **2000**, *287*, 460–462.
420. Tanner, M. J.; Brookhart, M.; DeSimone, J. M. *J. Am. Chem. Soc.* **1997**, *119*, 7617–7618.
421. Britovsek, G. J. P.; Bruce, M.; Gibson, V. C.; Kimberley, B. S.; Maddox, P. J.; Mastroianni, S.; McTavish, S. J.; Redshaw, C.; Solan, G. A., Stromberg, S., *et al. J. Am. Chem. Soc.* **1999**, *121*, 8728–8740.
422. Stahl, S. S.; Labinger, J. A.; Bercaw, J. E. *Angew. Chem., Int. Ed.* **1998**, *37*, 2181–2192.
423. Lin, M. R.; Shen, C. Y.; Garcia-Zayas, E. A.; Sen, A. *J. Am. Chem. Soc.* **2001**, *123*, 1000–1001.
424. Shen, C. Y.; Garcia-Zayas, E. A.; Sen, A. *J. Am. Chem. Soc.* **2000**, *122*, 4029–4031.
425. Tellers, D. M.; Bergman, R. G. *J. Am. Chem. Soc.* **2000**, *122*, 954–955.
426. Periana, R. A.; Taube, D. J.; Gamble, S.; Taube, H.; Satoh, T.; Fujii, H. *Science* **1998**, *280*, 560–564.
427. Sadow, A. D.; Tilley, T. D. *J. Am. Chem. Soc.* **2003**, *125*, 9462–9475.
428. Schrock, R. R.; Osborn, J. A. *Inorg. Chem.* **1970**, *9*, 2339–2343.
429. Hlatky, G. G.; Turner, H. W.; Eckman, R. R. *J. Am. Chem. Soc.* **1989**, *111*, 2728–2729.
430. Piers, W. E. *Chem. Eur. J.* **1998**, *4*, 13–18.
431. Bochmann, M. *Top. Catal.* **1999**, *7*, 9–22.
432. Zhou, Z. X.; Facey, G.; James, B. R.; Alper, H. *Organometallics* **1996**, *15*, 2496–2503.
433. Zhou, Z. X.; James, B. R.; Alper, H. *Organometallics* **1995**, *14*, 4209–4212.
434. Amer, I.; Alper, H. *J. Am. Chem. Soc.* **1990**, *112*, 3674–3676.
435. Winter, R. F.; Hornung, F. M. *Inorg. Chem.* **1997**, *36*, 6197–6204.
436. Dai, C. Y.; Robins, E. G.; Scott, A. J.; Clegg, W.; Yufit, D. S.; Howard, J. A. K.; Marder, T. B. *Chem. Commun.* **1998**, 1983–1984.
437. Westcott, S. A.; Blom, H. P.; Marder, T. B.; Baker, R. T. *J. Am. Chem. Soc.* **1992**, *114*, 8863–8869.
438. Westcott, S. A.; Taylor, N. J.; Marder, T. B.; Baker, R. T.; Jones, N. J.; Calabrese, J. C. *J. Chem. Soc., Chem. Commun.* **1991**, 304–305.
439. Chen, Y. F.; Wu, G.; Bazan, G. C. *Angew. Chem., Int. Ed.* **2005**, *44*, 1108–1112.
440. Lee, B. Y.; Bazan, G. C.; Vela, J.; Komon, Z. J. A.; Bu, X. H. *J. Am. Chem. Soc.* **2001**, *123*, 5352–5353.
441. Lu, C. C.; Peters, J. C. *J. Am. Chem. Soc.* **2004**, *126*, 15818–15832.
442. Betley, T. A.; Peters, J. C. *Angew. Chem., Int. Ed.* **2003**, *42*, 2385–2389.
443. Betley, T. A.; Peters, J. C. *Inorg. Chem.* **2002**, *41*, 6541–6543.
444. Lu, C. C.; Peters, J. C. *J. Am. Chem. Soc.* **2002**, *124*, 5272–5273.
445. Rankin, M. A.; McDonald, R.; Ferguson, M. J.; Stradiotto, M. *Angew. Chem., Int. Ed.* **2005**, *44*, 3603–3606.
446. Stradiotto, M.; Cipot, J.; McDonald, R. *J. Am. Chem. Soc.* **2003**, *125*, 5618–5619.
447. Mazet, C.; Kohler, V.; Pfaltz, A. *Angew. Chem., Int. Ed.* **2005**, *44*, 4888–4891.
448. Sawamura, M.; Ito, Y. *Chem. Rev.* **1992**, *92*, 857–871.
449. Rowlands, G. J. *Tetrahedron* **2001**, *57*, 1865–1882.
450. Shibasaki, M.; Kanai, M.; Funabashi, K. *Chem. Commun.* **2002**, 1989–1999.
451. Van Den Beuken, E. K.; Feringa, B. L. *Tetrahedron* **1998**, *54*, 12985–13011.
452. Kanai, M.; Kato, N.; Ichikawa, E.; Shibasaki, M. *Synlett* **2005**, 1491–1508.
453. Shibasaki, M.; Kanai, M. *Chem. Pharm. Bull.* **2001**, *49*, 511–524.
454. Shibasaki, M. *Enantiomer* **1999**, *4*, 513–527.
455. Clapham, S. E.; Hadzovic, A.; Morris, R. H. *Coord. Chem. Rev.* **2004**, *248*, 2201–2237.
456. Borovik, A. S. *Acc. Chem. Res.* **2005**, *38*, 54–61.
457. Noyori, R.; Kitamura, M.; Ohkuma, T. *Proc. Nat. Acad. Sci.* **2004**, *101*, 5356–5362.

458. Shvo, Y.; Czarkie, D.; Rahamim, Y.; Chodosh, D. F. *J. Am. Chem. Soc.* **1986**, *108*, 7400–7402.
459. Casey, C. P.; Bikzhanova, G. A.; Cui, Q.; Guzei, I. A. *J. Am. Chem. Soc.* **2005**, *127*, 14062–14071.
460. Csjernyik, G.; Ell, A. H.; Fadini, L.; Pugin, B.; Baeckvall, J.-E. *J. Org. Chem.* **2002**, *67*, 1657–1662.
461. Sandoval, C. A.; Ohkuma, T.; Muniz, K.; Noyori, R. *J. Am. Chem. Soc.* **2003**, *125*, 13490–13503.
462. Noyori, R.; Okhuma, T. *Angew. Chem., Int. Ed.* **2001**, *40*, 40–73.
463. Yamakawa, M.; Ito, H.; Noyori, R. *J. Am. Chem. Soc.* **2000**, *122*, 1466–1478.
464. Abdur-Rashid, K.; Clapham, S. E.; Hadzovic, A.; Harvey, J. N.; Lough, A. J.; Morris, R. H. *J. Am. Chem. Soc.* **2002**, *124*, 15104–15118.
465. Blum, Y.; Czarkie, D.; Rahamim, Y.; Shvo, Y. *Organometallics* **1985**, *4*, 1459–1461.
466. Menashe, N.; Salant, E.; Shvo, Y. *J. Organomet. Chem.* **1996**, *514*, 97–102.
467. Menashe, N.; Shvo, Y. *Organometallics* **1991**, *10*, 3885–3891.
468. Casey, C. P.; Johnson, J. B. *J. Am. Chem. Soc.* **2005**, *127*, 1883–1894.
469. Casey, C. P.; Singer, S. W.; Powell, D. R.; Hayashi, R. K.; Kavana, M. *J. Am. Chem. Soc.* **2001**, *123*, 1090–1100.
470. Laxmi, Y. R. S.; Baeckvall, J.-E. *Chem. Commun.* **2000**, 611–612.
471. Huerta, F. F.; Laxmi, Y. R. S.; Baeckvall, J.-E. *Org. Lett.* **2000**, *2*, 1037–1040.
472. Persson, B. A.; Huerta, F. F.; Baeckvall, J.-E. *J. Org. Chem.* **1999**, *64*, 5237–5240.
473. Persson, B. A.; Larsson, A. L. E.; Le Ray, M.; Baeckvall, J.-E. *J. Am. Chem. Soc.* **1999**, *121*, 1645–1650.
474. Larsson, A. L. E.; Persson, B. A.; Baeckvall, J.-E. *Angew. Chem., Int. Ed. Engl.* **1997**, *36*, 1211–1212.
475. Samec, J. S. M.; Baeckvall, J.-E. *Chem. Eur. J.* **2002**, *8*, 2955–2961.
476. Larsen, P. L.; Gupta, R.; Powell, D. R.; Borovik, A. S. *J. Am. Chem. Soc.* **2004**, *126*, 6522–6523.
477. MacBeth, C. E.; Gupta, R.; Mitchell-Koch, K. R.; Young, V. G., Jr.; Lushington, G. H.; Thompson, W. H.; Hendrich, M. P.; Borovik, A. S. *J. Am. Chem. Soc.* **2004**, *126*, 2556–2567.
478. Gupta, R.; Borovik, A. S. *J. Am. Chem. Soc.* **2003**, *125*, 13234–13242.
479. Zart, M. K.; Sorrell, T. N.; Powell, D.; Borovik, A. S. *Dalton Trans.* **2003**, 1986–1992.
480. Larsen, P. L.; Parolin, T. J.; Powell, D. R.; Hendrich, M. P.; Borovik, A. S. *Angew. Chem., Int. Ed.* **2003**, *42*, 85–89.
481. MacBeth, C. E.; Larsen, P. L.; Sorrell, T. N.; Powell, D.; Borovik, A. S. *Inorg. Chim. Acta* **2002**, *341*, 77–84.
482. Gupta, R.; MacBeth, C. E.; Young, V. G., Jr.; Borovik, A. S. *J. Am. Chem. Soc.* **2002**, *124*, 1136–1137.
483. MacBeth, C. E.; Hammes, B. S.; Young, V. G., Jr.; Borovik, A. S. *Inorg. Chem.* **2001**, *40*, 4733–4741.
484. MacBeth, C. E.; Golombek, A. P.; Young, V. G., Jr.; Yang, C.; Kuczera, K.; Hendrich, M. P.; Borovik, A. S. *Science* **2000**, *289*, 938–941.
485. Shirin, Z.; Hammes, B. S.; Young, V. G., Jr.; Borovik, A. S. *J. Am. Chem. Soc.* **2000**, *122*, 1836–1837.
486. Hammes, B. S.; Young, V. G., Jr.; Borovik, A. S. *Angew. Chem., Int. Ed.* **1999**, *38*, 666–669.
487. Lucas, R. L.; Powell, D. R.; Borovik, A. S. *J. Am. Chem. Soc.* **2005**, *127*, 11596–11597.
488. Yeh, C.-Y.; Chang, C. J.; Nocera, D. G. *J. Am. Chem. Soc.* **2001**, *123*, 1513–1514.
489. Collman, J. P.; Decreau, R. A. *Org. Lett.* **2005**, *7*, 975–978.
490. Liu, S.-Y.; Nocera, D. G. *J. Am. Chem. Soc.* **2005**, *127*, 5278–5279.
491. Collman, J. P.; Fu, L. *Acc. Chem. Res.* **1999**, *32*, 455–463.
492. Chang, C. J.; Chang, M. C. Y.; Damrauer, N. H.; Nocera, D. G. *Biochim. Biophys. Acta Bioenerg.* **2004**, *1655*, 13–28.
493. Chang, C. J.; Chng, L. L.; Nocera, D. G. *J. Am. Chem. Soc.* **2003**, *125*, 1866–1876.
494. Cukier, R. I.; Nocera, D. G. *Annu. Rev. Phys. Chem.* **1998**, *49*, 337–369.
495. Collman, J. P.; Gagne, R. R.; Halbert, T. R.; Marchon, J. C.; Reed, C. A. *J. Am. Chem. Soc.* **1973**, *95*, 7868–7870.
496. Chang, C. K.; Sotiriou, C.; Wu, W. *J. Chem. Soc., Chem. Commun.* **1986**, 1213–1215.
497. Chang, C. K.; Bag, N.; Guo, B.; Peng, S.-M. *Inorg. Chim. Acta* **2003**, *351*, 261–268.
498. Chang, C. K.; Liang, Y.; Aviles, G.; Peng, S.-M. *J. Am. Chem. Soc.* **1995**, *117*, 4191–4192.
499. Chang, C. K.; Aviles, G.; Bag, N. *J. Am. Chem. Soc.* **1994**, *116*, 12127–12128.
500. Lindsey, J. S.; Wagner, R. W. *J. Org. Chem.* **1989**, *54*, 828–836.
501. Lindsey, J. S. Synthesis of *meso*-Substituted Porphyrins. In *Porphyrin Handbook*; Kadish, K. M., Smith, K. M., Guilard, R., Eds.; Academic Press: San Diego, CA, 2000; Vol. 1, pp 45–118.
502. Chng, L. L.; Chang, C. J.; Nocera, D. G. *Org. Lett.* **2003**, *5*, 2421–2424.
503. Larrow, J. F.; Jacobsen, E. N. *Top. Organomet. Chem.* **2004**, *6*, 123–152.
504. Cozzi, P. G. *Chem. Soc. Rev.* **2004**, *33*, 410–421.
505. Vogt, M. The Application of Perfluorinated Polyethers for Immobilization of Homogeneous Catalysts. Ph.D. Thesis, Rheinisch-Westfälischen Technischen Hochschule, Aachen, Germany, 1991.
506. Horvath, I. T.; Rabai, J. *Science* **1994**, *266*, 72–75.
507. Gladysz, J. A.; Curran, D. P. *Tetrahedron* **2002**, *58*, 3823–3825.
508. Horvath, I. T. *Acc. Chem. Res.* **1998**, *31*, 641–650.
509. Fish, R. H. *Chem. Eur. J.* **1999**, *5*, 1677–1680.
510. Pozzi, G.; Shepperson, I. *Coord. Chem. Rev.* **2003**, *242*, 115–124.
511. Curran, D.; Lee, Z. *Green Chem.* **2001**, *3*, G3–G7.
512. Rabai, J.; Szlavik, Z.; Horvath, I. T. Chemistry in fluorous biphasic systems. In *Handbook of Green Chemistry and Technology*; Clark, J., Macquarrie, D., Eds.; Blackwell: Oxford, 2002; pp 502–523.
513. Hope, E. G.; Stuart, A. M. *J. Fluorine Chem.* **1999**, *100*, 75–83.
514. Sheldon, R. A. *Pure Appl. Chem.* **2000**, *72*, 1233–1246.
515. Gladysz, J. A.; Curran, D. P.; Horvath, I. T. *Handbook of Fluorous Chemistry;* Wiley-VCH: Weinheim, 2004.
516. Pozzi, G.; Cavazzini, M.; Quici, S.; Maillard, D.; Sinou, D. *J. Mol. Catal. A: Chem.* **2002**, *182–183*, 455–461.
517. Fache, F. *New J. Chem.* **2004**, *28*, 1277–1283.
518. Pozzi, G.; Cinato, F. *Chem. Commun.* **1998**, 877–878.
519. Bayardon, J.; Sinou, D. *Tetrahedron Lett.* **2003**, *44*, 1449–1451.
520. Pozzi, G.; Montanari, F.; Quici, S. *Chem. Commun.* **1997**, 69–70.
521. Horvath, I. T.; Kiss, G.; Cook, R. A.; Bond, J. E.; Stevens, P. A.; Rabai, J.; Mozeleski, E. J. *J. Am. Chem. Soc.* **1998**, *120*, 3133–3143.
522. Jiao, H.; Le Stang, S.; Soos, T.; Meier, R.; Kowski, K.; Rademacher, P.; Jafarpour, L.; Hamard, J.-B.; Nolan, S. P.; Gladysz, J. A. *J. Am. Chem. Soc.* **2002**, *124*, 1516–1523.

523. Alvey, L. J.; Meier, R.; Soos, T.; Bernatis, P.; Gladysz, J. A. *Eur. J. Inorg. Chem.* **2000**, 1975–1983.
524. Bhattacharyya, P.; Croxtall, B.; Fawcett, J.; Fawcett, J.; Gudmunsen, D.; Hope, E. G.; Kemmitt, R. D. W.; Paige, D. R.; Russell, D. R., Stuart, A. M., *et al. J. Fluorine Chem.* **2000**, *101*, 247–255.
525. Hughes, R. P.; Trujillo, H. A. *Organometallics* **1996**, *15*, 286–294.
526. Curran, D. P.; Wang, X.; Zhang, Q. *J. Org. Chem.* **2005**, *70*, 3716–3719.
527. Curran, D. P. *Synlett* **2001**, 1488–1496.
528. Tzschucke, C. C.; Markert, C.; Glatz, H.; Bannwarth, W. *Angew. Chem., Int. Ed.* **2002**, *41*, 4500–4503.
529. Dinh, L. V.; Gladysz, J. A. *Angew. Chem., Int. Ed.* **2005**, *44*, 4095–4097.
530. Darr, J. A.; Poliakoff, M. *Chem. Rev.* **1999**, *99*, 495–541.
531. Jessop, P. G.; Ikariya, T.; Noyori, R. *Chem. Rev.* **1999**, *99*, 475–493.
532. Leitner, W. *Appl. Organomet. Chem.* **2000**, *14*, 809–814.
533. Leitner, W. *Acc. Chem. Res.* **2002**, *35*, 746–756.
534. Musie, G.; Wei, M.; Subramaniam, B.; Busch, D. H. *Coord. Chem. Rev.* **2001**, *219–221*, 789–820.
535. Prajapati, D.; Gohain, M. *Tetrahedron* **2004**, *60*, 815–833.
536. Smart, N. G.; Carleson, T.; Kast, T.; Clifford, A. A.; Burford, M. D.; Wai, C. M. *Talanta* **1997**, *44*, 137–150.
537. DeSimone, J. M.; Guan, Z.; Elsbernd, C. S. *Science* **1992**, *257*, 945–947.
538. Kainz, S.; Koch, D.; Baumann, W.; Leitner, W. *Angew. Chem., Int. Ed. Engl.* **1997**, *36*, 1628–1630.
539. Grubbs, R. H. *Tetrahedron* **2004**, *60*, 7117–7140.
540. Schrock, R. R. *J. Mol. Catal. A: Chem.* **2004**, *213*, 21–30.
541. Schrock, R. R.; Hoveyda, A. H. *Angew. Chem., Int. Ed.* **2003**, *42*, 4592–4633.
542. Grubbs, R. H. *Adv. Synth. Catal.* **2002**, *344*, 569.
543. Schrock, R. R. *Adv. Synth. Catal.* **2002**, *344*, 571–572.
544. Greco, J. B.; Peters, J. C.; Baker, T. A.; Davis, W. M.; Cummins, C. C.; Wu, G. *J. Am. Chem. Soc.* **2001**, *123*, 5003–5013.
545. Peters, J. C.; Odom, A. L.; Cummins, C. C. *Chem. Commun.* **1997**, 1995–1996.
546. Enriquez, A. E.; White, P. S.; Templeton, J. L. *J. Am. Chem. Soc.* **2001**, *123*, 4992–5002.

1.03
General Classification of Organometallic Reactions

D Rabinovich, The University of North Carolina at Charlotte, Charlotte, NC, USA

1.03.1 Introduction

The inherent structural and bonding diversity of inorganic and organometallic compounds goes hand in hand with the variety of reactivity patterns associated with them, many of which have no parallel in organic chemistry. Although a mechanism is only a hypothesis or model proposed to explain experimental data, the understanding and verification of plausible reaction mechanisms is essential to the continued health and development of the field. Building on the basic concepts described in Chapters 1.01 and 1.02, an overview of the fundamental reaction types pertaining to inorganic and organometallic chemistry is presented here.

In general, organometallic reactions can be subdivided into two large groups, namely, those occurring at the metal (substitutions, oxidative additions, and reductive eliminations) and those involving modification of ligands, whether those changes take place at the metal or not (insertions/deinsertions and nucleophilic/electrophilic additions and abstractions). Although condensing such a broad topic into a few pages is both a challenge and a necessity due to space limitations, excellent sources of information are available for those seeking to expand on the material covered in this chapter. The book by Collman *et al.* (1987) continues to be an invaluable resource[1] and so are a number of organometallic chemistry textbooks published within the last decade or so.[2–5] A handful of monographs dealing primarily with mechanistic aspects of inorganic and organometallic chemistry[6–10] have also been published since COMC2 (1995) was released. Last but not least, a concerted effort has been made to include at the end of the chapter a combination of seminal papers on specific topics, useful reviews, and recent references from the primary literature.

1.03.2 Substitution Reactions

1.03.2.1 General Considerations

Substitution reactions involve the replacement of a ligand in the first coordination sphere of a metal center by another, without an overall change in the metal's oxidation state, coordination number, or electron count (Equation (1)).[11–15] The ligands X and Y that take part in the exchange are typically Lewis bases, including inorganic and organic donor groups (e.g., NH_3, halides, CO, phosphines) and solvent molecules.

$$MX_n + Y \longrightarrow MX_{n-1}Y + X \quad (1)$$

Ligand substitution reactions are among the simplest yet the most common and important elementary transformations in inorganic and organometallic chemistry and can be found in a myriad of stoichiometric and catalytic processes of industrial significance. For examples, see Chapter 1.04. These reactions permeate many areas of current research interest, ranging from the use of hemilabile ligands in supramolecular chemistry[16–20] to the development of improved olefin polymerization catalysts containing weakly coordinating anions.[21–25] The displacement of water molecules bound to metal ions is also critical in many bioinorganic systems, including the catalytic activity of most zinc enzymes[26,27] and the application of gadolinium(III)-based contrast agents for magnetic resonance imaging (MRI).[28–33] Substitution reactions in organometallic compounds containing an odd number of electrons (typically 17 or 19) have been meticulously studied since such paramagnetic species, often generated photochemically or electrochemically, tend to exhibit an increased reactivity relative to their electronically saturated analogs.[34–41]

The detailed investigation of ligand-displacement processes in transition metal carbonyl complexes, ever since the pioneering studies of Basolo in the 1960s, has played a key role in our current understanding of these fundamental reactions.[42–45] Both ligand- and metal-based effects have been thoroughly surveyed and have contributed to rationalize viable mechanistic pathways for substitution reactions.[46] The classification of ligand-substitution mechanisms was first proposed by Langford and Gray[47] and subsequently refined by Merbach.[48,49] It is now widely accepted that ligand-substitution reactions can be divided into three general categories of stoichiometric mechanisms: associative (A), where an intermediate of higher coordination number can be detected, dissociative (D), where an intermediate of lower coordination number can be observed, and interchange (I), where there is no kinetically discernible intermediate (Scheme 1). In addition, there are two subtypes of intermediate mechanisms: those with a predominantly associative activation mode (a) and those with a predominantly dissociative activation mode (d). In the first case, the reaction rate is sensitive to the nature of the incoming group, whereas in the second case the reaction rate is essentially unaffected by the variation of the entering ligand. Significantly, there is a continuum of transition states for the interchange mechanisms where the degree of bond formation between the new ligand and the complex ranges from substantial (I_a mechanism) to negligible (I_d mechanism).[42–45] This situation is akin to organic nucleophilic substitutions, where the actual mechanism for a given reaction usually lies somewhere in between the S_N1 and S_N2 extremes.

The elucidation of a substitution reaction mechanism depends on reliable kinetic and thermodynamic data obtained by measuring changes in the reaction rate as a function of a chemical property (e.g., concentration, pH, ionic strength, solvent polarity) or physical quantity (e.g., temperature). The determination of an empirical rate law, the observation of steric or electronic effects induced by the entering, spectator, or leaving groups, and the estimation of activation parameters from variable-temperature experiments (i.e., $\Delta H^{\ddagger}$ and $\Delta S^{\ddagger}$) contribute to the adjudication of a plausible mechanism for a given reaction.

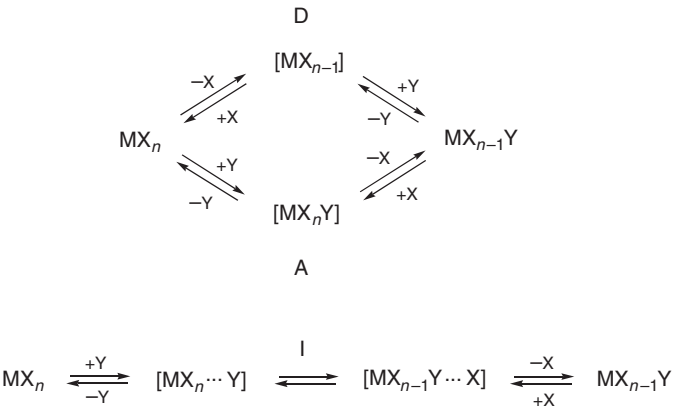

Scheme 1

In the case of solvent-exchange reactions, including those pertaining to aqueous metal ions, accurate mechanisms are particularly difficult to ascertain with standard experimental methods, particularly since rate constants span nearly 20 orders of magnitude.[50–52] However, variable-pressure techniques (e.g., stopped-flow kinetics, high-pressure NMR spectroscopy) and the measurement of activation volumes ($\Delta V^{\ddagger}$) have often shed light on such systems.[53–55]

The two main substitution mechanisms (A and D) will be described here using representative square-planar and octahedral complexes, the main features of which could be easily extrapolated to other coordination numbers or geometries. As a general guideline, it should also be mentioned that Taube proposed that complexes having substitution half-lives ($t_{1/2}$) shorter than 30 s could be considered labile while those with longer $t_{1/2}$ could be regarded as inert.[56] Computational methods have also been successfully applied to the study of a variety of substitution and rearrangement mechanisms in transition metal complexes.[57]

1.03.2.2 Ligand Substitution in Coordinatively Unsaturated Complexes

The associative substitution mechanism (A) is typical of 16-electron square-planar metal ions having a d^8-electron configuration, including Rh(I), Ir(I), Ni(II), Pd(II), Pt(II), and Au(III). The reduced steric hindrance and the availability of an empty p_z orbital perpendicular to the molecular plane are factors that promote the rate-determining nucleophilic attack of an additional ligand to form an 18-electron five-coordinate intermediate, which rapidly ejects the leaving group to yield the final product (Equation (2)).[58–63] In agreement with this mechanism, negative entropies of activation ($\Delta S^{\ddagger} \approx -10$ to -15 eu) and a marked dependence on the nature of both the incoming and leaving groups are typically observed. The rate law has two terms and can be written as rate $= (k_1 + k_2[Y])[MX_4]$, an expression which, under pseudo first-order conditions (i.e., $[Y] >> [MX_4]$), could be simplified to rate $= (k_{obs})[MX_4]$.[64]

$$MX_4 + Y \underset{k_2}{\overset{k_1}{\rightleftharpoons}} [MX_4Y] \xrightarrow{k_3} MX_3Y + X \qquad (2)$$

In the course of an associative substitution, the 18-electron square-pyramidal species, formed initially upon attack of the square planar complex by the nucleophile, readily rearranges to a trigonal bipyramidal (tbp) intermediate. Rotation of the incoming ligand (Y), the leaving group (X), and its original *trans* partner (L_t), with all three ligands now occupying the equatorial plane, is facile (Scheme 2).

Based on the principle of microscopic reversibility, whereby a reversible reaction must proceed by the same proposed mechanism in both the forward and reverse directions, the tbp intermediate generates a new square pyramidal species in which the leaving group is located in the apical position. Departure of the leaving group results in the rapid formation of the square planar substitution product. It is clear that the labilization or increased rate of substitution exerted on the ligand opposite to a given coordinated group (i.e., the *trans* effect)[65] has a conspicuous role on these reactions. This explains why associative substitutions in metal complexes proceed, unlike their typical S_N2 counterparts in organic chemistry, with retention of configuration at the atom bearing the leaving group (M or C, respectively). Furthermore, the interconversion of square pyramidal and tbp geometries is the key feature of the mechanism for the exchange of axial and equatorial ligands in tbp complexes, a process known as Berry pseudorotation.[66,67]

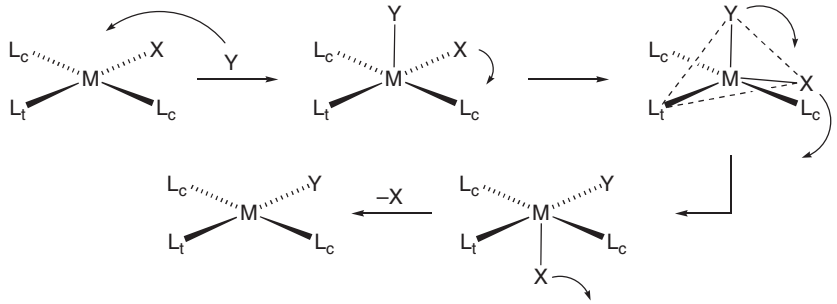

Scheme 2

It is also worth noting that ligand substitution reactions in square planar transition metal complexes are quite important in medicinal inorganic chemistry. The biological activity of the potent anti-tumor drug *cis*-diamminedichloroplatinum(II) (cisplatin) relies on the efficient displacement of the two labile chloro ligands present in *cis*-$Pt(NH_3)_2Cl_2$ by two water molecules before the complex binds to DNA.[68–75] Literally, thousands of related mononuclear and multinuclear Pt(II) and Pt(IV) compounds have been synthesized over the years with the goal of developing cancer treatment agents with better specificity and less pernicious side-effects.[76–81] Furthermore, several isoelectronic (d^8) square planar complexes of Rh(I), Pd(II), and Au(III) have also been prepared and their cytotoxicity probed with the same goal in mind.[82–88]

1.03.2.3 Ligand Substitution in 18-Electron Complexes

The dissociative substitution mechanism (D) is commonly found for electronically saturated (18-electron) complexes, the best studied of which have historically been octahedral Co(III) derivatives (i.e., Werner-type species) and, to a lesser degree, Cr(III), Ru(III), and Rh(III) compounds.[89–92] Interestingly, a variety of octahedral Ru(II) and Ru(III) complexes, including those of general formulas $[RuCl_4L_2]^-$, $RuCl_3(dmso)_2(L)$, and $[RuCl_4(dmso)(L)]^-$ (L = nitrogen donor ligand), have also been studied as potential anticancer agents.[93–96]

Organometallic dissociative substitutions, like their associative counterparts for square-planar complexes, have been investigated in detail primarily for octahedral transition metal carbonyl complexes.[42–45] They involve the initial rate-limiting separation of one ligand (X) from the substrate to give an electronically unsaturated (16-electron) distorted tbp intermediate, followed by rapid binding of the nucleophile (Y) to give the substituted product (Equation (3), where $k_3 > k_2$).

$$MX_6 \underset{+X,\ k_2}{\overset{-X,\ k_1}{\rightleftharpoons}} [MX_5] \xrightarrow[\text{fast}]{+Y,\ k_3} MX_5Y \qquad (3)$$

Although the stereochemistry in dissociative substitution reactions is not always conserved due to the presence of a rather distorted five-coordinate intermediate, positive values of $\Delta S^{\ddagger}$ (10–15 eu) and a pseudo-first-order rate law (rate = $(k_{obs})[MX_6]$) that clearly resembles that for associative substitutions are typically observed. Electronic and steric factors that affect organometallic dissociative substitutions, including the metal's charge, electron count, position in the periodic table, and electron configuration and also ligand *trans* effects, have been carefully investigated.[46,97]

Substitution reactions on electronically saturated complexes may also follow an associative pathway that does not involve the generation of a high-energy 20-electron intermediate. Such seemingly counterintuitive mechanism entails the reaction of complexes bearing ligands capable of undergoing rearrangements that reduce their electron count and thereby allow the associative substitution pathway to take place. A classic example is the nitrosyl (NO) ligand, which could behave as a three-electron donor and exhibit a linear geometry or, alternatively, relocate a pair of electrons to the nitrogen atom, act as a one-electron donor, and display a bent structure (Equation (4)).[98,99]

$$\underset{\substack{\text{linear (3-e}^-\text{) NO}\\ \text{18-e}^-\text{ complex}}}{Co(CO)_3(NO)} \xrightarrow{PR_3} \underset{\substack{\text{bent (1-e}^-\text{) NO}\\ \text{18-e}^-\text{ complex}}}{[Co(CO)_3(PR_3)(NO)]} \xrightarrow{-CO} \underset{\substack{\text{linear (3-e}^-\text{) NO}\\ \text{18-e}^-\text{ complex}}}{Co(CO)_2(PR_3)(NO)} \qquad (4)$$

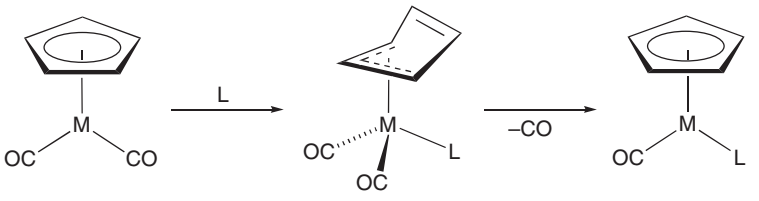

Scheme 3

Important families of electronically saturated compounds that are also susceptible to partake in associative substitution reactions are those containing polyhapto π-ligands such as cyclopentadienyl (Cp, η^5-C_5R_5) and indenyl (Ind, η^5-C_9R_7). These ligands possess the ability to set aside a pair of electrons in their five-membered rings and "slip" to a bonding mode of lower hapticity (η^3), sometimes referred to as the π-allyl–ene form. This ring-slippage mechanism allows the metal to accommodate temporarily an additional donor ligand while still maintaining its 18-electron count and is therefore critical in a variety of substitution reactions.[15,42–45,98–103] For example, an η^5- to η^3-ring slippage occurs in the reaction of the dicarbonyl complexes (η^5-C_5H_5)M(CO)$_2$ (M = Co, Rh, Ir) with a phosphine or a phosphite to give the corresponding monosubstituted products (η^5-C_5H_5)M(CO)(L) (Scheme 3).

Ring slippage in indenyl complexes has a significantly more dramatic effect on substitution reaction rates, which sometimes increase by as much as 10 orders of magnitude (!) relative to those observed for their cyclopentadienyl analogs. A term originally coined by Basolo,[104,105] the so-called indenyl effect was originally attributed to the full aromatization of the fused six-membered ring in the transition state, thought to stabilize the ene portion of the allyl–ene transition state (Scheme 4). However, the more facile η^5-to-η^3-haptotropic shift observed in indenyl complexes may (more realistically) be related to differences in bond-dissociation energies, which have been probed using both calorimetric and computational studies.[106–109] The stabilization of the η^3-intermediate is enhanced even more in the case of fluorenyl ligands (Flu, η^5-$C_{13}H_9$) since they have two fused benzene rings flanking the central cyclopentadienyl moiety. In addition, the steric effect of methyl substituents on these π-ligands has been analyzed for analogous reactions so that an approximate order of relative rates of substitution has been established: η^5-$C_{13}H_9 > \eta^5$-$C_9H_7 >> \eta^5$-$C_9Me_7 > \eta^5$-$C_5H_5 > \eta^5$-C_5Me_5.[110]

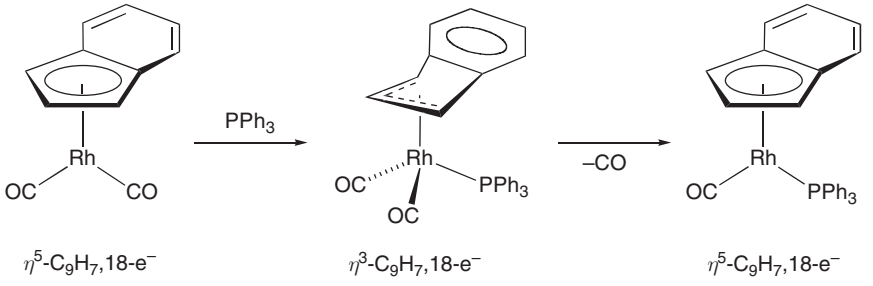

Scheme 4

Arene-displacement reactions of both aromatic hydrocarbons and heterocyclic systems are also envisioned to occur via an associative mechanism in which stepwise changes of hapticity in the unsaturated ligand take place.[111–113] Kinetic studies and the isolation or spectroscopic observation of solvated dihapto (η^2-) and tetrahapto (η^4-) intermediates have led to a proposed "unzipping" mechanism where the 18-electron count in each step is conserved (Scheme 5). While not nearly as common as η^6-arene derivatives, several complexes bearing η^2-arene and η^4-arene ligands have been independently synthesized and structurally characterized.[114–117] These hapticity shifts have been implicated in substitution reactions of arene complexes in general and may be of particular relevance in the homogeneous transition metal-catalyzed hydrogenation of aromatic hydrocarbons.[118–120] Furthermore, recent research efforts have been directed at exploring the role of soluble transition metal nanoclusters[121] and the potential use of ionic liquids as solvents[122] in these reactions.

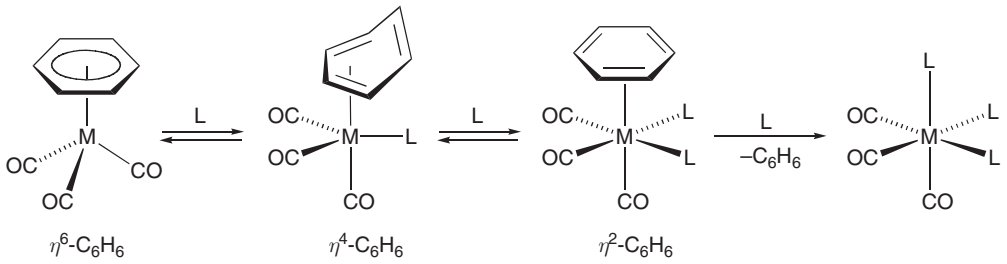

Scheme 5

1.03.3 Oxidative Addition and Reductive Elimination Reactions

1.03.3.1 Oxidative Addition: General Considerations

Oxidative addition reactions (and their reverse, reductive eliminations) are among the most important elementary transformations in organometallic chemistry and also play a key role in many stoichiometric and catalytic processes. Oxidative additions commonly involve the addition of a neutral molecule (X–Y) to a single metal center (M), resulting in the formation of new M–X and M–Y bonds and an increase by two units in the metal's oxidation state, electron count, and coordination number (Equation (5)). Although oxidative additions and reductive eliminations are in principle reversible reactions, the position of the equilibrium, which is governed by the overall thermodynamics of the species involved (i.e., the relative strengths of the bonds broken and formed), is often completely shifted to one of the sides.

$$L_nM + X-Y \underset{\text{reductive elimination}}{\overset{\text{oxidative addition}}{\rightleftharpoons}} L_nM\begin{matrix}X\\Y\end{matrix} \qquad (5)$$

The nature of the overall oxidative addition process, regardless of the exact mechanism involved (see Section 1.03.3.2), typically requires that the starting metal complex is electronically and coordinatively unsaturated or that such a species is generated by dissociation of a two-electron donor ligand prior to the oxidative addition step. Furthermore, the metal must have both nonbonding electron density available for donation to the incoming ligand ($d^n \geq 2$) and a stable oxidation state that is two units higher. Thus, oxidative additions are particularly favorable for electron-rich (i.e., low-valent) late transition metals such as Rh(I), Ir(I), or Pt(0).

A variety of substrates, including both electrophilic (e.g., X_2, RX, HX) and non-electrophilic (e.g., H_2, RH, R_3SiH) molecules, are susceptible to oxidative addition and result in the complete cleavage of the participating single bonds (Table 1).[123] Accordingly, the addition of alkyl halides (RX) or dihydrogen to the square planar Ir(I) compound

Table 1 Representative molecules susceptible to oxidative addition

Complete bond cleavage	*Incomplete bond cleavage*
X–X H_2, Cl_2, Br_2, I_2, RSSR, ArSeSeAr, R_2BBR_2	O_2, SO_2
C–C C_2Ph_6, PhCN	RC≡CR[1], $F_2C{=}CF_2$, $(NC)_2C{=}C(CN)_2$
H–X HCl, HBr, HI, C_6F_5OH, H_2O, H_2S, NH_3, PH_3, ROH, $(RO)_2BH$, C_6H_6, $C_6F_5NH_2$, RC≡CH, HCN, RCO_2H, C_6F_5H, CH_4, RCHO, R_3SiH, $HSiCl_3$, $PhGeH_3$, GeH_4	
C–X MeI, C_6H_5Br, CH_2Cl_2, CCl_4, MeCOCl, PhCOCl, ROR^1, R_2S, RCN, ArCN,	RN=C=O, RN=C=S, $RN{=}C{=}NR^1$ $R_2C{=}C{=}O$, CS_2, CF_3CN, epoxides
M–X $HgCl_2$, $Hg(O_2CCF_3)_2$, MeHgCl, Ph_2BX, PhSeX, R_nECl_{4-n} (E = Si, Sn; $n = 0, 1, 2, 3$)	

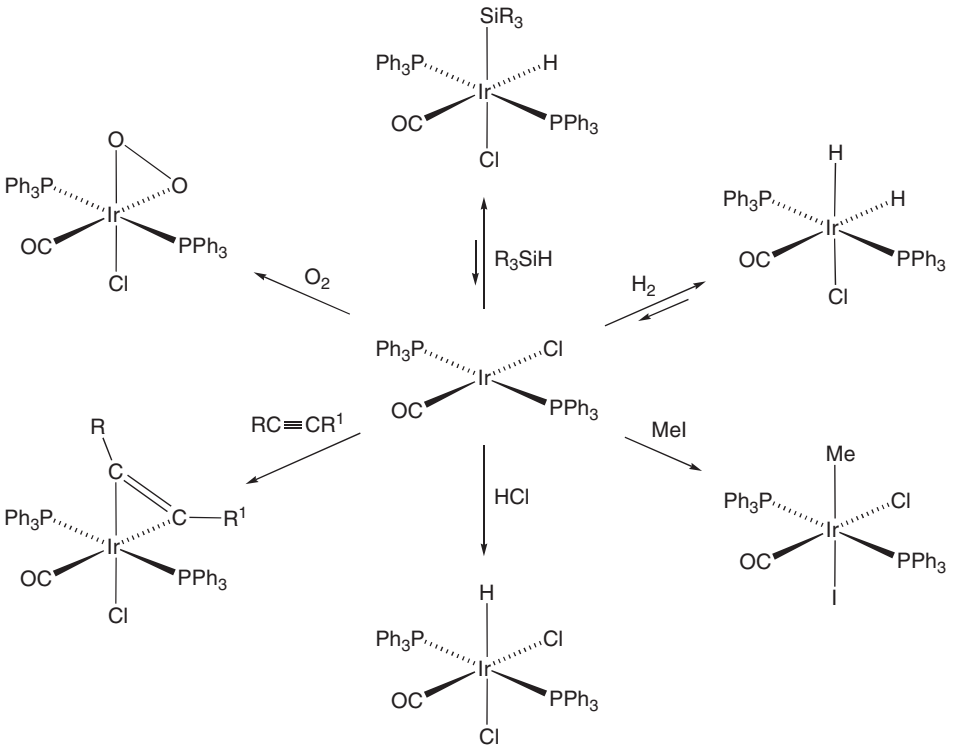

Scheme 6

trans-Ir(PPh_3)$_2$(CO)Cl (Vaska's complex) produces the octahedral Ir(III) derivatives Ir(PPh_3)$_2$(CO)(R)(X)Cl or Ir(PPh_3)$_2$$H_2$(CO)Cl, respectively (Scheme 6). The oxidative addition of unreactive bonds (e.g., C–F) or polarized molecular fragments containing atoms other than carbon (e.g., B–X) is a research area of great current interest. In this regard, recent advances include the activation and functionalization of fluorocarbons,[124–127] described in more detail in Chapter 1.26, and the development of new protocols for the syntheses of boryl (M–BR_2) and borylene (M═BR) complexes.[128–130] Significantly, the first direct oxidative addition of ammonia (NH_3) to form the stable amido hydride complex (PCP)Ir(NH_2)H, where PCP is a sterically demanding tridentate "pincer" ligand, has also been reported recently.[131,132]

A number of unsaturated molecules may occasionally also add oxidatively to a metal center and lead to products in which the original atoms are not completely detached. For example, the formation of side-on peroxo or metallacyclopropene complexes has been observed upon addition of dioxygen or alkynes to suitable precursors (Scheme 6). It is also important to note that even though most oxidative additions occur under kinetic control and follow a *cis*-stereochemistry, a variety of electronic and structural features and the availability of different mechanistic pathways may promote subsequent ligand rearrangements.

1.03.3.2 Mechanisms of Oxidative Addition

1.03.3.2.1 Three-center concerted additions

The oxidative addition of molecules having nonpolar or marginally polar σ-bonds (e.g., H–H, C–H, Si–H) usually requires the presence of an empty metal *d* orbital for binding of the substrate before the actual bond-breaking step takes place. The intermediate σ-complexes thus generated are sometimes stable and can be isolated but back-donation of electron density from the metal to the σ^* orbital is often sufficient to induce bond scission and the formation of the oxidized addition product via a three-center transition state (Equation (6)).

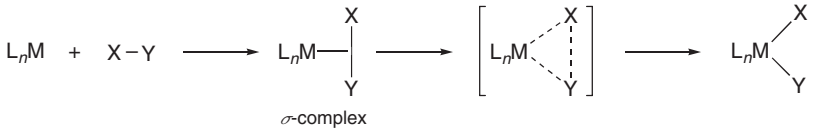

(6)

Given the importance of catalytic hydrogenation reactions, it is not surprising that the oxidative addition of H_2 to metal centers is among the best-studied systems. The prototypical reaction of H_2 with Vaska's complex to yield the Ir(III) dihydride derivative $Ir(PPh_3)_2H_2(CO)Cl$ (Scheme 6) displays second-order kinetics, a negative entropy of activation (i.e., an observation consistent with the intermediacy of a σ-complex), overall *cis*-stereochemistry, and negligible solvent effects.

Hundreds of dihydrogen complexes have been isolated and thoroughly studied to date,[133–137] and many borane, silane, germane, and related σ-complexes have also been synthesized and structurally characterized.[138–142] An overview of the synthesis, structures and reactivity of dihydrogen and other σ-complexes is presented in Chapter 1.24. In contrast, the preparation of stable alkane complexes remains elusive, with only a limited number of transient species having been observed using matrix isolation techniques, time-resolved spectroscopic methods, or low-temperature NMR spectroscopy[143–145] or probed indirectly measuring isotope effects (see also Section 1.03.3.6).[146] The field of C–H bond activation is nevertheless one of the most challenging and vibrant areas of research in modern organometallic chemistry.[147–160] For a review of the main features of C–H bond activation chemistry, see Chapter 1.25. The development of new oxidation catalysts for the selective functionalization of saturated hydrocarbons (e.g., the selective conversion of methane to methanol) is arguably one of its ultimate practical goals.[161–167] Interestingly, recent applications of C–H bond activation methodologies extend beyond the traditional realm of organometallic chemistry and embrace such diverse topics as the synthesis of complex organic molecules[168–172] and the advantageous use of molecular recognition effects and supramolecular chemistry in homogeneous catalysis.[173,174]

1.03.3.2.2 Nucleophilic (S_N2) reactions

The reaction of square-planar 16-electron complexes with polarized molecules such as methyl, benzyl, allyl, and acyl halides features a rate-determining step that is akin to the classic bimolecular nucleophilic substitution (S_N2) mechanism of organic chemistry. Direct attack by the metal complex (i.e., the nucleophile) on the least electronegative atom (C_α) of the electrophile (RX) results in displacement of the leaving group (X), which often (but not always) recombines with the cationic intermediate to yield the oxidative addition product (Scheme 7). The relative positions of the R and X groups in the product (i.e., *cis*- or *trans*-stereochemistry) depend on a variety of factors, including the *trans*-effect exerted by the newly bound electrophile in the charged intermediate.

The inversion of configuration at the carbon bearing the leaving group and the observation of second-order kinetics, large negative entropies of activation (−40 to −50 eu), and a rate increase with solvent polarity are diagnostic attributes of this mechanism and are consistent with the generation of a polarized transition state and the formation of a charged intermediate. Furthermore, the same reactivity patterns as in organic S_N2 reactions are also at work, particularly with regard to the steric hindrance ($CH_3X > RCH_2X > R_2CHX >> R_3CX$) and nucleophilicity of the leaving groups ($CF_3SO_3 > I > Br > Cl >> F$). An industrially important example of this mechanism is the rhodium-catalyzed carbonylation of methanol to form acetic acid (i.e., the Monsanto acetic acid process), in which the rate-determining step involves the formation of the six-coordinate complex $[Rh(CO)_2(Me)I_3]^-$ via the oxidative addition of iodomethane to the active catalyst $[Rh(CO)_2I_2]^-$.

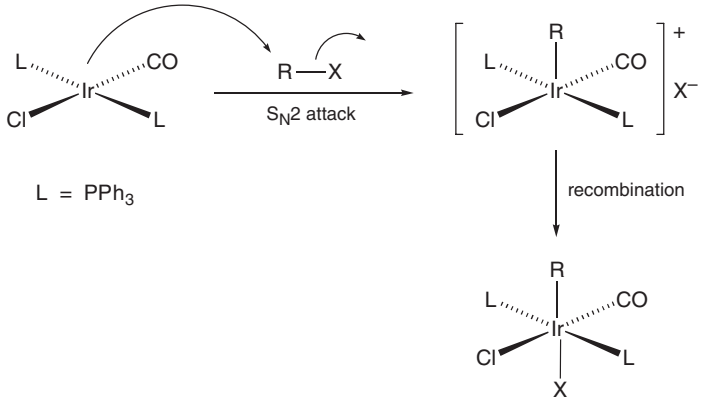

Scheme 7

1.03.3.2.3 Radical mechanisms

Oxidative additions that proceed via radical intermediates are very sensitive to the nature of the complex and the organic substrate, the overall reaction conditions, and the presence of paramagnetic impurities, all of which may affect the reproducibility and interpretation of experimental data.[175,176] While the study of radical mechanisms is less systematic than those of concerted or nucleophilic reactions, two main radical pathways have been identified: non-chain and chain processes. The radical non-chain mechanism has been proposed to take place during the addition of certain alkyl halides RX (R = Me, CH_2Ph, CH_2OMe, allyl) to zerovalent complexes such as $Pt(PPh_3)_3$.[177] The key feature is the one-electron oxidation of the metal by RX, which results in the formation of M^+ and RX^-, followed by transfer of X^- to the metal and liberation of an alkyl radical R· (Equation (7)). The pair of radicals generated during the reaction (R· and ·MX) finally recombines to yield the formal oxidative addition product RMX. Electron-rich metal centers and weaker RX bonds (R–I > R–Br > R–Cl) accelerate these reactions but, unlike the S_N2 mechanism described in the previous section, so does the generation of stable, sterically protected organic radicals (3° > 2° > 1°). Unlike the radical-chain mechanism described below, non-chain processes are unaffected by the presence of radical initiators or scavengers.

$$:M + RX \longrightarrow {\cdot}M^+ + {\cdot}RX^- \longrightarrow {\cdot}MX + R{\cdot} \longrightarrow RMX \qquad (7)$$

The radical-chain mechanism has been established for the reaction of the electron-rich iridium(I) trimethylphosphine complex $Ir(PMe_3)_2(CO)Cl$ with some unactivated alkyl halides (e.g., EtBr), vinyl and aryl halides, and α-halo esters.[178–181] In this mechanism, a small amount of an organic radical (R·) is first generated during an induction period, a process usually facilitated by radical initiators (Ini·) such as a trace amount of oxygen or a peroxide. The subsequent propagation steps involve the fast addition of the alkyl radical to Ir(I) to form the metalloradical RIr(II), which in the rate-determining step abstracts a halogen atom from RX to regenerate the chain carrier R· and produce the overall oxidative addition iridium(III) product RIrX (Equation (8)). The coupling of two alkyl radicals to produce R_2 is the most common chain-termination process and limits the number of possible catalytic cycles. Evidence to support the radical-chain pathway for oxidative addition reactions includes the sensitivity to both radical initiators (e.g., BZP, AIBN) and inhibitors (e.g., galvinoxyl), structural effects that are consistent with the stability of the alkyl radicals generated in the rate-determining step (3° > 2° > 1°), and complete loss of stereospecificity at the reacting carbon atom.

$$R \xrightarrow{Ini\cdot} R\cdot \xrightarrow{M} RM\cdot \xrightarrow[slow]{RX} RMX + R\cdot \qquad (8)$$

1.03.3.2.4 Ionic mechanisms

The stepwise addition of a proton and a halide may also occur in the reaction of certain metal complexes with hydrogen halides. In the most common case, the initial protonation of a basic metal center is followed by addition of a free halide anion. The cationic intermediate could sometimes be isolated if the conjugate acid of a poorly nucleophilic ("non-coordinating") anion (e.g., HBF_4, HPF_6) is used in the reaction (Equation (9)).[182] Alternatively, it has been found that electrophilic or cationic complexes are occasionally attacked first by the halide and subsequently protonated to generate the product of formal oxidative addition (Equation (10)).[183]

$$\underset{\text{18-e}^-\text{, tetrahedral}}{Pt(PPh_3)_4} \underset{}{\overset{-PPh_3}{\rightleftharpoons}} Pt(PPh_3)_3 \xrightarrow{H^+} \underset{\text{16-e}^-\text{, sq. planar}}{[HPt(PPh_3)_3]^+} \xrightarrow[-PPh_3]{Cl^-} \underset{\text{16-e}^-\text{, sq. planar}}{HPt(PPh_3)_2Cl} \qquad (9)$$

$$\underset{\text{16-e}^-\text{, sq. planar}}{[Ir(cod)(PPh_3)_2]^+} \xrightarrow{Cl^-} \underset{\text{18-e}^-\text{, trig. bipyramidal}}{IrCl(cod)(PPh_3)_2} \xrightarrow{H^+} \underset{\text{18-e}^-\text{, octahedral}}{[IrHCl(cod)(PPh_3)_2]^+} \qquad (10)$$

1.03.3.3 Sigma-bond Metathesis

The activation of C–H bonds by early transition metals or *f*-block elements in their highest possible formal oxidation states, for some of which the first direct observations of methane activation were verified,[184–186] is particularly interesting from a mechanistic point of view since their d^0- (or d^0f^n-) electron configurations preclude any of the

oxidative addition pathways described above.[187,188] Bercaw coined the term "σ-bond metathesis" in 1987 to describe this type of reaction and carried out a thorough investigation of the reactivity of permethylscandocene complexes Cp^*_2ScR (R = H, alkyl, aryl) toward a range of aliphatic and aromatic hydrocarbons.[189,190] Mechanistically, σ-bond metathesis by a coordinatively unsaturated, highly electrophilic metal center occurs via a four-center, four-electron transition state in which two bonds break and two bonds form in a concerted fashion (Equation (11)). Detailed density functional theory (DFT) studies on the activation of C–H and H–H bonds have provided a computational basis for these processes[191–195] and beautiful examples of σ-bond metathesis of Si–H bonds in the reactions of hydrosilanes with scandium(III) and zirconium(IV) alkyl complexes have also been recently disclosed.[196,197]

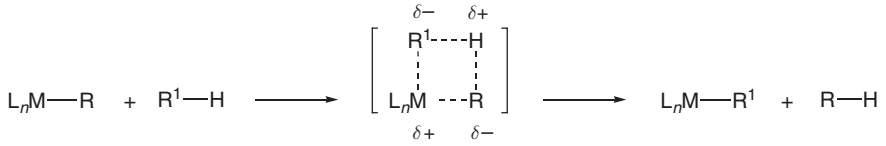

(11)

A fascinating new strategy to enable pseudo-"oxidative addition" reactions at d^0-transition metal centers, in which the addition takes place at the metal but the oxidation is actually ligand-based, has also been recently uncovered.[198] Illustrating this novel approach, the reaction of a zirconium(IV) bis(amidophenolate) complex $Zr(ap)_2(THF)_2$ with elemental chlorine yields the bis(iminosemiquinone) derivative $Zr(isq)_2Cl_2$, still a zirconium(IV) complex, arising from the one-electron oxidation of each of the two bidentate supporting ligands and the formal addition of two chlorides to the metal center.

1.03.3.4 Reductive Elimination

Reductive elimination, the reverse of oxidative addition, typically involves the excision of two adjacent (*cis*-) ligands from a single metal center with the concomitant decrease by two units in its oxidation state, electron count, and coordination number (Equation (12)).[199] The reaction is favored for metals in relatively high oxidation states, particularly if bulky ligands that promote the relief of steric hindrance or good π-acceptor groups (e.g., CO) that could help stabilize the reduced metal are present. The rate of the reaction is also enhanced by the presence of a positive charge, which may be originated by chemical or electrochemical oxidation,[200–205] or by the generation of a coordinatively unsaturated, more electrophilic metal center by the thermally or photolytically induced dissociation of a ligand prior to reductive elimination.[206–211]

(12)

Reductive elimination is typically the last step in a variety of stoichiometric and catalytic transformations and is thus important in the synthesis of a host of organic molecules of industrial and biological significance. Many fundamental carbon–carbon bond-forming processes,[212–214] including the palladium-mediated cross-coupling of organic electrophiles with organoboranes (the Suzuki–Miyaura reaction)[215–221] or organostannanes (the Stille reaction),[222–224] rely on the reductive elimination of two organometallic fragments in the final step of the catalytic cycle for product formation. Intensive research efforts since the mid-1990s have also been directed at developing efficient protocols for C–N, C–O, and C–S bond-forming reductive eliminations and, in general, the metal-catalyzed preparation of amines, ethers, sulfides, and related species.[225–235]

Based on the principle of microscopic reversibility, most reductive eliminations go through a three-center transition state akin to that postulated for the concerted pathway in oxidative additions and, accordingly, proceed with retention of stereochemistry at the leaving group. Whereas dissociation of a ligand before reductive elimination is commonly observed for octahedral d^6-complexes such as those of Rh(III), Ir(III), Pd(IV), and Pt(IV), the corresponding reactions of square-planar d^8-species, including Ni(II) and Pd(II) derivatives, may undergo either dissociative, nondissociative, or associative pathways.[236]

1.03.3.5 Bimetallic Systems

Oxidative additions and reductive eliminations at dinuclear metal complexes have both similarities and differences with those occurring in monometallic systems. In general, the interactions between metals and ligands in bimetallic systems lead to unique reactivity patterns that are not simply the sum of those exhibited by their separate mononuclear components.[237,238] The addition or elimination of two ligands to or from two metal centers usually involves a change by one unit in the oxidation state and electron count for each of the metals involved (Equation (13)). However, a change in coordination number depends on whether a metal–metal bond is cleaved, retained, or formed in the reaction and on the fate of the remaining ligands. Thus, the Mn–Mn bond is broken in the reaction of $Mn_2(CO)_{10}$ with Br_2 to give $Mn(CO)_5Br$ but each manganese atom remains roughly octahedral. Conversely, a new Co–Co bond forms when two $HCo(CO)_4$ fragments cooperatively undergo reductive elimination of dihydrogen and form $Co_2(CO)_8$. On the other hand, the coordination number increases by one when the cobalt(II) complex $[Co(CN)_5]^{3-}$ is oxidized by an alkyl halide (RX) to give the two cobalt(III) fragments $[RCo(CN)_5]^{3-}$ and $[XCo(CN)_5]^{3-}$. Interesting examples of one-site addition two-metal oxidation reactions have also been reported.[239–241]

$$L_nM{-}ML_n \quad (\text{or } 2ML_n) \xrightarrow{X{-}Y} L_nM{-}X + L_nM{-}Y \tag{13}$$

1.03.3.6 Oxidative Cleavage, Reductive Coupling, and Related Reactions

Oxidative cleavage and reductive coupling are two fundamental redox processes that involve respectively the fragmentation or coalescence of one or more ligands, usually within the coordination sphere of a single metal center. These elementary transformations could be easily understood in the context of the three-center concerted mechanisms for oxidative addition and reductive elimination discussed already (Sections 1.03.3.2 and 1.03.3.4, respectively). Thus, an oxidative addition could be envisioned as a composite of an association step (i.e., the binding of the incoming ligand to generate a σ-complex) followed by an oxidative cleavage reaction (Equation (14)).[242] Similarly, a reductive elimination could be regarded as the combination of a reductive coupling and a dissociation reaction.

$$L_nM + X{-}Y \underset{\text{dissociation}}{\overset{\text{association}}{\rightleftharpoons}} \underset{\sigma\text{-complex}}{L_nM(X)(Y)} \underset{\text{reductive coupling}}{\overset{\text{oxidative cleavage}}{\rightleftharpoons}} L_nM(X)(Y) \tag{14}$$

It is important to note that the terms "oxidative" and "reductive" in all of these reactions refer to changes in the formal oxidation state of the metal whereas the terms "addition", "elimination", "coupling", and "cleavage" reflect structural modifications affecting one or more ligands. Since the oxidative or reductive nature of a process depends on the formal oxidation state of the metal before and after the reaction, the assignment of formal oxidation states should be practiced with care, especially in cases where more than one bonding scheme is possible (e.g., L vs. X_2 for an alkene).[243] In this regard, Green's thorough classification of covalent compounds of the transition metals (i.e., the popular "MLX" formalism), while dismissing the concept of formal oxidation states, provides a helpful benchmark for understanding bonding motifs in such compounds.[244]

Although the oxidative cleavage and reductive coupling of ligands are both intramolecular events, the use of external reagents or the nature of the co-ligands may often play a role in the overall reaction and the thermodynamic stability of the final products. For example, addition of excess *tert*-butylisocyanide to the tungsten(IV) complex $W(PMe_3)_4(Te)_2$ promotes the reductive coupling of the two terminal tellurido ligands and results in the formation of the tungsten(II) ditellurido derivative $W(PMe_3)(CNBu^t)_4(\eta^2\text{-}Te_2)$ (Scheme 8).[245]

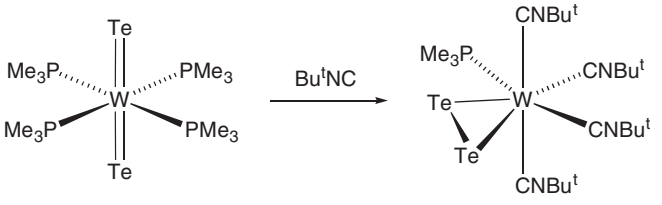

Scheme 8

Oxidative coupling and reductive cleavage are yet two additional reaction types in which the names reflect metal-based redox changes.[246] In this regard, the metal-catalyzed reactions of carbon monoxide with other donor molecules such as isonitriles (RNC), carbynes (CR), alkenes, and alkynes, often referred to in the literature as "reductive couplings" to reflect the transformations affecting the ligands, frequently involve metal-based oxidations and should therefore be more appropriately described as oxidative couplings.[247–253] Examples of "reductive coupling" of simple organic nitriles to give bridging diimido or diiminato ligands bound to two metal centers that have been formally oxidized by one or two electrons have also been described recently.[254,255] In this "metallocentric" view of reactivity patterns, a bis(ethylene) complex that yields a metallacyclopentane derivative is undergoing an oxidative coupling since the metal has been formally oxidized by two units, the two alkene ligands have (reductively) coupled, and the coordination number remains the same (Equation (15)). Regardless of semantics, the coupling of "C_1" building blocks to synthesize more elaborate organic molecules has been extensively investigated and is quite important in the context of C–C bond-forming reactions.

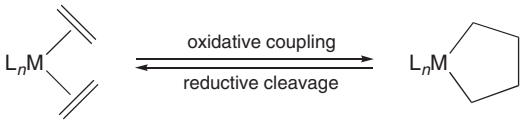

(15)

1.03.4 Insertion and Elimination Reactions

1.03.4.1 Insertion Reactions: General Considerations

Insertion reactions typically involve the combination of an anionic ligand (X) and an unsaturated molecule (AB) within the coordination sphere of a metal to generate a new ligand that, unlike reductive eliminations or substitutions, remains attached to the metal.[256–260] There are two fundamental types of insertion reactions; those in which the metal and the X ligand end up bound to the same atom (1,1- or α-insertions)[261] (Equation (16)) and those in which they end up on adjacent atoms (1,2- or β-insertions)[262] (Equation (17)). A variety of unsaturated molecules are capable of undergoing insertion reactions (see Section 1.03.4.4) but the most important ones from an industrial perspective are carbon monoxide and olefins, which are the archetypical examples of 1,1- and 1,2-insertions, respectively. Although insertion reactions and their microscopic reverses, known generically as eliminations, are potentially reversible, only one of the directions in the equilibrium is usually thermodynamically viable.

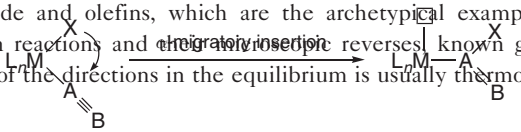

(16)

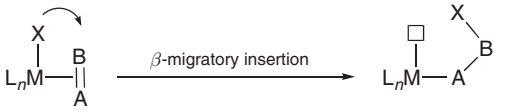

(17)

It is important to note that while the term "insertion" accurately describes the overall product of the reaction, it is mechanistically misleading since there is ample evidence that the molecule to be inserted actually coordinates to the metal before reacting further. In addition, there are compelling experimental data suggesting that the group X actually migrates to the coordinated AB molecule and, consequently, these reactions are more appropriately envisioned as ligand migratory insertions, an alternative name commonly found in the literature.

Migratory insertions require a *cis*-disposition of the AB and X ligands, which upon reaction create a vacant two-electron site ("□") at the metal center. Thus, while the formal oxidation state of the metal does not change during the insertion reaction, the electron count decreases by two and the coordination number is one unit lower. Under normal conditions, the open coordination site is subsequently occupied by an additional ligand, which effectively traps the insertion product and regenerates the original electron count and coordination number.

1.03.4.2 Carbonyl Insertion Reactions

The insertion of carbon monoxide into a metal–alkyl (or metal–aryl) bond to give an acyl (or aroyl) complex M–C(O)R is one of the best-studied reactions in organometallic chemistry (Equation (18)).[263–268] The hydroformylation of alkenes (i.e., the oxo process)[269–272] and the carbonylation of methanol (i.e., the BASF and Monsanto acetic acid processes)[273–275] are two examples of massive industrial operations that involve the insertion of CO into a metal–carbon bond in their catalytic cycles. Furthermore, there has been an upsurge of interest in the function of the ubiquitous enzyme acetyl–CoA synthase (ACS) since the molecular structure of the so-called A-cluster, responsible for the assembly of an acetate moiety at a nickel center, was recently elucidated using X-ray crystallography.[276–281]

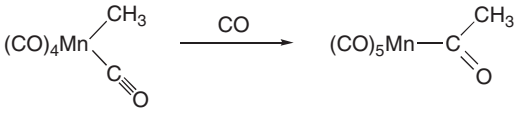

(18)

The mechanism of carbonylation of M–C bonds has been firmly established based on elegant experimental and theoretical studies carried out with both $MeMn(CO)_5$ and $Mn(CO)_5(COMe)$.[264,282–285] Of the three basic mechanistic possibilities (i.e., CO insertion, CO migration, and methyl migration), only the latter was found to be consistent with all the kinetic and isotope labeling (^{13}CO) data available, including the observation that the process is intramolecular (i.e., the acyl forms from a CO already bound to the metal) and that the external CO ligand is usually added *cis* to the acyl group. The addition of Lewis acids like BF_3 or $AlCl_3$ and the use of coordinating polar solvents are factors that accelerate the migration of the alkyl group, which can also be promoted by chemical or photochemical oxidation of a catalytic amount of the starting 18-electron complex.[286]

The versatility of CO as a synthon also stems from its ability to undergo insertion reactions into a variety of metal–heteroatom bonds. The migratory insertion of CO into transition metal–hydride bonds, while thermodynamically unfavorable, generates metal–formyl complexes M–C(O)H (Equation (19)), a few examples of which have been isolated independently.[287,288] This reaction is assumed to be a key step in both the homogeneous and heterogeneous catalytic hydrogenation (i.e., reduction) of CO, including the Fischer–Tropsch synthesis of hydrocarbons[289–294] and the Union Carbide process for the preparation of ethylene glycol from syngas.[295,296]

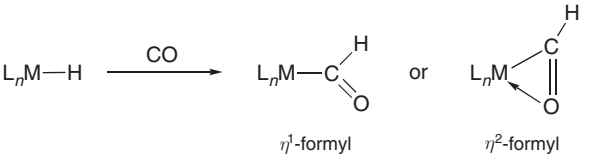

(19)

Carbon monoxide also reacts with metal hydroxide (M–OH) or alkoxide (M–OR) complexes[297–300] to give hydroxycarbonyl (metallacarboxylic acid) [M–C(O)OH] or alkoxycarbonyl (metallacarboxylate) [M–C(O)OR] derivatives, respectively (Equation (20)). Although several examples of these types of compounds are now known,[301–311] not all have been synthesized by the straightforward migratory insertion of CO into M–OH or M–OR bonds. Some alkoxycarbonyl complexes, for instance, have been obtained by esterification of a hydroxycarbonyl precursor or by the direct reaction of a carbonyl complex with an alkali metal alkoxide. Furthermore, a dissociative mechanism whereby the initial displacement of CO by a weakly bound aryl oxide ligand is followed by the nucleophilic attack of the latter on a carbonyl ligand to give the expected aryloxycarbonyl product has been considered for the carbonylation of certain late transition metal aryloxide complexes.[312,313]

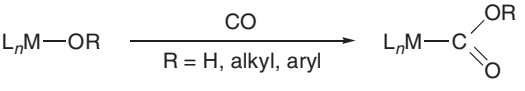

(20)

The preparation of metal carbamoyl [M–C(O)NR_2] and silaacyl [M–C(O)SiR_3] derivatives by the migratory insertion of CO in the appropriate metal amide (M–NR_2) or silyl (M–SiR_3) complexes is also precedented.[263–268,314–316] Although CO reacts with metal–acyl bonds to give α-ketoacyl compounds,[317] this and related reactions that appear to be double carbonylations but do not actually involve two consecutive CO migratory insertions have also been reported.[318]

1.03.4.3 Alkene Insertions

The insertion of alkenes into M–H or M–C bonds is one of the common methods used for the generation of metal alkyl complexes and is a crucial step in a variety of catalytic processes, most importantly the Ziegler–Natta polymerization of olefins.[22,319–325] In these intramolecular reactions, a coordinated alkene undergoes a concerted 1,2-insertion via a planar cyclic transition state, leaving behind an open coordination site (Equation (21)).[326,327] Binding of a new olefin molecule and subsequent cycles of alternating migratory insertion and alkene coordination lead to polymer chain growth (i.e., the Cossee mechanism).[328] Agostic complexes[329,330] may also play a key role as intermediates since they could be responsible for lowering the activation barrier for the insertion step and also contribute to define the product's stereochemistry.[331]

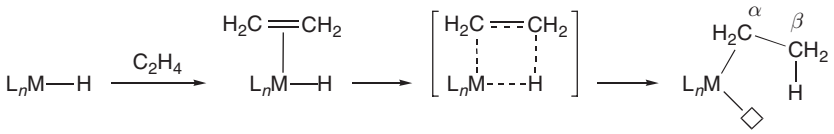

(21)

The hydrozirconation of alkenes using Cp_2ZrHCl (Schwartz's reagent) is another important application of olefin insertion chemistry.[332] The Zr–H bond in the zirconocene derivative reacts with terminal alkenes at the least sterically hindered position (i.e., an anti-Markovnikov addition) and the resulting zirconium alkyl complex could be readily functionalized to a variety of alkyl halides and alcohols (Equation (22)).[333–335] Similarly, terminal alkynes and 1,3-dienes react with Cp_2ZrHCl to give *cis*-vinyl and γ,δ-unsaturated alkyl complexes, respectively. The insertion of an alkene into one of the B–H bonds in diborane (B_2H_6) to give an organoborane derivative, which is typically oxidized to an alcohol using hydrogen peroxide in aqueous base, is also one of the most versatile and thoroughly studied methods for the conversion of olefins to alcohols (i.e., hydroboration reactions).[336–340]

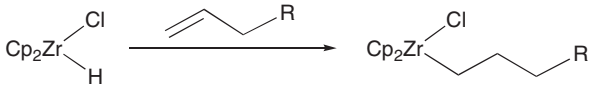

(22)

Alkenes may also insert into the Pd–C bonds of some palladium acyl complexes,[341,342] an important reaction that has been successfully applied to the synthesis of polyketones of general formula $[–CH_2CH_2C(O)–]_n$ via the alternating co-polymerization of CO and ethylene (Scheme 9).[343–347]

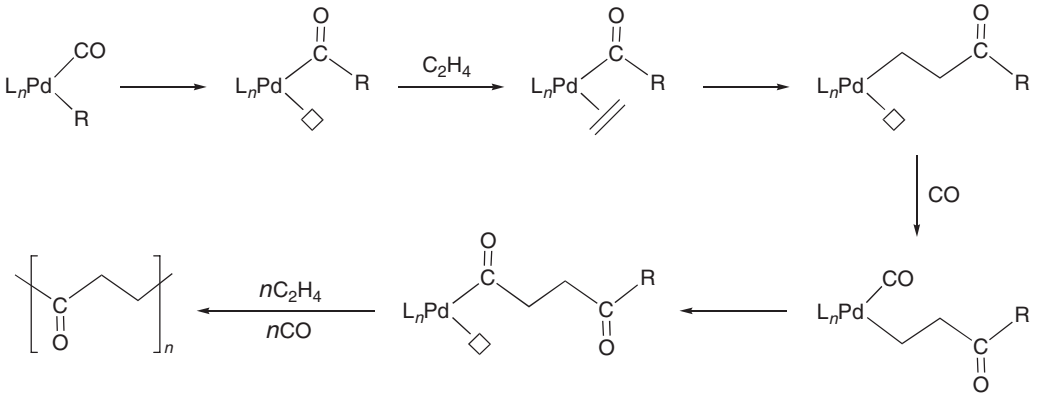

Scheme 9

1.03.4.4 Other Insertion Reactions

Although CO and alkenes are the most prominent substrates participating in migratory insertions, a variety of additional molecules are also susceptible to undergo such reactions.[348,349] For example, both alkyl and aryl isonitriles (RNC) readily insert into M–C or M–H bonds to generate iminoacyl or formimidoyl derivatives, respectively

(Equation (23)).[266,350–353] Even though CO and RNC are isoelectronic species, the latter tends to be more reactive and consequently multiple insertions into M–C bonds are more common than for acyl complexes. Similarly, the insertion of an alkyne into an M–C bond gives a vinyl derivative.

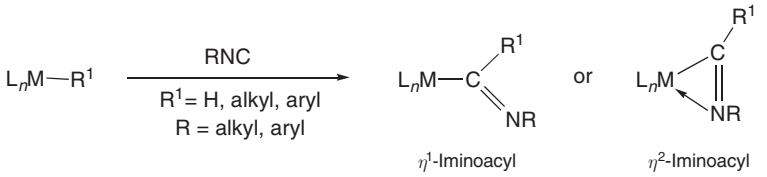

(23)

The synthesis and coordination chemistry of carbon dioxide complexes has attracted a lot of attention over the years[354,355] and their reactivity, not surprisingly, includes several types of 1,2-migratory insertion reactions.[356–359] Thus, CO_2 inserts into a variety of M–X bonds (X = H, C, O, N, P, S, Si) to yield the corresponding M–OC(O)X products, often following the initial formation of a π-complex (Scheme 10).

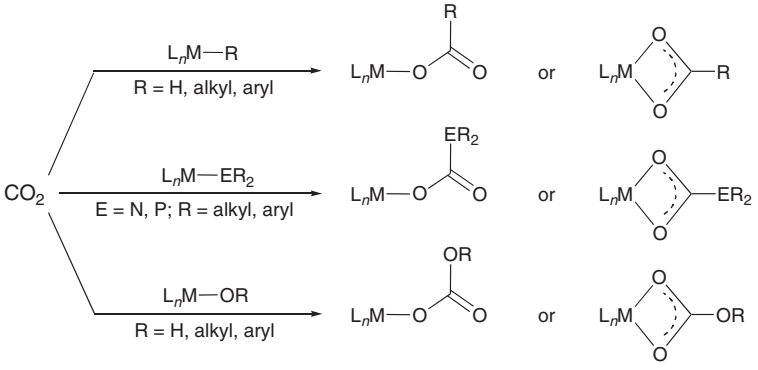

Scheme 10

The reaction of CO_2 with a metal hydride produces formate complexes M–OC(O)H, not formyl derivatives M–C(O)OH, and the insertion into M–C bonds gives the appropriate carboxylate compounds M–OC(O)R. In a similar fashion, the reactions with M–OH and M–OR (R = alkyl, aryl) generate the corresponding bicarbonate M–OC(O)OH and carbonate M–OC(O)OR species, respectively. The reaction of CO_2 with a zinc hydroxide moiety is particularly important in biological systems, namely, for the reversible hydration of CO_2 to HCO_3^- catalyzed by Zn(II) in carbonic anyhdrases.[26,360,361] Moreover, it has been postulated that the insertion of CO_2 into M–O bonds is essential in the co-polymerization of CO_2 and epoxides and in the preparation of cyclic carbonates and polycarbonates.[362,363] In a similar vein, the insertion of CO_2 into the M–N bond of both main group and transition metal dialkylamides (M–NR_2) yields the corresponding carbamate complexes M(O_2CNR_2).[364]

Other electrophilic heterocumulenes (e.g., CS_2, RNCO, RNCS, SO_2) are also subject to insertion reactions. Accordingly, the insertion of CS_2 into the M–N bond in metal dialkylamides produces dithiocarbamate derivatives[365] and the reaction of SO_2 with M–C bonds gives sulfinate complexes resulting from either 1,1-insertion [M–OS(O)R] or 1,2-insertion [M–S(R)O_2].[366–368] Rare examples of insertion of dioxygen into Pt–H bonds to generate remarkably stable hydroperoxide derivatives L_nPt–OOH have also been reported.[369,370]

1.03.4.5 Elimination Reactions

The microscopic reverse of migratory insertions, known as deinsertions, extrusions, or (most commonly) eliminations, involves the fragmentation of a ligand within the coordination sphere of a metal and the generation of a new complex with the same formal oxidation state but the electron count increased by two and the coordination number one unit higher (unless the eliminated group also dissociates). Since elimination requires a vacant site at the metal, an electronically saturated (18-electron) complex will not undergo such reactions unless another ligand dissociates

first. The most important type of elimination, in which the group to be eliminated is in the β-position relative to the metal, is called a β-elimination and is formally the reverse of a 1,2-insertion (Equation (24)).

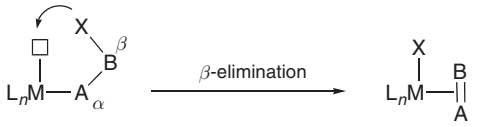

(24)

The elimination of a hydrogen atom from the β-position is commonly found in the decomposition of metal alkyl complexes, whereby a hydrido alkene derivative is generated. Thus, common strategies to prevent the decomposition of alkyl complexes include the use of organic groups lacking β-hydrogens such as methyl, neopentyl, benzyl, phenyl, and trimethylsilylmethyl ($-CH_2SiMe_3$). Complexes having alkyl ligands with electron-withdrawing substituents (e.g., fluorinated alkyls) also tend to be fairly robust and do not readily decompose.[124–127]

Alternative decomposition pathways for alkyl and other ligands that do not have β-hydrogens often entail the cleavage of a C–H bond in the α-, γ-, or even δ-positions. A methyl group, for example, may undergo an α-elimination, which can be regarded as the microscopic reverse of a 1,1-migratory insertion, to generate a hydrido methylene complex (Equation (25)).

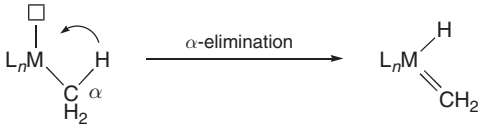

(25)

1.03.5 Reactions on Coordinated Ligands

1.03.5.1 General Considerations

The ability to enhance or modify the reactivity of unsaturated organic molecules upon their coordination to a metal center is one of the salient features of synthetic and mechanistic organometallic chemistry. Unlike previous sections in this chapter, the reactions described below occur directly at coordinated ligands, with the metal playing an important role in the activation of the substrates but without directly interacting with the reagents. The attacking groups can have either nucleophilic or electrophilic character and molecular fragments could be either added to or removed from existing ligands and therefore the reactions described below will be discussed accordingly. Excluded from this classification are single-electron pathways, that is, the ligand-centered reactivity of organometallic radicals and the reaction of organic free radicals with metal complexes.[34–41,371]

1.03.5.2 Nucleophilic Additions

Carbon monoxide and electron-rich π-ligands such as alkenes, polyenes, and arenes, which do not normally react with nucleophiles, are rendered more susceptible to nucleophilic attack upon coordination to a metal. There are several factors that contribute to decreasing the electron density at the metal and increasing the reactivity of a coordinated ligand, including (i) the presence of an overall positive charge or other electron-withdrawing ligands on the complex and (ii) the display of coordinative saturation, which makes a direct attack at the metal less likely.

CO is particularly reactive toward nucleophiles when coordinated to an electron-deficient metal center, where the degree of backbonding to the CO's π^* orbitals is limited. In the classic synthesis of Fischer (heteroatom-stabilized) carbenes, an organolithium reagent attacks a CO and generates an acyl intermediate, which is subsequently alkylated to give the final product (Equation (26)). The presence of a positive charge in $[Mn(CO)_6]^+$ makes it significantly more sensitive to nucleophilic attack than its isoelectronic and isosteric analog $Mo(CO)_6$, so even weaker nucleophiles such as water or alcohols can be used to prepare the corresponding metallacarboxylic acid or ester derivatives.

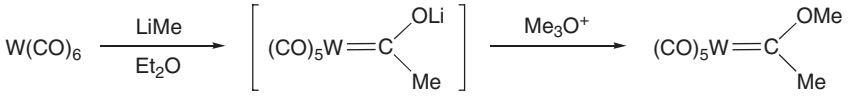

(26)

The nucleophilic addition to polyene (e.g., alkene, diene, arene) and polyenyl (e.g., allyl, cyclopentadienyl) ligands has contributed significantly to the numerous and unique applications organometallic reagents have in organic synthesis.[372–375] The catalytic oxidation of olefins to carbonyl compounds (e.g., the palladium-mediated conversion

of ethylene to acetaldehyde) in the Wacker process is a prime example of nucleophilic addition chemistry applied in a large industrial scale.[376,377]

Although polyenes are typically subject to electrophilic attack in the free state, they are rendered amenable to nucleophilic attack as coordinated ligands, a fascinating reversal in chemical reactivity usually referred to by the German term "umpolung". It is important to note that nucleophiles (Nu^-) usually add to the external face of an arene ligand (i.e., an "*exo*-" attack) and tend to reduce the hapticity of the ligands to which they add (Scheme 11).

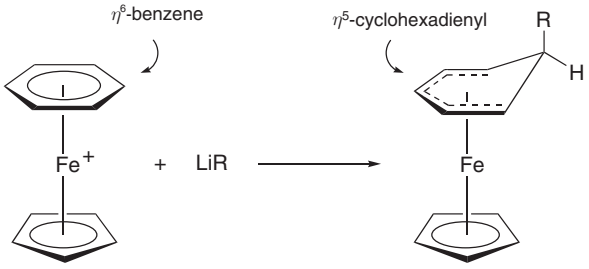

Scheme 11

Davies *et al*. have developed a succinct set of guidelines to predict the most favorable position of nucleophilic attack on electronically saturated cationic metal complexes bearing more than one unsaturated hydrocarbon ligand.[378] In essence, the so-called DGM rules state that (i) polyenes (L_n-type ligands) are more reactive than polyenyls (L_nX-type ligands; see also Scheme 11); (ii) open or acyclic ligands react before closed or cyclic ligands; and (iii) addition to the terminal position occurs in all polyenes and most polyenyls.[379,380]

1.03.5.3 Nucleophilic Abstractions

A nucleophile may extract a cationic fragment such as a proton (H^+) or an alkyl group (R^+) from a coordinated ligand, and therefore these reactions can be regarded as deprotonations and dealkylations, respectively. They are not particularly common processes since the reduced metal complexes are typically poor leaving groups but an interesting example involves the deprotonation of the iridium hydride complex $Cp^*Ir(PMe_3)H_2$ to give a strongly basic iridate derivative.[381] Another beautiful example of ligand deprotonation involves the preparation of the first complex containing a terminal carbide ligand, $[\{Ar(R)N\}_3Mo{\equiv}C{:}]^-$, by reacting the methylidyne complex $\{Ar(R)N\}_3Mo{\equiv}CH$ with benzyl potassium.[382,383]

The nucleophilic abstraction of an acyl group is much more important and is perhaps best exemplified by the multifarious palladium(0)-catalyzed carbonylation reactions of organic halides.[384,385] Aryl, benzyl, vinyl, and heterocyclic halides are carbonylated to esters, amides, or aldehydes in the presence of alcohols, primary amines, or H_2, respectively, but unfortunately the mechanistic intricacies of these reactions are still not fully understood (Scheme 12). Similarly, disodium tetracarbonylferrate ($Na_2Fe(CO)_4$, Collman's reagent) is a synthetically valuable complex used in the preparation of esters from hydrocarbon halides via nucleophilic acyl abstraction reactions.[386]

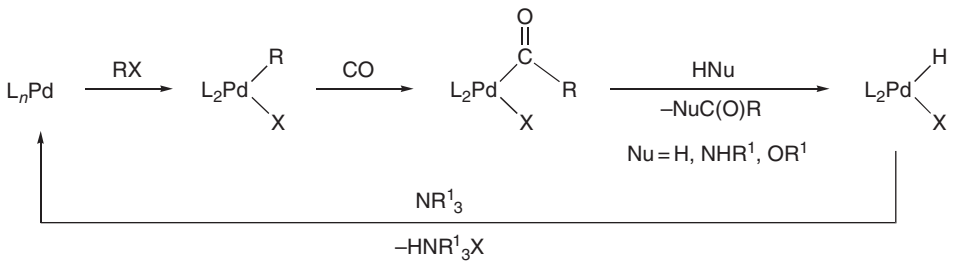

Scheme 12

1.03.5.4 Electrophilic Additions

Electrophilic species such as H^+ or Me^+ may also add directly to a metal or to a coordinated ligand rather than abstract a nucleophile (Section 1.03.5.3) and, as such, these additions can be regarded as protonation or alkylation reactions.[387–393] In contrast to the addition of a nucleophile (Nu^-), the net result of adding an electrophile (E^+) to a polyene is the reduction of electron density at the ligand, which is compensated in part by the interaction with an additional metal-based lone pair. Thus, an effective increase in hapticity takes place and a polyenyl ligand containing a delocalized π-system with one additional carbon atom is generated, for example, the transformation of an η^4-diene to an η^5-cyclohexadienyl (Scheme 13).

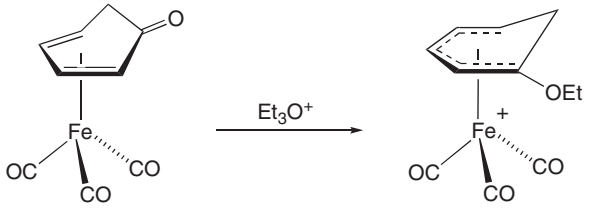

Scheme 13

Factors that promote the electrophilic attack to coordinated ligands are usually based on the generation of an electron-rich metal center. This could be a consequence of several bonding features, including (i) a zero or negative overall charge on the complex, (ii) a low formal oxidation state for the metal, and (iii) the presence of good donor ligands that strengthen the degree of backbonding and increase the electron density at the ligand to be attacked.

Protonation of ligands is a simple yet versatile method to accomplish a variety of fundamental transformations in coordination chemistry, from the synthesis of dihydrogen complexes starting from metal hydride precursors[133–137,395–396] to the generation of N_2H_x species with different degrees of unsaturation during the reduction of dinitrogen to ammonia (i.e., nitrogen fixation).[397–402]

1.03.5.5 Electrophilic Abstractions

The removal of a negatively charged fragment like a hydride (H^-) or an alkyl anion (R^-) from a coordinated ligand by an electrophile (E^+) is also a widely applied synthetic strategy in inorganic and organometallic chemistry. Common electrophiles include metal ions such as Hg(II) and organic species like the triphenylmethyl (trityl) cation Ph_3C^+, which has been used to prepare, for example, the unusual cationic methylene complex $[Cp_2Re{=}CH_2]^+$ (Scheme 14).[403]

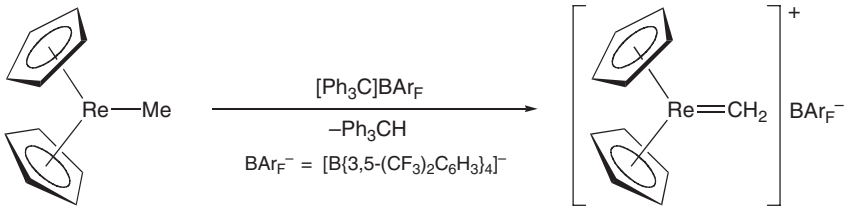

Scheme 14

Abstraction of an anionic molecular fragment from a coordinated ligand by an electrophile, much like the addition of an electrophile, sometimes results in the generation of a new ligand with an expanded hapticity. Thus, hydride abstraction from a methylene group in a polyene ligand forms a polyenyl ligand with an additional carbon atom in the conjugated π-system, as in the conversion of an η^6-cyclooctatriene to an η^7-cyclooctatrienyl (Scheme 15).

Electrophiles do not have to be cations: tris(pentafluorophenyl)borane $B(C_6F_5)_3$ and related Lewis acids are very efficient hydride and alkyl anion abstractors and have found important applications as co-catalysts in the homogeneous Ziegler–Natta polymerization of olefins.[21–25,404–406] The quest for better activators with potential

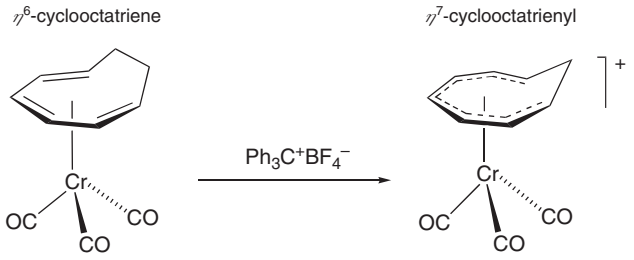

Scheme 15

applications in metallocene-based alkene polymerizations continues and the synthesis and reactivity of novel, highly electrophilic borinium, borenium, and boronium cations $[R_2BL_n]^+$ (where $n = 0$, 1, or 2, respectively) has been reviewed recently.[407]

References

1. Collman, J. P.; Hegedus, L. S.; Norton, J. R.; Finke, R. G. *Principles and Applications of Organotransition Metal Chemistry*; University Science Books: Mill Valley, 1987.
2. Crabtree, R. H. *The Organometallic Chemistry of the Transition Metals*, 4th ed.; Wiley: Hoboken, 2005.
3. Spessard, G. O.; Miessler, G. L. *Organometallic Chemistry*; Prentice-Hall: Upper Saddle River, 1997.
4. Hill, A. F. *Organotransition Metal Chemistry*; Royal Society of Chemistry/Wiley: New York, 2002.
5. Mathey, F.; Sevin, A. *Molecular Chemistry of the Transition Elements*; Wiley: New York, 1996.
6. Atwood, J. D. *Inorganic and Organometallic Reaction Mechanisms*, 2nd ed.; VCH: New York, 1997.
7. Jordan, R. B. *Reaction Mechanisms of Inorganic and Organometallic Systems*, 2nd ed.; Oxford University Press: New York, 1998.
8. Tobe, M. L.; Burgess, J. *Inorganic Reaction Mechanisms*; AddisonWesley Longman: New York, 1999.
9. Hay, R. W. *Reaction Mechanisms of Metal Complexes*; Horwood Publishing: Chichester, 2000.
10. Asperger, S. *Chemical Kinetics and Inorganic Reaction Mechanisms*, 2nd ed.; Kluwer Academic/Plenum Publishers: New York, 2003.
11. Richens, D. T. *Chem. Rev.* **2005**, *105*, 1961–2002.
12. Burgess, J.; Hubbard, C. D. *Adv. Inorg. Chem.* **2003**, *54*, 71–155.
13. Howell, J. A. S.; Burkinshaw, P. M. *Chem. Rev.* **1983**, *83*, 557–599.
14. Basolo, F. *Coord. Chem. Rev.* **1990**, *100*, 47–66.
15. Basolo, F. *Isr. J. Chem.* **1986**, *27*, 233–240.
16. Slone, C. S.; Weinberger, D. A.; Mirkin, C. A. *Prog. Inorg. Chem.* **1999**, *48*, 233–350.
17. Gianneschi, N. C.; Masar, M. S. III; Mirkin, C. A. *Acc. Chem. Res.* **2005**, *38*, 825–837.
18. Holliday, B. J.; Mirkin, C. A. *Angew. Chem., Int. Ed.* **2001**, *40*, 2022–2043.
19. Allgeier, A. M.; Mirkin, C. A. *Angew. Chem., Int. Ed.* **1998**, *37*, 894–908.
20. Braunstein, P.; Naud, F. *Angew. Chem., Int. Ed.* **2001**, *40*, 680–699.
21. Krossing, I.; Raabe, I. *Angew. Chem., Int. Ed.* **2004**, *43*, 2066–2090.
22. Chen, E. Y.-X.; Marks, T. J. *Chem. Rev.* **2000**, *100*, 1391–1434.
23. Lupinetti, A. J.; Strauss, S. H. *Chemtracts Inorg. Chem.* **1998**, *11*, 565–595.
24. Reed, C. A. *Acc. Chem. Res.* **1998**, *31*, 133–139.
25. Strauss, S. H. *Chem. Rev.* **1993**, *93*, 927–942.
26. Parkin, G. *Chem. Rev.* **2004**, *104*, 699–767.
27. Auld, D. S. *BioMetals* **2001**, *14*, 271–313.
28. Caravan, P.; Ellison, J. J.; McMurry, T. J.; Lauffer, R. B. *Chem. Rev.* **1999**, *99*, 2293–2352.
29. Aime, S.; Botta, M.; Terreno, E. *Adv. Inorg. Chem.* **2005**, *57*, 173–237.
30. Raymond, K. N.; Pierre, V. C. *Bioconjugate Chem.* **2005**, *16*, 3–8.
31. Maiocchi, A. *Mini Rev. Med. Chem.* **2003**, *3*, 845–859.
32. Gries, H. *Top. Curr. Chem.* **2002**, *221*, 1–24.
33. Sherry, A. D.; Zhang, S.; Woods, M. In *Medicinal Inorganic Chemistry*; Sessler, J. L., Doctrow, S. R., McMurry, T. J., Lippard, S. J., Eds.; American Chemical Society: Washington, 2005; Chapter 10, pp 151–165.
34. Astruc, D. *Acc. Chem. Res.* **1991**, *24*, 36–42.
35. Astruc, D. *Chem. Rev.* **1988**, *88*, 1189–1216.
36. Baird, M. C. *Chem. Rev.* **1988**, *88*, 1217–1227.
37. Pariya, C.; Theopold, K. H. *Curr. Sci.* **2000**, *78*, 1345–1351.
38. Tyler, D. R. *Prog. Inorg. Chem.* **1988**, *36*, 125–194.
39. Pevear, K. A.; Banaszak Holl, M. M.; Carpenter, G. B.; Rieger, A. L.; Rieger, P. H.; Sweigart, D. A. *Organometallics* **1995**, *14*, 512–523.
40. Trogler, W. C. *Int. J. Chem. Kinet.* **1987**, *19*, 1025–1047.
41. Sun, S.; Sweigart, D. A. *Adv. Organomet. Chem.* **1996**, *40*, 171–214.
42. Basolo, F. *J. Organomet. Chem.* **1990**, *383*, 579–586.
43. Basolo, F. *Polyhedron* **1990**, *9*, 1503–1535.

44. Darensbourg, D. J. *Adv. Organomet. Chem.* **1982**, *21*, 113–150.
45. Albers, M. O.; Coville, N. J. *Coord. Chem. Rev.* **1984**, *53*, 227–259.
46. Atwood, J. D. *J. Organomet. Chem.* **1990**, *383*, 59–69.
47. Langford, C. H.; Gray, H. B. *Ligand Substitution Processes*; W. A. Benjamin: New York, 1966.
48. Merbach, A. E. *Pure Appl. Chem.* **1982**, *54*, 1479–1493.
49. Merbach, A. E. *Pure Appl. Chem.* **1987**, *59*, 161–172.
50. Helm, L.; Merbach, A. E. *Chem. Rev.* **2005**, *105*, 1923–1959.
51. Helm, L.; Nicolle, G. M.; Merbach, A. E. *Adv. Inorg. Chem.* **2005**, *57*, 327–379.
52. Helm, L.; Merbach, A. E. *Adv. Inorg. Chem.* **2003**, *54*, 1–69.
53. van Eldik, R.; Dücker-Benfer, C.; Thaler, F. *Adv. Inorg. Chem.* **2000**, *49*, 1–58.
54. Helm, L.; Merbach, A. E. *J. Chem. Soc., Dalton Trans.* **2002**, 633–641.
55. Drljaca, A.; Hubbard, C. D.; van Eldik, R.; Asano, T.; Basilevsky, M. V.; le Noble, W. J. *Chem. Rev.* **1998**, *98*, 2167–2289.
56. Taube, H. *Chem. Rev.* **1952**, *50*, 69–126.
57. Rotzinger, F. P. *Chem. Rev.* **2005**, *105*, 2003–2037, and references therein.
58. Cross, R. J. *Chem. Soc. Rev.* **1985**, *14*, 197–223.
59. Banerjee, P. *Coord. Chem. Rev.* **1999**, *190–192*, 19–28.
60. Basolo, F. *Coord. Chem. Rev.* **1996**, *154*, 151–161.
61. Basolo, F.; Pearson, R. G. *Mechanisms of Inorganic Reactions*, 2nd ed.; Wiley: New York, 1967; Chapter 5, pp 351–453.
62. Tobe, M. L.; Burgess, J. In *Inorganic Reaction Mechanisms*; Addison Wesley Longman: New York, 1999; pp 70–112.
63. Cross, R. J. *Adv. Inorg. Chem.* **1989**, *34*, 219–292.
64. Huheey, J. E.; Keiter, E. A.; Keiter, R. L. In *Inorganic Chemistry: Principles of Structure and Reactivity*, 4th ed.; HarperCollins College Publishers: New York, 1993; pp 540–542.
65. Basolo, F.; Pearson, R. G. *Prog. Inorg. Chem.* **1962**, *4*, 381–453.
66. Berry, R. S. *J. Chem. Phys.* **1960**, *32*, 933–938.
67. Ugi, I.; Marquarding, D.; Klusacek, H.; Gillespie, P.; Ramirez, F. *Acc. Chem. Res.* **1971**, *4*, 288–296.
68. Reedijk, J. *Proc. Natl. Acad. Sci. USA* **2003**, *100*, 3611–3616.
69. Reedijk, J. *Coord. Chem. Rev.* **2005**, *249*, 2845–2853.
70. Jamieson, E. R.; Lippard, S. J. *Chem. Rev.* **1999**, *99*, 2467–2498.
71. Bruhn, S. L.; Toney, J. H.; Lippard, S. J. *Prog. Inorg. Chem.* **1990**, *38*, 477–516.
72. Lippert, B., Ed. *Cisplatin: Chemistry and Biochemistry of a Leading Anticancer Drug*; Wiley-VCH: New York, 1999.
73. Lippert, B. *Prog. Inorg. Chem.* **1989**, *37*, 1–97.
74. Kelland, L. R. In *Uses of Inorganic Chemistry in Medicine*; Farrell, N. P., Ed.; Royal Society of Chemistry: Cambridge, 1999; Chapter 7, pp 109–123.
75. Barnes, K. R.; Lippard, S. J. In *Metal Ions in Biological Systems, Vol. 42: Metal Complexes in Tumor Diagnosis and as Anticancer Agents*; Sigel, A., Sigel, H., Eds.; Dekker: New York, 2004; Chapter 5, pp 143–177.
76. Wheate, N. J.; Collins, J. G. *Coord. Chem. Rev.* **2003**, *241*, 133–145.
77. Farrell, N.; Spinelli, S. In *Uses of Inorganic Chemistry in Medicine*; Farrell, N. P., Ed.; Royal Society of Chemistry: Cambridge, 1999; Chapter 8, pp 124–134.
78. Lippert, B. *Coord. Chem. Rev.* **1999**, *182*, 263–295.
79. Farrell, N. In *Metal Ions in Biological Systems, Vol. 42: Metal Complexes in Tumor Diagnosis and as Anticancer Agents*; Sigel, A., Sigel, H., Eds.; Dekker: New York, 2004; Chapter 8, pp 251–296.
80. Hall, M. D.; Hambley, T. W. *Coord. Chem. Rev.* **2002**, *232*, 49–67.
81. Hall, M. D.; Dolman, R. C.; Hambley, T. W. In *Metal Ions in Biological Systems, Vol. 42: Metal Complexes in Tumor Diagnosis and as Anticancer Agents*; Sigel, A., Sigel, H., Eds.; Dekker: New York, 2004; Chapter 9, pp 297–322.
82. Navarro, M.; Peña, N. P.; Colmenares, I.; González, T.; Arsenak, M.; Taylor, P. *J. Inorg. Biochem.* **2006**, *100*, 152–157.
83. Giovagnini, L.; Ronconi, L.; Aldinucci, D.; Lorenzon, D.; Sitran, S.; Fregona, D. *J. Med. Chem.* **2005**, *48*, 1588–1595.
84. Katsaros, N.; Anagnostopoulou, A. *Crit. Rev. Onc. Hemat.* **2002**, *42*, 297–308.
85. Tiekink, E. R. T. *Crit. Rev. Onc. Hemat.* **2002**, *42*, 225–248.
86. Rajput, J.; Moss, J. R.; Hutton, A. T.; Hendricks, D. T.; Arendse, C. E.; Imrie, C. *J. Organomet. Chem.* **2004**, *689*, 1553–1568.
87. Shaw, F. C. III *Chem. Rev.* **1999**, *99*, 2589–2600.
88. Marcon, G.; Messori, L.; Orioli, P. *Expert Rev. Anticancer Ther.* **2002**, *2*, 337–346.
89. Lay, P. A. *Coord. Chem. Rev.* **1991**, *110*, 213–233.
90. Swaddle, T. W. *Comments Inorg. Chem.* **1991**, *12*, 237–258.
91. Basolo, F.; Pearson, R. G. In *Mechanisms of Inorganic Reactions*, 2nd ed.; Wiley: New York, 1967; Chapter 3, pp 124–246.
92. Tobe, M. L.; Burgess, J. In *Inorganic Reaction Mechanisms*; Addison Wesley Longman: New York, 1999; pp 128–204.
93. Clarke, M. J.; Zhu, F.; Frasca, D. R. *Chem. Rev.* **1999**, *99*, 2511–2533.
94. Clarke, M. J. *Coord. Chem. Rev.* **2003**, *236*, 209–233.
95. Alessio, E.; Mestroni, G.; Bergamo, A.; Sava, G. In *Metal Ions in Biological Systems, Vol. 42: Metal Complexes in Tumor Diagnosis and as Anticancer Agents*; Sigel, A., Sigel, H., Eds.; Dekker: New York, 2004; Chapter 10, pp 323–351.
96. Keppler, B. K.; Lipponer, K.-G.; Stenzel, B.; Kratz, F. In *Metal Complexes in Cancer Therapy*; Keppler, B. K., Ed.; VCH: New York, 1993; pp 187–220.
97. Coe, B. J.; Glenwright, S. J. *Coord. Chem. Rev.* **2000**, *203*, 5–80.
98. Basolo, F. *Coord. Chem. Rev.* **1982**, *43*, 7–15.
99. Basolo, F. *Inorg. Chim. Acta* **1985**, *100*, 33–39.
100. Basolo, F. *Pure Appl. Chem.* **1988**, *60*, 1193–1196.
101. Basolo, F. *New J. Chem.* **1994**, *18*, 19–24.
102. O'Connor, J. M.; Casey, C. P. *Chem. Rev.* **1987**, *87*, 307–318.
103. Merola, J. S.; Kacmarcik, R. T.; Van Engen, D. *J. Am. Chem. Soc.* **1986**, *108*, 329–331.
104. Rerek, M. E.; Ji, L.-N.; Basolo, F. *J. Chem. Soc., Chem. Commun.* **1983**, 1208–1209.
105. Ji, L.-N.; Rerek, M. E.; Basolo, F. *Organometallics* **1984**, *3*, 740–745.

106. Calhorda, M. J.; Romão, C. C.; Veiros, L. F. *Chem. Eur. J.* **2002**, *8*, 868–875.
107. Veiros, L. F. *Organometallics* **2000**, *19*, 3127–3136.
108. Calhorda, M. J.; Veiros, L. F. *Coord. Chem. Rev.* **1999**, *185–186*, 37–51.
109. Calhorda, M. J.; Veiros, L. F. *Comments Inorg. Chem.* **2001**, *22*, 375–391.
110. Rerek, M. E.; Basolo, F. *J. Am. Chem. Soc.* **1984**, *106*, 5908–5912.
111. Butler, I. S.; Uhm, H. L. *Comments Inorg. Chem.* **1988**, 7, 1–16.
112. Muetterties, E. L.; Bleeke, J. R.; Sievert, A. C. *J. Organomet. Chem.* **1979**, *178*, 197–216.
113. Traylor, T. G.; Stewart, K. J.; Goldberg, M. J. *J. Am. Chem. Soc.* **1984**, *106*, 4445–4454.
114. Harman, W. D. *Coord. Chem. Rev.* **2004**, *248*, 853–866.
115. Harman, W. D. *Coord. Chem. Rev.* **2000**, *206–207*, 3–61.
116. Harman, W. D. *Chem. Rev.* **1997**, *97*, 1953–1978.
117. Thompson, R. L.; Lee, S.; Rheingold, A. L.; Cooper, N. J. *Organometallics* **1991**, *10*, 1657–1659, and references therein.
118. Muetterties, E. L.; Bleeke, J. R. *Acc. Chem. Res.* **1979**, *12*, 324–331.
119. Dyson, P. J. *Dalton Trans.* **2003**, 2964–2974.
120. Parshall, G. W.; Ittel, S. D. In *Homogeneous Catalysis*, 2nd ed.; Wiley: New York, 1993; pp 180–183.
121. Widegren, J. A.; Finke, R. G. *J. Mol. Catal. A* **2003**, *191*, 187–207.
122. Geldbach, T. J.; Dyson, P. J. *J. Organomet. Chem.* **2005**, *690*, 3552–3557.
123. Cotton, F. A.; Wilkinson, G.; Murillo, C. A.; Bochmann, M. In *Advanced Inorganic Chemistry*, 6th ed.; Wiley: New York, 1999; pp 1171–1194.
124. Jasim, N. A.; Perutz, R. N.; Whitwood, A. C.; Braun, T.; Izundu, J.; Neumann, B.; Rothfeld, S.; Stammler, H.-G. *Organometallics* **2004**, *23*, 6140–6149.
125. Kiplinger, J. L.; Richmond, T. G.; Osterberg, C. E. *Chem. Rev.* **1994**, *94*, 373–431.
126. Braun, T.; Perutz, R. N. *Chem. Commun.* **2002**, 2749–2757.
127. Burdeniuc, J.; Jedlicka, B.; Crabtree, R. H. *Chem. Ber:Recl.* **1997**, *130*, 145–154.
128. Aldridge, S.; Coombs, D. L. *Coord. Chem. Rev.* **2004**, *248*, 535–559.
129. Braunschweig, H.; Colling, M. *Coord. Chem. Rev.* **2001**, *223*, 1–51.
130. Smith, M. R. III *Prog. Inorg. Chem.* **1999**, *48*, 505–567.
131. Zhao, J.; Goldman, A. S.; Hartwig, J. F. *Science* **2005**, *307*, 1080–1082.
132. Braun, T. *Angew. Chem., Int. Ed.* **2005**, *44*, 5012–5014.
133. Esteruelas, M. A.; Oro, L. A. *Chem. Rev.* **1998**, *98*, 577–588.
134. Kubas, G. J. *Catal. Lett.* **2005**, *104*, 79–101.
135. Kubas, G. J. *Metal Dihydrogen Complexes and σ-Bond Complexes*; Kluwer Academic/Plenum Publishers: New York, 2001.
136. Heinekey, D. M.; Oldham, W. J., Jr. *Chem. Rev.* **1993**, *93*, 913–926.
137. Jessop, P. G.; Morris, R. H. *Coord. Chem. Rev.* **1992**, *121*, 155–284.
138. Kubas, G. J. *Adv. Inorg. Chem.* **2004**, *56*, 127–177.
139. Crabtree, R. H. *Angew. Chem., Int. Ed. Engl.* **1993**, *32*, 789–805.
140. Nikonov, G. I. *Adv. Organomet. Chem.* **2005**, *53*, 217–309.
141. Lin, Z. *Chem. Soc. Rev.* **2002**, *31*, 239–245.
142. Vincent, J. L.; Luo, S.; Scott, B. L.; Butcher, R.; Unkefer, C. J.; Burns, C. J.; Kubas, G. J.; Lledós, A.; Maseras, F.; Tomàs, J. *Organometallics* **2003**, *22*, 5307–5323.
143. Hall, C.; Perutz, R. N. *Chem. Rev.* **1996**, *96*, 3125–3146.
144. Sun, X.-Z.; Grills, D. C.; Nikiforov, S. M.; Poliakoff, M.; George, M. W. *J. Am. Chem. Soc.* **1997**, *119*, 7521–7525.
145. Geftakis, S.; Ball, G. E. *J. Am. Chem. Soc.* **1998**, *120*, 9953–9954.
146. Jones, W. D. *Acc. Chem. Res.* **2003**, *36*, 140–146.
147. Goldberg, K. I.; Goldman, A. S., Eds. *Activation and Functionalization of C–H Bonds*; American Chemical Society: Washington, DC, 2004.
148. Crabtree, R. H. *J. Organomet. Chem.* **2004**, *689*, 4083–4091.
149. Jia, C.; Kitamura, T.; Fujiwara, Y. *Acc. Chem. Res.* **2001**, *34*, 633–639.
150. Crabtree, R. H. *J. Chem. Soc., Dalton Trans.* **2001**, 2437–2450.
151. Dyker, G. *Angew. Chem., Int. Ed.* **1999**, *38*, 1698–1712.
152. Lersch, M.; Tilset, M. *Chem. Rev.* **2005**, *105*, 2471–2526.
153. Jones, W. D. *Inorg. Chem.* **2005**, *44*, 4475–4484.
154. Labinger, J. A.; Bercaw, J. E. *Nature* **2002**, *417*, 507–514.
155. Crabtree, R. H. *Chem. Rev.* **1995**, *95*, 987–1007.
156. Schneider, J. J. *Angew. Chem., Int. Ed. Engl.* **1996**, *35*, 1068–1075.
157. Arndtsen, B. A.; Bergman, R. G.; Mobley, T. A.; Peterson, T. H. *Acc. Chem. Res.* **1995**, *28*, 154–162.
158. Shilov, A. E.; Shul'pin, G. B. *Activation and Catalytic Reactions of Saturated Hydrocarbons in the Presence of Metal Complexes*; Kluwer Academic Publishers: Boston, 2000.
159. Fekl, U.; Goldberg, K. I. *Adv. Inorg. Chem.* **2003**, *54*, 259–320.
160. Sakaki, S. *Topics Organomet. Chem.* **2005**, *12*, 31–78.
161. Periana, R. A.; Bhalla, G.; Tenn, W. J. III; Young, K. J. H.; Liu, X. Y.; Mironov, O.; Jones, C. J.; Ziatdinov, V. R. *J. Mol. Catal. A: Chem.* **2004**, *220*, 7–25.
162. Labinger, J. A. *J. Mol. Catal. A: Chem* **2004**, *220*, 27–35.
163. Chepaikin, E. G. *Kinet. Catal.* **2004**, *45*, 307–328.
164. Wolf, D. *Angew. Chem., Int. Ed.* **1998**, *37*, 3351–3353.
165. Periana, R. A.; Taube, D. J.; Gamble, S.; Taube, H.; Satoh, T.; Fujii, H. *Science* **1998**, *280*, 560–564.
166. Stahl, S. S.; Labinger, J. A.; Bercaw, J. E. *Angew. Chem., Int. Ed.* **1998**, *37*, 2180–2192.
167. Shilov, A. E.; Shteinman, A. A. *Acc. Chem. Res.* **1999**, *32*, 763–771.
168. Sames, D. In *Activation and Functionalization of C–H Bonds*; Goldberg, K. I., Goldman, A. S., Eds.; American Chemical Society: Washington, DC, 2004; Chapter 9, pp 155–168.
169. O'Malley, S. J.; Tan, K. L.; Watzke, A.; Bergman, R. G.; Ellman, J. A. *J. Am. Chem. Soc.* **2005**, *127*, 13496–13497.
170. Kakiuchi, F.; Chatani, N. *Adv. Synth. Catal.* **2003**, *345*, 1077–1101.

171. Tobisu, M.; Chatani, N. *Angew. Chem., Int. Ed.* **2006**, *45*, 1683–1684.
172. Jun, C.-H.; Lee, J. H. *Pure Appl. Chem.* **2004**, *76*, 577–587.
173. Fiedler, D.; Leung, D. H.; Bergman, R. G.; Raymond, K. N. *Acc. Chem. Res.* **2005**, *38*, 349–358.
174. Crabtree, R. H. *Dalton Trans.* **2003**, 3985–3990.
175. Halpern, J. *Pure Appl. Chem.* **1986**, *58*, 575–584.
176. Lappert, M. F.; Lednor, P. W. *Adv. Organomet. Chem.* **1976**, *14*, 345–399.
177. Hall, T. L.; Lappert, M. F.; Lednor, P. W. *J. Chem. Soc., Dalton Trans.* **1980**, 1448–1456.
178. Labinger, J. A.; Osborn, J. A. *Inorg. Chem.* **1980**, *19*, 3230–3236.
179. Labinger, J. A.; Osborn, J. A.; Coville, N. J. *Inorg. Chem.* **1980**, *19*, 3236–3243.
180. Paonessa, R. S.; Thomas, N. C.; Halpern, J. *J. Am. Chem. Soc.* **1985**, *107*, 4333–4335.
181. Kaim, W. *Top. Curr. Chem.* **1994**, *169*, 231–251.
182. Crabtree, R. H.; Quirk, J. M.; Fillebeen-Khan, T.; Morris, G. E. *J. Organomet. Chem.* **1979**, *181*, 203–212.
183. Ashworth, T. V.; Singleton, J. E.; de Waal, D. J. A.; Louw, W. J.; Singleton, E.; van der Stok, E. *J. Chem. Soc. Dalton Trans.* **1978**, 340–347.
184. Bruno, J. W.; Marks, T. J.; Morss, L. R. *J. Am. Chem. Soc.* **1983**, *105*, 6824–6832.
185. Watson, P. L. *J. Am. Chem. Soc.* **1983**, *105*, 6491–6493.
186. Watson, P. L.; Parshall, G. W. *Acc. Chem. Res.* **1985**, *18*, 51–56.
187. Rothwell, I. P. *Polyhedron* **1985**, *4*, 177–200.
188. Rothwell, I. P. In *Selective Hydrocarbon Activation*; Davies, J. A., Watson, P. L., Liebman, J. F., Greenberg, A., Eds.; VCH: New York, 1990; Chapter 3, pp 43–78.
189. Thompson, M. E.; Baxter, S. M.; Bulls, A. R.; Burger, B. J.; Nolan, M. C.; Santarsiero, B. D.; Schaefer, W. P.; Bercaw, J. E. *J. Am. Chem. Soc.* **1987**, *109*, 203–219.
190. Piers, W. E.; Shapiro, P. J.; Bunel, E. E.; Bercaw, J. E. *Synlett* **1990**, 74–84.
191. Ziegler, T.; Folga, E.; Berces, A. *J. Am. Chem. Soc.* **1993**, *115*, 636–646.
192. Perrin, L.; Maron, L.; Eisenstein, O. In *Activation and Functionalization of C–H Bonds*; Goldberg, K. I., Goldman, A. S., Eds.; American Chemical Society: Washington, 2004; Chapter 7, pp 116–133.
193. Coperet, C.; Grouiller, A.; Basset, M.; Chermette, H. *ChemPhysChem* **2003**, *4*, 608–611.
194. Hyla-Kryspin, I.; Gleiter, R. *J. Mol. Catal. A* **2000**, *160*, 115–124.
195. Sakaki, S. *Top. Organomet. Chem.* **2005**, *12*, 31–78.
196. Sadow, A. D.; Tilley, T. D. *J. Am. Chem. Soc.* **2005**, *127*, 643–656.
197. Wu, F.; Jordan, R. F. *Organometallics* **2005**, *24*, 2688–2697.
198. Blackmore, K. J.; Ziller, J. W.; Heyduk, A. F. *Inorg. Chem.* **2005**, *44*, 5559–5561.
199. Ozawa, F. *Curr. Meth. Inorg. Chem.* **2003**, *3*, 479–512.
200. Koo, K.; Hillhouse, G. L. *Organometallics* **1995**, *14*, 4421–4423.
201. Han, R.; Hillhouse, G. L. *J. Am. Chem. Soc.* **1997**, *119*, 8135–8136.
202. Lin, B. L.; Clough, C. R.; Hillhouse, G. L. *J. Am. Chem. Soc.* **2002**, *124*, 2890–2891.
203. Fooladi, E.; Tilset, M. *Inorg. Chem.* **1997**, *36*, 6021–6027.
204. Pedersen, A.; Tilset, M.; Folting, K.; Caulton, K. G. *Organometallics* **1995**, *14*, 875–888.
205. Burk, M. J.; Staley, D. L.; Tumas, W. *J. Chem. Soc., Chem. Commun.* **1990**, 809–810.
206. Procelewska, J.; Zahl, A.; Liehr, G.; van Eldik, R.; Smythe, N. A.; Williams, B. S.; Goldberg, K. I. *Inorg. Chem.* **2005**, *44*, 7732–7742, and references therein.
207. Crumpton-Bregel, D. M.; Goldberg, K. I. *J. Am. Chem. Soc.* **2003**, *125*, 9442–9456.
208. Jensen, M. P.; Wick, D. D.; Reinartz, S.; White, P. S.; Templeton, J. L.; Goldberg, K. I. *J. Am. Chem. Soc.* **2003**, *125*, 8614–8624.
209. Williams, B. S.; Goldberg, K. I. *J. Am. Chem. Soc.* **2001**, *123*, 2576–2587.
210. Bartlett, K. L.; Goldberg, K. I.; Borden, W. T. *J. Am. Chem. Soc.* **2000**, *122*, 1456–1465.
211. Goldberg, K. I.; Yan, J.; Breitung, E. M. *J. Am. Chem. Soc.* **1995**, *117*, 6889–6896.
212. Culkin, D. A.; Hartwig, J. F. *Organometallics* **2004**, *23*, 3398–3416.
213. Culkin, D. A.; Hartwig, J. F. *Acc. Chem. Res.* **2003**, *36*, 234–245.
214. Beletskaya, I. P.; Cheprakov, A. V. In *Comprehensive Coordination Chemistry II*; McCleverty, J. A., Meyer, T. J., Eds.; Elsevier: San Diego, 2004; Chapter 9.6, pp 305–368.
215. Suzuki, A. *Chem. Commun.* **2005**, 4759–4763.
216. Miyaura, N.; Suzuki, A. *Chem. Rev.* **1995**, *95*, 2457–2483.
217. Suzuki, A. *J. Organomet. Chem.* **1999**, *576*, 147–168.
218. Kotha, S.; Lahiri, K.; Kashinath, D. *Tetrahedron* **2002**, *58*, 9633–9695.
219. Bellina, F.; Carpita, A.; Rossi, R. *Synthesis* **2004**, 2419–2440.
220. Miyaura, N. *Top. Curr. Chem.* **2002**, *219*, 11–59.
221. Miyaura, N. In *Metal-Catalyzed Cross-Coupling Reactions*, 2nd ed.; de Meijere, A., Diederich, F., Eds.; Wiley: New York, 2004, Vol. 1, Chapter 2, pp 41–123.
222. Espinet, P.; Echavarren, A. M. *Angew. Chem., Int. Ed.* **2004**, *43*, 4704–4734.
223. Farina, V.; Krishnamurthy, V.; Scott, W. J. *Org. React.* **1997**, *50*, 1–652.
224. Fugami, K.; Kosugi, M. *Top. Curr. Chem.* **2002**, *219*, 87–130.
225. Hartwig, J. F. *Acc. Chem. Res.* **1998**, *31*, 852–860.
226. Hartwig, J. F. *Angew. Chem., Int. Ed.* **1998**, *37*, 2046–2067.
227. Yang, B. H.; Buchwald, S. L. *J. Organomet. Chem.* **1999**, *576*, 125–146.
228. Wolfe, J. P.; Wagaw, S.; Marcoux, J.-F.; Buchwald, S. L. *Acc. Chem. Res.* **1998**, *31*, 805–818.
229. Dehli, J. R.; Legros, J.; Bolm, C. *Chem. Commun.* **2005**, 973–986.
230. Dick, A. R.; Kampf, J. W.; Sanford, M. S. *J. Am. Chem. Soc.* **2005**, *127*, 12790–12791.
231. Bedford, R. B.; Cazin, C. S. J.; Holder, D. *Coord. Chem. Rev.* **2004**, *248*, 2283–2321.
232. Macgregor, S. A.; Neave, G. W.; Smith, C. *Faraday Discuss.* **2003**, *124*, 111–127.
233. Hartwig, J. F. In *Comprehensive Coordination Chemistry II*; McCleverty, J. A., Meyer, T. J., Eds.; Elsevier: San Diego, 2004; Chapter 9.7, pp 369–398.

234. Muci, A. R.; Buchwald, S. L. *Top. Curr. Chem.* **2002**, *219*, 131–209.
235. Jiang, L.; Buchwald, S. L. In *Metal-Catalyzed Cross-Coupling Reactions*, 2nd ed.; de Meijere, A., Diederich, F., Eds.; Wiley: New York, 2004; Vol. 2, Chapter 13, pp 699–760.
236. Crabtree, R. H. In *The Organometallic Chemistry of the Transition Metals*, 4th ed.; Wiley: Hoboken, 2005; Chapter 6, and references therein, pp 170–175.
237. Qin, C. J.; Gavrilova, A.; Bosnich, B. *Pure Appl. Chem.* **2001**, *73*, 221–226.
238. Bosnich, B. *Inorg. Chem.* **1999**, *38*, 2554–2562.
239. Gavrilova, A. L.; Bosnich, B. *Inorg. Chim. Acta* **2003**, *352*, 24–30.
240. Gavrilova, A. L.; Qin, C. J.; Sommer, R. D.; Rheingold, A. L.; Bosnich, B. *J. Am. Chem. Soc.* **2002**, *124*, 1714–1722.
241. Incarvito, C.; Rheingold, A. L.; Gavrilova, A. L.; Qin, C. J.; Bosnich, B. *Inorg. Chem.* **2001**, *40*, 4101–4108.
242. Churchill, D. G.; Janak, K. E.; Wittenberg, J. S.; Parkin, G. *J. Am. Chem. Soc.* **2003**, *125*, 1403–1420.
243. For a lucid discussion of oxidation state ambiguities, see: Crabtree, R. H. In *The Organometallic Chemistry of the Transition Metals*, 4th ed.; Wiley: Hoboken, 2005; Chapter 2, pp 29–41.
244. Green, M. L. H. *J. Organomet. Chem.* **1995**, *500*, 127–148.
245. Rabinovich, D.; Parkin, G. *J. Am. Chem. Soc.* **1993**, *115*, 9822–9823.
246. Elschenbroich, C.; Salzer, A. In *Organometallics: A Concise Introduction*, 2nd ed.; VCH: New York, 1992; pp 412–414.
247. Mayr, A.; Bastos, C. M. *Prog. Inorg. Chem.* **1992**, *40*, 1–98.
248. Mayr, A.; Hoffmeister, H. *Adv. Organomet. Chem.* **1991**, *32*, 227–324.
249. Mayr, A. *Comments Inorg. Chem.* **1990**, *10*, 227–266.
250. Vrtis, R. N.; Lippard, S. J. *Isr. J. Chem.* **1990**, *30*, 331–341.
251. Carnahan, E. M.; Protasiewicz, J. D.; Lippard, S. J. *Acc. Chem. Res.* **1993**, *26*, 90–97.
252. Alt, H. G. *Angew. Chem., Int. Ed. Engl.* **1991**, *30*, 1119.
253. Filippou, A. C.; Lungwitz, B.; Kociok-Kohn, G. *Eur. J. Inorg. Chem.* **1999**, 1905–1910.
254. Tsai, Y.-C.; Stephens, F. H.; Meyer, K.; Mendiratta, A.; Gheorghiu, M. D.; Cummins, C. C. *Organometallics* **2003**, *22*, 2902–2913, and references therein.
255. Cross, J. L.; Garrett, A. D.; Crane, T. W.; White, P. S.; Templeton, J. L. *Polyhedron* **2004**, *23*, 2831–2840, and references therein.
256. Cavell, K. J. *Coord. Chem. Rev.* **1996**, *155*, 209–243, and references therein.
257. Soderberg, B. C. In *Comprehensive Organometallic Chemistry II*; Abel, E. W., Stone, F. G. A., Wilkinson, G., Eds.; Elsevier: Oxford, 1995; Vol. 12, Chapter 3.5, pp 241–297.
258. Berke, H.; Hoffmann, R. *J. Am. Chem. Soc.* **1978**, *100*, 7224–7236.
259. Yamamoto, A. *J. Chem. Soc., Dalton Trans.* **1999**, 1027–1037.
260. Parkin, G.; Bunel, E.; Burger, B. J.; Trimmer, M. S.; Van Asselt, A.; Bercaw, J. E. *J. Mol. Catal.* **1987**, *41*, 21–39.
261. Kayaki, Y.; Yamamoto, A. *Curr. Meth. Inorg. Chem.* **2003**, *3*, 373–409.
262. Espinet, P.; Albéniz, A. C. *Curr. Meth. Inorg. Chem.* **2003**, *3*, 293–371.
263. Wojcicki, A. *Adv. Organomet. Chem.* **1973**, *11*, 87–145.
264. Calderazzo, F. *Angew. Chem., Int. Ed. Engl.* **1977**, *16*, 299–311.
265. Kuhlmann, E. J.; Alexander, J. J. *Coord. Chem. Rev.* **1980**, *33*, 195–225.
266. Durfee, L. D.; Rothwell, I. P. *Chem. Rev.* **1988**, *88*, 1059–1079.
267. Ojima, I. *Chem. Rev.* **1988**, *88*, 1011–1030.
268. Ford, P. C.; Rokicki, A. *Adv. Organomet. Chem.* **1988**, *28*, 139–217.
269. Kamer, P. C. J.; van Rooy, A.; Schoemaker, G. C.; van Leeuwen, P. W. N. M. *Coord. Chem. Rev.* **2004**, *248*, 2409–2424.
270. Trzeciak, A. M.; Ziolkowski, J. J. *Coord. Chem. Rev.* **1999**, *190–192*, 883–900.
271. Frohning, C. D.; Kohlpaintner, C. W.; Bohnen, H.-W. In *Applied Homogeneous Catalysis with Organometallic Compounds*, 2nd ed.; Cornils, B., Herrmann, W. A., Eds.; Wiley-VCH: Weinheim, 2002, Vol. 1, Chapter 2.1.1, pp 31–103.
272. Pruett, R. L. *Adv. Organomet. Chem.* **1979**, *17*, 1–60.
273. Forster, D. *Adv. Organomet. Chem.* **1979**, *17*, 255–267.
274. Thomas, C. M.; Süss-Fink, G. *Coord. Chem. Rev.* **2003**, *243*, 125–142.
275. Torrence, P. In *Applied Homogeneous Catalysis with Organometallic Compounds*, 2nd ed.; Cornils, B., Herrmann, W. A., Eds.; Wiley-VCH: Weinheim, 2002; Vol. 1, Chapter 2.1.2.1, pp 104–136.
276. Harrop, T. C.; Mascharak, P. K. *Coord. Chem. Rev.* **2005**, *249*, 3007–3024.
277. Hegg, E. L. *Acc. Chem. Res.* **2004**, *37*, 775–783.
278. Drennan, C. L.; Doukov, T. I.; Ragsdale, S. W. *J. Biol. Inorg. Chem.* **2004**, *9*, 511–515.
279. Lindahl, P. A. *J. Biol. Inorg. Chem.* **2004**, *9*, 516–524.
280. Brunold, T. C. *J. Biol. Inorg. Chem.* **2004**, *9*, 533–541.
281. Riordan, C. G. *J. Biol. Inorg. Chem.* **2004**, *9*, 542–549.
282. Crabtree, R. H. In *The Organometallic Chemistry of the Transition Metals*, 4th ed.; Wiley: Hoboken, New Jersey, 2005; pp 185–187.
283. Spessard, G. O.; Miessler, G. L. In *Organometallic Chemistry*; Prentice-Hall: Upper Saddle River, 1997; pp 192–197.
284. Marynick, D. S.; Derecskei-Kovacs, A. *J. Am. Chem. Soc.* **2000**, *122*, 2078–2086.
285. Calderazzo, F.; Noack, K. *Coord. Chem. Rev.* **1966**, *1*, 118–125.
286. Prock, A.; Giering, W. P.; Greene, J. E.; Meirowitz, R. E.; Hoffman, S. L.; Woska, D. C.; Wilson, M.; Chang, R.; Chen, J.; Magnuson, R. H., *et al. Organometallics* **1991**, *10*, 3479–3485.
287. Gladysz, J. A. *Adv. Organomet. Chem.* **1982**, *20*, 1–38.
288. Reinartz, S.; Brookhart, M.; Templeton, J. L. *Organometallics* **2002**, *21*, 247–249, and references therein.
289. Maitlis, P. M. *J. Organomet. Chem.* **2004**, *689*, 4366–4374.
290. Masters, C. *Adv. Organomet. Chem.* **1979**, *17*, 61–103.
291. Overett, M. J.; Hill, R. O.; Moss, J. R. *Coord. Chem. Rev.* **2000**, *206–207*, 581–605.
292. Van der Laan, G. P.; Beenackers, A. A. C. M. *Catal. Rev., Sci. Eng.* **1999**, *41*, 255–318.
293. Schulz, H. *Appl. Catal. A* **1999**, *186*, 3–12.
294. Herrmann, W. A. In *Applied Homogeneous Catalysis with Organometallic Compounds*, 2nd ed.; Cornils, B., Herrmann, W. A., Eds.; Wiley-VCH: Weinheim, 2002; Vol. 2, Chapter 3.1.8, pp 808–822.

295. Pruett, R. L. *Ann. N. Y. Acad. Sci.* **1977**, *295*, 239–248.
296. Dombek, B. D. *J. Chem. Educ.* **1986**, *63*, 210–212.
297. Fulton, J. R.; Holland, A. W.; Fox, D. J.; Bergman, R. G. *Acc. Chem. Res.* **2002**, *35*, 44–56.
298. Bryndza, H. E.; Tam, W. *Chem. Rev.* **1988**, *88*, 1163–1188.
299. Macgregor, S. A.; Neave, G. W. *Organometallics* **2004**, *23*, 891–899.
300. Bradley, D. C.; Mehrotra, R. C.; Rothwell, I. P.; Singh, A. *Alkoxo and Aryloxo Derivatives of Metals*; Academic Press: San Diego, 2001.
301. Cámpora, J.; Palma, P.; del Río, D.; Álvarez, E. *Organometallics* **2004**, *23*, 1652–1655.
302. Dockter, D. W.; Fanwick, P. E.; Kubiak, C. P. *J. Am. Chem. Soc.* **1996**, *118*, 4846–4852.
303. Angelici, R. J. *Acc. Chem. Res.* **1972**, *5*, 335–341.
304. Bennett, M. A.; Jin, H.; Willis, A. C. *J. Organomet. Chem.* **1993**, *451*, 249–256.
305. Lee, D. W.; Jensen, C. M.; Morales-Morales, D. *Organometallics* **2003**, *22*, 4744–4749.
306. Torresan, I.; Michelin, R. A.; Marsella, A.; Zanardo, A.; Pinna, F.; Strukul, G. *Organometallics* **1991**, *10*, 623–631.
307. Katz, N. E.; Szalda, D. J.; Chou, M. H.; Creutz, C.; Sutin, N. *J. Am. Chem. Soc.* **1989**, *111*, 6591–6601.
308. Gibson, D. H.; Ding, Y.; Andino, J. G.; Mashuta, M. S.; Richardson, J. F. *Organometallics* **1998**, *17*, 5178–5183.
309. Ruiz, J.; Martínez, M. T.; Florenciano, F.; Rodríguez, V.; López, G.; Pérez, J.; Chaloner, P. A.; Hitchcock, P. B. *Inorg. Chem.* **2003**, *42*, 3650–3661.
310. Fernandez, M. J.; Rodriguez, M. J.; Oro, L. A. *J. Organomet. Chem.* **1992**, *438*, 337–342.
311. Bryndza, H. E. *Organometallics* **1985**, *4*, 1686–1687.
312. Kapteijn, G. M.; Dervisi, A.; Verhoef, M. J.; van den Broek, M. A. F. H.; Grove, D. M.; van Koten, G. *J. Organomet. Chem.* **1999**, *517*, 123–131.
313. Rees, W. M.; Churchill, M. R.; Fettinger, J. C.; Atwood, J. D. *Organometallics* **1985**, *4*, 2179–2185.
314. Takemoto, S.; Oshio, S.; Kobayashi, T.; Matsuzaka, H.; Hoshi, M.; Okimura, H.; Yamashita, M.; Miyasaka, H.; Ishii, T.; Yamashita, M. *Organometallics* **2004**, *23*, 3587–3589.
315. Fox, D. J.; Bergman, R. G. *J. Am. Chem. Soc.* **2003**, *125*, 8984–8985.
316. Campion, B. K.; Falk, J.; Tilley, T. D. *J. Am. Chem. Soc.* **1987**, *109*, 2049–2056.
317. Geoffroy, G. L.; Sheridan, J. B.; Bassner, S. L.; Kelley, C. *Pure Appl. Chem.* **1989**, *61*, 1723–1729.
318. Yamamoto, A.; Ozawa, F.; Osakada, K.; Huang, L.; Son, T.; Kawasaki, N.; Doh, M.-K. *Pure Appl. Chem.* **1991**, *63*, 687–696.
319. Coates, G. W.; Waymouth, R. M. In *Comprehensive Organometallic Chemistry II*; Abel, E. W., Stone, F. G. A., Wilkinson, G., Eds.; Elsevier: Oxford, 1995, Vol. 12, Chapter 12.1, pp 1193–1208.
320. Collman, J. P.; Hegedus, L. S.; Norton, J. R.; Finke, R. G. In *Principles and Applications of Organotransition Metal Chemistry*; University Science Books: Mill Valley, 1987; Chapter 11, pp 577–617.
321. Coates, G. W.; Hustad, P. D.; Reinartz, S. *Angew. Chem., Int. Ed.* **2002**, *41*, 2236–2257.
322. Mecking, S. *Angew. Chem., Int. Ed.* **2001**, *40*, 534–540.
323. Gibson, V. C.; Spitzmesser, S. K. *Chem. Rev.* **2003**, *103*, 283–315.
324. Kaminsky, W., Ed. *Metalorganic Catalysts for Synthesis and Polymerisation*; Springer-Verlag: Berlin, 1999.
325. Janiak, C. In *Metallocenes*; Togni, A., Halterman, R. L., Eds.; Vol. 2, Chapter 9, pp 547–623.
326. Silanes, I.; Ugalde, J. M. *Organometallics* **2005**, *24*, 3233–3246.
327. Rappé, A. K.; Skiff, W. M.; Casewit, C. J. *Chem. Rev.* **2000**, *100*, 1435–1456.
328. Cossee, P. *J. Catal.* **1964**, *3*, 80–88.
329. Brookhart, M.; Green, M. L. H. *J. Organomet. Chem.* **1983**, *250*, 395–408.
330. Brookhart, M.; Green, M. L. H.; Wong, L.-L. *Prog. Inorg. Chem.* **1988**, *36*, 1–124.
331. Grubbs, R. H.; Coates, G. W. *Acc. Chem. Res.* **1996**, *29*, 85–93.
332. Schwartz, J.; Labinger, J. A. *Angew. Chem., Int. Ed. Engl.* **1976**, *15*, 333–340.
333. Wipf, P.; Takahashi, H.; Zhuang, N. *Pure Appl. Chem.* **1998**, *70*, 1077–1082.
334. Wipf, P.; Kendall, C. *Top. Organomet. Chem.* **2005**, *8*, 1–25.
335. Wipf, P.; Jahn, H. *Tetrahedron* **1996**, *52*, 12853–12910.
336. Vaultier, M.; Carboni, B. In *Comprehensive Organometallic Chemistry II*; Abel, E. W., Stone, F. G. A., Wilkinson, G., Eds.; Elsevier: Oxford, 1995, Vol. 11, Chapter 5, pp 191–276.
337. Brown, H. C. *Organic Synthesis Via Boranes*; Wiley: New York, 1975.
338. Ramachandran, P. V., Brown, H. C., Eds. *Organoboranes for Syntheses*; American Chemical Society: Washington, DC, 2001.
339. Beletskaya, I.; Pelter, A. *Tetrahedron* **1997**, *53*, 4957–5026.
340. Omae, I. In *Applications of Organometallic Compounds*; Wiley: New York, 1998; Chapter 6, pp 91–106.
341. Ledford, J.; Shultz, C. S.; Gates, D. P.; White, P. S.; DeSimone, J. M.; Brookhart, M. *Organometallics* **2001**, *20*, 5266–5276.
342. Groen, J. H.; Delis, J. G. P.; van Leeuwen, P. W. N. M.; Vrieze, K. *Organometallics* **1997**, *16*, 68–77.
343. Drent, E.; van Broekhoven, J. A. M.; Budzelaar, P. H. M. In *Applied Homogeneous Catalysis with Organometallic Compounds*, 2nd ed.; Cornils, B., Herrmann, W. A., Eds.; Wiley-VCH: Weinheim, 2002, Vol. 1, Chapter 2.3.4, pp 344–361.
344. Bianchini, C.; Meli, A. *Coord. Chem. Rev.* **2002**, *225*, 35–66.
345. Nozaki, K.; Hiyama, T. *J. Organomet. Chem.* **1999**, *576*, 248–253.
346. Drent, E.; Budzelaar, P. H. M. *Chem. Rev.* **1996**, *96*, 663–681.
347. Sen, A. *Acc. Chem. Res.* **1993**, *26*, 303–310.
348. Cotton, F. A.; Wilkinson, G.; Murillo, C. A.; Bochmann, M. In *Advanced Inorganic Chemistry*, 6th ed.; Wiley: New York, 1999; pp 1207–1228.
349. Crabtree, R. H. In *The Organometallic Chemistry of the Transition Metals*, 4th ed.; Wiley: Hoboken, 2005; Chapter 7, pp 183–204.
350. Sebastian, A.; Royo, P.; Gómez–Sal, Pilar; Ramírez de Arellano, C. *Eur. J. Inorg. Chem.* **2004**, 3814–3821.
351. Martins, A. M.; Ascenso, J. R.; de Azevedo, C. G.; Dias, A. R.; Duarte, M. T.; da Silva, J. F.; Veiros, L. F.; Rodrigues, S. S. *Organometallics* **2003**, *22*, 4218–4228.
352. Thorn, M. G.; Lee, J.; Fanwick, P. E.; Rothwell, I. P. *J. Chem. Soc., Dalton Trans.* **2002**, 3398–3405.
353. Ong, T.-G.; Wood, D.; Yap, G. P. A.; Richeson, D. S. *Organometallics* **2002**, *21*, 1–3.
354. Gibson, D. H. *Chem. Rev.* **1996**, *96*, 2063–2095.
355. Leitner, W. *Coord. Chem. Rev.* **1996**, *153*, 257–284.
356. Yin, X.; Moss, J. R. *Coord. Chem. Rev.* **1999**, *181*, 27–59.
357. Pandey, K. K. *Coord. Chem. Rev.* **1995**, *140*, 37–114.

358. Darensbourg, D. J.; Kudaroski, R. A. *Adv. Organomet. Chem.* **1983**, *22*, 129–168.
359. Gibson, D. H. In *Comprehensive Coordination Chemistry II*; McCleverty, J. A., Meyer, T. J., Eds.; Elsevier: San Diego, 2004; Chapter 1.30, pp 595–602.
360. Duda, D. M.; McKenna, R. In *Handbook of Metalloproteins*; Messerschmidt, A., Cygler, M., Bode, W., Eds.; Wiley: Hoboken, 2004; Vol. 3, pp 249–263.
361. Tripp, B. C.; Smith, K.; Ferry, J. G. *J. Biol. Chem.* **2001**, *276*, 48615–48618.
362. Darensbourg, D. J.; Holtcamp, M. W. *Coord. Chem. Rev.* **1996**, *153*, 155–174.
363. Coates, G. W.; Moore, D. R. *Angew. Chem., Int. Ed.* **2004**, *43*, 6618–6639.
364. Dell'Amico, D. B.; Calderazzo, F.; Labella, L.; Marchetti, F.; Pampaloni, G. *Chem. Rev.* **2003**, *103*, 3857–3897.
365. Hogarth, G. *Prog. Inorg. Chem.* **2005**, *53*, 71–561.
366. Wojcicki, A. *Adv. Organomet. Chem.* **1974**, *12*, 31–81.
367. Ryan, R. R.; Kubas, G. J.; Moody, D. C.; Eller, P. G. *Struct. Bond.* **1981**, *46*, 47–100.
368. Mews, R.; Lork, E.; Watson, P. G.; Görtler, B. *Coord. Chem. Rev.* **2000**, *197*, 277–320.
369. Wick, D. D.; Goldberg, K. I. *J. Am. Chem. Soc.* **1999**, *121*, 11900–11901.
370. Denney, M. C.; Smythe, N. A.; Cetto, K. L.; Kemp, R. A.; Goldberg, K. I. *J. Am. Chem. Soc.* **2006**, *128*, 2508–2509.
371. Torraca, K. E.; McElwee-White, L. *Coord. Chem. Rev.* **2000**, *206–207*, 469–491.
372. Pike, R. D.; Sweigart, D. A. *Coord. Chem. Rev.* **1999**, *187*, 183–222.
373. McDaniel, K. F. In *Comprehensive Organometallic Chemistry II*; Abel, E. W., Stone, F. G. A., Wilkinson, G., Eds.; Elsevier: Oxford, 1995; Vol. 12, Chapter 6.1, pp 601–622.
374. Harrington, P. J. In *Comprehensive Organometallic Chemistry II*; Abel, E. W., Stone, F. G. A., Wilkinson, G., Eds.; Elsevier: Oxford, 1995; Vol. 12, Chapter 8.2, pp 797–804.
375. Semmelhack, M. F. In *Comprehensive Organometallic Chemistry II*; Abel, E. W., Stone, F. G. A., Wilkinson, G., Eds.; Elsevier: Oxford, 1995; Vol. 12, Chapter 9.1, pp 979–1015.
376. Takacs, J. M.; Jiang, X. *Curr. Org. Chem.* **2003**, *7*, 369–396.
377. Jira, R. In *Applied Homogeneous Catalysis with Organometallic Compounds*, 2nd ed.; Cornils, B., Herrmann, W. A., Eds.; Wiley-VCH: Weinheim, 2002, Vol. 1, Chapter 2.4.1, pp 386–405.
378. Davies, S. G.; Green, M. L. H.; Mingos, D. M. P. *Tetrahedron* **1978**, *34*, 3047–3077.
379. Crabtree, R. H. *The Organometallic Chemistry of the Transition Metals*, 4th ed.; Wiley: Hoboken, 2005; pp 213–217.
380. Spessard, G. O.; Miessler, G. L. In *Organometallic Chemistry*; Prentice-Hall: Upper Saddle River, 1997; pp 213–219.
381. Peterson, T. H.; Golden, J. T.; Bergman, R. G. *Organometallics* **1999**, *18*, 2005–2020.
382. Peters, J. C.; Odom, A. L.; Cummins, C. C. *Chem. Commun.* **1997**, 1995–1996.
383. Greco, J. B.; Peters, J. C.; Baker, T. A.; Davis, W. M.; Cummins, C. C.; Wu, G. *J. Am. Chem. Soc.* **2001**, *123*, 5003–5013.
384. Skoda-Földes, R.; Kollár, L. *Curr. Org. Chem.* **2002**, *6*, 1097–1119, and references therein.
385. Heck, R. F. *Pure Appl. Chem.* **1978**, *50*, 691–701.
386. Collman, J. P. *Acc. Chem. Res.* **1975**, *8*, 342–347.
387. Henderson, R. A. *Angew. Chem., Int. Ed. Engl.* **1996**, *35*, 946–967.
388. Kuhlman, R. *Coord. Chem. Rev.* **1997**, *167*, 205–232.
389. Kuhlman, R.; Streib, W. E.; Huffman, J. C.; Caulton, K. G. *J. Am. Chem. Soc.* **1996**, *118*, 6934–6945.
390. Papish, E. T.; Rix, F.; Spetseris, N.; Norton, J. R.; Williams, R. D. *J. Am. Chem. Soc.* **2000**, *122*, 12235–12242.
391. Miedaner, A.; Raebiger, J. W.; Curtis, C. J.; Miller, S. M.; DuBois, D. L. *Organometallics* **2004**, *23*, 2670–2679.
392. Angelici, R. J. *Acc. Chem. Res.* **1995**, *28*, 51–60.
393. Bullock, R. M. *Comments Inorg. Chem.* **1991**, *12*, 1–33.
394. Kimmich, B. F. M.; Bullock, R. M. *Organometallics* **2002**, *21*, 1504–1507.
395. Bautista, M. T.; Bynum, L. D.; Schauer, C. K. *J. Chem. Educ.* **1996**, *73*, 988–991.
396. Papish, E. T.; Magee, M. P.; Norton, J. R. In *Recent Advances in Hydride Chemistry*; Peruzzini, M., Poli, R., Eds.; Elsevier: Amsterdam, 2001; Chapter 2, pp 39–74.
397. Shaver, M. P.; Fryzuk, M. D. *Adv. Synth. Catal.* **2003**, *345*, 1061–1076.
398. Pool, J. A.; Lobkovsky, E.; Chirik, P. J. *Nature* **2004**, *427*, 527–530.
399. Schrock, R. R. *Chem. Commun.* **2003**, 2389–2391.
400. Yandulov, D. V.; Schrock, R. R. *Science* **2003**, *301*, 76–78.
401. Nishibayashi, Y.; Iwai, S.; Hidai, M. *Science* **1998**, *279*, 540–542.
402. Schrock, R. R. *Acc. Chem. Res.* **2005**, *38*, 955–962.
403. Heinekey, D. M.; Radzewich, C. E. *Organometallics* **1999**, *17*, 51–58.
404. Erker, G. *Dalton Trans.* **2005**, 1883–1890.
405. Piers, W. E. *Adv. Organomet. Chem.* **2005**, *52*, 1–76.
406. Piers, W. E.; Chivers, T. *Chem. Soc. Rev.* **1997**, *26*, 345–354.
407. Piers, W. E.; Bourke, S. C.; Conroy, K. D. *Angew. Chem., Int. Ed.* **2005**, *44*, 5016–5036.

1.04
Reaction Mechanisms of Multistep Catalytic Cycles

G G Stanley, Louisiana State University, Baton Rouge, LA, USA

1.04.1 Introduction

Every catalytic cycle is composed of fundamental (or elementary) reaction steps that convert the reactant(s) into a product. In the case of a *d*- or *f*-block catalyst, the starting metal complex bonds with the reactants and usually couples them together to form the product. Although the metal complex undergoes a series of transformations, it eventually must reform the starting catalyst complex that can then initiate another catalytic reaction. Because the initial catalyst species is regenerated at the end of the catalytic reaction, catalytic mechanisms are typically written as cycles proceeding in a clockwise fashion. One exception to this is for polymerization catalysis where the product after each insertion of monomer is different. Each step in a catalytic cycle is formally in equilibrium, but many authors simplify this with a single arrow pointing in the direction of the forward reaction.

This chapter will briefly review the fundamental organometallic reactions that play a key role in almost all metal-catalyzed processes. It will then apply these reaction steps to explain currently accepted mechanisms for some major catalytic cycles: hydrogenation, hydroformylation, methanol carbonylation, Pd-catalyzed coupling reactions, and alkene polymerization and metathesis. Each of these catalytic reactions is covered in considerably more detail in later chapters, so the discussion here will be limited to relating and using the various fundamental reactions to build up and describe multistep catalytic cycles.

An important caveat to remember is that currently accepted core mechanisms for the catalytic cycles discussed will be used. A common rule of thumb is that one cannot prove that a proposed mechanism is correct. All the catalytic reactions discussed here have been extensively studied and the mechanisms shown fit the known data, but remain as "proposed" mechanisms. Probing the detailed mechanism of a catalytic cycle can be exceedingly difficult. Many of the fundamental reactions shown to construct the catalytic cycles are assumed to be occurring based on more than 50 years of organometallic research and many stoichiometric examples.

1.04.2 Fundamental Reactions

There are a relatively small number of fundamental organometallic/inorganic reaction types used to describe multistep catalytic cycles (cf. Refs: 1, 1a–1d). These are covered in detail in Section 1.04.1, but will be briefly reviewed

here. They fall into five major reaction classes:

(i) ligand dissociation/association (substitutions),
(ii) oxidative addition/reductive elimination,
(iii) hydrogenolysis/4-center concerted reactions and heterolytic H_2 activation,
(iv) migratory insertion/elimination, and
(v) nucleophilic/electrophilic reagent attack on a coordinated ligand.

Of these, the first four typically play the biggest roles in the major catalytic cycles discussed in this chapter. Electron counting plays an important role in identifying some of these reaction types (especially oxidative addition and reductive elimination), and the ionic method of electron counting will be used in this chapter.

1.04.3 Ligand Dissociation/Association (Substitutions)

The simplest type of reaction is ligand dissociation (loss) and association (addition). These reactions are critically important for opening up free coordination sites on a metal center, coordinating reactant(s), and the ultimate loss of the product from the metal center. When dealing with an 18-electron ($18e^-$) starting catalyst complex, it is almost universally accepted that unless the reactants are already coordinated, the first step in any catalytic cycle needs to be dissociation of one of the existing ligands. This is usually the one with the weakest metal–ligand (M–L) bond. The *trans*-$RuCl_2(dmpe)_2$ (dmpe = $Me_2PCH_2CH_2PMe_2$) complex in Equation (1) is $18e^-$ and considered saturated, that is, it does not have any low-lying empty orbitals that an incoming ligand can coordinate to. Therefore, one of the existing ligands needs to dissociate before any incoming reactant can coordinate to the metal center. The strongly donating dmpe chelated groups imply that the most easily lost ligand is one of the chlorides to generate the five-coordinate cationic $16e^-$ complex shown. This complex can now add another ligand via a ligand-association (addition) reaction.

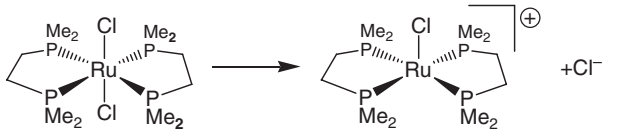

(1)

The higher reactivity of square-planar $16e^-$ d^8 Rh(I) and Pd(II) complexes arises from the fact that there is an open axial $5p_z$-orbital that ligands can directly bind to forming five-coordinate $18e^-$ systems (Equation (2)). The coordination of a fifth ligand is, however, weakened by the presence of the filled $4d_{z^2}$ orbital in these d^8-complexes.

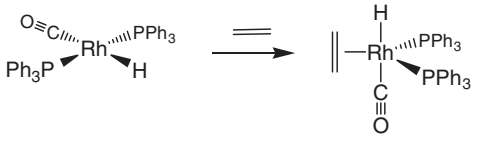

(2)

Ir(I) and especially Pt(II) square-planar $16e^-$ d^8-complexes have less of a tendency to add a fifth axial ligand due to the greater spatial extent of the filled $5d_{z^2}$ orbital that provides a more effective "block" of ligands wanting to coordinate to the empty $6p_z$-orbital. Relativistic effects become quite important for Ir and Pt raising the energy of the filled $5d_{z^2}$-orbital and contracting the empty $6p_z$-orbital, thus accentuating the blocking effect of the filled $5d_{z^2}$ orbital for the coordination of axial ligands. Thus, the ligand-substitution mechanism for $PtCl_2(PPh_3)_2$ is more likely to proceed via the dissociative substitution shown on the top part of Equation (3) (PPh_3 loss is also possible). This likely proceeds via the $14e^-$ three-coordinate T-shaped cationic intermediate and not via the $18e^-$ five-coordinate complex shown on the bottom pathway.

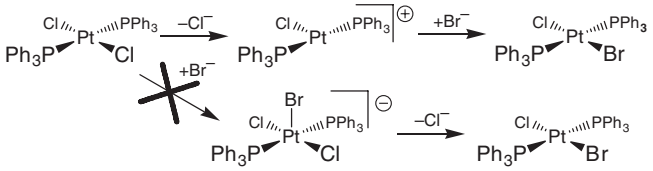

(3)

Steric effects can also promote ligand-dissociation pathways in $16e^-$ square-planar d^8-complexes, as shown in Equation (4). Here, the steric strain of having three fairly bulky PPh_3 groups (cone angle = 145°) promotes the dissociation of one to form a far more reactive trigonal-planar $14e^-$ complex.

(4)

1.04.4 Oxidative Addition/Reductive Elimination Reactions

An oxidative addition reaction is one in which a ligand adds to a metal center with an electron count of d^2 or higher, and in doing so oxidizes the metal, typically by $2e^-$. The two electrons are transferred from the metal center to the coordinating ligand breaking a covalent bond (σ or π) and forming two new anionic centers. At least one of these new anionic ligand centers ends up bonded to the metal center.

There are two main classes of molecules (substrates) that can perform oxidative additions to metal centers: non-electrophilic and electrophilic. Oxidative addition reactions with either class of substrates are favored by metal complexes that are more electron rich. Common non-electrophilic substrates are H_2, Si–H bonds, P–H bonds, S–H bonds, B–H bonds, N–H bonds, S–S bonds, C–H bonds, alkenes, and alkynes. An important criterion for these non-electrophillic substrates is that they require a sterically accessible open coordination site on the metal ($16e^-$ configuration or lower) onto which they need to pre-coordinate before initiating the oxidative addition to the metal center. For these substrates, both ligand atoms typically become cisoidally coordinated to the metal center after the oxidative addition as anionic σ-donors (subsequent ligand rearrangements, of course can occur). H_2 is the most important and common for catalysis and a well-studied reaction is shown in Equation (5).

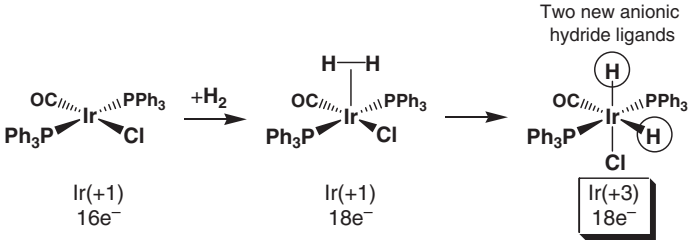

(5)

Alkenes and alkynes typically coordinate by simple σ-donation of their π-system to the metal center. But if the metal complex is electron rich enough and/or the alkene/alkyne has electron-withdrawing groups, oxidative addition can occur to form metallacyclopropanes (for alkenes) or metallacyclopropenes (for alkynes). An example of this is shown in Figure 1 for three Pt-alkene complexes that span the range from simple $2e^-$ neutral σ-donation of their π-system to the metal, to what most organometallic chemists consider a formal oxidative addition of the alkene to make a metallacyclopropane with two anionic carbon donors coordinated to the oxidized Pt center. Note that the presence of the four electron-withdrawing cyano groups on the alkene helps promote the formal oxidative addition reaction.

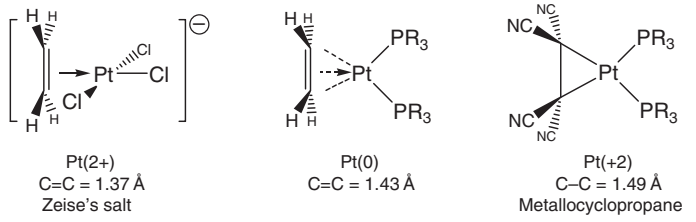

Figure 1 Three Pt complexes that show increasing longer C═C bonds (PR_3 = alkylated phosphines). The alkene in the middle complex is considered to be π-backbonding enough to the Pt center to reduce the C═C bond order to about 1.5. The tetracyanoethylene ligand in the right-most complex has performed an oxidative addition to the Pt center to form a dianionic ligand.

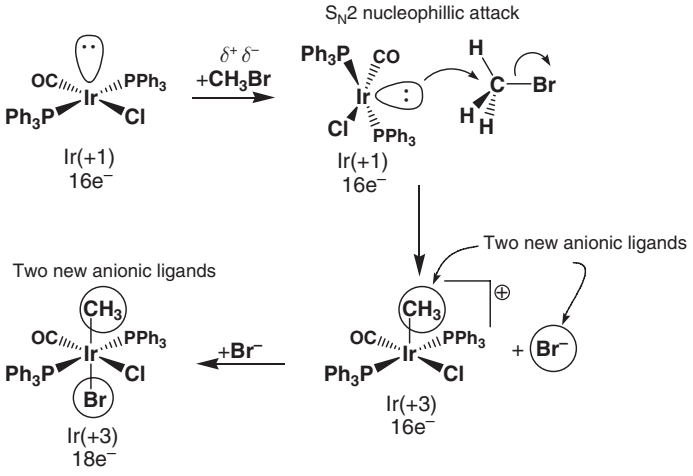

Figure 2 Proposed mechanism for the oxidative addition of CH_3Br to $IrCl(CO)(PPh_3)_2$, illustrating how the *trans*-orientation of the methyl and bromide groups occurs.

Electrophilic substrates include X_2 (X = halogen), RX (R = alkyl, vinyl, alkynyl), ArX (Ar = aryl), HX, and O_2. The most important of these for common catalytic reactions are RX and ArX. These have been extensively studied and one example is shown in Figure 2.

Electrophilic ligands differ from the non-electrophilic substrates in that they do not necessarily need a low-lying empty orbital on the metal center in order to pre-coordinate necessary for oxidative addition. Although the Ir complex shown in Figure 2 does have an empty p_z orbital, this is not believed to play an important role in the oxidative addition reaction. An example with an 18e$^-$ complex is shown in Equation (6).

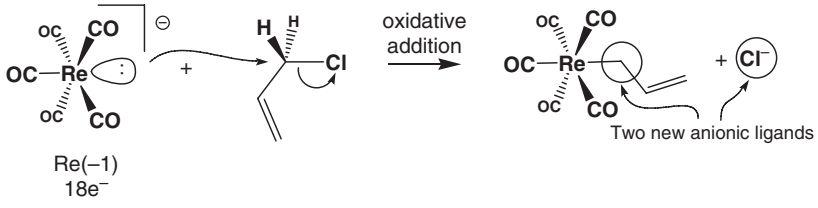

(6)

The dihalogens (F_2, Cl_2, Br_2, I_2) can often oxidize an 18e$^-$ saturated metal center (d^2 or higher electronic configuration) even when the metal is sterically protected via outer shell electron-transfer reactions. However, these are not common substrates in catalytic reactions.

Consider the reaction shown in Equation (7). The Cr center on the right now has two new anionic alkyl ligands forming a metallacyclopentane ring system. This is an oxidative addition, but in forming a new bond between the two ethylene ligands (and losing the original double bonds),[1] we have coupled the two ligands together. While this is an oxidative addition, there is a special term for this type of reaction called "oxidative coupling." The metal is being oxidized to create two new anionic ligands, but the original two neutral ligands also form a new σ-bond between them, instead of fragmenting apart to make two new independent anionic ligands. The driving force for this reaction is the formation of a new C–C σ-bond (stronger than a π-bond) and the creation of two new strongly donating anionic ligands that can better donate to the metal even though one has technically lowered the electron count.

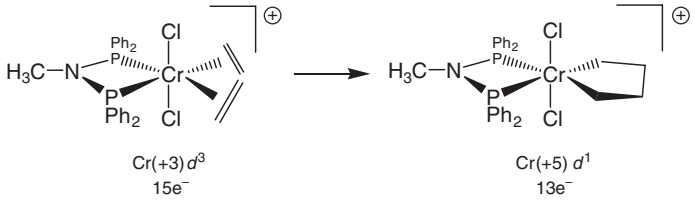

(7)

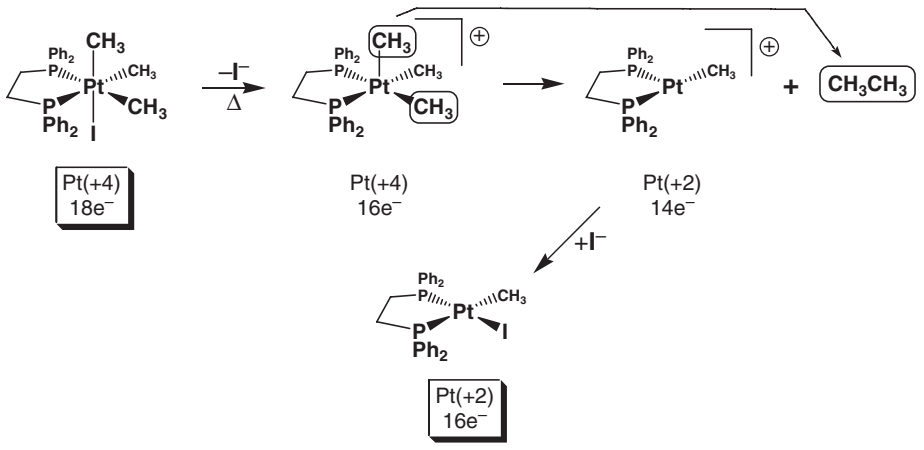

Figure 3 Reductive elimination of CH_3CH_3 in this Pt complex is promoted by initial dissociation of an iodide ligand to generate a cationic $16e^-$ system. Goldberg, K. I.; Yan, J.; Breitung, E. M. *J. Am. Chem. Soc*. **1995**, *117*, 6889.

A reductive elimination reaction is just the reverse of an oxidative addition. It is a reaction in which two *cisoidal* anionic ligands on a metal center couple together. Each anionic ligand pushes one electron back onto the metal center (in the case of a monometallic complex) to reduce it by $2e^-$. The coupled anionic ligands then usually fall off the metal center as a neutral molecule in a separate ligand-dissociation step (often assumed). Reductive eliminations are favored by electron-deficient metal centers (cationic, $16e^-$ or lower counts, electron-withdrawing ligands). An example of this is shown in Figure 3.[2]

1.04.5 Hydrogenolysis (Four-center Concerted Reactions) and Heterolytic Cleavage of H_2

The d^0-metal complexes naturally cannot perform oxidative addition reactions. These complexes, however, can react with H_2 in a four-center concerted fashion, as shown in Equation (8). This type of reaction is called hydrogenolysis. It occurs most commonly with alkyl and halide ligands on d^0-metal centers reacting with H_2. An empty coordination site on the metal center is required in order to pre-coordinate the H_2 ligand.

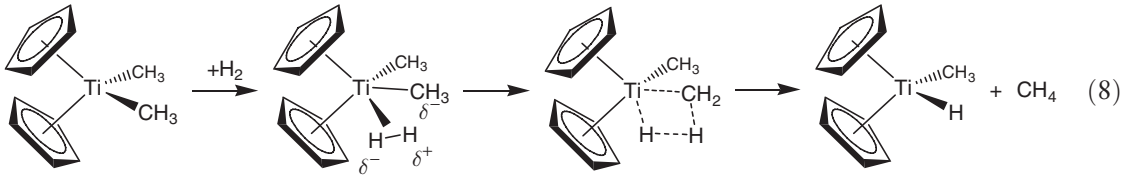

A fundamentally similar reaction is the heterolytic cleavage of H_2 by a metal center and a base to generate a hydride ligand (H^-) coordinated to the metal center and H^+ trapped by the base. Heterolytic cleavage does not involve an oxidation of the metal center and can occur on d^0 or higher systems. Ru complexes, for example, are believed to often activate H_2 in this fashion. Figure 4 shows two possible mechanisms for accomplishing this for $RuCl_2(PPh_3)_3$. The bottom pathway is the commonly proposed mechanism with an end-on coordination of H_2 to an empty coordination site on the Ru followed by base interaction to complete the polarization of the H_2 into H^- coordinated to the metal, and H^+ abstracted by the base.

However, one can also consider this a hydrogenolysis mechanism as shown on the top pathway in Figure 4 with subsequent trapping of the HCl by base to prevent facile backreactions. In many ways hydrogenolysis can be

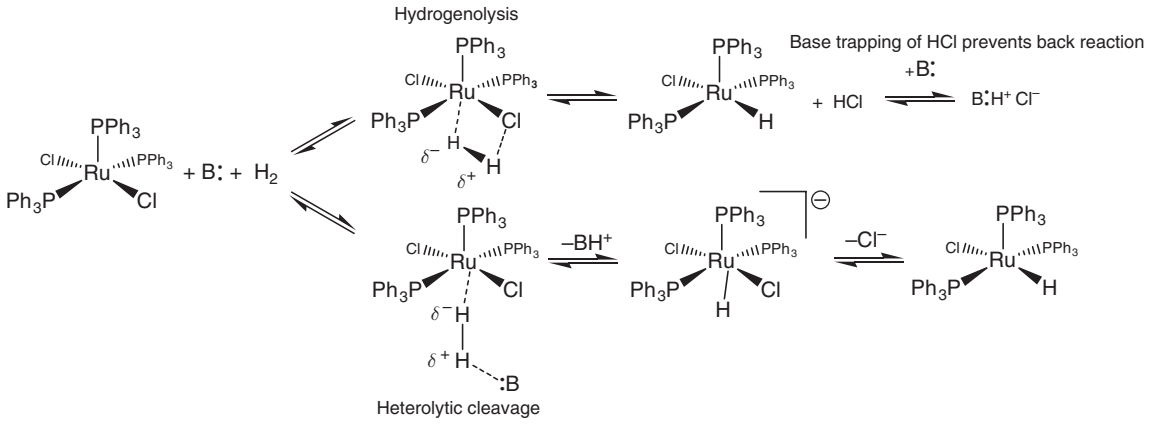

Figure 4 Two possible ways of activating H_2 on an Ru complex without doing an oxidative addition. Top pathway is hydrogenolysis, while the bottom mechanism is heterolytic cleavage.

considered an "intramolecular" heterolytic activation of H_2. If a system requires the addition of a base to assist in the formation of the M–H, one usually labels that reaction a heterolytic H_2 activation.

1.04.6 Migratory Insertions and Eliminations

A migratory insertion reaction is when a *cisoidal* anionic and neutral ligand on a metal complex couple together to generate a new coordinated anionic ligand. An example of the migratory insertion of a CO and methyl group is shown in Equation (9) to produce an acyl ligand.

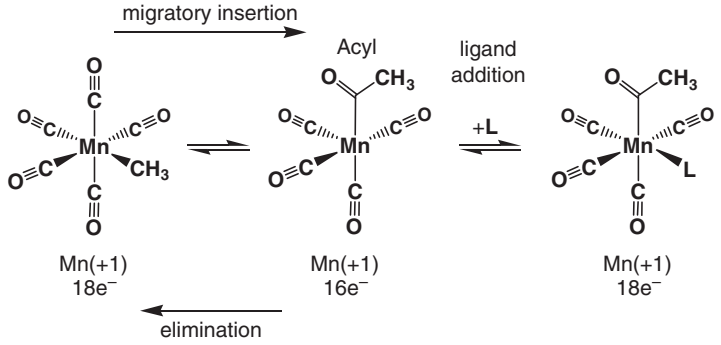

(9)

This new anionic ligand is composed of the original neutral and anionic species now bonded to one another. There is generally no change in the oxidation state or *d*-electron count of the metal center. But the overall electron count on the metal decreases by $2e^-$. The empty orbital generated by the migratory insertion reaction can enable the reverse of a migratory insertion reaction, which is called an elimination reaction. To stop (or inhibit) the reverse elimination reaction from occurring after a migratory insertion, one often adds a ligand to coordinate to this empty orbital. This is sometimes called a trapping ligand. Migratory insertions are usually favored on more electron-deficient metal centers.

The following are common anionic and neutral ligands that can do migratory insertion reactions with one another: (i) anionic—H^-, R^- (alkyl), Ar^- (aryl), $acyl^-$, CR_2^{2-} (alkylidenes), O^{2-} (oxo) and (ii) neutral–CO, alkenes, alkynes, carbenes. Note that the neutral ligands all need to have some unsaturation and need to lose one of their π-bonds in order to form a new σ-bond with the anionic ligand. CO and alkyl migratory insertions are extremely important and are often generically referred to as carbonylation reactions. Hydride and CO migratory insertions to produce formyl groups are not common due to the thermodynamic instability of the formyl–metal interaction.

Alkene and hydride/alkyl migratory insertions are also extremely important in catalytic reactions and form the basis for most polymerization reactions, an example of which is shown in Figure 5.

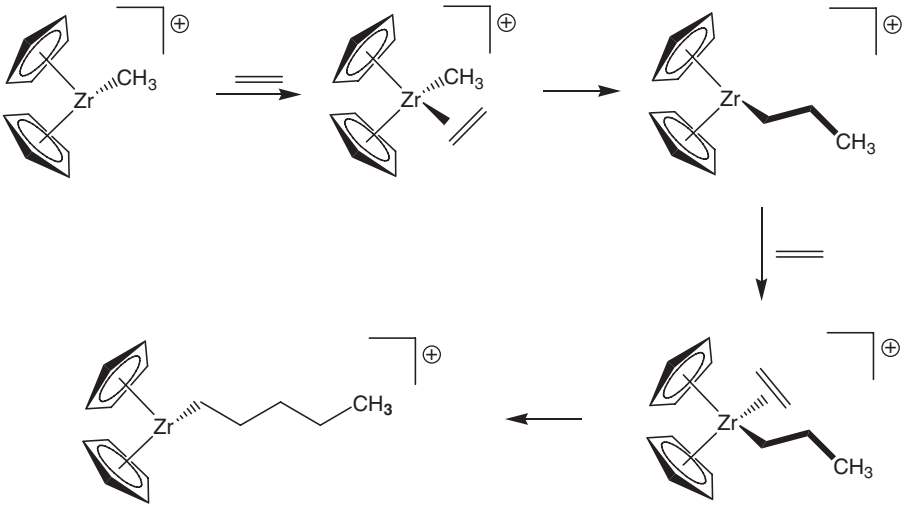

Figure 5 Ethylene ligand addition followed by migratory insertion forms a new propyl alkyl ligand. Further ligand additions of ethylene followed by migratory insertions lead to chain growth (oligomerization or polymerization).

An alkene and a hydride usually react via a migration of the hydride to the coordinated alkene ligand, as shown in Equation (10). The backward reaction is called a β-hydride elimination and is usually quite favorable if there is an empty orbital *cis* to the alkyl ligand.

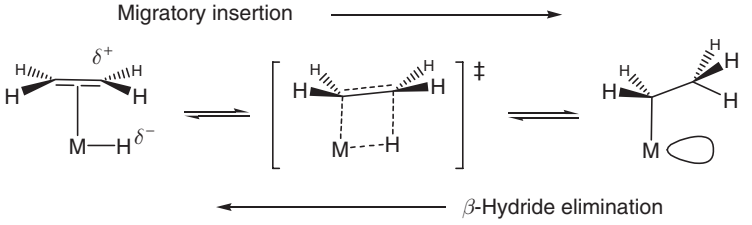

(10)

Equation (11) illustrates an intramolecular migratory insertion of an acyl with an alkyne to generate a lactone ring system.

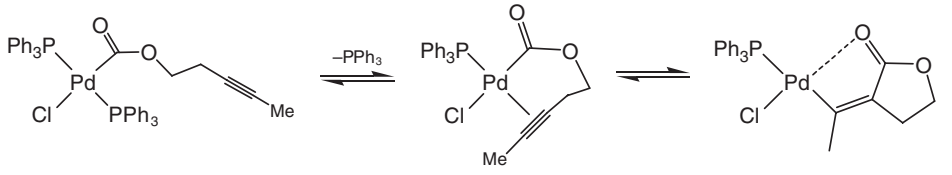

(11)

Alkylidenes (and alkylidynes) can react with alkenes (or alkynes) to produce metallacyclobutanes (or metallacyclobutenes), as shown in Equation (12). This is the key first step in alkene (olefin) metathesis.

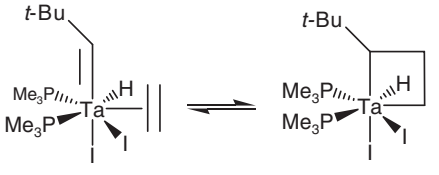

(12)

Carbenes can react with anionic ligands like alkyl groups to make longer chain alkyls, as shown in Equation (13) (* by the Cp ring indicates Cp*).

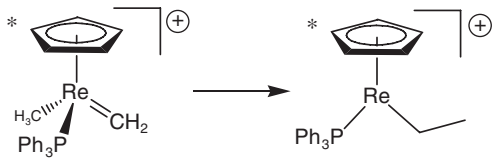

(13)

There can be some ambiguity in dealing with carbenes and alkylidenes with regard to electron counting. In equation (12), we consider the alkylidiene as a dianionic $4e^-$ donor ligand performing a migratory insertion with a neutral alkene to make a dianionic metallacyclobutane. No change in metal oxidation state is observed. In equation (13), the carbene can be treated as a neutral $2e^-$ donor that reacts with the anionic methyl group to make a new anionic propyl ligand. No change in metal oxidation state is observed. However, if one considered the carbene ligand in equation (13) to be a dianionic alkylidene ligand, then the Re center is going from Re(V) to Re(III) (d^2 to d^4). This then does not fit the general definition of a migratory insertion not changing the metal oxidation state or *d*-electron count. If we wanted to use a dianionic alkylidene ligand in equation (13), then one might characterize that reaction to be a reductive coupling. Similarly, treating the alkylidene ligand in equation (12) as a neutral carbene leads one to recategorize that reaction as an oxidative coupling (Ta(III) to Ta(V)).

Elimination reactions are just the opposite of migratory insertions. The most common reactions are summarized in Figure 6. If one electron counts the carbene in Figure 6 as an alkylidene, then the reaction would be called a C–H oxidative addition to the metal center.

A key point for elimination reactions is that one must have an empty orbital that is *cisoidal* to the group that one is doing the elimination reaction on. Alternatively, there must be a *cis*-labile ligand that can easily dissociate to open up an empty orbital to allow the elimination.

1.04.7 Hydrogenation Catalysis Mechanisms

Hydrogenation is one of the simplest catalytic reactions that makes use of the four main reaction types (ligand addition/dissociation, oxidative addition/reductive elimination, hydrogenolysis/heterolytic H_2 activation, and migratory insertions). Wilkinson's catalyst, $RhCl(PPh_3)_3$, and related variants, have been extensively studied and represent an excellent starting point for examining multistep catalytic mechanisms (cf. Ref: 3, 3a–3f). The proposed and generally accepted mechanism for Wilkinson's catalyst is shown in Figure 7.

The loss of PPh_3 from the sterically crowded $RhCl(PPh_3)_3$ is facile and the three-coordinate $RhCl(PPh_3)_2$ species is almost 900 times more reactive toward H_2 relative to the tris-phosphine starting complex. The rate-determining step, however, is the coordination of the alkene or the migratory insertion of the alkene and hydride to produce the Rh–alkyl intermediate.

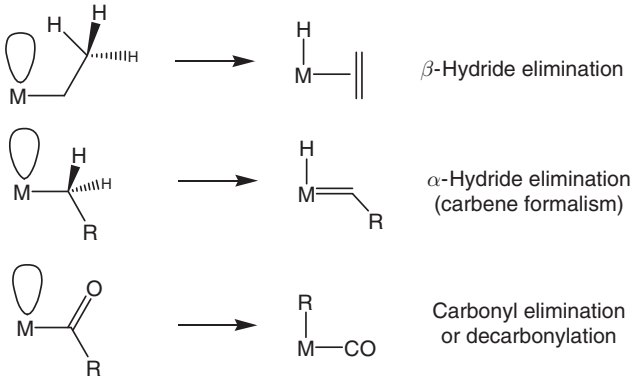

Figure 6 Some common elimination reactions.

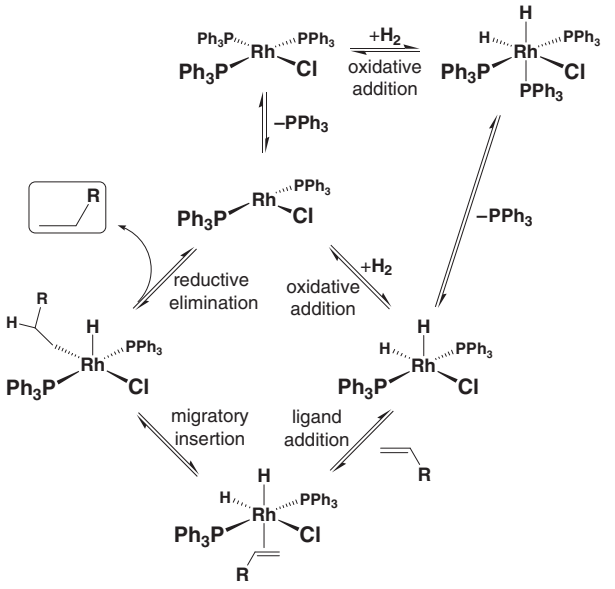

Figure 7 Proposed hydrogenation cycle for Wilkinson's catalyst, $RhCl(PPh_3)_3$.

All hydrogenation catalysts that operate via the oxidative addition of H_2 to the metal center to produce a dihydride have fundamentally similar mechanisms. The alkene can be already coordinated to the metal center prior to the H_2 oxidative addition, so long as there is still an empty coordination site available for binding the H_2 molecule to the metal center. Migratory insertion of one of the hydride ligands and coordinated alkene then produces an alkyl. If the alkyl is *trans* to the remaining hydride ligand, a ligand rearrangement has to occur to orient them *cis* to one another. The final step is reductive elimination of the alkyl and remaining hydride ligand, followed by dissociation of the saturated alkane product.

Table 1 lists turnover frequencies (TOFs) for three hydrogenation catalysts based on Rh and Ir complexes. The cationic $[Rh(nbd)(PPh_3)_2]^+$ (nbd = norbornadiene) catalyst was developed by Osborn and Schrock,[4] while the highly active $[Ir(nbd)(py)(PCy_3)]^+$ (py = pyridine) catalyst was discovered by Crabtree and co-workers.[5] These all function via the same mechanistic concepts presented in Figure 7. The higher activities of the cationic Rh and Ir catalysts are a result of their electron deficiency (higher electrophilicity) that favors alkene coordination (generally the rate determining step), migratory insertion, and the reductive elimination steps. The effect of increasing steric bulk of the coordinating alkene can also be seen from Table 1. The high activity for the Ir catalyst for even the most sterically hindered tetramethylethylene substrate can be explained by the very open environment about the metal.

Ru hydrogenation catalysts can also exhibit high activity, but are believed to generally operate via base-assisted heterolytic activation of the hydrogen. Figure 4 previously showed how the active monohydride catalyst species $RuHCl(PPh_3)_3$ could be generated via either hydrogenolysis (followed by base trapping of the HCl produced) or direct base-assisted heterolytic H_2 cleavage. Figure 8 illustrates the two possible mechanistic pathways for

Table 1 Turnover frequencies (TOFs) and subtrate dependence for three group 9 hydrogenation catalysts[5]

Catalyst	*Alkene substrates and TOF* (h^{-1})			
	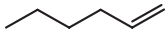		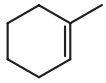	
$RhCl(PPh_3)_3$	650	700	13	
$[Rh(nbd)(PPh_3)_2]PF_6$	4,000	10		
$[Ir(nbd)(py)(PCy_3)]PF_6$	6,500	4,800	3,800	4,000

nbd = norbornadiene, py = pyridine.

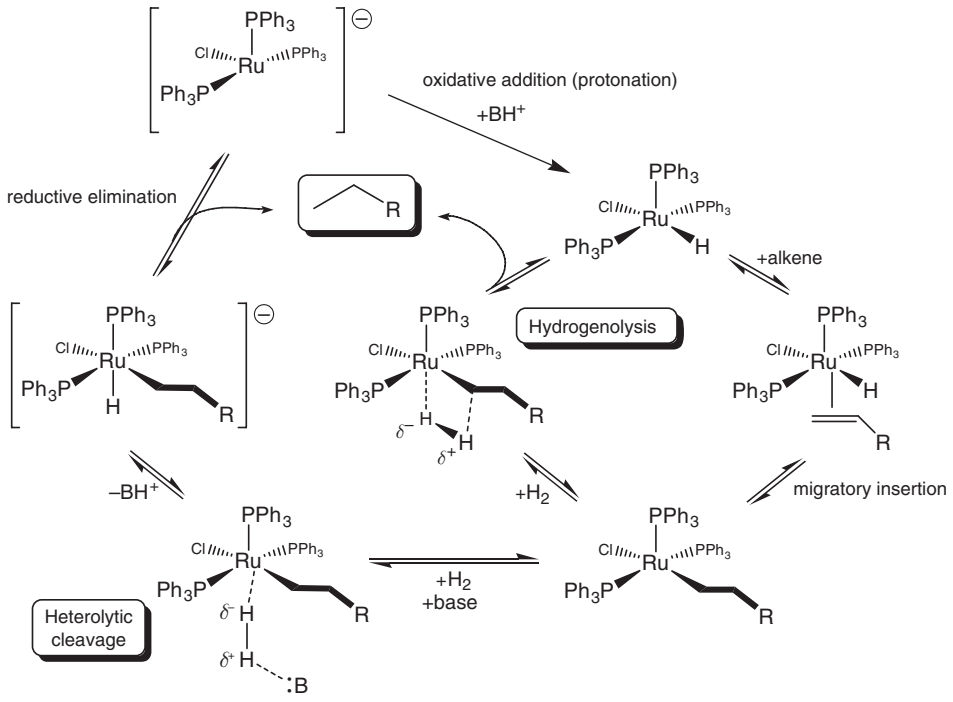

Figure 8 Proposed mechanism for Ru hydrogenation catalysis showing both hydrogenolysis (center) and base-assisted heterolytic H_2 activation pathways (left side).

Ru-catalyzed hydrogenation. They only differ by how the H_2 coordinates and reacts on the metal center. The central hydrogenolysis path has the H_2 binding to the metal and then forming a four-center transition state with the alkyl ligand leading to dissociation of the saturated alkane and regeneration of the $RuHCl(PPh_3)_3$ starting catalyst. The other pathway branches off to the left side of the cycle and involves the base-assisted heterolytic cleavage of H_2 to give an anionic $[RuHCl(alkyl)(PPh_3)_2]^-$ complex. Reductive elimination of the alkane product leads to an anionic Ru(0) complex, $[RuCl(PPh_3)_3]^-$, that can then be protonated to produce the starting catalyst. This protonation step is also classified as formal oxidative addition of H^+ to the Ru(0) center generating the Ru(II)–hydride catalyst. One can argue that the direct hydrogenolysis mechanism is more attractive as it avoids a reductive elimination from the fairly electron-rich anionic $[RuHCl(alkyl)(PPh_3)_2]^-$ complex that is formed on the heterolytic pathway.

The final type of hydrogenation cycle involves what is believed to be pure hydrogenolysis as it uses a d^0-lanthanide catalyst (Figure 9).[6] Marks and coworkers reported the extraordinary activity of $(Cp^*_2LuH)_2$ for the hydrogenation of alkenes and alkynes.[6] The monometallic complex catalyzes the hydrogenation of 1-hexene with a TOF $\approx 120{,}000\,h^{-1}$ at 1 atm H_2, 25 °C (estimated from low-temperature runs). This is one of the most active hydrogenation catalysts known. Although Lu(III) has an $f^{14}d^0$ configuration, the *f*-electrons are low enough in energy that they can not participate in any oxidative addition reactions. Thus, the proposal that the Lu center activates H_2 via a four-center hydrogenolysis mechanism.

1.04.8 Hydroformylation Catalysis Mechanisms

Hydroformylation (Equation (14)) is one of the very largest homogeneous catalytic reactions carried out by industry making over 15 billion pounds of aldehyde products each year. These are subsequently hydrogenated to alcohols or oxidized to carboxylic acids. There are several recent excellent reviews on hydroformylation catalysis (cf. Refs: 7, 7a–7c). Industry is generally more interested in the linear aldehyde product, and much of hydroformylation catalyst development work has been directed at increasing the linear to branched regioselectivity (L : B, also referred to as normal to iso), reaction rates, and catalyst stability (lifetime). There are three main hydroformylation catalysis

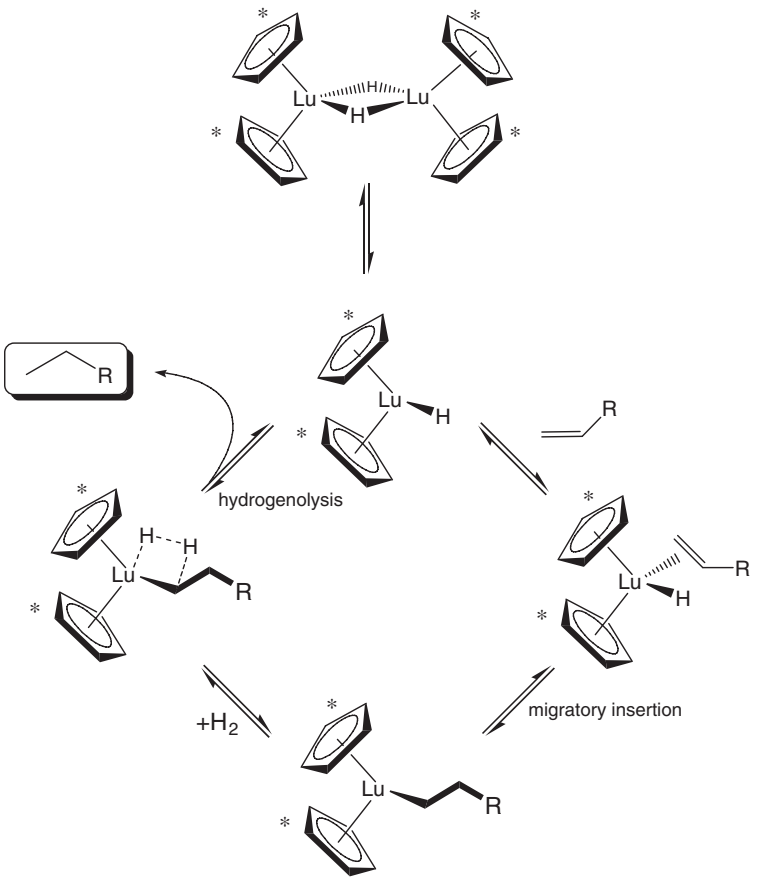

Figure 9 Proposed Lu-catalyzed hydrogenation cycle (* by the Cp rings indicates Cp* ligands). Jeske, G.; Lauke, H.; Mauermann, H.; Schumann, H.; Marks, T. J. *J. Am. Chem. Soc*. **1985**, *107*, 8111.

systems used in industry today: the original $HCo(CO)_4$ catalyst, the Shell phosphine-modified Co system, and the Union Carbide/BASF/Celanese Rh/PPh_3 process. The Pt/Sn hydroformylation catalyst system has also been fairly extensively studied, although it is much slower and less selective.

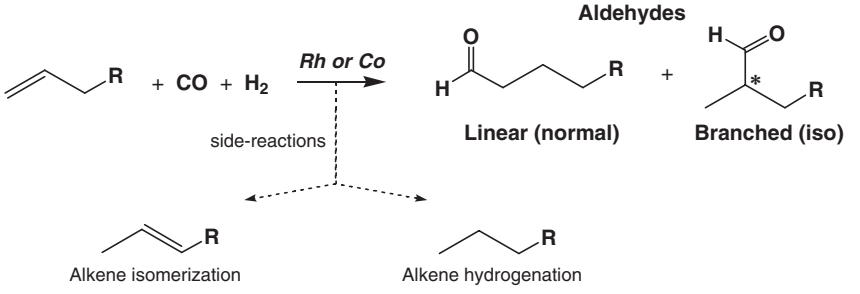

(14)

Heck proposed the first widely accepted mechanism for $HCo(CO)_4$-catalyzed hydroformylation in 1960 (Figure 10) (cf. Refs: 8, 8a). All hydroformylation mechanisms have essentially the same sequence of steps to convert alkene, CO, and H_2 into aldehyde product. Figure 10 shows both the production of linear and branched aldehyde products. The key regioselectivity step is the migratory insertion of the hydride and alkene ligands. If the hydride adds to the internal carbon of the double bond, the linear alkyl intermediate is formed. If the hydride adds to the terminal carbon of the double bond, the branched alkyl intermediate is produced. Although these steps are in equilibrium and can interconvert, the subsequent migratory insertion of CO to make the linear or branched acyl intermediate is typically fast and the regioselectivity of the product is believed to be set by the initial selectivity of the alkene–hydride

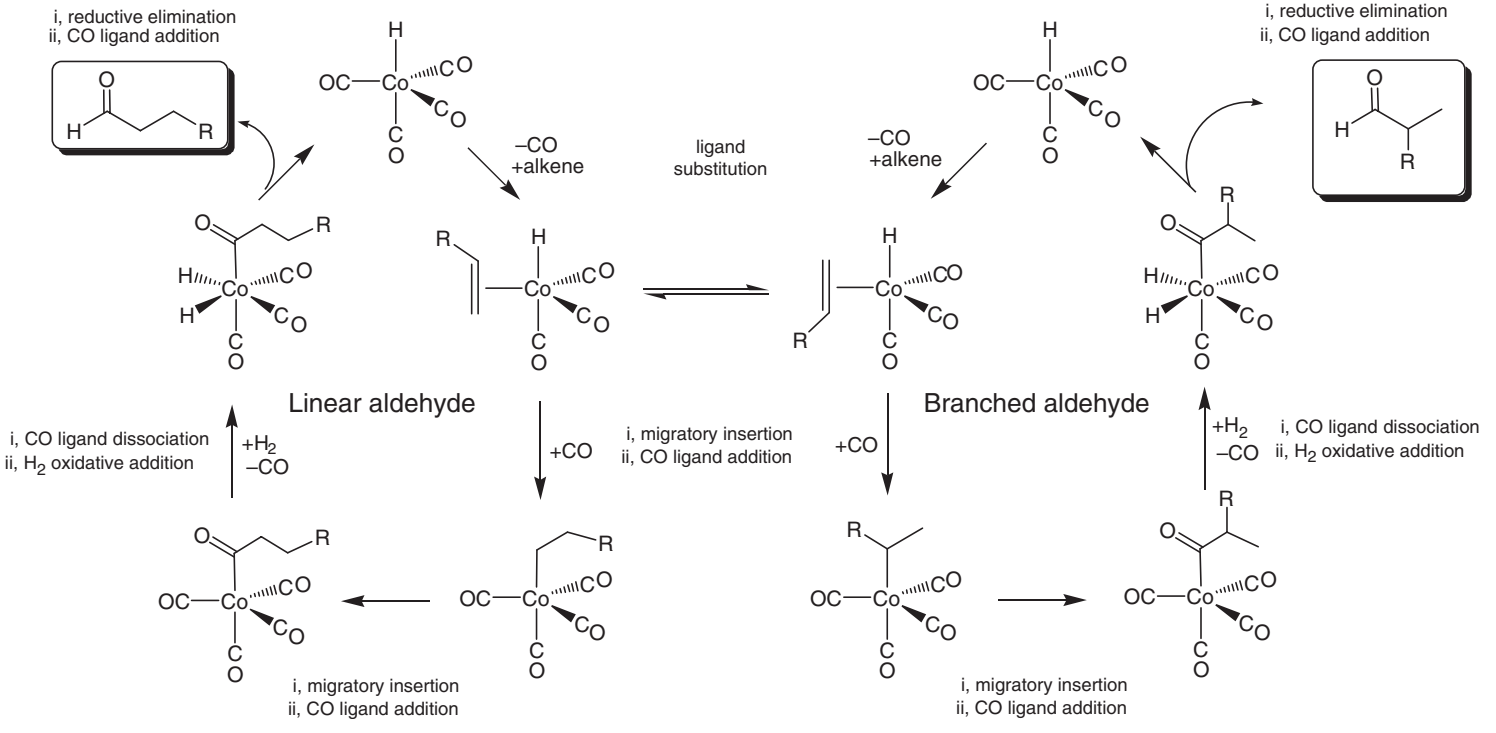

Figure 10 Cobalt-catalyzed hydroformylation cycle proposed by Heck showing both linear and branched aldehyde mechanisms.

migratory insertion step. The linear regioselectivity of this step is favored by increasing the steric bulk of one or more of the ligands on the metal center.

A somewhat unusual aspect of hydroformylation is that the CO reactant is a considerably better ligand than H_2 or alkene, and capable of saturating the metal center and inhibiting catalysis. The metal–carbonyl bond strength is dependent on the electron "richness" of the metal center, which, in turn, is strongly affected by the other ligands and their donor/acceptor properties. The addition of a phosphine ligand increases the sterics around the metal center favoring the more desirable linear aldehyde product. However, the stronger σ-donor and weaker π-acceptor properties of a phosphine ligand increases the electron density on the metal center promoting stronger M–CO bonding. This slows hydroformylation reaction rates by favoring saturated $18e^-$ complexes and making it harder for alkene or H_2 to react with the metal center.

Shell Chemical developed the phosphine-modified Co system in order to increase the L : B aldehyde regioselectivity.[9] The proposed mechanism is shown in Figure 11 and has the same sequence of reaction steps as $HCo(CO)_4$. The main difference is that the one electron-rich alkylated phosphine ligand is coordinated to the metal. This increases the steric environment about the cobalt center giving L : B aldehyde regioselectivities around 8 : 1 compared to the unmodified $HCo(CO)_4$ system that only gives L : B regioselectivities of 2 : 1 to a maximum of about 4 : 1. The phosphine also increases the Co–CO bond strength via increased π-backbonding to the more electron-rich metal center. The $HCo(CO)_3(PR_3)$ catalyst is, therefore, more stable than $HCo(CO)_4$ and can operate under lower pressures (75 vs. 250 bar). The higher stability of the $HCo(CO)_3(PR_3)$ catalyst also translates as lower reactivity for hydroformylation, so fairly high temperatures are still needed (180 °C).

The other important effect of the phosphine ligand is to increase the basicity of the cobalt hydride. This, coupled with the fairly high operating temperature, allows the $HCo(CO)_3(PR_3)$ catalyst to also function as an effective aldehyde hydrogenation catalyst to produce alcohol. This is generally a desirable reaction, as the aldehyde is typically hydrogenated in a separate reactor using a heterogeneous catalyst to produce the final alcohol product. One does have to watch out for unwanted hydrogenation of alkene starting material, but this can be controlled to an acceptable extent by increasing the CO pressure. The aldehyde hydrogenation cycle is also shown in Figure 11.

The Rh/PPh_3 hydroformylation catalyst system was developed approximately simultaneously by Geoffrey Wilkinson (and students),[10] Union Carbide, BASF, and Celanese. This catalyst system has been extensively studied, and the key species is $HRh(CO)(PPh_3)_2$. Once again the core mechanism is the same as that discussed previously for the cobalt systems and shown in Figure 12. Rhodium catalysts are approximately 1,000 times faster than ones based on cobalt (Rh is also about 1,000 times more expensive). Thus, rhodium catalysts can be run at considerably milder pressures and temperatures (8–10 bar, 125 °C), which dramatically reduces the capital expenditures for industrial plant construction. The increased activity of Rh over Co mainly derives from the stronger electronic preference of

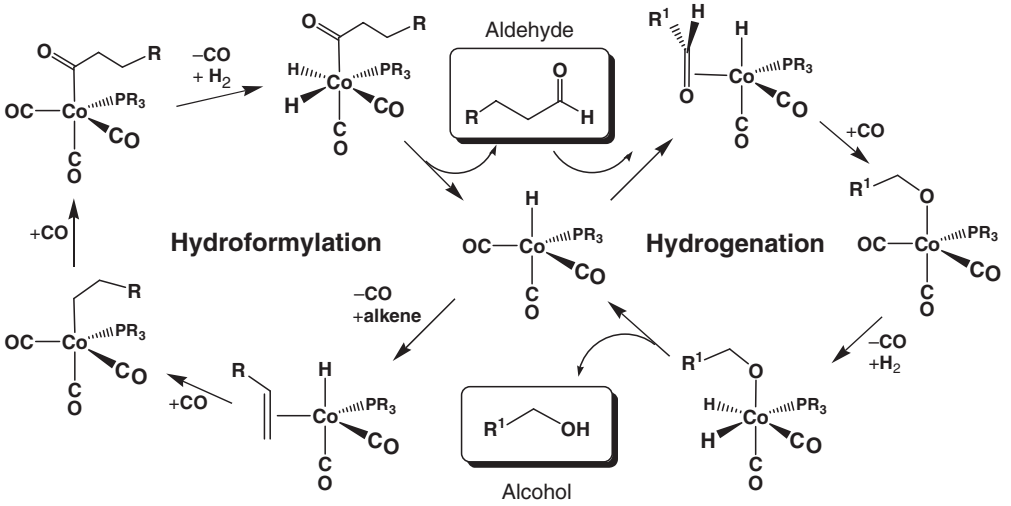

Figure 11 Proposed cobalt–phosphine hydroformylation and aldehyde hydrogenation cycles showing the dominant linear product selectivity.

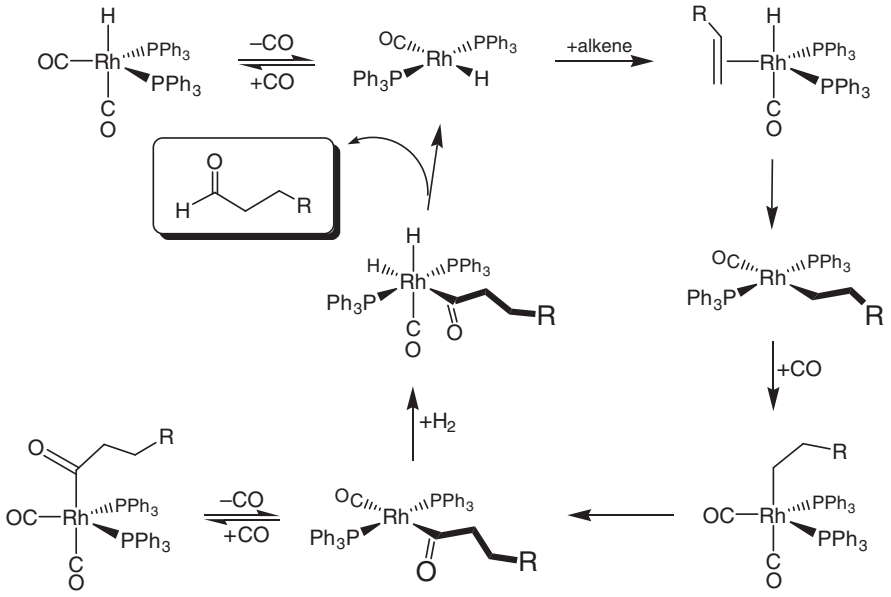

Figure 12 Proposed Rh–PPh_3 hydroformylation cycles showing linear product selectivity.

Rh(I) complexes to adopt stable $16e^-$ square-planar coordination geometries. Although a fifth ligand can readily add to make $18e^-$ complexes, there is a far greater tendency for the rhodium center for ligand dissociation to return to the more reactive $16e^-$ configuration. The considerably higher tendency for Rh to form these reactive $16e^-$ square-planar systems is the key to the far higher catalyst activity relative to cobalt.

Figure 12 shows the formation of the saturated $18e^-$ complexes $HRh(CO)_2(PPh_3)_2$ and $Rh(acyl)(CO)_2(PPh_3)_2$ on the left side of the cycle. The relatively facile dissociation of CO (or PPh_3) is extremely important to get the catalyst back on the active cycle to react with alkene or H_2. The rate-determining step for most good Rh hydroformylation catalysts is alkene coordination to the metal or the subsequent migratory insertion reaction with hydride to form the alkyl intermediate. Electron-rich donating alkylated phosphines are typically very bad for Rh hydroformylation because they increase the electron density on the rhodium center enough to favor strong Rh–CO π-backbonding that makes the $18e^-$ five-coordinate saturated complexes too stable and non-reactive.

Roy Pruett and Union Carbide patented (and obtained the licensing rights for) the key discovery that a large excess of PPh_3 ligand is necessary to produce a reasonably stable and selective $HRh(CO)(PPh_3)_2$ catalyst system. The various four-coordinate catalyst species that can form with their relative activities and selectivities are shown in Figure 13. Pruett realized that PPh_3 is not a particularly strong binding ligand, but that using a large excess of PPh_3 would shift the phosphine-dissociation equilibrium back toward the highly selective, but less active bis-phosphine catalyst. This is LeChatelier's principle in action. More of the inactive tris-phosphine complex is also produced, but for most of the industrial applications that use the Rh/PPh_3 catalyst, good L : B aldehyde regioselectivity (8 : 1 to 20 : 1) is very important. The typical industrial hydroformylation processes have an Rh concentration around 1 mM with a minimum PPh_3 concentration of 0.4 M, or a 400-fold excess of PPh_3 ligand. When higher L : B regioselectivities are required, the PPh_3 in solution can increase up to 50% by solution weight.

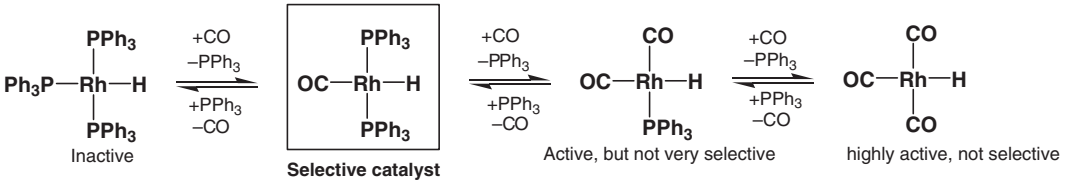

Figure 13 $HRh(CO)_x(PPh_3)_{3-x}$ ($x = 0$–3) species formed by CO/PPh_3 ligand-substitution equilibria.

1.04.9 Carbonylation of Methanol to Acetic Acid

The second largest homogeneous industrial process using rhodium catalysts is the carbonylation of methanol to produce acetic acid (Equation (15)). This was developed by Roth and Forster at Monsanto in the 1970s and is still commonly referred to as the Monsanto acetic acid process (even though BP purchased this technology in 1986). This highly active and efficient catalyst system completely replaced the previously used far less active and selective cobalt technology.

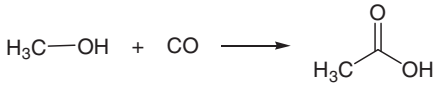

(15)

The mechanism has been studied extensively by Forster (cf. Ref: 11, 11a), and is an unusual double catalysis cycle involving an HI-catalyzed transformation of CH_3OH into the reactive CH_3I species and the Rh-catalyzed carbonylation of CH_3I (Figure 14). The initial step is reaction of methanol with HI to produce CH_3I, which then does an oxidative addition to $[RhI_2(CO)_2]^-$ to produce the Rh(III) complex $[RhI_3(CH_3)(CO)_2]^-$ (this is the rate-determining step). Migratory insertion of CO and methyl makes the acyl intermediate. Reductive elimination of the acyl iodide regenerates the starting $[RhI_2(CO)_2]^-$ catalyst. Reaction of the acyl–iodide with water generates acetic acid and 1 equiv. of HI.

There are several interesting features to this catalytic cycle. CO is not a part of the rate-determining reaction step, so the process has very little dependence on CO pressure. Nor is there any inhibitory effect of CO on the catalysis, as seen in hydroformylation. Furthermore, the oxidative addition of CH_3I to $[RhI_2(CO)_2]^-$ is not slowed by ligand-association reactions to make $18e^-$ five-coordinate complexes. This is due to the S_N2-like nature of the oxidative addition reaction that does not need an empty coordination site on the metal center. In fact, the addition of another iodide anion to $[RhI_2(CO)_2]^-$ produces the more electron-rich dianionic $18e^-$ catalyst species $[RhI_3(CO)_2]^{2-}$, which is more reactive for the oxidative addition of CH_3I. Researchers at Celanese independently figured this out and were able to patent the iodide-promoted "low water" variant of the $[RhI_2(CO)_2]^-$-catalyzed acetic acid process that they currently operate. The excess LiI used in the Celanese process also dramatically reduces precipitation of RhI_3 that can be a limiting factor in the original Monsanto catalytic system. The Monsanto process is sometimes referred to as the "high water" system due to the higher concentrations of water used to minimize the RhI_3 catalyst precipitation/deactivation problem. However, the increased water use causes other problems such as consumption of CO via water-gas shift catalysis and increased reactor corrosion due to the HI present.

BP announced a "new" iridium-catalyzed commercial system in 1999 called Cativa (cf. Ref: 12, 12a). This is shown in Figure 15 and is mechanistically the same as the original $[RhI_2(CO)_2]^-$-catalyzed system. In fact, Forster (Monsanto) studied this system in considerable detail along with the Rh catalyst that they commercialized.[13] Although the fundamental mechanism is the same, there are some important differences tied into electronic effects and the stronger Ir–ligand bonding.

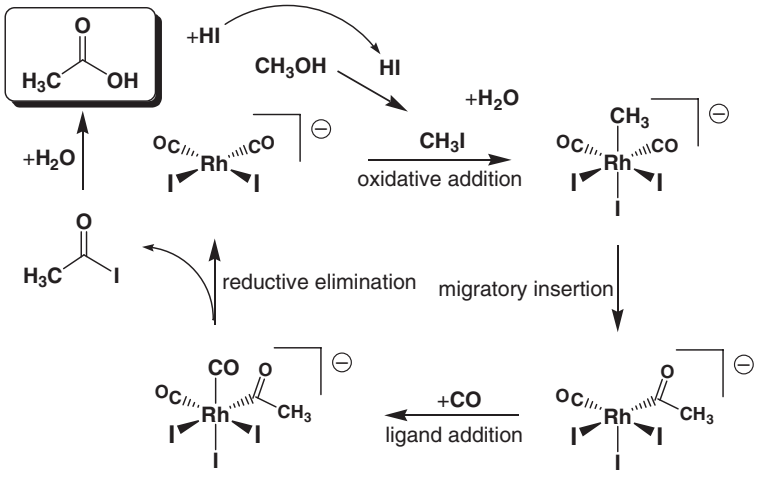

Figure 14 Proposed catalytic cycle for the $[RhI_2(CO)_2]^-$ and HI-catalyzed carbonylation of methanol to acetic acid.

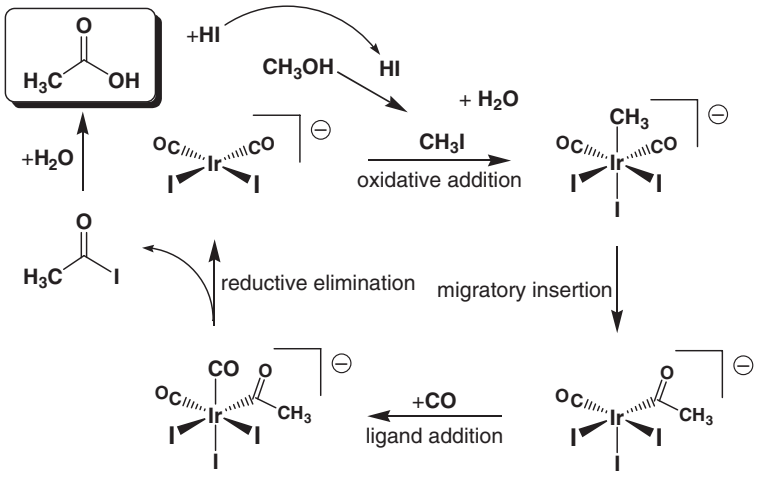

Figure 15 Proposed catalytic cycle for the $[IrI_2(CO)_2]^-$ and HI-catalyzed carbonylation of methanol to acetic acid.

The rate-determining step for the Ir cycle is now the migratory insertion of CO and the methyl group to make the acyl intermediate. The lower electronegativity of Ir (vs. Rh) increases the rate of the oxidative addition step (excess iodide increases this even futher), but the stronger metal–ligand bonding and higher electron density on the $[IrI_3(CH_3)(CO)_2]^-$ slow down, fairly substantially, the CO–methyl migratory insertion step. BP found that by adding iodide-abstracting agents, they could remove an iodide from the acyl species to generate the neutral $16e^-$ five-coordinate complex $IrI_2(CH_3)(CO)_2$ that was considerably more active with regard to the migratory insertion reaction.[12a] The Ir system allows them to operate under "low water" conditions and avoid problems associated with the original rhodium-based Monsanto system.

1.04.10 Palladium-Catalyzed Coupling Reactions

There are a host of palladium-catalyzed C–C coupling reactions that have been developed since the mid-1960s, but only a couple of specific examples will be covered here (cf. Ref: 14, 14a). Tsuji discovered Pd-catalyzed π-allyl and carbon nucleophile coupling reactions in 1965.[15,16] Mizoroki[17] and Heck[18] separately developed vinylic coupling reactions (Equation (16)) in the early 1970s, and this is commonly referred to as a Heck reaction or coupling.

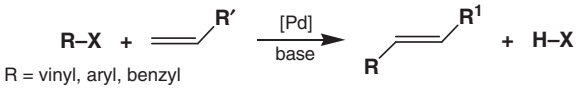

(16)

The coupling of organoboron compounds with R–X (R = aryl, alkenyl, alkynyl) is another popular Pd-catalyzed reaction (Equation (17)) called the Suzuki–Miyaura[19] coupling reaction (or often just the Suzuki reaction).[20]

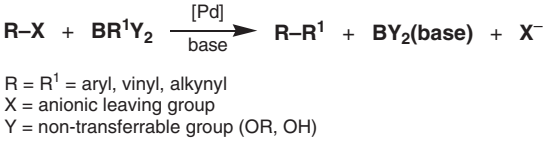

(17)

Although most Pd-catalyzed couplings involve a reactive organohalide as one of the reagents (aryl bromides being one of the most popular), the direct activation of aryl C–H bonds is known using a $Pd(OAc)_2$ catalyst, although these couplings often require more forcing conditions.

The mechanisms of Pd-catalyzed couplings are generally closely related and involve oxidative addition of the R–X bond to the Pd(0) center, coordination of the second reagent, migratory insertion of the two leading to C–C coupling, β-hydride elimination and product dissociation, reductive elimination of H–X (base trapping) to regenerate the starting Pd catalyst. Two proposed mechanisms for the Heck coupling are shown in Figure 16.

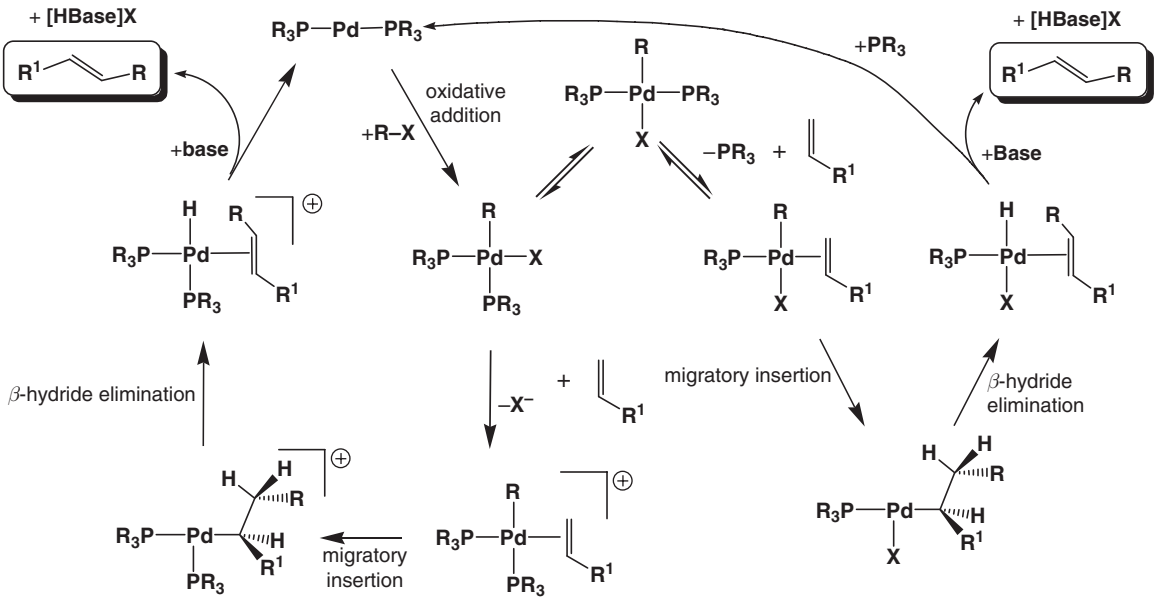

Figure 16 General catalytic cycle for a Pd(0)-catalyzed Heck coupling of R–X and an alkene showing cationic cycle (X^- dissociation, left) and neutral cycle (PR_3 dissociation, right).

Base is almost always required for Pd-catalyzed coupling reactions in order to trap out the H–X released in the final reductive elimination step or to abstract a proton from a cationic Pd–hydride (both shown in Figure 16). This generates one equivalent of salt per equivalent of product, which is not a problem for laboratory scale reactions, but certainly does limit the applicability of these coupling reactions for larger scale industrial processes.

The oxidative addition step of the R–X species to the Pd(0) center has been studied in some detail, and it has been proposed that it proceeds by an oxidative insertion.[21] This is an oxidative addition reaction where both atoms of the substrate interact with the metal center and end up *cisoidal* to the metal as anionic ligands. The oxidative addition of H_2 to most metals, for example, can be considered an oxidative insertion reaction.

Pd(II) precursors are often used in these catalytic reactions, which lead to the ongoing question about how reduction to the Pd(0) species occurs. Alcohol solvent, NEt_3 base, and phosphine ligands have all been proposed to be reducing agents for producing the active Pd(0) catalyst species. There also exists the possibility of having a Pd(II)–Pd(IV) catalysis cycle with a similar sequence of steps.[22]

1.04.11 Polymerization and Metathesis

The most commonly accepted mechanism for polymer chain growth on a transition metal catalyst is the very simple migratory insertion mechanism, initially proposed by Piet Cossee[23] (Royal Shell labs) in 1964 and shown in Figure 17.

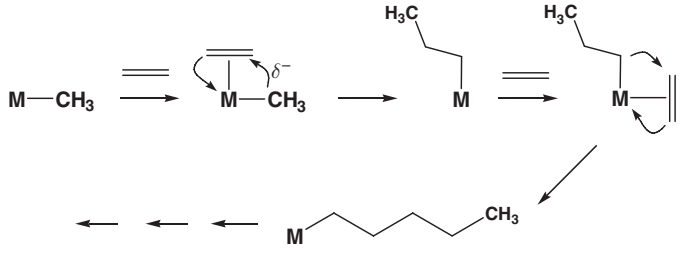

Figure 17 Cossee migratory insertion mechanism for alkene polymerization.

In many careful mechanistic studies on early and late transition metal polymerization catalysts, this is the mechanism that fits the experimental data best.

The only real competing mechanism proposed for alkene polymerization is the alkylidiene–metallacyclobutane pathway proposed in 1978 by Green and Rooney (shown in Figure 18).[24] This mechanism starts with an intramolecular α-C–H bond oxidative addition to the metal to generate an alkylidene–hydride species. Coordination of alkene to an empty *cisoidal* orbital is followed by a migratory insertion to produce the metallacyclobutane intermediate. Reductive elimination of the metal–hydride with chain-branched alkyl carbon gives one a new linear alkyl group that is two carbons longer. One can also have reductive elimination of the hydride with what is drawn as the *trans*-alkyl group in Figure 18 to produce a branched carbon chain.

Schrock has demonstrated that the Ta-based ethylene polymerization system shown in Figure 19 is likely to proceed via the Green–Rooney alkylidene mechanism.[25] They based this on their observation of the metallacyclobutane intermediate at low temperatures in the NMR. However, the alkylidene–metallacyclobutane mechanism does not appear to operate for most metal-based polymerization catalysts.

Late transition metal oligiomerization catalysts have been known for many years. Well-characterized group 8 polymerization catalysts were reported by Brookhart in 1998 and Gibson in 1999.[26,27] These catalysts operate via the simple Cossee alkene addition and migratory insertion mechanism. A key in preparing an efficient polymerization catalyst was the realization that the facile β-hydride eliminations occurring on group 8 metals (especially Ni and Pd) lead to an associative displacement problem that short-circuited the chain growth pathway (Figure 20). When a

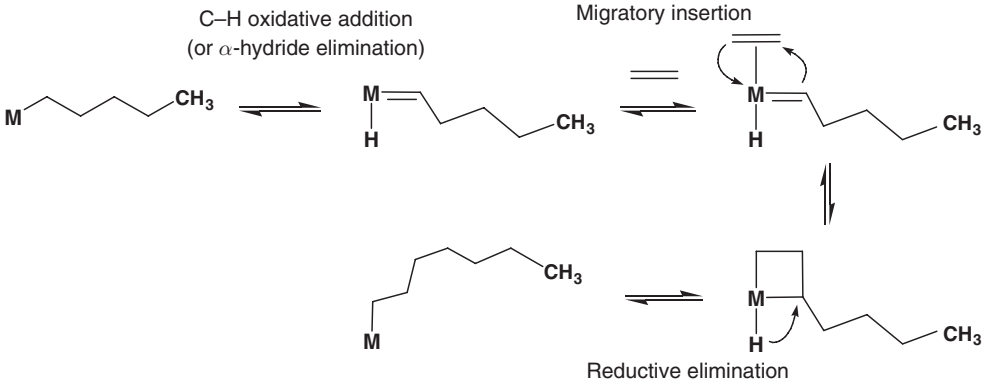

Figure 18 Green–Rooney alkylidene mechanism for alkene polymerization.

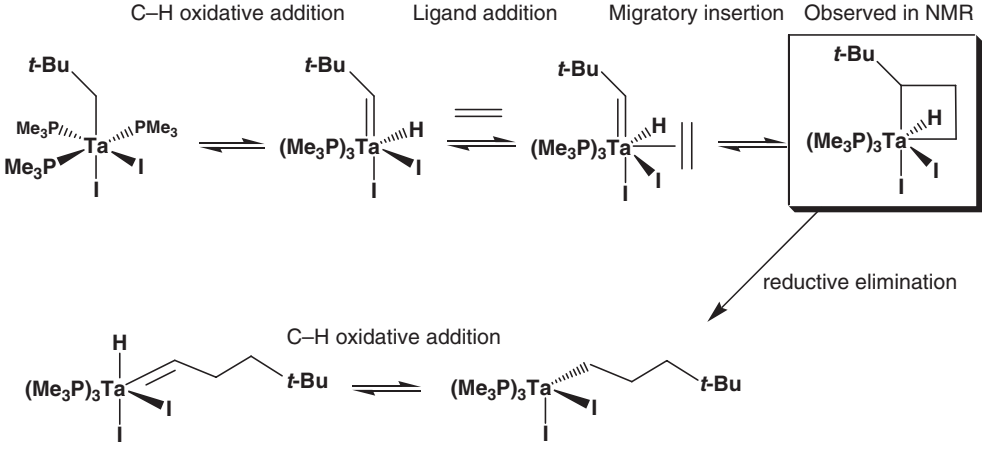

Figure 19 Proposed mechanism for ethylene polymerization by $TaI_2(CH_2\text{–}t\text{-Bu})(PMe_3)_2$.

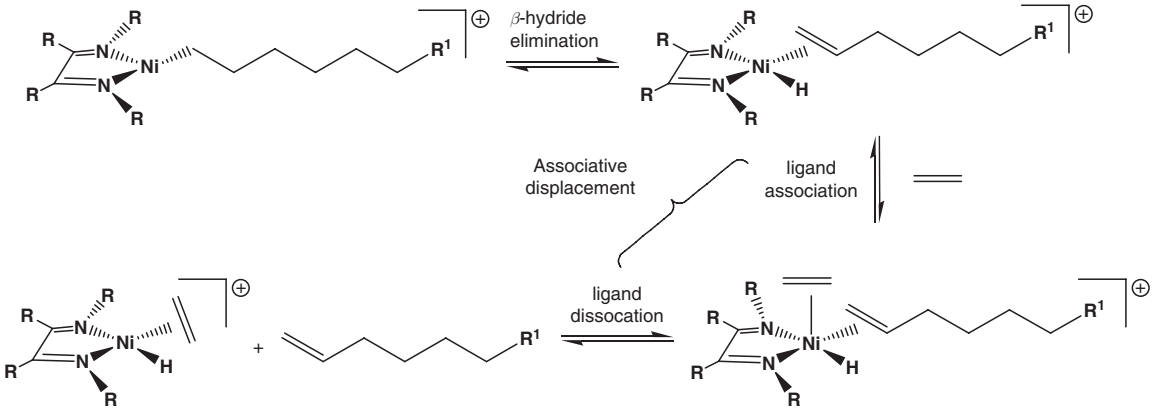

Figure 20 The associative displacement problem on Ni polymerization catalysts. By using very bulky R groups Brookhart blocked out the axial coordination site, thus preventing small ethylene molecules from associatively displacing the longer coordinated alkene formed from β-hydride elimination.

growing polymer alkyl chain does a β-hydride elimination from a three-coordinated catalyst species, a four-coordinate hydride–alkene is formed. A small olefin can easily coordinate to the axial metal site leading to a less stable five-coordinate complex. This promotes loss of the longer alkene chain leading to termination of the chain growth. By placing extremely bulky R groups on the diimine ligand, Brookhart was able to effectively block both axial coordination sites while still allowing equatorial alkene coordination.

An unusual aspect of Brookhart's Ni and Pd polymerization catalysts was that they could produce highly branched polyethylene, with the amount of branching controlled in large part by the ethylene pressure. Mechanistic studies indicated that facile β-hydride eliminations on these catalysts under lower ethylene pressures enabled a "chain-walking" isomerization process shown in Figure 21. This leads to branching (sometimes extensive) of the growing

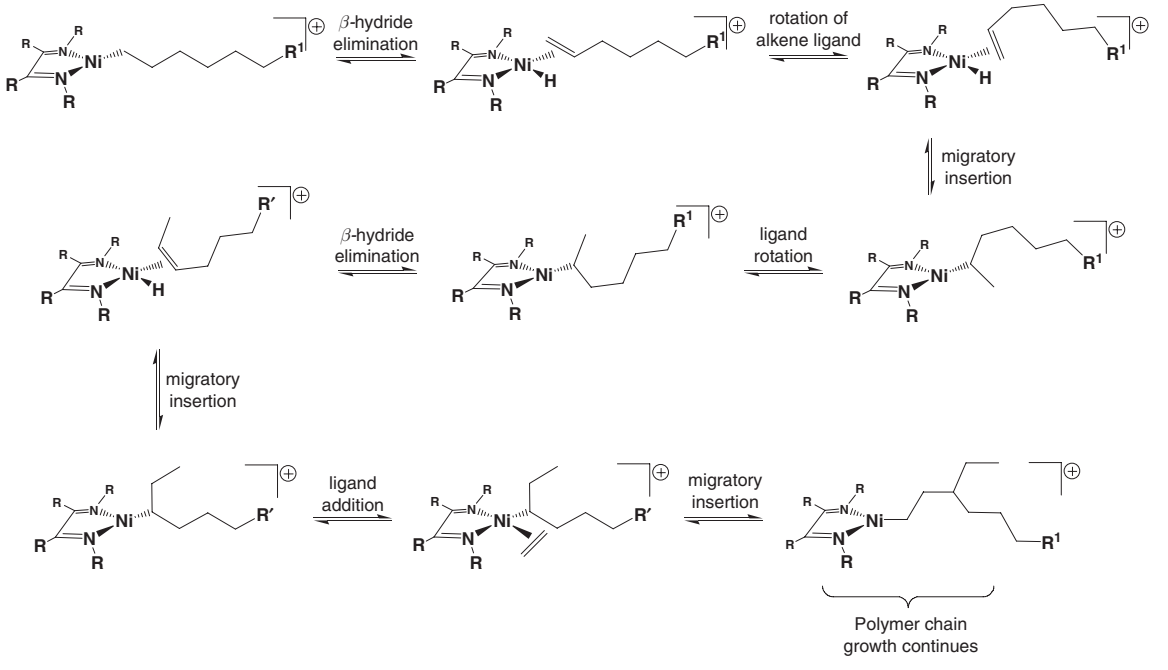

Figure 21 Proposed chain-walking mechanism that leads to branched polyethylene.

polymer chain. Under higher ethylene pressures, the empty coordination site needed for β-hydride elimination is more rapidly filled by an ethylene leading to more linear chain growth.

There is another mechanism for polymerization related to the Green–Rooney alkylidene pathway that can operate when one deals with cyclic alkenes. This is called ring-opening metathesis polymerization (ROMP) (cf. Ref: 28, 28a), and the first commercial product was prepared by CdF Chimie from norbornene (Equation (18)) using a heterogeneous catalyst based on MoO_3 supported on alumnia.

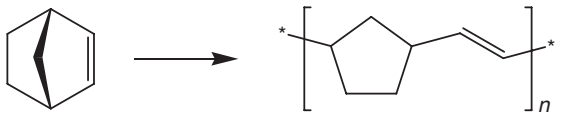

(18)

ROMP works best on cyclic alkenes that have some ring strain to drive the ring-opening process and minimize possible ring-closing reactions. A proposed mechanism for the ROMP of norbornene using a Cp_2Ti center is shown in Figure 22. In this mechanism, we consider the alkylidene as a dianionic ligand, so the reaction with the alkene is considered a migratory insertion. The subsequent elimination reaction can proceed in two ways, backward (nonproductive) and forward, which opens the norbornene ring and extends the polymer chain.

One can also perform acyclic diene metathesis (ADMET) polymerization using longer chain α,ω-dienes, which is basically a specialized type of metathesis catalysis. The general reaction and mechanism is shown in Figure 23 and relies on the loss of ethylene from the reaction mixture to drive the reaction to high couplings and molecular weights. The internal double bonds generated are not as reactive as the terminal double bonds for the metathesis reaction.

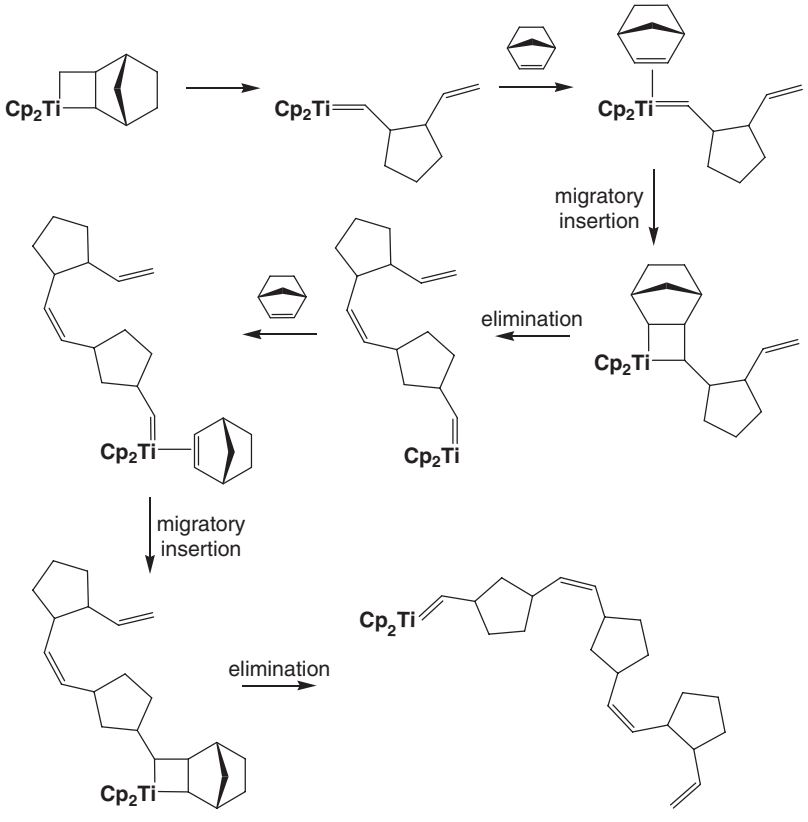

Figure 22 Proposed ring-opening metathesis polymerization (ROMP) of norbornene.

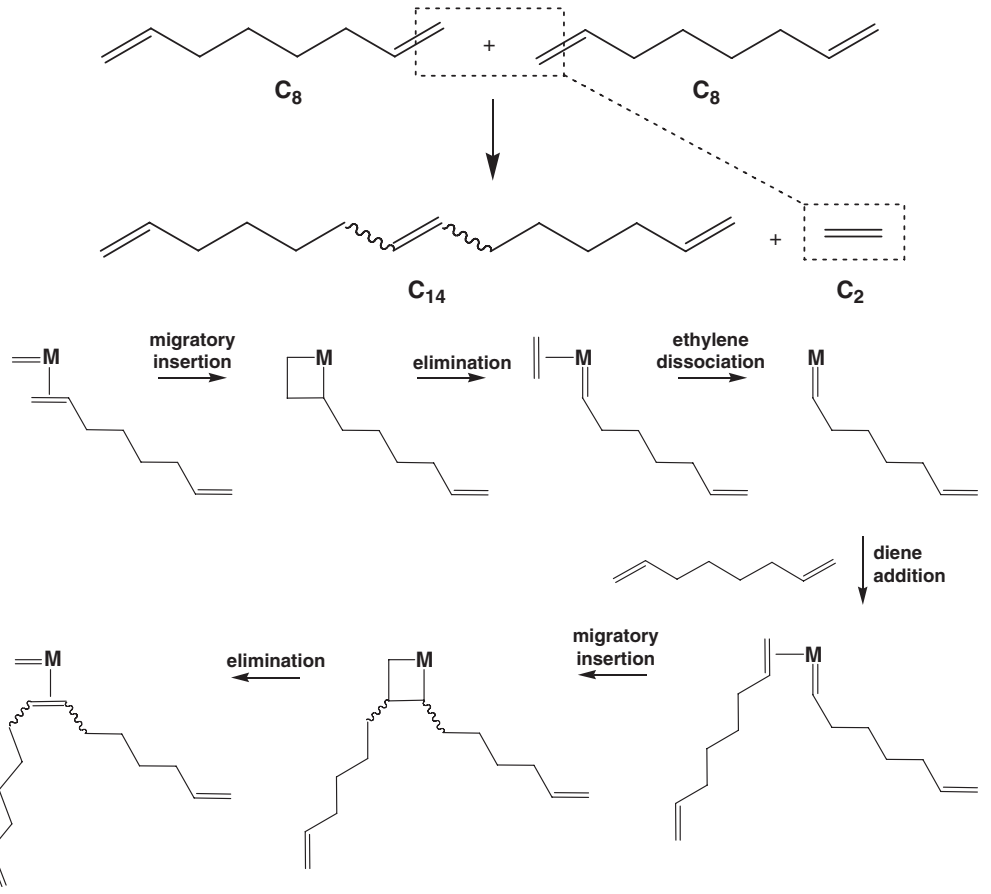

Figure 23 General reaction and mechanism for acyclic diene metathesis (ADMET) polymerization.

1.04.12 Conclusions

The examples covered in this chapter demonstrate that multistep catalytic cycles are simply composed of the following mixture of elementary organometallic reaction steps: (i) ligand addition/dissociation, (ii) oxidative addition/reductive elimination, (iii) hydrogenolysis (four-center concerted reactions, heterolytic H_2 activation), and (iv) migratory insertion/elimination. The vast majority of catalytic reactions can be described using these basic reactions.

References

1. Cf. Colman, J. P.; Hegedus, L. S.; Norton, J. R.; Finke, R. G. *Principles and Applications of Organotransition Metal Chemistry*, 2nd ed.; University Science Books: Mill Valley, CA, 1987.
1a. Crabtree, R. H. *The Organometallic Chemistry of the Transition Metals*, 3rd ed.; Wiley-Interscience: New York, 2001.
1b. Elschenbroich, C.; Salzer, A. *Organometallics*; VCH: Weinheim, 1989.
1c. Spessard, G. O.; Miessler, G. L. *Organometallic Chemistry*; Prentice-Hall: Saddle River, NJ, 1996.
1d. Lukehart, C. M. *Fundamental Transition Metal Organometallic Chemistry*; Brooks/Cole: Monterey, CA, 1985.
2. Goldberg, K. I.; Yan, J.; Breitung, E. M. *J. Am. Chem. Soc.* **1995**, *117*, 6889.
3. Cf. Osborn, J. A.; Jardine, F. H.; Young, J. F.; Wilkinson, G. *J. Chem. Soc. A.* **1966**, 1711.
3a. Jardine, F. H.; Osborn, J. A.; Wilkinson, G. *J. Chem. Soc. A.* **1967**, 1574.
3b. Halpern, J.; Wong, C. S. *Chem. Commun.* **1973**, 629.
3c. Harmon, R. E.; Gupta, S. K.; Brown, D. J. *Chem. Rev.* **1973**, *73*, 21.
3d. Chan, A. S. C.; Halpern, J. *J. Am. Chem. Soc.* **1980**, *102*, 838.
3e. Halpern, J. *J. Organomet. Chem.* **1980**, *200*, 133.
3f. Rylander, P. N. *Hydrogenation Methods*; Academic Press: London, 1990.
4. Osborn, J. A.; Schrock, R. R. *J. Am. Chem. Soc.* **1971**, *93*, 3089.
5. Crabtree, R. H. *Acc. Chem. Res.* **1979**, *12*, 331.

6. Jeske, G.; Lauke, H.; Mauermann, H.; Schumann, H.; Marks, T. J. *J. Am. Chem. Soc.* **1985**, *107*, 8111.
7. Cf. Freixa, Z.; Van Leeuwen, P. W. N. M. *J. Chem. Soc., Dalton Trans.* **2003**, 1890.

7a. Gleich, D. Hydroformylation. In *Applied Homogeneous Catalysis with Organometallic Compounds*, 2nd ed.; Cornils, B., Herrmann, W. A, Eds.; Wiley-VCH: Weinheim, 2002; Vol. 2, pp 727–737.

7b. van Leeuwen, P. W. N. M.; Claver, C. *Rhodium Catalyzed Hydroformylation*; Kluwer: Dordrecht, 2000.

7c. Cornils, B. In *New Syntheses with Carbon Monoxide*; Falbe, J., Ed. Springer: Berlin, 1980.

8. Breslow, D. S.; Heck, R. F. *Chem. Ind. (London)* **1960**, 467–468.

8a. Heck, R. F.; Breslow, D. S. *J. Am. Chem. Soc.* **1961**, *83*, 4023.

9. Slaugh, L. H.; Mullineaux, R. D. *J. Organometal. Chem.* **1968**, *13*, 469.
10. Evans, D.; Osborn, J. A.; Wilkinson, G. *J. Chem. Soc. A* **1968**, 3133.
11. Forster, D. *J. Am. Chem. Soc.* **1976**, *98*, 846.

11a. Forster, D. *Adv. Organomet. Chem.* **1979**, *17*, 255.

12. Sunley, G. J.; Watson, D. J. *Catal. Today* **2000**, *58*, 293.

12a. Haynes, A.; Maitlis, P. M.; Morris, G. E.; Sunley, G. J.; Adams, H.; Badger, P. W.; Bowers, C. M.; Cook, D. B.; Elliott, P. I. P.; Ghaffar, T., *et al. J. Am. Chem. Soc.* **2004**, *126*, 2847.

13. Forster, D. *J. Chem. Soc., Dalton Trans.* **1979**, 1639.
14. Cf. Heck, R. F. *Palladium Reagents in Organic Synthesis*; Academic Press: London, 1985.

14a. Tsuji, J. *Palladium Reagents and Catalysts*; Wiley: West Sussex, 1995.

15. Tsuji, J.; Takahashi, H.; Morikawa, M. *Tetrahedron Lett.* **1965**, 4387.
16. Tsuji, J. *Acc. Chem. Res.* **1969**, *2*, 144.
17. Mizoroki, T.; Kori, K.; Ozaki, A. *Bull. Chem. Soc. Jpn.* **1971**, *44*, 581.
18. Heck, R. F.; Nolley, J. P. *J. Org. Chem.* **1972**, *37*, 2320.
19. Miyaura, N.; Suzuki, A. *Chem. Commun.* **1979**, 866.
20. Suzuki, A. *Acc. Chem. Res.* **1982**, *15*, 178.
21. Hieringer, W. Heck Reaction. In *Applied Homogeneous Catalysis with Organometallic Compounds*, 2nd ed.; Cornils, B., Herrmann, W. A., Eds.; Wiley-VCH: Weinheim, 2002; Vol. 2, pp 721–727.
22. Shaw, B. L. *New. J. Chem.* **1998**, 77.
23. Cossee, P. *Tetrahedron Lett.* **1960**, 12.
24. Ivin, K. J.; Rooney, J. J.; Stewart, C. D.; Green, M. L. H.; Mahtab, R. *Chem. Commun.* **1978**, 604.
25. Turner, H. W.; Schrock, R. R. *J. Am. Chem. Soc.* **1982**, *104*, 2331.
26. Brookhart, M.; Haupman, E. *J. Am. Chem. Soc.* **1998**, *120*, 4050.
27. Britovsek, G. J. P.; Bruce, M.; Gibson, V. C.; Kimberley, B. S.; Maddox, P. J.; Mastroianni, S.; McTavish, S. J.; Redshaw, C.; Solan, G. A., Stromberg, S., *et al. J. Am. Chem. Soc.* **1999**, *121*, 8728.
28. Cf. Schrock, R. R. *Acc. Chem. Res.* **1990**, *24*, 158.

28a. Grubbs, R. H.; Tumas, W. *Science* **1989**, *243*, 907.

1.05
Mechanistic Aspects of Olefin-polymerization Catalysis

W E Piers, University of Calgary, Calgary, AB, Canada
S Collins, University of Akron, Akron, OH, USA

1.05.1 Introduction and Scope

Since the beginnings of organometallic chemistry with the discovery of Zeise's salt in 1825, and its structural elucidation in the 1950s,[1] the transformation of olefins into useful molecules and materials by transition metal catalysis has been a primary driver in the development of modern organometallic chemistry. This is particularly true of the past 50 years following the seminal discoveries of Ziegler[2,2a] and Natta[3] concerning the effect of transition metals on the "aufbau" reaction, and the birth of today's multi-billion dollar worldwide plastics industry. While heterogeneous catalysts have dominated commercial processes for plastics production, homogeneous organometallic compounds have gradually been making gains due to the high level of control over selectivity afforded by these well-defined systems. A deep understanding of the mechanisms by which they operate has contributed to their effective deployment and the development of catalysts that selectively produce polymeric materials not available using heterogeneous catalysts. The drive to understand the mechanisms of action for these catalysts at a molecular level has contributed to the advancement of organometallic chemistry as a discipline, bringing to bear the classic tools of physical organic chemistry to elucidate the mechanisms of these important transformations.

While coordination polymerization of ethylene and other aliphatic olefins is arguably the most-studied and emphasized mechanism by which organotransition metals mediate polymerization reactions, ring-opening metathesis

polymerization (ROMP) and group-transfer polymerizations are other well-studied mechanisms by which metal complexes knit together olefinic monomers into useful polymeric materials. Furthermore, some transition metal complexes are effective initiators of more traditional anionic, cationic, or radical-based pathways.

Each of these is a distinct mechanism by which organometallic compounds conduct polymerization catalysis. In this chapter, we discuss aspects of each of these mechanisms, highlighting seminal mechanistic organometallic papers, and illustrating how a deep mechanistic understanding of the propagation step in the polymerization process has impacted catalyst development. Typically, polymerization processes are described in terms of three basic steps: initiation of polymerization, propagation, and chain transfer or termination steps. To narrow the scope of our discussion, we will focus primarily on the propagation or initiation steps of each mechanism, that is, the steps that result in olefin enchainment; mechanisms of termination and chain-transfer steps will not be discussed in any detail.

1.05.2 Polymerization by Migratory Olefin Insertion

1.05.2.1 Introduction

Single-site olefin-polymerization catalysts are discrete, molecular compounds bearing at least a metal–carbon linkage that is susceptible to an olefin-insertion reaction, that regenerates the metal–alkyl group for further enchainments (Scheme 1). While metallocenes based on group 4 metals, and, to a lesser extent, group 3 metals and lanthanides, are the most well understood family of such compounds, the "post-metallocene" era is well underway and many families of single-site catalysts are now known. The area has been extensively reviewed[4] and much is known about the mechanism of these catalysts *vis-à-vis* olefin polymerization. At the core of the mechanism is the insertion of an olefinic double bond into a reactive M–C bond.

Early mechanistic studies on the migratory insertion of C═C into M–H bonds lead to a detailed picture of the transition state for this model reaction for the propagating step in olefin polymerization. Bercaw *et al.* carried out landmark studies that showed that olefin insertion into the M–H bonds of group 3 and 5 metallocenes proceed via a concerted, four-centered transition state **1**. Studies utilizing d^2-niobocenes $Cp_2Nb(H)(\eta^2\text{-}CH_2CHR)$ ($Cp = C_5H_5$, C_5Me_5; R = H, CH_3, *p*-X–C_6H_4) showed that insertion rates were depressed when R or X is electron withdrawing relative to R = H, suggesting that the polarization in the four-centered ring depicted and the hydrogen transferred have hydridic character.[5,5a] This interpretation was corroborated by sister studies in the d^0-decamethylscandocene manifold, where the microscopic reverse reaction, β-hydride elimination, was studied.[6] Similar conclusions were put forward in an earlier study by Halpern *et al.* in a late metal system based on rhodium.[7] Thus, a fairly unified picture of this fundamental reaction emerged from these early studies.

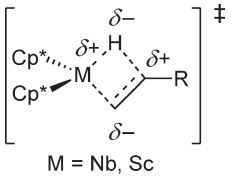

1

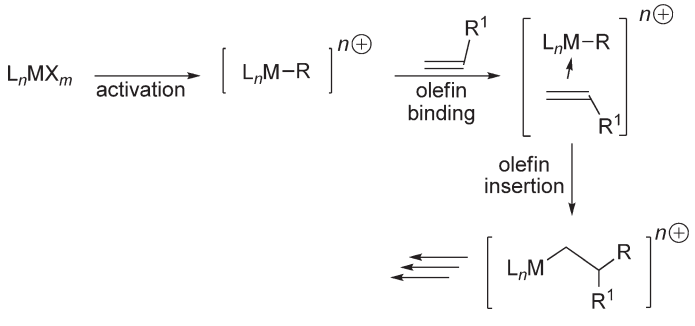

Scheme 1

It was generally recognized during this period, however, that olefin-insertion reactions into analogous M–C bonds were higher barrier processes, since the orbitals involved in the four-centered transition state of **1** are now comprised completely of the more directional sp^2- or sp^3-hybridized orbitals. Classic studies by Brookhart *et al.* using cationic piano-stool cobalt compounds **2**, $\{Cp^*[(MeO)_3P]CoCH_2CH_3\}+[BF_4]$, demonstrated that insertion of ethylene into the Co–C bond of suitably activated precursors were not only possible, but quite facile in suitable compounds.[8] At his time, the role of agostic C–H interactions in the insertion process also began to be appreciated[9] and Brookhart postulated that systems in which β-agostic structures characterized the ground state might serve as flags for compounds with a propensity to insert olefins into their M–C bonds. This has proved to be a useful hypothesis over the years, as many active olefin-polymerization catalysts based on metals from across the periodic table exhibit ground state β-agostic structures.

The generalized picture for the steps necessary in the olefin enchainment process by homogeneous transition metal complexes given in Scheme 1 is reasonably well understood for a number of families of olefin-polymerization catalysts. Once activated, the catalyst must capture an olefin monomer, forming a metal–olefin complex that may or may not be observable, from which the insertion transition state is accessed. Upon insertion, an active metal–alkyl species is regenerated and the polymerization continues. The relative energy of each species along this reaction coordinate is dependent on the formal electron count at the metal, the structure of the supporting ligands, and even the nature of the weakly coordinating anion. We consider two general classes of catalyst, the d^0-early metal catalysts and d^n-metal-based catalysts.

1.05.2.2 d^0-Olefin-polymerization Catalysts

Olefin-polymerization catalysts based on d^0-metals (early transition metals) are a commercially important class of catalysts that are probably the most well-understood systems currently known. The metallocenes are the most common, but variations on the supporting ligand set are numerous.

Because these are d^0-metals, olefin binding relies mainly on the fact that these metals are highly Lewis acidic, and can attract olefins through donation of the pair of π-electrons associated with the C=C double bond. Backbonding from the metal to the ligand is, of course, not possible in these systems, and as a result, the olefin–metal complex is not generally stable enough to isolate or observe. Nonetheless, there are several systems in which model d^0-olefin complexes have been observed and studied, revealing aspects of their structure and the energetics of olefin binding in close analogs of the olefin complexes that are postulated to lie along the reaction coordinate for olefin-polymerization catalysts. Some representative examples are shown in Scheme 2.[10–13] The groups of Casey and Jordan in particular have made significant advances in our understanding of these systems using the neutral decamethylyttrocene framework **7** and **8**, and [14–15] and the more catalytically relevant group 4 metal cations **9**,[16] **10**,[17] **11**,[18] **12**,[19] and **13**.[20] Bercaw has similarly studied complexes β-silyl complexes exemplified by **14**.[21,21a] Collectively, these studies reveal the following concerning olefin binding and the properties of these intermediates in d^0-olefin-polymerization catalysts.

(i) Olefin binding to d^0-metals is unsymmetrical, resulting in polarization of the olefin bond such that positive charge develops on the β-carbon. This is manifested by downfield chemical shifts for both the hydrogen and carbon atoms of the internal position. In cases where structural data are available, the $M–C_{terminal}$ bond distance is 0.1–0.2 Å shorter than the $M–C_{internal}$ distance, in agreement with most computed structures for such adducts. Furthermore, binding is aided by the incorporation of silyl groups β to the internal carbon, which helps to disperse the developing positive charge on this carbon engendered upon binding. This is entirely consistent with the picture developed for the transition state of olefin insertion into M–H shown in **1** above.

(ii) The strength of olefin binding, as judged by measured barriers to olefin dissociation and equilibrium measurements between free and bound olefin, is stronger in the cationic systems than in the neutral decamethylyttrocene systems.

(iii) Olefin binding is relatively insensitive to the nature of the alkyl group on the metal in the systems **8**. Although somewhat counterintuitive, this observation is rationalized on the basis of the relative energies of α- (higher energy) versus β- (lower energy) agostic ground-state structures, which must be disrupted to accommodate olefin binding.

(iv) In both the neutral and cationic systems, despite the possibility of electronic stabilization of developing positive charge on the β-carbon, olefin binding is generally weaker for more substituted olefins ($R^1 \neq H$ in Scheme 1), indicating that steric effects dominate the olefin binding process.

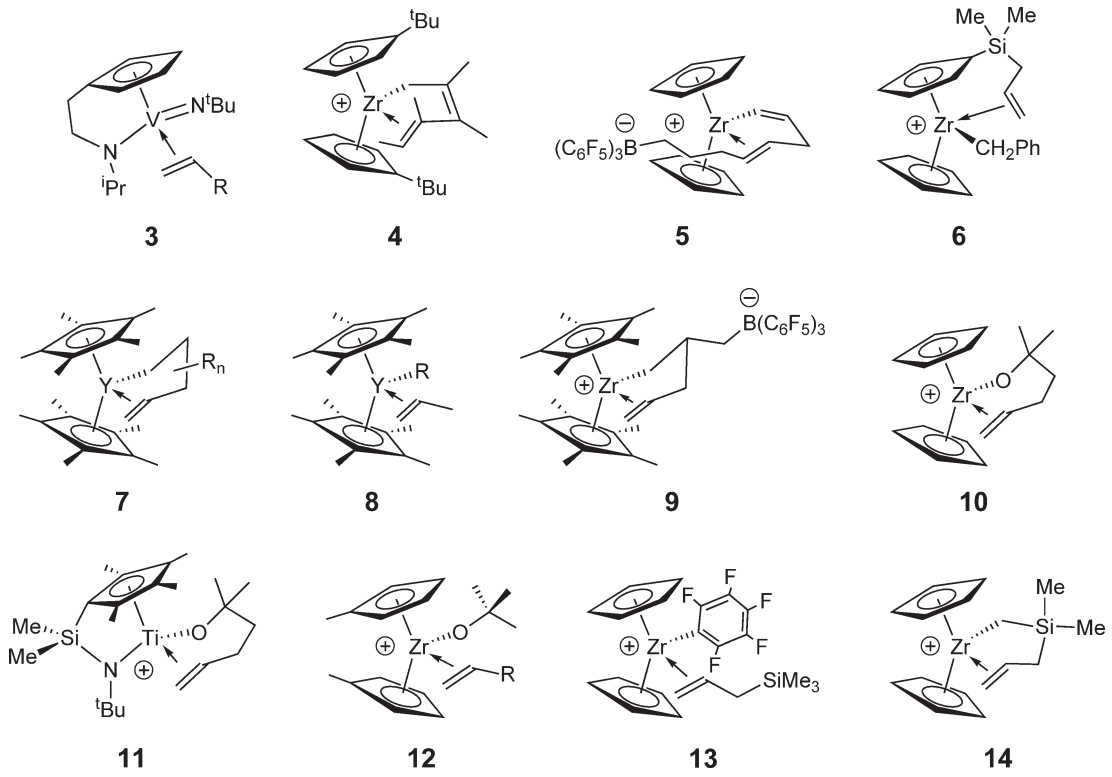

Scheme 2

(v) In the chelated systems **7**, **9–11**, and **14**, dynamic NMR studies allow for study of olefin face exchange, a highly relevant process to stereospecific olefin polymerization. This process does not appear to be influenced by the nature of the anion in the cationic systems, and both dissociative and non-dissociative mechanisms (involving vinyl C–H σ-complexes) have been identified as being operative.

(vi) Relative to the barrier for insertion, dissociation of olefin is generally lower in energy, particularly for bulky alkyl groups (R in Scheme 1) resulting in rapid association/dissociation equilibria prior to enchainment.

In summary, olefin binding is slightly to moderately exothermic, and occurs reversibly prior to migration of the M–alkyl group to the coordinated olefin. This migratory process is aided by the polarization induced in the coordinated olefin bond, which renders the β-carbon more susceptible to nucleophilic attack. Incoming olefin generally needs to displace a ground-state agostic interaction of some sort, usually β-agostic interactions, but sometimes α-C–H donors if the β-carbon is disubstituted. These features of olefin binding to d^0-metals are in excellent agreement with the picture that emerges from computational investigations of this process.[22,22a–22c]

As depicted in Scheme 1, once olefin is bound, the migratory insertion step that constitutes the actual enchainment process can occur via migration of the M–R group to the β-carbon of the coordinated olefin via a transition state akin to that observed for olefin insertion into M–H, **1** (see Scheme 3).[23] This mechanism was first formulated by Cossee and Arlman,[24,24a] but the lack of direct observation of such a reaction led to modified proposals involving other primary organometallic reactions. The so-called Green–Rooney mechanism[25,25a] (Scheme 3) invoked α-elimination to form an alkylidene hydride, which could couple with an olefinic monomer via a [2 + 2]-cycloaddition (see Section 6.01.3), yielding an alkyl hydride which rapidly undergoes reductive elimination, effecting overall olefin insertion. Of course, since α-elimination is formally an oxidative process, this mechanism is problematic for d^0-metals; nonetheless, elements from both of these proposals constitute our current understanding of the mechanism of olefin insertion into d^0-M–C bonds. Rather than a full α-elimination, the mechanism invokes agostic interactions in the reaction.

The most active olefin-polymerization catalysts have not just one but two available empty orbitals proximal to the alkyl group that initiate chain growth through olefin insertions. One orbital accommodates the incoming olefin

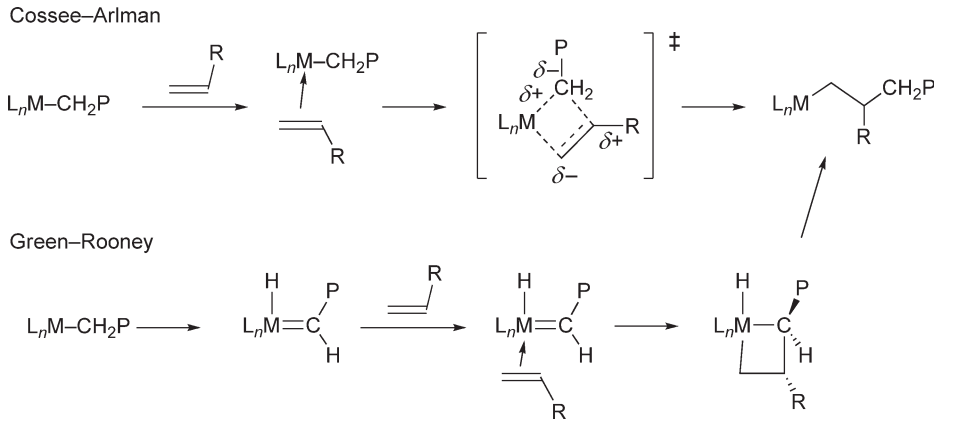

Scheme 3

monomer, while the other is able to receive the sigma-bonding electrons of α, β, and γ C–H bonds, stabilizing crucial intermediates or transition states along the reaction coordinate. These interactions also serve to rigidify structures, improving catalyst performance in stereospecific polymerizations. For example, the transition state for propene insertion into the Zr–CH_2P bond of the C_2-symmetric catalyst shown in **15** is stabilized by an α-agostic interaction between one of the diastereotopic C–H bonds of the α-methylene group and the cationic Zr center. The C–H bond chosen for this interaction is the one that allows the growing polymer chain to occupy an open quadrant of space as defined by the C_2-ligand environment.[26,26a,27] This directs the incoming propene to approach with its Si face (for the transition state depicted), such that the propene methyl group is oriented *trans* to the C–C bond of the metal alkyl. While this directs the propene methyl group up into the other open quadrant, it is the *trans*-orientation across the incipient C–C bond that is the most stereodirecting interaction in this transition state. Thus, the α-agostic interaction reinforces the stereochemistry-regulating properties of the ligand.[28,28a]

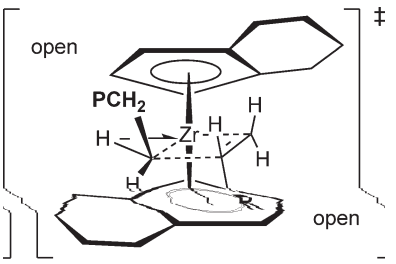

PCH_2 and **R**-oriented *trans*

15

The influence of the agostic interaction on the stereochemical outcome of olefin insertion formed the basis for obtaining experimental evidence for α-agostic stabilization of olefin-insertion transition states via Grubbs' isotopic perturbation of stereochemistry experiment,[29] a variation of which is shown in Scheme 4. Diastereomeric transition states for the hydrocyclization[30] or hydrodimerization[31] of appropriately deuterium-labeled α,ω-dienes or α-olefins are only accessed if α-agostic interactions are important, and the isotope effect is able to perturb the ratio of diastereomeric isotopomers. Furthermore, the effect is only observed in systems where olefin insertion, rather than olefin binding, is rate limiting;[23] examples of systems where olefin binding is not rate limiting are not implicated via this probe, although an α-agostic interaction may be important in the subsequent rapid olefin-insertion step, and isotope effects of 1.00 ± 0.02 are observed. Interestingly, the α-agostic mechanism is also implicated by the observed differences in molecular weight of the polymers produced from polymerization of (*E*)-1-propene-d_1 versus (*Z*)-1-propene-d_1.[32,32a] In cases where α-agostic isotope effects are observed, they are on the order of $k_H/k_D = 1.2$–1.3. Finally, several computational investigations also implicate agostic interactions along the olefin-insertion reaction coordinate, providing significant stabilization of the transition state for insertion.[33]

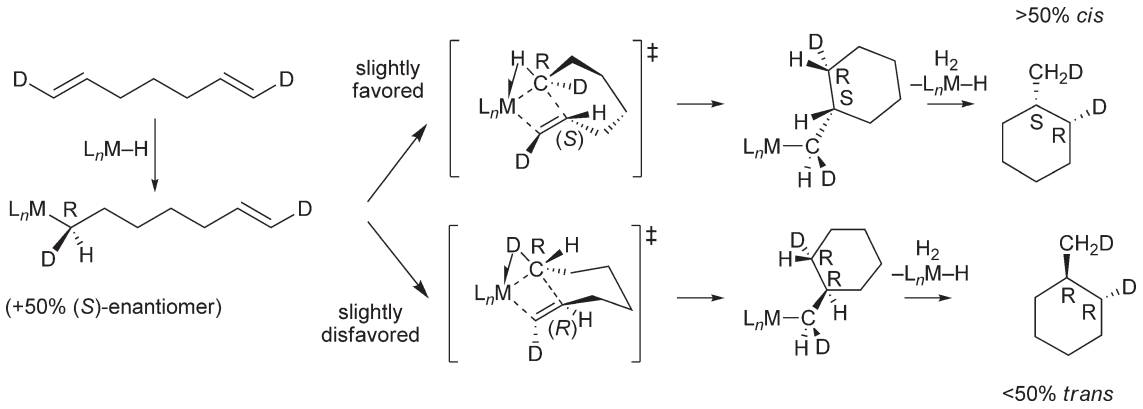

Scheme 4

1.05.2.3 d^n-Olefin-polymerization Catalysts

While the highly electrophilic cationic d^0-catalysts described above are highly active and effective catalysts for α-olefin polymerization, they are generally not compatible with polar functions. Late, d^n-metal-based catalysts offer the potential for greater functional group tolerance, but until recently could not compete in terms of activity with the early transition metal catalysts. Currently, however, there are several classes of catalysts based on mid- to late transition metals (exemplified by the catalysts **16**,[34,34a] **17**,[35,35a–35g] **18**,[36,36a,36b] **19**,[37] **20**,[38,38a–38d] and **21**[39,39a–39c] shown in Scheme 5) that not only compete with the early metals, but have unique properties that allow for greater scope in monomer tolerance and tunable polymer microstructures. The many variations of late metal catalysts have been reviewed elsewhere;[40,40a–40c] for the purposes of this treatment, we will focus on the most well-understood ones from a mechanistic perspective, Brookhart's cationic Ni and Pd diimine catalysts **16** (Scheme 5).

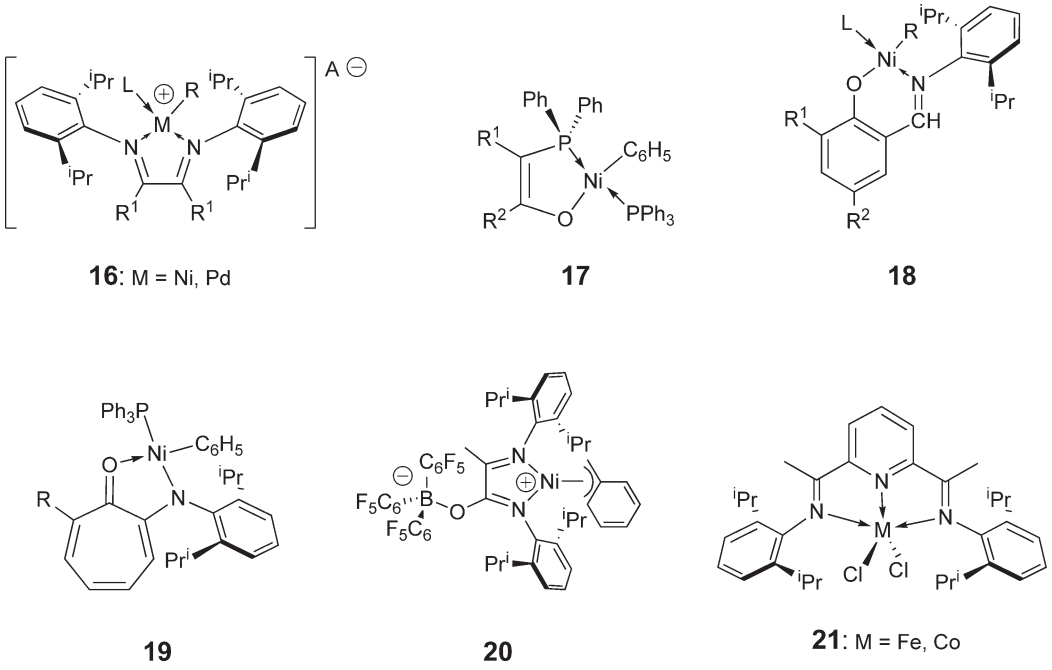

16: M = Ni, Pd

17

18

19

20

21: M = Fe, Co

Scheme 5

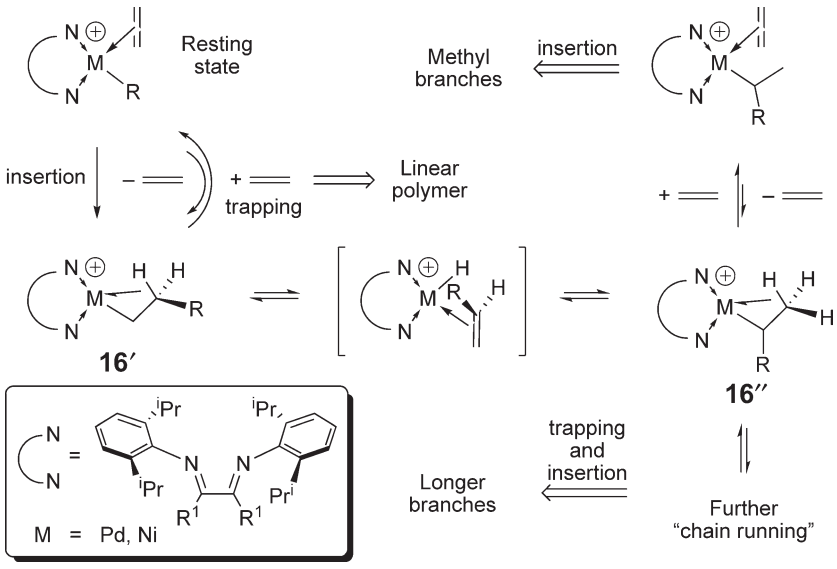

Scheme 6

The general mechanistic picture for catalysts **16** is depicted in Scheme 6. The key mechanistic features of this catalytic system include the following:

(i) Unlike the d^0-catalysts described above, in these systems, the resting state of the catalyst is the cationic alkyl–olefin complex; although the metal remains quite electrophilic due to the positive charge, sufficient backbonding is possible from these d^8-metals to stabilize the olefin complex. The olefin is likely oriented perpendicular to the square plane of the metal complex in the ground state, but rotates and inserts into the M–C bond via a standard four-center insertion transition state. The steric bulk of the diimine ligand is key in lowering the barrier to insertion by raising the ground-state energy of the olefin–alkyl resting states. Furthermore, Ziegler has shown[41,41a,42] that the bulky *ortho*-substituents on the *N*-aryl groups significantly raise the barrier to chain termination by β-hydrogen transfer to coordinated monomer by sterically blocking the two axial coordination sites in these square-planar complexes. This elevates these systems to olefin-polymerization catalysts from the oligomerization mediators typically found with less bulky ligand environments.

(ii) The product of insertion is a highly dynamic β-agostic cationic alkyl **16′**, which may isomerize via the olefin–hydride species shown in Scheme 6 (not observed) to secondary alkyl derivatives **16″**. When these are trapped with olefin monomer, subsequent insertions give methyl or longer alkyl branches. The extent of branching can be controlled using different metals and by varying the ethylene pressure.

(iii) Dissociation of olefin from the resting state occurs to access the β-agostic structures and the "chain-running" manifold, potentially resulting in extensive isomerization prior to the next insertion.

(iv) Insertion barriers are 4–5 kcal mol^{-1} lower for M = Ni than M = Pd, making the Ni systems significantly more active than the Pd congeners. On the other hand, chain running in the Ni systems has a substantially higher barrier than in the analogous Pd catalyst. The combination of these two effects results in much more highly branched polymers when Pd-based catalysts are used.

1.05.2.4 Polymerization of Polar Monomers via Coordination Polymerization Mechanisms

While cationic catalysts **16** are an effective and important class of catalysts, their electrophilicity still hampers their ability to tolerate polar functions. The less electrophilic neutral **17–19** and zwitterionic **20** nickel catalysts have been examined in an effort to enhance compatibility with polar monomers and co-monomers. Again, bulky ligands are necessary not only to promote olefin insertion, but also to discourage ligand-redistribution reactions resulting in deactivated bis-ligand complexes and decomposition products. For a typical neutral Ni(II) system, such as **19**, Brookhart has shown that the mechanism involves (i) associative displacement of the PR_3 ligand by ethylene to

give an olefin alkyl complex and (ii) insertion to give a β-agostic alkyl species that may isomerize or be trapped by olefin or PR_3. In these systems, trapping by L is generally rapid relative to isomerization, and the resting state of the catalyst is in most cases the PR_3 complex. In some cases, addition of phosphine scavengers enhances the activity of the catalyst, but also leads to shorter catalyst lifetimes. Since the *N*,*O*- or *P*,*O*-ligands are not symmetric, insertion from the olefin–alkyl complex takes on added complexity due to the possibility of isomerism (Scheme 7). Ziegler has shown[43,43a] that the insertion barrier from the less stable isomer, where the alkyl chain is *trans* to N, **19″**, is lower than insertion from the thermodynamically more stable *trans O*-isomer **19′**. The barrier to interconversion of **19′** and **19″** is significantly smaller than the insertion barriers and so insertion likely takes place from the less stable isomer **19″**.

While some of these late metal-based catalysts are reportedly able to incorporate polar monomers via an insertion mechanism,[44,44a–44d] direct evidence for this is rare, and some of these examples[36,45] involve monomers in which the polar function is relatively far removed from the olefinic locus of insertion. Polar monomers such as acrylates or vinyl halides, in which the polar group is directly bonded to the olefinic moiety to be inserted, are the most desirable polar monomers for incorporation, but provide several challenges to be overcome if a coordination insertion process is to be viable (Scheme 8). The first obstacle involves the preference of binding for the substrate; for olefin insertion to take place, it is clear that the olefinic moiety must bind at some point to the metal center. Since the catalysts for olefin polymerization are generally electrophilic in nature, there is a tendency for polar monomers to preferentially bind the metal through the polar function in a σ-bonding mode. Thus, there must be at least an equilibration to the π-bound form involving the olefin function, if not a clear preference for π-bonding, in order for insertion to take place at appropriate rates. Assuming a π-bound complex, from which insertion can take place, is accessible, the next challenge involves control of the regiochemistry of insertion. Vinyl monomers with polar groups generally exhibit a tendency to undergo kinetic 2,1-insertion, since the polarity of the four-centered transition state (see Scheme 3 above) disfavors electron-withdrawing groups in the β-position.[5–7] These 2,1-products, however, may undergo isomerization to the 1,2-isomer, with the polar group now on the β-carbon, and facile β-polar group-elimination processes often ensue,[46–47a] poisoning the catalyst toward further reactivity. Intermediates in Scheme 8 that contain β-hydrogens could also potentially undergo β-hydrogen elimination, forming Heck-type products; for simplicity, these reactions are not depicted in Scheme 8. In other instances, the polar group simply forms a stable chelate to the metal from the β-position, blocking the vacant coordination site necessary to take up further equivalents of monomer.[48] In yet another scenario, the polar group can facilitate oligomerization of catalyst sites by binding to the vacant site of a separate catalyst molecule.[49,49a,49b] All of these proclivities have a tendency to preclude further steps in a polymerization reaction.

Finally, even if one can design a catalyst that effectively binds the polar monomer through the olefin, and regioselectively inserts the monomer to an alkyl with a polar group that is relatively stable toward isomerization or oligomerization processes, a final challenge is likely to be encountered. The electron-withdrawing nature of the polar group tends to raise the barrier toward its migration to a coordinated olefin, since it is significantly less nucleophilic than an unfunctionalized alkyl ligand. Thus, while it may be possible to exert some control on the insertion of the polar co-monomer into M–C bonds, subsequent insertions of aliphatic olefins or polar co-monomers may be prohibited by the presence of the polar substituents, even if it is non-chelating. Thus, the polymerization or co-polymerization of olefins with polar substituents (particularly acrylates) remains a significant challenge for single-site catalysts that operate via a migratory-insertion mechanism. One way in which metal catalysts may circumvent some of these difficulties is via polymerization by group-transfer mechanisms, discussed in Section 6.01.4.

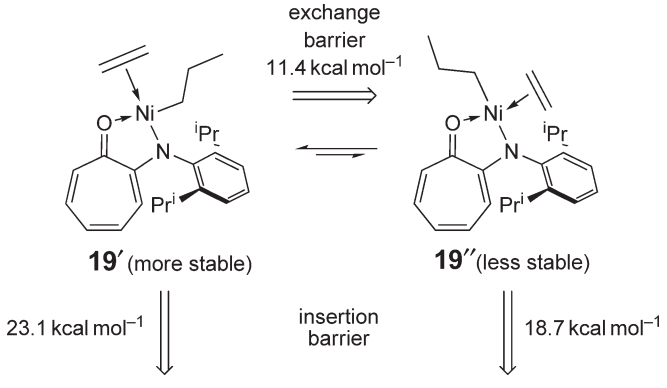

Scheme 7

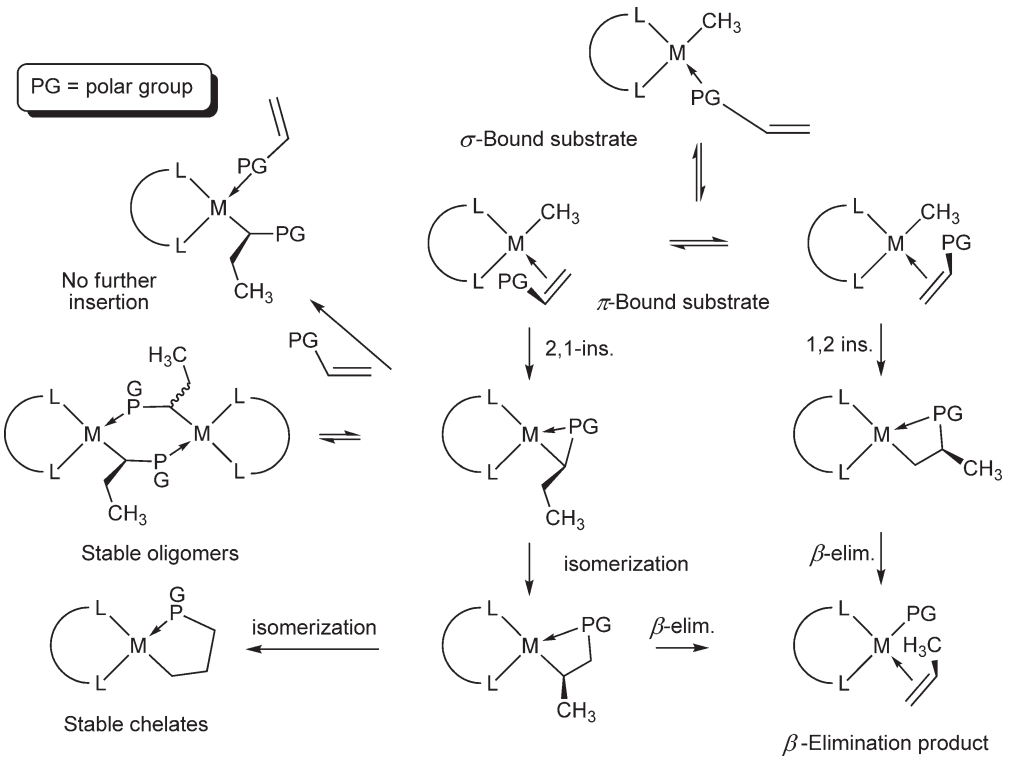

Scheme 8

1.05.3 Polymerization by Olefin Metathesis

1.05.3.1 Introduction

A second fundamental organometallic reaction that can lead to enchainment or condensation of olefinic monomers is the olefin metathesis reaction, one of the most powerful metal-catalyzed bond breaking/making reactions available today. The development of this reaction again has its roots in the 1950s when ill-defined heterogeneous mixtures of tungsten or molybdenum halides and tin or aluminum-based alkylating agents were observed to catalyze the reaction. Little was known about the mechanism of the process for many years after its discovery, but eventually consensus was reached concerning the Chauvin mechanism[50] involving metal–carbene (alkylidene) complexes undergoing reversible [2 + 2]-cycloaddition reactions with olefins, completing metathesis via metallacyclobutane intermediates as shown in Scheme 9.

The metathesis reaction may be used to produce a range of polymers by two processes (Scheme 10). Cyclic olefins with a threshold level of ring strain can be polymerized via ROMP chain process. Under appropriate conditions, certain acyclic dienes can be polymerized in a condensation process known as acyclic-diene metathesis polymerization, or ADMET. The elimination of a volatile olefin byproduct (usually ethylene) provides a driving force for the latter process, while alleviation of ring strain is the primary driver in ROMP. Because ADMET is a condensation

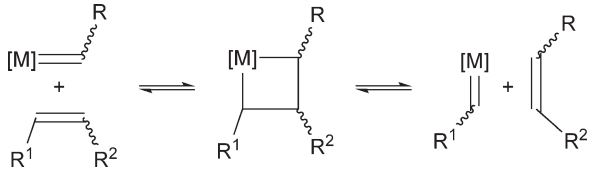

Scheme 9

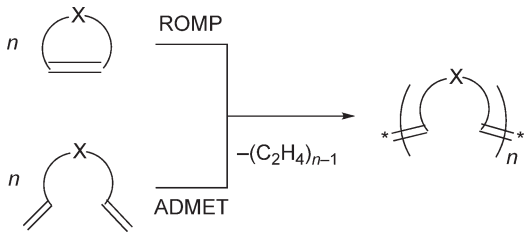

Scheme 10

polymerization, high molecular weight (MW) polymers require almost complete conversion of monomer that is highly pure. ROMP reactions are somewhat more tolerant of impurities and produce generally higher MW polymers.

Since the discovery of olefin metathesis, the intervening years have seen enormous amounts of activity in the area, both in terms of catalyst development and commercial applications. These advances have been chronicled extensively in a number of reviews[51,51a–51g] and monographs[52,52a] to which the reader is referred for more detail. Here, we detail the mechanism of olefin metathesis via discussions of the two most prominent classes of homogeneous olefin-metathesis catalysts, the Mo,W-based Schrock alkylidenes,[53] exemplified by commercially available **22**, and the Ru-based Grubbs-type catalysts,[54] represented by the so-called Grubbs generation 1 and 2 catalysts **23** and **24**. These two examples embody the culmination of extensive research programs and are model case studies in catalyst design. In both cases, ligand tuning to optimize the properties of the reactive metal carbene serve to flatten the energy surface of carbene–metallacyclobutane interconversion, allowing for facile olefin metathesis and minimization of potential side-reactions[55] of both the carbene (e.g., cyclopropanation) and the metallacyclobutane (e.g., reductive elimination or β-hydride elimination).

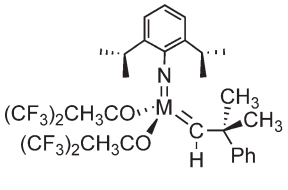

22: M = Mo, W
Schrock

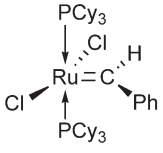

23
Grubbs generation 1

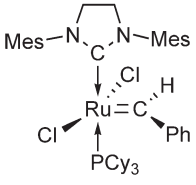

24
Grubbs generation 2

1.05.3.2 Schrock Catalysts

The four-coordinate Schrock catalysts are comprised of a high oxidation state group 6 metal, supported by a bulky imido ligand to prevent bimolecular decomposition, two bulky but electronically tunable alkoxide ligands, and a reactive alkylidene ligand, again preferably somewhat bulky to improve catalyst stability. *Syn*- and *anti*-rotomers exist depending on the orientation of the alkylidene ligand relative to the imido ligand (Scheme 11), with the *syn*-isomer generally more stable due to the possibility of a stabilizing α-agostic interaction between the metal and the alkylidene C–H bond that is possible in this isomer but not in the *anti*-form. The relative stabilities, rates of interconversion, and relative rate of reaction with olefinic substrates of these two rotomers is dependent mainly on the nature of the alkoxide ligands. To the extent that the approach of olefin to the metal for each of these isomers has the potential to influence the overall stereochemistry of ROMP polymers[56] and other asymmetric metathesis reactions,[57,57a] knowledge of these details for each catalyst variant is critical.

In the cases examined in detail either experimentally[51] or computationally,[58,58a–58c] coordination of the olefin occurs via attack at a CNO face of the pseudo-tetrahedral metal center. The olefin/alkylidene intermediate is generally not observed in these systems, but proceeds readily to the metallacyclobutane, which in many cases has been observed.[57,57a,59,59a,59b] The geometry of the five-coordinate metallacyclobutane is either distorted trigonal bipyramidal or square pyramidal, both of which have been observed, sometimes simultaneously. Structural studies on stable metallacyclobutenes generated from **22** and its derivatives indicate that the four-membered ring assumes a butterfly conformation with the dihedral angle between the planes defined by C_α–M–C_α and C_α–C_β–C_α ranging

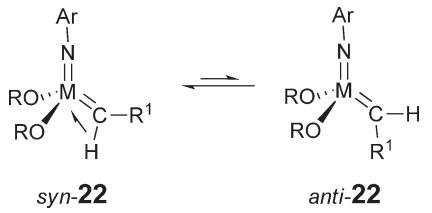

Scheme 11

from 25° to 37°. Low-field chemical shifts in both the ^{13}C and ^{1}H NMR spectra for the α-carbons (80–90 ppm) and hydrogens (3–4 ppm), and high-field shifts for the β-carbons (−5 to 5 ppm) and hydrogens (0–0.75 ppm) constitute the spectroscopic signatures for these moieties. In the most active catalysts, these compounds readily undergo retro-cyclization to regenerate an active alkylidene and complete the metathesis event.

Schrock catalysts **22** are highly active, effective catalysts, not only for ROMP and ADMET, but also other useful types of olefin-metathesis reactions. However, due to their relatively high electrophilicity, they do not tolerate polar functions well. Nonetheless, they have been effectively employed in complex organic synthetic applications, and have been modified to effect enantioselective reactions with high selectivity. Ruthenium-based Grubbs catalysts were developed to increase the range of functional groups in which metathesis could be performed.

1.05.3.3 Grubbs Catalysts

The ruthenium carbene catalysts **23**[60,60a] and **24**[61] are two of the most widely used members of a large family of commercially available olefin-metathesis catalysts with this general structure. In comparison to Schrock catalysts, they have typically lagged in terms of activity, but their superb functional group tolerance has fueled their wide popularity among polymer and organic chemists alike.[54] While **24** exhibits relatively high activity, recent variations on this motif have furnished catalysts with comparable or better activities than the prototypical Schrock catalyst **22** (see below).[62,62a]

The primary reason for the lower activities generally observed in Grubbs catalysts stems from the initiation step necessary to access the catalytic manifold for olefin metathesis. The mechanism by which these catalysts mediate metathesis is quite well understood,[63,63a] and the salient features are shown in Scheme 12. While the catalyst precursors **23** and **24** are 16-electron species, and therefore capable of taking up an olefinic substrate, uptake of olefin followed by metathesis via an 18-electron manifold via an "associative" mechanism accounts for less than 5% of the metathesis in a typical application.[63] Instead, the bulk of the catalysis occurs from the 14-electron alkylidene, **25**,

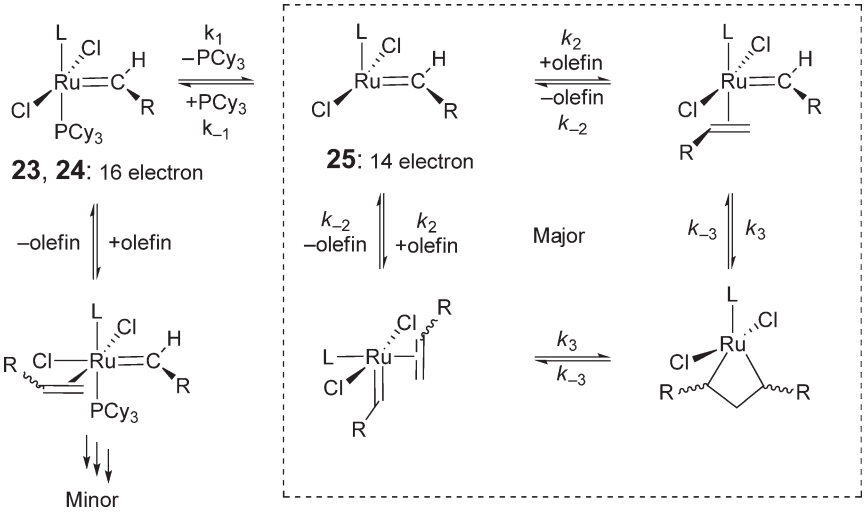

Scheme 12

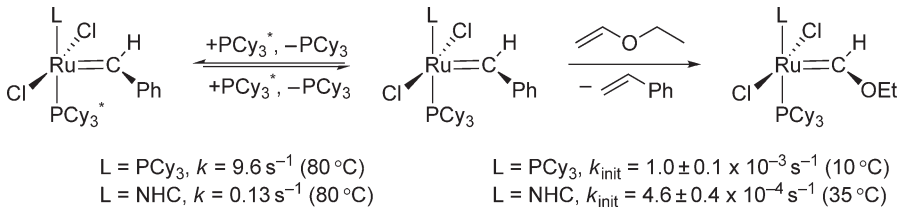

Scheme 13

produced upon rate-limiting, dissociative loss of phosphine from the ruthenium center, the initiation step in the reaction. The necessity for initiation in this way differentiates these Grubbs catalysts from the more active Schrock catalysts, which enter the catalytic cycle directly.

That initiation involves dissociative substitution of a phosphine ligand from catalysts **23** and **24** (rather than associative displacement) is indicated by several experimental observations.[63,63a] Metathesis activity for these catalysts is severely depressed in the presence of excess PR_3. The $\Delta S^{\ddagger}$ values for degenerate phosphine exchange in these systems are ≈13 eu, indicative of a dissociative mechanism (via the 14-electron alkylidene **25**) for this process. Furthermore, the rate of this exchange is identical to the rate of initiation (when corrected for temperature), as measured by the irreversible reaction of **23** and **24** with ethyl vinyl ether (Scheme 13). Thus, the propensity for PR_3dissociation is directly related to a given catalyst's ability to initiate and enter the catalytic cycle shown within the dotted lines of Scheme 12.

Counterintuitively, however, the rate of initiation is not necessarily directly proportional to the overall activity of a given catalyst for olefin metathesis. This is demonstrated by the measured phosphine-exchange and initiation rates for first-generation **23** versus the more active second-generation IH_2Mes-substituted catalyst **24** given in Scheme 13. As can be seen, the less active catalyst **23** initiates approx. 10 times faster than **24**, a result mirrored in the phosphine-exchange rates measured at a different temperature. In an elegant kinetic study, Grubbs *et al.*[63a] have shown that it is not how fast the catalyst precursor loses phosphine that governs overall activity, but the relative affinity of the 14-electron active species for PR_3 versus olefin substrate as measured by the ratio k_{-1}/k_2 (as defined in Scheme 12). This ratio can be determined from plots of $1/k_{init}$ versus [PR_3]/[ethyl vinyl ether] using the model reaction shown to the right of Scheme 13. For **23**, this ratio is $\approx 10^4$ times larger than the same ratio for **24**, indicating that the greater efficacy of the IH_2Mes-substituted catalyst stems from the fact that its 14-electron species has a much higher relative affinity for the olefin substrate than the recently departed phosphine ligand. Although the IH_2Mes ligand thus discourages phosphine dissociation relative to PCy_3, it renders the resulting active species much more olefinophilic than the analogous species derived from the generation 1 catalyst **23**. While initiation is slower for **24**, a greater proportion of the available ruthenium is engaged in the productive 14-electron manifold.

Until recently, none of the intermediates within the dotted line of Scheme 12 have been directly observed in solution, although the 14-electron alkylidenes have been detected via mass spectrometry in the gas phase,[64,64a] and model compounds for this[65] and the other[66] proposed species have been reported. Recently, Piers and Romero reported a family of 14-electron phosphonium alkylidene compounds[67] via protonation of the ruthenium carbides shown in Scheme 14, originally reported by Heppert and co-workers.[68] Phosphonium alkylidenes **26** are remarkably air and moisture tolerant, and exhibit excellent thermal stability when the phosphonium moiety is derived from PCy_3 and the counteranion is a weakly coordinating arylborate. The structures of several examples have been determined via X-ray crystallography, and show that the orientation of the phosphonium alkylidene is orthogonal to that found in the parent Grubbs catalyst precursors, such that the PR_3 group essentially lies underneath the ligand remaining on the ruthenium center, hampering anion coordination to the metal even in the case of the triflate salts.

These catalysts are extremely active olefin-metathesis mediators, rivaling or exceeding the activities observed for Schrock catalysts, presumably because the phosphine dissociation initiation event has been obviated. Here, initiation consists of olefin binding, as indicated by the large negative $\Delta S^{\ddagger}$ of −55(6) eu observed for the reaction of **26** (L = H_2IMes, A = $B(C_6F_5)_4$) with 2-*iso*-propoxystyrene (Scheme 14). The orientation of the phosphonium alkylidene in the ground-state structure probably means that rotation about the Ru=C bond by ≈90° is also part of this initiation step.[69] Low-temperature monitoring of these reactions by NMR spectroscopy gives evidence for the presence of observable intermediates, and when **26** is reacted with ethylene at below −40 °C, smooth conversion to a 14-electron ruthenacyclobutane is observed (Scheme 15).[70]

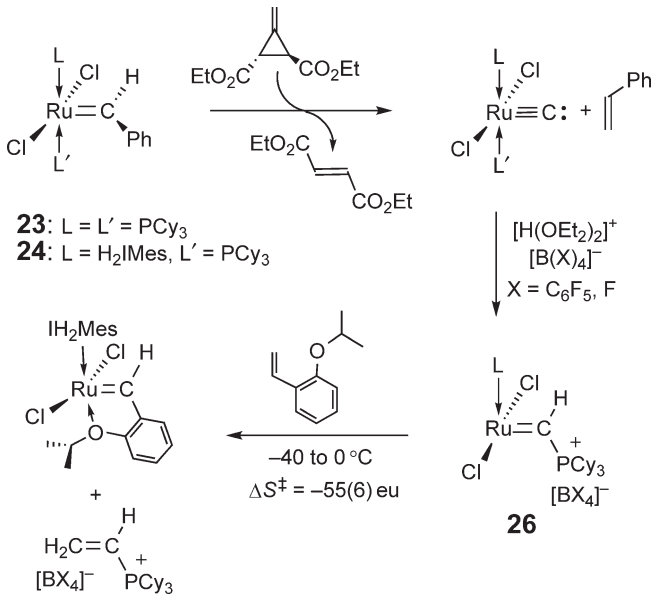

Scheme 14

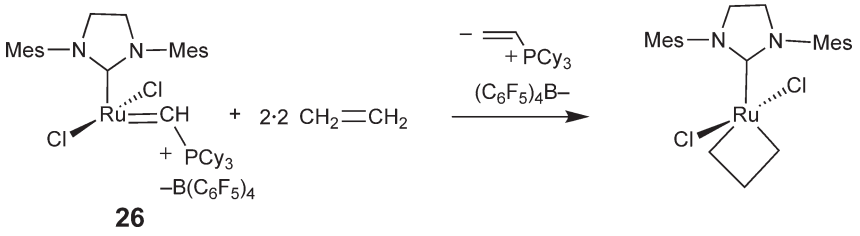

Scheme 15

Like the tungstenacyclobutanes formed from *22* and ethylene, low-field chemical shifts in both the ^{13}C and ^{1}H NMR spectra for the α-carbons (94.0 ppm) and hydrogens (6.6 ppm), and high-field shifts for the β-carbon (2.2 ppm) and hydrogens (−2.6 ppm) are observed for this metathesis-active ruthenacyclobutane. All of the NMR data are consistent with a C_{2v}-symmetric structure, as shown, providing the first non-computational data concerning the geometry of this crucial intermediate in ruthenium-mediated olefin metathesis.

While the basic Chauvin mechanism of olefin metathesis has been appreciated and acknowledged for some time, the studies on both Schrock and Grubbs type catalysts show that the knowledge of the mechanistic steps necessary to access Chauvin-metathesis intermediates, and details concerning the structures and geometries of these intermediates, can lead to ever-improving and selective catalysts for this important polymerization reaction.

1.05.4 Polymerization by Group Transfer

1.05.4.1 Introduction

Group-transfer polymerization (GTP) was discovered by scientists at DuPont and involves the conjugate Michael addition of an enol silane or related compound to acrylate or methacrylate monomers under the influence of an activator.[71] The process is related to anionic polymerization but the species involved are believed to feature a high degree of covalent character in the transition state for chain growth.

Thus, one should expect similar behavior for transition metal enolates where there is significant covalent character to the M–O (or M–C) bond. This section will focus on polymerization of (meth)acrylate esters by group 4 metallocene (or the related group 3 and lanthanocene[72,72a–72v]) initiators where the mechanism of this process is analogous to the classical GTP process. Of course, the polymerization of (meth)acrylates by other transition metal complexes has been reported frequently in the literature; however, in many cases the mechanisms of these processes are less well understood or involve free radical or other forms of initiation. Recent examples of other transition metal-mediated methyl methacrylate (MMA) polymerization processes that "may" proceed via a GTP or anionic mechanism are given.[73,73a–73i]

GTP of acrylate and methacrylate esters using group 4 metallocene initiators dates back to the early work of Hertler and Farnham at DuPont where neutral enolate complexes of Zr and Ti were found to initiate polymerization of MMA.[74] It is unclear that this early report actually involves metal-mediated GTP, since subsequent work has generally found these types of neutral enolate complexes to be inactive for MMA polymerization (*vide infra*). On the other hand, many titanocene (and to a lesser extent, zirconocene) complexes are competent photo-initiators of free-radical polymerization of (meth)acrylates;[75,75a,75b] so, this complication should be borne in mind.

There are two limiting mechanisms for the GTP of meth(acrylate) esters using group 4 (or lanthanide) initiators. One involves *in situ* (or prior) formation of an enolate complex (neutral for lanthanide/group 3 elements but positively charged for group 4 complexes) and propagation via an unimolecular pathway involving conjugate addition of the enolate to coordinated monomer to form a cyclic intermediate. Displacement of the ester group by monomer completes the propagation sequence, generically displayed in Scheme 16.[72,72a–72v,76,76a–76v]

The second mechanism, which has been documented for group 4 initiators,[5,77,77a–77l] involves Michael addition of a neutral enolate complex (either preformed or generated *in situ*) to monomer, activated by coordination to a second (cationic) metal center, in a bimolecular process. Displacement of the ester group from the dinuclear intermediate thus formed completes the propagation sequence (Scheme 17). Note that the two metals exchange identities in forming the dinuclear intermediate depicted in Scheme 17.

In this section, we will review the features that are important for propagation via either mechanism and the evidence for each. The focus will be on methacrylate polymerization, and for applications of this chemistry to polymer synthesis, the reader is referred to the primary literature.[72,72a–72v,76,76a–76v,5,77,77a–77l]

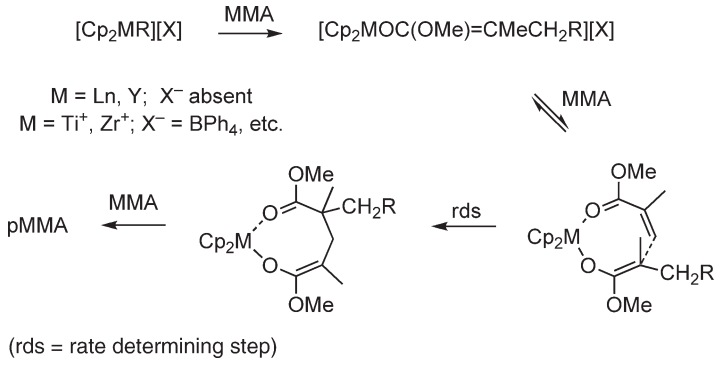

Scheme 16

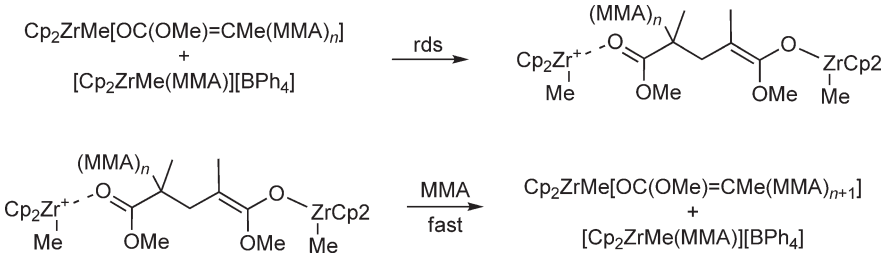

Scheme 17

1.05.4.2 Propagation via the Unimolecular Process

The evidence for this process is based on the pioneering work of Yasuda and co-workers who succeeded in isolating the cyclic ester intermediate in the case of $[Cp^*_2SmH]_2$-initiated polymerization of MMA and showed that it was an equally competent initiator of polymerization.[72,72a] While kinetic studies were not immediately forthcoming, there seems little doubt that the mechanism is as depicted in Scheme 16. This process is living and quite rapid even at low temperature where highly syndiotactic PMMA is formed via a chain end control mechanism. If one initiates ethylene polymerization using these or related lanthanocene complexes, it is possible to subsequently form block co-polymers by the addition of MMA.[72g,72t] The co-polymers are contaminated with both PE and PMMA homopolymer because the ethylene polymerization process is not living but the resulting chain-transfer products are active initiators of MMA polymerization.

Although it has been known for some time that the isoelectronic group 4 enolates are less reactive initiators of MMA polymerization,[76] and it has been presumed that the mechanism of this process is analogous,[76,76a–76v] it is not until quite recently that this reaction has been examined with the same level of mechanistic rigor. Polymerization of MMA by [*rac*-en(Ind)$_2$ZrMe][MeBR$_3$] or [*rac*-en(Ind)$_2$Zr{OC(O^{i}Pr)=CMe$_2$}(THF)][MeBR$_3$] (R = C_6F_5) provides isotactic PMMA whose microstructure is consistent with a site-control mechanism.[76u] The kinetics of this polymerization are first order in both monomer and enolate initiator, consistent with the mechanism depicted in Scheme 16, where the cyclic enolate/ester intermediate (which was spectroscopically characterized) is the resting state, and intramolecular Michael addition is rate determining.

Table 1 lists the discrete group 4 metallocene or related initiators that are either known or presumed to produce PMMA by this mechanism. In the case of chiral or prochiral initiators, often the microstructure of the resulting polymer, particularly if it is consistent with a site-control mechanism, is a reliable indicator of mechanism. In other cases, this assumption is less certain, and often the mechanism is presumed to be analogous. In the case of the CGCTi complexes studied by Chen and co-workers, the unimolecular pathway is followed,[76q] but syndiotactic PMMA is produced by a chain-end control mechanism.

The factors which are important in determining whether polymerization occurs by this mechanism with group 4 initiators revolve around two issues. In the case of metal–alkyl initiators, the initial conjugate addition of M–R to monomer to generate the cationic enolate may be rate determining and/or complicated by side-reactions (Scheme 18). A closely connected issue relates to the thermal stability versus reactivity of the cationic enolate formed (or preformed) under the conditions of the polymerization. Either or both of these effects can conspire to prevent polymerization, particularly at ambient temperature where metal alkyls or related initiators are typically evaluated.

For example, it is generally accepted that the prototypical complex [Cp$_2$ZrMe(THF)][BPh$_4$] is an ineffective initiator, largely because it does not add to MMA to form a cationic enolate complex. This is based on both experimental observation[76,76a–76v,5,77,77a–77l] as well as theoretical study.[78,78a] That the cationic enolate that would be generated *in situ* through this initial reaction is competent for polymerization is revealed by the early work of Collins and co-workers using preformed [Cp$_2$Zr{OC(OMe)=CMe$_2$}(THF)][BPh$_4$].[76]

On the other hand, metal alkyls featuring weakly coordinating counteranions where the ion pairs are thermally stable at ambient temperature, and where MMA is the strongest donor in the system, are competent (although sometimes inefficient) initiators. Thus, [Cp$_2$ZrMe][MeB(C_6F_5)$_3$] is an effective initiator of MMA at room temperature as are a number of other related complexes (Table 1). Donor ligands such as THF often strongly inhibit polymerization, especially when present in greater than stoichiometric amounts; in unhindered initiators, this may relate to the known ability of this donor to interact with both empty frontier orbitals in these complexes.[79]

Table 1 Group 4 metallocene or related initiators

Metal Alkyl Initiators	*Metal Enolate Initiators*
[Cp$_2$ZrMe][MeB(C_6F_5)$_3$]	[Cp$_2$Zr{OC(OMe)=CMe$_2$}(THF)][BPh$_4$]
[Me$_2$CCp$_2$ZrMe][MeB(C_6F_5)$_3$]	[Cp$_2$Zr{OC(O^{i}Pr)=CMe$_2$}(THF)][MeB(C_6F_5)$_3$]
[Me$_2$CCp$_2$ZrMe(THF)][BPh$_4$]	[Cp$_2$Zr{OC(O^{t}Bu)=CMe$_2$}(THF)][MeB(C_6F_5)$_3$]
[Me$_2$CCp(Ind)ZrMe][MeB(C_6F_5)$_3$]	[Cp$_2$Zr{OC(O^{t}Bu)=CMe$_2$}(THF)][B(C_6F_5)$_4$]
[Me$_2$CCp(Ind)ZrMe(THF)][BPh$_4$]	[en(Ind)$_2$Zr{OC(OiPr)=CMe$_2$}(THF)][MeB(C_6F_5)$_3$]
[Me$_2$Si(Ind)$_2$ZrMe][MeB(C_6F_5)$_3$]	[Me$_2$Si(η-C_5Me_4)(^{t}BuN)Ti{OC(O^{i}Pr)=CMe$_2$}(THF)][MeB(C_6F_5)$_3$]
[en(Ind)$_2$ZrMe][[MeB(C_6F_5)$_3$]	[Me$_2$Si(η-C_5Me_4)(^{t}BuN)Zr{OC(O^{t}Bu)=CMe$_2$}(THF)][B{C_6H_3(CF_3)$_2$}$_4$]
[Me$_2$Si(η-C_5Me_4)(^{t}BuN)TiMe][MeB(C_6F_5)$_3$]	

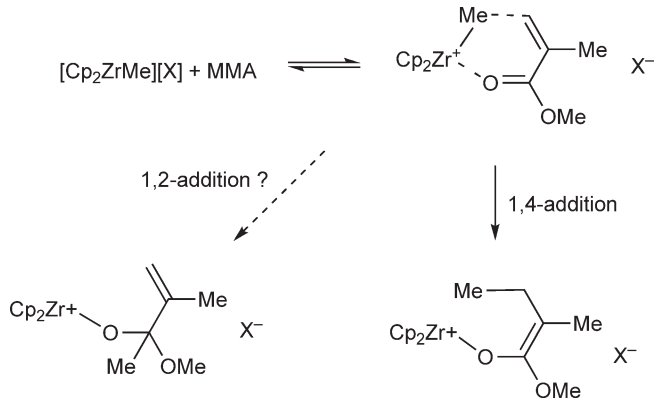

Scheme 18

Frequently, the efficiency of the metal–alkyl initiators is quite low (<50%); while this may be related to scavenging issues, it is also possible that competitive 1,2-addition of M–R to monomer is responsible for this observation (Scheme 18). There has been limited fundamental study of this initial reaction considering its importance for successful polymerizations; part of the difficulty is that the initial reaction is often slow compared to subsequent conjugate additions of monomer to the enolate complex.

As for preformed cationic enolate complexes, one decomposition pathway has been conclusively identified. Enolates derived from 3° alkyl esters are prone to loss of alkene to form cationic carboxylate complexes (Scheme 19).[76d,76t,77l] Since donors such as THF partially impede this process, prior coordination of the ester oxygen may precede elimination. By the same token, the unhindered enolate $[Me_2Si(\eta\text{-}C_5Me_4)(^tBuN)Zr\{OC(O^tBu)=CMe_2\}(THF)][B\{C_6H_3(CF_3)_2\}_4]$ decomposes at temperatures above −20 °C to form the cationic carboxylate complex, even in the presence of excess THF,[80] while the more hindered $[Cp_2Zr\{OC(O^tBu)=CMe_2\}(THF)][X]$ {X = BPh_4,[81] $MeB(C_6F_5)_3$,[76t] $B(C_6F_5)_4$[76t]} complexes are more robust. Enolates derived from 1-adamantyl esters are resistant to this elimination process and thus have improved thermal stability at room temperature.[82] It would appear that the enolate initiators studied by Chen and co-workers, which are derived from 2° alkyl esters, and feature the weakly stabilizing $MeB(C_6F_5)_3$ counteranion, currently represent an optimal combination of stability coupled with reactivity.

Of course, following initiation, the propagating enolate features an OMe group in the case of MMA polymerization. There is, surprisingly, little known about the stability/reactivity of these important species. Part of this may relate to the difficulty in preparing suitable precursors as neutral enolates featuring this group are susceptible to β-alkoxide elimination, again particularly when the metal complex is unhindered.[76d]

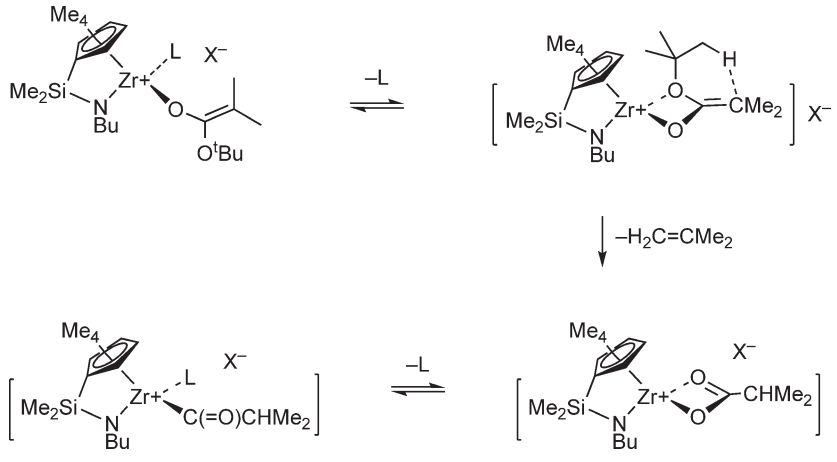

Scheme 19

It is clear that polymerization of MMA via the unimolecular mechanism offers the greatest prospect for both control of polymer MWD, commoner sequence distributions, as well as tacticity. As chiral and prochiral group 4 metallocene complexes are more readily available than their group 3 or lanthanide analogs, we can expect continued effort in this area will eventually lead to a wide range of applications to polymer synthesis.

1.05.4.3 Propagation via the Bimolecular Process

Propagation via this mechanism has been conclusively demonstrated in the case of neutral group 4 alkyl initiators in combination with cationic alkyls. It was discovered during a fairly circuitous mechanistic study of the parent system $[Cp_2ZrMe(THF)][BPh_4]/Cp_2ZrMe_2$.[76,77,77a] The mechanism has also been shown or is presumed to be operative for polymerizations involving excess Cp_2ZrMe_2 and *in situ* generation of the cationic alkyl using *inter alia* $[R_3NH][BPh_4]$, $[PhMe_2NH][B(C_6F_5)_4]$, and $B(C_6F_5)_3$.[77b,77h,77i] Also, preformed dinuclear complexes of the type $[(Cp_2ZrMe)_2(\mu\text{-}Me)][MeB(o\text{-}C_6F_5\text{-}C_6F_4)_3]$ appear to operate via this process.[77c] Generally speaking, partially *s*-PMMA is produced using initiators of this type and whose microstructure is consistent with a chain-end control mechanism.

Since initiation in this system can be inefficient and slow relative to propagation, synthesis of narrow MWD polymers is generally not possible unless preformed neutral enolate complexes are used. Here again, kinetic study has revealed that propagation is independently first order in neutral enolate and cationic alkyl, consistent with the mechanism shown in Scheme 17.[77a,77d,77i,77j]

Although not widely advertised, this propagation step is more rapid than the unimolecular process, and where comparative studies have been made, it dominates at low temperature as long as excess neutral enolate is present.[77l] What is generally not known is to what extent this pathway is important for metallocene initiators other than the parent system. In one of the few studies to carefully examine this issue, Höcker and co-workers demonstrated that the C_1-symmetric complex $[Me_2C(Cp)IndZrMe(THF)][BPh_4]$ produced isotactic PMMA by a site control mechanism, whereas in the presence of the corresponding neutral enolate $[Me_2C(Cp)IndZrMe\{O(O^tBu){=}CMe_2]$, partially syndiotactic PMMA was exclusively produced by a more rapid chain-end control process.[76e,g] On the other hand, with sterically hindered complexes, such as *rac*- or [*S*]-en$(H_4Ind)_2ZrMe_2$, and *in situ* activation with $[Bu_3NH][BPh_4]$, the use of excess dialkyl had little effect on either the rate or stereochemical outcome of polymerization.[76,81]

Recently, the use of a *bona fide* dinuclear enolate initiator for MMA polymerization was reported.[77l] Kinetic studies reveal that the rate of polymerization was first order in dinuclear enolate and zero order in monomer consistent with a mechanism where intramolecular Michael addition is rate determining and the resting state is the acyclic dinuclear intermediate **A** (Scheme 20). Despite the kinetic advantage in converting a bimolecular process into a unimolecular one, this dinuclear enolate was less reactive than mixtures of neutral and cationic enolate complexes at identical concentrations. This was attributed to reduced nucleophilicity of the neutral enolate moiety in **A**, as a result of delocalization of charge through the μ-oxo bridge linking the two metal centers.

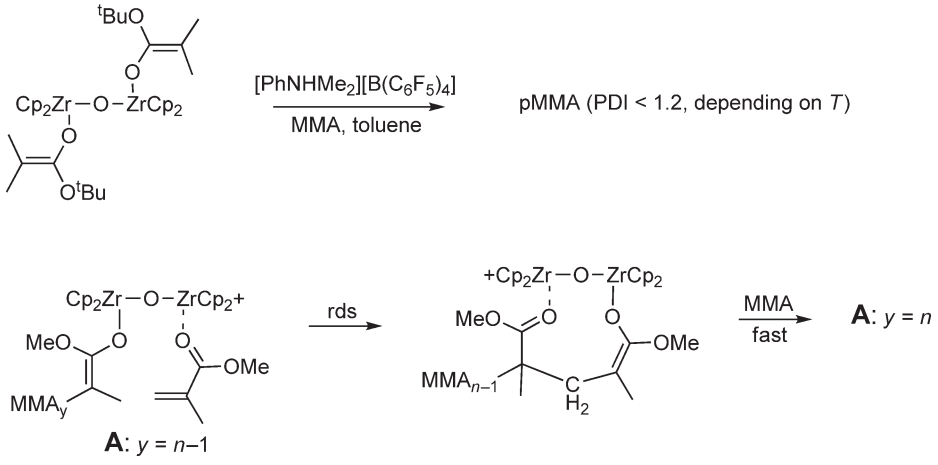

Scheme 20

This kind of approach, particularly if it could be used to control polymer tacticity, might be a useful alternative to polymerizations involving mononuclear initiators as propagation is definitely more rapid than that involving mononuclear, cationic enolate complexes of similar structure.

1.05.5 Polymerization by Other Mechanisms

1.05.5.1 Introduction

The preceding sections have dealt with polymerization by either insertion or GTP mechanisms. Of course, vinyl monomers are also polymerizable by radical, anionic, or cationic mechanisms. In this short section, we summarize the processes which are reasonably well understood from a mechanistic viewpoint, and which involve the intervention of transition metal alkyls (or hydrides), either during initiation, propagation, or chain transfer/termination. A much larger class of polymerization reactions where redox-active transition metal complexes are used to mediate radical polymerizations by reversible atom transfer (ATRP) or other means has been extensively and recently reviewed from a mechanistic perspective[83,83a–83g] and will only be briefly mentioned here.

1.05.5.2 Polymerization Involving Radical Mechanisms

The Kharasch addition reaction involving the addition of organic halides (or related compounds) to activated alkenes in the presence of redox active metal complexes, and involving either thermal or photochemical initiation, has long been known.[84] In the presence of excess alkene, polymerization is observed. This process serves as the basis for living free-radical polymerization through the mechanism of ATRP. As shown in Scheme 21, reversible halogen (or other labile group) abstraction, accompanied by single-electron oxidation of the metal complex, generates a small concentration of free radicals which propagate via the usual means.

Provided the rate of capture of the propagating radicals by metal halide is faster than the rate of radical recombination (or disproportionation), quasi-living conditions are achieved, and a controlled synthesis of polymers or (block) co-polymers is possible. It is now reasonably well understood what factors are important in governing both the rate and equilibrium involved in reversible halogen abstraction,[83,83a–83g] and while organometallic complexes, particularly of Ru[85,85a–85f] and Ni,[86] have been employed in ATRP, the complexes have generally featured (π-bound or related spectator ligands which block undesirable side-reactions and/or positively influence the redox couple summarized in Scheme 21. A striking development is the dual role of Grubbs/Herrmann (NHC)Ru–carbene complexes which can be used for both ATRP and ROMP.[85,85a–85f]

A smaller but quite useful class of free-radical polymerization reactions are those involving catalytic chain transfer (CCT).[83,87,87a,87b] Here, initiation can be achieved by conventional thermal or photochemical means, using a free-radical initiator, while a transition metal complex is intimately involved in chain transfer usually through hydride abstraction from the propagating radical (Scheme 22). The resulting metal hydride features a thermally labile bond and so can reinitiate chain growth through homolysis of this bond following by addition of H$^{\cdot}$ to monomer. As long as the tendency for the resulting metal-centered radical to dimerize (or otherwise decompose[88,88a,88b]) is low compared to its rate of reaction with propagating free radicals, effective chain transfer, which is catalytic in transition metal complex, is achieved.

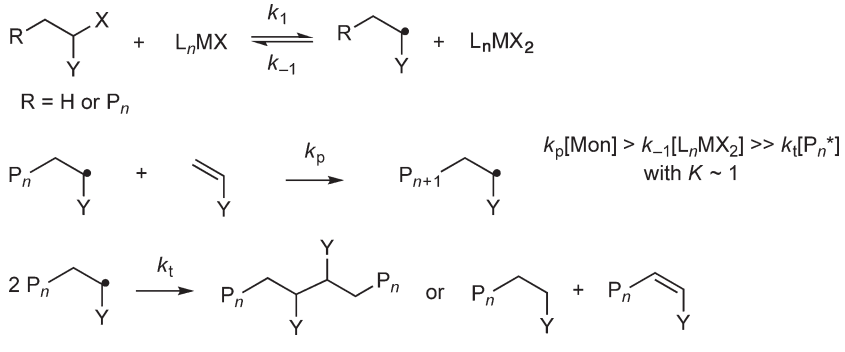

Scheme 21

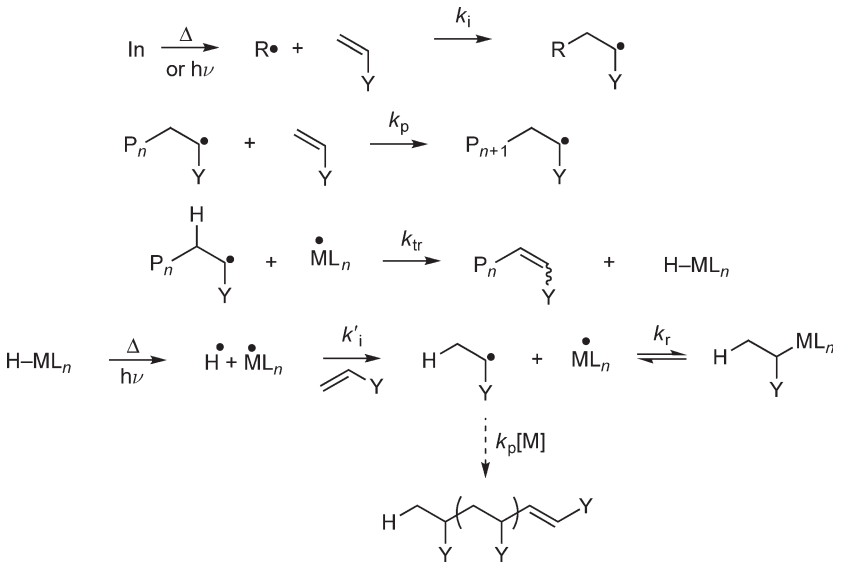

Scheme 22

Competing side-reactions include recombination of the propagating radicals with the metal-centered radical to form a metal alkyl.[89,89a] If the latter process is reversible, quasi-living conditions can be achieved using metal alkyls as initiators—this reaction actually predates ATRP as a living-polymerization method but has not achieved the same utility due to the need for prior formation of metal alkyls.[90,90a–90h] CCT process is chiefly important in the synthesis of macromonomers since the resulting oligomeric products feature terminal unsaturation, useful in the synthesis of graft or other co-polymers.

1.05.5.3 Polymerization Involving Cationic Mechanisms

A growing class of polymerization reactions involve the use of an electron-deficient and usually positively charged metal alkyl (or related complex) to initiate cationic polymerization of susceptible monomers such as isobutene, styrene, dienes, or polar monomers such as vinyl ethers or carbazoles.[91,91a–91d] Some of these monomers, especially vinyl ethers, are so susceptible to polymerization via a cationic mechanism[93] that it is doubtful that a metal alkyl is required, as long as the metal complex is highly Lewis acidic (for recent examples of metal alkyl-mediated vinyl ether polymerizations, see Refs: 92, 92a, and 92b). Examples of cationic polymerization of both vinyl ethers and even styrene, elicited by transition metal electrophiles devoid of metal–carbon bonds, are well known.[94,94a] Polymer tacticity or quasi-living behavior, etc., is not necessarily a good indicator of a change in mechanism (to coordination) as tactic and living poly(vinyl ethers) can be prepared using conventional Lewis acids.[95,95a,95b]

Since the metal alkyl is only involved in initiation of chain growth while subsequent propagation and chain transfer (usually involving chain transfer to monomer via hydride abstraction[93]) are usually very rapid, it is generally not possible to determine the fate of the metal alkyl in such polymerizations. End-group analyses provide evidence for a cationic propagation and chain-transfer mechanism,[96] but the initiator moiety is not detected unless the process is at least quasi-living under the conditions studied.[95,95a,95b]

In a recent study on isobutene polymerization, Bochmann and co-workers examined the reaction of dinuclear, zirconocene hydride initiators with isobutene (and related olefins) at low T.[97] The final product shown in Scheme 23 results from insertion and C–H activation of 3 equiv. of monomer per molecule of dinuclear initiator; one of the monomers is hydrogenated in this process.

Further addition of monomer led to consumption of this material and formation of polymer; it is unclear how this occurs, and what is typically proposed involves electrophilic attack of the metal (or metal–alkene complex) on monomer to generate a carbocation which then rapidly propagates.[91,91a–91d] In the system studied by Bochmann and co-workers, an alternate mechanism involving C–H activation of monomer (which could conceivably generate a

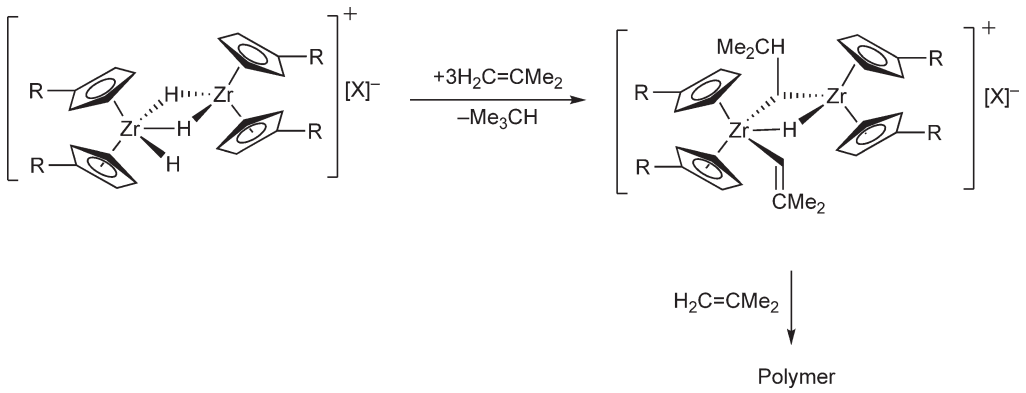

Scheme 23

reactive proton in the absence of competing alkane elimination) to form a π-allyl complex (a common reaction pathway for early metal alkyls and isobutene[98,98a]) was excluded.

Some insight into the mechanism of vinyl ether polymerization using cationic Pd–diimine complexes is provided by recent work of Jordan and co-workers.[99] They noted that reaction of the [(α-diimine)PdMe(OEt_2)][$B(C_6F_5)_4$] complex with vinyl ethers afforded the π-allyl complex [(α-diimine)Pd(η-C_3H_5)][$B(C_6F_5)_4$] and alcohol by the process of 1,2-insertion, β-alkoxide elimination to form propene, and C–H activation of propene by the cationic alkoxide complex thus formed. Addition of excess vinyl ether resulted in cationic polymerization, although how initiation occurs was not discovered. This provides another example that insertion/C–H activation chemistry may be a prelude to cationic propagation in those systems involving metal–alkyl initiators.

1.05.5.4 Polymerization Involving Anionic Mechanisms

Anionic polymerization is closely related to group-transfer polymerization, and distinguishing between the two processes in the case of metal–alkyl-mediated polymerization of polar monomers such as acrylates[100,100a] or acrylonitrile[101,101a,101b] is not trivial.[102] In this short section, we focus on transition metal- or lanthanide-mediated polymerizations involving styrene and dienes. Anionic polymerization of both monomers is well known,[103] and one might expect transition metal or lanthanide alkyls with a high degree of ionic character for the M–C bonds to initiate polymerization via this mechanism.

There has been fairly intense activity focusing on the use of neutral and anionic organolanthanide complexes for polymerization of diene-,[104,104a–104n] and to a lesser extent, styrene-based monomers.[105,105a–105h] In the former case, the focus is on the synthesis of poly(butadiene) and especially poly(isoprene) with high *cis*-1,4-content. Both organolanthanide (II) and (III) complexes have been employed where the former are thought to initiate polymerization via single-electron transfer to (coordinated) monomer. In some cases, particularly for dienes, these processes are at least quasi-living, and the synthesis of di-block co-polymers, usually with polar monomers, such as methacrylates or lactones[104f,104j] is possible.

It is unclear that an anionic mechanism is involved, since, frequently, the same initiators are also competent for diene– or styrene–olefin co-polymerization, which likely involves a coordination mechanism.[104d,104g,104k,105] On the other hand, very few of these studies use isolated metal alkyls,[104n,104k,105,105a–105e] which are often isolated as "ate" complexes with lithium or magnesium salts, and often an activation procedure is involved; so, there may be more than one type of species present when *in situ* generation is employed.

An exciting development in this area is the recent use of $CpTiR_3$ complexes[106,106a–106c] to co-polymerize dienes with styrene to furnish block or blocky co-polymers of, for example, butadiene and syndiotactic poly(styrene) (*s*-PS).[107] It is largely accepted that a [$Cp^*Ti^{III}R$][X] species is responsible for styrene polymerization,[108,108a,108b] forming *s*-PS via a 2,1-insertion mechanism; at sufficiently low *T*, the η-benzyl intermediates appear sufficiently stable toward β-elimination such that block co-polymers can be prepared.

A fairly large number of well-defined late metal complexes are competent for diene polymerization, (Fe,[109,109a,109b,] Co,[109c–109f] Ni[109g–109i]) often in a quasi-living fashion, but it is believed that a conventional insertion

mechanism involving π- and σ-allyl intermediates is involved, and a range of microstructures (i.e., 1,2- vs. 1,4-insertion) are produced.

1.05.6 Conclusions

The variety of mechanisms by which organotransition metals are able to enchain olefins is reflected in the diverse chemistry discussed above. While much progress has been observed over the past 10–15 years, many challenges remain, including evermore active and selective catalysts, particularly those which are able to handle olefinic monomers with polar functions.

References

1. Seyferth, D. *Organometallics* **2001**, *20*, 2.
2. Ziegler, K.; Holzkamp, E.; Breil, H.; Martin, H. *Angew. Chem.* **1955**, *67*, 426.
2a. Ziegler, K.; Holzkamp, E.; Breil, H.; Martin, H. *Angew. Chem.* **1955**, *67*, 541.
3. Natta, G.; Pino, P.; Corradini, P.; Danusso, F.; Mantica, E.; Mazzanti, G.; Moraglio, G. *J. Am. Chem. Soc.* **1955**, *77*, 1708.
4. Frontiers in metal-catalyzed polymerization. *Chem. Rev.* **2000**, *100*, 1167–1681.
5. Doherty, N. M.; Bercaw, J. E. *J. Am. Chem. Soc.* **1985**, *107*, 2670.
5a. Burger, B. J.; Santarsiero, B. D.; Trimmer, M. S.; Bercaw, J. E. *J. Am. Chem. Soc.* **1988**, *110*, 3134.
6. Burger, B. J.; Thompson, M. E.; Cotter, W. D.; Bercaw, J. E. *J. Am. Chem. Soc.* **1990**, *112*, 1566.
7. Halpern, J.; Okamoto, T.; Zakcharieve, A. *J. Mol. Catal.* **1976**, *2*, 65.
8. Schmidt, G. F.; Brookhart, M. *J. Am. Chem. Soc.* **1985**, *107*, 1443.
9. Brookhart, M.; Green, M. L. H.; Wong, L. L. *Prog. Inorg. Chem.* **1988**, *36*, 1.
10. Witte, P. T.; Meetsma, A.; Hessen, B.; Budzelaar, P. H. M. *J. Am. Chem. Soc.* **1997**, *119*, 10561.
11. Horton, A. D.; Orpen, A. G. *Organometallics* **1992**, *11*, 8.
12. Karl, J.; Dahlmann, M.; Erker, G.; Bergander, K. *J. Am. Chem. Soc.* **1998**, *120*, 5643.
12a. Temme, B.; Karl, J.; Erker, G. *Chem. Eur. J.* **1996**, *2*, 919.
12b. Erker, G.; Noe, R.; Krüger, C.; Werner, R. *Organometallics* **1992**, *11*, 4164.
13. Galakov, M. V.; Heinz, G.; Royo, P. *J. Chem. Soc. Chem. Commun.* **1998**, 17.
14. Casey, C. P.; Hallenbeck, S. L.; Pollock, D. W.; Landis, C. R. *J. Am. Chem. Soc.* **1995**, *117*, 9770.
14a. Casey, C. P.; Hallenbeck, S. L.; Wright, J. M; Landis, C. R. *J. Am. Chem. Soc.* **1997**, *119*, 9680.
14b. Casey, C. P.; Fisher-Klein, J.; Fagan, M. A. *J. Am. Chem. Soc.* **2000**, *122*, 4320.
14c. Casey, C. P.; Lee, T.-Y.; Tunge, J. A.; Carpenetti, D. W. II, *J. Am. Chem. Soc.* **2001**, *123*, 10762.
15. Casey, C. P.; Tunge, J. A.; Lee, T.-Y.; Fagan, M. A. *J. Am. Chem. Soc.* **2003**, *125*, 2641.
16. Casey, C. P.; Carpenetti, D. W., II. *Organometallics* **2000**, *19*, 3970.
17. Carpentier, J.-F.; Wu, Z.; Lee, C. W.; Strömberg, S.; Christopher, J. N.; Jordan, R. F. *J. Am. Chem. Soc.* **2000**, *122*, 7750.
18. Carpentier, J.-F.; Maryin, V. P.; Luci, J.; Jordan, R. F. *J. Am. Chem. Soc.* **2001**, *123*, 898.
19. Stoebenau, E. J., III; Jordan, R. F. *J. Am. Chem. Soc.* **2003**, *125*, 3222.
20. Stoebenau, E. J., III; Jordan, R. F. *J. Am. Chem. Soc.* **2004**, *126*, 11170.
21. Brandow, C. G.; Mendiratta, A.; Bercaw, J. E. *Organometallics* **2001**, *20*, 4253.
21a. Casey, C. P; Carpenetti, D. W., II; Sakurai, H. *Organometallics* **2001**, *20*, 4262.
22. Margl, P.; Deng, L.; Ziegler, T. *Top. Catal.* **1999**, 7, 187.
22a. Castonguay, L. A.; Rappé, A. K. *J. Am. Chem. Soc.* **1992**, *114*, 5832.
22b. Yoshida, T.; Koga, N.; Morokuma, K. *Organometallics* **1996**, *15*, 766.
22c. Prosenc, M. H.; Brintzinger, H. H. *Organometallics* **1997**, *16*, 3889.
23. For an extremely lucid summary of the mechanism of olefin insertion into d^0 M-C bonds, see Grubbs, R. H.; Coates, G. W. *Acc. Chem. Res.* **1996**, *29*, 85.
24. Cossee, P. *J. Catal.* **1964**, *3*, 80.
24a. Arlman, E. J.; Cossee, P. *J. Catal.* **1964**, *3*, 99.
25. Green, M. L. H. *Pure Appl. Chem.* **1978**, *50*, 27.
25a. Ivin, K. J.; Rooney, J. J.; Stewart, C. D.; Green, M. L. H.; Mahtab, R. *J. Chem. Soc., Chem. Commun.* **1978**, 604.
26. Prosenc, M. H.; Janiak, C.; Brintzinger, H. H. *Organometallics* **1992**, *11*, 4036.
26a. Röll, W.; Brintzinger, H. H.; Rieger, B.; Zolk, R. *Angew. Chem., Int. Ed. Engl.* **1990**, *29*, 279.
27. Gilchrist, J. H.; Bercaw, J. E. *J. Am. Chem. Soc.* **1996**, *118*, 12021.
28. Kaminsky, W.; Külper, K.; Brintzinger, H. H.; Wild, F. W. R. P. *Angew. Chem., Int. Ed. Engl.* **1985**, *24*, 507.
28a. Gilchrist, J. H.; Bercaw, J. E. *J. Am. Chem. Soc.* **1996**, *118*, 12021.
29. Clawson, L.; Soto, J.; Buchwald, S. L.; Steigerwald, M. L.; Grubbs, R. H. *J. Am. Chem. Soc.* **1990**, *112*, 1289.
30. Piers, W. E.; Bercaw, J. E. *J. Am. Chem. Soc.* **1990**, *112*, 9406.
31. Kraudelat, H.; Brintzinger, H. H. *Angew. Chem., Int. Ed. Engl.* **1990**, *29*, 1412.
32. Leclerc, M. K.; Brintzinger, H. H. *J. Am. Chem. Soc.* **1995**, *117*, 1651.
32a. Leclerc, M. K.; Brintzinger, H. H. *J. Am. Chem. Soc.* **1996**, *118*, 9024.
33. Janiak, C. *J. Organomet. Chem.* **1993**, *452*, 63.
34. Tempel, D. J.; Johnson, L. K.; Huff, R. L.; White, P. S.; Brookhart, M. *J. Am. Chem. Soc.* **2000**, *122*, 6686.
34a. Leatherman, M. D.; Svejda, S. A.; Johnson, L. K.; Brookhart, M. *J. Am. Chem. Soc.* **2003**, *125*, 3086.

35. Klabunde, U.; Ittel, S. D. *J. Mol. Catal.* **1987**, *41*, 123.
35a. Klabunde, U.; Mülhaupt, R.; Herskovitz, T.; Janowicz, A. H.; Calabrese, J.; Ittel, S. D. *J. Polym. Sci.* **1987**, *25*, 1989.
35b. Keim, W.; Howaldt, F. H.; Goddard, R.; Krüger, C. *Angew. Chem., Int. Ed. Engl.* **1978**, *17*, 466.
35c. Wilke, G. *Angew. Chem., Int. Ed. Engl.* **1988**, *27*, 185.
35d. Keim, W.; Appel, R.; Storeck, A.; Krüger, C.; Goddard, R. *Angew. Chem., Int. Ed. Engl.* **1981**, *20*, 116.
35e. Keim, W.; Appel, R.; Gruppe, S.; Knoch, F. *Angew. Chem., Int. Ed. Engl.* **1987**, *26*, 1012.
35f. Ostoja, S. K. A.; Witte, J. *Angew. Chem., Int. Ed. Engl.* **1985**, *24*, 599.
35g. Heinicke, J.; Koesling, M.; Brüll, R.; Keim, W.; Pritzkow, H. *Eur. J. Inorg. Chem.* **2000**, 299.
36. Younkin, T. R.; Connor, E. F.; Henderson, J. I.; Friedrich, S. K.; Grubbs, R. H.; Bansleben, D. A. *Science* **2000**, *287*, 460.
36a. Wang, C.; Friedrich, S.; Younkin, T. R.; Li, R. T.; Grubs, R. H.; Bansleben, D. A.; Day, M. W. *Organometallics* **1998**, *17*, 3149.
36b. Waltman, A. W.; Younkin, T. R.; Grubbs, R. H. *Organometallics* **2004**, *23*, 5121.
37. Jenkins, J. C.; Brookhart, M. *J. Am. Chem. Soc.* **2004**, *126*, 5827.
38. Komon, Z. J. A.; Bu, X.; Bazan, G. C. *J. Am. Chem. Soc.* **2000**, *122*, 1830.
38a. Komon, Z. J. A.; Bu, X.; Bazan, G. C. *J. Am. Chem. Soc.* **2000**, *122*, 12379.
38b. Komon, Z. J. A.; Bazan, G. C. *Macromol. Rapid Commun.* **2001**, *22*, 467.
38c. Lee, B. Y.; Bazan, G. C.; Vela, J.; Komon, Z. J. A.; Bu, X. *J. Am. Chem. Soc.* **2001**, *123*, 5352.
38d. Lee, B. Y.; Bu, X.; Bazan, G. C. *Organometallics* **2001**, *20*, 5425.
39. Small, B. L.; Brookhart, M.; Bennett, A. M. A. *J. Am. Chem. Soc.* **1998**, *120*, 4049.
39a. Small, B. L.; Brookhart, M. *J. Am. Chem. Soc.* **1998**, *120*, 7143.
39b. Britovsek, G. J. P.; Gibson, V. C.; Kimberley, B. S.; Maddox, P. J.; McTavish, S. J.; Solan, G. A.; White, A. J. P.; Williams, D. J. *Chem. Commun.* **1998**, 849.
39c. Britovsek, G. J. P.; Bruce, M.; Gibson, V. C.; Kimberley, B. S.; Maddox, P. J.; Mastroianni, S.; McTavish, S. J.; Redshaw, C.; Solan, G. A., Stromberg, S., *et al. J. Am. Chem. Soc.* **1999**, *121*, 8728.
40. Britovsek, G. J. P.; Gibson, V. C.; Wass, D. F. *Angew. Chem., Int. Ed. Engl.* **1999**, *38*, 428.
40a. Gibson, V. C.; Spitzmesser, S. K. *Chem. Rev.* **2003**, *103*, 283.
40b. Ittel, S. D.; Johnson, L. K.; Brookhart, M. *Chem. Rev.* **2000**, *100*, 1169.
40c. Boffa, L. S.; Novak, B. M. *Chem. Rev.* **2000**, *100*, 1479.
41. Deng, L.; Woo, T. K.; Cavallo, L.; Margl, P. M.; Ziegler, T. *J. Am. Chem. Soc.* **1997**, *119*, 6177.
41a. Woo, T. K.; Blöchl, P. E.; Ziegler, T. *J. Phys. Chem.* **2000**, *104*, 121.
42. Froese, R. D. J.; Musaev, D. G.; Morokuma, K. *J. Am. Chem. Soc.* **1998**, *120*, 1581.
43. Michalak, A.; Ziegler, T. *Organometallics* **2003**, *22*, 2069.
43a. Chan, M. S. W.; Deng, L.; Ziegler, T *Organometallics* **2000**, *19*, 2741.
44. Johnson, L. K.; Mecking, S.; Brookhart, M. *J. Am. Chem. Soc.* **1996**, *118*, 267.
44a. Mecking, S.; Johnson, L. K.; Wang, L.; Brookhart, M. *J. Am. Chem. Soc.* **1998**, *120*, 888.
44b. Stibrany, R. T.; Schultz, D. N.; Kacker, S.; Patil, A. O.; Baugh, L. S.; Rucker, S. P.; Zushma, S.; Berluche, E.; Sissano, J. A. *Macromolecules* **2003**, *36*, 8584.
44c. He, X.; Yao, Y.; Luo, X.; Zhang, J.; Liu, Y.; Zhang, L.; Wu, Q. *Organometallics* **2003**, *22*, 4952.
44d. Britovsek, G. J. P.; Gibson, V. C.; Spitzmesser, S. K.; Tellman, K. P; White, A. J. P.; Williams, D. J. *J. Chem. Soc., Dalton Trans.* **2002**, 1159.
45. Diamanti, S. J.; Ghosh, P.; Shimizu, F.; Bazan, G. C. *Macromolecules* **2003**, *36*, 9731.
46. Stockland, R. A., Jr.; Jordan, R. F. *J. Am. Chem. Soc.* **2000**, *122*, 6315.
46a. Shen, H.; Jordan, R. F. *Organometallics* **2003**, *22*, 2080.
46b. Stockland, R. A., Jr.; Foley, S. R.; Jordan, R. F. *J. Am. Chem. Soc.* **2003**, *125*, 796.
46c. Strazisar, S. A.; Wolczanski, P. T. *J. Am. Chem. Soc.* **2001**, *123*, 4728.
46d. Kraft, B. M.; Jones, W. D. *J. Am. Chem. Soc.* **2002**, *124*, 8681.
46e. Clot, E.; Megret, C.; Kraft, B. M.; Eisenstein, O.; Jones, W. D. *J. Am. Chem. Soc.* **2004**, *126*, 5647.
47. Shen, H.; Jordan, R. F. *Organometallics* **2003**, *22*, 1878.
47a. Foley, S. R.; Stockland, R. A., Jr.; Shen, H.; Jordan, R. F *J. Am. Chem. Soc.* **2003**, *125*, 4350.
48. Szabo, M. J.; Jordan, R. F.; Michalak, A.; Piers, W. E.; Weiss, T.; Yang, S.-Y.; Ziegler, T. *Organometallics* **2004**, *23*, 5565.
49. Wu, F.; Foley, S. R.; Burns, C. T.; Jordan, R. F. *J. Am. Chem. Soc.* **2005**, *127*, 1841.
49a. Groux, L. F.; Weiss, T.; Reddy, D. N.; Chase, P. A.; Piers, W. E.; Ziegler, T.; Parvez, M.; Benet-Buchholz, J. *J. Am. Chem. Soc.* **2005**, *127*, 1854.
49b. Yang, S.-Y.; Szabo, M. J.; Michalak, A.; Weiss, T.; Piers, W. E.; Jordan, R. F.; Ziegler, T. *Organometallics* **2005**, *24*, 1242.
50. Hérisson, J.-L.; Chauvin, Y. *Makromol. Chem.* **1971**, *141*, 161.
51. Schrock, R. R. *Tetrahedron* **1999**, *55*, 8141.
51a. Buchmeiser, M. R. *Chem. Rev.* **2000**, *100*, 1565.
51b. Kingsbury, C. L.; Mehrman, S. J.; Takacs, J. M. *Curr. Org. Chem.* **1999**, *3*, 497.
51c. Randall, M. L.; Snapper, M. L. *J. Mol. Catal. A* **1998**, *133*, 29.
51d. Ivin, K. J. *J. Mol. Catal. A* **1998**, *133*, 1.
51e. Grubbs, R. H.; Chang, S. *Tetrahedron* **1998**, *54*, 4413.
51f. Pariya, C.; Jayaprakash, K. N.; Sarkar, A. *Coord. Chem. Rev.* **1998**, *168*, 1.
51g. Naota, T.; Takaya, H.; Murahashi, S.-I. *Chem. Rev.* **1998**, *98*, 2599.
52. Ivin, K. J.; Mol, J. C. *Olefin Metathesis and Metathesis Polymerization*; Academic Press: London, 1997.
52a. Grubbs, R. H., Ed.; In *Handbook of Metathesis*; Wiley-VCH: Weinheim, 2003; Vol. 1-3.
53. Schrock, R. R. *Acc. Chem. Res.* **1990**, *23*, 158.
54. Trnka, T. M.; Grubbs, R. H. *Acc. Chem. Res.* **2001**, *34*, 18.
55. Grubbs, R. H. In *Comprehensive Organometallic Chemistry I*; Wilkinson, G., Stone, F. G. A., Abel, E. W., Eds.; Pergamon: Oxford, 1982; Vol. 8, 499.
56. O'Dell, R.; McConville, D. H.; Hofmeister, G. E.; Schrock, R. R. *J. Am. Chem. Soc.* **1994**, *116*, 3414.
57. Tsang, W. C. P.; Hultzsch, K. C.; Alexander, J. B.; Bonitatebus, P. J., Jr.; Schrock, R. R.; Hoveyda, A. H. *J. Am. Chem. Soc.* **2003**, *125*, 2653.
57a. Tsang, W. C. P.; Jamieson, J. Y.; Aeilts, S. L.; Hultzsch, K. C.; Schrock, R. R.; Hoveyda, A. H. *Organometallics* **2004**, *23*, 1997.

58. Goumans, T. P. M.; Ehlers, A. W.; Lammertsma, K. *Organometallics* **2005**, *24*, 3200.
58a. Folga, E.; Ziegler, T. *Organometallics* **1993**, *12*, 325.
58b. Monteyne, K.; Ziegler, T. *Organometallics* **1998**, *17*, 5901.
58c. Wu, Y.-D.; Peng, Z.-H. *J. Am. Chem. Soc.* **1997**, *119*, 8043.
59. Feldman, J.; Murdzek, J. S.; Davis, W. M.; Schrock, R. R. *Organometallics* **1989**, *8*, 2260.
59a. Feldman, J.; Davis, W. M.; Thomas, J. K.; Schrock, R. R. *Organometallics* **1990**, *9*, 2535.
59b. Feldman, J.; Schrock, R. R. *Prog. Inorg. Chem.* **1991**, *39*, 1.
60. Schwab, P.; France, M. B.; Ziller, J. W.; Grubbs, R. H. *Angew. Chem., Int. Ed. Engl.* **1995**, *34*, 2039.
60a. Schwab, P.; Grubbs, R. H.; Ziller, J. W. *J. Am. Chem. Soc.* **1996**, *118*, 100.
61. Scholl, M.; Ding, S.; Lee, C. W.; Grubbs, R. H. *Org. Lett.* **1999**, *1*, 953.
62. Wakamatsu, H.; Blechert, S. *Angew. Chem., Int. Ed.* **2002**, *41*, 794.
62a. Wakamatsu, H.; Blechert, S. *Angew. Chem., Int. Ed.* **2002**, *41*, 2403.
63. Dias, E. L.; Nguyen, S. T.; Grubbs, R. H. *J. Am. Chem. Soc.* **1997**, *119*, 3887.
63a. Sanford, M. S.; Love, J. A.; Grubbs, R. H. *J. Am. Chem. Soc.* **2001**, *123*, 6543.
64. Adlhart, C.; Volland, M. A. O.; Hofmann, P.; Chen, P. *Helv. Chim. Acta* **2000**, *83*, 3306.
64a. Adlhart, C.; Chen, P. *Helv. Chim. Acta* **2000**, *83*, 2192.
65. Sanford, M. S.; Henling, L. M.; Day, M. W.; Grubbs, R. H. *Angew. Chem., Int. Ed.* **2000**, *39*, 3451.
66. Tallarico, J. A.; Bonitatebus, P. J., Jr.; Snapper, M. L. *J. Am. Chem. Soc.* **1997**, *119*, 7157.
67. Romero, P. E.; Piers, W. E.; McDonald, R. *Angew. Chem., Int. Ed.* **2004**, *43*, 6161.
68. Carlson, R. G.; Gile, M. A.; Heppert, J. A.; Mason, M. H.; Powell, D. R.; Vander, V. D.; Vilain, J. M. *J. Am. Chem. Soc.* **2002**, *124*, 1580.
69. Straub, B. F. *Angew. Chem., Int. Ed.* **2005**, *44*, 5974.
70. Romero, P. E.; Piers, W. E. *J. Am. Chem. Soc.* **2005**, *127*, 5032.
71. Webster,; Owen, W. *Adv. Polym. Sci.* **2004**, *167*, 1.
72. Yasuda, H.; Yamamoto, H.; Yokota, K.; Miyake, S.; Nakamura, A. *J. Am. Chem. Soc.* **1992**, *114*, 4908.
72a. Yasuda, H.; Yamamoto, H.; Yamashita, M.; Yokota, K.; Nakamura, A.; Miyake, S.; Kai, Y.; Kanehisa, N. *Macromolecules* **1993**, *26*, 7134.
72b. Boffa, L. S.; Novak, B. M. *Macromolecules* **1994**, *27*, 6993.
72c. Giardello, M. A.; Yamamoto, Y.; Brard, L.; Marks, T. J. *J. Am. Chem. Soc.* **1995**, *117*, 3276.
72d. Boffa, L. S.; Novak, B. M. *Macromolecules* **1997**, *30*, 3494.
72e. Yasuda, H.; Ihara, E.; Hayakawa, T.; Kakehi, T. *J. Macromol. Sci., Pure Appl. Chem.* **1997**, *A34*, 1929.
72f. Knjazhanski, S. Y.; Elizalde, L.; Cadenas, G.; Bulychev, B. M. *J. Organomet. Chem.* **1998**, *568*, 33.
72g. Desurmont, G.; Tokimitsu, T.; Yasuda, H. *Macromolecules* **2000**, *33*, 7679.
72h. Qian, C.; Nie, W.; Sun, J. *Organometallics* **2000**, *19*, 4134.
72i. Zhang, L.; Zhou, X.; Cai, R.; Weng, L. *J. Organomet. Chem.* **2000**, *612*, 176.
72j. Qian, C.; Zou, G.; Chen, Y.; Sun, J. *Organometallics* **2001**, *20*, 3106.
72k. Yasuda, H. *J. Polym. Sci., Part A: Polym. Chem.* **2001**, *39*, 1955.
72l. Arndt, S.; Beckerle, K.; Hultzsch, K. C.; Sinnema, P.-J.; Voth, P.; Spaniol, T. P.; Okuda, J. *J. Mol. Cat. A: Chem.* **2002**, *190*, 215.
72m. Bala, M. D.; Huang, J.; Zhang, H.; Qian, Y; Sun, J.; Liang, C. *J. Organomet. Chem.* **2002**, *647*, 105.
72n. Qi, G.; Nitto, Y.; Saiki, A.; Tomohiro, T.; Nakayama, Y.; Yasuda, H. *Tetrahedron* **2003**, *59*, 10409.
72o. Kirillov, E.; Toupet, L.; Lehmann, C. W.; Razavi, A.; Carpentier, J.-F. *Organometallics* **2003**, *22*, 4467.
72p. Woodman, T. J.; Schormann, M.; Bochmann, M. *Organometallics* **2003**, *22*, 2938.
72q. Woodman, T. J.; Schormann, M.; Hughes, D. L.; Bochmann, M. *Organometallics* **2003**, *22*, 3028.
72r. Qian, Y.; Bala, M. D.; Yousaf, M.; Zhang, H.; Huang, J.; Sun, J.; Liang, C. *J. Mol. Catal. A: Chem.* **2002**, *188*, 1.
72s. Qian, C.; Zou, G.; Jiang, W.; Chen, Y.; Sun, J.; Li, N. *Organometallics* **2004**, *23*, 4980.
72t. Yasuda, H.; Desurmont, G. *Polym. Int.* **2004**, *53*, 1017.
72u. Woodman, T. J.; Schormann, M.; Hughes, D. L.; Bochmann, M. *Organometallics* **2004**, *23*, 2972.
72v. Simpson, C. K.; White, R. E.; Carlson, C. N.; Wrobleski, D. A.; Kuehl, C. J.; Croce, T. A.; Steele, I. M.; Scott, B. L.; Young, V. G., Jr., Hanusa, T. P., *et al. Organometallics* **2005**, *24*, 3685.
73. Matsuo, Y.; Mashima, K.; Tani, K. *Angew. Chem., Int. Ed.* **2001**, *40*, 960.
73a. Ihara, E.; Tanaka, S.; Itoh, T.; Inoue, K. *Polymer J.* **2003**, *35*, 972.
73b. Siemeling, U.; Koelling, L.; Kuhnert, O.; Neumann, B.; Stammler, A.; Stammler, H. G.; Fink, G.; Kaminski, E.; Kiefer, A.; Schrock, R. R. *Z. Anorg. Allg. Chem.* **2003**, *629*, 781.
73c. Feng, S.; Roof, G. R.; Chen, E. Y.-X. *Organometallics* **2002**, *21*, 832.
73d. Ihara, E.; Amamoto, M.; Inoue, K. *Polym. Bull.* **2003**, *50*, 213.
73e. Ihara, E.; Todaka, T.; Inoue, K. *J. Polym. Sci., Part A: Polym. Chem.* **2003**, *42*, 31.
73f. Kim, I.; Hwang, J.-M.; Lee, J. K.; Ha, C. S.; Woo, S. I. *Macromol. Rapid Commun.* **2003**, *24*, 508.
73g. Britovsek, G. J. P.; Gibson, V. C.; Spitzmesser, S. K.; Tellmann, K. P.; White, A. J. P.; Williams, D. J. *J. Chem. Soc., Dalton Trans.* **2002**, 1159.
73h. Li, X.-F.; Li, Y.-G.; Li, Y.-S.; Chen, Y.-X.; Hu, N.-H. *Organometallics* **2005**, *24*, 2502.
73i. Albeniz, A. C.; Espinet, P.; Lopez-Fernandez, R. *Organometallics* **2003**, *22*, 4206.
74. Farnham, W. B.; Hertler, W. U.S. Patent 4,728,706, 1988.
75. Puzin, Y. I.; Prokudina, E. M.; Yumagulova, R. Kh.; Muslukhov, R. R.; Kolesov, S. V. *Dokl. Akad. Nauk* **2002**, *386*, 211.
75a. Bhattacharjee, M.; Patra, B. N. *Polymer* **2004**, *45*, 3111.
75b. Polo, E.; Barbieri, A.; Traverso, O. *New J. Chem.* **2004**, *28*, 652.
76. Collins, S.; Ward, D. G.; Suddaby, K. H. *Macromolecules* **1994**, *27*, 7222.
76a. Soga, K.; Deng, H.; Yano, T.; Shiono, T. *Macromolecules* **1994**, *27*, 7938.
76b. Deng, H.; Shiono, T.; Soga, K. *Macromolecules* **1995**, *28*, 3067.
76c. Shiono, T.; Saito, T.; Saegusa, N.; Hagihara, H.; Ikeda, T.; Deng, H.; Soga, K. *Macromol. Chem. Phys.* **1998**, *199*, 1573.
76d. Nguyen, H.; Jarvis, A. P.; Lesley, M. J. G.; Kelly, W. M.; Reddy, S. S.; Taylor, N. J.; Collins, S. *Macromolecules* **2000**, *33*, 1508.
76e. Stuhldreier, T.; Keul, H.; Höcker, H. *Macromol. Rapid Commun.* **2000**, *21*, 1093.
76f. Cameron, P. A.; Gibson, V.; Graham, A. J. *Macromolecules* **2000**, *33*, 4329.
76g. Frauenrath, H.; Keul, H.; Höcker, H. *Macromolecules* **2001**, *34*, 14.

76h. Bolig, A. D.; Chen, E. Y.-X. *J. Am. Chem. Soc.* **2001**, *123*, 7943.
76i. Jin, J.; Chen, E. Y.-X. *Organometallics* **2002**, *21*, 13.
76j. Jin, J.; Wilson, D. R.; Chen, E. Y.-X. *Chem. Commun.* **2002**, 708.
76k. Bolig, A. D.; Chen, E. Y.-X. *J. Am. Chem. Soc.* **2002**, *124*, 5612.
76l. Jin, J.; Chen, E. Y.-X. *Macromol. Chem. Phys.* **2002**, *203*, 2329.
76m. Chen, E. Y.-X.; Cooney, M. J. *J. Am. Chem. Soc.* **2003**, *125*, 7150.
76n. Jin, J.; Mariott, W. R.; Chen, E. Y.-X. *J. Polym. Chem., Part A: Polym. Chem.* **2003**, *41*, 3132.
76o. Karanikolopoulos, G.; Batis, C.; Pitsikalis, M.; Hadjichristidis, N. *Macromol. Chem. Phys.* **2003**, *204*, 831.
76p. Batis, C.; Karanikolopoulos, G.; Pitsikalis, M.; Hadjichristidis, N. *Macromolecules* **2003**, *36*, 9763.
76q. Rodriguez-Delgado, A.; Mariott, W. R.; Chen, E. Y.-X. *Macromolecules* **2004**, *37*, 3092.
76r. Strauch, J. W.; Faure, J.-L.; Bredeau, S.; Wang, C.; Kehr, G.; Frohlich, R.; Luftmann, H.; Erker, G. *J. Am. Chem. Soc.* **2004**, *126*, 2089.
76s. Bolig, A. D.; Chen, E. Y.-X. *J. Am. Chem. Soc.* **2004**, *126*, 4897.
76t. Lian, B.; Toupet, L.; Carpentier, J.-F. *Chem. Eur. J.* **2004**, *10*, 4301.
76u. Rodriguez-Delgado, A.; Chen, E. Y.-X. *Macromolecules* **2005**, *38*, 2587.
76v. Lian, B.; Lehmann, C. W.; Navarro, C.; Carpentier, J.-F. *Organometallics* **2005**, *24*, 2466.
77. Collins, S.; Ward, D. G. *J. Am. Chem. Soc.* **1992**, *114*, 5460.
77a. Li, Y.; Ward, D. G.; Reddy, S. S.; Collins, S. *Macromolecules* **1997**, *30*, 1875.
77b. Rhodes, L. F.; Goodall, B. L.; Collins, S. Reaction injection molding (RIM) of methyl (meth)acrylate and related monomers using Group-4 catalysts. U.S. Patent 5,668,234 1997, 10 pp.
77c. Chen, Y.-X.; Metz, M. V.; Li, L.; Stern, C. L.; Marks, T. J. *J. Am. Chem. Soc.* **1998**, *120*, 6287.
77d. Bandermann, F.; Ferenz, M.; Sustmann, R.; Sicking, W. *Macromol. Symp.* **2000**, *161*, 127.
77e. Bandermann, F.; Ferenz, M.; Sustmann, R.; Sicking, W. *Macromol. Symp.* **2001**, *174*, 247.
77f. Karanikolopoulos, G.; Batis, C.; Pitsikalis, M.; Hadjichristidis, N. *Macromolecules* **2001**, *34*, 4697.
77g. Wang, J.; Odian, G.; Haubenstock, H. *Polym. Prepr.* **2003**, *44*, 673.
77h. Wang, J.; Haubenstock, H.; Odian, G. *Polym. Prepr.* **2003**, *44*, 675.
77i. Ferenz, M.; Bandermann, F.; Sustmann, R.; Sicking, W. *Macromol. Chem. Phys.* **2004**, *205*, 1196.
77j. Karanikolopoulos, G.; Batis, C.; Pitsikalis, M.; Hadjichristidis, N. *J. Polym. Sci., Part A: Polym. Chem.* **2004**, *42*, 3761.
77k. Stojcevic, G.; Kim, H.; Taylor, N. J.; Marder, T. B.; Collins, S. *Angew. Chem., Int. Ed.* **2004**, *43*, 5523.
77l. Kostakis, K.; Mourmouris, S.; Pitsikalis, M.; Hadjichristidis, N. *J. Polym. Sci., Part A: Polym. Chem.* **2005**, *43*, 3337.
78. Hölscher, M.; Keul, H.; Höcker, H. *Macromolecules* **2002**, *35*, 8194.
78a. Hölscher, M.; Keul, H.; Höcker, H. *Chem. Eur. J.* **2001**, *7*, 5419.
79. Jordan, R. F. *Adv. Organomet. Chem.* **1991**, *32*, 325.
80. Nguyen, H. M. Sc. Thesis, The University of Waterloo, Waterloo, NE 2000.
81. Ward, D. G. Ph. D. Thesis, The University of Waterloo, Waterloo, NE 1995.
82. Stojcevic, G. M. Sc. Thesis, The University of Akron, Akron, OH 2004.
83. Barner-Kowollik, C.; Davis, T. P.; Stenzel, M. H. *Polymer* **2004**, *45*, 7791.
83a. Pintauer, T; McKenzie, B.; Matyjaszewski, K. *ACS Symp. Ser.* **2003**, *854*, 130.
83b. Matyjaszewski, K. *Ibid. ACS Symp. Ser.* **2003**, *854*, 2.
83c. Lowe, A. B.; McCormick, C. L. *Aust. J. Chem.* **2002**, *55*, 367.
83d. Matyjaszewski, K. *Macromol. Symp.* **2002**, *183*, 71.
83e. Cunningham, M. F. *Prog. Polym. Sci.* **2002**, *27*, 1039.
83f. Matyjaszewski, K. *Curr. Org. Chem.* **2002**, *6*, 67–82.
83g. Matyjaszewski, K.; Xia, J. *Chem. Rev.* **2001**, *101*, 2921.
84. Studer, A. *Chem. Eur. J.* **2001**, *7*, 1159.
85. Delaude, L.; Demonceau, A.; Noels, A. F. *Top. Organomet. Chem.* **2004**, *11*, 155.
85a. Opstal, T.; Couchez, K.; Verpoort, F. *Adv. Synth. Catal.* **2003**, *345*, 393.
85b. Delaude, L.; Delfosse, S.; Demonceau, A.; Richel, A.; Noels, A. F. *NATO Sci. Ser., II* **2003**, *122*, 87.
85c. Delfosse, S.; Richel, A.; Simal, F.; Demonceau, A.; Noels, A. F.; Tutusaus, O.; Nunez, R.; Vinas, C.; Teixidor, F. *ACS Symp. Ser.* **2003**, *854*, 116.
85d. Demonceau, A.; Simal, F.; Noels, A. F. *NATO Sci. Ser., II* **2002**, *56*, 227.
85e. Simal, F.; Sebille, S.; Hallet, L.; Demonceau, A.; Noels, A. F. *Macromol. Symp.* **2000**, *161*, 73.
85f. Simal, F.; Jan, D.; Demonceau, A.; Noels, A. F. *ACS Symp. Ser.* **2000**, *768*, 223.
86. Gossage, R. A.; van de Kuil, L. A.; van Koten, G. *Acc. Chem. Res.* **1998**, *31*, 423.
87. Heuts, J. P. A.; Roberts, G. E.; Biasutti, J. D. *Aust. J. Chem.* **2002**, *55*, 381.
87a. Gridnev, A. A.; Ittel, S. D. *Chem. Rev.* **2001**, *101*, 3611.
87b. Bon, S. A. F.; Morsley, D. R.; Waterson, J.; Haddleton, D. M.; Lees, M. R.; Horne, T. *Macromol. Symp.* **2001**, *165*, 29.
88. Tang, L.; Norton, J. R. *Macromolecules* **2004**, *37*, 241.
88a. Tang, L.; Papish, E. T.; Abramo, G. P.; Norton, J. R.; Baik, M.-H.; Friesner, R. A.; Rappé, A. *J. Am. Chem. Soc.* **2003**, *125*, 10093.
88b. Abramo, G. P.; Norton, J. R. *Macromolecules* **2000**, *33*, 2790.
89. Roberts, G. E.; Barner-Kowollik, C.; Davis, T. P.; Heuts, J. P. A. *Macromolecules* **2003**, *36*, 1054.
89a. Roberts, G. E.; Heuts, J. P. A.; Davis, T. P. *Macromolecules* **2000**, *33*, 7765.
90. Lu, Z.; Fryd, M.; Wayland, B. B. *Macromolecules* **2004**, *37*, 2686.
90a. Li, Y.; Wayland, B. B. *Chem. Commun.* **2003**, 1594.
90b. Li, Y.; Wayland, B. B. *Macromol. Rapid Commun.* **2003**, *24*, 307.
90c. Li, Y.; Basickes, L.; Wayland, B. B. *Polym. Prepr.* **2001**, *42*, 200.
90d. Shim, A. K.; Harwood, H. J. *Ibid. Polym. Prepr.* **1999**, *40*, 132.
90e. Gridnev, A. A.; Ittel, S. D.; Wayland, B. B.; Fryd, M. *Organometallics* **1996**, *15*, 5116.
90f. Ittel, S. D.; Gridnev, A. A.; Wayland, B. B.; Fryd, M. *Polym. Prepr.* **1994**, *35*, 704.
90g. Arvanitopoulos, L. D.; Greuel, M. P.; Harwood, H. J. *Ibid. Polym. Prepr.* **1994**, *35*, 549.
90h. Greuel, M. P.; Harwood, H. J. *Ibid. Polym. Prepr.* **1992**, *32*, 545.
91. Baird, M. C. *Can. J. Chem.* **2003**, *81*, 330.

91a. Bochmann, M.; Lancaster, S. J.; Hannant, M. D.; Rodriguez, A.; Schormann, M.; Walker, D. A.; Woodman, T. J. *Pure Appl. Chem.* **2003**, *75*, 1183.
91b. Baird, M. C. *Chem. Rev.* **2000**, *100*, 1471.
91c. Bochmann, M. *Top. Catal.* **1999**, *7*, 9.
91d. Ewart, S. W.; Baird, M. C. *Top. Catal.* **1999**, *7*, 1.
92. Kim, I.; Ha, Y. S.; Ha, C.-S. *Macromol. Rapid Commun.* **2004**, *25*, 1069.
92a. Kawaguchi, T.; Sanda, F.; Masuda, T. *J. Polym. Sci, Part A: Polym. Chem.* **2002**, *40*, 3938.
92b. Albietz, P. J., Jr.; Yang, K.; Lachicotte, R. J.; Eisenberg, R. *Organometallics* **2000**, *19*, 3543.
93. Kennedy, J. P.; Maréchal, E. *Carbocationic Polymerization*; Wiley: New York, 1982; p 510.
94. Chen, C.-L.; Chen, Y.-C.; Liu, Y.-H.; Peng, S.-M.; Liu, S.-T. *Organometallics* **2002**, *21*, 5382.
94a. Jiang, Z.; Sen, A. *Organometallics* **1993**, *12*, 1406.
95. Katayama, H.; Kamigaito, M.; Sawamoto, M. *J. Polym. Sci., Part A: Polym. Chem.* **2001**, *39*, 1258.
95a. Ouchi, M.; Kamigaito, M.; Sawamoto, M. *J. Polym. Sci., Part A: Polym. Chem.* **2001**, *39*, 1060.
95b. Ouchi, M.; Kamigaito, M.; Sawamoto, M. *Macromolecules* **1999**, *32*, 6407.
96. Barsan, F.; Karam, A. R.; Parent, M. A.; Baird, M. C. *Macromolecules* **1998**, *31*, 8439.
97. Garratt, S.; Carr, A. G.; Langstein, G.; Bochmann, M. *Macromolecules* **2003**, *36*, 4276.
98. Al-Humydi, A.; Garrison, J. C.; Mohammed, M.; Youngs, W. J.; Collins, S. *Polyhedron* **2005**, *24*, 1234.
98a. Carr, A. G.; Dawson, D. M.; Thornton-Pett, M.; Bochmann, M. *Organometallics* **1999**, *18*, 2933.
99. Luo, S.; Jordan, R. F. Reactions of vinyl ethers with cationic Pd(II) alkyl complexes; Abstract. Paper. 230th *ACS National Meeting* 2005 INOR-329.
100. Boffa, L. S. *ACS Symp. Ser.* **2000**, *760*, 1.
100a. Davis, T. P.; Haddleton, D. M.; Richards, S. N. *J. Macromol. Sci., Rev. Macromol. Chem. Phys.* **1994**, *C34*, 243.
101. Yang, P.; Chan, B. C. K.; Baird, M. C. *Organometallics* **2004**, *23*, 2752.
101a. Schaper, F.; Foley, S. R.; Jordan, R. F. *J. Am. Chem. Soc.* **2004**, *126*, 2114.
101b. Arndt, S.; Beckerle, K.; Hultzsch, K. C.; Sinnema, P.-J.; Voth, P.; Spaniol, T. P.; Okuda, J. *J. Mol. Cat. A: Chem.* **2002**, *190*, 215.
102. Quirk, R. P.; Ren, J.; Bidnger, G. *Makromol. Chem., Macromol. Symp.* **1993**, *67*, 351.
103. Hsieh, H. L.; Quirk, R. P. *Anionic Polymerization. Principles and Practical Applications*; Dekker: New York, 1996.
104. Osakada, K.; Takeuchi, D. *Adv. Polym. Sci.* **2004**, *171*, 137.
104a. Hou, Z.; Wakatsuki, Y. *Coord. Chem. Rev.* **2002**, *231*, 1.
104b. Hou, Z.; Wakatsuki, Y. *J. Organomet. Chem.* **2002**, *647*, 61.
104c. Evans, W. J.; Champagne, T. M.; Giarikos, D. G.; Ziller, J. W. *Organometallics* **2005**, *24*, 570.
104d. Boisson, C.; Monteil, V.; Ribour, D.; Spitz, R.; Barbotin, F. *Macromol. Chem. Phys.* **2003**, *204*, 1747.
104e. Kaita, S.; Hou, Z.; Nishiura, M.; Doi, Y.; Kurazumi, J.; Horiuchi, A. C.; Wakatsuki, Y. *Macromol. Rapid Commun.* **2003**, *24*, 179.
104f. Dong, W.; Endo, K.; Masuda, T. *Macromol. Chem. Phys.* **2003**, *204*, 104.
104g. Bonnet, F.; Barbier-Baudry, D.; Dormond, A.; Visseaux, M. *Polym. Intern.* **2002**, *51*, 986.
104h. Friebe, L.; Nuyken, O.; Windisch, H.; Obrecht, W. *Macromol. Chem. Phys.* **2002**, *203*, 1055.
104i. Maiwald, S.; Sommer, C.; Muller, G.; Taube, R. *Macromol. Chem. Phys.* **2002**, *203*, 1029.
104j. Dong, W.; Masuda, T. *J. Polym. Sci., Part A: Polym. Chem.* **2002**, *40*, 1838.
104k. Barbier-Baudry, D.; Bonnet, F.; Domenichini, B.; Dormond, A.; Visseaux, M. *J. Organomet. Chem.* **2002**, *647*, 167.
104l. Bonnet, F.; Visseaux, M.; Barbier-Baudry, D.; Dormond, A. *Macromolecules* **2002**, *35*, 1143.
104m. Evans, W. J.; Giarikos, D. G.; Ziller, J. W. *Organometallics* **2001**, *20*, 5751.
104n. Maiwald, S.; Weissenborn, H.; Sommer, C.; Muller, G.; Taube, R. *J. Organomet. Chem.* **2001**, *640*, 1.
105. Okuda, J.; Arndt, S.; Beckerle, K.; Hultzsch, K. C.; Voth, P.; Spaniol, T. P. In *Organometallic Catalysts and Olefin Polymerization*; Blom, R., Ed.; Springer: Berlin, 2001, p 156.
105a. Luo, Y.; Baldamus, J.; Hou, Z. *J. Am. Chem. Soc.* **2004**, *126*, 13910.
105b. Trifonov, A. A.; Fedorova, E. A.; Fukin, G. K.; Bochkarev, M. N. *Eur. J. Inorg. Chem.* **2004**, 4396.
105c. Kirillov, E.; Lehmann, C. W.; Razavi, A.; Carpentier, J.-F. *J. Am. Chem. Soc.* **2004**, *126*, 12240.
105d. Hou, Z.; Zhang, Y.; Nishiura, M.; Wakatsuki, Y. *Organometallics* **2003**, *22*, 129.
105e. Voth, P.; Arndt, S.; Spaniol, T. P.; Okuda, J.; Ackerman, L. J.; Green, M. L. H. *Organometallics* **2003**, *22*, 65.
105f. Tanaka, K.; Furo, M.; Ihara, E.; Yasuda, H. *J. Polym. Sci., Part A: Polym. Chem.* **2001**, *39*, 1382.
105g. Barbier-Baudry, D.; Blacque, O.; Hafid, A.; Nyassi, A.; Sitzmann, H.; Visseaux, M. *Eur. J. Inorg. Chem.* **2000**, 2333.
105h. Bogaert, S.; Carpentier, J.-F.; Chenal, T.; Mortreux, A.; Ricart, G. *Macromol. Chem. Phys.* **2000**, *201*, 1813.
106. Schellenberg, J.; Tomotsu, N. *Prog. Polym. Sci.* **2002**, *27*, 1925.
106a. Zhang, H.; Nomura, K. *J. Am. Chem. Soc.* **2005**, *127*, 9364.
106b. Lopez-Sanchez, J. A.; Lamberti, M.; Pappalardo, D; Pellecchia, C. *Macromolecules* **2003**, *36*, 9260.
106c. Naga, N.; Imanishi, Y. *J. Polym. Sci., Part A: Polym. Chem.* **2003**, *41*, 939.
107. Ban, H. T.; Tsunogae, Y.; Shiono, T. *J. Polym. Sci., Part A: Polym. Chem.* **2005**, *43*, 1188.
108. Bonoldi, L.; Abis, L.; Fiocca, L.; Fusco, R.; Longo, L.; Simone, F.; Spera, S. *J. Mol. Catal. A: Chem.* **2004**, *219*, 47.
108a. Mahanthappa, M. K.; Waymouth, R. M. *J. Am. Chem. Soc.* **2001**, *123*, 12093.
108b. Pellecchia, C.; Grassi, A. *Top. Catal.* **1999**, *7*, 125.
109. Nakayama, Y.; Baba, Y.; Yasuda, H.; Kawakita, K.; Ueyama, N. *Macromolecules* **2003**, *36*, 7953.
109a. Ricci, G.; Morganti, D.; Sommazzi, A.; Santi, R.; Masi, F. *J. Mol. Catal. A: Chem.* **2003**, *204–205*, 287.
109b. Bazzini, C.; Giarrusso, A.; Porri, L. *Macromol. Rapid Commun.* **2002**, *23*, 922.
109c. Ricci, G.; Forni, A.; Boglia, A.; Sommazzi, A.; Masi, F. *J. Organomet. Chem.* **2005**, *690*, 1845–1854.
109d. Ricci, G.; Forni, A.; Boglia, A.; Motta, T.; Zannoni, G.; Canetti, M.; Bertini, F. *Macromolecules* **2005**, *38*, 1064–1070.
109e. Ricci, G.; Forni, A.; Boglia, A.; Motta, T. *J. Mol. Catal. A: Chem.* **2005**, *226*, 235–241.
109f. Thiele, S. K.-H.; Wilson, D. R. *J. Macromol. Sci., Polym. Rev.* **2003**, *C43*, 581–628.
109g. Suzuki, H.; Matsumura, S.; Satoh, Y.; Sogoh, K.; Yasuda, H. *React. Funct. Polym.* **2004**, *59*, 253–266.
109h. Barnes, D. A.; Benedikt, G. M.; Goodall, B. L.; Huang, S. S.; Kalamarides, H. A.; Lenhard, S.; McIntosh, L. H., III; Selvy, K. T.; Shick, R. A.; Rhodes, L. F. *Macromolecules* **2003**, *36*, 2623–2632.
109i. Wilke, G.; Eckerle, A. Cyclooligomerizations and Cyclo-co-oligomerizations of 1,3-dienes. In *Applied Homogeneous Catalysis with Organometallic Compounds*; Cornils, B., Herrmann, W. A., Eds.; VCH, Weinheim, Germany; Vol. 1, 358.

1.06
Metathesis Reactions

J W Herndon, New Mexico State University, Las Cruces, NM, USA

1.06.1 Overview and Historical

This review focuses on the scope, limit, and modes of metathesis reactions. Metathesis reactions became an important tool in synthetic organic chemistry after the introduction of stable carbene complex catalysts. This article focuses on more recent metathesis processes that are initiated by these complexes. Alkene metathesis has served as an extremely valuable method to prepare compounds useful for diverse areas such as polymer chemistry, synthetic organic chemistry, and bioorganic chemistry. The Nobel prize in chemistry for 2005 was awarded to three pioneers in the field of metathesis, J. L. Chauvin, R. H. Grubbs, and R. R. Schrock. This article is not a totally comprehensive listing of all metathesis reactions; however, numerous comprehensive reviews of metathesis reactions have appeared.[1,1a] In addition, comprehensive surveys of transition metal carbene complexes and carbyne complexes, common catalysts for metathesis, are published annually.[2] As many examples as possible have been incorporated into this article; however, many aspects of metathesis are well developed, particularly, ring-closing metathesis, and their use in organic synthesis has become rather routine. The number of examples illustrating these processes is vast,[3] and thus only selected examples of these reactions can be presented. The article first discusses metathesis reactions using alkenes, followed by co-metathesis of alkenes with alkynes, followed by alkyne metathesis.

The general reaction equation for alkene metathesis in a simple system, cross-metathesis of two different disubstituted alkenes, is depicted in Scheme 1. In this reaction, a transition metal catalyst establishes equilibrium between the starting alkenes, the (*E*)- and (*Z*)-stereoisomers of all possible substituent combinations, and ethylene. Related reaction processes have also been reported for alkynes (alkyne metathesis) and for combinations of alkenes and alkynes (enyne metathesis). Alkyne metathesis is less well developed compared to alkene metathesis and enyne metathesis. This review has been organized according to the basic modes of metathesis depicted in Scheme 2. Alkene metathesis is the more developed process and numerous examples of all the variants have been reported. Alkyne metathesis is less well developed and three variants exist: alkyne cross-metathesis, alkyne metathesis polymerization, and ring-closing alkyne metathesis.

At first glance, a reaction producing the diverse array of products depicted in Scheme 1 would appear to be of limited utility; however, many examples of selective and synthetically useful alkene metathesis reactions have been reported. Although the reaction is in theory an equilibrium process, it can become a very useful method in some situations. Circumstances that give rise to selective metathesis reactions include: (i) if one reaction product is significantly more stable than all of the other species, thus driving the reaction to a single product, (ii) if the catalyst is not equally reactive to all of the species in the reaction, and thus the reaction never reaches true equilibrium, or (iii) if one or more of the products can leave the system, and thus shift the equilibrium. All of the synthetically useful metathesis processes exploit one or more of these features in the reaction design. The modes of metathesis depicted in Scheme 2 represent cases where selective reactions have been documented.

The mechanism of alkene metathesis has been well studied. The generally accepted mechanism is depicted in Scheme 3, using the hypothetical dimerization of 1-butene to 3-hexene as an example, and using the undefined

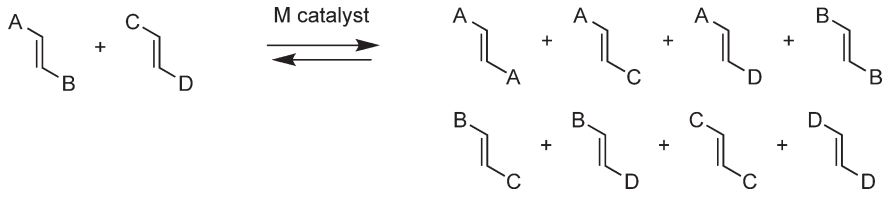

Scheme 1 General equation for alkene metathesis.

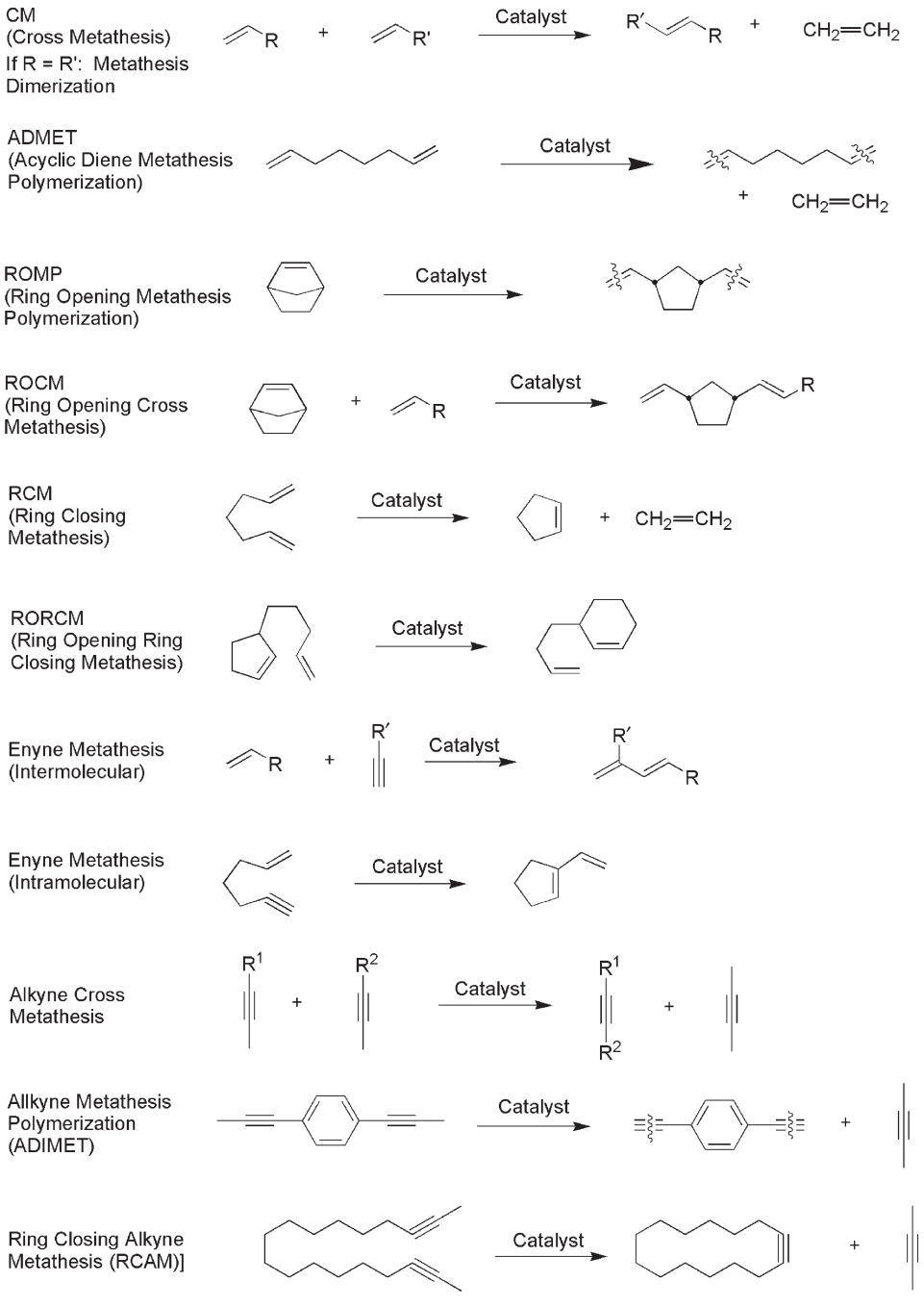

Scheme 2 Common modes of successful metathesis reactions.

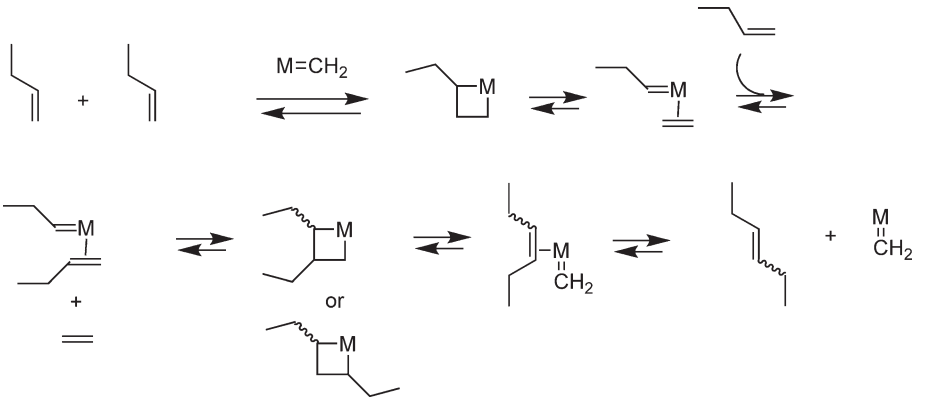

Scheme 3 Detailed mechanism for alkene cross-metathesis.

carbene complex ($M=CH_2$) as the catalyst. The mechanism depicted in Scheme 3 is commonly known as the Chauvin mechanism,[4] and involves a series of reversible [2 + 2]-cycloaddition processes between alkenes and carbene complexes. Although there are numerous reversible steps involved in the mechanism, the reactions are all driven toward the production of the ultimate products ((*E*)- and (*Z*)-3-hexene) by expulsion of the gaseous product ethylene from the system.

A metal carbene complex ($M=CH_2$) is the catalytically active species in the alkene metathesis reaction. The earliest alkene metathesis catalysts were not carbene complexes, but mechanistic proposals suggested that these catalysts would generate carbene complexes during the reaction. These early catalysts almost exclusively involve the combination of a high oxidation state early transition metal complex and a main group organometallic species, most often an organotin, organoaluminum, or organotitanium reagent. A common initiator of metathesis reactions, tetramethyltin and tungsten(VI) oxychloride, can form a metal carbene complex **2** through transmetallation followed by α-hydride elimination (Scheme 4).[5,5a] Most of the newer alkene metathesis catalysts are in fact transition metal carbene complexes. Each of the individual steps of alkene metathesis has been demonstrated using stoichiometric reaction process, and metal carbene complex intermediates or metallacyclobutanes have been detected or isolated from metathesis processes. Some of the seminal experiments establishing the mechanism for alkene metathesis are depicted in Scheme 5. The first example of a metathesis reaction between a carbene complex and an alkene is the coupling of tungsten carbene complex **3** with enol ethers (e.g., **4**) to produce the Fischer carbene complex **5** and 1,1-diphenylethylene **6**.[6] Carbene complex **3** is also the first discreet carbene complex to catalyze alkene metathesis.[7,7a] A related metathesis process occurs between alkylidenetantalum complex **7** (formed via an α-hydride elimination) and carbonyl compounds to afford an olefination product (e.g., **9**) and the metal oxide **10**.[8] Coupling of a carbene complex precursor (**11** or Tebbe's reagent) with norbornene affords metallacyclobutane **12**, which can undergo a metathesis polymerization reaction in the presence of excess norbornene.[9] In addition to experimental studies, there have been numerous theoretical calculations reported for alkene metathesis reactions.[10,10a–10m]

The advent of stable carbene complex catalysts has had a profound effect on the general utility of alkene metathesis. Early metathesis catalysts displayed a low tolerance for functional groups, and successful metathesis reactions were primarily restricted to relatively unfunctionalized substrates. Early demonstrations that discreet carbene complex catalysts could initiate alkene metathesis[7,7a,9,11] inspired the development new transition metal carbene complex catalysts. Some of the more commonly employed alkene metathesis initiators are depicted in

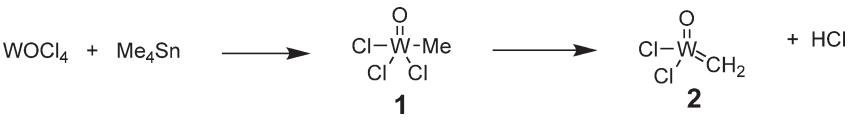

Scheme 4 Hypothetical generation of a carbene complex from a traditional metathesis catalyst system.

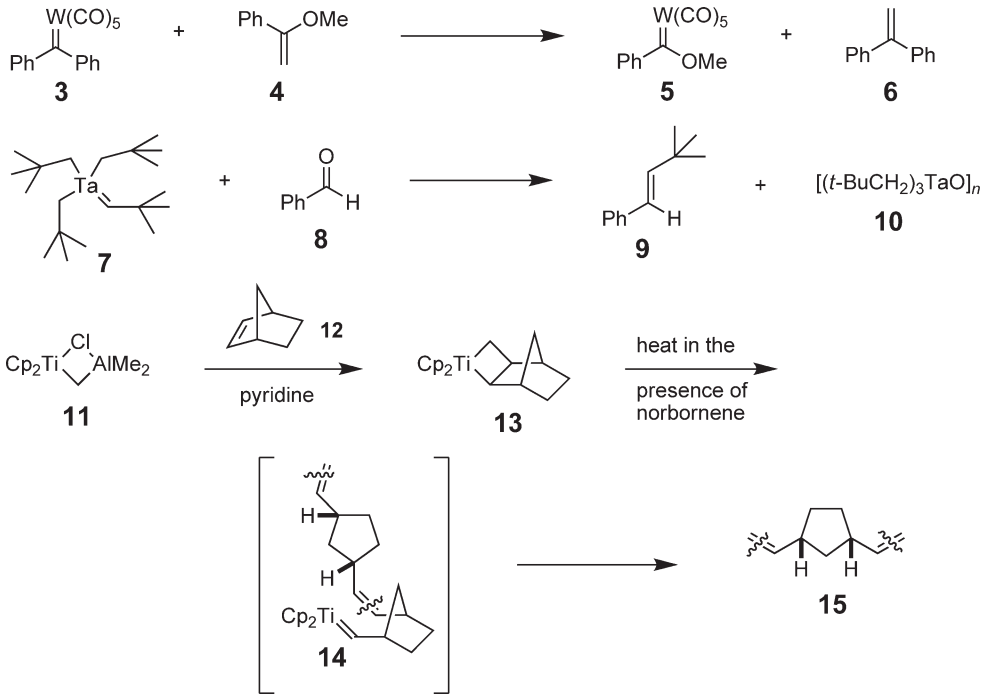

Scheme 5 Early uses of carbene complexes in metathesis-like reactions.

Figure 1. In the early 1990s the molybdenum catalyst **17** (commonly called the Schrock catalyst)[12] was introduced, followed by the ruthenium catalyst **16** (commonly called Grubbs catalyst).[13] The molybdenum catalyst was more reactive but the ruthenium catalyst was easier to handle. Further efforts to develop more reactive and user-friendly catalysts have been quite successful. Noted examples are depicted in Figure 1 and include catalyst **18** (commonly called the second-generation Grubbs catalyst),[14] an unsaturated analog **19**,[15] catalysts that feature a chelating ligand (e.g., **20** and **21**),[16,16a,16b] the *in situ* prepared indenylcarbene complex **22**,[17] the cationic carbene complex **23** featuring a chelating diphosphine ligand,[18] bromopyridine catalyst **24**,[19] and a tethered analog of Grubbs catalyst II **25** that is especially effective for the preparation of cyclic ring-opening metathesis polymerization (ROMP) polymers.[20] In addition to the catalysts depicted, numerous derivatives have been prepared to maximize their performance in aqueous systems (e.g., **26**)[21,21a] and in ionic liquids (e.g., **27**).[22,22a] Numerous polymer-bound analogs of these catalysts (e.g., **28**)[23,23a] have also been developed. Among the ruthenium catalysts, those that feature an *N*-heterocyclic carbene ligand are among the most active. Various chiral and optically pure catalysts that are useful for asymmetric alkene metathesis have also been developed; representative examples have been depicted in Figure 2.[24,24a–24e]

A detailed mechanistic study was undertaken in order to better understand the enhanced level of activity of various ruthenium carbene complex catalysts.[25] The mechanism for the early steps in a metathesis reaction is depicted in Scheme 6. Catalyst **16** undergoes phosphine dissociation nearly twice as fast as catalyst **18**. The enhanced rate of metathesis for catalyst **18** was attributed to the rate of reaction of intermediate **36** with alkenes versus reaction with phosphine to regenerate the starting complex (i.e., the k_2/k_{-1} ratio). Several other factors were observed to increase the rate of phosphine dissociation but did not necessarily lead to better metathesis catalysts. The factors include: (i) replacement of PCy_3 by PPh_3 in catalyst **16**, (ii) replacement of chlorines by iodines, and (iii) presence of a large and electron-donating group at the carbene carbon.[26] A comparison of complexes differing only in the phosphine ligands revealed that more bulky phosphine ligands (i.e., those with larger cone angles) and more electron-donating phosphine ligands result in a more reactive olefin metathesis catalyst.[27] A similar comparison of halide ligands showed that the catalyst reactivity decreases in the order Cl > Br ≫ I. Steric and electronic effects of the halide and phosphine ligands appear to work in opposite directions. Theoretical studies of ligand and substituent effects in ruthenium alkylidenes were also reported.[28]

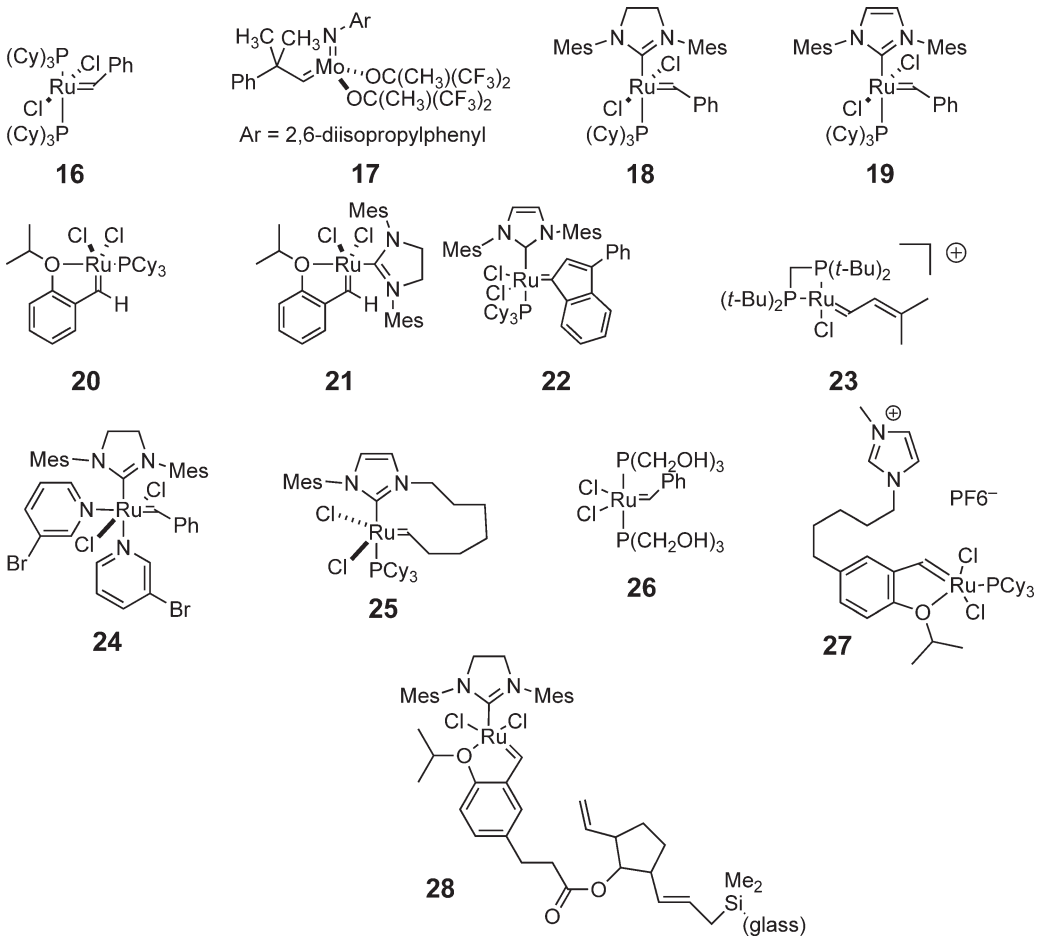

Figure 1 Representative alkene metathesis catalysts.

1.06.2 Cross-Metathesis

The simplest form of metathesis is cross-metathesis, involving the intermolecular reaction of two alkene units in the presence of a metathesis catalyst. Cross-metathesis of two dissimilar monosubstituted alkenes, the most common situation in cross-metathesis, is represented by the general reaction equation in Scheme 7. This reaction can hypothetically lead to ethylene and *E*/*Z* mixtures of three different 1,2-disubstituted alkenes. The desired product is usually the "mixed" product **42**. If the two R groups are identical, a "metathesis dimerization" or "homodimerization" occurs; ethylene and the homodimerization product are the only possible products. Cross-metathesis is an energetically neutral reaction, and is driven to completion by the escape of ethylene from the reaction mixture. If R^1, $R^2 = Me$, ΔH for the reaction is $+2.8\,kJ\,mol^{-1}$, and ΔG is $+4.9\,kJ\,mol^{-1}$.[29]

In the general equation for alkene cross-metathesis depicted in Scheme 7, the major competing process is homodimerization metathesis of the reactant alkenes (i.e., formation of **43** and **44**). The first examples of successful cross-metatheses involved the reaction of one alkene with a large excess of another alkene to circumvent this side-reaction. The reactions depicted in Scheme 8 represent two extreme cases. Throughout this chapter metathesis reactions will not have the catalyst specified; unless otherwise noted all of the metathesis reactions are initiated by one of the carbene complex catalysts in Figure 1. Coupling of **45** and **46** requires a large excess of alkene **45**, while a nearly 1 : 1 ratio of **48** and **49** provides a high yield of cross-metathesis products. As more examples of this reaction began to accumulate, a better understanding of the scope and limitations and general predictability of cross-metathesis reactions developed. An observation of numerous cross-metathesis processes has led to a predictive model for success in cross-metathesis reactions.[30] The essence of this model

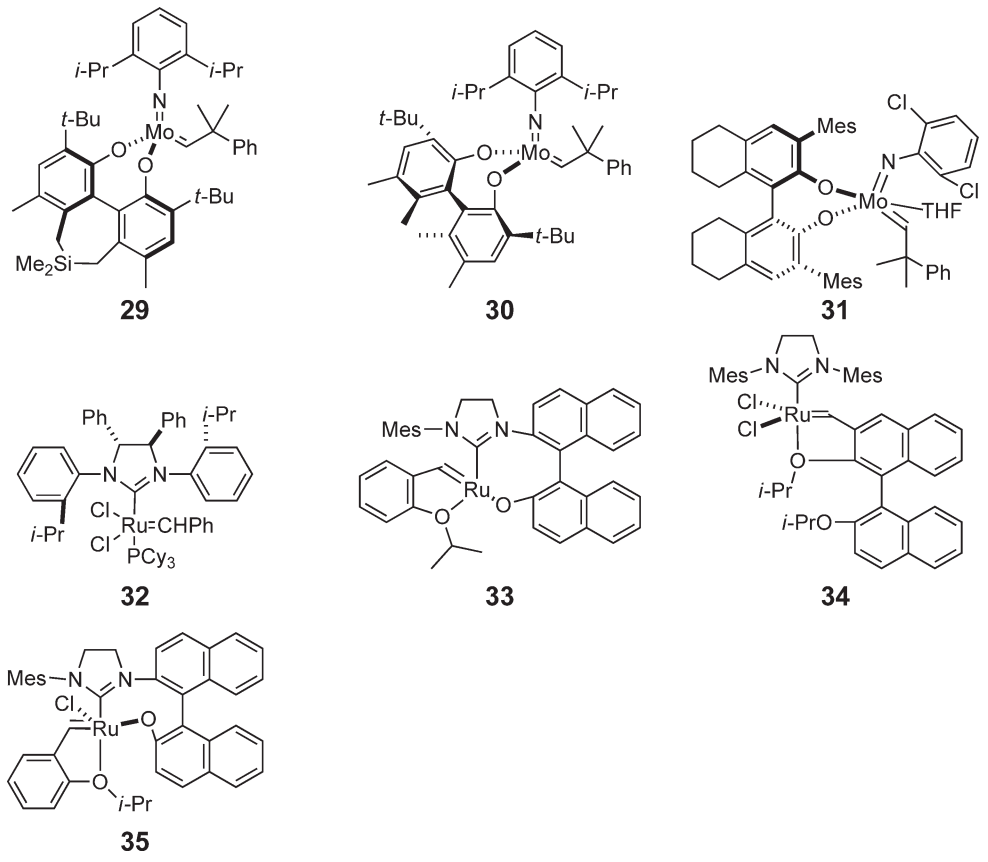

Figure 2 Representative catalysts for asymmetric alkene metathesis.

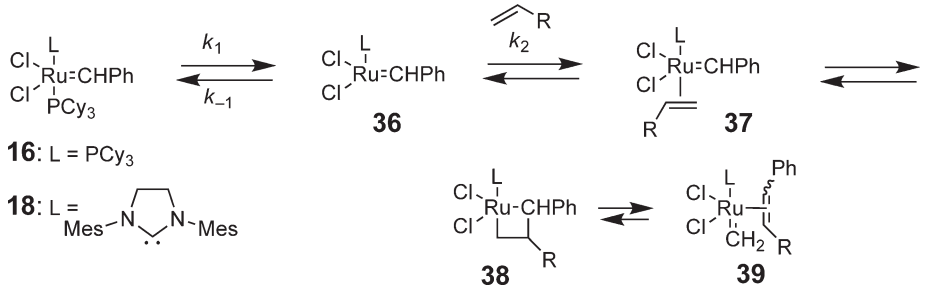

Scheme 6 Mechanism-based comparison of the first- and second-generation Grubbs catalysts.

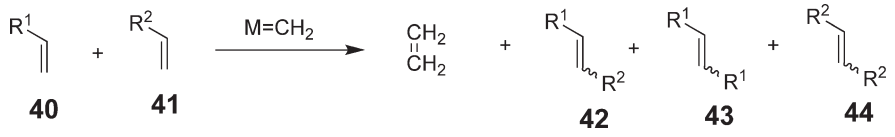

Scheme 7 Hypothetical reaction products from cross-metathesis of dissimilar alkenes.

is that alkenes can be divided into four general types: (i) those that undergo rapid homodimerization, (ii) those that undergo slow homodimerization, (iii) those that do not undergo homodimerization, and (iv) those that do not undergo cross-metathesis. This model predicts that successful cross-metathesis will occur under the following scenarios: (i) the cross-metathesis of two type-one alkenes will require a large excess of one of the partners;

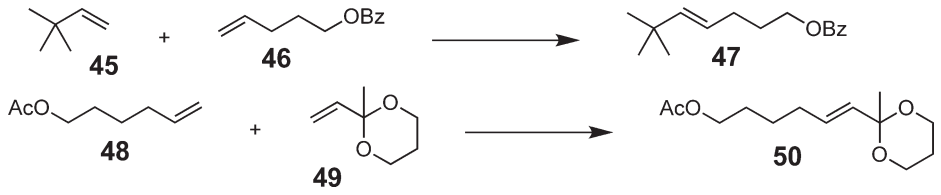

Scheme 8 Extremes of cross-metathesis.

(ii) selective cross-metathesis can be achieved using type-one alkenes with either type-two or type-three alkenes, since the type-one homodimers can engage in secondary cross-metathesis reactions—type-three alkenes became useful only with the advent of more reactive catalysts (e.g., **18**); (iii) selective cross-metathesis can be observed in the coupling of type-two alkenes with type-three alkenes. The various types of alkenes can be summarized as: type-one—monosubstituted alkenes that are not hindered or do not contain strongly electron-withdrawing groups; type-two—hindered monosubstituted alkenes or unhindered electron-deficient alkenes; type-three—1,1-disubstituted alkenes, unhindered trisubstituted alkenes, vinyl sulfones, and vinyl phosphonates; and type-four—vinyl nitro compounds and sterically hindered alkenes. Cross-metathesis typically affords mixtures of (*E*)- and (*Z*)-alkenes. In general, the highest selectivity for (*E*)-alkenes is observed with the most reactive metathesis catalysts. This has been attributed to secondary metathesis of the product alkenes and the greater reactivity of metathesis catalysts with (*Z*)-alkenes.[31] Representative examples of successful cross-metathesis and metathesis homodimerization are depicted in Scheme 9 and include the following alkene combinations: (i) alkenes **52** and **53** for total synthesis of zaragozic acid C;[32] (ii) two complex alkenes **55** and **56** for amphidinolide T1 total synthesis;[33] (iii) various alkenes (e.g., **58**) and vinylphosphine oxides (e.g., **59**), and metathesis dimerization of vinylphosphine oxides;[34] (iv) metathesis dimerization of various allyl–Cp titanium complexes (e.g., **61**);[35] (v) vinylboronates (e.g., **64**) and monosubstituted alkenes featuring a high degree of oxygenation (e.g., **63**);[36] (vi) simple alkenes (e.g., **66**) and ···,δ-unsaturated Fischer carbene complexes (e.g., **67**);[37,37a] (vii) homodimerization of ethyl oleate **69** using a traditional catalyst system;[38] (viii) dimerization of *O*-allyl carbohydrate derivatives (e.g., **71**);[39] and (ix) chemoselective cross-metathesis involving acrolein **74** and diene **73**, which features two monosubstituted alkene units.[40]

In addition to cross-metathesis for making small molecules, the cross-metathesis of 1,*n*-dienes can lead to polymeric materials (Scheme 10). This process is known as acyclic diene metathesis polymerization, or ADMET polymerization. In theory, ADMET polymerization is competitive with ring-closing metathesis (RCM), and most of the successful examples of ADMET involve the use of dienes where the RCM process would produce an unfavorable ring size. Some examples of ADMET polymerization are depicted in Scheme 10, and include: (i) amino acid-containing dienes (e.g., **75**),[41] (ii) boronate-linked dienes **77**,[42] (iii) 1,4-divinyl-2,5-bis(heptyloxy)-benzene **79**,[43] and (iv) phosphazine-containing dienes (e.g., **81**).[44]

1.06.3 Ring-Opening Metathesis

The general equations for ring-opening metathesis (ROM) are depicted in Scheme 11. Ring-opening metathesis can be divided into two general reaction processes, co-metathesis with an acyclic alkene or ring-opening metathesis polymerization (ROMP). The overall process is thermodynamically favorable if there is relief of ring strain during the metathesis (ROCM) process, and thus most of the examples of successful ROM reactions involve the opening of strained ring systems. The co-metathesis of ethylene and norbornene is quite exothermic ($\Delta H = -70.5\,\mathrm{kJ\,mol^{-1}}$, $\Delta G = -32.1\,\mathrm{kJ\,mol^{-1}}$).[29] By far, most of the reported examples of ROM involve a norbornene ring.

The most mature aspect of ROM is ROMP. Especially active in this reaction are norbornene and oxanorbornene derivatives. Reactions provide "living" polymers, which can be reacted with other metathesizable alkenes or can be terminated through reaction with aldehydes (using the Schrock catalyst) or enol ethers (using the Grubbs catalyst). The reaction is highly tolerant of functional groups, and has frequently been utilized for the immobilization of organic reagents.[45,45a] Representative substrates that have been subjected to ROMP are depicted in Figure 3 and include: (i) acid chloride-substituted norbornenes (e.g., **87**) for preparation of a solid-phase nucleophile scavenger,[46] (ii) (tris)norbornene monomers (e.g., **88**) for synthesis of STAR co-polymers,[47] (iii) norbornenes containing a palladium-ligated system (e.g., **89**),[48] (iv) dinorbornenes (e.g., **90**) for the cross-linking of ROMP polymers,[49]

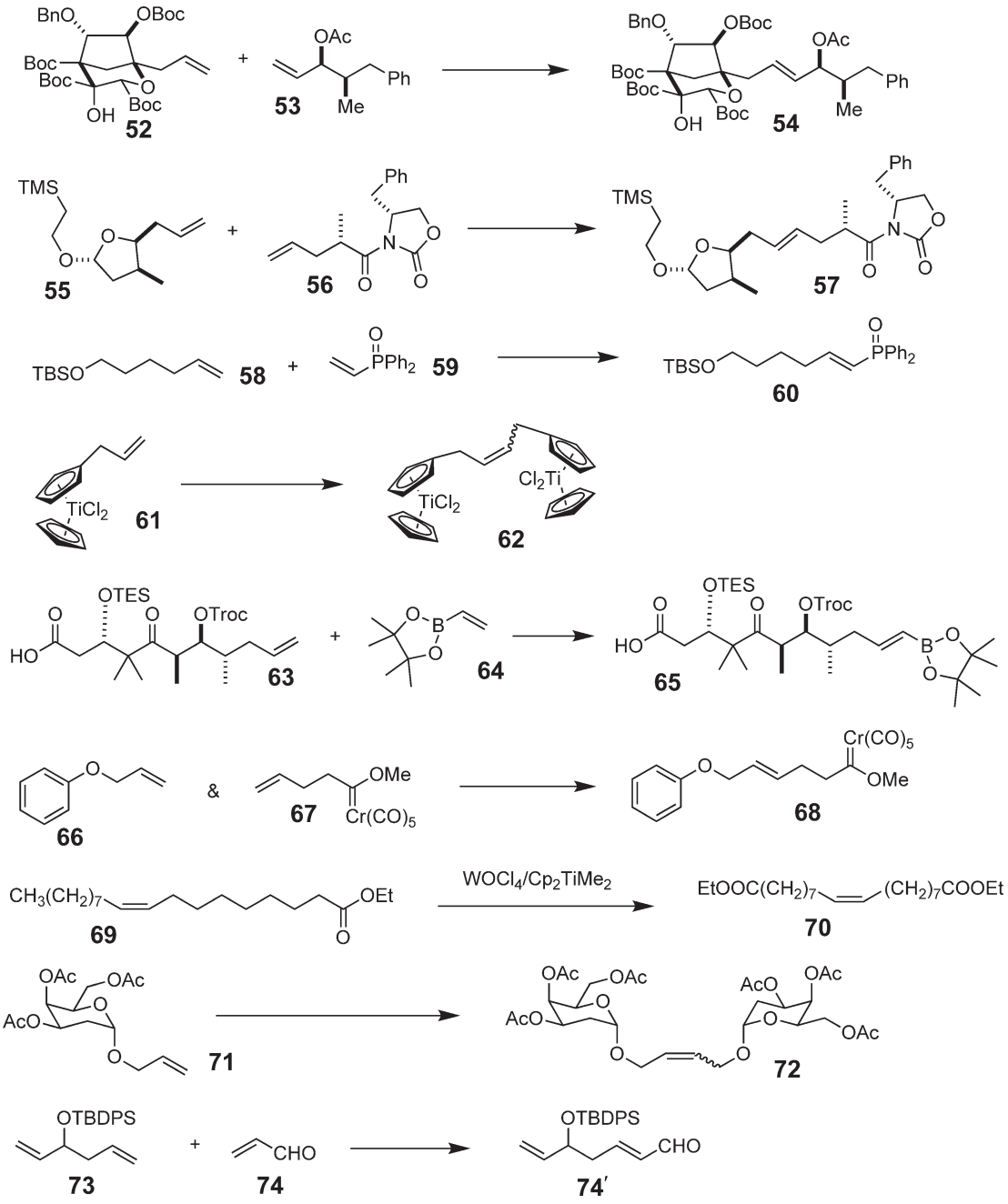

Scheme 9 Reprentative examples of cross-metathesis and metathesis homodimerization.

(v) norbornene derivatives featuring a thymidine ring associated with a 1,6-diamidopyridine derivative **91**,[50] (vi) norbornene derivatives containing chelating pyridine ligands (e.g., **92**),[51] and (vii) norbornenes linked to complex arenes (e.g., **93**), which afford liquid crystalline polynorbornenes.[52] In many cases, the random thermodynamic nature of metathesis reactions has been instrumental in the combinatorial design of biologically relevant molecules. Examples include the ROMP of various carbohydrate-linked norbornene derivatives (e.g., **94**) for the design of single multivalent biological receptors.[53,53a] Other ring systems that have been subjected to ROMP reactions include cyclobutenes (e.g., **95** and **96**),[54,54a] benzvalene **97**,[55] cyclooctatetraene,[56] eight-membered ring alkenes (e.g., **98**),[57] and cyclopentenes.[58,58a]

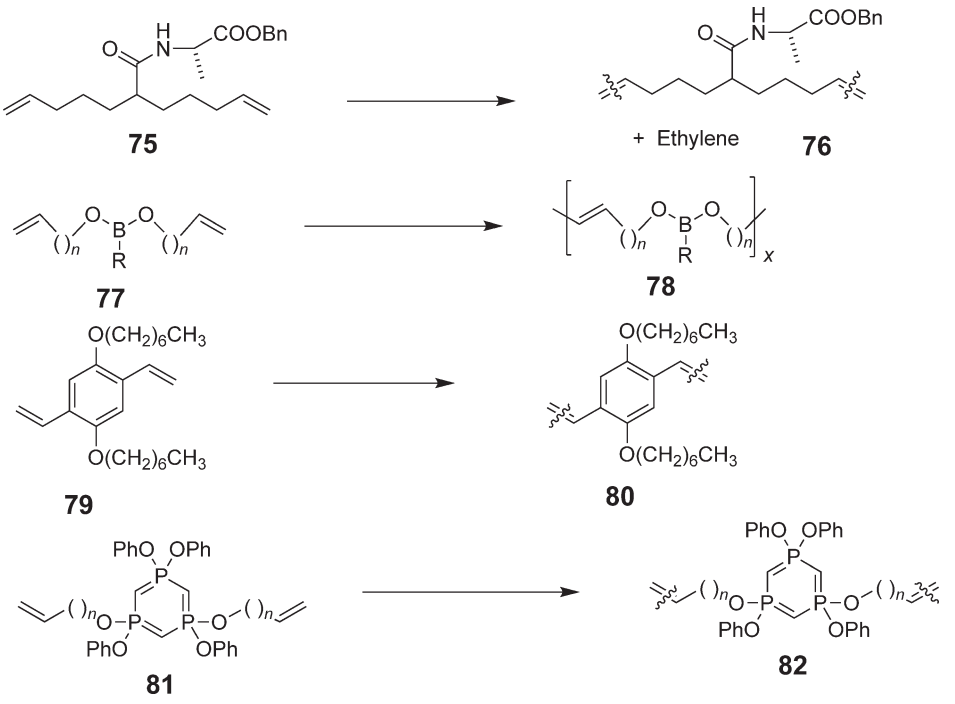

Scheme 10 Representative examples of acyclic diene metathesis (ADMET) polymerization.

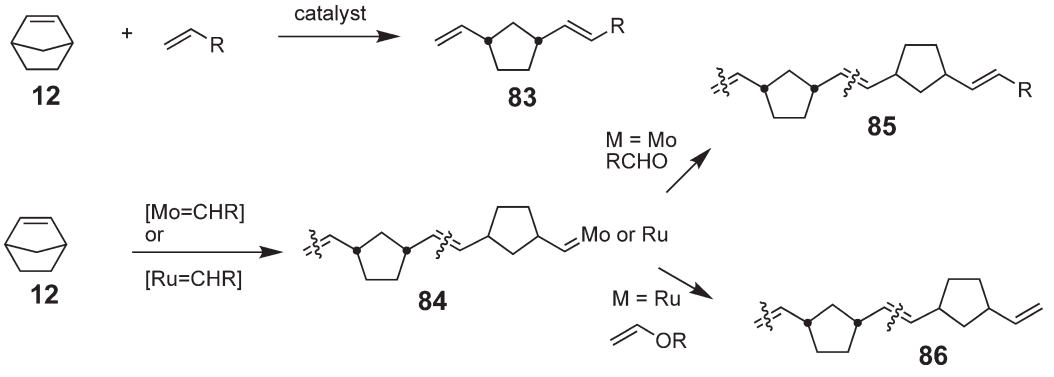

Scheme 11 General mechanistic equation for ring-opening metathesis polymerization (ROMP).

In addition to ROMP, ROM has proved to be very useful in the formation of non-polymeric materials through co-metathesis of a strained alkene and an acyclic alkene (ring-opening cross-metathesis or ROCM). Representative examples of ROCM are depicted in Scheme 12. A very high degree of regioselectivity favoring the more hindered isomer was observed in the ROCM of oxanorbornene **99** and various heteroatom-substituted alkenes (e.g., vinyl acetate).[59] Co-metathesis of cyclopropenone ketal **103** and a monosubstituted alkene **104** was a critical step in a short total synthesis of bistramide A.[60] A stereodivergent synthesis of all 15 F_2 isoprostanes was developed utilizing of bicyclo[3.2.0]heptane ring systems (e.g., **106**) as the key step.[61] Asymmetric ROCM was reported for *meso*-norbornene derivates (e.g., **109**) and allylboranes (e.g., **110**), using a chiral and optically pure molybdenum carbene complexes (e.g., **111**) as catalysts.[62] A high degree of enantioselectivity was observed in the co-metathesis of oxabicyclo[3.2.1]octane derivative **113** in the presence of chiral ruthenium carbene complex **33**.[63] A ring expansion was observed in the ROCM of oxanorbornene **115** and butadiene.[64] This process likely occurs through an ROCM to afford **116** followed by RCM.

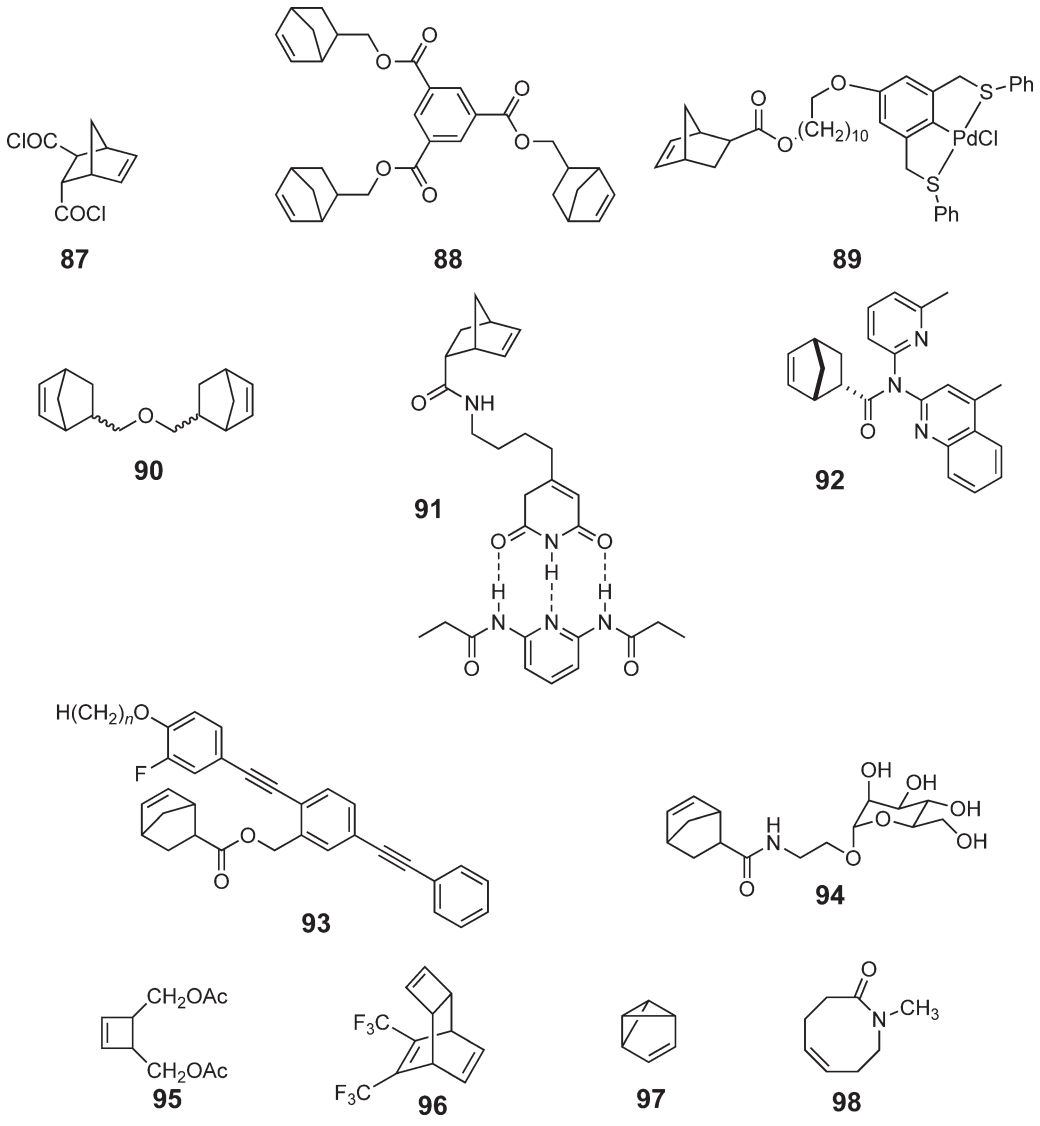

Figure 3 Representative substrates for the ROMP reaction.

1.06.4 Ring-Closing Metathesis

The general equation and mechanism for RCM is depicted in Scheme 13. The feasibility of this reaction is due to a combination of thermodynamic and kinetic factors. Ethylene can escape from the system to drive the reaction to completion. The conversion of 1,6-heptadiene into cyclopentene and ethylene is slightly endothermic ($\Delta H = +10.4\,\text{mol}^{-1}$); however, the reaction is favorable when entropy is considered ($\Delta G = -26.5\,\text{kJ mol}^{-1}$).[29] Most of the successful examples involve the intramolecular coupling of two monosubstituted alkene units, and the reaction proceeds with evolution of ethylene; however, there are numerous successful RCM reactions that involve the formation of non-gaseous alkene byproducts. Recent advances in catalyst design have enabled the use of more highly substituted alkenes in the RCM reaction. The reaction also affords a product that is more highly substituted than either of the reactant alkenes, which is thus less reactive to the metathesis catalysts than either of the starting alkenes. The reaction is nearly universally successful in the formation of five- through seven-membered rings from bis(monosubstituted alkene) precursors. The reaction is less reliable for the formation of eight- and larger membered ring systems, although there are numerous examples where this process is successful. A general trend is that successful medium ring formation requires favorable conformational factors to promote the ring closure.

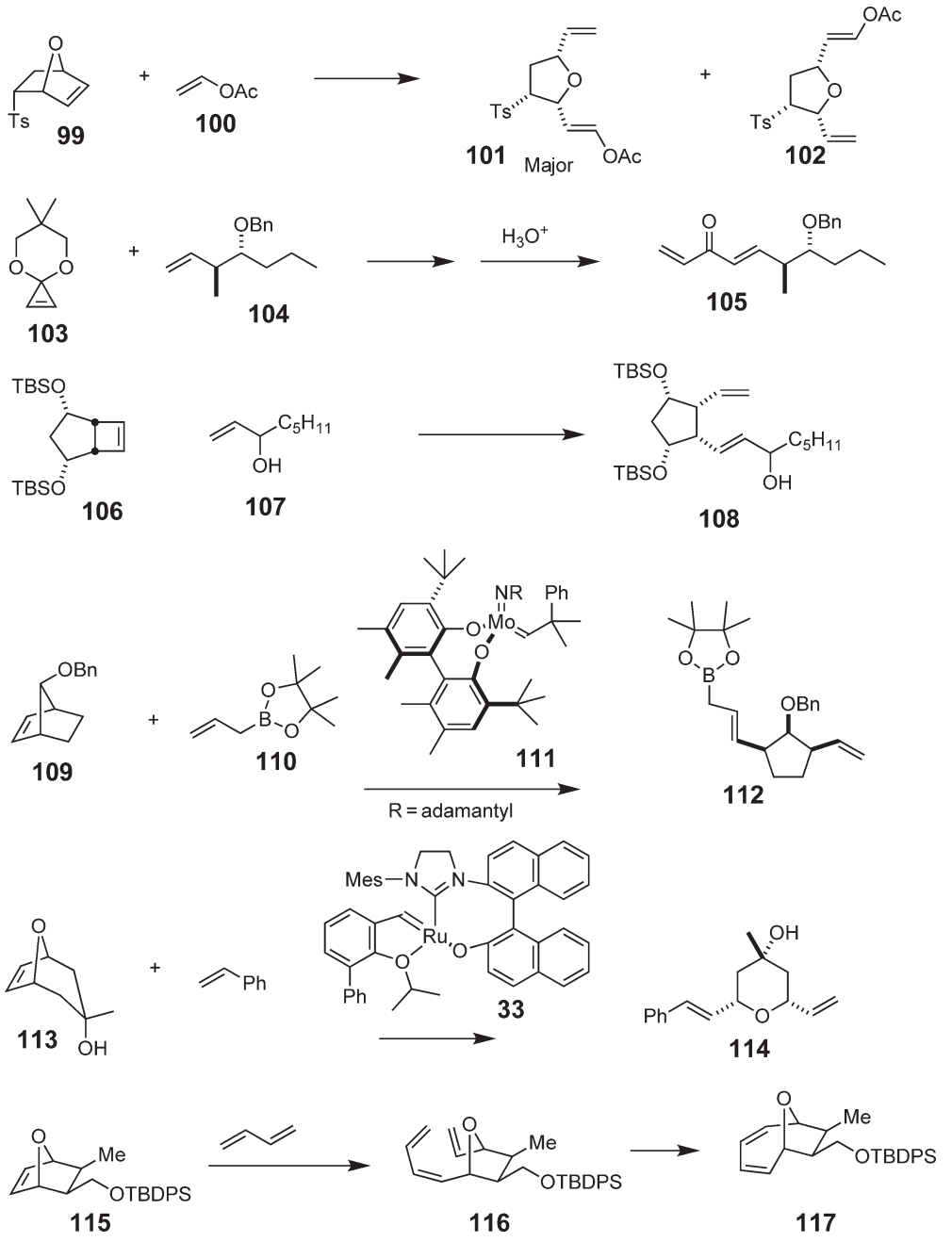

Scheme 12 Representative examples of ring-opening cross-metathesis (ROCM).

Macrocyclic rings are often formed efficiently under high dilution conditions; however, intermolecular metathesis processes (i.e., homodimerization and ADMET polymerization) are often competing processes.

The RCM reaction is remarkably reliable and functional group tolerant. Nearly every functional group known has been tested for its compatibility with the ruthenium-catalyzed RCM reaction. Some representative compounds prepared using RCM reactions are depicted in Figure 4, and include: (i) the five-membered ring system of triquinane derivatives (e.g., **118**),[65] (ii) the strained compound featuring an "inside-out" ring **119** present in ingenol,[66] (iii) six–nine-membered ring oxygen heterocycles (e.g., **120**) for total synthesis of ciguatoxin/brevitoxin and related compounds,[67] (iv) highly functionalized cyclopentenols (e.g., **121**) for total synthesis of pentenomycin,[68]

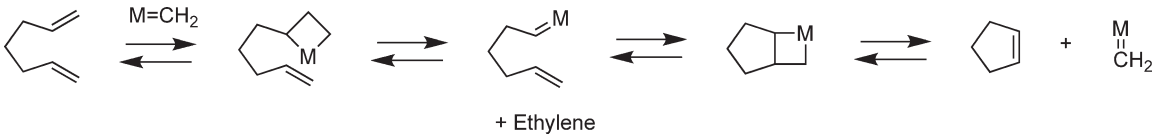

Scheme 13 General mechanistic equation for ring-closing metathesis (RCM).

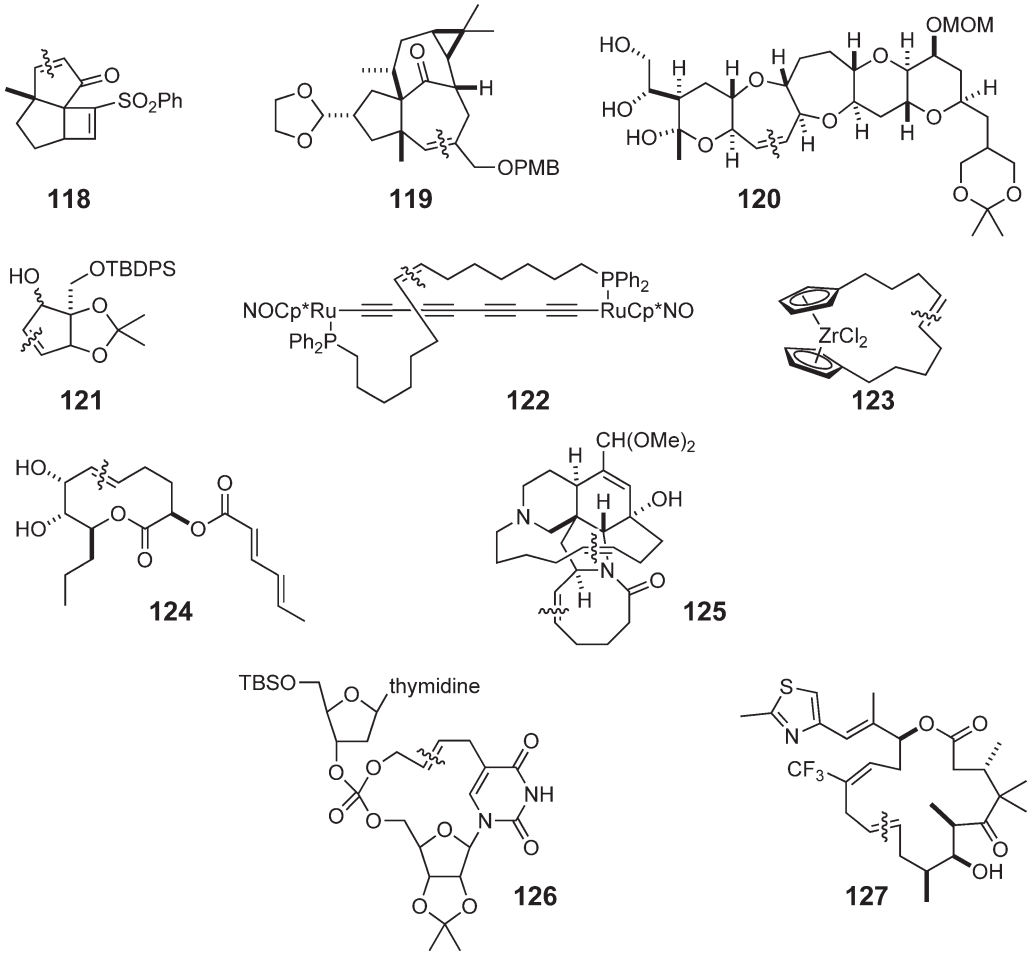

Figure 4 Representative products of the RCM reaction (newly formed bond in parentheses).

(v) metallacyclic sterically shielded all carbon-bridged dirhenium complexes (e.g., **122**),[69] (vi) bridging zirconacene derivatives (e.g., **123**),[70] (vii) a 10-membered ring lactone (e.g., **124**) for total synthesis of ascidiatrienolide A,[71] (viii) an eight-membered ring cyclic lactam and a macrocyclic amine (e.g., **125**) in two separate RCM reactions for the total synthesis of manzamine A,[72] (ix) a nucleoside that features a tether between a phosphate ester and the amine base (e.g., **126**),[73] and (x) macrocyclic compounds (e.g., **127**) for the total synthesis of epothilone derivatives.[74]

Numerous examples of the RCM reaction have been demonstrated for substrates that contain three or more alkene groups. Examination of these substrates reveals several interesting features that allow for their reliable use in the synthesis of complex molecules. General trends noted are as follows: (i) less substituted alkenes are more likely to participate in metathesis reactions and (ii) RCM reactions that lead to five- or six-membered rings are generally more favorable than other ring sizes. Numerous substrates that feature diastereotopic alkenyl groups undergo the RCM reaction with a moderate to high degree of diastereoselectivity; some representative examples of diastereoselective metathesis are depicted in Scheme 14, and include: (i) diastereoselective RCM with the *cis*-vinyl group of

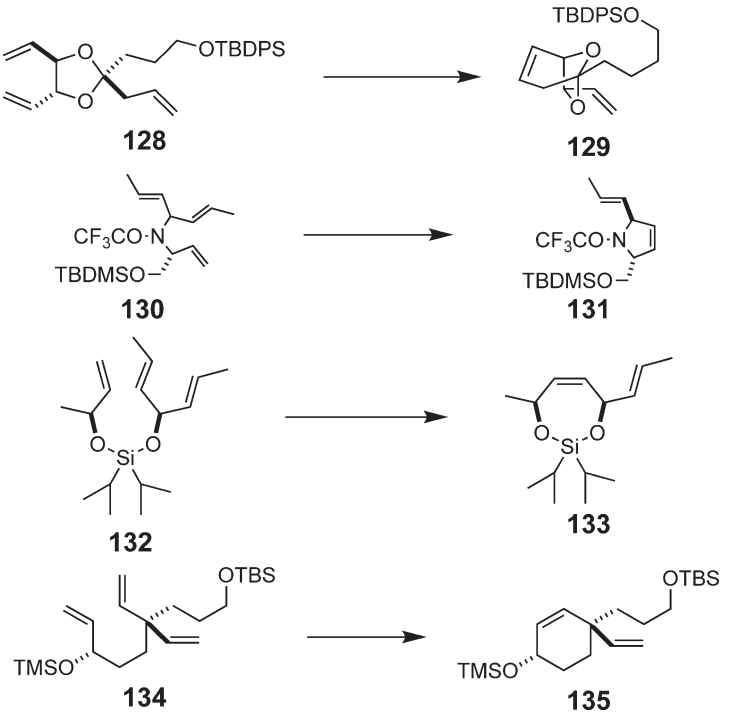

Scheme 14 Representative diastereoselective RCM reactions.

C_2-symmetric alcohol-derived ketal **128**,[75] (ii) stereoselective synthesis of dihydropyrroles through diastereoselective metathesis on the substrate **131**, featuring diastereotopic propenyl groups (e.g., **132**),[76] (iii) diastereoselective synthesis of cyclic siloxanes (e.g., **133**) from precursors containing diastereotopic propenyl groups,[77] and (iv) moderately diastereoselective formation of six-membered rings (e.g., **135**) from triene derivatives that contain diastereotopic vinyl groups (e.g., **134**).[78] Numerous substrates that feature three or more unhindered alkene groups undergo the RCM reaction with a high degree of selectivity for formation of a specific ring system. Selected examples are depicted in Scheme 15 and include: (i) a preference for cyclizing one alkene connected to the phosphorus via a carbon and one connected via an oxygen in the RCM reaction alkene-containing phosphonates (e.g., **136**),[79] (ii) synthesis of chelating phosphine–metal complexes (e.g., **140**) from RCM of bis(remote alkenyl)phosphine complexes (e.g., **139**) instead of the complexes featuring cyclic phosphine ligands (e.g., **141**),[80] and (iii) formation of bicyclic δ-lactams (e.g., **143**) in competition with formation of *N*-cyclopentenyl–γ-lactams (e.g., **144**) in RCM of acyclic amide–tetraene derivatives (e.g., **142**).[81] In one example, the use of relative reactivity of different alkene substitution patterns allows for the preparation of a macrocycle **146** over a five-membered ring.[82,82a] A "metathesis relay" system (Scheme 16) has been demonstrated for the activation of a sluggish system through the placement of a reactive alkene in a favorable proximity to a less reactive alkene.[83] In the RCM reaction in Scheme 16, an initial RCM generates methylcyclopentene **151** and carbene complex **150**, which then undergoes a second intramolecular metathesis to form the cyclic oxane **152**. Several examples depict selective cyclization at the less substituted end of the conjugated diene system. For example, formation of macrocyclic esters (e.g., **154** Scheme 17) via RCM of a conjugated diene (e.g., **153**) occurs efficiently without formation of the smaller ring compound **155**.[84] One example, RCM of tetraene **156**, involves a selective reaction in the internal alkenes, presumably as a result of ring size thermodynamics—this process occurs with excision of 1,3-butadiene.[85] The product distribution in this reaction can be controlled by the catalyst.

Although numerous examples of successful RCM reactions have been demonstrated, a few limitations and/or side-reactions have been uncovered. Some cases where the RCM reaction proceeds with complications are depicted in Scheme 18. Sometimes RCM reactions are competitive with alkene isomerization. For example, the unexpected formation of **162** from precursor **160** was attributed to alkene isomerization (affording **161**), followed by RCM to afford the ring-contracted compound **162**.[86] Later investigators went on to exploit this observation for the synthesis of cyclic enol ethers.[87,87a] Treatment of the allyl ether **164** with a ruthenium carbene complex catalyst affords the RCM

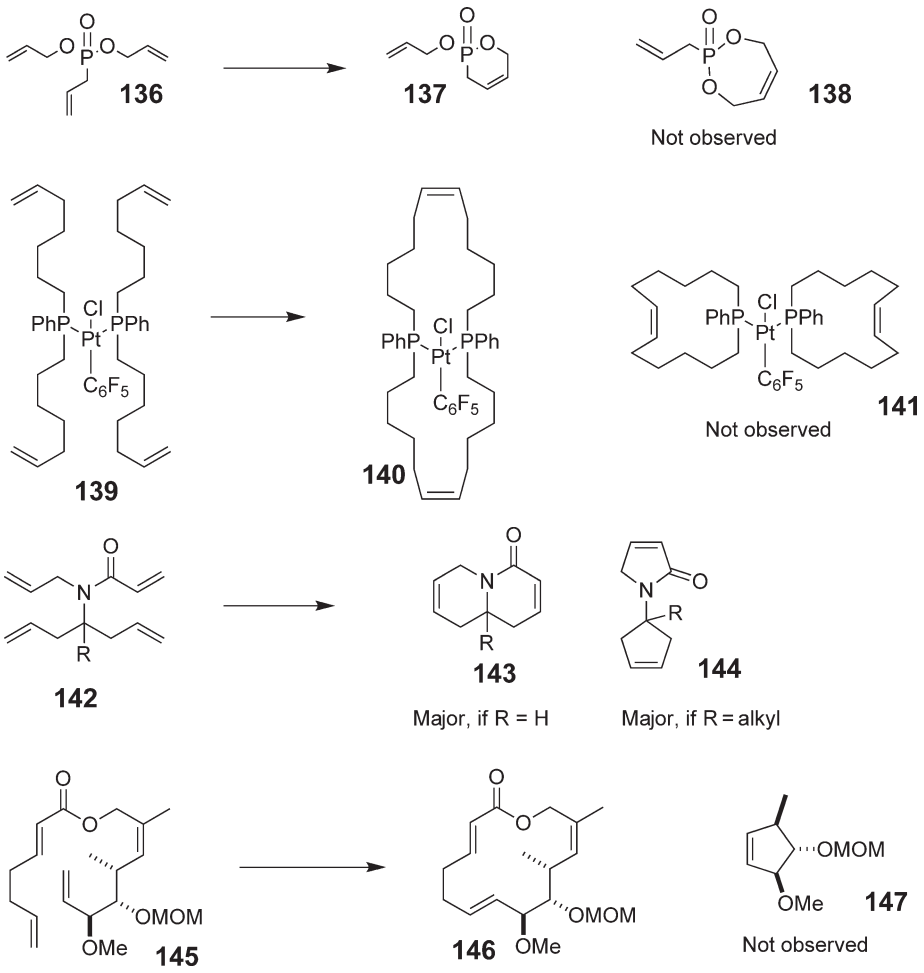

Scheme 15 Reprentative selective RCM reactions using polyene precursors.

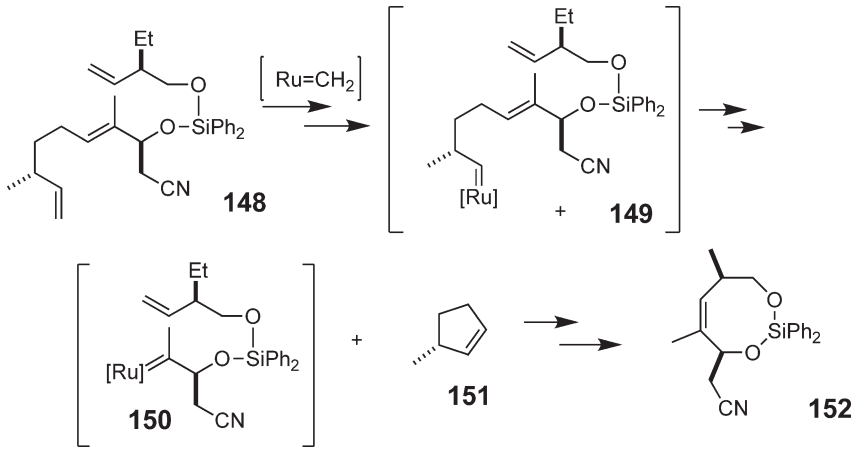

Scheme 16 Olefin metathesis using a relay system.

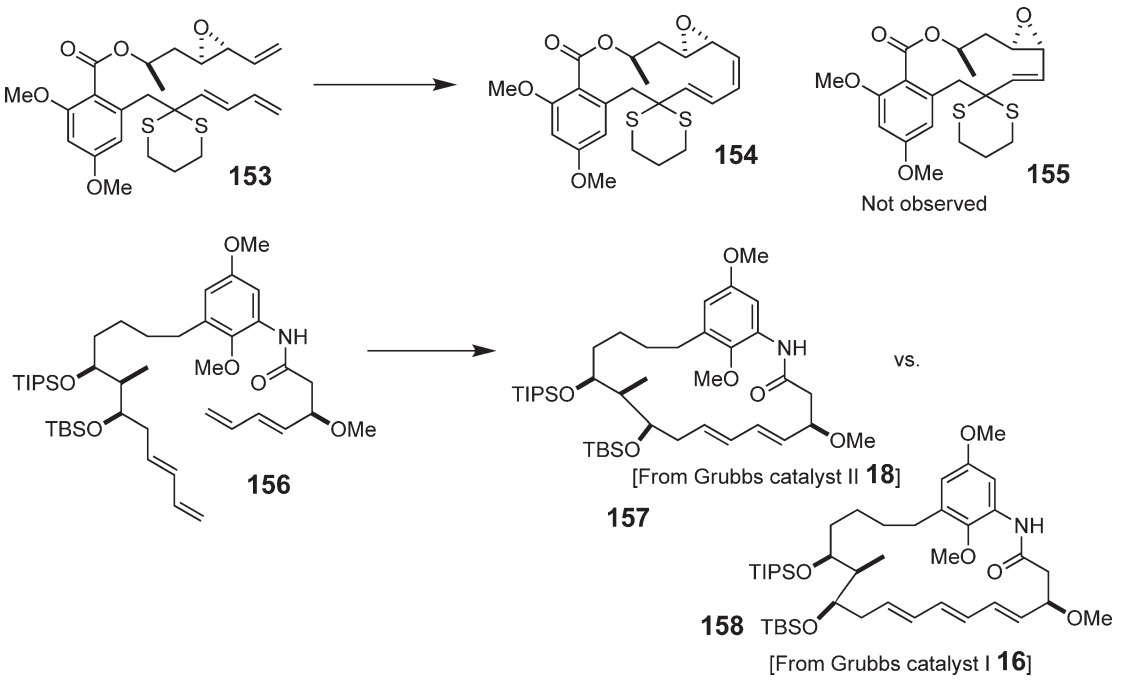

Scheme 17 Representative ring size selective RCM reactions using conjugated diene precursors.

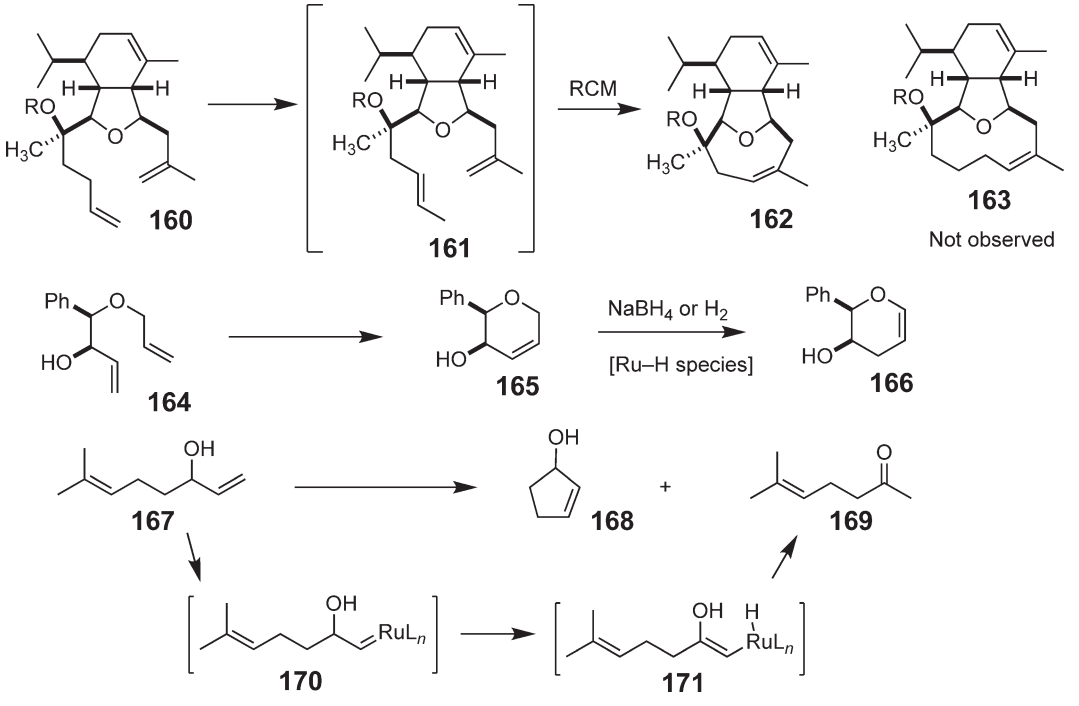

Scheme 18 Representative side-reactions occurring in competition with RCM.

product **165**. This side-reaction has been attributed to the formation of metal hydrides, and the process can be suppressed through the addition of metal hydride scavengers (e.g., benzoquinone).[88] Treatment of the crude reaction mixtures with hydrogen or sodium borohydride *in situ* converts the metathesis catalyst into an alkene isomerization catalyst, and the enol ether **166** is obtained from the reaction.[89] This modified catalyst can also function as a

hydrogenation catalyst. Attempted RCM of certain allylic alcohols (e.g., **167**) led to the methyl ketone (e.g., **169**) and the expected RCM product **168**[90,90a] Reaction of other secondary allylic alcohols that lack the second alkene with Grubbs catalysts led to primarily the methyl ketone analogous to **169**. A tertiary allylic alcohol analog of **167** (linalool) underwent the RCM reaction efficiently. Formation of the methyl ketone is a stoichiometric process. The pathway in Scheme 18, involving isomerization of carbene intermediate **170** to the enol **171**, was proposed for the formation of **169**.

Asymmetric RCM has been demonstrated using chiral molybdenum and tungsten carbene complex catalysts,[24,24a–24e] and more recently some degrees of success have been demonstrated using chiral ruthenium carbene complexes.[91,91a–91c] Some examples of asymmetric RCM are depicted in Scheme 19. Both asymmetric RCM using precursors that contain diastereotopic alkenes (e.g., **172** and **175**)[92,92a] as well as kinetic resolutions of racemic dienes (i.e., **178**)[93] have been demonstrated. Remarkable degrees of enantioselectivity have been demonstrated in many of these systems. The origins of stereoselectivity in ruthenium-catalyzed asymmetric alkene metathesis have also been studied theoretically, and were attributed to the chiral folding of the *N*-bonded aromatic groups of the *N*-heterocyclic carbene ligand.[94]

Tandem CM-RCM (see Scheme 20) can be employed for the synthesis of complex ring systems from simple starting materials. A very noteworthy example of this reaction serves as the cornerstone for the total synthethis of the natural product cyclindrocyclophane.[95,95a] The CM-RCM reaction of diene **182** was completely selective for formation of the head-to-tail isomer **183**. The selectivity was attributed to thermodynamic control; the head-to-head dimer **184** is considerably less stable. In an effort to synthesize pyrenophorin derivatives, the formation of cyclic dimers (e.g., **186**) and trimers (e.g., **187**) from treatment of acrylate ester–alkene derivatives (e.g., **185**) with various ruthenium metathesis catalysts was examined.[96,96a] The product distribution was very time and concentration dependent; higher concentrations favor the trimer over the dimer.

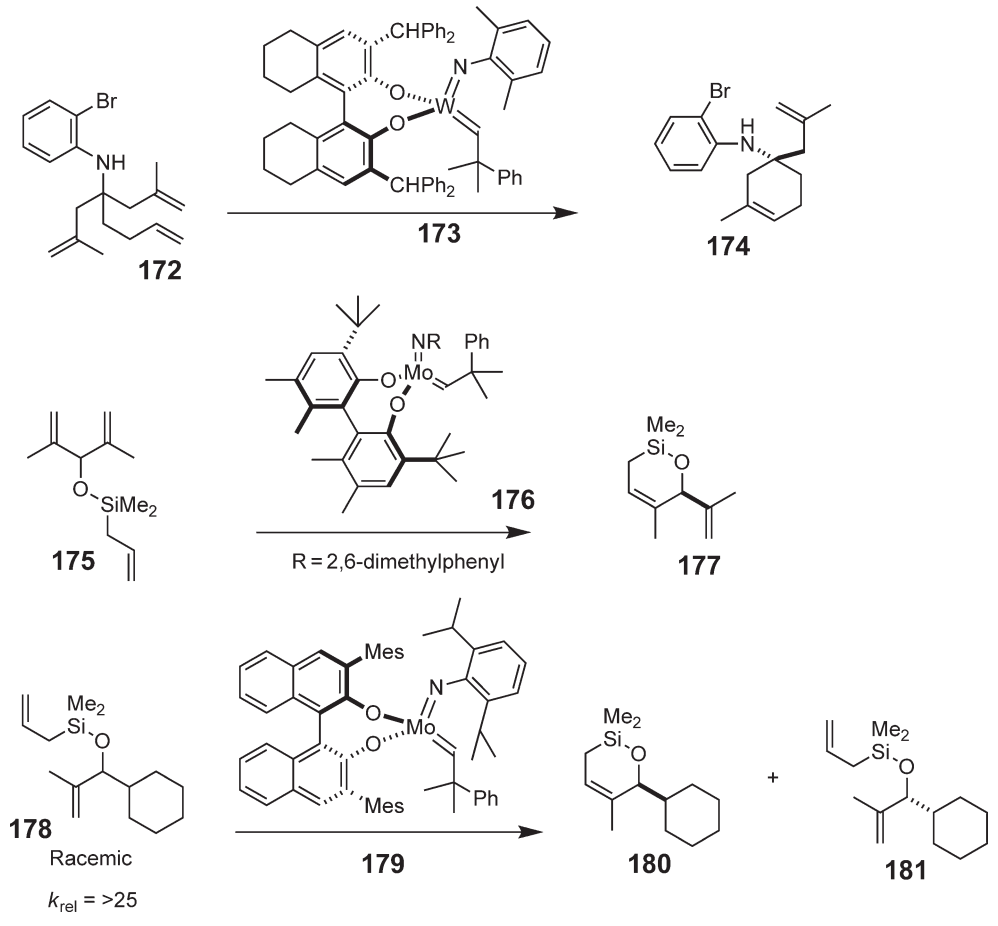

Scheme 19 Representative examples of enantioselective RCM.

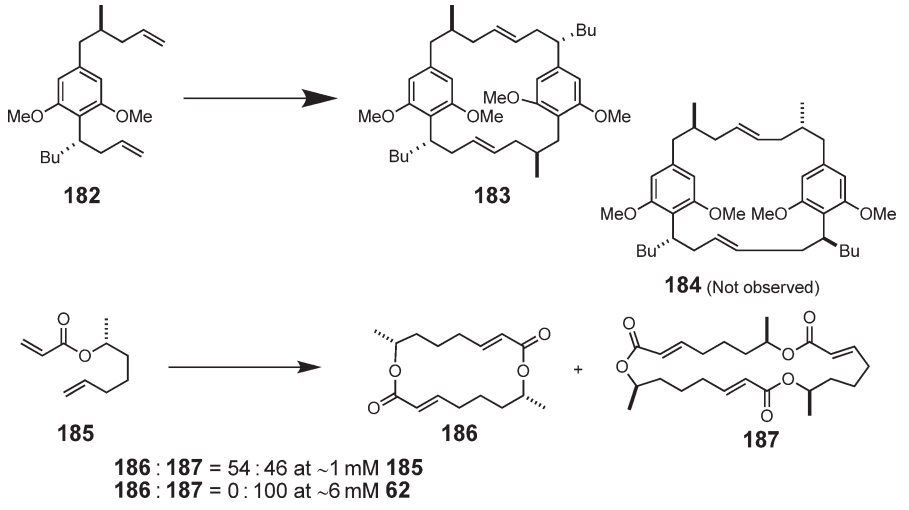

Scheme 20 Representative examples of tandem CM-RCM.

When one of the alkene partners of an RCM reaction is already cyclic, a metathesis isomerization or tandem ring opening–ring closing metathesis (RO-RCM) or ring-rearrangement metathesis (RRM) can occur if the new ring is more stable than the original ring system. Examples of this process are depicted in Scheme 21 and include: (i) the conversion of oxygenated dihydropyrrole derivative **188** into the six-membered ring compound **189**,[97] (ii) conversion

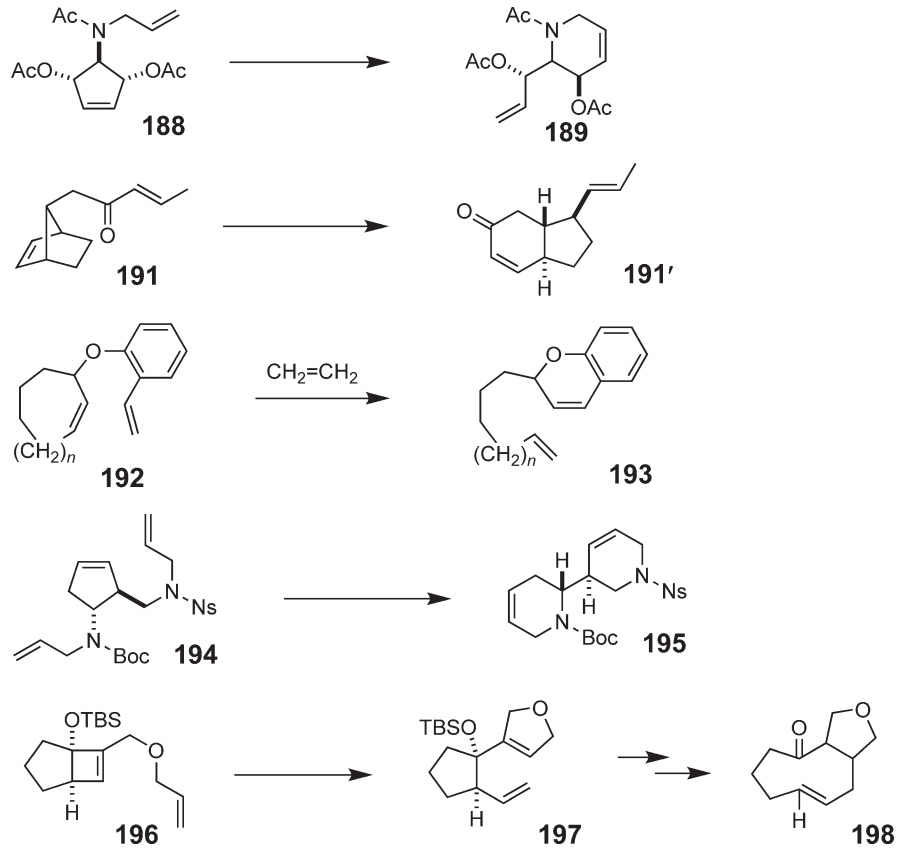

Scheme 21 Representative examples of ring-rearrangement metathesis (RRM).

of norbornene derivative **191** into the *trans*-hydrindane derivative **191′**,[98] (iii) isomerization of styryl allyl ethers (e.g., **192**) to the analogous benzene-fused oxygen hetereocycles (e.g., **193**),[99] (iv) conversion of monocyclic triene derivative **194** into the bicyclic ring-expanded product **195** in a tandem process involving one ROM and two RCMs,[100]and (v) RRM of allyloxymethylcyclobutenes (e.g., **196**) followed by oxy-Cope rearrangement as a general method for medium-sized ring synthesis.[101]

1.06.5 Enyne Metathesis

Treatment of an alkyne/alkene mixture with ruthenium carbene complexes results in the formation of diene derivatives without the evolution of byproducts; this process is known as enyne cross-metathesis (Scheme 22). An intramolecular version of this reaction has also been demonstrated, sometimes referred to as enyne RCM. The yield of this reaction is frequently higher when ethylene is added to the reaction mixture. The preferred regiochemistry is opposite for enyne cross-metathesis and enyne RCM. The complex mechanistic pathways of Scheme 22 have been employed to account for the observed products of the enyne RCM reaction. Several experiments have shown that initial reaction is at the alkene and not the alkyne.[102] The regiochemistry of enyne RCM can be attributed to the inability to form highly strained intermediate **B** from intermediate carbene complex **A** in the "alkene-first" mechanism. Enyne metathesis is a thermodynamically favorable process, and thus is not a subject to the equilibrium constraints facing alkene cross-metathesis and RCM. In a simple bond energy analysis, the π-bond of an alkyne is

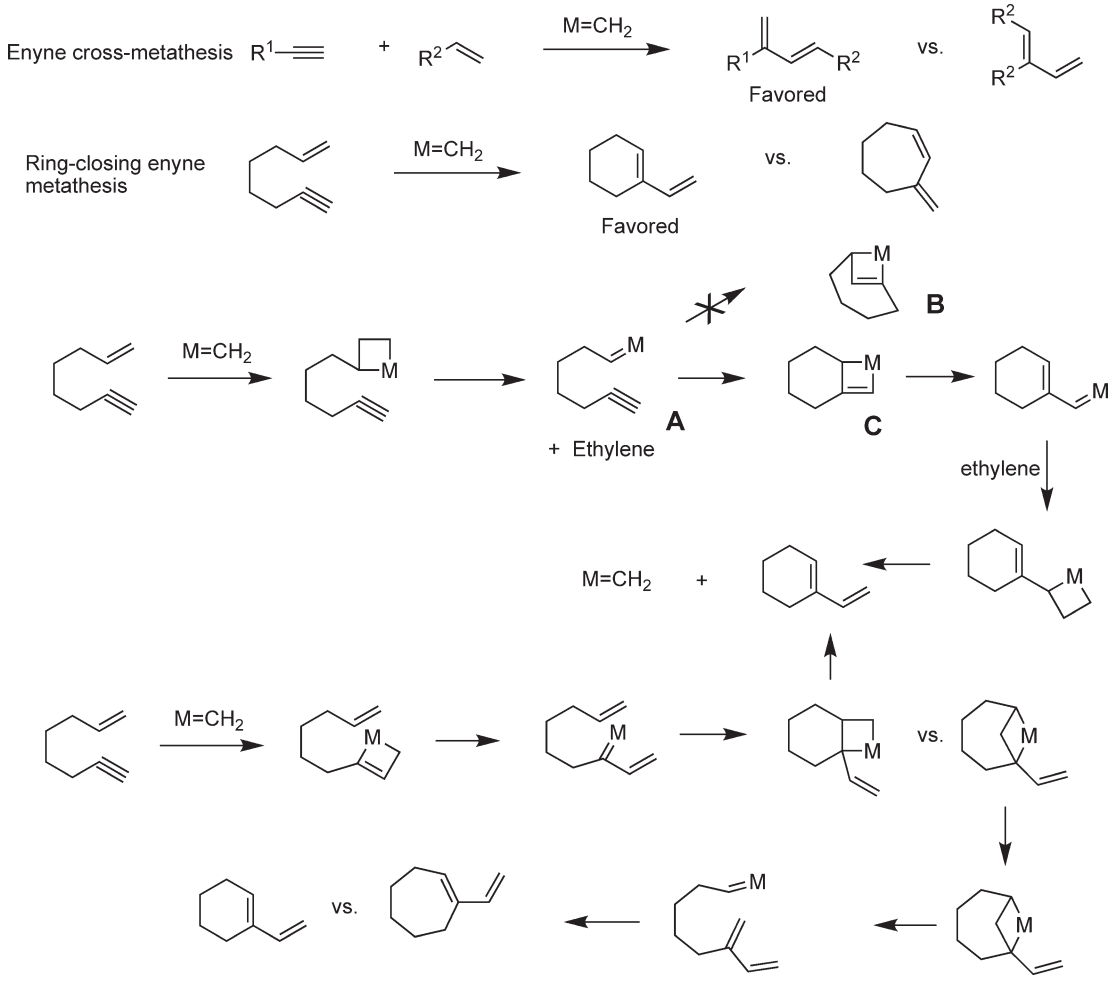

Scheme 22 General and mechanistic equations for enyne metathesis.

replaced by a C–C σ-bond. The coupling of acetylene and ethylene to produce 1,3-butadiene is both exothermic and exergonic ($\Delta H = -157\,\text{kJ mol}^{-1}$, $\Delta G = -113\,\text{kJ mol}^{-1}$).[29]

There are many examples of successful enyne cross-metathesis.[103] The regiochemistry of the process involving terminal alkynes and monosubstituted alkenes is consistent, as indicated by the products of Scheme 23, where the original alkyne substituent is at the 3-position and the original alkene substituent is at the 1-position. The alternate regioisomer is typically not observed. Mixtures of (*E*)- and (*Z*)-alkenes are typically obtained; however, the proportion of the (*E*)-isomer increases with more active catalysts and/or with extended reaction time.[31] Representative examples of intermolecular enyne metathesis are depicted in Scheme 23 and include: (i) co-metathesis of polymer-bound allylsilane **200** and monosubstituted alkynes to provide polymer-bound diene **201**,[104] (ii) synthesis of the diene-linked disaccharide **204** via co-metathesis of O-propargyl carbohydrate **202** and O-allyl carbohydrate **203**,[105] (iii) co-metathesis of the alkyne–tosylate **206** with the allylic ether **205**,[106]and (iv) a regio- and stereoselective process involving silylated alkene **209**.[107]A novel cycloaddition process is observed in the co-metathesis of mono-substituted alkynes and 1,5-hexadiene (Scheme 24).[108]The reaction leads to a mixture of cyclohexadienes (e.g., **212**) and acyclic trienes (e.g., **213**). The acyclic trienes were obtained as exclusively the (*E*)-isomer. Presumably, enyne metathesis initially produces an *E*/*Z* mixture of triene **213**. The (*Z*)-isomer then undergoes an RCM to afford cyclohexadiene derivative **212**. The (*E*)-isomer is inert to further metathesis. The yields of this process are improved by the use of 1,5-cyclooactadiene in place of 1,5-hexadiene.[109] A novel ring-expansion process (e.g., formation of **218**,

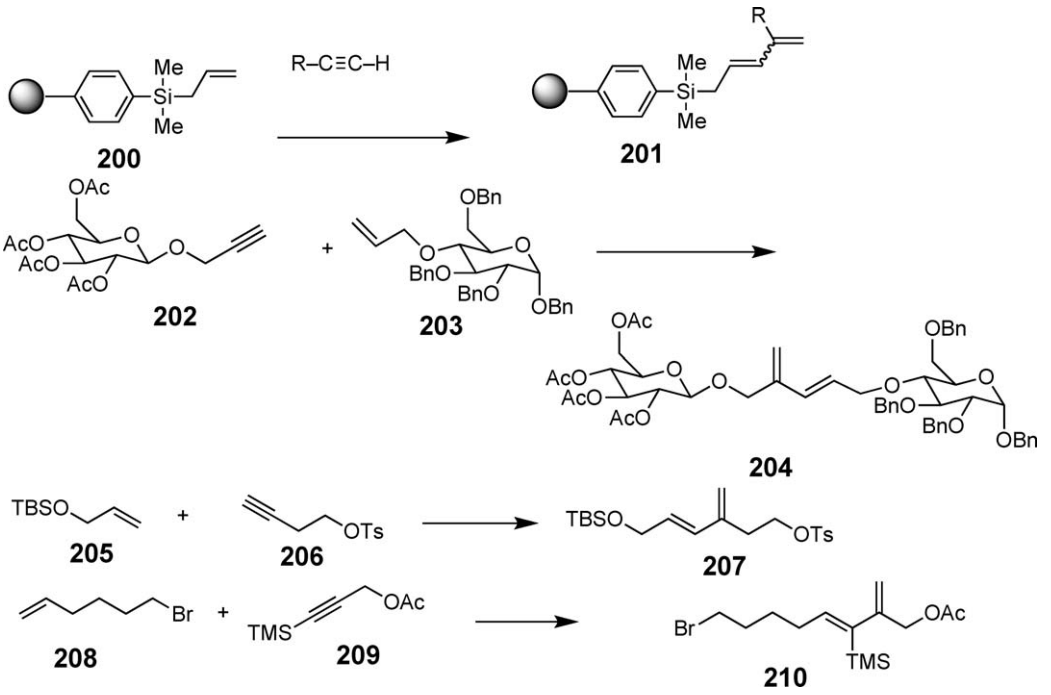

Scheme 23 Representative examples of enyne cross-metathesis.

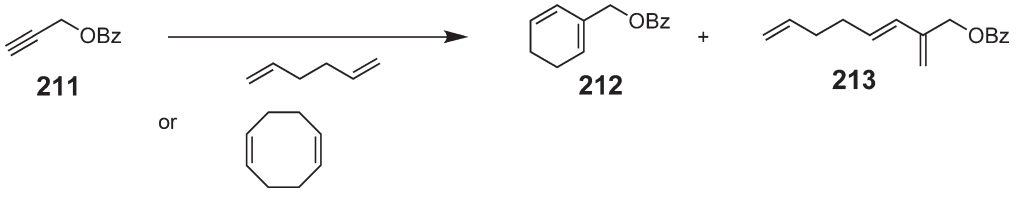

Scheme 24 Cycloaddition through tandem enyne cross-metathesis-RCM.

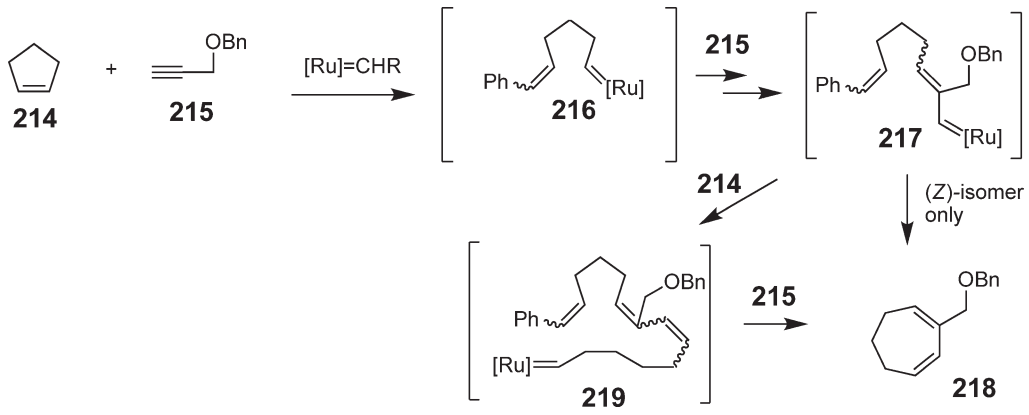

Scheme 25 Ring expansion through tandem enyne cross-metathesis-RCM.

Scheme 25) was observed when cyclic alkenes (e.g., **214**) were treated with ruthenium carbene complex **18** in the presence of terminal alkynes (e.g., **215**).[110] A mechanism involving initial ROM, followed by alkyne insertion of the intermediate carbene complex, followed by RCM from intermediate **217**, was proposed. In order to account for the unexpectedly high yield (the yield is higher than the anticipated $E:Z$ selectivity in the formation of **217**) of the process, a second source of the observed product involving metathesis of an additional mole of cyclopentene from intermediate **217** was suggested.

Numerous examples of enyne RCM have been documented.[103] The ring size limitations noted for RCM pretty much parallel those for enyne metathesis. Representative examples of ring-closing enyne metathesis are depicted in Scheme 26 and include: (i) formation of bicyclic amine derivative **221** through intramolecular enyne metathesis of substrate **220**,[111] (ii) formation of α,β-unsaturated ketones (e.g., **224**) via enyne metathesis employing silyloxyalkynes (e.g., **222**) followed by hydrolysis,[112] (iii) synthesis of butadienyl-substituted cycloalkenes (e.g., **226**) through intramolecular metathesis of a conjugated enyne and a monosubstituted alkene,[113] (iv) synthesis of cyclic siloxane–dienes (e.g., **228**) using a non-carbene–ruthenium catalyst,[114] (v) synthesis of diene–cyclic amine derivatives through enyne metathesis of *N*-allyl–*N*-propargyl–*N*-sulfonamide derivatives (e.g., **229**, Scheme 12) in an ethylene atmosphere,[115] (vi) formation of cyclohexadienes (e.g., **232**) in an intramolecular enyne metathesis ring expansion,[116] (vii) formation of cyclic ethers present in ciguatoxin and related compounds (e.g., **234**),[117] and (viii) tandem enyne metathesis and cross-metathesis.[118,118a] As noted in the examples in Scheme 26 that feature monosubstituted alkenes, the regiochemistry is usually opposite to that for intermolecular enyne metathesis. This is due to the regiochemistry of alkyne insertion noted in Scheme 22. Conversion of intermediate carbene complex **A** into metallacyclobutene **B** does not occur due to ring strain. Carbene complex **A** converts into metallacyclobutene **B**, which eventually provides the observed reaction products.[119] Formation of the alternate regioisomer is occasionally observed. For example, intramolecular enyne metathesis of **235** (Scheme 27) results in both five- and six-membered ring metathesis products.[120] Formation of the six-membered ring product **237** was proposed to arise through initial reaction of a methylene–ruthenium complex intermediate with the alkyne via the "alkyne-first" pathway (see Scheme 22). If the ring is sufficiently large, the regioisomer matching the intermolecular system is obtained. For example, atropoisomer-selective formation of the *p*-cyclophane-conjugated diene **239** for total synthesis of longithorone was observed upon exposure of **238** to a metathesis catalyst.[121]

Additional aspects of enyne metathesis are depicted in Scheme 28. The conjugated diene products of enyne metathesis can undergo Diels–Alder reactions. Enyne metathesis—Diels–Alder can even be performed as a one-pot tandem reaction process, as exemplified by enyne metathesis of **240** in the presence of maleic anhydride.[122,122a] Totally intramolecular enyne metathesis Diels–Alder sequences have been demonstrated[121] (e.g., the conversion of **244** into **246**).[123] Enyne RCM of substrate **247** affords stereochemically pure **248** due to kinetic resolution during metathesis.[124] A process equivalent to enyne metathesis that proceeds through a non-carbene mechanism has been demonstrated using platinum chloride as a catalyst.[125] In addition to routine observations, some other interesting side-reactions have been noted (Scheme 29). Competitive cross-metathesis with ethylene and intramolecular enyne metathesis were observed in the treatment of substrate **249** with catalyst **16** and ethylene.[126] Cyclopropane ring opening was observed in the attempted enyne metathesis of substrate **253**, resulting in alkylidenecyclopentene **254**.

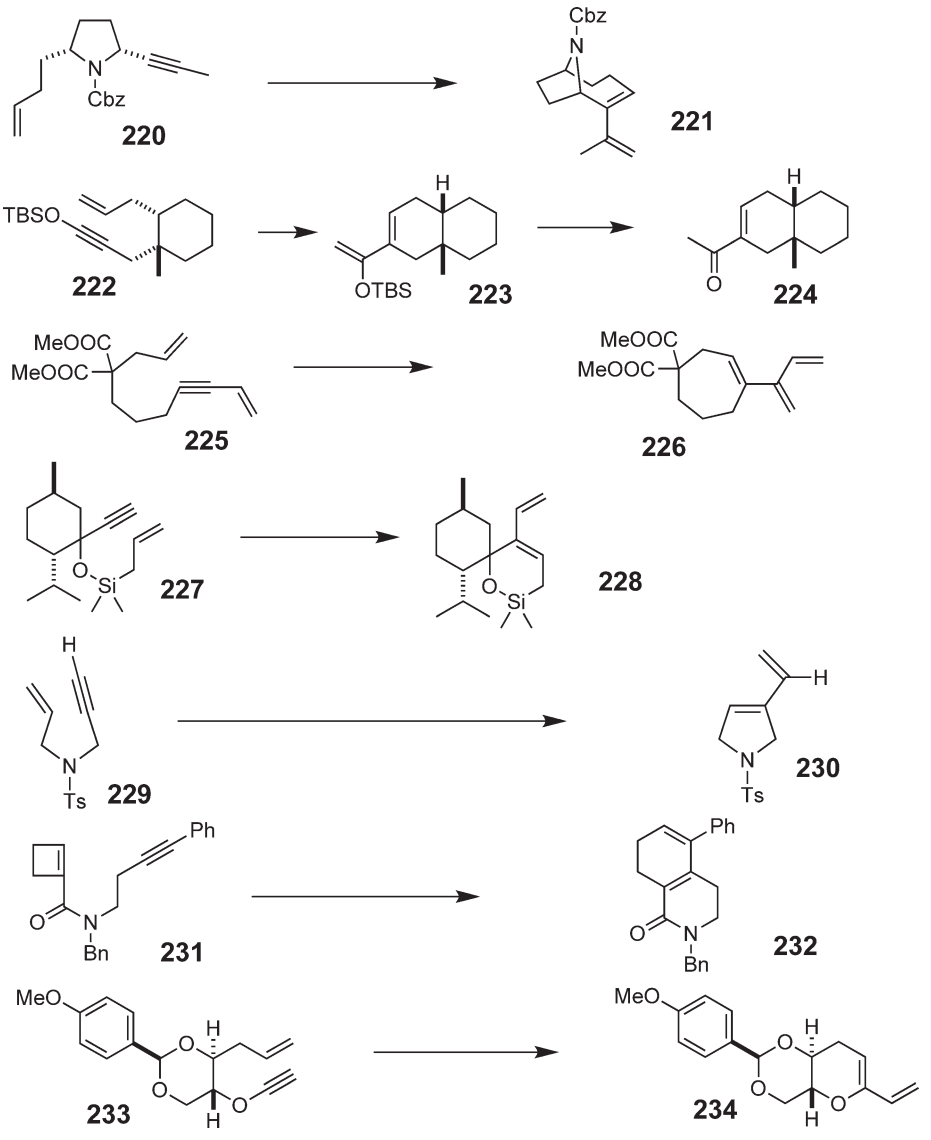

Scheme 26 Representative examples of enyne RCM.

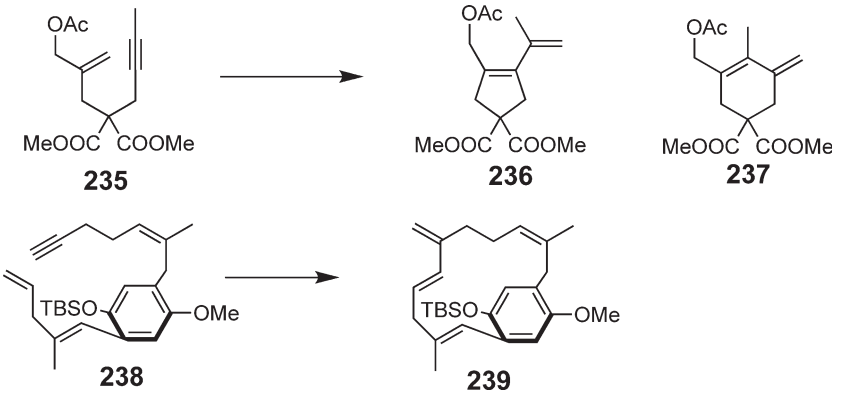

Scheme 27 Representative examples of enyne RCM proceeding with alternate regioselectivity.

Enyne metathesis RCM can be performed in tandem with RCM using appropriately spaced diene–yne substrates. Many examples of this reaction featuring various degrees of complexity have been reported. Representative examples of tandem enyne metathesis-RCM are depicted in Scheme 30 and include: (i) formation of the fused bicyclic compound **257** from dienyne **255** for securinine total synthesis,[127] (ii) synthesis of cyclic ethers (e.g., **261** and **262**) from diene–alkynes (e.g., **258**) and control of the product distribution through alkene substitution pattern,[128] and (iii) double tandem RCM-enyne metatheses (conversion of **263** into **266**) of appropriate polyene–polyyne systems.[129] A simultaneous intermolecular/intramolecular enyne metathesis process using diynes (e.g., **267**) and allylsilane **268** afforded conjugated triene derivatives (e.g., **270**).[130] Cyclopropanation was observed as a side-reaction in the tandem enyne metathesis RCM of diene–yne **271**.[131]

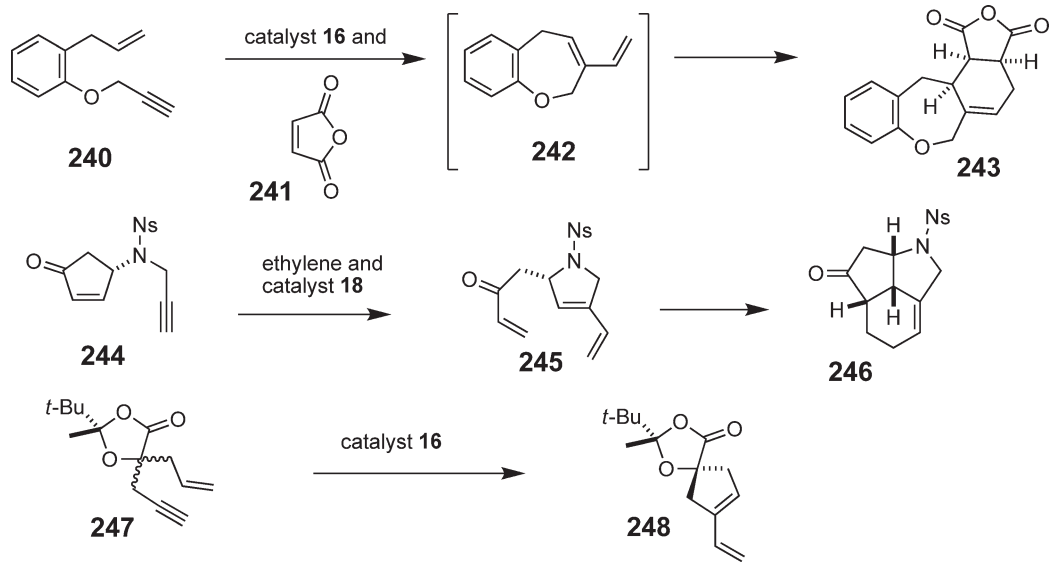

Scheme 28 Complex enyne RCM reactions.

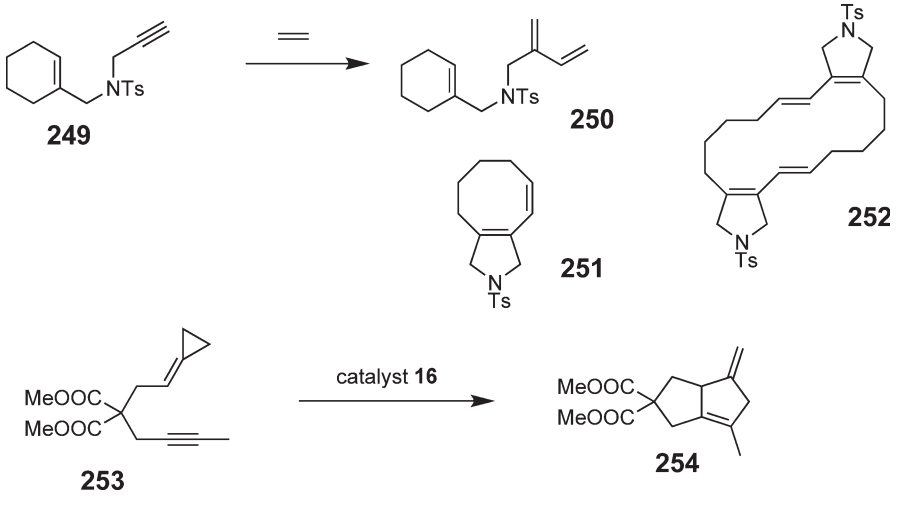

Scheme 29 Side-reactions competing with enyne RCM.

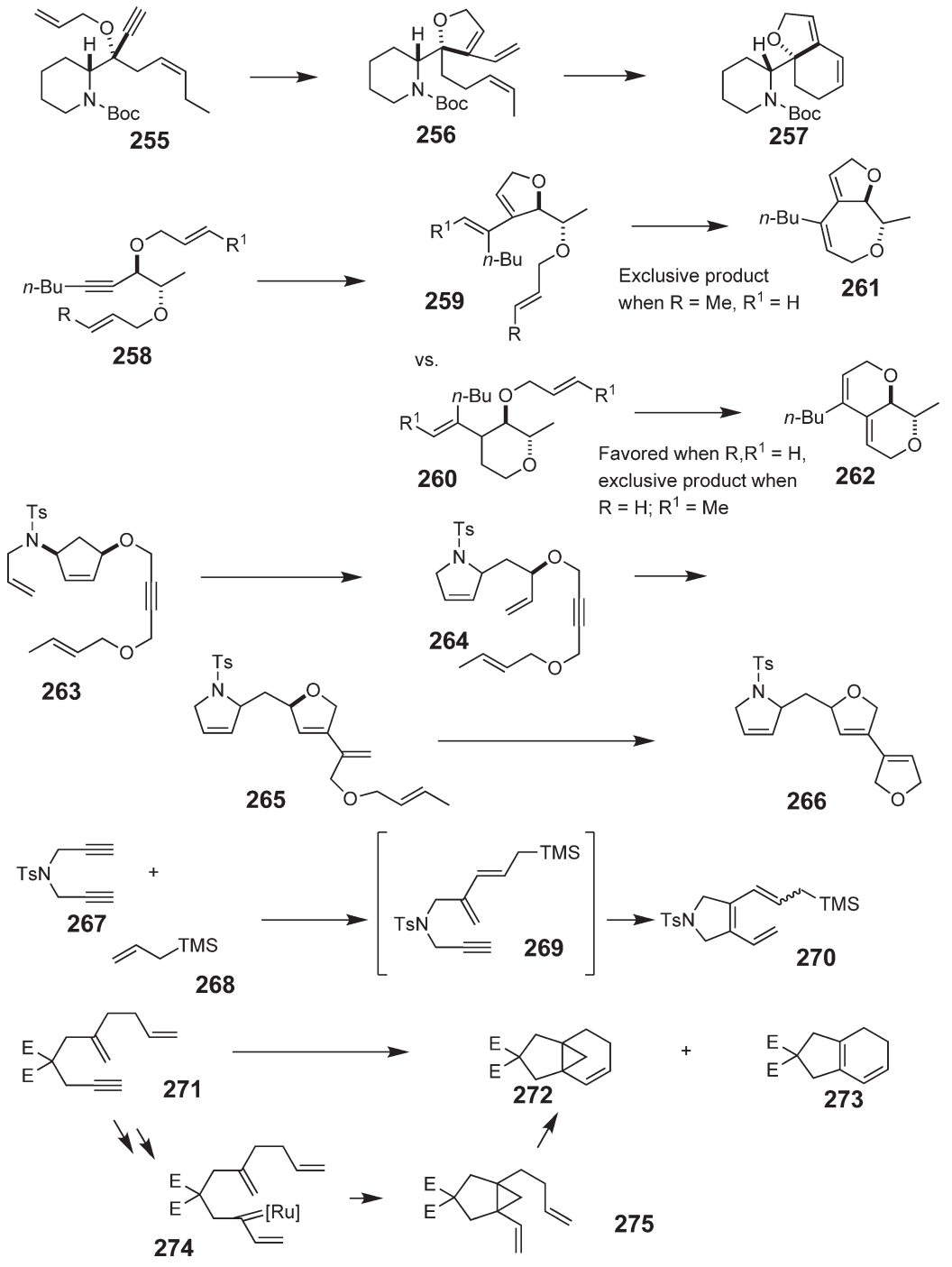

Scheme 30 Representative examples of enyne metathesis reactions occurring in tandem with other metathesis modes.

1.06.6 Alkyne Metathesis

The general equation and mechanism for alkyne metathesis is depicted in Scheme 31. Alkyne metathesis is considerably less well developed in comparison to alkene metathesis.[132] Carbyne complexes or carbyne complex precursors are among the most effective alkyne metathesis catalysts; representative catalysts are depicted in Scheme 32. Tungsten carbyne complex **276**[133] is one of the earliest alkyne metathesis catalysts, and has frequently been employed to initiate

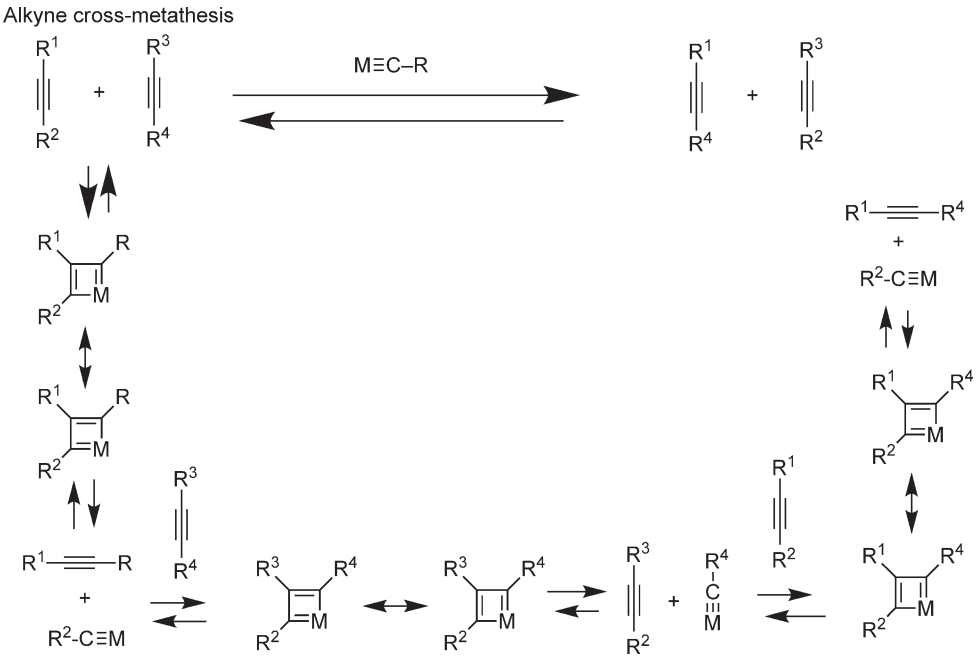

Scheme 31 General and mechanistic equation for alkyne metathesis.

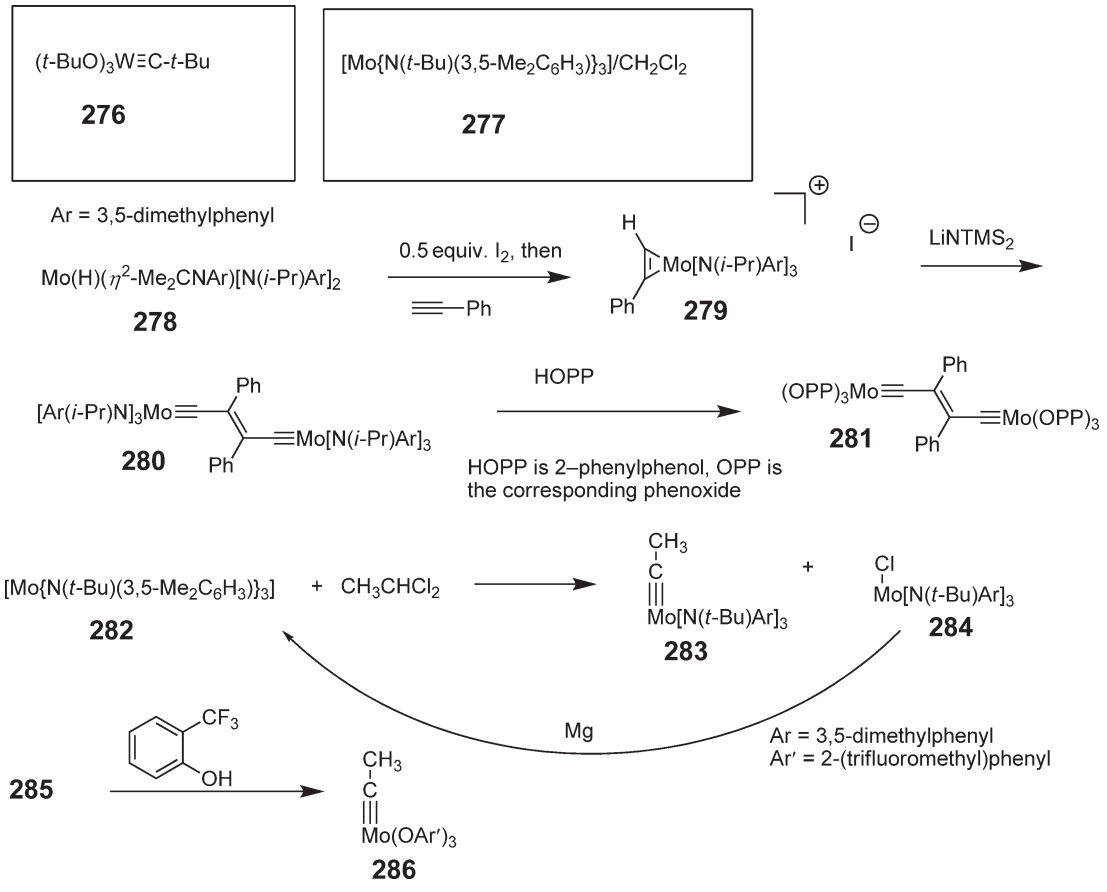

Scheme 32 Development of new catalysts for alkyne metathesis.

alkyne metathesis reactions. The system of molybdenum hexacarbonyl in the presence of phenol derivatives has also been utilized with varying degrees of success.[134,134a] Among the most effective catalysts are molybdenum(IV) amido complexes (e.g., **277**) in the presence of geminal dihalides, which generate carbyne complexes *in situ*. The conversion of derivatives of **277** into actual molybdenum carbyne complexes **281**,[135] **283**, and **286**,[136] and their subsequent use in alkyne metathesis was recently reported.

Alkyne metathesis is generally restricted to internal alkynes, and is driven to completion by the evolution of gaseous 2-butyne. Representative examples of alkyne cross-metathesis are depicted in Scheme 33, and include: (i) dimerization of alkynylbenzoic acid derivative **287**,[136] (ii) alkyne cross-metathesis of **289** and bis(trimethylsilyl)acetylene,[137] (iii) cross-metathesis of enyne **291** and various alkynes and metathesis dimerization of **291**,[138] and (iv) formation of high molecular weight alkyne-containing polymers through acyclic diyne metathesis (ADIMET) polymerization of acyclic diynes (e.g., **293**)[139,139a,140] using the molybdenum hexacarbonyl/2-chlorophenol system.

Ring-closing alkyne metathesis was reported in 1998 for the first time.[141] Only large rings where the alkyne is stable within a ring can be formed through alkyne metathesis. An additional useful feature of alkyne metathesis is that the cyclic alkyne product can lead to the cyclic alkene with a high degree of *cis*-stereoselectivity after hydrogenation. Representative examples of ring-closing alkyne metathesis are depicted in Scheme 34, and include: (i) preparation of compound **297** in stereochemically pure form via ring-closing alkyne metathesis of diyne **295** followed by hydrogenation,[142] (ii) ring-closing alkyne metathesis using substrate **298** and molybdenum catalyst **277**

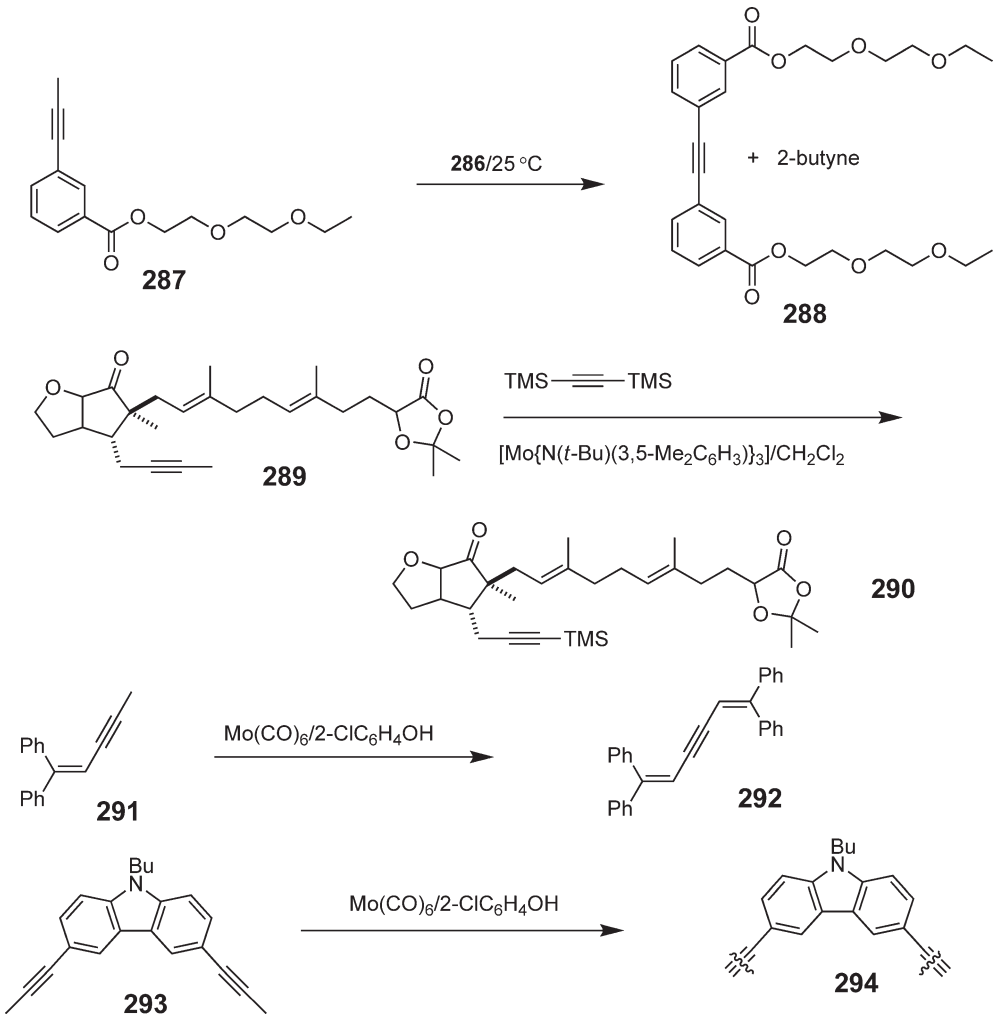

Scheme 33 Representative examples of alkyne cross-metathesis and acyclic diyne metathesis (ADIMET) polymerization.

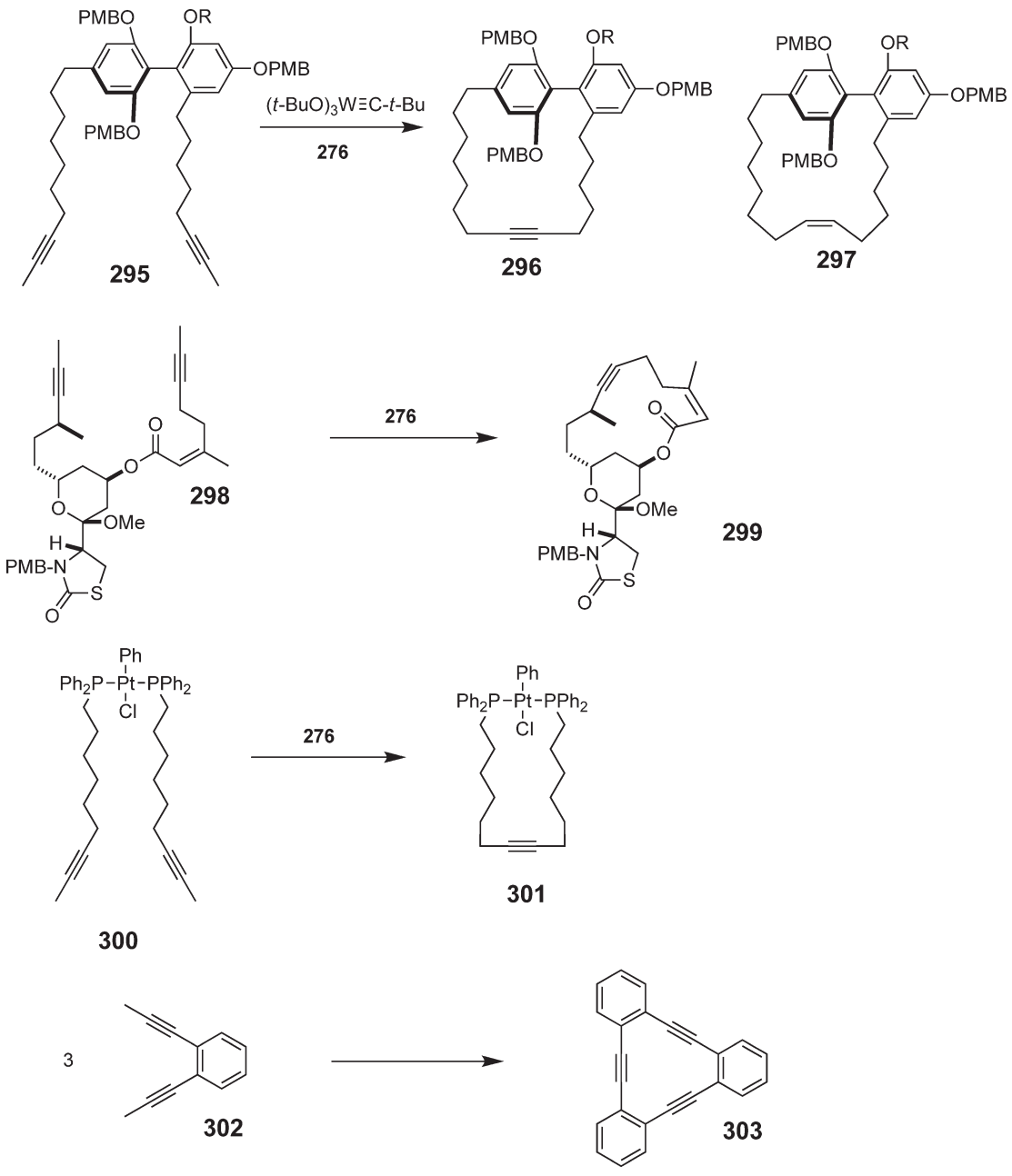

Scheme 34 Representative examples of ring-closing alkyne metathesis.

for the total synthesis of latrunculin B,[143] (iii) ring-closing alkyne metathesis of various 7-nonynylphosphine complexes (e.g., **300**) using tungsten carbyne complex **276** to afford macrocycle-bridged diphosphine complexes (e.g., **301**),[144] and (iv) a metathesis trimerization of 1,2-bis(1-propynyl)benzene **302**.[145]

References

1. Astruc, D. *New J. Chem.* **2005**, *29*, 42–56.
1a. Connon, S. J.; Blechert, S. *Top. Organomet. Chem.* **2004**, *11*, 93–124.
1b. Grubbs, R. H. *Tetrahedron* **2004**, *60*, 7117–7140.
1c. Diver, S. T.; Giessert, A. J. *Chem. Rev.* **2004**, *104*, 1317–1382.

1d. Schrock, R. R.; Hoveyda, A. H. *Angew. Chem., Int. Ed.* **2003**, *42*, 4592–4633.
1e. Grubbs, R. H.; Trnka, T. M.; Sanford, M. S. *Curr. Meth. Inorg. Chem.* **2003**, *3*, 187–231.
1f. Connon, S. J.; Blechert, S. *Angew. Chem., Int. Ed.* **2003**, *42*, 1900–1923.
1g. Poulsen, C. S.; Madsen, R. *Synthesis* **2003**, 1–18.
2. For the most recent survey see: Herndon, J. W. *Coord. Chem. Rev.* **2005**, *249*, 999–1083.
3. For more details on "ring-closing metathesis" refer to the search engine Scifinder (http://www.cas.org).
4. Herrison, J. L.; Chauvin, Y. *Makromol. Chem.* **1971**, *141*, 161–176.
5. Cundari, T. R.; Gordon, M. S. *Organometallics* **1992**, *11*, 55–63.
5a. Rappe, A. K.; Goddard, W. A. III *J. Am. Chem. Soc.* **1982**, *104*, 448–456.
6. Casey, C. P.; Burkhardt, T. J. *J. Am. Chem. Soc.* **1974**, *96*, 7808–7809.
7. McGinnis, J.; Katz, T. J.; Horowitz, S. *J. Am. Chem. Soc.* **1976**, *98*, 605–606.
7a. Use of this catalyst for the initiation of alkene metathesis was recently reviewed. Katz, T. J. *Angew. Chem. Int. Ed.* **2005**, *44*, (Early view).
8. Schrock, R. R. *J. Am. Chem. Soc.* **1974**, *96*, 6796–6797.
9. Gilliom, L. R.; Grubbs, R. H. *J. Am. Chem. Soc.* **1986**, *108*, 733–742.
10. Wu, Y. D.; Peng, Z. H. *Inorg. Chim. Acta* **2003**, *345*, 241–254.
10a. Fomine, S.; Martinez Vargas, S.; Tlenkopatchev, M. A. *Organometallics* **2003**, *22*, 93–99.
10b. Tlenkopatchev, M. A.; Vargas, S. M.; Fomine, S. *Tetrahedron* **2002**, *58*, 4817–4824.
10c. Vyboishchikov, S. F.; Bühl, M.; Thiel, W. *Chem. Eur. J.* **2002**, *8*, 3962–3975.
10d. Adlhart, C.; Chen, P. *Angew. Chem., Int. Ed.* **2002**, *41*, 4484–4487.
10e. Handzlik, J.; Ogonowski, J. *NATO Science Series, II: Mathematics, Physics and Chemistry* **2002**, *69*, 417–422.
10f. Handzlik, J.; Ogonowski, J. *J. Mol. Catal. A* **2001**, *175*, 215–225.
10g. Tlenkopatchev, M.; Fomine, S. *J. Organomet. Chem.* **2001**, *630*, 157–168.
10h. Aagaard, O. M.; Meier, R. J.; Buda, F. *J. Am. Chem. Soc.* **1998**, *120*, 7174–7182.
10i. Wu, Y.; Peng, Z. *J. Amer. Chem. Soc.* **1997**, *119*, 8043–8049.
10j. Benson, M. T.; Cundari, T. R. *Int. J. Quantum Chem.* **1997**, *65*, 987–996.
10k. Adlhart, C.; Chen, P. *J. Am. Chem. Soc.* **2004**, *126*, 3496–3510.
10l. Suresh, C. H.; Koga, N. *Organometallics* **2004**, *23*, 76–80.
10m. Bernardi, F.; Bottoni, A.; Miscione, G. P. *Organometallics* **2003**, *22*, 940–947.
11. Kress, J.; Wesolek, M.; Osborn, J. A. *J. Chem. Soc., Chem. Commun.* **1982**, 514–516.
12. Schrock, R. R.; Murdzek, J. S.; Bazan, G. C.; Robbins, J.; DiMare, M.; O'Regan, M. *J. Am. Chem Soc.* **1990**, *112*, 3875–3886.
13. Schwab, P.; France, M. B.; Ziller, J. W.; Grubbs, R. H. *Angew. Chem., Int. Ed.* **1995**, *34*, 2039–2041.
14. Scholl, M.; Ding, S.; Lee, C. W.; Grubbs, R. H. *Organic Lett.* **1999**, *1*, 953–956.
15. Huang, J.; Stevens, E. D.; Nolan, S. P.; Petersen, J. L. *J. Am. Chem. Soc.* **1999**, *121*, 2674–2678.
16. Garber, S. B.; Kingsbury, J. S.; Gray, B. L.; Hoveyda, A. H. *J. Am. Chem. Soc.* **2000**, *122*, 8168–8179.
16a. Gessler, S.; Randl, S.; Blechert, S. *Tetrahedron Lett.* **2000**, *41*, 9973–9976.
16b. Kingsbury, J. S.; Harrity, J. P. A.; Bonitatebus, P. J., Jr.; Hoveyda, A. H. *J. Am. Chem. Soc.* **1999**, *121*, 791–799.
17. Jafarpour, L.; Schanz, H.-J.; Stevens, E. D.; Nolan, S. P. *Organometallics* **1999**, *18*, 5416–5419.
18. Hofmann, P.; Volland, M. A. O.; Hansen, S. M.; Eisenträger, F.; Gross, J. H.; Stengel, K. *J. Organomet. Chem.* **2000**, *606*, 88–92.
19. Love, J. A.; Morgan, J. P.; Trnka, T. M.; Grubbs, R. H. *Angew. Chem., Int. Ed.* **2002**, *41*, 4035–4037.
20. Bielawski, C. W.; Benitez, D.; Grubbs, R. H. *J. Am. Chem. Soc.* **2003**, *125*, 8424–8425.
21. Maynard, H. D.; Grubbs, R. H. *Tetrahedron Lett.* **1999**, *40*, 4137–4140.
21a. Gallivan, J. P.; Jordan, J. P.; Grubbs, R. H. *Tetrahedron Lett.* **2005**, *46*, 2577–2580.
22. Yao, Q.; Zhang, Y. *Angew. Chem. Int. Ed.* **2003**, *42*, 3395–3398.
22a. Audic, N.; Clavier, H.; Manduit, M.; Guillermin, J. C. *J. Am. Chem. Soc.* **2003**, *125*, 9248–9249.
23. Kingsbury, J. S.; Garber, S. B.; Giftos, J. M.; Gray, B. L.; Okamoto, M. M.; Farrer, R. A.; Fourkas, J. T.; Hoveyda, A. H. *Angew. Chem. Int. Ed.* **2001**, *40*, 4251–4256.
23a. Randl, S.; Buschmann, N.; Connon, S. J.; Blechert, S. *Synlett* **2001**, 1547–1550.
24. Alexander, J. B.; Schrock, R. R.; Davis, W. M.; Hultzsch, K. C.; Hoveyda, A. H.; Hauser, J. H. *Organometallics* **2000**, *19*, 3700–3715.
24a. Zhu, S. S.; Cefalo, D. R.; La, D. S.; Jamieson, J. Y.; Davis, W. M.; Hoveyda, A. H.; Schrock, R. R. *J. Am. Chem. Soc.* **1999**, *121*, 8251–8259.
24b. Schrock, R. R.; Jamieson, J. Y.; Dolman, S. J.; Miller, S. A.; Bonitatebus, P. J., Jr.; Hoveyda, A. H. *Organometallics* **2002**, *21*, 409–417.
24c. Seiders, T. J.; Ward, W.; Grubbs, R. H. *Org. Lett.* **2001**, *3*, 3225–3228.
24d. Van Veldhuizen, J. J.; Garber, S. B.; Kingsbuty, J. S.; Hoveyda, A. H. *J. Am. Chem. Soc.* **2002**, *124*, 4954–4955.
24e. Van Veldhuizen, J. J.; Gillingham, D. G.; Garber, S. B.; Kataoka, O.; Hoveyda, A. H. *J. Am. Chem. Soc.* **2003**, *125*, 12502–12508.
25. Sanford, M. S.; Ulman, M.; Grubbs, R. H. *J. Am. Chem. Soc.* **2001**, *123*, 749–750.
26. Sanford, M. S.; Love, J. A.; Grubbs, R. H. *J. Am. Chem. Soc.* **2001**, *123*, 6543–6554.
27. Dias, E. L.; Nguyen, S. T.; Grubbs, R. H. *J. Am. Chem. Soc.* **1997**, *119*, 3887–3897.
28. Benson, M. T.; Cundari, T. R. *Int. J. Quantum Chem.* **1997**, *65*, 987–996.
29. This number was calculated based on Hartree-Frock energy minimization and frequency calculations for acetylene, ethylene, propene, *E* 2-butene, norbornene, *cis* 1,3-divinylcyclopentene, and 1,6-heptadiene using Gaussian 03. The -31G* basis set was used. Frisch, M. J.; Trucks, G. W.; Schlegel, H. B.; Scuseria, G. E.; Robb, M. A.; Cheeseman, J. R.; Zakrzewski, V. G.; Montgomery, J. A.; Stratmann, R. E.; Burant, J. C., *et al.* Gaussian, Inc., Pittsburgh, PA, 1998.
30. Chatterjee, A. K.; Choi, T. L.; Sanders, D. P.; Grubbs, R. H. *J. Am. Chem. Soc.* **2003**, *125*, 11360–11370.
31. Geissert, A. J.; Diver, S. T. *J. Org. Chem.* **2005**, *70*, 1046–1049.
32. Nakamura, S.; Hirata, Y.; Kurosaki, T.; Anada, M.; Kataoka, O.; Kitagaki, S.; Hashimoto, S. *Angew. Chem., Int. Ed.* **2003**, *42*, 5351–5355.
33. Ghosh, A. K.; Li, C. *J. Am. Chem. Soc.* **2003**, *125*, 2374–2375.
34. Demchuk, O. M.; Pietrusiewicz, K. M.; Michrowska, A.; Grela, K. *Org. Lett.* **2003**, *5*, 3217–3220.
35. Sierra, J. C.; Hüerländer, D.; Hill, M.; Kehr, G.; Erker, G.; Fröhlich, R. *Chem. Eur. J.* **2003**, *9*, 3618–3622.
36. Njaradson, J. T.; Biswas, K.; Danishefsky, S. J. *Chem. Comm.* **2002**, 2759–2761.
37. Zhang, L.; Herndon, J. W. *Tetrahedron Lett.* **2002**, *43*, 4471–4473.
37a. Hazra, D.; Sarkar, A. *Indian J. Chem.* **2003**, *42A*, 2398–2405.

38. Tsuji, J.; Hashiguchi, S. *Tetrahedron Lett.* **1980**, *21*, 2955–2958.
39. Kirschning, A.; Chu, G. W.; Jaunzems, J.; Jesberger, M.; Kalesse, M.; Lindner, M. *Tetrahedron* **2004**, *60*, 3505–3521.
40. Bouzbouz, S.; Simmons, R.; Cossy, J. *Org. Lett.* **2004**, *6*, 3465–3467.
41. Hopkins, T. E.; Wagener, K. B. *Macromolecules* **2004**, *37*, 1180–1189.
42. Wolfe, P. S.; Wagener, K. B. *Macromolecules* **1999**, *32*, 7961–7967.
43. Peetz, R.; Strachota, A.; Thorn-Csányi, E. *Macromol. Chem. Phys.* **2003**, *204*, 1439–1450.
44. Allcock, H. R.; Kellam, E. C., III. *Macromolecules* **2002**, *35*, 40–47.
45. Barrett, A. G. M.; Hopkins, B. T.; Koebberling, J. *Chem. Rev.* **2002**, *102*, 3301–3323.
45a. Harned, A. M.; Zhang, M.; Vedantham, P.; Mukherjee, S.; Herpel, R. H.; Flynn, D. L.; Hanson, P. R. *Aldrichim. Acta* **2005**, *38*, 3–16.
46. Moore, J. D.; Byrne, R. J.; Vedantham, P.; Flynn, D. L.; Hanson, P. R. *Org. Lett.* **2003**, *5*, 4241–4244.
46a. Zhang, M.; Moore, J. D.; Flynn, D. L.; Hanson, P. R. *Org. Lett.* **2004**, *6*, 2657–2660.
47. Connor, E. F.; Sundberg, L. K.; Kim, H. C.; Cornelissen, J. J.; Magbitang, T.; Rice, P. M.; Lee, V. Y.; Hawker, C. J.; Volksen, W.; Hedrick, J. L., *et al. Angew. Chem., Int. Ed.* **2003**, *42*, 3785–3788.
48. Pollino, J. M.; Stubbs, L. P.; Weck, M. *Macromolecules* **2003**, *36*, 2230–2234.
49. Lee, B. S.; Mahajan, S.; Clapham, B.; Janda, K. D. *J. Org. Chem.* **2004**, *69*, 3319–3329.
50. Drechsler, U.; Thibault, R. J.; Rotello, V. M. *Macromolecules* **2002**, *35*, 9621–9623.
51. Silberg, J.; Schareina, T.; Kempe, R.; Wurst, K.; Buchmeiser, M. R. *J. Organomet. Chem.* **2001**, *622*, 6–18.
52. Kim, G. H.; Pugh, C.; Cheng, S. Z. D. *Macromolecules* **2000**, *33*, 8983–8991.
53. Gestwicki, J. E.; Strong, L. E.; Kiessling, L. L. *Angew. Chem., Int. Ed.* **2000**, *39*, 4567–4570.
53a. Gestwicki, J. E.; Cairo, C. W.; Strong, L. E.; Oetjen, K. A.; Kiessling, L. L. *J. Am. Chem. Soc.* **2002**, *124*, 14922–14933.
54. Lapinte, V.; De Fremont, P.; Montembault, V.; Fontaine, L. *Macromol. Chem. Phys.* **2004**, *205*, 1238–1245.
54a. Dounis, P.; Feast, W. J.; Widawski, G. *J. Mol. Catal. A* **1997**, *115*, 51–60.
55. Swager, T. M.; Dougherty, D. A.; Grubbs, R. H. *J. Am. Chem. Soc.* **1988**, *110*, 2973–2974.
56. Scherman, O. A.; Rutenberg, I. M.; Grubbs, R. H. *J. Am. Chem. Soc.* **2003**, *125*, 8515–8522.
57. Baran, J.; Bogdanska, I.; Jan, D.; Delaude, L.; Demonceau, A.; Noels, A. F. *J. Mol. Catal. A* **2002**, *190*, 109–116.
58. Maishal, T. K.; Mondal, B.; Puranik, V. G.; Wadgaonkar, P. P.; Lahiri, G. K.; Sarkar, A. *J. Organomet. Chem.* **2005**, *690*, 1018–1027.
58a. Lee, L. W.; Register, R. A. *Polymer* **2004**, *45*, 6479–6485.
59. Liu, Z.; Ranier, J. D. *Org. Lett.* **2005**, *7*, 131–133.
60. Statsuk, A. V.; Kozmin, S. A. *J. Am. Chem. Soc.* **2004**, *126*, 9546–9547.
61. Schrader, T. O.; Snapper, M. L. *J. Am. Chem. Soc.* **2002**, *124*, 10998–10999.
62. Tsang, W. C. P.; Jernelius, J. A.; Cortez, G. A.; Weatherhead, G. S.; Schrock, R. R.; Hoveyda, A. H. *J. Am. Chem. Soc.* **2003**, *125*, 2591–2596.
63. Gillingham, D. G.; Kataoka, O.; Garber, S. B.; Hoveyda, A. H. *J. Am. Chem. Soc.* **2004**, *126*, 12288–12290.
64. Takao, K. I.; Yasui, H.; Yamamoto, S.; Sasaki, D.; Kawasaki, S.; Watanabe, G.; Tadano, K. I. *J. Org. Chem.* **2004**, *69*, 8789–8795.
65. Ito, H.; Hasegawa, M.; Takeraka, Y.; Kobayashi, T.; Iguchi, K. *J. Am. Chem. Soc.* **2004**, *126*, 4520–4521.
66. Nickel, A.; Maruyama, T.; Tang, H.; Murphy, P. D.; Greene, B.; Yusuff, N.; Wood, J. L. *J. Am. Chem. Soc.* **2004**, *126*, 16300–16301.
67. Zakarian, A.; Batch, A.; Holton, R. A *J. Am. Chem. Soc.* **2003**, *125*, 7822–7824.
68. Ramana, G. V.; Rao, B. V. *Tetrahedron Lett.* **2003**, *44*, 5103–5105.
69. Horn, C. R.; Martín-Alvarez, J. M.; Gladysz, J. A. *Organometallics* **2002**, *21*, 5386–5393.
70. Hüerländer, D.; Kleigrewe, N.; Kehr, G.; Erker, G.; Fröhlich, R. *Eur. J. Inorg. Chem.* **2002**, 2633–2642.
71. Fürstner, A.; Schlede, M. *Adv. Synth. Catal.* **2002**, *344*, 657–665.
72. Humphrey, J. M.; Liao, Y.; Ali, A.; Rein, T.; Wong, Y. L.; Chen, H. J.; Coutney, A. K.; Martin, S. F. *J. Am. Chem. Soc.* **2002**, *124*, 8584–8592.
73. Børsting, P.; Sørenson, A. M.; Nielsen, P. *Synthesis* **2002**, 797–801.
74. Rivkin, A.; Yoshimura, F.; Garbada, A. E.; Cho, Y. S.; Chou, T. C.; Dong, H.; Danishefsky, S. J. *J. Am. Chem. Soc.* **2004**, *126*, 10913–10922.
75. Keller, V. A.; Martinelli, J. R.; Streiter, E. R.; Burke, S. D. *Org. Lett.* **2002**, *4*, 467–470.
76. Huwe, C. W.; Blechert, S. *Synthesis* **1997**, 61–67.
77. Evans, P. A.; Cui, J.; Buffone, G. P. *Angew. Chem., Int. Ed.* **2003**, *42*, 1734–xx.
78. Fukuda, Y.; Shindo, M.; Shishido, K. *Org. Lett.* **2003**, *5*, 749–751.
79. Hanson, P. R.; Stoianova, D. S. *Tetrahedron Lett.* **1998**, *39*, 3939–3942.
80. Bauer, E. B.; Ruwwe, J.; Martín-Alvarez, J. M.; Peters, T. B.; Bohling, J. C.; Hampel, F. A.; Szafert, S.; Lis, T.; Gladysz, J. A. *Chem. Commun.* **2000**, 2261–2262.
81. Ma, S.; Ni, B. *Org. Lett.* **2002**, *4*, 639–641.
82. Njardson, J. T.; Gaul, C.; Shan, D.; Huang, X. Y.; Danishefsky, S. J. *J. Am. Chem. Soc.* **2004**, *126*, 1038–1040.
82a. Gaul, C.; Njardson, J. T.; Shan, D.; Dorn, D. C.; Wu, K. D.; Tong, W. P.; Huang, X. Y.; Moore, M. A. S.; Danishefsky, S. J. *J. Am. Chem. Soc.* **2004**, *126*, 11326–11337.
83. Hoye, T. R.; Jeffrey, C. S.; Tennakoon, M. A.; Wang, J.; Zhao, N. *J. Am. Chem. Soc.* **2004**, *126*, 10210–10211.
84. Garbaccio, R. M.; Stochel, S. J.; Baeschlin, D. K.; Danishefsky, S. J. *J. Am. Chem. Soc.* **2001**, *123*, 10903–10908.
85. Evano, G.; Schaus, J. V.; Panek, J. S. *Org. Lett.* **2004**, *6*, 525–528.
86. Joe, D.; Overman, L. E. *Tetrahedron Lett.* **1997**, *38*, 8635–8638.
87. Schmidt, B. *J. Org. Chem.* **2004**, *69*, 7672–7687.
87a. Sutton, A. E.; Seigal, B. A.; Finnegan, D. F.; Snapper, M. L. *J. Am. Chem. Soc.* **2002**, *124*, 13390–13391.
88. Hong, S. H.; Sanders, D. P.; Lee, C. W.; Grubbs, R. H. *J. Am. Chem. Soc.* **2005**, *127*, 17160–17161.
89. Drouin, S. D.; Zamanian, F.; Fogg, D. E. *Organometallics* **2001**, *20*, 5495–5497.
90. Hoye, T. R.; Zhao, H. *Org. Lett.* **1999**, *1*, 169–172.
90a. Hoye, T. R.; Zhao, H. *Org. Lett.* **1999**, *1*, 1123–1125.
91. Seiders, T. J.; Ward, D. W.; Grubbs, R. H. *Org. Lett.* **2001**, *3*, 3225–3228.
91a. Gillingham, D. G.; Kataoka, O.; Garber, S. B.; Hoveyda, A. H. *J. Am. Chem. Soc.* **2004**, *126*, 12288–12290.
91b. Van Veldhuizen, J. J.; Gillingham, D. G.; Garber, S. B.; Kataoka, O.; Hoveyda, A. H. *J. Am. Chem. Soc.* **2003**, *125*, 12502–12508.
91c. Van Veldhuizen, J. J.; Garber, S. B.; Kingsbury, J. S.; Hoveyda, A. H. *J. Am. Chem. Soc.* **2002**, *124*, 4954–4955.
92. Dolman, S. J.; Schrock, R. R.; Hoveyda, A. H. *Org. Lett.* **2003**, *5*, 4899–4902.

92a. Tsang, W. C. P.; Hultzsch, K. C.; Alexander, J. B.; Bonitatebus, P. J., Jr.; Schrock, R. R.; Hoveyda, A. H. *J. Am. Chem. Soc.* **2003**, *125*, 2652–2666.
93. Zhu, S. S.; Cefalo, D. R.; La, D. S.; Jamieson, J. Y.; Davis, W. M.; Hoveyda, A. H.; Schrock, R. R. *J. Am. Chem. Soc.* **1999**, *121*, 8251–8259.
94. Costabile, C; Cavallo, L. *J. Am. Chem. Soc.* **2004**, *126*, 9592–9600.
95. Smith, A. B., III; Adams, C. M.; Kozmin, S. A.; Paone, D. V. *J. Am. Chem. Soc.* **2001**, *123*, 5925–5937.
95a. Smith, A. B., III; Adams, C. M.; Kozmin, S. A. *J. Am. Chem. Soc.* **2001**, *123*, 990–991.
96. Fürstner, A.; Thiel, O. R.; Ackermann, L. *Organic Lett.* **2001**, *3*, 449–451.
96a. Lee, C. W.; Grubbs, R. H. *J. Org. Chem.* **2001**, *66*, 7155–7158.
97. Song, L.; Duesler, E. N.; Mariano, P. S. *J. Org. Chem.* **2004**, *69*, 7284–7293.
98. Holtsclaw, J.; Koreeda, M. *Org. Lett.* **2004**, *6*, 3719–3722.
99. Harrity, J. P. A.; Visser, M. S.; Gleason, J. D.; Hoveyda, A. H. *J. Am. Chem. Soc.* **1997**, *119*, 1488–1489.
100. Schandt, M.; Blechert, S. *J. Org. Chem.* **2003**, *68*, 2913–2920.
101. White, B. H.; Snapper, M. L. *J. Am. Chem. Soc.* **2003**, *125*, 14901–14904.
102. Galan, B. R.; Giessert, A. J.; Keister, J. B.; Diver, S. T. *J. Am. Chem. Soc.* **2005**, *127*, 5762–5763.
103. Diver, S. T.; Giessert, A. J. *Chem. Rev.* **2004**, *104*, 1317–1382.
104. Schuster, M.; Blechert, S. *Tetrahedron Lett.* **1998**, *39*, 2295–2298.
105. Schürer, S. C.; Blechert, S. *Chem. Commun.* **1999**, 1203–1204.
106. Rodríguez-Conesa, S.; Candal, P.; Jiménez, C.; Rodriguez, J. *Tetrahedron Lett.* **2001**, *42*, 6699–6702.
107. Kim, M.; Park, S.; Maifeld, S. V.; Lee, D. *J. Am. Chem. Soc.* **2004**, *126*, 10242–10243.
108. Smulik, J. A.; Diver, S. T. *Tetrahedron Lett.* **2001**, *42*, 171–174.
109. Kulkarni, A. A.; Diver, S. T. *J. Am. Chem. Soc.* **2004**, *126*, 8110–8111.
110. Kulkarni, A. A.; Diver, S. T. *Org. Lett.* **2003**, *5*, 3463–3466.
111. Brenneman, J. B.; Martin, S. F. *Org. Lett.* **2004**, *6*, 1329–1331.
112. Reddy, D. S.; Kozmin, S. *J. Org. Chem.* **2004**, *69*, 4860–4862.
113. Kang, B.; Kim, D. H.; Do, Y.; Chang, S. *Org. Lett.* **2003**, *5*, 3041–3043.
114. Le Nôtre, J.; Martinez, A. A.; Dixneuf, P. H.; Bruneau, C. *Tetrahedron* **2003**, *59*, 9425–9432.
115. Mori, M.; Sakakibara, N.; Kinoshita, A. *J. Org. Chem.* **1998**, *63*, 6082–6083.
116. Mori, M.; Wakamatsu, H.; Tonogaki, K.; Fujita, R.; Kitamura, T.; Sato, Y. *J. Org. Chem.* **2005**, *70*, 1066–1069.
117. Clark, J. S.; Elustando, F.; Trevitt, G. P.; Boyall, D.; Robertson, J.; Blake, A. J.; Wilson, C.; Stammen, B. *Tetrahedron* **2002**, *58*, 1973–1982.
118. Lee, H. Y.; Kim, H. Y.; Tae, H.; Kim, B. G.; Lee, J. *Org. Lett.* **2003**, *5*, 3439–3442.
118a. Royer, F.; Vilain, C.; Elkaïm, L.; Grimaud, L. *Org. Lett.* **2003**, *5*, 2007–2009.
119. Hanson, E. C.; Lee, D. *J. Am. Chem. Soc.* **2004**, *126*, 15074–15080.
120. Kitamura, T.; Sato, Y.; Mori, M. *Adv. Synth. Catal.* **2002**, *344*, 678–693.
120a. Kitamura, T.; Sato, Y.; Mori, M. *Chem. Comm.* **2001**, 1258–1259.
121. Layton, M. E.; Morales, C. A.; Shair, M. D. *J. Am. Chem. Soc.* **2002**, *124*, 773–775.
122. Ackermann, L.; Bruneau, C.; Dixneuf, P. H. *Synlett* **2001**, 397–399.
122a. Moreno-Mañas, M.; Pleixats, R.; Santamaria, A. *Synlett* **2001**, 1784–1786.
123. Fukumoto, H.; Esumi, T.; Ishihara, J.; Hatekeyama, S. *Tetrahedron Lett.* **2003**, *44*, 8047–8049.
124. Rapado, L. P.; Bulugahapitiva, V.; Renaud, P. *Helv. Chim. Acta* **2000**, *83*, 1625–1632.
125. Fürstner, A.; Stelzer, F.; Szillat, H. *J. Am. Chem. Soc.* **2001**, *123*, 11863–11869.
126. Mori, M.; Kuzuba, Y.; Kitamura, T.; Sato, Y. *Org. Lett.* **2002**, *4*, 3855–3858.
127. Honda, T.; Namiki, H.; Kaneda, K.; Mizutani, H. *Org. Lett.* **2004**, *6*, 87–89.
128. Wu, C. J.; Madhushaw, R. J.; Liu, R. S. *J. Org. Chem.* **2003**, *68*, 7889–7892.
129. Zuercher, W. J.; Scholl, M.; Grubbs, R. H. *J. Org. Chem.* **1998**, *63*, 4291–4298.
130. Stragies, R.; Schuster, M.; Blechert, S. *Chem. Commun.* **1999**, 237–238.
131. Peppers, B. T.; Diver, S. T. *J. Am. Chem. Soc.* **2004**, *126*, 9524–9525.
132. Fürstner, A.; Davies, P. W. *Chem. Commun.* **2005**, 2307–2320.
133. Wengrovius, J. H.; Sancho, J.; Schrock, R. R. *J. Am. Chem. Soc.* **1981**, *103*, 3932–3934.
134. Brizius, G.; Bunz, U. H. F. *Org. Lett.* **2002**, *4*, 2829–2831.
134a. Grela, K.; Ignatowska, J. *Org. Lett.* **2002**, *4*, 3747–3749.
135. Blackwell, J. M.; Figueroa, J. S.; Stephens, F. H.; Cummins, C. C. *Organometallics* **2003**, *22*, 3351–3353.
136. Zhang, W.; Krafft, S.; Moore, J. S. *Chem. Commun.* **2003**, 832–833.
137. Chan, J.; Jamison, T. F. *J. Am. Chem. Soc.* **2004**, *126*, 10682–10691.
138. Brizius, G.; Bunz, U. H. F. *Org. Lett.* **2002**, *4*, 2829–2831.
139. Wilson, J. N.; Steffen, W.; McKenzie, T. G.; Lieser, G.; Oda, M.; Neher, D.; Bunz, U. H. F. *J. Am. Chem. Soc.* **2002**, *124*, 6830–6831.
139a. Brizius, G.; Kroth, S.; Bunz, U. H. F. *Macromolecules* **2002**, *35*, 5317–5319.
140. Chen, S.; Michael, W. D.; Johnson, T. E. *Polym. Mater. Sci. Eng.* **2002**, *86*, 45–46.
141. Fürstner, A.; Seidel, G. *Angew. Chem., Int. Ed. Engl.* **1998**, *37*, 1734–1736.
142. Fürstner, A.; Stelzer, F.; Rumbo, A.; Krause, H. *Chem. Eur. J.* **2002**, *8*, 1856–1871.
143. Fürstner, A.; De Souza, D.; Parra-Rapado, L.; Jensen, J. T. *Angew. Chem., Int. Ed.* **2003**, *42*, 5358–5360.
144. Bauer, E. B.; Szafert, S.; Hampel, F.; Gladysz, J. A. *Organometallics* **2003**, *22*, 2184–2186.
145. Miljanić, O. S.; Vollhardt, K. P. C.; Whitener, G. D. *Synlett* **2003**, 29–34.

1.07
Experimental Methods and Techniques: Basic Techniques

D A Vicic, and G D Jones, University of Arkansas, Fayetteville, AR, USA

1.07.1 Introduction

A good deal of the chemistry described in this collective edition of *Comprehensive Organometallic Chemistry* is about organometallic complexes in reduced oxidation states. Such complexes tend to be extremely air-sensitive, and the reader should be aware that sophisticated laboratory techniques were required to prepare and characterize these

compounds. Many of the organometallic transformations needed to be monitored by air-sensitive techniques, and if care was not taken to exclude atmospheric oxygen, the unwanted formation of metal oxides would have prevented a lot of the new and exciting chemistry described throughout this edition from being discovered. Advanced anaerobic laboratory techniques are usually handed down from the experienced user to the novice, but in the absence of lineage of experienced predecessors a written guide is invaluable to getting started in the lab. While there have been entire books and manuscripts devoted to the subject of the manipulation of air-sensitive compounds,[1–7] many of them are now out of print and not easily accessible to the newer student or researcher. The intent of this chapter is not to replace these resources, but to provide an updated and consolidated guide to the first year graduate student or novice in the field.

Note about safety—There are many hazards associated with the use of a vacuum and positive pressures of inert gases with the glassware described throughout this chapter, and anyone attempting the following techniques should thoroughly prepare for all of the hazards that are involved.

1.07.2 High Vacuum and Schlenk Lines

1.07.2.1 High Vacuum Line

Perhaps the most important tool a chemist will need to work with air-sensitive compounds is a double manifold that will permit the introduction of both vacuum and inert gases. High vacuum and Schlenk lines contain such manifolds and can aid in most air-sensitive techniques. There are three major differences between a high vacuum and Schlenk line:

(i) Ground-glass and/or O-ring joints are used to connect reaction vessels on a high vacuum line whereas flexible tubing is typically used on a Schlenk line.
(ii) A diffusion pump is commonly used in series with a mechanical forepump on a high vacuum line to achieve lower pressures for more air-sensitive compounds.
(iii) High vacuum lines are typically used to manipulate volatiles while Schlenk lines are more amenable to the transfer of bulk solutions.

Since high vacuum and Schlenk lines possess double manifolds, many of the operations that are performed on them are similar. However, based on our lab's experience, high vacuum lines are ideal for removing/transferring solvents and drying solids, whereas a Schlenk line is superior for cannula transfers and for working under positive pressures of nitrogen. Therefore, depending on the nature of the research, one or both of the above lines may be needed. General aspects of the two lines are provided below.

The basic components of a high vacuum line include:

(i) *The double manifold*. A basic diagram of a double manifold is shown in Figure 1. It is constructed so that the ports, or "workstations," are connected to both a vacuum line and nitrogen/argon line via a three-way valve. The valves themselves can be designed for ground-glass stopcocks, which require greasing to prevent leaks, or for polytetrafluoroethylene (PTFE) stopcocks that have greaseless Teflon or O-ring seals. A manifold equipped with PTFE valves is shown in Figure 1, and glassware containing these types of valves will be described in more detail throughout this chapter.

Double manifolds can now be purchased commercially through a variety of vendors. However, for heavy users, it is still ideal to have a glassblower customize a manifold to meet individual laboratory specifications and needs. If a custom manifold is built, care must be taken to ensure that the glass walls are thick enough to safely maintain pressures ranging from approximately 10^{-4} to 900 torr. Leaks in a high vacuum line can be detected with the use of a Tesla coil, which provides a high voltage, high frequency spark. The electrical discharge is passed over suspected areas of the vacuum line that contain a pinhole leak, and a bright blue spark is produced at the location of the leak. Tesla coils should not be used on thin glass or on dewars, as punctures may occur from the high concentration of voltage.

One optional, but highly recommended accessory to a double manifold is an active pressure gauge that monitors the pressure in the vacuum line. Since leaks from the line can ruin experiments with air-sensitive compounds, it is critical to be aware of the status of the vacuum at all times. A traditional mercury McLeod gauge can provide accurate readings of pressure, but thermocouple and Pirani gauges can more quickly and

continuously monitor changes in pressure. When incorporating active pressure gauges, it is advisable to have a valve which can isolate the gauge from the vacuum line in case the volatile solvents contain chemicals that could react with and damage the sensors in the gauge itself.

Another optional accessory related to the active gauges is a U-shaped mercury manometer like that shown in Figure 2. Such a manometer is constructed with a long, thin U-shaped column that is filled with mercury and then tacked onto a backing support equipped with a ruler so that one can measure pressures usually handled by standard laboratory glassware (1 atm of gas pushes the mercury 760 mm). Typically, the length of one column is about 850 mm to account for over-pressurizing, and a small reservoir can be added to the columns to minimize mercury spilling. An example of how this simple U-shaped manometer can be used to introduce gases into an NMR tube is described in Section 1.07.4.5.

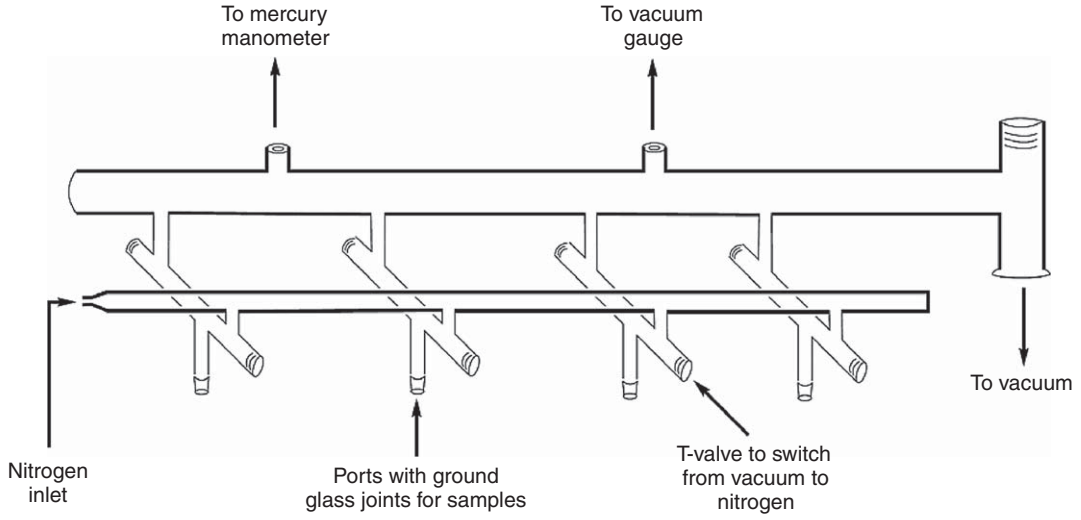

(a)

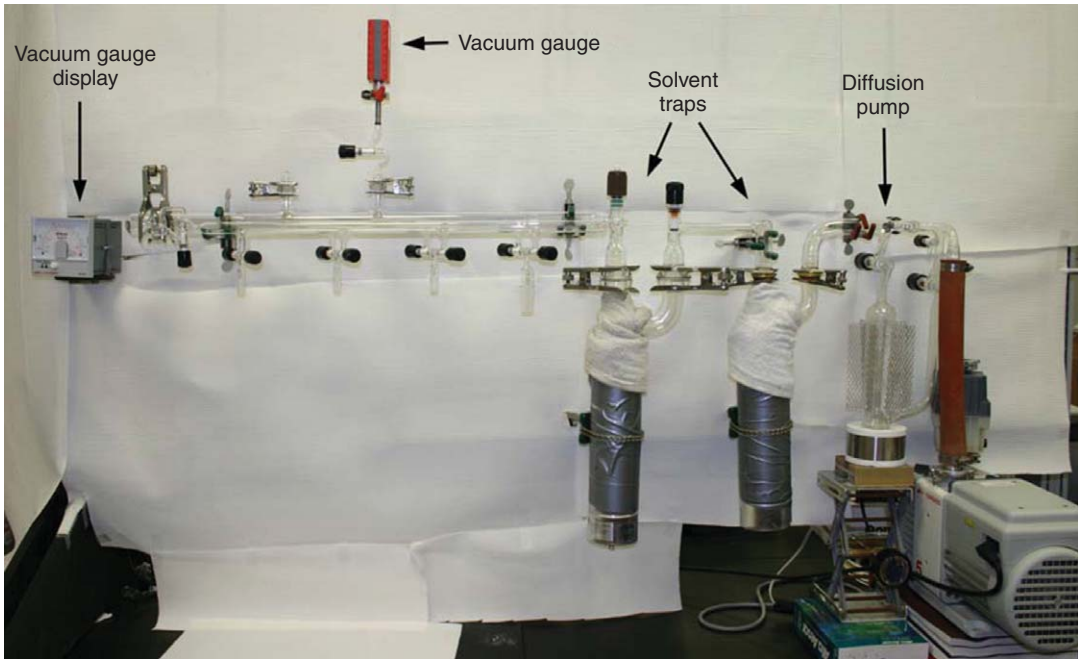

(b)

Figure 1 (a) Schematic diagram of a standard double manifold. (b) Photo of an actual high vacuum line system.

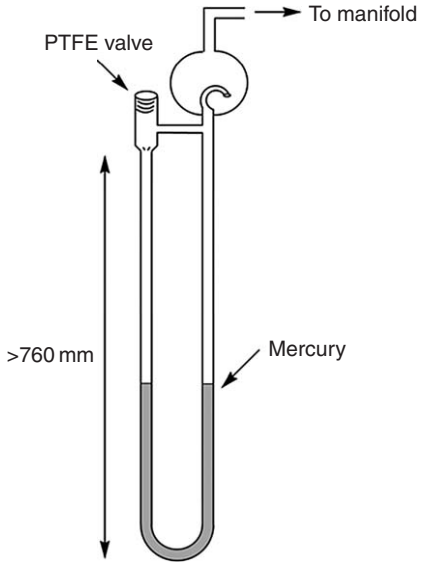

Figure 2 Diagram of a U-shaped mercury manometer for reliably introducing 1 atm of gas into a reaction vessel attached to a high vacuum line. Initially, both sides of the U-shaped column are evacuated along with the rest of the high vacuum manifold. Once a high vacuum has been obtained, the PTFE valve on the manometer is closed, and the high vacuum line is isolated from the vacuum source. Then the gas of choice is introduced into the main manifold until the mercury level advances 760 mm. The manifold is now charged with 1 atm of gas.

The nitrogen/inert gas line of a double manifold can have a number of different designs. The first major consideration is that the inert gas inlet has to be regulated so that pressure does not build up and explode the glass manifold. A dual-stage regulator attached to the inert gas tank is the primary means of controlling pressure. In addition to the regulator, bubblers can be linked to the line to not only provide a pressure release system but also to provide a means to monitor the general flow of nitrogen in the line. Oftentimes one has to introduce the inert gas from a manifold into an evacuated reaction flask. This becomes a tricky process, especially if a bubbler is employed on the nitrogen line, since one has to take care that oil and/or air does not surge into the line once it is opened to the evacuated flask. A common method to avoid such a situation is to use reasonably high positive pressures of nitrogen (being careful not to exceed the safety limits of the glass!) and opening the valve to the evacuated flask slowly enough so that the oil does not flow back into the line. If introduction of inert gas from a manifold into an evacuated reaction flask is a common procedure, then a pressure release bubbler that contains a check-valve (or "firestone valve") to prevent oil or air from surging into the flask may be a good investment.

(ii) *The solvent traps*. Solvent traps are necessary on a vacuum apparatus to prevent organic solvents from ultimately reaching the vacuum pump, where they can mix with and degrade the pump oil. This degradation can be harmful to the pumps, especially direct drive pumps, where the vanes are susceptible to freezing. To prevent these situations from occurring, two, often three, liquid nitrogen traps are placed between the main double manifold where solvents enter the line and the vacuum/diffusion pumps. The traps are designed to be removable, and are separated from the main line and pumps through a series of valves. Figure 3 shows a typical arrangement of two traps in series.

Some solvents have extremely low melting points, so multiple traps are needed to ensure that organic vapors will not reach the pumps. The traps need to be removable so that the condensed solvents can eventually be discarded, and can range in sizes depending on the volumes of solvents being condensed. While the bigger traps are useful in evaporating large amounts of solvents, they also require larger amounts of liquid nitrogen to keep the solvents condensed. Figure 4 shows two sizes of solvent traps. A spare glass trap is handy for rapidly getting the vacuum line up and running while the condensed solvents in the removed trap melt. A spare trap is also recommended to avoid downtime in the event that one trap breaks and needs to be repaired by a glassblower.

(iii) *The vacuum pumps*. A series of two vacuum pumps maintain low pressures on the high vacuum line. The rough forepump usually consists of a direct drive or belt-driven pump which is ultimately exhausted to a fume hood.

Figure 3 Two solvent traps in series. The left trap is connected to the manifold by O-ring joints while the right trap is connected through ball and socket joints.

Because the rough pump can only bring the pressure in a vacuum line down to $\sim 10^{-3}$ torr, placement of a diffusion pump in between the rough pump and the vacuum line helps achieve pressures down to 10^{-4} torr.

Both mercury and oil diffusion pumps are commercially available. The oil-based pumps achieve lower pressures but need to have their oil changed on a regular basis. The mercury-based pumps can go years without having to be changed; however, the health hazards of mercury have led to a general decline in their use. Fan-cooled

Figure 4 Solvent traps can be designed to handle both small (left) and large (right) amounts of solvent.

diffusion pumps are preferred for settings that often require maintenance on the chilled water supply since they do not have to be shut down during any maintenance procedures. The manufacturers of diffusion pumps typically supply instructions with the equipment, so their operational details will not be discussed further in this review.

1.07.2.1.1 Operation of a high vacuum line

Transport of air-sensitive materials to and from a double manifold requires that samples be placed in flasks containing isolation valves which can be linked to the manifold ports. The use of custom-designed one-piece flasks (Figure 5) is perhaps the best way to avoid leaks throughout an air-free manipulation; however, equipping a laboratory with only one-piece flasks is extremely expensive. A more versatile solution is to purchase or design resealable adaptors which can readily attach cheap commercially available glassware to the double manifold. These adaptors are typically designed by a glassblower by means of fusing a resealable PTFE valve to joints that match the manifold and the flask. The adaptors also minimize expenses in the lab, since if a reaction flask breaks, the only piece of equipment that needs to be replaced is commercially available. An example of a round bottom flask attached to a workstation on a high vacuum line via a custom-made adaptor is shown in Figure 6.

1.07.2.1.2 Solvent removal

Now that the basic components of a high vacuum line have been described, it is worth describing in detail the use of a vacuum line for a common laboratory scenario. Take, for instance, a case where a sample needs to be placed on a manifold for solvent evacuation and then later removed without ever being exposed to the air. Such a scenario is common after working up reactions inside a glovebox. The first step in the process is to attach a resealable adaptor to the round bottom flask containing the sample and stir bar (taking care to grease the joints on the adaptor and to close the PTFE valve) in the glovebox. Then, the flask that has been fitted with the adaptor is secured to a port on a double manifold with Keck clips (or rubber bands, or pinch clamps, etc.), and a stir plate is placed below the flask. Next, while leaving the valve on the adaptor closed, the valve on the manifold port is opened to vacuum to remove the air that is trapped between the port and the adaptor valve. Once the pressure on the active gauge display returns to low pressure, the valve on the adaptor can be opened to evaporate the solvent. Evaporation to dryness can be confirmed by monitoring the pressure with the gauge. Once low pressure has again been obtained, the valves on both the manifold port and adaptor are closed. This process seals the flask under a vacuum. The flask with the adaptor can finally be released from the manifold by removing the Keck clip holding the adaptor to the line, opening the nitrogen

Figure 5 (a) Example of a standard taper round bottom flask and its adaptor for use on a high vacuum line. (b) Example of a one-piece flask designed for use on a high vacuum line.

Figure 6 A round bottom flask fitted with an adaptor and attached to a high vacuum line.

valve on the manifold port, and gently pulling the adaptor from the manifold. Since the valve on the adaptor is closed, the sample still remains under vacuum. Now the flask with the sealed adaptor can be brought back into the glovebox (Section 1.07.5.2) and opened under an inert atmosphere for further manipulations. At this point in the process it is advisable to empty the solvent trap of the high vacuum line into the appropriate waste container to ready the line for the next user or application.

1.07.2.1.3 Degassing of a solution

One of the most effective ways to degas a solution is on a high vacuum line using what is referred to as the "freeze–pump–thaw" method. Here a solution containing a stir bar is attached to the vacuum line with the aid of an adaptor as shown in Figure 6. A vacuum is applied up to the PTFE valve of the adaptor, and a dewar of liquid nitrogen is then used to freeze the solution in the flask. Once the solution is frozen, the PTFE valve of the adaptor is opened to the vacuum and any gas that is in the headspace of the frozen solution is evacuated. The gas removal can be confirmed with the use of a pressure gauge. Once a low pressure has been obtained, the PTFE valve of the adaptor is closed and the frozen solution is allowed to thaw. A warm water bath placed on top of a stir plate can be used to facilitate the thawing process. The thawing of the solution allows for any trapped gas bubbles to escape into the headspace of the flask. Repeating this freeze–pump–thaw cycle three times provides quite reliable degassing of standard size reaction flasks.

1.07.2.1.4 Quantitative gas transfers

Another useful feature of a high vacuum line is the ability to transfer precise amounts of gas. For such an operation, a flask of known volume (usually a one-piece flask to prevent leaks) is attached to a workstation and evacuated on a high vacuum line. Then, as described in Figure 2, 1 atm of desired gas is introduced into the system, and the valve of the volumetric flask is closed once the flask contains 1 atm of gas. The number of moles of gas in the volumetric flask can then be determined from the ideal gas law. Introduction of this known quantity of gas into another reaction vessel can then be performed by standard vacuum transfer techniques (Section 1.07.4.4).

At this point it should be mentioned that care must be taken to distinguish between condensable and non-condensable gases. The temperatures involved in gas transfers on a high vacuum line are low enough that many common gases such as methane, ethane, ethylene, O_2, CO, CO_2, can readily condense in a liquid nitrogen cooled

reaction vessel. If the vessel is a closed system, then upon warming of the condensed gas an explosion is likely to ensue. Thus, it is important to only transfer known volumes of condensable gases that are capable of being held safely by the reaction vessel. A rule of thumb is that as long as the volumetric flask is smaller than the available volume of the reaction flask where the gas is being transferred (assuming 1 atm), then pressure will not build up upon warming of the transferred gas. Another common mistake is to forget to remove a liquid nitrogen dewar from a receiving flask or trap once a vacuum has been turned off. Oxygen from the air can condense in such vessels and cause explosions once a sufficiently warm temperature has been achieved.

1.07.2.2 Schlenk Lines

Schlenk lines contain the same double manifold that can be found on high vacuum lines, but are designed to carry out more dynamic techniques such as cannula transfers or operations that require joining multiple pieces of Schlenk ware. Thus, quite often the workstations on a Schlenk line are not standard taper ground-glass joints but rather hose connections for flexible tubing. Since Schlenk lines typically do not have an additional diffusion pump in series with the forepump, they are also more mobile and amenable to fume hood use. Thus, reactions that use low temperature cooling baths or need to be refluxed under a nitrogen atmosphere are typically performed with the aid of a Schlenk line. A huge selection of commercially available Schlenk glassware allows one to perform just about any operation under the exclusion of oxygen, and some basic techniques are described throughout the remainder of this chapter.

1.07.3 Methods of Practical Anaerobic Experimentation

1.07.3.1 Glassware and Preparations

The glassware for air-sensitive experimentation is not only varied but is also constantly evolving. New materials and designs permit safer experimentation and quicker manipulations. Moreover, since double manifolds can easily permit the introduction of inert gases and vacuum to a flask, even standard laboratory glassware can be easily adapted to allow for air-sensitive operations. The Schlenk tube (Figure 7) is the prototypical flask used in air-sensitive operations. It consists of a reservoir to hold samples/solvents and a valve to attach the flask to a source of nitrogen or vacuum. The valves can have greaseless Teflon or O-ring seals or may also be constructed from a ground-glass stopcock that needs to be greased for an airtight seal. The Schlenk tubes also have standard taper ground-glass joints to allow for a variety of connections to other pieces of glassware.

Figure 7 A commercially available Schlenk tube containing a PTFE valve. The valve, tube, and ground-glass joint sizes may vary.

Before introducing an air-sensitive compound into a reaction vessel, the inside of the reaction vessel needs to be placed under an inert atmosphere. On a Schlenk line, this is usually achieved through a number of "pump–fill" cycles. The first step in a pump–fill cycle consists of attaching the vessel to the flexible tubing that is linked to a workstation on the double manifold. The vessel is then sealed with a greased ground-glass stopper. Septa should not be used to seal flasks that must be evacuated because they do not hold a vacuum very well and may even be sucked inside the flask, exposing the compound to air. Septa are generally used only for manipulations that involve positive pressures of nitrogen. A possible exception is the use of inverted joints with septa of the correct size. These combinations lead to sufficiently tight seals that are difficult for the septa to penetrate. Once the flask is sealed and attached to the Schlenk line, the flask is evacuated by opening the workstation valve for the vacuum line on the double manifold. After a substantial amount of oxygen has been removed from the flask, the valve to the vacuum source is closed and the vessel is filled with inert gas by opening up the valve to the nitrogen manifold on the Schlenk line. These pump–fill cycles are repeated at least three times to ensure that the vessel is air-free. A second method for removing oxygen involves flushing an empty flask with an inert gas to displace any oxygen. This method works best with argon, which is heavier than oxygen, but can be employed with nitrogen as long as no part of the apparatus is bypassed by its flow.

Once an inert atmosphere has been achieved in the vessel, the ground-glass stopper can be replaced by a rubber septum so that cannula transfers, syringe additions, or other manipulations involving positive pressures of nitrogen can be facilitated. The exchange of a glass stopper by a rubber septum is achieved by exerting a positive pressure of nitrogen on the flask. The pressure should be large enough to gently force out the ground-glass stopper and prevent any atmospheric gases from entering the flask. To guarantee that the system is producing a strong enough positive pressure, connect a piece of tubing to a vent needle that is plunged into the septum on one end and to an oil bubbler on the other end. When the septum is placed on the flask, bubbles should be appearing in the bubbler. Once the septum has been secured to the flask, the pressure is then adjusted so the septum will not pop off (not a problem when using inverted joints).

1.07.3.2 Additions and Cannula Transfers

Additions to compounds under an inert atmosphere can occur in a variety of ways. Four common methods include:

(i) rapid addition of air-stable solids under a positive pressure of nitrogen,
(ii) addition of air-sensitive solids via solid addition funnels,
(iii) liquid or gas additions via syringes, and
(iv) cannula transfer of liquids.

If a solid that is not air sensitive needs to be added to a reaction vessel, then (under a strong positive pressure of nitrogen) the septum or stopper may be removed and the solid can be added directly with a spatula. Often a powder funnel is placed over the opening before the addition to prevent the solids from sticking to the joints or to the sides of the flask.

The addition of air-sensitive solids is trickier and is best performed in a glovebox or glovebag. However, if these are unavailable, or not amenable to the experiment on hand (like variable temperature additions), then commercially available solid addition funnels may suffice. The commercially available addition funnels are not always rigorously air free, however. A simple, more rigorously air-free alternative is a ground-glass sidearm such as that shown in Figure 8 in which one end is fused-closed. With this custom-made accessory, the solids rest on the slanted sidearm and are then added by carefully tapping the sidearm allowing the solids to slowly fall into the flask.

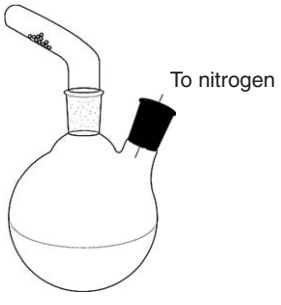

Figure 8 A simple sidearm extender fused at one end can make a good solid addition apparatus.

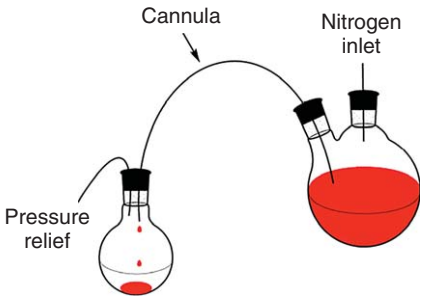

Figure 9 Schematic diagram representing the correct operation of a cannula for the transferring of voluminous liquids.

When using a syringe for solution additions and withdrawals, the syringe is often initially purged multiple times by inserting it into the septum of the flask, slowly drawing up the inert gas of the system, and expelling the gas outside of the system. This needs to be done under a positive pressure of nitrogen, because anytime gas or liquid is withdrawn from a system a partial vacuum is created that needs to be filled with inert gas before oxygen leaks into the system. This fact should be especially kept in mind when withdrawing air-sensitive reagents packed in Sure/Seal™ containers. If a secondary needle to an inert gas source is not inserted into a Sure/Seal™ container while the solution is withdrawn from another syringe, then upon removal of the withdrawing syringe, oxygen will rush into the container and contaminate the reagent. Once a syringe is filled with a liquid, it is usually adequate to quickly insert the syringe into the rubber septum of the reaction vessel and release the contents into the flask. Small volumes of gases may also be added to a vessel under similar conditions, with the only additional requirement of employing gas-tight syringes.

A cannula is especially useful in transferring copious amounts of liquids. It is simply a hollow piece of Teflon or stainless-steel tubing containing double-tipped non-coring ends. In other words, it is a double-ended needle. To transfer solvents or solutions, a cannula is inserted into a solution in one flask that has a positive pressure of nitrogen above it. The other end is then inserted into a receiving flask containing a pressure relief (Figure 9). A cannula transfer operates by forcing nitrogen into the solution vessel through a septum causing a buildup of pressure. Because of this pressure buildup, new septa should be used whenever possible, as older septa tend to leak and could slow down the transfer process. The pressure buildup forces the liquid in the solution vessel through the cannula needle and into the receiving flask in order to relieve the pressure. It is very important to relieve the pressure in the receiving flask through an extra syringe needle vent or bubbler. The rate of addition can be controlled by adjusting the flow rate of nitrogen entering the flask or by adjusting the rate at which pressure is relieved. Adjusting pressure relief is possible through the use of a bubbler containing a pinch clamp attached to its tubing. The transfer can be stopped altogether simply by removing the submerged cannula from the liquid. Cannulation of a solution from a suspended mixture can also be performed by securing filter paper or a sintered filter over one end of the cannula needle.[7]

1.07.3.3 Filtering and Washing

By far, the quickest and easiest method of filtering and washing air-sensitive compounds is by standard benchtop methods inside of a glovebox. For filtration outside of a glovebox, a variety of Schlenk-ware is available to filter reaction flasks without ever exposing the system to oxygen. Filtration can also be performed on a high vacuum line by means of a swivel frit. The swivel frit is composed of a fritted glass funnel with connections for both a reaction flask and a receiving flask. The frit is also constructed with a double manifold connection and a valve that can control the flow of pressure on both sides of the frit. A diagram of a typical swivel frit and its attachment to a high vacuum line are shown in Figure 10.

To perform a swivel frit filtration, the frit is turned upside down (swiveled) and a slight vacuum is applied through control of the manifold workstation valve to "pull" the solution through the frit where it is collected in the receiving flask. The sidearm bypass valve of the swivel frit is closed during the filtering procedure. The solvents may also be "pushed" through the frit by using a positive pressure of nitrogen from the manifold. Alternatively, the solvents may also be pushed through the frit by heating the reaction flask with a heat gun, or they can be pulled through by cooling the receiving flask in a low temperature bath.

(a)

(b)

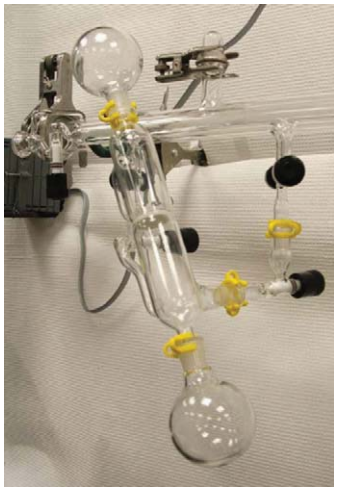

(c)

Figure 10 (a, b) Different views of a swivel frit designed to be used on a high vacuum line with the use of an adaptor. (c) Picture of a swivel frit/round bottom flask assembly attached to a high vacuum line with the use of an adaptor.

The insoluble material collected on the fritted disk of the swivel frit can then be washed using some clever vacuum transfer techniques. First, the solution in the receiving flask is degassed by several freeze–pump–thaw cycles. Then, the solution is warmed with stirring on a water bath, and the sidearm valve of the swivel frit is opened. Next the top flask is swabbed with a dry ice/acetone slurry. A good swab can be constructed from pipe-cleaner wrapped around the tip of a spatula. "Clean" solvent from the filtrate should then condense at the cold, swabbed areas of the top flask. Upon warming, this condensed solvent will run down the sides of the swivel frit and effectively wash the solid material. At this point the sidearm valve can be closed again and the filtration process can be repeated.

1.07.3.4 Crystallization

Schlenk and high vacuum line techniques can be used to perform standard protocols of crystallization such as concentration of solvent, cannula transfer of solvent in which the solute is not soluble, and cooling of a solution to a temperature that leads to precipitation of the solute. In effect, slowing down each of these techniques will produce

larger crystals which could be used for X-ray diffraction experiments. There are advantages and disadvantages to growing X-ray quality crystals with organometallic compounds. One advantage is that most organometallic compounds contain at least one heavy atom, which can aid in recovering phase information in a diffraction experiment. However, the fact that most organometallic compounds are also air sensitive requires some extra care and specialized techniques to both grow and mount crystals. Common methods of crystal growth for organometallic compounds are described below.

1.07.3.4.1 Vapor diffusion

Vapor diffusion is one of the best methods to grow large crystals from a minimum amount of material. This method involves taking a concentrated solution of your sample, say in a small test tube, and placing the test tube inside of a larger Schlenk tube that contains a solvent to precipitate your compound. The Schlenk tube is then sealed tightly and the apparatus is left undisturbed throughout the crystal growth process. Crystals will grow by means of slow vapor diffusion of precipitating solvent from the outer Schlenk tube into the smaller test tube. The same technique can be performed inside of a glovebox using a small vial placed inside a larger one, taking care that the outer vial is equipped with a Teflon-lined or chemically resistant cap. The precipitating solvent should have a lower boiling point than that used in the inner vial. Figure 11 shows a typical setup for vapor diffusion crystal growth inside of a Schlenk tube.

1.07.3.4.2 Solvent layering

This is a simple method by which a precipitating solvent is added slowly enough to a concentrated solution of a sample so that layers form. The vessel is then allowed to stand undisturbed while the two layers slowly mix causing crystal growth. The slow addition of solvent can be achieved in a glovebox by placing a pipette tip on the inner side of the vial containing a solution of the sample and slowly pipetting in the precipitating solvent. With a Schlenk flask, slow addition of the solvent can be achieved by careful cannula transfer of the precipitating solvent from another flask. This method takes practice, and care must be taken so that the flow of the solvent is slow and runs down the side of the Schlenk tube to prevent rapid mixing. The solvent layering method is often combined with the slow cooling process to prevent decomposition of thermally sensitive compounds.

Figure 11 Picture of a vapor diffusion setup for crystal growth inside a Schlenk tube. Solvents are colored for better visual aid.

1.07.3.4.3 Slow cooling

This method works well for compounds that are highly soluble in hydrocarbon solvents. Here, the idea is to cool a concentrated solution of a sample as slowly as possible to produce large crystals. This might be achieved by placing a Schlenk tube containing a solution of the material in a plastic or Styrofoam container before placing in a refrigerator. The only complication with this technique is that care must be taken to ensure the integrity of any valves throughout the cooling process. Grease may freeze and produce channels for oxygen to enter the flask, and PTFE valves can contract causing leaks. Hence, a glovebox fitted with a refrigerator or freezer is ideal for this crystal growing technique.

1.07.3.4.4 Crystal selection and mounting

Once a batch of X-ray quality crystals is in hand, it is usually standard practice to transfer the crystals to a microscope slide in order to choose the best crystal to mount on the diffractometer. With air-sensitive compounds, the easiest way to achieve this is to decant the crystallizing solvent and immerse the crystals in a dense and degassed oil such as Paratone-N, so they can be removed from a vial or Schlenk tube and placed on a slide. The oil forms a protective layer around the crystals that usually prevents oxygen from reacting with the crystals in the amount of time it takes to select and mount the crystal. Paratone-N is an especially nice oil for low temperature crystallography because it is also a cryoprotectant that becomes sufficiently hard upon cooling to −50 °C that additional glue or epoxy is not needed to mount the crystals to glass fibers throughout the data collection.

1.07.3.5 Chromatography

Under appropriate conditions, column chromatography can be performed on air-sensitive organometallic compounds. Cannula transfer techniques allow chromatography to be done on the more stable compounds without the need for custom-made glassware. For these cases, a standard column is packed dry in the fume hood and then a septum and vent needle are attached. Degassed solvents are subsequently cannulated into the column and the adsorbent is packed tightly under a positive pressure of nitrogen. Eluted bands are then collected under Schlenk-type conditions.

If access to a glovebox is available, chromatography on the more air-sensitive compounds can be performed quite readily. Gravity elution is often necessary, but if the glovebox is equipped with either a supplemental nitrogen or vacuum inlet, then flash chromatography would be possible. Figure 12 shows one possible adaptation of standard glassware to perform flash chromatography inside a glovebox using a vacuum source.

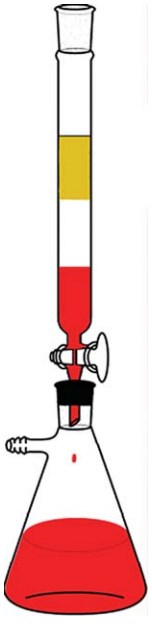

Figure 12 Exploiting a vacuum inlet for flash column chromatography inside a glovebox. The tip of the column is fitted with neoprene filter adapters in order to have a good seal with a standard filter flask. With plenty of solvent on the column and in reserve, a controlled vacuum is then applied to the filter flask in order to rapidly elute the various fractions.

Column chromatography of the highly fragile compounds requires additional care. Sometimes, the adsorbent needs to be prepped before introducing a solution containing an organometallic compound. The author's group has found that, in general, organometallic compounds are quite stable toward activated aluminum oxide (Brockman I, ~150 mesh) that has been heated to 200 °C on a high vacuum line for 2 days before being used. The enhanced stability is perhaps due to the removal of trace amounts of oxygen, water, and/or acid. This rigorous preparation of the adsorbent does not always prevent decomposition, however, and for the extremely sensitive compounds low temperature column chromatography can be performed using columns containing an additional jacket for circulated coolants.[8]

1.07.4 NMR Spectroscopy of Air-Sensitive Compounds

1.07.4.1 Introduction

NMR spectroscopy is routinely used to characterize new compounds, monitor reaction kinetics, measure magnetic susceptibilities,[9] and quantify chemical yields. NMR spectroscopy is also a major technique used to follow exploratory organometallic reactions since thin layer chromatography of fragile, air-sensitive compounds can either be impossible or too tedious. Thus, a wide range of techniques and equipment have been developed to facilitate the use of NMR spectroscopy with air-sensitive compounds. Some essential air-free techniques for a novice in the field are described below.

1.07.4.2 Glassware Involved

The four most widely used NMR tubes used for organometallic chemistry include those equipped with a resealable J. Young valve, those that can be permanently flame-sealed, those containing screw-caps, and standard NMR tubes fitted with a small rubber septum. The most expensive but most versatile NMR tube for manipulating air-sensitive complexes is the one equipped with a J. Young valve (Figure 13). This threaded valve not only forms a tight seal that can be readily opened and closed, but is also designed to attach to a high vacuum line for further manipulations. The high vacuum line capability allows for quantitative transfer of volatiles and gases in and out of the NMR tube.

Permanently sealed NMR tubes are ideal for situations that might cause a J. Young-type NMR tube to leak over time. One such situation involves low temperature reactions in a cold room that may cause the PTFE seal on a J. Young-type NMR tube to contract and leak. Another area of use for a sealed NMR tube is for NMR-scale reactions that take weeks to months to complete. A leak-free environment is thus assured by a permanent glass seal. Sealed tubes also make good NMR reference tubes, as the solvents inside a flame-sealed NMR tube will not evaporate.

Sealing NMR tubes can be done on a high vacuum line using an NMR tube that has been fused to a ground-glass joint assembly (Figure 14). Typically, the NMR tube is loaded with the air-sensitive sample and deuterated solvent inside of a glovebox. Then a high vacuum line adaptor is attached to the ground-glass joint and the whole apparatus is removed from the glovebox and attached to the high vacuum line. Upon cooling the solution to −196 °C, the NMR tube is evacuated. The reduced pressure in the NMR tube causes the walls to collapse upon

Figure 13 Top of a J. Young NMR tube (left), a J. Young valve (center), and a manifold adapter for a J. Young NMR tube (right).

Figure 14 An NMR tube blown to a standard taper ground-glass joint.

treatment of the upper section of the tube with a cool flame from a glass-blowing torch. A torch which uses natural gas (or propane) and oxygen is best, as a hydrogen/oxygen torch produces flames that are too hot. The sample solution is always kept at −196 °C throughout the flame-sealing process to maintain low pressures in the vacuum line and to prevent ignition of the solvent in the event of a crack in the NMR tube during the flame-sealing process. The flame sealing should also be performed using shaded glassblowing goggles that provide protection against the sodium flare. Once a seal has been made, it is advisable to turn off the oxygen gas and anneal the tube with the natural gas flame. Annealing should be continued until a thin carbon black deposit appears on the surface of the glass. Since the glass of a sealed NMR tube may have additional stress points remaining, the solution should be allowed to warm to room temperature behind proper shielding. Moreover, if the sealed NMR tube is to be subsequently heated in the NMR spectrometer, testing the integrity of the tube by brief heating in an oil bath is recommended to prevent damage to the NMR probe.

Sealing NMR tubes has been made easier by the introduction of commercially available sealing adaptors, which allow one to tip off standard NMR tubes without the need of additional sealing to ground-glass or O-ring joints. Commercially available NMR tubes that are constricted on one end to allow for rapid and symmetrical flame sealing are also available, and a device to conveniently seal and open NMR tubes under air-free conditions has been described elsewhere.[10]

The use of screw-capped tubes (Figure 15) is a rapid way to seal an NMR tube inside of a glovebox, although these tubes cannot be adapted to versatile high vacuum line techniques. Screw-capped tubes contain small seals that permit the introduction of fluids by either syringe or cannula to avoid contamination. The seals on screw-cap NMR tubes are not as tight as for J. Young valves, and should only be used for mildly air-sensitive compounds.

Figure 15 Screw-capped septum NMR tube.

Figure 16 An NMR tube fitted with a small rubber septum.

Attachment of a rubber septum to a standard NMR tube (Figure 16) is the least expensive method for manipulating air-sensitive organometallic compounds. This method works well for sample preparations inside a glovebox. Like a screw-capped tube, one can inject or transfer liquids via cannula liquid into the tube. Caution must be used when attaching a septum to an NMR tube because the thin-walled tube has the potential of breaking.

1.07.4.3 Deuterated Solvent Preparation

Rigorous drying and degassing of the deuterated solvent must typically be performed before exposure to an organometallic compound. Deuterated solvent is placed in a round bottom flask containing a stir bar and the appropriate drying reagent, and multiple freeze–pump–thaw cycles are performed to remove any dissolved gases in the solvent. Stirring the degassed solvents overnight over a large amount of drying agent (or until a color indicator confirms dryness) is usually adequate. Once the solvent is dry, small quantities can be vacuum transferred directly into an NMR tube on a high vacuum line (see below). Alternatively, the bulk dried and degassed solvent can be vacuum transferred into one-piece greaseless ampoules such as those shown in Figure 17 for long-term storage.

1.07.4.4 Transfer of Deuterated Solvents

Although deuterated solvents can be stored in a glovebox and simply pipetted into NMR tubes, there is a risk of contamination from vapors from other solvents that might also be present in the glovebox atmosphere. Purging a glovebox with copious amounts of nitrogen may help reduce contamination of the deuterated solvent. An alternative and cleaner method for transfer of deuterated solvent involves the use of a high vacuum line according to the following basic protocol: an ampoule containing dried and degassed deuterated solvent (like that shown in Figure 17) is placed on a high vacuum line and the manifold is evacuated up to the needle valve of the ampoule.

Figure 17 Air-free ampoules used for deuterated solvent storage and transfer.

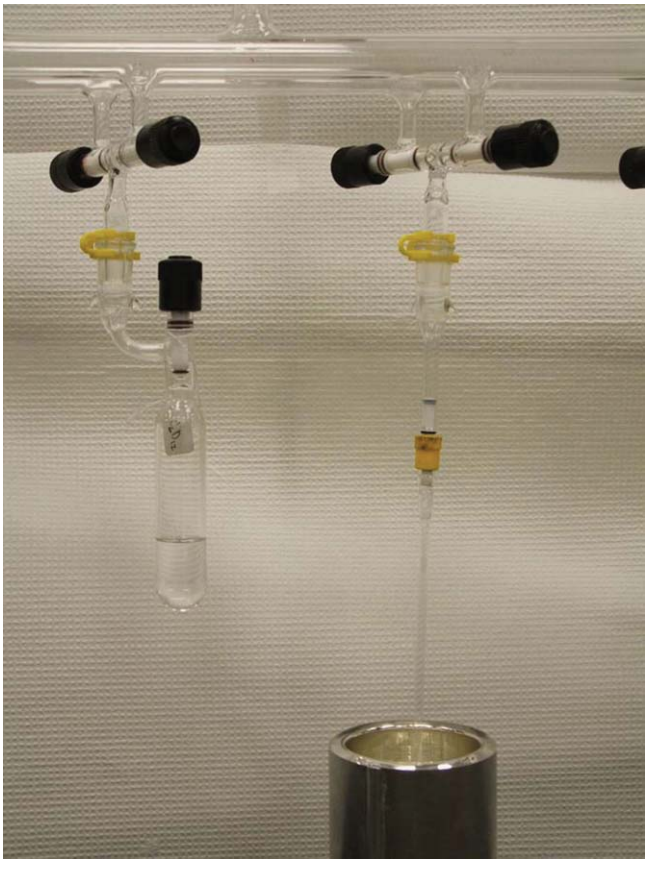

Figure 18 Typical setup for transferring deuterated solvents on a high vacuum manifold.

An NMR tube containing a J. Young valve is also placed on the manifold (Figure 18) and fully evacuated. A dewar containing liquid nitrogen is then placed under the NMR tube and the bottom portion of the NMR tube is chilled. Next, the main valve to the vacuum source on the high vacuum line is closed, creating a static vacuum between the ampoule and the NMR tube. Immediately after the line is isolated from the vacuum source, the needle valve on the ampoule containing the deuterated solvent is opened. The temperature difference causes the solvent from the ampoule to be transferred into the chilled NMR tube. Once an appropriate amount of solvent has been transferred, the valves on both the ampoule and the NMR tube are closed, and the manifold can be evacuated once again. The NMR tube is then carefully thawed, usually with organic solvents like acetone, to prevent cracking. The rate of transfer of deuterated solvent will depend upon its vapor pressure, the temperature of the solvent pot (a hot water bath could facilitate transfer), and the ultimate pressure in the vacuum line.

1.07.4.5 Transfer of Gases into an NMR Tube

The transfer of 1 atm of gas into a J. Young NMR tube is most easily accomplished on a high vacuum line with the aid of a U-shaped manometer (Figure 2). During the transfer of gas, the manometer, the NMR tube, and a hose connection to the gas regulator will all be attached to the vacuum manifold. However, before the gas transfer, the solution in the NMR tube must be freeze–pump–thawed to ensure that there is no residual nitrogen atmosphere in the tube. Care must also be taken to thaw the deuterated solution before the gas transfer, so an excess of gas is not condensed into the tube, which may lead to an explosion. Once the vacuum line is charged with 1 atm of gas, the J. Young valve is opened briefly to allow the gas to enter the tube, and then the valve is closed.

1.07.5 Glovebag and Glovebox Techniques

1.07.5.1 The Glovebag

The glovebag allows chemists to manipulate air-sensitive compounds while maintaining an inert atmosphere less expensively than a glovebox. Glovebags are commercially available plastic bags containing hand ports that permit a variety of temporary solutions to many air-sensitive applications. One advantage glovebags have over gloveboxes is the ability to quickly introduce more expensive inert gases such as argon. This feature comes in handy when working with such compounds like lithium metal, which cannot be handled under a nitrogen atmosphere. Glovebags are also more mobile than gloveboxes, and may be employed in small rooms or over various pieces of equipment. For instance, air-sensitive solids can also be conveniently weighed with a glovebag by placing the entire balance inside the bag. This procedure would eliminate the need for storing air-sensitive reagents permanently inside of a glovebox.

Techniques needed for using a glovebag are quite simple. First, make sure there are no holes in the glovebag prior to use. Any wires or tubing that span that plastic membrane should be sealed to reduce the infiltration of atmospheric air inside the bag, which could be potentially dangerous. This can simply be done by wrapping the exit ports with excess Parafilm®. Before opening air-sensitive complexes in the glovebag, purge multiple times to assure an inert atmosphere in the glovebag. Keep a constant pressure of gas to assure no other gases are entering the glovebag. Once one has finished using the glovebag, the air-sensitive compounds should be resealed and the glovebag opened to remove the contents. Glovebags can be reused as long as the plastic integrity of the glovebag is not compromised.

1.07.5.2 The Glovebox

1.07.5.2.1 Introduction

The inert atmosphere glovebox allows one to handle air-sensitive compounds without having to use complicated Schlenk-like glassware. This greatly reduces the amount of time needed to perform anaerobic reactions, especially those involving a lot of manipulations of solids. A wide range of gloveboxes are commercially available, and can come with a custom number of glove ports, refrigerators, cold wells, electrical leads, built-in solvent taps, etc. These amenities further facilitate the workup of air-sensitive organometallic reactions, and the glovebox has evolved from a place to just store air-sensitive solids to a full benchtop replacement. Glovebox work is also ideal for training new students in the field of organometallic chemistry, as chemical fires can be minimized because of the "leak-free," low-oxygen-level environment.

1.07.5.2.2 Glovebox catalyst and atmosphere

Gloveboxes maintain their inert atmosphere either by constant purging of the box with a positive pressure of inert gas, or by removing the moisture and oxygen from the inert atmosphere of the glovebox by recycling an inert atmosphere though a catalyst. If properly maintained, a glovebox can provide an inert atmosphere with oxygen levels less than 1 ppm. For gloveboxes that are not on a constant purge, it is important to realize that any volatile materials that are brought into the box have a certain vapor pressure and can eventually contribute to the glovebox atmosphere. This partial evaporation of solvents inside the box can in turn contaminate other solids and reagents that are stored inside the box. For instance, THF use in a glovebox may interfere with the synthesis of extremely oxophilic and solvent-free lanthanide complexes. However, solvent mixing can be minimized by regular purging of a glovebox under a rapid flow of inert gas, and it is ultimately up to the discretion of the user whether to permit solvent use in a glovebox. Another disadvantage of using solvents in the box is that, over time, solvents can interfere with the ability of the regeneration catalyst to remove oxygen and water and can also limit the lifetime of any oxygen and water sensors that are in use. Regeneration cycles on contemporary gloveboxes do contain extended evacuation cycles which aid in solvent removal from the catalyst bed. Nevertheless, some volatiles absolutely cannot be used in the glovebox because they will permanently poison the catalyst, and the owner should refer to the glovebox manual for a list of chemicals that should be avoided. Typically for gloveboxes employing copper-based catalysts, the following volatiles should be avoided: amines, halogenated solvents, alcohols, phosphines, and thiols. One can also minimize exposure of the catalyst to certain volatiles simply by isolating the catalyst from the atmosphere by closing the circulation valves during solvent use, and then thoroughly purging the atmosphere before the valves are reopened. The term "dry box" is often used for gloveboxes that are set aside to be solvent-free.

1.07.5.2.3 Monitoring the environment of a glovebox

The integrity of the atmosphere of a glovebox can be tested by a few classic methods. The light bulb test estimates the total amount of oxygen inside the box by the time it takes a light bulb filament to burn out when exposed to the glovebox atmosphere. Exposure of the filament to the atmosphere can be achieved by etching a hole in a standard light bulb. If the filament burns out in less than 6 hours, the oxygen/moisture levels are greater than 5 ppm. If the filament burns for days (or weeks!), then the oxygen/moisture levels are between 1 and 5 ppm (see Vac-Atm glovebox instruction manual). For more precise calculation, the filament lifetime relative to ppm oxygen levels can even be calibrated.[11]

A chemical test for the residual moisture levels of a glovebox can be performed with a bottle of titanium tetrachloride ($TiCl_4$). If upon the opening of the bottle a white smoke is immediately produced, it quickly indicates the presence of moisture in the glovebox atmosphere. Chemical tests, while rapid and inexpensive, also may evolve HCl or other impurities that could harm the catalyst. Consequently, purging of the atmosphere with nitrogen should be performed immediately after chemical testing of the glovebox environment. Gloveboxes may also be purchased with convenient digital oxygen and water sensors, and retrofitting older gloveboxes with the newer sensors has become relatively inexpensive. Such sensors can rapidly and continuously monitor the glovebox atmosphere and are highly recommended.

1.07.5.2.4 Sources of impurities

Maintaining an air- and moisture-free box is a constant struggle. Major sources of impurities stem from leaks, normal diffusion of air and moisture into the glovebox atmosphere, and outgassing from porous materials. Leaks can occur anywhere there is a bad seal; however, the major source of leaks in a glovebox is from tears or puncture holes in the rubber gloves. If a small hole is found in the glove, then a simple bicycle repair kit or electric tape can be used as temporary repair. Larger holes in gloves require the gloves to be replaced, so often a set of replacement gloves are kept in the laboratory in case of an emergency. Replacement gloves come as one-piece bonded gloves or two-piece sleeve/glove combinations. The two-piece units provide the convenience of quick, easy glove replacement without having to remove or replace the entire sleeve from the glove box.

Diffusion of air into a glovebox is usually only a concern for gloveboxes containing a large amount of glove ports or a significant amount of plastic construction. Diffusion of air and moisture is accelerated by heavy use, and body heat can increase diffusion of air, and sweat can contribute to diffusion of moisture through the rubber gloves. Typically, there is nothing much one can do to prevent normal diffusion of air and moisture from occurring, so more attention is placed on maintaining an active regeneration catalyst to maintain an inert environment. One can, however, minimize a good deal of contaminants that may arise from the slow outgassing of porous materials. Cork rings, pencils, paper, and other wood-based materials are to be avoided inside a box. If one desires to use Kimwipes or other cloth materials, they should at least be evacuated overnight inside the antechamber before being brought inside.

1.07.5.2.5 Antechamber

The primary disadvantage of a glovebox is that some time is needed to bring materials in and out of a glovebox. The antechamber is the chamber separating the inside of the glovebox from the outside environment. In order to bring items into the glovebox, the outer antechamber door is opened (making sure that the inner door is closed), the contents are placed inside the antechamber, the outer door is closed, and a vacuum is applied to remove oxygen. The amount of time the antechamber is pumped down depends both upon the size of the antechamber and the speed of the vacuum pump, but the time may be shortened by multiple pump–fill cycles using the inert atmosphere inside of the box as the filling gas. Mini-antechambers can usually be found on modern-day gloveboxes, and allow one to bring smaller items into the glovebox more rapidly. Once the antechamber is adequately air-free from multiple pump–fill cycles, a final refill is performed and the contents can be brought through the inner antechamber door.

One complication that arises from the need to use pump–fill cycles to bring items into the glovebox is that any solvent or solution that is brought into the glovebox must be degassed on a vacuum line and/or placed in a thick-walled container to prevent the explosion of the flask from the pressure differential of the evacuated antechamber. An example of a thick-walled flask used to bring bulk solvents into a glovebox is shown in Figure 19. This flask contains two ports which can be connected to both a solvent still and a high vacuum line, allowing the direct transfer of the solvent from a still to the flask under anaerobic conditions. Thus, before this flask is placed in the antechamber, the contents are already under vacuum and the seals are strong enough to survive the pump–fill cycles of the

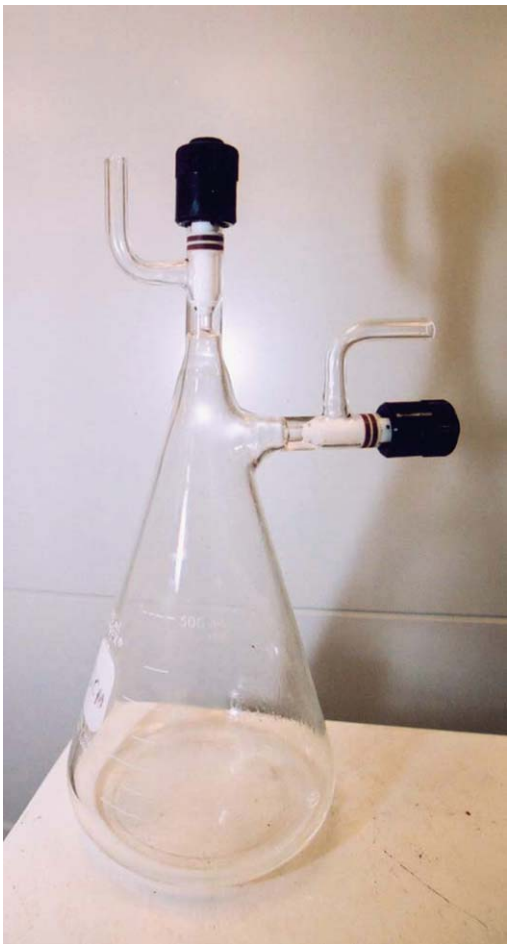

Figure 19 A thick-walled flask used to bring solvents into the glovebox.

antechamber. An additional note is that flasks containing solvent that are sealed with a septum typically cannot survive the pump–fill cycles as the pressure differential will pop off the septum, even if it is secured with wire reinforcements.

1.07.5.2.6 Miscellaneous glovebox techniques

A very useful optional feature of modern-day gloveboxes is the integrated cold well (Figure 20). The cold well contains an external dewar which can be filled with liquid nitrogen or other cooling agents to permit low temperature operations inside of a glovebox. Cold wells are especially nice for low temperature crystallizations, which can be combined with filtration techniques (see below) to rapidly work up reactions under air-free conditions. Combined with a recirculation pump that can handle organic materials, these cold wells can also permit refluxing operations to be performed inside of a glovebox using anhydrous solvent as a cooling fluid. A comparable and inexpensive system that enables the cooling of reactions inside a glovebox without the use of a cold well has previously been described.[12]

Vacuum filtration can be performed in a glovebox after a few minor adjustments. Assuming a port for standard pipe fittings is available on a glovebox, a filtration device can be built that uses a solenoid valve connected to a foot switch on the exterior of the glovebox port, and linked to a safety valve containing a hose connection on the inside of the box (Figure 21). A flexible hose can then be employed for connecting the external vacuum pump to standard filter flasks. Such a setup allows the operator to use both hands inside of the glovebox for performing delicate operations while maintaining control of the vacuum with the foot switch.

Figure 20 Picture of a Vacuum Atmospheres Co. (VAC) glovebox equipped with a cold well.

Figure 21 Picture of a pipe fitting adapted for vacuum filtration use inside a glovebox. The solenoid valve controls an opening to a vacuum source through a foot switch (not shown).

References

1. Lay, P. A. Argon line techniques for the electrochemical generation and manipulation of air-sensitive compounds: an electrochemical Zwickel flask. *J. Chem. Ed.* **1988**, *65*, 1017.
2. Wayda, A. L.; Darensbourg, M. Y., Eds. *Experimental Organometallic Chemistry, A Practicum in Synthesis and Characterization*; American Chemical Society: Chicago, 1987; Vol. 357.
3. Guillo, N.; Perrio, S. General techniques for handling air-sensitive compounds. *Transition Metals in Organic Synthesis*; Oxford University Press: Oxford, 1997; pp 205–214.
4. Ashby, E. C.; Schwartz, R. D. Glove box system for the manipulation of air sensitive compounds. *J. Chem. Ed.* **1974**, *51*, 65–68.
5. Leal, J. P. Manipulation of air-sensitive compounds. *Bol. Soc. Port. Quim.* **1995**, *59*, 56–61.
6. Neilson, A. J. Manipulations of air and moisture sensitive compounds. *Chemistry in New Zealand* **1985**, *49*, 11–14.
7. Shriver, D. F.; Drezdzon, M. A. *The Manipulations of Air-Sensitive Compounds*, 2nd ed.; Wiley: New York, 1986.
8. Buck, R. C.; Brookhart, M. S. In *Experimental Organometallic Chemistry, A Practicum in Synthesis and Characterization*; Wayda, A. L., Darensbourg, M. Y., Eds.; American Chemical Society: Chicago, 1987; Vol. 357, pp 27–29.
9. Sur, S. K. Measurement of magnetic susceptibility and magnetic moment of paramagnetic molecules in solution by high-field Fourier transform NMR spectroscopy. *J. Magn. Reson.* **1989**, *82*, 169–173.
10. Bergman, R. G.; Buchanan, J. M.; McGhee, W. D.; Periana, R. A.; Seidler, P. F.; Trost, M. K.; Wenzel, T. T. In *Experimental Organometallic Chemistry, A Practicum in Synthesis and Characterization*; Wayda, A. L., Darensbourg, M. Y., Eds.; American Chemical Society: Chicago, 1987; Vol. 357, pp 227–229.
11. Eubanks, I. D.; Abbott, F. J. Gas purification and pressure control system for inert atmosphere boxes. *Anal. Chem.* **1969**, *41*, 1708–1709.
12. Schwartz, J.; Cannon, K. In *Experimental Organometallic Chemistry, A Practicum in Synthesis and Characterization*; Wayda, A. L., Darensbourg, M. Y., Eds.; American Chemical Society: Chicago, 1987; Vol. 357, pp 156–157.

1.08
Metal Vapor Synthesis: Principles and Practice

F G N Cloke, University of Sussex, Brighton, UK
P L Arnold, University of Nottingham, Nottingham, UK

Dedication

In memory of Peter Timms (1937–2005), the pioneer of MVS.

1.08.1 Introduction

The simplicity and directness of the approach of using metal atoms and a neutral hydrocarbon to generate organometallic species has made the technique of metal vapor synthesis (MVS) a powerful tool. The origins of the technique lie in the matrix isolation studies on trapping of radicals or high temperature species in low-temperature inert gas matrices pioneered by Pimentel, Linevsky, and others in the late 1950s.[1,1a] The first synthetic use of the vapor of a

normally involatile element was described by Skell who studied the reactions of arc-generated carbon vapor,[2] and it is now more than 30 years since the pioneering work of Timms who reported the first preparative co-condensation routes to organometallics.[3] Since then, the technology behind the apparatus employed for the formation of such metal–ligand species has progressed significantly. In this chapter, we will look briefly at underlying physical and experimental principles of the MVS technique, and then focus our attention on the design, construction, and operation of typical experimental setups.

1.08.2 Principles of the MVS Technique – Thermodynamic and Kinetic Considerations

In principle, an obvious synthetic route to an organometallic complex containing a zerovalent metal is via the co-condensation of the metal atoms with the appropriate ligand molecules. The use of metal atoms in this way gives a twofold advantage over solution techniques as shown in Figure 1. The combined factors described here result in a reduction of the overall energy barrier to any metal–ligand bond forming reaction.

The thermodynamic advantages stem from the more negative free energy of formation of the product of a metal atom reaction (ΔG_g in Figure 1) than that of one synthesized by solution or solid-state techniques (ΔG_s). The discrepancy in total free energy of the two processes is approximately the heat of sublimation of the metal in favor of the metal atom process (B → D instead of A → D). Since the heat of sublimation of a metal can be as high as 837 kJ mol^{-1} (the value for tungsten), the energetic advantage of using atoms can be considerable.

The kinetic activation energy barrier is removed by using a metal atom unencumbered by surrounding ligands that constrain the route available for approaching ligands. The activation energy required for a metal atom and substrate vapor to reach the transition state, TS, ($\Delta G^{\ddagger}_g$) is lower than the activation energy input required to excite the metal and ligands from the solid state ($\Delta G^{\ddagger}_s$). Numerically, this is also by an amount approximating to the heat of sublimation of the metal (B → C instead of A → C). This affords the main kinetic advantage over solution or solid-state techniques. It should be noted that the atoms in the generated metal vapor are not "hot" in a thermal sense although they may have a residual excess energy (e.g., translational) after leaving the bulk metal source. However, the kinetic energy of a species derived from a 3000 °C source is approximately 25 kJ mol^{-1} (≈ 0.25 eV), which is a trivial contribution to the overall energy of the reaction.

1.08.3 Principles of the MVS Technique – Overview of Experimental Requirements

The essential features of the MVS experiment are summarized in Figure 2 below.

The "metal atom source" is typically a furnace operating in a vacuum system; a variety of heating methods for metal vaporization are available, which will be discussed in detail in Section 1.08.4. Operation under vacuum (a) aids

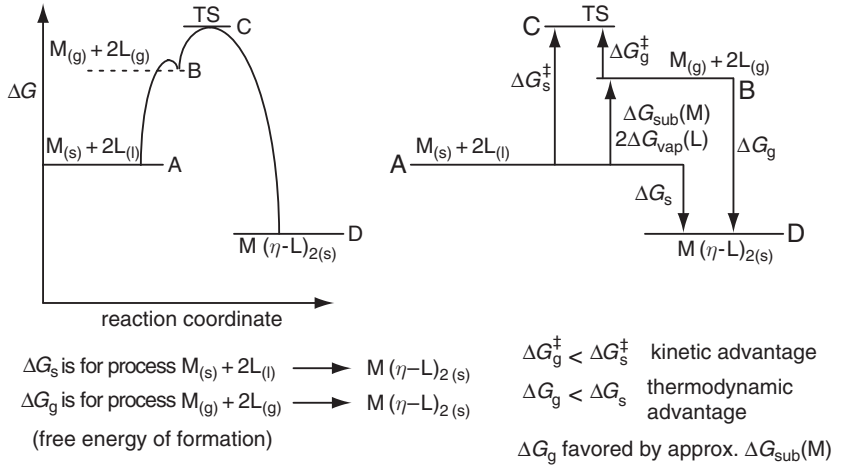

Figure 1 Thermodynamic and kinetic advantages incurred by a reaction using metal vapor over solution or solid-state techniques. Reproduced with permission from the *Journal of Chemical Education*, **1972**, *49*(11).

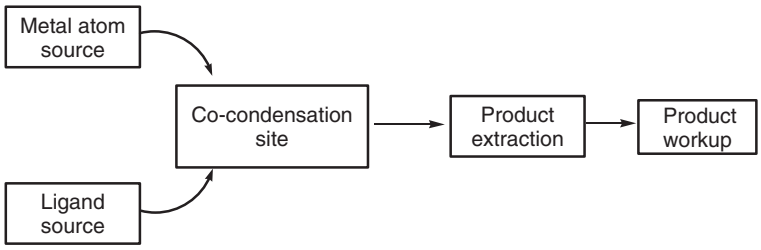

Figure 2 Flow diagram of MVS experiment.

metal vaporization and, most importantly (b) ensures that atoms proceed from the furnace to the reaction site by an essentially collision-free path. The latter puts an upper limit on the operating-system pressure of ca. 10^{-3} mbar.

The "co-condensation site" (Section 1.08.5) is usually the walls of an evacuated glass or metal reactor cooled to liquid nitrogen temperature (77 K) where metal atoms and ligand vapor co-condense to form a solid matrix, thus in a sense mimicking the matrix-isolation experiment, although here the metal atoms are clearly "isolated" in a reactive matrix. In order to statistically minimize recombination of metal atoms back to bulk metal in the matrix and improve product yields, the ligand is usually employed in considerable excess (>10 : 1) over metal. However, in some cases, low ligand : metal ratios may lead to unusual products, for example, the triple-decker sandwich compound [$Cr_2(\eta$-$C_6Me_3H_3)_2(\mu$-η,η-$C_6Me_3H_3)$].[4] Cryogenic temperatures are also usually required in order to keep the vapor pressure of the ligand low ($<10^{-4}$ mbar) and compatible with a relatively long mean free path for the metal atoms. Consequently for ligands of relatively low volatility (e.g., tri-*t*-butylbenzene) it is often possible to use dry ice (200 K) as the refrigerant. This also has an advantage in that the ratio of reaction velocities for product formation versus recombination of metal atoms back to bulk metal increases with temperature, thus potentially increasing product yields. Conversely there are some ligands of potential interest (e.g., CO, CH_4) whose vapor pressures, even at 77 K, are too high to be compatible with the MVS experiment. In principle, one could employ an alternative refrigerant such as liquid hydrogen (B.Pt. 20 K) or liquid neon (B.Pt. 27 K) – liquid helium has a too low heat capacity to be useful – although safety and cost considerations render their use impracticable.

The "ligand source" is simply a nozzle or other vapor dispersion device to introduce volatile co-reactants or gases into the vacuum system and thence to the co-condensation site; co-condensation of metal vapors with solutions of involatile substrates requires special techniques, which will be discussed in Section 1.08.6.

"Product extraction" and "workup" typically involve standard organometallic techniques for the manipulation of air-sensitive compounds, although removal of excess (sometimes relatively involatile) ligand and rapid separation of product from finely divided bulk metal are important considerations (Section 1.08.7).

1.08.4 The Metal Atom Source: Vaporization Techniques and Furnace Design

There are a large number of techniques available for the vaporization of metals and other refractory materials most of whose origins lie in the vacuum-coating industry, although not all are suitable for the MVS experiment (certainly without modification). Table 1 shows the melting point and temperatures at which the vapor pressure is such as to achieve preparative scale evaporation rates (ca. 1 gm hr^{-1} cm^{-2}) under high vacuum conditions (10^{-5} mbar) for metals of interest, together with suitable vaporization methods (*vide infra*).

The various evaporation techniques will now be discussed, together with their limitations and applicability in the context of the MVS experiment.

1.08.4.1 Resistance Heating

This is probably the simplest and most economic method, and was used very effectively by Timms in his original work on MVS of organometallics.[3] The metal evaporant is contained in an alumina (or other refractory oxide) crucible, which is electrically heated by a tungsten or molybdenum wire element wound around the outside of the crucible, (see Figures 3(a) and Figure 4): provision of a tantalum radiation shield cuts down heat loss (Figure 4). A variation on this method employs evaporation from an Mo, W or Ta boat as illustrated in Figure 3(b), and shown in Figure 4.

Table 1 Melting points, vaporization temperatures and suitable vaporization techniques for metals

	Element	*MPt.*	T_{vap}	*Suitable vaporization technique; comments*
3d	Sc	1539	1470	e-beam
	Ti	1660	1830	e-beam
	V	1900	1950	e-beam
	Cr	1860	1480[a]	resist.
	Mn	1242	1020[a]	resist.
	Fe	1536	1570	resist.
	Co	1495	1630	resist.
	Ni	1453	1610	resist.
	Cu	1083	1320	resist.
	Y	1526	1700	e-beam
4d	Zr	1850	2550	e-beam
	Nb	2470	2820	e-beam
	Mo	2620	2610	e-beam, wire
	Tc	2140	2650	e-beam
	Ru	2430	2470	e-beam
	Rh	1966	2130	e-beam
	Pd	1552	1530	resist. or e-beam
	Ag	961	1060	resist.
	La	920	1800	e-beam
5d	Hf	2330	2510	e-beam
	Ta	2980	3140	e-beam
	W	3410	3320	e-beam, wire
	Re	3180	3150	e-beam
	Os	3030	3040	e-beam
	Ir	2454	2550	e-beam
	Pt	1770	2150	e-beam
	Au	1063	1440	resist.
f	Ce	795	2000	e-beam
	Pr	935	1600	e-beam
	Nd	1024	1700	e-beam
	Sm	1072	850[a]	resist.
	Eu	826	700[a]	resist.
	Gd	1312	1800	e-beam
	Tb	1356	1700	e-beam
	Dy	1407	1200[a]	resist.
	Ho	1461	1300[a]	resist.
	Er	1497	1500	e-beam
	Tm	1545	950[a]	resist.
	Yb	824	550[a]	resist.
	Lu	1652	1900	e-beam
	Th	1842	2200	e-beam
	U	1132	2300	e-beam. Very long liquid range; best from URe_2 alloy
s	Li	180	625	resist.
	Na	98	355	resist.
	K	63	265	resist.
	Be	1287	1385	resist.
	Mg	650	510	resist.
	Ca	842	680	resist.
	Sr	777	625	resist.
	Ba	727	715	resist.
p	Al	660	1350	resist. BN crucible
	Ga	30	1280	resist.
	In	157	1080	resist.
	Tl	304	700	resist.
	Ge	938	1540	resist.
	Sn	232	1420	resist.
	Pb	327	830	resist.

[a]Sublimes.
MPt. (°C) = melting point of bulk metal. T_{vap} (°C) = temperature at which evaporation rate is 1 $gh^{-1}\,cm^{-2}$.
e-beam = electron beam gun, resist. = resistively heated crucible, wire = resistively heated wire.

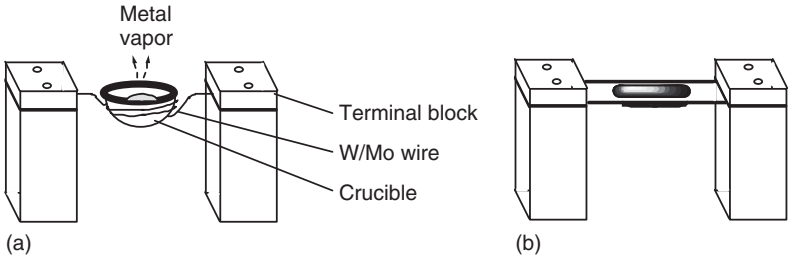

Figure 3 Diagram of resistance furnace for metal evaporation from a heated crucible (a) or a metal boat (b).

Figure 4 Various apparata for metal containment for resistive heating (from left to right): small molybdenum crucible; tantalum boat; alumina crucible inside coiled tungsten winding, shown positioned between two electrical terminal blocks; tantalum heat shield surround for crucible; alumina crucible in shielded and insulated tungsten winding.

Power to such a furnace is typically provided from the secondary output of a 24 V/100 A transformer, controlled by a variac or phase angle controller on the primary input.

This method is clearly limited to vaporization temperatures below that at which the crucible material itself either vaporizes or melts, and in effect places an upper limit of around 1700 °C for alumina crucibles. Molten, electropositive elements (e.g., aluminum and several lanthanides) will also chemically react with oxide crucibles, although aluminum is readily vaporized from boron nitride crucibles (see Sections 1.08.4.2–1.08.4.5 for containerless methods). Metal boats, in principle, achieve somewhat higher temperatures (although they lose a lot of heat by radiation and may require currents in excess of 250 A) and can be useful for metals which sublime.

Vaporization directly from resistively heated wires is possible for elements which sublime readily under vacuum and has been employed to generate small amounts (ca. 200 mg) of molybdenum and tungsten vapors using the setup illustrated in Figure 5.[5] Similarly, titanium may be vaporized from Ti–Mo alloy wires – the working basis of the titanium sublimation pump used in the UHV field. Small amounts of uranium vapor have also been generated from a resistively heated tungsten wire coil coated with molten uranium, and used for the synthesis of $[U(\eta\text{-}C_8H_8)_2]$.[6]

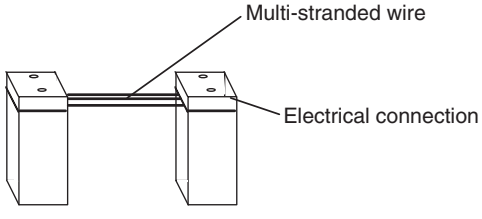

Figure 5 Evaporation of metal vapor from a wire.

1.08.4.2 Electric Arcs

This is the first of the so-called "containerless" methods, which obviate the problems of crucible contamination, in which an electric arc is struck between two conducting electrodes. This evaporation technique was used in the original carbon vapor experiments by Skell[2] and, most strikingly, in the more recent syntheses of C_{60} and higher fullerenes.[7] However, control of the arc can prove difficult and the problem of evaporation of fragments rather than atoms of evaporant arises, so the method has not been applied to MVS.

1.08.4.3 Laser Beam Heating

Laser evaporation was originally employed by von Gustorf:[8] the beam from a 200 W Nd-doped laser passed through a "gas window" (a stream of inert gas in the window area ensures that it remains uncoated with evaporant) and was focused on to the metal sample contained in a water-cooled copper crucible (i.e., another example of a containerless method). The main drawback of this method is that reflectivity of the incident laser radiation increases with surface temperature (thus requiring elevated power levels), so that it is not a generally useful method for the more refractory metals.

1.08.4.4 Sputtering

Simple diode sputtering uses a plate of the material to be evaporated as the cathode (which is usually water cooled) in a glow discharge of argon at a pressure of ca. 10^{-2}–10^{-1} mbar; the Ar^+ ions so produced bombard the evaporant target and eject the material. This process does not produce single metal atoms, rather small metal clusters, and so is not useful for "metal atom" synthesis. Of more potential interest in the latter context is magnetron sputtering, in which the Ar^+ ions are magnetically focused on to the target, and which operates at a much lower pressure (ca. 10^{-4}–10^{-3} mbar). An MVS apparatus based on vaporization by magnetron sputtering has been designed.[9]

1.08.4.5 Electron Beam Vaporization

The electron-beam furnace is widely used industrially, and offers good temperature control and the ability to vaporize metals, non-metals, and ceramics at temperatures of up to 4000 °C. Such a furnace was originally used by Green and Young in a rotary apparatus (*vide infra*) for the synthesis of bis(η-arene)titanium complexes.[10] The essential features of the furnace are shown in Figure 6.

A beam of thermionic electrons from a resistively heated tungsten filament is electrostatically focused on to the metal sample, which is sitting on a water-cooled copper hearth (i.e., a containerless method). In the original apparatus of Green and Young, the furnace was of a conventional, commercial design, in which the focusing was achieved by an electrically earthed hearth with the filament, focusing ring, and furnace lid biased to a high negative potential (0 to −7 kV, electron beam current 0–250 mA; power output 0 to −1.4 kW). However, there was evidence for damage to ligands/products, especially at the high operating potentials required for refractory elements such as tungsten, by reflected electrons from the metal sample. This led to the development of the positive hearth electron-beam furnace, in which the hearth is maintained at a high "positive" potential and the filament, focusing ring, and furnace lid at "earth" potential.[11,11a] Studies showed no secondary electron emission from the latter arrangement, and a dramatic

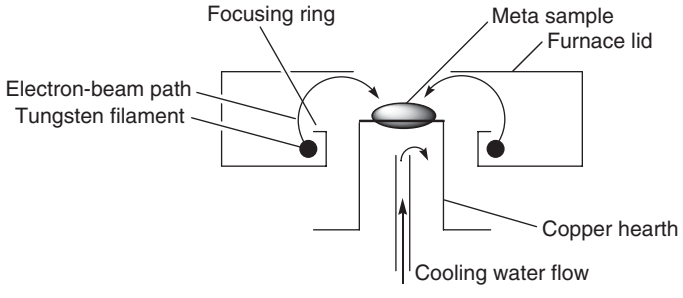

Figure 6 Schematic of electrostatically focused electron-beam furnace.

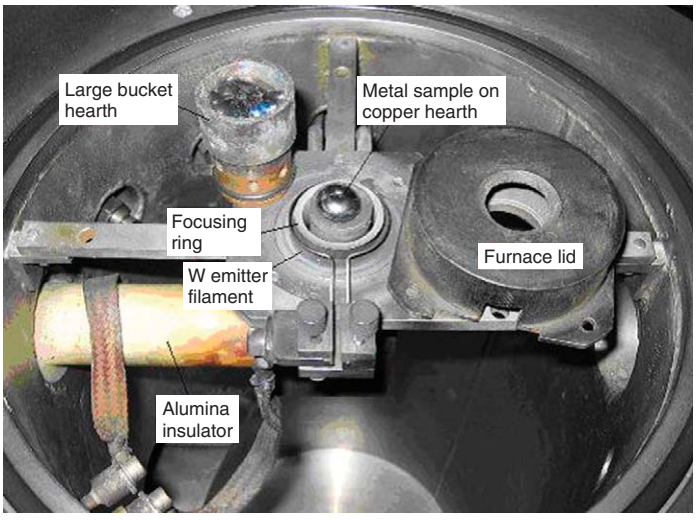

Figure 7 10 kW positive hearth electron-beam furnace.

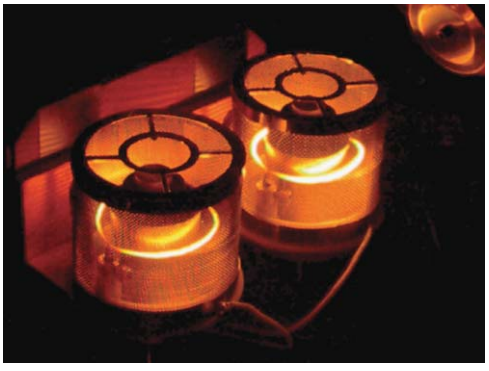

Figure 8 Twin electron-beam furnaces with skeleton lids.

improvement in yield for the synthesis of [W(η-toluene)$_2$]: 3% for the conventional earthed hearth furnace and 30% for the positive hearth furnace.[12] A 10 kW (0–+10kV, 0–1000 mA) positive hearth electron-beam furnace (in the apparatus of Figure 21, *vide infra*) is shown in Figure 7.

The electron-beam furnaces discussed thus far rely on electrostatic focusing of the electron beam by the geometry of the focusing ring and furnace lid; however, this arrangement leads to the deposition of up to 40% of the vaporized metal within the confines of the furnace. The vaporized metal available for reaction can be increased somewhat by the use of a "skeleton" furnace lid (Figure 8). Also, deposition of certain metals (particularly lanthanides) onto the emitter filament lowers its work function, which can cause instability in some electron-beam power supplies; use of a power supply with electronic feedback from the beam current to control the filament heating current obviates this problem. Industrial scale electron beam furnaces use magnetic focusing of the electron beam from a remote emitter filament onto a completely open hearth; such a furnace has been employed in the large scale, cryopumped, MVS machine built at the Los Alamos National Laboratories.[13]

1.08.4.6 Measurement of Evaporation Rates, Purification of Metal Samples, and "Problem" Metals

An estimate of metal evaporation rate is usually based on experience (power settings for a given evaporation rate for electron-beam and resistance furnaces are usually fairly reproducible), coupled with the intensity of the color of the

co-condensate when using a glass reactor. A more sophisticated approach has been employed by Ozin, with the use of a quartz crystal microbalance at grazing incidence to the metal-vapor flux.[14]

Commercially available metals (typically in the form of ingots, rods, slugs, etc.) often contain volatile or gaseous impurities associated with the refining process, which can cause the sample to erupt when using electron-beam evaporation. Thus, while it is possible to purchase vacuum-remelted evaporation slugs (at considerable expense), premelting of any metal, which melts before evaporation, in a separate operation prior to the co-condensation experiment, is advisable.

Electron-beam evaporation of metals, with vaporization temperatures in excess of 2000 °C, which have long liquid ranges (i.e., large $\Delta_{T_{vap}-T_{mpt}}$) requires elevated power levels due to the high and efficient conduction of the electron-beam energy to the water-cooled hearth via the liquid metal. This can be problematic for Zr, La, Ce, and U ($\Delta_{T_{vap}-T_{mpt}} = 700$, 900, 1195, and 1170 °C, respectively, see Table 1) in particular. In fact, while uranium is vaporized industrially for isotope separation on a very large scale, even the 10 kW furnace of Figure 7 will not vaporize it on a synthetically useful scale. However, uranium may be readily evaporated from the uranium–rhenium alloy of composition URe_2 using such a furnace.

1.08.5 Vacuum System and Reactor Design

1.08.5.1 Vacuum System

The design and construction of the vacuum system for MVS is largely dependent on whether a static or rotating reactor is used, the choice of vaporization method, and the scale of operation.

For "resistance-heated furnaces" on a modest scale (e.g., a 1–5 l reactor), a simple, trapped, diffusion-pumped apparatus constructed of stainless steel or glass capable of achieving $<10^{-4}$ mbar is sufficient.

For "electron-beam vaporization", a working vacuum of around 10^{-5} mbar with high pumping speed must be achievable, otherwise arcs and discharges within the furnace will seriously disrupt the experiment. For small-scale apparatus, diffusion pumps are adequate; however, for "large-scale" co-condensation experiments, degradation of the diffusion-pump fluid by the inevitable ingress of ligand vapor (even on a well-trapped pumping system) can be problematic. Alternative pumping systems in the form of cryopumps and turbomolecular pumps have both been employed. Cryopumps offer very high pumping speeds for water and other condensables; however, they rely on cryosorption by charcoal at 10 K for pumping of hydrogen, and this pumping stage can become contaminated by volatile ligands during pump regeneration, thus degrading performance. Modern turbomolecular pumps are very reliable, and versions are available suitable for use in highly corrosive environments (e.g., the semiconductor and coating industries), which, when coupled with a corrosion-resistant mechanical pump, make them ideal for the MVS application.

"Rotating reactors" clearly require a high vacuum rotating seal, through which power leads and other services for the furnace and ligand distribution system must pass. In the original design of Green and Young, a modified Buchi rotary-evaporator seal was employed,[10] and Timms has used a double o-ring seal system with additional external pumping between the seals.[15] Commercial MVS machines based on these designs use ferrofluidic seals for improved reliability and vacuum performance. It is important that the bore of the seal be fairly large (>75 mm) in order not to reduce the pumping speed to the reactor, especially when using an electron-beam furnace.

1.08.5.2 Reactor Design

"Glass reactors" offer the considerable advantage of being able to visually monitor the progress of the co-condensation experiment. The most straightforward setup for a static apparatus uses a round-bottom flask (1–5 l) immersed in a bath of coolant.[16] Glass bell jars, ranging in size from 6 to 50 l, equipped with a removable, insulated cooling jacket, are also used (particularly with electron-beam evaporation[12]). A convenient design employs a bell jar constructed from commercially available 15 or 30 cm diameter QVF glass pipeline with a ground-glass flange equipped with a Viton L-gasket for the vacuum seal (see Figure 9). Note that it is important to maintain this seal area at ambient temperature, since freezing of the L-gasket or O-ring by the reactor coolant will result in loss of vacuum; this is conveniently achieved by the use of silicone rubber-insulated heating tape (Figure 9). Rotating MVS setups typically use round-bottom flasks of 2–10 l in size (*vide infra*).

For large-scale reactors (>50 l), "metal" construction is preferable for safety reasons. Figure 10 shows a 75 l reactor, consisting of a copper bell jar housed in a glass vacuum chamber (60 cm diameter × 90 cm high); liquid nitrogen, or

Figure 9 6 l glass reactor and cooling jacket.

Figure 10 75 l copper reactor.

other coolant, is passed through the copper tubing soldered to the outside of the copper bell jar. This arrangement also essentially "Dewarizes" the co-condensation surface and minimizes coolant loss. However, it has been found that use of a "metal" co-condensation surface can have a deleterious effect on product yields for some compounds (e.g., $[Hf(\eta\text{-}C_6H_6)_2(PMe_3)]$[17]), for reasons which remain unclear.[18]

1.08.6 Ligand Introduction Systems

1.08.6.1 Volatile Ligands

Since gases disperse extremely rapidly in a vacuum system, dispersion of the vapors of volatile ligands onto the co-condensation surface is easily achieved by the use of a simple (preferably baffled) nozzle ("showerhead," see

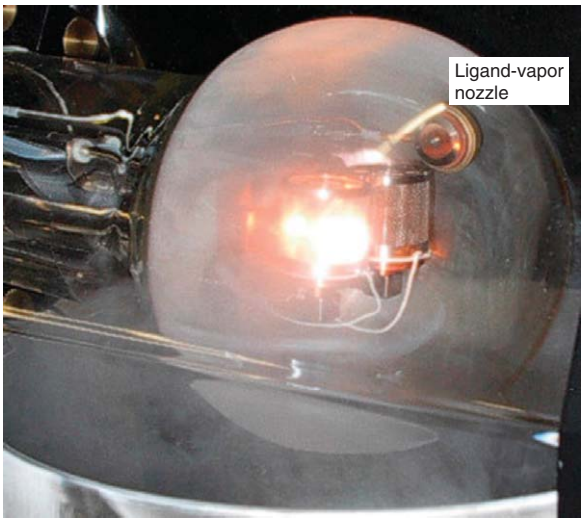

Figure 11 Ligand-vapor nozzle in rotating apparatus.[14]

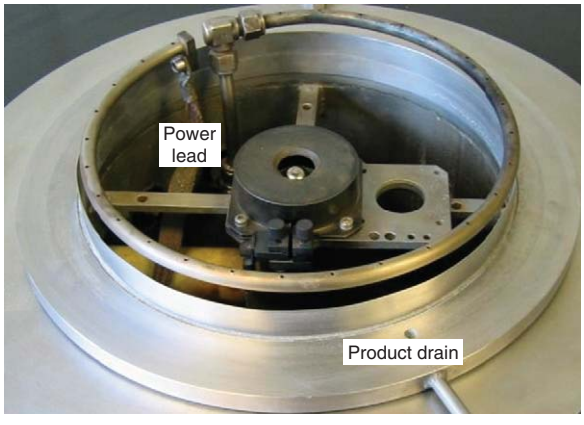

Figure 12 Electrically heatable gas ring.[13]

Figure 11) for static and rotating reactors based on round-bottom flasks, or a perforated tubular metal ring ("gas ring") for bell jar reactors (see Figure 12). While radiant heat from the furnace may be sufficient, additional electrical heating of the nozzle or gas ring may be required for ligands of relatively low volatility (e.g., 1,3,5-tri-*t*-butylbenzene). Ligand vapor introduction is usually commenced a short while prior to metal evaporation to facilitate removal of the co-condensate from the reactor walls after warm up. Ligands which do not form a glass on freezing (e.g., benzene) can produce weak, non-adherent matrices, which may flake off the reactor walls during co-condensation. This problem may be ameliorated by silylating the walls of glass reactors, or by admixing with, for example, hexane, although the latter approach may adversely affect yields.

Condensable "gases," for example, PF_3, as used by Timms in one of the first MVS reactions (that of Fe atoms with PF_3 to yield $[(PF_3)_3Fe(PF_2)_2Fe(PF_3)_3])$,[19] must be introduced via a high-vacuum needle valve, although measurement of gas-flow rate is difficult without the use of a mass-flow transducer. A range of homoleptic PF_3 complexes of first-row transition metals was subsequently synthesized in this way: $[M(PF_3)_n]$, M = Cr, Mo, $n = 6$; M = Fe, $n = 5$; M = Co_2, $n = 8$; M = Ni, Pd, $n = 4$.[20] The MVS technique proved in all cases to be a better synthetic route to these complexes than traditional high-pressure methods.[21] The gases PF_3 and CO have similar π-acidity but only PF_3 lends itself to macroscale co-deposition, since CO has a considerable vapor pressure at 77 K (*vide supra*). However, CO (or other reactive gases) can be introduced at the "end" of the reaction in addition to dinitrogen or argon, while the co-condensate warms to room temperature. Thus, the complex $[Ru(CO)(\eta^4\text{-}C_6H_{10})_2]$ was isolable from the co-condensate formed between ruthenium atoms and dimethylbutadiene after allowing the matrix to warm up under an atmosphere of CO.[22]

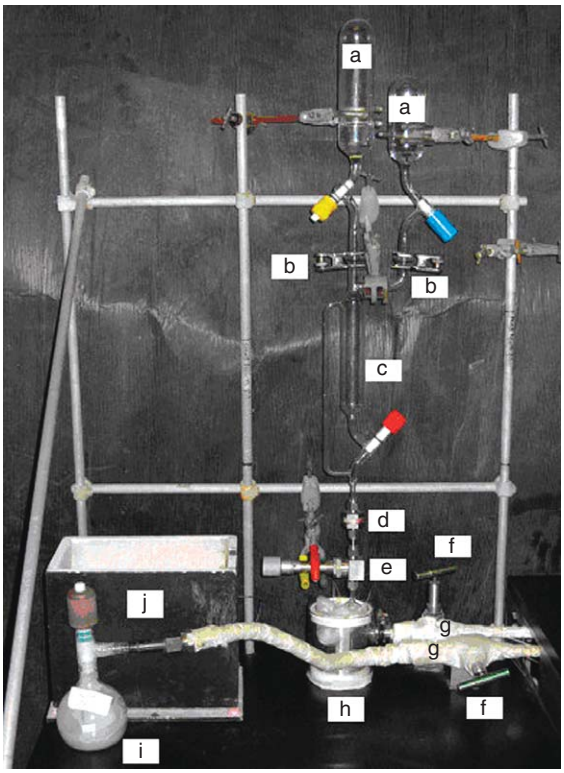

Figure 13 Photograph of typical ligand-inlet system. Liquid: (a) liquid ligand reservoir, (b) Young's greaseless ball-joint with Kalrez o-rings, (c) flow-rate monitoring section, (d) filter, (e) precision, stainless steel bellows needle valve, (f) high-vacuum bellows valve, (g) heated bellows ligand-inlet tube, (h) heated vaporization chamber. Solid: (j) insulated hotbox for ligand flask (i) ligand flask.

Volatile "liquid ligands," or solutions thereof, may be introduced from a gravity-fed system of the type shown in Fig. 13. The additional capillary-armed measuring section shown in the photograph allows for fine control over the rate of ligand addition. The heated chamber at the bottom is used to ensure complete vaporization of the ligand; the use of relatively high-melting-point liquids, such as benzene, which can freeze in the needle valve due to evaporative cooling, is facilitated by maintaining a relatively high pressure in this chamber.

"Solid ligands" with an appreciable vapor pressure at temperatures up to 150 °C can be introduced as vapor from a heated flask via a heated manifold, as shown in Figure 13, with the rate of introduction controlled by a high vacuum bellows valve; the operating pressure in the vacuum chamber during co-condensation can be used as a guide to the rate of introduction. In order to avoid blockage of the inlet system by solid ligands, it is important that the whole of the introduction system (including the gas ring or nozzle) is maintained at a suitable elevated temperature. Outside the vacuum system, this is most easily achieved by the use of heating tapes, monitored by thermocouples whose output is ideally fed back to solid-state temperature controllers. Nozzles may be electrically heated by a "button heater," and a stainless steel gas ring (and associated pipe work) within the vacuum system may be conveniently heated by making use of the natural electrical resistance of stainless steel and passage of a low-voltage electric current (0–30 A) (see Figure 12).

1.08.6.2 Involatile Liquids and Solutions of Involatile Solids

Involatile liquid ligands, or solids that can be dissolved in a suitable solvent, may be sprayed onto the walls of a rotating reactor, using the "rotary atomizer" device shown in Figure 14. A solution or liquid is introduced from a storage vessel via a stainless steel needle valve through a stainless steel capillary tube onto a rotating PTFE cone or disk driven by a small electric motor. This generates a spray of fine ligand droplets which is deposited as a band of co-condensate with the metal vapor as the flask rotates.

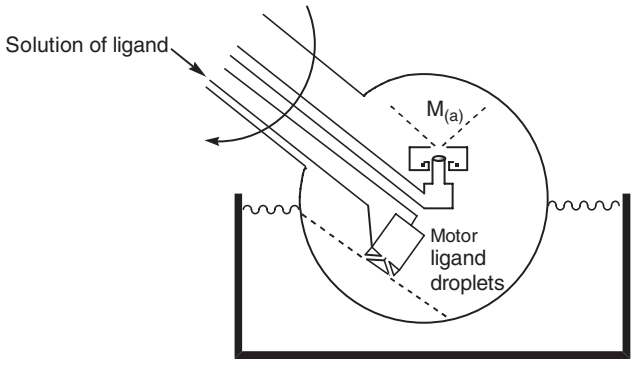

Figure 14 Rotating cone device for introduction of involatile liquids.

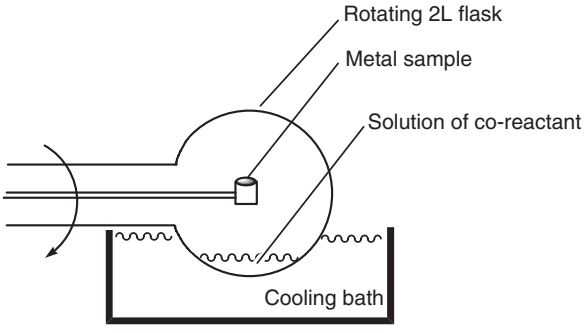

Figure 15 Condensation of metal vapors into solutions.

This technique was particularly successful for the introduction of aluminum alkyl halides into co-condensates of first-row transition metal vapors and butadiene/arene mixtures to catalyze butadiene telomerization reactions.[23] The oligomers produced were significantly different from the products produced by heterogeneous catalyst slurry systems.

An alternative to spraying the ligand is to prefill the rotating reaction flask with a cooled, mobile pool of involatile liquid – a potential ligand in a solvent or a pure liquid ligand with suitably low vapor pressures ($<10^{-3}$ mbar) at a convenient temperature. This approach has been employed by Timms for the condensation of resistively vaporized Cr into methylphenylsiloxane polymers at 273 K,[24,24a] for the synthesis of $[Fe(COD)_2]$,[15] and for the synthesis of bis(η-arene) and bis(η-naphthalene) complexes of Ti, V, Cr, and Mo by condensation of K atoms into solutions of the appropriate metal halides in THF-arene or-naphthalene solutions at 160 K, as shown in Figure 15.[25]

Adaption of this technique to electron-beam vaporization requires additional cryocooling around the furnace in order to maintain a sufficiently low vacuum in the furnace area; using this approach, both $[V(\eta\text{-}C_6H_5Me)_2]$ and $[Mo(\eta\text{-}C_6H_5Me)_2]$ have been prepared by condensation of the metal atoms into a solution of toluene in methylcyclohexane at 150 K.[14]

A potential drawback of this general method (and indeed any co-condensation experiment involving an excess of a ligand of low volatility) is that it can be difficult to extract fragile organometallic complexes from the large excess of involatile material.

1.08.7 Product Recovery Techniques

1.08.7.1 Extraction of the Co-condensate

At the end of the reaction, the coolant bath is drained; at this stage it is often useful, particularly for valuable ligands, for example, $^tBuC{\equiv}P$,[26] to employ a separate outlet in the co-condensation apparatus that allows the *in situ* recovery of ligands with high vapor pressures via a standard 10^{-3} mbar vacuum system and pre-traps prior to product removal. Otherwise, an inert gas (dinitrogen or argon) is introduced while the reaction vessel is allowed to warm to room

temperature. For rotating and small-scale static reactors, the products may be extracted via cannula into a Schlenk flask; for the bell jar apparatus of Figure 21, a stopper in the top of the vessel and a gutter at the base of the vessel (see also Figure 12) allow for extraction and washing of the crude product from the reactor with a suitable inert solvent, and collection in a large Schlenk vessel connected to the product drain. With appropriate use of lagging and solid carbon dioxide, products that are thermally stable at temperatures around −70 °C may also readily be isolated, but recovery of excess ligand may not be possible. For example, the zero-valent bis(η-arene) lanthanide complex [Sm(η-$C_6H_3Bu^t_3)_2$] is only stable at low temperatures, unlike the other lanthanide metal analogs, but isolation at −78 °C allowed its identity to be confirmed by low-temperature UV-Vis spectroscopy.[27]

1.08.7.2 Removal of Unreacted Metal

Caution. Many finely divided metals are pyrophoric and, if solvent residues are also present, are a significant fire risk.

The crude product mixture invariably contains quantities of metal powders which can readily be removed by filtration through a pad of Celite on a glass sinter. Careful removal is especially important if product decomposition is catalyzed by metal particles, for example, [Ti(η-$C_6H_6)_2$] (which undergoes autocatalytic decomposition in solution in the presence of finely divided Ti).[10]

1.08.7.3 Recovery of Unreacted Ligand

For volatile liquid ligands, ligand recovery is most easily achieved from the crude reaction mixture after filtration to remove the excess metal by removal under reduced pressure into a liquid-nitrogen trap. Similarly, solid ligands may be recovered by the use of a large-scale sublimation apparatus, such as that shown in Figure 16, which is suitable for 10–20 g batches of sublimable solids.

As mentioned in Section 1.08.6.2, separation of the product from a large excess of a relatively involatile ligand may be problematic, particularly for thermally sensitive products. However, in some cases, chemical methods may be employed: for example, the co-condensation of Mo, W, or Re vapors with pentamethylcyclopentadiene affords the hydrides, [M(η-$C_5Me_5)H_n$], M = Mo, W, $n = 2$; M = Re, $n = 1$, which may be isolated from the somewhat intractable excess of C_5Me_5H by protonation into aqueous HCl and subsequent deprotonation of the separated aqueous phase.[28]

Figure 16 High-vacuum sublimation apparatus for recovery of volatile solid ligands; RBF diameter 100 mm.

1.08.8 Experimental and Commercial Systems

In this section, we exemplify the design considerations for MVS equipment discussed above with a range of experimental and commercial apparatus.

1.08.8.1 Small-scale Static Reactors with Resistance Heating

Figure 17 shows simple resistance-heated apparatus, based on a 1 l round-bottom flask.

1.08.8.2 Rotary Reactors with Electron-beam or Resistance Heating

A schematic of a rotating apparatus, based on a 10 l round-bottom flask, with electron-beam heating (1.4 kW maximum) is shown in Figure 18. Figure 19 shows the synthesis of $[Ti(\eta\text{-}C_6H_5Me)_2]$[10] on this equipment.

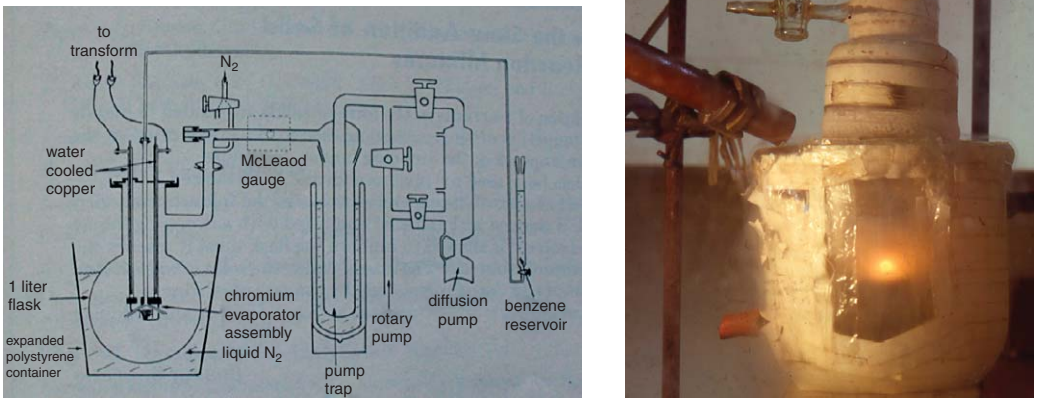

Figure 17 Small-scale, diffusion-pumped static systems: (a) schematic of apparatus for synthesis of $[Cr(\eta\text{-}C_6H_6)_2]$ (reproduced with permission from *J. Chem. Educ*. **1972**, *49*(11), 782–784, © 1972 Division of Chemical Education, Inc.); (b) co-condensation of Cr atoms with cycloheptatriene.

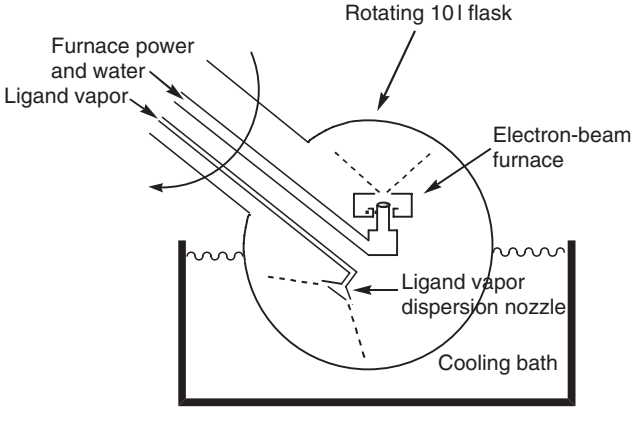

Figure 18 Rotary reactor with electron-beam heating.

Figure 19 Synthesis of [Ti(η-$C_6H_5Me)_2$].

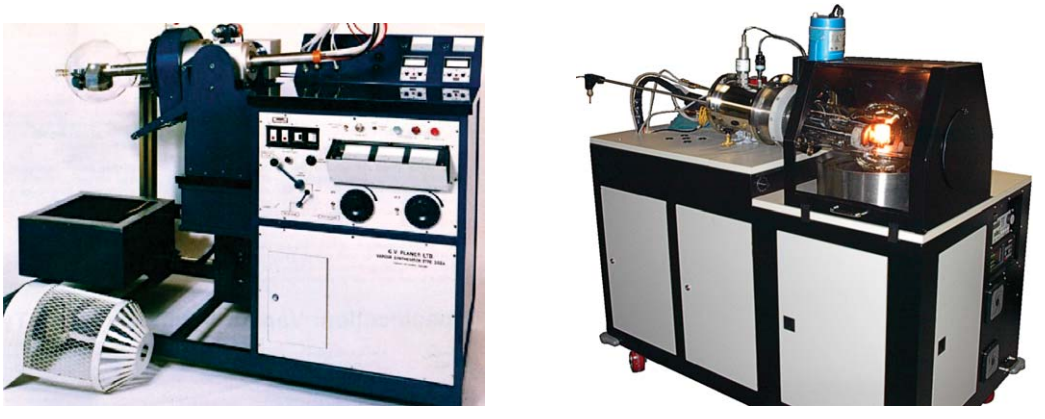

Figure 20 Commercial rotating MVS machines.

Figure 20 shows commercial, rotating MVS machines equipped with twin electron-beam furnaces, suitable for both co-condensation reactions and condensation of metal vapors into solutions (Section 1.08.6.2).

1.08.8.3 Intermediate-scale Static Reactor with Electron-beam or Resistive Heating

A static, turbopumped, bell jar apparatus with electron-beam heating (10 kW maximum) is shown in Figure 21. Both 6 l (for exploratory synthesis) and 50 l (for larger-scale synthesis) bell jars may be accommodated. Figure 22 shows a photograph, taken from above, of this apparatus during the synthesis of [Ho(η-$C_6H_3Bu^t_3)_2$].[29] The liquid-nitrogen level has been allowed to drop so that the shoulders of the glass bell jar and the glowing lump of Ho on the hearth are visible. Under an argon atmosphere, the central metal nut on the

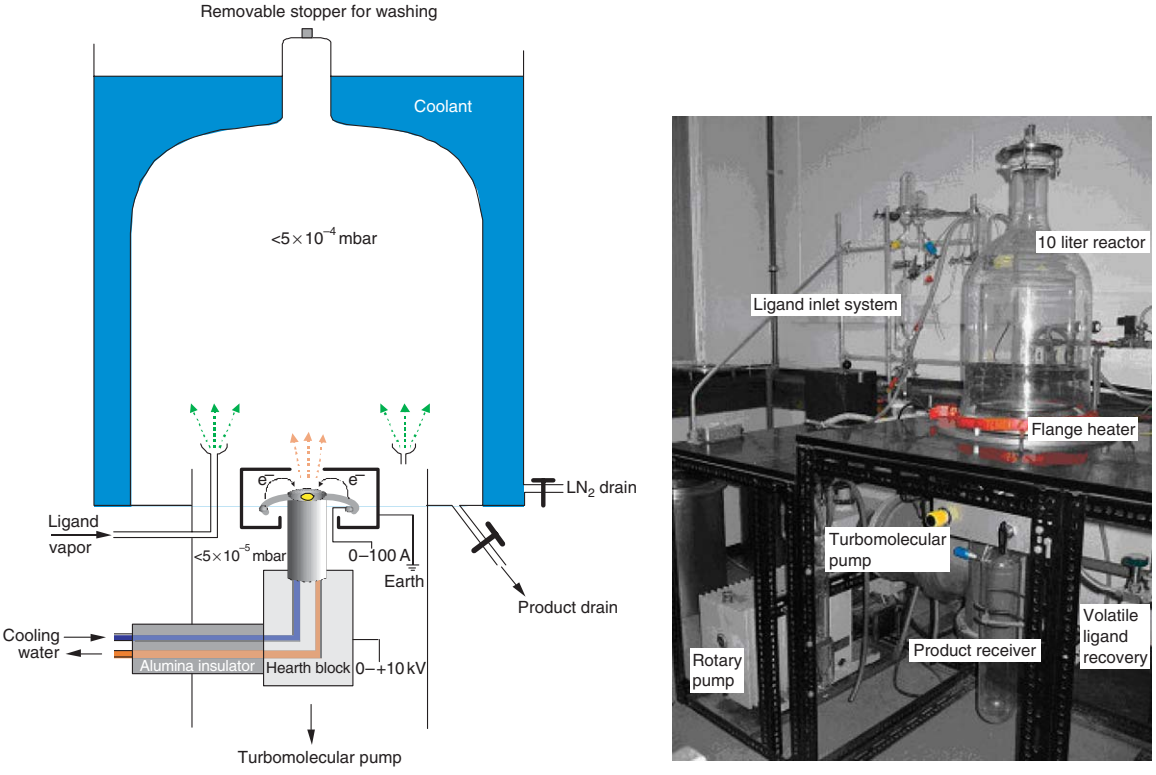

Figure 21 Turbopumped static apparatus with electron-beam heating.

Figure 22 Synthesis of [Ho(η-$C_6H_3Bu^t_3$)$_2$].

top plate may be removed and replaced with a rubber septum to allow solvent washing of the walls by cannula transfer.

1.08.8.4 Large-scale Reactor with Electron-beam Heating

Finally, Figure 23 shows a large-scale, cryopumped system with a 75 l metal reactor (discussed in Section 1.08.5.2) and a 10 kW electron-beam furnace. This apparatus is capable of synthesizing [Ti(η-C_6H_5Me)$_2$] on a scale of 20 g/run and [W(η-C_6H_5Me)$_2$] on a scale of 5–7 g/run.[30,30a]

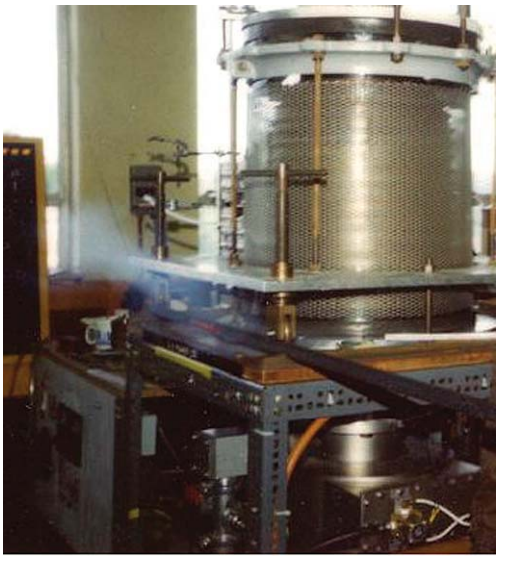

Figure 23 Large-scale cryopumped system with electron-beam vaporization.

1.08.9 Milestones in MVS

We conclude by presenting a brief, historical list of MVS-generated organometallics, which represents (in the view of the authors) important advances in technique and scope of ligand–atom reactions, or particularly significant compounds.

The first organometallics by MVS (1969)[3]

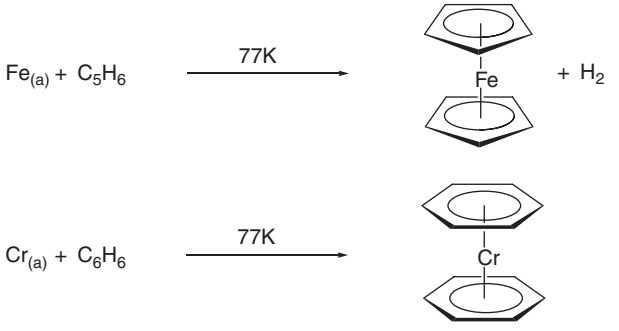

Tris(butadiene)molybdenum and tungsten (1974)[5]

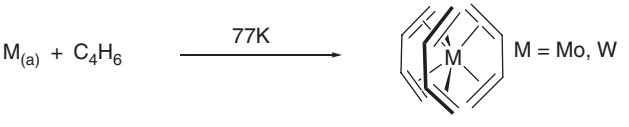

Condensation of metal atoms into solutions (1974)[14,15,24,25]

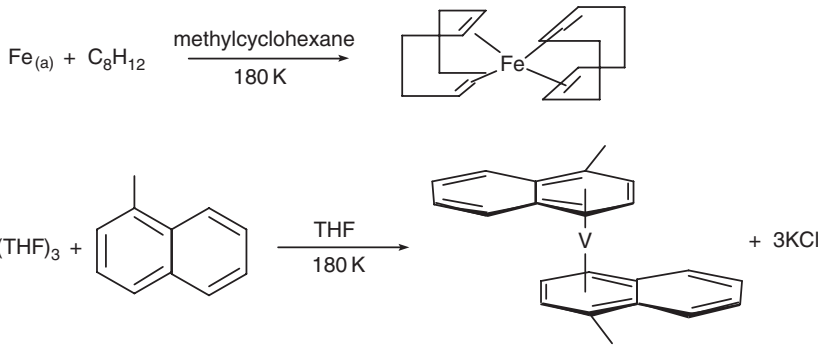

The first use of electron-beam vaporization in MVS: bis(η-benzene)titanium (1975)[10]

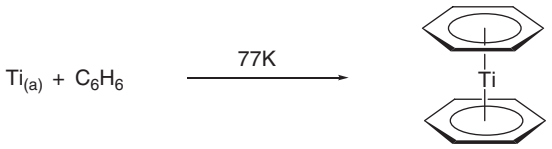

Development of +ve hearth electron-beam furnace: bis(η-benzene)tungsten (1978)[11]

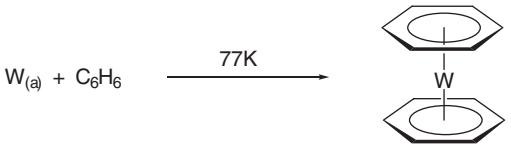

Refractory metal zerovalent bis(η-arene) complexes (1981)[12]

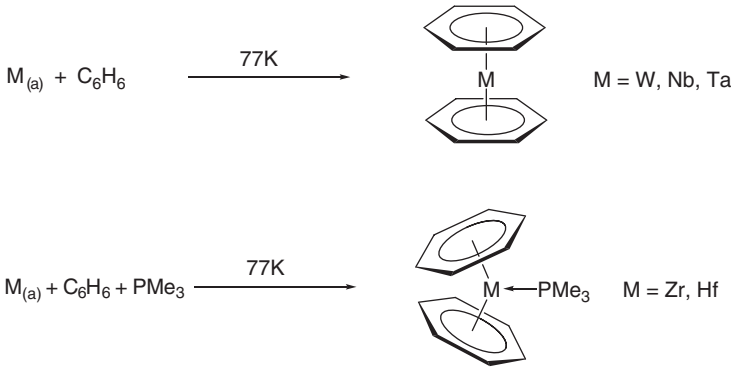

Ligand fragmentation – oxalyl chloride as a precursor to metal carbonyl halides (1982)[31]

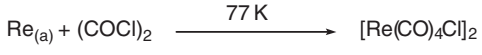

C–H activation by rhenium atoms (1984)[32,32a]

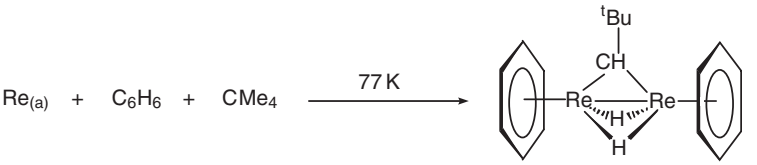

Heteroarene complexes (1986)[33]

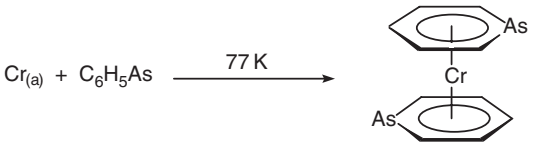

Triple-decker arene complexes (1986)[4]

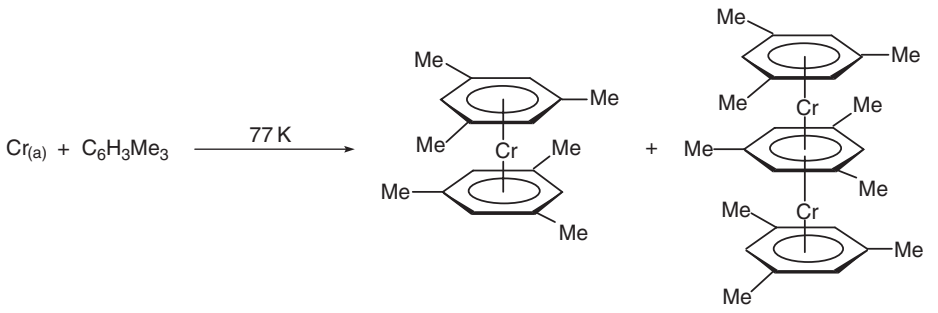

The first lanthanide(0) complexes (1987)[34,34a]

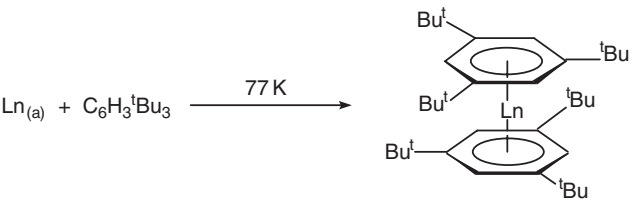

Ln = Sc, Y, La, Pr, Nd, Sm, Gd, Tb, Dy, Ho, Er, Lu

Cyclization of a phosphaalkyne to form Sc(I) and Sc(II) sandwich complexes (1996)[30]

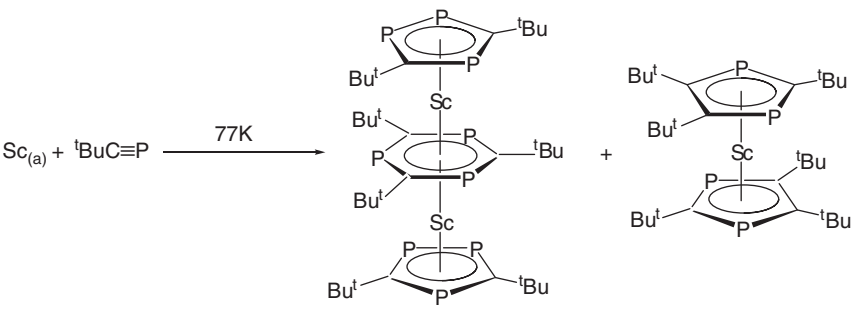

References

1. Pimentel, G. C. *Spectrochem. Acta* **1958**, *12*, 94.
1a. Linevsky, M. J. *J. Chem. Phys.* **1961**, *34*, 587.
2. Skell, P. S. *J. Am. Chem. Soc.* **1963**, *85*, 1023.
3. Timms, P. L. *J. Chem. Soc., Chem. Commun.* **1969**, 1033.
4. Lamanna, W. M.; Britton, D. *J. Am. Chem. Soc.* **1986**, *108*, 2096.
5. Skell, P. S.; van Dam, E. M.; Silvon, M. P. *J. Am. Chem. Soc.* **1974**, *96*, 626.
6. Graves, V.; Lagowski, J. J.; Simons, L. H. *Chem. Eng. News* **1974**, 26.
7. Krätschmer, W.; Lamb, L.; Fostiropoulos, K.; Huffman, D. R. *Nature* **1990**, *347*, 354.
8. von Gustorf, E. K.; Jaenicke, O.; Polansky, O. E. *Angew. Chem., Int. Ed. Engl.* **1972**, *11*, 532.
9. Bradley, J. S. *Personal Communication*, 1987.
10. Anthony, M. T.; Green, M. L. H.; Young, D. *J. Chem. Soc., Dalton Trans.* **1975**, 1419.
11. Cloke, F. G. N.; Green, M. L. H.; Morris, G. E. *J. Chem. Soc., Chem. Commun.* **1978**, 72.
11a. Timms, P. L. *Angew. Chem., Int. Ed. Engl.* **1975**, *14*, 273.
12. Cloke, F. G. N.; Green, M. L. H. *Dalton Trans.* **1981**, 1938.
13. Watkin, J. L.; Sattelberger, A. P. *Personal Communication*, 1988.
14. Ozin, G. A.; Andrews, M. P.; Francis, C. G.; Huber, H. X.; Molnar, K. *Inorg. Chem.* **1990**, *29*, 1068.
15. Mackenzie, R.; Timms, P. L. *J. Chem. Soc., Chem. Comm.* **1974**, 650.
16. Timms, P. L. *J. Chem. Educ.* **1972**, *49*, 782.
17. Cloke, F. G. N.; Green, M. L. H. *J. Chem. Soc., Chem. Commun.* **1979**, 127.
18. Cloke, F. G. N.; Green, M. L. H. unpublished observations.
19. Klabunde, K. J. *Chemistry of Free Atoms and Particles*; Academic Press: London,1980, Chapter 4; pp 48–81.
20. Timms, P. L. *J. Chem. Soc., A* **1970**, 2526.
21. Kruck, T. *Angew. Chem., Int. Ed. Engl.* **1967**, *6*, 53.
22. Cox, D. N.; Roulet, R.; Chapuis, G. *Organometallics* **1985**, *4*, 2001.
23. Akhmedov, V. M.; Anthony, M. T.; Green, M. L. H.; Young, D. *J. Chem. Soc., Dalton Trans.* **1975**, 1412.
24. Francis, C. G.; Timms, P. L. *J. Chem. Soc., Chem. Comm.* **1977**, 466.
24a. Young, D.; D. Phil. Thesis, University of Oxford, 1974.
25. Hawker, P. N.; Timms, P. L. *J. Chem. Soc., Dalton Trans.* **1983**, 1123.
26. Arnold, P. L.; Cloke, F. G. N.; Hitchcock, P. B.; Nixon, J. F. *J. Am. Chem. Soc.* **1996**, *118*, 7630.
27. Arnold, P. L.; Petrukhina, M. A.; Bochenkov, V. E.; Shabatina, T. I.; Zagorskii, V. V.; Sergeev, G. B.; Cloke, F. G. N. *J. Organomet. Chem.* **2003**, *688*, 49.
28. Cloke, F. G. N.; Day, J. P.; Green, J. C.; Morley, C. P.; Swain, A. C. *J. Chem. Soc., Dalton Trans.* **1991**, 789.
29. Cloke, F. G. N. *Chem. Soc. Rev.* **1993**, 17.
30. Green, M. L. H. *J. Organomet. Chem.* **1980**, *200*, 119.
30a. Cloke, F. G. N.; Hitchcock, P. B.; Nixon, J. F.; Vickers, D. M. *J. Organomet. Chem.* **2001**, *635*, 201.
31. Brown, P. R.; Cloke, F. G. N.; Green, M. L. H.; Tovey, R. C. *J. Chem. Soc., Chem. Commun.* **1982**, 519.
32. Bandy, J. A.; Cloke, F. G. N.; Green, M. L. H.; O'Hare, D.; Prout, C. K. *J. Chem. Soc., Chem. Commun.* **1984**, 240.
32a. Green, J. C.; Green, M. L. H.; O'Hare, D.; Watson, R. R.; Bandy, J. A. *J. Chem. Soc., Dalton Trans.* **1987**, 391.
33. Elschenbroich, C.; Kroker, J.; Massa, W.; Ashe, A. J., III. *Angew. Chem., Int. Ed. Engl.* **1986**, *25*, 571.
34. Brennan, J. G.; Cloke, F. G. N.; Sameh, A. A.; Zalkin, A. *J. Chem. Soc., Chem. Commun.* **1987**, 1668.
34a. Anderson, D.; Cloke, F. G. N.; Cox, P. A.; Edelstein, N.; Green, J. C.; Pang, T.; Sameh, A. A.; Shalimoff, G. *J. Chem. Soc., Chem. Commun.* **1989**, 53.

1.09 Organometallic Photochemistry, Synthetic Aspects and Applications

D R Tyler, University of Oregon, Eugene, OR, USA

1.09.1 Introduction

The emerging themes in organometallic photochemistry over the past 10–15 years include the following:

(i) The development and use of faster kinetics techniques that take advantage of new laser technologies.[1,2] These techniques permit the routine observation of chemical and physical processes even at the femtosecond timescale.

(ii) The exploitation of faster, more accurate, and more reliable calculations, primarily using advances in density functional theory (DFT) methods, to interpret photochemical reactions.[3]
(iii) The exploration of new reaction media, examples being super-critical CO_2, ionic liquids, and confining media such as zeolites and cages.[4,5]
(iv) The photochemistry of supramolecular complexes.[6]
(v) The development of methods to photochemically cleave selected bonds in a molecule.[7]
(vi) The recognition that electronic spin is an important parameter in determining the reactivity of photogenerated intermediates.

The following sections describe general aspects of organometallic photochemistry with examples that emphasize these emerging themes. General reviews[8,9] that discuss other aspects of the field are available, as are a number of more specialized reviews.[10–17]

1.09.2 Excited States of Organometallic Complexes

A variety of excited states are found in organometallic complexes, and each type is generally associated with a characteristic photoprocess. To explain reactivities and mechanisms, it is useful therefore to identify the excited state involved. To facilitate discussion, the generic molecular orbital diagram in Figure 1 is presented, showing the interaction of n ligand orbitals with a metal atom. The ligands are also shown with empty π^* orbitals, which is typical for most ligands found in organometallic complexes. Note that the interaction of n ligand σ-orbitals with the metal orbitals forms n M–L σ (bonding) molecular orbitals, which are predominantly ligands in character, and n M–L σ^* (antibonding) molecular orbitals, which are predominantly metals in character. The $9-n$ remaining valence orbitals on the metal are generally involved in π-backbonding to the empty π^* orbitals on the ligands. As shown in the figure, π-backbonding stabilizes the $9-n$ metal orbitals and increases the energy of the ligand π^* orbitals.

1.09.2.1 Ligand Field Excited States and Photochemistry

In ligand field (LF) transitions (also known as *d–d* transitions; labeled 1 in Figure 1), a π-bonding or non-bonding *d*-orbital is deoccupied and a metal–ligand antibonding orbital (also primarily *d* in character) is occupied. The result is a weakening of

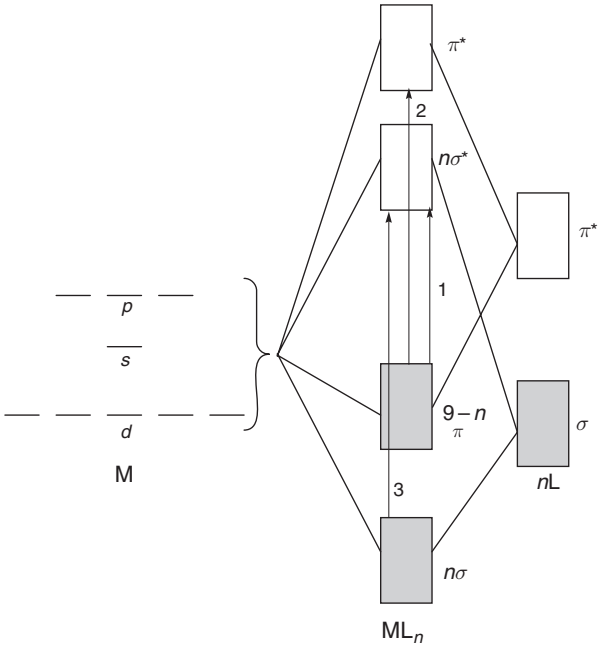

Figure 1 Molecular orbital diagram for the interaction of a metal with *n* ligands. The electronic transitions are: 1, LF (*d–d*); 2, MLCT; and 3, LMCT. Shading indicates filled orbitals.

the metal–ligand bond, which is generally assumed to lead to metal–ligand bond dissociation. Typical examples of this behavior include the photodissociation of metal–CO bonds in most metal carbonyl complexes (Equation (1)).

$$ML_m(CO)_n \xrightarrow{h\nu} ML_m(CO)_{n-1} + CO \quad (1)$$

$ML_m(CO)_n$ = $Fe(CO)_5$, $Re(CO)_5Cl$, $CpV(CO)_4$, (η^6-mesitylene)$Mo(CO)_3$, and numerous others

Recent DFT calculations on $Cr(CO)_6$, however, suggest that low-energy metal-to-ligand charge-transfer (MLCT) excited states (see below) rather than LF states are responsible for the photodissociation of a Cr–CO bond in this complex.[18–21] This result has important implications because the $M(CO)_6$ molecules (M = Cr, Mo, W) are typically cited as the prototypical examples of an LF excitation leading to M–CO bond dissociation. Based on the example of the $M(CO)_6$ complexes, if M–L bond photodissociation is observed with a particular molecule, it has frequently been assumed that the excited state involved was an LF excited state. The DFT results with $Cr(CO)_6$ suggest that a reassessment of the role of LF states in metal–ligand bond photodissociation is necessary. Overall, these DFT results demonstrate three important points: (i) it is not necessary to excite LF states in order to induce M–L photodissociation; (ii) conversely, M–L photodissociation does not imply an LF excited state (in fact, as every photochemist knows, it is incorrect to infer an excited state based on the photoreactivity of a molecule); and (iii) DFT methods have advanced to the point that the results of these calculations are deemed reliable by the photochemistry community even in the absence of direct spectroscopic confirmation of the DFT results. (Electronic structural studies of organometallic complexes are very often not definitive because the absorption bands are broad and overlapping. Calculations have, therefore, always played an important role in helping to interpret the electronic spectra of these complexes.)

Another example of M–L bond dissociation following LF excitation is provided by the photochemistry of $CpFe(\eta^6$-arene$)^+$. LF excitation of this molecule labilizes one bond to the arene and the initial product is $CpFe(\eta^4$-arene$)^+$ (Equation (2)).[22,23] Subsequent reactions lead to cleavage of the other Fe–arene bonds and the formation of $CpFe(solvent)_3^+$. The utility of this photoreaction is discussed later.

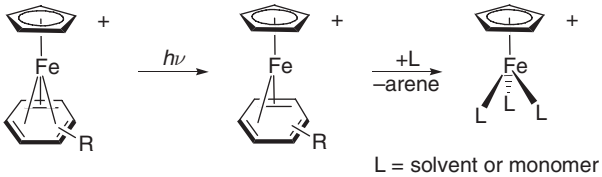

(2)

L = solvent or monomer

Theoretical considerations show that, in general, M–L bond heterolysis should occur when dative bonds are weakened by LF excitation.[24] (In fact, metal–ligand bond homolysis following LF excitation is rare. Most examples of homolysis involve ligand-to-metal charge-transfer (LMCT) excitations, see below.) But, whether M–L heterolysis is caused by LF, MLCT, or Rydberg excitation (see below), it is interesting to note that the heterolysis is generally not dependent on the phase of the reaction (gas, liquid, matrix). Differences do occur, however, in the extent of ligand loss. Generally, multiple M–L bond dissociations can occur in the gas-phase UV photolysis of organometallics, because the molecule has no straightforward way to dissipate the excess energy. For example, $Fe(CO)_2$ and $Fe(CO)_3$ are typical net reaction products in the gas-phase UV photolysis of $Fe(CO)_5$, whereas $Fe(CO)_4$ is formed in the liquid phase and in matrices, where transfer of excess energy to the medium is possible. Note, however, it is generally believed that the $Fe(CO)_2$ and $Fe(CO)_3$ products form in the gas phase by sequential loss of CO from $Fe(CO)_5$, and not by the concerted loss of several ligands.[25]

Another point to note is that a change in the spin state can occur when a ligand is dissociated from a complex. Typical of this behavior is the photochemical formation of triplet $Fe(CO)_4$ following loss of a CO ligand from (singlet) $Fe(CO)_5$[25,26] (Equation (3)) and the formation of triplet Cp_2W from $Cp_2W(H)_2$ (Equation (4)).[27]

$$Fe(CO)_5 \xrightarrow{h\nu} {}^3Fe(CO)_4 + CO \quad (3)$$

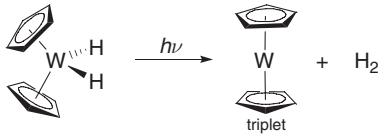

(4)

One important consequence of triplet-state intermediates is that subsequent reactions of these species may have larger than expected energy barriers because of necessary spin-state changes on the pathway to singlet products.

A final point is that incorporation of organometallic species into polymers does not change their photochemistry, assuming the electronic structure of the species is not extensively altered by the polymer. For example, if photochemical M–L bond dissociation occurs as a result of irradiation of a molecule, then that reactivity is also observed when the molecule is incorporated in a polymer. An example is the photochemical substitution reaction shown in Equation (5).[28]

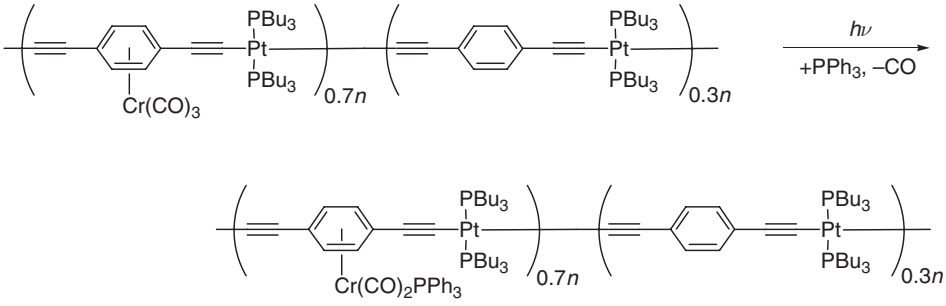

(5)

1.09.2.2 Metal-to-ligand Charge-transfer Excited States

Charge-transfer (CT) transitions are those in which a large fraction of an electronic charge is transferred from one region of a molecule to another. For example, in an MLCT (transition 2 in Figure 1; Equation (6)), an electron moves from an orbital that is primarily metal in character to one that is mainly ligand in character. Other common types of charge transfer include LMCT (transition 3 in Figure 1) and charge-transfer to solvent (CTTS). Charge-transfer excited states of organometallics typically lead to redox reactions, but as discussed in the previous section, MLCT excitations are also responsible for the M–L photodissociations observed in many complexes.

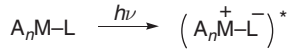

(6)

Of the various types of charge-transfer, MLCT transitions (Equation (6)) are the most important in organometallic photochemistry, because the types of ligands found in organometallic complexes typically have low-energy π-acceptor orbitals and the MLCT transitions are therefore at lower energy than the other types of charge-transfer transitions. Also, the metal centers in organometallic compounds are generally in low oxidation states, which makes them easier to oxidize than reduce. MLCT reactivity in organometallics has been thoroughly reviewed.[29,30] An example of MLCT reactivity is given in Equation (7).

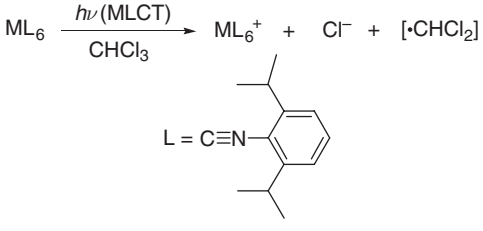

(7)

The mechanism for this reaction is shown in Scheme 1. Note that the essential feature in the mechanism is quenching of the MLCT excited state by electron transfer to chloroform, a step facilitated by the fact that in the MLCT excited state, the "reduced" ligand is susceptible to electrophilic attack. Thus, note the net oxidation of the metal in the reaction scheme. It has been suggested that ligand substitution can occur by associative attack of an entering nucleophile on the oxidized metal center. In fact, when L is the less bulky C≡NPh ligand in Equation (7), a Cl atom is transferred from $CHCl_2^-$ to the metal to form ML_6Cl^+ as the product.

$$ML_6 \xrightarrow{h\nu\,(MLCT)} ML_6^*$$

$$ML_6^* + CHCl_3 \longrightarrow ML_6^{+}\cdots CHCl_3^{-}$$

$$ML_6^{+}\cdots CHCl_3^{-} \longrightarrow ML_6^{+} + CHCl_3^{-}$$

$$CHCl_3^{-} \longrightarrow Cl^{-} + {\bullet}CHCl_2$$

Scheme 1 Oxidation mechanism of ML_6 (L = CNAr; Ar = 2,6-diisopropylphenyl) following MLCT excitation.

1.09.2.3 Ligand-to-metal Charge Transfer

Two important exceptions to the generalization that LMCT transitions occur at high energy in organometallic complexes occur in complexes with non-dative (covalent) metal–ligand bonds, and in complexes with high oxidation-state metal centers. As an example of the former, complexes with M–alkyl bonds oftentimes have photochemically accessible σ (M–alkyl) → metal CT states. Depopulation of the σ (M–alkyl) orbital will weaken and break the metal–alkyl bond. (This type of transition corresponds to transition 3 in Figure 1.) An example of this type of photoreactivity is provided by coenzyme B_{12} and its numerous model complexes (Equation (8)).

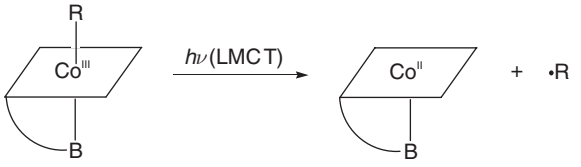

(8)

In this case, LMCT excitation forms R· and a Co(II) metal center. Note, this is formally a redox reaction. An example of LMCT reactivity in a high oxidation-state complex occurs on irradiation of Cp_2TiCl_2. The Cp → Ti CT state leads to the intermediate formation of Cp and $CpTiCl_2$ radicals.[31]

1.09.2.4 Metal–Metal Bond Localized Transitions

Many organometallic complexes have a framework of metal–metal bonds, and several types of electronic transitions are associated with orbitals contained in this framework.[32] For example, excitation from a metal–metal bonding to a metal–metal antibonding orbital is denoted as a $\sigma_{M-M} \rightarrow \sigma_{M-M}^*$ transition, or more simply just as $\sigma \rightarrow \sigma^*$. Transitions from non-bonding d orbitals are also possible in these complexes, and they are referred to as $d\pi \rightarrow \sigma^*$ transitions, because the d-orbital being depopulated typically has π-type symmetry with respect to the metal–metal bond. In both transitions, a metal–metal antibonding orbital is occupied, which should weaken the metal–metal bonding. In fact, it is observed experimentally that both $\sigma \rightarrow \sigma^*$ and $d\pi \rightarrow \sigma^*$ excited states lead to homolytic cleavage of the metal–metal bond and consequently, to the formation of metal radicals (Equation (9)).

$$L_nM{-}ML_n \underset{}{\overset{h\nu}{\rightleftharpoons}} 2\dot{M}L_n$$
$$ML_n = Mn(CO)_5,\ Re(CO)_5,\ Co(CO)_4,\ CpFe(CO)_2,\ CpMo(CO)_3,\ CpW(CO)_3,\ Pd(CNMe)_3^{+} \tag{9}$$

The metal radicals can be trapped, either with traditional metal-radical traps such as alkyl halides (Equation (10)) or with ligands to yield 19-electron complexes (Equation (11)).

$$\dot{M}L_n + R{-}X \longrightarrow L_nM{-}X + R{\bullet} \tag{10}$$

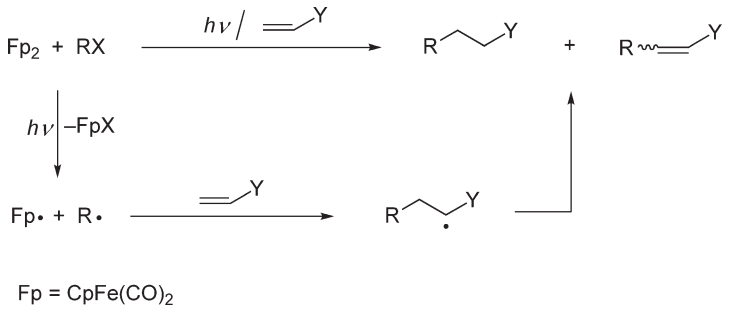

Scheme 2

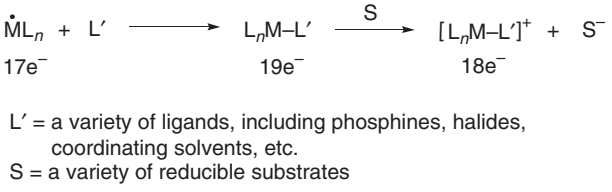

(11)

The 19-electron complexes are short-lived species, but their formation and reactivity has been observed by picosecond timescale infrared spectroscopy.[33] Their dominant mode of reactivity is electron transfer to yield a more stable 18-electron complex. In the absence of a metal-radical trap, the two metal radicals produced by M–M photolysis can recombine and no net reaction will take place.[34–37]

Metal–metal bond photolysis has found practical synthetic use in C–C bond-forming reactions. The metal-trapping reaction (Equation (10)) is used to generate an organic radical, which subsequently reacts with an alkene to form saturated and/or unsaturated products (Scheme 2).[38] Giese has extensively developed this reaction for synthetic purposes, and reports that $Cp_2Fe_2(CO)_4$ and $Mn_2(CO)_{10}$ are both practical M–M bond precursors in these reactions.[38] The method is also valuable for carrying out intramolecular cyclization reactions (Equation (12)).

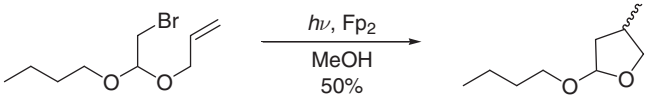

(12)

1.09.2.5 Other Excited States

Many ligands have characteristic electronic transitions and these transitions are still present when the ligands are coordinated to a metal. For example, $Re_2(CO)_8L_2$ (L_2 = 1,10-phenanthroline) has a phenanthroline-centered $\pi \rightarrow \pi^*$ transition at essentially the same wavelength as uncoordinated 1,10-phenanthroline. Such transitions are often referred to as intraligand transitions. Rydberg transitions are another type of excitation found in organometallic complexes. Located in the far ultraviolet or the vacuum UV, these transitions involve electronic excitations to atomic orbitals that are higher in energy than the valence-shell molecular orbitals. These transitions are frequently high enough in energy to dissociate multiple ligands when the molecules are irradiated in the gas phase where the molecules have no competing mechanisms for dissipating the energy. These excited states are particularly useful in the photochemical deposition of metallic thin films where the loss of all ligands is required.

1.09.3 Reactions

A key use of photochemistry in organometallic chemistry is to activate metal centers for reactivity. Oftentimes, such activation consists solely of creating a vacant coordination site by photochemical M–L bond cleavage. In other cases,

an intact excited state of the metal complex is involved in the reaction. The sections below make a catalog of the typical photochemical reactions of organometallic complexes.

1.09.3.1 Reactions Subsequent to Heterolytic Metal–Ligand Bond Cleavage

As discussed in the preceding sections, LF, MLCT, and Rydberg excitations of organometallic molecules can lead to heterolysis of an M–L bond. Such activation has been exploited in a number of ways, as the following sections describe.

1.09.3.1.1 Oxidative-addition preceded by photochemically induced ligand loss

Oxidative addition of a substrate to a photochemically generated coordinatively unsaturated species is widespread. Recent examples of this reactivity are shown in Equations (13) and (14).[39]

(13)

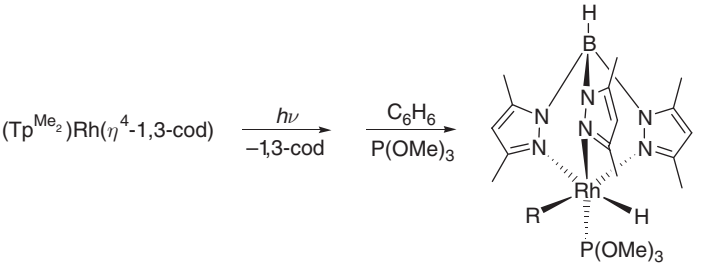

(14)

An area of particularly intense interest is the activation of C–H bonds. A number of papers have reviewed this chemistry,[40] and several important points have emerged that are relevant to the photochemical activation of the metal center.[41] The first point is that the spin state of the photochemically generated intermediate (i.e., the coordinatively unsaturated species) is important. Recent mechanistic studies showed that singlet states initially form σ-agostic complexes before oxidative addition occurs, while triplet states react directly to give the oxidative-addition product. The reaction with the singlet-state species is consequently slower than with the triplet species.

1.09.3.1.2 Linkage isomerism for photochromic behavior

Photochemical M–L bond dissociation has been exploited for the design of photochromic materials.[42] Conceptually, the idea is to use a complex with a photodissociable, non-chelatable, bifunctional ligand. Irradiation of the complex at one wavelength dissociates the ligand, which then reacts–backreacts with the coordinatively unsaturated molecule at the other coordination site on the ligand, that is, a photochemical linkage isomerism has occurred. If the two molecules have different colors, then irradiation at a different wavelength can reform the original molecule and the system is photochromic. Burkey demonstrated this reactivity with complexes of the type $Cp'Mn(CO)_2L$, where L is a functionalized pyridine ligand (Scheme 3).[42]

A key to this reactivity is the solvent cage, which keeps the photogenerated fragments from diffusing apart so that they can recombine. The importance of the solvent's effect in controlling photochemical and thermal reactivity in organometallic reaction systems has been discussed,[34,35] and photochemical studies of organometallic molecules showed that the ratio of diffusive separation (k_d) to recombination (k_c) of two particles is controlled by the mass of the particles and the surface area of the particles ($k_d/k_c \approx m^{1/2}$ (surface area)$^{-1}$).

1.09.3.1.3 Photochemistry of coordinatively unsaturated species

An intriguing report described formation of triplet state $CpMn(CO)_2$ in an Ar matrix at 10 K according to the following reaction scheme.[43] The structural assignments were based on an excellent agreement between the experimental infrared spectra and those computed using DFT (Equation (15)).

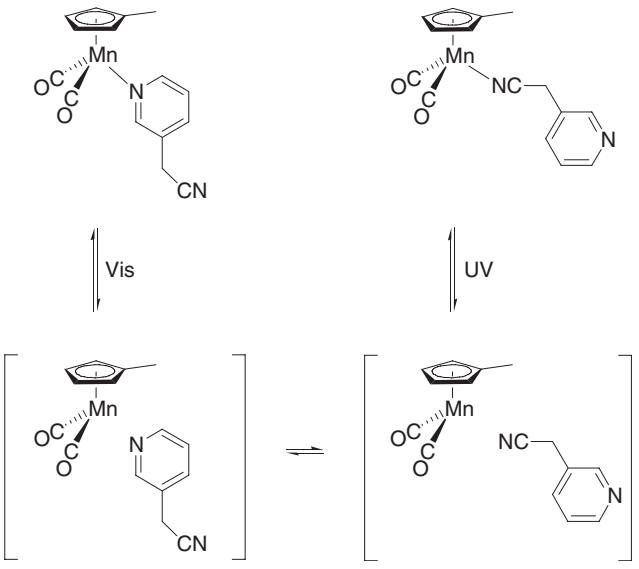

Scheme 3

$$CpMn(CO)_3 \xrightarrow[\text{Ar, 10 K}]{h\nu} {}^1[CpMn(CO)_2] \underset{\text{dark, Ar, 10 K}}{\overset{h\nu}{\rightleftharpoons}} {}^3[CpMn(CO)_2] \qquad (15)$$

No full paper has been published yet, but this report suggests that the triplet states of coordinatively unsaturated species might be formed and trapped by photochemical excitation in low-temperature matrices. Although these reactions would be of limited synthetic usefulness, the important point is that the ability to stabilize intermediates at low temperature has proved to be an invaluable method for obtaining spectroscopic data about suspected photochemical intermediates. In fact, as this example demonstrates, low-temperature generation and spectroscopic characterization of unstable species at low temperature, used in conjunction with DFT calculations, is a powerful combination for the mechanistic interpretation of reactions.

1.09.3.2 Oxidative Addition to Excited States

Four-coordinate square-planar molecules are coordinatively unsaturated and can frequently undergo oxidative addition reactions without prior ligand loss. This feature has been exploited in the photochemical carbonylation of alkyl and aryl hydrocarbons. In a detailed study, Goldman showed that hydrocarbons oxidatively add to the excited state of *trans*-$Rh(CO)(PMe_3)_2Cl$ to give a six-coordinate species that undergoes a subsequent photochemical reaction to form the CO insertion product.[44] Later work[45] using TRIR confirmed that the excited state of $Rh(CO)(PMe_3)_2Cl$ reacted with RH, and also showed that Rh–CO bond dissociation occurs when $Rh(CO)(PMe_3)Cl$ is irradiated. However, the three-coordinate intermediate thus formed is not involved in the carbonylation pathway. Further confirmation of these results was obtained by irradiation of $Rh(CO)(PMe_3)Cl$ and related species in frozen organic glasses[46] where a long-lived species was observed by IR spectroscopy that was tentatively assigned to a non-planar, triplet-excited state. The assignment to this species was reinforced by DFT calculations, again demonstrating the powerful combination of low-temperature photochemistry and DFT to investigate mechanisms.

1.09.3.3 Photochemically Induced Electron Transfer

Photochemical electron-transfer reactions of organometallic molecules have been extensively studied for both synthetic and theoretical/mechanistic purposes.[16] Among the most common photochemical electron-transfer reactions are those involving MLCT excitation, followed by electron transfer of the ligand-localized electron to an oxidizing solvent. Examples of this reactivity are given in other sections (see Equation (7) above and Scheme 12

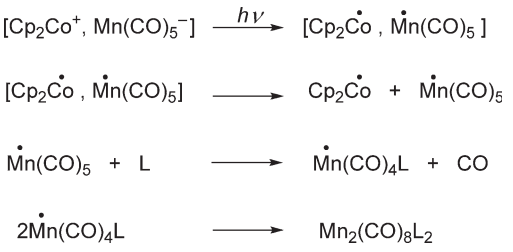

Scheme 4

below). Another common reaction category involves photochemically initiated charge transfer in an electron donor–acceptor pair (Scheme 4). In addition to their usefulness as a convenient way to generate reactive intermediates, these reactions provide useful mechanistic information about electron-transfer theories.[47] As discussed below, they are also particularly useful for synthetic purposes in the initiation of ionic polymerization reactions.[48]

In another type of reaction, direct electron transfer to the solvent is a consequence of CTTS excitation. This reactivity is observed in oxidizing solvents such as CCl_4 (Equation (16)).[49] In some instances, CTTS excitation leads to solvated electrons rather than solvent reduction. An example is provided by irradiation of $Fe(CO)_4^{2-}$ in glasses of aqueous NaOH at 77 K.[50]

$$Cp_2Fe^{II} + CCl_4 \xrightarrow{h\nu\,(CTTS)} [Cp_2Fe^{III}]^+ + Cl^- + {\cdot}CCl_3 \qquad (16)$$

1.09.3.4 Adaptive Quantum Control for Selective Bond Cleavage

A long-range goal in photochemistry is to selectively break certain bonds while leaving others intact. The applications to synthesis of such an ability would be far-reaching, if not astounding, because specific target molecules could be selectively synthesized in high yield with minimal byproducts. Selective bond cleavage is one possible application of the recently developed technique called "adaptive quantum control."[7,51,52] In this technique, specifically shaped femtosecond laser pulses, optimized by a feedback algorithm, are used to manipulate the interaction of light with molecules by using frequency- and time-domain quantum mechanical interference phenomena. Understandably, the technique was first applied to relatively simple molecules, but of late the technique has been applied to the control of more complex organometallic molecules. In a seminal study, the technique was applied to the $CpFe(CO)_2Cl$ molecule, and it was shown that the branching ratio of the two pathways giving CpFe(CO)Cl and FeCl products can be controlled (Equation (17)).[7,53]

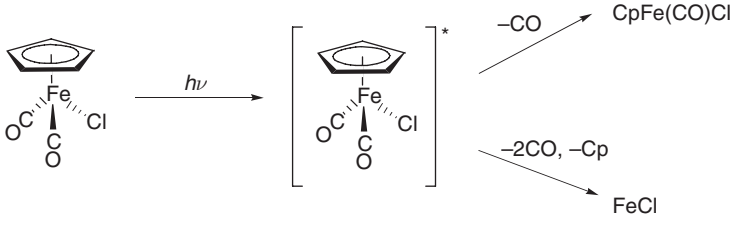

(17)

Control experiments showed that the usual experimental methods for controlling the products in a photochemical reaction such as wavelength, light intensity, and chirp control (in the case of laser irradiation) were not effective in controlling the product distribution in this system. (The authors of this study stress that other specific bond cleavage reactions could have been selected but the two chosen were simply picked as examples to demonstrate the applicability of the technique.) The method has several drawbacks for practicing organometallic chemists. First, a relatively sophisticated fs laser system and its associated hardware and software are required for "coherent control" of the laser pulses. Second, application of the method to molecules in solution presents additional challenges (compared to the more common gas-phase experiments).[51] Obviously, extension to solution-phase work is required before the technique will be practical for organometallic chemists.

1.09.4 Applications

1.09.4.1 Applications of Laser Methods to Mechanistic Studies

Photochemists have been interested in short time domains ever since the first flash lamp-powered flash photolysis systems provided data about reaction events on the millisecond timescale. In recent years, the introduction of Ti-sapphire laser systems has shortened the observation window to events that occur on the femtosecond timescale. Data acquisition in early experiments relied on UV–Vis detection, but a problem was that electronic spectra of the intermediate species formed in organometallic photochemical reactions are not definitive.[2] In fact, with the advent of faster laser systems, a particular problem is that it is often difficult to determine if a spectrum is attributable to an excited state or to an intermediate. To identify the species observed by electronic spectroscopy, it was common to carry out the reactions in a low-temperature matrix with the hope that the species would be stabilized at low temperature and could be definitively identified by infrared spectroscopy.[54–56] Because of the usefulness of infrared spectroscopy, a considerable effort has gone into the construction of apparatuses over the past decade for identifying intermediates by infrared and Raman spectroscopy on the fast timescale. Excellent overviews of these techniques for organometallic chemists have appeared.[2,57–59] A particularly interesting example of the type of detailed mechanistic information that can be obtained using Fourier transform infrared (FTIR) is the finding that recombination of photochemically generated (^{n}BuCp)Mo(CO)$_3$ radicals occurs to give a non-equilibrium mixture of *trans*- and *gauche*-[(^{n}BuCp)Mo(CO)$_3$]$_2$.[60] Rate constants for the radical–radical recombination ($\approx 10^9$–10^{10} $M^{-1}s^{-1}$ in various solvents) and the kinetics of the *gauche*-to-*trans* isomerization were also determined (Scheme 5).

Advances in data acquisition now make it possible to obtain rate constants on the ps, and even fs, timescale. On these timescales, it is also possible to observe the "physical" processes that occur during a photochemical reaction, examples being the observation of vibrational cooling of the Mn(CO)$_5$ radical following photolysis of Mn$_2$(CO)$_{10}$ ($\tau \approx 500$ ps),[61] the vibrational cooling of M(CO)$_5$ (M = Cr, Mo, W) following dissociation of a CO ligand from M(CO)$_6$, and the vibrational cooling of M(CO)$_6$ following geminate recombination of M(CO)$_5$ and CO.[62]

The power of time-resolved IR (TRIR) methods to solve mechanistic quandaries is superbly demonstrated in a study of the photochemical *fac–mer* isomerization of the Mn(Br)(CO)$_3$(*i*Pr-DAB) complex (*i*Pr-DAB = N,N′-di-*i*Pr-1,4-diazabutadiene) (Scheme 6).[2] Time-resolved visible absorption showed an initial species with λ_{max} at 605 nm formed within 400 fs following excitation. This species decayed with an 11 ps lifetime accompanied by the appearance of the product with identical kinetics. Based on this evidence alone, it was not possible to differentiate between two mechanistic interpretations: (i) the 605 nm transient is an excited state and the 11 ps process is concerted CO loss and Br movement, or (ii) the 605 nm species is the CO loss primary photoproduct and the 11 ps process is the axial → equatorial Br movement. Subsequent experiments with picosecond TRIR showed that the IR bands of the 605 nm species were shifted to lower frequencies relative to the starting complex, a result interpreted as consistent only with the assignment of the species to the CO loss species and not the excited state. Note that a slower 22 ps process was attributed to coordination of a pyridine solvent molecule to the Mn(Br)(CO)$_2$(*i*Pr-DAB) intermediate.

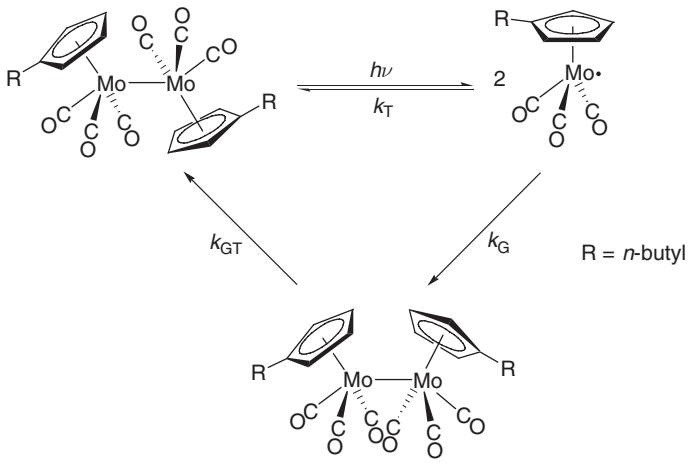

Scheme 5

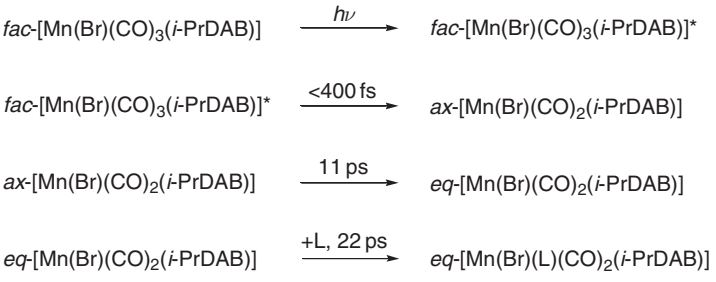

Scheme 6

Another fascinating demonstration of TRIR and time-resolved optical spectroscopy was the determination that photoexcitation of $Mn(CO)_5(COCH_3)$ forms an intermediate with structure C in weakly coordinating solvents but with structure S in more strongly donating solvents.[63,64] Spectroscopic assignments were confirmed by comparing the TRIR spectra to those obtained at low temperature in similar solvents.

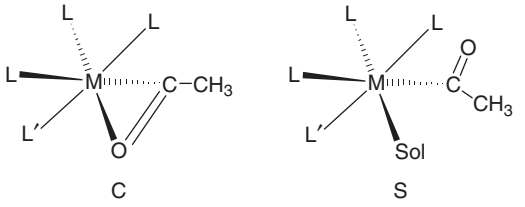

1.09.4.2 Applications of Photochemistry to the Synthesis of Organometallic Molecules

1.09.4.2.1 Ligand substitution following ligand loss

The most common application of photochemistry in the syntheses of organometallic complexes is in ligand substitution reactions where an initial photochemical step is used to create a vacant coordination site (Equation (18)). Many of these reactions will also occur thermally, but the advantages of photochemistry are that milder conditions can often be used than in the corresponding thermal reactions, and the photochemical reactions are generally more selective than their thermal counterparts.

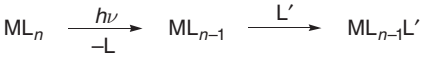

(18)

Although the ligand substitution products are potentially appealing, more often than not it is the reactivity that occurs subsequent to substitution that makes these reactions interesting. An example is the synthesis of organometallic acetylido complexes shown in Equation (19).[65]

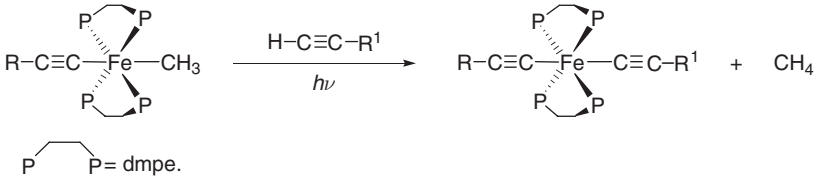

(19)

Data suggested that the reaction proceeded by the initial cleavage of an Fe–P bond, as shown in Scheme 7. Subsequent photochemical reactions gave even longer acetylide chains.

1.09.4.2.2 Photochemical reactions that differ from the thermal reactions

Photochemical reactions that give products different than the corresponding thermal reactions are of particular interest and use in synthesis. Differences arise because photochemical reactivity is controlled by the properties of the relevant excited state, whereas thermal reactivity is determined by the properties of the ground electronic state.

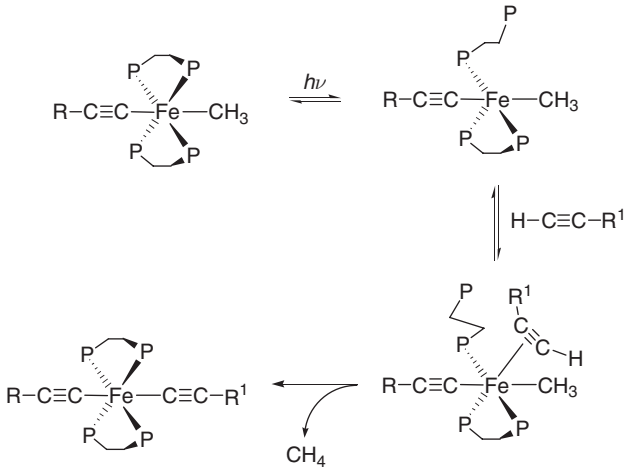

Scheme 7

Examples of dramatic differences in the photochemical and thermal reactivity are found with metal carbonyl clusters. Typically, electronic excitation of these molecules leads to metal–metal bond cleavage with consequent partial or complete fragmentation of the cluster.[66–68] In contrast, the thermal reactions of these clusters typically proceed by metal–ligand bond cleavage with retention of the cluster framework.[69,70] (Note, however, that by careful selection of irradiation wavelength and solvent, it is frequently possible to prepare either photofragmentation or photosubstitution products.[66] With metal carbonyl clusters, low-energy excitation generally leads to fragmentation, while higher energy excitation leads to M–CO bond dissociation, as well as some fragmentation.) An example of fragmentation versus M–CO bond dissociation is found in the photochemical and thermal chemistry of the $Ru_3(CO)_9(PPh_3)_3$ cluster (Scheme 8).[71] Irradiation of this molecule in the presence of substrates such as H_2, CO, olefins, and acetylenes generally forms mononuclear complexes, whereas the thermal reactions retain the cluster network.

Photochemical fragmentation of a cluster leads to coordinatively unsaturated species that are valuable synthetic intermediates in the preparation of a wide range of organometallic complexes. A synthetically useful procedure is to

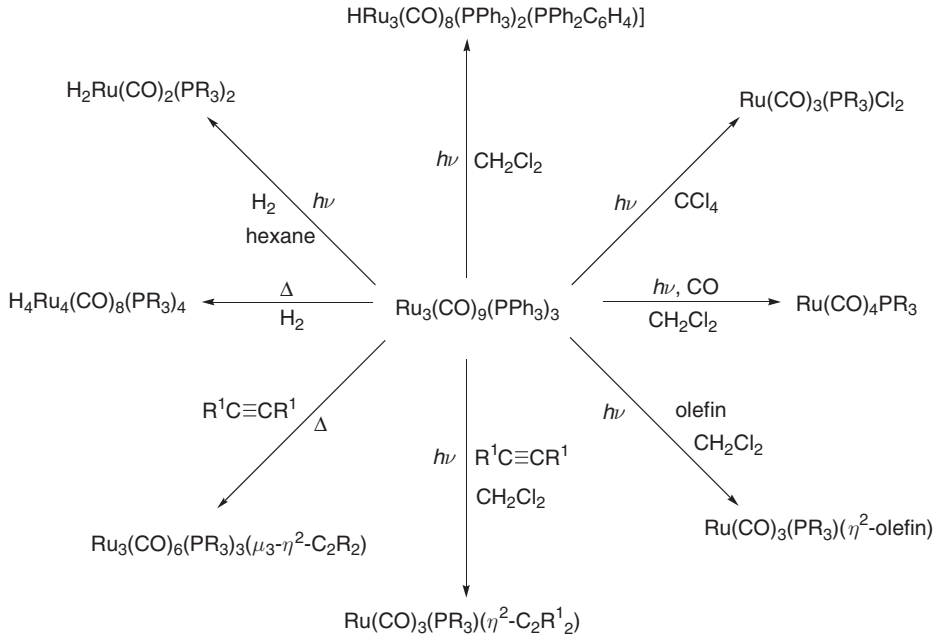

Scheme 8

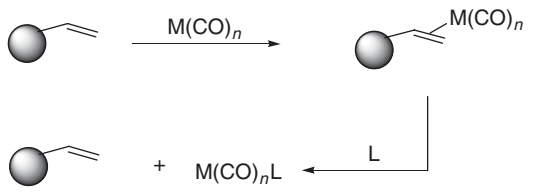

Figure 2 Concept for the preparation and use of polymer-supported organometallic fragments. Reprinted with permission from Leadbearer, N. E.; Sharp, E. L. *Organometallics* **2003**, *22*, 4167–4169. © (2003) American Chemical Society.

capture these fragments with olefins. Because the olefin ligands are labile, these complexes are effectively sources of the coordinatively unsaturated species. However, the olefin complexes are generally air and light sensitive, and they typically decompose on removal of the solvent. In addition, they have a tendency to react in bimolecular reactions to give unreactive species. To circumvent this problem, Leadbetter has described a process whereby the fragments (e.g., $Ru(CO)_4$ from $Ru_3(CO)_{12}$; $Mo(CO)_5$ from $Mo(CO)_6$) are generated in the presence of a polymer with pendant olefin groups.[72] The resulting materials are stable and useful for syntheses. The utility of these materials as a source of coordinatively unsaturated fragments was demonstrated by showing that ligand substitution for the coordinated olefin was relatively facile (Figure 2).

1.09.4.2.3 Photochemical reactions in the presence of oxygen

Oxygen must generally be excluded in the photochemical reactions of organometallics because the excited states and intermediates react with oxygen to form metal oxides. However, under certain conditions, this oxidation reactivity can be controlled to produce metal oxide products that still have organometallic ligands.[73–75] Examples are the synthesis of $(CpV)_mO_n$ clusters by irradiation of $CpV(CO)_4$ in the presence of controlled amounts of oxygen,[76] and the synthesis of Cp^*MoO_2Cl from $Cp^*Mo(CO)_3Cl$ (Equations (20) and (21)).[75]

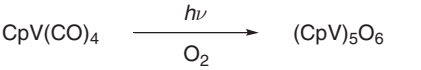

(20)

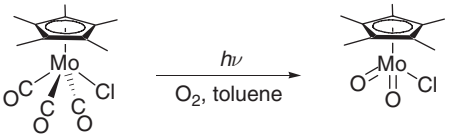

(21)

1.09.4.2.4 Photochemistry of metal hydrides

Photochemical elimination of H_2 is a general reaction of organometallic di- and polyhydrides (e.g., Equation (4)).[77] The elimination of H_2 results in a coordinatively unsaturated species that can react in the ways typical of a coordinatively unsaturated species, for example, with a ligand, in an electron-transfer reaction, with another coordinatively unsaturated molecule, in an oxidative addition reaction, etc. Extensive early research showed that MLCT excited states give rise to the photochemical elimination of H_2.

An interesting synthetic application of photochemistry was the attempted generation and trapping of an η^2-H_2 complex by irradiation of *trans*-$CpRe(CO)_2(H)_2$ at low temperature.[78] The expectation here was not necessarily that the photochemistry would directly convert the complex to a metastable state having an η^2-H_2 ligand, but rather that the η^2-H_2 complex might be in equilibrium with the photogenerated *cis*-isomer. However, although the *trans*- → *cis*-isomerization was observed, no η^2-H_2 complex was detected (Equation (22)).

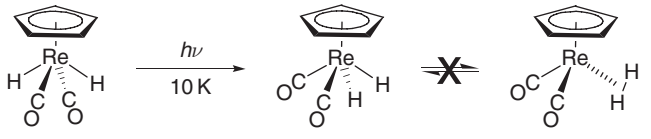

(22)

Furthermore, it was speculated that loss of H_2 was not observed because the low-temperature matrix (methylcyclohexane glass) prevented dissociative ligand loss, and allowed the isomerization reaction channel to predominate.

In this regard, it is noted that the photochemical reactivity and excited-state dynamics of organometallic hydride complexes are frequently studied by rigorous calculation methods, because the hydride ligand is small, which permits more accurate calculations.[79–81] With regard to these calculations, the questions of most interest to organometallic photochemists concern the identification of the excited states and the partitioning of the reactivity between different pathways. Whereas current calculation methods such as DFT do an excellent job in identifying excited states, recent computational results on metal hydride systems make it clear that an extremely detailed knowledge of the potential energy-surface topology is essential for an understanding of the excited-state dynamics (such as the partitioning of the reactivity between different pathways).[82] The problem for the experimentalist is that features such as energy barriers cannot be predicted using an intuitive approach based on relatively simple concepts such as the character of the orbitals involved in an excitation. The suggestion has been made that more calculations on well-chosen model systems will eventually bring to light the generalizations that will make the results of high-end calculations useful for the experimentalist.[82]

1.09.4.2.5 Photochemical reactions of carbene complexes

A vast amount of synthetic work has been done on the photochemistry of Cr and Mo Fischer carbene complexes in the presence of doubly bonded substrates to give cycloaddition products. This chemistry has been comprehensively reviewed,[83,84] and the salient points are the following. The photochemistry of metal carbene complexes (using light with $\lambda \approx 400$ nm) originates from an MLCT excited state, involving electronic excitation from a non-bonding metal-centered orbital to a π^*-orbital that is carbene–carbon *p*-orbital centered. The resulting MLCT excited state has ketene-like reactivity, and the interpretation of this reactivity is that excitation promotes the reversible insertion of a *cis*-CO ligand into the metal–carbon double bond. The result is a short-lived metallacyclopropanone/metal-bound ketene intermediate (Equation (23)).

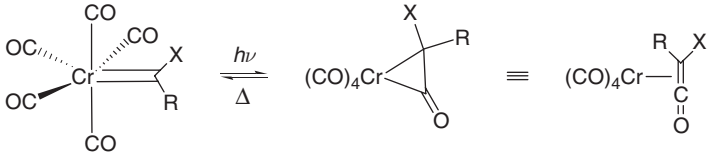

(23)

In the presence of appropriate substrates (i.e., substrates that normally undergo reactions with ketenes), the ketene fragment is transferred from the metal to the substrates. In the absence of reactive substrates, the CO is deinserted and the carbene complex is regenerated, leading to no net reaction. With regard to the CO insertion, note that it has been shown that one-electron oxidation of a metal center promotes insertion of CO into M–C bonds.[85,86] Because MLCT excitation is effectively a one-electron oxidation of the metal, the mechanistic interpretation of ketene formation proposed above is reasonable. An alternative explanation invokes an intermediate with a lone pair on the reduced carbene ligand attacking an electrophilic CO ligand (Equation (24)).[29]

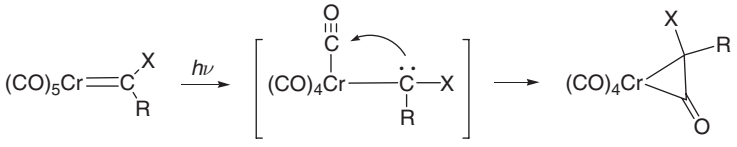

(24)

The photochemical generation of the ketene intermediates has been exploited for a variety of synthetic purposes. Thus, photolysis of chromium alkoxycarbene complexes in the presence of imines produces *β*-lactams, in good to excellent yields, with high diastereoselectivity, and few byproducts (Equation (25)).

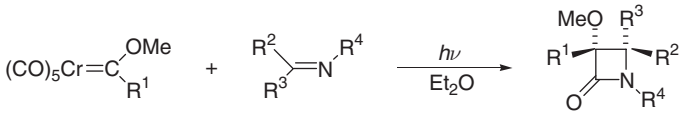

(25)

Likewise, the ketene intermediates undergo highly stereoselective cycloadditions with electron-rich olefins to give cyclobutanones (Equation (26)). Among scores of other reactions, they react with aldehydes to produce *β*-lactones and

with ylides to form captodative allenes. Chromium aminocarbenes are also important intermediate complexes in the synthesis of α-amino esters from amides. In fact, Hegedus has summarized the reactivity of these species by noting that they "undergo all of the reactions for which classically generated free ketenes are famous, and (they) often enjoy greater selectivity and tolerance for the presence of functionality."[84]

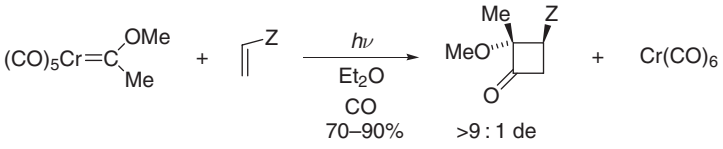

(26)

Z = Ph, CH_2OAc, OEt, NHAc, alkyl, and others.

1.09.4.2.6 Photochemical reactions of carbyne complexes

The photochemistry of metal carbyne complexes is in many ways similar to the photochemistry of metal carbene complexes, but the reactions have not been developed or become as synthetically useful as the photochemistry of metal carbene complexes. Among reported reactions are couplings with ancillary CO ligands to form ketenyl complexes, protonation of the carbyne carbon, insertions into C–H bonds, addition of the carbyne carbon to an alkyne to produce a cyclopropenyl complex, and electron-transfer reactions.[87]

As with metal carbenes, the photoactive state is proposed to be MLCT. Interpretation of the reactivity suggests that this excited state, or the intermediate derived from it, is bent, as shown by the pathway for the protonation reaction of $(CO)(PPh_3)_2(Cl)Os{\equiv}CPh$ in Scheme 9.[88]

Rapid CO migration in the excited state to form an η^2-ketenyl intermediate is proposed to occur in other reactions, as shown in Schemes 10 and 11.

As with many other complexes, MLCT excitation of metal carbyne complexes can lead to electron-transfer reactions. An example is the oxidation of $Cp(P(OMe)_3)_2Mo{\equiv}CPh$ in $CHCl_3$; the reaction proceeds through an unusual 17-electron metal carbyne intermediate (Scheme 12).[87]

1.09.4.3 Applications of Organometallic Complexes in Photocatalysis

Photocatalysis refers to a process in which light and a catalyst complex bring about or accelerate a chemical reaction. The subject area has been extensively reviewed, and numerous examples of synthetically useful photocatalytic transformations have been cataloged and tabulated.[89–91] Photocatalysis is also useful for the activation of small

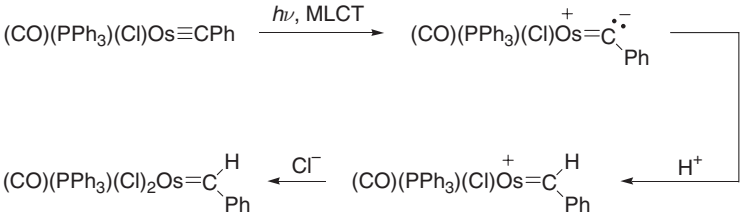

Scheme 9

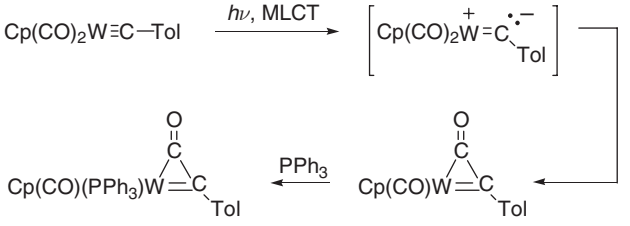

Scheme 10

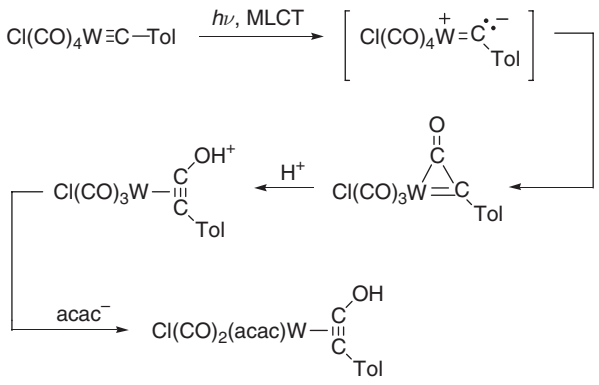

Scheme 11

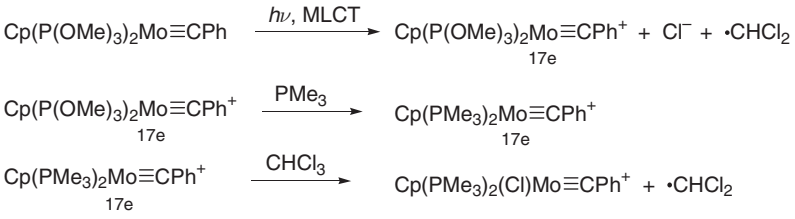

Scheme 12

molecules, and these reactions have likewise been extensively tabulated and reviewed.[92] The list of useful transformations and small molecule reactions includes the following: (i) geometric isomerization of alkenes; (ii) allylic [1,3] hydrogen shifts; (iii) cycloaddition of alkenes; (iv) dimerization and trimerization of alkenes; (v) polymerization of alkenes (radical, cationic, and anionic); (vi) skeletal rearrangement of alkenes; (vii) metathesis of alkenes; (viii) hydrogenation of alkenes; (ix) additions to alkenes; (x) additions to C═X; k) aliphatic substitution; (xi) aromatic substitution; (xii) vinyl substitution; (xiii) alkene oxidation; (xiv) alcohol oxidation; (xv) arene oxidation; (xvi) oxidative decarbonylation; (xvii) amine oxidation; (xviii) sulfide oxidation; (xix) benzaldehyde oxidation; (xx) dehydrogenation; and (xxi) hydrosilylation reactions.[90]

Photochemists divide photocatalytic reactions into two categories, those that are catalytic in photons and those that are not. Selected examples that demonstrate fundamental principles and synthetic utility will be discussed here.[89] A typical role of the photon in a reaction that is catalytic in photons is to generate a vacant coordination site. An example is the $Fe(CO)_5$-catalyzed isomerization of olefins, shown in Scheme 13, where photodissociation of an Fe–CO bond generates $Fe(CO)_4$.[93]

Another example of a reaction that is catalytic in photons is the $Cp'Pt(CH_3)_3$-catalyzed hydrosilylation of olefins (Equation (27)). In this reaction, $\sigma(Pt–CH_3) \rightarrow Pt$ charge transfer is proposed to homolyze a $Pt–CH_3$ bond, leading to radicals that catalyze the reaction in a chain process.[94] Note that the quantum yields for reactions that are catalytic in photons can be greater than one, because many product molecules can be formed once the true catalyst is photochemically generated. The kinetics of these systems frequently show an induction period.

$$R_3Si–H + H_2C{=}CHR^1 \xrightarrow{h\nu,\ Cp'Pt(CH_3)_3} R_3Si–CH_2\text{-}CH_2R^1 \qquad (27)$$

Another role of photoexcitation is to produce a long-lived excited state that is photochemically active. An example is the previously discussed carbonylation of arenes and alkanes using *trans*-$RhCl(CO)(PMe_3)_2$.[44] Photocatalytic reactions involving a long-lived excited-state catalyst are rare because most excited states of organometallic complexes are not long lived enough to undergo bimolecular reactions with a substrate. An interesting extension of

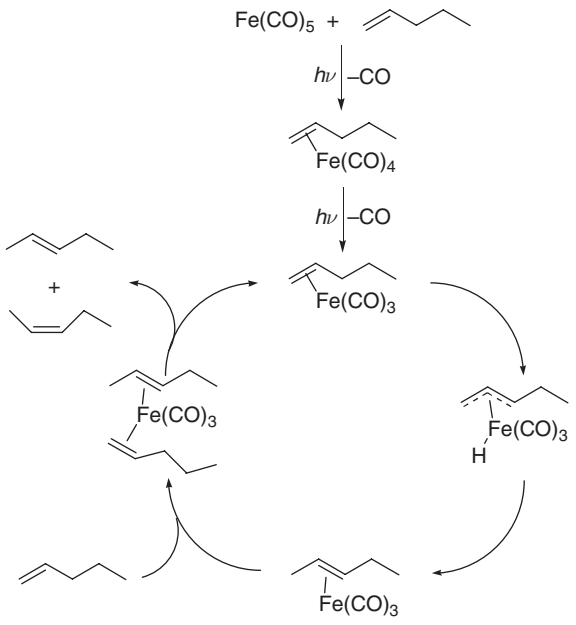

Scheme 13 Reprinted with permission from Kutal, C. Photosensitive Metal-Organic Systems: An Overview. In *Photosensitive Metal-Organic Systems, Mechanistic Principles and Applications*; Kutal, C., Serpone, N., Eds.; Advances in Chemistry Series 238; American Chemical Society: Washington, DC, 1993; pp 1–25. © (1993) American Chemical Society.

the work with *trans*-RhCl(L)$(PMe_3)_2$ was to use dense CO_2 as the reaction medium and CH_4 as the substrate (Equation (28)):[95]

$$CH_4 + CO \xrightarrow[\text{dense } CO_2]{h\nu,\ RhCl(CO)(PR_3)_2} CH_3CHO \qquad (28)$$

The chief advantages to using dense CO_2 as the reaction medium were claimed to be its inertness, its general ability to dissolve the reactants, and its easy separation from the reaction mixture. No mechanistic work was reported, but the same mechanism as previously proposed in alkane solvents was suggested, that is, the key step was oxidative addition to the excited state of the metal complex. The CO_2/Rh complex system was also reported to be an effective photocatalytic system for the dehydrogenation of cyclooctane.

Photocatalytic reactions using organometallic complexes as photocatalysts have found significant use in organic synthesis. Among the many types of reactions that have been investigated are C–C bond-forming reactions, including alkylation, carbonylation, photocyclization, and photocycloaddition reactions; C–H activation reactions; reduction reactions; isomerization reactions; and polymerization reactions.[89]

Metal radicals formed by photolysis of metal–metal bonded dimers are catalysts for the substitution of metal hydride complexes.[90] The proposed photocatalytic cycle is shown in Scheme 14.

An emerging area of study in the area of photocatalysis is the development and investigation of new polymerization photocatalysts. Early work showed that ferricenium, generated by irradiation into the CTTS band of ferrocene in CCl_4, was a catalyst for the radical polymerization of vinyl monomers (Equation (29)).[96]

$$Cp_2Fe + CCl_4 \rightleftharpoons [Cp_2Fe, CCl_4] \xrightarrow{h\nu} Cp_2Fe^+ + CCl_4^- \longrightarrow \cdot CCl_3 + Cl\cdot \qquad (29)$$

Recent work has shown that a similar strategy, using a ferrocene → ethyl α-cyanoacrylate CTTS excitation, can be used for anionic polymerization of the ethyl α-cyanoacrylate (Scheme 15).[96]

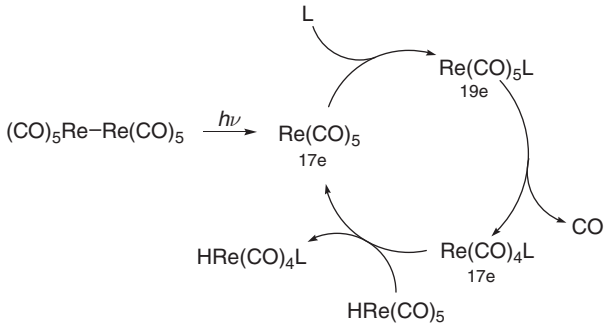

Scheme 14

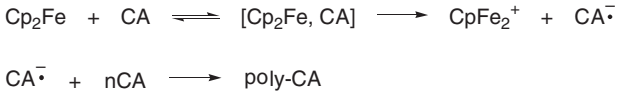

Scheme 15

Substitution of the Cp rings on ferrocene with benzoyl lowers the energy of the MLCT-excited states, and changes the photochemistry from electron transfer to substitution (Equation (30)).

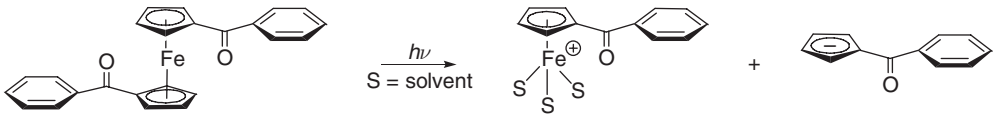

(30)

It was argued that the MLCT excited state has a change in hapticity (from η^5 to η^4), and this facilitates solvent attack on the Fe center, leading to loss of a $CpR^{-\bullet}$ ligand. The anion thus produced efficiently initiates the anionic polymerization of ethyl α-cyanoacrylate. It was likewise shown that cationic polymerizations could be initiated by LF excitation of $CpFe(\eta^6\text{-arene})^+$ complexes.

The photocatalytic reduction of CO_2 to CO using supramolecular organometallic complexes has been described.[97] In particular, irradiation of $[(dmb)_2Ru^{II}(bpyC_3bpy)Re^{I}(CO)_3Cl]^{2+}$ (dmb = 4,4′-dimethyl-2,2′-bipyridine) in DMF/TEOA solution (DMF = N,N-dimethylformamide; TEOA = triethanol amine) containing a sacrificial electron source gave CO. The mechanism (Scheme 16) was proposed to involve initial excitation to an MLCT excited state of the Re moiety. Electron transfer then occurs from the reduced bpy ligand bonded to the Re center to the bpy ligand bonded to the Re center. The latter species is the catalyst for the CO_2 reduction reaction.

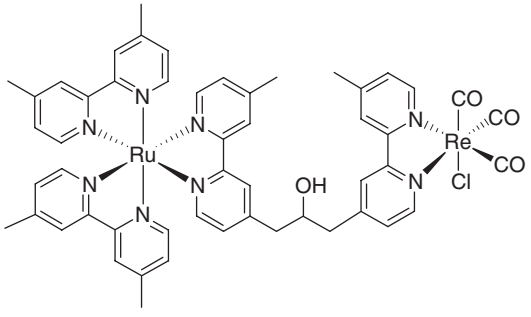

$[(dmb)_2Ru^{II}(bpyC_3bpy)Re^{I}(CO)_3Cl]^{2+}$

This work demonstrates the principle of using a supramolecular complex containing both a photosensitizer and a catalytically active site, and is conceptually related to the "antenna effect" used in energy-storage reactions.[98] The advantage of the supramolecular complexes was demonstrated by comparing the turnover numbers for the

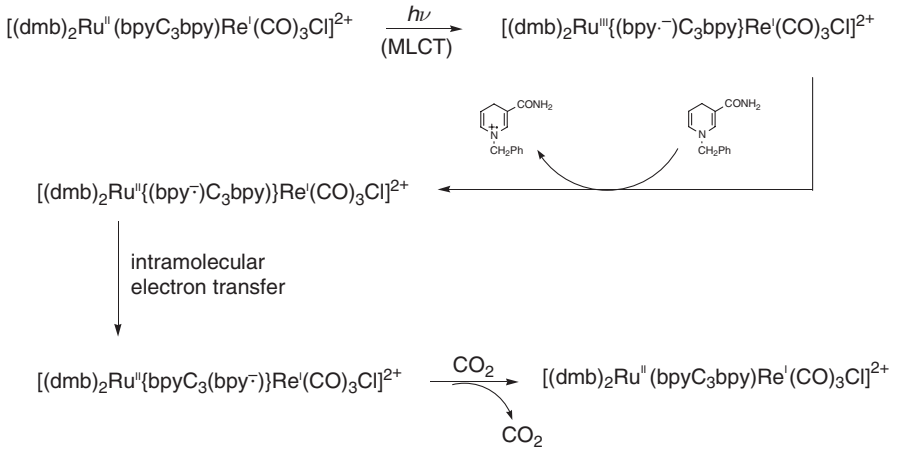

Scheme 16

supramolecular complexes to solutions containing 1 : 1 ratios of analogous mononuclear Re and Ru complexes; the turnover numbers for the supramolecular complexes were considerably larger. In designing a supramolecular complex for photocatalysis, a number of factors must be considered, including the energetics of the intramolecular electron transfer (it cannot be endothermic), the rates of electron transfer in the various steps, and the extent of electronic communication between the photosensitizer and the catalyst moiety.

1.09.4.4 Applications of Organometallic Photochemistry to Polymers

1.09.4.4.1 Organometallic molecules as photoinitiators

Organometallic molecules have been used as photoinitiators in cationic, anionic, and radical (chain) polymerization reactions. Examples of each type abound, but only selected examples will be discussed here because the fundamental principle is the same in each case: irradiation is used to generate an intermediate species (an ion or a radical species) that can initiate a polymerization reaction.

1.09.4.4.1.(i) Cationic initiation

The complexes used to initiate cationic polymerization have photolabile ligands.[99,100] Among the most commonly studied initiators are those that have photodissociable arene ligands. An example is the $CpFe(C_6H_6)^+$ complex. This molecule and related ones have relatively low-energy LF absorption bands. Irradiation into these bands leads to loss of the arene ligand (Equation (2)). The coordinatively unsaturated species thus produced acts as a Lewis acid to bond monomers. Following coordination of a monomer, polymerization occurs by the usual cationic polymerization mechanism. Note that the arene ligand in $CpFe(C_6H_6)^+$ can be varied and derivatized so as to change the absorption spectrum. This allows for control of the wavelength used in the photochemical polymerization process and also of the extinction coefficient of the absorbing band.

In principle, any organometallic molecule that loses a dative ligand in a photochemical heterolysis reaction is a potential catalyst for this type of polymerization. Other common catalysts are $(\eta^5\text{-}C_6H_7)Fe(CO)_3^+$ and $CpFe(CO)_2L^+$ (L = various phosphines or other ligands). The former molecule, in particular, is exceptionally reactive. When these molecules are irradiated, an M–CO bond is dissociated; the coordinatively unsaturated species thus produced reacts with, for example, an epoxide monomer, and polymerization proceeds via a standard ring-opening pathway.

1.09.4.4.1.(ii) Anionic initiation

Kutal has reported that MLCT excitation of benzoyl-substituted ruthenocenes leads to anionic polymerization of ethyl 2-cyanoacrylate (Equation (31)).[101] These complexes do not undergo ligand loss as a result of MLCT excitation, and it was suggested that the charge redistribution in the excited state allowed the complex to act as an anionic initiator.

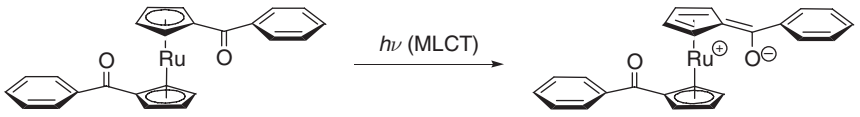

(31)

1.09.4.4.1.(iii) Radical initiation

Molecules that produce radicals upon excitation are capable of initiating radical chain-polymerization reactions of vinyl monomers.[102,102a] Organometallics produce radicals in numerous ways, and several of these methods are outlined in the following reactions.

1.09.4.4.1.(iii).(a) Homolysis of a metal–carbon bond

In either of the cases in Equation (32) or (33), it is likely that an LMCT ($\sigma_{ligand} \rightarrow M$) transition is responsible for the M–C bond homolysis.

$$Mn(CO)_5CH_3 \xrightarrow{h\nu} \bullet Mn(CO)_5 + \bullet CH_3 \quad (32)$$

$$MR_4 \xrightarrow{h\nu} \bullet MR_3 + \bullet R \quad (33)$$

M = Ti, Zr; R = neopentyl.

1.09.4.4.1.(iii).(b) Homolysis of a metal–metal bond

In this reaction, a metal radical is produced by homolysis of the metal–metal bond (Equation (34)). A typical behavior of metal radicals is halogen atom abstraction from an alkyl halide, such as CCl_4 (Equation (35)). The CCl_3 radical thus produced can then react with a vinyl monomer to initiate a polymerization reaction.

$$Re_2(CO)_{10} \xrightarrow{h\nu} 2 \bullet Re(CO)_5 \quad (34)$$

$$\bullet Re(CO)_5 + CCl_4 \longrightarrow Re(CO)_5Cl + \bullet CCl_3 \quad (35)$$

1.09.4.4.1.(iii).(c) Heterolysis of a metal–ligand bond

Somewhat surprisingly, even M–L heterolyses can lead to initiation of radical chain reactions. In these reactions, the key feature is again the formation of CCl_3 radicals (Equation (36)).

$$W(CO)_6 \xrightarrow[-CO]{h\nu} W(CO)_5 \xrightarrow{CCl_4} [W(CO)_5Cl] + \bullet CCl_3 \quad (36)$$

1.09.4.4.2 Polymers containing organometallic molecules in the backbone

Organometallic molecules have been incorporated into polymer backbones for a variety of reasons.[103,104] In general, the photochemistry of the molecules in the polymers is the same as the discrete molecules. One example has already been mentioned in Equation (5). In another example, metal–metal bonds are cleaved homolytically with visible light in polymeric materials that have organometallic metal–metal bonds along the backbone (e.g., Scheme 17; compare to Equation (9)).[105]

The photochemistry above has been demonstrated with a variety of polymers, including polyurethanes, polyureas, vinyl polymers, and polyamides (e.g., see structure **1**).

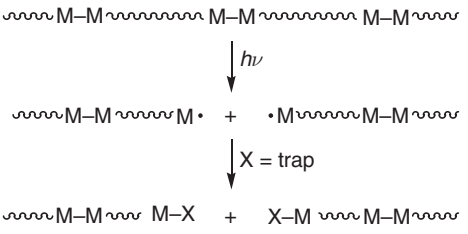

Scheme 17 Reprinted with permission from Male, J. L.; Lindfors, B. E.; Covert, K. J.; Tyler, D. R. *Macromolecules* **1997**, *30*, 6404–6406. © (1997) American Chemical Society.

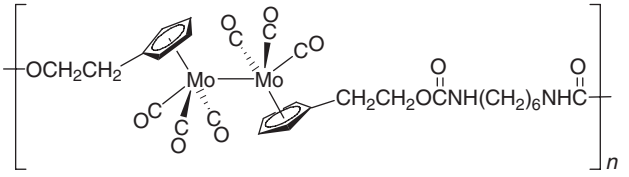

1

In general, the qualitative photochemical behavior of organometallics incorporated in polymers is the same as that of the discrete molecules.

1.09.4.4.3 Organometallics for monitoring polymerization reactions

An emerging use for organometallics in polymers is for real-time monitoring of polymerization reactions.[106] The emission spectra of many organometallic species are sensitive to environmental rigidity, and this feature has been exploited to monitor the curing processes of both thermoset and photosensitive polymers. Typical of the complexes used in these systems are $W(CO)_4L$ and *fac*-$Re(CO)_3L$, where L is bpy or phen (phen = 1,10-phenanthroline).

1.09.4.5 Applications to the Deposition of Thin Films and Wires

Organometallic complexes are finding increased use as precursors in the photochemical processes that sustain the present-day microelectronics industries.[107] In particular, laser photochemical vapor deposition (LPCVD) using organometallic complexes has become an important process for the deposition of metal surfaces and wires. The basic technique is to irradiate a volatile organometallic complex such that all of its ligands dissociate, leaving the metal to be deposited. Numerous examples have been reported, including the deposition of Zn from $ZnEt_2$, Mo from $Mo(CO)_6$, Fe from $Fe(CO)_5$, Pd and Pt from $M_2(CNMe)_6^{2+}$,[108] Cr from $Cr(CO)_6$, and W from $W(CO)_6$. A list of compounds frequently used in LPCVD has been published.[107]

One of the major applications of organometallic photochemistry to materials chemistry is in the photochemical deposition of thin films.[107,109] In the photochemical film-deposition process, a thin metal film is deposited on a substrate surface by using light to dissociate the ligands from an organometallic complex. During the irradiation, the organometallic molecule can either be adsorbed to the substrate surface (Equation (37)) or it can be in the gas phase above the substrate (Equation (38)).

$$ML_{n(\text{adsorbed})} \xrightarrow{h\nu} M_{(s)} + nL \tag{37}$$

$$ML_{n(g)} \xrightarrow{h\nu} M_{(s)} + nL \tag{38}$$

The specific compounds used in these studies depend on the type of thin film desired. Thus, in the semiconductor industry, molecules such as $Ga(CH_3)_3$ and AsH_3 are irradiated. If thin films of transition metals are needed, then molecules such as $Fe(CO)_5$, $W(CO)_6$, or $Cr(CO)_6$ are used. In each case, the photochemical principle is the same: the organometallic molecule is irradiated and the ligands are dissociated, leaving behind the naked metal atom to form

the thin film on the substrate surface. As discussed previously, the types of excited states leading to ligand dissociation include LF, LMCT, and Rydberg excited states.

In modern photochemical thin film-deposition processes, the light source for the process is typically a laser. The light beam can be perpendicular to the substrate surface or parallel to the surface. The perpendicular orientation is used in maskless direct-writing processes (e.g., for circuits), because it gives sharply defined deposition areas while the parallel irradiation method is used to deposit films over a large area. The fate of the ligands in these photoreactions is of some concern. Ideally, the organic material that makes up the ligands is simply vaporized and not deposited with the metals. In fact, carbon and sometimes other elements are often deposited, and one of the prime areas of technological research is to find ways to minimize these co-depositions.

Specific organometallic molecules used in photochemical deposition studies include SiH_4 and Si_2H_6 for the deposition of silicon, SiO_2, or Si_3N_4; $AlMe_3$, $GeMe_3$, and $InMe_3$ are used to prepare the respective metal films. In combination with group 15 alkyls and hydrides (e.g., PH_3, AsH_3, PMe_3), these same group 13 alkyls are used to prepare 13–15 semiconductors such as GaP, InP, and GaAs. Group 2 alkyls and group 16 alkyls are used to make 2–16 semiconductors (e.g., $CdMe_2$ with $TeEt_2$ will produce CdTe). One of the advantages of using a photodeposition method to prepare these materials is that the materials with various compositions can be prepared by varying the starting materials, and by varying the amounts present. For example, ternary materials such as AlGaAs are produced by adding a third material to the starting mixture of gases. Alloys are produced in a similar fashion.

In addition to forming thin films of metals or semiconductor materials on the surface of a substrate, photolytic degradation of organometallics can also be used to form metal particles within a transparent substrate.[110] For example, one of the techniques for doing surfaced-enhanced Raman spectroscopy (SERS) is to adsorb molecules on silver or gold particles (colloids) contained within silica gel or a xerogel. Standard techniques for depositing the gold or silver within the gel generally include some heating, which has numerous disadvantages. Recently, however, it was demonstrated that UV irradiation of $Au(CH_3)_2$(tfac) or $Au(CH_3)_2$(hfac) dissolved in the gel materials led to gold clusters within the gel and that these materials were suitable for SERS (tfac = trifluoroacetylacetonato; hfac = hexafluoroacetylacetonato). In this case, the advantages of the photochemical deposition process over the thermal methods include the ability to pattern the deposit and to control the gold particle size by controlling the photolysis time.

References

1. Leadbeater, N. E. *Comm. Inorg. Chem.* **1998**, *20*, 57–82.
2. Vlcek, A., Jr.; Farrell, I. R.; Liard, D. J.; Matousek, P.; Towrie, M.; Parker, A. W.; Grills, D. C.; George, M. W. *J. Chem. Soc., Dalton Trans.* **2002**, 701–712.
3. Bursten, B. E.; Drummond, M. L.; Li, J. *Faraday Discuss.* **2003**, *124*, 1–24.
4. Poliakoff, M.; Turner, J. J. *Advances in Spectroscopy* **1995**, *23*, 275–306.
5. Poliakoff, M.; George, M. W. *J. Phys. Org. Chem.* **1998**, *11*, 589–596.
6. Carassiti, V. *Coord. Chem. Rev.* **1993**, *125*, 351–360.
7. Assion, A.; Baumert, T.; Bergt, M.; Brixner, T.; Kiefer, B.; Seyfried, V.; Strehle, M.; Gerber, G. *Science* **1998**, *282*, 919–922.
8. Bitterwolf, T. E. *J. Organomet. Chem.* **2004**, *689*, 3939–3952.
9. Roundhill, D. M. *Photochemistry and Photophysics of Metal Complexes*; Plenum: New York, **1994**.
10. Bitterwolf, T. E. *Coord. Chem. Rev.* **2001**, *211*, 235–254.
11. Bitterwolf, T. E. *Coord. Chem. Rev.* **2000**, *206–207*, 419–450.
12. Ford, P. C.; Laverman, L. E. In *High Pressure Chemistry*; van Eldik, R., Klacher, F. G., Eds.; Weiley: Weinheim, 2002; pp 184–222.
13. Lees, A. J. *Coord. Chem. Rev.* **2001**, *211*, 255–278.
14. Farrell, I. R.; Vlcek, A., Jr., *Coord. Chem. Rev.* **2000**, *208*, 87–101.
15. Vogler, A.; Kunkely, H. *Coord. Chem. Rev.* **2000**, *200–202*, 991–1008.
16. Vlcek, A. *Coord. Chem. Rev.* **2000**, *200–202*, 933–978.
17. Vogler, A.; Kunkely, H. *Comm. Inorg. Chem.* **1999**, *21*, 149–163.
18. Baerends, E. J.; Rosa, A. *Coord. Chem. Rev.* **1998**, *177*, 97–125.
19. Rosa, A.; Baerends, E. J.; van Gisbergen, S. J. A.; van Lenthe, E.; Groeneveld, J. A.; Snijders, J. G. *J. Am. Chem. Soc.* **1999**, *121*, 10356–10365.
20. Pollak, C.; Rosa, A.; Baerends, E. J. *J. Am. Chem. Soc.* **1997**, *119*, 7324–7329.
21. Pierloot, K.; Tsokos, E.; Vanquickenborne, L. G. *J. Phys. Chem.* **1996**, *100*, 16545–16550.
22. Chrisope, D. R.; Park, K. M.; Schuster, G. B. *J. Am. Chem. Soc.* **1989**, *111*, 6195–6201.
23. Gill, T. P.; Mann, K. R. *Inorg. Chem.* **1980**, *19*, 3007–3010.
24. Armentrout, P. B.; Simons, J. *J. Am. Chem. Soc.* **1992**, *114*, 8627–8633.
25. Leadbeater, N. *Coord. Chem. Rev.* **1999**, *188*, 35–70.
26. Portius, P.; Yang, J.; Sun, X.-Z.; Grills, D. C.; Matousek, P.; Parker, A. W.; Towrie, M.; George, M. W. *J. Am. Chem. Soc.* **2004**, *126*, 10713–10720.
27. Green, J. C.; Harvey, J. N.; Poli, R. *J. Chem. Soc., Dalton Trans.* **2002**, 1861–1866.
28. Morisaki, Y.; Chen, H.; Chujo, Y. *J. Organomet. Chem.* **2004**, *689*, 2684–2689.
29. Vogler, A.; Kunkely, H. *Coord. Chem. Rev.* **2004**, *248*, 273–278.
30. Vlcek, A., Jr., *Coord. Chem. Rev.* **1998**, *177*, 219–256.

31. Harrigan, R. W.; Hammond, G. S.; Gray, H. B. *J. Organomet. Chem.* **1974**, *81*, 79–85.
32. Meyer, T. J.; Caspar, J. V. *Chem. Rev.* **1985**, *85*, 187–218.
33. Kling, M. F.; Cahoon, J. F.; Glascoe, E. A.; Shanoski, J. E.; Harris, C. B. *J. Am. Chem. Soc.* **2004**, *126*, 11414–11415.
34. Male, J. L.; Lindfors, B. E.; Covert, K. J.; Tyler, D. R. *J. Am. Chem. Soc.* **1998**, *120*, 13176–13186.
35. Schutte, E.; Weakley, T. J. R.; Tyler, D. R. *J. Am. Chem. Soc.* **2003**, *125*, 10319–10326.
36. Covert, K. J.; Askew, E. F.; Grunkemeier, J.; Koenig, T.; Tyler, D. R. *J. Am. Chem. Soc.* **1992**, *114*, 10446–10448.
37. Braden, D. A.; Parrack, E. E.; Tyler, D. R. *Coord. Chem. Rev.* **2001**, *211*, 279–294.
38. Giese, B.; Thoma, G. *Helv. Chim. Acta* **1991**, *74*, 1135–1142.
39. Ferrari, A.; Merlin, M.; Sostero, S.; Ruegger, H.; Venanzi, L. M. *Helv. Chim. Acta* **1999**, *82*, 1454–1457.
40. Goldman, A. S.; Goldberg, K. I. In *Activation and Functionalization of C–H Bonds*; Goldman, A. S., Goldberg, K. I., Eds.; ACS Symposium Series; American Chemical Society, Washington, D.C., 2004; Vol. 885, pp 1–43.
41. Lees, A. J.; Purwoko, A. A. *Coord. Chem. Rev.* **1994**, *132*, 155–160.
42. To, T. T.; Barnes, C. E.; Burkey, T. J. *Organometallics* **2004**, *23*, 2708–2714.
43. Ball, E. S.; Kemnitz, C. R.; McMahon, R. J. *Book of Abstracts, 217th ACS National Meeting*, Anaheim, *CA, USA, March 21–25*, 1999, INOR-062.
44. Rosini, G. P.; Boese, W. T.; Goldman, A. S. *J. Am. Chem. Soc.* **1994**, *116*, 9498–9505.
45. Bridgewater, J. S.; Netzel, T. L.; Schoonover, J. R.; Massick, S. M.; Ford, P. C. *Inorg. Chem.* **2001**, *40*, 1466–1476.
46. Bitterwolf, T. E.; Scallorn, W. B.; Bays, J. T.; Weiss, C. A.; Linehan, J. C.; Franz, J.; Poli, R. *J. Organomet. Chem.* **2002**, *652*, 95–104.
47. Kochi, J. K. *Adv. Phys. Org. Chem.* **1994**, *29*, 185–272.
48. Kutal, C.; Yamaguchi, Y.; Ding, W.; Sanderson, C. T.; Li, X.; Gamble, G.; Amster, I. J. In *Photoinitiated Polymerization*; Belfield, K. D., Crivello, J. V., Eds.; ACS Symposium Series; American Chemical Society, Washington, D.C., 2003; Vol. 847, pp 332–350.
49. Vogler, A.; Kunkely, H. *Coord. Chem. Rev.* **1998**, *177*, 81–96.
50. Kunkely, H.; Vogler, A. *J. Organomet. Chem.* **1992**, *431*, C42–C44.
51. Brixner, T.; Gerber, G. *ChemPhysChem* **2003**, *4*, 418–438.
52. Gordon, R. J.; Zhu, L.; Seideman, T. *Acc. Chem. Res.* **1999**, *32*, 1007–1016.
53. Bergt, M.; Brixner, T.; Dietl, C.; Kiefer, B.; Gerber, G. *J. Organomet. Chem.* **2002**, *661*, 199–209.
54. Brough, S.-A.; Hall, C.; McCamley, A.; Perutz, R. N.; Stahl, S.; Wecker, U.; Werner, H. *J. Organomet. Chem.* **1995**, *504*, 33–46.
55. Perutz, R. N. *Pure Appl. Chem.* **1998**, *70*, 2211–2220.
56. Downs, A. J. In *Low Temperature Molecular Spectroscopy*; Fausto, R., Ed.; NATO ASI Series, Series C: Mathematical and Physical Sciences, Kluwer Academic Publishers, Dordrecht, The Netherlands, 1996; Vol. 483, pp 45–93.
57. Ford, P. C.; Bridgewater, J. S.; Lee, B. *Photochem. Photobiol.* **1997**, *65*, 57–64.
58. George, M. W.; Poliakoff, M.; Turner, J. J. *Analyst* **1994**, *119*, 551–560.
59. Kuimova, M. K.; Alsindi, W. Z.; Dyer, J.; Grills, D. C.; Jina, O. S.; Matousek, P.; Parker, A. W.; Portius, P.; Sun, X. Z., Towrie, M., *et al. J. Chem. Soc., Dalton Trans.* **2003**, 3996–4006.
60. Linehan, J. C.; Yonker, C. R.; Addleman, R. S.; Autrey, S. T.; Bays, J. T.; Bitterwolf, T. E.; Daschbach, J. L. *Organometallics* **2001**, *20*, 401–407.
61. Steinhurst, D. A.; Baronavski, A. P.; Owrutsky, J. C. *Chem. Phys. Lett.* **2002**, *361*, 513–519.
62. Lian, T.; Bromberg, S. E.; Asplund, M.; Yang, H.; Harris, C. B. *J. Phys. Chem.* **1996**, *100*, 11994–12001.
63. Ford, P. C.; Bridgewater, J. S.; Massick, S.; Marhenke, J. *Catal. Today* **1999**, *49*, 419–430.
64. Boese, W.; McFarlane, K.; Lee, B.; Rabor, J.; Ford, P. C. *Coord. Chem. Rev.* **1997**, *159*, 135–151.
65. Field, L. D.; Turnbull, A. J.; Turner, P. *J. Am. Chem. Soc.* **2002**, *124*, 3692–3702.
66. Leadbeater, N. E. *J. Chem. Soc., Dalton Trans.* **1995**, 2923–2934.
67. Ford, P. C. *J. Organomet. Chem.* **1990**, *383*, 339–356.
68. Grevels, F. W. Photochemistry of Organo-metal Carbonyls: Stereochemical and Catalytic Aspects. In *NATO ASI Series, Series C: Mathematical and Physical Sciences*; Kochanski, E., Ed.; Kluwer Academic Publishers, Dordrecht, The Netherlands, 1992; Vol. 376, pp 141–171.
69. Coville, N. J.; Stolzenberg, A. M.; Muetterties, E. L. *J. Am. Chem. Soc.* **1983**, *105*, 2499–2500.
70. Stolzenberg, A. M.; Muetterties, E. L. *J. Am. Chem. Soc.* **1983**, *105*, 822–827.
71. Leadbeater, N. E.; Jones, C. *Transition Met. Chem.* **2000**, *25*, 99–107.
72. Leadbeater, N. E.; Sharp, E. L. *Organometallics* **2003**, *22*, 4167–4169.
73. Almond, M. J.; Atkins, R. W. *J. Mol. Struct.* **1998**, *449*, 99–109.
74. Almond, M. J.; Atkins, R. W.; Orrin, R. H. *J. Chem. Soc., Dalton Trans.* **1994**, 311–313.
75. Trost, M. K.; Bergman, R. G. *Organometallics* **1991**, *10*, 1172–1178.
76. Hino, K.; Inokuchi, Y.; Kosugi, K.; Sekiya, H.; Hosokoshi, Y.; Inoue, K.; Nishi, N. *J. Phys. Chem. B* **2002**, *106*, 1290–1293.
77. Geoffroy, G. L.; Wrighton, M. S. *Organometallic Photochemistry*; Academic Press: New York, **1979**.
78. Casey, C. P.; Tanke, R. S.; Hazin, P. N.; Kemnitz, C. R.; McMahon, R. J. *Inorg. Chem.* **1992**, *31*, 5474–5479.
79. Daniel, C.; Kolba, E.; Lehr, L.; Manz, J.; Schroeder, T. *J. Phys. Chem.* **1994**, *98*, 9823–9830.
80. Daniel, C.; Heitz, M. C.; Lehr, L.; Schroeder, T.; Warmuth, B. *Int. J. Quantum Chem.* **1994**, *52*, 71–88.
81. Heitz, M. C.; Finger, K.; Daniel, C. *Coord. Chem. Rev.* **1997**, *159*, 171–193.
82. Vlcek, A., Jr., *Chemtracts: Inorg. Chem.* **1994**, *6*, 306–313.
83. Hegedus, L. S. *Acc. Chem. Res.* **1995**, *28*, 299–305.
84. Hegedus, L. S. *Tetrahedron* **1997**, *53*, 4105–4127.
85. Magnuson, R. H.; Meirowitz, R.; Zulu, S. J.; Giering, W. P. *Organometallics* **1983**, *2*, 460–462.
86. Collman, J. P.; Hegedus, L. S.; Norton, J. R.; Finke, R. G. In *Principles and Applications of Organotransition Metal Chemistry*; University Science Books: Mill Valley, California, 1987; p 373.
87. Leep, C. J.; Kingsbury, K. B.; McElwee-White, L. *J. Am. Chem. Soc.* **1988**, *110*, 7535–7536.
88. Sheridan, J. B.; Pourreau, D. B.; Geoffroy, G. L.; Rheingold, A. L. *Organometallics* **1988**, *7*, 289–294.
89. Kutal, C. In *Homogeneous Photocatalysis*; Chanon, M., Ed.; Wiley: New York, 1997; Vol. 2, pp 135–168.
90. Heumann, A.; Chanon, M. In *Applied Homogeneous Catalysis with Organometallic Compounds*; Cornils, B., Herrmann, W. A., Eds.; Wiley-VCH Verlag GmbH, 2002; 2nd Ed., Vol. 3, pp 1060–1078.
91. Serpone, N., Pelizzetti, E., Eds. In *Photocatalysis: Fundamentals and Applications*; Wiley: New York, 1989.
92. Chanon, F.; Chanon, M. In *Photocatalysis: Fundamentals and Applications*; Serpone, N., Pelizzetti, E., Eds.; Wiley: New York, 1989; pp 489–540.

93. Kutal, C. *Adv. Chem. Ser.* **1993**, *238*, 1–25.
94. Jakubek, V.; Lees, A. J. *Inorg. Chem.* **2004**, *43*, 6869–6871.
95. Choi, J.-C.; Kobayashi, Y.; Sakakura, T. *J. Org. Chem.* **2001**, *66*, 5262–5263.
96. Kutal, C.; Yamaguchi, Y.; Ding, W.; Sanderson, C. T.; Li, X.; Gamble, G.; Amster, I. J. *ACS Symp. Ser.* **2003**, *847*, 332–350.
97. Gholamkhass, B.; Mametsuka, H.; Koike, K.; Tanabe, T.; Furue, M.; Ishitani, O. *Inorg. Chem.* **2005**, *44*, 2326–2336.
98. Balzani, V.; Ceroni, P.; Juris, A.; Venturi, M.; Campagna, S.; Puntoriero, F.; Serroni, S. *Coord. Chem. Rev.* **2001**, *219–221*, 545–572.
99. Klingert, B.; Riediker, M.; Roloff, A. *Comm. Inorg. Chem.* **1988**, *7*, 109–138.
100. Hendrickson, W. A.; Palazzotto, M. C. *Adv. Chem. Ser.* **1993**, *238*, 411–430.
101. Sanderson, C. T.; Quinlan, J. A.; Conover, R. C.; Johnson, M. K.; Murphy, M.; Dluhy, R. A.; Kutal, C. *Inorg. Chem.* **2005**, *44*, 3283–3289.
102. Curtis, H.; Irving, E.; Johnson, B. F. G. *Chem. Br.* **1986**, *22*, 327–328.
102a. Curtis, H.; Irving, E.; Johnson, B. F. G. *Chem. Br.* **1986**, *22*, 330.
103. Abd-El-Aziz, A. S.; Carraher, C. E. Jr.; Pittman, C. U. Jr.; Sheats, J. E.; Zeldin, M., Eds.; *Macromolecules Containing Metal and Metal-Like Elements, Volume1*; Wiley: Hoboken, N.J., 2003.
104. Abd-El-Aziz, A. S.; Carraher, C. E. Jr.; Pittman, C. U. Jr.; Sheats, J. E.; Zeldin, M., Eds.; *Macromolecules Containing Metal and Metal-Like Elements, Volume 2: Organoiron Polymers*; Wiley: Hoboken, N.J., 2004.
105. Tyler, D. R. *Coord. Chem. Rev.* **2003**, *246*, 291–303.
106. Lees, A. J. *Coord. Chem. Rev.* **1998**, *177*, 3–35.
107. Sato, H. *Appl. Organomet. Chem.* **1989**, *3*, 363–382.
108. Kubiak, C. P.; Broeker, G. K.; Granger, R. M.; Lemke, F. R.; Morgenstern, D. A. In In *Advances in Chemistry Series;* ; Kutal, C. Serpone, N., Eds.; American Chemical Society, Washington, D.C.; 1993; Vol. 238, pp 165–184.
109. Herman, I. P. *Chem. Rev.* **1989**, *89*, 1323–1357.
110. Akbarian, F.; Dunn, B. S.; Zink, J. I. *J. Phys. Chem.* **1995**, *99*, 3892–3894.

1.10 Studying Highly Reactive Organometallic Complexes with Infrared Spectroscopy: Matrix Isolation, Liquefied Noble Gases, Supercritical Fluids, and Time-resolved IR Spectroscopy

M W George and P Portius, The University of Nottingham, Nottingham, UK

1.10.1 Introduction

Although IR spectroscopy is used as a rapid analytical tool in organometallic chemistry, characterization of compounds usually relies upon standard techniques such as NMR and X-ray crystallography. The answer to the question as to why use a more classical method such as IR spectroscopy as a major characterization technique is that it provides information which would not readily be obtainable from other more standard techniques. NMR and X-ray crystallography are difficult to apply when probing the structure and dynamics of unstable molecules. However, recent developments combining photochemistry with either low-temperature NMR spectroscopy[1–6] or fast time-resolved single crystal X-ray crystallography[7–19] or extended X-ray absorption fine structure (EXAFS)[20] may mean that this statement will no longer be true in future as these techniques evolve.

In most cases, no single spectroscopic technique or experimental approach provides "all" the answers to a particular problem. In this chapter we will show how a range of experimental techniques have been used to probe organometallic reactive intermediates. Given that reactive organometallic complexes are unstable, there are two experimental approaches to study them: (i) by prolonging their lifetime at low temperatures (e.g., matrix isolation or liquefied noble gases) so that they can be characterized using conventional spectroscopy (e.g., Fourier transform infrared spectroscopy (FTIR)) or (ii) by probing their "natural" lifetime at room temperature (RT) using very rapid detection methods (e.g., flash photolysis). At first we outline three different experimental approaches which have utilized IR spectroscopy to probe short-lived organometallic species and which have been the subject of several reviews, namely matrix isolation,[21–30] liquefied noble gases,[31–36] and fast time-resolved IR spectroscopy.[37–50] The aim of this chapter is not to give an exhaustive review of all studies characterizing highly reactive organometallic species, but rather give an outline of how these techniques are used in a few exemplifying areas, which probe series of reactions or complexes.

1.10.2 Low-Temperature Techniques—Matrix Isolation

The use of matrix isolation to study unstable molecules has a long history and there have been several reviews of the general technique[51–56] and its application to organometallic chemistry.[57–61] The key concept here is that the unstable molecules are generated in a matrix cage where they are surrounded by a large number of unreactive host matrix atoms or molecules at cryogenic temperatures (4–20 K), which form a rigid framework such that a pair of unstable species cannot come together and combine via a bimolecular reaction. However, even the most innocent of matrix materials, such as Xe or alkanes, are "potential" ligands for unsaturated organometallic complexes (see below). A further advantage of using matrix isolation techniques is that at low temperatures the unstable molecules have very

little energy to decompose by unimolecular reactions. There are several variations on the basic matrix isolation technique, each of which has distinct advantages and disadvantages. Noble gases are commonly used as the matrix material at very low temperatures and they have the advantage that they have no IR or UV/Vis absorption bands to interfere with spectroscopic monitoring of a reaction. IR bands of species trapped in noble gas matrices are extremely sharp, although they may be split into several lines due to solid-state effects. A typical matrix-isolation experiment for studying organometallic intermediates involves a gas mixture, which is deposited on a cold surface. A precursor complex is co-condensed with a significant excess of matrix gas, and the species of interest is generated by photolysis of the matrix-isolated precursor. Very low temperatures are used to form "rigid" matrices from gases such as Ar (e.g., 20 K), and hence extremely unstable species can be identified. The first major limitation to this technique is that preparation of the matrix involves deposition of the parent molecules from the gas phase onto a cold spectroscopic window and hence the molecules under study must therefore be volatile, which may involve the sample being heated in order to provide sufficient vapor pressure. A method to avoid heating is laser ablation, which has been successfully used for studying the interaction of metal atoms with small ligands such as CO, ethane, and benzene.[22]

The gas matrix approach is also limited because the matrix sublimes at extremely low temperature (i.e., 40 K for Ar); it is not possible to warm the matrix and follow reactions of intermediates up to RT. Frozen glasses[62,63] at 77 K (e.g., EPA – a mixture of Et_2O, pentane and EtOH) have been used since the 1930s to probe unstable species. Frozen hydrocarbon solutions or nujol mulls[23,64] are often much better suited to be studied using IR spectroscopy due to the spectral window they offer and their chemical inertness under photochemical conditions. Such glasses have an advantage over traditional gas matrices in that the cold matrix is produced by freezing a solution, initially at RT; this means that the molecule under study does not need to be volatile. Once intermediates are generated in hydrocarbon matrices, it is possible to follow the reactions of the intermediate up to RT. However, hydrocarbon matrices have the disadvantages of a limited spectral range in the infrared due to the absorptions from the glass material and the IR bands are much broader than in noble gas matrices.

Some of the advantages of noble gas and hydrocarbon matrices have been combined by the use of polymer films as matrix material (e.g. polyethylene PE),[58,65–75] which like hydrocarbon matrices allow the reactions of intermediates to be followed up to RT, and the available spectral window in the polymer is much wider than hydrocarbon matrices due to thinner optical path lengths. Furthermore, the use of polymers as hosts overcomes many of the significant limitations when applying the matrix-isolation technique to study homogeneously catalyzed reactions such as hydroformylation. There are major difficulties in trying to use the matrix-isolation approach to probe homogeneously catalyzed reactions: for example, how to trap all the components of a reaction mixture (substrates and catalysts) in close proximity in the matrix, ensuring that matrix can be varied over a sufficiently wide temperature range so that reaction intermediates can be identified at low temperature and warming can induce reactions within the matrix. The temperature limitations of the matrix-isolation technique can be avoided using PE as a matrix for studying photochemical reactions over a wide temperature range (20–300 K).[76,77] This approach has been advanced further by the development of a high-pressure cell, which can be pressurized with gases such as hydrogen but can still operate over a wide temperature range (see Figure 1).[74]

Another advantage of this approach is that reactive gases can be changed rapidly and efficiently during a particular experiment, and the products can be recovered and analyzed at the end of the reaction by gas chromatography–mass spectrometry (GC–MS).[58]

1.10.3 Low-Temperature Techniques—Liquefied Noble Gases

Liquefied noble gases such as Ar, Kr, or Xe are particularly attractive solvents for studying highly reactive organometallic complexes and reactive intermediates at cryogenic temperatures. They are ideal solvents for spectroscopic investigations since they have no absorptions over the spectral region from far infrared to vacuum UV. Modest pressures can be used to produce considerable liquid ranges. Liquefied noble gases also have the advantage over noble gas matrices in that there are no multiple guest-trapping sites and this simplifies the interpretation of the IR spectra.

The most important drawback of these solvents is that, in conventional use, they cannot be used to study the highly reactive species that can be observed using matrix isolation. Another drawback of using these solvents is the low solubility of most analytes, but this can be compensated by long path lengths that can range from 1–2 cm[31,34,79,80] to several meters.[31] Such long path lengths mean that it is possible to obtain even very weak absorptions which, in the absence of more direct methods such as X-ray crystallography or NMR spectroscopy, may provide a definitive assignment. Following early matrix isolation work,[81] liquid Xe experiments demonstrated that photolysis of $M(CO)_6$ (M = Cr, Mo, or W) in H_2-doped liquid Xe at −70 °C produces $M(CO)_5(H_2)$.[82,83] The mode of coordination

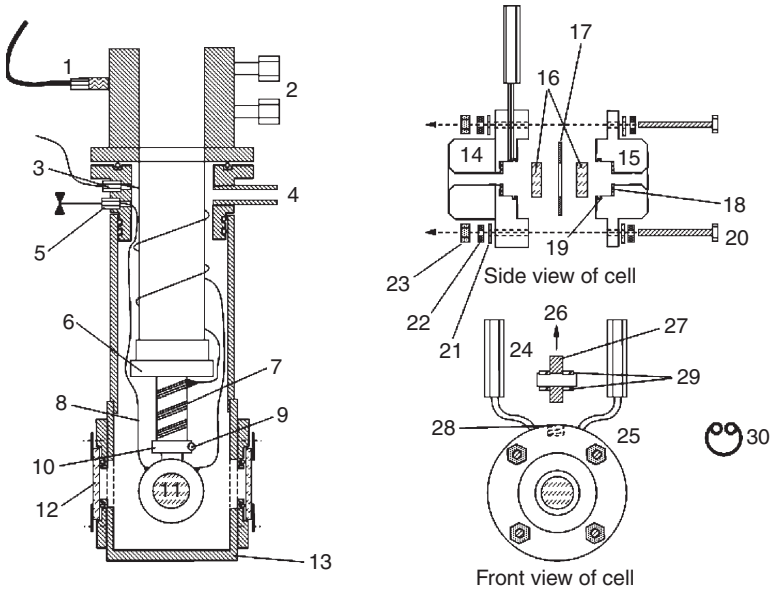

Figure 1 Matrix apparatus as used in Nottingham: (1) valve power supply, (2) helium pressure connections to compressor, (3) silicon diode and heater lead-through, (4) pump-out port, (5) gas inlet port, (6) cold station, (7) heater and thermocouple wires, (8) stainless steel tube, (9) silicon diode, (10) very cold station and heater sleeve, (11) cell, (12) photolysis and spectroscopic windows, for an experiment the cell is turned by 90° towards the windows, (13) vacuum shroud, (14) large half of cell, (15) small half of cell, (16) IR optical windows, (17) lead seal, (18) indium window seal, (19) circlip retainer groove, (20) bolt, (21) steel washer, (22) spring washer, (23) nut, (24) femal–femal union, (25) steel tubing, (26) to very cold station, (27) threaded copper stud, (28) threaded hole in large half of cell to receive stud, (29) indium joints, (30) circlip, which fits in groove and retains windows.

of dihydrogen was confirmed as a non-classical dihydrogen complex by direct observation of the ν(H–H) band and the corresponding ν(H–D) and ν(D–D) bands, when the experiment was repeated with HD or D_2 (Figure 2).

The relative stabilities of these dihydrogen complexes in liquid Xe are W > Cr ≫ Mo. $Cr(CO)_5(H_2)$ and $W(CO)_5(H_2)$ have recently been characterized by NMR in solution at 190–220 K.[83] After the initial liquefied Xe work on $Cr(CO)_5(H_2)$, subsequent matrix experiments characterized dihydrogen complexes using ν(H–H) IR bands and identified a range of complexes including $M(Cp)H(CO)_2(H_2)$ (M = Mo or W)[84,85] and $CoX(CO)_3(H_2)$ (X = H or Me).[86] Photolysis of metal carbonyls in liquefied noble gases has been a successful approach in the charaterization of a range of highly reactive dihydrogen complexes including $V(CO)_5(H_2)$,[87] $M(Cp)(CO)_3(H_2)$ (M = V or Nb),[87] $M(CO)_{5-n}(olefin)_n(H_2)$ ($n = 1$ or 2; M = Cr, Mo, or W),[88–90] $Cr(\eta^6\text{-}C_6H_6)(CO)_2(H_2)$,[91] $Fe(CO)(H_2)(NO)_2$,[92] $Fe(CO)_2(\eta^4\text{-}C_4H_4)(H_2)$,[91] and $Co(CO)_2(H_2)(NO)$.[92]

1.10.4 Room Temperature Techniques—Fast Time-Resolved Infrared Spectroscopy

The detection of short-lived transient species is often achieved by flash photolysis where an extremely short flash of UV/Vis radiation from a laser generates a high concentration of transient species, and a second probe beam monitors any changes that occur after the flash. Traditionally, UV/Vis spectroscopy has been used as a detection method. However, time-resolved infrared spectroscopy (TRIR), a combination of UV flash photolysis and fast IR detection, also has a long history.[39] There are several different approaches to fast IR spectroscopy and the method of choice depends upon the timescale of the reaction. Measurements on the nanosecond to millisecond timescale are obtained using point-by-point techniques or by step-scan FTIR. In the point-by-point approach, a continuous wave IR laser (CO or diode) or globar is used as the IR source, which is tuned to one particular IR frequency (Figure 3).[39]

The change in IR absorbance following the laser flash is monitored using a fast IR detector(HgCdTe or InSb), thus producing an IR kinetic trace at the chosen IR frequency. The IR frequency is changed and the measurement can be repeated. TRIR spectra at a certain time delay are built up in a point-by-point fashion by plotting the change in absorbance versus wave number. A limitation of the point-by-point approach for obtaining TRIR spectra is that it is

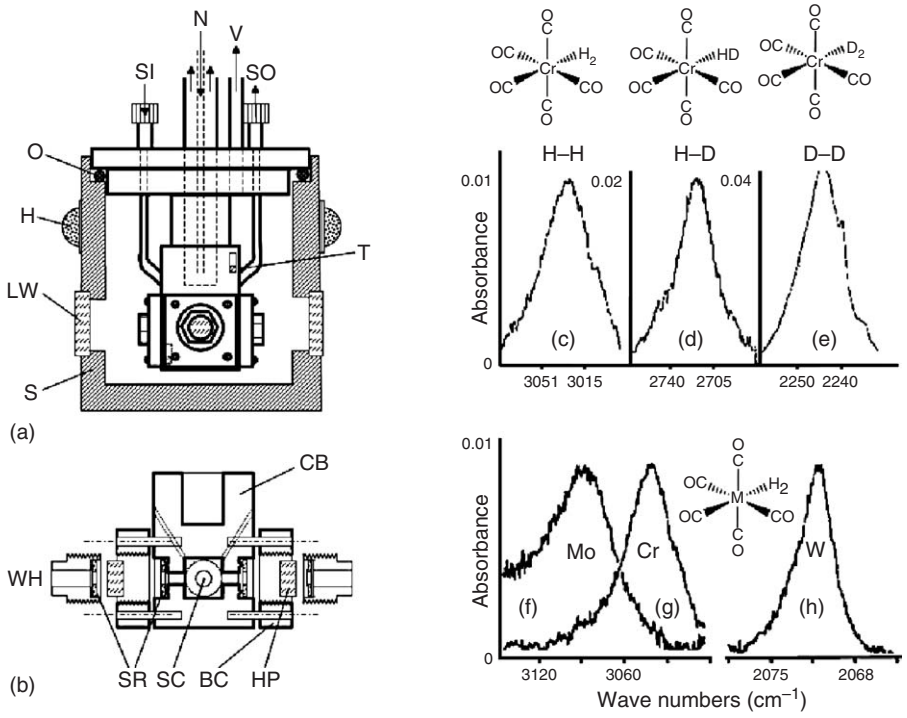

Figure 2 (a) Four-port low-temperature high-pressure cell with N – liquid N_2 flow in; V – vacuum; SI – solution in; SO – solution out; O – O ring; H – heater cartridges; T – thermocouple; LW – low-pressure IR window; S – aluminum shroud; (b) schematic diagram showing cell design with CB – copper cell body; WH – window holder; SR – sealing ring; SC – sample compartment; BC – brass collar; HP – high-pressure IR window. IR absorption bands due to the (c) ν(HH); (d) ν(HD); and (e) ν(DD) stretches of the non-classical dihydrogen complexes $Cr(CO)_5(H_2)$, $Cr(CO)_5(HD)$, and $Cr(CO)_5(D_2)$. IR absorption bands due to the ν(HH) stretches of $M(CO)_5(HH)$ complexes for M = (f) Mo; (g) Cr; and (h) W. Adapted from Upmacis, R. K.; Poliakoff, M.; Turner, J. J. *J. Am. Chem. Soc.* **1986**, *108*, 3645–3651.

extremely labor intensive, and the coverage of a larger IR spectral range ($>200\,cm^{-1}$) is an arduous task. An alternative approach to IR laser-based TRIR spectroscopy on the nanosecond timescale is time-resolved step-scan FTIR, which is advantageous since the entire mid-IR region is covered allowing for a simultaneous measurement at all wave numbers while maintaining the high-throughput and multiplex advantages of FTIR.[37] The time-resolved step-scan FTIR technique involves the movable mirror of the interferometer being displaced in a stepwise manner. At each mirror position, the time-dependent change in IR intensity is measured following excitation, producing time-dependent interferograms (Figure 4). Fourier transformation of an interferogram at a particular time delay following excitation yields the spectral intensity changes at that particular time slice and this can be easily converted to the corresponding absorption spectrum. This process can be repeated at a variety of time delays following excitation generating a series of time-resolved spectra. Kinetic traces can be obtained by plotting the change in absorbance at any frequency as a function of time.

The time resolution of the point-by-point and step-scan FTIR approaches is limited by the rise time of the fast IR detector used in the experiment (ca. 10 ns). However, many photochemical and photophysical events take place on the sub-nanosecond timescale, which require a faster technique. Ultrafast IR spectroscopy is a variant of the pump–probe technique, where time resolution is achieved by spatially delaying the probe pulse with respect to the pump pulse (Figure 5).

Ultrafast IR spectroscopy is constantly improving with the advancement of solid-state lasers.[93] Currently, such fs/ps IR spectrometers are based around a solid-state Ti:sapphire oscillators/amplifier, which provides ultrashort pulses at ca. 800 nm. The advantages of these lasers are that they provide a source of short and high repetition rate pulses, which are inherently stable and which maintain their near transform-limited broadband characteristics ($>100\,cm^{-1}$ FWHM). The Ti : sapphire laser is used to pump an optical parametric amplifier (OPA) and the IR light is generated by difference frequency mixing, in non-linear crystals, of the signal and idler produced by OPA. The residual 800 nm light can be used to produce tunable pump pulses across the UV/Vis region. Changes in IR absorption at various pump–probe time delays can be monitored by dispersing the IR on MCT (HgCdTe) infrared linear array detectors.

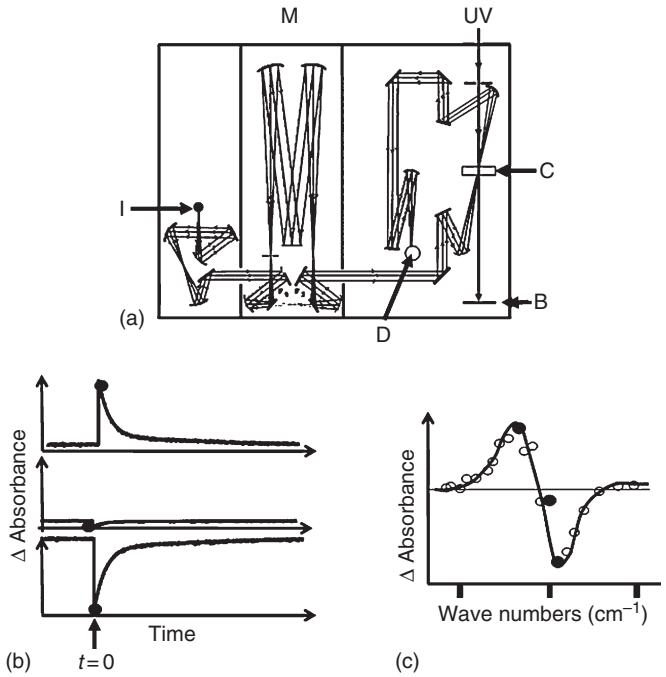

Figure 3 (a) Schematic layout of an IR diode laser-based TRIR spectrometer where I – IR laser diode; M – monochromator; C – cell; D – MCT IR detector; UV – UV or visible laser pulse; and B – beamstop. The ''point-by-point'' TRIR approach is achieved by (b) recording the change in IR absorbance following the UV/visible laser flash at one specific IR frequency. Repeating this measurement at different IR wavelengths generates a series of TRIR decay traces. (c) Plotting the change in IR absorbance versus wave number for a given time delay (Δt) after the laser flash ($t = 0$) produces a TRIR spectrum at that time delay.

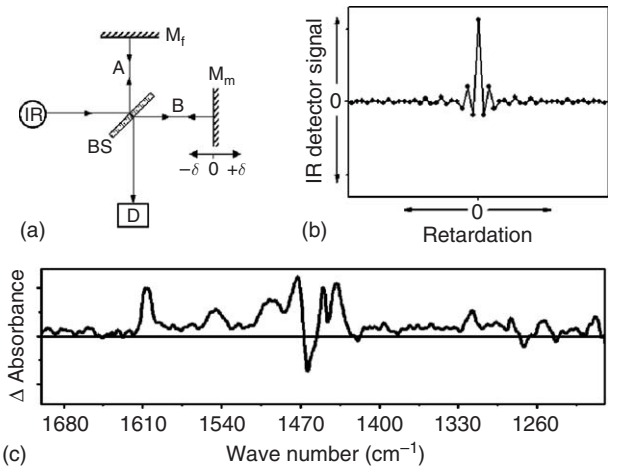

Figure 4 (a) Schematic diagram of a Michelson interferometer in a typical FTIR spectrometer where BS – beamsplitter; D – IR detector; IR – IR source; M_f – fixed mirror; M_m – moving mirror. The principle of time-resolved step-scan FTIR involves stopping the moving mirror of the FTIR and recording the change in IR absorbance at all wavelengths at one specific mirror position. Repeating this measurement at different mirror positions generates a series of time-resolved data at different mirror positions. A time-resolved interferogram (b) can be produced by plotting IR detector signal versus retardation for a given time delay (Δt) after the laser flash. Fourier transformation of this interferogram generates the TRIR spectrum (c) for a given time delay. The resulting spectrum covers the entire IR region and we illustrate this point showing the excited state IR spectrum (1200–1700 cm^{-1}) obtained 100 ns after the UV/Vis photolysis of $[Ru(bpy)_3]Cl_2$ in CD_3CN. The negative bands result from depletion of parent absorptions and the positive bands are due to the IR fingerprint of the excited state.

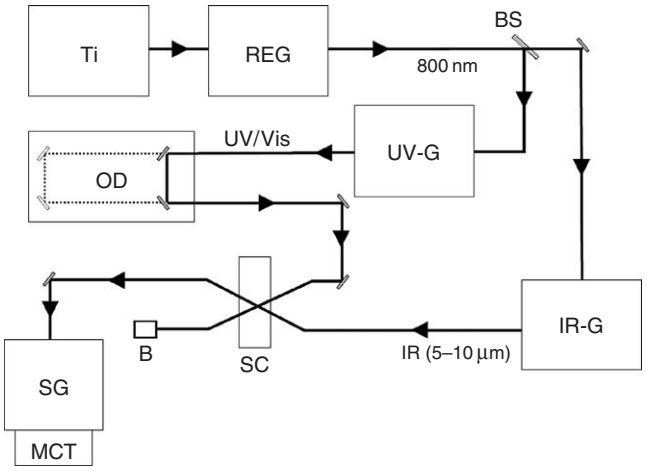

Figure 5 Schematic setup for a femtosecond time-resolved IR spectrometer consisting of Ti – Ti : sapphire laser; REG – regenerative amplifier; BS – beamsplitter; OD – optical delay; SG – spectrograph(s); MCT – (multi-element) MCT IR detector(s); SC – sample cell; B – beamstop; IR-G – IR generation using OPA laser and difference frequency mixing; UV-G – UV/Vis generation by OPA laser or using harmonics of the fundamental laser.

As stated in the introduction, we do not aim to provide an exhaustive review of all studies but highlight how these techniques can be used to provide understanding of reaction mechanisms, and the study of highly reactive complexes, by covering two case studies on: (i) alkane and noble gas complexes and C–H activation and (ii) the photochemistry of $Fe(CO)_5$.

1.10.5 Alkane and Noble Gas Complexes and C–H Activation

The conversion of alkanes, particularly methane, to more useful and complex products is one of the "Holy Grails" of chemistry. The insertion of metals into C–H bonds was first discovered by Chatt and Davidson in 1965 during their examination of the thermal reactions of low-valence ruthenium complexes.[94] A large number of organometallic complexes have been shown to activate alkane C–H bonds since the photochemically induced insertion of a transition metal into alkane C–H bonds was discovered almost simultaneously by Graham[95] and Bergman.[96]

$$Rh(Cp)(CO)_2 \xrightarrow[\text{alkane}]{h\nu} Rh(Cp)(CO)(\text{alkane}) \rightarrow Rh(Cp)(CO)(H)(\text{alkyl})$$

A typical reaction is the photochemical oxidative addition of alkanes to complexes such as $Rh(Cp)(CO)_2$, which occurs via initial loss of CO followed by σ-coordination of the alkane before oxidative addition.

C–H activation has been extensively reviewed[97–103] and here we will focus on the different techniques pertinent to this chapter that have contributed to probing the C–H mechanism. The first example of alkane σ-coordination was demonstrated by Perutz and Turner using matrix isolation.[104,104a,105] Photolysis of $Cr(CO)_6$ in a CH_4 matrix at 20 K generated $Cr(CO)_5(CH_4)$ which was characterized by IR and UV visible spectroscopy. $Cr(CO)_6$ is octahedral and the C–O stretching should contain only one IR active mode. Figure 6 shows the one band of $Cr(CO)_6$ at 1985 cm^{-1} in a CH_4 matrix, which is split by matrix effects. UV photolysis of $Cr(CO)_6$ generated free CO and a $Cr(CO)_5$ fragment with three ν(CO) IR bands at 1932, 1962, and 2088 cm^{-1} and a visible absorption at 489 nm. The $Cr(CO)_5$ species was demonstrated to be $C_{4\nu}$ symmetric by analysis of IR spectra following irradiation of ^{13}CO-substituted $Cr(CO)_6$.[104a] The key to the discovery of coordination of CH_4 to the $Cr(CO)_5$ fragment came from repeating the experiment in different gas matrices where the visible absorption of $Cr(CO)_5$ was very sensitive to the matrix, varying from 489 nm observed in CH_4 to 624 nm in Ne. Proof that this difference was due to coordination of matrix and not general solvent effects came from mixed matrix experiments, for example, Ne/2% Xe.[104] In these experiments two visible absorptions were observed similar to the pure matrices demonstrating stereospecific interactions, thus identifying alkane and noble gase complexes such as $Cr(CO)_5(CH_4)$ and $Cr(CO)_5Xe$.

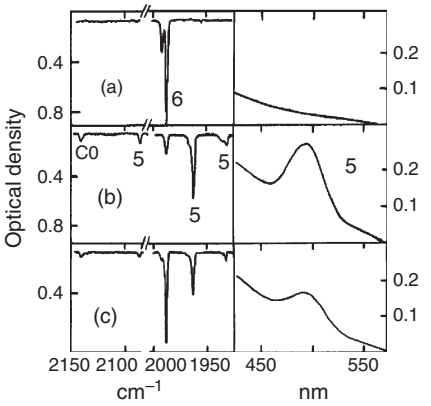

Figure 6 (a) IR and visible spectra obtained following deposition of $Cr(CO)_6$ (6) in a CH_4 matrix at 20 K; resulting spectra obtained after (b) 15 s photolysis with unfiltered Hg arc showing the production of $Cr(CO)_5$ (5) and CO and, (c) 2 min photolysis with filtered light from Hg arc ($\lambda > 375$ nm) showing regeneration of $Cr(CO)_6$. Adapted from Perutz, R. N.; Turner, J. J. *J. Am. Chem. Soc.* **1975**, *97*, 4791–4800.

Although the developments of alkane/noble gas chemistry and C–H activation have continued to occur, in parallel, we will focus initially on the σ-coordination of the alkane before looking at oxidative addition. Flash photolysis of $Cr(CO)_6$ in cyclohexane solution gave[106] a UV/Vis band at 503 nm, which was understood to be $Cr(CO)_5$(cyclohexane) by analogy with the results in CH_4 matrices. More evidence for the coordination of the alkane to the $Cr(CO)_5$ moiety was provided when the flash photolysis experiments were repeated in the weakly coordinating perfluorocyclohexane solvent. The transient absorption band obtained in perfluorocyclohexane was similar in wavelength to that previously observed in Ne matrix (which is presumably an extremely weak coordinating ligand) and shifted significantly compared to more strongly coordinating alkanes.[107,108] Since then numerous investigations into the reaction of photochemically generated alkane complexes have been carried out, both in solution and in the gas phase,[109–115] using TRIR. Metal alkane bond strengths were found to be in the order of 10–15 kcal mol^{-1} from both gas phase TRIR experiments[111,114] and solution-based photoacoustic calorimetery measurements.[116–119] The alkane complexes formed via solvation of 16-electron intermediates have lifetime which can vary considerably for seemingly similar complexes. For example, $Cr(CO)_5$(*n*-heptane) and $Mo(CO)_5$(*n*-heptane) both have lifetimes of approximately 15 μs, while the corresponding $W(CO)_5$(*n*-heptane) has a lifetime more than an order of magnitude longer (ca. 200 μs) under similar conditions.[120] The analogous first-row early transition metal alkane complexes increase in reactivity, $V(Cp)(CO)_3$(*n*-heptane) decaying on the nanosecond timescale. The following order was found: $V(Cp)(CO)_3$(*n*-heptane) > $Cr(\eta^6\text{-}C_6H_6)(CO)_2$(*n*-heptane) > $Mn(Cp)(CO)_2$(*n*-heptane) (see Figure 7).[121]

TRIR experiments found $Re(Cp)(CO)_2$(*n*-heptane) to be long-lived at RT,[122] which led to the characterization of $Re(Cp)(CO)_2$(cyclopentane) by NMR spectroscopy.[2,3] NMR studies on $Re(Cp)(CO)_2$(pentane) were able to characterize the binding of three different C–H groups within the alkane complex, which is important when considering the mechanism of C–H activation (see later). Some evidence for the coordination of alkanes has also been obtained from crystallographic studies.[123,124]

Organometallic noble gas complexes have also been identified in the gas phase and in solution. $M(CO)_5L$ and $Cp^*Rh(CO)L$ (M = Cr, W; L = Xe, Kr) have been identified in liquid Xe or Kr using rapid-scan FTIR[125,126] and TRIR, respectively. At RT TRIR measurements in the gas phase characterized a range of complexes such as $M(CO)_5Xe$ (M = Cr, Mo, or W) and kinetic measurements afforded metal–noble gas bond strengths to be estimated.[127] Noble gas complexes can be observed in fluid solution at RT following irradiation of metal carbonyls in supercritical Xe (sc Xe) (Figure 8(a)). The lifetime of the short-lived organometallic noble gas complexes also varies depending on the metal and the nature of ligand in a similar way as in alkane complexes. The reaction of $M(CO)_5L$ with CO for $M(CO)_5Xe$ and $M(CO)_5Kr$ (M = Cr, Mo, and W) shows that the reactivity for each complex was in the order Kr > Xe and Cr ≈ Mo > W (Figure 7(b)).

The reactivity of $M(Cp)(CO)_nXe$ complexes, for instance, is in the order Re < Rh < Mn < Ta ~ Nb.[128–130] $Re(Cp)(CO)_2Xe$ was shown to be relatively long-lived at RT in scXe solution at RT and in liquid Xe at 170 K.[122,128] This led to the characterization[1] of $Re(^iPrCp)(CO)(PF_3)Xe$ by NMR, and the ^{129}Xe chemical shift

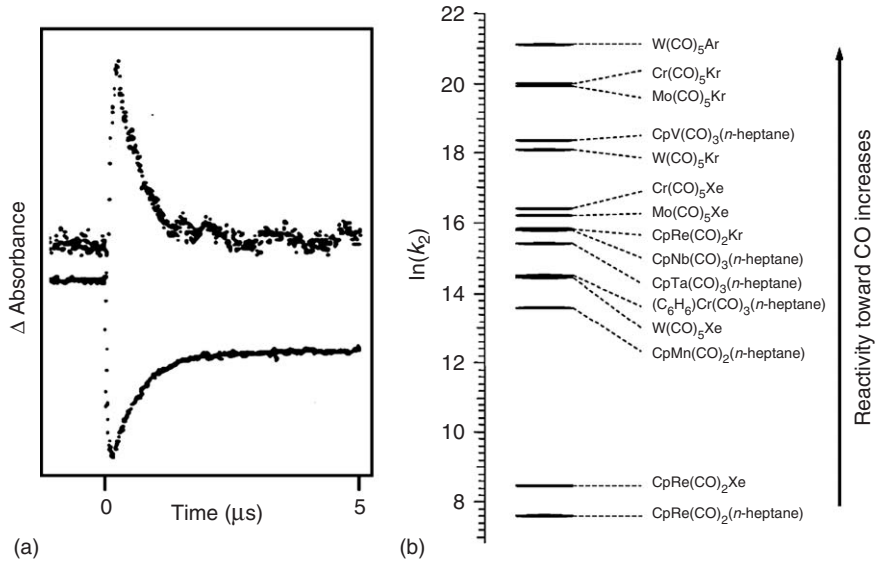

Figure 7 (a) Time-resolved IR traces showing the decay of the ''instantaneously'' generated $V(Cp)(CO)_3$(*n*-heptane) and the recovery of the parent complex $V(Cp)(CO)_4$ obtained following the photolysis of $V(Cp)(CO)_4$ in *n*-heptane, and; (b) a schematic representation of the reactivity towards carbon monoxide of a series of alkane and noble gas complexes obtained by plotting $\ln(k_2)$, where k_2 is the respective second-order rate constant for the reaction of the complex with CO.

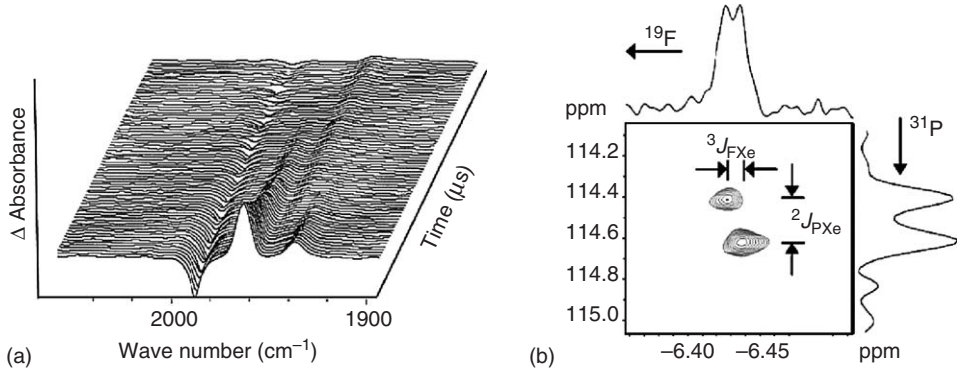

Figure 8 (a) Step-scan FTIR spectrum after 355 nm photolysis of $W(CO)_6$ dissolved in scXe (1500 psi, 298 K) in the presence of 50 psi of CO. The spectra are displayed every 500 ns. The negative band indicates depletion of the parent and the positive bands produced immediately after the flash are assigned to the ν(C–O) vibrations of $W(CO)_5Xe$. (b) 2D ^{19}F–^{31}P heteronuclear single quantum coherence shift-correlated NMR spectrum of ^{129}Xe-labelled $Re(^iPrCp)(CO)(PF_3)Xe$ recorded following photolysis of $Re(^iPrCp)(CO)_2(PF_3)$ in liquefied Xe at 163 K. Adapted from Ball, G. E.; Tamim, A.; Geftakis, S.; George, M. W.; Lawes, D. J.; Portius, P.; Rourke, J. P. *Proc. Natl. Acad. Sci.* **2005**, *102*, 1853–1858.

(−6179 ± 3 ppm at 163 K) shows that coordinated Xe is significantly shielded with respect to free Xe (Figure 8(b)). The coupling constants between coordinated ^{129}Xe and both the ^{19}F and ^{31}P nuclei present have confirmed the identity of the compound. The occurrence of atomic xenon as a discrete ligand in a selection of cationic gold and mercury inorganic complexes has been demonstrated by crystallography,[131–134] and theoretical studies[135] had previously predicted high stability of such cationic gold complexes.

Early studies on C–H activation reactions were performed using matrix isolation. Photochemical reactions of a range of complexes ($M(Cp)(CO)_2$; M = Ir, Rh, Co, R = H or CH_3) in a variety of matrices (CH_4, CD_4, Ar, and Ar doped with ^{13}CO)[136] were investigated. For example, the photolysis of $Rh(Cp)(CO)_2$ in an Ar matrix results in the

loss of CO to form CpRh(CO). When the matrix was doped with ^{13}CO exchange of the CO ligands took place resulting in the formation of Rh(Cp)(^{13}CO)(CO) and Rh(Cp)(^{13}CO)$_2$. In a CH_4 matrix the adduct Rh(Cp)(CO)(CH_4) together with the C–H activated product Rh(Cp)(CO)(CH_3)H was observed. These observations provided evidence that the 16-valence-electron complex is indeed the primary photoproduct, which then coordinates to the matrix. In solution, Rh(Cp)(CO)(C_6H_{11})H was identified in neat cyclohexane at ambient temperature using TRIR.[137] The time resolution of the TRIR apparatus used in this study meant that the transformation of the alkane precursor into the final C–H activated product could not be determined and the formation of Rh(Cp)(CO)(C_6H_{11})H occurred within less than 400 ns after flash. Rh(Cp)(CO) was identified at RT in the gas phase.[138] Photolysis of ca. 0.4 torr Rh(Cp)(CO)$_2$ in argon buffer gas at ambient temperature resulted in initial bleaching of the parent infrared absorption and a new band of a photoproduct at 1985 cm^{-1} appeared. On the basis of the work in matrices, the latter band was assigned to the coordinatively unsaturated 16-valence-electron CO loss product Rh(Cp)(CO) which directly compares to Rh(Cp)(CO) in an Ar matrix. In the presence of alkanes, such as neopentane, this band rapidly decays accompanied by the concomitant oxidative addition. All observed reaction rates are within an order of magnitude of the calculated gas-kinetic values. Therefore, reactions occurred on nearly every collision.

Further insight into these reactions came from irradiation of Rh(Cp^*)(CO)$_2$ in a noble gas solution (krypton or xenon).[139] A monocarbonyl species was generated, exhibiting only one ν(CO) band. In the absence of any other reactant this species had a surprisingly long lifetime in xenon. Repeating this experiment in liquefied krypton resulted in a new transient species, which was much more reactive. The intermediates were assigned to Rh(Cp^*)(CO)Xe and Rh(Cp^*)(CO)Kr, respectively. When cyclohexane was added to the sample, Rh(Cp^*)(CO)Kr decayed at a rate dependent on the alkane concentration. Furthermore, a new species was observed, which grew in with the same rate as the krypton complex decayed. This species was assigned to the alkyl hydride complex Rh(Cp^*)(CO)(c-C_6H_{11})H complex. At this stage a σ-bound alkane complex was proposed for the first time, which was assumed to be in equilibrium with the noble gas complex. The kinetic data for the photo-induced reaction of Rh(Cp^*)(CO)$_2$ with linear and cyclic alkanes support a strong influence of the alkane structure on the binding affinity toward the rhodium center in Rh(Cp^*)(CO).[140]

Picosecond TRIR spectroscopy has been used to follow the formation of Rh(Cp)(CO)$_2$ in neat alkane solution at RT.[141] The reactive monocarbonylalkane complex, Rh(Cp)(CO)(c-C_6H_{12}), was characterized following irradiation of Rh(Cp)(CO)$_2$ in cyclohexane solution (Figure 9). The TRIR spectrum obtained shows that the parent ν(CO) bands (1985 and 2048 cm^{-1}) are clearly bleached at early time.

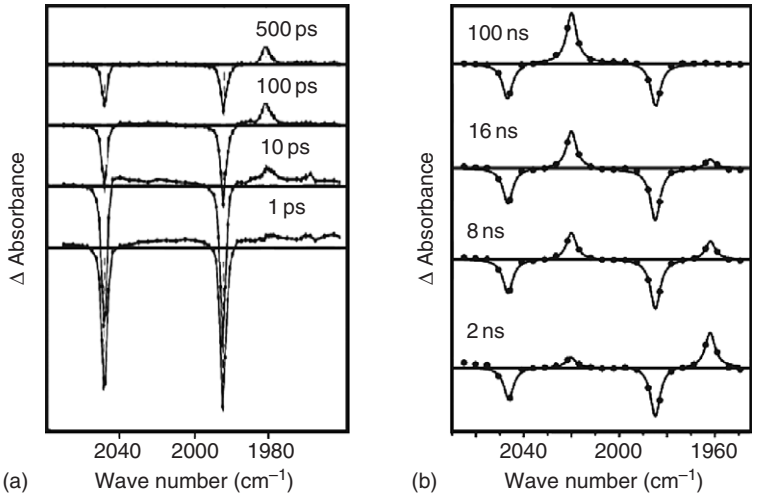

Figure 9 (a) ps-Time-resolved IR spectra of Rh(Cp)(CO)$_2$ in cyclohexane after photolysis. From Asbury, J. B.; Ghosh, H. N.; Yeston, J. S.; Bergman, R. G.; Lian, T. *Organometallics* **1998**, *17*, 3417–3419. A broad featureless transient is observed in the TRIR spectra taken 1 ps after the flash which was assigned to electronic and/or vibrationally excited states. These states decay to reveal a band shifted to lower wave number relative to the parent absorptions, which can be assigned to the alkane complex Rh(Cp)(CO) (cyclohexane). Rh(Cp)(CO)(cyclohexane) is stable up to 500 ps. (b) Previously unpublished ns-Time-resolved IR spectra from our laboratory, of Rh(Cp)(CO)$_2$ in *n*-hexane, which are used to illustrate that after photolysis the ν(CO) IR band of CpRh(CO)(*n*-hexane) decays between 2–100 ns while the band of Rh(Cp)(CO)(hexyl)H grows in.

About 75% of the bleached absorptions recover within 200 ps, which shows that 25% loss of the parent molecules were driven to the CO loss channel, since no long-lived non-dissociative excited states were present. This result was consistent with earlier quantum yield measurements.[142,143] The "naked" 16-valence-electron complex Rh(Cp)(CO) was not directly observed. The early time ps-TRIR spectra show broad featureless transient absorptions due to the formation of electronically and vibrationally excited states. On the nanosecond timescale, Rh(Cp)(CO)(alkane) converts to Rh(Cp)(CO)(alkyl)H. We have recently repeated these experiments and these data are shown in Figure 9, from which the rate of C–H activation from the solvated intermediates can be measured.

Although we have focused on the photochemistry of $Rh(Cp')(CO)_2$ ($Cp' = Cp$ or Cp^*) so far, the most complete understanding of C–H reactions came in parallel TRIR studies on $Rh(Tp^*)(CO)_2$ ($Tp^* = HB(3,5'\text{-}Me_2pyrazol\text{-}1\text{-}yl)_3$, and extensive reviews cover this work.[41] We choose this example since this investigation built upon matrix-isolation and liquid Xe studies. A combination of ultrafast TRIR and ns-step-scan FTIR spectroscopy was used to unravel the mechanism of alkane C–H activation by $Rh(Tp^*)(CO)_2$.[144,145] An alkane complex was formed within the earliest accessible time (10 ps) after photolysis. This complex was generated in a vibrationally excited state which, following relaxation to the ground vibrational state (23 ps), decayed ($\tau = 200$ ps) with concurrent formation of a new intermediate. The latter was assigned to the partly dechelated (κ^2-Tp^*)Rh(CO) (solvent) complex, which is characterized by one new transient IR band at 1992 cm^{-1}. This assignment was confirmed by analogous experiments using $Rh(Bp^*)(CO)_2$ ($Bp^* = HB(3,5\text{-}Me_2pyrazol\text{-}1\text{-}yl)_2$).[146] On the ns-timescale step-scan TRIR measurements proved that Rh(κ^2-Tp^*)(CO) (cyclohexane) converts ($\tau = 230$ ns) into the final C–H activated product, Rh(κ^3-Tp^*)(CO)(cyclohexyl)H, which has a characteristic ν(CO) IR band at 2032 cm^{-1}.

This section on organometallic alkane and noble gas complexes and C–H activation has shown that all three techniques of matrix isolation, liquefied noble gases, and TRIR spectrsoscopy have played an important role in the characterization of intermediates and the elucidation of reaction mechanisms. For both organometallic alkane and noble gas complexes, the initial characterization of these highly reactive organometallic complexes was obtained from matrix-isolation experiments. Elucidation of the reactivity of these complexes using TRIR in solution led to the generation of alkane and xenon complexes which were sufficiently long-lived to allow characterization by NMR spectroscopy. The intermediates involved in C–H activation of complexes such as $Rh(Cp')(CO)_2$ were initially characterized using a combination of matrix-isolation and infrared spectroscopy. TRIR measurements in both neat alkanes at RT and in liquefied noble gases allowed the key steps of this reaction to be monitored in real time.

The second case study we wish to describe concerns the photochemistry of $Fe(CO)_5$. How spin states affect organometallic reactivity is a fundamental question that is key to many areas of inorganic chemistry, and $Fe(CO)_5$ is a prototypical molecule for the investigation of such effects.[147,148] Low-temperature matrix-isolation experiments on $Fe(CO)_5$ were able to characterize the structure of several unsaturated intermediates.[149–151] $Fe(CO)_5$ was deposited in dilute Ar, CH_4, or SF_6 matrices at ca. 10 K. UV irradiation generated mainly triplet $Fe(CO)_4$ ($^3Fe(CO)_4$). Figure 10 shows the results obtained following irradiation of $Fe(CO)_5$ in an SF_6 matrix. The IR spectrum of $^3Fe(CO)_4$ was consistent with a C_{2v} structure, and quantum mechanical calculations[152] found the C_{2v} structure to be the energetic minimum on the potential energy surface of ground state $Fe(CO)_4$.

The most intriguing feature of $Fe(CO)_4$ is that it exists in a triplet ground state. This was confirmed experimentally by measuring the magnetic circular dichroism (MCD) of matrix isolated $^3Fe(CO)_4$. The MCD spectrum of $^3Fe(CO)_4$ unlike $Fe(CO)_5$ showed significant changes over the temperature range 5–25 K indicative of a paramagnetic species.[151] Another intriguing result is the observation that $^3Fe(CO)_4$ was not observed to react with the matrix in an argon matrix. However, in both CH_4 or Xe matrices irradiation with IR light facilitates a reaction of $Fe(CO)_4$ with the matrix resulted in formation of $^1Fe(CO)_4(CH_4)$ and $^1Fe(CO)_4Xe$. The latter reaction is accompanied by changes in position and relative intensities of the $Fe(CO)_4$ IR absorption bands due to subtle changes in the geometry of the $Fe(CO)_4$ fragment in the newly formed complex $Fe(CO)_4L$, $L = CH_4$ or Xe. Thus, a spin change is occurring in this reaction.

Photolysis of $Fe(CO)_5$ in the gas phase under low pressure at RT allows the photochemistry of $Fe(CO)_5$ to be probed in the absence of any reactive species. Photolysis of a mixture of $Fe(CO)_5$ and a buffer gas was investigated[153–162] with TRIR (Figure 11).

In the gas phase, the photolysis of $Fe(CO)_5$ can result in the loss of more than one CO ligand, and the degree of CO loss largely depends on the wavelength of the laser light; this is usually not observed in the condensed phase where the excess energy remaining in the molecule is lost to the solvent rather than effecting a second ligand loss. The transient IR spectrum of $Fe(CO)_4$ in the gas phase was similar to those observed for $^3Fe(CO)_4$ in frozen Ne matrix. $^3Fe(CO)_4$ reacted relatively slow with added CO in the gas phase reflecting the spin forbidden nature of such a transformation. This finding can be compared to experiments, where $M(CO)_5$, $M = Cr$, Mo, W under similar conditions reacted much faster with CO. The formation of $Fe_2(CO)_8$ in a reaction of $Fe(CO)_5$ with $Fe(CO)_3$ was also observed in the gas phase. However, it was still not clear according to which pathway the formation of the

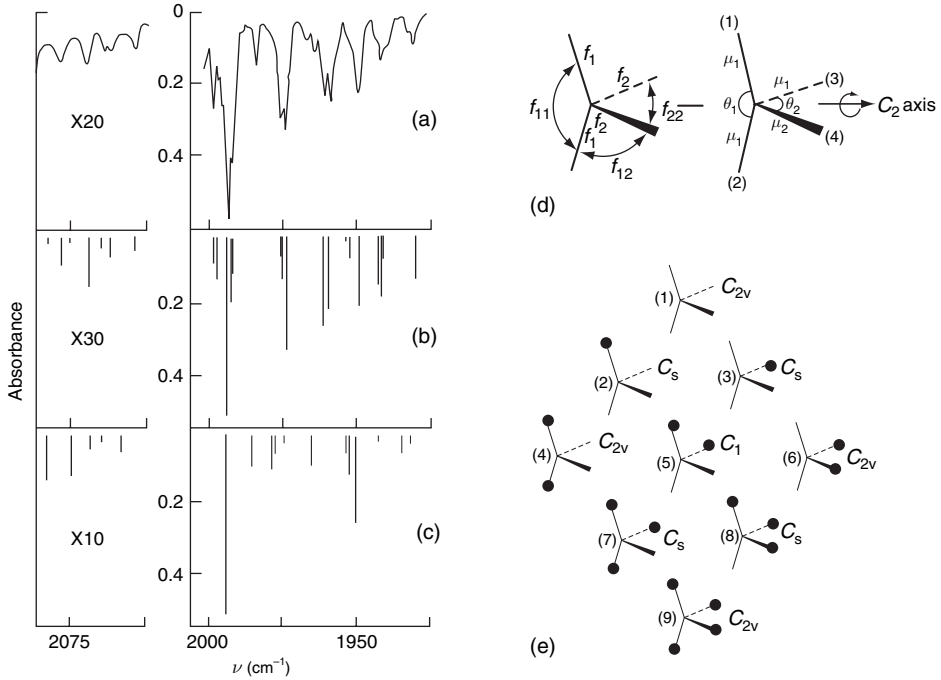

Figure 10 (a) IR spetrum of $Fe(CO)_4$ in an SF_6 matrix obtained following photolysis of ^{13}CO enriched $Fe(CO)_5$. The calculated IR spectrum assuming either a (b) $C_{2\nu}$ and (c) $C_{3\nu}$ symmetry. (d) Labeling of energy-factored CO force constants and dipole moments in $C_{2\nu}$ $Fe(CO)_4$. (e) The nine possible $Fe(^{12}CO)_{4-x}(^{13}CO)_x$ molecules and their symmetries. From Poliakoff, M.; Turner, J. J. *J. Chem. Soc., Dalton Trans.* **1974**, 2276–2285.

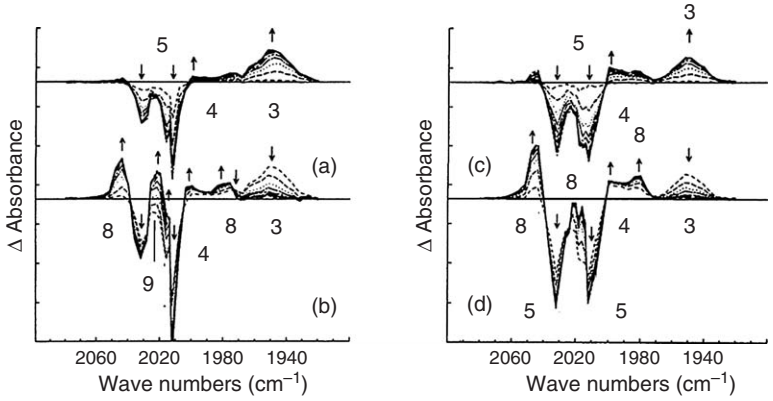

Figure 11 Time-resolved IR spectra generated upon 351 nm photolysis of $Fe(CO)_5$ in the gas phase. The photolysis flow contained 80 mtorr $Fe(CO)_5$ and 3 torr (a, b) or 30 torr (c, d) argon buffer gas. The TRIR spectra are shown in either 50 ns intervals (a) and (c) or 400 ns intervals (b) and (d). The arrows indicate the direction of change in IR absorbance. The following assignments were made: $Fe(CO)_5$ (5), excited $^1Fe(CO)_4$ (4), $Fe(CO)_3$ (3), unbridged $Fe_2(CO)_8$ (8), and an isomer of $Fe_2(CO)_9$ (9). Adapted from Ryther, R. J., Weitz, E. *J. Phys. Chem.* **1991**, *95*, 9841–9852.

$^3Fe(CO)_4$ proceeds, that is, $Fe(CO)_5 \rightarrow$ excited $^1Fe(CO)_5 \rightarrow {}^1Fe(CO)_4 \rightarrow {}^3Fe(CO)_4$, or $Fe(CO)_5 \rightarrow$ excited $^1Fe(CO)_5 \rightarrow$ excited $^3Fe(CO)_5 \rightarrow {}^3Fe(CO)_4$. $^1Fe(CO)_4$ was not observed in the low-temperature matrix experiments. Femtosecond UV laser excitation with time-of-flight mass spectrometric detection was able to show that photolysis of $Fe(CO)_5$ at 267 nm proceeds via an excited singlet state to yield (in ca. 30 fs) $Fe(CO)_4$, initially in an excited singlet state, which then rapidly decays to the lowest singlet state.[163] Ultrafast electron diffraction experiments were able to determine a more precise structure of $^1Fe(CO)_4$ and confirm the singlet pathway.[164]

The bond angles and bond lengths of $^1Fe(CO)_4$ were very similar to those determined by matrix investigations for $^1Fe(CO)_4(CH_4)$, where methane is only very weakly bound. However, it is worth mentioning that although the most advanced techniques were employed, due to the timing of all experiments carried out up to this point, it was impossible to determine experimentally the energy gap between singlet and triplet $Fe(CO)_4$, and the singlet–triplet conversion of $Fe(CO)_4$ was not directly monitored in these experiments. In solution, the formation of $^1Fe(CO)_4$(cyclohexane) at RT was followed by microsecond TRIR, and the IR spectrum was similar to that which had been previously reported for $^1Fe(CO)_4(CH_4)$ in a CH_4 matrix at 12 K.[165]

More recently, TRIR experiments demonstrated the formation of both $^1Fe(CO)_4$(cyclohexane) and $Fe(CO)_3$(cyclohexane) following the absorption of one UV photon, that is, one photon causes the loss of "two" CO groups in the condensed phase. Both $^1Fe(CO)_4$(cyclohexane) and $Fe(CO)_3$(cyclohexane) readily react with $Fe(CO)_5$, forming $Fe_2(CO)_9$ and $Fe_2(CO)_8$, respectively.[166] On the picosecond timescale, $^3Fe(CO)_4$ was characterized[161] by IR bands at 1965 and 1987 cm^{-1}. In another TRIR study in MeOH the conversion of $^3Fe(CO)_4$ to $^1Fe(CO)_4$(MeOH) was shown to occur within 50 ps.[167] The direct conversion of $^3Fe(CO)_4$ into $^1Fe(CO)_4$(heptane) has been subsequently monitored to be much slower and found to be 13 ns, showing that the triplet to singlet conversion is strongly dependent on the nature of the solvent.[168] Furthermore, in these experiments the ultrafast formation of $Fe(CO)_3$ was observed. The combination of TRIR and supercritical fluids allowed the reactivity of $^3Fe(CO)_4$ to be probed in Ar, Xe, and CH_4 solutions at RT, that is, applying the strategy of the original matrix-isolation experiments using the varying coordination ability of the token ligand in solution at RT. This allows analogous experiments to the original matrix-isolation experiments, particularly the possibility of performing doped experiments, for example, Ar with various amounts of added Xe or CH_4, to investigate the chemistry of the more strongly coordinating Xe and CH_4 ligands. In xenon, $^3Fe(CO)_4$ decays at the same rate as $^1Fe(CO)_4Xe$ rises. In supercritical Ar, $^3Fe(CO)_4$ was formed but no reaction with the Ar solvent was observed and $^3Fe(CO)_4$ reacted with CO to reform the parent. However, doping supercritical Ar with Xe resulted in $^3Fe(CO)_4$ reacting with Xe to form $^1Fe(CO)_4Xe$ in supercritical Ar (Figure 12). Analogous results were obtained using supercritical Ar doped with CH_4.

The understanding of spin-forbidden reactions of organometallic reactions continues to be the subject of continued activity, particularly the theoretical understanding of such reactions.[169] However, there is only a limited amount of experimental data available in order to benchmark such theoretical calculations of spin crossing and reactivity. Recent picosecond TRIR measurements have provided valuable insight into how spin-forbidden reactions affect other first-row organometallic metal carbonyl species,[170,171] and it is likely that the combination of matrix isolation and TRIR will continue to produce important information for this class of reactions.

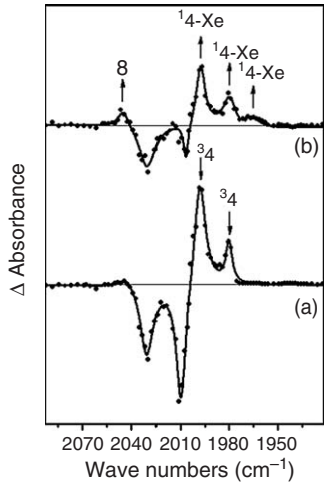

Figure 12 TRIR spectra obtained (a) 50 ns and (b) 500 ns following photolysis (266 nm) of $Fe(CO)_5$ in supercritical Ar (4500 psi) at RT, doped with Xe (400 psi) and CO (30 psi). (^{3}4 = $^3Fe(CO)_4$; ^{1}4-Xe = $^1Fe(CO)_4Xe$ and 8 = $Fe_2(CO)_8$). Adapted from Portius, P.; Yang, J.; Sun, X. Z.; Grills, D. C.; Matousek, P.; Parker, A. W.; Towrie, M.; George, M. W. *J. Am. Chem. Soc.* **2004**, *126*, 10713–10720.

References

1. Ball, G. E.; Tamim, A.; Geftakis, S.; George, M. W.; Lawes, D. J.; Portius, P.; Rourke, J. P. *Proc. Natl. Acad. Sci.* **2005**, *102*, 1853–1858.
2. Lawes, D. J.; Geftakis, S.; Ball, G. E. *J. Am. Chem. Soc.* **2005**, *127*, 4134–4135.
3. Geftakis, S.; Ball, G. E. *J. Am. Chem. Soc.* **1998**, *120*, 9953–9954.
4. Godard, C.; Callaghan, P.; Cunningham, J. L.; Duckett, S. B.; Lohman, J. A. B.; Perutz, R. N. *Chem. Commun.* **2002**, 2836–2837.
5. Schott, D.; Callaghan, P.; Dunne, J.; Duckett, S. B.; Godard, C.; Goicoechea, J. M.; Harvey, J. N.; Lowe, J. P.; Mawby, R. J.; Müller, G.; Perutz, R. N.; Poli, R.; Whittlesey, M. K. *Dalton. Trans.* **2004**, 3218–3224.
6. Dunne, J. P.; Blazina, D.; Aiken, S.; Carteret, H.; Duckett, S. B.; Jones, J. A.; Poli, R.; Whitwood, A. C. *Dalton. Trans.* **2004**, 3616–3628.
7. Vorontsov, I. I.; Kovalevsky, A. Y.; Chen, Y. S.; Graber, T.; Gembicky, M.; Novozhilova, I. V.; Omary, M. A.; Coppens, P. *Phys. Rev. Lett.* **2005**, *94*, 193003.
8. Coppens, P.; Vorontsov, I. I.; Graber, T.; Gembicky, M.; Kovalevsky, A. Y. *Acta Crystallogr., Sect. A* **2005**, *61*, 162–163.
9. Cole, J. M. *Acta Crystallogr., Sect. A* **2004**, *60*, 472–479.
10. Coppens, P.; Gerlits, O.; Vorontsov, I. I.; Kovalevsky, A. Y.; Chen, Y. S.; Graber, T.; Gembicky, M.; Novozhilova, I. V. *Chem. Commun.* **2004**, 2144–2145.
11. Coppens, P.; Vorontsov, I. I.; Graber, T.; Kovalevsky, A. Y.; Chen, Y.-S.; Wu, G.; Gembicky, M.; Novozhilova, I. V. *J. Am. Chem. Soc.* **2004**, *126*, 5980–5981.
12. Cole, J. M. *Chem. Soc. Rev.* **2004**, *33*, 501–513.
13. Moffat, K. *Chem. Rev.* **2001**, *101*, 1569–1581.
14. Coppens, P.; Novozhilova, I. V. *Faraday Discuss.* **2003**, *122*, 1–11.
15. Cole, J. M.; Raithby, P. R.; Wulff, M.; Schotte, F.; Plech, A.; Teat, S. J.; Bushnell-Wye, G. *Faraday Discuss.* **2003**, *122*, 119–129.
16. Coppens, P. *Chem. Commun.* **2003**, 1317–1320.
17. Novozhilova, I. V.; Volkov, A. V.; Coppens, P. *J. Am. Chem. Soc.* **2003**, *125*, 1079–1087.
18. Yasuda, N.; Uekusa, H.; Ohashi, Y. *Bull. Chem. Soc. Jpn* **2004**, 77, 933–944.
19. Hoshino, M.; Sekine, A.; Uekusa, H.; Ohashi, Y. *Chem. Lett.* **2005**, 1228–1229.
20. Bressler, C.; Chergui, M. *Chem. Rev.* **2004**, *104*, 1781–1812.
21. Andrews, L. *Chem. Soc. Rev.* **2004**, *33*, 123–132.
22. Willson, S. P.; Andrews, L. Matrix Isolation Infrared Spectroscopy. In *Handbook of Vibrational Spectroscopy*; Chalmers, J. M., Griffiths, P. R., Eds.; Wiley: Chichester, UK, 2002; Vol. 2, pp 1342–1351.
23. Bitterwolf, T. E. Photochemistry of Inorganic Molecules in Hydrocarbon Matrices. In *Handbook of Vibrational Spectroscopy*; Chalmers, J. M., Griffiths, P. R, Eds.; Wiley: Chichester, UK, 2002; Vol. 4, pp 3137–3151.
24. Andrews, L.; Citra, A. *Chem. Rev.* **2002**, *102*, 885–911.
25. Himmel, H. M.; Downs, A. J.; Greene, T. M. *Chem. Rev.* **2002**, *102*, 4191–4241.
26. Zhou, M. F.; Andrews, L.; Bauschlicher, C. W. *Chem. Rev.* **2001**, *101*, 1931–1961.
27. Downs, A. J.; Greene, T. M. *Adv. Inorg. Chem.* **1999**, *46*, 101–171.
28. Dunkin, I. R. *Matrix-Isolation Techniques A Practical Approach*; Oxford University Press: Oxford, **1998**.
29. Almond, M. J. *Chem. Soc. Rev.* **1994**, *23*, 309–317.
30. Hitam, R. B.; Mahmoud, K. A.; Rest, A. J. *Coord. Chem. Rev.* **1984**, *55*, 1–29.
31. Bulanin, M. O. Liquefied Gases as Solvents for Vibrational Spectroscopy. In *Handbook of Vibrational Spectroscopy*; Chalmers, J. M., Griffiths, P. R., Eds.; Wiley: Chichester, UK, 2002; Vol. 2, pp 1329–1341.
32. Turner, J. J.; Poliakoff, M.; Howdle, S. M.; Jackson, S. A.; McLaughlin, J. G. *Faraday Discuss.* **1988**, *86*, 271–284.
33. Poliakoff, M.; Turner, J. J. Organometallic Photochemistry in Liquefied and Supercritical Noble Gas Solution. In *Molecular Cryospectroscopy Advances in Spectroscopy*; Clark, R. J. H., Hester, H. E., Eds.; Wiley: New York, 1995; Vol. 23, pp 275–304.
34. Bulanin, M. O. *J. Mol. Struct.* **1995**, *347*, 73–82.
35. Nibbering, E. T. J.; Fidder, H.; Pines, E. *Annu. Rev. Phys. Chem.* **2005**, *56*, 337–367.
36. Grills, D. C.; Turner, J. J.; George, M. W. In *Comprehensive Coordination Chemistry II*; McCleverty, J. A., Meyer, T. J., Eds.; Elsevier: Oxford, 2003; Vol.2, pp 91–101.
37. Smith, G. D.; Palmer, R. A. Fast Time-resolved Mid-infrared Spectroscopy Using Step-scan Interferometer. In *Handbook of Vibrational Spectroscopy*; Chalmers, J. M., Griffiths, P. R., Eds.; Wiley: Chichester, UK, 2002; Vol. 1, pp 625–640.
38. Hashimoto, M.; Yuzawa, T.; Kato, C.; Iwata, K.; Hamaguchi, H.-O. Fast Time-resolved Mid-infrared Spectroscopy using Grating Spectrometers. In *Handbook of Vibrational Spectroscopy*; Chalmers, J. M., Griffiths, P. R., Eds.; Wiley: Chichester, UK, 2002; Vol. 1, pp 666–676.
39. Grills, D. C.; George, M. W. Fast and Ultrafast Time-resolved Mid-infrared Spectrometry using Lasers. In *Handbook of Vibrational Spectroscopy*; Chalmers, J. M., Griffiths, P. R., Eds.; Wiley: Chichester, UK, 2002; Vol. 1, pp 677–692.
40. McFarlane, K.; Lee, B.; Bridgewater, J.; Ford, P. C. *J. Organomet. Chem.* **1998**, *554*, 49–61.
41. Yang, H.; Kotz, K. T.; Asplund, M. C.; Wilkens, M. J.; Harris, C. B. *Acc. Chem. Res.* **1999**, *32*, 551–560.
42. Ford, P. C.; Bridgewater, J. S.; Lee, B. *Photochem. Photobiol.* **1997**, *65*, 57–64.
43. Weitz, E. *J. Phys. Chem.* **1994**, *98*, 11256–11264.
44. George, M. W.; Poliakoff, M.; Turner, J. J. *Analyst* **1994**, *119*, 551–560.
45. Yuzawa, T.; Kato, C.; George, M. W.; Hamaguchi, H.-O. *Appl. Spectrosc.* **1994**, *48*, 684–690.
46. Weitz, E.; Wells, J. R.; Ryther, R.; House, P. G. Bond Energies and Reaction. In *Laser Chemistry of Organometallics*; Chaiken, J., Ed.; ACS Symposium Series 530; American Chemical Society: Washington, DC, 1993; pp 147–163.
47. Ford, P. C.; Belt, S. T. *Adv. Chem. Ser.* **1992**, *238*, 27–43.
48. Iwata, K.; Hamaguchi, H.-O. *Appl. Spectrosc.* **1990**, *44*, 1431–1437.
49. Seder, T.; Ouderkirk, A.; Church, S.; Weitz, E. In *High Energy Processes in Organometallic Chemistry*; Suslick, K. S., Ed.; ACS Symposium Series; American Chemistry Society: Washington, DC, 1987; Vol. 333, pp 81–98.
50. Poliakoff, M.; Weitz, E. *Adv. Organomet. Chem.* **1986**, *25*, 277–316.
51. Almond, M. J.; Wiltshire, K. S. *Annu. Rep. Prog. Chem., Sect. C: Phys. Chem.* **2001**, *97*, 3–60.

52. Downs, A. J. In *Low Temperature Molecular Spectroscopy*; Fausto, R., Ed.; NATO ASI Series, Series C: Kluwer: Dordrecht, 1996; Vol. 483, pp 1–93.
53. Almond, M. J.; Downs, A. J. *Adv. Spectrosc.* **1989**, 1–511.
54. see: Almond, M. J., Ed. *Short-lived Molecules*; Ellis Horwood: New York 1990.
55. Perutz, R. N. *Annu. Rep. Prog. Chem., Sect. C: Phys. Chem.* **1986**, *83*, 157–191.
56. Turner, J. J. In *Photoprocesses in Transition Metal Complexes, Biosystems and Other Molecules, Experiment and Theory*; Kochanski, E., Ed.; Kluwer: NATO ASI Series, Series C; Kluwer: Dordrecht, 1992; Vol. 376, pp 125–140.
57. Perutz, R. N. *Chem. Rev.* **1985**, *85*, 97–127.
58. Poliakoff, M.; George, M. W. *J. Phys. Org. Chem.* **1998**, *11*, 589–596.
59. Perutz, R. N. *Pure Appl. Chem.* **1998**, *70*, 2211–2220.
60. Perutz, R. N. *Chem. Soc. Rev.* **1993**, *22*, 361–369.
61. Turner, J. J.; Burdett, J. K.; Perutz, R. N.; Poliakoff, M. *Pure Appl. Chem.* **1977**, *49*, 271–285.
62. Hill, R. H.; Wrighton, M. S. *Organometallics* **1985**, *4*, 413–415.
63. Hill, R. H.; Wrighton, M. S. *Organometallics* **1987**, *6*, 632–638.
64. Mascetti, J.; Rest, A. J. *J. Chem. Soc., Chem. Commun.* **1987**, 221–222.
65. Hitam, R. B.; Hooker, R. H.; Mahmoud, K. A.; Narayanaswamy, R.; Rest, A. J. *J. Organomet. Chem.* **1981**, *222*, C9–C13.
66. Hooker, R. H.; Mahmoud, K. A.; Rest, A. J.; Alt, H. G. *J. Organomet. Chem.* **1991**, *419*, 101–112.
67. Zhang, J.; Sun, X.-Z.; Poliakoff, M.; George, M. W. *J. Organomet. Chem.* **2003**, *678*, 128–133.
68. Zhang, J.; Poliakoff, M.; George, M. W. *Organometallics* **2003**, *22*, 1612–1618.
69. Childs, G. I.; Cooper, A. I.; Nolan, T. F.; Carrott, M. J.; George, M. W.; Poliakoff, M. *J. Am. Chem. Soc.* **2001**, *123*, 6857–6866.
70. Clarke, M. J.; Cooper, A. I.; Howdle, S. M.; Poliakoff, M. *J. Am. Chem. Soc.* **2000**, *122*, 2523–2531.
71. Goff, S. E. J.; Nolan, T. F.; George, M. W.; Poliakoff, M. *Organometallics* **1988**, *17*, 2730–2737.
72. Clarke, M. J.; Howdle, S. M.; Jobling, M.; Poliakoff, M. *J. Am. Chem. Soc.* **1994**, *116*, 8621–8628.
73. Cooper, A. I.; Poliakoff, M. *Chem. Phys. Lett.* **1993**, *212*, 611–616.
74. Molvinger, K.; Childs, G. I.; Jobling, M.; Roper, M.; George, M. W.; Poliakoff, M. *Chem. Lett.* **2000**, 1260–1261.
75. Childs, G. I.; Gallagher, S.; Bitterwolf, T. E.; George, M. W. *J. Chem. Soc., Dalton Trans.* **2000**, 4534–4541.
76. Rest, A. J. *J. Mol. Struct.* **1990**, *222*, 87–93.
77. Hooker, R. H.; Mahmoud, K. A.; Rest, A. J. *J. Chem. Soc., Dalton Trans.* **1990**, 1231–1241.
78. Childs, G. I.; Cooper, A. I.; Nolan, T. F.; Carrott, M. J.; George, M. W.; Poliakoff, M. *J. Am. Chem. Soc.* **2001**, *123*, 6857–6866.
79. Maier, W. B. II; Holland, R. F. *J. Chem. Phys.* **1980**, *72*, 6661–6677.
80. Andrea, R. R.; Luyten, H.; Vuurman, M. A.; Stufkens, D. J.; Oskam, A. *Appl. Spectrosc.* **1986**, *40*, 1184–1190.
81. Sweany, R. L. *J. Am. Chem. Soc.* **1985**, *107*, 2374–2379.
82. Upmacis, R. K.; Gadd, G. E.; Poliakoff, M.; Simpson, M. B.; Turner, J. J.; Whyman, R.; Simpson, A. F. *J. Chem. Soc., Chem. Commun.* **1985**, 27–30.
83. Upmacis, R. K.; Poliakoff, M.; Turner, J. J. *J. Am. Chem. Soc.* **1986**, *108*, 3645–3651.
84. Sweany, R. L. *J. Am. Chem. Soc.* **1986**, *108*, 6986–6991.
85. Sweany, R. L. *Organometallics* **1986**, *5*, 385–386.
86. Sweany, R. L.; Russell, F. N. *Organometallics* **1988**, *7*, 719–727.
87. George, M. W.; Haward, M. T.; Hamley, P. A.; Hughes, C.; Johnson, F. P. A.; Popov, V. K.; Poliakoff, M. *J. Am. Chem. Soc.* **1993**, *115*, 2286–2299.
88. Jackson, S. A.; Upmacis, R. K.; Poliakoff, M.; Turner, J. J.; Burdett, J. K.; Grevels, F. W. *J. Chem. Soc., Chem. Commun.* **1987**, 678–680.
89. Jackson, S. A.; Hodges, P. M.; Poliakoff, M.; Turner, J. J.; Grevels, F. W. *J. Am. Chem. Soc.* **1990**, *112*, 1221–1233.
90. Hodges, P. M.; Jackson, S. A.; Jacke, J.; Poliakoff, M.; Turner, J. J.; Grevels, F. W. *J. Am. Chem. Soc.* **1990**, *112*, 1234–1244.
91. Howdle, S. M.; Healy, M. A.; Poliakoff, M. *J. Am. Chem. Soc.* **1990**, *112*, 4808–4813.
92. Gadd, G. E.; Upmacis, R. K.; Poliakoff, M.; Turner, J. J. *J. Am. Chem. Soc.* **1986**, *108*, 2547–2552.
93. see: Fayer, M. D., Ed. *Ultrafast Infrared and Raman Spectrscopy*; Marcel Dekker: New York 2001.
94. Chatt, J.; Davidson, J. M. *J. Chem. Soc.* **1965**, 843–855.
95. Hoyano, J. K.; Graham, W. A. G. *J. Am. Chem. Soc.* **1982**, *104*, 3723–3725.
96. Janowicz, A. H.; Bergman, R. C. *J. Am. Chem. Soc.* **1982**, *104*, 352–354.
97. Labinger, J. A.; Bercaw, J. E. *Nature* **2002**, *417*, 507–514.
98. Crabtree, R. H. *J. Chem. Soc., Dalton Trans.* **2001**, 2437–2450.
99. Shilov, A. E.; Shul'pin, G. B. *Chem. Rev.* **1997**, *97*, 2879–2932.
100. Schneider, J. J. *Angew. Chem., Int. Ed. Engl.* **1996**, *35*, 1068–1075.
101. Lersch, M.; Tilset, M. *Chem. Rev.* **2005**, *105*, 2471–2526.
102. Crabtree, R. H. *J. Organomet. Chem.* **2004**, *689*, 4083–4091.
103. Crabtree, R. H. *Chem. Rev.* **1985**, *85*, 245–269.
104. Perutz, R. N.; Turner, J. J. *J. Am. Chem. Soc.* **1975**, *97*, 4791–4800.
104a. Perutz, R. N.; Turner, J. J. *Inorg. Chem.* **1975**, *14*, 262–270.
105. Hall, C.; Perutz, R. N. *Chem. Rev.* **1996**, *96*, 3125–3146.
106. Kelly, J. M.; Gustorf, E. K. v. *J. Chem. Soc., Chem. Commun.* **1973**, 105–106.
107. Bonneau, R.; Kelly, J. M. *J. Am. Chem. Soc.* **1980**, *102*, 1220–1221.
108. Kelly, J. M.; Long, C.; Bonneau, R. *J. Phys. Chem.* **1983**, *87*, 3344–3349.
109. House, P. G.; Weitz, E. *J. Phys. Chem. A* **1997**, *101*, 2988–2995.
110. Tanaka, H.; Jyoo, M.; Ishikawa, Y.; Arai, S. *J. Phys. Chem.* **1995**, *99*, 4558–4565.
111. Wells, J. R.; House, P. G.; Weitz, E. *J. Phys. Chem.* **1994**, *98*, 8343–8351.
112. Jyoo, M.; Tanaka, H.; Omiya, K.; Ishikawa, Y.; Arai, S. *Bull. Chem. Soc. Jpn.* **1993**, *66*, 3618–3626.
113. Ishikawa, Y.; Hackett, P. A.; Rayner, D. M. *J. Phys. Chem.* **1989**, *93*, 652–657.
114. Brown, C. E.; Ishikawa, Y.; Hackett, P. A.; Rayner, D. M. *J. Am. Chem. Soc.* **1990**, *112*, 2530–2536.
115. Ishikawa, Y.; Brown, C. E.; Hackett, P. A.; Rayner, D. M. *Chem. Phys. Lett.* **1988**, *150*, 506–510.
116. Jiao, T. J.; Leu, G. L.; Farrell, G. J.; Burkey, T. J. *J. Am. Chem. Soc.* **2001**, *123*, 4960–4965.

117. George, M. W.; Haward, M. T.; Hamley, P. A.; Hughes, C.; Johnson, F. P. A.; Popov, V. K.; Poliakoff, M. *J. Am. Chem. Soc.* **1993**, *115*, 2286–2299.
118. Burkey, T. J. *J. Am. Chem. Soc.* **1990**, *112*, 8329–8333.
119. Morse, J. M.; Parker, G. H.; Burkey, T. J. *Organometallics* **1989**, *8*, 2471–2474.
120. Breheny, C. J.; Kelly, J. M.; Long, C.; O'Keefe, S.; Pryce, M. T.; Russell, G.; Walsh, M. M. *Organometallics* **1998**, *17*, 3690–3695.
121. Childs, G. I.; Grills, D. C.; Sun, X. Z.; George, M. W. *Pure Appl. Chem.* **2001**, *73*, 443–444.
122. Sun, X. Z.; Grills, D. C.; Nikiforov, S. M.; Poliakoff, M.; George, M. W. *J. Am. Chem. Soc.* **1997**, *119*, 7521–7525.
123. Evans, D. R.; Drovetskaya, T.; Bau, R.; Reed, C. A.; Boyd, P. D. W. *J. Am. Chem. Soc.* **1997**, *119*, 3633–3634.
124. Castro-Rodriguez, I.; Nakai, H.; Gantzel, P.; Zakharov, L. N.; Rheingold, A. L.; Meyer, K. *J. Am. Chem. Soc.* **2003**, *125*, 15734–15735.
125. Simpson, M. B.; Poliakoff, M.; Turner, J. J.; Maier, W. B. II; McLaughlin, J. G. *J. Chem. Soc., Chem. Commun.* **1983**, 1355–1357.
126. Weiller, B. H. *J. Am. Chem. Soc.* **1992**, *114*, 10910–10915.
127. Wells, J. R.; Weitz, E. *J. Am. Chem. Soc.* **1992**, *114*, 2783–2787.
128. Grills, D. C.; George, M. W. *Adv. Inorg. Chem.* **2001**, *52*, 113–150.
129. Grills, D. C.; Sun, X. Z.; Childs, G. I.; George, M. W. *J. Phys. Chem. A* **2000**, *104*, 4300–4307.
130. Childs, G. I.; Colley, C. S.; Dyer, J.; Grills, D. C.; Sun, X. Z.; Yang, J.; George, M. W. *J. Chem. Soc., Dalton Trans.* **2000**, 1901–1906.
131. Seidel, S.; Seppelt, K. *Science* **2000**, *290*, 117–118.
132. Drews, T.; Seidel, S.; Seppelt, K. *Angew. Chem.* **2002**, *41*, 454–456.
133. Hwang, I.-C.; Seidel, S.; Seppelt, K. *Angew. Chem.* **2003**, *42*, 4392–4395.
134. Seppelt, K. *Z. Anorg. Allg. Chem.* **2003**, *629*, 2427–2430.
135. Schröder, D.; Schwarz, H.; Hruák, J.; Pyykkö, P. *Inorg. Chem.* **1998**, *37*, 624–632.
136. Rest, A. J.; Whitwell, I.; Graham, W. A. G.; Hoyano, J. K.; McMaster, A. D. *J. Chem. Soc., Dalton Trans.* **1987**, 1181–1190.
137. Belt, S. T.; Grevels, F. W.; Klotzbuecher, W. E.; McCamley, A.; Perutz, R. N. *J. Am. Chem. Soc.* **1989**, *111*, 8373–8382.
138. Wasserman, E. P.; Moore, C. B.; Bergman, R. G. *Science* **1992**, *255*, 315–318.
139. Weiller, B. H.; Wasserman, E. P.; Bergman, R. G.; Moore, C. B.; Pimentel, G. C. *J. Am. Chem. Soc.* **1989**, *111*, 8288–8290.
140. McNamara, B. K.; Yeston, J. S.; Bergman, R. G.; Moore, B. D *J. Am. Chem. Soc.* **1999**, *121*, 6437–6443.
141. Asbury, J. B.; Ghosh, H. N.; Yeston, J. S.; Bergman, R. G.; Lian, T. *Organometallics* **1998**, *17*, 3417–3419.
142. Purwoko, A. A.; Drolet, D. P.; Lees, A. J. *J. Organomet. Chem.* **1995**, *504*, 107–113.
143. Dunwoody, N.; Lees, A. J. *Organometallics* **1997**, *16*, 5770–5778.
144. Bromberg, S. E.; Yang, H.; Asplund, M. C.; Lian, T.; McNamara, B. K.; Kotz, K. T.; Yeston, J. S.; Wilkens, M.; Frei, H.; Bergman; R. G.; Harris, C. B. *Science* **1997**, *278*, 260–263.
145. Asplund, M. C.; Snee, P. T.; Yeston, J. S.; Wilkens, M. J.; Payne, C. K.; Yang, H.; Kotz, K. T.; Frei, H.; Bergman, R. G.; Harris, C. B. *J. Am. Chem. Soc.* **2002**, *124*, 10605–10612.
146. Yeston, J. S.; McNamara, B. K.; Bergman, R. G.; Moore, C. B. *Organometallics* **1998**, *17*, 3442–3446.
147. Poliakoff, M.; Turner, J. J. *Angew. Chem.* **2001**, *40*, 2809–2812.
148. Leadbeater, N. *Coord. Chem. Rev.* **1999**, *188*, 35–70.
149. Poliakoff, M.; Turner, J. J. *J. Chem. Soc., Dalton Trans.* **1973**, 1351–1357.
150. Poliakoff, M.; Turner, J. J. *J. Chem. Soc., Dalton Trans.* **1974**, 2276–2285.
151. Barton, T. J.; Grinter, R; Thomson, A. J.; Davis, B; Poliakoff, M. *J. Chem. Soc., Chem. Commun.* **1977**, 841–842.
152. Burdett, J. K. *J. Chem. Soc., Faraday Trans.* **1974**, 1599–1613.
153. Cedeno, D. L.; Weitz, E. *Organometallics* **2005**, *24*, 1233–1241.
154. Ryther, R. J.; Weitz, E. *J. Phys. Chem.* **1991**, *95*, 9841–9852.
155. Wang, J. Q.; Long, G. T.; Weitz, E. *J. Phys. Chem. A* **2001**, *105*, 3765–3772.
156. House, P. G.; Weitz, E. *J. Phys. Chem. A* **1997**, *101*, 2988–2995.
157. House, P. G.; Weitz, E. *Chem. Phys. Lett.* **1997**, *266*, 239–245.
158. Wang, W. H.; Narducci, A. A.; House, P. G.; Weitz, E. *J. Am. Chem. Soc.* **1996**, *118*, 8654–8657.
159. Gravelle, S. J.; Vandeburg, L. J.; Weitz, E. *J. Phys. Chem.* **1993**, *97*, 5272–5283.
160. Hayes, D. M.; Weitz, E. *J. Phys. Chem.* **1991**, *95*, 2723–2727.
161. Ouderkirk, A. J.; Weitz, E. *J. Chem. Phys.* **1983**, *79*, 1089–1091.
162. Ouderkirk, A. J.; Wermer, P.; Schultz, N. L.; Weitz, E. *J. Am. Chem. Soc.* **1983**, *105*, 3354–3355.
163. Trushin, S. A.; Fuss, W.; Kompa, K. L.; Schmid, W. E. *J. Phys. Chem. A* **2000**, *104*, 1997–2006.
164. Ihee, H.; Cao, J. M.; Zewail, A. H. *Angew. Chem.* **2001**, *40*, 1532–1536.
165. Grevels, F. W. In *Photoprocesses in Transition Metal Complexes, Biosystems and Other Molecules. Experiment and Theory*; Kochanski, E., Ed.; NATO ASI Series, Series C; Kluwers: Dordrecht, 1992; Vol. 376, pp 141–171.
166. Bachler, V.; Grevels, F. W.; Kerpen, K.; Olbrich, G.; Schaffner, K. *Organometallics* **2003**, *22*, 1696–1711.
167. Snee, P. T.; Payne, C. K.; Mebane, S. D.; Kotz, K. T.; Harris, C. B *J. Am. Chem. Soc.* **2001**, *123*, 6909–6915.
168. Portius, P.; Yang, J.; Sun, X. Z.; Grills, D. C.; Matousek, P.; Parker, A. W.; Towrie, M.; George, M. W. *J. Am. Chem. Soc.* **2004**, *126*, 10713–10720.
169. Poli, R.; Harvey, J. N. *Chem. Soc. Rev.* **2003**, *32*, 1–8.
170. Snee, P. T.; Payne, C. K.; Kotz, K. T.; Yang, H.; Harris, C. B. *J. Am. Chem. Soc.* **2001**, *123*, 2255–2264.
171. Snee, P. T.; Yang, H.; Kotz, K. T.; Payne, C. K.; Harris, C. B. *J. Phys. Chem. A* **1999**, *103*, 10426–10432.

1.11 Organometallic Electrochemistry: Thermodynamics of Metal–Ligand Bonding

M Tilset, University of Oslo, Oslo, Norway

1.11.1 Background and Scope

A quantitative insight into the energetics of chemical bonding is crucial to the understanding of organometallic chemistry. Information about bond strengths and related parameters helps an understanding of reaction mechanisms and aids the development of new catalytic systems or improvement of existing ones. A wide range of methods is available for obtaining relevant thermodynamic data.[1–3] Electrochemical techniques have proved to be particularly valuable in this respect during the last couple of decades.

Electrochemical methods have diverse applications in chemistry – synthesis, catalysis, thermodynamics, kinetics, mechanistic studies, to mention a few. Electrochemistry was well developed for studies of relevance to organometallic chemistry prior to COMC (1995), but there was no separate section devoted to the topic in that work. However, excellent books and reviews have been published that summarize aspects of organometallic electrochemistry.[4–6]

In this chapter, the application of electrochemical techniques in organometallic chemistry will be presented with specific focus on utilization of electrode potential data to extract thermodynamic quantities pertaining to metal–ligand bonding energetics. Many readers may be unfamiliar with the electrochemical methods, and therefore the most widely used technique to obtain the required electrode potential data – cyclic voltammetry (CV) – will be briefly described. The derived bond energy data will be no better than the underlying electrode potential data, and therefore some issues which, in the author's view, are particularly relevant to ensure that data are obtained as accurately and correctly as possible will be discussed. For a more in-depth discussion of CV and other electrochemical techniques, the reader is referred to selected textbooks and reviews.[7–11]

Following the brief description of the CV method, the thermochemical cycles that constitute the basis for extraction of bond energy data will be reviewed. The application of these cycles on real systems will be surveyed, and comprehensive tabulations of bond energy data that have been acquired with these methods are provided. Some chemical implications are discussed in brief, but a critical review and comparison with bond energy data obtained by alternative methods is outside the scope of this chapter. Finally, recent, selected applications where the thermodynamic data have played an interesting role in reactivity studies will be highlighted. The use of such data in experimental design and interpretation is only limited by the creativity of the practitioner!

It must be emphasized that the thermochemical cycles that will be discussed are generally applicable and have counterparts in organometallic, organic, and inorganic chemistry. The emphasis of this chapter will necessarily focus on organometallic systems; it is however appropriate and relevant to refer the reader to emerging and exciting developments in the study of reactions between inorganic compounds and organic molecules without the explicit involvement of organometallic species.[12–15]

1.11.2 Basics of CV

1.11.2.1 CV – Selected Relevant Issues

1.11.2.1.1 The reversible cyclic voltammogram

We will initially consider a process in which a species **A** undergoes oxidation to the oxidized form $\mathbf{A}^+$ (Equation (1)) at a potential E°, arbitrarily set at zero in the voltammograms that are depicted. The oxidized species is assumed to be stable on the measurement timescale.

$$\mathbf{A} \rightleftharpoons \mathbf{A}^+ + e^- \tag{1}$$

The convention will be adhered to where anodic (oxidizing) potentials and oxidation currents are taken as positive. A cyclic voltammogram of the simplest form is obtained as the current versus electrode potential response when the potential of a stationary, planar working electrode is cycled at a certain scan rate ν ($\mathrm{V\,s^{-1}}$) from a starting potential well below $E^\circ(\mathbf{A}/\mathbf{A}^+)$ to a potential well above E°, and then back again. Thus, the electrode-generated species is generated and detected at the same electrode, and the adjustable timeframe of the scan makes it possible to obtain E° data even for transient species. Figure 1 shows a cyclic voltammogram for this process. Certain features are characteristic of this voltammogram, for example, the peak potentials are scan rate independent, and the reversible electrode potential $E^\circ(\mathbf{A}/\mathbf{A}^+)$ can be taken as the midpoint between the peak potentials $E_{p,a}$ and $E_{p,c}$. The separation between the peaks, $\Delta E_p = 2.3RT/nF$, is 59 mV at 25 °C. The two peak currents $i_{p,a}$ and $i_{p,c}$ have equal magnitudes provided that the latter is measured from the adjusted baseline for the cathodic scan. The magnitude of the anodic peak current is given as $i_{p,a} = 2.69 \times 10^5 A D^{1/2} \nu^{1/2} C_{A^*}$, where A is the electrode area, D is the diffusion coefficient of **A**, and C_{A^*} is the bulk concentration of **A**. Thus, the peak current will increase as the square root of the scan rate ν, a

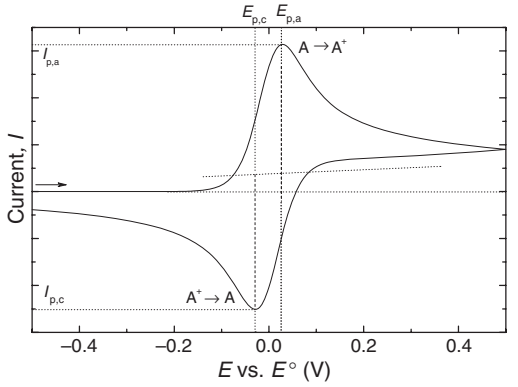

Figure 1 Cyclic voltammogram for a reversible one-electron oxidation.

characteristic of the diffusion-controlled process. This is the simplest reversible voltammogram from which the E° value that is required for derivation of bond energy data is readily obtained.

In many situations, such readily interpretable ideal or near-ideal voltammograms are not obtained. There are numerous factors that can distort the voltammogram from this ideal shape, of which three will be briefly and qualitatively discussed here: chemical irreversibility, electrochemical irreversibility, and solution resistance iR drop. Textbooks have an in-depth coverage of these issues.[7,8,11]

1.11.2.1.2 Chemical irreversibility

We now consider a one-electron oxidation followed by a homogeneous follow-up reaction that consumes the electrode-generated species $\mathbf{A}^+$ according to an unspecified mechanism with an associated rate constant k (Equation (2)). Chemical quasi-reversibility or irreversibility will manifest itself in the voltammogram if the electrode-generated species $\mathbf{A}^+$ has a lifetime comparable to or shorter than the measurement timescale.

$$\begin{aligned} \mathbf{A} &\rightleftharpoons \mathbf{A}^+ + e^- \\ \mathbf{A}^+ &\xrightarrow{k} \text{Products} \end{aligned} \qquad (2)$$

This is illustrated in Figure 2. An increased rate of the follow-up reaction first leads to a decrease of the cathodic peak current. Importantly, as long as a true cathodic peak is observed, E° is quite well approximated by the midpoint between the two peak potentials. As the follow-up reaction proceeds at a greater rate, the cathodic peak vanishes and

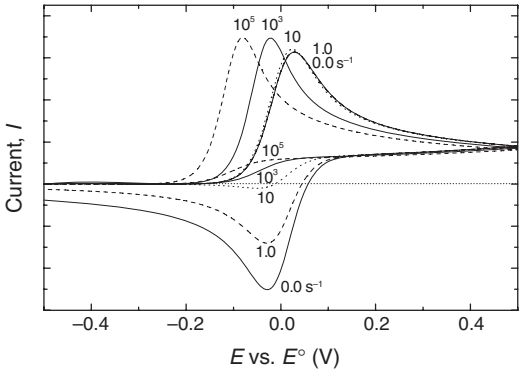

Figure 2 Cyclic voltammograms for a one-electron oxidation of **A** followed by a first-order homogeneous reaction that consumes electrode-generated $\mathbf{A}^+$. The numbers are rate constants (s^{-1}) and a voltage scan rate $\nu = 1.0\,V\,s^{-1}$ is assumed. The decrease in cathodic current and the increasing kinetic potential shift are evident as the rate of the follow-up reaction increases.

the anodic peak undergoes a shift in a direction opposite of the scan direction, in this example in the cathodic (negative) direction. The voltammetric wave is now chemically irreversible. Under such circumstances, the observed peak potential $E_{p,a}$ can deviate considerably from what was its position for $k = 0$, and this will introduce uncertainties in the derived thermochemical data. The magnitude of the so-called kinetic potential shift of the wave away from the true reversible position depends on the rate of the homogeneous reaction (relative to the voltage scan rate ν) as well as the mechanism of the reaction. If the rate and the mechanism are known, the displacement can be calculated or obtained from simulations so that appropriate corrections can be made to the data, but more often than not, such mechanistic and kinetic data are not available. In principle, chemical irreversibility can be circumvented by outrunning the follow-up reaction simply by increasing the scan rate ν. The relatively simple electrochemistry equipment that is found in many laboratories may not allow sufficiently high scan rates, and most certainly not the acquisition of high-quality voltammograms under such conditions. Extremely high scan rates require the use of smaller electrodes (microelectrodes or even ultramicroelectrodes[16–19]) and specialized instrumentation; a detailed discussion of this is outside the scope of this chapter.

1.11.2.1.3 Electrochemical irreversibility ("non-Nernstian" electron transfer)

The analysis in Sections 1.11.2.1.1 and 1.11.2.1.2 pertains to situations in which the electron transfer at the electrode surface is rapid relative to the measurement timescale. This ensures that the Nernst equilibrium ratio between the concentrations of $\mathbf{A}$ and $\mathbf{A}^+$ at the electrode surface is established at every instant, despite the constantly changing potential of the electrode, hence the term "Nernstian electron transfer". However, the electron-transfer event may itself be inherently slow, a commonly encountered phenomenon if significant structural changes accompany the electron transfer. The terms quasi-reversible and even irreversible electron transfer are used to describe this situation. The electrode potential essentially changes too fast for the perturbed Nernst equilibrium to be re-established. This manifests itself as a broadening of the voltammogram: the peak potential for the oxidation of $\mathbf{A}$ shifts in the anodic direction, and the corresponding peak for the reduction of $\mathbf{A}^+$ conversely shifts in the cathodic direction. The peak-to-peak separation ΔE_p now becomes greater than the ideal 59 mV for the Nernstian process. This effect becomes more pronounced at higher voltage scan rates ν. Importantly, the midpoint between the peaks still serves as a reasonable estimate for the true E° value as long as ΔE_p is not extremely large.

1.11.2.1.4 Uncompensated solution resistance

Electrochemistry on organometallic systems is usually performed in organic solvents that are not particularly good conductors of electric current. Despite the use of high concentrations of a supporting electrolyte, the extent of electrolyte ionization may be low due to pronounced ion pairing; the overall effect is that the internal solution resistance of the medium is significant. This applies especially to solvents of low dielectric constant including dichloromethane, THF, and others. The effect of the solution resistance, the so-called "iR drop", that exists between the reference electrode and the working electrode, is that the voltammograms undergo broadening with concomitant shifts of the anodic and cathodic peak potentials away from each other, in a manner that superficially resembles the broadening caused by non-Nernstian behavior as discussed in Section 1.11.2.1.3. The effect of solution resistance becomes adverse at higher currents and hence at high voltage scan rates ν, but in contrast to the non-Nernstian broadening of the waves, this effect can at least to some extent be counteracted by the use of smaller electrodes. Most modern potentiostats have electronic circuitry that is intended to compensate for the iR drop. In practice, complete or correct iR compensation is difficult to achieve, in particular, for the less polar solvents that are commonly used.

1.11.2.1.5 Real-life complex voltammograms and digital simulations

The CV shape is determined by the interplay between processes that occur in solution (diffusion, homogeneous reactions) and at the electrode surface (adsorption, electron transfer). The combined effect of chemical irreversibility, non-Nernstian electron transfer, uncompensated solution resistance, and factors not even discussed here (multi-electron transfer, multiple redox-active species, double-layer charging, adsorption, non-linear diffusion, etc.,) can be a voltammogram that appears to be seriously distorted compared with the reversible voltammogram in Figure 1. In such cases, it is a far from trivial exercise to extract the thermodynamically meaningful E° value for the process under study with the desired accuracy. It is possible to perform digital simulations of these processes, and all the complications discussed are readily implemented.[20,21] DIGISIM®, a commercially available software (developed by Bioanalytical Systems Inc., West Lafayette, IN, USA), is extremely fast and powerful and even offers the possibility to optimize the fit between simulated and experimental voltammograms. While this is a wonderful feature, it is important to be aware

of the fact that the great number of adjustable parameters that are involved in complicated cases may give rise to a multitude of equally good fits of the simulated voltammograms to experimental data, resulting in a range of acceptable values for E°, rate constants, and other parameters. This situation applies, in particular, to those instances in which the voltammograms are completely irreversible in the chemical sense, as pointed out in the context of organometallic reactivity by the author [22] and others.[23]

1.11.2.1.6 A simple electrochemical cell assembly

Handling of air sensitive and/or moisture sensitive compounds that require great care from the experimentalist is routine in organometallic chemistry. Accordingly, sophisticated electrochemical cells and cell assemblies have been devised to ensure that inert conditions are maintained. The electrochemical cell is frequently installed inside an inert-atmosphere drybox as an extra precaution. Needless to say, frequent change of samples and reagents as well as maintaining (and adjusting) a stable cell temperature will be a rather cumbersome exercise. In the author's experience, even for most of the air sensitive systems encountered, it suffices to use a simple electrochemical cell construction that can easily be operated outside the drybox. The three-electrode cell assembly shown in Figure 3 is a ~2.5–3 cm outer diameter test tube with a ground-glass joint, equipped with a Teflon stopper through which are drilled four tight-fitting holes for inserting the three electrodes and an inert gas inlet tube for purging/stirring the solution and maintaining an atmosphere of purified argon inside the cell, and an additional hole that functions as a gas outlet. Stationary conditions are achieved in the solution by withdrawing the inert gas inlet tube to the headspace and reducing the argon flow. Samples, solvents, and so on can easily be added using a standard syringe and Schlenk techniques. The solvent level in the cell can be maintained if the inert gas is pre-saturated with solvent vapors by passing it through a solvent-filled bubbler, and the cell temperature can be conveniently varied by immersing the tube into a temperature-conditioned bath.

1.11.2.2 Electrode Potential References, Solvents, Electrolytes, and their Influence on E° Data

A survey of the literature, old and recent, reveals that electrochemical experiments are conducted under widely different conditions. Reported electrode potentials for one given compound can vary significantly even under apparently quite similar conditions when published values from different sources are compared. Frequently, this can be caused by erroneous reporting of data or improper conversion of electrode potentials from the scale of one reference electrode to another. Furthermore, the use of different solvents, supporting electrolytes, and physical reference electrodes adds other, physically well understood, reasons why E° data differ, and in many instances *should* actually differ considerably. It is important at least to understand these effects, and if possible to make reasonable corrections for them. Obviously, there is a definite need to standardize as much as possible the way in which electrode potential data are reported. Errors or discrepancies in E° values will easily lead to significant errors in derived bond energy data.

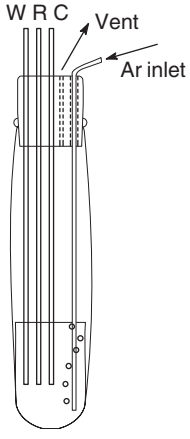

Figure 3 Simple electrochemical cell made from a test tube, a Teflon stopper, reference (R), working (W), and counter (C) electrodes, and an inert gas purge inlet tube.

1.11.2.2.1 Electrode potential references

The normal hydrogen electrode (NHE) is the primary reference electrode and is used to define the accepted scale of standard potentials in aqueous media. It is also one of the most reproducible electrodes that are available. The hydrogen electrode has been successfully employed in dipolar aprotic solvents;[8] however, it is not frequently used. The aqueous saturated calomel electrode (SCE), connected to the electrolyte under study by a non-aqueous salt bridge, has become the reference electrode of choice for most investigators. Whether it is the SCE that is used, or any other suitable reference electrode for a given solvent,[8] junction potentials will exist between the reference electrode and the electrolyte under study. These junction potentials will affect electrode potential measurements and will vary from one solvent/electrolyte system to another. In addition, the instability of the SCE in non-aqueous solvents has been noted.[24,25]

Therefore, reliable internal references are needed for accurate determination of redox potentials. Desired properties for such a reference standard are[26] (i) constant difference in solvation energies for both members of the redox couple, (ii) fast electron-transfer kinetics, (iii) high stability of both members of the redox couple, and (iv) a conveniently located E° value. IUPAC has recommended the use of the Cp_2Fe/Cp_2Fe^+ (Fc) couple[27] despite the fact that this couple has an E° value that is highly solvent and electrolyte dependent, in the range 0.16–0.56 V versus SCE.[28] The variations are primarily but not exclusively due to solvation and ion-pairing effects of the Cp_2Fe^+ ion. The Fc couple does fulfill the other requirements and has therefore been commonly adapted, being readily available at low cost. Every practitioner of non-aqueous voltammetry is strongly encouraged to measure E°(Fc) versus their chosen reference electrode, be it SCE or any other reference, and report the voltammetric data either relative to Fc or relative to their reference while explicitly reporting E°(Fc) versus the reference electrode under the experimental conditions. This procedure also provides an easy check that the reference electrode is stable and in acceptable working condition.

In a most valuable review, Connelly and Geiger[28] have critically reviewed redox potential data for a wide range of important redox couples and electron-transfer reagents in different solvents.

1.11.2.2.2 Solvents and electrolytes and their impact on chemical reversibility and E° data

CV is usually done with substrate concentrations in the mM range. The redox process that occurs at the working electrode often generates species – radicals, ions, or both – that are reactive and short lived. Traces of impurities in the solvent or supporting electrolyte (at a typical concentration of 0.1 M and above) can significantly shorten the lifetimes of these species. The supporting electrolyte and the solvent are both present in a large excess compared to the substrate; procedures for the prerequisite solvent and electrolyte purification have been summarized.[8]

Dipolar, nucleophilic or coordinating solvents (MeCN, DMSO, and DMF are widely used) and coordinating anions will significantly decrease the lifetimes of many cationic electrode-generated species. A reduction of solvent polarity is therefore often desirable. This is clearly at odds with the desire to conduct current with minimum solution resistance (see Section 1.11.2.1.4) – common electrolytes have low solubilities in low-polarity solvents and tend to form ion pairs rather than conducting, free ions. Supporting electrolytes of the $Bu_4N^+X^-$ type, where X^- is a large, weakly coordinating[29,30] anion such as $B(C_6F_5)_4^-$ or $B[C_6H_3(CF_3)_2]_4^-$ have been recently promoted as excellent, albeit more expensive, alternatives to the more traditional electrolytes with $X = ClO_4^-$, BF_4^-, or PF_6^-.[31,32] The relative "innocence" of PF_6^- relative to BF_4^- and ClO_4^- in dichloromethane was noted earlier for the oxidation of $(C_6H_6)Cr(CO_3)$ and other π-arene compounds.[33] Considering the chemical safety issues that arise with the use of perchlorate salts, and taking into account the ready availability of attractive alternatives, *there is no reason at all that perchlorate salts should be the default electrolytes for non-aqueous electrochemistry today*. The use of $Bu_4N^+B(C_6F_5)_4^-$ and $Bu_4N^+B[C_6H_3(CF_3)_2]_4^-$ as electrolytes has now established that numerous electrode reactions which were previously believed to be chemically irreversible can indeed be made chemically reversible.[34,35] Furthermore, these new electrolytes have solubility characteristics that give improved solution conductivity, which allows CV to be conducted in increasingly less polar solvents, at lower temperatures, and at faster scan rates ν with less signal broadening due to iR drop. Thus, CV can now be performed with great success using solvents of as low polarity as $C_6H_5CF_3$,[36,37] C_6H_5F,[38] and even Et_2O and *t*BuOMe.[32] For these new solvent/electrolyte systems, it is of course still imperative that the advice to standardize the reference electrode relative to the accepted standard Cp_2Fe is followed.

In addition to acting as a convenient medium for dissolving complexes and conducting current, the chosen solvent with its dissolved supporting electrolyte will also influence the thermodynamics of any redox reaction through its capacity to stabilize various oxidation states differently through solvation. For example, consider the two successive one-electron transfer processes in Equation (3). Here, $E^\circ(\mathbf{A}/\mathbf{A}^+)$ will tend to decrease ("**A** is more readily oxidized")

in a more polar solvent because the charged, oxidized part of the redox couple, $\mathbf{A}^+$, gains more stabilization by improved solvation than neutral **A** does. On the other hand, $E°(\mathbf{A}^-/\mathbf{A})$ will increase ("**A** is more readily reduced") because it is the reduced, charged part of the couple, $\mathbf{A}^-$, that will gain more stabilization in a more polar solvent. Related effects are anticipated as a consequence of changing the identity of the supporting electrolyte, and even of changing its concentration; the direction of $E°$ changes caused by ion-pairing effects will of course depend on the charges in the redox couple as well as the identities of both the anion and the cation of the supporting electrolyte.

$$\mathbf{A}^- \underset{+e^-}{\overset{-e^-}{\rightleftharpoons}} \mathbf{A} \underset{+e^-}{\overset{-e^-}{\rightleftharpoons}} \mathbf{A}^+ \qquad \begin{matrix} E°(\mathbf{A}^-/\mathbf{A}) & E°(\mathbf{A}/\mathbf{A}^+) \end{matrix} \tag{3}$$

Ruiz and Astruc have recently considered these effects for the $\mathbf{A}/\mathbf{A}^+$ charge type of redox couples in a systematic study of the redox potentials of Cp_2Fe, Cp^*_2Fe, $Cp^*_2Co^+$, and $Cp^*Fe(C_6Me_6)$ in a wide range of solvents.[26] As would be expected for the reasons discussed above, all redox potentials, measured against SCE, showed a pronounced dependence on the solvent/electrolyte being used – the range of $E°$ values versus SCE spanned a range as great as 0.27 V for a given redox couple in the solvents DMF, MeCN, THF, CH_2Cl_2, DMSO, and DME with 0.1 M $Bu_4N^+PF_6^-$ as the supporting electrolyte. However, the differences between the redox potentials for the permethylated species were quite insensitive to solvent changes, whereas the redox potential for ferrocene relative to the others was highly solvent dependent. Similarly, the difference between $E°$ for Cp_2Fe/Cp_2Fe^+ and $Cp^*_2Fe/Cp^*_2Fe^+$ in CH_2Cl_2 varied by as much as 0.065 V when the electrolyte (0.1 M) was varied in the series $Bu_4N^+X^-$ with $X = PF_6$, BF_4, Br, Cl, HSO_4. A slight electrolyte concentration dependence of ca. 0.020 V was even noted between electrolyte concentrations of 0.1 and 0.4 M. All these variations are a consequence of more pronounced solvation and ion-pairing changes for the small Cp_2Fe/Cp_2Fe^+ couple than for the much larger permethylated redox couples. On this basis, the permethylated species were suggested as candidates for a new redox scale as a better, less error-prone alternative than ferrocene itself. An important advantage of these references will be that changes in $E°$ data for a given investigated compound from one solvent to another will mostly reflect the impact of solvation changes on the particular compound in question, rather than on the reference compound.

Geiger and co-workers recently[39] described a striking manifestation of related solvent/electrolyte effects: the differences in $E°$ for the first and second reversible oxidation waves of bis(fulvalene)dinickel, $(\eta^5{:}\eta^5\text{-}C_{10}H_8)_2Ni_2$ or Fv_2Ni_2, changed from 0.212 V in anisole/0.1 M $Bu_4N^+Cl^-$ to 0.850 V in dichloromethane/0.02 M $Na^+B[C_6H_3(CF_3)_2]_4^-$. Noticeably, $E°(Fv_2Ni_2/Fv_2Ni_2^+)$, referenced against Fc, was relatively solvent/electrolyte insensitive, indicating that the Fc reference redox couple and the substrate redox couple responded similarly to solvent/electrolyte changes.

The importance of conducting experiments that establishes $E°$ for a readily available standard compound under the actual measurement conditions cannot be overstated. If this is consistently done, many of the problems that are encountered when comparing electrode potential data from different sources in the literature can be diminished. Quantitative bond energy data that are derived from electrode potentials will obviously benefit from such a standardization – note that the 0.4 V span that is found for $E°$(Fc) versus SCE[28] translates to an astonishing possible error in bond energies of about 40 kJ mol^{-1} merely as a consequence of flawed comparisons of electrode potentials that have been measured in two different solvents!

1.11.3 Bonding Energetics from Electrode Potential Data

A covalently bonded complex M–X can be envisioned to undergo M–X bond cleavage by the three modes depicted in Scheme 1. Here, Equation (4) represents the homolytic bond cleavage that defines the BDE, normally defined in enthalpy terms – as will be the case in all tabulated values here. Equations (5) and (6) in Scheme 1 are the two corresponding heterolytic bond cleavage processes. The processes are interrelated by the electron affinities (EAs) and ionization potentials (IPs) of the radicals $M^\cdot$ and $X^\cdot$ in the gas phase. In solution, EA and IP are replaced by the corresponding electrode potentials (multiplied by the Faraday constant).

The relationship between the homolytic and heterolytic processes in different oxidation states of M–X has been summarized by Wayner and Parker[40] in the form of the mnemonic in Scheme 2. Horizontal reactions represent electron-transfer processes, vertical ones are homolytic processes, and diagonal ones are heterolytic processes. The energy change for a particular reaction can be written as the sum of energy changes for transformations that add up to the same overall reaction. Square schemes in which two constituent reactions are electron-transfer processes will be of

Reaction			Energy change	
M–X	⟶	$M^{\cdot} + X^{\cdot}$	BDE(M–X)	(4)
M–X	⟶	$M^{-} + X^{+}$	BDE(M–X) – EA($M^{\cdot}$) + IP($X^{\cdot}$)	(5)
M–X	⟶	$M^{+} + X^{-}$	BDE(M–X) + IP($M^{\cdot}$) – EA($X^{\cdot}$)	(6)

Scheme 1 Modes of cleavage of a covalent M–X bond.

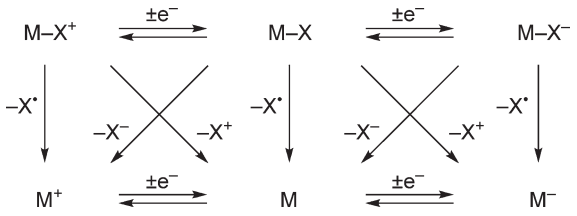

Scheme 2 Interrelation between homolytic and heterolytic bond cleavage reactions. Adapted from Wayner, D. D. M.; Parker, V. D. *Acc. Chem. Res.* **1993**, *26*, 287–294, with permission from American Chemical Society.

particular relevance here. The thermochemical cycles normally lead to relative, rather than absolute, bond energy data. Fortunately, in many cases, it is possible to extract absolute data through the use of reliable anchoring points.

Landmark contributions by Breslow and co-workers[41–43] introduced the use of thermochemical cycles based on electrode potential data to organic chemistry in their determination of pK_a data for weak carbon acids. The methods were modified, adapted, and further developed by others and have been extensively reviewed.[39,44–46] Some of the applications in organometallic chemistry that are described in the following have also been reviewed.[47]

1.11.4 M–H Bond Dissociation Energies (BDEs) in Stable Metal Hydrides

1.11.4.1 Thermochemical Cycle for M–H BDE Determination

The thermochemical cycle in Scheme 3 can be used to determine M–H bond dissociation energies (BDEs) of metal hydrides.[48] The required quantities are the thermodynamic acidity (pK_a) of the metal hydride MH and the oxidation potential for the corresponding base M^-, $E°(M^-/M)$, both in the same solvent (solv). The thermochemical cycle and its underlying parameters are based on Bordwell's method for determination of C–H BDEs.[49] The constant term C in Equation (7), Scheme 3 contains contributions from the H^+/H_2 electrode potential in the solvent under consideration, H_2 dissociation, $H^{\cdot}$ solvation, conversion of electrode potentials to the Fc scale, and entropy contributions that convert the free-energy based quantities (BDE_G) obtained from $E°$ and pK_a data to enthalpy-based BDEs. These terms have been extensively discussed and evaluated.[48,50] Equation (7), Scheme 3 is the simple equation that is used

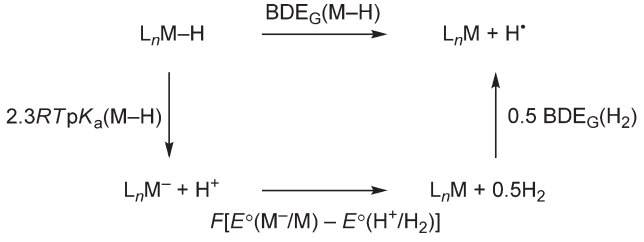

$$BDE = 2.3RTpK_a(M–H, solv) + FE°(M^-/M,solv) + C \quad (7)$$

Scheme 3 Thermochemical cycle for determination of M–H bond dissociation energies. The quantity C in Equation (7), when electrode potentials and pK_a data are obtained in the same solvent and $E°(M^-/M)$ is referenced to the Cp_2Fe/Cp_2Fe^+ scale, is 249 kJ mol^{-1} (solv = MeCN) and 308 kJ mol^{-1} (solv = DMSO).

for determining the M–H BDE. The constant term C is 249 kJ mol^{-1} when pK_a and $E°$(M$^-$/M) data are determined in acetonitrile and $E°$ is referred to the Fc scale. The corresponding C term for DMSO is 308 kJ mol^{-1} and the difference is largely due to improved solvation of H^+ in DMSO relative to MeCN.[50] (Note that this and other thermochemical cycles can also be used in "reverse" – for example, from Equation (7), Scheme 3, pK_a values can be determined from BDE and $E°$, and $E°$ can be estimated from pK_a and BDE data.)

It is obviously desirable to have reversible $E°$(M$^-$/M) data for use with Equation (7), Scheme 3. Irreversible waves are frequently encountered for the oxidation of metal carbonyl anions, in part due to the fact that the corresponding 17-electron radicals undergo rapid dimerizations; corrections for kinetic potential shifts are then required but kinetic data are not always available. The validity of the method when truly reversible potentials are available has been confirmed by the fact that Cr–H BDEs that were determined for $CpCr(CO)_3H$ and $CpCr(CO)_2(PPh_3)H$ using this method were identical, to within 2 kJ mol^{-1}, to values that were independently determined by calorimetry.[51] The cyclic voltammograms for the M$^-$/M couples in these cases were fully reversible and hence the $E°$ data could be obtained without the need to make corrections for kinetic potential shifts. The accuracy of BDEs derived from chemically irreversible electrode processes will depend on the goodness of the corrections; quasi-reversible or irreversible (non-Nernstian) electron transfer complicates matters even further.

1.11.4.2 M–H BDE Data for Stable Metal Hydrides in Acetonitrile

Acetonitrile has been used for the determination of metal–hydride acidities by equilibrium measurements[52] and is an excellent solvent for electrochemistry, so a great number of investigations have been performed into this solvent. Table 1 gives a comprehensive list of M–H BDE data for metal carbonyl and cyclopentadienyl hydrides that have

Table 1 Metal–hydride BDEs, pK_a's, and oxidation potentials for the corresponding bases for metal carbonyl and cyclopentadienyl hydrides in acetonitrile

Entry	*Metal hydride M–H*	pK_a(*M–H*)	$E°$(*M*$^-$/*M*)[a] (V vs. Fc)	*BDE*(*M–H*) (kJ mol^{-1})	*References*
1	$CpCr(CO)_3H$	13.3	−0.69	257	48
2	$CpCr(CO)_2[P(OMe)_3]H$	21.1[c]	−1.11	262	54
3	$CpCr(CO)_2(PPh_3)H$	21.8	−1.29	250	50,54
4	$CpCr(CO)_2(PEt_3)H$	25.8[c]	−1.51	251	54
5	$Cp^*Cr(CO)_3H$	16.1[c]	−0.83	261	54
6	$TpCr(CO)_3H$	<8	−0.82	<215	55
7	$Tp'Cr(CO)_3H$		−0.86		55
8	$CpMo(CO)_3H$	13.9	−0.50[b]	290	48
9	$Cp^*Mo(CO)_3H$	17.1	−0.71[b]	287	48
10	$TpMo(CO)_3H$	10.7	−0.52	260	55
11	$Tp'Mo(CO)_3H$	9.7	−0.58	248	55
12	$CpW(CO)_3H$	16.1	−0.49[b]	303	48
13	$CpW(CO)_2(PMe_3)H$	26.6	−1.23[b]	291	48
14	$CpW(CO)_2(PMe_3)H_2^+$	>9	0.16	>316	56
15	$TpW(CO)_3H$	14.4	−0.58	275	55
16	$Tp'W(CO)_3H$	12.9	−0.65	260	55
17	$Mn(CO)_5H$	14.1	−0.56[b]	285	48
18	$Mn(CO)_4(PPh_3)H$	20.4	−0.87[b]	286	48
19	$Re(CO)_5H$	21.1	−0.69[b]	313	48
20	$CpFe(CO)_2H$	19.4	−1.35[b]	239	48
21	$Fe(CO)_4H_2$	11.4	−0.40[b]	283	48
22	$CpRu(CO)_2H$	20.2	−1.06[b]	272	48
23	$Cp^*_2OsH^+$	9.9	−0.06	298	57
24	$Co(CO)_4H$	8.3	−0.27[b]	278	48
25	$Co(CO)_3(PPh_3)H$	15.4	−0.72[b]	272	48
26	$Co(CO)_3[P(OPh)_3]H$	11.3	−0.49[b]	273	48

[a] $E°$ data from reversible voltammograms unless otherwise noted.
[b] Oxidation peak potentials in irreversible voltammograms. Kinetic potential shifts were applied before use in Equation (7), Scheme 3.
[c] pK_a data calculated from calorimetrically determined BDE data using Equation (7), Scheme 3.

been determined with the thermochemical cycle in Scheme 3. Note that, for entries 2, 4, and 5, calorimetrically determined BDEs have been used to calculate pK_a data from Equation (7), Scheme 3. Most electrode processes in Table 1 were irreversible and are corrected for dimerization kinetics. The uncertainties that can still exist in such cases are illustrated by later findings, suggested by digital simulations, that the original $E°$ values for the oxidations of $CpW(CO)_3^-$ and $CpMo(CO)_3^-$ should be adjusted ca. 90 mV to more negative values, meaning that the BDEs in Table 1 (entries 8 and 12) might be overestimated by 8 kJ mol^{-1}.[22] Subsequent to this,[53] an investigation of the reductions of $CpM(CO)_3^{\cdot}$ (M = Cr, Mo, W) by photomodulated voltammetry in DMF led to the conclusion that the original W (but not Mo and Cr) $E°$ value should be adjusted 115 mV to more positive values, requiring an increase of the tabulated BDE in entry 12 by 11 kJ mol^{-1}!

The data in Table 1 reveal some clear trends. The M–H BDEs consistently decrease within a group in the order third row > second row > first row. Furthermore, for a given metal, the BDE is rather insensitive to modest changes of the ligands, for example, the replacement of Cp^* for Cp, or phosphine for a CO, ligand. Inspection of the data reveals that this is caused by opposite, canceling effects from the pK_a and the $E°(M^-/M)$ terms, that is, increased M^- basicity is accompanied by a decrease in $E°(M^-/M)$ to the same extent in energy terms when ligand electronic effects are changed.

The bonding energetics of bis(diphosphine) metal hydrides of group 9 and 10 metals have been recently studied in detail. These species give rise largely to reversible voltammograms in acetonitrile, and uncertainties due to kinetic potential shifts and other corrections are therefore not introduced. Table 2 gives a comprehensive list of reported BDE data. As in Table 1, there is a trend (although with exceptions) that BDEs increase downward in the periodic table. Significant coordination geometry changes when going from five-coordinate to four-coordinate species probably significantly influence the data. It was pointed out that $(diphosphine)_2Ni–H^+$ BDE data correlate quite well with $E°(M/M^+)$,[58] but not with $E°(M^+/M^{2+})$, probably reflecting the coordination geometry issues. A creative use of combined proton transfer, hydride transfer, and H_2 heterolytic cleavage equilibria allowed the determination of 11 out of 12 possible modes of Co–H bond cleavage processes of $H_2Co(dppe)_2^+$ and monohydride derivatives.[59]

Table 2 Metal–hydride BDEs, pK_a's, and oxidation potentials for the corresponding bases for bis(diphosphine) metal hydrides in acetonitrile

Entry	*Metal hydride M–H$^+$*	pK_a(*M–H$^+$*)	$E°(M/M^+)$ (V vs. Fc)	*BDE*(*M–H$^+$*) (kJ mol^{-1})	*References*
1	$H_2Co(dppe)_2^+$	22.8	−1.16	263[a]	59
2	$HCo(dppe)_2$	38.1[c]	−2.03	268[a]	59
3	$HCo(dppe)_2(MeCN)^{2+}$	11.3	−0.70	242[a]	59
4	$H_2Rh(depx)_2^+$	30.6	−1.26	299[a]	60
5	$HRh(depx)_2$	51.5[c]		316[a,c]	60
6	$HNi(dppv)_2^+$	13.2	−0.83	241[a]	58
7	$HNi(dppe)_2^+$	14.2	−0.88	246	61
8	$HNi(dmpp)_2^+$	23.9	−1.33	258	61
9	$HNi(dedpe)_2^+$	20.2	−1.08	257[a]	58
10	$HNi(depp)_2^+$	23.3	−1.34	229[a]	62
11	$HNi(depe)_2^+$	23.8	−1.29	261	61
12	$HNi(dmpe)_2^+$	24.3	−1.35	254	61
13	$HNi(PNP)_2^+$	22.2	−1.24	253[a]	63
14	$HPd(depe)_2^+$	23.2	−1.24[b]	259[a]	64
15	$HPd(depp)_2^+$	22.9	−1.22	259[a]	64
16	$HPd(depx)_2^+$	19.8	−1.02	260[a]	64
17	$HPd(depPE)_2^+$	18.3	−0.92	261[a]	64
18	$HPd(EtXanthphos)_2^+$	18.5	−0.94	260[a]	64
19	$HPt(EtXanthpos)_2^+$	27.3	−0.97	310[a]	65
20	$H_2Pt(EtXanthphos)_2^{2+}$	6.8	0.23	306[a]	65

[a]A $T\Delta S°$ term of 21 kJ mol^{-1} has been added[66] to the BDEG data provided in the reference.
[b]Estimated from E vs. pK_a correlation data.[64]
[c]See reference for the actual thermochemical cycle used.
dppe = $Ph_2PCH_2CH_2PPh_2$, depx = 1,2-$(Et_2PCH_2)_2C_6H_4$, dppv = $Ph_2PCHCHPPh_2$, dmpp = $Me_2PCH_2CH_2CH_2PMe_2$, dedpe = $Et_2PCH_2CH_2PPh_2$, depp = $Et_2PCH_2CH_2CH_2PEt_2$, depe = $Et_2PCH_2CH_2PEt_2$, dmpe = $Me_2PCH_2CH_2PMe_2$, PNP = $MeN(CH_2PEt_2)_2$, depPE = bis(2-(diethylphosphino)phenyl)ether, EtXanthphos = 9,9-dimethyl-4,5-bis(diethylphosphino)xanthene.

1.11.4.3 M–H BDE Data Determined in 1,2-Dichloroethane

Acetonitrile can be used for acid/base equilibrium measurements only within a certain range of substrate pK_a values, limited at the high end by onset of solvent deprotonation and at the low end by substrate autodissociation. These limitations can be overcome by the use of less polar solvents, such as dichloromethane, THF, and 1,2-dichloroethane (DCE). Although a rigorous 1 : 1 relationship between the pK_a scales in two different solvents never exists, it is often assumed that pK_a differences between structurally related species are nearly constant when a series is compared in two different solvents. If the acidity of at least one compound can be determined in both solvents, then the two scales are at least loosely anchored to each other. Angelici[67] has performed systematic studies of relative acidities of cationic metal hydrides in DCE by calorimetric measurements of the heat of protonation (ΔH_{MH+}) of neutral precursor complexes with triflic acid (Equation (8)). The advantage of using this medium and the technique is that thermochemical data are available for metal hydrides that are too weakly acidic to be investigated by equilibrium measurements in acetonitrile. Permethylosmocene Cp^*_2Os, the equilibrium protonation of which has been studied in acetonitrile (Table 1, entry 23), was included and provides a common anchoring point for the two solvent scales.[57] Differences in pK_a values for $Cp^*_2OsH^+$ and other hydrides M–H in acetonitrile can be related to differences in heat of protonation data through the relationship $2.3RT\Delta pK_a = -\Delta\Delta H_{MH+} + T\Delta\Delta S_{MH+}$. On the presumption that $\Delta\Delta S_{MH+} = 0$, this leads to $\Delta pK_a = -\Delta\Delta H_{MH+}/2.3RT$, or $-\Delta\Delta H_{MH+} = 5.70\Delta pK_a\ \text{kJ mol}^{-1}$ at 25 °C, that is, a slope of 5.70 is predicted for a plot of $-\Delta H_{MH+}$ versus pK_a data for a series of complexes. If $Cp^*_2OsH^+$ is used as an anchoring point, ΔH_{MH+} (DCE) can be converted to pK_a (acetonitrile) data which in conjunction with the pertinent $E°(M/M^+)$ electrode potential gives access to M–H BDEs for the cationic hydrides using Equation (7), Scheme 3. Wang and Angelici proposed Equation (9) for the determination of M–H BDEs based on ΔH_{MH+} data in DCE and $E°(M/M^+)$ data, measured in DCE relative to the SCE reference.[68] Table 3 lists the BDE data that were derived from the combined calorimetry and voltammetry measurements. The uncertainties arising from largely irreversible voltammograms are of course as relevant here as for the data in Table 1.

$$L_nM \xrightarrow[DCE]{CF_3SO_3H} L_nM{-}H^+ \qquad \Delta H_{reaction} = \Delta H_{MH+} \tag{8}$$

$$BDE(M{-}H^+) = -\Delta H_{MH+} + FE°(L_nM/L_nM^+) + 139\ \text{kJ mol}^{-1} \tag{9}$$

The BDE data in Table 3 clearly exhibit trends that are similar to those seen in Table 1, that is, BDEs decrease in the order third > second > first row. Furthermore, the canceling effect of the contributions from the metal basicity and oxidation terms renders the BDEs relatively invariant to modest changes in the ligand environment as long as steric factors remain similar.

1.11.4.4 M–H BDE Data Determined in THF and Dichloromethane

Morris and co-workers and others have described the protonation of a variety of group 8 hydrides. Relative acidities of the resulting cationic dihydride or dihydrogen complexes were established by proton-transfer equilibrium measurements in dichloromethane, THF, and acetone. All data were linked to the aqueous scale using the aqueous pK_a of Cy_3PH^+ as an anchor. Electrochemical measurements giving rise mostly to broadened and chemically irreversible waves were conducted in these solvents and were referenced to Fc in the respective solvents. Equation (7), Scheme 3 was modified with a value for the constant C of 276 kJ mol^{-1} based on the pseudo-aqueous pK_a data and $E°$ data referring to Fc in the pertinent solvent. The derived BDE data are included in Table 4. Some concern regarding the underlying assumptions has been expressed;[47] different experimental conditions have led in some cases to quite different BDE data (cf. entries 1 and 2). Note that some of the entries in Table 4 pertain to cationic dihydride complexes whereas others are cationic dihydrogen complexes. Sometimes, these two isomeric forms co-exist; since they give the same conjugate base upon deprotonation, their BDEs and pK_a's must be very similar. For the dihydrogen complexes, the BDEs can be considered to reflect properties of the H–H rather than the M–H bond; the BDEs are well below the H–H BDE of 436 kJ mol^{-1} in H_2(g),[69] reflecting the activation of the H–H bond by the metal not only toward heterolysis[70] but also toward homolysis.

Table 3 Metal–hydride BDEs, and heats of protonation and oxidation potentials of the corresponding bases in DCE[68]

Entry	*Metal hydride M–H*$^+$	$-\Delta H_{MH+}$ (kJ mol^{-1})	$E°(M/M^+)$[a] (V vs. SCE)	*BDE*(*M–H*$^+$) (kJ mol^{-1})
1	$HCr(CO)_2(dppm)_2^+$	107	−0.12	234
2	$HMo(CO)_2(arphos)_2^+$	100	0.28	266
3	$HMo(CO)_2(dppe)_2^+$	115	0.24	277
4	$HMo(CO)_2(dppm)_2^+$	124	0.18	281
5	$HW(CO)_3(PMePh_2)_3^+$	63	0.48[b]	249
6	$HW(CO)_3(PEtPh_2)_3^+$	71	0.45[b]	254
7	$HW(CO)_3(PEt_2Ph)_3^+$	77	0.41[b]	255
8	$HW(CO)_3(PMe_3)_3^+$	82	0.40[b]	259
9	$HW(CO)_3(PEt_3)_3^+$	105	0.28[b]	271
10	$HW(CO)_2(dppm)_2^+$	132	0.14	285
11	$HW(CO)_3(tripod)^+$	44	0.72	253
12	$HW(CO)_3(triphos)^+$	70	0.63	270
13	$HCp^*Re(CO)_2(PMe_2Ph)^+$	77	0.84[b]	297
14	$HCp^*Re(CO)_2(PMe_3)^+$	84	0.80[b]	300
15	$HFe(CO)_3(PPh_3)_2^+$	59	0.55[b]	251
16	$HFe(CO)_3(PMePh_2)_2^+$	74	0.49[b]	260
17	$HFe(CO)_3(PMe_2Ph)_2^+$	89	0.45[b]	272
18	$HFe(CO)_3(PMe_3)_2^+$	97	0.41[b]	277
19	$HFe(CO)_3(dppp)^+$	88	0.31[b]	257
20	$HFe(CO)_3(dppm)^+$	100	0.40[b]	278
21	$Cp^*_2RuH^+$	79	0.68[b]	285
22	$CpRu(PMe_3)_2(I)H^+$	86	0.56	279
23	$CpRu(dppm)H_2^+$	121	0.37	296
24	$CpRu(dppe)H_2^+$	121	0.31	290
25	$CpRu(PPh_3)_2H_2^+$	124	0.23[b]	286
26	$Cp^*_2OsH^+$	111	0.51[b]	300
27	$CpOs(PPh_3)_2(Br)H$	68	0.59[b]	264
28	$CpOs(PPh_3)_2(Cl)H^+$	82	0.58[b]	278
29	$CpOs(PPh_2Me)_2(Br)H^+$	85	0.51[b]	273
30	$CpOs(PMe_3)_2(Br)H^+$	123	0.34[b]	295
31	$CpOs(PPh_3)_2H_2^+$	156	0.13[b]	308
32	$CpIr(CO)[P(p\text{-}C_6H_4CF_3)_3]H^+$	117	0.60	314
33	$CpIr(CO)[P(p\text{-}C_6H_4F)_3]$	125	0.53	315
34	$CpIr(CO)(PPh_3)H^+$	126	0.50	313
35	$CpIr(CO)(PPh_2Me)H^+$	132	0.45	315
36	$CpIr(CO)(PMe_2Ph)H^+$	136	0.41	315
37	$CpIr(CO)(PMe_3)H^+$	139	0.37	314
38	$CpIr(CO)(PEt_3)H^+$	138	0.35	311
39	$CpIr(CO)(PCy_3)H^+$	137	0.35	310
40	$CpIr(CS)(PPh_3)H^+$	111	0.51	300
41	$CpIr(COD)H^+$	95	0.69	301
42	$(C_5H_4Me)Ir(COD)H^+$	101	0.61	299
43	$(1,2,3\text{-}C_5H_2Me_3)Ir(COD)H^+$	110	0.54	302
44	$(C_5Me_4H)Ir(COD)H^+$	115	0.47	300
45	$Cp^*Ir(COD)H^+$	119	0.45	302
46	$Cp^*Ir(CO)[P(p\text{-}C_6H_4CF_3)_3]H^+$	141	0.30	310
47	$Cp^*Ir(CO)[P(p\text{-}C_6H_4Cl)_3]H$	154	0.20	313
48	$Cp^*Ir(CO)(PPh_3)H^+$	155	0.09	303
49	$Cp^*Ir(CO)(PPh_2Me)H^+$	155	0.08	303
50	$Cp^*Ir(CO)(PMe_3)H^+$	159	0.07	305
51	$Cp^*Ir(CO)_2H^+$	90	0.72	298

[a]Irreversible voltammograms unless otherwise noted.
[b]Reversible voltammogram.
dppm = $Ph_2PCH_2PPh_2$, arphos = $Ph_2AsCH_2CH_2AsPh_2$, tripod = $MeC(CH_2PPh_2)_3$, triphos = $PhP(CH_2PPh_2)_2$.

Table 4 Metal–hydride BDEs, pseudo-aqueous pK_a's, and oxidation potentials for the corresponding bases in THF or dichloromethane

Entry	*Metal hydride* MH_2^+	p$K_a(MH_2^+)$	$E(MH/MH^+)$ (V vs. Fc)	$BDE(MH_2^+)$ (kJ mol^{-1})	*References*
1	*trans*-$CpRu(PPh_3)_2H_2^+$	8.0	−0.20	303	71
2	*trans*-$CpRu(PPh_3)_2H_2^+$	8.3	−0.36	289	72
4	$Cp^*Ru(dppm)H_2^+$	8.8	−0.25	302	73
4	$Cp^*Ru(dppm)(\eta^2\text{-}H_2)^+$	9.2	−0.25	306	73
5	*trans*-$CpOs(PPh_3)_2H_2^+$	13.4	−0.38	316	72
6	*trans*-$CpOs(dppm)H_2^+$	10.0	−0.16	318	72
7	*cis*-$CpOs(dppm)H_2^+$	10.9	−0.16	323	72
8	*trans*-$CpOs(dppe)H_2^+$	11.8	−0.17	327	72
9	*cis*-$CpOs(dppe)H_2^+$	9.9	−0.17	316	72
10	*trans*-$CpOs(dppp)H_2^+$	13.4	−0.35	319	72
11	$TpRu(PPh_3)_2(\eta^2\text{-}H_2)^+$	7.6	−0.12	308	72
12	$TpOs(PPh_3)_2(\eta^2\text{-}H_2)^+$	8.9	−0.22	306	72
13	*trans*-$HRu(dtfpe)_2(\eta^2\text{-}H_2)^+$	10.0	0.40	372	71
14	*trans*-$HRu(dppe)_2(\eta^2\text{-}H_2)^+$	15.0	−0.20	343	71
15	*trans*-$ClRu(dppe)_2(\eta^2\text{-}H_2)^+$	6.0	−0.12	299	73
16	*trans*-$HRu(depe)_2(\eta^2\text{-}H_2)^+$	17.5	−0.40	338	71,73
17	*trans*-$HRu(dppf)_2H_2^+$	4.4	−0.63	240	73
18	*trans*-$HOs(dtfpe)_2(\eta^2\text{-}H_2)^+$	9.2	0.10	339	71
19	*trans*-$HOs(dppe)_2(\eta^2\text{-}H_2)^+$	13.6	−0.20	335	71
20	*trans*-$ClOs(dppe)_2(\eta^2\text{-}H_2)^+$	7.4	−0.13	306	74
21	*trans*-$BrOs(dppe)_2(\eta^2\text{-}H_2)^+$	5.4	−0.11	296	74
22	*trans*-$HOs(depe)_2(\eta^2\text{-}H_2)^+$	17.3	−0.60	317	71
23	*trans*-$(MeCN)Os(dppe)_2(\eta^2\text{-}H_2)^{2+}$	−2.0	0.58	321	74

dtfpe = $(4\text{-}CF_3C_6H_4)_2PCH_2CH_2P(4\text{-}CF_3C_6H_4)_2$, dppf = $(\eta^5\text{-}C_5H_4PPh_2)_2Fe$, dppp = $Ph_2PCH_2CH_2CH_2PPh_2$.

1.11.5 M–H Hydride Donor Strengths (Hydricities)

1.11.5.1 Thermochemical Cycles for M–H Hydricity Determination

DuBois and co-workers introduced the thermochemical cycle in Scheme 4 as a means to determine the hydride donor power (ΔG°_{H-}), or hydricity, of a cationic metal hydride.[61] The method requires the knowledge of metal–hydride acidity (pK_a) data and the electrode potentials for the oxidation of the metal–hydride conjugate base to two-electron oxidized counterpart, either by two successive one-electron processes (Equation (10), Scheme 4), or by one two-electron process (Equation (11), Scheme 4). The thermochemical cycle is derived from one that was introduced by Parker and co-workers for use in organic systems.[75] The accuracy of values on an absolute scale rests upon the

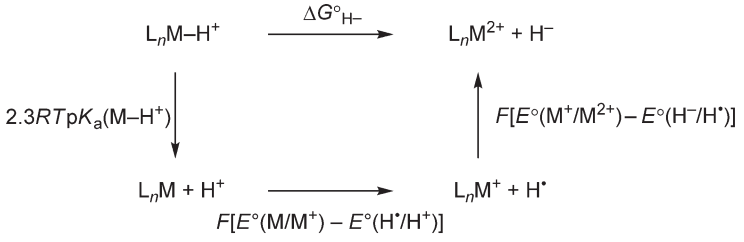

$$\Delta G^\circ_{H-} = 2.3RT\text{p}K_a(\text{M–H}^+,\text{solv}) + F[E^\circ(\text{M/M}^+,\text{solv}) + E^\circ(\text{M}^+/\text{M}^{2+},\text{solv})] + C \quad (10)$$

$$\Delta G^\circ_{H-} = 2.3RT\text{p}K_a(\text{M–H}^+,\text{solv}) + 2FE^\circ(\text{M/M}^{2+},\text{solv}) + C \quad (11)$$

Scheme 4 Thermochemical cycle for determination of metal–hydride hydricities from pK_a and electrode potential data. The quantity C in Equations (10) and (11), when electrode potentials and pK_a data are obtained in the same solvent and E° data are referred to the Cp_2Fe/Cp_2Fe^+ scale, is 333 kJ mol^{-1} (solv = MeCN) and 387 kJ mol^{-1} (solv = DMSO).

$$L_nM^{2+} + B + H_2 \overset{K_{het}}{\rightleftharpoons} L_nM{-}H^+ + BH^+ \quad (12)$$

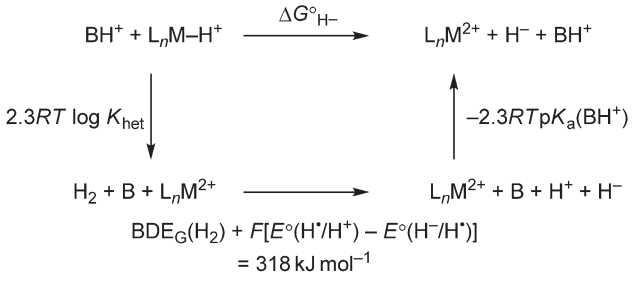

$$\Delta G^\circ_{H-} = 2.3RT \log K_{het} - 2.3RTpK_a(BH^+) + 318\ \text{kJ mol}^{-1} \quad (13)$$

Scheme 5 Thermochemical cycle for the determination of metal–hydride hydricities by heterolytic cleavage of H_2 in the presence of a metal hydride and a base. The term 318 kJ mol^{-1} represents the hydricity of H_2 in MeCN.

derivation of a value for $E^\circ(H^-/H^\cdot)$ in the solvent of choice. The constant term C differs from that in Equation (7), Scheme 3 in subtracting $T\Delta S$ for the hydrogen atom and adding $FE^\circ(H^-/H^\cdot)$ versus Fc.[66] The method has been used to establish a hydride acceptor scale for a wide range of carbenium ions,[66] which again have served as indicator references for determination of hydricities of group 5 (Nb, Ta)[76] and 6 (Mo, W)[77–79] hydrides by hydride-transfer equilibrium and calorimetric measurements.

It has also been demonstrated that metal–hydride hydricities can be determined from equilibrium measurements of base-induced, metal-promoted heterolytic cleavage of H_2. This method requires only the measurement of the equilibrium constant for heterolysis of H_2 in the presence of a base B with known basicity (Equation (12), Scheme 5). This technique does not require electrode potential measurements, but the thermochemical cycle that is shown in Scheme 5 reveals an obvious relationship to the cycles which have already been discussed; the constant term of 318 kJ mol^{-1} in Equation (13), Scheme 5 which yields the hydricity is derived from the $H^-/H^\cdot$ and $H^\cdot/H^+$ redox couples.

1.11.5.2 M–H Hydricity Data

Table 5 gives a comprehensive list of metal–hydride hydricities that have been determined with Equation (10) or Equation (11), Scheme 4 while hydricity data that have been determined with Equation (13), Scheme 5 are listed in Table 6. There is an excellent agreement between equivalent data obtained by these two methods. The data (the lower the number, the better the H^- donor) indicate that high hydride donating power for a given metal is favored by basic phosphine substituents and by smaller chelate rings. Larger rings cause a tetrahedral distortion and therefore destabilization of the ideally square-planar structures of the M(diphosphine)$_2^{2+}$ products of the hydride donation. A similar influence of the ring size on the pK_a data is not seen; it is therefore possible to independently influence the hydricity by chelate ring size variations.[65] The order of hydricities parallel trends in $E^\circ(M/M^{2+})$ but not trends in pK_a. For the Ni complexes (their homolytic BDEs as well as hydricities can be determined because the intermediate (diphosphine)$_2$Ni$^+$ oxidation state is observable by voltammetry), it is seen that the Ni–H BDEs correlate with $E^\circ(M/M^+)$ whereas ΔG°_{H-} data correlate with $E^\circ(M^+/M^{2+})$.[58,61] The entries for HM(PNP)$_2^+$ and HM(depe)$_2^+$ (M = Ni, Pd, Pt) in Tables 5 and 6 reveal a periodic trend in hydride donor powers that decrease in the order Pd > Pt > Ni. The metal–hydride acidities decrease in the order Pd ~ Ni > Pt. Thus, there is no direct, periodic correlation between hydricity and basicity among these group 10 metal complexes. It is surmised that the fact that Pd exhibits excellent proton and hydride donor properties may be related to the higher reactivity and catalytic activity that is seen for second-row transition metal complexes.[80]

The hydricity data established using the thermochemical cycles have been utilized in conjunction with hydride-transfer equilibrium measurements between various organometallic and organic molecules.[78,79]

Table 5 Metal–hydride acidities, conjugate base oxidation potentials, and hydricities in acetonitrile

Entry	*Metal hydride M–H*$^+$	pK_a (*M–H*$^+$)	$E°(M/M^+)$ (V vs. Fc)	$E°(M^+/M^{2+})$ (V vs. Fc)	$E°(M/M^{2+})$ (V vs. Fc)	$\Delta G°_{H-}$ (kJ mol^{-1})	*References*
1	$HCo(dppe)_2$	38.1	−2.02	−1.56		205	59
2	$HCo(dppe)_2^+$	23.6	−1.56	−0.70		250	59
3	$HRh(dppb)_2$	35.0[c]			−2.02	142[c]	81
4	$HNi(dppv)_2^+$	13.2	−0.83	−0.52		278	58
5	$HNi(dppe)_2^+$	14.2	−0.88	−0.70		262	61
6	$HNi(dmpp)_2^+$	23.9	−1.33	−0.89		256	61
7	$HNi(dedpe)_2^+$	20.3	−1.08	−0.99		250	58
8	$HNi(depp)_2^+$	23.3	−1.34	−0.58		281	62
9	$HNi(depe)_2^+$	23.8	−1.29	−1.16		234	61
10	$HNi(PNP)_2^+$	22.2	−1.24	−0.64		276	63
11	$HNi(dmpe)_2^+$	24.3			−1.35	212	61
12	$HPd(depe)_2^+$	23.2	−1.24[b]		−1.48	181	64
13	$HPd(PNP)_2^+$	22.1[c]			−1.21	214[c]	80
14	$HPd(depp)_2^+$	22.9	−1.22		−1.22	229	64
15	$HPd(depx)_2^+$	19.8	−1.02	−0.92		257	64
16	$HPd(depPE)_2^+$	18.3	−0.92	−0.73		278	64
17	$HPd(EtXanthphos)_2^+$	18.5	−0.94	−0.55		295	64
18	$HPt(PNP)_2^+$	27.6[c]			−1.36	229[c]	80
19	$HPt(dmpp)_2^+$	30.4[a]			−1.51	212	62
20	$HPt(depe)_2^+$	29.7[a]			−1.63	185	62
21	$HPt(dmpe)_2^+$	31.1[a]			−1.73	178	62
22	$HPt(dppe)_2^+$	22.2			−1.24	221	61
23	$HPt(EtXanthphos)_2^+$	27.3	−0.97	−0.81		318	65

[a]Originally reported pK_a values (Ref: 61) have been revised upward resulting in the listed $\Delta G°_{H-}$ data.
[b]Estimated from *E* vs. pK_a correlation data.
[c]pK_a value was determined from $\Delta G°_{H-}$ and $E°$ data.
dppb = $(Ph_2P)_2C_6H_4$.

Table 6 Hydricities of metal hydrides determined by base-induced metal-promoted heterolytic splitting of H_2 in acetonitrile

Entry	*Metal hydride M–H*$^+$	*Base B*	p$K_a(BH^+)$	K_{het}	$\Delta G°_{H-}$ (kJ mol^{-1})	*References*
1	$H_2Co(dppe)_2^+$	2,4-dichloroaniline	8.0	1.1	272	59
2	$HRh(dppb)_2$	$HPt(dmpp)_2^+$	30.4	2.4	142	81
3	$H_2Rh(depx)_2^+$	thioacetamide, benzamide	4.7, 3.7	0.13, 0.08	300[a]	60
4	$HRh(depx)_2$				190[b]	60
5	$HNi(dmpp)_2^+$	*p*-bromoaniline	9.6	0.016	253	62
6	$HNi(depp)_2^+$	2,4-dichloroaniline	8.0	7.7	277	62
7	$HNi(depe)_2^+$	anisidine	11.3	0.00052	234	62
8	$HNi(dmpe)_2^+$	triethylamine	18.5	0.49	213	62
9	$HPd(PNP)_2^+$				214[c]	80
10	$HPt(dmpp)_2^+$	triethylamine	18.5	1.7	213	62
11	$HPt(depp)_2^+$	morpholine	16.6	2.9	226	62
12	$HPt(dmpe)_2^+$	tetramethylguanidine	23.3	0.0089	176	62
13	$HPt(PNP)_2^+$	triethylamine	18.5	790	229	80

[a]Free energy of MeCN coordination during H^- transfer is included in the value which is therefore not transferable to other solvents.
[b]See reference for actual thermochemical cycle used.
[c]From hydride transfer equilibrium with $Pt(PNP)_2^{2+}$.

1.11.6 Consequences of One-electron Oxidation on M–H Bonding Energetics

1.11.6.1 Thermochemical Cycles for Determining Acidities and BDEs of One-electron Oxidized Metal Hydrides

The thermochemical cycle in Scheme 6 has been used to estimate the effect of a one-electron oxidation on the thermodynamic acidities of metal hydrides.[56] The method has been similarly used on organic systems.[82] Measurement of the oxidation potentials for the metal hydride and its conjugate base gives access to relative pK_a values for the metal hydride and its one-electron oxidized counterpart through Equation (14), Scheme 6. In many reported cases, one (or even both) electrode potentials are obtained from chemically irreversible voltammograms, with consequential uncertainties in the derived thermodynamic data. Table 7 gives a comprehensive list of M–H pK_a data comparing MH and MH^+ species as determined with this thermochemical cycle.

The thermochemical cycle in Scheme 7 has been used to estimate the effect of a one-electron oxidation on the BDEs of metal hydrides.[54,55] Similar methods have been applied to the study of C–H bonds.[83] Accurate determination of the BDE data through Equation (15), Scheme 7 requires electrode potential data for the oxidation of the parent metal hydride and of the metal fragment that is formed by its homolytic M–H cleavage. Table 7 gives a list of compounds that have been investigated. For entries 1–20, at least one of the underlying electrode potentials was for a chemically irreversible process; entries 21–24 are based entirely on reversible voltammograms.

1.11.6.2 Acidity and BDE Data of One-electron Oxidized Metal Hydrides

Table 7 summarizes BDE and pK_a data for metal hydrides whose BDEs and/or pK_a's have been experimentally compared in two adjoining oxidation states using the thermochemical cycles in Scheme 6 and Scheme 7. The data reveal that metal–hydride acidities increase by 15–30 pK_a units as a consequence of a one-electron oxidation; as might be expected, the increase is greatest for complexes that bear a positive charge before the oxidation and for those that bear electron-withdrawing ligands. Interestingly, the M–H bonds are weakened also in the homolytic sense (albeit to a lesser extent than toward H^+ loss) as a consequence of the one-electron oxidation. This applies to the oxidation of neutral as well as cationic (entry 24) closed-shell hydrides. It may be a contributing factor that homolysis of closed-shell species inevitably leads to metallaradicals, whereas homolysis of the one-electron oxidized species leads to an even-electron species which can gain stabilization by electron pairing; however, the spin state of the product will undoubtedly be important.[84]

1.11.6.3 Effect of One-electron Oxidations on M–X Bond Energies (X = Me, Halogen)

A straightforward adjustment of Scheme 7 by substituting "M–X" for "M–H" gives a thermochemical cycle that determines the effect of changing the oxidation state on the M–X BDE of any metal–X complex. Equation (16), Scheme 8 gives the pertinent expression and the only electrochemical parameters that are needed to provide relative M–X BDEs are $E°(M/M^+)$ and $E°(M–X/M–X^+)$ – that is, the consequences of a one-electron oxidation can be assessed for any M–X species provided that the two redox processes can be evaluated.

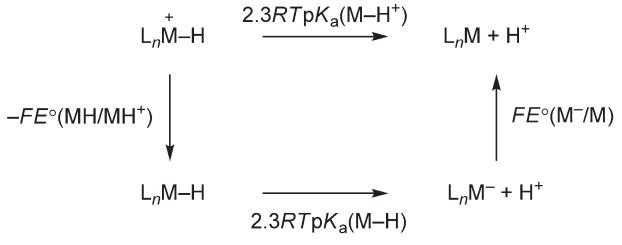

$$\Delta pK_a = pK_a(M–H^+) – pK_a(M–H) = (F/2.3RT)\,[E°(M^–/M) – E°(MH/MH^+)] \quad (14)$$

Scheme 6 Thermochemical cycle for the determination of the effect of one-electron oxidations on metal hydride acidities.

Table 7 pK_a and BDE data (kJ mol^{-1}) of metal hydrides and their one-electron oxidized analogs

Entry	*Metal hydride M–H*	$pK_a(M–H)$	$pK_a(M–H^+)$	ΔpK_a	*BDE(M–H)* (kJ mol^{-1})	*BDE(M–H$^+$)* (kJ mol^{-1})	*ΔBDE* (kJ mol^{-1})	*References*
1	$CpCr(CO)_3H$	13.3	−9.5	22.8	257	233	24	56
2	$CpCr(CO)_2(P(OMe)_3)H$	21.1	−2.4	23.5	262	216	46	54
3	$CpCr(CO)_2(PEt_3)H$	25.8	0.5	25.3	251	213	38	54
4	$CpCr(CO)_2(PPh_3)H$	21.8	−2.1	23.9	250	208	42	54
5	$Cp^*Cr(CO)_3H$	16.1	−7.2	23.3	261	227	34	54
6	$TpCr(CO)_3H$	<8			<215			55
7	$Tp'Cr(CO)_3H$	<8			<212			55
8	$CpMo(CO)_3H$	13.9	−6.0	19.9	290			56
9	$TpMo(CO)_3H$	10.7	−8.2	18.9	260	233	27	55
10	$Tp'Mo(CO)_3H$	9.7	−9.5	19.2	248	223	25	55
11	$CpW(CO)_3H$	16.1	−3.0	19.1	303			56
12	$CpW(CO)_2(PMe_3)H$	26.6	5.1	21.5	291			56
13	$TpW(CO)_3H$	14.4	−5.4	19.8	275	241	34	55
14	$Tp'W(CO)_3H$	12.9	−6.7	19.6	260	231	29	55
15	*trans*-$Cr(CO)_2(dppm)_2H^+$			30.0				85
16	*trans*-$Cr(CO)_2(dppe)_2H^+$			29.5				85
17	*trans*-$Mo(CO)_2(dppm)_2H^+$			27.9				85
18	*trans*-$Mo(CO)_2(dppe)_2H^+$			26.2				85
19	*trans*-$W(CO)_2(dppm)_2H^+$			28.8				85
20	*trans*-$W(CO)_2(dppe)_2H^+$			25.4				85
21	$Cp^*Fe(dppe)H$						51	86
22	$HCo(dppe)_2$	38.1	23.6	14.5	268[a]	229[a]	38	59
23	$HRh(depx)_2$	51.5	33.5[b]	18.0	316[a]	224[a,b]	92	60
24	$HPt(EtXanthphos)_2^+$	27.3	7.1	20.2	310[a]	209[a]	101	65

[a]A $T\Delta S°$ term of 21 kJ mol^{-1} has been added[66] to the BDE_G data given in the reference.
[b]See reference for thermochemical cycle that was used.

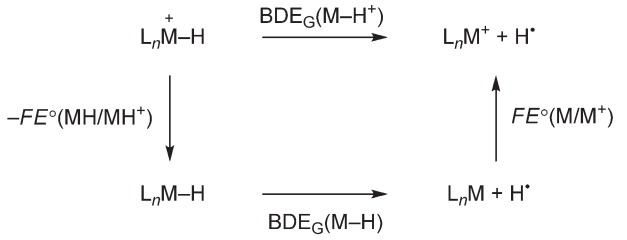

$$\Delta BDE = BDE(M–H^+) – BDE(M–H) = F\,[E°(M/M^+) – E°(MH/MH^+)] \quad (15)$$

Scheme 7 Thermochemical cycle for the determination of the effect of one-electron oxidations on metal hydride BDEs. It is assumed that $T\Delta S$ contributions to the two homolytic processes cancel.

$$\Delta BDE = BDE(M–X^+) – BDE(M–X) = F[E°(M/M^+) – E°(MX/MX^+)] \quad (16)$$

A thermochemical cycle can also be constructed to estimate differences in the heterolytic bond energies for removal of X^- from two neighboring oxidation states (Equation 17, Scheme 8).

Despite the simplicity of these schemes, data for such processes are still scarce. The sterically crowded, electron-rich $Cp^*Fe(dppe)$ moiety supports iron complexes in a great number of oxidation states and with electron counts from

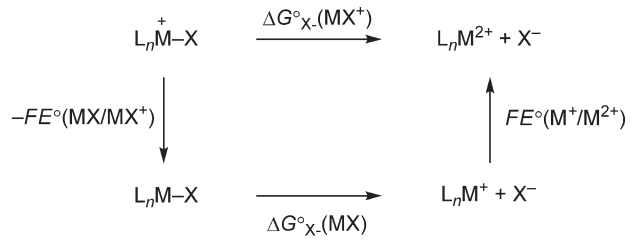

$$\Delta\Delta G°_{X\text{-}} = \Delta G°_{X\text{-}}(MX^+) - \Delta G°_{X\text{-}}(MX) = F\,[E°(M^+/M^{2+}) - E°(MX/MX^+)] \quad (17)$$

Scheme 8 Thermochemical cycle for the determination of differences in heterolytic bond energies for two adjoining oxidation states.

Table 8 Cyclic voltammetry[a] and derived ΔBDE data for Cp*Fe(dppe) complexes in THF/0.2M Bu_4NPF_6[38]

Compound FeX	$E°(FeX/FeX^+)$ (V vs. Fc)	$E°(FeX^+/FeX^{2+})$ (V vs. Fc)	$\Delta BDE(FeX/FeX^+)$ (kJ mol^{-1})	$\Delta BDE(FeX^+/FeX^{2+})$ (kJ mol^{-1})	$\Delta\Delta G°_{Fe–X}(FeX/FeX^+)$ (kJ mol^{-1})
$Cp^*Fe(dppe)^{\cdot}$	−1.27	−0.29			
$Cp^*Fe(dppe)H$	−0.75	0.75[b]	51	100	−44
$Cp^*Fe(dppe)Me$	−0.88	0.56[b]	38	82	−57
$Cp^*Fe(dppe)F$	−0.82	0.69	43	94	−52
$Cp^*Fe(dppe)Cl$	−0.62	0.82	63	107	−32
$Cp^*Fe(dppe)Br$	−0.58	0.81	67	106	−28
$Cp^*Fe(dppe)I$	−0.54	0.78	71	103	−24

[a]Reversible voltammograms unless otherwise noted.
[b]Peak potential for irreversible oxidation.

15 to 19. The relative BDEs of $Cp^*Fe(dppe)X$ complexes (X = H, Me, F, Cl, Br, I) have been investigated for the neutral Fe(II), monocationic Fe(III), and dicationic Fe(IV) oxidation states.[38,86] Table 8 gives the pertinent electrode potentials – all $E°$ values except that for generating the $Cp^*Fe(dppe)H^{2+}$ from its stable monocation precursor arise from chemically reversible, near-Nernstian cyclic voltammograms. Interestingly, the electrochemical data exhibit an "inverse halide order" – the ease of oxidation of MX to MX^+ decreases in the order F > Cl > Br > I, contrary to what might be anticipated from the electronegativities of X alone.[87–89] This phenomenon, experimentally manifested in diverse ways, has been interpreted in terms of X-to-M $p(\pi)$ to $d(\pi)$ bonding involving electron-pair donation from X to M,[90] with F rather unexpectedly acting as the best π-donor. This view was challenged when DFT calculations established that in the $Cp^*Fe(dppe)$ system, $p(\pi)$–$d(\pi)$ bonding was only a minor contributor to the effect, which was largely interpreted in terms of electrostatic (crystal field) interactions,[38] a notion that has later been supported by others.[91] The data show that the Fe–X bonds for all σ-bonded X ligands investigated in the $Cp^*Fe(dppe)$ series are homolytically weakened as a consequence of the one-electron oxidation. These findings were supported by IR $\nu_{Fe–X}$ data and DFT calculations; taken together with crystallography data for Fe–Cl and Fe–Cl^+, the Fe–X bonds appear to be shorter, yet homolytically weaker, in the Fe–X^+ species than in Fe–X. In a different system, not subjected to electrochemical investigation, it was suggested on the basis of IR and DFT results that the W–H bond in $Cp^*W(dppe)H_3$ is homolytically strengthened upon one-electron oxidation.[92] The oxidative heterolytic strengthening of the Fe–X bond toward dissociation of X^- is largely due to charge effects.[38]

1.11.7 Metal–Metal Bond Energies

Dinuclear complexes are ubiquitous to organometallic chemistry and serve as ultimate precursors for a wide range of compounds. Knowledge of their M–M BDEs would be extremely useful since the data could serve as anchors upon which other M–X BDEs could be based. Pugh and Meyer[93] (COMC 1995, Volume 6, 1.2.1.2.) devised a redox equilibration technique that enables the determination of M–M bond strengths. While this methodology apparently has not been further exploited since COMC (1995), it is nevertheless presented in Scheme 9 for the sake of completeness. The formal redox potential $E°(M_2/2M^-)$ for Equation (18), Scheme 9 was derived (Equation (19),

$$L_nM\text{–}ML_n + Red \underset{}{\overset{K_{eq}}{\rightleftharpoons}} 2L_nM^- + Red^+ \quad (18)$$

$$E^{\circ\prime}(M_2/2M^-) = E^{\circ}(Red/Red^+) + (RT/2F)\ln K_{eq} \quad (19)$$

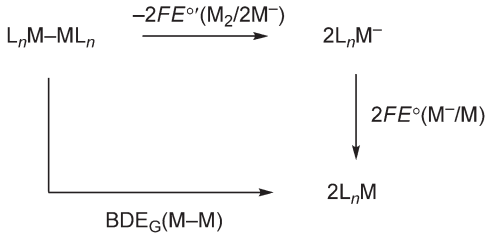

$$BDE_G(M\text{–}M) = 2FE^{\circ}(M^-/M) - 2FE^{\circ\prime}(M_2/2M^-) \quad (20)$$

Scheme 9 M–M BDE from redox equilibrium and electrode potential measurements.

Scheme 9) from measured redox equilibrium constants using suitable reducing agents "Red". The potentials were combined with the anion oxidation potentials to give the M–M BDE_G value from Equation 20, Scheme 9. The BDE_G data ($Mn_2(CO)_{10}$, 117 kJ mol^{-1}; $Cp_2Mo_2(CO)_6$, 92 kJ mol^{-1}; $Cp_2Fe_2(CO)_4$, 105 kJ mol^{-1}) can be converted to enthalpy-based BDE values if the entropy changes are available; this resulted in a Mn–Mn BDE of 159 kJ mol^{-1}. It is noteworthy that reversible anion oxidation potentials for this purpose were obtained by rapid-scan CV at 5000 V s^{-1} with a 10 μm electrode (although very broadened waves were observed).

1.11.8 Energetics of Ligand C–H Bonding

The coordination of a ligand at a metal center dramatically influences the properties of the ligand. This is a major reason why metal-mediated, stoichiometric or catalytic, transformations have gained their present prominent position in chemistry. Despite this fact, relatively few quantitative studies of bonding energetics in relevant systems have been probed by electrochemical methods.

1.11.8.1 C–H BDEs in π-Coordinated Ligands

The thermochemical cycle that led to Equation (7), Scheme 3 was a modification of a cycle that was devised for estimating C–H BDEs in organic molecules. Accordingly, it is directly applicable to investigate the properties of C–H bonds in coordinated ligands.

Zhang and Bordwell[94] evaluated the effects of η^6-coordination of fluorene at $Cr(CO)_3$, $Mn(CO)_3^+$, and $CpFe^+$ moieties in DMSO (Equation (21)). Coordination at the electron-withdrawing metal centers increased the acidity of fluorene by 5.6, 16.9, and 8.0 pK_a units, respectively. On the other hand, the C–H BDEs remained rather constant around 335 kJ mol^{-1}. Presumably, the opposing contributions from basicity and anion oxidation potentials cause a cancelation of effects in much the same way as was seen for simple ligand replacements at metal hydrides in Section 1.11.4.

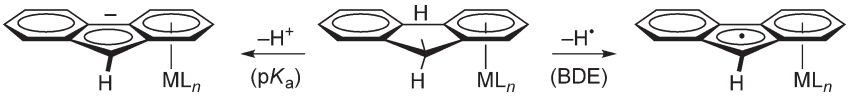

(21)

Similar effects were noted by Astruc and co-workers[95,96] who quantified the effect on benzylic C–H bond strengths and acidities when substituted η^6-coordinated arenes C_6Me_6, $C_6H_5CH_2Ph$, $C_6H_5CHPh_2$, and fluorene were coordinated at the $CpFe^+$ (all arenes) or Cp^*Fe^+ (C_6Me_6 only) moieties. For example, the pK_a of hexamethylbenzene was lowered by 14 units upon coordination at $CpFe^+$ (Equation (22)) according to equilibrium measurements in DMSO.

The benzylic C–H BDE was calculated from a modified Equation (7), Scheme 3 using $E^{\circ}(Cp^{*}Fe(C_6Me_5{=}CH_2)^{0/+})$ and the C value for DMSO, and remained essentially unchanged at 362 kJ mol^{-1}.

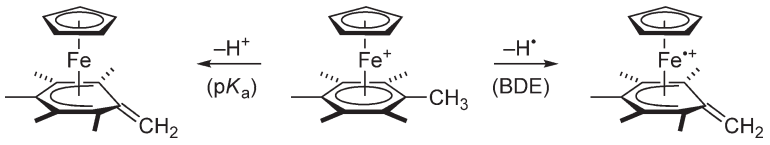

(22)

The capacity of the Cp(*)Fe(arene) moieties to stabilize multiple oxidation states[97] made it possible to quantify C–H acidities and BDEs of the coordinated arenes in several adjoining oxidation states. Table 9 summarizes the pertinent thermochemical data, while Scheme 10 depicts the data for the $CpFe(C_6Me_6)$ series in particular. In Table 9, entries 1–5 are the reference compounds that have readily measured E° values for the reduction as well as for the oxidation, while their pK_a's were established by proton-transfer equilibrium measurements with bases of known pK_a. Their conjugate bases, entries 26–30, are also stable and provided well-defined E° data for the reductions and mostly irreversible waves for the oxidations. The derivation of pK_a and BDE data was based on variations in Schemes 3–5. For example, the benzylic BDE of entry 1 is obtained from its pK_a and the oxidation potential for its conjugate base (entry 26) using a modified Equation (7), Scheme 3, with the C value for DMSO. The pK_a data for the other oxidation states are obtained from the pertinent electrode potentials and a modified Equation (14), Scheme 6, and the BDE data are similarly obtained using a modified Equation (15), Scheme 7. This strategy provided pK_a and benzylic C–H BDE values for the series of complexes in which the oxidation state of Fe ranges from 0 to +4, with electron counts from 20 to 16. Assumptions and approximations lead to significant uncertainties in BDEs and pK_a's that are derived from E° data involving highly charged species (see the original paper for a discussion), but the data nevertheless allow some conclusions to be drawn regarding systematic trends:[97] (i) Arene coordination at the $CpFe^{+}$ and $Cp^{*}Fe^{+}$ moieties enhance the benzylic C–H acidity by 12–14 pK_a units while the BDEs are rendered essentially unchanged in the cationic 18e species. (ii) The neutral 19-electron (19e) species have acidities comparable to the parent hydrocarbons whereas the BDEs are lowered by ca. 88 kJ mol^{-1} presumably because loss of H$^{\cdot}$ gives a stable 18e species. (iii) The acidities decrease by 18 pK_a units in the 20e species because of the negative charge while the BDEs are essentially unchanged from their values in the 19e species. (iv) The acidities are enhanced by ca. 40 pK_a units in the 17e dications compared to the 18e species, and the BDEs are the weakest in the series. (v) The acidities increase by another 40–50 pK_a units in the 16e triply charged cations.

1.11.8.2 C–H BDEs in σ-Coordinated Ligands

There appear to be remarkably few quantitative studies pertaining to C–H BDEs in σ-coordinated ligands.

1.11.8.2.1 C–H BDE of an Nb acetyl ligand

Bruno and co-workers[23] measured the pK_a of the α-C–H bond in the acyl ligand of $Cp'_2NbCl(\eta^2\text{-}COCHEtPh)^{+}$ as 10.4 by equilibrium measurements in MeCN, a value considerably lower than that for regular ketones (Equation (23)). The irreversible oxidation of the conjugate base, the neutral ketene complex (left), occurred at 0.24 V versus Fc. Modified Equation (7), Scheme 3 then yielded a C–H BDE of the coordinated acyl group of 343 kJ mol^{-1}, subject to uncertainty due to an unknown kinetic potential shift. The BDE is in the range that is typical for comparably substituted ketones.[101] Thus, metal coordination of the acyl group significantly enhanced the C–H acidity but did not homolytically weaken the C–H bond compared to ordinary ketones.[23]

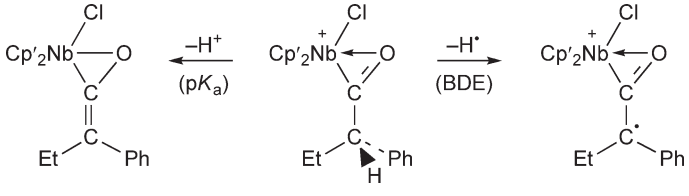

(23)

Table 9 Redox potentials, pK_a, and benzylic BDE data for Cp(*)Fe(arene) complexes in five oxidation states[96]

Entry		*Compound L_nFe*	*$E°(L_nFe^-/L_nFe)$* (V vs. Fc)	*$E°(L_nFe/L_nFe^+)$* (V vs. Fc)	*p$K_a(L_nFe)$* (DMSO)	*C–H BDE* (kJ mol^{-1})
1	18e	$CpFe(\eta^6\text{-}C_6Me_6)^+$	−1.99	1.25	29.2	362
2		$Cp^*Fe(\eta^6\text{-}C_6Me_6)^+$	−2.22	1.03	31.4	347
3		$CpFe(\eta^6\text{-}C_6H_5CH_2Ph)^+$	−1.80	1.61	20.0[98]	347
4		$CpFe(\eta^6\text{-}C_6H_5CHPh_2)^+$	−1.74	1.61	18.2	345
5		$CpFe(\eta^6\text{-fluorene})^+$	−1.77	1.49	14.6[94]	335
6	19e	$CpFe(\eta^6\text{-}C_6Me_6)$	−2.77	−1.99	43.5	282
7		$Cp^*Fe(\eta^6\text{-}C_6Me_6)$	−3.00	−2.22	46.4	272
8		$CpFe(\eta^6\text{-}C_6H_5CH_2Ph)$	−2.55	−1.80	32.9	248
9		$CpFe(\eta^6\text{-}C_6H_5CHPh_2)$	−2.56	−1.74	32.5	242
10		$CpFe(\eta^6\text{-fluorene})$	−2.69	−1.77	23.9	220
11	20e	$CpFe(\eta^6\text{-}C_6Me_6)^-$		−2.77	61.4	285
12		$Cp^*Fe(\eta^6\text{-}C_6Me_6)^-$		−3.00	61.4	282
13		$CpFe(\eta^6\text{-}C_6H_5CH_2Ph)^-$		−2.55	46.2	249
14		$CpFe(\eta^6\text{-}C_6H_5CHPh_2)^-$		−2.56	46.5	248
15		$CpFe(\eta^6\text{-fluorene})^-$		−2.69	32.8	184
16	17e	$CpFe(\eta^6\text{-}C_6Me_6)^{2+}$	1.25	2.83	−11.6	202
17		$Cp^*Fe(\eta^6\text{-}C_6Me_6)^{2+}$	1.03	2.61	−8.5	201
18		$CpFe(\eta^6\text{-}C_6H_5CH_2Ph)^{2+}$	1.61	3.19	−18.5	203
19		$CpFe(\eta^6\text{-}C_6H_5CHPh_2)^{2+}$	1.61	3.19	−19.1	197
20		$CpFe(\eta^6\text{-fluorene})^{2+}$	1.49	3.07	−20.0	213
21	16e	$CpFe(\eta^6\text{-}C_6Me_6)^{3+}$	2.83		−53.7	
22		$Cp^*Fe(\eta^6\text{-}C_6Me_6)^{3+}$	2.61		−50.5	
23		$CpFe(\eta^6\text{-}C_6H_5CH_2Ph)^{3+}$	3.19		−71.5	
24		$CpFe(\eta^6\text{-}C_6H_5CHPh_2)^{3+}$	3.19		−72.0	
25		$CpFe(\eta^6\text{-fluorene})^{3+}$	3.07		−68.6	
26		$CpFe(\eta^6\text{-}C_6Me_5CH_2)$	−2.80, −3.58	−1.16, −0.41		
27		$Cp^*Fe(\eta^6\text{-}C_6Me_5CH_2)$	−3.11, −3.89	−1.34, −0.59		
28		$CpFe(\eta^6\text{-}C_6H_5CHPh)$	−2.56, −3.31	−0.67, 0.05		
29		$CpFe(\eta^6\text{-}C_6H_5CPh_2)$	−2.61, −3.43	−0.68, 0.07		
30		$CpFe(\eta^6\text{-fluorenyl})$	−2.32, −3.24	−0.56, 0.19		
31		$PhCH_3$			43[99]	366[100]
32		Ph_2CH_2			32.3[99]	343[49]
33		Ph_3CH			30.6[99]	339[49]
34		Fluorene			22.6[99]	335[49]

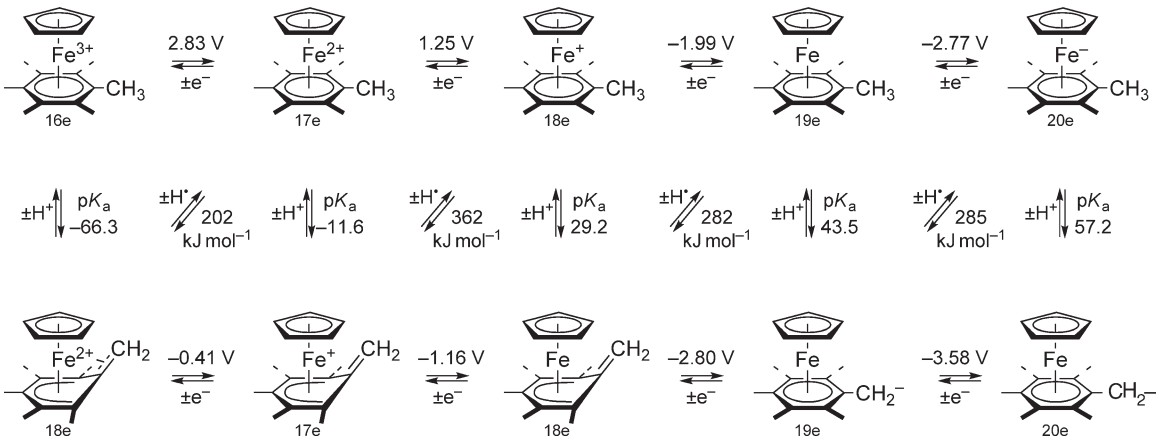

Scheme 10 Interrelation and energetics of electron transfer, proton transfer, and hydrogen atom transfer reactions of $CpFe(C_6Me_6)^n$ complexes in five different oxidation states. Adapted from Trujillo, H. A.; Casado, C. M.; Ruiz, J.; Astruc, D. *J. Am. Chem. Soc.* **1999**, *121*, 5674–5686, with permission from American Chemical Society.

1.11.8.3 C–H BDE of an Nb Methoxy Ligand

The methoxy group of $Cp'_2Nb(Cl)(OCH_3)^+$ (Equation (24)) has a pK_a of 10.1 in MeCN – some 50 units lower than the pK_a of $PhOCH_3$. The conjugate base, the neutral formaldehyde complex (left), was reversibly oxidized at −0.07 V versus Fc, resulting by modified Equation (7) from Scheme 3 in a C–H BDE of 301 kJ mol^{-1} in the coordinated methoxy group.[23] Thus, the Nb center has weakened the C–H bond by a substantial 92 kJ mol^{-1} when compared to the C–H BDE of 393 kJ mol^{-1} in methanol.[102]

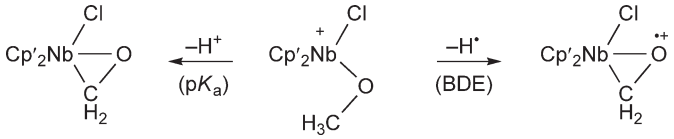

(24)

1.11.8.3.1 C–H BDEs of Re formyl ligands

The hydride complex $HPt(dmpe)_2^+$ (Table 5, entry 21 and Table 6, entry 12) reversibly transferred H^- to $CpRe(NO)(CO)(PMe_3)^+$ (Equation (25)). From equilibrium measurements, the hydricity of $CpRe(NO)(PMe_3)(CHO)$ was determined to be 185 kJ mol^{-1}. This served as an anchoring point for the determination of formyl ligand hydricities ΔG°_{H-} in the range 185–230 kJ mol^{-1} for a series of Mn, Re, and Ru formyl complexes.[103] The Re carbonyl cations underwent reversible reduction by CV and the C–H BDEs in the coordinated formyl ligands could be determined with the thermochemical cycle in Scheme 11 (see also Equations (26) and (27)). The formyl C–H BDEs that were measured are listed in Table 10. The BDEs are essentially constant in this series of complexes as a result of compensating contributions from ligand electronic effects on Re–CHO hydricities and E°(M–CO/M–CO$^+$). The data corroborate the common perception that formyl complexes have inherently weak H–CO bonds; these bonds are indeed weakened by about 140 kJ mol^{-1} compared with typical bond strengths in aldehydes.

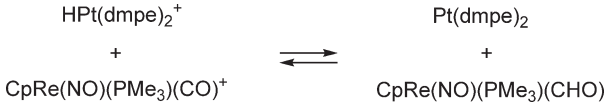

(25)

1.11.9 Selected Applications

1.11.9.1 Hydrogenation of Carbon Monoxide

The hydricities of $HW(CO)_4L^-$ (L = CO, $P(OMe)_3$, PPh_3) have been established by equilibrium and calorimetry measurements in acetonitrile, and the mechanism and thermodynamics of their hydride transfer to $Cp^*Re(NO)(PMe_3)(CO)^+$ to yield $Cp^*Re(NO)(PMe_3)(CHO)$ was investigated.[78] The thermodynamic data on hydricities of metal hydrides and metal formyl complexes enabled DuBois and co-workers to design a system that hydrogenates a CO ligand with H_2 as the hydrogen source.[103] In this system, $Pt(dmpp)^{2+}$ heterolytically activates H_2 rapidly in the presence of "proton sponge" (1,8-bis(dimethylamino)naphthalene) as a base. The resulting Pt hydride,

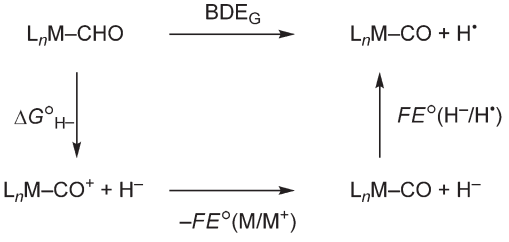

$$BDE_G = \Delta G^\circ_{H-} - F[E^\circ(M/M^+) + E^\circ(H^-/H^\bullet)] = \Delta G^\circ_{H-} - FE^\circ(M/M^+) - 109\ \text{kJ mol}^{-1} \quad (26)$$

$$BDE = BDE_G + T\Delta S^\circ = \Delta G^\circ_{H-} - FE^\circ(M/M^+) - 88\ \text{kJ mol}^{-1} \quad (27)$$

Scheme 11 Thermochemical cycle for the determination of C–H BDEs of coordinated formyl ligands. The constant terms apply when electrode potentials are referenced to the Fc couple in acetonitrile.

Table 10 C–H BDEs and hydricities of metal formyl complexes

Formyl M–CHO	$E^{\circ}(M\text{–}CO/M\text{–}CO^{+})$ (V vs. Fc)	*Formyl hydricity*[103] ΔG°_{H-} (kJ mol^{-1})	*Formyl C–H BDE*[103] (kJ mol^{-1})
CpRe(NO)(CO)(CHO)	−0.88	230	227[a]
Cp^{*}Re(NO)(CO)(CHO)	−0.97	220	226[a]
CpRe(NO)(PPh_3)(CHO)	−1.34	195	236[a]
CpRe(NO)(PMe_3)(CHO)	−1.46	185	237[a]
CpRe(NO)(PEt_3)(CHO)	−1.46	183	236[a]
R-CHO (R = H, Me, CF_3, Ph)			368–385[102,104]

[a]A $T\Delta S^{\circ}$ term of 21 kJ mol^{-1} has been added[66] to the BDE_G data given in the reference in order to provide enthalpy-based BDEs.

$HPt(dmpp)^{+}$, has a thermodynamic and kinetic hydricity that is sufficient for the transfer of H^{-} to coordinated CO in $CpRe(NO)(CO)_2^{+}$ and $Cp^{*}Re(NO)(CO)_2^{+}$ to give the respective Re formyl complexes (Equation (28)). The overall reaction is in principle catalytic with respect to Pt. Although the yields were low (9%), the design of this system demonstrated how access to relevant thermodynamic data may facilitate rational catalyst design.

$$\begin{aligned} &H_2 + Pt(dmpp)_2^{2+} + Base \longrightarrow HPt(dmpp)_2^{+} + BaseH^{+} \\ &HPt(dmpp)_2^{+} + CpRe(NO)(CO)_2^{+} \longrightarrow Pt(dmpp)_2^{2+} + CpRe(NO)(CO)(CHO) \end{aligned} \tag{28}$$

1.11.9.2 Stability of Metal Hydrides toward Disproportionation and H_2 Loss

The combination of acidity and hydricity data for metal hydrides can be used to evaluate and better understand factors that govern stabilities of metal hydrides with respect to disproportionation and H_2 loss. It is obvious that a metal hydride will be unstable with respect to deprotonation in the presence of a base B if the pK_a of BH^{+} is greater than the pK_a of the metal hydride. Similarly, Equation (13), Scheme 5 can be used to determine whether a metal hydride with a known hydricity will react with an acid BH^{+} of known pK_a to generate H_2. Thus, the pK_a of the acid that causes Equation (12), Scheme 5 to be in equilibrium with $K_{het} = 1$ will be given by pK_{BH+} in Equation (29). Acids that have a pK_a below this value will protonate the corresponding metal hydride to give H_2. Thus, it is possible to predict a range of pK_a's for acids and bases in whose presence a metal hydride will be thermodynamically stable with respect to protonation/H_2 loss and with respect to deprotonation.[58]

$$pK_{BH+} = (318 - \Delta G^{\circ}_{H-})/5.70 \tag{29}$$

This stability range of pK_a's has been evaluated for Ni[58] and Pd[64,80] hydrides. For the Ni hydrides, the pK_a stability range encompasses 6–13 pK_a units depending on the particular ligand system. On the other hand, the fact that many Pd hydrides are good acids and good hydride donors (see Section 1.11.5.2) causes these Pd hydrides to be stable toward acids and bases only in a narrow pK_a range, offering an explanation for the frequently encountered difficulty of isolating such Pd hydrides.[80] For example, $HPd(dppe)_2^{+}$ was prepared from $Pd(dppe)_2$ and triflic acid in THF, from which it precipitated.[105] Upon dissolution in acetonitrile, the Pd hydride underwent disproportionation to form H_2, $Pd(dppe)_2$, and $Pd(dppe)_2^{2+}$. The acidity and hydricity data for $HPd(dppe)_2^{+}$ are not known. However, data for $HPd(PNP)_2^{+}$ (Table 5, entry 13) lead to a narrow (4 pK_a units) stability window for this hydride in the presence of acids or bases.[80] Similarly, the pK_a of $HPd(depe)_2^{+}$ (Table 5, entry 12) is 23.2 and pK_{BH+} according to Equation (29) is 23.9; consistent with this, $HPd(depe)_2^{+}$ is unstable with respect to disproportionation and indeed establishes the equilibrium in Equation (30) in benzonitrile solution.[64]

$$Pd(depe)_2 + Pd(depe)_2^{2+} + H_2 \rightleftharpoons 2HPd(depe)_2^{+} \tag{30}$$

1.11.9.3 Reactions Related to Enzyme Catalysis

The formal transfer of hydride is a fundamental reaction in biological catalysis. The Re formyl complex CpRe(NO)(CO)(CHO), the hydricity of which was determined by equilibrium measurements (Equation (25)), engaged in a reversible hydride transfer with an NAD/NADH model system, $BzNAD^{+}$/BzNADH (Equation (31)).

This allowed the determination of a new and significantly revised value, $\Delta G^{\circ}_{H-} = 247\,\text{kJ mol}^{-1}$, for the hydricity of BzNADH in acetonitrile.[79] Interestingly, this value was in turn used to re-evaluate the hydricities of $CpMo(CO)_3H$ derivatives in acetonitrile.[79]

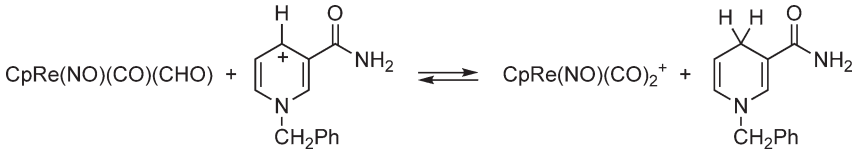

(31)

The Ni complex $Ni(PNP)_2^{2+}$ was investigated as a potential functional model for the NiFe class of hydrogenases.[63] The molecular design comprises the bis(diphosphine)Ni motif that enabled heterolytic activation of H_2 in the presence of bases, as well as a built-in base at the two bridging N atoms of the chelate ligand. Proton-transfer equilibrium measurements established the pK_a of $HNi(PNP)_2^+$ as 22.2 in acetonitrile (Table 5, entry 10); a second protonation occurred in the presence of stronger acids and resulted in the *N*-protonated complex $HNi(PNP)(PNHP)^{2+}$ with a pK_a of 10.6 for the N–H proton. The first pK_a and electrochemical data established the hydricity ΔG°_{H-} as 276 kJ mol^{-1} from Equation (10), Scheme 4; inserting ΔG°_{H-} and the second (N–H) pK_a into Equation (13), Scheme 5 leads to the prediction that, based on thermodynamics, $Ni(PNP)_2^{2+}$ should be capable of heterolytically cleaving H_2 using its own built-in N-base as the proton acceptor with $\Delta G^{\circ}_{reaction} = -21\,\text{kJ mol}^{-1}$ in acetonitrile. Indeed, this prediction was corroborated by experiment (Equation (32)). An investigation of the CV behavior of $HNi(PNP)_2^+$ was consistent with the overall reactivity in Scheme 12. Here, oxidation of $HNi(PNP)_2^+$ gives the Ni(+3) species $HNi(PNP)_2^{2+}$ which transfers the Ni–H proton to the N atom of the PNP ligand. External NEt_3 as a base effects deprotonation from the ligand N–H, yielding $Ni(PNP)_2^+$ which undergoes a second oxidation to furnish $Ni(PNP)_2^{2+}$. This species is capable of activating H_2, which after another deprotonation by external NEt_3 closes the cycle. The overall Scheme 12 is the Ni-catalyzed electrooxidation of H_2 to protons. The catalytic nature of the system was demonstrated with bulk electrolysis of acetonitrile solutions of $Ni(PNP)_2^{2+}$ in the presence of H_2 and NEt_3 at potentials sufficiently high to oxidize $HNi(PNP)_2^+$. 15 mol H^+ were produced per mol catalyst after 6 h. No enhanced (catalytic) currents were observed by CV; the apparent slowness of the reaction was attributed to inefficient reaction between $Ni(PNP)_2^{2+}$ and H_2 on the voltammetric timescale.

(32)

1.11.10 Square Schemes and Redox-Induced Structural Changes

Square schemes related to those discussed in the previous sections have been applied to investigate kinetic, thermodynamic, and mechanistic aspects of redox-induced structural changes in organometallic complexes. The topic has been recently reviewed[106–108] and will be illustrated with only one recent example as a demonstration of principle. The general features of the method are given in Scheme 13. Here, **A** and **B** represent two isomeric,

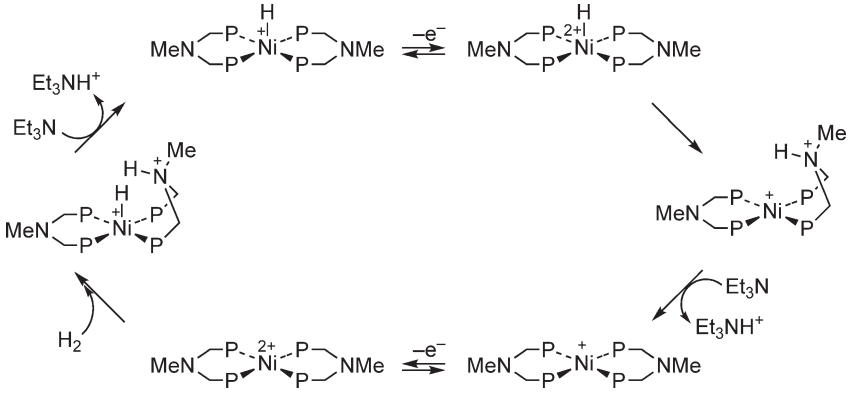

Scheme 12 Proposed mechanism for Ni-catalyzed electrooxidation of H_2 to protons.[63]

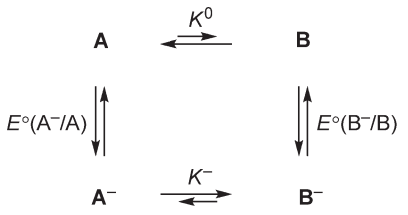

$$-2.3RT \log K^0 = F[E°(B^-/B) - E°(A^-/A)] - 2.3RT \log K^- \quad (33)$$

$$\log (K^0/K^-) = 16.9[E°(B^-/B) - E°(A^-/A)] \quad (34)$$

Scheme 13 Generalized square scheme for redox-induced isomerizations.

equilibrating forms of a metal complex. Whereas **A** is the thermodynamically preferred isomer in the oxidized form, it is $\mathbf{B}^-$ that is preferred in the reduced state. The reduction of **A** to give $\mathbf{B}^-$ may occur via **B** in a stepwise fashion, as depicted here, or in a one-step process in which the structural changes occur in concert with the electron transfer (the latter is a situation that typically may cause non-Nernstian electron transfer).[109] The energetics of the process obtained from the square scheme is given by Equation (33), Scheme 13 and leads to the ratio between the equilibrium constants K^0 and K^- in Equation (34), Scheme 13.[108] Thus, if $E°(\mathbf{A}^-/\mathbf{A})$ and $E°(\mathbf{B}^-/\mathbf{B})$ can be measured or estimated, the relative magnitudes of the two K values can be determined. The analysis of such a scheme is often far from trivial as it usually involves the interpretation of complex voltammograms being characterized by non-Nernstian electron transfer, homogeneous reaction kinetics in both oxidation states, competing reaction pathways, cross electron transfer between **A** and $\mathbf{B}^-$, and so on. A full analysis usually requires the use of complementary electrochemical techniques and digital simulation of the voltammetry response, and will not be described here.

As an example, consider the neutral $(\eta^5\text{-}C_5Ph_5)Rh(\eta^4\text{-}C_8H_8)$ complex (Scheme 14) which prefers the 1,5- rather than 1,3-bonding of the cyclooctatetraene ligand with an estimated equilibrium constant $K(1,5/1,3)^0 = 65$.[109] Upon reduction, rapid isomerization for which the kinetics was elucidated occurs to provide the preferred 1,3-bonding in the anion; $K(1,5/1,3)^- = 1.2 \times 10^{-5}$. The ratio between the two K values corresponds to an $E°$ difference of 0.395 V between $E°(1,3/1,3^-)$ and $E°(1,5/1,5^-)$. This translates to a stabilization of the anionic Rh(0) species by 38 kJ mol^{-1} by the 1,3-coordination mode compared to the 1,5-mode, relative to the situation in the neutral Rh(+1) complex.

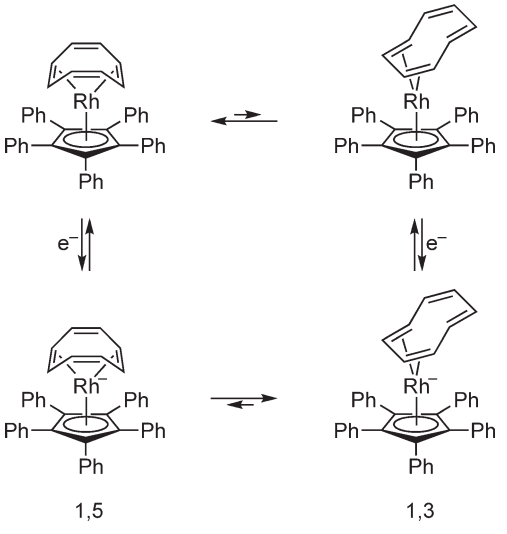

Scheme 14 Square scheme for redox-induced isomerization of $(\eta^5\text{-}C_5Ph_5)Rh(\eta^4\text{-}C_8H_8)$.

References

1. da Piedade, M. E. M. *Energetics of Stable Molecules and Reactive Intermediates*; NATO Science Series; Kluwer: Dordrecht, 1999; Vol. C535.
2. Simões, J. A. M. *Energetics of Organometallic Species*; NATO Science Series; Kluwer: Dordrecht, 1992; Vol. C367.
3. Marks, T. J. *Bonding Energetics in Organometallic Compounds*; ACS Symposium Series 428; American Chemical Society: Washington, DC, 1990.
4. Balzani, V. *Electron Transfer in Chemistry: Organic, Organometallic, and Inorganic Molecules*; Wiley-VCH: New York, 2001; Vol. 2.
5. Astruc, D. *Electron Transfer and Radical Processes in Transition-Metal Chemistry*; VCH: Weinheim, 1995.
6. Pombeiro, A. J. L.; McCleverty, J. A. *Molecular Electrochemistry of Inorganic, Bioinorganic and Organometallic Compounds*; NATO Science Series; Kluwer: Dordrecht, 1993; Vol. C385.
7. Bard, A. J.; Faulkner, L. R. *Electrochemical Methods: Fundamentals and Applications*, 2nd ed.; Wiley: New York, 2001.
8. Sawyer, D. T.; Sobkowiak, A.; Roberts, J. L., Jr. *Electrochemistry for Chemists*, 2nd ed.; Wiley: New York, 1995.
9. Hammerich, O. Methods for Studies of Electrochemical Reactions. In *Organic Electrochemistry*; 4th ed.; Lund, H., Hammerich, O., Eds.; Dekker: New York, 2001; pp 95–182.
10. Evans, D. H. *Chem. Rev.* **1990**, *90*, 739–751.
11. Kissinger, P. T.; Heineman, W. R. *Laboratory Techniques in Electroanalytical Chemistry*, 2nd ed.; Dekker: New York, 1996.
12. Mayer, J. M. *Annu. Rev. Phys. Chem.* **2004**, *55*, 363–390.
13. Mayer, J. M. *Acc. Chem. Res.* **1998**, *31*, 441–450.
14. Bryant, J. R.; Mayer, J. M. *J. Am. Chem. Soc.* **2003**, *125*, 10351–10361.
15. Larsen, A. S.; Wang, K.; Lockwood, M. A.; Rice, G. L.; Won, T. J.; Lovell, S.; Sadilek, M.; Turecek, F.; Mayer, J. M. *J. Am. Chem. Soc.* **2002**, *124*, 10112–10123.
16. Wightman, R. M.; Wipf, D. O. *Acc. Chem. Res.* **1990**, *23*, 64–70.
17. Battaglini, F.; Calvo, E. J.; Doctorovich, F. *J. Organomet. Chem.* **1997**, *547*, 1–21.
18. Andrieux, C. P.; Hapiot, P.; Saveant, J. M. *Chem. Rev.* **1990**, *90*, 723–738.
19. Heinze, J. *Angew. Chem., Int. Ed. Engl.* **1993**, *32*, 1268–1288.
20. Gosser, D. K., Jr. *Cyclic Voltammetry: Simulation and Analysis of Reaction Mechanisms*; VCH: New York, 1993.
21. Rudolph, M.; Reddy, D. P.; Feldberg, S. W. *Anal. Chem.* **1994**, *66*, 589A–600A.
22. Tilset, M. *Inorg. Chem.* **1994**, *33*, 3121–3126.
23. Kerr, M. E.; Zhang, X.-M.; Bruno, J. W. *Organometallics* **1997**, *16*, 3249–3251.
24. Hills, G. J. *Reference Electrodes*; Ives, D., Janz, J. G., Eds.; Academic Press: New York, 1961.
25. Coetzee, J. F.; Padmanabhan, G. R. *J. Phys. Chem.* **1962**, *66*, 1708–1713.
26. Ruiz, J.; Astruc, D. *C. R. Acad. Sci. Paris, Ser. 2c* **1998**, *1*, 21–27.
27. Gritzner, G.; Kuta, J. *Pure Appl. Chem.* **1984**, *56*, 461–466.
28. Connelly, N. G.; Geiger, W. E. *Chem. Rev.* **1996**, *96*, 877–919.
29. Strauss, S. H. *Chem. Rev.* **1993**, *93*, 927–942.
30. Reed, C. A. *Acc. Chem. Res.* **1998**, *31*, 133–140.
31. Gassman, P. G.; Sowa, J. R., Jr.; Hill, M. G.; Mann, K. R. *Organometallics* **1995**, *14*, 4879–4885.
32. LeSuer, R. J.; Geiger, W. E. *Angew. Chem., Int. Ed.* **2000**, *39*, 248–250.
33. Stone, N. J.; Sweigart, D. A.; Bond, A. M. *Organometallics* **1986**, *5*, 2553–2555.
34. Camire, N.; Nafady, A.; Geiger, W. E. *J. Am. Chem. Soc.* **2002**, *124*, 7260–7261.
35. Trupia, S.; Nafady, A.; Geiger, W. E. *Inorg. Chem.* **2003**, *42*, 5480–5482.
36. Ohrenberg, C.; Geiger, W. E. *Inorg. Chem.* **2000**, *39*, 2948–2950.
37. LeSuer, R. J.; Buttolph, C.; Geiger, W. E. *Anal. Chem.* **2004**, *76*, 6395–6401.
38. Tilset, M.; Fjeldahl, I.; Hamon, J.-R.; Hamon, P.; Toupet, L.; Saillard, J. Y.; Costuas, K.; Haynes, A. *J. Am. Chem. Soc.* **2001**, *123*, 9984–10000.
39. Barriere, F.; Camire, N.; Geiger, W. E.; Mueller-Westerhoff, U. T.; Sanders, R. *J. Am. Chem. Soc.* **2002**, *124*, 7262–7263.
40. Wayner, D. D. M.; Parker, V. D. *Acc. Chem. Res.* **1993**, *26*, 287–294.
41. Breslow, R.; Chu, W. *J. Am. Chem. Soc.* **1973**, *95*, 411–418.
42. Breslow, R.; Grant, J. L. *J. Am. Chem. Soc.* **1977**, *99*, 7745–7746.
43. Jaun, B.; Schwarz, J.; Breslow, R. *J. Am. Chem. Soc.* **1980**, *102*, 5741–5748.
44. Bordwell, F. G.; Zhang, X. M. *Acc. Chem. Res.* **1993**, *26*, 510–517.
45. Bordwell, F. G.; Satish, A. V.; Zhang, S.; Zhang, X.-M. *Pure Appl. Chem.* **1995**, *67*, 735–740.
46. Arnett, E. M.; Flowers, R. A. II *Chem. Soc. Rev.* **1993**, *22*, 9–15.
47. Tilset, M. The Thermodynamics of Organometallic Systems Involving Electron-Transfer Paths. In *Electron Transfer in Chemistry*; Balzani, V., Ed.; Wiley-VCH: New York, 2001; Chapter 3, pp 677–713.
48. Tilset, M.; Parker, V. D. *J. Am. Chem. Soc.* **1989**, *111*, 6711–6717; **1990**, *112*, 2843 (corrigendum).
49. Bordwell, F. G.; Cheng, J. P.; Harrelson, J. A., Jr. *J. Am. Chem. Soc.* **1988**, *110*, 1229–1231.
50. Parker, V. D.; Handoo, K. L.; Roness, F.; Tilset, M. *J. Am. Chem. Soc.* **1991**, *113*, 7493–7498.
51. Kiss, G.; Zhang, K.; Mukerjee, S. L.; Hoff, C. D.; Roper, G. C. *J. Am. Chem. Soc.* **1990**, *112*, 5657–5658.
52. Kristjansdottir, S. S.; Norton, J. R. *Transition Metal Hydrides*; Dedieu, A., Ed.; VCH: Weinheim, 1992; pp 309–359.
53. Barbini, D. C.; Tanner, P. S.; Francone, T. D.; Furst, K. B.; Jones, W. E., Jr. *Inorg. Chem.* **1996**, *35*, 4017–4022.
54. Tilset, M. *J. Am. Chem. Soc.* **1992**, *114*, 2740–2741.
55. Skagestad, V.; Tilset, M. *J. Am. Chem. Soc.* **1993**, *115*, 5077–5083.
56. Ryan, O. B.; Tilset, M.; Parker, V. D. *J. Am. Chem. Soc.* **1990**, *112*, 2618–2626.
57. Pedersen, A.; Skagestad, V.; Tilset, M. *Acta Chem. Scand.* **1995**, *49*, 632–635.
58. Berning, D. E.; Miedaner, A.; Curtis, C. J.; Noll, B. C.; DuBois, M. C. R.; DuBois, D. L. *Organometallics* **2001**, *20*, 1832–1839.
59. Ciancanelli, R.; Noll, B. C.; DuBois, D. L.; DuBois, M. R. *J. Am. Chem. Soc.* **2002**, *124*, 2984–2992.
60. Raebiger, J. W.; DuBois, D. L. *Organometallics* **2005**, *24*, 110–118.
61. Berning, D. E.; Noll, B. C.; DuBois, D. L. *J. Am. Chem. Soc.* **1999**, *121*, 11432–11447.
62. Curtis, C. J.; Miedaner, A.; Ellis, W. W.; DuBois, D. L. *J. Am. Chem. Soc.* **2002**, *124*, 1918–1925.

63. Curtis, C. J.; Miedaner, A.; Ciancanelli, R.; Ellis, W. W.; Noll, B. C.; Dubois, M. R.; Dubois, D. L. *Inorg. Chem.* **2003**, *42*, 216–227.
64. Raebiger, J. W.; Miedaner, A.; Curtis, C. J.; Miller, S. M.; Anderson, O. P.; DuBois, D. L. *J. Am. Chem. Soc.* **2004**, *126*, 5502–5514.
65. Miedaner, A.; Raebiger, J. W.; Curtis, C. J.; Miller, S. M.; DuBois, D. L. *Organometallics* **2004**, *23*, 2670–2679.
66. Zhang, X.-M.; Bruno, J. W.; Enyinnaya, E. *J. Org. Chem.* **1998**, *63*, 4671–4678.
67. Angelici, R. J. *Acc. Chem. Res.* **1995**, *28*, 51–60.
68. Wang, D.; Angelici, R. J. *J. Am. Chem. Soc.* **1996**, *118*, 935–942.
69. *CRC Handbook of Chemistry and Physics*; 85th ed.; Lide, D. R., Ed.; CRC Press: Boca Raton, 2005.
70. Kubas, G. J. *J. Organomet. Chem.* **2001**, *635*, 37–68.
71. Cappellani, E. P.; Drouin, S. D.; Jia, G.; Maltby, P. A.; Morris, R. H.; Schweitzer, C. T. *J. Am. Chem. Soc.* **1994**, *116*, 3375–3388.
72. Ng, W. S.; Jia, G.; Hung, M. Y.; Lau, C. P.; Wong, K. Y.; Wen, L. *Organometallics* **1998**, *17*, 4556–4561.
73. Chin, B.; Lough, A. J.; Morris, R. H.; Schweitzer, C. T.; D'Agostino, C. *Inorg. Chem.* **1994**, *33*, 6278–6288.
74. Schlaf, M.; Lough, A. J.; Maltby, P. A.; Morris, R. H. *Organometallics* **1996**, *15*, 2270–2278.
75. Cheng, J.; Handoo, K. L.; Parker, V. D. *J. Am. Chem. Soc.* **1993**, *115*, 2655–2660.
76. Sarker, N.; Bruno, J. W. *Organometallics* **2001**, *20*, 55–61.
77. Sarker, N.; Bruno, J. W. *J. Am. Chem. Soc.* **1999**, *121*, 2174–2180.
78. Ellis, W. W.; Ciancanelli, R.; Miller, S. M.; Raebiger, J. W.; DuBois, M. R.; DuBois, D. L. *J. Am. Chem. Soc.* **2003**, *125*, 12230–12236.
79. Ellis, W. W.; Raebiger, J. W.; Curtis, C. J.; Bruno, J. W.; DuBois, D. L. *J. Am. Chem. Soc.* **2004**, *126*, 2738–2743.
80. Curtis, C. J.; Miedaner, A.; Raebiger, J. W.; DuBois, D. L. *Organometallics* **2004**, *23*, 511–516.
81. Price, A. J.; Ciancanelli, R.; Noll, B. C.; Curtis, C. J.; DuBois, D. L.; DuBois, M. R. *Organometallics* **2002**, *21*, 4833–4839.
82. Bordwell, F. G.; Cheng, J. P. *J. Am. Chem. Soc.* **1989**, *111*, 1792–1795.
83. Griller, D.; Simoes, J. A. M.; Mulder, P.; Sim, B. A.; Wayner, D. D. M. *J. Am. Chem. Soc.* **1989**, *111*, 7872–7876.
84. Poli, R. *J. Organomet. Chem.* **2004**, *689*, 4291–4304.
85. Marken, F.; Bond, A. M.; Colton, R. *Inorg. Chem.* **1995**, *34*, 1705–1710.
86. Tilset, M.; Hamon, J.-R.; Hamon, P. *Chem. Commun.* **1998**, 765–766.
87. Bartlett, I. M.; Carlton, S.; Connelly, N. G.; Harding, D. J.; Hayward, O. D.; Orpen, A. G.; Ray, C. D.; Rieger, P. H. *Chem. Commun.* **1999**, 2403–2404.
88. Aston, G. M.; Badriya, S.; Farley, R. D.; Grime, R. W.; Ledger, S. J.; Mabbs, F. E.; McInnes, E. J. L.; Morris, H. W.; Ricalton, A.; Rowlands, C. C., *et al. J. Chem. Soc., Dalton Trans.* **1999**, 4379–4388.
89. Hascall, T.; Rabinovich, D.; Murphy, V. J.; Beachy, M. D.; Friesner, R. A.; Parkin, G. *J. Am. Chem. Soc.* **1999**, *121*, 11402–11417.
90. Caulton, K. G. *New J. Chem.* **1994**, *18*, 25–41.
91. Mezzetti, A.; Becker, C. *Helv. Chim. Acta* **2002**, *85*, 2686–2703.
92. Pleune, B.; Morales, D.; Meunier-Prest, R.; Richard, P.; Collange, E.; Fettinger, J. C.; Poli, R. *J. Am. Chem. Soc.* **1999**, *121*, 2209–2225.
93. Pugh, J. R.; Meyer, T. J. *J. Am. Chem. Soc.* **1992**, *114*, 3784–3792.
94. Zhang, S.; Bordwell, F. G. *Organometallics* **1994**, *13*, 2920–2921.
95. Trujillo, H. A.; Casado, C. M.; Astruc, D. *J. Chem. Soc., Chem. Commun.* **1995**, 7–8.
96. Trujillo, H. A.; Casado, C. M.; Ruiz, J.; Astruc, D. *J. Am. Chem. Soc.* **1999**, *121*, 5674–5686.
97. Astruc, D. *Acc. Chem. Res.* **2000**, *33*, 287–298.
98. Terrier, F.; Vichard, D.; Chatrousse, A. P.; Top, S.; McGlinchey, M. J. *Organometallics* **1994**, *13*, 690–697.
99. Bordwell, F. G. *Acc. Chem. Res.* **1988**, *21*, 456–463.
100. Zhang, X.-M.; Bordwell, F. G. *J. Am. Chem. Soc.* **1994**, *116*, 4251–4254.
101. Bordwell, F. G.; Zhang, X. M.; Filler, R. *J. Org. Chem.* **1993**, *58*, 6067–6071.
102. McMillen, D. F.; Golden, D. M. *Annu. Rev. Phys. Chem.* **1982**, *33*, 493–532.
103. Ellis, W. W.; Miedaner, A.; Curtis, C. J.; Gibson, D. H.; DuBois, D. L. *J. Am. Chem. Soc.* **2002**, *124*, 1926–1932.
104. Niiranen, J. T.; Gutman, D.; Krasnoperov, L. N. *J. Phys. Chem.* **1992**, *96*, 5881–5886.
105. Aresta, M.; Dibenedetto, A.; Amodio, E.; Papai, I.; Schubert, G. *Inorg. Chem.* **2002**, *41*, 6550–6552.
106. Geiger, W. E. *Acc. Chem. Res.* **1995**, *28*, 351–357.
107. Bond, A. M.; Colton, R. *Coord. Chem. Rev.* **1997**, *166*, 161–180.
108. Pombeiro, A. J. L.; Guedes da Silva, M. F. C.; Lemos, M. A. N. D. *Coord. Chem. Rev.* **2001**, *219–221*, 53–80.
109. Shaw, M. J.; Hyde, J.; White, C.; Geiger, W. E. *Organometallics* **2004**, *23*, 2205–2208.

1.12 Applications of Sonochemistry and Microwaves in Organometallic Chemistry

D J Casadonte, Jr. and Z Li, Texas Tech University, Lubbock, TX, USA
D M P Mingos, University of Oxford, Oxford, UK

1.12.1 Introduction

1.12.1.1 The Physical and Chemical Action of Ultrasound in Solution

Sonochemistry (the study of the use of both low- and high-intensity ultrasound (LIU and HIU) to drive chemical reactions) has become a significant research field in recent years (for examples See Ref: 1, 1a–1f). Ultrasound refers to that portion of the acoustic spectrum beyond the limits of human hearing, typically within the range from 20 kHz to 10 MHz.[2] When ultrasound is transmitted through a liquid, high-energy events are produced through acoustic cavitation, that is, the generation, growth, and nearly adiabatic implosion of vacuoles in solutions.[3] If LIU (power densities typically in the range of 0–5 W cm^{-2})[22] is deployed through a solution, the resulting cavitation sites oscillate about a mean radius which is sensitive to the frequency of ultrasound,[4,4a–4c] and produce modest internal temperatures and pressures before reabsorption.[5] This process is known as stable cavitation. When a solution undergoes interaction with HIU, the bubbles produced oscillate and grow through a non-linear process known as rectified diffusion[6] until they are out of resonance with the acoustic field, and then undergo adiabatic collapse in a process known as transcient cavitation.[3] The short collapse lifetimes (<100 ps)[7,7a] and high dynamic pressures (>100 atm)[8] generated during transcient cavitation are largely responsible for the extreme temperatures (ranging from 800 to 15,000 K or even higher),[7,7a,9,9a,9b] enormous momentum transfers,[10] and rapid quenching rates[11] observed upon bubble collapse. Indeed, the physical extrema generated using ultrasound have led to the production of a variety of species not observed using thermal or photochemical means, and, as such, sonochemistry occupies a unique niche in modern chemistry.[12] The extreme energy infused during cavity collapse often leads to the production of light. This process is known as sonoluminescence, and is one of the current methods used for estimating the extreme temperatures generated in the bubbles during implosion.[9,9a,9b] Indeed, the temperatures and pressures that occur during cavitation have recently been implicated in efforts toward producing fusion using ultrasound, that is, sonofusion.[9,9b]

Whereas in homogeneous systems the collapse of the bubbles produced during cavitation occurs symmetrically, in heterogeneous solid–liquid systems the bubbles tend to collapse in the direction of the particle surface, creating high-speed microjets.[13] These microjets impinge upon the surface with the full temperature and pressure of the collapsing bubble and cause erosion (via interparticle collision) and localized melting. Microstreaming of the liquid at the surface of the particle due to the sonic field creates turbulent flow that can significantly improve mass transport in the solution. Enormous momentum transfers are observed during heterogeneous sonochemical activity due to interparticle collisions. In studies involving the sonochemical formation of transition metal coatings through interparticle collisions, localized melt temperatures nearing 4,000 °C have been observed.[14,15]

Ultrasound has been used to produce a variety of effects not observed in thermal or photochemical transformations.[16] For example, Wurtz-type coupling of organic halides or organometallic chlorides using lithium wire at room temperature proceeds at a convenient rate only in the presence of an ultrasonic field.[17] Ultrasound has been used to accelerate the Reformatsky reaction and produces lactams as well as the traditional coupling products.[18] Indeed, the use of HIU to facilitate the kinetics of organic reactions has been studied for over three decades.[19] Within the domain of inorganic and materials chemistry, ultrasound has proved to be useful in the generation of hydrogenation[20,21] and hydrodesulfurization[22] (HDS) catalysts, metallic glasses,[11,23] intercalation compounds,[24] and ceramic systems.[25] The largest application of sonochemistry has been in the remediation of contaminants in aqueous media.[26–34]

Ultrasound offers several potential advantages compared with the more traditional synthetic routes. Among these include (i) the use of mild ambient temperatures to protect reactants which might be thermally unstable; (ii) enhanced mixing and transport properties; (iii) the ability to generate unique, high-energy intermediates; and (iv) the production of materials normally associated with physical extrema, for example molten metals and plasmas, with relatively nominal energy input. Indeed, the energy efficiency of sonochemistry (i.e. the amount of useful

product produced per kilowatt hour of electricity input) can be as high as 100 times that of analogous thermal or photochemical processes.[35]

The use of HIU to fashion nanometer-scale compounds is expanding almost exponentially.[1] This is in part due to the efficacy of ultrasound as an energy source for the formation of nanophasic materials. Since the temperature of the bubble interior at cavity collapse cools by 10^2–10^4 K in a timescale from 10^{-6}–10^{-11} s, cooling rates of 10^8–10^{15} Ks^{-1} are possible. Excited-state atoms present in the bubbles upon cavitation collapse that are coalescent do not have time to generate large lattices, and can only form nanoscaled amorphous or (assuming the presence of nucleation sites) nanocrystalline materials.

There are three general mechanisms by which ultrasound-generated nanometric materials are largely produced. The first involves atomization of volatile substrates to generate high-energy species that then coalesce to form the desired product. This strategy has been employed in the synthesis of FeP (*vide infra*).[36] The second mechanism involves the production or activation of reducing agents capable of performing subsequent chemistry.[37] Activation of reducing metals occurs by the removal of deleterious surface deposits or the production of metal sands as well as by the formation of such compounds as M_yX_z, where X is a main group element or organic species. These first two mechanisms may employ any of a number of techniques used in nanostructured materials production (e.g., the use of reverse micelles, *vide infra*) for specific size control. The third mechanism for material production involves reaction by either homolytic or heterolytic bond cleaveage. This synthetic strategy has been explored, for example, in the ultrasound-assisted formation of polysilyne supramolecules.[38]

1.12.1.2 The Interaction of Ultrasound and Organometallic Compounds

Numerous reviews have been written during the past 20 years concerning the action of ultrasound in both the synthesis of and reaction with organometallic compounds, including the alkali metals.[19,39,39a–39c] The principal applications of ultrasound in organometallic chemistry since 1993 involve: (i) the pyrolysis of metal carbonyl compounds in the formation of nanomaterials; (ii) the generation of metal atom sonoluminescence from the sonolysis of metal carbonyl compounds; (iii) the synthesis of new carbonyl compounds, especially as intermediates in catalysis such as in the Pauson–Khand (P–K) reaction; (iv) the use of organometallic compounds as precursors for the formation of materials; (v) metal insertion reactions involving the formation of metal–carbon bonds; (vi) the facilitation of organic reactions such as the Barbier and Reformatsky reactions; and (vii) direct organometallic synthesis. This chapter examines recent organometallic sonochemistry within the context of the products generated and the mechanistic aspects and intermediates produced.

1.12.2 Metal Carbonyl Sonochemistry

1.12.2.1 Ultrasound-induced Pyrolysis of Metal Carbonyl Compounds

The pyrolysis of metal carbonyl compounds to produce amorphous and nanometric materials has been investigated by several authors since the initial discovery of this effect in 1991.[40] Volatile organometallic precursors decompose in the collapsing bubbles to produce high-energy metal atoms that agglomerate or interact with support media (polymer, alkane, silica, etc.) to produce individual nanoparticles or coatings. The high rates of cooling (ca. 10^{10} $K\,s^{-1}$) inhibit crystallization processes, and insure that the particles formed are, fundamentally, nanometric in size. The decomposition rates for the organometallic compounds depend on a variety of factors, including, among others, the vapor pressure of the precursor, solvent vapor pressure, and the nature of the ambient gas. To achieve high yields, the substrate vapor pressure should be high to insure that a relatively high concentration of the reactive species is present in the bubble at collapse. Coincidently, the vapor pressure of the solvent should be relatively low, to produce peak temperatures. The ambient gas should also typically be one that has a high polytropic ratio, such as Ar.

Experiments involving the pyrolytic decomposition of varying dilutions of $Fe(CO)_5$ in decane yielded a dull gray powder which was comprised of nanoparticulate iron.[41] The size of the particles depended upon the initial concentration of the iron pentacarbonyl, but were typically in the range of 50–250 nm, with smaller particles appearing in more dilute solutions. The magnetic moment varied also as a function of concentration, with pure $Fe(CO)_5$ having a magnetic moment of 42.5 emu g^{-1} and the most dilute solution possessing a magnetic moment of 12 emu g^{-1}.

The sonication of 0.015 M $Fe(CO)_5$ in decalin for 6 h has also been shown to yield amorphous iron.[42] Upon consolidation by vacuum hot pressing, the resulting iron was shown by XRD to be α-Fe, with an average particle size

of the nanocrystallites of 40 nm. Although the as-prepared sample displayed a porous coral morphology, the sample displayed a homogeneous and smooth microstructure upon consolidation. The sonochemically prepared iron had a high Rockwell C (RC) hardness (37) compared to the value of 4–5 RC for conventional iron.

Suslick and co-workers have produced nanostructured materials by the sonically induced pyrolysis of a variety of metal carbonyl and substituted carbonyl compounds.[43–48] $Fe(CO)_5$ was sonicated in dry decane at 0 °C under argon for 3 h for the synthesis of nanometric Fe. The resulting iron nanoparticles had an average size of 20 nm, which consisted of aggregates of individual iron particles with a mean size of 4–6 nm. Differential scanning calorimetric measurements show a single disorder–order transition at 308 °C. The resulting iron proved to be a soft ferromagnet, with a saturation magnetization of 173 g^{-1} and a Curie temperature >580 K.[47] The effective magnetic moment was measured to be 1.7μ_B and was consistent with a random packing model for the amorphous nanoparticulate material. The nanometric iron was 10 times more active than commercially available 5 μm iron for the Fischer–Tropsch hydrogenation of carbon monoxide. When pentacarbonyl iron(0) was sonicated in decane in the presence of silica gel, the gel was coated with amorphous iron. TEM analysis indicated that the particle size of the coating iron ranged from 3 to 8 nm. This coated silica was 10 times more active as a Fischer–Tropsch catalyst than commercially available supported iron, and had high activity at low temperatures (<250 K), especially for $>C_5$ hydrocarbon production. The enhanced reactivity was attributed to the amorphous nature of the catalyst (leading to high surface coverage) and the large number of defect sites present.

A method for the production of stable iron colloids in solution has been developed.[48–50] Sonication of $Fe(CO)_5$ in the presence of a polyvinylpyrrolidone (PVP) stabilizer yielded an iron colloid with a particle size ranging from 3 to 8 nm, while sonication in oleic acid yielded colloids with a uniform size of 8 nm. Heating of the resulting colloids yielded bcc-Fe. The colloids were superparamagnetic, with a saturation magnetization of 101 emu g^{-1}, compared to a saturation magnetization of 123 emu g^{-1} for a typical iron-based ferrofluid.

Sonication may be used as a means of producing core-shell-type vesicles in solution.[51] Application of HIU to a solution of iron pentacarbonyl and chlorotrimethylsilane in decaline, followed by pentane washing, centrifugation, and drying under vacuum, produced micron-sized vesicles containing monodispersed spindles of $FeCl_2$ and the tetrahydrate. The vesicles were roughly 1.5–4.2 μm, and the spindles displayed an average length of approximately 450 nm. The ratio of the length to the diameter of the spindles was roughly 1 : 10. Infrared and thermal gravimetric analysis were consistent with a membrane structure for the vesicles that was composed of dimethylsiloxane polymers. The mechanism for the formation of the vesicles was found to be complex. The first step involved the formation of nanometric Fe from the pyrolysis of the pentacarbonyl iron(0). This was followed by attachment of the chlorotrimethylsilane on the surface of the freshly prepared iron. Water present in air and in decaline which was not anhydrous reacted with the chlorotrimethylsilane to form HCl and trimethyl silanol. The HCl functioned to oxidize the iron to iron(II) chloride, whereas the trimethyl silanol dimerized to form hexamethyldisiloxane. The latter process was presumably catalyzed by the presence of the newly prepared iron dichloride. Subsequent repetition of the above reactivity sequence generated the chains of the dimethylsiloxane polymer that comprised the membrane.

Gedanken and Sivakumar have attempted to quantify the effects of molar concentration and power density on the sonolytic decomposition of $Fe(CO)_5$ in decalin in the presence of oxygen to yield amorphous Fe_2O_3.[52] They have observed that low concentrations of iron pentacarbonyl resulted in a higher percent conversion of the carbonyl to the oxide, and that at a 0.02 M concentration of $Fe(CO)_5$ the yield approached 100%. This behavior assumed that Raoult's law held for the two-component mixture, and that the overall vapor pressure, all other things being equal, was controlled by the mole fraction of iron pentacarbonyl present. The lower the mole fraction of $Fe(CO)_5$, the lower the overall vapor pressure and the higher the peak temperature in the cavity. Power density (defined as the amount of power dissipated in joules per unit volume (here, ml) to bring about a desired sonochemical product) displayed a parabolic behavior, with the maximum power density values ranging between 1.15×10^4 and 2.56×10^4 J ml^{-1}. The minimum power density required to initiate the reaction of $Fe(CO)_5$ in decalin (i.e., the threshold power density) was 1.1×10^4 J ml^{-1}. When power and concentration effects were combined into an expression that Gedanken termed the sonochemical yield, a 0.81 M solution under optimum power conditions provided the maximum yield of iron(II) oxide.

1.12.2.2 Sonochemical Decomposition of Mixed Metal Carbonyl Species

Mixed metal Fe–Co alloys of variable composition have been prepared by the sonication of controlled stoichiometries of $Fe(CO)_5$ and $Co(CO)_3(NO)$.[43] These compounds were chosen as precursors because of their solubility and high vapor pressure. Similar results have been obtained in a mixed-phase reaction by the sonication of $Fe(CO)_5$ and $Co_2(CO)_8$, both in decane and using $Fe(CO)_5$ as the sonication medium.[53,53a] The resulting mixed metal alloys were

effective dehydrogenation and hydrogenolysis catalysts toward cyclohexene after treatment with hydrogen to generate a consistent catalytic surface. The alloyed catalysts showed intermediate activity toward hydrogenolysis relative to the pure metals, and superior dehydrogenation.

1.12.2.3 Sonochemical Formation of Metal Carbides

The sonication of molybdenum hexacarbonyl in hexadecane produced a black powder that has been characterized as fcc-Mo_2C.[43] The carbide was produced by the concurrent ultrasonic disproportionation of the carbonyl moiety to carbon and carbon dioxide. The resulting molybdenum carbide was contaminated with oxygen, although this could be removed by treatment with heated CH_4/H_2. The material consisted of porous agglomerates of ~2 nm particles. After reduction, the particle size increased slightly to 3 nm. The carbide was effective in the dehydrogenation of cyclohexene without hydrocarbon cracking. No hydrogenation products were observed. The catalytic behavior of the sonochemically produced molybdenum carbide closely matched that of platinum rather than ruthenium, to which it has often been compared.

1.12.2.4 Sonochemical Formation of Nanostructured Steel

The production of M50 nanostructured steel (4.0% Cr, 4.5% Mo, 1.0% V, 0.8% c, and 89.3% Fe) has been achieved by the sonication of a mixed metal organometallic system containing $Fe(CO)_5$, $Cr(Et_xC_6H_{6-x})_2$, $Mo(Et_xC_6H_{6-x})_2$, and $V(CO)_6$ in the appropriate molar ratios in dry decalin for 7 h.[54] The resulting black powder was amorphous with a porous morphology. Upon compaction, α-Fe was observed in the XRD spectrum. The resulting microstructures were homogeneous, with only minor segregation of V as determined by EDAX analysis. Further analysis of the compacted material by TEM indicated a distribution of particle sizes from 5 to 70 nm. A very fine precipitate was also observed, corresponding to Mo_2C.

M50 steel has also been prepared using a surfactant.[55,56] Without the presence of a surfactant, the M50 steel was highly agglomerated with a particle size of ~5–10 nm. However, upon addition of surfactant, the sonochemically produced particles were discrete and deglomerated, with a mean particle size of 2 nm.

1.12.2.5 Sonochemical Synthesis of HDS Catalysts from Metal Carbonyls

Ultrasound has been used in the fabrication of nanostructured MoS_2 through the sonication of $Mo(CO)_6$ and S in 1,2,3,5-tetramethylbenzene.[57] The resulting material had a porous amorphous structure, in contrast to conventional MoS_2, which has a plate-like structure and which is often used as a lubricant. The TEM lattice fringes for both materials were identical (interlayer spacing of 0.62 ± 0.01 nm), although the sonochemically prepared material showed more edge defects, consistent with the differences in morphology. The sonochemically prepared molybdenum sulfide was an excellent HDS catalyst. It was 5 times more active than the conventionally prepared MoS_2 in the HDS of thiophene and was competitive with RuS_2 and ReS_2, although was significantly less expensive to prepare. The conventionally prepared HDS catalysts showed high selectivity for the formation of butene from thiophene, whereas the sonochemically produced MoS_2 produced more butane.

Suslick and co-workers have developed Co–Mo–S/Al_2O_3, Ni–Mo–Al_2O_3, and Co–Ni–Mo–S/Al_2O_3 supported catalysts for the hydrodesulfurization of thiophene and bidenzothiophene.[58] The synthesis of the catalysts again involved $Mo(CO)_6$ as the molybdenum source and $Co_2(CO)_8$ rather than cobalt carbonyl nitrosyl as the precursor for Co formation on the alumina surface. Rather than employing $Ni(CO)_4$, which is highly toxic, as the source of nickel, the alumina was first soaked in an aqueous solution of a nickel hydrazine carboxylate complex, $Ni(N_2H_5)(N_2H_3COO)_3$, for 1 h and then heat-treated under 10% H_2 in He at 300 °C for 2 h. Decomposition of the nickel compound yielded ~3 nm nanocrystals on the surface of the alumina. STEM-XEDS studies indicated that the active catalytic component resided on the outside surface of the support. The Co–Ni–Mo–S/Al_2O_3 supported catalyst showed enhanced HDS of thiophene relative to either the Co- or Ni-promoted sonochemical or commercially prepared catalysts. Activation of the Ni and Co catalysts by H_2 increased its HDS activity by removal of edge sulfur atoms, leaving more active coordinatively unsaturated surface atoms. The principal products of the promoted catalysts were C_4 hydrocarbons, with a marked selectivity for butanes. The HDS of dibenzothiophene principally resulted in the generation of biphenyl, with the Co-supported catalyst being 4 times and the Ni catalyst being 2 times, respectively, more effective than commercial catalysts.

The formation of mixed metal Mo–Co oxide HDS catalysts on the MCM support occurs in a sequential reaction by first depositing the molybdenum oxide followed by pyrolysis of $Co(CO)_3NO$ to disperse the Co over the Mo-covered support.[59] The option of co-sonicating the molybdenum carbonyl and cobalt carbonyl nitrosyl concurrently yields catalysts with poorly reproducible stoichiometries. The resulting catalyst (13 wt.% CoO and 43 wt.% MoO_3) was examined as an HDS catalyst for dibenzothiophene, and was found to display 1.7 times greater activity than a commercial Co–Mo–Al catalyst.

1.12.2.6 Sonochemical Synthesis of Phosphine Semiconductor Materials

Whereas the reaction of metal carbonyl and phosphine species with low vapor pressures produces phosphine-substituted metal carbonyl compounds,[60] sonication of liquid metal carbonyl compounds such as $Fe(CO)_5$ with volatile phosphines can lead to nanometric solid pyrolysis products. The ultrasound-induced pyrolysis of iron pentacarbonyl in the presence of high-vapor-pressure aliphatic phosphines produced FeP, a semiconductor material with a bandgap that lies in the infrared.[36] Casadonte and sweet sonicated a 1 : 1 molar ratio of $Fe(CO)_5$ and either triethylphosphine or trimethylphosphine for 5 h either in neat or in decane solvent to produce a black pyrophoric species. The resulting particles with a spongy morphology were 10–15 μm agglomerates of nanometric FeP particles. Annealing of the samples at 950 °C produced crystalline FeP as determined by XRD analysis.

1.12.2.7 Sonochemical Synthesis of Metal Oxides

The placement of metal oxides on silica surfaces has been achieved through the sonication of mononuclear metal carbonyls and metal carbonyl nitrosyls in decalin in the presence of a slurry of non-porous silica microspheres.[61,62] The addition of Al-MCM-41 material with an average pore size of 8.3 nm and a surface area of 840 $m^2 g^{-1}$ increased the deposition of MoO_3 by an order of magnitude relative to the production of the oxide by sonication of $Mo(CO)_6$ in oxygenated decalin. The mechanism for the enhancement involved a deposition–precipitation process, where the molybdenum carbonyl underwent a decomposition–oxidation reaction in decalin to yield MoO_x species that were anchored to the surface through Mo–O–Si bridges. The resulting MoO_x moieties were hydrated from water molecules formed, with decalin acting as the proton source. The MoO_x, which was anchored to the surface of the support, was also capable of interacting with the microjets formed in the heterogeneous sonication process. The effect was to push the metal oxide into the pores of the support, as observed by XPS spectroscopy.

Gedanken and co-workers have recently surveyed the literature concerning the sonochemical formation of mesoporous metal oxides.[64,65] A variety of inorganic precursors were available to prepare specific metal oxide species. For example, sonication of $[Co(acac)(OMe)(MeOH)]_4$ yielded mesoporous Co_3O_4 with a specific surface area of 70 $m^2 g^{-1}$. Sonolysis of iron(II) ethoxide in CTAB surfactant generated Fe_2O_3 with 100–200 nm particle size and 2–5 nm pores. Both were effective catalysts for the oxidation of cyclohexane. Mesoporous SnO_2 produced by this method from the analogous ethoxide has found utility as an electrode in dye-sensitized solar cell studies using large bandgap semiconductors.

1.12.3 Metal Carbonyl Sonoluminescence

The sonoluminesence of mono- and dinuclear metal carbonyls in silicone oil including $Fe(CO)_5$, $Cr(CO)_6$, $Mo(CO)_6$, $W(CO)_6$, $Mn_2(CO)_{10}$, and $Co_2(CO)_8$ has been investigated by Suslick *et al.*[66] Atomic emission was observed from the metals, indicative of the high temperatures produced by cavitation. The presumed mechanism involved pyrolysis of the metal carbonyl compound to generate excited-state metal atoms in the cavity, followed by activation through collision with a third vapor-phase molecule in the system. Individual atomic emission lines were not well resolved. Rather, the peaks were broadened due to the high pressures produced upon cavitation collapse. The intensity of the emission followed the pattern Cr > Mo > Fe > W >> Mn, Co.

The effective temperature that was resolved from metal carbonyl sonoluminescence (5,150 ± 300 K for Fe, 4,700 ± 400 K for Cr, and 4,750 ± 400 K for Mo) was in excellent agreement with the peak temperature obtained by sonication of silicone oil under argon.[67] The peak temperature of the bubble could be controlled by the addition of hydrocarbon gases (C_1–C_3) to the solutions. As the mole fraction of the gas increased and as the polytropic ratio decreased, the anticipated temperature from adiabatic compression decreased.

1.12.4 Pauson–Khand (P–K) Sonochemistry

The use of both LIU and HIU has been shown to increase the efficiency of the P–K reaction, which involves the formation of cyclopentenone from the annulation of a cobalt alkynyl carbonyl complex and an alkene. The use of low-power ultrasound, as for example, from a cleaning bath, although capable of producing intramolecular P–K reactions, generated relatively low cyclization yields.[68] The motivation for the use of high intensity came from its ability, as previously described, to effectively decarbonylate metal carbonyl and substituted metal carbonyl complexes. Indeed, HIU produced by a classic horn-type sonicator has been shown to be capable of facile annulation of norbornene and norbornadiene in under 10 min in the presence of a trimethylamine or trimethylamine *N*-oxide dihydrate (TMANO) promoter, with the latter promoter producing cleaner product mixtures.[69] This methodology also proved effective in the enhancement of the P–K reaction with less strained alkenes such as 2,5-dihydrofuran and cyclopentene, as well as the less reactive alkenes *p*-fluorostyrene and cycloheptene. The mechanism has been postulated to involve decarbonylation of the cobalt carbonyl alkyne, followed by coordination by the amine to the vacant coordination sites on the cobalt.

1.12.5 Pyrolysis of Non-Carbonyl Organometallic Compounds

The sonochemical pyrolysis of organometallic palladium precursors has been used in a successful synthetic strategy for the production of nanostructured activated Pd on carbon black.[70] Ultrasonic irradiation of tris-μ-[dibenzylideneacetone]dipalladium in mesitylene under argon for 3 h at dry ice-acetone temperature yielded a black powder that Gedanken and co-workers have characterized as consisting of ~80 nm porous agglomerates of ~1–5 nm particles with a flake-like morphology. The average surface area of the Pd–carbon compound was approximately 85 $m^2 g^{-1}$, with a disorder–order transition evident at 400 °C by calorimetry. The phase transition was broad rather than sharp as was expected for pure metals due to the presence of atomic carbon. Once the Pd–C was heated to 400 °C, fcc-Pd was detected. X-ray photoelectron spectroscopy indicated that the structure of the amorphous material prior to heating was core-shell, with a palladium core of ~20 Å surrounded by a carbon shell, also ~20 Å. Gedanken posited that the reaction producing this unusual structure occurred at the interfacial region between the bubble and the bulk owing to the low vapor pressure of the substrate at the dry ice-acetone temperature, which inhibited its inclusion into the bubble. The mechanism was postulated as a two-step process, with palladium–ligand cleavage (producing palladium atoms) followed by pyrolysis of the dibenzylideneacetone ligand to produce a carbon shell. The palladium–carbon nanoparticles were active catalysts for the Heck reaction of bromobenzene with styrene, and were highly stable in organic solvents.

1.12.6 Sonochemical Metal-Organic Reactions

The role of the solvent beyond vapor pressure considerations in the formation of nanocrystalline materials has been demonstrated by Xie *et al.* in the synthesis of silver, copper, and lead selenides.[71] When $AgNO_3$, $PbCl_2$, or CuI were reacted with ethylenediamine (en) in an ultrasonic cleaning bath at 18 kHz for 10 h, the corresponding selenides were produced. The PbSe formed were large nanocrystals (~150 nm). The authors indicated that the lack of coordination of en to the lead ions provided for unrestrained growth. In contrast, $[Cu(en)_n]^+$ is a stable complex in en solution ($k = 10^{10.8}$). The resulting complex ions could be linked by hydrogen bonding and self-assemble during sonication to form the oriented 30–150 nm CuSe which was observed. Silver was intermediate in this regard, forming a complex with en with a lower stability constant ($k = 10^{7.7}$), so that the particle size was reduced, but no orientation of the resulting 70 nm crystals was observed.

1.12.7 Sonochemical Metal Insertion Reactions

Metal insertion reaction can be categorized as organic substrates, usually organic halides, reacting with metal or organometallic catalysts by undergoing oxidative addition. The metal atom, as a result, is inserted between the organic group and the halide atom, as shown in Equation (1). In this mechanism, the A–B bond is broken to form M–A and M–B bonds. The oxidation state (OS), coordination number (CN), and electron count (in the case of organometallic catalysts) of the metal, all increase by 2 units during the reaction.

$$R-X+M \rightarrow R-M-X \quad (1)$$

$$\Delta OS = +2$$

$$\Delta CN = +2$$

The highly versatile intermediate R–M–X allows further reactions with an organic partner or it can obtain a second organic ligand from another metal (transmetallation). Hence, organic compounds can be formed by a reductive elimination mechanism.

When only one unit can be changed between the metal oxidation state, coordination number, and electron accounts, two metal atoms are required to form R–M species (Equation (2)). Equation (2) is also favorable for lithium metal, but the remaining alkali metals are limited due to the possibility of Wurtz coupling.[72]

$$R-X+2M \rightarrow R-M+M-X \quad (2)$$

$$\Delta OS = +1$$

$$\Delta CN = +1$$

Metal-insertion reactions form the basis for a variety of organic reactions that are metal catalyzed. These are discussed below.

1.12.7.1 Metal Activation

An induction time is generally observed when performing reactions involving organic reagents and metals. The metal is often passivated by oxide, hydroxide, carbonate, and even nitride (in the case of lithium) coatings on the surface. Metal activation using ultrasound irradiation has been investigated and is very well reviewed.[73,73a–75] It is now accepted that the effect of ultrasonic cavitation on solid surfaces promotes the activation. When the bubble is in the vicinity of a solid surface, spherical implosion of a bubble no longer occurs. Instead, an asymmetric collapse of the cavity generates a liquid jet directly pointed at the surface, with the velocity of the jet tip greater than 100 m s^{-1} and with pressure up to 10^4 bar.[76] The impingement of such jets generates enough energy so that it creates a localized erosion (even melting), and surface pitting, as evidenced by morphological changes of the metal surfaces. Recently, Lauterborn and Ohl discovered that at least three shock waves are generated as a result of the collapse of a jet interacting with the residual bubbles.[77]

The second mechanism of cavitation-induced surface damage is the impact of the shock waves launched by bubbles collapse.[73a] In a liquid–solid slurry, as the shock waves pass over particles that are very close to one another, particles accelerate with high velocity and collide with each other. The speeds are estimated at 100–500 m s^{-1} for particles that are ~10 μm in diameter. Two scenarios are proposed.[78,79] If the particle collision is direct, metal particles, such as zinc, can weld together because the high-speed collision releases enough energy to melt the contacting surface. If the particles collide at a glancing angle, the tribomechanical effect from the collision results in removal of surface materials, which lead to the exposure of a fresh metal surface.

The mechanical properties of the metals, the coating, and their interaction also play a role in the process in metal activation. Two mechanisms, shown in Scheme 1, were proposed according to the hardness of the metal.[74,80] Soft metals, such as alkali metals (hardness <0.6 Mohs[81]), undergo permanent plastic deformation to form powders. For harder metals (<2.7 Mohs, e.g., magnesium and aluminum), only superficial layers were deformed. Nevertheless, if

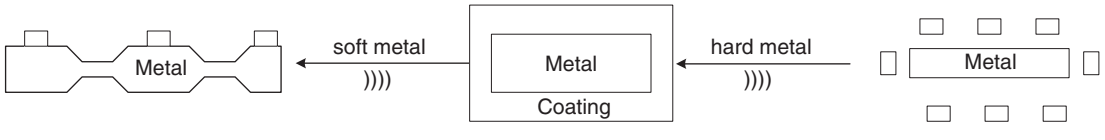

Scheme 1 Ultrasonic effect on coated metal.

the geometry of the metal below the surface is changed, a fresh metal surface will be revealed, because the coating (which is non-ductile and more brittle than metal itself) in general is broken to reveal the substructure.

For harder metals with a hardness greater than 2.7 Mohs, the adhesiveness of oxides on the metals must be taken into account. Metals such as zinc, copper, and nickel can have their coating oxides removed by energetic cavitational shock waves. Suslick *et al.*[82,82a] observed changes in atomic composition on the surfaces of nickel powder using Auger spectroscopy, indicating the loss of the oxide coating. For those metals with hard, adhesive oxides, for example, molybdenum and tungsten, sonochemical activation is no longer observed.[73a]

Alex *et al.*[83] reported that the smaller the initial particles, the less significant the ultrasonic breakage becomes. Examining particles of copper and lead in the range of 50 μm revealed that small particles have too low an inertia to make the cavitation shock effective, assuming that the size of a cavitation bubbles as 150 μm at 20 kHz. These results suggest that the surface cleaning of very fine metallic suspensions might be difficult.

1.12.7.2 The Facilitation of Organic Reactivity

Ultrasound can be used to improve many heterogeneous organic and organometallic reactions with metals in terms of ease of reaction, substantially improved yields, and much shorter reaction times.[84,85] In many cases, sonochemical methods initiate the reaction by activating the metal surface, producing the organometallic intermediates *in situ* so that a distinct preparation step can be avoided and reactions can be conducted with simpler procedures and better efficiency. Furthermore, not only does sonication marginally depend on the dryness of the solvent,[86,87] which is an important factor in the synthesis of Grignard reagents, but it can also prevent metal passivation by reaction products recoating the surface, as shown by studies on electrodes in the presence of ultrasound.[88,89]

The facilitation of ultrasound in many organic reactions involving metals before 1998 has been reviewed by Luche and colleagues.[74,90] In many reactions that involve organic halides reacting with metals, mechanisms which do not involve a direct carbon-to-metal bond have found more general acceptance. In this chapter, these reactions are excluded and only new reports that are not covered in Refs: 71 and 90 are discussed.

1.12.7.2.1 Metal insertion in organic reactions forming C–C bonds

Organometallic reagents can be prepared either in an ultrasonic cleaning bath or with probe sonication without previous metal activation. The induction period is suppressed or at least largely shortened. Such a synthesis can be carried out *in situ* and used as reagents for subsequent reactions, saving time and allowing for the possibility of preparing and reacting reagents with labile stability in a single step.

1.12.7.2.1.(i) Barbier–Grignard-type reactions

The Barbier–Grignard-type reactions are usually referred as a transformation in which the organometallic reagents serve as nuclophiles to lead to carbon–carbon bond formations (Equation (3)).[91]

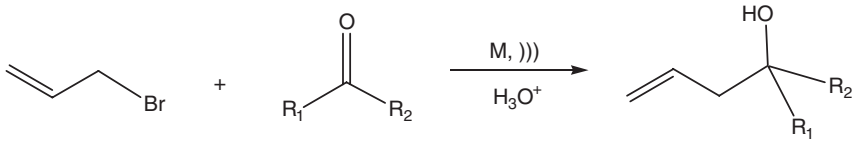

(3)

Lee *et al.*[92] reported the synthesis of homopropargyl alcohol using propargyl bromide reacting with ketones and aldehydes with zinc and 1,2-diiodoethane. The authors reported a shorter reaction time and better yield under ultrasonic irradiation. Single homopropargyl alcohols with good to excellent yields were obtained when propargyl bromide reacted with aldehydes, and allenyl alcohols were also obtained as byproducts when reacted with ketones, shown in Scheme 2.

In attempts to prepare homoallyl alcohol in an environmental friendly process, Andrews and co-workers reported its synthesis using a solvent-free method mediated by tin under ultrasound.[93] Experiments showed that the alcohols were produced in excellent yields with aldehydes but that no products were produced using ketones. However, the existence of toxic allyltin compounds in the final products prevented the method from being applied downstream in fine chemical applications. On the other hand, according to Wang *et al.*,[94] carbonyl allylation reactions mediated by $SnCl_2$ in aqueous solution without a Lewis acid under ultrasonic irradiation were successfully carried out.

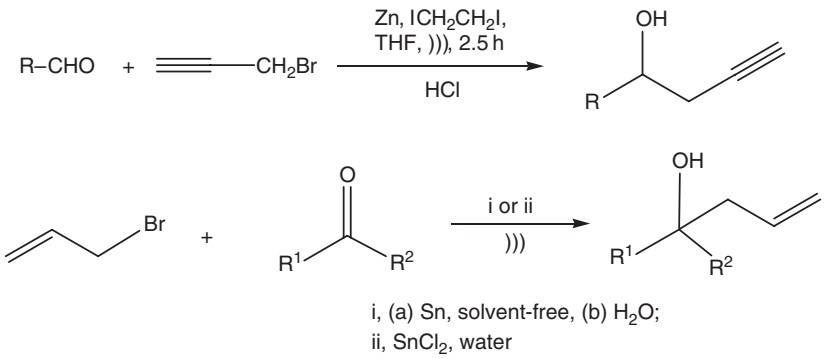

Scheme 2

1.12.7.2.1.(ii) Reformatsky reactions

The Reformatsky reaction (Equation (4)) with aldehydes can be achieved in almost quantitative yield using either a low-intensity cleaning bath[95] (LIU) or a high-intensity probe sonicator (HIU),[96] which makes this reaction one of the first organometallic reactions studied under ultrasonic irradiation because of the difficulties in metal activation under silent conditions.

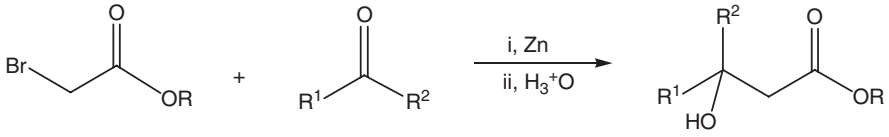

(4)

The ultrasound-assisted Reformatsky reaction was used in reactions involving hexafluoropropylene oxide.[97] The authors noticed that the yield of 2-fluoro-2-trifluoro-methyl-3-hydroxylpropanoate was improved from 37% to 54% using a cleaning bath. Recently, Ross and Bartsch reported successful syntheses of β-hydroxyesters using phenyl ketones, α-bromoesters, zinc dust, and catalytic amount of iodine under high-intensity ultrasonic irradiation with good to quantitative yield.[98] The authors found that the reaction was mainly dependent upon the stoichiometry of Zn dust, and that sterically bulky alkyl groups on the ketone affected the yields dramatically. In a subsequent study on imines with α-bromoesters,[99] it was discovered that the product, generated in good yield, was either β-lactam or β-aminoester exclusively, depending on the identity of the imine. Experiments showed that groups with different electronic properties attached to the N atom may determine the product.

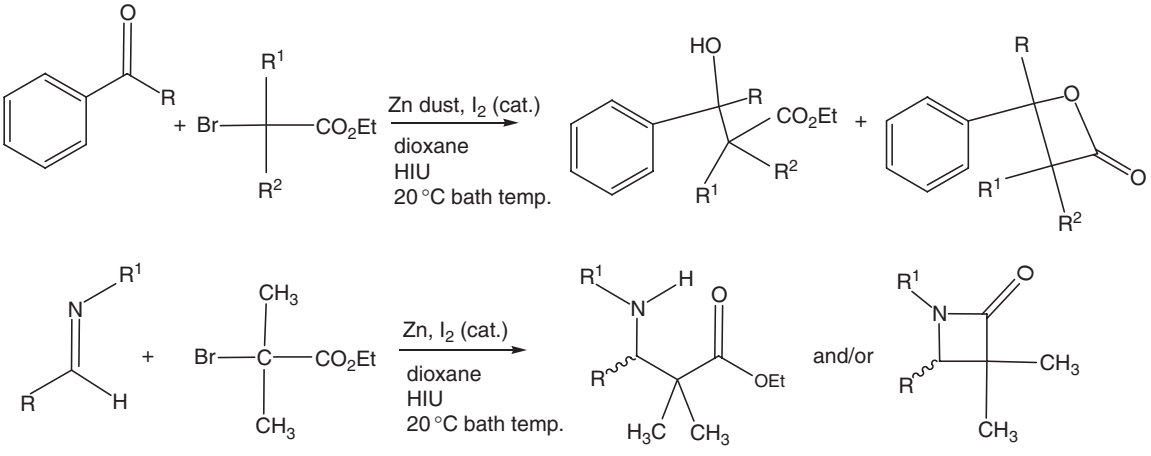

Scheme 2 Reformatsky reaction reported by Ross and Bartsch.[98,99]

1.12.7.2.1.(iii) Ullmann-type coupling reactions

The Ullmann reaction (Equation (5)) occurs at a lower temperature and shorter time in almost quantitative yield with probe sonication.[100] This reaction has been previously reviewed.[74]

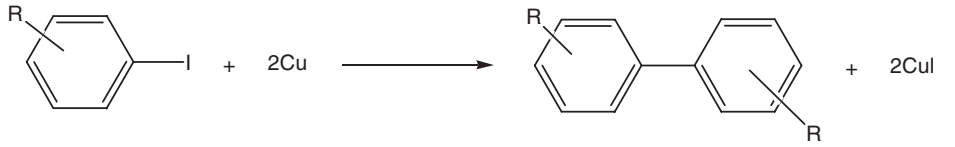

(5)

Having observed the improvement using ultrasound in the cross-coupling of *o*-halobenzoic acids and substituted benzoamines with copper, or Cu/Zn under probe sonication,[101] Galy and co-workers successfully synthesized acridine derivatives using this method (Scheme 3).[102] In order to replace dry organic solvents with more environmentally benign ones, Pellón *et al.* extended the synthesis of halobenzoic acid and alkylamine in the presence of water as a solvent with copper under probe sonication.[103] In most cases, the yields were 20% greater than those resulting from classic heating.

1.12.7.2.1.(iv) Simmons–Smith reaction

Sonochemically activated metals greatly improve the reaction of CH_2X_2 (X = Br, I) with olefin to produce cyclopropane derivatives, as shown in Equation (6).

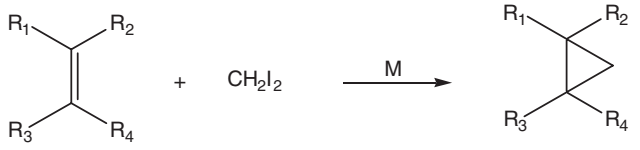

(6)

The reaction conditions of cyclopropanation of enoxylsilane (R_1, R_2 = H; R_3 = Ph; R_4 = $OSiM_3$) with dihalomethane were studied by Sun and Li,[104] and the results showed that CuCl promoted the reaction significantly.

Zhu carried out the cycloaddition of C_{60} and methanofullerene dihalides, $C_{60}(CX_2)$ (X = Cl, Br, I), with Mg in the ionic liquid 1-butyl-3-methylimidazolium tetrafluoroborate [BMIM]BF_4 with a yield of 55–84%, in contrast to 6–21% yield in THF under sonication (Scheme 4).[105] Only [6,6]-ring junction cycloaddition isomers of C_{121} were detected, showing the cyclopropane configuration on the connecting C atom.

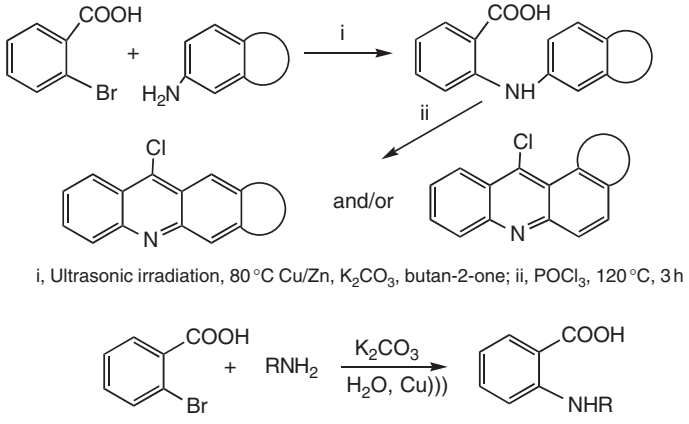

Scheme 3 Ullmann reaction reported by Galy[101,102] and Pellón.[103]

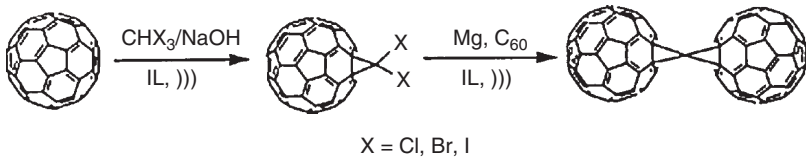

Scheme 4 C_{60} cycloaddition reactions promoted by ultrasound.

1.12.7.2.2 Catalytic organic reactions

Catalytic organic reaction systems, especially heterogeneous catalytic organic reaction systems, are a most industrially important class of reactions. Besides the erosion, surface activation, and collision between catalyst particles, the nonlinear coupling of acoustic waves causes the enhancement of molecular motion of the liquid phase, leading to an enhanced mixing effect in solution.[106] Such effects reduce or even eliminate the thickness of diffusion layers in the vicinity of a solid surface, largely improving catalytic ability by accelerating adsorption and desorption processes as well as mass transfer to and from the catalyst.

1.12.7.2.2.(i) Coupling reactions

Suzuki reactions, especially those friendly to the environment, that involve ultrasonic irradiation have been reviewed recently.[107] Cravotto and co-workers carried out ligand-free Pd/C-catalyzed Suzuki cross- and homo-couplings in either water or DMF using high-intensity ultrasound.[108] In combination with microwave (MW) irradiation, further improvements in yields and reaction time were achieved. The authors also reported that Ullmann homocoupling mediated by zinc also occurred, with CO_2 bubbling into the reaction. The failure of 3-arylation of 3-bromo-4-hydroxycoumarin using the Suzuki procedure under oxygen atmosphere irradiated by ultrasound was investigated,[109] and a mechanism was proposed.

Besides the study on Suzuki cross-coupling reactions (Scheme 5) in the ionic liquid 1,3-di-n-butyl-imidazolium tetrafluoroborate ([BBIM][BF_4]) catalyzed by palladium prepared *in situ* in a cleaning bath,[110] Srinivasan and co-workers reported ligand-free Pd-catalyzed couplings between aryl halides and terminal alkyne[111]

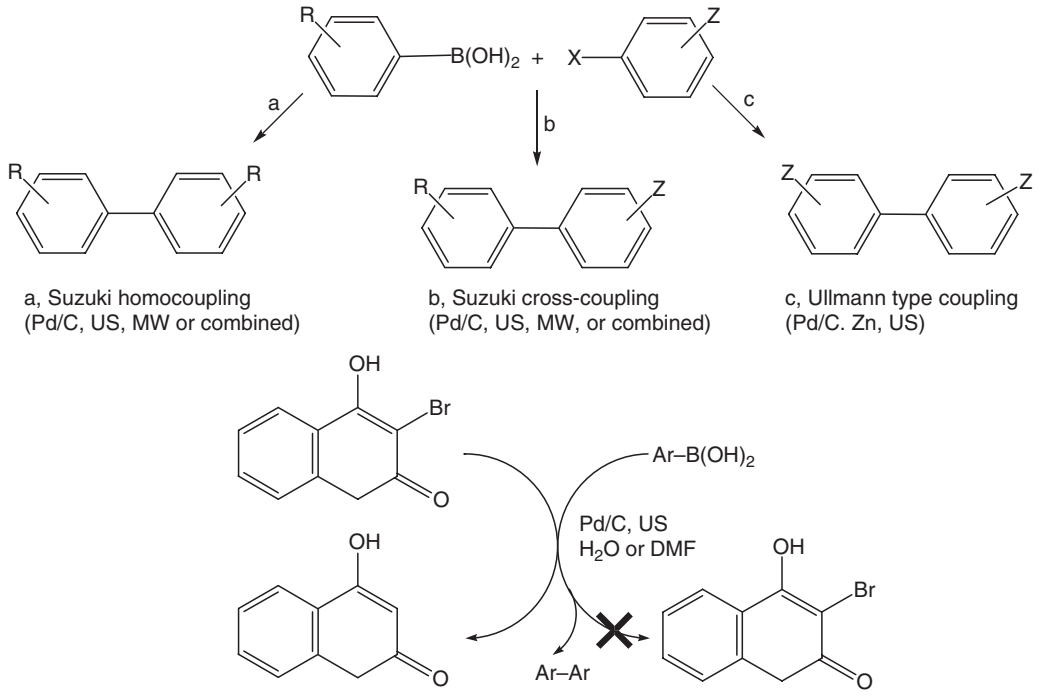

Scheme 5 Suzuki coupling reactions.

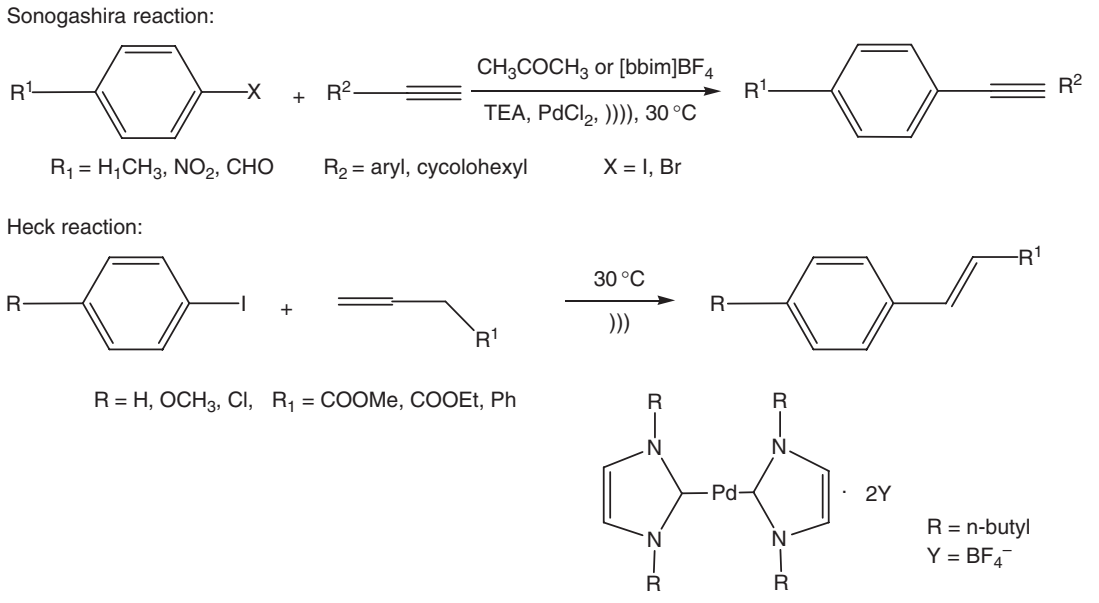

Scheme 6 Sonogashira and Heck reactions.

(Sonogashira reaction) or terminal acetylenes[112] (Heck reaction) in ionic liquids using a cleaning bath. The authors proposed that a Pd–bis-carbene complex, shown in Scheme 6, was formed and was consequently reduced into Pd black in both reactions, with palladium particle sizes of 1–12 nm, as determined by TEM.

Ambulgekur *et al.* investigated the leaching of Pd off the support during the reaction, by examining the Heck reaction under ultrasound.[113] Besides noticing that the reaction was accelerated by ultrasound, the authors reported that the Pd/C catalyst can be reduced by sodium formate and redeposited, so that the catalyst can be recycled twice.

1.12.7.2.2.(ii) Other catalytic organic reactions

Some catalytic organic reactions, for example, hydrogenations, dechlorinations, were reviewed recently.[114] Boudjouk *et al.* found that ultrasonic irradiation accelerated the hydrosilylation of alkenes in the presence of Pt/C with good to excellent yields at ~30 °C under atmospheric pressure, while higher temperature above (100 °C) and pressure (over 3 bar) were usually required in silent reaction (Equation (7)).[115] The mechanism of hydrosilylation involves the insertion of a catalytic metal atom between the Si–H bond, followed by insertion of an alkene into the M–H bond, followed by reductive elimination of alkylsilane, so that C=C is reduced to C–C.[116] Hydrosilylation can be extended to the C=O bond as well. The reduction of 2-substituted cyclohexanones to alcohol with shorter reaction time and higher yields was reported by Felföldi *et al.* via hydrosilylation with Wilkinson's complex as the catalyst in an ultrasonic cleaning bath.[117]

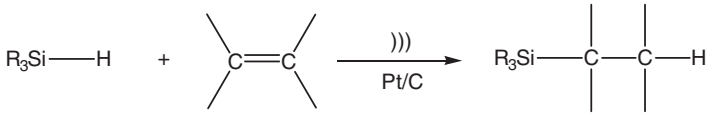

(7)

1.12.7.3 In Organometallic Synthesis

Metal-insertion reactions in organometallic synthesis, as one of the results of metal activation, have been comprehensively reviewed by Luche and co-workers.[74,90,118] In this section, the focus is on main group metals.

Organostannanes are the important reagents for the Stille coupling reaction. Zhao *et al.*[119] reported improved syntheses of various organostannanes in almost quantitative yields using stannane halides, Mg metal, and an initiator in an ultrasonic cleaning bath compared to the syntheses using bis(alkyltin)oxide reported by Lee and Dai (Scheme 7).[120] The treatment of Bu_3SnCl and Mg irradiated by ultrasound resulted in the formation of $Bu_3Sn–SnBu_3$. However, the reaction failed with alkenyl halide.

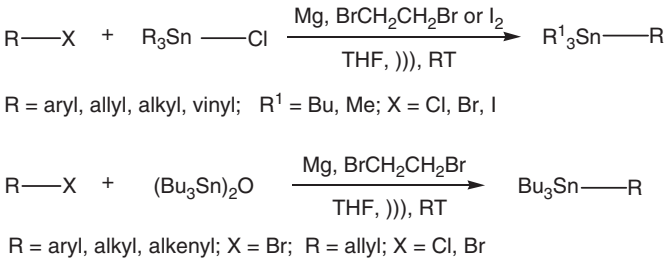

Scheme 7 Organostannanes synthesized by Zhao *et al.*[119] and Lee and Dai.[120]

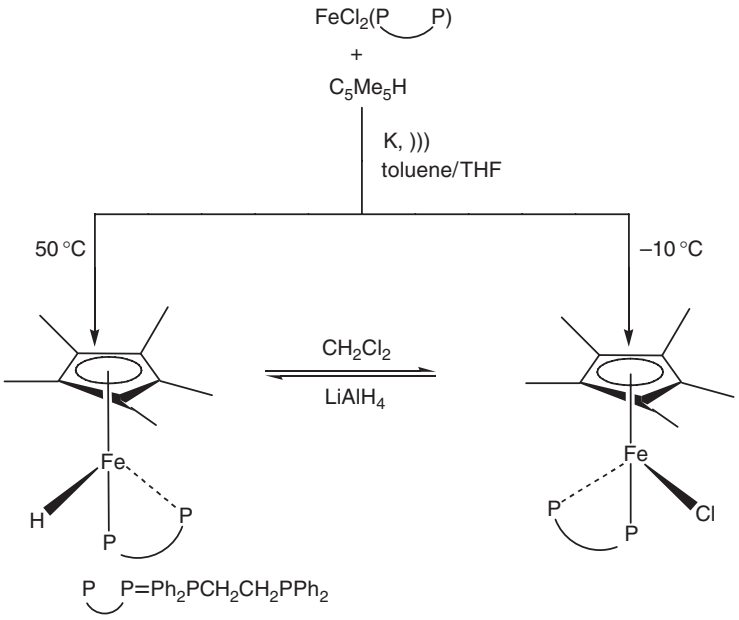

Scheme 8 Synthesis and conversion of $(C_5Me_5)Fe^{III}(dppe)X$ (X = Cl, H).

In the study of $(C_5Me_5)Fe^{III}(dppe)R$ 17-electron complexes (dppe: $Ph_2PCH_2CH_2PPh_2$; 1,2-bis(diphenylphosphino)-ethane), Roger *et al.* used potassium slurry pulverized by HIU reacting with pentamethylcyclopentadiene (C_5Me_5H; Cp^*H) and $Fe(dppe)Cl_2$ to prepare $Fe(C_5Me_5)(dppe)X$ and $Fe(C_5Me_5)(dppe)H$, depending on the reaction temperature (Scheme 8).[121] As experiments revealed that C_5Me_5K and iron halide did not yield the products, the authors speculated that a transient Fe(dppe) intermediate inserts into the C_5Me_5–H bond.[122] The authors also used a potassium slurry to produce metallates from the dimer, and these *in situ* metallates reacted with alkyl halides to give excellent yields.[123] Green *et al.* developed a facile sonochemical synthesis of $RGaI_2$ using molten Ga, I_2, and RX under HIU with good yield.[124] Furthermore, sonication of molten Ga and I_2 in the absence of alkyl halide resulted in a pale green powder, which was "surprisingly reactive and behaved as a monovalent gallium system."[124] Sonochemically prepared GaI has become such a versatile reagent that it has been utilized in several areas of organic and gallium cluster synthesis.[125] Anandhi used GaI reacted with Cp^*K to form [Cp^*Ga/GaI] reagent in the study of Ga–Au clusters.[126]

1.12.8 Organometallic Compounds and Ultrasound

As mentioned earlier, the synthesis, properties, and reactivity of organometallic compounds under ultrasound were reviewed by Suslick,[39b] and later by Luche *et al.*,[74,90] and Walton and Mason.[127] In this section, the focus is on organometallic compounds that are not covered by the above reviews.

In the study of Rh complexes as catalysts in the hydroformylation of alkenes, Kostas *et al*. used ultrasound in the replacement of bridging-chloro ligands with aryloxide and carboxylate respectively, and generated good yields.[128] In the synthesis and characterization of organopalladium complexes containing a fluoro ligand, the replacement of iodo with a fluoro ligand using ultrasound gave almost quantative yield.[129] Neto *et al*. reported that cyclopentadieneothallium, an air stable reagent used as transmetallation agent for cyclopentadienide transfer, was obtained in nearly quantitative yields and in practically pure form using alternating periods of sonication and magnetic stirring, starting with TlSO4, KOH, and cyclopentadiene in aqueous solution.[130]

Besides using sonochemistry as a means of promoting the pyrolysis of metal carbonyl compounds, ultrasound has been effective in the preparation of supramolecular organobismuth–transition metal carbonyls.[131] The compound $[n\text{-BuBiFe(CO)}_4]_\infty$ has been formed by the reaction of *n*-BuBr and $[Et_4N]_3[Bi\{Fe(CO)_4\}_4]$ in an ultrasonic cleaning bath in MeCN, followed by acidification. The reaction has been postulated to involve an ultrasound-generated radical mechanism.[131]

1.12.9 Preparation of Catalysts Using Ultrasound

Ultrasound irradiation has been used in the process of catalyst preparation. Acoustic irradiation increases the dispersion of the active metal on the support,[132] depassivates the metal, and reduces the particle size to nanometer scale.[133] In the case of palladium supported on active carbon prepared under ultrasound with extremely high surface area, not only was a greater metal dispersion achieved, but a larger penetration of metal inside the pores of the support and an easier elimination of chloride ion were observed as well.[134,135]

Ultrasound-assisted catalyst preparation has been reviewed elsewhere;[74,114,133] some recent developments in the production of catalysts that were not covered in these review are discussed here.

Bartók and co-workers reported considerable to great improvement on enantioselectivity in hydrogenation of ethyl pyruvate[136] and trifluoromethyl ketones[137] using Pt/Al_2O_3 catalyst pretreated by ultrasound. After reporting that nanostructured MoS_2 with high surface area that were synthesized by the reaction of $Mo(CO)_6$ and sulfur under horn sonication showed higher catalytic ability in hydrodesulfurication (HDS) to thiophene (*vide supra*),[57] Suslick and co-workers synthesized MoS_2/Al_2O_3 as well as Co- and Ni-promoted MoS_2/Al_2O_3 using the same technique.[58] Recently, in addition to their efforts in preparing hollow nanospheres of MoS_2 and hollow nanocrystals of MoO_3 by leaching of a silica support with fluoric acid,[138] the Suslick group has continued to synthesize porous MoS_2 using ultrasonic spray pyrolysis, in an attempt to reach even higher surface area and better HDS catalytic ability.[139]

1.12.10 Applications of Microwave Dielectric Heating

1.12.10.1 The Physical Basis

Advances in chemistry have depended not only on the discovery of new classes of reagents, but also on new modes of introducing energy into chemical reactions. The previous section described the applications of ultrasound to chemical reactions and this section discusses the applications of MW dielectric heating. The two processes are often confused and it should be stressed from the outset that the mechanism of interaction, the temperatures induced, and the consequences are very different.

The first reliable device for generating fixed-frequency MW radiation was designed by Randall and Booth at the University of Birmingham, UK, during World War II. MW radiation is a part of the broader electromagnetic spectrum and it was well known that infrared and visible light accelerated chemical reactions, and therefore when it was first observed that microwave radiation was able to heat foodstuffs it did not come as a complete surprise. The first patent for MW dielectric heating was filed by the Raytheon Company in 1946 and commercial MW ovens became available in 1947.

Although MW dielectric heating had been applied to analytical problems, for example, acid digestion, drying, sintering, ashing, extraction, and protein hydrolysis, it was not exploited for chemical syntheses until the late 1980s.[140] Subsequently, there has been[141–143] an exponential growth of publications devoted to the subject. From the original publications in 1986, it has been calculated that approximately 500 papers a year were being published in 1997, and by 2002 this had risen to more than 1,300 papers a year.

From the early days, it was recognized that the rapid heating of foodstuffs in MW cavity arose because of their high water content and the consequent efficient conversion of microwave energy into thermal energy by water molecules.[144] The advantages of MW dielectric heating for drying were recognized in the 1950s and 1960s.[144] The

development of MW dielectric heating for the digestion and drying of analytical processes was also recognized, and specially designed MW applicators for chemical analyses were produced commercially by the CEM Corporation in 1978.[140] These applications utilized the interactions between MW energy (2.45 GHz) and aqueous solutions to accelerate acid digestion and they made an important contribution to improving the overall efficiency of the process.

There were also reports in the materials literature during the 1970s of MW dielectric heating being used for ceramics' processing and calcining.[145] Examples of encapsulating radioactive samples in inorganic glasses using MW dielectric heating were also patented. During this time, the application of MW dielectric heating in chemical laboratories remained very limited. The mistaken belief that the MW dielectric heating arose exclusively from specific interactions between MW radiation and water molecules contributed to this lack of interest. Early measurements by von Hippel [146] at MIT had established that there were other chemicals capable of coupling effectively with MWs, but these results did not percolate into the chemical consciousness. The important observation that it was possible to use MW energy to accelerate reactions in organic solvents resulted from empirical observations rather than theoretical considerations, but nonetheless represented an important development for synthetic chemistry. Following on from the important observations by Gedye, Majetich and their co-workers in 1986,[147,148] the use of MW dielectric heating in organic, inorganic, and organometallic chemistry has expanded very rapidly, and now there are more than 4,000 papers describing the application of this technique for the synthesis of new compounds. The early papers in this field[141] used either domestic MW ovens, adapted versions of them, or cavities initially designed for analytical science, and their use raised many questions and speculations concerning the mechanism by which chemical reactions were accelerated. The technical problems associated with the safe containment of flammable organic liquids, sometimes under pressurized conditions, required the development of accurate and reliable temperature and pressure measurement.

1.12.10.2 MW Radiation—Energy Ranges and Frequencies Available for Dielectric Heating

The MW region of the electromagnetic spectrum corresponds to wavelengths of 1 cm–1 m (30 GHz–300 MHz). The wavelengths of 1 cm–25 cm are also used extensively for RADAR and telecommunications, and by international agreement, only the frequencies 2.45 GHz (12.2 cm) and 900 MHz (33.3 cm) are available for dielectric heating unless rigorous precautions are taken to limit the leakage of stray MW radiation. Domestic and commercially available MW applicators for chemical purposes generally operate at 2.45 GHz (12.2 cm), and the vast majority of the literature pertaining to chemical applications of MW dielectric heating has been presented for this frequency.

In the gas phase, small molecules with permanent dipole moments interact with MW energy, and they display a well-defined spectrum which may be used to define the moment of inertia of the molecule. In this phase, the rotation of molecules is quantized and the transitions between the energy levels may be observed as sharp lines in the MW spectrum as long as the molecule has a permanent dipole moment. The spectral lines are very sharp and lines as close as 1 MHz apart may be distinguished. At low pressures, the mean free paths of the molecules are large and consequently the lifetimes of the excited states are long. However, as the pressure is increased, the lifetimes of the excited states are reduced, and this leads progressively to broader bands. In liquids, the continuum of rotational states generated for a very large ensemble of frequently interacting molecules means that the phenomenon loses its identity as a quantum mechanical description and the rotational motions become less distinguishable from translational processes. Therefore, in the solution phase, the physical phenomenon associated with MW dielectric heating is not appropriately considered as a quantum-mechanical phenomenon and may be interpreted using classical electromagnetic theory. The interaction between MW radiation and solutions of polar molecules may be adequately described using classical models which may be derived from Maxwell's equations. It is a collective property which occurs in a semiclassical manner and involves aggregates of molecules. The rotations at one molecule influence the translational and rotational motions of neighboring molecules via intermolecular interactions. These are greatest when the intermolecular forces arise from hydrogen bonding and strong dipole–dipole interactions. Rotations at one center are therefore capable of raising the translational energies of adjacent molecules, and when this phenomenon is repeated across the sample, the temperature of the whole solution rises. The large mean free paths in the gas phase prevent this from happening in the gas phase. The only feature common to the gas-phase and the solution-phase interactions of molecules with the MW radiation is that it is essential that the molecules have a permanent dipole moment.[149,149a,150]

1.12.10.3 Theoretical Basis

1.12.10.3.1 Relaxation times of solvents

The theoretical basis of MW dielectric heating has been thoroughly reviewed elsewhere,[149,149a,150] and therefore only a brief summary of the important points is presented in this chapter. The important parameter in deciding the extent of interaction between MW radiation and a particular solvent is the average rotational frequency, or its inverse, the "average relaxation time." Debye first proposed that this relaxation time depended on the size of the molecule and the nature of the intermolecular forces. In the Debye interpretation, for a spherical molecule with a radius r rotating in a viscous continuum, the relaxation time, τ, is defined as

$$\tau = 4\pi r^3 \eta / kT$$

In this expression, the size of the molecule is identifiable as the volume element, and the intermolecular forces, which may have contributions from dipole–dipole, induced dipole–dipole, and hydrogen bonding effects, are represented by the viscosity, η. The relaxation time is temperature dependent since the molecules rotate faster as the temperature is increased. If we compare a series of molecules with similar hydrogen bonding capabilities, then there is a reasonable correlation between molecular size and the average relaxation time; however, if the viscosity varies significantly, then the Debye expression is not so predictive. For the great majority of liquids, a broad relaxation peak is observed, and therefore it represents a continuum of the rotations/translations of the molecule and the envelope cannot be designated to specific bond rotations.

For simple aliphatic alcohols, the relaxation time increases with molecular weight from 50 to approximately 1,000 ps, in agreement with the Debye expression. The relaxation time envelope is spread over approximately 10^3 Hz and the width of the relaxation peak at half height is approximately 10^2 Hz, and therefore the efficiency of energy conversion is not very frequency dependent. For example, although the relaxation time for water is 9.04 ps, the operating frequency for dielectric heating corresponds to a maximum relaxation time of 65 ps. Therefore, it happens that a whole range of organic molecules have relaxation time profiles which incorporate a relaxation time of 65 ps and hence are able to couple effectively with MW energy with a frequency of 2.45 GHz. These data support the empirical observation of many synthetic chemists who have noted that a wide range of polar organic solvents heat rapidly in an MW cavity operating at 2.45 GHz.[147,148]

The average relaxation time is temperature dependent, and for EtOH, the relaxation time decreases from 270 to 49 ps as the temperature rises from 10 to 70 °C . Therefore, the alcohol couples more effectively with the MW source at 2.45 GHz as the temperature increases. Such a situation is ripe for superheating the solvent, since the extent of conversion increases as the temperature rises. It also follows that some organic solvents with very long relaxation times at room temperature may initially appear to be unsuitable candidates for dielectric heating, but since the match becomes more favorable with temperature, they may behave as effective couplers as the temperature rises, that is, after a slow start they may heat very well very rapidly.

The solvents which do not have hydrogen bonding capabilities have much shorter relaxation times and lower viscosities. This reduces the interaction of molecules in the rotational process which are responsible for the MW coupling, and therefore they will generally not heat as effectively in a MW cavity. The dielectric properties of organic solvents are also influenced by the presence of solvated ions, which provide an alternative mechanism for dielectric heating which is akin to resistive heating.[140] Therefore, reactions which produce ionic products can experience more efficient coupling with the MWs as the reaction proceeds. Also, it is the prime mechanism for heating in ionic liquids.

1.12.10.3.2 Loss tangents

The more formal theoretical basis of MW dielectric heating can be defined in terms of the real and imaginary components of the dielectric constant, and these data have been presented and analyzed for a wide range of common organic solvents elsewhere.[149,149a] The dielectric analysis of the interactions of MWs with biological materials has increased in importance in recent years, and Craig has provided an excellent summary of the relevant data.[150]

In summary, MW dielectric heating of polar solvents occurs most effectively when the average relaxation time comes into resonance with the MW frequency. It is not a quantum-mechanical effect, and the large width of the relaxation time envelope ensures that it is not a very specific effect, but one that can be used for a wide range of polar organic solvents. A reasonable match with the MW energy is sufficient for effective coupling to occur and the efficient conversion into thermal energy.

1.12.10.4 Single and Multimode Cavities and Containment Issues

The initial chemical research was done in domestic MW ovens. These were engineered for thoroughly cooking relatively large food samples, and it was essential to kill all the bacteria in all the parts by heating it evenly to a sufficiently high temperature.[144] In a multimode cavity, the energy from the magnetron is used to create many alternative wave patterns in the cavity, and rotation of the sample or rotating reflectors (mode stirrers) encouraged a more or less even energy distribution. Speculative synthetic chemistry involves smaller samples, and given that the wavelength of the MWs is approximately 12.2 cm, it was found that they did not necessarily experience even heating. The temperature observed was very size dependent for samples with volumes in the range 1–25.0 cm^3. In a single mode cavity, only a single standing waveform is generated, and it is possible to optimize the absorption of energy using tuning devices. Therefore, as equipments specifically designed for synthesis became available, they have been based increasingly on single mode cavity technologies. The tuning of the cavity has been automated using computer software and the heating rates have become much more predictable and reliable. The tuning is important because the wave patterns are influenced by the dielectric properties and the dimensions of the sample placed within the cavity. The single mode cavities are also based on closed systems—the chemicals are contained either in a Teflon or glass container. The closed nature of the system means that the pressure builds up as the reacting samples are heated, and therefore it is also important for reasons of safety to monitor the pressure within the vessel.[141] It has become commonplace to operate at 2–20 atm pressure, and this of course leads to an increase in the boiling point of the solvent. The conditions commonly generated in custom-designed chemical reactors are summarized in Table 1.[151]

The availability of modern automated single mode cavities which feature rapid parallel throughput with full sequential reaction control has made a major impact on the field and in particular in the early drug discovery area.[152–154] They provide the possibility of preprogramming both liquid dispensing, heating time and reaction temperature, and lead to optimized reaction conditions. According to the Arrhenius equation, an increase in reaction temperature of 100 °C leads to a reduction of the rate constant by 10^3, and this translates into a contraction in the total time for a reaction from 24 h to less than a minute.

The introduction of volatile and inflammable organic solvents into an MW cavity adjacent to a magnetron which may spark in its off–on duty cycle has to be handled with care if explosions are to be avoided. There are a range of materials including glasses and plastics which are transparent to MWs and which may be used as containment vessels as long as they are not attacked by the solvents. Teflon is particularly attractive in this regard since it is not attacked by any of the organic solvents and is thermally stable up to 270 °C. Teflon vessels may be encased in very robust Kevlar outer containers if they are used under extreme pressures.[155–157] Thick-walled glass may be used safely up to about 20 atm pressure as long as the vessels are not too large, that is, greater than 100 cm^3.[157] The development of ports which give access to the MW cavity have been developed, which enable organic solvents to be refluxed safely at atmospheric pressures using MW radiation[156] and also for the introduction of thick-walled glass pressure vessels.[157]

1.12.10.5 Temperature Control and Monitoring

In the 1980s, it was commonplace to make chemical experiments with domestic MW ovens; however, since they were produced as cheaply as possible for mass domestic markets, they rarely incorporated temperature monitoring as a feature.[158,158a] This resulted in some novel observations, but not reproducible science. It was eventually recognized that the most reliable and least intrusive way of monitoring the temperature was based on fluoro-optic fiber technology (Luxtron)—however, such systems initially cost several times as much as the cavity itself. Once

Table 1 Operating temperatures and pressures for some common organic solvents in a microwave cavity

Solvent	*Conventional boiling point* (°C)	*Operating temperature in the microwave cavity* (°C)	*Pressure* (bar)
Water	100	220	16
Methanol	65	160	17
Ethanol	78	180	16
DMF	153	250	5
CH_2Cl_2	40	140	15
CH_3CN	86	200	10
Acetone	56	150	5

introduced, it was possible to have several optical probes working simultaneously, and therefore it was possible to establish simultaneously the temperature at several points in the reaction vessel.[159]

The application of infrared pyrometry and optical fiber temperature measurements had an important influence on the development of the understanding of the chemical acceleration of reactions in MW fields, because it established for the first time that even at atmospheric pressures, water and commonly used organic solvents did not boil at their thermodynamically determined temperatures, but at significantly higher temperatures.[159,160] Baghurst and Mingos[159] described these higher boiling temperatures as "nucleation-limited boiling points" (NLBP) and suggested that many of the previously speculated MW effects could be attributed to the higher reaction temperatures achieved in an MW cavity. The boiling phenomenon in an MW cavity is kinetically controlled, and higher temperatures were required in order to bring into action a sufficient number of nucleation sites to get efficient boiling. The volumetric nature of the MW dielectric heating phenomenon, that is, the simultaneous heating through the whole volume as long as the penetration depth is larger than the cross-section of the vessel, and the large heating rates induced meant that the nucleation sites on the surface of the vessel, which are so important in the initial stages of bubble formation for boiling, are not sufficiently numerous to allow the boiling to commence at the thermodynamically dictated point. Table 2[20] gives some typical nucleation-limited boiling points for organic solvents. It should be noted that the "nucleation-limited boiling points" could be affected by treatment of the glass surface and the introduction of surfactants. In contrast, the elevation of the boiling points may be reduced by introducing more nucleation sites, for example, by having boiling chips or scratching the surface of the reaction vessel. These studies also established how to introduce ports into the MW cavity, which could be safely used for the entry and exit of gases, and tubes.[156]

The elevation of boiling point can be enhanced by allowing the pressure to rise in the vessel, and when this rises to 10 atm pressure, the solvent boils at approximately 100 °C above the conventional boiling point (see Table 1). Translated into the Arrhenius expression, this means that the rate constant for a reaction may be increased by approximately 10^3. The great majority of the rate enhancements of reactions in solution using MW radiation may be attributed to the nucleation-limited and superheating effects described above. Indeed, when the temperature of a reaction which is studied in MW cavity reaction is carefully and accurately measured, the rates are found to correspond closely to those found for the same reaction under conventional heating conditions.[158,161–163] There is little evidence of specific or quantum-mechanically based phenomenon for accelerating solution reactions when they have been studied under carefully controlled conditions. Nevertheless, the very different temperature profiles associated with MW heating makes it a very attractive and convenient method for carrying out inorganic and organic reactions under "flash heating" conditions, that is, reactions where the energy is inputted very rapidly for short periods of time (see Figure 1). This allows the attainment of a high temperature very quickly, followed by rapid cooling at the end of the reaction. These conditions can yield high conversion rates for reactions with large activation energies, lower yields of decomposition products, and alternative isomer distributions.

The development of equipment specifically designed for chemical reactions[152–154] has removed many of the uncertainties which plagued the early days of the subject. It is now generally possible to measure the temperature and pressure of the reaction as it proceeds. The pressure may be measured by inserting a tube in the reaction vessel and using a transducer to measure the pressure buildup. In the early days of Parr pressure vessels based on Kevlar and PTFE, there was no temperature or pressure control, and it was possible to develop high pressures in the reactor vessel and suffer the consequences of the resultant explosions.

Table 2 Heating rates and nucleation-limited boiling points for solvents under microwave conditions

Solvent	*Heating rate* (°C s^{-1})	*Conventional b.p.*(°C)	*NLBP* (°C)	*Difference* (°C)
H_2O	1.01	100	104	4
EtOH	2.06	79	103	24
MeOH	2.11	65	84	19
CH_2Cl_2	2.16	40	55	15
THF	2.04	66	81	15
MeCN	2.36	82	100	18
Me_2CO	2.23	56	81	25
diglyme	2.17	162	175	13

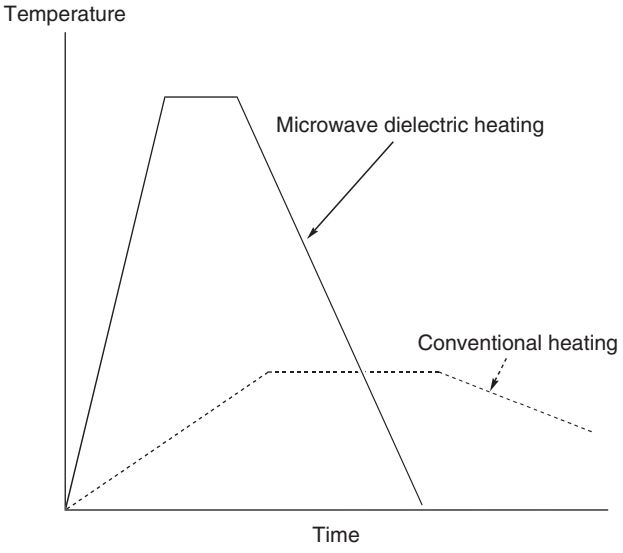

Figure 1 A schematic illustration of the differences in temperature–time profiles for conventional and microwave dielectric heating. Particularly noteworthy are the far higher heating and cooling rates and the greater reaction temperatures achieved. Since at these higher temperatures the rate of reaction is much larger, it is not necessary to hold the reaction at this temperature for an extended period of time. Since the rate of reaction depends exponentially on temperature, the translation of these profiles into product yields as a function of time will magnify these effects.

The ability to measure the temperature reliably has allowed the examination of the rates of heat transfer in mixtures of solvents. For example, if water is mixed in small quantities of benzene or toluene, it is found that the whole solvent mixture heats up very rapidly. This strongly suggests that even if the initial coupling occurs between the MWs and the water molecules, the energy is rapidly transmitted to the whole of the solvent. Therefore, the proposal found in some publications that somehow the MW energy is stored selectively in a particular type of molecule or bond grouping within a molecule is unlikely.[164,164a]

1.12.10.6 Comparison of MW, Conventional, and Ultrasound

It is clear from the discussion above that MW dielectric heating is a non-quantum-mechanical effect, and leads to volumetric heating of the samples. Therefore, it is necessary to question whether it has any significant advantages compared to conventional heating of chemical reactants. There are significant differences in the mode of interaction, and these may confer advantages for dielectric heating; however, the effects require a greater understanding of the temperature profile and the nature of the interaction.

(i) MW coupling can lead to much higher heating rates than those that can be achieved using resistive heating. Using very cheap and readily available MW cavities, heating rates of 2–4 °C[159] or more per second may be readily achieved in a multimode cavity and higher rates in a single mode focused cavity. Such heating rates are more difficult to achieve using conventional heating. For small samples the volumetric nature of dielectric heating produces large heating rates throughout the sample. Reactions on solid supports are frequently associated even with high heating rates if the support material couples effectively.

(ii) The volumetric MW heating is more efficient than conductive heating and may lead to considerable energy savings.[160]

(iii) The very different temperature profiles for MW and conventional heating may lead to an alternative distribution of chemical products in the reaction. The MW energy is introduced into the reactor remotely, and therefore there is no direct contact between the energy source and the sample undergoing heating. This promotes not only much higher heating, but also higher cooling rates. A schematic illustration of the differences in temperature profiles for thermal and MW heating is given in Figure 1. Therefore, MW dielectric heating is akin to a flash heating process. These different profiles may lead to significantly different products, particularly if the product distribution is controlled by complex kinetics.

(iv) Chemicals and the containment materials for chemical reaction do not interact equally with the commonly used MW frequencies for dielectric heating, and consequently a certain degree of selective heating may result. Specifically, it is possible to cool the outside of the vessel with a coolant that is transparent to MWs (solid CO_2, liquid N_2, or a cooled air stream) and thereby have cold walls which still allow the MW energy to penetrate and heat the reactants, which are MW active.[165–166] The effects of simultaneously MW heating while cooling the sample has provoked some controversy, and the subject is discussed more fully in Refs: 165 and 166. Metal powders, which form a fluidized bed in a counter stream of gas, can be made to interact very strongly with the MWs, rapidly heat, and thereby react with the gases which are transparent to MWs. Therefore, the reaction is induced by a very selective interaction between metal and MWS.[167–170] The reactions of metal powders with organic ligands have also been investigated (see 13.10.1.6).

(v) Selective heating of one component of a miscible solvent mixture does not lead to high thermal gradients in solution. For example, when a mixture of MeOH (2%), which has a high loss factor, and benzene (98%), which is transparent to MWs, are exposed to an MW field, the whole mixture heats up very rapidly. Since the MW dielectric heating process promotes translations by rotations of neighboring molecules, the benzene molecules are also rapidly heated. Therefore, it is not possible to store the MW energy selectively either within parts of a molecule or in the active molecules of such a two-component mixture. This observation has led to the suggestion that polar molecules can act as "molecular radiators" and transfer the MW energy to the apolar solvent which is transparent to MWs. The "molecular radiator" may actually be one of the molecules participating in the reaction.[171,172] Inert compounds, which efficiently couple to microwaves but are not soluble in the solvents, for example, graphite, inorganic oxides, etc., may also be used as "susceptors" to transfer the MW energy to the solvent system.[173–175] Ionic liquids have not only been used to study MW-assisted reactions, but also have proved to be very effective susceptors.[174,175] More generally, interest has been shown in the use of ionic liquids as solvents for MW dielectric heating.

(vi) There have been some interesting results on two-phase immiscible systems, for example, chloroform/water. An attempted Hoffman elimination when studied in water at 105 °C leads to unwanted polymerization, but when performed in water/chloroform, it leads to a high yield of the predicted product. This results because of a temperature differential between the chloroform (50 °C) and water (110 °C) layers under MW heating conditions. The fact that the product is soluble in $CHCl_3$ and therefore effectively removed from the hotter region[176,176a,177] is an important contributing factor.

(vii) As discussed above, boiling is a kinetic as well as a thermodynamic process, and therefore solvents heated rapidly under MW conditions often boil at elevated temperatures, even though they remain contained under 1 atm pressure. The precise elevation of this nucleation-limited boiling point depends on the power input, the occurrence of effective stirring, and the limitation of the number of nucleation sites, for example, by having smooth surfaces and no boiling chips. This effect can be enhanced by allowing the pressure to rise above atmospheric.

(viii) In solid samples the rate of energy transport is reduced, and consequently the development of "hot spots" is more significant. A careful analysis of heterogeneous catalysis suggests that "hot spot" formation around the catalyst not only enhances the reaction rate but also may contribute to shifts in the equilibrium constant.[178] Loupy and co-workers[179,179a] have utilized this difference in order to study reactions of organic compounds on solid supports such as alumina and silica. Such solvent-free reactions have proved to have widespread applications, and have been proposed as effective means of performing green synthetic organic chemistry.[174]

(ix) In sonochemistry, microcavitation effects result in very high temperatures over relatively small volumes, whereas in MW dielectric heating it is the solvent or support material which experiences the major temperature rise, and the temperatures achieved are in the normal range associated with chemical reactions, that is, room temperature to 400 °C rather than thousands of degrees. Therefore, in both cases, reaction times may be diminished but the mechanisms involved are quite different.

(x) The microcavitation effects associated with ultrasound cause the cleaning of surfaces and breaking up of crystalline samples, both of which increase the surface area of a sample and thereby increase the rates of reaction. These effects are much less pronounced in MW dielectric heating, because of the mediation of the solvent and the lower temperatures involved. An interesting difference between the two methods has been noted for the intercalation reactions of $VOPO_4$, which are accelerated under MW and sonochemistry conditions; in the former case, the crystallinity of the samples is retained to a greater extent during the process.[180]

In summary, it is apparent that the application of dielectric heating to chemical reactions may result in different reaction rates and product distributions, and chemists can also take advantage of the remote nature of the interaction.

To maximize the difference between MW and conventional heating, one needs to use relatively high power levels and thereby develop a temperature profile which ramps up and cools off more quickly than conventional heating and work under conditions where high pressures may develop. This may mean working outside the bounds of conventional equilibrium conditions.

It is therefore not surprising that there have been a number of suggestions in the literature which ascribe for the differences between conventional and MW heating to "specific MW effects." A recent review has satisfactorily summarized the current controversial position.[164] "Specific MW" effects are defined as accelerations in rate that cannot be achieved or duplicated by conventional heating, but which are still attributed to thermal effects. This contrasts with "non-thermal" MW effects, where the enhanced reaction rates cannot be understood in terms of purely thermal/kinetic effects and may result from direct interactions with the electric field. It is generally agreed that photons in the MW region are not sufficiently energetic to result in direct bond breaking since their energies are 10^{-5}–10^{-6} times the energy of a bond. They are also unlikely to induce very energetic rotational levels of specific groups. Furthermore, the electric field strengths arising from the MWs are not sufficiently large to induce organization of molecules at the molecular level. It has been suggested that athermal effects may originate from:[143,164]

(i) Changes in the pre-exponential factor of the Arrhenius expression due to preferential orientation of molecules in the transition state because of the electric field component of the MW radiation.
(ii) Decrease in the entropy of activation of the reaction because of the ordering of the solvent in the MW field.
(iii) Intervention of microscopic but very localized high temperatures as a result of the MW heating.
(iv) Some have even suggested that the oscillating magnetic component of the MWs may make a contribution.

However, direct evidence for these suggestions is currently not available, and the circumstantial evidence is neither overwhelming nor definitive. The recent development of *in situ*, real time monitoring of MW-accelerated reactions by Raman spectroscopy will perhaps provide answers to the important questions.[177] Loupy[143] has proposed that the non-thermal effects depend on the reaction medium, that is, solvent-free or polar or non-polar solvent, the polarity of the transition state, and the position of the transition state along the reaction coordinate. He has suggested that "specific" MW effects are more apparent in apolar solvents and those reactions which have late transition states.

However, where the rates of reactions and product distributions of organic solution reactions have been studied under carefully controlled conditions, the yields appear to be identical and independent of the mode of heating. In the solid state, hot spot formation can be a more serious issue, especially if the solid is inhomogeneous and one component has a much higher loss tangent than the second, but even there it remains a thermal effect responsible for the rate enhancement, although it is much more difficult to satisfactorily model the results using elementary kinetic theory.

1.12.10.7 Applications to Organometallic Syntheses

The application of MW dielectric heating to organometallic and coordination chemistry was pioneered by Mingos and Baghurst, in the late 1980s.[141] Subsequently, it has been demonstrated that a wide range of organometallic synthons may be conveniently and rapidly made in high yields using MW dielectric heating.[181–187] Mingos and Baghurst also developed open reflux systems which could be adapted from domestic MW ovens and used safely for the synthesis of organometallic compounds.[156] Extensions of this methodology to other transition metal organometallic compounds have been reported by a number of research groups, and Schemes 9, 10 and 11 illustrate the flexibility of this methodology for synthesizing a wide range of compounds from group 6 metal hexacarbonyls.[182,183] This development makes the technique sufficiently safe and reproducible to be used routinely in undergraduate laboratory classes. If these reactions are performed using solvents with high loss tangents, reasonably large acceleration rates are observed, primarily due to the nucleation-limited boiling phenomenon discussed before.

Green and Danks have also used the technique to study the reactions of metal carbonyls of the group 6 metals and aza-butadience complexes of iron.[181,184–186] Danks has also studied the synthesis of cyclopentadienyl bis-phosphine ruthenium complexes of the type [RuCp(dppm)SR] (R = Ph, CH_2CH_2Ph, CH_2(2-furyl), CH_2CO_2Et, etc.) from $[RuCp(PPh_3)_2Cl]$ using conventional heating and MWs in a focused monomode reactor. A considerable decrease in reaction times was observed, although both techniques gave comparable yields.[186]

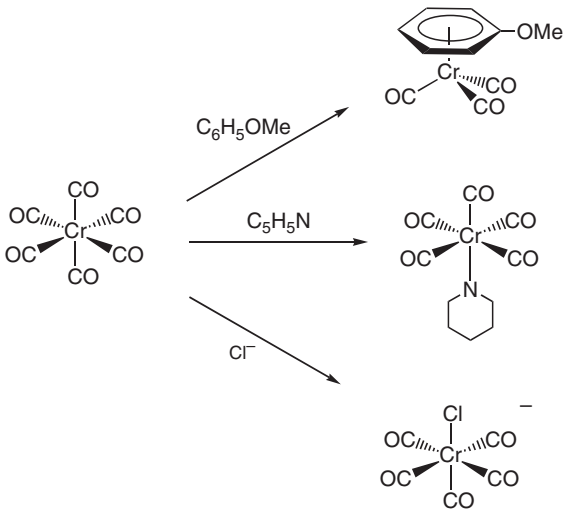

Scheme 9

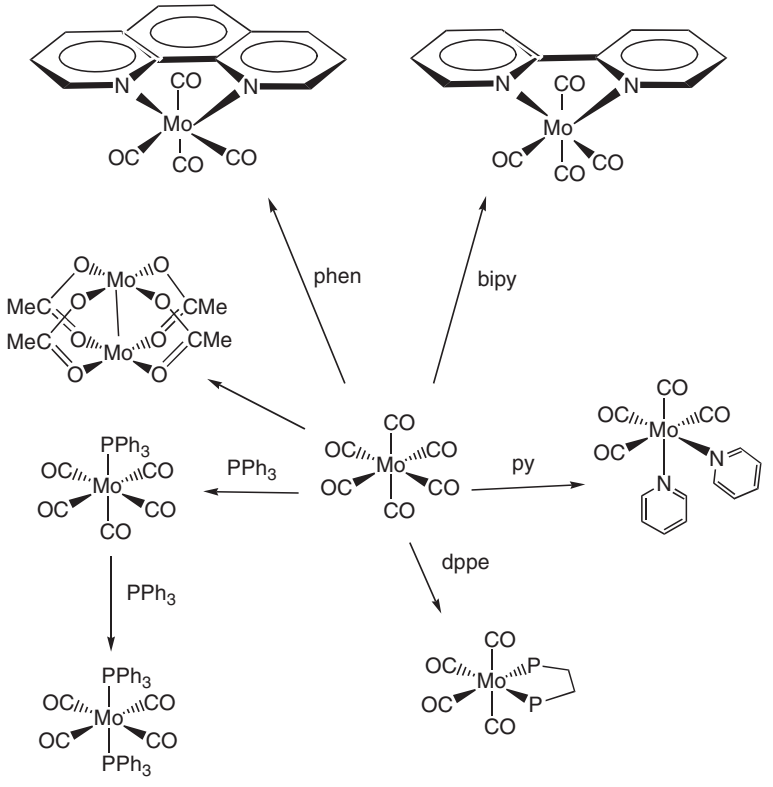

Scheme 10

The application of the MW technique to main group organometallic compounds was pioneered by McWhinnie and his co-workers, and some specific examples are given in Scheme 12.[188] More recently, the technique has been used in the synthesis of organosilanes and germanes,[189,190] and the method has been applied to accelerate the synthesis of aryl Grignard reagents.[191]

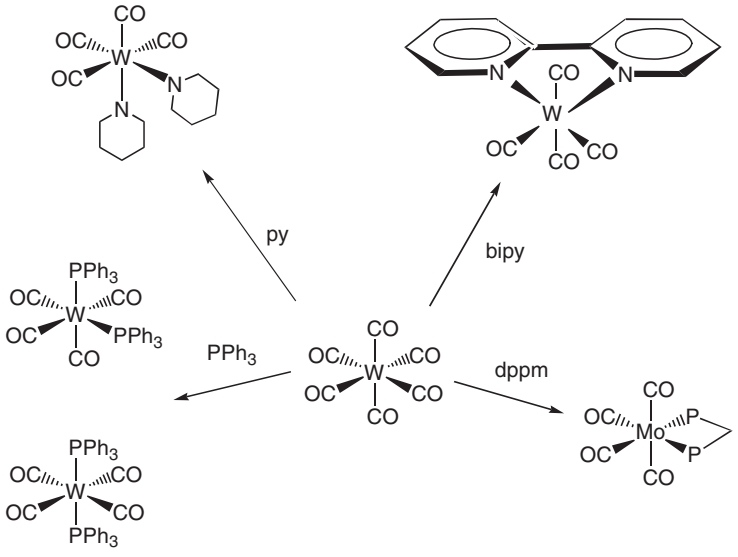

Scheme 11

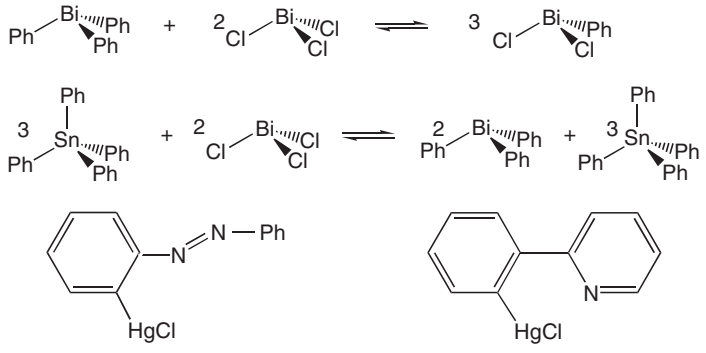

Scheme 12

1.12.10.8 Organometallic Reactions Involving Metal Powders

The reactions of metal powders with organic ligands to generate organometallic compounds have been widely studied, and the reduction of sparking phenomena in the presence of organic solvents has been investigated.[168–170] Schemes 13 and 14 provide some specific examples of the application of metal powders in organometallic transformations.[192–195] Although this application is counter-intuitive, it can nonetheless be used effectively for the synthesis of sandwich compounds and the generation of carbene intermediates.

Roberts *et al.*[192–196] have made a detailed study of the synthesis of (η-arene)(η-cyclopentadienyl)iron(II) salts using MW dielectric heating. The reactions were carried out in a conventional MW oven, but modified to permit simultaneous cooling using solid carbon dioxide, which is transparent to MWs because of the absence of a dipole moment. The MW technique reduced the reaction times the $AlCl_3$-mediated ligand exchange with ferrocene, in the presence of aluminum powder (to prevent ferricinium ion formation), from several hours to a few minutes, and generally higher yields were observed. 1,2,4-Trichlorobenzene proved to be an excellent solvent for such reactions; zinc and copper were also effective, but nickel and tin failed to promote the reaction. Arylamine complexes were also made in high yields. Complexes of triphenylphosphine were also reported, and decomplexation of the free ligands was obtained by irradiating a mixture of the complexes and graphite.

MW-mediated synthesis of [(η-arene)$(CO)_3$Mn][PF_6] salts was also reported, and a bis-complexed triphenylphosphine iron sandwich complex was obtained from the $AlCl_3$-catalyzed ligand-exchange reaction between

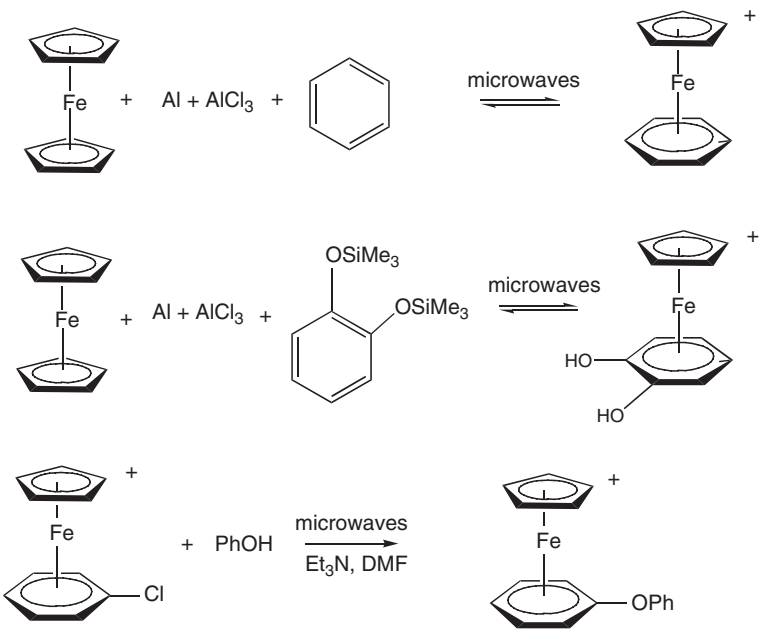

Scheme 13

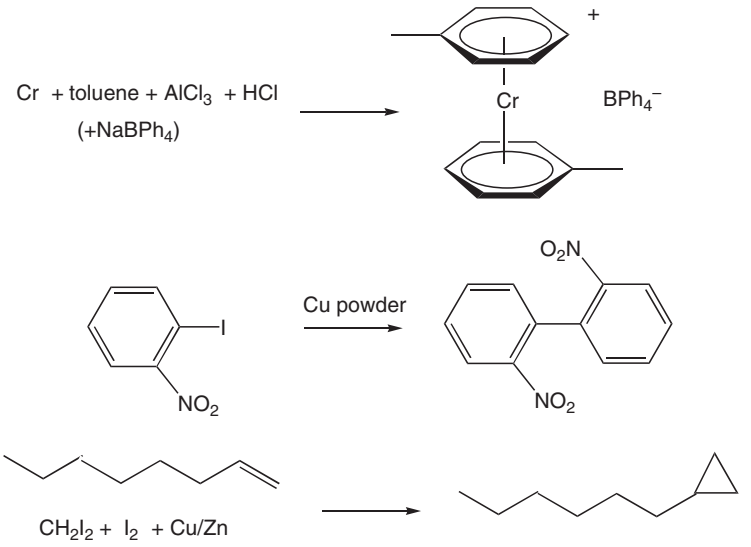

Scheme 14

$[M(CO)_4(PPh_3)_2]$ complexes (M = Cr, Mo, or W) and ferrocene.[193] In a recent study, it has been shown that the combination of ferrocene and $AlCl_3$ resulted in the highest temperatures for this class of reaction, and it has been proposed that a highly dipolar intermediate involving ferrocene and $AlCl_3$ may be responsible.[196] It was also noted that the reaction times of the displacement reactions of halobenzene complexes by phenols could be reduced from several hours to a few minutes. It was necessary to protect the phenols in order to obtain high yields.

Refs: 197–199 provide examples of organometallic compounds being synthesized without solvents on dry supports—a technique which has been widely used in organic chemistry. In these specific examples, ferrocenylenones and ferocenoate esters and amides were synthesized, the latter from ferrocenoyl fluoride.

1.12.10.9 Applications in Organic Syntheses Catalyzed by Organometallic Compounds

The general availability of specialized equipment, which had been designed specifically for organic syntheses, has led to the widespread application of the technique to organic reactions catalyzed by organometallic reagents (see Refs: 200–202 for an overview of the subject). Organometallic catalysis, in general, and palladium-catalyzed reactions, specifically, have been widely studied under MW conditions, because they frequently involve long reflux times under thermal conditions. The special features of flash MW heating have resulted in a number of innovations, for example, the generation of reacting gases *in situ*. In addition, the organic chemists have developed catalytic protocols that deliver impressive ee's even at the high temperatures which are encountered in an MW cavity. Nevertheless, the problems associated with transition metal catalysts, such as air and moisture sensitivity, expensive metals and ligands, remain. These applications have recently been reviewed by Olofsson and Larhed,[201] and, specifically, the following classes of reactions have been widely studied: Suzuki couplings, Negishi couplings, Heck couplings, cyanation and Sonogashira reactions, asymmetric molybdenum allylic alkylations, P–K reactions. Specific examples of these reactions are given in Scheme 15, and the relevant references are summarized in Table 3. A detailed analysis of the Heck reaction under thermal and MW conditions has been reported by Solabannavar *et al.*[225]

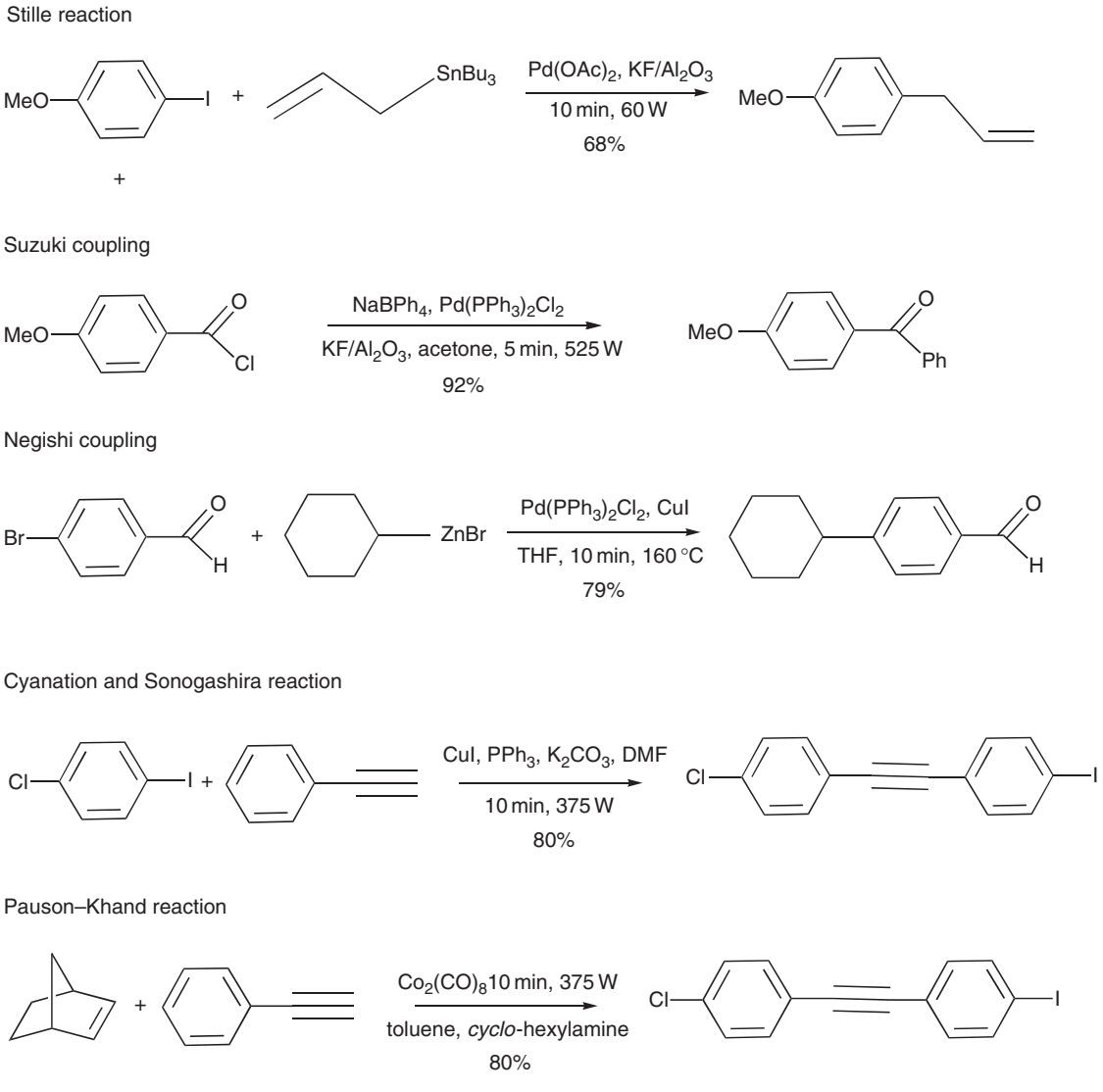

Scheme 15

Table 3 Examples of organic transformations catalyzed by transition metals studied under microwave conditions

Class of reaction	*References*
Stille coupling	203–206
Suzuki coupling	207–219
Negishi coupling	220
Heck coupling	221–234
Cyanation and Sonogahira reactions	235–238
Carbon heteroatom couplings	239–245
Asymmetric molybdenum alkylations and palladium allylations	246–254
Carbonyl sources	255–257
Pauson–Khand reactions	258,259
Ring-closing metathesis	260–262

MW energy has been shown to accelerate the reduction of many key functional groups in organic chemistry, and Danks and Wagner[265] have recently reviewed the area. In many examples, mild reagents and reaction conditions have been developed, and it has been demonstrated that the technique is widely applicable for the reduction of sensitive substrates; the use of supported reagents has reduced the need for solvents and permitted shorter reaction times. The higher yields of products have also simplified the work-up procedures.

The classes of functional groups which have been reduced and widely studied include: carbon–carbon multiple bonds,[264] carbonyl groups,[265] nitrogen-containing functional groups,[266,267] such as imines, nitro groups, hydrazones, and hydrazides. A number of reductions in organic chemistry require the addition of gases under high pressures, for example, catalytic hydrogenation or carbonylation, which require specialized techniques. The addition of solid hydrogen donors has allowed hydrogenation reactions to be performed in normal reaction vessels, and this has facilitated the application of MW dielectric heating to such processes. Metal carbonyls and formamide have been used as sources of carbon monoxide, although the latter generates not only carbon monoxide, but also ammonia. This can be advantageous in the synthesis of benzamides from arylhalides (see Table 3).[255–257]

Solvent-free reactions, particularly on mineral supports, have been widely developed following on from the pioneering work of Loupy and his group.[179] These reactions have proved to have a strong impact on the development of safe and efficient reduction processes. In these dry reactions, the MW energy is absorbed by the solid support as well as the reagent itself, thus allowing fast and homogeneous heating of the reactants. This would not have been possible with conventional thermal heating because of the poor thermal conductivity of solid powders. Ley and Kappe have reviewed MW-assisted solid-phase syntheses in organic chemistry and the integration of MW-assisted syntheses and solid-supported reagents.[268–271]

Lead drug compound synthesis using the current knowledge of medicinal chemistry represents a significant bottleneck in the discovery chain. MW-accelerated chemistry has proved to be invaluable for the pharmaceutical industry in reducing the timescale of this process. Therefore, pharmacentical companies have invested heavily in robot-assisted MW technology.[274–278] The time saving associated with the use of MW-assisted accumulation of compound libraries was tested by giving two independent researchers the task of making a target compound. The one who had access to an MW synthesizer achieved the desired target in 2 working days and with an 88% overall yield, whereas the one limited to using conventional thermal methods spent 37 working days and achieved an overall yield of only 4%.

1.12.10.10 Coordination Compounds

The technique has been widely applied to the synthesis of coordination compounds, but they fall outside the scope of this chapter, and the reader is referred to other recent sources.[273] Mingos and co-workers demonstrated that the synthesis of coordination compounds of very inert metal ions with d^3-and d^6-electronic configurations which generally require reaction times involving days could be reduced significantly using MW dielectric heating. Therefore, the technique has many possibilities for synthesizing coordination compounds which are precursors to organometallic compounds.[274–278] Also, it is noteworthy that the reactions of metal powders suspended as fluidized beds can be induced to react with gases such as chlorine, dioxygen, and ammonia on exposure to MWs and can lead to the synthesis of important starting materials on a large scale.

1.12.10.11 Heterogenous Catalytic Processes

In the area of solid-state chemistry, MW dielectric heating has been widely used to reduce the timescales of synthetic reactions, and as early as 1989, the thermal runaway associated with certain solids was utilized to synthesize high-temperature superconducting ceramics. The technique has also been used to study in detail heterogeneous catalytic processes.[279–289] "Hot spot" formation appears to be an important feature of the interaction of the MWs with the solid support materials which are impregnated with the catalyst, because the latter couple much more efficiently. The conversion efficiency of MW reactions is much higher than that for comparable thermal reactions and this has been attributed to hot spot formation, and it is estimated that the regions around the catalysts may be 100–200 °C higher than the temperature of the support material. These hot spots may be as large as 10 μm.

1.12.10.12 Fullerenes and Carbon Nanotubes

Refs: 290–294 summarize some recent applications of microwaves to fullerenes and also for the functionalization of nanotubes.[295,296]

1.12.10.13 MW Dielectric Heating in Combination with Other Energy Sources

Instrumentation for combining MW dielectric heat with sonochemistry, UV irradiation, and electrochemistry has been developed in recent years, and the subject has been reviewed by Roberts and Strauss.[297–301]

MW dielectric heating does not always lead to dramatic rate increases, but the simple convenience of the technique is likely to make it a standard one in the future. MW reactors are no longer viewed as the last resort for recalcitrant chemical reactions, but now frequently seen as the first choice for performing chemical reactions.

Acknowledgments

D. M. P. Mingos acknowledges the Alexander von Humboldt Foundation for its support.

References

1. See, for example, the following reviews: Gedanken, A. *Ultrason. Sonochem.* **2004**, *11*(2), 47–56.
1a. Ince, N. H.; Tezcani, G.; Belen, R. K.; Apikyan, I. G. *Appl. Catal., B* **2001**, *29*(3), 167–176.
1b. Adewuyi, Y. G. *Ind. Eng. Chem. Res.* **2001**, *40*(22), 4681–4715.
1c. Mason, T. J. *Ultrason. Sonochem.* **2000**, *7*(4), 145–149.
1d. Luche, J-L.; Fauvarque, J. *Info. Chim. Mag.* **2000**, *417*, 90–96.
1e. Mason, T. J. *Chem Soc. Rev.* **1997**, *26*(6), 443–451.
1f. Colarusso, P.; Serpone, N. *Res. Chem. Intermed.* **1996**, *22*(1), 61–89.
2. Mason, T. J., *Practical Sonochemistry – Users Guide to Applications in Chemistry and Chemical Engineering*; Ellis Horwood: New York, 1991; p 4.
2a. Mason, T. J., *Practical Sonochemistry – Users Guide to Applications in Chemistry and Chemical Engineering*; Ellis Horwood: New York, 1991; p 64.
3. Suslick, K. S., Ed. *Ultrasound: Its Chemical, Physical, and Biological Effects*; 1998; VCH: New York; Chapter 1.
4. Devin, C. *J. Acoust. Soc. Am.* **1959**, *31*, 1654.
4a. Casadonte, D. J., Jr.; Flores, M.; Petrier, C. *Ultrasonic Sonochemistry*, **2005**, *12*(3), 147–152.
4b. Wayment, D. G.; Casadonte, D. J. Jr. *Ultrasonics Sonochemistry* **2002**, *9*, 189–195.
4c. Wayment, D. G.; Casadonte, D. J. Jr. *Ultrasonics Sonochemistry* **2002**, *9*, 251–257.
5. Riesz, P. *Adv. Sonochem.* **1991**, *2*, 26.
6. Suslick, K. S.; Price, G. J. *Annu. Rev. Mater. Sci.* **1999**, *29*, 295–326.
7. Barber, B. P. Putterman, *Nature* **1991**, *352*, 318–320.
7a. Gompf, B.; Gunther, R.; Nick, G.; Pecha, R.; Eisenmenger, W. *Phys. Rev. Letts.* **1997**, *79*, 1405–1408.
8. Gaitan, D. F.; Crum, L. A.; Church, C. C.; Roy, R. A. *J. Acoust. Soc. Am.* **1992**, *91*, 3166–3183.
9. Flannigan, D. J.; Suslick, K. S. *Nature* **2005**, *434*(7029), 52–55.
9a. Didenko, Y. T.; McNamara, W. B.; Suslick, K. S. *Nature* **2001**, *407*, 877–879.
9b. Taleyarkhan, R.. P; West, C. D.; Cho, J. S.; Lahey, R. T.; Nigmatulin, R. I.; Block, R. C. *Science* **2002**, *295*, 1868–1873.
10. Sweet, J. D.; Casadonte, D. J., Jr. *J. Trib.* **1998**, *120*(3), 641–643.
11. Suslick, K. S.; Choe, S.-B.; Cichowlas, A. A.; Grinstaf, M. W. *Nature* **1991**, *353*, 414–416.
12. Suslick, K. S. *Sci. Amer.* **1989**, 62–68.
13. Lauterborn, W.; Hentschel, W. *Ultrasonics* **1985**, *24*, 59–65.
14. Sweet, J. D.; Casadonte, D. J., Jr. *Chem. Materials,* **1994**, *6*, 2113–2117.
15. Casadonte, D. J., Jr.; Sweet, J. D.; Vedamuthu, M. S. *Ultrasonics* **1994**, *32*(6), 477–480.
16. Suslick, K. S.; Schubert, P. S.; Goodale, J. W. *J. Am. Chem. Soc.* **1981**, *103*, 7342–7344.

17. Han, B. H.; Boudjouk, P. *Tetrahedron Lett.* **1981**, *22*(39), 3813–3814.
18. Ross, N. A.; Bartsch, R. A. *J. Heterocycl. Chem.* **2001**, *38*, 1255–1258.
19. Luche, J. L., Ed. *Synthetic Organic Sonochemistry*; Plenum: New York, 1998; 431 pp.
20. Suslick, K. S.; Casadonte, D. J., Jr.; Choe, S. B.; Cichowlas, A. A.; Doktycz, S. J.; Ghosh, C. K.; Grinstaff, M. W. *Mat. Res. Soc. Proc. EA-24* **1990**, 209–212.
21. Suslick, K. S.; Casadonte, D. J., Jr. *J. Am. Chem. Soc.*, **1987**, *109*, 3459–3461.
22. Uzcanga, I.; Bezverkhyy, I.; Afanasiev, P. *Chem. Mater.* **2005**, *17*, 3575–3577.
23. Casadonte, D. J., Jr.; Sweet, J. D. *205th ACS National Meeting*, Denver, CO, USA, 1993.
24. Chatakondu, K.; Green, M. L. H.; Thompson, M. E.; Suslick, K. S. *J. Chem. Soc., Chem. Comm.* **1987**, 900–901.
25. Kumar, R. V.; Elgamiel, R.; Palchik, O.; Gedanken, A.; Norwig, J. *J. Cryst. Growth* **2003**, *250*, 409–417.
26. Zhang, G.; Hua, I., **2000**, *34(8)*, 1529–1534.
27. Hua, I.; Hoffmann, M. R. *Environ. Sci. Technol.* **1996**, *30*, 864–871.
28. Hoffman, M. R.; Hua, I.; Höchemer, R. H. *Ultrason. Sonochem.* **1996**, *3*(3), S163–S172.
29. Petrier, C.; Jeunet, A.; Luche, J. L.; Reverdy, G. **1992**, *114*, 3148–3150
30. Kotronarou, A.; Mills, G.; Hoffmann, M. *Environ. Sci. Technol.* **1992**, *26*(7), 1460–1462.
31. Kotronarou, A.; Mills, G.; Hoffmann, M. *J. Phys. Chem.* **1991**, *95*, 3630–3638.
32. Cheung, H. M.; Bhatnagar, A.; Jansen, G. *Environ. Sci. Technol.* **1991**, *25*(8), 1510–1512.
33. Serpone, N.; Terzian, R.; Hidaka, H.; Pelizzeti, E. *J. Phys. Chem.* **1994**, *98*(10), 2634–2640.
34. Petrier, C.; Casadonte, D. J., Jr. *Advances in Sonochemistry*; Elsevier: Amsterdam, 2000; Vol. 6, pp 91–110.
35. Suslick, K. S. In *High Energy Processes in Organometallic Chemistry*; Suslick, K. S., Ed. American Chemical Society: Washington, D.C, 1987; p 191.
36. Sweet, J. D.; Casadonte, D. J., Jr. *Ultrason. Sonochem.*, **2001**, *8*, 97–101.
37. Jones, J.; Cheshire, M.; Casadonte, D. J., Jr.; Phifer, C. *Org. Letts.* **2004**, *6*(12), 1915–1917.
38. Thomes, W. J., Jr.; Simmons-Potter, K.; Phifer, C. C.; Potter, B. G., Jr.; Jamison, G. M.; Jones, J. E.; Casadonte, D. J., Jr. *J. App. Phys.* **2004**, *96*(11), 6313–6318 and references therein.
39. Suslick, K. S. In *High Energy Processes in Organometallic Chemistry*; Suslick, K. S., Ed.; American Chemical Society: Washington, D.C., 1987; p 196.

39a. Henglein, A. *Ultrasonics* **1987**, *25*, 7–18.

39b. Suslick, K. S. *Adv. Organomet. Chem.* **1986**, *25*, 73–120.

39c. Mason, T. J.; Lorimar, J. P. *Sonochemistry: Theory, Application and Uses of Ultrasound in Chemistry*; Wiley: New York, 1988.

40. Suslick, K. S.; Choe, S. B.; Cichowlas, A. A.; Grinstaff, M. W. *Nature* **1991**, *353*, 414–416.
41. Cao, X.; Koltypin, Y.; Kataby, G.; Prozorov, R.; Gedanken, A. *J. Mater. Res.* **1995**, *10*, 2952.
42. Gonsalves, K. E.; Rangarajan, S. P.; Garcia-Ruiz, A.; Law, C. C. *J. Mater. Sci. Lett.* **1996**, *15*, 1261.
43. Suslick, K. S.; Hyeon, T.; Fang, M. *Chem. Mater.* **1996**, *8*, 22172–2179.
44. Hyeon, T.; Fang, M.; Suslick, K. S. *J. Am. Chem.. Soc.* **1996**, *118*, 5492–5493.
45. Suslick, K. S. *MRS Bull.* **1995**, 29.
46. Suslick, K. S. In *Handbook of Heterogeneous Caatalysis*; Ertl, G., Knozinger, H., Weitkamp, J., Eds.; Vol. 3, Chapter 8.6, pp 1350–1357.
47. Suslick, K. S.; Didenko, Y.; Fang, M. M.; Hyeon, T.; Kolbeck, K. J.; McNamara, W. B., III; Mdleleni, M. M.; Wong, M. *Phil. Trans. Roy. Soc. London A* **1999**, *357*, 335–353.
48. Suslick, K. S.; Fang, M.; Hyeon, T. *J. Am. Chem. Soc.* **1996**, *118*, 11960–11961.
49. Grinstaff, M. W.; Salamon, M. B.; Suslick, K. S. *Phys. Rev.* **1993**, *B 48*, 269.
50. Bellisent, R.; Galli, G.; Grinstaff, M. W.; Migliardo, P.; Suslick, K. S. *Phys. Rev.* **1993**, 15797–15800.
51. Palchik, O.; Kataby, G.; Mastai, Y.; Gedanken, A. *Adv. Mater.* **1999**, *11*, 1289–1292.
52. Sivakumar, M.; Gedanken, A. *Ultrason. Sonochem.* **2004**, *11*, 373–378.
53. Sweet, J. D. Ph.D. Dissertation, Texas Tech University, Lubbock, 1998.

53a. Casadonte, D. J., Jr.; Sweet, J. D. *205th National Meeting of the American Chemical Society*, Denver, CO, USA, April, 1993.

54. Gonsalves, K. E.; Rangarajan, S. P.; Law, C. C.; Garcia-Ruiz, A.; Chow, G. M. *NanoStruct. Mater.* **1997**, *9*, 169–172.
55. Gonsalves, K. E.; Rangarajan, S. P. *J. Appl. Polym. Sci.* **1997**, *64*, 2667.
56. Gonsalves, K. E.; Li, H.; Perez, R.; Santiago, P.; Jose-Yacaman, M. *Coor. Chem. Rev.* **2000**, *206–207*, 607–630.
57. Mdleleni, M. M.; Hyeon, T.; Susklick, K. S. *J Am. Chem. Soc.* **1998**, *120*, 6189–6190.
58. Dhas, N. A.; Ekhtiarzadeh, A.; Suslick, K. S *J. Am. Chem. Soc.* **2001**, *123*, 8310–8316.
59. Landau, M. V.; Vradman, L.; Herskowitz, M.; Koltypin, Y.; Gedanken, A. *J. Catal.*, **2001**, *22*–36.
60. Suslick, K. S.; Hammerton, D. A.; Cline, R. E. *J. Am. Chem. Soc.* **1986**, *108*, 5641.
61. Dhas, N. A.; Gedanken, A. *J. Phys. Chem. B*, **1997**, *101*, 9495.
62. Dhas, N. A.; Gedanken, A. *Chem. Mater.*, **1997**, *9*, 3144.
64. Kesavan, V.; Dhar, D.; Koltypin, Y.; Perkas, N.; Palchik, O.; Gedanken, A.; Chandrasekaran, S. *Pure Appl. Chem.*, **2001**, *73*, 85–91.
65. Srivastava, D. N.; Perkas, N.; Zaban, A.; Gedanken, A. *Pure Appl. Chem*, **2002**, *74*, 1509–1517.
66. Suslick, K. S.; Flint, E. B.; Grinstaff, M. W.; Kemper, K. A. *J. Phys. Chem.* **1993**, *97*, 3098–3099.
67. McNamara, W. B., III; Didenko, Y.; Suslick, K. S. *Nature* **1999**, *401*, 772–775.
68. Jamison, T. F.; Shambayati, S.; Crowe, W. E.; Schreiber, S. L. *J. Am. Chem. Soc.* **1997**, *119*, 4353.
69. Ford, J. G.; Kerr, W. J., Kirk, G. G.; Lindsay, D. M.; Middlemiss, D. *Synlett.* **2000**, *10*, 1415–1418.
70. Dhas, N. A.; Cohen, H.; Gedanken, A. *J. Phys. Chem. B* **1997**, *101*, 6834–6838.
71. Li, B.; Xie, Y.; Huang, J.; Qian, Y. *Ultrason. Sonochem.* **1999**, *6*, 217–220.
72. Wardell, J. L. In *Comprehensive Organometallic Chemistry I*; Wilkinson, G., Stone, F. G. A., Able, E., Eds.; Pergamon: Oxford, 1982; Vol. 1, Chapter 2, pp 43–120.
73. Suslick, K. S.; Doktycz, S. J. In *Advances in Sonochemistry*; JAI Press: London, 1990; Vol. 1, pp 197–230.

73a. Suslick, K. S. In *Encyclopedia of Inorganic Chemistry*; King, R. B. Ed.; Wiley: New York, 1994; Vol. 7, pp 3890–3905.

74. Citas, P.; Luche, J.-L. In *Synthetic Organic Sonochemistry*; Luche, J.-L., Ed.; Plenum: New York, 1998; pp 167–234.

74a. Luche, L.-J.; Cintas, P. In *Active Metals: Preparation, Characterisation, Application*; Fürstner, A., Ed.; VCH: Weinheim, 1996; pp 133–190.

75. Pugin, B.; Turner, A. T. *Advances in Sonochemistry*; JAI Press: London, 1990; Vol. 1, pp 81–118.

76. Lepoint, T.; Lepoint-Mullie, F. Theoretical Bases. In *Synthetic Organic Sonochemistry*; Luche, J.-L., Ed.; Plenum: New York, 1998; pp 1–50.
77. Lauterborn, W.; Ohl, C. D. *Ultrason. Sonochem.* **1997**, *4*, 65–67.
78. Doktycz, S. J.; Suslick, K. S. *Science* **1990**, *247*, 1067–106.
79. Suslick, K. S.; Price, G. I. *Annu. Rev. Mater. Sci.* **1999**, *29*, 295–326.
80. Luche, J.-L. *Ultrason. Sonochem.* **1994**, *1*, S111–S118.
81. Samsonov, G. V. *Handbook of the Physicochemical Properties of the Elements*; IFI/Plenum: New York, 1968; Chapter 6, pp 387–445.
82. Suslick, K. S.; Casadonte, D. J., Jr. *J. Am. Chem. Soc.* **1987**, *109*, 3459–3461.

82a. Suslick, K. S.; Casadonte, D. J., Jr.; Doktycz, S. J. *J. Solid State Ionics* **1989**, *32–33*, 444–452.

83. Alex, C. C. T.; Goh, N. K.; Chia, L. S. *J. Chem. Soc. Chem. Commum.* **1995**, 201.
84. van Eldik, R.; Hubbard, C. C. *Chemistry Under Extreme or Non-classical Conditions*; Wiley: New York, 1997.
85. Marguilis, M. A. *High Energy Chem.* **2004**, *38*, 135–142.
86. Luche, J.-L.; Damiano, J. C. *J. Am. Chem. Soc.* **1980**, *102*, 7927–7928.
87. Tuulmets, A.; Kaubi, K.; Heinoja, K. *Ultrason. Sonochem.* **1995**, *2*, S75–S78.
88. Compton, R. G.; Eklund, J. C.; Page, S. D.; Sanders, G. H. W.; Booth, J. *J. Phys. Chem.* **1994**, *98*, 12410–12414.
89. Benhacene, A.; Labbé, P.; Pétrier, C.; Reverdy, G. *New J. Chem.* **1995**, *19*, 989–995.
90. Pétrier, C.; Luche, J.-L. In *Synthetic Organic Sonochemistry*; Luche, J.-L., Ed.; Plenum: New York, 1998; pp 51–106.
91. Li, C.-J. *Tetrahedron* **1996**, *52*, 5643–5668.
92. Lee, A. S.-Y.; Chu, S.-F.; Chang, Y.-T.; Wang, S.-H. *Tetrahedron Lett.* **2004**, *45*, 1551–1553.
93. Andrews, P. C.; Peatt, A. C.; Raston, C. L. *Tetrahedron Lett.* **2002**, *43*, 7541–7543.
94. Wang, J.; Yuan, G.; Dong, C.-Q. *Chem. Lett.* **2004**, *33*, 286–287.
95. Han, B. H.; Boudjouk, P. J. *J Org. Chem.* **1982**, *47*, 5030–5032.
96. Suslick, K. S.; Doktycz, S. J. *J. Am. Che. Soc.* **1989**, *111*, 2342–2344.
97. Coe, P. L.; Löhr, M.; Rochin, C. *J. Chem. Soc., Perkin Trans. 1* **1998**, 2803–2811.
98. Ross, N. A.; Bartsch, R. A. *J. Org. Chem.* **2003**, *68*, 360–366.
99. Ross, N. A.; MacGregor, R. R.; Bartsch, R. A. *Tetrahedron* **2004**, *60*, 2035–2041.
100. Lindly, J.; Lorimer, J. P.; Mason, T. J. *Ultrasonics* **1986**, *24*, 292–293.
101. Hanoun, J.-P.; Galy, J.-P.; Tenaglia, A. *Synth. Commun.* **1995**, *25*, 2443–2448.
102. Robin, M.; Pique, V.; Faure, R.; Galy, J.-P. *J. Heterocycl. Chem.* **2002**, *39*, 1083–1085.
103. Pellón, R. F.; Estévez-Braun, A.; Docampo, M. L. Martín, A.; Ravelo, A. G. *Synlett* **2005**, 1606–1608.
104. Sun, H.-Z.; Li, J.-S. *Chin. J. Org. Chem.* **1998**, *18*, 550–556.
105. Zhu, Y. *J. Phys. Chem. Solids* **2004**, *65*, 349–353.
106. Ragaini, V.; Bianchi, C. L. In *Synthetic Organic Sonochemistry*; Luche, J.-L., Ed.; Plenum: New York, 1998; pp 235–262.
107. Bai, L.; Wang, J.-X. *Curr. Org. Chem.* **2005**, *9*, 535–553.
108. Cravotto, G.; Beggiato, M.; Penoni, A.; Palmisano, G.; Tollari, S.; Lévêque, J.-L.; Bonrath, W. *Tetrahedron Lett.* **2005**, *46*, 2267–2271.
109. Cravotto, G.; Palmisano, G.; Tollari, S.; Nano, G. M.; Penoni, A. *Ultrason. Sonochem.* **2005**, *12*, 91–94.
110. Rajagopal, R.; Jarikote, D. V.; Srinivasan, K. V. *Chem Commun.* **2002**, 616–617.
111. Deshmukh, R. R.; Rajagopal, R.; Srinivasan, K. *Chem. Commun.* **2001**, 1544–1545.
112. Gholap, A. R.; Venkatesan, K.; Pasricha, R.; Daniel, T.; Lahoti, R. J.; Srinivasan, K. V. *J. Org. Chem.* **2005**, *70*, 4869–4872.
113. Ambulgekur, G. V.; Bhanage, B. M.; Damant, S. D. *Tetrahedron Lett.* **2005**, *46*, 2483–2485.
114. Toukoniity, B.; Mikkola, J.-P.; Muzin, D. Yu.; Salmi, T. *Appl. Catal. A: General* **2005**, *279*, 1–22.
115. Han, B.-H.; Boudjouk, P. *Organometallics* **1983**, *2*, 769–771.
116. Crabtree, R. H. In *The Organometallic Chemistry of the Transition Metals*, 2nd Ed.; Wiley: New York, 1994; Chapter 9, 206–235.
117. Felföldi, K.; Szőri, K.; Török, B.; Bartók, M. *Ultrason. Sonochem.* **2000**, *7*, 15–17.
118. Loupy, A.; Luche, J. L. In *Synthetic Organic Sonochemistry*; Luche, J.-L. Ed.; Plenum: New York, 1998; pp 107–166.
119. Zhao, Z.-Q.; Sun, B.; Peng, L.-Z.; Li, Y.; Li, Y.-L. *Chin. J. Chem.* **2004**, *22*, 1382–1383.
120. Lee, A. S. Y.; Dai, W. C. *Tetrahedron* **1997**, *53*, 859–868.
121. Roger, C.; Marseilli, P.; Salus, C.; Hamon, J.-R.; Lapinte, C. *J. Organomet. Chem.* **1987**, *336*, C13–C16.
122. Roger, C.; Hamon, P.; Toupet, L.; Rebaâ, H.; Saillard, J.-Y.; Hamon, J.-R.; Lapinte, C. *Organometallics* **1991**, *10*, 1045–1054.
123. Roger, C.; Tudoret, M.-J.; Guerchais, V.; Lapinte, C. *J. Organomet. Chem.* **1989**, *365*, 347–350.
124. Green, M. L. H.; Mountford, P.; Smout, G. J.; Speel, S. R. *Polyhedron* **1990**, *22*, 2763–2765.
125. Baker, R. J.; Jones, C. *Dalton Trans.* **2005**, 1341–1348.
126. Anandhi, U.; Sharp, P. R. *Angew. Chem., Int. Ed.* **2004**, *43*, 6128–6131.
127. Walton, D. J.; Mason, T. J. In *Synthetic Organic Sonochemistry*; Luche, J.-L., Ed.; Plenum: New York, 1998; pp 263–300.
128. Kostas, I. D.; Vallianatou, K. A.; Kyritsis, P.; Zedník, J. Vohlídal, J. *Inorg. Chim. Acta.* **2004**, *357*, 3084–3088.
129. Pilon, M. C.; Grushin, V. V. *Organometallics* **1998**, *17*, 1774–1781.
130. Neto, A. F.; Borges, A. D. L.; Miller, J.; Darin, V. A. *Synth. React. Inorg. Met. Org. Chem.* **1997**, *27*, 1299–1314.
131. Shieh, M.; Liou, Y.; Miao-Hsing, H.; Rung-Tsang, C.; Shioq-Jane, Y.; Shie-Ming, P.; Gene-Hsiang, L. *Angew. Chem., Int. Ed.* **2002**, *41*, 2384–2386.
132. Bianchi, C. L.; Carli, R.; Lanzani, S.; Lorenzetti, D.; Vergani, G.; Ragani, V. *Catal. Lett.* **1993**, *22*, 319–325.
133. Mason, T. J.; Lorimer, J. P. *ibid*, 2002; Chapter 3, pp 75–130.
134. Gigannantonio, R.; Ragaini, V.; Magni, P. *J. Catal.* **1994**, *146*, 103–115.
135. Ragaini, V.; Gigannantonio, R.; Magni, P.; Lucarelli, L.; Leofanti, G. *J. Catal.* **1994**, *146*, 116–125.
136. Török, B.; Felföldl, K.; Szakonyi, G.; Balázski, K.; Bartók, M. *Catal. Lett.* **1998**, *52*, 81–84.
137. Balázsik, K.; Török, B.; Felföldl, K.; Bartók, M. *Ultrason. Sonochem.* **1999**, *5*, 149–155.
138. Dhas, N. A.; Suslick, K. S. *J. Am Chem. Soc.* **2005**, *127*, 2368–2369.
139. Skrabalak, S. E.; Suslick, K. S. *J. Am Chem. Soc.* **2005**, *127*, 9990–9991.
140. Kappe, C. O.; Stadkler, A. *Microwaves in Organic and Medicinal Chemistry*; Wiley-VCH: Weinheim, 2005. (provides an excellent source of previous reviews).
141. Mingos, D. M. P.; Baghurst, D. R. *Chem. Soc. Rev.* **1991**, *20*, 1–45.
142. Lidstom, P.; Tierney, J. P., Eds. *Microwave-assisted Organic Synthesis*; Blackwell: Oxford, 2004.

143. Loupy, A., Ed. *Microwaves in Organic Synthesis*; Wiley-VCH: Weinheim, 2002.
144. Metaxas, A. C.; Meredith, R. J. *Industrial Microwave Heating*; Peter Perigrinis: London, 1983.
145. Sutton, W. H. *Am. Ceram. Soc. Bull.* **1989**, *68*, 376–386.
146. Von Hippel, A. R., *Dielectric Materials and Applications*; MIT Press: Cambridge, 1954.
147. Gedye, R.; Smith, F.; Westaway, K.; Ali, H.; Balderisa, L.; Laberge, L.; Roasell, J. *Tetrahedron Lett.* **1986**, *27*, 279–282.
148. Giguere, R. J.; Bray, T. L.; Duncan, S. N.; Majetich, G. *Tetrahedron Lett.* **1986**, *28*, 4945–4948.
149. Gabriel, C.; Gabrield, S.; Grant, E. H.; Halstead, B. D. J.; Mingos, D. M. P. *Chem. Soc. Rev.* **1998**, *27*, 213–223.
149a. Mingos, D. M. P. *Microwave-assisted Organic Synthesis*; Lidston, P., Tierney, J. P., Eds.; Blackwell: Oxford, 2004; pp 1–22.
150. Craig, D. Q. M. *Dielectric Aspects of Pharmacological Systems*; Taylor and Francis: London, 1995.
151. These data were supplied by Biotage (previously Personal Chemistry) Kunsgaten 76,SE-753 18 Uppsala,Sweden.; similar data are available from the other manufacturers listed below.
152. CEM Corporation, PO Box 200, Mathews NC 28106-0200, United States.
153. Biotage (previously Personal Chemistry), Kunsgaten 76, SE-753 18 Uppsala, Sweden.
154. Milestone Inc., 160B Shelton Rd., Monroe, CT 06468, United States.
155. Baghurst, D. R.; Mingos, D. M. P.; Watson, M. J. *J. Organomet. Chem.*, **1989**, *368*, C43–C45.
156. Baghurst, D. R.; Mingos, D. M. P. *J.Organomet.Chem.* **1990**, *384*, C57–C60.
157. Baghurst, D. R.; Mingos, D. M. P. *J. Chem. Soc. Dalton. Trans.* **1992**, 1151–1158.
158. Pollington, S. D.; Bond, G.; Moyes, R. B.; Whan, D. A.; Candlin, J. P.; Jennings, J. R. *J. Org. Chem.* **1991**, *56*, 1313–1314.
158a. Pollington, S. D.; Bond, G.; Moyes, R. B.; Whan, D. A. *Chem. Ind.* **1991**, *18*, 686–687.
159. Baghurst, D. R.; Mingos, D. M. P. *J. Chem. Soc., Chem. Commun.* **1992**, 674–677 and reference to Hoopy, T., Neas, E., and Magetich, G.
160. Gronnow, M. J.; White, R. J.; Clarke, R. J.; Maquarie, D. J. *Org. Process. Res. Dev.* **2005**, *9*, 516–518.
161. Raner, K. D.; Strauss, C. R.; Vyskoc, F.; Mokbel, L. *J. Org. Chem.*, **1993**, *58*, 950.
162. Raner, K. D.; Strauss, C. R. *J. Org. Chem.*, **1992**, *57*, 62.
163. Gedye, R. N.; Rank, W.; Westaway, K. *Can. J. Chem.*, **1991**, *69*, 79.
164. de la Hoz, A.; Diaz-Ortez, A.; Moreno, A. *Chem. Soc. Rev.*, **2005**, *34*, 164–178.
164a. Kappe, C. O.; Dallinger, D. *Nature Drug., Discov.* **2005**, 1.
165. Hayes, B. L. *Microwave Synthesis at the Speed of Light*; CEM Publications: Mathews, 2002; p 2005.
166. Leadbeater, N. E.; Pillsbury, S. J.; Shanahan, E.; Williams, V. A. *Tetrahedron*, **2005**, *61*, 3565–3585.
167. Dabirmnesh, Q.; Roberts, R. M. G. J. *Organomet. Chem.*, **1993**, *460*, C28–C29.
168. Whittaker, A. G.; Mingos, D. M. P. *J. Chem. Soc., Dalton Trans.*, **2002**, 3967–3970.
169. Whittaker, A. G.; Mingos, D. M. P. *J. Chem. Soc., Dalton Trans.*, **1992**, 2751–2752.
170. Whittaker, A. G.; Harrison, A.; Oakley, G. S.; Youngson, I. D.; King, S.; Heenan, R. *Rev. Sci. Instr.* **2001**, *72*, 173–176.
171. Baghurst, D. R.; Cooper, S. R.; Greene, D. L.; Mingos, D. M. P.; Reynolds, S. M. *Polyhedron* **1990**, *9*, 893–895.
172. Steinker, A.; Stadlet, A.; Mayer, S. F.; Faber, K.; Kappe, C. O. *Tetrahedron Lett.*, **2001**, *42*, 6283.
173. Garrigues, B; Laurent, R.; Laporte, C.; Laporterie, A.; Dubac, J. *Liebigs. Ann. Chem.*, **1996**, 743.
174. Ley, S. V.; Leach, A. G.; Storer, R. T. *J. Chem. Soc., Perkin Trans.1*, **2001**, 358–361.
175. Leadbeater, N. E.; Torrenius, H. M. *J. Org. Chem.* **2002**, *67*, 3145–3148.
176. Strauss, C. R.; Trainor, R. W. *Aust. J. Chem.*, **1995**, *48*, 1665–1992.
176a. Raner, K. D.; Strauss, C. R.; Trainor, R. W. *J. Org. Chem.* **1995**, *60*, 2456–2460.
177. Pivonka, D. A.; Empfield, J. R., *Appl. Spect.* **2004**, *58*, 41–46.
178. Zhang, X.; Hayward, D. O.; Mingos, D. M. P. *Catal. Lett.* **2003**, *88*, 33–38.
179. Pereux, L.; Loupy, A. *Tetrahedron* **2001**, *57*, 9199–9223.
179a. Loupy, A.; Maurel, F.; Sabatie-Gogova, A. *Tetrahedron*, **2004**, *60*, 1683.
180. Chatakondu, K.; Green, M. L. H.; Reynolds, S. M.; Mingos, D. M. P. *J. Chem. Soc., Chem. Commun.* **1989**, 1515–1517.
181. Van Atta, S. L.; Duclos, B. A.; Green, D. B. *Organometallics* **2000**, *19*, 2397–2399.
182. Hogarth, G. B.; Ardon, M.; Hayes, P. D. *J. Chem. Educ.* **2002**, *79*, 1249–1251.
183. Ardon, M.; Hogarth, G. B.; Oscroft, D. J. *J. Organomet. Chem.*, **2004**, *689*, 2429–2435.
184. Kuhnert, N.; Danks, T. N. *Green Chem.* **2001**, *3*, 68–75.
185. Desai, B.; Danks, T. N.; Wagner, G. *J. Chem. Soc. Dalton Trans.* **2003**, 2544–2549.
186. Kuhnert, N.; and Danks, T. N. *J. Chem. Res., Synop.* **2002**, 66–68.
187. Stoddart, M. W.; Brownie, J. H.; Baird, M. C.; Schmider, H. L. *J. Organomet. Chem.* **2005**, *690*, 3440–3450.
188. Ali, S.; Bond, S. P.; Mbogo, S. A.; McWhinnie, W. R.; Watts, P. M. *J. Organomet. Chem.* **1989**, *371*, 11–13.
189. Laurent, R.; Laporterie, A.; Dubac, J.; Berlan, J. *Organometallics* **1994**, *13*, 2493–2495.
190. Singh, R. V.; Jain, M.; Deshmukh, C. N. *Appl. Organomet. Chem.* **2005**, *19*, 879–886.
191. Gold, H.; Larhed, M.; Nilsson, P. *Synlett.*, **2005**, *10*, 1596–1600.
192. Dabirmanesh, Q.; Fernando, S.; Roberts, R. M. G. *J. Chem. Soc. Perkin Trans. I*, **1995**, 743–749.
193. Dabirmanesh, Q.; Roberts, R. M. G. *J. Organomet. Chem.* **1997**, *542*, 99–103.
194. Brown, R. A.; Fernando, S.; Roberts, R. M. G. *J. Chem. Soc. Perkin Trans. I*, **1994**, 197–201.
195. Fernando, S.; Roberts, R. M. G. *J. Organomet. Chem.* **1994**, *474*, 133–141.
196. Roberts, R. M. G., *J. Organomet. Chem.* **2006**, *691*, 2641–2647.
197. Villemin, D.; Martin, B.; Puciova, M.; Toma, S. *J. Organomet. Chem.* **1994**, *484*, 27–31.
198. Spinella, A.; Caruso, T.; Pastore, U.; Ricart, S. *J. Organomet. Chem.* **2003**, *684*, 266–268.
199. Imrie, C.; Elago, R. T.; Williams, N.; McCleland, C. W.; Engelbrecht, P *J. Organomet. Chem.* **2005**, *690*, 4959–4966.
200. Dankwardt, J. W. *J. Organomet. Chem.* **2005**, *690*, 932–938.
201. Olofsson, K.; Larhed, M. In *Microwave-assisted Organic Synthesis*; Lidstom, P., Tierney, J. P., Eds.; Blackwell: Oxford, 2004; pp 23–41.
202. Kappe, C. O. *Angew. Chem., Int. Ed.*, **2004**, *43*, 6250–6284.
203. De La Hoz, A.; Diaz-Ortiz, A.; Moreno, A. *Curr. Top. Org. Chem.* **2004**, *8*, 903–918.
204. Villemin, D.; Caillot, F. *Tetrahedron Lett.*, **2001**, *42*, 639–642.
205. Skoda-Foldes, R.; Pfeiffer, P.; Horvarth, J.; Tuba, Z.; Kollar, L. *Steroids* **2002**, *67*, 709–713.
206. Elander, N.; Jones, J. R.; Lu, S. Y.; Stone-Elander, S. *Chem. Soc. Rev.*, **2000**, *29*, 239–249.

207. Samuelsson, L.; Langstrom, B. *J. Labelled Compd. Radiopharm.*, **2002**, *46*, 263–272.
208. Wang, J. X.; Wei, B. G.; Hu, Y. L.; Lui, Z. X.; Yang, Y. H. *Synth. Commun.*, **2001**, *31*, 3885–3890.
209. Appukkuttan, P.; Dehaen, W.; Van der Eyken, E. *J. Org. Lett.*, **2005**, *7*, 2723–2726.
210. Wang, J. X.; Yang, Y. H.; Wei, B. G.; Hu, Y. L.; Fu, Y. *Bull. Chem. Soc. Jpn.*, **2002**, *75*, 1381–1382.
211. Kabalka, G. W.; Wang, L.; Pagni, R. M.; Hair, C. M.; Namboori, V. *Synthesis*, **2003**, 217–222.
212. Gong, Y.; He, W. *Org. Lett.*, **2002**, *4*, 3803–3805.
213. Noteberg, D.; Hamelink, E.; Hulten, L.; Wahlgren, M.; Vrang, L. *J. Med. Chem.*, **2003**, *46*, 734–746.
214. Noteberg, D.; Schaal, W.; Hamelink, E.; Vrang, L.; Larhed, M. *J. Comb. Chem.*, **2003**, *5*, 456–464.
215. Blettner, C. G.; Konig, W. A.; Stenzel, W.; Schotten, T. *J. Org. Chem.*, **1999**, *64*, 3885–3890.
216. Leadbeater, N. E.; Marco, M. *Org. Lett.*, **2002**, *4*, 2973–2976.
217. Leadbeater, N. E.; Marco, M. *J. Org. Chem.*, **2003**, *68*, 888–892.
218. Nambroodiri, V. V.; Varma, R. S. *Green Chem.*, **2001**, *3*, 146–148.
219. Luo, G. L.; Chen, L.; Poindexter, G. S. *Tetrahedron Lett.*, **2002**, *43*, 5739–5742.
220. Melucci, M.; Barbarella, G.; Sotgiu, G. *J. Org. Chem.*, **2002**, *67*, 8877–8884.
221. Ohberg, L.; Westman, J. *Synlett.*, **2001**, 1893–1896.
222. Ley, S. V.; Leach, A. G.; Storer, R. I. *J. Chem. Soc., Perkin Trans. 1*, **2001**, 358–361.
223. Van der Eycken, E.; Appukkuttan, P.; De Borggraeve, W.; Dehaen, W.; Dallinger, D. *J. Org. Chem.*, **2002**, *67*, 7904–7907.
224. Alonso, S.; Beletskaya, I. P.; Yus, M. *Tetrahedron* **2005**, *61*, 117711–11835.
225. Vallin, K. S. A.; Emilsson, P.; Larhed, M.; Hallberg, A. *J. Org. Chem.*, **2002**, *67*, 6243–6246.
226. Solabannavar, S. B.; Desai, U. V.; Mane, R. B. *Indian J. Chem., Sect. B. Org.* **2004**, *43B*, 2235–2237.
227. Cabri, W.; Candiani, I., *Acc. Chem. Res.* **1995**, *28*, 2–7.
228. Xu, L. J.; Chen, W. P.; Ross, J.; Xiao, J. L. *Org. Lett.* **2001**, *3*, 295–297.
229. Varma, R. S.; Namboodiri, V. V. *Chem. Comm.*, **2001**, *7*, 643–644.
230. Law, M. C.; Wong, K. Y.; Chan, T. H. *Green Chem.* **2002**, *4*, 328–330.
231. Choudray, B. M.; Madhi, S.; Chowdari, N. S.; Kantam, M. L.; Sreedhar, B. *J Am. Chem. Soc.* **2002**, *124*, 14127–14136.
232. Wang, J. X.; Liu, Z. X.; Hu, Y. L.; Wei, B. G.; Bai, L., *Synth. Commun.* **2002**, *32*, 1607–1614.
233. Larhed, M.; Hallberg, A. In *Handbook of Organopalldium Chemistry for Organic Synthesis*; Negishi, E.-I., Ed.; Wiley: New York, 2002; Vol. 1, pp 1133–1178.
234. Loiseleur, O.; Meier, P.; Pfaltz, A. *Angew. Chem., Int. Ed. Engl.* **1996**, *35*, 200–202.
235. Nilsson, P.; Gold, H.; Larhed, M.; Hallberg, A. *Synthesis* **2002**, 1611–1614.
236. Alterman, M.; Hallberg, A. *J. Org. Chem.* **2000**, *65*, 7984–7989.
237. Zhang, A.; Meumeyer, J. L. *Org. Lett.* **2003**, *5*, 201–203.
238. Arvela, R. K.; Leadbeater, N. E.; Torenius, H. M.; Tye, H. *Org. Biomol. Chem.* **2003**, *1*, 1119–1121.
239. Sorensen, U. S.; Pombo-Villar, E. *Tetrahedron* **2005**, *61*, 2697–2703.
240. Wang, J. X.; Liu, Z. X.; Hu, Y. L.; Wei, B. G.; Kang, L. Q. *Synth. Commun.* **2002**, *32*, 1937–1945.
241. Yang, B. H.; Buchald, S. L. *J. Organomet. Chem.*, **1999**, *576*, 125–146.
242. Hartwig, J. F. *Angew. Chem., Int. Ed. Engl.* **1998**, *37*, 2047–2067.
243. Sharifi, A.; Hosseinzadeh, R.; Mirzaei, M. *Mon. Chem.* **2002**, *133*, 329–332.
244. Wan, Y. Q.; Alterman, M.; Hallberg, A. *Synthesis* **2002**, 1597–1600.
245. Wang, T.; Magnin, D. R.; Hamann, L. G. *Org. Lett.* **2003**, *5*, 897–900.
246. Stadler, A.; Kappe, C. O. *Org. Lett.* **2002**, *4*, 3541–3543.
247. Trost, B. M.; Hachiva, I. *J. Am. Chem. Soc.* **1998**, *120*, 1104–1105.
248. Trost, B. M.; Van Vranken, D. L. *Chem. Rev.* **1996**, *96*, 395–422.
249. Bremberg, U.; Lutsenko, S.; Kaiser, N. F.; Larhed, M.; Hallberg, A. *Synthesis*, **2000**, 1004–1008.
250. Kaiser, N.-F. K.; Bremberg, U.; Larhed, M.; Moberg, C.; Hallberg, A. *J. Organomet. Chem.* **2000**, *603*, 2–5.
251. Sebahar, H. L.; Yoshida, K.; Hegedus, L. S. *J. Org. Chem.*, **2002**, *67*, 3788–3795.
252. Belda, O.; Kaiser, N. F.; Bremberg, U.; Larhed, M.; Hallberg, A. *J. Org. Chem.*, **2000**, *65*, 5668–5870.
253. Trost, B. M.; Andersen, N. G. *J. Am. Chem. Soc.*, **2002**, *124*, 14320–14321.
254. Belda, O.; Moberg, C. *Synthesis*, **2002**, 1601–1606.
255. Larsen, R. D. *Curr. Opin. Drug Discov. Dev.* **1999**, *2*, 651–667.
256. Wannberg, J.; Larhed, M. *J. Org. Chem.* **2003**, *68*, 5750–5753.
257. Georgsson, J.; Hallberg, A.; Larhed, M. *J. Comb. Chem.*, **2003**, *5*, 350–352.
258. Wan, Y. Q.; Alterman, M.; Larhed, M.; Hallberg, A. *J. Org. Chem.*, **2002**, *67*, 6232–6235.
259. Wan, Y. Q.; Alterman, M.; Larhed, M.; Hallberg, A. *J. Comb. Chem.*, **2003**, *5*, 82–84.
260. Iqbal, M.; Vyse, N.; Dauvergne, J.; Evans, P. *Tetrahedron Lett.* **2002**, *43*, 7859–7862.
261. Fischer, S.; Groth, U.; Jung, M.; Schneider, A. *Tetrahedron Lett.*, **2002**, *43*, 2023–2026.
262. Kaiser, N. F. K.; Bremberg, U.; Larhed, M.; Moberg, C.; Hallberg, A. *Angew. Chem., Int. Ed.* **2000**, *39*, 3595.
263. Garbacci, S.; Desai, B.; Lavaster, O.; Kappe, C. O. *J. Org. Chem.* **2003**, *68*, 9136.
264. Grigg, R.; Martin, W.; Morris, J.; Sridharan, V. *Tetrahedron Lett.* **2003**, *44*, 4899.
265. Danks, T. N.; Wagner, G. In *Microwave-assisted Organic Synthesis*; Lidstom, P., Tierney, J. P., Eds.; Blackwell: Oxford, 2004; pp 75–98.
266. Banik, B. K.; Barakat, K. J.; Wagle, D. R.; Manhas, M. S.; Bose, A. K. *J. Org. Chem.* **1999**, *64*, 5746–5753.
267. Varma, R. S.; Saini, R. K. *Tetrahedron Lett.* **1997**, *38*, 4337–4338.
268. Varma, R. S.; Dahiya, R. *Tetrahedron* **1998**, *54*, 6293–6298.
269. Lakar, D. D.; Gohain, M.; Prajapati, D.; Sandhu, J. S. *New. J. Chem.* **2002**, *26*, 193–195.
270. Baxendale, I. R.; Lee, A-L.; Ley, S. V. In *Microwave-assisted Organic Synthesis*; Lidstom, P., Tierney, J. P., Eds.; Blackwell: Oxford, 2004; pp 133–176.
271. Stadler, A.; Kappe, C. O. In *Microwave-assisted Organic Synthesis*; Lidstom, P., Tierney, J. P., Eds.; Blackwell: Oxford, 2004; pp 177–221.
272. Sarko, C. In *Microwave-assisted Organic Synthesis*; Lidstom, P., Tierney, J. P., Eds.; Blackwell: Oxford, 2004; pp 222–235.
273. Harrison, A.; Whittaker, A. G. *Comprehensive Co-ordination Chemistry*, McCleverty, J. A., Meyer, T., Eds.; 2003; pp 741–745.
274. Mingos, D. M. P.; Greene, D. L. *Transit. Met. Chem.* **1991**, *16*, 71–72.

275. Whittaker, A. G. *Educ. Chem.* **2002**, 134–136.
276. Saito, K.; Matsusue, N.; Kanno, H.; Kamada, Y.; Takahashi, H.; Matsumura, T. *Jpn. J. Appl. Phys. Part 1* **2004**, *43*, 2733–2734.
277. Amarante, D.; Cherian, C.; Emmel, C.; Chen, H-Y.; Dayal, S.; Koshy, M.; Megehee, E. G. *Inorg. Chim. Acta.* **2005**, *358*, 2231–2238.
278. Safari, N.; Jamaat, P. R.; Pirouzmand, M.; Shabani, A. *J. Porphr. Phthalocya.* **2004**, *8*, 1209–1213.
279. Zhang, X.; Hayward, D. O.; Mingos, D. M. P. *Catalysis Lett.* **2003**, *88*, 33–38.
280. Zhang, X.; Hayward, D. O.; Mingos, D. M. P. *J. Chem. Soc. Chem. Commun.* **1999**, 975–976.
281. Zhang, X.; Hayward, D. O.; Mingos, D. M. P. *Ind. Eng. Chem. Res.* **2001**, *40*, 2810–2817.
282. Zhang, X.; Hayward, D. O.; Lee, C.; Mingos, D. M. P. *Appl. Catal. B: Environmental* **2001**, *33*, 137–148.
283. Zhang, X.; Hayward, D. O.; Mingos, D. M. P. *Catal. Lett.* **2002**, *84*, 225–233.
284. Chen, C-L.; Weng, H-S. *Appl. Catal. B: Environmental* **2005**, *55*, 115–122.
285. Zhang, X.; Lee, C. S.-M; Hayward, D. O.; Mingos, D. M. P. *Catal. Lett.* **2003**, *88*, 129–139.
286. Zhang, X.; Lee, C. S.-M.; Mingos, D. M. P.; Hayward, D. O. *Appl. Catal. A: General* **2003**, *249*, 151–164.
287. Will, H.; Scholz, P.; Ondruschka, B. *Top. Catal.* **2004**, *29*, 175–182.
288. Will, H.; Scholz, P.; Ondruschka, B. *Chem. Ing. Tech.* **2004**, *76*, 272–275.
289. Will, H.; Scholz, P.; Ondruschka, B. *Chem. Eng. Technol.* **2004**, *27*, 113–122.
290. Zholobenko, V. L.; House, E. R *Catal. Lett.* **2003**, *89*, 35–40.
291. Will, H.; Scholz, P.; Ondruschka, B. *Chem. Ing. Tech.* **2002**, *74*, 1057–1067.
292. Langa, F.; De la Cruz, P.; Espildora, E.; De la Hoz, A. Proceedings of Electrochemical Society; *Fullerenes 2000: Functionalized Fullerenes* 2000; Vol. 9, pp 168–178.
293. Langa, F.; de la Cruz, P.; Espildora, E.; Garcia, J. J.; Perez, M. C.; de la Hoz, A. *Carbon* **2000**, *38*, 1641–1646.
294. Langa, F.; De la Cruz, P.; De la Hoz, A.; Espildora, E.; Cossio, F. P.; Lecea, B. *J. Org. Chem.*, **2000**, *65*, 2499–2507.
295. Wang, Y.; Iqbal, Z.; Mitra, S. *J. Am. Chem. Soc.* **2006**, *128*, 95–99.
296. Wang, Y.; Iqbal, Z.; Mitra, S. *Carbon* **2005**, *43*, 1015–1020.
297. Robert, B. A.; Strauss, C. R. In *Microwave-assisted Organic Synthesis*; Lidstom, P., Tierney, J. P., Eds.; Blackwell: Oxford, 2004; pp 177–221.
298. Muench, J.; Herrmann, R.; Schwieger, W. *Chem. Eng. Technol.* **2005**, *28*, 672–676.
299. Peng, Y.; Song, G. *Green Chem.* **2001**, *3*, 302–304.
300. Chemat, S.; Aouabed, A.; Bartels, P. V.; Esveld, D. C.; Chemat, F. *J. Microwave Power Electromagn.* **1999**, *34*, 55.
301. Compton, R. G.; Coles, B. A.; Marken, F. *J. Chem. Soc., Chem. Commun.* **1998**, 2595–2596.

1.13 High-throughput Organometallic Chemistry: Chemical Approaches, Experimental Methods, and Screening Techniques

V Murphy, Symyx Technologies, Santa Clara, CA, USA

1.13.1 Introduction

During the mid-1980s, a highly competitive pharmaceutical industry was motivated to accelerate the drug discovery process. Organic synthesis directed toward discovery of new pharmacologically active molecules was a time-consuming, labor-intensive process with a low probability of success. The synthetic chemist making tens to hundreds of molecules per year in a serial fashion was faced with an overwhelmingly complex relationship between molecular structure and desirable biological interactions. High-efficiency biological assays had been proposed many years earlier to facilitate more rapid screening,[1] but the synthesis of the requisite number of candidate molecules was a huge bottleneck. A new concept emerged: combinatorial chemistry, defined as the simultaneous synthesis of collections (libraries) of structurally distinct molecules, was introduced as a technique to accelerate discovery research.[2] Clever synthetic strategies such as the solid-phase "split-pool" approach subsequently enabled the concurrent synthesis of many thousands of molecules.[3,3a–3g] When combined with a suitable high-throughput biological assay, combinatorial chemistry afforded the opportunity to perform experiments at rates many orders of magnitude faster than conventional approaches, which would in theory greatly improve the probability of success. Early approaches were motivated by the synthesis of very large numbers of compounds, attainable with little to no purification, but the structural diversity of the molecules was restricted by a limited number of amenable chemical routes. The initial success rates proved to be lower than anticipated. Such experiences catalyzed a fundamental shift in strategy, which spawned the development of new parallel chemistries and creative synthetic techniques designed to better address specific biological targets. Candidate libraries, often smaller in size, were targeted to maximize the opportunity for desirable biological interactions. The benefits from such a focused approach became apparent through an increased pipeline of pharmacologically active molecules in clinical development, and a significant decrease in the time from target identification to the generation of useful leads. Initially confronted with skepticism and resistance, combinatorial organic chemistry has evolved into a well-established and broadly adopted discipline with a very successful track record.[4,4a,5,5a–5c]

In the mid-1990s, several reports suggested that the philosophy of combinatorial chemistry could be extended into other non-biological areas. Schultz[6,6a] first described and exemplified the combinatorial approach to the discovery of new materials, while Ellman, and subsequently several other groups, demonstrated the possibilities for extending the concept into the area of catalysis.[7,8,8a,8b,9] Combinatorial or high-throughput approaches to the synthesis of organometallic compounds began to develop with homogeneous catalysis as the principle area of interest (the term "high-throughput" has been adopted preferentially within the field of organometallic chemistry, likely because the number of library members synthesized is typically much lower when compared with the number of library members synthesized by initial combinatorial approaches reported within the pharmaceutical industry[3,3a–3g]). In fact, a review of the literature since COMC (1995) reveals that practically all reports associated with high-throughput organometallic chemistry were centered on making discoveries in the field of homogeneous catalysis.[10] The focus on catalysis is not surprising. Analogous to the situation in the field of drug discovery, the discovery and development of new homogeneous catalysts is impeded by a limited understanding of the complex relationships between molecular structure and catalytic performance. A typical free energy surface for a catalytic cycle is complicated, and the ability to predict catalytic properties is, not surprisingly, very limited. For example, one cannot readily predict which new metal–ligand combinations will lead to active catalyst classes and, even for existing well-studied catalysts, simple ligand modifications can lead to profound and unpredictable effects. The conventional approach of designing, synthesizing, screening, and optimizing catalysts one at a time therefore remains a perilously slow trial-and-error process, which offers no guarantee of success. With a seemingly limitless structural landscape, and unpredictable structure–performance relationships, high-throughput approaches are unquestionably attractive.

As with the case in the pharmaceutical industry, high-throughput approaches for catalyst discovery were initially confronted with healthy skepticism and resistance. One of the reasons is perhaps associated with the compromises that often need to be made to carry out a successful high-throughput experiment. The high-throughput synthesis and screening of organometallic catalyst libraries is typically performed at smaller scales in order to accommodate arrays of reaction vessels. Smaller reaction vessels, microliter reaction volumes, and the effects of scaling down catalyst concentrations all raise questions of experiment quality and relevance to larger scales. Moreover, control of process conditions (e.g., temperature, stirring) can be challenging. In particular, for catalysis involving gaseous reactants, mass-transfer limitations can be accentuated because of the difficulties of achieving efficient stirring within a confined array format, thus potentially obscuring the true properties of the catalysts.[11]

Perhaps the most contentious issue centers on the synthesis of the candidate organometallic catalysts in library format. Traditionally, the organometallic chemistry student is trained to purify and meticulously characterize every new organometallic compound before subjecting it to further experimentation. While such an approach

unquestionably provides excellent training, it is simply not amenable to a high experimental throughput. The synthesis and screening of libraries of organometallic compounds usually precludes the synthesis, isolation, and characterization of each library member. For a high experimental throughput, the experiments must be approached in a different manner. Most of the reports chronicled within this chapter adopt a "mix and screen" approach in which ligands are contacted *in situ* with reactive metal complexes and the product(s) are screened without compound isolation or purification. Understandably, this approach seems less than satisfying in the face of more traditional training. For example, complexation efficiencies can be expected to vary significantly depending upon the properties of the ligands, coordination modes may be uncertain, mixtures will certainly form, and in some instances no reactions will take place at all.[12,13] What are the implications and benefits of screening such mixtures? Although many of these issues have now been ingeniously addressed, experimental compromises often go hand-in-hand with the high-throughput approach, and it is little wonder that such approaches were initially confronted with skepticism.

The issues raised in the preceding paragraphs illustrate that it is naive to suppose that high-throughput catalyst discovery is simply a case of assembling a collection of molecules and screening them to find the catalyst of interest. The high-throughput experiment is fraught with challenges that must be addressed skillfully in order to produce results with meaningful information. For example, if "mix and screen" approaches are to be deployed for high-throughput synthesis, then the complexation conditions need to be chosen very carefully. Multiple chemical routes and reaction conditions should be included in the experimental design to maximize the probability of accessing the targeted catalyst candidates. All experimental protocols and reaction conditions should be scrutinized closely, and validated wherever possible by "rediscovering" known catalysts using the high-throughput protocols. Any compromises should be considered fully before resultant experimental data are subjected to interpretation and used to design follow-up experiments. In summary, sustainable high-throughput workflows are challenging to construct, and catalysts that meet desired performance criteria are usually found through carefully planned rounds of synthesis, screening, and intelligence gathering.

The breadth of topics covered in the first COMC chapter to address this important topic reveals how rapidly high-throughput approaches to the syntheses and screening of organometallic compounds have developed. Clever chemical approaches, elaborate parallel chemical reactors, and a diverse range of rapid analytical techniques all combine to testify a broadening interest within academic and industrial institutions. The reports reviewed in this chapter reveal that high-throughput approaches have led to the discovery of new catalyst structures that would likely not have been uncovered using more conventional approaches. The examples illustrate the utility of pooled, rapid-serial and parallel high-throughput approaches. Pooled approaches, in which candidate catalysts are screened together in a one reactor and subjected to necessary deconvolution techniques to identify the particular catalyst of interest, can obviate the need for sophisticated parallel reactors. Rapid-serial or parallel approaches place more challenging demands on the reactor capabilities, but avoid the need to develop a deconvolution technique. Whichever approach is considered, it is clear that new catalysts can now be discovered at extraordinary rates, and moreover, much of the periodic table can be addressed: from high-valent cationic group (IV) metal alkyl complexes for olefin polymerization to low-valent, redox-active, chiral, late-metal complexes for enantioselective transformations. As with traditional approaches, intelligent chemical strategies and thoughtful experimental protocols, when applied correctly, can produce incredible results.

1.13.1.1 Chapter Scope and Organization

This chapter is intended to provide a comprehensive review of the advances made in this field since its inception in 1995. The principal focus is the field of combinatorial or high-throughput organometallic chemistry, defined here as the simultaneous synthesis of organometallic molecules for whatever purpose. It is the intent to adhere to the traditional definition of an organometallic compound, although as will be seen, in many high-throughput approaches compounds are not isolated, and the generation of the M–C bonds may often only be inferred from the putative mechanism of a catalytic cycle. The intention is to be inclusive wherever possible. High-throughput approaches directed toward inorganic coordination compounds are not within the scope of this chapter. Furthermore, the uses of single organometallic catalysts to prepare libraries of organic molecules are not addressed here. Both of these topics have been reviewed extensively elsewhere.[5,5a–5c,14]

It is no coincidence that high-throughput approaches have advanced in concert with new reactor designs and rapid analytical techniques. Elaborate parallel reactors have been reported and utilized for catalyst discovery and process optimization and, in addition, a host of rapid analytical techniques is now available for product analysis. Significant advances are highlighted throughout the chapter, and Sections 1.13.4 and 1.13.5 provide the reader with references to

all of the advances made in these important areas. The organization of the topics covered in this chapter reflects the dominance of studies focused on discovering new catalysts for the transformation of organic molecules. Sections are grouped into types of organic transformations addressed with high-throughput approaches utilizing arrays of organometallic molecules. Table 1 provides a global summary of the reports highlighted in this chapter.

1.13.1.2 Related Literature Reviews

Since the mid-1990s, high-throughput approaches to the discovery of new catalysts and new materials have advanced sufficiently to warrant multiple literature reviews.[15–28] Jandeleit and co-workers,[15] and Woo and co-workers,[16] have previously reviewed the field of high-throughput materials science and catalysis, while many groups have published broad reviews in the area of homogeneous catalysis.[14,17–24] Additionally, Hoveyda and co-workers,[25,25a–25f] Ding and co-workers,[26] Gennari and Piatulli,[27] Snapper and Traverse,[28] Reetz,[29] Merritt,[30] and Burgess and Porte,[31] have all reviewed high-throughput approaches to the discovery of new catalysts for asymmetric transformations.

1.13.2 High-throughput Approaches to Catalyst Discovery

1.13.2.1 Olefin Polymerization

The polyolefin industry continues to seek improvements and differentiation in catalyst performance features such as productivity, temperature stability, co-monomer incorporation capability, co-polymer sequence distribution control, stereochemical control, molecular weight capability, and the ability to co-polymerize new monomer combinations. In order to set up a high-throughput approach for the discovery of new olefin polymerization catalysts, significant challenges need to be addressed. For example, the parallel synthesis of high-valent cationic metal alkyl complexes is very challenging, since traditional synthetic routes and resultant yields are highly sensitive to the nature of the supporting ligands and reaction conditions. Furthermore, such complexes are typically very sensitive to water and oxygen, and upon activation the resultant catalysts will often decompose in the absence of monomer. Additionally, the difficulties associated with performing controlled polymerization reactions are well known and must be considered. Changes in solution viscosity, exotherms arising from the polymerization events and polymer precipitation, can all impact mass-transfer efficiencies and obscure accurate catalyst performance ranking. Consequently, olefin polymerization reactions are typically performed in sophisticated autoclaves with mass flow controllers and good mechanical stirring to ensure efficient gas–liquid mass transfer. Furthermore, a suitable method for temperature control is necessary to manage exotherms, and a reaction quenching mechanism is necessary to control the extent of reaction (and avoid polymer precipitation). Confronted with such technical difficulties, it would seem that olefin polymerization catalysis is far from an ideal candidate for the high-throughput approach. However, several groups have now reported successful high-throughput experiments using a wide variety of chemical approaches and polymerization reactor designs.

The first example of a high-throughput approach to the synthesis and screening of organometallic compounds for olefin polymerization was reported by workers at Symyx Technologies.[32,32a] Building off the catalyst discovery reported by Brookhart,[33,33a] the Symyx team developed a parallel synthesis and screening protocol for a library of 96 polystyrene-bound 1,2-diimine nickel and palladium complexes. The key synthetic intermediate, a polystyrene-bound 1,2-diketone, was converted into a 48-membered 1,2-diimine library through a condensation reaction with 48 electronically and sterically diverse anilines (Equation (1)).

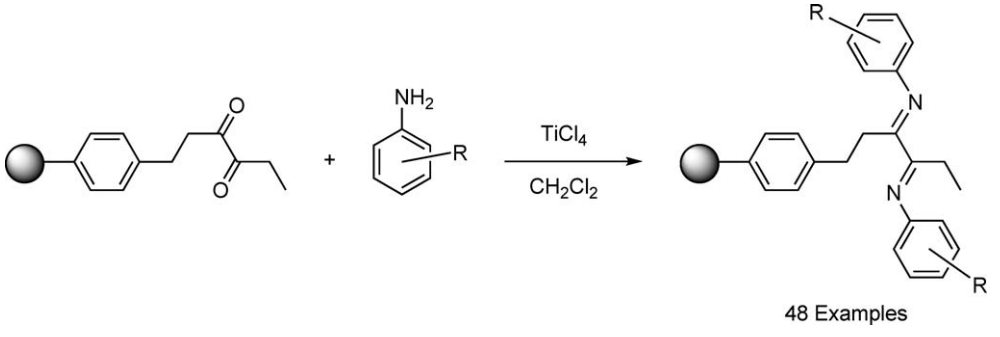

(1)

Table 1 Efficacy of two room temperature Heck catalysts discovered in Hartwig's high-throughput screen

Chemical transformation	*Ligand array description*	*Metals*	*Reactor format and conditions*	*Rapid analytical technique*	*Comments*	*Year*	*References*
Olefin polymerization							
Ethylene polymerization	48 Polystyrene-supported 1,2-diimines	Ni, Pd	Symyx PPR®, 5 ml, RT, 50 psi C_2H_4	GPC (M_W)	Proof of concept for HT approaches	1998	32
Ethylene polymerization	Eight 1,2-diimines	Pd	Pooled in single vessel, excess C_2H_4, −10 °C	ESI-MS	Proof of concept; catalyst performance in line with literature	1999	49
Propylene polymerization	12 Salicylaldimines, 2 : 1 ligand metal ratio	Ti	Pooled in single vessel, 150 ml, RT, 2.7 atm C_3H_6	Selective extraction of pooled products and library deconvolution	New syndiospecific Ti catalyst discovered	2000	38
Ethylene polymerization	200 Salicylaldimines	Cr	Reactor not specified, 1.5 ml, RT, 1 bar C_2H_4	[a]	New highly active Cr catalyst discovered	2002	36
1-Octene polymerization	23 Diverse ligands	Zr, Hf	Sealed 96 glass vial array, 250 µl, 75 °C, (120 µl 1-octene)	Automated yield, GPC (M_W)	New amide–ether Hf catalyst family identified	2003	12
Ethylene-1-octene co-polymerization	96 Amine–ether ligands	Hf	Symyx PPR®, 6 mL, 130 °C, (0.25 ml 1-octene), 100 psi C_2H_4	Automated yield, GPC (M_W), FTIR (composition)	Amide–ether Hf catalysts identified; catalysts on par with commercially relevant systems	2003	12
Ethylene–norbornene co-polymerization	16 1,2-Diimines	Pd	Conventional reactor, 200 ml, 30 °C, (6.6 ml norbornene) 6 bar C_2H_4	[b]	Catalyst performance strongly dependent upon structure	2003	44
Propylene polymerization	10 Salicylaldimines, 2 : 1 ligand : metal ratio (Target structures: $[L^a][L^b]TiCl_2$)	Ti	Pooled in single vessel, 150 ml, 0 °C, 2.7 atm C_3H_6	Pooled GPC (M_W) and library deconvolution	New heteroligated Ti catalyst discovered	2004	39
Ethylene polymerization	47 Imido ligands, derived from amines (Target structures: $Ti(NR)(Me_3[9]aneN_3)Cl_2$)	Ti	Custom eight-well pressure reactor, 62 ml, 100 °C, 7 bar C_2H_4	[a]	New highly active Ti catalyst discovered	2004	40

(*Continued*)

Table 1 (Continued)

Chemical transformation	*Ligand array description*	*Metals*	*Reactor format and conditions*	*Rapid analytical technique*	*Comments*	*Year*	*References*
Norbornene polymerization	Four Pyrazoyl–pyridine ligands	Ni, Pd, Co	Custom eight-well reactor, 10 ml, 30 °C, (1.28 g norbornene)	[b]	New active catalysts identified	2004	42
Ethylene polymerization	~30 1,2-Dimines, ~90 2,6-Diimino-pyridines	Fe	Custom eight-well pressure reactor, 30 ml, 50 °C, 10 bar C_2H_4	[b]	Results consistent with previous reports	2004	45
Ethylene polymerization	205 Salicylaldimines	Cr	24-Well Radley reactor,[c] 2 ml, RT, 1 atm C_2H_4	Reaction solutions tared and then re-weighed post polymerization (without stripping solvent)	A series of structurally distinct catalysts identified	2005	37
Ethylene polymerization	Series of small salicylaldimine focus libraries (~20 ligands)	Cr	Schlenk tube, 100 ml, RT, 1 atm C_2H_4	[b]	Cr catalysts optimized for low and high M_W polyethylene	2005	37
Coupling and addition reactions							
Sonogashira coupling	Seven diverse ligands	Ru, Ni, Co, Fe, Pd	Array of 96 vials, 250 µl, 50 °C	TLC with quantitative image analysis	The first example of an Ru catalyst for Sonogashira coupling identified	2004	55
Aryl–amine coupling	119 Diverse phosphine and heterocyclic carbene ligands	Pd	Sealed glass 96-well microtiter plate, 50 µl, 70 °C	FRET technique, fluorescence plate reader	Series of Pd/ligand combinations shown to be effective	2003	58
Hydroamination: aniline plus cyclohexadiene	11 Simple phosphines	Ni, Pd, Ru, Rh, Ir	Sealed glass 96-well microtiter plate, 50 µl, RT	Colorimetric assay	A general, high yielding Pd catalyst discovered	2001	61
Hydroamination: alkylamines plus functionalized olefins	11 Simple phosphines	Ni, Pd, Ru, Rh, Ir	Sealed glass 96-well microtiter plate, 50 µl, RT	Colorimetric assay	Variety of high-yielding catalysts discovered	2001	62
Heck coupling of solid-supported aryl bromides and chlorides with fluorescent olefins	45 Diverse phosphines	Pd	Sealed glass 96-well microtiter plate, 165 µl, 100 °C	UV lamp	Two Pd catalysts identified, highly effective for aryl chlorides	1999	63

Heck coupling through C–H bond activation	Four metal complexes, no added ligands	Pd, Ru	Chemspeed ASW 2000[d], ~3–5 ml, 20–80 °C	GC-MS	Selective catalyst identified to couple acrylates and aryl amides	2002	64
Heck coupling of derivatized substrates for FRET screen	96 Diverse phosphines	Pd	Sealed glass 96-well microtiter plate, 50 µl, 70 °C	FRET technique, fluorescence plate reader	Room temperature Heck catalyst discovered	2003	56
α-arylation of cyanoesters: derivatized substrates for FRET screen	113 Diverse phosphine and heterocyclic carbene ligands	Pd	Sealed glass 96-well microtiter plate, 50 µl, 70 °C	FRET technique, fluorescence plate reader	Catalyst identified to couple cyanoacetate with a variety of aryl halides	2001	59
Ullmann ether synthesis: 2-bromoaniline plus various alcohols	96 diverse pyridine-based ligands	Cu	Septa-sealed glass vials on an orbital shaker, 450 µl, 80 °C	GC	Two high yielding Cu catalysts identified (yields >50%)	2000	66
Ullmann ether synthesis: 2-bromoaniline plus various alcohols	Three pyridine-based focus libraries (total 94 ligands)	Cu	Septa-sealed glass vials on an orbital shaker, 450 µl, 80 °C	GC	Improved systems identified, including ligands previously unreported for Ullmann coupling	2000	66
Suzuki coupling of aryl chlorides	P-functionalized aminopyridines (~20 ligands)	Ni,Pd	Parallal apparatus installed in glove box[h]	GC	Multiple high yielding Ni and Pd catalysts identified	2002	67
Annulation reaction for the formation of γ-carbolines	Seven Pd-ligand combinations, 11 Bases	Pd	Array of 96 sealed glass tubes 120 µl, 110 °C	Parallel capillary electrophoresis	Several catalyst systems identified	2000	70
Hydrosilylation: derivatized substrate for colorimentric screen	12 Isolated metal complexes	Ir, Pd	Custom 60-well teflon plate, 300 µl, RT	Colorimetric assay	New Pd catalyst identified	1998	71
Hydrosilylation of acetophenone	40 Polystyrene-supported aminophosphine–phosphinites	Rh	Custom 76-well plate 400, µl, RT	GC	New Rh catalyst identified	2002	72

(*Continued*)

Table 1 (Continued)

Chemical transformation	*Ligand array description*	*Metals*	*Reactor format and conditions*	*Rapid analytical technique*	*Comments*	*Year*	*References*
Hydroformylation of 1-octene	16 "Base-paired" ligands, four Phosphine-functionalized aminopyridines, and four phosphine-functionalized isoquinolones	Rh	Reactor details not specified, 10 bar 1 : 1 CO/H_2	GC	Active "base-pair" ligands identified	2005	73
Allylic alkylation of diethyl malonate	Eight diverse ligands	Mn, Fe, Co, Ni, Cu, Ru, Rh, Pd, Ir, La	Microtiter plate[h] RT	Colorimetric assay	First non-phosphine Ir catalyst identified	1999	74
Olefin metathesis	Seven diverse ligands	Fe, Ru, Pd, Ir	Array of 96 1 ml tubes 300 µl, 70 °C	TLC with quantitative image analysis	Unexpected outcome, olefin isomerization catalyst identified	2003	76
Tandem olefin isomerization–Claisen rearrangement	Seven diverse ligands	Ru, Ir	Array of 96 tubes 350 µl, 70 °C	TLC with quantitative image analysis	Ru catalyst identified	2005	77
Enantioselective reactions							
$Et_2Zn + RCHO$	10 2-Pyrrolidinemethanol ligands	Zn	[e]	[b]	Proof of concept for HT approaches	1995	7
$Et_2Zn + RCHO$	Five chiral diols and five chiral nitrogen ligands as chiral "additives" for asymmetric activation	Zn	24-well plate of polypropylene tubes ~300 μL, 0 °C	HPLC-CD	ee values up to >99% (100% conversion)	1999	84
$Et_2Zn + RCHO$	Five racemic amino alcohols 10 chiral amino alcohol "activators" to induce asymmetric catalysis	Zn	24-well plate of polypropylene tubes, ~400 µl, 0 °C	HPLC-CD	ee values up to 93% (>90% conversion)	2001	92b
Hydrogenation of 3-alkylidene-lactams	32 Chiral phosphines	Ru, Rh, Ir	Array of 96 glass vials in a pressure chamber 360 μL, RT or 40 °C, 65 psi H_2	Chiral HPLC	Ir catalyst identified with ee 91% (>99% conversion)	2002	97
Transfer hydrogenation of aromatic ketones	10 Amino alcohols	Ru	Sealed NMR tubes	^{13}C NMR	Proof of concept for rapid NMR technique	2002	90a

Hydrogenation of (*Z*)-*β*-(acylaminoacrylates)	One optimized chiral phosphoramidite used in combination with six others (target structures: $[(L^{a*})(L^{b*})Rh]BF_4$)[f]	Rh	Array of 88 glass tubes housed in an autoclave, ~3 ml, RT, 10 bar H_2	Chiral GC	ee values up to 91% (>99% conversion)	2003	99
Hydrogenation of acetamidoacrylates	Six chiral phosphonites, eight chiral phosphites, one chiral phosphoramidite (target structures: $[(L^{a*})(L^{b*})Rh]BF_4$)[f]	Rh	Schlenk flask array, ~11 ml, RT, 1.3 bar H_2	Chiral HPLC or GC	high ee values (>95%) for a variety of substrates	2003	101
Hydrogenation of acetamidoacrylates	Two chiral phosphonites, two chiral phosphites, one chiral phosphoramidite, 9 achiral ligands (target structures: $[(L^{a*})(L^{b*})Rh]BF_4$)[f]	Rh	Schlenk flask array, ~11 ml, RT, 1.3 bar H_2	Chiral HPLC or GC	Reversal of ee compared to Ref: 101	2003	102
Hydrogenation of 1,3-oxazoldines	48 Chiral phosphorus-based ligands	Rh	Glass vials in a 1 l autoclave, 500 µl, RT, 40 bar H_2	Chiral HPLC	ee values up to ~80% obtained	2003	104
Hydrogenation of methyl *N*-acetamido acrylate	Eight chiral phosphites and eight chiral phosphoramidites (target structures: $[(L^{a*})(L^{b*})Rh]BF_4$)	Rh	Library screened under H_2 purge, RT[h]	Chiral GC	ee values up to 94% (>99% conversion)	2004	100
Hydrogenation of *N*-acylenamines	Three chiral phosphonites, five chiral phosphites, two chiral phosphines (target structures: $[(L^{a*})(L^{b*})Rh]BF_4$)[f]	Rh	Schlenk flask array, ~11 ml, RT, 1.3 bar H_2	Chiral HPLC or GC	ee values up to 97% (>99% conversion)	2004	101c
Hydrogenation of (*Z*)-*β*-(acylamino acrylates)	Seven chiral phosphonites, five chiral phosphites, one chiral phosphoramidite (target structures: $[(L^{a*})(L^{b*})Rh]BF_4$)[f]	Rh	Array of glass vials, 2.5 ml, RT, 60 bar H_2	Chiral HPLC or GC	ee values up to 99% (>99% conversion)	2004	101a
Hydrogenation of (*Z*)-*β*-(acylamino acrylates)	32 Chiral phosphoramidites	Rh	Premix-multi reactor[g], 6 bar H_2	Chiral GC	ee values up to 95% TOF 150 hr^{-1}	2004	98

(*Continued*)

Table 1 (Continued)

Chemical transformation	*Ligand array description*	*Metals*	*Reactor format and conditions*	*Rapid analytical technique*	*Comments*	*Year*	*References*
Hydrogenation of various substrates	20 Planar chiral diphosphines covalently attached to an arene chromium tricarbonyl framework	Rh	Two Formats:[h] (i) glass vials, 1 bar H_2, RT, (ii) high pressure 80 bar H_2, RT	[h]	Several promising new catalysts identified, ee values up to 82%	2004	105
Transfer hydrogenation of acetophenone	Nine chiral amines	Ru	6 ml, RT[h]	Capillary GC	Several promising new catalysts identified, ee values up to 89%	2005	103
Hydroformylation of pooled substrates (styrene, vinyl acetate, and allyl cyanide)	Nine chiral phosphites	Ru	Endeavor eight-well reactor[j]; 4 ml, 35 or 100 °C, 150 psi 1 : 1 H_2/CO	Chiral GC	Rh catalyst identified, ee values up to 88% for vinyl acetate (branched/linear ratio >100 : 1)	2004	114
Allylic substitution: 1,3-diphenylpropenyl acetate plus dimethylmalonate	13 Phosphine oxazolines	Pd	Array of 1 ml polypropylene tubes, 430 µl, RT	Chiral HPLC	Pd catalyst identified, ee values up to 94%	1998	117d
Allylic substitution reaction: cyclopentenyl acetate plus dimethylmalonate	136 Phosphines bound to β-turn peptides linked to a solid support	Pd	Array of vials[h], ~2 ml, RT	NMR	Pd catalyst identified, ee values up to 95%	2004	117a
Allylic substitution reactions: chiral allylic esters plus diethylmalonate	60 Phosphorus-based ligands	Pd	~250 µl, RT	ESI-MS	Pd catalyst identified with ee values higher than previously reported	2004	82e
Hydrosilylation of various ketones	32 Nitrogen-containing chiral phosphites	Rh	Array of glass vials, 100 µl, RT	ESI-MS and chip-based DIOS-MS	Pd catalyst identified ee values up to 88%	2003	82e

[a]Activities were obtained through product yields, not known if automated procedures were used.
[b]Conventional analytical methods employed.
[c]http://www.radleys.com.
[d]http://www.chemspeed.com.
[e]Conventional laboratory equipment employed.
[f]L* = chiral ligand.
[g]www.premex-reactorag.ch.
[h]Details limited.
[i]http://argonaut.biotage.com.

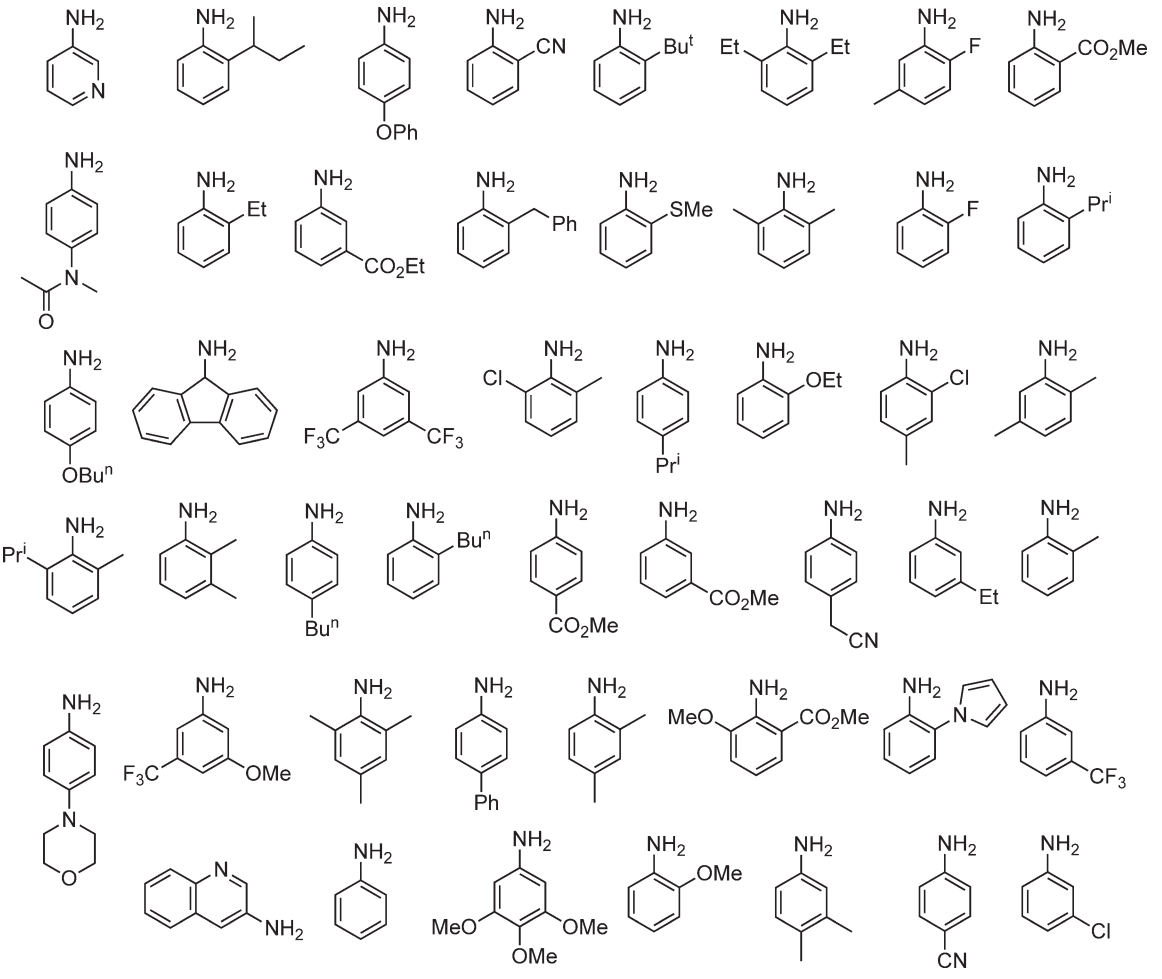

The ligand library was then divided into two parts and converted into 48 nickel and palladium complexes through one-step reactions with $(DME)NiBr_2$ and (COD)PdMeCl (where DME = 1,2-dimethoxyethane and COD = cyclooctadiene)(Equation (2)).

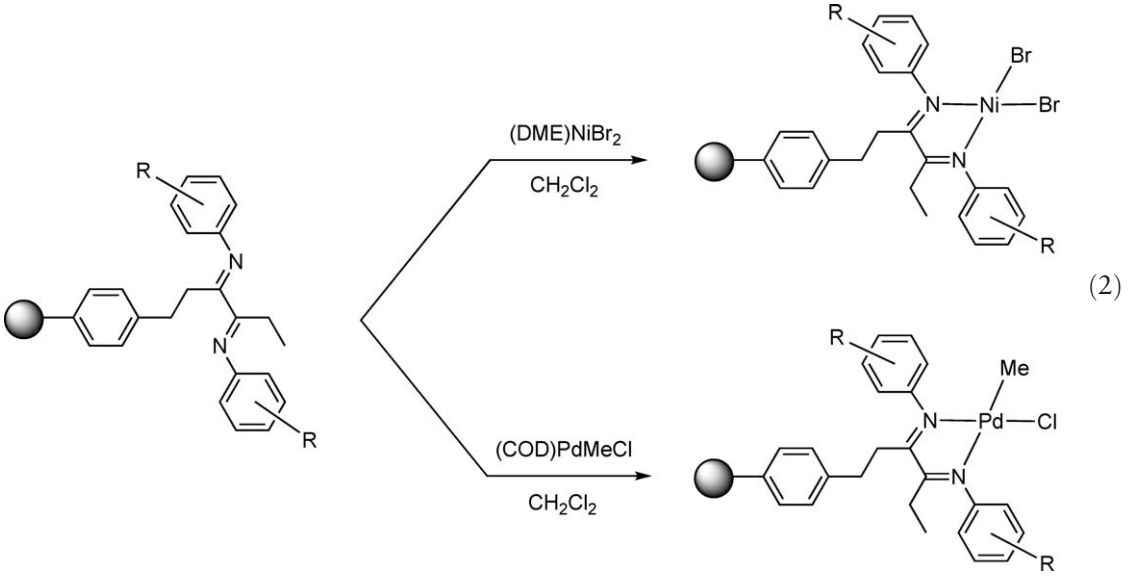

(2)

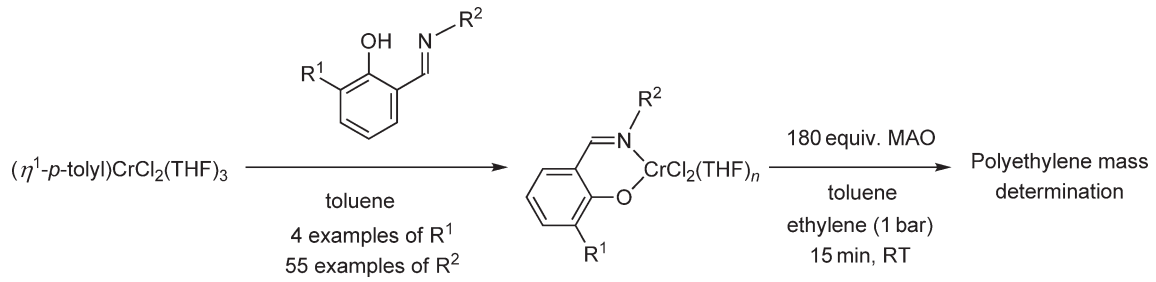

Scheme 1

The supported nickel catalyst precursors were activated with 300 equiv. of MAO (MAO = methylaluminoxane), while the palladium catalyst precursors were activated with $Na[B(3,5\text{-}(CF_3)_2C_6H_3)_4]$. The catalysts were then screened for their ability to polymerize ethylene (60 psi, room temperature) using a new parallel pressure reactor.[34,34a] For the first time, the efficacy of a high-throughput, parallel approach for synthesizing and screening olefin polymerization catalysts was demonstrated. However, despite this nice illustration of ligand diversity, no significant catalyst discoveries emerged from the Symyx study. The report also demonstrated an interesting pooled approach involving a chemical encoding strategy in which polystyrene-bound Ni(II) and Pd(II) complexes were encoded with cleavable tertiary amine tags. The two encoded complexes were activated and screened for ethylene polymerization activity in the same reactor. After the pooled polymerization, individual polymer particles were selected and chemically treated to cleave their amine tags. Subsequent analysis using HPLC revealed the identity of the amine, thus associating the polymer particle with identity of the catalyst. Müllen and co-workers at the Max-Planck Institute have also reported a pooled screening approach in which silica-supported catalysts were encoded with fluorescent dyes.[35] First, solutions of various metallocene–MAO mixtures were contacted with silica, exposed to the appropriate dye, and dried to produce the encoded, supported catalysts. After pooled polymerizations, the resultant polymer particles were analyzed by UV spectroscopy to identify the fluorescent tag, and hence the metallocene. Encoding strategies open possibilities for high-throughput screening in a single reactor, thus eliminating the need for sophisticated parallel reactors.

Gibson and co-workers at BP have also reported a high-throughput approach, directed toward the optimization of newly discovered salicylaldimine chromium polyethylene catalysts.[36] In this study, a ca. 200-membered salicylaldimine ligand library was synthesized using simple condensation reactions between four bulky salicylaldehydes and 55 commercially available amines. The bulky salicylaldehyde building blocks were chosen on the basis of previous screening studies. The chromium complexes were formed *in situ* by contacting the ligands (5 µmol) with the reactive chromium complex $(\eta^1\text{-}p\text{-tolyl})CrCl_2(THF)_3$ (5 µmol in 1.5 ml toluene). The solutions were activated with MAO and stirred under an ethylene atmosphere (1 bar) for 15 min at room temperature (Scheme 1). Although the authors do not specify the reactor format, simple reaction vessels would accommodate such mild screening conditions. Catalyst activity was determined by polyethylene yield, and a new highly active chromium catalyst **1** was discovered from the study.

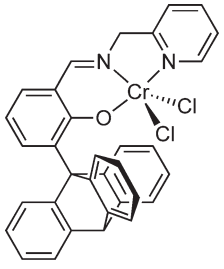

1

As previously discussed, there are known difficulties associated with performing olefin polymerizations. Changes in solution viscosity, reaction exotherms, and polyethylene precipitation can all enhance mass-transfer limitations and obscure accurate catalyst performance ranking. However, with these caveats in mind, it is noteworthy that the information content from the aforementioned studies was still high, and a new highly active chromium catalyst was uncovered with a surprising structure.

In a subsequent study, the Gibson/BP team further optimized the salicylaldimine chromium catalysts identified in the initial high-throughput screening experiments.[37] The six most active catalysts were first tested at larger scales, and the

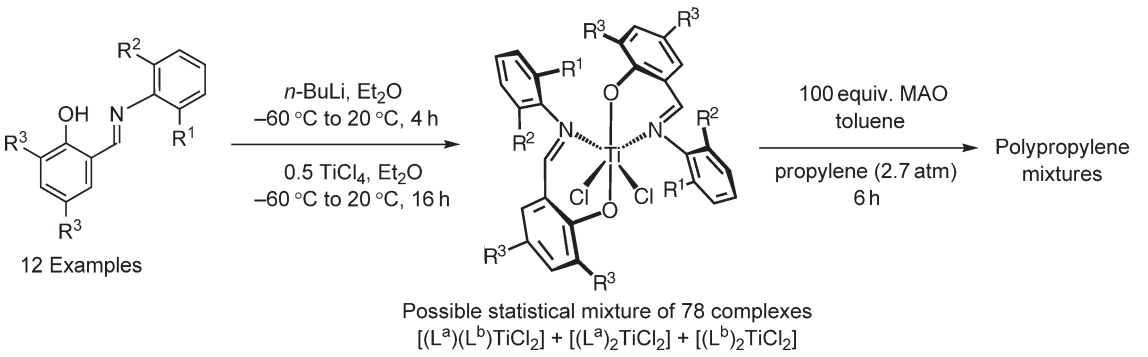

Scheme 2

relative activities identified in the initial high-throughput screen were reproduced. The authors then prepared a series of small focus libraries centered around three structurally distinct regions of activity identified in the initial high-throughput screen. The focus library synthesis and screening was carried out along with conventional organometallic synthesis and structural characterization to fortify the high-throughput approach. The focus libraries confirmed that chromium catalysts comprising bidentate anthryl-substituted salicylaldimine ligands, bearing small primary or secondary alkyls bound to the imino nitrogen, produced linear, high molecular weight polyethylene with high productivities. A second category of chromium catalyst was discovered, containing a tridentate salicylaldimine ligand with the bulky *ortho*-triptycyl substituent with pendant pyridylmethyl **1** or quinolyl donors bound to the imine nitrogen. These catalysts were reported to be thermally robust oligomerization catalysts producing linear α-olefins with extremely high productivities.

The Coates group has also reported a high-throughput approach utilizing salicylaldimine ligands.[38] The purpose of this study was to examine the efficacy of a high-throughput pooled approach to the discovery of stereospecific polypropylene catalysts. A collection of 12 bidentate salicylaldimine ligands was pooled in solution, deprotonated and reacted with 0.5 equiv. $TiCl_4$, producing a library with potentially 78 homoligated and heteroligated metal–ligand complexes (Scheme 2). To demonstrate that a statistical mixture of 78 compounds was likely, the authors reacted equal amounts of two deprotonated salicylaldimine ligands with $TiCl_4$ and observed the presence of three complexes in a 1 : 2 : 1 statistical mixture (by ^{1}H NMR). The authors reasoned that any polypropylene polymers produced from the catalyst pool would represent a stereochemical recording of the polymerization events. Under the polymerization conditions chosen, atactic polymers are amorphous and highly soluble, while syndiotactic and isotactic polymers are crystalline and highly insoluble. It was therefore reasoned that product deconvolution through selective extraction procedures should reveal the identity of any catalyst exhibiting stereocontrol.

The pooled library of salicylaldimine–titanium products was combined with MAO and 150 ml toluene in a pressure vessel, and screened at 20 °C under 2.7 atm of propylene for 6 h. Although 90% of the polymers produced were determined to be atactic through extraction experiments with diethylether, the remaining 10% of the polymers produced were found to contain insoluble syndiotactic polypropylene. Small subsets of the complex libraries were then resynthesized and screened in order to ascertain the particular metal–ligand combination responsible for the stereocontrol. The authors concluded the study by identifying and isolating a new syndiospecific propylene polymerization catalyst **2**.

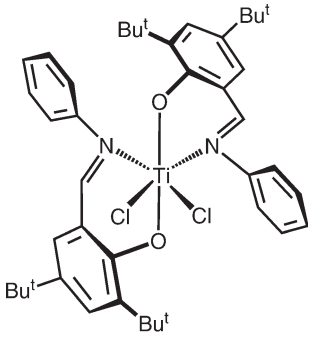

2

In a subsequent study, the Coates team reported the use of a pooled approach to identify heteroligated bis(salicylaldimine) titanium complexes ([$(L^a)(L^b)TiCl_2$]) with enhanced catalytic performance's properties relative to either of the homoligated systems, $(L^a)_2TiCl_2$ or $(L^b)_2TiCl_2$.[39] Interestingly, the authors had previously determined that a pure heteroligated complex had exhibited higher activity and produced polypropylene with higher molecular weight when compared with either of the homoligated complexes. Product polymers from the individual catalyst runs suggested that the ligands were not scrambling under polymerization conditions. For the pooled catalyst study, 10 ligands were chosen, potentially proving access to 45 heteroligated complexes and 10 (previously studied) homoligated complexes. The study was specifically designed to probe the effect of progressively increasing fluorine substitutions on the *N*-aryl group of the salicylaldimine ligand. Subsets of five-membered ligand libaries were complexed as previously described and screened in a pressure vessel under mild conditions (0 °C, 30 psi propylene, 3 h), and the resultant polymer mixtures were analyzed by GPC to determine the molecular weight profiles. The GPC traces from the pooled libraries were sufficiently informative to enable the discovery of a variety of higher activity, heteroligated complexes with higher molecular weight capabilities than the previously studied homoligated complexes. The study demonstrates that a straightforward, high-yielding chemical synthesis combined with a carefully considered screening protocol can provide experimental results rich with information.

Mountford and co-workers have reported high-throughput synthesis and screening techniques to discover seven highly active ethylene polymerization catalysts.[40] A library of 47 imidotitanium compounds of the formula Ti(NR)-$(Me_3[9]aneN_3)Cl_2$ (R = alkyl or aryl; $Me_3[9]aneN_3$ = 1,4,7-trimethyltriazacyclononane) were first prepared in array format in two steps using semiautomated parallel procedures (Equation (3)).

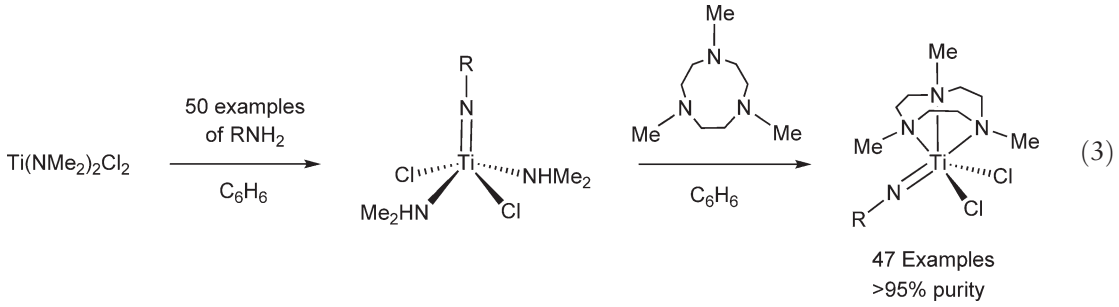

The compounds were then screened at an industrially relevant 100 °C using MAO activation in custom-built, eight-well pressure reactors (62 ml pentamethylheptane solvent; 7 bar ethylene; 10 min polymerization time). A systematic study of catalyst diversity revealed the unpredictable effects of imido group-substitution patterns on the catalyst performance. The first highly active, high-temperature group (IV) imido-based ethylene polymerization catalysts were reported. The Mountford report is a nice illustration of the utility of general, high-yielding coordination chemistry to access catalyst diversity and systematically probe structure–activity relationship (SAR) within an interesting family of compounds (Figure 1).

In 2003, workers at Symyx Technologies reported the first fully integrated methodology for the discovery and optimization of olefin polymerization catalysts using high-throughput approaches.[12] The goal of the study was to find catalysts capable of producing high molecular weight ethylene-1-octene co-polymers in an industrial high-temperature solution process. It is known that insertion barriers for α-olefins are higher than for ethylene, and catalysts capable of polymerizing α-olefins would be predicted to co-polymerize ethylene with the α-olefin. The authors therefore rationalized that an assessment of activated metal–ligand complexes for their ability to homopolymerize 1-octene would serve as a meaningful screen for new catalyst discovery. The Symyx report introduced a staged screening approach comprising high-throughput primary and secondary screening techniques utilizing liquid-handling robotics and rapid polymer characterization methods. Microliter-scale 1-octene primary screening polymerization experiments were carried out with arrays of ligands that were contacted with the reactive metal complexes, $M(CH_2Ph)_4$ (M = Zr, Hf), and subjected to multiple activation conditions in the presence of 1-octene. In this example, the primary screen was performed in 250 µl reaction volumes within arrays of 1 ml glass vials (Figure 2).

The primary screening methods were first validated using a commercially relevant polyolefin catalyst, and implemented rapidly to discover a new amide–ether hafnium catalyst [η^2-(N,O)–(2-MeO–C_6H_4)(2,4,6-$Me_3C_6H_2$)N]Hf(CH_2Ph)$_3$. Larger-scale secondary screening experiments were performed on a focused 96-membered amine–ether library using a custom-built 48-well parallel polymerization reactor, in which each polymerization event can be monitored in real time under conditions that provided meaningful information about the performance capabilities of each catalyst at high temperatures and high pressures. The results demonstrated high-temperature

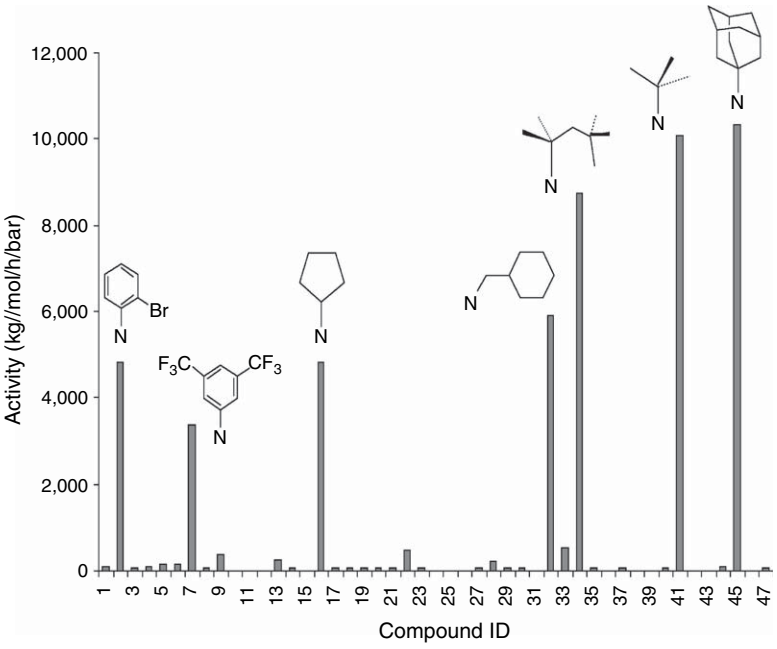

Figure 1 Polyethylene structure-activity dependence upon imido group for compounds of the formula Ti(NR)(Me_3[9]aneN$_3$)Cl_2. Reproduced by permission of The Royal Society of Chemistry.

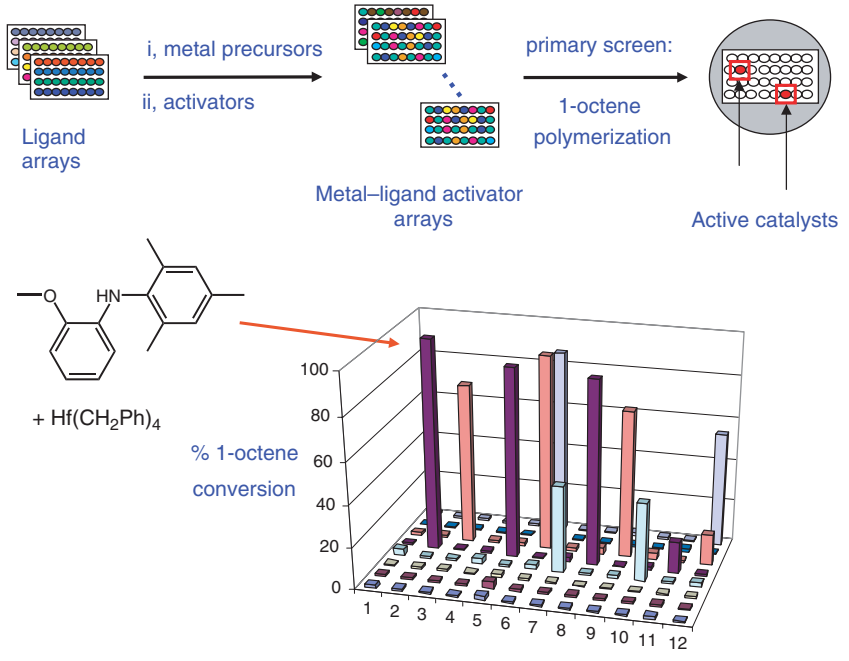

Figure 2 The Symyx 1-octene primary screening workflow from polyolefin catalyst discovery.

ethylene-1-octene co-polymerization capabilities for this catalyst class, and led to catalysts with significant performance improvements over the initial primary screening discovery (Figure 3). Importantly, conventional one gallon batch reactor co-polymerizations performed using selected amide–ether hafnium compounds confirmed the performance features of this new catalyst class, thus validating the overall high-throughput approach and demonstrating the utility of small-scale array-based polymerizations. The work is significant because it represents the first example of a

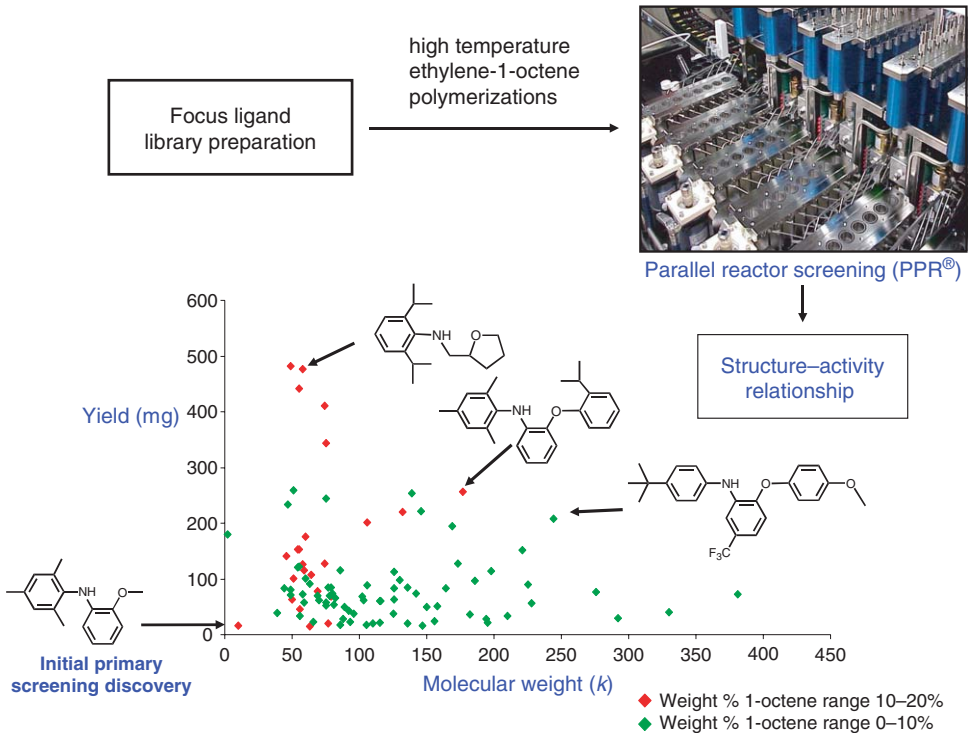

Figure 3 Structure–performance relationship for 96 amine-ether/Hf($CH_2C_6H_5$)$_4$ combinations (ethylene-1-octene copolymerizations performed at 130 °C).

new catalyst family discovered and optimized using high-throughput approaches supported by rapid synthesis, liquid-handling robotics, custom-designed software, sophisticated parallel polymerization reactors, and specially developed rapid polymer characterization techniques.

A most significant example, which was also provided by the Symyx team, deployed the same methodology to uncover an entirely new family of isospecific propylene polymerization catalysts. The Symyx team, in collaboration with Dow Chemical, discovered and developed a new catalyst class, and a new commercial solution process for the production of isotactic polypropylene-based elastomers and plastomers.[41,41a–41d]

Woo and co-workers reported a rapid way to conduct catalyst synthesis and screening using automated techniques and a parallel polymerization reactor.[42] Four pyrazolyl-pyridine ligands were prepared and complexed with (DME)$NiBr_2$, (COD)$PdCl_2$, and $CoCl_2 \cdot 6H_2O$ using a Chemspeed automated synthesizer.[43] The 12 complexes were then activated with MAO (125 equiv.) and screened for their ability to polymerize norbornene using a custom, eight-well parallel polymerization reactor (10 ml reaction volume). Polymerization activity was noted for several nickel and palladium complexes. Kaminsky and Keisewetter have reported a similar approach.[44]

A related approach was reported by workers at HTE,[45] who prepared a diverse set of tridendate diiminopyridine ligands, also using a Chemspeed automated synthesizer. The ligands were complexed to Fe(II) and Fe(III) halides, and the products were activated with 5,000 equiv. of MAO and screened for their ability to polymerize ethylene using a custom, eight-well parallel polymerization reactor (30 ml reaction volume; 10 bar ethylene). In total, 402 polymerization runs were performed with an experimental throughput of 40 polymerizations per week. Conventional polymer analysis techniques were employed, and the results were consistent with previously reported trends for this catalyst family.[46]

Other reports have emerged discussing the use of parallel approaches to optimize catalyst performance. For example, Bazan and collaborators at Symyx have reported the use of the parallel polymerization reactor and the rapid polymer characterization techniques, previously described,[12] to perform a tandem catalysis experiment in which three well-defined catalysts were pooled and coordinated to produce a wide range of branched polyethylenes from a single monomer (ethylene).[47] The high-throughput screening infrastructure comprising the parallel reactor, liquid-handling robots and rapid polymer characterization tools was essential for optimizing reaction conditions and probing the effects of catalyst compositions on the polymer properties. Coughlin *et al.* have recently described a convenient gas manifold and associated reactor design that accommodates different reactor vessel sizes (70–300 ml) in addition to multi-well

arrays (20 ml per well). The authors demonstrate the utility of the parallel reactor to identify the most favorable process conditions to prepare low molecular weight isotactic polypropylene with a high occurrence of olefinic end groups.[48,48a]

Chen has introduced a mechanism-based approach to high-throughput screening of olefin polymerization catalysts.[49,49a,49b] The technique uses an electrospray ionization tandem mass spectrometer to assay trapped cationic organometallic intermediates during an olefin polymerization reaction. Olefin polymerization catalysts can be activated in the presence of monomer, quenched with a trapping agent, and then introduced through an electrospray into the mass spectrometer. Analysis of the intermediates can then reveal kinetic properties such as rates of initiation, chain propagation, and termination for a given catalyst. The authors claim that the monomer uptake rate and resultant polymer molecular weight can be predicted for each catalyst for a given set of polymerization conditions. Furthermore, the mass spectrometry technique was extended to include a higher-throughput, pooled approach to catalyst screening.

A variety of other reports and reviews discussing high-throughput approaches to olefin polymerization and polymer property screening have also appeared, although no examples of high-throughput organometallic approaches are given in these reports.[50–53]

1.13.2.2 Cross-Coupling and Addition Reactions

Recent advances in this area have provided a suite of catalyst options for cross-coupling and addition reactions.[54,54a,54b] However, a survey of the literature reveals that choosing the appropriate catalyst and reaction conditions for a desired reaction can be a difficult process. Changing from one reaction substrate to another can turn a productive catalyst into an ineffective one. With choices in ligand, metal, ligand/metal ratio, solvent(s), temperature, base (where used), and other components (where used), these chemistries also represent an exercise in multi-dimensional experimental space with an unpredictable outcome. Cross-coupling and addition reaction chemistries are therefore extremely well suited to high-throughput approaches. As an illustration, Equation (4) depicts a generic C–N coupling reaction along with the typical elements of experimental diversity.

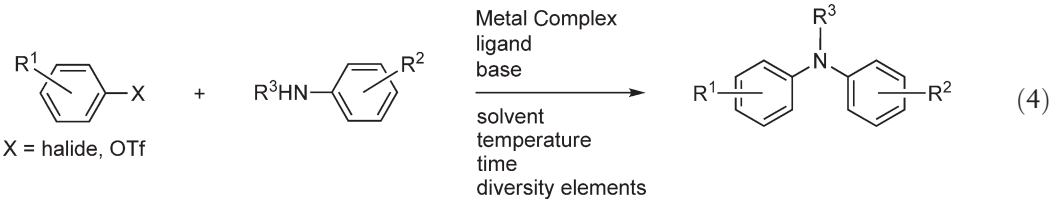

(4)

With simple reaction vessels, an efficient method to assemble and manipulate reagents, a means of temperature control, and a rapid method for product-composition analysis, cross-coupling, and addition chemistries can readily be addressed in a high-throughput manner. The following reports illustrate the efficacy of the high-throughput approach.

1.13.2.3 Sonogashira Coupling

Lavastre and co-workers have recently reported a high-throughput approach to the discovery of new organometallic catalysts for the Sonogashira coupling reaction.[55] Using a microtiter plate format, the report describes the screening of seven simple ligands with 11 metal complexes for the reactions shown in Equation (5).

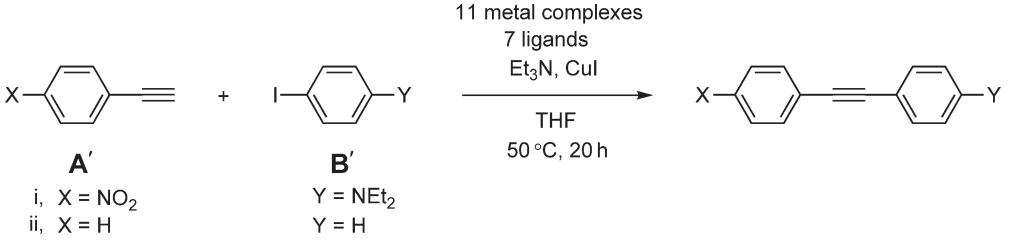

(5)

Solutions of the ligands (50 µl; 0.02 M in THF) and metal complexes (50 µl; 0.01 M in THF) were first dispensed into the microtiter plate with a multi-channel pipette. After allowing 1 h for complexation, 50 µl of a solution containing the substrates (**A′** and **B′** in Equation (5); 0.5 M) and copper iodide (0.01 M) was added to each of the

vials, along with 100 µl of Et_3N. The vials were closed and the microtiter plate was heated at 50 °C for 20 h. For the product analysis, quantitative TLC was set up with image analysis software to provide a simple and effective way to measure reaction conversions. Quantification was made possible using model solutions to first optimize the appropriate sample concentration and volume for deposition onto the TLC plate, and then to calibrate the procedure. The results of this high-throughput screening procedure were unanticipated; (η^6-1-Me–4-Pr^i–C_6H_4)(PPh_3)$RuCl_2$ was discovered as the first ruthenium-based catalyst for the Sonogashira coupling reaction.

1.13.2.4 Aryl–Amine Coupling

In 2001, Hartwig and co-workers described the use of fluorescence resonance energy transfer (FRET) as a method to quantify the formation of covalent bonds formed from metal-catalyzed coupling events.[56] The FRET technique was leveraged from biological assay screening where it is often used to measure non-covalent binding constants.[57,57a] FRET occurs due to overlap of a fluorescence emission band of one (donor) molecule with an excitation band of a second neighboring (acceptor) molecule. Under the appropriate conditions, the fluorescence emission from a solution containing free donors, and associated donors and acceptors, will be inversely proportional to the mole fraction of associated molecules. For the discovery of new catalysts for the aryl amination reaction, Hartwig exploited the FRET concept by tethering a fluorophore donor to an amine, and an acceptor molecule to an aryl bromide (Equation (6)).[58] The donor and acceptor molecules were chosen to be tolerant to the conditions of catalysis. The relative emission intensity could then be converted directly into coupled product yield. For this high-throughput study, 119 ligands comprising 11 diverse structural families were chosen, including 39 previously untested ligand structures.

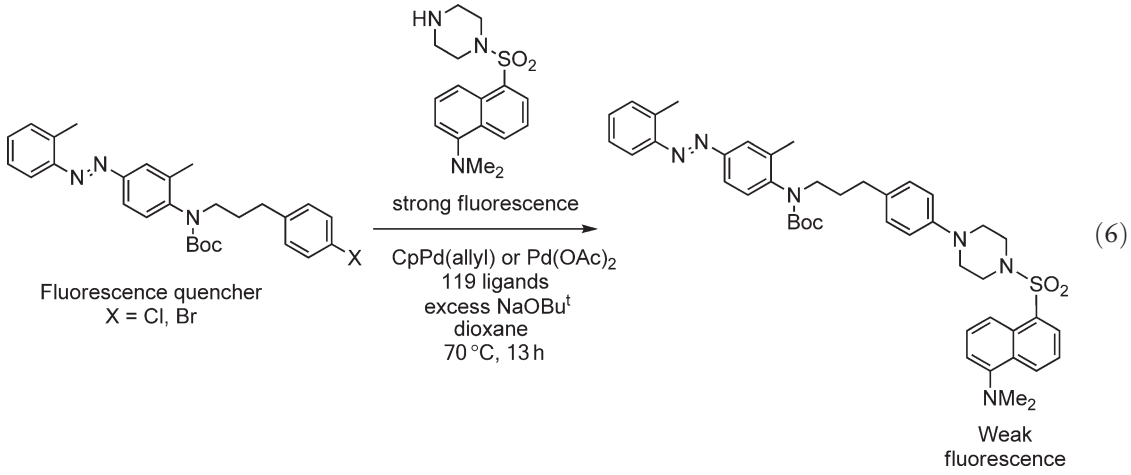

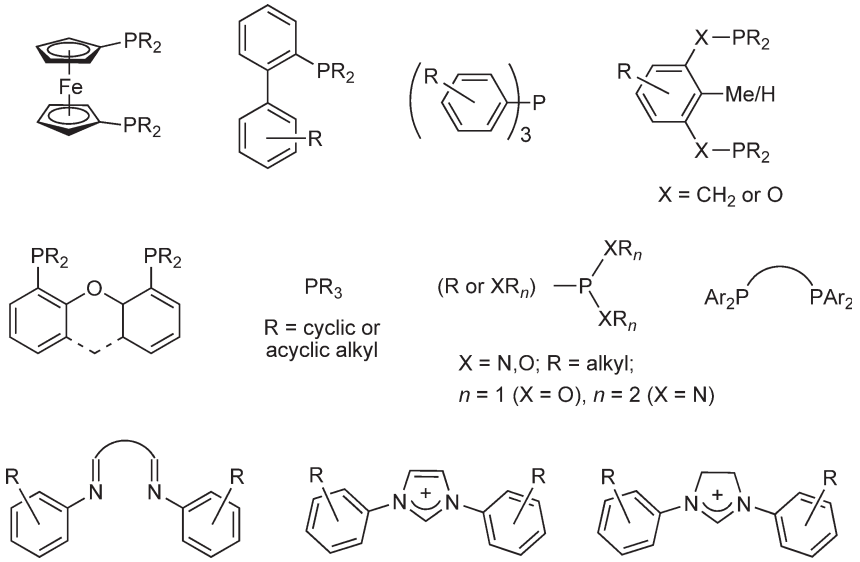

A 96-well microtiter was loaded sequentially with ligands (3 mol% (relative to the substrates to be coupled) for monodentate ligands; 1.5 mol% for bidentate ligands), fluorophore (7.5 μmol), dye (7.5 μmol), $NaOBu^t$ (1.5 equiv.), and CpPd(allyl) or $Pd(OAc)_2$ (3 mol%), to produce a total reaction volume of 50 μl. In addition to the conditions shown in Equation (6), the authors also exploited the microtiter plate format to examine the influence of various solvents and bases upon the reaction yields. A whole series of Pd/ligand combinations were shown to be effective for the coupling reactions studied. The Hartwig group had previously exploited the FRET-based screening approach to uncover effective catalysts for two different classes of coupling reactions, namely, the Heck reaction and the arylation of cyanoacetates (refer to Sections 1.13.2.6 and 1.13.2.7).[56,59] Additionally, a Symyx group has also reported a high-throughput approach to the discovery of new palladium-based catalysts for the amination of aryl iodides, bromides, and chlorides.[60]

1.13.2.5 Hydroaminations Reactions

The Hartwig group has also described a spectroscopic technique to uncover new organometallic catalysts for the hydroamination of 1,3-dienes.[61,61a] The initial reaction of interest was the addition of aniline to cyclohexadiene. In this study, a simple colorimetric spot test was used to detect the presence of unreacted aniline. 2-Furaldehyde is known to undergo an acid-catalyzed condensation and subsequent ring opening with aniline to produce a distinctive red product. Diversity was expressed with 11 phosphines in combination with seven metal complexes (comprising commercially available Ni, Pd, Ru, Rh, and Ir complexes). The ligand and metal complex combinations were contacted with aniline, cyclohexadiene, and trifluoracetic acid (TFA) and shaken on an orbital shaker for 4 h. The subsequent furaldehyde spot test revealed a simple and effective catalyst from a $PPh_3/[(\eta^3\text{-allyl})PdCl]_2$ combination. Upon scale up, this catalyst proved to be high yielding for a diverse series of aniline additions to cyclohexadiene and other 1,3-dienes. Inspired by the seemingly broad applicability of the catalyst, the authors screened the reaction in the presence of five well-known chiral phosphines producing enantioselective catalysts with ee values up to 95%. In a subsequent report, the Hartwig group used the same high-throughput screening and spot test method to develop a series of catalysts for the addition of primary and secondary amines to a variety of functionalized olefins.[62]

1.13.2.6 The Heck Reaction

A FRET-based strategy (refer to Section 1.13.2.4) was employed to discover catalysts for the reaction between a styrenic olefin fluorophore donor and an aryl halide tethered to an acceptor molecule.[56] The FRET-based approach was an extension of a previously reported fluorescence-based screen for new and improved palladium-based Heck catalysts.[63] The purpose of this FRET study was to uncover a palladium catalyst for room-temperature Heck reactions. The study evaluated the use of 96 phosphines, similar in structural diversity to the phosphines within the ligand set shown in Ref: 58 (Equation (6)). All reactions contained a 1 : 1 ratio of tethered olefin and aryl bromide, 2.5 equiv. of Et_3N as the base, and 5 mol% of CpPd(allyl) and ligand. Screening was conducted in a 96-well microtiter plate sealed with a Viton gasket and heated at 70 °C for 15 h. Samples were then analyzed using an automated fluorescence plate reader. A total of 15 diverse ligands generated catalysts that produced product yields >70%. The two ligands that generated the most active catalysts were tested at room temperature and found to be effective for a variety of substrates considered to be both activated and deactivated for the Heck reaction (Equation (7) and Table 2). The results from the use of the two ligands (L1 and L2) are shown in Table 2.

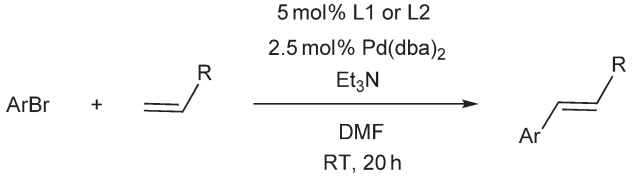

(7)

The results of the study once again confirm the unpredictable nature of this chemistry and underscore the advantages offered by the high-throughput approach.

Several other high-throughput approaches have also been reported.[64,65,65a] In a collaboration between DSM and the University of Amsterdam, van Leeuvan and co-workers have reported using a parallel approach to the discovery of catalysts for the Heck coupling of aniline derivatives, in which *ortho*-directed metallation of the aniline serves as the entry point to the catalytic cycle, potentially replacing the need for an aryl halide.[64] Parallel screening was conducted

Table 2 General summary of the high-throughput screening strategies highlighted in this chapter

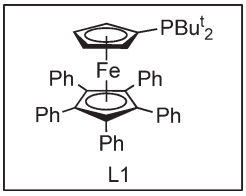

L1

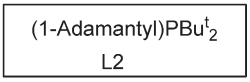

L2

R	*Ar*	*Yield* (%)
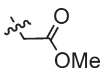	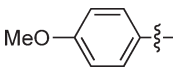	91
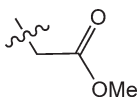	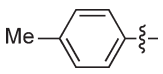	91
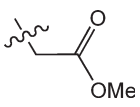	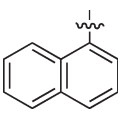	95
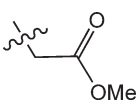	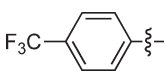	88
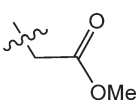	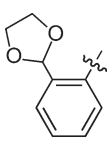	89
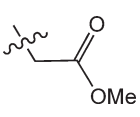	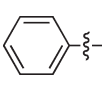	94
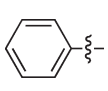	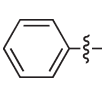	93
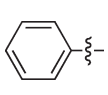	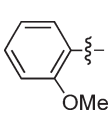	99
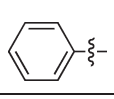	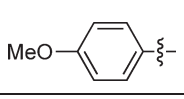	94

using a Chemspeed automated synthesizer and conventional gas chromatography-mass spectrometry (GC-MS) analysis.[43] A variety of palladium-based catalysts were shown to be effective for Heck coupling of *n*-butylacrylate with various aryl amides.

In 1999, Blackmond and Pfalts from the Max-Planck Institute introduced a rapid screening protocol based upon reaction calorimetry.[65,65a] In the absence of significant side-reactions, heat-flow monitoring can provide a rapid measurement of activity and a multi-dimensional kinetic profile of the catalyst candidate for the reaction of interest.

Through consecutive injections of small aliquots of reaction components and subsequent monitoring of the resultant heat flow, the authors were able to compile information about induction periods, reaction rates, and catalyst lifetimes for a Heck coupling reaction between an aryl bromide and *n*-butylcinnamate. The technique readily distinguished the performances of three structurally distinct catalysts, and resulted in the identification of a particularly active palladium catalyst with an interesting nitrogen-based ligand.

1.13.2.7 α-Arylation of Carbonyl/Cyano Derivatives

Hartwig and co-workers once again exploited the high-throughput approach and FRET screening to uncover new palladium catalysts for the arylation of α-cyanoacetates.[59] The approach was very similar to those described for the aryl amination and Heck coupling reactions previously described (refer to Sections 1.13.2.4 and 1.13.2.6). The authors uncovered effective catalysts for this transformation, introducing substituted ethyl cyanoacetates as new and versatile synthons.

1.13.2.8 Ullmann Ether Synthesis

In 1990, Hauptmann and co-workers at DuPont reported a thoughtful high-throughput approach to the synthesis and screening of a 96-membered pyridine-based library for the discovery and optimization of homogeneous copper catalysts for challenging Ullmann ether coupling reactions.[66] The particular reaction chosen for the study (Equation (8)) involved an electron-rich, unprotected aniline, 2-Br–4,6-$Me_2C_6H_2NH_2$, a very challenging substrate for Ullmann ether coupling, and a chemical problem of particular interest to DuPont.

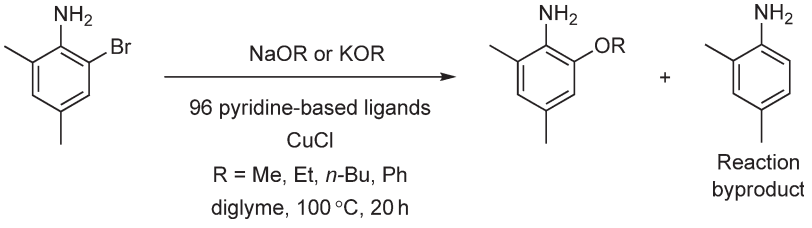

(8)

Of the 96 pyridine-based ligands chosen for the discovery of new catalysts for this reaction, 79 were chosen with attention to: (i) electron-donating and electron-withdrawing capabilities (σ and π), (ii) steric encumbrance around the donating atoms, (iii) variation in hapticities, (iv) bite-angle for multidentate ligands, and (v) secondary coordination sphere considerations. Additionally, 17 ligands were reported to be randomly selected, for example, containing structural features outside of considerations (i)–(v). Catalyst solutions were prepared by combining solutions of CuCl (150 µl, 0.02 M in CH_3CN) and ligands (150 µl, 0.02 M in either MeOH or benzotrifluoride) in 2 ml vials using a Bohdan automated liquid handler. Solvents were first removed under a nitrogen purge and then the resultant compositions were dried further under vacuum. To each vial, sequentially, was then added 150 µl solutions of aniline (0.40 M in diglyme), biphenyl as an internal standard (0.00125 M), and alkoxide or aryloxide salts (0.60 M in diglyme). The vials were then placed on an orbital shaker at the desired temperature (ca. 100 °C) until the end of the run (ca. 20 h). Following the reaction, solutions were diluted with 0.8 ml of toluene and analyzed using a conventional GC fitted with an autosampler. Promising "hits" were obtained for methoxylation, ethoxylation, butoxylation, and phenoxylation reactions (however, reactions were sluggish in the case of secondary or tertiary alkoxides). The ligands selected on the basis of the criteria (i)–(v) generally performed better than the ligands chosen outside of these criteria, although some interesting exceptions were noted. Focused libraries were then screened for the methoxylation and phenoxylation reactions, leading to improved results in both cases, and the identification of promising ligand systems previously unreported for the Ullmann reaction. The overall study demonstrates the value of the high-throughput approach, as the authors conclude that it would have been impossible to predict which ligands would produce best combination of yield and a low concentration of undesirable side-products. The DuPont study represents a good example of a high-throughput approach to both discover and optimize new catalysts.

1.13.2.9 Suzuki Couplings

Several high-throughput approaches for the discovery of new or improved organometallic catalysts for Suzuki coupling reactions have been reported.[67–69] Kempe and Schareina have reported the synthesis and screening of a

small library of phosphine-substituted aminopyridines for a variety of Suzuki couplings using the more challenging ArCl-based substrates.[67] A variety of effective palladium and nickel catalysts were discovered in this study. Additionally, Colacot and co-workers at Johnson Matthey have described both solution-phase and polymer-supported high-throughput approaches for the discovery of new catalysts for Suzuki coupling.[68,68a]

1.13.2.10 Intramolecular Coupling Reactions

An interesting example of a high-throughput approach to optimize a palladium-catalyzed annulation reaction was presented by Yeung and co-workers (Equation (9)).[70]

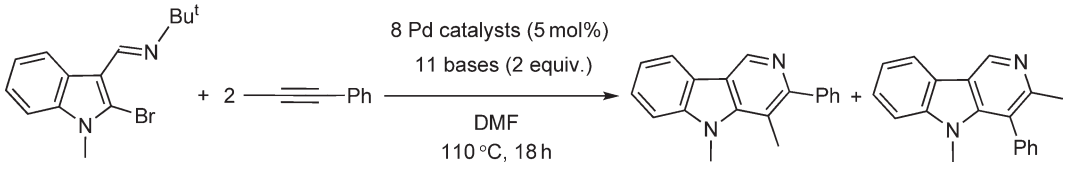

(9)

The reactions were run on a 5 µmol scale in 120 µl total reaction volume through the use of 6 mm o.d. glass tubes that were sealed at one end and arranged in a 96-well format. Reagents, including an internal standard, were added by pipette either as dimethylformamide (DMF) solutions or slurries. Interestingly, for the product analysis, the authors employed a custom-built multiplexed capillary array electrophoresis technique coupled with absorption detection. Injection volumes were 10–100 nl, taken directly from the reaction mixture. Separation protocols were first established for the reactants and products, and then all 88 samples from the high-throughput experiment were injected and run in 1 h. Figure 4 shows the capillary electrophoresis output from the 88 injections.

The output illustrated in Figure 4 enables quantitative extraction of yield, selectivity, and kinetic information for all of the individual reactions. Although no significant discoveries were made, this is a good example of a clever analytical technique used for the benefit of high-throughput organometallic chemistry.

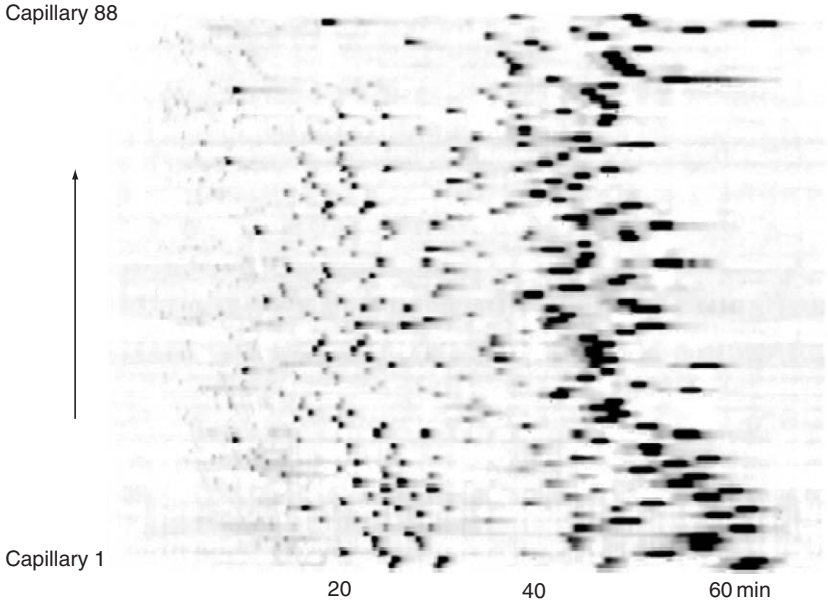

Figure 4 Capillary electrophoresis output from 88 palladium-catalyzed annulation reactions. Reproduced by permission of Journal of Combinatorial Chemistry.

1.13.2.11 Hydrosilylation

Crabtree and co-workers have reported an approach in which the unsaturated bonds to be hydrosilylated were conjugated to electron-donor and -acceptor groups, leading to highly colored complexes.[21c,21e,71,71a] Upon hydrosilylation, the conjugation is disrupted, which causes the color to diminish. Using a 60-well array of 1 ml reactors generated by drilling holes in a Teflon block, the authors used solutions of the dye and Ph_2SiH_2 to screen 12 potential catalysts, and identified several systems that caused bleaching of the color. Control experiments demonstrated that the catalyst activity ranking was the same when conventional substrates were used, and a palladium complex not previously known to catalyze this reaction was identified. The technique reported is a creative one, although given the unpredictable nature of catalysis, direct screening of the actual substrates of interest would clearly be preferable, and the advances reported in rapid analytical techniques (refer to Section 1.13.5) would now make this possible. A high-throughput approach to the discovery of catalysts for asymmetric hydrosilylation reactions is also described in Section 1.13.3.4. In 2002, Lavastre and Morken[72] reported a solid-phase approach, in which a library of 40 multidentate aminophosphine–phosphinite ligands was prepared on polystyrene beads using a split-and-pool method, in which each ligand was chemically encoded with a photocleavable tag.[9] To prepare the ligand library, 40 amino alcohols were first attached to the encoded polystyrene beads, and treated with diphenylchlorophosphine to generate the aminophosphine–phosphinite functionality. After treatment with $[Rh(COD)Cl]_2$, the resultant beads were treated with methanol for 1 h in order to cleave the Rh–Cl bond and generate a cationic species. From the resultant collection of orange beads, 76 were selected at random and placed in a homemade 76-well plate attached to a vortex stirrer. The beads were then treated with 400 µl of a stock solution containing Ph_2SiH_2 and acetophenone (0.5 M in CH_2Cl_2; theoretical catalyst loading 0.05 mol%). After vortexing for 40 h, the reactions were quenched with 20 µl HCl (10% in 150 µl acetone) and extracted with diethyl ether. Reaction products were then analyzed by GC. The highest activity catalysts were then subjected to decoding in order to identify the nature of the catalyst. While many examples of active catalysts were identified, the most active systems were derived from very simple amino alcohols. The Lavastre and Morken study highlights a useful high-throughput technique to identify effective supported catalysts that can be readily separated from reaction products.

1.13.2.12 Hydroformylation

In 2005, Breit and co-workers described an interesting approach in which an array of bidentate phosphines was assembled using a hydrogen bonding strategy.[73] Inspiration for the concept came from adenine–thymine (AT) base pairing within a DNA structure. As a model for the AT base pair, the aminopyridine/isoquinolone system was selected. From four phosphine-functionalized 2-aminopyridines and four phosphine-functionalized isoquinolones, a set of 16 Rh bidentate ligand combinations was generated by mixing the components with $Rh(CO)_2(acac)$ (ligand pair to Rh ratios 10 : 10 : 1; Scheme 3).

The resultant formulations were tested for their potential to catalyze the hydroformylation of 1-octene. The screening was conducted in toluene at 80 °C under 10 bar of a 1 : 1 H_2/CO mixture (details of the reactor hardware

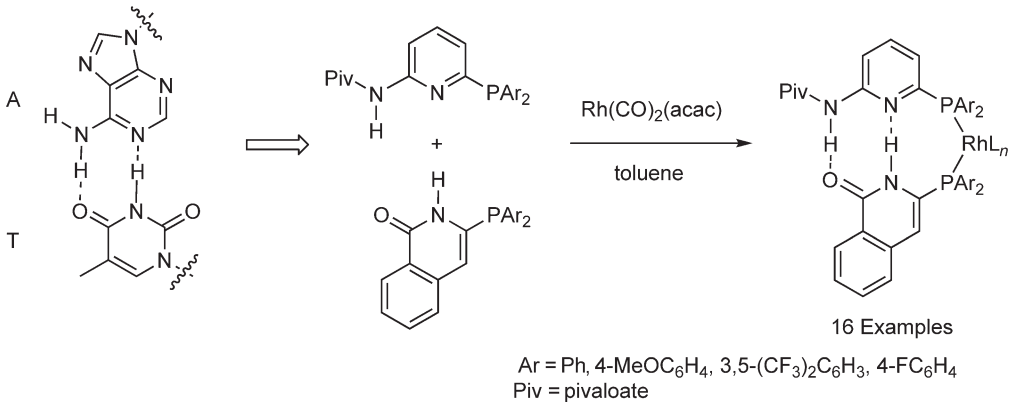

Scheme 3

were not disclosed). Multiple systems were identified with high activities, and ratios of linear to branched products were observed to be as high as 96 : 4. Importantly, catalyst performance responded to structural changes, and the authors conclude by stating that application of this interesting approach to asymmetric catalysis is a next logical step. A high-throughput approach to the discovery of catalysts for asymmetric hydroformylation of olefins to branched aldehydes is also described in Section 1.13.3.5.

1.13.2.13 Addition of Nucleophiles to Allylic Esters

In 1999, Lavastre and Morken reported a visual colorimetric screen for the detection of effective organometallic catalysts for the allylic alkylation of diethylmalonate.[74] The colorimetric technique was based upon trapping a 1-naphthol elimination product of the reaction with a diazonium salt (Scheme 4).

The authors used a 96-well microtiter plate to run the high-throughput screen. In a glove box, eight ligands were dispensed along the rows, and 11 metal salts were dispensed along the columns of the microtiter plate (one column was reserved as a no-metal control). A solution containing the diethyl malonate and 1-naphthyl allyl carbonate substrates (substrates : metal = 100 : 1) was then dispensed across the microtiter plate. After 2 h, a solution of the diazonium salt was added to image the plate, and the resultant microtiter plate appearance is shown in Figure 5.

While the visual appearance of the products was sufficient to identify the active catalysts, the authors employed a parallel UV plate reader to quantify the results. The rhodium catalysts identified provided encouragement that metals other than palladium could be developed for this transformation, and in a subsequent experiment, the colorimetric technique was used to discover the first non-phosphine-based iridium catalyst for allylic alkylations. A high-throughput approach to the discovery of catalysts for asymmetric allylic alkylations is also described in Section 1.13.3.6.

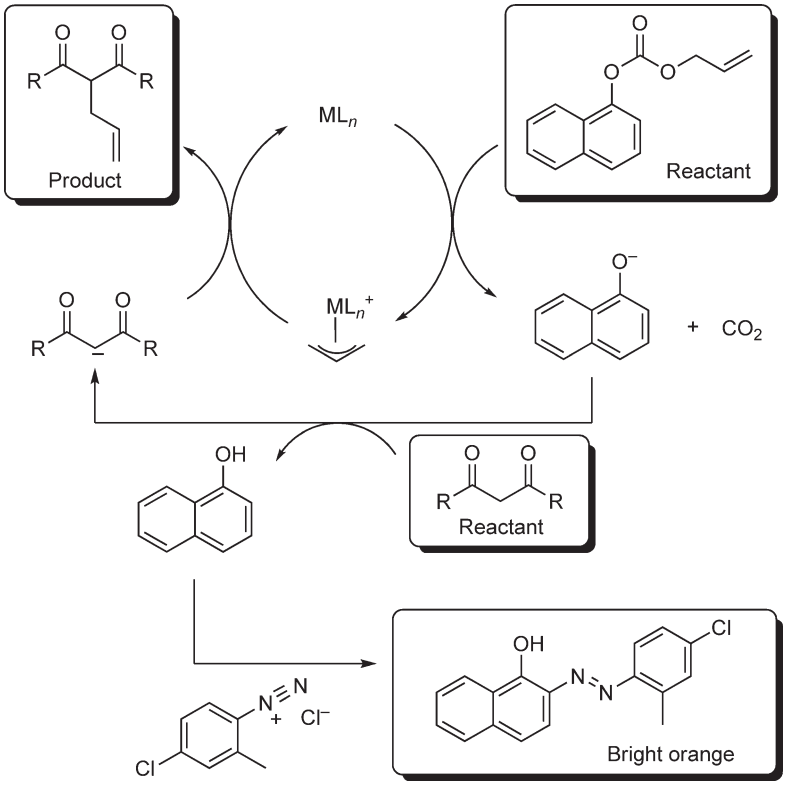

Scheme 4

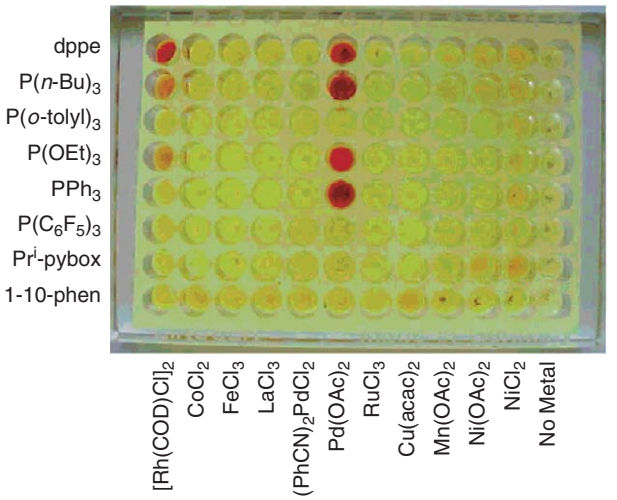

Figure 5 Colorimetric microtiter plate screen for the allylic alkylation of diethylmalonate. Reproduced by permission of Angewandte Chemie.

1.13.2.14 Olefin Metathesis

Using the electrospray ionization tandem mass spectrometer screening technique (ESI-MS) described in Section 1.13.2, Huber and Chen described a pooled approach to the synthesis and screening of ruthenium-based ring-opening metathesis polymerization (ROMP) catalysts.[49b,49c] Starting from a lead structure originally reported by Hofmann,[75,75a] $(PCy_3)_2RuCl_2(CHC_6H_5)$ was dissolved in CH_2Cl_2, and then treated with various chelating diphosphines, tetrabutylammonium halides, and styrene derivatives to generate a pooled catalyst library (exact details not provided). The use of a polar solvent enables the generation of small quantities of cationic complexes through heterolysis of the metal–halide bonds (a formal charge is necessary for the ESI-MS technique). The mixture was then injected into the tandem mass spectrometer, which comprised several distinct regions. The solutions are first passed through a heated capillary into the mass spectrometer, where desolvation occurs. The ions then enter a first-quadruple region, where they are separated by their m/z ratio and passed into an octapole region, with serves as reaction chamber where the ions are subjected to collisions with neutral gases. In this study, vinyl ether was introduced into the octapole region of the instrument. Reaction products pass through to a second quadrupole region where they are again separated by m/z ratio before detection. The extent of reaction during the finite residence time in the octapole region is taken as measure of reaction rate, thus enabling catalyst comparisons. From the pooled library, the authors were able to select the most active catalyst and confirm the results in scaled-up solution-phase ROMP experiments.

Lavastre and co-workers also set up a high-throughput approach to discover new catalysts for the ring-closing metathesis (RCM) of a diolefin.[76] Catalyst diversity was expressed through the combination of seven ligands and nine metal complexes arranged in a microtiter plate. Thin layer chromatography (TLC) was used to analyze the reaction contents directly.[55] Although the desired ring-closed product was not detected from this library, an unexpected iridium-based olefin isomerization catalyst was identified.

1.13.2.15 Tandem Olefin Isomerization–Claisen Rearrangement

Dixneuf and co-workers have recently described a high-throughput approach to discover catalysts for the conversion of 1,7- and 1,6-dienyl ethers into γ,δ-unsaturated aldehydes.[77] The high-throughput approach built off a previous discovery that $Ru_3(CO)_{12}$, when used in combination with a bulky imidazolium salt and Cs_2CO_3, was an effective tandem catalyst capable of converting natural monoterpenoids into new sesquiterpenoids.[78] For the high-throughput study, 96 tubes, housed in an argon dry box were charged with six ruthenium compounds and one iridium compound, each used in combination with four ligands and two bases. Screening was conducted in 350 µl toluene

at 80 °C. The most effective catalyst was (COD)Ru(η^3-methallyl)$_2$, which was reproduced on a larger scale and found to be effective without the need for additional ligands.

1.13.3 High-throughput Approaches to the Discovery of Organometallic Catalysts for Enantioselective Reactions

As with the other areas of catalysis reviewed in this chapter, the discovery of new classes of enantioselective organometallic catalysts is hampered because of a limited understanding of the complex relationships between molecular structure and catalytic performance. In addition to the need for high productivity, the catalyst must promote stereoselectivity, which can rely upon an ability to select between transition state energy differences of 1–2 kcal mol^{-1}. As expressed by Knowles in his 1983 review article stated,[79] "Since achieving 95% ee only involves energy differences of about 2 kcal, which is no more than the barrier encountered in a simple rotation of ethane, it is unlikely that before the fact one can predict what kind of ligand structures will be effective." Furthermore, enantioselective catalysts are often substrate specific, and even with closely related substrates, they may not be as effective. Such difficulties, coupled with an ever increasing need for enantiomerically pure compounds for pharmaceutical purposes, provided a strong argument for the development of high-throughput approaches for the discovery of new organometallic catalysts for enantioselective reactions.[25–31]

The reaction products from a catalytic enantioselective reaction needed to be analyzed to ascertain both conversion and enantioselectivity, and consequently, significant analytical developments were required before high-throughput approaches could be adopted. Initial studies focused on small libraries with the use of conventional analytical techniques such as HPLC and GC.[7] However, it was soon apparent that a more rapid screening capability for enantioselectivity was an absolute necessity if the potential of the high-throughput approach was to be realized. Following these initial studies, a variety of new and ingenious analytical methods were reported, and these techniques now provide us with a host of rapid screening options. High-throughput analytical techniques for the analysis of asymmetric reactions have now been reported using fluorescence imaging,[80] liquid crystal doping,[81] mass spectrometry,[82,82a–82e] infrared thermography,[83,83a–83c] circular dichroism,[84] enzymatic techniques,[85,85a] antibody detection,[86] indicator displacement,[87] parallel chiral capillary array electrophoresis,[70,88,88a] IR spectroscopy,[89] and isotope labeling in combination with flow-through NMR.[90,90a–90c] Additionally, the more traditional techniques such as HPLC and GC have been modified to improve throughput.[91] The introduction of these rapid analytical techniques represent some of the most important advances to this field. With such an impressive portfolio of rapid screening options, high-throughput approaches to the discovery of organometallic catalysts for a broad array of enantioselective reactions are now possible. A variety of studies utilizing these new techniques are illustrated in the following sections.

1.13.3.1 Addition of Nucleophiles to Prochiral Aldehydes

The traditional approach to the discovery of enantioselective catalysts is an iterative process involving the synthesis and screening of chiral ligands of high enantiopurity. Once the chiral ligands have been bound to the metal, screening takes place and after the evaluation of the results, the next generation of chiral ligands is designed and prepared. In a seminal study in 1995, Ellman reported a general solid-phase synthesis of a small library of substituted 2-pyrrolidine–alcohol ligands, which were contacted with Et_2Zn and screened directly for their ability to promote the stereoselective addition of Et_2Zn to various aldehydes.[7] Although the library was small, and the products were analyzed by conventional techniques, the results were promising enough to suggest that a "mix and screen" high-throughput approach offered great potential for the discovery of new enantioselective organometallic catalysts. The addition of Et_2Zn to prochiral aldehydes in the presence of chiral ligand library has since served as a model reaction to study a variety of high-throughput approaches.[92,92a,93,93a]

An interesting strategy was later reported by Ding and co-worker,[92a] who attempted to induce asymmetric catalysis through the addition of a chiral ligand or "activator" to a racemic catalyst.[94,94a,94b] Recognizing that the synthesis of enantiopure ligands would be a troublesome bottleneck for a high-throughput approach, Ding and co-worker used an approach in which an enantiopure ligand (L*) is used in combination with racemic ligands (L) to prepare a catalyst ML(L*). The conformations of the enantiomers in ML become diastereotopic in ML(L*), and therefore differ in energy. If the interactions between L and L* are strong, and the chiral ligand can bind in a selective diastereomeric

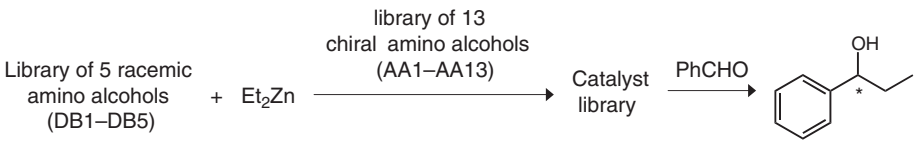

Figure 6 Ding's high throughput strategy for the discovery of catalysts for the asymmetric addition of Et_2Zn to benzaldehyde.

form, asymmetric induction can result. The advantage of such an approach is that promising catalysts can be optimized through the synthesis of racemic ligands, instead of an enantiopure ligand.

The Ding approach used a combination of five racemic amino alcohols, and 13 chiral amino alcohols to generate a chiral catalyst library comprising 65 members (Figure 6).

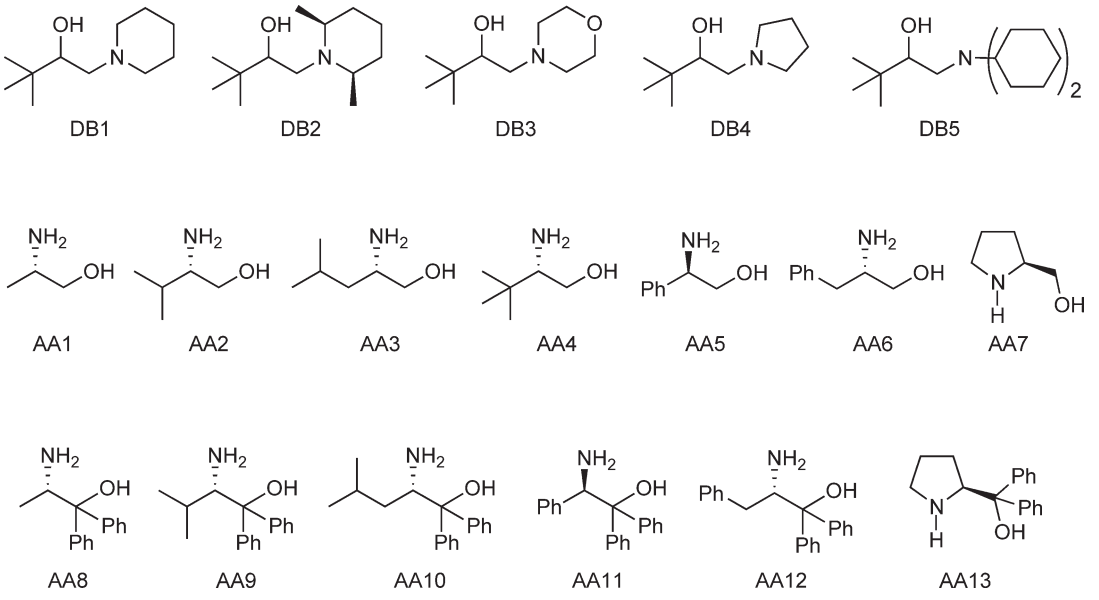

The high-throughput screening was carried out in a 24-well plate containing 1.5 ml polypropylene tubes. The chiral catalysts (AA; 50 µl; 0.1 M in CH_2Cl_2) and racemic catalysts (DB; 50 µl; 0.2 M in CH_2Cl_2) were introduced in the tubes along with Et_2Zn (300 µl; 1.0 M in hexane). The resultant mixture was held at 0 °C for 30 min, prior to addition of benzaldehyde (11 µl; 0.1 M). After a 24 h reaction time, the reactions were quenched with NH_4Cl (aq.), extracted with hexane, and analyzed by HPLC-CD.[77] Results shown in Figure 7 illustrate that the more promising ligand combinations originate from the chiral ligands containing bulky tertiary alcohol groups. The most promising combinations were then further optimized, in parallel, by adjusting the ligand ratios and reaction temperature. At a reaction temperature of −40 °C, the combination of AA13/DB2 produced (*S*)-1-phenylpropanol with a yield of >95% with up to 93% ee. Various catalyst combinations also proved to be effective for enantioselective ethylation of a variety of other prochiral aldehydes.

Prior to the Ding report, Mikami and co-workers[84] reported a similar high-throughput approach, in which the principle of asymmetric activation for the same nucleophilic addition was pursued through the combination of chiral diols and chiral, bidentate nitrogen-based ligands. The concept is centered on the notion that improvements in catalyst efficiency and enantioselectivity can be achieved through the appropriate choice of a chiral additive. The chiral catalyst library was prepared and screened in a manner similar to the Ding report with HPLC-CD as the analytical tool. Catalysts comprising diol/dimine combinations discovered in the high-throughput screen were further optimized to identify conditions to promote full conversions with >99% ee.

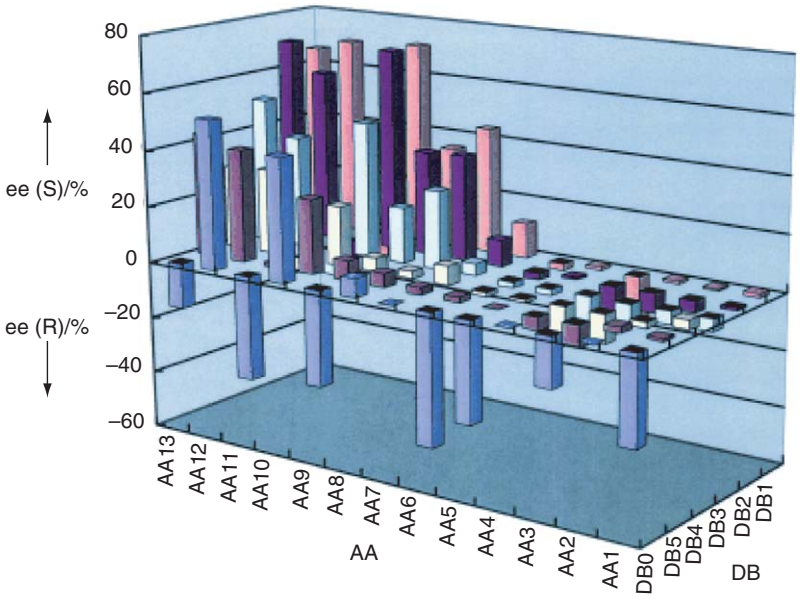

Figure 7 High-throughput catalyst screening results for asymmetric addition of Et_2Zn to benzaldehyde. Reproduced by permission of Angewandte Chemie.

1.13.3.2 Enantioselective Hydrogenation

As specified earlier in this chapter, high-throughput approaches, directed toward reactions requiring the diffusion of gases into liquids, face the problem of providing efficient mixing on a small scale. Since enantioselective hydrogenation reactions typically operate on kinetic control, these reactions can indeed be susceptible to pressure and mass transport effects. In fact, it has even been suggested that ee values reported from early library-based screening were deceptively low because of such effects.[95,95a] Parallel reactor formats that provide good heat and mass transport in small volumes are not widely available (although many have been custom designed, see Section 1.13.4), and the reaction format is therefore something that needs consideration before high-throughput approaches are adopted.(for a list of commercially available equipment directed toward parallel synthesis and screening, see Ref: 11 and 50a, respectively.)[95a] In spite of such difficulties, numerous groups have reported high-throughput approaches for the discovery of new organometallic catalysts for this industrially important reaction,[96] and even with the aforementioned caveats, the results suggest that the high-throughput approach offers tremendous benefits.[89,90a,90b,97–106]

In 2002, Bristol-Meyers researchers, Yue and Nugent, successfully utilized a high-throughput approach for the asymmetric hydrogenation of 3-alkylidene-2-piperidones, providing an attractive industrial route to pharmacologically important 3-alkylpiperidines (Equation (10)).[97] Thirty-two chiral phosphines were screened *in situ* with four rhodium complexes: $[Rh(C_2H_4)_2Cl]_2$, $[Rh(COD)_2]BF_4$, $[Rh(COD)_2]OTf$, and $[Rh(COD)Cl]_2$; two iridium complexes: $[Ir(COD)_2]BF_4$, and $[Ir(COD)Cl]_2$; and two ruthenium complexes: $(COD)Ru(\eta^3\text{-methallyl})_2$ (used in combination with 2HBr to generate $LRuBr_2$ *in situ*), and $(COD)Ru(\eta^3\text{-methallyl})_2$ (used in combination with 1 equiv. $BF_3 + 1$ equiv. HBF_4 to generate $[(COT)LRuH]BF_4$ *in situ*; COT = cyclooctatetraene).

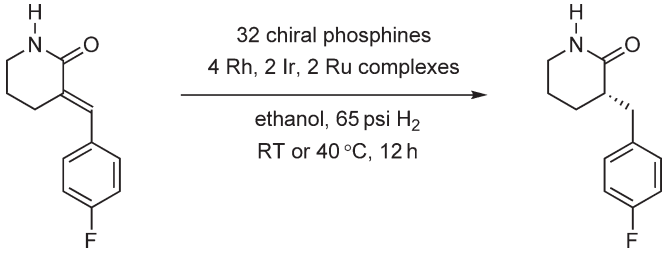

(10)

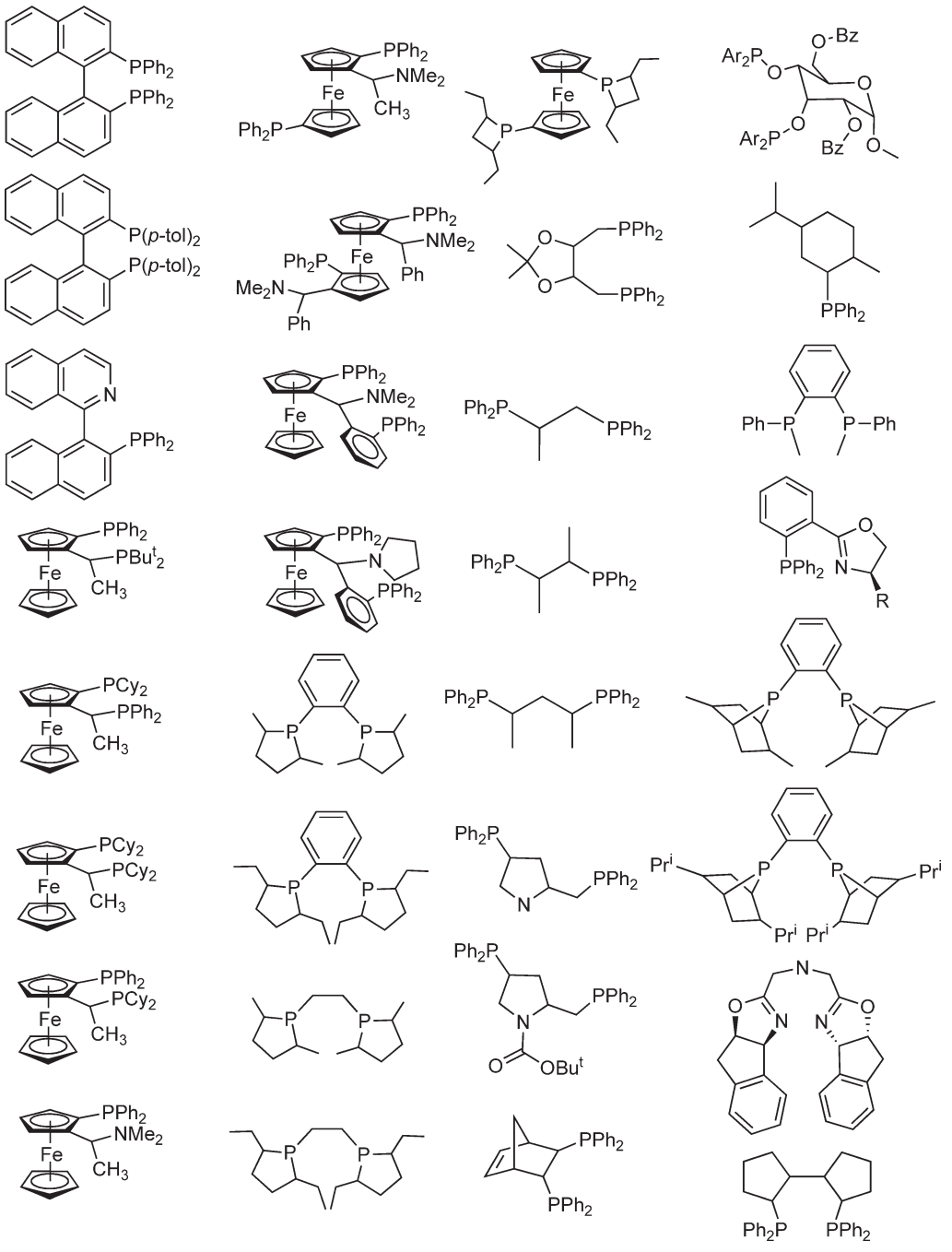

Screening was conducted in array format with 96 × 1 ml glass vials housed within a glove box. Each vial was charged with aliquots of three stock solutions: (i) 30 µl of ligand (10 mM solution in toluene); (ii) 30 µl of metal complex (9 mM solution in ethanol or THF); and (iii) 300 µl of 3-(*p*-fluorobenzylidene)valerolactam (90 mM solution in ethanol; substrate to catalyst ratio = 100 : 1). The array was covered with an airtight seal and removed from the glove box. The system was flushed with H_2 and pressurized to 65 psi for 12 h at room temperature (for Rh and Ir) or 40 °C (for Ru). Stirring was maintained using a modified commercial vortexing unit, and product analysis was conducted by chiral HPLC (initial catalyst screening was conducted at Symyx Technologies). The highest enantioselectivity was observed for the combination of $[Ir(COD)_2]BF_4$ with 2,4-bis(diphenylphosphino)pentane (BDPP), which produced the desired 3-(*p*-fluorobenzyl)piperidine with full conversion and 91% ee. The authors expressed great surprise in the

results, which contradicted an emerging hypothesis that, for asymmetric induction, structural rigidity is a beneficial feature (especially for chelating diphosphines).[108] Using such a hypothesis, BDPP would have been anticipated to perform poorly, since it is known to possess a highly flexible backbone. Impressively, the authors used the results of the study to successfully prepare (*S*)-(+)-3-(*p*-fluorobenzyl)piperidine on an industrial 20 kg scale. The conclusions from these results raise an important point: if new catalyst design criteria are centered upon incomplete or speculative theories, then inevitably opportunities for breakthrough discoveries will be missed.

In the same year, Morken and co-worker introduced a high-throughput assay based upon the use of an isotopically labeled reactant coupled with a rapid NMR technique that can be used to analyze reactions *in situ* without the need for quenching and product work-up.[90] The authors took advantage of the fact that enantiotopic groups are rendered diastereotopic if a neighboring prochiral group undergoes a reaction to generate a chiral center. To explore the utility of the NMR assay, the authors examined the asymmetric transfer hydrogenation of a prochiral ketone with a library of 10 amino alcohols and three ruthenium sources (Equation (11)).

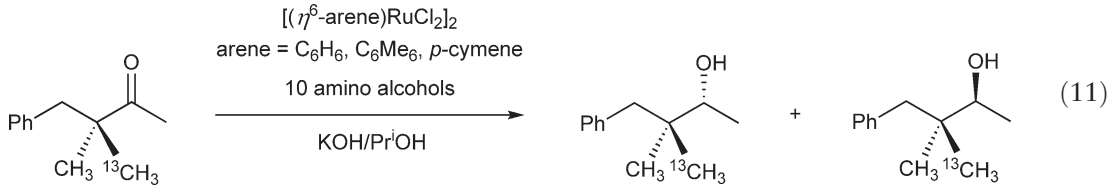

(11)

A 3 × 10 array of 1 ml glass vials containing small stir bars was assembled. Using stock solutions, 0.56 µmol of $\{[\eta^6\text{-arene}]RuCl_2\}_2$ (arene = benzene, *p*-cymene, C_6Me_6) and 2.24 µmol ligand were transferred to each reaction vial and diluted to 0.28 ml with isopropanol. The vials were sealed and heated to 82 °C for 30 min, whereupon 0.21 ml of a 0.26 M stock solution of the ketone was added, followed by 67 µl of 0.084 M KOH in isopropanol. Each sample was then transferred to an NMR tube and sealed for the duration of the experiment. After shimming on the first samples, subsequent samples were analyzed by ^{13}C NMR (15 s per analysis) to provide conversion and enantioselectivity data for each library member over a range of reaction times, thereby obviating the need for reaction sampling or quenching for timed analyses. The authors discovered that the combination of $\{[\eta^6\text{-}C_6Me_6]RuCl_2\}$ with chiral primary alcohols produced the highest level of enantioselectivity for this reaction.

Historically, conventional wisdom, coupled with a large number of reports, have suggested that chiral bidentate ligands are a necessary component of an effective enantioselective hydrogenation catalyst.[109,110] However, fairly recent reports demonstrate that monodentate ligands can be just as effective, and high-throughput approaches to explore the more accessible monodentate ligand space are particularly attractive.[98,98a,98b,99] In 2004, de Vries and co-workers reported a fully automated protocol for the synthesis and screening of a 32-membered phosphoramidite library for the asymmetric hydrogenation of amino acid precursors.[98] Before describing the de Vries approach, it is worth commenting that the automated synthesis of ligands is a difficult process that is not commonly adopted. Since high-purity ligands are desired, the rate-determining step in the synthesis of a ligand is nearly always the purification, and so an automated parallel synthesis will not be effective if laborious downstream separations are required. High-yielding chemical routes and/or clever purification strategies are therefore very important, and utilizing such approaches to express structural diversity for catalyst discovery remains a significant challenge. The de Vries report illustrates a simple and effective one-step nucleophilic displacement reaction to prepare a diverse series of 1,1′-binaphthalene-2,2′-diol (BINOL)-based monodentate phosphoramidites.

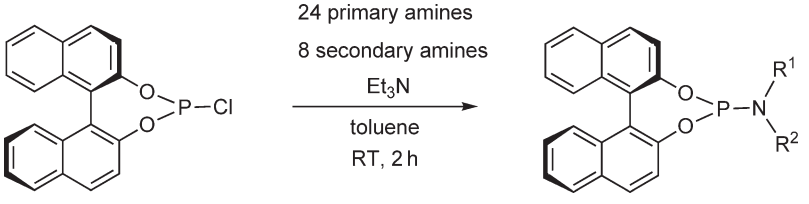

(12)

As can be seen in Equation (12), the only likely byproduct is HCl, and this can easily be trapped with a base and filtered away to leave the desired ligand without any need for further purification steps. Stock solutions of the amines, (*R*)-2,2′-binaphthol–chlorophosphite and 1 equiv. of Et_3N were dispensed using a liquid-handling robot into a 96-well microtiter plate. The 32 reaction mixtures were vortexed using an orbital shaker for 2 h and filtered to generate 32 ligand solutions.[111] An aliquot of each solution was transferred to each of two sets of 32 vials which contained

$[Rh(COD)_2]BF_4$ (ligand to rhodium ratio = 2 : 1) for screening against two unsaturated amino acid precursors. The hydrogenation reactions were performed at room temperature under 6 bar H_2 for 1 h using a Premix 96-multi reactor,[112] and conversion and ee values were determined using capillary GC. Several ligands were observed to impart ee values >90%, in good agreement with the values obtained from purified ligands prepared in a traditional manner. The authors claim that this protocol allows the preparation and subsequent screening of 96 ligands reactions over the course of just 2 days.

As previously described, catalyst sites comprising two ligands on a single metal center provides an opportunity for the high-throughput synthesis and screening of heteroligated complexes.[39,84,92a] Several independent groups have reported approaches in which mixtures of two chiral monodentate ligands were treated with $[Rh(COD)_2]BF_4$ in attempts to prepare and screen complexes of the type $[(L^a)(L^b)Rh]BF_4$. The resultant formulations were then screened against a variety of unsaturated substrates. Feringa and co-workers,[99] Gennari and co-workers,[100] and the Reetz group at the Max-Planck Institute have all reported the screening of mixtures of BINOL-based phosphonites, phosphates, and phosphoramidites.[101,101a–101c] All of the reports identify heteroligated systems that outperformed the respective homoligated analogs, showing that such an approach is a worthy one. In an attempt to exploit the asymmetric activation approach previously reported by Mikami,[84,94,94a,94b] the Reetz group also reported an approach in which mixtures of chiral and achiral ligands were contacted with $[Rh(COD)_2]BF_4$.[102] Intriguingly, reversals of enantioselectivity were observed for certain heteroligated complexes (relative to the chiral homoligated complexes).

1.13.3.3 Enantioselective Hydroamination

Palladium-based catalysts for enantioselective hydroamination reactions were discovered by extending the results of a high-throughput screening approach directed toward the discovery of non-selective hydroamination catalysts, reported by the Hartwig group in 2001. The approach taken by Hartwig and co-workers is described in Section 1.13.2.5.[61,61a,62]

1.13.3.4 Enantioselective Hydrosilylation

Multiple groups have reported high-throughput approaches for the discovery of catalysts for asymmetric hydrosilylation reactions.[82d,113d] Using a mass spectrometry technique for the determination of ee, Finn and co-workers employed a high-throughput screening approach to uncover catalysts for the enantioselective hydrosilylation of ketones, for the ultimate purpose of synthesizing chiral alcohols.[82d] The Scripps group used a one-pot procedure for the synthesis of a 21-membered library of chiral phosphite ligands with pendant amine functionalities. The ligand solutions (25 µl, 0.01 mmol) were first contacted with a solution of $[(COD)RhCl]_2$ (25 µl, 0.0025 mmol) in a dry box, and stirred for 1 h followed by the addition of 1-naphthyl methyl ketone (25 µl, 0.05 mmol). After cooling the reaction mixtures at −30 °C for 20 min, the hydrosilylation reactions were initiated by the addition of diphenylsilane (25 µl, 0.08 mmol), and agitated on a rotary evaporator in the dry box overnight, before the addition of 900 µl benzene as a diluent to quench the reactions. For the analysis, a 25 µl aliquot from each of the reaction products was removed to a separate vial and treated sequentially with CsF (as a suspension in THF) to cleave the silanes and produce chiral alcohols, and 120 µl (24 µmol) of mass-tagged chiral carboxylic acids to derivatize and mass differentiate the resultant products as esters. The product conversions and ee values were then analyzed by ESI-MS. Initial results from the ESI-MS technique were compared to those obtained from chiral HPLC for validation purposes. The first round of screening identified promising catalysts, and a modified set of 11 ligands were subsequently prepared to gain further insight into the structure–activity relationships. The most effective catalysts were then screened against a group of seven prochiral ketones using a chip-based desorption/ionization on silica (DIOS) mass spectrometry technique.[113,113a–c] Using this technique, the products were derivatized as mass-differentiated esters as described above, but aliquots of the product solutions (0.1–0.5 µl) were then deposited on a porous silicon plate prior to MS analysis. The data collection rate was reduced from 5 min to 10 s per sample. The best rhodium catalyst identified converted prochiral ketones into chiral alcohols with full conversions and ee values around 75%.

1.13.3.5 Enantioselective Hydroformylation

Klosin and co-workers at Dow Chemical have reported a parallel protocol for the screening of asymmetric hydroformylation reactions of styrene, vinyl acetate, and allyl cyanide.[114,114a,114b] In a one-pot, multiple substrate screening method introduced by Kagan,[115,115a] an Endeavor eight-cell reactor[116] was used to screen 48 different rhodium

catalysts (comprising nine chiral phosphite ligands) against pooled mixtures of the three olefins (144 discrete reactions). In order to facilitate the analysis of the complex product mixture obtained from a pooled substrate approach, two chiral GC methods were developed. Additionally, to ensure that the presence of the additional olefins did not influence the catalyst performance, a series of control experiments were performed on the individual olefins. The Dow study led to the discovery of a rhodium catalyst comprising a bidentate phosphite ((*S*,*S*)-Kelliphite) that produced hydroformylated vinyl acetate with an unprecedented >100 : 1 branched : linear ratio and 88% ee.

1.13.3.6 Enantioselective Addition of Nucleophiles to Allylic Esters

Multiple groups have reported high-throughput approaches for the discovery of catalysts for asymmetric allylic alkylations.[82e,117,117a–117d,118] Inspired by the ESI-MS technique described in Sections 1.13.2.1 and 1.13.2.14,[49,49a–49c] Pfaltz and co-workers devised a high-throughput ESI-MS screen to resolve chiral allylic esters through palladium-catalyzed allylic substitution reactions.[82e] Pfaltz reasoned that the catalytic resting states (palladium allyl cations) for this reaction could exist in sufficient quantities to be observable by MS. However, since the intermediates from enantiomeric allylic esters would have the same molecular weight, they would be indistinguishable by their mass spectra. Cleverly, Pfaltz chose to vary substituents (methyl vs. ethyl) remote to the two chiral allylic esters in order to provide intermediates with distinct molecular weights (Scheme 5). As an initial test, the authors treated an equimolar mixture of the two chiral allylic esters with an achiral palladium catalyst and showed that the ESI-MS spectrum indeed showed the expected signals corresponding to the allyl intermediates **A** and **B** with equal intensity. The equivalent experiment with a chiral ligand showed a strong bias toward one of the two intermediates (**A** : **B** = 9 : 91; a control experiment using the same chiral ligand with inversely substituted methyl and ethyl groups produced the reverse ratio **A** : **B** = 91 : 9).

The authors reasoned that transitions states of the first and second steps of this catalytic cycle would be geometrically similar, and consequently, the kinetic resolution identified from the first step should translate through to a high enantioselectivity for the final product. This assumption was confirmed from kinetic analysis of a

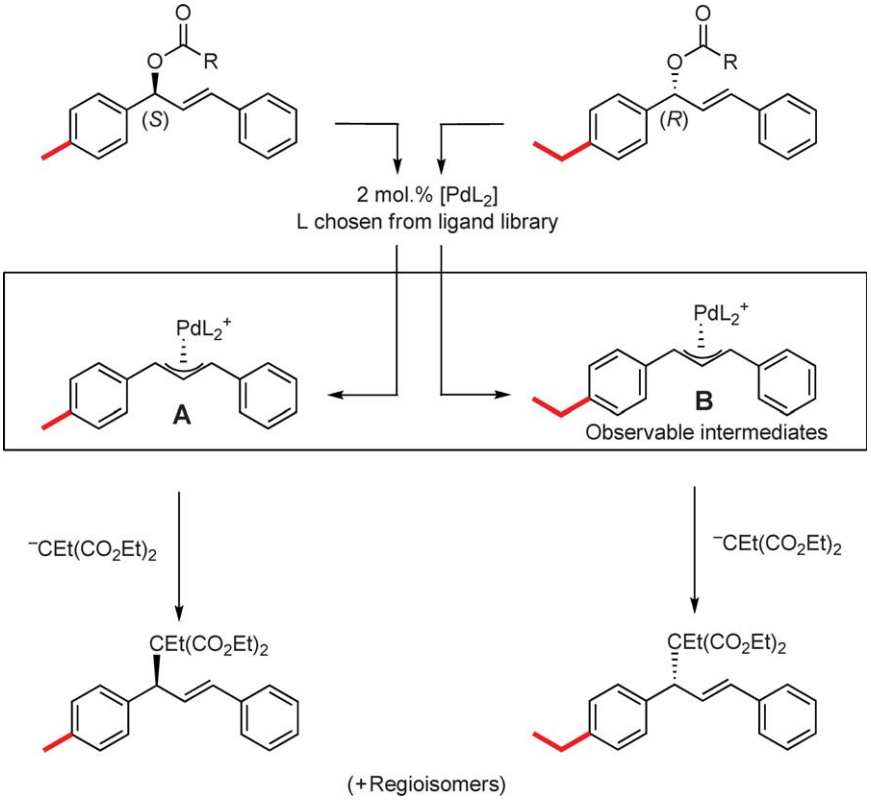

Scheme 5

preparative reaction using diethylethylmalonate as the nucleophile. Using the ESI-MS screening technique, the authors were able to screen up to 10 chiral catalysts per hour. From a library of 60 phosphorus-based ligands, a highly selective ligand **3** was identified producing a ratio of **A**:**B** = 100:1, significantly higher than selectivities previously reported for this reaction.

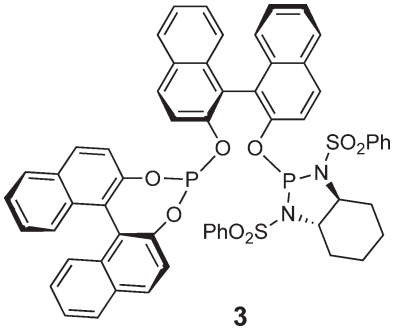

3

Having demonstrated the utility of the technique, the authors attempted a pooled approach in which five catalyst precursors were combined with the two chiral allylic esters at −78 °C. The low temperature was necessary to avoid ligand scrambling, but the authors demonstrate that provided the molecular ion signals do not overlap, ESI-MS can be used very effectively to screen pooled catalysts.

Gilbertson and co-workers have reported a peptide-based high-throughput approach in which a library of 136 polymer-supported diphosphines, linked predominantly through a β-turn peptide motif, were screened in the presence of $[(\eta^3\text{-allyl})PdCl]_2$, for their ability to catalyze the enantioselective addition of dimethylmalonate to cyclopentenyl acetate.[117,117a–117d] The screening results revealed the importance of the β-turn motif for asymmetric induction. Optimization experiments generated catalysts with ee values up to 95%, comparable to the best catalysts known for this reaction.

1.13.4 Reactor Technology

The examples highlighted in the previous sections illustrate the utility of pooled, rapid-serial, and parallel approaches to high-throughput screening. While pooled approaches have taken advantage of traditional reactor designs, rapid-serial and parallel approaches have utilized a variety of designs, ranging from simple arrays of glass vials, to sophisticated assemblies of computer-controlled reactor arrays, to precision-machined rapid-serial microreactors. One feature that is common to all of these approaches is an adaptation to smaller scale. In order to work in a high-throughput manner, chemistries are performed at scales much lower than used in a traditional laboratory reactor. Clearly, if the results from the high-throughput experiment are to be exploited, chemistries at these scales need to be calibrated with well-studied examples and shown to correlate in some meaningful way to traditional scales. The science of microreactor design for miniaturized chemical reactions is a separate and lively field of research that will not be addressed here, but the reader will certainly need to seek advice from this field if a new small scale high-throughput reactor technology is being designed.[119] The purpose of this section is to provide the necessary background references and to highlight recent examples of reactor designs that have been used in the field of high-throughput organometallic chemistry (for a list of commercially available equipment directed toward parallel synthesis and screening, see Ref: 11 and 50a, respectively).

Depending on the chemistry under scrutiny, an array of glass vials may represent a perfectly suitable microreactor design. For example, homogeneous liquid-phase chemical reactions with non-volatile components may be addressed adequately in an array of vials. For chemistries where more demanding conditions are required, several groups have reported impressive, custom-built microreactor designs. A Dow Chemical team has recently described a rapid-serial "electrothermal microreactor" designed to assess polyolefin catalyst performance at high temperature (175 °C) and pressure (400 psi) within a tubular reactor containing a series of temperature sensors.[120] Measurable exotherms were correlated to the differences in the nascent activity of two well-studied polyolefin catalysts. de Bellefon and co-workers also describe a tubular microreactor that is preceded by a micromachined mixing stage.[95,95a,121] During operation, two carrier liquids flow continuously through the apparatus and the catalyst and substrate are pulsed into the carrier stream and mixing stage. The apparatus was first used to screen eight allylic alcohol isomerization catalysts, and then further extended to accommodate a gaseous stream for two-phase reactions. The authors propose

a throughput capability of 500 samples per day for enantioselective hydrogenation reactions. Researchers at Symyx have recently described a fully automated parallel pressure reactor.[12,34,34a] The instrument consists of 48 individually controlled high-pressure batch reactors where each reactor possesses its own pressure and temperature control and gaseous feed line. The whole assembly is mounted in a dry box to sustain a uniform inert atmosphere and consistently low background impurity level. Solid-supported or solution-phase catalysts are prepared and manipulated robotically in arrays of glass vials situated alongside the reactor. With the computer-controlled reactor at temperature and pressure equilibrium, the catalysts are injected into each reactor cell (ca. 5 ml reaction volume) and monitored in real time through pressure and temperature monitors. Concerning the mass transport issues mentioned in Sections 1.13.2 and 1.13.3.2, the gas–liquid diffusion kinetics within the Symyx reactor can immediately be compared to the kinetics of catalysis to ensure that reactions are not diffusion limited. Thus, 48 individual reaction events can be monitored in real time under conditions that provide meaningful information about the performance capabilities of each catalyst at high temperatures (up to 200 °C) and pressures (up to 500 psig) for both solution-phase and slurry-phase reactions. More recently, this instrument has been further developed to accommodate 12 separate reagent addition channels that enable semicontinuous microliter reagent additions at high pressures.[122]

Coughlin and co-workers have recently described a convenient gas manifold and associated reactor design that accommodates different reactor vessel sizes (70–300 ml) in addition to multi-well arrays (20 ml).[48,48a] The simple design represents an alternative to highly sophisticated systems that can be prohibitively expensive for many laboratories. The multi-well design can be used to perform seven simultaneous polymerizations. The reactor utility was demonstrated using literature catalysts for ethylene and propylene polymerizations. A team from Bayer has also recently reported a parallel reactor design.[123] Mülhaupt and co-workers have recently report a fully automated single polymerization reactor with a series of carousels used to deliver catalyst solutions and collect resultant polymer products.[50,50a–50f] The authors claim that initial scoping polymerizations are performed in a commercially available Chemspeed parallel reactor,[43] a process which provides appropriate candidates for the larger scale automated single reactor (300 ml). The throughput is specified at 120 polymerizations per day, provided that the unit can be operated continuously over a 24 h period. Additionally, the authors provide a convenient list of commercially available parallel reactors. Finally, a variety of other groups have now reported examples of microreactor designs that are amenable to high-throughput screening.[124–131]

1.13.5 Rapid Analytical Techniques

The collection of rapid analytical techniques that is now available to support high-throughput organometallic chemistry is impressive. For example, within the field of olefin polymerization, the advent of the high-throughput approach has necessarily led to the development of a suite of rapid polymer characterization techniques. Rapid GPC,[132] rapid spectroscopic techniques,[50b,50d,133,133a,133b,134] and a variety of techniques to measure physical and mechanical properties,[135,136,136a,136b,137] all combine to provide powerful analytical capabilities that can now serve the throughput and scale of state-of-the-art parallel polymerization reactor technologies (see also the techniques described within Refs: 50 and 51, respectively). Additionally, for the analysis of small molecules, the list of available analytical methods continues to grow rapidly.[138,139] The list of techniques reported include fluorescence imaging[63,63a] (see also Ref: 63 for an example of the use of fluorescence imaging for achiral transformations), liquid crystal doping,[81] mass spectrometry,[82,82a–82e] infrared thermography,[83,83a–83c] circular dichroism,[84] enzymatic techniques,[85,85a] antibody detection,[86] indicator displacement assays,[87] parallel chiral capillary array electrophoresis,[70,88,88a] IR spectroscopy,[89] and isotope labeling in combination with flow-through NMR,[90,90a–90c] rapid HPLC,[91] rapid GC,[91] reaction calorimetry,[65,65a] and quantitative, image-based TLC.[55,76] Many examples of high-throughput approaches highlighted within this chapter have utilized creative inferential screens which require for example, specially designed reaction substrates with spectroscopic handles, or post-reaction derivatization. Rapid screening capabilities have now clearly advanced to the point where future high-throughput approaches can focus on a preferred approach: namely the direct analysis of the specific reactions of interest.

1.13.6 Conclusions

It is hoped that the breadth of chemical approaches, experimental methods, and screening techniques described in this chapter provide the reader with a clear picture of the status of the field of high-throughput organometallic chemistry. Practically, all reports are associated with making advances in the field of catalysis. When considered

collectively, the reports reviewed in this chapter challenge the notion that high-throughput catalyst discovery is simply a case of assembling a collection of molecules and screening them to find the catalyst of interest. The high-throughput experiment presents many challenges that must be addressed skillfully in order to produce results with meaningful information. Sustainable high-throughput workflows are challenging to construct, and the most effective approaches are usually centered on carefully planned rounds of synthesis, screening, and intelligence gathering. From the combined advances reported in high-throughput synthetic approaches, reactor technologies, and rapid analytical techniques, it is clear that high-throughput approaches are evolving rapidly in academic and industrial settings. It is appropriate to conclude that since COMC (1995), the field of organometallic chemistry has been fortified with a powerful new research strategy.

Acknowledgments

The author would like to express sincere gratitude to Drs. Keith Hall, Dawn Verdugo, and Guang Zhu who have kindly set aside time to read and improve this contribution.

References

1. Lees, K. A.; Tootill, J. P. R. *Analyst* **1955**, *80*, 531–535.
2. Nicolaou, K. C.; Hanko, R.; Hartwig, W. Combinatorial Chemistry in Perspective. In *Handbook of Combinatorial Chemistry, Drugs, Catalysts, Materials*; Nicolaou, K. C., Hanko, R., Hartwig, W., Eds.; Wiley-VCH: Weinheim, 2002; pp 3–9.
3. Furka, Á.; Sebestyén, F.; Asgedom, M.; Dibó, G. *Proceedings of the 14th International Congress of Biochemistry*, Prague, Czechoslovakia, 1988.
3a. Furka, Á.; Sebestyén, F.; Asgedom, M.; Dibó, G. *Proceedings of the 14th International Congress of Biochemistry*, VSP, Utrecht, The Netherlands, 1988, *13*, 47.
3b. Furka, Á.; Sebestyén, F.; Asgedom, M.; Dibó, G. *Int. J. Peptide Prot. Res.* **1991**, *37*, 487–493.
3c. Lam, K. S.; Salmon, S. E.; Hersh, E. M.; Hruby, V. J.; Kazmirsky, W. M.; Knapp, R. J. *Nature* **1991**, *354*, 82–84.
3d. Brenner, S.; Lerner, R. A. *Proc. Natl. Acad. Sci.* **1992**, *89*, 5381–5383.
3e. Nielsen, S. B.; Janda, K. D. *J. Am. Chem. Soc.* **1993**, *115*, 9812–9813.
3f. Needels, M. C.; Jones, D. G.; Tate, E. H.; Heinkel, G. L.; Kochersperger, L. M.; Dower, W. J.; Barrett, R. W.; Gallop, M. A. *Proc. Natl. Acad. Sci.* **1993**, *90*, 10700–10704.
3g. Ohlmeyer, M. H. J.; Swanson, R. N.; Dillard, L. W.; Reader, J. C.; Asouline, G.; Kobayashi, R.; Wigler, M.; Still, W. C. *Proc. Natl. Acad. Sci.* **1993**, *90*, 10922–10926.
4. Merritt, A. T.; Gerritz, S. W. *Curr. Opin. Chem. Biol.* **2003**, *7*, 305–307.
4a. Golebiowski, A.; Klopfenstein, S. R.; Portlock, D. E. *Curr. Opin. Chem. Biol.* **2003**, *7*, 308–325.
5. Nicolaou, K. C., Hanko, R., Hartwig, W., Eds. *Handbook of Combinatorial Chemistry, Drugs, Catalysts, Materials*; Wiley-VCH: Weinheim, 2002.
5a. Bräse, S.; Köbberling, J.; Griebenow, N. Organopalladium Reactions in Combinatorial Chemistry. In *Handbook of Organopalladium Chemistry for Organic Synthesis*; Negishi, E., de Meijere, A., Eds.; Wiley-Interscience: New York, 2002; pp 3031–3126.
5b. Fenniri, H., Ed. *Combinatorial Chemistry*; Oxford University Press: Oxford, 2000.
5c. Terrett, N. K. *Combinatorial Chemistry*; Oxford University Press: Oxford, 1998.
6. Xiang, X.-D.; Sun, X.; Briceño, G.; Lou, Y.; Wang, K.-A.; Chang, H.; Wallace-Freedman, W. G.; Chen, S-W.; Schultz, P. G. *Science* **1995**, *268*, 1738–1740.
6a. Briceño, G.; Chang, H.; Sun, X.; Schultz, P. G.; Xiang, X.-D. *Science* **1995**, *270*, 273–275.
7. Liu, G.; Ellman, J. A. *J. Org. Chem.* **1995**, *60*, 7712–7713.
8. Burgess, K.; Lim, H.-L.; Porte, A. M.; Sulikowski, G. A. *Angew. Chem., Int. Ed.* **1996**, *35*, 220–221.
8a. Burgess, K.; Moye-Sherman, D.; Porte, A. M. *Conference Proceedings: Molecular Diversity and Combinatorial Chemistry: Libraries and Drug Discovery*; Chaiken, I. M., Janda, K. D., Eds.; Coronado, California, January 28–February 2, 1996; American Chemical Society: Washington, 1996.
8b. Menger, F. M.; Eliseev, A. V.; Migulin, V. A. *J. Org. Chem.* **1995**, *60*, 6666–6667.
9. Gilbertson, S. R.; Wang, X. *Tetrahedron Lett.* **1996**, *37*, 6475–6478.
10. Scifinder 2002 Version. www. cas. org
11. De Bellefon, C. *NATO Science Series, II Mathematics, Physics and Chemistry*; 2002; Vol. 69, pp 71–83.
12. Boussie, T. R.; Diamond, G. M.; Goh, C.; Hall, K. A.; LaPointe, A. M.; Leclerc, M. K.; Lund, C.; Murphy, V.; Shoemaker, J. A. W., Tracht, U., *et al. J. Am. Chem. Soc.* **2003**, *125*, 4306–4317.
13. Weinburg, W. H.; Turner, H. W. Impact of High-Throughput Screening Technologies on Chemical Catalysis. In *High-Throughput Screening in Chemical Catalysis, Technologies, Strategies and Applications*; Hagemeyer, A., Strasser, P., Volpe, A. F. Jr., Eds.; Wiley-VCH: Weinheim, 2004; pp 1–17.
14. Reetz, M. T. Combinatorial methods in catalysis by metal complexes. In *Comprehensive Coordination Chemistry II*; McCleverty, J. A., Meyer, T. J., Eds.; Elsevier Ltd., Oxford, 2004; Vol 9, pp 509–548.
15. Jandeleit, B.; Schaefer, D. J.; Powers, T. S.; Turner, H. W.; Weinberg, W. H. *Angew. Chem., Int. Ed.* **1999**, *38*, 2494–2532.
16. Woo, S. I.; Kim, K. W.; Cho, H. Y.; Kwang, S.; Jeon, M. K.; Tarte, N. H.; Kim, T. S.; Mahmood, A. *QSAR Comb.l Sci.* **2005**, *24*, 138–154.
17. Wennemers, H. Combinatorial Methods for the Discovery of Catalysts. In *Highlights in Bioorganic Chemistry*; Schmuck, C., Wennemers, H., Eds.; Wiley-VCH: Weinheim, 2004; pp 436–445.
18. Stambuli, J. P.; Hartwig, J. F. *Curr. Opin. Chem. Biol.* **2003**, *7*, 420–426.
18a. Murphy, V.; Volpe, A. F., Jr.; Weinberg, W. H. *Curr. Opin. Chem. Biol.* **2003**, *7*, 427–433.
18b. Gilbertson, S. R. *Chemtracts* **2003**, *16*, 560–566.

18c. de Vries, J. G.; de Vries, A. H. M. *Eur. J. Org. Chem.* **2003**, 799–811.
19. Archibald, B.; Brümmer, O.; Devenney, M.; Gorer, S.; Jandeleit, B.; Uno, T.; Weinberg, W. H.; Weskamp, T. Combinatorial Methods in Catalysis. In *Handbook of Combinatorial Chemistry, Drugs, Catalysts, Materials*; Nicolaou, K. C., Hanko, R., Hartwig, W., Eds.; Wiley-VCH: Weinheim, 2002; pp 885–990.
20. Lavastre, O.; Pinault, N.; Mincheva, Z. *NATO Science Series, II Mathamatics, Physics and Chemistry*; 2002; Vol. 69, pp 135–151.
20a. Xu, L.; Baillie, C.; Chen, W.; Xiao, J. *NATO Science Series, II Mathamatics, Physics and Chemistry*; 2002; Vol. 69, pp 279–290.
21. Dahmen, S.; Bräse, S. *Synthesis* **2001**, *10*, 1431–1449.
21a. Wennemers, H. *Comb. Chem. & High Throughput Screening* **2001**, *4*, 273–285.
21b. Gilbertson, S. R. *Prog. Inorg. Chem.* **2001**, *50*, 433–471.
21c. Crabtree, R. H. *Chem. Commun.* **1999**, 1611–1616.
21d. Loch, J. A.; Crabtree, R. H. *Pure Appl. Chem.* **2001**, *73*, 119–128.
22. Gennari, F.; Seneci, P.; Miertus, S. *Catal. Rev. -Sci. Eng.* **2000**, *42*, 385–402.
23. Kuntz, K. W.; Snapper, M. L.; Hoveyda, A. H. *Curr. Opin. Chem. Biol.* **1999**, *3*, 313–319.
24. Francis, M. B.; Jamison, T. F.; Jacobsen, E. N. *Curr. Opin. Chem. Biol.* **1998**, *2*, 422–428.
25. Hoveyda A. H.; Murphy, K. E. *Comprehensive Asymmetric Catalysis Supplement*; 2004; Vol. 1, pp 171–187.
25a. Hoveyda.; Amir, H. Diversity-Based Identification of Efficient Homochiral Organometallic Catalysts for Enantioselective Synthesis. In *Handbook of Combinatorial Chemistry*; Nicolaou, K. C., Hanko, R., Hartwig, W., Eds.; Wiley-VCH: Weinheim, 2002; pp 991–1016.
25b. Snapper, M. L.; Hoveyda, A. H. Combinatorial Approaches to Chiral Catalyst Discovery. In *Combinatorial Chemistry*; 2000; pp 433–455.
25c. Shimizu, K. D.; Snapper, M. L.; Hoveyda, A. H. Combinatorial Approaches. In *Comprehensive Asymmetric Catalysis I-III*; Jacobsen, E. N., Pfaltz, A., Yamamoto, H., Eds.; Springer-Verlag: Berlin, 1999; pp 1389–1399.
25d. Hoveyda, A. *Chem. Biol.* **1999**, *6*, R305–R308.
25e. Shimizu, K. D.; Snapper, M. L.; Hoveyda, A. H. *Chem. Eur. J.* **1999**, *4*, 1885–1889.
25f. Hoveyda, A. H. *Chem. Biol.* **1998**, *6*, R187–R191.
26. Ding, K.; Haifeng, D.; Yuan, Y.; Long, J. *Chem. Eur. J.* **2004**, *10*, 2872–2884.
27. Gennari, C.; Piatulli, U. *Chem. Rev.* **2003**, *103*, 3071–3100.
28. Traverse, J. F.; Snapper, M. L. *Drug Discov. Today* **2002**, 7, 1002–1012.
29. Reetz, M. T. *Angew. Chem., Int. Ed.* **2001**, *40*, 284–310.
30. Merritt, A. Combinatorial Approaches to Asymmetric Catalyst Discovery. In *Rodd's Chemistry of Carbon Compounds Volume V*; Sainsbury, M., Ed. Elsevier Science B.V. 2001; pp 259–274.
31. Burgess, K.; Porte, A. M. *Advances in Catalytic Processes*; 1997; Vol. 2, pp 69–82.
32. Boussie, T. R.; Coutard, C.; Turner, H.; Murphy, V.; Powers, T. S. *Angew. Chem., Int. Ed.* **1998**, *37*, 3272–3275.
32a. Boussie, T. R.; Murphy, V.; Hall, K. A.; Dales, C.; Petro, M.; Carlson, E.; Turner, H.; Powers, T. S. *Tetrahedron* **1999**, *55*, 11699–11710.
33. Johnson, L. K.; Killian, C. M.; Brookhart, M. *J. Am. Chem. Soc.* **1995**, *117*, 6414–6415.
33a. Ittel, S. D.; Johnson, L. K.; Brookhart, M. *Chem Rev.* **2000**, *100*, 1169–1203.
34. Turner, H.; Dales, C. G.; Van Erden, L.; van Beek, J. A. M. U.S. Patent 6,306,658, October 23, 2001. (See also, U.S. Patents 6,455,316, 6,582,116, 6,548,116, 6,489,168; E.P. 1069942 and C.A. 2381014.)
34a. Dales, G. C.; Troth, J. R.; Higashihara, K. S.; Diamond, G.; Murphy, V.; Chandler, W. H., Jr.; Frank, T. G.; Freitag, C. J.; Huffman, D. E.P. 226,867, 2002. (See also, U.S. Patents 6,485,692 and 6,566,461.)
35. Stork, M.; Herrmann, A.; Nemnich, T.; Klapper, M.; Müllen, K. *Angew. Chem., Int. Ed.* **2000**, *39*, 4367–4369.
36. Jones, D. J.; Gibson, V. C.; Green, S. M.; Maddox, P. J. *Chem. Commun.* **2002**, 1038–1039.
37. Jones, D. J.; Gibson, V. C.; Green, S. M.; Maddox, P. J.; White, A. J. P.; Williams, D. J. *J. Am. Chem. Soc.* **2005**, *127*, 11037–11046.
38. Tian, J.; Coates, G. W. *Angew. Chem., Int. Ed.* **2000**, *39*, 3626–3629.
39. Mason, A. F.; Coates, G. W. *J. Am. Chem. Soc.* **2004**, *126*, 10798–10799.
40. Adams, N.; Arts, H. J.; Bolton, P. D.; Cowell, D.; Dubberley, S. R.; Friederichs, N.; Grant, C. M.; Kranenburg, M.; Sealey, A. J.; Wang, B., *et al. Chem. Commun.* **2004**, 434–435.
41. Boussie, T. R.; Diamond, G. M.; Goh, C.; Hall, K. A.; LaPointe, A. M.; Leclerc, M.; Lund, C.; Murphy, V. U.S. Patent 6,750,345, June 14, 2004.
41a. Boussie, T. R.; Diamond, G. M.; Goh, C.; Hall, K. A.; LaPointe, A. M.; Leclerc, M.; Lund, C.; Murphy, V. U.S. Patent 6,713,577, 30 March 2004.
41b. Boussie, T. R.; Brümmer, O.; Diamond, G.; Goh, C.; LaPointe, A. M.; Leclerc, M. K.; Shoemaker, J. A. World Pat. Appl. 091262, 2003.
41c. Boussie, T. R.; Diamond, G. M.; Goh, C.; Hall, K. A.; LaPointe, A. M.; Leclerc, M.; Murphy, V.; Shoemaker, J. A. W.; Turner, H.; Rosen, R. K., *et al. Angew. Chem., Int. Ed.* **2006** (in press.).
41d. See www.dow.com\versify.
42. Cho, H. Y.; Hong, D. S.; Jeong, W. D.; Gong, Y.-D.; Woo, S. I. *Macromol. Rapid Commun.* **2004**, *25*, 302–306.
43. See Chemspeed Technologies. http://www.chemspeed.com.
43a. For a list of commercially available equipment directed towards parallel synthesis and screening, see Refs. 11 and 50a.
44. Keisewetter, J.; Kaminsky, W. *Chem. Eur. J.* **2003**, *9*, 1750–1758.
45. Kolb, P.; Demuth, D.; Newsam, J. M.; Smith, M. A.; Sundermann, A.; Schunk, S. A.; Bettonville, S.; Bruelet, J.; Francios, P. *Macromol. Rapid Commun.* **2004**, *25*, 280–285.
46. For a recent review of non-metallocene olefin polymerization catalysts, see Gibson, V. C.; Spitzmesser, S. K. *Chem. Rev.* **2003**, *103*, 283–316.
47. Komon, Z. J. A.; Diamond, G. M.; Leclerc, M. K.; Murphy, V.; Okazaki, M.; Bazan, G. C. *J. Am. Chem. Soc.* **2002**, *124*, 15280–15285.
48. Constable, G. S.; Gonzalez-Ruiz, R. A.; Kasi, R. M.; Coughlin, E. B. *Macromolecules* **2002**, *35*, 9613–9616.
48a. Focante, F.; Gonzalez-Ruiz, R. A.; Coughlin, E. B. *Polymeric Materials: Science and Engineering*; 2003; Vol. 89, pp 553–554.
49. Hinderling, C.; Chen, P. *Angew. Chem., Int. Ed.* **1999**, *38*, 2253–2256.
49a. Hinderling, C.; Chen, P. *Chimia* **2000**, *54*, 232–235.
49b. Chen, P. *Angew. Chem., Int. Ed.* **2003**, *42*, 2832–2847.
49c. Huber, M. *PharmaChem* **2002**, 14–17.
50. Tuchbreiter, A.; Marquardt, J.; Kappler, B.; Honerkamp, J.; Mülhaupt, R. *Macromol. Symp.* **2004**, *213*, 327–333.
50a. Tuchbreiter, A.; Marquardt, J.; Kappler, B.; Honerkamp, J.; Kristen, M. O.; Mülhaupt, R. *Macromol. Rapid Commun.* **2003**, *24*, 47–62.
50b. Kappler, B.; Tuchbreiter, A.; Faller, D.; Liebetraut, P.; Horbelt, W.; Timmer, J.; Honerkamp, J.; Mülhaupt, R. *Polymer* **2003**, *44*, 6179–6186.
50c. Tuchbreiter, A.; Kappler, B.; Stockmann, R.; Mülhaupt, R.; Honerkamp, J. *Macromol. Mater. Eng.* **2003**, *288*, 29–34.

50d. Tuchbreiter, A.; Marquardt, J.; Zimmermann, J.; Walter, P.; Mülhaupt, R. *J. Comb. Chem.* **2001**, *3*, 598–603.
50e. Tuchbreiter, A.; Mülhaupt, R. *Macromol. Symp.* **2001**, *173*, 1–20.
50f. Tuchbreiter, A.; Kappler, B.; Honerkamp, J.; Mülhaupt, R. *Dechema Monographien* **2001**, *137*, 323–334.
51. Zhang, H.; Hoogenboom, R.; Meier, M. A. R.; Schubert, U. S. *Meas. Sci. Technol.* **2005**, *16*, 203–211.
51a. Adams, N.; Schubert, U. S. *QSAR and Combi. Sci.* **2005**, *24*, 155–158.
51b. Hoogenboom, R.; Meier, M. A. R.; Schubert, U. S. *Mat. Res. Soc. Symp. Proc.* **2004**, *804*, 83–94.
51c. Meier, M. A. R.; Schubert, U. S. *J. Mater. Chem.* **2004**, *14*, 3289–3299.
51d. Meier, M. A. R.; Hoogenboom, R.; Schubert, U. S. *Macromol. Rapid Commun.* **2004**, *25*, 21–33.
51e. Hoogenboom, R.; Meier, M. A. R.; Schubert, U. S. *Macromol. Rapid Commun.* **2003**, *24*, 15–32.
51f. Hoogenboom, R.; Schubert, U. S. *J. Polym. Sci. Part A* **2003**, *41*, 2425–2434.
52. Gruter, G. J. M.; Graham, A.; McKay, B.; Gilardoni, F. *Macromol. Rapid Commun.* **2003**, *24*, 73–80.
53. Meredith, J. C. *J. Mater. Chem.* **2003**, *38*, 4427–4437.
54. de Meijere, A., Diederich, F., Eds. *Metal-Catalyzed Cross-Coupling Reactions*; Wiley-VCH: Weinheim, 2004.
54a. Negishi, E., de Meijere, A., Eds. *Handbook of Organopalladium Chemistry for Organic Synthesis*; Wiley-Interscience: New York, 2002.
54b. Cornils, B., Herrmann, W. A., Eds. *Applied Homogeneous Catalysis with Organometallic Compounds*; Wiley-VCH: Weinheim, 2002.
55. Garbacia, S.; Touzani, R.; Lavastre, O. *J. Comb. Chem.* **2004**, *6*, 297–300.
56. Stambuli, J. P.; Stauffer, S. R.; Shaughnessy, K. H.; Hartwig, J. F. *J. Am. Chem. Soc.* **2001**, *123*, 2677–2678.
57. Stryer, L.; Haugland, R. P. *Proc. Natl. Acad. Sci.* **1967**, *58*, 719–726.
57a. Wu, P.; Brand, L. *Anal. Biochem.* **1994**, *218*, 1–13.
58. Stauffer, S. R.; Hartwig, J. F. *J. Am. Chem. Soc.* **2003**, *125*, 6977–6985.
59. Stauffer, S. R.; Beare, N. A.; Stambuli, J. P.; Hartwig, J. F. *J. Am. Chem. Soc.* **2001**, *123*, 4641–4642.
60. Bei, X.; Uno, T.; Norris, J.; Turner, H. W.; Weinberg, W. H.; Guram, A. S. *Organometallics* **1999**, *18*, 1840–1853.
61. Löber, O.; Kawatsura, M.; Hartwig, J. F. *J. Am. Chem. Soc.* **2001**, *123*, 4366–4367.
61a. Pawlas, J.; Nakao, Y.; Kawatsura, M.; Hartwig, J. F. *J. Am. Chem. Soc.* **2002**, *124*, 3669–3679.
62. Kawatsura, M.; Hartwig, J. F. *Organometallics* **2001**, *20*, 1960–1964.
63. Shaughnessy, K. H.; Kim, P.; Hartwig, *J. Am. Chem. Soc.* **1999**, *121*, 2123–2132.
63a. For another example of a fluorescence-based screen, see Copeland, G. T.; Miller, S. J. *J. Am. Chem. Soc.* **1999**, *121*, 4306–4307.
64. Boele, M. D. K.; van Strijdonck, G. P. F.; de Vries, A. H. M.; Kamer, P. C. J.; de Vries, J. G.; van Leeuwen, P. W. N. M. *J. Am. Chem. Soc.* **2002**, *124*, 1586–1587.
65. Blackmond, D. G.; Rosner, T.; Pfaltz, A. *Org. Process Res. Dev.* **1999**, *3*, 275–280.
65a. Blackmond, D. G. *Angew. Chem., Int. Ed.* **2005**, *44*, 4302–4320.
66. Fagan, P. J.; Hauptman, E.; Shapiro, R.; Casalnuovo, A. *J. Am. Chem. Soc.* **2000**, *122*, 5043–5051.
67. Schareina, T.; Kempe, R. *Angew. Chem., Int. Ed.* **2002**, *41*, 1521–1523.
68. Colacot, T. J.; Gore, E. S.; Kuber, A. *Organometallics* **2002**, *21*, 3301–3304.
68a. Colacot, T. J.; Shea, H. A. *Org. Lett.* **2004**, *6*, 3731–3734.
69. IJpeij, E. G.; Beijer, F. H.; Arts, H. J.; Newton, C.; de Vries, J. G.; Gruter, G.-J. M. *J. Org. Chem.* **2002**, *67*, 169–176.
70. Zhang, Y.; Gong, X.; Zhang, H.; Larock, R. C.; Yeung, E. S. *J. Comb. Chem.* **2000**, *2*, 450–452.
71. Cooper, A. C.; McAlexander, L. H.; Lee, D.-H.; Torres, M. T.; Crabtree, R. H. *J. Am. Chem. Soc.* **1998**, *120*, 9971–9972.
71a. Dieguez, M.; Collomb, M. N.; Crabtree, R. H. *J. Organomet. Chem.* **2000**, *608*, 146–152.
72. Lavastre, O.; Morken, J. P. *New J. Chem.* **2002**, *26*, 745–749.
73. Breit, B.; Seiche, W. *Angew. Chem., Int. Ed.* **2005**, *44*, 1640–1643.
74. Lavastre, O.; Morken, J. P. *Angew. Chem., Int. Ed.* **1999**, *38*, 3163–3165.
75. Hansen, S. M.; Rominger, F.; Metz, M.; Hofmann, P. *Chem. Eur. J.* **1999**, *5*, 557–566.
75a. Hansen, S. M.; Volland, M. A. O.; Rominger, F.; Eisenträger, F.; Hofmann, P. *Angew. Chem., Int. Ed.* **1999**, *38*, 1273–1276.
76. Lavastre, O.; Touzani, R.; Garbacia, S. *Adv. Synth. Catal.* **2003**, *345*, 974–977.
77. Le Nôtre, J.; Touzani, R.; Lavastre, O.; Bruneau, C.; Dixneuf, P. H. *Adv. Synth. Catal.* **2005**, *347*, 783–791.
78. Le Nôtre, J.; Brissieux, L.; Sémeril, D.; Bruneau, C.; Dixneuf, P. H. *Chem. Commun.* **2002**, 1772–1773.
79. Knowles, W. S. *Acc. Chem. Res.* **1983**, *16*, 106–112.
80. Korbel, G. A.; Lalic, G.; Shair, M. D. *J. Am. Chem. Soc.* **2001**, *123*, 361–362.
80a. See also Ref. 63 for an example for the use of fluorescence imaging for achiral transformations.
81. van Delden, R. A.; Feringa, B. L. *Angew. Chem., Int. Ed.* **2001**, *40*, 3198–3200.
82. Reetz, M. T.; Becker, M. H.; Klein, H.-W.; Stockigt, D. *Angew. Chem., Int. Ed.* **1999**, *38*, 1758–1761.
82a. Guo, J.; Wu, J.; Siuzdak, G.; Finn, M. G. *Angew. Chem., Int. Ed.* **1999**, *38*, 1755–1758.
82b. Schrader, W.; Eipper, D.; Pugh, J.; Reetz, M. T. *Can. J. Chem.* **2002**, *80*, 626–632.
82c. Horeau, A.; Nouaille, A. *Tetrahedron Lett.* **1990**, *31*, 2707–2710.
82d. Yao, S.; Meng, J.-C.; Siuzdak, G.; Finn, M. G. *J. Org. Chem.* **2003**, *68*, 2540–2546.
82e. Markert, C.; Pfaltz, A. *Angew. Chem., Int. Ed.* **2004**, *43*, 2498–2500.
83. Taylor, S. J.; Morken, J. K. *Science* **1998**, *280*, 267–270.
83a. Reetz, M. T.; Becker, M. H.; Kühling, K. M.; Holzwarth, A. *Angew. Chem. Int. Ed.* **1998**, *37*, 2647–2650.
83b. Reetz, M. T.; Becker, M. H.; Liebl, M.; Fürstner, A. *Angew. Chem., Int. Ed.* **2000**, *39*, 1236–1239.
83c. Millot, N.; Borman, P.; Anson, M. S.; Campbell, I. B.; Macdonald, S. J. F.; Mahmoudian, M. *Org. Process Res. Dev.* **2002**, *6*, 463–470.
84. Ding, K.; Ishii, A.; Mikami, K. *Angew. Chem., Int. Ed.* **1999**, *38*, 497–501.
85. Abato, P.; Seto, C. T. *J. Am. Chem. Soc.* **2001**, *123*, 9206–9207.
85a. Dey, S.; Karukurichi, K. R.; Shen, W.; Berkowitz, D. B. *J. Am. Chem. Soc.* **2005**, *127*, 8610–8611.
86. Taran, F.; Gauchet, C.; Mohar, B.; Meunier, S.; Valleix, A.; Renard, P. Y.; Créminon, C.; Grassi, J.; Wagner, A.; Mioskowski, C. *Angew. Chem., Int. Ed.* **2002**, *41*, 124–127.
87. Zhu, L.; Anslyn, E. V. *J. Am. Chem. Soc.* **2004**, *126*, 3676–3677.
88. Reetz, M. T.; Kuhling, K. M.; Deege, A.; Hinrichs, H.; Belder, D. *Angew. Chem., Int. Ed.* **2000**, *39*, 3891–3893.
88a. Doolen, R. D.; Cong, P. U.S. Patent 6,462,816, October 8, 2002. (See also U.S. Patents 6,531,041, 6,544,396, 6,572,750, and 6,799,628.)
89. Petra, D. G.; Reek, J. N. H.; Kramer, P. C. J.; Schoemaker, H. E.; van Leewwn, P. W. N. M. *Chem. Commun.* **2000**, 683–684.

89a. Reetz, M. T. *Chem. Eur. J.* **2003**, *9*, 3882–3887.
90. Evans, M. A.; Morken, J. P. *J. Am. Chem. Soc.* **2002**, *124*, 9020–9021.
90a. Reetz, M. T.; Eipper, A.; Tielmann, P.; Mynott, R. *Adv. Synth. Catal.* **2002**, *344*, 1008–1016.
90b. Reetz, M. T.; Tielmann, P.; Eipper, A.; Ross, A.; Schlotterbeck, G. *Chem. Commun.* **2004**, 1366–1367.
90c. This concept was previously utilized in the field of olefin polymerization, see Gilchrist, J. H.; Bercaw, J. E. *J. Am. Chem. Soc.* **1996**, *118*, 12021–12028.
91. Reetz, M. T.; Kühling, K. M.; Wilensek, S.; Husmann, H.; Häusig, U. W.; Hermes, M. *Catal. Today* **2001**, *67*, 389–396.
92. Mikami, K.; Angelaud, R.; Ding, K.; Ishii, A.; Tanaka, N.; Sawada, N.; Kudo, K.; Senda, M. *Chem. Eur. J.* **2001**, *7*, 730–737.
92a. Long, J.; Ding, K. *Angew. Chem., Int. Ed.* **2001**, *40*, 544–547.
93. Wolf, C.; Hawes, P. A. *J. Org. Chem.* **2002**, *67*, 2727–2729.
93a. Wolf, C.; Francis, C. J.; Hawes, P. A.; Shah, M. *Tetrahedron* **2002**, *13*, 1733–1741.
94. Mikami, K.; Yamanaka, M. *Chem. Rev.* **2003**, *103*, 3369–3400.
94a. Mikami, K.; Korenaga, T.; Matsukawa, S.; Ding, K.-L.; Long, J. *Chin. J. Chem.* **2001**, *19*, 545–557.
94b. Walsh, P. J.; Lurain, A. E.; Balsells, J. *Chem. Rev.* **2003**, *103*, 3297–3344.
95. de Bellefon, C.; Tanchoux, N.; Caravieilhes, S.; Grenouillet, P.; Hessel, V. *Angew. Chem., Int. Ed.* **2000**, *39*, 3442–3445.
95a. de Bellefon, C.; Pestre, N.; Lamouille, T.; Grenouillet, P.; Hessel, V. *Adv. Synth. Catal.* **2003**, *345*, 190–193.
96. Chen, B.; Dingerdissen, U.; Krauter, J. G. E.; Lansink Rotgerink, H. G. J.; Möbus, K.; Ostgard, D. J.; Panster, P.; Riermeier, T. H.; Seebald, S.; Tacke, T., *et al. Appl. Catal., A* **2005**, *280*, 17–46.
97. Yue, T.-Y.; Nugent, W. A. *J. Am. Chem. Soc.* **2002**, *124*, 13692–13693.
98. Lefort, L.; Boogers, J. A. F.; de Vries, A. H. M.; de Vries, J. G. *Org. Lett.* **2004**, *6*, 1733–1735.
98a. de Vries, A. H. M.; Boogers, J. A. F.; van den Berg, M.; Peña, D.; Minnaard, A. J.; Feringa, B. L.; de Vries, J. G. *PharmaChem* **2003**, 33–36.
98b. van den Berg, M.; Peña, D.; Minnaard, A. J.; Feringa, B. L.; Lefort, L.; Boogers, J. A. F.; de Vries, A. H. M.; de Vries, J. G. *Chim. Oggi.* **2004**, 18–21.
99. Peña, D.; Minnaard, A. J.; Boogers, J. A. F.; de Vries, A. H. M.; de Vries, J. G.; Feringa, B. L. *Org. Biomol. Chem.* **2003**, *1*, 1087–1089.
100. Monti, C.; Gennari, C.; Piarulli, U. *Tetrahedron Lett.* **2004**, *45*, 6859–6862.
101. Reetz, M. T.; Sell, T.; Meiswinkel, A.; Mehler, G. *Angew. Chem., Int. Ed.* **2003**, *42*, 790–793.
101a. Reetz, M. T.; Xiaoguang, Li. *Tetrahedron* **2004**, *60*, 9709–9714.
101b. Reetz, M. T. *Chim. Oggi.* **2003**, *21*, 5–8.
101c. Reetz, M. T.; Mehler, G.; Meiswinkel, A. *Tetrahedron: Asymmetry* **2004**, *15*, 2165–2167.
102. Reetz, M. T.; Mehler, G. *Tetrahedron Lett.* **2003**, *44*, 4593–4596.
103. Sortais, J.-B.; Ritleng, V.; Voelklin, A.; Holuigue, A.; Smail, H.; Barloy, L.; Sirlin, C.; Verzijl, G. K. M.; Boogers, J. A. F., de Vries, A. H. M., *et al. Org. Lett.* **2005**, *7*, 1247–1250.
104. Tararov, V. I.; Kadyrov, R.; Monsees, A.; Riermeier, T. H. *Adv. Synth. Catal.* **2003**, *345*, 239–245.
105. Braun, W.; Salzer, A.; Spindler, F.; Alberico, E. *Appl. Catal., A* **2004**, *274*, 191–203.
106. Xu, G.; Gilbertson, S. R. *Tetrahedron Lett.* **2003**, *44*, 953–955.
107. Zhu, G.; Coa, P.; Jiang, Q.; Zhang, X. *J. Am. Chem. Soc.* **1997**, *119*, 1799–1800.
108. Jiang, Q.; Jiang, Y.; Xiao, D.; Cao, P.; Zhang, X. *Angew. Chem., Int. Ed.* **1998**, *37*, 1100–1103.
108a. Togni, A.; Breutel, C.; Schnyder, A.; Spindler, F.; Landert, H.; Tijani, A. *J. Am. Chem. Soc.* **1994**, *116*, 4062–4066.
108b. Inoguchi, K.; Achiwa, K. *Synlett* **1991**, *1*, 49–51.
109. Komarov, I. V.; Börner, A. *Angew. Chem., Int. Ed.* **2001**, *40*, 1197–1200.
110. Noyori, R. *Asymmetric Catalysis in Organic Synthesis*; Wiley: New York, 1994.
111. Microtiter plates with embedded filters are commercially available, see Whatman. http://www.whatman.com./www.whatman.com.
112. See premex reactorag. http://www.premex-reactorag.ch/www.premex-reactorag.ch/e/spezialloesungen/prohukteneuheiten/.
113. Shen, Z.; Yao, S.; Crowell, J. E.; Siuzdak, G.; Finn, M. G. *Isr. J. Chem.* **2002**, *41*, 313–316.
113a. Wei, J.; Buriak, J.; Siuzdak, G. *Nature* **1999**, *399*, 243–246.
113b. Shen, Z.; Thomas, J. J.; Averbuj, C.; Broo, K. M.; Engelhard, M.; Crowell, J. E.; Siuzdak, G. *Anal. Chem.* **2001**, *73*, 612–619.
113c. Thomas, J. J.; Shen, Z.; Crowell, J. E.; Finn, M. G.; Siuzdak, G. *Proc. Natl. Acad. Sci. USA.* **2001**, *98*, 4932–4937.
113d. Moreau, C.; Frost, C. G.; Murrer, B. *Tetrahedron Lett.* **1999**, *40*, 5617–5620.
114. Cobley, C. J.; Klosin, J.; Qin, C.; Whiteker, G. T. *Org. Lett.* **2004**, *6*, 3277–3280.
114a. Cobley, C. J.; Gardner, K.; Klosin, J.; Praquin, C.; Hill, C.; Whiteker, G. T.; Zanotti-Gerosa, A.; Petersen, J. L.; Abboud, K. A. *J. Org. Chem.* **2004**, *69*, 4030–4040.
114b. Clark, T. P.; Landis, C. R.; Freed, S. L.; Klosin, J.; Abboud, K. A. *J. Am. Chem. Soc.* **2005**, *128*, 5040–5042.
115. Kagan, H. B. *J. Organomet. Chem.* **1998**, *567*, 3–6.
115a. Satyanarayana, T.; Kagan, H. B. *Adv. Synth. Catal.* **2005**, 737–748.
116. Biotage. http://www.biotage.com/
117. Gilbertson, S. R.; Collibee, S. E.; Agarkov, A. *J. Am. Chem. Soc.* **2000**, *122*, 6522–6523.
117a. Agarkov, A.; Greenfield, S. J.; Ohishi, T.; Collibee, S. E.; Gilbertson, S. R. *J. Org. Chem.* **2004**, *69*, 8077–8085.
117b. Gilbertson, S. R.; Satoshi, Y. *Tetrahedron Lett.* **2004**, *45*, 3917–3920.
117c. Greenfield, S. J.; Agarkov, A.; Gilbertson, S. R. *Org. Lett.* **2003**, *5*, 3069–3072.
117d. Porte, A. M.; Reibenspies, J.; Burgess, K. *J. Am. Chem. Soc.* **1998**, *120*, 9180–9187.
118. Gilbertson, S. R.; Chang, C.-W. T. *J. Org. Chem.* **1998**, *63*, 8424–8431.
119. Hessel, V.; Hardt, S.; Löwe, H. *Chemical Micro-Process Engineering*; Wiley-VCH: Weinheim, 2004.
120. Nielsen, C. A.; Chrisman, R. W.; LaPointe, R. E.; Miller, T. E., Jr. *Anal. Chem.* **2002**, *74*, 3112–3117.
121. de Bellefon, C.; Abdallah, R.; Lamouille, T.; Pestre, N.; Caravieilhes, S.; Grenouillet, P. *Chimia* **2002**, *56*, 621–626.
122. Freitag, C. J.; Hajduk, D.; Nielsen, R. B.; Safir, A.; Tiede, R. U.S. Patent 6,306,658, May 20, 2003, (6,566,461).
123. Jähn, P.; Wiessmeier, G.; Krumbach, B.; Rose, R.; Seibert, T.; Krautkrämer, R. E.P. 1 256378, 2002.
124. Keil, F. J. *Chem. Eng. Sci.* **2004**, *59*, 5473–5478.
125. Pennemann, H.; Hessel, V.; Kost, H.-J.; Löwe, H.; de Bellefon, C.; Pestre, N.; Lamouille, P; Grenouillet, P. *International Conference on Process Intensification for the Chemical Industry, 5th*, Maastricht, Netherlands, October 13–15, 2003, 137–147.
126. Pennemann, H.; Hessel, V.; Löwe, H. *Chem. Eng. Sci.* **2004**, *59*, 4789–4794.
127. Snyder, D. A.; Noti, C.; Seeberger, P. H.; Schael, F.; Bieber, T.; Rimmel, G.; Ehrfeld, W. *Helv. Chim. Acta.* **2005**, *88*, 1–9.

128. Haswell, S. J.; Watts, P. *Green Chem.* **2003**, *5*, 240–249.
129. Zech, T.; Claus, P.; Hönicke, D. *Chimia* **2002**, *56*, 611–620.
130. Brändi, C.; Maiwald, P.; Schröer, J. *Chimia* **2003**, *57*, 284–289.
131. Bergh H. S.; Guan, S. U.S. Patent, 6,902,934, June 7, 2005.
132. Safir, A.; Petro, M.; Nielson, R. B.; Lee, T. S.; Fréchet, J. M. J. U.S. Patent 6,475,391, November 5, 2002. (See also, U.S. 6406632, 6,416,663 and 6,260,407.)
133. Boussie, T. R.; Devenney, M. EP 1 160262, 2001.
133a. Potyrailo, R. A.; Wroczynski, R. J.; Lemmon, J. P.; Flanagan, W. P.; Siclovan, O. P. *J. Comb. Chem.* **2003**, *5*, 8–17.
133b. Leugers, A.; Neithamer, D. R.; Sun, L. S.; Hetzner, J. E.; Hilty, S.; Hong, S.; Krause, M.; Beyerlein, K. *J. Comb. Chem.* **2003**, *5*, 238–244.
134. Drenski, M. F.; Mignard, E.; Alina, A. M.; Reed, W. F. *J. Comb. Chem.* **2004**, *6*, 710–716.
135. Hajduk, D. A.; Carlson, E.; Srinivasan, R. U.S. Patent 6,484,567, November 6, 2002.
136. Kossuth, M. B.; Hajduk, D. A.; Freitag, C.; Varni, J. *Macromol. Rapid Commun.* **2004**, *25*, 243–248.
136a. Hajduk, D. A.; Carlson, E.; Freitag, J. C.; Kolosov, O. U.S. Patent 6,664,067 December 16, 2003.
136b. Schneider, K.; Zafeiropoulos, N. E.; Häußler, L.; Stamm, M. *Macromol. Rapid Commun.* **2004**, *25*, 355–359.
137. Stafford, C. M.; Guo, S.; Harrison, C.; Chiang, M. Y. M. *Rev. Sci. Instrum.* **2005**, *76*, 062207/1–062207/5.
138. Yan, B., Ed. *Analysis and Purification Methods in Combinatorial Chemistry*; Wiley: Hoboken, 2004.
139. Yan, B., Ed. *Analytical Methods in Combinatorial Chemistry*; Technomic: Lancaster, 2000.

1.14
Photoelectron Spectroscopy

J C Green, University of Oxford, Oxford, UK

1.14.1 Introduction

Photoelectron (PE) spectroscopy measures the binding energies of electrons in molecules. In combination with theoretical calculations, it provides a powerful insight into the detailed electronic structure of molecules. This chapter introduces basic aspects of the technique and provides a wide variety of examples where studies of organometallic compounds have been particularly fruitful.

When molecules are irradiated with monoenergetic photons of sufficient energy ($h\nu$) to initiate ionization, the ejected electrons show a distribution of kinetic energies (KEs). The KE of the photoelectrons is related to their ionization energies (IEs) by Einstein's equation:

$$h\nu = \mathrm{IE} + \mathrm{KE}$$

PE spectra are displayed as plots of the number of ionized electrons versus their IEs and commonly show discrete bands. The PE bands provide a direct measurement of the accessible energy states of the molecular ion. In an orbital approximation, these ion states can be regarded as resulting from ejection, by a photon, of an electron from an occupied molecular orbital (MO). Thus, PE bands map directly onto occupied levels of an MO diagram (Figure 1).

IEs are fundamental thermodynamic quantities. They are closely related to electrode potentials, which quantify solution ionization, help determine gas phase proton affinities, and are key factors in electron-transfer reactions. Knowledge of molecular IE aids in the understanding of reactivity. They can be used to measure effects of chemical substitution, for example, changes of ligands, metals, or functional groups.

PE spectroscopy has also been a significant factor in the development of quantum chemistry. IEs provide electronically sensitive benchmarks against which different computational methods may be tested. Conversely, quantum chemistry, especially density functional theory (DFT), has been invaluable in the assignment of PE spectra.

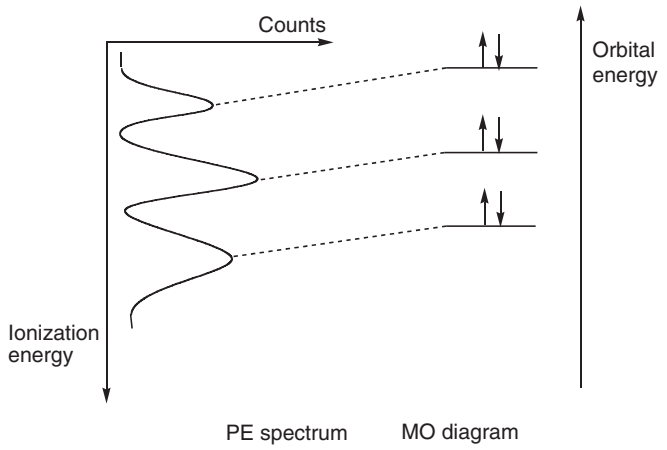

Figure 1 Diagram denoting the relation between the principal bands of a PE spectrum and the occupied MOs of a molecule. A PE spectrum is plotted as the number of electrons (counts) against their ionization energy (IE).

For more detailed accounts of the technique and its applications, the reader is referred to a number of excellent texts and review articles.[1–13] This account aims to illustrate its use in the context of organometallic molecules.

1.14.2 Some Experimental Considerations

Gas phase PE spectroscopy commonly uses a helium discharge lamp as a photon source. This provides intense monochromatic radiation with a photon energy of 21.2 eV, sufficient to ionize the valence electrons of a molecule. The atomic transition involved is between the $2p$ and the $1s$ orbitals of He. He discharge lamps can also be engineered to produce another spectral line resulting from the same transition in the He ion. This has a higher energy of 40.8 eV. X-ray sources are used to ionize core electrons. This branch of PE spectroscopy is known as XPS and is mostly applied to surfaces. The most versatile light sources for PE spectroscopy are synchrotrons, which can produce highly intense monochromatic radiation all the way from the IR to the soft X-ray region.

The IE of a molecule is independent of the photon energy. One major advantage of using a synchrotron source is that the PE band intensities are dependent on the photon energy, and additional information on electronic structure may be derived from studies of the variation of band intensities with photon energy.[12] Even the limited intensity information accessible from the two lines of a He discharge lamp can aid spectral assignment.

For measurement of PE spectra in the gas phase, a sample must sublime without decomposition. Though this is a severe restriction in the case of classical complexes that are frequently charged, a very wide range of organometallic compounds are sufficiently thermally stable to generate a vapour pressure in the gas phase of 10^{-2} bar; even small clusters have been investigated. Though other complexes can be studied in the solid state, bandwidths are larger and calibration is less reliable, so a gas phase measurement is preferred.

1.14.3 Spectral Features and Interpretation

When a photon causes ionization from a molecule, M, the molecular ion, M^+, may be formed in the ground state or a number of excited states:

$$M \xrightarrow{h\nu} M^+$$

A PE spectrum, therefore, displays the energy levels of the molecular ion as a series of bands. The bands may show vibrational structure. The spectral transition is governed by the Franck–Condon principle. Ionization of an electron takes place on a much faster timescale than molecular vibrations, so the nuclei are frozen during the transition. If the ion has a different ground-state geometry from the molecule, it is most probable that it is formed in a vibrationally

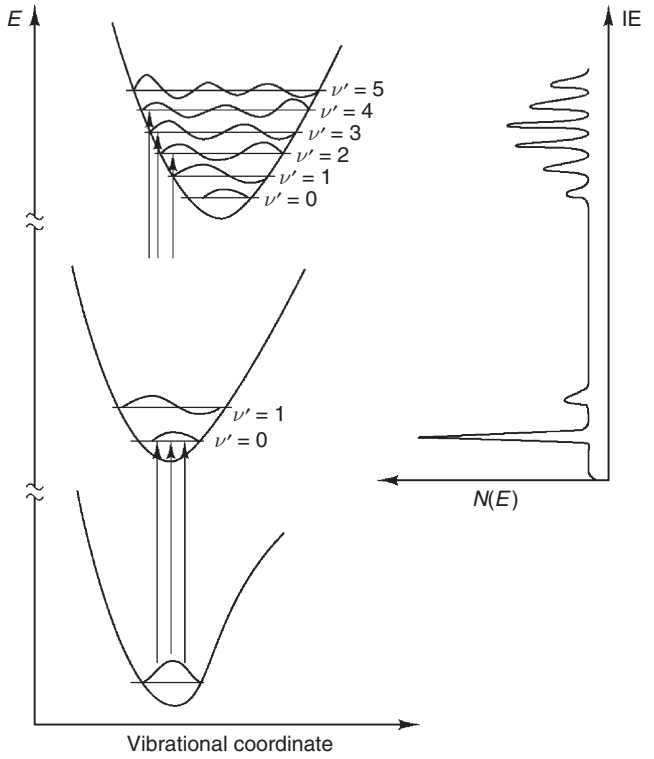

Figure 2 The lowest potential curve represents the energy of the ground state against a vibrational coordinate; the upper two curves represent excited states. Transitions occur with no change in geometry according to the Franck–Condon principle. Excitation to the first excited state involves removal of a non-bonding electron, hence, there is no change in geometry between the molecule and ion's ground states, and the ion is formed principally in the lowest vibrational level. The corresponding fine structure for the first PE band is indicated on the right. Excitation to the second ion state involves a significant geometry change between the two ground states, consequently a strong vibrational progression is seen in the associated PE band with the vertical ionization (most probable transition) corresponding with the fourth vibrational level. Reproduced from *Photoelectron Spectroscopy*, 2nd edn (J. H. D. Eland, Ed.), Butterworths, London, 1984, with permission.

excited state. The most probable transition for each band is termed the vertical IE. Figure 2 illustrates the formation of a molecular ion in two electronic states.

The lower energy ground state has a similar geometry to the molecule, so the molecular ion is formed mainly in its lowest vibrational state. The excited ion state has a longer bond distance than the molecule, so the ion is formed in a number of vibrational states, that with $\nu' = 3$ being the most probable. The resulting PE spectrum is also shown. The separation of the vibrational levels gives the frequency of a normal mode of the molecular ion. Further information can be obtained by comparing the ion frequencies with those of the molecule. If the ion state is formed by removal of a non-bonding electron, the ionic vibrational frequency will be very close to that of the ground-state molecule.

If the target molecule has high symmetry and an electron is ionized from a degenerate pair of orbitals, the associated PE band may show structure associated with splitting of the ion state. The cause of this may be Jahn–Teller splitting as the associated ion state will be non-degenerate; this is most common when the degenerate orbitals are bonding and the ion experiences considerable structural distortion. A complex vibronic band profile results. If the degenerate orbitals are localized on a heavy atom, spin–orbit splitting of the associated ion state will be the primary cause of splitting and ion states of different angular momentum will result.

These points are nicely illustrated by the series of tetrahedral molecules $M(CH_3)_4$ (M = C, Si, Ge, Pb), where the first PE band (A) originates from the M–C t_2 bonding orbitals (Figure 3).[14] For the lighter elements, the band shows unresolved vibronic structure but for Pb it splits into two components, $^2U_{3/2}$ (A') and $^2E_{1/2}$ (A''). The a_1 band (C) shows clear vibrational structure, when M = C, the principal progression being the a_1 C–H deformation mode.

For a closed-shell molecule, the primary accessible ion states correspond with holes in the occupied valence orbitals of the molecule. However, if a molecule has an open-shell configuration, exchange splitting often causes this simple correlation to break down. For example, if a molecule were to have a b^2a^1 configuration, a doublet ground state

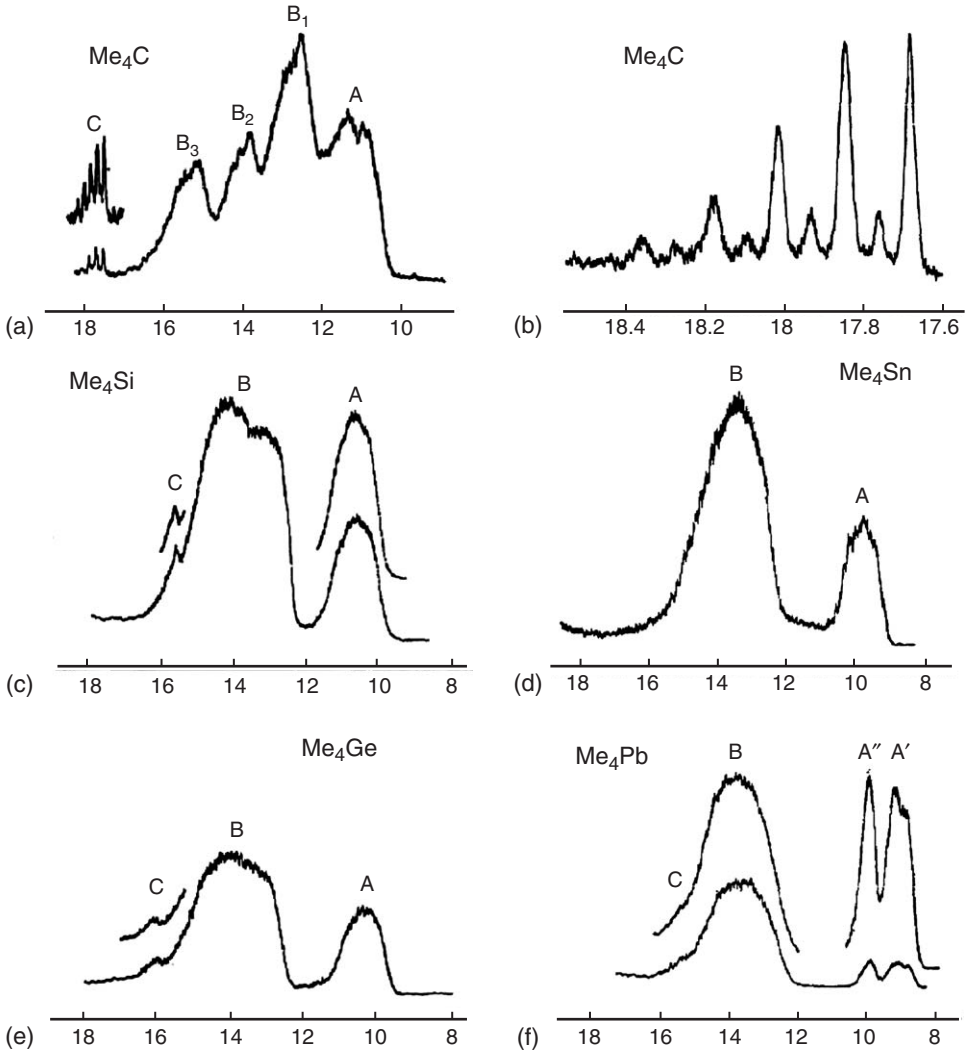

Figure 3 He I PE spectra of EMe_4 (E = C (a), Si (c), Sn (d), Ge (e), Pb (f).[14] The lowest IE band corresponds to ionization from the upper t_2-orbitals largely localized on the E–C bonds. For E = Pb (5), the t_2-band is split by spin–orbit coupling with the U component showing further Jahn–Teller splitting. The highest sharp band shown corresponds to an a_1 ionization. For C, this shows vibrational structure (b). Adapted with permission of Royal Society of Chemistry from Evans, S.; Green, J. C.; Joachim, P. J.; Orchard, A. F.; Turner, D. W.; Maier, J. P. *J. Chem. Soc., Faraday Trans. 2* **1972,** *68*, 905.

where orbital a is occupied by just one electron and orbital b by two electrons, then ionization of an electron from orbital b may result in either a singlet or triplet ground state (Figure 4).

Such complex spectra are found for open-shell metallocenes.[15,16] Whereas ferrocene has two bands arising from ionization of its d-electron configuration, $e_2^4a_1^2$, chromocene, with a triplet ground state and an $e_2^3a_1^1$ configuration, has four d-bands in its PE spectrum. The rules governing the number and intensity of bands from open-shell molecules are complex but well documented.[17]

1.14.4 Intensity Variations

The probability of photoionization to an ion state is termed a PE "cross section," commonly denoted σ. As PE flux is a function of the angle of observation of the PEs, measurements of band intensities are made at a "magic angle" where the intensity is independent of the angular parameter, β. The cross section is then directly proportional to the band intensity. Direct photoionization is controlled by the dipole selection rule, but as a free electron can assume any

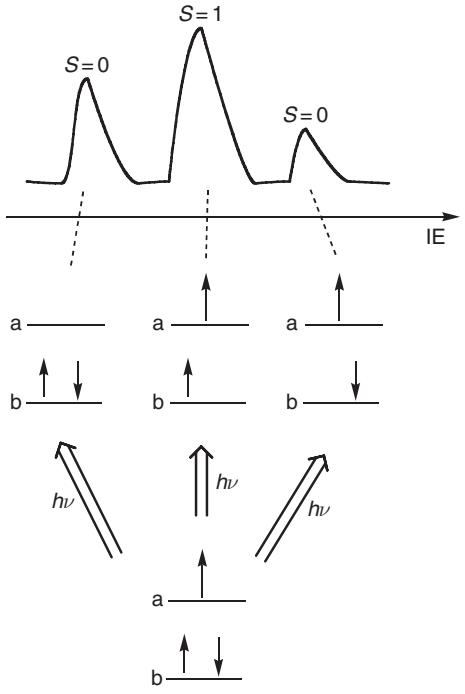

Figure 4 Diagram showing ionization from a molecule with a b^2a^1 configuration ($S = 1/2$) to three states with $S = 0$, $S = 1$, and $S = 0$, and the three associated bands in the PE spectrum. If orbitals *b* and *a* have similar ionization cross sections, the relative intensity of the bands would be 2 : 3 : 1.

l-value, all one-electron photoionizations are allowed, and PE cross sections for particular ion states are all of the same order of magnitude. They vary with the photon energy used, and the variation is characteristic of the nature of the vacated orbital. In favorable circumstances, the photon energy dependence of the cross section of a band is like the signature of the originating MO. The nature of that signature depends on the type of atomic orbitals (AOs) that go to make up the MO. Thus, ideally, cross-section studies can provide a firm basis for band assignment and also reveal details of molecular bonding.[6,12]

The model on which most interpretations of molecular cross sections are based is that of Gelius.[18] It makes a simplifying assumption that the cross section for an MO is determined only by the cross section of the AO constituting the MO. The weight of an AO's contribution is given by the square of its coefficient in the MO concerned. The model is valid when the contribution of the overlap electron density to the cross section is negligible and the effects of the anisotropy of the molecular ion potential on the outgoing electron wave function are small. Both these conditions are most likely to hold when the PE kinetic energy is high. At low photon energies, molecular effects on ionization cross sections are well documented, but even in these regions atomic effects are evident and the Gelius model provides a good basis for molecular cross-section interpretation.

Thus, in order to evaluate the photon energy dependence of molecular cross sections, we need to have a good appreciation of the range of atomic cross-section variations. These latter are well understood and a useful compilation of calculated atomic cross sections for direct photoionization exists.[19]

A cross section is usually highest near the ionization threshold and thereafter it decreases with increasing photon energy. As the KE of the PE increases, its wavelength decreases, and the electron wave becomes more oscillatory. As a consequence, the positive and negative parts of the dipole matrix element with the vacated orbital tend to cancel one another and the cross section suffers rapid decay. The rate of decay can be characteristic of the AO ionized, for example, H 1*s* orbitals decay more rapidly with photon energy than C 2*p*. Figure 5 shows calculated cross sections for the 2*p* orbitals of B to Ne.

Other variations superimposed on the decay can also be characteristic. For orbitals with a radial node, there is a minimum in the cross section, known as a Cooper minimum. At some photon energy, the contributions from the inner

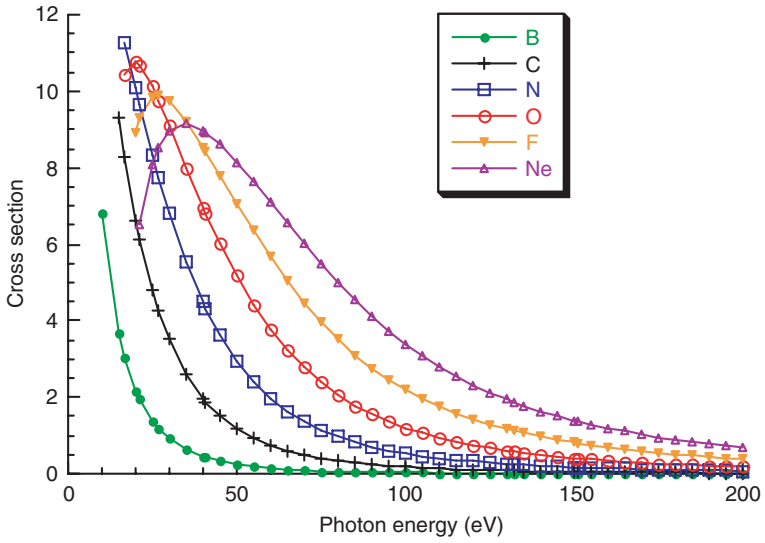

Figure 5 Calculated ionization cross sections for the atomic 2*p* orbitals of the elements B to Ne.[19]

and outer parts of the orbital will tend to cancel one another. This phenomenon is responsible for the rapid decay of the 3*p* cross sections for the elements Si to Cl (Figure 6). With such minima, the photon energy may be tuned to minimize the contribution from certain types of orbitals to a PE spectrum.

Orbitals with high angular momentum, that is, *d*- or *f*-orbitals, often have maxima in their ionization cross sections some way above threshold (Figure 7). This is in contrast to *s*- and *p*-orbitals where maxima, if they exist, tend to be very close to the threshold. As a consequence, changes in relative band intensity between He I and He II spectra can often be used in distinguishing between metal and ligand bands. This feature has been particularly useful in distinguishing *d*- and *f*-bands in the PE spectra of transition metal compounds.

Perhaps the most dramatic departure from monotonic decay of a cross section occurs for *d*- and *f*-electron cross sections at photon energies near those necessary for the excitation of particular core electrons. At these photon energies, indirect ionization can occur and may dominate the cross section in these regions. For example, for first row transition metals, excitation of a 3*p* core electron to an empty 3*d* level can result in the ionization of a 3*d* electron. The ionization borrows intensity from the resonant absorption. The resonant transition is strongest when the levels have the same principal quantum number ($\Delta n = 0$); the transition increases the angular momentum quantum number by 1 ($\Delta l = +1$) and the excited orbital and the ejected electron have the same *l*-value which must be high, namely 2 or 3. These so-called giant resonances are particularly useful in identifying *d*- or *f*-bands or covalency involving such orbitals.

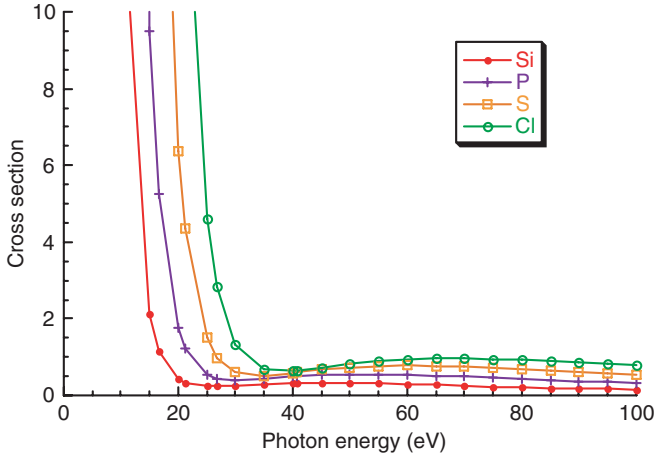

Figure 6 Calculated ionization cross sections for the atomic 3*p* orbitals of the elements Si to Cl.[19]

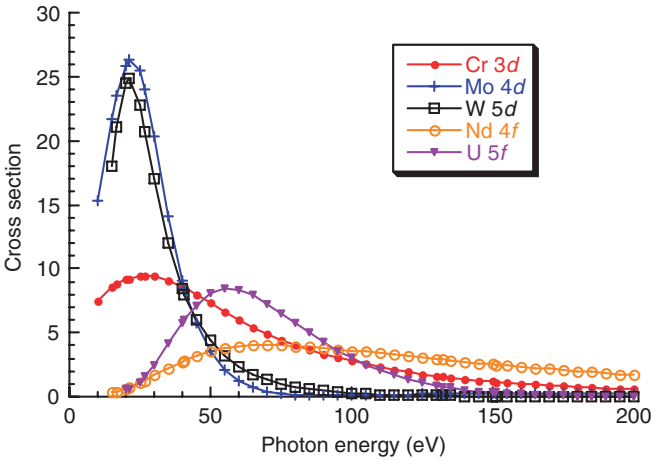

Figure 7 Calculated ionization cross sections for the atomic $(n-1)d$ orbitals of the elements Cr, Mo, W, and the $(n-2)f$ orbitals of the elements Nd and U.[19]

1.14.5 Metal Carbonyls

The group 6 metal octahedral hexacarbonyls have PE spectra where the *d*-band, resulting from ionization of the t_{2g}^6 configuration, is well separated from ionizations that arise principally from ligand orbitals (Figure 8).[20,21]

The vertical IE of the *d*-band varies little going down the group. The *d*-band for $W(CO)_6$ shows spin–orbit splitting. In this case, the E'' state is more stable than the U' state as the splitting is *d*-based (with $Pb(CH_3)_4$ it was *p*-based and the energy ordering is the reverse). The *d*-bands on close examination also show vibrational structure.[22]

The cross-section variation with photon energy of the *d*-bands illustrates the giant resonances discussed above (Figure 9).[21] The energy region at which the core *np* electrons are known to ionize are marked with arrows. There are two energies arising by the spin–orbit splitting of the core hole; this increases as the metal gets heavier. The resonant excitations to the empty *nd* orbitals occur in these regions and the consequent effects on the ionization cross sections are large. For $W(CO)_6$, the giant resonance has a split structure due to these spin–orbit effects.

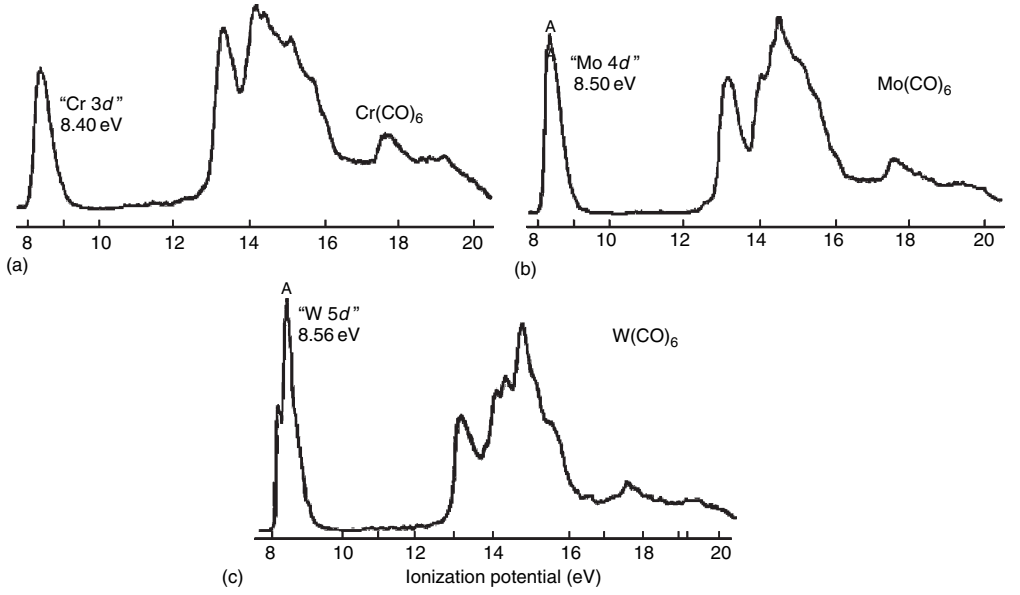

Figure 8 He I PE spectra of $M(CO)_6$ (M = (a) Cr, (b) Mo, (c) W).[20] Adapted with permission of Royal Society of Chemistry from Higginson, B. R.; Lloyd, D. R.; Burroughs, P.; Gibson, D. M.; Orchard, A. F. *J. Chem. Soc., Faraday. Trans. 2* **1973**, *69*, 1659.

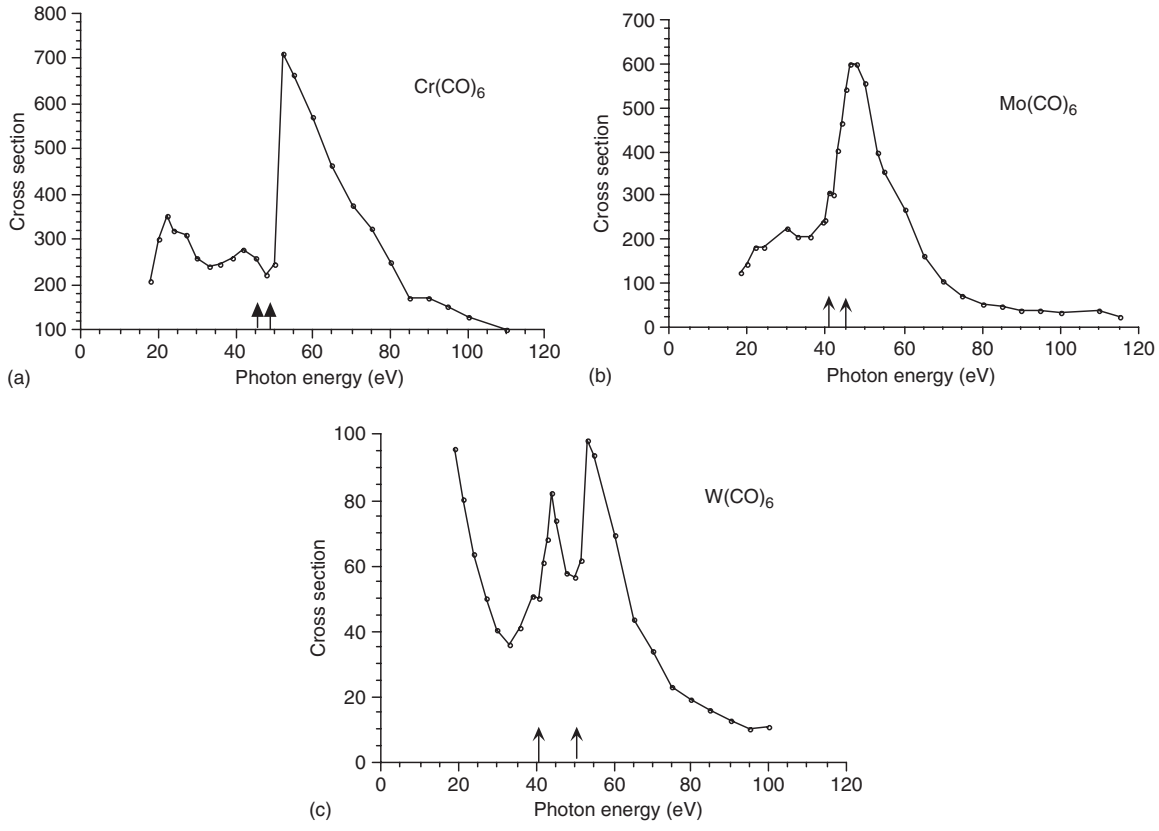

Figure 9 Relative partial photoionization cross sections (RPPICS) of the *d*-bands of $M(CO)_6$ (M = Cr (a), Mo (b), W (c)). The arrows indicate the energies at which the $(n-1)p$ core electrons ionize; two energies are a consequence of the spin–orbit splitting of the core hole.[21] Adapted with permission of The American Chemical Society from Cooper, G.; Green, J. C.; Payne, M. P.; Dobson, B. R.; Hillier, I. H. *J. Am. Chem. Soc.* **1987**, *109*, 3836.

The lowest energy ligand band (~13 eV) is assigned to the t_{1u} combination of the CO 5σ orbitals. Other ligand bands overlap so as to make experimental assignment difficult.

The *d*-bands for $V(CO)_6$,[23] $Fe(CO)_5$,[24] and $Ni(CO)_4$[24] are shown in Figure 10. $V(CO)_6$ is an octahedral molecule with a t_{2g}^5 configuration and an open-shell structure. On ionization, $^3T_{1g}$, $^1T_{2g}$, ^1E_g, and $^1A_{1g}$ ion states are formed. The

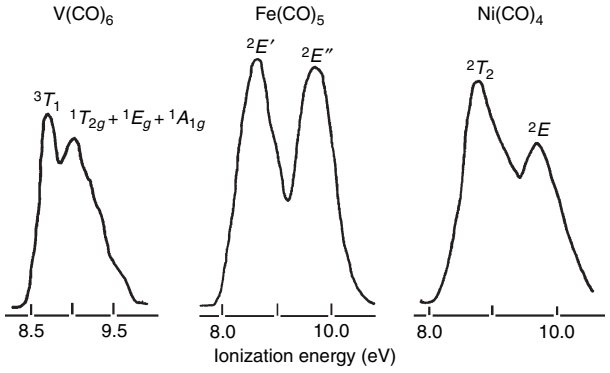

Figure 10 PE spectra showing the *d*-bands of $V(CO)_6$,[23] $Fe(CO)_5$, and $Ni(CO)_4$[24] together with the band assignments. In the case of $V(CO)_6$, the *d*-band structure is caused by exchange coupling, for $Fe(CO)_5$ and $Ni(CO)_4$ by ligand field splitting. Adapted with permission of The American Chemical Society from Evans, S.; Green, J. C.; Orchard, A. F.; Saito, T.; Turner, D. W. *Chem. Phys. Lett.* **1969**, *4*, 361 and Lloyd, D. R.; Schlag, E. W. *Inorg. Chem.* **1969**, *8*, 2544.

triplet state is the lowest in energy and is assigned to the lowest energy maximum; the singlet states overlap and give rise to the rest of the *d*-band structure. For the closed-shell molecules, the *d*-bands reflect directly the configurations. $Fe(CO)_5$, with its trigonal-bipyramidal geometry and an $e'^4\,e''^4$ configuration, shows two bands of approximately equal intensity. $Ni(CO)_4$ has a tetrahedral-structure and an $e^4t_2^6$ configuration and shows two bands of intensity ratio around 3 to 2 corresponding to $^2T_2$ and ^2E ion states, respectively, the former being the lower in energy.

1.14.6 Metallocenes

The PE spectra of the bis-cyclopentadienyl metal complexes, MCp_2, illustrate how, in addition to information on metal electrons, information on bonding orbitals can be obtained. The PE spectra of the group 8 metallocenes, with 18-electron closed-shell configurations, are shown in Figure 11.[25,26]

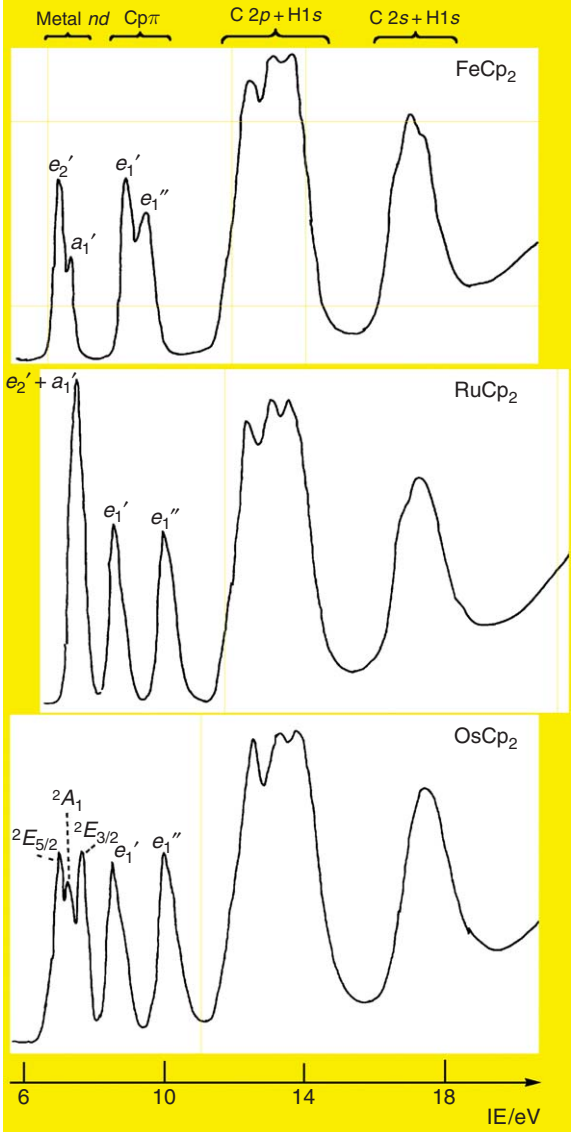

Figure 11 PE spectra of $FeCp_2$, $RuCp_2$, and $OsCp_2$ measured with a photon energy of 27 eV.[26] Assignment of the *d* and top ligand ionizations are given for an eclipsed D_{5h} structure. Note the increased separation between the e_1' and e_1'' bands for the second and third row transition metals as a consequence of increased covalent bonding. Adapted with permission of Taylor & Francis from Cooper, G.; Green, J. C.; Payne, M. P. *Mol. Phys.* **1988**, *63*, 1031.

The ionizations below 8 eV arise from the six *d*-electrons which occupy e_2'($d(x^2-y^2)$ $d(xy)$ based) and a_1'($d(z^2)$ based) orbitals (Figure 12). For $FeCp_2$, the 2 to 1 intensity structure of the *d*-band makes the assignment straightforward. In the spectrum of $RuCp_2$, the two bands overlap. For $OsCp_2$, spin–orbit splitting of the $^2E'$ ion state leads to three bands, the resulting $J = 5/2$ and $J = 3/2$ ion states lying above and below the $^2A_1'$ state with $J = 1/2$.

All three group 8 metallocenes exhibit two bands between 8.5 and 11 eV. These two bands are principally ligand-based ionizations and arise from in-phase (e_1') and out-of-phase (e_1'') combinations of the HOMOs of the Cp rings (Figure 12). The e_1' orbitals have fairly constant IEs descending the group (Table 1). This is a consequence of their non-bonding characteristics; they have the same symmetry as the metal $p(x)$ and $p(y)$ orbitals which are too high in energy to mix significantly with the ligand orbitals. In contrast, the IEs of the e_1'' orbitals increase down the group. In this case, overlap with the metal $d(xz)$ and $d(yz)$ orbitals is significant and this orbital is the principal source of bonding in transition metal MCp_2 compounds.

Evidence for this covalent interaction is provided by variable photon energy PE spectroscopy (VPEPES).[26] The giant resonance in the *d*-band for $RuCp_2$ is particularly strong (Figure 13). At a photon energy of 27 eV, the e_1' and e_1'' bands are of equal intensity. At the photon energy at which the *d*-band has maximum intensity ($h\nu = 55$ eV), the e_1'' band is significantly more intense than the e_1' as a result of the 4*d* contribution to the associated MO. The

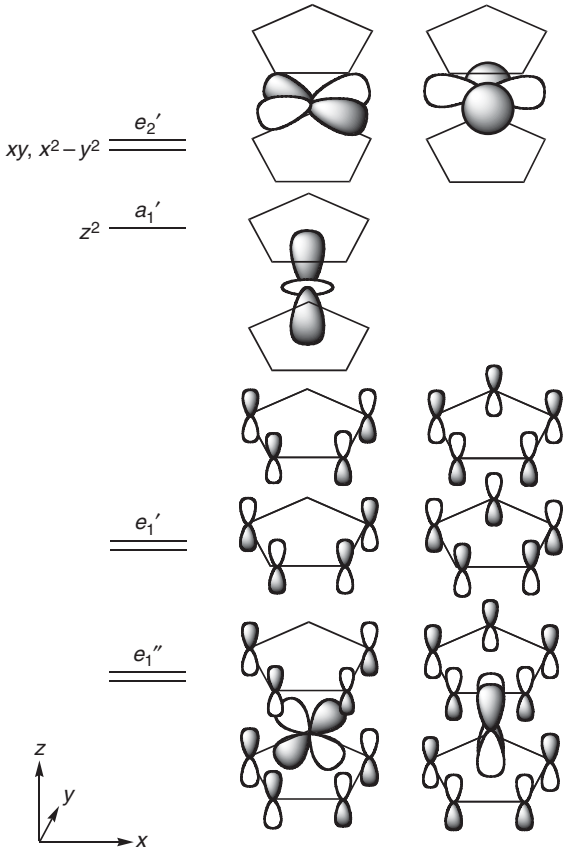

Figure 12 Occupied MOs for a group 8 metallocene of D_{5h} symmetry.

Table 1 Vertical IEs (eVs) of the principal PE bands of $FeCp_2$, $RuCp_2$, and $OsCp_2$[25,26]

Ion state	$^2E_2'$	$^2A_1'$	$^2E_1'$	$^2E_1''$
$FeCp_2$	6.88	7.23	8.72	9.14
$RuCp_2$	7.45	7.45	8.51	9.93
$OsCp_2$	7.15 (5/2) 7.81 (3/2)	7.42	8.63	10.02

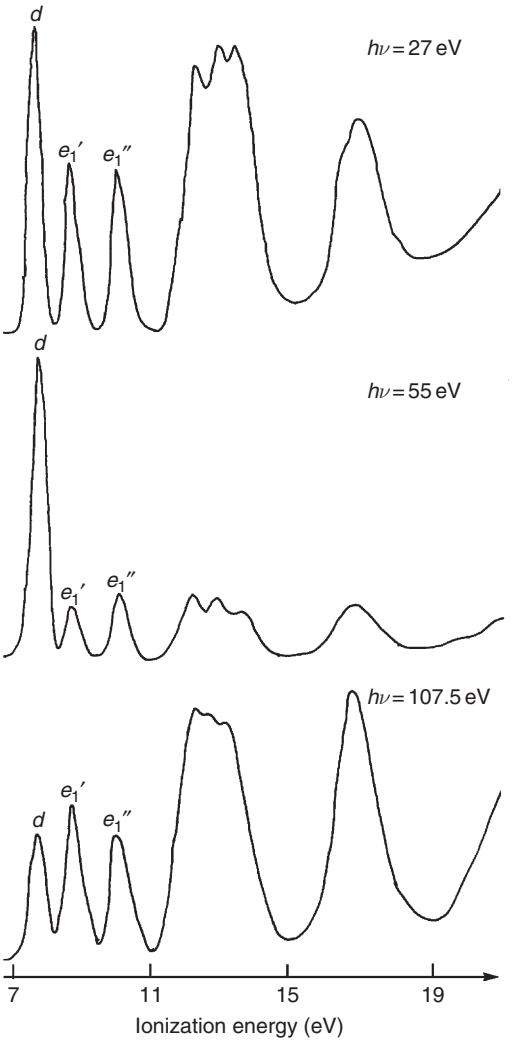

Figure 13 PE spectra of $RuCp_2$ at 27, 55, and 107.5 eV.[26] The *d*-band varies strongly in intensity; 55 eV corresponds to the maximum in the giant resonance of the 4*d* band and 107.5 eV is close to the 4*d* Cooper minimum. The e_1'' band shares some of the intensity changes of the *d*-band as a result of the covalent character of the associated orbital. Adapted with permission from Cooper, G.; Green, J. C.; Payne, M. P. *Mol. Phys.* **1988**, *63*, 1031.

situation is reversed at photon energies around 107.5 eV, at which point the *d*-band passes through a Cooper minimum, the e_1'' band cross section drops below that of the e_1' band. Thus, the cross section of the MO of mixed Ru 4*d* and C 2*p* character shows behavior intermediate between that of its two parents.

For the closely related pentadienyl compounds, or open metallocenes, **I** and **II**, PE spectroscopy has shown interesting differences in electronic structure from the closed analogs.[27,28]

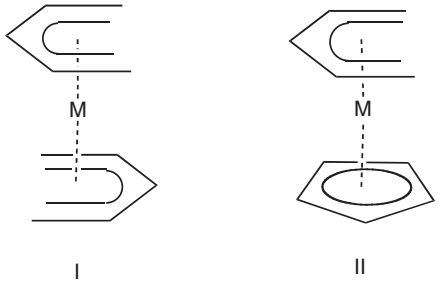

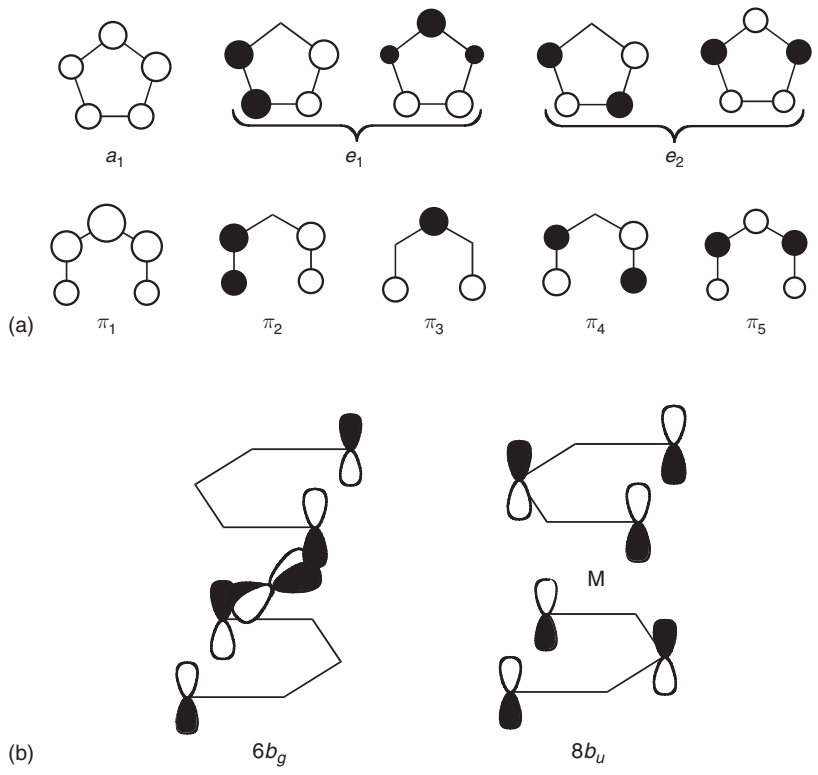

Figure 14 (a) Relation between the π-orbitals of C_5H_5 and C_5H_7. Breaking of the C–C bond stabilizes those orbitals that are antibonding across this interaction and destabilizes the orbitals that are bonding across this interaction. (b) Representations of the $6b_g$ and $8b_u$ orbitals of the open metallocenes.[27]

Only methyl-substituted compounds had sufficient thermal stability for PE studies. Opening the ring lifts the degeneracy of the ligand π-orbitals resulting in spectra of greater complexity than those of MCp_2. They have been assigned successfully using semi-empirical calculations on the Fe derivatives coupled with a Green's function technique for calculating IE,[27] as well as He I/He II intensity arguments for the dimethyl half-open metallocenes, **II**, of Fe, Ru, and Os.[28] The PE spectral studies helped establish the *trans*-structure of compounds of class **I**. The principal difference is greater backdonation to the open pentadienyl ligand. The LUMO of the pentadienyl ligand, related to the e_2-orbitals of Cp, is more stable than the latter as a result of decrease in the antibonding character on opening the ring (Figure 14a). Thus, it mixes with the metal $d(xy)$ orbital, which, because of the lower symmetry, is also able to orient to achieve maximum overlap with the terminal C $p\pi$-orbitals, forming the $6b_g$ orbital in the case of **I**. As a consequence, its IE is higher than that of the other two d-orbitals. Opening the ring and removing a bonding interaction from one of the parent e_1 orbitals of Cp results in the destabilization of the $8b_u$ orbital compared with the e_1' orbitals of MCp_2 (Figure 14). Thus, it has a lower IE and in the case of compounds of type **I** it is proposed that a reversal of order between the metal and ligand ionizations takes place with the $8b_u$ orbital having a lower IE than the $6b_g$ (Figure 14). Overall the first IE is higher than the analogous MCp_2 compounds.

1.14.7 Bis-Allyl Nickel, Palladium, and Platinum

In some senses, the bis-allyl complexes of the group 10 metals are the simplest of the transition metal sandwich compounds in that they have the fewest number of atoms, but their PE spectra have been notoriously difficult to assign, especially that of Ni.[29–32] One reason is that the metal d-electrons are more closely bound as a result of a high effective nuclear charge at the end of the transition series and, as a consequence, they have IEs similar to the upper ligand orbitals. Much experimental work, including methyl substitution, He I and He II spectra[31] and synchrotron studies,[32] has gone into cutting down the options for band assignment. A wide variety of theoretical studies have also

had their input; *ab initio* calculations give low-lying metal orbitals and Koopmans' theorem in these cases gives a poor account of the IE ordering.[33,34] Green's function methods[31,35] and ΔSCF calculations give better agreement with experiment as do Xα-SW methods.[32]

Figure 15 presents He I and high energy spectra for $M(\eta\text{-}C_3H_5)_2$ (M = Ni, Pd, Pt). One seeks to assign eight ionization processes, four that are principally ligand based and four from the metal d^8-configuration. In the case of $Pt(\eta\text{-}C_3H_5)_2$, eight separate maxima are identifiable and intensity changes mark out bands 2 to 5 as metal ionizations. The remaining bands are assigned as indicated in Figure 16.

From intensity changes band 7 shows signs of partial metal character and so is assigned to the b_g orbital which is the principal metal ligand-bonding orbital. Bands 6 and 8 are derived from the most stable π MO of the allyl ligand, and assigned to the b_u and a_g obitals, respectively. Band 1 is assigned to the ligand non-bonding a_u MO. It shows a low cross section at high photon energies indicating its C 2*p* origin. $Pd(\eta\text{-}C_3H_5)_2$ has a similar IE assignment. In this case, the b_u and b_g bands overlap giving rise to band 6.

There is still some dispute concerning the assignment of the PE spectrum of $Ni(\eta\text{-}C_3H_5)_2$. Bands 1 and 2 are generally agreed to comprise four ionizations, three of metallic character and the fourth the a_u ionization. VPEPES[32] indicates bands 1, 2, and 3 to be from orbitals with high metallic character and it is argued from branching ratio data that the deconvoluted area corresponding to band 2 contains the a_u band. Shifts on methylation and Green's function[31] calculations indicate that the a_u ionization lies under band 1.

In common with the metallocene spectrum, it is evident that the IEs of the metal ligand bonding orbital increase down the group as a consequence of increased covalent interaction. The trends in the average metal IE is Ni < Pd ~ Pt. The spread of the metal ionizations increases down the group, in line with the expectations from ligand field splitting; the increase from Pd to Pt is probably also assisted by second-order spin–orbit coupling in the third transition series element.[36]

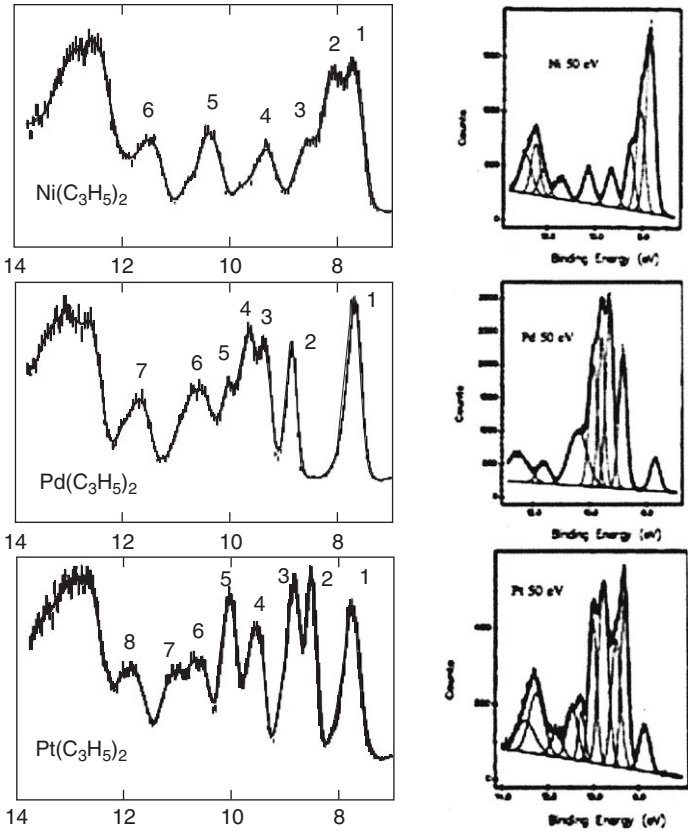

Figure 15 PE spectra of $M(\eta^3\text{-}C_3H_5)_2$ (M = Ni, Pd, Pt). On the left are the He I spectra[31] and on the right the spectra measured with a photon energy of 50 eV.[32] The *d*-bands are relatively more intense at the higher photon energy. Adapted with permission of Verlag Helvetica Chimica Acta AG from Boehm, M. C.; Gleiter, R.; Batich, C. B. *Helv. Chim. Acta* **1980**, *63*, 990 and Li, X.; Bancroft, G. M.; Puddephatt, R. J.; Liu, Z. F.; Hu, Y. F.; Tan, K. H. *J. Am. Chem. Soc.* **1994**, *116*, 9543.

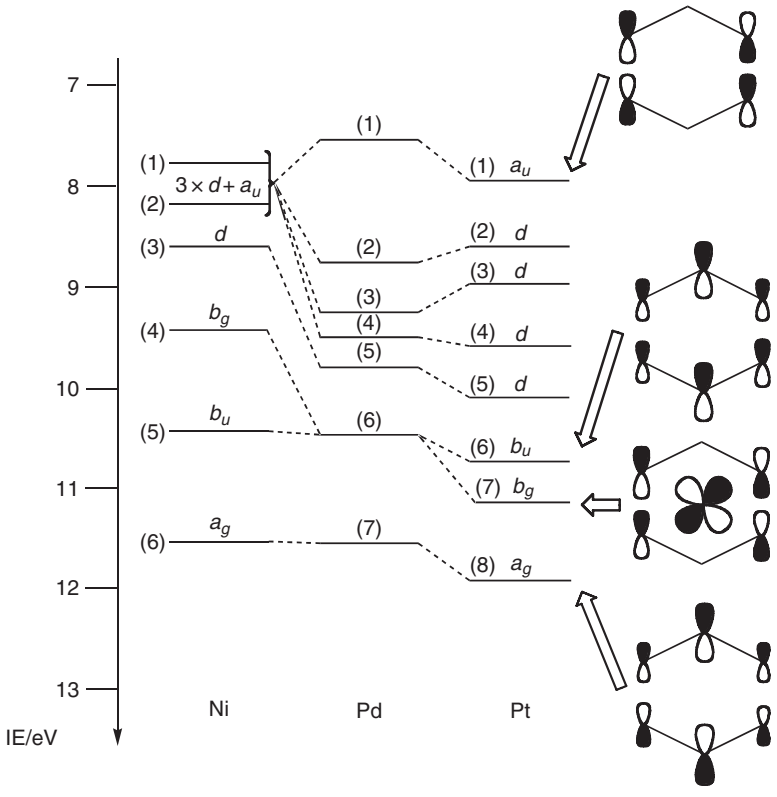

Figure 16 Assignment and correlation of IE of PE bands for $M(\eta^3\text{-}C_3H_5)_2$ in the series M = Ni, Pd, Pt. The numbers refer to the spectral band labels in Figure 15. On the right, representations of the associated orbitals are given.[31,32]

1.14.8 Ligand Additivity Effects, Ligand Field Effects, and Core–Valence Ionization Correlations

The capability to measure the binding energy of electrons from individual orbitals has led to detailed studies of how ligands affect these binding energies. The ligand additivity model for IE proposes that the shift in metal *d*-ionization energy is directly proportional to the number and type of ligand substitutions at the metal center.[37] The major testing bed of this principle has been the group 6 carbonyl series $M(CO)_{6-n}L_n$.[38,39] These allow the separation of ligand σ- and π-effects. For example, in the C_{4v} symmetry of an $M(CO)_5L$ complex, the shift in energy of the $d(xy)$ ionization (b_2) is affected by the total donor capacity of the ligand, whereas the $d(xz)$ and $d(yz)$ IEs (e) are also sensitive to the π-acceptor ability of L. This leads to a splitting of the t_{2g} band of the parent octahedral carbonyl into two bands of relative intensity 2 : 1. In the case of W, the e-band is split by spin–orbit coupling and the effect of L on the spin–orbit splitting may also be probed. Complexes with other symmetries may be similarly analyzed.

IE shifts for the metal *d*-orbitals toward lower energy have been observed for the series $Mo(CO)_{6-n}(PR_3)_n$[39] and $W(CO)_{6-n}(PR_3)_n$,[38] where CO has been replaced by a stronger σ-donor but weaker π-acceptor. Comparison of splitting patterns in monosubstituted, *cis*-, *trans*-, *mer*-, and *fac*- isomers confirmed the validity of the ligand additivity model. The series showed the alkyl phosphines studied to be stronger σ-donors than CO, in the order $PMe_3 < PEt_3 <$ P-*n*-Bu_3, with PEt_3 being more similar to P-*n*-Bu_3 than PMe_3. All essentially had the same π-acceptor capacity, inferior to that of CO. Studies of the d^6 18-electron complexes of the type $CpM(CO)_2L$, where M = Cr, Mn, and Fe, extend ligand comparisons to a broader range.[40] Though these compounds lack the high symmetries of the substituted octahedral carbonyl complexes, their pseudo-octahedral nature enables a similar decomposition into σ- and π-effects. Table 2 gives a comparison of the π-bonding capacity of a series of ligands analyzed in this way. The parameter listed, ΔE_s, is a measure of the net π-interaction of the ligand with a $CpM(CO)_2$ fragment and the series is normalized to a value of zero for H as the ligand.

Table 2 Comparison of the π-bonding capacity (ΔE_s) of a series of ligands[40]

Metal	*Ligand*	ΔE_s (eV)	*References*
Cr	NO	−1.48	83
Mn	CO	−0.69	84
Mn	η^2-MeC≡CMe	−0.69	85
Mn	η^2-H_2C=CH_2	−0.69	86
Mn	SO_2	−0.69	87
Mn	N_2	−0.33	88
Mn	PMe_3	−0.30	89
Fe	$SiCl_3$	−0.17	90
Mn	NH_3	−0.14	88
Fe	CN	−0.09	91
Fe	Me	−0.02	92
Fe	H	0.00	93
Fe	Cl	0.08	92
Fe	$SiMe_3$	0.10	94
Fe	C≡CH	0.10	95
Fe	C≡CBu^t	0.24	95
Fe	C≡C—C≡CH	0.26	96

Table 3 Values for the ratio of valence to core IE shift for a series of Mo and W carbonyl phosphine compounds[41,42]

Core ionization	*Mo* $3d_{5/2}$	*W* $4d_{5/2}$	*W* $4f_{7/2}$	*P* 2*p*
$\Delta E_{valence}/\Delta E_{core}$	0.74 ± 0.06	0.86 ± 0.03	0.86 ± 0.03	0.73 ± 0.04

High resolution gas phase core spectra of $Mo(CO)_{6-n}(PR_3)_n$[41] and $W(CO)_{6-n}(PR_3)_n$[42] have established that the ligand additivity principle extends to core ionizations. This work helps establish the core–valence ionization correlation model which states that the binding energy shift of a non-bonding valence orbital localized on a particular atom for related molecules should be eight-tenths of that atom's core binding energy shift between the two molecules.[43]

$$\Delta E_{valence} = 0.8\Delta E_{core}$$

The values found in the above two studies (Table 3) are consistent with this principle. For the W series, fine structure in addition to spin–orbit coupling, resulting from ligand field splittings and vibrational coupling is detected in both the W 5*d* and W 4*f* regions.

1.14.9 Effects of Methyl Substitution

The effect of methyl substitution in the carbocyclic rings of sandwich compounds on the IE of valence bands is given in Table 4.[3]

All shifts are to lower IE in comparison with the unsubstituted derivatives. The presence of two methyl groups in a metallocene (one on each ring) has a fairly uniform effect on the *d*-ionizations, but decreases the ligand ionizations

Table 4 The effect of methyl substitution on the IE of sandwich compounds, where M is a *d*-block transition metal. Values give the average shift (in eV) to lower IEs relative to the IE of the unsubstituted compound [3]

Orbital	$M(\eta\text{-}C_5H_4Me)_2$	$M(\eta\text{-}C_6H_5Me)_2$	$M(\eta\text{-}C_6H_3Me_3)_2$	$M(\eta\text{-}C_5Me_5)_2$
a_{1g}	0.19	0.18	0.33	0.95
e_{2g}	0.18	0.28	0.54	0.88
e_{1g}^*	0.22			0.77
e_{1u}	0.26	0.36	0.77	1.25
e_{1g}	0.24	0.22	0.78	1.11

slightly more. However, when two methyl groups are substituted in a bis-arene compound, the effect on the e_{2g} IE is significantly greater than that on the a_{1g} IE. This reflects the higher ligand content of the e_{2g} orbital. Again the ligand bands show larger shifts. The M(η-$C_5Me_5)_2$ (MCp^*_2) compounds show shifts roughly five times those of the M(η-$C_5MeH_4)_2$ (MCp'_2) compounds, whereas the bis-mesitylene compounds have shifts only twice those of the bis-toluene complexes.

In the $CpMn(CO)_3$, $Cp'Mn(CO)_3$, $Cp^*Mn(CO)_3$ complexes, the shift in ring e_1 IE per methyl substitution is about -0.24 eV.[7] In this case, comparison with the C 1*s* core shifts is possible and demonstrates that the bulk of the shift is a result of hyperconjugative interaction with the methyl groups, the inductive effect playing only a minor role.

1.14.10 Effect of Ring Size on IE and Bonding

The influence of ring size on metal ligand interactions is well demonstrated by considering variations in the IE of metal sandwich compounds.[3] The principal bonding interactions in metal sandwich compounds are between the metal $d(xz)$ and $d(yz)$ orbitals and the ring e_1 π-orbitals and between the metal $d(xy)$ and $d(x^2-y^2)$ orbitals and the ring e_2 π-orbitals. As the ring size of the ligand increases, the e_1 and e_2 π-orbitals become more stable with the consequences that the e_1-interaction becomes less bonding and the e_2-interaction more so. The $d(z^2)$ orbital (a_1) is non-bonding.

Comparisons of IE are made most effectively between isoelectronic compounds, which necessitate a change in metal as well as ring size along a series. Several plots showing such IE trends are given in Figures 17a and 17b.

The a_1 IE increases rapidly across a series as the atomic number of the metal increases. As this orbital has largely metal character, this increase can be correlated with a stabilization of the metal *d*-orbital energies with the increase in nuclear charge. The variation in the e_2 IE is both less regular and less marked, which is understandable in terms of its composite nature. As far as the ring contribution to the e_2 orbital is concerned, the e_2 IE should decrease across the series as the ring size decreases. Superimposed on this decrease will be an increase due to the metal contribution as the metal orbitals become more stable. The net effect is to produce an irregular variation. It is significant in this context that Cr(η-C_5H_5)(η-C_7H_7) has a higher e_2 IE than Cr(η-$C_6H_6)_2$ and the same is true for the Nb analogs; the stabilizing effect of one C_7H_7 ring on these orbitals outweighs that of two C_6H_6 rings. In the 17-electron series, the separation of the $^3E_2$ and $^1E_2$ ion states decreases with ring size. This is also consistent with greater localization of the e_2 electrons on the metal for the smaller rings. For the series M(η-C_5H_5)(η-C_nH_n), the upper e_1 IE stays almost

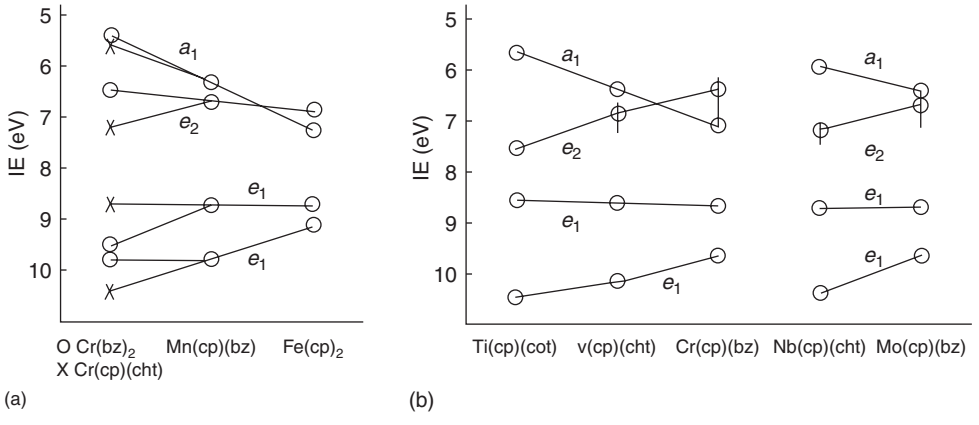

Figure 17 Variations in IE of sandwich compounds: (a) 18-electron compounds, varying metal and ring; (b) 17-electron compounds, varying metal and ring (for the e_2-orbital, a weighted average of the $^3E_2$ and $^1E_2$ states is plotted; the bar denotes the exchange splitting.[3] cp = (η-C_5H_5), bz = (η-C_6H_6), cht = (η-C_7H_7), cot = (η-C_8H_8). NB: IE increases down the page corresponding to a stabilization of the associated orbital. Reproduced with permission of Springer Verlag from Green, J. C. *Struct. Bond.* **1981**, *43*, 37.

constant throughout, whereas the lower e_1-orbital IE decreases with decrease in ring size, following the rise in ring orbital energy.

1.14.11 *d*-Electron Band Ionization Energy (DEBIE) Series

PE spectroscopy of transition metal complexes affords the opportunity to compare the effect of a wide range of ligands on the *d*-electron band ionization energy (DEBIE). The comparison is inevitably a bit rough and ready as the metal d^n-configuration itself has significant effects especially in the case of open-shell compounds. Rather than averaging *d*-electron energies, the first IE is used for comparison as it is the most thermodynamically significant parameter. Table 5 gives the first IEs of a series of homoleptic compounds of V, Cr, and Fe. The DEBIE series can be used for quantitative comparative assessment of the effect of a ligand on the electron richness of a metal. It should be borne in mind that $1\,\text{eV} = 96.4\,\text{kJ mol}^{-1}$ so that the range of DEBIE spanned for Cr, for example, is around $450\,\text{kJ mol}^{-1}$.

Perhaps the most striking fact to emerge from such a comparison is that the DEBIE of a metal bears absolutely no relation to its oxidation state. For example, complexes with metals in their zero oxidation state span the whole series.

The lowest members of the DEBIE series, those with first IE < 6.5 eV, are the sandwich molecules. Interestingly, homoleptic amido compounds have comparable IEs, the low IE being a result of the π-donor ability of alkyl amido ligands. Silyl amido compounds fall in the middle range of the series (6.5 < IE < 8.0 eV), for example, $Cr[N(SiMe_3)_2]_3$ has a first IE 1.64 eV higher than $Cr[N(CHMe_2)_2]_3$. The Cr complex of the *tris*-triamido amine ligand, CrN_3N' ($N_3N' = (tert\text{-}BuMe_2SiNCH_2CH_2)_3N$), which has one alkyl and one silyl substituent on each amido goup has an intermediate IE. The power of Si substituents in attenuating the π-donor power of amido ligands is well illustrated. The top of the series where first IEs lie above 8.0 eV is shared between the strong π-acceptors, CO and PF_3, and the electronegative fluorinated acetyl acetonate ligands and chloride. PF_3 is demonstrated to be a superior acceptor to CO as is also evident when comparing the spectra of $Ni(CO)_4$ and $Ni(PF_3)_4$.[44]

The DEBIE series may be used predictively to estimate the IE of mixed ligand compounds. An example of this is the comparison of $Cr(\eta\text{-}C_6H_6)_2$ (5.4 eV) with $Cr(CO)_6$ (8.5 eV) to predict a first IE of ~7 eV for $Cr(\eta\text{-}C_6H_6)(CO)_3$. The experimental value is 7.42 eV.

Table 5 The DEBIEs (eV) for selected complexes of V, Cr, and Fe

Complex	*V*	*Cr*	*Fe*	*References*
$M(\eta\text{-}C_6H_3Me_3)_2$	5.33	5.01		97
$M(\eta\text{-}C_6H_5Me)_2$	5.82	5.24		97
$M(\eta\text{-}C_6H_6)_2$	5.95	5.40		97
MCp^*_2	5.87	4.93	5.88	16
MCp'_2	6.60	5.53	6.72	15
MCp_2	6.78	5.70	6.88	15
$M(NEt_2)_4$	6.2	5.90		V[98] Cr[99]
$M[N(CHMe_2)_2]_4$		6.30		99
$M(N_3N')$		7.14	7.08	100
$M(CH_2CMe_3)_4$		7.25		101
$M(CH_2SiMe_3)_4$		7.26		101
$M(\eta\text{-}C_3H_5)_3$		7.26		102
$M(acac)_3$		7.46	8.10	103
$M[N(SiMe_3)_2]_3$		7.58	7.78	Cr[104] Fe[105]
$M(CO)_n$	7.52 ($n = 6$)	8.5 ($n = 6$)	8.6 ($n = 5$)	V[23] Cr[20] Fe[106]
$M(tfa)_3$		8.58	9.18	103
$M(PF_3)_n$		9.26 ($n = 6$)	8.83 ($n = 5$)	107
$M(hfa)_3$	8.68	9.53	10.13	108
MCl_4	8.82			109

$Cp^* = C_5Me_5$, $Cp' = C_5H_4Me$, $Cp = C_5H_5$, $N_3N' = (tert\text{-}BuMe_2SiNCH_2CH_2)_3N$, $acac = H_3CCOCHCOCH_3$, $tfa = F_3CCOCHCOCH_3$, $hfa = F_3CCOCHCOCF_3$.

1.14.12 Vibrational Structure

Observation of vibrational structure in the PE spectra of large organometallic molecules is rare because of the large number of vibrational modes that may be excited, the low frequencies of many of the vibrational modes, and the lack of resolution in conventional spectrometers. Techniques such as "zero electron kinetic energy" (ZEKE) spectroscopy have been successful in resolving vibrational structure on small molecules but have not been successfully extended to organometallics as yet. Those spectra that show vibrational structure have proved informative.

The PE spectra of CpRe(NO)(CO)H, Cp^*Re(NO)(CO)H, and Cp^*Re(NO)(CO)D exhibit resolved vibrational structures in the σ(Re–H) and σ(Re–D) ionizations assignable to the Re–H and Re–D stretch in the corresponding cationic states (Figure 18).[45]

The cationic Re–H and Re–D stretching frequencies are lowered in each case in comparison to those corresponding to the neutral molecule. This experimental information can be used to evaluate quantitatively the changes in Re–H bonding and equilibrium bond distance upon removal of an electron. For all three of these molecules, Franck–Condon analysis of the observed vibrational structure indicates that the Re–H or Re–D equilibrium bond distance is lengthened by about 0.25 Å on ionization. The deduction that the Re–H bond orbital is localized is confirmed by theoretical calculations.

Vibrational structure can aid band assignment. The first band of the PE spectrum of CpNiNO shows a vibrational progression of 1855($\pm$81) cm^{-1}. The ν(NO) stretching mode of the neutral molecule has an energy of 1832 cm^{-1}, suggesting that it is this mode that is excited on ionization and that the HOMO has some NO antibonding character. If the band is fitted with three asymmetric Gaussians over a photon energy range, their relative band areas are constant confirming that this band should be assigned to a single ion state (Figure 19).[46]

Calculations confirm that the associated HOMO, $8e_1$, is an in-phase combination of the $2\pi^*$ orbital of NO (29%) with the cyclopentadienyl e_1 π-orbitals (49%) mixed with some Ni character (22%, of which 15% is *d*-based) (Figure 20).

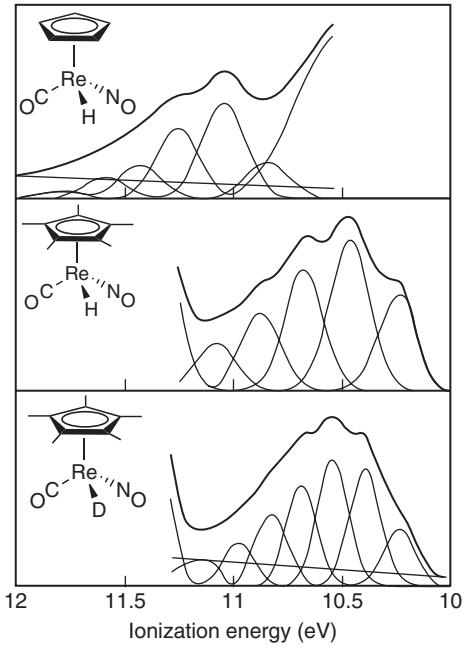

Figure 18 Re–H(D) bonding PE bands of CpReH(NO), Cp*ReH(NO), and Cp*ReD(NO).[45] Vibrational structure corresponding to an Re–H(D) stretching mode is apparent, which has been fitted with Gaussian peaks. Adapted with permission of The American Chemical Society from Lichtenberger, D. L.; Gruhn, N. E.; Rai-Chaudhuri, A.; Renshaw, S. K.; Gladysz, J. A.; Jiao, H.; Seyler, J.; Igau, A. *J. Am. Chem. Soc.* **2002**, *124*, 1417.

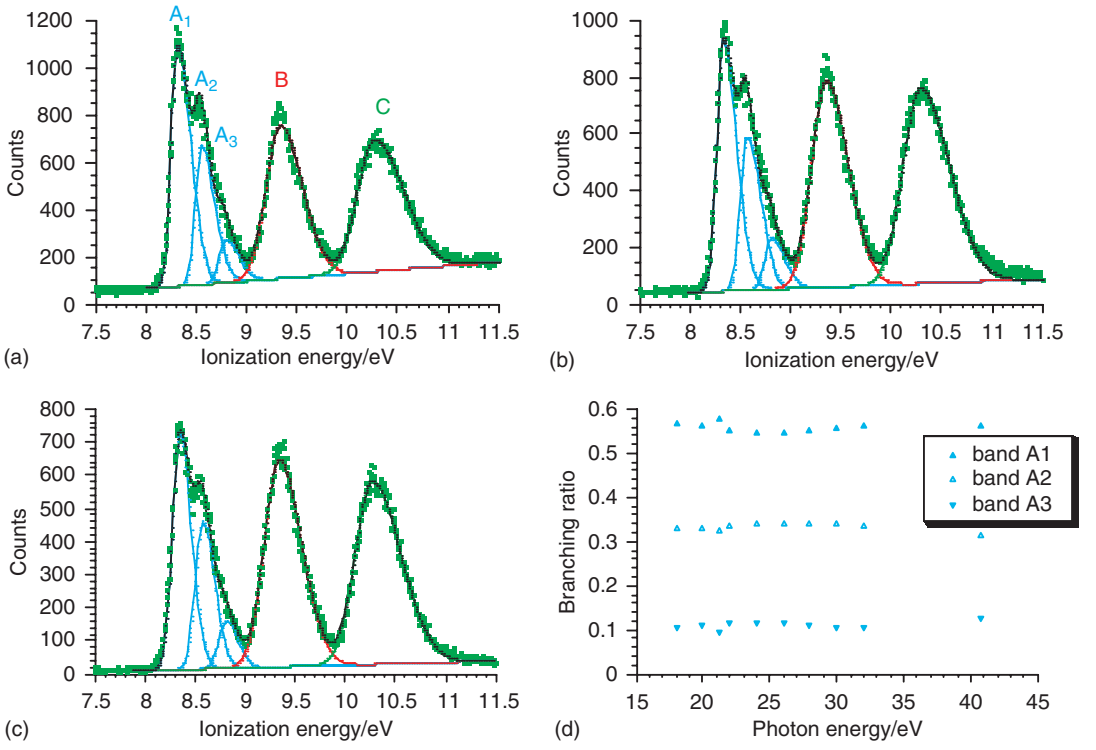

Figure 19 PE spectra of CpNiNO measured at (a) 18 eV, (b) 22 eV, and (c) 28 eV. The first band shows three vibrational components corresponding to an NO stretching mode. Branching ratios of the three components (d) are constant over the photon energy range indicated. The points at 40.8 eV correspond to an He II spectrum.[46] Adapted with permission of The American Chemical Society from Field, C. N.; Green, J. C.; Mayer, M.; Nasluzov, V. A.; Rösch, N.; Siggel, M. R. F. *Inorg. Chem.* **1996**, *35*, 2504.

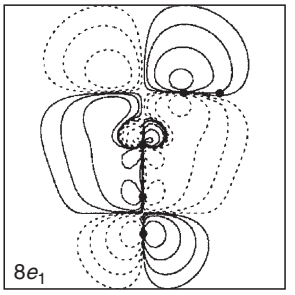

Figure 20 Contour plot for the HOMO of CpNiNO, $8e_1$, showing its NO π^* antibonding character. Removal of an electron from this orbital excites the NO stretching mode.[46] Adapted with permission of The American Chemical Society from Field, C. N.; Green, J. C.; Mayer, M.; Nasluzov, V. A.; Rösch, N.; Siggel, M. R. F. *Inorg. Chem.* **1996**, *35*, 2504.

1.14.13 Ligand Field Splittings of Core Levels

The primary splitting of core levels is by a spin–orbit mechanism. Ligand field splitting was first resolved and characterized on the Zn 3*d* core level of $Zn(Me)_2$ and the Cd 4*d* core level of $Cd(Me)_2$ using He I and He II radiation Figure 21.[11,47]

The magnitude of this splitting was found to be very sensitive to the ligand in the Zn and Cd analogs of the above two molecules. The splitting increased in the order $Cl < Br < I < Me < Et < nPr < Me_3SiCH_2$. This increase can be

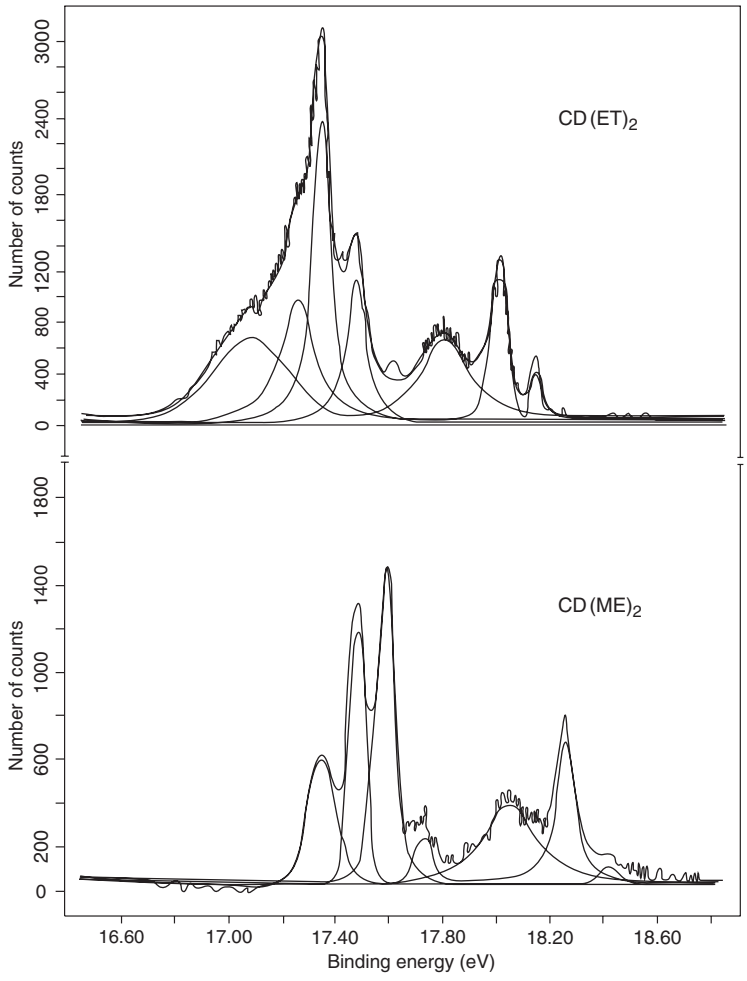

Figure 21 Spin–orbit and ligand field splitting of the 4*d* core orbitals of $CdMe_2$ and $CdEt_2$.[11,47] Reproduced with permission of The American Institute of Physics from Bancroft, G. M.; Creber, D. K.; Basch, H. *J. Chem. Phys.* **1977**, *67*, 4891.

readily attributed to an increase in valence p_z ($4p_z$ for Zn and $5p_z$ for Cd) electron density in the above order. The order is consistent with the accepted order of increasing donor strength for these ligands. Such splittings have been observed at higher photon energies using high resolution synchrotron radiation on a host of mostly inorganic Br, I, and Xe compounds, and they have been useful for obtaining the gas phase structure and bonding in these molecules, for example, the gas phase structure of XeF_6.[48]

1.14.14 PE spectra of Lanthanide and Actinide Organometallics

The PE spectra of bis-cyclooctatetraene uranium(IV) (uranocene) and thorium(IV) (thorocene) have certainly represented a cornerstone in the studies of the electronic structures of *f*-elements (Figure 22).[49–52] In particular, initially, combined He-I/He-II PE spectroscopy[51] and subsequently VPEPES[52] have provided unambiguous evidence of a dominant role played in the metal–ligand bonding by both 5*f* and 6*d* orbitals. The low energy region of the spectrum of thorocene has two bands whereas that of uranocene shows three bands; the extra band for uranocene is associated with the *f*-electrons. The other two bands are assigned to the e_{2u} and the e_{2g} orbitals, but from the He- I spectrum it is not obvious which is which.

The ionization cross section of the first band of uranocene (the *f*-band) shows a dramatic rise to a delayed maximum at 40 eV and subsequently resonance structure between 95 and 120 eV (Figure 23). Assignment of the second and third bands is readily made from their cross sections. Both decay with an increase in photon energy, as expected for C

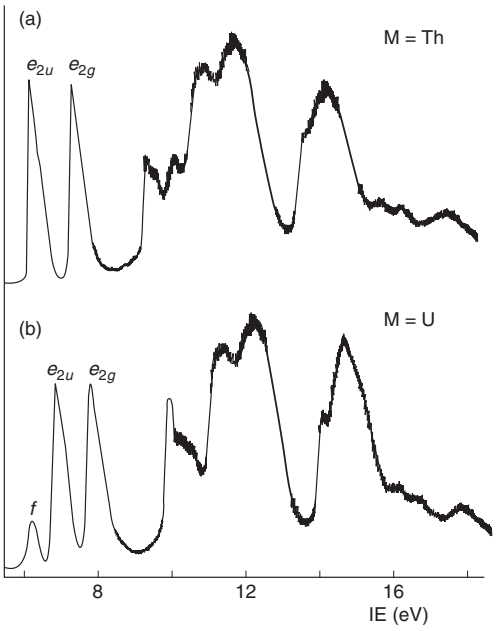

Figure 22 He I PE spectra of (a) Th(η-C_8H_8)$_2$ and (b) U(η-C_8H_8)$_2$.[51] Adapted with permission of Royal Society of Chemistry from Clark, J. P.; Green, J. C. *J. Chem. Soc., Dalton Trans*. **1977**, 505.

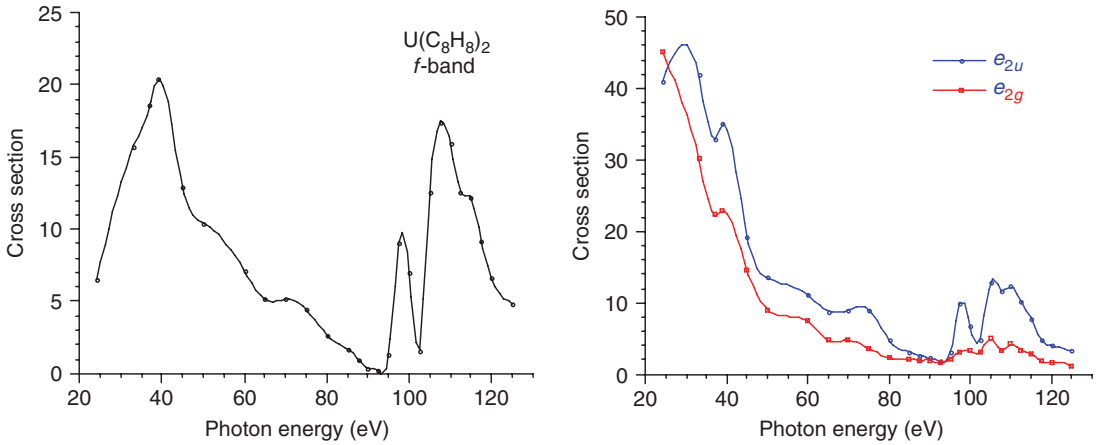

Figure 23 Relative partial photoionization cross sections for the 5*f*, e_{2u}, and e_{2g} bands of U(η-C_8H_8)$_2$. The 5*f* band shows a delayed maximum at 40 eV and resonance structure on the regions of 5*d* to 5*f* excitation. The e_{2u} band also mirrors these features as a result of a 5*f* contribution to the e_{2u} orbital. Adapted with permission of American Chemical Society from Brennan, J. G.; Green, J. C.; Redfern, C. M. *J. Am. Chem. Soc.* **1989**, *111*, 2373.

2*p* based ionizations; however, the second band shows features that mirror the delayed maximum and the resonant structure of the *f*-band, thus establishing that this ionization arises from the e_{2u} orbitals and that the associated MO has *f*-orbital covalency.

The higher IE band is therefore assigned to the e_{2g} orbital, the inference being that this is the more stable of the e_2 orbitals as a consequence of the 6*d* orbitals forming stronger bonds to the rings.

Some ring-substituted uranocenes[53,54] have been scrutinized and a similar bonding model assessed by PE spectra. Finally PE spectra of di-π-(8)annulenecerium(IV), cerocene, are similar to those of thorocene, and spectroscopic/

theoretical Xα-SW data are consistent with ring–metal bonding having substantial covalency with significant 4*f* contributions.[55] Tetrahedral tetrakis(cyclopentadienyl)actinide complexes, unlike many other cyclopentadienyls, have a particularly crowded environment and thus have no structural counterparts in the *d*-block metals. Both, the simpler M(η-C_5H_5)$_4$[56] and the ring-substituted M(η-C_5H_4Me)$_4$[57] (M = Th, U), complexes have been studied. Three bands associated with ionizations of Cp e_1 π-character are readily identified and can be treated with T_d symmetry as being associated with t_1, t_2, and e MO. He-I and He-II spectra show the third band to have the greatest intensity increase from He I to He II photon energy. Xα-SW calculations suggest that the first ligand band is from MOs of t_1-symmetry that are stabilized by *f*-orbital covalency. The second and third bands are assigned with t_2- and e-ionizations, respectively, which have a *d*-orbital contribution to the associated MOs.[56,57] Thus, in this case, the band with a *d*-contribution appears to gain more intensity with increase in photon energy. It is likely that there is a breakdown of the Gelius model in this case. It had been demonstrated that *d*-bands of metallocenes have strong shape resonances around 40 eV[12] and such a feature in the *e*-band cross section could account for the anomalous He II intensity. This case history underlines the desirability of studying intensity changes over a broad range of photon energies as is provided by synchrotron radiation.

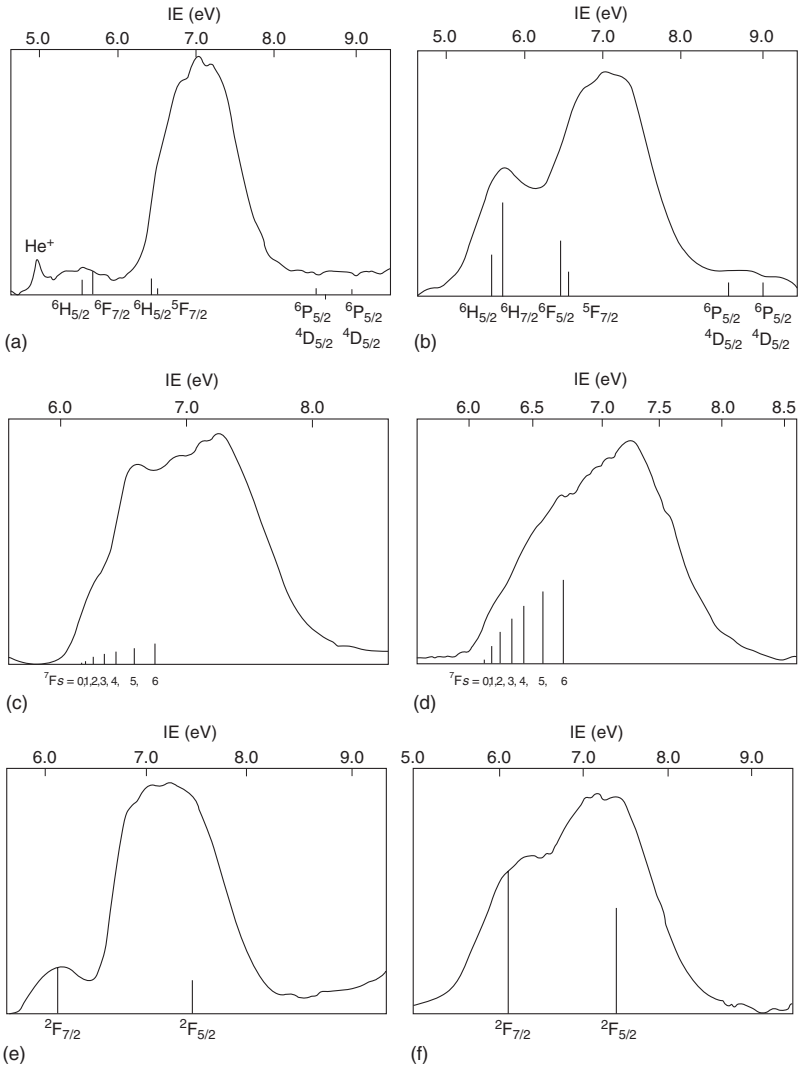

Figure 24 He I (on left) and He II (on right) PE spectra of $LnCp^*_2$ (Ln = (a)(b) Sm (c)(d) Eu (e)(f) Yb). The sticks mark predicted ion states and their relative intensities. The band centered on 7.0 eV, most apparent in the He I spectra, is due to Cp^* e_1 π ionizations.[64] Adapted with permission of Royal Society of Chemistry from Andersen, R. A.; Boncella, J.; Green, J. C.; Burns, C. J.; Hohl, D.; Rœsch, N. *J. Chem. Soc., Chem. Commun.* **1986**, 405.

Compounds of the stoichiometry $MCp^*_2X_2$ provide an opportunity to compare actinides with *d*-block elements. Several such species have been studied both by gas phase PE experiments as well as by theoretical approaches. Thus, the first comparative study of the PE spectra of a series of transition metal and actinide organometallic compounds with exactly the same ligand array was carried out on $MCp^*_2X_2$ (M = Zr, Th, U, and X = CH_3 and Cl) complexes.[58] Comparable bonding was found along the series with smaller differences than encountered in the parent series involving transition elements. The major differences between Zr and the actinides are due to the involvement of 5*f* in the bonding.

Further studies have extended the range of X ligands, examined MCp_3X analogs and also examined analogous indenyl complexes.[59–63] Xα-SW calculations proved invaluable in both spectral assignment and interpretation.

It is much more difficult to detect 4*f* ionizations in the spectra of lanthanide complexes. Cross sections are very low at He I photon energies and when the lanthanide is in the oxidation state (III), the 4*f* band will normally lie under a ligand ionization. However, for the $LnCp^*_2$ (Ln = Sm, Eu, and Yb) with an oxidation state of II, the 4*f* band precedes the ligand ionizations and gives bands of low intensity in the He I spectra, which show large relative intensity increases with He II photons.[64] Ionization of *f*-electrons gives complex band structure; the selection rules for direct ionization are well documented.[17] The theoretical patterns are indicated by sticks in Figure 24.

In a series of Ln(III) complexes, $Cp^*_2LnCH(SiMe_3)_2$ and $(Me_2SiCp'')_2LnCH(SiMe_3)_2$ ($Cp'' = \eta^5$-$(CH_3)_4C_5$; Ln = La, Ce, Nd, Sm, Lu), the f-bands have been detected in the He II spectra and their IEs are consistent with a gradual energetic stabilization of 4*f* orbitals across the lanthanide series.[110]

1.14.15 Metal–Metal Bonded Species and Clusters

The ability of PE spectroscopy to interrogate the whole range of valence orbitals of a molecular system has proved invaluable in investigating the electronic structure of metal–metal multiple bonds and small metal clusters. In the organometallic field, most attention has been focused on metal carbonyl dimers and small clusters, and their derivatives, on account of the high stability and volatility of these species.[5] Metal chalcogen clusters of stoichiometry $M_4Cp_4E_4$ (E = O, S, Se) have also proved viable and fruitful candidates for PE spectroscopy.[65,66]

A simple example illustrates the type of information available. The clusters $Os_3(CO)_{12}$ and $Re_3H_3(CO)_{12}$ are isoelectronic, and both have a triangle of metal atoms each bonded to four terminal CO groups. The Re cluster has three hydrogens bridging the edges of the metal triangle. Overall, both molecules possess D_{3h} symmetry.

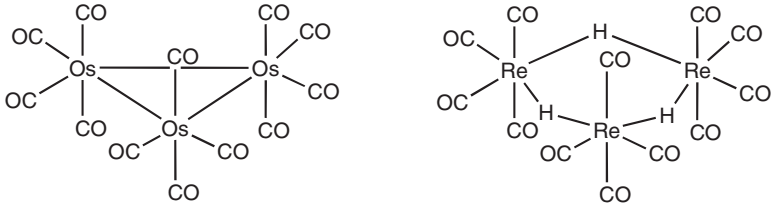

He I PE spectra of both molecules are shown in Figure 25.[67–70] Ionization bands from the a_1' and e' Os–Os bonding orbitals lie at lower IE than those from the metal *d*-electrons involved in Os to CO backbonding. The a_1' orbital has the lowest IE, and the e' band is split by spin–orbit coupling. In the isoelectronic Re_3H_3 cluster, the Re to CO backbonding electrons ionize at lower IE than in the Os_3 case, because Re has the lower nuclear charge. The cluster a_1' and e' bonding orbitals, however, are stabilized by just under 4 eV with their IE lying above the main *d*-band. Thus, the cluster bonding is more robust. He II spectra confirm the assignment and indicate a high degree of localization of the Re_3H_3 cluster orbitals on the hydrogen atoms.

With less symmetric clusters, DV-Xα calculations have proved invaluable in assigning spectra and revealing electronic structure. The combined techniques have been used to study the (μ_2-L)-M_2 and (μ_2-L)$_2$-M_2 subunits, where L = CO,[71–74] CH_2,[72,75,76] PR_2,[77] and (μ_3-L)-M_3 subunits where L = alkyne,[78–80] alkynyl,[70] and CR.[81,82] These studies reveal the relative importance of direct M–M versus delocalized M–L multicentered interactions. One important factor is the π-acceptor ability of the bridging ligand. For example, in $[FeCp(CO)_2]_2$, an M–M bond is practically absent but in the case of a ligand lacking low lying acceptor orbitals, as for example PR_2, the major electron pairing mechanism is by direct metal–metal interaction.

The analogy between the interaction of organic fragments with small clusters and with metal surfaces has also been explored.

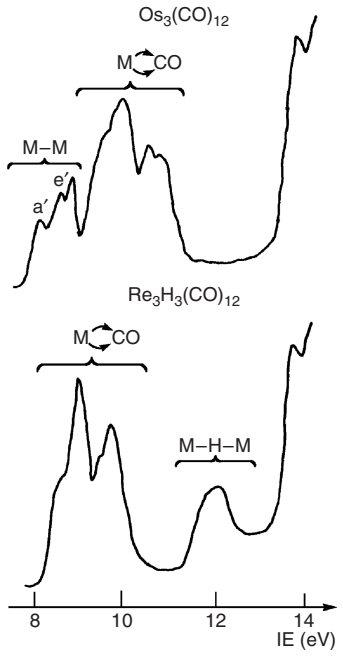

Figure 25 He I PE spectra of $Re_3H_3(CO)_{12}$ and $Os_3(CO)_{12}$. Assignments are indicated for the Os–Os and Re–H–Re cluster bonding electrons, the latter being stabilized by the edge-bridging hydrogens. Assignment of the metal to CO backbonding electrons is also indicated.[69] Adapted with permission of The American Chemical Society from Green, J. C.; Mingos, D. P. M.; Seddon, E. A. *Inorg. Chem.* **1981**, *20*, 2595.

1.14.16 Conclusions

PE spectroscopy enables direct observation of a full range of valence and core electron binding energies. The information is directly related to the electronic descriptions of chemical bonding generated by MO theory. Sources of chemical bonding may be investigated and categorized in terms of the AOs combining to form MOs. For both *d*-and *f*-block transition metal complexes, ligand field effects and exchange interactions may be observed. Ligand additivity effects and core–valence ionization correlations have been established. Ligands can be ordered according to their π-acceptor/donor capacity and to their DEBIEs. The latter are shown to bear no relation to the oxidation state of a metal. Bonding in small clusters, and the interaction of such clusters with organic fragments, have been explored in combination with DV-Xα calculations.

Such studies have underpinned and provided bench marks for much of the development of modern electronic structure theory.

Acknowledgments

This chapter is dedicated to the memory of Tony Orchard with whom the author has shared many adventures in the early days of the application of PE spectroscopy to inorganic molecules. The author gratefully acknowledges the advice and assistance of the following colleagues in the preparation of this chapter: Mike Bancroft, Luciano Fragala, Rolf Gleiter, Gaetano Granozzi, Dennis Lichtenberger, Gabor Balazs, Nilay Hazari, Jason Holland, Navaratnarajah Kuganathan, and Emma Sceats.

References

1. Cowley, A. H. *Prog. Inorg. Chem.* **1979**, *26*, 46.
2. Cauletti, C.; Furlani, C. *Struct. Bond.* **1978**, *35*, 119.
3. Green, J. C. *Struct. Bond.* **1981**, *43*, 37.
4. van Dam, H.; Oskam, A. *Trans. Metal. Chem.* **1985**, *9*, 125.

5. Granozzi, G.; Casarin, M. In *Topics in Physical Organometallic Chemistry*; Gielen, M., Ed.; Freund Publishing House: Israel, 1989; Vol. 3.
6. Green, J. C. *Acc. Chem. Res.* **1994**, *27*, 131.
7. Lichtenberger, D. L.; Kellogg, G. E. *Acc. Chem. Res.* **1987**, *20*, 379.
8. Lichtenberger, D. L.; Copenhaver, A. S. In *Bonding Energetics in Organometallic Compounds*; Marks, T. J., Ed.; ACS Symposium Series, American Chemical Society: Washington, DC, 1990; Vol. 428.
9. Gruhn, N. E.; Lichtenberger, D. L. In *Inorganic Electronic Structure and Spectroscopy; Vol. II: Applications and Case Studies*; Lever, A. B. P., Solomon, E. I., Eds.;, Wiley: New York, 1999.
10. Li, X.; Bancroft, G. M.; Puddephatt, R. J. *Acc. Chem. Res.* **1997**, *30*, 213.
11. Bancroft, G. M.; Hu, Y. F. In *Inorganic Electronic Structure and Spectroscopy I*; Solomon, E. I., Lever, A. B. P., Eds.; Wiley: New York, 1999; Vol. 1.
12. Green, J. C.; Decleva, P. *Coord. Chem. Rev.* **2005**, *249*, 209.
13. Green, J. C. In *Encyclopedia of Inorganic Chemistry*; King, R. B., Ed.; Wiley: Chichester, 2005; Vol. 6.
14. Evans, S.; Green, J. C.; Joachim, P. J.; Orchard, A. F.; Turner, D. W.; Maier, J. P. *J. Chem. Soc., Faraday Trans. 2* **1972**, *68*, 905.
15. Evans, S.; Green, M. L. H.; Jewitt, B.; King, G. H.; Orchard, A. F. *J. Chem. Soc. Farad. II* **1974**, *70*, 356.
16. Cauletti, C.; Green, J. C.; Kelly, M. R.; Powell, P.; van Tilborg, J.; Robbins, J.; Smart, J. *J. Electron. Spectrosc. Relat. Phenom.* **1980**, *19*, 327.
17. Cox, P. A. *Struct. Bond.* **1975**, *24*, 59.
18. Gelius, U.; Siegbahn, K. *Faraday. Discuss., Chem. Soc.* **1972**, *54*, 257.
19. Yeh, J. J.; Lindau, I. *At. Data Nucl. Data Tables* **1985**, *32*, 1.
20. Higginson, B. R.; Lloyd, D. R.; Burroughs, P.; Gibson, D. M.; Orchard, A. F. *J. Chem. Soc., Faraday. Trans. 2* **1973**, *69*, 1659.
21. Cooper, G.; Green, J. C.; Payne, M. P.; Dobson, B. R.; Hillier, I. H. *J. Am. Chem. Soc.* **1987**, *109*, 3836.
22. Hubbard, J. L.; Lichtenberger, D. L. *J. Am. Chem. Soc.* **1982**, *104*, 5026.
23. Evans, S.; Green, J. C.; Orchard, A. F.; Saito, T.; Turner, D. W. *Chem. Phys. Lett.* **1969**, *4*, 361.
24. Lloyd, D. R.; Schlag, E. W. *Inorg. Chem.* **1969**, *8*, 2544.
25. Evans, S.; Green, M. L. H.; Jewitt, B.; Orchard, A. F.; Pygall, C. F. *J. Chem. Soc., Faraday. Trans. 2* **1972**, *68*, 1847.
26. Cooper, G.; Green, J. C.; Payne, M. P. *Mol. Phys.* **1988**, *63*, 1031.
27. Boehm, M. C.; Eckert-Maksić, M.; Ernst, R. D.; Wilson, D. R.; Gleiter, R. J. *J. Am. Chem. Soc.* **1982**, *104*, 2699.
28. Gleiter, R.; Hyla-Krispin, I.; Ziegler, M. L.; Sergeson, G.; Green, J. C.; Stahl, L.; Ernst, R. D. *Organometallics* **1989**, *8*, 298.
29. Lloyd, D. R.; Lynaugh, N. In *Electron Spectroscopy*; Shirley, D. E., Ed.; Amsterdam: North Holland, 1972; 445.
30. Batich, C. D. *J. Am. Chem. Soc.* **1976**, *98*, 7585.
31. Boehm, M. C.; Gleiter, R.; Batich, C. B. *Helv. Chim. Acta* **1980**, *63*, 990.
32. Li, X.; Bancroft, G. M.; Puddephatt, R. J.; Liu, Z. F.; Hu, Y. F.; Tan, K. H. *J. Am. Chem. Soc.* **1994**, *116*, 9543.
33. Veillard, A. *J. Chem. Soc. D* **1969**, 1022.
34. Rohmer, M.-M.; Veillard, A. *J. Chem. Soc., Chem. Commun.* **1973**, 250.
35. Boehm, M. C.; Gleiter, R. *Theor. Chim. Acta* **1980**, *57*, 315.
36. Boehm, M. C.; Gleiter, R. *Angew. Chem., Int. Ed. Engl.* **1983**, *22*, 329.
37. Bursten, B. E. *J. Am. Chem. Soc.* **1982**, *104*, 1299.
38. Bancroft, G. M.; Dignard-Bailey, L.; Puddephatt, R. J. *Inorg. Chem.* **1984**, *23*, 2369.
39. Bursten, B. E.; Darensbourg, D. J.; Kellogg, G. E.; Lichtenberger, D. L. *Inorg. Chem.* **1984**, *23*, 4361.
40. Lichtenberger, D. L.; Gruhn, N. E.; Renshaw, S. K. *J. Mol. Struct.* **1997**, *405*, 79.
41. Lichtenberger, D. L.; Kellogg, G. E.; Landis, G. H. *J. Chem. Phys.* **1985**, *83*, 2759.
42. Wu, J.; Bancroft, G. M.; Puddephatt, R. J.; Hu, Y. F.; Li, X.; Tan, K. H. *Inorg. Chem.* **1999**, *38*, 4688.
43. Jolly, W. L. *Acc. Chem. Res.* **1983**, *16*, 370.
44. Green, J. C.; King, D. I.; Eland, J. H. D. *Chem. Commun.* **1970**, 1121.
45. Lichtenberger, D. L.; Gruhn, N. E.; Rai-Chaudhuri, A.; Renshaw, S. K.; Gladysz, J. A.; Jiao, H.; Seyler, J.; Igau, A. *J. Am. Chem. Soc.* **2002**, *124*, 1417.
46. Field, C. N.; Green, J. C.; Mayer, M.; Nasluzov, V. A.; Rösch, N.; Siggel, M. R. F. *Inorg. Chem.* **1996**, *35*, 2504.
47. Bancroft, G. M.; Creber, D. K.; Basch, H. *J. Chem. Phys.* **1977**, *67*, 4891.
48. Cutler, J. N.; Bancroft, G. M.; Bozek, J. D.; Tan, K. H.; Scrobilgen, G. J. *J. Am. Chem. Soc.* **1991**, *113*, 9125.
49. Clark, J. P.; Green, J. C. *J. Organomet. Chem.* **1976**, *112*, C14.
50. Fragala, I.; Condorelli, G.; Zanella, P.; Tondello, E. *J. Organomet. Chem.* **1976**, *122*, 357.
51. Clark, J. P.; Green, J. C. *J. Chem. Soc., Dalton Trans.* **1977**, 505.
52. Brennan, J. G.; Green, J. C.; Redfern, C. M. *J. Am. Chem. Soc.* **1989**, *111*, 2373.
53. Bruno, G.; Ciliberto, E.; Fischer, R. D.; Fragala, I.; Spiegl, A. W. *Organometallics* **1982**, *1*, 1060.
54. Green, J. C.; Payne, M. P.; Streitwieser, A., Jr. *Organometallics* **1983**, *2*, 1707.
55. Streitwieser, A., Jr.; Kinsley, S. A.; Rigsbee, J. T.; Fragala, I. L.; Ciliberto, E. *J. Am. Chem. Soc.* **1985**, *107*, 7786.
56. Green, J. C.; Kelly, M. R.; Long, J. A.; Kanellakopulos, B.; Yarrow, P. I. W. *J. Organomet. Chem.* **1981**, *212*, 329.
57. Bursten, B. E.; Casarin, M.; Dibella, S.; Fang, A.; Fragala, I. L. *Inorg. Chem.* **1985**, *24*, 2169.
58. Ciliberto, E.; Condorelli, G.; Fagan, P. J.; Manriquez, J. M.; Fragala, I. L.; Marks, T. J. *J. Am. Chem. Soc.* **1981**, *103*, 4755.
59. Arduini, A. L.; Malito, J.; Takats, J.; Ciliberto, E.; Fragala, I.; Zanella, P. *J. Organomet. Chem.* **1987**, *326*, 49.
60. Vittadini, A.; Casarin, M.; Ajo, D.; Bertoncello, R.; Ciliberto, E.; Gulino, A.; Fragala, I. L. *Inorg. Chim. Acta* **1986**, *121*, L23.
61. Gulino, A.; Ciliberto, E.; Di Bella, S.; Fragala, I. L.; Seyam, A. M.; Marks, T. J. *Organometallics* **1992**, *11*, 3248.
62. Gulino, A.; Di Bella, S.; Fragala, I. L.; Casarin, M.; Seyam, A. M.; Marks, T. J. *Inorg. Chem.* **1993**, *32*, 3873.
63. Fragala, I. L.; Goffart, J.; Granozzi, G.; Ciliberto, E. *Inorg. Chem.* **1983**, *22*, 216.
64. Andersen, R. A.; Boncella, J.; Green, J. C.; Burns, C. J.; Hohl, D.; Rœsch, N. *J. Chem. Soc., Chem. Commun.* **1986**, 405.
65. Bandy, J. A.; Davies, C. E.; Green, J. C.; Green, M. L. H.; Prout, K.; Rodgers, D. P. S. *J. Chem. Soc., Chem. Commun.* **1983**, 1395.
66. Davies, C. E.; Green, J. C.; Kaltsoyannis, N.; MacDonald, M. A.; Qin, J.; Rauchfuss, T. B.; Redfern, C. M.; Stringer, G. H.; Woolhouse, M. G. *Inorg. Chem.* **1992**, *31*, 3779.
67. Green, J. C.; Seddon, E. A.; Mingos, D. M. P. *Chem. Commun.* **1979**, 94.
68. Ajo, D.; Granozzi, G.; Tondello, E.; Fragala, I. *Inorg. Chim. Acta* **1979**, *37*, 191.
69. Green, J. C.; Mingos, D. P. M.; Seddon, E. A. *Inorg. Chem.* **1981**, *20*, 2595.

70. Granozzi, G.; Tondello, E.; Bertoncello, R.; Aime, S.; Osella, D. *Inorg. Chem.* **1983**, *22*, 744.
71. Granozzi, G.; Tondello, E.; Benard, M.; Fragala, I. *J. Organomet. Chem.* **1980**, *194*, 83.
72. Andreocci, M. V.; Bossa, M.; Cauletti, C.; Paolesse, R.; Ortaggi, G.; Vondrak, T.; Piancastelli, M. N.; Casarin, M.; Dalcolle, M.; Granozzi, G. *J. Organomet. Chem.* **1989**, *366*, 343.
73. Granozzi, G.; Casarin, M.; Ajo, D.; Osella, D. *J. Chem. Soc., Dalton Trans.* **1982**, 2047.
74. Granozzi, G.; Tondello, E.; Ajo, D.; Faraone, F. *J. Organomet. Chem.* **1982**, *240*, 191.
75. Granozzi, G.; Tondello, E.; Casarin, M.; Ajo, D. *Inorg. Chim. Acta* **1981**, *48*, 73.
76. Bender, B. R.; Bertoncello, R.; Burke, M. R.; Casarin, M.; Granozzi, G.; Norton, J. R.; Takats, J. *Organometallics* **1989**, *8*, 1777.
77. Rizzi, G. A.; Granozzi, G.; Casarin, M.; Basato, M. *Organometallics* **1987**, *6*, 2536.
78. Granozzi, G.; Tondello, E.; Casarin, M.; Aime, S.; Osella, D. *Organometallics* **1983**, *2*, 430–434.
79. Busetti, V.; Granozzi, G.; Aime, S.; Gobetto, R.; Osella, D. *Organometallics* **1984**, *3*, 1510.
80. Aime, S.; Bertoncello, R.; Busetti, V.; Gobetto, R.; Granozzi, G.; Osella, D. *Inorg. Chem.* **1986**, *25*, 4004.
81. Granozzi, G.; Tondello, E.; Ajo, D.; Casarin, M.; Aime, S.; Osella, D. *Inorg. Chem.* **1982**, *21*, 1081.
82. Casarin, M.; Ajo, D.; Lentz, D.; Bertoncello, R.; Granozzi, G. *Inorg. Chem.* **1987**, *26*, 465.
83. Lichtenberger, D. L.; Hubbard, J. L. *Inorg. Chem.* **1984**, *24*, 3835.
84. Calabro, D. C.; Hubbard, J. L.; Blevins, C. H. II; Campbell, A. C.; Lichtenberger, D. L. *J. Am. Chem. Soc.* **1981**, *103*, 6839.
85. Pang, L. S. K. *Diss. Abstr. Int. B* **1986**, *46*, 3839.
86. Calabro, D. C.; Lichtenberger, D. L. *J. Am. Chem. Soc.* **1981**, *103*, 6846.
87. Campbell, A. C. M.S. Thesis, University of Arizona, Tuczon, Arizona, 1979
88. Lichtenberger, D. L.; Fenske, R. F. *J. Organomet. Chem.* **1976**, *117*, 253.
89. Lichtenberger, D. L.; Rai-Chaudhuri, A. *Inorg. Chem.* **1990**, *29*, 975.
90. Lichtenberger, D. L.; Rai-Chaudhuri, A. *J. Am. Chem. Soc.* **1993**, *113*, 2923.
91. Hubbard, J. L. *Diss. Abstr. Int. B* **1983**, *43*, 2203.
92. Lichtenberger, D. L.; Fenske, R. F. *J. Am. Chem. Soc.* **1976**, *98*, 50.
93. Renshaw, S. K. *Diss. Abstr. Int. B* **1992**, *51*, 5259.
94. Lichtenberger, D. L.; Rai-Chaudhuri, A. *J. Am. Chem. Soc.* **1991**, *113*, 2923.
95. Lichtenberger, D. L.; Renshaw, S. K.; Bullock, R. M. *J. Am. Chem. Soc.* **1993**, *115*, 3276.
96. Lichtenberger, D. L.; Rai-Chaudhuri, A.; Wong, A.; Tagge, C. D. *Organometallics* **1993**, *12*, 3522.
97. Evans, S.; Green, J. C.; Jackson, S. E.; Higginson, B. *J. Chem. Soc., Dalton Trans.* **1974**, 304.
98. Gibbins, S. G.; Lappert, M. F.; Pedley, J. B.; Sharp, G. J. *J. Chem. Soc., Dalton Trans.* **1975**, 72.
99. Chisholm, M. H.; Cowley, A. H.; Lattman, M. *J. Am. Chem. Soc.* **1980**, *102*, 46.
100. Metcalfe, J. Part II Thesis, University of Oxford, Oxford 1995.
101. Evans, S.; Green, J. C.; Jackson, S. E. *J. Chem. Soc., Faraday. Trans. 2* **1973**, *69*, 191.
102. Green, J. C.; Seddon, E. A. *J. Organomet. Chem.* **1980**, *198*, C61.
103. Evans, S.; Hamnett, A.; Orchard, A. F.; Lloyd, D. R. *Farad. Discuss. Chem. Soc.* **1972**, *54*, 227.
104. Green, J. C.; Payne, M. P.; Seddon, E. A.; Andersen, R. A. *J. Chem. Soc., Dalton Trans.* **1982**, 887.
105. Lappert, M. F.; Pedley, J. B.; Sharp, G. J.; Bradley, D. C. *J. Chem. Soc. Dalton Trans.* **1976**, 1737.
106. Symon, D. A.; Waddington, T. C. *J. Chem. Soc., Dalton Trans.* **1975**, 2140.
107. Muller, J.; Fenderl, K.; Mertschenck, B. *Chem. Ber.* **1971**, *104*, 700.
108. Evans, S.; Hamnett, A.; Orchard, A. F. *J. Coord. Chem.* **1972**, *2*, 57.
109. Egdell, R. G.; Orchard, A. F.; Lloyd, D. R.; Richardson, N. V. *J. Electron. Spectrosc. Relat. Phenom.* **1977**, *12*, 415.
110. Di Bella, S.; Gulino, A.; Lanza, G.; Fragala, I. L.; Stern, D.; Marks, T. J. *Organometallics* **1994**, *13*, 3810.

1.15 Dynamic NMR Spectroscopy in Organometallic Chemistry

J W Faller, Yale University, New Haven, CT, USA

1.15.1 Introduction

When molecular interconversions occur at rates that affect the NMR line shapes in generally accessible temperature ranges, the observed spectrum is said to be a "dynamic NMR" or DNMR spectrum, even though it is the molecular system that is dynamic. Examinations of DNMR spectra allow determination of rates and elucidation of mechanisms. This approach was first applied to intramolecular rearrangements of organometallics 40 years ago in a series of investigations of these "stereochemically non-rigid organometallic compounds".[1–6] The compounds were designated as fluxional[7] in situations where equivalent structures of these non-rigid compounds interconverted via a series of bond angle changes, rotations of ligands, or bond-breaking and bond-making reactions. Cotton's retrospective description of these early developments provides a review of the early work.[8]

A book prepared in the mid-1970s summarizes many of the essential elements of DNMR spectroscopy,[9] and subsequent reviews related to organometallics[10–16] provide further updated information. The older review by Mann[10]and his recent book[17] are particularly valuable resources in this area. Studies of dynamics by NMR have often been carried out using detailed calculations of the line shapes that vary with temperature;[18] nevertheless, magnetization transfer[13,19–22] and newer two-dimensional (2D) methods can often provide more comprehensive information.[17,23,24]

1.15.2 Activation Energies and DNMR

1.15.2.1 DNMR Line Shapes and Rates

A common observation is that an η^5-cyclopentadienyl ligand appears as a singlet in the ^{1}H NMR, even though one would note that the protons in a given conformation may not be equivalent. This is attributed to rapid rotation of the Cp and a very low barrier for rotation of this ligand. The barrier is sufficiently low that it can rarely be measured in solution. Barriers in the range of 20–100 kJ mol^{-1} tend to produce observable effects in the NMR in generally accessible temperature ranges. When metal complexes with unpaired electrons are synthesized, the EPR can occasionally provide information on low barriers owing to the larger separations in frequency of the resonances. In the case of 19-electron (η^5-C_5Ph_4H)Mo(CO)$_2$(bis-diphenylphosphinomaleic anhydride), where the electron resides predominantly on the ligand, the barrier for ring rotation was ~12 kJ mol^{-1} at 25 °C.[25] Sufficiently bulky substituents on the rings and metal can increase the barriers in diamagnetic compounds appreciably so that the NMR line shapes are affected.[26,27] The line shapes observed in these and other dynamic NMR systems are a function of rate of exchange between environments with different chemical shifts and can be calculated readily with small computers.[18,28–32] Some features of a simple example of spectral dependence on the rate constant will be reviewed to provide a background for discussion. For two-site exchange, increasing the rate will first broaden the resonances; then the resonances will coalesce and then finally sharpen to a narrow resonance (see Figure 1). Often, the rate change will be induced by raising the temperature of the sample. In the initial phases of broadening, the additional half-width (W') of the resonance produced from the exchange is proportional to the rate constant for leaving that site (Equation (1)). At equilibrium, the forward and reverse rate must be equal; hence for a 2 : 1 ratio of intensities, the rate constants for leaving each site must be in a ratio of 1 : 2. The greater broadening of the lower population site is evident in Figure 1.

$$k = \pi W' \tag{1}$$

After coalescence, the width depends on the rate and the reciprocal square of the separation of the resonances (Figure 1). The crucial observation is that if the resonances in the absence of exchange have a greater separation, it will take a higher temperature and exchange rate to average them completely. Therefore, although the initial broadening that is observed is independent of the separation or the field strength, the broadening observed after coalescence is field dependent. Experimentally, one may observe a slightly broadened resonance at ambient temperature, but upon lowering the temperature it will broaden and decoalesce, finally exhibiting sharp resonances that were averaged at the higher temperature. The stage where changes in the spectrum are no longer apparent is designated as the limiting low-temperature spectrum. This does not mean that exchange has stopped, but merely that the rate has dropped below the temperature at which it affects the NMR spectrum ($k \sim 0.03\ s^{-1}$).

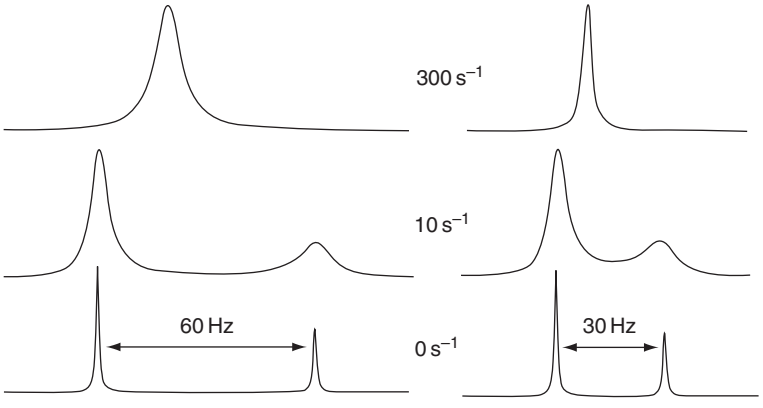

Figure 1 The effect of rate of exchange on line shapes of resonances with a population ratio of 2 : 1. The rate constant shown is that for leaving the site with the larger population.

Table 1 Approximate free energies of activation determined by the temperature at which a low-temperature limiting spectrum in observed[a]

T (°C)	$\Delta G^{\ddagger}$ (kcal mol^{-1})	$\Delta G^{\ddagger}$ (kJ mol^{-1})
−160	6.1	25
−120	8.4	35
−80	10.7	45
−40	13.0	54
0	15.3	64
40	17.6	74
80	20.0	84
120	22.3	93
160	24.7	103

[a]The most accurate values are obtained at the temperature where broadening just becomes perceptible in ^{1}H NMR.

The temperature at which coalescence occurs upon raising the temperature is known as the coalescence temperature, T_c, and there is a simple formula for determining the rate at this point for "equal" population sites. Using coalescence temperature formulas may be, however, subject to serious errors owing to uncertainty in the chemical shift separations in the absence of exchange. This is particularly evident when small chemical shift separations are involved and the shifts vary with temperature. Thus, kinetics studies purporting to have some reasonable degree of accuracy require extrapolating chemical shift separations from low temperature limits through the high-temperature limits.

As an example of the difficulties that can be encountered, an analysis of DNMR spectra relevance that was carried out in 1964 suggested a barrier to rotation in $(\eta^5\text{-}C_5H_5)Rh(C_2H_4)_2$ ~25 kJ mol^{-1}.[33] This original study did not take into account the variations in chemical shifts with temperature, thus gaving an anomalously low activation energy for a process which showed initial line broadening at ca. −15 °C and a coalescence temperature of ≈50 °C for resonances separated by 110 Hz. A subsequent re-evaluation of the activation energies, including approximations for coupling,[34] found an activation energy of 46 kJ mol^{-1}. The advantages of using initial broadening rather than coalescence to estimate the barrier are evident, since this approach yields a barrier of ~45 kJ mol^{-1}.

If one assumes that, when raising the temperature above the low-temperature limit, broadening just becomes perceptible, approximately when the peak broadens by 1 Hz, this would imply a rate constant ~0.3 s^{-1}, and a free energy of activation can be determined at this temperature (T_1). Reference to Table 1 indicates approximate free energies associated with DNMR spectra indicated by this approach.

Fitting of observed line shapes to calculated line shapes provides a method of determining rates.[35] Calculation of the line shapes including coupling can be carried out using available computer programs;[18,28–32] however, one must take care in relating the "rate" used in the programs to the chemically relevant pseudo-first-order rate constant for a particular chemical process that exchanges nuclei. The "rate" entered in a program is likely to be the "overall" or "absolute" rate, which represents the sum of departures from all sites. This "rate" must be divided by the concentrations or populations of individual sites in order to obtain the rate constant for departure from a particular site. This problem has been discussed for some complicated cases by Green *et al.*,[36] and the topic was also covered in other reviews.[12,16] Green's approach focuses on an overall rate constant, k_{chem}, but there are alternative choices to that approach; nevertheless, a reliable check is provided by comparing results from computer calculations with those from Equation (1) for an elementary step in the exchange to assure consistency. In most cases, difficulties can be eliminated by cleanly defining the rate constant for departures of nuclei from a given site.

1.15.2.2 Magnetization Transfer and Rates

An alternative to line-shape analysis is the determination of rate constants via spin saturation transfer (SST).[19,37–39] The simplest experiment involves irradiating the resonance of a site that is slowly exchanging with another ($k \sim 0.1$–1 s^{-1}). If sufficient power is used to saturate the resonance, the intensity of the other site will decrease in a manner that

depends on the rate constants and the relaxation time of that site. For multiple sites, analysis of the relative intensities of the sites involves analysis of the magnetization entering or leaving a particular site (Equation (2)).

$$\frac{dM_z^A}{dt} = \frac{M_0^A - M_z^A}{T_{1A}} - k_{A-other}M_z^A + k_{BA}M_z^B + k_{CA}M_z^C + \cdots \quad (2)$$

The first term accounts for normal relaxation at the site in the absence of external irradiation which describes the return to the original magnetization at site A, $M_0{}^A$. The second term accounts for magnetization leaving site A and going to other sites. The subsequent terms describe magnetization arriving at site A from other sites. With saturation of a resonance of another site, the magnetization at that site will be zero and $M_z{}^A$ will decrease from $M_0{}^A$ to a constant value at which time the derivative will be zero, and a steady state of magnetization at site A will be observed. This value will represent the consequence of the attempt of the system to return $M_z{}^A$ to $M_0{}^A$ via relaxation, the loss of magnetization owing to transfer to other sites, and gain of magnetization owing to transfer into the site from other sites. This equation and analogous ones for other sites allow determination of the rate constants. If one follows the approach to equilibrium after applying the saturating r.f. or (less easily) the return to M_0 after removing it, one can evaluate the relaxation times as well. Generally, the values of the individual relaxation times can be determined independently via the usual 180°–τ–90° pulse sequence. One should note that if exchange also occurs, the measured relaxation time is a composite of both exchange and T_1. (In fact, in this experiment, cross-relaxation can yield a different value for T_1 from that in a soft pulse experiment.) Although the relaxation times would be expected to vary with temperature somewhat, it is generally useful to measure the T_1's at a lower temperature where site exchange is insignificant to determine the relative magnitudes of T_1 for each site. Measurement of T_1 from selective inversion of an individual resonance and comparing it to that of T_1 from the usual inversion of all resonances can give an estimate of the dipolar relaxation contribution. The nuclear Overhauser effects can also be measured at a lower temperature to see if cross-relaxation will be significant. One needs the values at the temperature at which the experiment is carried out, but the lower temperature results will indicate potential problems. Equation (2) does not take account of the cross-relaxations from dipolar effects which give rise to the Overhauser effect, and this can lead to significant errors at slow rates of site exchange. Thus, although SST experiments allow extension of rate determinations for systems where line broadening is too small to be useful, there are potential problems in the rate determination owing to cross-relaxation. Therefore, it is often useful to carry out the SST experiment when some broadening is present in order to minimize the contribution of cross-relaxation. This also has the advantage of providing a determination of $k_{A\ -\ other}$ using Equation (1). The important point to be recognized here is that cross-relaxation can cause significant errors in rate constant determinations, particularly at slower rates of exchange. If cross-relaxation is significant and it is ignored, then determination of activation parameters from variation in temperature will not yield either the correct slope or the intercept, and a pronounced systematic error will be produced in the values of $\Delta H^{\ddagger}$ and $\Delta S^{\ddagger}$. Methods of evaluation of relaxation effects can be found in several reviews.[22,24,40]

An alternative is the use of soft pulse techniques which invert the magnetization at one site and then follow the evolution of magnetization at frequent time intervals thereafter. This approach is currently known as spin inversion transfer (SIT) or multisite magnetization transfer (MMT).[13,20–22] This approach is probably the most informative with regard to elucidation of pathways in multi-site exchanges, which involve sequential migrations between sites. It has similar problems with respect to cross-relaxation and is also best carried out when exchange is fast compared to cross-relaxation. The determination of individual rates has been discussed in several reviews.[13,22,41] For more complex cases, recasting Equation (2) in terms of the magnetization in each site as elements of a vector and a relaxation matrix and considering terms involving $M_0 - M_z$ rather than M_z is done. Using the difference avoids problems with superposition of a resonance being superimposed on resonances from impurities or non-exchanging nuclei.

These SIT or MMT methods are particularly useful for determining pathways of rearrangement and are useful in the slow exchange region. Although not used extensively for small molecules, there are methods that are appropriate for determining very fast rates after the coalescence and narrowing of resonances. The measurement of the spin-lattice relaxation times or rates in the rotating frame, $T_{1\rho}$ or $R_{1\rho}$, allows the calculation of fast exchange rates.[42–47]

1.15.2.3 2D DNMR Methods

Assignment of NMR based on proximity of nuclei often uses the 2D NMR method known as nuclear Overhauser effect spectroscopy (NOESY). The pulse sequence involves a 90° pulse followed by a delay, which is incremented to provide the second dimension, a second 90° pulse followed by a mixing time, τ_m, and a final 90° pulse followed by

collection of the free induction decay. The mixing time is a delay which allows the NOE to build up. Cross-peaks are observed in the 2D spectra where a significant NOE is induced between nearby nuclei. When site exchange occurs during the mixing time, cross-peaks are also observed between sites involved in the exchange. An experiment which is designed to observe the exchange uses the same pulse sequence as the NOESY experiment but one which alters the mixing time to optimize the correlations from exchange is known as EXSY. NOESY spectra are often plotted using magnitude mode, which takes the square root of the sum of the squares of the imaginary and real components of the transformed spectra. This removes the phase information and produces all positive peaks. If this is done, one cannot distinguish cross-peaks arising from NOE versus those from exchange. Retaining the phase information allows one to distinguish them with positive peaks corresponding to exchange and negative peaks corresponding to NOE. Nevertheless, if a cross-peak is affected by both, it could disappear. A prudent approach usually involves increasing the temperature until the exchange rate is fast relative to the cross-relaxation rate and adjusting the mixing time appropriately.

The actual rate constants can be determined by analyzing volumes of cross-peaks,[23,48] but 1D methods generally would appear to give more accurate results.[49,50] An alternative 2D method to NOESY, ROESY, can be useful with somewhat larger molecules and in special cases. The recent review by Bain[24] is particularly useful for information on the details of rate determination by newer methods.

1.15.3 Mechanism of Metal Migrations Around Rings

The first uses of NMR line-shape analysis were for the determination of rates of rearrangement. Comparison of line-shape differences for certain resonances, however, can provide information about mechanisms of rearrangement. In the classic case of $(\eta^5\text{-Cp})\text{Fe(CO)}_2(\eta^1\text{-Cp})$,[1] where this approach was first used for an organometallic rearrangement mechanism, an AA′BB′X spectrum was observed for the η^1-Cp ring. The observation that the A portion of the spectrum broadened differently than the B portion provided definitive evidence that the path involved a rearrangement in which the iron moved from one carbon to the immediately adjacent carbon, rather than randomly to other positions, or across the ring. Many examples for different migrations of metals about ring systems have followed.[15,51,52] The compounds which exhibited migration around the rings were originally called "ring whizzers", but "haptotropic" or "metallotropic" rearrangements appear to be currently accepted jargon. Reference to the recent review by Minkin *et al.*[15] provides a comprehensive review of the literature up to 2003. An informative study of rearrangement mechanisms of several cycloheptatrienyl complexes was published in 2002 by Muhandiram *et al.*[53] This study illustrates the use of various DNMR methods. A 1,2-shift was shown to be the mode of rearrangement in $(\eta^3\text{-}C_7H_7)\text{Re(CO)}_4$ using primarily SIT (MMT),[53] but this system serves to indicate the way the various methods could be used (Scheme 1). If one considers the environments of nuclei after the shift, one will note that nuclei in A, B, and C sites all move to a different environment, whereas nuclei in one of the D sites remain in a D environment. Since line widths reflect the lifetime in a given environment (Equation (1)), the D resonance will not broaden as much as those for the B or C environments. Thus, the line shapes can be used to determine the mechanism of this using either ^{1}H or, more conveniently, ^{13}C NMR spectroscopy.[54]

If the A resonance is saturated in an SST experiment, the B resonance intensity will decrease more than that of the C resonance, and the D resonance will decrease the least (if all of the relaxation times are effectively the same).

The SIT experiment more dramatically shows the preference for a 1,2-shift. After the magnetization in site A is inverted, the intensities of the resonance for sites B, C, and D are initially the same. When $k_{AB} = 5\,s^{-1}$ at 224 K, the magnetization at B drops rapidly as the magnetization increases from negative to positive at A as a result of negative magnetization being transferred to B. The magnetization at B goes through a minimum after ~0.1 s. The magnetization at B is also being transferred to C, so that its magnetization also decreases with time and then returns to

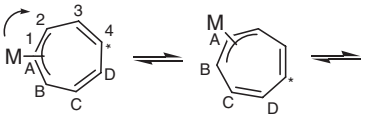

M = Re(CO)$_4$

1

Scheme 1

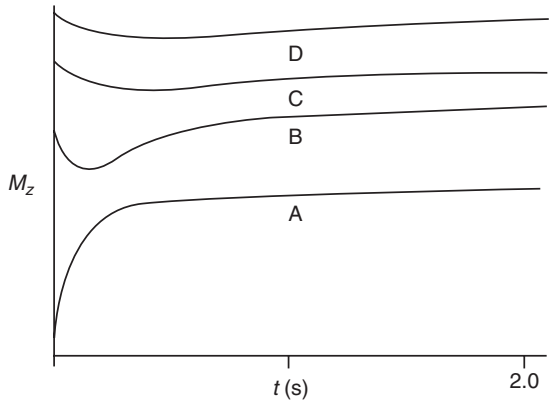

Figure 2 SIT experiment where magnetization is inverted at site A and then transferred to sites B, C, and D for a 1,2-shift in a compound like **1**.

equilibrium with the minimum for C occurring after that for B. A similar situation is also observed at D owing to magnetization transfer from C to D. These features are illustrated in Figure 2.

An analogous analysis showed that only 1,3-shifts occur in $(\eta^5\text{-}C_7H_7)Re(CO)_3$.[53] In contrast, a mixture of 1,2- and 1,3-shifts occurs in $(\eta^5\text{-}C_7H_7)Os(CO)_2SnPh_3$,[53] where the rates of the two processes are similar, and yield $k_{12} = 5.5\,s^{-1}$ and $k_{13} = 7.9\,s^{-1}$ at 10 °C. In this case, the other methods would also show this superposition of two processes. SST, however, is significantly better when there is a significant difference between the two rates. This generally would be observed as a deviation in observed and calculated magnetizations as a function of time after the initial inversion pulse of one resonance in least-squares analysis, if only one process was assumed. A difference of a factor of three is not immediately obvious, but can be detected with careful analysis. Reference to the examples in the paper by Takats and co-workers is recommended for an in-depth analysis.[53]

1.15.4 Inter-Ring Metal Migrations

Metal migration is not restricted to a single ring, and there has been considerable interest in inter-ring haptotropic shifts.[14,55] Often the barriers are over 125 kJ mol^{-1}, so that conventional NMR rather than DNMR studies are used to measure rates in these cases; nevertheless, there are a number of cases where DNMR studies have been effective.

Inter-ring shifts ($\Delta G^{\ddagger} \sim 85$ kJ mol^{-1}) as well as intra-ring shifts ($\Delta G^{\ddagger} \sim 35$ kJ mol^{-1}) have been observed for nickel complexes of anthracene (Scheme 2).[56]

Inter-ring shifts have also been studied using line-shape analysis of ^{13}C NMR in palladium phenylene derivatives (Scheme 3).[57,58]

Values for $\Delta G^{\ddagger}$ of 89.5 kJ mol^{-1}, $\Delta^{\ddagger}$ of 87.4 kJ mol^{-1}, and $\Delta S^{\ddagger}$ of -5.4 J K^{-1} were determined (90 °C). The value of $\Delta S^{\ddagger}$ was $\sim$0 J K^{-1}, as is often observed for rearrangements of neutral compounds, but not necessarily for ionic compounds with significant ion pairing.

Although DNMR provides information on the site exchange information and some aspects of the mechanism, one must often rely on theory to provide details of the path. Fortunately, modern DFT methods are now available to provide the details with some confidence. In the case of inter-ring dynamics, there are questions regarding whether

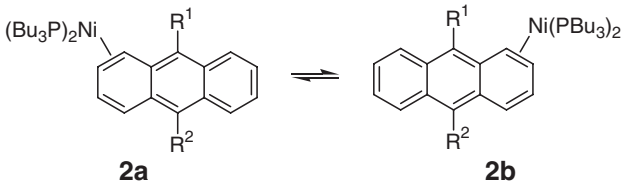

2a **2b**

Scheme 2

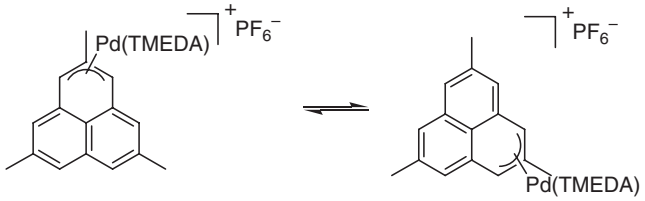

Scheme 3

the fluxionality takes place through direct movement from one ring to the next across the bond joining them, cruising around the inner edge like ring whizzers, or making excursions toward the outer edge of the ring to give exocyclic intermediates (Scheme 4).[55,57,59]

Another system which has undergone extensive investigation is the fluorenylchromium anions. This further illustrates the importance of ion pairing in the observed rates of rearrangement in ionic species.[14,60] In THF solution, there is significant ion pairing and there is a large negative entropy of activation ($\Delta H^{\ddagger} = 65.6\,\mathrm{kJ\,mol^{-1}}$; $\Delta S^{\ddagger} = -81.9\,\mathrm{J\,K^{-1}}$), whereas in the presence of a crown ether, there is a near-zero entropy of activation ($\Delta H^{\ddagger} = 89.0\,\mathrm{J\ mol^{-1}}$; $\Delta S^{\ddagger} = 0.8\,\mathrm{J\,K^{-1}}$). This has been attributed to the ion binding on top of the five-membered ring in **5** and to the carbonyl in **6**, but the ions being separated in the presence of the crown ether (Scheme 5).

An inter-ring η^5–η^5-haptotropic shift of an $Mn(CO)_3$ fragment in an anionic dibenzopentalene has also been observed in the interconversion of **7** and **8** using line-shape analysis of the methyl resonances (Scheme 6).[61] Reference to the review of Oprunenko[14] is recommended for a comprehensive treatment of intra-ring haptotropic rearrangements.

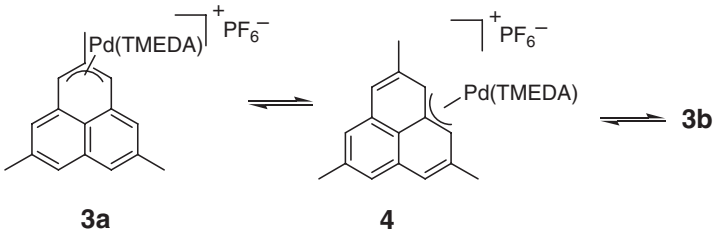

Scheme 4

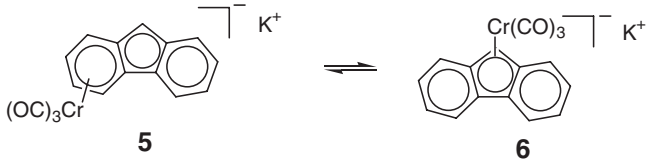

Scheme 5

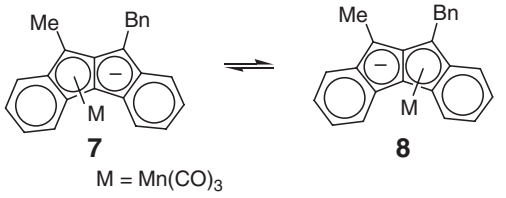

Scheme 6

1.15.5 Conformational Interconversions in Metal Complexes with Cycloalkenyl Rings

In the rearrangements of the cycloheptatrienyl complexes discussed above, the mechanism of the metal moving about the ring was the focus of the attention. One must also consider that conformations of the ring relative to the other ligands on the metal can exist. Although $(\eta^5\text{-}C_7H_7)Os(CO)_2SnPh_3$ exists predominantly as a single symmetrical isomer, the ruthenium analog[53] exists as a symmetrical conformer and two enantiomers of an unsymmetrical conformer. Magnetization transfer in the range of 178–183 K showed only transfer to analogous or equivalent positions in the other isomers, but no significant rate of migration around the ring. In the unsymmetrical isomer, the protons in the ring are diastereotopic. Equal magnetization transfer from site 3 in **9s** to 3′ and 3″ in **9a** or **9a** with minima was observed at equal times after inversion of site 3; however, inversion of site 3′ produced a faster drop in the magnetization at site 3 in **9s** and an earlier minimum than observed for 3″. This shows that racemization of **9a** occurs predominantly via conversion into **9s** rather than direct interconversion of **9a** to **9a**′. Detailed analysis showed that the rate constant for conversion of **9a** into **9s** is ~40 times larger than that for **9a** into **9a**′ (Scheme 7).

1.15.6 Restricted Rotation of η^1-Rings

Bagioni *et al.* noted that the ^{31}P NMR of $(\eta^1\text{-fluorenyl})Mn(CO)_3[P(Et)_3]_2$, **10**, had non-equivalent phosphines,[62] suggesting a stable unsymmetrical conformer. McGlinchey and co-workers observed a similar situation with a cpp analog, **11**.[63]

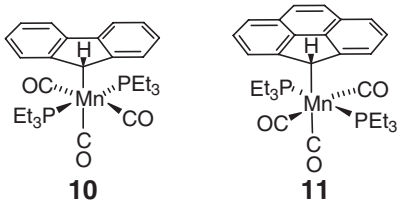

Although one might consider line-shape analysis, decomposition of **11** above 60 °C prevented this over a wide temperature range. The ^1H NMR of the ring protons is diastereotopic and overlapped, but the methane hydrogen on the carbon attached to manganese retains its coupling to phosphorus in the temperatures up to decomposition, indicating that intermolecular exchange of phosphines is not occurring rapidly (see below). The ^1H NMR is fairly well resolved at 30 °C, but shows slight broadening, which suggests a barrier ~70 kJ mol^{-1} (Table 1). The ^{31}P spectra showed a 461 Hz chemical separation at 300 MHz, indicating that an averaged ^{31}P resonance would not be observed before decomposition. The magnetization transfer methods are thus ideal for observing exchange and measuring rates in situations where raising the temperature to use complete line-shape analysis is precluded by decomposition/stability considerations.

Two 2D EXSY spectra for **11** are illustrated in Figure 3. Note that a mixing time of 25 ms is insufficient to allow enough magnetization transfer to occur to observe cross-peaks; however, a τ_m of 50 ms clearly shows the cross-peaks between the methylenes and methyls in the different environments.

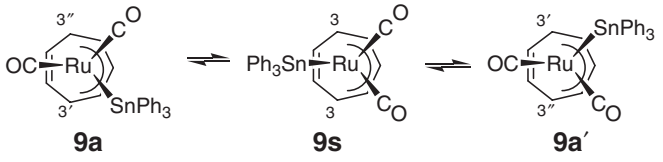

Scheme 7

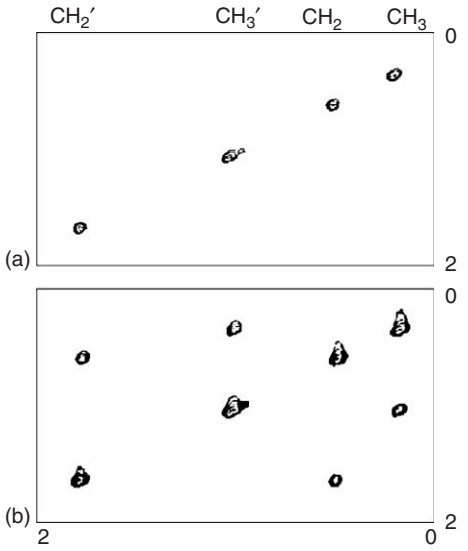

Figure 3 EXSY spectra for **11**: (a) τ_m of 25 ms; (b) τ_m of 50 ms.

1.15.7 Tripodal Rotations of η^5-Cyclopentadienyl, η^6-Arene, and Similar Ligands

Although rotations of η^5-cyclopentadienyl ligands usually involve barriers less than 20 kJ mol^{-1}, suitable substitutions on the rings and metal can increase the barriers to sufficient magnitude to be measured by DNMR. McGlinchey has been very active in this area, and reference to his reviews is recommended.[26,27,64] The fluxionality of the tripodal rotation of the Fe(CO)(L)(R) group in **12** has a barrier of 38 kJ mol^{-1} (Scheme 8). A higher barrier process inverts the configuration of the helical conformation of the phenyl groups between *M* and *P*. With unsymmetrical substitution of the ring, different rotamers can be observed in complexes such as **13** at low temperature (Scheme 9).[65]

A high degree of substitution is not necessarily required, as hindered rotation has been observed in *para*-substituted arenes. For example, in (1,4-C_6H_4–Pr^i_2)Fe(CO)($SiCl_3$)$_2$, **14**, there are two arene proton resonances observed at −120 °C, indicative of hindered rotation. At −40 °C, they coalesce into a singlet reflecting a barrier of 11 kcal mol^{-1}.[66] *p*-Cymene is frequently used with ruthenium complexes owing to the ready availability of [(1,4-C_6H_4–Me,Pr^i)$RuCl_2$]$_2$. Hindered rotation of the arene has been observed in a number of (*p*-cymene)Ru complexes. It is particularly important to recognize this possibility because hindered rotation of the ring produces diastereomers related to arene orientation that might be mistaken for diastereomers arising from different configurations at the chiral metal center.[67]

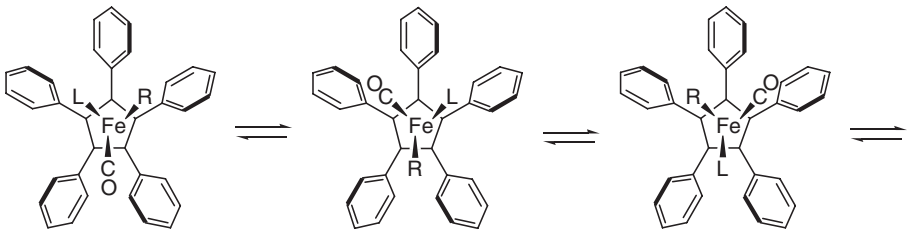

(*M*)-**12a** (*M*)-**12b** (*M*)-**12c**

Scheme 8

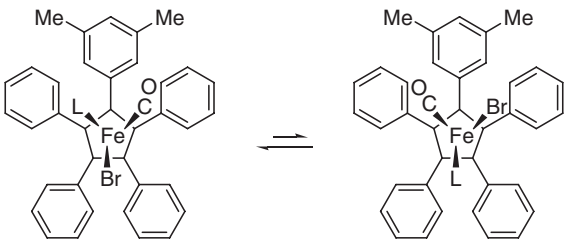

13a
Major

13b
Minor

Scheme 9

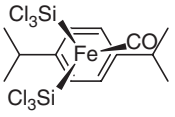

14

1.15.8 Pseudo-Rotations of η^4-Dienes and η^3-Allyls

The stereodynamics of η^4-diene and η^3-allyl complexes are likely to be of importance in understanding their reactivity, as these complexes are used in many synthetic strategies.[68,69] Although an η^3-cyclopropenyl may be considered to rotate about a metal-centroid axis, rearrangements of conformers in η^4-diene complexes, such as **15** and **16** (Schemes 10 and 11), may be considered as motions involving a pseudo-rotation of a five-coordinate or seven-coordinate metal complex with a bidentate diene. [70–74] This can account for presence of an allyl rotation in **17** (Scheme 12), but absence of it in **18**, where **18** can be considered as based on a non-fluxional tetrahedron or octahedron. A theoretical analysis of the allyl fluxionality in **17** and **18** has recently been published.[75] Formation of an η^1-allyl allows an alternative to rotation for interconversion of *exo*- and *endo*-isomers and characterized by interchange of *syn*- and *anti*-protons. This is a well-documented process which is particularly important in asymmetric catalysis using Pd allyls (Scheme 13).[12,16,76,77]

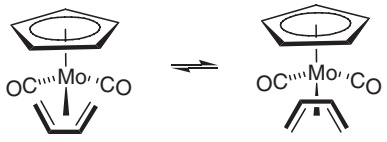

endo-**15a** *exo*-**15b**

Scheme 10

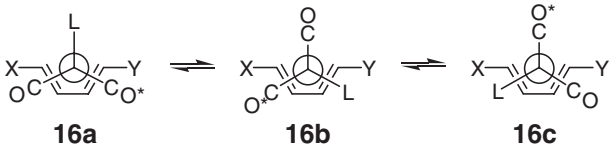

16a **16b** **16c**

Scheme 11

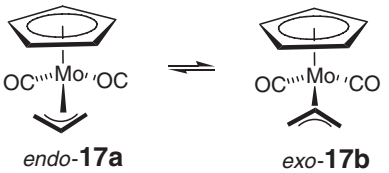

Scheme 12

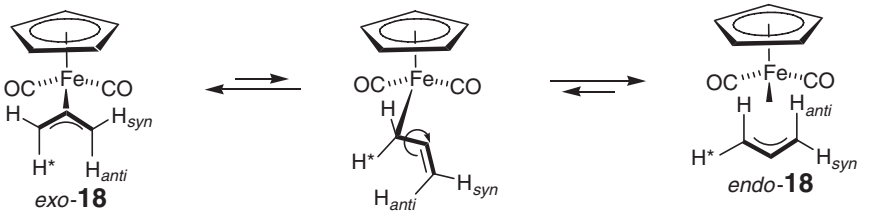

Scheme 13

1.15.9 Olefin Interconversions

Some of the earliest DNMR observed for organometallics involved the planar rotation of olefins.[33,34] This process effectively involves a rotation about an axis from the metal to the midpoint of an η^2-alkene and is sometimes called a propeller rotation. In unsymmetrical metal complexes, there is the possibility of several conformers based on orientations of the olefin. This can generally be attributed to differing donor properties of non-equivalent *d*-orbitals on the metal created by the other ligands.[78,79] The faces of many substituted olefins are enantiotopic, and binding to the metal produces enantiomers or diastereomers.[80] Notably, the chirality of the olefin–metal moiety is not changed by rotation of the olefin. The conformations of olefins in organometallics and their interconversions can be an important factor in regio- and stereocontrol in mechanisms of insertions of other ligands and in polymerizations.[81–84] The potential for interconversion of enantiotopic faces of olefins is particularly important in asymmetric catalysis and control of stereochemistry of reactions. The potential for epimerization of an olefin–metal moiety, such as that shown in **19**, however, exists (Scheme 14).

Although intramolecular olefin rotation is quite common, it does not provide a path for inversion of stereochemistry. Inversion usually occurs via dissociation of the olefin. Generally, one expects the metal to be restricted to one side of the ring; however, the results observed by Gladysz[85] for olefins and Harman[86,87] with aromatics indicate that there is a real possibility of migration to the opposite face via an agostic C–H intermediate. This has been termed an "end-run" or "flip" of the olefin, and has been implicated in olefin derivatives of zirconocene involved in polymerizations.[84,88]

Both olefin rotation and acetylene have been extensively studied, and reviews cover many of the details.[10,12,16] Some significant recent observations will be briefly mentioned. Early observations suggested that fluorinated olefins had high barriers to rotation, which seems to be generally true, but some compounds have shown low barriers for their rotation.[89,90] Correlations of propeller rotation barriers with electronic factors, carbonyl stretches, andRh NMR[103] have been observed, which argue for a strong electronic component defining the barriers to rotation.[91,92] Studies of olefin rotation rates in a series of $CpFe(CO)_2[\eta^2\text{-}CH_2C(H)NH(p\text{-}C_6H_4X)]$ showed that increasing electron donation from the aniline moiety facilitated olefin bond rotation.[93]

Several other processes can occur with different barriers, giving sequential or simultaneous averaging in the DNMR spectra. An instructive example is $[Ir(^{13}CO)(diphos)(ethylene)_2]^+$, **20**, which has been studied by ^1H, ^{13}C,

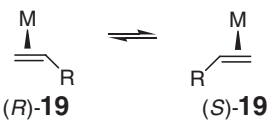

Scheme 14

and ^{31}P DNMR.[94] At the slow exchange limit (−90 °C), four ethylene proton resonances are observed. Upon raising the temperature, a propeller rotation in the trigonal-bipyramidal complex averages two environments to yield an AA′BB′ pattern in the $^{1}H\{^{31}P\}$ spectrum. A second dynamic process averages the ^{31}P resonances in the ^{31}P NMR leading to coalescence at −10 °C. Similarly, the ^{31}P–^{13}C coupling in the ^{13}C NMR averages, and the ^{1}H NMR also shows averaging of the non-equivalent protons for the diphos backbone ($\Delta G^{\ddagger} \sim 46\,kJ\,mol^{-1}$). This can be attributed to a pseudo-rotation of the trigonal-bipyramidal structure. At higher temperatures, exchange with free ethylene occurs.

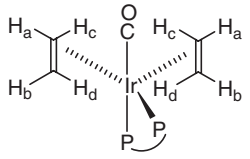

20

1.15.10 Apparent Rotations and Hemilability

As discussed above, the rotation of a (1,3-diene)$Fe(CO)_3$ complex may be considered as a pseudo-rotation of a five-coordinate iron complex. There are situations where DNMR spectra are observed for 1,5-diene complexes. If five-coordinate complexes are involved, these may also be viewed as pseudo-rotations; however, rotation in four-coordinate 1,5-cyclooctadiene complexes, **21**, is not expected (Scheme 15).

Intermolecular ligand exchange can give the impression that the ligand has rotated, as is often observed when X = halide and Y = phosphine. Equilibria with a $[CODIrY]_2$ dimer formed via dissociation of the X ligand often provide a pathway. A second-order path via attack on iridium to form a fluxional five-coordinate intermediate may also provide a route for interconversion of **21a** and **21b**. Intramolecular routes can also be observed if the XY donor combination is a hemilabile ligand, **22** (Scheme 16).

The detection of hemilability is rather difficult. With complete dissociation of a phosphine ligand, coupling of other ligands to the ^{31}P is averaged because after dissociation of a ^{31}P with spin +1/2, a ^{31}P with spin −1/2 can return, and this averages the components of the doublet arising from coupling to ^{31}P. If the ^{31}P is tethered in a hemilabile ligand and the ^{31}P with the same spin returns, the frequency of the resonance would not change; hence, the coupled nucleus would not be affected, if only a small fraction of the species with the unbound tethered ligand were present.

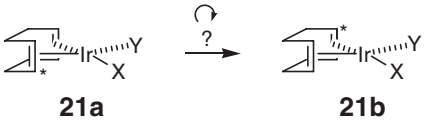

21a **21b**

Scheme 15

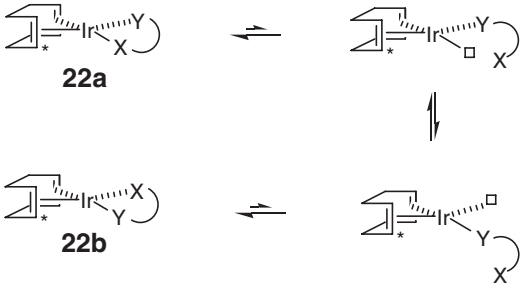

22a

22b

Scheme 16

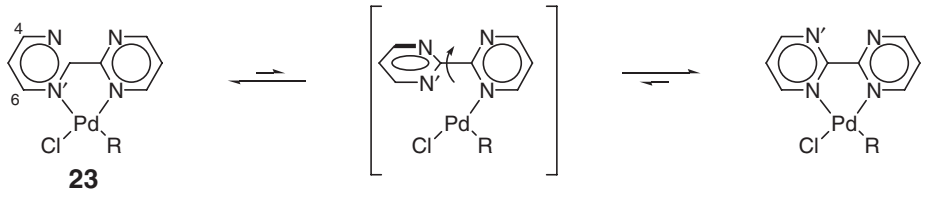

23

Scheme 17

One approach to detecting hemilability is to provide an alternative donor within the ligand. The 2,2′-bipyrimidyl ligand **23** is useful in this regard (Scheme 17).[95] Interconversion of the H4 and H6 is indicative of the Pd–N bond rupture. This approach for detection of Pd–N bond rupture has also been used for pyrazolylpyrimidines and trisubstituted triazines.[96–101]

Dimethylamino groups also provide a convenient probe of hemilability.[102] If the metal–nitrogen bond ruptures, rapid pyramidal inversion at the nitrogen interchanges the methyl groups, and their environments are interchanged upon reforming the M–N bond. The "apparent" rotation of the ligands in (η^3-$C_{10}H_{15}$)Pd(TMEDA) **24** in the presence of chloride was investigated using EXSY spectra.[95] The methyl groups were assigned using NOE experiments. At −15 °C, exchange of the methyl groups on the same nitrogen occurred rapidly. This shows that the chloride can promote Pd–N bond rupture, and is consistent with the formation of a four-coordinate arm-off TMEDA complex.

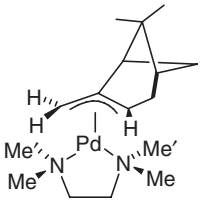

24

The "apparent" rotation of the ligands in (η^3-$C_{10}H_{15}$)Pd(Me_2NCH_2py) **25** was also investigated using EXSY (Scheme 18).[103] The important features are that: (i) *N*-methyl groups exchange between isomers, "but not within a given isomer" and (ii) the *anti*-protons of the allyl exchange between isomers, but not with the *syn*-protons. This requires that the Pd–NMe_2 bond is not ruptured. The observation can be accommodated by: (i) rupture of the py–N–Pd bond, (ii) rotation about the Pd–*N*(Me_2) bond, (iii) isomerization within the T-shaped intermediate and (iv) reformation of the py–N–Pd bond. It can also be accommodated by a rupture of the more substituted Pd–allyl bond and rearrangement of the T-shaped intermediate. Ultimately, this experiment shows that neither the Pd–CH_2 nor Pd–NMe_2 is broken in the process.

Cationic phosphine methylplatinum(II) complexes containing 2,9-dimethyl–1,10-phenanthroline (dmphen) exhibit fluxionality owing to hemilability of the dmphen (**26**, Scheme 19).[104] Apparently, this is the route involved with some counterions, but others, such as Cl^-, involve nucleophilic attack to form a five-coordinate intermediate, which could rearrange via either a κ^1- or a κ^2-intermediate. One should note that **26** is not planar and the rings make a significant

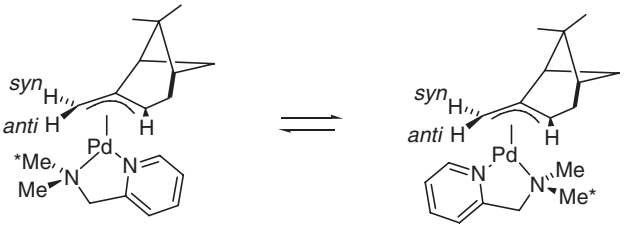

25

Scheme 18

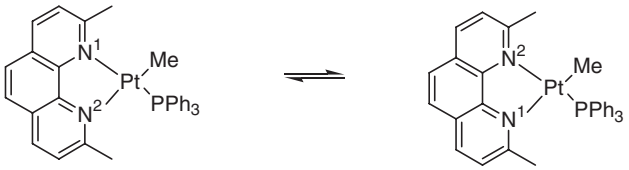

26

Scheme 19

angle relative to the Pt square plane. This feature makes the molecules chiral, so that enantiomers are also interconverted via a fluxional process, although these particular experiments could not detect racemization.

1.15.11 Carbene Rotation

The symmetry of the *p*-orbital in a carbene ligand is analogous to that of a π^*-orbital of an alkene and consequently, similar orientation effects are expected for carbene complexes as found in alkene complexes[78] in electronically asymmetric complexes. Typical examples of conformational isomerism are synclinal **27** and anticlinal **27**. The extensive studies of rotational barriers and conformational preferences by Brookhart[105] and Gladysz[106,107] provide leading references to earlier work. The conformational isomers control the stereochemistry of reactions of the carbene. Variations in ligands produce a significant variation in barriers to rotation in amido complexes, such as TpMo(=CHR)(NAr)(CH_3), **28**, and TpMo(=CHR)(NAr)(OTf), **29**.[108] Other arylamido complexes show correlations of rotational rates in alkylidenes with electron-donating ability of alkoxide substituents.[109] Other examples have been covered in reviews.[110,111]

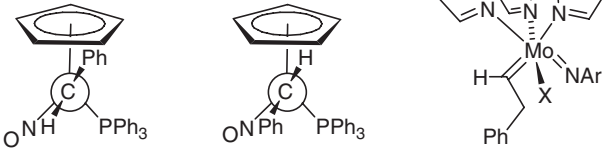

Synclinal **27** Anticlinal **27** **28**: X = Me **29**: X = OTf

Barriers to carbene rotation in *N*-heterocyclic carbenes (NHCs) appear to be dominated by steric interactions, and they have been observed in square-planar complexes using the diastereotopic protons in benzyl, butyl, and ethyl derivatives. For example, **30** shows diastereotopic methylenes owing to a lack of a mirror plane through the Ir–C(carbene) plane, and averaging of the methylene protons at higher temperatures indicates a 67 kcal mol^{-1} barrier to rotation.[112] Steric interactions influencing barriers have also been observed in other cases and allow observation of rotamers with unsymmetrically substituted NHCs or triazolinylidenes.[113–115]

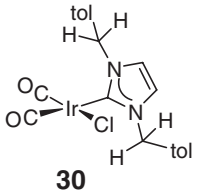

30

DNMR also reveals hindered rotations about single bonds in addition to rotation about the M=C bond in some conventional carbene complexes, such as **26**–**28**. Restricted rotation around the C–C bond between the *ipso*-carbon and the α-carbon in both Fe=CHAr and Ru=CHAr was observed with $\Delta G^{\ddagger} \sim 40$–$50$ kJ mol^{-1}.[106,116,117]

1.15.12 Hindered C–C, P–C, M–P, and M–C Rotation and Atropisomerism

Substituted biaryls can show sufficient restricted rotation about C–C bonds to allow the isolation of axially chiral complexes that do not racemize (atropisomers). In ligands based on atropisomers, such as BINAP **30**, the chirality of the backbone controls the chirality of the phenyl groups on the phosphines and produce chiral environment at the metal in asymmetric catalysts. In BIPHEP, **31**, the barrier for atropisomerization is not high enough to prevent racemization. The barrier can be measured by observing the exchange between diastereotopic nuclei in the phenyl groups.[118] This requires temperatures well above 30 °C and the rotation about the phenyl C–P bonds is rapid at this temperature. Separate resonances for the *ortho*-protons of the diastereotopic phenyl groups are observed. These resonances average at high temperature yielding a barrier of 105 kJ mol^{-1} for racemization of the biphenyl backbone. Once the BIPHEP is coordinated, the barrier for racemization is slowed further, and if the complex has been resolved, it can be used for catalysis.[119]

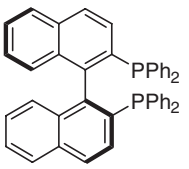

31

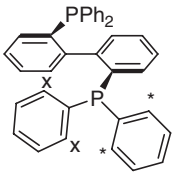

32

DNMR can also be observed associated with rotations about metal–P single bonds in ligands, as well as P–C bonds. These generally involve barriers significantly less than 60 kJ mol^{-1}. Bulky phosphines often show barriers ~40 kJ mol^{-1} for conformer interconversions involving M–P bonds. Effects from these restricted rotations are usually observed below room temperature, but they can be a nuisance if one is trying to observe other processes that occur at lower temperatures.[67] Under many circumstances, rotations about P–C and M–C bonds would occur rapidly enough that the resonances of the rotamers would be averaged; however, the use of higher field NMR spectrometers often results in incomplete averaging. Since the rate at which resonances will coalesce and sharpen depends on the reciprocal square of the chemical shift difference, higher fields yield many instances where M–P and P–C conformational effects are a source of broadening in spectra observed below 0 °C. Although such barriers are low, there have been extensive studies of hindered rotation in P–M bonds.[80,120–127] Generally, higher barriers involve phosphines containing bulky substituents, such as *t*-butyl, *o*-tolyl, and mesityl groups. Broad resonances can even be observed at room temperature in some cases, such as Pt(mesityl$_2$PH)$_2$(Et)(I).[124] With sufficient congestion, PPh_3 can show restricted rotation at low temperatures (~40 kJ mol^{-1}), for example, Cp*Ir(pz)$_2$(PPh_3)[127] and *trans*-[PtX(Me$_2$—phen–κ^1-*N*)-(PPh_3)$_2$]X.[128]

Restricted rotation about the P–C bonds in phosphine ligands also produces conformational isomers that lead to observations of DNMR spectra, usually below room temperature.[124,125,128–134]

Preferred conformations of phenyl groups attached to phosphorus can be induced by the chirality of the backbone with chiral ligands. Thus, idealized right- or left-handed propeller chirality can be observed, **33**. The hindered rotation of the axial phenyl group and its conformation was implicated in determining the high stereoselectivity of a BINAP catalyst enantioselective hydroformylation; furthermore, hindered phenyl rotation has been observed in several BINAP complexes.[135–137] In the simplest example, (BINAP)$PdCl_2$, non-equivalent *ortho*- and *meta*-^{1}H resonances of one phenyl group are near coalescence at 25 °C and only become sharp multiplets (at 400 MHz) on heating to 70 °C. [136] In addition to 180° rotations averaging *ortho*- and *meta*-^{1}H and -^{13}C resonances, there is the potential for partial rotations that would invert the propeller chirality that could average resonances of different rotamers or diastereomers.

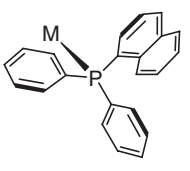

(*P*)-**33**

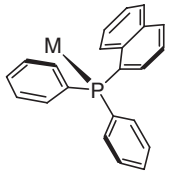

(*M*)-**33**

Hindered rotation of metal–aryl complexes can also produce atropisomerism,[138,139] and isomerism similar to that observed for restricted rotation of carbenes can be observed. For example, for **34**, a 57 : 43 ratio of rotamers (diastereomers) is observed.

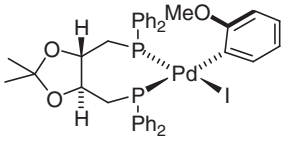

34a

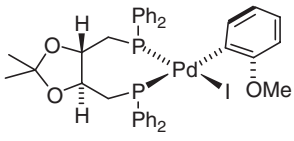

34b

More than one dynamic process can occur in many systems. Five different processes occurring over the $\Delta G^{\ddagger}$ range of 7.7–13.4 were observed for the triphenylphosphine/trimesityliridum(III) system.[140] This includes: (i) P–C rotation of one ring, (ii) P–C rotation of a different ring, (iii) racemization of the propeller chirality of the Ir(mesityl)$_3$ portion of the complex with PPh_3, (iv) PPh_3 dissociation, and (v) Ir–C complete rotation in the free Ir(mesityl).

The potential importance of many of these types of conformational interconversion may be found in the asymmetric olefin metathesis catalysts recently developed by Grubbs.[141,142] A key intermediate formed after loss of 3-bromopyridine or Cy_3P would have structure **35**. The orientation of the aromatic rings could be influenced by other substituents (R^1) on the *N*-heterocyclic carbine. Those rings would, in turn, select a preference of location of R^3 in the conformation of the alkylidene. Finally, the preferred orientation and reactivity of the olefin with substituents R^4 would serve to control regiochemistry and stereochemistry. Thus, the dynamics and conformational preferences of the types which have been discussed are crucial for the understanding of the reactivity of this system.

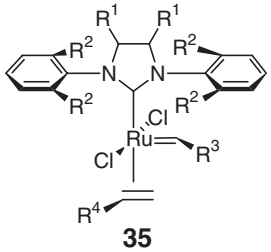

35

1.15.13 H Migrations

The making and breaking of C–H and M–H bonds are key steps in important metal-catalyzed reactions, such as hydrogenations, hydrosilylations, C–H activations, and Fischer–Tropsch reactions. Insertion of an alkene into a metal–hydride bond and the reverse, β-hydride elimination, are key steps in some of these processes (see Equation (3)). Occasionally, compounds exist as an agostic complex, which may be viewed as a key intermediate in these reaction paths. Brookhart has carried out extensive DNMR studies of these processes and agostic interactions.[143–146]

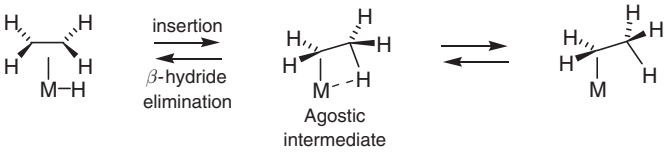

(3)

Hydride-to-olefin migrations were observed as early as 1971,[147] but there are more informative simple examples based on $[Cp^*Rh(L)(ethylene)(H)]^+$.[148–152] The stable structure is the ethylene hydride, and propeller rotation of the ethylene occurs with a barrier of ~40 kJ mol^{-1} in the complex with L = $(MeO)_3P$. This rotation averages the ^{13}C resonances of the ethylene, but since there is a stereogenic Rh center, the protons are diastereotopic and two sets average independently. At higher temperatures, however, the alkene protons average with the hydride, indicating a $\Delta G^{\ddagger}_{234} \sim 55$ kJ mol^{-1} for the insertion, which presumably proceeds via the agostic intermediate. When L is another alkene rather than a phosphine or phosphite in $[Cp^*Rh(L)(ethylene)(H)]^+$, the agostic complex is the stable form.

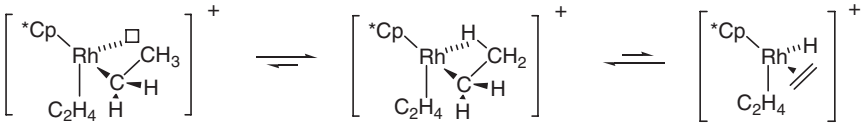

36b **36a** **36c**

Scheme 20

Thus, $[Cp^*Rh(ethylene)_2H]^+$, **36c**, where propeller rotation of the olefin which averages the termini can occur, is a transition state or intermediate in the fluxionality exhibited by $[Cp^*Rh(ethylene)(CH_2CH_2\text{–}\mu\text{-}H)]^+$, **36a**. An in-place rotation of the methyl group in **36a** could occur or conversion to a normal ethyl group **36b** would allow rapid rotation of the methyl and averaging of all of the methyl protons (Scheme 20).[151] More recent SIT studies have investigated similar processes in $(Me_3P)_3Co(ethylene)H$.[153]

Analogous situations exist with allyl hydrides and propene complexes, agostic propene, propene hydrides, and isopropyl complexes.[36,149] Exchange of hydride with methylene carbene is relevant to the Fischer–Tropsch reaction, and one of the early uses of SIT was used in studies of this exchange.[154,155] Recent studies of bimetallic systems that involve interchange of hydride with the hydrogen of a methylene have also been studied by DNMR.[156,157]

There has been intense interest in recent years in another area involving metal hydrides that concerns DNMR arising from exchange of nuclei in complexes containing both hydride and dihydrogen ligands.[40,158–160] The first example of this was reported by Crabtree[161] for $[(benzoquinolyl)(PPh_3)_2Ir(H_2)(H)]^+$. In most cases, it appears that the mechanism involves the formation of a very low concentration intermediate of trihydride. These studies can be complicated by factors other than those encountered in earlier discussions. The short H–H bonds in the dihydrogen complexes give rise to short T_1 relaxation times from dipolar effects. This can cause difficulties in spin saturation transfer experiments and in T_1 determinations; also, exchange with hydrides (SIT) can artificially lengthen the observed T_1 of the dihydrogen and shorten that of the hydride. Sometimes, trihydride species can also give rise to quantum mechanical exchange phenomena which produce incredibly large couplings between the hydrogen nuclei.[162–164]

1.15.14 CSA and Apparent DNMR

There can be a number of surprises in the binding of ligands and a situation that is increasingly observed is that of the metal bonding to the arene rings in BIPHEP and BINAP ligands, as well as triphenylphosphine. Although this feature is now well recognized, a bizarre binding in the phenyl-substituted tris(3-*tert*-butylpyrazolyl)borato complex $[PhTp(Bu^t)]Tl$ is observed where the Tl interacts with the nitrogen attached directly to the boron via a *p*-orbital component of the aromatic π-system of the pyrazolyl. This molecule is non-rigid, and at low temperatures one can observe two isomers.[165]

In contrast, in other substituted pyrazolylborates that are bound in the normal κ^3-*N,N,N*-mode, one would not expect non-rigidity in a Tl complex. Nevertheless, one observes temperature dependence in the shape of the resonances of nuclei coupled to Tl.[205] At first, this might be interpreted as intermolecular exchange; however, the rate of change with temperature is unusual and the initial broadening region is field dependent (note that Equation (1) has no field dependence). The broadening and averaging which increase with field (actually the square of the field) arise from averaging of the lines associated with Tl(+1/2) and Tl(−1/2) spins owing to relaxation of Tl nuclei from chemical shift anisotropy effects.[166]

Another situation where this arises is in platinum complexes where CSA causes the Pt satellites[195] to average, whereas resonances attached to Pt ($I = 0$) remain sharp.[167] A different case where some lines broaden and others stay sharp, but which does not involve CSA, is the appearance of spectra in which nuclei are coupled to ^{31}P, and there is an intramolecular exchange of phosphines.[168] In this situation, exchange of $P^A(\alpha)$ with $P^B(\alpha)$ results in no net change in effective field or frequency for nuclei in the complex coupled to them. However, exchange of $P^A(\alpha)$ with $P^B(\beta)$ does result in a frequency change, and these resonances will broaden and coalesce with those associated with $P^A(\beta)$ with $P^B(\alpha)$ Hence, within a doublet of doublets, two of the resonances will broaden and two will remain sharp. Either the inner or outer lines will average, depending on the relative signs of the coupling constants.

1.15.15 A Brief Survey of Leading References on DNMR in Other Systems

Many of the topics covered in this summary of DNMR studies were chosen owing to their relevance to selectivity in catalysis. In the space available for this article, there were a number of areas that have been studied extensively, but could not be covered in detail. Leading references for some of these areas follow. Fluxionality is generally associated with five- and seven-coordinate complexes; however, there are a number of six-coordinate complexes that show DNMR.[169–174] Some formally square four-coordinate structures are also fluxional.[168] Rearrangement of metal clusters and carbonyls which are bound to them have also been studied extensively.[175–178] DNMR is not limited to solutions and can also be studied in solid materials.[179] DNMR has also been observed with supramolecular complexes.[23] Calixarene complexes based on Ir(I) and Rh(I) complexes also show dynamic motions associated with encapsulation of other molecules.[180] Although not an organometallic, a study of ring inversion in Fe(III) porphyrins provides a particularly well-documented discussion of the methodologies that can be applied to DNMR.[181]

1.15.16 Comments and Conclusions

The following comments represent the opinions of this author on the use of DNMR. The most accurate rates can be determined by analysis of line shapes, particularly in the region before coalescence. Pathways are best determined using SIT methods, whereas EXSY methods provide a convenient presentation for demonstrating which sites interchange. When any of these methods are used to evaluate activation parameters other than $\Delta G^{\ddagger}$ from variations of rates with temperature, there is a strong possibility of systematic errors. Owing to variations of chemical shifts with temperature in line-shape analysis and the differing importance of cross-relaxation in SST, SIT, or MMT experiments at different rates, there can be significant errors in the evaluation of $\Delta S^{\ddagger}$. If $\Delta S^{\ddagger}$ differs significantly from zero for an intramolecular process in a neutral compound, it is probably more prudent to check for experimental errors, before rationalizing the result. In most cases, evaluating $\Delta G^{\ddagger}$ from initial line broadening and Equation (1) will provide a reliable value and may well be sufficient for most applications.

References

1. Bennett, M. J.; Cotton, F. A.; Davison, A.; Faller, J. W.; Lippard, S. J.; Morehouse, S. M. *J. Am. Chem. Soc.* **1966**, *88*, 4371–4376.
2. Cotton, F. A.; Faller, J. W.; Musco, A. *J. Am. Chem. Soc.* **1966**, *88*, 4506–4507.
3. Cotton, F. A.; Davison, A.; Faller, J. W. *J. Am. Chem. Soc.* **1966**, *88*, 4507–4509.
4. Bratton, W. K.; Cotton, F. A.; Davison, A.; Musco, A.; Faller, J. W. *Proc. Natl. Acad. Sci. USA* **1967**, *58*, 1324–1328.
5. Cotton, F. A.; Faller, J. W.; Musco, A. *Inorg. Chem.* **1967**, *6*, 179–182.
6. Faller, J. W.; Davison, A. *Inorg. Chem.* **1967**, *6*, 182–184.
7. Doering, W. E. V.; Roth, W. R. *Angew. Chem., Int. Ed.* **1963**, *75*, 27–30.
8. Cotton, F. A. *J. Organomet. Chem.* **1975**, *100*, 29–41.
9. Jackman, L. M.; Cotton, F. A. *Dynamic Nuclear Magnetic Resonance*; Academic Press: New York, 1975.
10. Mann, B. E. *Adv. Organomet. Chem* **1988**, *28*, 397–457.
11. Abel, E. W.; Orrell, K. G. In *Encyclopedia of Inorganic Chemistry*; King, R. B., Ed.; Wiley: New York, 1994; pp 2581–2615.
12. Faller, J. W. In *Encyclopedia of Inorganic Chemistry*; King, R. B., Ed.; Wiley: New York, 1994; pp 3914–3933.
13. Orrell, K. G. *Ann. Rep. NMR Spectroc.* **1999**, *37*, 1–74.
14. Oprunenko, Y. F. *Russ. Chem. Rev.* **2000**, *69*, 683–704.
15. Minkin, V. I.; Mikhailov, I. E.; Duchenko, G. A.; Zsunke, A. *Russ. Chem. Rev.* **2003**, *71*, 867–898.
16. Faller, J. W. In *Encyclopedia of Inorganic Chemistry*; King, R. B., Ed.; Wiley: New York, 2005 (in press).
17. Akitt, J.; Mann, B. E. *NMR and Chemistry*, 4th ed.; Stanley Thornes: Cheltenham, 2000.
18. Binsch, G.; Kessler, H. *Angew. Chem., Int. Ed.* **1980**, *19*, 411–428.
19. Faller, J. W. In *Determination of Organic Structures by Physical Methods*; Nachod, F. C., Zuckerman, J., Eds.; Academic Press: New York, 1973; Vol. V, p 75.
20. Dahlquist, F. W.; Longmuir, K. J.; Duvernet, R. B. *J. Magn. Reson.* **1975**, *17*, 406–410.
21. Alger, J. R.; Prestegard, J. H. *J. Magn. Reson.* **1977**, *27*, 137.
22. Muhandiram, D. R.; McClung, R. E. D. *J. Magn. Reson.* **1987**, *71*, 187–192.
23. Perrin, C. L.; Dwyer, T. J. *Chem. Rev.* **1990**, *90*, 935–967.
24. Bain, A. D. *Prog. Nucl. Magn. Reson. Spectrosc.* **2003**, *43*, 63–103.
25. Mao, F.; Philbin, C. E.; Weakley, T. J. R.; Tyler, D. R. *Organometallics* **1990**, *9*, 1510–1516.
26. Brydges, S.; Harrington, L. E.; McGlinchey, M. J. *Coord. Chem. Rev.* **2002**, *233*, 75–105.
27. McGlinchey, M. J. *Can. J. Chem.* **2001**, *79*, 1295–1309.
28. Budzelaar, P. H. M. *gNMR*; Adept Scientific: Bethesda, MD, USA, 1999.
29. Reich, H. J. *J. Chem. Educ.* **1995**, *72*, 1086.

29a. Reich, H. J. *J. Chem. Ed. Software* **1996**, *3D*(2).

30. Stephenson, D. S.; Binsch, G. *DNMR5: Iterative Nuclear Magnetic Resonance Program for Unsaturated Exchange Boradened Band Shapes Institue of Organic Chemistry, University of Munich, Munich, FRG, QCPE 365 (1978) and 569*.
31. Brown, J. H.; Bushweller, C. H. *QCPE Bulletin* **1983**, *3*, 103 (http://www.qcpe.chem.indiana.edu).
32. Sandstrom, J. *Dynamic NMR Spectroscopy*; Academic Press: New York, 1982.
33. Cramer, R. *J. Am. Chem. Soc.* **1964**, *86*, 217–222.
34. Cramer, R.; Kline, J. B.; Roberts, J. D. *J. Am. Chem. Soc.* **1969**, *91*, 2519–2524.
35. Bain, A. D.; Rex, D. M.; Smith, R. N. *Magn. Reson. Chem.* **2001**, *39*, 122–126.
36. Green, M. L. H.; Wong, L. L.; Sella, A. *Organometallics* **1992**, *11*, 2660–2668.
37. Hoffman, R. A.; Forsen, S. *Prog. Nucl. Magn. Reson. Spectrosc.* **1966**, *1*, 15.
38. Jarek, R. L.; Flesher, R. J.; Shin, S. K. *J. Chem. Educ.* **1997**, *74*, 978–982.
39. Morris, G. A.; Freeman, R. *J. Mag. Reson.* **1978**, *29*, 433–462.
40. Bakmutov, V. I. *Practical NMR Relaxation for Chemists*; Wiley: New York, 2005.
41. Grassi, M.; Mann, B. E.; Pickup, B. T.; Spencer, C. M. *J. Magn. Reson.* **1986**, *69*, 92–99.
42. Deverell, C.; Morgan, R. E.; Strange, J. H. *Mol. Phys.* **1970**, *18*, 553–557.
43. Massi, F.; Johnson, E.; Wang, C. Y.; Rance, M.; Palmer, A. G. *J. Am. Chem. Soc.* **2004**, *126*, 2247–2256.
44. Palmer, A. G. *Chem. Rev.* **2004**, *104*, 3623–3640.
45. Trott, O.; Palmer, A. G. *J. Magn. Res.* **2004**, *170*, 104–112.
46. Braun, S.; Kalinowski, H.-O.; Berger, S. *150 and More Basic NMR Experiments*; Wiley-VCH: New York, 1998; p 150.
47. Palmer, A. G.; Kroenke, C. D.; Loria, J. P. In *Methods in Enzymology, Pt B*; 2001; Vol. 339, pp 204–238.
48. Orrell, K. G.; Sik, V.; Stephenson, D. *Prog. Nucl. Magn. Reson. Spectrosc.* **1990**, *22*, 141–208.
49. Bain, A. D.; Cramer, J. A. *J. Magn. Reson. Ser. A* **1996**, *118*, 21–27.
50. Bain, A. D.; Cramer, J. A. *J. Phys. Chem.* **1993**, *97*, 2884–2887.
51. Jutzi, P. *Chem. Rev.* **1986**, *86*, 983–996.
52. Mann, B. E. *Chem. Soc. Rev.* **1986**, *15*, 167–187.
53. Muhandiram, D. R.; Kiel, G. Y.; Aarts, G. H. M.; Saez, I. M.; Reuvers, J. G. A.; Heinekey, D. M.; Graham, W. A. G.; Takats, J.; McClung, R. E. D. *Organometallics* **2002**, *21*, 2687–2704.
54. Heinekey, D. M. Ph. D. Dissertation, University of Alberta, 1982 (discussed in ref Mundiriham).
55. Albright, T. A.; Hofmann, P.; Hoffmann, R.; Lillya, C. P.; Dobosh, P. A. *J. Am. Chem. Soc.* **1983**, *105*, 3396–3411.
56. Stanger, A.; Weismann, H. *J. Organomet. Chem.* **1996**, *515*, 183–191.
57. Woell, J. B.; Boudjouk, P. *J. Organomet. Chem.* **1979**, *172*, C43–C46.
58. Nakasuji, K.; Yamaguchi, M.; Murata, I.; Nakanishi, H. *J. Am. Chem. Soc.* **1986**, *108*, 325–327.
59. Calhorda, M. J.; Goncalves, I. S.; Goodfellow, B. J.; Herdtweck, E.; Romao, C. C.; Royo, B.; Veiros, L. F. *New J. Chem.* **2002**, *26*, 1552–1558.
60. Ceccon, A.; Gambaro, A.; Agostini, G.; Venzo, A. *J. Organomet. Chem.* **1981**, *217*, 79–89.
61. Ustynyuk, Y. A.; Trifonova, O. I.; Oprunenko, Y. F.; Mstislavskiy, V. I.; Gloriozov, I. P.; Ustynyuk, N. A. *Organometallics* **1990**, *9*, 1707–1709.
62. Biagioni, R. N.; Lorkovic, I. M.; Skelton, J.; Hartung, J. B. *Organometallics* **1990**, *9*, 547–551.
63. Decken, A.; Rigby, S. S.; Girard, L.; Bain, A. D.; McGlinchey, M. J. *Organometallics* **1997**, *16*, 1308–1315.
64. McGlinchey, M. J. *Adv. Organomet. Chem.* **1992**, *34*, 285–325.
65. Li, L. J.; Decken, A.; Sayer, B. G.; McGlinchey, M. J.; Bregaint, P.; Thepot, J. Y.; Toupet, L.; Hamon, J. R.; Lapinte, C. *Organometallics* **1994**, *13*, 682–689.
66. Hansen, V. M.; Batchelor, R. J.; Einstein, F. W. B.; Male, J. L.; Pomeroy, R. K.; Zaworotko, M. J. *Organometallics* **1997**, *16*, 4875–4881.
67. Faller, J. W.; Parr, J.; Lavoie, A. R. *New J. Chem.* **2003**, *27*, 899–901.
68. Knolker, H.-J.; al, e. *Pure Appl. Chem.* **2001**, *73*, 1075–1086.
69. Trost, B. M.; Crawley, M. L. *Chem. Rev.* **2003**, *103*, 2921–2943.
70. Faller, J. W.; Rosan, A. M. *J. Am. Chem. Soc.* **1976**, *98*, 3388–3389.
71. Faller, J. W.; Rosan, A. M. *J. Am. Chem. Soc.* **1977**, *99*, 4858–4859.
72. Faller, J. W.; Incorvia, M. J. *J. Organomet. Chem.* **1969**, *19*, P13-P16.
73. Faller, J. W.; Murray, H. H.; White, D. L.; Chao, K. H. *Organometallics* **1983**, *2*, 400–409.
74. Howell, J. A. S.; Walton, G.; Tirvengadum, M. C.; Squibb, A. D.; Palin, M. G.; McArdle, P.; Cunningham, D.; Goldschmidt, Z.; Gottlieb, H.; Strul, G. *J. Organomet. Chem.* **1991**, *401*, 91–123.
75. Ariafard, A.; Bi, S.; Lin, Z. *Organometallics* **2005**, *24*, 2241–2244.
76. Mackenzie, P. B.; Whelan, J.; Bosnich, B. *J. Am. Chem. Soc.* **1985**, *107*, 2046–2054.
77. Faller, J. W.; Stokes-Huby, H. L.; Albrizzio, M. A. *Helv. Chim. Acta* **2001**, *84*, 3031–3042.
78. Schilling, B. E. R.; Hoffmann, R.; Faller, J. W. *J. Am. Chem. Soc.* **1979**, *101*, 592–598.
79. Gladysz, J. A.; Boone, B. J. *Angew. Chem., Int. Ed.* **1997**, *36*, 551–583.
80. Pu, J. Q.; Peng, T. S.; Mayne, C. L.; Arif, A. M.; Gladysz, J. A. *Organometallics* **1993**, *12*, 2686–2698.
81. Sillars, D. R.; Landis, C. R. *J. Am. Chem. Soc.* **2003**, *125*, 9894–9895.
82. Yoder, J. C.; Bercaw, J. E. *J. Am. Chem. Soc.* **2002**, *124*, 2548–2555.
83. Carpentier, J. F.; Maryin, V. P.; Luci, J.; Jordan, R. F. *J. Am. Chem. Soc.* **2001**, *123*, 898–909.
84. Prosenc, M. H.; Brintzinger, H. H. *Organometallics* **1997**, *16*, 3889–3894.
85. Peng, T. S.; Gladysz, J. A. *J. Am. Chem. Soc.* **1992**, *114*, 4174–4181.
86. Brooks, B. C.; Meiere, S. H.; Freidman, L. A.; Carrig, E. H.; Gunnoe, T. B.; Harman, W. D. *J. Am. Chem. Soc.* **2001**, *123*, 3541–3550.
87. Harman, W. D. *Coord. Chem. Rev.* **2004**, *248*, 853–866.
88. Stoebenau, E. J.; Jordan, R. F. *J. Am. Chem. Soc.* **2004**, *126*, 11170–11171.
89. Curnow, O. J.; Hughes, R. P.; Rheingold, A. L. *J. Am. Chem. Soc.* **1992**, *114*, 3153–3155.
90. Hughes, R. P.; Curnow, O. J.; Rose, P. R.; Zheng, X. M.; Mairs, E. N.; Rheingold, A. L. In *Inorganic Fluorine Chemistry*; ACS Symposium Series, Oxford University Press USA, New York, 1994; Vol. 555, pp 252–264.
91. Friedman, L. A.; Meiere, S. H.; Brooks, B. C.; Harman, W. D. *Organometallics* **2001**, *20*, 1699–1702.
92. Akermark, B.; Blomberg, M. R. A.; Glaser, J.; Ohrstrom, L.; Wahlberg, S.; Warnmark, K.; Zetterberg, K. *J. Am. Chem. Soc.* **1994**, *116*, 3405–3413.
93. Matchett, S. A.; Zhang, G. R.; Frattarelli, D. *Organometallics* **2004**, *23*, 5440–5449.

94. Albietz, P. J.; Cleary, B. P.; Paw, W.; Eisenberg, R. *Inorg. Chem.* **2002**, *41*, 2095–2108.
95. Gogoll, A.; Ornebro, J.; Grennberg, H.; Backvall, J. E. *J. Am. Chem. Soc.* **1994**, *116*, 3631–3632.
96. Elguero, J.; Fruchier, A.; delaHoz, A.; Jalon, F. A.; Manzano, B. R.; Otero, A.; GomezdelaTorre, F. *Chem. Ber.* **1996**, *129*, 589–594.
97. Carrion, M. C.; Guerrero, A.; Jalon, F. A.; Manzano, B. R.; de la Hoz, A.; Claramunt, R. M.; Milata, V.; Elguero, J. *Inorg. Chem.* **2003**, *42*, 885–895.
98. Elguero, J.; Guerrero, A.; de la Torre, F. G.; de la Hoz, A.; Jalon, F. A.; Manzano, B. R.; Rodriguez, A. *New J. Chem.* **2001**, *25*, 1050–1060.
99. Gomez-de la Torre, F.; de la Hoz, A.; Jalon, F. A.; Manzano, B. R.; Rodriguez, A. M.; Elguero, J.; Martinez-Ripoll, M. *Inorg. Chem.* **2000**, *39*, 1152–1162.
100. Milata, V.; Claramunt, R. M.; Cabildo, P.; Santa Maria, M. D.; Cornago, P.; Infantes, L.; Cano, F. H.; Elguero, J. *Heterocycles* **2001**, *55*, 905–924.
101. FernandezGalan, R.; Jalon, F. A.; Manzano, B. R.; RodriguezdelaFuente, J.; Vrahami, M.; Jedlicka, B.; Weissensteiner, W.; Jogl, G. *Organometallics* **1997**, *16*, 3758–3768.
102. Gomez-de la Torre, F.; Jalon, F. A.; Lopez-Agenjo, A.; Manzano, B. R.; Rodriguez, A. *Organometallics* **1998**, *17*, 4634–4644.
103. Albinati, A.; Kunz, R. W.; Ammann, C. J.; Pregosin, P. S. *Organometallics* **1991**, *10*, 1800–1806.
104. Romeo, R.; Fenech, L.; Scolaro, L. M.; Albinati, A.; Macchioni, A.; Zuccaccia, C. *Inorg. Chem.* **2001**, *40*, 3293–3302.
105. Brookhart, M.; Liu, Y. M.; Goldman, E. W.; Timmers, D. A.; Williams, G. D. *J. Am. Chem. Soc.* **1991**, *113*, 927–939.
106. Kiel, W. A.; Buhro, W. E.; Gladysz, J. A. *Organometallics* **1984**, *3*, 879–886.
107. Wang, Y.; Gladysz, J. A. *Chem. Ber.* **1995**, *128*, 213–220.
108. Vaughan, W. M.; Abboud, K. A.; Boncella, J. M. *Organometallics* **1995**, *14*, 1567–1577.
109. Hansen, H. D.; Nelson, J. H. *Inorg. Chim. Acta* **2003**, *352*, 4–8.
110. Herndon, J. W. *Coord. Chem. Rev.* **2003**, *243*, 3–81.
111. Bernasconi, C. F. *Chem. Soc. Rev.* **1997**, *26*, 299–307.
112. Chianese, A. R.; Li, X. W.; Janzen, M. C.; Faller, J. W.; Crabtree, R. H. *Organometallics* **2003**, *22*, 1663–1667.
113. Enders, D.; Gielen, H.; Runsink, J.; Breuer, K.; Brode, S.; Boehn, K. *Eur. J. Inorg. Chem.* **1998**, 913–919.
114. Enders, D.; Gielen, H. *J. Organomet. Chem.* **2001**, *617*, 70–80.
115. Herrmann, W. A.; Weskamp, T.; Bohm, V. P. W. *Adv. Organomet. Chem.* **2001**, *48*, 1–69.
116. Brookhart, M.; Studabaker, W. B.; Humphrey, M. B.; Husk, G. R. *Organometallics* **1989**, *8*, 132–140.
117. Brookhart, M.; Tucker, J. R.; Husk, G. R. *J. Organomet. Chem.* **1980**, *193*, C23–C26.
118. Desponds, O.; Schlosser, M. *Tetrahedron Lett.* **1996**, *37*, 47–48.
119. Becker, J. J.; White, P. S.; Gagne, M. R. *J. Am. Chem. Soc.* **2001**, *123*, 9478–9479.
120. Mann, B. E.; Masters, C.; Shaw, B. L.; Stainbank, R. E. *J. Chem. Soc. D: Chem. Commun.* **1971**, 1103–1103.
121. Bushweller, C. H.; Lourandos, M. Z. *Inorg. Chem.* **1974**, *13*, 2514–2515.
122. Bushweller, C. H.; Rithner, C. D.; Butcher, D. J. *Inorg. Chem.* **1986**, *25*, 1610–1616.
123. Brunner, H.; Oeschey, R.; Nuber, B. *J. Chem. Soc., Dalton Trans.* **1996**, 1499–1508.
124. Pelczar, E. M.; Nytko, E. A.; Zhuravel, M. A.; Smith, J. M.; Glueck, D. S.; Sommer, R.; Incarvito, C. D.; Rheingold, A. L. *Polyhedron* **2002**, *21*, 2409–2419.
125. Hughes, R. P.; Laritchev, R. B.; Williamson, A.; Incarvito, C. D.; Zakharov, L. N.; Rheingold, A. L. *Organometallics* **2003**, *22*, 2134–2141.
126. Canepa, G.; Brandt, C. D.; Ilg, K.; Wolf, J.; Werner, H. *Chem. Eur. J.* **2003**, *9*, 2502–2515.
127. Carmona, D.; Oro, L. A.; Lamata, M. P.; Jimeno, M. L.; Elguero, J.; Belguise, A.; Lux, P. *Inorg. Chem.* **1994**, *33*, 2196–2203.
128. Fanizzi, F. P.; Lanfranchi, M.; Natiel, G.; Tiripicchio, A. *Inorg. Chem.* **1994**, *33*, 3331–3339.
129. Faller, J. W.; Johnson, B. V. *J. Organomet. Chem.* **1975**, *96*, 99–113.
130. Jones, W. D.; Feher, F. J. *Inorg. Chem.* **1984**, *23*, 2376–2388.
131. Howell, J. A. S.; Yates, P. C.; Palin, M. G.; McArdle, P.; Cunningham, D.; Goldschmidt, Z.; Gottlieb, H. E.; Hezronilangerman, D. *J. Chem. Soc., Dalton Trans.* **1993**, 2775–2780.
132. Vicente, J.; Chicote, M. T.; Lagunas, M. C.; Jones, P. G.; Ahrens, B. *Inorg. Chem.* **1997**, *36*, 4938–4944.
133. Kovacs, I.; Baird, M. C. *Organometallics* **1995**, *14*, 4084–4091.
134. Faller, J. W.; Chase, K. J. *Organometallics* **1995**, *14*, 1592–1600.
135. Kollar, L.; Sandor, P.; Szalontai, G. *J. Mol. Catal.* **1991**, *67*, 191–198.
136. Ammann, C. J.; Pregosin, P. S.; Ruegger, H.; Albinati, A.; Lianza, F.; Kunz, R. W. *J. Organomet. Chem.* **1992**, *423*, 415–430.
137. Deeming, A. J.; Speel, D. M.; Stchedroff, M. *Organometallics* **1997**, *16*, 6004–6009.
138. Brown, J. M.; Pereztorrente, J. J.; Alcock, N. W. *Organometallics* **1995**, *14*, 1195–1203.
139. Alcock, N. W.; Brown, J. M.; Pereztorrente, J. J. *Tetrahedron Lett.* **1992**, *33*, 389–392.
140. Jacobi, B. G.; Laitar, D. S.; Pu, L. H.; Wargocki, M. F.; DiPasquale, A. G.; Fortner, K. C.; Schuck, S. M.; Brown, S. N. *Inorg. Chem.* **2002**, *41*, 4815–4823.
141. Trnka, T. M.; Morgan, J. P.; Sanford, M. S.; Wilhelm, T. E.; Scholl, M.; Choi, T. L.; Ding, S.; Day, M. W.; Grubbs, R. H. *J. Am. Chem. Soc.* **2003**, *125*, 2546–2558.
142. Costabile, C.; Cavallo, L. *J. Am. Chem. Soc.* **2004**, *126*, 9592–9600.
143. Brookhart, M.; Green, M. L. H.; L.-L, W *Prog. Inorg. Chem.* **1988**, *36*, 1.
144. Shultz, L. H.; Brookhart, M. *Organometallics* **2001**, *20*, 3975–3982.
145. Liu, W. J.; Brookhart, M. *Organometallics* **2004**, *23*, 6099–6107.
146. Leatherman, M. D.; Svejda, S. A.; Johnson, L. K.; Brookhart, M. *J. Am. Chem. Soc.* **2003**, *125*, 3068–3081.
147. Tebbe, F. N.; Parshall, G. W. *J. Am. Chem. Soc.* **1971**, *93*, 3793.
148. Werner, H.; Feser, R. *J. Organomet. Chem.* **1982**, *232*, 351–370.
149. Bennett, M. A.; McMahon, I. J.; Pelling, S.; Brookhart, M.; Lincoln, D. M. *Organometallics* **1992**, *11*, 127–138.
150. Brookhart, M.; Lincoln, D. M.; Bennett, M. A.; Pelling, S. *J. Am. Chem. Soc.* **1990**, *112*, 2691–2694.
151. Brookhart, M.; Lincoln, D. M.; Volpe, A. F.; Schmidt, G. F. *Organometallics* **1989**, *8*, 1212–1218.
152. Brookhart, M.; Lincoln, D. M. *J. Am. Chem. Soc.* **1988**, *110*, 8719–8720.
153. Wadepohl, H.; Kohl, U.; Bittner, M.; Koppel, H. *Organometallics* **2005**, *24*, 2097–2105.
154. Threlkel, R. S.; Bercaw, J. E. *J. Am. Chem. Soc.* **1981**, *103*, 2650–2659.
155. Burger, B. J.; Santarsiero, B. D.; Trimmer, M. S.; Bercaw, J. E. *J. Am. Chem. Soc.* **1988**, *110*, 3134–3146.

156. Torkelson, J. R.; Antwi-Nsiah, F. H.; McDonald, R.; Cowie, M.; Pruis, J. G.; Jalkanen, K. J.; DeKock, R. L. *J. Am. Chem. Soc.* **1999**, *121*, 3666–3683.
157. Dell'Anna, M. M.; Trepanier, S. J.; McDonald, R.; Cowie, M. *Organometallics* **2001**, *20*, 88–99.
158. Gusev, D. G.; Berke, H. *Chem. Ber.* **1996**, *129*, 1143–1155.
159. Jessop, P. G.; Morris, R. H. *Coord. Chem. Rev.* **1992**, *121*, 155–284.
160. Kubas, G. J. *Metal Dihydrogen and Sigma-bond Complexes: Structure, Theory and Reactivity*; Kluwer: New York, 2001.
161. Crabtree, R. H.; Lavin, M.; Bonneviot, L. *J. Am. Chem. Soc.* **1986**, *108*, 4032–4037.
162. Sabo-Etienne, S.; Chaudret, B. *Chem. Rev.* **1998**, *98*, 2077–2091.
163. Limbach, H. H.; Ulrich, S.; Grundemann, S.; Buntkowsky, G.; Sabo-Etienne, S.; Chaudret, B.; Kubas, G. J.; Eckert, J. *J. Am. Chem. Soc.* **1998**, *120*, 7929–7943.
164. Scheurer, C.; Wiedenbruch, R.; Meyer, R.; Ernst, R. R.; Heinekey, D. M. *J. Chem. Phys.* **1997**, *106*, 1–10.
165. Kisko, J. L.; Hascall, T.; Kimblin, C.; Parkin, G. *J. Chem. Soc., Dalton Trans.* **1999**, 1929–1935.
166. Ghosh, P.; Desrosiers, P. J.; Parkin, G. *J. Am. Chem. Soc.* **1998**, *120*, 10416–10422.
167. Anklin, C.; Pregosin, P. S. *Magn. Reson. Chem.* **1985**, *23*, 671–675.
168. Tsuji, Y.; Nishiyama, K.; Hori, S.; Ebihara, M.; Kawamura, T. *Organometallics* **1998**, *17*, 507–512.
169. Pomeroy, R. K.; Vancea, L.; Calhoun, H. P.; Graham, W. A. G. *Inorg. Chem.* **1977**, *16*, 1508–1514.
170. He, X. M.; Hartwig, J. F. *Organometallics* **1996**, *15*, 400–407.
171. Asali, K. J.; Smit, J. P.; Ladogana, S.; Dobson, G. R. *Inorg. Chem. Commun.* **1998**, *1*, 87–89.
172. Bottomley, L. D.; Clark, R. J.; Berger, T. G. *Polyhedron* **1989**, *8*, 2125–2129.
173. Darensbourg, D. J.; Gray, R. L. *Inorg. Chem.* **1984**, *23*, 2993–2996.
174. Darensbourg, D. J.; Darensbourg, M. Y.; Gray, R. L.; Simmons, D.; Arndt, L. W. *Inorg. Chem.* **1986**, *25*, 880–882.
175. Corbett, J. D. *Chem. Rev.* **1985**, *85*, 383–397.
176. McGlinchey, M. J.; Girard, L.; Ruffolo, R. *Coord. Chem. Rev.* **1995**, *143*, 331–381.
177. ElAmouri, H.; Gruselle, M. *Chem. Rev.* **1996**, *96*, 1077–1103.
178. Adams, R. D.; Captain, B.; Pellechia, P. J.; Zhu, L. *Inorg. Chem.* **2004**, *43*, 7243–7249.
179. Duer, M. J. *Ann. Rep. NMR Spectroc.* **2001**, *43*, 1–58.
180. Obora, Y.; Liu, Y. K.; Jiang, L. H.; Takenaka, K.; Tokunaga, M.; Tsuji, Y. *Organometallics* **2005**, *24*, 4–6.
181. Yatsunyk, L. A.; Ogura, H.; Walker, F. A. *Inorg. Chem.* **2005**, *44*, 2867–2881.

1.16 Parahydrogen-induced Polarization in Organometallic Chemistry

R S Eisenberg and D Fox, University of Rochester, Rochester, NY, USA

1.16.1 Introduction

1.16.1.1 Parahydrogen and Orthohydrogen: Two Spin Isomers of Dihydrogen

Due to the nuclear spin of a proton, molecular hydrogen (dihydrogen) exists as two spin isomers, *para*- and *ortho*-hydrogen. The *para*-isomer of hydrogen (p-H_2) possesses an antisymmetric spin configuration with wave function ($\alpha\beta - \beta\alpha$) while the *ortho*-spin isomer (o-H_2) is actually threefold degenerate with symmetric spin wave functions of $\alpha\alpha$, $\beta\beta$, and ($\alpha\beta + \beta\alpha$). While p-H_2 is thermodynamically more stable than o-H_2, the energy difference is small enough that at ambient temperature the ratio of p-H_2 : o-H_2 is near the high-temperature limit, and determined mainly by the degeneracy of the configurations, ca. 1 : 3. However, at lower temperatures, the greater stability of p-H_2 leads to a shift of the equilibrium ratio, resulting in a nearly 1 : 1 ratio at 77 K and essentially pure p-H_2 below 20 K (Table 1).[1,2] While interconversion between the spin isomers of hydrogen is symmetry forbidden, addition of species such as paramagnetic metal salts or activated charcoal to a hydrogen sample readily catalyzes orthohydrogen/parahydrogen interconversion to give the equilibrium distribution at the particular sample temperature. This phenomenon can be exploited for the enrichment of hydrogen in the *para*-spin state by cooling hydrogen in the presence of such a catalyst before use. Many groups, including ours, generate hydrogen enriched in the *para*-spin state to ~50% by using liquid nitrogen (77 K) to cool a bulb containing a paramagnetic catalyst filled with H_2. The

Table 1 Percentages of *para*- and *ortho*-hydrogen at various temperatures

Temperature (K)	*para-hydrogen* (%)	*ortho-hydrogen* (%)
0	100	0
20	99.82	0.18
75	51.86	48.14
150	28.54	71.46
273	25.13	74.87
High temp. limit	25.00	75.00

degree of enrichment in parahydrogen can be written as: $f = (1/3)(4x_p - 1)$, where x_p is the fraction of H_2 that is p-H_2.[3] Use of liquid nitrogen as a coolant results in an enrichment of $f = 0.33$. Duckett and co-workers have demonstrated that it is possible to generate virtually pure parahydrogen ($f = 1$) by cooling to temperatures of 20 K or less while passing H_2 over activated charcoal.[4] It is important to note that in the absence of a catalyst, hydrogen enriched in the *para*-spin state will maintain its enrichment for several days, even at room temperature.

1.16.1.2 Theory of Parahydrogen-induced Polarization (PHIP) and Its Mechanistic Significance

Dihydrogen enriched in the *para*-spin state has proved to be an extremely useful part of the toolbox of mechanistic organometallic chemistry when used in conjunction with NMR spectroscopy for probing mechanisms of transformations involving hydrogen addition. Resulting product resonances of the added hydrogen atoms may be seen in enhanced absorption and emission, and the phenomenon has been termed parahydrogen-induced polarization, or PHIP. The basis of PHIP may be understood in its essence as follows. When p-H_2 adds in a "pairwise" manner to a system (i.e., a metal complex or an unsaturated organic substrate), the spins of the hydrogen atoms may remain correlated. If the added protons become magnetically distinct in the product, the correlation between these two nuclei can lead to an overpopulation of the product $\alpha\beta$ and $\beta\alpha$ spin states relative to $\alpha\alpha$ and $\beta\beta$ as compared with a Boltzmann distribution of those spins obtained using normal hydrogen with its ca. 1 : 3 mixture of p-H_2 and o-H_2 (Figure 1). Overpopulation of the $\alpha\beta$ and $\beta\alpha$ spin states occurs since the $(\alpha\beta - \beta\alpha)$ spin state of p-H_2 transfers only to these states in the product. The selective population of the $\alpha\beta$ and $\beta\alpha$ spin states leads to enhanced signal intensity

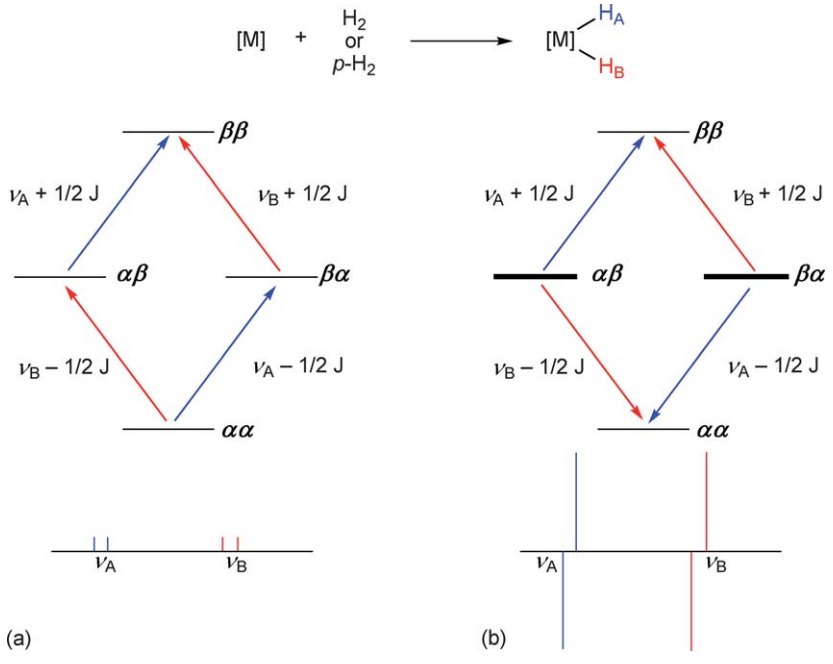

Figure 1 Energy level diagram for product of addition of H_2 to a metal center: (a) Boltzmann distribution; (b) p-H_2 derived distribution.

and characteristic emission/absorption (E/A) or absorption/emission (A/E) doublets in the ^{1}H NMR spectrum of the product (Figure 1). The last decade and a half has seen the publication of several reviews concerning many aspects of the theory and applications of parahydrogen and PHIP.[2,5–9] In this chapter, we will discuss several important goals that have been achieved using the PHIP phenomenon: (i) the unambiguous determination that pairwise addition of H_2 to a metal center or an organic substrate has occurred, (ii) differentiation between mechanisms involving two or more different ways of activating dihydrogen, (iii) assessment qualitatively or quantitatively of the rate of exchange of added dihydrogen with free H_2, (iv) the observation and identification of intermediates and other reaction species formed in very small concentrations, (v) the transfer of polarization to other nuclei, and (vi) the rapid acquisition of two-dimensional (2D) NMR spectra by indirect detection of X nuclei using the added protons of a parahydrogen molecule.

1.16.2 Late Transition Metal Reactions with Parahydrogen

1.16.2.1 Mechanistic Studies Involving Dihydrogen Addition to Late Metal Centers

A fundamental mode of reactivity in organometallic chemistry is the oxidative addition of dihydrogen to a metal center. The reaction proceeds in a concerted manner through a triangular MH_2 transition state with M–H bond formation occurring as the H–H bond is weakened and ultimately cleaved. In order for this reaction to proceed, the metal center needs to be coordinatively unsaturated. The orbital interactions that lead to dihydrogen oxidative addition have been studied extensively on a theoretical basis, and involve a synergic interaction consisting of donation from the filled H_2 σ-bonding orbital into a vacant orbital on the metal center and backbonding from a filled metal $d\pi$-orbital into the H_2 σ^*-antibonding function. This manner of dihydrogen reactivity and activation lends itself in a very straightforward manner to the use of p-H_2 and PHIP.

1.16.2.1.1 d^8–d^6 Oxidative addition with iridium systems

Some of the earliest examples of PHIP in oxidative addition chemistry involved the reaction of p-H_2 with *trans*-$IrCl(CO)(PPh_3)_2$ (Vaska's complex) and its related analogs IrX(CO)(PP), where X is halide and PP is a bidentate diphosphine.[3,10,11] For example, the addition of p-H_2 to IrBr(CO)(dppb) **1**, (dppb = 1,2-*bis*(diphenylphosphino)-benzene) formed a dihydride species, the ^{1}H NMR spectrum of which showed enhanced hydride signals at −8.73 and −9.32 ppm for the hydride ligands *trans* to P and CO, respectively (Equation (1)).[11] The signal enhancement of the hydride signals was estimated to be approximately 12. Later work showed that it was possible to obtain far greater signal enhancements relative to other resonances in the system when smaller quantities of sample were used. In the case of IrBr(CO)(dppe) **2**, (dppe = 1,2-*bis*(diphenylphosphino)ethane), a 4.6 mg sample under 3 atm p-H_2 yielded a 40-fold enhancement, while 0.3 mg gave a 95-fold enhancement.[12] In these PHIP spectra, each of the ^{31}P-coupled hydride resonances appeared as an emission/absorption antiphase doublet from H/H coupling that is often not resolved using normal hydrogen. While depletion of p-H_2 enrichment (relative to the normal or Boltzmann ratio of parahydrogen : orthohydrogen) in the solution was observed by the loss of polarization in the hydride signals over time (~3 min), the authors found that the loss of *para*-enrichment in the H_2 "above" the solution occurred more slowly: thus, a vigorous shaking of the sample led to re-establishment of the polarization seen in the initial ^{1}H NMR spectrum when a new spectrum was acquired immediately after reinsertion of the NMR tube into the spectrometer.

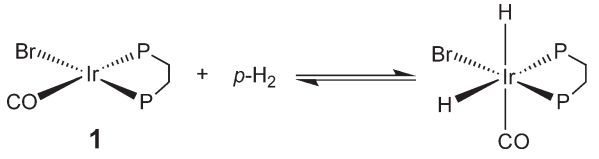

(1)

Additionally, the non-Boltzmann spin populations obtained from the use of p-H_2 that led to PHIP, as shown in Figure 1, have been used to enhance the signal from associated X nuclei such as the ^{31}P resonances of the diphosphine donors by polarization transfer.[11,12] In this way, a signal enhancement of greater than sevenfold was obtained in the ^{31}P resonances of the $IrH_2Br(CO)(dppe)$ system relative to those seen after polarization had waned. If signal amplitude increases as the square of the number of scans, then a sevenfold increase in the intensity of the ^{31}P

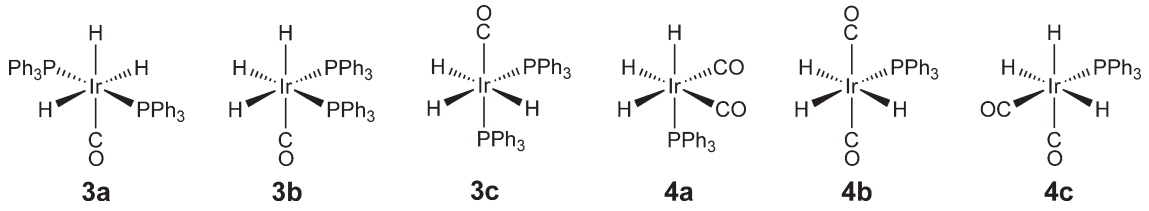

Scheme 1

resonances would correspond to the acquisition of 49 scans of the same sample under normal hydrogen. Such an increase in signal intensity of X nuclei resonances without an increased number of scans makes PHIP a very useful method for analyzing H_2 addition products. In the same study based on the formation of $IrH_2Br(CO)(dppe)$ with *p*-H_2, polarization transfer to ^{13}C in the carbonyl ligand was also achieved.[12] Specifically, a ^{13}C NMR spectrum obtained using a 0.3 mg sample of IrBr(CO)(dppe) under *p*-H_2 revealed the unlabeled carbonyl (^{13}C in natural abundance) signal after only 32 scans. The enhancement of signal seen in this system was approximately 18 times greater than the ^{13}C carbonyl resonance produced from a more concentrated sample containing ^{13}C-labeled CO. The extent of enhancement was such that >5,000 scans would have been needed to obtain a comparable signal from an unlabeled sample without parahydrogen-related effects.

PHIP made possible the rapid characterization of thermally and photochemically generated complexes $IrH_3(CO)_{3-x}(PPh_3)_x$ ($x = 1-3$).[13] Illustrated in Scheme 1 are the possible isomers that can form by *cis* oxidative addition when $x = 2$ or 1. The trihydride $IrH_3(CO)(PPh_3)_2$ had been shown previously to exist in solution as two isomers, one with *trans*-phosphines and *mer*-hydrides **3a**, and the other with *cis*-phosphines and *fac*-hydrides **3b**.[14] Duckett and co-workers found that under parahydrogen, the hydride resonances of **3a** and **3b** exhibited PHIP enhancement, indicative of facile exchange of these systems with dihydrogen dissolved in solution.[13] While no resonances corresponding to **3c** were seen, both hydrides of isomers **3a** and **3b** showed polarization. Mechanistically, this means that for **3a**, H_2 reductive elimination and oxidative readdition involves only one of the mutually *trans*-hydrides and the hydride *trans* to CO, as the mutually *trans*-hydrides are unable to eliminate together. Likewise, for complex **3b**, the dominant H_2 reductive elimination/oxidative addition pathway involves one hydride *trans* to PPh_3 and the other hydride *trans* to CO. For **3a** and **3b**, the addition of H_2 proceeds, respectively, through *trans*- and *cis*-$IrH(CO)(PPh_3)_2$, such that the added hydrogen atoms become inequivalent in the product, and the transition state is trigonal bipyramidal with CO in an equatorial position along with the adding H_2 molecule. This position for CO makes its π^*-orbitals more able to withdraw electron density from the IrH_2 fragment with consequent weakening of the H–H bond and reduction of the barrier for oxidative addition.[15] For the addition of H_2 to *cis*-$IrH(CO)(PPh_3)_2$ to generate **3c**, a trigonal-bipyramidal transition state with CO in the axial position would be required, and the absence of **3c** is consistent with the notion that such a transition state would be unfavorable.

It was also found that addition of *p*-H_2 to the coordinatively saturated species $IrH(CO)_2(PPh_3)_2$ at 333 K led to the formation of the dicarbonyl complex **4a** as well as the related monocarbonyl trihydrides **3a** and **3b**. The former is generated by loss of PPh_3 and addition of H_2 (Equation (2)) as opposed to CO loss and H_2 addition that give **3a** and **3b**. Other experiments showed that addition of *p*-H_2 to $IrH(CO)(PPh_3)_3$ gave enhanced resonances for **3a** and **3b** and no resonances for **4a** (Equation (3)), while photolysis of **3a** and **3b** in C_6D_6 for 5 min yielded resonances corresponding to **3a**, **3b**, and **4a** as well as several new species. Gradient-assisted COSY{^{31}P} and HMQC experiments were used to determine that **3c** and **4b**, which are unstable under thermal conditions, were two of the species formed under photolytic conditions (Equation (4)). Complexes **3c** and **4b** could not have been observed using normal hydrogen.

$$IrH(CO)_2(PPh_3)_2 \xrightarrow[\text{heat}]{H_2} \mathbf{3a} + \mathbf{3b} + \mathbf{4a} \quad (2)$$

$$IrH(CO)(PPh_3)_3 \xrightarrow[\text{heat}]{H_2} \mathbf{3a} + \mathbf{3b} \quad (3)$$

$$\mathbf{3a} + \mathbf{3b} \xrightarrow[h\nu]{H_2} \mathbf{3c} + \mathbf{4a} + \mathbf{4b} \quad (4)$$

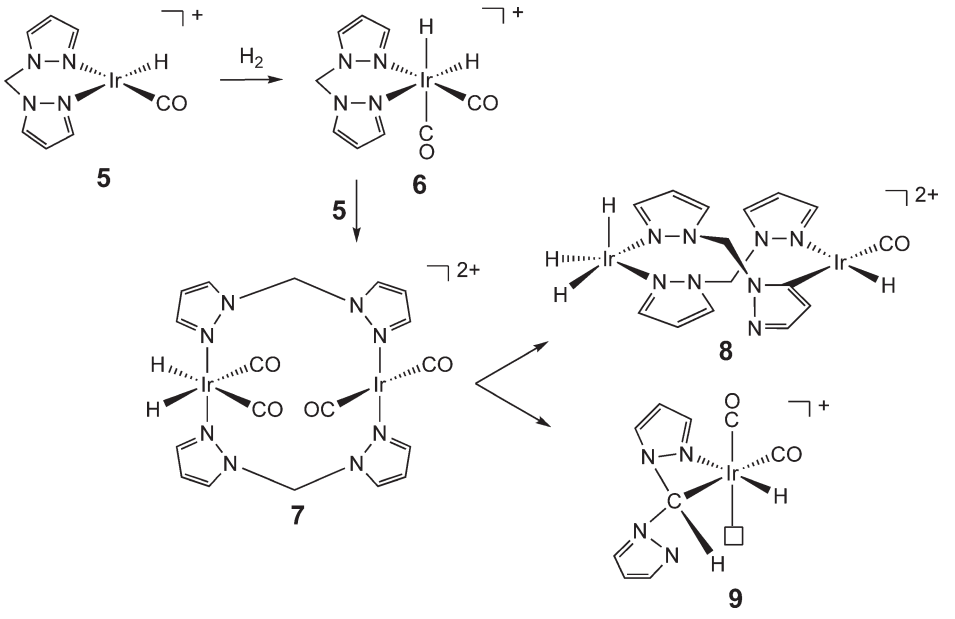

Scheme 2

The enhanced signals resulting from the addition of *p*-H_2 can often appear in a series of products even though *p*-H_2 only adds directly to the first product formed. For example, Duckett *et al.* saw four products from a "cascade" of reactions upon addition of *p*-H_2 to [$Ir(CO)_2$(BPM)][BPh_4] **5**, (BPM = bis(pyrazol-1-yl)methane, Scheme 2).[16] All of the products shown in Scheme 2 **6**–**9** exhibited enhanced signals due to PHIP in the ^{1}H NMR spectrum and the identities of the products were confirmed using ^{13}C- and ^{15}N-labeled **5** and 2D NMR spectroscopy. Interestingly, the signal enhancement for complex **8** was of very short duration, indicating limited exchange with free *p*-H_2. The absence of PHIP for certain systems as well as its presence in others can also shed light on the mechanism of a particular transformation. For example, Albietz *et al.* found that addition of *p*-H_2 to the cationic iridium trifluoromethyl complex $Ir(CF_3)(CO)(dppe)(DIB)^{2+}$, where DIB = *o*-diiodobenzene, led to PHIP in the resonances of the final system product $IrH_2(CO)_2(dppe)^+$ (the counterion for both of these complexes was tetrakis(3,5-bis(triflouromethyl)phenyl)borate).[17] Subsequent labeling studies revealed that the second CO in the product originated from the CF_3 ligand in the starting complex. The fact that initial reaction of the trifluoromethyl complex with H_2 did not generate PHIP and that transformation of anionic CF_3 ligands to CO had been identified previously as acid promoted[18–26] led to the conclusion that the initial rapid reaction of $Ir(CF_3)(CO)(dppe)(DIB)^{2+}$ with H_2 proceeded by heterolytic splitting of dihydrogen with liberation of H^+, rather than by PHIP-producing oxidative addition. The overall reaction is shown as Equation (5).

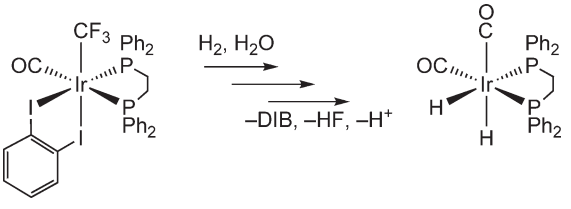

(5)

An important application of the signal enhancement of PHIP is the ability to characterize species that are present only transiently, and, therefore, in very small quantities. Although there are few examples of dihydrogen addition to anionic iridium complexes, *p*-H_2 does allow for the study of this process. Upon addition of *p*-H_2 to (Bu_4N)[$IrBr_2(CO)_2$] **10**, two hydrides corresponding to (Bu_4N)[$IrH_2Br_2(CO)_2$] **11** appeared in the ^{1}H NMR spectrum (Equation (6)).[27] Significantly, there was no evidence for **11** upon addition of normal H_2 to complex **10**, indicating that the equilibrium shown in Equation (6) greatly favored complex **10**. A more complex and interesting situation arose when $SnBr_2$ was added to **10** because this gave both the *cis*- and *trans*-tribromostannyl

derivatives $[IrBr_x(SnBr_3)_{2-x}(CO)_2]^-$ (**12**, $x = 1$; **13**, $x = 0$). When *p*-H_2 was added to a solution of **10** treated with 0.5 equiv. $SnBr_2$, the major species in the ^1H NMR spectrum was **14**, which was assigned as the kinetic isomer from the product of oxidative addition of H_2 to **12**-*cis* (Equation (7)); the stereochemistry of **14** was assigned using both the hydride chemical shifts and the magnitude of their $^{117,119}Sn$ satellites. At greater ratios of $SnBr_2$/**10** and higher temperatures, other product isomers resulted, as shown in Scheme 3. In these experiments, PHIP allowed for the observation of kinetic products, which were produced most rapidly, and characterization of more thermodynamically stable products that formed more slowly. Of the different possible dihydride isomers, only **15** was not seen, even with the use of ^{13}CO that would remove the equivalence of the two hydrides. On the other hand, other products with equivalent dihydride ligands **16** and **17** were rendered PHIP-active with spin-active $^{117}Sn/^{119}Sn$ or ^{13}C nuclei, and were observed directly.

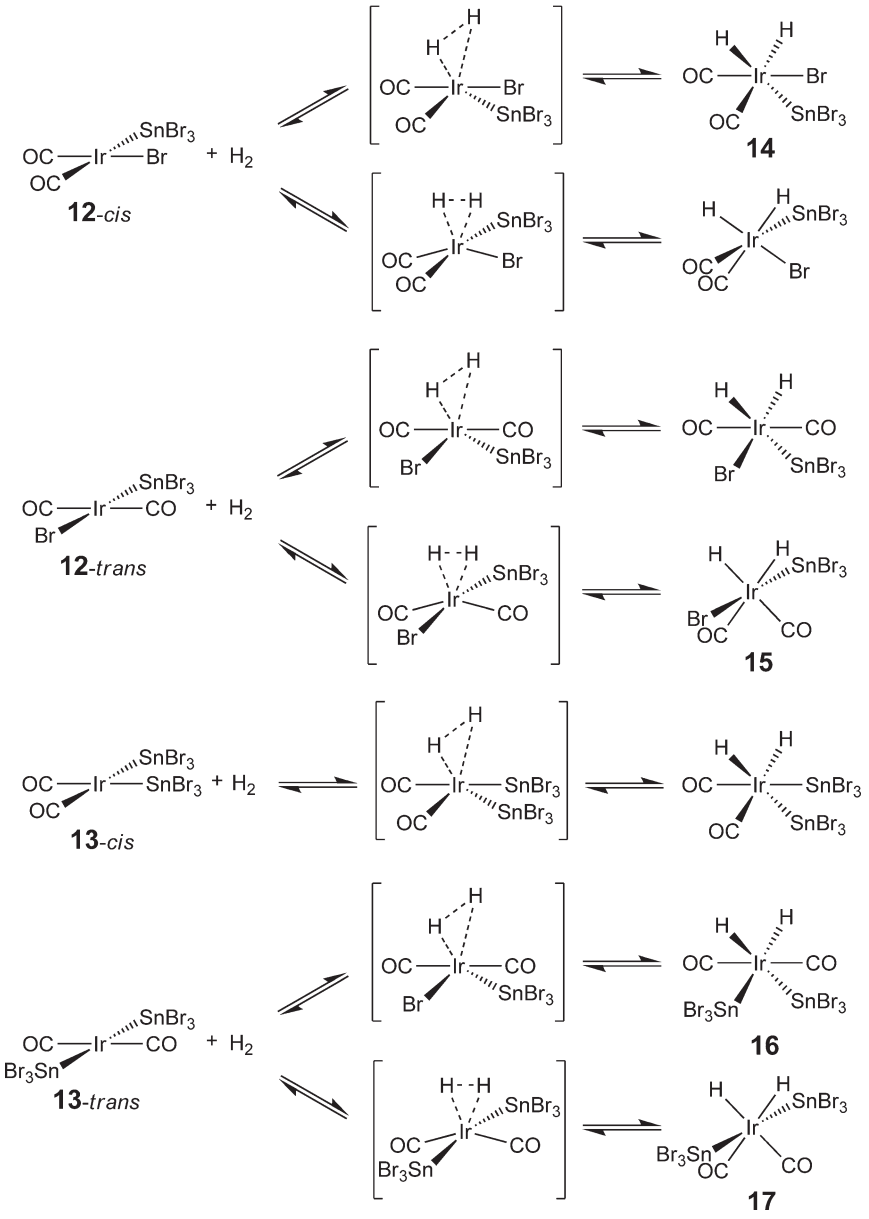

Scheme 3

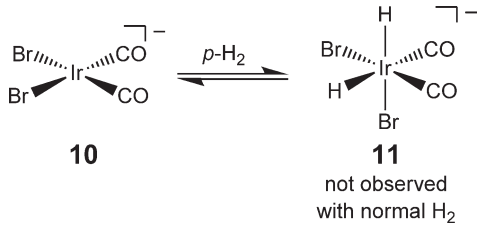

(6)

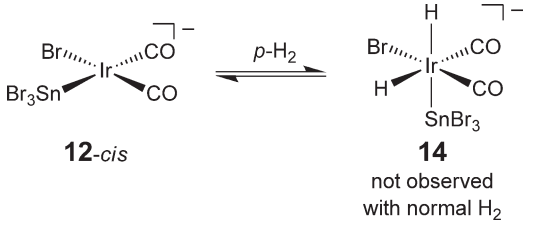

(7)

1.16.2.1.2 d^8–d^6 Oxidative addition with rhodium systems

The signal enhancements of PHIP make possible the observation of previously unknown species. An excellent example is the addition of *p*-H_2 to *trans*-RhCl(CO)$(PPh_3)_2$ **18**. While its iridium analog (Vaska's complex) oxidatively adds H_2 to form a dihydride complex, the corresponding reaction with **18** had not been reported. However, a ^{1}H NMR spectrum of complex **18** under 3 atm *p*-H_2 revealed two hydride signals at −19.31 and −19.66 ppm.[28] Significant to the interpretation of this result were the similarity of chemical shifts of the two hydride resonances and the lack of additional splitting in the ^{1}H and ^{31}P NMR spectra when ^{13}CO was used. Both of these results indicated that the simple oxidative addition product, $RhH_2Cl(CO)(PPh_3)_2$, was not the species detected (similar observations were obtained with the bromo and iodo analogs of **18**). While there was no coupling of the hydride signals to ^{13}C in the product, the authors demonstrated that CO was a necessary component of the detected species since the same product was found in the reaction of $[Rh(\mu\text{-}Cl)(PPh_3)_2]_2$ with *p*-H_2 only in the presence of a CO source such as 1-butanal (a good decarbonylation substrate); a different species, identified as $[RhH_2(PPh_3)_2(\mu\text{-}Cl)_2Rh(PPh_3)_2]$, was formed in the absence of 1-butanal. This information led to the formulation of the product as a dinuclear species **19**, which had not been identified previously in this reaction using normal H_2 (Equation (8)). The formation of this dinuclear rhodium complex highlights the usefulness of PHIP in the detection and identification of dihydride species formed in minute quantities.

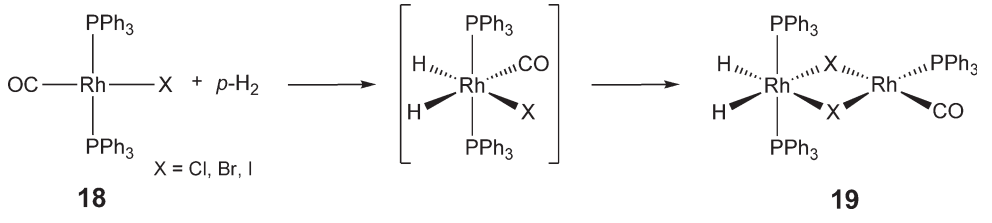

(8)

Further work with $RhX(CO)(PR_3)_2$ (R = Me, Ph; X = Cl, Br, I) complexes and *p*-H_2 using combinations of ^{1}H, ^{13}C, ^{31}P, and ^{103}Rh NMR spectroscopies were reported in 1999.[29] When *p*-H_2 was added to mixtures of these complexes, species containing mixed halide bridges, $RhH_2(PPh_3)_2(\mu\text{-}X)(\mu\text{-}Y)Rh(CO)(PPh_3)$ (X, Y = Cl, Br, I; $X \neq Y$), were detected using PHIP. Interestingly, it was found that when X or Y = I, the only isomer seen in the spectra contained the μ-iodide-bridging ligand in the position *trans* to the CO ligand of the Rh(I) center (Equation (9)). However, when the mixed μ-chloride/μ-bromide complex was produced in the same manner, two isomers were seen. The mechanism of this transformation was determined using combinations of the mononuclear rhodium complexes in varying ratios. Multinuclear and 2D NMR methods were essential to the careful identification of the mixed products. The mechanism for the transformation is shown in Scheme 4. Additionally, 2D NMR spectroscopic experiments yielded strong evidence that hydride exchange processes in these complexes were intramolecular (Scheme 5).[29]

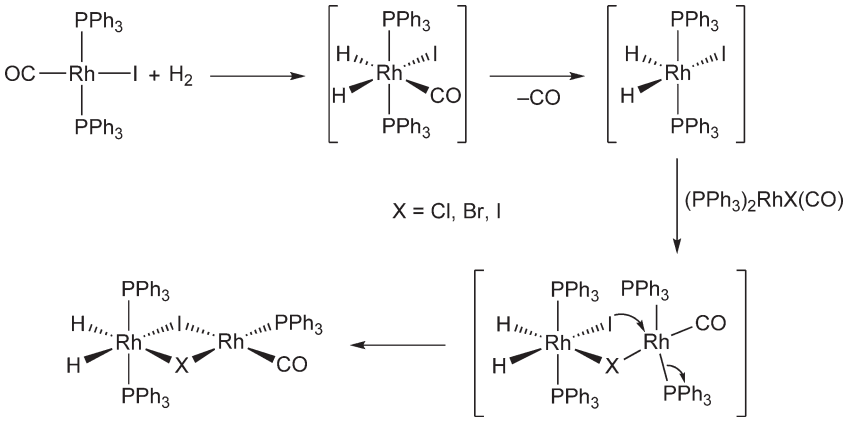

Scheme 4

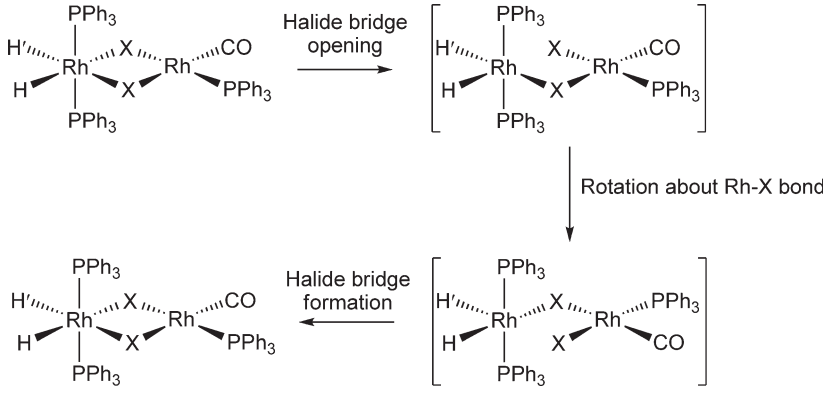

Scheme 5

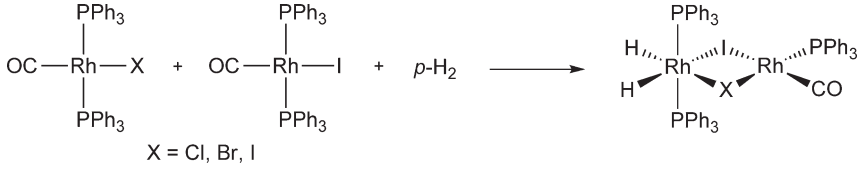

(9)

Bargon and Koch observed similar dinuclear complexes of rhodium upon addition of *p*-H_2 to $[Rh(NBD)Cl]_2$ (NBD = 2,5-norbornadiene) in the presence of tertiary phosphines.[30] While addition of H_2 to complexes containing PPh_2Me formed only the mononuclear product $RhH_2Cl(PPh_2Me)_3$, use of PMe_3 and $PPhMe_2$ complexes led to dinuclear complexes related to those of Schemes 4 and 5, as shown in Scheme 6.

1.16.2.1.3 d^{10}–d^8 Oxidative addition with platinum systems

While the preparation of Pt(II) dihydrides under H_2 has long been presumed to occur through oxidative addition, evidence for such a process has not always been compelling. Part of the ambiguity in the mechanism of this process stemmed from the fact that the formation of Pt(II) dihydrides often involved reductions using hydride sources.[31] Additionally, experiments involving H/D exchange to form d_1-isotopomers of the dihydrides generated uncertainty about a mechanism involving pairwise addition.[32] PHIP provided the definitive evidence to confirm H_2 activation to give Pt(II) dihydride products by oxidative addition.[33] Upon addition of *p*-H_2 to 0.4 mg $PtH_2(Ph_2PCH_2CH(Me)OPPh_2)$ in toluene-d_8, the ^{1}H NMR spectrum showed large PHIP-enhanced signals for the

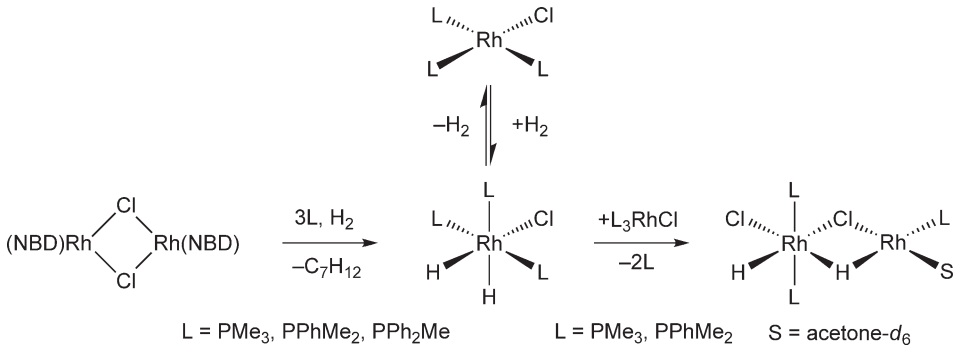

Scheme 6

two hydride signals at −0.282 and −0.014 ppm (Equation (10)). In this system, signal enhancement at $t = 2.3$ min was greater than 900-fold, leading to an estimate of signal enhancement at $t = 0$ of about 1600-fold—the largest signal enhancement yet observed. (Note that a 900-fold signal enhancement requires 810,000 times the number of scans in the absence of parahydrogen effects.) These results were clear evidence for the pairwise addition of H_2 to the platinum center. Additionally, the signal enhancement of PHIP allowed for the collection of 2D modified ^{1}H–^{31}P and ^{1}H–^{195}Pt HMQC correlation spectra on less than 1 mg of sample in only 2–5 min, efficiency that would not be possible without using *p*-H_2. The modification done to the pulse sequence for HMQC is the use of an initial 45° pulse in place of the standard 90° pulse.[34] In HMQC spectra, X nuclei are detected indirectly through the ^{1}H nuclei with which they couple, and for the complexes described here, these ^{1}H nuclei are supplied by parahydrogen upon addition.

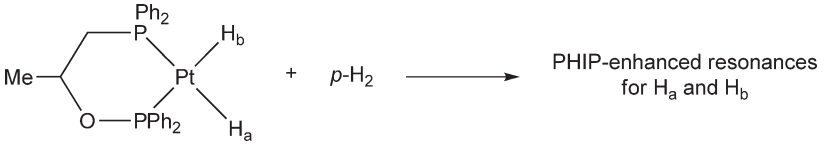

(10)

1.16.2.1.4 Oxidative addition with group 8 systems

Parahydrogen was used to great effect in the observation of minor isomers of $RuH_2(CO)_2L_2$ containing inequivalent hydride ligands (L = $AsMe_2Ph$, PMe_2Ph, PMe_3; L_2 = dppe).[35,36] It was shown that the three isomers illustrated in Scheme 7 are all possible (two of them had not been observed before these experiments with *p*-H_2). The dppe complex adopts a ccc geometry, and upon reaction with *p*-H_2 at 323 K, PHIP-enhanced resonances appeared for both hydride ligands. The polarization decayed within 10 min, indicating rapid exchange with free H_2. Additionally, the observation of PHIP indicated that the intermediate to which free H_2 added was diamagnetic, since interaction with a triplet intermediate would be expected to eliminate the parahydrogen enrichment. Interestingly, reaction of *p*-H_2 with $M(CO)_3$(dppe) (M = Fe, Ru) under photolytic conditions to form $MH_2(CO)_2$(dppe) demonstrated that while the intermediate was diamagnetic in the ruthenium system (PHIP was observed), the key intermediate species in the iron system was more likely a triplet (no PHIP was observed).[37] With L = $AsMe_2Ph$, both hydride signals were enhanced by "1,035 times" for the ccc isomer, while the hydride resonance of the cct-L isomer unexpectedly showed

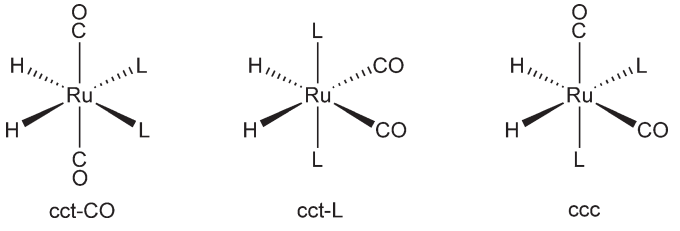

Scheme 7

enhancement (of 60-fold) even though the two hydride ligands are equivalent.[35] The authors suggested that the unusual enhancement in the cct-L isomer could be the result of the inequivalence of the hydrides in the ccc isomer. In this system, 1- and 2D EXSY spectra were used in conjunction with *p*-H_2 to detect a third isomer, cct-CO, and it was determined that the cct-L, ccc, and cct-CO isomers are present in solution in a ratio of 54 : 45 : 1.[36] When L = PMe_2Ph, the cct-L isomer predominates, although the ccc isomer is observed quite clearly when *p*-H_2 is employed. Only the cct-L isomer was observed under normal H_2 even after 10,000 scans when L = PMe_3; however, the ccc isomer was easily detected under *p*-H_2 at 333 K using only four scans. The work by Duckett and co-workers using the above ruthenium complexes demonstrated for the first time that *p*-H_2 enhancements were possible in ruthenium systems, and these enhancements were subsequently used to characterize species that could not have been observed conveniently without PHIP.

Oxidative addition of dihydrogen to metal carbonyl clusters and exchange of the resulting hydrides with free H_2 were also found to be amenable to PHIP investigation despite the increased complexity of the systems and their reaction chemistry. Aime *et al.* were able to show that two pathways were operative in the reaction of $Os_3(\mu\text{-}H)_2(CO)_{10}$ **20** with dihydrogen using both H_2/D_2 exchange experiments and *p*-H_2.[38] Under *p*-H_2, the ^{1}H NMR spectrum showed strong polarization for the bridging hydrides of **20**, indicating that pairwise exchange of H_2 did occur. However, under deuterium, the D_2 and HD isotopomers of **20** formed, indicating that simple pairwise transfer was not the only process in operation. The authors determined that consecutive reactions were occurring, as shown in Equations (11) and (12) (*H–H* is either D_2 or *p*-H_2; $k_1 = 3.7 \pm 0.3 \times 10^{-5}\,s^{-1}$; $k_2 = 2.2 \pm 0.2 \times 10^{-5}\,s^{-1}$). Note that although the hydride ligands in the osmium clusters discussed above are equivalent, their resonances in the ^{1}H NMR spectrum are still strongly enhanced by PHIP. This effect is attributed to an intermediate species having inequivalent hydride ligands formed during the exchange with free *p*-H_2.[39] We will discuss a related observation in the context of hydroformylation later in the chapter.

$$\underset{\textbf{20}}{Os_3(\mu\text{-}H)_2(CO)_{10}} + {}^*H\text{–}H^* \xrightarrow{k_1} Os_3(\mu\text{-}H)(\mu\text{-}{}^*H)(CO)_{10} + {}^*H\text{–}H \quad (11)$$

$$Os_3(\mu\text{-}H)(\mu\text{-}{}^*H)(CO)_{10} + {}^*H\text{–}H^* \xrightarrow{k_2} Os_3(\mu\text{-}{}^*H)_2(CO)_{10} + {}^*H\text{–}H \quad (12)$$

1.16.2.2 Hydrogenation Chemistry

1.16.2.2.1 Rhodium-catalyzed hydrogenation

Since a critical step in many catalytic hydrogenations of unsaturated organic substrates by transition metal complexes is the oxidative addition of dihydrogen to the active catalyst, PHIP can be used in the study of the mechanism of these reactions. In hydrogenation reaction systems, polarization in resonances corresponding to the hydride ligands of catalytic intermediates and other species formed in minor concentrations can be seen, as well as polarization in the resonances of organic products of some hydrogenations. One of the earliest examples of hydrogenation studies using PHIP showed polarization in the products of the reaction of phenylacetylene, styrene-d_8, propylene-d_6, and ethylene-d_4 with *p*-H_2 in the presence of $[Rh_3H_2Cl_2(CO)_2((Ph_2PCH_2)_2\text{-}PPh)_2]^+$ as the catalyst.[10]

The existence of PHIP in the resonances of hydrogenation products provides unambiguous evidence that the transfer of hydrogen atoms to the organic substrate occurs in a pairwise manner, as opposed to a non-pairwise addition mechanism in which the added H atoms come from two different H_2 molecules. Subsequent work investigated the mechanistic differences between various catalysts that promoted pairwise addition. Under identical conditions for phenylacetylene hydrogenation, weak PHIP signals disappeared quickly (7–10 min) when $RhCl(PPh_3)_3$ was used as the catalyst, while for $Rh(cod)(dppe)^+$ (cod = 1,5-cyclooctadiene) as the catalyst, much stronger PHIP signals were seen and polarization was readily regenerated when the sample was removed from the probe, shaken, and reinserted into the spectrometer over numerous cycles.[40] In the former system, mixing the solution with the H_2 atmosphere above it did not bring back PHIP after 7–10 min, indicating rapid conversion of *para*-enriched H_2 back to the equilibrium mixture of the *ortho*- and *para*- spin states via reversible oxidative addition of H_2 to the Rh center competitive with the catalytic hydrogenation. However, in the latter system, the catalysis proceeded by rapid, reversible olefin binding followed by slower irreversible dihydrogen activation to lead to the product. The absence of facile, reversible H_2 oxidative addition for this catalyst system

meant that the *para*-enrichment of the dihydrogen atmosphere was maintained for longer than was found for Wilkinson's catalyst, $RhCl(PPh_3)_3$.

A more exciting application of PHIP for the mechanistic study of catalytic hydrogenations was the ability to observe and characterize intermediate species previously proposed but not directly detected. In 1994, Duckett *et al.* reported dihydride–olefin complexes of rhodium during the hydrogenation of those olefins using $RhCl(PPh_3)_3$ as catalyst under *p*-H_2.[41] The expected mononuclear complexes were present, as were dirhodium species $[RhH_2(PPh_3)_2(\mu\text{-}Cl)_2Rh(PPh_3)(olefin)]$ **21** that had been neither proposed nor seen previously (Scheme 8). Complete characterization of complexes **21** was achieved using *p*-H_2 and HMQC spectroscopy.[42] The HMQC experiments demonstrated that hydride ligands were coupled to two different ^{31}P nuclei when the hydrogenation of terminal olefins (olefin = stilbene, **21a**; 4-methylstyrene, **21b**; 4-chlorostyrene, **21c**; 1-hexene, **21d**) was studied, while during the hydrogenation of *cis*-stilbene and 1,1-diphenylethylene, similar species with only equivalent *trans*-phosphines were observed (**21e** and **21f**, respectively). These results with primary prochiral olefins and symmetrical diphenylethylenes helped to support the proposed structures for **21a–f**. Despite their presence during catalysis, however, complexes **21** were not thought to be intermediates in the principal mechanism of catalysis.

Further studies by Bargon and co-workers used PHIP to obtain evidence for coordination of styrene hydrogenation products to rhodium through the arene group.[43] Upon reaction of styrene and *p*-H_2, with $[Rh(cod)(dppbu)]BF_4$ as catalyst (dppbu = 1,4-*bis*(diphenylphosphino)butane), polarized resonances for the ethyl resonances of the ethylbenzene product appeared in the ^1H NMR spectrum in addition to resonances further upfield with the same coupling constants. The fact that the former resonances were downfield relative to those of free ethylbenzene led to the suggestion that the ethylbenzene product remained bound to the Rh center immediately after it was produced (Scheme 9). (The iridium analogs of these complexes are thermodynamically stable and had been isolated and

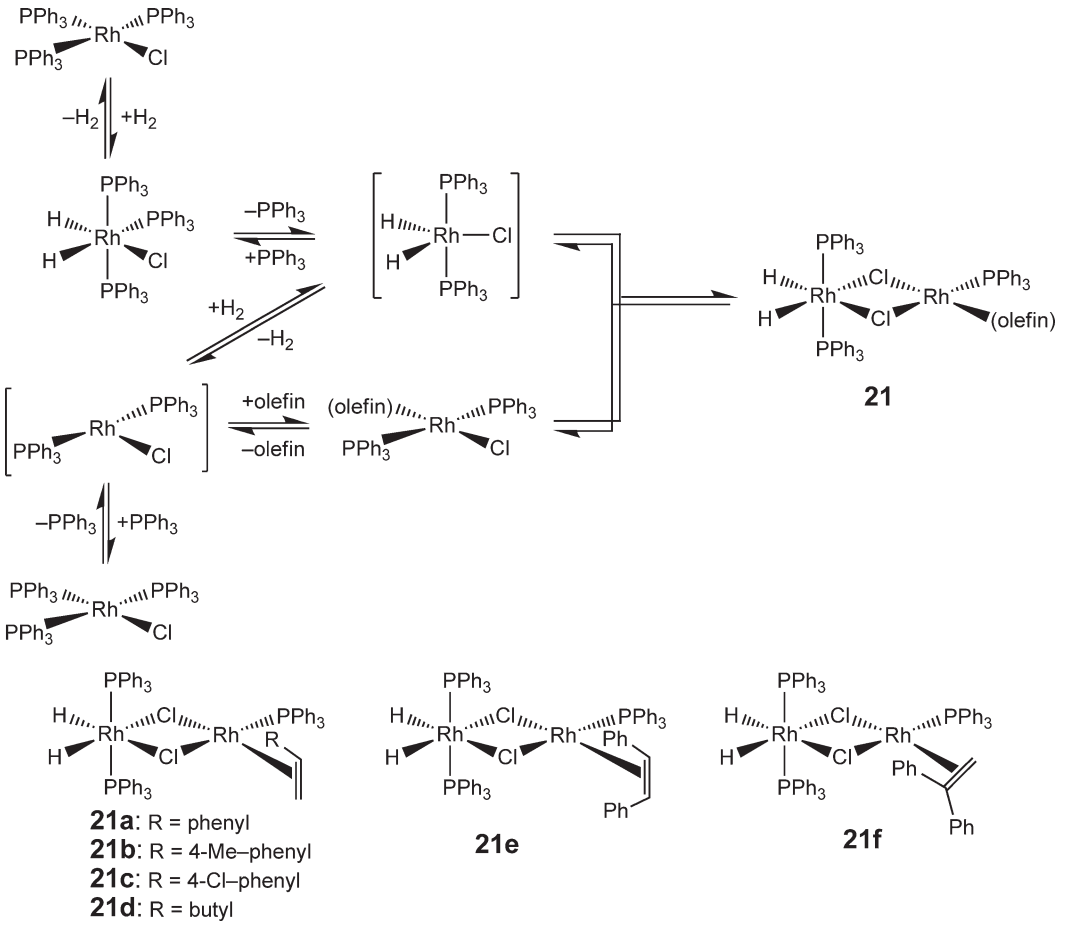

Scheme 8

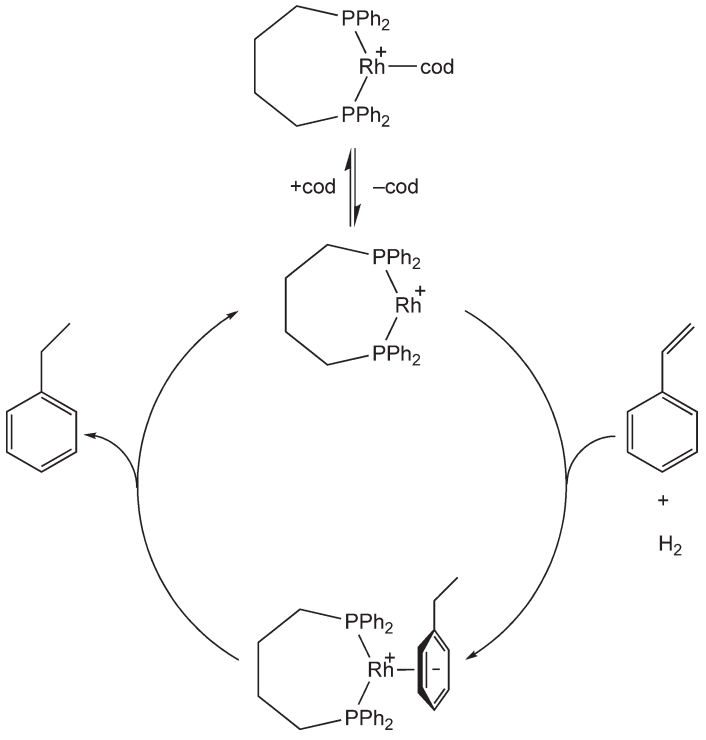

Scheme 9

characterized previously by Crabtree *et al.*[44]) When the chiral catalyst [Rh(cod)((*R*)-(*S*)-JOSIPHOS)]BF_4 was employed for the hydrogenation of 3-methylstyrene with *p*-H_2, polarized resonances corresponding to two diastereomeric species were observed, as were similar resonances for free 1-ethyl-3-methylbenzene (Equation (13)). Diastereomers were only possible by face selective binding of the 1-ethyl-3-methylbenzene product.

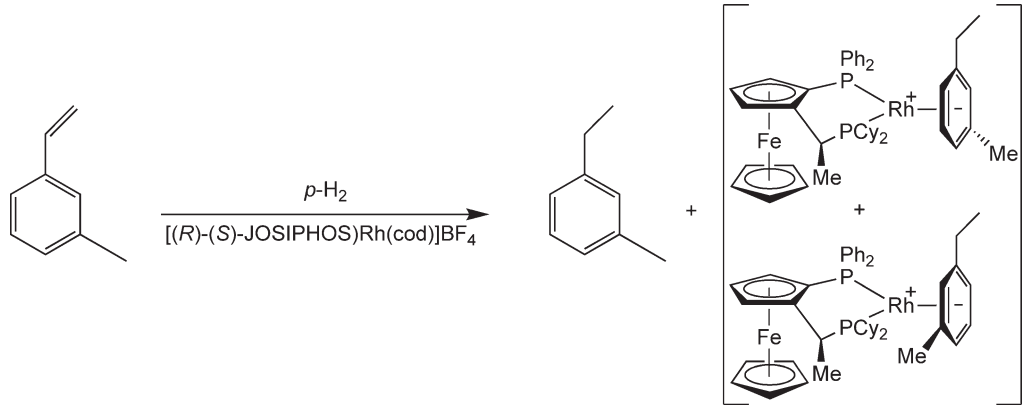

(13)

While the above experiments demonstrated that the rate of detachment of the ethylbenzene product was surprisingly slow after the hydrogenation of styrene, quantitative analysis of PHIP signals was shown to be useful for the determination of the rates of catalytic hydrogenation. Chinn and Eisenberg studied the hydrogenation of ethyl (*Z*)-α-acetamidocinnamate (EAC) to form *N*-acetyl-(*R*)-phenylalanine ethyl ester ($EACH_2$) using [Rh(NBD)-(chiraphos)]BF_4 (chiraphos = 2,3-*bis*(diphenylphosphino)butane) as the catalyst (Equation (14)).[45] Upon the addition of *p*-H_2, polarized resonances corresponding to H_a and H_c of Equation (14) were found to be of similar intensity in absorption/emission/absorption/emission (A/E/A/E) patterns, while the resonance corresponding to H_b was of weaker intensity and opposite phase (E/A/E/A). These observations were consistent with *cis*-addition of H_2 to the substrate. Kinetic information in this system was determined by following the decay of polarization of

resonances H_a and H_b (decay of the H_c resonance could not be followed accurately due to overlap with solvent). Interestingly, the time dependence of the polarization decay agreed with the rate of hydrogenation measured by integration of unpolarized product signals. The decay of polarization was determined to occur much more slowly than would be predicted solely based on spin-lattice relaxation alone, indicating that newly polarized product was formed as the previously formed product underwent rapid relaxation. The time dependence for the concentration of polarized product ($[^*EACH_2]$) was approximated as $[^*EACH_2] = A_0 \exp(-k_2[Rh]_T t)$ where $A_0 = \{k_2[Rh]_T/(k_1 - (k_2[Rh]_T))\}$; k_1 is the rate constant for relaxation of $^*EACH_2$, and k_2 is the rate constant for hydrogenation.

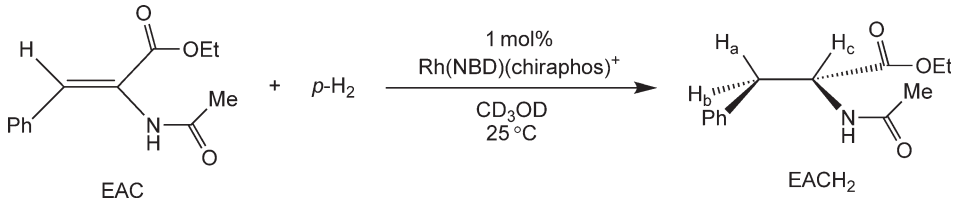

(14)

Bargon and co-workers also studied the kinetics of rhodium-catalyzed hydrogenations by analyzing the rate of polarization decay.[46] The methodology of Chinn and Eisenberg discussed above was used to determine the rates of alkyne hydrogenations using $[Rh(cod)(dppbu)]BF_4$ catalyst (k_{HYD}, Equation (15)). The hydrogenation of various styrenes was also studied, and the authors were able to determine the rate of detachment of hydrogenated product from the Rh center (k_{OFF}) in addition to the hydrogenation rate (k_{HYD}), as shown in Scheme 10. Both of these constants could be determined because the ethyl resonances were polarized for the bound product as well as the free product. The values of k_{HYD} and k_{OFF} were calculated for substrates with different *para*-substituents, and the results showed that as the electron-donating ability of the substituent increased, the hydrogenation rate increased while the rate of product detachment decreased. These observations were consistent with stronger bonding between the arene and the Rh center of the catalyst, thus giving an increase in K (and therefore k_{HYD}) and a decrease in k_{OFF} (see Scheme 10).

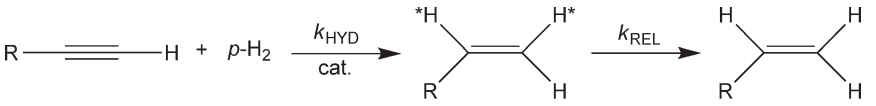

(15)

R = Ph, Me_3C, Me_3Si, Ph_3Si
k_{REL} = rate of relaxation of the polarized hydrogens

In addition to kinetic applications, Bargon and co-workers also used the $[Rh(cod)(dppbu)]BF_4$ catalytic hydrogenation system for the transfer of polarization from PHIP-active ^1H nuclei in the product to all of the carbon atoms in the products of alkyne hydrogenation.[47] For example, in addition to the alkene carbon atoms,

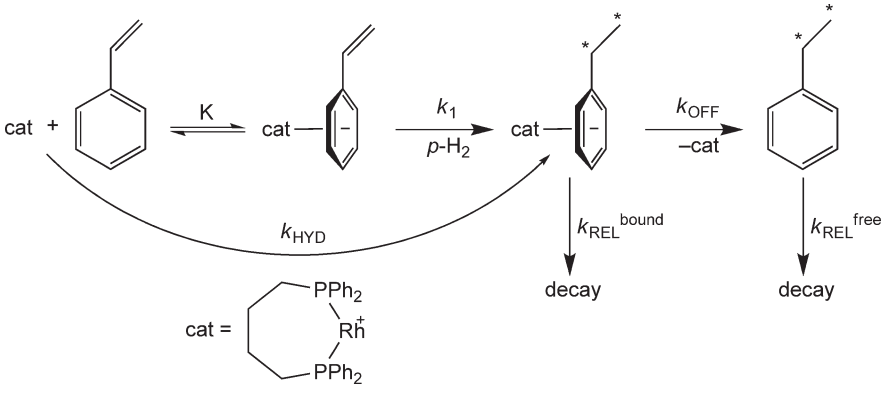

Scheme 10

polarization was transferred to the quaternary and methyl carbons of *tert*-butylethylene and the phenyl carbons of styrene. Similar results were observed for 1-, 2-, and 3-hexyne, and 4-octyne. These ^{13}C NMR spectra were obtained using just *one scan* with very good signal-to-noise ratios. Transfer of polarization to all carbon nuclei was possible because the hydrogenation occurred rapidly outside the magnetic field of the NMR spectrometer. In this very low magnetic field, the difference in resonance frequency between ^{1}H and ^{13}C was small relative to their coupling constants, which allowed for facile transfer of polarization.[47] This technique can permit the extremely efficient acquisition of ^{13}C NMR spectra. (No signals were observed for the starting material because these species were not PHIP-active.)

Aime *et al*. also demonstrated polarization transfer in the [Rh(cod)(dppbu)]BF_4-catalyzed hydrogenation system, in this case transferring polarization from the ^{1}H nuclei to ^{2}H via ^{13}C in the hydrogenation of acetylene-d_2 and ethylene-d_4. A single-scan ^{2}H NMR spectrum was recorded immediately after insertion of the sample into the NMR spectrometer to give polarized resonances for free ethylene-d_2 and ethane-d_4 (the products of acetylene-d_2 and ethylene-d_4 hydrogenation, respectively).[48] In the hydrogenation of ethylene-d_4, signal enhancements of 560 times were achieved for the deuterium resonance of ethane-d_4. Work from the same group also noted that PHIP occurred upon addition of p-H_2 to cod with [Rh(cod)(dppbu)]BF_4 as the catalyst in both the aliphatic *and* olefinic resonances of free cyclooctene product.[49] Although one might initially conclude that exchange between p-H_2 and the olefinic protons was the cause of polarization, there was no signal in the olefin region of the ^{2}H NMR spectrum when the hydrogenation was undertaken with D_2. Therefore, NOE transfers within a substrate hydrogenated with p-H_2 and within metal–hydride complexes best explained the data.

1.16.2.2.2 Ruthenium-catalyzed hydrogenation

PHIP has been used as a valuable tool for the determination of relative rates of ruthenium-catalyzed hydrogenations. For example, hydrogenation of styrene-d_8 and ethylene-d_4 with p-H_2 using $RuH_4(PPh_3)_3$ resulted in characteristic absorption/emission PHIP signals in the ^{1}H NMR spectrum corresponding to ethylbenzene.[50] However, in the hydrogenation of methyl acrylate and several alkynes, the outcome was quite different: "net" polarization occurred, in which the signals were completely in enhanced emission or enhanced absorption. This "net" polarization was consistent with hydrogenation outside the magnetic field of the NMR spectrometer.[51] The authors concluded that the hydrogenation of methyl acrylate and alkynes was more rapid than hydrogenation of styrene and ethylene using the $RuH_4(PPh_3)_3$ catalyst. In halogenated solvents, there was a large reduction in PHIP enhancement under otherwise identical hydrogenation conditions. Additionally, hydrogenation using $RuHCl(PPh_3)_3$ under p-H_2 yielded products with PHIP-enhanced signals in the ^{1}H NMR spectrum with significantly lower intensity than those seen with $RuH_4(PPh_3)_3$. Further experiments demonstrated that $RuHCl(PPh_3)_3$ was not directly involved in the catalysis, but instead $RuH_2(PPh_3)_3$ (in undetectable quantity) was likely the active hydrogenation catalyst. The large difference in PHIP signal intensity between the two catalysts supports this notion. Interestingly, hydrogenation of olefins with electron-withdrawing substituents such as acrylonitrile and tetracyanoethylene by $RuHCl(PPh_3)_3$ occurred extremely rapidly with no PHIP in the ^{1}H NMR spectrum, consistent with the conclusion that pairwise transfer of H_2 was not the major operative pathway for hydrogenation by this catalyst with these substrates. However, conclusions like this merit additional testing using non-PHIP methods.

As with the mononuclear system described above, changes in solvent polarity can have a significant effect on the active catalytic species when triruthenium clusters are used as catalysts. Upon addition of p-H_2 to $[Ru_3(CO)_{10}(dppe)]$ **22** and diphenylacetylene in $CDCl_3$, two enhanced signals corresponding to complex **23** in the ^{1}H NMR spectrum at −14.36 and +7.25 ppm appeared (Equation (16)).[52] The hydride resonance was coupled to two equivalent ^{31}P centers and the vinyl center. The spectrum also showed enhanced signals for *cis*-stilbene. EXSY experiments confirmed that there was direct magnetization transfer from **23** to *cis*-stilbene, indicating that the complex was actively involved in the hydrogenation process. When $[Ru_3(CO)_8(dppe)_2]$ **24** was used as the catalyst, only normal signals for *cis*-stilbene appeared, indicating that the catalysis occurred at a significantly slower rate. This trend was consistent with previous observations that catalysts with monodentate phosphines are more active, and that substrate binding is inhibited by the dppe ligand. Interestingly, when clusters **22** and **24** were used as catalysts in toluene-d_8 instead of $CDCl_3$, there were no cluster-based hydride resonances in the ^{1}H NMR spectrum, although hydrogenation of diphenylacetylene was evident by the appearance of normal signals corresponding to *cis*-stilbene. The only hydride product observed was identified as $[RuH_2(CO)_2(dppe)]$, indicating that the dppe ligand did not stabilize the ruthenium cluster under the reaction conditions.

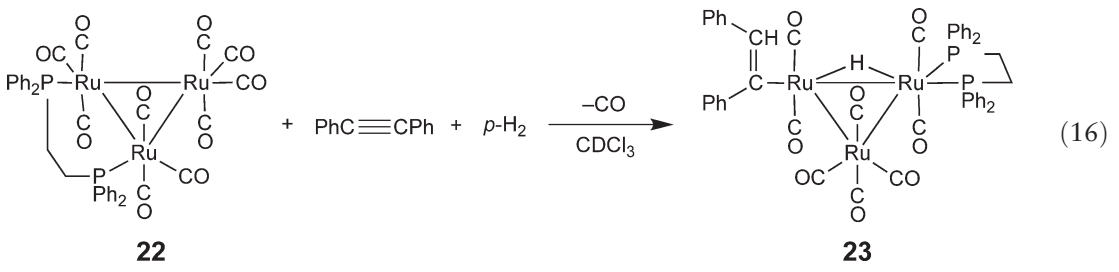

(16)

1.16.2.2.3 Platinum- and palladium-catalyzed hydrogenation

Bargon and co-workers first reported the use of PHIP in the study of alkyne-hydrogenation reactions catalyzed by platinum complexes in 1997 with Pt(alkyne)$(PPh_3)_2$, Pt$(C_2H_4)(PPh_3)_2$ + alkyne, and PtHCl$(PMePh_2)_2$ + $SnCl_2$ + alkyne systems.[53] In all three systems, hydrogenations using *p*-H_2 led to PHIP, indicating pairwise transfer of H_2. In the Pt/Sn system, the occurrence of PHIP was surprising since the reaction was generally thought to go through a two-step non-pairwise mechanism involving insertion of substrate into the Pt–H followed by hydrogenolysis of a Pt–alkenyl intermediate,[54] a process that would not be expected to yield any polarization with *p*-H_2. The fact that there was polarization was consistent with the possibility that a Pt(0) species was involved in the PHIP-producing mechanism of hydrogenation.

More recently, Duckett and co-workers reported on the mechanism of diphenylacetylene hydrogenation by a palladium catalyst bearing a very bulky phosphine ligand.[55] An interesting aspect of the work presented in this communication was its demonstration that, as also mentioned above in the context of the triruthenium system,[52] PHIP can be observed in the organic ligands of organometallic species that do not contain hydride ligands, which may represent an important complement to the large body of work involving PHIP in metal–dihydride species. The hydrogenation of diphenylacetylene with *p*-H_2 to form both *cis*- and *trans*-stilbene was studied using Pd$(OTf)_2$(bcope) **25** (OTf = trifluoromethanesulfonate; bcope = $(C_8H_{14})PCH_2CH_2P(C_8H_{14})$) as catalyst. The Pd–alkyl species that displayed PHIP-enhanced signals may account for the isomerization of *cis*-stilbene to the *trans*-isomer (Scheme 11).

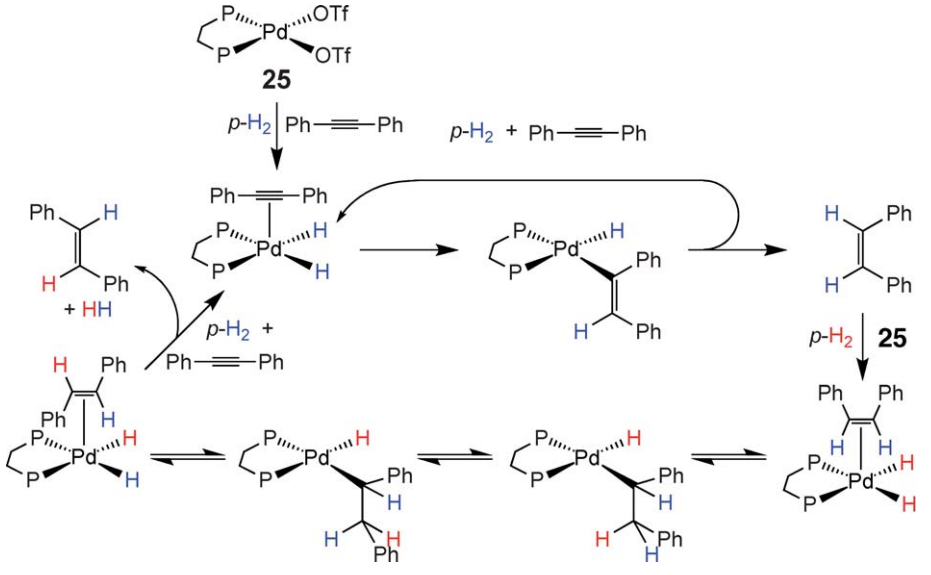

Scheme 11

1.16.2.3 Hydroformylation Chemistry

Hydroformylation is the largest scale industrial reaction based on homogeneous catalysis in which H_2 is a reactant.[56–64] A number of different metal catalyst systems have been employed for the reaction, including Rh(I) phosphine and phosphite carbonyl hydrides,[65–67] and platinum phosphine chlorides activated by $SnCl_2$ and $Co_2(CO)_8 + PR_3$.[60] At present, the Rh systems are most extensively used for both linear and branched aldehyde products. The reaction has been studied mechanistically with key steps involving olefin coordination, insertion into the M–H bond, migratory insertion of CO to generate a metal acyl, H_2 oxidative addition to form an acyl–dihydride intermediate, and reductive elimination of aldehyde product. The formation of branched product is central to asymmetric hydroformylation, in which interest has increased greatly.[58,68–78] Some catalysts have been developed that exhibit very respectable ee's in the hydroformylation of styrene.[77–79] In mechanistic terms, attention has been paid to key catalytic steps that determine the rate of reaction, and for asymmetric catalysis, its enantioselectivity, but important catalytic intermediates such as the key acyl–dihydride species have remained elusive to direct observation.[80–84]

Recently, several reports have appeared in which PHIP has been used to probe the mechanism of, and look for intermediates in model reactions related to, catalytic hydroformylation. Two of these studies focused on the detection and identification of species formed in small quantities,[85,86] while a third involved the discovery of an unexpected parahydrogen effect.[87]

The first of two hydroformylation studies by Duckett and co-workers involved the study of the stoichiometric reaction of $Ir(\eta^3\text{-}C_3H_5)(CO)(PPh_3)_2$ **26** with *p*-H_2 and CO.[85] Under *p*-H_2, **26** was found to generate two new species assigned to different isomers of $IrH_2(\eta^3\text{-}C_3H_5)(CO)(PPh_3)$ in a 1 : 1.8 ratio as a result of phosphine loss and oxidative addition of *p*-H_2 (Equation (17)); this process did not occur in the presence of excess PPh_3. At elevated temperatures, further reaction was observed, leading to the *mer*- and *fac*-isomers of $IrH_3(CO)(PPh_3)_2$, as well as propane and propene, all of which exhibited PHIP enhanced resonances. The PHIP results for propene and propane indicated that reversible interconversions between $IrH_2(\eta^3\text{-allyl})$, $IrH(\eta^2\text{-propene})$, and Ir(propyl) species were occurring readily to transfer the polarized protons into the propene and propane detected experimentally.

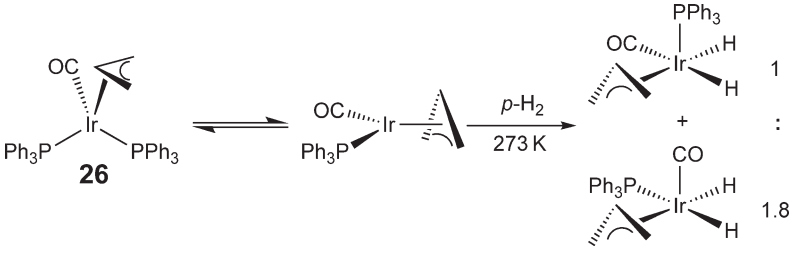

(17)

Under a 2 : 1 ratio of CO and *p*-H_2 (3 atm), the allyl complex **26** was seen to generate the alkyl dihydride **27** and acyl dihydride **28** with PHIP-enhanced hydride signals in the ^{1}H NMR spectrum; assignment of the complexes was supported using ^{13}C-labeling and HMQC methods to correlate the hydride signals with either a single terminal carbonyl resonance or those of the acyl and terminal carbonyl ligands, respectively (Scheme 12). There was also a PHIP-enhanced signal for **27** corresponding to the Ir-bound methylene proton of the $\eta^1\text{-}C_3H_5$ ligand, which required reversible generation of a propene–hydride intermediate. Further warming led to production of the hydroformylation products $CH_3CH_2CH_2CHO$ and $CH_3CH(CH_3)CHO$.

Duckett and co-workers have also studied PHIP in hydroformylation with a related cobalt η^3-allyl model system, for which no Co–H intermediates or products were detected.[86] When a 1 : 2 mixture of CO and *p*-H_2 (3 atm) was added to $Co(\eta^3\text{-}C_3H_5)(CO)_2(PCy_3)$ **29** at 363 K, a ^{1}H NMR spectrum and a ^{1}H–^{1}H COSY experiment revealed enhanced resonances corresponding to a linear propyl group and an isopropyl group. Use of ^{13}CO showed that these were metal-bound species (**30** and **31**, respectively; see Scheme 13). The linear and branched aldehyde products also displayed enhanced signals, as shown in Scheme 13. The high signal strengths of the aldehyde products allowed their production to be monitored even at very early reaction times. A mechanism involving reversible formation of $CoH(\eta^2\text{-}$propene) and Co(propyl) species was put forward to account for the polarization seen in all of the alkyl resonances of intermediate species and products. These studies underscore the ability of PHIP to: (i) aid in the study of intermediate organometallic species even when no metal hydride ligands are observed directly and (ii) monitor product formation due to the increased signal obtained using *p*-H_2.

In 2002, work from the authors' laboratory revealed a different parahydrogen-related effect in a model hydroformylation system. The initial observation was made in the reaction of $Pt(COEt)Cl(PPh_3)_2 + SnCl_2$ with *p*-H_2 that

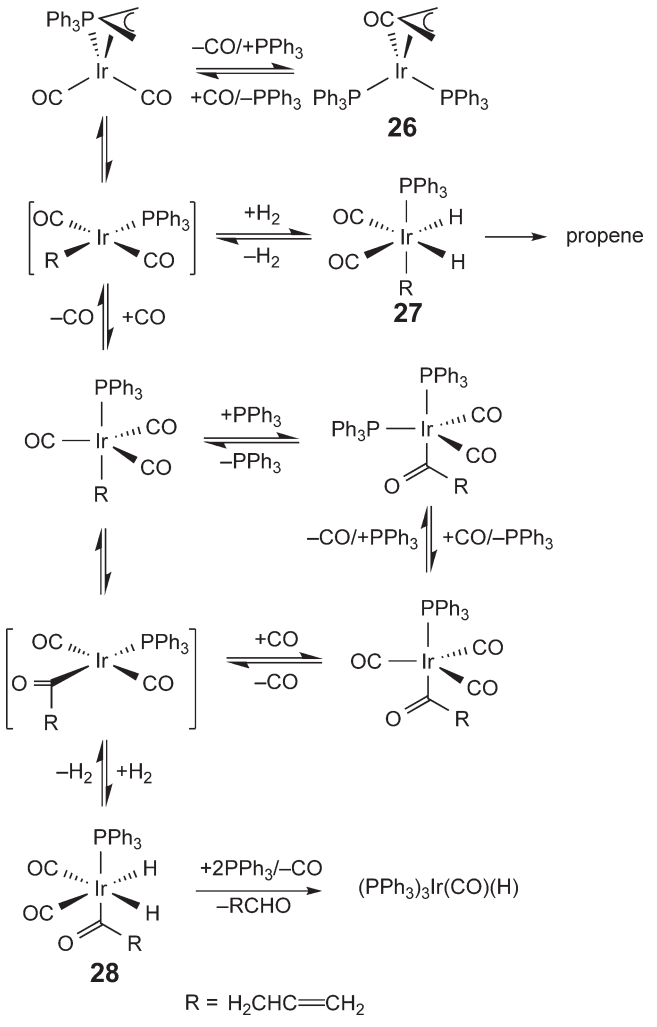

Scheme 12

led to a ^{1}H NMR spectrum in which the product aldehyde resonance was in emission only—a result referred to as oneH-PHIP.[87] This unusual and unexpected observation was followed up with work on the previously reported model system Ir(COEt)(CO)$_2$(dppe) **32** (dppe = bis(diphenylphosphino)ethane), from which propanal is generated upon reaction with H_2 and for which the acyl dihydride **33** had been identified using normal H_2.[88] When the reaction was conducted with parahydrogen, it was found to produce aldehyde emission only when conditions were such that second order effects were seen in some of the resonances of the acyl dihydride. This in turn led to an interpretation of one H-PHIP based on: (i) second-order mixing to alter the parahydrogen-induced non-Boltzmann spin populations in the acyl–dihydride intermediate and (ii) stereoselective reductive elimination of EtCHO from **33**, that is, the aldehyde product contained specifically H_b from **33** (Scheme 14). The latter arises because of the steric constraint of the dppe ligand and the *cis*-nature of C–H reductive elimination from the metal center. Variation of temperature and solvent (benzene-d_6/acetone-d_6 in different ratios) changed the chemical shift difference between the two hydride resonances of **33** that in turn altered any second-order effects, leading to corresponding changes in the oneH-PHIP resonance. In all cases, the signal enhancement of oneH-PHIP was smaller than that of conventional PHIP.

The basis of oneH-PHIP is proposed to result from second-order mixing of $\alpha\beta$ and $\beta\alpha$ spin states, leading to one level with slightly greater $\alpha\beta - \beta\alpha$ (*para*) character and the other with slightly greater $\alpha\beta + \beta\alpha$ (*ortho*) character. (The $\alpha\beta$ and $\beta\alpha$ states can be viewed as linear combinations of equally weighted *para*- and *ortho*- (T_0) spin functions.) Therefore if one of the levels has slightly greater *para*-character, it will acquire a greater population from reaction

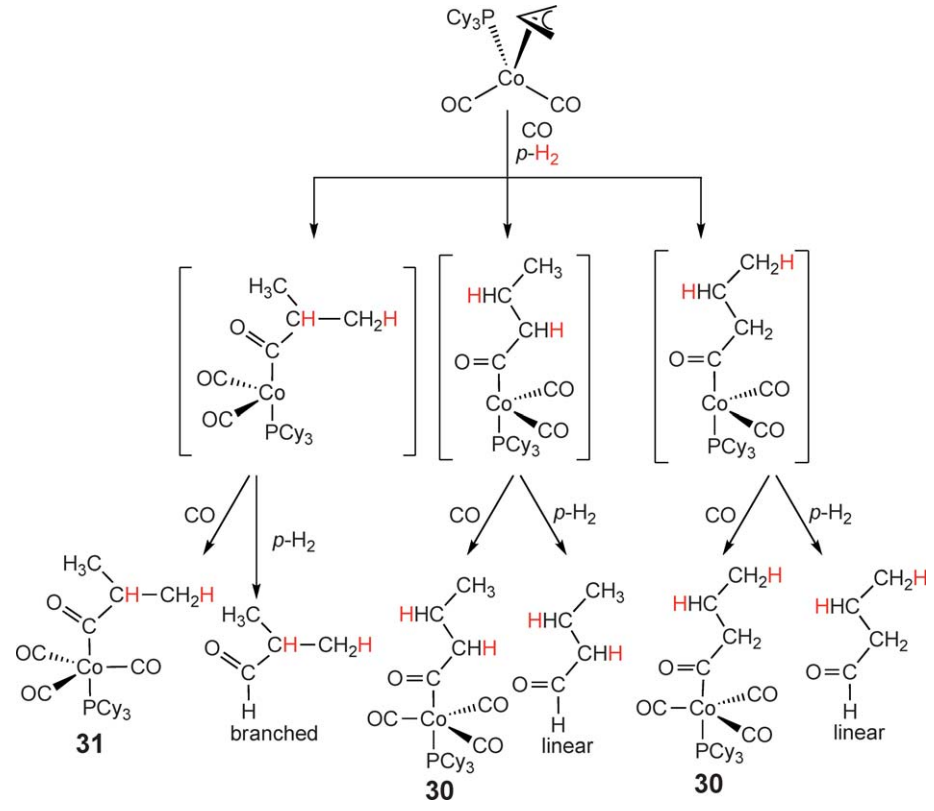

Scheme 13

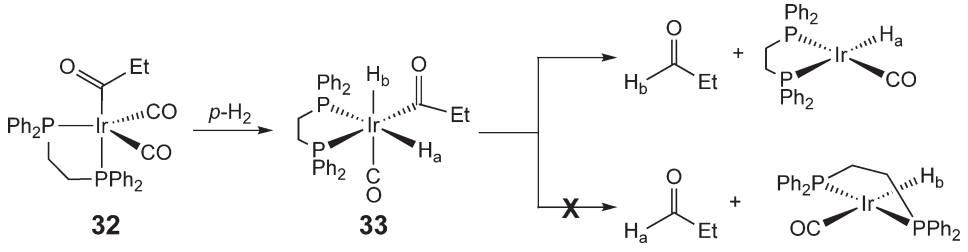

Scheme 14

with *para*-enriched H_2, and upon stereoselective reductive elimination involving only one of the two hydrides of **33**, polarization in the aldehyde resonance will be seen.

1.16.3 Parahydrogen Addition to Tantalocene Complexes

Prior to 1997, the occurrence of PHIP in systems involving early transition metal complexes was unknown, but over the past decade, it has been found and used with success in tantalocene chemistry.

1.16.3.1 Reaction of Parahydrogen with Tantalocene–Benzyne and –Phenyl Complexes

Previous work by Bercaw and co-workers showed that the addition of dihydrogen to the tantalocene–benzyne complex **34** resulted first in the tantalocene–phenyl dihydride **35**, followed by formation of the trihydride **36** and benzene (Scheme 15).[89–92] Although these transformations were thought to proceed via intermediate Ta(III) species

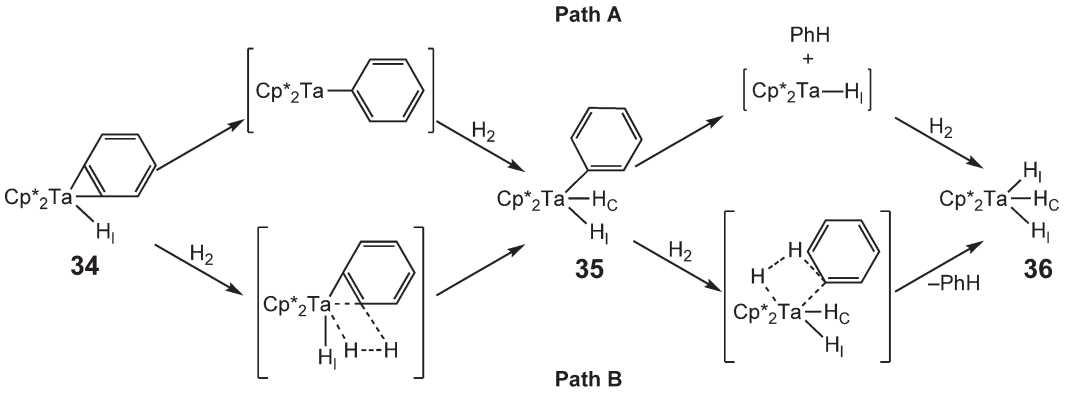

Scheme 15

(Scheme 15, path A), in part based on magnetization transfer experiments, the use of *p*-H_2 had the potential to determine unequivocally whether this hypothesis was the case, or if an alternative concerted σ-bond metathesis mechanism (Scheme 15, path B) was operative. Addition of *p*-H_2 to complex **34** resulted in PHIP-enhanced signals for both of the hydride ligands of **35**, consistent with pairwise addition of dihydrogen to an intermediate Ta(III)–phenyl species (path A) rather than by direct reaction of H_2 to the formally Ta(V)–benzyne complex (path B).[93] Over time, the final trihydride product **36** forms with PHIP-enhanced resonances for the new hydride ligands denoted as H_c for central and H_l for lateral positions in the bent metallocene complex. A second H_l ligand exists for **36** that would not show polarization. The second oxidative addition proceeds via prior reductive elimination of benzene from **35** to give a Ta(III)–hydride species followed by a *cis*-concerted reaction of this Ta(III) species with H_2. The observation of PHIP in this reaction proves unequivocally that the oxidative addition of H_2 gives a *cis*-dihydride product, even for an early metal species (Scheme 15).

1.16.3.2 Reaction of Parahydrogen with a Tantalocene–Alkylidene Complex

Hydrogenation chemistry similar to that seen for the benzylidene complex **34** was also found to occur for the methylidene–hydride complex **37**. Again, the sole organometallic product is tantalocene trihydride **36** formed through hydrogen addition and methane loss. As for the reaction of **34** with H_2, two mechanisms can be envisaged, one proceeding by a Ta(III) methyl species and H_2 oxidative addition (path A) and the other involving a concerted [2 + 2]-addition (path B), as shown in Scheme 16. The latter is akin to a σ-bond metathesis mechanism, and was thought to be possible since the formally Ta(V)–methylidene complex **37** was unable to undergo oxidative addition without prior rearrangement. PHIP was used by Bregel *et al.* to determine which mechanism, path A or path B of Scheme 16, was operative in this transformation.[94] In the case of path A, polarization would be expected in the two hydride resonances of the methyl–dihydride complex **38** after oxidative addition to the Ta(III) intermediate, while path B would result in polarization in one of the hydride resonances and the methyl resonance after concerted

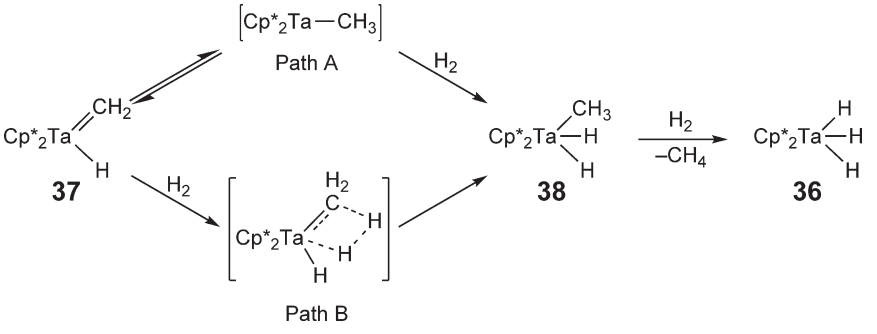

Scheme 16

addition. It was notable that the methyl dihydride **38** had not been observed previously, although α-insertion to form the Ta(III) methyl species from **37** had been noted through magnetization transfer. Upon addition of *p*-H_2 to the methylidene hydride **37**, there was polarization of both resonances of the final trihydride product **36**, as well as polarized resonances at 2.73 and 0.57 ppm, which were assigned to the methyl–dihydride complex **38**. While the ^{1}H chemical shifts for **38** were similar to those of the hydride ligands for phenyl dihydride **35**, it was not immediately clear whether the resonances corresponded to two Ta–H ligands or to one Ta–H and one Ta–CH_3. However, addition of *p*-H_2 to complex **37** labeled with ^{13}C in the alkylidene ligand yielded ^{13}C–^{1}H couplings too small to represent one-bond coupling (~11 and ~3 Hz), indicating that the polarized resonances corresponded to the two hydride ligands and not a hydride and CH_3 proton. Therefore, the observation of **38**, which would have been impossible without the use of PHIP, led to the conclusion that addition of H_2 to complex **37** proceeded through a Ta(III) intermediate, as illustrated in path A of Scheme 16.

1.16.3.3 Reaction of Parahydrogen with a Tantalum–Dinitrogen Complex

Reaction of H_2 with the dinuclear tantalum–dinitrogen complex $(Cp^*_2TaCl)_2(\mu\text{-}N_2)$ **39** at 60 °C was found to result in the formation of both the unsymmetrical and symmetrical isomers of $Cp^*_2TaH_2Cl$ (**40** and **41**, respectively; Scheme 17).[95] Complex **40** displayed two hydride signals (doublets) at 6.7 and 5.1 ppm in the ^{1}H NMR spectrum, while **41** had one singlet hydride signal at 7.1 ppm. Upon addition of *p*-H_2 to **39** at 75 °C, acquisition of the ^{1}H NMR spectrum revealed strong polarization for the hydride resonances of **40** (signal enhancement of greater than 1,000-fold was observed). However, no polarization for **41** was found (PHIP requires that the hydrogen atoms that originate in the *p*-H_2 molecule be inequivalent in the product). The strong polarization seen in the unsymmetrical dihydride **40** (coupled with experiments in which addition of H_2 to $Cp^*_2TaCl(THF)$ at room temperature gave **40** only, followed by **41** over time; Equation (18)) was consistent with initial formation of **40** followed by slower isomerization to give an equilibrium mixture with **41**.

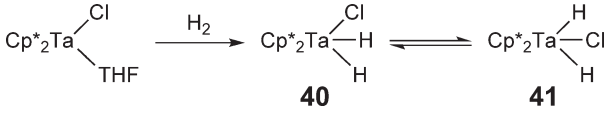

(18)

1.16.4 Conclusion

In this chapter, we have summarized work from a number of laboratories that demonstrates that PHIP is a useful tool for the study of mechanistic organometallic chemistry. While the enhanced signals of PHIP provide nominally simple evidence for pairwise addition of H_2, PHIP can be employed in many cases to determine much more complicated aspects of reaction mechanisms involving hydrogen addition. It is important to note, however, that PHIP has yet to be observed in σ-bond metathesis reactions or in metal–dihydrogen complexes.

PHIP provides conclusive evidence for oxidative additions in d^{10}–d^8 (Pt(0)), d^8–d^6 (Ir(I), Rh(I), Ru(0)), and d^2–d^0 (Ta(III)) systems through polarization of the hydride resonances in the resulting dihydride complexes. These experiments make possible the observation of minor isomers of species and also enable the authors to reach important mechanistic conclusions that could not be obtained or supported using traditional methods.

Mechanistic studies of hydrogenation and hydroformylation chemistry were undertaken using complexes of group 8, 9, and 10 metals as catalysts. The exploration of hydrogenation reactions led to the observation of reaction intermediates through polarization of metal hydride resonances as well as polarization in the resonances of hydrogenation products, both free and still bound to the catalyst. Hydroformylation reactions were studied using parahydrogen with both model systems and active catalysts. The use of parahydrogen allowed for the observation of

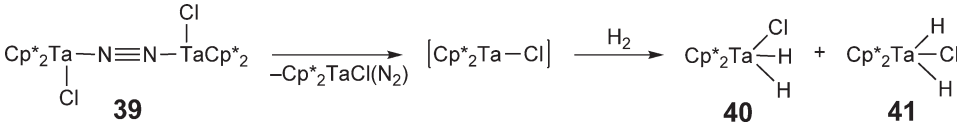

Scheme 17

intermediate dihydride species as well as metal–alkyl complexes through the enhanced resonances that appeared in the ^{1}H NMR spectra acquired over the course of the hydroformylation reactions. Additionally, an unusual phenomenon by which the aldehydic proton of the product aldehyde was in enhanced emission or absorption in Pt and Ir systems was described (oneH-PHIP).

A very exciting use of the signal enhancement of PHIP is the transfer of the resulting polarization to heteronuclei. This application permits the acquisition of NMR spectra of heteronuclei such as ^{13}C, ^{31}P, and ^{2}H in much less time than could be achieved otherwise. In systems where this process can be used, the course of a reaction can be followed using the NMR spectra of X nuclei in addition to ^{1}H NMR spectra, since these spectra can be acquired very rapidly. Similarly, the use of parahydrogen allows for the rapid acquisition of 2D NMR spectra by indirect detection of X nuclei using the added protons of p-H_2.

Acknowledgment

We wish to thank the National Science Foundation for support of PHIP-related research conducted in the authors' laboratory over the years.

References

1. Farkas, A. *Orthohydrogen, Parahydrogen and Heavy Hydrogen*; Cambridge University Press: New York, 1935.
2. Duckett, S. B.; Sleigh, C. J. *Prog. Nucl. Magn. Reson. Spectrosc.* **1999**, *23*, 71–92.
3. Bowers, C. R.; Weitekamp, D. P. *J. Am. Chem. Soc.* **1987**, *109*, 5541.
4. Duckett, S. B. Personal communication.
5. Eisenberg, R. *Acc. Chem. Res.* **1991**, *24*, 110–116.
6. Eisenberg, R.; Eisenschmid, T. C.; Chinn, M. S.; Kirss, R. U. Parahydrogen-induced Polarization and Polarization Transfer in Hydrogenation and Oxidative Addition Reactions. In *Homogeneous Transition Metal Catalyzed Reactions*; Moser, W. R., Slocum, D. W., Eds.; American Chemical Society: Washington, DC, 1992; pp 47–74.
7. Natterer, J.; Bargon, J. *Prog. Nucl. Magn. Reson. Spectrosc.* **1997**, *31*, 293–315.
8. Bowers, C. R. Sensitivity Enhancement Utilizing Parahydrogen. In *Encyclopedia of Nuclear Magnetic Resonance*; Grant, D. M., Harris, R. K., Eds.; Wiley: Chichester, 2002; pp 750–770.
9. Duckett, S. B.; Blazina, D. *Eur. J. Inorg. Chem.* **2003**, 2901–2912.
10. Eisenschmid, T. C.; Kirss, R. U.; Deutsch, P. P.; Hommeltoft, S. I.; Eisenberg, R.; Bargon, J.; Lawler, R. G.; Balch, A. L. *J. Am. Chem. Soc.* **1987**, *109*, 8089–8091.
11. Eisenschmid, T. C.; McDonald, J.; Eisenberg, R.; Lawler, R. G. *J. Am. Chem. Soc.* **1989**, *111*, 7267–7269.
12. Duckett, S. B.; Newell, C. L.; Eisenberg, R. *J. Am. Chem. Soc.* **1993**, *115*, 1156–1157.
13. Hasnip, S.; Duckett, S. B.; Taylor, D. R.; Taylor, M. J. *Chem. Commun.* **1998**, 923–924.
14. Harrod, J. F.; Yorke, W. J. *Inorg. Chem.* **1981**, *20*, 1156–1159.
15. Collman, J. P.; Hegedus, L. S.; Norton, J. R.; Finke, R. G. *Principles and Applications of Organotransition Metal Chemistry*; University Science Books: Mill Valley, 1987.
16. Duckett, S. B.; Field, L. D.; Messerle, B. A.; Shaw, W. J.; Soler, L. P. *J. Chem. Soc., Dalton Trans.* **2000**, 2251–2253.
17. Albietz, P. J.; Houlis, J. F.; Eisenberg, R. *Inorg. Chem.* **2002**, *41*, 2001–2003.
18. Brothers, P. J.; Roper, W. R. *Chem. Rev.* **1988**, *88*, 1293–1326.
19. Appleton, T. G.; Berry, R. D.; Hall, J. R.; Neale, D. W. *J. Organomet. Chem.* **1989**, *364*, 249–273.
20. Clark, G. R.; Hoskins, S. V.; Roper, W. J. *J. Organomet. Chem.* **1982**, *234*, C9–C12.
21. Burrell, A. K.; Clark, G. R.; Rickard, C. E. F.; Roper, W. R. *J. Organomet. Chem.* **1994**, *482*, 261–269.
22. Hughes, R. P.; Rose, P. R.; Rheingold, A. L. *Organometallics* **1993**, *12*, 3109–3117.
23. Hughes, R. P.; Lindner, D. C.; Rheingold, A. L.; Liable-Sands, L. M. *J. Am. Chem. Soc.* **1997**, *119*, 11544–11545.
24. Crespi, A. M.; Shriver, D. F. *Organometallics* **1985**, *4*, 1830–1835.
25. Koola, J. D.; Roddick, D. M. *Organometallics* **1991**, *10*, 591–597.
26. Richmond, T. G.; Crespi, A. M.; Shriver, D. F. *Organometallics* **1984**, *3*, 314–319.
27. Permin, A.; Eisenberg, R. *Inorg. Chem.* **2002**, *41*, 2451–2458.
28. Duckett, S. B.; Eisenberg, R. *J. Am. Chem. Soc.* **1993**, *115*, 5292–5293.
29. Morran, P. D.; Duckett, S. B.; Howe, P. R.; McGrady, J. E.; Colebrooke, S. A.; Eisenberg, R.; Partridge, M. G.; Lohman, J. A. B. *J. Chem. Soc., Dalton Trans.* **1999**, 3949–3960.
30. Koch, A.; Bargon, J. *Inorg. Chem.* **2001**, *40*, 533–539.
31. Moulton, C. J.; Shaw, B. L. *J. Chem. Soc., Chem. Commun.* **1976**, 365–366.
32. Schwartz, D. J.; Andersen, R. A. *J. Am. Chem. Soc.* **1995**, *117*, 4014–4025.
33. Jang, M.; Duckett, S. B.; Eisenberg, R. *Organometallics* **1996**, *15*, 2863–2865.
34. Duckett, S. B.; Barlow, G. K.; Partridge, M. G.; Messerle, B. A. *J. Chem. Soc., Dalton Trans.* **1995**, 3427–3429.
35. Duckett, S. B.; Mawby, R. J.; Partridge, M. G. *J. Chem. Soc., Chem. Commun.* **1996**, 383–384.
36. Schott, D.; Sleigh, C. J.; Lowe, J. P.; Duckett, S. B.; Mawby, R. J.; Partridge, M. G. *Inorg. Chem.* **2002**, *41*, 2960–2970.
37. Schott, D.; Callaghan, P.; Dunne, J.; Duckett, S. B.; Godard, C.; Goicoechea, J. M.; Harvey, J. N.; Lowe, J. P.; Mawby, R. J., Müller, G., *et al. Dalton Trans.* **2004**, 3218–3224.
38. Aime, S.; Dastru, W.; Gobetto, R.; Reineri, F.; Russo, A.; Viale, A. *Organometallics* **2001**, *20*, 2924–2927.

39. Aime, S.; Gobetto, R.; Canet, D. *J. Am. Chem. Soc.* **1998**, *120*, 6770–6773.
40. Kirss, R. U.; Eisenberg, R. *J. Organomet. Chem.* **1989**, *359*, C22–C26.
41. Duckett, S. B.; Newell, C. L.; Eisenberg, R. *J. Am. Chem. Soc.* **1994**, *116*, 10548–10556.
42. Colebrooke, S. A.; Duckett, S. B.; Lohman, J. A. B.; Eisenberg, R. *Chem. Eur. J.* **2004**, *10*, 2459–2474.
43. Giernoth, R.; Huebler, P.; Bargon, J. *Angew. Chem., Int. Ed.* **1998**, *37*, 2473–2475.
44. Crabtree, R. H.; Mellea, M. F.; Quirk, J. M. *J. Chem. Soc., Chem. Commun.* **1981**, 1217–1218.
45. Chinn, M. S.; Eisenberg, R. *J. Am. Chem. Soc.* **1992**, *114*, 1908–1909.
46. Hubler, P.; Giernoth, R.; Kummerle, G.; Bargon, J. *J. Am. Chem. Soc.* **1999**, *121*, 5311–5318.
47. Stephan, M.; Kohlmann, O.; Niessen, H. G.; Eichhorn, A.; Bargon, J. *Magn. Reson. Chem.* **2002**, *40*, 157–160.
48. Aime, S.; Gobetto, R.; Reineri, F.; Canet, D. *J. Chem. Phys.* **2003**, *119*, 8890–8896.
49. Aime, S.; Canet, D.; Dastru, W.; Gobetto, R.; Reineri, F.; Viale, A. *J. Phys. Chem. A* **2001**, *105*, 6305–6310.
50. Kirss, R. U.; Eisenschmid, T. C.; Eisenberg, R. *J. Am. Chem. Soc.* **1988**, *110*, 8564–8566.
51. Pravica, M. G.; Weitekamp, D. P. *Chem. Phys. Lett.* **1988**, *145*, 255–258.
52. Prestwich, T. G.; Blazina, D.; Duckett, S. B.; Dyson, P. J. *Eur. J. Inorg. Chem.* **2004**, 4381–4387.
53. Klages, S.; Permin, A. B.; Petrosyan, V. S.; Bargon, J. *J. Organomet. Chem.* **1997**, *545–546*, 201–205.
54. James, B. R. *Homogeneous Hydrogenation*; Wiley: New York, 1973.
55. Dunne, J. P.; Aiken, S.; Duckett, S. B.; Konya, D.; Almeida Lenero, K. Q.; Drent, E. *J. Am. Chem. Soc.* **2004**, *126*, 16708–16709.
56. Parshall, G. W.; Ittel, S. D. *Homogeneous Catalysis. The Applications and Chemistry of Catalysis by Soluble Transition Metal Complexes*, 2nd ed.; Wiley: New York, 1992.
57. Pruett, R. L. Hydroformylation. In *Advances in Organometallic Chemistry: Catalysis and Organic Syntheses*; Stone, F. G. A., West, R., Eds.; Academic Press: New York, 1979; Vol. 17, p 1.
58. Buisman, G. J. H.; Kamer, P. C. J.; van Leeuwen, P. W. N. M. *Tetrahedron: Asymmetry* **1993**, *4*, 1625–1634.
59. van Koten, G.; van Leeuwen, P. W. N. M. Homogeneous Catalysis with Transition Metal Complexes. In *Catalysis: An Integrated Approach*; van Santen, R. A., van Leeuwen, P. W. N. M., Moulijn, J. A., Averill, B. A., Eds.; Elsevier: Amsterdam, 1999; pp 289–342.
60. Ungvary, F. *Coord. Chem. Rev.* **2002**, *228*, 61–82.
61. Riley, D. P.; Tremont, S. J. Homogeneous Catalysis of Organic Reactions by Complexes of Metal Ions. In *Mechanisms of Inorganic and Organometallic Reactions*; Twigg, M. V., Ed.; Plenum: New York, 1988; pp 335–374.
62. Buisman, G. J. H.; Martin, M. E.; Vos, E. J.; Klootwijk, A.; Kamer, P. C. J.; van Leeuwen, P. W. N. M. *Tetrahedron: Asymmetry* **1995**, *6*, 719–738.
63. van Leeuwen, P. W. N. M.; Roobeek, C. F. *J. Organomet. Chem.* **1983**, *258*, 343–350.
64. Cotton, F. A.; Wilkinson, G. *Advanced Inorganic Chemistry*, 5th ed.; Wiley: New York, 1988; pp 1455.
65. Claver, C.; van Leeuwen, P. W. N. M. Asymmetric Hydroformylation. In *Rhodium Catalyzed Hydroformylation*; van Leeuwen, P. W. N. M., Claver, C., Eds.; Kluwer: Amsterdam, 2000, p 284.
66. van Leeuwen, P. W. N. M. Introduction to Hydroformylation: Phosphorus Ligands in Homogeneous Catalysis. In *Rhodium Catalyzed Hydroformylation*; van Leeuwen, P. W. N. M., Claver, C., Eds.; Kluwer: Amsterdam, 2000; pp 1–13.
67. van Leeuwen, P. W. N. M.; van Koten, G. *Stud. Surf. Sci. Catal.* **1993**, *79*, 199–248.
68. Nozaki, K.; Takaya, H.; Hiyama, T. *Top. Catal.* **1998**, *4*, 175–185.
69. Breit, B. *Acc. Chem. Res.* **2003**, *36*, 264–275.
70. Kamer, P. C. J.; van Strijdonck, G. P. F.; Reek, J. N. H.; van Leeuwen, P. W. N. M. *Syn. Methods Organomet. Inorg. Chem.* **2002**, *10*, 42–63.
71. Stanley, G. G. *Adv. Cat. Processes* **1997**, *2*, 221–243.
72. Wink, D. J.; Kwok, T. J.; Yee, A. *Inorg. Chem.* **1990**, *29*, 5006–5008.
73. Cuny, G. D.; Buchwald, S. L. *J. Am. Chem. Soc.* **1993**, *115*, 2066–2068.
74. Sakai, N.; Nozaki, K.; Mashima, K.; Takaya, H. *Tetrahedron: Asymmetry* **1992**, *3*, 583–586.
75. Laneman, S. A.; Stanley, G. G. Homogeneous Bimetallic Hydroformylation Catalysis: Two Metals are Better Than One. In *Homogeneous Transition Metal Catalyzed Reactions*; Moser, W. R., Slocum, D. W., Eds.; American Chemical Society: Washington, DC, 1992; pp 349–366.
76. Babin, J. E.; Whiteker, G. T. U.S. Patent 5,260-938, 1994.
77. Nozaki, K.; Sakai, N.; Nanno, T.; Higashijima, T.; Mano, S.; Horiuchi, T.; Takaya, H. *J. Am. Chem. Soc.* **1997**, *119*, 4413–4423.
78. Deerenberg, S.; Kamer, P. C. J.; van Leeuwen, P. W. N. M. *Organometallics* **2000**, *19*, 2065–2072.
79. Sakai, N.; Mano, S.; Nozaki, K.; Takaya, H. *J. Am. Chem. Soc.* **1993**, *115*, 7033–7034.
80. Casey, C. P.; Whiteker, G. T.; Melville, M. G.; Petrovich, L. M.; Gavney, J. A.; Powell, D. R. *J. Am. Chem. Soc.* **1992**, *114*, 5535–5543.
81. Casey, C. P.; Petrovich, L. M. *J. Am. Chem. Soc.* **1995**, *117*, 6007–6014.
82. Casey, C. P.; Paulsen, E. L.; Beuttenmueller, E. W.; Proft, B. R.; Petrovich, L. M.; Matter, B. A.; Powell, D. R. *J. Am. Chem. Soc.* **1997**, *119*, 11817–11825.
83. Casey, C. P.; Paulsen, E. L.; Beuttenmueller, E. W.; Proft, B. R.; Matter, B. A.; Powell, D. R. *J. Am. Chem. Soc.* **1999**, *121*, 63–70.
84. Oswald, A. A.; Hendriksen, D. E.; Kastrup, R. V.; Mozeleski, E. J. Electronic Effects on the Synthesis, Structure, Reactivity, and Selectivity of Rhodium Hydroformylation Catalysts. In *Homogeneous Transition Metal Catalyzed Reaction*; Moser, W. R., Slocum, D. W., Eds.; American Chemical Society: Washington, DC, 1992; pp 395–418.
85. Godard, C.; Duckett, S. B.; Henry, C.; Polas, S.; Toose, R.; Whitwood, A. C. *Chem. Commun.* **2004**, 1826–1827.
86. Godard, C.; Duckett, S. B.; Polas, S.; Tooze, R.; Whitwood, A. C. *J. Am. Chem. Soc.* **2005**, *127*, 4994–4995.
87. Permin, A. B.; Eisenberg, R. *J. Am. Chem. Soc.* **2002**, *124*, 12406–12407.
88. Deutsch, P. P.; Eisenberg, R. *Organometallics* **1990**, *9*, 709–718.
89. van Asselt, A.; Burger, B. J.; Gibson, V. C.; Bercaw, J. E. *J. Am. Chem. Soc.* **1986**, *108*, 5347–5349.
90. Parkin, G.; Bunel, E.; Burger, B. J.; Trimmer, M. S.; van Asselt, A.; Bercaw, J. E. *J. Mol. Catal.* **1987**, *41*, 21–39.
91. Trimmer, M. S. Ph.D. Thesis, California Institute of Technology, Pasadena, CA, 1989.
92. Antonelli, D. M.; Schaefer, W. P.; Parkin, G.; Bercaw, J. E. *J. Organomet. Chem.* **1993**, *462*, 213–220.
93. Millar, S. P.; Zubris, D. L.; Bercaw, J. E.; Eisenberg, R. *J. Am. Chem. Soc.* **1998**, *120*, 5329–5330.
94. Bregel, D. C.; Oldham, S. M.; Eisenberg, R. *J. Am. Chem. Soc.* **2002**, *124*, 13827–13832.
95. Bregel, D. C.; Oldham, S. M.; Lachicotte, R. J.; Eisenberg, R. *Inorg. Chem.* **2002**, *41*, 4371–4377.

1.17 Solid-state NMR Spectroscopy in Organometallic Chemistry

R E Wasylishen and G M Bernard, University of Alberta, Edmonton, AB, Canada

1.17.1 Introduction

Nuclear magnetic resonance (NMR) spectroscopy has become an indispensable technique for the characterization of molecules in most areas of chemical research, including organometallic chemistry. Until recently, most NMR studies in the latter area of research have been of diamagnetic compounds dissolved in isotropic solvents. Although much information can be gained from such studies, there are many benefits to investigations of organometallic complexes in the solid state via NMR.[1] For some compounds, solution NMR is not possible, as they may either be insoluble or decompose upon dissolution. Furthermore, many organometallic compounds are fluxional, particularly when dissolved in isotropic liquids.[2] Although molecular dynamics may also influence the NMR spectra obtained from solid samples, this behavior is more readily investigated by variable-temperature solid-state NMR, since one is not restricted to temperatures dictated by the solvent. In the absence of X-ray or neutron diffraction data, solid-state NMR provides an important method for characterizing organometallic compounds. When diffraction data are available, solid-state NMR provides a valuable link between the structure observed in the solid state and that for the compound in solution. For example, solid-state NMR may be used to verify that a compound that has been subjected to solution NMR studies maintains the same structure as that determined in the solid state via X-ray crystallography. Perhaps most important, the orientation dependence of interactions such as magnetic shielding, spin–spin coupling, and the electric field gradient (EFG), can be investigated by solid-state NMR spectroscopy.

Until recently, most NMR studies of solids have involved spin-1/2 nuclei, particularly ^{13}C, ^{15}N, ^{29}Si, and ^{31}P.[1,3–6] Since over 70% of magnetically active nuclei are quadrupolar (i.e., they have nuclear spin $I > 1/2$), a wealth of information about organometallic compounds is potentially available from solid-state NMR investigations of these isotopes. The advent of high-field NMR magnets ($B_0 > 17.6$ T, corresponding to ^{1}H frequencies of 750 MHz or greater) combined with the development of new NMR techniques and hardware, such as NMR probes capable of spinning samples rapidly about the magic angle, have rendered most diamagnetic compounds containing NMR-active isotopes, as well as ligand nuclei of paramagnetic compounds, accessible to the solid-state NMR spectroscopist.

The objective of this chapter is to provide an overview of current solid-state NMR techniques for the study of organometallic compounds. Although the techniques discussed here are applicable to such studies, actual examples are not restricted to organometallic compounds. Recent applications of solid-state NMR techniques are also presented, but a complete review of the literature is beyond the scope of this chapter; review articles are cited when available. In Section 2, the fundamental concepts required for a basic understanding of solid-state NMR spectroscopy are presented. The discussion of the NMR techniques is divided into three sections: NMR of spin-1/2 nuclei (Section 3), NMR of quadrupolar nuclei (Section 4) and NMR of ligand nuclei in paramagnetic compounds (Section 5). Finally, some recent applications of solid-state NMR in organometallic chemistry are highlighted (Section 6).

1.17.2 Background

A brief overview of the theory describing the NMR spectra obtained for solid samples is presented below. An understanding of fundamental NMR concepts, as presented in several introductory texts,[7–13] is assumed.

1.17.2.1 Chemical Shift Tensors

The magnetic shielding experienced by a nucleus is described by a second-rank tensor, represented by a 3×3 matrix.[14] Although the shielding tensor is comprised of symmetric and antisymmetric components,[15] the latter generally do not have a measurable effect on NMR spectra[16] and hence will not be considered further here. The symmetric portion of the shielding tensor may be described by six parameters: the three diagonal elements of the tensor, σ_{xx}, σ_{yy}, and σ_{zz}, as well as three off-diagonal elements, $\sigma_{xy} = \sigma_{yx}$, $\sigma_{xz} = \sigma_{zx}$, and $\sigma_{yz} = \sigma_{zy}$. However, more commonly, the tensor is described in terms of its principal axis system (PAS) in which the off-diagonal elements are zero and the three diagonal elements, referred to as the principal components, are designated by $\sigma_{11} \leq \sigma_{22} \leq \sigma_{33}$. Hence, for practical purposes, the shielding tensor may be fully described by three principal components and by three Euler angles that describe the orientation of the PAS in the molecular framework.

In the preceding, the σ_{ii} describe the magnetic shielding of the nucleus relative to that for the bare nucleus, and consequently are known as the components of the absolute shielding tensor.[17] Experimentally, one measures the principal components of the chemical shift (CS) tensor relative to the frequency of a standard sample.[18]

$$\delta_{ii,\text{sample}}(\text{ppm}) = \frac{(\nu_{ii,\text{sample}} - \nu_{\text{iso,ref}})(\text{Hz})}{(\nu_{\text{iso,ref}})(\text{MHz})} \tag{1}$$

where $\nu_{ii,\text{sample}}$ is the resonance frequency for a given principal component of the shielding tensor of the sample and $\nu_{\text{iso,ref}}$ is the isotropic resonance frequency for the reference compound. Although this equation is well known, errors in referencing are not uncommon. In particular, some commercial software programs incorrectly calculate $\delta_{ii,\text{sample}}$ using the spectrometer's transmitter frequency for $\nu_{\text{iso,ref}}$; this may introduce an error in the ppm scale if the observed frequency is significantly different from that of the reference compound, a common occurrence when acquiring NMR spectra for metal nuclei or of ligand nuclei in paramagnetic compounds (*vide infra*). By convention, CS tensor components are reported in ppm, such that $\delta_{11} \geq \delta_{22} \geq \delta_{33}$. The CS tensor is directly related to the magnetic shielding according to: [17]

$$\delta_{ii} = \frac{\sigma_{\text{ref}} - \sigma_{ii}}{1 - \sigma_{\text{ref}}} \tag{2}$$

For nuclei of elements in the first or second row of the periodic table, $\sigma_{\text{ref}} \ll 1$, such that $\delta_{ii} \approx \sigma_{\text{ref}} - \sigma_{ii.}$ Absolute magnetic shielding tensor components can be determined if σ_{ref} is known;[17] however, it is more common to determine the CSs of the principal components relative to that of a reference compound. Gustavsson and Mårtensson-Pendrill have shown that the current values for the magnetogyric ratios (γ) of heavier nuclei are subject to significant error since σ_{ref} is not known accurately for these.[19]

NMR spectra are usually referenced on the δ scale according to Equation (1). However, when comparing nuclear magnetic properties of different isotopes, frequencies are sometimes expressed in MHz on the Ξ scale.[18] On this scale, the frequency of the reference compound for the nucleus of interest is referenced to the ^{1}H frequency of TMS, in a dilute solution (volume fraction <1%) in chloroform, in a magnetic field such that its frequency would be exactly 100 MHz. Harris *et al.*[18] list Ξ values for many isotopes in various reference compounds that are extremely valuable to experimentalists.

In the absence of spin–spin interactions, the NMR spectrum of an isolated spin-1/2 nucleus for a sample in solution consists of a single peak, since rapid molecular tumbling leads to averaging of the magnetic shielding tensor. However, in solid-state NMR, one usually acquires spectra for powder samples, generally consisting of randomly-oriented microcrystals. As an example of the NMR spectra obtained in such cases, the carbon CS tensor for ethylene is considered.[20] For crystals oriented such that B_0 is perpendicular to the plane described by ethylene, an NMR peak at 24 ppm is obtained (Figure 1, upper trace). As illustrated in this figure, very different values are obtained for crystals oriented such that B_0 is either parallel to the C–C bond, or in the plane of the molecule but perpendicular to this bond. An NMR spectrum of a stationary powder is the sum of contributions from all microcrystals in the sample (Figure 1, lower trace).[6,16] Although one may obtain NMR spectra from single crystals and directly determine the principal components of the CS tensor,[21,22] such experiments are often impractical since they are time consuming, and suitable single crystals are often difficult to grow. However, the principal components may be determined from the spectrum of a stationary powder sample; in the absence of any other interactions, these may be obtained directly from the shoulders and the discontinuity in the spectrum, as illustrated in the lower trace of Figure 1. In addition, the principal components may sometimes be determined from the spinning-sideband pattern of NMR spectra acquired with slow magic angle spinning (MAS) samples, using the methods of Herzfeld and Berger[23] or of Maricq and Waugh.[24]

While the procedure outlined above yields the principal components of the CS tensor, NMR spectra of isolated spins in powder samples generally do not contain information about the orientation of the CS tensor in the molecular framework. This may sometimes be deduced from those determined for similar compounds, or from the local molecular symmetry. In our lab, we have often relied on the dipolar CS method,[25–27] which uses the orientation dependence of the dipolar interaction[28] between a spin pair to orient the principal components of the CS tensor relative to the dipolar vector. Remaining ambiguities in the tensor orientation may be resolved via first-principles calculations.[29,30]

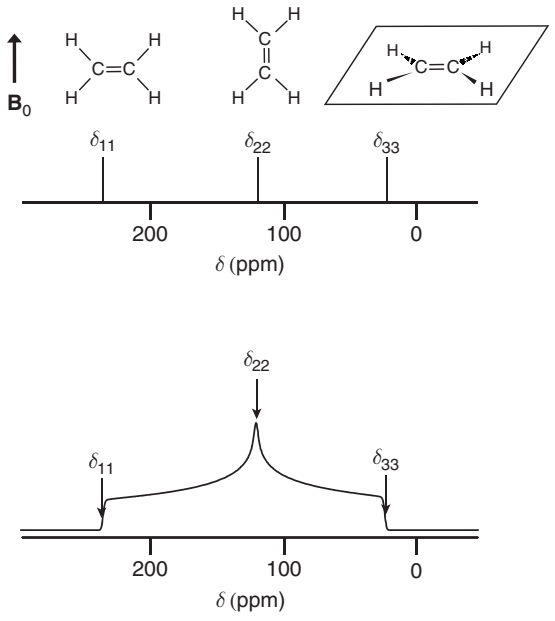

Figure 1 Carbon-13 NMR spectra expected for ethylene based on the CS tensor parameters reported by Zilm *et al.*, $\delta_{11} = 234$, $\delta_{22} = 120$, and $\delta_{33} = 24$ ppm.[20] The upper trace is that expected for a sample containing three crystals placed such that the ethylene is in the orientations illustrated above the peaks with B_0 as indicated. The lower trace is the ^{13}C NMR spectrum expected for a stationary powder sample.

In the ensuing discussion, three parameters will be used to describe the CS tensors.[31] The isotropic CS, δ_{iso}, is the average of the three principal components of the CS tensor:

$$\delta_{iso} = \tfrac{1}{3}(\delta_{11} + \delta_{22} + \delta_{33}) \tag{3}$$

Because of solvent effects, the value for δ_{iso} measured in the solid state usually differs slightly from that obtained for the same sample in solution. The span, Ω, and the skew, κ, are also used to describe the CS tensor:

$$\Omega = \delta_{11} - \delta_{33} \tag{4}$$

$$\kappa = \frac{3(\delta_{22} - \delta_{iso})}{\Omega} \tag{5}$$

Values for κ range from 1.0 ($\delta_{11} = \delta_{22}$) to -1.0 ($\delta_{22} = \delta_{33}$). Unfortunately, the conventions and choice of parameters used to describe CS tensors measured by NMR are not universally agreed upon. See the articles by Harris[32] and by Jameson[33] for a discussion of this issue.

1.17.2.2 The Quadrupolar Interaction

For an ensemble of crystallographically equivalent nuclei with spin I, $2I$ NMR transitions take place. For most elements, the most abundant spin-active isotope is quadrupolar with half-integer spin. For these nuclei, spectroscopists usually focus on the $m_I = 1/2 \rightarrow m_I = -1/2$ transition since it is not perturbed by the first-order quadrupolar interaction (i.e., to a first approximation, this transition behaves like that for a spin-1/2 nucleus, see below). Hence, an overview of the theory for half-integer spin quadrupolar nuclei is presented here. For a thorough description of the theory for the quadrupolar interaction, readers are referred to numerous texts and reviews on the topic.[34–40]

Nuclei, unless at sites of high symmetry (e.g., $T_{d,}$ O_h), experience an EFG, which is described by a second-rank tensor. In its PAS, the principal components of this tensor are defined such that $|eq_{zz}| \geq |eq_{yy}| \geq |eq_{xx}|$. Because the tensor is traceless and symmetric, only two parameters are required to describe the principal components of the EFG, eq_{zz} and the asymmetry parameter:

$$\eta_Q = \frac{q_{xx} - q_{yy}}{q_{zz}} \tag{6}$$

where $0 \leq \eta_Q \leq 1$. EFGs have no effect on the NMR spectra of spin-1/2 nuclei, since the nuclear charge distribution for these nuclei is spherically symmetric. However, nuclei with spin $I > 1/2$ have an asymmetric nuclear charge distribution, described by the nuclear quadrupole moment, Q, which may interact with the EFG.[36,37,40] This interaction generally dominates the NMR spectra of quadrupolar nuclei.

The magnitude of the nuclear quadrupolar interaction, in frequency units, is described by the quadrupolar coupling constant, C_Q:

$$C_Q = \frac{e^2 Q q_{zz}}{h} \tag{7}$$

where h is Planck's constant. A convenient parameter when discussing the NMR spectra of quadrupolar nuclei is the so-called quadrupolar frequency, ν_Q:

$$\nu_Q = \frac{3C_Q}{2I(2I-1)} \tag{8}$$

In the absence of a magnetic field, one can, in principle, characterize the EFG tensor using nuclear quadrupolar resonance, (NQR),[41] microwave,[42] or zero-field NMR[43] spectroscopy. The quadrupolar interaction also manifests itself in NMR spectra. Obtaining NMR spectra for nuclei where the Larmor frequency, ν_0, is less than or approximately equal to ν_Q is generally challenging; this is not considered further here, although we note that quadrupolar parameters may sometimes be determined indirectly via NMR in such cases (see Section 4.3). In the ensuing discussion, the line shapes obtained for NMR spectra of quadrupolar nuclei in the case where $\nu_0 \gg \nu_{Q,}$ known as the high-field approximation, are considered.

The NMR transition frequencies for quadrupolar nuclei are generally discussed in terms of first- and second-order perturbation theory where the quadrupolar interaction is treated as a perturbation of the Zeeman interaction.[3,4,36,37,44] Although the central transition (CT) is not perturbed by the first-order quadrupolar interaction, the remaining $2I-1$ single-quantum transitions (i.e., the satellite transitions (STs)) are perturbed by both the first- and second-order quadrupolar interactions (*vide infra*).

1.17.2.2.1 NMR spectra for the satellite transitions of half-integer quadrupolar nuclei

To a good approximation, powder NMR line shapes for the STs of quadrupolar nuclei may be understood by first-order perturbation theory; thus, we first consider these transitions. To first order, the transition frequencies, $\nu_Q(m_I,m_I-1)$, expected for a quadrupolar nucleus, are given by

$$\nu_Q(m_I,m_I-1) = \nu_0 - \frac{\nu_Q}{4}(1-2m_I)(3\cos^2\beta - 1 + \eta_Q \sin^2\beta \cos 2\alpha) \tag{9}$$

where α and β are polar angles orienting B_0 in the PAS of the EFG tensor (Figure 2) and m_I ranges from I to $-I+1$. Figure 3 illustrates the ^{27}Al ($I = 5/2$) NMR spectrum obtained for $KAl(SO_4)_2{\cdot}12H_2O$.[45] The lower traces show the calculated spectrum, as well as the four STs calculated for this spin-5/2 system. Obtaining complete powder NMR spectra for quadrupolar nuclei, particularly for stationary samples, is usually impractical since the spectra often span hundreds of kHz. Exceptions are the nuclei that have small nuclear quadrupole moments such

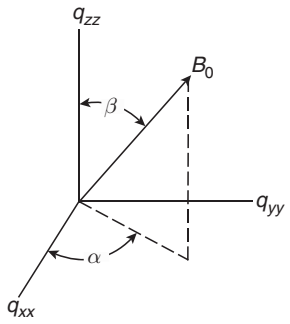

Figure 2 Polar angles describing the orientation of B_0 in the PAS of the EFG tensor.

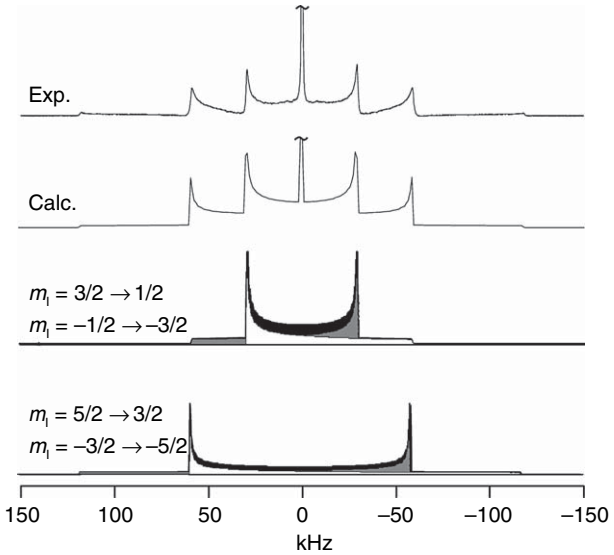

Figure 3 Aluminum-27 NMR spectrum of a stationary sample of aluminum potassium sulphate dodecahydrate acquired at 7.05 T (upper trace). Shown below this spectrum is the calculated spectrum, assuming $C_Q = 395$ kHz and $\eta_Q = 0.0$. The peak from the central transition is truncated in both the experimental and calculated spectra. The lower two traces are the satellite transitions contributing to the total spectrum. The frequency of the central transition was arbitrarily set to 0.0.

as ^{2}H ($I = 1$), ^{6}Li ($I = 1$), or ^{133}Cs ($I = 7/2$). However, as will be shown in the following section, the orientation dependence of the EFG also manifests itself in the NMR spectra of the CT for half-integer quadrupolar nuclei.

Although the first-order quadrupolar interaction dominates the line shape for the STs of quadrupolar nuclei, the second-order interaction (*vide infra*) also contributes to their line shapes and peak positions, particularly when considering the NMR spectra of MAS samples. Figure 4 illustrates an ^{27}Al NMR spectrum of an MAS sample of $Al(acac)_3$.[45] The breadth of the spinning sideband pattern, ±900 kHz, demonstrates the effect of the first-order quadrupolar interaction for a nucleus with a significant quadrupolar coupling, 3.03 MHz.[46] The expansion of the region near 450 kHz is that near the edge of the range covered by the $m_I = 3/2 \rightarrow m_I = 1/2$ and the $m_I = -1/2 \rightarrow m_I = -3/2$ transitions. Thus, the peaks arising from the $m_I = 5/2 \rightarrow m_I = 3/2$ and the $m_I = -3/2 \rightarrow m_I = -5/2$ transitions dominate. The second-order quadrupolar interaction accounts for the distinctive line shape seen for the peaks of the $m_I = 5/2 \rightarrow m_I = 3/2$ and the $m_I = -3/2 \rightarrow m_I = -5/2$ transitions, as well as for the separation of the peaks arising from each transition. A similar pattern is seen in the expansion of the region near −200 kHz, although in this case, the peaks for the $m_I = 3/2 \rightarrow m_I = 1/2$ and the $m_I = -1/2 \rightarrow m_I = -3/2$ transitions are more intense.

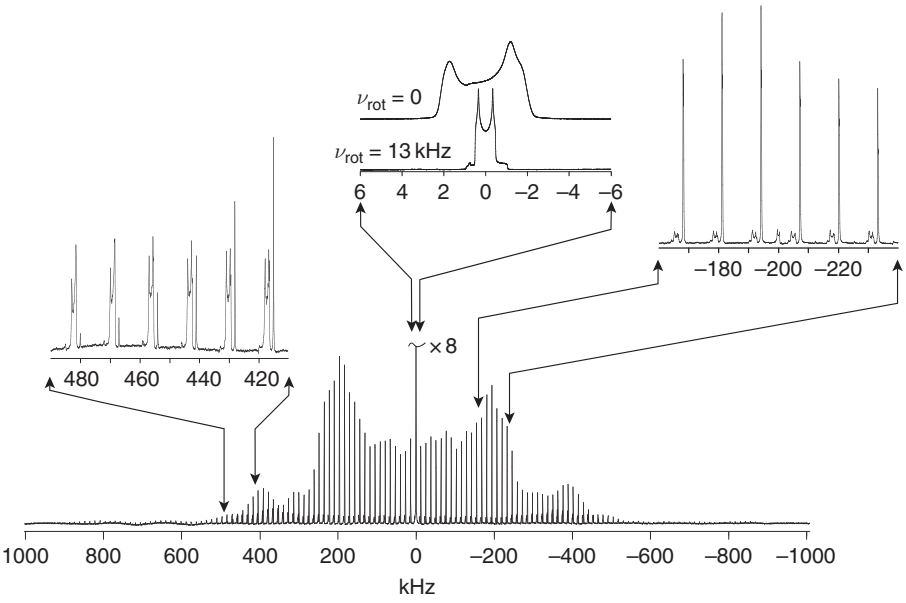

Figure 4 Aluminum-27 NMR spectra of Al(acac)$_3$ acquired at 7.05 T.[45] All spectra were obtained with $\nu_{rot} = 13$ kHz except for the upper trace of the central transition, which is that of a stationary sample. The small peak at approximately 750 Hz in the spectrum of the central transition of the MAS sample arises from the $m_I = 3/2 \rightarrow m_I = 1/2$ and the $m_I = -1/2 \rightarrow m_I = -3/2$ transitions. The small peak at −200 kHz in the expansion on the right is an artefact. Note that the expansions illustrated here were obtained from separate NMR experiments. The corresponding regions in the lower trace are similar to the expansions obtained for MAS samples, but have lower resolution since the wide sweep width required the use of a lower digital resolution.

1.17.2.2.2 The central transition for NMR spectra of half-integer quadrupolar nuclei

To first order, the CT for half-integer quadrupolar nuclei is not perturbed by the quadrupolar interaction (Equation (9)); however, second-order perturbation theory is typically required to properly describe the line shape and position of the CT. For the case where the EFG tensor is axially symmetric (i.e., $\eta_Q = 0.0$) and in the absence of anisotropic magnetic shielding, the frequencies, $\nu_Q(1/2, -1/2)$, for the CT of a stationary powder sample are given by[34]

$$\nu_Q(1/2,-1/2) = \frac{1}{16}\frac{\nu_Q^2}{\nu_0}\left[I(I+1)-\frac{3}{4}\right](1-\cos^2\beta)(1-9\cos^2\beta) \tag{10}$$

Because of the angular dependence of the second-order quadrupolar interaction, the CT contains a distinctive line shape that can be used to deduce C_Q and η_Q. Another important consequence of the second-order term is the dependence of the line shapes on the term ν_Q^2/ν_0. Since ν_Q is invariant to the applied magnetic field while ν_0 scales linearly with B_0, acquiring NMR spectra at higher applied magnetic fields results in significant line narrowing in the absence of anisotropic magnetic shielding. Figure 5 illustrates the CT ^{11}B NMR spectra of hexamethylborazine acquired with MAS at three different applied magnetic fields.[47] However, readers must be aware that the NMR spectra of quadrupolar nuclei may be broadened at higher B_0 values if the anisotropic magnetic shielding is significant, particularly for stationary samples.[48,49] Nevertheless, acquiring NMR spectra at high magnetic fields, when practical, may allow the resolution of multiple sites, and facilitates obtaining spectra of MAS samples for which the spinning sidebands do not interfere with those of the central peak. The expression defining the line shape of the CT for nuclei where the EFG tensor is not axially symmetric (i.e., $\eta_Q \neq 0$) is more complicated;[34] however, the second-order broadening also depends on ν_Q^2/ν_0.[34] For a stationary sample, the breadth of the CT, $\Delta\nu_{CT}$, is given by

$$\Delta\nu_{CT} = \frac{(\eta_Q^2 + 22\,\eta_Q + 25)}{144\,\nu_0}\left[\frac{9C_Q^2}{[(2I)(2I-1)]^2}\right]\left[I(I+1)-\frac{3}{4}\right] \tag{11}$$

Clearly, a smaller C_Q, a higher spin number or a higher applied magnetic field reduces the breadth of the CT.

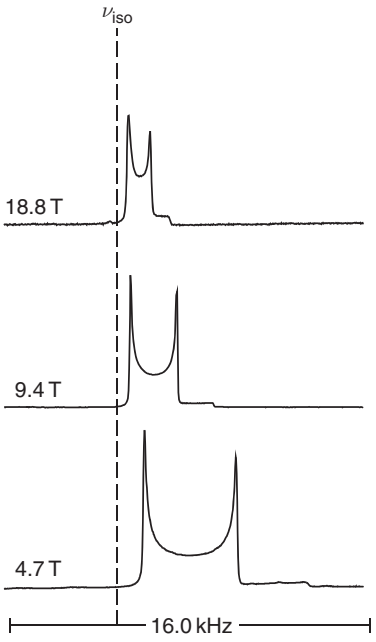

Figure 5 Boron-11 NMR spectra of an MAS sample of solid hexamethylborazine acquired at various applied magnetic fields. Reprinted, with permission from: Forgeron, M. A. M.; Bryce, D. L.; Wasylishen, R. E.; Rösler, R. *J. Phys. Chem. A* **2003**, *107*, 726–735. © 2003 American Chemical Society.

Unlike spectra for spin-1/2 nuclei, determining δ_{iso} does not merely entail a determination of the center of mass of the NMR spectrum of a stationary sample, nor is it simply the CS for the isotropic peak of a spectrum obtained with MAS. This is because the quadrupole interaction also results in a shift, $\Delta\nu_{m,m-1}$, in the frequency of the NMR transitions. The shift of the CT is given by

$$\Delta\nu_{1/2,-1/2} = \nu_{iso} - \frac{\nu_Q^2}{30\,\nu_0}\left[I(I+1) - \frac{3}{4}\right]\left(1 + \frac{\eta^2}{3}\right) \tag{12}$$

where ν_{iso} is the isotropic CS in frequency units. Note that the quadrupolar shift also is field dependent, as illustrated in Figure 5, where $\Delta\nu_{1/2,-1/2}$ decreases with increasing B_0. The second-order quadrupolar interaction also results in a shift in the position of the STs;[50] this effect generally is only detected in the spectra of MAS samples, for example, see the insets to Figure 4.

As a consequence of the different angular dependencies of the two terms describing the line shape for half-integer quadrupolar nuclei (Equation (10)), there is no single spinning angle that will average the second-order quadrupolar interaction.[51] Hence, a distinctive line shape is obtained for the CT, regardless of spinning frequency or angle, although the peaks are narrowed compared to those obtained from stationary samples. As shown in the expansion of the CT in Figure 4, MAS can reduce the line width while maintaining the distinctive line shapes from which the quadrupolar parameters may be derived. Since the anisotropic magnetic shielding for $Al(acac)_3$ is small,[46] the line narrowing in the spectra of the MAS sample is almost entirely due to partial averaging of the second-order quadrupolar interaction.

In this section, the effects of the quadrupolar interaction on NMR spectra of quadrupolar nuclei have been considered. Additional information about the environment around quadrupolar nuclei may be obtained from the anisotropic magnetic shielding, which often also contributes to the NMR spectra of quadrupolar nuclei. For example, the relative orientations of the CS and EFG tensors may be determined.[52] Since these two interactions have opposite responses to differences in the applied magnetic field (second-order broadening decreases with increasing B_0 while that arising from anisotropy in the magnetic shielding increases), acquiring NMR spectra at two or more applied magnetic fields often allows the spectroscopist to separate the two interactions. In addition, if ν_{rot} is sufficiently rapid,

the anisotropy in the magnetic shielding is averaged by MAS. In such cases, simulation of the spectrum yields the quadrupolar parameters; the CS tensor parameters may then be determined from an analysis of the stationary spectrum.

1.17.2.2.3 Selective excitation

Radiofrequency (r.f.) pulses on quadrupolar nuclei are generally classified as "selective" or "non-selective".[39,44,53,54] A "hard" pulse (i.e., a pulse which simultaneously excites all NMR transitions) is non-selective. Although Kentgens and co-workers have recently demonstrated a microcoil capable of r.f. fields in excess of 1 MHz,[55] current commercial NMR coils typically have r.f. field strengths of less than 200 kHz, significantly less than the breadth of most line shapes encountered in solid-state NMR investigations of quadrupolar nuclei. Thus, in most cases, one obtains selective excitation. Hence, most NMR studies of half-integer quadrupolar nuclei entail selectively exciting the CT.[56] Selective excitation of this transition leads to an effective nutation frequency $\nu_{\text{r.f.}}^{\text{eff}}$:

$$\nu_{\text{r.f.}}^{\text{eff}} = \left(I + \frac{1}{2}\right)\nu_{\text{r.f.}} \tag{13}$$

Thus, if $\nu_{\text{r.f.}}$ is calibrated on a sample dissolved in an isotropic solution or on a solid sample where all $2I$ transitions appear at a single frequency (e.g., a quadrupolar nucleus in a site of cubic symmetry), one must recognize that the nutation frequency for the CT of a sample with a significant C_{Q} will be enhanced according to Equation (13) compared to that obtained from the calibration sample. For example, Figure 6 illustrates ^{23}Na ($I = 3/2$) NMR spectra[45] of a mixture of NaCl and $NaNO_2$, which have C_{Q}'s of 0.0 and 1.1 MHz,[57] respectively, acquired as a function of the excitation pulse time, p.w. As expected from Equation (13), the 90° pulse width for ^{23}Na of $NaNO_2$ is approximately 50% that for NaCl. The term "selective", although commonly used, is misleading. When acquiring NMR spectra of quadrupolar nuclei for powder samples, some crystallites (i.e., those with $\beta \approx 54.7°$ in Equation (9)) are oriented such that satellite transitions appear at the same spectral frequency as that for the CT.

1.17.2.3 Receptivity Considerations for Solid-state NMR Studies

In solution NMR spectroscopy, the receptivity, D, of a nucleus is often used to assess the suitability of a given isotope for NMR studies.[7] D depends on the magnetogyric ratio, γ, of the nucleus and on the natural abundance, C, of the isotope: $D = |\gamma^3|C[I(I + 1)]$. However, in solid-state NMR spectroscopy of half-integer quadrupolar nuclei, one usually only excites the CT, so that the effective D is less than that observed for NMR of solutions. Although γ and C are important when considering the suitability of a particular isotope for solid-state NMR studies, many other factors must also be considered.

For spin-1/2 nuclei, relaxation times and large anisotropies in the magnetic shielding may render data acquisition difficult even if the nucleus has a favorable receptivity. For example, a comparison of the receptivities for ^{13}C and ^{195}Pt would suggest that the latter nucleus is more suitable for NMR studies. Yet there have been few reports of ^{195}Pt

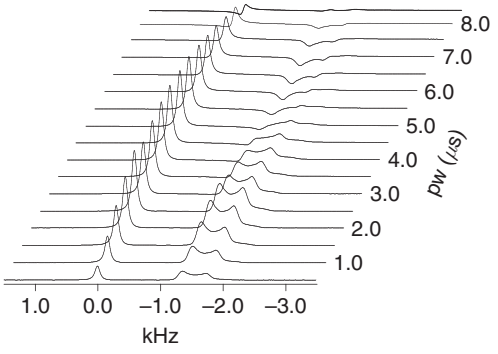

Figure 6 Sodium-23 NMR spectra of a mixture of 20% NaCl (0.0 kHz) and 80% $NaNO_2$ (−1.5 kHz), acquired with single-pulse excitation, plotted as a function of the pulse duration, p.w.[45] Each spectrum was acquired with a spinning frequency of 10 kHz at 7.05 T with a 60 s recycle delay and $\gamma B_1/2\pi \approx 60$ kHz; eight transients were co-added.

NMR spectra of solid samples since its NMR signal is usually spread over several thousand ppm, a consequence of the large magnetic shielding anisotropy typical for ^{195}Pt.[58] For example, the span for K_2PtCl_4 is greater than 10 000 ppm.[59] On the other hand, techniques such as cross-polarization (CP; *vide infra*) facilitate the acquisition of NMR spectra for apparently challenging nuclei such as ^{15}N.

For quadrupolar nuclei, the nuclear quadrupole moment, Q, as well as the Sternheimer anti-shielding factor,[60] should be considered. However, the most important factor is the environment about the nucleus, since this determines the magnitude of the quadrupolar coupling[61,62] and of the magnetic shielding anisotropy. Thus, acquiring NMR spectra for an apparently challenging isotope may still be practical if the NMR signal is not dispersed greatly by these interactions. For example, despite a significant Q, low γ, and low natural abundance, the feasibility of solid-state ^{99}Ru NMR spectroscopy has recently been demonstrated, particularly for ^{99}Ru in sites of octahedral or near-octahedral symmetry.[63]

1.17.2.4 Spectral Simulations and Computational NMR

An important part of the analysis of solid-state NMR spectra is the simulation of the experimental spectra to extract the NMR parameters.[64] In our lab, we have found the programs SIMPSON[65] and WSOLIDS[66] particularly useful. The latter program, written in our laboratory, uses the space-tiling method of Alderman and co-workers.[67] Recently, the new simulation program SPINEVOLUTION was described.[68] The program MXQET has been used to simulate ^{2}H NMR spectra influenced by molecular dynamics.[69] Other programs used to calculate NMR spectra for various spin systems include NMRLAB,[70] γ-COMPUTE,[71] STARS,[72] and MathNMR.[73]

Computation of NMR parameters using modern quantum chemistry methods (e.g., *ab initio* methods that start with the Hartree–Fock approximation, density functional theory) has become an important tool to complement the data obtained from an analysis of NMR spectra of solid samples.[74–76] The technique has been used extensively to verify conclusions drawn from complex NMR spectra and to complement or help rationalize incomplete NMR data. For example, orientations for CS tensors are difficult to determine from the experimental spectra of powder samples; thus, computational NMR has been used to propose orientations of tensors for which the principal components were determined experimentally.[30,77] The development of new theoretical methods, improved algorithms, and the rapid growth in the capacities of computers have greatly increased the ability of investigators to calculate CS and EFG tensors.[78] Despite these advances, calculations of CS tensors for organometallic complexes remain challenging, particularly in cases where the metal[76,79–83] and ligand nuclei[76,79,81–83] are subject to relativistic effects. Hence, this remains an area of intensive research; see the articles by Yates *et al.*[84] and Autschbach[85] for recent progress. Recently, Willans *et al.* used relativistic density functional theory calculations to propose orientations for the ^{139}La CS and EFG tensors for a series of lanthanum coordination compounds.[86] Pickard and co-workers have calculated the ^{17}O NMR parameters for SiO_2 polymorphs[87] as well as the ^{13}C, ^{14}N, ^{15}N, ^{17}O, and ^{35}Cl EFG or CS tensors, or both, for some amino acids[88] and their salts using density functional theory. By adopting periodic boundary conditions, intermolecular contributions are included in the calculation, improving their accuracy.

1.17.3 NMR of Spin-1/2 Nuclei

In this section, the acquisition of NMR spectra for spin-1/2 nuclei in diamagnetic compounds is discussed; see Section 5 for a discussion of NMR spectroscopy on paramagnetic complexes. Obtaining NMR spectra for spin-1/2 isotopes in solid samples became practical with the development of two widely used techniques: MAS[3,5,89–91] and CP under the Hartmann–Hahn matching condition.[5,92–94] These techniques have been discussed extensively.[56,95–98] Below, the acquisition of NMR spectra for abundant-spin ligand nuclei (^{1}H and ^{19}F), as well as the direct observation of the NMR signals from spin-1/2 metal nuclei, are discussed.

The NMR literature on spin-1/2 ligand nuclei in organometallic complexes has been reviewed extensively. See the review by Pregosin and Rüegger[99] for a discussion of NMR of spin-1/2 metal nuclei. Until recently, Mann has published an annual review of the NMR literature in the series *Spectroscopic Properties of Inorganic and Organometallic Compounds*.[100] See also Nelson's review of the ^{31}P NMR literature for the phosphines of transition metal complexes[101] and the review of solid-state ^{13}C NMR spectroscopy of unsaturated ligands by Bernard and Wasylishen.[102] In addition, readers should consult the articles by Jameson and de Dios in *Specialist Periodical Reports* published by the Royal Society of Chemistry.[74] An annual review of solid-state NMR, published by Aliev and Law[103] since 2001 and by Smith prior to this,[104] is also highly recommended. A useful compilation of anisotropic CS data prior to 1994 has been published by Duncan.[105] The recent textbooks by Duer[95] and MacKenzie and Smith[106] provide excellent introductions to many NMR techniques.

Several two-dimensional (2-D) NMR techniques commonly used by solution NMR spectroscopists have also been used in solid-state NMR investigations.[107] For example, ^{31}P *J*-resolved NMR spectra were used by Wu and Wasylishen to investigate some rhodium(I) phosphine complexes.[108]

1.17.3.1 ^{1}H and ^{19}F NMR Spectroscopy

Until recently, the strong ^{1}H–^{1}H dipolar interactions, R_{DD} (^{1}H,^{1}H), rendered most solid-state ^{1}H NMR experiments impractical. Two approaches have been developed to address this problem: spinning samples very rapidly at the magic angle, and the use of homonuclear decoupling pulse sequences. MAS at frequencies, ν_{rot}, up to 70 kHz,[109] has allowed the direct observation of ^{1}H NMR spectra, since R_{DD}(^{1}H,^{1}H) is significantly averaged at such spinning frequencies.[110–112] This experiment is an attractive option since it can be carried out with sample volumes of less than 10 μl, it can be implemented easily using single-pulse excitation, and the favorable NMR conditions for ^{1}H mean that NMR spectra can usually be acquired quickly. This approach, combined with multiple-quantum coherences,[113] has been used to obtain high resolution ^{1}H NMR spectra of solid samples. If spinning samples at such high frequencies is either undesirable or impractical, schemes have been developed that allow homonuclear decoupling of ^{1}H. In the CRAMPS (combined rotation and multiple pulse spectroscopy) experiment,[4,114,115] spinning the sample at moderate frequencies averages the anisotropy in the proton or fluorine magnetic shielding, while a series of $\pi/2$ pulses averages the homonuclear dipolar coupling. Pulse sequences used for CRAMPS include MREV-8[4,16,116] and BR-24.[4,117] The CRAMPS experiment requires that the pulse sequence be executed during a time period that is significantly less than that required for one rotor cycle; thus, these experiments are restricted to relatively slow MAS frequencies (<3 kHz). Recently, Emsley and co-workers have shown that the DUMBO[118] and eDUMBO[119,120] pulse sequences yield high-resolution ^{1}H NMR spectra at slow and fast MAS frequencies.[121] Vega and co-workers have implemented a pulse sequence based on the phase-modulated Lee–Goldburg scheme that allows the acquisition of 1-D ^{1}H NMR spectra with high spinning frequencies ($\nu_{rot} > 14$ kHz) as well as 2-D ^{1}H–^{1}H and ^{1}H–^{13}C correlation NMR spectra.[122]

Another abundant isotope with a high magnetogyric ratio that has proved to be challenging for solid-state NMR spectroscopists is ^{19}F ($\Xi = 94.094$ MHz). A recent review by Ulrich on solid-state ^{19}F NMR is highly recommended.[123] The applications discussed above for the acquisition of ^{1}H NMR spectra of solids may in principle be applied to ^{19}F, but there are additional factors that must be considered. A large bandwidth is often required to fully excite ^{19}F, since this isotope has a large CS range. The large CS range may also complicate homonuclear decoupling. In addition, the similar magnetogyric ratios, and thus similar NMR frequencies, for ^{1}H and ^{19}F means that acquiring ^{1}H-decoupled ^{19}F NMR spectra is not the routine double resonance experiment that is often carried out in solid-state NMR labs.[124,125] Suitable filters are required to isolate the ^{19}F signals from those of ^{1}H, and corrections for the Bloch–Siegert shift in the ^{19}F NMR spectra, induced by irradiation close to the observed frequency, must be applied.[123,125] Another minor difficulty is that typical probe and rotor components often contain ^{19}F, which may give rise to a significant background signal. For samples containing ^{1}H, CP from ^{1}H to ^{19}F will negate this problem, since probe components are generally polyfluorinated to minimize background ^{13}C NMR signals.[126,127]

Cherryman and Harris have investigated organotin fluorides, R_3SnF, through the acquisition of ^{1}H-decoupled ^{19}F NMR spectra, as well as through the indirect observation of ^{19}F through a ^{119}Sn{^{19}F} HETCOR experiment.[128] From the measured Sn–F dipolar coupling and from the Sn–F bond lengths, which were known from X-ray diffraction experiments, the authors estimate that the anisotropy in the **J** tensor, ΔJ(^{119}Sn, ^{19}F), is −3150 and −2950 Hz for the two sites of Mes_3SnF; the authors report that the errors in ΔJ are significant, preventing an assignment of the values to specific NMR sites. Based on calculations on a model compound, Feindel and Wasylishen predicted a value for ΔJ of −1872 Hz for this compound.[129]

1.17.3.2 Indirect Detection

The indirect detection of insensitive nuclei through the observation of abundant-spin NMR signals (usually ^{1}H) has been used extensively in solution NMR studies.[130] Because the ^{1}H peaks in NMR spectra of solid samples are generally broad, the technique has not been widely applied to solid-state NMR studies.[131] Several techniques have been devised to circumvent this problem. Ishii and Tycko demonstrated that significant enhancements of the ^{15}N NMR signal is possible through indirect ^{1}H detection, combined with rapid MAS and high applied magnetic fields.[131] The authors found that, with indirect detection, the sensitivity of the ^{15}N signal is comparable to that of ^{13}C. Khitrin and Fung have used multiple periods of CP combined with incremented evolution periods to yield a large sensitivity enhancement for the indirect detection of low natural-abundance isotopes in stationary samples.[132]

Using this technique, the authors obtained a ^{2}H NMR spectrum of a stationary sample of tetramethylbenzene at natural abundance in approximately 40 h.

1.17.3.3 NMR of Spin-1/2 Metal Nuclei

The properties of the metal isotopes with spin $I = 1/2$ are summarized in many texts and articles.[18,99,133] The reviews by von Philipsborn[134] and by Pregosin and Rüegger[99] on the NMR literature of spin-1/2 metal isotopes are recommended; see also the article by Davies and Dutremez on the NMR literature concerning *d*- and *p*-block metal isotopes.[133] Dybowski and Neue have reviewed the literature for ^{207}Pb NMR of solids,[135] and Smith has reviewed the NMR on low-γ spin-1/2 isotopes.[136] Early NMR papers for a specific isotope are particularly helpful when undertaking a series of experiments, since these report the pitfalls that the spectroscopists may encounter. See, for example, articles by Challoner and Sebald[58] for a discussion of ^{195}Pt CP/MAS NMR, by Merwin and Sebald for a discussion of ^{89}Y NMR[137] and of ^{183}W CP/MAS NMR,[138] and by Eichele *et al.*, [139] for a discussion of ^{199}Hg CP/MAS. Readers are referred to articles by Rabe and Sebald[140] and by Keates and Lawless[141] for a discussion of ^{171}Yb CP/MAS NMR, as well as that by Mao *et al.* for an example of solid-state NMR spectra of a ^{171}Yb complex obtained with single-pulse excitation.[142] Phillips *et al.* recently demonstrated the practicality of undertaking ^{103}Rh CP/MAS experiments.[143] When attempting CP to a rare spin-1/2 isotope that has not been previously investigated, some researchers first optimize conditions with an isotope that has a similar NMR frequency (and hence a similar Hartmann–Hahn matching profile) but a higher natural abundance. For example, before attempting the first ^{109}Ag{^{1}H} CP experiment, Merwin and Sebald[144] optimized the Hartmann–Hahn matching condition through an ^{89}Y CP experiment,[137] since the frequency for ^{89}Y is only 250 kHz greater than that for ^{109}Ag on the Ξ scale.

Although there have been numerous solid-state NMR experiments involving spin-1/2 metal nuclei, these are not always routine. For example, many metal isotopes fall outside the ^{15}N to ^{31}P tuning range typical for most broadband solid-state MAS probes, corresponding to $\Xi = 10.1$–40.5 MHz. For low-γ nuclei, much of the NMR signal may be lost due to probe ringing (i.e., the probe dead time). For isotopes that are readily accessible and not hampered by inordinately long dead times, two other factors must be considered. In single-pulse excitation experiments, long spin-lattice (T_1) relaxation times for the nucleus under consideration may preclude acquisition of NMR spectra in a reasonable time. As well, many metal isotopes have very large CS ranges and thus often have a large span. Such nuclei often yield spectra with broad spinning sideband patterns. Although it is tempting to increase ν_{rot} when acquiring spectra of samples with large spans, sample heating during rapid spinning may lead to shifts in the resonance frequencies and to line broadening due to temperature gradients in the rotor.[145] For example, the sensitivity of ^{207}Pb CSs to temperature has led to the use of $Pb(NO_3)_2$ as an "NMR thermometer".[146–148] Based on the ^{119}Sn NMR CSs as a function of ν_{rot}, Langer *et al.* concluded that the temperature of samples in 2.5 mm o.d. rotors spinning at 35 kHz increased by 30–40 K.[149]

Experimental techniques for performing CP experiments from ^{1}H to high-γ nuclei ($\Xi > 10$ MHz) have been discussed extensively.[56,98,150,151] The benefits of the technique are twofold: the recycle delays for the CP technique depend on the ^{1}H T_1 relaxation times, which are usually much shorter than those for the metal nuclei, and the enhancement factor, up to γ_H/γ_X, seems to make the technique particularly appealing for low-γ nuclei. However, these experiments are generally not routine. At values of ν_{rot} that approach the ^{1}H–^{1}H dipolar interactions, the Hartmann–Hahn matching profile is split into a series of sidebands separated by the spinning frequency.[150,152–155] Thus, although spinning the sample rapidly may be desirable since many metal nuclei have a large CS anisotropy (CSA), determining the optimum Hartmann–Hahn matching condition under these conditions can be challenging. Techniques such as variable-amplitude CP (VACP)[154] and ramped CP[156] have been developed to facilitate optimizing the Hartmann–Hahn matching conditions. A further difficulty is that very long contact times are required for CP when the ^{1}H–metal dipolar interactions are small, such as those encountered when attempting CP to low-γ nuclei; thus spectroscopists must proceed with caution and be aware of the limitations of their hardware when undertaking such experiments.

Despite these difficulties, there have been several reports of CP to low-γ nuclei. For example, Penner and Li have recently proposed the use of silver methanesulfonate as a setup sample for ^{109}Ag{^{1}H} CP experiments.[157] The authors found that the optimum contact time is greater than 60 ms, similar to values reported by Merwin and Sebald in an earlier ^{109}Ag{^{1}H} CP experiment on silver lactate and other organometallic silver compounds.[144] The latter authors[144] suggest that the ^{1}H spin-lattice relaxation time in the rotating frame,[7] $T_{1\rho}$, be determined prior to attempting the CP experiment, since unfavorable $T_{1\rho}$ values may render the experiment impossible regardless of contact time.

A common method of determining the principal components of a CS tensor is to obtain an NMR spectrum of a stationary powder sample.[56] The accurate determination of these parameters requires uniform excitation of the entire spectrum, something that is impractical for many heavy nuclei which may have spans in excess of 1000 ppm.

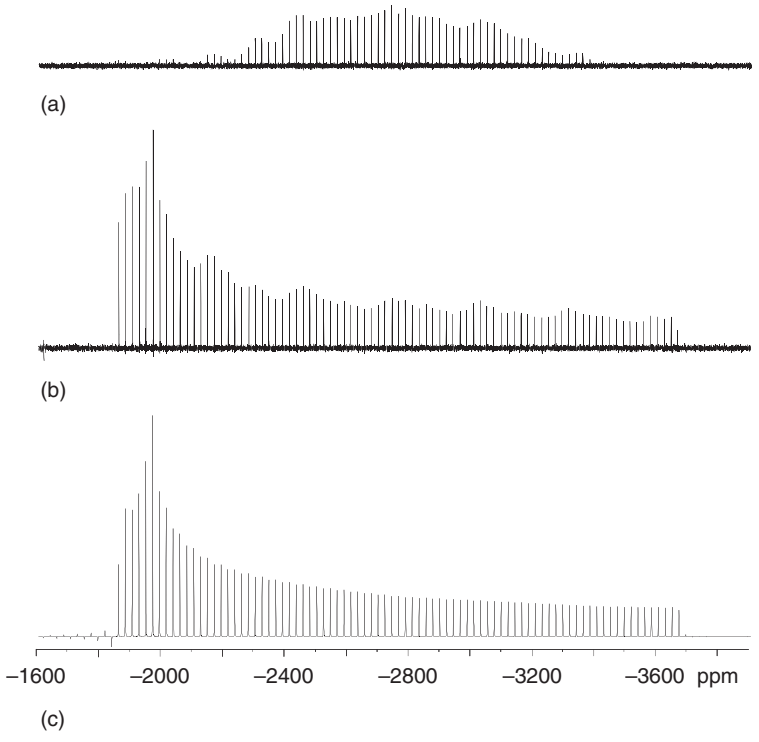

Figure 7 Hg-199 NMR spectra of $Hg(CH_3COO)_2$ acquired at 11.75 T: (a) central subspectrum acquired with CP-CPMG; (b) spectrum acquired with CP-CPMG (this spectrum is the sum of nine subspectra, each separated by 25.7 kHz and with 16 transients added for each); (c) simulated spectrum. Reprinted with permission from: Siegel, R.; Nakashima, T. T.; Wasylishen, R. E. *J. Phys. Chem. B* **2004**, *108*, 2218–2226. © 2004 American Chemical Society.

Recently, Siegel *et al.*[158,159] as well as Schurko and co-workers[160] demonstrated that the Carr–Purcell Meiboom–Gill (CPMG) experiment may be used as an enhancement technique to efficiently provide NMR spectra in much less experimental time. The technique yields NMR spectra with a series of spikes (referred to as spikelets) that emulate the powder pattern expected from a stationary sample. Another important benefit of the technique is that it avoids sample heating that might occur if the sample was spinning. The technique can be combined with other enhancement techniques, such as CP and decoupling via two-pulse phase modulation (TPPM)[161] to further reduce the experimental time. Several subspectra may be acquired with varying transmitter offsets, then added or overlain to yield an NMR spectrum that one would expect for a sample with uniform excitation. Figure 7 illustrates a ^{199}Hg NMR spectrum acquired with CP-CPMG.[158] Siegel *et al.* found that a modified CPMG pulse sequence[158] provides improved homonuclear decoupling compared to that obtained with the original CPMG pulse sequence. Although the NMR spectra obtained with CPMG are similar to those obtained with MAS, one important distinction is that with this technique, individual NMR sites are not readily resolved, since the positions of the peaks in a spectrum acquired with CPMG depend on the transmitter frequency and the spikelet spacing, rather than on ν_{rot} and the isotropic CSs.

1.17.3.4 Obtaining CS Tensors from Complex Spectra

By spinning samples rapidly about the magic angle, one obtains NMR spectra with only isotropic peaks. Although this is often desirable, particularly for systems containing multiple sites, most of the information about the nuclear environment that is encoded in the CS tensor is lost. For systems with multiple sites, obtaining NMR spectra of stationary samples does not always resolve this problem, since the anisotropic shielding may result in extensive overlap in the spectra.

As already mentioned, the most common technique for recovering anisotropic CS information is to spin the sample at rates much less than the span (in frequency units);[23,24] however, when one has multiple sites, spectral overlap may be unavoidable. Another technique that has been used to address this problem is variable-angle spinning (VAS).[162]

By spinning samples at angles other than the magic angle, the anisotropic information is reintroduced, albeit scaled from that obtained in the absence of sample spinning. For fast VAS, one obtains an NMR spectrum with an identical pattern to that obtained from a stationary sample, but scaled in the frequency domain by the factor $(1/2)(3\cos^2\theta - 1)$, where θ is the angle of rotation relative to B_0.[162] Thus, one may obtain NMR spectra that are sufficiently scaled to avoid overlap and that maintain the distinctive line shape from which the principal components of the CS tensors may be determined. The value for θ from which the scaling factor is determined is verified with a calibration sample for which the dependence of the line shape on θ is known. Besides reintroducing the CSA, the indirect spin–spin coupling (J) between crystallographically equivalent but magnetically distinct nuclei, not detected by fast MAS, is reintroduced by fast VAS.[163,164]

Other techniques have been developed that reintroduce the CSA while still spinning the sample at the magic angle.[165] In the magic angle hopping (MAH) technique,[166] the sample is "hopped" in 120° increments about the magic angle. In this 2-D experiment, one obtains the isotropic peaks along one axis, and the spectrum of a stationary sample along the other. The individual powder patterns containing the CS tensor data may be obtained by examining the appropriate projection. In the magic angle turning (MAT) experiment,[167] the same effect is achieved with much less complicated hardware by spinning the sample very slowly about the magic angle (e.g., 30 Hz), while a series of rotor-synchronized pulses is applied.

1.17.4 NMR Spectroscopy of Quadrupolar Nuclei

1.17.4.1 Acquisition of NMR Spectra of the Central Transition of Half-integer Spin Quadrupolar Nuclei

The majority of quadrupolar isotopes have half-integer spin. Because the CT of such nuclei is not broadened to first order by the quadrupolar interaction (Section 2.2.2), most NMR data on these nuclei have been obtained from an analysis of the CT.[40,168] Hence, the discussion on techniques below focuses on these experiments. See the reviews by Smith and van Eck[168] and by Kentgens[169] for a discussion of techniques for the acquisition of NMR spectra of the CT of half-integer quadrupolar nuclei, as well as that by Smith for a review of NMR studies on low-γ quadrupolar nuclei.[136] See also the review of the literature up to 1992 on *d*- and *p*-block metal nuclei.[133]

1.17.4.1.1 Spin echoes

Generally, one cannot obtain undistorted NMR spectra of the CT of half-integer quadrupolar nuclei with single-pulse excitation, since the FID decay time is often a significant portion of the receiver dead time and the probe ringing time. This problem is often circumvented by using spin echoes,[39,170] which refocus the NMR signal to a period after the probe and receiver dead times;[56,171] for the CT, this is usually a Hahn-echo (90°–τ–180°–τ–acquire).[171] A particular benefit of the technique is that the CT may be selectively excited by using a soft pulse (Section 2.2.3). Bodart *et al.* have reported instructions for minimizing line shape distortions in NMR spectra of the CT for stationary samples.[172] Echoes may also be used in NMR experiments with MAS samples; the delay between the excitation and refocusing pulses must be synchronized with ν_{rot} in this case.

Uniform excitation of the entire spectral region is not always possible, since the spectra may span hundreds of kHz. As for the CPMG experiment discussed above (Section 3.3), this problem can be overcome by acquiring several subspectra with different frequency offsets. Recently, Schurko and co-workers demonstrated that undistorted ^{27}Al NMR spectra of CTs which span up to 700 kHz, in a series of three- and five-coordinate aluminum compounds, may be acquired using a frequency-stepped acquisition method.[173] These spectra were acquired using the Hahn-echo or quadrupolar CPMG (QCPMG; *vide infra*) techniques.

1.17.4.1.2 The quadrupolar Carr–Purcell Meiboom–Gill technique

The breadth of the CT in an NMR spectrum of a half-integer quadrupolar nucleus increases with C_Q^2, and also depends on the spin quantum number I, decreasing as I increases (Equation (11)).[34,56] Acquiring spectra that cover a large spectral range is often difficult and time consuming. To overcome this problem, Nielsen and co-workers proposed a technique based on the CPMG experiment.[174] In this experiment, known as the QCPMG technique, a $\pi/2$ pulse, followed by a train of π-pulses, leads to a train of echoes, provided the T_2 relaxation time is sufficiently long. As for the CPMG method, this experiment yields NMR spectra that contain spikelets which mimic the powder pattern of a stationary sample. Because the total intensity of the spectrum is concentrated into these spikelets rather

than being dispersed over the entire spectral region, and because several echoes are acquired simultaneously, spectra may be obtained in much less time than with conventional echo experiments.

Since the second-order quadrupolar interaction is partially averaged by MAS, an improvement in resolution and sensitivity may be achieved by combining QCPMG with MAS;[175] however, one must spin the sample at a frequency comparable to the breadth of the second-order quadrupolar broadening. The pulse sequence is simply that for the QCPMG experiment,[174] preceded by a rotor-synchronized solid-echo pulse, and with an increase in the sampling period to allow full decay of the FID. Larsen *et al.* demonstrated the technique by acquiring ^{87}Rb NMR spectra of Rb_2SO_4 via quadrupolar-echo MAS and QCPMG-MAS experiments; the latter technique yielded a sevenfold increase in sensitivity.[175]

Obtaining useful titanium NMR spectra poses unique challenges for the spectroscopist due to the nuclear properties of the two magnetically active isotopes for this atom: ^{47}Ti ($I = 5/2$, $\Xi = 5.6375$ MHz, $Q = 30.2$ fm^2, natural abundance = 7.44%) and ^{49}Ti ($I = 7/2$, $\Xi = 5.6390$ MHz, $Q = 24.7$ fm^2, natural abundance = 5.41%).[18] With similar NMR frequencies and natural abundances and with large quadrupolar moments, one generally obtains broad overlapping patterns for the CTs arising from the two isotopes. Recently, Larsen and co-workers demonstrated that the different spin numbers can be used to obtain NMR spectra for each isotope.[54] This is accomplished by using the different nutation frequencies for the two isotopes Equation (13) in a modified QCPMG experiment.

1.17.4.1.3 Signal enhancement techniques

With the increasing importance of solid-state NMR spectroscopy of half-integer quadrupolar nuclei, there has been considerable recent interest in developing techniques to enhance signal intensity for the CT via population transfer. The recent review by Siegel *et al.* is recommended.[176]

The double frequency sweep (DFS) technique was developed to simultaneously invert the population of the energy levels associated with the STs and thus to enhance the CT of half-integer quadrupolar nuclei.[176–178] The technique involves the use of frequency sweeps that either diverge from or converge toward the CT; these sweeps are achieved using waveform generators. Kentgens and Verhagen demonstrated the technique with ^{23}Na ($I = 3/2$) NMR spectroscopy by applying DFS on a single crystal of $NaNO_3$;[177] enhancements of up to 3.0 (the theoretical maximum, $2I$) were obtained. Siegel *et al.*[176] have examined the sensitivity of the signal enhancement of the CT in ^{87}Rb NMR spectra of stationary powder samples of $RbClO_4$ as a function of the r.f. amplitude and of the sweep duration, using DFS. Enhancements of approximately 2.5 were obtained, whether weak ($\gamma B_1/2\pi = 10$–20 kHz) or stronger ($\gamma B_1/2\pi > 30$ kHz) r.f. fields were used. However, shorter sweep times are required if stronger r.f. fields are used.

In the rotor-assisted population transfer (RAPT) experiment,[179] a series of pulses is applied with alternating phases.[176] This leads to a saturation of the energy levels for the STs, and to an enhancement of the CT. For spin-3/2 nuclei, the CT is enhanced by approximately a factor of 2; the maximum enhancement for saturation of the STs is $I + 1/2$. Madhu *et al.* obtained enhancements of approximately 2.5 (compared to a maximum possible enhancement of 3.0) when they applied RAPT to two $I = 5/2$ isotopes: ^{17}O and ^{27}Al.[180] In this case, the $m_I = 5/2 \rightarrow m_I = 3/2$ and the $m_I = -3/2 \rightarrow m_I = -5/2$ transitions were saturated, followed by saturation of the $m_I = 3/2 \rightarrow m_I = 1/2$ and the $m_I = -1/2 \rightarrow m_I = -3/2$ transitions and by observation of the CT.

Another method of achieving a population transfer from the STs to the CT is through the use of hyperbolic secant (HS) pulses.[176,181] See the articles by Garwood and co-workers[182,183] for a detailed discussion of HS pulses. Siegel *et al.*[181] investigated the efficiency of HS pulses by acquiring ^{23}Na NMR spectra of a single crystal of $NaNO_3$, as well as ^{87}Rb NMR spectra of an MAS powder sample of $RbClO_4$. A maximum enhancement approaching the theoretical limit was achieved for both experiments. The HS pulses were also used by these authors to enhance the CT in a rotor-synchronized ^{87}Rb QCPMG experiment. Comparison with the other population transfer techniques, DFS and RAPT, suggests that HS pulses offer the greatest enhancement (Figure 8). The applicability of the technique to $I = 5/2$ isotopes has recently been demonstrated.[184] Maximum achievable enhancements by population transfer experiments may be diminished if the spin-lattice relaxation times are short.

The most widely used technique for enhancement of the NMR signal from spin-1/2 nuclei in the solid state, CP/MAS, has not been widely applied to quadrupolar nuclei. In some cases, the rapid relaxation induced by the quadrupolar interaction leads to shorter T_1 relaxation times for the quadrupolar nuclei than for the protons (or other abundant spin-1/2 nuclei), negating one of the advantages of CP/MAS. A more serious concern is that the highly anisotropic CP dynamics for half-integer quadrupolar nuclei[151,185] render the experimental setup particularly challenging. NMR spectra obtained under such conditions should therefore be interpreted with caution since the resulting powder NMR line shapes may be distorted.[185] Hence, most applications of CP to quadrupolar nuclei have been restricted to spectral editing techniques.[151,186,187] For example, Lim and Grey demonstrated that the

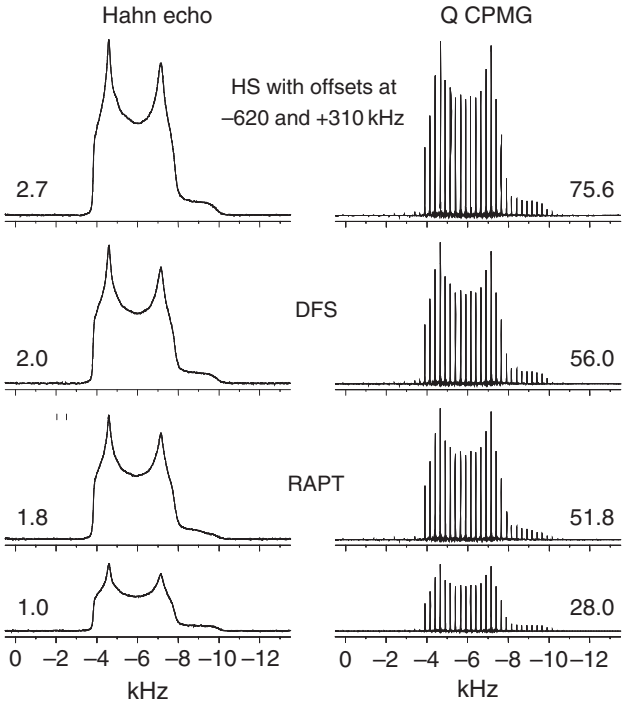

Figure 8 Comparison of the ^{87}Rb NMR signal intensity of an MAS powdered sample of $RbClO_4$ obtained with the Hahn echo (left) and QCPMG (right) experiments. The bottom traces are obtained with no enhancement; those above were obtained with the indicated enhancement techniques. Reprinted from: Siegel, R.; Nakashima, T. T.; Wasylishen, R. E. *Chem. Phys. Lett.* **2004**, *388*, 441–445, with permission from Elsevier.

Hartmann–Hahn matching condition for triple-quantum CP is very dependent on the crystallite orientation.[188] Wiench *et al.* have used $^{31}P \rightarrow {}^{27}Al$ CP with multiple-quantum HETCOR to correlate the aluminum and phosphorus nuclei in $AlPO_4$-14.[189] The practicality of CP between half-integer spin quadrupolar nuclei has also been demonstrated.[190,191]

1.17.4.1.4 Multiple-quantum MAS

The second-order broadening of the CT peaks of quadrupolar nuclei was a major factor discouraging the routine acquisition of NMR spectra of quadrupolar nuclei, since it is very difficult to resolve peaks that arise from two or more sites with standard echo techniques. In 1988, two techniques, double rotation, DOR,[192] and dynamic-angle spinning, DAS,[193] were developed to address this problem.[194] In the DAS experiment, which is a 2-D technique, the rotor is switched rapidly between the two axes to average the first- and second-order quadrupolar interactions. The DOR experiment attempts to average these interactions by simultaneously spinning the sample about the two axes. Because 1-D spectra are acquired with DOR, this technique is less time consuming. Although these methods show promise,[195] numerous technical difficulties remain. In 1995, Frydman and Harwood introduced the multiple-quantum MAS (MQMAS) method.[196] Because this technique also yields high resolution NMR spectra of half-integer quadrupolar nuclei, but with hardware that generally is available in solid-state NMR labs (probes capable of MAS, high-power amplifiers), it has become the method of choice for most spectroscopists. Readers are referred to the numerous review articles on the topic.[171,197–204]

Since the introduction of MQMAS, much effort has been expended on developing methods to enhance the signal of the CT, and thus to extend the utility of the technique. A common signal enhancement technique is fast amplitude modulation (FAM).[198,205] Shaped pulses,[206] including the HS pulses introduced above,[207] as well as DFS[178,208] have been used for signal enhancement in MQMAS experiments. Kwak *et al.*[209,209a] have combined RAPT with the rotationally induced coherence transfer (RIACT-II) scheme of Griffin and co-workers.[210] The authors found that applying RAPT before RIACT-II improved the sensitivity of the MQMAS experiment by a factor of 2, but that application of RAPT before conventional MQMAS resulted in a reduction in the sensitivity of the experiment by a

factor of 0.6. Gan and Kwak have recently shown that significant improvements in sensitivity may also be achieved through the soft-pulse-added mixing (SPAM) method.[211] The procedure entails adding several coherence transfer pathways constructively; see the article by Amoureux *et al.* for a detailed discussion of the technique.[212] Gan and Kwak[211] also used the multiplex phase cycling method of Ivchenko *et al.*[213] to simultaneously acquire signals from multiple coherence transfer pathways. Fernandez and co-workers[214] have recently shown that a significant gain in sensitivity may be achieved by combining the multiplex phase cycling and SPAM techniques. The authors also demonstrated that simultaneous recording of 3Q and 5Q MAS experiments is possible, although the signal-to-noise ratio is poor. Nevertheless, the technique offers potential for future development. A promising recent development is the application of optimal control theory to improve the excitation scheme in MQMAS experiments.[215] The authors found that the scheme yields a 50% improvement in the sensitivity of the MQMAS experiment.

The MQMAS technique has been combined with other NMR techniques to provide correlation information. For example, Iijima *et al.*[216] recently used $^{31}P\{^{27}Al\}$ MQMAS/HETCOR NMR to study the structure of amorphous $AlPO_4$. The technique yields a 2-D spectrum with the isotropic ^{27}Al and ^{31}P peaks along the F_1 and F_2 dimensions, respectively, allowing a determination of the connectivity between the nuclei.

1.17.4.1.5 Satellite-transition MAS

In 2000, Gan[217] proposed the 2-D satellite transition MAS (STMAS) experiment[218] as an alternative to MQMAS. Readers should not confuse this technique, which is used to observe the CT, with methods for the direct observation of the NMR signals from the STs, discussed in Section 4.2. The STMAS experiment establishes a correlation between the STs and CTs by using a two- or three-pulse sequence to excite the STs, then transferring the coherence to the CT. This has the effect of removing the higher-order terms defining the CT, yielding isotropic peaks. To excite the STs, short hard pulses are recommended. Gan and co-workers have published a summary of the procedure required to optimize experimental conditions for the STMAS experiment.[219] Recently, Dowell *et al.* have demonstrated that the technique may be applied to low-γ nuclei, such as ^{39}K and ^{25}Mg.[220] Based on experimental results and numerical calculations, the authors suggest that STMAS is the preferred technique for the acquisition of high resolution NMR spectra for low-γ nuclei.

A major disadvantage of the STMAS experiment as originally formulated was that the magic angle had to be set with very high accuracy. For example, a deviation of more than 0.004° in the adjustment of the magic angle would result in a broadening of more than 100 Hz for the CT of a nucleus with $\nu_Q = 250$ kHz and $\nu_0 = 100$ MHz.[221] Antonijevic and Bodenhausen have recently published a technique for the precise setting of the magic angle.[222] Also Ashbrook and Wimperis have reported the pulse sequence SCAM-STMAS (self-compensates for angle misset) that compensates for inaccurate setting of the magic angle.[221,223] In the pulse sequence, a pulse is introduced in the middle of the t_1 period that transfers the coherence between the two STs for a spin-3/2 nucleus. Since any first-order broadening that remains from an offset in the magic angle is equal in magnitude but opposite in sign for the two transitions, the unwanted broadening is refocused. The authors show that first-order broadening is refocused even for deviations from the magic angle of greater than 1°, although in such cases, second-order broadening and, if present, the effects of CSA are reintroduced.[223] The authors also demonstrated that the technique may be applied to spin-5/2 and spin-7/2 nuclei.[223]

Another difficulty with the original STMAS experiment is the presence of large diagonal peaks in the 2-D spectra, arising from a correlation of the CT peaks from the two axes; there are also smaller diagonal peaks arising from the STs. In 2003, Kwak and Gan introduced double-quantum filtered STMAS (DQF-STMAS)[224] to address this problem. By using a π-pulse that is selective for the CT, the various single-quantum coherences are converted to different pathways; the undesired CT–CT and ST–CT transitions may then be filtered through the selection of an appropriate phase cycling scheme.

Several of the sensitivity-enhancement techniques that have been successfully applied to MQMAS are also suitable for STMAS. For example, Amoureux and co-workers have incorporated SPAM with DQF-STMAS.[225,226] Other techniques, such as multiplex phase cycling,[211] that have been used successfully with MQMAS, may also be applicable to STMAS.

1.17.4.1.6 Other techniques

The preceding was an overview of some of the recent techniques employed to investigate half-integer quadrupolar nuclei. Readers should consult the excellent annual reviews to keep abreast of the new techniques in this rapidly developing field.[74,103] Here, we briefly mention some other techniques that readers interested in investigating quadrupolar nuclei might find helpful.

With QPASS, one obtains a spectrum equivalent to that which would be obtained at an infinite spinning rate.[227,228] Fyfe *et al.* have demonstrated that through-bond connections involving quadrupolar nuclei can be determined using the INEPT experiment.[229] Kao and Grey employed the $^{27}Al \rightarrow {}^{31}P$ INEPT experiment to investigate the Me_3P–$AlCl_3$ complex in the NaX zeolite.[230] Off-resonance nutation NMR spectroscopy is an easily implemented technique that allows the spectroscopist to investigate samples containing nuclei with a range of nuclear quadrupole coupling constants.[231,232]

Several methods have been developed that yield structural information based on the dependence of the dipolar interaction on the internuclear separation.[233–235] These include rotational echo double resonance (REDOR),[236,237] multiple-quantum rotational echo double resonance (MQ-REDOR),[238] transfer of populations in double resonance (TRAPDOR),[239] and rotational echo adiabatic passage double resonance (REAPDOR).[240] Kalwei and Koller have presented a comparison of the latter two techniques applied to the determination of H–Al separations in zeolites.[241] Zhou *et al.* have used a combination of techniques, including REDOR and TRAPDOR, to investigate the Al/P ratio in some aluminophosphates.[242]

Although MAS reduces the breadth of the CT in NMR spectra of half-integer quadrupolar nuclei, the angular dependence of the second-order quadrupolar interaction is such that spinning the sample rapidly about angles other than the magic angle may be more effective at narrowing the line widths.[51,168,243–246] A minimum width in the CT peak is achieved by setting the rotor spinning axis at an angle ranging from 60° to 70° relative to B_0; the actual value depends on the value of η_Q. However, spinning samples off the magic angle also reintroduces any anisotropy in the magnetic shielding (Section 3.4) as well as any dipolar interactions, if not removed by r.f. irradiation. Hence, the technique is useful only in cases where the latter interactions are negligible. The technique has nevertheless been applied in some investigations. For example, Kroeker *et al.*[247] used the results of a ^{133}Cs ($I = 7/2$) VAS experiment to investigate the relative orientations of the CS and EFG tensors for ^{133}Cs of $CsCd(SCN)_3$. Kentgens and co-workers have used the reintroduction of the dipolar interaction arising from spinning samples away from the magic angle in homonuclear correlation experiments for quadrupolar nuclei.[248]

1.17.4.2 Acquisition of NMR Spectra of the Satellite Transitions for Quadrupolar Nuclei

The STs of quadrupolar nuclei contain a wealth of information; indeed, for integer-spin quadrupolar nuclei, these are the only transitions available to the NMR spectroscopist. Because the NMR signals from the STs are subject to the first-order quadrupolar interaction, they often are dispersed over hundreds of kHz for stationary powder samples, precluding conventional acquisition of NMR spectra.

In most cases, ν_{rot} is much less than ν_Q; thus, the NMR spectra of MAS samples arising from the STs are defined by a series of spinning sidebands, the envelope of which emulates the powder pattern expected for a stationary sample. The primary difficulties with obtaining such spectra are: (i) the total intensity of the STs may be distributed over hundreds of spinning sidebands, resulting in low intensities for individual sidebands, and (ii) uniform excitation of the entire spectral region may not be possible. Notwithstanding these difficulties, satellite transition spectroscopy (SATRAS)[249] has been used to obtain spectra of STs, from which information about the nucleus of interest may be derived (see Figure 4 for an example of a ^{27}Al SATRAS spectrum). Samoson[50] showed that accurate values for δ_{iso} may be obtained from the determination of the relative shifts for the CTs and STs. Because the line widths for the spinning sidebands of some of the STs are narrowed significantly (e.g., for $I = 5/2$ nuclei, the line widths of the sidebands for the $m_I = 3/2 \rightarrow m_I = 1/2$ and the $m_I = -1/2 \rightarrow m_I = -3/2$ transitions are narrowed by a factor of approximately 3 compared to that for the CT), Jäger showed that the technique may be used to identify separate sites with different C_Q and δ_{iso} values.[250] Recent applications of SATRAS include ^{23}Na and ^{27}Al NMR investigations of natural sodalite,[251] a ^{27}Al investigation of aluminum chlorofluoride,[252] and a ^{99}Ru investigation of some diamagnetic Ru-containing compounds.[63]

Jakobsen and co-workers reported a strategy for obtaining ^{14}N ($I = 1$) NMR spectra of some simple amino acids in the solid state.[253] Obtaining a well-resolved spinning sideband manifold required careful optimization of experimental parameters,[254] including stable sample spinning (±1 Hz) using a pressure-stabilized air supply, and precise setting of the magic angle. Spectra were acquired without ^1H decoupling, since the low-pass filter that would have been needed for decoupling adversely affected the ^{14}N r.f. bandwidth. The ^{14}N quadrupolar parameters were obtained through simulation of the NMR spectra of MAS samples; the software accounts for the non-uniform excitation of the spectra, and also includes the effects of anisotropic nitrogen shielding[254] and the second-order cross term between the quadrupolar coupling and the anisotropic shielding.[255]

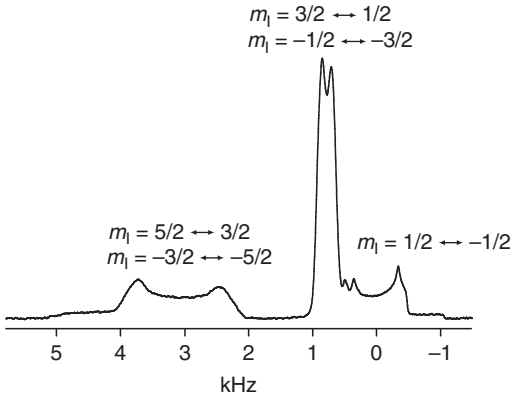

Figure 9 Rotor-synchronized ^{27}Al NMR spectrum for Al(acac)$_3$ acquired at 7.05 T with $\nu_{rot} = 15$ kHz.[45] The dwell time was 66.7 μs and a 67.25 μs preacquisition delay was used; 2048 transients were added.

Although spinning samples rapidly enough to remove the first-order broadening in the STs is usually impractical, the effect may nevertheless be removed by setting the spectral width equal to ν_{rot}. In the absence of filters, the spinning sidebands are then folded onto the centerband of the ST.[256] This yields a spectrum consisting of one peak for each ST and one for the CT. As for SATRAS, this technique helps determine δ_{iso} and to resolve multiple sites in a spectrum, but, because the entire NMR signal from a given ST is aliased into a single peak, it provides far greater intensity. As for all experiments involving high-order spinning sidebands, the technique is sensitive to the setting of the magic angle.[218] One must also ensure that the first point of the FID is at the top of a rotary echo. This is easily accomplished by varying the preacquisition delay such that a maximum signal is observed. Figure 9 illustrates the rotor-synchronized ^{27}Al NMR spectrum for Al(acac)$_3$.[45] By employing a double-quantum filter,[224] Ashbrook and Wimperis also demonstrated that one may obtain NMR spectra where only the $m_I = 3/2 \rightarrow m_I = 1/2$ and the $m_I = -1/2 \rightarrow m_I = -3/2$ transitions are detected.[256]

STs may also be observed via single crystal NMR experiments.[21,22] The EFG and CS tensors may be characterized by obtaining NMR spectra of single crystals as a function of the orientation of the crystal relative to B_o. For a single crystal with a unique NMR site, one observes $2I$ peaks, whose positions vary as a function of the crystal orientation relative to B_0 – the degree of variation depends on the magnitude of C_Q and of the anisotropy in the magnetic shielding. Such experiments require large single crystals which are not always available. In a recent ^{11}B investigation of borates, Hansen *et al.* [257] determined the boron CS tensors for borax based on the sum frequencies for the $m_I = 3/2 \rightarrow m_I = 1/2$ and the $m_I = -1/2 \rightarrow m_I = -3/2$ transitions. As for most single crystal NMR experiments, a goniometer probe was used for the preceding analysis;[257] such specialized equipment is not always available in solid-state NMR labs. In a ^{59}Co NMR study of hydrated and dehydrated $\pm$[Co(en)$_3$]Cl$_3$, Ueda *et al.* demonstrated that accurate NMR parameters for quadrupolar nuclei may be obtained from a single crystal in an MAS probe,[258] provided one of the crystallographic axes can be identified so that the orientation of that axis is known when the crystal is placed in the NMR rotor; spectra are then obtained as a function of the rotor position. Although an analysis of single crystal NMR data of the STs is probably the most accurate method of determining quadrupolar parameters, readers should be aware that these parameters, as well as the anisotropy in the magnetic shielding, may also be determined by analyzing single crystal NMR data of only the CT.[259]

1.17.4.3 Indirect Determination of Quadrupolar Parameters

In the absence of a significant C_Q, the indirect spin–spin interaction between quadrupolar and spin-1/2 nuclei manifests itself in the spectrum of the latter as a multiplet consisting of $2I + 1$ evenly spaced peaks. However, if ν_Q is a significant fraction of ν_0, the spin states for the quadrupolar nucleus are not quantized precisely in the direction of B_0 and hence MAS does not completely average the dipolar interaction between the nuclei. The effect, referred to as residual dipolar coupling, [234,260–262] manifests itself as distortions in the multiplet structure in the NMR spectrum of a spin-1/2 nucleus (Figure 10),[263] giving rise to unequal spacings between adjacent peaks and distinctive line shapes for the individual peaks.[264] The exact spacing and line shapes depend on the magnitudes of C_Q, R_{eff},[28] J_{iso}, the orientation of the dipolar vector relative to the EFG tensor, and most importantly, on the ratio ν_Q/ν_0. Thus, a

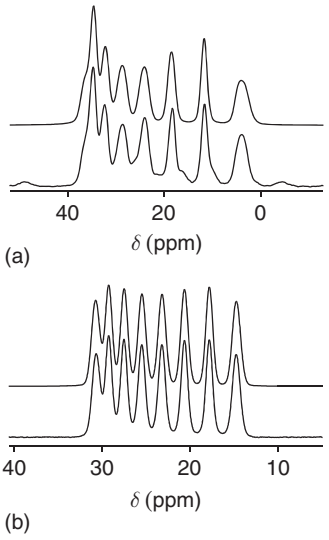

Figure 10 Calculated and experimental ^{31}P NMR spectra of P(*p*-tol)$_3$Co(DH)$_2$Cl acquired at (a) 4.7 T and (b) 9.4 T. Reprinted, with permission from: Schurko, R. W.; Wasylishen, R. E.; Moore, S. J.; Marzilli. L. G.; Nelson, J. H. *Can. J. Chem.* **1999**, *77*, 1973–1983. © 1999 NRC Press.

simulation of the NMR spectra of the spin-1/2 nucleus allows the indirect determination of the parameters for the quadrupolar nucleus; however, there are numerous parameters describing the line shape. The effect is more pronounced in spectra acquired at lower applied magnetic field strengths, a consequence of the dependence of the spectra on ν_Q/ν_0 (compare, for example, Figures 10(a) and 10(b)). This fact may aid in the determination of the quadrupolar parameters.

Even in cases where the quadrupolar parameters can be determined from direct observation of the quadrupolar nuclei, the residual dipolar coupling may be used to determine important molecular properties. For example, based on the magnitude of the residual dipolar coupling between ^{13}C and $^{10/11}$B determined from a simulation of the ^{13}C NMR spectra of MAS samples, Forgeron *et al.* determined that, at room temperature, the borazine rings of hexamethylborazine undergo rapid jumps about the molecular C_3 axis.[47]

The efficient relaxation of quadrupolar nuclei in solution generally results in self-decoupling, such that quadrupolar effects are generally not observed in NMR spectra of spin-1/2 nuclei. Self-decoupling may also be a factor in NMR spectra of solid samples;[263,265] this often manifests itself as an asymmetric line shape. By decreasing the temperature, the T_1 relaxation time of the quadrupolar nucleus may increase sufficiently to allow acquisition of NMR spectra where the effects of residual dipolar coupling are sufficiently resolved.[263]

The residual dipolar coupling also manifests itself in NMR spectra of dipolar-coupled quadrupolar spin pairs.[234,266,267] Wu and Yamada also observed residual dipolar coupling attributed to the ^{14}N–^{11}B dipolar interaction in the ^{11}B NMR spectra of MAS samples of triethanolamine borate.[268] More recently, the effect of the ^{14}N–^{11}B, ^{11}B–^{11}B, and ^{55}Mn–^{55}Mn residual dipolar interactions on the ^{11}B and ^{55}Mn NMR line shapes acquired through MQMAS were also demonstrated.[266]

1.17.5 NMR of Paramagnetic Systems

Multinuclear magnetic resonance studies of paramagnetic molecules dissolved in isotropic fluids is a well-developed area of research. An extremely valuable early textbook, *NMR of Paramagnetic Molecules, Principles and Applications*, was published in 1973.[269] More recently, other textbooks focusing on paramagnetic molecules in solution have appeared.[270–272] In contrast, NMR investigations of paramagnetic solids, particularly of molecules of interest to organometallic chemists, have received much less attention. Here, we mention only a few reviews and key papers in this area. We are unaware of NMR studies of metal nuclides in paramagnetic systems that would be of interest to

organometallic chemists; therefore, this section is restricted to a discussion of NMR investigations of the ligand nuclei. An article by Köhler is highly recommended.[273] In addition, readers should refer to the biennial reports on the current NMR literature of paramagnetic systems, currently reviewed by Sharp.[274]

1.17.5.1 NMR of the Ligand Nuclei for Paramagnetic Compounds

The CSs of the ligand nuclei in a paramagnetic molecule can be shifted by hundreds of ppm compared to a diamagnetic analog. As well, the NMR peaks in paramagnetic systems can be significantly broadened – in some cases beyond detection. The CS of the ligand nuclei in paramagnetic species can generally be described by Equation (14).

$$\delta_T^{exp} = \delta_T^{dia} + \delta_T^{cont} + \delta_T^{dip} \tag{14}$$

Here, $\delta_T{}^{exp}$ is the observed CS, $\delta_T{}^{dia}$ is the shift that would be observed if the molecule were diamagnetic, $\delta_T{}^{cont}$ is the contact shift, and $\delta_T{}^{dip}$ is the dipolar or pseudo-contact shift.

The contact shift arises from delocalization of unpaired electron spin density, generally localized on a metal, to the ligand nuclei, and it depends inversely on temperature and directly on $\rho_{\alpha,\beta}$, the Fermi contact spin density at the nucleus under NMR observation. The spin density, $\rho_{\alpha,\beta}$, represents the net imbalance between α and β electron spins at the nucleus of interest; positive and negative spin densities correspond to high- and low-frequency contact shifts, respectively.

The term $\delta_T{}^{dip}$ is the dipolar or pseudo-contact shift and is typically smaller than $\delta_T{}^{cont}$ and is proportional to the square of the anisotropy in the electron g-tensor as well as to r^{-3}, where r is the electron–nucleus separation. Equations describing the relationship between $\delta_T{}^{dip}$ and g-tensors, etc., can be found elsewhere.[270–273]

For the organometallic chemist interested in paramagnetic systems, the recent publications of Köhler and co-workers are essential reading. High resolution ^{13}C NMR spectra of several paramagnetic metallocenes have been acquired and interpreted.[275,276] As well, the results of ^{13}C and ^{15}N MAS studies of the Prussian-blue precursors, $Cs_2K[Fe(CN)_6]$ and $Cs_2K[Mn(CN)_6]$, have been described.[277] Paramagnetic cyanide complexes have also been investigated by Takeda and his group.[278] This research group has also used solid-state NMR to study the spin-density distribution of the ferromagnetic coordination polymer, $Ni(NCS)_2(Him)_2$.[279] Liu *et al.*,[280] as well as Ishii and co-workers,[281] have demonstrated the advantages of acquiring NMR spectra of paramagnetic complexes using the fastest possible spinning speeds. Oldfield and co-workers have reported ^{1}H, ^{13}C, ^{15}N, and ^{19}F NMR CSs in paramagnetic metalloporphyrins and metalloproteins.[282] The latter study included density functional theory computations of Fermi contact spin density which assisted the interpretation of the experimental results. Several chapters in the recent text edited by Kaupp *et al.* discuss the calculations of hyperfine coupling constants relevant to the interpretation of solid-state NMR data on paramagnetic systems.[283] See, for example, the chapter by Moon and Patchkovskii.[284] Rinkevicius *et al.* have also discussed the calculation of nuclear magnetic shielding in paramagnetic molecules.[285]

1.17.6 Selected Applications of Solid-State NMR in Organometallic Chemistry

Solid-state NMR provides researchers with an opportunity to obtain much more fundamental information intimately related to the electronic and molecular structure of organometallic compounds than does conventional solution NMR measurements. In particular, magnetic shielding tensors can be characterized for both spin-1/2 nuclei and quadrupolar nuclei. For the latter, EFG tensors can also be measured. These tensors provide information about the orientation dependence of magnetic shielding and EFGs at nuclei and are sensitive probes of the nuclear environment. In molecular fragments containing two or more NMR-active nuclei, it is possible, in principle, to measure spin–spin coupling tensors, which provide information about the mechanisms by which nuclei communicate. As mentioned in Section 1, solid-state NMR is ideally suited to investigate dynamic systems. Finally, the technique enables one to examine atoms or molecules on surfaces or compounds that are insoluble or ones that lose their integrity on dissolution. In this section, we briefly illustrate some of these applications.

1.17.6.1 Carbon-shielding Tensors in η^2-Coordinated Transition Metal Complexes of Alkenes and Alkynes

It has long been known that upon coordinating an alkene to a late transition metal, the alkene carbon magnetic shielding increases.[286] On the other hand, when an alkyne is coordinated to a late transition metal, the carbon nuclei of the alkyne become less shielded. What is the origin of this curious behavior? As described below, the answer becomes clear when one characterizes the carbon tensors of model ligands and their transition metal complexes (Figure 11).[30] Qualitatively, in the case of η^2-olefin complexes, one no longer has low-lying unoccupied molecular orbitals with the correct symmetry localized on the coordinated carbon to mix with the occupied molecular orbitals. As a result, the paramagnetic contribution to the magnetic shielding of the carbon nuclei is diminished and they become more shielded.[287] In the case of acetylenes, one must recognize that for the uncoordinated ligand, the paramagnetic contribution to shielding, when the applied field is along the C≡C bond, is small (it is zero in the case of acetylene). Upon coordination to a metal, the symmetry is broken and deshielding due to the paramagnetic term becomes important. Several low-lying virtual orbitals contribute to the carbon-shielding tensor – the shielding along two principal components decreases while that along the other component increases; overall, there is a net deshielding. Further details can be found in the paper by Harris *et al.*[30] The articles by Grutzner[288] and Duer[96] are recommended for a qualitative discussion of carbon shielding in ethylene. Experimental data for Zeise's salt have been presented by Huang *et al.*,[289] Ding and McDowell,[290] and Bernard *et al.*[287] Other key references to solid-state NMR investigations of carbon CS tensors in metal–olefin complexes include the work of Gay and Young,[291] and Oldfield and co-workers.[292]

1.17.6.2 Phosphorus Magnetic Shielding Tensors of General Phosphido Ligands in Transition Metal Complexes

Phosphorus-containing ligands are often an integral part of organometallic compounds. The favorable NMR properties of ^{31}P make it an ideal nucleus for the investigation of organometallic compounds containing phosphorus.[293] Carty and co-workers have outlined the various bonding modes of phosphido complexes and highlighted trends in phosphorus CSs deduced from extensive solution ^{31}P NMR investigations.[294] The range of isotropic phosphorus CSs in phosphido complexes are known to exceed 1500 ppm, but how does the shielding depend on the orientation of the phosphorus-containing moiety in the applied magnetic field? For example, the ^{31}P NMR spectrum of the solid cluster $Ru_8(CO)_{21}(\mu_6\text{-P})(\mu_4\text{-PPh})(\mu_2\text{-PPh}_2)$ obtained with MAS (Figure 12) illustrates the problem.[295] The spinning sidebands arising from the three phosphorus ligands in this particular complex extend over 1200 ppm! Analysis of the

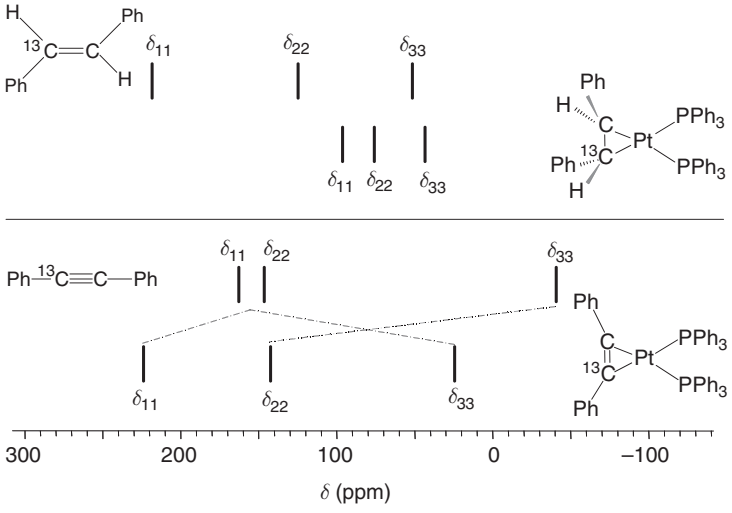

Figure 11 Summary of the effects on the CS tensors of alkynyl carbons caused by η^2-bonding to platinum. The dashed lines in the lower portion of the figure indicate CS tensor components that are oriented in the same approximate direction. Reprinted with permission from: Harris, K. J.; Bernard, G. M.; McDonald, C.; McDonald, R.; Ferguson, M. J.; Wasylishen R. E. *Inorg. Chem.* **2006**, *45*, 2461–2473. © 2006 American Chemical Society.

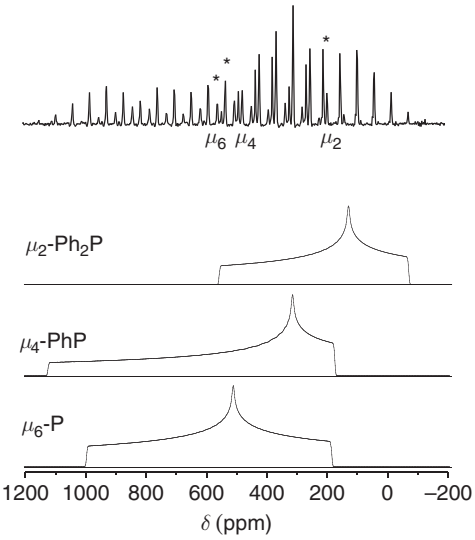

Figure 12 Phosphorus-31 NMR spectrum of $Ru_8(CO)_{21}(\mu_6\text{-P})(\mu_4\text{-}PPh)(\mu_2\text{-}PPh_2)$ obtained at 4.7 T and $\nu_{rot} = 4.5$ kHz (upper trace). The asterisks indicate the isotropic peaks for the three ^{31}P sites. The lower traces are simulations of the ^{31}P NMR powder patterns expected for each site in a stationary sample, based on the principal components of the phosphorus CS tensors as reported in Ref: 295. Reprinted with permission from: Eichele, K.; Wasylishen, R. E.; Corrigan, J. F.; Taylor, N. J.; Carty, A. J. *J. Am. Chem. Soc.* **1995**, *117*, 6961–6969. © 1995 American Chemical Society.

experimental spectrum indicates that the shielding powder patterns for the μ_2-PPh_2, μ_4-PPh, and μ_6-P ligands span 620, 944, and 807 ppm, respectively. Why are the phosphorus CSs of these complexes so anisotropic while those of group 6 transition metal complexes of phospholes such as 5-phenyldibenzophosphole (DBP) exhibit small anisotropies?[296] For example, the spans for (DBP)$Cr(CO)_5$, (DBP)$Mo(CO)_5$, and (DBP)$W(CO)_5$ are less than 160 ppm.[296] Eichele and co-workers have addressed this question by performing numerous single crystal ^{31}P NMR investigations of phosphorus-containing ligands in organometallic compounds.[295,297–299] In addition to providing high-quality experimental data that serve as benchmarks for modern computational quantum chemistry calculations, these studies attempt to provide qualitative explanations using orbital pictures familiar to experimental chemists. Finally, the results of this research clearly demonstrate that the information available from shielding tensors far exceeds that obtained from their isotropic values. For a summary of quantum chemical calculations of phosphorus magnetic shielding tensors in transition metal complexes, see the paper by Feindel and Wasylishen.[300]

1.17.6.3 Characterization of Metal-shielding and EFG Tensors for Quadrupolar Nuclei

As mentioned elsewhere in this chapter, most NMR-active nuclei are half-integer spin quadrupolar nuclei and many of these are isotopes of important metals in organometallic chemistry (e.g., $^{47/49}$Ti, ^{51}V, ^{55}Mn, ^{59}Co, ^{91}Zr, $^{95/97}$Mo, $^{99/101}$Ru). Granger has provided an excellent summary of solution NMR studies of quadrupolar transition metal NMR.[301] See also the contributions by Lewinski, [302] Pettinari,[303] Appleton,[304] Rehder,[305] and Kolehmainen.[306]

Here we present an interesting example that demonstrates both the advantages as well as some special considerations in conducting solid-state NMR experiments on half-integer spin quadrupolar nuclei. The ^{95}Mo ($I = 5/2$) NMR spectrum of solid mesitylenetricarbonyl–molybdenum(0) obtained with MAS at 18.8 T (800 MHz ^{1}H NMR frequency) is shown in Figure 13.[49] First, one must realize that this spectrum arises solely from the $m_I = 1/2 \rightarrow m_I = -1/2$ transition; the STs are too spread out and consequently too weak to be observed in a reasonable time. Second, note that at a first glance, the spectrum appears analogous to what one would expect from a spin $I = 1/2$ nucleus with an axially symmetric CS tensor. Indeed, the ^{95}Mo nuclear quadrupolar coupling constant, C_Q, is sufficiently small, 0.95 ± 0.15 MHz, to cause only minor perturbations of the CT at this high field. The ^{95}Mo NMR line shape of the CT is completely dominated by the anisotropic molybdenum magnetic shielding, as indicated by the span, 775 ± 30 ppm. Analysis of the spectrum further indicated that the largest component of the EFG tensor is coincident with the component of the magnetic shielding tensor in the direction of maximum shielding, perpendicular to the plane of the cyclopentadienyl rings. It is important to reiterate that the analysis of NMR spectra of half-integer spin quadrupolar nuclei in solids will

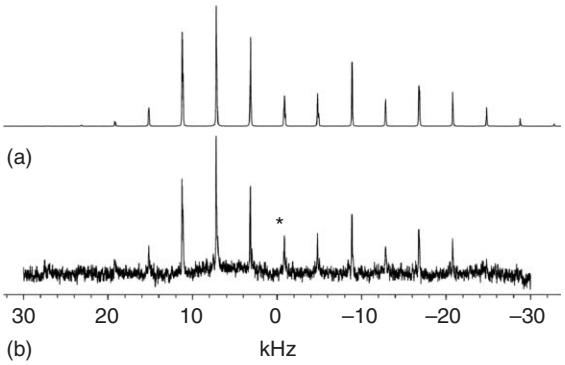

Figure 13 Simulated (a) and experimental (b) ^{95}Mo NMR spectra of the central transition of solid mesitylenetricarbonyl–molybdenum(0) obtained at 18.8 T with $\nu_{rot} = 4.000$ kHz. The asterisk denotes the center band.

generally benefit from studies at more than one applied magnetic field since, in frequency units, the shielding scales linearly with the field strength, while the perturbation due to the second-order quadrupolar interaction scales as the inverse of the applied magnetic field.

Metallocenes have been of interest to spectroscopists for some time, because of their unusual structures and many useful applications. With the availability of high applied magnetic fields and the development of new techniques, as discussed in Section 4, many metal isotopes in metallocenes are now accessible to the solid-state NMR spectroscopist. The research group of Schurko has been particularly active in this area, having investigated numerous metallocenes through the acquisition of solid-state NMR spectra of the metal centers in the decamethylaluminocenium cation,[307] some decamethylcyclopentadienyl boron complexes,[308] some sodium metallocenes,[309] bis(cyclopentadienyl)magnesium,[310] some polymeric potassium metallocenes,[311] and some half-sandwich Nb(I) and Nb(V) complexes.[312]

Zirconocene complexes have received considerable attention owing to their importance in organic syntheses.[313] In 2004, Hung and Schurko investigated bis(cyclopentadienyl)dichlorozirconium(IV) via solid-state ^{91}Zr ($I = 5/2$) NMR spectroscopy.[314] Through the use of the QCPMG experiment, enhanced with either DFS or RAPT (Section 4.1.3), the authors obtained high-quality ^{91}Zr NMR spectra for both stationary and MAS samples. Despite the presence of a significant ^{91}Zr background NMR signal from the ZrO_2 rotors used in the experiment, the authors were able to determine the principal components of the ^{91}Zr CS and EFG tensors. They found that ^{91}Zr has a significant anisotropic shielding, $\Omega = 475$ ppm, and that $C_Q = 6.35$ MHz. On the basis of these experimental results and those obtained with either Hartree–Fock or density functional theory calculations, orientations of the CS and EFG tensors were proposed (Figure 14).

1.17.6.4 Dynamics in Transition Metal Carbonyls – Iron Pentacarbonyl

NMR has been a tremendously powerful technique to study systems which are dynamic.[315–317] A classic example is iron pentacarbonyl where rapid axial–equatorial exchange of carbonyl ligands in this trigonal-bipyramidal structure is

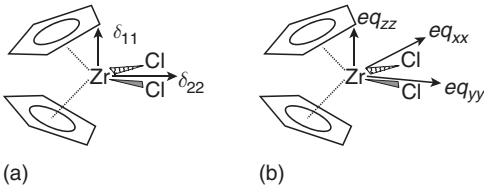

Figure 14 Approximate orientations of the (a) Zr chemical shift and (b) EFG tensors for Cp_2ZrCl_2.[314] The δ_{11} component is perpendicular to the plane defined by the Zr and Cl atoms, while δ_{22} bisects the angle formed by these atoms; δ_{33} is approximately perpendicular to the plane of the page. The largest component of the EFG, eq_{zz} is coincident with δ_{11}, while eq_{xx} and eq_{yy} are in the plane defined by the Zr and Cl atoms, forming angles of approximately 13° and 19°, respectively, with the nearest Zr–Cl bond.

Table 1 Carbon and oxygen CS tensor principal components for $Fe(CO)_5$[a]

Site	δ_{11} (ppm)	δ_{22} (ppm)	δ_{33} (ppm)	δ_{iso} (ppm)	Ω (ppm)	κ
C_{axial}	345	345	−30	215	375	1.000
$C_{equatorial}$	354	341	−60	207	414	0.971
O_{axial}	588	588	28	401	560	1.000
$O_{equatorial}$	627	545	−25	362	652	0.842

[a]From Ref: 320.

known to be extremely rapid both in the gas phase and in solution. In fact, exchange has never been "stopped" in solution; that is, separate ^{13}C or ^{17}O NMR peaks have not been observed for the equatorial and axial carbons or oxygen nuclei in an isotropic solution. On the other hand, separate ^{13}C and ^{17}O NMR peaks have been observed for these sites in solid-state NMR studies.[318–320] In 1989, Hanson succeeded in resolving separate peaks for the axial and equatorial carbons of solid $Fe(CO)_5$ at temperatures of −38 °C or lower.[318] From the ^{13}C CS difference, approximately 8 ppm, the axial–equatorial exchange rate was estimated to be less than $10^2\,s^{-1}$ at −38 °C. The investigation of molecules such as iron pentacarbonyl is particularly challenging because of the extremely lengthy spin-lattice relaxation times. For example, at −60 °C, $T_1(^{13}C)$ for this molecule has been estimated to be approximately 32 min.[321]

More recently, Oldfield and co-workers characterized both the carbon and oxygen magnetic shielding tensors for the axial and equatorial carbonyl groups of iron pentacarbonyl.[320] For both carbon and oxygen, the equatorial sites are more shielded and have larger spans than the corresponding axial sites (see Table 1). These results, together with the results obtained for several other transition metal clusters, are discussed in detail by Oldfield and co-workers.[320] Finally, it is important to note that transition metal carbonyls typically have relatively small ^{17}O nuclear quadrupolar coupling constants and thus are ideally suited for solid-state ^{17}O NMR studies (for $Fe(CO)_5$, the axial and equatorial oxygens have C_Q values of (+)1.17 and (−)1.87 MHz, respectively).[320]

The dynamics in many other systems of interest to organometallic chemists have been studied. For example, the stereochemical non-rigidity of titanium tetracyclopentadienyl has been investigated by Heyes and Dobson;[322] more recently, Munson and co-workers used variable-temperature 1-D and 2-D ^{13}C CP/MAS NMR to study the dynamics of monohaptocyclopentadienyl rings of hafnium and titanium tetracyclopentadienyl in the solid state.[323] It is hoped that the references provided here will serve as a useful starting point to the solid-state NMR literature dealing with dynamics in organometallic systems.

1.17.6.5 Solid-state NMR Studies of Supported Organometallics

For many years now, researchers have been interested in using solid-state NMR to investigate atoms and molecules immobilized on surfaces.[324] For example, Fyfe and co-workers demonstrated the feasibility of solid-state ^{31}P CP/MAS NMR in investigating transition metal complexes immobilized on solid supports.[325–328] In 1994, Reven reviewed solid-state NMR research involving supported organometallics;[329] since that time, exciting applications continue to appear in the literature. For example, Copéret and co-workers have used the 2-D ^1H–^{13}C HETCOR solid-state NMR to characterize a well-defined alkylidyne complex of molybdenum supported on silica.[330] The compound, $Mo(\equiv C\text{-}t\text{-}Bu)(CH_2\text{-}t\text{-}Bu)_3$, was grafted on a silica surface and the resulting surface complex, $[(\equiv SiO)Mo(\equiv C\text{-}t\text{-}Bu)(CH_2\text{-}t\text{-}Bu)_2]$, was subsequently unequivocally identified. Recently, this same group of researchers, together with Schrock and co-workers, used state-of-the-art solid-state NMR techniques including 2-D ^1H–^1H NMR spectroscopy to characterize $[(\equiv SiO)Mo(=NAr)(=CH\text{-}t\text{-}Bu)(CH_2Bu\text{-}t)]$, a well-defined heterogeneous catalyst for olefin metathesis.[331]

Ahn and Marks have employed solid-state ^{13}C CP/MAS NMR to investigate the chemistry of several organotantalum hydrocarbyl/alkylidene complexes supported on high surface area oxides.[332] In some cases, chemisorption resulted in the formation of cation-like species, for example, $Cp^*Ta(^{13}CH_3)_3^+$.

Scott and co-workers recently reported applying IR, ^{13}C, and ^{29}Si solid-state CP/MAS NMR to investigate catalyst/co-catalyst/support interactions in silica-supported olefin polymerization catalysts based on Cp^*TiMe_3.[333] Finally, we mention the research of Lindner *et al.* on supported organometallic complexes.[334]

1.17.7 Concluding Remarks

An overview of the recent developments in solid-state NMR applicable to studies of organometallic compounds has been presented. The rapid pace of development in this field is expected to continue – combined with new hardware, the utility of solid-state NMR in the investigation of organometallic complexes will continue to grow. Until recently, the wealth of information available from these techniques have been neglected, since the methods were often viewed as "exotic" or of little practical interest to anyone but physical chemists. We hope that the overview of NMR techniques presented here will convince researchers that solid-state NMR spectroscopy can be a valuable tool which can be used in their investigations.

Acknowledgments

The authors thank members of the solid-state NMR group at the University of Alberta for many helpful comments in the preparation of this manuscript. Research in the lab has been possible thanks to the financial support of the Natural Sciences and Engineering Research Council (NSERC) of Canada, Alberta Ingenuity, and the University of Alberta.

Nomenclature

B_0	applied magnetic field
C	natural abundance
C_Q	nuclear quadrupolar coupling constant
D	receptivity
e	electron charge
eq_{ii}	principal components of the electric field gradient tensor, with $i = x$, y, or z
I	nuclear spin quantum number
J	indirect spin–spin coupling
Q	nuclear quadrupole moment
R_{DD}	dipolar coupling constant
R_{eff}	effective dipolar coupling[28]
T_1	spin-lattice relaxation time
α, β	polar angles describing the orientation of B_0 relative to the EFG tensor
γ	magnetogyric ratio
δ_{ii}	principal components of the chemical shift tensor, with $i = 1$, 2, or 3
δ_{iso}	isotropic chemical shift
$\delta_{\text{T}}^{\text{cont}}$	contact chemical shift
$\delta_{\text{T}}^{\text{dia}}$	chemical shift in the absence of paramagnetic effects
$\delta_{\text{T}}^{\text{dip}}$	dipolar or pseudo-contact shift
$\delta_{\text{T}}^{\text{exp}}$	experimental chemical shift for nuclei in paramagnetic compounds
ΔJ	antisotropy in the indirect spin–spin coupling tensor[28]
$\Delta\nu_{1/2,-1/2}$	second-order quadrupolar shift in the NMR frequency of the central transition
$\Delta\nu_{CT}$	total breadth of the NMR central transition
η_Q	asymmetry in the electric field gradient tensor
κ	skew in the chemical shift tensor
ν_0	Larmor frequency
ν_Q	nuclear quadrupole frequency
ν_{rot}	spinning frequency of an NMR sample
Ξ	frequency of the nucleus of interest in the reference compound, relative to that of ^{1}H of TMS in $CDCl_3$ set to exactly 100.0000 MHz
$\rho_{\alpha,\beta}$	Imbalance in the α- and β-spin electrons
σ_{ii}	Principal components of the magnetic shielding tensor, with $i = 1$, 2, or 3
Ω	Span of a chemical shift tensor

References

1. Fyfe, C. A. *Solid State NMR for Chemists*; C.F.C. Press: Guelph, 1983.
2. Cotton, F. A. *Acc. Chem. Res.* **1968**, *1*, 257–265.
3. Mehring, M. *Principles of High Resolution NMR in Solids*, 2nd ed.; Springer-Verlag: Berlin, 1983.
4. Gerstein, B. C.; Dybowski, C. R. *Transient Techniques in NMR of Solids: An Introduction to Theory and Practice*; Academic Press: Orlando, 1985.
5. Stejskal, E. O.; Memory, J. D. *High Resolution NMR in the Solid State: Fundamentals of CP/MAS*; Oxford University Press: Oxford, 1994.
6. Schmidt-Rohr, K.; Spiess, H. W. *Multidimensional Solid-state NMR and Polymers*; Academic Press: London, 1994.
7. Harris, R. K. *Nuclear Magnetic Resonance Spectroscopy: A Physicochemical View*; Pitman: London, 1983.
8. Günther, H. *NMR Spectroscopy*, 2nd ed.; Wiley: Chichester, 1995.
9. Hore, P. J. *Nuclear Magnetic Resonance*; Oxford University Press: Oxford, 1995.
10. Braun, S.; Kalinowski, H.-O.; Berger, S. *100 and More Basic NMR Experiments*; VCH: New York, 1996.
11. Claridge, T. D. W. High-resolution NMR Techniques in Organic Chemistry. In *Tetrahedron Organic Chemistry Series*; Baldwin, J. E., Williams, R. M., Eds.; Pergamon: Amsterdam, 1999; Vol. 19.
12. Akitt, J. W.; Mann, B. E. *NMR and Chemistry: An Introduction to Modern NMR Spectroscopy*, 4th ed.; Stanley Thornes: Cheltenham, 2000.
13. Keeler, J. *Understanding NMR Spectroscopy*; Wiley: Chichester, 2005.
14. Duer, M. J. The Basics of Solid-state NMR. In *Solid-state NMR Spectroscopy: Principles and Applications*; Duer, M. J., Ed.; Blackwell: Oxford, 2002; Chapter 1, pp 3–72.
15. Anet, F. A. L.; O'Leary, D. J. *Conc. Magn. Reson.* **1991**, *3*, 193–214.
16. Haeberlen, U. High Resolution NMR in Solids: Selective Averaging. In *Advances in Magnetic Resonance*; Supplement 1; Waugh, J. S., Ed.; Academic Press: New York, 1976, pp 1–190.
17. Jameson, C. J. Chemical Shift Scales on an Absolute Basis. In *Encyclopedia of Nuclear Magnetic Resonance*; Grant, D. M., Harris, R. K., Eds.; Wiley: Chichester, 1996; Vol. 2, pp 1273–1281.
18. Harris, R. K.; Becker, E. D.; Cabral de Menezes, S. M.; Goodfellow, R.; Granger, P. *Pure Appl. Chem.* **2001**, *73*, 1795–1818.
19. Gustavsson, M. G. H.; Mårtensson-Pendrill, A.-M. *Phys. Rev. A* **1998**, *58*, 3611–3618.
20. Zilm, K. W.; Conlin, R. T.; Grant, D. M; Michl, J. *J. Am. Chem. Soc.* **1980**, *102*, 6672–6676.
21. Kennedy, M. A.; Ellis, P. D. *Conc. Magn. Reson.* **1989**, *1*, 35–47.
22. Kennedy, M. A.; Ellis, P. D. *Conc. Magn. Reson.* **1989**, *1*, 109–129.
23. Herzfeld, J.; Berger, A. E. *J. Chem. Phys.* **1980**, *73*, 6021–6030.
24. Maricq, M. M.; Waugh, J. S. *J. Chem. Phys.* **1979**, *70*, 3300–3316.
25. Zilm, K. W.; Grant, D. M. *J. Am. Chem. Soc.* **1981**, *103*, 2913–2922.
26. Power, W. P.; Wasylishen, R. E. *Ann. Rep. NMR Spectrosc.* **1991**, *23*, 1–84.
27. Eichele, K.; Wasylishen, R. E. *J. Magn. Reson. Ser. A* **1994**, *106*, 46–56.
28. Wasylishen, R. E. Dipolar & Indirect Coupling Tensors in Solids. In *Encyclopedia of Nuclear Magnetic Resonance*; Grant, D. M., Harris, R. K., Eds.; Wiley: Chichester, 1996; Vol. 3, pp 1685–1695.
29. Wasylishen, R. E. Characterization of NMR Tensors via Experiment and Theory. In *Calculation of NMR and EPR Parameters: Theory and Applications*; Kaupp, M., Bühl, M., Malkin, V. G., Eds.; Wiley-VCH Verlag GmbH: Weinheim, 2004; Chapter 27, pp 433–447.
30. Harris, K. J.; Bernard, G. M.; McDonald, C.; McDonald, R.; Ferguson, M. J.; Wasylishen, R. E. *Inorg. Chem.* **2006**, *45*, 2461–2473.
31. Mason, J. *Solid State Nucl. Magn. Reason.* **1993**, *2*, 285–288.
32. Harris, R. K. *Solid State Nucl. Magn. Reson.* **1998**, *10*, 177–178.
33. Jameson, C. J. *Solid State Nucl. Magn. Reson.* **1998**, *11*, 265–268.
34. Amoureux, J. P.; Fernandez, C.; Granger, P. Interpretation of Quadrupolar Powder Spectra: Static and MAS Experiments. In *Multinuclear Magnetic Resonance in Liquids and Solids–Chemical Applications*; Granger, P., Harris, R. K., Eds.; NATO ASI Series C: Mathematical and Physical Sciences; Kluwer: Dordrecht, 1990; Vol. 322, Chapter XXII, pp 409–424.
35. Freude, D.; Haase, J. *NMR Basic Princ. Prog.* **1993**, *29*, 1–90.
36. Man, P. P. Quadrupolar Interactions. In *Encyclopedia of Nuclear Magnetic Resonance*; Grant, D. M., Harris, R. K., Eds.; Wiley: Chichester, 1996; Vol. 6, pp 3838–3848.
37. Vega, A. J. Quadrupolar Nuclei in Solids. In *Encyclopedia of Nuclear Magnetic Resonance*; Grant, D. M., Harris, R. K., Eds.; Wiley: Chichester, 1996; Vol. 6, pp 3869–3889.
38. Freude, D. Quadrupolar Nuclei in Solid-state Nuclear Magnetic Resonance. In *Encyclopedia of Analytical Chemistry. Applications, Theory and Instrumentation*; Meyers, R. A., Ed.; Wiley: Chichester, 2000; Vol. 14, pp 12188–12224.
39. Man, P. P. Quadrupole Couplings in Nuclear Magnetic Resonance, General. In *Encyclopedia of Analytical Chemistry: Applications, Theory and Instrumentation*; Meyers, R. A., Ed.; Wiley: Chichester, 2000; Vol. 14, pp 12224–12265.
40. Duer, M. J.; Farnan, I. Quadrupole Coupling: Its Measurement and Uses. In *Solid-state NMR Spectroscopy: Principles and Applications*; Duer, M. J., Ed.; Blackwell: Oxford, 2002; Chapter 4, pp 179–215.
41. Lucken, E. A. C. *Nuclear Quadrupole Coupling Constants*; Academic Press: London, 1969.
42. Bryce, D. L.; Wasylishen, R. E. *Acc. Chem. Res.* **2003**, *36*, 327–334.
43. Zax, D. B. Zero Field NMR. In *Encyclopedia of Nuclear Magnetic Resonance*; Grant, D. M., Harris, R. K., Eds.; Wiley: Chichester, 1996; Vol. 8, pp 5052–5063.
44. Abragam, A. *The Principles of Nuclear Magnetism*; Oxford University Press: Oxford, 1961.
45. Bernard, G. M.; Wasylishen, R. E. unpublished results.
46. Schurko, R. W.; Wasylishen, R. E.; Foerster, H. *J. Phys. Chem. A* **1998**, *102*, 9750–9760.
47. Forgeron, M. A. M.; Bryce, D. L.; Wasylishen, R. E.; Rösler, R. *J. Phys. Chem. A* **2003**, *107*, 726–735.
48. Eichele, K.; Chan, J. C. C.; Wasylishen, R. E.; Britten, J. F. *J. Phys. Chem. A* **1997**, *101*, 5423–5430.
49. Bryce, D. L.; Wasylishen, R. E. *Phys. Chem. Chem. Phys.* **2002**, *4*, 3591–3600.
50. Samoson, A. *Chem. Phys. Lett.* **1985**, *119*, 29–32.
51. Oldfield, E.; Schramm, S.; Meadows, M. D.; Smith, K. A.; Kinsey, R. A.; Ackerman, J. *J. Am. Chem. Soc.* **1982**, *104*, 919–920.
52. Power, W. P.; Wasylishen, R. E.; Mooibroek, S.; Pettitt, B. A.; Danchura, W. *J. Phys. Chem.* **1990**, *94*, 591–598.
53. Man, P. P.; Klinowski, J.; Trokiner, A.; Zanni, H.; Papon, P. *Chem. Phys. Lett.* **1988**, *151*, 143–150.

54. Larsen, F. H.; Farnan, I.; Lipton, A. S. *J. Magn. Reson.* **2006**, *178*, 228–236.
55. Yamauchi, K.; Janssen, J. W. G.; Kentgens, A. P. M. *J. Magn. Reson.* **2004**, *167*, 87–96.
56. Bryce, D. L.; Bernard, G. M.; Gee, M.; Lumsden, M. D.; Eichele, K; Wasylishen, R. E. *Can. J. Anal. Sci. Spectrosc.* **2001**, *46*, 46–82.
57. Kundla, E.; Samoson, A.; Lippmaa, E. *Chem. Phys. Lett.* **1981**, *83*, 229–232.
58. Challoner, R.; Sebald, A. *Solid State Nucl. Magn. Reson.* **1995**, *4*, 39–45.
59. Sparks, S. W.; Ellis, P. D. *J. Am. Chem. Soc.* **1986**, *108*, 3215–3218.
60. Slichter, C. P. Principles of Magnetic Resonance. In *Springer Series in Solid-state Sciences 1*, 3rd ed.; Fulde, P., Ed.; Springer-Verlag: Berlin, 1990; Chapter 10, pp 485–502.
61. Akitt, J. W.; McDonald, W. S. *J. Magn. Reson.* **1984**, *58*, 401–412.
62. Han, O. H.; Oldfield, E. *Inorg. Chem.* **1990**, *29*, 3666–3669.
63. Ooms, K. J.; Wasylishen, R. E. *J. Am. Chem. Soc.* **2004**, *126*, 10972–10980.
64. Higinbotham, J.; Marshall, I. *Ann. Rep. NMR Spectrosc.* **2001**, *43*, 59–120.
65. Bak, M.; Rasmussen, J. T.; Nielsen, N. C. *J. Magn. Reson.* **2000**, *147*, 296–330.
66. Eichele, K.; Wasylishen, R. E. *WSOLIDS NMR Simulation Package*; University of Alberta, Edmonton, 2001.
67. Alderman, D. W.; Solum, M. S.; Grant, D. M. *J. Chem. Phys.* **1986**, *84*, 3717–3725.
68. Veshtort, M.; Griffin, R. G. *J. Magn. Reson.* **2006**, *178*, 248–282.
69. Greenfield, M. S.; Ronemus, A. D.; Vold, R. L.; Vold, R. R.; Ellis, P. D.; Raidy, T. E. *J. Magn. Reson.* **1987**, *72*, 89–107.
70. Sun, B.; Griffin, R. G. unpublished.
71. Hohwy, M.; Bildsøe, H.; Jakobsen, H. J.; Nielsen, N. C. *J. Magn. Reson.* **1999**, *136*, 6–14.
72. Skibsted, J.; Nielsen, N. C.; Bildsøe, H.; Jakobsen, H. J. *J. Am. Chem. Soc.* **1993**, *115*, 7351–7362.
73. Jerschow, A. *J. Magn. Reson.* **2005**, *176*, 7–14.
74. Jameson, C. J.; de Dios, A. C. Theoretical and Physical Aspects of Nuclear Shielding. In *Nuclear Magnetic Resonance*; Webb, G. A., Ed.; Specialist Periodical Reports; Royal Society of Chemistry: Cambridge, 2005; Vol. 34, Chapter 2, pp 57–86. See also articles by these authors in previous issues in this annual series.
75. Gauss, J.; Stanton, J. F. *Adv. Chem. Phys.* **2002**, *123*, 355–422.
76. Kutzelnigg, W. Fundamentals of Nonrelativistic and Relativistic Theory of NMR and EPR Parameters. In *Calculation of NMR and EPR Parameters: Theory and Applications*; Kaupp, M., Bühl, M., Malkin, V. G., Eds.; Wiley-VCH Verlag GmbH: Weinheim, 2004; Chapter 5, pp 43–82.
77. de Dios, A. C.; Roach, J. L.; Walling, A. E. The NMR Chemical Shift: Local Geometry Effects. In *Modeling NMR Chemical Shifts*; Facelli, J. C., de Dios, A. C., Eds.; ACS Symposium Series 732; American Chemical Society: Washington, DC, 1999; Chapter 16, pp 220–239.
78. Facelli, J. C. Shielding Calculations. In *Encyclopedia of Nuclear Magnetic Resonance: Advances in NMR*; Grant, D. M., Harris, R. K., Eds.; Wiley: Chichester, 2002; Vol. 9, pp 323–333.
79. Autschbach, J.; Ziegler, T. Relativistic Computation of NMR Shieldings and Spin–Spin Coupling Constants. In *Encyclopedia of Nuclear Magnetic Resonance. Advances in NMR*; Grant, D. M., Harris, R. K., Eds.; Wiley: Chichester, 2002; Vol. 9, pp 306–323.
80. Autschbach, J. Calculation of Heavy-nucleus Chemical Shifts: Relativistic All-electron Methods. In *Calculation of NMR and EPR Parameters. Theory and Applications*; Kaupp, M., Bühl, M., Malkin, V. G., Eds.; Wiley-VCH Verlag GmbH: Weinheim, 2004; Chapter 14, pp 227–247.
81. Melo, J. I.; Ruiz de Azua, M. C.; Giribet, C. G.; Aucar, G. A.; Romero, R. H. *J. Chem. Phys.* **2003**, *118*, 471–486.
82. Vaara, J.; Manninen, P.; Lantto, P. Perturbational and ECP Calculation of Relativistic Effects in NMR Shielding and Spin–Spin Coupling. In *Calculation of NMR and EPR Parameters: Theory and Applications*; Kaupp, M., Bühl, M., Malkin, V. G., Eds.; Wiley-VCH Verlag GmbH: Weinheim, 2004; Chapter 13, pp 209–226.
83. Autschbach, J. *Struct. Bond.* **2004**, *112*, 1–48.
84. Yates, J. R.; Pickard, C. J.; Payne, M. C.; Mauri, F. *J. Chem. Phys.* **2003**, *118*, 5746–5753.
85. Autschbach, J. *Theor. Chem. Acc.* **2004**, *112*, 52–57.
86. Willans, M. J.; Feindel, K. W.; Ooms, K. J.; Wasylishen, R. E. *Chem. Eur. J.* **2006**, *12*, 159–168.
87. Profeta, M.; Mauri, F.; Pickard, C. J. *J. Am. Chem. Soc.* **2003**, *125*, 541–548.
88. Gervais, C.; Dupree, R.; Pike, K. J.; Bonhomme, C.; Profeta, M.; Pickard, C. J.; Mauri, F. *J. Phys. Chem. A* **2005**, *109*, 6960–6969.
89. Lowe, I. J. *Phys. Rev. Lett.* **1959**, *2*, 285–287.
90. Andrew, E. R. *Prog. Nucl. Magn. Reson. Spectrosc.* **1971**, *8*, 1–39.
91. Samoson, A. Extended Magic-angle Spinning. In *Encyclopedia of Nuclear Magnetic Resonance: Advances in NMR*; Grant, D. M., Harris, R. K., Eds.; Wiley: Chichester, 2002; Vol. 9, pp 59–64.
92. Hartmann, S. R.; Hahn, E. L. *Phys. Rev.* **1962**, *128*, 2042–2053.
93. Pines, A.; Gibby, M. G.; Waugh, J. S. *J. Chem. Phys.* **1972**, *56*, 1776–1777.
94. Pines, A.; Gibby, M. G.; Waugh, J. S. *J. Chem. Phys.* **1973**, *59*, 569–590.
95. Duer, M. J. Essential Techniques for Spin-1/2 Nuclei. In *Solid-state NMR Spectroscopy. Principles and Applications*; Duer, M. J., Ed.; Blackwell: Oxford, 2002; Chapter 2, pp 73–110.
96. Duer, M. J. Shielding and Chemical Shift. In *Solid-state NMR Spectroscopy Principles and Applications*; Duer, M. J., Ed.; Blackwell: Oxford, 2002; Chapter 5, pp 216–235.
97. Duer, M. J. Solid State NMR. In *Solid State Organometallic Chemistry: Methods and Applications*; Gielen, M., Willem, R, Wrackmeyer, B., Eds.; Wiley: Chichester, 1999 Physical Organometallic Chemistry; Vol. 2, Chapter 6, pp 227–277.
98. Taylor, R. E. *Conc. Magn. Reson. Part A* **2004**, *22A*, 37–49.
99. Pregosin, P. S.; Rüegger, H. Nuclear Magnetic Resonance Spectroscopy. In *Comprehensive Coordination Chemistry II*; McCleverty, J. A., Meyer, T. J., Lever, A. B. P., Eds.; Elsevier: Amsterdam, 2004; Vol. 2, pp 1–35.
100. Mann, B. E. Nuclear Magnetic Resonance Spectroscopy. In *Spectroscopic Properties of Inorganic and Organometallic Compounds*; Davidson, G., Ed.; A Specialist Periodical Report; Royal Society of Chemistry: Cambridge, 1997; Vol. 30, Chapter 1; pp 1–209.
101. Nelson, J. H. *Conc. Magn. Reson.* **2002**, *14*, 19–78.
102. Bernard, G. M.; Wasylishen, R. E. NMR Studies of Ligand Nuclei in Organometallic Compounds—New Information from Solid-state NMR Techniques. In *Unusual Structures and Physical Properties in Organometallic Chemistry*; Gielen, M., Willem, R., Wrackmeyer, B., Eds.; Wiley: Chichester, 2002 Physical Organometallic Chemistry; Vol. 3, Chapter 4, pp 165–205.
103. Aliev, A. E.; Law, R. V. Solid State NMR Spectroscopy. In *Nuclear Magnetic Resonance*; Webb, G. A., Ed.; Specialist Periodical Reports; Royal Society of Chemistry: Cambridge, 2005; Vol. 34, Chapter 7, pp 253–327. See also articles by these authors in previous issues in this annual series.

104. Smith, M. E. Solid State NMR. In *Nuclear Magnetic Resonance*; Webb, G. A., Ed.; Specialist Periodical Reports; Royal Society of Chemistry: Cambridge, 2000; Vol. 29, Chapter 7, pp 251–315. See also articles by this author in earlier issues in this annual series.
105. Duncan, T. M. *Principal Components of Chemical Shift Tensors: A Compilation*, 2nd ed.; Farragut Press: Chicago, 1994.
106. MacKenzie, K. J. D.; Smith, M. E. *Multinuclear Solid-state NMR of Inorganic Materials*; Elsevier: Oxford, 2002.
107. Wu, G.; Wasylishen, R. E. *Organometallics* **1992**, *11*, 3242–3248.
108. Wu, G.; Wasylishen, R. E. *Inorg. Chem.* **1992**, *31*, 145–148.
109. Samoson, A.; Tuherm, T.; Past, J.; Reinhold, A.; Anupõld, T.; Heinmaa, I. *Top. Curr. Chem.* **2005**, *246*, 15–31.
110. Filip, C.; Hafner, S.; Schnell, I.; Demco, D. E.; Spiess, H. W. *J. Chem. Phys.* **1999**, *110*, 423–440.
111. Hafner, S.; Spiess, H. W. *Conc. Magn. Reson.* **1998**, *10*, 99–128.
112. Samoson, A.; Tuherm, T.; Gan, Z. *Solid State Nucl. Magn. Reson.* **2001**, *20*, 130–136.
113. Schnell, I.; Spiess, H. W. *J. Magn. Reson.* **2001**, *151*, 153–227.
114. Gerstein, B. C.; Pembleton, R. G.; Wilson, R. C.; Ryan, L. M. *J. Chem. Phys.* **1977**, *66*, 361–362.
115. Gerstein, B. C. CRAMPS. In *Encyclopedia of Nuclear Magnetic Resonance*; Grant, D. M., Harris, R. K., Eds.; Wiley: Chichester, 1996; Vol. 3, pp 1501–1509.
116. Rhim, W.-K.; Elleman, D. D.; Vaughan, R. W. *J. Chem. Phys.* **1973**, *58*, 1772–1773.
117. Burum, D. P.; Rhim, W. K. *J. Chem. Phys.* **1979**, *71*, 944–956.
118. Sakellariou, D.; Lesage, A.; Hodgkinson, P.; Emsley, L. *Chem. Phys. Lett.* **2000**, *319*, 253–260.
119. Brown, S. P.; Lesage, A.; Elena, B.; Emsley, L. *J. Am. Chem. Soc.* **2004**, *126*, 13230–13231.
120. Elena, B.; de Paëpe, G.; Emsley, L. *Chem. Phys. Lett.* **2004**, *398*, 532–538.
121. Lesage, A.; Sakellariou, D.; Hediger, S.; Eléna, B.; Charmont, P.; Steuernagel, S.; Emsley, L. *J. Magn. Reson.* **2003**, *163*, 105–113.
122. Vinogradov, E.; Madhu, P. K.; Vega, S. *Chem. Phys. Lett.* **2002**, *354*, 193–202.
123. Ulrich, A. S. *Prog. Nucl. Magn. Reson. Spectrosc.* **2005**, *46*, 1–21.
124. Ando, S.; Harris, R. K.; Scheler, U. Fluorine-19 NMR of Solids Containing Both Fluorine and Hydrogen. In *Encyclopedia of Nuclear Magnetic Resonance. Advances in NMR*; Grant, D. M., Harris, R. K., Eds.; Wiley: Chichester, 2002; Vol. 9, pp 531–550.
125. Hodgkinson, P. *Prog. Nucl. Magn. Reson. Spectrosc.* **2005**, *46*, 197–222.
126. Harris, R. K.; Carss, S. A.; Chambers, R. D.; Holstein, P.; Minoja, A. P.; Scheler, U. *Bull. Magn. Reson.* **1995**, *17*, 37–45.
127. Doty, F. D. Probe Design & Construction. In *Encyclopedia of Nuclear Magnetic Resonance*; Grant, D. M., Harris, R. K., Eds.; Wiley: Chichester, 1996; Vol. 6, pp 3753–3762.
128. Cherryman, J. C.; Harris, R. K. *J. Magn. Reson.* **1997**, *128*, 21–29.
129. Feindel, K. W.; Wasylishen, R. E. *Magn. Reson. Chem.* **2004**, *42*, S158–S167.
130. Bax, A.; Griffey, R. H.; Hawkins, B. L. *J. Magn. Reson.* **1983**, *55*, 301–315.
131. Ishii, Y.; Tycko, R. *J. Magn. Reson.* **2000**, *142*, 199–204.
132. Khitrin, A. K.; Fung, B. M. *J. Magn. Reson.* **2001**, *152*, 185–188.
133. Davies, J. A.; Dutremez, S. *Coord. Chem. Rev.* **1992**, *114*, 201–247.
134. von Philipsborn, W. *Chem. Soc. Rev.* **1999**, *28*, 95–105.
135. Dybowski, C.; Neue, G. *Prog. Nucl. Magn. Reson. Spectrosc.* **2002**, *41*, 153–170.
136. Smith, M. E. *Ann. Rep. NMR Spectrosc.* **2001**, *43*, 121–175.
137. Merwin, L. H.; Sebald, A. *J. Magn. Reson.* **1990**, *88*, 167–171.
138. Merwin, L. H.; Sebald, A. *Solid State Nucl. Magn. Reson.* **1992**, *1*, 45–47.
139. Eichele, K.; Kroeker, S.; Wu, G.; Wasylishen, R. E. *Solid State Nucl. Magn. Reson.* **1995**, *4*, 295–300.
140. Rabe, G. W.; Sebald, A. *Solid State Nucl. Magn. Reson.* **1996**, *6*, 197–200.
141. Keates, J. M.; Lawless, G. A. *Organometallics* **1997**, *16*, 2842–2846.
142. Mao, X.; Zhao, X.; Ye, C.; Wang, S. *Solid State Nucl. Magn. Reson.* **1994**, *3*, 107–110.
143. Phillips, B. L.; Houston, J. R.; Feng, J.; Casey, W. H. *J. Am. Chem. Soc.* **2006**, *128*, 3912–3913.
144. Merwin, L. H.; Sebald, A. *J. Magn. Reson.* **1992**, *97*, 628–631.
145. Webb, A. G. *Ann. Rep. NMR Spectrosc.* **2002**, *45*, 1–67.
146. van Gorkom, L. C. M.; Hook, J. M.; Logan, M. B.; Hanna, J. V.; Wasylishen, R. E. *Magn. Reson. Chem.* **1995**, *33*, 791–795.
147. Bielecki, A.; Burum, D. P. *J. Magn. Reson. A* **1995**, *116*, 215–220.
148. Mildner, T.; Ernst, H.; Freude, D. *Solid State Nucl. Magn. Reson.* **1995**, *5*, 269–271.
149. Langer, B.; Schnell, I.; Spiess, H. W.; Grimmer, A.-R. *J. Magn. Reson.* **1999**, *138*, 182–186.
150. Reinhard, S.; Blümel, J. *Magn. Reson. Chem.* **2003**, *41*, 406–416.
151. Amoureux, J.-P.; Pruski, M. *Mol. Phys.* **2002**, *100*, 1595–1613.
152. Stejskal, E. O.; Schaefer, J.; Waugh, J. S. *J. Magn. Reson.* **1977**, *28*, 105–112.
153. Meier, B. H. *Chem. Phys. Lett.* **1992**, *188*, 201–207.
154. Peersen, O. B.; Wu, X.; Kustanovich, I.; Smith, S. O. *J. Magn. Reson. Ser. A* **1993**, *104*, 334–339.
155. Michel, D.; Engelke, F. *NMR Basic Princ. Prog.* **1994**, *32*, 69–125.
156. Metz, G.; Wu, X.; Smith, S. O. *J. Magn. Reson. Ser. A* **1994**, *110*, 219–227.
157. Penner, G. H.; Li, W. *Solid State Nucl. Magn. Reson.* **2003**, *23*, 168–173.
158. Siegel, R.; Nakashima, T. T.; Wasylishen, R. E. *J. Phys. Chem. B* **2004**, *108*, 2218–2226.
159. Siegel, R.; Nakashima, T. T.; Wasylishen, R. E. *Conc. Magn. Reson. Part A* **2005**, *26A*, 62–77.
160. Hung, I.; Rossini, A. J.; Schurko, R. W. *J. Phys. Chem. A* **2004**, *108*, 7112–7120.
161. Bennett, A. E.; Rienstra, C. M.; Auger, M.; Lakshmi, K. V.; Griffin, R. G. *J. Chem. Phys.* **1995**, *103*, 6951–6958.
162. Sethi, N. K. Variable Angle Sample Spinning. In *Encyclopedia of Nuclear Magnetic Resonance*; Grant, D. M., Harris, R. K., Eds.; Wiley: Chichester, 1996; Vol. 8, pp 4904–4908.
163. Wu, G.; Wasylishen, R. E. *J. Chem. Phys.* **1994**, *100*, 4828–4834.
164. Wu, G.; Wasylishen, R. E. *J. Chem. Phys.* **1994**, *100*, 5546–5549.
165. Hu, J. Z.; Wang, W.; Pugmire, R. J. Magic Angle Turning & Hopping. In *Encyclopedia of Nuclear Magnetic Resonance*; Grant, D. M., Harris, R. K., Eds.; Wiley: Chichester, 1996; Vol. 5, pp 2914–2921.
166. Bax, A.; Szeverenyi, N. M.; Maciel, G. E. *J. Magn. Reson.* **1983**, *52*, 147–152.
167. Gan, Z. *J. Am. Chem. Soc.* **1992**, *114*, 8307–8309.

168. Smith, M. E.; van Eck, E. R. H. *Prog. Nucl. Magn. Reson. Spectrosc.* **1999**, *34*, 159–201.
169. Kentgens, A. P. M. *Geoderma* **1997**, *80*, 271–306.
170. Solomon, I. *Phys. Rev.* **1958**, *110*, 61–65.
171. Chan, J. C. C. *Conc. Magn. Reson.* **1999**, *11*, 363–377.
172. Bodart, P. R.; Amoureux, J.-P.; Dumazy, Y.; Lefort, R. *Mol. Phys.* **2000**, *98*, 1545–1551.
173. Tang, J. A.; Masuda, J. D.; Boyle, T. J.; Schurko, R. W. *Chem. Phys. Chem.* **2006**, *7*, 117–130.
174. Larsen, F. H.; Jakobsen, H. J.; Ellis, P. D.; Nielsen, N. C. *J. Phys. Chem. A* **1997**, *101*, 8597–8606.
175. Larsen, F. H.; Jakobsen, H. J.; Ellis, P. D.; Nielsen, N. C. *J. Magn. Reson.* **1998**, *131*, 144–147.
176. Siegel, R.; Nakashima, T. T.; Wasylishen, R. E. *Conc. Magn. Reson. Part A* **2005**, *26A*, 47–61.
177. Kentgens, A. P. M.; Verhagen, R. *Chem. Phys. Lett.* **1999**, *300*, 435–443.
178. Iuga, D.; Schäfer, H.; Verhagen, R.; Kentgens, A. P. M. *J. Magn. Reson.* **2000**, *147*, 192–209.
179. Yao, Z.; Kwak, H.-T.; Sakellariou, D.; Emsley, L.; Grandinetti, P. J. *Chem. Phys. Lett.* **2000**, *327*, 85–90.
180. Madhu, P. K.; Pike, K. J.; Dupree, R.; Levitt, M. H.; Smith, M. E. *Chem. Phys. Lett.* **2003**, *367*, 150–156.
181. Siegel, R.; Nakashima, T. T.; Wasylishen, R. E. *Chem. Phys. Lett.* **2004**, *388*, 441–445.
182. Garwood, M.; DelaBarre, L. *J. Magn. Reson.* **2001**, *153*, 155–177.
183. Tannús, A.; Garwood, M. *NMR Biomed.* **1997**, *10*, 423–434.
184. Siegel, R.; Nakashima, T. T.; Wasylishen, R. E. *Chem. Phys. Lett.* **2006**, *421*, 529–533.
185. Barrie, P. J. *Chem. Phys. Lett.* **1993**, *208*, 486–490.
186. Ashbrook, S. E.; Wimperis, S. *Chem. Phys. Lett.* **2001**, *340*, 500–508.
187. Ashbrook, S. E.; Wimperis, S. *J. Magn. Reson.* **2000**, *147*, 238–249.
188. Lim, K. H.; Grey, C. P. *Chem. Phys. Lett.* **1999**, *312*, 45–56.
189. Wiench, J. W.; Tricot, G.; Delevoye, L.; Trebosc, J.; Frye, J.; Montagne, L.; Amoureux, J.-P.; Pruski, M. *Phys. Chem. Chem. Phys.* **2006**, *8*, 144–150.
190. Chan, J. C. C.; Bertmer, M.; Eckert, H. *Chem. Phys. Lett.* **1998**, *292*, 154–160.
191. Eastman, M. A. *J. Magn. Reson.* **1999**, *139*, 98–108.
192. Samoson, A.; Lippmaa, E.; Pines, A. *Mol. Phys.* **1988**, *65*, 1013–1018.
193. Llor, A.; Virlet, J. *Chem. Phys. Lett.* **1988**, *152*, 248–253.
194. Chmelka, B. F.; Zwanziger, J. W. *NMR Basic Princ. Prog.* **1994**, *33*, 79–124.
195. For a recent application of DOR, see: Kentgens, A. P. M.; van Eck, E. R. H.; Ajithkumar, T. G.; Anupõld, T.; Past, J.; Reinhold, A.; Samoson, A. *J. Magn. Reson.* **2006**, *178*, 212–219.
196. Frydman, L.; Harwood, J. S. *J. Am. Chem. Soc.* **1995**, *117*, 5367–5368.
197. Rocha, J.; Morais, C. M.; Fernandez, C. *Top. Curr. Chem.* **2004**, *246*, 141–194.
198. Goldbourt, A.; Madhu, P. K. *Ann. Rep. NMR Spectrosc.* **2005**, *54*, 81–153.
199. Rocha, J.; Morais, C. M.; Fernandez, C. *Clay Miner.* **2003**, *38*, 259–278.
200. Frydman, L. Fundamentals of Multiple-quantum Magic-angle Spinning NMR on Half-integer Quadrupolar Nuclei. In *Encyclopedia of Nuclear Magnetic Resonance: Advances in NMR*; Grant, D. M., Harris, R. K., Eds.; Wiley: Chichester, 2002; Vol. 9, pp 262–274.
201. Amoureux, J.-P.; Pruski, M. Advances in MQMAS NMR. In *Encyclopedia of Nuclear Magnetic Resonance: Advances in NMR*; Grant, D. M., Harris, R. K., Eds.; Wiley: Chichester, 2002; Vol. 9, pp 226–251.
202. Goldbourt, A.; Madhu, P. K. *Monatsh. Chem.* **2002**, *133*, 1497–1534.
203. Medek, A.; Frydman, L. *J. Braz. Chem. Soc.* **1999**, *10*, 263–277.
204. Pruski, M.; Fernandez, C.; Lang, D. P.; Amoureux, J.-P. *Catal. Today* **1999**, *49*, 401–409.
205. Madhu, P. K.; Goldbourt, A.; Frydman, L.; Vega, S. *J. Chem. Phys.* **2000**, *112*, 2377–2391.
206. Ding, S.; McDowell, C. A. *Chem. Phys. Lett.* **1997**, *270*, 81–86.
207. Siegel, R.; Nakashima, T. T.; Wasylishen, R. E. *Chem. Phys. Lett.* **2005**, *403*, 353–358.
208. Kentgens, A. P. M.; Iuga, D.; Kalwei, M.; Koller, H. *J. Am. Chem. Soc.* **2001**, *123*, 2925–2926.
209. Kwak, H.-T.; Prasad, S.; Yao, Z.; Grandinetti, P. J.; Sachleben, J. R.; Emsley, L. *J. Magn. Reson.* **2001**, *150*, 71–80.

209a. See also the erratum:Kwak, H.-T.; Prasad, S.; Yao, Z.; Grandinetti, P. J.; Sachleben, J. R.; Emsley, L. *J. Magn. Reson.* **2001**, *153*, 151–154.

210. Wu, G.; Rovnyak, D.; Griffin, R. G. *J. Am. Chem. Soc.* **1996**, *118*, 9326–9332.
211. Gan, Z.; Kwak, H.-T. *J. Magn. Reson.* **2004**, *168*, 346–351.
212. Amoureux, J. P.; Delevoye, L.; Steuernagel, S.; Gan, Z.; Ganapathy, S.; Montagne, L. *J. Magn. Reson.* **2005**, *172*, 268–278.
213. Ivchenko, N.; Hughes, C. E.; Levitt, M. H. *J. Magn. Reson.* **2003**, *160*, 52–58.
214. Malicki, N.; Mafra, L.; Quoineaud, A.-A.; Rocha, J.; Thibault-Starzyk, F.; Fernandez, C. *Solid State Nucl. Magn. Reson.* **2005**, *28*, 13–21.
215. Vosegaard, T.; Kehlet, C.; Khaneja, N.; Glaser, S. J.; Nielsen, N. C. *J. Am. Chem. Soc.* **2005**, *127*, 13768–13769.
216. Iijima, T.; Kanehashi, K.; Saito, K.; Hatakeyama, M.; Nemoto, T.; Shimizu, T.; Ohki, S. *Chem. Lett.* **2005**, *34*, 1380–1381.
217. Gan, Z. *J. Am. Chem. Soc.* **2000**, *122*, 3242–3243.
218. Ashbrook, S. E.; Wimperis, S. *Prog. Nucl. Magn. Reson. Spectrosc.* **2004**, *45*, 53–108.
219. Huguenard, C.; Taulelle, F.; Knott, B.; Gan, Z. *J. Magn. Reson.* **2002**, *156*, 131–137.
220. Dowell, N. G.; Ashbrook, S. E.; Wimperis, S. *J. Phys. Chem. B* **2004**, *108*, 13292–13299.
221. Ashbrook, S. E.; Wimperis, S. *J. Am. Chem. Soc.* **2002**, *124*, 11602–11603.
222. Antonijevic, S.; Bodenhausen, G. *Angew. Chem. Int. Ed.* **2005**, *44*, 2935–2938.
223. Ashbrook, S. E.; Wimperis, S. *J. Magn. Reson.* **2003**, *162*, 402–416.
224. Kwak, H.-T.; Gan, Z. *J. Magn. Reson.* **2003**, *164*, 369–372.
225. Amoureux, J.-P.; Flambard, A.; Delevoye, L.; Montagne, L. *Chem. Commun.* **2005**, 3472–3474.
226. Amoureux, J. P.; Delevoye, L.; Fink, G.; Taulelle, F.; Flambard, A.; Montagne, L. *J. Magn. Reson.* **2005**, *175*, 285–299.
227. Massiot, D.; Montouillout, V.; Fayon, F.; Florian, P.; Bessada, C. *Chem. Phys. Lett.* **1997**, *272*, 295–300.
228. Massiot, D.; Montouillout, V.; Fayon, F.; Florian, P.; Bessada, C. *J. Chim. Phys.* **1998**, *95*, 270–279.
229. Fyfe, C. A.; Wong-Moon, K. C,; Huang, Y.; Grondey, H. *J. Am. Chem. Soc.* **1995**, *117*, 10397–10398.
230. Kao, H.-M.; Grey, C. P. *J. Magn. Reson.* **1998**, *133*, 313–323.
231. Kentgens, A. P. M. *J. Magn. Reson. Ser. A* **1993**, *104*, 302–309.
232. Kentgens, A. P. M. *Prog. Nucl. Magn. Reson. Spectrosc.* **1998**, *32*, 141–164.
233. van Eck, E. R. H.; Janssen, R.; Maas, W. E. J. R.; Veeman, W. S. *Chem. Phys. Lett.* **1990**, *174*, 428–432.

234. Jerschow, A. *Monatsh. Chem.* **2002**, *133*, 1481–1496.
235. Gullion, T.; Vega, A. J. *Prog. Nucl. Magn. Reson. Spectrosc.* **2005**, *47*, 123–136.
236. Gullion, T.; Schaefer, J. *J. Magn. Reson.* **1989**, *81*, 196–200.
237. Fyfe, C. A.; Mueller, K. T.; Grondey, H.; Wong-Moon, K. C. *Chem. Phys. Lett.* **1992**, *199*, 198–204.
238. Fernandez, C.; Lang, D. P.; Amoureux, J. P.; Pruski, M. *J. Am. Chem. Soc.* **1998**, *120*, 2672–2673.
239. Grey, C. P.; Vega, A. J. *J. Am. Chem. Soc.* **1995**, *117*, 8232–8242.
240. Chopin, L.; Vega, S.; Gullion, T. *J. Am. Chem. Soc.* **1998**, *120*, 4406–4409.
241. Kalwei, M.; Koller, H. *Solid State Nucl. Magn. Reson.* **2002**, *21*, 145–157.
242. Zhou, D.; Xu, J.; Yu, J.; Chen, L.; Deng, F.; Xu, R. *J. Phys. Chem. B* **2006**, *110*, 2131–2137.
243. Ganapathy, S.; Schramm, S.; Oldfield, E. *J. Chem. Phys.* **1982**, *77*, 4360–4365.
244. Lefebvre, F.; Amoureux, J.-P.; Fernandez, C.; Derouane, E. G. *J. Chem. Phys.* **1987**, *86*, 6070–6076.
245. Ajoy, G.; Ramakrishna, J. *Solid State Nucl. Magn. Reson.* **1995**, *4*, 77–100.
246. Ajoy, G.; Ramakrishna, J. *Solid State Nucl. Magn. Reson.* **1995**, *4*, 125–142.
247. Kroeker, S.; Eichele, K.; Wasylishen, R. E.; Britten, J. F. *J. Phys. Chem. B* **1997**, *101*, 3727–3733.
248. Ajithkumar, T. G.; van Eck, E. R. H.; Kentgens, A. P. M. *Solid State Nucl. Magn. Reson.* **2004**, *26*, 180–186.
249. Jakobsen, H. J.; Skibsted, J.; Bildsøe, H.; Nielsen, N. C. *J. Magn. Reson.* **1989**, *85*, 173–180.
250. Jäger, C. *J. Magn. Reson.* **1992**, *99*, 353–362.
251. Ding, S.; McDowell, C. A. *Chem. Phys. Lett.* **2001**, *333*, 413–418.
252. Krahl, T.; Stösser, R.; Kemnitz, E.; Scholz, G.; Feist, M.; Silly, G.; Buzaré, J.-Y. *Inorg. Chem.* **2003**, *42*, 6474–6483.
253. Giavani, T.; Bildsøe, H.; Skibsted, J.; Jakobsen, H. J. *J. Magn. Reson.* **2004**, *166*, 262–272.
254. Giavani, T.; Johannsen, K.; Jacobsen, C. J. H.; Blom, N.; Bildsøe, H.; Skibsted, J.; Jakobsen, H. J. *Solid State Nucl. Magn. Reson.* **2003**, *24*, 218–235.
255. Jakobsen, H. J.; Bildsøe, H.; Skibsted, J.; Giavani, T. *J. Am. Chem. Soc.* **2001**, *123*, 5098–5099.
256. Ashbrook, S. E.; Wimperis, S. *J. Magn. Reson.* **2005**, *177*, 44–55.
257. Hansen, M. R.; Vosegaard, T.; Jakobsen, H. J.; Skibsted, J. *J. Phys. Chem. A* **2004**, *108*, 586–594.
258. Ueda, T.; Bernard, G. M.; McDonald, R.; Wasylishen, R. E. *Solid State Nucl. Magn. Reson.* **2003**, *24*, 163–183.
259. Vosegaard, T.; Massiot, D.; Gautier, N.; Jakobsen, H. J. *Inorg. Chem.* **1997**, *36*, 2446–2450.
260. Alarcón, S. H.; Olivieri, A. C.; Harris, R. K. *Solid State Nucl. Magn. Reson.* **1993**, *2*, 325–334.
261. Harris, R. K.; Olivieri, A. C. *Prog. NMR Spectrosc.* **1992**, *24*, 435–456.
262. Bain, A. D.; Dumont, R. S. *Can. J. Anal. Sci. Spectrosc.* **2001**, *46*, 176–181.
263. Schurko, R. W.; Wasylishen, R. E.; Moore, S. J.; Marzilli, L. G.; Nelson, J. H. *Can. J. Chem.* **1999**, *77*, 1973–1983.
264. Eichele, K.; Wasylishen, R. E.; Grossert, J. S.; Olivieri, A. C. *J. Phys. Chem.* **1995**, *99*, 10110–10113.
265. Schurko, R. W.; Wasylishen, R. E.; Nelson, J. H. *J. Phys. Chem.* **1996**, *100*, 8057–8060.
266. Wi, S.; Frydman, L. *J. Chem. Phys.* **2000**, *112*, 3248–3261.
267. Wi, S.; Frydman, V.; Frydman, L. *J. Chem. Phys.* **2001**, *114*, 8511–8519.
268. Wu, G.; Yamada, K. *Chem. Phys. Lett.* **1999**, *313*, 519–524.
269. La Mar, G. N., Horrocks, W., DeW. Jr.; Holm, R. H., Eds.; *NMR of Paramagnetic Molecules, Principles and Applications*, Academic Press: New York, 1973.
270. Bertini, I.; Luchinat, C. *NMR of Paramagnetic Molecules in Biological Systems*. Physical Bioinorganic Chemistry Series, Number 3; Lever, A. B. P., Gray, H. B., Eds.; Benjamin/Cummings: Menlo Park, 1986.
271. Bertini, I.; Luchinat, C. NMR of Paramagnetic Substances. In *Coordination Chemistry Reviews*; Lever, A. B. P., Ed.; Elsevier: Amsterdam, 1996; Vol. 150.
272. Bertini, I., Luchinat, C., Parigi, G., Eds.; *Solution NMR of Paramagnetic Molecules*, Elsevier: Amsterdam, 2001.
273. Köhler, F. H. Probing spin densities by the use of NMR Spectroscopy. In *Magnetism: Molecules to Materials*; Miller, J. S., Drillon, M., Eds.; Wiley-VCH: New York, 2001; Vol. 1, pp 379–430.
274. Sharp, R. R. Paramagnetic NMR. In *Nuclear Magnetic Resonance*; Webb, G. A., Ed.; Specialist Periodical Reports; Royal Society of Chemistry: Cambridge, 2005; Vol. 34, Chapter 15; pp 553–596.
275. Heise, H.; Köhler, F. H.; Herker, M.; Hiller, W. *J. Am. Chem. Soc.* **2002**, *124*, 10823–10832.
276. Heise, H.; Köhler, F. H.; Xie, X. *J. Magn. Reson.* **2001**, *150*, 198–206.
277. Köhler, F. H.; Lescouëzec, R. *Angew. Chem., Int. Ed.* **2004**, *43*, 2571–2573.
278. Watanabe, R.; Ishiyama, H.; Maruta, G.; Takeda, S. *Polyhedron* **2005**, *24*, 2599–2606.
279. Maruta, G.; Takeda, S. *Polyhedron* **2005**, *24*, 2424–2430.
280. Liu, K.; Ryan, D.; Nakanishi, K.; McDermott, A. *J. Am. Chem. Soc.* **1995**, *117*, 6897–6906.
281. Ishii, Y.; Wickramasinghe, N. P.; Chimon, S. *J. Am. Chem. Soc.* **2003**, *125*, 3438–3439.
282. Mao, J.; Zhang, Y.; Oldfield, E. *J. Am. Chem. Soc.* **2002**, *124*, 13911–13920.
283. Kaupp, M.; Bühl, M.; Malkin, V. G. In *Calculation of NMR and EPR Parameters. Theory and Applications*; Wiley-VCH Verlag GmbH: Weinheim, 2004.
284. Moon, S.; Patchkovskii, S. First-principles Calculations of Paramagnetic NMR Shifts. In *Calculation of NMR and EPR Parameters: Theory and Applications*; Kaupp, M., Bühl, M., Malkin, V. G., Eds.; Wiley-VCH Verlag GmbH: Weinheim, 2004; Chapter 20, pp 325–338.
285. Rinkevicius, Z.; Vaara, J.; Telyatnyk, L.; Vahtras, O. *J. Chem. Phys.* **2003**, *118*, 2550–2561.
286. Chisholm, M. H.; Clark, H. C.; Manzer, L. E.; Stothers, J. B. *J. Am. Chem. Soc.* **1972**, *94*, 5087–5089.
287. Bernard, G. M.; Wasylishen, R. E.; Phillips, A. D. *J. Phys. Chem. A* **2000**, *104*, 8131–8141.
288. Grutzner, J. B. Chemical Shift Theory. Orbital Symmetry and Charge Effects on Chemical Shifts. In *Recent Advances in Organic NMR Spectroscopy*; Lambert, J. B., Rittner, R., Eds.; Norell Press: Landisville, 1987; Chapter 2, pp 17–42.
289. Huang, Y.; Gilson, D. F. R.; Butler, I. S. *J. Chem. Soc., Dalton Trans.* **1992**, 2881–2883.
290. Ding, S.; McDowell, C. A. *Chem. Phys. Lett.* **1997**, *268*, 194–200.
291. Gay, I. D.; Young, G. B. *Organometallics* **1996**, *15*, 2264–2269.
292. Havlin, R.; McMahon, M.; Srinivasan, R.; Le, H.; Oldfield, E. *J. Phys. Chem. A* **1997**, *101*, 8908–8913.
293. Quin, L. D., Verkade, J. G., Eds.; *Phosphorus-31 NMR Spectral Properties in Compound Characterization and Structural Analysis*; VCH: New York, 1994.

294. Carty, A. J.; MacLaughlin, S. A.; Nucciarone, D. Stereochemistry of Metal Complexes: Phosphido Bridging Ligands. In *Phosphorus-31 NMR Spectroscopy in Stereochemical Analysis: Organic Compounds and Metal Complexes*; Verkade, J. G., Quin, L. D., Eds.; Methods in Stereochemical Analysis 8; VCH: Deerfield Beach, 1987; Chapter 16, pp 559–619.
295. Eichele, K.; Wasylishen, R. E.; Corrigan, J. F.; Taylor, N. J.; Carty, A. J. *J. Am. Chem. Soc.* **1995**, *117*, 6961–6969.
296. Eichele, K.; Wasylishen, R. E.; Kessler, J. M.; Solujić, L.; Nelson, J. H. *Inorg. Chem.* **1996**, *35*, 3904–3912.
297. Eichele, K.; Wasylishen, R. E.; Maitra, K.; Nelson, J. H.; Britten, J. F. *Inorg. Chem.* **1997**, *36*, 3539–3544.
298. Eichele, K.; Ossenkamp, G. C.; Wasylishen, R. E.; Cameron, T. S. *Inorg. Chem.* **1999**, *38*, 639–651.
299. Eichele, K.; Wasylishen, R. E.; Corrigan, J. F.; Taylor, N. J.; Carty, A. J.; Feindel, K. W.; Bernard, G. M. *J. Am. Chem. Soc.* **2002**, *124*, 1541–1552.
300. Feindel, K. W.; Wasylishen, R. E. *Can. J. Chem.* **2004**, *82*, 27–44.
301. Granger, P. Quadrupolar Transition Metal & Lanthanide Nuclei. In *Encyclopedia of Nuclear Magnetic Resonance*; Grant, D. M., Harris, R. K., Eds.; Wiley: Chichester, 1996; Vol. 6, pp 3889–3900.
302. Lewinski, J. Heteronuclear NMR Applications (B, Al, Ga, In, T1). In *Encyclopedia of Spectroscopy and Spectrometry*; Lindon, J. C., Tranter, G. E., Holmes, J. L., Eds.; Academic Press: London, 2000; Vol. 1, pp 691–703.
303. Pettinari, C. Heteronuclear NMR Applications (Ge, Sn, Pb). In *Encylopedia of Spectroscopy and Spectrometry*; Lindon, J. C., Tranter, G. E., Holmes, J. L., Eds.; Academic Press: London, 2000; Vol. 1, pp 704–717.
304. Appleton, T. G. Heteronuclear NMR Applications (La–Hg). In *Encylopedia of Spectroscopy and Spectrometry*; Lindon, J. C., Tranter, G. E., Holmes, J. L., Eds.; Academic Press: London, 2000; Vol. 1, pp 718–722.
305. Rehder, D. Heteronuclear NMR Applications (Sc–Zn). In *Encylopedia of Spectroscopy and Spectrometry*; Lindon, J. C., Tranter, G. E., Holmes, J. L., Eds.; Academic Press: London, 2000; Vol. 1, pp 730–740.
306. Kolehmainen, E. Heteronuclear NMR Applications (Y–Cd). In *Encylopedia of Spectroscopy and Spectrometry*; Lindon, J. C., Tranter, G. E., Holmes, J. L., Eds.; Academic Press: London, 2000; Vol. 1, pp 740–750.
307. Schurko, R. W.; Hung, I.; Macdonald, C. L. B.; Cowley, A. H. *J. Am. Chem. Soc.* **2002**, *124*, 13204–13214.
308. Schurko, R. W.; Hung, I.; Schauff, S.; Macdonald, C. L. B.; Cowley, A. H. *J. Phys. Chem. A* **2002**, *106*, 10096–10107.
309. Willans, M. J.; Schurko, R. W. *J. Phys. Chem. B* **2003**, *107*, 5144–5161.
310. Hung, I.; Schurko, R. W. *Solid State Nucl. Magn. Reson.* **2003**, *24*, 78–93.
311. Widdifield, C. M.; Schurko, R. W. *J. Phys. Chem. A* **2005**, *109*, 6865–6876.
312. Lo, A. Y. H.; Bitterwolf, T. E.; Macdonald, C. L. B.; Schurko, R. W. *J. Phys. Chem. A* **2005**, *109*, 7073–7087.
313. Broene, R. D.; Buchwald, S. L. *Science* **1993**, *261*, 1696–1701.
314. Hung, I.; Schurko, R. W. *J. Phys. Chem. B* **2004**, *108*, 9060–9069.
315. Bain, A. D. *Prog. Nucl. Magn. Reson. Spectrosc.* **2003**, *43*, 63–103.
316. McGlinchey, M. J. *Can. J. Chem.* **2001**, *79*, 1295–1309.
317. Aime, S.; Milone, L. *Prog. Nucl. Magn. Reson. Spectrosc.* **1977**, *11*, 183–210.
318. Hanson, B. E. *J. Am. Chem. Soc.* **1989**, *III*, 6442–6443.
319. Hanson, B. E.; Whitmire, K. H. *J. Am. Chem. Soc.* **1990**, *112*, 974–977.
320. Salzmann, R.; Kaupp, M.; McMahon, M. T.; Oldfield, E. *J. Am. Chem. Soc.* **1998**, *120*, 4771–4783.
321. Spiess, H. W.; Grosescu, R.; Haeberlen, U. *Chem. Phys.* **1974**, *6*, 226–234.
322. Heyes, S. J.; Dobson, C. M. *J. Am. Chem. Soc.* **1991**, *113*, 463–469.
323. Munson, E. J.; Douskey, M. C.; De Paul, S. M.; Ziegeweid, M.; Phillips, L.; Separovic, F.; Davies, M. S.; Aroney, M. J. *J. Organomet. Chem.* **1999**, *577*, 19–23.
324. Slichter, C. P. *Ann. Rev. Phys. Chem.* **1986**, *37*, 25–51.
325. Bemi, L.; Clark, H. C.; Davies, J. A.; Fyfe, C. A.; Wasylishen, R. E. *J. Am. Chem. Soc.* **1982**, *104*, 438–445.
326. Clark, H. C.; Davies, J. A.; Fyfe, C. A.; Hayes, P. J.; Wasylishen, R. E. *Organometallics* **1983**, *2*, 177–180.
327. Fyfe, C. A.; Clark, H. C.; Davies, J. A.; Hayes, P. J.; Wasylishen, R. E. *J. Am. Chem. Soc.* **1983**, *105*, 6577–6584.
328. Clark, H. C.; Fyfe, C. A.; Hayes, P. J.; McMahon, I.; Davies, J. A.; Wasylishen, R. E. *J. Organomet. Chem.* **1987**, *322*, 393–404.
329. Reven, L. *J. Mol. Catal.* **1994**, *86*, 447–477.
330. Saint-Arroman, R. P.; Chabanas, M.; Baudouin, A.; Copéret, C.; Basset, J.-M.; Lesage, A.; Emsley, L. *J. Am. Chem. Soc.* **2001**, *123*, 3820–3821.
331. Blanc, F.; Copéret, C.; Thivolle-Cazat, J.; Basset, J.-M.; Lesage, A.; Emsley, L.; Sinha, A.; Schrock, R. R. *Angrew. Chem., Int. Ed.* **2006**, *45*, 1216–1220.
332. Ahn, H.; Marks, T. J. *J. Am. Chem. Soc.* **2002**, *124*, 7103–7110.
333. Scott, S. L.; Church, T. L.; Nguyen, D. H.; Mader, E. A.; Moran, J. *Top. Catal.* **2005**, *34*, 109–120.
334. Lindner, E.; Al-Gharabli, S.; Warad, I.; Mayer, H. A.; Steinbrecher, S.; Plies, E.; Seiler, M.; Bertagnolli, H. *Z. Anorg. Allg. Chem.* **2003**, *629*, 161–171.

1.18 High Pressure NMR and IR Spectroscopy in Organometallic Chemistry

C L Dwyer, Research and Development, Sasol Technology, Sasolburg, South Africa

1.18.1 Introduction

Organometallic species have particular relevance as the mediators of homogeneous catalytic reactions for the production of commodity or specialty chemicals.[1] While a range of analytical techniques may be employed for the precise characterization of discrete organometallic complexes which can be synthesized and isolated, it is often not these complexes which are the active catalysts. With some exceptions, such analytical techniques are also typically applied under ambient conditions in an inert environment. However, under typical catalytic conditions of elevated temperature and/or pressure, and in the presence of reactive gases, liquids, and/or solids, such organometallic pre-catalysts may be converted into a range of derivatives. These new species are typically fluxional and interconvert with changes in reaction conditions and concentrations of reagents and products, as required from any catalytically active species. They may also be thermodynamically stable end products which are catalytically inactive, or species which are active for a transformation other than that which is desired. Identification of these diverse species and an understanding of how they can be manipulated by varying reaction conditions is an integral part of understanding a catalytic process, and the first step toward rational control and optimization of catalyst activity, selectivity, and lifetime.

High pressure nuclear magnetic resonance spectroscopy (HP-NMR)[2–5] and high pressure infrared spectroscopy (HP-IR)[6–8] are two valuable techniques for the *in situ* observation of organometallic species under typical catalytic conditions. While numerous spectroscopic studies of organometallic complexes have been carried out,[9,10] relatively few have been performed at the generally high temperatures and pressures required for effective catalysis, thereby making extrapolation of the behavior of an organometallic precursor to a real catalyst at typical operating conditions very difficult. In particular, HP-NMR and HP-IR allow the observation of key catalytic intermediates and inactive catalyst sinks, and allow the researcher to understand the effect of changing process parameters on the catalyst equilibria.[11,12] The techniques are applicable to reactions where at least one of the reagents is a reactive gas and

where above-ambient pressures are required, for example, hydroformylation (synthesis gas), carbonylation (CO), and hydrogenation (H_2). Transition metal hydrides and carbonyls modified by phosphines or other heteroatomic ligands are therefore the catalytic species most commonly observed by these techniques. It is a fact that much of the development of the high pressure instrumentation and use of these techniques was either carried out in industry or by academics closely aligned with an industrial partner. This is perhaps surprising due to the fundamental nature of the information generated. However, the techniques are very much focused on the study of real catalysis, and should be an integral part of catalytic process development.

It should be remembered that these techniques may not be able to identify all catalytic intermediates in a cycle. Unless special techniques are employed, it is often only the longer-lived (i.e., less reactive) organometallic species within the catalytic cycle which are observed, as well as persistent species which lie outside the catalytic cycle. However, the value of these techniques should not be underestimated, as a variety of important process issues can be studied:

- The resting state may change depending on the reaction conditions; hence, it may actually be possible to determine a number of the catalytic intermediates. Information on which step within the cycle is rate limiting, and how to manipulate these intermediates may provide crucial insights as to how the reaction can be directed toward higher activities or selectivities.
- It is important to understand how the organometallic precursor enters the catalytic cycle, to ensure that as much as possible of the valuable metal is converted into catalytically active species. This is of major importance for process efficiency and lower catalyst costs. In some cases this transformation occurs readily in the reaction medium, but in other cases it may be advisable to preform the active catalyst in a separate reaction vessel to avoid unwanted side-reactions, or to ensure that formation of the active catalyst is not rate limiting.
- The end fate of the catalyst is also critical.[13] Side-reactions which consume catalytic intermediates can be identified, and conditions can be optimized to minimize catalyst deactivation. Irreversible reactions to inactive species lead to a steady decline in active catalyst concentrations unless a continuous top-up of catalyst is introduced. It also means that a catalyst purge is required to avoid accumulation of inactive species in the system. Both are costly exercises, as catalyst costs increase, and a purge always results in product losses.
- Catalyst equilibria are affected by changing reaction parameters such as temperature and pressure; thus, a suitable operating window can be identified where the catalyst is stable, active, and selective. The concentrations of the various reagent and product molecules are another critical variable, where solvent, acid/base (Brønsted), and ligating (Lewis) properties of the molecules may dramatically influence the nature and behavior of the catalyst. Ligating organics can have a stabilizing effect on the catalyst, but can also act as inhibitors (by retarding activity) or poisons (irreversible interaction with catalyst). Solvents are often not necessary for catalytic processes, but where required can be selected to stabilize or promote the catalyst. In a batch reaction, the concentration of organic reagents is constantly changing; therefore, the catalyst performance can also change significantly with time. In continuous operation at steady state, the concentration of all components is constant, or viewed in another way, the conversion of starting materials is constant with time. This provides a more uniform environment for the catalyst, and an understanding of the effect of reaction components on the catalyst may help determine an optimum conversion at which the process can be run.
- Additives are frequently employed to enhance catalyst performance. These often facilitate conversion of a pre-catalyst to an active species, or help to stabilize a reactive catalytic intermediate. The exact nature of the additive–catalyst interaction can often be studied using such *in situ* techniques.

As with all analytical techniques, HP-NMR and HP-IR have certain advantages and limitations. HP-NMR suffers from relatively low sensitivity; thus, reactions at low catalyst concentrations can be difficult to study without very long scan times. Paramagnetic complexes such as those of chromium and iron are also very difficult to study. However, it is a versatile technique because specific nuclei of interest can be targeted, and data from chemical shifts and coupling constants can provide a wealth of information regarding the nature of organometallic species. ^{1}H and ^{13}C NMR can provide valuable information on species such as transition metal hydrides and carbonyls, but may not be appropriate when observing species under catalytic conditions, as the resonances tend to be dwarfed by the signals corresponding to the organic reagents, particularly when looking for slow-relaxing metal carbonyl resonances. It is when observing the resonances of the metals and ligands themselves that the true value of HP-NMR can be demonstrated.[14] In particular ^{31}P NMR[10,15,16] is a powerful tool for observing the phosphine-modified organometallic complexes which are frequently used in catalysis due to their versatility toward both structural and electronic modification. Spectra are generally fairly simple, and chemical shifts, coupling constants (P–P, P–H, and P–M), and peak shapes can provide

detailed information on catalyst structure, properties, and dynamic processes such as ligand exchange. Transition metals can also be observed directly if they have suitable nuclides for observation.[17,18] Organometallic complexes of such transition metals usually have very large chemical shift ranges, and variation of the coordinating ligands can lead to significant changes in the observed spectra. However, such measurements sometimes require specialized probes with wider spectral ranges, making NMR of this nature non-routine. A further advantage of HP-NMR is that absolute quantification of catalytic intermediates is made possible by the use of resonance integrals and an internal standard.

HP-IR has a greater sensitivity and can be used to detect very low concentrations of organometallic species in solution. It also has a much shorter timescale, so information on reactive intermediates (not just resting states) is possible under catalytic conditions. However, IR spectra are generally far more complex than NMR spectra as specific functional groups cannot always be analyzed. Quantification of reaction mixtures is also generally more difficult, as bands often overlap. However, for specific classes of organometallics which have characteristic spectral regions, HP-IR can provide unique information. Most notably, metal carbonyls have been a major focus of HP-IR research due to the characteristic and usually well-defined metal–carbonyl stretching frequencies. HP-IR has also been used extensively in heterogeneous catalysis, mostly for the study of absorbates on solid surfaces rather than discrete organometallic species, and accordingly will not be dealt with in this chapter.[9]

When used in conjunction, HP-NMR and HP-IR are often complementary and can give a more complete picture of catalyst behavior. Coupled with molecular modeling[19] and experimental results from catalyst synthesis and catalytic testing, these tools allow researchers to move away from empirical optimizations of catalyst performance and toward rational and iterative design of improved catalyst systems.

1.18.2 HP-NMR Instrumentation

HP-NMR was first carried out by Benedek and Purcell in the 1950s in order to investigate various physical properties of liquids under hydrostatic pressure.[20] Essentially, this involves applying direct mechanical pressure on a liquid sample by means of a hydraulic press or similar equipment. Their probe, made of a non-magnetic beryllium–copper alloy, was designed for use with an electromagnet and spurred publications in the area during the 1970s.[2,21] Later improvements included the use of a more heat-resistant titanium alloy[2] and a Teflon piston and cap.[22] While such studies are of limited use to the organometallic chemist, many of the principles in the design of such equipment are of relevance to organometallic complexes where the high pressure is usually applied by the introduction of a reactive gas. Two types of systems predominate, namely those employing modified high pressure probes and those using pressurizable NMR tubes. NMR probes with diamond anvil cells have also been developed for solid-state NMR at very high pressures, but are beyond the scope of this review.[23,24]

1.18.2.1 Glass and Sapphire Tubes

The simplest systems are the pressurizable tubes as they can be used in most high frequency commercial NMR probes. Resolutions therefore tend to be very good, and are improved by the ability to spin the tube. As early as the 1960s, several researchers were using thick-walled sealed pyrex[25,26] or borosilicate[27,28] tubes. However, safety concerns were paramount. The higher the required pressure, the thicker the tube wall was required to be, resulting in progressively poorer resolution. Merbach[29] and others[30] described the use of chemical resistant polyimide (Vespel) tubes at pressures up to 1000 bar. However, difficult alignment of the tube led to spinning sidebands, and after several reuses the tubes required replacing due to deformation. Other groups have reported the use of tubes constructed of high performance polymers for supercritical fluid applications up to pressures of 400 bar.[31,32]

In the mid-1980s, Roe[33] made a significant improvement on these systems by using a single crystal sapphire tube fastened to a titanium head. Such tubes can withstand high pressures (up to 130 bar) at elevated temperatures (150 °C), giving improved resolutions over the corresponding glass analogs. The titanium head also allows easier control of pressurization by means of a valve and gas inlet port. As these Roe tubes are significantly heavier than normal NMR tubes, a higher spinner air pressure is required. Alternatively, if spinning is not required the tube can be manually lowered into the probe to the correct depth. The weak point in the design is that the titanium head is glued onto the tube, and this glue can perish upon continued exposure to chemical vapors. Accordingly, it is recommended that such tubes be inspected and sent for pressure testing on a regular basis. An alternative design is to employ *o*-rings made of teflon or other chemical/heat resistant materials to isolate the reaction solution from the glue.[34] Such *o*-rings are also subject to slow deterioration, but are much easier to inspect and replace. The tube is typically loaded

Figure 1 Roe cell and gas manifold.

with reagents via syringe, placed in a suitable spinner, and then in a safety shield. The whole setup can be placed in a fumehood and pressurized by connecting to a gas manifold fitted with a pressure regulator (Figure 1). Once pressurized, the shield and tube are fitted on top of the magnet, and the cell can be lowered into the probe. In this way the operator is never directly exposed to the pressurized tube. Further safety issues are discussed elsewhere.[2,35,36] Variations on this design are dealt with in several publications.[37]

Despite their simplicity and ease of use, there are several notable limitations of these tubes. For instance, there is no way of stirring the tube contents, so mass transfer limitations can affect the behavior of the organometallic species. This is particularly problematic in reactions where one is consuming a reactive gas, as partial pressures do not remain constant with time. In addition, the gas may take quite some time to reach equilibrium concentrations in the liquid phase, due to the small surface area for dissolution. This is not as problematic when the gas has a high solubility in the organic solvent (e.g., ethylene), but gases such as carbon monoxide may take a very long time to permeate through the liquid. Accordingly, it is advisable to leave the cell under gas pressure for an adequate period of time before taking spectra, or to employ a gentle shaking system to facilitate dissolution. The effectiveness of these steps can be determined by measuring NMR spectra of the solution with time and monitoring how long it takes for the resonances corresponding to the reactive gas to reach equilibrium concentrations. Alternatively, a color change of a suitable indicator which reacts with the gas of interest can indicate the progress of dissolution down the tube. In some instances, slow mass transfer may actually allow the researcher to observe more reactive intermediates by slowing down a normally rapid reaction in the cycle. A further limitation is that the system under observation is a closed one. Therefore, it is important to calculate in advance what pressure to introduce to the cell at ambient temperature to afford the desired pressure in the NMR tube at the final temperature of interest. It also follows that as the reaction proceeds, the pressure in the system will change as gas is consumed and perhaps also formed. For safety reasons it is critical that the maximum possible pressure in this system under reaction conditions is estimated before proceeding with an experiment. To address this issue, Bai *et al.* have reported a variation of the sapphire tube where pressure can be controlled independent of the temperature.[38] In a similar vein, Elsevier and co-workers have reported the use of a sapphire tube fitted with a pressure sensor.[39]

1.18.2.2 Modified Probes

With the advent of superconducting magnets, new high pressure probes were designed for wide bore magnets. Heaton and co-workers published the first such example, with a probe capable of handling up to 850 bar but with an upper temperature limit of only 25 °C due to hydrogen embrittlement.[40–42] This probe was made of a titanium alloy pressure vessel with a sample insert. Temperature was controlled by means of copper cooling coils. In 1987, Jonas and van der Velde reported a probe with improved sensitivity which also allowed stirring of the sample cell.[43] Rathke took the design a step further with the introduction of highly sensitive toroidal detection probes.[44–46] The toroid coils may be located next to the pressure vessel with little signal loss from coupling with the metal vessel, and are capable of delivering excellent resolutions. The liquid reaction mixture can be either in an enclosed system, or circulated through the probe from an autoclave. Iggo and co-workers have reported a novel flow cell which combines the advantages of efficient mixing of the probe systems with the ease of use of the sapphire tubes.[47] The flow cell can operate up to 175 °C and 200 bar and consists of a sapphire cell sealed at both ends to titanium flanges, and placed within a wide bore magnet. Reactive gases are bubbled through the liquid in the cell at controlled flow rates and pressures, thereby achieving the mixing required to ensure adequate mass transfer. Numerous groups have reported modifications of these systems for various applications.[48–51]

In general, these modified probes give more accurate data on real catalysis as they are not closed systems, and constant partial pressures of reactive gases can be maintained. However, they are not so easy to use, require a wide bore magnet, and also usually a dedicated NMR.

1.18.3 HP-IR Instrumentation

In the 1970s, HP-IR for homogeneous catalysis was generally carried out in modified autoclaves, using either transmission or reflectance cells to obtain the spectrum.[6] Typical transmission cells require the use of suitable windows built into the autoclave body which can withstand both high pressures and chemical exposures (Figure 2). The autoclave sits within the body of the IR spectrometer, and can be connected to gas and liquid supplies as

Figure 2 High pressure IR transmission cell.

required. The weak point in the design is the windows themselves, and care should be taken to inspect and replace them frequently to avoid damage to the spectrometer. Transmission can take place directly through the autoclave body, but spectral acquisition is sometimes hampered if there is excessive turbulence in the reaction mixture due to stirring. To alleviate this, the reaction mixture in a standard autoclave can be periodically routed through an external loop which passes through the high pressure transmission cell of the spectrometer.[52–55] Whyman's group has used such cells for a range of applications.[6,56,57] Suppes and McHugh have developed a variable-volume HP-IR cell specifically for supercritical fluid applications.[58] An elegant combination of flash photolysis with HP-IR has allowed Ford and co-workers to directly observe short-lived reactive intermediates in several reaction systems.[59,60] A modified cuvette has also been reported, which can take a pressure of around 180 bar.[61]

The use of cylindrical internal reflectance cells for HP-IR was pioneered by Moser and further modified by others.[62–64] This method involves the use of an optically transparent internal reflectance crystal (typically ZnS, ZnSe, sapphire). Due to the inherently short path length, the method is not as sensitive as transmission-based IR, and a Fourier transform infrared (FTIR) spectrometer is therefore generally required. In addition, the type of crystal may need to be changed depending on the reaction of interest, as the optics may be corroded by some reagents or catalysts. However, as the path length is fixed regardless of conditions, it is much easier to quantify catalyst species, and unlike transmission systems the cells can also be used for the study of liquid–solid and gas–liquid–solid mixtures.[63]

1.18.4 Application to Homogeneous Catalysis and Coordination Chemistry

1.18.4.1 Cobalt

As early as 1938, Otto Roelen discovered hydroformylation when observing the formation of aldehydes in the presence of cobalt carbonyls.[65] Cobalt carbonyls[66]are extremely effective catalysts for a variety of carbonylation reactions,[67,68] but have been largely overlooked in recent years due to the overwhelming research efforts into rhodium and iridium chemistry. However, cobalt affords a much cheaper catalyst and is still attractive from an industrial perspective. HP-NMR and HP-IR studies of such catalysts have recently been reviewed.[11]

As with all of these systems, cobalt carbonyls can be used either with or without further modifying ligands, but the unmodified cobalt carbonyl catalysts generally require much harsher operating conditions: high CO pressures are required to stabilize the active catalyst, and under these conditions higher temperatures are required to increase reaction rates to acceptable levels. Phosphine ligands stabilize the catalyst and allow milder conditions to be employed;[69] however, they also increase the hydrogenation capability of the catalyst. This is advantageous as the aldehyde product is hydrogenated directly to the desired alcohol end product in the hydroformylation reactor, but loss of alkene feed to alkane byproducts is a significant and undesirable side-reaction. Use of phosphine-modified cobalt carbonyls also results in an improved ratio of normal to iso products due to better steric control of alkene insertion. The basic mechanism for hydroformylation of alkenes with $HCo(CO)_4$ was initially proposed by Heck and Breslow in the early 1960s.[70] Although some specific aspects of the mechanism have been disputed, the basics of the catalytic sequence and key intermediates proposed therein have been confirmed by a range of experimental and mechanistic investigations, including HP-NMR and HP-IR. This mechanism (Scheme 1; $L = CO, PR_3$) is also generally accepted for phosphine-modified catalysts:

- The catalyst precursor $HCo(CO)_3L$ **1** enters the cycle by loss of a CO ligand.
- Coordination of an alkene to the coordinatively unsaturated $HCo(CO)_2L$ **2** followed by insertion leads to the formation of an alkylcobalt intermediate **3**.
- Recoordination of CO followed by alkyl migration leads to the formation of an acylcobalt species **4**.
- Hydrogenolysis of this species (either by H_2 or by $HCo(CO)_3L$) releases the aldehyde product and liberates $HCo(CO)_2L$ which can carry on the cycle.

In the early 1970s, Whyman[71,72] reported the behavior of unmodified cobalt carbonyls under a pressure of synthesis gas (syngas; mixture of H_2 and CO) using HP-IR. In this study, he showed that $Co_2(CO)_8$ could be readily converted to $HCo(CO)_4$ under the reaction conditions of 290 bar syngas and 150 °C. Upon addition of 1-octene the spectrum changed significantly, with disappearance of $HCo(CO)_4$ corresponding to the appearance of a strong aldehyde absorbance and further acyl bands which were attributed to the acylcobalt intermediate $Co(COR)(CO)_4$. Upon varying the H_2 : CO ratio, the proposed acyl species increased with an increase in CO partial pressure, further

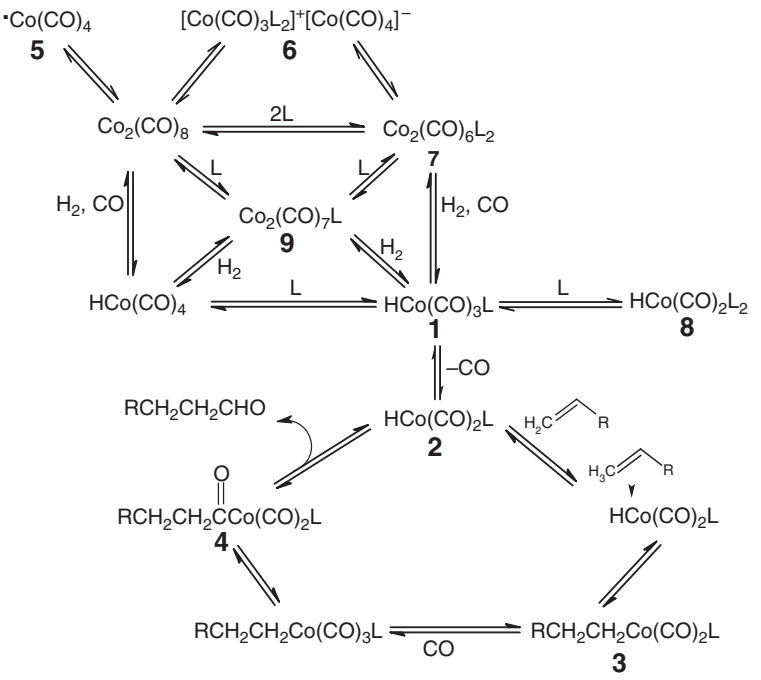

Scheme 1 Catalyst preforming and hydroformylation cycle with unmodified and phosphine-modified cobalt carbonyl catalysts (L = CO, PR_3).

supporting this assignment. This suggests that hydrogenolysis of the acyl species is rate determining for this reaction. In contrast, HP-IR spectra obtained for hydroformylation of internal alkenes only showed the starting $HCo(CO)_4$ complex, suggesting that alkene insertion becomes rate determining for sterically less available alkenes.

Another early paper dealing with HP-IR of $HCo(CO)_4$ and related compounds under hydroformylation conditions challenges Heck and Breslow's assertion that the acylcobalt species **4** reacts with hydrogen to release the aldehyde product.[73] In their studies, the authors observed an increase of $Co_2(CO)_8$ during reaction, which they ascribed to the reaction of $HCo(CO)_4$ with the acylcobalt intermediate. They reported that $HCo(CO)_4$ was the major cobalt species observed during reaction with 1-pentene, due to slow reaction of the incoming alkene with the coordinatively unsaturated $HCo(CO)_3$ species. The rate of formation of $HCo(CO)_4$ from the $Co_2(CO)_8$ precursor was reported to be slower than the rate of hydroformylation, and in contrast to Whyman,[71] no evidence was found for presence of an acylcobalt intermediate. In a later paper by Mirbach,[74] the findings on the hydrogenolysis step were refuted. HP-IR and HP-UV studies indicated a faster reaction rate for the reaction of the acylcobalt species with hydrogen than with $HCo(CO)_4$. The slow formation of $HCo(CO)_4$ from dicobaltoctacarbonyl was however confirmed.

The seemingly contradictory results from these three papers can possibly be accounted for by comparing reaction conditions. Whyman[71] undertook his investigations at much higher syngas pressures, which would favor both cleavage of the starting dicobaltoctacarbonyl and formation of an acyl species. This emphasizes how sensitive all of the transformations of these complexes are to temperature and pressure changes, and care should be taken when trying to extrapolate between different studies.

Further studies on unmodified cobalt catalysis have been carried out by several groups. Roe[75] studied CO exchange reactions of $Co_2(CO)_8$ and $Co(COCH_3)(CO)_4$ using HP-NMR with ^{13}C magnetization techniques. The acyl complex showed quick incorporation of ^{13}CO for the carbonyl ligands but much slower scrambling of the acyl resonance, indicating that further reaction of the acyl intermediate is preferred to deinsertion of the acyl carbonyl group. Pino *et al.*[76] used HP-IR to study the activation of hydrogen under hydroformylation conditions. They demonstrated that reaction of an acylcobalt species under hydrogen pressure afforded aldehyde product as well as an unknown cobalt species. This was attributed to the highly reactive and coordinatively unsaturated species $HCo(CO)_3$ which initiates the hydroformylation cycle. Pretzer and Kobylinski[77] reported the use of HP-IR to study methanol homologation with iodide-promoted cobalt carbonyls. $Co(CO)_4^-$ was confirmed as the key intermediate during catalysis, and catalyst deactivation at higher I/Co levels was observed. Mirbach[78] studied the interaction of conjugated dienes with

$Co_2(CO)_8$ and $HCo(CO)_4$ using HP-IR. A cobalt carbonyl–butadiene complex and an allylcobalt carbonyl species were formed from the reaction of butadiene with $Co_2(CO)_8$. Reaction with $HCo(CO)_4$ gradually afforded an alkenyl complex which reacted to form further byproducts. The reaction of cobalt carbonyls with hydrogen or deuterium, and the stoichiometric interaction of the resultant hydride with alkenes has also been studied with HP-IR.[79–81] Ojima[82] reported HP-IR studies into Co–Rh bimetallic carbonyl catalysts, and observed a $CoRh(CO)_7$ species which was active for hydroformylation–amidocarbonylation.

Using their toroid NMR probe coupled with a high pressure cell,[44] the group of Rathke and Klingler at the Argonne National Laboratory have published several reports of the behavior of unmodified cobalt carbonyls in supercritical CO_2-(sCO_2).[45,83,84] What also makes their work unique is the use of ^{59}Co NMR in conjunction with the usual ^{1}H and ^{13}C NMR. The first paper described the hydroformylation of propylene in sCO_2.[45] Under conditions of no stirring, it was revealed that the usual mass transfer issues when dealing with gas–liquid systems were overcome in sCO_2, while no obvious differences in catalytic behavior were evident. In a separate paper,[83] equilibrium constants were determined for the reaction of $Co_2(CO)_8$ with H_2 in sCO_2, to afford the hydridocobalttetracarbonyl pre-catalyst. Results were similar to those observed in non-polar organic solvents. An intriguing ^{59}Co NMR study[84] on hydride transfer between $Co_2(CO)_8$ and $HCo(CO)_4$ in sCO_2 revealed that the exchange is a facile process observable by line broadening and eventual coalescene of the two cobalt resonances. It was also shown to be specific to these two species: $Co_4(CO)_{12}$ and $MnCo(CO)_9$ introduced to the same reaction mixture showed no line broadening. Various arguments and evidence were presented to show that oxidative addition of the hydride to $Co_2(CO)_7$ is not a key step in this exchange process. Instead, the thermolytic cleavage of $Co_2(CO)_8$ to two hydroformylation active $^{\bullet}Co(CO)_4$ radicals (**5**, Scheme 1) was proposed. In support of this theory, the authors cite work by Pino[85] where odd isotope distributions from deuterium-labeling experiments suggested the presence of some unidentified active cobalt species. These and further studies of cobalt carbonyls in supercritical fluids applied to CO hydrogenation and methanol homologation have been reviewed.[86]

Phosphine-modified cobalt carbonyls were extensively studied by Shell in the 1960s,[87] and are employed industrially in the large-scale production of detergent alcohols. In early years, tributylphosphine was the ligand of choice and the focus of much high pressure spectroscopy. Whyman[71,88] published HP-IR studies which showed that $Co_2(CO)_8$ and PBu_3 reacted to initially afford a disproportionated salt (**6**, Scheme 1, L = PBu_3). This salt was converted to a bis(phosphine) dimer **7** at higher temperatures. Under hydrogen pressure at high temperatures, the dimer was converted to a modified hydride **1**, which initiated catalysis by loss of CO. Under catalytic conditions, the two predominant species observed were $Co_2(CO)_6(PBu_3)_2$ and $HCo(CO)_3(PBu_3)$. No trace of an acyl intermediate was seen, suggesting that initial alkene coordination and insertion was rate limiting. At high ligand concentrations, the bis(phosphine)hydride $HCo(CO)_2(PBu_3)_2$ **8** was observed, while the monosubstituted dimer $Co_2(CO)_7(PBu_3)$ **9** was observed at low ligand concentrations. Penninger[89] determined equilibrium constants at different temperatures for a number of these interconversions using HP-IR. Complementary to Whyman's HP-IR studies, Rathke and co-workers[90] described the HP-NMR behavior of the $Co_2(CO)_8/PBu_3$ system. The salt (**6**, Scheme 1, L = PBu_3), mono- and disubstituted dimers **9** + **7**, and hydride **1** were observed, and factors affecting their equilibria were investigated. Salt formation was found to be favored at lower temperatures and with polar solvents, including the typical alcohol products.

Ford's group[60,91] probed the synthesis and reactivity of acylcobalt intermediates with PPh_3 as a ligand. The coordinatively unsaturated $Co(COCH_3)(CO)_2PPh_3$ intermediate was characterized, and could be converted to $Co(CH_3)(CO)_3PPh_3$ under ambient CO pressures, while at higher pressures the fully coordinated $Co(COCH_3)(CO)_3PPh_3$ was also observed. A recent paper by Rathke and co-workers[92] described the use of a fluorous phosphine ligand for hydroformylation in sCO_2.

The development and implementation of the eicosyl phobane ligand (EP, **10**, [3.3.1] and [4.2.1] isomers) by Shell[93] opened a further avenue of research. This sterically bulky, basic phosphabicycloalkane ligand derived from cyclooctadiene afforded alcohols with a superior product linearity, and resulted in lower losses of alkene feedstock to paraffins via hydrogenation. In recent years, Sasol Technology developed an alternative modified cobalt hydroformylation technology based on another phosphabicycloalkane ligand (Lim, **11** (Lim = 4,8-dimethyl-2-octadecyl-2-phosphabicyclo[3.3.1]nonane)) derived from (*R*)-(+)-limonene.[94] High pressure spectroscopy studies on the Co/EP catalyst were not reported by Shell, but have recently been reported in a review by Dwyer and co-workers at Sasol[95] which describes detailed HP-NMR studies into cobalt carbonyl catalysts derived from both EP and Lim. Under various reaction conditions, the salt (**6**, Scheme 1, L = Lim, EP), mono- and disubstituted dimers **9** + **7**, and hydride **1** were identified for both Lim and EP catalysts. Resonances assigned to a disubstituted hydride **8** and acylcobalt species **4** were also observed. The effect of added iron carbonyls on the cobalt catalyst equilibria was investigated, and it was shown that iron effectively scavenged both free ligand in the reaction solution as well as ligand from the cobalt complexes. Differences in the reactivity of the Lim diastereomers as observed by HP-NMR were subsequently proved by autoclave experiments using a pure Lim diastereomer.[96] Behavior of a linear acylcobalt

Lim derivative was also studied using HP-NMR, and a mechanism for the formation of branched aldehyde products was proposed.[96] Further work published by Crause *et al.*[97] described the effect of variation of the Lim alkyl chain. HP-NMR and HP-IR studies, combined with molecular modeling and autoclave experiments, showed that the primary factor governing performance of these ligands was the extent of phosphine-modified versus unmodified catalysis. Control of catalyst equilibria in favor of cobalt–phosphine species resulted in improved product linearities, but slower reaction rates.

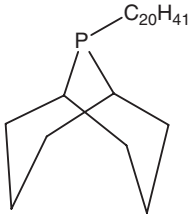

10a

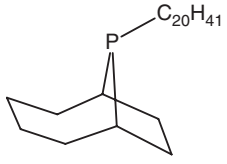

10b

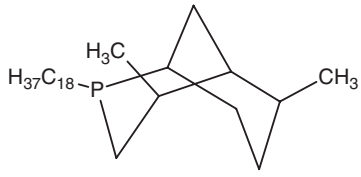

11

1.18.4.2 Rhodium

Rhodium-based homogeneous catalysts have found widespread application in a variety of processes, including hydroformylation of alkenes,[98–100] methanol carbonylation to acetic acid (the Monsanto process),[101] and various hydrogenation and C–H activation reactions.

The chemistry of unmodified rhodium carbonyls has been extensively studied.[102,103] In the early 1980s, researchers at Union Carbide published several reports of the reactivity of rhodium carbonyl clusters under syngas pressure.[104–106] Whereas $HCo(CO)_4$ had been observed by several groups at high syngas pressures,[71,89] the corresponding rhodium hydride had proved elusive. Starting with $Rh_4(CO)_{12}$, the authors studied the effect of temperature and carbon monoxide pressure on the formation of $Rh_2(CO)_8$ using HP-IR (Scheme 2).[104,106] Even at CO pressures above 1300 bar, small traces of $Rh_4(CO)_{12}$ remained. Upon addition of hydrogen to this mixture (4.5 CO : 1 H_2), the absorbances of $Rh_2(CO)_8$ decreased, those of $Rh_4(CO)_{12}$ increased, and a new species was observed. Significant peak overlap made identification of this species from the original IR spectrum rather difficult, but Fourier subtractions of the spectra for the di- and tetranuclear complexes were carried out to simplify the spectrum. The remaining peaks were assigned to $HRh(CO)_4$ **12**, based on excellent correlation with the data for the corresponding cobalt and iridium hydrides. The relative instability of the rhodium hydride in this triad was reported based on its greater tendency to reform the tetranuclear cluster when subjected to small increases in CO pressure. The performance of higher rhodium carbonyl clusters, including those containing encapsulated heteroatoms, was investigated for ethylene glycol synthesis under syngas pressure.[105] HP-IR studies again provided information on the active species during the reaction. Around the same time, King *et al.* reported studies of rhodium carbonyls during hydroformylation of ethylene.[107] At elevated syngas pressures in the presence of ethylene, the unstable alkyl species **13** was observed, while the rhodium–alkene complex **14** was observed under similar conditions but in the absence of CO. Heaton *et al.*[108] used ^{13}C HP-NMR to study the conversion of $[Rh_{12}(CO)_{30}]^{2-}$ to $[Rh_5(CO)_{15}]^-$. Equatorial edge-bridging carbonyls were observed, as well as very slow exchange of the remaining carbonyls on the NMR timescale.

More recently, Garland has carried out detailed studies on the use of $Rh_4(CO)_{12}$ in a range of hydroformylation reactions. The reaction of $Rh_4(CO)_{12}$ with various terminal, internal, branched, and cyclic alkenes under elevated temperatures and syngas pressures led to the formation of a range of acylrhodium intermediates $RCORh(CO)_4$,

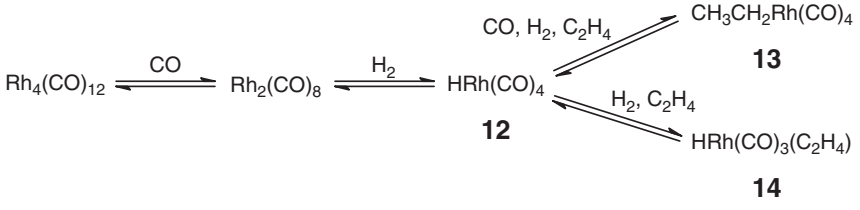

Scheme 2 Unmodified rhodium carbonyl equilibria.

which were characterized by HP-IR.[109] The intermediates were assigned trigonal bipyramidal geometry with the acyl carbonyl in an axial position. Relative rates of reaction were determined for all alkenes, and it was shown that the rate-determining step for these unmodified systems was the entry of $Rh_4(CO)_{12}$ into the catalytic cycle. Branched internal alkenes did not react at all under the conditions employed. Depending on the alkene structure, a number of different acyl isomers and stereoisomers were also observed. In a similar study,[110] the reaction of $Rh_4(CO)_{12}$ with various substituted alkynes under CO and syngas pressure afforded new dirhodium–alkyne complexes. The stability of these complexes even under H_2 pressure supports the observation of alkynes as poisons for such catalysts. Further investigations of poisoning with conjugated dienes indicated that the rhodium intermediates react preferentially with trace amounts of dienes in an alkene feed, and new resonances observed by HP-IR were attributed to various mononuclear rhodium allyl complexes.[111] Reactive intermediates for hydroformylation of cyclohexene,[112] ethylene,[113,114] and styrene[115] substrates were also reported.

Rhodium carbonyl/iodide systems are used industrially in the carbonylation of methanol to acetic acid.[116] Initial work to elucidate the reaction mechanism was carried out by Forster and Dekleva at Monsanto.[117] Using HP-IR, Maitlis determined that $[Rh(CO)_2I_2]^-$ is the predominant species under reaction conditions, and confirmed that oxidative addition of methyl iodide to this species is rate determining.[118] The reaction of this key intermediate with methyl iodide was also investigated, and compared to the corresponding iridium species. While the iridium system underwent oxidative addition to form an alkyl complex much more rapidly than rhodium, it was found that subsequent migratory insertion to afford the acyl intermediate was much faster for rhodium due to the inherent instability of the alkylrhodium complex. Fontaine *et al.*[119] also observed $[Rh(CO)_2I_2]^-$ as the catalyst resting state for the conversion of methyl formate to methyl acetate or acetaldehyde.

Triphenylphosphine-modified rhodium catalysts for hydroformylation were discovered by Wilkinson in the late 1960s, and a mechanism for the reaction was proposed involving a hydridorhodium dicarbonyl with two phosphine ligands as the active catalyst.[120] Soon thereafter, HP-IR and catalytic studies of $RhCl(CO)(PPh_3)_3$ and $HRh(CO)(PPh_3)_3$ were carried out by Morris and Tinker.[121] $RhCl(CO)(PPh_3)_3$ reacted slowly with alkenes, and was the predominant species observed under syngas pressure. At higher CO pressures, bands corresponding to $RhCl(CO)_2(PPh_3)_2$ were observed. In contrast, the hydride precursor afforded rapid hydroformylation under mild conditions. At room temperature two new rhodium species were seen under syngas pressure, $HRh(CO)_2(PPh_3)_2$ and $[Rh(CO)_2(PPh_3)_2]_2$, which upon heating afforded an unidentified species speculated to be a dinuclear compound. Moser[122] and van Leeuwen and Claver[123] also observed $HRh(CO)_2(PPh_3)_2$ in studies on hydroformylation of 1-hexene and 1-octene, respectively. Bianchini used HP-NMR to evaluate the catalyst equilibria for the hydroformylation of 1-hexene with $HRh(CO)(PPh_3)_3$.[124] Under syngas pressure, the starting complex was readily converted to the diphosphine $HRh(CO)_2(PPh_3)_2$, and an acylrhodium intermediate was also observed. Upon releasing pressure, a series of rhodium dimers were observed. More recently, Caporali *et al.*[125] compared the hydroformylation of 1-hexene and cyclohexene using $HRh(CO)(PPh_3)_3$, and found from HP-IR that different rate-determining steps applied in each case, namely alkene insertion for the sterically demanding internal alkene, and hydrogenolysis of the acyl intermediate in the case of the terminal alkene. van Leeuwen[126] investigated the poisoning effect of a range of typical alkene impurities on $HRh(CO)_2(PPh_3)_2$. Using HP-IR, he observed the formation of inactive carboalkoxyrhodium species arising from the reaction of the catalyst with enones. Poliakoff[127] reported HP-IR studies on unmodified and PPh_3-modifed rhodium (acetylacetonate (acac)) complexes in a polyethylene matrix. HP-IR and HP-NMR studies on other monodentate phosphines, particularly those effective in alternative solvents, are summarized in Table 1.

The use of bidentate phosphine ligands has vastly expanded the scope of rhodium-catalyzed hydroformylation. Monodentate phosphines afford good performance in industrial processes, but need to be used in large excesses

Table 1 HP-IR and HP-NMR studies of rhodium-catalyzed hydroformylation and carbonylation using monodentate phosphines other than PPh_3

Ligand	*Substrate*	*Solvent*	*Method*	*References*
PEt_3	Allylic halides	EtOH	HP-NMR	128
TPPTS[a]	Alkenes	H_2O	HP-NMR	129
TPPTS		H_2O	HP-NMR	130
$P(p\text{-}PhCF_3)_3$	Ethylene	Liquid CO_2	HP-NMR	131
$P[(CH_2)_x(CF_2)_yCF_3]_3$	1-Decene	Toluene/$C_6F_{11}CF_3$	HP-NMR	132
$P[Ph(3,5\text{-}CF_3)]_3$	Ethylene	sCO_2	HP-IR	133

[a]Triphenylphosphine trisulfonate.

to stabilize the rhodium hydride.[98] Bidentate ligands afford superior stabilization at lower ligand concentrations, and their bite angles[134] allow control of the geometry of the accepted trigonal bipyrimidal hydride complex, by enforcing either diequatorial (ee, **15**) or equatorial apical (ea, **16**) coordination of the phosphine.[98,135,136] This allows much better control of hydroformylation selectivities, with ee-coordinated bidentates generally affording superior product linearities. 2,2′-Bis(diphenylphosphinomethyl)-1,1′-binaphthyl (BISBI) **17**, 9,9-dimethyl-4,5-bis(diphenylphosphino)xanthene (Xantphos) **18**, ferrocenyl-based diphosphines **19**, 1,2-bis(diphenylphosphino)ethane (DIPHOS) **20**, 2,2′-bis(biphenylphosphino)-1,1′-binaphthyl (BINAP) **21**, and variations of these ligands have been studied extensively.[98,]

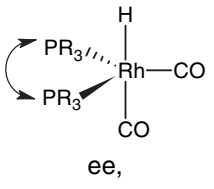

ee,

15

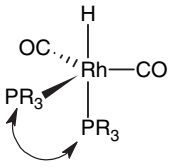

ea,

16

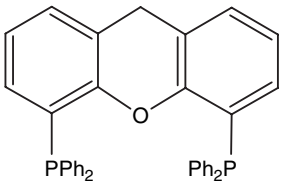

17

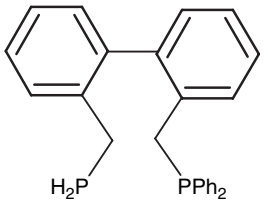

18

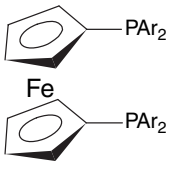

19

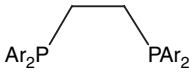

20

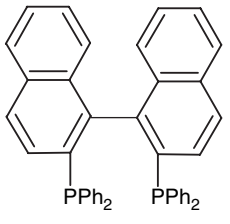

21

van Leeuwen and Claver dominate the literature regarding high pressure spectroscopic studies in this area. van Leeuwen[137] reported a study on a series of xantphos-type ligands, where variations of the backbone were synthesized to afford ligands with different bite angles. HP-IR spectra for $HRh(CO)_2$(P–P) complexes clearly demonstrated the presence of ee and ea isomers in differing ratios. ^{13}CO-labeled complexes were also prepared and the rate of ^{13}CO exchange was determined under syngas pressure by IR. A similar study was carried out on a range of thixantphos ligands,[138] where HP-NMR and HP-IR indicated increasing ee isomer formation with more electron-withdrawing ligands. The primary species observed during hydroformylation were the $HRh(CO)_2$(P–P) complexes, suggesting alkene coordination was rate limiting with these systems. Phenoxaphosphino- and phenothiaphosphino-modified xantphos ligands[139,140] afforded almost exclusively the ee geometry. Catalysts using these ligands showed unsurpassed hydroformylation and isomerization activity, believed to arise from very rapid CO dissociation, as observed by ^{13}CO-labeling studies at high pressure using rapid scanning IR. This was the first reported example of formation of a terminal aldehyde from an internal alkene.[140] In a variation from the usual ^{31}P NMR studies, Elsevier[141] reported the ^{103}Rh shifts for rhodium hydrides of a range of bidentate phosphines using heteronuclear multiple quantum correlation (HMQC) sequences.

These diphosphine ligands are often suitable or can be modified for use in biphasic systems. Sulfonation of xantphos led to a suitable water-soluble ligand [2,7-bis(SO_3Na)-xantphos], which was employed for hydroformylation of propylene, 1-hexene, and 4-styrene sulfonate.[142] HP-NMR confirmed that the diphosphine adopted the desired ee configuration. A rhodium–sulfoxantphos complex was employed for hydroformylation of 1-octene in $[bmim]PF_6$, where bmim = 1-butyl-3-methyl-imidazolium.[143] High pressure studies showed that the ee–ea ratio was sensitive to temperature and syngas pressure variations, but not to hydrogen partial pressure.

Asymmetric hydroformylation of styrene has been studied with a range of bidentate phosphines. van Leeuwen[144] reported phosphorus-chiral ferrocenyl-based diphosphines, the hydride complexes of which showed varying ee–ea ratios depending on ligand basicity, as determined by HP-IR and HP-NMR. This contrasted to the clear ea preference shown by complexes of the achiral 1,1′-bis(diphenylphosphino)ferrocene (dppf) ligand. Claver and van Leeuwen[145–147] investigated BDPP [(2*S*,4*S*)-bis(diphenylphosphino)pentane] and CHIRAPHOS [(2*R*,3*R*)-bis(diphenylphosphino)butane] for the same transformation. High pressure spectroscopic data for the catalytic species

Table 2 HP-NMR and HP-IR studies of rhodium complexes based on diphosphites and other ligands

Ligand types	*Ligand precursors*	*References*
Diphosphites	Bisphenols	158–160
Diphosphites	Carbohydrates	161
Diphosphites	Binaphthols	162
Phosphine–phosphites	Bisphenols	163
Diphosphonites	Phenols	164
Phosphorus diamides	Biuret	165,166
Phosphorus amidites	Pyrroles	167,168
Linear tridentate phosphine		169
Tetradentate phosphine		170
Bis(imidazolium) carbene		171

present during hydroformylation were correlated with the observed enantiomeric excesses determined for the reaction product, and a number of resting states were observed which were dependent on syngas pressure. Nozaki *et al.*[148] recently employed (*R*,*S*)-BINAPHOS and a methoxy derivative thereof to induce enantioselectivity, and studied the active catalytic species by HP-IR. Claver has also reported the rhodium-catalyzed aqueous biphasic hydroformylation of substituted styrenes using the tetrasulfonated ligands 1,3-bis(diphenylphosphino)propane tetrasulfonate (dpppts) and (2*S*,4*S*)-bis(diphenylphosphino)pentane tetrasulfonate ((*S*,*S*)-bdppts). HP-NMR and HP-IR studies confirmed the formation of $HRh(CO)_2$(P–P) in a basic medium, but under neutral conditions the sulfonated bdpp ligand afforded $[Rh(bdppts)_2]^{2+}$, and afforded poorer catalytic results.

Phosphite ligands, more particularly bulky monophosphites, afford significantly improved reaction rates for hydroformylation of alkenes. In addition, they are less prone to oxidation, and are generally easy to synthesize. The rate enhancement is ascribed to the fact that steric bulk generally results in the formation of more reactive monophosphite rhodium hydrides. Reactions of triphenyl phosphite-modified tetranuclear rhodium carbonyls were studied by multinuclear NMR and IR.[149] Under CO or syngas pressure, the clusters fragmented to dinuclear species, and no evidence was found for hydride formation. Crous *et al.*[150] studied catalysts based on the bulky tris(2,4-di-*tert*-butylphenyl)phosphite. It has been suggested that only monophosphite rhodium hydride species [$HRh(CO)_3$(phosphite)] should form with sterically demanding phosphites.[151,152] However, Crous and co-workers found that significant quantities of $HRh(CO)_2(phosphite)_2$ also formed with this ligand, and they studied the effect of changing pressure and ligand concentration on the equilibrium between mono- and disubstituted hydrides using HP-NMR and HP-IR. The effect of the rhodium precursor on catalyst preforming was also investigated, with $Rh_4(CO)_{12}$ giving the cleanest and quickest conversion to active hydrides.

Diphosphites have the advantage of higher selectivities, but generally afford slower reaction rates.[153] Again, van Leeuwen and Claver are leaders in this area, and some of their key papers describing high pressure studies are summarized in Table 2. Further work is summarized in a review.[154] A variety of alternative mono- and bidentate ligands have also been studied under hydroformylation conditions (Table 2). In general, all of these papers discuss the formation of the active catalyst from the precursors, as well as the nature and geometry of the active intermediates and resting states. High pressure studies of heterobimetallic complexes of rhodium with other metals have also been carried out using a range of ligands.[155–157]

High pressure spectroscopic studies of hydrogenation and other catalytic processes using rhodium catalysts have been carried out by several groups and are summarized in Table 3.

Table 3 High pressure spectroscopic studies of rhodium complexes for applications other than carbonylations

Application	*Substrate*	*Ligands*	*Method*	*References*
Hydrogenation	Indole	Triphos[a]	HP-NMR	172
Hydrogenation	Quinoline	Triphos	HP-NMR	173
Hydrogenation	Indoles	Diphosphines	HP-NMR	174
Hydrogenation	Alkenes	acac[b]	HP-IR	175
Hydrogenation/hydrogenolysis	Benzothiophene	Sulfos[c]	HP-NMR	176
Hydrogenolysis	Epoxides	Chiral sulfonated phosphines	HP-NMR	177
Hydroaminomethylation	Alkenylamines	Fluorinated ligands	HP-NMR	178

[a]Triphos = Bis(2-diphenylphosphinoethyl)phenylphosphine, $MeC(CH_2PPh_2)_3$.
[b]acac = acetylacetone.
[c]Sulfos = $-O_3S(C_6H_4)CH_2C(CH_2PPh_2)_3$.

1.18.4.3 Iridium

Iridium complexes are well known as hydrogenation and carbonylation catalysts, exhibiting similar behavior to rhodium and cobalt in terms of formation and reaction of metal carbonyls and hydrides.[179,180]

HP-NMR and HP-IR studies of the hydrogenation of several substrates have been reported.[181,182] Bianchini[181] reported an orthometallated iridium dihydride as an effective catalyst precursor for the enantioselective hydrogenation of 2-methylquinoxaline. HP-NMR showed that this pre-catalyst enters the catalytic cycle by deorthometallation rather than by reductive elimination of hydrogen. The enantioselective hydrogenation of imines with cationic iridium complexes in supercritical CO_2 was studied using HP-IR and HP-NMR.[182] The counter ion played an important role in enantioselectivity, and the effect of various reaction parameters, particularly the substrate itself, on the nature of the catalytically active species was investigated. Bianchini[183] described the reactivity of a novel cationic tetrahydrido iridium complex, $[(triphos)Ir(H_2)(H)_2]^+BF_4^-$. The complex was extremely labile in solution, and could only be isolated as a solid by reaction of hydrogen with solid $[(triphos)Ir(C_2H_4)(H)_2]^+BF_4^-$. Characterization of the complex in solution could only be achieved by means of HP-IR and HP-NMR under hydrogen pressure. Detailed NMR studies indicated that the complex was octahedral, with the hydrides and dihydrogen *trans* to a facially coordinated triphos ligand. Hydrogenation of thiophenes to thiols was studied by Bianchini using 16-electron iridium and rhodium hydrides with triphos ligands.[184] The rhodium complex afforded only hydrogenation products, while the iridium complex also afforded hydrodesulphurization products. HP-NMR was employed to assist in elucidating the mechanism of these reactions.

Carbonylations of alkenes with iridium carbonyls have not been studied as extensively as the corresponding methanol carbonylations. However, as far back as 1975, Whyman[185] carried out detailed HP-IR investigations of the behavior of $HIr(CO)_3P^iPr_3$ under syngas pressures in the presence of alkenes (Scheme 3). This fairly stable mononuclear complex was readily formed from a tetranuclear iridium cluster at high temperatures and syngas pressures, and was active for hydroformylation of alkenes. As observed with the Co/PBu_3 system,[71] under typical hydroformylation conditions, $HIr(CO)_3P^iPr_3$ **22** was the only species observed. Whyman investigated the effect of sequentially introducing reactive gases to this complex, in an attempt to mimic the sequence of proposed intermediates within the hydroformylation catalytic cycle. At 14 bar of ethylene and 50 °C, the $HIr(CO)_3(P^iPr_3)$ absorptions decreased and new peaks were observed, consistent with the formation of an ethyliridium complex **23**. The wave numbers correlated well when compared to the corresponding methylcobalt complex. The reaction mixture was depressurized to remove excess ethylene, and pressurized again with 200 psi of carbon monoxide at the same temperature. Again new peaks were evident, this time corresponding to the formation of an acyliridium species **24**. Once more, CO pressure was vented and the solution was pressurized under 200 psi of hydrogen. The acyliridium absorbances disappeared, and peaks corresponding to $HIr(CO)_3(P^iPr_3)$ reappeared, along with a carbonyl peak at 1730 cm^{-1} corresponding to propionaldehyde. The presence of additional absorbances was ascribed to the presence of $H_3Ir(CO)_2P^iPr_3$ **25**, which was observed previously for the corresponding PPh_3 complexes.[186] Upon replacing hydrogen with CO, these peaks disappeared. Upon repeating the same stepwise addition of gases, the same observations were made, and the propionaldehyde resonance increased after each sequence, confirming completion of the catalytic cycle and production of the desired product. This is an excellent example of catalysis in slow motion.

More recently, Merbach[187] used HP-NMR and HP-IR to study the reactions of typical alcohol carbonylation catalysts with alkenes. In particular, the reactivity of *cis*-$[Ir(CO)_2I_2]^-BPh_4^+$ was examined and compared to that of the corresponding rhodium complex. Under elevated CO pressures, both rhodium and iridium complexes were

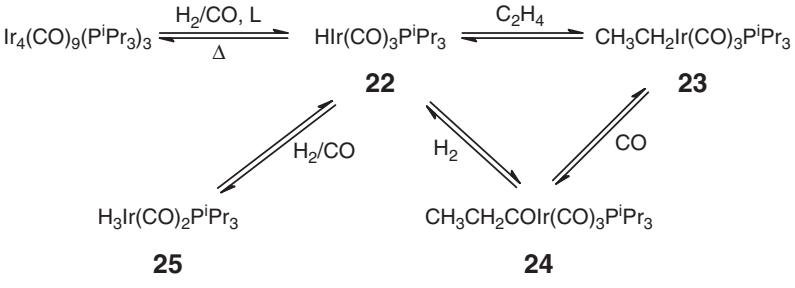

Scheme 3 Phosphine-modified iridium carbonyl equilibria.

converted to the neutral $[M(CO)_3I]$ complex. However, the equilibrium lies far to the left in the case of the rhodium complex, which would exist largely in anionic form under catalytic conditions. The complexes were also studied under hydrogen pressure, as hydrogen is produced *in situ* during the carbonylation process. The major products were *cis*,*cis*,*cis*-$[Ir(H)_2(CO)_2I_2]^-$ and *cis*,*trans*,*cis*-$[Ir(H)_2(CO)_2I_2]^-$, with a minor amount of *cis*,*cis*,*trans*-$[Ir(H)_2(CO)_2I_2]^-$. The CO exchange process was also investigated for these $[M(CO)_2I_2]^-$complexes using ^{13}C HP-NMR.[188]

In the 1970s and 1980s, Forster and co-workers at Monsanto studied phosphine-free iridium iodide systems under CO pressure using HP-IR.[189,190] This groundbreaking work followed on from similar studies with rhodium,[117] and laid the foundation for BP's Cativa process.[191,192] By careful investigation of IR spectra obtained under catalytic conditions followed by synthesis of proposed species, Forster obtained a comprehensive picture of the catalytic cycle as well as of various side-reactions of the intermediates and pre-catalysts. Whereas the rate-limiting step in the rhodium-catalyzed process is the oxidative addition of CH_3I to $[Rh(CO)_2I_2]^-$, with the corresponding iridium system it is the further reaction of $[CH_3Ir(CO)_2I_3]^-$ via substitution of an iodide by CO that is rate limiting. Therefore, under typical operating conditions the main iridium species observed by HP-IR during catalysis was $[CH_3Ir(CO)_2I_3]^-$. Higher CO partial pressures increased the reaction rate, while addition of ionic iodide to the reaction mixture slowed the reaction rate, supporting a dissociative mechanism for the iodide displacement by CO. A neutral species $[Ir(CO)_3I]$ predominated in the HP-IR at low concetrations of water and iodide. This species was also active for the carbonylation reaction, but in this case oxidative addition of CH_3I to $[Ir(CO)_2I]$ was found to be rate determining.

Maitlis[193] reported the identification of a key intermediate in the methanol carbonylation cycle. The facial $[Ir(CO)_3I_2(CH_3)]$ complex was observed with HP-IR and HP-NMR upon reaction of dimer $[Ir(CO)_2I_2(CH_3)]_2$ with CO. The kinetics of CO insertion of the methyl tricarbonyl complex to the corresponding acyl species was studied, lending support to its proposed role within the catalytic cycle. Recently, a mechanistic study was published by the group of Maitlis and workers at BP,[194] which also included investigations on the effect of promoters for this reaction. Interactions in the complex reaction cycles were explored by HP-NMR and HP-IR. As reported by Forster, under reaction conditions the main species observed by HP-IR was $[CH_3Ir(CO)_2I_3]^-$. However, as the reaction progressed, the characteristic bands for this species decreased, and peaks corresponding to $[Ir(CO)_2I_4]^-$ appeared. This species sits outside the catalytic cycle and is regarded as an inactive form of iridium. It accumulates in the mixture as water concentration decreases, as it can no longer be effectively reduced to $[Ir(CO)_2I_2]^-$ to maintain the catalytic cycle. At very low water concentrations, neutral intermediates $[Ir(CO)_3I]$ and $[Ir(CO)_3I_3]$ were observed. Addition of iodide salts minimized consumption of $[CH_3Ir(CO)_2I_3]^-$ to $[Ir(CO)_2I_4]^-$ but inhibited the reaction rate. In catalytic runs, addition of a neutral ruthenium iodocarbonyl promoter was observed to dramatically enhance reaction rates. Zinc, gallium, and indium iodides afforded similar improvements. When studying reaction mixtures promoted by ruthenium using HP-IR, it was found that the predominant ruthenium species was $[Ru(CO)_3I_3]^-$. The counter ion is believed to be H_3O^+. The authors proposed that the promoters modulate HI concentrations in the reaction mixture by acting as Bronsted acid catalysts and accelerate reaction of HI with methyl acetate to form methyl iodide.

1.18.4.4 Nickel

Nickel carbonyls have a long and well-studied history, and are particularly suitable for IR studies due to their characteristic nickel carbonyl stretching frequencies.[195,196] Beattie *et al.*[197] studied the interconversions of nickel carbonyl cluster compounds using HP-IR. Starting from the dianion $[Ni_6(CO)_{12}]^{2-}$, they demonstrated that the cluster was converted to other cluster compounds at room temperature under moderate CO and syngas pressures via an $[Ni_5(CO)_{12}]^{2-}$ intermediate. At 100 °C, the primary product was $Ni(CO)_4$.

Moser[198,199] carried out HP-IR studies on the nickel-catalyzed carbonylation of methanol using his CIR reactor.[63] Methanol carbonylation is more commonly performed with highly active rhodium and iridium catalysts.[118] However, nickel is significantly cheaper than both of these metals, and thus there is a significant incentive to understand and implement such catalysts industrially. Nickel generally requires fairly harsh conditions (250–300 °C; 200 atm) to effect this conversion, but the use of organotin and organophosphorus promoters can significantly reduce operating conditions.[200] Moser's studies focused on the identification of catalytic intermediates using a nickel phosphine catalyst, and also probed the effect of ligand electronics and steric bulk on catalyst performance. In initial studies using an NiI_2–PPh_3–LiI–MeI system, Moser observed that while $Ni(CO)_4$ absorbances were very strong at the start and end of a catalytic run, almost no nickel carbonyl peaks were observed during the run at high reaction rates. He

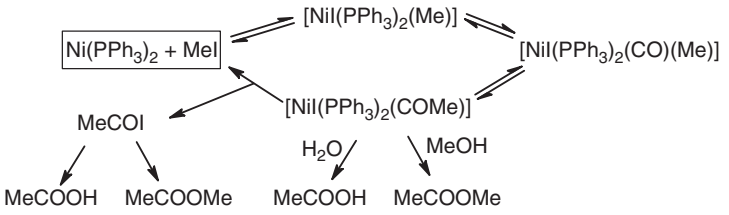

Scheme 4 Nickel carbonylation chemistry.

attributed this to the active catalytic species containing no Ni–CO bond, in disagreement with most prior postulates which place $Ni(CO)_4$ and $[Ni(CO)_3I]^-$ as key intermediates in the catalytic cycle. Further evidence for this theory is that changes in reaction rate due to changing process parameters do not correlate with concurrent changes in the $[Ni(CO)_3I]^-$ concentration. Moser suggests that the key catalytic step is the reversible oxidative addition of MeI to $Ni(PPh_3)_2$ (Scheme 4). Rapid CO addition then occurs to form a pentacoordinate intermediate, followed by methyl migration to form a nickel acyl species, and either reductive elimination to form acetyl iodide, or trapping of the acyl intermediate with water or methanol to afford acetic acid or methyl acetate. Acetyl iodide itself is not observed, suggesting that it is either immediately consumed by reaction with water or methanol, or that the products are formed by direct reaction of the acylnickel intermediate. $Ni(PPh_3)_2$ was observed in the IR spectra, further supporting this mechanism. None of the other postulated intermediates were detected, as they presumably react away faster than the oxidative addition step. Another interesting observation was the extent of phosphonium salt formation under the reaction conditions, which could be clearly oberved in the HP-IR. PPh_3 readily reacted with methyl iodide, and only a proportion of the PPh_3 was available for binding to nickel. Understandably, increasing the ligand concentration resulted in a decrease in reaction rate due to lowering of the MeI concentration by reaction with the phosphine. The nature of the phosphine was found to affect the reaction rate and phosphonium salt equilibrium, and phosphines which shifted the equilibrium to free phosphine afforded improved catalysis.

1.18.4.5 Palladium

Palladium is a well-known mediator of carbonylation chemistry, including hydroformylation, hydroesterification, hydrocarboxylation, and CO–alkene co-polymerization.[201,202] These reactions proceed via an acylpalladium intermediate, which is then intercepted by an appropriate reagent (hydrogen, alcohol, water, or alkene) to afford the desired product. As all these reactions require an alkene and CO at elevated temperatures and pressures, control of selectivity in these reactions is essential. It has been clearly demonstrated that bidentate ligands are required to enforce CO–alkene co-polymerization, while monodentate ligands are generally selective toward the former reactions. However, bidentate ligands can also be tuned to give the monomeric acyl products, depending on the steric (particularly P–P bridge length) and electronic properties of the ligand. Such systems lend themselves to high pressure *in situ* studies.

van Leeuwen and co-workers[203] made a series of neutral and cationic palladium methyl complexes with bidentate phosphine ligands and investigated the influence of ligands and counter ions on CO insertion. The rate of reaction of neutral complexes $(P–P)Pd(CH_3)Cl$ with CO was measured in a sapphire HP-NMR tube at a pressure of 25 bar (P–P = 1,2-bis(diphenylphosphino)ethane (dppe), 1,3-bis(diphenylphosphino)propane (dppp), 1,4-bis(diphenylphosphino)butane (dppb), dppf). The dppe complex showed no CO insertion at −38 °C, and only a relatively slow insertion to $(P–P)Pd(COCH_3)Cl$ at 32 °C. The other complexes underwent facile insertion at the lower temperature, with the dppf complex giving a slightly lower rate than dppp and dppb. Upon depressurization, the acyl complexes slowly decarbonylated back to the starting methyl complexes, but Pd(0) and other unidentified decomposition products were also observed. The ionic complexes $[(P–P)Pd(CH_3)(CH_3CN)]^+SO_3CF_3^-$ were prepared from the corresponding neutral complexes by treatment with $AgSO_3CF_3$ and CH_3CN, and were studied with HP-NMR under CO pressure in an identical manner. The dppe and dppp complexes readily and cleanly afforded the expected acyl complexes $[(P–P)Pd(COCH_3)(CH_3CN)]^+SO_3CF_3^-$. The CO insertion reaction of the dppf cationic complex proceeded reasonably, but several unidentified low intensity resonances were also observed. Synthesis of the starting dppb cationic complex was not so straightforward, and in addition to the expected *cis*-complex, resonances were observed corresponding to *trans*-complexes. It was proposed that dppb is bridging between two palladium centers, resulting in the formation of oligomeric complexes. Such behavior of dppb has been previously documented.[204] Upon

pressurizing with CO, the mixture of dppb cationic complexes afforded two acyl products which showed no P–H coupling, and were assigned to oligomeric complexes. Unlike the parent methyl complex, no trace of a *cis*-product was observed, which was ascribed to the stronger *trans*-influence of the acyl group. Upon release of CO pressure, all four cationic acyl complexes smoothly decarbonylated.

In similar work using HP-NMR, Elsevier[205] reported the first *in situ* identification of *cis*-alkyl(carbonyl)palladium complexes at low temperatures under a pressure of CO. It was also shown that a complex such as $[Pd(CH_3)(CO)\{(S,S)\text{-bdpp}\}]^+BF_4^-$ [(*S*,*S*)-bdpp = (2*S*,4*S*)-bis(diphenylphosphino)pentane] is not an intermediate in the insertion of CO into a Pd–OMe bond, although it is an exclusive intermediate for insertion into a Pd–Me bond. Pelagatti *et al.*[206] reported the synthesis of a range of neutral and cationic palladium–methyl complexes based on a hydrazone ligand [HPNO = 2-(diphenylphosphino)benzaldehye benzoyl hydrazone] which can coordinate in a bi- or tridentate manner. They studied the CO insertion reaction of these complexes using HP-NMR, and also investigated the stability of the resulting acyl complexes upon releasing CO pressure. Van Koten[207] used HP-NMR and HP-IR to identify unstable CO insertion products from a number of methyl- and arylpalladium complexes containing tridentate N-N′-N ligands. Results from NMR studies in combination with *ab initio* calculations were used to compare associative and dissociative pathways for the CO insertion.

Bianchini[208] recently published a review article dealing with mechanistic aspects of the alternating co-polymerization of ethylene and CO, focusing particularly on HP-IR and HP-NMR studies. His own studies in this area are particularly noteworthy. A simple yet effective ligand for this reaction is dppp. Bianchini[209] investigated the effect of substitution of the C_3 backbone on the reaction, and also investigated the nature of the active species with such ligands under catalytic conditions using HP-NMR in sapphire tubes. It was shown that the only NMR–visible phosphorus-containing species were Pd(II) compounds of the form $Pd(P–P)X_2$. Catalytic runs in methanol showed that the introduction of alkyl groups in the 1,3-positions of the phosphine linker afforded improved results, and NMR studies indicated that both steric and electronic factors were responsible. Further studies looked at the combination of bidentate P–P and N–N ligands for such complexes.[210] A combination of *meso*-dbpp and 2,2′-bipyridine afforded the best results. Aqueous biphasic palladium catalysis using a water-soluble diphosphine **26** has been studied for this reaction using HP-NMR in D_2O.[211] When combined with an organic acid (*p*-toluenesulfonic acid) and oxidant (1,4-benzoquinone), this water-soluble catalyst system is highly active. As observed in other studies,[209] Bianchini confirmed by HP-NMR that $Pd(P–P)X_2$ complexes were the only catalytic species visible during catalysis, and postulated that these act as a resting state which delivers active palladium hydride species to the catalytic cycle by reaction with water or acid. In two further papers, the effects of the ligand and the solvent were investigated.[212,213] In contrast to the earlier study in methanol, substituents on the 1,3-bridge positions of dppp had little or no effect on catalysis in dichloromethane. Using HP-NMR, palladium hydroxo complexes $[Pd(OH)(P–P)]_2^{2+}$ were observed to form in the presence of trace amounts of water, but these were also found to be catalytically active, converting to the expected $[Pd(P–P)]^{2+}$ species during the reaction. The hydroxo complexes were shown to be products arising from chain transfer by protonolysis, which proceeds via an enolate mechanism.

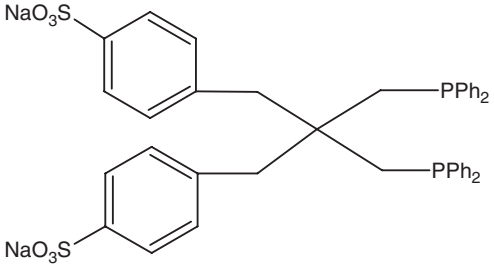

26

Luo *et al.*[214] used both HP-IR and HP-NMR in their studies of CO–ethylene co-polymerization. Using a Pd(II)/dppp/CF_3COOH catalyst system under CO pressure, they detected three palladium–carbonyl absorptions in the IR spectrum, and linked these to three intermediates in the proposed mechanism. In addition, ^1H NMR revealed the presence of coordinated ethylene and a palladium–methylene species (Pd–CH_2–). The co-polymerization of CO with propylene was investigated using the unsymmetrical phosphine–phosphite bidentate ligand, (R,S)-BINAPHOS.[215] Two major resting states of the catalyst were observed by HP-NMR, namely alkylpalladium and acylpalladium species which are believed to correspond to $[Pd(COR)(BINAPHOS)(CO)]^+[BF_4]^-$ and $[Pd(CH_2CHCH_3(CO)R)(BINAPHOS)]^+[BF_4]^-$.

Hydroesterification, also known as methoxycarbonylation when the reaction is carried out in the presence of methanol, is an effective route for the production of esters directly from alkenes.[216] Bianchini and co-workers[217] have reported HP-NMR studies for methyl propionate synthesis using dppf and an octamethyl dppf derivative (dppomf) as ligands. HP-NMR studies of the carbonylation of styrene have been reported by several groups.[218–220] A review[218] summarizing the mechanistic knowledge around hydroxycarbonylation of styrene also describes HP-NMR studies carried out by the authors, where palladium acyl and hydride species were observed, and the mechanism controlling regioselectivity was examined. Iggo and co-workers[219] employed HP-NMR for studies of the asymmetric alternating co-polymerization of styrene with CO using BINAPHOS as ligand. By running the experiments under both diffusion and reaction-controlled conditions to observe a number of possible intermediates, they propose the 1,2-insertion of styrene into a Pd–acyl bond as the key catalytic step.

1.18.4.6 Ruthenium and Osmium

Ruthenium is one of the most versatile catalytic metals, and organometallic ruthenium complexes have been used for C–H activation, carbonylation, hydrogenation, oxidation, and metathesis. Ruthenium hydrides and carbonyl compounds are typically the species studied with *in situ* spectroscopy, and demonstrate interesting behavior under a pressure of reactive gas.

Iggo[47] has described the cleavage of a ruthenium–rhodium dinuclear species **27** using an HP-NMR flow cell and studying the ^{31}P NMR spectra under a pressure of carbon monoxide. At low CO pressures, the complex exists as a metal–metal bonded complex with two bridging carbonyls and a bridging bidentate phosphine. Upon increasing the CO pressure to 30 bar, new resonances corresponding to intermediate (**28**, Scheme 5) were observed, where the metal–metal bond has cleaved, and carbonyls are no longer bridging, but the charged metal centers are still linked via the bridging bidentate phosphine. Upon increasing the CO pressure to 90 bar, **28** cleaved further to afford charged mononuclear species **29** and **30**. The presence of **30** was confirmed by HP-IR spectra under the same conditions. Upon releasing the CO pressure to 15 bar the reaction was found to be totally reversible. This study emphasizes the importance of analysis under real conditions to fully understand catalyst behavior. Interestingly, the complex was previously investigated using HP-IR;[221] however, the intermediate **28** was not observed. This further highlights the benefits of employing two techniques in conjunction, to compensate for the limitations of each.

Bianchini reported several studies of ruthenium phosphine catalysts under hydrogen pressure using HP-NMR with sapphire tubes. These catalysts were investigated for the hydrogenation of indole,[172] benzothiophene,[222] and acetylacetone.[223] The ruthenium tris(acetonitrile) complex $[Ru(MeCN)_3(triphos)]BPh_4$ was employed for the benzothiophene study.[222] At elevated hydrogen pressures (>5 bar), the acetonitrile ligands were converted to a

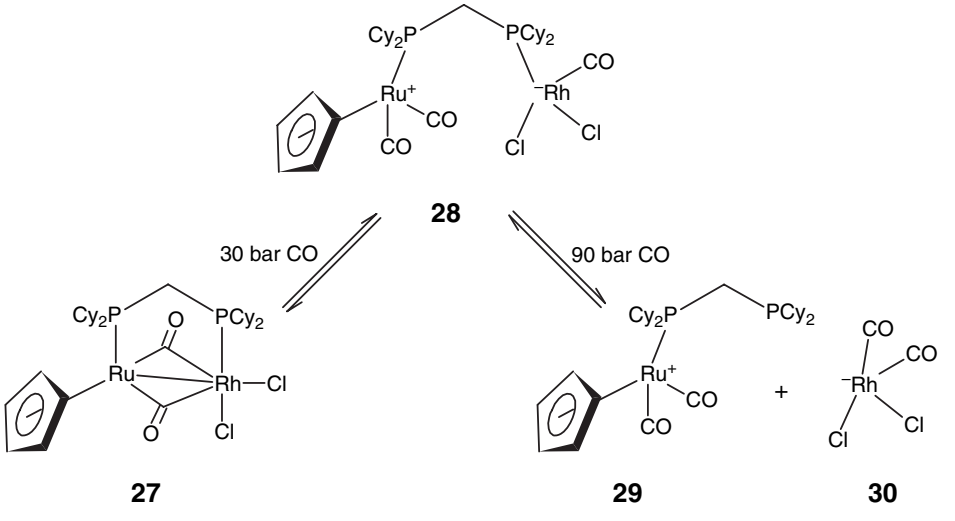

Scheme 5 Interconversions of a ruthenium-rhodium dinuclear species.

Table 4 Other HP-NMR and HP-IR investigations of ruthenium complexes

Application	*Substrate*	*Organometallics observed*	*Method*	*References*
Carbonylation	Piperidine	$Ru_3(CO)_{12}$, $Ru(CO)_5$	HP-IR	224
Carbonylation		Ru/Os carbonyls, hydrides, clusters	HP-IR	225
Hydrogenation	Benzene	Hydridoruthenium cluster	HP-NMR	226
C–C coupling/hydrogenation	Syngas	Bimetallic Ru–Rh complexes	HP-IR	157
Hydrogenation	CO_2	Ru hydrides and formates	HP-NMR	227
C–H cleavage/C–C coupling	Ar═O	Ru hydrides	HP-NMR	228
Dimerization	C_2H_4	Ru bis(ethylene) complex	HP-NMR	229,229a,229b

mixture of NH_3, $EtNH_2$ and Et_2NH, and Et_3N, while the starting ruthenium complex was converted to a series of hydrides which incorporated these amines as well as the hydrogenated substrate, 2,3-dihydrobenzo[b]thiophene (DHBT), as ligands. Below 5 bar of hydrogen pressure, acetonitrile was not hydrogenated, and the primary catalytic product was [HRu(MeCN)(triphos)(η^1-S-DHBT)]BPh_4. However, all of these Ru(II) hydrides were shown to be active for the hydrogenation reaction. In the presence of water, inactive Ru(II) acetate complexes formed, presumably via hydrolysis of the acetonitrile ligands. Enantioselective hydrogenation of acetylacetone to (2*R*,4*R*)-2,4-pentanediol was achieved using a ruthenium catalyst with a chiral diphosphine ligand.[223] HP-NMR investigations revealed that the only observable species during catalysis is a non-classical ruthenium polyhydride dimer.

Other high pressure IR and NMR studies carried out on ruthenium complexes are summarized in Table 4.

1.18.4.7 Other Metals

While the vast majority of HP-NMR and HP-IR research has focused on the typical carbonylation metals, the behavior of several other organometallic species under a gas pressure has been investigated. Hoff and co-workers[230] used HP-IR to investigate the effect of hydrogen and nitrogen pressure on solutions of $Cr(CO)_3(PCy_3)_2$. Although no reaction was observed at room temperature and pressure, the corresponding dihydrogen and dinitrogen complexes were observed at elevated pressures. Additionally, it was shown that hydrogen binds more strongly than nitrogen, in contrast to the results obtained for similar Mo and W complexes. Millar *et al.*[231] investigated the coordination mode of molecular hydrogen to the same chromium carbonyl complex under hydrogen pressure using ^{31}P and ^{1}H NMR. As seen by Hoff, dihydrogen complex (η^2-H_2)$Cr(CO)_3(PCy_3)_2$ was formed, and kinetics for this reversible binding was determined. Surprisingly, the classical dihydride species was not observed under the conditions investigated. Such complexes are important intermediates in catalytic hydrogenation reactions.

Reaction of Cp_2^*TiR complexes with CO was studied with HP-IR.[232] The coordinatively saturated $Cp_2^*TiR(CO)$ products can react further at elevated temperatures to afford Ti(II) and Ti(IV) disproportionation products, driven by the formation of the stable 18-valence electron $Cp_2^*Ti(CO)_2$ species. Detection of an unstable titanium(III) carbonyl has also been achieved using HP-IR.[233]

Ford[234] used HP-IR to investigate an acyliron migratory insertion intermediate formed by flash photolysis. Thus, flash photolysis of (η^5-Cp)$Fe(CO)_2C(O)CH_3$ affords coordinatively unsaturated (η^5-Cp)$Fe(CO)C(O)CH_3$. Trapping of the latter with CO in the reverse reaction was studied, and the second-order rate constant could be determined for this reaction under the high CO pressures employed. Variable-temperature studies allowed calculation of activation parameters for methyl migration. Iron cluster compounds have been studied for the carbonylation of methanol to methyl formate.[235] Consistent kinetics and a first-order dependence on cluster concentration confirmed the HP-IR results which showed that the cluster remained intact through the catalytic process.

Poliakoff[236] studied the photocatalytic hydrogenation of dimethylfumarate using low temperature HP-IR by investigating the behavior of a dimethylfumarate–iron carbonyl species in the presence of hydrogen. A dihydrogen intermediate was observed, and dimethylsuccinate was formed upon further warming. In the same study,[236] Poliakoff also investigated the hydrogenation of norbornadiene using molybdenum and chromium carbonyls. Iqbal[237] studied the reaction of $LMo(CO)_2(\eta^5$-$C_5H_5)$ complexes with CO at elevated temperatures and pressures using HP-IR. Molybdenumhexacarbonyl was the main product observed, and several intermediates were identified.

Table 5 Ligand exchange studies of metal complexes

Ligand	*Metal*	*Nuclide*	*Application*	*References*
Mg	H_2O	^{17}O	Exchange process	241
Ti	DMF[a]	^{1}H,^{17}O	Exchange process	242
	H_2O	^{17}O	Exchange process	243
	DMSO[c]	^{1}H	Exchange process	244
V	DMSO	^{1}H	Exchange process	245
	H_2O	^{17}O	Exchange process	246,
	MeCN, DMF, DMA	^{17}O	Exchange process	247
Nb, Ta	MeCN, Me_2O, Me_2S	^{1}H	Exchange process	248
Mn, Re	H_2O	^{17}O, ^{1}H	Exchange process	249,250
Fe	H_2O	^{17}O	Iron porphyrins	251
	DMSO, DMF, MeOH	^{1}H	Exchange process	252
Mn, Fe	DMF	^{13}C,^{17}O	Exchange process	253
Ru	H_2O, MeCN	^{1}H,^{17}O	Exchange process	254
Co	MeCN	^{13}C	Exchange process	255
Co, Ni	MeCN	^{13}C	Exchange process	256
Rh	MeCN, H_2O	^{1}H	Exchange process	257
Ni	MeOH	^{1}H	Exchange process	258
Ni, Pd, Pt	H_2O	^{17}O	Exchange process	259–261
Pd	DMF, DMA, MeCN	^{1}H	Exchange process	262
	DMS[b]	^{1}H	Exchange process	263
Pt	DMSO, DMS	^{1}H	Exchange process	264
	DMSO	^{1}H	Exchange process	265
Cu	H_2O, DMF	^{1}H,^{17}O	Exchange process	266
Al, Ga	H_2O	^{17}O	Exchange process	267,268
	DMSO, DMF	^{1}H	Exchange process	269
Sn	DMS	^{1}H,^{119}Sn	Exchange/isomerization	270
Sb	RCN, ROR, $RCONH_2$	^{1}H	Exchange	271
Ln (Tb–Tm)	H_2O	^{17}O	Exchange process	272
Ln	DMF	^{1}H	Exchange process	273
La	H_2O	^{139}La	Exchange process	274
Eu	H_2O	^{17}O	MRI imaging	275
Gd	H_2O	^{17}O	MRI imaging	276–279

[a]DMF = Dimethyl formamide.
[b]DMS = Dimethyl sulfate.
[c]DMSO = Dimethyl sulfoxide.

Kegl *et al.* used HP-NMR to investigate the behavior under syngas and CO pressure of three square-planar platinum diphosphine complexes with potential as hydroformylation catalysts.[238] A platinum hydride and cationic platinum complexes were observed.

The reaction of a range of alkali earth and lanthanide decamethylmetallocenes under CO pressure was studied using HP-IR.[239] Monocarbonyl complexes were formed for all metals except barium and magnesium, and equilibrium constants were calculated.

Merbach is the undisputed leader with regard to the theory of ligand exchange processes of metal complexes under hydrostatic pressure. Water, solvent, and ligand exchange has been studied extensively for a range of transition metal complexes using ^{17}O, ^{1}H, ^{13}C, and multinuclear HP-NMR.[240] The kinetics and mechanisms of the exchange processes, *cis–trans* isomerization, and the rotational dynamics of the ligands were investigated. In addition, a series of papers dealt with water exchange of Gd and Eu complexes suitable for use as magnetic resonance imaging (MRI) contrast agents. These, and a number of other HP-NMR studies of ligand exchange processes, are summarized in Table 5.

1.18.5 Other Applications

High pressure NMR and IR spectroscopy have been used for a variety of other applications, not strictly relevant to organometallic chemistry. However, a brief summary of some of these applications is given for completeness with some representative references (Table 6).

Table 6 Other applications of HP-NMR and HP-IR

Application	*Applications*	*References*
^{129}Xe High pressure MAS NMR	Heterogeneous catalysis, coke formation	280–282
	Pore analysis	
Conformational analysis	Proteins	283–285
	Organic molecules	286–288
Physical properties of systems	Gas solubilities and properties	289,290
	Solid-state gas analysis	291,292
Molecular dynamics	H-bonding, solvent interactions	293,294
Membrane chemistry	Diffusion	295,296

1.18.6 Summary

It is evident from the abundant literature in this area that high pressure NMR and IR spectroscopy are extremely valuable tools for scientists wishing to gain a better understanding of empirical experimental data. Continuing improvements in hardware and data manipulation techniques will further increase the usefulness and scope of the obtained data. While of interest to generic coordination chemistry studies, it is the use of such techniques for studies of homogeneous catalysis which demonstrates their true value. Coupled with other *in situ* analytical techniques and molecular modeling, they provide a powerful tool to explain the fundamental origins of observed catalyst behavior under process conditions. Although much fundamental information can be obtained, such information has many practical implications and these technologies are therefore being used as a standard tool in industry to assist with rational catalyst and process design.

References

1. Cornils, B.; Herrmann, W. A. *J. Catal.* **2003**, *216*, 23–31.
2. Horváth, I. T.; Millar, J. M. *Chem. Rev.* **1991**, *91*, 1339–1351.
3. Mann, B. E. NMR Spectroscopy in the Liquid and Gas Phase. *Spectroscopic Properties of Inorganic and Organometallic Compounds*; Royal Society of Chemistry, 2003; Vol. 36, pp 1–121.
4. Jonas, J. *NATO Sci. Ser., Ser. E* **1999**, *358*, 231–259.
5. Ballard, L.; Jonas, J. *Annu. Rep. NMR Spectrosc.* **1997**, *33*, 115–150.
6. Whyman, R. *Laboratory Methods in Vibrational Spectroscopy*; Willis, H. A., Van der Mass, J. H., Miller, J. G. J., Eds.; Wiley: New York, 1987.
7. Sherman, W. F. *Bull. Soc. Chim. Fr.* **1982**, *9–10*, 347–369.
8. Sherman, W. F. *J. Mol. Struct.* **1984**, *113*, 101–116.
9. Ryczkowski, J. *Catal. Today* **2001**, *68*, 263–381.
10. Meek, D. W.; Mazanec, T. J. *Acc. Chem. Res.* **1981**, *14*, 266–274.
11. Damoense, L.; Datt, M.; Green, M.; Steenkamp, C. *Coord. Chem. Rev.* **2004**, *248*, 2393–2407.
12. Whyman, R. *Chem. Tech.* **1991**, *21*, 414–419.
13. van Leeuwen, P. W. N. M. *Appl. Catal., A.* **2001**, *212*, 61–81.
14. Roe, D. C. *ACS Symp. Ser.* **1987**, *357*, 204–222.
15. Quin, L. D.; Verkade, J. G. *Phosphorus-31 NMR Spectral Properties in Compound Characterization and Structural Analysis*; VCH: New York, 1994; pp 201–252.
16. Dixon, K. R. *Multinuclear NMR*; Mason, J., Ed.; Plenum Press: New York, 1987; pp 369–402.
17. Rehder, D.; Goodfellow, R. J. *Multinuclear NMR*; Mason, J., Ed.; Plenum Press: New York, 1987; pp 479–590.
18. Friebolin, H. *Basic One- and Two-Dimensional NMR Spectroscopy*; VCH: Weinheim, 1993; pp 36–39.
19. Torrent, M.; Solà, M.; Frenking, G. *Chem. Rev.* **2000**, *100*, 439–493.
20. Benedek, G. B.; Purcell, E. M. *J. Chem. Phys.* **1954**, *22*, 2003.
21. Jonas, J. *Rev. Sci. Instrum.* **1972**, *43*, 643–646.
22. Earl, W. L.; Vanni, H.; Merbach, A. E. *J. Magn. Reson.* **1978**, *30*, 571–576.
23. Lee, S.-H.; Luszcynski, K.; Norberg, R. E.; Conradi, M. S. *Rev. Sci. Instrum.* **1987**, *58*, 415–417.
24. Bertani, R.; Mali, M.; Roos, J.; Brinkmann, D. *Rev. Sci. Instrum.* **1992**, *63*, 3303–3306.
25. Gordon, S.; Dailey, B. P. *J. Chem. Phys.* **1961**, *34*, 1084–1086.
26. Raynes, W. T.; Buckingham, A. D.; Bernstein, H. J. *J. Chem. Phys.* **1962**, *36*, 3481.
27. Jameson, A. K.; Jameson, C. J.; Gutowsky, H. S. *J. Chem. Phys.* **1970**, *53*, 2310.
28. Jameson, C. J.; Jameson, A. K.; Cohen, S. M. *J. Chem. Phys.* **1973**, *59*, 4540.
29. Vanni, H.; Earl, W. L.; Merbach, A. E. *J. Magn. Reson.* **1987**, *29*, 11.
30. Kinrade, S. D.; Swaddle, T. W. *J. Magn. Reson.* **1988**, *77*, 569.
31. Wallen, S. L.; Schoenbachler, L. K.; Dawson, E. D.; Blatchford, M. A. *Anal. Chem.* **2000**, *72*, 4230–4234.
32. Umecky, T.; Kanakubo, M.; Ikushima, Y.; Saito, N.; Yoshimura, J.; Yamazaki, H.; Yana, J. *Chem. Lett.* **2002**, *5*, 118–119.

33. Roe, D. C. *J. Magn. Reson.* **1985**, *63*, 388–391.
34. Horváth, I. T.; Ponce, E. C. *Rev. Sci. Instrum.* **1991**, *62*, 1104–1105.
35. Robert, J. M.; Evilia, R. F. *Anal. Chem.* **1988**, 2035–2040.
36. Roe, D. C. *Organometallics* **1987**, *6*, 942–946.
37. Yamada, H.; Nishikawa, K.; Honda, M.; Shimura, T.; Akasaka, K.; Tabayashi, K. *Rev. Sci. Instrum.* **2001**, *72*, 1463–1471.
38. Bai, S.; Taylor, C. M.; Mayne, C. L.; Pugmire, R. J.; Grant, D. M. *Rev. Sci. Instrum.* **1996**, *67*, 240–243.
39. Gaemers, S.; Luyten, H.; Ernsting, J. M.; Elsevier, C. J. *Magn. Reson. Chem.* **1999**, *37*, 25–30.
40. Heaton, B. T.; Jonas, J.; Eguchi, T.; Hoffman, G. A. *J. Chem. Soc., Chem. Commun.* **1981**, 331–332.
41. Heaton, B. T.; Strona, L.; Jonas, J.; Eguchi, T.; Hoffman, G. A. *J. Chem. Soc., Dalton Trans.* **1982**, 1159–1164.
42. Jonas, J.; Hasha, D. L.; Lamb, W. J.; Hoffmann, G. A.; Eguchi, T. *J. Magn. Res.* **1981**, *42*, 169–172.
43. van der Velde, D. G.; Jonas, J. *J. Magn. Reson.* **1987**, *71*, 480–483.
44. Rathke, J. W. *J. Magn. Reson.* **1989**, *85*, 150–152.
45. Rathke, J. W.; Klingler, R. J.; Krause, T. R. *Organometallics* **1991**, *10*, 1350–1355.
46. Rathke, J. W.; Klingler, R. J.; Gerald, R. E. II; Kramarz, K. W.; Woelk, K. *Prog. Nucl. Magn. Reson. Spectrosc.* **1997**, *30*, 209–253.
47. Iggo, J. A.; Shirley, D.; Tong, N. C. *New. J. Chem.* **1998**, 1043–1045.
48. Amita, F.; Oka, H.; Mukaide, M.; Urasaki, Y.; Takegoshi, K.; Terao, T.; Kajimoto, O. *Rev. Sci. Instrum.* **2004**, *75*, 467–471.
49. Castro, P.; Delsuc, M.-A. *Magn. Reson. Chem.* **1998**, *36*, 833–838.
50. Ballard, L.; Yu, A.; Reiner, C.; Jonas, J. *J. Magn. Reson.* **1998**, *133*, 190–193.
51. Favre, P.; Frei, U.; Marek, D.; Metz, F. *Eur. Pat. Appl.* EP 692719 A1, Jan 17, 1996.
52. Morris, D. E.; Tinker, H. B. *Rev. Sci. Instrum.* **1977**, *43*, 1024–1028.
53. Alemdaroglu, N. H.; Penninger, J. L. M.; Oltay, E. *J. Mol. Catal.* **1967**, *1*, 27–33.
54. Noack, K. *Spectrochim. Acta, Part A* **1968**, *24*, 1917.
55. Vidal, J. L.; Walker, W. E. *Inorg. Chem.* **1980**, *19*, 896.
56. Whyman, R.; Hunt, K. A.; Page, R. W.; Rigby, S. *J. Phys. E* **1984**, *17*, 559–561.
57. Rigby, W.; Whyman, R.; Wilding, K. *J. Phys. E* **1970**, *3*, 572–573.
58. Suppes, G. J.; McHugh, M. A. *Rev. Sci. Instrum.* **1989**, *60*, 666–669.
59. DiBenedetto, J. A.; Ryba, D. W.; Ford, P. C. *Inorg. Chem.* **1989**, *28*, 3503–3507.
60. Massick, S. M.; Buttner, T.; Ford, P. C. *Inorg. Chem.* **2003**, *42*, 575–580.
61. Hagen, J. *Chem. Labor Betr.* **1977**, *28*, 125–128.
62. Moser, W. R. *Adv. Chem. Ser.* **1992**, *230*, 3–18.
63. Moser, W. R.; Cnossen, J. E.; Wang, A. W.; Krouse, S. A. *J. Catal.* **1985**, *95*, 21–32.
64. Yokoyama, C.; Kanno, Y.; Takahashi, M.; Ohtake, K.; Takahashi, S. *Rev. Sci. Instrum.* **1993**, *64*, 1369–1370.
65. Roelen, O. Ger. Patent DE 849,548, 1938.
66. Sweany, R. L. Cobalt. In *Comprehensive Organometallic Chemistry II*; Abel, A. W., Stone, G. A., Wilkinson, G., Eds.; Elsevier, 1995; Vol. 8, pp 114.
67. Wender, I.; Pino, P. *Organic Syntheses via Metal Carbonyls*; Wiley: New York, 1977.
68. Falbe, J. *New Syntheses with Carbon Monoxide*; Springer-Verlag: Berlin, 1980.
69. Slaugh, L. H.; Mullineaux, R. D. *J. Organomet. Chem.* **1968**, *13*, 469–477.
70. Heck, R. F.; Breslow, D. S. *J. Am. Chem. Soc.* **1961**, *83*, 4023–4027.
71. Whyman, R. *J. Organomet. Chem.* **1974**, *81*, 97–106.
72. Whyman, R. *J. Chem. Soc., Chem. Commun.* **1970**, 1194–1195.
73. Alemdaroğlu, N. H.; Penninger, J. L. M.; Oltay, E. *Monatsh. Chem.* **1976**, *107*, 1153–1165.
74. Mirbach, M. F. *J. Organomet. Chem.* **1984**, *265*, 205–213.
75. Roe, D. C. *Organometallics* **1987**, *6*, 942–946.
76. Pino, P.; Major, A.; Spindler, F.; Tannenbaum, R.; Bor, G.; Horváth, I. T. *J. Organomet. Chem.* **1991**, *417*, 65–76.
77. Pretzer, W. R.; Kobylinski, T. P. *Ann. N. Y. Acad. Sci.* **1980**, *333*, 58–66.
78. Mirbach, M. F. *Transition Met. Chem.* **1984**, *9*, 465–468.
79. Mirbach, M. F. *Inorg. Chim. Acta* **1984**, *88*, 209–211.
80. Tannenbaum, R.; Bor, G. *Inorg. Chim. Acta* **1992**, *201*, 87–93.
81. Tannenbaum, R.; Bor, G. *J. Mol. Catal. A* **2004**, *215*, 33–43.
82. Ojima, I.; Okabe, M.; Kato, K.; Kwon, H. B.; Horváth, I. T. *J. Am. Chem. Soc.* **1988**, *110*, 150–157.
83. Rathke, J. W.; Klingler, R. J.; Krause, T. R. *Organometallics* **1992**, *11*, 585–588.
84. Klingler, R. J.; Rathke, J. W. *J. Am. Chem. Soc.* **1994**, *116*, 4772–4785.
85. Pino, P. *Ann. N. Y. Acad. Sci.* **1983**, *415*, 111–128.
86. Rathke, J. W.; Kramarz, K. W.; Klingler, R. J.; Chen, M. J.; Fremgen, D. E.; Gerald, R. E. II *Trends Organomet. Chem.* **1999**, *3*, 201–209.
87. Slaugh, L. H.; Mullineaux, R. D. *J. Organomet. Chem.* **1968**, *13*, 469–477.
88. Whyman, R. *J. Chem. Soc., Dalton Trans.* **1972**, 1375–1381.
89. van Boven, M.; Alemdaroğlu, N. H.; Penninger, J. L. M. *J. Organomet. Chem.* **1975**, *84*, 65–74.
90. Kramarz, K. W.; Klingler, R. J.; Fremgen, D. E.; Rathke, J. W. *Catal. Today* **1999**, *49*, 339–352.
91. Massick, S. M.; Rabor, J. G.; Elbers, S; Marhenke, J; Bernhard, S; Schoonover, J. R.; Ford, P. C. *Inorg. Chem.* **2000**, *39*, 3098–3106.
92. Chen, M. J.; Klingler, R. J.; Rathke, J. W.; Kramarz, K. W. *Organometallics* **2004**, *23*, 2701–2707.
93. Mason, R. F.; van Winkle, J. L. U.S. Patent US 3,400,163, 1968.
94. Steynberg, J. P.; Govender, K.; Steynberg, P. J. WO Patent 014248, 2002.
95. Dwyer, C. L.; Assumption, H.; Coetzee, J.; Crause, C.; Damoense, L.; Kirk, M. *Coord. Chem. Rev.* **2004**, *248*, 653–669.
96. Polas, A.; Wilton-Ely, J. D. E. T.; Slawin, A. M. Z.; Foster, D. F.; Steynberg, P. J.; Green, M. J.; Cole-Hamilton, D. J. *J. Chem. Soc., Dalton Trans.* **2004**, 4669–4677.
97. Crause, C.; Bennie, L.; Damoense, L.; Dwyer, C. L.; Grove, C.; Grimmer, N.; Janse van Rensburg, W.; Kirk, M. M.; Mokheseng, K. M., Otto, S., *et al. J. Chem. Soc., Dalton Trans.* **2003**, 2036–2042.
98. van Leeuwen, P. W. M. N.; Claver, C. Rhodium Catalyzed Hydroformylation. In *Catalysis By Metal Complexes*; James, B. R., van Leeuwen, P. W. M. N., Eds.; Kluwer Dordrecht, 2000; Vol. 22.

99. Pruett, R. L. *Adv. Organomet. Chem.* **1979**, *17*, 1–60.
100. Cornils, B. In *New Syntheses with Carbon Monoxide*; Falbe, J., Ed.; Springer-Verlag: Berlin, 1980; pp 1–225.
101. Roth, J. F.; Craddock, J. H.; Hershman, A.; Paulik, F. E. *Chem. Technol.* **1971**, 600.
102. Hughes, R. P. Rhodium. In *Comprehensive Organometallic Chemistry I*; Wilkinson, G., Stone, G. A., Abel, E. W., Eds.; Pergamon: Oxford, 1982; pp 277–540.
103. Sharp, P. R. Rhodium. In *Comprehensive Organometallic Chemistry II*; Abel, A. W., Stone, G. A., Wilkinson, G., Eds.; Elsevier: Oxford, 1995; Vol. 8, pp 115–302.
104. Vidal, J. L.; Schoening, R. C.; Walker, W. E. *ACS Symp. Ser.* **1981**, *155*, 61–83.
105. Vidal, J. L.; Walker, W. E. *Inorg. Chem.* **1980**, *19*, 896–903.
106. Vidal, J. L.; Walker, W. E. *Inorg. Chem.* **1981**, *20*, 249–254.
107. King, R. B.; King, A. D., Jr.,; Iqbal, M. Z.; Tanaka, K. *Ann. N. Y. Acad. Sci.* **1980**, *333*, 74–79.
108. Heaton, B. T.; Jonas, J.; Eguchi, T.; Hoffman, G. A. *J. Chem. Soc., Chem. Commun.* **1981**, 331–332.
109. Liu, G.; Volken, R.; Garland, M. *Organometallics* **1999**, *18*, 3429–3436.
110. Liu, G.; Garland, M. *Organometallics* **1999**, *18*, 3457–3467.
111. Liu, G.; Garland, M. *J. Organomet. Chem.* **2000**, *608*, 76–85.
112. Feng, J.; Garland, M. *Organometallics* **1999**, *18*, 1542–1546.
113. Liu, G.; Garland, M. *J. Organomet. Chem.* **2000**, *613*, 124–127.
114. Li, C.; Guo, L.; Garland, M. *Organometallics* **2004**, *23*, 2201–2204.
115. Feng, J.; Garland, M. *Organometallics* **1999**, *18*, 417–427.
116. Howard, M. J.; Jones, M. D.; Roberts, M. S.; Taylor, S. A. *Catal. Today* **1993**, *18*, 325.
117. Dekleva, T. W.; Forster, D. *J. Am. Chem. Soc.* **1985**, *107*, 3565–3567.
118. Maitlis, P. M.; Haynes, A.; Sunley, G. J.; Howard, M. J. *J. Chem. Soc., Dalton Trans.* **1996**, 2187–2196.
119. Fontaine, M.; Castanet, Y.; Mortreux, A.; Petit, F. *J. Catal.* **1997**, *167*, 324–336.
120. Evans, D.; Osborn, J. A.; Wilkinson, G. *J. Chem. Soc. (A)* **1968**, 3133–3134.
121. Morris, D. E.; Tinker, H. B. *Chem. Tech.* **1972**, 554–559.
122. Moser, W. R.; Papite, C. J.; Brannon, D. A.; Duwell, R. A.; Weininger, S. J. *J. Mol. Catal.* **1987**, *41*, 271–292.
123. Diéguez, M.; Claver, C.; Masdeu-Bultó, A. M.; Ruiz, A.; van Leeuwen, P. W. M. N.; Schoemaker, G. C. *Organometallics* **1999**, *18*, 2107–2115.
124. Bianchini, C.; Lee, H. M.; Meli, A.; Vizza, F. *Organometallics* **2000**, *19*, 849–853.
125. Caporali, M.; Frediani, P.; Salvini, A.; Laurenczy, G. *Inorg. Chim. Acta* **2004**, *357*, 4537–4543.
126. Walczuk, E. B.; Kamer, P. C. J.; van Leeuwen, P. W. N. M. *Angew. Chem., Int. Ed.* **2003**, *42*, 4665–4669.
127. Zhang, J.; Poliakoff, M.; George, M. W. *Organometallics* **2003**, *22*, 1612–1618.
128. Payne, M. J.; Cole-Hamilton, D. J. *J. Chem. Soc., Dalton Trans.* **1997**, 3167–3175.
129. Monflier, E.; Bricout, H.; Hapiot, F.; Tilloy, S.; Aghmiz, A.; Masdeu-Bulto, A. M. *Adv. Synth. Catal.* **2004**, *346*, 425–431.
130. Horvath, I. T.; Kastrup, R. V.; Oswald, A. A.; Mozeleski, E. J. *Catal. Lett.* **1989**, *2*, 85–90.
131. Yonker, C. R.; Linehan, J. C. *J. Organomet. Chem.* **2002**, *650*, 249–257.
132. Horvath, I. T.; Kiss, G.; Cook, R. A.; Bond, J. E.; Stevens, P. A.; Rabai, J.; Mozeleski, E. J. *J. Am. Chem. Soc.* **1998**, *120*, 3133–3143.
133. Haji, S.; Erkey, C. *Tetrahedron* **2002**, *58*, 3929–3941.
134. Freixa, Z.; van Leeuwen, P. W. N. M. *J. Chem. Soc., Dalton Trans.* **2003**, 1890–1901.
135. Casey, C. P.; Whiteker, G. T.; Melville, M. G.; Petrovich, L. M.; Gavney, J. A.; Powell, D. R. *J. Am. Chem. Soc.* **1992**, *114*, 5535–5543.
136. Casey, C. P.; Whiteker, G. T. *Isr. J. Chem.* **1990**, *30*, 299–304.
137. van der Veen, L. A.; Keeven, P. H.; Schoemaker, G. C.; Reek, J. N. H.; Kamer, P. C. J.; van Leeuwen, P. W. N. M.; Lutz, M.; Spek, A. L. *Organometallics* **2000**, *19*, 872–883.
138. van der Veen, L. A.; Boele, M. D. K.; Bregman, F. R.; Kamer, P. C. J.; van Leeuwen, P. W. N. M.; Goubitz, K.; Fraanje, J.; Schenk, H.; Bo, C. *J. Am. Chem. Soc.* **1998**, *120*, 11616–11626.
139. Bronger, R. P. J.; Kamer, P. C. J.; van Leeuwen, P. W. N. M. *Organometallics* **2003**, *22*, 5358–5369.
140. van der Veen, L. A.; Kamer, P. C. J.; van Leeuwen, P. W. N. M. *Organometallics* **1999**, *18*, 4765–4777.
141. Bregman, F. R.; Ernsting, J. M.; Muller, F.; Boele, M. D. K.; van der Veen, L. A.; Elsevier, C. J. *J. Organomet. Chem.* **1999**, *592*, 306–311.
142. Schreuder, G. M.; Kamer, P. C. J.; van Leeuwen, P. W. N. M. *J. Mol. Catal. A* **1998**, *134*, 243–249.
143. Silva, S. M.; Bronger, R. P. J.; Freixa, Z.; Dupont, J.; van Leeuwen, P. W. N. M. *New J. Chem.* **2003**, *27*, 1294–1296.
144. Nettekoven, U.; Kamer, P. C. J.; Widhalm, M.; van Leeuwen, P. W. N. M. *Organometallics* **2000**, *19*, 4596–4607.
145. del Rio, I.; de Lange, W. G. J.; van Leeuwen, P. W. N. M.; Claver, C. *J. Chem. Soc., Dalton Trans.* **2001**, 1293–1300.
146. del Rio, I.; Pamies, O.; van Leeuwen, P. W. N. M.; Claver, C. *J. Organomet. Chem.* **2000**, *608*, 115–121.
147. Castellanos-Páez, A.; Castillón, S.; Claver, C.; van Leeuwen, P. W. N. M.; de Lange, W. G. J. *Organometallics* **1998**, *17*, 2523–2552.
148. Nozaki, K.; Matsuo, T.; Shibahara, F.; Hiyama, T. *Organometallics* **2003**, *22*, 594–600.
149. Brown, D. T.; Eguchi, T.; Heaton, B. T.; Iggo, J. A.; Whyman, R. *J. Chem. Soc., Dalton Trans.* **1991**, 677–683.
150. Crous, R.; Datt, M.; Foster, D.; Bennie, L.; Steenkamp, C.; Huyser, J.; Kirsten, L.; Steyl, G.; Roodt, A. *J. Chem. Soc., Dalton Trans.* **2005**, 1108–1116.
151. Polo, A.; Real, J.; Claver, C.; Castillón, S.; Bayón, J. C. *J. Chem. Soc., Chem. Commun.* **1990**, 600–601.
152. Jongsma, T.; Challa, G.; van Leeuwen, P. W. N. M. *J. Organomet. Chem.* **1991**, *421*, 121–128.
153. van Rooy, A.; Orij, E. N.; Kamer, P. C. J.; van Leeuwen, P. W. N. M. *Organometallics* **1995**, *14*, 34–43.
154. Kamer, P. C. J.; van Rooy, A.; Schoemaker, G. C.; van Leeuwen, P. W. N. M. *Coord. Chem. Rev.* **2004**, *248*, 2409–2424.
155. Fornies-Camer, J.; Masdeu-Bulto, A. M.; Claver, C.; Tejel, C.; Ciriano, M. A.; Cardin, C. J. *Organometallics* **2002**, *21*, 2609–2618.
156. Casado, M. A.; Perez-Torrente, J. J.; Ciriano, M. A.; Oro, L. A.; Orejon, A.; Claver, C. *Organometallics* **1999**, *18*, 3035–3044.
157. Whyman, R.; Gilhooley, K.; Rigby, S.; Winstanley, D. *ACS Symp. Ser.* **1987**, *328*, 108–124.
158. van Rooy, A.; Kamer, P. C. J.; van Leeuwen, P. W. N. M.; Goubitz, K.; Fraanje, J.; Veldman, N.; Spek, A. L. *Organometallics* **1996**, *16*, 835–847.
159. Buisman, G. J. H.; van der Veen, L. A.; Kamer, P. C. J.; van Leeuwen, P. W. N. M. *Organometallics* **1997**, *16*, 5681–5687.
160. van Rooy, A.; Kamer, P. C. J.; van Leeuwen, P. W. N. M. *J. Organomet. Chem.* **1997**, *535*, 201–207.
161. Dieguez, M.; Pamies, O.; Ruiz, A.; Claver, C. *New. J. Chem.* **2002**, *26*, 827–833.
162. Uriz, P.; Fernandez, E.; Ruiz, N.; Claver, C. *Inorg. Chem. Commun.* **2000**, *3*, 515–519.

163. Deerenberg, S.; Kamer, P. C. J.; van Leeuwen, P. W. N. M. *Organometallics* **2000**, *19*, 2065–2072.
164. van der Vlugt, J. I.; Sablong, R.; Magusin, P. C. M. M.; Mills, A. M.; Spek, A. L.; Vogt, D. *Organometallics* **2004**, *23*, 3177–3183.
165. van der Slot, S. C.; Kamer, P. C. J.; van Leeuwen, P. W. N. M.; Fraanje, J.; Goubitz, K.; Lutz, M.; Spek, A. L. *Organometallics* **2000**, *19*, 2504–2515.
166. van der Slot, S. C.; Kamer, P. C. J.; van Leeuwen, P. W. N. M.; Iggo, J. A.; Heaton, B. T. *Organometallics* **2001**, *20*, 430–441.
167. van Rooy, A.; Burgers, D.; Kamer, P. C. J.; van Leeuwen, P. W. N. M. *Recl. Trav. Chim. Pays-Bas* **1996**, *115*, 492–498.
168. van der Slot, S. C.; Duran, J.; Luten, J.; Kamer, P. C. J.; van Leeuwen, P. W. N. M. *Organometallics* **2002**, *21*, 3873–3883.
169. Bianchini, C.; Frediani, P.; Meli, A.; Peruzzini, M.; Vizza, F. *Chem. Ber. Recl.* **1997**, *130*, 1633–1641.
170. Carter, R. D.; Howell, D. K.; Peng, W.-J.; Train, S. G.; Treleaven, W. D.; Stanley, G. G. *Angew. Chem., Int. Ed.* **1996**, *35*, 2253–2256.
171. Poyatos, M.; Uriz, P.; Mata, J. A.; Claver, C.; Fernandez, E.; Peris, E. *Organometallics* **2003**, *22*, 440–444.
172. Barbaro, P; Bianchini, C.; Meli, A.; Moreno, M.; Vizza, F. *Organometallics* **2002**, *21*, 1430–1437.
173. Bianchini, C.; Barbaro, P.; Macehi, M.; Meli, A.; Vizza, F. *Helv. Chim. Acta* **2001**, *84*, 2895–2923.
174. Ball, G. E.; Cullen, W. R.; Fryzuk, M. D.; Henderson, W. J.; James, B. R.; MacFarlane, K. S. *Inorg. Chem.* **1994**, *33*, 1464–1468.
175. Zhang, J.; Sun, X.-Z.; Poliakoff, M.; George, M. W. *J. Organomet. Chem.* **2003**, *678*, 128–133.
176. Bianchini, C.; Meli, A.; Patinec, V.; Sernau, V.; Vizza, F. *J. Am. Chem. Soc.* **1997**, *119*, 4945–4954.
177. Bakos, J.; Orosz, A.; Cserepi, S.; Toth, I.; Sinou, D. *J. Mol. Catal. A* **1997**, *116*, 85–97.
178. Wittmann, K.; Wisniewski, W.; Mynott, R.; Leitner, W.; Kranemann, C. L.; Rische, T.; Eilbracht, P.; Kluwer, S.; Ernsting, J. M.; Elsevier, C. J. *Chem. Eur. J.* **2001**, *7*, 4584–4589.
179. Leigh, J. G.; Richards, R. L. Iridium. In *Comprehensive Organometallic Chemistry I*; Wilkinson, G., Stone, F. G. A., Abel, E. W., Eds.; Pergamon: Oxford, 1982; Vol. 5, pp 541–628.
180. Atwood, J. D. Iridium. In *Comprehensive Organometallic Chemistry II*; Abel, A. W., Stone, F. G. A., Wilkinson, G., Eds.; Elsevier: Oxford, 1995; Vol. 8, pp 303–417.
181. Bianchini, C.; Barbaro, P.; Scapacci, G.; Farnetti, E.; Graziani, M. *Organometallics* **1998**, *17*, 3308–3310.
182. Kainz, S.; Brinkmann, A.; Leitner, W.; Pfaltz, A. *J. Am. Chem. Soc.* **1999**, *121*, 6421–6429.
183. Bianchini, C.; Moneti, S.; Peruzzini, M.; Vizza, F. *Inorg. Chem.* **1997**, *36*, 5818–5825.
184. Bianchini, C.; Meli, A.; Sanchez-Delgado, R. A. *ACS Symp. Ser.* **1996**, *653*, 187–196.
185. Whyman, R. *J. Organomet. Chem.* **1975**, *94*, 303–309.
186. Malatesta, L.; Angoletta, M.; Conti, F. *J. Organomet. Chem.* **1971**, *33*, C33.
187. Churlaud, R.; Frey, U.; Metz, F.; Merbach, A. E. *Inorg. Chem.* **2000**, *39*, 4137–4142.
188. Churlaud, R.; Frey, U.; Metz, F.; Merbach, A. E. *Inorg. Chem.* **2000**, *39*, 304.
189. Forster, D. *J. Chem. Soc., Dalton Trans.* **1979**, 1639.
190. Forster, D.; Hershman, A.; Morris, D. E. *Catal. Rev. – Sci. Eng.* **1981**, *23*, 89–105.
191. Sunley, G. J.; Watson, D. J. *Catal. Today* **2000**, *58*, 293–307.
192. Jones, J. H. *Platinum Met. Rev.* **2000**, *44*, 94.
193. Ghaffar, T.; Adams, H.; Maitlis, P. M.; Haynes, A.; Sunley, G. J.; Baker, M. J. *Chem. Commun.* **1998**, 1023–1024.
194. Haynes, A.; Maitlis, P. M.; Morris, G. E.; Sunley, G. J.; Adams, H.; Badger, P. W.; Bowers, C. M.; Cook, D. B.; Elliott, P. I. P., Ghaffar, T. *et al. J. Am. Chem. Soc.* **2004**, *126*, 2847–2861.
195. Jolly, P. W. Nickel Catalyzed Carbonylation and Related Reactions. In *Comprehensive Organometallic Chemistry I*; Wilkinson, G., Stone, F. G. A., Abel, E. W., Eds.; Pergamon: Oxford, 1982; Vol. 8, pp 799–938.
196. Jolly, P. W. Nickel Tetracarbonyl and Lewis-base Nickel Carbonyl Compounds. In *Comprehensive Organometallic Chemistry I*; Wilkinson, G., Stone, F. G. A., Abel, E. W., Eds.; Pergamon: Oxford, 1982; Vol. 6, pp 3–36.
197. Beattie, J. K.; Hambley, T. W.; Masters, A. F.; Meyer, J. T. *Inorg. Chim. Acta* **1993**, *213*, 49–55.
198. Moser, W. R.; Marshik-Guerts, B. J.; Okrasinski, S. J. *J. Mol. Catal. A* **1999**, *143*, 57–69.
199. Moser, W. R.; Marshik-Guerts, B. J.; Okrasinski, S. J. *J. Mol. Catal. A* **1999**, *143*, 71–83.
200. Rizkala, N. *ACS Symp. Ser.* **1987**, *328*, 61.
201. Trost, B. M.; Verhoeven, T. R. Organopalladium Compounds in Organic Synthesis and Catalysis. In *Comprehensive Organometallic Chemistry I*; Wilkinson, G., Stone, F. G. A., Abel, E. W., Eds.; Pergamon: Oxford, 1982; Vol. 8, pp 799–938.
202. Drent, E.; Budzelaar, P. H. M. *Chem. Rev.* **1996**, *96*, 663–681.
203. Dekker, G. P. C. M.; Elsevier, C. J.; Vrieze, K.; van Leeuwen, P. W. N. M. *Organometallics* **1992**, *11*, 1598–1603.
204. Sanger, A. R. *J. Chem. Soc., Dalton Trans.* **1979**, 1971–1972.
205. Toth, I.; Elsevier, C. J. *J. Am. Chem. Soc.* **1993**, *115*, 10388–10389.
206. Pelagatti, P.; Bacchi, A.; Carcelli, M.; Costa, M.; Fruhauf, H.-W.; Goubitz, K.; Pelizzi, C.; Triclistri, M.; Vrieze, K. *Eur. J. Inorg. Chem.* **2002**, 439–446.
207. Markies, B. A.; Wijkens, P.; Dedieu, A.; Boersma, J.; Spek, A. L.; van Koten, G. *Organometallics* **1995**, *14*, 5628–5641.
208. Bianchini, C.; Meli, A.; Oberhauser, W. *J. Chem. Soc., Dalton Trans.* **2003**, 2627–2635.
209. Bianchini, C.; Lee, H. M.; Meli, A.; Moneti, S.; Vizza, F.; Fontani, M.; Zanello, P. *Macromolecules* **1999**, *32*, 4183–4193.
210. Bianchini, C.; Lee, H. M.; Barbaro, P.; Meli, A.; Moneti, S.; Vizza, F. *New J. Chem.* **1999**, *23*, 929–938.
211. Bianchini, C.; Lee, H. M.; Meli, A.; Moneti, S.; Patinec, V.; Petrucci, G.; Vizza, F. *Macromolecules* **1999**, *32*, 3859–3866.
212. Bianchini, C.; Lee, H. M.; Meli, A.; Oberhauser, W.; Peruzzini, M.; Vizza, F. *Organometallics* **2002**, *21*, 16–33.
213. Bianchini, C.; Meli, A.; Mueller, G.; Oberhauser, W.; Passaglia, E. *Organometallics* **2002**, *21*, 4965–4977.
214. Luo, H.-K.; Kou, Y.; Wang, X.-W.; Li, D.-G. *J. Mol. Catal. A* **2000**, *151*, 91–113.
215. Nozaki, K.; Hiyama, T.; Kacker, S.; Horvath, I. T. *Organometallics* **2000**, *19*, 2031–2035.
216. Ojima, I.; Eguchi, M.; Tzamarioudaki, M. Transition Metal Hydrides: Hydrocarboxylation, Hydroformylation and Asymmetric Hydrogenation. In *Comprehensive Organometallic Chemistry II*; Abel, A. W., Stone, F. G. A., Wilkinson, G., Eds.; Elsevier: Oxford, 1995; Vol. 12, pp 9–38.
217. Bianchini, C.; Meli, A.; Oberhauser, W.; van Leeuwen, P. W. N. M.; Zuideveld, M. A.; Freixa, Z.; Kamer, P. C. J.; Spek, A. L.; Gusev, O. V.; Kal'sin, A. M. *Organometallics* **2003**, *22*, 2409–2421.
218. del Rio, I.; Claver, C.; van Leeuwen, P. W. N. M. *Eur. J. Inorg. Chem.* **2001**, 2719–2738.
219. Iggo, J. A.; Kawashima, Y.; Liu, J.; Hiyama, T.; Nozaki, K. *Organometallics* **2003**, *22*, 5418–5422.
220. Bianchini, C.; Mantovani, G.; Meli, A.; Oberhauser, W.; Bruggeller, P.; Stampfl, T. *J. Chem. Soc., Dalton Trans.* **2001**, 690–698.

221. Bearman, P. S.; Smith, A. K.; Tong, N. C.; Whyman, R. *Chem. Commun.* **1996**, 2061–2062.
222. Bianchini, C.; Meli, A.; Moneti, S.; Oberhauser, W.; Vizza, F.; Herrera, V.; Fuentes, A.; Sanchez-Delgado, R. A. *J. Am. Chem. Soc.* **1999**, *121*, 7071–7080.
223. Bianchini, C.; Barbaro, P.; Scapacci, G.; Zanobini, F. *Organometallics* **2000**, *19*, 2450–2461.
224. Liu, G.; Hakimifard, M.; Garland, M. *J. Mol. Catal. A* **2001**, *168*, 33–37.
225. Nicholls, J. N.; Farrar, D. H.; Jackson, P. F.; Johnson, B. F. G.; Lewis, J. *J. Chem. Soc., Dalton Trans.* **1982**, 1395–1400.
226. Laurenczy, G.; Faure, M.; Vieille-Petit, L.; Suss-Fink, G.; Ward, T. R. *Adv. Synth. Catal.* **2002**, *344*, 1073–1077.
227. Yin, C.; Xu, Z.; Yang, S.-Y.; Ng, S. M.; Wong, K. Y.; Lin, Z.; Lau, C. P. *Organometallics* **2001**, *20*, 1216–1222.
228. Buskens, P.; Giunta, D.; Leitner, W. *Inorg. Chim. Acta* **2004**, *357*, 1969–1974.
229. Cusanelli, A.; Frey, U.; Marek, D.; Merbach, A. E. *Spectrosc. Eur.* **1997**, *9*, 22.
229a. Cusanelli, A.; Frey, U.; Marek, D.; Merbach, A. E. *Spectrosc. Eur.* **1997**, *9*, 24.
229b. Cusanelli, A.; Frey, U.; Marek, D.; Merbach, A. E. *Spectrosc. Eur.* **1997**, *9*, 26–27.
230. Gonzalez, A. A.; Mukerjee, S. L.; Chou, S.-J.; Kai, Z.; Hoff, C. D. *J. Am. Chem. Soc.* **1988**, *110*, 4419–4421.
231. Millar, J. M.; Kastrup, R. V.; Melchior, M. T.; Horvath, I. T. *J. Am. Chem. Soc.* **1990**, *112*, 9643–9645.
232. Tacke, M.; Oskam, A.; Stufkens, D. J.; Teuben, J. H.; Luinstra, G. A.; de Wolf, J. M.; Tacke, C. *J. Mol. Struct.* **1997**, *408–409*, 499–505.
233. Ballintine, T. A.; Schmulbach, C. D. *J. Organomet. Chem.* **1978**, *164*, 381–390.
234. Massick, S. M.; Ford, P. C. *Organometallics* **1999**, *18*, 4362–4366.
235. Guzman-Jiminez, I. Y.; van Hal, J. W.; Whitmire, K. H. *Organometallics* **2003**, *22*, 1914–1922.
236. Childs, G. I.; Cooper, A. I.; Nolan, T. F.; Carrott, M. J.; George, M. W.; Poliakoff, M. *J. Am. Chem. Soc.* **2001**, *123*, 6857–6866.
237. Iqbal, M. Z. *Arab. J. Sci. Eng.* **1981**, *6*, 91–94.
238. Kegl, T.; Kollar, L.; Radics, L. *Inorg. Chim. Acta.* **1997**, *265*, 249–254.
239. Selg, P.; Brintzinger, H.; Schultz, M.; Andersen, R. A. *Organometallics* **2002**, *21*, 3100–3107.
240. Merbach, A. E. *NATO ASI Ser., Ser. C* **1987**, *197*, 311–331.
241. Bleuzen, A.; Pittet, P.-A.; Helm, L.; Merbach, A. E. *Magn. Reson. Chem.* **1997**, *35*, 765–773.
242. Dellavia, I.; Helm, L.; Merbach, A. E. *Inorg. Chem.* **1992**, *31*, 2230–2233.
243. Hugi, A. D.; Helm, L.; Merbach, A. E. *Inorg. Chem.* **1987**, *26*, 1763–1768.
244. Dellavia, I.; Helm, L.; Merbach, A. E. *Inorg. Chem.* **1992**, *31*, 4151–4154.
245. Dellavia, I.; Sauvageat, P. Y.; Helm, L.; Ducommun, Y.; Merbach, A. E. *Inorg. Chem.* **1992**, *31*, 792–797.
246. Hugi, A. D.; Helm, L.; Merbach, A. E. *Helv. Chim. Acta* **1985**, *68*, 508–521.
247. Ducommun, Y.; Zbinden, D.; Merbach, A. E. *Helv. Chim. Acta* **1982**, *65*, 1385–1390.
248. Vanni, H.; Merbach, A. E. *Inorg. Chem.* **1979**, *18*, 2758–2762.
249. Ducommun, Y.; Newman, K. E.; Merbach, A. E. *Helv. Chim. Acta* **1979**, *62*, 2511–2516.
250. Grundler, P. V.; Salignac, B.; Cayemittes, S.; Alberto, R.; Merbach, A. E. *Inorg. Chem.* **2004**, *43*, 865–873.
251. Schneppensieper, T.; Zahl, A.; van Eldik, R. *Angew. Chem., Int. Ed.* **2001**, *40*, 1678–1680.
252. Meyer, F. K.; Monnerat, A. R.; Newman, K. E.; Merbach, A. E. *Inorg. Chem.* **1982**, *21*, 774–778.
253. Cossy, C.; Helm, L.; Merbach, A. E. *Helv. Chim. Acta* **1987**, *70*, 1516–1525.
254. Rapaport, I.; Helm, L.; Merbach, A. E.; Bernhard, P.; Ludi, A. *Inorg. Chem.* **1988**, *27*, 873–879.
255. Monnerat, A.; Moore, P.; Newman, K. E.; Merbach, A. E. *Inorg. Chim. Acta* **1981**, *47*, 139–145.
256. Helm, L.; Meier, P.; Merbach, A. E.; Tregloan, P. A. *Inorg. Chim. Acta* **1983**, *73*, 1–9.
257. Pittet, P.-A.; Dadci, L.; Zbinden, P.; Abou-Hamdan, A.; Merbach, A. E. *Inorg. Chim. Acta* **1993**, *206*, 135–140.
258. Earl, W. L.; Meyer, F. K.; Merbach, A. E. *Inorg. Chim. Acta* **1977**, *25*, 91–92.
259. Ducommun, Y.; Earl, W. L.; Merbach, A. E. *Inorg. Chem.* **1979**, *18*, 2754–2758.
260. Frey, U.; Grove, D. M.; van Koten, G. *Inorg. Chim. Acta* **1998**, *269*, 322–325.
261. Helm, L.; Elding, L. I.; Merbach, A. E. *Helv. Chim. Acta* **1984**, *67*, 1453–1460.
262. Hallinan, N.; Besancon, V.; Forster, M.; Elbaze, G.; Ducommun, Y.; Merbach, A. E. *Inorg. Chem.* **1991**, *30*, 1112–1114.
263. Tubino, M.; Merbach, A. E. *Inorg. Chim. Acta* **1983**, *71*, 149–153.
264. Frey, U.; Helm, L.; Merbach, A. E.; Romeo, R. *J. Am. Chem. Soc.* **1989**, *111*, 8161–8165.
265. Ducommun, Y.; Helm, L.; Merbach, A. E.; Hellquist, B.; Elding, L. I. *Inorg. Chem.* **1989**, *28*, 377–379.
266. Powell, D. H.; Furrer, P.; Pittet, P.-A.; Merbach, A. E. *J. Phys. Chem.* **1995**, *99*, 16622–16629.
267. Hugi-Cleary, D.; Helm, L.; Merbach, A. E. *J. Am. Chem. Soc.* **1987**, *109*, 4444–4450.
268. Hugi-Cleary, D.; Helm, L.; Merbach, A. E. *Helv. Chim. Acta* **1985**, *68*, 545–554.
269. Ammann, C.; Moore, P.; Merbach, A. E.; McAteer, C. H. *Helv. Chim. Acta* **1980**, *63*, 268–276.
270. Knight, C. T. G.; Merbach, A. E. *Inorg. Chem.* **1985**, *24*, 576–581.
271. Kessler, J. E.; Knight, C. T. G.; Merbach, A. E. *Inorg. Chim. Acta* **1986**, *115*, 85–89.
272. Cossy, C.; Helm, L.; Merbach, A. E. *Inorg. Chem.* **1989**, *28*, 2699–2703.
273. Pisaniello, D. L.; Helm, L.; Meier, P.; Merbach, A. E. *J. Am. Chem. Soc.* **1983**, *105*, 4528–4536.
274. Ducommun, Y.; Helm, L.; Laurenczy, G.; Merbach, A. E. *Inorg. Chim. Acta* **1989**, *158*, 3–4.
275. Burai, L.; Toth, E.; Moreau, G.; Sour, A.; Scopelliti, R.; Merbach, A. E. *Chem. Eur. J.* **2003**, *9*, 1394–1404.
276. Toth, E.; Helm, L.; Kellar, K. E.; Merbach, A. E. *Chem. Eur. J.* **1999**, *5*, 1202–1211.
277. Toth, E.; Burai, L.; Brucher, E.; Merbach, A. E. *J. Chem. Soc., Dalton Trans.* **1997**, 1587–1594.
278. Powell, D. H.; Ni Dhubhghaill, O. M.; Pubanz, D.; Helm, L.; Lebedev, Y. S.; Schlaepfer, W.; Merbach, A. E. *J. Am. Chem. Soc.* **1996**, *118*, 9333–9346.
279. Toth, E.; Pubanz, D.; Vauthey, S.; Helm, L.; Merbach, A. E. *Chem. Eur. J.* **1996**, *2*, 1607–1615.
280. Miyoshi, T.; Takegoshi, K.; Terao, T. *Macromolecules* **2002**, *35*, 151–154.
281. Ueda, T.; Eguchi, T.; Nakamura, N.; Wasylishen, R. E. *J. Phys. Chem. B* **2003**, *107*, 180–185.
282. Ren, X.; Stapf, S.; Kuhn, H.; Demco, D. E.; Blumich, B. *Magn. Reson. Imaging* **2003**, *21*, 261–268.
283. Ballard, L.; Jonas, J. High-pressure NMR Spectroscopy of Proteins. In *Biological Systems Under Extreme Conditions*; Taniguchi, Y., Stanley, H. E., Ludwig, H., Eds.; Springer: Berlin, 2002; pp 75–100.
284. Akasaka, K. *Pure Appl. Chem.* **2003**, *75*, 927–936.
285. Akasaka, K.; Li, H.; Dubovskii, P.; Kalbitzer, H.-R.; Yamada, H. *NATO Sci. Ser. A* **2001**, 77–92.

286. Yamada, H.; Yonehara, S.; Tanaka, S.; Muro, F.; Watanabe, A.; Nishikawa, K. *J. Am. Chem. Soc.* **2001**, *123*, 279–284.
287. Campbell, D. M.; Mackowiak, M.; Jonas, J. *J. Chem. Phys.* **1992**, *96*, 2717–2723.
288. Imashiro, F.; Saika, A.; Yamada, H.; Sera, A. *Chem. Lett.* **1981**, 247–250.
289. Ohlin, C. A.; Dyson, P. J.; Laurenczy, G. *J. Chem. Soc., Chem. Commun.* **2004**, 1070–1071.
290. Helbk, M.; Hafskjold, B.; Dysthe, D. K.; Sorland, G. H. *J. Chem. Eng. Data* **1996**, *41*, 598–603.
291. van der Putten, D.; Prins, K. O.; Kortbeek, P. J.; Trappeniers, N. J. *J. Phys. C* **1987**, *20*, 3161–3173.
292. Nijman, A. J.; Trappeniers, N. J. *Physica B* **1978**, *95*, 147–162.
293. Vardag, T. M.; Luedemann, H. D. *Chem. Phys.* **1988**, *128*, 527–535.
294. Jonas, J. *Ber. Bunsen-Ges. Phys. Chem.* **1990**, *94*, 307–315.
295. Jayakody, J. R. P.; Stallworth, P. E.; Mananga, E. S.; Farrington-Zapata, J.; Greenbaum, S. G. *J. Phys. Chem. B* **2004**, *108*, 4260–4262.
296. Prosser, R. S.; Luchette, P. A.; Westerman, P. W.; Rozek, A.; Hancock, R. E. W. *Biophys. J.* **2001**, *80*, 1406–1416.

1.19
Kinetics Studies

R van Eldik and C D Hubbard, Universität Erlangen-Nürnberg, Erlangen, Germany

1.19.1 Introduction

Tremendous progress has been made in preparation of an abundance of organometallic compounds as attested to by the contents of journals dedicated to organometallic chemistry, and earlier versions of this series.[1,1a] Likewise, reactions of organometallic compounds are very widely described. The drive to understand reactions of organometallic compounds with the prospect of exploiting some of them for applications of industrial significance has led to considerable growth in mechanistic studies. Indeed, investigations of catalysis of important organic reactions by organometallic compounds are increasingly in evidence in chemical literature. The level of activity suggests that

many features of both catalytic and non-catalytic reactions of organometallic compounds are not yet fully understood. In fact, some processes involving activating particular bonds in organic molecules with a view of converting the substrate to other (more valuable) compounds have provided serious challenges in terms of success and comprehension. At an initial stage of understanding, many organometallic reactions can be divided into one of several classifications of mechanism. These mechanisms may be inferred from the nature of the starting reagents and a thorough characterization of the product(s), and in cases where intermediates can be detected or isolated, experimental analysis can be conducted. Additional mechanistic insight can sometimes be obtained by examining the consequences of changing the solvent, varying the temperature, varying a substituent, or other pertinent experimental parameters. In other subfields of chemistry, a most comprehensive profile of the overall mechanism can be established when interpretation of results of a complete kinetics investigation is added to the understanding brought about by other findings. Organometallic reaction mechanisms are no different, although it is recognized that many reactions are multistep, are not stoichiometrically simple or clean, and several products can ensue. Nevertheless, in suitable cases, a well-designed kinetics investigation can be of inestimable value to an understanding of the mechanism. This, in turn, can lead to modifying or tuning the system to deliver a more favorable yield and possibly more quickly, with a more desired product(s) outcome, and with potential economic benefit.

In this contribution, kinetics studies of organometallic reactions with the general objectives cited above will be highlighted. The methods and techniques normally involved in these investigations will be described briefly. Many of the methods are the same or similar to those applied in kinetics studies of organic, inorganic, or bioinorganic reactions. A few, perhaps less widely known, techniques will be emphasized. Following this section, examples from the organometallic literature will be provided. The massive volume of organometallic chemistry reported per annum means that the reactions whose kinetics have been examined and described here will necessarily be a selection, and compounds involving all metals in organometallic chemistry cannot be included. An approach that would represent a traditional way of covering organometallic mechanisms will not be adopted. Reactions reported recently, grouped, when possible, by the metal involved, will be presented. This does not imply that a classification according to substitution and insertion, oxidative addition and reductive elimination, intramolecular exchanges and isomerizations, and homogeneous catalysis of organic reactions by transition metal complexes would not be employed in a more comprehensive report. Perforce, the choice of reactions for inclusion is subjective and carries no connotation that reactions not described are unimportant. Progress in insight from theoretical treatment of organometallic reaction mechanisms will be introduced.

1.19.2 Kinetics: Background

1.19.2.1 Theory

Chemical kinetics are the subject matter of several books and of sections of standard works of physical chemistry.[2,3] Monographs that are specifically concerned with inorganic and organometallic kinetics and mechanisms have appeared.[4–7]In addition, for many years, a series devoted to a periodic updating of reports on the kinetics and mechanisms of inorganic and organometallic reactions also appeared.[8] Hence, the topic of kinetics itself, the development of rate equations, and their analysis and interpretation will not, in general, be treated further. There will be a necessity in cases of certain variables in kinetics investigations to elaborate further. This contribution will be focusing mostly, but not exclusively, on homogeneous reactions in liquid solutions, and where gases are involved, these are introduced into the liquid phase. Some time will be devoted to relevant reactions in supercritical fluids (SCFs). Parameters that can be derived from experimental kinetics results are those customarily obtained from application of transition state theory.

1.19.2.2 Experimental Variables

Experimental variables that may be applied in kinetics studies in organometallic chemistry would be concentrations of reactants, solvent, or solvent mixture (changing the dielectric constant), temperature, and, in some instances, hydrostatic pressure. In the case of solvent change, the theory of Kirkwood can be considered,[9] and variation of temperature can be treated employing the Eyring equation.[10] A separate brief account of the value and significance of employing the pressure variable will be provided. When an aqueous medium is employed, and ionic species are reactants or are thought to be involved in the rate-determining step, variation of the ionic strength can be informative. In many cases the ionic strength may exceed the level for which Debye–Hückel theory is applicable.[11,11a] Therefore,

use of the Brønsted–Bjerrum equation would not be permitted.[12] In systems in aqueous media where ionizable groups are present in reactants, a standard pH-dependence study can be conducted to reveal their pK_a values, and ascertain their importance in terms of the overall kinetics profile and mechanism. When the reactants allow appropriate systematic substitution, kinetics measurements of a related series of reactions can be treated according to a relevant graphical treatment on the basis of an implied linear free energy relationship (LFER). However, a particular LFER can be applied only when the reacting system mirrors precisely the system upon which substituent constants were derived. An indication of the nature of the transition state may be inferred from a proper application of the LFER approach. In appropriate cases substitution of different isotopes of elements from those present in reactants or solvent can be carried out. This may illustrate, from an analysis of the kinetics results, which particular bond(s) is (are) broken during the reaction, or, in the case of deuterium oxide for protium oxide solvent substitution, whether or not proton transfer is involved in the rate-determining and/or a pre-equilibrium step. However, use of these straightforward principles and relationships and experimental variations may often be thwarted by complexities of the reaction system; these can include incomplete reactions, multistep reactions, pre-equilibrium reactions, additional side-reactions, and other processes that preclude a straightforward analysis of results.

The consequences of using elevated pressures in kinetics investigations of solution reactions can be treated by an extension of the thermodynamic parameters relevant to equilibria, that is, by using transition state theory.[10] Prior to the development of the latter, a theory of the effect of hydrostatic pressure on reaction rates had been formulated at the beginning of the last century.[13] Relatively few investigators possess the facilities to conduct experiments at high hydrostatic pressures. Hence, there is less general familiarity with the relevant theory and the experimental practice. Hence, a few facts are supplied here[14] and later in the following section. If a reaction is characterized by a rate constant k at ambient pressure and by k_p at various elevated pressures p, then the relationship between them is given by $\ln k_p = \ln k_0 - (\Delta V^{\neq}/RT)\cdot p$, where k_0 is the rate constant at zero pressure, but for all intents and purposes is the same as the rate constant at ambient pressure, a pressure of 0.1 MPa (a pressure of 1 bar $= 10^5$ pascal (Pa)), since the effect of hydrostatic pressure on reaction rate constants is not very pronounced. In this equation, T is the absolute temperature, R is the ideal gas constant, and $\Delta V^{\neq}$ is the volume of activation. The latter is the difference between the partial molar volumes of the transition state and the reactant state. Thus, if the rate constant has been acquired over a range of pressure, a plot of $\ln k_p$ versus p, if linear, can yield the volume of activation, which will be negative for a reaction accelerated by pressure and positive for a reaction that is retarded by pressure. The pressure range needed to access this parameter successfully and with reasonable precision is generally up to 150 MPa. Particularly, if the solvent is water, there is rarely any detection of curvature in such plots, meaning that the volume of activation is independent of pressure. The effect of pressure on solvent properties, besides the effect on reaction kinetics, is more likely to manifest itself in non-aqueous solvents and at pressures beyond the range cited above.[15,16] These aspects and the treatment of systems, where the volume of activation depends on pressure, have been dealt with thoroughly in other sources and are not of great pertinence here.[16–18] The meaning and interpretation of volumes of activation will be treated together with other derived parameters in the sections below. However, although the volume of activation can be a very valuable diagnostic indicator of mechanism, the fact that it is in most cases composed of two contributions, interpretation is not always unequivocal. One contribution relates to changes in volume that arise as a consequence of bond-breaking or bond-making steps as the transition state is reached. Such changes and any others associated with volume changes of the reacting molecules or ions themselves are known as intrinsic volume changes. A second and often significant contribution is that arising from volume changes caused by solvation changes; these arise particularly when charge is increased or decreased in passage from the reactant to the transition state. The nature of the products will be indicative of the possible charged nature or not of the activated complex in the transition state. An increase in solvation by a developing charge species is termed an electrostriction increase and a loss of electrostriction occurs upon charge neutralization or reduction. Hence,

$$\Delta V^{\neq} = \Delta V^{\neq}{}_{\text{intr}} + \Delta V^{\neq}{}_{\text{solv}} \tag{1}$$

It is possible that the two contributions could be unequal or equal and opposite in sign, so that an overall value can mask the two contributions. Consequently, except for reactions such as solvent exchange, where there is no net reaction and the solvation component is essentially zero, each case for which $\Delta V^{\neq}$ is obtained must be treated individually and on its own merits. If a reacting system has a moderate driving force and hence reaches an equilibrium position, it may be possible to determine the equilibrium constant as a function of temperature and pressure yielding ΔG, ΔH, ΔS, and $\Delta V_{(\text{reaction})}$. Knowledge of these parameters complements the characterization of the system obtained from kinetics investigations. The last parameter may be obtained also from determining the volume of activation for a reaction in both

directions, since $\Delta V_{(\text{reaction})} = \Delta V^{\neq}_{(\text{forward})} - \Delta V^{\neq}_{(\text{reverse})}$. Typical values of volumes of activation for organic, organometallic, inorganic, and bioinorganic reactions can be viewed in extensive compilations.[19–21]

In some organometallic reactions, pressures of gases (usually in a much lower range of pressure than the range for kinetic studies at various hydrostatic pressures) are varied so that upon introduction to a reacting system, the potential for different reaction yields and mechanisms can be explored.[22]

1.19.3 Kinetics: Experimental Aspects

1.19.3.1 General and Practical Considerations

Methods and techniques for following the kinetics of reactions in solution have been presented in a wide variety of sources. For reactions at ambient pressure, and at temperatures at, or close to, ambient, and of convenient half-lives (for example, $t_{1/2} > 10$ min), the only limitation would be the lack of a suitable property of reactant or product for monitoring a concentration change. In almost all cases, the concentration is monitored through the means of a physical property linearly related to concentration, rather than by aliquot sampling, and if necessary, quenching the reaction, and chemical analysis to determine concentration of a reactant or product. For pressures other than ambient, special methods are required; these have been described.[15,16,23–25] The most enduring of devices of those presented for use in conventional time-range chemical kinetics at elevated pressures is the pillbox cell.[26] This can be fitted into a pressurizable housing in the cell compartment of a spectrophotometer. The pressurizing system is a standard array of high-pressure valves and a high-pressure pump system. The pillbox housing and hence the pillbox contents can be thermostatted (see Figures 1 and 2). The filling and operating techniques have been described elsewhere.[16,26] The

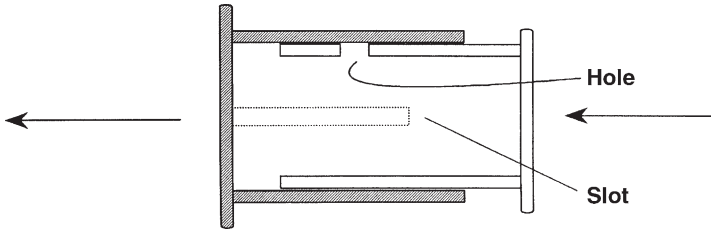

Figure 1 Schematic presentation of a ''pillbox'' optical cell for measurements on solutions at high hydrostatic pressures. The slot and hole allow the pillbox cell to be filled and extra liquid to be released on closing the cell.

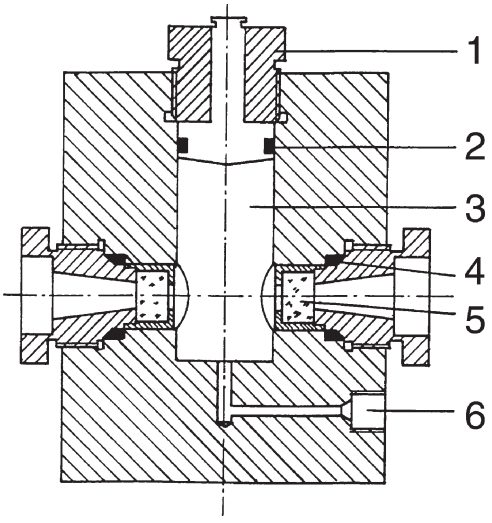

Figure 2 Schematic view of a two-window high-pressure cell to accommodate the pillbox optical cell for pressures up to 200 MPa: 1 – pressure plug; 2 – O-ring; 3 – reaction compartment; 4 – Δ-and-O-ring; 5 – sapphire window; 6 – pressure connection.

pressurizing liquid surrounds the windows of the cell and is chosen because it is transparent with respect to the monitoring method. The specific properties frequently monitored in organometallic reactions will be described in association with the selection of reactions in the following sections.

For reactions at ambient pressure but with a half-life ranging from a few minutes to the milli-, micro-, or nanosecond timescales, special monitoring methods are required. The history of development of these special methods for fast reactions can be tracked through appropriate literature.[27–30] Some commercial instruments currently available (e.g., a stopped-flow spectrophotometer), while offering greater sensitivity, semi-automation features, and modern data-treatment methods than original instruments, are based fundamentally on the early designs. Many applications of fast reaction methods have been to inorganic and bioinorganic reactions, but in principle the methods are equally suited to organometallic chemistry reactions in solution. There is additional focus in the literature upon the specialized equipment needed to be available when reactions that are rapid are also to be studied at pressures above ambient pressure. There is abundant literature to provide the technical aspects of these kinetics methods as may be applied generally in chemistry.[16,23–26,31–33] It is worth noting that many reactions of coordination compounds, when the central metal ion is a transition metal ion, are very labile, and hence there has been a tremendous growth in special fast reaction methods and techniques for their study. Relatively, organometallic reactions overall are less labile and therefore there is less emphasis on these special methods. Indeed, the most common relaxation technique, the temperature-jump method,[27,27a,28] in most configurations, can only operate with an aqueous medium and a moderate concentration of electrolyte. These clearly are conditions that could not be employed for kinetics studies of organometallic reactions requiring non-aqueous solvents, even if the reaction were to be in the milli- or microsecond time range. The most widely used method for rapid reactions is the stopped-flow (SF) method in which reactants are flowed together, and passed through a special mixer; the flow is stopped quickly ($\sim$2 ms), and the reaction progress of the mixed solution is followed by a suitable monitoring method. Reactions in the second to millisecond range may be observed; however, resort to more dilute solutions and to low temperatures, for second-order reactions and particularly for non-aqueous solvents, respectively, can position the reaction rate of faster reactions within the scope of time range of the device. In principle, with cryostatic capability, reactions in non-aqueous solvents of suitable melting point can be observed at temperatures down to 183 K ($-90\,^{\circ}$C). The SF method requires turbulent flow and is not well suited for studying reactions in mixed solvents or in viscous liquids. The method may also have limitations if reactants of widely varying concentrations are to be mixed, especially if high concentrations of added electrolytes or buffer agents relative to reactant concentrations are used. Somewhat similar SF devices have been developed for studying reactions at elevated pressures (HPSF – high-pressure stopped flow).[34–40] The reaction dead time is usually longer. Ambient- and elevated-pressure SF devices are commercially available; the former are fairly common laboratory currency and widely used, while the expense and complexity of the latter have restricted use to relatively few laboratories, or where "home-built" apparatus is employed. Examples of HPSFs (suppliers of HPSF are TgK Scientific Limited, Bradford-on-Avon, Wiltshire, UK, and Hikari High-Pressure Machinery Co., Ltd., Hiroshima, Japan) are shown in Figures 3 and 4; the original literature may be consulted regarding the design, construction, and operating features.

Other rapid reaction devices, the range of relaxation methods for example, except for the flash photolytic method, have not been used prolifically in organometallic chemistry relative to inorganic and bioinorganic chemistry.

1.19.3.2 Monitoring Methods

In discussing methods of following reaction kinetics, it is useful to subclassify them in terms of reaction initiation methods.

1.19.3.2.1 Thermal methods

The preponderance of reactions in this field is initiated by simply mixing reactants together, or otherwise initiating reactions at a temperature that ideally allows the kinetics to be conveniently followed. In the vast majority of systems, monitoring of the reaction progress would be by one, or occasionally more, spectroscopic methods. For slow reactions at ambient pressure, UV/visible and IR spectrometers would typically be employed. Monitoring the kinetics of solution reactions by IR spectroscopy could require special thermostatted cells of suitable path lengths. A setup for such procedures when UV/visible absorbance bands are utilized would be expected to be routine for investigators. Provided a suitable magnetically active nucleus is present in the reacting system, nuclear magnetic resonance (NMR) spectroscopic measurements can be made, although the time between reaction initiation and monitoring may be slightly longer than in the other two forms of spectroscopy. If a high resolution NMR spectrometer would be required

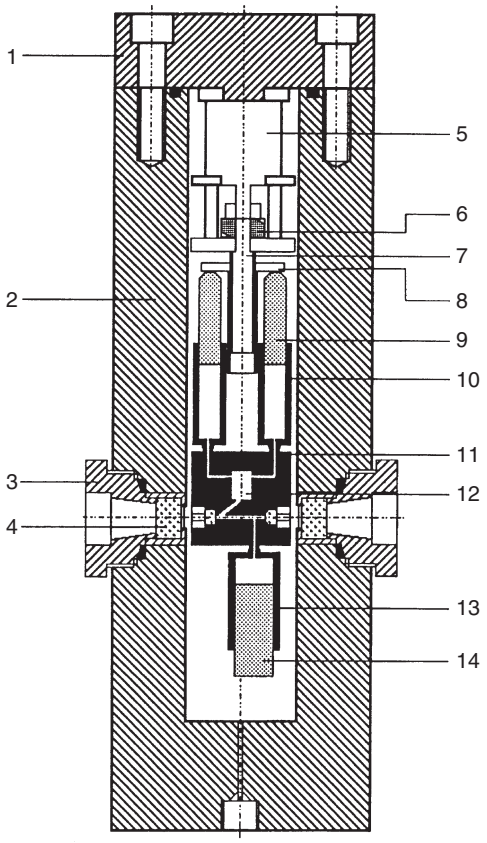

Figure 3 Schematic presentation of a high-pressure stopped-flow unit: 1 – lid to overall unit; 2 – outer vessel; 3 – window holder; 4 – quartz windows; 5 – electric motor; 6 – motor actuator; 7 – stopped-flow unit-positioning rod; 8 – syringe driving plate; 9 – drive syringe (inner); 10 – drive syringe (outer); 11 – block holding windows, mixer and syringe attachment points; 12 – mixing jet; 13 – stop syringe (outer); 14 – stop syringe (inner).

to monitor a reaction, and the reaction could also be followed by UV/visible and IR spectroscopies, from an economic standpoint, an investigator would probably choose one or both of the latter techniques.

For kinetics experiments at elevated pressures, specialized equipment and spectrometer cells or NMR tubes and probes would be required. Some of these that have been used for application of high hydrostatic pressures (HPNMR – high-pressure nuclear magnetic resonance spectroscopy) upon solution reactions have been described in detail in several sources.[41–49] Many kinetics studies applying HPNMR are solvent exchange reactions on metal ions, either fully solvated or partially solvated, and containing other coordinated ligands. When relevant properties permit, the mechanism of water or other solvent exchange reactions in organometallic chemistry can also be studied by HPNMR spectroscopy, for example, water exchange on $[Rh(\eta^5\text{-}C_5Me_5)(H_2O)_3]^{2+}$.[48a] However, an organometallic reaction whose kinetics can be studied by ambient pressure NMR spectroscopy could, if the reaction kinetics are reasonably straightforward, be studied by HPNMR to yield additional mechanistic information. Examples of probes for HPNMR are illustrated in Figure 5.

Another type of reaction requiring high-pressure technology is one in which a considerable quantity of a gas is needed in a solution, and consequently a high gas pressure above the solution is required. Such reactions commonly involve high pressures of CO or H_2, an organic substrate, and an organometallic compound as a catalyst. Adaptation of an NMR spectrometer for following reactions in this category or for detecting intermediates has been described in pioneering works,[50,51] and in updated reports.[52,53] For moderate pressures, sapphire sample tubes can be used.[54] A very recent authoritative account describes HPNMR cells for this type of reaction as well as for hydrostatic pressures and reactions in SCFs.[49] Another significant and recent development for investigations of gas/liquid reactions, for reactions in SCFs, and gas-phase reactions has been reported.[55] The key feature of the new probe is a cylindrical pressure vessel that serves as a toroid cavity detector (TCD) for NMR spectroscopy. The design features, advantages of the design, and the

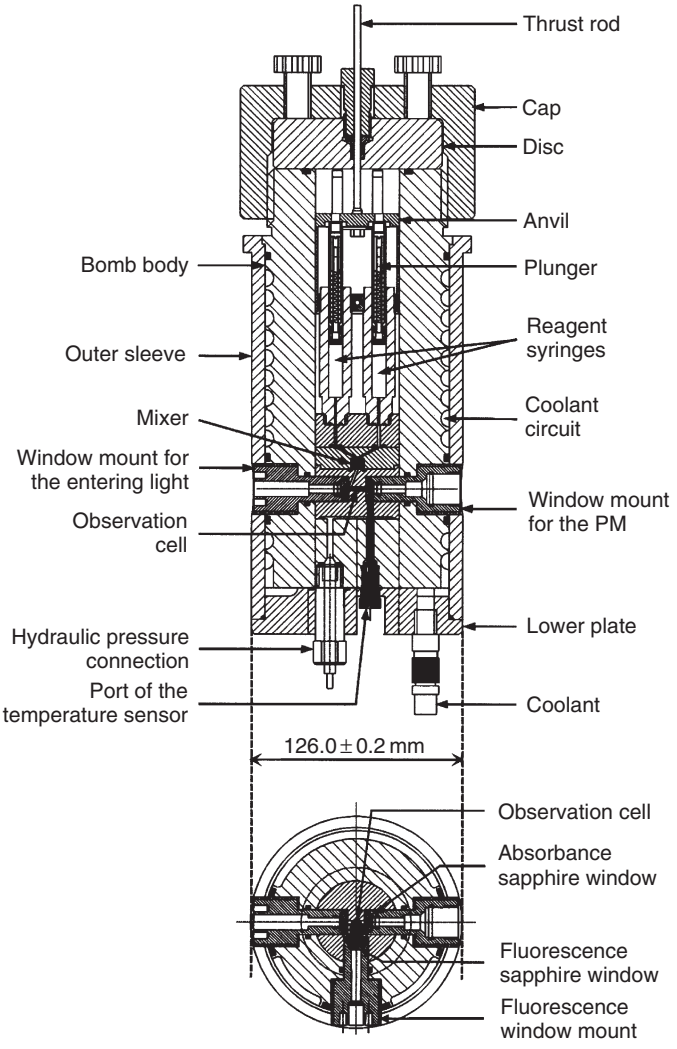

Figure 4 Schematic presentation of the commercially available Hi-Tech HPSF-56 high-pressure stopped-flow unit.

considerations of suitable materials for the TCD and the combination of the TCD with an autoclave, known as the toroid cavity autoclave (TCA), have been described thoroughly.[55] Schematic diagrams of the TCA are available.[55]

The use of parahydrogen as a high-sensitivity spin label in NMR spectroscopy was proposed almost 20 years ago.[56] Parahydrogen-induced polarization (PHIP) as a technique has become widespread in catalyzed hydrogenation reactions, and its application in the TCA designed for gas/liquid reactions and for reactions in SCFs has been reported.[55] In principle, reaction kinetics can be followed using the TCA device, and in hydrogenation reactions applying the PHIP approach. Various applications of PHIP NMR spectroscopy have been described.[57]

Apparatus suitable for use with high pressures combined with IR monitoring (HPIR – high-pressure infrared spectroscopy) has been designed.[58,59] A wide variety of catalytic reactions involving organometallic reactions have been studied using HPIR.[60] This latest account includes the technical aspects and the various types of cells that have been devised. A special cell made of copper, into which gases can be introduced at any time, and which possesses CaF_2 windows for *in situ* FTIR monitoring, has been designed and constructed.[61] It has been used in conjunction with the polymer matrix technique (*vide infra*).[61] Another cell for *in situ* HP monitoring employs a modified autoclave; this apparatus has been used in methanol carbonylation catalysis studies.[54]A review of recent advances in applying HPNMR and HPIR techniques to metal-catalyzed hydroformylation reactions provides a comprehensive literature on the subject.[62]

In inorganic and bioinorganic chemistry reaction kinetics studies, a frequently exploited property is UV/visible absorbance. However, other spectroscopic methods such as detection of fluorescence, monitoring optical rotation, or

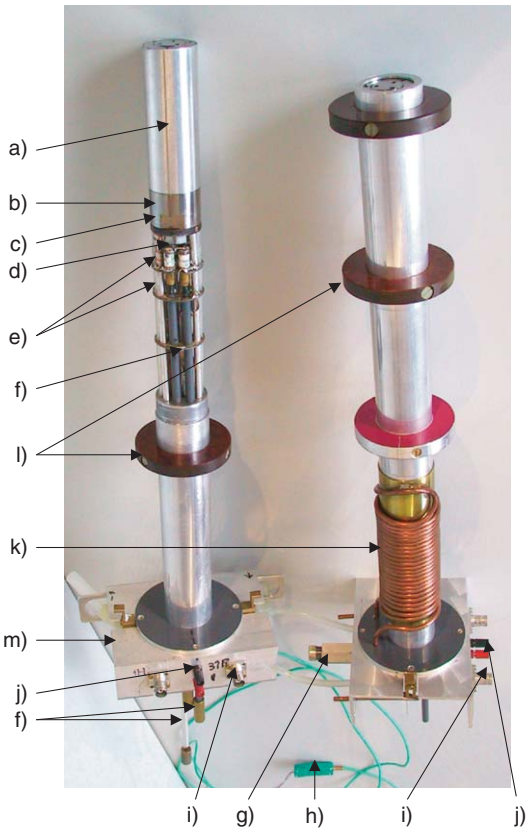

Figure 5 Photograph of two narrowbore probeheads: a) aluminum jacket sealing the double helix used for thermostatting; b) high-pressure vessel; c) platform carrying the autoclave; d) capacitors; e) capacitor platforms; f) tuning rods; g) high-pressure connector; h) thermocouple; i) BNC connector; j) Pt-100 connector; k) copper tubing; l) widebore adapter; m) base plate for cell mounting.

circular dichroism signals could be, or have been, employed in conventional time range or rapid reaction kinetics. UV/visible monitoring is not as ubiquitous in organometallic chemistry. Electrical conductivity changes have been exploited to follow reaction kinetics, but except for certain media, this method cannot be expected to find wide application in organometallic chemistry.

1.19.3.2.2 Radiation methods

The principal method under this subheading is the photochemical initiation of reaction. The purpose of photoinitiation could be either to cause further photochemical reactions or initiate a process that is followed by a thermal reaction. Common methods of monitoring the subsequent processes are UV/visible spectrophotometry or time-resolved IR (TRIR), whether the reaction is fast or slow, or at ambient or elevated pressures. In some highly specialized fields, reactions are not initiated by a flash of the flash photolysis method, but by a laser, and subsequent processes can be in the micro- or nano- or picosecond range. The detailed technical aspects of such apparatus are beyond the scope of this article, but references are cited for reader's examination.[63,64] Sophisticated apparatus such as the high-pressure/variable temperature cell and flow system enable fine details of mechanisms to be delineated in suitable reactions.[65] Examples of reactions in this genre will be described below.

A second but relatively uncommon form of reaction initiation by radiation is by pulse radiolysis. The method requires very specialized equipment. A critical aspect of the method involves knowing with confidence which species have been generated by the pulse, and therefore what are the reaction consequences of its generation. A second important aspect is that in the high-pressure mode, the design of a cell must permit sufficient radiation to be incident upon it. The latter aspect has been accomplished and successful application reported.[24,66] UV/visible absorbance signals constitute the most usual monitoring method.

1.19.3.2.3 Electrochemical methods

Application of electrochemical methods can be suitable for certain oxidation–reduction reactions. Both homogeneous and heterogeneous electron transfer reactions have been investigated electrochemically. The technique and apparatus can range from reasonably standard cyclic voltammetry[67] and rapid scan voltammetry[68] to quite specialized arrangements.[69–74] In the latter case, the method often needs to be adapted to the context of a particular reaction. An example of high-pressure electrochemistry apparatus is shown in Figure 6.

Approaches to both ambient- and elevated-pressure kinetics measurements have been reported, although the specialized nature of the apparatus means that practice in this subfield is restricted to a few laboratories.

1.19.3.3 Supercritical Fluids

Supercritical fluids (SCFs) have become of increasing significance in the past two decades for several reasons. However, it should be recognized that scf's have been a subject of research for some time.[75] Supercritical carbon dioxide and supercritical water have been investigated extensively as media for application in solvent-free chemistry processes and, therefore, suggesting to some people, green chemistry. They have also been used in environmental remediation. SCFs offer opportunities to carry out novel chemistry and have been shown to be media for study of organic, inorganic, and organometallic reactions. Authoritative reports contain examples of applications in organometallic chemistry.[76–79] Carrying out preparative or mechanistic chemistry in an SCF is not a trivial technical exercise. Consequently detailed kinetics studies are not particularly common. Where reaction kinetics have been studied in an SCF, the experimental method is very specialized, the apparatus modular and usually home built, and modified to be suitable for the particular system. Some very rapid reactions have been characterized kinetically. Complete details of the practical issues in these studies are beyond the scope of this contribution, but many aspects are treated in articles dedicated to reactions in SCFs, and applications cited below can be consulted for facts regarding instruments and their specifications. Reactions in SCFs are not contained in a separate applications section.

1.19.3.4 Ionic Liquids

Depending on the properties of a particular ionic liquid and the chemical reaction itself, conducting kinetics experiments may present different technical challenges from those encountered studying reactions in aqueous solutions or other solvents. For example, ionic liquids containing nuclei commonly used for NMR spectroscopy may hamper that particular avenue of monitoring of the reaction itself. Another property that may present difficulty is viscosity of the medium. For conventional time-range experiments, this may not be an issue, but, for example, in SF applications, the conditions for correct flow characteristics impose limits on the viscosity range of the medium. It would appear that each potential reaction and properties of the ionic liquid in question would have to be examined to

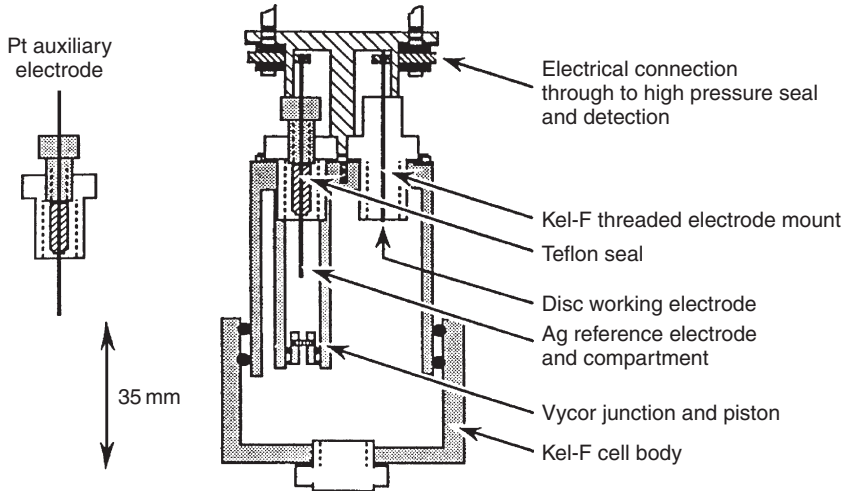

Figure 6 High-pressure electrochemical cell. (Reproduced with permission Sachinidis, J. I., Shalders, R. D. and Tregloan P. A. *Inorganic Chemistry*, Figure 1, p. 6182, *33*, 1994. The American Chemical Society.)

enable suitable experimental design to take place. There is a wealth of literature,[80–82] and a special issue devoted to organometallic chemistry in ionic liquids is forthcoming.[83] Reaction mechanisms could be changed relative to that followed when carrying out the same reaction in a conventional solvent. Indeed, catalytic effects have been noted. Nevertheless, although considerable attention has been paid to these liquids, relatively few kinetics or detailed mechanistic studies have been reported. An example of the practical aspects in a kinetics study including scrupulous purification of an ionic liquid and exclusion of moisture is available.[84]

1.19.3.5 Computational Aspects

The magnitude of the task of modeling organometallic reactions theoretically means that point-by-point kinetics cannot be expected. However, progress has been made in estimating whether key intermediates predicted experimentally are reasonable computationally. Results from relevant studies will be cited.

1.19.4 Selected Recent Kinetics Studies in Organometallic Chemistry

In this section, abbreviations, formulae, terminology, and nomenclature are almost always those used in the literature cited.

1.19.4.1 Organochromium

Chromium-based catalytic reagents have become established as highly active, selective, and thermally stable toward ethene trimerization.[85] However, only recently have specific chromium catalysts been characterized (by single crystal X-ray diffraction and NMR spectroscopy), and a more systematic investigation of the mechanism of trimerization been initiated.[85] Prominent examples are $(PNP^{OMe})CrPh_3$ and $(PNP^{OMe})Cr(o,o'$-biphenyldiyl)Br[$PNP^{OMe} = (o$-MeO-$C_6H_4)_2PN(Me)P(o$-MeO-$C_6H_4)_2$]. When the former compound is activated with $H(Et_2O)_2B[C_6H_3(CF_3)_2]_4$, effective turnover and selectivity to yield 1-hexene are observed. The latter requires to be converted to a cationic form to yield, upon exposure to ethene, *o*-vinylbiphenyl and 1-hexene. Analysis of the trimerization of partially deuterated ethenes afforded an insight into the mechanistic process. Using either *cis*- or *trans*-dideuterioethene, a single geometric isomer is observed with the stereochemistry of the double bond opposite to that of the ethene starting material. The product distribution indicated a kinetic isotope effect of 2.4 at room temperature. Various pathways producing this k_H/k_D value were presented. Trimerization of *gem*-dideuterioethene gave rise to a kinetic isotope effect of 1.3, consistently it was argued, with the irreversible formation of a chromium cycloheptane intermediate.

The use of organometallic compounds as chain-transfer catalysts in free-radical polymerization has been widely studied.[86] One objective is the production of polymers with terminal vinyl groups and lower molecular weight components compared with polymerization in the absence of chain-transfer catalysts. Complexes of cobalt(II) have been used as effective catalysts, but the instability of the intermediate cobalt hydride does not permit firm establishment of the reaction mechanism. To address this issue, several chromium compounds have been applied as catalysts for the polymerization of methylmethacrylate (MMA) and styrene.[87] The temperature dependence of the rate constant k_{tr} for free-radical polymerization of MMA for catalyzed chain transfer by $(C_5Ph_5)Cr(CO)_3$ has been determined using the Mayo equation.[88]

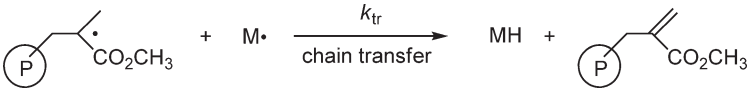

(2)

Over the range of temperature studied, k_{tr} decreased with temperature, which implied that abstraction of hydrogen from the chain carrying radical does not occur in a single step. Hence, it was suggested that a caged radical pair is formed associatively. A combination of ^1H NMR spectroscopy and UV spectrophotometry was used to study the kinetics and thermodynamics of $H^\cdot$ transfer from the chromium compound $(\eta^5\text{-}C_5R_5)Cr(CO)_3H$ (R = Ph, Me, H) to MMA or styrene. This is the follow-up step, with the hydride being removed from MH, and reaction with a monomer to start a new chain follows.

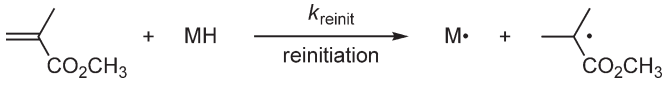

(3)

The effect of steric bulk of the hydride could be examined. Computer simulations were used and considerable complexities in the mechanism were revealed.[87]

1.19.4.2 Organomanganese

Understanding structural changes induced by electron transfer in metal complexes is important in a variety of applications. Determining the relative rates of change of the structural and redox processes can assist in understanding the mechanisms. However, more studies are required on the kinetics of these processes in solid-state/adsorbed systems for comparison of the solution and solid-phase processes to improve clarity.[68] A suitable system for such a study emanates from the discovery from electrochemical studies on manganese derivatives that isomerization can be oxidatively induced. The electrochemical properties associated with the oxidation of the *cis*- and *trans*-isomers of the 18-electron octahedral-type complex $[Mn(CN)(CO)_2\{P(OPh)_3\}(Ph_2PCH_2PPh_2)]$ in solution and immobilized on an electrode surface in the solid state have been investigated.[89] Rapid scan voltammetry has been used to monitor the kinetics of the *cis–trans* isomerization in both phases.[68] In homogeneous solution the rate constant for the isomeric conversion was independent of solvent and concentration, whereas in the solid-state electrolysis was strongly dependent on the identity of supporting electrolyte anion. Organic solvents, for example, acetonitrile, dimethylformamide, and tetrahydrofuran, upon being added to the aqueous electrolyte medium, enhanced the voltammetric response for either manganese compound attached to an electrode surface, and the effect was reversible. This was explained by suggesting that the incorporation of solvent into the lattice facilitates the rate of the charge neutralization process, which involves the transport of the anion from the solution to the solid phase. The effect noted with different anions could be correlated with their lipophilicity. It was reasoned that anions high on the lipophilicity scale are allowed facile ingress and egress to the immobilized solid during electrolysis/charge neutralization. Other instances of correlations with the lipophilicity scale were cited. The solvent independence of the isomerization rate in solution and the fact that the reaction was observed with an appreciable rate in the solid phase were interpreted in terms of a twist mechanism for the conformational change rather than the latter occurring via a dissociative (metal–ligand bond-breaking) process.

1.19.4.3 Organoiron

Although the mechanism of the photolysis of $Fe(CO)_5$ has been investigated extensively, some features remain unresolved. A wide-ranging study aimed at unraveling the photochemistry of $Fe(CO)_5$ in solution has been reported. Time-resolved infrared spectroscopy apparatus referred to earlier, and that available at the Rutherford Appleton Laboratory, were used to monitor events in the nano- and picosecond ranges following photochemical initiation.[64] The photochemistry of $Fe(CO)_5$ was studied in *n*-heptane, scAr, scXe, and $scCH_4$. The C_{2v}-symmetric triplet $^3Fe(CO)_4$ and singlet $Fe(CO)_3$(solvent) are the primary photoproducts formed in the first few picoseconds. In *n*-heptane, $scCH_4$, and scXe, $^3Fe(CO)_4$ decays to form $^1Fe(CO)_4S$, where S is *n*-heptane, $scCH_4$, or scXe, and also reacts to form $Fe_2(CO)_9$. Conversion of $^3Fe(CO)_4$ to the solvent-associated species has been monitored, and the kinetic parameters are $k_{heptane}$ $7.8 \times 10^7\ s^{-1}$, k_{scCH_4} $5 \times 10^6\ s^{-1}$, and k_{scXe} $2.1 \times 10^7\ s^{-1}$ at 298 K. The rate constant k_{CO} for the reaction of $^3Fe(CO)_4$ with CO in scAr has also been determined: $k_{CO} = 1.2 \times 10^7\ dm^3\ mol^{-1}\ s^{-1}$. The relative yield $^3Fe(CO)_4/^1Fe(CO)_4S$ decreased in the order *n*-heptane > scXe > $scCH_4 \gg$ scAr. Pressure-dependent measurements in scAr and $scCH_4$ indicated an influence of solvent density on this ratio. These kinetic parameters and spectroscopic results have not been obtained previously and represent a valuable increase in understanding of the photochemistry of $Fe(CO)_5$ in solution.

Considerable clarity has been brought to the subject of the mechanism and modeling of the self-exchange reactions of metallocenes by an investigation of the reaction between $[(\eta^5\text{-}C_5(CH_3)_5)_2Fe^+]$ ($DmFc^+$) and $[(\eta^5\text{-}C_5(CH_3)_5)_2Fe]$ ($DmFc^0$) in deuterated acetone, dichloromethane, and acetonitrile.[72] The counterions were either hexafluorophosphate or tetrafluoroborate. Values of the exchange rate constant k_{ex} were obtained from ^1H NMR spectroscopic measurements at ambient and elevated pressures. Only very marginal effects of ion pairing were encountered. Values of $\Delta V^{\neq}$ were distinctly negative, −8.5 to $-8.9\ cm^3\ mol^{-1}$ in $(CD_3)_2CO$, and −6.3 to $-7.2\ cm^3\ mol^{-1}$ in CD_2Cl_2. (Practical limitations precluded fully quantitative results for the reaction in CD_3CN.) The small variations arise when different concentrations or counterions are used. The various contributions to $\Delta V^{\neq}$ in terms of an extension to Marcus–Hush theory were carefully examined with particular reference to non-aqueous solvents. It was concluded that the results were entirely consistent with a two-sphere activation model and it was not necessary to invoke solvent dynamics in the explanation. This high-pressure study was able to counter arguments that solvent dynamics[91] were involved in this type of electron self-exchange.

In a related study, the volume of reaction, the volume of activation for diffusion ($\Delta V_{diff}^{\neq}$), and the volume of activation obtained from the standard electrode reaction rate constant at various pressures have been determined for the decamethylferrocene ($DmFc^{+/0}$) system, in several non-aqueous solvents.[91] The decamethylated ferrocene couple was chosen, rather than the unmethylated couple, because of its large size and low charge of the positive ion, offering minimization of complicating Coulombic interactions, such as ion pairing. The unmethylated $Fc^{+/0}$ couple is also less stable due to the rigor of the electrochemical experimental conditions required. A further objective planned was to compare the pressure effects on the corresponding outer-sphere bimolecular electron-transfer (self-exchange) rate constants in homogeneous solution with those on the non-aqueous electrode kinetics. The reaction volumes ΔV_{cell} could be expressed as a linear function of the term Φ (the Drude–Nernst relation, $\Phi = (1/\varepsilon)(\delta \ln \varepsilon/\delta P)_T$, where ε is the solvent dielectric constant). $\Delta V_{diff}^{\neq}$ ranged from +7 to +17 $cm^3\ mol^{-1}$ for the $DmFc^{+/0}$ system and generally increased with solvent viscosity. The values of $\Delta V_{el}^{\neq}$ for the electrode reaction of $DmFc^{+/0}$ were positive and, within experimental uncertainty, correspond to the relevant values of $\Delta V_{diff}^{\neq}$; this is in distinct contrast to the negative $\Delta V_{exp}^{\neq}$ values for the electron self-exchange reactions in homogeneous solution. It was concluded that the electrode reactions were subject to solvent dynamical control. There was an extensive discussion of the unsatisfactory relationship between the radii of the electro-active species according to the Drude–Nernst and Stokes–Einstein equations and those related to crystallographic radii.

Phosphine-functionalized ferrocenes are important compounds in homogeneous catalytic processes. Chiral derivatives are of particular interest for asymmetric catalysis. Such compounds containing two planar chiral units may exhibit *rac*- and *meso*-isomers. Conversion of one isomer to another would require one of the ferrocenyl rings to flip over and coordinate to the iron atom by the other face.

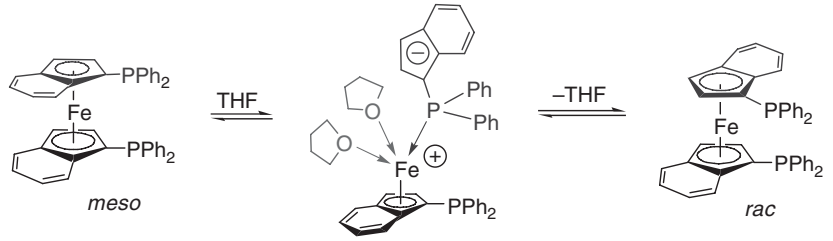

(4)

Only recently, this type of conversion has been observed in phosphine-functionalized ferrocenes.[92] In tetrahydrofuran, at room temperature, the bis-planar chiral ferrocenyldiphosphine, bis(1-(diphenylphosphino)-η^5-indenyl)iron(II), isomerizes from the *meso*- to the *fac*-isomer. In order to understand the mechanism, the reaction has been studied by adding other solvents, adding salts, varying the temperature and pressure, and judicious isotopic substitution within the reactant. The isomerization was accelerated by increases in temperature or pressure and in the presence of salts such as $LiClO_4$ or LiCl, but retarded by the presence of non-coordinating solvents. The reaction is facilitated by the coordinating THF solvent, and is vital since there is no reaction in 100% chloroform. Participation by the Cl^- ion as a nucleophile could be ruled out since the reaction is accelerated in the presence of both $LiClO_4$ and LiCl. The kinetics of isomerization were followed by ^{31}P NMR spectroscopy, leading to $\Delta H^{\neq} = 57 \pm 4\ kJ\ mol^{-1}$, $\Delta S^{\neq} = -145 \pm 15\ J\ mol^{-1}\ K^{-1}$, and $\Delta V^{\neq} = -12.9 \pm 0.8\ cm^3\ mol^{-1}$. The fate of the substituted deuterium atoms, the activation parameters, solvent, and salt effects could be analyzed to conclude that isomerization proceeds via an associative solvent-mediated ring-slipping process, resulting in dechelation of the indenide and coordination of the phosphine in the key intermediate species. Following this, the indenide is coordinated by the other face, forming the other isomer. The significance of the ring-slipping process and racemization in homogeneous catalysis was discussed.

1.19.4.4 Organocobalt

A series of related reports have appeared on the equilibria between five- and six-coordinate species and possible adduct formation in Co(III) corrinoids,[93] on the thermodynamic and kinetic properties for what is termed the base-on/base-off equilibration of alkyl cobalamins,[94] and on the kinetics and thermodynamics of parallel equilibria of alkyl-13-epicobalamins.[95] In the first report, the pressure dependence of the UV/visible spectra of the five-coordinate (yellow)/six-coordinate (red) equilibrium for both methylcobalamin and vinylcobinamide was obtained. Water is the ligand that converts the five- to a six-coordinate species. The reaction volumes were obtained from the pressure dependence of the equilibrium constant. The values of ΔV of -12.5 ± 1.2 and $-12.5 \pm 1.0\ cm^3\ mol^{-1}$ for the methyl and vinyl complexes are close to the values $\pm 13\ cm^3\ mol^{-1}$ advocated and accepted for the displacement or

introduction of a water molecule in limiting D or A mechanism.[96] Initial experiments with both vinylcobinamide (five-coordinate) and dicyanocobinamide (six-coordinate) showed that adducts were formed with a selection of various added solutes, consistent with their positions in the lyotropic series. It was suggested that the solute species are probably located within the hydrophobic cylinder surrounding the cobalt ion.

The base-on/base-off equilibration of a series of alkylcobalamins (XCbl) has been studied to investigate the influence of the electronic nature of X on an important equilibrium in which axially coordinated dimethylbenzimidazole moiety (DMBz) is displaced by water (the base-off form) and is protonated. The DMBz group is substituted in the biological cycle. Equilibrium and kinetics spectrophotometric measurements, as a function of temperature and pressure, and as a function of acid concentration for the equilibration base-on/base-off kinetics, could be analyzed to show that the base-off form of different XCbl species has different coordination.[94] AdoCbl and ethylcobalamin are mainly five coordinate, whereas the H_2O-, CN^-- and CF_3-cobalamins have little base-off form and exist mainly as six-coordinate species. There is an equilibrium mixture of the five- and six-coordinate species when $X = CH_3$, CH_2Br, and CH_2CF_3. The acid-dependence measurements provided evidence for an acid-catalyzed dechelation of DMBz pathway. The properties of structurally modified analogs of AdoCbl were considered to be insightful for understanding the chemistry of the unmodified coenzyme **1**.

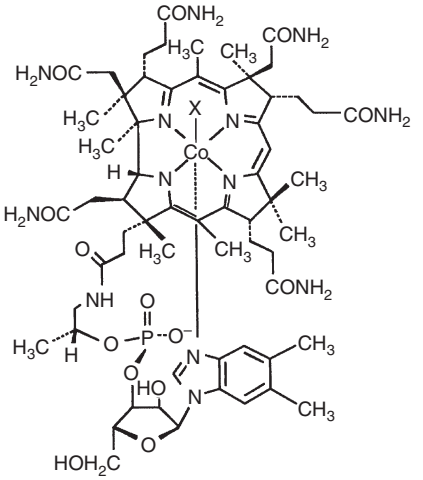

1

Two derivatives ($X = NCCH_2^-$ and CN^-) of the epimer obtained by epimerization at C13, in which the *e*-propionamide side chain adopts an upwardly axial configuration, have been used for a thorough examination of the kinetics of the cyanation reaction. The CN^- concentration and the temperature and pressure were varied in SF spectrophotometric measurements.[95] Epimerization has a sensitive influence on the kinetics of displacement of DMBz first by water and then by cyanide ion, and the rate of substitution was reduced compared with that for an XCbl. Saturation kinetics for DMBz displacement were observed at high [CN^-]. Activation parameters for the limiting rate constant were $\Delta S^{\neq} = +77 \pm 4$ and $+82 \pm 4\,J\,mol^{-1}\,K^{-1}$ and $\Delta V^{\neq} = +13.3 \pm 1.0$ and $+14.8 \pm 1.2\,cm^3\,mol^{-1}$ for the $NCCH_2^-$ and CN^- epimers, respectively, values that indicated a limiting D mechanism. A limiting D mechanism was also proposed for the kinetics of displacement of DMBz by CN^- in XCbl, where $X = \beta$-$NCCH_2$ and CN^- to form $NCCH_2(CN)$Cbl and $(CN)_2$Cbl, respectively. Saturation kinetics were obtained at high [CN^-], and again, significantly positive entropies and volumes of activation were established. This report included a formulation of general mechanistic principles for these types of reactions.[97]

The kinetics of substitution reactions of various cobaloximes have been investigated.[98] One purpose was to develop a comprehensive mechanistic picture for bio-relevant compounds. The kinetics of axial water substitution by cysteine in the cobaloxime system *trans*-$RCo(Hdmg)_2(H_2O)$ with $R = cyclo$-C_5H_9, CH_3CH_2, CH_3, $C_6H_5CH_2$, C_6H_5, and CF_3CH_2, and dmg = dimethylglyoxime have been examined.

$$trans\text{-}RCo(Hdmg)_2(H_2O) + L \rightarrow trans\text{-}RCo(Hdmg)_2(L) + H_2O \qquad (5)$$

Five-coordinate species have been inferred from results of studies on co-enzyme B_{12} in aqueous medium and on alkylcobaloximes in non-coordinating solvents, but the evidence here, principally residing in the magnitude of $\Delta V^{\neq}$

values, was that the mechanism is dissociative interchange, that is, no five-coordinate species are involved. Some mechanistic variation was implied by the absence of an isokinetic plot, and by the CF_3CF_2-containing compound undergoing substitution by an interchange mechanism ($\Delta V^{\neq} = 0.1\,cm^3\,mol^{-1}$). It was also concluded that all activation parameters are influenced by a combination of steric and electronic factors.

In a very similar study that exploits the influence of a single cobalt–carbon bond on the substitution lability of organocobalt(III) complexes, the kinetics of ligand substitution of S in *trans*-$RCo(Hdmg)_2S$ by imidazole, 1,2,4-triazole, *N*-methylimidazole, 5-chloro-1-imidazole, NO_2^-, Ph_3P, Ph_3As, and Ph_3Sb (R = CH_3, $PhCH_2$; S = H_2O, CH_3OH) have been monitored by SF spectrophotometry.[99] Except for Ph_3As and Ph_3Sb as entering nucleophiles, the reactions proceeded to completion under the conditions applicable, with the kinetic measurements yielding second-order rate constants. A reverse solvolysis reaction was in evidence for reactions with Ph_3As and Ph_3Sb. The activation parameters determined from the temperature and pressure dependences of the kinetic parameters for the substitution reaction, specifically positive $\Delta S^{\neq}$ and $\Delta V^{\neq}$ values, were interpreted as evidence for a dissociatively activated substitution mechanism. Variation in the magnitude of the positive value of the volume of activation reflected a variation in the extent of dissociative character of the mechanism; this pattern depended upon the nature of R and the entering nucleophile. The pressure dependence of the rate of the reverse solvolysis reaction, in the case of displacement of Ph_3As by methanol, could be determined. A value of $+15.9\,cm^3\,mol^{-1}$ was obtained for the volume of activation, reflecting the larger partial molar volume for the dissociating Ph_3As ligand. A volume profile for the reaction was constructed and this is shown in Figure 7.

The volume profile is a visualization of the volume changes accompanying reaction and can be combined with profiles recording Gibbs free energy, enthalpy, and entropy changes during reaction. In this case, a more detailed analysis of the volume profile, beyond noting that the overall reaction volume is negative ($-5.3\,cm^3\,mol^{-1}$), is precluded as there is a degree of uncertainty as to the distribution of contributions in the measured volume of activation in the forward direction between the volume change associated with precursor complex formation and the volume change of the actual ligand interchange. The magnitudes of the volumes of activation in both directions indicated possible operation of limiting D mechanisms. However, from this report and others cited, the lability of alkyl cobalt(III) complexes is amenable through variation of the R group, of the chelating ligand, and of the substituting ligand, to systematic tuning.

The effect of various alkyl substituents in the *trans*-position of the cobalt(III) center of cobalamins on the kinetics and thermodynamics of their substitution reactions has been undertaken to bring clarity to the mechanistic scheme.[100] The cobalamins studied were cyanocobalamin (vitamin B_{12}) and aquacobalamin (vitamin B_{12a}) and the complex formed when the cyano or water ligand in these species is replaced by 3′-deoxyadenosyl. This perspective article included a compilation of a large volume of research on this subject. It demonstrated the key role of the alkyl group in controlling the equilibrium between five- and six-coordinate species, relating to these species' potential participation in

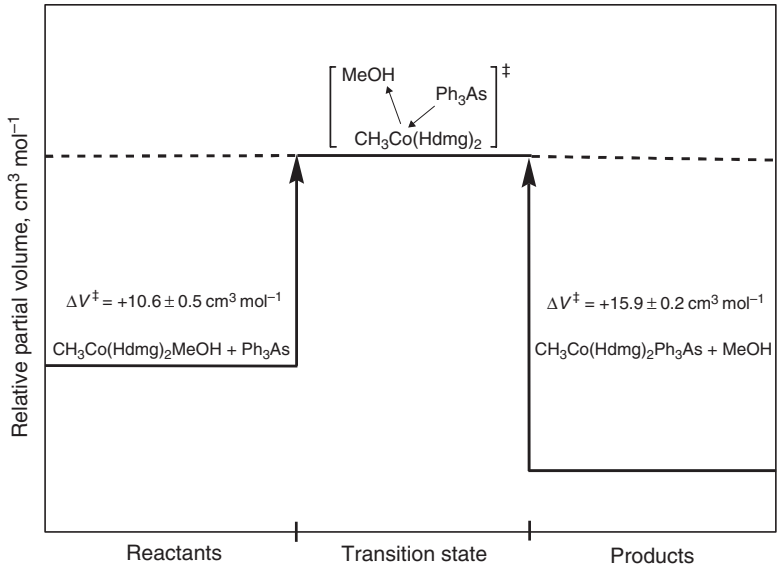

Figure 7 Volume profile for the reversible reaction *trans*-$[Co(Hdmg)_2(CH_3)MeOH] + Ph_3As \rightleftharpoons$ *trans*-$[Co(Hdmg)\text{-}(CH_3)Ph_3As] + MeOH$. (Reproduced with permission from Alzoubi, B. M., Liehr, G. and van Eldik, R. *Inorganic Chemistry*, Figure 6, p. 6097, *43*, 2004. The American Chemical Society.)

ligand-substitution reactions.[100] The mechanistic value of parameters derived from kinetics measurements at elevated pressures was also emphasized. It has become evident that the nature of the cobalt–carbon bond and the character of the group or substituent supplying the carbon atom to that bond are critically important. Employing UV/visible and ^{1}H NMR spectroscopies, it has also been shown ($\Delta V^{\neq} = -4.5\,\mathrm{cm^3\,mol^{-1}}$) that, for the reaction of co-enzyme B_{12} with cyanide ion, the rate-determining step involves solvent-assisted heterolytic cleavage of the Co–carbon bond.[101]

1.19.4.5 Organozirconium

Kinetic studies on the dissociation of $Al(CH_3)_3$ from $[Cp_2M(\mu\text{-}CH_3)_2Al(CH_3)_2]^+[B(C_5H_5)_4]^-$ (M = Ti, Zr, Hf) have been conducted in an effort to provide insight into the mechanism of transfer of alkyl groups from M to Al.[102] Transfer is expected to occur when Zr, for example, is used to catalyze chain growth in aluminum alkyls and when Zr is used to catalyze carboalumination of olefins. The catalytically active species is thought to be a coordinatively unsaturated cationic species Cp_2Zr^+–CH_3, which can be trapped by aluminum alkyls to form the adduct, shown:

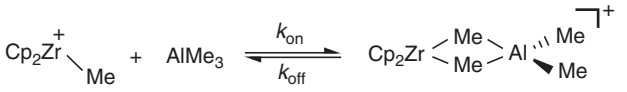

(6)

The equilibrium lies to the right, and the rate constants determined, in C_6D_6, by ^{1}H NMR spectroscopy are those for the regeneration of the catalytically active species. Exchange between the methyl groups of free $Al(CH_3)_3$ and those in the heterobimetallic species was slow on the NMR timescale. The rate constants (presumably obtained at an unstated room temperature) were independent of the value of $[Al(CH_3)_3]$ and decreased in the order Ti > Zr > Hf, which was reasonable if the dissociation involves breaking a metal–ligand bond. Kinetics experiments conducted with substrates in which Cp had been replaced by ethenebis(indenyl) (EBI) or ethenebis(tetrahydroindenyl) indicated that the zirconocene methyl cation will be a superior carboalumination catalyst.

1.19.4.6 Organomolybdenum

The hexacarbonylmolybdenum compound $Mo(CO)_6$ has been proposed to be important as the metal-bearing precursor active in the selective homogeneous hydrocarbonylation of ethene.[103] Although present in small steady-state concentration, the solvated pentacarbonyl species $Mo(CO)_5(S)$ was proposed as an intermediate in the formation of the chain-carrying complexes responsible for ethene hydroxycarbonylation pathways. An investigation of the reactivity and characteristics of this intermediate in cyclohexane solution has been initiated employing time-resolved-optical (TRO) and TRIR spectroscopies.[104] The species is generated by flash photolysis of $Mo(CO)_6$. The initial reaction sequence indicates loss of CO followed by cooling and trapping by solvent of the vibrationally excited pentacoordinate intermediate to yield $Mo(CO)_5(S)$.

$$\begin{gathered} Mo(CO)_6 + h\nu \rightarrow [Mo(CO)_5]^* + CO \\ [Mo(CO)_5]^* + S \rightarrow Mo(CO)_5(S) \end{gathered} \tag{7}$$

The kinetics of the reaction of this product with a mixture of CO and *n*-PrBr (halocarbons are used as promoters in the molybdenum-catalyzed hydroxycarbonylation mechanisms) have been monitored. Analysis of the results of TRO spectroscopy showed that the transient decay could be fitted differently depending on the CO concentration, and two reactions could be distinguished. One was the reaction of $Mo(CO)_5(S)$ with CO to reform $Mo(CO)_6$ and the other was the reaction of the hexacarbonyl to yield $Mo_2(CO)_{11}$. These findings were consistent with earlier results. In the presence of *n*-PrBr, the value of k_{obs} increased linearly with increasing [*n*-PrBr], yielding $k_{RBr} = (5.3 \pm 0.7) \times 10^7\,\mathrm{dm^3\,mol^{-1}\,s^{-1}}$ and the non-zero intercept of $(5.2 \pm 0.6) \times 10^4\,\mathrm{s^{-1}}$, equal to the value of k_{obs} in the absence of *n*-PrBr for $P_{CO} = 1$ atm. Higher pressures of CO could be used in parallel TRIR experiments with the special high-pressure/variable temperature cell. The activation parameters derived from k_{CO} measurements were $\Delta H_{CO}^{\neq} = 33 \pm 3\,\mathrm{kJ\,mol^{-1}}$ and $\Delta S_{CO}^{\neq} = -7 \pm 11\,\mathrm{J\,mol^{-1}\,K^{-1}}$ extracted for the reaction

$$\begin{gathered} Mo(CO)_5(S) + CO \rightarrow Mo(CO)_6 + S \\ S = \text{cyclohexane} \end{gathered} \tag{8}$$

Interpretation of these values, taking into account $Mo(CO)_5$–alkane bond energy values, led to the proposal of an interchange mechanism, in which there is considerable Mo–(S) bond breaking as the transition state is reached.

1.19.4.7 Organoruthenium

There have been several reports of the effect of chelate ring size on metal-catalyzed C–C bond-forming reactions such as hydroformylation, allylic substitution, and hydrocyanation.[105,106] Chelate ring size and bond-angle effects have been cited in reactions involving palladium complexes. As part of an investigation of the examination of various phosphines for catalytic use, the rates at which ruthenium complexes of the type CpRu(P–P)H (P–P = a chelating diphosphine) undergo hydride transfer to an iminium cation have been determined.[107] The compound containing the ions is 1-(1-phenylethylidene)pyrrolidinium tetrafluoroborate. Five chelating ligands were incorporated within a parent ruthenium compound providing P–Ru–P bite angles ranging from 72° to 94°. The kinetics were monitored by ^{1}H NMR spectroscopy in CD_2Cl_2 with varying minor quantities of CH_3CN. The observed second-order rate constants decreased by at least one order of magnitude for each additional carbon in the backbone of the chelating diphosphine ligand. An explanation was offered that the smaller chelate ring allowed more space for approach of the iminium cation. It was proposed that electronic factors control hydride transfer rates when other ligands are present in molybdenum compounds. The fact that the rate of hydride transfer was independent of [CH_3CN] suggested that the rate-determining step is the forward reaction where C^+ is a general cation, a suggestion supported by arguments involving orbital energies.

$$CpRu(P–P)H + C^+ \rightarrow CpRu(P–P)^+ + CH \quad (9)$$

Functionalization of aromatic C–H bonds leading to C–C or C–heteroatom is an important objective. The ruthenium compound [$(PCy_3)Ru(H_2)_2(H_2)_2$(IMes)], where IMes = 1,3-bis(2,4,6-trimethylphenyl)imidazol-2-ylidene, exhibits a unique reactivity toward aromatic C–H bonds giving rise to regioselective H/D exchange.[109] Subsequently, catalytic properties of this ruthenium complex for H/D exchange and coupling reactions of aromatic ketones with ethene as the olefinic reaction partner have been investigated.[109] Monitoring of reaction progress was carried out employing ^{1}H, ^{13}C, and ^{31}P high-pressure NMR spectroscopies. Mechanistic proposals were presented on the basis of chemo- and regioselectivities of the H/D exchange process and C–C bond formation. It was concluded that the C–H bond activation and C–C bond formation do not involve the same intermediate. A more detailed kinetic study may be anticipated and this could provide additional insight into the mechanism of this important ruthenium compound-catalyzed process.

Ruthenium complexes have been applied in a wide variety of hydrogenation reactions. However, less success has been reported in the ruthenium-catalyzed hydrogenolysis of esters.[110] It was argued that an active catalyst would need sufficient electron density on the ruthenium center to enhance the nucleophilicity of the intermediate hydride toward the carbonyl group. The latter is of lower polarity than that in a ketone. A sample substrate, dimethyloxalate, was readily converted to the methylglycolate by a mixture of PPh_3 with $Ru(acac)_3$.[111] However, ethane-1,2-diol was not obtained. Several mono-, bi-, and terdentate *P*- and *N*-ligands were evaluated for catalytic effectiveness. The most effective was a catalyst produced *in situ* from $Ru(acac)_3$ with the facially coordinating terdentate phosphine ligand, $CH_3C(CH_2PPh_2)_3$. Reactions were carried out in an autoclave and product analyses performed by ^{1}H NMR spectroscopy and gas chromatography. Kinetics studies of reactions were not described; however, in principle, there is scope for unraveling the mechanism, and that for a complex that is selective for the semi-hydrogenolysis product, methyl glycolate.

1.19.4.8 Organorhodium

Rhodium and ruthenium complexes of 2,2′-bis(diphenylphosphino)-1,1′-binaphthyl (BINAP) have frequently been used as catalysts for enantioselective hydrogenation of olefins and ketones.[112–114] From consideration of the literature on this subject, it was proposed that the presence of a mono-oxidized BINAP in an organometallic catalyst could have interesting consequences.[115] Accordingly, Rh(BINAP)(CO)Cl was prepared, and upon reaction with O_2, (BINAP(O))Rh(CO)Cl was formed. These compounds were authenticated by X-ray crystallography, and IR and NMR spectroscopies. The kinetics of this reaction were monitored by solution (chloroform was the solvent) IR spectroscopy. In the absence of added CO, the oxygenated compound was formed in about 50% yield. $BINAP(O)_2$ and CO_2 are also produced. Plots of k_{obs} (from loss of reactant) versus [O_2] at various temperatures yielded

second-order rate constants, and $\Delta H^{\neq} = 61\,\text{kJ mol}^{-1}$ and $\Delta S^{\neq} = 64\,\text{J mol}^{-1}\,\text{K}^{-1}$. The latter parameters together with other considerations led to the proposal that the first step of the reaction mechanism probably involves dioxygen coordination to the rhodium complex, forming a short-lived η^2-rhodium dioxygen intermediate. A series of experiments with the objective of understanding the catalytic oxidation of BINAP was conducted by reacting (BINAP)Rh(CO)Cl with a 1 : 1 $CO : O_2$ gas mixture in the presence of excess BINAP. The relative amounts of BINAP(O) and BINAP$(O)_2$ produced were influenced by solvents.

The reactions of P-donor nucleophiles with the metal carbonyl cluster Rh_4CO_{12} have been studied over a considerable time period.[116–119] It is widely accepted that the reaction is associative. This latest investigation[120] is aimed at quantifying the effects of the electronic and steric properties of the nucleophiles upon the kinetic parameters. A rapid substitution reaction step using an excess of the nucleophile was monitored by SF spectrophotometry. Second-order rate constants were obtained from the variation of the pseudo-first-order rate constants with nucleophile concentration. Contributions to these constants from the properties σ-basicity, a steric effect, π-activity, and, in addition, an aryl effect of the nucleophiles were assessed in a multi-parameter equation. The outcome is a successful understanding of the relative reactivities of many P-donors toward the rhodium cluster. The data were also represented by a three-dimensional potential energy surface.

The kinetics of oxidative addition of methyl iodide to complexes of rhodium(I) have been monitored by FTIR spectroscopy.[121] Dramatic ligand effects found in the rate of migratory CO insertion in complexes of the type $[Rh(CO)(L\text{–}L)I_2CH_3]$ (L–L = $Ph_2PCH_2P(S)Ph_2$, $Ph_2PCH_2CH_2PPh_2$),[122,123] in part, prompted the later study to examine, and possibly quantify, steric crowding effects on reaction rates.[121] Methyl iodide oxidative addition to [Rh(CO)(diimine)I], where diimine = $ArN{=}C(CH_3)C(CH_3){=}NAr$, usually in CH_2Cl_2, for seven variants of Ar was characterized by second-order kinetics, first order in each reactant concentration. The large negative $\Delta S^{\neq}$ values (in the range of -160 to $-200\,\text{J mol}^{-1}\,\text{K}^{-1}$) were consistent with highly ordered transition states for an S_N2 attack by the Rh(I) species on CH_3I. The rate constants were very sensitive to diimine steric bulk, varying over a range of three orders of magnitude. The rate constants exceeded in value those found for the carbonylation catalyst $[Rh(CO)_2I_2]^-$.[124] The subsequent migratory CO insertion reaction, when measurable, also demonstrated significant ligand steric effects that depended, in part, upon the distribution of the alkyl substituents and whether two groups adopt a conformation in which both are directed to the same axial site. The following is the general reaction scheme without specifying the diimine.

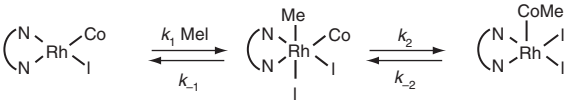

(10)

Complexes containing a free *N*-heterocyclic carbene (NHC) have been explored with a view of exploiting their properties in homogeneous catalysis.[125] However, relatively few quantitative studies of the fundamental reaction steps in the catalytic cycle have been reported. To address this shortcoming, a comprehensive kinetics study of the oxidative addition of methyl iodide to a rhodium(I) NHC complex has been conducted.[126] Reaction of $[Rh(CO)(L_{Me})_2I]$ (L_{Me} = 3,5-dimethylimidazoline-2-ylidene) with a large excess of methyl iodide can be monitored by FTIR spectroscopy. The decay of the band due to the reactant and the growth of the band due to the product (an Rh(III) acetyl complex), $[Rh(L_{Me})_2I_2(COMe)]$, formed from the facile migratory CO insertion after the oxidative addition of CH_3I can both be followed. Upon removal of excess CH_3I, the residue reformed the reactant in CH_2Cl_2 solution, a process that could be monitored by IR and ^{1}H NMR spectroscopies. From a plot of k_{obs} versus $[CH_3I]$, a net forward rate constant of $3.0 \times 10^{-4}\,\text{mol}^{-1}\,\text{dm}^3\,\text{s}^{-1}$ at 293 K was obtained.

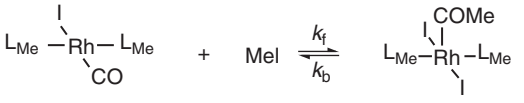

(11)

The equilibrium constant could be determined at various temperatures yielding $\Delta H = -51 \pm 3\,\text{kJ mol}^{-1}$ and $\Delta S = -159 \pm 12\,\text{J mol}^{-1}\,\text{K}^{-1}$. Thus, the reaction is exothermic but has a negative entropy, consistent with an addition reaction. The activation parameters for the forward reaction are $\Delta H^{\neq} = 36\,\text{kJ mol}^{-1}$ and $\Delta S^{\neq} = -189\,\text{J mol}^{-1}\,\text{K}^{-1}$, typical for oxidative addition proceeding by an S_N2 mechanism. Uncertainty that these activation parameters might contain a contribution from the migratory insertion step was raised. Two methods of determining the activation parameters for the reverse reaction yielded almost identical results: $\Delta H^{\neq} = 87$ or 84 kJ mol^{-1} and $\Delta S^{\neq}$ -30 ± 10 or $-38 \pm 6\,\text{J mol}^{-1}\,\text{K}^{-1}$. A comparison was made with oxidative addition of CH_3I to $[Rh(CO)(PEt_3)_2I]$. The rate

constant for the latter process is 3.5 times larger than for the rhodium(I) NHC complex despite the latter having greater electron density on the Rh(I) center.[127] Thus, the implication is that the effective nucleophilicity of the rhodium(I) NHC complex toward CH_3I is lower. This was interpreted as a consequence of the ligand *N*-methyl substituents. The octahedral product of oxidative addition of the rhodium(I) NHC complex is also destabilized by steric effects. Clearly, the reactivity trend based on ligand electronic properties is dramatically influenced, in reverse, by steric constraints.

In a somewhat similar study, the kinetics of CH_3I addition to $[LRh^{I}(CO)]$ in CH_2Cl_2 solution, where L = bis(imino)carbazolide, to form the rhodium(III) complex $[LRh^{III}I(CO)CH_3]$, have been investigated by FTIR spectroscopy.[128] The second-order rate constant was found to be 5×10^4 faster than for reaction of $[RhI_2(CO)_2]^-$.

(12)

The large negative value of $\Delta S^{\neq}$ (-179 ± 11 J mol^{-1} K^{-1}) is consistent with a highly ordered transition state for attack on CH_3I by Rh(I) in an S_N2 mechanism. The nucleophilicity of $[LRh^{I}(CO)]$ toward CH_3I is the highest measured and recorded to date for an Rh(I) carbonyl complex. It appears that the mono-anionic donor set is responsible. It was noted that a square-planar Rh(I) complex that does not contain an electron-withdrawing carbonyl ligand imparts an even higher nucleophilicity.

In the context of exploring potential catalysts for the alternating co-polymerization of CO and alkenes to yield polyketones, the rhodium(III) complex $[Cp^*Rh(CO)_2CH_3][BF_4]$ has been prepared. Its attraction arose from the fact that the cation had been prepared as a reactive intermediate in the oxidative addition of CH_3I to $[Cp^*Rh(CO)_2]$.[129] The co-polymerization has usually been achieved using Pd(II) complexes containing bidentate *P*,*P* or *N*,*N* ligands.[130,131] Reaction of $[Cp^*Rh(CO)_2CH_3][BF_4]$ with strained alkenes, norbornadiene (nbe), norbornene (nbd), and dicyclopentadiene yielded the expected and stable products, which were isolated and fully characterized (IR spectra, and in two cases by X-ray crystallography).[132] The reactions of the complex with a ligand, alkene, or phosphine, were rapid and required an SF device equipped with IR monitoring capability. An excess of ligand was used and pseudo-first-order rate constants plotted against ligand concentrations showed a saturation pattern. Further analysis and a study of temperature dependence demonstrated that the methyl migration step is independent of the ligand, whether alkene or phosphine, and is characterized by $\Delta H^{\neq} = 72$ kJ mol^{-1} and $\Delta S^{\neq} = -16$ J mol^{-1} K^{-1}. The relative nucleophilicities toward the intermediate could be extracted from the kinetic data and were $PPh(CH_3)_2 > PPh_2(CH_3) > PPh_3 >$ nbd > nbe. It prevailed that replacing the Cp^* component with an indenyl ligand (Ind = η^5-$C_5(CH_3)_7$) gave more promise of a potential catalytic co-polymerization agent. Kinetic measurements, monitoring again by IR spectroscopy, were used to chart reaction progress including detection of intermediates. Determination of the structural features of the polymer produced was reported to be in progress.

A novel method of studying rhodium-catalyzed hydroformylation of 1-octene, 1-butene, propene, and ethene has been described. Polyethylene film is impregnated with the rhodium catalyst (either $[Rh(acac)(CO)_2]$ or $[Rh(acac)(CO)(PPh_3)]$) and substrate and subjected to a high pressure of hydrogen within a high-pressure, low-temperature copper cell especially developed for this and related reactions (*vide supra*).[133] The reaction can be monitored by IR spectroscopy and, potentially, intermediates can be detected. Detailed kinetic measurements were not reported, but importantly, using $[Rh(acac)(CO)_2]$ as the catalyst, the acyl-rhodium tetracarbonyl intermediate, $[RC(O)Rh(CO)_4]$, could be characterized by IR spectroscopy. In addition, when using the PPh_3-modified catalyst, the acyl-rhodium tricarbonyl triphenyl phosphine intermediates, $[RC(O)Rh(CO)_3(PPh_3)]$, were observed, and the IR spectra suggested a trigonal-bipyramidal structure with the acyl ligand and PPh_3 occupying the axial positions. The polymer matrix technique has also been applied in studies of the thermal reaction of $[Rh(acac)(CO)_2]$ with alkenes in the absence or presence of hydrogen at high pressure. Rhodium alkene complexes [Rh(acac)(CO)(alkene)] were produced and characterized by IR spectroscopy. In the presence of a high pressure of hydrogen, catalytic hydrogenation of the alkenes was achieved. The sequence ligand loss, binding of an alkene, oxidative addition of hydrogen to the metal center, insertion of the coordinated alkene into the M–H bond, and reductive elimination of the alkane was consistent with the observations. The [Rh(acac)(CO)] species was proposed as the active catalytic species.

The application in rhodium chemistry of ^{103}Rh NMR spectroscopy, pertinent to its current status, has recently been presented thoroughly.[134] A broad selection of rhodium compounds was included; for example, migration insertion reactions involving phosphine-induced phenyl migration onto coordinated carbon monoxide in [Rh(I)Cp*(C_6H_4–X)(CO)] to yield rhodium acyl species were studied. A good correlation of the kinetic data with δ(^{103}Rh) of the reaction products was found. This suggests that the substitution proceeds through a late transition state with a product-like intermediate. The review contained concluding comments that other aspects of the mechanism should be known, rather than only relying on ^{103}Rh shifts. Another reaction example cited was the oxidative addition reaction of [Rh$^{\text{I}}$(Br)(4′-(4-tertbutylphenyl)-2,2′ : 6′2″-terpyridine)] with various alkyl bromides, containing (mainly terminal) carbon–bromine bonds.[135] The products are soluble in organic solvents and have been characterized by ^{1}H, ^{13}C, ^{15}N, and ^{103}Rh NMR spectroscopies. UV/visible spectrophotometry was used to monitor the kinetics of the latter rhodium(I) complex with 1-bromodecane in ethanol; isobestic points were observed. Derived kinetics parameters were not reported and it was opined that the involvement of intermediates could not be ruled out.

Many investigators have drawn attention to the complexities involved in addressing the mechanisms of dissociative electron transfer processes.[67,136] The mechanism may be concerted or consecutive, and many reports on what is termed an electron-transfer square scheme have appeared. Choosing a suitable system for study to shed light on the mechanism has been debated. Promising systems cited were the hydrotris(pyrazolyl)borate complexes of rhodium, in which an Rh(I)/Rh(II) redox couple is linked to formation and disruption of an Rh–N σ-bond. The Rh(II) compounds display κ^3-bonding of Rh with one N from each pyrazolyl ring, resulting in five-coordinate 17-electron cations such as [Rh(CO)(PPh_3)Tp^{Me_2}]$^+$, Tp^{Me_2} = hydrotris(3,5-dimethylpyrazolyl)borate **2**, **3**.

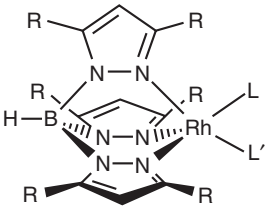

2

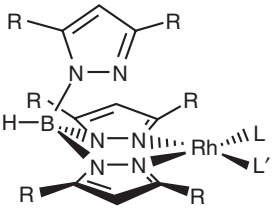

3

The neutral Rh(I) compounds [RhLL′Tp^{Me_2}], where L or L′ is a P-atom donor, CO, or another ligand, display either strictly κ^2-bonding to the Tp^{Me_2} ligand, resulting in a four-coordinate metal, or in an equilibrium between compound 2 and weak κ^3-Tp^{Me2} coordination. Changes in the ligands (either L or substituents on the Tp ring) affect the favored structures, with κ^2-coordination being favored by more bulky ligands. Compound 1 has L = CO, L′ = $P(OPh)_3$; compound 2 has L = CO, L′ = PPh_3; compound 3 has L = CO, L′ = PCy_3; and compound 4 has L = L′ = PPh_3, and R = Me.

Cyclic voltammetry experiments revealed contrasting voltammetric patterns for different compounds that ranged from qualitatively reversible to irreversible cyclic voltammograms, although the various derivatives undergo the same chemically reversible one-electron Rh(I)/Rh(II) redox reaction.

$$[\text{RhLL}'(\kappa^2\text{–Tp}^{\text{Me}_2})] \rightleftharpoons [\text{RhLL}'(\kappa^3\text{–Tp}^{\text{Me}_2})]^+ + \text{e}^- \qquad (13)$$

The electron transfer kinetics steps for compounds 3 and 4 of both the original oxidation and subsequent re-reduction processes are rate limiting, giving rise to totally irreversible heterogeneous charge-transfer reactions. These events were modeled by a square scheme.[136] The conclusion for these two compounds was that the overall process comprises a reversible sequence of intramolecular associative and dissociative electron transfer reactions involving formation and cleavage, respectively, of the Rh–N(2) apical bond. Compounds 1 and 2 exhibit a quasi-Nernstian pattern for which either a single step (concerted) process or a sequential process comprising relatively rapid reactions can be invoked. Structural differences were used to rationalize the differences. In compounds 3 and 4, the bulky L and L′ ligands impose steric constraints both on the electron transfer process and on the subsequent formation of the Rh–N(2) bond that is necessary to yield the square-pyramidal cationic Rh(II) oxidation product. In compound 1, the rhodium d_z^2 orbital is already pointed toward the N(2) position, thus minimizing the rearrangement energy necessary to form the Rh–apical N(2) bond.

A report, in which the reactivities of corresponding complexes of rhodium and iridium with respect to, principally, oxidative addition of methyl iodide are studied, is featured in the section on iridium compounds below.

1.19.4.9 Organopalladium

Following efforts to elucidate the mechanism of hydrocarbon functionalization (the Shilov system), attention was directed to exploiting oxidation of Pt(II) complexes by O_2 to circumvent the use of stioichiometric quantities of Pt(IV).[137,138] Since oxidation of arenes to phenols and alcohols to aldehydes or ketones had been accomplished using Pd catalysts and O_2, it was decided to apply an alternate strategy. The proposal involved a Pd(0)/Pd(II) redox couple and O_2 utilization, and studying the potential of Pd(II) effecting C–H activation and development of a catalytic cycle.[139] Analysis of the literature led these authors to select the Pd(II) complex [(α-diimine)Pd(CH_3)(H_2O)][BF_4] for an investigation of its intermolecular C–H activation.[140] The kinetics of the reaction of benzene with the Pd(II) complexes in the presence of O_2 were monitored by ^{1}H NMR spectroscopy. Trifluoroethanol-d_3 was used to replace H_2O in the reactant complex. Disappearance of the starting material occurred at the same rate as the production of the biphenyl product. Rate constants were determined for reaction of C_6H_6 and C_6D_6 and yielded a kinetic isotope effect of 4.1, indicating that a C–H bond cleavage step is rate determining. The fact that the reaction was inhibited by water implied that the coordinated H_2O is indeed displaced by trifluoroethanol solvent, before benzene coordination and subsequent C–H activation. A catalytic process was not observed but the method of O_2 activation holds promise for converting unactivated arenes to biaryls. Comparison and contrast with relevant platinum chemistry was discussed.

Other unrelated studies have compared and contrasted reactivities of the complexes of the second-row palladium with analogs of the third-row platinum.[141] The platinum-catalyzed methoxycarbonylation of ethene was monitored by *in situ* NMR spectroscopy for comparison with the corresponding palladium-catalyzed methoxycarbonylation of ethene to methylpropanoate. The latter reaction is involved in the production of methylmethacrylate. The platinum complex in question was [Pt(L–L)H(CH_3OH)][CF_3SO_3], where L–L = 1,2-($CH_2PBu^t_2$)$_2$(C_6H_4). Although the overall pathways for the two metal species were analogous, in the case of platinum, carbonyl complexes that are formed function as thermodynamic sinks for the reaction, effectively removing Pt from the catalytic cycle. The palladium system is highly active in contrast. The product-forming reactions are readily reversible in the Pt system. Together, these factors account for the low activity of Pt complexes in the methoxycarbonylation of ethene.

The participation of cationic diphosphine/diphosphane palladium complexes as catalysts for the co-polymerization of CO with alkenes and in the alkoxycarbonylation of alkenes has been studied extensively.[142] Quite recently, delineation of the initiation, propagation, and termination steps of the cycle has been reported.[143] The systems are very complex to permit readily detailed kinetics experiments. However, the mechanistic steps and reactivity of those steps have been established, by principally, NMR spectroscopic methods.

1.19.4.10 Organorhenium

Oxygen atom transfer (OAT) reactions catalyzed by oxorhenium(V) compounds have been comprehensively reviewed.[144] Some recent developments include a focus on nucleophilic assistance in this process, and a study in which the ligand-substitution reaction that precedes OAT is examined in detail.[145] In the former report, oxygen atom transfer from pyridine *N*-oxide to triphenylphosphine catalyzed by [CH_3ReO(mtp)PPh_3] (ReX), where mtpH_2 is 2-(mercaptomethyl)thiophenol, has been monitored. Reaction was carried out in benzene and following the absorbance of pyridine *N*-oxides, (PyO), by UV spectrophotometry. The rate law was established to be:

$$R = k_N[ReX][PyO]^2/[PPh_3] \quad (14)$$

In the presence of added nucleophiles N, the rate law became:

$$R = k_N[ReX][PyO][N]/[PPh_3] \quad (15)$$

A correlation approach based on the Hammett LFER, in which values of $\log(k_N^X/k_N^H)$ were plotted against σ_x values for each of the XC_5H_4N-added nucleophiles and yielded linear relationships with ρ values of -1.0 for 4-nitro-2-methylpyridine *N*-oxide and -2.6 for 4-methylpyridine *N*-oxide. The significance of these reaction constants was discussed.

The second report includes the preparation of new methyl(oxo)rhenium(V) complexes, [CH_3ReO(edt)(SPh)(PicH)], [CH_3ReO(edt)(SPh)(LutH)], and [CH_3ReO(edt)(SCN(CH_3)$_2$)] where edt is 1,2-ethanedithiolate, PicH is the 2-picoliniumH^+ species, and LutH is the 2,6-lutidiniumH^+ species.[146] Ligand-substitution reactions of these complexes with PPh_3 and pyridine were monitored kinetically, in $CHCl_3$, by conventional or SF spectrophotometry. These reactions and OAT reactions with pyridine *N*-oxides were followed under pseudo-first-order conditions with the

rhenium complexes in limiting concentration. Ligand substitution in which PPh_3 replaces PhSH follows second-order kinetics (first-order in each reactant), whereas when pyridine is displaced a complex rate law was found which includes the conversion of the cation. The neutral rhenium compound by contrast upon reaction with either PPh_3 or pyridine follows second-order kinetics. The OAT reactions yielded two or three distinct phases. Various reaction schemes were advanced to account for these observations. Coordination geometry around rhenium was considered. The cleavage of the O–Py bond is subject to nucleophilic assistance. Substituted pyridine *N*-oxides yielded massive (Hammett) rho values for both the first and second steps; potential causes and explanations were offered.

Following the unexpected observation that, providing perchlorate ions are absent, hydrogen gas is evolved upon mixing $(CH_3)Re^{VII}O_3$ with Eu^{2+} ions in acidic solution, a comprehensive study of the kinetics of this and other pertinent reactions was undertaken.[147] SF spectrophotometry and a recording gas microvolumeter for hydrogen gas evolution were the principal methods employed:

$$2Eu^{2+} + 2H^{+} \xrightarrow{MeReO_3} 2Eu^{3+} + H_2(g) \qquad (16)$$

A key intermediate was determined by spectrophotometric titration and required a $[Eu^{2+}]/[CH_3ReO_3]$ ratio of 3, and it was deduced that the intermediate is an Re(IV) species. A thorough analysis of kinetic parameters allowed postulation of a mechanism for evolution of hydrogen. It is formed from a reaction between an $H–Re^{V}O$ species and H^{+}. Comparable experiments with aqueous Cr(II) ions did not result in evolution of hydrogen. It was argued that this was a consequence of production of an inert derivative of Re(IV) and Cr(III), in which both metals possess d^3 electronic configurations **4**.

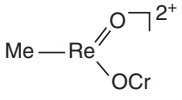

4

A complete scheme containing all the redox reactions and possible intermediate species was presented. In the presence of perchlorate ions, CH_3ReO_2 reduces perchlorate to chloride, confirming an earlier finding.

To address the question of rates of protonation of an oxo ligand of rhenium, it was proposed that a suitable stable, that is, not too labile, complex would be one in which the two butyne ligands in $[Re(O)(C_2H_5)(CH_3C{\equiv}CCH_3)_2]$ were replaced by a chelating diyne.[148] Accordingly, a complex [Re(O)I(2,7-nonadiyne)] was prepared and characterized. Upon mixing with CF_3SO_3H in CH_3CN at −40 °C in an SF apparatus, absorbance changes occurred and the resulting spectra were recorded typically over the range 380–600 nm. Two rate processes were observed and second-order rate constants extracted. These were presumed to relate to successive protonations. Using low temperature ^1H NMR spectroscopy, two doubly protonated intermediates were detected, each of which formed the product, $[Re(CH_3CN)_3(I)(2,7\text{-nonadiyne})]^{2+}$, which was characterized spectroscopically and by X-ray crystallography. During the conversion, the conformation of the diyne ligand changes from a "chair" to a "boat." The different observations from the two techniques (UV/visible and NMR spectroscopies) could be rationalized.

Many studies of the photophysics of rhenium diimine complexes have been carried out, but very little attention had been paid to the triplet ligand-field (^{3}LF) states (see Ref: **150** and references therein). Following the finding that rhenium polypyridine tricarbonyl complexes with a phosphorus ligand such as *fac*-$[Re(X_2bpy)(CO)_3(PR_3)]^{+}$ are readily photoactive ($X_2bpy = 4, 4'\text{-}X_2\text{-}2,2'$-bipyridine), a systematic investigation of the excitation, and consequences thereof, of nine of such complexes was conducted.[149] In acetonitrile solution, the substitution selectively yields the bis-carbonyl complexes, *cis*,*trans*-$[Re(X_2bpy)(CO)_2(PR_3)(CH_3CN)]^{+}$. The CH_3CN substitutes a CO ligand *trans* to the PR_3. These reactions, at the time, were the first examples of photo-induced ligand-substitution reactions of rhenium diimine tricarbonyl complexes via their ^{3}LF excited states. The photochemical states were described in terms of a Jablonski diagram. The substitution mechanism was found to be dissociative. Thermodynamic parameters have been obtained for the ^{3}LF excited states of the reactant complex, and were obtained from the data on temperature dependence for emission lifetimes and for the quantum yields of the photochemical reactions and emission. Measurement methods included UV–visible spectrophotometry, TRIR, emission spectroscopy, photochemical initiation, a multichannel spectrophotometer, and ^{13}C NMR spectroscopy.

1.19.4.11 Organoiridium

A comprehensive study of the role of metal-carbonyl complexes and metal iodides that act as promoters of the catalysis of methanol carbonylation by iridium complexes has been undertaken.[54] Kinetics aspects of this study involved *in situ* monitoring by IR of the contents of a modified autoclave system. A catalyst resting state was identified as *fac*,*cis*-$[Ir(CO)_2I_3(CH_3)]^-$. This species can undergo stoichiometric carbonylation to $[Ir(CO)_2I_3(COCH_3)]^-$, and this process is accelerated by substoichiometric amounts of neutral promoter species, examples of which are $[Ru(CO)_3I_2]_2$, InI_3, GaI_2, and ZnI_2. The rate increases are approximately proportional to promoter concentration in the promoter/iridium ratio of 0 to 0.2. Anionic complexes such as $[Ru(CO)_3I_3]^-$ do not promote the carbonylation process. A promoter appears to operate by abstracting an iodide ligand from the Ir center and allowing coordination of CO to give $[Ir(CO)_3I_2(CH_3)]$. Migratory CO insertion into the latter complex is about 700 times more rapid than into *fac*,*cis*-$[Ir(CO)_2I_3(CH_3)]^-$. These findings were supported by X-ray crystallographic studies, determination of activation parameters, and by HPNMR spectroscopy. *Ab initio* calculations indicated that the principal factor responsible for the more facile reaction was decreased π-back-donation to the carbonyl ligands in $[Ir(CO)_3I_2(CH_3)]$ relative to that in *fac*,*cis*-$[Ir(CO)_2I_3(CH_3)]$. Many other aspects and reactions relating to relevant catalysis cycles were also thoroughly examined.

The subject of carbonylation of methanol has been addressed in further studies from some of the same investigators.[150] This latter report examines comparative features regarding rates and mechanistic pathways for rhodium/iodide- and iridium/iodide-based processes. It has been shown earlier that oxidative addition of methyl iodide to the anionic $[Rh(CO)_2I_2]^-$ species is rate determining and that migratory CO insertion into $[Rh(CO)_2I_3(CH_3)]^-$ is relatively rapid.[124] In the Ir system, CH_3I oxidative addition to $[Ir(CO)_2I_2]^-$ is more than 100 times faster than it is for the Rh analog, and as indicated above, $[Ir(CO)_2I_3(CH_3)]^-$ is the catalyst resting state.[124,151,152] Carbonylation of $[Ir(CO)_2I_3(CH_3)]^-$ is rate limiting and occurs via substitution of an iodide ligand by CO to yield the neutral complex $[Ir(CO)_3I_2(CH_3)]$, which can be subject to rapid migratory CO insertion. Part of the emphasis in this study[150] was an examination of neutral complexes of rhodium in this context. In CH_3CN, reaction between the neutral rhodium(I) dimeric species $[Rh(CO)_2I]_2$ and CH_3I leads to stable Rh(III) acetyl products, for example, the iodide-bridged dimer $[Rh(CO)_2(NCCH_3)(COCH_3)I_2]_2$. This latter species and the precursor dimer can both be cleaved in CH_3CN to yield $[Rh(CO)_2(NCCH_3)I]$ and $[Rh(CO)(NCCH_3)_2(COCH_3)I_2]$, respectively. The kinetics of the reaction of the former complex with CH_3I are zeroth order in the concentration of the rhodium complex as monitored by IR spectroscopy, and participation of the anionic species $[Rh(CO)_2I_2]^-$ as an intermediate was invoked (based upon IR spectroscopy evidence). In other words, the rate-determining step is not a direct bimolecular reaction between the reactant species. From the analyses of all the results and species observed, it was argued that neutral Rh(III) methyl and acetyl complexes may be significant intermediates in Rh-catalyzed methanol carbonylation. To address the comparative properties, the kinetics of oxidative addition of CH_3I to $[Ir(CO)_2(NCCH_3)I]$ were monitored by IR spectroscopy. The reaction was determined to be first order in each reactant, and the second-order rate constant was found to be two orders of magnitude smaller than that also determined for the corresponding reaction of $[Ir(CO)_2I_2]^-$, reflecting the profound effect of removing an iodide ion. It was noted that the second-order rate constants for oxidative addition of the neutral $[Ir(CO)_2(NCCH_3)I]$ and the anionic $[Rh(CO)_2I_2]^-$ are very similar. Activation parameters for reaction of $[Ir(CO)_2(NCCH_3)I]$ and $[Ir(CO)_2I_2]^-$ were almost identical ($\Delta H^{\neq}$), but $\Delta S^{\neq}$ was much more negative for the former complex, which was suggested to be attributable to stronger solvation of the polar transition state derived from two neutral reactants.

A very recent report has addressed the longstanding issue of oxidative addition of ammonia.[153] The objective is to generate an amido hydride complex formed by cleavage of an N–H bond. Existing iridium chemistry was exploited to prepare a complex that would insert into the N–H bond of ammonia. A hydridoiridium amido complex containing a terdentate pincer-type ligand had been shown to form rapidly the N–H bond in an ammonia complex at room temperature by reductive elimination. It was reasoned that appropriate modification of the iridium complex could shift the thermodynamic balance from rapid formation to rapid cleavage of the N–H bond in ammonia. It was proposed that a pincer ligand with an aliphatic rather than an aromatic backbone would be more electron donating and therefore favor N–H insertion. When the complex shown (below, at left) was treated with ammonia in cyclohexane, a monomeric amido iridium complex was prepared rapidly in high yield. It was characterized by combustion analysis, X-ray diffraction, and by NMR spectroscopic methods. Kinetic studies were undertaken to establish the reaction pathway. Out of a possible four reaction routes, two were identified as the most likely. One was an associative path C in which NH_3 would react directly with the iridium complex, and the second would be a dissociative pathway D in which NH_3 would react with a 14-electron complex formed after the dissociation of the complexed olefin. ^{31}P NMR spectroscopy was used to monitor the reaction kinetics using various amounts of olefin

and ratios of ammonia to olefin. Isotopic-labeling studies were also conducted and provided useful criteria for mechanistic determination. Treatment of the results permitted the conclusion that the mechanism followed is dissociation of the olefin from the complex (path D) and NH_3 then reacts with the 14-electron iridium(I) fragment under neutral conditions.

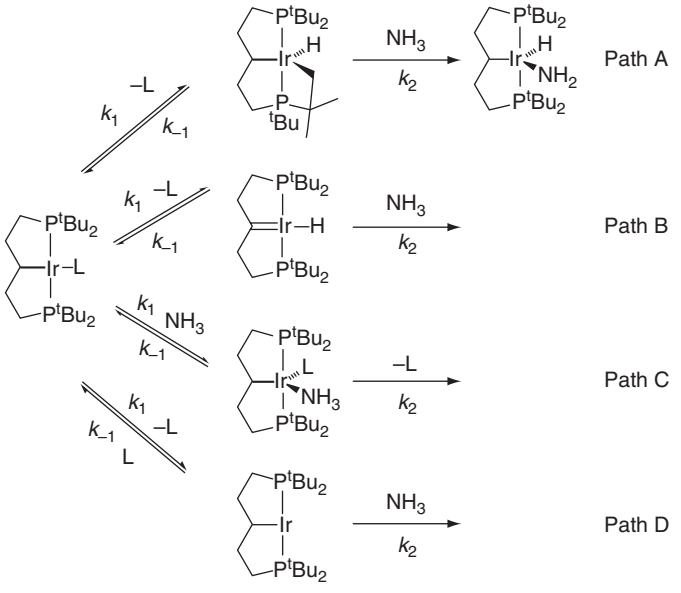

(17)

Thus, N–H bond cleavage in this system provides a foundation for the development of mild catalytic transformation of ammonia as in arene-oxidative amination and olefin hydroamination.

1.19.4.12 Organoplatinum

The subject of homogeneous hydrocarbon C–H bond activation and functionalization with platinum has been authoritatively reviewed, including literature reports up to and including most of 2003.[156] A notable example from earlier work presented evidence for an associative mechanism for benzene substitution at a platinum(II) center.[155] This report specifically addressed the mechanism in the first key step in the multistep catalytic cycle of a Shilov-type system.[156] The reaction of the platinum(II) methyl cation $[(N–N)Pt(CH_3)(solv)]^+$, (N–N) = ArN = C(Me)C(Me) = NAr, Ar = 2,6-$(CH_3)_2C_6H_3$, solv = H_2O or TFE, TFE = CF_3CH_2OH, with benzene in TFE/H_2O mixtures afforded the platinum(II) phenyl cation $[(N–N)Pt(C_6H_5)(solv)]^+$. To resolve the mechanism of the mode of entry of benzene into the coordination sphere, high-pressure kinetics studies were undertaken, monitoring UV/visible absorbance changes. The reaction was accelerated by pressure yielding a negative volume of activation. This was made up of a reaction volume term for the displacement of the coordinated water by TFE and a second term for the volume of activation for the activation of benzene by the TFE solvento complex. The latter could be obtained as $-9.5\,cm^3\,mol^{-1}$ which, together with the negative entropy of activation, supported clearly the operation of an associative mechanism.

The current status regarding oxidative addition and reductive elimination reactions involving platinum complexes has been described thoroughly in introducing a pivotal study of the mechanism of C–C and C–H alkane eliminations from octahedral complexes of Pt(IV).[157] Specifically, these authors[157] have addressed the mechanistic question whether the reductive elimination in the complexes chosen proceeds via a five-coordinate intermediate or by direct elimination. The platinum(IV) complexes, P_2PtMe_3R [P_2 = dppe ($PPh_2(CH_2)PPh_2$), dppbz (*o*-$PPh_2(C_6H_4)PPh_2$); R = CH_3, H], were among the complexes employed. Thermolysis of the complex when P_2 = dppe and R = CH_3, in C_6D_6, was monitored kinetically by ^1H NMR spectroscopy and required elevated temperatures (165–205 °C). A wealth of evidence suggested elimination of ethane occurred by a mechanism that involved dissociation of one end of the phosphine chelate to form a five-coordinate intermediate before C–C bond formation. A dramatic rate reduction

(two orders of magnitude) of the elimination of ethane occurred when the complex contained the more rigid biphosphine chelate, dppbz. The observation that *fac*-(dppe)$PtMe_3Et$ undergoes *fac*/*mer*-isomerization in conjunction with β–hydride elimination supports the opening of the dppe chelate prior to C–C coupling. Reductive elimination of methane from *fac*-(dppe)$PtMe_3H$ and *fac*-(dppbz)$PtMe_3H$ occurred at closer to ambient temperature and with almost identical rates and similar activation parameters ($\Delta H^{\neq}$ and $\Delta S^{\neq}$obtained in the 40–80 °C range). It was concluded, therefore, that these reactions occur directly from six-coordinate geometry, and are the first examples where mechanistic evidence points to direct reductive elimination from octahedral Pt(IV) alkyl complexes.

Five-coordinate alkyl Pt(IV) complexes have been proposed as short-lived intermediates in platinum-catalyzed alkane functionalization cycles. Hence, interest in preparing suitable complexes to enable their chemistry to be studied has arisen.[158] Novel five-coordinate platinum(IV) alkyl complexes with a variety of β-diiminate ligands have been prepared and have been shown to be useful precursors to unsaturated Pt(II) species for alkane.[158] Stoichiometric alkane dehydrogenation was observed using either a five-coordinate Pt(IV) species or an olefin hydride complex. Mechanistic proposals were based on ^{1}H NMR spectroscopic measurements and, in one case, on X-ray crystallographic characterization of a product. Kinetic details were not reported in this communication, but the systems hold potential promise, and conversion to a catalytic system may be feasible upon further investigation.

Although this communication[159] was included in a comprehensive review,[154] it is worth emphasizing the decisive way a well-designed and well-executed set of kinetics experiments can yield convincing evidence of a particular mechanistic route when more than one appears reasonable. Studies of the microscopic reverse of the C–H activation step in relevant platinum complex chemistry have been conducted. Diimine-$Pt^{II}(CH_3)_2$ complexes have been protonated in CH_3CN solution, whereby either a Pt(IV)-hydridomethyl complex is formed (direct protonation of platinum), or a Pt(II)-σ-methane species is produced. These two species undergo facile interconversion. The hydridomethyl complex is irreversibly trapped by CH_3CN to yield a six-coordinate species, whereas the σ-complex is associatively substituted by CH_3CN to eliminate CH_4. The product ratios could be determined by ^{1}H NMR spectroscopy, with the relative yield of the latter species decreasing with increasing CH_3CN concentration. From convincing arguments based on relative values of rate constants in these reactions, it could be concluded that the initial protonation occurs exclusively or mostly at Pt. It would then follow that, in the general Shilov mechanism, deprotonation must occur from a Pt(IV)-hydridomethyl complex rather than from a Pt(II)-σ-methane complex. Some time earlier, in considering the reaction of transition metal-hydride complexes with protons, it had been shown by a comprehensive kinetics study employing SF spectrophotometry and NMR spectroscopic methods that in the complex $CpW(CO)_2(P(CH_3)_3)H$, the site of protonation is the hydride ligand rather than the metal.[160] Clearly, different pathways may be anticipated in systems consisting of different metals with different surrounding ligands.

A systematic study of the microscopic reverse reaction of the C–H bond activation that occurs upon reaction of [K(κ^2-$Tp^{Me_2}Pt^{II}Me_2$)] with $B(C_6F_5)_3$ has been carried out.[161] The kinetics of C–H reductive elimination from [κ^3-$Tp^{Me_2}Pt^{IV}Me_2(H)$] in several solvents have been monitored by ^{1}H NMR spectroscopy. The nature of the platinum-containing product was noted to depend upon the solvent. The reductive elimination of CH_4 followed first-order kinetics characterized by rate constants that were nearly independent of solvent. Activation parameters obtained from measurements of temperature dependence were virtually the same in C_6D_6 and in toluene-d_8. That scrambling of hydrogen atoms between the methyl and hydride positions of the reactant complex occurs and the related energetics could be extracted from the kinetic data. A σ-methane complex [κ^2-$Tp^{Me2}Pt^{II}Me(CH_4)$], as a common intermediate in both the scrambling and reductive elimination processes, and the loss of methane by a dissociative process, were proposed. Clearly, pathways in these processes can vary, depending upon the metal, charge, and ligand set; many other substitution reactions at Pt(II) proceed by an associative mechanism.

An analysis of factors that could lead to enhanced tendency of a platinum(II) (or palladium(II)) complex to activate C–H bonds has led to the design and preparation of Pt(II) complexes that might exhibit such a property.[162] The complexes contain chelating pyridine NHC donors, *N*-(2-pyridyl)-R-pyridine-2-ylidene, where R = H, 4-*tert*-butyl, 4-dimethylamino, or 5-dimethylamino, and are abbreviated [(R-iso-bipy)$Pt(CH_3)L$][X^-], using R-iso-bipy to indicate the ligands are isomeric forms of 2,2′-bipyridine, and where L = SMe_2, DMSO, or CO, and X is tetrafluoromethanesulfonate (Otf^-) or [BPh_4^-]. X-ray crystallographically obtained structures, NMR parameters, and carbonyl stretching frequencies were examined to assess possible enhancement due to σ-donor and π-acceptor capabilities that could facilitate substitution of a *trans*-ligand. Degenerate DMSO exchange kinetics were determined using a ^{1}H NMR magnetization transfer kinetics method. Second-order rate constants ranged from 30 to 10^4 times greater than those for structurally similar cationic bis(nitrogen) donor complexes [(N–N)$Pt(CH_3)(DMSO)]^+$ and a neutral complex derived from cyclometallated 2-phenylpyridine [$(C_{11}H_8N)Pt(CH_3)(DMSO)$]. These accelerations were attributed primarily to stabilization of transition state energies and contributions from π-acceptors and weaker σ-donors. These conclusions were rationalized using orbital diagrams and examining the *trans*-influence of the carbene donor.

A wide-ranging study of several cyclometallated analogs of platinum(II) terpyridine/chloro complexes has been undertaken.[163] Crystal structures were determined, and substitution kinetics experiments in methanol were conducted. The nucleophiles Br^- and Cl^- were employed, and in two cases, [Pt(N-N-C)Cl] and [Pt(N-C-N)Cl], substitution kinetics with TU, DMTU, and TMTU were measured. N–N–CH is 6-phenyl-2,2′-bipyridine, N–CH–N is 1,3-di(2-pyridyl)benzene, TU is thiourea, and DMTU and TMTU are the dimethyl and tetramethyl analogs of TU. The complexes are schematically represented below **5**.

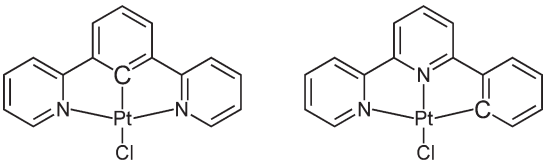

N–CH–N **5** N–N–CH

One principal objective of this study was an examination of the relationship between σ-donor and π-acceptor effects in Pt(II) chemistry. The much higher reactivity observed for the N–C–N compound was reflected in a 20 kJ mol^{-1} lower activation enthalpy than for the N–N–C compound. This was explained by citing the influence of the *trans*-phenyl group in destabilizing the ground state, thus facilitating cleavage of the leaving group to Pt bond. For the N–N–C compound, the activation enthalpy sequence was TMTU < DMTU ≈ TU, whereas for the N–C–N compound the relationship was TMTU < DMTU < TU, a sequence not in accord with expected reactivity trends. It was concluded that differences in activation entropies were responsible for the observed steric retardations. High hydrostatic pressure kinetics yielded negative volumes of activation for the three thiourea ligands reacting with the N–N–C and N–C–N compounds. A volume contraction occurs upon forming the transition state arising from the bond formation by the entering nucleophile, although this is partially offset by the geometry changing from square planar to trigonal bipyramidal. In the case of the N–C–N compound, the platinum–ligand bonds of the entering and leaving ligands are longer due to the *trans*-influence; thus, the observed $\Delta V^{\neq}$ values were less negative for the N–C–N reaction than for the reaction of the N–N–C compound where the corresponding bonds are shorter. From these results and copious literature on substitution reactions of Pt(II), it was concluded that the magnitude and direction of the *cis*-effect (as compared to the *trans*-effect of the same ligand) depend on the σ-donor strength, π-acceptor ability, and the steric property of the *cis*-ligand. The relative magnitudes of these factors and their subtle interplay have consequences for reactivities of these and related compounds.

In a related investigation, the roles of chelate substituents and the *cis*-σ-effect on the rate of ligand substitution at Pt(N–N–N) and Pt(N–N–C) centers were explored.[164] The terdentate ligands were 2,2′:6′,2″-terpyridine (terpy), 4′-Ph-terpy, 4′-(2‴-CF_3-Ph)-terpy, and 4′-(2‴-CF_3-Ph)-6-2,2′-bipy, and the remaining position was occupied by the chloro ligand. The rates of substitution of the chloro ligand by TU, DMTU, and TMTU were monitored as a function of incoming nucleophile concentration, temperature, and pressure by SF spectrophotometry. The reaction was first order in both platinum complex and nucleophile concentrations. The form of the rate law, together with the negative activation entropies and volumes, supported an associative substitution mechanism. Substitution in the terpy parent ligand did not affect the kinetic parameters significantly. The reaction was slower when a carbon σ-donor was in the *cis*-position than when an N σ-donor was present. This indicates a different situation from the effect of a Pt–C bond in the *trans*-position.

The acquisition of the volume of activation proved to be a valuable parameter for understanding the mechanism of substitution accompanied by isomerization in cyclometallated dimethylhalo-platinum(IV) complexes.[165] During the study of the substitution reactions of several *cis*-(CH_3/$S(CH_3)_2$)-arranged dimethylhaloplatinum(IV) complexes (PPh_3 substitutes the $S(CH_3)_2$ group), an intramolecular isomerization was detected in two cases. The latter process was monitored by low temperature ^1H and ^{31}P NMR spectroscopies and could be described as a very energetically demanding turnstile twist-type reorganization of the molecule, following a significant degree of dissociation of the ligand. The activation parameters were: $\Delta H^{\neq} \approx 100\,kJ\,mol^{-1}$, $\Delta S^{\neq} = +88$ and $+49\,J\,mol^{-1}\,K^{-1}$, and $\Delta V^{\neq} = +15$ and $+20\,cm^3\,mol^{-1}$. A substantial increase in volume in forming the transition state was therefore indicated. In other cases, *mer*/*fac* ratio dispositions introduced complexities.

Cationic platinum(II) complexes of the type $[(NN)Pt(CH_3)(CF_3CH_2OH)]^+$ have been used in mechanistic studies aimed at discovering new catalysts for selective hydrocarbon functionalization.[166] When excess benzene reacts with a mixture of $[(NN)Pt(CH_3)(CF_3CD_2OD)]^+$ and $[(NN)Pt(CH_2D)(CF_3CD_2OD)]^+$, where NN is $ArN=C(CH_3)–C(CH_3)=NAr$, a rapid reaction ensued, yielding second-order kinetics. Aromatic activation was not

observed when the corresponding reaction with mesitylene was studied, as exclusively benzylic activation occurred, affording $[(NN)Pt(CH_2C_6H_3(CH_3)_2)(CF_3CD_2OD)]^+$. Interestingly, *p*-xylene gave rise to both aromatic (Pt-2,5-$(CH_3)_2C_6H_4$) and benzylic ($Pt(CH_2C_6H_4CH_2)$) activation, although the former was converted to the latter by reaction of the former by *p*-xylene rather than by intramolecular isomerization. The observations were made that toluene reacts in an analogous manner to *p*-xylene. Kinetic isotope effects, different for sp^2 and sp^3 C–H bond activation, were not readily explained. Preference for benzylic C–H activation appeared to result from stabilizing η^3-bonding.

1.19.5 Examples of Kinetics Studies of Organometallic Reactions in Ionic Liquids

In order to probe the potential use of room temperature ionic liquids (RTILs) as media for transition metal-based catalysts, a study comparing the displacement rate of an RTIL with those for conventional solvents, each coordinated to a transitional metal center, has been undertaken.[167] It had been noted that kinetic studies of such reactions of RTILs have not been reported.[168] The system chosen was the chromium complex $[(C_6H_6)Cr(CO)_3]$, since it is readily converted by ultraviolet photolysis to $[(C_6H_6)Cr(CO)_2(solv)]$.[167]

$$[(C_6H_6)Cr(CO)_3] + solv + h\nu \rightarrow [(C_6H_6)Cr(CO)_2(solv)] + CO \quad (18)$$

Solvents that are weakly bound can then be replaced by a ligand L by a bimolecular exchange mechanism, characterized by a rate constant k_2.

$$[(C_6H_6)Cr(CO)_2(solv)] + L \rightarrow [(C_6H_6)Cr(CO)_2L] + solv \quad (19)$$

Laser flash-photolysis experiments were carried out on $[(C_6H_6)Cr(CO)_3]$ in cyclohexane, dichloroethane, methanol, and in the RTILs [bmim][PF_6] and [bmim][$(CF_3SO_2)_2N$], where bmim is the 1-*n*-butyl-3-methylimidazolium ion. Time-resolved spectra in the 300–700 nm range were obtained for displacement of cyclohexane (following its replacement of CO) and used to obtain first-order rate constants where L = acetonitrile. Rate constants obtained as a function of CH_3CN concentration yielded k_2 of $5.0 \times 10^7\,mol^{-1}\,dm^3\,s^{-1}$ at 25 °C. Displacements of $C_2H_4Cl_2$ and CH_3OH were estimated to occur with rate constants $\leq 10^4\,mol^{-1}\,dm^3\,s^{-1}$. When [bmim][$PF_6$] is the solvent, the time-dependent spectra revealed a more complex pattern. A species formed initially decayed via first-order kinetics with k_{obs} of $5 \times 10^6\,s^{-1}$. Since adventitious water was suspected of involvement, the kinetics experiment in [bmim][PF_6] was repeated using water-saturated [bmim][PF_6]. The spectrum of the product was identical and was generated more quickly ($k_{obs} = 8 \times 10^6\,s^{-1}$). This indicated that the final product was probably $[(C_6H_6)Cr(CO)_2(H_2O)]$ and a rate constant k_2 of $5 \times 10^6\,mol^{-1}\,dm^3\,s^{-1}$could be estimated for reaction of $[(C_6H_6)Cr(CO)_2(RTIL)]$ with water. A second-order rate constant of $3.8 \times 10^6\,mol^{-1}\,dm^3\,s^{-1}$ at 25 °C was determined for displacement of [bmim][PF_6] from $[(C_6H_6)Cr(CO)_2(RTIL)]$ by varying the concentration of CH_3CN in [bmim][PF_6], a value a factor of 50 times smaller than the diffusion controlled-reaction rate constant in this solvent. An analysis of the details of the spectra and other factors led to the suggestion that binding by the $[PF_6]^-$ anion was responsible for the spectrum at 20 ns. A tentative assignment was made of the order of Cr–solvent interaction: $C_6H_{12} < [bmim][PF_6] < C_2H_4Cl_2$. The potential application of RTILs in catalytic systems was discussed; although after the authors' findings in this study, they pointed out that extraneous water could represent a problem for use of RTILs as solvents in some catalytic systems. This report, however, demonstrated that [bmim][PF_6] can be displaced more easily from a vacant transition metal binding site than a low polarity solvent such as $C_2H_4Cl_2$. Additional experiments not discussed here showed that the lability of displacement could be tuned by variation of the anion of the RTIL. Further findings on this and similar systems in relation to catalytic systems can be anticipated.

The ionic liquid 1-butyl-3-methylimidazoliumbis(trifluormethylsulfonyl)amide, [bmim][bta], was rendered efficacious as a medium for kinetic studies following repeated purification and water-removal procedures.[84] The background purpose was to investigate the potential use of [bmim][bta] in platinum-based hydroformylation reaction studies. Specifically, the kinetics of reaction of the platinum(II) precursor complex *cis*-$[Pt^{II}(PPh_3)_2Cl_2]$ with $[SnCl_3]^-$ to form *cis*-$[Pt^{II}(PPh_3)_2Cl(SnCl_3)]$ and *cis*-$[Pt^{II}(PPh_3)_2(SnCl_3)_2]$ were monitored spectrophotometrically. The $[SnCl_3]^-$ species was supplied from the addition of a second ionic liquid, [bmim][bta], in at least 10-fold excess over the platinum complex concentration ($SnCl_2$ is poorly soluble in [bmim][bta]). The first of two steps observed was quite fast ($t_{1/2} \approx 50$ s) and followed first-order kinetics. The first-order rate constants were linearly dependent on the $[SnCl_3]^-$ concentrations. The derived second-order rate constant was $0.301 \pm 0.007\,mol^{-1}\,dm^3\,s^{-1}$. The thermal

activation parameters obtained were $\Delta H^{\neq} = 46 \pm 0.8\,\mathrm{kJ\,mol^{-1}}$ and $\Delta S^{\neq} = -100 \pm 3\,\mathrm{J\,K^{-1}\,mol^{-1}}$. The second step was much slower and could not yet be adequately characterized. The first step was suggested to involve nucleophilic substitution of Cl^- by $[SnCl_3]^-$ by an associative mechanism, deduced from the markedly negative entropy of activation. Thus, the first step yields the catalytically active complex *cis*-$[Pt^{II}(PPh_3)_2Cl(SnCl_3)]$. Another report[169] indicated the possible intervention of chloride ions as inhibiting catalytic activity in ionic liquids. It was suggested that the $[bta]^-$ anion has steric and solvating properties that would disfavor inhibition by chloride ions in [bmim][bta]. DFT calculations supported the conclusions from experimental results.

1.19.6 Organometallic Reactions: Pulse Radiolysis Initiation

Results from kinetics studies of organometallic reactions that have been initiated by pulse radiolysis are cited here in a separate section. Investigations are limited owing to the specialized nature of the detection and data acquisition systems and radiation source. The methods and techniques of pulse radiolysis have been shown to provide a useful tool for study of the properties of some transition metal complexes containing metal–carbon σ-bonds.[170] Such complexes can be intermediates in industrial catalytic processes and may be short-lived and of low steady-state concentration, and thus not amenable for study of their kinetic properties by more traditional methods. The range of reaction classes that have been studied by pulse radiolysis initiation is considerable. A simple systematic ordering of reaction types by metal or ligand nature is not readily devised because of the wide diversity of factors influencing whether corresponding reactions of compounds containing different central metals occur or are experimentally accessible. A leading authoritative review and the references cited therein may be consulted for more than this succinct overview.[170] Reaction types that have been identified and kinetics studies conducted include formation of metal–carbon σ-bonds and subsequent decomposition of the same or other transient complexes by heterolysis or homolysis of the metal–carbon bond. Sometimes oxidation of the transient species precedes homolysis. The methyl migration/CO insertion reaction of a Cu(I) complex has been studied. The kinetics of the participation of complexes containing metal–carbon σ-bonds in the reduction of alkenes have been reported. The approach to understanding the factors influencing the kinetics and mechanism of a particular process is a systematic variation of the metal, the organic moiety, and non-participating ligands. For example, in forming metal–carbon bonds, introducing steric hindrance within the organic moiety R in the formation of LM–R can have a significant retardation effect on the kinetics of bond formation. Likewise aqua ligands L (non-participating), when replaced by, for example, 2,5,8,11-tetramethyl-2,5,8,11-tetraazadecane, gave rise to a pronounced reduction in bond-formation rate constant. In general, reactions are very rapid, and rate constants may approach diffusion-controlled values.

1.19.7 Theoretical Studies of Kinetics of Organometallic Reactions

Computational chemistry has been applied to the Heck reaction.[171] The latter embraces a versatile method for generating new carbon–carbon bonds, and when using a Pd-based catalyst, the reaction couples an unsaturated carbon center, often from a vinyl or aryl group, to one end of an alkene double bond. The reaction has been studied under diverse conditions and with different catalysts. When using a Pd(0)/(II) couple, depending on the reaction conditions, the reaction can proceed through either what is termed a neutral cycle or a cationic cycle. There is considerable literature[172] on details of these mechanistic cycles and on the various reactants and auxiliary donors, often phosphines, connected to the Pd(0) species. Despite the volume of studies and many successful applications of Heck chemistry, simple predictive rules regarding regiochemistry, for example, have not been formulated. To address this, density functional theory (DFT) calculations of the transition-state structures and reaction barriers for the C–C coupling between monosubstituted η^2-olefins and η^1-vinyl for neutral $[PdI(PH_3)(vinyl)(RCHCH_2)]$ and the cationic $[Pd(H_2PCH_2PH_2)(vinyl)(RCHCH_2)]^+$ complexes, where R = OCH_3, CH_3, and CN, have been carried out.[173] They show that these (transition-state structures and reaction barriers) are relatively insensitive to the exact placement of the alkene but do depend significantly on the regiochemistry. This is independent of the pathway and is valid for $[PdRL_2(alkene)]^+$ and for [PdRIL(alkene)] (R = vinyl, L_2 = dppm (diphenylphosphinomethane), L = PH_3). It can be inferred that basic regiochemistry is already implicit in the electronic structure of the precursor metal complexes. A simple selectivity index Ω was developed on the basis of the electronic structure of the optimized precursor Pd complex. Since Ω is derived from the geometry optimization of the latter complexes, it can be extended to alkene substituents to provide a more rational approach for use of the intermolecular Heck reaction. Selectivity indices were obtained for 13 substituents. Larger Ω values operate for the cationic cycle conditions; Ω values are approximately

additive and can be used to predict the regiochemistry for disubstituted olefins. Computational methods and details as well as overall ramifications, specifications, and variations of Heck reaction chemistry were lucidly presented.[173]

The possible effect of spin-state changes in kinetics of organometallic reactions has been addressed with refined computations.[176] An extensive literature accompanies this subject and in addition to overall reviews,[175,176] a comprehensive update on the status of the topic has been provided.[174] The arguments in favor or otherwise of the concept of "spin blocking" as it affects the kinetics of organometallic reactions will not be repeated here. DFT calculations have been applied to two systems that have been studied experimentally in order to test the spin-blocking concept. The first was the oxidative addition of dihydrogen to a tungsten monohydride trisamido complex $[N_3N]WH$, where $N_3N = [(Me_3SiNCH_2CH_2)_3N]^{3-}$, a slow reaction, and a possible example of spin blocking.[177] The second was the reaction of addition of CO to a triplet, tris-pyrazolyl cobalt monocarbonyl, $Tp^{i\text{-}Pr,Me}Co(CO)$, where $Tp^{i\text{-}Pr,Me}$ = hydrotris(3-isopropyl-5-methylpyrazolyl)borato.[178] The latter reaction is rapid, and the rate constant approaches a diffusion-controlled rate constant value. It was concluded that spin blocking was absent and that ligand addition was not very different kinetically to spin-allowed reactions. The computations of singlet and triplet potential energy surfaces showed that the topology of the individual surfaces, as well as of the crossing regions between them, allow a rationalization of the observed reactivities. In short, the tungsten complex reaction with dihydrogen is spin-blocked with a high barrier due to the crossing between reactant triplet and product singlet surfaces. However, in contrast, addition of CO to the cobalt complex is fast because the triplet and singlet surfaces cross at low energy. It was noted that the impact on reaction rates (of spin blocking) depends markedly on the details of the potential energy surfaces and of the topology associated with their crossing. Furthermore, it was cautioned that the model developed would not permit generalization to all spin-forbidden processes.

Some computations that support experimental results have been discussed in various reports included in Section 1.19.4.

Acknowledgments

The authors gratefully acknowledge financial support from the Deutsche Forschungsgemeinschaft and Fonds der Chemischen Industrie, and the stimulating interaction with numerous graduate and postdoctoral co-workers over many years.

References

1. Wilkinson, G., Stone, F. G. A., Abel, E. W., Eds.; *Comprehensive Organometallic Chemistry I*; Pergamon: Oxford, 1982.
1a. Abel, E. W., Stone, F. G. A., Wilkinson, G., Eds.; *Comprehensive Organometallic Chemistry II*; Elsevier: Oxford, 1995.
2. Atkins, P. W.; de Paula, J. *Physical Chemistry*, 7th ed.; W. H. Freeman: New York, 2003.
3. Moore, J. W.; Pearson, R. G. *Kinetics and Mechanism*, 3rd ed.; Wiley-Interscience: New York, 1981.
4. Wilkins, R. G. *Kinetics and Mechanism of Reactions of Transition Metal Complexes*, 2nd ed.; VCH: Weinheim, 1991.
5. Espenson, J. H. *Chemical Kinetics and Reaction Mechanism*, 2nd ed.; McGraw-Hill: New York, 1996.
6. Jordan, R. B. *Reaction Mechanisms of Inorganic and Organometallic Systems*, 2nd ed.; Oxford University Press: Oxford, 1998.
7. Tobe, M. L.; Burgess, J. *Inorganic Reaction Mechanisms*; Addison Wesley Longman: Harlow, 1999.
8. Twigg, M. V., Ed.; *Mechanisms of Inorganic and Organometallic Reactions*; Plenum: New York, 1983–1994; Vols. 1–8.
9. Kirkwood, J. G. *J. Chem. Phys.* **1934**, *2*, 351.
10. Glastone, S.; Laidler, K. J.; Eyring, H. *The Theory of Rate Processes*; McGraw-Hill: New York, 1941.
11. Debye, P.; McAuley, J. *Physik. Z.* **1925**, *26*, 22.
11a. Hückel, E. *Physik. Z.* **1925**, *26*, 93.
12. Brønsted, J. N. *Z. Physik. Chem.* **1922**, *102*, 169.
12a. Bjerrum, N. *Z. Physik. Chem.* **1924**, *108*, 82.
13. Laidler, K. J. *Chemical Kinetics*, 2nd ed.; McGraw-Hill: New York, 1965, p 231.
14. Hamann, S. D. *Physico-Chemical Effects of Pressure*; Butterworth: London, 1957; Chapter 9.
15. Isaacs, N. S. *Liquid Phase High Pressure Chemistry*; John Wiley: Chichester, 1981.
16. van Eldik, R. In *Inorganic High Pressure Chemistry: Kinetics and Mechanism*; van Eldik, R., Ed.; Elsevier: Amsterdam, 1986; Chapter 1.
17. Eckert, C. A. *Annu. Rev. Phys. Chem.* **1972**, *23*, 239.
18. Jenner, G. *Angew. Chem., Int. Ed.* **1975**, *14*, 137.
19. Asano, T.; le Noble, W. J. *Chem. Rev.* **1978**, *78*, 407.
20. van Eldik, R.; Asano, T.; le Noble, W. J. *Chem. Rev.* **1989**, *89*, 549.
21. Drlijaca, A.; Hubbard, C. D.; van Eldik, R.; Asano, T.; Basilevsky, M. V.; le Noble, W. J. *Chem. Rev.* **1998**, *98*, 2167.
22. Heaton, B. T., Ed.; *Mechanisms in Homogeneous Catalysis*; Wiley-VCH: Weinheim, 2005.
23. van Eldik, R.; Hubbard, C. D. *S. Afr. J. Chem.* **2000**, *53*, 139.
24. van Eldik, R.; Hubbard, C. D. Effect of Pressure on Inorganic Reactions: Introduction and Mechanistic Applications. In *High Pressure Chemistry. Synthetic, Mechanistic and Supercritical Applications*; van Eldik, R., Klärner, F.-G., Eds.; Wiley-VCH: Weinheim, 2002; Chapter 1.

25. Wurche, F.; Klärner, F.-G. In *High Pressure Chemistry. Synthetic, Mechanistic and Supercritical Applications*; van Eldik, R., Klärner, F.-G., Eds.; Wiley-VCH: Weinheim, 2002; Chapter 2.
26. le Noble, W. J.; Schlott, R. *Rev. Sci. Instrum.* **1976**, *47*, 770.
27. Caldin, E. F. *Fast Reactions in Solution*; Blackwell Scientific: Oxford, 1964.

27a. Caldin, E. F. *The Mechanisms of Fast Reactions in Solution*; IOS Press: Amsterdam, 2001.

28. Eigen, M.; de Maeyer, L. In *Investigations of Rates and Mechanisms of Reactions*; Friess, S. L., Lewis, E. S., Weissberger, A., Eds.; Interscience: New York, 1963; Part II, Chapter 18.
29. Porter, G. In *Investigations of Rates and Mechanisms of Reactions*; Friess, S. L., Lewis, E. S., Weissberger, A., Eds.; Interscience: New York, 1963; Part II, Chapter 19.
30. Hague, D. N. *Fast Reactions*; Wiley: London, 1971.
31. van Eldik, R.; Hubbard, C. D. In *Chemistry under Extreme or Non-Classical Conditions*; van Eldik, R., Hubbard, C. D., Eds.; Wiley-Spektrum: New York/Heidelberg, 1997; Chapter 2.
32. van Eldik, R.; Hubbard, C. D. *High Pressure Chemistry: Principles, Technology, and Applications*; Kirk-Othmer Encyclopedia, Wiley: New York, 2005.
33. van Eldik, R.; Hubbard, C. D. Application of High Pressure in Inorganic and Bioinorganic Chemistry. In *Chemistry under Extreme Conditions*; Manaa, R. R., Ed.; Elsevier: Amsterdam, 2005; Chapter 4.
34. Heremans, K.; Snauwaert, J.; Rijkenberg, J. *Rev. Sci. Instrum.* **1980**, *51*, 806.
35. van Eldik, R.; Palmer, D. A.; Schmidt, R.; Kelm, H. *Inorg. Chim. Acta* **1981**, *50*, 131.
36. Ishihara, K.; Funahashi, S.; Tanaka, M. *Rev. Sci. Instrum.* **1982**, *52*, 1231.
37. Nichols, P. J.; Ducommun, Y.; Merbach, A. E. *Inorg. Chem.* **1983**, *22*, 3993.
38. Balny, C.; Saldana, J. L.; Dahan, N. *Anal. Biochem.* **1984**, *139*, 178.
39. van Eldik, R.; Gaede, W.; Wieland, S.; Kraft, J.; Spitzer, M.; Palmer, D. A. *Rev. Sci. Instrum.* **1993**, *64*, 1355.
40. Ishihara, K.; Kondo, Y.; Koizumi, M. *Rev. Sci. Instrum.* **1999**, *70*, 244.
41. Earl, W. L.; Vanni, H.; Merbach, A. E. *J. Magn. Reson.* **1978**, *30*, 571.
42. Voekel, G.; Lang, E.; Lüdemann, H.-D. *Ber. Bunsen-ges Phys. Chem.* **1979**, *83*, 722.
43. Sisley, M. J.; Yano, Y.; Swaddle, T. W. *Inorg. Chem.* **1982**, *21*, 1141.
44. Merbach, A. E. *Pure Applied. Chem.* **1987**, *59*, 161.
45. Moore, P. *Pure Applied Chem.* **1985**, *57*, 347.
46. Zahl, A.; Neubrand, A.; Aygen, S.; van Eldik, R. *Rev. Sci. Instrum.* **1994**, *65*, 882.
47. Zahl, A.; Igel, P.; Weller, M.; van Eldik, R. *Rev. Sci. Instrum.* **2004**, *75*, 3152.
48. Helm, L.; Merbach, A. E. *J. Chem. Soc., Dalton Trans.* 2002, 633.

48a. Dunand, F. A.; Helm, L.; Merbach, A. E. Solvent Exchange on Metal Ions. In *Adv. Inorg. Chem.*; van Eldik, R., Hubbard, CD., Eds.; Academic: San Diego, 2003; Vol 54, Chapter 1.

48b. Helm, L.; Nicolle, G. M.; Merbach, A. E. Water and Proton Exchange Processes on Metal Ions. In *Adv. Inorg. Chem.*; van Eldik, R., Ed.; Elsevier: San Diego, 2005; Vol. 57, Chapter 7.

49. Laurenczy, G.; Helm, L. High Pressure NMR Cells. In *Mechanisms in Homogeneous Catalysis*; Heaton, B. T. Ed.; Wiley-VCH: Weinheim, 2005; Chapter 2.
50. Heaton, B. T.; Jonas, J.; Eguchi, T.; Hoffman, G. A. *J. Chem. Soc., Chem. Commun.* **1981**, 331.
51. Heaton, B. T.; Strona, L.; Jonas, J.; Eguchi, T.; Hoffman, G. A. *J. Chem. Soc., Dalton Trans.* **1982**, 1159.
52. Iggo, J. A.; Shirley, D.; Tong, N. C. *New J. Chem.* **1998**, *22*, 1043.
53. Iggo, J. A.; Kawashima, Y.; Liu, J.; Hiyama.; Mozaki, K. *Organometallics* **2003**, *22*, 5418.
54. Haynes, A.; Maitlis, P. M.; Morris, G. E.; Sunley, G. J.; Adams, H.; Badger, P. W.; Bowers, C. M.; Cook, D. B.; Elliott, P. I. P.; Ghaffar, T., *et al. J. Am. Chem. Soc.* **2004**, *126*, 2847.
55. Niessen, H. G.; Trautner, P.; Wiemann, S.; Bargon, J.; Woelk, K. *Rev. Sci. Instrum.* **2002**, *73*, 1259.
56. Bowers, C. R.; Weitekamp, D. P. *Phys. Rev. Lett.* **1986**, *57*, 2645.
57. Giernoth, R. Hydrogenation. In *Mechanisms in Homogeneous Catalysis*; Heaton, B. T., Ed.; Wiley-VCH: Weinheim, 2005; Chapter 9.
58. Rigby, W.; Whyman, R.; Wilding, K. *J. Phys. E: Sci. Instrum.* **1970**, *3*, 1572.
59. Whyman, R. In *Laboratory Methods in Vibrational Spectroscopy*; Willis, H. A., Van der Maas, J. H., Miller, R. G. J., Eds.; Wiley: New York, 1987, p 289.
60. Haynes, A. The Use of High Pressure Infrared Spectroscopy to Study Catalytic Mechanisms. In *Mechanisms in Homogeneous Catalysis*; Heaton, B. T., Ed.; Wiley-VCH: Weinheim, 2005; Chapter 3.
61. Zhang, J.; Poliakoff, M.; George, M. W. *Organometallics* **2003**, *22*, 1612, and references *loc. cit.*
62. Damoense, L.; Datt, M.; Green, M.; Steenkamp, C. *Coord. Chem. Rev.* **2004**, *248*, 2393.
63. George, M. W.; Poliakoff, M.; Turner, J. J. *Analyst* **1994**, *119*, 551.
64. Portius, P.; Yang, J.; Sun, X.-Z.; Grills, D. C.; Matousek, P.; Parker, A. W.; Towrie, M.; George, M. W. *J. Am. Chem. Soc.* **2004**, *126*, 10713.
65. Kayran, C.; Richards, M.; Ford, P. C. *Inorg. Chim. Acta* **2004**, *357*, 143.
66. van Eldik, R.; Meyerstein, D. *Acc. Chem. Res.* **2000**, *33*, 207.
67. Geiger, W. E.; Ohrenberg, N. C.; Yeomans, B.; Connelly, N. G.; Emslie, D. J. H. *J. Am. Chem. Soc.* **2003**, *125*, 8680.
68. Hogan, C. F.; Bond, A. M.; Neufeld, A. K.; Connelly, N. G.; Llamas-Rey, E. *J. Phys. Chem. A* **2003**, *107*, 1274.
69. Doine, H.; Whitcombe, T. W.; Swaddle, T. W. *Can. J. Chem.* **1992**, *70*, 82.
70. Sachinidis, J. I.; Shalders, R. D.; Tregloan, P. A. *J. Electroanal. Chem. Interfacial Electrochem.* **1992**, *327*, 219.
71. Swaddle, T. W.; Tregloan, P. A. *Coord. Chem. Rev.* **1999**, *187*, 255.
72. Zahl, A.; van Eldik, R.; Matsumoto, M.; Swaddle, T. W. *Inorg. Chem.* **2003**, *42*, 3718.
73. Matsumoto, M.; Swaddle, T. W. *Inorg. Chem.* **2004**, *43*, 2724.
74. Matsumoto, M.; Neuman, N. L.; Swaddle, T. W. *Inorg. Chem.* **2004**, *43*, 1153.
75. Hannay, J. B.; Hogarth, J. *Proc. Roy. Soc.* **1880**, *30*, 178.
76. Ploiakoff, M.; George, M. W.; Howdle, S. M. Inorganic and Related Chemical Reactions in Supercritical Fluids. In *Chemistry Under Extreme or Non-Classical Conditions*; van Eldik, R., Hubbard, C. D., Eds.; Wiley-Spektrum: New York/Heidelberg, 1997; Chapter 5.
77. Hyde, J.; Leitner, W.; Poliakoff, M. Catalytic Reactions in Supercritical Fluids. In *High Pressure Chemistry. Synthetic, Mechanistic and Supercritical Applications*; van Eldik, R., Klärner, F.-G., Eds.; Wiley-VCH: Weinheim, 2002; Chapter 12.

78. Bonrath, W.; Karge, R. Application of Supercritical Fluids in the Fine Chemical Industry. In *High Pressure Chemistry. Synthetic, Mechanistic and Supercritical Applications*; van Eldik, R., Klärner, F.-G., Eds.; Wiley-VCH: Weinheim, 2002; Chapter 13.
79. Dinjus, E.; Kruse, A. Applications of Supercritical Water. In *High Pressure Chemistry. Synthetic, Mechanistic and Supercritical Applications*; van Eldik, R., Klärner, F.-G., Eds.; Wiley-VCH: Weinheim, 2002; Chapter 14.
80. Welton, T. *Coord. Chem. Rev.* **2004**, *248*, 21.

80a. Welton, T. *Coord. Chem. Rev.* **2004**, *248*, 2459.

81. Dupont, J.; DeSouza, R. F.; Suarez, P. A. Z. *Chem. Rev.* **2002**, *102*, 3667.
82. Wasserscheid, P., Welton, T., Eds.; *Ionic Liquids in Synthesis*; Wiley-VCH: Weinheim, 2003.
83. Special issue of *Journal of Organometallic Chemistry* devoted to organometallic chemistry in ionic liquids; **2005** 690.
84. Illner, P.; Zahl, A.; Puchta, R.; van Eikema Hommes, N.; Wasserscheid, P.; van Eldik, R. *J. Organomet. Chem.* **2005**, *690*, 3567.
85. Agapie, T.; Schofer, S. J.; Labinger, J. A.; Bercaw, J. E. *J. Am Chem. Soc.* **2004**, *126*, 1304, and references *loc. cit.*
86. Gridney, A. A.; Ittel, S. D. *Chem. Rev.* **2001**, *101*, 3659.
87. Tang, L.; Papish, E. T.; Abramo, G. P.; Norton, J. R.; Baik, M.-H.; Friesner, R. A.; Rappe, A. *J. Am. Chem. Soc.* **2003**, *125*, 10093.
88. Tang, L.; Norton, J. R.; Edwards, J. C. *Macromolecules* **2003**, *36*, 9716.
89. Connelly, N. G.; Geiger, W. E. *Chem. Rev.* **1996**, *96*, 877.
90. Nielson, R. M.; McManis, G. E.; Safford, L. K.; Weaver, M. J. *J. Phys. Chem.* **1989**, *93*, 2152.
91. Matsumoto, M.; Swaddle, T. W. *Inorg. Chem.* **2004**, *43*, 2724.
92. Curnow, O. J.; Fern, G. M.; Hamilton, M. L.; Zahl, A.; van Eldik, R. *Organometallics* **2004**, *23*, 906.
93. Hamza, M. S. A.; van Eldik, R.; Harper, P. L. S.; Pratt, J. M.; Betterton, E. A. *Eur. J. Inorg. Chem.* **2002**, 580.
94. Hamza, M. S. A.; Zou, X.; Brown, K. L.; van Eldik, R. *Eur. J. Inorg. Chem.* **2003**, 268.
95. Hamza, M. S. A.; Zou, X.; Brown, K. L.; van Eldik, R. *Dalton Trans.* **2003**, 2986.
96. Swaddle, T. W. *Rev. Phys. Chem. Jpn.* **1980**, *50*, 230.
97. Hamza, M. S. A.; Zou, X.; Brown, K. L.; van Eldik, R. *Dalton Trans.* **2003**, 3832.
98. Hamza, M. S. A.; Felluga, A.; Randaccio, L.; Tauzher, G.; van Eldik, R. *Dalton Trans.* **2004**, 287.
99. Alzoubi, B.; Liehr, G.; van Eldik, R. *Dalton Trans.* **2004**, 6093.
100. Hamza, M. S. A.; van Eldik, R. *Dalton Trans.* **2004**, 1.
101. Hamza, M. S. A.; Cregan, A. G.; Brasch, N. E.; van Eldik, R *Dalton Trans.* **2003**, 396.
102. Petros, R. A.; Norton, J. R. *Organometallics* **2004**, *23*, 5105.
103. Zoeller, J. R.; Buchanan, N. L.; Dickson, T. J.; Ramming, K. R. *Catal. Today* **1999**, *49*, 431.
104. Kayran, C.; Richards, M.; Ford, P. C. *Inorg. Chim. Acta* **2004**, *357*, 143.
105. van Leeuwen, P. W. N. M.; Kamer, P. C. J.; Reek, J. N. H.; Dierkes, P. *Chem. Rev.* **2000**, *100*, 2741.
106. Kamer, P. C. J.; van Leeuwen, P. W. N. M.; Reek, J. N. H. *Acc. Chem. Res.* **2001**, *34*, 895.
107. Guan, H.; Iimura, M.; Magee, M. P.; Norton, J. R.; Janak, K. E. *Organometallics* **2003**, *22*, 4084.
108. Six, C.; Beck, K.; Wegner, A.; Leitner, W. *Organometallics* **2000**, *19*, 4639.
109. Buskens, P.; Giunta, D.; Leitner, W. *Inorg. Chim Acta* **2004**, *357*, 1969.
110. Teunissen, H. T.; Elsevier, C. J. *Chem. Commun.* **1997**, 667.
111. van Engelen, M. C.; Teunissen, H. T.; de Vries, J. G.; Elsevier, C. J. *J. Mol. Catal. A: Chemical* **2003**, *206*, 185.
112. Proctor, G. *Asymmetric Synthesis*; Oxford UniversityPress: Oxford, 1996.
113. James, B. R. *Catal. Today* **1997**, *37*, 209.
114. Abdur-Rashid, K.; Lough, A. J.; Morris, R. H. *Organometallics* **2001**, *20*, 1047.
115. Bunten, K. A.; Farrar, D. H.; Poë, A. J.; Lough, A. *Organometallics* **2002**, *21*, 3344.
116. Poë, A. J.; Twigg, M. V. *J. Chem. Soc., Dalton Trans.* 1974, 1860.
117. Tolman, C. A. *Chem. Rev.* **1977**, *77*, 313.
118. Farrar, D. H.; Poë, A. J.; Zheng, Y. *J. Am. Chem. Soc.* **1992**, *114*, 5146.
119. Chen, L.; Poë, A. J. *Coord. Chem. Rev.* **1995**, *143*, 265.
120. Bunten, K. A.; Farrar, D. H.; Poë, A. J. *Organometallics* **2003**, *22*, 3448.
121. Gonsalvi, L.; Gaunt, J. A.; Adams, H.; Castro, A.; Sunley, G. J.; Haynes, A. *Organometallics* **2003**, *22*, 1047.
122. Gonsalvi, L.; Adams, H.; Sunley, G. J.; Ditzel, E.; Haynes, A. *J. Am. Chem. Soc.* **1999**, *121*, 11233.
123. Gonsalvi, L.; Adams, H.; Sunley, G. J.; Ditzel, E.; Haynes, A. *J. Am. Chem. Soc.* **2002**, *124*, 13597.
124. Haynes, A.; Mann, B. E.; Morris, B. E.; Maitlis, P. M. *J. Am. Chem. Soc.* **1993**, *115*, 4093.
125. Trnka, T. M.; Grubbs, R. H. *Acc. Chem. Res.* **2001**, *34*, 18.
126. Martin, H. C.; James, N. H.; Aitken, J.; Gaunt, J. A.; Adams, H.; Haynes, A. *Organometallics* **2003**, *22*, 4451.
127. Rankin, J.; Benyel, A. C.; Polle, A. D.; Cole-Hamilton, D. J. *J. Chem. Soc., Dalton Trans.* **1999**, 3771.
128. Gaunt, J. A.; Gibson, V. C.; Haynes, A.; Spitzmesser, S. K.; White, A. J. P.; Williams, D. J. *Organometallics* **2004**, *23*, 1015.
129. Kang, J. W.; Maitlis, P. M. *J. Organomet. Chem.* **1971**, *26*, 393.
130. Sen, A. *Acc. Chem. Res.* **1993**, *26*, 303.
131. Drent, E.; Budzelaar, P. H. M. *Chem. Rev.* **1996**, *96*, 663.
132. Haynes, A.; Haslam, C. E.; Bonnington, K. J.; Parish, L.; Adams, H.; Spey, S. E.; Marder, T. B.; Coventry, D. N. *Organometallics* **2004**, *23*, 5907.
133. Zhang, J.; Poliakoff, M.; George, M. W. *Organometallics* **2003**, *22*, 1612.
134. Ernsting, J. M.; Gaemers, S.; Elsevier, C. J. *Magn. Reson. Chem.* **2004**, *42*, 721.
135. De Pater, B. C.; Zijp, E. J.; Frühauf, H.-W.; Ernsting, J. M.; Elsevier, C. J.; Vrieze, K.; Budzelaar, P. H. M.; Gal, A. W. *Organometallics* **2004**, *23*, 269.
136. Geiger, W. E.; Ohrenberg, N. C.; Yeomans, B.; Connelly, N. G.; Emslie, D. J. H. *J. Am. Chem. Soc.* **2003**, *125*, 8680, and references *loc. cit.*
137. Rostovtsev, V. V.; Henling, L. M.; Labinger, J. A.; Bercaw, J. E. *Inorg. Chem.* **2002**, *41*, 3608.
138. Scollard, J. D.; Day, M. W.; Labinger, J. A.; Bercaw, J. E. *Helv. Chim. Acta.* **2001**, *84*, 3247.
139. References *loc. cit.* Ackerman, L. J.; Sadighi, J. P.; Kurtz, D. M.; Labinger, J. A.; Bercaw, J. E. *Organometallics* **2003**, *22*, 3884.
140. Ackerman, L. J.; Sadighi, J. P.; Kurtz, D. M.; Labinger, J. A.; Bercaw, J. E. *Organometallics* **2003**, *22*, 3884.
141. Wolowska, J.; Eastham, G. R.; Heaton, B. T.; Iggo, J. A.; Jacko, C.; Whyman, R. *Chem. Commun.* **2002**, 2784.
142. Drent, E.; Budzelaar, P. H. M. *Chem. Rev.* **1996**, *96*, 663.

143. Liu, J.; Heaton, B. T.; Iggo, J. A.; Whyman, R. *Angew. Chem., Int. Ed.* **2004**, *43*, 90.
144. Espenson, J. H. Oxygen Transfer Reactions: Catalysis by Rhenium Compounds. In *Adv. Inorg. Chem.*; van Eldik, R., Hubbard, C. D., Eds.; Academic Press: Amsterdam, 2003; Vol. 54, p158.
145. Vasbinder, M. J.; Espenson, J. H. *Organometallics* **2004**, *23*, 3355.
146. Shan, X.; Ellern, A.; Guzei, I. A.; Espenson, J. H. *Inorg. Chem.* **2004**, *43*, 3854.
147. Cai, Y.; Espenson, J. H. *Inorg. Chem.* **2005**, *44*, 489.
148. Han, Y.; Harlan, C. J.; Stoessel, P.; Frost, B. J.; Norton, J. R.; Miller, S.; Bridgewater, B.; Xu, Q. *Inorg. Chem.* **2001**, *40*, 2942.
149. Koike, K.; Okoshi, N.; Hori, H.; Takeuchi, K.; Ishitani, O.; Tsubaki, H.; Clark, I. P.; George, M. W.; Johnson, F. P. A.; Turner, J. J. *J. Am. Chem. Soc.* **2002**, *124*, 11448.
150. Haynes, A.; Maitlis, P. M.; Stanbridge, I. A.; Haak, S.; Pearson, J. M.; Adams, H.; Bailey, N. A. *Inorg. Chim. Acta* **2004**, *357*, 3027.
151. Ellis, P. R.; Pearson, J. M.; Haynes, A.; Adams, H.; Bailey, N. A.; Maitlis, P. M. *Organometallics* **1994**, *13*, 3215.
152. Pearson, J. M.; Haynes, A.; Morris, G. E.; Sunley, G. J.; Maitlis, P. M. *J. Chem. Soc., Chem Commun.* 1995, 1045.
153. Zhao, J.; Goldman, A. S.; Hartwig, J. F. *Science* **2005**, *307*, 1080.
154. Fekl, U.; Goldberg, K. I. Homogeneous Hydrocarbon C–H bond Activation and Functionalization with Platinum. In *Adv. Inorg. Chem.*; van Eldik, R., Hubbard, C. D., Eds.; Academic Press: Amsterdam, 2003; Vol. 54, p 260.
155. Procelewska, J.; Zahl, A.; van Eldik, R.; Zhong, H. A.; Labinger, J. A.; Bercaw, J. E. *Inorg. Chem.* **2002**, *41*, 2808.
156. Shilov, A.; Shulpin, G. B. *Chem. Rev.* **1997**, *97*, 2879.
157. Crumpton-Bregel, D. M.; Goldberg, K. I. *J. Am.Chem. Soc.* **2003**, *125*, 9442.
158. Fekl, U.; Kaminsky, W.; Goldberg, K. I. *J. Am. Chem. Soc.* **2003**, *125*, 15286.
159. Wik, B. J.; Lersch, M.; Tilset, M. *J. Am. Chem. Soc.* **2002**, *124*, 12116.
160. Papish, E. T.; Rix, F. C.; Spetseris, N.; Norton, J. R.; Williams, R. D. *J. Am. Chem. Soc.* **2000**, *122*, 12235.
161. Jensen, M. P.; Wick, D. D.; Reinartz, S.; White, P. S.; Templeton, J. L.; Goldberg, K. I. *J. Am. Chem. Soc.* **2003**, *125*, 8614.
162. Owen, J. S.; Labinger, J. A.; Bercaw, J. E. *J. Am. Chem. Soc.* **2004**, *126*, 8247.
163. Hofmann, A.; Dahlenburg, L.; van Eldik, R. *Inorg. Chem.* **2003**, *42*, 6528.
164. Jagyani, D.; Reddy, D.; Gertenbach, J. A.; Hofmann, A.; van Eldik, R. *Dalton Trans.* **2004**, 299.
165. Font-Bardia, M.; Gallego, C.; González, G.; Martinez, M.; Merbach, A. E.; Solans, X. *Dalton Trans.* **2003**, 1106.
166. Heyduk, A. F.; Driver, T. G.; Labinger, J. A.; Bercaw, J. E. *J. Am. Chem. Soc.* **2004**, *126*, 15034.
167. Swiderski, K.; McLean, A.; Gordon, C. M.; Vaughan, D. H. *Chem. Commun.* 2004, 590.
168. Zhao, D.; Wu, M.; Kou, Y.; Enze, M. *Catal Today* **2002**, *74*, 157.
169. Daguenet, C.; Dyson, P. J. *Organometallics* **2004**, *23*, 6080.
170. Masarwa, A.; Meyerstein, D. Properties of Transition Metal Complexes with Metal-Carbon Bonds in Aqueous Solutions as Studied by Pulse Radiolysis. In *Adv. Inorg. Chem.*; van Eldik, R., Ed.; Elsevier: San Diego, 2004; Vol. 55, p 272.
171. Heck, R. F. In *Comprehensive Organic Synthesis*; Trost, B. M., Fleming, I., Eds.; Pergamon Press: Oxford, 1991; Vol. 4.
172. For example, Soderberg, B. C. G. *Coord. Chem. Rev.* **2002**, *224*, 171.
173. Deeth, R. J.; Smith, A.; Brown, J. M. *J. Am. Chem. Soc.* **2004**, *126*, 7144.
174. Carreón-Macedo, J.-L.; Harvey, J. N. *J. Am. Chem. Soc.* **2004**, *126*, 5789.
175. Harvey, J. N.; Poli, R.; Smith, K. M. *Coord. Chem. Rev.* **2003**, *238*, 347.
176. Poli, R.; Harvey, J. N. *Chem. Soc. Rev.* **2003**, *32*, 1.
177. Schrock, R. R.; Shih, K. Y.; Dobbs, D. A.; Davis, W. M. *J. Am. Chem. Soc.* **1995**, *117*, 6609.
178. Detrich, J. L.; Reinaud, O. M.; Rheingold, A. L.; Theopold, K. H. *J. Am. Chem. Soc.* **1995**, *117*, 11745.

1.20 Isotope-labeling Studies and Kinetic and Equilibrium Isotope Effects in Organometallic Reactions

K E Janak, Reheis Inc., Berkeley Heights, NJ, USA

1.20.1 General Introduction

The investigation of the mechanism of reactions and chemical transformations mediated by metal complexes is at the core of organometallic chemistry. The purpose of this review is to delineate the ways that isotopic labeling has been used to provide insight into organometallic reaction mechanisms. A number of excellent reviews exist where the role of isotopic labels and corresponding isotope effects are discussed in terms of the relevance of such results to a specific type of reaction or area of interest.[1,1a] Specifically, a significant amount of attention will be paid to systems involving the interaction of H–H and C–H bonds with transition metal centers, with the intent of showing how the information gained from these studies can provide a guide to understanding and interpreting observed isotope effects.

An attempt has been made to provide a comprehensive overview of the use and interpretation of isotopes and isotope effects. Given the vast number of examples and the limitation of space, specific examples were chosen in order to give either a sense of the breadth and scope of the use of isotope labels or to highlight key concepts related to the isotope effects that result from the use of such labels. The reader is encouraged to consult the references provided for further examples. In addition, the use of isotopic labeling and the significance of isotope effects in bioinorganic systems and model systems has not been addressed due to space limitations. Excellent and thorough reviews on these topics exist, and the interested reader is also encouraged to consult these.[2,2a–2g]

1.20.2 Isotopic Labeling in Organometallic Systems Involving the Formation and Cleavage of C–H Bonds

1.20.2.1 Oxidative Addition and Reductive Elimination Reactions

The interaction of C–H bonds with transition metal centers has been the center of a significant amount of research over the past few decades.[3,3a–3d] The immense economic potential of efficiently activating and functionalizing alkane C–H bonds provides the primary impetus behind this research. Specifically, the presence of natural gas reserves globally represents a potentially important alternative to oil for energy and chemicals production. However, alkanes have generally been considered to be among the most difficult substrates for activation and functionalization. In fact, systems that effectively functionalize C–H bonds are rare and typically are not commercially viable on a large scale.[4,4a]

Nonetheless, one of the earliest applications of transition metal compounds involving alkane C–H bonds is the reaction of CrO_2Cl_2 with cyclohexane, known as the Etard reaction.[5] Since then, many other systems have been developed in order both to achieve C–H bond functionalization and to gain an understanding of the types of mechanisms involved in alkane activation.[6,6a–6e] Within these systems, isotopic labeling has played a key role in providing an understanding of such reaction mechanisms. Such labeling can be introduced in a variety of forms (e.g., ^2H and ^{13}C labels) and either in the complex or in the substrate that reacts with the complex.

Important reactions involving C–H bonds include the oxidative addition and reductive elimination of alkanes at transition metal centers. Fundamentally, oxidative addition reactions result in the increase in the oxidation state of the metal center upon cleavage of a substrate bond, whereas reductive elimination corresponds to a decrease in the oxidation state of the metal center and loss of substrate (Figure 1). In the case of a C–H bond, oxidative addition results in the concomitant formation of a metal alkyl and a metal hydride bond while reductive elimination results in the coupling of the metal alkyl and metal hydride to re-form the C–H bond and lose substrate, such as an alkane. The first reported example of C–H activation is attributed to Chatt, who observed intermolecular activation for naphthalene by a transiently generated [Ru(dmpe)$_2$] complex.[7] Soon afterward, Shilov reported one of the earliest examples of deuterium scrambling within a Pt(II) system that cleaved the C–H bond of methane.[8] Hydrogen–deuterium (H/D) exchange between methane and D_2O/CH_3CO_2D was observed, providing further evidence for the potential formation of a Pt(IV) alkyl intermediate. For many years, other well-defined examples of intermolecular alkane (versus arene) oxidative addition reactions remained elusive until this was achieved by Bergman using a cyclopentadienyl iridium phosphine system ([$Cp^*Ir(PMe_3)$]).[9] A variety of alkanes were shown to undergo intermolecular activation upon photolysis of $Cp^*Ir(H)_2PMe_3$, including methane. Since then, other systems have been developed in order to more fully understand alkane activation, including Ni, Os, Pt, Rh, Ru, and W.[10]

In order to gain information about the mechanism of reactions, organometallic chemists employ a variety of methods, including using isotopic substitution either on the metal complex or on the substrate. In the case of reactions involving C–H bonds, a label may be introduced at the metal hydride site, the metal alkyl site (in the form of ^2H, ^{13}C, or both), or in the free substrate (Scheme 1). The incorporation of an isotopic label has proved to be a particularly important component in investigating reaction mechanisms involving C–H bonds. Specifically, the ability to observe migrations of the label via spectroscopic techniques such as NMR and IR makes it a particularly powerful tool. In addition, the introduction of a label may result in dramatic kinetic and equilibrium isotope effects that can provide insight into the nature of the type of reaction mechanism that is operative for a given system (*vide infra*).

One of the earliest examples of the use of isotopic labeling involved the $Cp^*Rh(PMe_3)(CH_2CH_3)H$ system.[10] The introduction of ^2H at the metal hydride site revealed H/D exchange during the reductive elimination of ethane, but at a rate faster than overall ethane loss. In order to determine if the exchange process occurred via a β-hydride elimination

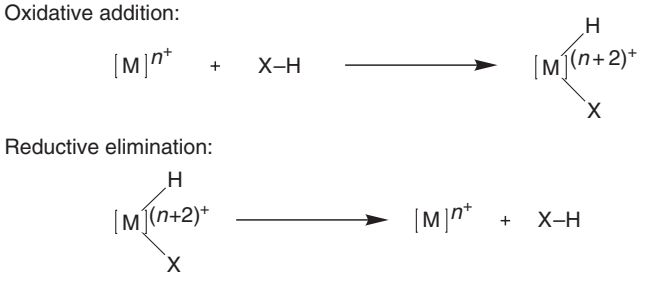

Figure 1 General description of oxidative addition and reductive elimination processes.

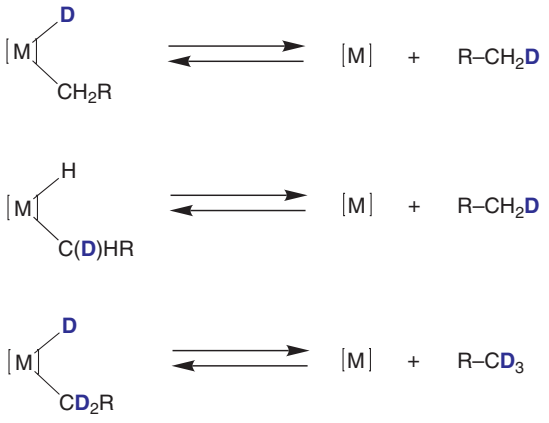

Scheme 1 Deuterium labeling in organometallic complexes and alkane oxidative addition/reductive elimination reactions.

mechanism, a doubly labeled complex was prepared with ^{2}H being incorporated at both the metal hydride site and the metal alkyl site and ^{13}C incorporated in the metal–carbon bond of the metal alkyl site (Scheme 2). Significantly, ^{13}C NMR revealed that the deuterium migrates with the ^{13}C label, ruling out β-hydride elimination as the mechanism of H/D exchange.

Similar studies have been employed in studying the reductive elimination of methane. Norton showed via ^{2}H labeling at the metal hydride site that H/D exchange occurs more rapidly than loss of methane within $Cp_2W(CH_3)H$.[11] Further, the intramolecularity of thermal methane elimination was confirmed by loss of methane at 82.9 °C from a benzene/acetonitrile solution of $Cp_2W(CD_3)D$ and $Cp_2W(^{13}CH_3)H$ to form the acetonitrile complex, $Cp_2W(\eta^2\text{-C,N-NCCH}_3)$. The principal isotopically labeled methanes observed were $^{13}CH_4$ ($40 \pm 6\%$), CD_4 ($42 \pm 6\%$), and CHD_3 ($14 \pm 6\%$). The CHD_3 is derived from the 12% $Cp_2W(CD_3)H$ present in the initial $Cp_2W(CD_3)D$. The analogous permethylated system $Cp^*_2W(CH_3)D$ also showed H/D exchange between the metal hydride and methyl C–H sites, but at rates more competitive with an overall loss of methane.[12] This type of exchange was also shown by Parkin in the *ansa*-bridged derivative, $[Me_2Si(C_5Me_4)_2]W(CH_3)H$, with an even larger difference between the rates of exchange and methane loss.[13] In both the Cp^*_2W and *ansa*–$[Me_2Si(C_5Me_4)_2]W$, no intermolecular activation of methane is observed while both inter- and intramolecular exchange occurs with Cp_2W.

Examples of intramolecular H/D exchange in isotopically labeled metal alkyl hydrides are not limited to metallocene- or cyclopentadienyl-based systems, however. Flood and co-workers investigated the oxidative addition and reductive elimination of alkanes within a $(PMe_3)_4Os(CH_2C(CH_3)_3)H$ system.[14,14a,14b] The complex eliminates neopentane upon thermolysis and C–H activates benzene in benzene solvent and benzene/cyclohexane solvent mixtures. Thermolysis in C_6D_6 and analysis by ^{2}H NMR revealed that only $86 \pm 4\%$ of the benzene-activated product, $(PMe_3)_4Os(C_6D_5)D$, was deuterated in the hydride site while mass spectral analysis showed that the eliminated *neo*pentane was $13 \pm 2\%$ neopentane-d_1. Significantly, the starting material shows no incorporation of deuterium throughout the reaction and the product exhibits no H/D exchange with C_6H_6. These labeling experiments established that both C_6H_6 and neopentane are present on the metal at the same time during the reaction, via a proposed seven-coordinate $(PMe_3)_3Os(CH_2C(CH_3)_3)(C_6D_5)(H)D$ intermediate.[14a] More recently, Bianchini *et al.* showed that the analogous triphos system $((Ph_2PCH_2CH_2)_3P)M$ (M = Ru, Os) intermolecularly activates the C–H bonds in alkanes, arenes, and other substrates, but these occur via an M(0) intermediate and the products are less stable with respect to reductive elimination.[15]

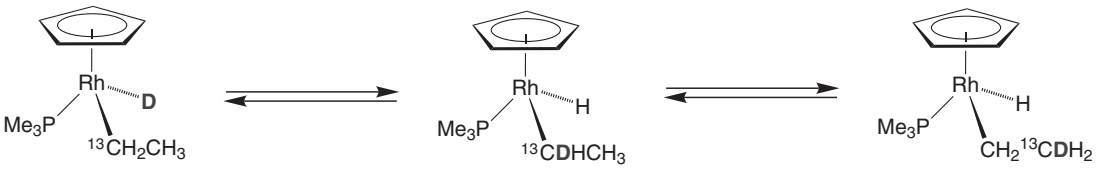

Scheme 2 Intramolecular rearrangement of deuterium in $CpRh(PMe_3)(^{13}CH_2CH_3)D$.

Other examples have involved systems containing "harder," less-polarizable ligands, such as the tridentate Cn and TACN ligands (Cn = 1,3,5-trimethyl-triazacylononane; TACN = 1,3,5-triazacyclononane). In particular, Flood has used these amine ligands in an effort to stabilize group VIII alkyl hydrides to the loss of alkane due to the reduced π-acidity of the nitrogen atoms relative to phosphine analogs.[16] Specifically, investigation of methane reductive elimination from the $[(Cn)Rh(PMe_3)(CH_3)D]^+$ complex using ^1H and ^{31}P NMR revealed that the complex intramolecularly exchanges deuterium between the metal hydride and methyl sites at 60 °C.[17] Significantly, loss of methane occurs at measurable rates at much higher temperature (80 °C) relative to its $Cp^*Rh(PMe_3)$ analogs.[18,18a] Further evidence of the stability toward loss of alkane imposed by the ligand system was shown by the isolation of a series of alkyl hydrides in the related $[(TACN)Rh(P(OMe)_3)(R)H]^+$ (R = Me, Et, Bu^n, n-C_6H_{13}, n-$C_{10}H_{21}$).[19] Loss of alkane occurs over a period of days at ~40 °C. Deuterium labeling of the metal hydride site revealed that exchange between the metal hydride and α-CH_2 site occurs at low temperature (4 °C) without loss of alkane. Upon further warming to 40 °C, deuterium is observed to incorporate into the terminal CH_3 group of the alkyl chain at rates faster than overall loss of alkane, even for the decyl group. Significantly, ^2H NMR revealed no incorporation of label into the methylene sites during the course of the reaction, ruling out β-hydride elimination as the mechanism for isotopic rearrangement. Further, the first-order rate constants for incorporation of deuterium from the α-CH_2 into the terminal CH_3 group decrease as a function of chain length, suggesting that the loss of alkane from the proposed intermediate σ-complexes becomes more competitive with respect to formation of the metal alkyl hydride with increasing chain length. However, additional studies indicate that alkyl chain structure plays a more complex role in such deuterium migrations/rearrangements within this system.[20]

Similarly, Jones has also investigated a series of alkyl hydrides within the $Tp^*Rh(CN(CH_2C(CH_3)_3))(R)H$ system (R = Me, Et, Pr^n, Pr^i, Bu^n, Bu^s, n-C_5H_{11}, n-C_6H_{13}).[21] Although there is some ambiguity concerning the "hardness" of Tp ligands relative to their isoelectronic Cp congeners,[22] the loss of alkane from this system occurs at higher temperatures than the analogous $Cp^*Rh(PMe_3)$ system, but at lower temperatures than the (Cn/TACN)Rh systems, indicating that it is less likely polarizable than the Cp^* ligand, but more polarizable than the Cn/TACN ligands. Nonetheless, labeling studies revealed that H/D exchange occurs between the hydride and α–CH_2 sites in the linear alkyl derivatives. Further, rearrangement to the terminus occurs in decreasing amounts from Et to n-C_6H_{13} and is concomitant with the loss of alkane. Most significantly, "no" H/D exchange occurs between the metal hydride sites and the α-CH_2 in the secondary alkyls (Pr^i, Bu^s). Further, these derivatives rearrange to the linear isomers faster than the overall loss of alkane occurs. These results were interpreted to be evidence that the selectivity observed in other systems[18a] for 1° CH_3's versus 2° CH_2's is both "kinetic" and "thermodynamic" in nature.

The ability of oxygen donor ligand systems to effect C–H activation reactions has been explored by Periana and co-workers. Reaction of $(acac)_2Ir(NC_5H_5)CH_3$ with C_6D_{12} results in the formation of an [Ir](cyclohexyl) complex and CH_3D, the latter being detected by GC-MS.[23] Although oxidative addition may be the mechanism for alkane exchange, resulting in the formation of an Ir(V) intermediate, a σ-bond methathesis mechanism could also be operative (Scheme 3).

Interestingly, catalytic H/D exchange is observed when the methyl complex is reacted with cylcohexane, CH_4, and n-octane in C_6D_6 solvent. Significantly, ^{13}C NMR analysis of the C_6D_6/n-octane reaction mixture shows ^2H incorporation into all of the 2° methylene and 1° methyl sites, with a slight isotopic preference for the 1° positions. Although no alkene complexes are observed on the NMR timescale during the course of the reaction, the possibility of non-productive β-hydride elimination was explored via ^2H and ^{13}C labeling studies. Preparation of the ^{13}C labeled $(acac)_2Ir(NC_5H_5)(^{13}CH_2CH_3)$ complex was achieved via reaction of $(\kappa^2$-acac$)_2(\eta^1$-C-acac$)Ir(OH_2)$ with

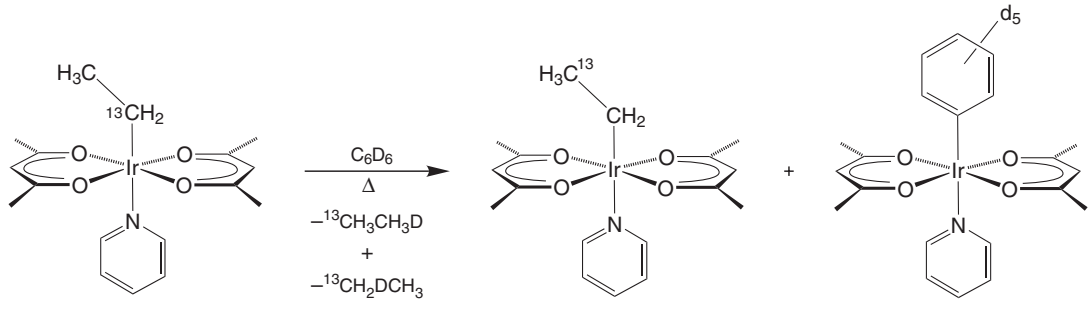

Scheme 3 Alkane C–H activation and $^2H/^{13}C$ labeling studies in $(acac)_2Ir(py)Et$.

$Zn(^{13}CH_2CH_3)_2$, followed by addition of pyridine.[23] If β-hydride elimination were occurring, then isomerization of the label from the α-carbon to the β-carbon position would be observed. Further, upon reaction in C_6D_6, isomerization would also result in separate regioisotopomers of ethane-d_1, $^{13}CH_3CH_2D$, and $^{13}CH_2DCH_3$. In fact, such isomerization was observed via ^{13}C NMR and GC-MS.

Bergman has also reported catalytic H/D exchange reactions in the $[Cp^*Ir(PMe_3)(CH_2Cl_2)Me]^+$ and $[Cp^*Ir(PMe_3)(CH_2Cl_2)H]^+$ systems.[24] Reaction of the $\{[Ir]H\}^+$ complex in C_6D_6 with a variety of alkanes shows catalytic deuterium incorporation into the C–H bonds of the substrate at low temperatures (−30 to −80°C), including >80% incorporation into CH_4 and ~80% into the α-CH_2 sites in THF and ~20% into the β-CH_2 sites. The methyl complex undergoes reversible methane activation, as evidenced by isotopic exchange between the ^{13}C labeled $\{[Ir]^{13}CH_3\}^+$ starting material and unlabeled CH_4. Evidence that these reactions proceed via Ir(V) intermediates rather than a σ-bond metathesis mechanism was provided by reaction with Ph_3SiH. Isolation of the cyclometallated product, $[Cp^*Ir(PMe_3)(\eta^2\text{-Si,C-Si}(C_6H_4)Ph_2)]^+$, revealed that an Ir(V) oxidation state was accessible in this system.[25]

As previously mentioned, one of the earliest discoveries of homogeneous C–H activation and functionalization of alkanes was discovered by Shilov.[8] In his initial studies, Shilov reported that solutions of $K_2[PtCl_4]$ in D_2O/CH_3CO_2D could incorporate deuterium into alkanes, even methane. Subsequent to this, he reported that addition of $H_2[PtCl_6]$ to the $K_2[PtCl_4]$ reaction mixture resulted in the oxidation of methane and other alkanes to alcohols and alkyl chlorides.[26] Significantly, the observed selectivity of $1° > 2° > 3°$ C–H bonds reflects what is reported in other systems.[18a,21]

Shilov's initial proposal for the mechanism of this Pt-catalyzed alkane oxidation involved:

(i) electrophilic activation of an alkane C–H bond by Pt(II);
(ii) 2-electron oxidation of Pt(II) to Pt(IV); and
(iii) reductive elimination of R–X (X = Cl, OH) to regenerate the Pt(II) catalyst.

More in-depth analysis of the mechanism can be found in other reviews.[27] The reaction and proposed mechanism sparked a considerable amount of interest in this type of system. Zamaschikov and co-workers prepared the alkyl platinum(IV) intermediate, $[Cl_5PtR]^{2-}$ (R = CH_3, CH_2CH_3, and $CH_2C(O)CH_3$), and monitored the kinetics of decomposition to form R–Cl and R–OH.[28] Subsequent studies by Bercaw and co-workers revealed that the R–X bond forming step proceeds via an S_N2-type mechanism.[29]

In addition, isotopic labeling studies by Bercaw's group provided evidence for inner-sphere two-electron transfer from R–Pt(II) to Pt(IV) to form the Pt(IV) alkyl intermediate. Examination of the oxidation of Zeise's salt by $[PtCl_6]^{2-}$ using isotopically labeled $Na_2[^{195}PtCl_6]$ and analysis via ^1H NMR revealed the ^{195}Pt satellites for Pt–CH_2CH_2OH to be only 33%, an intensity no greater than the naturally abundant ^{195}Pt.[29] This was interpreted as evidence for inner sphere, two-electron oxidation via chloride transfer, since an alkyl transfer mechanism would have resulted in an increase in intensity of the ^{195}Pt satellites relative to natural abundance.

Study of the C–H activation step remained particularly elusive, primarily due to the instability of Pt(IV) alkyl hydride complexes. Success in this area has involved the use of phosphine, nitrogen, and Tp ligands.[30] For example, Goldberg and Wick investigated the oxidative addition of alkanes to generate an isolable Pt(IV) alkyl hydride using $[(\kappa^2\text{-Tp}^*)Pt(CH_3)_2]^-$ and BCF (BCF = tris(pentafluorophenyl)borane).[31] Other attempts into the synthesis of $Pt^{IV}R(H)$ complexes have focused on protonation of Pt(II) alkyls. Reaction of $(tmeda)Pt(CH_3)_2$ in MeOH-d_4 resulted in the formation of multiple isotopologs of methane, $CH_{4-x}D_x$ (x = 0–4).[32] In addition, deuterium incorporation was observed in the starting material Pt–CH_3 ligands. The combination of these labeling results provides evidence for reversible formation and deprotonation of a $Pt^{IV}R(H)$ intermediate as well as a Pt(II) methane σ-complex.

Similar exchange processes using isotopic labels have been observed with Pt diimine complexes.[33,33a,33b] Tilset reported that methane C–H activation occurs at the aqua complex $[(N^f\text{–}N^f)Pt(CH_3)(H_2O)]^+[BF_4]^-$ ($(N^f\text{–}N^f)$ = ArN = CMe–CMe = NAr, where Ar = 3,5-$(CF_3)_2C_6H_3$) under mild conditions in 2,2,2-trifluoroethanol (TFE). The reaction between $[(N^f\text{–}N^f)Pt(CH_3)(H_2O)]^+$ and CD_4 led to extensive deuterium scrambling and formation of CH_nD_{4-n} isotopologs. Further, when the Pt complex was exposed to 20–25 bar of $^{13}CH_4$, ^{13}C incorporation into the Pt–CH_3 was readily observed by ^1H and ^{13}C NMR. When the dimethyl complex, $(N^f\text{–}N^f)Pt(CH_3)_2$, is treated with 1 equiv. of DOTf ($^-OTf = -O_3SCF_3$) in TFE-d_3, and CD_3CN is present, deuterium incorporation into the Pt–CH_3 is observed followed by loss of both CH_4 and CH_3D. Importantly, varying concentrations of CD_3CN resulted in differing relative amounts of methane isotopomers, CH_4 and CH_3D, produced as determined by integration of the ^1H NMR spectra. The data revealed that the $CH_4:CH_3D$ ratio decreased with increasing $[CD_3CN]$. This observation was rationalized as the result of an associative mechanism for the exchange of acetonitrile for methane in the proposed intermediate σ-complex, $[(N^f\text{–}N^f)Pt(CH_3)(\sigma\text{-}CH_4)]^+$. By the principle of microscopic reversibility, this implies that substitution of methane for MeCN at $[(N^f\text{–}N^f)Pt(CH_3)(NCMe)]^+$ should

occur associatively and that MeCN predissociation to provide a three-coordinate intermediate for methane elimination is not required, an issue of significant interest in Pt-mediated alkane functionalization reactions.[36]

Further, differences in C–H bond activation due to a different charge on the metal complex has been investigated in the related Pt-based systems, $(Ph_2X(CH_2PPh_2)_2)Pt(THF)Me]^+$.[34,34a] Significantly, larger deuterium kinetics isotope effects of the oxidative addition of benzene are observed for the Si-bridged cationic complex versus the B-bridged neutral complex (6.52 at 55 °C versus 1.26 at 45 °C, respectively). Further, while a ratio of 1 : 7.6 is observed for reductive elimination of CH_4/CH_3D in the cationic system, suggestive of the formation of an alkane σ-complex intermediate along the reaction coordinate, a ratio of 3.0 : 1 is observed in the neutral/zwitterionic system. Reversible, competitive cyclometallation of the B-Ph C–H bond was shown to account for the differences between the two systems, via preparation of the perdueterated ligand, $[(Ph\text{-}d_5)_2B(CH_2P(Ph\text{-}d_5)_2)_2]^-$, and observation of ^1H incorporation into the B–Ph ring rather than the P–Ph ring. Further, the protio ligand afforded observation of a cyclometallated Pt–H intermediate. However, the corresponding silane-ligated cationic system did not exhibit Si–Ph C–H bond activation.

Overall, labeling studies have provided many important details concerning the mechanisms of oxidative addition and reductive elimination of alkanes. Specifically, these studies have provided an abundance of data implicating the existence of alkane σ-complex intermediates and provided insight into the potential for effectively activating alkanes.

1.20.2.1.1 Alkane functionalization reactions

Isotopic labeling studies have proved to be useful in areas other than the investigation of alkane σ-complexes. As previously mentioned, one of the primary goals of C–H activation research has been to functionalize alkanes efficiently. Over the last 15 years, significant advances have been made, some of which involve oxidative addition and reductive elimination reaction mechanisms. For instance, Hartwig has shown that Cp^*Rh and Cp^*Ir complexes undergo catalytic borylation of alkanes via oxidative addition of alkane C–H bonds.[35,35a–35c] The likely intermediacy of $Cp^*M^v(Boryl)$ complexes is supported by the observation of H/D exchange at the metal hydride positions (M = Ir) with deuterated solvents (benzene-d_6, octane-d_{18}).[35c] In addition, Periana has shown that methane could be catalytically oxidized to methyl bisulfate ($MeOSO_3H$) and methanol without overoxidation via reaction of Pt and Hg salts in fuming sulfuric acid.[36,36a] The use of ^{13}C-labeled methane confirmed the absence of methyl sulfonic acid as well as over-oxidized products such as acetic acid. The mechanism of the reaction was suggested to occur via an electrophilic pathway involving a coordinatively unsaturated, 14-electron, T-shaped complex, $[(bpym)Pt(X)]^+$ (bpym = 2,2′-bispyrimidine), in contrast to the Pt-mediated C–H activations described by Tilset (*vide supra*). The existence of this intermediate was postulated based upon the observation of H/D exchange between deuterated solvent (D_2SO_4, CF_3CO_2D) and methane but no observed H/D exchange between solvent and the C–H bonds of the methyl group in the product methyl bisulfate.[36c]

Another area of interest with respect to alkane functionalization has been the catalytic dehydrogenation of alkanes in an effort to efficiently produce α-olefins.[37] In essence, the process of alkane dehydrogenation is the reverse of transition metal-catalyzed alkene hydrogenation. One of the earliest examples involved the dehydrogenation of cyclopentane and cyclooctane by $[(Me_2C(O))_2Ir(PPh_3)_2H_2]^+$.[38,38a] The resulting products were cyclopentadiene and cyclooctadiene iridium products. However, the reaction required a sacrificial hydrogen acceptor to produce favorable thermodynamics for the reaction due to the unfavorable enthalpic demands of dehydrogenation in the absence of such an acceptor. Rhenium and iridium polyhydride systems were later reported to dehydrogenate alkanes, with catalytic dehydrogenation of cycloalkanes being achieved with up to 70 turnovers.[39]

Important factors for achieving this type of reaction include:

(i) thermally stable complexes, in order to avoid catalyst decomposition;
(ii) the ability to produce coordinatively unsaturated intermediates, such as via ligand loss; and
(iii) the avoidance of using hydrogen acceptors to drive the reaction in order to make the process economical.

Reasonable success in these areas has been achieved primarily via "pincer"-type ligands using group VIII metals.[40,40a,40f] Jensen and Kaska reported that the Ir complex, $(PCP^{Bu^t})Ir$, catalytically dehydrogenates cycloalkanes at elevated temperature (150–200 °C) without catalyst decomposition.[41] The isopropyl-substituted phosphine pincer ligand was found to be more selective toward *n*-alkanes relative to the Bu^t analog, in addition to providing faster rates and higher turnover numbers for dehydrogenation.

In order to develop pincer complexes into efficacious systems for alkane dehydrogenation, information regarding the mechanism of dehydrogenation within these systems is necessary. Specifically, Goldman, Krogh-Jespersen, and co-workers[37,40,40a–40f] identified key steps in the dehydrogenation process, which include: (i) the regioselectivity of

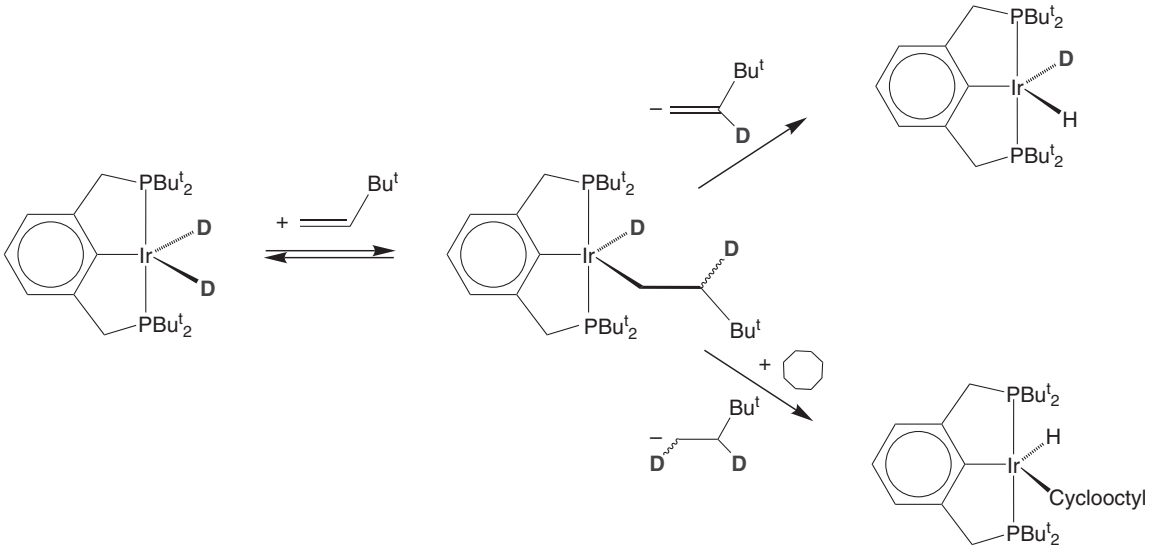

Scheme 4 ^{2}H labeling in the TBE hydrogenation by (PCP$^{Bu^t}$)IrH$_2$.

dehydrogenation, and (ii) the selectivity for the reactivity of primary (1°) versus secondary (2°) C–H bonds. Using the dehydrogenation of cyclooctane and *tert*-butyl ethylene (TBE) as a hydrogen acceptor as the prototypical dehydrogenation reaction within the (PCP)Ir system, key steps in the overall process were identified via deuterium labeling studies.[41,42] First, reaction of the iridium dihydride with TBE results in the formation of an Ir vinyl hydride complex that undergoes rapid exchange with free TBE on the NMR timescale. Use of the ^{2}H labeled dihydride complex showed that the initial rate of formation of the H/D exchanged product, $CH_2=C(D)Bu^t$ (TBE-β-d_1), was ~5 times greater than the formation of neohexane-d_2, CH_2D-$CHDBu^t$ (Scheme 4). This demonstrated that the rate-determining step for TBE hydrogenation is C–H reductive elimination. It was concluded, on the basis of microscopic reversibility, that C–H oxidative addition must be the rate-determining step of the reverse reaction, that is, the dehydrogenation of neohexane. Extension of this to less sterically encumbered linear alkanes as well as cycloalkanes indicates that β-hydride elimination was not the rate-determining step in the mechanism operative with these pincer complexes, an important difference between this and other, previously reported dehydrogenation systems.

1.20.2.2 σ-Bond Metathesis and 1,2-addition Reactions Involving C–H Bonds

Although oxidative addition reactions have received most attention in the area of C–H activation, many examples of C–H activation that do not involve formal oxidation at a metal center also exist. The general mechanistic descriptions for these types of processes are known as σ-bond metathesis and 1,2-additions. Since these reactions have in common the effect of not changing the formal oxidation of the metal, they will be discussed together in the following section. However, the terms will not be used interchangeably, as they are fundamentally different.

The first example of σ-bond metathesis was reported by Watson and Parshall using a Cp^*_2Lu system.[43] Evidence of this reaction type was provided by isotopic labeling studies. Cp^*_2LuMe was shown to undergo exchange with $^{13}CH_4$ in cyclohexane solvent. Importantly, the preference for activation of methane over cyclohexane provides another example of the greater selectivity of many metal-mediated C–H bond activation reactions for less substituted C–H bonds (1°, CH_4) versus more substituted ones (2°). Soon thereafter, Thompson and Bercaw showed that the scandocene complex, Cp^*_2Sc-R (R = CH_3, C_6H_5, $C_6H_4CH_3$, $CH_2C_6H_5$), also undergoes σ-bond metathesis reactions.[44] Reaction with dihydrogen results in the formation of Cp^*_2Sc-H. In fact, NMR studies show that the degenerate exchange reaction between Cp^*_2Sc-H and H_2 is fast on the NMR timescale, with an average signal observed for the Sc-H and H_2 even at −80 °C. H/D exchange between H_2, arene C–H bonds, and the 1° and 2° C–H bonds of alkanes was also observed via ^{1}H NMR spectroscopy. Reaction with toluene-d_8 showed that reaction with the aryl C–H bonds is ~60–70 times faster than with the methyl C–H bonds. A qualitative scale of reactivity toward H/D exchange was described, which indicated that reactivity correlated more closely with sterics (as well as the *s* character of the C–H bond) than the C–H bond dissociation energy of the substrate. A decreasing rate of H/D exchange with Cp^*_2Sc-D was observed

such that: H–H ≫ aryl C–H > (η^5-C_5Me_5), α-CH_2 in THF, PMe_3 > CH_4, $Si(CH_3)_4$, cyclopropane, $C_6H_5CH_3$ > CH_3-CH_2CH_3 ≫ β-CH_2 in THF, cyclopentane, cyclohexane, cyclooctane, $CH_3CH_2CH_3$. Hence, the order of reactivity with X–H substrates tend to follow the order H ≫ *sp*-C > sp^2-C ≫ sp^3-C in this system.

Intramolecular examples of σ-bond metathesis also exist.[45,45a] Rothwell and co-workers showed that the Ta complex, (2,6-diisopropyl phenoxide)$Ta(CH_3)_2$, thermally eliminates CH_4 to form the cyclometalated complex, (2,6-diisopropyl phenoxide)(η^1-C,O-$CH_2CH(CH_3)(C_6H_3O)(CH(CH_3)_2)$)$Ta(CH_3)_2$.[46] At least two mechanisms are possible for this transformation: (i) direct σ-bond metathesis of the 1° isopropyl C–H bond and the Ta–CH_3 bond; or (ii) intramolecular metathesis of two Ta–CH_3 ligands to form an intermediate carbene complex, Ta=CH_2, and methane, followed by a 1,2-addition across the Ta=CH_2 bond (*vide infra*) to form the cyclometallated product. In order to distinguish between these two reaction mechanisms, the perdeuterated complex, (2,6-diisopropyl phenoxide)$Ta(CD_3)_2$, was synthesized. If the first mechanism were operative, then thermolysis of the deuterated complex would result in the initial formation of CD_3H and incorporation of hydrogen in the product methyls would not be observed. The second mechanism, however, would initially result in the formation of CD_4 as well as hydrogen incorporation into the methyl ligands to form a Ta–CD_2H labeled product. In fact, the former mechanism was established based upon the observation of CD_3H formation and no Ta–CD_2H formation via ^{1}H NMR.

The first reports of early transition metal 1,2-additions and eliminations came from the Wolczanski and Bergman groups.[47,47a–47c] Thermolysis of $Cp_2Zr(CH_3)(N(H)Ph)$ in the presence of benzene resulted in the formation of the benzene C–H activated product, $Cp_2Zr(C_6H_5)(N(H)Ph)$.[47a] The proposed Zr imido intermediate, $Cp_2Zr(=N(Ph))$, could also be trapped with THF, aniline, and alkynes to form an imido THF complex, bis-anilido complex, and metallocyclobutene complex, respectively. Similarly, evidence for the formation of a reactive Zr oxo-complex was provided upon reaction of $Cp^*_2Zr(OH)Ph$ in the presence of trapping reagents such as nitriles and alkynes to form oxometallocycles.[48] The mechanism for benzene elimination was shown to be intramolecular by heating the isotopically labeled $Cp^*_2Zr(OD)Ph$ complex and analyzing the products via GC-MS: only C_6H_5D was observed.

These addition and elimination reactions are not limited to metallocene complexes. For example, Wolczanski showed that the Zr(IV) amido complexes, $(Bu^t_3SiNH)_3Zr$–R (R = CH_3, phenyl, cyclohexyl), undergo alkane elimination and exchange via a Zr(IV) imido intermediate.[47b] In C_6H_6 solution, $(Bu^t_3SiNH)_3Zr$–CH_3 formed $(Bu^t_3SiNH)_3Zr$–C_6H_5 concomitant with the release of CH_4. The intramolecular nature of this elimination reaction was demonstrated upon thermolysis of $(Bu^t_3SiNH)_3Zr$–CH_3 in C_6D_6, whereby 1 equiv. of CH_4 was generated. The rate of reaction was first order in $(Bu^t_3SiNH)_3Zr$–CH_3 and zero order in benzene, as monitored by ^{1}H NMR spectroscopy. Further, the final product was deuterated in both the amido and phenyl positions, forming $(Bu^t_3SiND)_3Zr$–C_6D_5. Conclusive evidence for the formation of an intermediate $(Bu^t_3SiND)_2Zr$=$NSiBu^t_3$ was provided by trapping experiments with added donor ligands, forming the isolated products $(Bu^t_3SiND)_2Zr$=$NSiBu^t_3$(L) (L = THF, Et_2O, NMe_3, PMe_3).[49] In addition, competition experiments showed that aryl C–H bond activation was favored over methane C–H activation both kinetically ($\Delta\Delta G^{\ddagger} = -3.4$ kcal mol^{-1}) and thermodynamically ($\Delta G^0 = -1.2$ kcal mol^{-1}). The studies provided a quantitative measurement of relative C–H bond activation selectivities such that the relative reactivities in this system were found to be: $Pr^cH \approx ArH$ [$\Delta\Delta G^{\ddagger} = 0.0$ kcal mol^{-1}] > MeH [$\Delta\Delta G^{\ddagger} = 3.4$ kcal mol^{-1}] > $PhCH_2H$ [$\Delta\Delta G^{\ddagger} = 4.0$ kcal mol^{-1}] > $SiBu^t_3$ cyclometallation [$\Delta\Delta G^{\ddagger} > 8.5$ kcal mol^{-1}] > EtH [$\Delta\Delta G^{\ddagger} = 8.9$ kcal mol^{-1}] > Bu^tCH_2H [$\Delta\Delta G^{\ddagger} > 9.3$ kcal mol^{-1}] > cyclohexane [$\Delta\Delta G^{\ddagger} > 11.2$ kcal mol^{-1}].

1,2-Addition and elimination reactions are also observed to occur with transition metal carbene complexes. Legzdins has shown that such a mechanism occurs in the elimination and addition of alkanes to group VI $Cp^*M(NO)R_2$ systems.[50] Such an intermediate alkylidene complex results from the thermolysis of $Cp^*W(NO)(CH_2CMe_3)_2$.[51,51a–51c] In the presence of benzene, the starting material eliminates neopentane and C–H activates benzene to form the corresponding $Cp^*W(NO)(C_6H_5)(CH_2CMe_3)$ complex. Reaction in C_6D_6 results in stereospecific deuterium incorporation into the synclinal methylene site of the product neopentyl alkyl ligand (Scheme 5). Definitive evidence for

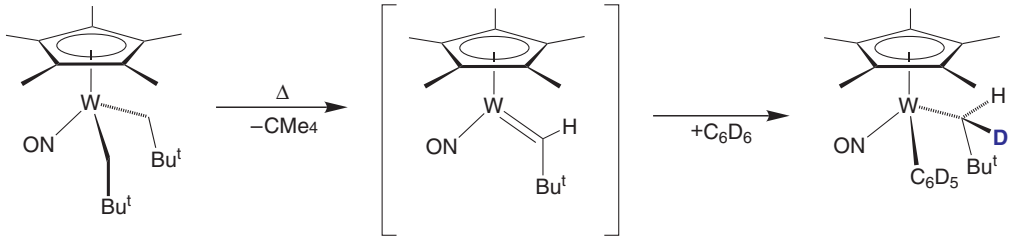

Scheme 5 1,2-alkane elimination and addition reactions in Cp*W(NO)(=C(H)CMe_3).

the formation of an alkylidene intermediate was provided by trapping experiments using PMe_3. Thermolysis of the bis-neopentyl complex in the presence of PMe_3 resulted in the formation of $Cp^*W(NO)(=C(H)CMe_3)(PMe_3)$. A variety of other substrates, including tetramethylsilane (TMS), methylcyclohexane, and mesitylene, were also shown to react to form the corresponding bis-alkyl, allyl hydride, and mixed mesityl/neopentyl complexes.

Interestingly, thermolysis of the α-deuterated derivative, $Cp^*W(NO)(CD_2CMe_3)_2$, undergoes intramolecular H/D exchange within the neopentyl ligands prior to neopentane elimination and product formation. This observation is consistent with the reversible formation of a $W(=C(D)CMe_3)(\sigma\text{-}CD_3CMe_3)$ intermediate that undergoes multiple C–H coupling/exchange reactions. Further evidence that intermediate arene π-complexes may also be formed during these reactions is provided by the observation of H/D exchange between phenyl C–H bonds and alkyl C–H bonds in the labeled complexes, $Cp^*W(NO)(CH_2CMe_3)(C_6D_5)$ and $Cp^*W(NO)(\eta^2\text{-}CH_2Ph)(C_6D_5)$. However, such exchange may also involve the formation of an intermediate benzyne complex, as shown for the Mo congener.[52] Thermolysis of $Cp^*Mo(NO)(C_6H_5)(CH_2CMe_3)$ in the presence of pyridine-d_5 results in the trapping of both an intermediate alkylidene complex, $Cp^*Mo(NO)(=C(H)CMe_3)(NC_5D_5)$, and an intermediate benzyne complex, $Cp^*Mo(NO)(\eta^2\text{-}C_6H_4)(NC_5D_5)$, as determined by ^1H NMR spectroscopy and the separation of the two pyridine complexes via fractional crystallization. Regardless, both mechanisms indicate the existence of an alkane σ-complex intermediate in these C–H activation reactions.

1.20.3 Isotope Effects Involving C–H and H–H Bonds

As exemplified in the previous sections, isotopic labels provide invaluable insight into the nature of reaction mechanisms. In addition to providing evidence for novel rearrangements (e.g., alkane migrations via σ-complexes) and distinguishing between different possible mechanisms (e.g., σ-bond methathesis versus carbene formation), the presence of a label can perturb the relative energetics of a system, thereby providing information concerning the kinetics and thermodynamics of the system of interest. These isotope effects are reflected as equilibrium isotope effects (EIEs) and kinetic isotope effects (KIEs) in various types of reactions, including many of the systems and reactions described earlier in this chapter. The following sections describe the insights and information gained within organometallic systems from both measured and calculated EIEs and KIEs.

1.20.3.1 Equilibrium Isotope Effects Involving the Coordination of C–H Bonds

EIEs provide invaluable information concerning both molecular structure and the determination of reaction mechanisms. EIEs are traditionally defined as the ratio of equilibrium constants for unlabeled and labeled reactants and products ($EIE = K_H/K_D$; Figure 2). For oxidative addition and reductive elimination reactions, the presence of intermediates along the reaction coordinate, such as alkane σ-complexes and agostic interactions, make these reactions multistep processes and hence, additional terms are necessary in order to more fully describe the overall mechanism.[13,21] Thus, reductive elimination may consist of a reductive coupling (rc) step followed by dissociation (d), whereas the microscopic reverse, oxidative addition, could consist of ligand association (a) followed by oxidative cleavage (oc), as illustrated in Scheme 6.

The measurement of the potentially different equilibrium constants for labeled and unlabeled reacting species provides the corresponding EIE for the reaction. In addition, evaluation of the vibrational frequencies of the participating species, either determined experimentally or computationally, allows for a more detailed understanding of the equilibrium reaction. This is typically achieved by calculating the EIE according to the expression: $EIE = K_H/K_D = SYM \cdot MMI \cdot EXC \cdot ZPE$, where SYM is the symmetry factor, MMI is the mass moment of inertia term, EXC is the excitation term, and ZPE is the zero point energy term (Figure 2).[53,53a] Hence, knowledge of the molecular structure and isotopically perturbed vibrations allows for the evaluation of the EIE.

Although studies that provide information on the EIEs for the coordination, oxidative addition, and reductive elimination of C–H bonds are rare, a few examples have been reported recently in the literature. Bergman and Moore reported substantially inverse EIEs ($K_H/K_D < 1$) for the coordination of cyclohexane (~0.1 at −100 °C) and neopentane (~0.07 at −108 °C) to $[Cp^*Rh(CO)]$, generated from the photolysis of $Cp^*Rh(CO)_2$ in Kr matrices.[54,54a,54b] In contrast, Geftakis and Ball reported a normal ($K_H/K_D > 1$) EIE for the coordination of cyclopentane to $[CpRe(CO)_2]$ (1.33 at −93 °C)[55] (Scheme 7). In this particularly novel experiment, the alkane σ-complex was generated *in situ* in the NMR probe at low temperature. Resonances corresponding to bound and unbound methylenes in the ^2H NMR spectrum were observed, making this the first transition metal alkane σ-complex observed on the NMR timescale.

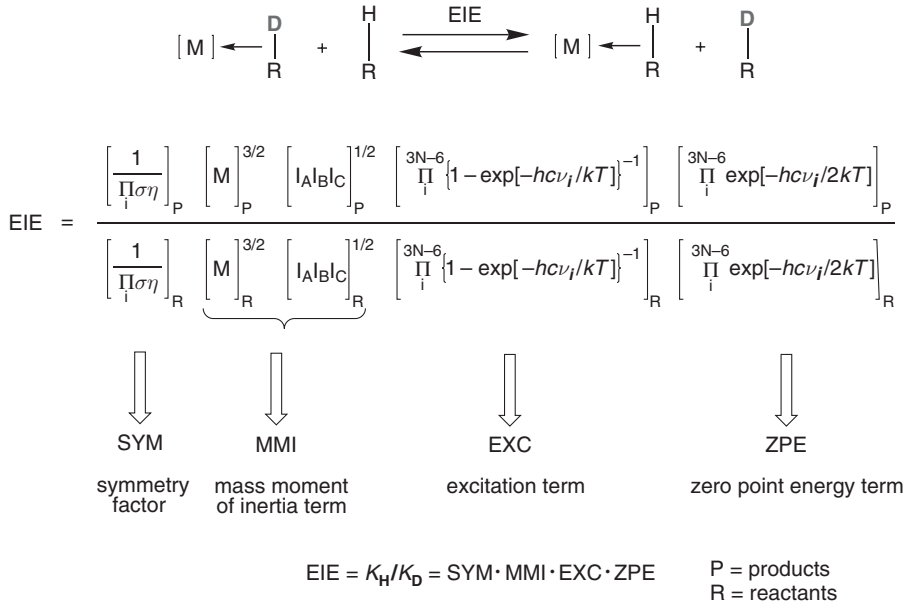

Figure 2 Calculation of equilibrium isotope effects in terms of SYM, MMI, EXC, and ZPE.

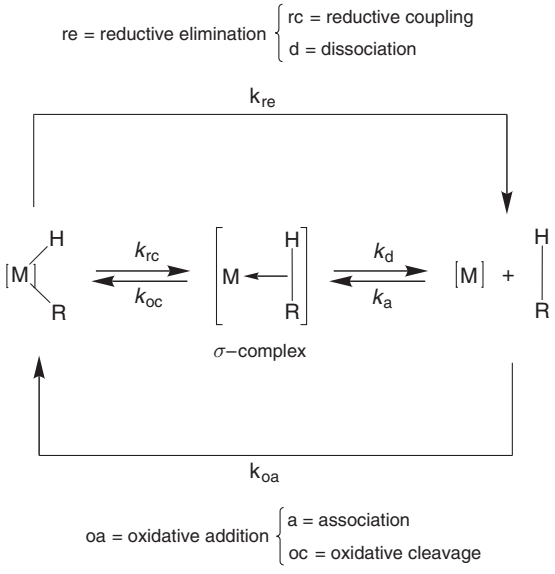

Scheme 6 Description of oxidative addition and reductive elimination reactions with alkane σ-complex intermediate.

In addition, EIEs for intermolecular coordination of alkanes have been explored computationally. The EIE for the coordination of CH_4 and CD_4 to {$[H_2Si(C_5H_4)_2]W$} to form the corresponding methane σ-complexes, $[H_2Si(C_5H_4)_2]W(\sigma\text{-}CH_4)$ and $[H_2Si(C_5H_4)_2]W(\sigma\text{-}CD_4)$, was calculated to be 1.45 at 100 °C and 1.57 at −100 °C. In contrast, Bender reported that the EIE for coordination of methane to $OsCl_2(PH_3)_2$ was 0.96 at 25 °C and 0.66 at −108 °C.[56] However, calculation of the temperature dependence of the EIE in the {$[H_2Si(C_5H_4)_2]W$} system revealed a surprising result: depending on the temperature both normal and inverse EIEs were obtained for coordination of methane in the same system. The transition from inverse to normal occurs upon raising the temperature above −170 °C in this system (Figure 3). Further, the EIE exhibits a maximum, rather than monotonically increasing or decreasing as a function of temperature. This behavior is the result of inverse ZPE and EXC terms that favor binding CD_4 versus CH_4 due to the creation of six new isotopically sensitive vibrations upon coordination of methane, generated

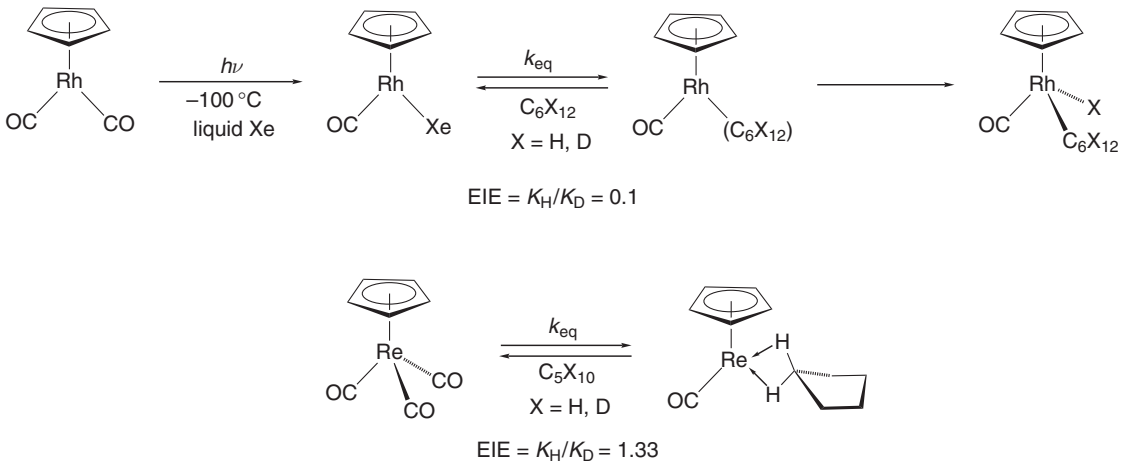

Scheme 7 Intermolecular EIEs for coordination of alkane.

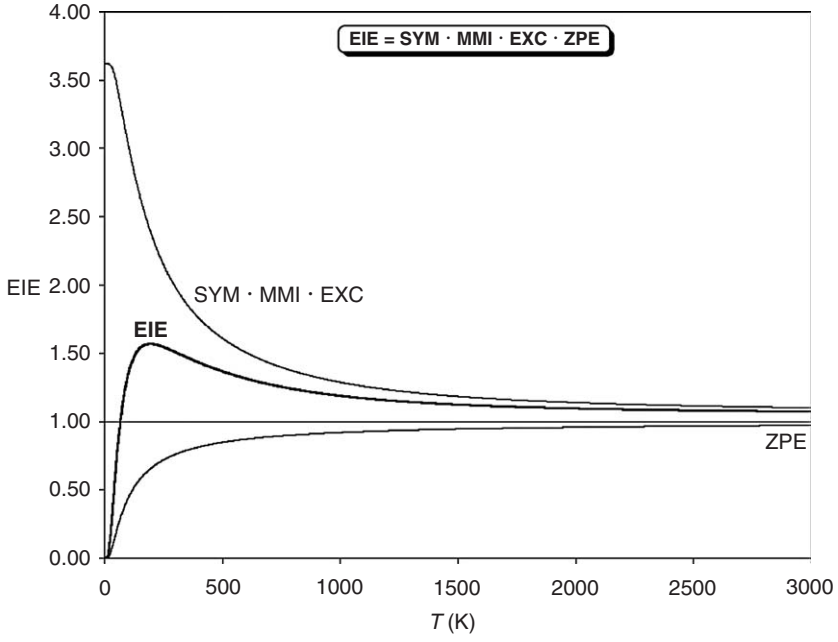

Figure 3 Calculated temperature dependence of the EIE for binding methane to $[H_2Si(C_5H_4)W]$.

from the six degrees of freedom associated with free methane. The ZPE corresponds closely to the enthalpy of the system, with inverse values (EIE < 1) indicating a positive $\Delta\Delta H^0$ as described in Figure 4, and normal values (EIE > 1) corresponding to a negative $\Delta\Delta H^0$. The EXC term is related to the vibrational entropy of the system and effectively attenuates the MMI component such that EXC approaches a limit of 1/MMI at infinite temperature. Ultimately, the ZPE term dominates at low temperatures and an inverse ZPE term will cause the EIE to be inverse at sufficiently low temperatures. However, at high temperatures, the MMI term dominates, causing the EIE to transition from an inverse value to a normal value. The MMI term is related to the entropy of the system, and must be large enough in comparison to the ZPE term in order for such a transition to occur. The SYM term is 1.00 in this reaction. For EIEs comparing isotopologues of different symmetry, this will have a dramatic effect. See Ref.: 61.The authors rationalized that other systems may exhibit a similar temperature dependence for the coordination of an alkane[53,53a], providing an explanation for the different experimental results reported in the $Cp^*Rh(CO)$ and $CpRe(CO)_2$. However, it was noted that whether or not this behavior is the proper description of alkane coordination within a system is dependent upon: (i) the nature of the σ-complex and its vibrational frequencies and (ii) the size of the alkane and, correspondingly, the magnitude of the

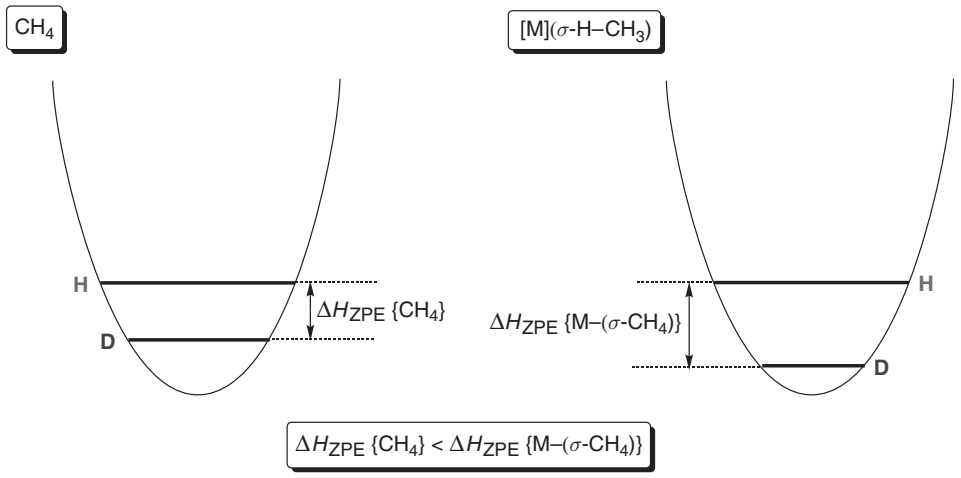

Figure 4 Depiction of a system in which the total ZPE stabilization in the σ-complex is greater than in free methane due to the additional vibrational modes gained upon coordination of methane.

MMI component. Furthermore, the presence of a maximum EIE is the result of an inverse ZPE term; if the ZPE term were >1, then a normal EIE would be observed at all temperatures.

Isotopic labeling of alkane substrates for the investigation of EIEs in intermolecular exchange reactions such as oxidative addition reactions, σ-bond metathesis reactions, and 1,2-addition reactions has also been explored by various research groups.[57,58,58a–58f] Wolczanski reported a variety of experimental and computational intermolecular EIEs within $(silox)_2(Bu^t_3SiN(D))TiR$ ($silox = Bu^t_3SiO–$) systems.[59] The EIEs for intermolecular 1,2-additions that involve cleavage of a C–H bond are all normal (EIE > 1). While the quantum mechanical calculations reproduce this trend, the calculations also reveal the complexity of the system. In all cases, the MMI term favors EIEs > 1. In other words, translational and rotational entropy favor deuterium to be present in the free alkane rather than in the metal complexes. Another common feature is that vibrational entropy (excitation) counters this term, favoring deuterium in the metal complex versus the free alkane. The authors discuss this phenomenon in detail, identifying the low frequency vibrations that contribute most significantly to this inverse term. Interestingly, while the EXC term is inverse for all the alkanes studied, the ZPE term is normal (>1) for all alkanes except methane and ethylene. According to the previous discussion concerning the temperature dependence of EIEs, this would imply that the EIE for 1,2-addition of methane would become inverse at sufficiently low temperature, in contrast to the other linear alkanes.

In contrast to the few examples of EIEs for intermolecular oxidative addition and reductive elimination of C–H bonds, there have been more examples of intramolecular EIEs (Scheme 8). One of the earliest reports of an intramolecular EIE was reported by Shapley and co-workers in the tri-osmium cluster, $(CO)_{10}Os_3(CH_2)H_2$.[60] Deuteration of the complex via reaction of $(CO)_{10}Os_3D_2$ with CH_2N_2 provided a mixture of hydridomethyl and dihyridomethylene tautomers in solution. Both simulation of the ^1H NMR data and neutron diffraction data revealed a preference for H over D in the metal hydride sites for both tautomers. The seminal study by Bergman and Periana reported the intramolecular EIE for M–H and α-C–H exchange within $Cp^*Ir(PMe_3)(CH_2CH_3)D$.[10] A value of 4.6 was obtained, indicating a preference for deuterium being in a C–H bond versus an M–H bond. Equilibrium values of 1.4 and 4.9 were found for intramolecular exchange within $Cp_2W(CD_3)H$ and $Cp_2W(CH_3)D$, respectively.[11] In the

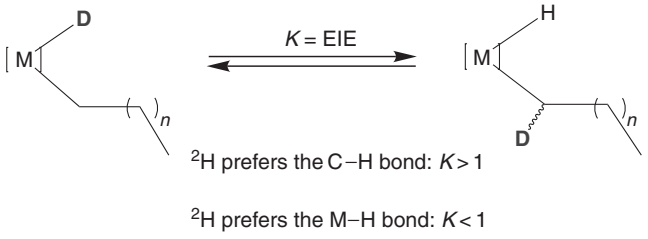

Scheme 8 Intramolecular EIE's resulting from H/D exchange between M(H) and α-CH sites.

absence of an EIE, equilibrium values of 3 would be expected for an [M](CH_3)H system while a value of 2 is expected for systems [M]($CH_2(CH_2)_nCH_3$)H systems due to statistical factors.

Site exchange within $\{Cp_2Re(CD_3)H\}^+$ was shown to occur at temperatures as low as −30 °C.[61] Similar to the Cp_2W system, the equilibrium constant measured was less than the statistical value of 3, $K = 1.0(0.1)$. Significantly, the equilibrium for the Re system was rapidly established at temperatures so that overall reductive elimination did not occur. Flood has also reported intramolecular EIEs for a variety of alkyl ligands in the (TACN)Rh and CnRh systems, which also undergo H/D exchange between the metal hydride and α-CH_x sites at rates much faster than overall alkane loss.[19] In the case of $[CnRh(PMe_3)(CH_3)D]^+$, a $K = 6.59$ was observed,[17] whereas a $K = 3.4$ was observed for $[(TACN)Rh(P(OMe)_3)(CH_2(CH_2)_4CH_3)D]^+$.[19]

Intramolecular EIEs for arene C–H oxidative addition reactions were first reported by Jones and Feher.[18,18a] Specifically, a value of 1.85 was reported for intramolecular exchange between the metal hydride and phenyl C–H sites within $Cp^*Rh(PMe_3)(C_6D_5)H$. The observation of a $K < 5$ reflects the preference for deuterium to occupy a phenyl C–H site versus an M–H site. Similarly, Parkin reported an intramolecular EIE of 1.96 for the interconversion of $[Me_2Si(C_5Me_4)_2]Mo(C_6H_2D_3)H$ and $[Me_2Si(C_5Me_4)_2]Mo(C_6H_3D_2)D$.[13] In fact, this also corresponds to the EIE for C–H versus C–D bond cleavage of $C_6H_3D_3$ by $\{[Me_2Si(C_5Me_4)_2]Mo\}$.

Since these exchange reactions are intramolecular, there is essentially no difference in the MMI terms in the EIE equation that describes the reaction. In other words, EIE ≈ SYM · ZPE · EXC for an intramolecular exchange. Hence, the EIEs associated with the exchanges consist of the vibrational terms, ZPE and EXC, and the symmetry term, SYM. Alternatively, one can consider the ZPE term to dominate the enthalpy component of the equilibrium, whereas the SYM and EXC terms contribute to the entropy of the exchange reaction. Due to the multiple C–H sites in the alkyl chain or aryl ligand (3 for methyl; 2 for the α-CH_2 of a linear alkyl chain, e.g., Bu^n; 5 for a phenyl ligand), the SYM term (i.e., entropy) will favor deuterium to be in the C–H site for an M(R)D system versus the M–H site. Hence, EIEs greater than or less than SYM reflect the isotopic site preference due to vibrational differences between the M–H and C–H bonds. Specifically, one would expect deuterium to populate the site that has the greatest zero point energy stabilization, that is, the stronger bond. This is readily understood if, for simplicity, a single M–H stretch and a single C–H stretch are considered. If $\nu_{M-H} > \nu_{C-H}$, then population of the M–H site by deuterium would result in lowering the energy of the system. Conversely, if $\nu_{M-H} < \nu_{C-H}$, as is typically observed from IR data of M–H compounds, then population of the C–H site by deuterium would result in a lower energy system (Figure 5). When considering multiple vibrational modes, it is the difference of the sum of the vibrations for each site (M–H vs. C–H) that will impact the magnitude and direction of the equilibrium and, hence, the EIE.

As indicated by the statistically corrected equilibrium constants in Table 1 for the reaction defined in Scheme 8, the values are all >1, revealing that deuterium prefers to be in the C–H site rather than the M–H site due to greater vibrational stabilization. This point has been appreciated by many authors, in particular with respect to both EIEs and KIEs associated with methane loss from M(CH_3)H systems.[10–13,14,14a,14b,17,18,18a,19,21,59]

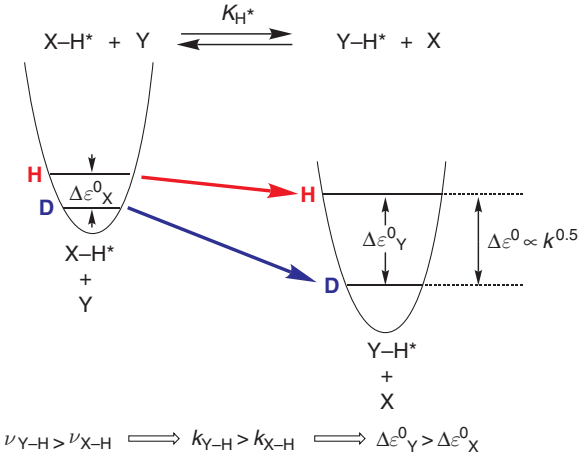

Figure 5 Expected equilibrium isotope effects based upon the relative frequencies of a single bond stretch.

Table 1 Intramolecular equilibrium isotope effects for M–H to α-CH_x exchange reactions

Transition metal system	*EIE*
$Cp^*Rh(D)(Et)(PMe_3)$	2.3
$Cp_2W(D)(CH_3)$	1.6
$Me_2Si(C_5Me_4)_2W(D)(CH_3)$	1.3
$Tp^*Rh(CNCH_2Bu^t)(D)(CH_3)$	2.1
$\{CnRh(D)(CH_3)(PMe_3)\}^+$	2.2
$\{(TACN)Rh(D)(CH_2(CH_2)_4CH_3)(P(OMe)_3)\}^+$	1.7

1.20.3.2 Kinetic Isotope Effects in the Oxidative Addition and Reductive Elimination of C–H Bonds

In addition to EIEs, the introduction of a label or multiple labels to a reagent or compound in a reaction can result in a perturbation of the rate of the reaction. These perturbations are known as kinetic isotope effects (KIEs). KIEs play a prominent role in the determination and evaluation of reaction mechanisms of organometallic complexes. This is particularly true with regard to transition metal-mediated oxidative addition and reductive elimination reactions of alkanes. Specifically, the KIEs measured for the reductive elimination of alkanes are some of the principal evidence for the existence of alkane σ-complex intermediates, in addition to the observation of deuterium exchange between hydride and alkyl sites (*vide supra*), as well as low temperature and room temperature flash kinetics studies.[54,54a,54b]

The effect of isotopic substitution on the rate of reductive elimination of alkanes has often focused on comparing the rate of alkane elimination for perdeuterated versus protio metal alkyl hydride complexes. Bergman reported the first example of an inverse KIE for the loss of cyclohexane-d_0 versus cyclohexane-d_{12} within the $Cp^*Ir(PMe_3)$ system.[9] The observed KIE, $K_H/K_D = 0.7$, indicated that loss of the perdeuterated substrate occurred faster than that of the protio species. Since then, other investigators have reported inverse KIEs for the reductive elimination of other alkanes, most prominently methane, as summarized in Table 2. These types of elimination reactions are not invariably characterized by inverse KIEs, however. For example, Whitesides reported a $K_H/K_D = 1.5$ for neopentane elimination from $(dcpe)Pt(CH_2CMe_3)H$ (dcpe = dicylcohexylphosphinoethane).[62,62a] Other examples include the large, normal KIEs observed for 1,2-addition to $\{(Bu^t{}_3SiO)_2Zr(=NSiBu^t{}_3)\}$.[59]

The initial fascination with these inverse KIEs centered around a mechanism for this observation. If one considers, for example, a single X–H bond, its corresponding vibration (stretch) cleavage of this bond would result in the same transition state for both the protio and deutero isotopomers (Scheme 9). Since the deuterated reactant isotopomer would have a lower zero point energy relative to the protio species, the comparison of the rates measured for the hypothetical cleavage of this bond would reflect the difference in the ground state zero point energy of the two species, because the ZPE in the transition state is the same for the hydrogen and deuterium isotopomers since this vibration is the reaction coordinate and corresponds to an imaginary frequency in the transition state. Hence, a normal KIE would be observed.[63] This is the type of scenario one might envisage for the irreversible loss of an alkane from an M–H versus an M–D compound.

Table 2 Inverse kinetic isotope effects for reductive elimination of alkane from transition metal centers

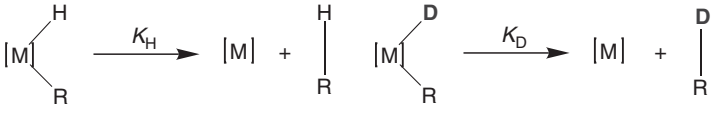

	Transition metal system	K_H/K_D
Bergman	$Cp^*Ir(H)(C_6H_{11})(PMe_3)$	0.75
	$Cp^*Rh(H)(Et)(PMe_3)$	0.5
Norton	$Cp_2W(H)(CH_3)$	0.74
Bercaw	$Cp^*{}_2W(H)(CH_3)$	0.70
	(tmeda)Pt(H)(CH_3)(Cl)	0.29
Heinekey	$\{Cp_2Re(H)(CH_3)\}^+$	0.8
Flood	$\{(TACN)Rh(H)(CH_3)(PMe_3)\}^+$	0.77

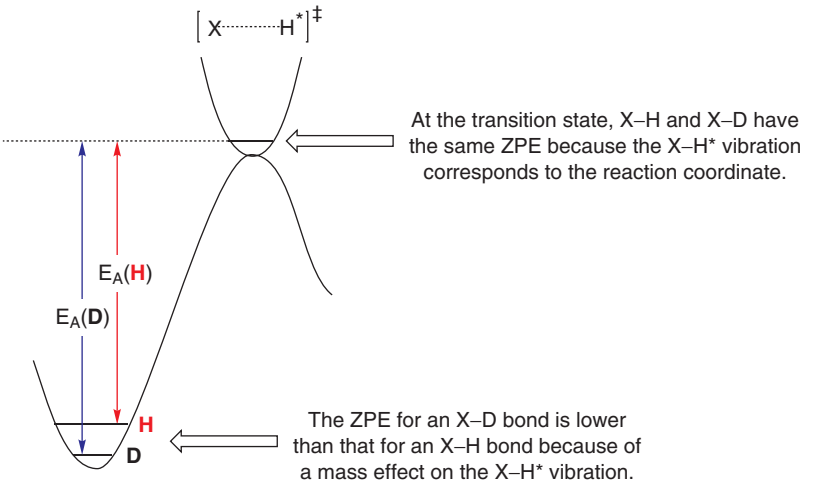

Scheme 9 Initial expectation of a normal primary deuterium kinetic isotope effect due to ground state energy differences.

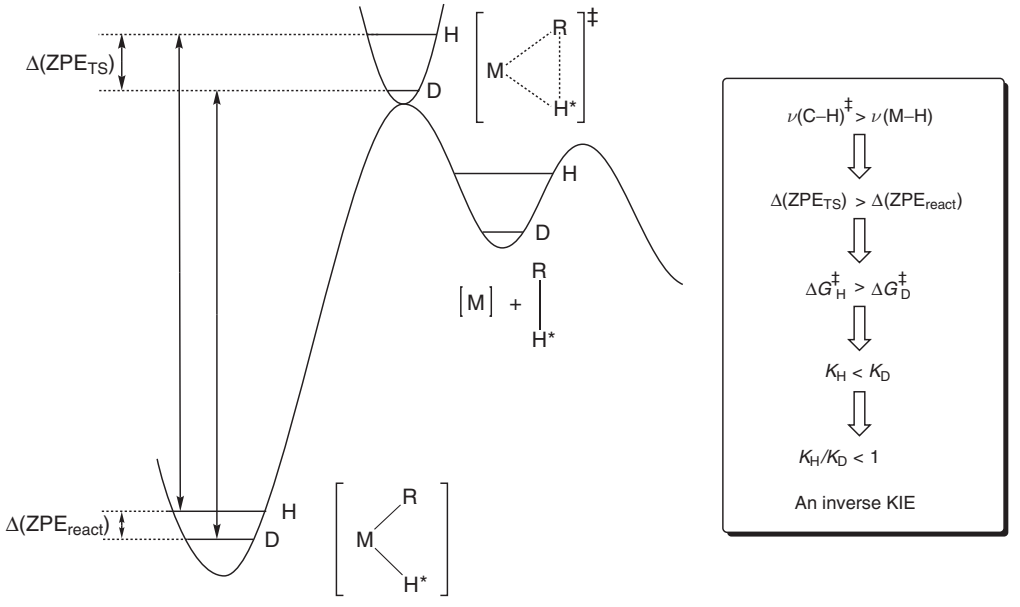

Figure 6 Energy surface corresponding to an inverse KIE for alkane loss due to a single-step reductive elimination.

Nonetheless, the observation of inverse KIEs for alkane elimination reactions indicates a greater complexity to those systems that exhibit them. Although an M–X (X = H, D) bond is being cleaved in the reductive elimination of alkane, a corresponding C–X bond is being formed. Hence, for a transition sate that is very late on the reaction coordinate (i.e., product-like), significant bond formation could result in a greater zero point energy difference for the isotopologs in the transition state relative to the ground state. Hence, if this scenario were operative, the observed inverse KIE would be the result of an inverse KIE on a "single" elementary step (Figure 6).

However, an alternative explanation can also account for the observed inverse isotope effects. As previously described, reductive elimination processes could be multistep reactions consisting of reductive coupling of an X–Y bond (C–H in the case of alkane activation) to form an intermediate, which may or may not be observed, followed by dissociation of substrate (alkane) (Figure 7). Hence, the rate constant for irreversible reductive elimination is a composite of the rate constants for reductive coupling (k_{rc}) to form the intermediate, oxidative cleavage (k_{oc}), resulting in decomposition of the intermediate to form starting material, and dissociation (k_d), such that $k_{obs} = k_{rc}k_d/(k_{oc} + k_d)$.[64]

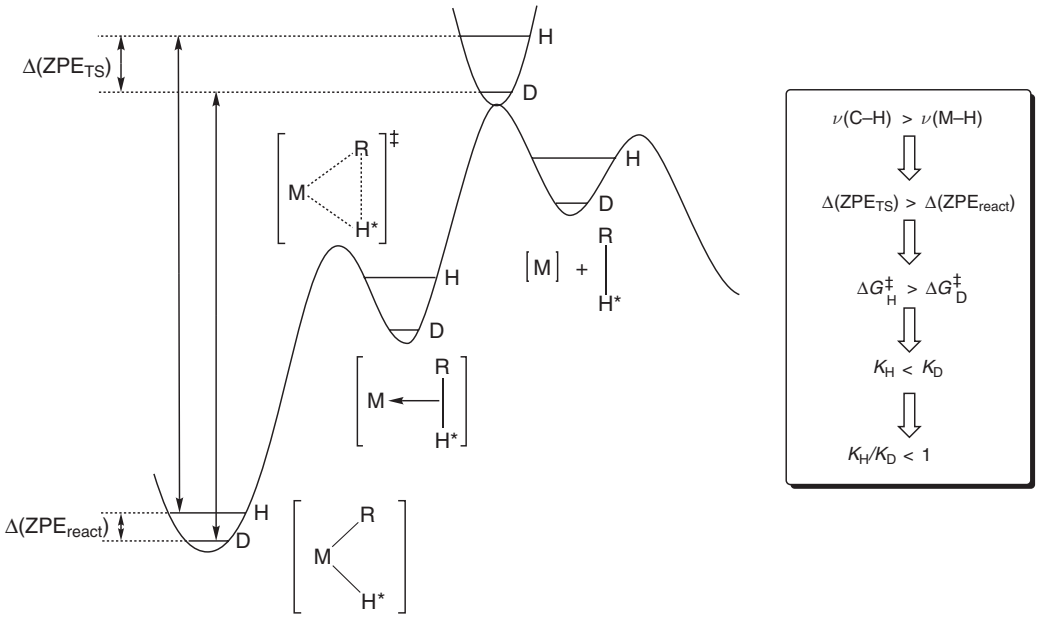

Figure 7 Energy surface corresponding to an inverse KIE for alkane loss due to pre-equilibrium formation of an alkane σ-complex intermediate.

The overall form of the free energy surface will depend on the relative magnitude of the individual rate constants such that: (i) if $k_d \gg k_{oc}$, the reductive coupling step becomes rate determining, $k_{obs} = k_{rc}$ or (ii) if $k_d \ll k_{oc}$, the dissociation of substrate becomes rate determining, $k_{obs} = (k_{rc}/k_{oc})k_d$. If the former scenario were operative, then the observed inverse KIEs for alkane elimination reactions would be due to a single-step inverse KIE, as described earlier. However, if an intermediate is formed prior to irreversible loss of alkane, then the KIE for reductive elimination is a composite of isotope effects on each of the individual steps of the reaction coordinate, that is, $K_H/K_D = [(k_{rcH}/k_{rcD})(k_{dH}/k_{dD})]/(k_{ocH}/k_{ocD})$.

Further, if the isotope effect for dissociation is negligible ($k_{dH}/k_{dD} \sim 1$), then the isotope effect on reductive elimination is dictated by the ratio of the isotope effect on reductive coupling to that of oxidative cleavage. This ratio essentially corresponds to the EIE on the interconversion of [M](R)H and [M](σ-RH). In the situation where an M–D bond is being broken and a C–D bond is being formed, the EIE would be predicted to be inverse because deuterium prefers to be located in the stronger bond (the C–D bond) due to a greater ZPE stabilization. Thus, for this type of reaction mechanism, an inverse KIE would be predicted for the overall reductive elimination of alkane. Essentially, the inverse EIE is transferred to the rate-determining step, and the observed inverse KIE for reductive elimination does not "require" an inverse KIE for a single step. In addition, the observation of intramolecular H/D exchange further substantiates the existence of intermediate alkane σ-complexes in the reductive elimination of C–H bonds and provides additional credence to the argument that the observed inverse KIEs are the direct result of the inverse EIEs for alkane σ-complex formation being transferred to the rate-determining step of alkane dissociation.

In spite of this, it has been recognized that the observation of an inverse KIE for loss of alkane does not *a priori* distinguish between the concerted or pre-equilibrium scenarios.[65] In addition, the existence of an inverse EIE for formation of an alkane σ-complex does not rule out the possibility of an inverse KIE for reductive coupling to form the σ-complex, since the EIE is simply the ratio of the forward (rc) and reverse (oc) KIEs. As shown in Figure 8, if the formation of the σ-complex is late and, correspondingly, if the transition state for reductive coupling is late on the reaction coordinate, it is entirely possible for $k_{rcH}/k_{rcD} < 1$. For instance, for an EIE = 0.5, a $k_{ocH}/k_{ocD} < 2.0$ necessitates a $k_{rcH}/k_{rcD} < 1$. In this regard, due to the challenges in measuring KIEs for oxidative addition of alkanes, few studies have determined the independent KIEs for either the oxidative cleavage or reductive coupling steps in alkane elimination reactions. Nonetheless, if at least two and/or three interdependent isotope effects (k_{rcH}/k_{rcD}, k_{rcH}/k_{rcD}, and/or K_H/K_D) are known, then the third can be obtained. In a particularly elegant series of experiments, Jones was able to measure typical KIEs for "both" the oxidative cleavage and reductive coupling of an alkane C–H bond within the [Tp*Rh($CNCH_2CMe_3$)] system.[21] Irradiation of the diimide complex, Tp*Rh($CNCH_2CMe_3$)($Me_3CCH_2N{=}C{=}NPh$), in C_6F_6 under 10 atm of CH_2D_2 at low temperature results in the initial formation of the corresponding methyl hydride and methyl deuteride isotopomers, [Rh](CHD_2)H and [Rh](CH_2D)D, in a ratio of

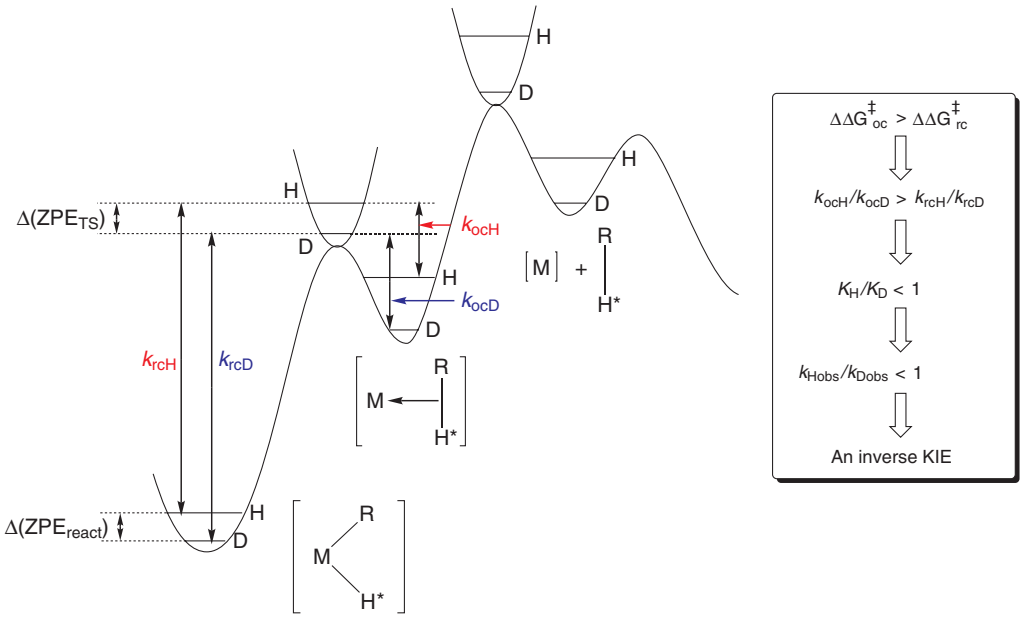

Figure 8 Free energy surface describing the kinetics for formation and decomposition of the σ-alkane intermediate.

4.3 : 1. This ratio reflects the KIE for oxidative cleavage and indicates that it is normal and large. Upon standing at 10 °C, the system undergoes equilibration such that a value of 1.7 : 1 was measured for the equilibrium ratio of [Rh](CHD$_2$)H/[Rh](CH$_2$D)D. This value represents the intramolecular isotope effect whereby deuterium favors the C–H site versus the M–H site. Significantly, it is in excellent agreement with the statistically adjusted value observed for the equilibration of Tp*Rh(CNCH$_2$CMe$_3$)(CH$_2$D)H and Tp*Rh(CNCH$_2$CMe$_3$)(CH$_3$)D ($K = 2.1$).

Most significantly, Jones was also able to directly determine the KIE for reductive coupling of a C–H bond. Thermolysis of the secondary alkyl hydride complex, Tp*Rh(CNCH$_2$CMe$_3$)(Pr^i)H, results in rearrangement to the *n*-propyl isomer, presumably via σ-complex intermediates, that is competitive with overall loss of propane. Kinetic modeling showed that a common intermediate from which the phenyl hydride and *n*-propyl products were formed was required in order to fit the kinetics data. Synthesis of the Tp*Rh(CNCH$_2$CMe$_3$)(Pr^i)D complex and subsequent thermolysis revealed that no incorporation of label into the 2° α-C–H site was observed during the course of the reaction. This is in contrast to other systems containing 2°cyclic alkyls.[9,66] Hence, the observed rate constant for disappearance of Tp*Rh(CNCH$_2$CMe$_3$)(Pr^i)X (X = H, D) represents the rate for the C–X reductive coupling step, k_{rc}. Ultimately, kinetic modeling of the rearrangements and loss of propane-d$_0$ and propane-d$_1$, respectively, provided the isotope effect for reductive coupling, $k_{rcH}/k_{rcD} = 2.1$, a normal KIE.

Since the EIE for intramolecular isomerization of the deuterium label between the M–H and C–H sites (after statistical corrections) is the ratio of the KIEs for oxidative cleavage and reductive coupling, the values obtained for the individual KIEs provide an EIE = 2.05 ($(k_{ocH}/k_{ocD})/(k_{rcH}/k_{rcD}) = 4.3/2.1$). This is in agreement with that obtained from the Tp*Rh(CNCH$_2$CMe$_3$)(CH$_3$)D complex isomerization ($K = 2.1$). Hence, this system provides definitive evidence that the EIE for intramolecular exchange in M(R)X (X = H, D) systems is the result of "normal" KIEs for both oxidative cleavage and reductive coupling of C–H bonds, but of differing magnitude.

This point has been further elucidated by Parkin within the *ansa*-tungstenocene system, [Me$_2$Si(C$_5$Me$_4$)$_2$]-W(CH$_3$)X (X = H, D).[13] Although no evidence of intermolecular methane exchange was observed and, hence, direct measurement of the KIEs for oxidative cleavage was unobtainable, it was reasoned that since intramolecular H/D exchange occurred at rates competitive with alkane loss, the kinetics analysis would be sensitive to the ratio of the isotope effects on the oxidative cleavage and reductive coupling steps for C–H and C–D bonds. In fact, poor nonlinear least-squares regression fits of the data resulted when $k_{rcH}/k_{rcD} < 1$. Further, DFT calculations on a model of this system, [H$_2$Si(C$_5$H$_4$)$_2$]W(CH$_3$)H, revealed that normal primary and secondary KIEs characterize this system from both the oxidative cleavage and reductive coupling steps, in agreement with the experimental analysis.[67]

The combination of the Tp*Rh and *ansa*-tungstenocene studies provides strong evidence that the inverse KIEs for CH$_4$ versus CD$_4$ reductive elimination observed in organometallic systems are not only due to an inverse EIE for reversible formation of an alkane σ-complex intermediate, but that the inverse EIE is the result of normal KIEs upon

the oxidative cleavage and reductive coupling steps. It is because the KIE for oxidative cleavage of a C–H versus a C–D bond is greater than that for reductive coupling that an overall inverse KIE for alkane-d_0 versus alkane-d_n loss is observed in other systems.

In contrast to the conclusions drawn from alkane addition and elimination studies, those involving arene C–H activation reveal a surprising result. As previously mentioned, the H/D exchange between the metal hydride and phenyl C–H sites in $Cp^*Rh(PMe_3)(C_6D_5)H$ results in an observed ratio of 2.7 : 2 : 2 : 1 for the M–H, *ortho*-, *meta*-, and *para*-sites, respectively, via ^1H NMR spectroscopy.[18,18a] This corresponds to an EIE = 0.37, with deuterium favoring the phenyl C–H versus the M–H site. Further, the existence of an arene complex intermediate was proposed in order to explain the different KIEs for intermolecular ($K_H/K_D = 1.0$ for C_6H_6 versus C_6D_6) and intramolecular ($K_H/K_D = 1.4$ for $C_6H_3D_3$) oxidative addition of benzene. In this regard, identical inter- and intramolecular KIEs ($K_H/K_D = 1.29$) were observed for oxidative addition of benzene to $[CnRh(PMe_3)(CH_3)H]^+$.[17] This was interpreted to indicate that if an intermediate existed on the path to benzene activation after reductive elimination of methane to form $[CnRh(PMe_3)]^+$, its formation must be rapidly reversible, with the C–H oxidative addition step being rate determining. Oxidative addition of benzene to the $\{Cp^*Ir(PMe_3)\}$ fragment also exhibits similar intramolecular ($K_H/K_D = 1.15$) and intermolecular ($K_H/K_D = 1.22$) KIE's.[68]

Nonetheless, since the EIE for interconversion of the aryl hydride and the arene complex is known for the $Cp^*Rh(PMe_3)$ system, and the KIE for oxidative cleavage of the arene C–H bond is determined, the KIE for reductive coupling of an arene C–H bond can be calculated via $k_{rcH}/k_{rcD} = (k_{ocH}/k_{ocD})K_{eq}$. The values give a $k_{rcH}/k_{rcD} = 0.52$, an inverse KIE. In light of the previous discussion, this result represents an unprecendented inverse KIE for a single step.

However, this result does not appear to be inherent to the reductive coupling of arene C–H bonds. Inverse intermolecular EIEs for C_6H_6 versus C_6D_6 exchange were obtained in the *ansa*-$[Me_2Si(C_5Me_4)_2]M$ system (M = Mo, W), with a $K = 0.53$ for Mo and $K = 0.66$ for W.[13] Generation of the intramolecular C–H activation "tuck-in" complex, $[Me_2Si(C_5Me_4)(\eta^6\text{-}C_5Me_3CH_2)]MH$, either via photolysis of the dihydride in C_6D_{12} at low temperature (M = Mo) or via thermolysis of the methyl hydride complex in C_6D_{12} (M = W), and subsequent reaction with C_6H_6, C_6D_6, or $C_6H_3D_6$ provided direct measurement of the KIE for oxidative cleavage of an arene C–H bond. In the Mo system, the inter- and intramolecular KIEs were large and normal ($K_H/K_D = 2.1$ and 2.6, respectively), whereas the W system exhibited no intermolecular KIE ($K_H/K_D = 1.0$) and a normal intramolecular KIE ($K_H/K_D = 1.4$). Reductive elimination of C_6H_6 or C_6D_6 from the corresponding phenyl hydride complexes resulted in KIEs (for reductive elimination) of 1.14 for the Mo system and 0.65 for the W system. Given that the inter- and intramolecular KIEs for oxidative addition were both similar and large in the Mo system, the KIE for reductive elimination was interpreted as directly probing the isotope effect for reductive coupling of the arene C–H bond. Using the intermolecular KIEs for oxidative addition and reductive elimination, an EIE = 0.54 was calculated, in agreement with the independently measured value. In contrast, the different KIEs for inter- and intramolecular C–H activation in the W system indicate that coordination of benzene is rate determining in the oxidative addition of benzene to *ansa*-$[Me_2Si(C_5Me_4)_2]W$, similar to the $Cp^*Rh(PMe_3)$ system, and in contrast to the Mo system. The ratio of the intermolecular KIEs for oxidative addition and reductive elimination gives an EIE = 0.65, again in agreement with the experimentally measured value. However, since the isotope effect for intramolecular oxidative addition represents the KIE for oxidative cleavage of the benzene C–H bond, the KIE for reductive coupling can be calculated, as described for the $Cp^*Rh(PMe_3)$ system, giving a $k_{rcH}/k_{rcD} = 0.91$. Thus, even for similar systems but with different metals, the isotope effect for reductive coupling of an arene C–H bond can be either normal or inverse.

Ultimately, the observation of KIEs for a reaction can provide significant insight into the mechanism that is operative, but the interpretation may require supplemental studies. Importantly, understanding the nature of the transition state for a particular reaction is crucial, and, in this regard, computational studies can supplement experimental investigations by providing insight into the evaluation of different hypotheses for explaining an observed KIE.

1.20.3.3 Isotope Effects Involving Dihydrogen

The reaction of dihydrogen with transition metal complexes is of fundamental importance in a wide range of stoichiometric and catalytic reactions.[69,69a–69h] As noted in earlier sections, the oxidative addition and reductive elimination of H_2 plays an intimate role in the functionalization of alkanes and other organometallic reactions. Consequently, the mechanisms of reactions of transition metals with dihydrogen have a central role in organometallic chemistry. Extensive reviews on this topic exist, and the reader is referred to these for a more thorough understanding of the topic.[70,70a–70d]

One type of interaction that has generated a significant amount of attention is that of dihydrogen acting as a ligand in transition metal complexes. The first example of dihydrogen acting as a ligand for a transition metal with a short H–H contact distance was reported by Kubas as the $W(PCy_3)_2(CO)_3(\eta^2\text{-}H_2)$ complex.[71] Initial evidence for the

coordinated H_2 came from IR data, with bands near 1570, 950, and 465 cm^{-1}. Upon substitution with D_2, the bands shifted to lower frequency. However, definitive proof came from cystallization of the complex under a D_2 atmosphere and subsequent neutron diffraction studies. An intact dihydrogen ligand (D–D = 0.84 Å) perpendicular to the C–W–C axis was identified. The presence of an intact, albeit weakened, H–H bond was also shown spectroscopically via the observation of H–D coupling ($^1J_{HD} = 33.5$ Hz) in the ^{1}H NMR spectrum when $W(PCy_3)_2(CO)_3$ was exposed to HD. Since $^2J_{HD}$ couplings for hydride–deuteride complexes are typically <5 Hz, and for HD the $^1J_{HD} = 43.2$ Hz, the large observed coupling provided proof of an intact H–H bond in the dihydrogen complexes.

Other examples of dihydrogen complexes have been studied under matrix isolation conditions, such as for $Cr(CO)_5(\eta^2\text{-}H_2)$ in liquid xenon[72,72a] and fast spectroscopy methods. IR spectroscopy under such conditions of the group VI pentacarbonyls, $M(CO)_5$ (M = Cr, Mo, W), indicates the existence of an H_2 ligand. Recently, the Cr and W derivatives have been observed via ^{1}H NMR, with $^1J_{HD} = 35.8$ and 35.3 Hz, respectively.[73] The cationic complex $[Re(CO)_5(\eta^2\text{-}H_2)]^+$ was also prepared, with an observed $^1J_{HD} = 33.9$ Hz.

Polyhydride systems have also been reported to have dihydrogen ligands. However, the presence of multiple sites and the possibility of fluxionality makes the identification of dihydrogen sites in these types of systems challenging. Crabtree proposed a "T_1 criterion" for distinguishing between classical M–H and non-classical $M(\eta^2\text{-}H_2)$ ligands.[74,74a] Conceptually, measurement of the spin-lattice (longitudinal) relaxation time provides a method to evaluate whether non-classical ligands are present because of the dependence of dipole–dipole relaxation on internuclear distances ($T_1 \propto r^6$).[75] Therefore, the close contact between hydrogen pairs in non-classical $M(\eta^2\text{-}H_2)$ ligands would result in much faster relaxation rates and, hence, application of the T_1 criterion suggests that fluxional polyhydrides with short T_1's should be characterized as having non-classical ligands. However, molecular motion influences the relaxation rate, so the minimum value of the T_1, which is independent of molecular motion, needs to be determined via the measurement of the temperature dependence of the T_1. However, all dipole–dipole interactions also need to be taken into account in order to accurately interpret the T_1 values as evidence of such ligands.[76]

Evaluation of the potential existence of dihydrogen ligands, therefore, has typically relied upon measurement of J_{HH} and J_{HD} coupling constants, as exemplified by the studies on the $W(PCy_3)_2(CO)_3(\eta^2\text{-}H_2)$ system. Recent studies, however, also indicate that determination of the existence of H_2 ligands based upon coupling constant data is also complex. For instance, the metallocene trihydrides, $[Cp_2WH_3]^+$ and $[Cp^*_2WH_3]^+$, are characterized by doublet and triplet resonances in the ^{1}H NMR ($^2J_{HH} = 8.5$ and 3 Hz, respectively), indicative of a classical hydride formulation.[77,77a,77b] In contrast to the tungstenocene complexes, the molybdenocene trihydride, $[Cp_2MoH_3]^+$, exhibits a singlet in the ^{1}H NMR at room temperature.[77a] Upon cooling to −70 °C, a highly second-order, static AB_2 spectrum was observed, with a $^2J_{HH(min)} = 1000$ Hz. This observation has been explained in terms of quantum mechanical exchange, whereby the $^2J_{HH}$ may be significantly greater than typical magnetic, scalar couplings such that $J_{obs} = J_{magnetic} - 2J_{ex}$.[78,78a–78e] The singlet at room temperature is the result of the temperature dependencies of the quantum mechanical exchange and classical site exchange.

Other systems have also been found to exhibit this type of quantum mechanical exchange. Chaudret and co-workers showed that $Cp^*Ru(PCy_3)H_3$ exhibits quantum mechanical exchange coupling (QMEC) at low temperature while also undergoing classical exchange at high temperatures.[79,79a] Similar exchange couplings were observed for the nuclei pairs in the corresponding isotopologs of the type $Cp^*Ru(PCy_3)H_xD_{3-x}$.[80] Interestingly, no kinetic deuterium isotope effects were observed for the classical exchange of hydride sites in this complex. In addition, while typical scalar couplings are observed for the tungstenocene trihydrides, QMEC is observed for the *ansa*-bridged $[Me_2Si(C_5H_5)_2WH_3]^+$ and $[Me_2C(C_5H_5)_2WH_3]^+$.[81,81a,81b] Significantly, the Me_2C-bridged complex exhibits the largest observed exchange couplings to date, with values for $J_{HH(min)}$ ranging from 2900 Hz at −130 °C to 16,000 Hz at −70 °C.

The observation of QMEC is not limited to classical polyhydride systems, however. The rotational dynamics of the coordinated dihydrogen ligand in non-classical systems is of interest, and labeling studies of such dynamics have revealed intriguing phenomena. For example, inelastic neutron scattering experiments provided a value of 1.9 kcal mol^{-1} for the barrier for rotation in $W(PCy_3)(CO)_3(\eta^2\text{–}H_2)$.[82] Similar studies showed a barrier of only 0.7 kcal mol^{-1} for H_2 rotation in $Mo(dppe)_2(CO)(\eta^2\text{-}H_2)$.[83] The first example of frozen rotation of the H_2 ligand on the NMR timescales was provided by Chaudret and co-workers in $[(Cp^{TMS})_2Nb(PMe_2Ph)(\eta^2\text{-}H_2)]^+$.[84] While both the H_2 and D_2 isotopologs exhibit a "single" peak in the NMR at all temperatures, preparation and analysis of the HD complex, $[(Cp^{TMS})_2Nb(PMe_2Ph)(\eta^2\text{-}HD)]^+$, resulted in the observation of two different rotamers in the ^{1}H NMR at −70 °C, corresponding to the *endo*- and *exo*-isomers of the dihydrogen complex. The barrier for rotation was determined to be 11.2 kcal mol^{-1}, significantly higher than the W and Mo systems. This was rationalized as being due to the absence of a filled *d*-orbital perpendicular to the H–H plane whereby π-back-bonding donation into the σ^* orbital of the H_2 ligand would lower the barrier for rotation. The observation of a single peak for the η^2-H_2 and η^2-D_2 ligands was proposed to be a manifestation of large J_{HH} and J_{DD} exchange

coupling constants within the AB spin system of the static dihydrogen ligand. Hindered rotation has also been observed using similar labeling studies for $[(Cp^{TMS})_2Nb(CNR)(\eta^2\text{-HD})]^+$ (R = Bu^t, Cy, Xylyl)[85] and the tantalocene complex, $[Cp_2Ta(CO)(\eta^2(HD)]^+$.[86] Recently, hindered rotation for the isotopically labeled *ansa*-molybdenocenes, $\{Me_2Si(C_5Me_4)_2Mo(\eta^2\text{-HD})H\}^+$ ($\Delta G^{\ddagger}_{rot} = 9.3\,kcal\,mol^{-1}$)[103] and $\{Me_2C(C_5H_4)_2Mo(\eta^2\text{-HD})D\}^+$ ($\Delta G^{\ddagger}_{rot} = 7.4\,kcal\,mol^{-1}$)[105], have also been reported.

Hence, deuterium labeling has proved to be critical to the observation and identification of non-classical dihydrogen ligands in transition metal complexes, including polyhydride systems. Ultimately, it also provides a means to evaluate the isotope effects related to dihydrogen activation and coordination in organometallic systems.

1.20.3.3.1 Isotope effects in the oxidative addition and reductive elimination of dihydrogen

In view of the discovery by Kubas of the existence of dihydrogen complexes, $[M(\eta^2\text{-}H_2)]$, a more complete understanding of the reactivity of metal hydride systems necessitates knowledge concerning both classical metal hydride $[M(H)_x]$ and non-classical metal dihydrogen $[M(\eta^2\text{-}H_2)_{x/2}]$ ligands. Further, as with alkane activation, the oxidative addition and reductive elimination of dihydrogen can be described as a composite of coordination/dissociation steps and oxidative cleavage/reductive coupling steps (Scheme 10). Likewise, as with C–H bonds, isotopic labeling of M–H ligands or use of D_2 has proved invaluable in providing a greater understanding of these types of reactions.[87]

Oxidative addition and reductive elimination reactions of dihydrogen have been known for a long time and is observed in a variety of systems.[69,69a–69h] As with alkanes, isotope effects have been observed for these processes. One of the first examples of an EIE for H_2 addition was reported by Bergman using the bimetallic complex, $Cp_2Ta(\mu\text{-}CH_2)_2Ir(CO)(PPh_3)$, to reversibly form the dihydride, $Cp_2Ta(\mu\text{-}CH_2)_2Ir(CO)(PPh_3)H_2$.[88] The equilibrium data for H_2 versus D_2 oxidative addition provided composite primary and secondary inverse EIEs ranging from 0.53 to 0.77 over the temperature range of 22–80 °C, indicating that oxidative addition of D_2 was preferred thermodynamically over oxidative addition of H_2 over this temperature range. Due to rapid exchange between the hydride sites and the bridging methylene C-H sites, the observed EIEs also have secondary isotope effect components. See Ref.: 88. The thermodynamic information provided from a van't Hoff plot gave $\Delta\Delta H^0$ ($\Delta H^0_D - \Delta H^0_H$) = (1.0 kcal mol^{-1} and $\Delta\Delta S^0$ (ΔS^0D − ΔS^0H) = −2.2 eu. Soon thereafter, Parkin reported inverse EIEs for the reaction of H_2 with $W(PMe_3)_4I_2$ to form $W(PMe_3)_4I_2H_2$ in C_6D_6 solvent.[89] An EIE = 0.63 at 60 °C was reported as well as thermodynamic data over the temperature range of 50–90 °C, giving a $\Delta\Delta H^0$ ($\Delta H^0_D - \Delta H^0_H$) = (1.9 kcal mol^{-1} and a $\Delta\Delta S^0$ ($\Delta S^0_D - \Delta S^0_H$) = (6 eu. The inverse EIE was rationalized as being due to the W–D bond being substantially stronger than the W–H bond (D(W–D) = 63.8 versus D(W–H) = 62.0 kcal mol^{-1}).[90,91] Further, the authors recognized that such an inverse EIE would not be predicted by consideration of only the observed W–H and W–D stretching frequencies, since the observed ν_{W-H} and ν_{W-D} stretching frequencies of 1961 and 1416 cm^{-1}, respectively, result in a zero point energy difference of only 273 cm^{-1}, which is less than the difference of 630 cm^{-1} between D_2 and H_2. In addition to the differences in the stretch frequencies, the differences associated with the bending modes of the dihydride were proposed to be responsible for the additional lowering of the zero point energy for $W(PMe_3)_4I_2D_2$ with respect to $W(PMe_3)_4I_2H_2$. Finally, it was further recognized that while the preference for D_2 oxidative addition was enthalpic in nature, entropic differences actually attempt to counter the inverse nature of the equilibrium deuterium isotope effect.

Soon thereafter, Goldman and Krogh-Jespersen re-examined the oxidative addition of H_2 within the Vaska system, $Ir(PPh_3)_2(CO)Cl$, both experimentally and computationally.[92,92a] An inverse EIE = 0.55 for oxidative addition of H_2 versus D_2 was observed experimentally at 25 °C, with the value being reproduced to good accuracy computationally (EIE_{calc} = 0.46). The authors analyzed the computational data in terms of the Wolfsberg formalism described earlier, that is EIE = SYM · MMI · EXC · ZPE. Inspection of the factors contributing to the EIEs from the DFT calculations revealed that the inverse value arises from an inverse contribution from the combined EXC and, especially, ZPE vibrational terms, which are countered by a normal MMI contribution. The large MMI value of 5.66 arises almost exclusively from the D_2/H_2 translational and rotational partition function ratios, since the masses and moments of inertia for the metal complexes are not significantly altered by deuterium substitution. The inverse EXC term (0.84) has a substantial contribution from the M–H and M–D bending vibrations of $[Ir]H_2$ and $[Ir]D_2$, since the high stretching vibrational frequencies do not have significantly populated excited states at moderate temperatures. The strongly inverse ZPE term (0.10) results from the magnitude of the zero point energy difference associated with the

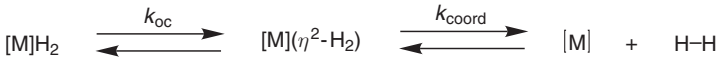

Scheme 10 Equilibrium reactions for metal-hydride metal-dihydrogen tautomerism and coordination of H.

[Ir]H_2 and [Ir]D_2 vibrations. Importantly, it was recognized that the presence of six isotope-sensitive vibrations in [Ir]X_2 (X = H, D) makes D_2 oxidative addition to Ir significantly more exothermic than H_2 addition. The important role of the four Ir–H bending modes in determining the final EIE was demonstrated by eliminating their frequencies from the calculations. The corresponding zero point energy difference is only 0.08 kcal mol^{-1} (cf. 1.39 kcal mol^{-1} for all frequencies), resulting in EXC and ZPE values of 0.92 and 0.89, respectively. Ultimately, the exclusion of the bending frequencies results in a normal and large EIE (=4.6).

A more complete understanding of the temperature dependence of EIEs for the oxidative addition of H_2 and D_2 was initially reported by Parkin.[93] DFT calculations were performed on the *ansa*-[$Me_2Si(C_5Me_4)_2W$] system via a computationally less intensive model, [$H_2Si(C_5H_4)_2W$]. It was reported that the temperature dependence of H_2 oxidative addition shows a trend similar to that of coordination of methane. That is, rather than either increasing or decreasing monotonically as a function of temperature, the oxidative addition of H_2 is characterized by a maximum, with temperatures below which an inverse EIE would be expected to be observed and temperatures above which a normal EIE would be observed.

Experimental evidence for this phenomenon was provided by using an analog of the thermally robust Vaska system, Ir($PMe_2Ph)_2$(CO)Cl.[94] The presence of the methyl groups in the phosphine ligands acts as an effective spectroscopic label by which the square-planar complex and octahedral dihydride could be distinguished via ^{1}H NMR spectroscopy. Independent measurement of each species for both the protio and deutero systems was necessary due to the fact that mixtures of Vaska-type IrH_2 and IrD_2 complexes undergo intermolecular isotopic exchange.[95,95a] At temperatures below 96 °C, inverse EIEs were observed, consistent with previous examples. However, "normal" EIEs were reported for temperatures "above" 96 °C, providing experimental evidence for a temperature-dependent transition of an EIE from "inverse" to "normal" within the same system (Figure 9). Furthermore, computational studies on the model Ir($PH_3)_2$(CO)Cl system both reproduced the result reported by Goldman and Krogh-Jespersen and predicted that such temperature-dependent behavior should be exhibited within this type of system. Importantly, the study demonstrated that at sufficiently high temperatures the greater entropy associated with D_2 versus H_2 offsets the enthalpic component arising from the formation of two Ir–H bonds, which produces five new vibrational modes, that favor an inverse EIE. Nonetheless, at low temperatures, the ZPE stabilization arising from these modes dominates, causing the EIE to be inverse, as is typically observed.

1.20.3.3.2 EIEs in the coordination of dihydrogen

In addition to the isotope effects associated with oxidative addition of dihydrogen, EIEs for binding H_2 have also garnered interest, in particular to gain an greater understanding of the nature of this type of interaction with a metal center. Regardless of the exact nature of the interaction, the EIEs reported for binding H_2 are typically inverse.[96,96a,96b] Early examples were reported for metal polyhydride systems. For example, a $K_H/K_D = 0.5$ was observed for

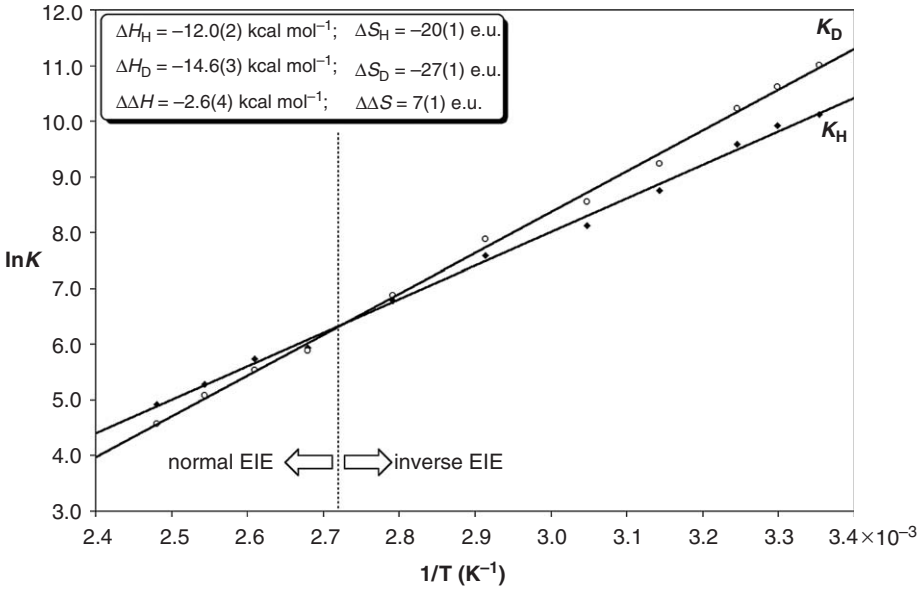

Figure 9 van't Hoff plot for the temperature dependence of H2 oxidative addition to Ir($PMe_2Ph)_2$(CO)Cl.

H_2 versus D_2 binding to $Ir(PPr^i_3)_2Cl_2H$.[96] Caulton reported an EIE = 0.37 for dihydrogen binding to the unsaturated complex, $Ir(PBu^t_2Ph)_2ClH_2$, to form $Ir(PBu^t_2Ph)_2ClH_2(\eta^2\text{-}H_2)$.[96a] Further, this is a rare example where the kinetics of H_2 binding has been determined. KIEs (k_{aH}/k_{aD}) = 1.8 and 6 at 25 and −50 °C, respectively, were measured for association of H_2 versus D_2. Similar KIEs were also observed for $W(PCy_3)_2(CO)_3(\eta^2\text{-}H_2)$ (1.7 at 25 °C), $Cr(CO)_5(\eta^2\text{-}H_2)$ (5 at ambient temperature), and $Ir(PCy_3)_2Cl_2H(\eta^2\text{-}H_2)$ (~7 at −70 °C).

In a seminal paper, Bender *et al.* reported the EIEs for H_2 versus D_2 binding to both $W(PCy_3)_2(CO)_3$ and $Cr(PCy_3)_2(CO)_3$ in THF solution.[97] Significantly, all of the isotopically sensitive vibrations were identified via IR and Raman spectroscopy for the $[W](\eta^2\text{–}H_2)$, $[W](\eta^2\text{–}D_2)$, and $[W](\eta^2\text{–}HD)$ isotopologs. The EIE was calculated according to the formalism expressed in earlier sections, except substituting the MMI term with the vibrational product (VP) term using the Teller–Redlich product rule: EIE = VP · EXC · ZPE. The value calculated for the W complex compared favorably with the experimental result ($EIE_{calc} = 0.78$ vs. $EIE_{expt} = 0.70$). The Cr analog also exhibited an inverse EIE ($K_H/K_D = 0.65$). The authors explained that if changes in the H–H (D–D) force constant were the major contributor to the EIE, then a normal EIE would be expected, since the D–D bond is 1.8 kcal mol^{-1} stronger than the H–H bond. However, the formation of five additional vibrational modes upon binding H_2 (Figure 10), including significant W–H interactions that resemble W–H stretches, results in an overall favorable enthalpy of binding D_2 versus H_2 that overcomes an unfavorable entropic barrier.

This point was further elucidated in DFT calculations for binding H_2 to the pentacarbonyl complex, $W(CO)_5$, to form $W(CO)_5(\eta^2\text{-}H_2)$.[98] Specifically, the full temperature dependence of the EIE was determined from the calculated frequencies, as well as the temperature dependence of the individual components of the EIE. A maximum EIE was explained to occur as a a result of the differing temperature dependencies of the ZPE and EXC terms. Further, the predicted transition from an inverse to a normal EIE is a result of the opposing enthalpic (ZPE) and entropic (SYM · MMI · EXC) components to the EIE. At low temperatures, the enthalpic term dominates, causing the EIE to be inverse in spite of the large entropy term. However, at high temperatures, the greater entropy associated with free D_2 versus H_2 dominates, resulting in a normal EIE. This is in accordance with the conclusions drawn by Bender *et al.* In fact, similar temperature-dependent behavior was predicted to occur within $W(PCy_3)_2(CO)_3(\eta^2\text{-}H_2)$, as shown using the experimentally determined frequencies (Figure 11).

Another aspect of EIEs related to metal–dihydrogen interactions pertains to dihydride–dihydrogen tautomerism. Specifically, the issue of whether deuterium prefers to be located in the classical (metal hydride) or non-classical (metal dihydrogen) site has garnered interest, partly because of differing results in the literature. One of the earliest reports of an EIE for this type of isomerism was in the $[Re(PMe_2Ph)_3(CO)H_4]^+$ system.[99] The presence of a non-classical tautomer, $[Re(PMe_2Ph)_3(CO)(\eta^2\text{-}H_2)H_2]^+$, was established from $T_{1\ min}$ experiments and the observation of a

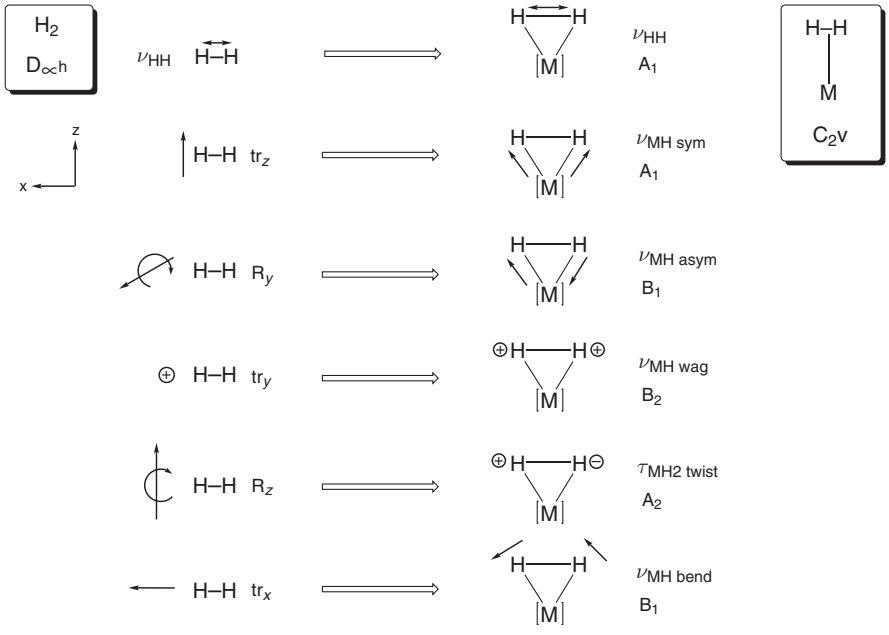

Figure 10 New vibrations generated upon coordination of H_2 to a metal center.

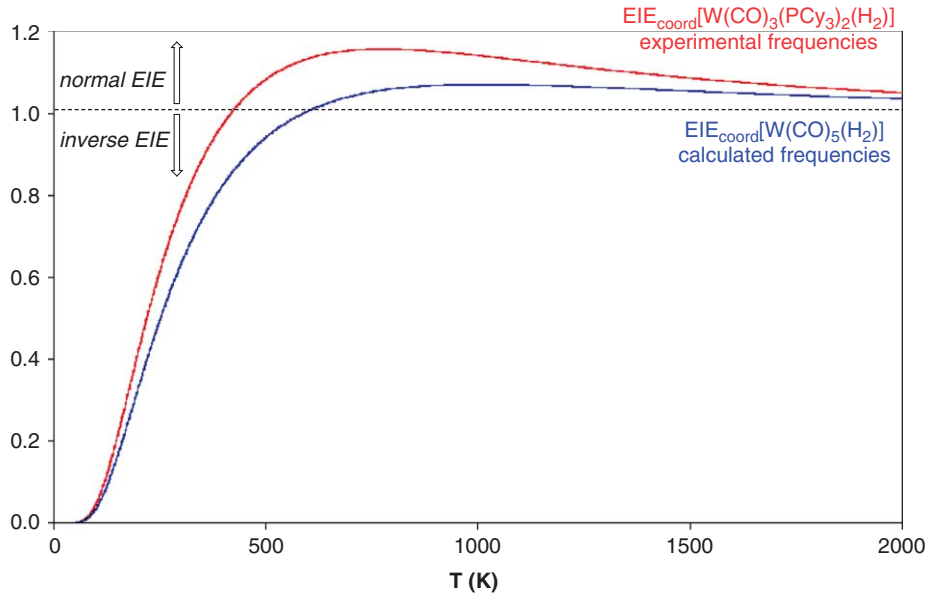

Figure 11 Temperature dependence of the EIE for coordination of H_2 to $W(PCy_3)_2(CO)_3$ and $W(CO)_5$.

$J_{HD(obs)} = 34$ Hz for the $[Re(PMe_2Ph)_3(CO)HD_3]^+$ isotopolog in the ^1H NMR spectrum. Although the classical tetrahydride isomer is preferred thermodynamically over the non-classical tautomer ($\Delta G^0 = -0.6$ kcal mol^{-1} for $\{[Re]H_4\}^+/\{[Re](\eta^2\text{-}H_2)H_2\}^+$), an EIE = 1.3 was found for the intramolecular isomerization within the non-classical tautomer of the [Re]-d_3 isotopolog, $[Re(PMe_2Ph)_3(CO)HD_3]^+$, for $\{[Re](\eta^2\text{-}HD)H_2\}^+/\{[Re](\eta^2\text{-}H_2)HD\}^+$. This was rationalized as a zero point energy stabilization of the dihydrogen site relative to the hydride site for deuterium. A similar EIE with deuterium favoring the non-classical dihydrogen site was also found for the equilibrium in $CpNb(CO)_3(\eta^2\text{-}H_2)/CpNb(CO)_3H_2$.[100]

However, experimental studies on $[Cp_2W(\eta^2\text{-}H_2)H]^+$ and $[TpIr(PMe_3)(\eta^2\text{-}H_2)H]^+$ indicate a preference for deuterium in the classical site. In an elegant series of NMR experiments, Heinekey showed that mixtures of $[TpIr(PMe_3)H_3]^+$, $[TpIr(PMe_3)H_2D]^+$, $[TpIr(PMe_3)HD_2]^+$ exhibit large, temperature-dependent downfield isotope shifts for the signal-average hydride resonances of the isotopologs corresponding to −10.37, −10.18, and −10.08 ppm, respectively.[101,101a] Assuming rapid exchange of the *endo*- and *exo*-dihydrogen sites via rotation of the dihydrogen ligand (Scheme 11), reported barriers to hydrogen rotation are typically low, except in d^2-systems, making the rotation of the dihydrogen ligand rapid on the NMR timescale. See, for example, Refs: 102,102a and that the M–H limiting chemical shift was upfield of the $M(\eta^2\text{-}H_2)$ chemical shift(s), the data allowed for the determination of the EIEs for deuterium site preference in both the $[TpIr(PMe_3)H_2D]^+$ and $[TpIr(PMe_3)HD_2]^+$ isotopologs ($EIE_{H2D} = 1.32$, $EIE_{HD2} = 1.26$). Heinekey rationalized that the observed isotopic perturbation of equilibrium and, correspondingly, the normal EIEs ($K > 1$) indicate that deuterium prefers the classical M–H site in this system. Preparation of the tritium analogs, $[TpIr(PMe_3)T_3]^+$, $[TpIr(PMe_3)T_2H]^+$, $[TpIr(PMe_3)TH_2]^+$ and analysis via both ^1H and ^3H NMR provided additional support for this conclusion.[101a] Evidence that only one type of species was present in solution, that is, the non-classical $\{[Ir](\eta^2\text{-}H_2)H\}^+$ tautomer versus the classical $\{[Ir]H_3\}^+$ tautomer, was provided by the observation that both the $[TpIr(PMe_3)H_3]^+$ and $[TpIr(PMe_3)T_3]^+$ species exhibit the same chemical shift in the ^1H and ^3H NMR, respectively. Different chemical shifts would be expected if two species (a trihydride vs. a dihydrogen hydride isomer) were present since an isotope effect on the tautomerism would be expected to perturb

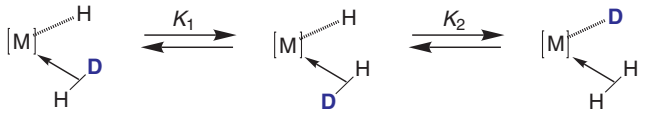

Scheme 11 Equilibrium reaction describing the intramolecular deuterium exchange between M(H) and $M(\eta^2\text{-}H_2)$ sites. For fast H_2 rotation, K_1 is assumed to be 1.

the energetics of the system so as to favor one species over the other for the two different isotopologs. Nonetheless, whereas the $[TpIr(PMe_3)T_2H]^+$ and $[TpIr(PMe_3)TH_2]^+$ isotopologs exhibit downfield chemical shifts in the ^1H NMR, similar to the $\{[Ir]H_xD_{3-x}\}^+$ system, the same species exhibit "upfield" chemical shifts relative to the $\{[Ir]T_3\}^+$ isotopolog, with the $\{[Ir]TH_2\}^+$ species having the greatest upfield shift. Since the M–H site was assumed to have the most upfield chemical shift, the observation that the $\{[Ir]TH_2\}^+$ species exhibited the largest shift was interpreted as further evidence that tritium and, by analogy, deuterium favor the classical site relative to the non-classical site.

It is important to note that these conclusions are based upon the assumption that the H_2 ligand chemical shifts lie downfield of the M–H chemical shift. However, deuterium labeling studies in the $\{Me_2Si(C_5Me_4)_2Mo(\eta^2\text{-}H_2)H\}^+$ system show the difficulty with this analysis.[103] At room temperature, signal-averaged chemical shifts were observed for the $\{[Mo]H_3\}^+$, $\{[Mo]H_2D\}^+$, and $\{[Mo]HD_2\}^+$ isotopologs. Upon cooling, decoalescence of the peaks corresponding to the $\{[Mo]H_2D\}^+$ and $\{[Mo]HD_2\}^+$ isotopologs is observed and attributed to freezing the rotation of the H_2 ligand in the complexes. A single peak is observed for the $\{[Mo]H_3\}^+$ isotopolog and was attributed to a large quantum mechanical exchange coupling constant for the η^2-H_2 species, which is quenched for the η^2HD isotopolog, in concert with rapid side-to-side motion of the central hydride that averages the Mo–H and *exo*-Mo(η^2-H_2) sites (Figure 12).[102,102a,104,104a,104b] Although the chemical shift of the *endo*-Mo(η^2-H_2) site was identified, the rapid side-to-side motion of this site results in only average chemical shifts for the other isomers and sites, precluding determination of whether deuterium prefers the classical or non-classical site via an isotopic perturbation of equilibrium, since there are multiple solutions for the individual chemical shifts that would satisfy the observed average chemical shift. Similar effects were also observed for the carbon-bridged *ansa*-molybdenocene, $\{Me_2C(C_5H_4)MoH_xD_{3-x}\}^+$.[105]

However, the relative magnitudes of the observed J_{HD} values for MH_2D and MHD_2 isotopologs can provide more conclusive indication of the preference for deuterium for either the classical or non-classical hydride sites. Specifically, a value of $J_{HD(obs)}[H_2D] > J_{HD(obs)}[HD_2]$ indicates that deuterium exhibits a greater than statistical preference to occupy the dihydrogen site, whereas a $J_{HD(obs)}[H_2D] < J_{HD(obs)}[HD_2]$ value indicates that deuterium favors the hydride site. Thus, the observation in the $\{TpIr(PMe_3)\ H_xD_{3-x}\}^+$ system of a $J_{HD(obs)} = 7.48$ Hz for the

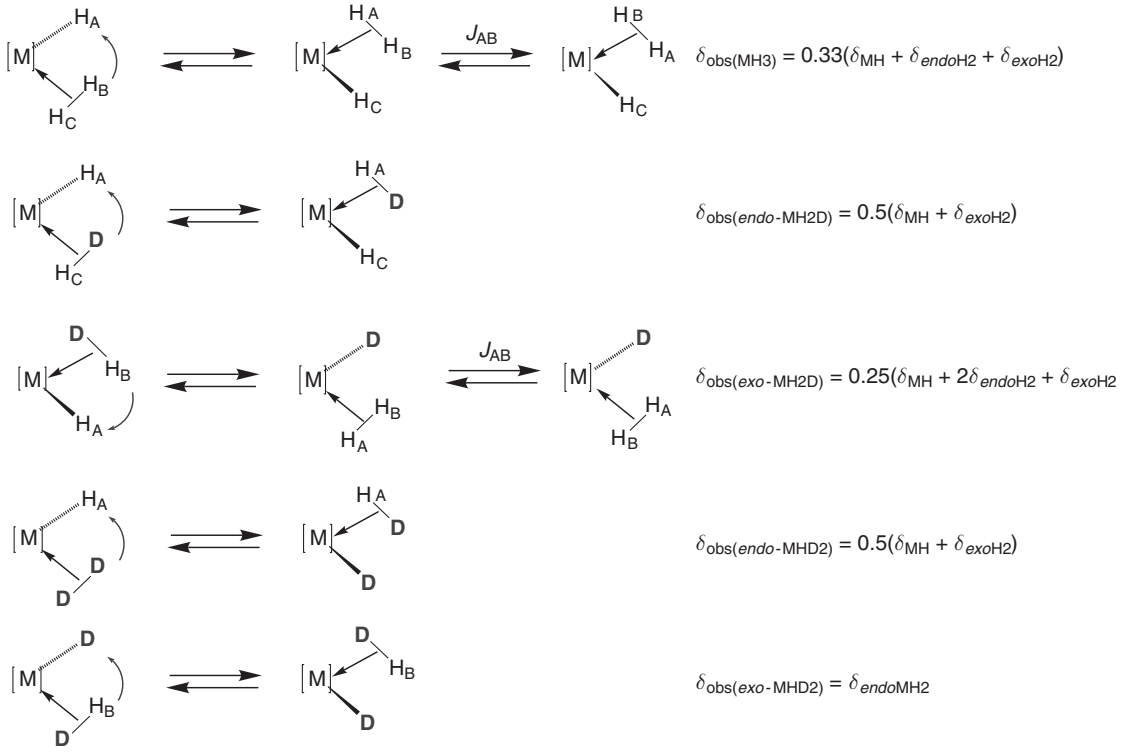

Figure 12 Site exchange mechanisms averaging M(H),*exo*-M(η^2–H_2), and *endo*-M(η^2–H_2) ^1H NMR chemical shifts at low temperature.

$\{[Ir]H_2D\}^+$ isotopolog and a $J_{HD(obs)} = 8.78$ Hz for the $\{[Ir]HD_2\}^+$ species at −33 °C is indicative of a preference for deuterium to occupy the classical site in this system, while the observation at 25 °C of a $J_{HD(obs)} = 8.0$ Hz for $\{[Mo]H_2D\}^+$ and a $J_{HD(obs)} = 7.8$ Hz for the $\{[Mo]H_2D\}^+$ provides evidence, albeit qualitative given the experimental uncertainty in the coupling constants (ca. ±0.5 Hz), for deuterium to prefer the dihydrogen site. However, DFT calculations on this system indicate that deuterium prefers the non-classical site and also reveals only slightly inverse EIEs at 25 °C, consistent with the experimental result.

Calculations on $W(CO)_3(PH_3)(\eta^2\text{-}H_2)/W(CO)_3(PH_3)H_2$ and $W(CO)_5(\eta^2\text{-}H_2)/W(CO)_5H_2$ indicate that deuterium prefers the non-classical site in these systems.[106,98] For the $W(CO)_5$ system, the primary source for this isotope effect centers on the ZPE term. Whereas five additional vibrational modes are formed for reactions involving either oxidative addition or coordination of H_2 to a metal, MH_2 and $M(\eta^2\text{-}H_2)$ systems have the same number of primary isotopically sensitive vibrations. Other isotopically sensitive vibrations may result due to vibrational coupling, but these are typically smaller in magnitude than the primary isotopically sensitive vibrations. Further, while the ZPE associated with the H–H fragment in $W(CO)_5(\eta^2\text{-}H_2)$ is greater than that in $W(CO)_5H_2$, the single most important mode corresponds to the high-energy H–H stretch in $W(CO)_5(\eta^2\text{-}H_2)$ ($\nu_{H-H} = 3330\,cm^{-1}$; $\nu_{D-D} = 2366\,cm^{-1}$), which becomes a low-energy symmetric bend in $W(CO)_5H_2$ ($\nu_{HMH} = 784\,cm^{-1}$; $\nu_{DMD} = 600\,cm^{-1}$). Hence, the ZPE differences for these vibrations favor deuterium occupying the non-classical site.

1.20.4 Isotope Labels in Polymerization Reactions

1.20.4.1 Ziegler–Natta Type Polymerization Reactions

The polymerization of olefins has long been one of the most industrially important applications of organometallic complexes.[107,108,108a–108d] The use of transition metals as catalysts ranges from early metal (e.g., Ti, Zr) Ziegler–Natta type polymerizations to late-metal single site catalysts as well as atom transfer radical polymerizations (ATRPs) and ring opening metathesis polymerizations (ROMPs).[109,109a–109c] Isotopic labeling has played a prominent role in elucidating polymerization reaction mechanisms and potentially important steps/factors for polymerization. As a classic example, evidence for the Chauvin mechanism for ring-closing/ring-opening metathesis was shown via intermolecular reaction of labeled and unlabeled dienes to produce mixtures of CH_2CH_2, CH_2CD_2, and CD_2CD_2, indicating that the mechanism for the metathesis reaction involved metal carbene intermediates.[110,110a]

One area of interest with regard to Ziegler–Natta polymerization has centered on the importance or role of intramolecular coordination of a C–H bond to a metal center to form a three-center two-electron bond, known as α-agostic interactions.[111] The presence of such interactions can often be determined from ^1H and ^{13}C NMR spectra. Specifically, the values of the $^1J_{CH}$ for an agostic bond is typically lower than those for unbridged C–H bonds.[112] Further, the agostic ^1H and ^{13}C chemical shifts often exhibit high-field shifts. These effects were observed for the α-agostic ethyl ligand in $(dmpe)TiCl_3(CH_2CH_3)$.[112] However, if the agostic alkyls are fluxional, and static spectra cannot be obtained via VT-NMR experiments, deuterium labeling studies can be employed for the identification and characterization of such interactions. Shapley's $Os_3(CO)_{10}(CH_2)H_2$ system was one of the earliest examples of such isotopic perturbation of resonance experiments.[60,113] Similar effects were also observed for the characterization of a Hf α-agostic complex.[114] $[Cp^*_2Hf(CHDC(H)Me_2)(PMe_3)]^+$ and $[Cp^*_2Hf(CH_2C(H)(CH_2D)Me)(PMe_3)]^+$ were generated via reaction of 2-Me-propene-1-d_1 with $Cp^*_2Hf(H)_2$ followed by protonolysis and trapping with PMe_3. Variable temperature ^1H NMR experiments revealed an isotope effect on the α-CH chemical shift between the α-CHD and α-CH_2 isotopomers of $\Delta\delta = 0.38$, 0.47, and 0.58 at −10, −50, and −90 °C, respectively. Further, the ^{13}C NMR revealed a $^1J_{C\alpha\text{-}H} = 91$ Hz for the α-CHD isotopomer, whereas a value of 100 Hz was observed for the α-CH_2 isotopomer.

Another area of interest has centered on the role that such α-agostic interactions may play in influencing the energetics of the transition state for olefin insertions. This is of consequence since such an interaction can have a profound influence on the tacticity of the growing alkyl chain.[115,115a] Initial studies by Grubbs *et al.* focused on the intramolecular cyclization of racemic titanocene 5-hexenyl-1-d_1, $Cp_2Ti(CHD(CH_2)_3CH_2{=}CH_2)Cl$.[116] Reaction with $EtAlCl_2$ at −100 °C resulted in both *cis*- and *trans*-$Cp_2Ti(CH_2(cyclopentane))Cl$ in a 1 : 1 ratio. In the absence of an α-agostic interaction in the transition state, the observed *cis* : *trans* ratio is expected to be 1 : 1, whereas an agostic interaction would favor the C–H versus the C–D bond and result in *cis* : *trans* ratio <1, since the interaction would orient the internal alkene such that an excess of the *trans*-isomer would be observed (Figure 13). Brintzinger, however, reported a ratio of 1.3 : 1 for the *erythro* : *threo* isomers of 5-Me-d_1-undecane-6-d_1 generated from insertion of 1-hexene-d_1 into $[Cp_2Zr(CHD(CH_2)_4CH_3)]^+$.[117] The product distribution was argued to be the result of an α-agostic interaction in the transition state, with the isotope effect for C–H versus C–D coordination being the source of the stereoselectivity.

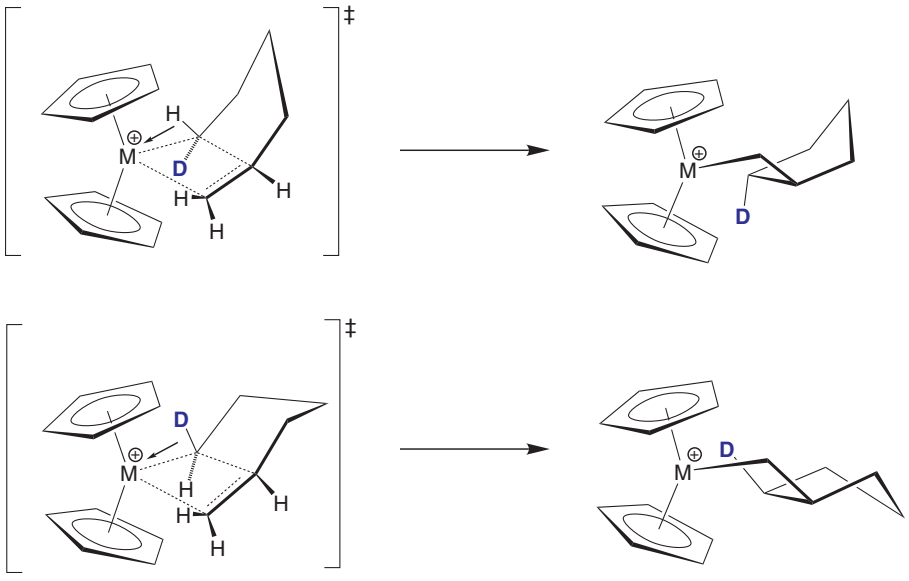

Figure 13 Deuterium isotope effect on the stereochemistry of intramolecular insertion due to an α-agostic interaction in the transition state.

Similar isotope effects for intramolecular cyclization were observed in the *ansa*-scandocene system, $Me_2Si(C_5Me_4)_2Sc(PMe_3)H$.[118] Reaction of 1,5-hexadiene-1,6-d_2 resulted in a *cis* : *trans* ratio of 1 : 1.23 for the two methylcyclopentane products. However, a *cis* : *trans* ratio of 1.12 : 1 was observed for the methylcyclohexanes generated from 1,6-heptadiene-1,7-d_2. Again, an isotope effect for preference of the C–H bond to occupy the α-agostic site in the transition state was rationalized as the source of the observed ratio. Whereas this would result in a preference for the *trans*-product over the *cis*-product due to the puckering conformation for the methylcyclopentane reaction, as in the Ti case, a chair conformation in the heptadiene reaction results in the opposite stereochemical preference (*cis* over *trans*), but due to the same type of α-agostic KIE.

In an effort to evaluate if such an effect might have been due to a steric isotope effect[63,14,14a,14b] rather than an isotope effect due to an agostic interaction, Bercaw investigated the insertion of 2-butyne-1,1,1-d_3, $CD_3C{\equiv}CCH_3$, into $(Cp^*–d_{15})_2Sc–CH_3$.[119] Presumably, if steric interactions between the incoming alkyne and the $Sc–CH_3$ dictated the stereochemistry of insertion, then the corresponding alkyne insertion product, $(Cp^*–d_{15})_2Sc–\dot{C}(CH_3{=}C(CH_3)(CD_3))$, would be formed preferentially to $(Cp^*–d_{15})_2Sc–(C(CD_3){=}C(CH_3)_2)$. The experiment revealed no measurable steric deuterium isotope effect, and the authors concluded that the isotope effects attributed to the agostic interactions were unlikely to be nascent effects from steric interactions.

Further, the influence of co-catalysts on both α- and β-deuterium isotope effects for alkene insertion has been studied. Stille and co-workers investigated these effects via competitive intramolecular six-membered ring formation within $Cp_2TiCl/MgCl_2$ and Cp_2TiCl/MAO co-catalyst systems.[120] A normal ($K_H/K_D > 1$) α-deuterium isotope effect of 1.22 was observed for the 2-propyl titanocene derivative using $MgCl_2$ as well as a normal β-deuterium isotope effect of 1.09. However, an "inverse" α-deuterium isotope effect of 0.88 and a normal β-deuterium isotope effect of 1.06 was observed using MAO. The authors suggested that the effect may be due to the existence of a ground state α-agostic interaction (versus a transition state interaction), possibly with the co-catalyst, which would render the deuterated species more reactive relative to the protio isotopolog.

The effect of agostic interactions on the uptake of olefin monomer was investigated in the C_2-symmetric zirconocene, $[rac\text{-}(CH_2)_2(C_5H_3(CH_2)_4)_2]ZrCl_2$.[121] The polymerization of *cis*- and *trans*-propene-d_1 resulted in polymers generated from the *trans*-isomer having molecular weights 1.3 times "greater" than those made from the *cis*-isomer. This was rationalized as being the measure of the relative rates of insertion of the two monomers, assuming the rates of chain transfer are equal for both isotopomers. Since the *trans*-isomer would result in a C–H bond oriented for an α-agostic interaction in the transition state while the *cis*-isomer places a C–D bond in this orientation, the faster rate of insertion would be due to a greater zero point energy stabilization in the transition state by the *trans*-isomer. Thus, depending on the system, the presence of α-agostic interactions and their effects on polymerization rates and tacticity may vary, but can be identified via isotope-labeling experiments.

1.20.4.2 Atom Transfer Radical Polymerization Type Reactions

Atom transfer radical polymerization (ATRP) reactions mediated by transition metals have also garnered interest.[109,109a–109c] Essentially, ATRP reactions are similar to traditional free-radical polymerization reactions in that they can be described by initiation, propagation, and chain-transfer steps involving carbon radicals. Transition metals mediate this process via redox processes ($M^{+n} \Rightarrow M^{+(n+1)}$) and promoting chain transfer by donation of a halide or hydrogen atom to the polymer radical.[122] Although it was originally assumed that transition metal ATRP operated via a mechanism similar to organic radical polymerizations, reports of ^{13}C KIEs (k^{12}_C/k^{13}_C) indicated that different mechanisms might be operative. For example, ^{13}C KIEs were studied for both the free-radical-initiated and the CuBr-mediated polymerization of methyl methacrylate.[123] The KIEs were measured using the technique introduced by Singleton[124] which allows for the measurement of multiple ^{13}C KIE's at "natural" abundance via ^{13}C NMR. While the investigators found similar KIEs for the β-carbon in the free-radical and Cu(I)-mediated polymerization reactions (1.045 and 1.050, respectively), they reported different α-carbon KIEs (1.002 versus 1.010). The different α-carbon KIEs were interpreted as evidence for a close interaction between the radical species and catalyst, either through coordination of the monomer to the metal prior to insertion or through the presence of radical cages during the course of the polymerization reaction.

However, further investigation of this reaction found identical ^{13}C KIEs (within statistical differences) for both the AIBN (free-radical) and Cu(I)-initiated processes.[125] DFT calculations reasonably reproduced the isotope effects and indicated that the α-carbon KIE was associated with the weakening of the two vibrational modes related to the $C_\alpha{=}C_\beta$ stretch in going from the alkene (1720 and 1395 cm^{-1}) to the transition state (1616 and 1322 cm^{-1}). The authors concluded that the previous report was statistically anomalous and that ATRP reactions exhibit identical chain-propagation steps as organic free-radical-initiated polymerizations.

Additional information regarding the relative rates of reinitiation, hydrogen atom transfer, and chain termination in this type of process has also been studied using M–H complexes as the radical source. Hence, deuterium isotope-labeling would prove useful to delineate such details in these systems. In this regard, Norton and co-workers studied the effect of steric bulk on the rate of radical reinitiation in $(Cp^R)Cr(CO)_3H$ (R = Ph, Me, H) mediated polymerization of methyl methacrylate.[126] Hydrogen atom transfer was studied via H/D exchange between the different Cr–H complexes and methyl methacrylate-d_5 and ^1H NMR analysis. The loss of the Cr–H was studied under pseudo-first-order conditions and allowed for the extraction of the rate for reinitiation in the different complexes. Ultimately, the rates of reinitiation were found to decrease on the order of $Cp > Cp^* > Cp^{Ph}$, a trend that was attributed primarily to steric effects resulting in an unfavorable entropic component for the kinetics of reinitiation.

1.20.5 Conclusions

Isotopic labeling is a fundamental experimental technique available to the organometallic chemist for the evaluation of reaction mechanisms. In addition to revealing novel rearrangements during the course of a reaction (e.g., alkane migrations via σ-complexes) and distinguishing between different possible mechansisms (e.g., σ-bond methathesis vs carbene formation), the use of isotope labels can result in perturbations of both the kinetic and thermodynamic outcomes of reactions. These perturbations are known as equilibrium isotope effects (EIEs) and kinetic isotope effects (KIs), which can be measured quantitatively via a variety of analytical techniques (e.g., IR and NMR spectroscopy). Experimental and computational investigation of reactions involving coordination of alkanes and dihydrogen, as well as C–H and H–H activation and elimination reactions, can exhibit complex effects. The research literature reveals that both normal (>1) and inverse (<1) effects may be observed for both KIEs and EIEs. In the case of EIEs, such reactions can exhibit temperature-dependent transitions of the EIEs, due to opposing enthalpic (ZPE) and entropic (SYM · MMI · EXC) components of the equilibria. However, the presence of opposing enthalpic and entropic components is not necessarily universal and is highly dependent upon the nature of the system and reaction of interest. For KIEs, experimentally observed inverse isotope effects have been shown to be composites of isotope effects on different steps (e.g., reductive coupling vs. oxidative cleavage) and do not require any single step to exhibit an inverse isotope effect. Nonetheless, a few systems appear to exhibit inverse isotope effects for a single step.[127] Thus, it is apparent that while isotopic labeling is crucial to understanding the reactivity of a particular system in greater detail, a thorough investigation of these effects is required in order to correctly interpret the effects and draw conclusions concerning mechanism of the reaction being investigated.

References

1. Bergman, R. G. *Accounts Chem. Res.* **1980**, *13*, 113–120.
1a. Weston, R. E. *Chem. Rev.* **1999**, *99*, 2115–2136.
2. Du Bois, J.; Mizoguchi, T. J.; Lippard, S. J. *Coord. Chem. Rev.* **2000**, *200*, 443–485.
2a. Guengerich, F. P.; Parikh, A.; Yun, C. H.; Kim, D.; Nakamura, K.; Notley, L. M.; Gillam, E. M. J. *Drug Metab. Rev.* **2000**, *32*, 267–281.
2b. Yoshizawa, K.; Kagawa, Y.; Shiota, Y. *J. Phys. Chem. B* **2000**, *104*, 12365–12370.
2c. Yoshizawa, K. *Coord. Chem. Rev.* **2002**, *226*, 251–259.
2d. Guallar, V.; Gherman, B. F.; Miller, W. H.; Lippard, S. J.; Friesner, R. A. *J. Am. Chem. Soc.* **2002**, *124*, 3377–3384.
2e. Baik, M. H.; Newcomb, M.; Friesner, R. A.; Lippard, S. J. *Chem. Rev.* **2003**, *103*, 2385–2419.
2f. Tshuva, E. Y.; Lippard, S. J. *Chem. Rev.* **2004**, *104*, 987–1011.
2g. Parkin, G. *Chem. Rev.* **2004**, *104*, 699–767.
3. Arndtsen, B. A.; Bergman, R. G.; Mobley, T. A.; Peterson, T. H. *Accounts Chem. Res.* **1995**, *28*, 154–162.
3a. Crabtree, R. H. *Chem. Rev.* **1995**, *95*, 987–1007.
3b. Shilov, A. E.; Shul′pin, G. B. *Chem. Rev.* **1997**, *97*, 2879–2932.
3c. Arakawa, H.; Aresta, M.; Armor, J. N.; Barteau, M. A.; Beckman, E. J.; Bell, A. T.; Bercaw, J. E.; Creutz, C.; Dinjus, E.; Dixon, D. A., *et al. Chem. Rev.* **2001**, *101*, 953–996.
3d. Crabtree, R. H. *J. Chem. Soc.-Dalton Trans.* **2001**, 2437–2450.
4. Crabtree, R. H. Current Ideas and Future-Prospects in Metal-Catalyzed Methane Conversion. In *Natural Gas Conversion II*; Curry-Hyde, H. E., Howe, R. F., Eds.; Elsevier: Amsterdam, 1994; Vol. 81, pp 85–92.
4a. Periana, R. A.; Taube, D. J.; Evitt, E. R.; Loffler, D. G.; Wentrcek, P. R.; Voss, G.; Masuda, T. A Novel, High-Yield System for the Oxidation of Methane to Methanol. In *Natural Gas Conversion II*; Curry-Hyde, H. E., Howe, R. F., Eds.; Elsevier: Amsterdam, 1994; Vol. 81, pp 533–544.
5. Etard, A. *Ann. Chim. Phys.* **1881**, *22*, 218.
6. Waltz, K. M.; He, X. M.; Muhoro, C.; Hartwig, J. F. *J. Am. Chem. Soc.* **1995**, *117*, 11357–11358.
6a. Gallo, R.; Lazzeri, V. *Appl. Catal. A-Gen.* **1996**, *146*, 87–106.
6b. Holtcamp, M. W.; Henling, L. M.; Day, M. W.; Labinger, J. A.; Bercaw, J. E. *Inorg. Chim. Acta* **1998**, *270*, 467–478.
6c. Grigoryan, E. A. *Kinet. Catal.* **1999**, *40*, 350–363.
6d. Labinger, J. A.; Bercaw, J. E *Nature* **2002**, *417*, 507–514.
6e. Crabtree, R. H. *J. Organomet. Chem.* **2004**, *689*, 4083–4091.
7. Chatt, J.; Davidson, J. M. *J. Chem. Soc.* **1965**, 843.
8. Gol'dshleger, N. F.; Tyabin, M. B.; Shilov, A. E.; Shteinman, A. A. *Zh. Fiz. Khim.* **1969**, *43*, 2174.
9. Janowicz, A. H.; Bergman, R. G. *J. Am. Chem. Soc.* **1983**, *105*, 3929–3939.
10. Periana, R. A.; Bergman, R. G. *Organometallics* **1984**, *3*, 508–510.
11. Bullock, R. M.; Headford, C. E. L.; Kegley, S. E.; Norton, J. R *J. Am. Chem. Soc.* **1985**, *107*, 727–729.
12. Parkin, G.; Bercaw, J. E. *Organometallics* **1989**, *8*, 1172–1179.
13. Churchill, D. G.; Janak, K. E.; Wittenberg, J. S.; Parkin, G. *J. Am. Chem. Soc.* **2003**, *125*, 1403–1420.
14. Desrosiers, P. J.; Shinomoto, R. S.; Flood, T. C. *J. Am. Chem. Soc.* **1986**, *108*, 1346–1347.
14a. Desrosiers, P. J.; Shinomoto, R. S.; Flood, T. C. *J. Am. Chem. Soc.* **1986**, *108*, 7964–7970.
14b. Shinomoto, R. S.; Desrosiers, P. J.; Gregory, T.; Harper, P.; Flood, T. C. *J. Am. Chem. Soc.* **1990**, *112*, 704–713.
15. Osman, R.; Pattison, D. I.; Perutz, R. N.; Bianchini, C.; Casares, J. A.; Peruzzini, M. *J. Am. Chem. Soc.* **1997**, *119*, 8459–8473.
16. Wang, L.; Sowa, J. R.; Wang, C. M.; Lu, R. S.; Gassman, P. G.; Flood, T. C. *Organometallics* **1996**, *15*, 4240–4246.
16a. Zhou, R. J.; Wang, C. M.; Hu, Y. H.; Flood, T. C. *Organometallics* **1997**, *16*, 434–441.
17. Wang, C. M.; Ziller, J. W.; Flood, T. C. *J. Am. Chem. Soc.* **1995**, *117*, 1647–1648.
18. Jones, W. D.; Feher, F. J. *J. Am. Chem. Soc.* **1986**, *108*, 4814–4819.
18a. Periana, R. A.; Bergman, R. G. *J. Am. Chem. Soc.* **1986**, *108*, 7332–7346.
19. Flood, T. C.; Janak, K. E.; Iimura, H.; Zhen, H. *J. Am. Chem. Soc.* **2000**, *122*, 6783–6784.
20. Flood, T. C.; Boothe, P. W.; Janak, K. E., unpublished results.
21. Northcutt, T. O.; Wick, D. D.; Vetter, A. J.; Jones, W. D *J. Am. Chem. Soc.* **2001**, *123*, 7257–7270.
22. Tellers, D. M.; Skoog, S. J.; Bergman, R. G.; Gunnoe, T. B.; Harman, W. D *Organometallics* **2000**, *19*, 2428–2432.
23. Bhalla, G.; Liu, X. Y.; Wong-Foy, A.; Jones, C. J.; Periana, R. A. Alkane C̆H Bond Activation by Ŏ Donor Ir Complexes. In *Activation and Functionalization of C̆H Bonds*, *ACS Symposium Series 885*; Goldberg, K. I., Goldman, A. S., Eds.; American Chemical Society: Washington, D.C., 2004.
24. Burger, P.; Bergman, R. G. *J. Am. Chem. Soc.* **1993**, *115*, 10462–10463.
25. Klei, S. R.; Tilley, T. D.; Bergman, R. G. *J. Am. Chem. Soc.* **2000**, *122*, 1816–1817.
26. Shilov, A. E. In *Activation and Functionalization of Alkanes*; Hill, C. L., Ed.; Wiley: New York, 1989; p 1.
27. Stahl, S. S.; Labinger, J. A.; Bercaw, J. E. *Angew. Chem., Int. Edit.* **1998**, *37*, 2181–2192 and references therein.
28. Zamashchikov, V. V.; Litvinenko, S. L.; Uzhik, O. N.; Galat, V. F. *Zh. Obs. Khim.* **1986**, *56*, 2417.
29. Luinstra, G. A.; Wang, L.; Stahl, S. S.; Labinger, J. A.; Bercaw, J. E. *J. Organomet. Chem.* **1995**, *504*, 75–91.
30. Hackett, M.; Ibers, J. A.; Whitesides, G. M. *J. Am. Chem. Soc.* **1988**, *110*, 1436–1448.
31. Wick, D. D.; Goldberg, K. I. *J. Am. Chem. Soc.* **1997**, *119*, 10235–10236.
32. Stahl, S. S.; Labinger, J. A.; Bercaw, J. E. *J. Am. Chem. Soc.* **1996**, *118*, 5961–5976.
33. Heiberg, H.; Johansson, L.; Gropen, O.; Ryan, O. B.; Swang, O.; Tilset, M. *J. Am. Chem. Soc.* **2000**, *122*, 10831–10845.
33a. Johansson, L.; Tilset, M.; Labinger, J. A.; Bercaw, J. E. *J. Am. Chem. Soc.* **2000**, *122*, 10846–10855.
33b. Johansson, L.; Tilset, M. *J. Am. Chem. Soc.* **2001**, *123*, 739–740.
34. Thomas, J. C.; Peters, J. C. *J. Am. Chem. Soc.* **2001**, *123*, 5100–5101.
34a. Thomas, J. C.; Peters, J. C. *J. Am. Chem. Soc.* **2003**, *125*, 8870–8888.
35. Waltz, K. M.; He, X. M.; Muhoro, C.; Hartwig, J. F. *J. Am. Chem. Soc.* **1995**, *117*, 11357–11358.
35a. Waltz, K. M.; Muhoro, C. N.; Hartwig, J. F. *Organometallics* **1999**, *18*, 3383–3393.

35b. Waltz, K. M.; Hartwig, J. F. *J. Am. Chem. Soc.* **2000**, *122*, 11358–11369.
35c. Kawamura, K.; Hartwig, J. F. *J. Am. Chem. Soc.* **2001**, *123*, 8422–8423.
36. Periana, R. A.; Taube, D. J.; Evitt, E. R.; Loffler, D. G.; Wentrcek, P. R.; Voss, G.; Masuda, T. *Science* **1993**, *259*, 340–343.
36a. Periana, R. A.; Taube, D. J.; Gamble, S.; Taube, H.; Satoh, T.; Fujii, H. *Science* **1998**, *280*, 560–564.
37. Labinger, J. A.; Bercaw, J. E. *Nature* **2002**, *417*, 507–514.
38. Crabtree, R. H.; Mellea, M. F.; Mihelcic, J. M.; Quirk, J. M. *J. Am. Chem. Soc.* **1982**, *104*, 107–113.
38a. Crabree, R. H.; Parnell, C. P.; Uriarte, R. J. *Organometallics* **1985**, *4*, 519–523.
39. Baudry, D.; Ephritikhine, M.; Felkin, H.; Zakrzewski, J. *J. Chem. Soc., Chem. Commun.* **1980**, 1243–1244.
40. Maguire, J. A.; Goldman, A. S. *J. Am. Chem. Soc.* **1991**, *113*, 6706–6708.
40a. McLoughlin, M. A.; Flesher, R. J.; Kaska, W. C.; Mayer, H. A. *Organometallics* **1994**, *13*, 3816–3822.
40b. Liu, F. C.; Pak, E. B.; Singh, B.; Jensen, C. M.; Goldman, A. S. *J. Am. Chem. Soc.* **1999**, *121*, 4086–4087.
40c. Haenel, M. W.; Oevers, S.; Angermund, K.; Kaska, W. C.; Fan, H. J.; Hall, M. B. *Angew. Chem., Int.* **2001**, *40*, 3596–3600.
40d. Krogh-Jespersen, K.; Czerw, M.; Goldman, A. S. *J. Mol. Catal. A-Chem.* **2002**, *189*, 95–110.
40e. Krogh-Jespersen, K.; Czerw, M.; Zhu, K. M.; Singh, B.; Kanzelberger, M.; Darji, N.; Achord, P. D.; Renkema, K. B.; Goldman, A. S. *J. Am. Chem. Soc.* **2002**, *124*, 10797–10809.
40f. Winter, A. M.; Eichele, K.; Mack, H. G.; Potuznik, S.; Mayer, H. A.; Kaska, W. C. *J. Organomet. Chem.* **2003**, *682*, 149–154.
41. Liu, F. C.; Pak, E. B.; Singh, B.; Jensen, C. M.; Goldman, A. S. *J. Am. Chem. Soc.* **1999**, *121*, 4086–4087.
42. Krogh-Jespersen, K.; Czerw, M.; Summa, N.; Renkema, K. B.; Achord, P. D.; Goldman, A. S. *J. Am. Chem. Soc.* **2002**, *124*, 11404–11416.
43. Watson, P. L.; Parshall, G. W. *Acc. Chem. Res.* **1985**, *18*, 51–56 and references therein.
44. Thompson, M. E.; Baxter, S. M.; Bulls, A. R.; Burger, B. J.; Nolan, M. C.; Santarsiero, B. D.; Schaefer, W. P.; Bercaw, J. E. *J. Am. Chem. Soc.* **1987**, *109*, 203–219.
45. Rothwell, I. P. *Acc. Chem. Res.* **1988**, *21*, 153–159.
45a. Schrock, R. R. *Chem. Rev.* **2002**, *102*, 145–180 and references therein.
46. Chamberlain, L. R.; Rothwell, I. P.; Huffman, J. C. *J. Am. Chem. Soc.* **1986**, *108*, 1502–1509.
47. Walsh, P. J.; Hollander, F. J.; Bergman, R. G. *J. Am. Chem. Soc.* **1988**, *110*, 8729–8731.
47a. Cummins, C. C.; Baxter, S. M.; Wolczanski, P. T. *J. Am. Chem. Soc.* **1988**, *110*, 8731–8733.
47b. Carney, M. J.; Walsh, P. J.; Hollander, F. J.; Bergman, R. G. *J. Am. Chem. Soc.* **1989**, *111*, 8751–8753.
47c. Walsh, P. J.; Hollander, F. J.; Bergman, R. G. *J. Am. Chem. Soc.* **1990**, *112*, 894–896.
48. Carney, M. J.; Walsh, P. J.; Hollander, F. J.; Bergman, R. G. *J. Am. Chem. Soc.* **1989**, *111*, 8751–8753.
49. Schaller, C. P.; Cummins, C. C.; Wolczanski, P. T. *J. Am. Chem. Soc.* **1996**, *118*, 591–611.
50. Chin, T. T.; Legzdins, P.; Trotter, J.; Yee, V. C. *Organometallics* **1992**, *11*, 913–922.
50a. Dryden, N. H.; Legzdins, P.; Rettig, S. J.; Veltheer, J. E. *Organometallics* **1992**, *11*, 2583–2590.
51. Legzdins, P.; Rettig, S. J.; Veltheer, J. E.; Batchelor, R. J.; Einstein, F. W. B. *Organometallics* **1993**, *12*, 3575–3585.
51a. Tran, E.; Legzdins, P. *J. Am. Chem. Soc.* **1997**, *119*, 5071–5072.
51b. Adams, C. S.; Legzdins, P.; McNeil, W. S. *Organometallics* **2001**, *20*, 4939–4955.
51c. Pamplin, C. B.; Legzdins, P. *Acc. Chem. Res.* **2003**, *36*, 223–233.
52. Wada, K.; Pamplin, C. B.; Legzdins, P. *J. Am. Chem. Soc.* **2002**, *124*, 9680–9681.
53. Wolfsberg, M. *Acc. Chem. Res.* **1972**, *5*, 225–233.
53a. Bender, B. R. *J. Am. Chem. Soc.* **1995**, *117*, 11239–11246.
54. Schultz, R. H.; Bengali, A. A.; Tauber, M. J.; Weiller, B. H.; Wasserman, E. P.; Kyle, K. R.; Moore, C. B.; Bergman, R. G. *J. Am. Chem. Soc.* **1994**, *116*, 7369–7377.
54a. Bengali, A. A.; Schultz, R. H.; Moore, C. B.; Bergman, R. G. *J. Am. Chem. Soc.* **1994**, *116*, 9585–9589.
54b. Bengali, A. A.; Arndsten, B. A.; Burger, P. M.; Schultz, R. H.; Weiller, B. H.; Kyle, K. R.; Moore, C. B.; Bergman, R. G. *Pure Appl. Chem.* **1995**, *67*, 281–288.
55. Geftakis, S.; Ball, G. E. *J. Am. Chem. Soc.* **1998**, *120*, 9953–9954.
56. Bullock, R. M.; Bender, B. R. Isotope Methods in Homogeneous Catalysis. In *Encyclopedia of Catalysis*; Horvath, I. T., Ed., Wiley-Interscience: Hoboken, NJ, 2002.
57. Tilley, T. D. *Acc. Chem. Res.* **1993**, *26*, 22–29.
58. Crellin, K. C.; Geribaldi, S.; Beauchamp, J. L. *Organometallics* **1994**, *13*, 3733–3736.
58a. Deelman, B. J.; Teuben, J. H.; Macgregor, S. A.; Eisensten, O. *New J. Chem.* **1995**, *19*, 691–698.
58b. Suginome, M.; Oike, H.; Shuff, P. H.; Ito, Y. *Organometallics* **1996**, *15*, 2170–2178.
58c. Irvine, G. J.; Lesley, M. J. G.; Marder, T. B.; Norman, N. C.; Rice, C. R.; Robins, E. G.; Roper, W. R.; Whittell, G. R.; Wright, L. J. *Chem. Rev.* **1998**, *98*, 2685–2722.
58d. Niu, S. Q.; Hall, M. B. *J. Am. Chem. Soc.* **1998**, *120*, 6169–6170.
58e. Castillo, I.; Tilley, T. D. *J. Am. Chem. Soc.* **2001**, *123*, 10526–10534.
58f. Thieuleux, C.; Coperet, C.; Dufaud, V.; Marangelli, C.; Kuntz, E.; Basset, J. M. *J. Mol. Catal. A-Chem.* **2004**, *213*, 47–57.
59. Slaughter, L. M.; Wolczanski, P. T.; Klinckman, T. R.; Cundari, T. R. *J. Am. Chem. Soc.* **2000**, *122*, 7953–7975.
60. Calvert, R. B.; Shapley, J. R.; Schultz, A. J.; Williams, J. M.; Suib, S. L.; Stucky, G. D. *J. Am. Chem. Soc.* **1978**, *100*, 6240–6241.
61. Gould, G. L.; Heinekey, D. M. *J. Am. Chem. Soc.* **1989**, *111*, 5502–5504.
62. Hackett, M.; Whitesides, G. M. *J. Am. Chem. Soc.* **1988**, *110*, 1449–1462.
62a. Hackett, M.; Ibers, J. A.; Jernakoff, P.; Whitesides, G. M. *J. Am. Chem. Soc.* **1986**, *108*, 8094–8095.
63. Lowry, T. H.; Richardson, K. S. In *Mechanism and Theory in Organic Chemistry*, 3rd ed.; Harper Collins: New York, 1987; Chapter 2; pp 233–240.
64. This is essentially the classic case of the steady-state approximation and pre-equilibrium conditions for a two-step reaction with a reversible step. See Espenson, J. H. *Chemical Kinetics and Reaction Mechanisms*, 2nd ed.; McGraw-Hill: New York, 1995; pp 77–90.
65. Jones, W. D. *Acc. Chem. Res.* **2003**, *36*, 140–146.
66. Janak, K. E. Ph.D. Thesis, University of Southern California, Los Angeles, CA, 2001.
67. Janak, K. E.; Churchill, D. G.; Parkin, G. *Chem. Commun.* **2003**, 22–23.
68. Peterson, T. H.; Golden, J. T.; Bergman, R. G. *J. Am. Chem. Soc.* **2001**, *123*, 455–462.
69. Green, M. A.; Huffman, J. C.; Caulton, K. G. *J. Organomet. Chem.* **1983**, *243*, C78–C82.
69a. Chinn, M. S.; Heinekey, D. M. *J. Am. Chem. Soc.* **1987**, *109*, 5865–5867.

69b. Kubas, G. J. *Acc. Chem. Res.* **1988**, *21*, 120–128.
69c. Crabtree, R. H. *Acc. Chem. Res.* **1990**, *23*, 95–101.
69d. Albeniz, A. C.; Heinekey, D. M.; Crabtree, R. H. *Inorg. Chem.* **1991**, *30*, 3632–3635.
69e. Maguire, J. A.; Goldman, A. S *J. Am. Chem. Soc.* **1991**, *113*, 6706–6708.
69f. Jessop, P. G.; Morris, R. H. *Coord. Chem. Rev.* **1992**, *121*, 155–284.
69g. Heinekey, D. M.; Oldham, W. J. *Chem. Rev.* **1993**, *93*, 913–926.
69h. Clapham, S. E.; Hadzovic, A.; Morris, R. H. *Coord. Chem. Rev.* **2004**, *248*, 2201–2237.
70. Kubas, G. J. *Metal Dihydrogen and σ-Bond Complexes: Structure, Theory, and Reactivity*; Kluwer/Plenum: New York, 2001.
70a. Lin, Z.; Hall, M. B. *Coord. Chem. Rev.* **1994**, *135/136*, 845–879.
70b. Hall, C.; Perutz, R. N. *Chem. Rev.* **1996**, *96*, 3125–3146.
70c. Maseras, F.; Lledos, A.; Clot, E.; Eisenstein, O. *Chem. Rev.* **2000**, *100*, 601–636.
70d. Heinekey, D. M.; Lledos, A.; Lluch, J. M. *Chem. Soc. Rev.* **2004**, *33*, 175–182.
71. Kubas, G. J.; Ryan, R. R.; Swanson, B. I.; Vergamini, P. J.; Wasserman, H. J. *J. Am. Chem. Soc.* **1984**, *106*, 451–452.
72. Upmacis, R. K.; Gadd, G. E.; Poliakoff, M.; Simpson, M. B.; Turner, J. J.; Whyman, R.; Simpson, A. F. *J. Chem. Soc., Chem. Commun.* **1985**, 27–30.
72a. Upmacis, R. K.; Poliakoff, M.; Turner, J. J. *J. Am. Chem. Soc.* **1986**, *108*, 3645–3651.
73. Heinekey, D. M. *J. Am. Chem. Soc.* **2005**, *127*, 850–851.
74. Crabtree, R. H.; Segmuller, B. E.; Uriarte, R. J. *Inorg. Chem.* **1985**, *24*, 1949–1950.
74a. Hamilton, D. G.; Crabtree, R. H. *J. Am. Chem. Soc.* **1988**, *110*, 4126–4133.
75. Bakhmutov, V. I.; Vorontsov, E. V. *Rev. Inorg. Chem.* **1998**, *18*, 183–221.
76. Desrosiers, P.; Cai, L.; Lin, Z.; Richards, R.; Halpern, J. *J. Am. Chem. Soc.* **1991**, *113*, 4173–4184.
77. Green, M. L. H.; McLeverty, J. A.; Pratt, L.; Wilkinson, G. *J. Chem. Soc. A* **1961**, 4854–4859.
77a. Heinekey, D. M. *J. Am. Chem. Soc.* **1991**, *113*, 6074–6077.
77b. Parkin, G.; Bercaw, J. E. *J. Chem. Soc.-Chem. Commun.* **1989**, 255–257.
78. Jones, D.; Labinger, J. A.; Weitekamp, J. *J. Am. Chem. Soc.* **1989**, *111*, 3087–3088.
78a. Zilm, K. W.; Heinekey, D. M.; Millar, J. M.; Payne, N. G.; Demou, P. *J. Am. Chem. Soc.* **1990**, *112*, 3088–3089.
78b. Heinekey, D. M.; Millar, J. M.; Koetzle, T. F.; Payne, N. G.; Zilm, K. W. *J. Am. Chem. Soc.* **1990**, *112*, 909–919.
78c. Zilm, K. W.; Heinekey, D. M.; Millar, J. M.; Payne, N. G.; Neshyba, S. P.; Duchamp, J. C.; Szczyrba, J. *J. Am. Chem. Soc.* **1990**, *112*, 920–929.
78d. Scheurer, C.; Wiedenbruch, R.; Meyer, R.; Ernst, R. R.; Heinekey, D. M. *J. Chem. Phys.* **1997**, *106*, 1–10.
78e. Sabo-Etienne, S.; Chaudret, B. *Chem. Rev.* **1998**, *98*, 2077–2091.
79. Arliguie, T.; Chaudret, B.; Devillers, J.; Poilblanc, R. *C. R. Acad. Sci. Paris, Ser. II* **1987**, *305*, 1523–1526.
79a. Arliguie, T.; Border, C.; Chaudret, B.; Devillers, J.; Poilblanc, R. *Organometallics* **1989**, *8*, 1308–1314.
80. Limbach, H. H.; Ulrich, S.; Gründemann, S.; Buntkowsky, G.; Sabo-Etienne, S.; Chaudret, B.; Kubas, G. J.; Eckert, J. *J. Am. Chem. Soc.* **1998**, *120*, 7929–7940.
81. Conway, S. L. J.; Dijkstra, T.; Doerrer, L. H.; Green, J. C.; Green, M. L. H.; Stephens, A. H. H. *J. Chem. Soc.-Dalton Trans.* **1998**, 2689–2695.
81a. Green, J. C.; Scottow, A. *New J. Chem.* **1999**, *23*, 651–655.
81b. Similar couplings are also observed for the *ansa*-$[Me_2Si(C_5Me_4)_2WH_3]^+$ complex, Parkin, G.; Janak, K. E. unpublished results.
82. Kubas, G. J.; Nelson, J. E.; Bryan, J. C.; Eckert, J.; Wisniewski, L.; Zilm, K. *Inorg. Chem.* **1994**, *33*, 2954–2960.
83. Kubas, G. J.; Burns, C. J.; Eckert, J.; Johnson, S. W.; Larson, A. C.; Vergamini, P. J.; Unkefer, C. J.; Khalsa, G. R. K.; Jackson, S. A.; Eisenstein, O. *J. Am. Chem. Soc.* **1993**, *115*, 569–581.
84. Jalón, F. A.; Otero, A.; Manzano, B. R.; Villaseñor, E.; Chaudret, B. *J. Am. Chem. Soc.* **1995**, *117*, 10123–10124.
85. Antiñolo, A.; Carrillo-Hermosilla, F.; Fajardo, M.; Garcia-Yuste, S.; Otero, A.; Camanyes, S.; Maseras, F.; Moreno, M.; Lledós, A.; Lluch, J. M. *J. Am. Chem. Soc.* **1997**, *119*, 6107–6114.
86. Sabo-Etienne, S.; Chaudret, B.; Abouelmakarim, H.; Barthelat, J. C.; Daudey, J. P.; Moise, C.; Leblanc, J. C. *J. Am. Chem. Soc.* **1994**, *116*, 9335–9336.
87. Bullock, R. M. In *Transition Metal Hydrides*; Dedieu, A., Ed. VCH: New York, 1992; pp 263–307.
88. Hostetler, M. J.; Bergman, R. G. *J. Am. Chem. Soc.* **1992**, *114*, 7629–7636.
89. Rabinovich, D.; Parkin, G. *J. Am. Chem. Soc.* **1993**, *115*, 353–354.
90. See Ref 34 in Hartwig, J. F.; Andersen, R. A.; Bergman, R. G *Organometallics* **1991**, *10*, 1875–1887.
91. The values were calculated on the basis of $D(\tilde{H}H) = 104.2$ kcal/mol and $D(\tilde{D}D) = 106.0$ kcal/mol. Weast, R. C., Ed.; *CRC Handbook of Chemistry and Physics* 70th ed.; CRC Press: Boca Raton, FL, 1989–1990; p F–199.
92. Werneke, M. F. Ph.D. Thesis, Clarkson College of Technology, Potsdam, NY, 1971.
92a. Abu-Hasanayn, F.; Krogh-Jespersen, K.; Goldman, A. S. *J. Am. Chem. Soc.* **1993**, *115*, 8019–8023.
93. Janak, K. E.; Parkin, G. *J. Am. Chem. Soc.* **2003**, *125*, 6889–6891.
94. Janak, K. E.; Parkin, G. *J. Am. Chem. Soc.* **2003**, *125*, 13219–13224.
95. Cleary, B. P.; Eisenberg, R. *Inorg. Chim. Acta* **1995**, *240*, 135–143.
95a. Shin, J. H.; Parkin, G. *J. Am. Chem. Soc.* **2002**, *124*, 7652–7653.
96. Gusev, D. G.; Bakhmutov, V. I.; Grushin, V. V.; Vol'pin, M. E. *Inorg. Chim. Acta* **1990**, *177*, 115–120.
96a. Hauger, B. E.; Gusev, D. G.; Caulton, K. G. *J. Am. Chem. Soc.* **1994**, *116*, 208–214.
96b. Bakhmutov, V. I.; Bertran, J.; Esteruelas, M. A.; Lledos, A.; Maseras, F.; Modrego, J.; Oro, L. A.; Sola, E. *Chem. Eur. J.* **1996**, *2*, 815.
97. Bender, B. R.; Kubas, G. J.; Jones, L. H.; Swanson, B. I.; Eckert, J.; Capps, K. B.; Hoff, C. D. *J. Am. Chem. Soc.* **1997**, *119*, 9179–9190.
98. Janak, K. E.; Parkin, G. *Organometallics* **2003**, *22*, 4378–4380.
99. Luo, X. L.; Crabtree, R. H. *J. Am. Chem. Soc.* **1990**, *112*, 6912–6918.
100. Haward, M. T.; George, M. W.; Hamley, P.; Poliakoff, M. *J. Chem. Soc., Chem. Commun.* **1991**, 1101–1103.
101. Heinekey, D. M.; Oldham, W. J. *J. Am. Chem. Soc.* **1994**, *116*, 3137–3138.
101a. Oldham, W. J.; Hinkle, A. S.; Heinekey, D. M. *J. Am. Chem. Soc.* **1997**, *119*, 11028–11036.
102. Jalón, F. A.; Otero, A.; Manzano, B. R.; Villaseñor, E.; Chaudret, B. *J. Am. Chem. Soc.* **1995**, *117*, 10123–10124.
102a. Sabo-Etienne, S.; Chaudret, B.; El Makarim, H. A.; Barthelat, J.; Daudey, J.; Ulrich, S.; Limbach, H.; Moïse, C. *J. Am. Chem. Soc.* **1995**, *117*, 11602–11603.
103. Janak, K. E.; Shin, J. H.; Parkin, G. *J. Am. Chem. Soc.* **2004**, *126*, 13054–13070.

104. Saboetienne, S.; Chaudret, B. *J. Am. Chem. Soc.* **1995**, *117*, 11602–11603.
104a. Manzano, B.; Jalon, F.; Matthes, J.; Sabo-Etienne, S.; Chaudret, B.; Ulrich, S.; Limbach, H. H. *J. Chem. Soc., Dalton Trans.* **1997**, 3153–3159.
104b. Gelabert, R.; Moreno, M.; Lluch, J. M. *Ber. Bunsen-Ges. Phys. Chem. Chem. Phys.* **1998**, *102*, 354–358.
105. Pons, V.; Conway, S. L. J.; Green, M. L. H.; Green, J. C.; Herbert, B. J.; Heinekey, D. M. *Inorg. Chem.* **2004**, *43*, 3475–3483.
106. Torres, L.; Moreno, M.; Lluch, J. M. *J. Phys. Chem. A* **2001**, *105*, 4676–4681.
107. Kaminsky, W., Sinn, H., Eds.; *Transition Metals and Organometallics as Catalysts for Olefin Polymerization*, Springer: Berlin, 1988.
108. Pino, P.; Mulhaupt, R. *Angew. Chem., Int. Ed. Engl.* **1980**, *19*, 857.
108a. Olabisi, O.; Atiqullah, M.; Kaminsky, W. *J. Macromol. Sci.-Rev. Macromol. Chem. Phys.* **1997**, *C37*, 519–554.
108b. Coates, G. W. *Chem. Rev.* **2000**, *100*, 1223–1252.
108c. Hlatky, G. G. *Chem. Rev.* **2000**, *100*, 1347–1376.
108d. Coates, G. W. *J. Chem. Soc., Dalton Trans.* **2002**, *4*, 467–475.
109. Patten, T. E.; Matyjaszewski, K. *Acc. Chem. Res.* **1999**, *32*, 895–903.
109a. Matyjaszewski, K.; Xia, J. *Chem. Rev.* **2001**, *101*, 2921–2990.
109b. Kamigaito, M.; Ando, T.; Sawamoto, M. *Chem. Rev.* **2001**, *101*, 3689–3745.
109c. Trnka, T. M.; Grubbs, R. H. *Acc. Chem. Res.* **2001**, *34*, 18–29.
110. Grubbs, R. H.; Burk, P. L.; Carr, D. D. *J. Am. Chem. Soc.* **1975**, *97*, 3265–3267.
110a. Katz, T. J.; Rothchild, R. *J. Am. Chem. Soc.* **1976**, *98*, 2519–2526.
111. Brookhart, M. W.; Green, M. L. H. *J. Organomet. Chem.* **1983**, *250*, 395–408.
112. Dawoodi, Z; Green, M. L. H.; Mtetwa, V. S. B.; Prout, K.; Schultz, A. J.; Williams, J. M.; Koetzle, T. F. *J. Chem. Soc., Dalton Trans.* **1986**, 1629–1637.
113. Saunders, M.; Jaffe, M. H.; Vogel, P. *J. Am. Chem. Soc.* **1971**, *93*, 2558–2559.
114. Guo, Z.; Swenson, D. C.; Jordan, R. F. *Organometallics* **1994**, *13*, 1424–1432.
115. Kaminsky, W.; Sinn, H. *Adv. Organomet. Chem.* **1980**, *18*, 99–149.
115a. Grubbs, R. H.; Coates, G. W. *Acc. Chem. Res.* **1996**, *29*, 85–93.
116. Clawson, L.; Soto, J.; Buchwald, S. L.; Steigerwald, M. L.; Grubbs, R. H. *J. Am. Chem. Soc.* **1985**, *107*, 3377–3378.
117. Krauledat, H.; Brintzinger, H. H. *Angew. Chem., Int. Ed. Engl.* **1990**, *29*, 1412–1413.
118. Piers, W. E.; Bercaw, J. E. *J. Am. Chem. Soc.* **1990**, *112*, 9406–9407.
119. Cotter, W. D.; Bercaw, J. E. *J. Organomet. Chem.* **1991**, *417*, C1–C6.
120. Barta, N. S.; Kirk, B. A.; Stille, J. R. *J. Am. Chem. Soc.* **1994**, *116*, 8912–8919.
121. Leclerc, M. K.; Brintzinger, H. H. *J. Am. Chem. Soc.* **1995**, *117*, 1651–1652.
122. Minisci, F. *Acc. Chem. Res.* **1975**, *8*, 165–171.
123. Harrisson, S.; Rourke, J. P.; Haddleton, D. M. *Chem. Commun.* **2002**, 1470–1471.
124. Singleton, D. A.; Thomas, A. A. *J. Am. Chem. Soc.* **1995**, *117*, 9357–9358.
125. Singleton, D. A.; Nowlan, D. T. III; Jahed, N.; Matyjaszewski, K. *Macromol.* **2003**, *36*, 8609–8616.
126. Tang, L. H.; Papish, E. T.; Abramo, G. P.; Norton, J. R.; Baik, M. H.; Friesner, R. A.; Rappe, A. *J. Am. Chem. Soc.* **2003**, *125*, 10093–10102.
127. Lo, H. C.; Haskel, A.; Kapon, M.; Keinan, E. *J. Am. Chem. Soc.* **2002**, *124*, 3226–3228.
127a. Lo, H. C.; Haskel, A.; Kapon, M.; Keinan, E. *J. Am. Chem. Soc.* **2002**, *124*(42), **2002**, 12626.

1.21
Structure and Bonding in Organometallic Compounds: Diffraction Methods

L Brammer and G M Espallargas, University of Sheffield, Sheffield, UK

1.21.1 Aims and Scope

In COMC (1982), the section on diffraction methods (Volume 9) comprised a listing of all structures determined by diffraction methods that were found in the other volumes of that edition. In COMC (1995), this listing was updated (Volume 13), and a comprehensive list of all compounds containing metal–carbon bonds and characterized by either X-ray, neutron, or electron diffraction methods was provided, thus encompassing the earlier listing.

As in these listings, the primary repository of structural data for organometallic compounds remains the Cambridge Structural Database ((CSD); for all references to crystal structure determinations, the CSD REFCODE is provided in parentheses in the References section),[1] which in its November 2005 release contains 355,064 structures, of which 2,229 contain *s*-block metal–carbon bonds, 37,433 contain *p*-block metal–carbon bonds (including B and Si), 75,631 contain *d*-block metal–carbon bonds, and 2,521 contain *f*-block metal–carbon bonds. Since 1993, the number of crystal structures determined by single crystal X-ray diffraction has grown enormously, in part due to faster computers and improved software and methodology for structure determination, but principally due to the introduction of charge-coupled device (CCD) area detectors in the mid-1990s. Therefore, the scope of this chapter is not to provide an updated comprehensive listing of all structure determinations. The CSD and its associated software provide a much better option for tailored searches and are the preferred method to locate structural data. However, a summary of the growth of structure determination and the aggregate numbers for organometallic compounds containing different metals is presented.

The main focus of the chapter will be on diffraction methods that at present account for a small number of structural studies compared to those determined by single crystal X-ray diffraction, namely single crystal neutron diffraction, X-ray and neutron powder diffraction, and charge density methods. A survey of compounds studied by these methods since 1993 is presented together with a summary of studies in which the CSD has been employed to derive chemical insight from and examine trends in intra- and intermolecular geometries. The chapter concludes with a brief look forward to how the methods discussed and other evolving approaches may become more important to organometallic chemists in the future.

1.21.2 Overview of Structure Determination Since 1993

As shown in Figure 1, the number of structure determinations reported per year has grown from ca. 3,000 in 1993 to well over 5,000 in 2004 (for 2005 data available in the November, 2005 CSD release are used and only represent structures determined in the early part of that year). The distribution of structures according to metal is given in Figure 2.

The introduction of CCD area detectors into many laboratories engaged in crystal structure determination as replacements for scintillation detectors has resulted in a major change in structure determination by single crystal X-ray diffraction, which accounts for most of the structures represented in Figures 1 and 2. CCD detectors are more sensitive than scintillation detectors, permitting data to be collected on smaller crystals. The current generation of CCD detectors permits data collection and structure determination in favorable cases for crystals with dimensions of 10–100 μm, whereas 200–500 μm were more typical crystal dimensions for use with scintillation detectors. As area detectors permit the simultaneous measurement of many diffraction intensities rather than sequential measurement

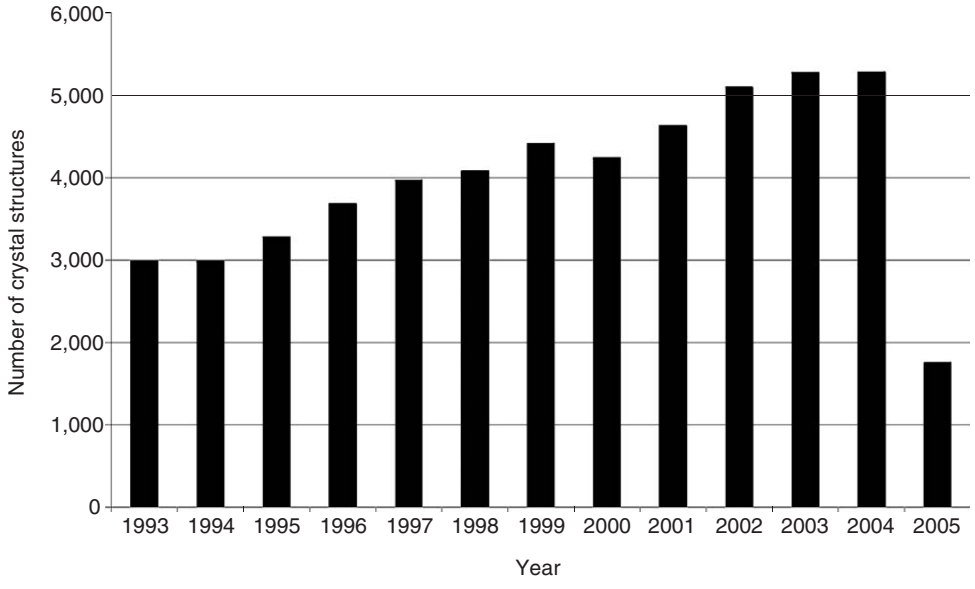

Figure 1 Number of structure determinations of organometallic compounds by year.

using a scintillation detector, it is also now feasible to measure data sets of high redundancy rather than measuring in one only asymmetric unit of reciprocal space as was more common using scintillation detectors. Such data result in greater accuracy and precision of intensity measurements and the option to make highly effective empirical corrections for absorption and other systematic errors. Use of area detectors also removes the necessity to determine the correct orientation matrix for the crystal before data collection and has led, with improvements in software, to the

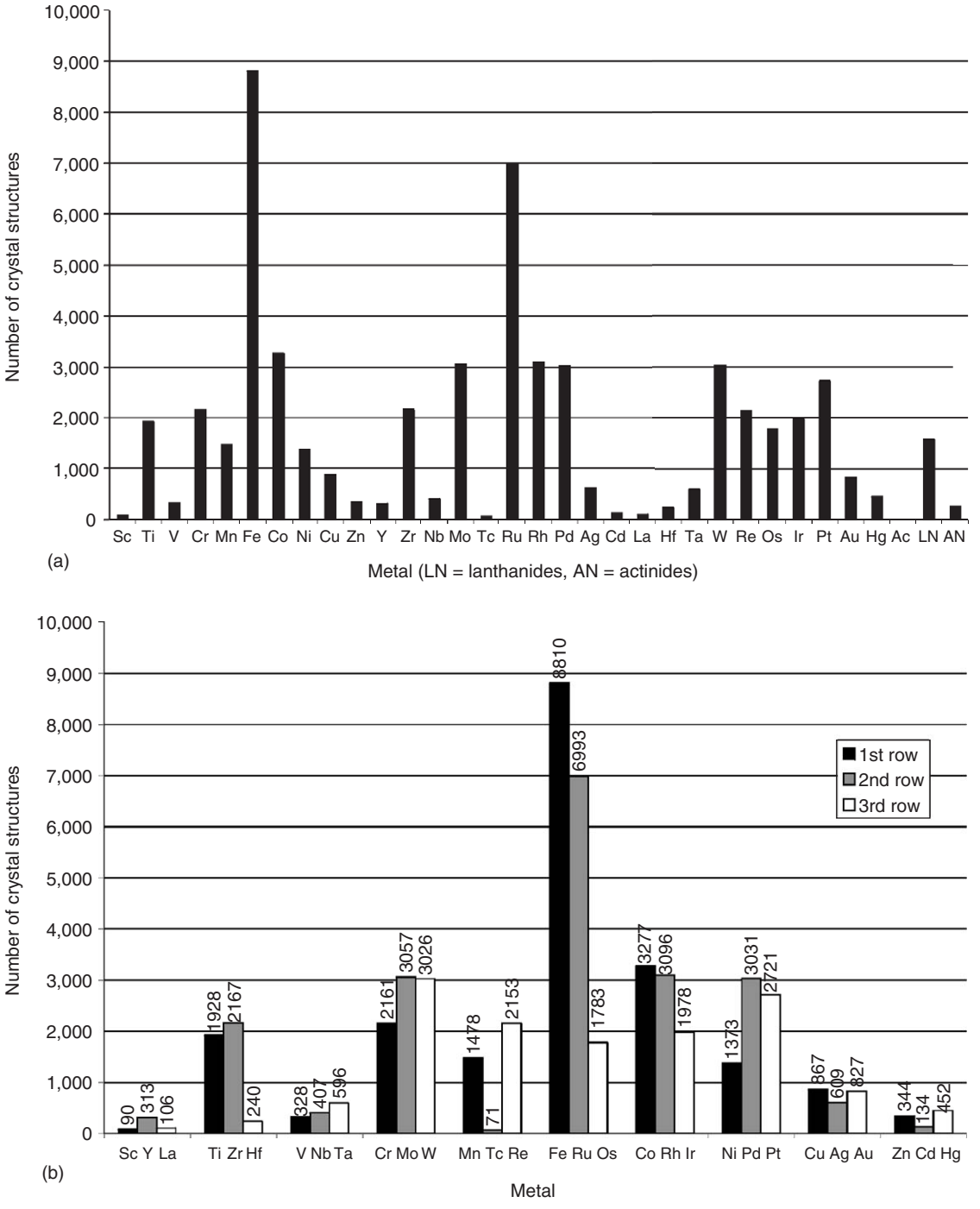

Figure 2 (a) Distribution of structures across *d*- and *f*-block metal complexes; (b) distribution of *d*-block structures by group; (c) distribution of *s*- and *p*-block structures by group.

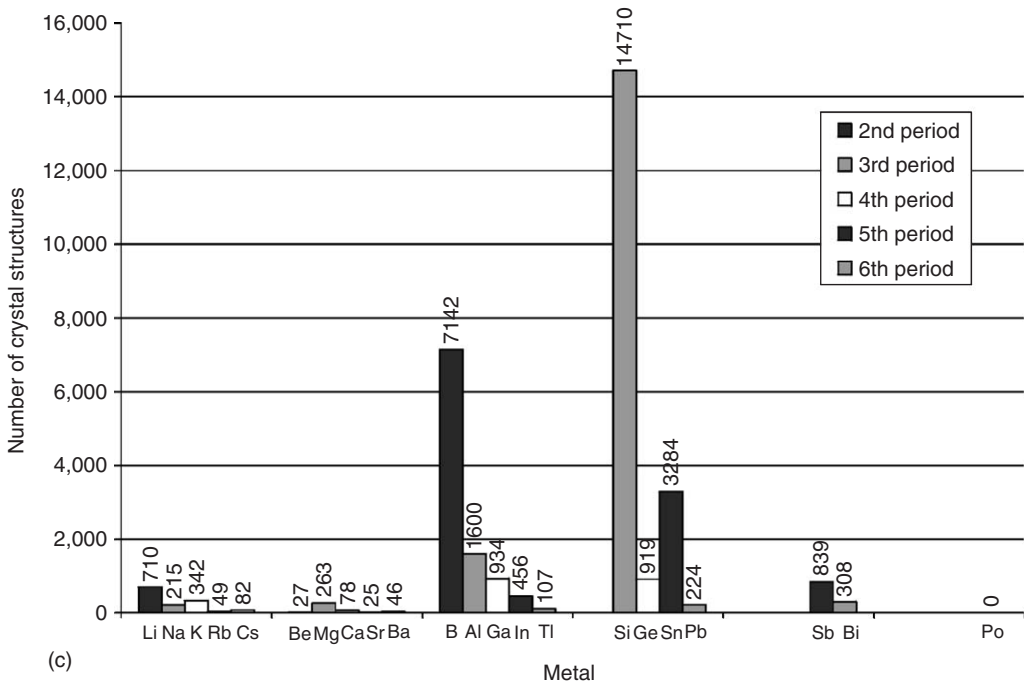

Figure 2 (*Continued*)

opportunity to determine many structures when the crystal used is twinned. Such samples often proved to be intractable problems or too time consuming when scintillation detectors were the principal detectors in use.

Overall, therefore, the introduction of CCD area detectors for laboratory X-ray diffraction has provided an opportunity to determine structures from samples that were previously not feasible or impractical (crystals too small or twinned). In addition, data quality and therefore structure quality have improved and data collection times have decreased. To organometallic chemists, who often rely upon crystal structure determination to characterize new and unusual ligand bonding where unambiguous spectroscopic characterization is difficult or impossible, this change is a great step forward.

1.21.3 Single Crystal Neutron Diffraction

The most common applications exploit the ability of neutron diffraction to provide accurate and precise light atom positions and displacement parameters, most emphatically for hydrogen atoms, which are poorly characterized by X-ray diffraction due to their weak scattering of X-rays relative to heavier elements. Neutron diffraction also often permits facile discrimination between elements of similar atomic number or isotopes of the same element. However, the low flux of neutrons currently available from most reactor or spallation neutron sources limits most neutron diffraction studies to crystals of volume 1 mm^3 or greater.

In the period 1993–2005, we have identified six single crystal neutron diffraction studies of compounds containing *s*-block metal–carbon bonds, 33 for *p*-block metals (including Si and B), 58 for *d*-block, and three for *f*-block metals (Figure 3).

The studies of *d*- and *f*-block metals are described briefly in Sections 3.1–3.9, whereas those containing *s*- and *p*-block metals are tabulated in Section 3.10. The primary purpose for the studies of *d*- and *f*-block metal complexes was accurate determination of hydrogen atom positions, most often for hydrogen atoms bonded to metal centers. These structures are organized according to the type of compound or chemical purpose of study and discussed briefly below. A further three dihydrogen complexes and 20 molecular metal hydride compounds in which no metal–carbon bond is present were also studied by neutron diffraction. Reviews of neutron diffraction studies of compounds containing M–H bonds or M···H interactions have been compiled by Bau and co-workers covering the period up to 1997.[2,2a]

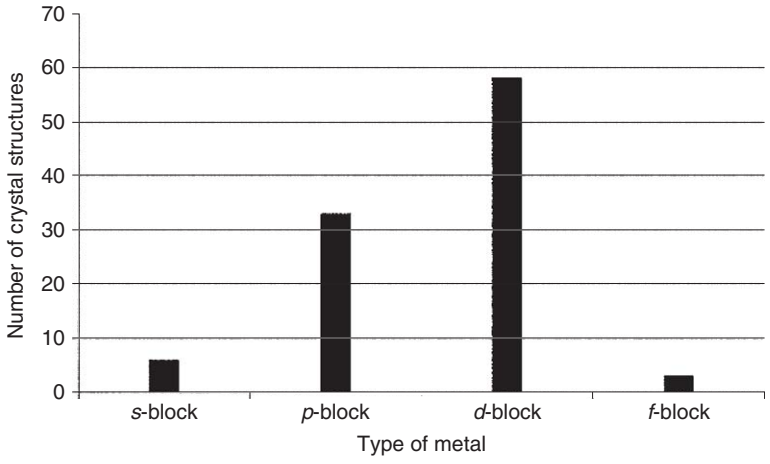

Figure 3 Distribution of neutron diffraction studies by type of metal.

1.21.3.1 Compounds with Dihydrogen Ligands

Six new crystal neutron structures of compounds with dihydrogen ligands were published. Of these, three can be classified as organometallic based upon the definition of containing a metal–carbon bond. Kubas and colleagues reported the structure of *trans*-[Mo(η^2-H_2)(CO){$(C_6D_5)_2PCH_2CH_2P(C_6D_5)_2$}]·4.5$C_6D_6$ **1**[3] and contrasted this with the corresponding dihydride complexes formed when more electron-donating phosphines are used (Scheme 1). The H–H distance is 0.736(10) Å (0.80–0.85 Å corrected for libration). Deuteration of the sample permitted an inelastic neutron scattering experiment, which enabled the very low barrier to dihydrogen rotation to be determined as 0.7 kcal mol^{-1}. The piano stool complex [Os(η^5-C_5Me_5)(η^2-H_2)H_2(PPh_3)]BF_4 **2** exhibits an elongated dihydrogen H–H distance of 1.014(11) Å.[4] Exchange of the classical and non-classical hydrogen atoms sites is observed by room-temperature ^{1}H NMR spectroscopy. As in **2**, the H_2 ligand in [Ru(η^2-H_2)(η^5-C_5Me_5)(dppm)]BF_4 **3** reported by Morris[5] lies parallel to the cyclopentadienyl ligand plane. In the latter case, this orientation maximizes metal–ligand π-overlap and results in an elongated H–H distance of 1.08(3) Å (1.10 Å corrected for libration). It is one of the few dihydrogen complexes where the presence of an elongated dihydrogen ligand has been established in the solid state and in solution (1.10(1) Å by T_1 NMR method). The three dihydrogen complexes containing no transition metal–carbon bonds are *trans*-[Ru(η^2-H_2)(H)$(dppe)_2$]BPh_4 **4**,[6] [Os(η^2-H_2)(κ^1-OC(O)Me)$(en)_2$]PF_6 **5**,[7] and *cis*-[Ir(η^2-H_2)(H)Cl_2(PPr^i_3)$_2$] **6**.[8]

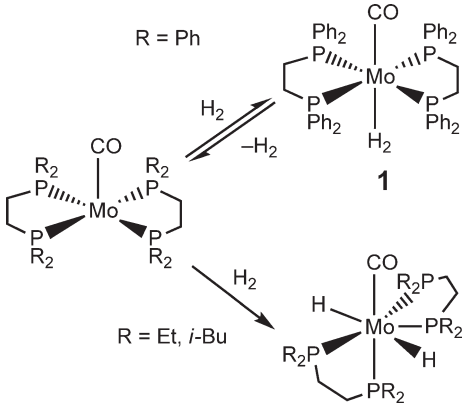

Scheme 1 Compound **1** (top) and the corresponding dihydride formed when more electron-donating phosphines are used.

Crabtree reported the structure of $[ReH_5(PPh_3)_3]\cdot C_8H_7N\cdot C_6H_6$ **7** which rather than containing a dihydrogen ligand contains an N–H···H–Re hydrogen bond (dihydrogen bond) of length 1.734(8) Å between indole and the polyhydride complex.[9]

1.21.3.2 Terminal Metal Hydrides

Lemke and Brammer reported the first terminal ruthenium hydrides to be characterized by neutron diffraction, $[RuH(\eta^5\text{-}C_5H_5)(PMe_3)_2]$ **8** (Ru–H 1.630(4) Å) and the dihydride obtained by protonation with HBF_4, $[RuH_2(\eta^5\text{-}C_5H_5)(PMe_3)_2]BF_4$ **9** (Ru–H 1.599(8); 1.604(9) Å).[10] The compounds are closely related to the dihydrogen complex **3**, and a full structural comparison of hydrides, dihydrides, and dihydrogen complexes $Cp'ML_2H$, $Cp'ML_2H^{2+}$, and $Cp'ML_2(H_2)^+$ has been provided.[11] The structure of $[MoH(\eta^5\text{-}C_5Me_5)(CO)_3]$ **10**,[12] reported together with a redetermination of the X-ray structure, corrects an original erroneous report (incorrect space group) and provides an accurate geometry (Mo–H 1.789(7) Å). A comparison of all $Cp'M(CO)_3LX$ structures establishes that the conformation of the piano stool complexes is determined by the steric rather than electronic interactions of the anionic ligand X. The neutron structure of $[MoH(\eta^5\text{-}C_5H_5)(CO)_3]$ **11**, was reported at the 1988 American Crystallographic Association meeting (Mo–H 1.720(5) Å),[13] but has not been published in the primary literature. A Mo–H distance of 1.69(5) Å was reported by Cummins in the study of a rare cyclometallation product, $[Mo(H)(\eta^2\text{-}Me_2C{=}NAr)\{N(Pr^i)Ar\}_2]$ (Ar = 3,5-$C_6H_3Me_2$) **12**,[14] in which an isopropylanilide ligand has undergone β-hydride elimination (Scheme 2).

The neutron structure of *cis*-$HMn(CO)_4PPh_3$ **13**[15] is only the second such characterization of a terminal Mn–H bond 1.573(2) Å, compared to 1.601(16) Å for β-$HMn(CO)_5$ **14**.[16] The study also reveals the presence of a weak intramolecular dihydrogen bond C–H···H–Mn (H···H 2.101(3) Å; C–H···H 129.0(2)°, Mn–H···H 126.5(1)°) suggestive of incipient orthometallation of a phenyl ring of the PPh_3 ligand. This compound was also the subject of an experimental charge density study, as described in Section 5.3. Bau has reported the most accurate metal hydride geometries to date for an FeH_2L_4 octahedral complex, $[FeH_2(CO)_2\{P(OPh)_3\}_2]$ **15**,[17] (Fe–H 1.521(2), 1.529(2) Å), which adopts a highly distorted octahedral coordination geometry (H–Fe–H 82.5(1)°; H···H 2.011(3) Å). The structure of $[K(18\text{-crown-6})][(PPh_3)_2ReH_6Cr(CO)_3]\cdot THF$ **16**[18] contains three terminal metal hydrides as well as three bridging hydrides, and those of $[(PEt_3)_2(Ph)Pt(\mu\text{-}H)PtH(PEt_3)_2]BPh_4$ **17**[19] and $[(PEt_3)_2(C_6Cl_5)Pt(\mu\text{-}H)Ag(H_2O)]CF_3SO_3$ **18**[20] contain both a terminal and bridging hydride. These compounds are discussed in Section 3.3. A final example in this section involves a structure redetermination[21] in which neutron diffraction has now established the absence of hydride ligands in contradiction to the original report in which a compound of composition $(Bu^n{}_4N)_2H_2\{Mo_2[Mo(CO)_4(PhPO_2)_2]_2\}$ with an unusually long quadruple bond was described.[22] The revised structure, $(Bu^n{}_4N)_2\{Mo_2[Mo(CO)_4(PhPO_2)_2]_2\}$ **19** exhibits an Mo≡Mo "triple" bond of typical length for this class of compound, 2.1874(7) Å, and is reported alongside X-ray structures of a new polymorph of this compound, a CH_2Cl_2 solvate and a THF adduct.[21]

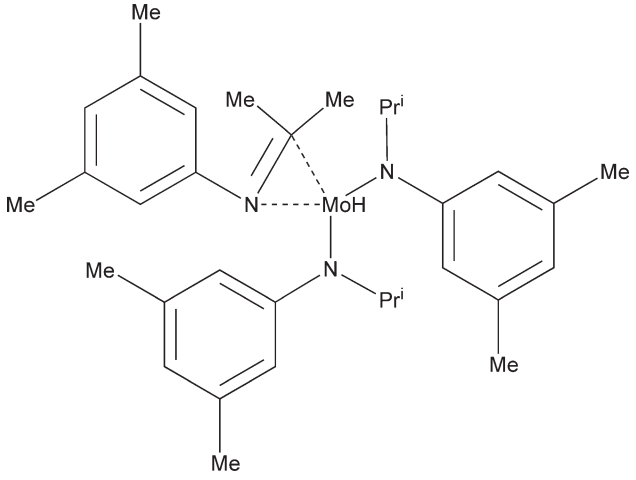

12

Scheme 2

1.21.3.3 Bridging Metal Hydrides

Seven neutron diffraction studies of bridging metal hydrides were reported (Table 1). Cations $[(PEt_3)_2(Ph)Pt(\mu\text{-}H)PtH(PEt_3)_2]^+$ (cation from **17**) and $[(PEt_3)_2(C_6Cl_5)Pt(\mu\text{-}H)Ag(H_2O)]^+$ (cation from **18**) contain both a single bridging hydride and a terminal platinum hydride. Cation $[\{(\eta^5\text{-}C_5H_3)_2(SiMe_2)_2\}Ru_2(CO)_4(\mu\text{-}D)]^+$ (cation from **20**) was studied in order to establish the steric accessibility of the hydride ligand (deuteride in the crystal structure) as part of studies of deptrotonation of this compound and related iron and osmium species to yield neutral metal–metal bonded products (Scheme 3).[23]

$[Ta_2(NMe_2)_6(\mu\text{-}H)_2(\mu\text{-}N\text{-}\eta^2\text{-}N,C\text{-}CH_2NMe)]$ **21** contains two bridging hydride ligands[24] and like **12** contains an η^2-imine ligand that results from β-hydride elimination of an amide ligand. The remaining three compounds studied have three hydride ligands bridging a metal–metal bond. $[(PPh_3)_2ReH_3(\mu\text{-}H)_3Cr(CO)_3]^-$ **16** can be viewed as a coordination of $[(PPh_3)_2ReH_6]^-$ to a $Cr(CO)_3$ moiety as a six-electron ligand via three Re–H bonds. Analogous examples are examined in the corresponding paper.[18] The neutron structure of $[\{Co(\eta^5\text{-}C_5Me_5)\}_2(\mu\text{-}H)_3]$ **22**[25] corrects an erroneous X-ray crystal structure which was described a few years earlier as containing an unsupported Co≡Co bond between the two Cp^*Co fragments. A related compound $[\{Co(\eta^5\text{-}C_5H_2Bu^t_3)\}_2(\mu\text{-}H)_3]$ **23** adopts a very similar structure,[26] and was refined successfully despite twinning in the crystals used. The report of this compound also contains a survey and analysis of structural patterns in $M(\mu\text{-}H)_nM$ systems ($n = 1, 2, 3, 4$).

1.21.3.4 Metal Cluster Hydrides

Three tetrahedral tetranuclear clusters containing hydride ligands have been studied. A fourth $[Re_4(\mu_3\text{-}H)_4(CO)_{12}]$ has been characterized by a combination of single crystal X-ray diffraction and powder neutron diffraction, and is discussed in Section 4.5. The study of $[PPN][HIr_4(CO)_9(\mu\text{-dppm})]$ **24** establishes that the hydride ligand is terminal (Ir–H 1.62(1) Å).[27] The paramagnetic cluster $[Cr_4(\eta^5\text{-}C_5Me_4Et)_4(\mu_2\text{-}H)_5(\mu_3\text{-}H)_2]$ **25** exhibits unusually strong intramolecular magnetic coupling leading to antiparallel alignment of three Cr(III) moments with one Cr(II) and a ground-state magnetic moment of $S = 7/2$.[28] The coupling is mediated by the bridging hydride ligands, and magnetic alignment is not disturbed appreciably even at room temperature, suggesting that metal hydrides may be useful

Table 1 Bridging hydride geometries

Compound	*M–H–M′*	*M–H* (Å)	*M′–H* (Å)	*M–H–M′* (°)	*References*
$[(PEt_3)_2(Ph)Pt(\mu\text{-}H)PtH(PEt_3)_2]BPh_4$ **17**	Pt–H–Pt	1.71(3)	1.74(3)	125(1)	19
$[(PEt_3)_2(C_6Cl_5)Pt(\mu\text{-}H)Ag(H_2O)]CF_3SO_3$ **18**	Pt–H–Ag	1.674(4)	1.831(5)	103.3(2)	20
$[\{(\eta^5\text{-}C_5H_3)_2(SiMe_2)_2\}Ru_2(CO)_4(\mu\text{-}D)]CF_3SO_3$ **20**	Ru–D–Ru	1.741(4)	1.768(5)	124.3(3)	23
$[Ta_2(NMe_2)_6(\mu\text{-}H)_2(\mu\text{-}N\text{-}\eta^2\text{-}N,C\text{-}CH_2NMe)]$ **21**	Ta–H–Ta	1.99(1)	1.98(1)	101.2(6) av.	24
		1.96(1)	1.92(1)		
$[K(18\text{-crown-6})][(PPh_3)_2ReH_3(\mu\text{-}H)_3Cr(CO)_3]\cdot THF$ **16**	Re–H–Cr	1.75(1)	1.94(2)	88.4(6)	18
		1.76(1)	1.95(2)	88.0(6)	
		1.74(1)	1.87(2)	91.0(7)	
$[\{Co(\eta^5\text{-}C_5Me_5)\}_2(\mu\text{-}H)_3]$ **22**	Co–H–Co	1.641(8)	1.641(8)	86.8(3)	25
$[\{Co(\eta^5\text{-}C_5H_2Bu^t_3)\}_2(\mu\text{-}H)_3]$ **23**	Co–H–Co	1.64(2)	1.64(2)	88.0(9)	26

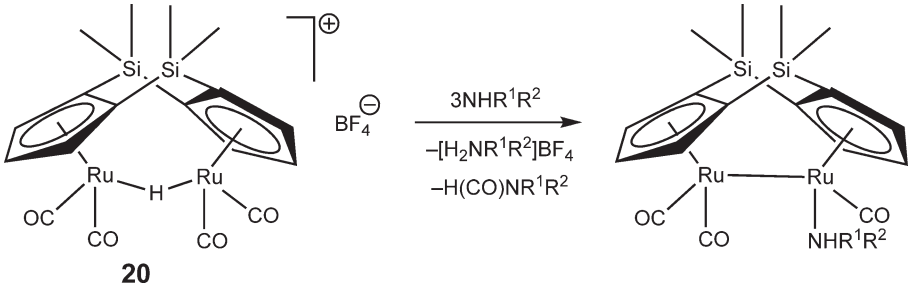

20

Scheme 3 Deprotonation of compound **20** yields metal–metal-bonded compound.

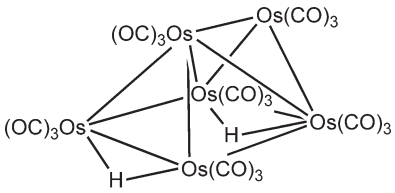

27

Scheme 4 Structure of $H_2Os_6(CO)_{18}$.

components of molecular magnetic materials. The structure of $[H_4Co_4(\eta^5\text{-}C_5Me_4Et)_4]$ **26** provides accurate characterization of a rare example of μ_3-hydride ligands, which occupy the four faces of the Co_4 tetrahedron (Co–H 1.749(7) Å; Co–H–Co 94.6(3)°).[29] The hexanuclear cluster $[H_2Os_6(CO)_{18}]$ **27** is unusual in adopting a non-octahedral cluster geometry,[30] in contrast to the isoelectronic analogs $[Os_6(CO)_{18}]^{2-}$ and $[HOs_6(CO)_{18}]^-$, which adopt octahedral cluster geometries. ^1H and ^{13}C NMR studies led Lewis and Johnson to suggest one edge-bridging hydride and one that is μ_3-H or μ_4-H, the latter being unprecedented.[31] Pauling later suggested two terminal hydrides[32] prior to Orpen's prediction based upon potential energy calculations that two edge-bridging hydrides should be present on the square face.[33,33a] The neutron diffraction study of **27** as a solvate, $[H_2Os_6(CO)_{18}]\cdot 0.5CH_2Cl_2$, confirms Orpen's prediction, as shown in Scheme 4.[30] The first report of an interstitial μ_5-hydride ligand arose when the cluster anion $[H_2Rh_{13}(CO)_{24}]^{3-}$ was crystallized as $(NH_4)_3[H_2Rh_{13}(CO)_{24}]\cdot CH_3COC_2H_5$ **28** ending a 20-year uncertainty regarding the hydride ligand coordination mode in this cluster.[34] Each hydride ligand is located in a separate square-pyramidal cavity. Four other square-pyramidal cavities remain unoccupied.

1.21.3.5 Agostic (C–H–M) and other 3c-2e E–H–M Interactions (E = B, Si, Sn)

Agostic interactions,[35,35a] three-center two-electron (3c-2e) interactions of a C–H bond with a metal center, can be regarded as snapshots along a reaction pathway for C–H bond activation at that metal center. Such interactions have been the subject of five studies. In three of these α-agostic interactions have been characterized. The alkylidene ligand in $[W(CHCH_3)Cl_2(CO)(PMe_3)_2]$ **29** exhibits a strong α-agostic interaction (W–H 1.922(6) Å) as evidenced by the highly elongated C–H bond (1.185(7) Å).[36] The neopentyl groups in $[W(\eta^5\text{-}C_5Me_5)(NO)(CH_2CMe_3)_2]$ **30** are each involved in an α-agostic interaction,[37] one being strong (W–H 2.233(6), C–H 1.153(6) Å, W–C–H 80.6(3)°; cf. C–H 1.070(8) Å for non-agostic methylene C–H), and the other very weak (W–H 2.582(6), C–H 1.083(7) Å, W–C–H 99.3(3)°; cf. C–H 1.094(6) Å for non-agostic methylene C–H). The structure of $[Mo(NC_6H_3Pr^i_2\text{-}2,6)_2Me_2]$ **31** provides only the second example of agostic interactions involving a methyl ligand.[38] Each methyl group is identified as having two α-agostic C–H–M interactions. The structure of $[RuCl_2\{PPh_2(2,6\text{-}Me_2C_6H_3)\}_2]$ **32** reveals δ-agostic interactions involving two C–H groups from the same methyl group on each of two xylene substituents, that is, CH_2 groups act as an electron donor instead of the more common single C–H bond (Scheme 5).[39]

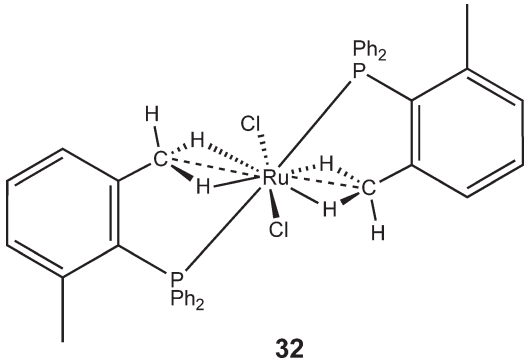

32

Scheme 5 Structure of **32**, showing δ-agostic interactions involving two CH_2 moieties.

These interactions stabilize the otherwise highly unsaturated 14-electron complex. The paper by Baratta and co-workers also examines the geometries of all interactions between methyl groups and metal centers through a survey of geometries found in the CSD for β-, γ-, δ-, and ε-agostic interactions as well as intermolecular contacts. The structures of organolanthanide complexes [Y(η^5-C_5Me_5)(OAr)CH($SiMe_3$)$_2$] (OAr = O-2,6-$C_6H_3Bu^t_2$) **33** and [La(η^5-C_5Me_5)(CH($SiMe_3$)$_2$)$_2$] **34** supported by density functional theory (DFT) calculations clearly show that β-Si–C interactions with the metal center take precedence over α-C–H or γ-C–H agostic interactions in relieving the unsaturation of the metal centers.[40] Elongation of the coordinated Si–C bonds is found, whereas no significant elongation is observed for either α-C–H or γ-C–H bonds that approach within 3.1 Å of the lanthanide metal centers.

In addition to these studies of C–H bond activation, five papers have been published in which analogous 3c-2e E–H–M interactions (E = B, Si, Sn) have been examined. The structure of the organotitaniumhydroborate $Cp_2Ti\{(\mu\text{-}H)_2\text{-}BC_8H_{14}\}$ **35** contains a Ti(μ-H)$_2$B ring, and is the first reported characterization of B–H–Ti interactions and of a Ti–H bond by neutron diffraction (Ti–H 1.90(2), 1.93(2) Å; B–H 1.33(1), 1.30(2) Å).[41] There have been three reports of compounds for which neutron diffraction was used in which potential Si–H–M interactions were investigated. [Mo(η^5-C_5Me_5)(dmpe)(H)($SiEt_2$)] **36** adopts a piano stool structure with significant Si···H interaction (1.68(1) Å) between the hydride ligand (Mo–H 1.85(1) Å) and the silylene ligand.[42] The structure of [Nb(η^5-C_5H_5)$_2$H($SiMe_2Cl$)$_2$] **37** shows that the hydride ligand (Nb–H 1.816(8) Å) lies directly between the two silyl ligands giving an Si···H separation of 2.056(3) Å (Scheme 6), which the authors interpret in terms of attractive Si···H interactions based upon supporting NMR data and DFT calculations.[43] In the closely related tantalum analog, [Ta(η^5-C_5H_5)$_2$(H)($SiMe_2H$)$_2$] **38** (Ta–H 1.79(2) Å, Si···H 2.19(2) and 2.19(2) Å), the geometry is interpreted as a simple disylyl–hydride complex with no significant Si···H interactions.[44] Finally, the compound [(η^6-C_7H_8)(μ-OH)(H)Fe{Sn[CH($SiMe_3$)$_2$]$_2$}$_2$] **39** (Scheme 7) and its isostructural cobalt analog are reported.[45] The former, characterized by neutron diffraction, exhibits an Fe–H bond length typical for a simple terminal hydride (1.575(8) Å), whereas Sn···H separations are long (2.482(9), 2.499(9) Å) and do not suggest any significant bonding interaction despite evidence to the contrary from solution-state NMR spectroscopy.

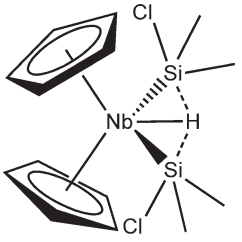

37

Scheme 6

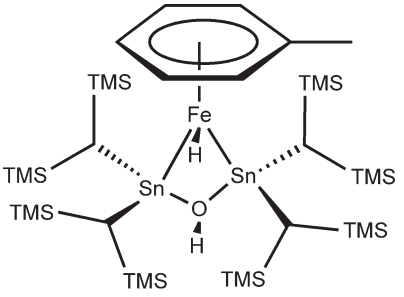

39

Scheme 7

1.21.3.6 Hydrogen Migration: Mechanism

In a series of papers, Ohashi and co-workers have used single crystal neutron diffraction to characterize the products of hydrogen(deuterium)-migration reactions that accompany isomerization of certain reactive ligands bound to bis(dimethylglyoximato)cobalt moieties upon UV irradiation, remarkably in single-crystal-to-single-crystal transformations.[46–49]

Site-selective deuteration of a cyanopropyl group enabled deuterium atom migration to be determined following isomerization from a 3-cyanopropyl to a 2-cyanopropyl ligand.[47] An analogous approach was taken to investigate inversion at the chiral carbon of coordinated 1-cyanoethyl ligands[48] and 1,2-bis(ethoxycarbony)ethyl ligands.[49] The mechanism was found to involve homolytic cleavage of the Co–C bond upon irradiation, followed by rotation of the dissociated radical and reformation of the Co–C bond. In an earlier study following irradiation of [(R)-1-cyanoethyl-*d*α][(S)-1-phenylethylamine]bis(dimethylglyoximato)cobalt(III) **40**, neutron diffraction established that partial deuterium migration from the α-carbon to the methyl group had taken place but without inversion at the chiral carbon atom.[50]

1.21.3.7 Metallocene and Metal–Arene Complexes

Two metallocene and one metal–arene complex have been studied by neutron diffraction. Brock and Fu have re-examined[51] the structural model for the high-temperature $P2_1/a$ phase of ferrocene by conducting rigid body refinements based upon the neutron data of Takasugawa and Koetzle at 173 and 298 K.[52] The rigid body model provides a better fit to the data than the original independent atom model and permits a three-site disorder description of the cyclopentadienyl rings. The study of $[U(\eta^5\text{-}C_5H_5)_3]Cl$ **41** focuses on the two phase transitions at 120 and 78 K, where the crystallographic symmetry is lowered upon reducing the temperature.[53] McMullan and colleagues investigated the structure of the $AgClO_4{\cdot}C_6H_6$ π-complex **42** at temperatures of 18, 78, and 158 K.[54] The Ag^+ ion is weakly coordinated to two of the six carbon atoms of the benzene molecule (Ag–C 2.565(1) Å at 18 K, 2.563(1) Å at 78 and 158 K).

1.21.3.8 Metal Alkyls

Evans and co-workers have reported the structure of $[Nd(AlMe_4)_3]{\cdot}0.5Al_2Me_6$ **43** in which the Nd complex is coordinated by three chelating $AlMe_4^-$ anions and remarkably each of the six bridging methyl groups adopts a trigonal-bipyramidal (five-coordinate) geometry.[55] Another remarkable study containing a metal–alkyl bond is that of vitamin B_{12} coenzyme which has been studied by neutron diffraction at 15 K.[56] Although the coenzyme structure is quite similar to that determined at 279 K by X-ray diffraction, the neutron study clearly establishes the location of the solvent water molecules and the hydrogen-bonded networks within the solvent. Single crystal X-ray and powder neutron diffraction methods have been combined to determine the structure of monomeric CH_3ReO_3 **44** and its crystal structure is found to be related to that of the polymeric form of empirical formula $\{H_{0.5}[(CH_3)_{0.92}ReO_3]_n\}$ **45**, which was established by a combination of X-ray powder diffraction and other analytical methods.[57]

1.21.3.9 Metal–Ligand Multiple Bonds

Solved from a twinned crystal, the structure of the *N*,*N*-diethylcyanamide adduct of $Cr(CO)_5$, $[Cr(CO)_5\{NCN(C_2H_5)_2\}]$ **46** was determined by neutron diffraction[58] as an initial step towards a charge density study of the bonding within the cyanamide ligand, which formally contains a sequence of double bonds $(OC)_5Cr{=}N{=}C{=}NEt_2$. Analysis of the structure shows a bond order greater than two between the N(α) and C(β), with bond orders between double and single for Cr–N and for C(β)–N(γ). The compound *trans*-[W(CH)(dmpe)$_2$Br] **47**[59] is the first methylidyne complex to be studied by neutron diffraction (here at 100 and 293 K). Although based upon data of moderately low resolution ($d > 0.88$ Å) the results unambiguously demonstrate the near linearity of the carbyne ligand (W–C–H 178.0(7)°; W≡C 1.750(12) Å, C–H 1.155(13) Å).

1.21.3.10 Compounds Containing Main Group Metal–Carbon Bonds

Table 2 provides a list of the compounds containing main group metal–carbon bonds whose structure has been determined by single crystal neutron diffraction.

Table 2 List of compounds containing s- or p-block metal–carbon bonds whose structures have been determined by single crystal neutron diffraction

Metal	*Name of the compound*	*References*	*CSD refcode*
Li, Si	Bis(μ_2-2-(bis(trimethylsilyl)methyl)pyridine-C,N) dilithium **48**	60, 61	CAWMUI12, CAWMUI13, CAWMUI15, CAWMUI16
Li, Al	(μ_6-Hydrido)hexakis(μ_4-(2-pyridyl)anilido)octalithium tetrakis(μ_2-methyl)tetra-*t*-butyl-dialuminium–lithium **49**	62	HOYNUE01 HOYNUE02
B	NH_4BPh_4 **50**	63	AMPHEB02, AMPHEB03
B	8-Dimethylamino-1-(dimethylammonio)naphthalene-10, 11-μH-7,8-dicarbanidoundecaborate(12) **51**	64	GUNHUS
B	*trans*-[Ru(η^2-H_2)(H)(dppe)$_2$]BPh_4 **4**	6	HINBOV01
B	Bis((μ_2-hydrido)dimesitylborane) **52**	65	JEBLUX01
B, Si	[U{N(SiMe$_3$)$_2$}$_2${N(SiMe$_3$)Si(Me)$_2$CH$_2$B(C$_6$F$_5$)$_3$}]·3.5C$_6$D$_6$ **53**	66	PUPMES01
B (also Ti)	$Cp_2Ti\{(\mu\text{-}H)_2BC_8H_{14}\}$ **35**	41	SUWSIM01
B (also Pt)	[(PEt$_3$)$_2$(Ph)Pt(μ-H)PtH(PEt$_3$)$_2$]BPh_4 **17**	19	WAZPUI01
B	Phenylnitronylnitroxide radical phenylboronic acid **54**	67	ZIGPAG02
Al (also Nd)	[Nd($AlMe_4$)$_3$]·0.5Al_2Me_6 **43**	55	YOSYAG01
Si	$Si(SiPr^i_3)_4$ **55**	68	COQYUC01
Si	$Si_2Pr^i_6$ **56**	68	HIDJUZ01
Si	(2-(Chlorodiisopropylsilyl)phenyl)diphenylphosphine **57**	69	EZUVOK
Si (also Y)	[Y(η^5-C_5Me_5)(OAr)CH(SiMe$_3$)$_2$] (OAr = O-2,6-C$_6$H$_3$Bu$^t_2$) **33**	40	JOPQUA
Si (also La)	[La(η^5-C_5Me_5){CH(SiMe$_3$)$_2$}$_2$] **34**	40	KADCUN01
Si (also Ta)	[Ta(η^5-C_5H_5)$_2$(H)(SiMe$_2$H)$_2$] **38**	44	KOKVOV01
Si, Sn (also Fe)	[(η^6-C_7H_8)(μ-OH)(H)Fe-{Sn[CH(SiMe$_3$)$_2$]$_2$}$_2$] **39**	45	LIMDUG
Si	(μ_2-Dinitrogen)-bis(μ_2-hydrido)-bis(phenylbis(dimethyl(phenylamino)silylmethyl) phosphino)ditantalum **58**	70	MIQDOF
Si (also Ru)	[{(η^5-C_5H_3)$_2$(SiMe$_2$)$_2$}$Ru_2(CO)_4$(μ-D)]CF_3SO_3 **20**	23	MUJQAJ
Si	(μ_2-Hydrido)-(μ_2-η^2,η^2-hydrogen-dinitrogen)-bis(2,2,6,6,8,8,12,12-octamethyl-4,10-diphenyl-1, 7-diaza-4,10-diphospha-2,6,8,12-tetrasilacyclododecane)dizirconium **59**	71	RIDJAP01
Si, Sb	(Me$_3$Si)$_2$C(H)Sb(H)Sb(H)CH(SiMe$_3$)$_2$ **60**	72	VIQVOG01
Si (also Mo)	[Mo(η^5-C_5Me_5)(dmpe)(H)(SiEt$_2$)] **36**	42	XAFZOU
Si (also Nb)	[Nb(η^5-C_5H_5)$_2$H(SiMe$_2$Cl)$_2$] **37**	43	ZEYVAA02

1.21.4 Powder Diffraction Studies

X-ray powder diffraction is widely used to establish crystallinity and phase purity of crystalline products. This is crucial in both an academic research laboratory setting and in industrial laboratories in the identification of polymorphic phases of a compound, which although having the same composition have different physical properties on account of their different crystal structures. Powder diffraction is also used to identify simple known products by matching measured powder patterns or sometimes key diffraction peaks with patterns from known compounds. Although *ab initio* structure solution from powder diffraction data has been pursued successfully by some research groups for many years, it is only since recent improvements in instrumentation, software, and greater access to high flux synchrotron X-ray sources have become available that the number of structures solved directly from X-ray powder diffraction data has begun to increase more rapidly (for some helpful reviews on *ab initio* structure determination by powder diffraction, see Refs: 73 and 73a–73c). It is important to note that molecular and intermolecular geometries determined by X-ray powder methods are generally much less precise and somewhat less accurate than those determined by single crystal diffraction studies. Typical structure refinements employ isotropic displacement parameters, and often a number of restraints or constraints are applied to molecular geometries. Neutron powder diffraction is less widely used for the same reasons that single crystal neutron diffraction studies are far fewer than corresponding X-ray studies. However, neutron powder diffraction can be vital when light atom positions are required or where isotopic distributions are needed.

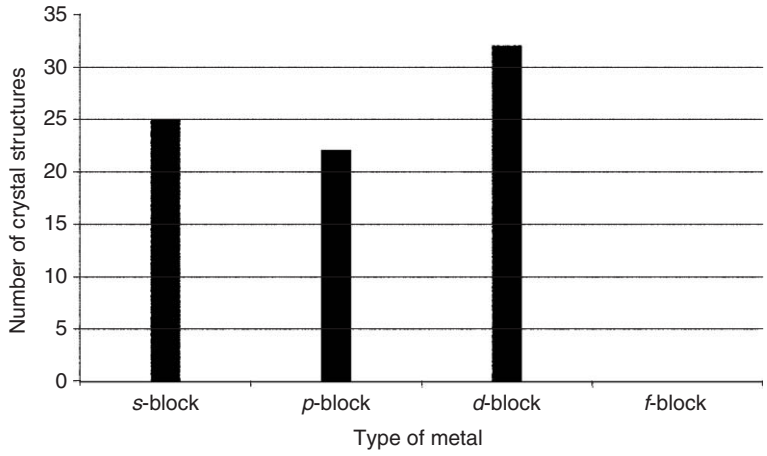

Figure 4 Distribution of powder diffraction studies by type of metal.

In the period 1993–2005, we have identified 25 powder diffraction studies of compounds containing *s*-block metal–carbon bonds, 22 for *p*-block metals including Si and B, 32 for *d*-block metals, but none for *f*-block metals (Figure 4). Structures containing bonds to carbon from *d*-block metals are organized according to the type of compound or chemical purpose of study and described briefly in Sections 4.1–4.5. Most were determined from laboratory powder X-ray data and subsequently refined using Rietveld methods. Where this is not the case, specific mention is made in the text. Structures containing *s*- and *p*-block metals are tabulated in Section 4.6 and organized by the element bound to carbon.

1.21.4.1 Catalysts and Compounds Related to Catalysis

The activity and selectivity of *fac*-$[Mo(CO)_3(Hpz)_3]$ **61** in alkyne cyclotrimerization and co-trimerization reactions have been investigated. Structure determination of **61**[74] identified the *fac*-octahedral coordination geometry (C–C and C–N bond lengths were constrained to 1.38 Å during refinement whereas M–C and C≡O bond lengths were restrained to 2.00 and 1.15 Å, respectively). Molecules are linked in the solid state via a number of N–H···O hydrogen bonds. Efforts to prepare late transition metal fluorides for comparison with catalytically active halide compounds and to examine the potential for homogeneous catalysts for metal-catalyzed fluorination reactions led to the reaction of $[Rh(\mu\text{-OH})(cod)]_2$ with 73% aqueous HF and initial assignment of the reaction product in the absence of diffraction data as polymer $[Rh(\mu\text{-F})(cod)]_n$. However, structure determination from laboratory X-ray powder diffraction data has enabled the compound to be correctly assigned as the novel salt $[Rh_3(\mu_3\text{-OH})_2(cod)_3](HF_2)$ **62** (Scheme 8) which forms a hydrogen-bonded polymer via μ_3-OH···F–H–F···HO(μ_3) chains of strong hydrogen bonds (Figure 5).[75]

Transition metal alkoxycarbonyl compounds are key intermediates in a number of metal-catalyzed processes involving alkanols and carbon monoxide. The square-planar palladium(II) complex, $[Pd(phen)(CO_2CH_3)_2]$ **63**, was determined in this context.[76] A compound isolated as a plausible intermediate in the catalytic reductive carbonylation of nitrobenzene (viz. $PhNO_2 + 3CO \rightarrow PhNCO + 2CO_2$) using palladium–phen-based catalysts was established by

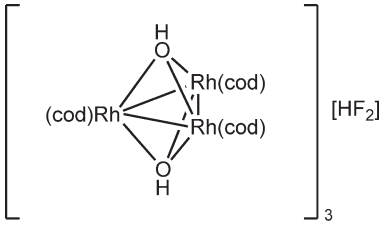

62

Scheme 8

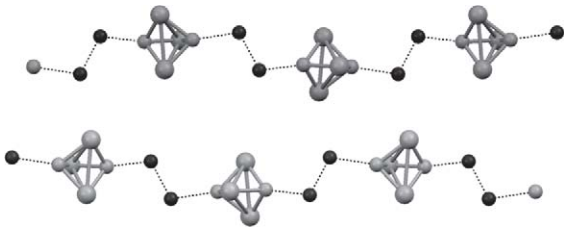

Figure 5 OH···F–H–F···HO hydrogen-bonded chains in crystal structure of compound **62**.

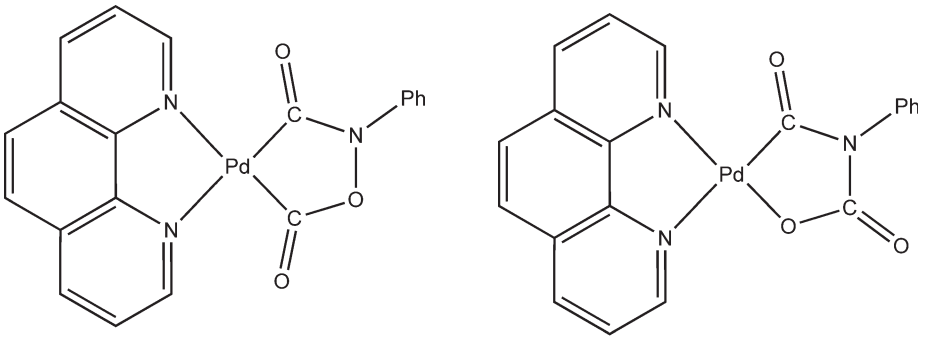

Scheme 9 (a) Correct structure of intermediate and (b) alternative proposed structure.

spectroscopic studies to be one of two isomers (Scheme 9). Although single crystals were not available, structure solution from powder data coupled with packing energy calculations permitted the ambiguity to be resolved. To simplify the powder diffraction analysis, the methyl homolog was used having first established that its spectroscopic characteristics were in accord with the original phenyl derivative. The compound [Pd(Phen)(C(O)N(Me)OC(O))] **64** was then successfully structurally characterized.[77]

1.21.4.2 Organometallic Polymers

Crystal structures of four organometallic polymers and a cyclic oligomer each containing transition metal atoms in the polymer backbone have been established using powder diffraction methods. The modified ferrocene polymer $\{[(C_5H_4BMe_2)_2Fe](4,4'\text{-bipy})\}_n$ **65** is propagated via N–B donor–acceptor bonds.[78] Its structure was determined using a model based on three translational and three orientational degrees of freedom combined with five variable torsion angles. All other structure parameters were constrained to typical literature values. Metal–metal bonds propagate the first structurally characterized example of a polymeric binary metal carbonyl compound, $[(Ru(CO)_4]_n$ **66**,[79] which was found to adopt a staggered conformation of carbonyl groups arranged in a square-planar manner about each Ru center (Figure 6). The Ru–Ru bond length was determined as 2.860(1) Å. Powder diffraction has also been

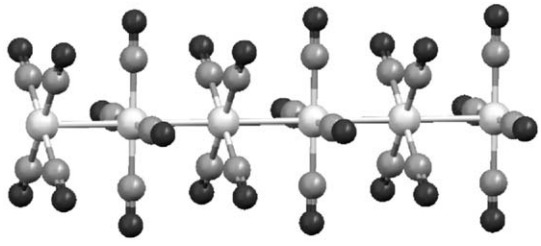

Figure 6 Molecular structure of compound **66**.

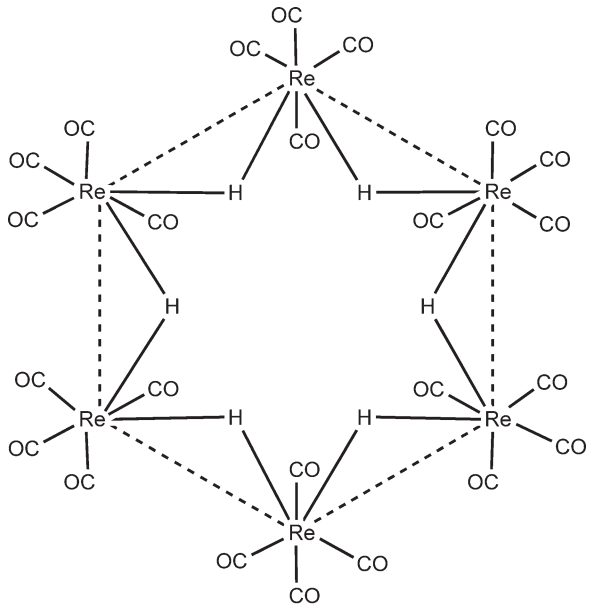

72

Scheme 10

used to establish the polymeric nature of a series of compounds of empirical formula $[Ru(L–L)(CO)_2]$ (L–L = phen **67**, 2,2′-bipy **68**, dmbpy **69**).[80] Each was prepared by electrocrystallization using controlled reduction of the corresponding $[Ru(L–L)(CO)_2Cl_2]Cl$ salt. Although powder patterns are very poor, models based on the previously established polymeric structure of **66** could be used to confirm the similar metal–metal-bonded polymeric structures of **67**–**69**. It is suggested that the poor-quality diffraction patterns arise from a random arrangement of monomers staggered by 45° or 135° along the chain and propagated by Ru–Ru bonds of length ca. 2.95 Å.

Using synchrotron radiation, the structure of $[Ru_2\{\mu_2{:}\mu_2\text{-}O_2PMe_2\}_2(CO)_4]_n$ **70**,[81] a polymer propagated via the dimethylphosphinate linkages between ruthenium centers, was determined at temperatures of 295 and 50 K. The phase transition between these phases lies around 220 K. The rhenium-containing polymer $[Re(\mu\text{-}H)(CO)_4]_n$ **71** and an analogous six-membered cyclic oligomer of $[Re(\mu\text{-}H)(CO)_4]_6$ **72** (Scheme 10) have been characterized and are described in terms of their isolobal analogy to polyethylene and cyclochexane, respectively.[82]

1.21.4.3 Metallocenes, Alkene, Alkyne, Acetylide, and Aryl Complexes

In addition to the polymeric material **65**, a number of other ferrocenyl compounds were characterized by X-ray powder diffraction. Tetraferrocenyl-[3]-cumulene, $(Fc)_2C{=}C{=}C{=}C(Fc)_2$ **73**, is one of a series of cumulene compounds prepared out of interest in molecular electronics and non-linear optics, where the role of the ferrocenyl groups is as redox active groups, electron donors, and steric protecting groups. Although the corresponding tetraferrocenyl-[*n*]-cumulenes ($n = 1$, 2, 4) could be characterized by single crystal diffraction, suitable crystals of **73** could not be obtained. The synchrotron X-ray powder diffraction study of **73** shows it to be disordered over two equally populated orientations.[83] Unusually, the ferrocenyl groups are in a *syn*-configuration (Scheme 11) rather than the up–down arrangement observed for related cumulenes. This is a rare example in which disorder has been satisfactorily modeled in a compound of this complexity using X-ray powder diffraction. The high quality of the synchrotron X-ray data is clearly important in the success of this structure determination. Also characterized using synchrotron data collected at NSLS, Brookhaven National Laboratory is the redox-active ferrocene-containing macrocycle **74** (Scheme 12), whose synthesis takes advantage of the facile formation of B–O and B–N bonds.[84] In this case, powder diffraction data alone were insufficient, but in combination with DFT calculations the structure was determined.

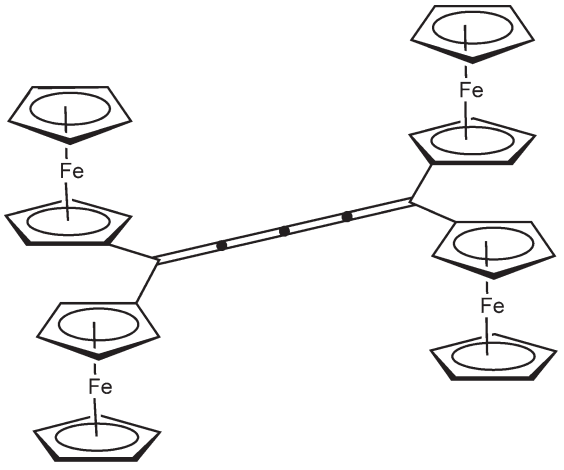

73

Scheme 11

Inclusion complexes in which inorganic framework materials incorporate metallocenes have been reported where structure solution from powder diffraction data has permitted not only characterization of the framework but also the location of the metallocene guest to be established. The structure of the silicate mineral fluoride dodecasil 1H (FDOH), serving as a host for [Co(η^5-$C_5H_4Me)_2$] **75**, was determined despite the availability of laboratory powder diffraction data of rather poor quality that permitted modeling of only the cage (based upon an earlier structure determination) and location of the cobalt atoms.[85] A starting model for Rietveld refinement of the carbon atoms was determined using a specifically parametrized force field calculation, which had previously been tested and refined using well-known structures of cobaltacene inclusion compounds of a similar type to **75**. The included [Co(η^5-$C_5H_4Me)_2$] adopts sixfold disorder within the cage, and its successful refinement even led to an improved model for the framework (Figure 7). The high-silicon zeolite, UTD-1, was the first of a new class of large pore zeolites obtained using [Cp^*_2Co]OH as the structure directing agent. Initial structural charaterization of the calcined product showed disorder in the framework. Thereafter, crystal growth in a fluoride medium was undertaken with a view to improving crystal quality based upon literature precedents. The structure of the resultant zeolite, UTD-1F, containing $[Cp^*_2Co]^+$ guests **76** has been determined[86] from synchrotron powder X-ray diffraction data obtained at ESRF, Grenoble, and is one of the largest structures to be determined *ab initio* by this method (69 independent non-hydrogen atoms). Remarkably, both the framework and the cobalticinium guests are ordered, with the organometallic guests situated in the 14-ring channels (Figure 8).

Martin and co-workers have reported the crystal structures of three adducts of ethylene with $CuAlCl_4$, namely, α-$(C_2H_4)CuAlCl_4$ **77**, β-$(C_2H_4)CuAlCl_4$ **78**, and $(C_2H_4)_2CuAlCl_4$ **79**.[87] The compounds have been further characterized by spectroscopic methods including solid-state NMR spectroscopy. The ethylene ligands coordinate to the Cu(I) center primarily through σ-donation. Structures of **78** and **79** were determined by single crystal diffraction methods, and a model has been proposed for **77** based on a partial structure solution from powder data. Coupled with spectroscopic studies, synchrotron powder diffraction studies of $CuAlCl_4$ under a pressure of C_2H_4 have been used to monitor and understand the sorption, desorption, and reversible binding of ethylene, and has provided mechanistic information (Scheme 13). Other alkene compounds discussed in Section 1.21.4 are cyclooctadiene complexes **62** (*vide supra*) and **87** (*vide infra*). A copper(I) alkyne complex has also been characterized by powder methods. Two polymorphic forms of Rb[$CuCl_2$(η^2-$HOCH_2C{\equiv}CCH_2OH$)] **80** are reported[88] and each shows η^2-alkyne coordination with a markedly bent alkyne geometry (C≡C–C 161–164°). Ruschewitz and co-workers have also reported a series of three tetrahedrally coordinated tetrakis(acetylide) complexes prepared under liquid ammonia conditions, $Rb_2[Zn(C_2H)_4]$ **81**, $Rb_2[Cd(C_2H)_4]$ **82**, and $Cs_2[Cd(C_2H)_4]$ **83**,[89] which are isostructural with the corresponding potassium salts, and the trigonal tris(acetylides) $[Ca(NH_3)_6][Cu(C_2H)_3]$ **84** and $Rb_2[Cu(C_2H)_3]{\cdot}NH_3$ **85**.[90] The crystal packing of a series of racket-shaped molecules, PhMX (M = metal, X = Cl, Br, I), has been examined, establishing that of the two packing arrangements one promotes crystal growth, whereas the other leads to a microcrystalline product. The crystal structure of the PhHgCl **86** determined from X-ray powder diffraction is reported.[91]

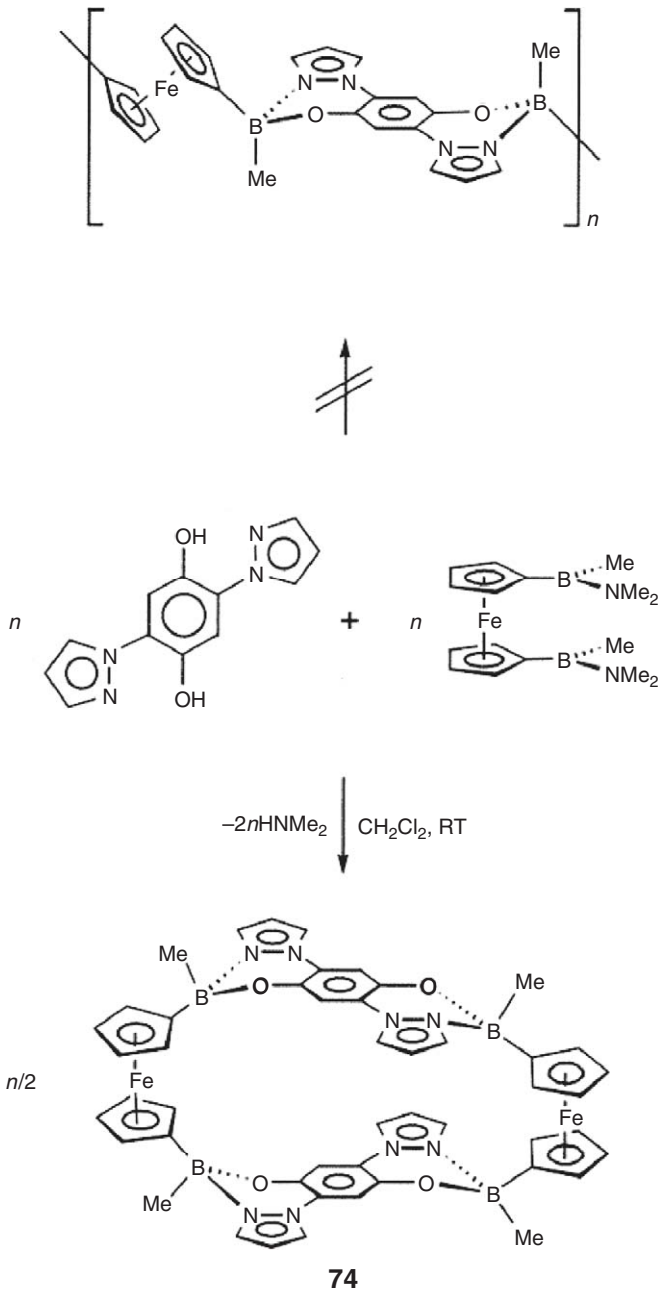

74

Scheme 12

1.21.4.4 Models for Reaction Intermediates

The crystal structure of $[(OC)_2Rh(\mu\text{-}Cl)_2Rh(cod)]$ **87** has been determined[92] as a model for the elusive intermediate $[(OC)_2Rh(\mu\text{-}OSiPh_3)_2Rh(cod)]$ in the conversion of $[(cod)Rh(\mu\text{-}OSiPh_3)_2Rh(cod)]$ into $[(OC)_2Rh(\mu\text{-}OSiPh_3)_2Rh(CO)_2]$. Both Rh centers in **87** adopt square-planar coordination geometries and are linked via the non-planar Rh_2Cl_2 core (Rh···Rh 3.252(7) Å). Close contacts with neighboring molecules occur via the less bulky $Rh(CO)_2$ ends of the molecules (Rh···Rh 3.55(1) Å). Ketonyl metal complexes are proposed as intermediates in numerous organic transformations. The structure of $K[Pt_2\{CH_2C(O)Me\}_6(\mu\text{-}Cl)_3]$ **88** was thus determined[93] as the first fully characterized acetonyl Pt(IV) complex and is unusual in being prepared from a combined normal and redox transmetallation reaction using an organomercury reagent.

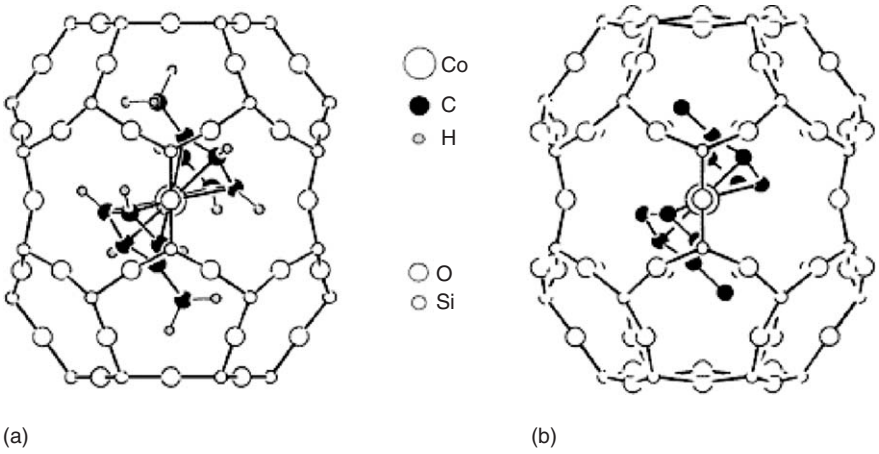

Figure 7 Cage of F-DOH showing (a) model for $[Co(\eta^5\text{-}C_5H_4Me)_2]$ determined by force field calculations and (b) one of six orientations for $[Co(\eta^5\text{-}C_5H_4Me)_2]$ determined from Rietveld refinement. Reproduced from Schneider, A. M.; Behrens, P. *Chem. Mater.* **1998**, *10*, 679–681 with permission of the American Chemical Society.

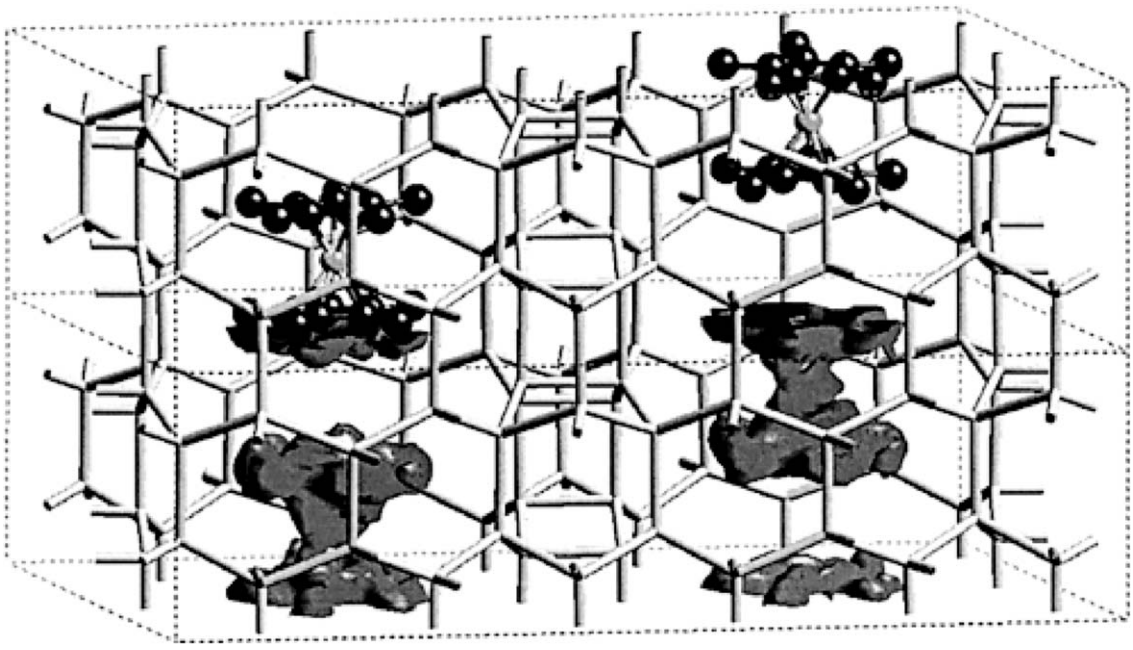

Figure 8 Arrangement of the $[(Cp^*)_2Co]^+$ guests in the 14-ring channels of UTD-1F showing electron density difference map for the cation carbon atoms in the lower unit cell and the final refined model for the cation in the upper unit cell. Reproduced from Wessels, T.; Baerlocher, C.; McCusker, L. B.; Creyghton, E. J. *J. Am. Chem. Soc.* **1999**, *121*, 6242–6247 with permission of the American Chemical Society.

1.21.4.5 Neutron Powder Diffraction

An earlier single crystal X-ray diffraction provided an accurate determination of the non-hydrogen atom positions in the tetrahedral cluster hydride complex $[Re_4(\mu_3\text{-}H)_4(CO)_{12}]\cdot 2C_6D_6$ **89**, but necessarily with much less accurate determinations of hydrogen atom positions.[94] Time-of-flight neutron powder data was then used to provide accurate location of hydrogen (and deuterium) atoms, and a combined refinement of the complete structure based upon simultaneous use of both sets of diffraction data was employed.[95]

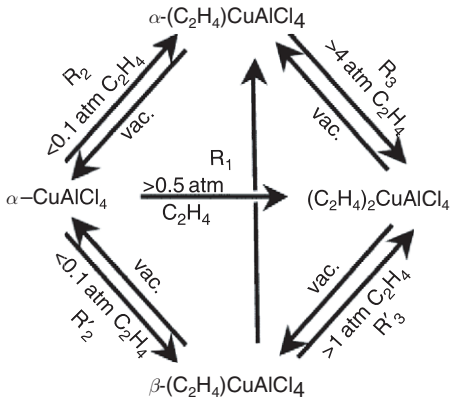

Scheme 13 Reproduced from Sullivan, R. M.; Liu, H.; Smith, D. S.; Hanson, J. C.; Osterhout, D.; Ciraolo, M.; Grey, C. P.; Martin, J. D. *J. Am. Chem. Soc*. **2003**, *125*, 11065–11079 with permission of the American Chemical Society.

Distances (Re–H 1.99(2) Å) and angles (Re–H–Re 94(1)°) involving the hydride ligands are not only determined more accurately but also with considerably greater precision (cf. Re–H 1.88(12) Å from single crystal X-ray diffraction alone). As noted in Section 3.8, an analogous approach has been used to determine the structure of monomeric CH_3ReO_3 **44**.[57]

1.21.4.6 Compounds Containing Main Group Metal–Carbon Bonds

Table 3 provides a list of the compounds containing main group metal–carbon bonds whose structure has been determined by powder diffraction.

1.21.5 Charge Denisty Studies

In an X-ray crystal structure determination, the electron density distribution in the crystal is modeled using a rather simple model based upon spherical free-atom densities for all atoms, modified only by refinement of anisotropic displacement parameters for non-hydrogen atoms. This approach, while highly successful in determining molecular and intermolecular geometries with good accuracy and precision, provides no information on more detailed aspects of the electron density distribution. Notably, the electron density associated with all atoms has marked asphericity due to perturbation of their valence electron shells arising from intramolecular, and to a lesser extent intermolecular, bonding. In charge density analyses, the aim is to provide a more accurate model for the electron density and thus derive valuable information about chemical bonding in the crystal. The charge density approach still involves an atom-centered model, but a more complex one, for the electron density. Core electrons are still treated as making a spherically symmetric contribution to the electron density about the atom. However, the valance shell electron density is modeled using parameters that describe the asphericity as a sum of spherical harmonic functions, the contribution of each being refined as part of the crystallographic least-squares model. The radial description of the valance charge density is also determined. In order for charge density models to be refined successfully, X-ray data measured to much higher resolution than for a structure determination is required (typically $d_{\min} < 0.5$ Å), and high redundancy of data is required for accurate and precise determination of X-ray intensities. Data are collected at low temperatures, most commonly at 100–150 K but increasingly at much lower temperatures as helium cryostats become more readily available, to reduce atomic motions and improve accuracy and deconvolution of the charge density from the atomic motions. Careful correction for systematic errors such as absorption or extinction is also crucial. Where hydrogen atoms are involved, it is helpful to be able to accurately determine the hydrogen atom positions and to describe the atomic displacements. This can be accomplished by a parallel neutron diffraction experiment.

In early experimental studies predominantly in the 1970s and 1980s, so-called deformation electron density studies were typically conducted. Thus, the electron density is modeled using the approach described above, and the electron density of a promolecule (procrystal), constructed by placing spherical free atoms densities at all atomic centers, is subtracted from the fully modeled density. The difference then shows the redistribution of electron density that arises due to chemical bond formation. This approach readily shows electron density buildup in the center of most covalent

Table 3 List of compounds containing s- or p-block metal–carbon bonds whose structures have been determined by powder diffraction

Metal	*Name of compound*	*References*	*CSD refcode*
Li	*catena*-($(\mu_2$-η^5,η^5-$C_5H_5)$Li) **90**	96	NIBSEW
Li	*catena*-($(\eta^5$-$C_5Me_5)$Li) **91**	97	SUWHEX
Li	*catena*-($(\mu_2$-η^5,η^5-Indenyl)lithium) **92**	98	XACROI
Na	*catena*-($(\mu_2$-η^5,η^5-$C_5H_5)$Na) **93**	98	NIBSIA
Na	*catena*-($(\mu_2$-η^5,η^5-$C_5Me_5)$Na) **94**	99	UCUKOS
Na	Disodium tris(9-fluenyl)sodium **95**	98	XACRUO
K	*catena*-($(\mu_3$-η^6,η^2-O-hydroxyphenolato) potassium) **96**	100	EVAVOM
K	*catena*-($(\mu_2$-η^5,η^5-$C_5H_5)$K) **97**	96,101	NIBSOG, NIBSOG01, NIBSOG02, NIBSOG03, NIBSOG04, NIBSOG05, NIBSOG06, NIBSOG07, NIBSOG08, NIBSOG09, NIBSOG10
Rb (also Zn)	Dirubidium *catena*-[$Zn(C_2H)_4$] **81**	89	ETUGIJ
Rb (also Cd)	Dirubidium *catena*-[$Cd(C_2H)_4$] **82**	89	ETUGOP
Rb	*catena*-($(\mu_3$-η^6,η^2-*O*-hydroxyphenolato) rubidium) **98**	100	EVAVUS
Rb	*catena*-($(\mu_2$-η^5,η^5-$C_5H_5)$Rb) **99**	102	TIQKEJ, TIQKEJ01
Cs (also Cd)	Dicesium *catena*-[$Cd(C_2H)_4$] **83**	89	ETUGEF
Cs	*catena*-($(\mu_2$-η^5,η^5-$C_5H_5)$Cs) **100**	103	RAVHUR
B	$(CH_2CH_2O)_{8n}\cdot n$$NaBPh_4$ **101**	104	EROCUJ
B (also Fe)	Bis(μ_2-η^5,η^5-ferrocenylene)bis(μ_2-2,5-bis (pyrazol-1-yl)benzene-1,4-diolato) tetrakis(methylboron) **74**	84	PUXYAI
B (also Fe)	*catena*-($(\mu_2$-*N*,*N*′-Bis($(\eta^5$–cyclopentadienyl)(dimethyl)boryl)-4, 4′-bipyridine)iron) **65**	78	QINGEZ
Al	H_3NAlMe_3 **102**	105	LINZOX
Al	*cyclo*-$(H_2NAlMe_2)_3$ **103**	106	SAJCUB01
Al	$Al_2(\mu$-$CD_3)_2(CD_3)_4$ **104**	107	TRMEAL03
Si	*catena*-Rh(μ-$O_2CCF_3)_4$Rh ($NC_5H_4SiPh_2C_5H_4N$) **105**	108	FELVEY
Si	$Si(SiMe_3)_3Bu^t$ **106**	109	HUSQAN, HUSQAN01
Si	$Si(SiMe_3)_2Bu^t_2$ **107**	109	HUSQIV, HUSQIV01
Si	2,5-Bis(trimethylsilyl)thiophene-*S*, *S*-dioxide **108**	110	QEZXOI01
Si	Tribenzylsilanol **109**	111	WEKRUZ
Si	$Si(SiMe_3)_4$ **110**	112	GUFMOJ, GUFMOJ01
Si	$C(SiMe_3)_4$ **111**	113	ZZZWNG01, ZZZWNG02, ZZZWNG03
Sn	$Si(SnMe_3)_4$ **112**	114	MEZDIE, MEZDIE01
Sn	$Ge(SnMe_3)_4$ **113**	114	MEZDOK, MEZDOK01

bonds and indicates the location of lone pairs of electrons. Over the past decade, most studies have begun to adopt the approach based on Richard Bader's quantum theory of atoms in molecules (QTAM or AIM).[115] Using this approach, the topology of the total electron density is analyzed and evaluated in terms of critical points (maxima, minima, and saddle points) in the electron density. Similar analyses of the Laplacian (2nd derivative or curvature) of the electron density can also provide valuable insight. This quantitative approach, originally developed for theoretical studies of the charge density, provides valuable benchmarks for different types of intra- and intermolecular interaction. However, organometallic compounds with many soft interactions can prove to be a considerable challenge to understand and quantify by this approach, and studies of this type will be at the cutting edge for some time to come.

A number of reviews on experimental charge density analysis have been published over the years,[116,116a–117a] some focusing specifically[117,117a] or containing substantial sections[116b] on organometallic compounds. More details on experimental methodology and the theoretical basis for charge density studies can be found in these sources. The following sections contain a survey of *d*-block metal organometallic compounds that have been studied by charge density analysis in the period 1993–2005.

1.21.5.1 Unsupported Metal–Metal Bonds

Some of the earliest charge density studies of organometallic compounds were conducted on simple dinuclear complexes, for which metal–metal bonding was one of the major aspects of the investigation.[118] Such investigations were deformation density studies, but the typical observation of very low deformation density along the metal–metal vector or indeed its absence entirely raised concerns about the interpretation of metal–metal bonding. A number of studies reported since 1997 as part of a resurgence in charge density studies coinciding with the development of CCD area detectors for X-ray diffraction have readdressed this issue. In some cases, redetermination of the charge density of compounds studied earlier has been undertaken. A case in point is the two recent studies of $[Mn_2(CO)_{10}]$ **114**,[119,119a,119b] which contains an unsupported metal–metal bond. In the study by Bianchi *et al.*[119,119a] at 120 K, modern QTAM methods were used to analyze the topology of the charge density. A bond path between the two Mn centers was observed with a bond critical point (bcp) at which the electron density had a value of 0.190(4) eÅ^{-3} indicating a direct bonding interaction between the metal centers. The authors interpreted the positive Laplacian value and negative energy density at the bcp in terms of a closed shell, that is, not shared (covalent), interaction between the two metals. The subsequent study by Farrugia and co-workers[119b] at 100 K showed good agreement between topological values of the charge density and those of the aforementioned study. The authors argue that the Mn–Mn bond is a shared (covalent) interaction on the basis of the negative energy density and that integration of the electron density over the interface between the two atoms (atomic basins) is perhaps a better indicator of the bonding interaction. In addition, the atomic graph (i.e., the charge concentration distribution) around Mn is very similar to that of *cis*-$HMn(CO)_4PPh_3$ **13** (*vide infra*) favoring a covalent description of Mn–Mn bonding. Qualitatively similar properties of the bcp on the Co–Co bond path were observed in $[Co_2(CO)_6(AsPh_3)_2]$ **115**.[120] However, Macchi and co-workers have questioned the routine interpretation of this interaction as a closed shell interaction. Using an improved analysis of the Laplacian at the bcp led them to an interpretation of the Co–Co bond as a shared interaction, in contrast to metal–ligand donor–acceptor interactions Co–As and Co–C. This study highlights the continued difficulty but improving methodology in interpreting the nature of bonding in metal complexes by charge density methods.

1.21.5.2 Bridged Metal–Metal Bonds

Two compounds with bridging carbonyls ligands, $[Co_2(\mu\text{-}C_4O_2H_2)(\mu\text{-}CO)(CO)_6]$($C_4O_2H_2$=5-oxofuran-2(5*H*)-ylidene) **116**[121,121a] and $[Co_4(\mu\text{-}CO)_3(CO)_8(PPh_3)]$ **117**,[122] and one with a semi-bridging carbonyl ligand, [PPN][$FeCo(CO)_8$] **118**,[123] have been studied. The Co–Co bond length in **116** is intermediate in length between $[Co_2(\mu\text{-}CO)_2(CO)_6]$ (2.37 Å) and $[Co_2(\eta^5\text{-}C_5H_5)_2(\mu\text{-}NO)_2]$ (2.53 Å), for both of which there has been ambiguity in both resulting from calculated electron densities regarding whether there is a direct Co–Co bond or whether bonding between the metals occurs via the bridging ligands. Two polymorphic forms of **116** have been studied. In the orthorhombic form, studied at 150 K, a direct Co–Co bond path is present, and the electron density at the bcp (0.76(6) eÅ^{-3}) exceeds that in **114** (Co–Co bond length 2.4222(3) Å). The topology of the electron density for the terminal CO ligands closely resembles those in $[Mn_2(CO)_{10}]$. C–H···O hydrogen bonds between molecules are also identified based upon the characteristics of the electron density. The study, at 120 K, of the triclinic form of **116** indicates that a slightly longer Co–Co bond (2.4402(2) Å) is associated with a slightly smaller electron density at the bcp (0.46(2) eÅ^{-3}). Overall, there is good agreement between the two polymorphic forms for charge density properties of all bonds and even for weak intermolecular interactions. $[Co_4(\mu\text{-}CO)_3(CO)_8(PPh_3)]$ **117** is a tetrahedral cluster compound analogous to $[Co_4(CO)_{12}]$, with three basal Co–Co bonds bridged by carbonyl ligands. The parent compound, however, is crystallographically unsuitable for a charge density study. The study of **117** permits comparison of bridged and unbridged Co–Co bonds. The latter exhibit bcp's indicative of a direct Co–Co interaction, whereas no bcp was observed for the carbonyl-bridged Co–Co bonds in basal plane of cluster. Metal–metal bonding in the basal plane of the cluster is therefore interpreted as being indirect, occurring via the bridging CO ligands. These interactions can be viewed as 3c-4e Co–C–Co bonds.

In their analysis of the charge density distribution in [PPN][$FeCo(CO)_8$] **118**, Macchi and co-workers have taken the opportunity not only to study a compound with a semi-bridging carbonyl ligand but also to examine the pathway for carbonyl ligand migration between two metal centers in terms of the charge density and derived bonding information. In geometric terms, this pathway can be examined using the collective data on bridging and terminal carbonyl compounds available in the CSD. Application of the structure correlation approach of Bürgi and Dunitz[124] is illustrated in Figure 9, and it demonstrates that there is smooth geometrical progression from terminal to semi-bridging to bridging and through the reverse sequence to terminal once more, completing the transfer of the ligand

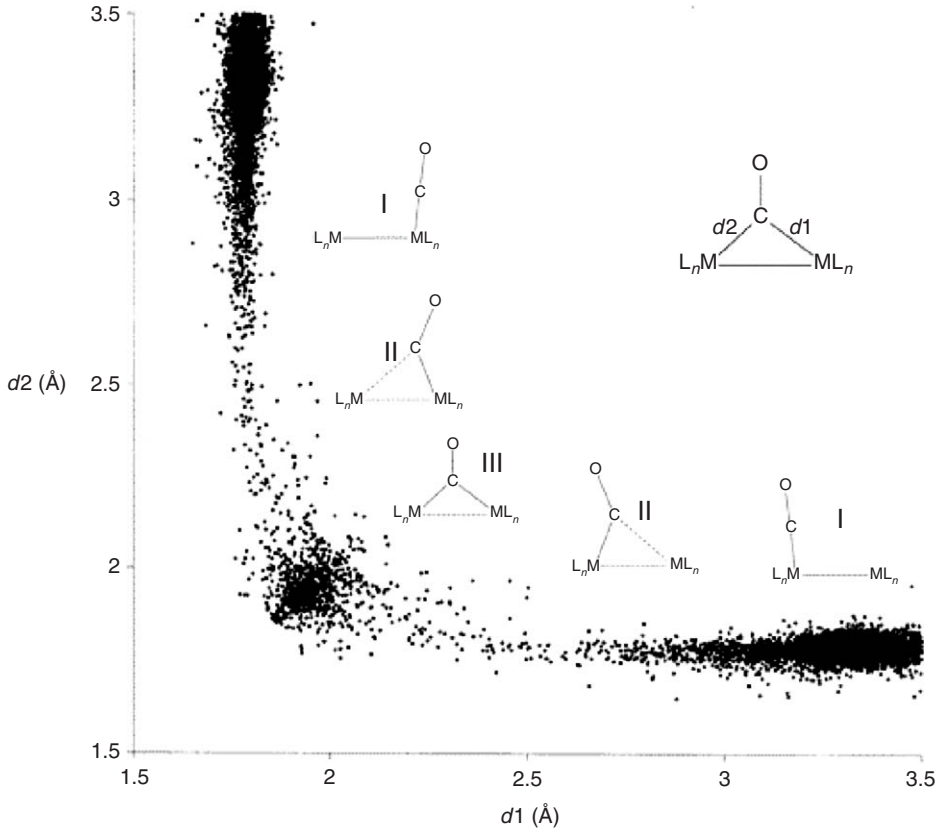

Figure 9 Structure correlation plot for the fragment M(CO)M (M = Fe, Co, Ni); each fragment retrieved from the CSD contributes to two (symmetrically related) points in configurational space. Reproduced from Macchi, P.; Garlaschelli, L.; Sironi, A. *J. Am. Chem. Soc.* **2002**, *124*, 14173–14184 with permission of the American Chemical Society. (An analogous plot was first presented by Orpen.[124]

from one metal center to another. Figure 10 shows the key features of the charge density distribution associated with the semi-bridging carbonyl region in **118**. In particular, the concentration of charge density can be seen in Figure 10(c) in the regions of the carbonyl lone pairs, and the absence of such concentration is apparent along the Co–Fe vector. A curved bond path is noted for the Fe–C interaction. The transfer of a carbonyl ligand between metal centers is examined by comparison of the electron density distribution in **118** with the terminal carbonyl ligands in **115** and the symmetrically bridging ligands found in **117** (Figure 11).

The smooth geometric transition from terminal to semi-bridging to bridging carbonyl ligand is reflected in direct interplay of M–M and M–CO bonding and indirect M···M and M···C characterized in terms of newly proposed indirect interaction indices derived from the charge density distribution. As in most of the experimental charge density studies discussed in Section 1.21.5, studies on comparative theoretical calculations of the charge density have been conducted. In this case, DFT calculations on a number of $[M_2(CO)_n]$ dimers allow a conceptual framework and quantitative evaluation of the changes in electron density distribution and thus bonding that occurs upon the change in bonding mode of a carbonyl ligand upon transfer between metal centers.

1.21.5.3 Metal Hydrides and Agostic Interactions

Two metal hydride complexes and two systems in which agostic interactions were a major focus of the study have been examined by experimental charge density analysis. The experimental charge density study of *cis*-$HMn(CO)_4PPh_3$ **13**[15] was first reported for a metal hydride compound. (Three earlier studies have been noted in a review article ($H_3Ru_3(CCl)(CO)_9$[125]) or in conference abstracts ($HMoCp(CO)_3$[13] and $HMn(CO)_5$[125a]), but not reported in full in the literature; for further details see Refs: 125 and 125a.) The geometry of this compound was

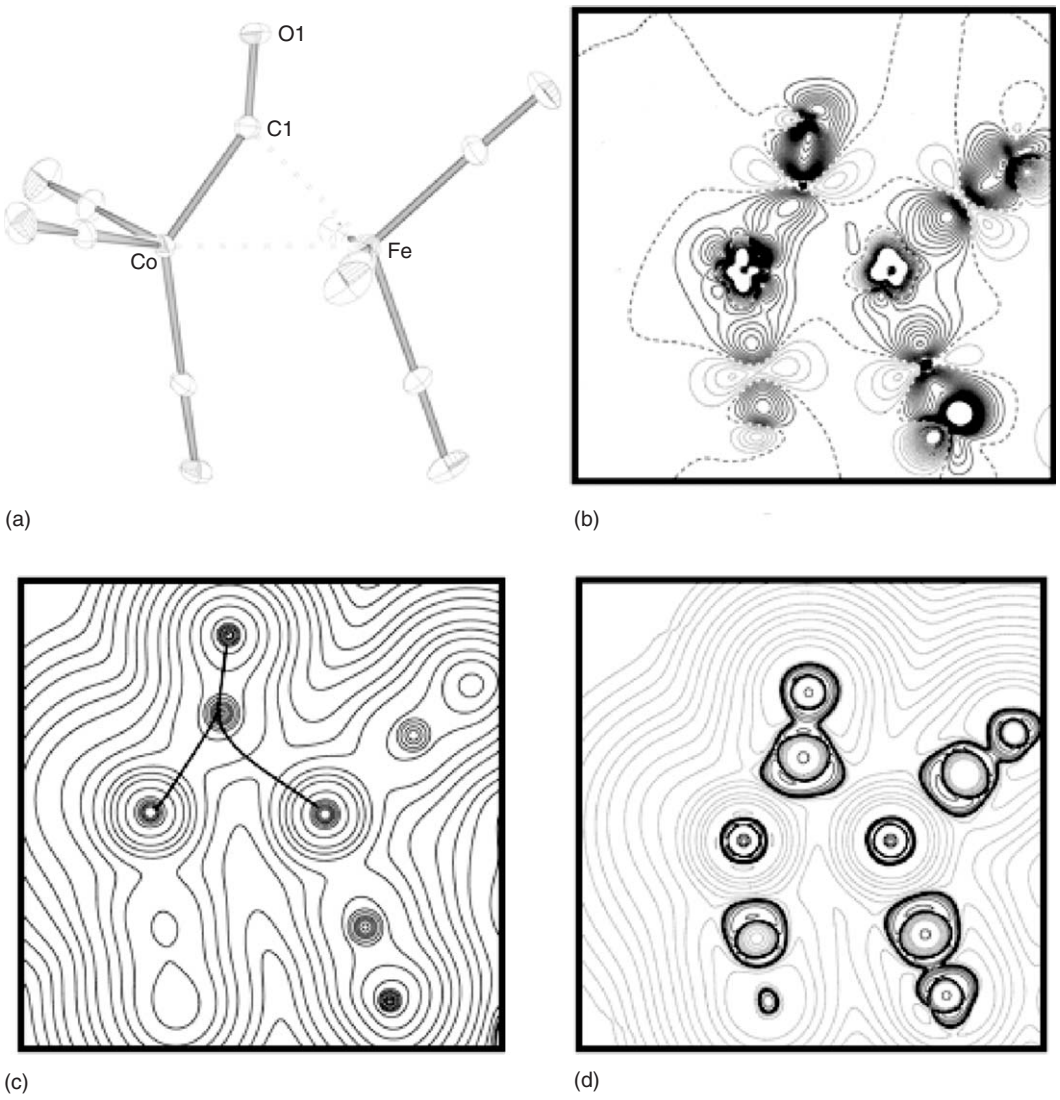

Figure 10 (a) Molecular structure of **118** shown with displacement ellipsoids of 50% probability; (b) deformation density plot (positive contours as solid lines, negative contours dashed lines; contour interval 0.05 eÅ^{-3}); (c) total electron density (exponential contours) with Co–C, Fe–C, and C–O bond paths shown; (d) Laplacian of the electron density, $\nabla^2\rho$, (exponential contours; negative contours as solid lines, positive contours as dashed lines). Reproduced from Macchi, P.; Garlaschelli, L.; Sironi, A. *J. Am. Chem. Soc.* **2002**, *124*, 14173–14184 with permission of the American Chemical Society.

discussed based on its neutron structure (Figure 12) in Section 3.2. Topological analysis of the charge density distribution and its Laplacian provides clear evidence for the expected σ-donor nature of hydride and phosphine ligands and the σ-donor/π-acceptor nature of the CO ligands, and shows the reduction in bond order for the CO ligands relative to free CO. Analysis of Mn *d*-orbital populations, derived from the populations of the Mn-centered spherical harmonic functions used to model its charge density, shows that these are higher than would be expected for a simple crystal field model, consistent with a degree of covalency in the M–L bonding. The C–H$\cdots$H–Mn dihydrogen bond (H$\cdots$H 2.101(3) Å) has been clearly identified from the charge density distribution as an interaction between the nucleophilic hydride ligand (monopole charge -0.4 e) and an electrophilic *ortho*-hydrogen atom (monopole charge $+0.3$ e) from the PPh_3 ligand. The H$\cdots$H bond path exhibits a bcp with very small electron density [0.066(5) eÅ^{-3}], as might be anticipated. The experimental charge density was also used to estimate the electrostatic component of the interaction energy as 5.7 kcal mol^{-1}, although it is noted that the total energy is expected to be less than this due to penetration and short-range repulsion effects.[126]

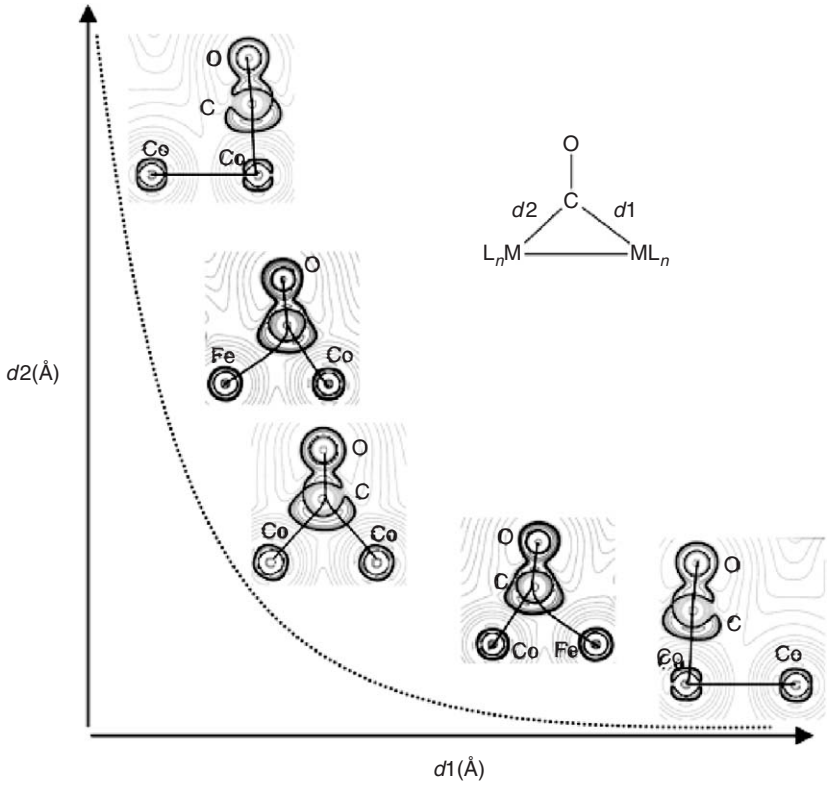

Figure 11 Same conformational space plot for Figure 9 shown here with $\nabla^2\rho$ distributions for unsupported, semi-bridged, and symmetrically bridged M–M bonds from **115**, **118**, and **117**, respectively. Reproduced from Macchi, P.; Garlaschelli, L.; Sironi, A. *J. Am. Chem. Soc.* **2002**, *124*, 14173–14184 with permission of the American Chemical Society.

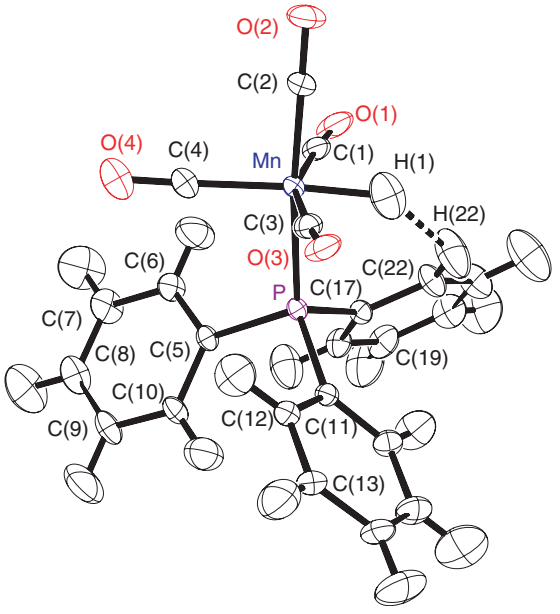

Figure 12 Molecular structure of **13** from the neutron diffraction study, showing the C–H···H–Mn dihydrogen bond. Reproduced from Abramov, Yu. A.; Brammer, L.; Klooster, W. T.; Bullock, R. M. *Inorg. Chem.* **1998**, *37*, 6317–6328 with permission of the American Chemical Society.

Using coordinates and displacement parameters from a prior neutron diffraction study at 20 K,[127] the charge density distribution of [K(crypt-222)][$Cr_2(\mu$-$H(CO)_{10}$] **119** has been determined from extensive X-ray diffraction data measured at 28 K.[128] Cr–H bond paths that are outwardly curved at the metal centers suggest an open rather than closed Cr–H–Cr bond, in contrast to the geometric designation of such bonds as closed. This observation also contrasts with the inwardly curved M–C bond paths for symmetrically bridging carbonyl ligands. A lower electron density at the bcp in each Cr–H bond (0.479(8), 0.446(8) eÅ^{-3}) is indicative of these bonds being weaker than terminal M–H bonds (e.g., ρ 0.65(2) eÅ^{-3} at bcp for **13**). DFT calculations of charge density are conducted on a wide range of Cr–H–X-bridged systems for comparison with **119** and for more complete understanding of bonding.

A facile interconversion pathway between staggered and eclipsed forms of the anion is also examined by computational methods. This variation in conformation is observed across the large range of salts of this anion that have been crystallographically characterized, indicating that "packing forces" can be sufficient to cause significant deformations of the anion geometry. Charge density studies of **118** and **119** have also very recently been extended into multiple temperature studies, permitting improved modeling of the atomic motions, which in turn has the potential to lead to more accurate charge densities.[129]

The extensively characterized β-agostic compound [$Ti(Et)Cl_3$(dmpe)] **120**[130,130a–130c] (Figure 13) has been studied by experimental charge density analysis at 105 K and by complementary DFT calculations.[131,131a] An indication of the C–C bond order comes from the observed density at the bcp (1.90(4) eÅ^{-3}), which is slightly larger than that calculated for the non-agostic ethyl group in $EtTiCl_3$ (1.606 eÅ^{-3}) and substantially smaller than that calculated for ethylene (2.326 eÅ^{-3}). The bcp in the Ti–H interaction is vanishingly small, suggesting that this may not be the best indicator of an agostic interaction. Curvature of the Ti–C_α bond path (path of maximum electron density between these atoms) is suggested as a more reliable indicator of the β-agostic interaction. The more extensive follow-up study,[131a] again supported again by DFT calculations, examines the concept of ligand opposed charge concentrations (LOCCs) at the metal center and the development of local sites of Lewis acidity in d^0-metal complexes. The importance of such sites in developing the β-agostic interaction in **120** is highlighted. A potential β-agostic interaction was investigated in [Zr(η^5-$CH_2C(Me)CHC(Me)CH_2$){$N(Pr^i)CHPhCH_2$(η^4-CMe═CH-CMe═CH_2)}] **121** by charge density analysis based on a synchrotron X-ray data set collected at 16 K.[132]

The molecular geometry (Zr–N–C 102.87(4)°, Zr···C 2.7601 (6) Å, Zr···H 2.4604(6) Å) suggests the possible presence of a β-agostic interaction involving the isopropyl group. (The esd for the hydrogen atom position is derived

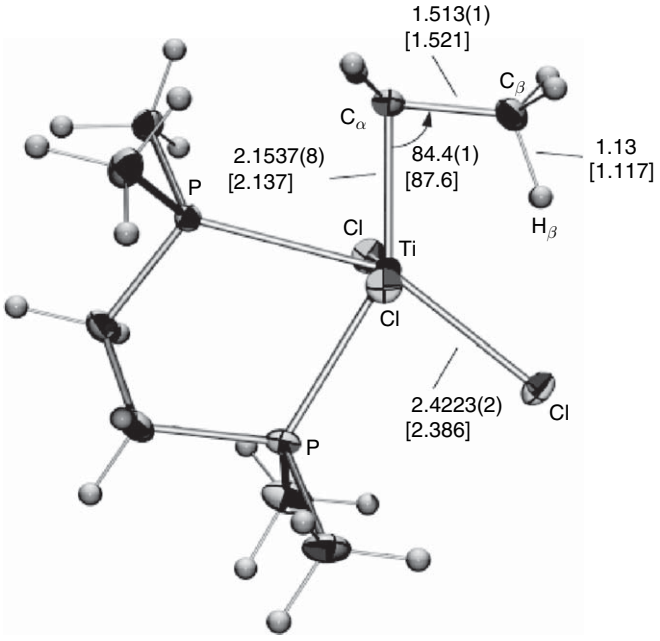

Figure 13 Molecular structure of **120** determined at 105 K and shown with 50% probability ellipsoids. Salient distances and angles are shown along with calculated values in square brackets. Reproduced from Scherer, W.; Sirsch, P.; Shorokhov, D.; Tafipolsky, M.; McGrady, G. S.; Gullo, E. *Chem. Eur. J.* **2003**, *9*, 6057–6070 with permission of the Wiley.

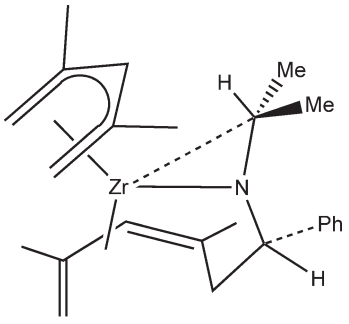

121

Scheme 14

from the carbon atom position. Hydrogen atom positions were obtained by isotropic refinement of low angle data then extension of the C–H vector to 1.08 Å.) However, the charge density study does not support this interpretation as there is no bond path between Zr and H, along with no lengthening of C–H bond from initial crystallographic refinements (and, indeed, no reduction in C–H coupling observed by NMR spectroscopy). Some caution is required here, given the absence of strong evidence for direct Ti···H interaction in the known agostic system **120**). The features of the charge density study of **121** are, however, fully consistent with the description of the proposed coordination and the interaction of the conjugated π-systems (Scheme 14).

1.21.5.4 Metal–Alkene Compounds

The study of $Ni(cod)_2$ **122**[133] confirms the Dewar–Chatt–Duncanson model of bonding for coordination the alkene units based on interpretation of the topology of the experimental charge density distribution. Specifically, Ni–C bond paths that are inwardly curved (σ-donation) but well separated (π-backdonation) are observed.

1.21.6 Crystallographic Database Studies

Since its establishment in the 1960s as a repository for crystallographic data on organic and metal-organic compounds, there have been numerous studies that have used geometric trends uncovered from systematic analysis of similar chemical fragments across large collections of crystal structures to derive useful chemical information.[134] Such information includes, for example, preferred geometries, both intra- and intermolecular, and mapping of reaction and conformational interconversion pathways using the structure correlation principle. Relatively few studies have been performed on organometallic systems. These are summarized below. Some related examples are also noted.

1.21.6.1 Studies of Intramolecular Geometries

In 1989, Orpen and co-workers reported a systematic survey of metal–ligand bond distances organized by metal, ligand, and bond type for *d*-block and *f*-block metals.[135,136] This tabulation was based on ca. 10,000 of the most accurate structures in the CSD at that time. Although heavily used, the tabulation has not been updated since that time. However, the need for a dynamically updated tabulation has been recognized in the release of the new Mogul database[137] by the Cambridge Crystallographic Data Centre (CCDC) and in the publication of the methodology to implement such a dynamically accessible tabulation for *d*-block and *f*-block metal complexes,[138] where identifying bond types is further complicated by ligand-bonding mode, metal oxidation state, and other issues such as Jahn–Teller distortions.

In a series of papers entitled Structural Systematics, Orpen and co-workers used the CSD to examine a number of geometric aspects of *d*-block metal complexes including torsional flexibility and conformer interconversion pathways for phosphine and diphosphine ligands, carbonyl ligand migration between metal centers (see also Figure 9,

Section 1.21.5.2), and metal site exchange in metal clusters. These studies were summarized in a review in 1993.[124] A subsequent paper undertook a quantitative analysis of the contributions to the variance observed in given molecular parameters, bond lengths, bond angles, and torsion angles.[139]

Thus, the total variance for a given parameter is $\sigma^2_{total} = \sigma^2_c + \sigma^2_p + \sigma^2_e$, where σ^2_c is the variance due to chemical environment (i.e., intramolecular effects); σ^2_c is due to intermolecular effects caused by crystal packing forces, and σ^2_e is simply the variance estimated from the crystallographic least-squares refinement. The intermolecular effects, for example, can be estimated from comparison of polymorphs, solvates, and crystal structures with more than one molecule in the asymmetric unit. The study found that crystal environment has a substantial effect on all aspects of molecular geometries. Thus, the total standard deviation for M–M and M–L bond lengths was found to be in the range 0.01–0.02 Å, L–M–L bond angles ca. 2° and far greater for torsion angles (e.g., up to 47° for PPh_3 ligands). These results have important consequences for the accuracy with which one should endeavor using methods such as theoretical calculations, to match molecular geometries that are obtained from crystal structures. The variation in particular geometries also provides some valuable insight into the flexibility of metal complexes, which also has a bearing on solution-phase behavior.

Although not specifically focused upon organometallic complexes, two other studies by Allen, Howard and co-workers should also be noted. In one case, the CSD has been used to map out the conformation space accessed by complexes of a particular coordination number,[140] and in the second case, the geometric pathway for addition of a ligand to linear $Hg^{II}L_2$ complexes has been examined.[141]

1.21.6.2 Hydrogen Bonding in Organometallic Compounds

In the mid-1990s, Braga and co-workers undertook a systematic study of hydrogen bonding of (largely organometallic) metal complexes. Hydrogen bond patterns and geometries involving –COOH, –OH, or –COOR groups[142] or amido groups[143] were found to be in close agreement with observations for crystals of organic compounds. In the latter case, a somewhat greater structural variability than for organic amides is observed, including interactions with ligated or solvent water molecules. The prevalence of C–H groups and of CO ligands in organometallic compounds was shown to give rise to an abundance of C–H···O hydrogen bonding in crystals of organometallic compounds. The CSD was used to examine such interactions involving bridged and terminal first-row metal carbonyls of *d*-block metals,[144] finding that variation of the metal atom does not affect these interactions.

A preferential interaction geometry with CO···H angles of ca. 140° was found for both terminal and bridging carbonyl ligands and attributed to the involvement of oxygen lone pairs. Average hydrogen bond distances (H···O) were found to decrease in the order $M(CO) > M_2(\mu_2\text{-}CO) > M_3(\mu_3\text{-}CO)$, consistent with greater π-backdonation to the carbonyl ligand resulting in increased basicity of the carbonyl oxygen atom. Bridging methylidyne (μ_3-CH) hydrogen-bond donors were also found to give rise to shorter C–H···O hydrogen bonds than methylene ligands (μ_2-CH_2).[145] Direct hydrogen-bonding interactions with metal centers were also investigated in an effort to identify potential M–H···O hydrogen bonds[146] and to provide geometric criteria to distinguish between 3c-4e N–H···M, O–H···M, and even C–H···M hydrogen bonds and possible 3c-2e intermolecular σ-bond complexation interactions of C–H groups.[147] Agostic interactions were also studied by these means.[148] This series of studies has been summarized in a number of subsequent reviews.[149,149a]

Although not a database study, using the structure correlation method[124] typically applied to sequences of structures, Brammer and co-workers have described the geometric pathway for proton transfer from an ammonium cation to the metal center of a $Co(CO)_3L^-$ anion (L = CO, phosphine) leading to the hydride complex $HCo(CO)_3L$ (Figure 14).[150] The pathway is based predominantly on crystal structures of a series of salts of the form $(R_2R^1NH)[Co(CO)_3L]$ (R = alkyl, R^1 = alkyl, H) in which the cation and anion are linked via a N–H···Co hydrogen bond. A separated pair of ions **A** with a tetrahedral anion represents the starting geometry of the protonation pathway and $HCo(CO)_3L$ complexes represent the hydride product **D**.

The wider implications of hydrogen bonding in the context of crystal engineering of organometallic compounds has also been examined[151] and is the subject of Chapter 12.11.

1.21.7 Future Developments

Crystallography and diffraction methods are continuously evolving. The introduction of CCD for single crystal X-ray diffraction has permitted significant improvements, not only in speed of data collection, but also in the accuracy and precision of the intensity measurements. It has become possible to study smaller crystals and more routinely obtain

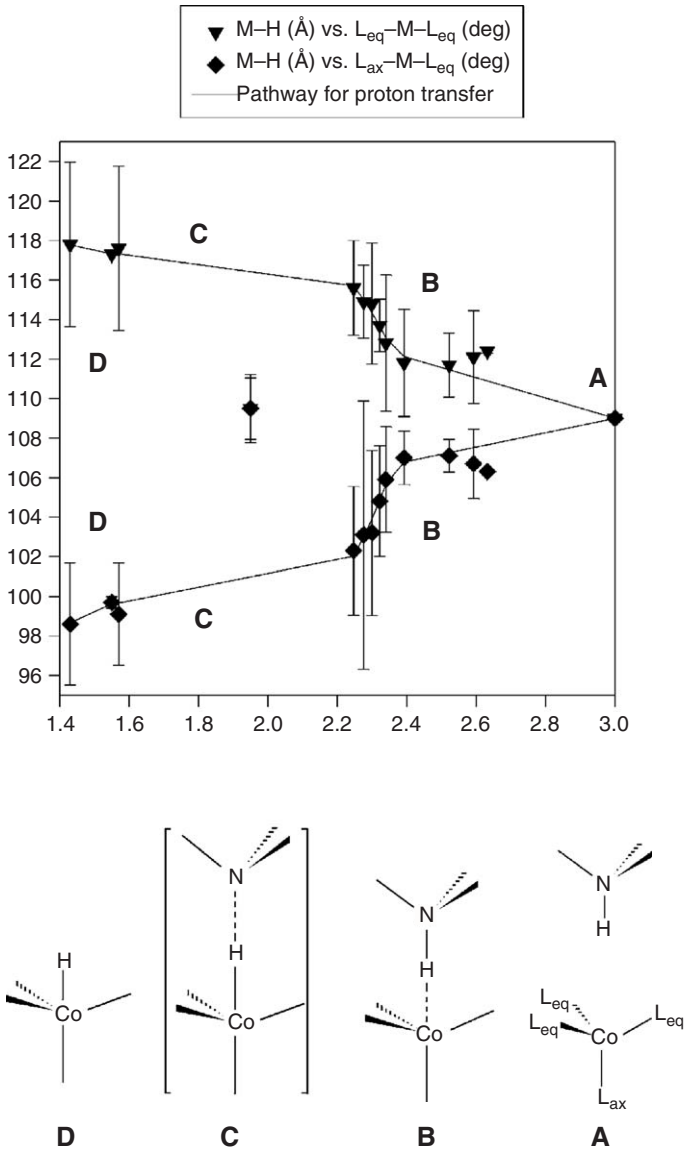

Figure 14 Structure correlation study modeling the pathway for protonation of the $Co(CO)_3L^-$ anion at the metal center. Reproduced from Brammer, L.; Mareque Rivas, J. C.; Spilling, C. D. *J. Organomet. Chem.* **2000**, *609*, 36–43 with permission of Elsevier Science S. A.

valuable and reliable structural information from twinned samples. New on the horizon is ready access to cryostats based on helium rather than (or in addition to) on nitrogen, permitting studies to be undertaken at temperatures as low as 30 K, and in some cases below 15 K. Studies of molecular crystals under pressure are also becoming more common. More synchrotron beam lines are being equipped for single crystal diffraction studies of small- and medium-sized unit cells, which encompass organometallic compounds. These facilities can permit studies upon crystals with dimensions in the 10–50 μm range. A similar transformation is on the horizon for neutron diffraction in ca. 2010. It is anticipated that the new instruments being planned or built will open single crystal neutron diffraction to studies upon crystals of dimensions of ca. 0.5 mm, little different to crystal sizes that were regularly employed for X-ray diffraction 20–30 years ago. Structure solution from powder diffraction is also reaching greater prominence. Both laboratory and synchrotron X-ray sources are already being used for structure determination of moderately complicated structures (10s of independent non-hydrogen atoms). Synchrotron radiation is also providing opportunities to undertake more advanced experiments such as time-resolved structural studies, crystallography of short-lived excited

state species, and, using the tunable wavelength, element or even oxidation-state specific diffraction. A survey of crystallographic and other structural techniques applied to organometallic and coordination compounds can be found in the Transactions of the 1995 American Crystallographic Association Meeting.[152] A 2004 special issue of *Chemical Society Reviews* devoted to crystallography[153] provides a valuable introduction to the many areas of development and applications of crystallography. Many crystallographic techniques which are quite specialist or esoteric now have the opportunity to develop into methods of importance to organometallic chemists in the future.

References

1. Allen, F. H. *Acta Crystallogr.* **2002**, *B58*, 380–388.
2. Bau, R; Teller, R. *Struct. Bond.* **1981**, *44*, 1–82.
2a. Bau, R.; Drabnis, M. H. *Inorg. Chim. Acta* **1997**, *259*, 27–50.
3. Kubas, G. J.; Burns, C. J.; Eckert, J.; Johnson, S. W.; Lamon, A. C.; Vergamini, P. J.; Unkefer, C. J.; Khalsa, G. R. K.; Jackson, S. A.; Eisenstein, O. *J. Am. Chem. Soc.* **1993**, *115*, 569–581 (WADSAV).
4. Gross, C. L.; Young, D. M.; Schultz, A. J.; Girolami, G. S. *J. Chem. Soc., Dalton Trans.* **1997**, 3081–3082 (NOLJIH).
5. Klooster, W. T.; Koetzle, T. F.; Jia, G.; Fong, T. P.; Morris, R. H.; Albinati, A. J. *Am. Chem. Soc.* **1994**, *116*, 7677–7681 (JOLWAI01).
6. Albinati, A.; Klooster, W. T.; Koetzle, T. F.; Fortin, J. B.; Ricci, J. S.; Eckert, J.; Fong, T. P.; Lough, A. J.; Morris, R. H.; Golombek, A. P. *Inorg. Chim. Acta* **1997**, *259*, 351 (HINBOV1).
7. Hasegawa, T.; Li, Z.; Parkin, S.; Hope, H.; McMullan, R. K.; Koetzle, T. F.; Taube, H. *J. Am. Chem. Soc.* **1994**, *116*, 4352 (PIYGAF).
8. Albinati, A.; Bakhmutov, V. I.; Caulton, K. G.; Clot, E.; Eckert, J.; Eisenstein, O.; Gusev, D. G.; Grushin, V. V.; Hauger, B. E., Klooster, W. T., *et al. J. Am. Chem. Soc.* **1993**, *115*, 7300 (PESFIC).
9. Wessel, J.; Lee, J. C., Jr.; Peris, E.; Yap, G. P. A.; Fortin, J. B.; Ricci, J. S.; Sini, G.; Albinati, A.; Koetzle, T. F., Eisenstein, O., *et al. Angew. Chem., Int. Ed.* **1995**, *34*, 2507 (ZIRFOV).
10. Brammer, L.; Klooster, W. T.; Lemke, F. R. *Organometallics* **1996**, *15*, 1721–1727 (ZEGYUF01, ZEGZAM01).
11. Brammer, L.; Lemke, F. R. *Organometallics* **1995**, *14*, 3980–3987.
12. Brammer, L.; Zhao, D.; Bullock, R. M.; McMullan, R. K. *Inorg. Chem.* **1993**, *32*, 4819–4824 (DOKTEC02).
13. Cameron, R. P.; Stevens, E. D.; Sweany, R. L.; Koetzle, T. F. *Am. Crystallogr. Assoc. Mtg.* **1988** Abstr. PB7.
14. Tsai, Y.-C.; Johnson, M. J. A.; Mindiola, D. J.; Cummins, C. C. *J. Am. Chem. Soc.* **1999**, *121*, 10426–10427 (VEQGED).
15. Abramov, Yu. A.; Brammer, L.; Klooster, W. T.; Bullock, R. M. *Inorg. Chem.* **1998**, *37*, 6317–6328 (CABNIC01).
16. LaPlaca, S. J.; Hamilton, W. H.; Ibers, J. A.; Davison, A. *Inorg. Chem.* **1969**, *8*, 1928.
17. Ho, N. N.; Bau, R.; Mason, S. A. *J. Organomet. Chem.* **2003**, *676*, 85–88 (QOSZON01).
18. Drabnis, M. H.; Bau, R.; Mason, S. A.; Freeman, J. W.; Ernst, R. D. *Eur. J. Inorg. Chem.* **1998**, 851–854 (PINYEQ).
19. Albinati, A.; Bracher, G.; Carmona, D.; Jans, J. H. P.; Klooster, W. T.; Koetzle, T. F.; Macchioni, A.; Ricci, J. S.; Thouvenot, R.; Venanzi, L. M. *Inorg. Chim. Acta* **1997**, *265*, 255–265 (WAZPUI01).
20. Albinati, A.; Chaloupka, S.; Demartin, F.; Koetzle, T. F.; Rüegger, H.; Venanzi, L. M.; Wolfer, M. K. *J. Am. Chem. Soc.* **1993**, *115*, 169–175 (JUTJOX01).
21. Cotton, F. A.; Daniels, L. M.; Liu, C. Y.; Murillo, C. A.; Schultz, A. J.; Wang, X. *Inorg. Chem.* **2002**, *41*, 4232–4238 (SIRCEB03).
22. Wong, E. H.; Valdez, C.; Gabe, E. V.; Lee, F. L. *Polyhedron* **1989**, *8*, 2339.
23. Ovchinnikov, M. V.; Wang, X.; Schultz, A. J.; Guzei, I. A.; Angelici, R. J. *Organometallics* **2002**, *21*, 3292–3296 (MUJQAJ).
24. Cai, H.; Chen, T.; Wang, X.; Schultz, A. J.; Koetzle, T. F.; Xue, Z. *Chem. Commun.* **2002**, 230–231 (IDUFOC02).
25. Lutz, F.; Bau, R.; Wu, P.; Koetzle, T. F.; Krüger, C.; Schneider, J. J. *Inorg. Chem.* **1996**, *35*, 2698–2700 (VUTHUN01).
26. Bortz, M.; Bau, R.; Schneider, J. J.; Mason, S. A. *J. Cluster Sci.* **2001**, *12*, 285–291 (RIVKIQ01).
27. Detti, S.; Forsyth, V. T.; Roulet, R.; Ros, R.; Tassan, A.; Schenk, K. J. *Z. Kristallogr.* **2004**, *219*, 47–53 (MAZHAW02).
28. Heintz, R. A.; Koetzle, T. F.; Ostrander, R. L.; Rheingold, A. L.; Theopold, K. H.; Wu, P. *Nature* **1995**, *378*, 359–362 (ZEYFOY).
29. Bau, R.; Ho, N. N.; Schneider, J. J.; Mason, S. A.; McIntyre, G. J. *Inorg. Chem.* **2004**, *43*, 555–558 (RIVKOW01).
30. Bau, R.; Mason, S. A.; Li, L.; Wong, W.-T. *J. Am. Chem. Soc.* **1997**, *119*, 11992–11993 (NUWCUD).
31. McPartlin, M.; Eady, C. R.; Johnson, B. F. G.; Lewis, J. *J. Chem. Soc., Chem. Commun.* **1976**, 883.
32. Pauling, L. *Proc. Nat. Acad. Sci. USA* **1977**, *74*, 5235.
33. Orpen, A. G. *J. Organomet. Chem.* **1978**, *159*, C1.
33a. Orpen, A. G. *J. Chem. Soc., Dalton Trans.* **1980**, 2509.
34. Bau, R.; Drabnis, M. H.; Garlaschelli, L.; Klooster, W. T.; Xie, Z.; Koetzle, T. F.; Martinengo, S. *Science* **1997**, *275*, 1099–1102 (REXWEW01).
35. Brookhart, M.; Green, M. L. H. *J. Organomet. Chem.* **1983**, *250*, 395.
35a. Brookhart, M.; Green, M. L. H.; Wong, L.-L. *Prog. Inorg. Chem.* **1988**, *36*, 1.
36. Bastos, C. M.; Lee, K. S.; Kjelsberg, M. A.; Mayr, A.; Van Engen, D.; Koch, S. A.; Franolic, J. D.; Klooster, W. T.; Koetzle, T. F. *Inorg. Chim. Acta* **1998**, *279*, 7–23 (VAZQAO01).
37. Bau, R.; Mason, S. A.; Patrick, B. O.; Adams, C. S.; Sharp, W. B.; Legzdins, P. *Organometallics* **2001**, *20*, 4492–4501 (PUWKUN01).
38. Cole, J. M.; Gibson, V. C.; Howard, J. A. K.; McIntyre, G. J.; Walker, G. L. P. *Chem. Commun.* **1998**, 1829–1830 (JITMUU).
39. Baratta, W.; Mealli, C.; Herdtweck, E.; Ienco, A.; Mason, S. A.; Rigo, P. *J. Am. Chem. Soc.* **2004**, *126*, 5549–5562 (GOYFOQ01).
40. Klooster, W. T.; Brammer, L.; Schaverien, C. J.; Budzelaar, P. H. M. *J. Am. Chem. Soc.* **1999**, *121*, 1381–1382 (JOPQUA and KADCUN01).
41. Ho, N. N.; Bau, R.; Plecnik, C.; Shore, S. G.; Wang, X.; Schultz, A. J. *J. Organomet. Chem.* **2002**, *654*, 216–220 (SUWSIM01).
42. Mork, B. V.; Tilley, T. D.; Schultz, A. J.; Cowan, J. A. *J. Am. Chem. Soc.* **2004**, *126*, 10428–10440 (XAFZOU).
43. Bakhmutov, V. I.; Howard, J. A. K.; Keen, D. A.; Kuzmina, L. G.; Leech, M. A.; Nikonov, G. I.; Vorontsov, E. V.; Wilson, C. C. *J. Chem. Soc., Dalton Trans.* **2000**, 1631–1635 (ZEYVAA02).
44. Tanaka, I.; Ohhara, T.; Niimura, N.; Ohashi, Y.; Jiang, Q.; Berry, D. H.; Bau, R. *J. Chem. Res.* **1999**, *14*, 180–192 (KOKVOV01).

45. Schneider, J. J.; Hagen, J.; Czap, N.; Krüger, C.; Mason, S. A.; Bau, R.; Ensling, J.; Gütlich, P.; Wrackmeyer, B. *Chem. Eur. J.* **2000**, *6*, 625–635 (LIMDUG).
46. Ohhara, T.; Uekusa, H.; Ohashi, Y.; Tanaka, I.; Kumazawa, S.; Niimura, N. *Chem. Lett.* **1998**, *27*, 365–366.
47. Ohhara, T.; Harada, J.; Ohashi, Y.; Tanaka, I.; Kumazawa, S.; Niimura, N. *Acta Crystallogr.* **2000**, *B56*, 245–253 (WISMEQ02).
48. Ohhara, T.; Uekusa, H.; Ohashi, Y.; Tanaka, I.; Kumazawa, S.; Niimura, N. *Acta Crystallogr.* **2001**, *B57*, 551–559 (CODXAU04 and RALBUB02).
49. Ohhara, T.; Ikeda, S.; Imura, H.; Uekusa, H.; Ohashi, Y.; Tanaka, I.; Niimura, N. *J. Am. Chem. Soc.* **2002**, *124*, 14736–14740 (COMBUB02).
50. Ohgo, Y.; Ohashi, Y.; Klooster, W. T.; Koetzle, T. F. *Enantiomer* **1997**, *2*, 241–248 (RACCYC03).
51. Brock, C. P.; Fu, Y. *Acta Crystallogr.* **1997**, *B53*, 928–938 (FEROCE26–FEROCE31).
52. Takasugawa, F.; Koetzle, T. F. *Acta Crystallogr.* **1979**, *B35*, 1074–1081.
53. Delapalme, A.; Raison, P.; Lander, G. H.; Rebizant, J.; Schweiss, P.; Kanellakopulos, B. *Z. Kristallogr.* **1994**, *209*, 727–732 (CYPUCL01).
54. McMullan, R. K.; Koetzle, T. F.; Fritchie, C. J., Jr. *Acta Crystallogr.* **1997**, *B53*, 645–653 (AGPCBE01–AGPCBE03).
55. Klooster, W. T.; Lu, R. S.; Anwander, R.; Evans, W. J.; Koetzle, T. F.; Bau, R. *Angew. Chem., Int. Ed.* **1998**, *37*, 1268–1270 (YOSYAG01).
56. Bouquiere, J. P.; Finney, J. L.; Lehmann, M. S.; Lindley, P. F.; Savage, H. F. J. *Acta Crystallogr.* **1993**, *B49*, 79–89 (DADCBL01).
57. Herrmann, W. A.; Scherer, W.; Fischer, R. W.; Blümel, J.; Kleine, M.; Mertin, W.; Gruehn, R.; Mink, J.; Boysen, H., Wilson, C. C., *et al. J. Am. Chem. Soc.* **1995**, *117*, 3231–3243 (YOXVAI).
58. Ohnet, M.-N.; Spasojević-de Biré, A.; Dao, N. Q.; Schweiss, P.; Braden, M.; Fischer, H.; Reindl, D. *J. Chem. Soc., Dalton Trans.* **1995**, 665–672 (EAMNCR01).
59. Ménoret, C.; Spasojević-de Biré, A.; Dao, N. Q.; Cousson, A.; Kiat, J.-M.; Manna, J. D.; Hopkins, M. D. *J. Chem. Soc., Dalton Trans.* **2002**, 3731–3736 (MUHNIM, MUHNIM01).
60. Scherer, W.; Sirsch, P.; Grosche, M.; Spiegler, M.; Mason, S. A.; Gardiner, M. G. *Chem. Commun.* **2001**, 2072 (CAWMUI12, CAWMUI13).
61. Scherer, W.; Sirsch, P.; Shorokhov, D.; McGrady, G. S.; Mason, S. A.; Gardiner, M. G. *Chem. Eur. J.* **2002**, *8*, 2324 (CAWMUI15, CAWMUI16).
62. Boss, S. R.; Cole, J. M.; Haigh, R.; Snaith, R.; Wheatley, A. E. H.; McIntyre, G. J.; Raithby, P. R. *Organometallics* **2004**, *23*, 4527 (HOYNUE01, HOYNUE02).
63. Steiner, T.; Mason, S. A. *Acta Crystallogr.* **2000**, *B56*, 254 (AMPHEB02, AMPHEB03).
64. Fox, M. A.; Goeta, A. E.; Howard, J. A. K.; Hughes, A. K.; Johnson, A. L.; Keen, D. A.; Wade, K.; Wilson, C. C. *Inorg. Chem.* **2001**, *40*, 173 (GUNHUS).
65. Entwistle, C. D.; Marder, T. B.; Smith, P. S.; Howard, J. A. K.; Fox, M. A.; Mason, S. A. *J. Organomet. Chem.* **2003**, *680*, 165 (JEBLUX01).
66. Muller, M.; Williams, V. C.; Doerrer, L. H.; Leech, M. A.; Mason, S. A.; Green, M. L. H.; Prout, K. *Inorg. Chem.* **1998**, *37*, 1315 (PUPMES01).
67. Pontillon, Y.; Akita, T.; Grand, A.; Kobayashi, K.; Lelievre-Berna, E.; Pecault, J.; Ressouche, E.; Schweizer, J. *J. Am. Chem. Soc.* **1999**, *121*, 10126 (ZIGPAG02).
68. Gasper, P. P.; Beatty, A. M.; Chen, T.; Haile, T.; Deqing, Lei.; Winchester, W. R.; Braddock-Wilking, J.; Rath, N. P., Klooster, W. T., *et al. Organometallics* **1999**, *18*, 3921 (COQYUC01, HIDJUZ01).
69. Quintard, D.; Keller, M.; Breit, B. *Synthesis* **2004**, 905 (EZUVOK).
70. Fryzuk, M. D.; Johnson, S. A.; Patick, B. O.; Albinati, A.; Mason, S. A.; Koetzle, T. F. *J. Am. Chem. Soc.* **2001**, *123*, 3960 (MIQDOF).
71. Basch, H.; Musaev, D. G.; Morokuma, K.; Fryzuk, M. D.; Love, J. B.; Seidel, W. W.; Albinati, A.; Koetzle, T. F.; Klooster, W. T., Mason, S. A., *et al. J. Am. Chem. Soc.* **1999**, *121*, 523 (RIDJAP01).
72. Balazs, G.; Breunig, H. J.; Lork, E.; Mason, S. A. *Organometallics* **2003**, *22*, 576 (VIQVOG01).
73. Masciocchi, N.; Sironi, A. *J. Chem. Soc., Dalton Trans.* **1997**, 4643.

73a. Poojary, D. M.; Clearfield, A. *Acc. Chem. Res.* **1997**, *30*, 414–422.

73b. Harris, K. D. M.; Tremaye, M.; Kariuki, B. M. *Angew. Chem., Int. Ed.* **2001**, *40*, 1626–1651.

73c. David, W. I. F.; Shankland, K.; Shankland, N. *Chem. Commun.* **1998**, 931.

74. Attilio Ardizzoia, G.; Brenna, S.; LaMonica, G.; Maspero, A.; Masciocchi, N. *J. Organomet. Chem.* **2002**, *649*, 173–180 (OGAZAX).
75. Vicente, J.; Gil-Rubio, J.; Bautista, D.; Sironi, A.; Masciocchi, N. *Inorg. Chem.* **2004**, *43*, 5665–5675 (BEXLUM01).
76. Santi, R.; Romano, A. M.; Garrone, R.; Millini, R. *J. Organomet. Chem.* **1998**, *566*, 37–43 (CIQGOY01).
77. Masciocchi, N.; Ragaini, F.; Cenini, S.; Sironi, A. *Organometallics* **1998**, *17*, 1052–1057 (PUNBEF).
78. Dinnebier, R. E.; Wagner, M.; Peters, F.; Shankland, K.; David, W. I. F. *Z. Anorg. Allg. Chem.* **2000**, *626*, 1400–1405 (QINGEZ).
79. Masciocchi, N.; Moret, M.; Cairati, P.; Ragaini, F.; Sironi, A. *J. Chem. Soc., Dalton Trans.* **1993**, 471–475 (SUFBOK).
80. Masciocchi, N.; Sironi, A.; Chardon-Noblat, S.; Deronzier, A. *Organometallics* **2002**, *21*, 4009–4012 (XUHZOP).
81. Barnes, C. M.; Scott Bohle, D.; Dinnebier, R. E.; Madsen, S. K.; Stephens, P. W. *Inorg. Chem.* **1997**, *36*, 5793–5798 (NULZID and NULZOJ).
82. Masciocchi, N.; D'Alfonso, G.; Garavaglia, L.; Sironi, A. *Angew. Chem., Int. Ed.* **2000**, *39*, 4478–4480 (HUBWOQ and HUBWUW).
83. Dinnebier, R. E.; Schweiger, M.; Bildstein, B.; Shankland, K.; David, W. I. F.; Jobst, A.; van Smaalen, S. *J. Appl. Cryst.* **2000**, *33*, 1199–1207 (ESOQAE).
84. Dinnebier, R. E.; Ding, L.; Ma, K.; Neumann, M. A.; Tanpipat, N.; Leusen, F. J. J.; Stephens, P. W.; Wagner, M. *Organometallics* **2001**, *20*, 5642–5647 (PUXYAI).
85. Schneider, A. M.; Behrens, P. *Chem. Mater.* **1998**, *10*, 679–681 (SIHQUV).
86. Wessels, T.; Baerlocher, C.; McCusker, L. B.; Creyghton, E. J. *J. Am. Chem. Soc.* **1999**, *121*, 6242–6247 (LIVWIW).
87. Sullivan, R. M.; Liu, H.; Smith, D. S.; Hanson, J. C.; Osterhout, D.; Ciraolo, M.; Grey, C. P.; Martin, J. D. *J. Am. Chem. Soc.* **2003**, *125*, 11065–11079 (OLEBEM and OLEBIQ).
88. Slyvka, Y. I.; Mykhalichko, B. M.; Davydov, V. N. *Zh. Neorg. Khim.* **2003**, *48*, 1500–1506 (IWULUH and IWULUH01).
89. Cremer, U.; Ruschewitz, U. *Z. Anorg. Allg. Chem.* **2004**, *630*, 337 (ETUGIJ, ETUGOP and ETUGEF).
90. Cremer, U.; Disch, S.; Ruschewit, U. *Z. Anorg. Allg. Chem.* **2004**, *630*, 2304 (QAKGAL and QAKGEP).
91. Fayos, J.; Artioli, G.; Torres, R. *J. Crystallogr. Spectrosc. Res.* **1993**, *23*, 595–600 (JAHHOP01).
92. Corradi, E.; Masciocchi, N.; Pályi, G.; Ugo, R.; Vizi-Orosz, A.; Zucchi, C.; Sironi, A. *J. Chem. Soc., Dalton Trans.* **1997**, 4651–4655 (PAWZUI).
93. Vicente, J.; Arcas, A.; Fernández-Hernández, J. M.; Sironi, A.; Masciocchi, N. *Chem. Commun.* **2005**, 1267–1269 (YAPXAP).
94. Wilson, R. D.; Bau, R. *J. Am. Chem. Soc.* **1976**, *98*, 4687.
95. Masciocchi, N.; D'Alfonso, G.; Kockelmann, W.; Schafer, W.; Sironi, A. *Chem. Commun.* **1997**, 1903–1904 (NIWROA).

96. Dinnebier, R. E.; Behrens, U.; Olbrich, F. *Organometallics* **1997**, *16*, 3855 (NIBSEW and NIBSOG).
97. Dinnebier, R. E.; Schneider, M.; van Smaalen, S.; Olbrich, F.; Behrens, U. *Acta Crystallogr.* **1999**, *B55*, 35 (SUWHEX).
98. Dinnebier, R. E.; Neander, S.; Behrens, U.; Olbrich, F. *Organometallics* **1999**, *18*, 2915 (XACROI, NIBSIA and XACRUO).
99. Tedesco, C.; Dinnebier, R. E.; Olbrich, F.; van Smaalen, S. *Acta Crystallogr.* **2001**, *B57*, 673 (UCUKOS).
100. Couhorn, U.; Dronskowski, R. *Z. Anorg. Allg. Chem.* **2003**, *629*, 2554 (EVAVOM and EVAVUS).
101. Dinnebier, R. E.; van Smaalen, S.; Olbrich, F.; Carlson, S. *Inorg. Chem.* **2005**, *44*, 964 (NIBSOG01, NIBSOG02, NIBSOG03, NIBSOG04, NIBSOG05, NIBSOG06, NIBSOG07, NIBSOG08, NIBSOG09 and NIBSOG10).
102. Dinnebier, R. E.; Olbrich, F.; van Smaalen, S.; Stephens, P. W. *Acta Crystallogr.* **1997**, *B53*, 153 (TIQKEJ and TIQKEJ01).
103. Dinnebier, R. E.; Olbrich, F.; Bendele, G. M. *Acta Crystallogr.* **1997**, *C53*, 699 (RAVHUR).
104. Staunton, E.; Christie, A. M.; Andreev, Y. G.; Slawin, A. M. Z.; Bruce, P. G. *Chem. Commun.* **2004**, 148 (EROCUJ).
105. Muller, J.; Ruschewitz, U.; Indris, O.; Hartwig, H.; Stahl, W. *J. Am. Chem. Soc.* **1999**, *121*, 4647 (LINZOX).
106. Dinnebier, R. E.; Muller, J. *Inorg. Chem.* **2003**, *42*, 1204 (SAJCUB01).
107. Dikarev, E. V.; Chernyshev, V. V.; Shpanchenko, R. V.; Filatov, A. S.; Petrukhina, M. A. *Dalton Trans.* **2004**, 4120 (FELVEY).
108. Wunschel, M.; Dinnebier, R. E.; Carlson, S.; Bernatowicz, P.; van Smaalen, S. *Acta Crystallogr.* **2003**, *B59*, 60 (HUSQAN, HUSQAN01, HUSQIV and HUSQIV01).
109. Tedesco, E.; Kariuki, B. M.; Harris, K. D. M.; Johnston, R. L.; Pudova, O.; Barbarella, G.; Marseglia, E. A.; Gigli, G.; Cingolani, R. *J. Solid State Chem.* **2001**, *161*, 121 (QEZXOI01).
110. Lightfoot, P.; Glidewell, C.; Bruce, P. G. *J. Organomet. Chem.* **1994**, *466*, 51 (WEKRUZ).
111. McGrady, G. S.; Turner, J. F. C.; Ibberson, R. M.; Prager, M. *Organometallics* **2000**, *19*, 4398 (TRMEAL03).
112. Dinnebier, R. E.; Dollase, W. A.; Helluy, X.; Kummerlen, J.; Sebald, A.; Schmidt, M. U.; Pagola, S.; Stephens, P. W.; van Smaalen, S. *Acta Crystallogr.* **1999**, *B55*, 1014 (GUFMOJ and GUFMOJ01).
113. Dinnebier, R. E.; Dollase, W. A.; Helluy, X.; Kummerlen, J.; Sebaid, A.; Schmidt, M. U.; Pagola, S.; Stephens, P. W.; van Smaalen, S. *Acta Crystallogr.* **1999**, *B55*, 1014 (ZZZWNG01, ZZZWNG02 and ZZZWNG03).
114. Dinnebier, R. E.; Bernatowicz, P.; Helluy, X.; Sebald, A.; Wunschel, M.; Fitch, A.; van Smaalen, S. *Acta Crystallogr.* **2002**, *B58*, 52 (MEZDIE, MEZDIE01, MEDZOK and MEDZOK01).
115. Bader, R. F. W. *Atoms in Molecules: A Quantum Theory*; Oxford University Press: Oxford, 1990.
116. Coppens, P. *X-ray charge densities and chemical bonding*; IUCr Texts on Crystallography; Oxford University Press: Oxford, 1997.
116a. Coppens, P. *Angew. Chem., Int. Ed.* **2005**, *44*, 6810–6811.
116b. Koritsanszky, T. S.; Coppens, P. *Chem. Rev.* **2001**, *101*, 1583–1627.
116c. Spackman, M. A. *Ann. Rep. Prog. Chem., Sect. C, Phys. Chem.* **1997**, *94*, 177–207.
117. Angermund, K.; Claus, K. H.; Goddard, R.; Krüger, C. *Angew. Chem., Int. Ed.* **1985**, *24*, 237–247.
117a. Macchi, P.; Sironi, A. *Coord. Chem. Rev.* **2003**, *238–239*, 383–412.
118. For example, Martin, M.; Rees, B.; Mitschler, A. *Acta Crystallogr.* **1982**, *B38*, 6–15.
119. Bianchi, R.; Gervasio, G.; Marabello, D. *Chem. Commun.* **1998**, 1535–1536.
119a. Bianchi, R.; Gervasio, G.; Marabello, D. *Inorg. Chem.* **2000**, *39*, 2360–2366.
119b. Farrugia, L. J.; Mallinson, P. R.; Stewart, B. *Acta Crystallogr.* **2003**, *B59*, 234–247.
120. Macchi, P.; Proserpio, D. M.; Sironi, A. *J. Am. Chem. Soc.* **1998**, *120*, 13429–13435.
121. Bianchi, R.; Gervasio, G.; Marabello, D. *Helv. Chim. Acta* **2001**, *84*, 722–734 (orthorhombic phase).
121a. Bianchi, R.; Gervasio, G.; Marabello, D. *Acta Crystallogr.* **2001**, *B57*, 722–734 (triclinic phase).
122. Macchi, P.; Garlaschelli, L.; Martinengo, S.; Sironi, A. *J. Am. Chem. Soc.* **1999**, *121*, 10428–10429.
123. Macchi, P.; Garlaschelli, L.; Sironi, A. *J. Am. Chem. Soc.* **2002**, *124*, 14173–14184.
124. Orpen, A. G. *Chem. Soc. Rev.* **1993**, *22*, 191–197.
125. Coppens, P. *Coord. Chem. Rev.* **1985**, *65*, 285.
125a. Cameron, R. P.; Stevens, E. D.; Sweany, R. L. *Am. Crystallogr. Assoc. Mtg.* **1990** Abstr. PD07.
126. Spackman, M. A.; Weber, H. P.; Craven, B. M. *J. Am. Chem. Soc.* **1988**, *110*, 775–782.
127. Pederson, J. L.; Brown, R. K.; Wiliams, J. M. *Inorg. Chem.* **1981**, *20*, 158–165.
128. Macchi, P.; Donghi, D.; Sironi, A. *J. Am. Chem. Soc.* **2005**, *127*, 16494–16504.
129. Macchi, P.; Sironi, A. *Acta Crystallogr.* **2004**, *A60*, 502–509.
130. Dawoodi, Z.; Breen, M. L. H.; Mtetwa, V. L. B.; Prout, C. K. *J. Chem. Soc., Chem. Commun.* **1982**, 802.
130a. Dawoodi, Z.; Breen, M. L. H.; Mtetwa, V. L. B.; Prout, C. K.; Schultz, A. J.; Williamns, J. M.; Koetzle, T. F. *J. Chem. Soc., Dalton Trans.* **1986**, 1629.
130b. Cotton, F. A.; Petrukhina, M. A. *Inorg. Chem. Commun.* **1998**, *1*, 195.
130c. Scherer, W.; Priermeier, T.; Haaland, A.; Volden, H. V.; McGrady, G. S.; Downs, A. J.; Boese, R.; Bläser, D. *Organometallics* **1998**, *17*, 4406.
131. Scherer, W.; Hieringer, W.; Spiegler, M.; Sirsch, P.; McGrady, G. S.; Downs, A. J.; Haaland, A.; Pedersen, B. *Chem. Commun.* **1998**, 2471–2472.
131a. Scherer, W.; Sirsch, P.; Shorokhov, D.; Tafipolsky, M.; McGrady, G. S.; Gullo, E. *Chem. Eur. J.* **2003**, *9*, 6057–6070.
132. Pillet, S.; Wu, G.; Kulsomphob, V.; Harvey, B. G.; Ernst, R. D.; Coppens, P. *J. Am. Chem. Soc.* **2003**, *125*, 1937–1949.
133. Macchi, P.; Proserpio, D. M.; Sironi, A. *J. Am. Chem. Soc.* **1998**, *120*, 1447–1455.
134. For illustrative examples of applications of the CSD, see: Allen, F. H.; Taylor, R. *Chem. Soc. Rev.* **2004**, *33*, 463–475.
135. Orpen, A. G.; Brammer, L.; Allen, F. H.; Kennard, O.; Watson, D. G.; Taylor, R. *J. Chem. Soc., Dalton Trans.* **1989**, S1–S83.
136. See also, the related survey of bond lengths in organic compounds: Allen, F. H.; Kennard, O.; Watson, D. G.; Brammer, L.; Orpen, A. G.; Taylor, R. *J. Chem. Soc., Perkin Trans. 2* **1987**, S1–S19.
137. Bruno, I. J.; Cole, J. C.; Kessler, M.; Luo, J.; Motherwell, W. D. S.; Purkis, L. H.; Smith, B. R.; Taylor, R.; Cooper, R. I., Harris, S. E., *et al. J. Chem. Inf. Comput. Sci.* **2004**, *44*, 2133–2144.
138. Harris, S. E.; Orpen, A. G.; Bruno, I. J.; Taylor, R. *J. Chem. Inf. Comput. Sci.* **2005**, *45*, 1727–1748.
139. Martín, A.; Orpen, A. G. *J. Am. Chem. Soc.* **1996**, *118*, 1464–1470.
140. Yao, J. W.; Copley, R. C. B.; Howard, J. A. K.; Allen, F. H.; Motherwell, W. D. S. *Acta Crystallogr.* **2001**, *B57*, 251–260.
141. Allen, F. H.; Mondal, R.; Pitchford, N. A.; Howard, J. A. K. *Helv. Chim. Acta* **2003**, *86*, 1129–1139.
142. Braga, D.; Grepioni, F.; Sabatino, P.; Desiraju, G. R. *Organometallics* **1994**, *13*, 3532–3543.
143. Biradha, K.; Desiraju, G. R.; Braga, D.; Grepioni, F. *Organometallics* **1996**, *15*, 1284–1295.

144. Braga, D.; Grepioni, F.; Biradha, K.; Pedireddi, V. R.; Desiraju, G. R. *J. Am. Chem. Soc.* **1995**, *117*, 3156–3166.
145. Braga, D.; Grepioni, F.; Tedesco, E.; Wadepohl, H.; Gebert, S. *J. Chem. Soc., Dalton Trans.* **1997**, 1727–1732.
146. Braga, D.; Grepioni, F.; Tedesco, E.; Biradha, K.; Desiraju, G. R. *Organometallics* **1996**, *15*, 2692–2699.
147. Braga, D.; Grepioni, F.; Biradha, K.; Desiraju, G. R. *J. Chem. Soc., Dalton Trans.* **1996**, 3925–3930.
148. Braga, D.; Grepioni, F.; Tedesco, E.; Biradha, K.; Desiraju, G. R. *Organometallics* **1997**, *16*, 1846–1856.
149. Braga, D.; Grepioni, F.; Desiraju, G. R. *J. Organomet. Chem.* **1997**, *548*, 33–43.
149a. Braga, D.; Grepioni, F. *Acc. Chem. Res.* **1997**, *30*, 81–87.
150. Brammer, L.; Mareque Rivas, J. C.; Spilling, C. D. *J. Organomet. Chem.* **2000**, *609*, 36–43.
151. Braga, D.; Grepioni, F.; Desiraju, G. R. *Chem. Rev.* **1998**, *98*, 1375–1405.
152. Brammer, L., Ed. Structural tools in organometallic and coordination chemistry;. *Trans. Am. Crystallogr. Assoc.* **1995**, *35*.
153. *Chem. Soc. Rev.* **2004**, *33*, 463–565 (entire issue 8).

1.22 Structure and Bonding in Organometallic Compounds: Organometallic Thermochemistry

J A Martinho Simões and M E Minas da Piedade, Universidade de Lisboa, Lisboa, Portugal

1.22.1 Introduction

Thermochemical studies of organometallic compounds can be traced back to at least as early as 1887, when Guntz reported the "heat of formation" of $ZnEt_2$ ($Et = C_2H_5$), obtained by using a precursor of the modern reaction–solution calorimeter.[1] Actually, the work of Guntz was presented at the *Académie des Sciences (Paris)* by Berthelot, who, two years later, investigated the thermochemistry of $HgMe_2$ ($Me = CH_3$), $HgEt_2$, and $HgPh_2$, with an ancestor of the static-bomb combustion calorimeter.[2] During the first half of the twentieth century only a handful of organometallic compounds were studied: the landmark compilation of Bichowsky and Rossini, published in 1936,[3] included five organometallic compounds and, in the words of Skinner,[4] "no data of real value appeared until after the end of World War II." By the mid-1960s, however, enthalpies of formation and vaporization/sublimation had been reported for various alkyl and/or aryl compounds of Li, Zn, Cd, Hg, B, Al, Ga, Si, Ge, Sn, Pb, As, Sb, Bi, and Se.[5] Some metallocenes and carbonyls of V, Cr, Mn, Fe, Mo, W, and Ni had also been studied.[5] From then on, the growth of thermochemical data for organometallic compounds was mainly fostered by the boom of transition-element, lanthanide, and actinide organometallic chemistry. A major impulse was provided by a debate in the 1970s, concerning the "strength" of transition metal–carbon bonds. Homoleptic species $(MR_n)_x$, where M is a transition metal and R a σ-hydrocarbyl ligand, seemed to be very difficult to prepare and the known compounds showed a high thermal instability (e.g., $TiMe_4$ is reported to decompose a few degrees above 195 K and WMe_6 decomposes explosively at room temperature).[6,7] In contrast, numerous $(MR_n)_x$ derivatives of the main group elements were found to be stable at room temperature.[8] These observations led to the general belief that transition metal–carbon bonds were weak,[9] a view that was challenged by the groups of Wilkinson and Lappert, who independently suggested that the instability of the transition metal σ-hydrocarbyls had a mechanistic origin.[8,10] These authors pointed out that β-elimination (Scheme 1) was an important channel for the thermal decomposition of transition metal σ-hydrocarbyls and that stable complexes could often be prepared by using ligands without β-hydrogen atoms (e.g., Me_3CCH_2, Me_3SiCH_2, and $PhCH_2$ ($Ph = C_6H_5$)). As illustrated in Scheme 1, the β-elimination pathway does not involve the simple cleavage of the M–C σ-bond, since there is a simultaneous formation of an incipient metal–hydrogen bond. Hence, the strength of the M–C σ-bond should not be inferred from the decomposition temperature of the compound. This controversy motivated several research groups to investigate the magnitude and trends of transition metal–carbon

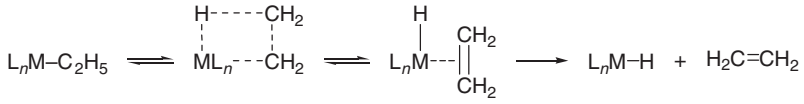

Scheme 1

bond dissociation enthalpies, a goal that was rapidly extended to other types of bonds and to a variety of problems in bonding energetics and reactivity.

This chapter was not written for (the few) experts in the field of organometallic thermochemistry. The contents selected for this overview had in mind those chemists who need to use thermochemical values to predict stability or reactivity and may welcome some clear guidelines about the appropriate use of data. Another important choice was concerned with the amount of data to be included in the form of tables or graphic representations. Hard copy databases, of any sort, are clearly old-fashioned resources. They have been gradually replaced by electronic databases, enabling much faster searches and allowing to keep the contents permanently updated (which is particularly important for thermochemical databases; see below). It was, therefore, decided to include a minimum of data and use the available space to review concepts, experimental methodologies, available databases, empirical estimation schemes, and to discuss some important applications.

What type of compounds will be covered in this overview? Strictly, only compounds which have at least one metal–carbon bond (with the exception of metal carbides) are called organometallic. However, this definition was not adopted in this chapter because many families of compounds that are relevant in organometallic chemistry would not be included (e.g., alkoxides). By "metal" we mean any element from groups 1 (except hydrogen), 2, 3 (including lanthanides and actinides), 4, 5, 6, 7, 8, 9, 10, 11, 12, 13 (except boron), 14 (except carbon and silicon), and 15 (antimony and bismuth only). Most of the available thermochemical data for all these species are freely available in a single on-line database: the *NIST Chemistry WebBook*.[11] Unless stated otherwise, all the data included in this chapter were quoted from that reference.

Finally, a brief comment on nomenclature. The word "energetics," rather than "thermochemistry," is frequently preferred nowadays to emphasize the fact that the basic quantities used in this field were not necessarily obtained through the determination of heat. "Thermochemistry," however, is still well imbedded in the scientific community and both designations will be used throughout this chapter.

1.22.2 Chemical Stability: Thermodynamics versus Kinetics

As mentioned in Section 1.22.1, the assessment of the stability of a compound or of a certain type of chemical bond is at the heart of many organometallic thermochemistry studies. But how is stability put on quantitative grounds? In general, a compound is said to be stable if its chemical composition and structure do not change with time. This notion of stability, however, only makes sense if the physical and chemical conditions in which the compound exists are specified. The yellow solid $MoCp_2H_2$, for example, apparently survives forever at 298 K under 1 bar of pure nitrogen, but it quickly decomposes in the presence of oxygen, yielding black powder after a few seconds.

Thermodynamics provides the concepts and framework to quantify the type of stability generally known as thermodynamic stability. According to the second law of thermodynamics, the driving force of a reaction at constant temperature and pressure is given by the corresponding Gibbs energy change, $\Delta_r G$, spontaneous reactions having $\Delta_r G < 0$. The value of $\Delta_r G$ is a sum of two terms:[12]

$$\Delta_r G = \Delta_r G^o + RT \ln Q \tag{1}$$

where $\Delta_r G^o$ represents the Gibbs energy of the reaction in the standard state ($p = 1$ bar), R is the gas constant ($R = 8.31451\,\mathrm{J\,K^{-1}\,mol^{-1}}$), T is the absolute temperature, and Q represents the reaction quotient, which has the general form:

$$Q = \prod_i (\alpha_i / \alpha_i^o)^{\nu_i} \tag{2}$$

In Equation (2), α_i is a quantity that measures the amount of the species i present in the system, α_i^o represents the value of that quantity under standard state conditions, and ν_i is the corresponding stoichiometric coefficient. Depending on the thermodynamic model chosen to describe i, α_i may be a partial pressure, molar fraction, concentration, activity, etc.; and because stoichiometric coefficients are negative for reactants and positive for products Q is normally written as a ratio. For example, in the case of the reaction,[13]

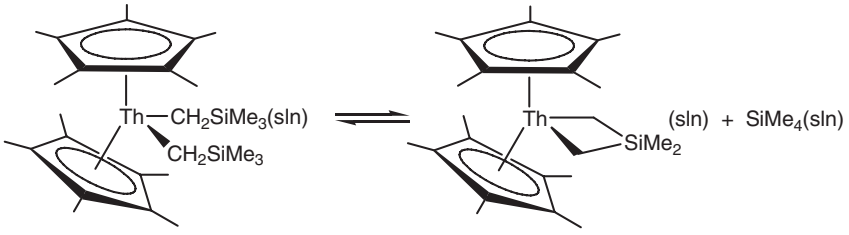

(3)

studied in cyclohexane, the reaction quotient may be written as

$$Q = \frac{[\overline{\mathrm{Th(Cp^*)_2(CH_2SiMe_2CH_2)}}]\,[\mathrm{SiMe_4}]}{[\mathrm{Th(Cp^*)_2(CH_2SiMe_3)_2}]} \tag{4}$$

where the α_i values are given as the molar concentrations of $\overline{\mathrm{Th(Cp^*)_2(CH_2SiMe_2CH_2)}}$, $\mathrm{Th(Cp^*)_2(CH_2SiMe_3)_2}$, and $\mathrm{SiMe_4}$, respectively, $\alpha_i^o = 1\ \mathrm{mol\ dm^{-3}}$ for all reactants and products, and $\nu_i = 1$ for the products and -1 for the reactant.

At the beginning of a reaction the amounts of reactants in the system largely exceed the amounts of products and $Q << 1$. Hence, $RT \ln Q << 0$ and $|RT \ln Q| > |\Delta_r G^o|$, leading to $\Delta_r G < 0$ regardless of $\Delta_r G^o$ being positive or negative. In this case, a tendency toward an increase of the concentration of the products will always exist. Under equilibrium conditions $\Delta_r G = 0$ and[12]

$$\Delta_r G^o = -RT \ln K \tag{5}$$

where K represents the equilibrium constant (i.e., the value of Q when equilibrium has been attained). As K reflects the maximum yield of the reaction at a given temperature and pressure, a large positive value of $\Delta_r G^o$ indicates stability, that is, the reaction yield will be negligible and for all practical purposes the compound will not react. Conversely, instability will be characterized by a large negative value of $\Delta_r G^o$. Thus, although, strictly speaking, the thermodynamic stability of a compound should be discussed in terms of $\Delta_r G$ (i.e., by considering both Q and $\Delta_r G^o$), normally this stability is strongly dependent on the position of the equilibrium, which is solely determined by $\Delta_r G^o$. Therefore, the thermodynamic stability of a molecule is usually discussed on the basis of $\Delta_r G^o$ only.

The standard Gibbs energy of a reaction is related to the corresponding enthalpy, $\Delta_r H^o$, and entropy, $\Delta_r S^o$, by

$$\Delta_r G^o = \Delta_r H^o - T\Delta_r S^o \tag{6}$$

In some cases experimental values of $\Delta_r H^o$ and $\Delta_r S^o$ are available, but in general these data are calculated using experimental or estimated values of the standard enthalpies of formation, $\Delta_f H^o$, and entropies, S^o, of all species involved in the reaction. It should also be pointed out that most organometallic reactions of interest occur in solution at temperatures not far from ambient, and that under these conditions the enthalpy term in Equation (6) is often dominant. Therefore, thermodynamic stability trends of organometallic compounds can frequently be analyzed solely in terms of $\Delta_r H^o$. When necessary, however, computational chemistry calculations or simple estimation schemes can normally be used to predict $\Delta_r S^o$ with an acceptable accuracy.[14,15]

Thermodynamic stability or instability is blind to the kinetic aspects of the decomposition pathway, since the values of $\Delta_r G^o$ and $\Delta_r H^o$ are only determined by the initial and final states of the reaction. Hence, a species that is predicted to be thermodynamically unstable under certain physical and chemical conditions may not decompose at all, simply because the rate of the process is very slow, due to a high activation energy.[16] This is called kinetic stability. A kinetically stable compound may be a thermodynamically unstable species whose transformation into some thermodynamically more stable product is hindered by the existence of a high activation barrier. Although at

first glance the relation between kinetic and thermodynamic stability does not appear to be significant, a bridge between both concepts can sometimes be built, since under equilibrium conditions the rates of the forward (ν_1) and reverse (ν_{-1}) reactions are equal. For example, the rates of the forward and reverse processes in reaction (3) can be written as

$$\nu_1 = k_1\left[\mathrm{Th(Cp^*)_2(CH_2SiMe_3)_2}\right] \tag{7}$$

$$\nu_{-1} = k_{-1}[\overline{\mathrm{Th(Cp^*)_2(CH_2SiMe_2CH_2)}}][\mathrm{SiMe_4}] \tag{8}$$

and if 1 mol dm^{-3} is selected as the standard state for the concentrations of reactants and products, then

$$K = \frac{k_1}{k_{-1}} \tag{9}$$

Equation (9) is valid if, as in the case of reaction (3), the partial orders of the reagents in the forward and reverse reactions equal their molecularities (i.e., the number of species involved in the process).[16] This is true for all elementary reactions and, depending on the mechanism, for some composite reactions also. According to the thermodynamic formulation of conventional transition-state theory, the rate constant of an elementary reaction is given by[16]

$$k = \frac{k_B T}{h}\exp\frac{\Delta^{\ddagger}G^{o}}{RT} \tag{10}$$

where k_B and h are the Boltzmann and Planck constants, respectively, and $\Delta^{\ddagger}G^{o}$ represents the Gibbs energy of activation. Combining Equations (5), (9), and (10), it is possible to conclude that

$$\Delta_r G^{o} = \Delta^{\ddagger}G_1^{o} - \Delta^{\ddagger}G_{-1}^{o} \tag{11}$$

where $\Delta^{\ddagger}G_1^{o}$ and $\Delta^{\ddagger}G_{-1}^{o}$ represent the Gibbs energies of activation for the forward and reverse reactions, respectively. Based on Equation (11), it is possible to understand why sometimes the kinetic and thermodynamic stability parallel one another. Since the quantities $\Delta_r G^{o}$, $\Delta^{\ddagger}G_1^{o}$, and $\Delta^{\ddagger}G_{-1}^{o}$ are not independent, as illustrated in Figure 1, a lower activation Gibbs energy (kinetic instability) may correspond to a more exergonic process (thermodynamic instability). However, this is only strictly true for elementary reactions and more often than not the parallel trend is not observed.

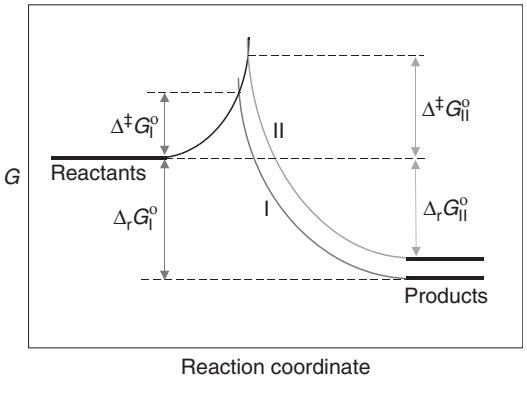

Figure 1 Gibbs energy profile illustrating the relationship between the decrease in energy of activation and the exergonicity of a reaction. Reaction II has a larger Gibbs energy of activation and is less exergonic than reaction I.

1.22.3 Thermochemical Measurements of Bond Strengths

A large number of organometallic thermochemistry studies were focused on the stability of chemical bonds rather than the stability of molecules as a whole. In this case, stability is associated with a strong bond and instability with a weak bond. Thermochemical measurements of bond strengths are normally given in terms of bond dissociation enthalpies, bond enthalpy terms, and, more infrequently, intrinsic bond enthalpies. Consider, for example, the molecule $MoCp_2Me_2$. The molybdenum–methyl bond dissociation enthalpy, DH^o(Mo–Me), corresponds to the standard enthalpy of the process:

$$MoCp_2Me_2(g) \rightarrow MoCp_2Me(g) + Me(g) \tag{12}$$

where a single Mo–Me bond is cleaved at constant temperature (usually 298.15 K) in the ideal gaseous state.

The molybdenum–methyl mean bond dissociation enthalpy, $\langle DH^o\rangle$ (Mo–Me), is related to the standard enthalpy of the reaction

$$MoCp_2Me_2(g) \rightarrow MoCp_2(g) + 2Me(g) \tag{13}$$

with $\langle DH^o\rangle$ (Mo–Me) $= \Delta_r H^o$ (13)/2.

The Mo–Cp and Mo–Me bond enthalpy terms, E (Mo–Cp) and E (Mo–Me), respectively, are defined in terms of the process:

$$MoCp_2Me_2(g) \rightarrow Mo(g) + 2Cp(g) + 2Me(g) \tag{14}$$

with $\Delta_r H^o$ (14) $= 2E$ (Mo–Cp) $+ 2E$ (Mo–Me).

Finally, the definition of the molybdenum–methyl intrinsic bond enthalpy or bond snap enthalpy, E_s (Mo–Me), is illustrated in Scheme 2. The asterisks in $MoCp_2Me^*$ and Me^* designate fragments retaining their original geometry in the precursor complex, and ER_1 and ER_2 are the reorganization energies associated with the relaxation of $MoCp_2Me^*$ and Me^* to originate $MoCp_2Me$ and Me in their ground states, respectively. Scheme 2 leads to E_s (Mo–Me) $= DH^o$ (Mo–Me) $- ER_1 - ER_2$. The values of the reorganization energies are not experimentally available, but can be estimated through computational chemistry calculations.

Note that bond dissociation enthalpies can also be used to calculate reaction enthalpies. For example, the enthalpy of the reaction

$$MoCp_2Me_2(g) + Cl_2(g) \rightarrow MoCp_2Cl_2(g) + C_2H_6(g) \tag{15}$$

is given by

$$\begin{aligned}\Delta_r H^o(15) = {} & 2\langle DH^o\rangle(\text{Mo–Me}) + DH^o(\text{Cl–Cl}) \\ & -2\langle DH^o\rangle(\text{Mo–Cl}) - DH^o(\text{Me–Me})\end{aligned} \tag{16}$$

According to the definition of bond dissociation enthalpy given above, reactants and products in reaction (12) must be in the ideal gas phase, where intermolecular interactions do not exist. There are many literature examples, however, where bond dissociation enthalpies have been reported in solution. Thus, the standard enthalpy of the reaction

$$MoCp_2Me_2(sln) \rightarrow MoCp_2Me(sln) + Me(sln) \tag{17}$$

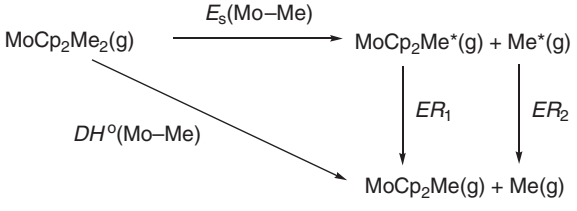

Scheme 2

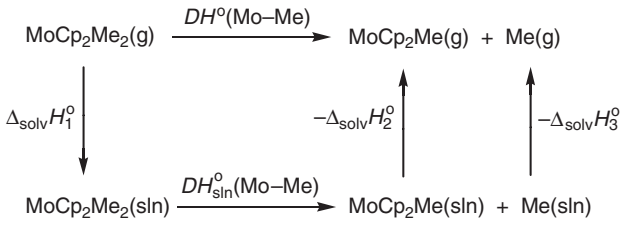

Scheme 3

represents DH^{o}_{sln}(Mo–Me). The relationship between DH^{o}(Mo–Me) and DH^{o}_{sln}(Mo–Me) is shown in Scheme 3, which translates into equation

$$DH^{o}(\text{Mo–Me}) = DH^{o}_{sln}(\text{Mo–Me}) + \Delta_{solv}H^{o}_{1} - \Delta_{solv}H^{o}_{2} - \Delta_{solv}H^{o}_{3} \tag{18}$$

It can be concluded from Equation (18) that DH^{o}(Mo–Me) = DH^{o}_{sln}(Mo–Me) when the solvation terms cancel out. This is seldom observed in practice, but there is some experimental evidence that the solvation effect may be largely canceled when the enthalpy of a reaction such as

$$MoCp_2Me_2(sln) + Cl_2(sln) \rightarrow MoCp_2Cl_2(sln) + C_2H_6(sln) \tag{19}$$

is considered:

$$\begin{aligned}\Delta_r H^{o}\,(19) = {} & 2\langle DH^{o}_{sln}\rangle(\text{Mo–Me}) + DH^{o}_{sln}(\text{Cl–Cl}) \\ & - 2\langle DH^{o}_{sln}\rangle(\text{Mo–Cl}) - DH^{o}_{sln}(\text{Me–Me}) \\ \approx {} & 2\langle DH^{o}\rangle(\text{Mo–Me}) + DH^{o}(\text{Cl–Cl}) \\ & - 2\langle DH^{o}\rangle(\text{Mo–Cl}) - DH^{o}(\text{Me–Me})\end{aligned} \tag{20}$$

1.22.4 The Tools of Organometallic Thermochemistry

The bond strengths and other quantities previously mentioned can sometimes be directly measured. However, they are often derived by conjugating a large variety of data (enthalpy of formation, equilibrium constant, Gibbs energy, proton affinity, electron affinity, ionization energy, standard electrode potential, activation energy, etc.) through appropriate thermodynamic cycles. The experimental determination of these quantities is usually a very specific task since the method of choice is not only dependent on the nature of the required information but also on the chemical composition, physical state, electrical charge, lifetime, and even the amount of the compound available for study. Many experimental methods have therefore been used in organometallic thermochemistry, and new methodologies are still being developed. Figure 2 gives a pictorial overview of some of the most representative ones and emphasizes the fact that the prediction of new data is also an important organometallic thermochemistry tool. Hence, three main "taxonomic" categories can be distinguished: (i) condensed phase methods; (ii) gas phase methods; and (iii) estimation methods. Only a brief survey of these methods will be made here, since they have been covered in the various reviews and monographs mentioned throughout this section. A good starting point to study the experimental methods is a review which discusses the procedures and approximations used in the derivation of the thermochemical data of interest from the directly measured quantities.[17]

Condensed phase methods include several calorimetric, equilibrium, kinetic, and electrochemical techniques. Combustion calorimetry in oxygen has been the most widely used technique to obtain enthalpies of formation of organic substances.[18–20] It has, however, played a much less important role in the study of organometallic compounds due to a number of limitations.[21–24] In principle, the complete oxidation of an organometallic compound in a water-saturated oxygen atmosphere ($p_{O_2} \approx 3$ MPa), to generate products of the combustion of the organic part of the molecule (e.g., CO_2, H_2O, NO_3^-) and a metallic oxide, would appear to be a promising general reaction to determine enthalpies of formation of organometallic substances. In practice, the experiments are seldom that simple. Many

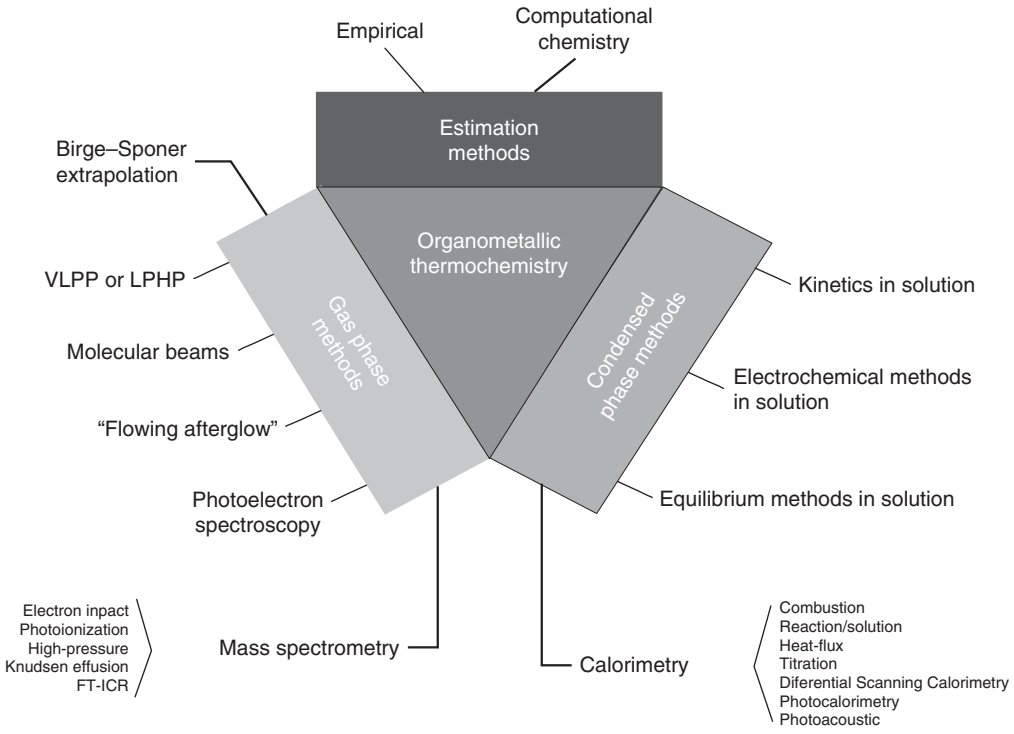

Figure 2 Some representative methods used in organometallic thermochemistry studies.

organometallic compounds are sensitive to oxygen and moisture and it may be difficult to ascertain that no decomposition of the sample occurs prior to combustion. This problem can sometimes be overcome by closing the sample in a container (e.g., polyethene bag or ampule), which burns during the calorimetric experiment. Yet, there is a cost to be paid in the precision of the measurements since the compound contributes a smaller fraction than usual to the observed change in combustion energy. Organometallic compounds usually exhibit problems of explosion on ignition and incomplete combustion. The use of combustion aids (e.g., benzoic acid, hydrocarbon oil, or the container protecting the sample from oxygen and moisture) can assist in moderating the combustion reaction and in ensuring the complete combustion of the organic part of the molecule. The inorganic products formed, however, are seldom simple stoichiometric oxides and an accurate characterization of the final state of the combustion process can be extremely difficult to achieve. Static-bomb combustion calorimetry has been advocated as a broad-spectrum method to obtain enthalpies of formation of organometallic compounds by the Nizhniy Novgorod thermodynamics group (Russia).[24] Nevertheless, it is generally agreed that this method is only adequate to study compounds of Hg and Sn.[22]

Some of the problems mentioned above may be eliminated by using the moving-bomb technique. In most modern instruments of this type, after the flame of the combustion reaction becomes extinguished, the bomb is simultaneously rotated about its axial and longitudinal axis. The rotation promotes an efficient contact between a suitable solution initially placed inside the bomb and all the other bomb contents, making it possible to obtain a mixture of homogeneous composition in the final state, with all solid residues formed dissolved. Finding such a solution is perhaps the major difficulty in the application of the moving-bomb method.[25] Reliable results have been obtained by the moving-bomb method for Si, Ge, As, Bi, and Pb organometallic compounds and also for Mn_2CO_{10} and WCp_2Cl_2.[22]

One of the major limitations of conventional macroscale combustion calorimetry is the amount of sample needed to determine the enthalpy of formation of a compound. Typically, samples of mass 0.5–1.0 g per experiment are used, and according to normal thermochemical practice a minimum of five results are needed to obtain the enthalpy of formation of a given compound. Enthalpies of combustion are also large and a high degree of purity of the sample (typically >99.9%) is necessary to attain an acceptable accuracy and precision. Only a limited number of organometallic compounds can, therefore, be obtained in the quantities and state of purity required for combustion measurements. Microcombustion calorimetry techniques requiring much smaller samples (<100 mg) have been slow to

develop.[23] Ferrocene is the only organometallic compound studied up to now at the microscale level and the obtained results are of poor accuracy.[26]

The determination of enthalpies of reaction in solution, using isoperibol reaction–solution calorimetry, is often the easiest and most accurate method of determining enthalpies of formation of organometallic compounds. Many types of isoperibol reaction–solution calorimeters have been developed,[27,28] some of which have been specifically designed for anaerobic operation.[29–31] The reaction or solution process under study is usually started by breaking a thin-walled glass ampule containing the sample, in an appropriate solution containing a second reagent that reacts with the compound under study. Alternatively, a solution of the sample may be introduced in the calorimeter via an automatic burette so that a titration may be performed.[29] Much less amount of sample per experiment is required (typically <100 mg) than in macrocombustion calorimetry. Problems of analysis of the final products are largely eliminated since a homogeneous solution is obtained in the final state (except in cases where precipitates are formed). The enthalpies of reaction to be measured (per gram of reactant) are normally significantly smaller than typical enthalpies of combustion (sometimes by a factor of 100), making the method less demanding than combustion calorimetry in terms of accuracy, precision, and purity of the sample. The accuracy of the method is essentially determined by chemical factors, such as reaction yields, which are less than 100%. Provided the reactions selected are clean, rapid (ca. 5 min), and quantitative, very reliable results can usually be obtained. The enthalpy of formation of a compound can only be derived from reaction–solution calorimetry results if a number of auxiliary data have been measured (solution enthalpies of reactants and products) and if the enthalpies of formation of the remaining reactants and products are available (which is often not the case). However, even when these conditions are not met, the enthalpy of reaction can still provide information on individual bond dissociation enthalpies in solution. This was illustrated above in the case of reaction (19) and Equation (20).

Another approach which has been developed by Skinner and co-workers is the measurement of enthalpies of thermal decomposition or halogenation by high-temperature heat-flux calorimetry.[32–39] In this procedure, a known mass of sample contained in a small glass capillary at room temperature is dropped into the sample cell of a high-temperature Calvet microcalorimeter while an identical but empty capillary is simultaneously dropped into a reference cell. This differential procedure allows the measurement of the heat effect associated solely with the process taking place in the sample cell. Both cells are kept at the same constant temperature. The sample cell may initially be empty if one wishes to study a thermal decomposition or contain I_2 or Br_2 vapor if the measurement of an enthalpy of a halogenation reaction is desired. This technique has the advantage that very small samples (ca. 5 mg) are required for each measurement. In addition, it can often be used for measuring the enthalpies of vaporization or sublimation of the organometallic complexes. However, thermal decomposition or high-temperature halogenation reactions may not yield simple products. Where it has been possible to compare the results of carefully performed high-temperature heat-flux calorimetry experiments with those of other methods, the agreement has generally been good.[35]

Differential scanning calorimetry (DSC) has been employed to obtain enthalpies of thermal decomposition of organometallic substances.[40] Details of the data treatment to extract $\Delta_r H^o$ from the obtained results have been discussed.[41] Sometimes information on the reaction kinetics can simultaneously be derived from the same data used to compute $\Delta_r H^o$.[42] In addition, the method can also be used to obtain enthalpies of phase transitions (fusion, vaporization, sublimation) and other thermodynamic properties, such as heat capacities.[40] All measurements are done by monitoring the change of the difference between the heat flow rate or power to a sample (S) and to a reference material (R), as a function of time or temperature, while both S and R are subjected to a controlled temperature program.[40,43–45] The DSC method requires only small samples (ca. 1–10 mg) but, on the other hand, the accurate determination of the final state of the thermal decomposition reaction may be a major problem.

A number of photocalorimeters have been applied to study radiation-activated processes involving organometallic compounds. In general, these instruments are "classical" (reaction–solution, heat-flux or DSC) calorimeters to which an optical system has been adapted. Comprehensive reviews of photocalorimetric methods, including examples of applications to organometallic systems, have been published by Teixeira.[46,47]

All calorimetric methods mentioned up to now are adequate to study reactions with durations that range from a few seconds to days. Photoacoustic calorimetry (PAC) enables the study of very rapid processes such as radical–molecule reactions in solution. In the basic design of a photoacoustic calorimeter, a solution of the sample is continuously passed through a UV–VIS absorption flow cell. A pulse from a laser is fired at the cell and part of its energy is absorbed by the photoreactive sample, initiating the reaction of interest, while the remaining excess laser energy is deposited in the solution as heat. The abrupt and localized heating causes the solution to expand locally, thus producing a wave that propagates through the fluid at the speed of sound. This wave is detected by an ultrasonic piezoelectric microphone connected to an oscilloscope. The corresponding amplitude can be related to the heat deposited in

solution through appropriate calibration of the apparatus, and the enthalpy of the reaction of interest, $\Delta_r H$, is derived from an energy balance which, in the absence of secondary reactions or energy loss by fluorescence, may be written as

$$E_m = \Delta_{obs}H + \Phi_r \Delta_r H \tag{21}$$

In Equation (21) E_m is the molar energy input corresponding to the laser photon energy $N_A h\nu$, $\Delta_{obs}H$ is the amount of heat dissipated in solution, and Φ_r is the reaction quantum yield. The basic theory of the photoacoustic effect was described by Tam and Patel[48,49] and the use of the photoacoustic calorimety technique as a thermochemical tool was recently examined.[50,51] Applications to organometallic thermochemistry were reviewed by Braslavski and Heibel.[52] The method has provided a significant amount of information on the bonding energetics of compounds of main group elements. Important studies on organotransition metal species have also been made, but several complicating factors are involved in this case, namely considerable solvation effects in the coordinatively unsaturated complexes formed in the reactions, lack of reliable values for quantum yields, and the occurrence of secondary reactions.

Equilibrium and kinetic techniques have also been applied to thermochemical studies of organometallic compounds in solution. The equilibrium approach consists in measuring the equilibrium constant (K) of a well-characterized process as a function of the temperature.[53] This can be achieved by a large variety of methods, such as NMR, FT-IR, and UV–Vis. A van't Hoff analysis of the obtained results leads to $\Delta_r H^o$ and $\Delta_r S^o$ for the process under study.[54–56] This analysis usually assumes that $\Delta_r H^o$ is constant over the temperature range covered by the experiments. Thus, in principle, the accuracy of the obtained $\Delta_r H^o$ values is poorer than when direct measurements by calorimetry are performed.[57–59] Typical problems of the application of this method to organometallic compounds are: (i) the difficulty in finding simple and rapid equilibria; (ii) the inaccuracy associated with the measurement of very large or very small equilibrium constants; (iii) and the thermal instability of some of the species involved, which precludes the measurement of K over a sufficiently wide temperature range. A review that covers the application of the equilibrium method to organometallic compounds (although with emphasis on the entropic term) has been published.[11,14]

The kinetic methodologies involve fitting the Arrhenius or Eyring equations[16] to rate constant (k) and temperature data to yield the activation enthalpies of processes such as (M = metal; L, X = ligands):

$$L_nM\text{–}X(sln) \underset{k_{-1}}{\overset{k_1}{\rightleftharpoons}} L_nM(sln) + X(sln) \tag{22}$$

The corresponding enthalpies of reaction, which in this case coincide with DH^o_{sln} (M–X), can be derived as

$$\Delta_r H^o = \Delta^{\ddagger}H^o_1 - \Delta^{\ddagger}H^o_{-1} \tag{23}$$

where $\Delta^{\ddagger}H^o_1$ and $\Delta^{\ddagger}H^o_{-1}$ represent the enthalpies of activation for the forward and reverse processes. Some of the drawbacks of this approach are common to those of the equilibrium method. For example, the thermal instability of some of the species involved may hinder the measurement of k over a sufficiently wide temperature range. Often more important, however, is the fact that the derived reaction enthalpies usually rely on a number of hypotheses or approximations that are difficult to assess and take into account.[60–62] For example, the results may be based on an assumed mechanism for the reaction under investigation, the value of $\Delta^{\ddagger}H^o_{-1}$ is ignored or estimated as 8–13 kJ mol^{-1} (for diffusion-controlled recombination reactions), and the parameters necessary to model radical cage effects are frequently not available.[60–62]

Thermodynamic cycles involving standard electrode potentials obtained by cyclic voltammetry have also been used to provide thermochemical information on organometallic compounds.[63–65] This so-called electrochemical method leads to Gibbs energies of reaction in solution, from which bond dissociation enthalpies may be derived using a number of auxiliary data that are often estimated. For example, the derivation of a metal–hydrogen bond dissociation enthalpy in an L_nMH species requires; (i) an estimate of the reduction potential of H^+ in the same solvent where the experiments were carried out; (ii) an estimate of the solvation entropies of L_nMH, L_nM, and H; and (iii) the knowledge of the pK_a of L_nMH.[17,64]

A large number of methods are used to obtain gas-phase thermochemical information on organometallic compounds and only a fraction is indicated in Figure 2. The majority of them involve ions, since they are easier to detect and their kinetic energies are easier to control (by means of electric and magnetic fields) than neutral molecules.[66–68] Information on neutral species can, however, be obtained from ion thermochemistry results, through thermodynamic cycles based on appearance energies (AE), ionization energies (E_i), electron affinities (E_{ea}), proton affinities (PA), gas-phase acidities ($\Delta_{acid}H^o$), etc.[66,68,69] This is illustrated in Schemes 4 and 5, which enable the calculation of several

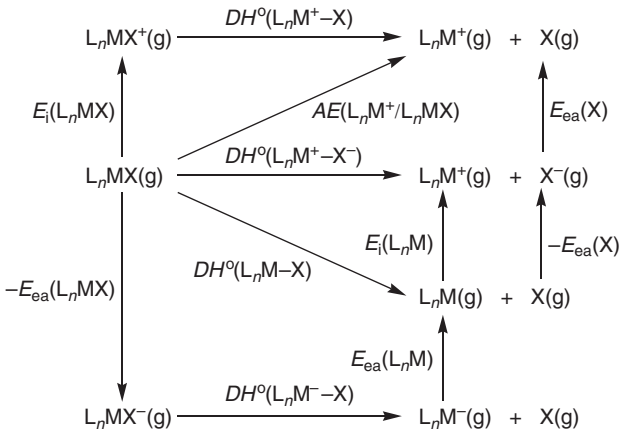

Scheme 4

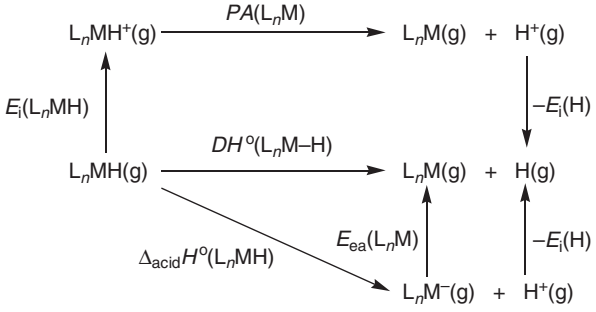

Scheme 5

types of $L_nM–X$ or $L_nM–H$ bond dissociation enthalpies. Thus, from Scheme 4 the following equations can be derived:

$$DH^o(L_nM–X) = DH^o(L_nM^+–X^-) - E_i(L_nM) + E_{ea}(X) \quad (24)$$

$$DH^o(L_nM–X) = DH^o(L_nM^+–X) + E_i(L_nMX) - E_i(L_nM) \quad (25)$$

$$DH^o(L_nM–X) = DH^o(L_nM^-–X) - E_{ea}(L_nMX) + E_{ea}(L_nM^-) \quad (26)$$

$$DH^o(L_nM–X) = AE(L_nM^+/L_nMX) - E_i(L_nM) \quad (27)$$

Scheme 5 leads to

$$DH^o(L_nM–H) = PA(L_nM) + E_i(L_nMH) - E_i(H) \quad (28)$$

$$DH^o(L_nM–X) = \Delta_{acid}H^o(L_nMH) + E_{ea}(L_nM) - E_i(H) \quad (29)$$

Many ionization energies of neutral organometallic species, L_nMX, have been measured by electron impact mass spectrometry (EIMS):[69–72]

$$L_nMX(g) + e^-(g) \rightarrow L_nMX^+(g) + 2e^-(g) \quad (30)$$

In these experiments E_i is obtained from an ionization efficiency curve (i.e., a plot of the ion intensity against the electron energy) as the minimum electron energy required for ionization. The identification of this threshold is difficult, particularly when polyatomic molecules are studied and non-monoenergetic electron beams are used. Thus, unpredictable uncertainties of 10–50 kJ mol^{-1} or more may be associated with many of the early EIMS values of E_i

reported for organometallic compounds.[73] A better alternative in terms of accuracy is provided by photoelectron spectroscopy (PES), including several coincidence and zero electron kinetic energy (ZEKE) methods, or by photoionization mass spectrometry (PIMS).[66,68,74] Both methods refer to the process:

$$L_nMX(g) + h\nu \rightarrow L_nMX^+(g) + e^-(g) \tag{31}$$

In photoelectron spectroscopy the photon energy is fixed at a value higher than $E_i(L_nMX)$ and the kinetic energy of the ejected electron is measured, while in the PIMS method the energy of the photon is varied until the onset of L_nMX^+ production is detected.

Photoionization has a number of advantages over electron impact ionization, such as greater sensitivity and thresholds that are easier to define. In coincidence photoelectron techniques (e.g., photoelectron photoion coincidence spectroscopy, PEPICO, and threshold photoelectron photoion coincidence spectroscopy, TPEPICO), the photoelectron and the photoion formed in the ionization process are detected simultaneously, thus providing information on the nature and energies of the ionized products.[66,68,75,76]

Photoelectron spectroscopy of anions and photodetachment thresholds for the loss of an electron by an anion yield electron affinities according to[66,68]

$$L_nMX^-(g) + h\nu \rightarrow L_nMX(g) + e^-(g) \tag{32}$$

Appearance energies may be obtained by electron impact mass spectrometry[73]

$$L_nMX(g) + e^-(g) \rightarrow L_nM^+(g) + X(g) + 2e^-(g) \tag{33}$$

or from dissociative photoionization threshold experiments:[77]

$$L_nMX(g) + h\nu \rightarrow L_nM^+(g) + X(g) + e^-(g) \tag{34}$$

As mentioned above, photoionization methods usually lead to more accurate results than the electron impact ionization techniques.

A significant fraction of the reported thermochemical data on charged organometallic compounds comes from Fourier-transform ion cyclotron resonance (FT-ICR) experiments. In this method, positive or negative ions are generated from a volatile precursor and trapped inside a cell by means of electric and magnetic fields. The ions can be stored for periods of up to several seconds (delay period) under cyclotron movement, at pressures below 1.3×10^{-4} Pa. While trapped they can react with neutrals, such as the parent molecule or other substances deliberately introduced in the system through leak valves or pulsed valves. Mass spectra at different delay times can be recorded. Kinetic or equilibrium information about the reaction can therefore be obtained by following the concentration of a particular reactant or product ion as a function of time. These studies may lead, for example, to equilibrium and rate constants, proton affinities, gas-phase acidities, ionization energies, electron affinities, and bond dissociation enthalpies. Many of the thermochemical data on organometallic compounds obtained by FT-ICR rely on the bracketing method. The fundamental assumption of this technique is that if a reaction is observed in the FT-ICR experiment, then its $\Delta_r H^o$ is less than ca. 8 kJ mol^{-1}.[78] The species of interest is successively reacted with a series of reference compounds with known values of the thermochemical property of interest (e.g., bond dissociation enthalpy, electron affinity, proton affinity). The reference compounds are ordered according to the value of that property and a "yes" or "no" process is used to indicate whether they have reacted or not with the compound under study. Low and high limits for the unknown thermochemical property of the compound can then be established.

Dissociation energies for a variety of metal–ligand bonds in coordinatively unsaturated organometallic molecules have been obtained by guided ion-beam mass spectrometry (GIBMS) techniques.[79–82] In this case, the threshold energies (E_o) for the endothermic reactions (M^+ = bare metal ion; L = ligand of interest; X = fragment of the precursor molecule LX)

$$M^+(g) + LX(g) \rightarrow ML^+(g) + X(g) \tag{35}$$

$$ML^+(g) + Xe(g) \rightarrow M^+(g) + L(g) + Xe(g) \tag{36}$$

are obtained from plots of the ion intensities against the kinetic energies of the reactants. Assuming that there are no activation barriers for the reverse reactions, these results lead to the bond dissociation enthalpies at zero kelvin, $DH_0^o(M^+–L)$, as

$$DH_0^o(M^+–L) = DH_0^o(L–X) - E_0(35) \tag{37}$$

$$DH_0^o(M^+–L) = E_0(36) \tag{38}$$

where E_o (35) and E_o (36) represent, respectively, the threshold energies for reactions (35) and (36). The values of $DH_{298}^o(M^+–L)$ can subsequently be derived after the appropriate thermal corrections are accounted for. The threshold of the reaction

$$M^+(g) + LX(g) \rightarrow ML(g) + X^+(g) \tag{39}$$

affords the bond dissociation enthalpy in the neutral species ML as

$$DH_0^o(M–L) = DH_0^o(L–X) + E_i(L) - E_i(M) - E_0(39) \tag{40}$$

Flowing afterglow (FA) techniques have been used to measure several thermochemical properties of neutral species, among them anion and electron affinities, acidities, and bond dissociation enthalpies.[83–85] Ions are generated from a suitable precursor by a variety of means (e.g., electron impact), and carried by a flow of helium gas through a long (ca. 1 m) tubular reactor coupled to a mass spectrometer detector for ion analysis. Several inlets placed along the tube, or a moveable injector, are used to introduce neutral reactant gases. The ion–molecule reactions occur at pressures of ca. 100 Pa, thus thermalizing the ions by their multiple collisions with the inert carrier gas. The steady-state concentration of the ions of interest can be monitored as a function of time, by varying the neutral inlet position at fixed flow rate or the neutral flow rate at fixed inlet position, thus affording kinetic and equilibrium information on the observed ion–molecule reactions.

Another technique that has been applied to thermochemical studies of organometallic species is commonly known as kinetic energy release distribution (KERD).[86,87] In this method, the translational energy distribution (the KERD) of a given fragment resulting from the exothermic decomposition of a metastable ion in the field-free region of, for example, a reverse geometry double focusing mass spectrometer

$$(L_nMX^+)^*(g) \rightarrow L_nM^+(g) + X(g) \tag{41}$$

is determined. Fitting the observed distribution by using, for example, statistical phase space theory may lead to $DH_0^o(M^+–L)$.

Knudsen cell mass spectrometry, also known as high-temperature mass spectrometry, has been widely used to study the thermochemistry of simple species, including diatomic metal carbides, hydrides, nitrides, oxides, sulfides, diatomic molecules containing two transition metal atoms, and MC_n clusters.[88–94] More complex molecules have also been investigated.[95] A Knudsen cell can be viewed as a reactor with a small and very thin hole in one of the walls.[96] If the area of the hole is sufficiently small, the number of reactant and product molecules effusing through it will be negligible compared to those existing inside the cell. Thus, to a very good approximation, equilibrium can be attained in a properly designed Knudsen cell. The relative concentrations of all species in equilibrium inside the cell, and therefore the equilibrium constant, may be determined by mass spectrometric analysis of the effusing vapor. Measurements of the equilibrium constant as a function of the temperature subsequently lead to the corresponding $\Delta_r H^o$ and $\Delta_r S^o$ values.

High-pressure mass spectrometry[86,97–99] and pulsed high-pressure mass spectrometry[100–104] have also been a source of thermochemical data for organometallic compounds (e.g., proton affinities, electron affinities, and bond dissociation enthalpies). The essential difference between both techniques is the fact that in the former the reactants are produced outside the collision cell.

Kinetic studies of pyrolysis processes in the gas phase have been an important source of bond dissociation enthalpy data for organometallic neutral molecules. In the case of very low pressure pyrolysis (VLPP),[105] a precursor molecule

L_nMX undergoes unimolecular decomposition by collision with the walls of a Knudsen cell flow reactor maintained at constant temperature:

$$L_nMX(g) \rightarrow L_nM(g) + X(g) \quad (42)$$

The rate constant, k, of the process under study is obtained by monitoring the composition of the effusing vapor as a function of time, by mass spectrometry. Measurements of k as a function of the temperature afford the activation energy from which a bond dissociation enthalpy may be derived. The experiments are carried out at low pressure (ca. 0.1 Pa) and keeping the residence times of the reactant mixture in the reactor small. This ensures that each L_nMX molecule essentially collides with the cell walls and not with another precursor molecule or decomposition fragment, thus avoiding complicating bimolecular reactions. An important problem in VLPP studies of organometallic compounds is the possible occurrence of competing processes involving catalytic decomposition pathways of L_nMX at the cell walls. This difficulty is removed in laser-powered homogeneous pyrolysis (LPHP) experiments where the precursor is thermally activated by collision with a bath gas.[106–109]

Bond dissociation enthalpies for many diatomic neutral molecules including, for example, metal hydrides, have been obtained by the Birge–Sponer extrapolation method.[110,111] This method is based on the analysis of the vibrational energy levels in a molecule obtained from spectroscopic studies.

As mentioned above, empirical estimation schemes and computational chemistry calculations provide essential contributions to narrow the gap between the available thermochemical data and the number of molecules for which data have not been experimentally determined. The comprehensive review of these methods is outside the scope of this work. Overviews of representative contributions from empirical schemes[14,112–114] and computational chemistry calculations[113,115] to organometallic thermochemistry have recently been published.

1.22.5 Energetics of Some Key Elementary Reactions

The thermodynamic analysis of a complex chemical process has both the advantage and the limitation of being concerned only with the reactants and products of the reaction. This blindness to the mechanistic details ensures that the analysis is correct even if the model designed for the path is not, but misses all the important chemical events that account for the transformation of the molecules. This point can be illustrated through Scheme 6, which represents the catalytic cycle of alkene hydrogenation. While the net thermodynamic efficiency of the process is only dictated by the enthalpies of formation of the olefin, hydrogen, and the alkane, its feasibility depends on the thermodynamics of each "elementary" step.

In this section we will apply some of the concepts mentioned above to discuss the energetics of a number of relevant elementary reactions. The required bond enthalpy values will be taken from Table 1 and the entropy values from the literature or estimated. It is worth pointing out that $T\Delta_r S^o$ terms are often disregarded in similar discussions, mainly because most enthalpy data are obtained by calorimetric methods, rather than by van't Hoff plots. However, they may determine the thermodynamics of organometallic reactions and therefore should always be considered. As mentioned above, there is a very simple method to estimate entropy terms.[14] This method will be used in the following discussion. The temperature will always be referred to 298 K, unless stated otherwise.

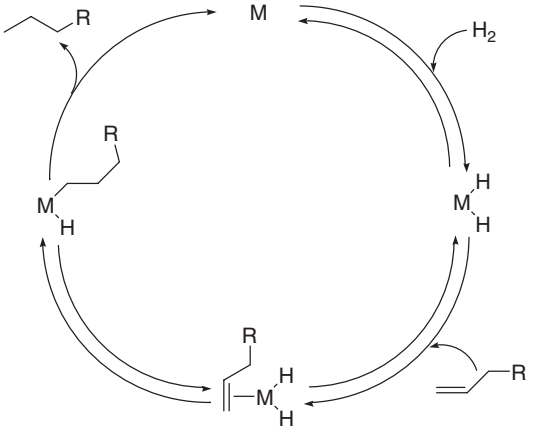

Scheme 6

Table 1 Bond dissociation enthalpies, $\langle DH^\circ \rangle$ (M–R) or DH° (M–R)[a]

	R					
Molecule[b]	*H*	*Me*	*Et*	*Bu*	*Ph*	*Bz*
RH[c]	436	439	421	418	465	368
$Th(Cp^*)_2R_2$	390	339	318	307	372	
$U(Cp^*)_2R_2$	(340)	300			(330)	251
$Ti(Cp)_2R_2$		298			332	237
$Zr(Cp^*)_2R_2$	330	284	(266)	(263)	312	
$Hf(Cp^*)_2R_2$	340	306		274	(332)	
$Nb(Cp)_2R_2$		263				
$Cr(Cp)(CO)_3R$	258					
$Cr(CO)_3(PCy_3)_2(H_2)$	31[d]					
$Mo(Cp)(CO)_3R$	280	203	185			154
$Mo(Cp)_2R_2$	257	172	156	154		
$Mo(CO)_3(PCy_3)_2(H_2)$	27[d]					
$W(Cp)(CO)_3R$	339					
$W(Cp)_2R_2$	311	221			(247)	
$W(CO)_3(PCy_3)_2(H_2)$	40[d]					
$Mn(CO)_5R$	245	190			207	129
$Re(CO)_5R$		220				
$Fe(CO)_4H_2$	272					
$Ru(oep)R_2$			91			
$Co(CO)_4H$	227					
$Co(dmg)_2(py)R$		138				136
$Rh(Cl)[P(o\text{-tolyl})_3]_3H_2$	242					
Rh(oep)R	259					
$Rh(Cp^*)(PMe_3)(R)H$		D2		(D2 − 28)	D2 + 55	
$Ir(Cl)(CO)(PPh_3)_2R_2$	247					
$Ir(Cl)(CO)(PCy_3)_2H_2$	240					
$Ir(Cl)(CO)[P(OPh)_3]_2H_2$	244					
$Ir(I)(CO)(PCy_3)_2H_2$	256					
$Ir(I)(CO)[P(OPh)_3]_2H_2$	224					
$Ir(Cl)(CO)(PMe_3)_2(I)R$	D1	D1 − 103	D1 − 113			D1 − 138
$Ir(Cp^*)(PMe_3)R_2$	310	243			330	
cis-$Pt(PEt_3)_2R_2$		269			(298)	
trans-$Pt(PEt_3)_2(Cl)H$	307		206			
trans-$Pt(PPh_3)_2(Cl)H$	(307)					

[a]Data in kJ mol^{-1}. Values quoted from Ref: 124, except for the dihydrogen group 6 complexes.[126,127] Estimates are in parentheses. Other estimates are given in text.
[b]Cp = η^5-cyclopentadienyl, Cp* = η^5-pentamethylcyclopentadienyl, Cy = cyclohexyl, dmgH = dimethylglyoxime, oep = octaethylporphyrin, py = pyridine, tolyl = MeC_6H_4.
[c]To ensure thermochemical consistency, the H–H and C–H bond dissociation enthalpies were also quoted from Ref: 124. In the cases of ethane, butane, benzene, and toluene, these are not the most updated values (see, for instance, Blanksby, S. J.; Ellison, G. B. *Acc. Chem. Res.* **2003**, *36*, 255), but the (upward) adjustments are smaller than the uncertainties of the metal–carbon bond dissociation enthalpies.
[d]DH° (M–H_2).

1.22.5.1 Hydrogen Activation

The three basic modes of hydrogen activation by a transition metal complex (M, ML, M_2, or MX) are illustrated by reactions (43)–(46).[116,117] A *cis*-oxidative addition of H_2 to the metal center(s) occurs in (43)–(45), whereas (46) is commonly described as heterolytic splitting of H_2:

$$M + H_2 \rightarrow MH_2 \quad (43)$$

$$ML + H_2 \rightarrow MH_2 + L \quad (44)$$

$$M_2 + H_2 \rightarrow 2MH \tag{45}$$

$$MX + H_2 \rightarrow MH + HX \tag{46}$$

The homolytic cleavage of the H–H bond requires an enthalpy of 436 kJ mol^{-1} and the entropy term of reaction (43) is estimated as $T\Delta_r S^o(43) \approx -40$ kJ mol^{-1}. Thus, for example, for an equilibrium constant equal to 0.5, $\Delta_r G^o(43) = -1.7$ kJ mol^{-1} implying $-\Delta_r H^o(43) = 2\langle DH^o\rangle(\text{M–H}) - DH^o(\text{H–H}) \approx 42$ kJ mol^{-1} or $\langle DH^o\rangle(\text{M–H}) = 239$ kJ mol^{-1}. The values in Table 1 are usually higher, thus indicating that reaction (43) should occur with a good yield, under relatively mild conditions, for a large variety of complexes.[117] While this is so for many coordinatively unsaturated molecules, for example, square-planar d^8 complexes, it is not observed when the metal center is coordinatively saturated. In this case, the oxidative addition requires a previous dissociation of a ligand L, reaction (44), which can be energetically demanding. Examples of the above processes are provided by reactions (47) and (48).[116] In reaction (47) the iridium center is unsaturated and the hydrogen activation occurs at room temperature and atmospheric pressure:

$$Ir(Cl)(CO)(PPh_3)_3(sln) + H_2(sln) \rightarrow Ir(Cl)(CO)(PPh_3)_3H_2(sln) \tag{47}$$

$$Os(CO)_4(PPh_3)(sln) + H_2(sln) \rightarrow Os(CO)_3(PPh_3)H_2(sln) + CO(sln) \tag{48}$$

By contrast, the H_2 addition in reaction (48) requires drastic temperature and pressure conditions (373 K, 80 atm). The thermodynamic analysis of both processes can be made with a bit of speculation in the case of reaction (48). The enthalpy of reaction (47), $\Delta_r H^o(47) = DH^o(\text{H–H}) - 2\langle DH^o\rangle(\text{Ir–H}) = 436 - 2\times 247 = -58$ kJ mol^{-1}, leads to $\Delta_r G^o(47) = -18$ kJ mol^{-1}, by assuming $T\Delta_r S^o(47) \approx -40$ kJ mol^{-1}. On the other hand, although the enthalpy of reaction (48) is predicted to be less exothermic (ca. -4 kJ mol^{-1}), the entropy term $T\Delta_r S^o(48)$ becomes favorable (ca. $+28$ kJ mol^{-1}) due to the high entropy of carbon monoxide, yielding $\Delta_r G^o(48) = -32$ kJ mol^{-1}. If this estimate is correct,[118,119] the fact that both $\Delta_r G^o(47)$ and $\Delta_r G^o(48)$ imply large equilibrium constants indicates that the severe experimental conditions for the synthesis of the osmium dihydride do not stem from the net thermodynamics of the reaction, but rather have a kinetic origin (cleavage of a strong Os–CO bond).

The enthalpy balance of hydrogen addition to a binuclear complex M_2 (reaction (45)), given by $\Delta_r H^o(45) = DH^o(\text{M–M}) + DH^o(\text{H–H}) - 2DH^o(\text{M–H})$, is less exothermic than $\Delta_r H^o(43)$, due to the cleavage of the metal–metal bond. The entropy term, however, is more favorable: $T\Delta_r S^o(45) \approx 4$ kJ mol^{-1}. Let us take some examples, involving the complexes $[M(Cp)(CO)_3]_2$ (M = Cr, Mo, and W), $Mn_2(CO)_{10}$, $Co_2(CO)_8$, and $[Rh(oep)]_2$. The enthalpies of reactions (49)–(54), as derived from data in Table 1 and from $DH^o(\text{M–M}) = 66$ (M = Cr), 136 (Mo), 234 (W), 159 (Mn), 64 (Co), and 69 (Rh) kJ mol^{-1}, lead to $\Delta_r H^o(49) = -14$ kJ mol^{-1}, $\Delta_r H^o(50) = 12$ kJ mol^{-1}, $\Delta_r H^o(51) = -8$ kJ mol^{-1}, $\Delta_r H^o(52) = 105$ kJ mol^{-1}, $\Delta_r H^o(53) = 46$ kJ mol^{-1}, and $\Delta_r H^o(54) = -13$ kJ mol^{-1}:

$$[Cr(Cp)(CO)_3]_2(sln) + H_2(sln) \rightarrow 2Cr(Cp)(CO)_3H(sln) \tag{49}$$

$$[Mo(Cp)(CO)_3]_2(sln) + H_2(sln) \rightarrow 2Mo(Cp)(CO)_3H(sln) \tag{50}$$

$$[W(Cp)(CO)_3]_2(sln) + H_2(sln) \rightarrow 2W(Cp)(CO)_3H(sln) \tag{51}$$

$$Mn_2(CO)_{10}(sln) + H_2(sln) \rightarrow 2Mn(CO)_5H(sln) \tag{52}$$

$$Co_2(CO)_8(sln) + H_2(sln) \rightarrow 2Co(CO)_4H(sln) \tag{53}$$

$$[Rh(oep)]_2(sln) + H_2(sln) \rightarrow 2Rh(oep)H(sln) \tag{54}$$

With exception of the manganese and cobalt complexes, the Gibbs energies of these reactions are therefore negative or close to zero. The value for H_2 addition to $Co_2(CO)_8$ relies on the enthalpies of formation of the complexes,[11] and disagrees with the results of several direct measurements of $\Delta_r H^o(53)$, namely 13.4, 26.4, 27.6, and 13.0 kJ mol^{-1}.[11,120–122] The lower values, ca. 13 kJ mol^{-1}, may be more accurate than the value of 46 kJ mol^{-1}, since they lead to $DH^o(\text{Co–H}) = 244$ kJ mol^{-1}, which is in better agreement with a more recent electrochemical result, $DH^o(\text{Co–H}) = 278$ kJ mol^{-1},[11,123] than the value in Table 1. The only striking result from the above analysis is

therefore the one for the manganese complex. $\Delta_r G^o(52) \approx 101\,kJ\,mol^{-1}$ suggests that $Mn_2(CO)_{10}$ would not be a hydrogenation catalyst precursor, which is contrary to experimental observation. It is important to note that although the absolute values of DH^o(Mn–Mn) and DH^o(Mn–H) are controversial,[124] they are interrelated, so that $\Delta_r H^o(52)$ (which can actually be derived from the enthalpies of formation of the complexes)[11] does not change if a different (but consistent) pair of values is selected. There being no reason to question the accuracy of the thermochemical results (enthalpies of formation), the value for $\Delta_r H^o(52)$ thus suggests that the mechanism of the catalytic hydrogenation by $Mn(CO)_5H$ does not involve the direct addtion of H_2 to $Mn_2(CO)_{10}$.

The net thermodynamic result of an alternative mechanism for the formation of metal monohydrides, the termolecular reaction (55),[116,117] is identical to reaction (45) if a previous cleavage of the metal–metal bond is required:

$$2M + H_2 \rightarrow 2MH \tag{55}$$

If this step is not needed, or can be achieved by external (e.g., photochemical) means, then the formation of MH becomes very favorable: $\Delta_r G^o(55) < 0$ despite the entropy term $T\Delta_r S^o(55) \approx -44\,kJ\,mol^{-1}$, since $\Delta_r H^o(55) = DH^o(H–H) - 2DH^o(M–H)$ is rather exothermic (see data in Table 1).

The formation of monohydrides via the heterolytic splitting of H_2 (reaction (46)) can be illustrated by reaction (56). Here, the entropy term $T\Delta_r S^o(56)$ is expected to be small, ca. $4\,kJ\,mol^{-1}$, but the enthalpy change is estimated as $\Delta_r H^o(56) = DH^o(Pt–Cl) + DH^o(H–H) - DH^o(Pt–H) - DH^o(H–Cl) \approx -14\,kJ\,mol^{-1}$. An important driving force of the reaction is therefore the stabilization of the proton by the basic ligand X (in this case X = Cl):

$$cis\text{-}Pt(PPh_3)_2Cl_2(sln) + H_2(sln) \rightarrow cis\text{-}Pt(PPh_3)_2(Cl)H(sln) + HCl(sln) \tag{56}$$

A likely intermediate in hydrogen activation reactions, including heterolytic splitting, is a hydrogen species where H_2 is η^2-bonded to the metal center. The first stable dihydrogen molecule (and recognized as such) has been isolated by Kubas *et al.* in 1983,[125] and some thermochemical studies on this type of molecules have appeared since then.[11,126,127] The enthalpy of reaction (57), $\Delta_r H^o(57) = -30.5$, -27.2, and $-40.2\,kJ\,mol^{-1}$ for M=Cr, Mo, and W, respectively, measures $DH^o(M–H_2)$:

$$M(CO)_3(PCy_3)_2(sln) + H_2(g) \rightarrow M(CO)_3(PCy_3)_2(H_2)(sln) \tag{57}$$

The entropy terms were also determined as -32 and $-30\,kJ\,mol^{-1}$ for the chromium and molybdenum reactions, leading to $\Delta_r G^o(57)$ values close to zero. As remarked by Hoff and co-workers,[126,127] this is in keeping with the reversibility of the above reaction for the three metals.

An appropriate question at this stage is why the hydrogen addition in reaction (57) does not proceed to the metal dihydride:

$$M(\eta^2–H_2) \rightleftarrows MH_2 \tag{58}$$

Indeed the bond data in Table 1 would suggest that this transformation should be rather exothermic, particularly for the tungsten complex. It is known that the bonding of H_2 to the metal center involves electron donation from the H_2 σ-orbital to the empty metal fragment σ-orbital and some back donation into the H_2 σ^*-orbital. A strong backdonation weakens the H–H bond and favors the dihydride formulation. Strong π-acid ligands, such as CO, coordinated to the metal, will compete for this electron backdonation, stabilizing the η^2-H_2 complex. As stated by Kubas and co-workers,[128] a fine balance of steric and electronic factors dictates whether a H_2 complex is stable at room temperature or proceeds to the dihydride. An example where the equilibrium (58) has been observed concerns the complexes $W(CO)_3[P(i\text{-}Pr)_3]_2(H_2)$ and $W(CO)_3[P(i\text{-}Pr)_3]_2H_2$:

$$W(CO)_3[P(i\text{-}Pr)_3]_2(H_2)(sln) \rightleftarrows W(CO)_3[P(i\text{-}Pr)_3]_2H_2(sln) \tag{59}$$

Where Pr stands for C_3H_7. Proton NMR experiments at several temperatures have shown that the relative stability of the dihydride increases at higher temperatures. A thermodynamic analysis of the reaction led to $\Delta_r H^o(59) = 5.0 \pm 2.5\,kJ\,mol^{-1}$ and $T\Delta_r S^o(59) \approx 1.5 \pm 2.6\,kJ\,mol^{-1}$.[129] As $\Delta_r H^o(59) = DH^o(W–H_2) + DH^o(H–H) - 2\langle DH^o\rangle(W–H)$, the above value of $DH^o(W–H_2)$ yields $\langle DH^o\rangle(W–H) = 236\,kJ\,mol^{-1}$. This tungsten–hydrogen mean bond dissociation enthalpy in the W(II) seven-coordinate complex is about $100\,kJ\,mol^{-1}$ lower than $DH^o(W–H)$ in $W(Cp)(CO)_3H$, where the metal is in the same oxidation state!

The observation of equilibrium (59) and the dramatic decrease of tungsten–hydrogen bond enthalpy in a seven-coordinate molecule are useful to emphasize our present ignorance about the "fine details" of metal–hydrogen bonding energetics in transition metal complexes. What we do know, based on experimental measurements, is almost limited to the fact that those bond dissociation enthalpies in a given group usually increase with atomic number. We also have some quantitative evidence that there is a marked decrease of DH^{o}(M–H) with increasing oxidation state of the metal (see data for group 6 $M(Cp)_2H_2$ and $M(Cp)(CO)_3H$ complexes in Table 1) and with increasing coordination number. This last conclusion, which is of course valid only if the oxidation state of the metal does not change, relies on the above calculation for the seven-coordinate tungsten complex and on the experimental values for the Ir(III) complexes $Ir(Cl)(CO)(PPh_3)_2H_2$ and $Ir(Cp^*)(PMe_3)H_2$ in Table 1.

Quantitative studies on how the nature and number of spectator ligands affect the values of DH^{o}(M–H) or $\langle DH^{o}\rangle$(M–H) are clearly needed, since these factors often determine the failure or success of hydrogen activation. For example, the above thermodynamic analysis of reaction (43) indicated that $\langle DH^{o}\rangle$(M–H) $\geq 239\,\mathrm{kJ\,mol^{-1}}$ for the process to be observed. The value reported for the hydrogenated Vaska's complex, $Ir(Cl)(CO)(PPh_3)_2H_2$, exceeds this limit by only $8\,\mathrm{kJ\,mol^{-1}}$, suggesting that the analogous rhodium molecule $Rh(Cl)(CO)(PPh_3)_2$ may not activate hydrogen.[130,131] Indeed it does not,[116] but other similar rhodium(I) complexes do, as for example $Rh(Cl)[P(p\text{-tolyl})_3]_3$ (see Table 1) and Wilkinson's catalyst $Rh(Cl)(PPh_3)_3$. The replacement of CO by a phosphine in these systems may therefore yield stronger rhodium–hydrogen bonds. The increase must however be small, because the catalytic hydrogenation process would be difficult if $\langle DH^{o}\rangle$(M–H) were too high. It must be noted that the suggested thermodynamic stabilization of metal–hydrogen bonds in the above complexes upon CO substitution is not in line with experimental data for the complexes $W(Cp)(CO)_2(L)H$ (L=CO, PMe_3), $Mn(CO)_4(L)H$ (L=CO, PPh_3), and $Co(CO)_3(L)H$ (L=CO, PPh_3, $P(OPh)_3$), which show negligible variations in DH^{o}(M–H) when CO is replaced by phosphine or phosphite.[11,123,132] Yet, this trend probably cannot be generalized for different metals and/or different ligand environments. It is instructive, for instance, to compare $\langle DH^{o}\rangle$(Ir–H) in the series of complexes $Ir(X)(CO)(PCy_3)_2H_2$ and $Ir(X)(CO)[P(OPh)_3]_2H_2$ (Table 1). While for X = Cl, $\langle DH^{o}\rangle$(Ir–H) is similar for the phosphine and phosphite complexes, in the case of X = I, $\langle DH^{o}\rangle$(Ir–H) is $32\,\mathrm{kJ\,mol^{-1}}$ higher for the complex with the basic cyclohexylphosphine ligand.

1.22.5.2 Intermolecular Carbon–Hydrogen Activation

As observed with reaction (43), the oxidative addition of methane to an unsaturated metal center, reaction (60), has a very negative entropy term, $T\Delta_r S^{o}(60) \approx -44\,\mathrm{kJ\,mol^{-1}}$:

$$M + CH_4 \rightarrow M(Me)H \qquad (60)$$

This implies that the reaction will be favorable ($\Delta_r G^{o}(60) < 0$) only if $\Delta_r H^{o}(60) = DH^{o}(\mathrm{Me–H}) - DH^{o}(\mathrm{M–H}) - DH^{o}(\mathrm{M–Me}) < -44\,\mathrm{kJ\,mol^{-1}}$, that is, the sum of metal–carbon and metal–hydrogen bond dissociation enthalpies must exceed the carbon–hydrogen bond dissociation enthalpy in methane, $439\,\mathrm{kJ\,mol^{-1}}$, by that amount. Taking a middle range value for DH^{o}(M–H), $250\,\mathrm{kJ\,mol^{-1}}$ (Table 1), one concludes that DH^{o}(M–Me) should be higher than ca. $230\,\mathrm{kJ\,mol^{-1}}$.

The metal–methyl mean bond dissociation enthalpies in the main-group homoleptic molecules, MMe_n, vary from $131\,\mathrm{kJ\,mol^{-1}}$ in $ZnMe_2$ to $283\,\mathrm{kJ\,mol^{-1}}$ in $AlMe_3$.[133] Thus, the above value for DH^{o}(M–Me) in a transition metal complex is not particularly high, suggesting that many coordinatively unsaturated transition metal complexes would activate methane.

Another way of looking into the thermodynamic possibility of intermolecular C–H activation is by considering the difference between metal–hydrogen and metal–carbon bond dissociation enthalpies, DH^{o}(M–H) – DH^{o}(M–Me). It has been concluded above that a given unsaturated metal complex would activate methane if $DH^{o}(\mathrm{M–H}) \approx 250\,\mathrm{kJ\,mol^{-1}}$ and $DH^{o}(\mathrm{M–Me}) \geq 230\,\mathrm{kJ\,mol^{-1}}$. Data in Table 1 reveal, however, that the differences DH^{o}(M–H) – DH^{o}(M–Me) range from about $40\,\mathrm{kJ\,mol^{-1}}$ to $100\,\mathrm{kJ\,mol^{-1}}$, respectively, for early and for late transition metals. Although M–Me bonds have stronger σ-bonding interactions than M–H bonds, the dominant contribution comes from repulsive steric interaction energies. These are also higher in the case of methyl ligands, but are reduced for the more electropositive early transition metals, due to the high polarity of M–Me bonds. This effect is clearly observed in ionic gaseous fragments MMe^{+} and MH^{+}, where $DH^{o}(\mathrm{M^{+}–Me})$ are often higher than $DH^{o}(\mathrm{M^{+}–H})$.[124]

As metal–methyl bonds are considerably weaker than metal–hydrogen bonds and DH^{o}(Me–H) ≈ DH^{o}(H–H), it is not surprising that reaction (60) is unfavorable for many complexes that readily activate hydrogen (reaction (43)). Consider, for instance, the complex Ir(Cl)(CO)$(PMe_3)_2$. The enthalpy of reaction (61) can be estimated as 39 kJ mol^{-1} by assuming that D1 (Table 1) is about 250 kJ mol^{-1}, leading to DH^{o}(Ir–Me) ≈ 150 kJ mol^{-1}. This value for $\Delta_r H^{o}$ (61), together with $T\Delta_r S^{o}$ (61) ≈ −44 kJ mol^{-1}, gives $\Delta_r G^{o}$ (61) ≈ 83 kJ mol^{-1}:

$$\mathrm{Ir(Cl)(CO)(PMe_3)_2(sln) + CH_4(sln) \rightarrow Ir(Cl)(CO)(PMe_3)_2(Me)H(sln)} \qquad (61)$$

The addition of methane to the binuclear complexes of reactions (49)–(54) is also endothermic, as can easily be concluded from an analysis similar to the one made for those reactions. If, however, the enthalpy balance does not involve the cleavage of metal–metal bonds (see discussion of reaction (55)), then some of those unsaturated fragments may be able to activate methane. This can be illustrated by considering reaction (62) (M = Cr, Mo, W), for which $\Delta_r H^{o}$ (62) = DH^{o}(Me–H) − DH^{o}(M–H) − DH^{o}(M–Me) and $T\Delta_r S^{o}$ (62) ≈ −47 kJ mol^{-1}:

$$\mathrm{2M(Cp)(CO)_3(sln) + CH_4(sln) \rightarrow M(Cp)(CO)_3Me(sln) + M(Cp)(CO)_3H(sln)} \qquad (62)$$

Data for DH^{o}(Cr–Me) and DH^{o}(W–Me) are not available, but they can be estimated by assuming that the difference DH^{o}(M–H) − DH^{o}(M–Me) is constant for this triad of complexes (77 kJ mol^{-1}). The values derived for the Gibbs energies, $\Delta_r G^{o}$ (62) ≈ 44 kJ mol^{-1}, 3 kJ mol^{-1}, and −115 kJ mol^{-1}, respectively, for Cr, Mo, and W, show a dramatic difference from first to second and third row metal complexes. Indeed, as remarked in the previous section for metal–hydrogen bonds, metal–carbon bond dissociation enthalpies in a given group are also expected to increase with atomic number, and with decreasing oxidation of the metal center and its coordination number. First row metal complexes are thus poor candidates for methane activation, as evidenced by the data in Table 1. Second row unsaturated metal centers may however give thermodynamically stable methyl hydrides (see, e.g., the cases of $Zr(Cp^{*})_2R_2$ and $Nb(Cp)_2R_2$).

An interesting example concerning a second row complex is provided by reaction (63),[116] which is known to occur with a reasonable yield, albeit quite slowly and at high temperature (400 K), suggesting that $\Delta_r G^{o}$ (63) is close to zero.

$$\mathrm{[Rh(oep)]_2(sln) + PhCH_3(sln) \rightarrow Rh(oep)Bz(sln) + Rh(oep)H(sln)} \qquad (63)$$

where Bz stands for $C_6H_5CH_2$. A net thermodynamic analysis, $\Delta_r H^{o}$ (63) = DH^{o}(Rh–Rh) + DH^{o}(Bz–H) − DH^{o}(Rh–Bz) − DH^{o}(Rh–H), can be made as follows. The value DH^{o}(Rh–Rh) = 69 kJ mol^{-1} has already been quoted in Section 1.22.5.1. The rhodium–benzyl bond dissociation enthalpy is not known, but a rule of thumb for estimating metal–carbon σ-bond dissociation enthalpies in a series of analogous compounds, if at least one value is available, is to consider that the differences DH^{o}(M–R) − DH^{o}(M–R^1) parallel DH^{o}(R–H) − DH^{o}(R^1–H).[134–137] While this approximation seems to hold for many ligands, inspection of the data in Table 1 shows that DH^{o}(M–Me) − DH^{o}(M–Bz) are always lower than DH^{o}(Me–H) − DH^{o}(Bz–H) = 71 kJ mol^{-1}. In the case of group 9 complexes, the difference is even surprisingly small for Co(dmg)$_2$(py)R, 2 kJ mol^{-1}, and about 25 kJ mol^{-1} for Ir(Cl)(CO)$(PMe_3)_2$(I)R. If a difference of ca. 20 kJ mol^{-1} is accepted for DH^{o}(Rh–Me) − DH^{o}(Rh–Bz) and DH^{o}(Rh–H) − DH^{o}(Rh–Me) is in the range of 80–100 kJ mol^{-1}, then $\Delta_r H^{o}$ (63) lies between 19 and 39 kJ mol^{-1} (the entropy term is small). Although this result is higher than one should expect on the basis of experimental observation, it is in qualitative agreement with the high temperature required by reaction (63). Moreover, there is evidence that the above estimate for DH^{o}(Rh–H) − DH^{o}(Rh–Me) may be an upper limit. Sherry and Wayland have measured the equilibrium constant of reaction (64) in benzene, at three temperatures (353, 373, and 393 K), and calculated $\Delta_r H^{o}$ (64) ≈ −54.4 ± 6.3 kJ mol^{-1}.[138,139]

$$\mathrm{2Rh(tmp)(sln) + CH_4(sln) \rightarrow Rh(tmp)Me(sln) + Rh(tmp)H(sln)} \qquad (64)$$

where tmp stands for 5,10,15,20-tetrakis(2,4,6-trimethylphenyl)porphyrinato dianion. This implies that DH^{o}(Rh–H) + DH^{o}(Rh–Me) ≈ 493 kJ mol^{-1}. If DH^{o}(Rh–H) in the tetramesitylporphyrinato complex is similar to DH^{o}(Rh–H) in Table 1 (i.e., 259 kJ mol^{-1}), then DH^{o}(Rh–Me) ≈ 234 kJ mol^{-1}, that is, a surprisingly small difference of only 25 kJ mol^{-1} is observed. Reaction (64) is also interesting because it illustrates the thermodynamic feasibility of methane activation by two metal centers when the metal–metal bond is virtually non-existent. In the present case this is due to the considerable steric requirements of the ligand tetramesitylporphyrinato, as compared with octaethylporphyrinato.[139]

Before proceeding with the thermodynamic discussion of intermolecular C–H activation on the basis of data from Table 1, it is appropriate to make a few comments. The conclusion that $\Delta_r H^o$ (60) must be more exothermic than $-44\,kJ\,mol^{-1}$ implies that $DH^o(M–Me) + DH^o(M–H) \geq 483\,kJ\,mol^{-1}$. It must be noted, however, that these bond dissociation enthalpies refer to process (65) and that there are no values in Table 1 (or elsewhere) that can be assigned to this stepwise reaction:

$$M(Me)H \rightarrow MMe + H \rightarrow M + Me + H \tag{65}$$

For example, the values for $W(Cp)_2H_2$ and $W(Cp)_2Me_2$ refer to the mean bond dissociation enthalpies, $\langle DH^o\rangle(W–H)$ and $\langle DH^o\rangle(W–Me)$. Two assumptions have thus to be used in order to predict the energetics of reaction (60) or (65). First, it is considered that $\langle DH^o\rangle(W–H) \approx DH^o[W(Cp)_2(Me)–H]$; second, $\langle DH^o\rangle(W–Me)$ is identified with $DH^o[W(Cp)_2–Me]$. Although there is no direct experimental evidence in support of these assumptions, they may be reasonable (within ca. $20\,kJ\,mol^{-1}$) for the methyl hydride complexes.[140]

A difficulty that is probably more important than the previous approximations is that many values in Table 1 are anchored in other bond dissociation enthalpies (usually metal–halogen or metal–oxygen), which are estimates. Although most of these estimates look sensible, they may affect the accuracy of the analysis by some 20 or $30\,kJ\,mol^{-1}$.[124]

Bearing in mind the above warnings, data in Table 1 predict that methane activation must be rather efficient for third row *d*-element and *f*-element $M(Cp')_2$ species ($Cp' = Cp$ or Cp^*). For instance, the Gibbs energy of reaction (66) is estimated as $-49\,kJ\,mol^{-1}$, which corresponds to a 100% yield of the methyl hydride complex:

$$W(Cp)_2(sln) + CH_4(sln) \rightarrow W(Cp)_2(Me)H(sln) \tag{66}$$

The reality is, however, different: the photochemically generated $W(Cp)_2$ prefers to react with itself and forms a dimer where each tungsten is bonded to a hydrogen atom and to a Cp ring of the other tungstenocene moiety.[141] The efficiency of this competitive reaction is likely to be mainly kinetic rather than thermodynamic. Although the estimate for $\Delta_r G^o$ (66) could be questioned (recall that it relies on anchored bond enthalpy values), it seems to be in line with the fact that the compounds $W(Cp)_2(Me)H$ and $W(Cp^*)_2(Me)H$ are stable at room temperature.[142,143] The effect of methyl groups in cyclopentadienyl rings on metal–ligand bond dissociation enthalpies is predicted to be small.[123,124]

Third row unsaturated complexes are, in principle, the best candidates to activate methane, but this depends, a good deal, on the environment of the metal center and its oxidation state. The unfavorable thermodynamics of reaction (61) contrasts with the easy intermolecular C–H activation observed in reaction (67),[144–146] for which $\Delta_r G^o$ (67) is estimated as $-70\,kJ\,mol^{-1}$, by using data in Table 1 and $T\Delta_r S^o$ (67) $\approx -44\,kJ\,mol^{-1}$:

$$Ir(Cp^*)(PMe_3)(sln) + CH_4(sln) \rightarrow Ir(Cp^*)(PMe_3)(Me)H(sln) \tag{67}$$

The species $Ir(Cp^*)(PMe_3)$, which is generated by photolysis of $Ir(Cp^*)(PMe_3)H_2$, reacts also with other aliphatic hydrocarbons. In the absence of steric or strain effects, the energetics of these reactions are expected to be similar to that of reaction (67), since $DH^o(M–R) - DH^o(M–R^1) \approx DH^o(R–H) - DH^o(R^1–H)$. For example, in the case of cyclohexyl, $DH^o(Ir–Me) - DH^o(Ir–Cy) = 34\,kJ\,mol^{-1}$ compares with $DH^o(Me–H) - DH^o(Cy–H) = 39\,kJ\,mol^{-1}$.[124,147]

The high value for $\langle DH^o\rangle(Pt–Me)$ in *cis*-$Pt(PEt_3)_2Me_2$ (Table 1) suggests that the oxidative addition of methane would be rather favorable. If a difference of ca. $70\,kJ\,mol^{-1}$ is accepted for $DH^o(Pt–H) - DH^o(Pt–Me)$, the reaction will be $170\,kJ\,mol^{-1}$ exothermic! However, this seems to be in contradiction with the thermal instability of $Pt(PR_3)_2(Me)H$ complexes. For example, $Pt(PPh_3)_2(Me)H$ loses methane at temperatures above 250 K, which is an indication that the reductive elimination is kinetically and thermodynamically favorable.[148] The problem may simply lie on the fact that the platinum–ligand bond dissociation enthalpies are anchored in a value for $DH^o(Pt–Cl)$ which can be too high. Theoretical calculations involving the model compound $Pt(PH_3)_2$ have shown that the oxidative addition of methane is $24\,kJ\,mol^{-1}$ endothermic.[149]

While the intermolecular activation of alkanes has been observed for a relatively small number of systems, the equivalent reaction for arenes is known for a larger variety of unsaturated transition metal centers. This may be somewhat puzzling from a thermodynamic viewpoint, since, for example, $DH^o(Ph–H)$ is higher than $DH^o(Me–H)$ by $26\,kJ\,mol^{-1}$, but it must be recalled that if $DH^o(M–Ph) - DH^o(M–Me)$ is also close to ca. $26\,kJ\,mol^{-1}$, there will be no

difference in the overall energetics of alkane and arene activation. For early transition metal and *f*-metal complexes in Table 1, it is noted that DH^{o}(M–Ph) – DH^{o}(M–Me) are indeed in the range of 26 kJ mol^{-1}. Thus, for example, in the case of reaction (68), DH^{o}(W–Ph) ≈ 247 kJ mol^{-1} and $\Delta_r H^{o}$(68) ≈ −93 kJ mol^{-1}.

$$W(Cp)_2(sln) + C_6H_6(sln) \rightarrow W(Cp)_2(Ph)H(sln) \quad (68)$$

Using $T\Delta_r S^{o}$(68) ≈ −44 kJ mol^{-1}, $\Delta_r G^{o}$(68) ≈ −49 kJ mol^{-1} is finally obtained, that is, the energetics of reactions (66) and (68) are comparable. A possible reason for the different reactivity of arenes and alkanes is that an arene may have a kinetic advantage over an alkane by forming a strong η^2-bond with the metal. The electron backdonation from the metal to the antibonding π^* orbitals of the arene weakens the C(sp^2)–H bond and favors the formation of the aryl hydride. While this kinetic explanation may account, by itself, for the preference of arene addition, it is observed in Table 1 that for late transition metal complexes the differences DH^{o}(M–Ph) – DH^{o}(M–Me) are substantially higher than DH^{o}(Ph–H) – DH^{o}(Me–H). This trend will, of course, imply that benzene activation is thermodynamically favorable, relative to methane activation.

A thorough discussion of arene versus alkane oxidation along the above lines was made by Jones and Feher,[150] and illustrated with kinetic and thermochemical data for the complex Rh(Cp*)(PMe_3), an unsaturated species which is known to activate both aliphatic and aromatic C–H bonds. This feature is not surprising if the result for $\Delta_r G^{o}$(67) ≈ −70 kJ mol^{-1} is recalled and one considers that rhodium–ligand bonds are ca. 20 kJ mol^{-1} weaker than iridium–ligand bonds in analogous complexes.[130]

The experimental Gibbs energy of reaction (69) was determined as 36 kJ mol^{-1} at 256 K, showing that the equilibrium is indeed shifted to the left:[150]

$$Rh(Cp^*)(PMe_3)(Ph)H(sln) + PrH(sln) \rightarrow Rh(Cp^*)(PMe_3)(Pr)H(sln) + PhH(sln) \quad (69)$$

As $T\Delta_r S^{o}$(69) ≈ 0 kJ mol^{-1}, DH^{o}(Rh–Ph) – DH^{o}(Rh–Pr) ≈ 83 kJ mol^{-1}, a value that is substantially higher than DH^{o}(Ph–H) – DH^{o}(Pr–H) = 47 kJ mol^{-1}. In addition to the net thermodynamic stabilization of the phenyl hydride complex, Jones and Feher have provided good evidence that the rate determining step of benzene activation is an η^2-coordination of a C–C bond to the metal center, that is, the C–H bond is not directly involved. This coordination can be quite strong, as suggested by an upper limit reported for DH^{o}(Rh–C_2H_4) in Rh(Cp)(C_2H_4)$_2$, 130 kJ mol^{-1},[124] and also by reaction (70), observed by Jones and Dong (K_{70} = 2.0 in hexane).[151] Using D2 in Table 1 as ca. 220 kJ mol^{-1} and DH^{o}(Rh–$C_{10}H_7$) – DH^{o}(Rh–Ph) ≈ DH^{o}($C_{10}H_7$–H) – DH^{o}(Ph–H), one concludes that DH^{o}(Rh–η^2-$C_{10}H_8$) ≈ −$\Delta_r H^{o}$(70) + DH^{o}(Rh–Ph) + DH^{o}(Rh–H) – DH^{o}(Ph–H) ≈ 100 kJ mol^{-1}:

$$Rh(Cp^*)(PMe_3)(C_{10}H_7)H(sln) \rightarrow Rh(Cp^*)(PMe_3)(\eta^2\text{–}C_{10}H_8)(sln), \quad C_{10}H_8 = \text{naphthalene} \quad (70)$$

The Gibbs energy pathway of reaction (69) was presented by Jones and Feher,[150] showing that arene activation in the rhodium system is preferred by thermodynamic rather than kinetic reasons (the activation barriers differ by only 2 kJ mol^{-1}). The Rh–η^2-C_6H_6 bond dissociation enthalpy is estimated as ca. 70 kJ mol^{-1}, in line with the above value for DH^{o}(Rh–η^2-$C_{10}H_8$).

Despite the convincing evidence provided by Jones and Feher, it cannot be concluded that the formation of an η^2-intermediate is a general feature of C(sp^2)–H activation. As remarked for reaction (70), the η^2-naphthalene complex is more stable than the naphthyl hydride, hence cannot be an intermediate of naphtalene activation by the rhodium species. Another example was given by Bergman and Stoutland, who found that by heating the vinyl hydride Ir(Cp*)(PMe_3)(C_2H_3)H in cyclohexene or benzene, at temperatures above 443 K, the complex was completely converted into Ir(Cp*)(PMe_3)(η^2-C_2H_4).[152] This thermodynamic stability of the ethylene complex relative to the vinyl hydride rules out its role as an intermediate in the oxidative addition of C_2H_4. An Ir···H–C_2H_3 linear approach and an η^2-C–H transition state have been suggested for this process.[153]

It is believed that the C–H oxidative addition of an aliphatic hydrocarbon proceeds also through an η^2-coordination (in this case of a C–H bond) to the metal.[148,154] Energetic data for this type of bonding, often called agostic[155] and similar to the one referred above for the η^2-H_2 complexes, are still very scarce. Photoacoustic calorimetry experiments involving the complexes M(CO)$_5$(heptane) revealed, however, that DH^{o}(M–heptane) in the triad M = Cr, Mo, and W are within a fairly narrow range (40, 36, and 56 kJ mol^{-1}, respectively),[156] suggesting that similar values should be observed for other metal centers. Thus, there seems to be no dramatic difference between the energetics of η^2-benzene and η^2-heptane coordination!

Hydrocarbons can also be activated through reactions that do not involve an oxidative addition to an unsaturated metal complex but rather proceed by a four-centered mechanism. This is usually called heterolytic activation of C–H bonds because these bonds are polarized ($C^{\delta-}$–$H^{\delta+}$) in the transition state, by action of an electrophilic metal and a basic ligand.[116,117,148] A most interesting example of this approach is given by reaction (71), which occurs under mild conditions (333 K in cyclohexane).[157]

$$\overbrace{\mathrm{Th(Cp^*)_2(CH_2CMe_2CH_2)(sln)}} + \mathrm{CH_4(sln)} \longrightarrow \mathrm{Th(Cp^*)_2(CH_2CMe_3)Me(sln)} \qquad (71)$$

The driving force for the reactivity of the thoracyclobutane complex lies in the strain of the metallacycle, which can be estimated as ca. 60 kJ mol^{-1} by comparing DH°(Th–C) = 274 kJ mol^{-1} in this complex with DH°(Th–CH_2CMe_3) = 302 kJ mol^{-1} in $Th(Cp^*)_2(CH_2CMe_3)_2$.[124] The enthalpy of reaction (71), $\Delta_r H^\circ(71) \approx DH^\circ$(Th–C) + DH°(Me–H) − DH°(Th–Me) − DH°(C–H) ≈ −44 kJ mol^{-1}, together with $T\Delta_r S^\circ(71) \approx -44$ kJ mol^{-1}, gives $\Delta_r G^\circ(71) \approx 0$ kJ mol^{-1}. Values in the same range are observed for the reaction with ethane and benzene, reflecting the nearly parallel trend followed by DH°(Th–R) and DH°(R–H).

The role of strain destabilization of the above thorium metallacycle, allowing methane activation, is also appreciated by noting that reaction (72) is thermoneutral and $\Delta_r G^\circ(72) \approx 44$ kJ mol^{-1}.

$$\overbrace{\mathrm{Th(Cp^*)_2(CH_2SiMe_2CH_2)(sln)}} + \mathrm{CH_4(sln)} \longrightarrow \mathrm{Th(Cp^*)_2(CH_2SiMe_3)Me(sln)} \qquad (72)$$

The larger silicon atom reduces the strain to ca. 34 kJ mol^{-1}, as indicated by DH°(Th–C) = 318 kJ mol^{-1} in the metallacycle complex and DH°(Th–CH_2SiMe_3) = 335 kJ mol^{-1} in $Th(Cp^*)_2(CH_2SiMe_3)_2$.[124,157]

Steric effects can also drive C–H activation. The thorium–neopentyl bond is about 16 kJ mol^{-1} weaker than expected on the basis of DH°(Th–Me) − DH°(Th–CH_2CMe_3) ≈ DH°(Me–H) − DH°(Me_3CCH_2–H) = 21 kJ mol^{-1}.[124] Reaction (73), for which the entropic term must be small, is predicted to be 16 kJ mol^{-1} exothermic.[124,157]

$$\mathrm{Th(Cp^*)_2(CH_2CMe_3)Me(sln) + CH_4(sln) \rightarrow Th(Cp^*)_2Me_2(sln) + CMe_4(sln)} \qquad (73)$$

1.22.5.3 Intramolecular Carbon–Hydrogen Activation

Cyclometallation reactions involving the cleavage of C–H bonds can be represented by Equation (74). The process, which is also described as an intramolecular oxidative addition of the C–H bond to the metal center, has an enthalpy change given by, $\Delta_r H^\circ(74) \approx DH^\circ(\mathrm{M-C}) + DH^\circ(\mathrm{C-H}) - DH^\circ(\mathrm{M-C})_1 - DH^\circ(\mathrm{M-C})_2 - DH^\circ(\mathrm{M-H})$ where the subscripts 1 and 2 indicate product bond dissociation enthalpies.

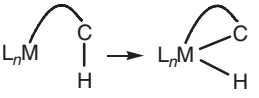

(74)

In the absence of noticeable strain in the metallacycle, DH°(M–C) ≈ DH°(M–C)$_1$. Therefore, $\Delta_r H^\circ(74) \approx DH^\circ$(C–H) − DH°(M–C)$_2$ − DH°(M–H), a balance that is similar to the one made for the intermolecular C–H activation (reaction (60)). In the present case, however, the weight of the entropy term is expected to be smaller than for reaction (60), −44 kJ mol^{-1}. As entropy effects are responsible for many thermodynamically unfavorable reactions surveyed in Section 1.22.5.2, it is thus not surprising that cyclometallations are so common and that they often compete with intermolecular C–H activations.

Note, however, that the entropy changes associated with cyclometallations must be negative, since, for example, a number of internal rotation degrees of freedom are lost. Although these changes are difficult to predict in most cases, some reliable estimates are possible, particularly those involving the cyclization of an alkyl chain. For instance, based on the available evidence, $T\Delta_r S^\circ$ becomes more negative with the size of the chain.[14] The formation of a small metallacycle will therefore be entropically more favorable than a large one, but strain effects vary in opposite direction.

The competition between intra- and intermolecular C–H activation has been discussed by Crabtree[148] and his main conclusions are summarized here: (i) alkane activation is kinetically favored, while cyclometallation is usually the thermodynamic preferred pathway; (ii) higher steric congestion favors cyclometallation, whereas intermolecular activation is more likely in less congested systems. Let us illustrate these points by using the unsaturated complexes $Ir(Cp^*)(PMe_3)$ and $Ir(Cp^*)(PPh_3)$. Both activate benzene (reactions (75) and (76)), but the products of the latter are a 1 : 1 mixture of the phenyl hydride complex and a four-membered metallacycle:[158]

$$Ir(Cp^*)(PMe_3)(sln) + C_6H_6(sln) \rightarrow Ir(Cp^*)(PMe_3)(Ph)H(sln) \tag{75}$$

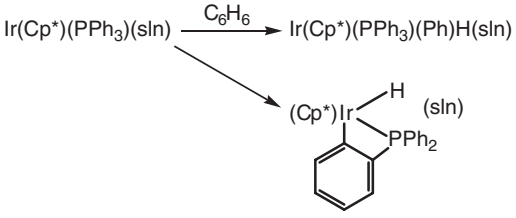

(76a)

(76b)

Using $T\Delta_rS^o(75) \approx -44\,kJ\,mol^{-1}$ and $\Delta_rH^o(75) \approx \Delta_rH^o(76a) \approx DH^o(Ph–H) - DH^o(Ir–Ph) - DH^o(Ir–H) \approx -175\,kJ\,mol^{-1}$, $\Delta_rG^o(75) \approx \Delta_rG^o(76a) \approx -131\,kJ\,mol^{-1}$. The enthalpy balance of reaction (76b) is hard to make due to the lack of data, but if it is arbitrarily assumed that $T\Delta_rS^o(76b)$ plus the strain in the four-membered metallacycle do not exceed $40\,kJ\,mol^{-1}$, then $\Delta_rG^o(76a)$ will be comparable to $\Delta_rG^o(76b)$. By contrast, it may be expected that the strain in a three-membered metallacycle (such as the one observed if cyclometallation occurred in the PMe_3 complex) would be considerably higher, thus favoring the intermolecular oxidative addition.

Kinetic and thermodynamic data for reaction (77) have been reported by Jones and Feher.[159]

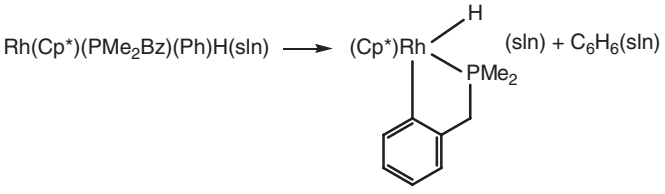

(77)

In this case it is noted that the intramolecular activation has a small thermodynamic preference relative to intermolecular activation, the opposite being observed for the kinetics of the reactions. The thermodynamic result looks sensible after the discussion made for reactions (75) and (76). The strain in the five-membered metallacycle (reaction (77)) is expected to be smaller than the entropy term associated with the reductive elimination of benzene and the cyclization. An upper limit for $T\Delta_rS^o(77)$, $40\,kJ\,mol^{-1}$, leads to $\Delta_rH^o(77) \leq 30\,kJ\,mol^{-1}$ ($\Delta_rG^o(77) = -10\,kJ\,mol^{-1}$).

Cyclometallations that involve the elimination of hydrogen or a hydrocarbon are usually entropy driven. For instance, the enthalpy of reaction (78), measured in benzene in the temperature range of 323–373 K,[55] is $15\,kJ\,mol^{-1}$ endothermic, but this is nearly offset by a positive entropy term.[14]

$$Sc(Cp^*)(C_5Me_4Pr)Ph(sln) \rightarrow \overline{Sc(Cp^*)(C_5Me_4CH_2CH_2CH_2)(sln)} + C_6H_6(sln) \tag{78}$$

$\Delta_rH^o(78)$ leads to a value of $DH^o[(Sc–C(sp^3)]$ which is about $62\,kJ\,mol^{-1}$ smaller than $DH^o(Sc–Ph)$,[124] suggesting a small strain in the metallacycle. Recall that $DH^o(Ph–H) - DH^o(Pr–H) = 47\,kJ\,mol^{-1}$.

The energetics of other intramolecular C–H activation reactions are known for several group 4 complexes (reactions (79)–(82)).[55,160] They all are endothermic, but have large and positive $T\Delta_rS^o$ terms.

$$Ti(Cp^*)_2Me(sln) \rightarrow Ti(Cp^*)Fv^*(sln) + CH_4(sln) \tag{79}$$

$$Ti(Cp^*)_2Ph(sln) \rightarrow Ti(Cp^*)Fv^*(sln) + C_6H_6(sln) \tag{80}$$

$$Hf(Cp^*)(C_5Me_4CH_2CH_2Me)H_2(sln) \longrightarrow \overbrace{Hf(Cp^*)(C_5Me_4CH_2CH_2CH_2)}H(sln) + H_2(sln) \quad (81)$$

$$Hf(Cp^*)(C_5Me_4CH_2Ph)H_2(sln) \longrightarrow \overbrace{Hf(Cp^*)(C_5Me_4CH_2C_6H_4)}H(sln) + H_2(sln) \quad (82)$$

Fv^* represents the fulvene group, $C_5Me_4CH_2$, which is believed to be $\eta^1:\eta^5$ rather than η^6-coordinated to the titanium atom. The Ti–C(sp^3) strained σ-bond was estimated as ca. 200 kJ mol^{-1},[160] to be compared with DH°(Ti–Bz) = 237 kJ mol^{-1} (Table 1). Reactions (79) and (80) are both endothermic, by 30 and 48 kJ mol^{-1}, respectively, but entropy terms must be large, possibly higher than 40 kJ mol^{-1}, explaining why the fulvene complex can be synthesized by thermolysis of the methyl and the phenyl precursors. $Zr(Cp^*)(C_5Me_4CH_2)Ph$ is another example of a strained fulvene complex.[161] Here DH°[Zr–C(sp^3)] was calculated as 195 kJ mol^{-1}, a result which is in line with the above one for the titanium complex. This value can also be compared with DH°[Zr–C(sp^3)] in the complexes $\overbrace{Zr(Cp^*)_2CH_2CHEt)_2}CH_2$ and $\overbrace{Zr(Cp^*)_2CH_2CH_2C_6H_4}$-*o*,[161] estimated as 261 and 282 kJ mol^{-1}, respectively.[124] Both are in the range of DH°(Zr–alkyl) ≈ 265 kJ mol^{-1} (Table 1), evidencing no strain in the zirconacyclopentane and zirconaindan metallacycles. Indeed, as remarked by Schock and Marks,[161] the latter cycle is even affected by a "negative" strain, due to reduced non-bonded repulsions relative to $Zr(Cp^*)_2(alkyl)_2$.

The strain in the metallacycles of reactions (81) and (82) should be smaller than in the fulvene complexes, reflecting Hf–C bond dissociation enthalpies closer to DH°(Hf–alkyl) and DH°(Hf–aryl). Δ_rH°(81) = 65 kJ mol^{-1} and Δ_rH°(82) = 35 kJ mol^{-1} yield DH°(Hf–H) – DH°(Hf–C) ≈ 83 and 6 kJ mol^{-1}, respectively. These values can be compared with DH°(Hf–H) – DH°(Hf–Pr) ≈ 55 kJ mol^{-1} and DH°(Hf–H) – DH°(Hf–Ph) ≈ 8 kJ mol^{-1}.[124] It thus appears that the metallacycle of reaction (81) has some degree of strain, which is somewhat surprising, whereas the same is not observed in the metallacycle of reaction (82). The endothermicity of both reactions is not quite offset by the entropy terms $T\Delta_rS^\circ$(81) = 51 kJ mol^{-1} (T = 365 K) and $T\Delta_rS^\circ$(82) = 28 kJ mol^{-1} (T = 359 K).[55] It is interesting to note that $T\Delta_rS^\circ$(81) is larger than would have been predicted, ca. 31 kJ mol^{-1}.

The energetics of γ-elimination reactions (83) and (84) have been investigated by Bruno *et al.* and both are endothermic, Δ_rH°(83) = 25 kJ mol^{-1} and Δ_rH°(84) = 15 kJ mol^{-1}.[162]

$$Th(Cp^*)_2(CH_2CMe_3)_2(cr) \longrightarrow (Cp^*)_2Th\begin{smallmatrix}H_2C\\ \\ H_2C\end{smallmatrix}CMe_2(cr) + CMe_4(l) \quad (83)$$

$$Th(Cp^*)_2(CH_2SiMe_3)_2(cr) \longrightarrow (Cp^*)_2Th\begin{smallmatrix}H_2C\\ \\ H_2C\end{smallmatrix}SiMe_2(cr) + SiMe_4(l) \quad (84)$$

The difference between these two results is due to a reduced strain in the silicon metallacycle (see discussion of reaction (72)). $T\Delta_rS^\circ$ is predicted as 26 kJ mol^{-1} for both reactions, enough to yield favorable Gibbs energy changes. Incidentally, this entropy estimate is in good agreement with the experimental value $T\Delta_rS^\circ$(84) = 25 kJ mol^{-1} (T = 353 K), measured by Smith *et al.*[13]

The above examples illustrate the roles of strain and entropy in the thermodymamics of cyclometallation and clarify the common misconception that this process is entropically neutral when no reductive elimination of hydrogen or hydrocarbon occurs. The thermodynamic competition between inter- and intramolecular C–H activation results from an interplay of those factors and, as pointed out by Crabtree,[148] also from sterical constraints. There are still too few energetic data to draw general conclusions, but it appears that cyclometallation may compete with intermolecular activation whenever the ring formation does not involve a considerable strain. Metals from the *d*- or the *f*-block are larger than carbon, so it is expected that, for example, the strain of a metallocyclobutane is dramatically reduced from the 110 kJ mol^{-1} observed in the corresponding hydrocarbon (see Section 1.22.5.4). It should, however, be recalled that the thermodynamic condition for intramolecular activation in the absence of strain is that the sum of metal–carbon and metal–hydrogen bond dissociation enthalpies must exceed the carbon–hydrogen bond dissociation

enthalpy plus the $|T\Delta_r S^o|$ term. This entropy term can be large, for example, −17 and −27 kJ mol^{-1}, respectively, for five- and six-membered aliphatic hydrocarbon rings.[14]

1.22.5.4 Carbon–Carbon Activation

The thermodynamics of intermolecular oxidative addition of C–C bonds to an unsaturated metal center is usually considered to be less favorable than C–H activation.[148] Take, for example, reactions (85) and (86), for which the entropy changes should be approximately identical:

$$M + C_2H_6 \rightarrow M(CH_3)_2 \tag{85}$$

$$M + C_2H_6 \rightarrow M(C_2H_5)H \tag{86}$$

$\Delta_r H^o$ (85) = DH^o(Me–Me) − 2$\langle DH^o\rangle$(M–Me) and $\Delta_r H^o$ (86) = DH^o(Et–H) − DH^o(M–Et) − DH^o(M–H). Using literature values for DH^o(Me–Me) = 378 kJ mol^{-1}, DH^o(Et–H) = 421 kJ mol^{-1} (Table 1) and assuming that $\langle DH^o\rangle$(M–Me) − DH^o(M–Et) ≈ 15 kJ mol^{-1}, the difference $\Delta_r H^o$ (85) − $\Delta_r H^o$ (86) is calculated as DH^o(M–H) − $\langle DH^o\rangle$(M–Me) − 58 kJ mol^{-1}. In other words, reaction (85) will be favorable when DH^o(M–H) − $\langle DH^o\rangle$(M–Me) is less than 58 kJ mol^{-1}. The result will not be much different if the same exercise is made with another linear hydrocarbon (e.g., butane), which indicates that C–C addition may be thermodynamically preferred over C–H activation for early transition elements and also for *f*-block metals. As discussed in Section 1.22.5.2 (see also Table 1), differences DH^o(M–H) − DH^o(M–Me) are usually larger for middle and late transition metals, implying that C–H activation is thermodynamically favored.

The above discussion is somewhat biased, in the sense that it excludes strain effects. If the reactant hydrocarbon is highly strained, the C–C bonds are expected to be more destabilized than C–H bonds. For instance, DH^o(C–C) in cyclopropane is only 249 kJ mol^{-1},[163] while DH^o(C–H) is about 440 kJ mol^{-1},[164] close to DH^o(Me–H). The formation of a strain-relieved metallocyclobutane may therefore be thermodynamically favored relative to C–H oxidation. A classical example of this strain relief concerns the complex $\overline{Pt(Cl)_2(py)_2CH_2CH_2CH_2}$ for which $\langle DH^o\rangle$(Pt–C) = 117 kJ mol^{-1}.[124] There is lack of reference data to derive a reliable value of the strain enthalpy, $\Delta_{st}H^o$, but a very crude estimate can be made by taking DH^o[Pt(Cp)(Me)$_2$–Me] = 163 kJ mol^{-1} and DH^o(Pt–Pr) ≈ DH^o(Pr–H) − DH^o(Me–H) + DH^o(Pt–Me) ≈ 146 kJ mol^{-1}. This suggests that $\Delta_{st}H^o \approx 2 \times 146 - 2 \times 117 = 58$ kJ mol^{-1} in the platinumcyclobutane ring, as compared with 115 kJ mol^{-1} in *cy*-C_3H_6.

A particularly elucidating example of C–C activation involves the reaction of the unsaturated rhodium center Rh(Cp*)(PMe$_3$) with cyclopropane (reaction (87)).

$$\begin{array}{l} Rh(Cp^*)(PMe_3)(sln) + cy\text{-}C_3H_6(sln) \\ \qquad\qquad \downarrow \\ Rh(Cp^*)(PMe_3)(cy\text{-}C_3H_5)H(sln) \longrightarrow \overline{Rh(Cp^*)(PMe_3)CH_2CH_2CH_2}(sln) \end{array} \tag{87}$$

The process is quantitative at 213 K, but the hydridocyclopropyl complex rearranges into the rhodiumcyclobutane compound when warmed to room temperature, rather than eliminating *cy*-C_3H_6.[165] Periana and Bergman remarked that this observation suggests that C–H activation in the rhodium system is kinetically preferred but the C–C activation product is the most stable from a thermodynamic point of view.

The activation of unstrained C–C bonds is difficult, as expected from the discussion following reactions (85) and (86). It is, however, possible to imagine other factors besides strain that can drive the process. In his review,[148] Crabtree illustrates this point with reaction (88).[166]

$$[Ir(\eta^4\text{-}C_5H_4Me_2)L_2]^+(cr) \rightarrow [Ir\eta^5\text{-}C_5H_4Me)(L)_2Me]^+(cr) \quad L = P(p\text{-}C_6H_4F) \tag{88}$$

Assuming that $DH^{o}(\text{Cp–Me}) \approx DH^{o}(\text{Cp–H}) - DH^{o}(\text{Bz–H}) + DH^{o}(\text{Bz–Me})$, the cleavage of the C_5H_4–Me bond in the cyclopentadienyl ring requires only ca. 290 kJ mol^{-1}, due to the resonance stabilization of the formed methylcyclopentadienyl. The difference between this value and $DH^{o}(\text{Ir–Me}) \approx 240\,\text{kJ mol}^{-1}$ must be compensated by the difference $DH^{o}(\text{Ir–}\eta^5\text{-}C_5H_4Me) - DH^{o}(\text{Ir–}\eta^4\text{-}C_5H_4Me_2)$ since the reaction occurs quantitatively by heating the crystalline reactant at 418 K under vacuum.[166]

The thermodynamic constraints of C–C activation do not necessarily mean that di- or polyalkyl metal compounds are unstable relative to the reductive elimination products. This can be confirmed in a number of cases with data from Table 1. For example, reaction (89) is predicted to be endothermic by about 64 kJ mol^{-1}, leading to $\Delta_r G^{o}(89) \approx 20\,\text{kJ mol}^{-1}$:

$$W(Cp)_2Me_2(g) \rightarrow W(Cp)_2(g) + C_2H_6(g) \tag{89}$$

An opposite conclusion is drawn for the molybdenum analog, whereas for early transition metals and *f*-elements the dialkyls are thermodynamically rather stable, as a result of strong metal–carbon bonds.

It is interesting to note that while the reductive elimination of ethane from the Pt(II) complex $Pt(PPh_3)_2Me_2$ is predicted to be endothermic (data from Table 1), the same is not observed in $Pt^{IV}(MeNC)_2Me_4$, which yields ethane at 396 K (reaction (90)):

$$\textit{cis}\text{-}Pt(MeNC)_2Me_4(cr) \rightarrow Pt(MeNC)_2Me_2(cr) + C_2H_6(g) \tag{90}$$

$\Delta_r H^{o}(90) = -94\,\text{kJ mol}^{-1}$ leads to $\langle DH^{o}\rangle(\text{Pt–Me}) = 142\,\text{kJ mol}^{-1}$.[167] This example illustrates once more the effect of oxidation and coordination numbers on the energetics of metal–ligand bonds. It must, however, be recalled that it is difficult to assess the accuracy of the values for the Pt(II) complex since they are anchored on an estimate for $DH^{o}(\text{Pt–Cl})$.

1.22.5.5 Olefin Insertion into Metal–Hydrogen and Metal–Alkyl Bonds

The general mechanism of insertion of an alkene into a metal–hydrogen or a metal–alkyl bond (reaction (91); R = H or alkyl) seems well established.[116] It consists of a coordination of the olefin to the metal, followed by the hydride or the alkyl migration to the olefin, yielding an alkyl complex. The process, which involves a planar four-centered transition state, requires that the metal center is coordinatively unsaturated.

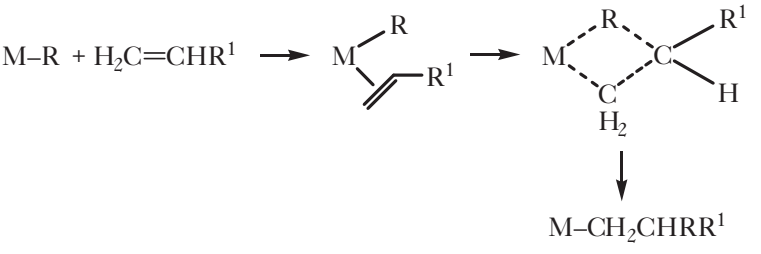

(91)

The net enthalpy balance of reaction (91) for $R = R^1 = H$, that is, ethylene insertion into a metal–hydrogen bond, is obtained as $\Delta_r H^{o}(91) = DH^{o}(\text{M–H}) - DH^{o}(\text{M–Et}) - DH^{o}(C_2H_4\text{–H}) = DH^{o}(\text{M–H}) - DH^{o}(\text{M–Et}) - 151\,\text{kJ mol}^{-1}$. Since $T\Delta_r S^{o}(91) \approx -40\,\text{kJ mol}^{-1}$,[14] the reaction will be thermodynamically favorable if $DH^{o}(\text{M–H}) - DH^{o}(\text{M–Et}) < 111\,\text{kJ mol}^{-1}$. Data in Table 1 show that this condition is indeed observed for most complexes, particularly in the case of *f*-elements and early transition metals, corresponding to the smallest differences $DH^{o}(\text{M–H}) - DH^{o}(\text{M–Et})$ (see Section 1.22.5.2). Consider, for instance, reactions (92)–(96), for which $\Delta_r H^{o}$ are −87, −56, −56, −38, and −50 kJ mol^{-1}, respectively. All values were calculated with data from Table 1:

$$Zr(Cp^{*})_2H_2(sln) + C_2H_4(sln) \rightarrow Zr(Cp^{*})_2(Et)H(sln) \tag{92}$$

$$Mo(Cp)_2H_2(sln) + C_2H_4(sln) \rightarrow Mo(Cp)_2(Et)H(sln) \tag{93}$$

$$Mo(Cp)(CO)_3H(sln) + C_2H_4(sln) \rightarrow Mo(Cp)(CO)_3Et(sln) \quad (94)$$

$$Ir(Cl)(CO)(PMe_3)_2(I)H(sln) + C_2H_4(sln) \rightarrow Ir(Cl)(CO)(PMe_3)_2(I)Et(sln) \quad (95)$$

$$\textit{trans}\text{-}Pt(PEt_3)_2(Cl)H(sln) + C_2H_4(sln) \rightarrow \textit{trans}\text{-}Pt(PEt_3)_2(Cl)Et(sln) \quad (96)$$

Note that these estimates must be fairly reliable, even for those cases where the bond dissociation enthalpies are relative to an anchor, since the value of the anchor cancels out when the difference DH^o(M–H) – DH^o(M–Et) is derived. Note also that some product compounds in the above type of reactions can be unstable relative to their reductive elimination products (e.g., $Mo(Cp)_2(Et)H$; see Section 1.22.5.2).

The thermodynamic driving force of olefin insertion into a metal–hydrogen bond is, of course, equal and with opposite sign to the thermodynamic barrier that prevents β-hydride elimination from the metal alkyl hydride compounds, that is, the reverse of reaction (91) (R = H; see Scheme 1). This decomposition mechanism will thus be more favorable for middle and late transition complexes, where metal–hydrogen bonds are much stronger than metal–alkyl bonds.

It is interesting to compare the energetics of two usual decomposition mechanisms of dialkyl complexes, reactions (97) and (98). In the first of these reactions, β-hydride elimination is followed by reductive elimination of ethane:

$$M(C_2H_5)_2 \rightarrow M(C_2H_5)H + C_2H_4 \rightarrow M + C_2H_4 + C_2H_6 \quad (97)$$

$$M(C_2H_5)_2 \rightarrow M + C_4H_{10} \quad (98)$$

The first step of reaction (97) is endothermic, but Δ_rH^o for the second is strongly dependent on the metal. As discussed in Section 1.22.5.2, it is expected to be exothermic for most first and second row transition metal complexes. In these cases, it is also predicted that Δ_rH^o(98) < 0 (see Section 1.22.5.4). Incidentally, a trend that obviously does not depend on the metal, since it relies exclusively on the enthalpies of formation and entropies of the product hydrocarbons, is that Δ_rH^o(97) exceeds Δ_rH^o(98) by 95 kJ mol^{-1} (or Δ_rG^o(97) = Δ_rG^o(98) + 53 kJ mol^{-1}). In other words, reductive elimination is always thermodynamically preferred over β-hydride elimination. In reality, however, the two processes often compete. Moreover, as remarked by Yamamoto, the decomposition pathways vary even for analogous complexes, such as *cis*-$Pd(PR_3)_2Et_2$ and *cis*-$Pt(PR_3)_2Et_2$.[168] The rate-determining step in both cases is the cleavage of a metal–phosphine bond, but whereas the Pd complex decomposes by reductive elimination, the Pt analog is thermolyzed through a β-elimination mechanism. The trend DH^o(Pd–Et) < DH^o(Pt–Et) must be determinant in lowering the activation barrier for the reductive elimination. A stronger platinum–ethylene bond, on the other hand, may contribute to a stabilization of the olefin intermediate of β-elimination (see reaction (91)). The intramolecular hydride migration to the olefin is quite facile, as indicated by the small number of known compounds that contain both olefin and hydride ligands.[116]

There are, unfortunately, very few "absolute" data for metal–alkene bond dissociation enthalpies, but they are expected to be much lower than metal–alkyl values. DH^o(Th–C_4H_6) in the complex $Th(Cp^*)_2(C_4H_6)$ is about 418 kJ mol^{-1}, or 209 kJ mol^{-1} per double bond. The difference between this value and $\langle DH^o\rangle$(Th–Me) in $Th(Cp^*)_2Me_2$, −130 kJ mol^{-1}, is in the range of DH^o(Mo–C_2H_4) – $\langle DH^o\rangle$(Mo–Me) ≈ −113 kJ mol^{-1} in the complexes $Mo(Cp)_2(C_2H_4)$ and $Mo(Cp)_2Me_2$.[124]

Let us now finally turn the attention toward reaction (91) for R = alkyl, say methyl, and R^1 = H. Δ_rH^o(91) = DH^o(M–Me) – DH^o(M–Pr) – DH^o(C_2H_4–Me) = DH^o(M–Me) – DH^o(M–Pr) – 103 kJ mol^{-1}. Therefore, Δ_rG^o(91) < 0 implies that DH^o(M–Me) – DH^o(M–Pr) < 63 kJ mol^{-1}, a condition that is fulfilled by any transition metal complex, since this difference is usually close to 20 kJ mol^{-1}. Moreover, as differences DH^o(M–Me) – DH^o(M–higher alkyl) are nearly constant throughout the periodic table, it is expected that olefin insertion into a metal–methyl bond is rather insensitive to the nature of the metal. It is also of interest to note that although these reactions are considerably more exothermic than β-hydride migrations (as shown by the enthalpies of reactions (99) and (93), ca. −83 kJ mol^{-1} and −56 kJ mol^{-1}, respectively), they are kinetically less favorable, in

keeping with the large number of stable complexes where an olefin and an alkyl group are both coordinated to the metal center:[116]

$$Mo(Cp)_2Me_2(sln) + C_2H_4(sln) \rightarrow Mo(Cp)_2(Me)Pr(sln) \quad (99)$$

1.22.6 Databases

A selected list of thermochemical databases, review articles, and monographs is presented in Tables 2 and 3. The comments included in these tables are intended as a guide to find data and to avoid thermochemical inconsistencies.

Table 2 A selection of thermochemical databases and reviews

Database	*Reference and comments*
Barin	Barin, I. *Thermochemical Data of Pure Substances* (2nd ed.); VCH: Weinheim, 1993. The 1st edition of this publication dates from 1973 (Barin, I.; Knackle, O. *Thermodynamic Properties of Inorganic Substances*; Springer-Verlag: Berlin, 1973). A supplement, co-authored by O. Kubaschewski, was released in 1977.
CATCH Tables	Pedley, J. B., Ed. *Computer Analysis of Thermochemical Data (CATCH Tables)*; School of Molecular Sciences, University of Sussex: Brighton, 1972, 1974. Includes data for compounds of Cr, Mo, and W, halogen, phosphorous, silicon, and nitrogen.
CHETAH	Harrison, B. K.; Madas, A.; Sharma, A. *CHETAH, Version 8.0. ASTM Computer Program for Chemical Thermodynamic and Energy Release Evaluation*; American Society for Testing and Materials: West Conshohocken, PA, 2005. (http://www.astm.org; http://www.southalabama.edu/engineering/chemical/chetah). The CHETAH program was developed for predicting both thermochemical properties and certain reactive chemical hazards associated with a pure chemical, a mixture of chemicals, or a chemical reaction. The estimation of thermochemical properties of gases and solid compounds is based on Benson's of group additivity method. The first version of this software package was released in 1976 under the leadership of W. H. Seaton, E. Freedman, and D. N. Treweek.
CODATA	Cox, J. D.; Wagman, D. D.; Medvedev, V. A., Eds. *CODATA Key Values for Thermodynamics*; Hemisphere: New York, 1989. This is possibly the primary source of thermochemical values and therefore it should be the starting point of all the other databases. The selections have been made by the "Task Group on Key Values for Thermodynamics" appointed in 1968 by the Committee on Data for Science and Technology (CODATA) of the International Council of Scientific Unions. Unfortunately, the number of species for which data are recommended in the final report is rather small (ca. 150).
Frenkel *et al.*	Frenkel, M.; Kabo, G. J.; Marsh, K. N.; Roganov, G. N.; Wilhoit, R. C. *Thermodynamics of Organic Compounds in the Gas State*; Thermodynamics Research Center: College Station, 1994. Volumes I and II. This database can be considered as an update of Stull, Westrum & Sinke (Stull, D. R.; Westrum, E. F., Jr.; Sinke, G. C. *The Chemical Thermodynamics of Organic Compounds*; Wiley: New York, 1969).
Glushko Tables I	Glushko, V. P., Ed. *Thermodynamic Properties of Individual Substances* (3rd ed.); Vols. 1–4; Nauka: Moscow, 1978–1982. This database offers an extensive discussion before the selection of each value. It is published in Russian, but the English translation and update of the first three volumes is now available (Gurvich Tables).
Glushko Tables II	Glushko, V. P., Ed. *Thermal Constants of Substances*; Vols. I–X; Academy of Science, USSR: Moscow, 1965–1982. This database may be considered the Russian equivalent of the *NBS 82 Tables*. It is only available in Russian.
Gurvich Tables	Gurvich, L. V.; Veyts, I. V.; Alcock, C. B., Eds. *Thermodynamic Properties of Individual Substances* (4th ed.); Vols. 1 and 2; Hemisphere: New York, 1989 and 1991. Vol. 3; CRC Press: Boca Raton, 1994. This database offers an extensive discussion before the selection of each value. It is the English translation and update of the first three volumes of *Glushko Tables*.
HSC Chemistry	Roine, A. *Outokumpu HSC Chemistry for Windows*, Version 5.1; Outokumpu Research Oy, Finland (http://www.outokumputechnology.com/pages/Page_____21758.aspx). This is a rather useful computer program that allows to make several types of calculations, including reaction enthalpies, heat balances, equilibrium compositions, and phase stability diagrams. The non-critically evaluated database contains HSC Chemistry 5.1 database contains enthalpy, entropy and heat capacity data for more than 17000 chemical species. Most of the species (some 60%) are inorganic ones.

(*Continued*)

Table 2 (Continued)

Database	*Reference and comments*
Majer & Svoboda	Majer, V.; Svoboda, V. *Enthalpies of Vaporization of Organic Compounds. A Critical Review and Data Compilation*; IUPAC Chemical Data Series No. 32; Blackwell: Oxford, 1985.
NBS 82	Wagman, D. D.; Evans, W. H.; Parker, V. B.; Schumm, R. H.; Halow, I.; Bailey, S. M.; Churney, K. L.; Nuttall, R. L. *The NBS Tables of Chemical Thermodynamic Properties: Selected Values for Inorganic and C_1 and C_2 Organic Substances in SI Units; J. Phys. Chem. Ref. Data* **1982**, *11*, Suppl. 2. The NBS 82 tables are still widely used, mainly because they contain data (e.g. solution enthalpies) not easily found in other databases.
NIST Chemistry WebBook	*NIST Chemistry WebBook*; NIST Standard Reference Database Number 69; Mallard, W. G.; Linstrom, P. J., Eds.; National Institute of Standards and Technology: Gaithersburg (http://webbook.nist.gov). The *NIST Chemistry WebBook* is probably the most extensive of all chemical compilations. It supersedes many of NIST databases and it is composed by several "chapters," some of which include thermochemical information of a variety of substances. It is regularly updated, either with new values or with new chapters. Not all of these chapters have thermochemical consistency. For instance, the *Neutral Thermochemical Data* quotes the standard enthalpies of formation directly from the original publications. However, as the experimental reaction enthalpies are also provided, the user can easily derive the "correct" values.
NIST S&P	Stein, S. S. *NIST Structures and Properties* (Version 2.0); NIST Standard Reference Database 25; National Institute of Standards and Technology: Gaithersburg, 1994. This useful and simple to use software package relies on Benson's group additivity scheme to estimate thermochemical data for organic compounds in the gas phase. It also contains values from several NIST databases, including *NIST Positive Ion Energetics* and *JANAF Tables*. The first version of *NIST S&P* is from 1991. The database is superseded by the *NIST Chemistry. WebBook*.
NIST Therm	Domalsky, E. S.; Hearing, E. D.; Hearing, V. J. Jr. *NIST Estimation of the Chemical Thermodynamic Properties for Organic Compounds at 298.15 K*; NIST Standard Reference Database 18; National Institute of Standards and Technology: Gaithersburg, 1994. Although the software is old-fashioned, this package is one of the best options to estimate thermochemical data for organic compounds in the gas and condensed phases. It relies on Benson's group additivity scheme, and contains also selected experimental values for a large number of organic compounds.
NIST-JANAF Tables	Chase, M. W. Jr. *NIST-JANAF Thermochemical Tables* (4th ed.); *J. Phys. Chem. Ref. Data* **1998**, Monograph No. 9. This is one of the most widely used thermochemical databases for inorganic compounds. The 1st and 2nd editions of *JANAF* (Joint Army, Navy and Air Force) *Tables* date from 1964 and 1971, respectively. Supplements of the latter were released in 1974, 1975, 1978, and 1982. The 3rd edition was published in 1985.
Pedley 94	Pedley, J. B. *Thermodynamic Data and Structures of Organic Compounds*; Thermodynamics Research Center Data Series, Vol I; Thermodynamics Research Center: College Station, 1994. This database supersedes those in Cox & Pilcher (Cox, J. D.; Pilcher, G. *Thermochemistry of Organic and Organometallic Compounds*; Academic Press: London, 1970), Pedley 77 (Pedley, J. B.; Rylance, J. *Sussex-N. P. L. Computer Analysed Thermochemical Data: Organic and Organometallic Compounds*; University of Sussex: Brighton, 1977), and Pedley 86 (Pedley, J. B.; Naylor, R. D.; Kirby, S. P. *Thermochemical Data of Organic Compounds*; Chapman and Hall: London, 1986). An empirical scheme, developed by the author, to estimate enthalpies of formation of organic compounds in gas and condensed phases, is also described.
Monographs and reviews[a]	*Reference and comments*
Angelici 95	Angelici, R. J. *Basicities of Transition Metal Complexes from Studies of their Heats of Protonation: A Guide to Complex Reactivity, Acc. Chem. Res.* **1995**, *28*, 51–60. Data included in the NIST Chemistry WebBook.
Benson 76	Benson, S. W. *Thermochemical Kinetics* (2nd ed.); Wiley: New York, 1976. This book contains a small database for organic and inorganic compounds. Its main value is, however, that it describes a group additivity scheme to estimate thermochemical data. An updated and extended list of group parameters is given in *NIST Therm* and *CHETAH*. The first edition of this classic work is from 1968.
Berkowitz *et al.* 94	Berkowitz, J.; Ellison, G. B.; Gutman, D. *Three Methods to Measure RH Bond* Energies, *J. Phys. Chem.* **1994**, *98*, 2744–2765. Contains a table with recommended R—H bond dissociation enhalpies and standard enthalpies of formation of radicals (at 0 K and 298.15 K).
Dias 94	Dias, P. B.; Minas da Piedade, M. E.; Martinho Simões, J. A. *Bonding and Energetics of Phosphorus (III) Ligands in Transition Metal Complexes, Coord. Chem. Rev.* **1994**, *135/136*, 737–807. Thermochemistry of transition metal-phosphorus bond. It also includes critically evaluated standard enthalpies of formation of phosphines and phosphites.

(*Continued*)

Table 2 (Continued)

Database	*Reference and comments*
Hill & Murray 93	Hill, J. O.; Murray, J. P. *Metal-Oxygen Thermochemical Bond Dissociation Enthalpies for Metal Pentane-2,4-dionate Complexes – A Review*, *Rev. Inorg. Chem.* **1993**, *13*, 157–181. Tables with standard enthalpies of formation and vaporization, and mean bond dissociation enthalpies.
Hoff 92	Hoff, C. D. *Thermodynamics of Ligand Binding and Exchange in Organometallic Reactions*; *Prog. Inorg. Chem*, **1992**, *40*, 503–561. A review on several aspects of the thermochemistry of metal-ligand bonds.
Kerr *et al*.	Strengths of Chemical Bonds, In *CRC Handbook of Chemistry and Physics*; CRC Press: Boca Raton. Tables with bond dissociation energies of diatomic molecules, bond dissociation enthalpies of polyatomic molecules, and standard enthalpies of formation of (mainly organic) radicals (at 298.15 K). The *CRC Handbook* is regularly updated, so the tables may vary according to the edition number.
Kristjánsdóttir & Norton 90	Kristjánsdóttir, S. S.; Norton, J. R. Acidity of Hydrido Transition Metal Complexes in Solution. In *Transition Metal Hydrides: Recent Advances in Theory and Experiment*; A. Dedieu, Editor; VCH: New York, 1990. Tables with pK_a values of some transition metal hydride complexes.
Luo 03	Luo, Y.-R. *Handbook of Bond Dissociation Energies in Organic Compounds*; CRC Press: Boca Raton, 2003.
Marks 90	Marks, T. J., Ed. *Bonding Energetics in Organometallic Compounds*; ACS Symposium Series No. 428: Washington, DC, 1990.
Marks 88	Marks, T. J., Ed. *Metal-Ligand Bonding Energetics in Organotransition Metal Compounds*; Polyhedron Symposia-in-Print No. 6; *Polyhedron* **1988**, 7, 1405–1637.
McMillen & Golden 82	McMillen, D. F.; Golden, D. M. *Hydrocarbon Bond Dissociation Energies*, *Ann. Rev. Phys. Chem.* **1982**, *33*, 493–532. This is one of the most cited sources of bond dissociation enthalpies at 298.15 K in organic compounds and standard enthalpies of formation of organic radicals. Most values, however, have been updated in other publications.
Nolan 94	Nolan, S. P. Bonding Energetics of Organometallic Compounds. In *Encyclopedia of Inorganic Chemistry*; John Wiley: New York, 1994. A review on application of metal-ligand bond dissociation enthalpy data to discuss several aspects of organometallic chemistry.
Nolan 95	Nolan, S. P. *Solution Thermochemistry of Ligand Substitution Reactions Involving Organoruthenium Complexes*, *Comments Inorg. Chem.* **1995**, *17*, 131–162. Reaction enthalpies in solution. Data included in the NIST Chemistry WebBook.
Simões	Martinho Simões, J. A., Ed. *Energetics of Organometallic Species*; Kluwer: Dordrecht, 1992
Squires 87	Squires, R. R. *Gas-Phase Transition Metal Negative Ion Chemistry*, *Chem. Rev.* **1987**, *87*, 623–646. Tables with electron affinities, proton affinities, and metal-ligand bond dissociation enthalpies.
Tel'noi & Sheiman 95	Tel'noi, V. I.; Sheiman, M. S. *Thermodynamics of Organoselenium and Organotellurium Compounds*, *Russ. Chem. Rev.* **1995**, *64*, 309–316. Tables with standard combustion and vaporization enthalpies, and standard enthalpies of formation. Data included in the NIST Chemistry WebBook.

[a]Not cited in the main text.

The choice of a given database as source of auxiliary values may not be straightforward, even for a thermochemist. A database should not be a mere collection of values quoted from the literature. It usually involves some critical assessment of those values and also an effort to present a "consistent" set of data. In a consistent database, all the standard enthalpies of formation have been recalculated from the original values reported for the reaction enthalpies, on the basis of a single set of auxiliary data which, itself, is internally consistent (and which should also be listed).

Consistency is a very important criterion, but factors such as the publication year, the assignment of an uncertainty to each value, and even the scientific reputation of the authors or the origin of the database do matter. Moreover, when calculating a reaction enthalpy from the standard enthalpies of formation of reactants and products, values from more than one database are frequently needed. The selection is therefore more complicated, and requires additional caution, to ensure thermochemical consistency.

Finally, when using a database with enthalpies of formation of ions, one should be aware of the two possible conventions used to derive those values: the so-called "thermal electron convention" or just "electron convention," and the "stationary electron convention" or the "ion convention." These conventions are related to the standard enthalpy of formation of an electron gas $\Delta_f H^o(e^-, g)$ and its thermal temperature correction from 0 to 298.15 K. A detailed description of the reasoning behind both conventions provided in the introductory chapter of a widely used data compilation.[69] In practical terms, one should be aware that the enthalpy of formation of an ion calculated by the electron convention will be 6.197 kJ mol^{-1} (= 2.5RT at 298.15 K) higher than the value derived by the ion convention. Therefore, we must be alert when using enthalpy of formation data from several sources, because they may have been derived by accepting either of those conventions.

Table 3 Contents of the databases selected in Table 2[a]

Database	*Contents*	*Form*	*Consistent*	$\Delta_f H^\circ$	$\Delta_f H^\circ$ (0 K)	*D*	$\Delta_{vap} H^\circ$	S°	C_p°	$H_T^\circ - H_{298}^\circ$	*PA*	E_1	*AE*	E_{ea}	*Errors*	*Exp. data*	*Refs.*
Barin	IN	P	✓	✓				✓	✓	✓							
CATCH tables	IN,OM	P	✓	✓			✓								✓	✓	✓
CHETAH	IN,O			✓				✓	✓	✓						✓	
CODATA	IN	P	✓	✓				✓		✓					✓	✓	✓
Frenkel *et al.*	IN,O	P	✓	✓				✓	✓	✓							✓
Glushko table I	IN,O,OM	P	✓	✓	✓		✓	✓	✓	✓					✓	✓	✓
Glushko tables II	IN,O,OM	P															
Gurvich tables	IN,O,OM	P	✓	✓	✓		✓	✓	✓	✓					✓	✓	✓
HSC chemistry	IN,O,OM	S		✓				✓	✓	✓						✓	✓
Majer and Svoboda	O	P					✓								✓	✓	✓
NBS 82	IN,O,OM	P,S	✓	✓	✓			✓	✓	✓							
NIST chemistry webbook	IN,O,OM	O		✓			✓	✓	✓		✓	✓	✓	✓	✓	✓	✓
NIST S&P	IN,O,OM	S	✓	✓				✓	✓			✓	✓		✓		✓
NIST therm	O	S	✓	✓				✓	✓								
NIST-JANAF tables	IN,O	P,S	✓	✓	✓		✓	✓	✓	✓					✓		✓
Pedley 94	O	P	✓	✓											✓		✓

[a]Explanation of the table: (i) A short designation of the database and its reference number. (ii) The types of compounds covered by the database (IN = inorganic; O = organic; OM = organometallic). (iii) The publishing medium (P = printed; S = software; O = on-line). (iv) The thermochemical consistency of the databases values (✓). The absence of a check mark indicates non-consistent data or that the comment is not appropriate. (v) The types of values reported in the database (standard enthalpies of formation at 298.15 and 0 K, bond dissociation energies or enthalpies at any temperature, standard enthalpy of vaporization or sublimation at 298.15 K, standard entropy at 298.15 K, standard heat capacity at 298.15 K, standard enthalpy differences between *T* and 298.15 K, proton affinity, ionization energy, appearance energy, and electron affinity). The absence of a check mark indicates that the data are not provided. However, that does not necessarily mean that they cannot be calculated from other quantities tabulated in the database. (vi) Uncertainties have been associated to each value (✓). The absence of a check mark indicates that no individual uncertainties have been assigned. (vii) The original (experimental) literature data are given in the database (✓). The absence of a check mark indicates that this information is not provided. (viii) The source of each value is indicated by literature references (✓). The absence of a check mark indicates that this information is not provided.

Nomenclature

E	= bond enthalpy term
K	= equilibrium constant
$\Delta_r G$	= Gibbs energy of reaction
$\Delta_r G^o$	= standard Gibbs energy of reaction
$\Delta^{\ddagger} G^o$	= standard Gibbs energy of activation
DH^o	= bond dissociation enthalpy
DH^o_{sln}	= solution-phase bond dissociation enthalpy
$\langle DH^o \rangle$	= mean bond dissociation enthalpy
$\langle DH^o_{sln} \rangle$	= solution-phase mean bond dissociation enthalpy
$\Delta_r H^o$	= standard enthalpy of reaction
$\Delta^{\ddagger} H^o$	= standard enthalpy of activation
$\Delta_r S^o$	= standard entropy of reaction

References

1. Guntz, A. *Comptes Rendus de l'Academie des Sciences* **1887**, *105*, 673–674.
2. Berthelot, M. P. E. *Comptes Rendus de l'Academie des Sciences* **1899**, *129*, 918–920.
3. Bichowsky, F. R.; Rossini, F. D. *The Thermochemistry of the Chemical Substances*; Reinhold: New York, 1936.
4. Skinner, H. A. *J. Chem. Thermodyn.* **1978**, *10*, 309–320.
5. Skinner, H. A. *Adv. Organomet. Chem.* **1964**, *2*, 49–114.
6. Bottrill, M.; Gavens, P. D.; Kelland, J. W.; McMeeking, J. In *Comprehensive Organometallic Chemistry I*; Wilkinson, G., Stone, F. G. A., Abel, E. W., Eds.; Pergamon: Oxford, 1982; Vol. 3, p 459.
7. Kirtley, S. W. In *Comprehensive Organometallic Chemistry I*; Wilkinson, G., Stone, F. G. A., Abel, E. W., Eds.; Pergamon: Oxford, 1982; Vol. 3, p 1308.
8. Davidson, P. J.; Lappert, M. F.; Pearce, R. *Chem. Rev.* **1976**, *76*, 219–242.
9. Jaffé, H. H.; Doak, G. O. *J. Chem. Phys.* **1953**, *21*, 196–200.
10. Wilkinson, G. In *Organometallic Chemistry (Proceedings of the 5th International Conference of Organometallic Chemistry, Moscow, 1971)*; IUPAC-Butterworths: London, 1972; pp 627–635.
11. Martinho Simões, J. A. In *NIST Chemistry WebBook, NIST Standard Reference Database Number 69*; Linstrom, P. J., Mallard, W. G., Eds.; National Institute of Standards and Technology: Gaithersburg, MD, March 2003.
12. Denbigh, K. *The Principles of Chemical Equilibrium*, 4th ed.; Cambridge University Press: Cambridge, 1981.
13. Smith, G. M.; Carpenter, J. D.; Marks, T. J. *J. Am. Chem. Soc.* **1986**, *108*, 6805–6807.
14. Minas da Piedade, M. E.; Martinho Simões, J. A. *J. Organomet. Chem.* **1996**, *518*, 167–180.
15. Watson, L. A.; Eisenstein, O. *J. Chem. Educ.* **2002**, *79*, 1269–1277.
16. Laidler, K. J. *Chemical Kinetics*, 3rd ed.; Harper & Row: New York, 1987.
17. Martinho Simões, J. A.; Ribeiro da Silva, M. A. V. In *Energetics of Stable Molecules and Reactive Intermediates*; Minas da Piedade, M. E., Ed.; Kluwer: Dordrecht, 1999; pp 1–28.
18. Rossini, F. D., Ed. *Experimental Thermochemistry*; Interscience: New York, 1956; Vol. 1.
19. Sunner, S., Mansson, M., Eds. *Combustion Calorimetry*; Pergamon: Oxford, 1979.
20. Hajiev, S. N. In *Thermochemistry and Equilibria of Organic Compounds*; Frenkel, M., Ed.; VCH: New York, 1993; Vol. 1, pp 7–169.
21. Good, W. D.; Scott, D. W. In *Experimental Thermochemistry*; Skinner, H. A., Ed.; Interscience: New York, 1962; Vol. 2, pp 57–75.
22. Pilcher, G. In *Energetics of Organometallic Species*; Martinho Simões, J. A., Ed.; Kluwer: Dordrecht, 1992; pp 9–34.
23. Minas da Piedade, M. E. In *Energetics of Stable Molecules and Reactive Intermediates*; Minas da Piedade, M. E., Ed.; Kluwer: Dordrecht, 1999; pp 29–53.
24. Rabinovich, I. B.; Nistranov, V. P.; Telnoy, V. I.; Sheiman, M. S. *Thermochemical and Thermodynamic Properties of Organometallic Compounds*; Begell House: New York, 1999.
25. Minas da Piedade, M. E.; Shaofeng, L.; Pilcher, G. *J. Chem. Thermodyn.* **1987**, *19*, 195–199.
26. Sabbah, R.; Perez, J. A. G. *Thermochim. Acta* **1997**, *297*, 17–32.
27. Skinner, H. A.; Sturtevant, J. M.; Sunner, S. In *Experimental Thermochemistry*; Skinner, H. A., Ed.; Interscience: New York, 1962; Vol. 2, pp 157–219.
28. Cordfunke, E. H. P.; Ouweltjes, W. In *Experimental Thermodynamics: Solution Calorimetry*; Marsh, K. N., O'Hare, P. A. G., Eds.; Blackwell: Oxford, 1994; Vol. 4, Chapter 14.
29. Bruno, J. W.; Stecher, H. A.; Morss, L. R.; Sonnenberger, D. C.; Marks, T. J. *J. Am. Chem. Soc.* **1986**, *108*, 7275–7280.
30. Leal, J. P.; Pires de Matos, A.; Martinho Simões, J. A. *J. Organomet. Chem.* **1991**, *403*, 1–10.
31. Diogo, H. P.; Minas da Piedade, M. E.; Martinho Simões, J. A.; Teixeira, C. *J. Organomet. Chem.* **2001**, *632*, 188–196.
32. Skinner, H. A.; Virmani, Y. *Rev. Roum. Chim.* **1972**, *17*, 467–470.
33. Connor, J. A.; Skinner, H. A.; Virmani, Y. *J. Chem. Soc., Faraday Trans. 1* **1972**, *68*, 1754–1763.
34. Brown, D. L. S.; Connor, J. A.; Leung, M. L.; Paz-Andrade, M. I.; Skinner, H. A. *J. Organomet. Chem.* **1976**, *110*, 79–89.
35. Connor, J. A. *Top. Curr. Chem.* **1977**, *71*, 71–110.
36. Connor, J. A.; Demain, C. P.; Skinner, H. A.; Zafarani-Moattar, M. T. *J. Organomet. Chem.* **1979**, *170*, 117–130.
37. Connor, J. A.; Zafarani-Moattar, M. T.; Bickerton, J.; El Saied, N. I.; Suradi, S.; Carson, R.; Al-Takhin, G.; Skinner, H. A. *Organometallics* **1982**, *1*, 1166–1174.
38. Al-Takhin, G.; Skinner, H. A.; Zaki, A. A. *J. Chem. Soc., Dalton Trans.* **1984**, 371–378.
39. Al-Takhin, G.; Connor, J. A.; Pilcher, G.; Skinner, H. A. *J. Organomet. Chem.* **1984**, *265*, 263–269.

40. McNaughton, J. L.; Mortimer, C. T. In *International Review of Science; Physical Chemistry Series 2, Thermochemistry and Thermodynamics*; Skinner, H. A., Ed.; Butterworths: London, 1975; Vol. 10, pp 1–44.
41. Beech, G.; Mortimer, C. T.; Tyler, E. G. *J. Chem. Soc. (A)* **1967**, 925–928.
42. Galwey, K.; Brown, M. E. In *Handbook of Thermal Analysis and Calorimetry. Principles and Practice*; Brown, M. E., Ed.; Elsevier: Amsterdam, 1998; Vol. 1, pp 147–224.
43. Hemminger, W.; Flammersheim, H.-J.; Höhne, G. W. H. *Differential Scanning Calorimetry: An Introduction for Practitioners*; Springer: New York, 1996.
44. Wunderlich, B. *Thermal Analysis*; Academic Press: San Diego, 1990.
45. Haines, P. J.; Reading, M.; Wilburn, F. W. In *Handbook of Thermal Analysis and Calorimetry. Principles and Practice*; Brown, M. E., Ed.; Elsevier: Amsterdam, 1998; Vol. 1, pp 279–361.
46. Teixeira, C.; Wadsö, I. *Netsu Sokutei* **1994**, *21*, 29–39.
47. Teixeira, C. In *Energetics of Stable Molecules and Reactive Intermediates*; Minas da Piedade, M. E., Ed.; Kluwer: Dordrecht, 1999; pp 105–136.
48. Patel, C. K. N.; Tam, A. C. *Rev. Mod. Phys.* **1981**, *53*, 517–550.
49. Tam, A. C. *Rev. Mod. Phys.* **1986**, *58*, 381–431.
50. Borges dos Santos, R. M.; Lagoa, A. L. C.; Martinho Simões, J. A. *J. Chem. Thermodyn.* **1999**, *31*, 1483–1510.
51. Correia, C. F.; Nunes, P. M.; Borges dos Santos, R. M.; Martinho Simões, J. A. *Thermochim. Acta* **2004**, *420*, 3–11.
52. Braslavsky, S. E.; Heibel, G. E. *Chem. Rev.* **1992**, *92*, 1381–1410.
53. Stull, D. R.; Westrum, E. F., Jr.; Sinke, G. C. *The Chemical Thermodynamics of Organic Compounds*; Wiley: New York, 1969.
54. Thompson, M. E.; Baxter, S. M.; Bulls, A. R.; Burger, B. J.; Nolan, M. C.; Santarsiero, B. D.; Schaefer, W. P.; Bercaw, J. E. *J. Am. Chem. Soc.* **1987**, *109*, 203–219.
55. Bulls, A. R.; Bercaw, J. E.; Manriquez, J. M.; Thompson, M. E. *Polyhedron* **1988**, *7*, 1409–1428.
56. Bryndza, H. E.; Domaille, P. J.; Tam, W.; Fong, L. K.; Paciello, R. A.; Bercaw, J. E. *Polyhedron* **1988**, *7*, 1441–1452.
57. Liu, Y. F.; Sturtevant, J. M. *Protein Sci.* **1995**, *4*, 2559–2561.
58. Naghibi, H.; Tamura, A.; Sturtevant, J. M. *Proc. Natl. Acad. Sci. USA* **1995**, *92*, 5597–5599.
59. Weber, G. *J. Phys. Chem.* **1995**, *99*, 1052–1059.
60. Koenig, T. W.; Hay, B. P.; Finke, R. G. *Polyhedron* **1988**, *7*, 1499–1516.
61. Bryndza, H. E.; Domaille, P. J.; Paciello, R. A.; Bercaw, J. E. *Organometallics* **1989**, *8*, 379–385.
62. Brinkmann, P. H. P.; Luinstra, G. A.; Saenz, A. *J. Am. Chem. Soc.* **1998**, *120*, 2854–2861.
63. Wayner, D. D. M.; Parker, V. D. *Acc. Chem. Res.* **1993**, *26*, 287–294.
64. Tilset, M. In *Energetics of Stable Molecules and Reactive Intermediates*; Minas da Piedade, M. E., Ed.; Kluwer: Dordrecht, 1999; pp 153–176.
65. Tilset, M.; Fjeldahl, I.; Hamon, J.-R.; Hamon, P.; Toupet, L.; Saillard, J.-Y.; Costuas, K.; Haynes, A. *J. Am. Chem. Soc.* **2001**, *123*, 9984–10000.
66. Ervin, K. M. *Chem. Rev.* **2001**, *101*, 391–444.
67. Operti, L.; Rabezzana, R. *Mass Spectrom. Rev.* **2003**, *22*, 407–428.
68. Armentrout, P. B., Ed. *Theory and Ion Chemistry in The Encyclopedia of Mass Spectrometry*; Elsevier: Amesterdam, 2003; Vol. 1.
69. Lias, S. G.; Bartmess, J. E.; Liebman, J. F.; Holmes, J. L.; Levin, R. D.; Mallard, W. G. *Gas-Phase Ion and Neutral Thermochemistry*; American Chemical Society and the American Institute of Physics for the National Institute of Standards and Technology: Washington, DC and New York, 1988.
70. Franklin, J. L.; Dillard, J. G.; Rosenstock, H. M.; Herron, J. T.; Draxl, K.; Field, F. H. *Ionization Potentials, Appearance Potentials, and Heats of Formation of Gaseous Positive Ions*; U.S. Department of Commerce, National Bureau of Standards: Washington, DC, 1969.
71. Rosenstock, H. M.; Draxl, K.; Steiner, B. W.; Herron, J. T. *J. Phys. Chem. Ref. Data* **1977**, *6*, *Suppl. 1*.
72. Levin, R. D.; Lias, S. G. *Ionization Potential and Appearance Potential Measurements, 1971–1981*; U.S. Department of Commerce, National Bureau of Standards: Washington, DC, 1982.
73. Rosenstock, H. M. *Int. J. Mass Spectrom. Ion Processes* **1976**, *20*, 139–190.
74. Berkowitz, J. *Photoabsorption, Photoionization, and Photoelectron Spectroscopy*; Academic Press: New York, 1979.
75. Baer, T. *Adv. Chem. Phys.* **1986**, *64*, 111–202.
76. Baer, T.; Sztaray, B.; Kercher, J. P.; Lago, A. F.; Bodi, A.; Skull, C.; Palathinkal, D. *Phys. Chem. Chem. Phys.* **2005**, *7*, 1507–1513.
77. Qi, F.; Yang, S.; Sheng, L.; Gao, H.; Zhang, Y.; Yu, S. *J. Chem. Phys.* **1997**, *107*, 10391–10398.
78. Talrose, V. L.; Vinogradov, P. S.; Larin, I. K. In *In Gas Phase Ion Chemistry*; Bowers, M. T., Ed.; Academic Press: New York, 1979; Vol. 1, pp 305–347.
79. Armentrout, P. B.; Georgiadis, R. *Polyhedron* **1988**, *7*, 1573–1581.
80. Armentrout, P. B.; Beauchamp, J. L. *Acc. Chem. Res.* **1989**, *22*, 315–321.
81. Armentrout, P. B. *Int. J. Mass Spectrom.* **2000**, *200*, 219–241.
82. Armentrout, P. B.; Clemmer, D. E. In *Energetics of Organometallic Species*; Martinho Simões, J. A., Ed.; Kluwer: Dordrecht, 1991; Vol. 367, pp 321–356.
83. Squires, R. R. *Chem. Rev.* **1987**, *87*, 623–646.
84. Graul, S. T.; Squires, R. R. *Mass Spectrom. Rev.* **1988**, *7*, 263–358.
85. Damrauer, R. *Organometallics* **2004**, *23*, 1462–1479.
86. Bowers, M. T.; Kemper, P. R.; van Koppen, P.; Wyttenbach, T.; Carpenter, C. J.; Weis, P.; Gidden, J. In *Energetics of Stable Molecules and Reactive Intermediates*; Minas da Piedade, M. E., Ed.; Kluwer: Dordrecht, 1999; pp 235–258.
87. Leyhn, B.; Lorquet, J. C. In *The Encyclopedia of Mass Spectrometry*; Armentrout, P. B., Ed.; Elsevier: Amsterdam, 2003; Vol. 1, pp 17–32.
88. Gingerich, K. A.; Haque, R. *J. Chem. Soc., Faraday Trans. 2* **1980**, *76*, 101–103.
89. Gupta, S. K.; Nappi, B. M.; Gingerich, K. A. *J. Phys. Chem.* **1981**, *85*, 971–976.
90. Haque, R.; Gingerich, K. A. *J. Chem. Phys.* **1981**, *74*, 6407–6414.
91. Ran, Q. S.; Schmude, R. W.; Gingerich, K. A.; Wilhite, D. W.; Kingcade, J. E. *J. Phys. Chem.* **1993**, *97*, 8535–8540.
92. Meloni, G.; Gingerich, K. A. *J. Chem. Phys.* **1999**, *111*, 969–972.
93. Meloni, G.; Gingerich, K. A. *J. Chem. Phys.* **2000**, *113*, 10978–10982.
94. Meloni, G.; Thomson, L. M.; Gingerich, K. A. *J. Chem. Phys.* **2001**, *115*, 4496–4501.
95. Krause, J. R.; Bidinosti, D. R. *Can. J. Chem.* **1975**, *53*, 628–632.
96. Margrave, J. L., Ed. *The Characterization of High-temperature Vapors*; Wiley: New York, 1967.
97. Kemper, P. R.; Bushnell, J.; von Helden, G.; Bowers, M. T. *J. Phys. Chem.* **1993**, *97*, 52–58.

98. Bushnell, J. E.; Kemper, P. R.; Maitre, P.; Bowers, M. T. *J. Am. Chem. Soc.* **1994**, *116*, 9710–9718.
99. Ekeberg, D.; Hagen, S. I.; Hvistendahl, G.; Schulze, C.; Uggerud, E.; Vedde, J. *Org. Mass Spectrom.* **1993**, *28*, 1547–1554.
100. Kebarle, P. *Annu. Rev. Phys. Chem.* **1977**, *28*, 445–476.
101. Sharpe, P.; Kebarle, P. *J. Am. Chem. Soc.* **1993**, *115*, 782–789.
102. Deng, H. T.; Kebarle, P. *J. Am. Chem. Soc.* **1998**, *120*, 2925–2931.
103. McMahon, T. B. In *Energetics of Stable Molecules and Reactive Intermediates*; Minas da Piedade, M. E., Ed.; Kluwer: Dordrecht, 1999; pp 259–280.
104. Peschke, M.; Blades, A. T.; Kebarle, P. *J. Am. Chem. Soc.* **2000**, *122*, 10440–10449.
105. Golden, D. M.; Spokes, G. N.; Benson, S. W. *Angew. Chem., Int. Ed. Engl.* **1973**, *12*, 534–546.
106. McMillen, D. F.; Lewis, K. E.; Smith, G. P.; Golden, D. M. *J. Phys. Chem.* **1982**, *86*, 709–718.
107. Lewis, K. E.; Golden, D. M.; Smith, G. P. *J. Am. Chem. Soc.* **1984**, *106*, 3905–3912.
108. Russell, D. K.; Mills, G. P.; Raynor, J. B.; Workman, A. D. *Chem. Vap. Deposition* **1998**, *4*, 61–67.
109. Russell, D. K.; Davidson, I. M. T.; Ellis, A. M.; Mills, G. P.; Pennington, M.; Povey, I. M.; Raynor, J. B.; Saydam, I. M. *Chem. Vap. Deposition* **1998**, *4*, 103–107.
110. Gaydon, A. G. *Dissociation Energies and Spectra of Diatomic Molecules*, 3rd ed.; Chapman and Hall: London, 1968.
111. Kerr, J. A.; Stoker, D. W. In *CRC Handbook of Chemistry and Physics*; Lide, D. R., Ed.; CRC Press: Boca Raton, FL, 2001–2002; pp 9.51–9.74.
112. Martinho Simões, J. A. In *Energetics of Organometallic Species*; Martinho Simões, J. A., Ed.; Kluwer: Dordrecht, 1992; pp 197–232.
113. Irikura, K. K.; Frurip, D. J., Eds. *Computational Thermochemistry. Prediction and Estimation of Molecular Thermodynamics*; ACS Symposium Series No. 677; American Chemical Society: Washington, DC, 1998.
114. Drago, R. S. *Applications of Electrostatic–Covalent Models in Chemistry*; Surfside: Gainesville, FLII, 1994.
115. Davidson, E. R., Ed. *Computational Transition Metal Chemistry. Chem. Rev.* **2000**, *100*, pp 351–818.
116. Collman, J. P.; Hegedus, L. S.; Norton, J. R.; Finke, R. G. *Principles and Applications of Organotransition Metal Chemistry*; Univertsity Science Books: Mill Valley, CA, 1987.
117. James, B. R. In *Comprehensive Organometallic Chemistry I*; Wilkinson, G., Stone, F. G. A., Abel, E. W., Eds.; Pergamon: Oxford, 1982; Vol. 8, Chapter 52.
118. An estimate for a similar reaction, although using different values for the bond dissociation enthalpies, also gives $\Delta_r H^\circ < 0$. See ref. 119.
119. Calderazzo, F. *Ann. N. Y. Acad. Sci.* **1983**, *415*, 37–46.
120. Ungváry, F. *J. Organomet. Chem.* **1972**, *36*, 363–370.
121. Alemdaroglu, N. H.; Penninger, J. M. L.; Oltay, E. *Monatsh. Chem.* **1976**, *107*, 1043–1053.
122. Bor, G. *Pure Appl. Chem.* **1986**, *58*, 543–552.
123. Tilset, M.; Parker, V. D. *J. Am. Chem. Soc.* **1989**, *111*, 6711–6717.
124. Martinho Simões, J. A.; Beauchamp, J. L. *Chem. Rev.* **1990**, *90*, 629–688.
125. Kubas, G. J. *Acc. Chem. Res.* **1988**, *21*, 120–128.
126. Gonzalez, A. A.; Hoff, C. D. *Inorg. Chem.* **1989**, *28*, 4295–4297.
127. Gonzalez, A. A.; Zhang, K.; Nolan, S. P.; Lopez de la Vega, R.; Mukerjee, S. L.; Hoff, C. D.; Kubas, G. J. *Organometallics* **1988**, *7*, 2429–2435.
128. Kubas, G. J.; Unkefer, C. J.; Swanson, B. I.; Fukushima, E. *J. Am. Chem. Soc.* **1986**, *108*, 7000–7009.
129. Khalsa, G. R. K.; Kubas, G. J.; Unkefer, C. J.; Van Der Sluys, L. S.; Kubat-Martin, K. A. *J. Am. Chem. Soc.* **1990**, *112*, 3855–3860.
130. This may be concluded from comparisons involving the enthalpies of oxidative addition of I_2, *o*-$O_2C_6Cl_4$, etc. to analogous Rh and Ir complexes. See refs. 11 and 131.
131. Burke, N. E.; Singhal, A.; Hintz, M. J.; Ley, J. A.; Hui, H.; Smith, L. R.; Blake, D. M. *J. Am. Chem. Soc.* **1979**, *101*, 74–79.
132. Kiss, G.; Zhang, K.; Mukerjee, S. L.; Hoff, C. D.; Roper, G. C. *J. Am. Chem. Soc.* **1990**, *112*, 5657–5658.
133. Pilcher, G.; Skinner, H. A. In *The Chemistry of the Metal–Carbon Bond*; Hartley, F. R., Patai, S., Eds.; Wiley: New York, 1982; pp 43–90.
134. Dias, A. R.; Martinho Simões, J. A.; Teixeira, C.; Airoldi, C.; Chagas, A. P. *J. Organomet. Chem.* **1987**, *335*, 71–83.
135. Dias, A. R.; Martinho Simões, J. A.; Teixeira, C.; Airoldi, C.; Chagas, A. P. *J. Organomet. Chem.* **1989**, *361*, 319–334.
136. Bryndza, H. E.; Fong, L. K.; Paciello, R. A.; Tam, W.; Bercaw, J. E. *J. Am. Chem. Soc.* **1987**, *109*, 1444–1456.
137. Pilcher, G. *Pure Appl. Chem.* **1989**, *61*, 855–860.
138. Wayland, B. B.; Ba, S.; Sherry, A. E. *J. Am. Chem. Soc.* **1991**, *113*, 5305–5311.
139. Sherry, A. E.; Wayland, B. B. *J. Am. Chem. Soc.* **1990**, *112*, 1259–1261.
140. Calhorda, M. J.; Dias, A. R.; Galvão, A. M.; Martinho Simões, J. A. *J. Organomet. Chem.* **1986**, *307*, 167–176.
141. Berry, M.; Elmitt, K.; Green, M. L. H. *J. Chem. Soc., Dalton Trans.* **1979**, 1950.
142. Cooper, N. J.; Green, M. L. H.; Mahtab, R. *J. Chem. Soc., Dalton Trans.* **1979**, 1557–1562.
143. Parkin, G.; Bercaw, J. E. *Organometallics* **1989**, *8*, 1172–1179.
144. This reaction is difficult to observe in common solvents due to practical problems related to the solubility of methane (see ref. 145). It readily occurs, however, in liquid xenon (see ref. 146).
145. Wax, M. J.; Stryker, J. M.; Buchanan, J. M.; Kovac, C. A.; Bergman, R. G. *J. Am. Chem. Soc.* **1984**, *106*, 1121–1122.
146. Sponsler, M. B.; Weiller, B. H.; Stoutland, P. O.; Bergman, R. G. *J. Am. Chem. Soc.* **1989**, *111*, 6841–6843.
147. Stoutland, P. O.; Bergman, R. G.; Nolan, S. P.; Hoff, C. D. *Polyhedron* **1988**, *7*, 1429–1440.
148. Crabtree, R. H. *Chem. Rev.* **1985**, *85*, 245–269.
149. Low, J. J.; Goddard, W. A., III. *J. Am. Chem. Soc.* **1986**, *108*, 6115–6128.
150. Jones, W. D.; Feher, F. J. *Acc. Chem. Res.* **1989**, *22*, 91–100.
151. Jones, W. D.; Dong, L. *J. Am. Chem. Soc.* **1989**, *111*, 8722–8723.
152. Stoutland, P. O.; Bergman, R. G. *J. Am. Chem. Soc.* **1988**, *110*, 5732–5744.
153. Silvestre, J.; Calhorda, M. J.; Hoffmann, R.; Stoutland, P. O.; Bergman, R. G. *Organometallics* **1986**, *5*, 1841–1851.
154. Periana, R. A.; Bergman, R. G. *J. Am. Chem. Soc.* **1986**, *108*, 7332–7346.
155. Brookhart, M.; Green, M. L. H. *J. Organomet. Chem.* **1983**, *250*, 395–408.
156. Morse, J. M., Jr.; Parker, G. H.; Burkey, T. J. *Organometallics* **1989**, *8*, 2471–2474.
157. Fendrick, C. M.; Marks, T. J. *J. Am. Chem. Soc.* **1986**, *108*, 425–437.
158. Janowicz, A. H.; Bergman, R. G. *J. Am. Chem. Soc.* **1983**, *105*, 3929–3939.
159. Jones, W. D.; Feher, F. J. *J. Am. Chem. Soc.* **1985**, *107*, 620–631.
160. Dias, A. R.; Salema, M. S.; Martinho Simões, J. A.; Pattiasina, J. W.; Teuben, J. H. *J. Organomet. Chem.* **1989**, *364*, 97–103.

161. Schock, L. E.; Marks, T. J. *J. Am. Chem. Soc.* **1988**, *110*, 7701–7715.
162. Bruno, J. W.; Marks, T. J.; Morss, L. R. *J. Am. Chem. Soc.* **1983**, *105*, 6824–6832.
163. Doering, W. v. E. *Proc. Natl. Acad. Sci. USA* **1981**, *78*, 5279–5283.
164. McMillen, D. F.; Golden, D. M. *Annu. Rev. Phys. Chem.* **1982**, *33*, 493–532.
165. Periana, R. A.; Bergman, R. G. *Organometallics* **1984**, *3*, 508–510.
166. Crabtree, R. H.; Dion, R. P. *J. Chem. Soc., Chem. Commun.* **1984**, 1260–1261.
167. Roy, S.; Puddephatt, R. J.; Scott, J. D. *J. Chem. Soc., Dalton Trans.* **1989**, 2121–2125.
168. Yamamoto, A. *Organotransition Metal Chemistry*; Wiley: New York, 1986.

1.23
The Application of Modern Computational Chemistry Methods to Organometallic Systems

T R Cundari, University of North Texas, Denton, TX, USA

1.23.1 Introduction

The last decade has seen a tremendous growth of computational chemistry, as applied to organometallic complexes. Simulation and modeling have proliferated to the point where they may be reasonably expected to approach in ubiquity experimental techniques such as infrared and NMR spectroscopy, and X-ray crystallography as tools for the analysis of organometallic species and reactions. Given recent advances in the field of computational chemistry, organometallic chemists may now even seriously consider the use of modeling and simulation in the design of novel systems and reactions, and for the planning of next-generation experiments. A simple testament to the growth of the field is the inclusion of an individual chapter devoted to the subject of computational organometallic chemistry in the current work. However, inspection of previous editions of this series is sufficient to validate the notion that organometallic chemists have long been very interested in fundamental questions of bonding, structure, and reactivity, in particular the differences and similarities of organometallics in relation to their purely organic congeners. In this context, computational chemistry (like other "traditional" experimental techniques) represents another weapon in the arsenal of organometallic chemists to understand this economically important, intellectually beguiling family of chemical species.

A variety of factors, technological and methodological, are responsible for the proliferation of theory applied to organometallic systems. Technological impetuses include the widespread availability of powerful, yet relatively inexpensive, computers, and easy-to-use, and dare one say almost fun, graphically based software tools. Programs such as GAMESS (General Atomic and Molecular Electronic Structure System),[1] Gaussian,[2] Jaguar,[3] MOLPRO (Molecular Properties Program),[4] and many others are now prevalent in chemistry departments across the globe. Each program has its own merits vis-à-vis the ease of use, the scope of computational methods it incorporates, and the tools available for analysis of calculational results. It is not the purpose of this chapter to delve into the pros and cons of each software package for computational organometallic chemistry. As is the case for experimental techniques, the choice of a particular software solution is often dictated by availability, cost issues, and the particular chemical problem the organometallic chemist wishes to study.

A combination of forces—scientific and social (e.g., greater familiarity with and acceptance of computers)—have pushed the state-of-the-art in computational chemistry to the point that organometallic chemists who are not full-time theorists can generate quality results with a reasonable effort on widely available software/hardware combinations and do so with a high degree of confidence. In this chapter, our goal is to provide some motivation for taking up this challenge, with emphasis on the challenges inherent in computational organometallic chemistry, as well as protocols that have been developed for dealing with these challenges. Theory and equations are thus kept at a minimum, while applications and practical advice are emphasized. The primary target audiences for the present chapter include: practicing experimental organometallic chemists who may wish to add computational chemistry to their experimental-analysis and design regimen; computational chemists who may wish to diversify into organometallics applications; early career researchers wishing exposure to a rapidly emerging field of research. We will discuss the most prevalent computational chemistry techniques applied to organometallic systems, and some of the pitfalls that may arise from their careless use. Many of the examples, views, and conclusions are colored by the experiences of the author's own research, and his extensive collaborations with many different experimentalists. As a result, many of the examples focus on transition metal organometallics, although the discussion is easily generalized to other families such as the *s*- and *p*-block metals, and *f*-block metals. However, the present discussion is in no way intended to overlook the huge, international scientific enterprise that is computational organometallic chemistry, one that has enjoyed the talents and enthusiasm of many excellent researchers.

1.23.2 The Challenge of Organometallics

Coming up through the ranks in the late 1980s, it struck me that two of the foremost books in the field of computational organometallic chemistry included the word "challenge" in their title.[5,5a] It remains to this day that the inclusion of a metal into a chemical system introduces computational challenges above and beyond those encountered in the modeling of compounds comprised of lighter main group elements common in organic and biological chemistry. Coupling the organic and metallic families of chemical entities into a single species, the organometallic thus encompasses the challenges of both. Conceptually, one can think of an organometallic as being comprised of a metallic or inorganic "core" surrounded by an organic "coating," as depicted schematically in Figure 1. As with any endeavor involving the modeling of two regions or phases, additional complications will arise in terms of modeling the interface of chemically different regions (Figure 1). In the following section, the general issues of computational chemistry (i.e., electron correlation and basis sets) are treated. Many of the issues discussed are pertinent to computational chemistry studies of any molecular system, organometallic or otherwise, but particular attention is given to those aspects relevant to computational organometallic chemistry.

1.23.3 General Computational Issues

The metallic core of many organometallics typically comprises a smaller subset of the total atoms than the organic periphery. The metallic core may be comprised of a single metal or a cluster of metal atoms, and the atoms directly attached to it, that is, the inner coordination sphere. For example, in the $Pt(P^tBu_3)_2$ complex shown in Figure 2, modeled by Svensson and co-workers,[6] of the 81 total atoms in the molecule, the metallic core is a scant three atoms (PtP_2), the remaining 78 atoms being the organic coating (six *tert*-butyl groups). Indeed, as we will discuss later, this conceptual partitioning of organometallics into organic and inorganic regions has led to some very exciting and important computational advances for the more efficient modeling of larger, and hence more experimentally relevant, organometallic complexes.[6]

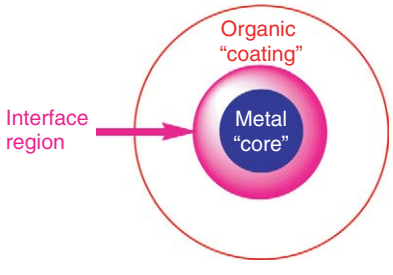

Figure 1 Cartoon showing inorganic core, organic coating, and interface region.

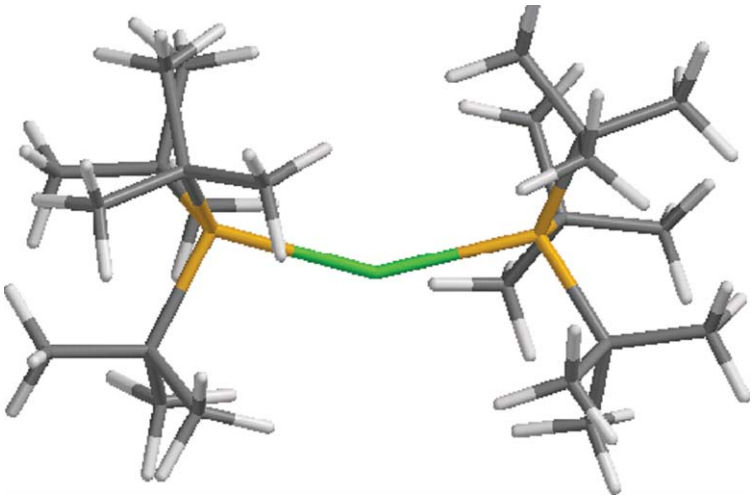

Figure 2 $Pt(P^tBu_3)_2$ Complex.[6] Pt (green), P (orange), C (gray), H (white).

Conformational complexity is often not as large a computational challenge for the inorganic core as it is for the organic periphery. This is a result of the smaller number of atoms that typically comprise the inorganic core, combined with the fact that the mobility of its atoms is often limited by the steric bulk and/or ligational requirements (e.g., if a chelate is formed) of the organic portion of the organometallic. That is not to say that conformational complexity is not an issue for inorganic species, but in fact it tends to manifest itself in different ways. In addition to the conformational and geometric (e.g., *cis*- vs. *trans*-olefins or *facial*- and *meridional*-octahedral complexes) isomerism prevalent in organic chemistry, metal complexes routinely display structural (e.g., tetrahedral vs. square planar vs. dodecahedral coordination for four-coordinate complexes), coordination (e.g., axial and equatorial coordination sites in a trigonal bipyramid), linkage (NCS^- vs. SCN^-, η^1-carboxylate vs. η^2-carboxylate, etc.), and "spin" (e.g., high- vs. intermediate- vs. low-spin states for partially filled *d*-shell electronic configurations) isomerism. Buda and co-workers have investigated a range of computational methods for rapid and reliable prediction of these forms of isomerism in organometallic complexes.[7,7a–7d] The interested reader is referred to the original papers for a discussion of techniques and the limitations of various conformational searching approaches applied to organometallics.

When giving seminars, many computational chemists show a qualitative graph highlighting two of the most important parameters in any calculational "experiment": treatment of electron correlation and basis-set completeness (Figure 3). Within most modern calculations, the choice of a Hamiltonian and basis set comprise the two most immediate and

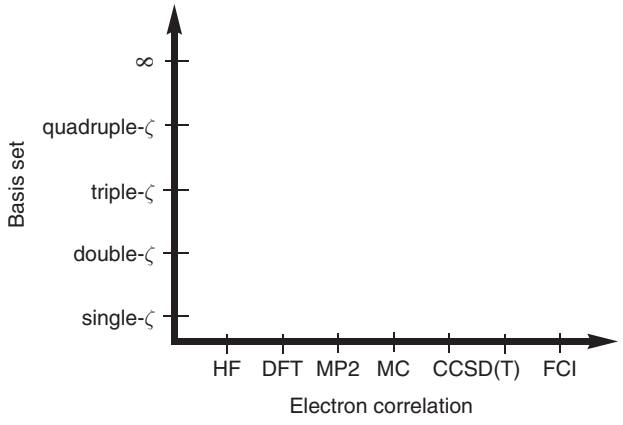

Figure 3 Qualitative diagram displaying increasing levels of electron correlation (abscissa) and basis-set size (ordinate). HF = Hartree–Fock; DFT = density functional theory; MP2 = second order Møller–plesset perturbation theory; MC = multi-configuration; CCSD(T) = coupled clusters with single, double, and perturbative triple excitations; FCI = full-configuration interaction.

important choices for the modeler. Semi-empirical quantum mechanics (SEQM) are an exception to this generalization as the selection of a semi-empirical model generally specifies both the Hamiltonian and the attendant basis sets. Of course, the ideal of infinite (or even near-infinite) basis sets and a complete account of electron correlation (i.e., full-configuration interaction, FCI) is achievable only for the smallest of molecules. Hence, the decision that must be made by the modeler is: how far must one proceed toward the upper right-hand corner of Figure 3 to achieve the desired accuracy with the minimum computational effort? As stressed throughout this chapter, the answer to this question is dependent not only on the particular organometallic system of interest, but also the task at hand. For example, if the organometallic chemist has a reasonably unambiguous crystal structure and wishes to qualitatively understand the electronic structure of the complex, then the demands of basis set and correlation are likely to be minimal, and a standard density functional calculation with a reasonable (say double-zeta-plus polarization) basis set is generally appropriate. If the goal is to confirm/deny the UV–VIS spectroscopic signature of a highly reactive, low-concentration putative catalytic intermediate, then one must trudge further to the upper right-hand corner of Figure 3, likely employing multi-configuration (MC) methods and extended basis sets (triplet-zeta-plus polarization-and-diffuse basis sets or larger) needed for the balanced description of a ground and one or more excited states.

1.23.4 Electron Correlation

As one goes further along the electron correlation axis (Figure 3), more and more complete (and hence more computationally expensive) treatments of electron correlation are incorporated. Electron correlation is a quantum effect that arises from the correlated motion of electrons, and is especially important for the correct description of many families of organometallic complexes. In practical terms of applications to organometallic chemistry, empirical observation of the literature yields the following chemical systems/properties for which an account of electron correlation is especially important in obtaining quantitative, and in some cases even qualitative, description:

(i) energetics, including those pertinent to spectroscopic transitions, but electron correlation is generally less important for geometries in many cases,
(ii) open-shell or paramagnetic systems, as compared to closed-shell or diamagnetic metal complexes,
(iii) organometallics of the first-row transition metals (in comparison to their heavier congeners),
(iv) low coordination number complexes,
(v) polymetallic clusters (vis-à-vis monometallic systems), especially those with direct metal–metal interaction,
(vi) heavier main group species (as compared to their lighter counterparts), and
(vii) classic Werner-type coordination complexes in relation to organometallic complexes.

While the organometallic chemist may take solace in the final generalization, the chemical characteristics listed above are those that frequently result in the presence of low-energy excited states, which exacerbates the electron correlation problem, for example, through the presence of partially filled *d*-electrons and/or weak ligand fields in *d*- and *f*-block organometallics.

Obviously, the modeling of organometallics that combines several of the aforementioned traits may be expected to be particularly difficult and requires special care to analyze the quality of the results, and assure that the treatment of electron correlation is appropriate for the system of interest. As an example, consider the following model of a Cr tetrameric "box" $[Cr(silox)Cl]_4$ (Figure 4), a complex studied by our group in collaboration with the experimental group of Professor Pete Wolczanski at Cornell University. The first notable thing from casual inspection of Figure 4 is that the usual approximation has been made of replacing the organic periphery with something more tractable: silox (OSi^tBu_3) → hydroxyl (OH). While it may be argued that the hydrogen atom and the tri-*tert*-butylsilyl group may be isolobal, their steric differences are indisputable, and the possible consequences of this on the computed results must always be kept in mind.

The chromous tetramer in Figure 4 displays several of the hallmarks of a highly correlated system: first-row transition metal, open-shell metal (each chromium is formally d^4-Cr(II)), and a polymetallic system. Moreover, the Cr···Cr distances (ca. 2.67–2.69 Å for adjacent chromium atoms in the tetramer) exist in an intermediate range between Cr–Cr bonds, such as in the metal and the non-interacting limit.[8] Previous calculations on a related complex $[Cr(\mu\text{-}CH_2SiMe_3)_2]_4$ with shorter Cr···Cr distances (2.33–2.40 Å) were reported for a singlet state using a restricted (i.e., α and β electrons are constrained to occupy identical spatial orbitals) density functional formalism.[9] For the Wolczanski tetramer, things are not so simple, due in large part to the longer Cr···Cr distances and hence weaker Cr···Cr interaction in the tetramer. The frontier orbitals of this tetramer are a densely packed (ca. 2.1 eV energy

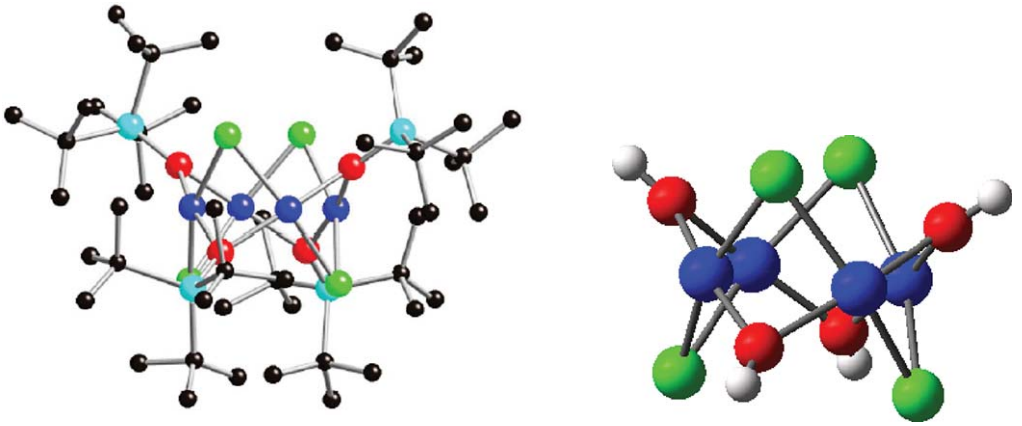

Figure 4 Wolczanski chromous(II) tetrameric "box." Experimental system (a) with hydrogens omitted for clarity, and computational model (b). Reprinted with permission from Sydora, O. L.; Wolczanski, P. T.; Lobkovsky, E. B.; Buda, C.; Cundari, T. R. *Inorg. Chem.* **2005**, *44*, 2606–2618. © 2005 American Chemical Society.

spread) array of chromium 3*d*-orbitals (Figure 5). The number of electronic configurations (referred to as configuration state functions, CSFs) that must be modeled increases tremendously as the multiplicity increases for even the minimal active space (the active space is those orbitals among which the electrons are rearranged in all possible combinations subject only to spatial and spin-symmetry restrictions): 1 CSF (mult = 17); 256 CSFs (mult = 15); 14,400 CSFs (mult = 13); 313,600 CSFs (mult = 11); 3,312,400 CSFs (mult = 9); 19,079,424 CSFs (mult = 7); 64,128,064 CSFs (mult = 5); 82,812,015 CSFs (mult = 3); 82,824,885 CSFs (mult = 1). For the minimal 16-orbital/16-electron (i.e., four *d*-electrons and four *d*-orbitals from each Cr(II) in the tetramer) active space, the highest spin (mult = 17) state can, of course, only be generated by a single, ferromagnetically coupled arrangement of the electrons. Even the singlet state is not so simple for the $[Cr(OH)Cl]_4$ "box," and indeed the sheer number of electron configurations (almost 83 million) needed for this description thwarted all attempts at its modeling using MC methods, even with the employment of symmetry constraints. In open-shell, polymetallic clusters, several groups, most notably that of Case, Noodleman and their co-workers, have successfully employed broken-symmetry density functional theory (BS-DFT) as a cost-effective alternative to MC calculations (for more details See Refs: 10,10a). These groups have reported many excellent studies of metal clusters, especially those germane to biological systems.

As in all cases, care must be employed in using any computational approximation or model. For example, in a study of the corresponding chromous dimer, $[Cr(\mu\text{-}OH)(OH)]_2$, it was feasible to study all possible multiplicities (1, 3, 5, 7, 9) with both BS-DFT and MC methods. For the chromous dimer, MC techniques, unlike the BS-DFT calculations, display a very dense network of states (within 4 kcal mol^{-1}) of differing multiplicity, and yielded a calculated magnetic susceptibility in good agreement with experiment.[11] Furthermore, the state splitting and magnetic susceptibility did not change much with respect to computational details of the MC calculation (e.g., using larger basis sets, and/or employing more elaborate active spaces, e.g., those providing for further correlation outside the primary active space of chromium *d*-electrons and *d*-orbitals). The latter exercise is a typical hallmark for a computational exercise that has converged with respect to basis set and correlation treatment. Convergence tests of both basis sets and correlation methods are as crucial in the computational chemistry study of new families of organometallics as are Beer's Law plots in spectroscopy, and one in which both the full- and part-time practitioner would be well advised to add to their regimen. Agreement with experiment, while more aesthetically pleasing than the alternative, cannot be the only criteria for assessing calculational quality. Convergence tests of both basis set and method are especially imperative for organometallic complexes.

In general, the treatment of electron correlation is more important for the inorganic, metal-containing "core" than it is for the organic "coating" of an organometallic. However, note that in traditional single theory-level calculations (as opposed to the hybrid methods that combine two or more levels of theory that are discussed later) the definition of a correlation treatment for one portion of the molecule requires the application of this treatment to the entire molecule. Put another way, if doing a calculation on 2,6-$Trip_2C_6H_3Tl$ (Trip = 2,4,6-$^{i}Pr_3C_6H_2$)[12,13] (Figure 6) requires an electron-correlation treatment for the Tl–C_{ipso} bond, then in a traditional calculation, this often more expensive

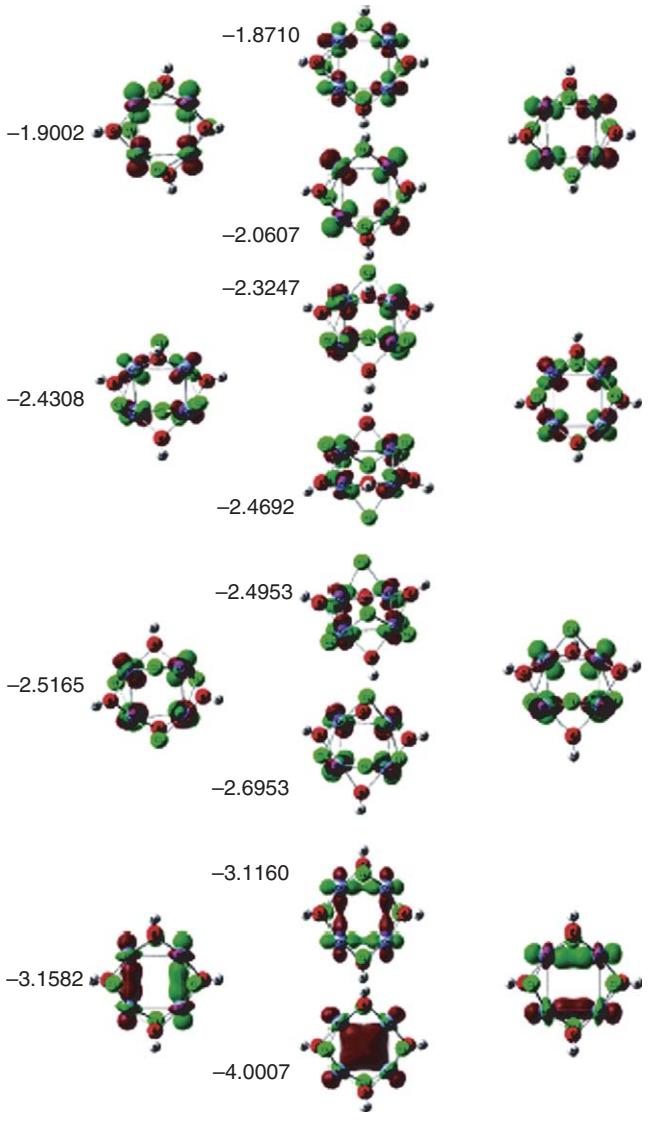

Figure 5 Frontier orbitals of $[Cr(\mu\text{-}Cl)(\mu\text{-}OH)]_4$. Orbital energies (eV) are determined at DFT level of theory for the high-spin multiplicity = 17 state.

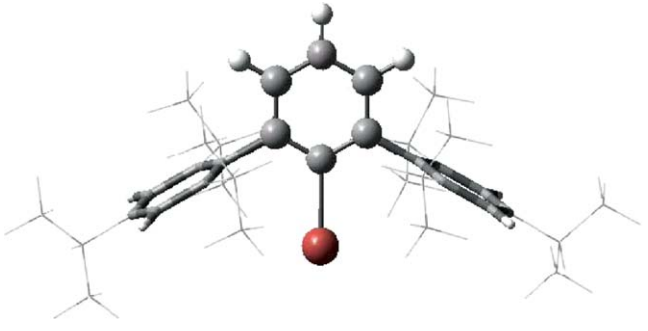

Figure 6 2,6-$Trip_2C_6H_3Tl$ complex.[12,13] Thallium–phenyl core is shown in a ball-and-stick representation; peripheral phenyl groups with a tube representation; isopropyl groups in wire frame.

level of theory must be applied as well to the organic remainder. As such, the quantum requirements needed to treat the metal core of an organometallic drags the entire molecule down with it. As alluded to above, such considerations have provided major impetus for the development of hybrid methods for individually modeling the organic and metallic subsets of the organometallic species.

There are several computational approaches that the organometallic chemist can employ in the treatment of electron correlation.

(i) Ignore it (e.g., employ Hartree–Fock (HF) calculations).
(ii) Add it after the fact in a perturbative fashion (e.g., a HF wave function as the reference to generate the second order Møller–Plesset perturbation theory (MP2) correction to the energy).
(iii) Use a parametrized method, for example SEQM, which given the fact that the parameters that describe nuclear and electronic interactions are often derived to reproduce experimental data, thus implicitly include electron correlation.
(iv) MC methods, which incorporate correlation by allowing electronic excitation from an active space to a set of erstwhile virtual orbitals, thus generate excited-state electronic configurations that mix into the reference (typically HF) electronic configuration.
(v) Use density functional theory (DFT).

We now discuss each of these methods in turn for the computational study of organometallic molecules.

1.23.5 Hartree-Fock Methods

Through the early 1990s, the majority of *ab initio* calculations reported for organometallics were of the Hartree–Fock (HF) variety. The HF method entails a single-electron configuration description of the organometallic species, and hence these methods provide no account of electron correlation between electrons of like spin. (For applications of Hartree-Fock theory to the electronic structure analysis of molecules see, for example, Refs: 44, 65.) As such, HF methods, although typically suitable for the organic coating of an organometallic, may present difficulties for the metal core. With the advent of DFT, HF calculations have largely gone the way of the slide rule—a quaint reminder of days gone by, a teaching tool, and a reminder to today's modelers how tough things were for previous generations.

One area in which HF-based calculations have remained robust is in the study of spectroscopy, although to some extent this is also being surpassed by density functional based approaches. Roques *et al.* used HF/6-31G* calculations to probe the excited-state magnetic properties of silicon organometallics.[14] Hung and Schurko employed both HF and Becke three-parameter and Lee–Yang–Parr hybrid functional (B3LYP) self-consistent field calculations to study the ^{25}Mg NMR properties of magnesium organometallics. Good agreement with experimentally derived NMR parameters was found for both HF and B3LYP methods in conjunction with double- and triple-zeta Pople-style basis sets such as 6-31G** and 6-311 + G**, respectively.[15] Zhang and co-workers employed HF theory and a variety of pure and hybrid density functionals to study the Mossbauer-derived isomer shifts of inorganic, organometallic, and biological iron complexes in a variety of formal oxidation and spin states. Qualitative agreement with experiment was found for HF methods, but the best agreement was seen for hybrid functionals such as B3LYP, which, of course, incorporate HF exchange into the density functional. Hence, HF calculations, when compared/contrasted with DFT calculations, may provide insight into the effects of electron correlation on the spectroscopic properties of organometallic species.

Parenthetically, in the author's own experience, HF calculations can aid in the treatment of the annoying issue of SCF convergence, which is a problem exacerbated in organometallic complexes for which low-energy excited states may be present. HF methods tend to possess better SCF convergence behavior than DFT methods. As a result, a useful strategy for difficult to converge cases is to first run a single-point HF calculation (with either the same basis set or a smaller basis set, e.g., leave off the polarization functions on the main group elements, or reduce from a triple-zeta to double-zeta valence basis set). This converged HF wave function can then be used to provide the density of an improved starting guess for a subsequent DFT calculation with the full basis set. Programs such as GAMESS[1] automatically employ such multistep strategies. Density functional calculations are first loosely SCF converged at the HF level, then loosely converged at the DFT level (by the employment of a coarse grid for DFT integrations), and then finally with the full-accuracy DFT integration grid. However, that is not to say that other programs cannot be used successfully in regard to difficult-to-converge organometallics. Gaussian[2] and MOLPRO,[4] for example, make it simple to chain together multiple calculations within a single input deck so that lower level (e.g., smaller basis set

and/or lower correlation treatment) calculations can be used to provide a starting wave function or density for more elaborate calculations with difficult-to-converge organometallic cases. Other programs, such as Jaguar,[3] employ different SCF initial-guess strategies specifically for organometallics that are quite successful. As always, the choice of program is a matter of availability, personal taste, and economics.

HF calculations are still employed as way-stations on the road to some other more expensive, higher-end calculation. For example, the HF wave function is used to provide the reference state for a perturbation-theory calculation (e.g., MP2[16]) or a MC calculation such as the highly popular, and near quantitative, coupled clusters method (viz., CCSD(T)).[17]

1.23.6 Perturbation Theory Methods

Perturbation theory (PT) methods, most notably the MP2 method and its higher order variants such as MP3 and MP4, have also receded in popularity with the advent of the more computationally efficient electron-correlation treatments available in density functional methods. Møller–Plesset (MP) calculations in the vast majority of cases are used for providing more accurate energetic quantities, and much less frequently for corrections to the wave function for property evaluation. The standard protocol for many computational studies of organometallics in the 1980s and 1990s entailed HF geometry optimization, followed by MP2 calculation of more accurate energetics at the stationary point thus obtained,[18] denoted MP2/basis set 2//HF/basis set 1 in the Pople notation. The notation MP2/basis set 2//HF/basis set 1 specifies that the level of theory (i.e., both basis set and method) after the double slash, HF/basis set 1 in the current example, is used for geometry optimization. Single-point energy calculations employing the MP2/basis set 2 are carried out at the stationary points (minima or transition states) determined at the HF/basis set 1 level of theory. Such a combined approach avoids the need to calculate the energy derivatives at the higher level of theory, which are often very expensive, or which early on in the development of computational chemistry were often not available. Basis set 1 and basis set 2 may or may not be equivalent. In a very interesting study of metal and ligand effects, Abu-Hasanayn and co-workers obtained excellent agreement with experimental thermodynamics using the higher order MP4(SDTQ) (i.e., Fourth order Møller–Plesset perturbation theory with single, double, triple, and quadruple excitations) for the study of H_2 oxidative-addition reactions as a function of ligand for a series of iridium Vaska-type complexes *trans*-$Ir(PH_3)_2(CO)X$ (X = univalent, anionic ligand), Table 1.[19,20] Modeling of kinetics, which is of course central to organometallic catalysis, requires an accurate modeling of transition states, for which correlation effects are typically more important than for the ground-state reactants and products they connect. Abu-Hasanayn *et al.* also employed the high-end perturbation theory method MP4(SDTQ) to study kinetic properties such as activation barriers and kinetic isotope effects.[21] Note that while energetic trends in Table 1 are reasonably well reproduced with HF and MP2 methods, the expansion of the PT to fourth order is needed for more quantitative agreement with experiment, and even at that expensive level of theory, the results are outside the window of chemical accuracy (typically taken as ± 1–2 kcal mol^{-1}) seen for computational organic chemistry. Further computational tests would be needed to ascribe the theory–experiment differences to deficiencies in the basis set, the correlation level, or the use of chemical models (e.g., replacement of experimental phosphines with parent PH_3).

Many textbook examples of the utilization of MP*n* calculations in organometallic chemistry can be found in the classic 1991 review by Koga and Morokuma.[18] DFT receives only scant mention in the Koga–Morokuma review. Olefin and carbonyl insertion, oxidative addition/reductive elimination, and many other prototypical organometallic reaction pathways of interest in catalysis and catalytic reactions are studied largely with HF, MP2, and MP2/HF approaches. Koga and Morokuma conclude their review by pointing out that for organometallics "...to obtain a reliable energetics, it is necessary to take into account the electron correlation effect, even if the single determinantal wave function is a good starting point."

One area in which MP*n* methods still maintain some degree of primacy over DFT in organometallic chemistry involves the modeling of metal–metal interactions, particularly those for which van der Waals and London/dispersion type interactions are often significant. Many studies have focused on organometallics of closed-shell d^{10}-metals due to their interesting photochemical and photophysical properties, especially Au(I), and the term aurophilic attraction has been coined to describe the gold–gold interaction. Standard density functional approaches often encounter difficulties in the modeling of van der Waals and London interactions.[22,22a] For these purposes, PT methods may be a better, but much more expensive, choice as compared to DFT. Wang and Schwarz recommended against the use of common gradient-corrected functionals for describing aurophilic interactions in Au(I) complexes.[23] This paper is an excellent "how-to" guide on method evaluation and calibration in computational organometallic chemistry as these researchers arrived at their conclusion on the basis of HF, MP2, and density functional (five functionals were tested)

Table 1 Calculated energies for addition of H2 to rhodium Vaska-type complexes

X	ΔE_{HF}[a]	ΔE_{MP2}[a]	ΔE_{MP4}[a]	ΔH_{exp}
$L = PH_3$				
F	−25.8	−20.3	−13.6	>−10
Cl	−34.2	−29.3	−22.0	−14[b]
Br	−36.2	−31.6	−24.1	−17[b]
I	−39.3	−35.0	−27.3	−19[b]
$L = PMe_3$				
Cl	−40.4	−30.9		−14[b]
I	−44.4	−33.4		−19[b]
$L = PH_3$(ECP-2)[c]				
Cl	−11.0	−18.0	−8.7	−14[b]
I	−15.2	−24.1	−14.4	−19[b]
$L = PH_3$				
CN	−38.8	−35.9	−28.3	−18[d]
H	−45.4	−38.6	−35.3	
CH_3	−36.1	−31.2	−23.2	
SiH_3	−48.9	−44.1	−35.1	
OH	−26.0	−19.8	−12.8	
SH	−37.0	−31.4	−23.7	
BH_4[e]	−44.6	−40.4	−32.2	
$L = NH_3$				
X = Cl	−29.3	−18.8	−13.8	
$L = AsH_3$				
X = Cl	−34.6	−29.9	−22.4	−15[f]

[a]ΔE given without ZPE corrections; "MP4" refers to MP4(STDQ) calculations.
[b]$L = PPh_3$; measured in chlorobenzene.
[c]Calculations carried out with the Ir(ECP-2) type potential.
[d]$L = PPh_3$; measured in benzene.
[e]Our previously reported values when $X = BH_4$ are in error.
[f]Estimated value.
Reprinted with permission from Abu-Hasanayn, F.; Goldman, A. S.; Krogh-Jespersen, K. *Inorg. Chem.* **1994**, *33*, 5122–5130. © 1993 American Chemical Society.

calculations. Pyykkö and co-workers studied interactions between heavy metal complexes of bis(cyclopentadienyl) and bis(pentamethylcyclopentadienyl) of the main group metal ions Tl(I) and In(I). The metal–metal attraction was found to be ca. 20 kJ mol^{-1} for Cp models and less (12–16 kJ mol) for larger Cp^* derivatives.[24] Pyykkö and co-workers have published extensively on aurophilic interactions and have even proposed a recipe for quantification of the aurophilic interaction as the difference between HF and MP2 binding energies.[25] Colacio *et al.*[26] have even hypothesized about the utilization of aurophilic attractions, which are thought to be on the order of weak hydrogen bonds, for crystal engineering of Au(I) complexes on the basis of MP2 calculations combined with relativistic pseudopotentials. Functionals that better model van der Waals interactions comprise an active area of research. For example, Grimme has reported empirically derived DFT functionals that include van der Waals interactions, and reported their application to organic examples.[27] Xu and Goddard have developed the X3LYP functional,[28] which better models hydrogen-bonded and van der Waals complexes than the popular B3LYP. Further development of such enhanced DFT approaches to organometallic complexes is of interest.

Perturbation methods, as the name implies, are built on the assumption that the excited states generated from the HF reference wave function are a perturbation or small correction to the overall wave function. Hence, the modeling of dynamical electron correlation and near-degeneracy effects (which is quite common for low coordination number organometallics) requires MC techniques, which are discussed in the following section. As an example, we take, from our study with the group of Holland (University of Rochester), the model three-coordinate, dinitrogen complex, L′FeNNFeL′(L′ = β-diketiminate model ligand), Figure 7.[29] From test calculations using MC methods, it is seen

State	ΔE_{rel} (kcal mol^{-1})
$^7B_3$	0.0
^5A	3.3
$^5B_3$	11.4
^3A	11.3
$^3B_3$	6.5
^1A	0.7

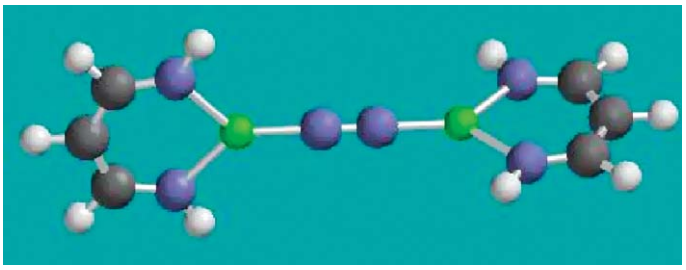

Figure 7 Low-energy electronic states of L′FeNNFeL′ as determined by MC techniques.

that there exists a dense manifold of a septet ground state ($^7B_3$) and five close energy-excited states of different multiplicities and symmetry: ^1A, ^5A, $^3B_3$, ^3A, and $^5B_3$. Such a state of affairs is clear proof that PT-based techniques will not be sufficient for the study of these systems.

It cannot be stressed enough that if the PT assumption is not valid, the wave functions and energies generated are not valid. Consider a simple ground-state description of an organometallic as a linear combination of the HF and excited state configurations (Equation (1)).

$$\psi \sim \psi_{HF} + \lambda \sum_{i} \psi_{es}(i) \tag{1}$$

There is no magic value of λ that allows one to state with complete confidence that the PT approximation will work. Even if one took a poll and came up with a consensus value of $\lambda = 10\%$, there remain problems with such a simplistic view. First, the appropriate calculation to determine λ is a MC wave function approach (e.g., as was done for the dinitrogen complex in Figure 7), which is much more expensive in general than PT calculations on comparably sized organometallics. Second, and more importantly, the appropriateness of the HF-reference wave function depends on the property of interest. If geometries are the point of interest for the organometallic chemist, then more "detritus" in the wave function can likely be tolerated. If energetic properties are paramount, then more stringent methods are typically required.

An easy and necessary test of the appropriateness of the PT approximation is simply to investigate important properties (energetic and spectroscopic quantities are preferred over geometric properties, as the latter are often quite insensitive to the computational details) both at the HF and MP2 level of theory. For example, imagine that one wishes to compare the stability of two organometallic isomers. At the HF level of theory (reasonable basis sets such as double-zeta-plus-polarization valence basis sets must always be employed in any test of method appropriateness), isomer A is substantially more stable than the isomer B (Figure 8). At the MP2 level of theory (same basis set used for both HF-geometry optimization and MP2 single-point energy evaluation), the energy ordering is substantially reversed. This is a clear indication that the PT approximation for one or both of the isomers is inappropriate, and one must investigate alternative approaches such as MC techniques.

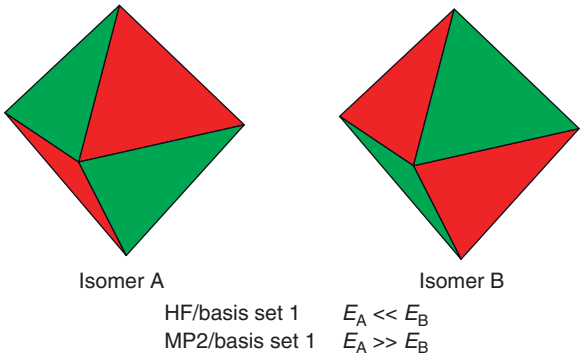

Figure 8 Simple test of the inappropriateness of the MP2 method.

In the present time, many issues in regard to the appropriateness of PT methods are obviated by the use of density functional methods, although this in no way reduces the need for calibration of the methods being used. Indeed, wave-function-based methods such as HF and MP2 are excellent choices along with DFT for conducting sensitivity analyses of calculated properties, as they are typically quick calculations and reasonably different in approach from density functional theory.

1.23.7 Multiconfiguration Techniques

From the point of view of the practitioner and user of computations, MC methods are similar in spirit to the PT techniques just outlined. In both cases, electron correlation is included by the mixing in of excited-state electronic configurations into a ground-state, single-configuration reference wave function. The main difference lies in that in MC methods, no mathematical approximations are made based on the assumption that there is a single dominant electronic configuration. Stated alternatively, there is, in theory, no upper bound on λ in Equation (1) for the appropriateness of MC wave functions. As MC techniques are variational, the magnitude of λ in Equation (1) will be small if the excited states are insignificant. If λ is indeed small, the computational organometallic chemist can then employ DFT and MP2 or even HF calculations with greater confidence. Of course, the extra flexibility of the MC wave function comes at a cost, and these costs are great computational expense in terms of memory, disk-storage space, and computing times. Given these issues, and the large size of many organometallics, MC techniques are often a method of last resort in computational organometallic chemistry.

A typical MC application in organometallic chemistry involves the calculation of very accurate energetics once a geometry has been obtained at a lower level of theory (nowadays, most typically DFT). Coupled-clusters methods are emerging as a best option within the MC universe for organometallic applications, but these calculations are very expensive, and often not feasible for the largest complexes. It is beyond the scope of this chapter to delve into the theory of coupled-clusters methods, but an excellent review by Crawford and Schaefer is available.[17] Also, Frenking and his group have published extensively in the field of computational organometallic chemistry, using a CCSD(T)// DFT protocol for the study of catalytic reactions.[30,30a] For example, Frenking carried out CCSD(T) calculations on $Fe(CO)_4L$ (L = ligand) geometries obtained with DFT to obtain accurate Fe–L bond-dissociation energies. These near-quantitative calculations were then combined with electronic structure analysis to describe the bond in terms of the classic Dewar–Chatt–Duncanson model.[31] Chemical vapor-deposition pathways of organometallics leading to Ta_2O_5 were also investigated with coupled-clusters methods (Figure 9).[32] Note in Figure 9 that while the ground

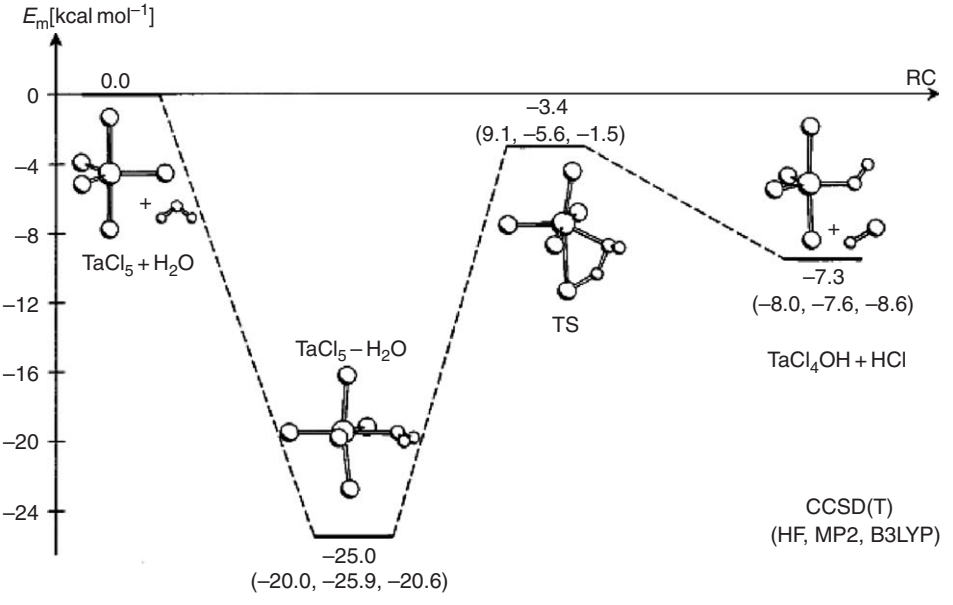

Figure 9 Potential energy surface for hydrolysis of $TaCl_5$. Energetics determined with HF, MP2, B3LYP, and coupled-clusters levels of theory. Reprinted with permission from Siodmiak, M.; Frenking, G.; Korkin, A. *J. Phys. Chem. A* **2000**, *104*, 1186–1195. © 2000 American Chemical Society.

state thermodynamics change little with methods (HF, MP2, and B3LYP results are reported along with CCSD(T)), the calculated activation barrier for hydrolysis shows considerable spread from -5.6 to $+9.1\,\mathrm{kcal\,mol^{-1}}$ (energies relative to separated reactants $TaCl_5$ and H_2O). Greater sensitivity to the level of theory for transition states versus ground states is typical and not unexpected. Hence, in the calculation of reaction coordinates for organometallic species, it is a good idea to use transition states as the "guinea pig" for basis-set and method convergence as they tend to be more sensitive gauges of convergence with respect to level of theory.

Non-coupled cluster techniques for generating MC wave functions exist and have been employed, for example, to study the bonding and structure of titanium hydrides[33] and titanium organometallics[34] by Gordon and co-workers. These papers also highlight that within the realm of computational chemistry, a sophisticated MC treatment is needed, in many cases to qualitatively describe the bonding of an organometallic.

Another common use of MC methods in metal chemistry involves the calculation of electronic spectra. In many cases, relaxation (in an orbital and geometric sense for the excited state) of the virtual orbitals is important, and hence the use of techniques such as MC methods that variationally optimize the virtual orbitals is essential for accurate reproduction of the spectroscopy of an organometallic. These methods, like all MC techniques, are computationally very intensive, and this often limits their application to very small model complexes. However, advances in software and hardware are constantly stretching the performance envelope of MC techniques. Roos and co-workers have reported MC studies pertinent to the spectroscopy of blue copper proteins[35] and plastocyanin,[36] and actinide complexes.[37]

MC methods are by no means "black box" even with the advent of modern computational-chemistry software. To some extent, this comment does not apply to CCSD(T) methods, as the default active space that excludes the core orbitals of the constituent atoms is often sufficient, and hence a good motivation for the use of coupled-clusters techniques by novices and experts alike. The hardest decision in the application of most MC methods is the choice of active space orbitals and electrons. The active space is comprised of the occupied orbitals (from which electrons are excited from) and the unoccupied orbitals (into which the electrons are excited). The active space should comprise those orbitals for which electron correlation is expected to be most important for describing the chemical reaction or spectroscopic event of interest. In an organometallic complex, the orbitals and electrons of a central metal are the typical focus as an active space. This is true, for example, for lanthanide organometallics, where the 4*f*-valence orbitals, and thus the electrons contained therein are largely localized on the metal (Figure 10).[38] However, any degree of covalency (which is more likely for organometallics than coordination complexes) will delocalize the frontier orbitals to a significant extent onto the ligand orbitals and thus complicate the selection of an appropriate active space.

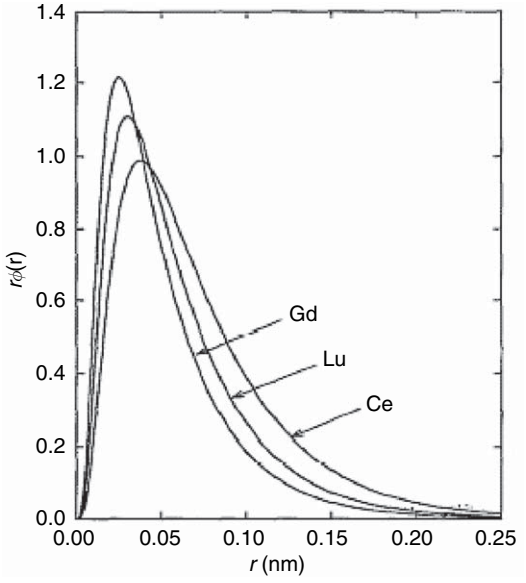

Figure 10 Plot of radial function ($r\phi$) versus distance (r) for 4*f*-orbitals of early (Ce^{+3}), middle (Gd^{+3}), and late (Lu^{+3}) trivalent lanthanide cations. Reprinted with permission from Cundari, T.R.; Stevens, W.J. *J. Chem. Phys.* **1993**, *98*, 5555–5565. © 1993, American Institute of Physics.

Returning to our chromous "box" example[11] (Figure 4), the active space was chosen to be comprised of the four *d*-orbitals and four d-electrons from each Cr(II) ion, yielding a total of 16 active orbitals and 16 active electrons for the tetramer. Just as easily, we could have relied on chemical intuition and selected an active space comprised of all five *d*-orbitals and the four *d*-electrons from each chromium(II), yielding an aggregate 20-orbital/16-electron active space for the tetramer. However, this active space is even larger and more unwieldy than the minimal 16/16 active space selected in the Wolczanski study.[11]

We continue this section by pointing out that calculations exist that combine (PT) and MC methods. For example, methods such as complete active space, second order perturbation theory (CASPT2)[39] and multi-configuration quasi-degenerate perturbation theory MCQDPT[40] use a MC wave function as the reference. PT, generally to second order, is used to estimate the contribution from excited states that arise from excitation outside the original active space of the MC calculation.

As a simple example of possible MC strategies that an organometallic chemist may wish to employ, consider a four-orbital, four-electron system such as a metal–carbon double bond in an alkylidene. The most expensive MC approach is the brute-force approach, generating all possible combinations among the four orbitals and four electrons (Figure 11). The maximum electronic excitation is quadruple excitation, that is, $\sigma^2\pi^2 \rightarrow \sigma^{*2}\pi^{*2}$, and the active space generates 20 possible CSFs for a singlet spin state without symmetry constraint. In a standard calculation, this translates into one reference state (typically the HF configuration) and 19 excited states. In the configuration interaction (CI) approximation, only the relative weights of the 20 CSFs are optimized; the orbitals contained within each CSF are frozen at their reference state. In a multi-configuration self-consistent field (MCSCF) calculation, the relative weights of the CSFs are optimized as are the orbitals for each CSF. In other words, the orbitals of the excited states are allowed to relax in MCSCF but not in CI. Of course, relaxation of the excited-state orbitals is more desirable in terms of wave function flexibility and expected accuracy, but as a result, MCSCF calculations are significantly more expensive than their CI counterparts.

Another approach to constructing an MC solution of the metal–carbon double bond might be to use chemical intuition and correlate only the π-orbital, that is, allow only those excited states generated from $\pi \rightarrow \pi^*$-excitation(s). The underlying assumption is that the energy gap between the π- and π^*-orbitals is much less than the energy gap between the σ- and σ^*-orbitals, and hence the former pair is expected to be more highly correlated. The maximum excitation level is now double excitation, and there are only three CSFs to be considered when correlating the π- and π^*-orbitals (π^2, $\pi\pi^*$, and π^{*2}), considerably less than the 20 CSFs generated when correlating both the metal–carbon σ- and π-bonds. As an indicator of how rapidly complete active space self-consistent field (CASSCF) expansions grow rapidly, if one was interested in studying an alkylidyne complex, correlating all six electrons and six orbitals contained in the metal–carbon triple bond would yield 175 CSFs. See also the above example of the explosive growth of the active-space side for the chromous tetramer. The take-home message is that only small increases in the number of orbitals and electrons in the MC active space quickly increase the number of CSFs that must be calculated, and thus the computational effort that must be expended.

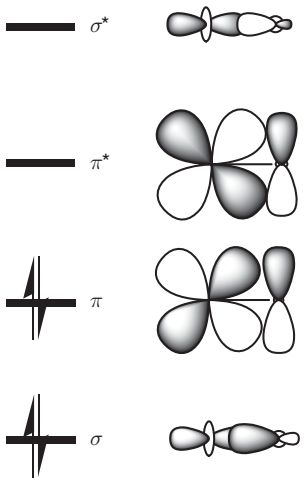

Figure 11 Four-orbital, four-electron active space of a metal–carbon double bond.

It is possible to include only a subset of excitations lower than the maximum, that is, the CASSCF/FORS (FORS = fully optimized reaction space) wave function. For example, employing a four-orbital/four-electron active space and permitting only single and double excitations would yield a wave function with 15 CSFs (instead of 20 CSFs); for the six-orbital/six-electron active space, the savings are greater: 55 CSFs with only single and double excitations from the reference state instead of 175 CSFs for the FORS/CASSCF wave function. There are a variety of reasons—computational and theoretical—to avoid MC wave functions other than FORS or CASSCF,[41] but wave functions with less than maximal excitation levels should only be used as a last resort for production calculations. While it is intuitively reasonable that excited states generated by higher levels of excitation from the reference ground state will lie very high in energy, it must always be remembered that there are a myriad of these states, and the aggregate of these many small contributions can add up to something chemically significant.

Another subset of the FORS/CASSCF wave function that has been especially successful in organometallic chemistry is the so-called generalized valence-bond (GVB) approach, pioneered by Goddard and his co-workers.[42,42a] Ostensibly, the method views molecules as a collection of two-center/two-electron bonds, which is inherently satisfying to the organometallic chemist in relation to the valence-bond pictures we have learned from our earliest days as chemists. Returning to our metal–carbon double bond case, one envisages in GVB the entire four-orbital/four-electron active space as a combination of two-orbital/two-electron subspaces. In the full MCSCF implementation, CSFs generated from excitation of an electron from the σ- to the π-space is permitted, but not so in GVB. Configurations are generated only within each subset, so that in the correlation of a double bond, only $\sigma \rightarrow \sigma^*$ and $\pi \rightarrow \pi^*$ excitations are allowed, but CSFs generated from neither $\sigma \rightarrow \pi^*$ nor $\pi \rightarrow \sigma^*$ excitation are permitted. The motivation lies in the observation that electrons tend to correlate within orbitals that share the same space, for example bonds with their antibond counterparts, and so GVB attempts to recover the maximum correlation energy with the smallest active space.

Returning to combined MC/PT methods, one may wish to correlate only the π-bond, and add other interactions $\sigma \rightarrow \sigma^*$, $\sigma \rightarrow \pi^*$, and/or $\pi \rightarrow \sigma^*$ in a perturbative fashion. In this way, the most highly correlated orbitals benefit from the full MC treatment, while contributions from less correlated orbitals are incorporated in a perturbative fashion. As with any application of perturbation theory, the results obtained are only reliable as long as the PT approximation is viable.

DFT may, at times, seem to stand for damn fine theory, and while it is, and rightly should be, the first tool usually taken out of the box, DFT is not a panacea for all organometallic complexes and applications. There are many cases where the extent of electron correlation is such that no dominant electron configuration exists and MC methods are essential. We conclude this brief section on MC methods with some general aphorisms for the practicing organometallic chemist who may either wish to employ MC techniques or needs to critically evaluate a paper in which such methods are employed.

(i) If at all chemically appropriate, avoid the use of MC techniques, whose expense and the involved nature of their rigorous implementation is such that they should only be tried after other simpler methods (HF, MP2, DFT) have been exhausted.

(ii) If the results suggest that MP2, DFT, or HF is insufficient, and if it is felt that one feel must use MC techniques, an expert should be consulted. Performing a successful MC study of an organometallic takes equal parts of luck, experience, science, and art.

(iii) If no experts are available or willing, the organometallic chemist must think long and hard about the appropriate active-space orbitals. Indeed, it may be argued that this is an area where the experimental chemist has an advantage over the theoretician, as most experimentalists generally have a good idea about the important structure and bonding features of their favorite organometallic molecule or reaction. Of course, one must always avoid biasing the calculation through use of chemical intuition alone. Questions to be asked include the following: what orbitals/electrons are involved in the chemical reaction? For example, if the reaction of interest is oxidative addition to a transition metal complex, then at a minimum the four orbitals and four electrons that comprise the σ-donation and π-backdonation, essential to the reaction, are needed (Figure 12). If the reaction of interest is sigma-bond metathesis (AB + CD $\rightarrow$ AD + CB), then the two bonds and two antibonds of the involved species, plus the four electrons contained therein, would make up the minimal active space. On the reactant side, the active space will be (σ_{AB}, σ_{CD}, σ^*_{AB}, σ^*_{CD}), and on the product side, the minimum active space orbitals are (σ_{AD}, σ_{CB}, σ^*_{AD}, σ^*_{CB}). If the goal is to compare and contrast a complex that can potentially activate by both of these mechanisms, then it is imperative that the active spaces be as balanced as possible, that is, one active-space choice should not generate a considerably larger number of CSFs than the other. If the target is spectroscopy, then the orbitals/electrons that are involved in the spectroscopic transition must be included as a minimum active space. If possible, tests starting with larger active

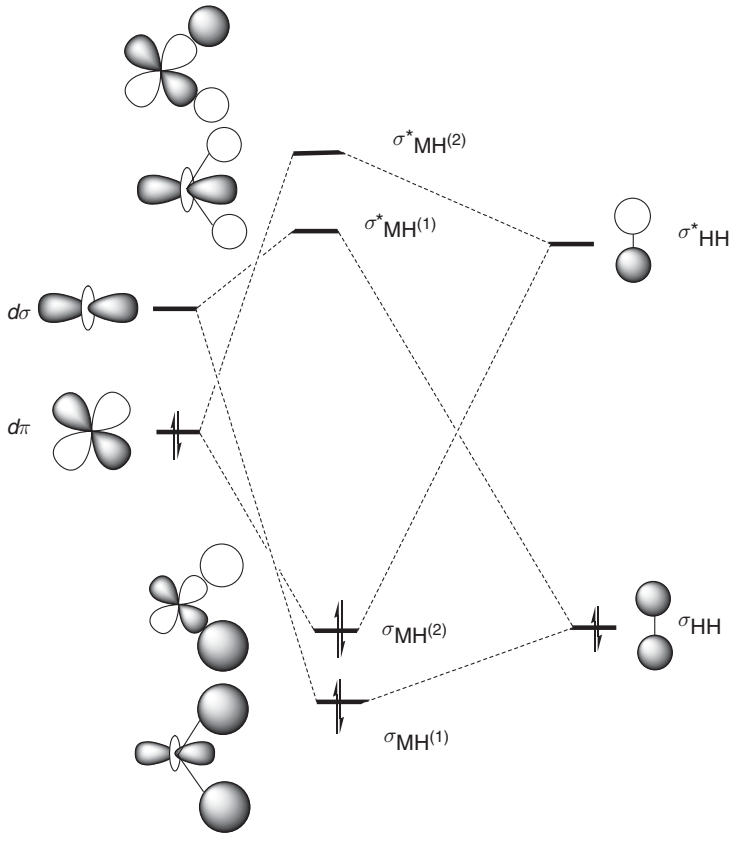

Figure 12 Qualitative MO diagram for oxidative addition. These orbitals and electrons would comprise a natural choice for an MC study of oxidative addition.

spaces and then progressively smaller active spaces should be carried out. For example, for a transition metal complex, one may wish to start by correlating the orbitals derived from the *nd*, $(n+1)s$, and $(n+1)p$, and then only the *nd* and $(n+1)s$, and finally the *nd*-only active space.

(iv) Our fourth recommendation continues on the last point in the preceding paragraph, that is, experiment with different active spaces to find one that is appropriate. Less expensive MC calculations such as configuration interaction—singles and doubles (CI-SD) can be quickly run with quite large active spaces to get a general idea of what the important correlating orbitals are, for example, the orbitals whose natural-orbital occupation numbers[41] are significantly different from zero or two. In general, one wishes to use larger and larger MC active spaces (better yet, one should start with the biggest active space one can get to work with hardware and software and then go smaller in active-space size) until there is a convergence in a property (or better yet properties) of interest.

(v) By no means try to save resources by coupling a small basis set with an extensive MC wave function and hope for some magical cancelation of errors. Moving in a horizontal or vertical fashion on the basis set/correlation map (Figure 3) is often a bad idea, the preferred direction is always diagonal.

An excellent review on MC methods is given by Schmidt and Gordon,[41] and the interested reviewer is directed to this paper before embarking on MC calculations.

1.23.8 Semi-empirical Quantum Mechanics

The usage of semi-empirical methods in the scientific literature has diminished over the past several years due to the increases in computing power that make higher-level calculations more and more feasible. However, these

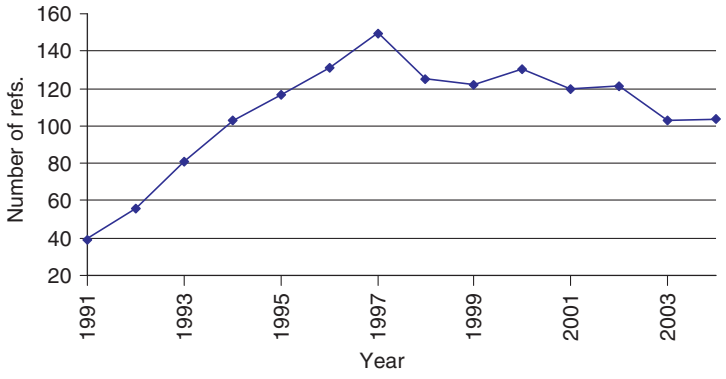

Figure 13 SciFinder "hits" containing the SEQM methods AM1 and PM3.

techniques remain popular (Figure 13), if for no other reason than they can provide the organometallic chemist with a quick insight into the structure and bonding of their system, with quick turnaround time while sitting in front of their personal computer. SEQM techniques are now most commonly coupled to GUI-based software,[43] which further facilitates their usage by those who are not full-time computational chemists. This ability to do desktop tinkering and run simple "what-if" scenarios has long been the purview of our organic colleagues, but is becoming possible in organometallic chemistry with the advent of programs such as Spartan and methods like PM3(tm) (parametrization method 3 for transition metal complexes).[43]

However, it is to be noted that SEQM, due to the inherent approximation of the methods, can often be faster to the wrong answer, and it is always wise to view the results with a good deal of skepticism, particularly for energetics, and to calibrate them as extensively as possible. However, the organometallic chemist should not ignore this family of techniques as their computational rapidity and ease of use make them an ideal option for "quick-and-dirty" calculations, for example, to probe the electronic structure of an organometallic complex of interest, to investigate several low-energy conformers, provide a starting guess for a higher level calculation, etc. It is the author's experience that SEQM methods generally either work (as long as they are not pushed beyond the limits of their approximations) or fail spectacularly. If they work, a pathway to the modeling of larger, generally more experimentally relevant complexes is opened. If not, little time is wasted as the largest calculations often take only minutes to a few hours on commodity-level personal computers. For example, before embarking on a DFT study of the photochemistry of gold(I) complexes, our group investigated the possibility of quickly predicting the structure of large $[Au(PR_3)_3]^+$ complexes (R = Me, Ph, Cy) with PM3(tm). In a few minutes on a 2 GHz PC, structures like those in Figure 14 resulted, showing evidence for unphysical C–H oxidative addition to the gold center. As a result, it was evident that PM3(tm) was a poor choice for initial geometry guesses of this family of gold(I)-phosphine complexes, and the task needed to be performed with full DFT (R = Me) or hybrid QM/MM (R = Ph, Cy) calculations.

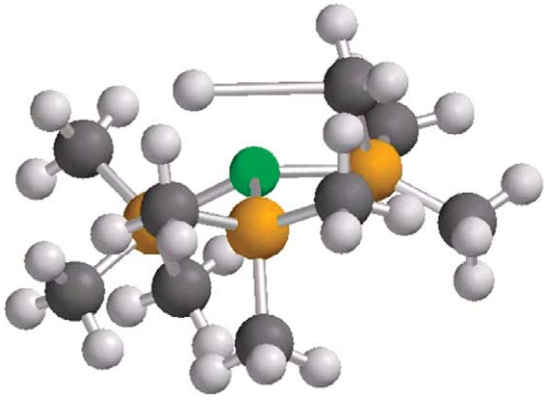

Figure 14 PM3(tm) geometry-optimized structure of $[Au(PMe_3)_3]^+$.

SEQM techniques, as their name implies, are quantum techniques that have as their basis the Schrödinger wave equation.[44] Unlike *ab initio* and density functional techniques, major approximations are made in the calculation of the various Hamiltonian matrix elements that describe the interactions among the nuclei and especially the electrons. The major computational expense in the calculation of the Hamiltonian matrix elements lies in the calculation of the electron–electron interactions. These are generally not only the most numerous Hamiltonian integrals to be evaluated, but also the most computationally expensive to calculate. As a result, much of semi-empirical methodology involves strategies to ameliorate the electron–electron problem. There are two common approaches employed in SEQM calculations. The first tact is to ignore those interactions deemed to be chemically less important, not only saving the time that would otherwise be spent on their calculation, but also the necessity of storing these integral results. Two popular routes to this end are the core-valence approximation (i.e., calculate only electron–electron interactions among valence electrons), or a distance-based screening. Given their $1/r$ dependence, electron–electron interactions between electrons in orbitals that are located on widely separated atoms may be assumed to be close to zero and thus ignored. As with any such approximation, one must worry that although the interactions are individually small, in their thousands (if not millions) they may add up to something chemically important.

A second type of approximation used in SEQM is the replacement of integrals with either parameters (which can then be varied to reproduce an experimental observable) or values directly derived from experimental techniques such as spectroscopy. In the historical evolution of SEQM, the latter approach was employed first and hence we focus on it in the subsequent section.

One of the earliest examples of using spectroscopic information in the parametrization of semi-empirical methods involves the granddaddy of all computational organometallic chemistry techniques, extended Hückel theory (EHT).[45,45a] In EHT, vertical orbital ionization potentials (VOIPs) are used to calculate the diagonal Hamiltonian matrix elements (H_{ii}) in an extended Hückel calculation. Once given these H_{ii}, it is possible to employ the Mulliken approximation to calculate off-diagonal Hamiltonian matrix elements ($H_{ij} = S_{ij}{}^{*}$ ave$(H_{ii}, H_{jj})^{*} k$), where k is a constant (typically in the 1.75–2 range), and S_{ij} is the overlap integral between atomic orbitals i and j. The extended Hückel method does not incorporate electron–electron interactions and, as such, cannot be used for computational tasks such as geometry optimization or discerning different electronic spin states. However, it would be impossible to overestimate the important contribution that Hoffmann, his colleagues, and those he inspired have made to understanding organometallic chemistry using the extended Hückel method.[46]

The extended Hückel method is quite transparent as a computational chemistry technique, with a minimum of fuss going on between the atomic orbitals that are fed in and the molecular orbitals that come out. The author recommends extended Hückel calculations highly to all his students and experimental collaborators as a first step in understanding the important interactions in an organometallic compound before going onto more quantitative (and hence much more expensive and thus also requiring more "baby-sitting") calculations. If, for example, one is going to undertake MC calculations, a quick EHT calculation of the frontier orbitals can provide some insight into the possibilities for active-space selection.

Another important value that remains in EHT is that the lack of electron–electron interactions means that all orbitals are treated on a more equal footing, even those with different occupation numbers (e.g., occupied and virtual orbitals), with their energy splittings determined by overlap and energy-match considerations. One must exercise care in comparing the orbital energies of SCF-based methods as the virtual (unoccupied) orbitals are less important in the variational optimization, since these orbitals are unoccupied and change only indirectly in response to changes in the occupied MOs. As a result, SCF methods may have artificially large energy gaps between occupied and unoccupied orbitals, although DFT seems to suffer less from this issue than HF-based techniques. A possible way around this orbital imbalance is very expensive, that is, the calculation of an MC wave function in which all possible electronic configurations are generated and variationally optimized, the so-called CASSCF or FORS wave function. Even in this case, the assignment of orbital energies to MOs derived from MC wave functions is problematic, although so-called EKT (extended Koopmans' theorem) techniques have been published.[47,47a]

The EHT wave function, in all its wonderful simplicity, evades many of these issues, and usually gives a qualitatively correct view of the frontier orbitals of many organometallics. For example, in a recent theory–experiment study of NO-bond scission, the group employed EHT calculations (for a qualitative understanding of the frontier orbitals (Figure 15) and active-space selection), density functional (geometry optimization) and MC wave functions (accurate energetics).[48] In the field of computationally organometallic chemistry, it is wise to use all tools at one's disposal, and not to neglect some due to their perceived age and infirmity. The EHT orbitals were used to understand the symmetry constraints on phosphorus–oxygen bond scission mediated by group 5 tris-silox complexes. The EHT molecular orbitals closely shadow those determined with *ab initio* and density functional methods in their LCAO-MO (LCAO-MO = linear combination of atomic orbitals–molecular orbitals) distribution and relative energy

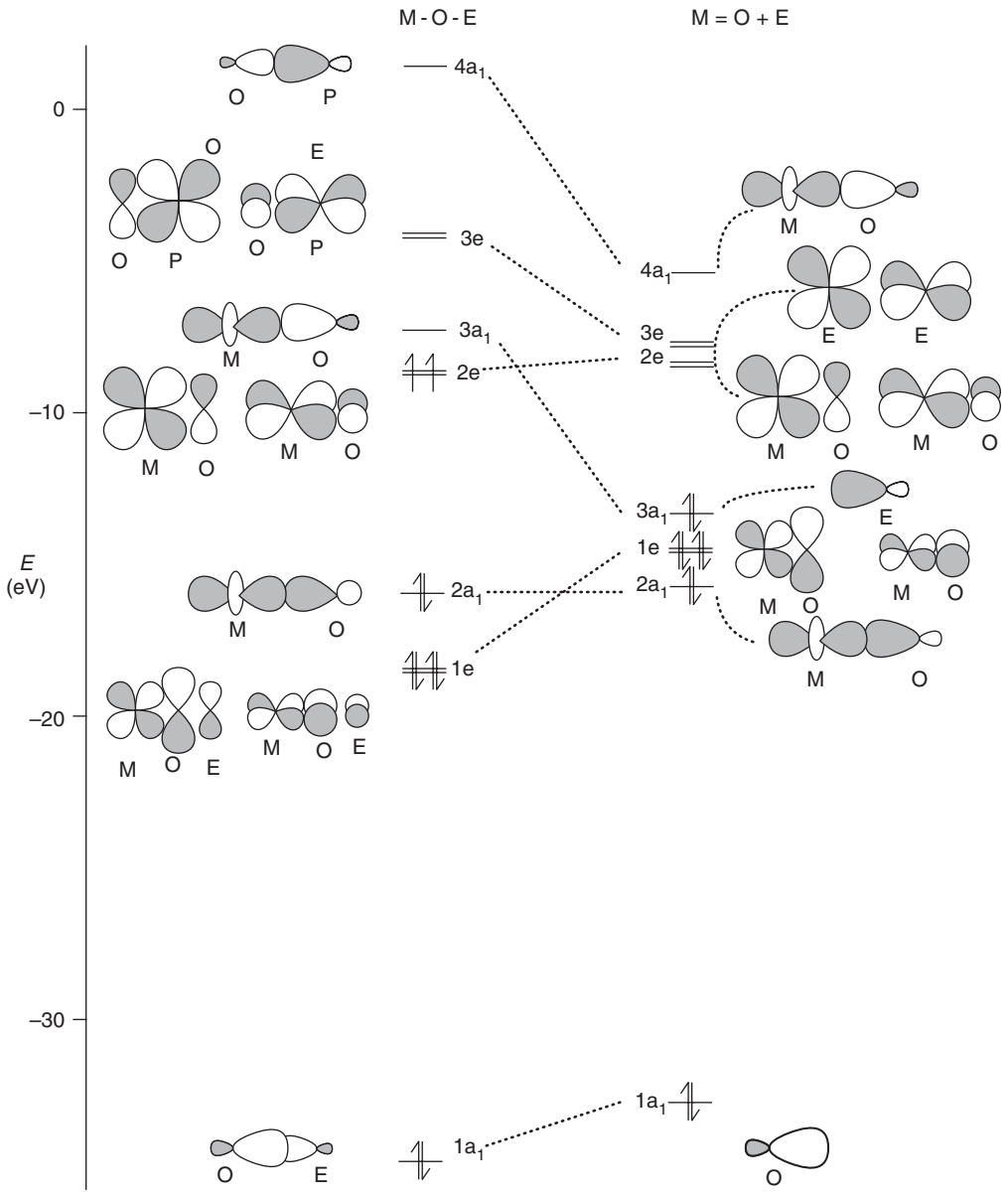

Figure 15 Orbital-correlation diagram for $L_nM + OE \rightarrow L_nM = O + E$ (E = substrate). Reprinted with permission from Viege, A. S.; Slaughter, L. M.; Lobkovsky, E. M.; Wolczanski, P. T.; Matsunaga, N.; Decker, S. A.; Cundari, T. R. *Inorg. Chem*. **2003**, *42*, 6204–6224. © 2003 American Chemical Society.

ordering, but without the complications inherent in comparing the energies of orbitals with differing occupation numbers in SCF-based calculations.

After EHT, the introduction of electron–electron interactions was the next logical step in SEQM methodology, and is typified by first-generation methods such as CNDO (complete neglect of differential overlap[49]) and INDO (intermediate neglect of differential overlap[50]), and their current progeny, most notably AM1[51] (Austin method 1) and PM3 (parametrization method 3).[52] The introduction of electron–electron interactions complicates the parametrization process. However, as a simple example of how spectroscopic information can be used to estimate an integral, consider the simple two-electron system (Figure 16) with an electron in each of two orbitals, ϕ_1 (with energy ε_1) and ϕ_2 (with energy ε_2). These electrons may be either singlet (right side of Figure 16) or triplet (left side of Figure 16) coupled. The energy of the singlet state can be given as $\varepsilon_1 + \varepsilon_2 + J_{12}$, where J_{12} represents the Coulomb repulsion

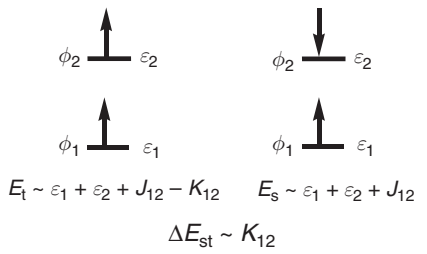

Figure 16 Graphical representation of the estimation of *K* (exchange integral) from singlet- and triplet-state energy differences.

between the electrons contained in orbitals ϕ_1 and ϕ_2. Similarly, the triplet state energy is $\varepsilon_1 + \varepsilon_2 + J_{12} + K_{12}$, where K_{12} denotes the quantum mechanical exchange between electrons of like spin. The singlet–triplet difference in energy is thus the exchange energy K_{12}. Assuming that both of these electronic states can be studied spectroscopically, one would then use the experimental energy difference, $\Delta E_{st} \sim K_{12}$, to estimate K_{12}. Orbital energies, ε_1 and ε_2, could be estimated, as in the EHT approach (*vide supra*), from VOIPs. In a similar, although admittedly much more complicated, fashion, the study of different electronic states can be utilized to generate other integrals needed for the SEQM calculation.

The more recent trend in SEQM theory is to select the parameters not from a one-to-one mapping of experimental observables, but to treat the parameters as variables that can be adjusted to reproduce an experimental observable. A classic example in this regard is the MNDO (modified neglect of differential overlap[53]) method, which was parametrized to reproduce experimental enthalpies of formation. The SEQM techniques currently in most widespread usage—AMI[51] and PM3[52]—are derived in a similar spirit. The AMI and PM3 methods are parametrized to predict different properties (bond lengths, bond angles, dipole moments, ionization potentials, etc.), primarily for organic entities, although PM3 incorporates in its training set are larger diversity of compounds, including compounds of the heavy main group elements.

The main issue in the application of SEQM methods to organometallics has been, not surprisingly, the metal, particularly the transition metals. The inclusion of *d*-orbitals adds a layer of complexity to the required integrals, as well as increases the number of integral parameters that are needed. Zerner's INDO method (ZINDO[54,55]) was one of the first of the modern semi-empirical methods to be applicable to transition metals. In the main, the use of the ZINDO approach is appropriate in those cases in which one has a geometry (e.g., from an X-ray structure or a highly related compound) and wishes to probe the electronic structure or spectroscopy of a target molecule. In general, the ZINDO method must be used with extreme caution for the optimization of organometallics geometries, and if it must be used for this task, it should be calibrated in detail by comparison with appropriate reference molecules. As mentioned above, the lack of electron–electron interaction terms in EHT precludes its use for discriminating among different spin states in organometallics. ZINDO is excellent for this purpose. In a study of technetium-based organometallics, the ZINDO method was able to correctly predict the correct ground-state multiplicity well over 90% of the time. (The biggest limitation of the ZINDO technique in relation to the PM3(tm) method arises from the more limited parametrization of elements for the former. See Ref: 7, 7a–7d.) Thus, one could envisage using ZINDO in a multi-tiered design and analysis protocol for organometallics to quickly establish the appropriate ground electronic states before embarking on more expensive *ab initio* methods. In a nice example of a multi-tiered computational approach, Ray used ZINDO to calculate the non-linear optical properties of ruthenium organometallics using geometries obtained with DFT.[56]

Perhaps, the most widely used SEQM approach nowadays in computational organometallic chemistry is the PM3(tm) Hamiltonian, developed and popularized by Wavefunction, Inc.,[57] and incorporated into easy-to-use programs such as Spartan. Voityuk has published on the AM1/*d*-method,[58,58a] although this has yet to see as widespread usage as PM3(tm). Likewise, MNDO(*d*) studies of Zn-triad complexes have been reported.[59,59a,59b] The PM3(tm) technique is now available for nearly all thirty *d*-block metals; PM3(tm) also incorporates parameters for many of the heavier main group elements, and thus permits quick calculation of numerous organometallic complexes. It is also worth pointing out that the specification of PM3(tm) for the calculation of an organometallic entails the PM3(tm) Hamiltonian for the transition metal (with its *spd*-valence) and PM3 (with its *sp*-valence) for the main group elements.

The PM3(tm) method is most appropriate for the calculation of geometries. Energetic quantities, absolute and relative, must be treated with extreme caution. However, as with any methodology, particularly those of a more

approximate nature, extensive calibration versus the best quality experimental data is imperative to establish the performance envelope of the method.

In a study of the predictive ability of PM3(tm) for the 19 transition metals then parametrized, Deng and Cundari[60] studied the ability of PM3(tm) for predicting geometries for more than a 1,000 prototypical transition metal complexes, including many organometallics. Based on this survey, some generalizations are appropriate. First, the PM3(tm) method tends to perform better for the early transition metals, and less well as one moves to the right in the transition series, especially within the first row of the transition series. Second, heavier transition metals, that is, those of the second and third series, yield better metric prediction that for complexes of the first transition series. Third, systems with polarized/dative metal–ligand bonds are typically less accurately predicted than complexes with covalent metal–ligand linkages. This implies, and the results corroborate this, that organometallic complexes will outperform coordination complexes with PM3(tm). Fourth, within the transition series, there is a decrease in accuracy for those metals from the upper right-hand side of the transition series, that is, iron, cobalt, nickel, and copper. Lindoy *et al.* have published a very interesting paper on ligand-binding specificity for nickel(II) complexes, and found that PM3(tm) was less effective than molecular-mechanics techniques.[61]

However, one should not assume that quality results cannot be achieved with PM3(tm), but the key is rigorous calibration. In addition to the Cundari–Deng study of PM3(tm) complexes, Bosque and Maseras have also published a survey of the utility of PM3(tm) for organometallic complexes.[62] As in the previous study, the quality of the PM3(tm) model is system specific, and the results range from good to poor. Despite the generalizations, maybe made from these and other papers, the message remains the same—when using approximate methods, the organometallic chemist must calibrate. One would not do a ^{1}H NMR without a TMS standard, and likewise one should not use computational methods, especially approximate techniques, without appropriate calibration.

Another important point to be emphasized in the use of PM3(tm) methods lies in the training set used for the development of the parameters. As PM3(tm) is primarily a commercial entity, the level of exposition of the method may be less than many are accustomed to when such pursuits were purely academic. The two main questions of importance in regard to the training set are: (a) What molecules or types of molecules were used in the training set? (b) What properties (geometries or energies or electronic properties or reactivity) were used to develop the parameters? For organometallics, the answer to the latter is most often geometries, which is appropriate because the identification of an appropriate geometry is the cornerstone of almost all computational-chemistry design and analysis scenarios. Geometry is also the most readily available information for calibration of a computational methodology due to the availability of large databases such as the Cambridge Structural Database (CSD).[63] It must, however, be kept in mind that geometries constitute one of the least method-dependent molecular properties, and, so, often do not change appreciably with theory, unless there is some underlying problem with the level of theory being used, the system is very weakly bound (e.g., in van der Waals complexes and in many classes of metal–metal bonded systems), or has many bonds far removed from typical equilibrium values (as is often the case in transition states). The latter observation is particularly relevant in a discussion of SEQM methods as these techniques are overwhelmingly calibrated on the basis of ground-state properties, and hence their utility for calculating transition state-dependent properties such as activation parameters, isotope effects, reaction rates, and so forth must be viewed as circumspect. Several groups, most notably Truhlar and co-workers, have investigated so-called reaction specific parameters (RSPs) for modeling the potential energy surfaces of biological and organic reactions,[64] although to our knowledge, no application to organometallics has been reported, but would be welcome.

With respect to question (a) above, wide chemical diversity is desirable, but one must often compromise by keeping the training set from being too large for computational efficiency reasons. Large training sets, although desirable in terms of the robustness of the resultant SEQM parameters, lend themselves to the multiple minimum problem in many parameter optimization strategies. In the research on the parametrization of the PM3(tm) Hamiltonian of technetium using genetic algorithms, we started our search using averaged parameters for the two metals flanking technetium, molybdenum and ruthenium.[65] The logic behind this choice is that the averaging would provide a starting point that is in the appropriate neighborhood of problem space. A training set too narrow can lead to poor generalization of the method when used in applications. For example, if the SEQM parameters for zinc are primarily developed by the study of two-coordinate, zinc(II) organometallics, such as $ZnMe_2$ and $ZnEt_2$, it would be a mistake to *a priori* expect it to be appropriate for four- and six-coordinate zinc coordination complexes. In the absence of such information about parametrization details in the original literature, calibrate versus whatever experimental data is of interest and available. Although one may object to calibrating one type of calculation against another, in the absence of experimental data, SEQM methods should then be calibrated against high-level *ab initio* and DFT results for representative model compounds.

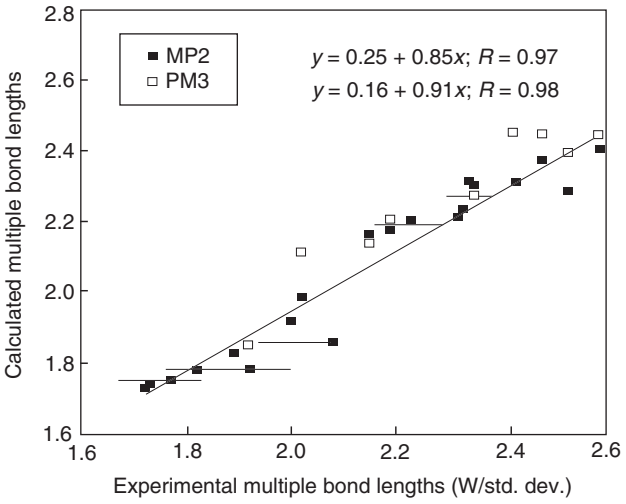

Figure 17 Comparison of PM3(tm)- and MP2-predicted metal–ligand multiple bond lengths for PM3(tm) semi-empirical Hamiltonian and the MP2 perturbation theory method. Reprinted with permission from Cundari, T. R.; Deng, J. PM3(tm) Analysis of Transition Metal Complexes; *J. Chem. Info. Comput. Sci.* **1999**, *39*, 376–381. © 1999 American Chemical Society.

Figure 17 shows a comparison of PM3(tm) and MP2 calculations (coupled with double-zeta-plus polarization effective core-potential basis sets) versus experiment.[60] While the MP2 results are superior to the PM3(tm) results (i.e., slope, intercept, and R value of best-fit line closer to one, zero, and one, respectively), the results are essentially comparable. Figure 17 is also worthy of further inspection as it includes the range of values found in the CSD, since metal–ligand bond lengths can change and do change with chemical environment. In this light, PM3(tm) and MP2 results in Figure 17 are statistically identical. Given the ability to identify numerous comparable bond lengths and angles for organometallic compounds, which comprise roughly half of the CSD, and the increasing speed possible with computational chemistry, it is advisable when studying new classes of compounds or testing new methods to go beyond the point-by-point comparisons of yore, and compare families of compounds with both theory and experiment. Such an approach not only gives more confidence in the methods employed, but also helps ensure that one has obtained the "right answer for the right reasons."

One of the less well appreciated tradeoffs in the SEQM approximations is particularly germane to organometallic chemistry modeling, that is, SEQM approximation may not only result in a loss of accuracy, but also flexibility, that is, the ability to reliably describe chemically disparate systems. This is especially important in organometallic chemistry, as metal systems are often found in a greater diversity of chemical states (oxidation state, coordination number, ligand and bond types, etc.) than their light main group counterparts. Indeed, this ability to stabilize different chemical states is the root cause of the utility of organometallic complexes in many areas of medicine, catalysis, and materials chemistry, and hence an issue that the modeler must meet head on. While *ab initio* and DFT methods, with suitable basis sets, can compare apples and oranges, it is often the case in SEQM methods that one must compare apples with apples for there to be any chance of reasonable success.

1.23.9 Basis Sets

Unlike SEQM methods, the use of *ab initio* and density functional techniques for modeling organometallics entails the choice of a method "and" a basis set. The combination of basis set and method defines the level of theory. Figure 3 depicts more and more complete basis-set treatments as one progresses along this hypothetical axis. The basis sets are the mathematical constructs that describe the motion and position of electrons. The larger the basis set, the more complete the treatment. As is usually the case in computational chemistry, a more complete treatment brings with it a greater computational expense.

Consideration of a *d*-block metal atom as an example suggests that three states are typically of chemical importance in their bonding: $d^n s^0$, $d^{n-1}s^1$, and $d^{n-2}s^2$ (Figure 18). In each case, the different occupation of the *nd*- and $(n+1)s$-atomic orbitals will result in their having different energies and sizes within each of the different atomic and atomic

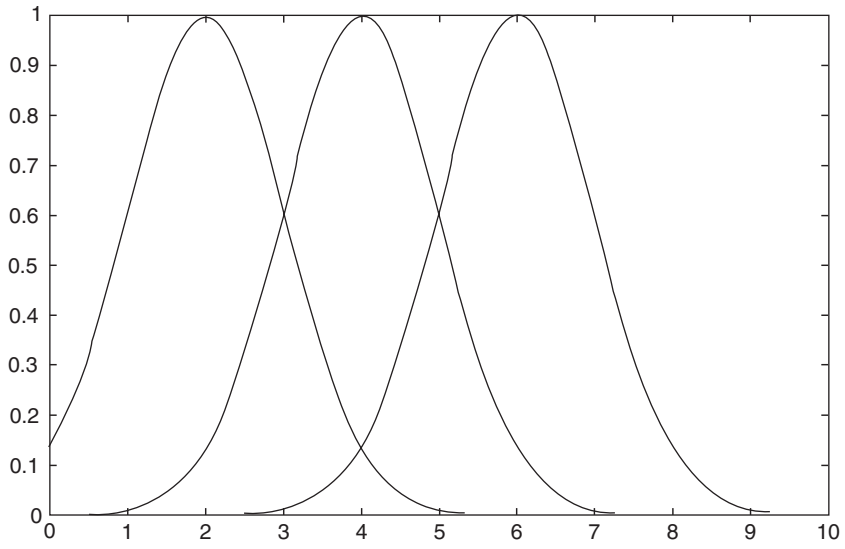

Figure 18 Qualitative picture of change in radial extent of metal *d*-orbitals in $d^n s^0$ (right), $d^{n-1}s^1$ (middle) and $d^{n-2}s^2$ (left) state. Abscissa is in arbitrary units of length; the radical expectation value is given on the ordinate.

ion states. The task is to describe the electronic states in a balanced fashion, as they can and do change in importance in response to the chemical environment. For example, one would expect that as the coordination number increases, the importance of $d^{n-2}s^2$ state will decline. To achieve this within the basis-set approximation, one must use split-valence basis sets, whereby the contribution each atomic state makes to the resultant molecule can be variationally optimized.

As with electron correlation, it is the metal that often requires a more elaborate basis set than the organic portion of an organometallic. However, modern software makes it easy to mix and match different basis sets of different sizes within a single calculation. Mixing basis sets is much more facile than mixing different correlation treatments within a single calculation. For example, returning to the 2,6-$Trip_2C_6H_3T1$ complex in Figure 6, one may naively assume that a large basis set can be applied to the thallium metal, with a smaller basis set for the carbon and hydrogen atoms. However, this approach will likely lead to a poor description of the organometallic. A more sophisticated approach might be to split the carbon atoms into two subsets—those either attached to the metal plus those that may interact (perhaps through π-arene interactions) with the metal, and those that are sufficiently remote from the metal so as to be considered non-interacting (for example, the isopropyl substituents in 2,6-$Trip_2C_6H_3Tl$, Figure 6). A larger basis set (double-zeta-plus-polarization or even larger, perhaps triple-zeta-plus-polarization-and-diffuse functions, if one wished to model the subtle metal–arene π-interactions) would then be applied to the former group of carbon atoms, and a smaller basis set to conserve computational resources for the non-interacting carbon atoms. A similar choice would then be appropriate for the hydrogen atoms.

However, caution is needed in the use of mixed or "spliced" basis sets. It is possible that the use of disparate basis set qualities for different regions of an organometallic may engender an imbalance in the basis set leading to a Robin Hood scenario. Those portions that are poor in basis set can "rob" basis functions from those rich in basis sets, particularly if the imbalance is great. This scenario is also particularly problematic for those atoms with mixed basis sets that are in proximity to each other, that is, at the interface region. Additionally, diffuse (small exponent, large in radial extent) basis functions are particularly prone to thievery by atoms with small basis sets.

Another basis-set issue that is particularly germane to the organometallic arena involves the lack of methodically developed, increasingly larger basis sets for metallic elements. Two well-known examples for the lighter main group elements are the classic Pople basis sets[66] and the newer correlation-consistent basis sets. The Pople basis sets start from very small, for example, a double-zeta representation such as 6-31G and become increasingly larger through the addition of *d*-polarization functions on the main group element (6-31G(*d*)) and hydrogen (6-31G(*d*,*p*)). The former are especially important in the description of the main group ligating atoms in metal–ligand bonds of an organometallic. Polarization functions on hydrogen are often more important for very accurate energetics, particularly in those cases in which hydrogen is directly interacting with the metal, say in a dihydrogen complex, or a C–H oxidative addition transition state.

For systems with a negative charge or substantial buildup of negative charge (which is very common in organometallic chemistry given the electropositivity of most metals and electronegativity of many ligating atoms), diffuse (small-exponent) basis sets can be added, yielding such Pople basis sets as 6–31 +G(*d*,*p*) or 6–31 ++G(*d*,*p*), the latter "++" designation indicating addition of diffuse functions to both main group elements and hydrogen, which would be warranted for hydridic hydrogen atoms. There is, of course, the possibility of expansion of the valence-orbital description, which is especially important given the near-universal use of Gaussian functions, say from double- to triple-zeta, 6–31G and 6–311G being two notable examples.

An alternative consistent set of basis sets is the so-called correlation-consistent basis sets developed by Dunning, Wilson, and their groups.[67] These are built up to not only saturate the radial portion on the wave function (by incrementally increasing the basis set from double- to triple- to quadruple-zeta and beyond), but also the angular portion of the basis set by adding higher and higher angular momenta function. These basis sets are very complete, and give near-complete basis-set (CBS) limit results for the largest members of this basis-set family, but are also very expensive, which precludes their use in many organometallic applications. Noteworthy within the realm of correlation-consistent basis sets is the research by Professor Kirk Peterson (Washington State University) to extend the correlation-consistent basis-set approach to *d*-block metals.[68,68a] Omary, Wilson, and co-workers have employed these basis sets to study the photophysics of mercury clusters.[69] The power of the correlation-consistent basis sets lies in their methodical increases in basis-set complexity, which allows for a rational assessment of basis-set (as opposed to method) effects on calculated properties. As a result, forthcoming research on correlation-consistent basis sets for metals is certainly of interest and will only ease the job of the organometallic modeler.

Basis-set augmentation for non-metal elements is quite standard; a double-zeta-plus-polarization valence-basis set should be considered a minimum choice, especially for atoms ligated directly to the metal. The choices for basis-set augmentation are less clear in many cases for metals. Two basis-set topics that the organometallic modeler should consider are (a) the need to add polarization (i.e., *f*) functions to the transition metal, and (b) the quality of the valence *p*-description. The literature suggests that the addition of *f*-functions to the basis sets of *d*-block metals is not as important as the addition of *d*-polarization functions to main group elements. In general, *f*-functions seem to be more important for energetics than geometries. One exception seen in the literature is the use of *f*-functions by Pyykkö to describe metallophilic interactions in d^{10}-coinage metal (silver and, especially, gold) assemblies.[25] Pyykkö specifies the necessity for two *f*-functions in gold complexes, one contracted *f*-function for metal–ligand interactions, and a diffuse one for describing the more long-range Au···Au interactions. A set of *f*-functions for the *d*-block metals is available through the research by Frenking and co-workers.[70] Other basis-set options can easily be obtained through the WalMart of basis sets, the Environmental and Molecular Sciences Laboratory's Gaussian Basis Set Order Form,[71] which comprises the Big Three of bookmarkable webpages of any serious computational organometallic chemist along with the likewise excellent WebElements[72] and NIST Webbook.[73]

Another basis set-related issue that has been discussed in the literature of computational organometallic chemistry is the necessity to augment the standard basis sets with an extra set of *p*-functions. Hall has contended that the standard valence basis sets for transition metals are insufficient, and has therefore developed with Couty the so-called Couty–Hall basis sets.[74] As with any case, when in doubt, try them out. It is an easy, and necessary, exercise to calibrate one's computational level of theory before proceeding into production calculations. In the absence of experimental data for calibration (do not forget, experiments can be wrong too), or literature precedence for related complexes, tests of basis-set convergence should be performed. The goal is to identify the most compact basis-set description needed for the task at hand.

1.23.10 Effective Core Potentials

In terms of theory development, two advances have revolutionized computational organometallic chemistry in the past decade or so: DFT and effective core potentials (ECPs). In this section we briefly treat ECPs, as this subject has been recently reviewed by Cundari *et al.*[75] and Frenking *et al.*[76]

ECPs, also referred to as pseudopotentials, like DFT have a long and storied history in areas such as solid-state chemistry and physics.[77] Apart from the computational savings obtained by replacing the chemically less-important core orbitals, and the electrons contained therein, ECPs accelerate the computational enterprise in another important fashion. It is now recognized that modeling the effects of relativity on electron motion of the heaviest elements,[78] and hence their resulting chemistry, is paramount in obtaining quantitatively, and indeed in many cases qualitatively, correct modeling of organometallic complexes involving the heaviest elements, for example, the *f*-block elements, the third-row transition metals, and 6*p*-main group metals. Pyykkö has written elegantly and at length about the

impact of relativistic effects in chemistry,[78] and the interested reader is directed to his excellent and highly readable reviews. At its most basic, relativistic effects arise from the interaction of electrons with nuclei. As core electrons are those with the highest probability of being found in the vicinity of the nucleus, it stands to reason that they display the largest direct relativistic effects. Hence, their replacement by an effective core potential goes a long way toward solving the relativity challenge; it is a classic case of addition by subtraction. Furthermore, relativistic effects like orbital contraction and expansion can be modeled by appropriate derivation of the field generated by the ECP. The most popular ECPs in use for organometallic computational chemistry are those of Hay and Wadt,[79] Stevens and co-workers,[80,80a] and the Stuttgart group.[81] The model core potential (MCP) approach of Klobukowski is an alternative to ECPs, and differs from the ECPs just mentioned in that the appropriate nodal properties of the valence basis sets are maintained.[82,82a]

Other relativistic effects such as spin-orbit coupling can also be addressed through the development of *j*-dependent ECPs, although in practice, most common codes use so-called average relativistic effective potentials (AREPs), which employ a *j*-weighted averaging scheme.[75,76] In sum, the ECP is a collection (ideally as small a collection as possible) of mathematical functions (Gaussians are commonly used as there is considerable experience in their use for calculating Hamiltonian integrals in molecular quantum mechanics) that mimic the role of the core electrons, that is, to act as a barrier to keep the valence electrons away from the core so that they can carry out the business of chemistry. Experience suggests that the different ECPs give comparable results as long as a comparable valence basis set is employed, and the choice should be dictated by availability of programs that have one or more of these ECP/valence basis-set schemes, and or literature precedence for their successful application to related organometallics.

In the use of ECPs, an important aspect for the organometallic chemist is the core–valence partitioning. This is often straightforward for the main group elements; the $ns^x np^v$-valence configuration is treated explicitly and the remaining orbitals with principal quantum number $n-1$ and lower are replaced by the ECP. However, some wrinkles are seen, even within the main group realm and the expert practitioner needs to be aware of them. First, the ECP integral routines are often less efficient than those developed for standard all-electron basis sets, and it often makes no sense to use an ECP approach unless many orbitals are being replaced, so that the savings due to the reduction in electron and orbitals more than compensates any ECP-integral efficiency. Thus, for example, for a study of $Ti(CH_3)_4$, an all-electron basis set is likely to be the best option. For $Zr(CH_3)_4$ or $Ti(SiH_3)_4$, an ECP approach would likely be the most efficient.

Second, many of the ECPs developed for the lightest main group elements are long in the tooth, and some care is needed in the evaluation of their suitability. For example, Gordon and Bode have shown that the replacement of the carbon all-electron basis set with a comparable ECP valence basis set yields bonds that are considerably too short.[83] In a study of thermodynamics of organometallic complexes, the differences in the accuracy of ECP methods were traced to the use of all-electron basis sets for light main group elements in one scheme, and ECPs for light main group elements in an alternative scheme.[84] So, be careful, and scrutinize those results. Always keep in mind that terminated normally is not the same as terminated correctly. If a few 0.01 Å in bond-length predictions is not a big deal, or one is comparing related series of complexes or reactions, then using ECPs for all heavy atoms (i.e., atoms other than hydrogen and helium) is likely to be appropriate. If greater accuracy is needed, then it is best to employ all-electron basis sets for elements up to neon. This mixed approach is standard operating procedure, for example, for programs such as Jaguar when Los Alamos National Laboratory (LANL) ECPs and basis sets are requested.[79]

As alluded to above, the core–valence partitioning is not always clear. Some problem cases that must be kept in mind include the following:

(i) Heavier *s*-block elements. The inclusion of outer core (also called semi-core) orbitals and electrons is often needed for the heavier alkaline and alkaline earth metals. For the alkaline earth metals, a classic case involves the proposal that these outer core electrons play in the distortion from the VSEPR (Valence Shell Electron Pair Repulsion) (i.e., linear) geometry for heavier AeX_2 species.[85] Stevens has mimicked the effect of the semi-core orbitals and electrons within the ECP approximation by the addition of so-called core-polarization potentials (CPPs).[86] Kwon and McKee have published a review of modeling of main group cyclopentadienyl complexes, including the heavier *s*-block elements.[87] Bridgeman has also published an interesting paper on modeling of *s*-block organometallics.[88] As with the Kwon–McKee book chapter, the emphasis is on Cp complexes, although many valuable pointers on modeling these organometallic complexes of these interesting elements can be extracted.

(ii) Lanthanides and Actinides. There have been effective core potentials developed in which the 4*f*-functions are not explicitly calculated, but rather their effect is mimicked by the potential.[89,89a] At first blush, this seems very extreme to the organometallic chemist, but further consideration suggests that it may be appropriate, given the small radial extent of the 4*f*-orbitals, Figure 10 (note that the radial maximum for the 4*f*-orbital of Gd^{+3} is close to that for

the Bohr hydrogen atom), and hence the extreme ionicity of lanthanide complexes, including lanthanide organometallics. In a very interesting paper, Rabbe and co-workers compared results for lanthanum–terpyridine complex using ECPs with and without 4*f*-functions explicitly incorporated into the valence space of the ECP and found similar calculational results.[90] Cundari and Sommerer compared and contrasted the kinetics and thermodynamics of lutetium-mediated H_2 activation with the other group 3 metals using a 68-electron (i.e., [Xe]$4f^{14}$) ECP for lutetium.[91] Li *et al.* have published a recent review of modeling of lanthanide complexes.[92] An older, although by no means less valuable, discourse on the modeling of actinide chemistry is available from Pepper and Bursten.[93] Bursten and co-workers have published extensively on actinide chemistry and the reader is directed there for a more in-depth discussion of the challenges of modeling these elements for which relativistic effects are of paramount significance.[94,94a]

(iii) Transition metals. The modeling of transition metal organometallics with emphasis on ECP methods has received a huge amount of attention, more so than probably any other family of organometallics.[18,75,76,95] (A few other reviews include Ref: 95a–95f.) One generalization based on experience worth emphasizing is that the use of ECPs for modeling transition metal organometallics must employ the semi-core approximation for reasonable results to be obtained. The replacement of the $(n-1)s^2(n-1)p^6$-electrons by the potentials yields ECPs that do not correctly reproduce the state splittings of the atoms and atomic ions. Happily, for most modern programs, the use of a transition metal ECP that employs the full-core approximation is either deprecated or not an option.

1.23.11 Density Functional Theory

DFT receives its own section as it is perhaps the most important theory advance in computational organometallic chemistry in the past decade.[96] Although widely used for decades in the solid-state chemistry and physics communities, DFT has only seen widespread implementation in generally available software for the modeling of molecular systems of greatest interest to most organometallic chemists in roughly the past decade. DFT now must be considered the first option in computational organometallic chemistry. In many routine (and not so routine) applications, DFT provides a computationally cost-effective and "black box" solution to the electron-correlation conundrum, which as we have stressed is especially problematic in many families of organometallic complexes.

DFT at its most essential involves a reformulation of the Hamiltonian to incorporate the effects of electron correlation neglected in the HF Hamiltonian that was long the standard in molecular-orbital calculations. Put simply, in the Schrödinger wave equation,

$$\hat{\mathrm{H}}\psi = \mathrm{E}\psi$$

electron correlation can be invoked either through altering the Hamiltonian $\hat{\mathrm{H}}$ (as DFT and SEQM methods do) or the wave function Ψ (as post-HFPT and MC methods do). The DFT approach, although not without its problems, is computationally efficient and, almost as importantly, DFT scales more favorably with basis-set size, on the order of N^{3-4}, where N is the number of basis functions. Thus, doubling the number of basis functions, engenders only an order of magnitude increase in the computational time. This may sound daunting, but MC techniques like MP and coupled-clusters methods typically scale in the N^{5-7} range, which means that doubling the basis set size yields a two orders of magnitude or greater increase in computational time. As a result, PT, MC, and, certainly, combined MC/PT methods are often limited within the realm of computational organometallic chemistry to small and perhaps experimentally less relevant models, large chemical systems with small basis sets (which as we advised above is very dangerous), or single-point calculations for the obtaining of accurate energetics at geometries determined with a lower level of theory.[97,97a]

It is not our purpose to discuss in detail the theory DFT, as there are many excellent reviews and books on that subject. Just a few examples of particular relevance to organometallic chemists apart from the myriad of applications that entail geometry optimization and reaction-coordinate evaluation include the use of DFT for prediction of ESR properties of metal complexes,[98] modeling heterogeneous catalysts,[99] time-resolved X-ray crystallography of metal complexes,[100] surface spectroscopy,[101] and photofragment spectroscopy.[102]

Density functional theory not only yields results that are of greater accuracy (in comparison to HF and, in many cases, even MP2 calculations), but it also permits the study of larger, more experimentally relevant organometallic complexes. It is not often in computational chemistry that one gets more and pays less for it, but DFT is that special circumstance. From the perspective of the computational organometallic chemist, the main issue is which density functional to use. It is amazing that from among the myriad of choices, the community has quickly converged on a

single uberfunctional, B3LYP. Indeed, it is worth noting that as a measure of the "popularity" of the B3LYP functional, the three papers detailing the B3LYP technique[103,103a,103b] occupy the top three positions in the 2003 list of most-cited chemistry articles.[104] Typing B3LYP into SciFinder yields almost 17,000 hits. Therefore, one can consider B3LYP as the *de facto* standard in current computational chemistry, for organometallic and indeed most molecular, chemical applications. B3LYP is a hybrid functional and thus incorporates into its Hamiltonian HF exchange as well as the more standard DFT exchange and correlation functionals. The "3" also signifies that B3LYP contains three parameters that modify the extent of correlation and exchange mixing, and these three parameters were obtained by optimization against a test set of molecules (read small and predominantly main group). As in agriculture, hybridization can result in a new strain that is stronger than the sum of its parts, and while researchers have addressed deficiencies in the standard B3LYP functional, for example, in modeling spin-state properties of *d*-block metal complexes,[105,105a] B3LYP remains king of the hill for organometallic chemistry applications.[103,103a,103b,104]

But, if B3LYP gives bad agreement with the experiment, what is an organometallic chemist going to do? Assuming the experiment is OK, which we know it is, and if calculation has been done correctly (remember, terminated normally is not the same as terminated correctly), some useful strategies include the following. First and foremost, try some other basis sets (see above). There is no sense in testing different computational techniques if basis-set convergence has not been achieved. Assuming the basis set is not the issue, step number two is to try different functionals. There is a bewildering array of functionals that can be found from a quick perusal of one's favorite computational-chemistry program. A particularly good strategy is to try a few pure functionals (i.e., those with no HF exchange) and compare with hybrid functionals. Popular pure functionals include BP86 and BLYP; in addition to B3LYP, another hybrid functional with considerable popularity is B3PW91. Third, dust the cobwebs off some non-DFT methods—HF and MP2. These calculations are reasonably quick and their comparison with DFT results can give some indication of the magnitude of the electron-correlation contribution to the property, chemical system, or reaction of interest. Such an integrated approach was done in a study by Buda *et al.* on the prediction of spin states in technetium complexes.[7,7a–7d] Fourth, add some MC calculations to the regimen. Techniques such as CI-SD and CCSD(T), if they are feasible for the size molecule and basis set employed, can be applied simply and without much need for human intervention. MC techniques like CASSCF and combined MC/PT generally require considerable human intervention for their correct application.

In computational organometallic chemistry, the density functional must often be viewed as an adjustable parameter. If similar and chemically reasonable results are obtained with different functionals, and with different wave function-based methods, this is typically a good indication that the computational techniques are reliably describing the underlying chemistry of the system at hand. In short, B3LYP is an excellent functional, but in the absence of literature precedence for its utility for the organometallic system of interest, it cannot be assumed to be infallible.

1.23.12 Hybrid Methods

In general, the needs of modeling the metal often dictate what methods are appropriate for the remainder of the organometallic complex. For example, if the electronic structure at the metal coordination sphere dictates an expensive MC solution for reliable modeling, then in a typical single-level calculation, this expensive MC level must also be applied to even the organic coating. The result is typically an infeasible or impossible computational exercise. As discussed above, organometallic complexes, by their very nature, are two-phase systems (Figure 1). They are quite often comprised of a small, inorganic core with a larger, organic coating. In many cases, the "action" takes place at the inorganic core, involving changes in spin state, geometry, ligation, formal oxidation state, bond breaking/making, etc. While its direct chemical reactivity may be limited, the organic coating is still important. Organic substituents are often employed to engender some degree of thermodynamic stability or metastability to permit experimental characterization or to produce some beneficial kinetic outcome vis-à-vis regiochemistry or stereochemistry via electronic or steric means.

The two-phase nature of organometallics has thus encouraged the use of so-called hybrid techniques for the efficient modeling of larger organometallic systems, allowing the organometallic chemist the opportunity to get beyond the embarrassing, but often very necessary, habit of pruning organic substituents back to hydrogen. In typical applications, a higher level of theory is used for modeling the inorganic core, and more approximate methods for the organic coating. In one of the most popular hybrid techniques, computationally inexpensive molecular mechanics (MM) approaches are used for the organic partition, and more expensive quantum mechanics (QM) techniques are applied to the metal and its inner coordination sphere.[106,106a] The most pressing issue in employing hybrid

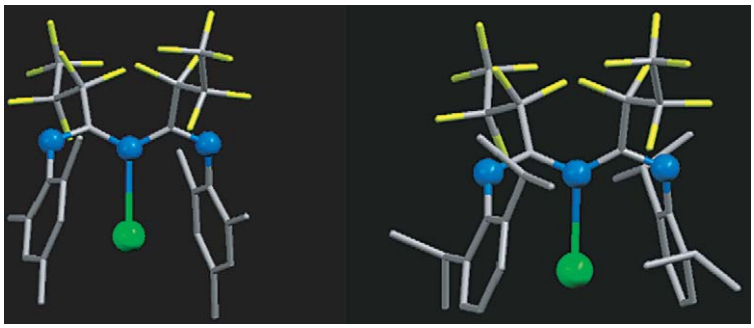

Figure 19 Two views of thallium(I) triazapentadienyl complex. Thallium (green), nitrogen (blue), carbon (grey), fluorine (yellow). Hydrogen atoms are omitted for clarity.

techniques is where to have the QM/MM partition. A good working rule is to partition QM/MM calculations only at single bonds to avoid cutting off important resonance effects, which may exert their influence over long distances. Of course, one must then worry about the neglect of inductive effects of the organic substituent. In the following paragraph, a typical example is given to highlight some of the decisions involved in the application of QM/MM models.

To reiterate, the goal in hybrid QM/MM calculations is to partition the organometallic such that the MM partition is that subset of chemical groups whose effect on the chemistry of interest is primarily steric rather than electronic in nature. As with all computational models, to assess the quality of the partitioning, calibration is needed. For example, in the modeling of thallium(I) triazapentadienyl complexes (Figure 19), the first (and computationally least expensive) model that may immediately suggest itself is to use QM techniques for the Tl and N_3C_2 backbone of the ligand.[107] However, test calculations indicate that it is not desirable to replace the phenyl substituents on the terminal nitrogen atoms, as these interact with thallium(I) through their π-cloud; comparison of calculations in which the Ar groups are and are not included in the MM partition show substantial changes in the bonding and geometry at the thallium center. Test calculations do reveal, however, that the isopropyl substituents can be placed into the MM partition with little change in the predicted geometry.

It is worth reminding the reader that in standard QM/MM applications, the default is to replace the MM portion with a hydrogen atom so that there are no open valences in the QM calculation of the truncated model. For example, in Morokuma's Pt-bis(tri-*tert*-butylphosphine), Figure 3, the most drastic (and hence quickest) QM/MM partitioning is to include only the Pt and P atoms in the QM region. The ONIOM (our own *n*-layered integrated molecular orbital and molecular mechanics) methodology for effecting the QM/MM calculation thus will perform a QM and MM calculation on the truncated model, $Pt(PH_3)_2$, and an MM calculation on the full complex, $Pt(P^tBu_3)_2$. The difference between the MM steric energy of $Pt(P^tBu_3)_2$ and $Pt(PH_3)_2$ thus gives a measure of the steric impact of the *tert*-butyl groups. Also, one may argue that P^tBu_3 is a good electron-donating phosphine due to the three alkyl substituents on phosphorus, and thus PH_3 is a poor electronic model given the subtle balance of σ-donation and π-backbonding manifested in organometallics with phosphine ligands. Thus, during the calibration phase, one would want to compare and contrast a partition scheme in which the *tert*-butyl methyl groups are replaced by hydrogen, resulting in a truncated PMe_3 model for the QM portion of the QM/MM calculations. Of course, this expanded partition will result in a slower calculation as compared to the PH_3 partition, but still will yield substantial savings over a full QM calculation on the P^tBu_3 complex.

Returning to the thallium complex in Figure 19, note that the carbon substituents are perfluoropropyl groups, which are expected to have a substantial electron-withdrawing inductive effect. In this case, the standard QM/MM replacement with hydrogen may be expected to be poor. However, the Gaussian program allows one to override the default and "cap" the resulting open valence on carbon with fluorine. The inductive effect of the fluorinated substituent on the thallium is smaller than the Tl–π-interactions, although not entirely negligible. For example, calculation of the Tl–π-interaction energy is $2\,\mathrm{kcal\,mol^{-1}}$ greater with the use of a hydrogen-capping atom than a fluorine-capping atom, suggesting that the C_3F_7 group decreases to some extent the acidity/electrophilicity of the Tl(I) anion, presumably aiding in stabilization of this low-coordinate Tl(I) complex.

We close this section by noting that the ONIOM strategy[106,106a] for hybrid calculations can also be applied to carry out QM/QM calculations. For example, another approach to modeling the inductive effect of the C_3F_7 groups of the

complex in Figure 3 would be to use a fast semi-empirical method such as AM1 or PM3. Indeed, one could envisage a three-tiered DFT/SEQM/MM approach, that is, DFT to describe the thallium atom and the carbon and nitrogen of the aza backbone, and the phenyl substituents on the terminal nitrogen atoms, SEQM to model the inductive effect of the C_3F_7 groups, and MM to model the steric consequences of the isopropyl substituents on the Ar groups. Another popular application of three-tiered ONIOM approaches is to investigate solvent effects. The first level of theory can describe the inorganic core of the organometallic, a second level of theory for the organic coating, and finally a third level of theory for modeling specific solvent molecules. Such an approach has seen substantial use in modeling biomolecules, and its application to organometallics would be of particular interest as there is considerable motivation for areas such as aqueous-phase catalysis, driven by the desire for more environmentally friendly, "green" chemistry.

1.23.13 Needs and Future Directions

Throughout this chapter we have highlighted some of the challenges in the field of computational organometallic chemistry. To a large extent, organometallic complexes combine the computational challenges that reflect both their organic and metallic parentage. Increases in computer power, the availability of easy-to-use software, and the development and implementation of more powerful methods have considerably narrowed the historical gap between modeling of organic and organometallic chemistry. Now, more than ever, the experimental organometallic chemist who wishes to add computation to their analysis protocols, as well as the computational chemist who desires to expand his expertise to organometallics, has a wider array of options—DFT, hybrid QM/MM techniques, ECPs, and so forth. We close this chapter by reiterating a major theme throughout, that is before embarking on production calculations, one must calibrate the techniques to be employed. The chemical diversity of organometallics demands this. The calibration process can be accomplished by evaluating literature results for related series of organometallics or similar types of reactions. In the absence of such results, it behooves the chemist to first do this calibration. For semi-empirical methods, it is best to limit oneself to the prediction of geometries and evaluation of electronic structure and bonding. Furthermore, for SEQM techniques, it is best to compare chemically similar species as opposed to those that are highly disparate in, for example, coordination number, ligand type, metal, formal oxidation state, etc. For *ab initio* and density functional techniques, the modeler must select both a suitable basis set and a Hamiltonian. A suite of tests with different combinations of basis sets and methods is needed to establish that the methods are correctly describing the underlying chemistry one wishes to better understand, and that the good agreement is not the result of fortuitous cancelation of errors from incomplete basis sets and inappropriate electron-correlation treatment. Furthermore, calibration should be carried out on as many different organometallic species as possible. For density functional approaches, try functionals other than B3LYP, in particular a menu of pure and hybrid functionals, HF and MP2 calculations to test their effect on the calculated properties of the organometallic systems of interest. The objective of these and any other calibrations is to see if there is convergence in calculated properties as one goes to more elaborate and complete theoretical treatments, and to establish the scheme that best combines accuracy and efficiency. In the application of hybrid QM/MM techniques, calibration calculations are needed to test not only the suitability of the different QM levels of theory and MM force fields, but also different partition schemes. In general, one wants to avoid splicing the QM and MM regions at anything other than a single bond. Further, experiment with different portions starting closest to the metal core and working out from that center until convergence in calculated properties is seen, keeping in mind that energetic properties are often much more sensitive to level of theory than metric parameters. Finally, to paraphrase my grandmother, "Don't use the same hammer for every job." In other words, there's a big, beautiful world of methods and techniques out there other than the B3LYP functional; experiment with them, and most of all, calibrate.

Acknowledgments

This contribution largely reflects the research experience of the author. For this experience he is grateful to his graduate and undergraduate students, faculty colleagues, and experimental collaborators at the University of North Texas (2002–present) and at the University of Memphis (1991–2001). The author also acknowledges generous support of his research by the National Science Foundation and the United States Department of Energy. Finally, but most importantly, the author thanks his wife, Mary E. Anderson, his light and inspiration.

References

1. Schmidt, M. W.; Baldridge, K. K.; Boatz, J. A.; Elbert, S. T.; Gordon, M. S.; Jensen, J. H.; Koseki, S.; Matsunaga, N.; Nguyen, K. A.; Su, S., *et al. J. Comput. Chem.* **1993**, *14*, 1347–1363.
2. Frisch, M. J.; Trucks, G. W.; Schlegel, H. B.; Scuseria, G. E.; Robb, M. A.; Cheeseman, J. R.; Zakrzewski, V. G.; Montgomery, J. A.; Stratmann, R. E.; Burant, J. C., *et al. Gaussian 98 (Revision A.1)*, Gaussian Inc., Pittsburgh PA, 2001.
3. Jaguar, version 5.5, Schrödinger, 1500 S. W. First Avenue, Suite 1180, Portland, OR 97201 (http://www.schrodinger.com).
4. MOLPRO, a package of *ab initio* programs designed by Werner, H. J.; Knowles, P. J.; Amos, R. D.; Bernhardsson, A.; Berning, A.; Celani, P.; Cooper, D. L.; Deegan, M. J. O.; Dobbyn, A. J.; Eckert, F.; Birmingham, UK, **2002**.
5. Salahub, D. R., Zerner, M. C., Eds.;*The Challenge of d and f Electrons: Theory and Computation*, ACS Symposium Series 394; American Chemical Society: Washington, DC 1988.

5a. Quantum Chemistry: The Challenge of Transition Metals and Coordination Chemistry; Veillard, A. *NATO ASI Ser., Ser. C* **1986**, *176*.

6. Svensson, M.; Humbel, S.; Froese, R. D. J.; Matsubara, T.; Sieber, S.; Morokuma, K. *J. Phys. Chem.* **1996**, *100*, 19357–19363.
7. Buda, C.; Burt, S. K.; Cundari, T. R.; Shenkin, P. S. *Inorg. Chem.* **2002**, *41*, 2060–2069.

7a. Ball, D. M.; Buda, C.; Cundari, T. R.; Gillespie, A. M.; White, D. P. *Inorg. Chem.* **2002**, *41*, 152–156.

7b. Buda, C.; Cundari, T. R. *J. Mol. Struct., THEOCHEM* **2004**, *686*, 137–145.

7c. Buda, C.; Cundari, T. R.; Flores, A. A. *J. Coord. Chem.* **2005**, *58*, 575–585.

7d. Buda, C.; Dinescu, A.; Kazi, A.; Cundari, T. R. *J. Chem. Info. Model.* **2005**, *45*, 965–970.

8. Cr-Cr distances are 2.498 Å in the metal. (http://www.webelements.com)
9. Schulzke, C.; Enright, D.; Sugiyama, H.; LeBlanc, G.; Gambarotta, S.; Yap, G. P. A.; Thompson, L. K.; Wilson, D. R.; Duchateau, R. *Organometallics* **2002**, *21*, 3810–3816.
10. See, for example, Li, J.; Noodleman, L.; Case, D. A. *Inorg. Electronic Struct. Spectosc.* **1999**, *1*, 661–724.

10a. Lovell, T.; Torres, R. A.; Han, W. G.; Liu, T.; Case, D. A.; Noodleman, L. *Inorg. Chem.* **2002**, *41*, 5744–5753.

11. Sydora, O. L.; Wolczanski, P. T.; Lobkovsky, E. B.; Buda, C.; Cundari, T. R. *Inorg. Chem.* **2005**, *44*, 2606–2618.
12. Niemeyer, M.; Power, P. P. *Angew. Chem., Int. Ed.* **1998**, *37*, 1277–1279.
13. For an integrated theory-experiment study of low-valent Tl(I) complexes see also Wright, R. J.; Brynda, M.; Power, P. P. *Inorg. Chem.* **2005**, *44*, 3368–3370.
14. Roques, N.; Gerbier, Ph.; Nakajima, S.; Teki, Y.; Guerin, C. *J. Phys. Chem. Solids* **2004**, *65*, 759–762.
15. Hung, I.; Schurko, R. W. *Solid State Nucl. Mag. Res.* **2003**, *24*, 78–93.
16. Møller, C.; Plesset, M. *Phys. Rev.* **1934**, *46*, 618–622.
17. Crawford, T. D.; Schaefer, H. F., III. *Rev. Comp. Chem.* **2000**, *14*, 33–136.
18. Koga, N.; Morokuma, K. *Chem. Rev.* **1991**, *91*, 823–842.
19. Abu-Hasanayn, F.; Goldman, A. S.; Krogh-Jespersen, K. *Inorg. Chem.* **1994**, *33*(22), 5122–5130.
20. See also: Factors influencing the thermodynamics of molecular hydrogen oxidation addition to Vaska-type complexes (*trans*-Ir(PR_3)$_2$(CO)X): predictions from *ab initio* calculations and experimental verification. Abu-Hasanayn, F.; Krogh-Jespersen, K.; Goldman, A. S. *Inorg. Chem.* **1993**, *32*, 495–496.
21. Abu-Hasanayn, F.; Goldman, A. S.; Krogh-Jespersen, K. *J. Phys. Chem.* **1993**, *97*, 5890–5896.
22. Wu, Q.; Yang, W. *J. Chem. Phys.* **2002**, *116*, 515–524.

22a. Andersson, Y.; Langreth, D. C.; Lundqvist, B. I. *Phys. Rev. Lett.* **1996**, *76*, 102–105.

23. Wang, S-G.; Schwarz Eugen, W. H. *J. Am. Chem. Soc.* **2004**, *126*, 1266–1276.
24. Pyykkö, P.; Straka, M.; Tamm, T. *Phys. Chem. Chem. Phys.* **1999**, *1*, 3441–3444.
25. Mendizabal, F.; Pyykkö, P.; Runeberg, N. *Chem. Phys. Lett.* **2003**, *370*, 733–740.
26. Colacio, E.; Lloret, F.; Kivekaes, R.; Ruiz, J.; Suarez-Varela, J.; Sundberg, M. R. *Chem. Comm.* **2002**, 592–593.
27. Grimme, S. *J. Comp. Chem.* **2004**, *25*, 1463–1473.
28. Xu, X.; Goddard, W. A., III. *Proc. Nat. Acad. Sci. USA* **2004**, *101*, 2673–2677.
29. Smith, J. M.; Lachicotte, R. J.; Pittard, K. A.; Cundari, T. R.; Lukat-Rodgers, G.; Rodgers, K. R.; Holland, P. L. *J. Am. Chem. Soc.* **2001**, *123*, 9222–9223.
30. Torrent, M.; Sola, M.; Frenking, G. *Chem. Rev.* **2000**, *100*, 439–494.

30a. Frenking, G. *Chem. Rev.* **2000**, *100*, 717–774.

31. Chen, Y.; Hartmann, M.; Frenking, G. *Z. Anorg. Allgem. Chem.* **2001**, *627*, 985–998.
32. Siodmiak, M.; Frenking, G.; Korkin, A. *J. Phys. Chem. A* **2000**, *104*, 1186–1195.
33. Aikens, C. M.; Gordon, M. S. *J. Phys. Chem. A* **2003**, *107*, 104–114.
34. Chung, G.; Gordon, M. S. *Organometallics* **2003**, *22*, 42–46.
35. Pierloot, K.; De Kerpel, J. O. A.; Ryde, U.; Olsson, M. H. M.; Roos, B. O. *J. Am. Chem. Soc.* **1998**, *120*, 13156–13166.
36. Pierloot, K.; De Kerpel, J. O. A.; Ryde, U.; Olsson, M. H. M.; Roos, B. O. *J. Am. Chem. Soc.* **1997**, *119*, 218–226.
37. Gagliardi, L.; Roos, B. O. *Inorg. Chem.* **2002**, *41*, 1315–1319.
38. Cundari, T. R.; Stevens, W. J. *J. Chem. Phys.* **1993**, *98*, 5555–5565.
39. Roos, B. O. *Acc. Chem. Res.* **1999**, *32*, 137–144.
40. Nakano, H. *J. Chem. Phys.* **1993**, *99*, 7983–7992.
41. Schmidt, M. W.; Gordon, M. S. *Ann. Rev. Phys. Chem.* **1998**, *49*, 233–266.
42. Goddard, W. A., III; Harding, L. B. *Ann. Rev. Phys. Chem.* **1978**, *29*, 363–396.

42a. Ohanessian, G.; Goddard, W. A., III *Acc. Chem. Res.* **1990**, *23*, 386–392.

43. Spartan modeling package, Wavefunction, Inc. 18401 Von Karman Avenue, Suite 370, Irvine, CA 92612, USA.
44. Pople, J. A.; Beveridge, D. L. *Approximate MO Theory*; McGraw-Hill: New York, 1970.
45. Hoffmann, R. *J. Chem. Phys.* **1963**, *39*, 1397–1412.

45a. See also Whangbo, M.-H. *Theor. Chem. Acc.* **2000**, *103*, 252–256.

46. Albright, T. A.; Burdett, J. K.; Whangbo, M. H. *Orbital Interactions in Chemistry*; Wiley: New York, 1985.
47. Morrison, R. C.; Zhou, Z.; Parr, R. G. *Theor. Chim. Acta* **1993**, *86*, 3–11.

47a. Pernal, K.; Cioslowski, J. *J. Chem. Phys.* **2001**, *114*, 4359–4361.

48. Veige, A. S.; Slaughter, L. M.; Wolczanski, P. T.; Matsunaga, N.; Decker, S. A.; Cundari, T. R. *J. Am. Chem. Soc.* **2001**, *123*, 6419–6420.
49. Pople, J. A.; Segal, G. A. *J. Chem. Phys.* **1966**, *44*, 3289–3296.
50. Pople, J. A.; Beveridge, D. L.; Dobosh, P. A. *J. Chem. Phys.* **1967**, *47*, 2026–2033.
51. Dewar, M. J. S.; Zoebisch, E. G.; Healy, E. F.; Stewart, J. J. P. *J. Am. Chem. Soc.* **1985**, *107*, 3902–3909.
52. Stewart, J. J. P. *J. Comp. Chem.* **1989**, *10*, 221–264.
53. Dewar, M. J. S.; Thiel, W. *J. Am. Chem. Soc.* **1977**, *99*, 4899–4907.
54. Bacon, A. D.; Zerner, M. C. *Thoer. Chim. Acta* **1979**, *53*, 21–54.
55. Anderson, W. P.; Cundari, T. R.; Drago, R. S.; Zerner, M. C. *Inorg. Chem.* **1990**, *29*, 1–3.
56. Ray, P. C. *Chem. Phys. Lett.* **2004**, *394*, 354–360.
57. The PM3(tm) method is contained within the Spartan modeling package, Wavefunction, Inc. 18401 Von Karman Avenue, Suite 370, Irvine, CA 92612 USA.
58. Voityuk, A. A.; Roesch, N. *J. Phys. Chem. A.* **2000**, *104*, 4089–4094.

58a. Voityuk, A. A. *227th ACS National Meeting*, Anaheim, CA, March 28–April 1, 2004, COMP-072.

59. Berweger, C. D.; Thiel, W.; van Gunsteren, W. F. *Proteins* **2000**, *41*, 299–315.

59a. Dorcak, V.; Krezel, A. *Dalton Trans.* **2003**, 2253–2259.

59b. Altun, A.; Golcuk, K.; Kumru, M. *Vibr. Spectr.* **2003**, *33*, 63–74.

60. Cundari, T. R.; Deng, J. PM3(tm) Analysis of Transition Metal Complexes; *J. Chem. Info. Comput. Sci.* **1999**, *39*, 376–381.
61. Adam, K. R.; Atkinson, I. M.; Lindoy, L. F. *J. Mol. Struct.* **1996**, *384*, 183–190.
62. Bosque, R.; Maseras, F. *J. Comput. Chem.* **2000**, *21*, 562–571.
63. 3D Search and Research using the Cambridge Structural Database; Allen, F.H.; Kennard, O. *Chem. Design Autom. News* **1993**, *8*, 31–37.
64. See, for example, Poulsen, T. D.; Garcia-Viloca, M.; Gao, J.; Truhlar, D. G. *J. Phys. Chem. B* **2003**, *i*, 9567–9578.
65. Cundari, T. R.; Deng, J.; Fu, W. *Intern. J. Quantum Chem.* **2000**, *77*, 421–432.
66. Hehre, W. J.; Radom, L.; Schleyer, P. v. R.; Pople, J. A. *Ab Initio Molecular Orbital Theory*; Wiley: New York, 1986.
67. See, for example, Dunning, T. H.; Peterson, K. A.; Wilson, A. K. *J. Chem. Phys.* **2001**, *114*, 9244–9253 and earlier papers by Dunning and Wlson in this series.
68. Peterson, K. A. Abstracts of Papers, *223rd ACS National Meeting*, Orlando, FL, United States, April 7–11, **2002**, COMP-088.

68a. Peterson, K. A. In *Recent Advances in Electron Correlation Methodology*; Wilson, A. K., Peterson, K. A., Eds.; American Chemical Society: Washington, DC, to be published.

69. Omary, M. A.; Sinha, P.; Bagus, P. S.; Wilson, A. K. *J. Phys. Chem. A* **2005**, *109*, 690–702.
70. Frenking, G.; Ehlers, A. W.; Boehme, M.; Dapprich, S.; Gobbi, A.; Hoellwarth, A.; Jonas, V.; Koehler, K. F.; Stegmann, R.; Veldkamp, A. *Chem. Phys. Lett.* **1993**, *208*, 111.
71. http://www.emsl.pnl.gov. Extensible Computational Chemistry Environment Basis Set Database, Version 02/25/04, as developed and distributed by the Molecular Science Computing Facility, Environmental and Molecular Sciences Laboratory which is part of the Pacific Northwest Laboratory, P.O. Box 999, Richland, Washington 99352, USA, and funded by the U.S. Department of Energy.
72. http://www.webelements.com. WebElements™, the periodic table on the WWW, URL: http://www.webelements.com/. Copyright 1993–2003 Mark Winter [The University of Sheffield and WebElements Ltd, UK]. All rights reserved.
73. http://webbook.nist.gov. Martinho Simões, J. A. Organometallic Thermochemistry Data. In NIST Chemistry WebBook, NIST Standard Reference Database Number 69, Eds. P. J. Linstrom and W. G. Mallard, March 2003, National Institute of Standards and Technology, Gaithersburg MD, 20899.
74. Couty, M.; Hall, M. B. *J. Comp. Chem.* **1996**, *17*, 1359–1370.
75. Benson, M. T.; Cundari, T. R.; Lutz, M. L.; Sommerer, S. O. *Rev. Comp. Chem.* **1996**, *8*, 145–202.
76. Frenking, G.; Antes, I.; Bohme, M.; Dapprich, S.; Ehlers, A. W.; Jonas, V.; Neuhaus, A.; Otto, M.; Stegmann, R., Veldkamp, A., *et al. Rev. Comp. Chem.* **1996**, *8*, 63–144.
77. Szasz, L. *Pseudopotential Theory of Atoms and Molecules*; Wiley: New York, 1985.
78. Pyykkö, P. *Chem. Rev.* **1988**, *88*, 563–594.
79. Hay, P. J.; Wadt, W. R. *J. Chem. Phys.* **1985**, *82*, 270–310.
80. Stevens, W. J.; Krauss, M.; Basch, H.; Jasien, P. G. *Can. J. Chem.* **1992**, *70*, 612–630.

80a. Cundari, T. R.; Stevens, W. J. *J. Chem. Phys.* **1993**, *98*, 5555–5565.

81. Wedig, W.; Dolg, M.; Stoll, H.; Preuss, H. In *Quantum Chemistry: The Challenge Transition Metals and Coordination Chemistry*. NATO ASI Series, Series C: Mathematical and Physical Sciences, **1986**, *176*, 79–89.
82. Lovallo, C. C.; Klobukowski, M. *J. Comp. Chem.* **2004**, *25*, 1206–1213.

82a. Lovallo, C. C.; Klobukowski, M. *J. Comp. Chem.* **2003**, *24*, 1009–1015.

83. Bode, B. M.; Gordon, M. S. *Theor. Chem. Acc.* **1999**, *102*, 366–376.
84. Cundari, T. R.; Ruiz Leza, H. A.; Grimes, T.; Steyl, G.; Waters, A.; Wilson, A. K. *Chem. Phys. Lett* **2005**, *401*, 58–61.
85. For a recent contribution to the study of non-VSEPR structures of alkaline earth dihalides see Levy, J. B.; Hargittai, M. *J. Phys. Chem.* **2000**, *104*, 1950–1958 and references therein.
86. Krauss, M.; Stevens, W. J. *J. Chem. Phys.* **1990**, *93*, 4236–4242.
87. Kwon, O.; McKee, M. L. In *Computational Organometallic Chemistry*; Cundari, T. R., Ed., Dekker: New York, 2001.
88. Bridgeman, A. J. *J. Chem. Soc., Dalton* **1997**, 2887–2893.
89. Dolg, M.; Stoll, H.; Preuss, H. *Theor. Chim. Acta* **1993**, *85*, 441–450.

89a. Dolg, M.; Stoll, H.; Savin, A.; Preuss, H. *Theor. Chim. Acta* **1989**, *75*, 173–194.

90. Rabbe, C.; Mikhalko, V.; Dognon, J. P. *Thoer. Chem. Acc.* **2000**, *104*, 280–283.
91. Cundari, T. R.; Sommerer, S. O.; Stevens, W. J. *Chem. Phys.* **1993**, *178*, 235–243.
92. Luo, Y.; Selvam, P.; Koyama, M.; Kubo, M.; Miyamoto, A. *Chem. Lett.* **2004**, *33*, 780–785.
93. Pepper, M.; Bursten, B. E. *Chem. Rev.* **1991**, *91*, 719–741.
94. Sonnenberg, J. L.; Hay, P. J.; Martin, R. L.; Bursten, B. E. *Inorg. Chem.* **2005**, *44*, 2255–2262.

94a. An older, but excellent reference on the degree of covalent in f-element organometallis is available in Burns, C. J.; Bursten, B. E. *Comm. Inorg. Chem.* **1989**, *9*, 61–93.

95. See, for example, and the other articles in this special issue Davidson, E. R. *Chem. Rev.* **2000**, *100*, 351–352.

95a. Cundari, T. R.; Gordon., M. S. *Coord. Chem. Rev.* **1996**, *147*, 87–115.

95b. Bursten, B. E.; Drummond, M. L.; Li, J. *Faraday Discussions* **2003**, *124*, 1–24.
95c. Ziegler, T.; Autschbach, J. *Chem. Rev.* **2005**, *105*, 2695–2722.
95d. Ziegler, T. *Can. J. Chem.* **1995**, *73*, 743–761.
95e. Ziegler, T. *Chem. Rev.* **1991**, *91*, 651–667.
95f. Tsipis, C. *Comm. Inorg. Chem.* **2004**, *25*, 19–74.
96. Koch, W.; Holthausen, M. C. A Chemists Guide to Density Functional Theory; Wiley-VCH: Weinheim, 2000.
97. Torrent, M.; Sola, M.; Frenking, G. *Chem. Rev.* **2000**, *100*, 439–494.
97a. Frenking, G. *Chem. Rev.* **2000**, *100*, 717–774.
98. Saladino, A. C.; Larsen, S. C. *Catal. Today* **2005**, *105*, 122–133.
99. Neyman, K. M.; Illas, F. *Catal. Today* **2005**, *105*, 2–16.
100. Coppens, P.; Novozhilova, I. V. *Int. J. Quantum. Chem.* **2005**, *101*, 611–623.
101. Nilsson, A.; Pettersson, L. *Surf. Sci. Rep.* **2004**, *55*, 49–167.
102. Metz, R. B. *Int. Rev. Phys. Chem.* **2004**, *23*, 79–108.
103. Becke, A. D. *J. Chem. Phys.* **1993**, *98*, 5648–5652.
103a. Lee, C.; Yang, W.; Parr, R. G. *Phys. Rev. B* **1988**, *37*, 785–789.
103b. Becke, A. D. *Phys. Rev.* **1998**, *A38*, 3098–3100.
104. This designation is from the Chemical Abstracts Service (CAS) for articles published in 2003 as pertains to journals covered by CAS, and under the subject heading of chemistry. The B3LYP articles (reference 103) occupy the most cited articles list for the years 1999 through 2003 (http://www.cas.org).
105. Reiher, M.; Salomon, O.; Hess, B. A. *Theo. Chem. Acc.* **2001**, *107*, 48–55.
105a. Salomon, O.; Reiher, M.; Hess, B. A. *J. Chem. Phys.* **2002**, *117*, 4729–4737.
106. Maseras, F. In *Computational Organometallic Chemistry*; Cundari, T. R., Ed., Dekker: New York, 2001.
106a. Maseras, F.; Morokuma, K. *J. Comp. Chem.* **1995**, *16*, 1170.
107. Dias, H. V. R.; Singh, S.; Cundari, T. R. *Angew. Chem.* **2005**, *44*, 4907–4910.

1.24
Dihydrogen and Other σ Bond Complexes

G J Kubas, Los Alamos National Laboratory, Los Alamos, NM, USA

1.24.1 Introduction

The discovery by Kubas and co-workers in 1984 of coordination of a dihydrogen molecule in $W(CO)_3(PR_3)_2(H_2)$ is the prototype for a new class of metal complexes commonly referred to as "σ-complexes."[1,2,2a–2c,3] Molecules containing only strong "inert" σ-bonds such as H–H had previously been believed to be incapable of stable binding, although metals readily break these bonds in catalysis, and σ-complexes were proposed as transients in both oxidative addition (OA) and reductive elimination (RE) processes, even for C–C bonds.[4] Metal hydrides formed by OA of H_2 are catalytic intermediates, and it is now clear that metal–H_2 and other σ-complexes can also be important in catalytic mechanisms.

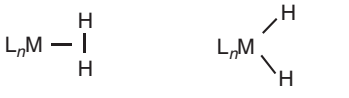

η^2-H_2 complex Dihydride complex

Remarkably, over 500 H_2 complexes are known (>1000 publications). M–H_2 and other σ-bond interactions are among the simplest yet most dynamic, complex, and enigmatic chemical topologies known. The H_2 molecule can bind/dissociate, undergo equilibrium splitting to dihydride, rapidly rotate about the M–H_2 axis, and exchange with *cis*-ligands, all on the same metal (Scheme 1).

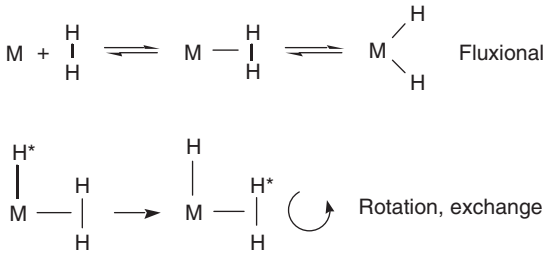

Scheme 1

Often these dynamics cannot be frozen out on the NMR timescale even at low temperature. The synergy and accord between experiment and theory concerning dynamics, structure, and bonding is exceptional.[3,5] The three-center interaction of a "bonding" electron pair with metal perfectly complements classical Werner and π complexes where ligands coordinate via nonbonding or π-electrons.

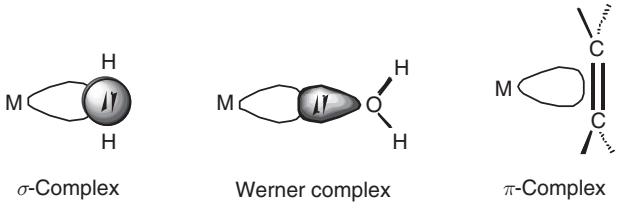

The side-on (η^2)-bonding in M-η^2-H_2 and other σ complexes (and the bonding in bridging hydrides/alkyls[6,6a]) is "nonclassical," by analogy to the three-center two-electron bonding in carbocations and boranes (Figure 1). Positively charged species, for example, CH_3^+ and H^+, are all strong electrophiles toward the weakly Lewis basic H_2, but transition metals are unique in stabilizing H_2 and other σ-bond complexes by M($d\pi$)–H_2(σ^*) "backdonation (BD)" (Figure 1), which is unavailable to main group atoms. The bonding is analogous[2a] to the Dewar–Chatt–Duncanson model[7,7a] for π-complexes, and H_2 is a good π-acceptor like ethylene. Importantly, the linkage in L_nM–H_2 is identifiable as "the" bond between two species capable of independent existence, in contrast to previously known intramolecular M···H–C interactions,[8,8a–8e] now commonly referred to as "agostic" interactions[8d] (Figure 1). A relevant example of the latter is interaction of an unsaturated 16e metal center with phosphine C–H bonds that relieve the electronic unsaturation in complexes such as the precursor to the first H_2 complex, $W(CO)_3(PR_3)_2$.[9]

A large variety of σ-bonds interact inter- or intramolecularly with metal centers.[3,10c]

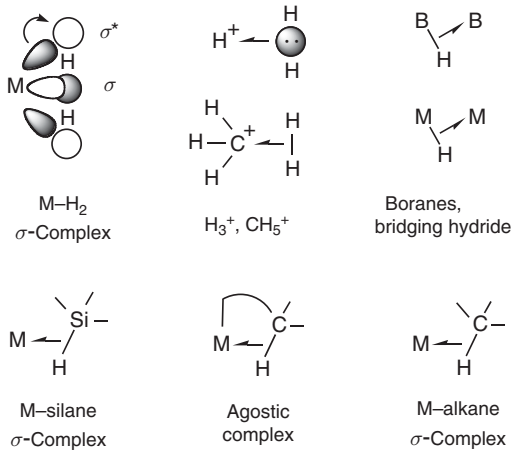

Figure 1 Examples of nonclassical three-center, two-electron (3c-2e) bonding.

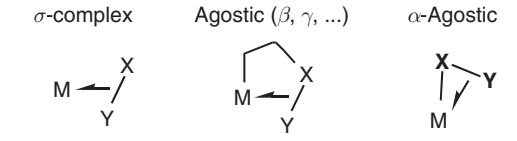

H–H, B–H, Ga–H	C–H, Si–H	C–H, Si–H
C–H, Si–H	B–H, N–H	S–H, P–H
Ge–H, Sn–H	C–C, Si–C	C–P, C–B, C–N

In principle any X–Y bond can coordinate to a metal center providing substituents at X and Y do not block access to M. σ-complexes have several favorable features in catalytic systems. Foremost is that the "oxidation state of M does not change" on binding of, for example, molecular H_2, whereas formation of a dihydride involves OA, that is, increasing the M oxidation state by two. H_2 ligands can also have far greater thermodynamic "and" kinetic acidity than hydrides, which is important in the ability of acidic H_2 ligands to protonate substrates such as olefins and N_2. Analogous increased acidity of C–H bonds in transient alkane complexes may be important in alkane activation such as conversion of methane to methanol. Although σ-complexes present a wealth of fascinating structure/bonding features, this article focuses mainly on basic principles, reactivity, and applications in catalysis.

1.24.2 Dihydrogen Complexes

1.24.2.1 Synthesis, Structure, and Properties of H_2 Complexes

H_2 is perhaps the most versatile ligand because it can act as both a Lewis acid (π-acceptor) and a Lewis base (σ-donor) to not only metals but main group species as well. Every metal from V to Pt forms H_2 complexes, although room temperature (RT)-stable V, Co, Ni, and Pd complexes have not been isolated.[2,2a–2c,3,5,10,10a–10h] Because H is difficult to locate crystallographically, an important NMR diagnostic for H_2 versus hydride coordination is J_{HD} for the HD isotopomer of an H_2 complex. J_{HD} for HD gas is 43 Hz, the maximum value ($d_{HD} = 0.74$ Å), and lower values represent proportionately shorter d_{HD} (Equation (1)). J_{HD} determined in solution correlates well with d_{HH} in the solid state via the empirical relationships developed by both Morris[11] and Heinekey:[12]

$$d_{HH} = 1.42 - 0.0167 J_{HD}\ \text{Å}\ \text{[Morris]}\ \text{or}\ d_{HH} = 1.44 - 0.0168 J_{HD}\ \text{Å}\ \text{[Heinekey]} \quad (1)$$

Input data include d_{HH} from both diffraction and solid-state NMR[13] measurements. For $W(CO)_3(P^iPr_3)_2(H_2)$, J_{HD} is 34 Hz, giving $d_{HH} = 0.86$–0.88 Å versus 0.89 Å from solid-state NMR and 0.82(1) Å from neutron diffraction (uncorrected for H_2 libration[14]). Short T_1 values for the H_2 ligand are also diagnostic[15] (e.g., 4 ms for the W complex), although care must be exercised in interpretation.[16,16a,16b,17] Inelastic neutron-scattering studies of H_2 rotation/libration provide definitive evidence for molecular H_2 binding and also $H_2 \rightarrow M$ backdonation but are difficult experimentally.[18]

The vibrational modes for $M(\eta^2\text{-}H_2)$ are distinct from those for hydrides, which have only two fundamental modes: ν(MH) at high energy and an M–H deformation at 700–900 cm^{-1}. However the initial routine IR spectrum of solid $W(CO)_3(PR_3)_2(H_2)$ additionally displayed an unusual low-energy band near 460 cm^{-1} that was the first clue to the novel structure here.[2b] This and other H_2 complexes were later found to have "six" fundamental modes: three stretches [ν(HH), $\nu_{as}(MH_2)$, $\nu_s(MH_2)$] plus three low-energy modes [two deformations and a torsion (H_2 rotation[18])].[1,2c,3] All shift to much lower frequencies on isotopic substitution with D_2. The frequency of most interest, ν_{HH}, is generally weak and often difficult to observe but is seen in a range, 2080–3200 cm^{-1}, considerably lower than that for free H_2, 4300 cm^{-1}. ν_{HH} is highly coupled with $\nu_{as}(MH_2)$, and the degree of bond activation does not correlate well with ν_{HH}. Because of the vibrational complexity, there is an inverse equilibrium isotope effect, that is, D_2 binds slightly more strongly than H_2.[2c,19]

Most H_2 complexes are low-valent octahedral d^6 systems, although $Re^{III}(N_3N_F)(H_2)$ is an exception.[20]

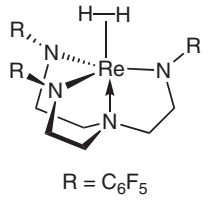

The value of J_{HD}, 17 Hz, indicates an elongated H–H bond (~1.15 Å, see below). A silane σ-complex (see Section 4) also forms. Paramagnetic σ-complexes are extremely rare, and an apparent high-spin H_2 complex has recently been reported.[21] Many H_2 complexes are cationic because the increased electrophilicity reduces BD that leads to H–H cleavage (see below). Neutral complexes normally contain at least one acceptor such as CO or a strong *trans*-effect ligand such as hydride to moderate BD. The first H_2 complexes stabilized only by nitrogen-donor ligands were $Tp^*RhH_2(H_2)$[22] (Tp^* = Me-substituted pyrazolyborate) and $[Os(NH_3)_5(H_2)]^{2+}$,[23] which has very long d_{HH} (1.34 Å) more characteristic of a dihydride. Complexes containing only aquo,[24] CO,[25,25a,25b] or carbon[26,26a] co-ligands are known, but in some cases are only marginally stable.

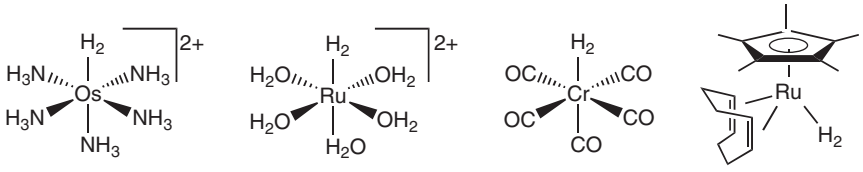

The highly acidic pentacarbonyl Cr complexes (and monophosphine and W derivatives) were recently observed by low-temperature NMR.[25,25a,25b] The first example of an H_2 complex with carbene co-ligands, $[Cp^*Ir(bis\text{-}carbene)(H_2)]^{2+}$, exhibits a much shorter H–H distance (1.04 Å) than its bis-phosphine analogs that contain highly elongated H_2 (1.45 Å).[26a]

Synthetic routes to H_2 complexes include reaction of H_2 with an unsaturated complex such as $W(CO)_3(PR_3)_2$ or displacement of weak solvento ligands, for example, CH_2Cl_2. Protonation of hydride complexes is common (Equation (2)).[10a,26,26a,27,28]

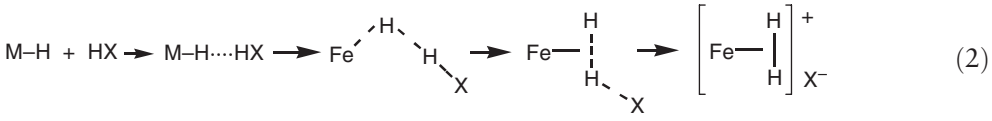

(2)

Reaction proceeds via observable hydrogen bonding of the acid,[28,29] which can be as weak, to the basic hydride. The group 8 triad gives many H_2 complexes, especially "half sandwich" type.[10g,26,26a]

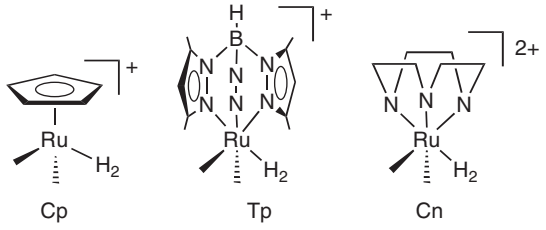

Isolable bis-H_2 complexes are rare, for example, $RuH_2(H_2)_2(PCy_3)_2$,[30,30a] $[RhH_2(H_2)_2(PCy_3)_2]^+$,[31] and $Tp^*RuH(H_2)_2$.[22] 16e $RuHX(H_2)(PCy_3)_2$ (X = Cl, I) reversibly adds a second H_2.[32,32a] Complexes with "two different η^2-coordinated σ-bonds" are known, for example, $RuH_2(\eta^2\text{-}H_2)(\eta^2\text{-}SiHPh_3)(PCy_3)_2$ and an analogous borane complex.[33,33a,33b] In the former[33] the bulky phosphines are in an unusual *cis*-configuration apparently because bonding interaction between Si and the hydride offsets steric repulsion between the phosphines.

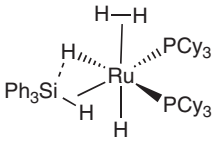

Such secondary interactions between silicon and hydrogen atoms (SISHAs) are hydrogen-bonding like and have been observed crystallographically in several other silane and H_2 complexes with *cis*-hydrides (see below).

Polynuclear H_2 complexes are few, primarily dinuclear Ru, Os, and Ir complexes with H_2 on only one M. Bridging-H_2 ligands have not been proved definitively. The properties of H_2 complexes vary greatly, depending on the degree of activation of the H_2 ligand toward dihydride. True H_2 complexes with short $d_{HH} < 1$ Å typically have reversibly bound H_2 ligands that exchange with D_2 and can give isotopic scrambling to HD. However, it is often difficult to determine conclusively whether or not a complex contains hydride or η^2-H_2, and some complexes lie in a "gray zone" ($d_{HH} = 1.4-1.6$ Å) between formulation as H_2 or dihydride complexes, for example, $[OsH_3(H_2)(PPhMe_2)_3]^+$ ($d_{HH} = 1.49(4)$ Å from neutron diffraction[34]). The accepted closest spacing in metal hydrides is 2.1 Å, although certain intermetallic rare earth hydrides display d_{HH} as low as 1.5 Å ("hydrogen-pairing" phenomena).[35,35a] At the other end of the spectrum lie weak "physisorption"-type interactions of H_2 with surfaces, bare metal ions, and main group compounds such as $MH_x(H_2)$ (M = B, Al, Mg; $x = 1$–3).[3,36] Theoretical calculations suggests that metal complexes can bind multiple H_2, and porous metal-organic framework species contain multiple H_2, all of which are being investigated for hydrogen-storage applications.[37,37a–37e]

1.24.2.2 Activation of Bound H_2 toward Homolytic Cleavage

BD is crucial in activating the H–H bond toward homolytic cleavage to a dihydride.[2,2a–2c,3,5] If BD becomes too strong, for example, by increasing electron-donor strength of co-ligands on M, the σ-bond cleaves to form a dihydride because of overpopulation of H_2 σ^*. There is a fine line between H_2 and dihydride coordination, and in some cases "equilibria" exist between the two forms in solution for $W(CO)_3(PR_3)_2(H_2)$ (R = *i*-Pr; $K = 0.25$) (Equation (3)).

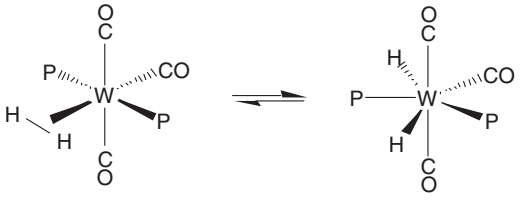

(3)

Sterics also play an important role: for less bulky R = Me the equilibrium lies completely to the right, that is, the complex is a "dihydride."[25b] The entire reaction coordinate for the activation of H_2 on a metal can be mapped out and related to the degree of M($d\pi$)–H_2(σ^*) BD, as dramatically observed in the remarkable "stretching" of the H–H distance, d_{HH}, within the large regime of L_nM–H_2 complexes.[3,10,10a–10h] Increasing the electron population of H_2(σ^*) via BD causes the H–H bond to elongate and eventually rupture, and examples of complexes with H–H distance (d_{HH}) varying from 0.82 to 1.6 Å (from crystallography and NMR) are known.

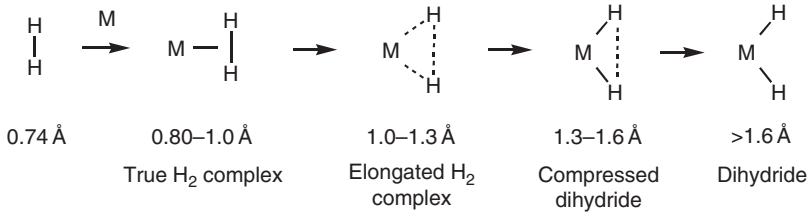

This arresting of the bond rupture process along its entire reaction coordinate is unprecedented in chemistry. Properties such as lability of the H_2 of the complexes can vary greatly depending on the metal, ancillary ligands, and other factors, and complexes with elongated and greatly elongated H–H bonds ("compressed dihydrides") are known.

Although the d_{HH} ranges shown are quite arbitrary, each category of complexes has distinct properties. The d_{HH} is relatively short (0.8–1 Å) and reversibly bound in "true" H_2 complexes best exemplified by $W(CO)_3(PR_3)_2(H_2)$, much as in physisorbed H_2. Elongated H_2 complexes[38,38a,38b] ($d_{HH} = 1-1.3$ Å) were first identified in 1991 in $ReH_5(H_2)(PR_3)_2$ where neutron diffraction showed a d_{HH} of 1.357(7) Å between two hydrides.[39] Complexes with such very long d_{HH} are now viewed as "compressed hydrides," with NMR features differing from elongated H_2 complexes, for example, J_{HD} increases with T for the former and decreases for the latter.[38a] These are relative terms since the H–H bond is always stretched on binding, and indeed a near "continuum" of d_{HH} exists.[3,38,38a,38b] This is most likely prototypical for all homolytic σ-bond activation processes on metals.

The activation of H_2 is very sensitive to the nature of M, L, and charge. Third-row M, strongly donating L, and neutral charge favors elongation or splitting of H–H, while first-row M, electron-withdrawing L, and positive charge shortens d_{HH}. The ligand *trans* to H_2 has a powerful influence: strong π-acceptors such as CO (and also strong σ-donors such as H) greatly reduce BD and normally keep $d_{HH} < 0.9$ Å. Conversely, mild σ-donors such as H_2O or π-donors such as Cl *trans* to H_2 elongate d_{HH} (0.96 – 1.34 Å), as dramatically demonstrated by the isomers below.[40]

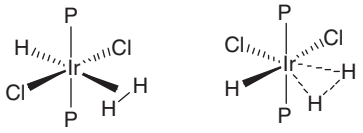

Recent experimental and calculational data indicate that the *cis*-Cl complex is actually a "compressed trihydride" ($d_{HH} \sim 1.5$ Å) in solution but in the solid state is an elongated H_2 complex ($d_{HH} = 1.11$ Å) due to Ir–Cl···H–Ir hydrogen bonding, illustrating the hypersensitivity of d_{HH} to both intra- and intermolecular effects.[41] Although the ligand *trans* to H_2 generally influences the activation of H_2 more than the *cis*-ligands, the isomers of electron-poor $Cr(CO)_4(PMe_3)(H_2)$ have similar J_{HD} (~34 Hz) and hence d_{HH} near 0.86 Å whether the H_2 is *trans* to CO or to PMe_3.[25a]

There is little H–H bonding interaction remaining for $d_{HH} > 1.1$ Å,[38,38a,38b] so at what point is the bond "broken?" Theoretical analyses suggest 1.48 Å, that is, twice the normal length.[42] Calculations also show that the energy barrier for stretching the H–H bond from 0.85 Å all the way to 1.6 Å is surprisingly low (on the order of one kcal mol^{-1}!) in certain "elongated" H_2 complexes, e.g. $[OsCl(H_2)(dppe)_2]^+$.[38,38a,38b] The H_2 molecule is extremely delocalized about Os, where the H atoms undergo large amplitude vibrational motion along the reaction coordinate for H–H breaking and also librate/rotate about the M–H_2 axis at a slower rate. Remarkably d_{HH} is both temperature and isotope dependent in $[CpM(diphosphine)(H_2)]^{n+}$ (M = Ru, Ir; $n = 1$, 2) type species with elongated H_2.[43,43a] These phenomena illustrate the amazing dynamic properties of η^2-H_2, which can even exhibit quantum mechanical behavior such as rotational tunneling[18] and quantum mechanical exchange coupling.[44]

Cis-interactions[5,45] play an important role as the nascent interaction in intramolecular hydrogen exchange processes (Scheme 2), which can be extremely facile. The intermediate is essentially a trihydrogen complex, which was initially proposed by Brintzinger as the key species in this direct hydrogen transfer process.[46] The possible existence of η^3-H_3 ligands has been examined theoretically by Burdett in his detailed studies of polyhydrogen species, H_n ($n = 3$–13).[47,48,48a] A trihydrogen complex has yet to be isolated, although there is experimental evidence for its intermediacy in a facile tautomerization process in $ReH_2(H_2)(CO)(PR_3)_3$ (Equation (4)).[49]

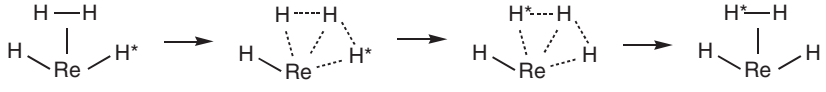

(4)

The $ReH(H_3)$ species is estimated to be no more than 10 kcal mol^{-1} less stable than the $ReH_2(H_2)$ complex. The H_3^- ligand is analogous to the π-allyl ligand in charge distribution and bonding properties (Scheme 2), illustrating a remarkable parallel between σ-bond coordination and π-bond coordination.[2a] OA to a trihydride would also produce exchange, but this is a much higher energy path as shown in *ab initio* calculations on $[FeH(H_2)(PR_3)_4]^+$ systems where experimentally H/H_2 scrambling is fast even at −140 °C.[50,51] A well-studied case is $IrClH_2(H_2)(P^iPr_3)_2$ where neutron scattering and solid-state ^1H NMR studies showed barriers of only 1.5 kcal mol^{-1} for hydrogen exchange, remarkably low for a solid-state process involving considerable structural rearrangements at less than 77 K.[52,53] The essential features of fluxionality among hydride and H_2 ligands are well reviewed by Gusev and others.[5,10b,54] More recent studies include H_2/hydride interchange in $[Cp_2MoH_3]^+$ and *ansa*-bridged analogs.[55,56]

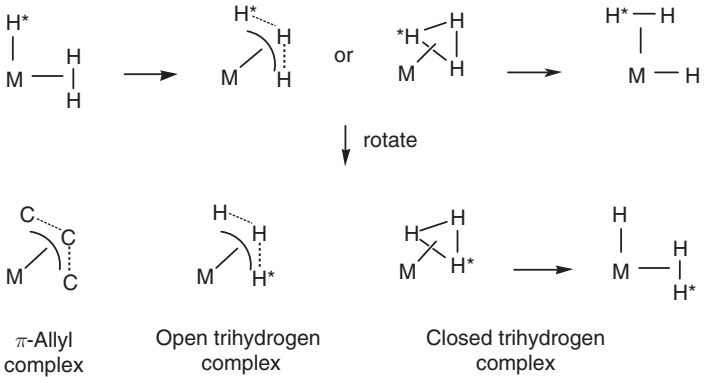

Scheme 2

1.24.2.3 Heterolytic Cleavage of Coordinated H–H

There are two distinct paths for cleavage of H–H (and X–H) bonds: homolysis to a dihydride (as above) and heterolysis, that is, breaking the H–H bond into H^+ and H^- fragment.[57–59] Both paths have been identified in catalytic hydrogenation and are available for other σ-bond activations. A proton can split off from the H_2 and migrate to either an external Lewis base (intermolecular) or a ligand/anion (intramolecular) as in Scheme 3.

On electron-poor cationic complexes, the H_2 ligand is highly acidic, that is, polarized toward $H^{\delta+}$–$H^{\delta-}$ where the highly mobile H^+ readily transfers. Free H_2 is an extremely weak acid with a pK_a near 35 in THF, but when H_2 is bound to a highly electrophilic cationic M, the acidity of H_2 gas can be increased spectacularly, up to 40 orders of magnitude. The pK_a of H_2 can become as low as −6 and the acidity of η^2-H_2 is as strong as that of sulfuric or triflic acid.[10b,10g,60] "Intramolecular" heterolysis involves proton transfer to a *cis*-ligand L (e.g., H or Cl) or to the counter-anion of a cationic complex. "Intermolecular" heterolysis involves protonation of an external base B to give a metal hydride (H^- fragment) and the conjugate acid of the base, HB^+, that is, the reverse of the protonation reaction used to synthesize H_2 complexes (all reactions in Scheme 1 can be reversible). Intramolecular heterolysis is related to "σ-bond metathesis" processes that can occur on less electrophilic M, especially d^0 systems (Equation (5)).[3,5]

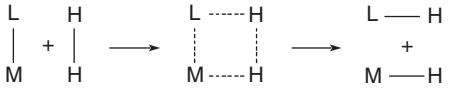

(5)

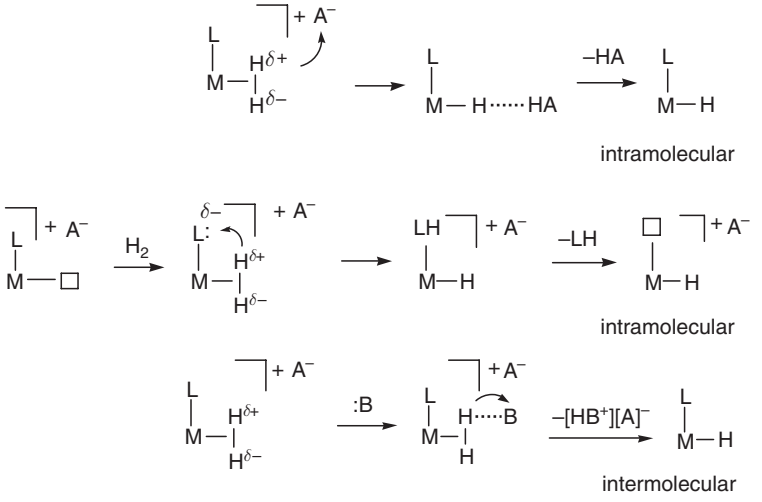

Scheme 3

Electron-deficient cationic and dicationic H_2 complexes with short d_{HH} (<0.9 Å) such as $[Cp^*Re(H_2)(CO)(NO)]^+$ and $[Re(H_2)(CO)_4(PR_3)]^+$ are among the most acidic complexes.[61,62] Positive charge and electron-withdrawing co-ligands such as CO, particularly when *trans* to H_2, greatly increase the acidity. An example of charge effect is provided by $W(CO)_3(PCy_3)_2(H_2)$, which is deprotonated only by strong bases but can be oxidized to $[W(CO)_3(PCy_3)_2(H_2)]^+$ that now can protonate THF.[63] Crabtree first demonstrated heterolysis of η^2-H_2 as in Scheme 3 by isotopic labeling studies to show that H_2 in $[IrH(H_2)(benzoquinoline)(PPh_3)_2]^+$ is deprotonated by LiR in preference to the hydride.[64] A milder base, NEt_3, specifically deprotonates the η^2-H_2 tautomer in an equilibrium mixture of $[CpRuH_2(dmpe)]^+$ and $[CpRu(H_2)(dmpe)]^+$, demonstrating the "greater kinetic acidity of the H_2 ligand than hydride."[65]

Intramolecular heterolysis of H_2 with elimination of HX is commonly observed under homogeneous conditions (Equation (6)).[66,67]

$$L_nMX + H_2 \rightarrow L_nMX(H_2) \rightarrow L_nMH\ [\text{or } L_nMH(H_2)] + HX \tag{6}$$

This is useful for preparative and catalytic chemistry, for example, a metal halide can be converted to a hydride in the presence of base or under phase-transfer or high-pressure conditions. Reversible proton transfer to pendant basic sites can also occur (Equation (7))[68] and is facilitated by hydrogen bonding interactions, for example, Equation (8) where the OH and IrH hydrogens scramble via rotation of the H_2 ligand.

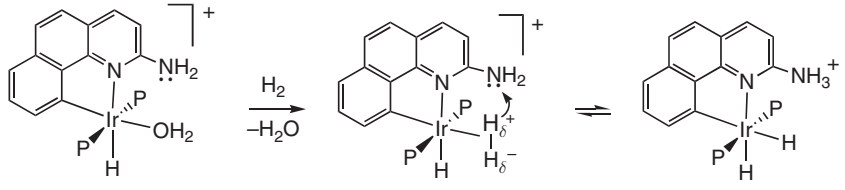

(7)

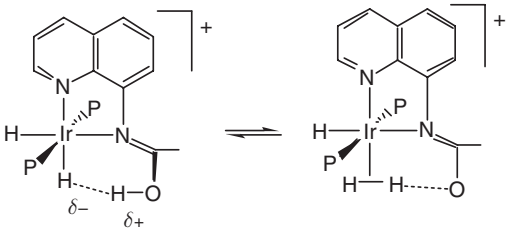

(8)

The H···H interactions (1.75–1.9 Å) in Equation (8) represent "unconventional hydrogen bonding" often referred to as "proton-hydride bonding" or "dihydrogen bonding" and include M–H···H–M′, M–H···H–X, and X–H···σ-interactions (X = C, N, P, O).[69–71,71a] These complexes represent intermediates in H_2 heterolysis and illustrate the basicity of the M–H bond and the acidity of η^2-H_2. H_2 heterolysis related to Equation (7) also occurs via proton transfer to nitrogen on dicationic TpRu complexes containing phosphinoamine ligands.[72]

Intermolecular heterolysis of H_2 is exemplified by the protonation of ethers by cationic electrophilic H_2 complexes often containing electron-withdrawing CO (Equations (9) and (10)).[73,74]

$$M-H + H^+ \rightarrow [M-H_2]^+ \xrightarrow{Et_2O} [M_2(\mu\text{-}H)]^+ + Et_2OH^+ + H_2 \quad M = Cp^*Ru(CO)_2 \tag{9}$$

$$[M'-CH_2Cl_2]^+ + H_2 \rightarrow [M'-H_2]^+ \xrightarrow{Pr_2O} [M'_2(\mu\text{-}H)]^+ + Pr_2OH^+ + H_2 \quad M' = Re(CO)_4(PR_3) \tag{10}$$

Hydride-bridged complexes often form even though the mononuclear hydride is known. A crucial initial step in heterolysis of σ-bonds is generation of a complex with either an unsaturated site or one occupied by a labile ligand, for example, H_2O in Equation (7) or CH_2Cl_2[74] as will be shown below.

1.24.2.4 Reactions of H_2 Complexes Relevant to Catalysis

1.24.2.4.1 Direct transfer of hydrogen from H_2 ligands

Dihydrogen complexes are now well-established catalysts or catalyst precursors for many chemical conversions, some of which lie at the interface between homogeneous and heterogeneous catalysis.[10h] A key question is whether η^2-H_2

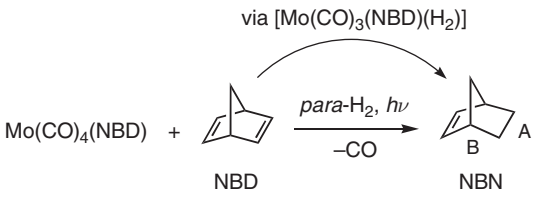

Scheme 4

"directly" transfers H atoms to substrates such as olefins (Equation (11)), that is, without the need for cleavage to the dihydride.

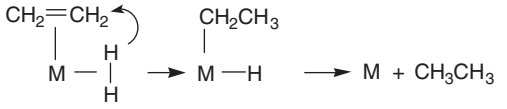

(11)

Proved examples, which can be viewed to involve initial intramolecular heterolysis of an H_2 ligand, are rare. Unstable but IR-detectable species such as $M(CO)_4$(norbornadiene)(H_2) are proposed intermediates for photocatalytic hydrogenation of norbornadiene to norbornene and nortricyclene involving direct reaction of H_2 ligands.[75–77] Evidence for direct transfer of η^2-H_2 to co-bound substrates is limited, but parahydrogen induced polarization (PHIP) provides crucial NMR evidence. The Mo-norbornadiene (NBD) complex in Scheme 4 forms an unstable H_2 complex on photolysis that is proposed to directly transfer H_2 to NBD to form norbornene (NBN).[76]

In situ NMR studies of the photocatayzed reaction show that the nuclear spin polarization from *para*-H_2 is transferred to protons at the A and B positions of the NBN product. This can only occur if the H–H bond in the presumed [$Mo(CO)_3$(NBD)(H_2)] intermediate is not first cleaved to dihydride ligands before the hydrogens are transferred to the coordinated NBD. [$Cp^*Ru(H_2)(NBD)]^+$ also gives intramolecular hydrogen transfer from H_2 to NBD.[77a] James and co-workers provide excellent evidence for a dinuclear H_2 complex transferring both hydrogens to styrene in DMA solution (Scheme 5; DMA = N,N-dimethylacetamide; PP = $Ph_2P(CH_2)_4PPh_2$)).[78]

A T-shaped 14e rhodium(I) complex containing a rigid P–C–P pincer ligand reversibly binds both H_2 and CO_2 and gives net insertion of CO_2 into the H_2 complex (Scheme 6),[79] the first demonstration of reaction of an H_2 complex with CO_2 and one of the clearest examples of direct reaction of η^2-H_2.

1.24.2.4.2 Catalytic hydrogenation on electrophilic complexes

Heterolytic activation of H_2 on electrophilic complexes is important in catalytic hydrogenation and dates back 70 years.[57] More recently, electrophilic activation of H_2 has been found to be valuable in "ionic hydrogenation" where a mixture of an organometallic hydride, for example, $CpMoH(CO)_3$, and a strong acid, for example, HO_3SCF_3, reduces sterically hindered olefins to alkanes via protonation to carbocations followed by hydride transfer from the metal hydride.[80,80a] It is likely that an acidic H_2 complex is involved in the proton-transfer step (Scheme 7).

The discovery by the recent Nobel laureate, Ryoji Noyori, of asymmetric hydrogenation of ketones to alcohols catalyzed by *trans*-$RuCl_2$[(*S*)-binap][(*S*,*S*)-dpen] (binap = [1,1′-binaphthalene-2,2′-diylbis(diphenylphosphane)];

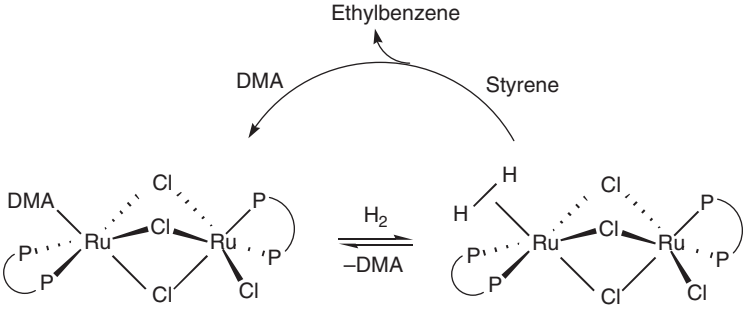

Scheme 5

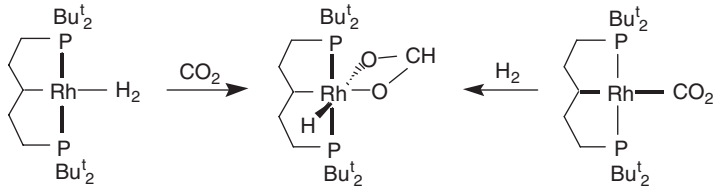

Scheme 6

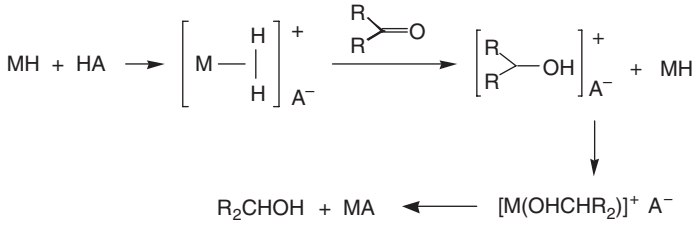

Scheme 7

dpen = diphenylethylenediamine) is one of the best examples of catalysis employing heterolysis of H_2.[81,81a] The reaction is quantitative within hours, gives enantiomeric excesses up to 99%, and shows high selectivity for carbonyl over olefin reduction. The non-classical bifunctional process involves ligand-assisted heterolytic splitting of H_2 to form a catalytically active Ru hydride as a key step (ligand-assisted heterolysis of the type M(amide) + H_2 → MH(amine) was found by Fryzuk[82,82a]). Similar heterolyses of H_2 ligands have been shown or proposed by Morris and others to be the critical step in the mechanism of related hydrogenations.[83,83a–83e] Calculational and experimental evidence suggests that heterolysis of a dihydrogen complex is key and is facilitated by alcohols, underscoring the importance of alcohol-containing solvents in promoting heterolysis of H_2 in metal bifunctional catalysis.[83d,83e]

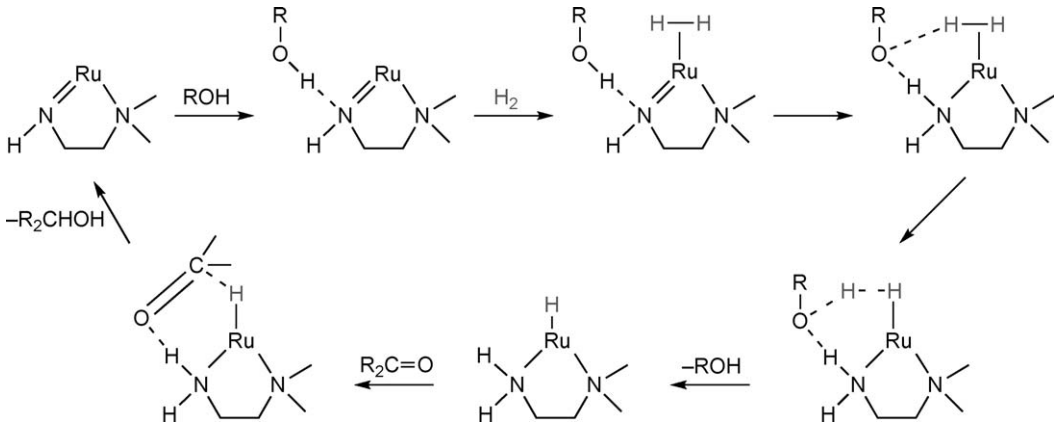

Heterolytic activation of H_2 can also trigger hydrogenolyses of C–F bonds on cationic Ir complexes with piano stool geometry (Equation (12)).[84,84a]

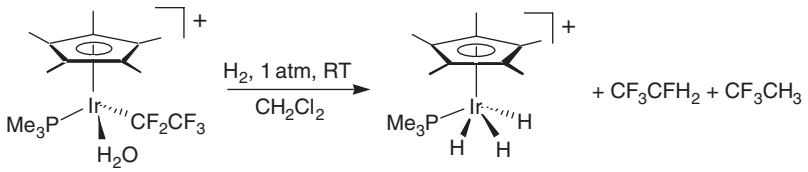

(12)

H_2 is proposed to displace H_2O and transfer a proton to an α-fluorine to eliminate HF and form a carbene ligand that is then hydrogenated to give fluorohydrocarbon products. Heterolysis of H_2 is also a key step in hydrogenation of CO_2 to formic acid in water catalyzed by $[(\eta^6\text{-}C_6Me_6)Ru(bipy)(H_2O)]SO_4$.[85]

1.24.2.4.3 Hydrogenation catalyzed by H_2 complexes in a precursor role

Many catalytic and stoichiometric reactions access H_2 complexes as "precursors."[10b,10d,10h,86] In the above examples of direct H_2 ligand reactions, open coordination sites for catalysis were often created by unusual rearrangements or dissociations. However, the presence of a hydride in addition to labile η^2-H_2 allows a straightforward path, and several catalysts possess $MH(H_2)$ (Scheme 8). The loss of H_2 opens a site for binding of unsaturated substrates, which in most cases are alkynes, alkenes, or ketones. The H_2 complex functions as a reservoir of unsaturation, stabilizing the catalyst system against decomposition. Catalysts include both neutral and cationic systems with labile H_2 such as $OsHCl(H_2)(CO)P_2$, $RuH_2(H_2)P_3$, $RuH_2(H_2)P_2$, $[MH(H_2)P_4]^+$ (M = Fe, Ru, Os), $[IrH_2(H_2)P_3]^+$, and $Tp^*RuH_2(H_2)$. Patented processes include hydrogenation of nitriles and nitro compounds catalyzed by $RuHCl(H_2)(PCy_3)_2$.[87,87a,87b] The versatile bis-H_2 complex, $RuH_2(H_2)_2(PCy_3)_2$ **1**, the chemistry of which has been reviewed,[30,30a] catalyzes a variety of reactions, for example, hydrogenation of arenes and the activated alkene, dimethylfumarate.[88] Reaction of **1** with ethylene leads to dehydrogenation of a Cy group on the phosphine to give **2** containing a cyclohexenyl group (Scheme 9).[89] This unusual species is a highly efficient catalyst for selective dehydrogenative silylation of ethylene into the vinylsilane $CH_2{=}CHSiEt_3$. Compound **1** catalyzes facile addition of ethylene to acetophenone and benzophenone to give mono- and di-addition products, for example, 2,2′-diethylbenzophenone (Murai reaction).[90,91] **1** can be used to prepare ruthenium carbenes used in ring-opening metathesis polymerization (ROMP).[92] ROMP followed by hydrogenation gives polyolefins inaccessible by other means.[93] The Grubbs-type catalyst, $RuCl_2(=CHPh)(PCy_3)_2$, readily transforms into potentially interconvertible dihydride, dihydrogen, and hydridochloro species under H_2. $OsHCl(H_2)(CO)(P^iPr_3)_2$ is a very active, selective catalyst for silylation of acetylenes (Equation (13)).[94]

$$HSiEt_3 + PhC{\equiv}CH \xrightarrow{60^\circ C} PhHC{=}CH(SiEt_3)(\text{trans- and cis-isomers}) \qquad (13)$$

η^2-H_2 and/or η^2-Si–H complexes could be relevant here, and the isolated complex $Os(SiEt_3)Cl(H_2)(CO)(P^iPr_3)_2$ is proposed to be an intermediate.

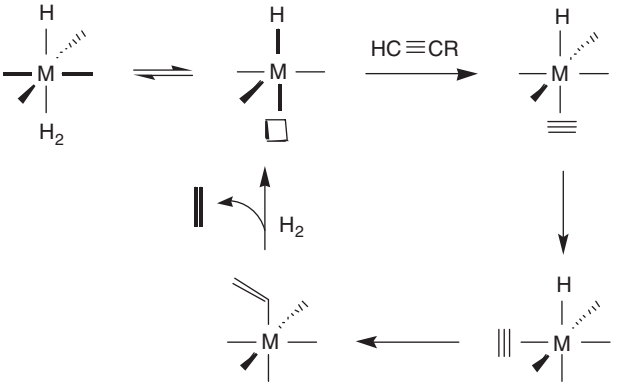

Scheme 8

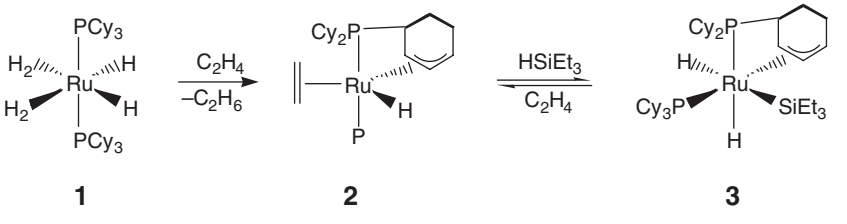

1 **2** **3**

Scheme 9

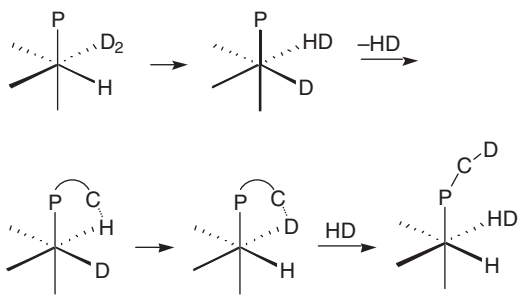

Scheme 10

1.24.2.4.4 Catalysis of isotopic exchange by H_2 complexes

Hydrogen-containing systems readily lend themselves to isotopic substitution by deuterium and tritium. Scrambling of H_2 and D_2 to form HD is often facile and can even occur over 18e H_2 complexes such as $W(CO)_3(PR_3)_2(H_2)$ even in the solid state at 1 atm.[20,95] The mechanism is enigmatic because there is ostensibly only one labile coordination site. Another remarkable solid–gas reaction is deuterium incorporation into the PMe_3 ligands of $[Fe(D_2)H(PMe_3)_4]^+$ (Scheme 10), which may involve agostic interactions where associative (σ-bond metathesis) or dissociative C–H bond activation occurs.[51]

Deuteration of alkyl groups under such mild conditions is rare. Exchanges involving deuterated solvents is also facile, for example, reaction of acetone-d_6 and $[RuCl(dppe)_2(H_2)]^+$ or $[OsH(H_2)(PP_3)]^+$ gives the HD isotopomer in 20 min and full deuteration of the H/H_2 ligands in hours.[67,96]

1.24.2.4.5 Dihydrogen binding on surfaces and in heterogeneous catalysis

Molecular binding of H_2 to solid materials and catalysts such as metal surfaces and small metal clusters is rare since formation of metal hydrides is favored. H_2 is observed by electron energy loss spectroscopy (EELS) to bind to a stepped Ni(510) surface containing unsaturated sites but not on the flat Ni(100) surface that lacks the requisite residual unfilled *d* states.[97,97a] Undoubtedly, such H_2 binding is the first step in H_2 dissociation on many other surfaces that form hydrides, for example, as similarly shown for Ni(111), Ni(100), Ni(110), and Pd(210).[98,98a] H_2 also ligates in small clusters such as $Cu_3(H_2)$ in Ar matrices,[99] and H_2 binds to similar species for M = Fe, Co, Ni, Pd at low temperature.[3] Monometallic species of these types have been studied by Andrews for many transition metals, including gold.[100]

Transition metal oxides, sulfides, and zeolitic materials are vital in many heterogeneous catalytic processes involving H_2 such as hydrotreatment of crude oils. Many oxides adsorb and activate H_2, including Cr_2O_3, Co_3O_4, V_2O_3, MnO, MgO, ZnO, and alumina even at 25 °C, some of which could have molecular binding. $(\eta^2\text{-}H_2)CrO_2$ and $(\eta^2\text{-}H_2)_2CrO_2$ have indeed been prepared by co-condensation of CrO_2 molecules with H_2 in argon at 11 K and photoisomerized to HCrO(OH), ostensibly via H_2 heterolysis.[101] Computational versus experimental studies of oxide surfaces relevant to heterogeneous catalysis have been reviewed.[102] $RuO_2(110)$ has recently been found to also bind H_2 non-dissociatively at 85 K ($\nu_{HH} = 2960\,cm^{-1}$).[103] Calculations indicate that $\delta_{HH} = 0.89$ Å and that the H_2 is 1.8 Å from the Ru atoms (cf. 0.94 Å and 1.81 Å respectively in *trans*-$RuH(H_2)(Ph_2PC_2H_4PPh_2)_2$[104]). These data suggest that, as for H_2 on Ni surfaces, the binding of H_2 to Ru is similar to that in organometallics. Metal sulfides also similarly activate H_2.[105,105a,105b] Hydrodesulfurization (HDS) catalysts vital to the petroleum industry contain sulfides, typically MoS_2.[105b] H_2 reacts with organometallic sulfides to give SH complexes that show exchange behavior (Equations (14) and (15)).[106–108]

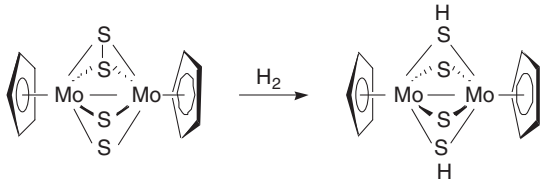

(14)

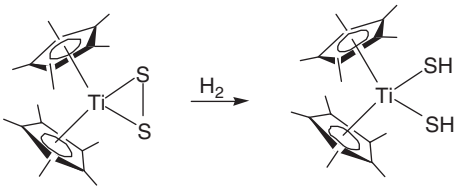

(15)

Although the mechanism of Equation (14) is unknown,[106] a four-center S_2H_2 transition state or a reduction coupled with proton transfer as in metalloenzymes can be envisioned. Activation of H_2 could be "sulfide ligand-based" in certain biological and industrial catalyst systems. Heterolysis of H_2 at the metal can directly be observed in thiolate complexes (Equation (16)).[109]

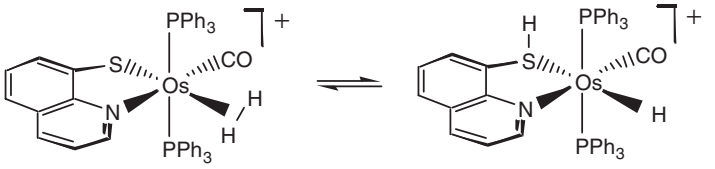

(16)

Zeolitic materials are also well utilized in catalysis and can bind H_2 molecularly.[110–111] Adsorption of H_2 onto the extraframework iron species in Fe-ZSM5 has been found to occur at 110 K where H_2 is strongly bound to Fe much as in H_2 complexes.[110] Research at the interface between heterogeneous and homogeneous catalysis[10h] includes employing H_2 interactions as probes for the catalytic binding sites in both regimes.[112–114] Heterogenization of the Rh(I) catalysts (sulfos)Rh(cod) and (sulfos)Rh(CO)$_2$ [sulfos = $-O_3S(C_6H_4)CH_2C(CH_2PPh_2)_3$; cod = cycloocta-1,5-diene] via controlled adsorption on partially dehydroxylated high surface area silica gives a grafted catalyst, (sulfos)Rh(cod)/SiO_2, active for alkene hydrogenation and hydroformylation.[112] Another example is the demonstration that complexes such as Ir(CO)Cl(PPh$_3$)$_2$ can catalyze *ortho–para* nuclear spin conversion of H_2 and hydrogenation of unsaturated compounds in both solution and in the solid state (as crystallites).[115]

1.24.2.4.6 Bioactivation of hydrogen in metalloenzymes

The intramolecular proton transfer from bound H_2 to sulfide or other Lewis-basic sites is a key step in the function of active sites in the metalloenzymes hydrogenase (H-ase) and possibly nitrogenase. H-ases are redox enzymes in microorganisms that catalyze interconversion of H_2 and protons to either utilize H_2 as an energy source or dispose excess electrons as H_2 (Equation (17)).[116,116a]

$$H_2 \rightleftharpoons 2H^+ + 2e^- \tag{17}$$

Biologically unprecedented CO and CN ligands are present in the dinuclear active site[117] of iron-only H-ases that are remarkably organometallic-like and presumably transiently bind and heterolytically split H_2, most likely at an octahedral site *trans* to bridging CO.[3,116,116a]

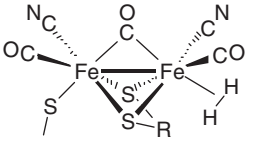

Even before H_2 complexes were isolated, heterolysis of a transient M–H_2 complex was proposed to occur in H-ases.[118,119] Catalysis of isotopic exchange of D_2 and water by H-ases and their models is consistent with H_2 heterolysis,[120] which would be favored by an active site with a mixture of CN donor and CO acceptor ligands. The strong *trans*-influence of CO favors reversible H_2 binding and heterolysis via proton transfer to proximal basic sites, for example, sulfido ligands and possibly amine functionality[116a] in the bridging R group.[3] Such intramolecular heterolysis occurs in organometallic complexes, for example, in Equations (7) and (16), and has recently been shown on an Fe complex with a pendant nitrogen base.[121] The first H_2 complex of a H-ase model, [Ru$_2$(μ-H)(μ-$S_2C_3H_6$)$_2$(H_2)(CO)$_3$(PCy$_3$)$_2$]$^+$, has recently been reported, albeit with Ru instead of Fe.[122] There is strong potential for H_2 fuel production via biomimetic chemistry based on H-ase.

Efforts to mimic the enigmatic structure and function of nitrogenases have been in progress for over 40 years in regard to producing ammonia or other nitrogen compounds from N_2.[123] An important feature of nitrogenase is that it also catalyzes isotopic exchange of D_2 and water, which occurs only in the presence of N_2. Sellmann and co-workers have studied model systems consistent with "N_2-dependent HD formation" where heterolysis of H_2 occurs on sulfur ligands.[124,124a] Other modeling studies have shown that protons can be transferred from acidic H_2 ligands in cationic Ru–H_2 complexes to N_2 ligands in $W(N_2)_2(P)_4$ complexes, in some cases forming ammonia (Equation (18)).[125,126]

$$cis\text{-}\left[W(N_2)_2(PMe_2Ph)_4\right] + trans\text{-}\left[RuCl(H_2)(dppe)_2\right]^+ \xrightarrow[55\,^\circ C,\ 24h]{H_2} NH_3 \qquad (18)$$

Heterolysis of H_2 was proposed to occur at Ru via nucleophilic attack of coordinated N_2 on bound H_2 where the bound N_2 is protonated and a hydride remains at Ru. Only a limited number of reactions of bound N_2 or nitride with H_2 are known,[123,127,127a,128,128a,128b] for example, Equation (19) which slowly occurs for a dinuclear Zr complex capped by macrocyclic ligands.[123,127,127a]

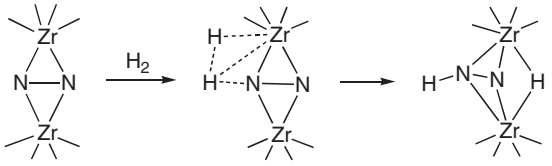

(19)

However, the reaction stopped at the stage of N_2H and no NH_3 was formed. Chirik recently found NH_3 is produced on reaction of H_2 with a similar μ-N_2 complex containing two methyl-substituted Cp ligands on each Zr.[128] Remarkably, side-on N_2 bonding and NH_3 production occurred only upon a seemingly insignificant change from pentamethylated to tetramethylated Cp ligands. A related hafnocene system hydrogenated the N_2 ligand but did not produce NH_3.[128a] Heterolysis of H_2 also occurs on an Fe(μ-N)Fe species to form Fe(μ-NH) (μ-H)Fe species, but NH_3 was not seen.[128b]

1.24.3 Silane σ-Complexes

1.24.3.1 Synthesis, Structure, and Properties of Silane Complexes

By analogy to H_2, hydrosilanes (R_3Si–H) can bind to M to form stable σ-complexes through Si–H bonds to give three-center two-electron M(η^2-Si–H) bonding (Equation (20)).

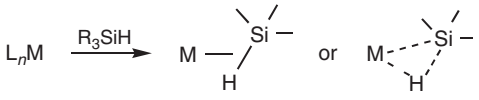

(20)

A major difference is that M–H–Si and M–H–X linkages are asymmetric, that is, look like hydride-bridged systems with M–H–Si near 90°. The bonding and activation of hydrosilanes have been extensively reviewed.[3,10c, 10f,129,129a,130,130a,130b] Theory supports a similar bonding picture for silane and H_2 complexes, although the Si–H bond is both a better σ-donor and a better π-acceptor than H–H (and especially C–H). Metal–silane bond energies can be larger than that for analogous M–H_2 (24 kcal mol^{-1} in (benzene)$Cr(CO)_2(HSiEt_3)$, cf. 17 kcal for the H_2 adduct and 21 kcal mol^{-1} for the THF adduct).[131,131a] Historically, the first silane complexes were reported by Graham and co-workers in 1969.[132,132a,132b] However the bonding was not immediately perceived to be non-classical in the clear-cut manner of M–H_2, and the true σ-complex nature was revealed only by a prolonged series of investigations by several researchers. Excellent accounts are given by Schubert,[129] who extensively studied $CpMn(CO)_2(\eta^2$-$HSiR_3)$ complexes, and Graham.[132b]

Silanes with multiple Si–H bonds usually coordinate through only one Si–H bond. The Si–H bond is activated toward cleavage remarkably similarly to H–H, and tautomeric equilibria can exist with the OA product in a system featuring the first example of a SiH_4 complex (see below).[133]

The Si–H bond, which is about twice as long as H–H, elongates on coordination to the same relative extent as H–H, and the energetics of binding, cleavage, and exchange with *cis*-hydrides are also similar. This would not have been expected based on the large difference in steric and electronic factors. H–H and Si–H bonds can simultaneously coordinate, as in $RuH_2(\eta^2$-$H_2)(\eta^2$-$SiHPh_3)(PCy_3)_2$.[33,33a,33b] The binding and activation of Ge–H and Sn–H bonds in

germanes[134] and stannanes[135] are also directly analogous to Si–H. The general principles of H–H activation can be applied to activation of all σ-X–H bonds. Silane complexes also model yet to be isolated alkane and methane complexes.

As for H_2 complexes a near continuum of degrees of "arrested" bond activation can exist, and the question of "where to draw the line in defining a molecular structure" has been addressed by Bader using the theory of atoms in molecules (AIM).[130b] The effects of variation in M/L sets can be similar to that for H_2 complexes, for example, $CpMn(CO)_2(HX)$ is a σ-complex for both X = H and SiR_3 while $CpRe(CO)_2(H)(X)$ is classical because of better BD from Re. Variations in the R substituents on Si can drastically affect Si–H activation regarding both homolysis and heterolysis. Electron-withdrawing R groups on $HSiR_3$ such as Cl promote OA to $MH(SiR_3)$ presumably because they lower the Si–H σ^* orbital energy, favoring increased BD. Conversely, donor substituents such as alkyls favor σ-coordination. Metal–silane interaction and activation can be finely tuned in several ways, leading at times to seemingly counterintuitive behavior, and unusual "interligand hypervalent interactions," M–H···SiX, can exist in some systems.[130a,136]

At least a dozen types of structures possess M(η^2-Si–H) interactions (Figure 2). Unlike H_2 complexes, about one third are dinuclear, although many contain α-agostic interactions similar to α-agostic C–H interactions.[8,8a–8e] Structure **XII** where X = P is directly analogous to that for M···H–C agostic interactions of phosphine organo groups. These types of interactions should be differentiated from those in **V**, **VIII**, and **IX**, which are true σ-complexes (silanes held to M "only" by 3c2e M–Si–H interaction). Whereas cationic H_2 complexes are common, cationic silane complexes are only rarely isolable because of facile Si–H heterolysis (see below). σ-silane complexes can be prepared by addition of silane to agostic, H_2, solvento, or 16e complexes (e.g., generated by dissociation of CO

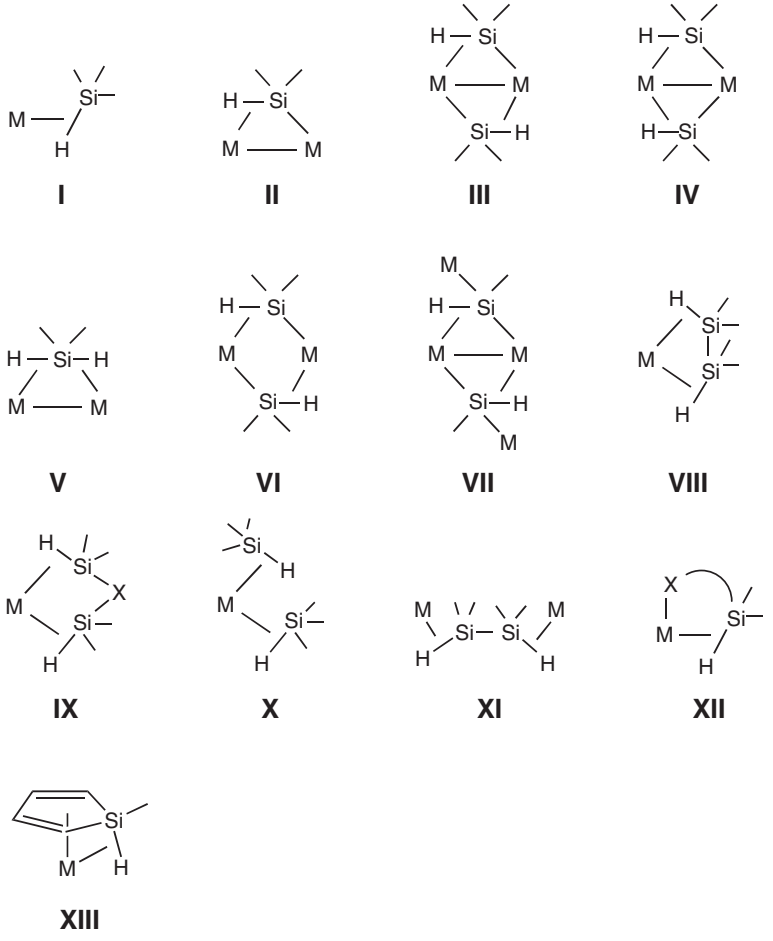

Figure 2 Structures of Si–H bond interaction with metal centers.

from $CpMn(CO)_3$). Reported d_{SiH} vary from 1.43–2.2 Å, compared to the average Si–H distance in free silanes, 1.48 Å. J_{SiH} in silane σ-complexes range from 22–80 Hz versus <20 Hz in silyl hydrides and ca 200 Hz in free silanes and are usually closer to those in OA products, that is, more analogous to J_{HD} in elongated H_2 complexes. Thus J_{SiH} does not correlate well with d_{SiH} or even the extent of OA.[3,129a] As for H_2 complexes, silane complexes are known for all group 5–10 metals, plus a group 4 complex,[137] $Cp_2Ti(SiH_2Ph_2)(PMe_3)$. Substitution of two *cis*-H_2 produced the first structurally characterized chelating bis-silane systems, $RuH_2[(SiHMe_2)_2X](PCy_3)_2$ (Equation (21)).[138,139]

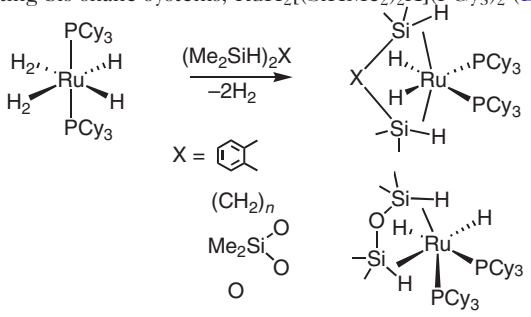

(21)

The bis(silane) ligand is strongly bound (d_{SiH} = 1.73–1.84 Å; cf 1.49 Å in the free disilanes) and cannot be displaced even by CO for X = C_6H_4. However for X = O, where the η^2-Si–H are *cis*, the opposite is true despite the fact that J_{SiH} is very low, 22 Hz, seemingly indicative of stretched Si–H.

The first stable SiH_4 complexes, $Mo(SiH_4)(CO)(PP)_2$ (PP = diphosphine), are important models for CH_4 binding/activation (Equation (22)).[133] Heating removes silane, which is bound more tightly than H_2 here. The η^2-coordination of one Si–H bond is confirmed by J_{SiH} = 35 and 50 Hz for R = Et (depe) and Ph respectively. X-ray studies did not locate the H atoms on the Si, but the coordination about Mo is similar to that in *cis*-$Mo(\eta^2$-H-$SiH_2Ph)$ (CO) $(depe)_2$,[140] where the H's were located. The bonding of only one Si–H bond in solid $Mo(SiH_4)(CO)(depe)_2$ is confirmed by IR, which shows three bands for terminal Si–H (2047, 1995, 1972 cm^{-1}) and one for the Mo–H–Si stretch at 1732 cm^{-1}. This pattern is similar to that for an analogous GeH_4 complex[134] and suggests that CH_4 probably also coordinates in η^2-H–C fashion. However the difference in electronegativity between Si and C and the consequent higher degree of BD to Si–H may invalidate direct comparison. Ge–H bonds undergo OA much more easily than Si–H, and in general, the ease of OA of H_2 is between that of germanes and silanes.[134] OA of C–H bonds is by far the least facile.

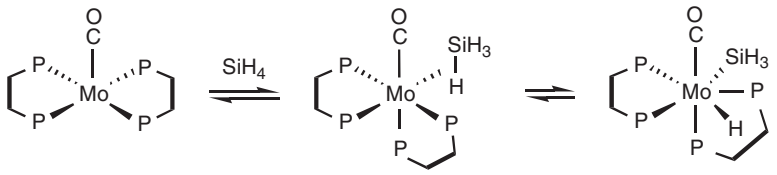

(22)

A novel μ-SiH_4 species shows coordination of all four Si–H,[141] which are quite elongated (1.69–1.73 Å). The d_{RuSi} (2.1875(4) Å) is among the shortest seen, even shorter than that in the silylene $[Cp^*(PMe_3)_2Ru{=}SiMe_3]^+$ (2.238(2) Å[142]) and is a consequence of the multiple σ-interactions. Such "trihapto" coordination of Si–H bonds in H_2SiR_2 to one metal has now been observed in a mononuclear Fe(II) hydride complex containing a tripodal tris(phosphino)borate ligand.[142a]

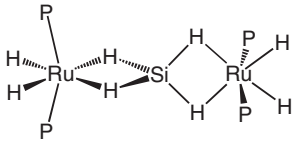

1.24.3.2 Reactions and Heterolytic Cleavage of Silane Complexes

Reactions of hydrosilanes have been reviewed[3,129a] and only major points concerning σ-silane complexes will be addressed. Hydrosilylation is directly analogous to hydrogenation, and the mechanisms are presumably the same.[143]

σ-bond metathesis and hydrogen transfer/exchange processes can also occur where SISHAs interactions reduce the barriers to such processes much as for H/H_2 exchanges above.[33] Chaudret has studied σ-ligand substitution mechanisms involving silanes and boranes, primarily for M = Ru(Equation (23)).[33a,33b]

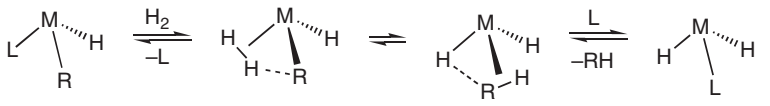

R = Si (H, B, C, etc.) (23)

The weak SISHA-type interactions (Si···H = 2.0–2.5 Å) play an important role as their breaking is responsible for the most energetically demanding step. They allow smooth variations leading to the formation of new σ-bonds without the necessity of decoordination of a ligand, which can be critical in catalytic reactions.

As for η^2-H_2, direct reaction of η^2-silane with a substrate is not well proven but is conceivable, especially in heterolysis processes which are very facile in cationic silane complexes. The electropositive Si (polarized $Si^{\delta+}$–$H^{\delta-}$) is highly activated toward elimination of a highly electrophilic silylium cation, R_3Si^+, that can abstract OH^- from trace water and fluoride from anions such as SbF_6 (Equation (24)).[144,145]

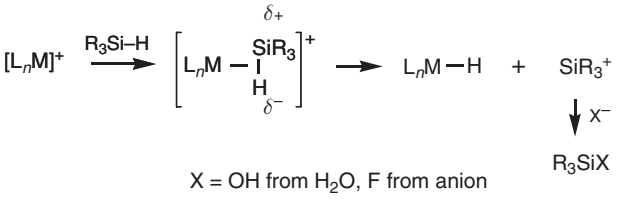

X = OH from H_2O, F from anion (24)

As initially proposed by Luo and Crabtree[144] and supported computationally, the cleavage is likely to be concerted, that is, the nucleophile attacks bound Si (Equation (25)).

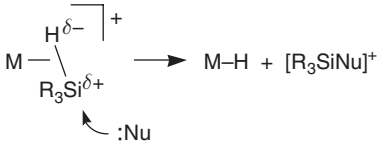

(25)

Silanes and H_2 generally have parallel reactivity, and silanes react with N_2 and sulfide ligands much like H_2 in Equations (15) and (19). 16e $[Re(NO)_2(PR_3)_2][BAr_F]$ ($BAr_F = [B\{C_6H_3(3,5\text{-}CF_3)_2\}_4]^-$) heterolytically cleaves both $SiHEt_3$ (Scheme 11) and H_2.[146] This is a rare case of silane heterolysis on a seemingly electron-rich species (formally d^8 Re^{-I}), although the strong π-acceptor NO increases the electrophilicity of the complex. Heterolysis of Et_3SiH in highly electrophilic *cis*-$Re(CO)_4(PR_3)(\eta^2\text{-}HSiEt_3)][A]$ (R = Ph, Cy) (Scheme 12)[147] is analogous to H_2 heterolysis,[74] and both produce a hydride-bridged dimer.

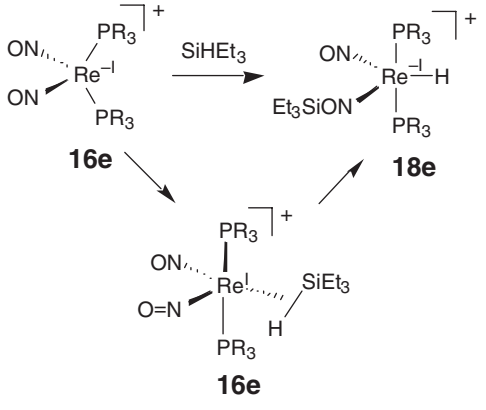

Scheme 11

A variety of Si species result from attack on the anion, and $(Et_3Si)_2O$ also forms from reaction of Et_3Si^+ with trace water (or nucleophilic attack of H_2O on bound silane). This is one of the few examples of Si–H heterolysis where the σ-complex was actually observed (by low T NMR) to be an intermediate. Another is $[(NN)Pd^{II}(Me)(\eta^2\text{-H–SiEt}_3)]^+$,[148] where $HSiEt_3$ displaces the pendant OMe on the diimine (Equation (26)).

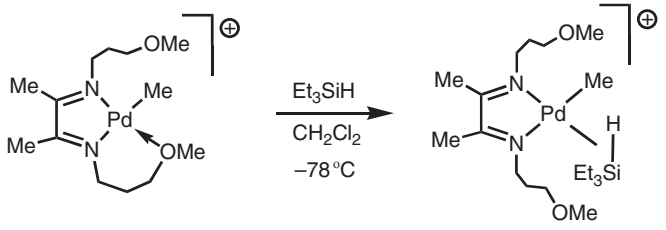

(26)

The complex is thermally unstable and rapidly decomposes to form Pd black and Et_3SiCl and $(Et_3Si)_2O$ initiated by attack on bound Si by solvent and trace H_2O.

The caged phosphite, $P(OCH_2)_3CMe$, is valuable for studies of the binding and electrophilic activation of silanes since it is a stronger acceptor than phosphines and increases metal Lewis acidity. $[Re(CO)_3\{P(OCH_2)_3CMe\}_2(HSiEt_3)]^+$ is a rare example of an isolable cationic silane complex (Equation (27)).[149]

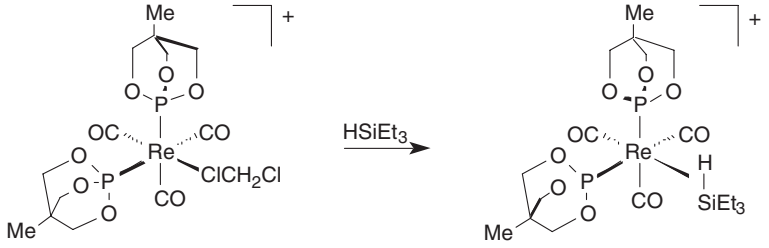

(27)

In contrast the more electrophilic tetracarbonyl, $[Re(CO)_4\{P(OCH_2)_3CMe\}(HSiEt_3)]^+$, and Mn analogs with *trans*-phosphites (see Section 1.24.3.3) give heterolysis of Si–H as in Scheme 12. Another stable cationic silane complex is $[CpRu(PMe_3)_2(HSiCl_3)][BAr_F]$, where an elongated d_{SiH} of 1.77(5) Å, indicates the bound silane is closer to homolysis than heterolysis.[150]

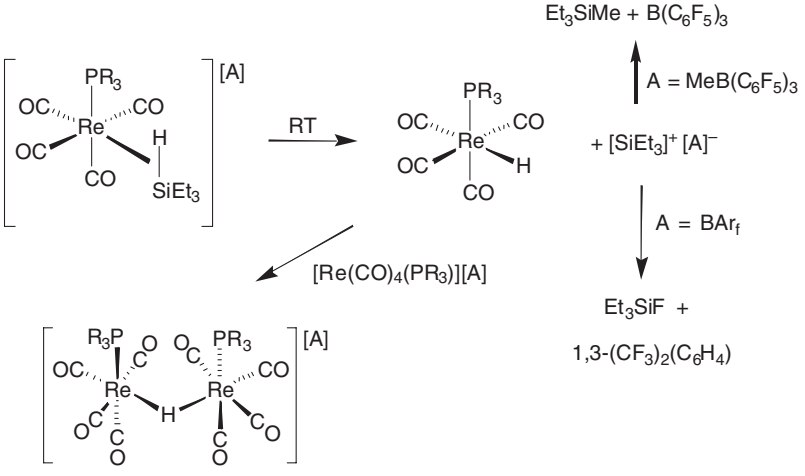

Scheme 12

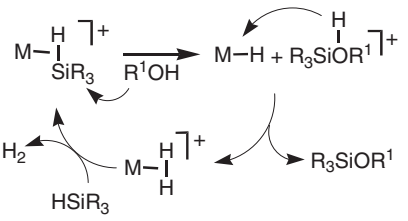

Scheme 13

1.24.3.3 Silane Alcoholysis

Alcoholysis of hydrosilanes (Equation (28)) is important for syntheses of silyl ethers and in protection of reactive OH groups in organic synthesis.[144]

$$R^1{}_3SiH + ROH \rightarrow R^1{}_3SiOR + H_2 \tag{28}$$

When heterolysis of $[IrH_2(\eta^2\text{-}HSiEt_3)_2(PPh_3)_2]SbF_6$ was carried out in the presence of alcohols, catalysis of silane alcoholysis occurred vigorously with high efficiency and selectivity via direct nucleophilic attack by ROH on Si as in Equation (25). $[CpFe(CO)(PR_3)(HSiEt_3)]BAr_F$ observable[151] by NMR at RT also catalyzes silane alcoholysis by phenol with turnover number of $80\,min^{-1}$.[152] Attack of ROH on bound Si was proposed to give a protonated silyl ether that could rapidly protonate M–H to form known $[CpFe(CO)(PR_3)(H_2)]^+$ (Scheme 13). The silane substrate then displaces H_2 to give back the starting silane complex as the rate-limiting step. This mechanism, which involves two different σ-complexes, $M(\eta^2\text{-Si–H})$ and $M(\eta^2\text{-}H_2)$, was supported by calculations showing that heterolysis is highly concerted: transformation of the silane complex to the H_2 complex could take place in a single step, avoiding a transient hydride.[153]

The caged-phosphite complex $[Mn(CO)_3\{P(OCH_2)_3CMe\}_2(CH_2Cl_2)][BAr_F]$ also catalyzes reaction of phenol with triethylsilane, presumably by a mechanism similar to that in Scheme 13 (Equation (29)).[154]

$$HSiEt_3 + PhOH \xrightarrow{Mn\text{–}CH_2Cl_2^+} Et_3SiOPh + H_2 \tag{29}$$

In an NMR tube reaction, ^1H NMR spectra recorded from -80 to $25\,^\circ C$ showed a broad signal at -9.23 ppm presumably due to an H_2 complex formed as an intermediate. After reaction was complete, NMR showed a triplet at -16.75 ppm corresponding to the silane σ-complex (from excess unreacted silane). Manganese carbonyl species such as $Mn(CO)_5(CH_3)$ and $[Mn(CO)_4Br]_2$ are also pre-catalysts for silane alcoholysis[155]and may operate via a similar pathway. Pentacarbonyl chromium(0) silane complexes also catalyze alcoholysis of silanes.[155a]

1.24.4 Alkane σ-Complexes and Relation to C–H Bond Activation

The quest for a stable alkane complex and conversion of light alkanes such as CH_4 in natural gas to liquid fuels, for example, methanol, are grand challenges.[156,157,157a,157b,158] CH_4 is intriguing because it could coordinate using up to three C–H bonds. However, alkanes are very poor ligands since they lack the backbonding ability of, for example, H_2, although form unstable complexes detected spectroscopically and have been shown to be intermediates in C–H cleavage.[156,157,157a,157b,158] "Intramolecular" (agostic) C–H coordination (Figure 1) is common,[8,8a–8e] although stabilized entropically, unlike an alkane σ-complex. Binding of alkanes to 16e fragments such as $Cr(CO)_5$ has been observed in matrices and by flash photolysis.[157,157a,157b,158] M–alkane binding energies are only $\sim 10\,kcal\,mol^{-1}$ versus $>20\,kcal\,mol^{-1}$ in H_2 and most other stable σ-complexes. Nonetheless, the first direct observation by NMR of a metal-alkane complex, $CpRe(CO)_2$(cyclopentane), was reported by Geftakis and Ball[159,159a,159b] in 1998 after $CpRe(CO)_2$(heptane) had been observed by time-resolved IR to have a long lifetime.[160] Key to this was an apparatus where an alkane solution of $CpRe(CO)_3$ at $-80\,^\circ C$ was continuously irradiated with UV light brought into an NMR tube via fiber optics (Equation (30)).

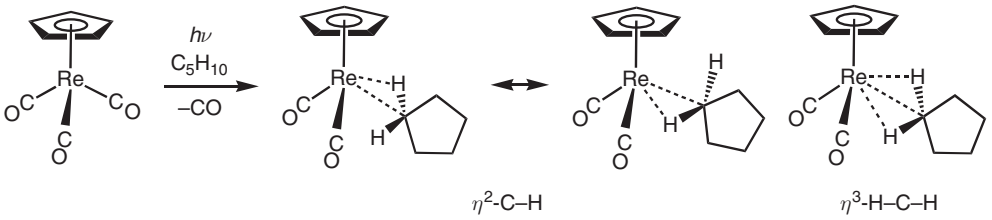

(30)

A high-field ^{1}H resonance at $\delta -2.32$ was assigned to one methylene of the bound cyclopentane and is a first-order quintet with $^3J_{HH} = 6.6$ Hz, consistent with four similar couplings to protons on adjacent carbons. Both protons attached to the same C are involved in binding to Re, where two rapidly exchanging η^2-C–H bonds interact with Re. Alternatively, an η^3-interaction is possible, but later studies of a pentane complex show that, as supported calculationally, binding is primarily through one C–H bond at any one instant.[159a] This bond rapidly exchanges with other bonds in the CH_3 or CH_2 unit that is attached to Re, with a slight preference for methylene C–H. J_{CH} for the bound C–H is 85 Hz versus 132 Hz in the unbound C–H. A related xenon complex was observed in liquid xenon.[159a]

Crystallographic studies of M–alkane interactions were reported for heptane associated with a double A-frame Fe-porphyrin complex[161] and for a cyclohexane–uranium system,[162] although host–guest effects may help hold the alkanes in place (no evidence for interaction in solution). However, crystallographic disorder in the Fe complex and a very long U···C distance prevented definitive characterization as true σ-complexes. Other evidence for alkane and arene binding comes from many sources. Bergman and co-workers have made exquisite use of liquefied rare gas solvents to obtain evidence for the intermediacy of alkane complexes in OA of alkanes by using ultrafast timescale techniques such as TRIR (time resolved infrared) in photolyses of $Cp^*Rh(CO)_2$.[163,163a] The binding affinities of different alkanes were strongly influenced by their size and structure. Larger alkanes interact more strongly with Rh than do smaller ones, and CH_4 does not appear to bind at all in competition with Kr. Ethane binds an order of magnitude less strongly than the longer chain alkanes, and cycloalkanes coordinate better than comparably sized linear alkanes. Similar TRIR evidence for alkane coordination to CpRh(CO) was seen in the gas phase,[164] and binding of alkanes to metal surfaces and CH_4 to Co atoms and monoxides such as FeO has also been seen spectroscopically.[165,165a,165b,165c]

Much of the understanding of C–H activation comes from mechanistic investigations of alkane "RE" from alkyl hydride complexes, the microscopic reverse of the OA, and other indirect signatures.[166,166a–166d,167–174] Several trails of evidence are left by transient alkane (or arene) σ-complexes, including observations that hydrogen exchange takes place between the hydride and alkyl ligands of isotopically labeled M(R)(H) prior to RE. Girolami found that the hydrogens of the alkyl and hydride ligands exchange at a rate sufficient to be dynamic on the NMR time scale.[172] In $[Cp^*Os(dmpm)(CH_3)(H)]^+$ the exchange is fast enough at $-100\,^\circ$C to give NMR signal broadening, but can be halted at $-120\,^\circ$C to give distinct Me and H resonances. This suggests (supported computationally[173]) that a methane complex $[Cp^*Os(dmpm)(CH_4)]^+$ is formed reversibly from the Me/H complex over 100 times per second. The mechanism of alkane RE from Tp′Rh(CNR)(R)H also showed indirect evidence for involvement of alkane complexes.[166,166d] For earlier metals, reaction of anionic $[L_3WH]K$ with primary alkyl halides provides evidence of alkane complexation (L = *t*-Bu_3SiN =).[174]

In 1969 Shilov observed Pt catalyzed conversion of MeOH to RCl and ROH in *aqueous solution* (Equation (31)).[175,175a]

$$CH_4 + [PtCl_6]^{2-} + H_2O(Cl^-) \xrightarrow[H_2O,\ 120\,^\circ C]{[PtCl_4]^{2-}} CH_3OH(CH_3Cl) + [PtCl_4]^{2-} + 2HCl \qquad (31)$$

This seminal discovery has led to considerable related studies that have been well reviewed,[157,157a,157b,175,175a,176,176a,176b,177] and only aspects dealing with evidence for σ complexes will be discussed. Shilov proposed a mechanism for the alkane oxidation consisting of three basic transformations (Equation (32)).

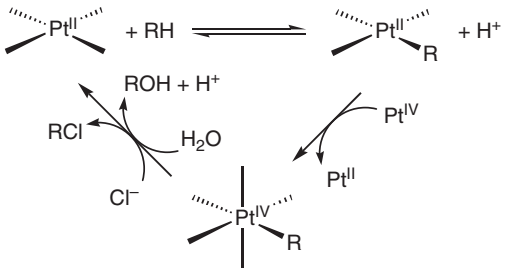

(32)

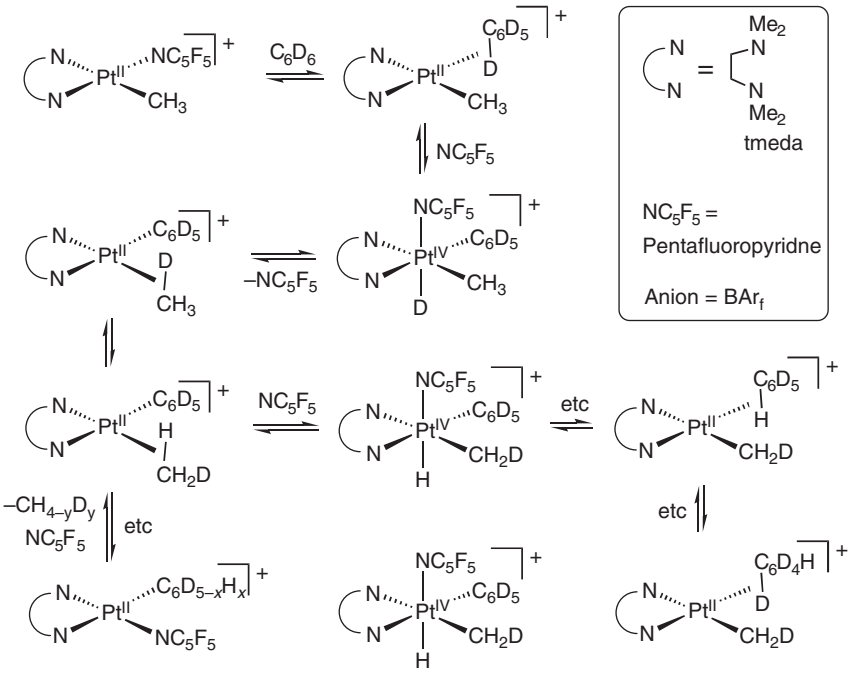

Scheme 14

Many features of the individual steps have only recently been identified, mainly through work by Bercaw and Labinger.[176,176a–176c] The first step determines both the rate and selectivity of the oxidation and is the most interesting in terms of σ complex participation, e.g. electrophilic displacement of a proton on the alkane by Pt^{II}, possibly via C–H heterolysis.[175a] Mechanistic information has been obtained by studying the microscopic reverse, i.e. protonolysis of alkylplatinum(II) complexes, and supports two paths: deprotonation of a transient Pt^{II}–alkane σ complex or OA of the C–H bond to give a Pt^{IV}(R) (H) complex that is subsequently deprotonated. Significantly, the complexes in deuterated acidic media give multiple H/D exchange into the alkyl positions prior to alkane elimination.[176,176a–176c] In the presence of D^+, deuterium incorporation into the alkyl is rationalized by the reversibility of the steps leading up to alkane elimination. The Pt-tmeda system in Scheme 14 is an excellent model and shows multiple exchange with hydrocarbon solvents.[178,178a]

Prolonged heating of $[Pt(CH_3)(NC_5F_5)(tmeda)][BAr_f]$ with benzene-d_6 gives NMR-observed methane isotopomers CH_4, CH_3D, CH_2D_2, CHD_3 which requires an intermediate with significant lifetime such as a σ complex. H/D isotopic exchange with benzene-d_6 similar to that in Scheme 14 is also seen in related complexes, and exchange reactions with CD_4 implicates methane σ-complexes as intermediates.[179,179a,179b] All aspects of C–H activation by Pt complexes have been well reviewed by Lersch and Tilset.[177]

Catalytic Hg^{II}, Pt^{II}, and Pd^{II} systems discovered by Periana *et al.*[180,180a,180b] represent a major advance for the direct, selective oxidation of CH_4, e.g. Scheme 15. At 200 °C in fuming sulfuric acid, methyl bisulfate can be obtained in 70% one-pass yield based on CH_4 (90% conversion, 81% selectivity) when X is HSO_4. Remarkably, the organic ligand is stable to hot H_2SO_4, probably because the uncoordinated nitrogens are protonated, reducing oxidative degradation. The mechanism may involve a 14e cationic complex that promotes rapid C–H heterolysis where a proton can rapidly transfer to either a cis ligand or the anion upon contact of alkane with Pt, similar to heterolysis of H_2. Theoretical calculations support a σ complex intermediate,[181,181a] and a clear example of reversible intramolecular heterolytic C–H cleavage at diazabutadiene ligands on iridium(III) has been reported.[182] Regardless of mechanism, the selective catalytic methane oxidation in 40–70% yields is unprecedented, and other types of methane hydroxylation may involve methane complexes.[182a]

1.24.5 Borane σ-Complexes

B–H σ complexes containing "neutral" borane ligands have recently been established and are distinct from borohydride complexes. Boranes such as BH_3 are Lewis acids but their base adducts such as $BH_3{\cdot}PR_3$ can act as σ ligands analogous to silanes.[183,183a,183b]

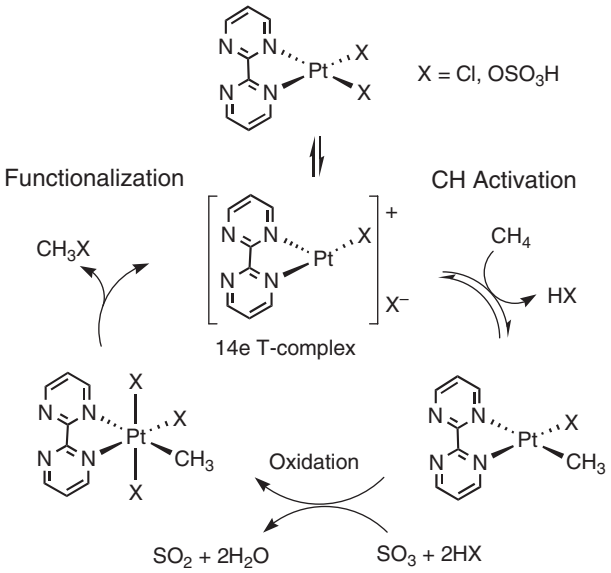

Scheme 15

The X-ray structures of group 6 pentacarbonyl species, $W(CO)_5(BH_3{\cdot}PMe_3)$ and a gallane analogue, $W(CO)_5(GaH_3{\cdot}$quinuclidine), the first Ga–H σ complex, show monodentate η^2-B–H and Ga–H coordination.[183,183a]

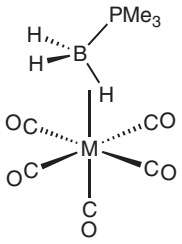

Related Cr and Ru complexes of the chelating phosphine-borane $HB_3{\cdot}$dppm are known.[183b] For the former, J_{BH} ranges from 80–87 Hz, about 10 Hz less than for free $BH_3{\cdot}L$. Because of fast BH scrambling these values are an average, and the actual J_{BH} for bound B–H is estimated to be ~60 Hz. This is ~65% of that in the free ligand, and comparable to the 50–80% reduction in J_{HD} in unstretched HD complexes[3] and the 74% reduction in J_{CH} for cyclopentane coordination[159,159a,159b] in $CpRe(CO)_2(C_5H_{10})$. d_{BH} ranges from 1.1–1.3 Å in B–H complexes and are not very meaningful because of large standard deviations. The M–H–B angles are near 130° in $M(CO)_5(BH_3{\cdot}PMe_3)$ and can be as high as 167°. These are much larger than the angles observed in M–H–Si σ complexes as well as the $Cp_2Ti(\eta^2\text{-HBcat})_2$ (Bcat = catecholborane) and related M–H–B σ complexes initially characterized by Hartwig that appear to the best examples of genuine η^2-BH σ complexes.[33a,185,185a–185c] Thus the bonding for these neutral borane ligands, while still bent, is closer to end-on than side-on as in BH_4^- complexes (M–H–B up to 162°). $RuH_2(\eta^2\text{-HBcat})$ $(\eta^2\text{-}H_2)$ $(PCy_3)_2$ contains both H_2 and borane ligands.[33a,185a] Ni(diphosphine) $(\eta^2\text{-}HBEt_2)$ species are rare examples of Ni σ complexes.[185b]

Although neutral, the above phosphine borane ligands contain four-coordinate boron when free and are more like BH_4^- ligands, i.e. more hydridic character than in the base-free HBcat complexes from which borane can be displaced as in Equation (33) to form, for example, a silane-borane σ-complex.[184]

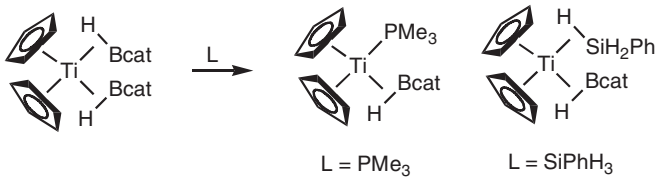

(33)

HBcat binding is thermodynamically favored over silane binding, partly because the borane is more Lewis acidic. $Cp^*RuH_2(Bpin)(SiR_3)$ (pin = pinacolato) contains boryl, silyl, and hydrido ligands and chooses to possess partial B–H bonding with Ru (rather than H–H or Si–H) and to eliminate borane faster than H_2 or silane.[185c] Similar borane binding to $CpM(CO)_2$ (M = Mn, Re) and Ru phosphine fragments is known where the borane can be displaced by silanes, stannanes, alkynes, and H_2.[33a,185,185a–185c] Metal-catalyzed hydroboration of C–C multiple bonds using such organoborane derivatives and coupling with alkanes to form linear alkylboranes has provided valuable applications in organic synthesis.[185,185a–185c,186,186a–186c,187,188] The cationic σ-borane complex $[Mn(CO)_4(PR_3)(BH_3{\cdot}PMe_3)]^+$ prepared by novel protonation of the neutral boryl complex $Mn(CO)_4(PR_3)(BH_2{\cdot}PMe_3)$ gives heterolytic cleavage of the B–H bond.[189] Solution decomposition (days) to $MnH(CO)_4(PR_3)$ and $[BH_2{\cdot}2PMe_3]^+$ suggested that the coordinated B–H cleaves into H^- and "$[BH_2{\cdot}2PMe_3]^+$" much as for silanes.

1.24.6 Other X–H and X–Y σ-Complexes

σ-bond interactions akin to α-agostic M–C–H interactions can exist for X–H groups where X is a classical lone-pair donor atom such as N, P, or S.[3,6a,10c] Metal centers can also interact with σ bonds not containing hydrogen ("hydrogen-free" X–Y σ complex).[3,10c,190] Many examples of C–C bond cleavage/coupling reactions are known and may proceed through a C–C σ complex[4,4a,191] such as observed[192,192a] in 14e titanium and related systems.

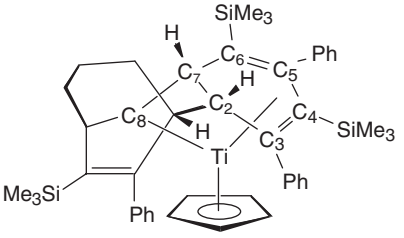

The saturated carbon C7 is only 2.293(7) Å from Ti (and C2 is 2.579(7) Å away). Remarkably C7 is closer to Ti than any of the bound olefinic carbons C4 and C5 (2.30–2.34 Å) and Cp carbons, clearly indicative of metal C–C bond interaction. Similar interactions have been found in electron-deficient metallocyclobutane complexes, $Cp^*_2M(CH_2)_2CHR$ (M = Ti and Zr but not 18e Mo and W analogues), which may have important implications in olefin polymerizations and metathesis.[192a] There is precedence for such interactions in an agostic C–Si interaction with Ti,[193] and other C–X interactions are known.

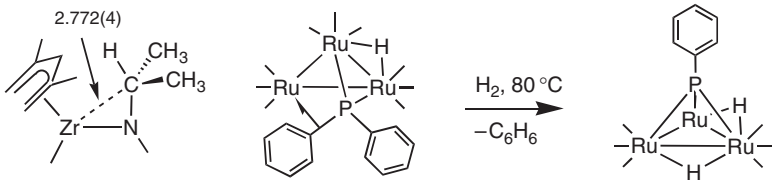

Agostic C–P interactions occur in phosphine complexes[6a] and in a trinuclear Ru cluster with a μ-phosphido interaction.[194] Reaction with H_2 cleaves $P–C_{Ph}$ to give benzene and a μ_3-phosphinidene complex shows that the C–P bond is activated as for other σ complexes. Si–Si bonds also coordinate,[190] including a unique tripalladium complex with six Si in the coordination sphere of the central Pd and initially believed to have an unprecedented Pd^{VI} oxidation state.[195] DFT studies showed formulation as a Pd^{II} Si–Si σ complex (also unprecendented) was correct,[196,196a] underscoring both the "multifarious"[10] and often well-concealed nature of H_2 and σ bond coordination.

References

1. Kubas, G. J.; Ryan, R. R.; Swanson, B. I.; Vergamini, P. J.; Wasserman, H. J. *J. Am. Chem. Soc.* **1984**, *106*, 451.
2. Kubas, G. J. *Acc. Chem. Res.* **1988**, *21*, 120.
2a. Kubas, G. J. *J. Organometal. Chem.* **2001**, *635*, 37.
2b. Kubas, G. J. *J. Chem. Soc., Chem. Commun.* **1980**, 61.
2c. Bender, B. R.; Kubas, G. J.; Jones, L. H.; Swanson, B. I.; Eckert, J.; Capps, K. B.; Hoff, C. D. *J. Am. Chem. Soc.* **1997**, *119*, 9179.

3. Kubas, G. J. *Metal Dihydrogen and σ–Bond Complexes*; Kluwer Academic/Plenum Publishers: New York, **2001**.
4. Brown, M. P.; Puddephatt, R. J.; Upton, C. E. E. *J. Chem. Soc., Dalton Trans.* **1974**, 2457.
4a. Hill, G. S.; Puddephatt, R. J. *Organometallics* **1998**, *17*, 1478.
5. Maseras, F.; Lledós, A.; Clot, E.; Eisenstein, O. *Chem. Rev.* **2000**, *100*, 601.
6. Baik, M.-H.; Friesner, R. A.; Parkin, G. *Polyhedron* **2004**, *23*, 2879.
6a. Braunstein, P.; Boag, N. M. *Angew. Chem., Int. Ed. Engl.* **2001**, *40*, 2427.
7. Dewar, M. J. S. *Bull. Soc. Chim. Fr.* **1951**, *18*, C79.
7a. Chatt, J.; Duncanson, L. A. *J. Chem. Soc.* **1953**, 2929.
8. LaPlaca, S. J.; Ibers, J. A. *Inorg. Chem.* **1965**, *4*, 778.
8a. Roe, D. M.; Bailey, P. M.; Moseley, K.; Maitlis, P. M. *J. Chem. Soc., Chem. Commun.* **1972**, 1273.
8b. Cotton, F. A.; Stanislowski, A. G. *J. Am. Chem. Soc.* **1974**, *96*, 5074.
8c. Trofimenko, J. *Prog. Inorg. Chem.* **1986**, *34*, 115.
8d. Brookhart, M.; Green, M. L. H.; Wong, L.-L. *Prog. Inorg. Chem.* **1988**, *36*, 1.
8e. Clot, E.; Eisenstein, O. *Struct. Bond.* **2002**, *113*, 1.
9. Wasserman, H. J.; Kubas, G. J.; Ryan, R. R. *J. Am. Chem. Soc.* **1986**, *108*, 2294.
10. McGrady, G. S.; Guilera, G. *Chem. Soc. Rev.* **2003**, *32*, 383.
10a. Heinekey, D. M.; Oldham, W. J., Jr. *Chem. Rev.* **1993**, *93*, 913.
10b. Jessop, P. G.; Morris, R. H. *Coord. Chem. Rev.* **1992**, *121*, 155.
10c. Crabtree, R. H. *Angew. Chem., Int. Ed. Engl.* **1993**, *32*, 789.
10d. Esteruelas, M. A.; Oro, L. A. *Adv. Organomet. Chem.* **2001**, *47*, 1.
10e. Jia, G.; Lin, Z.; Lau, C. P. *Eur. J. Inorg. Chem.* **2003**, 2551.
10f. Schneider, J. J. *Angew. Chem., Int. Ed. Engl.* **1996**, *35*, 1068.
10g. Jia, G.; Lau, C.-P. *Coord. Chem. Rev.* **1999**, *190–192*, 83.
10h. Kubas, G. *Catal. Lett.* **2005**, *104*, 79.
11. Maltby, P. A.; Schlaf, M.; Steinbeck, M.; Lough, A. J.; Morris, R. H.; Klooster, W. T.; Koetzle, T. F.; Srivastava, R. C. *J. Am. Chem. Soc.* **1996**, *118*, 5396.
12. Luther, T. A.; Heinekey, D. M. *Inorg. Chem.* **1998**, *37*, 127.
13. Zilm, K. W.; Millar, J. M. *Adv. Magn. Opt. Reson.* **1990**, *15*, 163.
14. Kubas, G. J.; Burns, C. J.; Eckert, J.; Johnson, S.; Larson, A. C.; Vergamini, P. J.; Unkefer, C. J.; Khalsa, G. R. K.; Jackson, S. A.; Eisenstein, O. *J. Am. Chem. Soc.* **1993**, *115*, 569.
15. Crabtree, R. H. *Acc. Chem. Res.* **1990**, *23*, 95.
16. Cotton, F. A.; Luck, R. L. *J. Chem. Soc., Chem. Commun.* **1988**, 1277.
16a. Bautista, M. T.; Earl, K. A.; Maltby, P. A.; Morris, R. H.; Schweitzer, C. T.; Sella, A. *J. Am. Chem. Soc.* **1988**, *110*, 7031.
16b. Desrosiers, P. J.; Cai, L.; Lin, Z.; Richards, R.; Halpern, J. *J. Am. Chem. Soc.* **1991**, *113*, 4173.
17. Gusev, D. G.; Kuhlman, R. L.; Renkema, K. H.; Eisenstein, O.; Caulton, K. G. *Inorg. Chem.* **1996**, *35*, 6775.
17a. Morris, R. H.; Wittebort, R. J. *Magn. Reson. Chem.* **1997**, *35*, 243.
18. Eckert, J.; Kubas, G. J. *J. Chem. Phys.* **1993**, *97*, 2378.
19. Janak, K. E.; Parkin, G. *Organometallics* **2003**, *22*, 4378.
20. Reid, S. M.; Neuner, B.; Schrock, R. R.; Davis, W. M. *Organometallics* **1998**, *17*, 4077.
21. Bart, S. C.; Lobkovsky, E.; Chirik, P. J. *J. Am. Chem. Soc.* **2004**, *126*, 13794.
22. Eckert, J.; Albinati, A.; Bucher, U. E.; Venanzi, L. M. *Inorg. Chem.* **1996**, *35*, 1292.
23. Hasegawa, T.; Li, Z.; Parkin, S.; Hope, H.; McMullan, R. K.; Koetzle, T. F.; Taube, H. *J. Am. Chem. Soc.* **1994**, *116*, 4352.
24. Aebischer, N.; Frey, U.; Merbach, A. E. *Chem. Comm.* **1998**, 2303.
24a. Grundler, P. V.; Yazyev, O. V.; Aebischer, N.; Helm, L.; Laurenczy, G.; Merbach, A. E. *Inorg. Chem. Acta* **2006**, *359*, 1795.
25. Matthews, S. L.; Pons, V.; Heinekey, D. M. *J. Am. Chem. Soc.* **2005**, *127*, 850.
25a. Matthews, S. L.; Heinekey, D. M. *J. Am. Chem. Soc.* **2006**, *1128*, 2615.
25b. Heinekey, D. M.; Law, J. K.; Schultz, S. M. *J. Am. Chem. Soc.* **2001**, *123*, 12728, [Note: $W(CO)_4(PMe_3)(H_2)$ and $W(CO)_5(H_2)$ were initially incorrectly formulated as dihydrides here; see ref 25 a,b].
26. Jia, G.; Lau, C. P. *J. Organomet. Chem.* **1998**, *565*, 37.
26a. Vogt, M.; Pons, V.; Heinekey, D. M. *Organometallics* **2005**, *24*, 1832.
27. Kuhlman, R. *Coord. Chem. Rev.* **1997**, *167*, 205.
28. Bakhmutov, V. I. *Eur. J. Inorg. Chem.* **2005**, 245.
29. Belkova, N. V.; Collange, E.; Dub, P.; Epstein, L. M.; Lemenovskii, D. A.; Lledós, A.; Maresca, O.; Maseras, F.; Poli, R., Revin, P. O., *et al. Chem. Eur. J.* **2005**, *11*, 873.
30. Sabo-Etienne, S.; Chaudret, B. *Coord. Chem. Rev.* **1998**, *178–180*, 381.
30a. Grellier, M.; Vendier, L.; Chaudret, B.; Albinati, A.; Rizzato, S.; Mason, S.; Sabo-Etienne, S. *J. Am. Chem. Soc.* **2005**, *127*, 17592.
31. Ingleson, M. J.; Brayshaw, S. K.; Mahon, M. F.; Ruggiero, G. D.; Weller, A. S. *Inorg. Chem.* **2005**, *44*, 3162.
32. Chaudret, B.; Chung, G.; Eisenstein, O.; Jackson, S. A.; Lahoz, F. J.; Lopez, J. A. *J. Am. Chem. Soc.* **1991**, *113*, 2314.
32a. Christ, M. L.; Sabo-Etienne, S.; Chaudret, B. *Organometallics* **1994**, *13*, 3800.
33. Hussein, K.; Marsden, C. J.; Barthelat, J.-C.; Rodriguez, V.; Conjero, S.; Sabo-Etienne, S.; Donnadieu, B.; Chaudret, B. *Chem. Comm.* **1999**, 1315.
33a. Lachaize, S.; Essalah, K.; Montiel-Palma, V.; Vendier, L.; Chaudret, B.; Barthelet, J.-C.; Sabo–Etienne, S. *Organometallics* **2005**, *24*, 2935.
33b. Atheaux, I.; Delpech, F.; Donnadieu, B.; Sabo-Etienne, S.; Chaudret, B.; Hussein, K.; Barthelat, J.-C.; Braun, T.; Duckett, S. B.; Perutz, R. N. *Organometallics* **2002**, *21*, 5347.
34. Johnson, T. J.; Albinati, A.; Koetzle, T. F.; Ricci, J.; Eisenstein, O.; Huffman, J. C.; Caulton, K. G. *Inorg. Chem.* **1994**, *33*, 4966.
35. Ghoshray, K.; Bandyopadhyay, B.; Sen, M.; Ghoshray, A.; Chatterjee, N. *Phys. Rev. B* **1993**, *47*, 8277.
35a. Sen, M.; Ghoshray, A.; Ghoshray, K.; Sil, S.; Chatterjee, N. *Phys. Rev. B* **1996**, *53*, 14345.
36. Main-group hydrides/H_2 compounds: Aldridge, S.; Downs, A. J. *Chem. Rev.* **2001**, *101*, 3305.
37. Gagliardi, L.; Pyykko, P. *J. Am. Chem. Soc.* **2004**, *126*, 15014.
37a. Zhao, Y.; Kim, Y.-H.; Dillon, A. C.; Heben, M. J.; Zhang, S. B. *Phys. Rev. Lett.* **2005**, *94*, 155504.
37b. Yildirim, T.; Ciraci, S. *Phys. Rev. Lett.* **2005**, *94*, 175501.

37c. Rosi, N. L.; Eckert, J.; Eddaoudi, M.; Vodak, D. T.; Kim, J.; O'Keeffe, M.; Yaghi, O. M. *Science* **2003**, *300*, 1127.
37d. Rowsell, J. L. C.; Yaghi, O. M. *Angew. Chem., Int. Ed.* **2005**, *44*, 4670.
37e. Forster, P. M.; Eckert, J.; Chang, J. S.; Park, S.-E.; Ferey, G.; Cheetham, A. K. *J. Am. Chem. Soc.* **2003**, *125*, 1309.
38. Heinekey, D. M.; Lledós, A.; Lluch, J. M. *Chem. Soc. Rev.* **2004**, *33*, 175.
38a. Gelabert, R.; Moreno, M.; Lluch, J. M. *Chem. Eur. J.* **2005**, *11*, 6315.
38b. Yousufuddin, M.; Wen, T. B.; Mason, S. A.; McIntyre, G. J.; Jia, G.; Bau, R. *Angew. Chem., Int. Ed.* **2005**, *44*, 7227.
39. Brammer, L.; Howard, J. A.; Johnson, O.; Koetzle, T. F.; Spencer, J. L.; Stringer, A. M. *J. Chem. Soc., Chem. Commun.* **1991**, 241.
40. Albinati, A.; Bakhmutov, V. I.; Caulton, K. G.; Clot, E.; Eckert, J.; Eisenstein, O.; Gusev, D. G.; Grushin, V. V.; Hauger, B. E., Klooster, W. T., *et al. J. Am. Chem. Soc.* **1993**, *115*, 7300.
41. Gusev, D. G. *J. Am. Chem. Soc.* **2004**, *126*, 14249.
42. Hush, N. S. *J. Am. Chem. Soc.* **1997**, *119*, 1717.
43. Law, J. K.; Mellows, H.; Heinekey, D. M. *J. Am. Chem. Soc.* **2002**, *124*, 1024.
43a. Gelabert, R.; Moreno, M.; Lluch, J. M.; Lledós, A.; Heinekey, D. M. *J. Am. Chem. Soc.* **2005**, *127*, 5632.
44. Sabo-Etienne, S.; Chaudret, B. *Chem. Rev.* **1998**, *98*, 2077.
45. Van Der Sluys, L. S.; Eckert, J.; Eisenstein, O.; Hall, J. H.; Huffman, J. C.; Jackson, S. A.; Koetzle, T. F.; Kubas, G. J.; Vergamini, P. J.; Caulton, K. G. *J. Am. Chem. Soc.* **1990**, *112*, 4831.
46. Brintzinger, H. H. *J. Organomet. Chem.* **1979**, *171*, 337.
47. Burdett, J. K.; Phillips, J. R.; Pourian, M. R.; Poliakoff, M.; Turner, J. J.; Upmacis, R. *Inorg. Chem.* **1987**, *26*, 3054.
48. Burdett, J. K.; Pourian, M. R. *Organometallics* **1987**, *6*, 1684.
48a. Burdett, J. K.; Pourian, M. R. *Inorg. Chem.* **1988**, *27*, 4445.
49. Luo, X.-L.; Crabtree, R. H. *J. Am. Chem. Soc.* **1990**, *112*, 6912.
50. Maseras, F.; Duran, M.; Lledos, A.; Bertran, J. *J. Am. Chem. Soc.* **1992**, *114*, 2922.
51. Gusev, D. G.; Hubener, R.; Burger, P.; Orama, O.; Berke, H. *J. Am. Chem. Soc.* **1997**, *119*, 3716.
52. Wisniewski, L. L.; Mediati, M.; Jensen, C. M.; Zilm, K. W. *J. Am. Chem. Soc.* **1993**, *115*, 7533.
53. Li, S.; Hall, M. B.; Eckert, J.; Jensen, C. M.; Albinati, A. *J. Am. Chem. Soc.* **2000**, *122*, 2903.
54. Gusev, D. G.; Berke, H. *Chem. Ber.* **1996**, *129*, 1143.
55. Pons, V.; Conway, S. L. J.; Green, M. L. H.; Green, J. C.; Herbert, B. J.; Heinekey, D. M. *Inorg. Chem.* **2004**, *43*, 3475.
56. Janak, K. E.; Shin, J. H.; Parkin, G. *J. Am. Chem. Soc.* **2004**, *126*, 13054.
57. Brothers, P. J. *Prog. Inorg. Chem.* **1981**, *28*, 1.
58. Morris, R. H. In *Recent Advances in Hydride Chemistry*; Peruzzini, M., Poli, R., Eds.; Elsevier: Amsterdam, 2001; pp 1–38.
59. Kubas, G. J. *Adv. Inorg. Chem.* **2004**, *56*, 127.
60. Morris, R. H. *Can. J. Chem.* **1996**, *74*, 1907.
61. Chinn, M. S.; Heinekey, D. M.; Payne, N. G.; Sofield, C. D. *Organometallics* **1989**, *8*, 1824.
62. Huhmann-Vincent, J.; Scott, B. L.; Kubas, G. J. *J. Am. Chem. Soc.* **1998**, *120*, 6808.
63. Bruns, W.; Kaim, W.; Waldhor, E.; Krejcik, M. *Inorg. Chem.* **1995**, *34*, 663.
64. Crabtree, R. H.; Lavin, M. *J. Chem. Soc., Chem. Commun.* **1985**, 794.
65. Chinn, M. S.; Heinekey, D. M. *J. Am. Chem. Soc.* **1987**, *109*, 5865.
66. Grushin, V. V. *Acc. Chem. Res.* **1993**, *26*, 279.
67. Chin, B.; Lough, A. J.; Morris, R. H.; Schweitzer, C.; D'Agostino, C. *Inorg. Chem.* **1994**, *33*, 6278.
68. Gruet, K.; Clot, E.; Eisenstein, O.; Lee, D. H.; Patel, B. P.; Macchioni, A.; Crabtree, R. H. *New. J. Chem.* **2003**, *27*, 80.
69. Lough, A. J.; Park, S.; Ramachandran, R.; Morris, R. H. *J. Am. Chem. Soc.* **1994**, *116*, 8356.
70. Crabtree, R. H.; Siegbahn, P. E. M.; Eisenstein, O.; Rheingold, A. L.; Koetzle, T. F. *Acc. Chem. Res.* **1996**, *29*, 348.
71. Custelcean, R.; Jackson, J. E. *Chem. Rev.* **2001**, *101*, 1963.
71a. Epstein, L. M.; Shubina, E. S. *Coord. Chem. Rev.* **2002**, *231*, 165.
72. Jimenez-Tenorio, M.; Palacios, M. D.; Puerta, M. C.; Valerga, P. *Organometallics* **2005**, *24*, 3088.
73. Chinn, M. S.; Heinekey, D. M.; Payne, N. G.; Sofield, C. D. *Organometallics* **1989**, *8*, 1824.
74. Huhmann-Vincent, J.; Scott, B. L.; Kubas, G. J. *J. Am. Chem. Soc.* **1998**, *120*, 6808.
75. Childs, G. I.; Cooper, A. I.; Nolan, T. F.; Carrott, M. J.; George, M. W.; Poliakoff, M. *J. Am. Chem. Soc.* **2001**, *123*, 6857.
76. Thomas, A.; Haake, M.; Grevels, F. W.; Bargon, J. *Angew. Chem. Int. Ed. Engl.* **1994**, *33*, 755.
77. Review: Jia, G.; Lin, Z.; Lau, C. P. *Eur. J. Inorg. Chem.* **2003**, 2551.
77a. Xue, P.; Zhu, J.; Liu, S. H.; Huang, X.; Ng, W. S.; Sung, H. H. Y.; Williams, I. D.; Lin, Z.; Jia, G. *Organometallics* **2006**, *25*.
78. Joshi, A. M.; MacFarlane, K. S.; James, B. R. *J. Organomet. Chem.* **1994**, *488*, 164.
79. Vigalok, A.; Ben-David, Y.; Milstein, D. *Organometallics* **1996**, *15*, 1839.
80. Bullock, R. M.; Song, J.-S.; Szalda, D. J. *Organometallics* **1996**, *15*, 2504.
80a. Guan, H.; Iimura, M.; Magee, M. P.; Norton, J. R.; Zhu, G. *J. Am. Chem. Soc.* **2005**, *127*, 7805, and references therein.
81. Noyori, R. *Angew. Chem., Int. Ed.* **2002**, *41*, 2008.
81a. Ohkuma, T.; Noyori, R. *J. Am. Chem. Soc.* **2003**, *125*, 13490.
82. Fryzuk, M. D.; MacNeil, P. A. *Organometallics* **1983**, *2*, 682.
82a. Fryzuk, M. D.; MacNeil, P. A.; Rettig, S. J. *J. Am. Chem. Soc.* **1987**, *109*, 2803.
83. Abdur-Rashid, K.; Clapham, S. E.; Hadzovic, A.; Harvey, J. N.; Lough, A. J.; Morris, R. H. *J. Am. Chem. Soc.* **2002**, *124*, 15104.
83a. Hamilton, R. J.; Leong, C. G.; Bigam, G.; Miskolzie, M.; Bergens, S. H. *J. Am. Chem. Soc.* **2005**, *127*, 4152.
83b. Hartmann, R.; Chen, P. *Angew. Chem., Int. Ed.* **2001**, *40*, 3581.
83c. Muniz, K. *Angew. Chem., Int. Ed.* **2005**, *44*, 6622.
83d. Hedberg, C.; Kallstrom, K.; Arvidsson, P. I.; Brandt, P.; Andersson, P. G. *J. Am. Chem. Soc.* **2005**, *127*, 15083.
83e. Casey, C. P.; Johnson, J. B.; Singer, S. W.; Cui, Q. *J. Am. Chem. Soc.* **2005**, *127*, 3100.
84. Hughes, R. P.; Smith, J. M. *J. Am. Chem. Soc.* **1999**, *121*, 6084.
84a. Hughes, R. P.; Willemsen, S.; Williamson, S.; Zhang, D. *Organometallics* **2002**, *21*, 3085.
85. Hayashi, H.; Ogo, S.; Fukuzumi, S. *Chem. Commun.* **2004**, 2714.
86. Esteruelas, M. A.; Oro, L. A. *Chem. Rev.* **1998**, *98*, 577.
87. Beatty, R. P.; Paciello, R. A., WO Patent 9623802, 1995.

87a. Beatty, R. P.; Paciello, R. A., WO Patent 9623803, 1995.
87b. Beatty, R. P.; Paciello, R. A., WO Patent 9623804, 1995.
88. Borowski, A. F.; Sabo-Etienne, S.; Christ, M. L.; Donnadieu, B.; Chaudret, B. *Organometallics* **1996**, *15*, 1427.
89. Christ, M. L.; Sabo-Etienne, S.; Chaudret, B. *Organometallics* **1995**, *14*, 1082.
90. Guari, Y.; Sabo-Etienne, S.; Chaudret, B. *J. Am. Chem. Soc.* **1998**, *120*, 4228.
91. Guari, Y.; Castellanos, A.; Sabo-Etienne, S.; Chaudret, B. *J. Mol. Catal. A* **2004**, *212*, 77.
92. Belderrain, T. R.; Grubbs, R. H. *Organometallics* **1997**, *16*, 4001.
93. Drouin, S. D.; Yap, G. P. A.; Fogg, D. E. *Inorg. Chem.* **2000**, *39*, 5412.
94. Esteruelas, M. A.; Oro, L. A.; Valero, C. *Organometallics* **1991**, *10*, 462.
95. Kubas, G. J.; Unkefer, C. J; Swanson, B. I.; Fukushima, E. *J. Am. Chem. Soc.* **1986**, *108*, 7000.
96. Bianchini, C.; Linn, K.; Masi, D.; Peruzzini, M.; Polo, A.; Vacca, A.; Zanobini, F. *Inorg. Chem.* **1993**, *32*, 2366.
97. Martensson, A.-S.; Nyberg, C.; Andersson, S. *Phys. Rev. Lett.* **1986**, *57*, 2045.
97a. Martensson, A.-S.; Nyberg, C.; Andersson, S. *Surf. Sci.* **1988**, *205*, 12.
98. Kresse, G. *Phys. Rev. B* **2000**, *62*, 8295.
98a. Schmidt, P. K.; Christman, K.; Kresse, G.; Hafner, J.; Lischka, M.; Gross, A. *Phys. Rev. Lett.* **2001**, *87*, 096103.
99. Hauge, R. H.; Margrave, J. L.; Kafafi, Z. H. *NATO ASI Ser., Ser. B* **1987**, *158* (Phys. Chem. Small Clusters), 787.
100. Andrews, L. *Chem. Soc. Rev.* **2004**, *33*, 123.
101. Zhou, M.; Zhang, L.; Shao, L.; Wang, W.; Fan, K.; Qin, Q. *J. Phys. Chem. A* **2001**, *105*, 10747.
102. Gronbeck, H. *Top. Catal.* **2004**, *28*, 59.
103. Wang, J.; Fan, C. Y.; Sun, Q.; Reuter, K.; Jacobi, K.; Scheffler, M.; Ertl, G. *Angew. Chem., Int. Ed. Engl.* **2003**, *42*, 2151.
104. Albinati, A.; Klooster, W. T.; Koetzle, T. F.; Fortin, J. B.; Ricci, J. S.; Eckert, J.; Fong, T. P.; Lough, A. J.; Morris, R. H.; Golombek, A. P. *Inorg. Chim. Acta* **1997**, *259*, 351.
105. Morris, R. H. Transition Metal Sulfides. *NATO ASI Ser., Ser. C* **1998**, *60*, 57.
105a. Bayon, J. C.; Claver, C.; Masdeu-Bulto, A. M. *Coord. Chem. Rev.* **1999**, *193–195*, 73.
105b. Startsev, A. N. *Cat. Rev.-Sci. Eng.* **1995**, *37*, 353.
106. Rakowski Dubois, M. *Chem. Rev.* **1989**, *89*, 1, and references therein.
107. Bianchini, C.; Mealli, C.; Meli, A.; Sabat, M. *Inorg. Chem.* **1986**, *25*, 4617.
108. Sweeney, Z. K.; Polse, J. L.; Andersen, R. A.; Bergman, R. G.; Kubinec, M. G. *J. Am. Chem. Soc.* **1997**, *119*, 4543.
109. Schlaf, M.; Lough, A. J.; Morris, R. H. *Organometallics* **1996**, *15*, 4423.
110. Mojet, B. L.; Eckert, J.; van Santen, R. A.; Albinati, A.; Lechner, R. E. *J. Am. Chem. Soc.* **2001**, *123*, 8147.
111. Eckert, J.; Nicol, J. M.; Howard, J.; Trouw, F. R. *J. Phys. Chem.* **1996**, *100*, 10646.
112. Bianchini, C.; Burnaby, D. G.; Evans, J.; Frediani, P.; Meli, A.; Oberhauser, W.; Psaro, R.; Sordelli, L.; Vizza, F. *J. Am. Chem. Soc.* **1999**, *121*, 5961.
113. Matthes, J.; Pery, T.; Grundemann, S.; Buntkowsky, G.; Sabo-Etienne, S.; Chaudret, B.; Limbach, H.-H. *J. Am. Chem. Soc.* **2004**, *126*, 8366.
114. Casty, G. L.; Matturro, M. G.; Myers, G. R.; Reynolds, R. P.; Hall, R. B. *Organometallics* **2001**, *20*, 2246.
115. Matthes, J.; Pery, T.; Grundemann, S.; Buntkowsky, G.; Sabo-Etienne, S.; Chaudret, B.; Limbach, H.-H. *J. Am. Chem. Soc.* **2004**, *126*, 8366.
116. Darensbourg, M. Y.; Lyon, E. J.; Smee, J. J. *Coord. Chem. Rev.* **2000**, *206–207*, 533.
116a. Darensbourg, M. Y.; Lyon, E. J.; Zhao, Z.; Georgakaki, I. P. *Proceedings of the National Academy of Sciences* **2003**, *100*, 3683.
117. Peters, J. W.; Lanzilotta, W. N.; Lemon, B. J.; Seefeldt, L. C. *Science* **1998**, *282*, 1853.
118. Henrici-Olive, G.; Olive, S. *J. Mol. Catal.* **1975/1976**, *1*, 121.
119. Crabtree, R. H. *Inorg. Chim. Acta* **1986**, *125*, L7.
120. Tye, J. W.; Hall, M. B.; Georgakaki, I. P.; Darensbourg, M. Y. *Adv. Inorg. Chem.* **2004**, *56*, 1.
121. Henry, R. M.; Shoemaker, R. K.; Newell, R. H.; Jacobsen, G. M.; DuBois, D. L.; Rakowski Dubois, M. *Organometallics* **2005**, *24*, 2481.
122. Justice, A. K.; Linck, R. C.; Rauchfuss, T. B.; Wilson, S. R. *J. Am. Chem. Soc.* **2004**, *126*, 13214.
123. Mackay, B. A.; Fryzuk, M. D. *Chem. Rev.* **2004**, *104*, 385.
124. Sellmann, D.; Fursattel, A.; Sutter, J. *Coord. Chem. Rev.* **2000**, *200–202*, 545.
124a. Sellmann, D.; Hille, A.; Heinemann, F. W.; Moll, M.; Reiher, M.; Hess, B. A.; Bauer, W. *Chem. Eur. J.* **2004**, *10*, 4214.
125. Jia, G.; Morris, R. H.; Schweitzer, C. T. *Inorg. Chem.* **1991**, *30*, 594.
126. Nishibayashi, Y.; Takemoto, S.; Iwai, S.; Hidai, M. *Inorg. Chem.* **2000**, *39*, 5946.
127. Fryzuk, M. D.; Love, J. B.; Rettig, S. J.; Young, V. G. *Science* **1997**, *275*, 1445.
127a. Basch, H.; Muaev, D. G.; Morokuma, K.; Fryzuk, M. D.; Love, J. B.; Seidel, W. W.; Albinati, A.; Koetzle, T. F.; Klooster, W. T., Mason, S. A., *et al. J. Am. Chem. Soc.* **1999**, *121*, 523.
128. Pool, J. A.; Lobkovsky, E.; Chirik, P. J. *Nature* **2004**, *427*, 527.
128a. Bernskoetter, W. H.; Olmos, A. V.; Lobkovsky, E.; Chirik, P. J. *Organometallics* **2006**, *25*, 1021.
128b. Brown, S. D.; Mehn, M. P.; Peters, J. C. *J. Am. Chem. Soc.* **2005**, *127*, 13146.
129. Schubert, U. *Adv. Organomet. Chem.* **1990**, *30*, 151.
129a. Corey, J. Y.; Braddock-Wilking, J. *Chem. Rev.* **1999**, *99*, 175.
130. Lin, Z. *Chem. Soc. Rev.* **2002**, *31*, 239.
130a. Nikonov, G. I. *Adv. Organomet. Chem.* **2005**, *53*, 217.
130b. Bader, R. F. W.; Matta, C. F.; Cortes-Guzman, F. *Organometallics* **2004**, *23*, 6253.
131. Bengali, A. A.; Fehnel, R. *Organometallics* **2005**, *24*, 1156.
131a. Howdle, S. M.; Healy, M. A.; Poliakoff, M. *J. Am. Chem. Soc.* **1990**, *112*, 4804.
132. Jetz, W.; Graham, W. A. G. *J. Am. Chem. Soc.* **1969**, *91*, 3375.
132a. Hoyano, J. K.; Graham, W. A. G. *J. Am. Chem. Soc.* **1969**, *91*, 4568.
132b. Graham, W. A. G. *J. Organomet. Chem.* **1986**, *300*, 81.
133. Luo, X.-L.; Kubas, G. J.; Burns, C. J.; Bryan, J. C.; Unkefer, C. J. *J. Am. Chem. Soc.* **1995**, *117*, 1159.
134. Huhmann-Vincent, J.; Scott, B. L.; Butcher, R.; Luo, S.; Unkefer, C. J.; Kubas, G. J.; Lledós, A.; Maseras, F.; Tomas, J. *Organometallics* **2003**, *22*, 5307.
135. See for example: Carleton, L. *Inorg. Chem.* **2000**, *39*, 4510.
136. Nikonov, G. I. *Organometallics* **2003**, *22*, 1597.

137. Spaltenstein, E.; Palma, P.; Kreutzer, K. A.; Willoughby, C. A.; Davis, W. M.; Buchwald, S. L. *J. Am. Chem. Soc.* **1994**, *116*, 10308.
138. Delpech, F.; Sabo-Etienne, S.; Chaudret, B.; Daran, J.-C. *J. Am. Chem. Soc.* **1997**, *119*, 3167.
139. Delpech, F.; Sabo-Etienne, S.; Daran, J.-C.; Chaudret, B.; Hussein, K.; Marsden, C. J.; Barthelet, J.-C. *J. Am. Chem. Soc.* **1999**, *121*, 6668.
140. Luo, X.-L.; Kubas, G. J.; Bryan, J. C.; Burns, C. J.; Unkefer, C. J. *J. Am. Chem. Soc.* **1994**, *116*, 10312.
141. Atheaux, I.; Donnadieu, B.; Rodriguez, V.; Sabo-Etienne, S.; Chaudret, B,; Hussein, K.; Barthelet, J.-C. *J. Am. Chem. Soc.* **2000**, *122*, 5664.
142. Grumbine, S. K.; Tilley, T. D.; Arnold, F. P.; Rheingold, A. L. *J. Am. Chem. Soc.* **1994**, *116*, 5495.
142a. Thomas, C. M.; Peters, J. C. *Angew. Chem. Int. Ed.* **2006**, *45*, 776.
143. Marciniec, B., Ed. *Comprehensive Handbook on Hydrosilylation*; Pergamon: Oxford, 1992.
144. Luo, X.-L.; Crabtree, R. H. *J. Am. Chem. Soc.* **1989**, *111*, 2527.
145. Reed, C. A. *Acc. Chem. Res.* **1998**, *31*, 325.
146. Llamazares, A.; Schmalle, H. W.; Berke, H. *Organometallics* **2001**, *20*, 5277.
147. Huhmann-Vincent, J.; Scott, B. L.; Kubas, G. J. *Inorg. Chim. Acta* **1999**, *294*, 240.
148. Fang, X.; Scott, B. L.; Watkin, J. G.; Kubas, G. J. *Organometallics* **2000**, *19*, 4193.
149. Fang, X.; Scott, B. L.; John, K. D.; Kubas, G. J. *Organometallics* **2000**, *19*, 4141.
150. Freeman, S. T. N.; Lemke, F. R.; Brammer, L. *Organometallics* **2002**, *21*, 2030.
151. Scharrer, E.; Chang, S.; Brookhart, M. *Organometallics* **1995**, *14*, 5686.
152. Chang, S.; Scharrer, E.; Brookhart, M. *J. Mol. Catal. A: Chem.* **1998**, *130*, 107.
153. Buhl, M.; Mauschick, F. T. *Organometallics* **2003**, *22*, 1422.
154. Fang, X.; Huhmann-Vincent, J.; Scott, B. L.; Kubas, G. J. *J. Organometal. Chem.* **2000**, *609*, 95.
155. Gregg, B. T.; Cutler, A. R. *Organometallics* **1994**, *13*, 1039.
155a. Matthews, S. L.; Pons, V.; Heinekey, D. M. *Inorg. Chem.* **2006**.
156. Arndtsen, B. A.; Bergman, R. G.; Mobley, T. A.; Peterson, T. H. *Acc. Chem. Res.* **1995**, *28*, 154.
157. Crabtree, R. H. *Chem. Rev.* **1995**, *95*, 987.
157a. Crabtree, R. H. *J. Chem. Soc., Dalton Trans.* **2001**, 2437.
157b. Crabtree, R. H. *J. Organomet. Chem.* **2004**, *689*, 4083.
158. Hall, C.; Perutz, R. N. *Chem. Rev.* **1996**, *96*, 3125.
159. Geftakis, S.; Ball, G. E. *J. Am. Chem. Soc.* **1998**, *120*, 9953.
159a. Lawes, D. J.; Geftakis, S.; Ball, G. E. *J. Am. Chem. Soc.* **2005**, *127*, 4134.
159b. Ball, G. E; Darwish, T. A.; Geftakis, S.; George, M. W.; Lawes, D. J.; Portius, P.; Rourke, J. P. *Proc. Natl. Acad. Sci.* **2005**, *102*, 1853.
160. Sun, X.-Z.; Grills, D. C.; Nikiforov, S. M.; Poliakoff, M.; George, M. W. *J. Am. Chem. Soc.* **1997**, *119*, 7521.
161. Evans, D. R.; Drovetskaya, T.; Bau, R.; Reed, C. A.; Boyd, P. D. W. *J. Am. Chem. Soc.* **1997**, *119*, 3633.
162. Castro-Rodriguez, I.; Nakai, H.; Gantzel, P.; Zakharov, L. Z.; Rheingold, A. L.; Meyer, K. *J. Am. Chem. Soc.* **2003**, *125*, 15734.
163. Bengali, A. A.; Arndtsen, B. A.; Burger, P. M.; Schultz, R. H.; Weiller, B. H.; Kyle, K. R.; Moore, C. B.; Bergman, R. G. *Pure Appl. Chem.* **1995**, *67*, 281.
163a. McNamara, B. K.; Yeston, J. S.; Bergman, R. G.; Moore, C. B. *J. Am. Chem. Soc.* **1999**, *121*, 6437.
164. Wasserman, E. P.; Moore, C. B.; Bergman, R. G. *Science* **1992**, *255*, 315.
165. Manner, W. L.; Hostetler, M. J.; Girolami, G. S.; Nuzzo, R. G. *J. Phys. Chem. B* **1999**, *103*, 6752.
165a. Perry, D. A.; Hemminger, J. C. *J. Am. Chem. Soc.* **2000**, *122*, 8079.
165b. Billups, W. E.; Chang, S.-C.; Hauge, R. H.; Margrave, J. L. *J. Am. Chem. Soc.* **1993**, *115*, 2039.
165c. Wang, G. J.; Chen, M. H.; Zhou, M. F. *J. Phys. Chem. A* **2004**, *108*, 11273.
166. Wick, D. D.; Reynolds, K. A.; Jones, W. D. *J. Am. Chem. Soc.* **1999**, *121*, 3974.
166a. Jones, W. D. *Acc. Chem. Res.* **2003**, *36*, 140.
166b. Vetter, A. J.; Flaschenriem, C.; Jones, W. D. *J. Am. Chem. Soc.* **2005**, *127*, 12315.
166c. Jones, W. D.; Vetter, A. J.; Wick, D. D.; Northcutt, T. O. *ACS Symp. Ser.* **2004**, *885 (Activation and Functionalization of C-H Bonds)*, 56–69.
166d. Vetter, A. J.; Flaschenriem, C.; Jones, W. D. *J. Am. Chem. Soc.* **2005**, *127*, 12315.
167. Stahl, S. S.; Labinger, J. A.; Bercaw, J. E. *J. Am. Chem. Soc.* **1996**, *118*, 5961.
168. Mobley, T. A.; Schade, C.; Bergman, R. G. *J. Am. Chem. Soc.* **1995**, *117*, 7822.
169. Green, J. C.; Jardine, C. N. *J. Chem. Soc. Dalton Trans.* **1998**, 1057.
170. Jensen, M. P.; Wick, D. D.; Reinartz, S.; White, P. S.; Templeton, J. L.; Goldberg, K. I. *J. Am. Chem. Soc.* **2003**, *125*, 8614.
171. Churchill, D. G.; Janak, K. E.; Wittenberg, J. S.; Parkin, G. *J. Am. Chem. Soc.* **2003**, *125*, 1403.
172. Gross, C. L.; Girolami, G. S. *J. Am. Chem. Soc.* **1998**, *120*, 6605.
173. Martin, R. L. *J. Am. Chem. Soc.* **1999**, *121*, 9459.
174. Schafer, D. F. II; Wolczanski, P. T. *J. Am. Chem. Soc.* **1998**, *120*, 4881.
175. Shilov, A. E.; Shul'pin, G. B. *Chem. Rev.* **1997**, *97*, 2879.
175a. Shilov, A. E.; Shul'pin, G. B. Activation and Catalytic Reactions of Saturated Hydrocarbons in the Presence of Metal Complexes. In *Catalysis by Metal Complexes*; James, B. R., Ed., Kluwer: Dordrecht, Boston, and London, 2000; Vol. 21.
176. Stahl, S. S.; Labinger, J. A.; Bercaw, J. E. *Angew. Chem., Int. Ed. Engl.* **1998**, *37*, 2181.
176a. Labinger, J. A.; Bercaw, J. E. *Nature* **2002**, *417*, 507.
176b. Heyduk, A. F.; Zhong, H. A.; Labinger, J. A.; Bercaw, J. E. *ACS Symp. Ser.* **2004**, *885 (Activation and Functionalization of C-H Bonds)*, 250–263.
176c. Owen, J. S.; Labing, J. A.; Bercaw, J. F. *J. Am. Chem. Soc.* **2006**, *128*, 2005.
177. Lersch, M.; Tilset, M. *Chem. Rev.* **2005**, *105*, 2471.
178. Stahl, S. S.; Labinger, J. A.; Bercaw, J. E. *J. Am. Chem. Soc.* **1995**, *117*, 9371.
178a. Stahl, S. S.; Labinger, J. A.; Bercaw, J. E. *J. Am. Chem. Soc.* **1996**, *118*, 5961.
179. Johansson, L.; Ryan, O. B.; Tilset, M. *J. Am. Chem. Soc.* **1999**, *121*, 1974.
179a. Heiberg, H.; Johansson, L.; Gropen, O.; Ryan, O. B.; Swang, O.; Tilset, M. *J. Am. Chem. Soc.* **2000**, *122*, 10831.
179b. Johansson, L.; Tilset, M.; Labinger, J. A.; Bercaw, J. E. *J. Am. Chem. Soc.* **2000**, *122*, 10846.
180. Periana, R. A.; Taube, D. J.; Evitt, E. R.; Loffler, D. G.; Wentrcek, P. R.; Voss, G.; Masuda, T. *Science* **1993**, *259*, 340.
180a. Periana, R. A.; Taube, D. J.; Evitt, E. R.; Loffler, D. G.; Wentrcek, P. R.; Voss, G.; Masuda, T. *Science* **1998**, *280*, 560.
180b. Periana, R. A.; Taube, D. J.; Evitt, E. R.; Loffler, D. G.; Wentrcek, P. R.; Voss, G.; Masuda, T. *Science* **2003**, *301*, 814.
181. Kua, J.; Xu, X.; Periana, R. A.; Goddard, W. A. III *Organometallics* **2002**, *21*, 511.

181a. Gilbert, T. M.; Hristov, I.; Ziegler, T. *Organometallics* **2001**, *20*, 1183.
182. Wik, B. J.; Romming, C.; Tilset, M. *J. Mol. Catal. A* **2002**, *189*, 23.
182a. Yoshizawa, K. *Acc. Chem. Res.* **2006**.
183. Shimoi, M.; Nagai, S.; Ichikawa, M.; Kawano, Y.; Katoh, K.; Uruichi, M.; Ogino, H. *J. Am. Chem. Soc.* **1999**, *121*, 11704.
183a. Ueno, K.; Yamaguchi, T.; Uchiyama, K.; Ogino, H. *Organometallics* **2002**, *21*, 2347.
183b. Merle, N.; Koicok-Kohn, G.; Mahon, M. F.; Frost, C. G.; Ruggerio, G. D.; Weller, A. S.; Willis, M. C. *J. Chem. Soc., Dalton Trans.* **2004**, 3883.
184. Muhoro, C. N; He, X.; Hartwig, J. F. *J. Am. Chem. Soc.* **1999**, *121*, 5033.
185. Schlecht, S.; Hartwig, J. F. *J. Am. Chem. Soc.* **2000**, *122*, 9435.
185a. Montiel-Palma, V.; Lumbierres, M.; Donnadieu, B.; Sabo-Etienne, S.; Chaudret, B. *J. Am. Chem. Soc.* **2002**, *124*, 5624.
185b. Crestani, M. G.; Munoz-Hernandez, M.; Arevalo, A.; Acosta-Ramirez, A.; Garcia, J. J. *J. Am. Chem. Soc.* **2005**, *127*, 18066.
185c. Cook, K. S.; Incarvito, C. D.; Webster, C. E.; Fan, Y.; Hall, M. B.; Hartwig, J. F. *Angew. Chem., Int. Ed.* **2004**, *43*, 5474.
186. He, X.; Hartwig, J. F. *J. Am. Chem. Soc.* **1996**, *118*, 1696.
186a. Hartwig, J. F.; Muhoro, C. N. *Organometallics* **2000**, *19*, 30.
186b. Chen, H.; Schlecht, S.; Semple, T. C.; Hartwig, J. F. *Science* **2000**, *287*, 1995.
186c. Webster, C. E.; Fan, Y.; Hall, M. B.; Kunz, D.; Hartwig, J. F. *J. Am. Chem. Soc.* **2003**, *125*, 858.
187. Musaev, D. G.; Mebel, A. M.; Morokuma, K. *J. Am. Chem. Soc.* **1994**, *116*, 10693.
188. Smith, M. R. III, *Prog. Inorg. Chem.* **1999**, *48*, 505.
189. Yasue, T.; Kawano, Y.; Shimoi, M. *Angew. Chem., Int. Ed.* **2003**, *42*, 1727.
190. Nikonov, G. I. *Angew. Chem., Int. Ed. Engl.* **2003**, *42*, 1335.
191. Rybtchinski, B.; Milstein, D. *Angew. Chem., Int. Ed. Engl.* **1999**, *38*, 870.
192. Tomaszewski, R.; Hyla-Kryspin, I.; Mayne, C. L.; Arif, A. M.; Gleiter, R.; Ernst, R. D. *J. Am. Chem. Soc.* **1998**, *120*, 2959.
192a. Harvey, B. G.; Mayne, C. L.; Arif, A. M.; Ernst, R. D. *J. Am. Chem. Soc.* **2005**, *127*, 16426.
193. Eisch, J. J.; Piotrowski, A. M.; Brownstein, S. K.; Gabe, E. J.; Lee, F. L. *J. Am. Chem. Soc.* **1985**, *107*, 7219.
194. MacLaughlin, S. A.; Carty, A. F.; Taylor, N. J. *Can. J. Chem.* **1982**, *60*, 87.
195. Chen, W.; Shimada, S.; Tanaka, M. *Science* **2002**, *295*, 308.
196. Aullon, G.; Lledos, A.; Alvarez, S. *Angew. Chem., Int. Ed. Engl.* **2002**, *41*, 1956.
196a. Scherer, E. C.; Kinsinger, C. R.; Kormos, B. L.; Thompson, J. D.; Cramer, C. J. *Angew. Chem., Int. Ed. Engl* **2002**, *41*, 1953.

1.25
Advances in Carbon–Hydrogen Activation

W D Jones, University of Rochester, Rochester, NY, USA

1.25.1 Introduction

This chapter presents developments in the activation and functionalization of carbon–hydrogen bonds that have been discovered since 1993. Major breakthroughs in hydrocarbon activation appeared in the early 1980s, and in the following decade, an explosion of discoveries was seen in new examples of metal complexes that could activate C–H bonds. Mechanisms for cleavage included oxidative addition, electrophilic cleavage, radical H-abstraction, and metal atom reactions, and several texts are available that summarize the first decade of this work.[1,2]

These early discoveries form the basis for the growth of this field over the last 15 years. Advances have been made in understanding the fundamental basis for C–H activation, including both intermediates involved and the bond strengths of the metal–carbon bonds that are formed. A detailed understanding of both oxidative addition and electrophilic activation of C–H bonds is now in hand. New discoveries of alkane and arene functionalization allow the formation of useful derivatives in synthetically useful quantities. Many new examples of the use of transition metal C–H activation in organic transformations are being reported.

In light of the rapid advancement of this field of organometallic chemistry, this chapter attempts to highlight the most significant reports of C–H activation in the last decade. Over 1,000 papers have been published since 1990 that deal with some aspect of C–H activation.[3] Figure 1 shows how the number of publications in this field has increased (based on the search using SciFinder), so it can be anticipated that developments in this field will continue to grow at a swift pace.

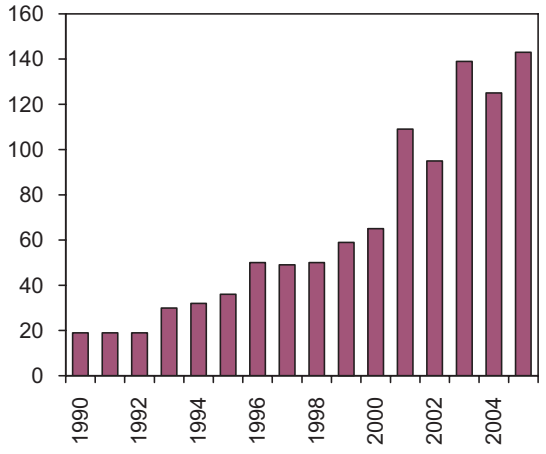

Figure 1 Annual number of publications on C–H activation.

1.25.2 Fundamental Aspects of C–H Bond Activation

1.25.2.1 Metal–Carbon Bond Strengths

The observation of C–H bond activation of alkanes via oxidative addition to iridium(I) and rhodium(I) complexes in 1982 sparked interest in expanding the scope and chemistry of metal complexes that could perform this reaction. One key aspect to understanding the possibility for this type of cleavage is to understand the thermodynamics of the process, which requires knowledge of the strength of the metal–carbon bond. More recent studies of trispyrazolylborate complexes have provided a range of relative metal–carbon bond strengths. These studies are paralleled by examinations of titanium and zirconium complexes that have widened the range even further.

The tris(3,5-dimethylpyrazolyl)borate(neopentylisocyanide)rhodium(I) fragment was reported to react with benzene to give a phenyl hydride product.[4] This reaction was extended to include activation of a number of alkanes using a carbodiimide derivative as a photochemical precursor (Equation (1)).[5,5a] The alkyl hydride products were found to be labile on the timescale of several hours, and conversion to the phenyl hydride complex could be monitored as a first-order reaction in benzene solvent, providing a measure of the barrier to reductive elimination ($\Delta G^{\ddagger}_{re}$) for each R group studied. In addition, irradiation of the carbodiimide complex in a mixture of two hydrocarbons provided a measure of the difference in the barriers to oxidative addition ($\Delta\Delta G^{\ddagger}_{oa}$). By combining these three values for any pair of hydrocarbons (as shown in Figure 2 for benzene vs. neohexene), one can obtain the thermodynamic preference (ΔG^{0}) for activation of one hydrocarbon over the other, even if this equilibrium could not be directly measured. This study showed that while the range of kinetic selectivities was quite small, the range of thermodynamic selectivities was quite large.

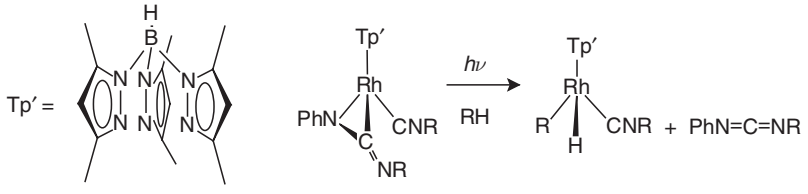

(1)

In addition, relative metal–carbon bond strengths were obtained by combination of the ΔG^{0} value with the difference in C–H bond strengths ($D_{rel} = \Delta G^{0} + D_{R–H} - D_{R'–H}$). A plot of the relative metal–carbon bond strength versus the C–H bond strength (Figure 3) shows that the increase in M–C bond strength is ~1.2 times greater than the increase in C–H bond strength, which provides the rational for why cleavage of stronger C–H bonds is preferred thermodynamically.

Another system in which metal–carbon bond strengths have been investigated in detail is the titanium system $(silox)_2Ti(NHSiBu^t_3)R$. These complexes lose hydrocarbon RH to generate transient $[Ti(silox)_2(=NSiBu^t_3)]$, which then adds a C–H bond from the solvent across the Ti=N bond (Equation (2)).[6] The equilibrium activation between two hydrocarbons could be directly measured in this system (ΔG^{0}), and construction of a ladder of stabilities was established for some 15 substrates.[7] In this system, relative metal carbon bond strengths could be directly obtained

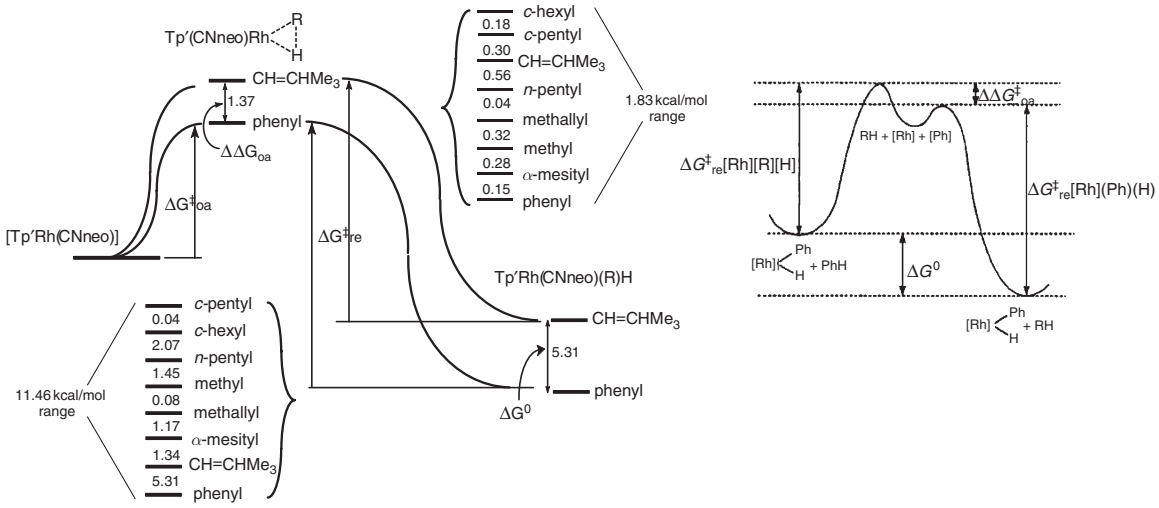

Figure 2 Use of reductive elimination barriers ($\Delta G^{\ddagger}_{re}$) and oxidative addition selectivities ($\Delta\Delta G^{\ddagger}_{oa}$) to determine thermodynamic preference for hydrocarbon activation (ΔG^0). Reprinted from Jones, W. D.; Wick, D. D. *Organometallics* **1999**, *18*, 495–505, with permission from the American Chemical Society.

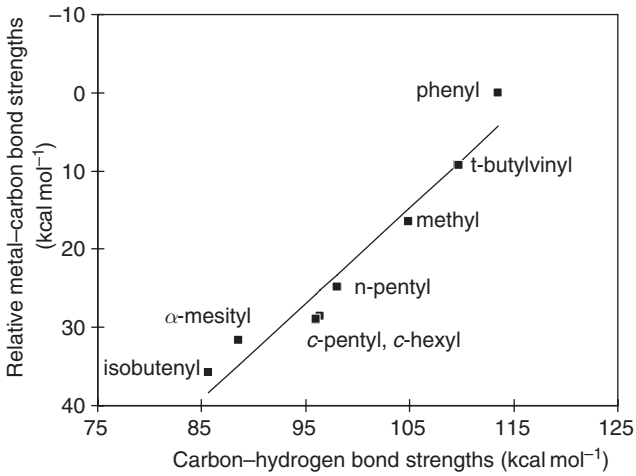

Figure 3 Relation between metal–carbon bond energies and C–H bond strengths in Tp′Rh(CNneopentyl)(R)H complexes. The slope of the line is 1.22. Reprinted from Jones, W. D.; Wick, D. D. *Organometallics* **1999**, *18*, 495–505, with permission from the American Chemical Society.

from ΔG^0 ($D_{rel} = \Delta G^0 + D_{RH} - D_{R'H}$), and kinetic selectivities could be obtained by combination of the rates of elimination of RH ($\Delta G^{\ddagger}_{re1}$, $\Delta G^{\ddagger}_{re2}$) and ΔG^0 ($\Delta\Delta G^{\ddagger}_{addn} = \Delta G^{\ddagger}_{re1} - \Delta G^{\ddagger}_{re2} + \Delta G^0$). A plot of Ti–C bond strength versus C–H bond strength is shown in Figure 4, in which a slope of 1.1 is observed for all data (slope = 1.36 excluding Ph, benzyl, mesityl, H), again providing evidence that differences in metal–carbon bond strengths exceed differences in C–H bond strengths by ~20%. The kinetic selectivities in the titanium system span a range of ~6 kcal mol^{-1}, much larger than in the [Tp′Rh(CNR)] system (1.6 kcal mol^{-1}), a difference that is attributed to the different transition states involved in C–H activation: direct addition of the C–H bond across the Ti=N bond in the former versus complexation of the alkane to form a σ-complex in the latter.

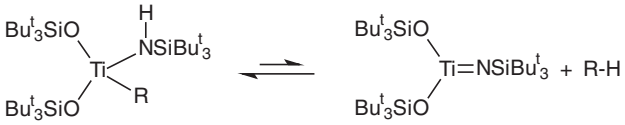

(2)

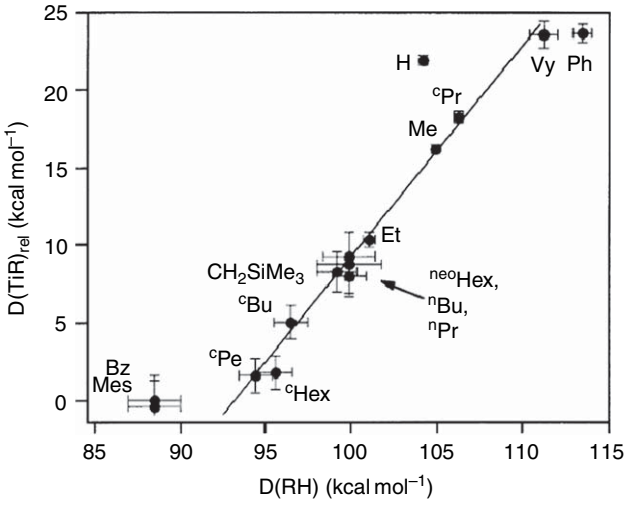

Figure 4 Relation between metal–carbon bond energies and C–H bond strengths in Ti(silox)$_2$(NHSiBu$^t_3$)R complexes. The slope of the line is 1.36, excluding Ph, benzyl, mesityl, and H. Reproduced from Bennett, J. L.; Wolczanski, P. T. *J. Am. Chem. Soc.* **1997**, *119*, 10696–10719, with permission from the American Chemical Society.

Other similar systems also showed an ability to determine relative metal–carbon bond strengths, although only for a limited set of hydrocarbon substrates. The tantalum intermediate [Ta(NHSiBu$^t_3$)(=NSiBu$^t_3$)$_2$] adds to the C–H bonds of benzene, toluene, and methane, and at 180 °C these products exchange hydrocarbons with the solvent, allowing ΔG^0 to be determined (Equation (3)).[8] For this limited set of data, the slope of a line correlating D_{M-C} with D_{C-H} has a slope of 1.0, indicating that metal–carbon and carbon–hydrogen bond strengths parallel each other for this metal complex. In the zirconium systems Zr(NHSiBu$^t_3$)$_3$R, which lose RH reversibly upon heating, remarkably little thermodynamic preference was seen between benzene, toluene (aromatic or benzylic C–H), methane, and cyclopropane (Equation (4)).[9] These observations are consistent with those seen in the tantalum system, where differences in M–C bond strengths are matched by the differences in C–H bond strengths.

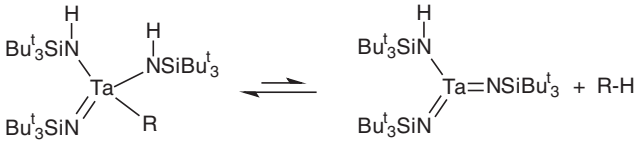

(3)

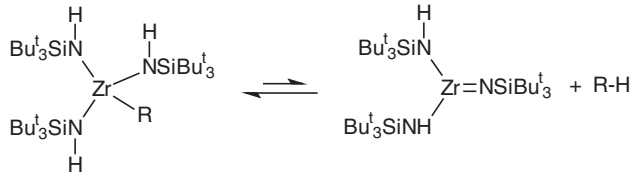

(4)

1.25.2.2 Alkane σ-complexes as Intermediates

1.25.2.2.1 Direct observation of alkane σ-complexes

In the activation of C–H bonds of hydrocarbons by either electrophilic or oxidative addition pathways, complexation of the alkane is believed to precede oxidative cleavage of the C–H bond.[10] In several cases, direct spectroscopic detection of these species (IR, NMR) has been possible, and provides further evidence for their presence beyond the early work with M(CO)$_5$ species in matrices[11] and solution by photoacoustic spectroscopy.[12]

Table 1 Equilibrium and rate constants of alkanes with [Cp*Rh(CO)] at −80 °C in liquid Kr

Alkane	K_{eq}	k_2 (s^{-1})
Ethane	14	28×10^5
Propane	140	11×10^5
Hexane	350	11×10^5
Octane	400	10×10^5
Cyclopentane	1,200	8.5×10^5
Cyclohexane	900	7.0×10^5
Cycloheptane	12,000	1.0×10^5
Cyclooctane	15,000	1.0×10^5

Reprinted from McNamara, B. K.; Yeston, J. S.; Bergman, R. G.; Moore, C. B. *J. Am. Chem. Soc.* **1999**, *121*, 6437–6443, with permission from the American Chemical Society.

Several studies using time resolved infrared spectroscopy (TRIR) have been reported for several metal carbonyl complexes in which transient σ-alkane complexes could be observed. Laser flash excitation of $Cp^*Rh(CO)_2$ in liquid krypton solution leads to the formation of a metal–krypton complex. In the presence of cyclohexane, $Cp^*Rh(CO)$(cyclohexyl)H is formed at a rate that is consistent with reversible formation of a σ-cyclohexane complex prior to oxidative cleavage of the C–H bond,[13] that is, krypton and cyclohexane compete for the vacant site on the metal. With neopentane-d_{12}, the IR signals for the krypton complex and the σ-alkane complex could just be distinguished, and both alkane equilibrium binding constants and oxidative cleavage rate constants could be determined (Equation (5)).[14,14a] Table 1 shows how K_{eq} and k_2 vary as a function of the nature of the alkane. In general, the longer alkanes are bound more favorably than the shorter alkanes, yet the C–H oxidative cleavage rates are the same for alkanes larger than ethane. The σ-alkane complexes of the type $Cp^*Rh(CO)$(alkane) were generally observed to have lifetimes of ∼1 μs at −80 °C. In contrast, the corresponding iridium complex was observed to undergo C–H oxidative cleavage in less than a few picoseconds.[15]

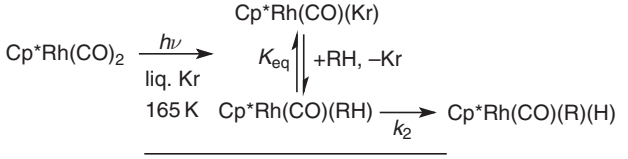

at 163 K:

R	K_{eq}	k_2 (s^{-1})
c-Hexyl	1,450	6.85×10^4
Neopentyl	1,180	3.90×10^4

(5)

Flash photochemical studies of the related tris(2,5-dimethylpyrazolyl)boratedicarbonyl-rhodium complex $Tp'Rh(CO)_2$ also provided evidence for the intermediacy of a σ-alkane complex prior to oxidative cleavage.[16,16a] In this case, two intermediates were observed, the first assigned as the σ-alkane complex with an η^3-Tp′ ligand that converts into a second σ-alkane complex with an η^2-Tp′ ligand in ∼200 ps. Oxidative cleavage was then seen to occur in ∼230 ns, with the concomitant reformation of the η^3-Tp′ (Equation (6)).

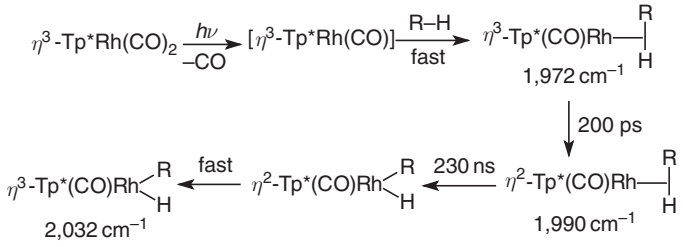

(6)

Irradiation of $CpRe(CO)_3$ in heptane solution was shown to produce transient species characterized as the σ-alkane complex $CpRe(CO)_2$(heptane) by TRIR. This complex underwent a second-order backreaction with CO to regenerate the starting complex. Similar complexes were observed upon irradiation of $CpV(CO)_4$, $CpNb(CO)_4$,

$CpTa(CO)_4$, $(C_6H_6)Cr(CO)_3$, $(C_6H_6)Mo(CO)_3$, $(C_6H_6)W(CO)_3$, and $CpMn(CO)_3$, but all of these had lifetimes at least 1,000× shorter than the rhenium complex.[17,17a]

Perhaps the strongest evidence for the formation of an alkane complex comes from the low temperature NMR experiments with $CpRe(CO)_3$. Irradiation at −80 °C in cyclopentane results in the formation of $CpRe(CO)_2$(c-pentane), for which a resonance for the CH_2 bound to the metal is observed in the NMR spectrum at δ −2.32, consistent with either a symmetrical binding of both hydrogens (η^2-H,H) or a rapid interchange between two σ-C–H (η^2-C,H) complexes.[18]

Irradiation in pentane solvent leads to the formation of three distinct species, assigned as coordination of rhenium to the methyl, α-methylene, and central methylene of pentane (Equation (7)).[19]

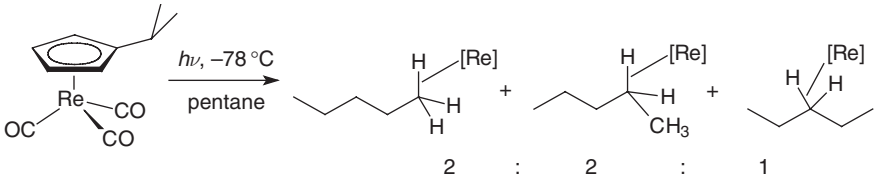

(7)

1.25.2.2.2 Indirect evidence for alkane σ-complexes

A number of studies have provided indirect evidence for σ-alkane complexes. One commonly used method is to prepare a metal alkyl deuteride complex that can then rearrange to an α-deuterioalkyl hydride complex prior to reductive elimination of alkane (Equation (8)). Complexes that have been found to undergo such rearrangements include $Cp^*_2W(CH_3)D$,[20,20a] $[(C_5H_4)_2CMe_2]W(CH_3)D$,[21] Tp′Rh(CNR)($CH_3$D),[22] (tacn)Rh($PMe_3$)($CH_3$)D,[23] and $Cp^*Ir(PMe_3)(R)D$.[24,24a] One example of hydride/methyl C–H interchange has been observed by spin saturation transfer between the two types of hydrogen nuclei in $[Cp^*Os(dmpm)(CH_3)H]^+$.[25]

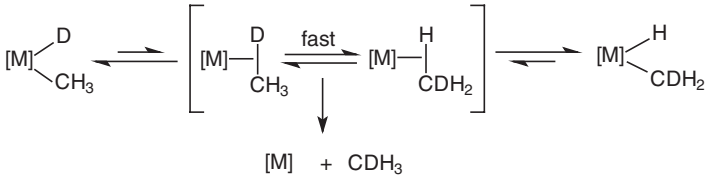

(8)

Alkane σ-complexes have also been invoked in the rearrangements of longer alkyl deuteride complexes. Flood reported the migration of a rhodium cation along a 10-carbon chain in the rearrangement of a deuterated triazacyclononane complex (Equation (9)). Migration into the α-position was seen to occur more rapidly.[26] A similar study was done in the migration in a series of alkyl complexes of Tp′Rh(CNneopentyl)(R)D, where R = methyl to *n*-hexyl. By simulation of the data in this study, the relative rates for the various processes available to a σ-alkane intermediate (dissociation, C–H oxidative cleavage, or migration) could be obtained. It was found that oxidative cleavage of the terminal methyl group was the fastest, followed by migration, followed by dissociation. Oxidative cleavage of a secondary C–H bond was by far the slowest process.[27]

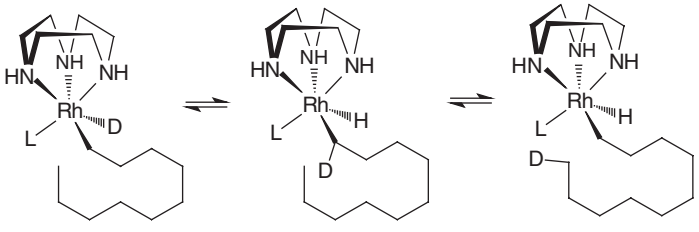

(9)

A related study was done in which the binding of the 16-electron rhodium fragment to methyl versus methylene groups was determined by competitions between pairs of alkanes, such as propane and pentane. It was established that a methylene group binds 1.5 times faster than a methyl group.[28]

1.25.2.2.3 Isotope effects in C–H bond activation

In studying the use of deuterium to monitor intramolecular interchanges of alkyl groups, several determinations of kinetic and thermodynamic isotope effects were made. In general, the thermodynamic preference is for isotopomers

with deuterium on carbon (the higher energy oscillator). Isotope effects on oxidative cleavage of alkanes are seen to be normal (i.e., >1), whereas isotope effects on reductive coupling are seen to be inverse (i.e., <1). In many cases examined, the observed kinetic isotope effect k_H/k_D on the overall process of alkane loss was *inverse*. ((i) Examples of inverse k_H/k_D for $Cp^*Ir(PMe_3)(H)(C_6H_{11})$ in C_6D_6 at 130 °C, 0.7(1), for $Cp^*Rh(PMe_3)(H)(C_2H_5)$ in toluene-d_8 at −30 °C, 0.5(1), for $Cp_2WH(CH_3)$ in CD_3CN at 72.6 °C, 0.75(4), for $Cp^*_2WH(CH_3)$ in C_6D_6 at 100 °C, 0.77(7), for $[Cp_2Re(H)(CH_3)][Cl]$ in CD_2Cl_2 at 9 °C, 0.8(1), for $[CnRh(PMe_3)(H)(CH_3)][BAr_4]$ in C_6D_6 at 75 °C, 0.74(2), and for (tmeda)$Pt(CH_3)(H)(Cl)$ in CH_3OH at −27 °C, 0.29, are given in Refs: 29, 29a, 29b, 29c, 29d, 29e, and 29f, respectively. (ii) Examples of normal k_H/k_D for $(PPh_3)_2Pt(Me)H$, 3.3, for $(PPh_3)_2$ $Pt(CH_2CF_3)H$, 2.2, and for $(Cy_2PCH_2CH_2PCy_2)Pt(CH_2CMe_3)$ H, 1.5 are given in Refs: 30, 30a, and 30b, respectively.) Hence, it became common to associate an inverse isotope effect with the intermediacy of a σ-alkane complex. Furthermore, since virtually all of this isotope effect would likely be associated with the C–H/C–D bond making/breaking step, rather than in the alkane dissociation step, the overall isotope effect for alkane loss was attributed to an "inverse equilibrium isotope" effect (i.e. $K_{eq}^{H/D} < 1$) separating the alkyl hydride complex from the σ-alkane complex.

Two recent articles describe details of the isotope effects in C–H activation. One separates the kinetic isotope effect on reductive coupling from that of oxidative cleavage by looking at the irreversible loss of propane from Tp′Rh(CNneopenyl)(*i*-propyl)D/H. The oxidative cleavage isotope effect was measured by irreversible activation of CH_2D_2. These separate measurements were combined to give an overall inverse equilibrium isotope effect on alkane loss.[31]

In a separate study, kinetic isotope effects were determined for the individual steps in methane loss from tungstanocene methyl hydride. These results were combined with theoretical studies that produced a complete picture for understanding isotope effects in terms of the contributing factors (zero point energy, mass moment of inertia, and excitation terms). The conclusion was that it is possible to observe either inverse or normal isotope effects, depending on the temperature at which the study is conducted.[32,32a]

1.25.3 Activation by Oxidative Addition

C–H activation by oxidative addition generally proceeds by generation of an unsaturated metal fragment in the presence of a hydrocarbon solvent. As intermediates in the C–H bond activation process, σ-alkane complexes have widely been proposed as described in the preceding section. Several new metal systems have been found to undergo oxidative addition to hydrocarbon C–H bonds.

The trimethyltriazacyclononanerhodium complex shown in Equation (10) undergoes reversible loss of methane and addition of $^{13}CH_4$ at 80 °C. In benzene, activation of the aryl C–H bond is seen.[33]

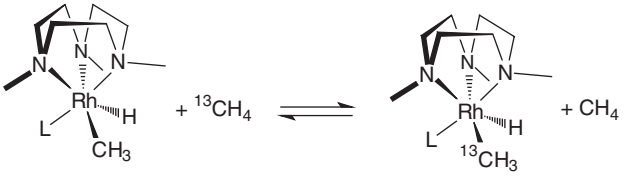

(10)

Several studies have examined substituted fluoroarenes in C–H activation. Reaction of the fragments $[CpRh(PMe_3)]$ and $[Cp^*Rh(PMe_3)]$ with fluoronated benzenes gives kinetic products in which the most accessible C–H bond is cleaved. Upon heating, conversion to a thermodynamic isomer is observed in which the number of *ortho*-fluorine substituents is maximized (Equation (11)).[34] Similar observations have been made with the related Cp and Cp^* rhenium carbonyl complexes.[35] Theoretical studies have shown that the number of *ortho*-fluorine substituents is directly related to the M-aryl bond strengths, accounting for these trends.[36,36a]

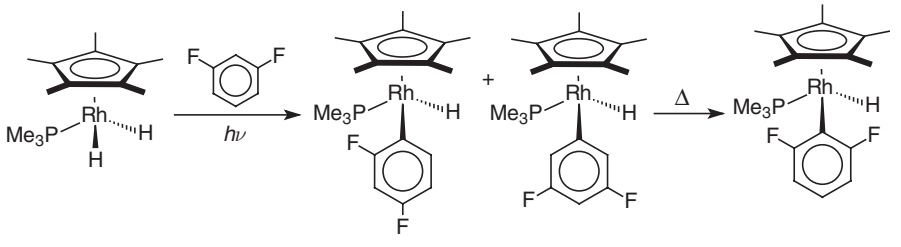

(11)

A trispyrazolylborate platinum complex was found to activate C–H bonds via a Pt(II)/Pt(IV) sequence. Removal of a methyl anion from $[(\eta^2\text{-Tp}')RhMe_2]^-$ leads to an unsaturated species that then adds to the hydrocarbon C–H bond (Equation (12)).[37] The related protonated species $Tp'PtMe_2H$ loses methane at 110 °C and then oxidatively adds benzene-d_6. The new methyl-phenyl-deuteride derivative then reversibly exchanges deuterium into the methyl group, indicating reversible methane activation.[38] In addition, the Pt–H bond can undergo reaction with oxygen to give a Pt–O–OH group.[39]

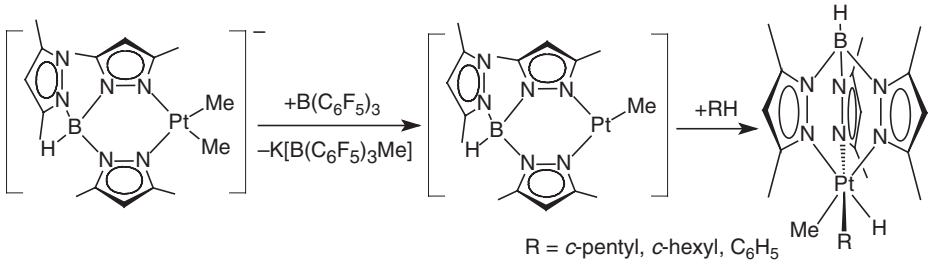

(12)

Related chemistry has been seen with $Tp'PtPhH_2$. Protonation of one arm of the Tp′ ligand induces reversible reductive coupling of phenyl and hydride to give an η^2-C_6H_6 complex (Equation (13)). This species was found to be in rapid equilibrium with the Pt(IV) phenyl dihydride complex.[40,40a] Addition of $B(C_6F_5)_3$ to the methyl dihydride induces loss of methane and activation of benzene solvent.[41]

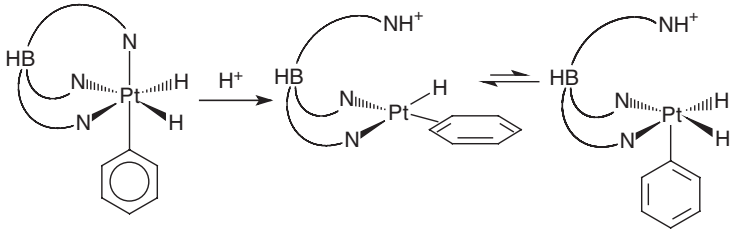

(13)

A study of a platinum β-diiminate (nacnac) complex provides evidence for oxidative addition to C–H bonds. Starting with a stable Pt(IV) trimethyl adduct, loss of ethane produces a reactive Pt(II) intermediate that metallates the ligand (Pt(II) → Pt(IV)) and reductively eliminates methane(Pt(IV) → Pt(II)). β-Elimination then generates an observable pendant olefin hydride complex. This species serves as a reversible source of the unsaturated Pt(II) intermediate, which can reversibly add to alkane solvent C–H or C–D bonds, permitting deuteration of the isopropyl groups of the ligand (Equation (14)).[42]

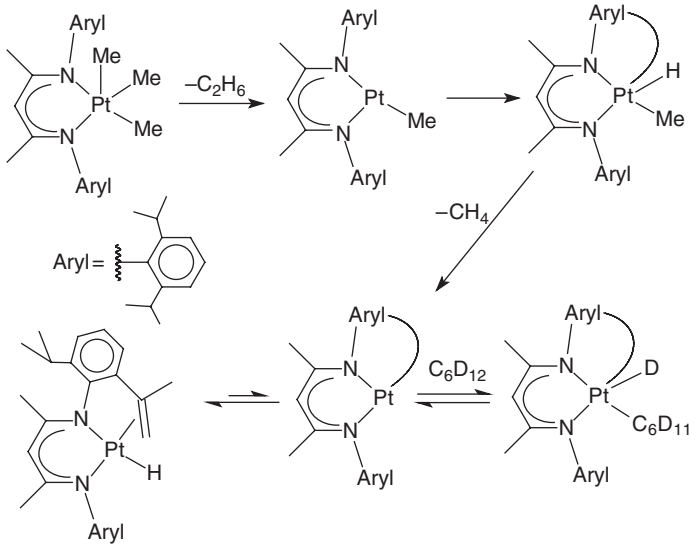

(14)

1.25.4 Electrophilic Activation of Carbon–Hydrogen Bonds

1.25.4.1 Studies Using Platinum Complexes

Among the earliest reports of alkane activation by a transition metal complex were the articles by Shilov in which Pt(II) served as a catalyst for methane oxidation and Pt(IV) served as a stoichiometric oxidant.[43] The mechanism of C–H activation was termed "electrophilic," as the cationic metal was postulated to interact with the electrons of the C–H bond which then lost a proton, forming a metal–carbon bond without a change in oxidation state. Oxidation of the complex by two electrons was then followed by nucleophilic attack at carbon, giving a functionalized hydrocarbon (Scheme 1).

Further studies on this chemistry have appeared in the 1990s from Bercaw and co-workers. For example, the oxidation of ethanol to ethylene glycol and propanol to propanediol has been reported.[44] The intermediate $[PtCl_3Me]^{2-}$ has been observed directly.[45] In addition, mechanistic studies have shed light on the intermediates in these reactions. Reaction of *cis*-dideuterio Zeise's salt with aqueous Pt(IV) leads to a β-hydroxyethyl complex of a single configuration (*d*,*l*) due to inversion at carbon upon attack of water on the coordinated ethylene. The next step in which chloride ion displaces the alkyl group, as in the Shilov system, was found to proceed by inversion of configuration, supporting an S_N2-type mechanism for this step (Equation (15)).[46]

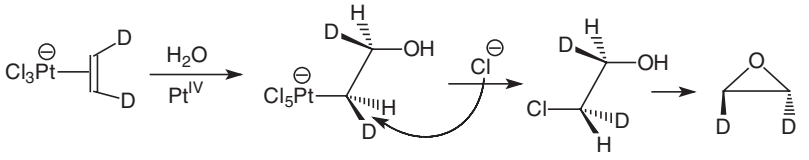

(15)

Mechanistic details of the oxidation step were also investigated. Reaction of enriched $[^{195}PtCl_6]^{2-}$ oxidant with $[PtCl_3(C_2H_4)]^-$ in water leads to initial formation of the Pt(II)-β-hydroxylethyl complex $[PtCl_3(CH_2CH_2OH)]^{2-}$, which then is oxidized to unlabeled $[PtCl_5(CH_2CH_2OH)]^{2-}$. Since the latter is not enriched, the hydroxyethyl group is not transferred during oxidation, and the oxidation must occur by electron, not alkyl group, transfer.[47] These studies together provide support for the original pathway proposed by Shilov, and a summary of this work has appeared.[48]

In order to work with more tractable systems, platinum–TMEDA complexes (TMEDA = tetramethylethylenediamine) have also been studied. Here, generation of Pt(IV) species from Pt(II) alkyl precursors results in reductive elimination of alkane (Scheme 2). The dimethylchloro Pt(IV) intermediate was found to be more stable than the methyldichloro intermediate. Inhibition studies demonstrate that chloride dissociation from the Pt(IV) intermediate precedes reductive elimination.[49]

Removal of chloride altogether from the Pt^{II}(TMEDA) methyl compound gives a cationic species that can activate methane reversibly.[50,50a] The weak donor perfluoropyridine is easily lost in this reaction.

The next development in electrophilic Pt chemistry came with the introduction of the diimine ligand, in which bulky aryl groups adjacent to the metal center prevent undesirable dimerization reactions. In analogy to the above chemistry with TMEDA, Tilset discovered that protonation of the a diiminedimethylplatinum(II) complex led to a cationic Pt(II) methyl species that could react with C–H aliphatic and aromatic bonds.[51,51a] In joint work with Bercaw, it was shown that the ancilliary solvent ligand adjacent to the methyl group played an important role in the facility of alkane activation, with strongly binding solvents inhibiting the activation (Equation (16)).[52] Trifluoroethanol was

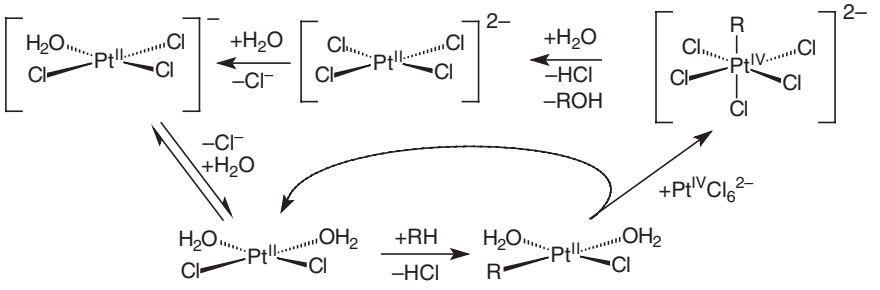

Scheme 1

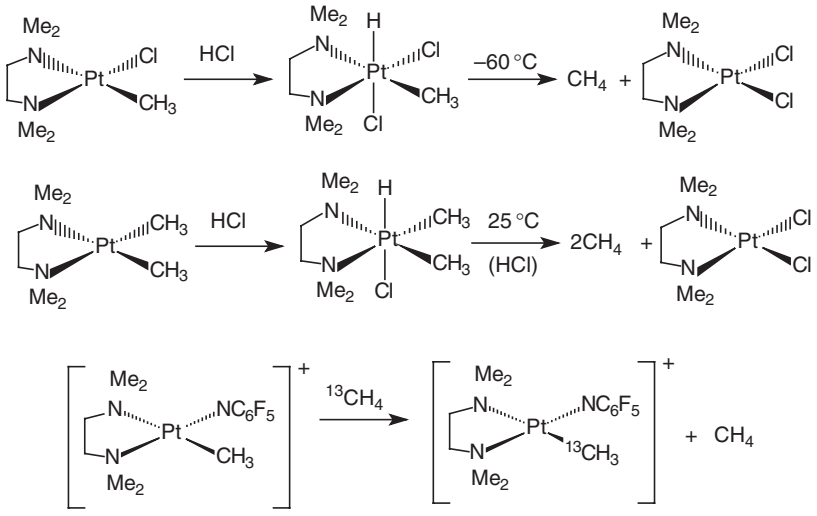

Scheme 2

found to bind weakest, and was the preferred ligand for C–H activation work. Water bound more tightly, and acetonitrile bound even more tightly. Acetonitrile was even found to undergo associative displacement of methane in the intermediate σ-methane species.[53,53a] A variety of aryl diimine ligands were examined, showing the effect of sterics on C–H activation selectivity in alkylated benzenes.[54] In one case, a π-benzene adduct could be observed prior to C–H activation. By studying the effect of [CH_3CN] on the protonation of the dimethyl precursor to the cation, it was demonstrated that the kinetic site of protonation was at the metal, and, by microscopic reversibility, methane activation must occur by way of a Pt(IV) dimethylhydrido intermediate. $B(C_6F_5)_3$ was also found to be capable of producing the Pt(II) methyl cation from the dimethyl complex by methide abstraction. A preference for benzylic C–H activation was seen, but was attributed to the formation of an η^3-benzyl product.[55]

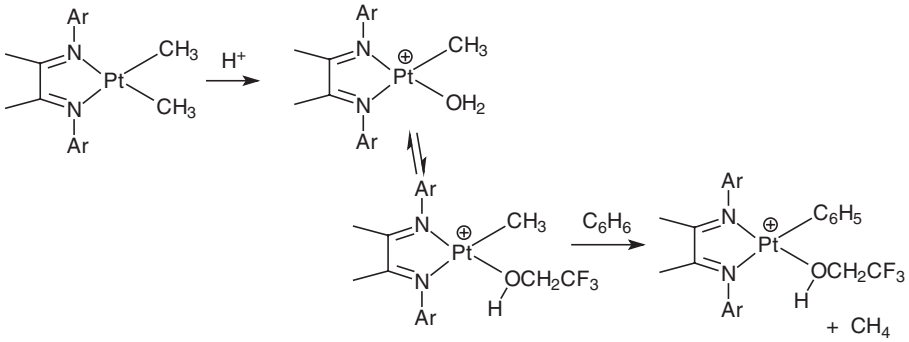

(16)

Periana discovered that use of bispyrimidine (bpym) as a ligand leads to stabilization of Pt(II) in the Shilov system. It was shown that Pt(0) would actually be taken back into solution using bpym in strongly acidic media. At 220 °C in sulfuric acid solution, he showed that Pt(bpym)$(OSO_3H)_2$ could catalyze the oxidation of methane to methylbisulfate (Scheme 3). The proposed mechanism involved methane activation by a Pt(II) cation and oxidation to Pt(IV) by SO_3 (formed in the hot H_2SO_4).[56]

Sen has also reported several alkane C–H activation and functionalization reactions using platinum(II). In a re-examination of the Pt(II)/Pt(IV)/H_2O Shilov system, he found that methane oxidation was about six times more rapid than methanol oxidation.[57] Reactions of ethane were found to proceed through a Zeise's salt intermediate, $[PtCl_3(C_2H_4)]^-$, leading to ethanol and ethylene glycol as major products.[58] Furthermore, in functionalized alkanes, terminal activation and functionalization followed the trend $CH_3CH_2OSO_3H > CH_3CH_2OPO_3H > CH_3CH_2CO_2H > CH_3CO_2H > CH_3CH_2CH_2OH$, confirming the low reactivity of alcohols.[59] In studies using Pt(II) and $CuCl_2$ in the presence of oxygen as oxidant, alkylsulfonic acids could be ω-hydroxylated catalytically (up to 50 turnovers).[60]

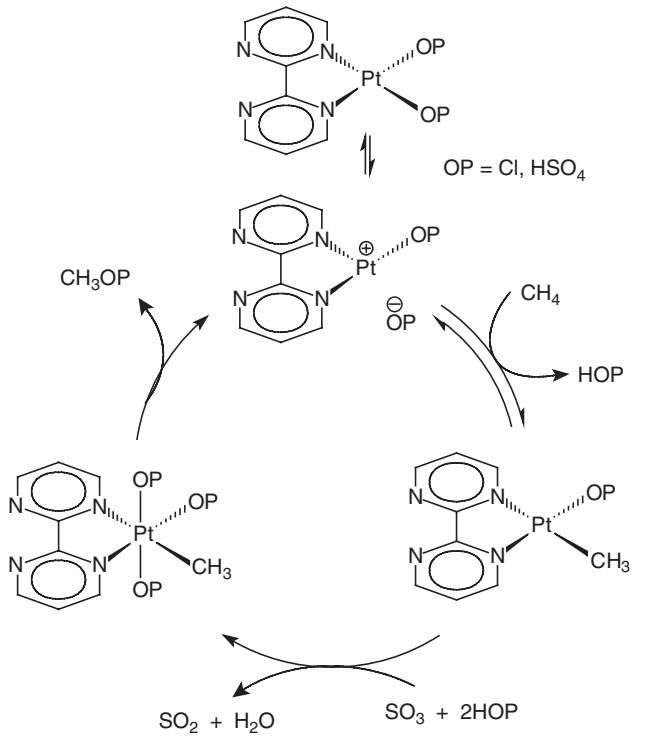

Scheme 3

1.25.4.2 Studies Using Iridium Complexes

In 1993 Bergman discovered that an iridium(III) methyl cation was capable of undergoing an exchange of the methyl group with other alkanes in a process that looked similar to the electrophilic activation of alkanes by Shilov's Pt(II) complex (Equation (17)).[61,61a] Theoretical treatment of this system provided evidence that the actual pathway involved oxidative addition of the alkane to give an Ir(V) dialkylhydride that then underwent reductive elimination of methane.[62,62a]

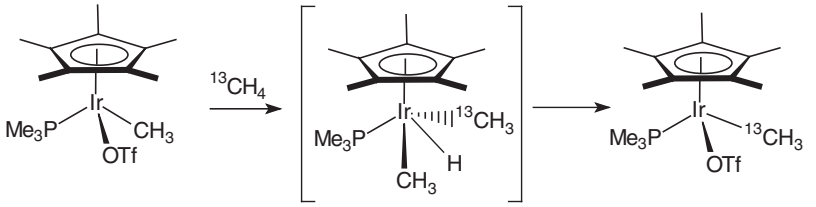

(17)

In 2000, Periana reported an Ir(III)(acac)$_3$ complex that could activate benzene and catalyze anti-Markovnikov additions of olefins to the aryl C–H bond.[63,63a] An iridium–phenyl complex was shown to be an intermediate.[64] This complex was converted to an Ir(III) derivative containing an iridium–methyl bond, a species which underwent alkane C–H activation (Equation (18)).[65]

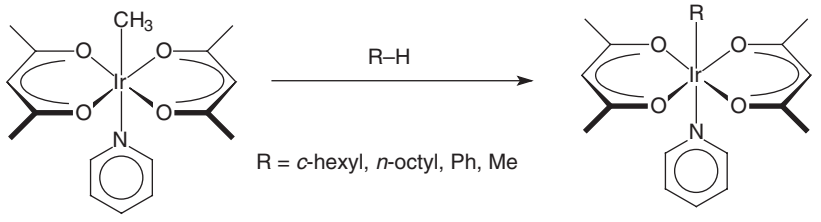

(18)

More recently, a bis-tropolonato iridium(III) methyl complex was found to undergo a similar metathesis with alkane C–H bonds.[66] This complex also catalyzed the anti-Markovnikov addition of olefins to arenes.[67]

1.25.4.3 Studies Using Other Metal Ions

Several other cationic metal systems have proved to be active in C–H bond activation and functionalization by way of electrophilic pathways. In 1993, Periana reported that $Hg(OSO_3H)^+$ could activate methane and then eliminate methylbisulfate. The reaction was catalytic at 180 °C, and gives 85% selectivity to the intermediate at 50% methane conversion with a turnover frequency of 10^{-3} per second.[68] Sen also studied Hg^{2+} and other catalysts (Pd^{2+}, Ce^{4+}, $S_2O_8^{2-}$) for methane oxidation to methylbisulfate in H_2SO_4 solvent. He observed that ethane oxidation gave up to 25% methylbisulfate, which led to the conclusion that radical processes were involved with this substrate to generate carbocations that could fragment.[60,69] These studies with the radical initiator $S_2O_8^{2-}$ leave open the question as to whether methane oxidation under these conditions proceeds by radical, electrophilic, or a combination of the two mechanisms.

Sen also reported the use of iodide-promoted $RhCl_3$ as a catalyst for the oxidative carbonylation to acetic acid. In this reaction, $[Rh(CO)_2I]_2$ is observed as an intermediate and oxygen is employed as the oxidant (Equation (19)). While this system is similar to the Monsanto system for the carbonylation of methanol, it was shown that methanol is not an intermediate. Oxidative carbonylation in the presence of $^{13}CH_3OH$ gave only unlabeled acetic acid plus $H^{13}COOH$.[70]

$$CH_4 + CO + O_2 \xrightarrow[KI,\ H_2O,\ 100\,^\circ C]{RhCl_3} CH_3COOH \qquad (19)$$

Palladium was also investigated for oxidative carbonylation using O_2 as oxidant, but now $CuCl_2$ was added to re-oxidize the palladium metal. These reactions were carried out in aqueous trifluoroacetic acid, and led to the formation of a mixture of methanol and its triflate ester.[71]

Flood looked at an intramolecular Pd(II) C–H cleavage in which the stereochemistry of the C–H activation was determined. The cyclometallation of (*R*)-(−)-8-(α-deuterioethyl)quinoline by K_2PdCl_4 led to the formation of a product in which net retention of configuration at carbon was observed (Equation (20)). A large kinetic isotope effect ($k_H/k_D = 44$) allowed selective activation of the C–H bond, and complexation with leucine provided a diastereotopic center for analysis.[72]

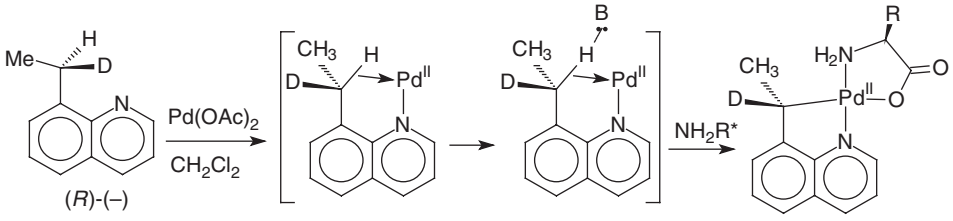

(20)

1.25.5 Alkane Dehydrogenation

1.25.5.1 Studies of L_2RhCl Systems

In the late 1980s, the complex $RhCl(CO)(PMe_3)_2$ was reported by Goldman to be able to photochemically dehydrogenate alkanes to give dihydrogen plus alkenes.[73] In the early 1990s this work was extended to thermal reactions carried out in the presence of dihydrogen, in which a sacrificial hydrogen acceptor was employed to keep the catalyst in its active form (Equation (21)).[74,74a] Extensive studies of this system with different phosphines showed that dimer formation led to catalyst deactivation.[75] This work was extended to a metal complex that did not require an acceptor to stoichiometrically dehydrogenate cyclooctane, $RhCl(CO)(P\text{-}i\text{-}Pr_3)_2$, an observation that would open up a whole new world of chemistry.[76] Jensen also reported that the related iridium complex could catalyze the transfer dehydrogenation between cyclooctane and *t*-butylethylene.[77]

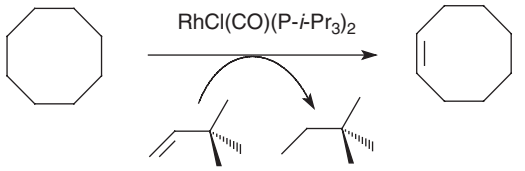

(21)

Goldman also discovered that these same complexes could catalyze the incorporation of CO into hydrocarbons to give aldehydes. Irradiation of $RhCl(CO)(PMe_3)_2$ in benzene in the presence of CO generated benzaldehyde by a two-photon mechanism involving an excited state that activated the benzene C–H bond, and a second photon that promoted the CO insertion.[78] The analogous photochemical reaction with alkanes also gave linear and branched aldehydes, the former arising from a two-photon cycle (one photon involving CO dissociation[79]) and the latter from a one-photon radical pathway.[80]

1.25.5.2 Studies Using Pincer Systems

Alkane dehydrogenation took a step forward in 1996 with the report of rhodium and iridium pincer complexes that could catalyze transfer hydrogenation. While the rhodium complex was found to be active but unstable, the iridium complex was stable even after a week at 200 °C. This permitted it to efficiently catalyze the transfer hydrogenation of cyclooctane to cyclooctene (12 t.o./min, Scheme 4).[81,81a] The reaction is inhibited by high concentrations of olefin, either the *t*-butylethylene acceptor or the cyclooctene product. Dinitrogen also inhibited the reaction.[82] A variety of other hydrocarbons were found to undergo transfer dehydrogenation using this catalyst and *t*-butylethylene as acceptor. Methylcyclohexane was converted to toluene, decalin was converted to naphthalene, ethylbenzene was converted to styrene, and THF was converted to furan and dihydrofuran.[83,83a] In addition, while the *t*-butylphosphine complex was not effective for dehydrogenation of linear alkanes, the isopropylphosphine derivative was found to produce substantial yields of 1-octene from octane at 150 °C. Over time, the amount of terminal olefin was seen to decrease as internal alkenes increased.[84,84a] The isopropylphosphine analog was also found to undergo transfer dehydrogenation of a variety of hydrocarbon substrates.[85] Tertiary aliphatic amines were found to undergo transfer dehydrogenation to give enamines,[86] whereas secondary aliphatic amines gave imines.[87] Aliphatic alcohols gave terminal aldehydes using *t*-butylethylene as acceptor.[88]

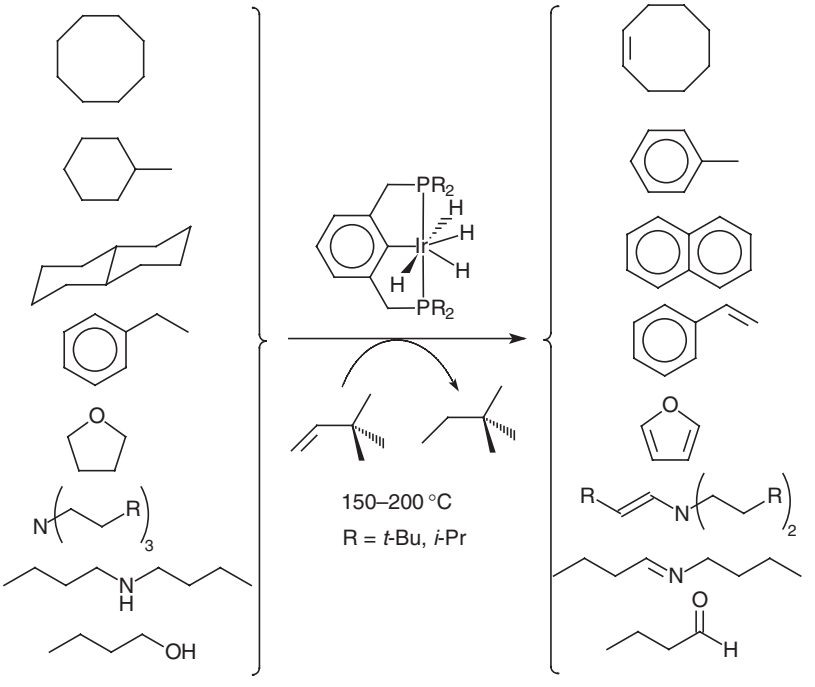

Scheme 4

When the iridium hydride is reacted with a hydrogen acceptor, simple oxidative addition adducts can be seen for aromatic and vinylic C–H containing substrates.[89] With nitrobenzene, although a thermodynamic preference is seen for an orthometallated chelate product, the kinetic preference is for *meta*- and *para*-C–H activation, which is then followed by rearrangement to the *ortho*-activated product, which in turn coordinates the nitro group. Hence, "chelate assistance" is found to have no kinetic benefit for C–H activation in this complex (Equation (22)).

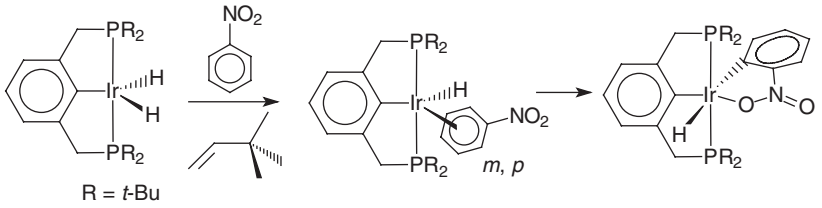

(22)

It was soon discovered that this iridium catalyst could also dehydrogenate alkanes without an olefin acceptor for the dihydrogen. Refluxing a solution of the iridium-*t*-butyl-pincer complex in cyclodecane under a flow of argon to remove the H_2 formed resulted in the formation of a solution approximately 0.4 M in cyclodecene over about 24 h. At this point, olefin inhibition of further dehydrogenation slows the rate of further reaction.[90] The isopropylphosphine catalyst performed acceptorless dehydrogenation at a rate of about 10× faster than the *t*-butylphosphine analog.[91]

Brookhart reported in 2004 that oxygen-linked modifications of the iridium–pincer complex led to very active catalysts for the transfer dehydrogenation of cyclooctane (Equation (23)).[92,92a,92b] These new catalysts are about an order of magnitude faster for transfer hydrogenation than the *t*-butylphosphine catalyst reported by Jensen and Goldman. In the absence of a hydrogen acceptor, the isopropylphosphinito complex has been reported to catalyze acceptorless dehydrogenation of undecane.[93]

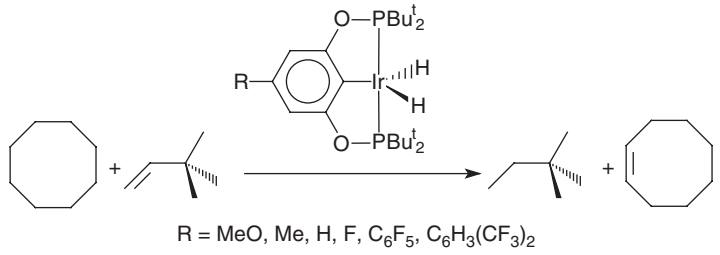

(23)

1.25.6 Termolecular Hydrocarbon Activation

The only system reported to undergo termolecular activation of hydrocarbons is the rhodium porphyrin system reported by Wayland in 1990. By increasing steric bulk by adding four xylyl groups to the porphyrin ligand, the dimerization of the Rh(II) metal centers was prevented. Two of these Rh(II) radical centers then approached methane to give a 1 : 1 ratio of Rh(III)-hydride and Rh(III)-methyl products.[94,94a] As this reaction involves organization of three centers for reaction, the entropy of activation was found to be large and unfavorable. More recently, Wayland has overcome this problem by linking the two xylyl-substituted porphyrin centers together with a hexyl linker. The reaction with methane now displays bimolecular kinetics and is much faster (Equation (24)).[95,95a] In a competitive reaction with methanol, methane activation was found to be 7.2 times faster.[96] Large isotope effects were seen in the activation of methane and methanol substrates.

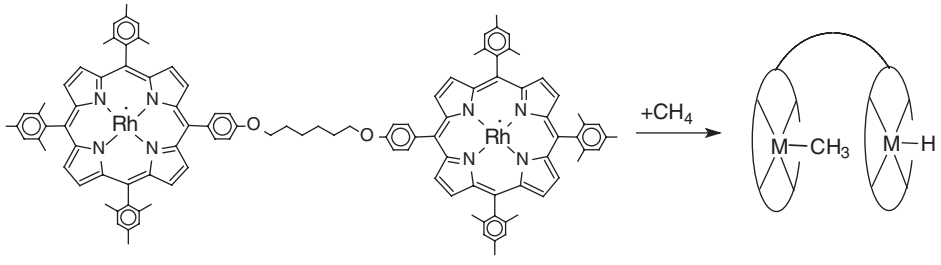

(24)

Also, reaction of a water-soluble sulfonated version of the rhodiumtetraxylylporphyrin-hydride has been examined with substituted olefins. Here, insertion occurs to give anti-Markovnikov products of the type (TSPP)Rh–CH_2CH_2X.[97]

1.25.7 C–H Bond Functionalization

1.25.7.1 Intermolecular Functionalization

Several examples of intermolecular C–H bond functionalization have appeared during the past decade. In addition to the oxidations reported above in Shilov-type systems, and the dehydrogenation of alkanes to make alkenes, catalytic systems have been developed to introduce functional groups into hydrocarbons.

One of the simplest examples is the alkylation of aromatics. As mentioned above, Periana reported an Ir(III)$(acac)_3$ complex that could activate benzene and catalyze anti-Markovnikov additions of olefins to the aryl C–H bond.[63,63a] In this reaction, a 61 : 39 ratio of linear : branched isomers was observed (Equation (25)). An iridium–phenyl complex was shown to be an intermediate.[64] Gem-disubstituted and acrylate olefins proved to be minimally reactive. More recently, a bis-tropolonato iridium(III) methyl complex was found to catalyze the anti-Markovnikov addition of olefins to arenes with slightly lower activity, but similar selectivity.[67]

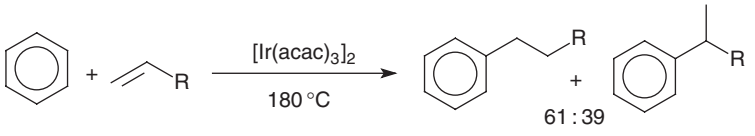

(25)

Gunnoe has also reported examples of catalytic aromatic alkylation using a ruthenium complex and olefins. With propylene and other terminal olefins, a ~1.6 : 1 preference for anti-Markovnikov addition was seen. The proposed mechanism involved olefin insertion into the metal–aryl bond followed by a metathesis reaction with benzene to give the alkylated aromatic and a new metal–phenyl bond (Equation (26)). DFT calculations supported the proposed non-oxidative addition mechanism.[98,98a] The work was extended to include catalytic alkylation of the α-position of thiophene and furan.[99] With pyrrole, insertion of the coordinated acetonitrile into the α-C–H bond was observed.[100] Gunnoe has also summarized recent developments in aromatic C–H transformations in synthesis using metal catalysts.[101]

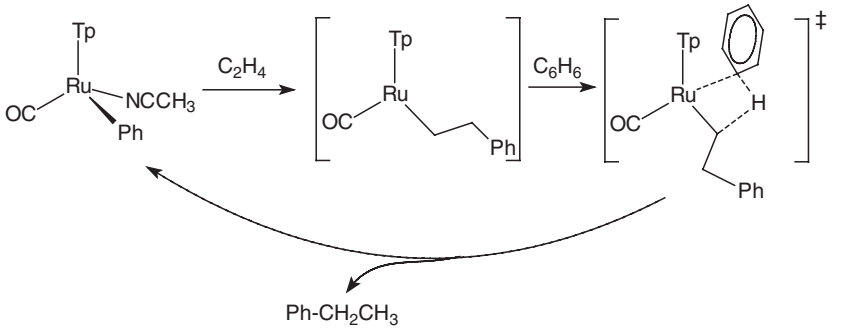

(26)

A number of reports have appeared in which boron is incorporated into a hydrocarbon. In 1994 Hartwig reported a stoichiometric reaction of $CpRu(PPh_3)_2Me$ with HBcat (cat = catechol) to give $CpRu(PPh_3)_2H$ and MeBcat. Phosphine dissociation was not required, and a four-centered transition state was postulated as an intermediate (Equation (27)).[102] It was also found that intermolecular functionalization of arenes was possible. $M(CO)_5$(Bcat) (M = Mn, Re) and $CpFe(CO)_2$(Bcat) were demonstrated to undergo a photochemical reaction in benzene to give 45–87% yields of Ph–Bcat. Olefin solvents (*t*-butylethylene and hexene) gave vinylcatecholboranes in 55–90% yields.[103,103a]

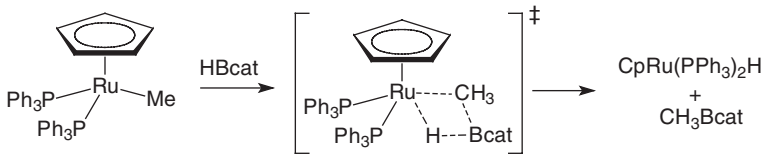

(27)

The work was extended to include stoichiometric alkane borylation by irradiation of $CpW(CO)_3(Bcat')$ in pentane (and other alkanes) to give *n*-pentyl–Bcat′ in 85% yield (cat′ = 3,5-dimethylcatechol). $CpM(CO)_2(Bcat')$ (where M = Fe, Ru) also gave borylated pentane, although in lower yields.[104,104a] While an initial mechanism involving alkane oxidative addition/alkylborane reductive elimination was proposed, a follow-up study with calculations showed a more involved metathesis mechanism.[105] As shown in Scheme 5, an initial alkane σ-complex leads to a borane B–H σ-complex. Rotation about the M–(σ-B–H) bond is followed by a metathesis of the boryl group back to the alkyl group, giving a functionalized alkylborane σ-complex. Smith reported borylation of cyclohexane and benzene using $Cp^*Ir(PMe_3)(R)H$ complexes and HBpin (pin = pinacol) or HBcat. Benzene was catalytically borylated at 150 °C with $Cp^*Ir(PMe_3)(Bpin)H$.[106]

A breakthrough was made in 1999 when Hartwig discovered that irradiation of $CpM(CO)_3$ (M = Mn, Re) in pentane solvent containing B_2pin_2 gave catalytic formation of *n*-pentyl–Bcat in 95% yield, along with HBpin in 32% yield ($CpRe(CO)_2(Bpin)_2$ was also isolated as an intermediate). Other alkanes showed similar reactivity, giving product in 75–100% yield (Equation (28)).[107] σ-B–H complexes of the $[CpM(CO)_2]$ fragments have been isolated and structurally characterized.[108] Soon after this discovery, an even cleaner catalyst was discovered for the catalytic borylation of alkanes. $Cp^*M(\eta^4\text{-}C_6H_6)$ (M = Rh, Ir) was found to catalyze the thermal reaction of octane with B_2pin_2 to give octyl–Bpin plus HBpin. The latter reacted with additional alkane to give more octyl–Bpin (net yield, 84%).[109] Calculations were consistent with a series of σ-metathesis exchanges leading to B–C bond formation.[110] Intermediates were isolated in these reactions, demonstrating that $Cp^*IrH_3(Bpin)$, $Cp^*IrH_2(Bpin)_2$, and $Cp^*IrH(Bpin)$ were all involved in the reaction.[111]

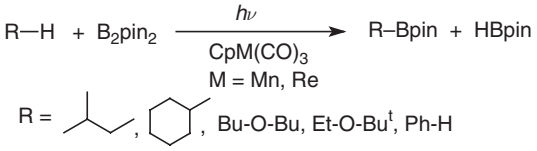

(28)

Smith has reported several catalytic arene borylations. A variety of substituted arenes were found to undergo borylation using $Cp^*Ir(PMe_3)(Bpin)H$ or $Cp^*Rh(\eta^4\text{-}C_6Me_6)$ as catalyst (Equation (29)).[112] It was also reported that the borylation could be carried out in 50–90% yield using dilute arene in cyclohexane solvent rather than in neat arene.[113] Smith also found that certain catalyst systems were tolerant of fluoro, chloro, and iodo groups.[114] Systems formed by reaction of (mesitylene)$Ir(Bpin)_3$ or (indenyl)Ir(COD) with dmpe or dppe were found to borylate not only benzene, but also di- and trifluorobenzene, dichlorobenzene, and iodobenzene. The halogen groups were intact in the arylboron products, demonstrating remarkable tolerance. The arylboron product could be oxidized with aqueous

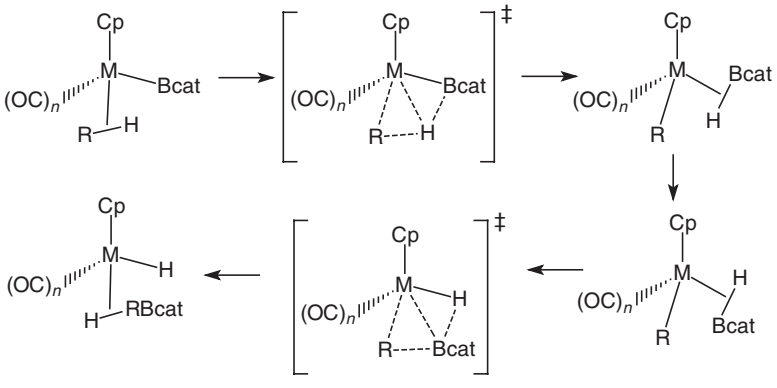

Scheme 5

ozone in acetone to give the corresponding halo-substituted phenols in 80–90%, thereby affording a one-pot synthesis of these derivatives.[115]

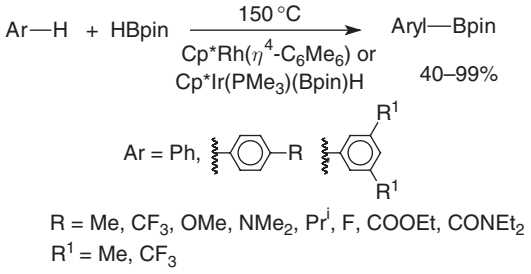

(29)

In 2002, Hartwig reported another system for borylation of aromatic substrates under mild conditions. Combination of $[IrCl(COD)]_2$ and bipyridine generates a catalyst for the borylation of alkyl-, alkoxy-, and chloro-substituted arenes by B_2pin_2 at 80 °C in 72–95% yield.[116] The catalyst was also effective for borylation of thiophene, furan, and pyrrole with di-*t*-butylbipyridine as the additive.[117] Indoles and pyridines also underwent reaction. It was discovered that the replacement of the chloride by hydroxide, phenoxide, or methoxide, gives the catalyst $[Ir(OR)(COD)]_2$ which now effects aromatic borylation at RT in the presence of di-*t*-butylpyridine and B_2pin_2 in hexane.[118,118a] This system is also effective for heterocycle borylation (thiophene, furan, pyrrole), and is tolerant of halogens and ester substitution on the aromatic ring.[119] Finally, Perutz has reported that this catalyst system is selective for borylation of the β-positions in naphthalene, just those that are most difficult to substitute.[120] Larger fused polycyclic aromatics also showed a preference for β-borylation.

In 2005, Hartwig reported that $Tp'PtMe_2H$ serves as a catalyst for the silylation of benzene at 200 °C.[121] This reaction was also found to work with $Tp'PtPh_2H$ and $Tp'PtMeH_2$ as catalysts.

1.25.7.2 Intramolecular Functionalization

A number of reports have appeared in which the C–H bond undergoing a functionalization reaction is in a molecule containing other functional groups. In many cases, these other functional groups are believed to participate in the reaction by binding the substrate and bringing the target C–H bond into proximity to the metal center. In other cases, the functional group activates a nearby C–H bond for reaction. Murai and Chatani have reported a number of examples in which ruthenium catalysts have been used for the insertion of olefins into the C–H bond *ortho* to a ketone, ester, imine, nitrile, or aldehyde functional group.[122] Equation (30) shows the scope of the reaction for aromatic ketones, giving excellent yields.[123] Heteroaromatic ketones also give good yields of products (Equation (31)). The reaction is tolerant of both electron-donating (NMe_2, OMe, CH_3, $OC(O)CH_3$) and electron-withdrawing (CF_3, CN, CO_2Me, F, OCF_3) groups. Aromatic esters[124,124a] and imines,[125] and aldehydes[126] undergo similar *ortho*-olefin insertions. Aromatic nitriles lead to double *ortho*-olefin insertions.[127] Olefinic C–H bonds in α,β-unsaturated ketones were also found to undergo a similar insertion reaction (Equation (32)).[128] Insertion of acetylenes into the *ortho*-ketone C–H bond has also been found to be efficient (Equation (33)).[129,129a]

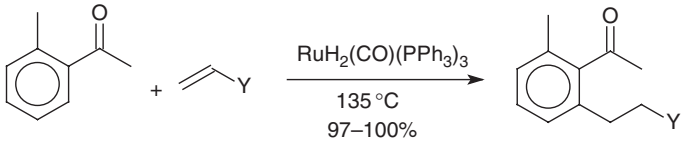

(30)

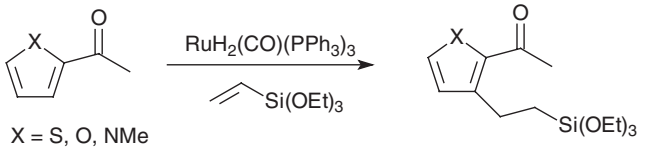

(31)

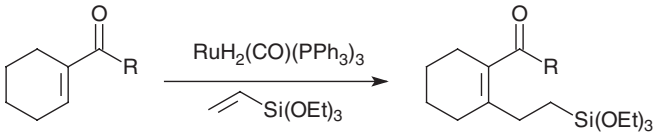

(32)

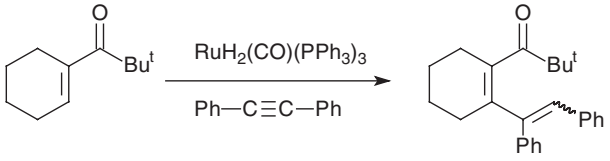

(33)

In addition to olefin insertion reactions, Murai and Chatani have also reported silylation using vinylsilanes or hydrosilanes. Reaction of 3-acetylthiophene with trimethylvinylsilane using $RuH_2(CO)(PPh_3)_3$ as catalyst gave the usual olefination product, whereas use of $Ru_3(CO)_{12}$ as catalyst led to silylation of the thiophene ring.[130] A mechanism involving olefin insertion into a ruthenium–hydride bond followed by β-silyl elimination was proposed to account for the coupling product (Equation (34)). While aromatic derivatives are not silylated using vinylsilane, use of hydrosilanes does give excellent yields of silylated product (Equation (35)).[131,131a]

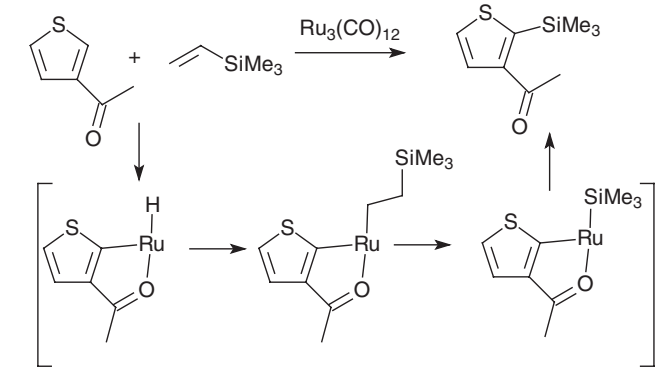

(34)

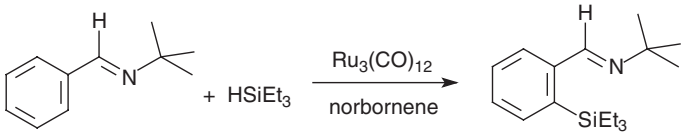

(35)

Bergman and Ellman have reported a number of examples of C–H activation followed by intramolecular olefin insertion. A variety of aryl imines possessing *meta*-olefinic substituents underwent cyclization in the presence of Wilkinson's catalyst to give annulated rings. The cyclization was successful with CH_2, O, or NR linkers attaching the olefin to the ring (Equation (36)).[132,132a] By employing a chiral phosphamidite ligand, the reaction could be carried out in quantitative yield and 88% ee.[133] The reaction was extended to intermolecular incorporation of olefins in good yield using a rhodium catalyst with $MgBr_2$ as a required additive (Equation (37)).[134,134a,134b] In addition to olefin insertion, coupling with aryl iodides could be effected (Equation (38)).[135]

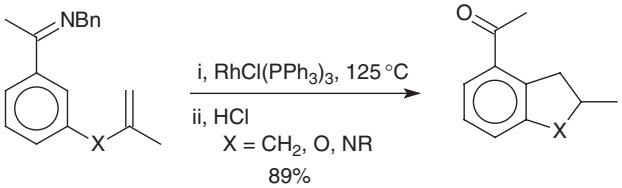

(36)

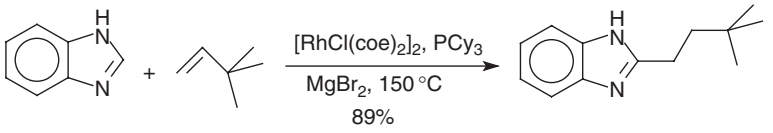

(37)

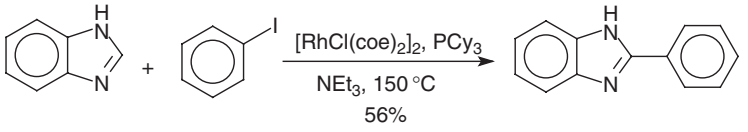

(38)

Miura has also published examples of arylation reactions directed by intramolecular C–H activation. Reaction of *o*-phenylphenol and phenyl iodide in the presence of palladium(II) leads to arylation of the remote ring (Equation (39)).[136,136a] Reaction of *o*-phenylphenol and methyl acrylate in the presence of palladium, copper, and molecular sieves leads to the formation of a tricyclic product (Equation (40)).[137] With benzoic acid and styrene, a lactone is formed (Equation (41)). Mori has reported that the α-C–H bond in thiophenes can be arylated in using aryl iodides in the presence of $PdCl_2(PPh_3)_2$ and silver ion.[138]

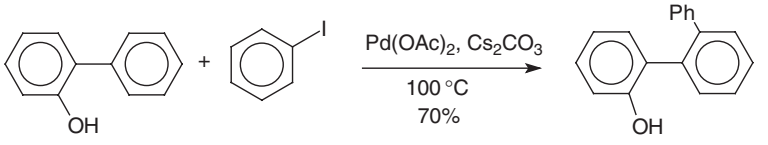

(39)

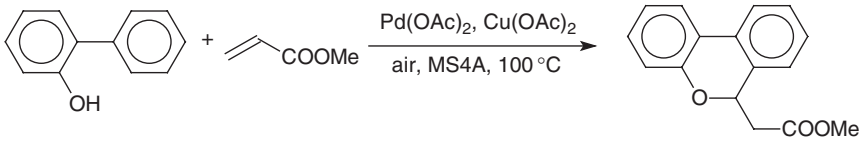

(40)

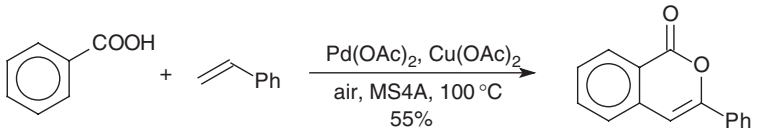

(41)

Another interesting intramolecular-directed functionalization has been investigated by Chang and co-workers. A pyridal formate group is used for hydroesterification of an olefin (Equation (42)).[139] Use of a benzyl ester in place of the pyridyl group gave 0% yield. Pyridyl formamides were also found to give hydroamidation products with high linear/branched ratios.[140]

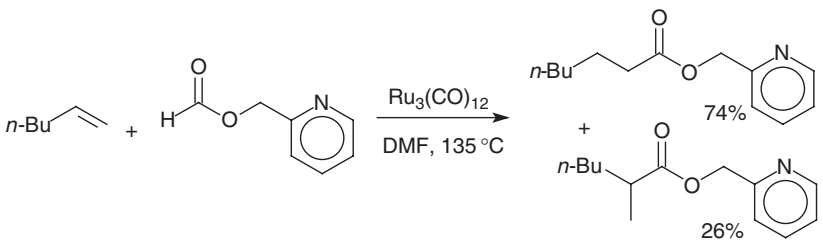

(42)

Kuninobu has found that benzaldimines undergo C–H activation and acetylene insertion to give indenes using a rhenium catalyst (Equation (43)).[141] A similar reaction with isocyanates gives rise to phthalimidine derivatives (Equation (44)).[142] This catalyst also efficiently permits insertion of terminal alkynes into the acidic C–H bond of 1,3-diketones to give branched vinyl products.[143]

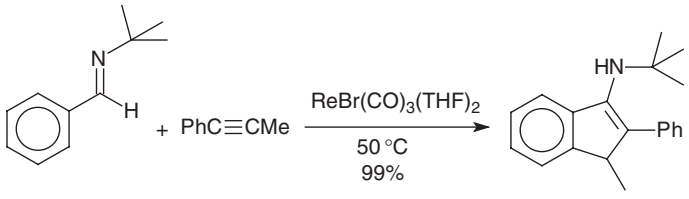

(43)

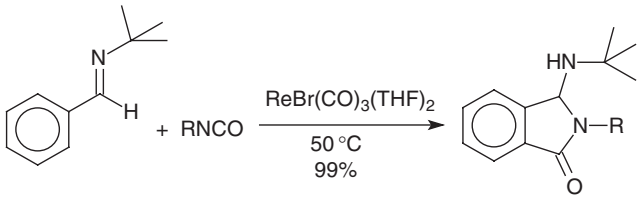

(44)

Sanford has reported the oxidative functionalization of sp^3- and sp^2-hybridized C–H bonds using directing groups. For example, 8-methyl quinoline can be oxidized to the benzylic acetate using Pd(II) and $PhI(OAc)_2$ oxidant (Equation (45)).[144] The compound 2-phenylpyridine is oxidized to the *ortho*-acetate under similar conditions (Equation (46)).[145] Using $Ph_2I^+BF_4^-$ as oxidant results in phenylation rather than acetylation.[146] Sanford also found that pinacalone O-methyl oximes undergo oxidation of the unactivated sp^3-C–H bond (Equation (47)).[147] These reactions proceed through Pd(IV) intermediates, which can be isolated in some cases.[148,148a]

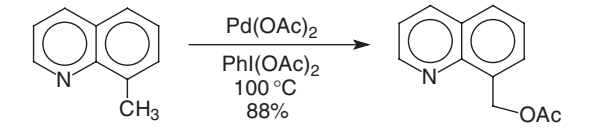

(45)

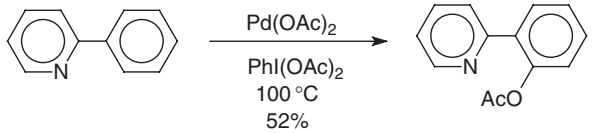

(46)

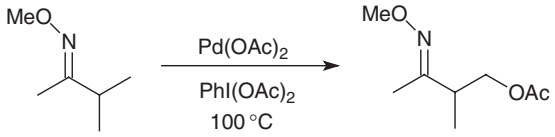

(47)

Sames has reported the use of $PtCl_4^{2-}/CuCl_2$ as catalyst for the functionalization of C–H bonds in alkyl chains attached to a functional group in water solvent. For example, *n*-butylamine can be hydroxylated (Equation (48)) and pentanoic acid is both hydroxylated and cyclized to give lactone products (Equation (49)).[149] A related platinum system was employed in the synthesis of the natural product Rhazinilam.[150,150a]

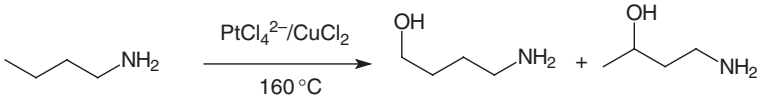

(48)

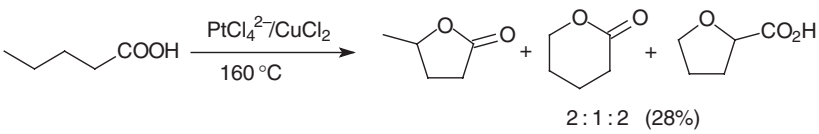

(49)

Sames also found that palladium(II) was effective for intermolecular functionalizations. Using an imine directing group, sp^3-C–H bonds could be activated and coupled with boron reagents to give elaborated organic products (Equation (50)).[151] In combination with the palladium catalyst and RMgX (to mask the N–H functionality), phenyl iodide was found to be capable of arylating indoles to afford a mixture of C-2 and C-3 products in 60–96% yield (Equation (51)).[152,152a] A rhodium catalyst system was later identified for C-2 selective arylation of free indoles and pyrroles that worked well even in the presence of the acidic N–H bonds (Equation (52))[153]

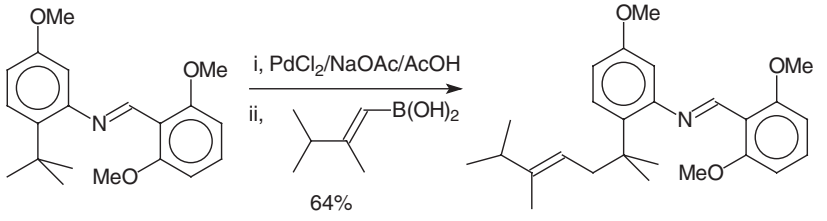

(50)

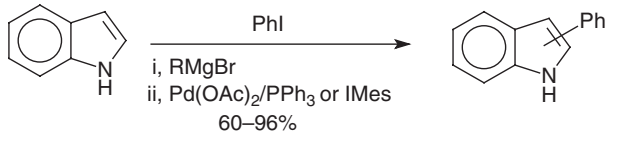

(51)

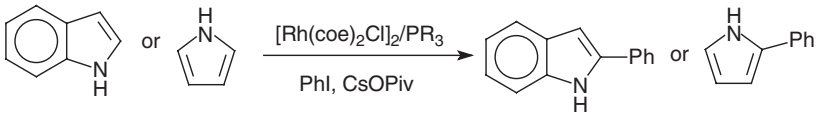

(52)

Du Bois has developed the use of $Rh_2(OAc)_4$ and oxidant $PhI(OAc)_2$ for the selective activation and amination of C–H bonds in functionalized molecules. A sulfonamide group has proved to be effective in several applications, as nucleophiles can displace this temporary directing group (Equation (53)).[154] This directing group/catalyst has been used for the synthesis of natural products such as manzacidins A and C[155] and (−)-tetrodotoxin.[156] The stereoselectivity of the reaction is for formation of the *syn*-product with observed selectivities in the range 3 : 1 to 15 : 1.[157] The amination product can also be alkynylated to introduce additional functionality.[158] The range of bonds to undergo cleavage with this dimeric rhodium catalyst includes α-ethers, benzylic, tertiary, and secondary C–H bonds, with α-ethers showing the greatest reactivity.[159] Du Bois recently reported an improved catalyst that contains a chelating diacid rather than simple acetate bridges. As little as 0.15% of this catalyst gives quantitative conversion of the sulfonamide to the cyclized product.[160]

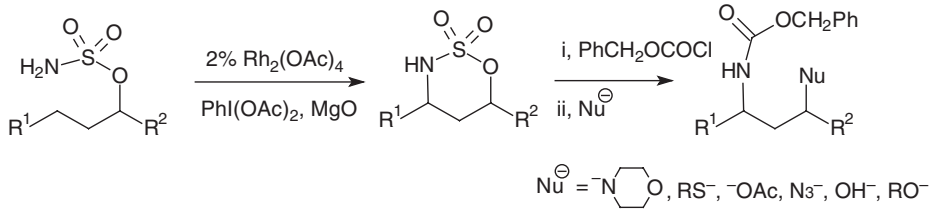

(53)

1.25.7.3 Alkane Metathesis

As mentioned above in Section 1.25.5.2, rhodium and iridium pincer complexes have been used to catalytically dehydrogenate alkanes, giving terminal olefins as the kinetic products. In a recent report by Goldman and Brookhart, the iridium Pincer complexes were combined with Schrock's alkylidene metathesis catalyst

$Mo[O(CF_3)_2CH_3]_2(=CHCMe_2PH)(=Naryl)$ to carry out *alkane metathesis*, a fundamentally new type of reaction for organometallic catalysis (Equation (54)).[161] Re_2O_7/Al_2O_3 also served as an effective co-catalyst for the metathesis portion of the reaction at 175 °C. This tandem catalytic was system was shown to convert decane solvent into a distribution of C_2–C_{30} alkanes. These systems have the pontential for substantial development in the near future.

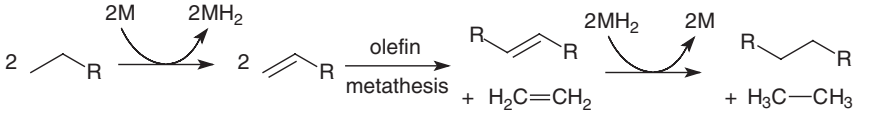

(54)

References

1. Hill, C. L., Ed. *Activation and Functionalization of Alkanes*; Wiley: New York, 1989.
2. Davies, J. A., Watson, P. L., Liebman, J. F., Greenberg, A., Eds.; *Selective Hydrocarbon Activation*; VCH: New York, 1990.
3. As determined by a search with SciFinder Scholar, (http://www.cas.org) 2004, American Chemical Society.
4. Jones, W. D.; Hessell, E. T. *J. Am. Chem. Soc.* **1992**, *114*, 6087–6095.
5. Jones, W. D.; Hessell, E. T. *J. Am. Chem. Soc.* **1993**, *115*, 554–562.

5a. Jones, W. D.; Wick, D. D. *Organometallics* **1999**, *18*, 495–505.

6. Bennett, J. L.; Wolczanski, P. T. *J. Am. Chem. Soc.* **1994**, *116*, 2179–2180.
7. Bennett, J. L.; Wolczanski, P. T. *J. Am. Chem. Soc.* **1997**, *119*, 10696–10719.
8. Schaller, C. P.; Wolczanski, P. T. *Inorg. Chem.* **1993**, *32*, 131–144.
9. Schaller, C. P.; Cummins, C. C.; Wolczanski, P. T. *J. Am. Chem. Soc.* **1996**, *118*, 591–611.
10. Hall, C.; Perutz, R. N. *Chem. Rev.* **1996**, *96*, 3125–3146.
11. Turner, J. J.; Burdett, J. K.; Perutz, R. N.; Poliakoff, M. *Pure Appl. Chem.* **1977**, *49*, 271.
12. Brown, C. E.; Ishikawa, Y.; Hackett, P. A.; Rayner, D. M. *J. Am. Chem. Soc.* **1990**, *112*, 2530–2536.
13. Schultz, R. H.; Bengali, A. A.; Tauber, M. J.; Weiller, B. H.; Wasserman, E. P.; Kyle, K. R.; Moore, C. B.; Bergman, R. G. *J. Am. Chem. Soc.* **1994**, *116*, 7369–7377.
14. Bengali, A. A.; Schultz, R. H.; Moore, C. B.; Bergman, R. G. *J. Am. Chem. Soc.* **1994**, *116*, 9585–9589.

14a. McNamara, B. K.; Yeston, J. S.; Bergman, R. G.; Moore, C. B. *J. Am. Chem. Soc.* **1999**, *121*, 6437–6443.

15. Asbury, J. B.; Hang, K.; Yeston, J. S.; Cordaro, J. G.; Bergman, R. G.; Lian, T. *J. Am. Chem. Soc.* **2000**, *122*, 12870–12871.
16. Bromberg, S. E.; Yang, H.; Asplund, M. C.; Lian, T.; McNamara, B. K.; Kotz, K. T.; Yeston, J. S.; Wilkens, M.; Frei, H.; Bergman, R. G., *et al. Science* **1997**, *278*, 260–263.

16a. Asplund, M. C.; Snee, P. T.; Yeston, J. S.; Wilkens, M. J.; Payne, C. K.; Yang, H.; Kotz, K. T.; Frei, H.; Bergman, R. G.; Harris, C. B. *J. Am. Chem. Soc.* **2002**, *124*, 10605.

17. Sun, X.-Z.; Grills, D. C.; Nikiforov, S. M.; Poliakoff, J.; George, M. W. *J. Am. Chem. Soc.* **1997**, *119*, 7521–7525.

17a. Childs, G. I.; Grills, D. C.; Sun, X. Z.; George, M. W. *Pure Appl. Chem.* **2001**, *73*, 443–447.

18. Geftakis, S.; Ball, G. E. *J. Am. Chem. Soc.* **1998**, *120*, 9953–9954.
19. Lawes, D. J.; Geftakis, S.; Gall, G. E. *J. Am. Chem. Soc.* **2005**, *127*, 4134–4135.
20. Bullock, R. M.; Headford, C. E. L.; Hennessy, K. M.; Kegley, S. E.; Norton, J. R. *J. Am. Chem. Soc.* **1989**, *111*, 3897–3908.

20a. Parkin, G.; Bercaw, J. E. *Organometallics* **1989**, *8*, 1172–1179.

21. Chernega, A.; Cook, J.; Green, M. L. H.; Labella, L.; Simpson, S. J.; Souter, J.; Stephens, A. H. H. *J. Chem. Soc., Dalton Trans.* **1997**, 3225–3243.
22. Wick, D. D.; Reynolds, K. A.; Jones, W. D. *J. Am. Chem. Soc.* **1999**, *121*, 3974–3983.
23. Wang, C.; Ziller, J. W.; Flood, T. C. *J. Am. Chem. Soc.* **1995**, *117*, 1647–1648.
24. Buchanan, J. M.; Stryker, J. M.; Bergman, R. G. *J. Am. Chem. Soc.* **1986**, *108*, 1537–1550.

24a. Mobley, T. A.; Schade, C.; Bergman, R. G. *J. Am. Chem. Soc.* **1995**, *117*, 7822–7823.

25. Gross, C. L.; Girolami, G. S. *J. Am. Chem. Soc.* **1996**, *120*, 6605–6606.
26. Flood, T. C.; Janak, K. E.; Iimura, M.; Zhen, H. *J. Am. Chem. Soc.* **2000**, *122*, 6783–6784.
27. Northcutt, T. O.; Wick, D. D.; Vetter, A. J.; Jones, W. D. *J. Am. Chem. Soc.* **2001**, *123*, 7257–7270.
28. Vetter, A. J.; Flaschenriem, C.; Jones, W. D. *J. Am. Chem. Soc.* **2005**, *127*, 12315–12322.
29. Buchanan, J. M.; Stryker, J. M.; Bergman, R. G. *J. Am. Chem. Soc.* **1986**, *108*, 1537–1550.

29a. Periana, R. A.; Bergman, R. G. *J. Am. Chem. Soc.* **1986**, *108*, 7332–7346.

29b. Bullock, R. M.; Headford, C. E. L.; Hennessy, K. M.; Kegley, S. E.; Norton, J. R. *J. Am. Chem. Soc.* **1989**, *111*, 3897–3908.

29c. Parkin, G.; Bercaw, J. E. *Organometallics* **1989**, *8*, 1172–1179.

29d. Gould, G. L.; Heinekey, D. M. *J. Am. Chem. Soc.* **1989**, *111*, 5502–5504.

29e. Wang, C.; Ziller, J. W.; Flood, T. C. *J. Am. Chem. Soc.* **1995**, *117*, 1647–1648.

29f. Stahl, S. S.; Labinger, J. A.; Bercaw, J. E. *J. Am. Chem. Soc.* **1996**, *118*, 5961–5976.

30. Abis, L.; Sen, A.; Halpern, J. *J. Am. Chem. Soc.* **1978**, *100*, 2915–2916.

30a. Michelin, R. A.; Faglia, S.; Uguagliati, P. *Inorg. Chem.* **1983**, *22*, 1831–1834.

30b. Hackett, M.; Ibers, J. A.; Whitesides, G. M. *J. Am. Chem. Soc.* **1988**, *110*, 1436–1448.

31. Jones, W. D. *Acc. Chem. Res.* **2003**, *36*, 140–146.
32. Janak, K. E.; Parkin, G. *J. Am. Chem. Soc.* **2003**, *125*, 6889–6891.

32a. Janak, K. E.; Churchill, D. G.; Parkin, G. *Chem. Commun.* **2002**, 22–23.

33. Wang, C.; Ziller, J. W.; Flood, T. C. *J. Am. Chem. Soc.* **1995**, *117*, 1647–1648.
34. Selmeczy, A. D.; Jones, W. D.; Partridge, M. G.; Perutz, R. N. *Organometallics* **1994**, *13*, 522–532.

35. Godoy, F.; Higgitt, C. L.; Klahn, A. H.; Oelckers, B.; Parsons, S.; Perutz, R. N. *J. Chem. Soc., Dalton Trans.* **1999**, 2039–2048.
36. Clot, E.; Oelckers, B.; Klahn, A. H.; Eisenstein, O.; Perutz, R. N. *Dalton Trans.* **2003**, 4065–4074.
36a. Clot, E.; Besora, M.; Maseras, F.; Mégret, C.; Eisenstein, O.; Oelckers, B.; Perutz, R. N. *Chem. Commun.* **2003**, 490–491.
37. Wick, D. D.; Goldberg, K. I. *J. Am. Chem. Soc.* **1997**, *119*, 10235–10236.
38. Jensen, M. P.; Wick, D. D.; Reinartz, S.; White, P. S.; Templeton, J. L.; Goldberg, K. I. *J. Am. Chem. Soc.* **2003**, *125*, 8614–8624.
39. Wick, D. D.; Goldberg, K. I. *J. Am. Chem. Soc.* **1999**, *121*, 11900–11901.
40. Reinartz, S.; White, P. S.; Brookhart, M.; Templeton, J. L. *J. Am. Chem. Soc.* **2001**, *123*, 12724–12725.
40a. Reinartz, S.; White, P. S.; Brookhart, M.; Templeton, J. L. *J. Am. Chem. Soc.* **2002**, *124*, 7249.
41. Reinartz, S.; White, P. S.; Brookhart, M.; Templeton, J. L. *Organometallics* **2001**, *20*, 1709–1712.
42. Fekl, U.; Kaminsky, W.; Goldberg, K. I. *J. Am. Chem. Soc.* **2003**, *125*, 15286–15287.
43. Gol′dshleger, N. F.; Tyabin, M. B.; Shilov, A. E.; Shteinman, A. A. *Zh. Fiz. Khim.* **1969**, *43*, 2174.
44. Labinger, J. A.; Herring, A. M.; Lyon, D. K.; Luinstra, G. A.; Bercaw, J. E.; Horvath, I. T.; Eller, K. *Organometallics* **1993**, *12*, 895–905.
45. Wang, L.; Stahl, S. S.; Labinger, J. A.; Bercaw, J. E. *J. Mol. Catal. A* **1997**, *116*, 269–275.
46. Luinstra, G. A.; Labinger, J. A.; Bercaw, J. E. *J. Am. Chem. Soc.* **1993**, *115*, 3004–3005.
47. Luinstra, G. A.; Wang, L.; Stahl, S. S.; Labinger, J. A.; Bercaw, J. E. *Organometallics* **1994**, *13*, 755–756.
48. Luinstra, G. A.; Wang, L.; Stahl, S. S.; Labinger, J. A.; Bercaw, J. E. *J. Organomet. Chem.* **1995**, *504*, 75–91.
49. Stahl, S. S.; Labinger, J. A.; Bercaw, J. E. *J. Am. Chem. Soc.* **1996**, *118*, 5961–5976.
50. Holtcamp, M. W.; Labinger, J. A.; Bercaw, J. E. *J. Am. Chem. Soc.* **1997**, *119*, 848–849.
50a. Holtcamp, M. W.; Henling, L. M.; Day, M. W.; Labinger, J. A.; Bercaw, J. E. *Inorg. Chim. Acta* **1998**, *270*, 467–478.
51. Johansson, L.; Ryan, O. B.; Tilset, M. *J. Am. Chem. Soc.* **1999**, *121*, 1974–1975.
51a. Heiberg, H.; Johansson, L.; Gropen, O.; Ryan, O. B.; Swang, O.; Tilset, M. *J. Am. Chem. Soc.* **2000**, *122*, 10831–10845.
52. Johansson, L.; Tilset, M.; Labinger, J. A.; Bercaw, J. E. *J. Am. Chem. Soc.* **2000**, *122*, 10846–10855.
53. Johansson, L.; Ryan, O. B.; Romming, C.; Tilset, M. *J. Am. Chem. Soc.* **2001**, *123*, 6579–6590.
53a. Johansson, L.; Tilset, M. *J. Am. Chem. Soc.* **2001**, *123*, 739–740.
54. Zhong, H. A.; Labinger, J. A.; Bercaw, J. E. *J. Am. Chem. Soc.* **2002**, *124*, 1378–1399.
55. Heyduk, A. F.; Driver, T. G.; Labinger, J. A.; Bercaw, J. E. *J. Am. Chem. Soc.* **2004**, *126*, 15034–15035.
56. Periana, R. A.; Taube, D. J.; Gamble, S.; Taube, H.; Satoh, T.; Fujii, H. *Science* **1998**, *280*, 560–564.
57. Sen, A.; Benvenuto, M. A.; Lin, M.; Hutson, A. C.; Basickes, N. *J. Am. Chem. Soc.* **1994**, *116*, 998–1003.
58. Hutson, A. C.; Lin, M.; Basickes, N.; Sen, A. *J. Organomet. Chem.* **1995**, *504*, 69–74.
59. Basickes, N.; Sen, A. *Polyhedron* **1995**, *14*, 197–202.
60. Lin, M.; Shen, C.; Garcia-Zayas, E. A.; Sen, A. *J. Am. Chem. Soc.* **2001**, *123*, 1000–1001.
61. Arndtsen, B. A.; Bergman, R. G. *Science* **1995**, *270*, 1970–1973.
61a. Burger, P.; Bergman, R. G. *J. Am. Chem. Soc.* **1993**, *115*, 10462–10463.
62. Strout, D. L.; Zaric, S.; Niu, S.; Hall, M. B. *J. Am. Chem. Soc.* **1996**, *118*, 6068–6069.
62a. Niu, S.; Hall, M. B. *J. Am. Chem. Soc.* **1998**, *120*, 6169–6170.
63. Matsumoto, T.; Periana, R. A.; Taube, D. J.; Yoshida, H. *J. Mol. Catal A* **2002**, *180*, 1–18.
63a. Matsumoto, T.; Taube, D. J.; Periana, R. A.; Taube, H.; Yoshida, H. *J. Am. Chem. Soc.* **2000**, *122*, 7414–7415.
64. Periana, R. A.; Liu, X. Y.; Bhalla, G. *Chem. Commun.* **2002**, *24*, 3000–3001.
65. Wong-Foy, A. G.; Bhalla, G.; Liu, X. Y.; Periana, R. A. *J. Am. Chem. Soc.* **2003**, *125*, 14292–14293.
66. Bhalla, G.; Periana, R. A. *Angew. Chem., Int. Ed.* **2005**, *44*, 1540–1543.
67. Bhalla, G.; Oxgaard, J.; Goddard, W. A., III; Periana, R. A. *Organometallics* **2005**, *24*, 3229–3232.
68. Periana, R. A.; Taube, D. J.; Evitt, E. R.; Loffler, D. G.; Wentrcek, P. R.; Voss, G.; Masuda, T. *Science* **1993**, *259*, 340–343.
69. Basickes, N.; Hogan, T. E.; Sen, A. *J. Am. Chem. Soc.* **1996**, *118*, 13111–13112.
70. Lin, M.; Sen, A. *Nature* **1994**, *368*, 613–615.
71. Lin, M.; Hogan, T.; Sen, A. *J. Am. Chem. Soc.* **1997**, *119*, 6048–6053.
72. Holcomb, H. L.; Nakanishi, S.; Flood, T. C. *Organometallics* **1996**, *15*, 4228–4234.
73. Maguire, J. A.; Boese, W. T.; Goldman, A. S. *J. Am. Chem. Soc.* **1989**, *111*, 7088–7093.
74. Maguire, J. A.; Goldman, A. S. *J. Am. Chem. Soc.* **1991**, *113*, 6706–6708.
74a. Maguire, J. A.; Petrillo, A.; Goldman, A. S. *J. Am. Chem. Soc.* **1992**, *114*, 9492–9498.
75. Wang, K.; Goldman, M. E.; Emge, T. J.; Goldman, A. S. *J. Organomet. Chem.* **1996**, *518*, 55–68.
76. Shih, K. C.; Goldman, A. S. *Organometallics* **1993**, *12*, 3390–3392.
77. Belli, J.; Jensen, C. M. *Organometallics* **1996**, *15*, 1532–1534.
78. Rosini, G. P.; Boese, W. T.; Goldman, A. S. *J. Am. Chem. Soc.* **1994**, *116*, 9498–9505.
79. Rosini, G. P.; Soubra, S.; Vixamar, M.; Wang, S.; Goldman, A. S. *J. Organomet. Chem.* **1998**, *554*, 41–47.
80. Rosini, G. P.; Zhu, K.; Goldman, A. *J. Organomet. Chem.* **1995**, *504*, 115–121.
81. Gupta, M.; Hagen, C.; Flesher, R. J.; Kaska, W. C.; Jensen, C. M. *Chem. Commun.* **1996**, 2083–2084.
81a. Gupta, M.; Hagen, C.; Flesher, R. J.; Kaska, W. C.; Jensen, C. M. *Chem. Commum.* **1996**, 2687.
82. Lee, D. W.; Kaska, W. C.; Jensen, C. M. *Organometallics* **1998**, *17*, 1–3.
83. Gupta, M.; Kaska, W. C.; Jensen, C. M. *Chem. Commun.* **1997**, 461–462.
83a. Gupta, M.; Hagen, C.; Kaska, W. C.; Cramer, R. E.; Jensen, C. M. *J. Am. Chem. Soc.* **1997**, *119*, 840–841.
84. Liu, F.; Pak, E. B.; Singh, B.; Jensen, C. M.; Goldman, A. S. *J. Am. Chem. Soc.* **1999**, *121*, 4086–4087.
84a. Renkema, K. B.; Kissin, Y. V.; Goldman, A. S. *J. Am. Chem. Soc.* **2003**, *125*, 7770–7771.
85. Jensen, C. M. *Chem. Commun.* **1999**, 2443–2449.
86. Kanzelberger, M.; Singh, B.; Czerw, M.; Krogh-Jespersen, K.; Goldman, A. S. *J. Am. Chem. Soc.* **2000**, *122*, 11017–11018.
87. Gu, X.-Q.; Chen, W.; Morales-Morales, D.; Jensen, C. M. *J. Mol. Catal. A* **2002**, *189*, 119–124.
88. Morales-Morales, D.; Redon, R.; Wang, Z.; Lee, D. W.; Yung, C.; Magnuson, K.; Jensen, C. M. *Can. J. Chem.* **2001**, *79*, 823–829.
89. Kanzelberger, M.; Singh, B.; Czerw, M.; Krogh-Jespersen, K.; Goldman, A. S. *J. Am. Chem. Soc.* **2000**, *122*, 11017–11018.
90. Xu, W.-W.; Rosini, G. P.; Krogh-Jespersen, K.; Goldman, A. S.; Gupta, M.; Jensen, C. M.; Kaska, W. C. *Chem. Commun.* **1997**, 2273–2274.
91. Liu, F.; Goldman, A. S. *Chem. Commun.* **1999**, 655–656.
92. Goettker-Schnetmann, I.; White, P.; Brookhart, M. *J. Am. Chem. Soc.* **2004**, *126*, 1804–1811.

92a. Goettker-Schnetmann, I.; White, P. S.; Brookhart, M. *Organometallics* **2004**, *23*, 1766–1776.
92b. Goettker-Schnetmann, I.; Brookhart, M. *J. Am. Chem. Soc.* **2004**, *126*, 9330–9338.
93. Morales-Morales, D.; Redon, R.; Yung, C.; Jensen, C. M. *Inorg. Chim. Acta* **2004**, *357*, 2953–2956.
94. Sherry, A. E.; Wayland, B. B. *J. Am. Chem. Soc.* **1990**, *112*, 1259–1261.
94a. Wayland, B. B.; Ba, S.; Sherry, A. E. *J. Am. Chem. Soc.* **1991**, *113*, 5305–5311.
95. Zhang, X.-X.; Wayland, B. B. *J. Am. Chem. Soc.* **1994**, *116*, 7897–7898.
95a. Cui, W.; Wayland, B. B. *J. Am. Chem. Soc.* **2004**, *126*, 8266–8274.
96. Cui, W.; Zhang, X. P.; Wayland, B. B. *J. Am. Chem. Soc.* **2003**, *125*, 4994–4995.
97. Fu, X.; Basickes, L.; Wayland, B. B. *Chem. Commun.* **2003**, 520–521.
98. Lail, M.; Bell, C. M.; Conner, D.; Cundari, T. R.; Gunnoe, T. B.; Petersen, J. L. *Organometallics* **2004**, *23*, 5007–5020.
98a. Lail, M.; Arrowood, B. N.; Gunnoe, T. B. *J. Am. Chem. Soc.* **2003**, *125*, 7506–7507.
99. Pittard, K. A.; Lee, J. P.; Cundari, T. R.; Gunnoe, T. B.; Petersen, J. L. *Organometallics* **2004**, *23*, 5514–5523.
100. Pittard, K. A.; Cundari, T. R.; Gunnoe, T. B.; Day, C. S.; Petersen, J. L. *Organometallics* **2005**, *24*, 5015–5024.
101. Goj, L. A.; Gunnoe, T. B. *Curr. Org. Chem.* **2005**, *9*, 671–685.
102. Hartwig, J. F.; Bhandari, S.; Rablen, P. R. *J. Am. Chem. Soc.* **1994**, *116*, 1839–1844.
103. Waltz, K. M.; He, X.; Muhoro, C.; Hartwig, J. F. *J. Am. Chem. Soc.* **1995**, *117*, 11357–11358.
103a. Waltz, K. M.; Muhoro, C. N.; Hartwig, J. F. *Organometallics* **1999**, *18*, 3383–3393.
104. Waltz, K. M.; Hartwig, J. F. *Science* **1997**, *277*, 211–213.
104a. Waltz, K. M.; Hartwig, J. F. *J. Am. Chem. Soc.* **2000**, *122*, 11358–11369.
105. Webster, C. E.; Fan, Y.; Hall, M. B.; Kunz, D.; Hartwig, J. F. *J. Am. Chem. Soc.* **2003**, *125*, 858–859.
106. Iverson, C. N.; Smith, M. R., III. *J. Am. Chem. Soc.* **1999**, *121*, 7696–7697.
107. Chen, H.; Hartwig, J. F. *Angew. Chem., Int. Ed. Engl.* **1999**, *38*, 3391–3393.
108. Schlecht, S.; Hartwig, J. F. *J. Am. Chem. Soc.* **2000**, *122*, 9435–9443.
109. Chen, H.; Schlecht, S.; Semple, T. C.; Hartwig, J. F. *Science* **2000**, *287*, 1995–1997.
110. Hartwig, J. F.; Cook, K. S.; Hapke, M.; Incarvito, C. D.; Fan, Y.; Webster, C. E.; Hall, M. B. *J. Am. Chem. Soc.* **2005**, *127*, 2538–2552.
111. Kawamura, K.; Hartwig, J. F. *J. Am. Chem. Soc.* **2001**, *123*, 8422–8423.
112. Cho, J.-Y.; Iverson, C. N.; Smith, M. R., III. *J. Am. Chem. Soc.* **2000**, *122*, 12868–12869.
113. Tse, M. K.; Cho, J.-Y.; Smith, M. R., III. *Org. Lett.* **2001**, *3*, 2831–2833.
114. Cho, J.-Y.; Tse, M. K.; Holmes, D.; Maleczka, R. E., Jr.; Smith, M. R., III. *Science* **2002**, *295*, 305–308.
115. Maleczka, R. E., Jr.; Shi, F.; Holmes, D.; Smith, M. R. *J. Am. Chem. Soc.* **2003**, *125*, 7792–7793.
116. Ishiyama, T.; Takagi, J.; Ishida, K.; Miyaura, N.; Anastasi, N. R.; Hartwig, J. F. *J. Am. Chem. Soc.* **2002**, *124*, 390–391.
117. Takagi, J.; Sato, K.; Hartwig, J. F.; Ishiyama, T.; Miyaura, N. *Tetrahedron Lett.* **2002**, *43*, 5649–5651.
118. Ishiyama, T.; Takagi, J.; Hartwig, J. F.; Miyaura, N. *Angew. Chem., Int. Ed. Engl.* **2002**, *41*, 3056–3058.
118a. Ishiyama, T.; Nobuta, Y.; Hartwig, J. F.; Miyaura, N. *Chem. Commun.* **2003**, 2924–2925.
119. Ishiyama, T.; Takagi, J.; Yonekawa, Y.; Hartwig, J. F.; Miyaura, N. *Adv. Synth. Catal.* **2003**, *345*, 1103–1106.
120. Perutz, R. N. *Chem. Commun.* **2005**, 2172–2174.
121. Tsukada, N.; Hartwig, J. F. *J. Am. Chem. Soc.* **2005**, *127*, 5022–5023.
122. Kakiuchi, F.; Murai, S. In *Topics Organometallic Chemistry*; Murai, S., Ed.; Springer: New York, 1999; Vol. 3, pp 47–80.
123. Murai, S.; Kakiuchi, F.; Sekine, S.; Tanaka, Y.; Kamatani, A.; Sonoda, M.; Chatani, N. *Nature* **1993**, *366*, 529–531.
124. Sonoda, M.; Kakiuchi, F.; Kamatani, A.; Chatani, N.; Murai, S. *Chem. Lett.* **1996**, *2*, 109–110.
124a. Kakiuchi, F.; Ohtaki, H.; Sonoda, M.; Chatani, N.; Murai, S. *Chem. Lett.* **2001**, *9*, 918–919.
125. Kakiuchi, F.; Yamauchi, M.; Chatani, N.; Murai, S. *Chem. Lett.* **1996**, *2*, 111–112.
126. Kakiuchi, F.; Sato, T.; Igi, K.; Chatani, N.; Murai, S. *Chem. Lett.* **2001**, *5*, 386–387.
127. Kakiuchi, F.; Sonoda, M.; Tsujimoto, T.; Chatani, N.; Murai, S. *Chem. Lett.* **1999**, *10*, 1083–1084.
128. Kakiuchi, F.; Tanaka, Y.; Sato, T.; Chatani, N.; Murai, S. *Chem. Lett.* **1995**, *8*, 679–680.
129. Kakiuchi, F.; Yamamoto, Y.; Chatani, N.; Murai, S. *Chem. Lett.* **1995**, *8*, 681–682.
129a. Kakiuchi, F.; Uetsuhara, T.; Tanaka, Y.; Chatani, N.; Murai, S. *J. Mol. Catal. A* **2002**, *182–183*, 511–514.
130. Kakiuchi, F.; Matsumoto, M.; Sonoda, M.; Fukuyama, T.; Chatani, N.; Murai, S. *Chem. Lett.* **2000**, *7*, 750–751.
131. Kakiuchi, F.; Igi, K.; Matsumoto, M.; Hayamizu, T.; Chatani, N.; Murai, S. *Chem. Lett.* **2002**, *3*, 396–397.
131a. Kakiuchi, F.; Igi, K.; Matsumoto, M.; Chatani, N.; Murai, S. *Chem. Lett.* **2001**, *5*, 422–423.
132. Thalji, R. K.; Ahrendt, K. A.; Bergman, R. G.; Ellman, J. A. *J. Org. Chem.* **2005**, *70*, 6775–6781.
132a. Thalji, R. K.; Ahrendt, K. A.; Bergman, R. G.; Ellman, J. A. *J. Am. Chem. Soc.* **2001**, *123*, 9692–9693.
133. Thalji, R. K.; Ellman, J. A.; Bergman, R. G. *J. Am. Chem. Soc.* **2004**, *126*, 7192–7193.
134. Tan, K. L.; Park, S.; Ellman, J. A.; Bergman, R. G. *J. Org. Chem.* **2004**, *69*, 7329–7335.
134a. Tan, K. L.; Bergman, R. G.; Ellman, J. A. *J. Am. Chem. Soc.* **2002**, *124*, 13964–13965.
134b. Wiedemann, S. H.; Bergman, R. G.; Ellman, J. A. *Org. Lett.* **2004**, *6*, 1685–1687.
135. Lewis, J. C.; Wiedemann, S. H.; Bergman, R. G.; Ellman, J. A. *Org. Lett.* **2004**, *6*, 35–38.
136. Satoh, T.; Kawamura, Y.; Miura, M.; Nomura, M. *Angew. Chem., Int. Ed. Engl.* **1997**, *36*, 174–182.
136a. Åhman, J.; Wolfe, J. P.; Troutman, M. V.; Palucki, M.; Buchwald, S. L. *J. Am. Chem. Soc.* **1998**, *120*, 1918.
137. Miura, M.; Tsuda, T.; Satoh, T.; Nomura, M. *Chem. Lett.* **1997**, 1103–1104.
138. Kobayashi, K.; Sugie, A.; Takahashi, M.; Masui, K.; Mori, A. *Org. Lett.* **2005**, *7*, 5083–5085.
139. Ko, S.; Na, Y.; Chang, S. *J. Am. Chem. Soc.* **2002**, *124*, 750–751.
140. Ko, S.; Han, H.; Chang, S. *Org. Lett.* **2003**, *5*, 2687–2690.
141. Kuninobu, Y.; Tokunaga, Y.; Kawata, A.; Takai, K. *J. Am. Chem. Soc.* **2006**, *128*, 202–209.
142. Kuninobu, Y.; Kawata, A.; Takai, K. *J. Am. Chem. Soc.* **2005**, *127*, 13498–13499.
143. Kuninobu, Y.; Kawata, A.; Takai, K. *Org. Lett.* **2005**, *7*, 3823–3825.
144. Dick, A. R.; Hull, K. L.; Sanford, M. S. *J. Am. Chem. Soc.* **2004**, *126*, 2300–2301.
145. Kalyani, D.; Sanford, M. S. *Org. Lett.* **2005**, *7*, 4149–4152.
146. Kalyani, D.; Deprez, N. R.; Desai, L. V.; Sanford, M. S. *J. Am. Chem. Soc.* **2005**, *127*, 7330–7331.
147. Desai, L. V.; Hull, K. L.; Sanford, M. S. *J. Am. Chem. Soc.* **2004**, *126*, 9542–9543.

148. Dick, A. R.; Kampf, J. W.; Sanford, M. S. *Organometallics* **2005**, *24*, 482–485.
148a. Dick, A. R.; Kampf, J. W.; Sanford, M. S. *J. Am. Chem. Soc.* **2005**, *127*, 12790–12791.
149. Dangel, B. D.; Johnson, J. A.; Sames, D. *J. Am. Chem. Soc.* **2001**, *123*, 8149–8150.
150. Johnson, J. A.; Sames, D. *J. Am. Chem. Soc.* **2000**, *122*, 6321–6322.
150a. Johnson, J. A.; Li, N.; Sames, D. *J. Am. Chem. Soc.* **2002**, *124*, 6900–6903.
151. Dangel, B. D.; Godula, K.; Youn, S. W.; Sezen, B.; Sames, D. *J. Am. Chem. Soc.* **2002**, *124*, 11856–11857.
152. Lane, B. S.; Brown, M. A.; Sames, D. *J. Am. Chem. Soc.* **2005**, *127*, 8050–8057.
152a. Lane, B. S.; Sames, D. *Org. Lett.* **2004**, *6*, 2897–2900.
153. Wang, X.; Lane, B. S.; Sames, D. *J. Am. Chem. Soc.* **2005**, *127*, 4996–4997.
154. Espino, C. G.; Wehn, P. M.; Chow, J.; Du Bois, J. *J. Am. Chem. Soc.* **2001**, *123*, 6935–6936.
155. Wehn, P. M.; Du Bois, J. *J. Am. Chem. Soc.* **2002**, *124*, 12950–12951.
156. Hinman, A.; Du Bois, J. *J. Am. Chem. Soc.* **2003**, *125*, 11510–11511.
157. Wehn, P. M.; Lee, J.; Du Bois, J. *Org. Lett.* **2003**, *5*, 4823–4826.
158. Fleming, J. J.; Fiori, K. W.; Du Bois, J. *J. Am. Chem. Soc.* **2003**, *125*, 2028–2029.
159. Fiori, K. W.; Fleming, J. J.; Du Bois, J. *Angew. Chem., Int. Ed.* **2004**, *43*, 4349–4352.
160. Espino, C. G.; Fiori, K. W.; Kim, M.; Du Bois, J. *J. Am. Chem. Soc.* **2004**, *126*, 15378–15379.
161. Goldman, A. S.; Roy, A. H.; Huang, Z.; Ahuja, R.; Schinski, W.; Brookhart, M. *Science*, **2006**, *312*, 257–261.

1.26
Transition Metal-mediated C–F Bond Activation

R N Perutz, University of York, York, UK
T Braun, Universität Bielefeld, Bielefeld, Germany

1.26.1 Introduction and Principles

The coordination and C–F bond activation of fluorocarbons at transition metals has developed strongly in the last few years. One stimulus for the investigations is the search for fundamental principles including understanding the nature of the metal–fluorine bond. By now it is recognized that the principles underlying C–F activation are significantly different from those underlying C–H bond activation. Another driver is the search for new routes to fluoroorganic and fluoroorganometallic compounds. It has been demonstrated that there are particular opportunities for syntheses involving removal of fluorine rather than the more conventional introduction of fluorine into an organic framework. With the enormous growth in the importance of cross-coupling has come the search for catalytic C–C coupling reactions involving C–F activation rather than the more usual cleavage of bonds to heavier halogens. There are now several examples of catalytic C–F activation including cross-coupling.

The work on C–F bond activation at transition metal complexes should be seen in the wider context of the innumerable applications of fluorinated organic molecules in areas as diverse as pharmaceuticals, enzyme substrate analogs, pesticides, catalysts, solvents, polymers, liquid crystals, refrigerants, etc.

Table 1 summarizes reviews relevant to C–F bond activation. The most important previous reviews of C–F activation are those of Kiplinger *et al.* in 1994[1] and of Burdeniuc *et al.* in 1997.[2] In light of these reviews, we have chosen the starting point for our detailed example sections as 1997.

Table 1 Reviews relevant to C–F bond activation

Year	*Author(s), reference*	*Topic*
1988	Brothers, Roper[3]	Dihalocarbene complexes
1990	Hughes[4]	Organotransition metal complexes with perfluorinated ligands
1993	Morrison[5]	Complexes of CF_3
1994	Kiplinger, Richmond, Osterberg[1]	C–F activation by metal complexes
1997	Burdeniuc, Jedlicka, Crabtree[2]	C–F activation
1997	Plenio[6]	Coordination chemistry of C–F bonds
1997	Murphy, Murugavel, Roesky[7]	Organometallic fluorides of *d*-block metals
1999	Richmond[8]	C–F activation
2000	Richmond[9]	C–F activation (very brief)
2002	Braun, Perutz[10]	C–F activation at nickel and rhenium complexes
2002	Alonso, Beletskaya, Yus[11]	Metal-mediated hydrodehalogenation
2003	Mazurek, Schwarz[12]	Gas-phase C–F activation
2003	Jones[13]	C–F activation at zirconium complexes
2005	Torrens[14]	C–F bond activation by platinum group complexes

For this review we limit the definition of C–F bond activation at transition metal centers to reactions involving cleavage of C–F bonds mediated by transition metals. The majority of such reactions involve a change in the primary coordination sphere of the metal. Nevertheless, the definition allows for enhancement of reactivity of C–F bonds even if the immediate coordination sphere of the metal is unchanged. Section 1.26.1 of our review sets out the principal modes of coordination of fluorinated molecules to transition metal centers and the principal pathways for C–F bond activation with one or two examples for each type. Section 1.26.2 provides a moderately comprehensive set of examples of intermolecular C–F bond activation organized by aromatic, alkene, and aliphatic C–F bonds and for the period 1997–2005. Section 1.26.3 follows the same pattern but for intramolecular C–F activation.

1.26.1.1 Coordination of Fluorinated Molecules

While coordination of fluorinated alkenes occurs via the C=C double bond, several coordination modes are known for fluorinated arenes including η^6-, η^4-, and η^2-coordination (Scheme 1). McGlinchey and Tan reported metal vapor synthesis of chromium bis(arene) compounds including $[Cr(\eta^6\text{-}C_6F_6)(\eta^6\text{-}C_6H_6)]$ in 1976,[15] while Timms *et al.* reported the reaction of tungsten atoms with hexafluorobenzene and the crystal structure of the resulting $[W(\eta^6\text{-}C_6F_6)_2]$.[16] With η^4-coordination, the hexafluorobenzene unit is distorted into a diene–ene structure with two carbons out of the plane of the remaining four as can be seen in the structures of $[Ru(\eta^6\text{-}C_6H_3Me_3)(\eta^4\text{-}C_6F_6)]$ or $[Ir(\eta^5\text{-}C_5Me_5)(\eta^4\text{-}C_6F_6)]$.[17,18]

Several examples of η^2-coordination of hexafluorobenzene at transition metal centers have been reported.[19] A detailed investigation on the structure and dynamics of rhenium hexafluorobenzene complexes was performed by Perutz.[19] The complex $[(\eta^5\text{-}C_5H_5)Re(CO)_2(\eta^2\text{-}C_6F_6)]$ shows the characteristic distortion of the fluorinated ligand from planarity in the crystalline state. The average dihedral angle between the C(1)F(1)C(2)F(2) plane and the plane of the benzene ring in this class of complex is 46° (see Scheme 2, the coordinated carbons are labeled C(1) and C(2)). IR and ^{19}F NMR spectroscopy of $[(\eta^5\text{-}C_5H_5)Re(CO)_2(\eta^2\text{-}C_6F_6)]$ reveal the occurrence of two separate dynamic processes in solution. At 184 K two rotamers are interconverted by rotation about the metal–C_6F_6 bond with $\Delta G^{\neq} = 36.7\,kJ\,mol^{-1}$. At higher temperature an intramolecular 1,2-shift of the site of the rhenium coordination has been identified by line broadening and EXSY NMR spectroscopy ($\Delta H^{\neq} = 57.6\,kJ\,mol^{-1}$, $\Delta S^{\neq} = -7\,kJ\,mol^{-1}$, Scheme 2).

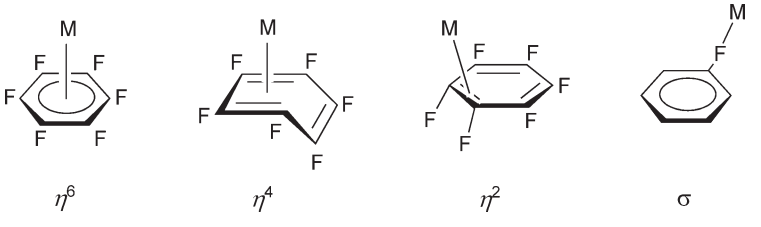

Scheme 1

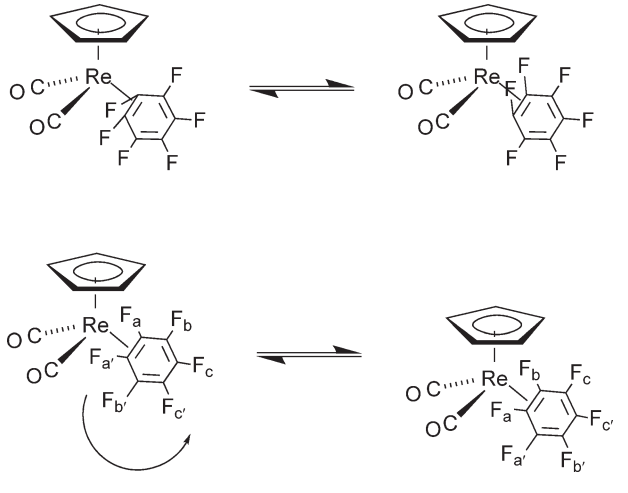

Scheme 2

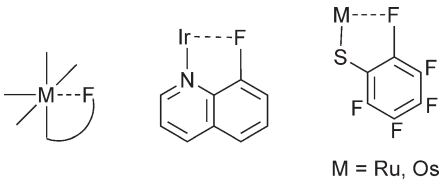

Scheme 3

Hessen and Teuben recently reported the decisive example of σ-F coordination of a fluoroarene with the X-ray structure of $[Ti(\eta^5\text{-}C_5Me_5)_2(\sigma\text{-}FC_6H_5)][BPh_4]$.[20] Its C–F bond is extended to 1.402(3) Å compared to 1.364(2) Å in fluorobenzene. It is notable that this is a d^1-system so electron repulsion is almost at a minimum; nevertheless, the fluorobenzene is displaced by THF. In 2005, the same authors reported an analog with chelating 1,2-difluorobenzene together with related scandium complexes.[21] Horton and Orpen observed intermolecular Zr···F–C interactions in the zirconocene complexes $[(\eta^5\text{-}C_5Me_5)_2ZrMe][B(4\text{-}C_6H_4F)_4]$.[22] The cationic thorium complex $[(\eta^5\text{-}C_5Me_5)ThMe][B(4\text{-}C_6F_5)_4]$ contains two Th···F–C bridges.[23]

Complexes with intramolecular M···F–C interactions also exist as stable entities, as has been highlighted by Plenio's review of the coordination chemistry of CF units.[6] Orpen *et al.* provide a critical account of how to assess short contacts in crystal structures.[24] The chelation of an aromatic C–F bond to iridium has been detected by ^{19}F NMR and X-ray crystallography in the 8-fluoroquinoline complex $[Ir(H)_2(PPh_3)_2(\kappa^2(N,F)\text{-}C_9H_6NF)]SbF_6$ (Scheme 3).[25] A comparable interaction has been observed in the solid-state structure of the paramagnetic complex $[Ru(\kappa^1\text{-}SC_6F_5)_2\{\kappa^2(S,F)\text{-}SC_6F_5\}(PMe_2Ph)_2]$ and its osmium analog.[26–28] The latter exhibits an Os···F distance of 2.531(6) Å with fluorine occupying the sixth coordination position of an octahedron around osmium (Scheme 3). However, in other cases of F···M chelates it has been argued that the geometry of the complexes imposes short metal–fluorine interactions and that they do not necessarily correspond to an attractive interaction.[29,30]

There is also well-documented evidence for short contacts between fluoroalkyl groups and transition metals in sterically crowded complexes. Studies of palladium tris(trifluoromethyl)phenyl complexes show that the contacts are probably non-bonding; the shortest Pd···F distance observed is 2.766 Å.[24] Significant intramolecular nickel–fluorine contacts to a fluoroalkyl CF_3 group are reported to exist in solution and in the solid state in *cis*-$[Ni\{2,4,6\text{-}C_6H_2(CF_3)_3\}_2(dme)]$. The Ni···F distances are 2.592(5) and 2.595(5) Å and the fluorine atoms occupy the axial positions of a distorted octahedron but are again argued to be non-bonding.[31] Close intramolecular fluorine–vanadium contacts of 2,4,6-tris(trifluoromethyl)phenyl groups have been detected in the solid state.[32] Direct intramolecular coordination of a fluorinated tripod ligand to yttrium has been observed in the solid state and in solution by detection of ^{89}Y–^{19}F coupling in the ^{19}F NMR spectrum.[33] Evidence for fluoroalkyl coordination to transition metals from matrix isolation spectroscopy and time-resolved spectroscopy in solution and gas phases has been reviewed by Richmond.[1]

1.26.1.2 Fundamental Processes of Intermolecular C–F Activation

We classify the fundamental processes of intermolecular C–F bond activation in the following six categories: (i) oxidative addition of fluorocarbon, (ii) M–C bond formation with HF elimination, (iii) M–C bond formation with fluorosilane elimination, (iv) hydrodefluorination of fluorocarbon with M–F bond formation, (v) nucleophilic attack on fluorocarbon, and (vi) defluorination of fluorocarbon (Scheme 4). Table 2 shows the occurrence of these processes for intermolecular C–F activation, classified according to the type of C–F bond. For instance, oxidative addition is a characteristic process for fluoroaromatics but not for fluoroalkanes, while defluorination is characteristic of fluoroalkanes but not fluoroaromatics. We include processes as intermolecular even if they involve coordination of the fluorocarbon in one of the modes in Section 1.26.1.1 prior to C–F bond breaking. Notice that processes (ii), (iii), and (iv) could be described as σ-bond metatheses; we have avoided this descriptor, since it has mechanistic connotations that are only appropriate in some cases. It should also be recognized that secondary processes may make some reactions awkward to classify under this scheme.

The energetics of C–F bond-activation reactions depend on the strength of the C–F bond as well as bond energies of the fluorine-containing products. While there is general agreement that C–F bonds are stronger than the C–H bonds of hydrocarbon analogs, determinations of C–F bond energies are limited in number, and there is sometimes significant disagreement between different methods. Table 3[34,34a,34b] lists H–X and F–X bond energies taken from a

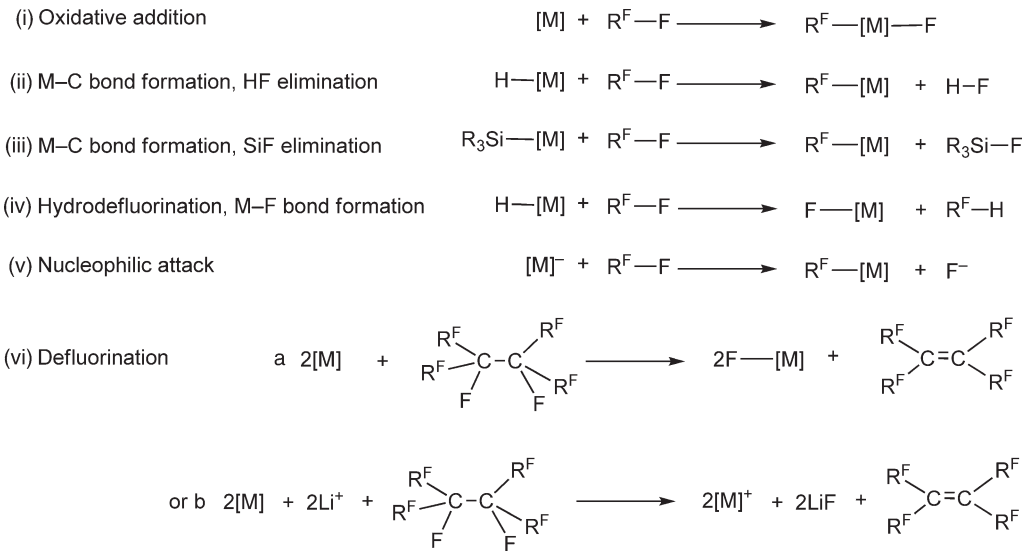

Scheme 4 Intermolecular C–F activation processes.

Table 2 Occurrence of intermolecular C–F activation processes

Entry	*Reaction(s)*	*Fluoroaromatic*	*Fluoroalkene*	*Fluoroalkyl*
(i)	Oxidative addition	Yes	?	No
(ii)	M–C bond formation, HF elimination	Yes	Yes	No
(iii)	M–C bond formation, fluorosilane elimination	Yes	Yes	No
(iv)	Hydrodefluorination, M–F bond formation	Yes	Yes	Yes
(v)	Nucleophilic attack	Yes	Yes	Rare
(vi)	Defluorination	No	No	Yes

Table 3 H–X and F–X bond energies (kJ mol^{-1})[a]

X	*H–X*	*F–X*
H	435.99	569.9
F	569.9	158.78
CH_3	438.89	472
CF_3	449.5	547
C_6H_5	473.1	533
C_6F_5	476.6	487[b]
R_3Zr	–	650.3[c]
R_3Si	396[d]	565[e]

[a]Unless otherwise stated, all values are taken from David, R. L. (ed.) In *CRC Handbook of Chemistry and Physics*; CRC Press LLC: Boca Raton, 2005.
[b]Note that much higher values for F–C_6F_5 are quoted elsewhere.
[c]Based on average bond energy of ZrF_4 in *NIST Webbook*.
[d]Kalinowski, I. J.; Gutman, D.; Krasnoperov, L. N.; Goumri, A.; Yuan, W.-J.; Marshall, P. *J. Phys. Chem*. **1994**, *98*, 9551.
[e]Huheey, J. E.; Keiter, E. A.; Keiter, R. L. *Inorganic Chemistry*, 4th ed.; Harper Collins: New York, 1993.

common compilation where possible. Oxidative addition is greatly assisted energetically by the formation of the M–F bond, even if the metals concerned have as many as 8 *d*-electrons, but literature on the factors determining the strength of M–F bonds is very limited (see also Section 1.26.2.1.3).[35,35a,36] Processes (ii), (iii), and (iv) are driven energetically by the formation of the strong H–F, Si–F, and M–F bonds, respectively. Many different reaction mechanisms may yield products corresponding to any one of these processes. At this stage, we are beginning to

understand the circumstances that lead to relatively low barriers to C–F bond activation; details will be found later in the review.

Functionalization of highly fluorinated molecules at transition metal centers is limited not only by the difficulty of C–F bond activation, but also by the well-established observations that metal–fluoroalkyl and metal–fluoroaryl bonds are stronger and much more kinetically inert than the corresponding metal–alkyl and metal–aryl bonds. Thus, migration, alkene metathesis, CO insertion, alkene insertion, α- and β-elimination of fluorinated substrates are all very challenging to achieve. The reactions described in this chapter form the reaction repertoire for the transition metal complexes interacting with fluorocarbons, a very different set from those for hydrocarbons.

The effect of fluorine substituents on the strength of a metal–aryl bond is graphically illustrated by theoretical calculations of bond energy correlations.[37] Fluorine substituents in the two positions *ortho* to the metal–fluorine bond are shown to have far more effect on the M–C bond energy than substituents in the *meta*- or *para*- positions; in the case of Re–C bonds this difference is calculated to be ca. 50 kJ mol^{-1}. These conclusions are borne out by experiment.

In the following sections, we illustrate the processes and their application to catalysis with a few examples, mostly chosen from the recent literature. We also remark briefly on the energetics and mechanisms of the reactions.

1.26.1.3 Prototype Examples of Intermolecular Activation of Fluorinated Aromatics

1.26.1.3.1 Oxidative addition

Oxidative addition of fluorinated aromatics to give metal(aryl) fluoro complexes has been observed frequently for complexes of group 10 metals, but rarely otherwise. The reactions include the insertion of an {Ni(PEt_3)$_2$} unit into a carbon–fluorine bond in hexafluorobenzene (Scheme 5). The very slow conversion (4 weeks) was initially reported by Fahey and Mahan;[38] full spectroscopic and crystallographic characterization of the product was performed by Perutz *et al*.[39] Mechanistic studies and density functional theory (DFT) calculations give strong evidence for precoordination of the aromatic substrate followed by a concerted oxidative addition.[35a,40,41] Oxidative addition has also been reported as the photochemically driven reaction for an Rh(η^2-C_6F_6) complex both in solution and in low-temperature matrices.[42]

The most effective precursors for C–F oxidative addition have proved to be very different from the typical precursors for C–H oxidative addition of arenes or alkanes. The best ones for C–F oxidative addition, such as {Ni(PEt_3)$_2$}, may not be active in C–H oxidative addition at all, bringing the advantage of selectivity for C–F over C–H bonds. In contrast, the best precursors for C–H oxidative addition, such as {Rh(η^5-C_5Me_5)(PMe_3)}, have a strong preference for C–H bonds over C–F bonds that curtails their application to C–F bond activation. Theoretical investigations have shown that the C–F bond activation may still be very energetically favorable in these systems, but a high kinetic barrier leads to the observed preference for C–H activation.[35,35a]

Oxidative addition of C–Cl bonds is usually preferred to C–F bond activation, but there are exceptions. Thus, the treatment of [Ni(COD)$_2$] (COD = 1,5-cyclooctadiene) with 5-chloro-2,4,6-trifluoropyrimidine in the presence of L (L = PCy_3, PPr^i_3, or PPh_3) effects the formation of the fluoro complexes *trans*-[NiF(4-$C_4N_2ClF_2$)(L)$_2$].[43,44] The only other example of the selective activation of a C–F bond in the presence of a C–Cl bond by a transition metal is the activation of the imine (C_6F_5)CH=NCH$_2$(2-ClC_6H_4) at a Pt(II) center, but with the carbon–halogen bonds at different rings.[45]

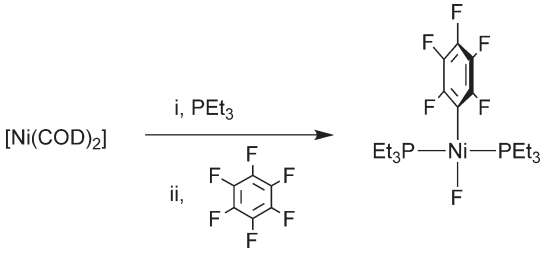

Scheme 5

1.26.1.3.2 M–C bond formation, HF elimination

A different approach to the activation of carbon–fluorine bonds involves the formation of HF when using metal hydrides as starting compounds. For instance, the reaction of *cis*-[Ru(H)$_2$(dmpe)$_2$] (dmpe = bis(dimethylphosphino)ethane) with hexafluorobenzene at −78 °C yields *trans*-[Ru(H)(C$_6$F$_5$)(dmpe)$_2$] (Scheme 6).[46] There is considerable evidence that this reaction proceeds via an electron-transfer pathway, but this mechanism should not be generalized.

1.26.1.3.3 M–C bond formation, fluorosilane elimination

In a comparable strategy, the formation of strong silicon–fluorine bonds can be applied as thermodynamic driving force for C–F activation generating fluorosilanes and metal aryls. A classic example was reported by Aizenberg and Milstein: treatment of the rhodium complex [Rh(SiPh$_3$)(PMe$_3$)$_3$] with hexafluorobenzene yields [Rh(C$_6$F$_5$)(PMe$_3$)$_3$] and FSiPh$_3$ (Scheme 7).[47]

1.26.1.3.4 Hydrodefluorination, M–F bond formation

Another strategy involves the use of metal hydrides to replace a fluorine at the fluoroorganic substrate by hydrogen while forming a metal–fluorine bond. Jones *et al.* demonstrated that treatment of [Zr(η^5-C$_5$Me$_5$)$_2$(H)$_2$] with hexafluorobenzene leads to a mixture of [Zr(η^5-C$_5$Me$_5$)$_2$(H)F] and the hydrodefluorination product pentafluorobenzene (Scheme 8). However, a second reaction pathway leads to the aryl complex [Zr(η^5-C$_5$Me$_5$)$_2$(H)(C$_6$F$_5$)].[48] This reaction is assisted by the great strength of the Zr–F bond.

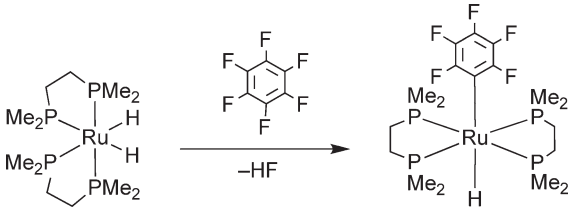

Scheme 6

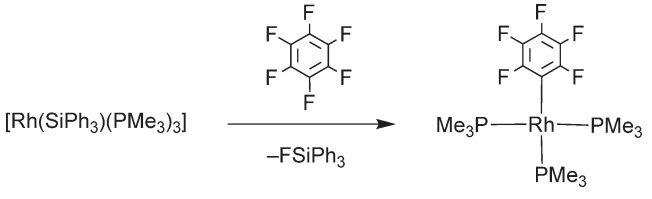

Scheme 7

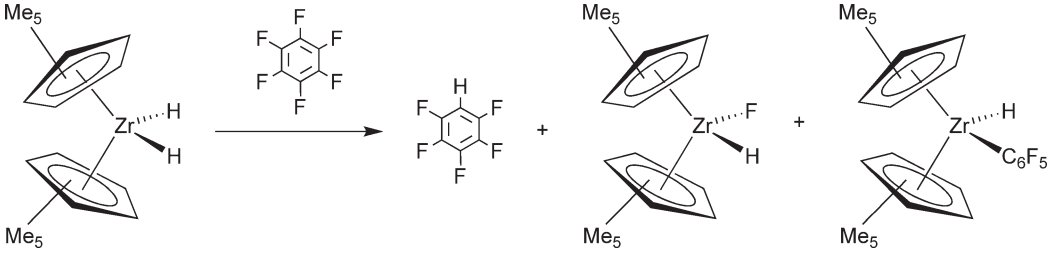

Scheme 8

1.26.1.3.5 Nucleophilic attack

Anionic metal complexes can replace a fluorine in an aromatic substrate by nucleophilic aromatic substitution. King showed as early as 1964 that $[Fe(\eta^5\text{-}C_5H_5)(CO)_2]^-$ reacts with hexafluorobenzene to furnish $[Fe(\eta^5\text{-}C_5H_5)(C_6F_5)(CO)_2]$ (Scheme 9).[49] Examples of nucleophilic attack may be disguised; for instance, an anionic metal complex is formed *in situ* in the base-promoted reaction of $[Rh(\eta^5\text{-}C_5Me_5)(H)_2(PMe_3)]$.[50]

1.26.1.4 Prototype Examples of Intermolecular Activation of Fluorinated Alkenes

1.26.1.4.1 Oxidative addition

Oxidative addition reactions of fluorinated alkenes are very rare. However, the rearrangement of the pentafluoro-propene complex $[IrCl(F_2C{=}CHCF_3)(PMe_3)_3]$ to yield $[IrClF(FC{=}CHCF_3)(PMe_3)_3]$ was mentioned in Richmond's review.[1]

1.26.1.4.2 M–C bond formation, HF elimination

Carbon–fluorine bonds of fluoroalkenes can be cleaved by reaction with metal hydrides to give HF and vinyl complexes. Thus, the rhodium compound $[Rh\{(Z)\text{-}CF{=}CF(CF_3)\}(PEt_3)_3]$ can be synthesized by regioselective C–F bond activation of hexafluoropropene at $[RhH(PEt_3)_3]$ in the presence of Et_3N/Cs_2CO_3 (Scheme 10 left).[51]

1.26.1.4.3 M–C bond formation, fluorosilane elimination

There is no simple analog of Milstein's reaction (Scheme 7) for reactions with fluorinated alkenes. The silyl complex *cis-fac*-$[Rh(H)_2(SiPh_3)(PEt_3)_3]$ is capable of the C–F activation of hexafluoropropene to afford $[Rh\{(Z)\text{-}CF{=}CF(CF_3)\}(PEt_3)_3]$ with elimination of $FSiPh_3$. The reaction may proceed via $[Rh(SiPh_3)(PEt_3)_3]$ and/or via $[RhH(PEt_3)_3]$ as intermediate (Scheme 10 right).[52]

1.26.1.4.4 Hydrodefluorination, M–F bond formation

Reaction of $[Zr(\eta^5\text{-}C_5Me_5)_2(H)_2]$ and hexafluoropropene at −40 °C leads to the hydrodefluorination product (*E*)-pentafluoropropene and the zirconium fluoride $[Zr(\eta^5\text{-}C_5Me_5)_2(H)F]$ (Scheme 11).[53]

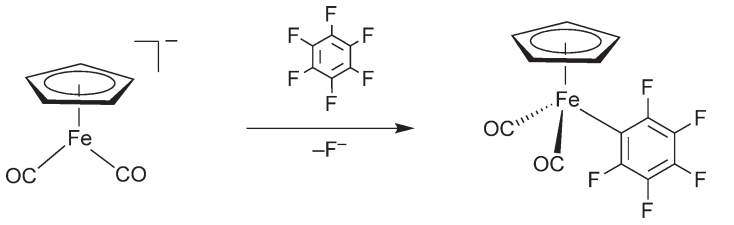

Scheme 9

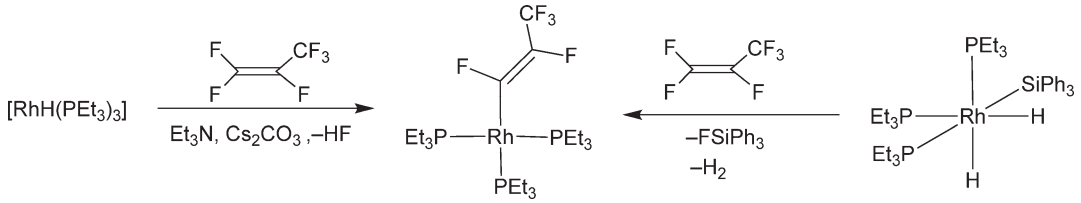

Scheme 10

Scheme 11

1.26.1.4.5 Nucleophilic attack

As has been shown for aromatic substrates, anionic metal complexes can also replace a fluorine in olefins. For instance, hexafluoropropene reacts with $[Fe(\eta^5\text{-}C_5H_5)(CO)_2]^-$ to give $[Fe(\eta^5\text{-}C_5H_5)\{FC{=}CF(CF_3)\}(CO)_2]$.[54]

1.26.1.5 Prototype Examples of Intermolecular Activation of Fluorinated Alkanes

1.26.1.5.1 Oxidative addition

Classical oxidative addition of a fluorinated alkane at a transition metal center still remains elusive. However, such a step is conceivable in catalytic cross-coupling reactions of primary alkyl fluorides.[55] The reactions of lanthanoid cations with CH_3F to form LnF^+ and $\cdot CH_3$ have been described as oxidative additions, but do not conform to our definition of oxidative addition.[56,57]

1.26.1.5.2 Hydrodefluorination, M–F bond formation

$[Zr(\eta^5\text{-}C_5Me_5)_2(H)_2]$ reacts with monofluorinated hydrocarbons such as fluorohexane to give $[Zr(\eta^5\text{-}C_5Me_5)_2(H)F]$ and/or $[Zr(\eta^5\text{-}C_5Me_5)_2F_2]$ and alkane through a radical chain mechanism (Scheme 12).[13]

1.26.1.5.3 Nucleophilic attack

The anionic rhodium complex $[Rh(dmgH)_2(PPh_3)]^-$ (dmg = dimethylglyoximato) reacts with $Br(CH_2)_2F$ to give the binuclear complex $[Rh(dmgH)_2(PPh_3)]_2(CH_2)_2$ (Scheme 13).[58] This is likely to proceed via attack of the metal anion on $[Rh(dmgH)_2(PPh_3)(CH_2CH_2F)]$.

1.26.1.5.4 Defluorination

In contrast to carbon–fluorine activation reactions of alkenes or aromatics, the conversion of fluorinated alkanes and cycloalkanes to alkenes and aromatics is well documented. For instance, Crabtree and Burdeniuc discovered metal-based photochemical systems which are useful for the defluorination of perfluorocarbons.[59–61] Irradiation of perfluoromethylcyclohexane or perfluoroisopentane in the presence of decamethylferrocene and LiOTf provides a route to prepare perfluoroalkenes (Scheme 14). These reactions conform to the general equation (vi)a (Scheme 4) with

Scheme 12

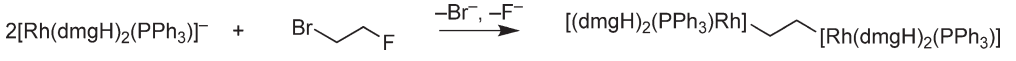

Scheme 13

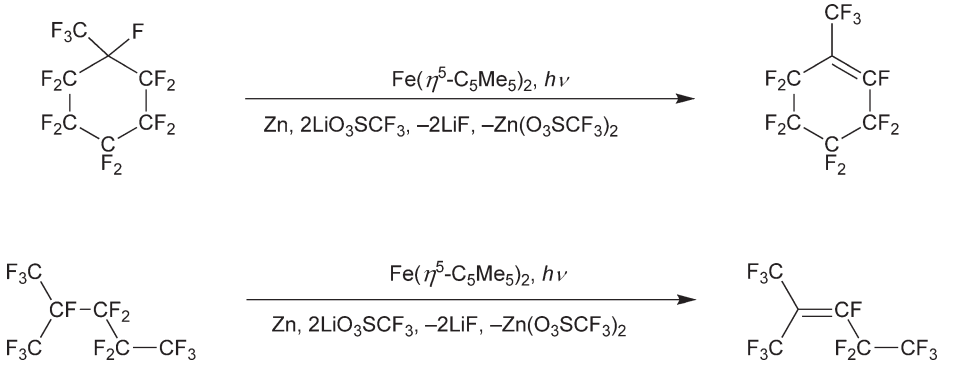

Scheme 14

decamethylferrocene as the reducing metal. The system can be made catalytic by using zinc to reduce the intermediate ferrocenium cation.

The reaction of ytterbocene with perfluorodecalin to form perfluoralkenes and $[Yb(\eta^5\text{-}C_5H_5)_2F]_3$ conforms to the alternative general equation for defluorination (equation (vi)a of Scheme 4).[62,63]

1.26.1.6 Fundamental Processes of Intramolecular C–F Activation

The fundamental processes of intramolecular C–F activation with directly bound fluoroalkyl or fluoroaryl groups are less easily generalized than their intermolecular counterparts. We have identified the following processes which are shown in Scheme 15: (i) [1,2]-F shift (α-fluoride elimination), (ii) [1,3]-F shift (β-fluoride elimination),

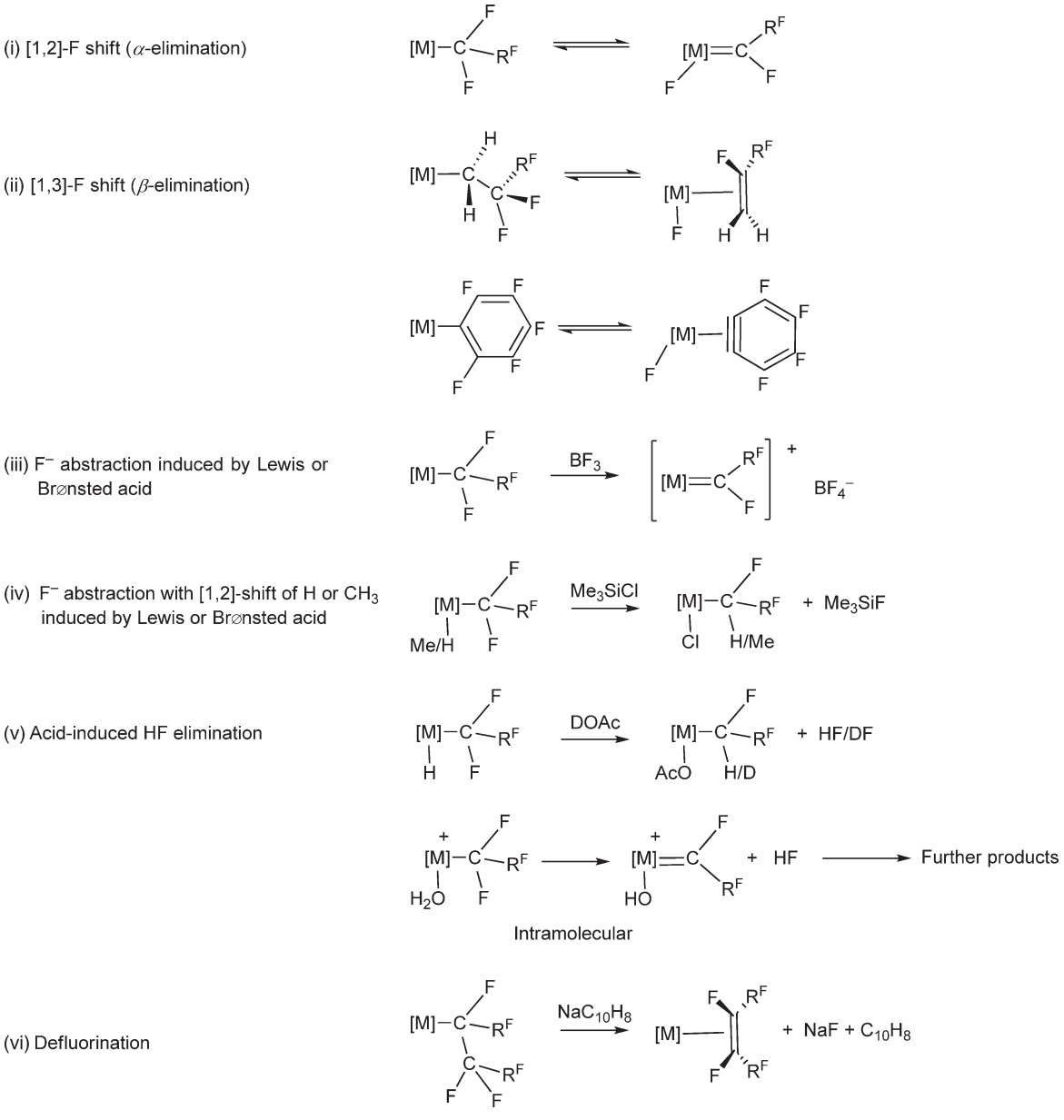

Scheme 15 Intramolecular C–F activation processes.

(iii) F^- abstraction induced by Lewis or Brønsted acid, (iv) F^- abstraction with H or CH_3 migration induced by Lewis or Brønsted acid, (v) acid-induced HF elimination, (vi) defluorination.

The fundamental processes for remote attack, that is, C–F activation on a pendant group remote from the metal, are limited to (vii) C–F oxidative addition and (viii) C–C coupling of two ligands with HF elimination.

1.26.1.7 Prototype Examples of α-activation of Metal Fluoroalkyls and Activation of Metal Fluoroaryls

1.26.1.7.1 [1,2]-Fluorine-to-metal and [1,3]-fluorine-to-metal shifts

The equivalent of oxidative addition for a metal fluoroalkyl is the [1,2]-fluorine shift in an M–CF_3 group, generating a metal difluorocarbene fluoride. This class of reaction is exemplified by the reaction of 16-electron $[ML_2(CO)(H)F]$ (M = Ru, L = PBu^t_2Me, or PPr^i_3, M = Os, L = PBu^t_2Me) with Me_3SiCF_3 in the presence of catalytic CsF to form $[ML_2(CO)(=CF_2)(H)F]$ (Scheme 16).[64] Although M=CF_2(F) complexes remain rarities, the [1,2]-F shift can be a reversible process in which the equilibrium may lie toward the carbene side.[64]

A [1,3]-fluorine shift of a fluoroalkyl ligand is implicated in the reactions of $[Zr(\eta^5\text{-}C_5Me_5)_2(H)_2]$ with fluoroalkenes, but the transient $[Zr(\eta^5\text{-}C_5Me_5)_2(H)F(alkene)]$ is not detected directly (Scheme 11). The corresponding [1,3]-fluorine shift of a pentafluorophenyl complex is implicated in the thermolysis of $[Zr(\eta^5\text{-}C_5Me_5)_2(H)(C_6F_5)]$ under hydrogen yielding $[Zr(\eta^5\text{-}C_5Me_5)_2F(C_6HF_4)]$ (Scheme 17). This reaction probably proceeds via a zirconium(η^2-tetrafluorobenzyne) complex.[65] When the reaction is conducted under vacuum, products are formed with η^6-tetramethylfulvene ligands derived by hydrogen elimination. Since these steps are associated with intermolecular reactions, especially hydrodefluorination, the reader is referred to Sections 1.26.1.4.4, 1.26.2.1.1, and 1.26.2.2.1.

1.26.1.7.2 Fluoride abstraction induced by Lewis or Brønsted acid

The α-C–F bond of metal fluoroalkyls is susceptible to electrophilic attack by Lewis and Brønsted acids; this is sometimes associated with M–fluoroalkyl π-backbonding. Fluoride may be abstracted from the α-position of metal fluoroalkyls with fluoride acceptors including H^+, BF_3, and SbF_5 to form metal difluorocarbene complexes, as in the conversion of $[Fe(\eta^5\text{-}C_5H_5)(CF_3)(CO)_2]$ to $[Fe(\eta^5\text{-}C_5H_5)(=CF_2)(CO)_2]BF_4$.[3]

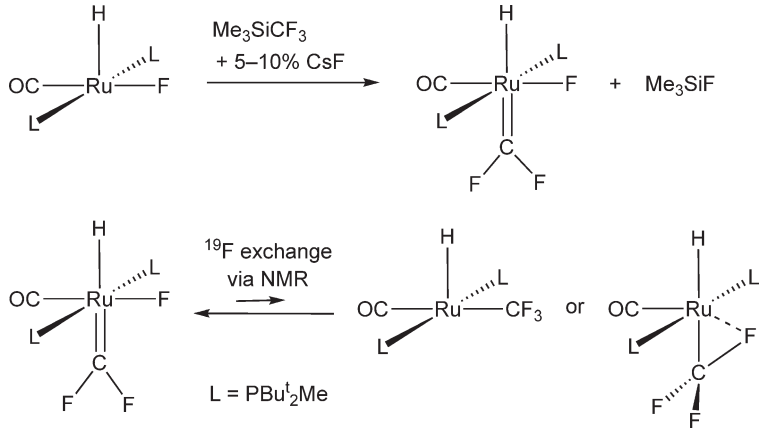

Scheme 16

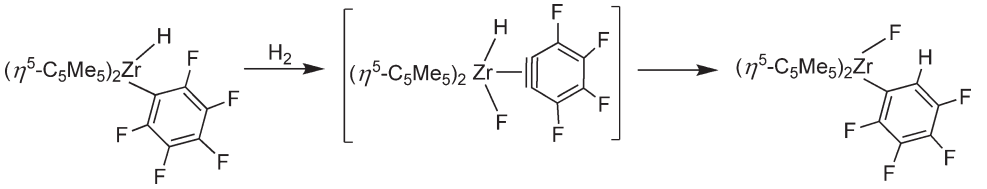

Scheme 17

1.26.1.7.3 Fluoride abstraction with [1,2]-shift of H or CH_3 induced by Lewis or Brønsted acids

A metal hydride (or alkyl) complex that also has fluoroalkyl ligands may react with a Lewis acid to induce fluoride abstraction and a shift of hydrogen (or methyl) onto the fluoroalkyl ligand (Scheme 18). Fluoride acceptors and Lewis acids such as Me_3SiCl and $[Ph_3C]OTf$ have been used. Similar reactions may occur with strong Brønsted acids such as triflic acid.[66,67]

1.26.1.7.4 Acid-induced HF elimination

Brønsted acids may react at the α-position of fluoroalkyls to abstract HF. The reaction may involve external H^+ attacking at the CF bond directly. The reaction may also have intramolecular character as in (1) attack by coordinated water or (2) initial attack by external acid on a metal hydride generating a dihydrogen complex as an intermediate (Schemes 19 and 15, equation (v)).

1.26.1.7.5 Defluorination

Defluorination of a perfluoroalkyl ligand has been achieved with sodium naphthalenide as a reducing agent but not with a transition metal-based reducing agent. An example is shown in Scheme 20.[68]

1.26.1.8 Prototype Examples of Intramolecular Activation of Remote C–F Bonds

The vast majority of the examples of remote C–F activation involve aromatic C–F bonds, and we restrict ourselves to them in this section.

1.26.1.8.1 Remote oxidative addition

Oxidative addition of a remote aromatic C–F bond on a nitrogen ligand was investigated in detail by Richmond *et al.* and is documented in his review: this remains one of the best examples in its class. The reaction of $[W(CO)_3(PrCN)_3]$

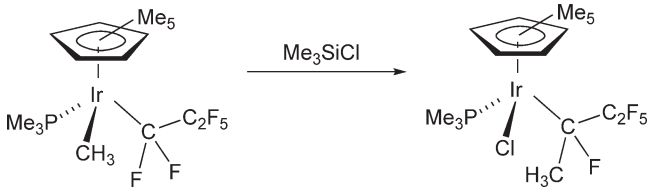

Scheme 18

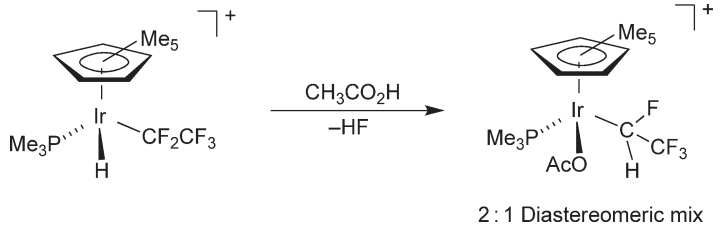

Scheme 19

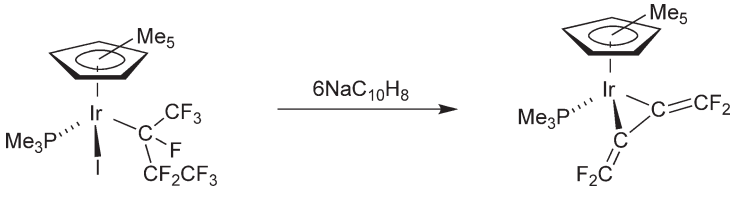

Scheme 20

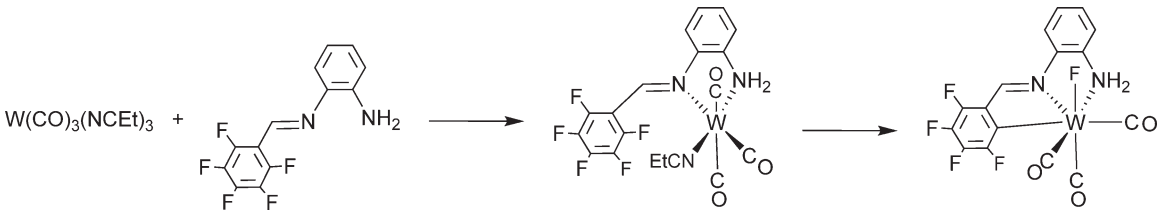

Scheme 21

with a chelating nitrogen ligand with a C_6F_5 substituent on the carbon of the Schiff base gives an oxidative addition product directly. However, it is possible to obtain the $[W(CO)_3(EtCN)(chelate)]$ complex and monitor its intramolecular conversion into the final product (Scheme 21).[1]

1.26.1.8.2 Remote C–C coupling with HF Elimination

Saunders *et al.* have studied the C–C coupling in rhodium and iridium complexes that links fluorinated aromatic substituents on phosphine ligands to the methyl substituents of cyclopentadienyl ligands. These reactions involve HF elimination and can be induced by heat or base. The most effective bases are proton sponge (1,8-bis(dimethylamino)naphthalene) and Bu_4NF. One example is shown in Scheme 22.[69–71]

1.26.1.9 Prototype Examples of Catalytic Conversions

Catalytic C–F activation has been demonstrated in several reactions. Most of the catalytic conversions involving the cleavage of a C–F bond achieve hydrodefluorination reactions (i.e., the replacement of fluorine by hydrogen) or cross-coupling reactions of fluorinated aromatics. Prominent exceptions consist of Murai's rhodium-catalyzed exchange reaction between fluorobenzenes (see Scheme 41) and a disilane as well as the amination of 2-fluoronitrobenzene.[72,73] At present, turnover numbers are invariably low and there are no detailed studies of kinetics and mechanism of catalytic C–F activation.

1.26.1.9.1 Hydrodefluorination reactions

Homogeneous hydrodefluorination reactions, which have been reported, use dihydrogen itself, tertiary silanes or alkoxides containing β-hydrogens as hydrogen source. Aizenberg and Milstein demonstrated the first catalytic activation of a C–F bond by transition metal complexes under mild conditions with the use of rhodium complexes as catalysts. The complex $[Rh(SiR_3)(PMe_3)_3]$ ($R_3 = Ph_3$ or $PhMe_2$) catalyzes the reaction of hexafluorobenzene with Ph_3SiH or $(EtO)_3SiH$ to give pentafluorobenzene.[47] Catalytic substitution of fluorine by hydrogen with turnover numbers up to 114 has also been demonstrated with hexafluorobenzene, H_2, and $[Rh(C_6F_5)(PMe_3)_3]$ as catalyst (Scheme 23).[74] The HF formed is trapped with triethylamine.

1.26.1.9.2 Cross-coupling reactions

Most of the catalytic cross-coupling reactions are based on the activation of a C–F bond of monofluorinated aromatic substrates. The Kumada–Corriu-, Suzuki-, and Stille-type reactions are catalyzed by nickel or palladium complexes.

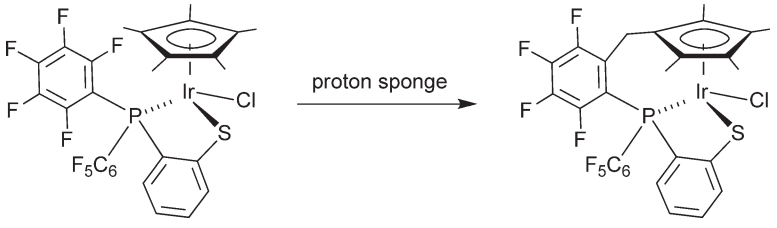

Scheme 22

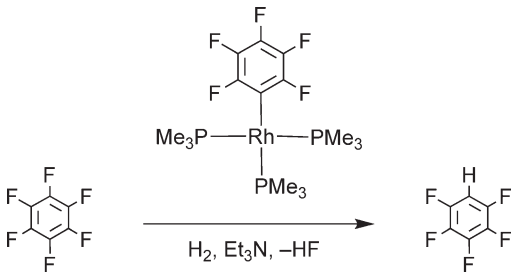

Scheme 23

In typical experiments 5–10% catalyst has to be employed. Conversions of pentafluoropyridine and 2,4,6-trifluoropyrimidine are also known, but turnover numbers are low.[44,75]

The first example of a cross-coupling reaction of a monofluorinated substrate was reported by Kumada and co-workers.[76] With 5% [$NiCl_2$(dmpe)], Pr^iMgCl and fluorobenzene could be converted into $Pr^iC_6H_5$ and $Pr^nC_6H_5$ with an overall yield of 62%. More recent outstanding examples consist of cross-coupling reactions of fluoroalkanes such as 1-fluorooctane with Grignard reagents using 3% $NiCl_2$ or $CuCl_2$ as catalyst and 1,3-butadiene as additive.[55]

1.26.2 Survey of Intermolecular C–F Bond Activation 1997–Mid 2005

1.26.2.1 Activation of Aromatic C–F Bonds

1.26.2.1.1 Group 4 metals and lanthanides

The reactions of zirconocene complexes with fluoroaromatics have complex mechanisms and several products are formed. As a result, they are hard to classify though some conform to the formal processes of hydrodefluorination with M–F bond formation (Scheme 4). When [$Zr(\eta^5\text{-}C_5H_5)_2(C_6F_5)_2$] is heated in the presence of C_6F_6, [$Zr(\eta^5\text{-}C_5H_5)_2F(C_6F_5)$], perfluorobiphenyl, and higher molecular weight linear oligomers are produced rapidly.[77] A radical chain mechanism has been proposed which is initiated by impurities in [$Zr(\eta^5\text{-}C_5H_5)_2(C_6F_5)_2$] or a radical initiator (Scheme 24).

The zirconium hydrides [$Zr(\eta^5\text{-}C_5H_5)_2(H)_2]_2$ and [$Zr(\eta^5\text{-}C_5H_5)_3(H)$] react with C_6F_6 to give [$Zr(\eta^5\text{-}C_5H_5)_2F(C_6F_5)$] as the major product along with [$Zr(\eta^5\text{-}C_5H_5)_2F_2$], C_6F_5H, and H_2 (Scheme 25).[77] Mechanistic studies are consistent with initial association between the metal center and C_6F_6 via fluorine. Such an interaction may lead to loss of H_2 and C–F oxidative addition or, alternatively, to a σ-bond metathesis pathway.[13,77]

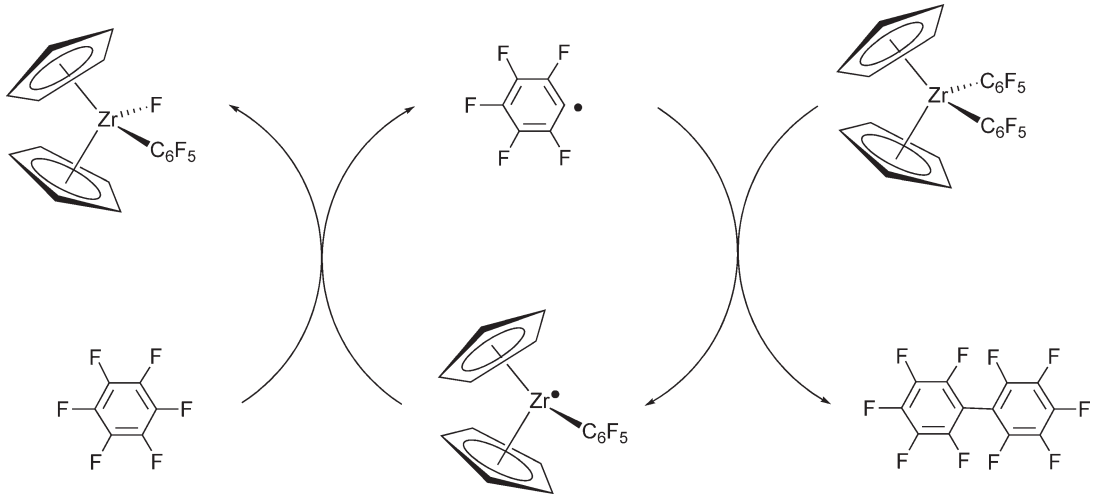

Scheme 24

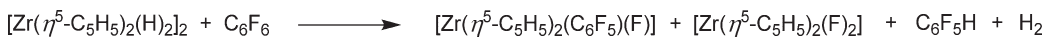

Scheme 25

$[Zr(\eta^5\text{-}C_5H_5)_2(H)_2]_2$ reacts with fluorobenzene to furnish a mixture of $[Zr(\eta^5\text{-}C_5Me_5)_2(H)F]$, benzene, and $[Zr(\eta^5\text{-}C_5Me_5)_2F(C_6H_5)]$.[78] Detailed studies indicate that dual hydrodefluorination pathways are operative. One involves hydride attack at the aromatic ring and subsequent fluoride abstraction to give $[Zr(\eta^5\text{-}C_5Me_5)_2(H)F]$ and benzene. Alternatively, initial *ortho*-C–H activation of fluorobenzene occurs, followed by β-fluoride elimination to generate a benzyne ligand, which then inserts into the Zr–H bond. The reactivity of $[Zr(\eta^5\text{-}C_5Me_5)_2(H)_2]$ toward higher fluorinated aromatics has also been investigated.[48] With hexafluorobenzene, a mixture of $[Zr(\eta^5\text{-}C_5Me_5)_2(H)F]$, $[Zr(\eta^5\text{-}C_5Me_5)_2(H)(C_6F_5)]$, and the hydrodefluorination product pentafluorobenzene has been obtained (Scheme 8). Comparable reactions have been found with perfluoronaphthalene, perfluorotoluene, and perfluorobiphenyl. For pentafluorobenzene, C–H activation is preferred over C–F activation, which occurs mainly in the *ortho*-position.

Reaction of $[Ce(Cp')_2H]$ ($Cp' = \eta^5$-1,3,4-$C_5H_2(CMe_3)_3$) with C_6F_6 yields $[Ce(Cp')_2F]$, H_2, and tetrafluorobenzyne which is trapped as a Diels–Alder adduct.[79] $[Ce(Cp')_2(C_6F_5)]$ has been detected as an intermediate. With C_6F_5H, activation of the C–H bond and of the C–F bond in the 4-position of the fluorinated substrate has been observed. The latter reaction leads to $C_6F_4H_2$ and $[Ce(Cp')_2F]$, conforming to equation (iv) of Scheme 4. DFT calculations have been used to explore the pathways leading to the observed products of the exergonic reactions. A key step for the C–F activation is the H/F exchange which transforms C_6F_6 and the cerium hydride into C_6F_5H and the cerium fluoride. The reaction starts with an η^1-*F*-C_6F_5 interaction which serves as a hook. The reaction then proceeds via a σ-bond metathesis where the fluorine in the *ortho*-position to the hook migrates toward the hydride with a low activation energy. As soon as C_6F_5H is formed, it can react with $[Ce(Cp')_2H]$ to give H_2 and $[Ce(Cp')_2(C_6F_5)]$. The latter slowly decomposes to give $[Ce(Cp')_2F]$ and tetrafluorobenzyne.

Reaction of La with $Hg(C_6F_5)_2$ and *N*,*N*′-bis(2,6-diisopropylphenyl)formamidine(HdippForm) in THF yields $[LaF(DiipForm)_2(THF)]$. The conversion presumably proceeds via $[La(C_6F_5)(DiipForm)_2]$, which forms $[LaF(DiipForm)_2(THF)]$ and tetrafluorobenzyne by β-fluoride elimination. The latter is trapped by THF and HdippForm to give the functionalized formamidine $DiippForm(CH_2)_4OC_6F_4H$.[80]

1.26.2.1.2 Groups 6–8 metals

UV irradiation of $[Re(\eta^5\text{-}C_5Me_5)(CO)_3]$ in the presence of hexafluorobenzene effects intermolecular C–F and intramolecular C–H activation generating $[Re(\eta^6\text{-}C_5Me_4CH_2)(C_6F_5)(CO)_2]$ in two isomeric forms (Scheme 26). A similar reaction with $C_6F_5CF_3$ gives $[Re(\eta^6\text{-}C_5Me_4CH_2)(C_6F_4CF_3)(CO)_2]$.[81] UV irradiation of $[Re(\eta^5\text{-}C_5Me_5)(CO)_3]$ in the presence of C_6HF_5 affords C–H activation yielding $[Re(\eta^5\text{-}C_5Me_5)(H)(C_6F_5)(CO)_2]$ as the principal product. The C–H activation products $[Re(\eta^5\text{-}C_5H_5)(H)(C_6F_5)(CO)_2]$ and $[Re(\eta^5\text{-}C_5H_5)(H)(C_6F_4H)(CO)_2]$ are generated with the cyclopentadienyl analog $[Re(\eta^5\text{-}C_5H_5)(CO)_3]$ and C_6HF_5 or $C_6H_2F_4$ (Scheme 26).[82] There are minor byproducts including bis(aryl) complexes produced by C–F activation of a second aromatic molecule as well as binuclear complexes, as shown in Scheme 26.

The reaction between $B(C_6F_5)_3$ and $[Fe(\eta^5\text{-}C_5H_5)Me(CO)_2]$ gives $[Fe(\eta^5\text{-}C_5H_5)\{C_6F_4C(O)Me\}(CO)]$ (Scheme 27).[83] Comparable conversions led to the formation of $[M(\eta^5\text{-}C_5H_5)\{C_6F_4C(O)Me\}(CO)_2]$ (M = Mo, W) using $[M(\eta^5\text{-}C_5H_5)Me(CO)_2]$ as starting compounds.

The hexahydride $[Os(H)_6(PPr^i_3)_2]$ is capable of activating *ortho*-C–F bonds of fluorinated aromatic ketones such as pentafluoroacetophenone, decafluorobenzophenone, 2,3,4,5,6-pentafluorobenzophenone, and 2,6 difluoroacetophenone to give osmium derivatives (Scheme 28).[84] 2,3,4,5-Tetrafluoroacetophenone and 2-fluoroacetophenone yield products of C–H activation. In contrast, DFT calculations suggest that *ortho*-C–F activation is thermodynamically preferred over *ortho*-C–H activation. Pentafluoroacetophenone has also been shown to undergo C–H activation at $[Os(H)_3(SnPh_2Cl)(PPr^i_3)\{PPr^i_2(CMe{=}CH_2)\}]$.[85]

1.26.2.1.3 Groups 9 and 10 metals

$[Rh(\eta^5\text{-}C_5Me_5)(H)_2(PMe_3)]$ reacts with C_6F_6, C_6F_5H, $C_{12}F_{10}$, or $C_{10}F_8$ in pyridine or pyridine/benzene to give the C–F cleavage products such as $[Rh(\eta^5\text{-}C_5Me_5)(C_6F_5)(H)(PMe_3)]$ (Scheme 29, fits equation (ii) of Scheme 4).[50] Kinetic studies reveal that the reaction has autocatalytic character, and fluoride anions are responsible for the catalysis. They act by deprotonating the rhodium dihydride, allowing nucleophilic attack (see Section 1.26.1.3.5).

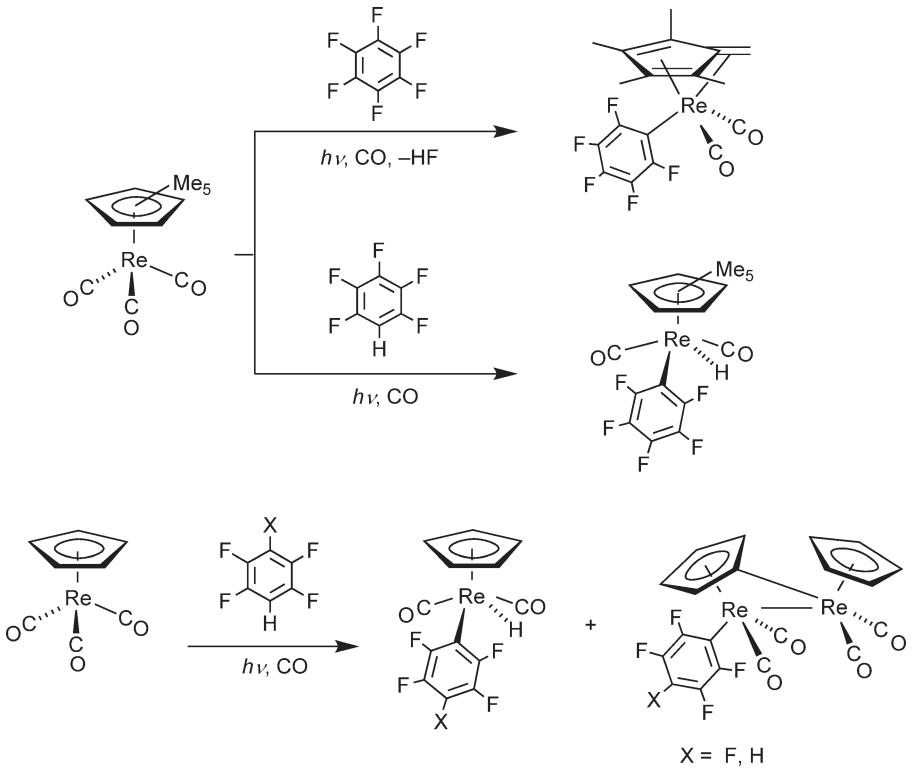

Scheme 26

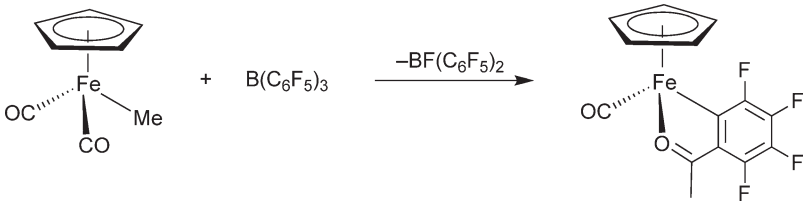

Scheme 27

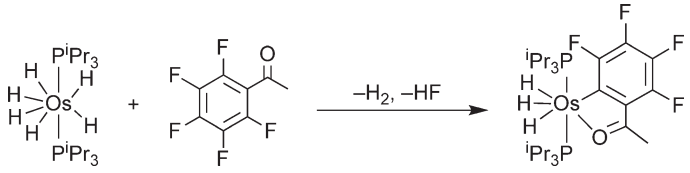

Scheme 28

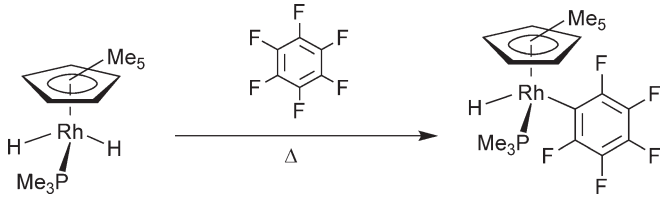

Scheme 29

DFT calculations have been carried out for the oxidative addition of a C–H or C–F bond in 1,4-difluorobenzene at $[Rh(\eta^5\text{-}C_5H_5)(PH_3)]$ or $[Os(CO)(PH_3)_2]$ in order to probe why the related experimental systems undergo C–H oxidative addition but not C–F oxidative addition.[35] The calculations reveal that for both systems C–F oxidative addition is thermodynamically preferred. For rhodium, the activation energy for C–F activation is considerably higher than for C–H activation suggesting that the inertness of this system toward C–F activation has a kinetic origin. The activation energy for C–H bond breaking is kept low by synchronous bond making in the transition state. In contrast, C–F bond cleavage is poorly compensated by bond making (Rh···F electron repulsion).

Reactions of $[RhH(PEt_3)_3]$ with pentafluoropyridine (C–F activation) or 2,3,5,6-tetrafluoropyridine (C–H activation) afford the activation product $[Rh(4\text{-}C_5NF_4)(PEt_3)_3]$ (Scheme 30).[29] Further reactions of $[Rh(4\text{-}C_5NF_4)(PEt_3)_3]$ are shown in Scheme 30.

The fast oxidative addition of fluorinated heteroaromatics such as pentafluoropyridine, or 2,4,6-trifluoropyrimidine at a nickel center giving *trans*-$[NiF(2\text{-}C_5NF_4)(PEt_3)_2]$, and *trans*-$[NiF(4\text{-}C_4N_2F_2H)(PEt_3)_2]$ in high yield has been reported (Scheme 31).[10,39,86–88] The intermolecular reactions are regioselective for the position adjacent to the nitrogen atom. Reactions of $[Ni(COD)_2]$ with 2,3,4,5-tetrafluoropyridine or 2,3,5,6-tetrafluoropyridine demonstrate the chemospecificity for C–F over C–H activation (Scheme 31). There is strong evidence that precoordination of the aromatic compounds at the nickel center is a crucial step in the activation of a C–F bond in the fluorinated aromatic systems.[35a] This is indicated

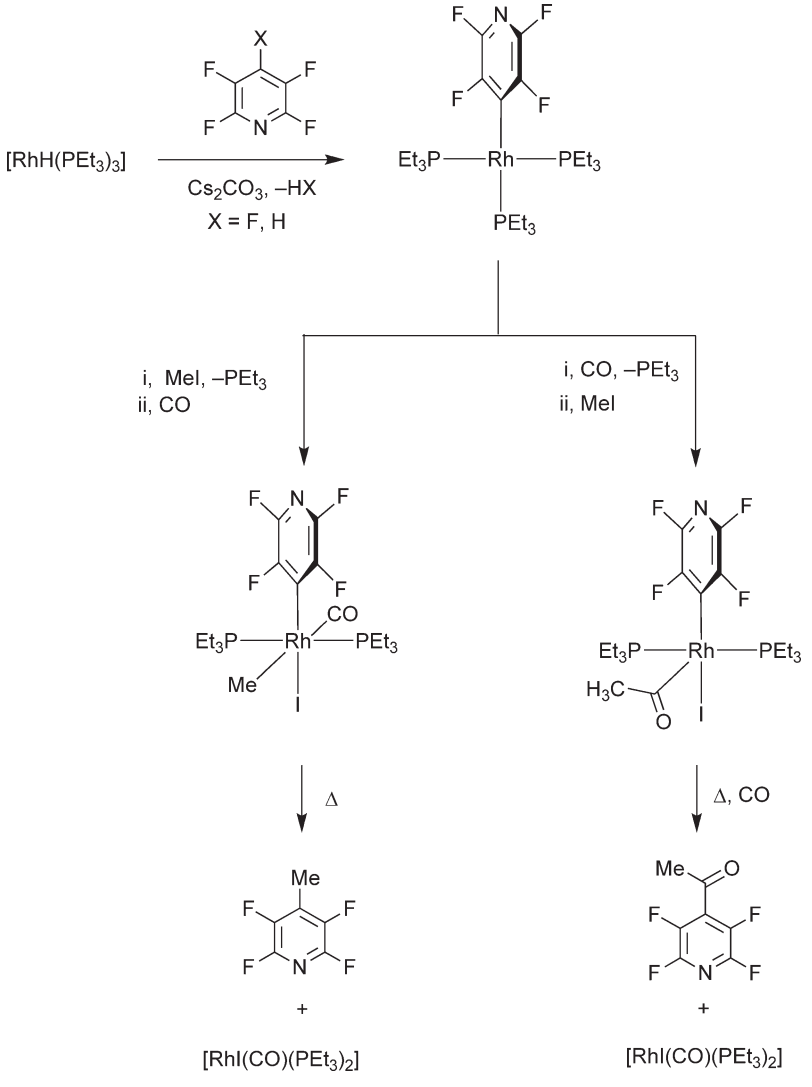

Scheme 30

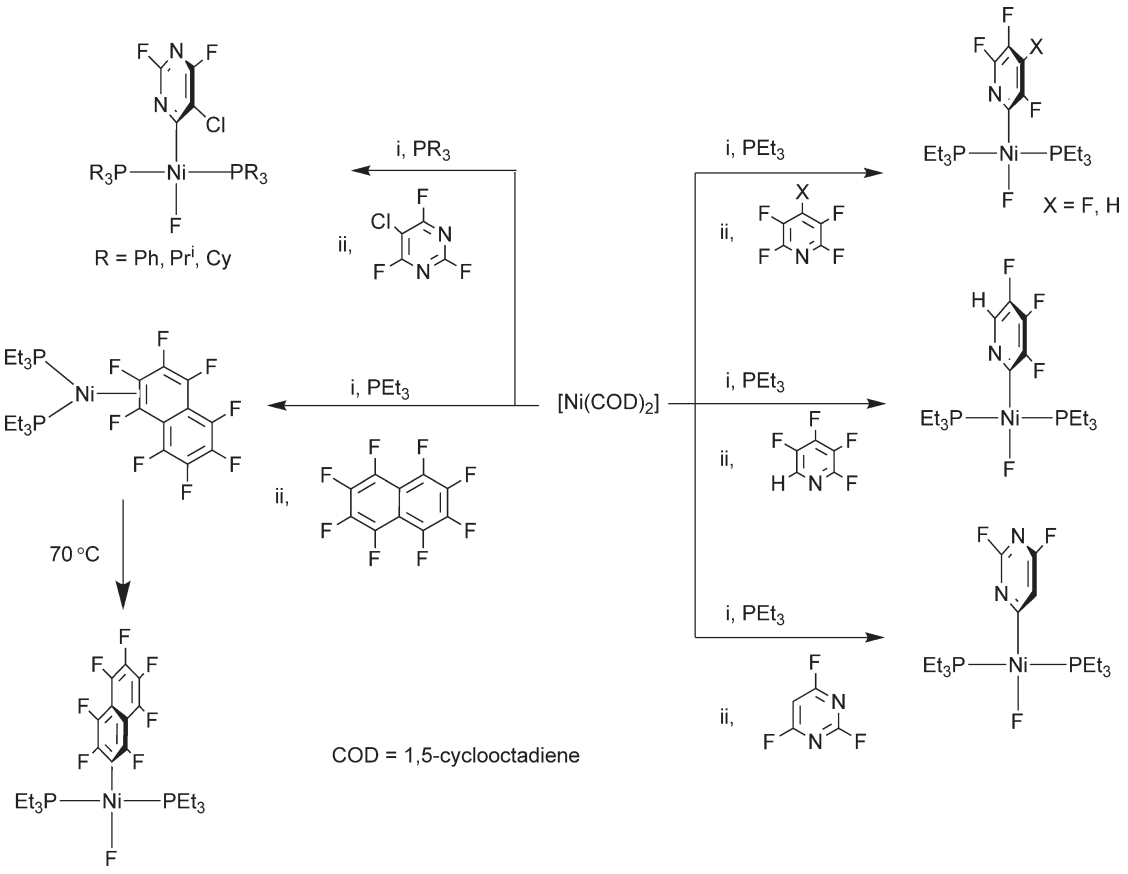

Scheme 31

by the observation of coordination and intramolecular activation of octafluoronaphthalene at $\{Ni(PEt_3)_2\}$ yielding initially $[Ni(\eta^2\text{-}1,2\text{-}C_{10}F_8)(PEt_3)_2]$, which can be converted into *trans*-$[NiF(2\text{-}C_{10}F_7)(PEt_3)_2]$ (Scheme 31).[40] The activation of a C–F bond in the presence of a much weaker C–Cl bond in 5-chloro-2,4,6-trifluoropyrimidine has also been accomplished to give *trans*-$[NiF(4\text{-}C_4N_2ClF_2)(PR_3)_2]$ (R = Ph, Pr^i, Cy) (Scheme 31).[43,44] The reactions of the fluorinated precursors at nickel provide access to organofluoro heterocycles that are otherwise inaccessible.[10,43,44,87,89] Thus, the synthesis of the methyl pyridyl complex *trans*-$[NiMe(2\text{-}C_5NF_4)(PEt_3)_2]$ from *trans*-$[NiF(2\text{-}C_5NF_4)(PEt_3)_2]$ allows the generation of new pyridine derivatives (Scheme 32).

The carbene complex $[Ni_2(Pr^i{}_2C_3N_2H_2)_4(COD)]$ activates the C–F bond of hexafluorobenzene to give $[NiF(C_6F_5)(Pr^i{}_2C_3N_2H_2)_2]$ within 1 h.[90] Reaction of $[NiEt_2(bpy)]$ (bpy = 2,2′-bypyridine) with hexafluorobenzene leads to the formation of $[Ni(C_6F_5)_2(bpy)]$.[91]

Reactions of pentafluoropyridine and 2,3,5,6-tetrafluoropyridine with $[Pd(PR_3)_2]$ and $[Pt(PR_3)_2]$ (R = Cy or Pr^i) take a different course with palladium or platinum compared to the results obtained at nickel (Scheme 33). The palladium complexes react with pentafluoropyridine at 100 °C to yield the fluoride complexes *trans*-$[PdF(4\text{-}C_5NF_4)(PCy_3)_2]$ and *trans*-$[PdF(4\text{-}C_5NF_4)(PPr^i{}_3)_2]$.[92] In contrast to the observations at nickel, the reactions occur at the 4-position. Treatment of the platinum(0) complexes $[Pt(PR_3)_2]$ with pentafluoropyridine in THF at ambient temperature yields $[Pt(Cy)(4\text{-}C_5NF_4)(PCy_3)(PFCy_2)]$ and $[Pt(Pr^i)(4\text{-}C_5NF_4)(PPr^i{}_3)(PFPr^i{}_2)]$. In this case, the heterocycle has also been activated in the 4-position (Scheme 33). However, in a remarkable rearrangement, the fluoride attacks one of the phosphorus atoms, and an alkyl group migrates from phosphorus to platinum. Reaction of $[Pt(PCy_3)_2]$ with 2,3,5,6-tetrafluoropyridine results in C–H activation to form *cis*-$[Pt(H)(4\text{-}C_5NF_4)(PCy_3)_2]$. The latter also forms during the reaction of $[Pt(PCy_3)_2]$ with C_5F_5N in hexane. There is a brief account of the reaction of $[M(PCy_3)_2]$ (M = Pd, Pt) with C_6F_6 in THF at 65 °C yielding *trans*-$[PdF(C_6F_5)(PCy_3)_2]$ and *trans*-$[Pt(Cy)(C_6F_5)(PCy_2F)(PCy_3)]$, that follow an analogous pathway to pentafluoropyridine.[36]

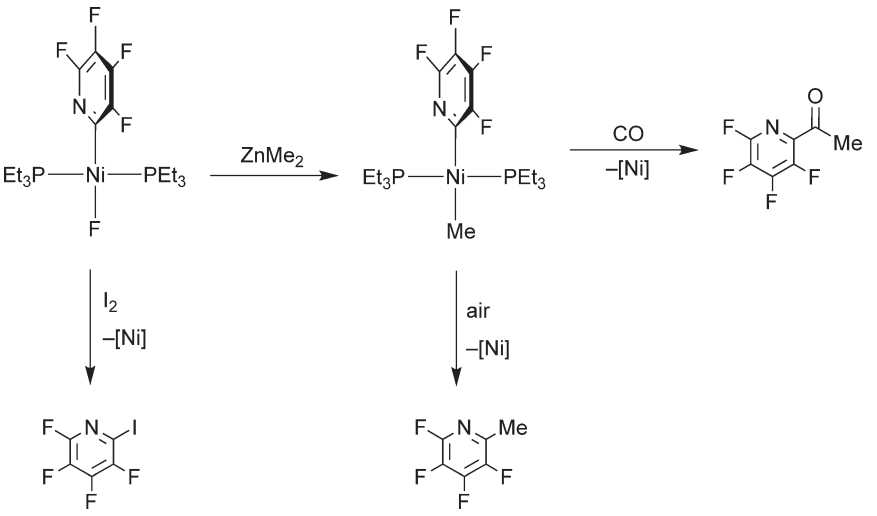

Scheme 32

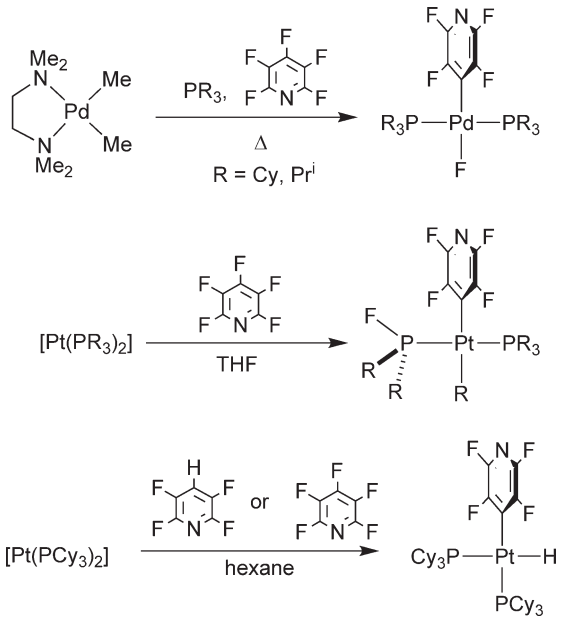

Scheme 33

The platinum dihydride complex *trans*-$[Pt(H)_2(PCy_3)_2]$ reacts with pentafluoropyridine at room temperature yielding a 1 : 1 : 1 mixture of *trans*-$[PtH(FHF)(PCy_3)_2]$, *trans*-$[PtH(C_5NF_4)(PCy_3)_2]$, and $[PtCy(4\text{-}C_5NF_4)(PCy_3)(PFCy_2)]$. Reaction of *trans*-$[Pt(H)_2(PCy_3)_2]$ with hexafluorobenzene in the presence of $[NMe_4]F$ yields the bifluoride complex *trans*-$[PtH(FHF)(PCy_3)_2]$ and *trans*-$[PtH(C_6F_5)(PCy_3)_2]$ in a ratio of 1 : 13.[93] $[PdMe_2(tmeda)]$ reacts with pentafluoropyridine in the presence of water and triethylamine to give the aryloxy compound $[PdMe(OC_5NF_4)(tmeda)]$.[94]

DFT calculations indicate that the oxidative addition reactions of a C–F bond in C_6F_6 at $\{Ni(H_2PCH_2CH_2PH_2)\}$ and $\{Pt(H_2PCH_2CH_2PH_2)\}$ proceed initially via exothermic formation of an η^2-arene complex.[35a] The C–F oxidative addition reaction is more exothermic at nickel than at platinum. The barrier for exothermic oxidative addition is higher at Pt than at Ni because of strong *d–p* repulsions in the transition state. Similar repulsive interactions lead to a relatively long Pt–F bond with a considerably lower stretching frequency in the oxidative addition product than for

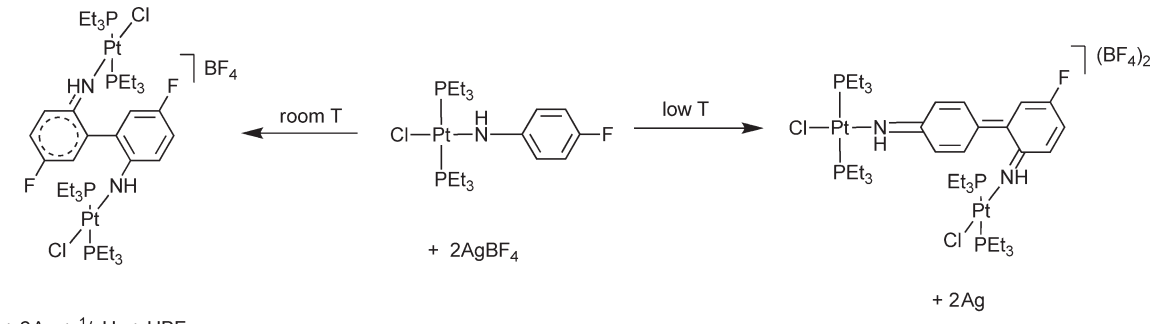

Scheme 34

the nickel analog. C–H bond activation of benzene at nickel is energetically unfavorable, whereas the corresponding process at platinum is comparable in exothermicity to the formation of the {Pt(η^2-C_6H_6)} adduct and has a very low barrier. Overall, C–F oxidative addition at nickel is strongly preferred energetically to C–H oxidative addition. For platinum, C–H and C–F oxidative additions are the kinetically and thermodynamically preferred processes, respectively.

Platinum arylamides can be coupled oxidatively with $AgBF_4$ by temperature-dependent C–F or C–H activation (Scheme 34).[95]

1.26.2.2 Activation of C–F Bonds of Alkenes

1.26.2.2.1 Groups 4 and 5 metals

Perfluoropropene reacts with [Zr(η^5-$C_5Me_5)_2(H)_2$] to give hydrodefluorination products with Zr–F bond formation; initial products are [Zr(η^5-$C_5Me_5)_2$(H)F] and [Zr(η^5-$C_5Me_5)_2$(H)(Pr^n)] (Scheme 35).[78] The latter reacts with hydrogen to form propane. [Zr(η^5-$C_5Me_5)_2(H)_2$] also reacts with allylic and vinylic C–F bonds of partially fluorinated alkenes such as 1,1-difluoroethene, 1,1-difluoromethylenecyclohexane, $CH_2{=}CF_2CF_2CF_2CF_3$, and 3,3,3-trifluoropropene to give hydrodefluorination products.[78,96] NMR studies at low temperature and deuterium labeling investigations give evidence for olefin coordination in the lateral positions of the metallocene followed by an insertion/β-fluoride elimination mechanism (see Section 1.26.1.4.4). DFT calculations for a reaction of hexafluoropropene with [Zr(η^5-$C_5H_5)_2(H)_2$] also support such a mechanism.[13,53] Watson and Caulton showed that vinyl fluoride reacts with [Zr(η^5-$C_5H_5)_2$(H)Cl] to give [Zr(η^5-$C_5H_5)_2$(F)Cl] and ethene as primary products.[97]

1-Fluorovinylzirconocene complexes have been prepared *in situ* by reactions of [Zr(η^5-$C_5H_5)_2Cl_2$]/BuLi with $F_2C{=}CHX$ (X = $Et_2NC(O)O$, PhO, $MeOC_6H_4O$, etc.) via C–F activation and applied in palladium-catalyzed cross-coupling reactions of aryl iodides.[98]

Exposure of fluoroethene to [Ta$(H)_2(OSiBu^t_3)_3$] yields [TaH(Et)$(OSiBu^t_3)_3$] and [TaH(F)$(OSiBu^t_3)_3$].[99] The latter is formed by insertion of the olefin into the metal–hydrogen bond followed by β-fluoride elimination. The ethene which is produced in turn gives the ethyl compound [TaH(Et)$(OSiBu^t_3)_3$].

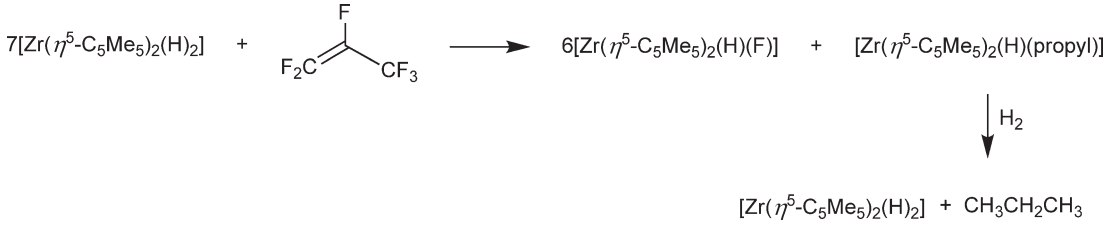

Scheme 35

1.26.2.2.2 Group 8 metals

$[Os(H)_3ClL_2]$ ($L = PPr^i_3$) reacts at room temperature with vinyl fluoride to produce $[OsH(F)(Cl)(\equiv CCH_3)L_2]$ and H_2.[100] The liberated H_2 converts vinyl fluoride into ethene and HF in a reaction catalyzed by $[Os(H)_3ClL_2]$. The intermediates $[OsH(Cl)(H_2)(H_2C{=}CHF)(L)_2]$, $[OsCl(F)(=CHMe)L_2]$, and $[OsH(Cl)(H_2)(C_2H_4)L_2]$ have been detected by low-temperature NMR spectroscopy (Scheme 36). DFT calculations of the potential energy and free energy at 298 K of possible intermediates have been performed. It is suggested that the reactions are catalyzed by HF. On scavenging the HF with Et_3N, $[Os(H)_2Cl(\equiv CCH_3)L_2]$ becomes the exclusive product. Reaction of $[Os(H)_3ClL_2]$ with $F_2C{=}CH_2$ produces $[Os(H)FCl(\equiv CCH_3)L_2]$ and HF.

The reaction of $(F_3C)_2C{=}C(F)(CF_2CF_3)$ with *cis*-$[Ru(H)_2(dmpe)_2]$ affords the bifluoride complex *cis*-$[RuF(FHF)(dmpe)_2]$, whereas reaction with $[Ru(H)_2(dcpe)_2]$ (dcpe = bis(dicyclohexylphosphino)ethane) yields the cation $[RuH(dcpe)_2]^+$ with $[(F_3C)_2C{=}C(O)CF_2CF_3]^-$ as anion.[101] When *cis*-$[Ru(H)_2(dmpe)_2]$ was treated with hexafluoropropene, the formation of *cis*-$[RuF(FHF)(dmpe)_2]$ was also observed. ^{19}F NMR spectroscopy revealed the presence of the hydrodefluorination products (*Z*)-$CF_3CF{=}CFH$, (*E*)-$CF_3CF{=}CFH$, and $CF_3CF{=}CH_2$ in a ratio of 4 : 1 : 3 (Scheme 37).

1.26.2.2.3 Group 9 metals

Reaction of $[Co_2(CO)_8]$ with $F_2C{=}C{=}CF_2$ affords the cluster compounds **A** and **B** (Scheme 38).[102] The latter is formed by fluoride abstraction giving a carbyne ligand. A nonacarbonyliron carbyne complex also reacts photochemically with $F_2C{=}C{=}CF_2$ forming the diferrallyl structure **C** and the cluster **D**.[103]

Rapid and regioselective C–F bond activation of hexafluoropropene occurs on reaction with $[RhH(PEt_3)_3]$ in the presence of Et_3N/Cs_2CO_3 giving $[Rh\{(Z)\text{-}CF{=}CF(CF_3)\}(PEt_3)_3]$ with loss of HF. Subsequent oxidative addition of hydrogen affords the rhodium(III) complex *cis-mer*-$[Rh(H)_2\{(Z)\text{-}CF{=}CF(CF_3)\}(PEt_3)_3]$. The latter converts in the presence of hydrogen into 1,1,1-trifluoropropane and the fluoro complexes $[RhF(PEt_3)_3]$ and *cis-mer*-$[Rh(H)_2F(PEt_3)_3]$ (Scheme 39).[51] On treatment of $[RhF(PEt_3)_3]$ and *cis-mer*-$[Rh(H)_2F(PEt_3)_3]$ with $HSiPh_3$, the complexes $[RhH(PEt_3)_3]$ and *cis-fac*-$[Rh(H)_2(SiPh_3)(PEt_3)_3]$ are obtained. The silyl compound is also capable of the C–F activation of hexafluoropropene to afford $[Rh\{(Z)\text{-}CF{=}CF(CF_3)\}(PEt_3)_3]$ (Schemes 10 and 39).[52,104] Activation of (*E*)-1,2,3,3,3-pentafluoropropene at $[RhH(PEt_3)_3]$ results in the formation of $[Rh\{(E)\text{-}C(CF_3){=}CHF\}(PEt_3)_3]$ and $[RhF(PEt_3)_3]$ together with the hydrodefluorination product (*Z*)-1,3,3,3-tetrafluoropropene.[52]

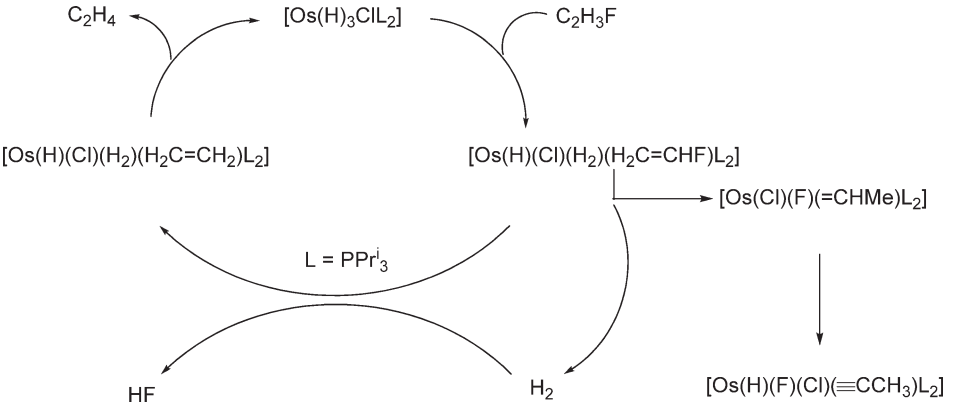

Scheme 36

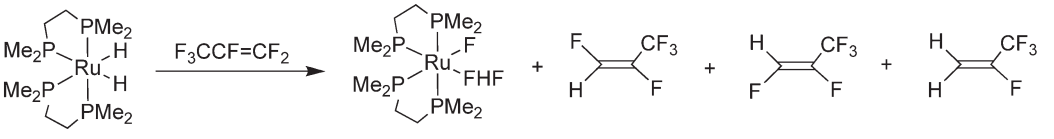

Scheme 37

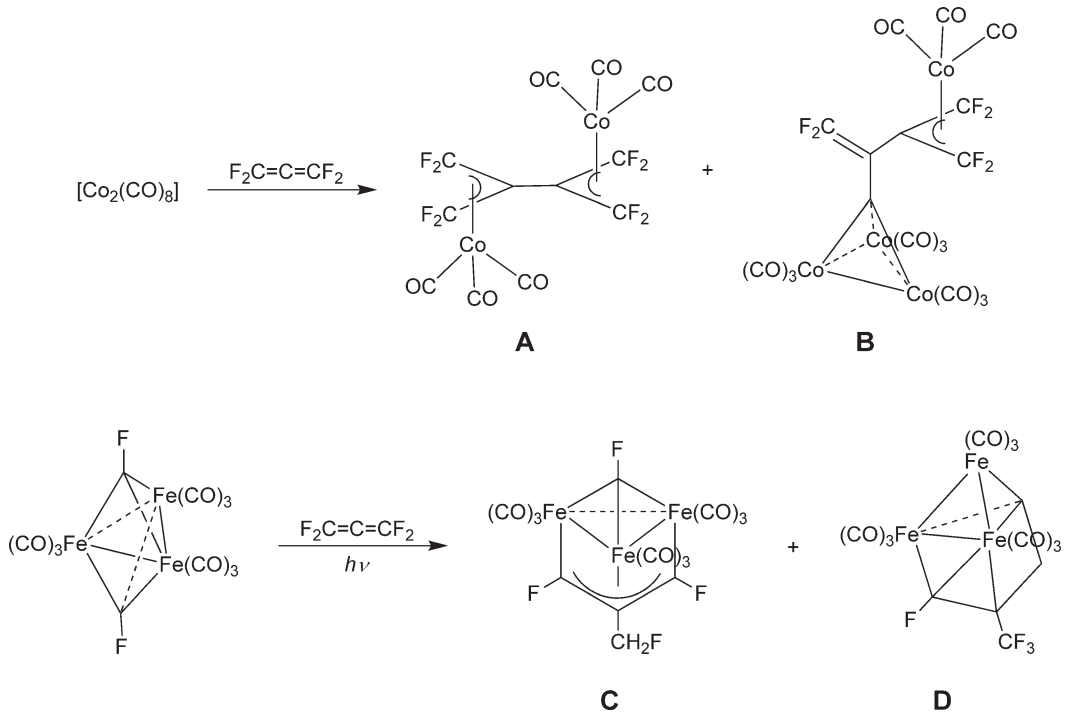

Scheme 38

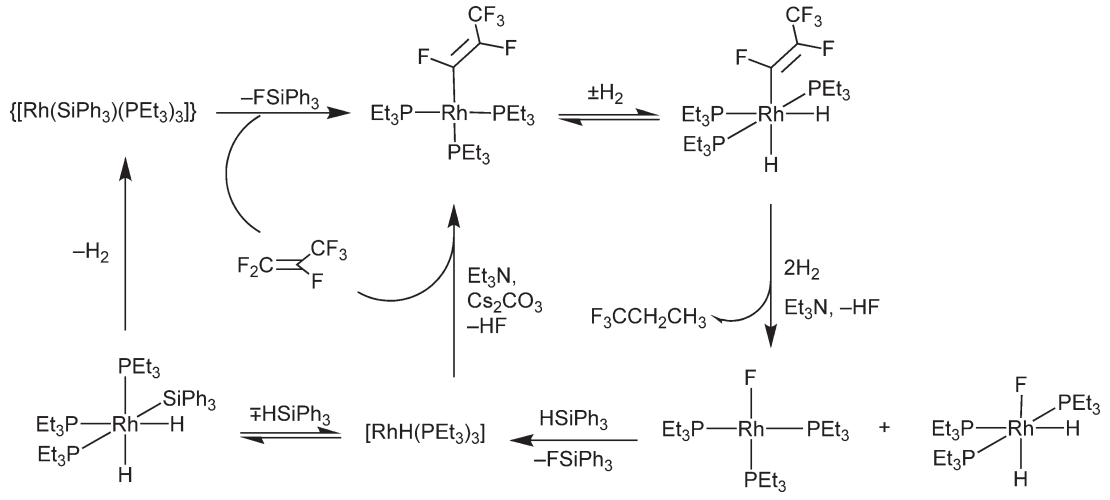

Scheme 39

Nucleophilic attack of the lithium iridate Li[Ir(η^5-C_5Me_5)(H)(PMe_3)] at hexafluoropropene gives the perfluoro-propenyl complex [Ir(η^5-C_5Me_5)(H){(*Z*)-CF═CF(CF_3)}(PMe_3)].[105] The iridate also reacts with 3,3,3-trifluoropropene to give the allyl complex [Ir(η^5-C_5Me_5)(H)(CH_2CH═CF_2)(PMe_3)].

1.26.2.3 Activation of Aliphatic C–F Bonds

[Zr(η^5-C_5Me_5)$_2$(H_2)] reacts with primary, secondary, and tertiary monofluorinated hydrocarbons such as fluorohexane, fluorocyclohexane, and fluoroadamantane to give [Zr(η^5-C_5Me_5)$_2$(H)F] and/or [Zr(η^5-C_5Me_5)$_2F_2$] and alkane through

a radical chain mechanism (Scheme 12).[13,78] While the former reacts at room temperature, elevated temperatures and the presence of H_2 were required for the latter two. The rate of hydrodefluorination is considerably reduced with CF_2H or CF_3 groups attached to the hydrocarbon. Dichlorofluoromethane also reacts with $[Zr(\eta^5\text{-}C_5Me_5)_2(H)_2]$ to yield the hydrodechlorinated product initially, and methane is formed after 1 day at ambient temperature. Difluorodichloromethane and difluorochloromethane give difluoromethane initially, but further conversion into methane requires prolonged heating to 120 °C under H_2.

Reaction of $[Yb(OAr)_2(THF)_3]$ (Ar = 2,6-Bu^t–4-R; R = H, Me, Bu^t) with perfluorodecalin at room temperature results in the formation of $[Yb(OAr)_2F(THF)]_2$.[63] Oxidation of $[Yb(\eta^5\text{-}C_5H_5)_2]$ with perfluorodecalin or perfluoro(methyl)cyclohexane in DME gives $[Yb(\eta^5\text{-}C_5H_5)_2F]_3$. An analogous reaction with $[Yb(\eta^5\text{-}C_5H_4Me)_2]$ leads to $[Yb(\eta^5\text{-}C_5H_4Me)_2F]_4$, while oxidation of $[Yb(\eta^5\text{-}C_5H_4Me)_2]$ or $[Yb(\eta^5\text{-}C_5H_5)_2(DME)]$ in THF provides $[Yb(\eta^5\text{-}C_5H_4Me)_2F(THF)]_2$ or $[Yb(\eta^5\text{-}C_5H_5)_2F(THF)]_2$, respectively.[62,63] For the latter reaction, perfluorodecalin converts into unsaturated fluorocarbons, whereas perfluoro(methyl)cyclohexane gives perfluorotoluene and three isomers of $HC_6F_4CF_3$.

The hydride $[Ce(Cp')_2H]$ ($Cp' = \eta^5\text{-}1,3,4\text{-}C_5H_2(CMe_3)_3$) reacts with CH_3F or CH_2F_2 to yield $[Ce(Cp')_2F]$ and CH_4.[106] It also reacts with CHF_3 to form $[Ce(Cp')_2F]$, H_2, 1,2,4- and 1,3,5-tri-*tert*-butylbenzene, but does not react with CF_4. Studies on the mechanism of the latter reaction suggest that the substituted benzenes result from reaction of the Cp′ ligand with a fluorocarbene fragment derived by α-fluoro abstraction from $[Ce(Cp')_2CF_3]$. The decomposition products and CH_2 and CHF arising from the activation of CH_3F or CH_2F_2 could also be trapped. DFT calculations show that the initial step is a C–H activation of the fluorinated substrates by $[Ce(Cp')_2H]$ that proceeds with a low barrier. The C–F bond activation is the rate-determining step, that is, the carbene ejection and its trapping by H_2 formed in the C–H activation. The calculations show that CF_4 does not react because of a high activation barrier.

Complete defluorination of 1,2,3,4-tetramethyl(trifluoromethyl)cyclopentadiene occurred on treatment with $[Ti(NMe_2)_4]$ to give $[Ti(\mu\text{-}NMe_2)(NMe_2)(\mu\text{-}F)F]_6$.[107] $C_5Me_4{=}C(NMe_2)_2$ was isolated as a byproduct.

The anionic rhodium complex $[Rh(dmgH)_2(PPh_3)]^-$ reacts with $Br(CH_2)_2F$ to give the binuclear complex $[Rh(dmgH)_2(PPh_3)]_2(CH_2)_2$ (Scheme 13).[58] No such reaction occurred with $BrCH_2F$ or $Br(CH_2)_3F$. In comparable transformations anionic cobalt gyloxime complexes were found to react with $BrCH_2CH_2CH_2F$, *trans*-1-bromo-2-fluorocyclohexane, or *trans*-1-bromo-2-fluorocyclopentane to give the (fluoroalkyl)compounds and also dehalogenated olefins.[108]

Calculations based on DFT suggest that the hypothetical activation of a carbon–fluorine bond in CF_4 at *trans*-$[IrCl(PH_3)_2]$ would occur via a concerted oxidative addition mechanism and not via a single electron transfer or an S_N2-type mechanism.[109] The calculations are not related to any known reaction, but it has also been concluded that a π-donor ligand and the heavier transition metal allow more facile oxidative addition for the complexes *trans*-$[M(X)(PH_3)_2]$ (M = Ir, Rh; X = H, CH_3, Cl).[110]

Perfluoroalkenes are obtained from perfluoroalkanes such as perfluorinated methylcyclohexane or 2-methylpentane by photoinduced electron transfer from decamethylferrocene in the presence of LiOTf. In the presence of Zn, the reactions become catalytic because the decamethylferrocenium ion can be reduced to decamethylferrocene (Scheme 14).[59–61]

Mercury photosensitization in the presence of NH_3 leads to partial defluorination and functionalization of a variety of perfluoroalkanes to give perfluoroalkyl imines, amines, and nitriles (Scheme 40).[111] Polytetrafluoroethylene can be surface functionalized by this method to give a hydrophilic surface. DFT studies suggest that the $[Hg^*(NH_3)_2]$ excited state complex may be involved as a key intermediate.

1.26.2.4 Intermolecular Activation of C–F Bonds in the Gas Phase

Carbon–fluorine bond activation and their mechanisms on surfaces and in the gas phase have been reviewed.[12] Hexafluoroacetone is activated in the gas phase by Cr^+ in the presence of water yielding a variety of products.[112] Comparable hydrolytic C–F bond activations have also been performed for monofluoroacetone, 1,1,1-trifluoroacetone, pentafluorobenzaldehyde, and 2,3,4,5,6-pentafluoroacetophenone.[113]

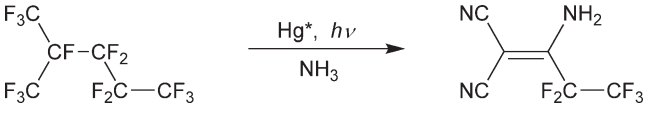

Scheme 40

DFT calculations for the activation of fluoromethane and fluorobenzene at Ce^+ and Ho^+ have been performed revealing a "harpoon-type" mechanism for the metal-mediated fluoride abstraction.[114] The reactions of the lanthanoid cations La^+ Ce^+, Pr^+, and Yb^+ with fluoromethane have also been investigated by DFT calculations. After coordination of Ln^+, electron transfer from Ln^+ to fluoromethane takes place, followed by formation of LnF^+ and a methyl radical.[56,57,115]

Mass spectrometric investigations which show gas-phase collisions of Nb^+ with hexafluoro- and tetrafluorobenzene have been reported. The reactions involve the transfer of four fluorine atoms to Nb.[116] A systematic study on the reactivity of transition metal cations toward hexafluorobenzene in the gas phase has been performed by inductively coupled plasma (ICP) tandem mass spectrometry.[117] Multiple fluorine atom abstraction dominates the chemistry observed for early transition metals, while association of hexafluorobenzene to the metal cation has been found for late transition metals.

1.26.2.5 Catalytic Activation of C–F Bonds

1.26.2.5.1 Hydrodefluorination and elimination of fluorosilanes

In this section, we emphasize homogeneous reactions. The hydrodefluorination of hexafluorobenzene, pentafluoropyridine, and octafluorotoluene with tertiary silanes is catalyzed by addition of three-coordinate diketiminatoiron(II) complexes including the fluoride derivative giving pentafluorobenzene, 2,3,5,6-tetrafluoropyridine, and heptafluoro-toluene in up to five turnovers.[118] The reaction is first order in each of silane, iron complex, and fluoroaromatic, but no unique mechanism can be deduced. Hydrodefluorination of fluorobenzene in refluxing THF was performed using $[Ni(acac)_2]$, *N,N*-dimesitylimidazolium chloride, and $NaOPr^i$ as the catalytic system.[119] Other monofluorinated aromatic systems, for example, fluoronaphthalenes, fluoropyridines, or fluorotoluene, have been used in similar hydrodefluorination reactions with alkoxides containing β-hydrogens as hydrogen source.[120]

Carbon–silicon bonds have been formed by catalytic conversions of functionalized fluorobenzenes such as fluoroacetophenones and (fluorophenyl)oxazolines with hexamethyldisilane using $[Rh(COD)_2]BF_4$ as catalyst (Scheme 41).[72]

Several catalytic hydrodefluorination heterogeneous reactions of aromatic compounds have been reported. 1-Fluoronaphthalene reacts with H_2 in the presence of 40% NaOH and catalytic amounts of $[Rh(H)Cl_2(PCy_3)_2]$ to give naphthalene.[121] The hydrodefluorination of 4-fluorotoluene, 3-fluoroanisole, and 4-fluoroaniline occurred in the presence of traces of air only. The reactions are presumably catalyzed by rhodium black that is formed under aerobic conditions. In another heterogeneous reaction, aqueous ammonia has been found to be a versatile medium for the selective hydrodefluorination of highly fluorinated aromatics by zinc.[122,123] The substrates include fluorinated benzoic acids, pentafluorobenzylalcohol, pentafluoropyridine, and hexafluorobenzene. Comparable reactions with the catalytic system $[NiCl_2(bpy)]$/Zn in DMF in the presence of water or ammonium chloride resulted in various hydrodefluorination products.[124]

1.26.2.5.2 Cross-coupling

Nickel-catalyzed Kumada–Corriu cross-coupling reactions of a variety of monofluorinated aromatics have been accomplished using nickel(0) complexes bearing the *N*-heterocyclic carbene ligand 1,3-di(2′6′-diisopropylphenyl)imidazolin–2-ylidene (Scheme 42).[125] The catalysts can also be prepared *in situ* from $[Ni(acac)_2]$ and an imidazolium salt.

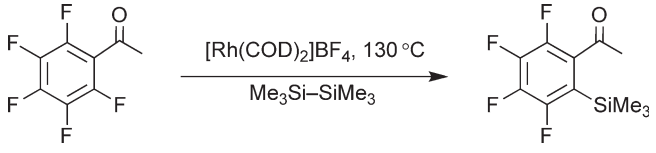

Scheme 41

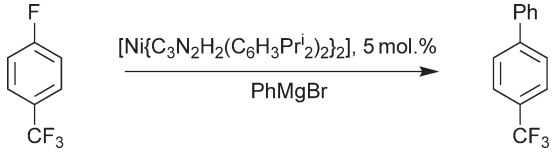

Scheme 42

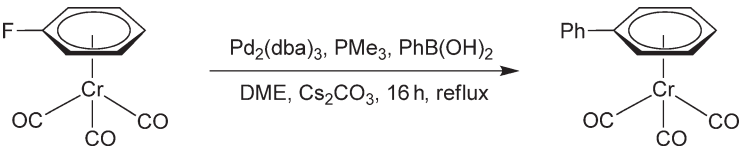

Scheme 43

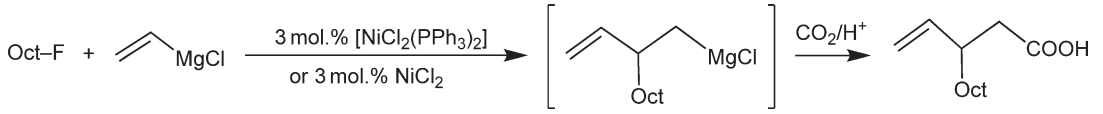

Scheme 44

Furthermore, various nickel- or palladium-catalyzed cross-coupling reactions of aryl Grignard reagents with aryl fluorides to give unsymmetrical biaryl compounds have been developed.[126,127] The investigations involve catalytic conversions under phosphine-free conditions using palladium [Pd(dba)$_2$] (dba = dibenzylideneacetone) as pre-catalyst. [(THF)$_4$Li$_4$Me$_8$Ni$_2$] can be used as a catalyst to couple 4-fluorotoluene with mesityl-MgBr.[128] Palladium complexes catalyze cross-coupling reactions of trifluorobenzenes producing mainly mono-coupled products while nickel catalysts afford di- or tri-coupled products. Palladium catalysts have been applied to a cross coupling reaction of 1,1-difluoro-2-naphthylethene with Zn(Tol)Cl to give 1-tolyl-1-fluoro- or 1,1-ditolyl-derivatives.[128a]

Nickel-catalyzed cross-coupling reactions of arylmagnesium halides with monofluorinated heterocycles have also been reported.[129] The cross-coupling reactions of pentafluoropyridine or 2,3,5,6-tetrafluoropyridine with tributylvinyltin affording 2-vinyl derivatives are catalyzed by *trans*-[NiF(2-C$_5$NF$_4$)(PEt$_3$)$_2$].[75] The reactions constitute the only examples of cross-coupling reactions of highly fluorinated aromatics which proceed via a C–F activation reaction. However, the nickel fluoro complex *trans*-[NiF(4-C$_4$N$_2$ClF$_2$)(PPh$_3$)$_2$] catalyzes Suzuki–Miyaura-type cross-coupling reactions of 5-chlorotrifluoropyrimidine with aromatic boronic acids yielding 5-chloro-2-fluoro-4,6-diarylpyrimidines. The conversions represent the first catalytic reactions mediated by transition metals that involve the cleavage of a C–F bond in the presence of a C–Cl bond.[44]

The catalytic system Pd$_2$(dba)$_3$/PMe$_3$/Cs$_2$CO$_3$ allows the cleavage of C–F bonds by Suzuki reactions of aryl fluorides.[130] The reactions are facilitated by coordination of a nitro group in the *ortho*-position to the fluorine. The amination, Stille coupling, and Suzuki coupling of electron-deficient 2-fluoronitrobenzenes is catalyzed most effectively by [Pd(PPh$_3$)$_4$].[73] DFT/B3LYP investigations revealed that palladium-catalyzed Stille and Suzuki couplings of aryl fluorides are facilitated by stabilization of the transition state by proximal oxyanions such as nitro groups.[131] These predictions were verified by further Suzuki and Stille couplings with, for example, 4-fluoro–3-nitrobenzaldehyde as substrate, and with [Pd(PPh$_3$)$_4$]/base as catalyst.[131]

It has been found that (η^6-fluoroarene)tricarbonylchromium complexes undergo Suzuki reactions with arylboronic acids to form (η^6-biaryl)tricarbonylchromium complexes in the presence of PMe$_3$/[Pd$_2$(dba)$_3$] and CsF or Cs$_2$CO$_3$ (Scheme 43).[132,133] Comparable Stille couplings have been developed.[133] DFT calculations have been performed modeling the insertion of {Pd(PH$_3$)$_2$} into the C–F bond in fluoroarenes and (η^6-fluoroarene)tricarbonylchromium.[134] A σ-complex could be located when 2,4-dinitro or 2-nitro substitution is present. No such intermediate could be located for the fluorobenzene complex, and only a concerted pathway was identified.

The nickel- or copper-catalyzed cross-coupling of primary fluoroalkanes with various Grignard reagents has been demonstrated.[55] The reactions proceed efficiently using 1-fluorooctane as substrate in the presence of 1,3-butadiene as additive. Kambe observed coupling of vinyl Grignard reagents and fluoroalkanes by C–F activation.[135] For instance, 1-fluorooctane can be converted into a 2-octylbutenyl Grignard reagent which can be used for further reactions (Scheme 44).

1.26.3 Survey of Intramolecular C–F Bond Activation 1997–Mid 2005

1.26.3.1 α-C–F and β-C–F Activation of Fluoroalkyl Groups

There are numerous complexes containing fluoroalkyl groups, but their enhanced reactivity at the α-C–F bond is only observed under specific circumstances, as has been demonstrated especially by Hughes *et al.*, and is illustrated by the prototypes in Section 1.26.1.7. Hughes' progress depended on conversion of the iodide and triflate derivatives

of the half-sandwich complexes [M(η^5-C_5Me_5)X(R^F)(PMe_3)] (M = Rh, Ir; X = I, OTf; R^F = CF_2CF_3, $CF_2CF_2CF_3$, $CF_2C_6F_5$, $CF(CF_3)_2$) to aqua cations and to hydrides. The aqua cations [M(η^5-C_5Me_5)(R^F)(PMe_3)(OH_2)]$^+$ are synthesized by reaction of the iodide derivatives with $AgBF_4$ in moist CH_2Cl_2. They exhibit short intramolecular O–H···F contacts with O···F distances in the range 2.8 to 2.9 Å.[136,137] The iridium hydride derivatives [Ir(η^5-C_5Me_5)H(R^F)(PMe_3)] are formed by reaction of the aqua cations with proton sponge, 1,8-bis(dimethylamino)-naphthalene, via a single-electron-transfer mechanism.[138] This is a very rare example of a reaction implicating migration of a pentafluoro group, converting an acyl complex to a carbonyl aryl complex.

The rhodium aqua cations [Rh(η^5-C_5Me_5)(R^F)(PMe_3)(OH_2)]$^+$ undergo hydrolysis of the fluoroalkyl ligand via attack by the coordinated water yielding carbonyl complexes. For instance, the perfluorobenzyl complex [Rh(η^5-C_5Me_5)($CF_2C_6F_5$)(PMe_3)(OH_2)]$^+$ reacts to form the [Rh(η^5-C_5Me_5)(C_6F_5)(PMe_3)(CO)]$^+$. The reaction involves proton transfer from coordinated water to form a perfluoroacyl complex, and its rate is dependent on the counterion as well as the solvent (see also reaction (v) of Scheme 15).[136]

The iridium aqua cations such as [Ir(η^5-C_5Me_5)(CF_2CF_3)(PMe_3)(OH_2)]$^+$ react with dihydrogen to release specific hydrofluorocarbons (here CF_3CFH_2 and CF_3CH_3) in a hydrogenolysis reaction that attacks the α-C–F bonds. The reaction and the proposed mechanism are illustrated in Scheme 45. The same products are obtained when the corresponding hydride complexes are reacted with triflic acid releasing HF.[139] If the hydride is treated with acetic acid, the reaction is arrested at the stage of [Ir(η^5-C_5Me_5)($CFHCF_3$)(PMe_3)(OAc)], which is formed as a mixture of two diastereomers (Scheme 19). In a neat application of isotope effects, it has been shown that the reaction of [Ir]D with CH_3CO_2H gives a different mixture of diastereomers from the reaction of the [Ir]H with CH_3CO_2D. These results are consistent with attack at the C–F bond by the external proton forming HF, followed by migration of hydride from the metal to make the new C–H bond.[66] The reader is also referred to extensive studies of the reaction of [Ir(η^5-C_5Me_5)(CF_2R)(H)(PMe_3)] (R = F, CF_3) with lutidinium salts.[140] While the iridium aqua cations undergo simple substitution of water by ammonia and phosphine, they react with H_2S at the α-C–F bonds to give metallacycles containing carbon and sulfur.[141]

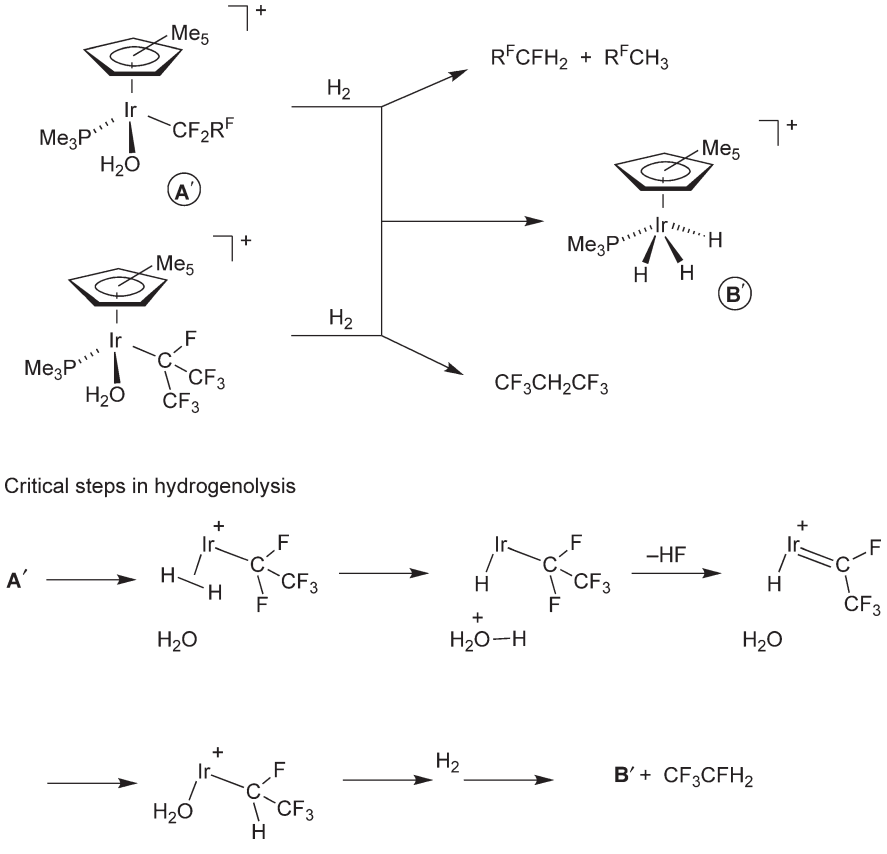

Scheme 45

In a reaction matching equation (iv) of Scheme 15, the methyl complex [Ir(η^5-C_5Me_5)($CF_2CF_2CF_3$)(CH_3)(PMe_3)] undergoes fluoride abstraction and [1,2]-methyl migration with lutidinium chloride to form a single diastereomer of [Ir(η^5-C_5Me_5)($CFMeCF_2CF_3$)Cl(PMe_3)] (Scheme 18).[67] In a closely related process, the vinyl analog reacts with lutidinium salts to form allyl complexes. With lutidinium iodide, the product is an η^1-allyl complex, but with [LuH][$BAr^F{}_4$], η^3-allyl complexes are formed. At sufficiently low temperature, the reaction is completely diastereoselective (Scheme 46).[142]

Removal of fluoride from [Ir(η^5-C_5Me_5)($COCF_3$)(H)(PMe_3)] with *t*-BuLi yields the difluoroketene complex [Ir(η^5-C_5Me_5)(η^2-*C*,*C*-$COCF_2$)(PMe_3)] together with [Ir(η^5-C_5Me_5)(PMe_3)(CO)] formed by elimination $LiCF_3$ (Scheme 47).[143] The tetrafluorobutatriene complex [Ir(η^5-C_5Me_5)(PMe_3)(2,3,-η^2-CF_2═CC═CF_2)] is formed by reductive defluorination of [Ir(η^5-C_5Me_5)($CF(CF_3)CF_2CF_3$)I(PMe_3)] with sodium naphthalene (Scheme 20).[68] Reductive defluorination reactions have also been used to form fluoroalkylidene complexes (see Section 1.26.3.2).

The conversion of an Ir–CF_3 group to an Ir–CO group of [Ir(CF_3)(CO)(dppe)($I_2C_6H_4$)] (dppe = bis(diphenylphosphino)ethane) by reaction with hydrogen (Scheme 48) has been attributed to the formation of an intermediate Ir═CF_2 complex that reacts with adventitious water.[144] Although the proposed mechanism is plausible, the authors do not appear to have considered mechanisms involving coordinated water attacking the CF_3 group as described above.

An Rh–CF_3 complex with a PCP pincer ligand also undergoes fluoride abstraction on reaction with Brønsted or Lewis acids but rearranges to form a CF_2 bridge between rhodium and the central carbon atom of the pincer ligand. The product can be described as an arenium difluoromethylene complex (Scheme 49). The reaction is thought to proceed via electrophilic abstraction of fluoride yielding a difluorocarbene complex as intermediate. This mechanism is consistent with the behavior of trifluoromethyl complexes described in Section 1.26.1.6. Notably, the methyl complex undergoes an analogous rearrangement.[145]

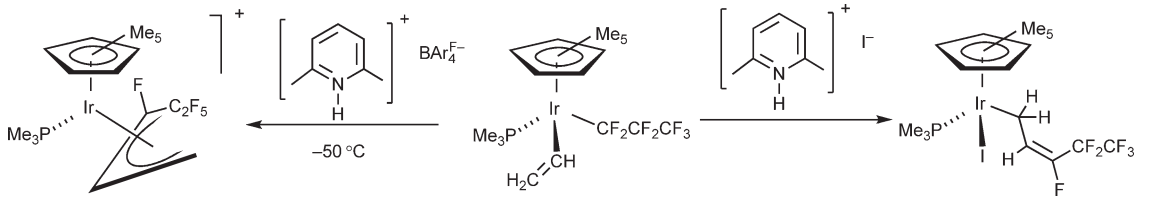

Scheme 46

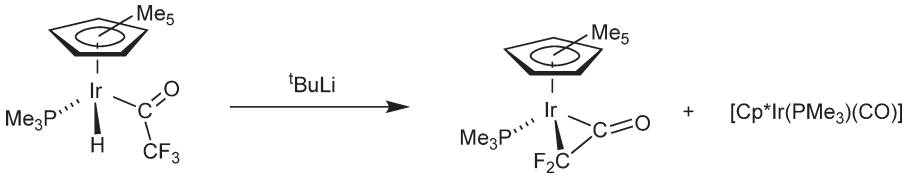

Scheme 47

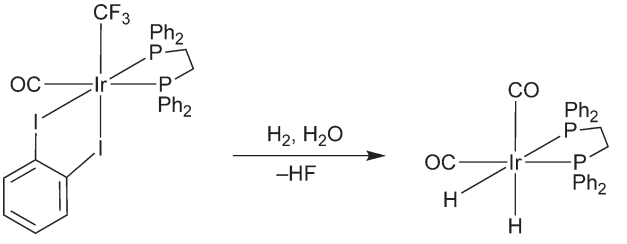

Scheme 48

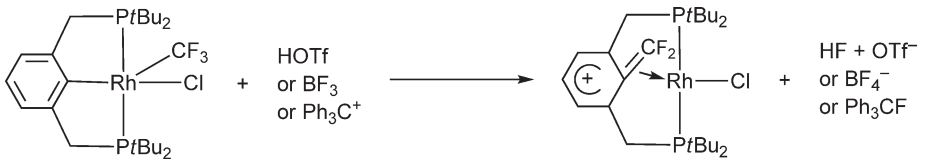

Scheme 49

Examples of interconversion of fluoroalkyl groups and fluoroalkylidene complexes are given in the succeeding section.

1.26.3.2 Fluorinated Alkyl to Alkylidene Interconversions

The interconversion of M–CF_3 groups and M=CF_2 (M = metal), especially via fluoride abstraction and addition, is well established.[3,5] Advances in the field have been made especially in the development of reactions involving α-F migration. Huang *et al*. reported the synthesis of 18-electron difluorocarbene complexes, [M(H)FL_2(CO)(=CF_2)], by reaction of 16-electron [M(H)FL_2(CO)] (M = Ru, L = PBu^t_2Me or PPr^i_3; M = Os, L = PBu^t_2Me) with Me_3SiCF_3 in the presence of catalytic CsF (Scheme 50).[64,146] These difluorocarbene complexes reveal several remarkable features. Exchange of the fluorine atoms in the CF_2 group of [Ru(H)FL_2(CO)(=CF_2)] with that in the metal fluoride is shown by ^{19}F spin saturation transfer. The exchange proceeds via the CF_3 isomer (Scheme 16) which

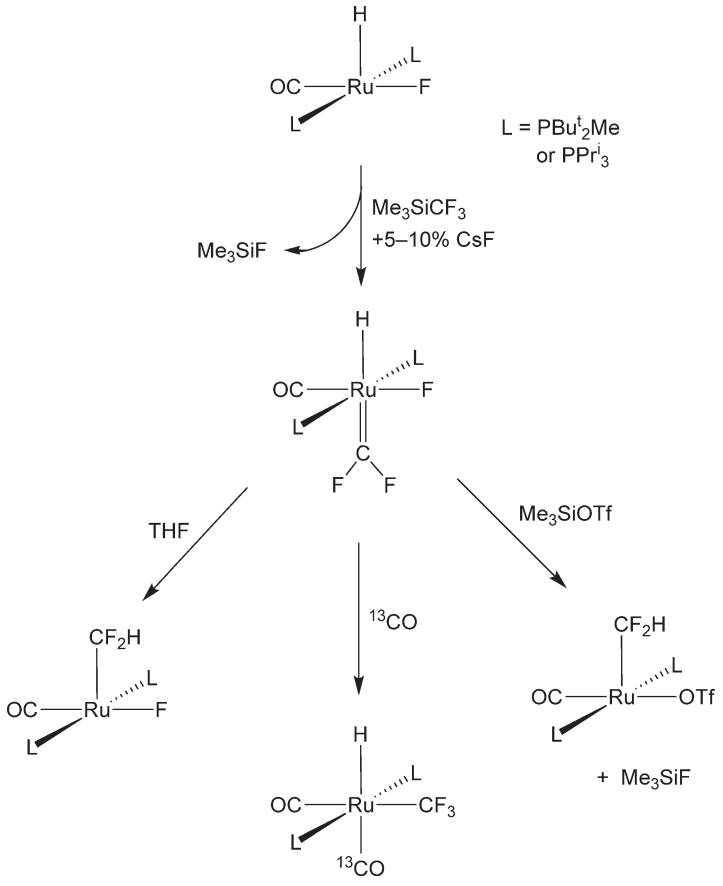

Scheme 50

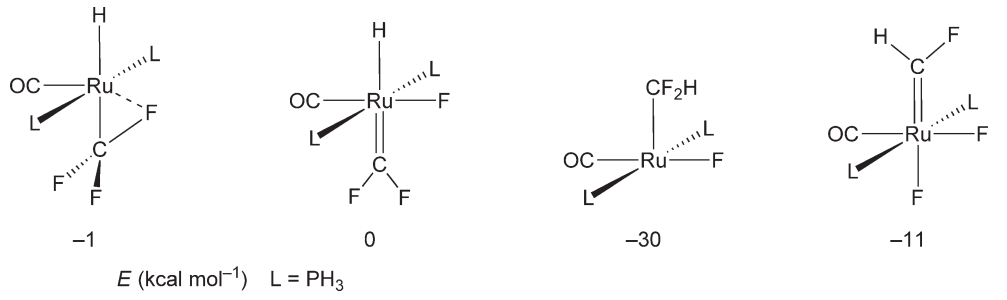

Scheme 51

may be trapped by reaction with CO or MeNC. The difluorocarbene complex isomerizes to a difluoromethyl complex, $[Ru(CF_2H)FL_2(CO)]$, in THF but not in benzene, a reaction that is triggered by phosphine dissociation. Reaction of the difluorocarbene complex with Me_3SiOTf removes fluoride, also initiating the conversion of the $Ru(=CF_2)H$ arrangement into an $Ru–CF_2H$ group (Scheme 50).

The osmium analog behaves in a significantly different way: $[Os(H)FL_2(CO)(=CF_2)]$ converts into 18-electron $[OsF_2L_2(CO)(=CFH)]$ on heating to 110 °C or on reaction with water at room temperature. An osmium difluoromethyl complex is formed only on reaction with CO, whereas CO is not required for the ruthenium analog.[64]

These reactions have also been studied by DFT. When the set of four ruthenium isomers is considered (Scheme 51), it becomes clear that the $[Ru(H)F(PH_3)_2(CO)(=CF_2)]$ is almost equienergetic with $[RuH(CF_3)(PH_3)_2(CO)]$. However, the fluorocarbene complex, $[RuF_2(PH_3)_2(CO)(=CFH)]$, is substantially more stable, and the difluoromethyl complex, $[Ru(CF_2H)F(PH_3)_2(CO)]$, is the most stable of all in accord with experiment. The calculated structure of $[RuH(CF_3)(PH_3)_2(CO)]$ shows a remarkable distortion of the CF_3 group in which one fluorine is brought close to the metal (2.626 Å) while extending its C–F bond (Scheme 51). This structure resembles that of an agostic alkyl, and clearly assists the α-fluorine elimination.[64]

A theoretical comparison of the migration ability of hydrogen and fluorine in the conversion of $[RuCl(CH_2X)(PH_3)_2]$ (X = H, F) to $[RuClX(PH_3)_2(=CH_2)]$ shows that the carbene is slightly more stable than the alkyl for X = F and slightly less stable for X = H at the DFT level. The activation energy for the migration of fluorine is shown to be substantially higher than for hydrogen, largely because of repulsion between the fluorine lone pairs and the electrons in the occupied *d*-orbitals.[147]

Hughes *et al.* have very recently demonstrated that fluoroalkyl complexes of iridium $[Ir(\eta^5\text{-}C_5Me_5)(CF_2R)(I)(PMe_3)]$ (R = F, CF_3, C_6F_5) can be converted into fluoroalkylidene complexes $[Ir(\eta^5\text{-}C_5Me_5)(=CFR)(PMe_3)]$ by reductive defluorination with sodium naphthalene or potassium graphite.[148]

1.26.3.3 Activation of Vinylic C–F Bond of Coordinated Fluoroalkenes and Fluorovinyl Groups

There are remarkably few examples of C–F bond activation of coordinated fluoroalkenes or fluorovinyl complexes. Those examples that are implicated during intermolecular reactions are covered in Section 1.26.2.2. Pétillon and Muir *et al.* have studied the rearrangements of a [perfluoro(sulfanyl)vinyl]diiron(I)hexacarbonyl complex that contains a $C=CF_2$ group σ-bonded to one iron and π-bonded to the other. This species undergoes several different rearrangements according to the nucleophile, all involving formal removal of fluoride from the CF_2 group. The ultimate position of the attacking nucleophile depends on its nucleophilicity, hardness, and the atom in question (S, N, O, and P nucleophiles have been tested).[149–152] The variety of outcomes is best covered in the 2002 paper.[152]

Reaction of methyllithium with a dinuclear iridium complex including a trifluorovinyl ligand results in replacement of a fluorine substituent at the β-position *trans* to the metal by a methyl group. It is argued that the reaction may be assisted by the second metal and may involve an alkylidene-bridged intermediate (Scheme 52).[153] The fluorine in the β-position in *trans*-$[Ni(CF=CF_2)(CNBu^t)(PEt_3)_2][BAr^F{}_4]$ can be replaced by a phosphine yielding, in the presence of $NaBAr^F{}_4$, the phosphonioethenyl complex *trans*-$[Ni\{CF=CF(PEt_3)\}(CNBu^t)(PEt_3)_2][BAr^F{}_4]_2$.[154]

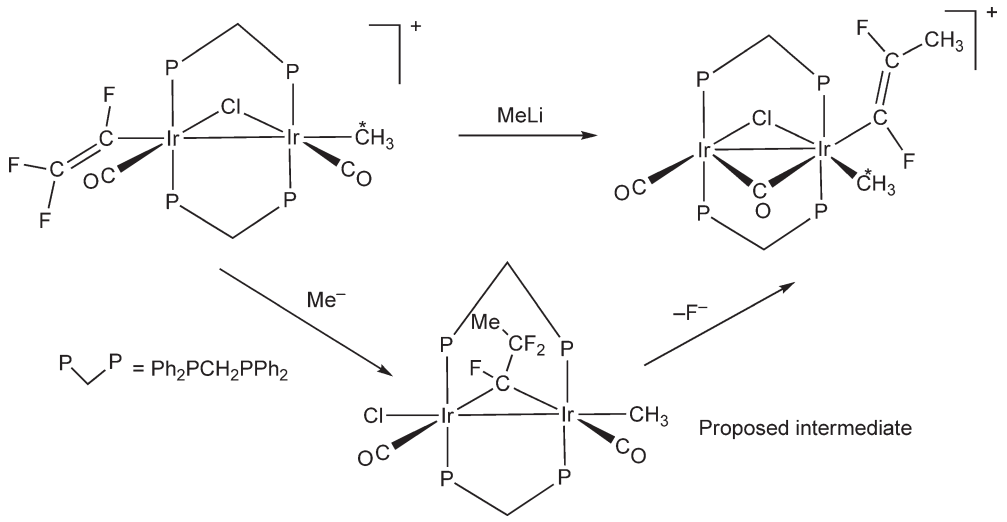

Scheme 52

1.26.3.4 Activation of *ortho*-C–F Bond of Pentafluorophenyl Complexes

The preceding sections have demonstrated the enhanced reactivity of the C–F bonds of fluoroalkyl groups when coordinated to a metal. The same principle can apply to the *ortho*-C–F bonds of M–C_6F_5 complexes. Hughes *et al.* have shown that [M(η^5-C_5Me_5)(H)(C_6F_5)(PMe_3)] (M = Rh, Ir) reacts with butyllithium to form η^2-tetrafluorobenzyne complexes (Scheme 53), the first examples of fluorinated benzyne complexes to be isolated. The mechanism of this reaction is unknown.[155,156] They are readily converted into tetrafluorophenyl derivatives by protonation.[157]

The formation of the η^2-tetrafluorobenzyne complexes is an example of β-fluoride abstraction. The corresponding β-elimination or [1,3]-fluorine-to-metal shift has been strongly implicated in the thermolysis of [Zr(η^5-C_5Me_5)$_2$(C_6F_5)H] at 100 °C under hydrogen that yields [Zr(η^5-C_5Me_5)$_2$(2,3,4,5-C_6F_4H)F]. Trapping experiments with durene reveal the presence of tetrafluorobenzyne, but a complex of tetrafluorobenzyne is likely to precede the free molecule.[65] Thermolysis of [Zr(η^5-C_5Me_5)$_2$(C_6F_5)H] at 80 °C under vacuum gave a ring-activated product, in addition, [Zr(η^5-C_5Me_5)(η^6-$C_5Me_4CH_2$)(C_6F_5)], with loss of H_2. The latter was synthesized independently and converted thermally into [Zr(η^5-C_5Me_5)(η^6-$C_5Me_4CH_2C_6F_4$)F]. This reaction implicates a further β-fluoride elimination and formation of another η^2-tetrafluorobenzyne intermediate.[65]

1.26.3.5 Activation of Remote Aromatic C–F Bonds

A variety of examples of remote intramolecular C–F bond activation have been discovered. All the recent examples involve fluorinated aromatic substituents that exhibit special reactivity including attack at the metal center. We divide the examples according to the atoms to which the fluoroaryl group is bonded, considering them in the order nitrogen, phosphorus, and sulfur.

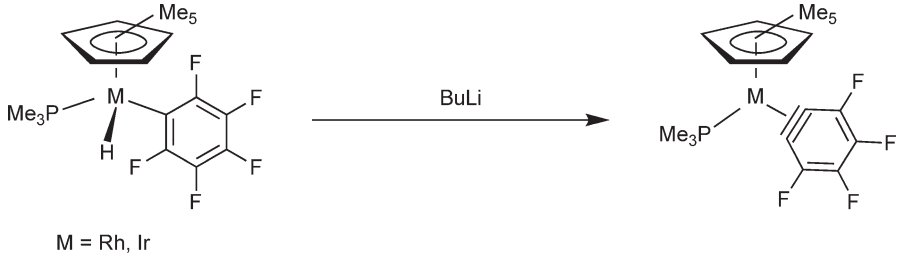

Scheme 53

1.26.3.5.1 Remote aromatic C–F bonds on nitrogen ligands

Berg *et al.* have exploited the photosensitivity of zirconium(IV) alkyls in a reaction of a zirconium dibenzyl complex that contains a chelating amido ligand with C_6F_5 substituents on nitrogen. The two products are dinuclear, one with a C_6F_4 group bound to nitrogen and zirconium and the other containing bridging fluorine ligands (Scheme 54).[158] Thus, the reaction is reminiscent of that of $[Zr(\eta^5\text{-}C_5Me_5)_2(H)_2]$ with fluorobenzene (see Section 2.1.1.1).

Crespo *et al.* established that Schiff bases with fluorinated aromatic substituents undergo intramolecular C–F bond activation with platinum(II) precursors to form cyclometallated Pt(IV) fluorides; this reaction occurs even with chlorine substituents on other neighboring aryl groups (Scheme 55).[159] In the most thorough kinetic study of C–F bond activation to date, Crespo *et al.* reported activation enthalpies, entropies, and volumes for these reactions and related C–H, C–Br, and C–Cl activation processes. They showed that the activation parameters vary smoothly, exhibiting strong correlation between entropy of activation and enthalpy of activation typical of an isokinetic relationship. The C–F activation reactions appeared at the extreme of the plot with small enthalpies, large negative entropies, and moderately negative volumes of activation. The authors conclude that the reactions proceed by a concerted oxidative addition mechanism with a three-center transition state in all cases.[160]

The principle of C–F activation at platinum(II) was extended to the reaction of Schiff bases with a pendant dimethylamino group. The reaction proceeded in analogous fashion, except that the final product showed that the acetone solvent had added across the imine double bond.[161] The same Schiff bases were used with a Pt(0) precursor, $Pt(dba)_2$, this time followed by workup with LiX (X = Cl, Br). Intramolecular C–F activation occurred when the substituent on the sp^2-carbon was C_6F_5, 2,4,6-$C_6H_2F_3$, 2,3,6-$C_6H_2F_3$, or 2,6-$C_6H_3F_2$. However, no C–F activation occurred with 2,4,5-$C_6H_3F_2$ or 2-C_6H_4F substituents.[162]

The reaction of $[Ni(COD)_2]$ with the imine, $C_6F_5CH{=}NCHMePh$, in the presence of LiBr and a phosphine or pyridine, L, yields an *ortho*-metallated product resulting from C–F oxidative addition and bromination at the metal: $[Ni\{(\kappa^2\text{-}C,N)\text{-}C_6F_4CH{=}NCHMePh\}BrL_n]$ ($n = 1$, L = 2,4,6-trimethylpyridine or $n = 2$, L = PMe_2Ph).[163]

1.26.3.5.2 Remote aromatic C–F bonds on phosphorus ligands

Saunders *et al.* have published an extensive series of papers on the coupling of ligands via dehydrofluorination at rhodium or iridium. The coupling reactions start with a fluorine substituent on the *ortho*-carbon of an aryl phosphine ligand and a methyl substituent on a cyclopentadienyl; removal of HF with proton sponge or simple heating results in C–C bond formation between these two groups and generation of a bifunctional ligand, $C_5Me_4CH_2\text{–}C_6F_4PR_2$. In

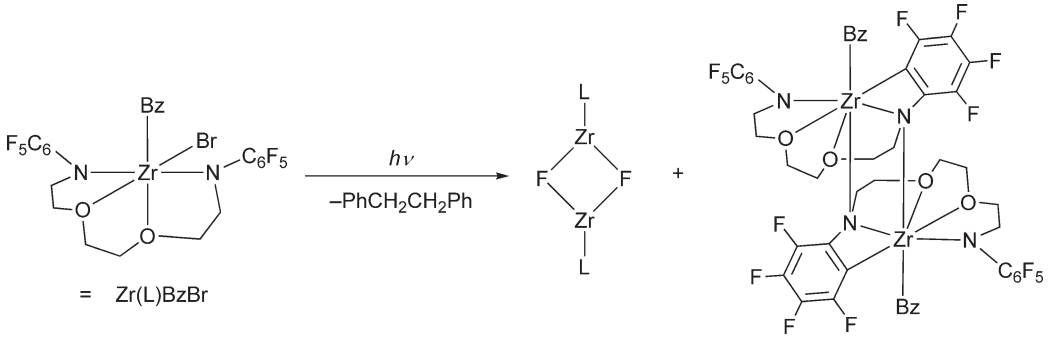

Scheme 54

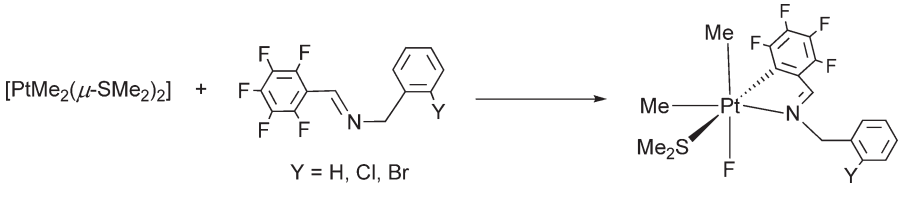

Scheme 55

some recent examples, the phosphine has been of the type $P(C_6F_5)_2(C_6H_4SMe)$ and the sulfur has also been bound to the metal (Scheme 22).[69–71] Alternatively, a chelating diphosphine has carried a single tetrafluoropyridyl group, $Ph_2PCH_2CH_2PPh(C_5NF_4)$.[164]

A related example concerns a platinum complex with phosphine and thiolate ligands that reacts via activation of a C_6F_5 substituent on phosphorus to couple a phosphorus ligand to a sulfur ligand forming a PtSCCP metallacycle.[165]

1.26.3.5.3 Remote aromatic C–F bonds on sulfur ligands

The osmium thiolate complex, $[Os(SC_6F_5)_3(PMe_2Ph)_2]$, exhibits a six-coordinate octahedral structure with an Os···F–C interaction to the 2-position of one of the C_6F_5 groups (Scheme 3).[28] The osmium complex reacts at the same position on thermolysis and is converted into a mixture of two complexes, both possessing a 1,2-$S_2C_6F_4$ dithiolate ligand, $[Os(SC_6F_5)_2(S_2C_6F_4)(PMe_2Ph)]$ and $[Os(C_6F_5)_2(S_2C_6F_4)(PMe_2Ph)_2]$. Although the reactions are complex, the significance of the Os···F–C interaction in the subsequent C–F cleavage is evident.

References

1. Kiplinger, J. L.; Richmond, T. G.; Osterberg, C. E. *Chem. Rev.* **1994**, *94*, 373–431.
2. Burdeniuc, J.; Jedlicka, B.; Crabtree, R. H. *Chem. Ber. Recl.* **1997**, *130*, 145–154.
3. Brothers, P. J.; Roper, W. R. *Chem. Rev.* **1988**, *88*, 1293–1326.
4. Hughes, R. P. *Adv. Organomet. Chem.* **1990**, *31*, 183–268.
5. Morrison, J. A. *Adv. Organomet. Chem.* **1993**, *35*, 211–239.
6. Plenio, H. *Chem. Rev.* **1997**, *97*, 3363–3384.
7. Murphy, E. F.; Murugavel, R.; Roesky, H. W. *Chem. Rev.* **1997**, *97*, 3425–3468.
8. Richmond, T. G. *Topics Organomet. Chem.* **1999**, *3*, 243.
9. Richmond, T. G. *Angew. Chem., Int. Ed.* **2000**, *39*, 3241–3244.
10. Braun, T.; Perutz, R. N. *Chem. Commun.* **2002**, 2749–2757.
11. Alonso, F.; Beletskaya, I. P.; Yus, M. *Chem. Rev.* **2002**, *102*, 4009–4091.
12. Mazurek, U.; Schwarz, H. *Chem. Commun.* **2003**, 1321–1326.
13. Jones, W. D. *Dalton Trans.* **2003**, 3991–3995.
14. Torrens, H. *Coord. Chem. Rev.* **2005**, *249*, 1957.
15. McGlinchey, M. J.; Tan, T. S. *J. Am. Chem. Soc.* **1976**, *98*, 2271–2275.
16. Barker, J. J.; Orpen, A. G.; Seeley, A. J.; Timms, P. L. *J. Chem. Soc., Dalton Trans.* **1993**, 3097–3102.
17. Martin, A.; Orpen, A. G.; Seeley, A. J.; Timms, P. L. *J. Chem. Soc., Dalton Trans.* **1994**, 2251–2255.
18. Bell, T. W.; Helliwell, M.; Partridge, M. G.; Perutz, R. N. *Organometallics* **1992**, *11*, 1911–1918.
19. Higgitt, C. L.; Klahn, A. H.; Moore, M. H.; Oelckers, B.; Partridge, M. G.; Perutz, R. N. *J. Chem. Soc., Dalton Trans.* **1997**, 1269–1280.
20. Bouwkamp, M. W.; de Wolf, J.; Morales, I. D.; Gercama, J.; Meetsma, A.; Troyanov, S. I.; Hessen, B.; Teuben, J. H. *J. Am. Chem. Soc.* **2002**, *124*, 12956–12957.
21. Bouwkamp, M. W.; Budzelaar, P. H. M.; Gercama, J.; Del Hierro Morales, I.; de Wolf, J.; Meetsma, A.; Troyanov, S. I.; Teuben, J. H.; Hessen, B. *J. Am. Chem. Soc.* **2005**, *127*, 14310–14319.
22. Horton, A. D.; Orpen, A. G. *Organometallics* **1991**, *10*, 3910–3918.
23. Yang, X. M.; Stern, C. L.; Marks, T. J. *Organometallics* **1991**, *10*, 840–842.
24. Bartolome, C.; Espinet, P.; Villafane, F.; Giesa, S.; Martin, A.; Orpen, A. G. *Organometallics* **1996**, *15*, 2019–2028.
25. Kulawiec, R. J.; Holt, E. M.; Lavin, M.; Crabtree, R. H. *Inorg. Chem.* **1987**, *26*, 2559–2561.
26. Catala, R. M.; Cruzgarritz, D.; Sosa, P.; Terreros, P.; Torrens, H.; Hills, A.; Hughes, D. L.; Richards, R. L. *J. Organomet. Chem.* **1989**, *359*, 219–232.
27. Arroyo, M.; Bernes, S.; Brianzo, J. L.; Mayoral, E.; Richards, R. L.; Rius, J.; Torrens, H. *Inorg. Chem. Commun.* **1998**, *1*, 273–276.
28. Arroyo, M.; Bernes, S.; Brianso, J. L.; Mayoral, E.; Richards, R. L.; Rius, J.; Torrens, H. *J. Organomet. Chem.* **2000**, *599*, 170–177.
29. Noveski, D.; Braun, T.; Neumann, B.; Stammler, A.; Stammler, H.-G. *Dalton Trans.* **2004**, 4106–4119.
30. Garcia, M. P.; Jimenez, M. V.; Lahoz, F. J.; Oro, L. A.; Tiripicchio, A.; Lopez, J. A. *J. Chem. Soc., Dalton Trans.* **1990**, 1503–1508.
31. Benedikt, G. M.; Goodall, B. L.; Iyer, S.; McIntosh, L. H.; Mimna, R.; Rhodes, L. F.; Day, C. S.; Day, V. W. *Organometallics* **2001**, *20*, 2565–2569.
32. Gibson, V. C.; Redshaw, C.; Sequeira, L. J.; Dillon, K. B.; Clegg, W.; Elsegood, M. R. J. *Chem. Commun.* **1996**, 2151–2152.
33. Memmler, H.; Walsh, K.; Gade, L. H.; Lauher, J. W. *Inorg. Chem.* **1995**, *34*, 4062–4068.
34. David, R. L. In *CRC Handbook of Chemistry and Physics*; CRC Press: Boca Raton, 2005.

34a. Kalinowski, I. J.; Gutman, D.; Krasnoperov, L. N.; Goumri, A.; Yuan, W.-J.; Marshall, P. *J. Phys. Chem.* **1994**, *98*, 9551.

34b. Huheey, J. E.; Keiter, E. A.; Keiter, R. L. *Inorganic Chemistry*, 4th ed.; Harper Collins: New York, 1993.

35. Bosque, R.; Clot, E.; Fantacci, S.; Maseras, F.; Eisenstein, O.; Perutz, R. N.; Renkema, K. B.; Caulton, K. G. *J. Am. Chem. Soc.* **1998**, *120*, 12634–12640.

35a. Reinhold, M.; McGrady, J. E.; Perutz, R. N. *J. Am. Chem. Soc.* **2004**, *126*, 5268–5276.

36. Macgregor, S. A.; Roe, D. C.; Marshall, W. J.; Bloch, K. M.; Bakhmutov, V. I.; Grushin, V. V. *J. Am. Chem. Soc.* **2005**, *127*, 15304–15321.
37. Clot, E.; Besora, M.; Maseras, F.; Mégret, C.; Eisenstein, O.; Oelckers, B.; Perutz, R. N. *Chem. Commun.* **2003**, 490–491.
38. Fahey, D. R.; Mahan, J. E. *J. Am. Chem. Soc.* **1977**, *99*, 2501–2508.
39. Cronin, L.; Higgitt, C. L.; Karch, R.; Perutz, R. N. *Organometallics* **1997**, *16*, 4920–4928.
40. Braun, T.; Cronin, L.; Higgitt, C. L.; McGrady, J. E.; Perutz, R. N.; Reinhold, M. *New J. Chem.* **2001**, *25*, 19–21.
41. Bach, I.; Pörschke, K. R.; Goddard, R.; Kopiske, C.; Kruger, C.; Rufinska, A.; Seevogel, K. *Organometallics* **1996**, *15*, 4959–4966.

42. Belt, S. T.; Helliwell, M.; Jones, W. D.; Partridge, M. G.; Perutz, R. N. *J. Am. Chem. Soc.* **1993**, *115*, 1429–1440.
43. Sladek, M. I.; Braun, T.; Neumann, B.; Stammler, H.-G. *J. Chem. Soc., Dalton Trans.* **2002**, 297–299.
44. Steffen, A.; Sladek, M. I.; Braun, T.; Neumann, B.; Stammler, H.-G. *Organometallics* **2005**, *24*, 4057–4064.
45. Crespo, M.; Martinez, M.; Sales, J. *J. Chem. Soc., Chem. Commun.* **1992**, 822–823.
46. Whittlesey, M. K.; Perutz, R. N.; Moore, M. H. *Chem. Commun.* **1996**, 787–788.
47. Aizenberg, M.; Milstein, D. *Science* **1994**, *265*, 359–361.
48. Kraft, B. M.; Jones, W. D. *J. Organomet. Chem.* **2002**, *658*, 132–140.
49. King, R. B.; Bisnette, M. B. *J. Organomet. Chem.* **1964**, *2*, 38–43.
50. Edelbach, B. L.; Jones, W. D. *J. Am. Chem. Soc.* **1997**, *119*, 7734–7742.
51. Braun, T.; Noveski, D.; Neumann, B.; Stammler, H.-G. *Angew. Chem., Int. Ed.* **2002**, *41*, 2745–2748.
52. Noveski, D.; Braun, T.; Schulte, M.; Neumann, B.; Stammler, H. G. *Dalton Trans.* **2003**, 4075–4083.
53. Clot, E.; Mégret, C.; Kraft, B. M.; Eisenstein, O.; Jones, W. D. *J. Am. Chem. Soc.* **2004**, *126*, 5647–5653.
54. Jolly, P. W.; Bruce, M. I.; Stone, F. G. A. *J. Chem. Soc.* **1965**, 5830–5837.
55. Terao, J.; Ikumi, A.; Kuniyasu, H.; Kambe, N. *J. Am. Chem. Soc.* **2003**, *125*, 5646–5647.
56. Zhang, D.; Liu, C.; Bi, S. *J. Phys. Chem. A* **2002**, *106*, 4153–4157.
57. Zhang, D. J.; Liu, C. B. *Chin. Chem. Lett.* **2002**, *13*, 359–362.
58. Rausch, M.; Bruhn, C.; Steinborn, D. *J. Organomet. Chem.* **2001**, *622*, 172–179.
59. Burdeniuc, J.; Chupka, W.; Crabtree, R. H. *J. Am. Chem. Soc.* **1995**, *117*, 10119–10120.
60. Burdeniuc, J.; Crabtree, R. H. *J. Am. Chem. Soc.* **1996**, *118*, 2525–2526.
61. Burdeniuc, J.; Crabtree, R. H. *Organometallics* **1998**, *17*, 1582–1586.
62. Deacon, G. B.; Harris, S. C.; Meyer, G.; Stellfeldt, D.; Wilkinson, D. L.; Zelesny, G. *J. Organomet. Chem.* **1998**, *552*, 165–170.
63. Deacon, G. B.; Meyer, G.; Stellfeldt, D. *Eur. J. Inorg. Chem.* **2000**, 1061–1071.
64. Huang, D. J.; Koren, P. R.; Folting, K.; Davidson, E. R.; Caulton, K. G. *J. Am. Chem. Soc.* **2000**, *122*, 8916–8931.
65. Kraft, B. M.; Lachicotte, R. J.; Jones, W. D. *Organometallics* **2002**, *21*, 727–731.
66. Hughes, R. P.; Willemsen, S.; Williamson, A.; Zhang, D. H. *Organometallics* **2002**, *21*, 3085–3087.
67. Hughes, R. P.; Zhang, D. H.; Zakharov, L. N.; Rheingold, A. L. *Organometallics* **2002**, *21*, 4902–4904.
68. Hughes, R. P.; Laritchev, R. B.; Zakharov, L. N.; Rheingold, A. L. *J. Am. Chem. Soc.* **2004**, *126*, 2308–2309.
69. Bellabarba, R. M.; Nieuwenhuyzen, M.; Saunders, G. C. *J. Chem. Soc., Dalton Trans.* **2001**, 512–514.
70. Bellabarba, R. M.; Saunders, G. C. *J. Fluorine Chem.* **2001**, *112*, 139–144.
71. Bellabarba, R. M.; Saunders, G. C. *Polyhedron* **2004**, *23*, 2659–2664.
72. Ishii, Y.; Chatani, N.; Yorimitsu, S.; Murai, S. *Chem. Lett.* **1998**, 157–158.
73. Kim, Y. M.; Yu, S. *J. Am. Chem. Soc.* **2003**, *125*, 1696–1697.
74. Aizenberg, M.; Milstein, D. *J. Am. Chem. Soc.* **1995**, *117*, 8674–8675.
75. Braun, T.; Perutz, R. N.; Sladek, M. I. *Chem. Commun.* **2001**, 2254–2255.
76. Kiso, Y.; Tamao, K.; Kumada, M. *J. Organomet. Chem.* **1973**, *50*, C12–C14.
77. Edelbach, B. L.; Kraft, B. M.; Jones, W. D. *J. Am. Chem. Soc.* **1999**, *121*, 10327–10331.
78. Kraft, B. M.; Lachicotte, R. J.; Jones, W. D. *J. Am. Chem. Soc.* **2001**, *123*, 10973–10979.
79. Maron, L.; Werkema, E. L.; Perrin, L.; Eisenstein, O.; Andersen, R. A. *J. Am. Chem. Soc.* **2005**, *127*, 279–292.
80. Cole, M. L.; Deacon, G. B.; Junk, P. C.; Konstas, K. *Chem. Commun.* **2005**, 1581–1583.
81. Klahn, A. H.; Oelckers, B.; Godoy, F.; Garland, M. T.; Vega, A.; Perutz, R. N.; Higgitt, C. L. *J. Chem. Soc., Dalton Trans.* **1998**, 3079–3086.
82. Godoy, F.; Higgitt, C. L.; Klahn, A. H.; Oelckers, B.; Parsons, S.; Perutz, R. N. *J. Chem. Soc., Dalton Trans.* **1999**, 2039–2047.
83. Chernega, A. N.; Graham, A. J.; Green, M. L. H.; Haggitt, J.; Lloyd, J.; Mehnert, C. P.; Metzler, N.; Souter, J. *J. Chem. Soc., Dalton Trans.* **1997**, 2293–2303.
84. Barrio, P.; Castarlenas, R.; Esteruelas, M. A.; Lledos, A.; Maseras, F.; Onate, E.; Tomas, J. *Organometallics* **2001**, *20*, 442–452.
85. Esteruelas, M. A.; Lledos, A.; Olivan, M.; Onate, E.; Tajada, M. A.; Ujaque, G. *Organometallics* **2003**, *22*, 3753–3765.
86. Archibald, S. J.; Braun, T.; Gaunt, J. A.; Hobson, J. E.; Perutz, R. N. *J. Chem. Soc., Dalton Trans.* **2000**, 2013–2018.
87. Braun, T.; Foxon, S. P.; Perutz, R. N.; Walton, P. H. *Angew. Chem., Int. Ed.* **1999**, *38*, 3326–3329.
88. Burling, S.; Elliott, P. I. P.; Jasim, N. A.; Lindup, R. J.; McKenna, J.; Perutz, R. N.; Archibald, S. J.; Whitwood, A. C. *Dalton Trans.* **2005**, 3686–3695.
89. Braun, T.; Parsons, S.; Perutz, R. N.; Voith, M. *Organometallics* **1999**, *18*, 1710–1716.
90. Schaub, T.; Radius, U. *Chem. Eur. J.* **2005**, *11*, 5024–5030.
91. Yamamoto, T.; Abla, M. *J. Organomet. Chem.* **1997**, *535*, 209–211.
92. Jasim, N. A.; Perutz, R. N.; Whitwood, A. C.; Braun, T.; Izundu, J.; Neumann, B.; Rothfeld, S.; Stammler, H. G. *Organometallics* **2004**, *23*, 6140–6149.
93. Jasim, N. A.; Perutz, R. N. *J. Am. Chem. Soc.* **2000**, *122*, 8685–8693.
94. Braun, T.; Rothfeld, S.; Schorlemer, V.; Stammler, A.; Stammler, H.-G. *Inorg. Chem. Commun.* **2003**, *6*, 752–755.
95. Albeniz, A. C.; Calle, V.; Espinet, P.; Gomez, S. *Chem. Commun.* **2002**, 610–611.
96. Kraft, B. M.; Jones, W. D. *J. Am. Chem. Soc.* **2002**, *124*, 8681–8689.
97. Watson, L. A.; Yandulov, D. V.; Caulton, K. G. *J. Am. Chem. Soc.* **2001**, *123*, 603–611.
98. Fujiwara, M.; Ichikawa, J.; Okauchi, T.; Minami, T. *Tetrahedron Lett.* **1999**, *40*, 7261–7265.
99. Strazisar, S. A.; Wolczanski, P. T. *J. Am. Chem. Soc.* **2001**, *123*, 4728–4740.
100. Ferrando-Miguel, G.; Gérard, H.; Eisenstein, O.; Caulton, K. G. *Inorg. Chem.* **2002**, *41*, 6440–6449.
101. Kirkham, M. S.; Mahon, M. F.; Whittlesey, M. K. *Chem. Commun.* **2001**, 813–814.
102. Lentz, D.; Willemsen, S. *Angew. Chem., Int. Ed.* **2001**, *40*, 2087–2091.
103. Lentz, D.; Willemsen, S. *J. Organomet. Chem.* **2002**, *641*, 215–219.
104. Noveski, D.; Braun, T.; Krückemeier, S. *J. Fluorine Chem.* **2004**, *125*, 959–966.
105. Peterson, T. H.; Golden, J. T.; Bergman, R. G. *Organometallics* **1999**, *18*, 2005–2020.
106. Werkema, E. L.; Messines, E.; Perrin, L.; Maron, L.; Eisenstein, O.; Andersen, R. A. *J. Am. Chem. Soc.* **2005**, *127*, 7781–7795.
107. Santamaria, C.; Beckhaus, R.; Haase, D.; Saak, W.; Koch, R. *Chem., Eur. J.* **2001**, *7*, 622–626.
108. Galinkina, J.; Rusanov, E.; Wagner, C.; Schmidt, H.; Strohl, D.; Tobisch, S.; Steinborn, D. *Organometallics* **2003**, *22*, 4873–4884.

109. Su, M. D.; Chu, S. Y. *J. Am. Chem. Soc.* **1999**, *121*, 1045–1058.
110. Su, M. D.; Chu, S. Y. *J. Am. Chem. Soc.* **1997**, *119*, 10178–10185.
111. Burdeniuc, J.; Siegbahn, P. E. M.; Crabtree, R. H. *New J. Chem.* **1998**, *22*, 503–510.
112. Mazurek, U.; Schroder, D.; Schwarz, H. *Angew. Chem., Int. Ed.* **2002**, *41*, 2538–2541.
113. Mazurek, U.; Koszinowski, K.; Schwarz, H. *Organometallics* **2003**, *22*, 218–225.
114. Hertwig, R. H.; Koch, W. *Chem., Eur. J.* **1999**, *5*, 312–319.
115. Zhang, D. J.; Zhang, C. Q.; Liu, C. B. *J. Organomet. Chem.* **2001**, *640*, 121–126.
116. Caraiman, D.; Koyanagi, G. K.; Cunje, A.; Hopkinson, A. C.; Bohme, D. K. *Organometallics* **2002**, *21*, 4293–4296.
117. Caraiman, D.; Koyanagi, G. K.; Bohme, D. K. *J. Phys. Chem. A* **2004**, *108*, 978–986.
118. Vela, J.; Smith, J. M.; Yu, Y.; Ketterer, N. A.; Flaschenriem, C. J.; Lachicotte, R. J.; Holland, P. L. *J. Am. Chem. Soc.* **2005**, *127*, 7857–7870.
119. Desmarets, C.; Kuhl, S.; Schneider, R.; Fort, Y. *Organometallics* **2002**, *21*, 1554–1559.
120. Kuhl, S.; Schneider, R.; Fort, Y. *Adv. Synth. Catal.* **2003**, *345*, 341–344.
121. Young, R. J.; Grushin, V. V. *Organometallics* **1999**, *18*, 294–296.
122. Laev, S. S.; Shteingarts, V. D. *J. Fluorine Chem.* **1999**, *96*, 175–185.
123. Laev, S. S.; Shteingarts, V. D. *Tetrahedron Lett.* **1997**, *38*, 3765–3768.
124. Frohn, H. J.; Adonin, N. Y.; Bardin, V. V.; Starichenko, V. F. *J. Fluorine Chem.* **2002**, *117*, 115–120.
125. Böhm, V. P. W.; Gstöttmayr, C. W. K.; Weskamp, T.; Herrmann, W. A. *Angew. Chem., Int. Ed.* **2001**, *40*, 3387–3389.
126. Dankwardt, J. W. *J. Organomet. Chem.* **2005**, *690*, 932–938.
127. Ackermann, L.; Born, R.; Spatz, J. H.; Meyer, D. *Angew. Chem., Int. Ed.* **2005**, *44*, 7216–7219.
128. Lamm, K.; Stollenz, M.; Meier, M.; Gorls, H.; Walther, D. *J. Organomet. Chem.* **2003**, *681*, 24–36.
128a. Saeki, T.; Takashima, Y.; Tamao, K. *Synlett* **2005**, 1771–1774.
129. Mongin, F.; Mojovic, L.; Guillamet, B.; Trecourt, F.; Queguiner, G. *J. Org. Chem.* **2002**, *67*, 8991–8994.
130. Widdowson, D. A.; Wilhelm, R. *Chem. Commun.* **2003**, 578–579.
131. Bahmanyar, S.; Borer, B. C.; Kim, Y. M.; Kurtz, D. M.; Yu, S. *Org. Lett.* **2005**, *7*, 1011–1014.
132. Widdowson, D. A.; Wilhelm, R. E. *Chem. Commun.* **1999**, 2211–2212.
133. Wilhelm, R.; Widdowson, D. A. *J. Chem. Soc., Perkin Trans. 1* **2000**, 3808–3813.
134. Jakt, M.; Johannissen, L.; Rzepa, H. S.; Widdowson, D. A.; Wilhelm, R. *J. Chem. Soc., Perkin Trans. 2* **2002**, 576–581.
135. Terao, J.; Watabe, H.; Kambe, N. *J. Am. Chem. Soc.* **2005**, *127*, 3656–3657.
136. Hughes, R. P.; Lindner, D. C.; Rheingold, A. L.; Liable-Sands, L. M. *J. Am. Chem. Soc.* **1997**, *119*, 11544–11545.
137. Hughes, R. P.; Lindner, D. C.; Smith, J. M.; Zhang, D. H.; Incarvito, C. D.; Lam, K. C.; Liable-Sands, L. M.; Sommer, R. D.; Rheingold, A. L. *J. Chem. Soc., Dalton Trans.* **2001**, 2270–2278.
138. Hughes, R. P.; Kovacik, I.; Lindner, D. C.; Smith, J. M.; Willemsen, S.; Zhang, D. H.; Guzei, I. A.; Rheingold, A. L. *Organometallics* **2001**, *20*, 3190–3197.
139. Hughes, R. P.; Smith, J. M. *J. Am. Chem. Soc.* **1999**, *121*, 6084–6085.
140. Garratt, S. A.; Hughes, R. P.; Kovacik, I.; Ward, A. J.; Willemsen, S.; Zhang, D. *J. Am. Chem. Soc.* **2005**, *127*, 15585–15594.
141. Hughes, R. P.; Smith, J. M.; Incarvito, C. D.; Lam, K. C.; Rhatigan, B.; Rheingold, A. L. *Organometallics* **2002**, *21*, 2136–2144.
142. Hughes, R. P.; Laritchev, R. B.; Zakharov, L. N.; Rheingold, A. L. *J. Am. Chem. Soc.* **2005**, *127*, 6325–6334.
143. Cordaro, J. G.; van Halbeek, H.; Bergman, R. G. *Angew. Chem., Int. Ed.* **2004**, *43*, 6366–6369.
144. Albietz, P. J.; Houlis, J. F.; Eisenberg, R. *Inorg. Chem.* **2002**, *41*, 2001–2003.
145. van der Boom, M. E.; Ben-David, Y.; Milstein, D. *J. Am. Chem. Soc.* **1999**, *121*, 6652–6656.
146. Huang, D. J.; Caulton, K. G. *J. Am. Chem. Soc.* **1997**, *119*, 3185–3186.
147. Gérard, H.; Davidson, E. R.; Eisenstein, O. *Mol. Phys.* **2002**, *100*, 533–540.
148. Hughes, R. P.; Laritchev, R. B.; Yuan, J.; A, G. J.; Rucker, A. N.; Rheingold, A. L *J. Am. Chem. Soc.* **2005**, *127*, 15020–15021.
149. Rumin, R.; Guennou, K.; Pétillon, F. Y.; Muir, K. W. *J. Chem. Soc., Dalton Trans.* **1997**, 1381–1386.
150. Rumin, R.; Guennou, K.; Pichon, R.; Pétillon, F. Y.; Muir, K. W.; Yufit, D. S. *J. Organomet. Chem.* **1997**, *533*, 177–185.
151. Guennou-de Cadenet, K.; Rumin, R.; Pétillon, F. Y.; Muir, K. W. *Organometallics* **2000**, *19*, 1912–1926.
152. de Cadenet, K. G.; Rumin, R.; Pétillon, F. Y.; Yufit, D. S.; Muir, K. W. *Eur. J. Inorg. Chem.* **2002**, 639–657.
153. Ristic-Petrovic, D.; Wang, M.; McDonald, R.; Cowie, M. *Organometallics* **2002**, *21*, 5172–5181.
154. Braun, T.; Blöcker, B.; Schorlemer, V.; Neumann, B.; Stammler, A.; Stammler, H.-G. *J. Chem. Soc., Dalton Trans.* **2002**, 2213–2218.
155. Hughes, R. P.; Williamson, A.; Sommer, R. D.; Rheingold, A. L. *J. Am. Chem. Soc.* **2001**, *123*, 7443–7444.
156. Hughes, R. P.; Laritchev, R. B.; Williamson, A.; Incarvito, C. D.; Zakharov, L. N.; Rheingold, A. L. *Organometallics* **2002**, *21*, 4873–4885.
157. Hughes, R. P.; Laritchev, R. B.; Williamson, A.; Incarvito, C. D.; Zakharov, L. N.; Rheingold, A. L. *Organometallics* **2003**, *22*, 2134–2141.
158. O'Connor, P. E.; Berg, D. J.; Barclay, T. *Organometallics* **2002**, *21*, 3947–3954.
159. Crespo, M.; Martinez, M.; Sales, J. *Organometallics* **1993**, *12*, 4297–4304.
160. Crespo, M.; Martinez, M.; de Pablo, E. *J. Chem. Soc., Dalton Trans.* **1997**, 1231–1235.
161. Lopez, O.; Crespo, M.; Font-Bardia, M.; Solans, X. *Organometallics* **1997**, *16*, 1233–1240.
162. Crespo, M.; Granell, J.; Font-Bardia, M.; Solans, X. *J. Organomet. Chem.* **2004**, *689*, 3088–3092.
163. Ceder, R. M.; Granell, J.; Muller, G. *J. Chem. Soc., Dalton Trans.* **1998**, 1047–1051.
164. Bellabarba, R. M.; Nieuwenhuyzen, M.; Saunders, G. C. *Organometallics* **2003**, *22*, 1802–1810.
165. Villanueva, L.; Arroyo, M.; Bernes, S.; Torrens, H. *Chem. Commun.* **2004**, 1942–1943.

1.27 Hydrodesulfurization and Hydrodenitrogenation

R A Sánchez-Delgado, Brooklyn College, NY, USA

1.27.1 Hydrodesulfurization and Hydrodenitrogenation

Hydrodesulfurization (HDS) is the reaction of organosulfur compounds with hydrogen over a catalyst leading to the extrusion of sulfur as H_2S with concomitant production of the corresponding hydrocarbon (Equation (1)). Hydrodenitrogenation (HDN) refers to the analogous removal of nitrogen from organonitrogen compounds to produce ammonia and hydrocarbons (Equation (2)). These are the means by which sulfur and nitrogen are removed from petroleum feedstocks in refineries; HDS and HDN are the most important and most thoroughly studied reactions of the complex "hydrotreating" process involved in fuel production.[1–3]

$$[R\text{–}S] + H_2 \xrightarrow{\text{cat.}} [R\text{–}H] + H_2S \quad (1)$$

$$[R\text{–}N] + H_2 \xrightarrow{\text{cat.}} [R\text{–}H] + NH_3 \quad (2)$$

Petroleum is a complex mixture of hydrocarbons containing varying amounts of heteroatoms. The most abundant is invariably sulfur, present in concentrations up to 5 wt.% in a variety of compounds; thiols, sulfides, and disulfides can be removed with relative ease, but thiophenes, benzothiophenes, and specially dibenzothiophenes (Figure 1) are more refractory as a result of their increased aromatic character. Of particular interest are 4,6-dialkyldibenzothiophenes, since they are the most difficult to degrade. Removal of such sulfur through "deep desulfurization" is a most demanding task for which a satisfactory solution has not yet been found. The nitrogen content of crudes is lower than the sulfur content, typically around 0.1 wt.%, although it may reach levels as high as 1 wt.%. Nitrogen is present predominantly in the heavier and cracked fractions, and the highly refractory molecules relevant to HDN are those derived from pyridine (py) and from pyrrole (Pyr) with one or several short-chain alkyl substituents, as well as higher polycyclic homologs (see Figure 1).

Organo- S- and N-compounds generate sulfur and nitrogen oxides (SO_x and NO_x) upon combustion; if released into the atmosphere, they are responsible for acid rain and other polluting effects. Therefore, environmental legislation imposes severe restrictions on the amounts of sulfur and nitrogen allowed in transportation fuels.[1–4b] Currently available technologies cannot fully meet these specifications, and therefore there is an urgent need for improved methods to produce cleaner fuels, specifically for the development of more efficient catalysts. "Promoted Mo catalysts" commonly employed in industry are composed of Co–Mo sulfides supported on γ-alumina; other useful combinations include Ni–Mo and Ni–W. Co–Mo catalysts are excellent for HDS and less active for HDN, which is better performed over Ni–Mo or Ni–W. Operating conditions for HDS range between 300–450 °C and 10–250 atm H_2 (1 atm = 101.325 kPa). Many other metal sulfides are active in HDS catalysis, and maximum activities are invariably found for Ru, Os, Rh, Ir; this is important in relation to organometallic HDS modeling, since a good proportion of such chemistry is concerned with Ru, Rh, and Ir complexes. Due to the higher C═N bond strength and the smaller atomic radius of N, the removal of nitrogen is more difficult to achieve. Strongly hydrogenating catalysts perform the best, the most commonly used being $NiMo/Al_2O_3$.

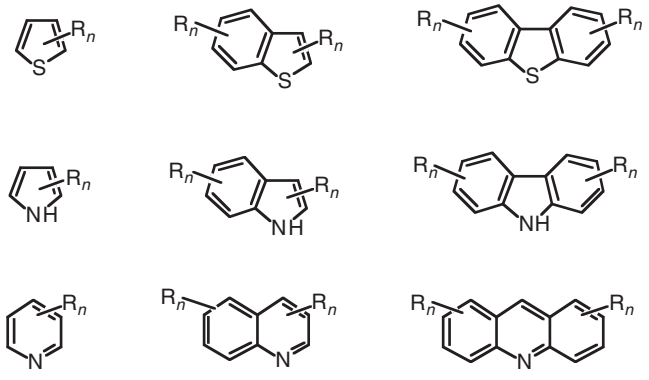

Figure 1 Important components of petroleum fractions.

A complicated set of reactions takes place during HDS and HDN, and large amount of work has been devoted to the study of their kinetics and mechanisms. The best-understood reaction within hydrotreating is no doubt HDS, particularly of thiophene (T), the most extensively used model compound. Mechanistic knowledge for benzothiophene (BT) and dibenzothiophene (DBT) has also advanced considerably, as have the mechanisms of HDN. Even for the simplest substrates HDS and HDN networks are complex, involving a number of elementary steps. An extensive literature on heterogeneous reaction mechanisms is available,[1–3] and there is a general agreement on some key fundamental steps that need to be taken into account in any mechanistic proposal, namely:

- the generation and the nature of the active sites,
- the dissociative adsorption of hydrogen on the surface of the catalyst,
- the chemisorption of the organosulfur or organonitrogen compound on the catalytic sites, and
- the reactions of the adsorbates: hydrogenation of unsaturated bonds and hydrogenolysis of C–S or C–N bonds.

Some examples of the most widely accepted reaction networks for important HDS and HDN model compounds are presented in Schemes 1 and 2, respectively.

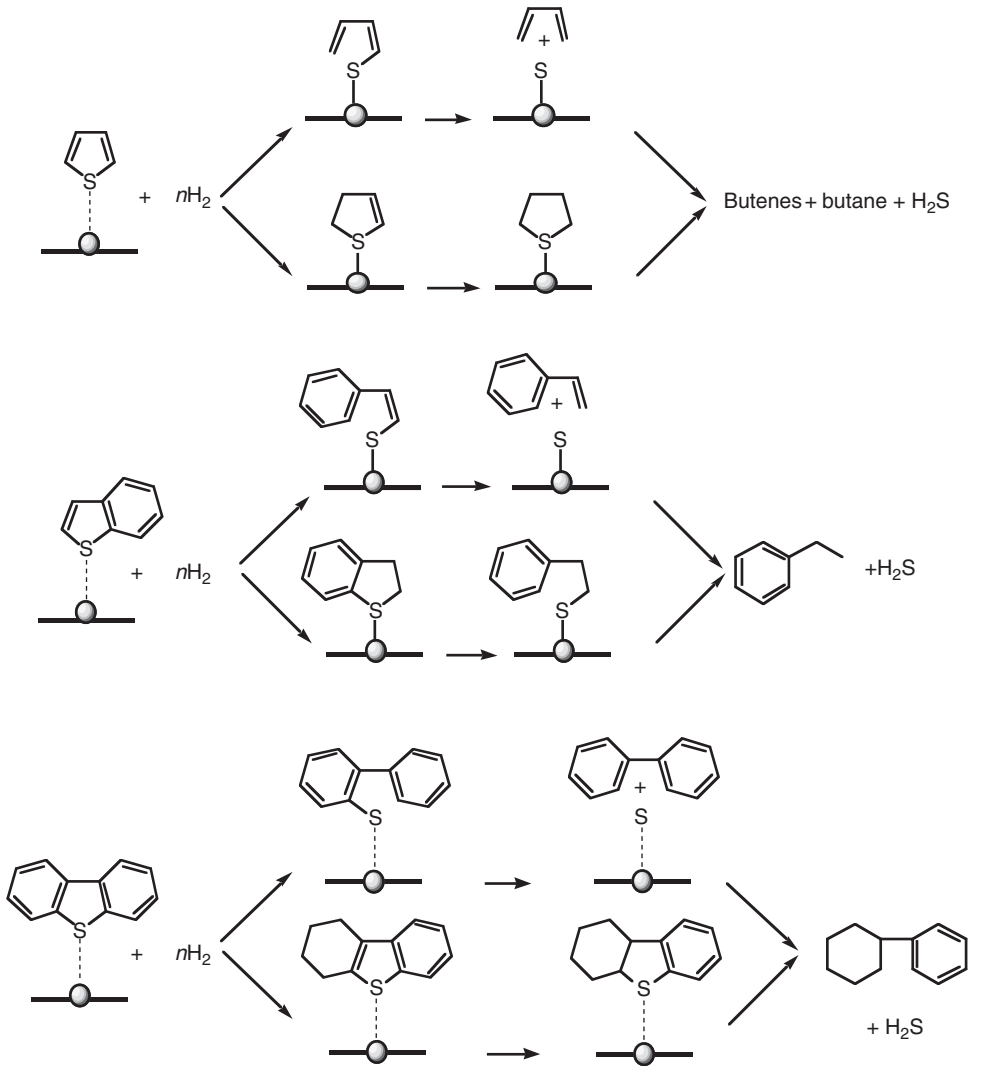

Scheme 1 General mechanisms of HDS of thiophene, benzothiophene, and dibenzothiophene on solid catalysts.

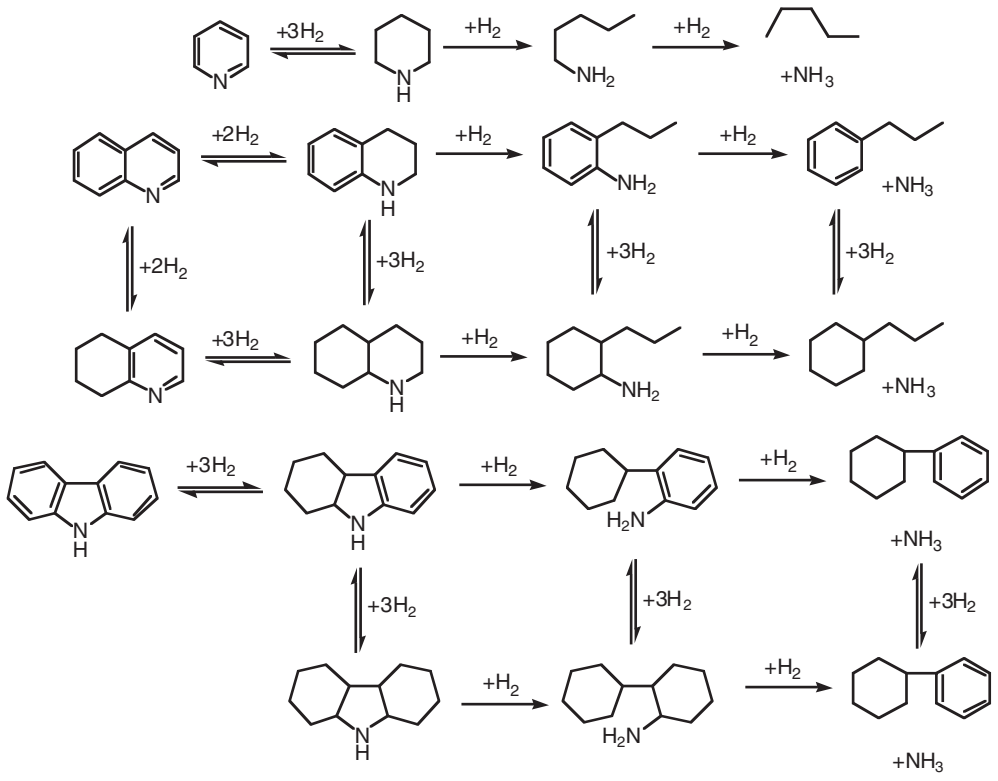

Scheme 2 General mechanisms of HDN of pyridine, quinoline, and carbazole on solid catalysts.

1.27.1.1 The Organometallic Modeling Approach

Even though the chemistry and engineering of HDS and HDN have been in continuous development and industrial application for decades, new environmental constraints have produced a resurgence of the field, particularly an intensified search for novel catalysts capable of meeting present and future standards for cleaner fuels. Despite impressive practical achievements over the last 40–50 years, new discoveries have been delayed by the lack of a better understanding of some key issues, notably the nature of HDS–HDN active sites on metal sulfide catalysts and the details of the elementary reactions implicated in the catalytic schemes. Within this context, organometallic chemistry has become an additional powerful tool for understanding the HDS[4–6,6a,6b] and HDN[4,4a,4b,7,7a] reactions. The possibility of preparing metal complexes of model substrates such as the thiophenes or the pyridines, stable enough to be characterized by NMR spectroscopy and X-ray diffraction, but at the same time sufficiently reactive to allow the detailed study of their reaction mechanisms, has provided an interesting possibility for connecting organometallic and surface chemistry in relation to a problem of fundamental interest and environmental and industrial importance. Prior to 1985, very few metal complexes of the thiophenes were known and virtually no mention of them could be found in the HDS literature. Today, a large number and variety of such compounds are known[4–6,6a,6b] and they have become of obliged reference in the heterogeneous HDS field. On the other hand, metal derivatives of N-donor ligands such as pyridines or amines have been extensively studied over the years but their relevance to HDN has only recently been recognized and reviewed.[4,4a,4b,7,7a] Some early proposals for the modes of adsorption of thiophenes, pyridines, and pyrroles on metal sulfides have now been probed by comparison with the structures of well-characterized metal complexes; this has allowed the identification of the most reasonable alternatives for reactive surface intermediates and of new possibilities not previously considered. Theoretical studies on well-defined complexes have also contributed to a clear and consistent picture of the bonding modes of organosulfur and organonitrogen compounds to catalytic metal centers. Thus, when results from molecular chemistry are combined with the information available from surface techniques and heterogeneous catalysis, the chemisorption of these compounds appears as a

well-understood phenomenon. This is no doubt one of the most important achievements of the organometallic modeling approach, as described in detail below.

A number of possible reaction schemes have been derived for heterogeneous HDS and HDN catalysis, based on sound experimental evidence and/or extensive calculations.[1–3] Because of the intrinsic complexity of the problem, some of key mechanistic points have remained speculative. By studying analogous reactions on discrete well-characterized transition metal complexes in solution, a better distinction of the most sensible reaction pathways from the less likely ones has become possible, especially in the case of HDS modeling. The new knowledge thus obtained can be extrapolated – no doubt with caution – to surface reactions. Perhaps more importantly, some patterns have emerged connecting some characteristics of the metal centers with the available or preferred modes of bonding of thiophenes, as well as with the specific reactions that such activated substrates may reasonably follow in each of these bonding situations. Similar considerations apply in the case of HDN-related substrates, but the advances in this direction are more modest. This chapter describes the major achievements of the organometallic modeling approach and attempts to build some conceptual bridges between molecular and surface chemistry in relation to HDS and HDN catalysis, following the outline of a previous monograph.[4] It is intended here to summarize the most important aspects of this chemistry published up to mid-2005.

1.27.2 Organometallic Models of the Hydrodesulfurization Reaction

1.27.2.1 Coordination and Activation of Thiophenes in Metal Complexes

In order to understand HDS reactions, it is important to define the ways in which thiophenes are bonded to metal centers on catalytic surfaces. A number of modes in which T interacts with surfaces have been proposed, the most important ones being the "one-point adsorption", that is, a strong interaction between the S atom and a "vacancy" on the surface, and the "multi-point adsorption" involving the S atom plus one or both of the C═C bonds in a delocalized π-bonding.[1–3] While it is difficult to experimentally obtain detailed information on the bonding of thiophenes to surface sites, several coordination modes of thiophenes have been authenticated in metal complexes (Figure 2).

Metal–T complexes have been widely studied by NMR spectroscopy, and a good number of X-ray structures are available, providing a sound basis for understanding the chemisorption of such entities by analogies between the bonding modes in complexes and the proposed chemisorption modes on solid catalysts; extensive calculations have also contributed to a better understanding of the electronic structures of metal thiophene complexes. Perhaps more importantly, some patterns have emerged concerning the reactivity associated with thiophenes in each particular bonding mode; this allows some interesting parallels to be drawn with the ways in which thiophenes are thought to be degraded on the active sites of heterogeneous HDS catalysts. In this section, the syntheses and structures of the most important types of metal complexes of the thiophenes will be described. Table 1 provides a fairly comprehensive list of known complexes of the thiophenes.

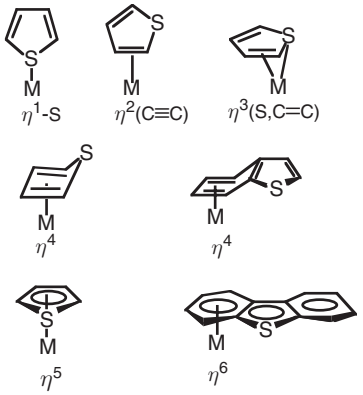

Figure 2 Bonding modes of thiophenes in metal complexes.

Table 1 Metal complexes of thiophenes

Complex	*Characterized by*	*References*
η^1S-bonded complexes		
$Cr(CO)_5$(Th) (Th = 2,5-Me_2T, BT, 3-MeBT)	NMR	8
$Cr(CO)_5$(DBT)	NMR + X-rays	8
$Mo(CO)_3$[2,5($Ph_2PCH_2CH_2)_2$T]	NMR + X-rays	9
$Mo(CO)_5$(DBT)	NMR	8
[$Me_2Si(C_5Me_4)$Mo(DBT)]	NMR + X-rays	10
$W(CO)_5$(Th) (Th = 2,5-Me_2T, BT)	NMR	8
$W(CO)_5$(DBT)	NMR + X-rays	8
$CpMn(CO)_2$(Th) (Th = 2,5-Me_2T, BT)	NMR	8
$CpMn(CO)_2$(DBT)	NMR + X-rays	8
$Cp^*Re(CO)_2$(T)	NMR + X-rays	11
$Cp'Re(CO)_2$(BTh) (BTh = BT, 2-MeBT, 3-MeBT)	NMR + X-rays	12
[$CpRe(NO)(PPh_3)$(Th)]BF_4 (Th = T, 2-MeT, 2,5-Me_2T, BT, 2-MeBT, 3-MeBT)	NMR	13
$Re_2(CO)_9$(BTh) (BTh = BT, 2-MeBT, 3-MeBT, 3,5-Me_2BT)		14
$CpFe(CO)_2$(T)]BF_4	NMR	15
[$CpFe(CO)_2$(2,5Me_2T)]PF_6	NMR	16
[$CpFe(CO)_2$(BT)]BF_4	NMR	15
[$CpFe(CO)_2$(DBT)]BF_4	NMR + X-rays	15
[$C_5H_4CH_2$–2-C_4H_3S)$Ru(PPh_3)_2$]BF_4	NMR + X-rays	17
$RuCl_2(Ph_2P$–DBT$)_2$	NMR + X-rays	18
$RuCl_2(Ph_2P$–DBT$)_2$(CO)	NMR + X-rays	18
$Ru(H)_2(H_2)(PCy_3)_2$(DBT)	NMR	19
[Cp′$Ru(CO)_n(PPh_3)_m$(Th)]BF_4 (Cp′ = Cp, Cp^*; n = 1,2; m = 1,0; Th = T, 2,5-Me_2T, 3-MeT, BT, Me_4T, DBT, 4-MeDBT, 4,6-Me_2DBT, 2,8-Me_2DBT)	NMR + X-rays	20
{$Co(CO)_2$[2,5($Ph_2PCH_2CH_2)_2$T]}BPh_4	NMR	9
{Rh(CO)[2,5($Ph_2PCH_2CH_2)_2$T]}BPh_4	NMR + X-rays	9
[$Ir(H)_2(PPh_3)_2$(Th)$_2$]PF_6 (Th = T, THT, BT, DHBT, DBT)	NMR + X-rays	21
Cp^*IrCl_2(DBT)	NMR + X-rays	22
η^2(C═C)-bonded complexes		
TpW(NO)(PMe3)(Th) (Th = T, 2-MeT, 2,5-Me_2T)	NMR + X-rays	23
$[Os(NH_3)_5(Th)]^{2+}$ (Th = 2-MeT, 3-MeT, 2,5Me_2T, 2-MeOT, BT)	NMR	24
$Cp^*Re(CO)_2$(BT)	NMR	12
η^3(S,C═C)-bonded complexes		
{(triphos)Ir[η^3(S,C═C)–BT]}$^+$ (triphos = $MeC(CH_2PPh_2)_3$)	NMR	25
η^4-Bonded complexes		
Cp^*Ir(Th) (Th = T, 2-MeT, 3-MeT, BT, DBT)	NMR	26
Cp^*Ir(2,5-Me_2T)	NMR + X-rays	27
Cp^*Ir(2,5-Me_2T·A) (A = BH_3, CH_3^+, CS_2, Ru(η^6-C_6H_6)Cl_2, $Fe(CO)_4$, $Co_4(CO)_{11}$, $Ru_3(CO)_{11}$, $Re_2(CO)_9$)	NMR + /or X-rays	28
$Cp^*Rh(Me_4T)$	NMR + X-rays	29
$Cp^*Rh[Me_4T·Fe(CO)_4]$	NMR + X-rays	29
$Cp^*Rh(Me_4T·O)$	NMR + X-rays	30
(η^6-C_6Me_6)Ru(Th) (Th = T, 2-MeT, 2,5-Me_2T, Me_4T)	NMR	31
(η^6-C_6Me_6)Ru[η^4-T·$Mo(CO)_5$]	NMR + X-rays	31, 32
(η^5-Me_4T)Ru(η^4-Me_4T)	NMR	31, 32
(η^5-Me_4T)Ru(η^4-$Me_4T·Fe(CO)_4$)	NMR + X-rays	31, 32
η^5-Bonded complexes		
$Cr(CO)_3$(T)	NMR + X-rays	33, 34
$Cr(CO)_3$(Th) (Th = T, 2-MeT, 3-MeT, 2,5-Me_2T, Me_4T, ...)	NMR	35–37
$Mo(PMe_3)_3$(T)	NMR	38
[$Mn(CO)_3$(Th)](OTf) (Th = T, 2-MeT, 2,5-Me_2T, Me_4T)	NMR	39, 40
Cp′Fe(Th) (Cp′ = Cp; Th = T, 2-MeT, 3-MeT, 2,5-Me_2T, Me_4T; Cp′ = Et-Cp; Th = 2,5-Me_2T, Me_4T)	NMR	41–43
[$Fe(Me_4T)_2$]$(PF_6)_2$	NMR	44
[Cp′Ru(Th)]X (Cp′ = Cp; X = BF_4; Th = T, 2-MeT, 3-MeT, 2,5-Me_2T, 2,3,5-Me_3T, Me_4T; Cp′ = Cp^*; X = PF_6; Th = T, 3-MeT, 2,5-Me_2T)	NMR	45–48

(*Continued*)

Table 1 (Continued)

Complex	*Characterized by*	*References*
$[Ru(Th)_2](X)_2$ ($(Th)_2 = (Me_4T)_2$, X = BF_4; Th_2 = T, 2-MeT, Me_4T, X = OTf	NMR	49
$[Ru(Th)_2](BF_4)_2$	NMR + X-rays	50
$[Ru(Me_4T)(p\text{-cymene})](BF_4)_2$	NMR	51
$[Ru(Me_4T)Cl_2]_2$	NMR + X-rays	49, 50
$Ru(Me_4T)Cl_2(PR_3)$	NMR	49
$Ru(Me_4T)Cl_2(H_2NTol)$	NMR	49
$[(Me_4T)Ru(Cl)]_3S(BF_4)$	NMR + X-rays	49
$[(Me_4T)Ru(L)_3](OTf)_2$ (L = H_2O, NH_3)	NMR + X-rays	50
$[Rh(T)(PPh_3)_2]PF_6$	NMR + X-rays	52
$[Rh(Th)(diene)]PF_6$ (Th = 2,5-Me_2T Me_4T; diene = COD, NBD)	NMR	51
$[Cp^*Rh(Th)][PF_6]_2$ (Th = T, Me_4T)	NMR	52, 53
$[Cp^*Ir(Th)][X]_2$ (Th = T, 2-MeT, 2,5-Me_2T, Me_4T; X = PF_6, BF_4)	NMR	49, 51, 53
η^6-Arene-bonded complexes		
$Cr(CO)_3(Th)$ (Th = BT, DBT, BNT)	NMR	54
$[Mn(CO)_3(Th)]BF_4$ (Th = 7-MeBT, 7-EtBT)	NMR	54
$[CpFe(Th)]PF_6$ (Th = BT, DBT)	NMR	54, 55
trans-$[(CpFe)_2(DBT)_2](PF_6)_2$	NMR	55
$[CpRu(Th)]PF_6$ (Th = BT, DBT)	NMR	54, 56
trans-$[(CpRu)_2(DBT)_2](PF_6)_2$	NMR + X-rays	57
$[(C_6Me_6)Ru(BT)_2](BF_4)_2$	NMR	54
$Co_4(CO)_9(DBT)$	NMR	58
$Cp^*M(Th)$ (M = Rh, Ir; Th = BT, 2-MeBT, 3-MeBT, 2,3-Me_2BT)	NMR	53

1.27.2.1.1 η^1-S-bonded metal thiophene complexes

η^1-S-bonded thiophenes are neutral 2e ligands. Some of the earliest proposals for the adsorption of T involved vertical bonding to the surface through the S atom only, and thus the characterization of η^1-S complexes has shed light on the "one-point adsorption" on solid catalysts. In all the X-ray structures available, the S atom is pyramidal, corresponding to approximate sp^3-hybridization, but the ring itself is planar and perturbed only by a slight lengthening of the C–S bonds. The T ring is invariably tilted away from a perpendicular arrangement at angles ranging from 16° in $[Me_2Si(C_5Me_4)Mo(DBT)]$[10] to 61° in $[CpRu(CO)(PPh_3)(2\text{-MeT})]BF_4$,[20,20a,20b] in agreement with spectroscopic studies of the adsorption of T on clean surfaces, which also concluded that it is tilted away from perpendicularity.[4,4a,4b] This is now accepted as a general phenomenon both in metal complexes and on surfaces, and it represents an important advance in connection with the early view of the vertical adsorption. Detailed calculations on the bonding in η^1-S complexes of thiophenes show that the interaction is predominantly a ligand-to-metal donation of electron density from orbitals concentrated on the sulfur lone pairs, in agreement with a small effect of coordination on the C–S bonds or on the ligand as a whole.[61,61a] The "π-acceptor" ability of T becomes important as the electron density on the metal increases, and this results in the weakening of the C–S bonds through backdonation into an antibonding π^*-orbital; this provides a reasonable pathway for the activation of T. Indeed, electron-rich metal fragments promote C–S bond scission of thiophenes. Tilting of the ring away from perpendicular binding avoids a repulsive interaction between filled ligand π-orbitals and an occupied d_π-metal orbital. The IR spectral features of η^1-S-bonded thiophene in complexes are very similar to those of thiophene adsorbed on sulfided Mo/Al_2O_3, and a detailed analysis of such spectra concludes that the S-only bonding causes C–S bond weakening, and therefore the most reasonable pathway for thiophene activation in HDS is η^1-S-bonding followed by C–S bond scission.[60]

Examples of S-bonded T complexes are available for Mn, Re, Cr, Mo, W, Fe, Ru, Co, Rh, and Ir; their syntheses are usually straightforward, involving addition of the thiophene to an unsaturated metal precursor or displacement of a labile ligand. The M–S bond is generally weak, the stability increasing along the trend thiophenes < benzothiophenes < dibenzothiophenes. This has limited the study of the transformations of η^1-bonded thiophenes, since ligand-exchange processes dominate the behavior of such compounds in solution. Some exceptions to this behavior are worth noting: $Cp^*(CO)_2Re(\eta^1S\text{–}T)$ reacts with $Fe_2(CO)_9$ to yield the thiophene-bridged bimetallic derivative $Cp^*(CO)_2Re(\mu\text{-}T)Fe(CO)_3$ **1** in which the T ligand remains η^1-S-bonded to Re but also binds in an η^4-fashion to the $Fe(CO)_3$ fragment.[62] Bases such as OH^- or Et_3N induce the activation of the C–H bond α to S in $[Cp^*(NO)(PPh_3)Re(\eta^1\text{-S–T})]^+$ to yield the corresponding 2-thienyl derivative.[13,13a] The equilibrium constants for

thiophene exchange in a series of Ru complexes $[Cp(CO)(L)Ru(\eta^1S\text{–}Th)]^+$ (L = CO, PPh_3; Th = T, 2-MeT, 3-MeT, 2,5-Me_2T, Me_4–T, BT, DBT), measured by NMR, show that increased methylation on the thiophene results in stronger binding to the metal and that steric effects are important for the stability of the complexes. η^1-S–BT and η^1-S–DBT complexes are also more stable than their T analogs, and tetrahydrothiophene (THT) binds 10^6 times more strongly than T. This is in parallel with trends reported for the adsorption and desulfurization of thiophenes on Co–Mo/Al_2O_3 catalysts.[5–5d] Also important in connection with HDS mechanisms, the S-bonded complex $Cp^*(\eta^1$-S–T)$Rh(PMe_3)$ is considered the key precursor toward insertion of the metal into the C–S bond from experimental and theoretical arguments.[63,63a]

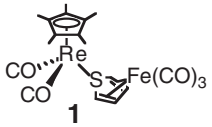

1

Complex $[Ir(H)_2(PPh_3)_2(T)_2]PF_6$ **2** and the analogs containing BT, DBT, THT, DHBT were obtained through the mild hydrogenation of $[Ir(COD)(PPh_3)_2]PF_6$ in the presence of the appropriate organosulfur ligand and characterized by X-ray diffraction for T, THT, DHBT.[21] In addition, $RuH_2(\eta^2\text{-}H_2)_2(PCy_3)_2$ reacts with DBT to yield $RuH_2(\eta^2\text{-}H_2)(\eta^1\text{-S–DBT})(PCy_3)_2$ **3**.[19] These complexes demonstrate that a single metal center can activate a hydrogen molecule and two thiophenes.

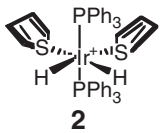

2

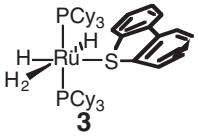

3

T complexes of Mo or W, the metals commonly used in heterogeneous catalysts, are scarce. Theoretical studies predict that $M(CO)_5(\eta^1$-S–T) (Mo[64], W[65]) should be stable, and the W derivative has been studied spectroscopically by following the kinetics of substitution of cyclohexane by T in $W(CO)_5$(cyclohexane).[65] Extremely labile $Mo(CO)_5(\eta^1$-S–DBT) and its 2,5-Me_2T **4** and BT analogs were obtained by photolysis of $Mo(CO)_6$ in the presence of the appropriate thiophene and characterized by NMR.[8] More stable Cr and W analogs $M(CO)_5(\eta^1$-S–Th) (M = Cr, Mo; Th = 2,5-Me_2T, BT and DBT) were obtained in a similar manner and characterized spectroscopically and crystallographically. The only crystal structure available of an Mo complex containing an η^1-S-bonded thiophenic ligand is that of *ansa*-$Cp_2''Mo(\eta^1$-S–DBT) **5**, prepared by photolysis of $Cp_2''Mo(H)_2$ in the presence of DBT.[10] This structure displays the usual features of η^1-S-bonded derivatives but with the smallest tilt angle θ observed so far (16°); this is most likely due to steric interactions between DBT and the methyl substituents on the Cp rings. The reaction can be reversed by the treatment of the DBT adduct with H_2 at 80 °C and 1 atm. No examples of η^1-S-bonded T complexes of Co or Ni, the other important metals in industrial HDS catalysts, have been reported.

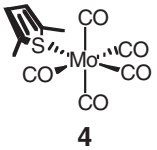

4

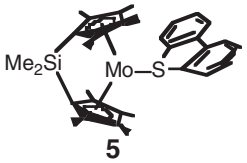

5

1.27.2.1.2 η^2-(C═C)-bonded metal thiophene complexes

Stable η^2-(C═C) complexes with thiophenes acting as olefin-like 2e ligands are very scarce. A series of complexes $TpW(NO)(PMe_3)(\eta^2$-(C═C)–Th) (Th = T, 2-MeT, 2,5-Me_2T) was obtained by reduction of $TpW(NO)(PMe_3)Br$ in the presence of the S-donor ligands; these compounds are particularly interesting in that they are rare examples of thiophene complexes of the HDS-useful metal W. The X-ray structure of the 2,5-Me_2T derivative is the only example for an η^2(C═C)-bonded T complex. These compounds also displayed a rich reactivity, mainly deriving from the enhanced basicity of the coordinated thiophenes, which promoted, for instance, the facile protonation at C2 and the mild hydrogenation of the uncoordinated C═C bond by Pd/C.[23]

Reduction of $[Os(NH_3)_5(OTf)]^{2+}$ in the presence of Th yields $\{Os(NH_3)_5[\eta^2(C{=}C)\text{–Th}]\}^{2+}$ (Th = 2-MeT, 3-MeT, 2,5-Me_2T, 2-MeOT, and BT), characterized spectroscopically.[24,24a] These complexes readily add

electrophiles to the S atom, and the resulting adducts react with nucleophiles (H^-, CN^-, OAc^-, py, $PrNH_2$, N_3^-, PPh_3, PhO^-, PhS^-) to yield the corresponding ring-opened η^2-4-(alkylthio)-1,3-butadiene complexes. In contrast, protonation of $\{Os(NH_3)_5[\eta^2(C{=}C)\text{–}Th]\}^{2+}$ with triflic acid proceeds via addition to the *exo*-side of the ring to give an η^2-2H–thiophenium product $\{Os(NH_3)_5[\eta^2(C{=}C)\text{–}Th{\cdot}H]\}^{2+}$.[66]

The complexes $Cp'Re(CO)_2[\eta^2(C{=}C)\text{–}BT]$ ($Cp' = Cp, Cp^*$) slowly interconvert with their η^1-S isomers in solution; the $\eta^2(C{=}C)$ form is favored by the presence of the more electron-donating Cp^* ligand. Introducing steric congestion and a stronger donor ability of the sulfur atom, as in 2-Me– and 3-MeBT, leads to the formation of the S-bonded isomers only. If the BT ligand is previously η^6-coordinated to $Cr(CO)_3$, reaction with $Cp(CO)_2Re(THF)$ leads exclusively to the $\eta^2(C{=}C)$ isomer of the Re moiety in the bimetallic product **6**, as a result of the greater π-acceptor ability of the C=C bond in the Cr complex. On the other hand, when the η^1–η^2 mixtures of $Cp'Re(CO)_2[\eta^2(C{=}C)\text{–}BT]$ are allowed to react with electrophiles, only the S atom coordinates to the incoming group, for example, Me_3O^+ produces $Cp'Re(CO)_2[\eta^2(C{=}C)\text{–}BT{\cdot}Me]$ while $W(CO)_5$ yields the *S*-adduct **7** exclusively.[12] Similarly, reaction of $Cp'Re(CO)_2(BT)$ with $Cp'Re(CO)_2(THF)$ gives a product containing the BT ligand-bound η^1-S to one $Cp'Re(CO)_2$ group and $\eta^2(C{=}C)$ to the other. In the reaction between $Cp^*Re(CO)_2(BT)$ and $CpRe(CO)_2(THF)$, the only product isolated contains the BT ligand-bound η^1-S to the $CpRe(CO)_2$ group and $\eta^2(C{=}C)$ to $Cp^*Re(CO)_2$, consistent with the more electron-rich metal fragment binding to the π-accepting olefin, while the less electron-rich one accepts electron density from the sulfur donor.

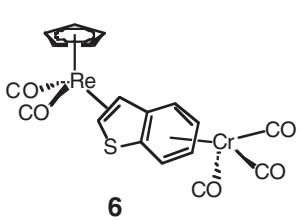

6

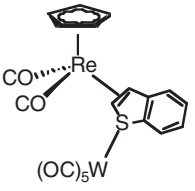

7

1.27.2.1.3 η^3(S,C=C)-bonded metal thiophene complexes

Only one example is available of a complex containing the 4e combination of η^1-S + $\eta^2(C{=}C)$ bonding at a single metal center, viz, $\{(triphos)Ir[\eta^3(S,C{=}C)\text{–}BT]\}^+$ **8** ($triphos = MeC(CH_2PPh_2)_3$).[25] This bonding mode coincides with the structure suggested in early "multi-point adsorption" proposals in heterogeneous catalysis. On refluxing in THF, further reaction takes place to break one C–S bond, which demonstrates that this type of coordination can be important for activating thiophenes toward ring opening. Density functional theory (DFT) calculations indicate that this η^3(S,C=C) bonding is more stable than the η^1-S or η^4-coordination modes of thiophene in $[(T)Ir(PH_3)_3]^+$ model complexes, and it is also more adequate for promoting C–S bond scission by d^8-ML_3 14e fragments.[67]

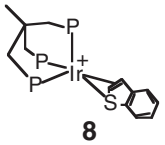

8

1.27.2.1.4 η^4-Bonded metal thiophene complexes

The diene-type η^4-bonding of Th ligands to transition metals (Th = T and its methylated derivatives) is infrequent. Ru, Rh, and Ir complexes containing η^4-bonded thiophenes with Cp or arene co-ligands have been synthesized by chemical or electrochemical reduction of the corresponding 18e η^5-Ru, -Rh, and -Ir precursors;[26–32] upon addition of two extra electrons to, for example, $Cp^*Ir(\eta^5\text{-Th})$, the π-thiophene ligand transforms into a 4e donor to avoid oversaturation at the metal. For instance, reduction of $Cp^*Rh(\eta^5\text{-}Me_4T)$ with Cp_2Co leads to $Cp^*Rh(\eta^4\text{-}Me_4T)$; one ring of $[Ru(\eta^5\text{-}Me_4T)_2]^{2+}$ is reduced in an analogous manner to yield a mixed η^5–η^4 species $[(\eta^5\text{-}Me_4T)Rh(\eta^4\text{-}Me_4T)]^{2+}$. Complexes of the higher homologs are exemplified by $Cp^*Ir(\eta^4\text{-BT})$ and $Cp^*Ir(\eta^4\text{-DBT})$, characterized by *in situ* NMR spectroscopy. The crystal structures of η^4-Th metal complexes invariably show the T ring highly distorted with the four carbon atoms coordinated to the metal, and the sulfur bending out of the plane. The C–S distances in η^4-Th derivatives are significantly longer than those measured in free thiophenes, indicating a significant perturbation of the ligand. The η^4-Th bonding is imposed by the electron count at the metal center, even if there are

no important spatial restrictions to accommodate the ligand in a flat η^5-bonding fashion. This type of bonding has been discussed at length;[61,61a] it resembles that of simple dienes but additionally it incorporates a substantial antibonding metal–sulfur interaction; thus, breaking one C–S bond may be viewed as a way of relieving the repulsive M–S interaction. Ring opening of thiophenes in $Cp^*Ir(\eta^4\text{-Th})$ is catalyzed by basic alumina or by triethylamine, or promoted by UV light.[26] Reaction of $Cp^*Ir(\eta^4\text{-Th})$ with H_2 also promotes ring opening.

η^4-Coordination renders the organosulfur molecules highly reactive; a common reaction of η^4-T metal complexes is the formation of adducts with Lewis acids binding to the S atom. For instance, $Cp^*Ir(\eta^4\text{-Me}_2\text{T})$ reacts with $M(CO)_nL_{6-n}$ (M = Cr, Mo, W) complexes to yield a series of derivatives $Cp^*Ir(\eta^4\text{-Me}_2\text{T})\cdot M(CO)_5$, where the thiophene is η^1-S-bonded to M. The η^4-complex also isomerizes in solution to the ring-opened form, which can also bind to $M(CO)_n$ fragments in a variety of ways.[68] Protonation of $(\eta^6\text{-}C_6Me_6)Ru(\eta^4\text{-T})$ gives a transient cationic thioallylic intermediate **9**, which evolves by C–S bond scission into a butadienethiolate ligand in **10** (Equation (3)).[69]

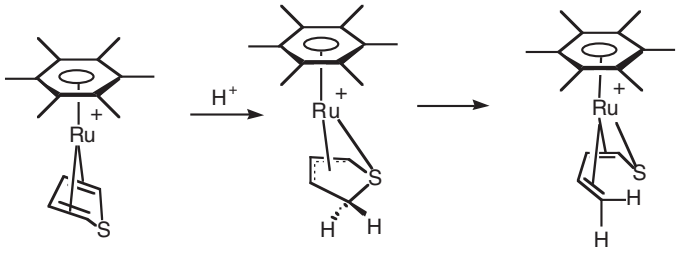

9 **10** (3)

1.27.2.1.5 η^5-Bonded metal thiophene complexes

Complexes containing η^5-bonded thiophenes, where the ring formally donates six electrons, are the most numerous and stable of the transition metal–thiophene derivatives (see Table 1). Examples are available for Cr, Mn, Re, Fe, Ru, Rh, and Ir. Curiously, $Cr(CO)_3(\eta^5\text{-T})$, the first π-thiophene metal complex reported in 1958,[33] is still the only case of a group 6 metal π-bonded to T; its X-ray structure was solved in 1965 albeit with a strong rotational disorder for the T ligand.[34] Early CNDO calculations predicted the stability of $Mo(CO)_3(\eta^5\text{-T})$, but attempts to synthesize it have failed, most likely due to its extreme lability in solution.[64] The first example of an Mo complex containing an η^5-bonded thiophene ligand, $Mo(PMe_3)_3(\eta^5\text{-T})$, has only recently become available from the reaction of $Mo(PMe_3)_6$ with T at room temperature.[38] No examples of η^5-T derivatives of W or of the promoter metals Co or Ni have been reported to date, and therefore many important synthetic challenges remain in this area.

The bonding in η^5-thiophene metal complexes resembles that of the Cp analogs, except that T is a poorer electron donor but a better acceptor than Cp; in addition, the presence of the larger S atom in T causes a slight tilting of the ring relative to a perfectly horizontal disposition (and in some cases a ring slip); consequently, thiophenes are less strongly bound to metals than Cp ligands.[61,61a] An interesting exception to the common case of d^6-complexes is $[(\eta^5\text{-T})Rh(PPh_3)_2]PF_6$ **11**, a rare example of a five-coordinated d^8-η^5-T complex prepared by hydrogenation of $[(COD)Rh(PPh_3)_2]PF_6$ in the presence of excess T. This compound provided the first non-disordered X-ray structure of a π-bonded metal–T complex.[52] The ring in this case is not only tilted as usual, but also slightly bent in what may be viewed as a unique case of an intermediate structure between a "normal" η^5- and an η^4-mode, in which the sulfur tends to be located away from the metal, but nevertheless remains coordinated to Rh in order to attain an 18e configuration. The energy level diagram of the PH_3 analog[61,61a] nicely accounts for these interesting features.

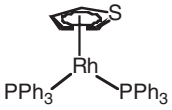

11

Methyl-substituted thiophenes bind more strongly to transition metals than the unsubstituted ligand, as illustrated by ligand-exchange reactions of $CpRu(\eta^5\text{-Th})$ complexes. The equilibrium constant measured by NMR increases by a factor of about 6 for each methyl group added on the thiophene;[47] benzene, BT, and DBT also displace T. These observations can be related to the inhibition effect of benzene and other aromatic hydrocarbons on HDS of BT over solid catalysts, ascribed to a stronger binding of arenes on metal sulfide surfaces as compared to common sulfur

heterocycles. The π-bonded T ring, particularly in cationic complexes, is activated as expected from electron donation to the metal center. For instance, H–D exchange is observed at the H(2,5) positions of T in CpRu(η^5-Th) complexes in CD_3OD in the presence of OD^-, while H(3,4) exchange takes place much more slowly, in agreement with an increased acidity of coordinated T; this is an interesting parallel to the trends observed for H–D exchange in T when D_2 is passed over conventional HDS catalysts.[46] Another appealing feature in relation to HDS mechanisms is the activation of π-bonded thiophenes in cationic complexes toward nucleophilic attack by hydrides to yield reactive intermediates such as **12** and **13**, which ultimately lead to hydrogenation of the C═C bonds[39] or to C–S bond breaking.[70] Neutral η^5-thiophene complexes do not suffer attack by nucleophiles but can be deprotonated with strong bases to yield 2-thienyl products.

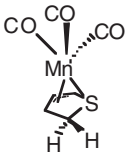

12

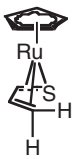

13

In summary, η^5-coordination does not produce a great alteration in the charge distribution on the T ring, and nucleophilic attack is observed only in positively charged complexes. It thus seems that it is the overall charge on the metal derivative rather than changes in the electronic structure of the bound thiophenes that leads to activation toward nucleophiles. It is clear from organometallic HDS models that most of the reactions of metal–T complexes with hydrogen leading to ring saturation or C–S bond breaking are associated with other types of thiophene bonding, especially η^1-S and η^2-(C═C). Thus, η^5-adsorption on surface sites, frequently invoked in the heterogeneous literature, is probably a peripheral situation, rather than a crucial phenomenon directly related to the actual HDS reactions.

1.27.2.1.6 η^6-Bonded metal benzothiophene and dibenzothiophene complexes

η^6-Coordination of arenes to 12e metal centers is well documented, as is the consequent activation of such aromatic fragments for further reactions.[71,71a] A number of complexes containing BT and DBT π-coordinated through the benzene ring are known, indicating a strong preference of these two ligands for this type of arene bonding. Examples are available for Cr, Mn, Fe, Ru, Co, Rh, and Ir, as shown in Table 1. Such structures are not of general relevance as HDS models, since they produce activation predominantly of the coordinated benzene ring toward nucleophilic attack.[72,72a] However, other aspects of the chemistry of η^6-bonded metal BT and DBT complexes are important in connection with HDS. In particular, 4-Me– and 4,6-Me_2DBT are desulfurized through prior hydrogenation of one or both of the arene rings,[1–3] and therefore the study of η^6-DBT complexes could be of use in developing new catalysts for reducing the arene moieties in this type of molecule. In addition, η^6-BT or DBT complexes such as $[Mn(CO)_3(\eta^6\text{-BT})]^+$ are activated toward C–S bond scission by a second metal center,[54,54a,54b] as discussed in Section 1.27.2.3.1.(iii). A related interesting class of η^6-bonded complexes involves thiametallacycles derived from ring opening of thiophenes acting as 6e donors.[68]

1.27.2.1.7 Metal η^1-S-bonded thiophene complexes as adsorbents for the removal of dibenzothiophenes

η^1-S-coordinated thiophenes are usually labile ligands in metal complexes, and this has been applied to model an extraction process of dibenzothiophenes, in which a mixture is desulfurized by removal of the intact sulfur compound and regeneration of the adsorbing complex. $[Ru(NH_3)_5(H_2O)]^+$ reacts with DBT or 4,6-Me_2DBT in DMF/H_2O solution to yield the corresponding $[Ru(NH_3)_5(\eta^1\text{-S-DBT})]^+$ derivatives. By increasing the water concentration, the reverse reaction can be induced to liberate the DBT and regenerate the aqua complex (Equation (4)). This has been used to desulfurize a model mixture containing toluene, hexanes, and 500 ppm of DBT. One extraction cycle removes 50% of DBT and five cycles bring the content down to 25 ppm; 4,6-Me_2DBT could also be removed but with lower efficiency. The complexes $[CpRu(CO)_2]BF_4$ and $[CpFe(CO)_2(\eta^2\text{-2-methylpropene})]BF_4$ perform similarly in solution or when supported on mesoporous silica, achieving 99% removal of DBT and 72% of 4,6-Me2DBT.[73,73a]

$$[Ru(NH_3)_5(H_2O)]^+ + DBT \rightleftharpoons [Ru(NH_3)_5(\eta^1\text{-S-DBT})]^+ + H_2O \quad (4)$$

1.27.2.1.8 Conclusion

The organometallic chemistry of thiophenes is now well developed; synthetic methods are available for a variety of metals and thiophenes, and the general structural trends are well established. The various bonding modes of thiophene ligands in metal complexes have been studied in detail, and a deep understanding of the interactions involved and the factors affecting them have been reached. Mo and W thiophene complexes have been reported but remain scarce and examples of Co and Ni derivatives are still lacking, so this remains as an important synthetic challenge. It is possible to draw some parallels between the coordination modes of thiophenes in complexes and the ways in which such molecules are adsorbed on surfaces. Each type of binding seems to be associated with a particular kind of reaction of the activated substrate in connection with HDS schemes.

1.27.2.2 Metal Complex–catalyzed Homogeneous Hydrogenation of HDS-relevant Aromatic Compounds

Hydrogenation reactions play a major role in hydrotreating. The general, HDS mechanisms shown in Scheme 1 include the partial or complete saturation of a thiophene ring and/or a benzene ring. Hydrogenation may precede C–S bond scission, but ring opening of the heterocycle may also take place prior to hydrogenation.[1–3]

Despite the impressive advances of homogeneous hydrogenation over recent decades, hydrogenation of simple arenes remains rather undeveloped in contrast with heterogeneous systems widely employed in industry and in research laboratories. Few organometallic complexes have been reported to catalyze the reduction of benzene and related molecules, and recent reviews indicate that most of them are not truly homogeneous but instead the hydrogenation ability is due to decomposition of the complexes into active metal nanoparticles or colloids, with the exception of d^0-Nb and -Ta hydride catalysts that appear to be truly homogeneous but are not related to HDS chemistry.[74,75] On the other hand, the homogeneous hydrogenation of polynuclear aromatic hydrocarbons may be achieved with a number of complexes such as $RuCl_2(PPh_3)_3$,[76] $Ru(H)_2(H_2)(PPh_3)_3$,[77,77a] $(\eta^6\text{-}C_6Me_6)_2Ru_2(\mu\text{-}H)_2(\mu\text{-}Cl)]Cl_2$,[78] and $[Rh(MeOH)_2(diphos)]^+$.[79] Here we will concentrate on the metal complex-catalyzed hydrogenation of HDS-related substrates, particularly of *S*-aromatic hydrocarbons, for which the number of catalysts and the level of understanding is growing; mechanistic details are related whenever possible to hydrogenation within HDS mechanistic networks. Other reviews are available on this subject.[4,4a,4b,80,80a,80b]

1.27.2.2.1 Thiophene hydrogenation

Examples of homogeneous hydrogenation of T or substituted analogs are very scarce. $Co_2(CO)_8$ slowly reduces T under forcing conditions,[81] but no mechanistic details are available, and the formation of active metal particles cannot be ruled out in this case. The first example of a well-defined system for the reduction of T to THT was $[Ir(H)_2(\eta^1\text{S-T})_2(PPh_3)_2]PF_6$ **3**,[82] which operates at atmospheric pressure and 80 °C, according to the mechanism depicted in Scheme 3. Some salient features of this cycle are as follows. (i) Activation of T and of H_2 on a single metal site, which has been considered in mechanistic models for heterogeneous reactions on Co–Mo–S sites. (ii) The regio- and stereospecific intramolecular transfer of hydrides to the η^1-S/η^2-bound T leading to an η^3-(S,C=C) thioallyl intermediate **14**, similar to one proposed in heterogeneous catalysis. (iii) 2,3-Dihydrothiophene (2,3-DHT) is the actual

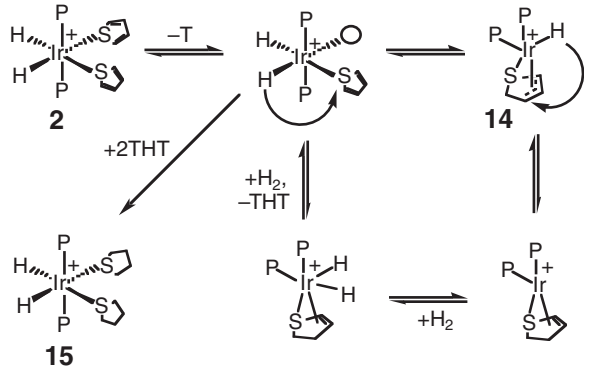

Scheme 3 The mechanism of homogeneous hydrogenation of thiophene by $[IrH_2(PPh_3)_2(\eta^1\text{S-T})_2]^+$.

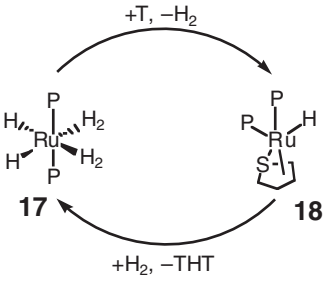

Scheme 4 Catalytic hydrogenation of thiophene by $RuH_2(H_2)_2(PCy_3)_2$.

intermediate toward ring saturation, in agreement with some proposals for heterogeneous T hydrogenation. (iv) Although the reaction is formally catalytic, turnover numbers are very low due to catalyst poisoning by strong binding of the product to the metal in $[Ir(H)_2(\eta^1\text{-S–THT})_2(PPh_3)_2]PF_6$ **15**. Methyl-substituted thiophenes react in an analogous manner as long as there is at least one unsubstituted carbon atom next to sulfur, but 2,5-Me_2T was unreactive.[4,4a,4b]

In a related set of stoichiometric reactions, T in $(\eta^5\text{-S–T})Mn(CO)_3^+$ was partially reduced by external hydride attack to yield $(\eta^3,\eta^1\text{-S–thioallyl})Mn(CO)_3$ **12**, followed by protonation to produce **16** with 2,3-DHT bonded to Mn through the sulfur atom and the remaining C═C bond (Equation (5)).[12]

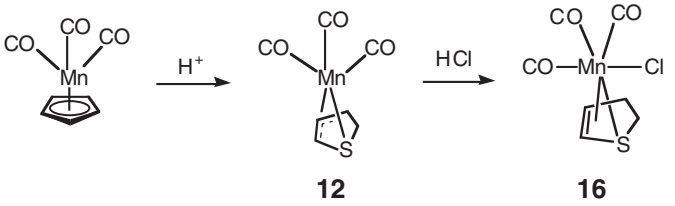

(5)

$RuH_2(\eta^2\text{-}H_2)_2(PCy_3)_2$ **17** reacts with T to yield the thioallyl derivative $[RuH(\eta^4\text{-(S,C)T–H})(PCy_3)_2]$ **18**, which upon further reaction with H_2 liberates THT and regenerates **17**. This forms the basis of the catalytic cycle shown in Scheme 4, and complex **17** is indeed the only efficient catalyst known for the mild homogeneous hydrogenation of T to THT (up to 50 turnovers in 17 h at 80 °C, 3 atm). 2-MeT is also catalytically converted into 2-MeTHT by **17** at rates about one order of magnitude slower than for T, while BT is hydrogenated to DHB at rates comparable to those observed for T.[19]

1.27.2.2.2 Benzothiophene hydrogenation

Hydrogenation of BT to DHBT takes place much more readily than reduction of T, since the C(2)═C(3) bond in this molecule behaves essentially as an olefin. Ru, Os, Rh, and Ir complexes efficiently catalyze the reduction of BT to DHBT under moderate reaction conditions. Examples of catalyst precursors include $RuCl_2(PPh_3)_3$,[76,83] $RuHCl(CO)(PPh_3)_3$,[83] $RuCl_3\cdot 3H_2O + TPPTMS$,[84,84a,84b] $[Ru(triphos)(MeCN)_3][BF_4]_2$,[85] $RuH_2(\eta^2\text{-}H_2)(PCy_3)_2$,[19] $OsHCl(CO)(PPh_3)_3$,[83] $RhCl(PPh_3)_3$,[75,83] $[Cp^*Rh(NCMe)_3][BF_4]_2$,[86] $[M(COD)(PPh_3)_2]PF_6$ (M = Rh, Ir),[83,87,88] Rh(COD)(sulphos),[89,89a] and $[Ru(sulphos)(MeCN)_3]SO_3CF_3$.[80,89,89a] The BT hydrogenation cycle for $[Cp^*Rh(NCMe)_3]^{2+}$,[90] as well as the kinetics and mechanisms for $[M(COD)(PPh_3)_2]PF_6$ (M = Rh, Ir),[87,88] and for $[(triphos)Ru(NCMe)_3][BF_4]_2$ [(triphos = $MeC(CH_2PPh_2)_3$] (the fastest homogeneous BT hydrogenation catalyst known)[85] have been elucidated in detail and previously reviewed.[4,4a,4b,80,80a,80b] The elementary steps involved are in clear parallel with olefin hydrogenation mechanisms, and the $\eta^1\text{-S} \Leftrightarrow \eta^2\text{-S}$ interconversion is generally accepted as the step leading to activation of the C═C bond of BT, required to enter the catalytic cycle. Scheme 5 depicts the generally accepted mechanisms for this reaction involving metal monohydride and dihydride complexes.

Some interesting key points common to the well-understood catalysts are as follows. (i) All effective BT hydrogenation catalysts are based on "HDS promoter metals" (Ru, Os, Rh, Ir), and they are specific for the hydrogenation of the S-containing ring, while saturation of the benzene ring has never been detected. (ii) In all the mechanisms elucidated in solution, coordination of BT occurs in an η^1-S or an η^2(C═C) fashion prior to hydrogen transfer. Although the olefin-type coordination has not been directly observed under catalytic conditions, the occurrence of the $\eta^1\text{-S} \leftrightarrow \eta^2$(C═C) equilibrium in metal BT complexes has been well established,[11] and this is now generally accepted

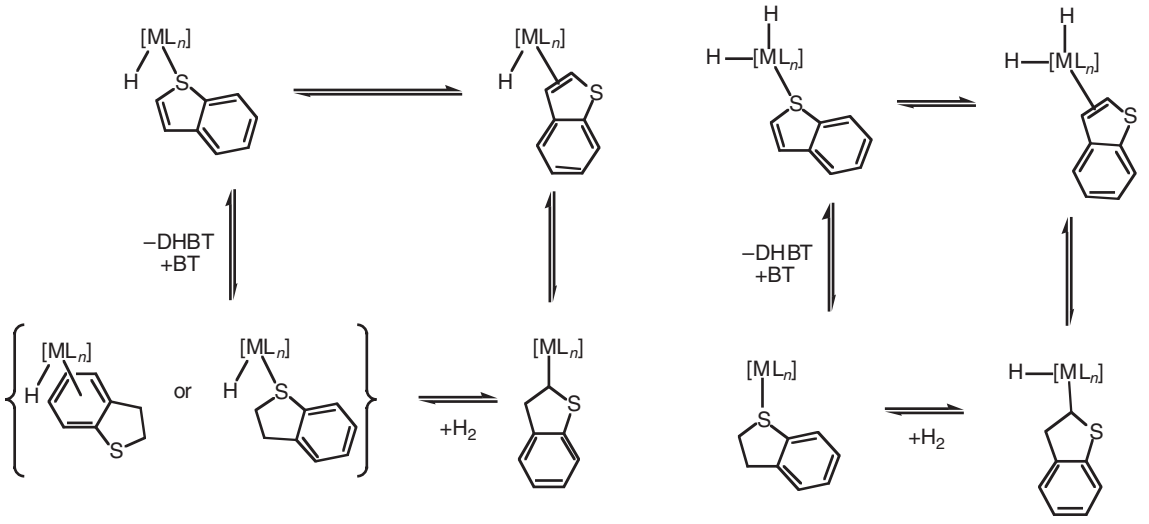

Scheme 5 General mechanisms of the homogeneous hydrogenation of benzothiophene.

in BT hydrogenation cycles. (iii) Calculations[87,91] indicate that the C(2) atom of BT is more negatively charged than C(3), and thus it should be more susceptible to electrophilic attack by the metal; therefore, a 2-benzothienyl intermediate is more likely to be involved in the catalytic cycle upon hydride migration from the metal to BT.

1.27.2.2.3 Aqueous-biphasic and solid-supported catalysts for benzothiophene hydrogenation as a pretreatment for HDS

Apart from the mechanistic considerations discussed above, metal complex-catalyzed hydrogenation of organosulfur compounds has potential for practical applications in connection with HDS of refined fuels or refinery cuts. A series of patents by INTEVEP, the Venezuelan petroleum research company,[84,84a,84b] describes the use of water-soluble catalysts for the biphasic reduction of benzothiophenes. The catalysts are generated *in situ* by reaction of $RuCl_3{\cdot}3H_2O$ with *m*-monosulfonated or trisulfonated triphenylphosphine (TPPMS, TPPTS) in the presence of a basic co-catalyst such as aniline or quinoline; the resulting mixtures hydrogenate BT at reasonably fast rates under 30 atm H_2 at 120 °C. This partial reduction of BT has been used for several consecutive cycles as a pretreatment for naphtha, which was subsequently subjected to mild HDS over conventional catalysts, thereby improving sulfur removal without compromising the benzene rings, which contribute to a high octane number. These systems operate through mechanisms involving similar features to those described in the preceding section, with, for example, $RuHCl(PPh_3)_2(aniline)_2$ as the active species entering the catalytic cycle. Other water-soluble catalysts have been developed[80,80a,80b] by using polydentate ligands such as $NaO_3S(C_6H_4)CH_2C(CH_2PPh_2)_3$ (Na sulphos, the sulfonated analog of triphos) and $NaO_3S(C_6H_4)CH_2)_2C(CH_2PPh_2)_2$ (Na_2DPPDS). The complexes [(sulphos)Rh(COD)], [(sulphos)Ru(NCMe)$_3$]-SO_3CF_3, and Na[{Ru(sulphos)}$_2$(μ-Cl)$_3$] catalyze BT hydrogenation under mild reaction conditions in aqueous biphasic media or when supported on silica. The solid-supported catalyst [(sulphos)Ru(NCMe)$_3$]SO_3CF_3/SiO_2 (Ru(II)/SiO_2) reduces BT at rates superior to those observed for homogeneous or liquid-biphasic systems, with excellent recyclability even when used in a BT-doped naphtha. Other heterocycles are also reduced. Similar materials containing Ru(0)/SiO_2 derived from $Ru_3(CO)_{12}$ did not hydrogenate BT.[80,80a,80b]

Further research into easily recoverable hydrogenation catalysts would be welcome, as a pretreatment for HDS of difficult thiophenic substrates. A particularly appealing possibility for practical applications in deep desulfurization would be the development of a two-stage process incorporating a highly active catalyst (liquid-biphasic or supported metal complex) for the hydrogenation of one or both of the benzene rings in, for example, 4,6-Me_2DBT, followed by mild HDS of the saturated product on conventional Co–Mo–S or similar catalysts, as shown in Scheme 6. Arene hydrogenation has been achieved with bimetallic materials combining molecular and nanostructured catalysts derived from Rh complexes on Pd/SiO_2[92,92a–92c] or [(sulphos)Rh(COD)]/Pd/SiO_2,[80,80a,80b] but no attempts have been disclosed of applications of this chemistry to deep HDS.

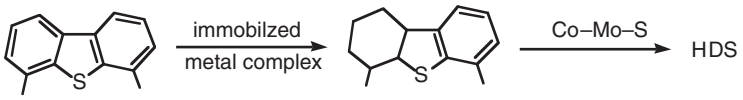

Scheme 6 A possible two-stage process for deep HDS.

1.27.2.3 C–S Bond Activation, Hydrogenolysis, and Desulfurization of Thiophenes by Metal Complexes

C–S bond breaking is the reaction responsible for desulfurization. Thus, understanding of the pathways through which such reactions take place is a key element in HDS modeling. A great proportion of the work has dealt with C–S bond rupture under mild conditions, which is induced by complexes of different metals and varied structures. The mechanisms of C–S activation are understood, and some homogeneous and supported catalysts for the hydrogenolysis and hydrodesulfurization of thiophenes have become available. The extensive mechanistic knowledge gained from organometallic models[4–6,6a,6b] represents a significant contribution to the understanding of the reaction networks in heterogeneous catalysts.

1.27.2.3.1 Stoichiometric ring opening, hydrogenolysis, and desulfurization of thiophenes

C–S bond energies of thiophenes are comparable to C–H bond energies. C–H bond activation is established for a variety of metal complexes through well-documented mechanisms; although less extensively developed, activation of C–S bonds by metal complexes has experienced an impressive growth in the last few years. Ring opening of thiophenes through oxidative addition of the C–S bond has been achieved via a concerted process or through reactions involving intermediates containing the thiophene molecule coordinated to the metal. The ring-opened η^2-(C,S) products have been characterized by use of NMR spectroscopy and X-ray crystallography, and theoretical studies have complemented the experimental data. The thiametallacycles may be described as containing a thiabutadiene fragment with localized C═C bonds as in structure **19** or as a delocalized thiametallabenzene ring as in **20**.

19 **20**

1.27.2.3.1.(i) C–S bond activation by complexes of cyclopentadienyl and related ligands

Pioneering mechanistic studies on C–S bond activation were performed with [$Cp^*Rh(PMe_3)$], generated by thermolysis of [$Cp^*Rh(PMe_3)(H)(Ph)$] or by photolysis of [$Cp^*Rh(PMe_3)(H)_2$].[63,63a] Upon thermal reaction with T, BT, or DBT, the unsaturated Rh fragment yielded the corresponding thiametallacycles $Cp^*Rh(PMe_3)[\eta^2$-(S,C)–Th] (Th = T, BT, DBT) (Equation (6)). The low-temperature photochemical experiment yielded the same thiametallacycles mixed with the corresponding 2-thienyl hydride complexes $Cp^*Rh(PMe_3)(H)(\eta^1$-C–Th) resulting from C–H activation; the latter slowly converted into the thermodynamically stable ring-opened product, demonstrating that C–S and C–H bond activation pose similar energy requirements; ring opening is preceded by η^1-S-coordination of T to Rh. Similar reactions with Me_xT, BT, and DBT invariably lead to activation of the unsubstituted C–S bond.[93]

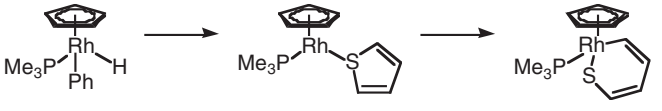

(6)

In a similar set of reactions, η^1-S-coordination of thiophene and benzothiophene followed by ring opening has been observed for $(PMe_3)_3Ir(Th)Cl$,[94] while the thermal and photochemical reactions of T with $Tp^*Rh(PMe_3)(C_2H_4)$ afford mixtures of the corresponding C–H and C–S activation products, with the former being the predominant species.[95] In a rare example of Co chemistry, $Cp^*Co(C_2H_4)_2$ activates the C–S bond of T, BT, and DBT, presumably through undetected η^1-S-bonded intermediates, to produce **21**.[96] The fragment [*ansa*-Cp_2''Mo] [$Cp_2'' = Me_2Si(C_5Me_4)_2$] generated by photolysis of [*ansa*-$Cp_2''Mo(H)_2$] readily inserts into the C–S bond of T and

BT to produce the corresponding ring-opened products, as exemplified for T in **22**.[10] No intermediates containing intact T or BT could be observed, although they are probably involved in this reaction, as suggested by the formation of the stable η^1-S-adduct $Cp_2''Mo(\eta^1$-S–DBT) **5**. The S-bonded derivative does not open the DBT ring but its reaction (80 °C) with T leads to the ring-opened T-derived product. These C–S bond-breaking reactions induced by Mo complexes are very important in connection with modeling MoS_2-based catalysts. Other interesting Cp systems used in HDS-related chemistry include $Cp^*Ir(\eta^4$-T), which isomerizes to the ring-opened isomer upon contact with basic alumina or triethylamine, or by UV irradiation.[26] $[Cp^*M(\eta^5$-$Me_2T)]^+$ (M = Rh, Ir) undergo a complex series of reactions with aqueous base leading to a variety of mononuclear and polynuclear products containing ring-opened ligands resulting from nucleophilic attack on the T ring and related reactions.[97] $[CpRu(\eta^5$-T)$]^+$ is attacked by H^- or other nucleophiles promoting C–S activation.[5–5d] $[W(NPh)\{o$-$(Me_3SiN)_2C_6H_4\}(C_5H_5N)_2]$ opens the rings of T, 2-MeT, and BT at 65 °C in toluene;[98] this represents a rare example of C–S activation induced by W, one of the most frequently used metals in heterogeneous HDS.

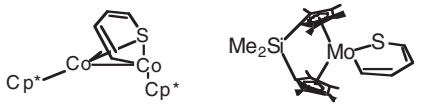

21 **22**

1.27.2.3.1.(ii) C–S bond activation by complexes with phosphine ligands

The fragments $[(triphos)Ir]^+$ or [(triphos)MH] (M = Rh, Ir), thermally generated from $[(triphos)Ir(\eta^4$-$C_6H_6)]^+$, $[(triphos)Ir(H)_2(C_2H_5)]$, or $[(triphos)Rh(H)_3]$ (triphos = $MeC(CH_2PPh_2)_3$) display a very rich HDS-related chemistry.[4–6,6a,6b] The unsaturated Rh and Ir triphos fragments readily add the C–S bonds of T,[99] BT,[25] DBT,[100] and some of their methylated derivatives,[101] leading to the corresponding thiametallacycles. The propensity of these Rh(I) and Ir(I) species to activate the C–S bond is related to the rigidity of the tripodal ligand. In particular, $[(triphos)Ir(\eta^4$-benzene)$]BF_4$ reacts with thiophene to give the ring-opened product $[(triphos)Ir(\eta^2$C,S-T$)]^+$, which has provided a complete stepwise HDS model reaction by sequential addition of thiophene, H^-, and H^+, as shown in Scheme 7.[99]

This illustrates the fact that electron-rich systems promote ring opening of thiophene and that addition of hydrogen can take place heterolytically via addition of hydride followed by protonation to produce 1,3-butadiene + H_2S, the primary products of thiophene HDS, as invoked in some heterogeneous mechanisms. This is not catalytic but it is an excellent model in which various elementary steps involved in the degradation of thiophene could be authenticated, in clear parallel with surface chemistry. An analogous set of reactions has been described for BT with the important difference that a stable intermediate **8** containing a unique η^3(S,C=C)-bonded BT was isolated. Above 40 °C, this intermediate converts into the ring-opened isomer $[(triphos)Ir(\eta^2$C,S-BT$)]^+$, characterized by X-ray diffraction.[25] The main reactions of the BT-derived metallacycle with H_2 or with H^-/H^+ couples, summarized in Scheme 8, lead to the formation of ethylbenzenethiolate, thereby modeling the hydrogenolysis of BT but not its complete HDS.[25] The extensive [(triphos)Ir] model chemistry shows that all the necessary steps for HDS of T or for hydrogenolysis of BT can be achieved without previously saturating the heterocyclic ring, in agreement with one of the commonly invoked

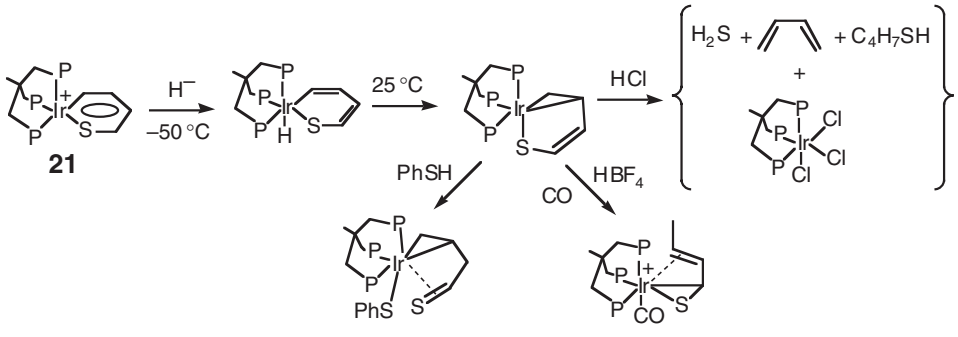

Scheme 7 Stepwise HDS of thiophene on Ir-triphos complexes.

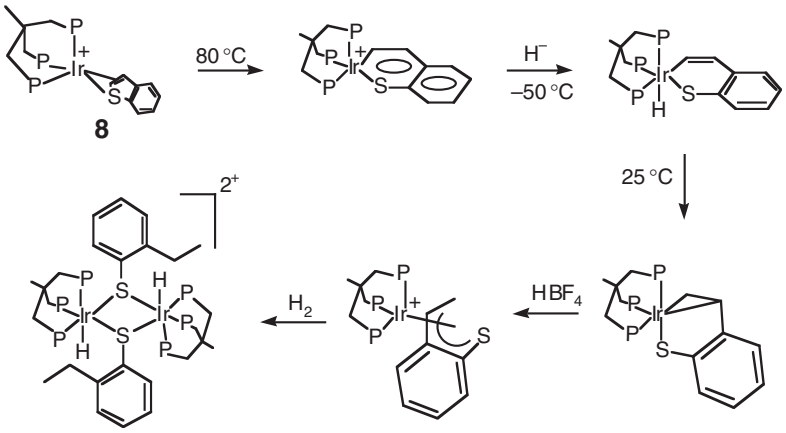

8

Scheme 8 Stepwise hydrogenolysis of benzothiophene on Ir-triphos complexes.

"desulfurization route" in HDS catalysis. Nevertheless, hydrogenolysis of the saturated cyclic thioether 2,3-DHBT also proceeds by use of $[(triphos)Ir(H)_2]^+$, in the presence of a strong base, to produce ethylbenzenethiol plus $[(triphos)Ir(H)_3]$. This demonstrates that even though presaturation of the thiophenic rings is not required for desulfurization, the C–S bonds of saturated cyclic thioethers can be broken by (triphos)Ir(III), geometrically very similar to but less electron rich than, the Ir(I) fragments that promote ring opening of thiophenes.

$ReH_7(PPh_3)_2$, in conjunction with 3,3-dimethyl-1-butene as a hydrogen acceptor, promotes hydrogenolysis of T through a stable thioallyl intermediate **23**, which upon photolysis affords the corresponding thiol. In contrast, if **23** is treated thermally, hydrogenation to THT is observed.[102]

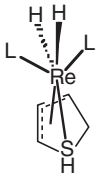

23

A set of reactions, which provides a nice model for heterogeneous Mo catalysts, involves C–S bond activation of T by $Mo(PMe_3)_6$ under very mild conditions to yield the butadienethiolate complex **24**. The formation of this species involves C–S bond activation and attack by a hydrogen atom from one PMe_3 ligand. Protonation of **24** regenerates PMe_3 and causes a change in conformation of the butadienethiolate ligand in **25** (see Equation (7)). The X-ray structures of these two derivatives are the only ones available of butadienethiolate–metal complexes, a class of compounds often alluded to in organometallic HDS modeling. Interestingly, $Mo(PMe_3)_3(\eta^5\text{-T})$ is formed as a minor product of this reaction but it does not interconvert with **24**.[38]

24 **25** (7)

The HDS-related chemistry of Pt phosphine complexes has been extensively developed.[103,103a–103f] $[PtL_n]$ ($L = PEt_3$, PMe_3; $L_2 = Ph_2PCH_2CH_2PPh_2$, dppe) reversibly insert into the C–S bond of T, BT, and DBT and their methylated derivatives to yield ring-opened products $[PtL_2(\eta^2\text{-C,S–Th})]$. The thiaplatinacycle derived from BT is about 10 times more stable than those derived from T or DBT, which are, in turn, similar to each other. Reaction of the PEt_3 thiametallacycle derived from DBT with Et_3SiH results in complete HDS to yield biphenyl plus $[Pt(PEt_3)_2(H)(SH)]$ (Scheme 9); upon exposure to HCl(g) the latter generates H_2S plus $Pt(PEt_3)_2Cl_2$ to complete the HDS scheme. Similar reactions were observed for the ring-opened products of T and BT, with relative rates BT > DBT >> T; this shows again that electron-rich metal centers are prone to oxidatively add C–S bonds.

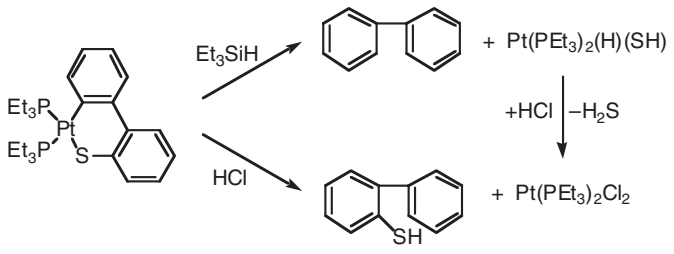

Scheme 9 Desulfurization and hydrogenolysis of dibenzothiophene on Pt-PEt_3 complexes.

In contrast to the reactions with hydrides, the interaction of the DBT and BT metallacycles with HCl produces the corresponding free thiols plus $PtCl_2(PEt_3)_2$, (Scheme 9). Thus, the hydridic or protonic character of the hydrogen atoms transferred to the ring-opened intermediates directs the reaction toward the Pt–C bond-breaking process followed by a second C–S bond rupture, or by a Pt–S bond scission, respectively. Methylated T, BT, and DBT also provide the corresponding thiaplatinacycles. Reaction of $Pt(PEt_3)_4$ with 4,6-Me_2DBT led to C–H activation only; nevertheless, the ring-opened product of 4,6-Me_2DBT (DMDBT) was obtained indirectly by reaction of $[PtCl_2(PEt_3)_2]$ with the substrate and Na metal under hydrogen at low pressure. If the PMe_3 and dppe PtL_2 analogs are used, complete HDS of DBT and 4-MeDBT to biphenyl and 3-Me–biphenyl, respectively, takes place under 20 atm H_2 at 100 °C.

Replacement of one PEt_3 ligand by a phosphite leads to new series of phosphine/phosphite or bis(phosphite) complexes; the differences in ability to promote HDS were accounted for in terms of donor–acceptor properties of the ligands involved in each case.[104] Thiophene substituted with groups other than alkyls (e.g., –Cl, –NO_2, –OMe, –OAc) also form thiaplatinacycles, which are notable in that they promote catalytic desulfurization. These substituted thiophenes also produced the first thiapalladacycles by reaction with the corresponding Pd–phosphine complexes, as well as Ni analogs.[105] 3,6-Dimethylthieno[3,2-*b*]thiophene also forms a thiaplatinacycle by activation of a C(vinyl)–S bond upon reaction with $[Pt(PEt_3)_4]$; 2,2′-bithiophene and 1-methyl-2-(2-thienyl)pyrrole react similarly but also promote C–H activation.[106]

The mild HDS of DBT by complexes of Ni, a widely used promoter metal in industrial catalysts, has also been reported.[107,107a–107c] As shown in Scheme 10, $[(dippe)NiH]_2$ [dippe = $(i\text{-}Pr_2PCH_2)_2$] readily reacts with DBT to release H_2 and insert into the C–S bond, yielding the thiametallacycle [(dippe)Ni(η^2-C,S–DBT)] **26**, which evolves

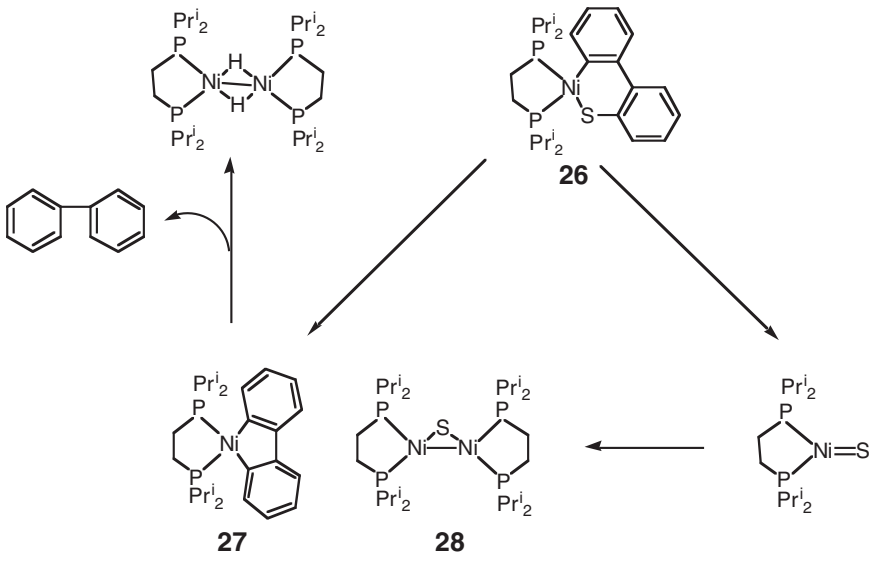

Scheme 10 Stepwise HDS of thiophene on Ir-triphos complexes.

into [(dippe)Ni(2,2′-biphenyl)] **27** and a transient mononuclear intermediate (dippe)$_2$Ni═S, which spontaneously dimerizes to [(dippe)$_2$Ni$_2$(μ-S)] **28**. The chemistry of **28** has been further explored as a model of reactions of NiS_2, widely used as a promoter in HDS.[108] Complex **12** reacts with H_2 at atmospheric pressure and room temperature to liberate biphenyl and regenerate the dimeric hydride, demonstrating that desulfurization can take place without participation of H_2 or H^+/H^- couples. Hydrogen seems to be required for this system only in the subsequent release of the desulfurized product, biphenyl, from **26**.

Analogous reactions of T and BT with [(dippe)NiH]$_2$ also allowed the isolation of C–S insertion products. On the other hand, 4-MeDBT produces a metallacycle from insertion into the C–S bond distal to the methyl group, which upon interaction with an excess of the Ni hydride under H_2 at 1 atm and 90 °C yields the HDS product 3-methylbiphenyl. No nickel insertion products could be identified in similar reactions with 4,6-Me$_2$DBT, but the reaction of the dimeric hydride with an excess of Me$_2$DBT under 1 atm H_2 at 90 °C did lead to the formation of the hydrodesulfurized product 3,3′-dimethylbiphenyl plus monomeric Ni(dippe)$_2$ as the only identifiable metal-containing species. In contrast, the reaction of the Pt analog [(dippe)PtH]$_2$ with 4,6-Me$_2$DBT afforded [(dippe)Pt(η^2-C,S–DMDBT)] **29**. This compound reacted further with an excess of the Pt hydride at 160 °C to yield the HDS product 3,3′-dimethylbiphenyl (Equation (8)) and presumably a sulfido-bridged dimer [(dippe)$_2$Pt$_2$(μ-S)], which decomposed under the reaction conditions. Analogous complexes originating from insertion of DBT and 4-MeDBT were also characterized for the Pt system, thus providing a nice family of complexes resulting from C–S activation of the dibenzothiophenes with varying degrees of methylation.[106]

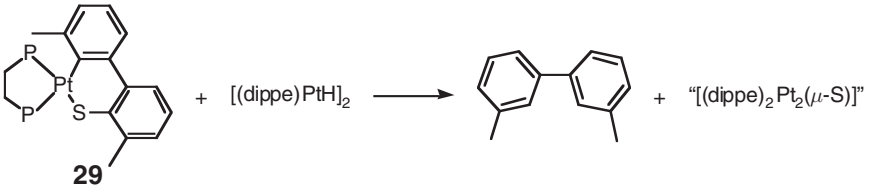

(8)

1.27.2.3.1.(iii) Reactions of thiophenes on polynuclear complexes

Multi-site reactions are important in heterogeneous catalysis, and it is likely that more than one metal center is needed to effect sulfur removal from organic molecules. Therefore, binuclear or polynuclear metal complexes are of interest in modeling HDS reactions in solution.[4–6,6a,6b,109] Thiophenes interact with $Fe_3(CO)_{12}$ in refluxing benzene to produce thiaferroles **30** through metal insertion into the less hindered C–S bond of the thiophene.[110,110a,110b] The thiaferroles are subsequently desulfurized to the corresponding ferroles **31** in refluxing benzene. Interaction of **30** with H_2 yields ethylbenzene and related thiols; the fate of the extracted sulfur is not clear. Dibenzothiophenes failed to undergo C–S bond activation under similar conditions. $Ru_3(CO)_{12}$ reacts with thiophenes and BT to give products analogous to **30**, together with some C–H activation products. In the case of 2-MeT, complex **32** was isolated. The X-ray structure displays the separated S atom capping an Ru triangle and the butadiene linked through two M–C σ-bonds to one Ru atom in the triangle and η^4 to a fourth "spiked" Ru center, in a remarkable "snapshot" of the desulfurization process as it takes place.[111,111a] Substituted BTs as well as DBT react with $Ru_3(CO)_{12}$ to yield related products, the most remarkable one being **33**, which upon reaction with H_2 releases biphenyl.[112]

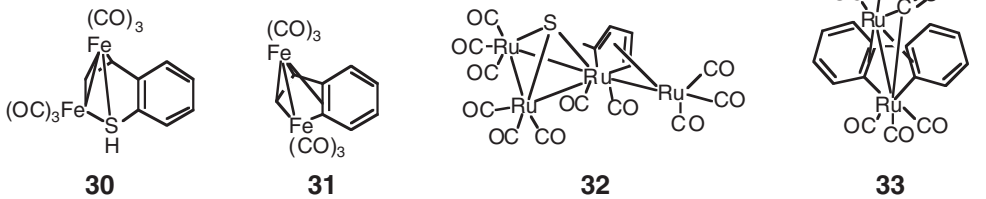

$(CpRu)_3(\mu\text{-H})_3(\mu_3\text{-H})_2$ breaks both C–S bonds of BT and DBT to yield ethylbenzene and biphenyl, respectively. In the case of BT, the reaction proceeds through an intermediate thiaruthenacyclohexadiene complex **34** formed through insertion of one Ru atom across the vinylic C–S bond. This intermediate evolves into a μ^3-alkylidene-μ^3-sulfido-bis(μ^2-hydrido) cluster **35**, which was further hydrogenated in THF at 80 °C and 7.2 atm H_2 for 1 week to produce ethylbenzene and $(Cp^*Ru)_3(\mu\text{-H})_3(\mu_3\text{-S})$. DBT is also cleaved by $(Cp^*Ru)_3(\mu\text{-H})_3(\mu_3\text{-H})_2$ in toluene at

110 °C over 8 days to yield biphenyl, plus the same μ^3-sulfido complex.[113] C–S bond-breaking reactions of saturated cyclic thioethers are favored when the sulfur atom bridges two metal centers [54].[114] For instance, thermolysis of $Os_3(CO)_{10}(THT)_2$ yields an intermediate **36** containing a butenethiolate ligand formed by ring opening of THT via an $Os_3(CO)_{10}(\mu^2$-THT).

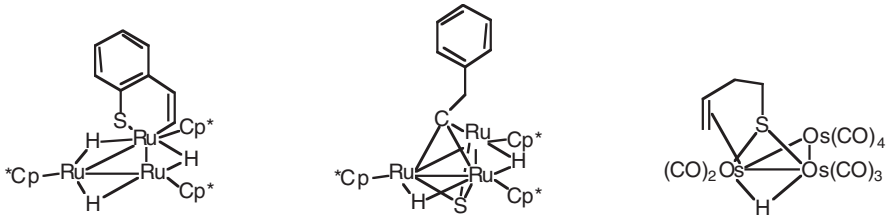

$Re_2(CO)_{10}$ reacts photochemically with T to yield complex **37** and with BT to yield **38**; several methyl-substituted BT analogs react in a similar way, via η^1-S-bonded intermediates. Under H_2, photolysis of $Re_2(CO)_{10}$ in the presence of 3,5-Me_2BT leads to a ring-opened partially hydrogenated ligand in **39**. Reaction of **38** with PMe_3 affords further ring-opened products **40**. Also, the non-photochemical reaction of $Re_2(CO)_{10}$ with BT, under a hydrogen atmosphere, produces an interesting cluster **41** containing BT molecules that have undergone hydrogenation and hydrogenolysis; the reaction mechanism involves prior formation of $H_4Re_3(CO)_{12}$, which is the species actually interacting with BT.[115,115a,115b]

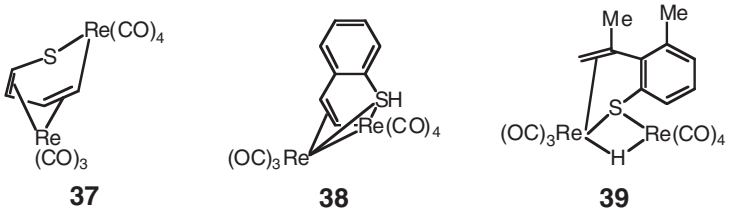

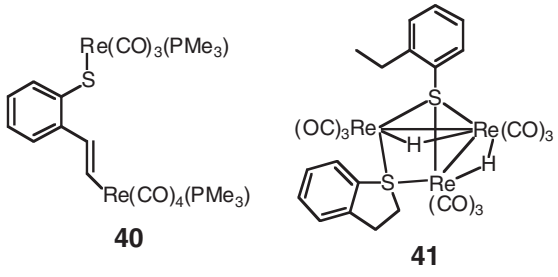

The reaction of $[Cp^*IrH_3]_2$ with T in the presence of *tert*-butylethylene as a hydrogen acceptor yields a product **42**, containing the separated sulfur atom and the butadiene fragment bridging the same two metal atoms, another remarkable "snapshot" of a desulfurization process taking place. The coordinated butadiene is readily displaced by CO to form $[Cp^*Ir(CO)]_2(\mu$-S); hydrogenation of **42** leads to butane, but the fate of the sulfur or of the metal complex were not clearly established. 2-MeT reacted similarly, but 2,5-Me_2T, BT and DBT failed to react. $[Cp^*IrHCl]_2$ also reacted with T or BT at 90 °C under H_2 to give thiolate-bridged products $[Cp^*IrCl]_2[(\mu$-H)-$(\mu$-$SBu^n)]$ and $[Cp^*IrCl]_2[(\mu$-H)$(\mu$-S)$(C_6H_4)Et]$, respectively, arising from hydrogenolysis of the thiophenic substrates; both of them could be completely desulfurized to butane or ethylbenzene by further reaction with hydrogen.[116,116a,116b] The sulfur-bridged dimer $Cl_3W(\mu$-$THT)_3WCl_3$ undergoes C–S bond cleavage upon attack by H^- to yield $Cl_3W(\mu$-$THT)_2(\mu$-$SBu^n)WCl_3$ **43** [55], in a rare case of homogeneous C–S bond scission by tungsten. Apparently, the acute W–S–W angle (ca. 62.5°) arising from a very short W–W bond contributes to weaken the C–S bonds.[117]

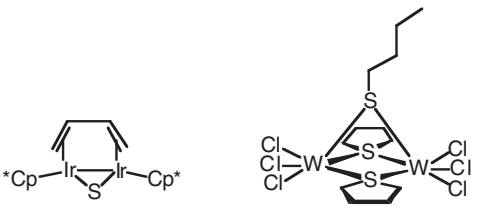

42 **43**

Industrial HDS catalysts are composed of at least two metals, and therefore heterobimetallic complexes are better models for HDS-related reactions. $Fe_3(CO)_{12}$ reacts with the η^4-activated thiophene in $Cp^*Rh(\eta^4\text{-T})$ via a stable intermediate **44**, containing the T ligand η^4-bonded to Cp^*Rh and η^1 to $Fe(CO)_4$, to yield a desulfurized bimetallic product **45** containing a ferrole unit π-bonded to Rh; both complexes were characterized by X-ray diffraction.[29] Similarly, $Cp^*Ir(\eta^2\text{-C,S–Th})$ (Th = 2,5-Me_2T) reacts with iron carbonyls through cleavage of both C–S bonds to produce compound **46**, containing the separated sulfur atom and organic fragment bonded to the metal framework.[5,5a–5d]

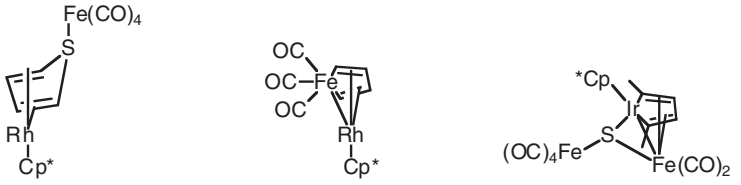

44 **45** **46**

Another case of bimetallic cooperative C–S bond activation involves the reaction the triphos–Rh BT-derived metallacycle with $W(CO)_5$ to yield the heterobimetallic sulfur-bridged species **47**, which upon thermolysis under H_2 (30 atm) induced HDS of BT to ethylbenzene, plus [(triphos)RhH(CO)] together with an insoluble "W–S material" (Equation (9)). This shows that the S-bridged Rh–W couple switches the reactivity from hydrogenolysis to hydrodesulfurization.[118]

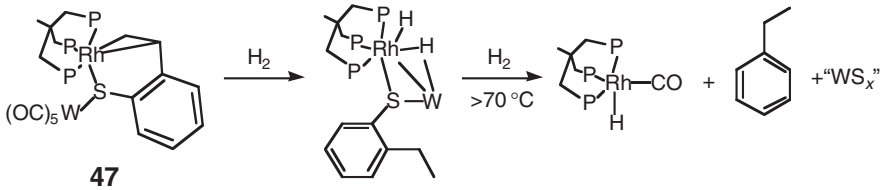

47 (9)

It is tempting to speculate whether the role of "promoter" HDS metals (Co, Ni) is the C–S activation of the thiophenes whereas the "catalytic" metal (group 6, Mo, W) would be responsible for the transfer of hydrogen to the activated substrate. This is a very likely pathway to be envisaged on metal sulfide surfaces where sulfides or thiolates bonded to two or more metal atoms are plentiful. However, this type of interaction is obviously unavailable in single-site complexes, and this could explain why ring opening is frequent but complete desulfurization is rare on mononuclear derivatives.

Another type of activation involves attack of a metal carbonyl fragment to a thiophene previously coordinated to another metal to yield bimetallic products, which display a rich reactivity, frequently involving C–S bond scission. Examples of this chemistry involve the reductive cleavage of $[Mn(CO)_3(\eta^5\text{-}Me_2T)]^+$ with a second Mn unit to produce **48**, which is subsequently hydrogenated to **49** as in Equation (10).[119]

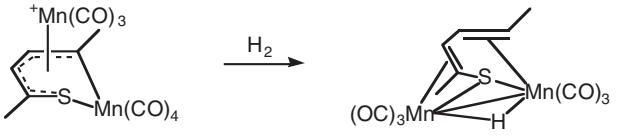

48 **49** (10)

Similarly, $Cp^*Ir(\eta^4\text{-}Me_2T)$ and its metallacyclic isomer undergo a series of interesting reactions with a variety of metal carbonyl fragments to yield heterobimetallic derivatives such as **50–52** (M = Cr, Mo, W), which further react to yield products of relevance to HDS modeling such as **53–55**.[20,20a,20b,68] The analogous complex containing the thiairidacycle π-bonded to $FeCp^+$ is attacked by H^- at the carbocyclic fragment, as in Equation (11); several other nucleophiles react similarly to yield related derivatives.[121]

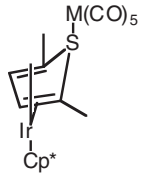

50

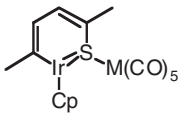

51

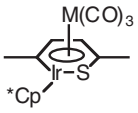

52

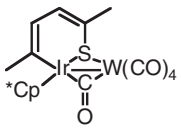

53

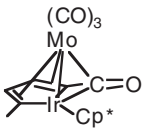

54

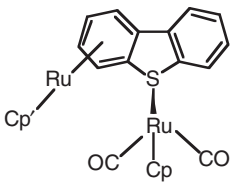

55

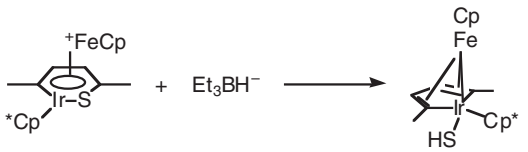

(11)

An interesting alternative makes use of the "remote activation" of the thiophene ring of BT and DBT produced by previous η^6-binding to a carbocyclic ring, to induce C–S bond activation by a second metal center under mild conditions, as exemplified in Equation (12) for an Mn/Pt combination. A variety of metal-containing fragments can produce this type of activation through η^6-bonding, and the second metal inserting into the C–S bond need not be identical to the one π-bonding the arene ring. For instance, $Pt(PPh_3)_2$, which does not react with free BT, readily inserts into the C(vinyl)–S bond of $(\eta^6\text{-BT})ML_n$ complexes, the ease of insertion following the order $ML_n = Ru(C_6Me_6)^{2+}$, $Mn(CO)_3^+ > FeCp^+$, $RuCp^+ \gg Cr(CO)_3$. The thiophene rings of alkylated BTs and DBTs previously activated by η^6-bonding to $Mn(CO)_3^+$ are also cleaved by $Pt(PPh_3)_2(C_2H_4)$. Reductive cleavage by use of cobaltocene under CO also leads to ring-opened bimetallic products through initial activation of the C(aryl)–S bond, followed by isomerization to a more stable configuration (Equation (13)). The latter reaction has been studied in detail, showing that the course of the reaction is markedly influenced by the substituents on BT.[54,54a,54b,122] A theoretical analysis of some of the reactions of thiophenes involving more than one metal center is available.[123]

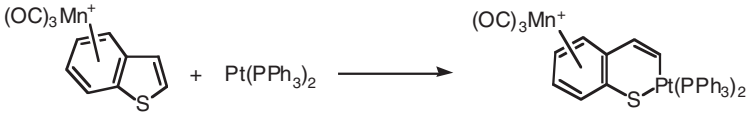

(12)

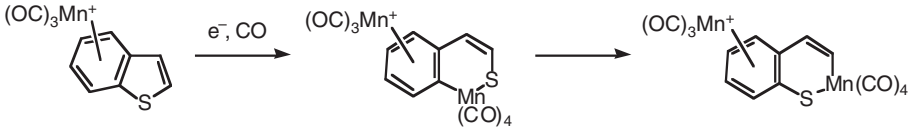

(13)

The closest models available for real HDS catalysts involve Co–Mo molecular clusters. The "butterfly"-shaped $[Cp'_2Mo_2Co_2S_3(CO)_4]$ ($Cp' = MeCp^-$) reacts with T in solution under hydrogen (150 °C, 15 atm) to produce the free C_4 hydrocarbons corresponding to HDS and a new cubane cluster $[Cp'_2Mo_2Co_2S_4(CO)_2]$ in which the extruded sulfur

has been incorporated (Equation (14)). This cubane cluster is converted back to the original one by reaction with CO yielding COS, thus completing a cyclic reaction; CO inhibits the forward desulfurization reaction and therefore the process cannot be rendered catalytic. The exact mechanism of thiophene HDS by use of these clusters is not clearly understood.[124] Nevertheless, extensive related mechanistic studies on the desulfurization of thiols and sulfides using the same cluster $Cp'_2Mo_2Co_2S_3(CO)_4$ allowed the main reaction pathways for desulfurization of these substrates to be understood, according to the overall mechanism represented in Scheme 11.[125]

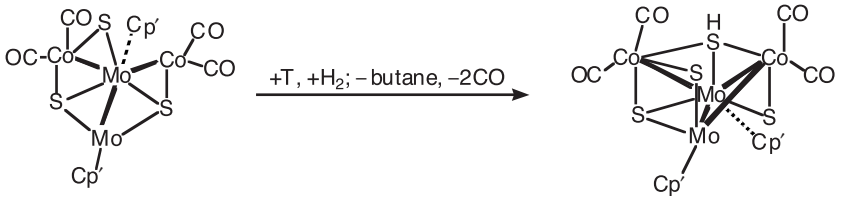

(14)

If this mechanism is combined with the reaction networks that have been worked out for the ring opening and hydrogenolysis of thiophenes by electron-rich late transition metal complexes, a very complete mechanistic model for heterogeneous HDS emerges. In addition, it is important to note that in this model, there are several low-energy steps related to breaking and forming C–S bonds, and that the proton is highly mobile. These features are also typical of Co–Mo–S HDS catalysts, which are very dynamic metal sulfide surfaces acting as reservoirs of protons and electrons. A further point of interest that emerges from Scheme 11 is the concept of "latent vacancies and sulfur mobility". The Co atom, which is the primary site of attack of thiols, in this case, is electronically saturated and the empty site required for the incoming thiol is formed only when needed through an energetically little demanding rearrangement of a quadruply bridging sulfide (bonded to 2Co + 2Mo atoms) into a triply bridging mode (bonding 1Co + 2Mo atoms). This is consistent with the Co–S bond (promoter metal) being weaker than the Mo–S bond. At the end of the HDS reaction, the cobalt loses the "extra ligand" and the quadruple bridge can be easily reconstructed. Within this framework, there is no need to invoke physical "vacancies", but a resting state of the cluster possessing latent vacancies. Although the distinction is rather subtle, the idea of "latent" or "potential" vacancies in a "resting state" rather than actual physically empty sites around electron-rich areas of space seems like an adequate and useful evolution of the classical concept of "anionic vacancies" in HDS catalysts.

Modeling substrate adsorption on Ni–Mo–S catalysts, the Ni atom in the unsaturated cubane-like cluster $[Me–Cp_3Mo_3S_4Ni]^+$ binds HDS-relevant molecules such as Me_2S, Et_2S, Bu^t_2S, THT, as well as HDN-related compounds such as pyridine and quinoline. No derivatives of thiophenes could be observed.[126]

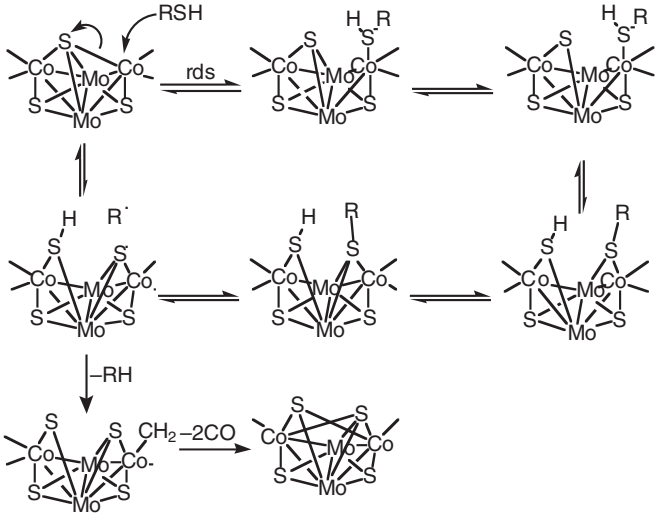

Scheme 11 Desulfurization of thiols on Co–Mo–S clusters. Reproduced from 'Organometallic modeling of the hydrodesulfurization and hydrodenitrogenation, by R. A. Sánchez-Delgado; in *Catalysis by Metal Complexes*; B. R. James and P. W. N. M. van Leeuwen, Eds.; Kluwer Academic Publishers: Dordrecht, Vol. 24, p. 126 (2002). With kind permission of Springer Science and Business Media.

1.27.2.3.2 Catalytic hydrogenolysis and hydrodesulfurization of thiophenes

A few well-defined molecular catalysts for the hydrogenolysis and HDS of thiophenic substrates to their corresponding thiols in solution are available.[4,4a,4b,6,6a,6b] The electron-rich fragments [(triphos)RhH] and [(triphos)RuH]$^-$ are efficient homogeneous hydrogenolysis catalysts; reactions are typically performed at 160 °C and 30 atm H_2, in the presence of strong bases such as NaOH or KO^{t}Bu, conditions that are well tolerated by the very stable triphos derivatives. The main reaction pathways have been elucidated by kinetic studies, high pressure *in situ* NMR measurements, and the isolation and independent syntheses of key intermediates, together with the extensive knowledge previously gained from stoichiometric modeling studies involving analogous (triphos)Ir complexes. The most important features of the catalytic cycles are exemplified in Scheme 12 for the hydrogenolysis of BT. It is interesting to point out that the S atom of the ring-opened intermediate readily binds to $W(CO)_5$ and the resulting heterobimetallic intermediate **47** reacts subsequently with H_2 achieving desulfurization, albeit in a non-catalytic way.

While the anionic Ru(0) complex [(triphos)RuH]$^-$ is active and selective for the conversion of BT into 2-ethylthiophenol,[101] the corresponding cationic Ru(II) species [(triphos)RuH]$^+$, with the same geometry but two electrons less, very efficiently saturates the thiophene ring of BT to form DHBT catalytically, but it is unable to break the C–S bonds.[85] This is a remarkable switch in selectivity brought about by a 2e difference between two otherwise very similar catalysts; this is consistent with electron-rich 16e fragments being particularly adapted for η^1-S-bonding and C–S bond scission of thiophenes, while electron-poorer more strongly electrophilic centers prefer the η^2(C═C) bonding leading to hydrogenation. The [(triphos)Ru]^x systems demonstrate that the selectivity of a metal site can be fine-tuned by a simple 2e variation while maintaining essentially the same geometrical characteristics around the active site. A Co–Mo–S surface is electron rich and it allows electrons to move freely, mainly through the sulfur bridges, which are easily formed, broken, and reconstructed. Other low-energy 2e redox pathways are available in metal sulfide surfaces, such as the interconversion of surface S_2^{2-}, S^{2-}, SH^-, etc., under HDS conditions; therefore, these organometallic systems provide important clues on how a single-surface geometric configuration containing few metal atoms and several forms of sulfur ligands can give rise to different types of reactivity. The hydrogenolysis of T, DBT, and dinaphthothiophene (DNT) can also be performed with the Rh-based catalyst.[127] This work has been extended to aqueous biphasic systems for BT hydrogenolysis, by use of Na–sulphos in combination with Rh, to generate active catalysts that are easily recovered through simple decantation. The Rh–sulphos derivative has also been grafted onto polystyrene/divinylbenzene affording effective and recyclable catalysts for BT hydrogenolysis under conditions analogous to the homogeneous reactions. This polymer-supported catalyst also promoted the complete HDS of BT to ethylbenzene, albeit with lower efficiency. Both Rh(I) and Ru(II) were attached to silica through strong hydrogen bonds, but these systems were not effective as they do not tolerate strong bases. A variation involving a triphos analog covalently linked to silica did result in active Ru and Rh heterogenized catalysts.[80,80a,80b]

The first homogeneous catalytic HDS reaction reported involved the conversion of DBT to biphenyl plus H_2S, together with some hydrogenolysis products by use of [(triphos)IrH], generated by thermolysis of [(triphos)IrH_2(Et)] in THF solution. The reaction proceeds slowly at 170 °C. The catalytic cycle (Scheme 13) was established from the isolation of most of the intermediates involved and the independent study of the individual reactions implicated.[100]

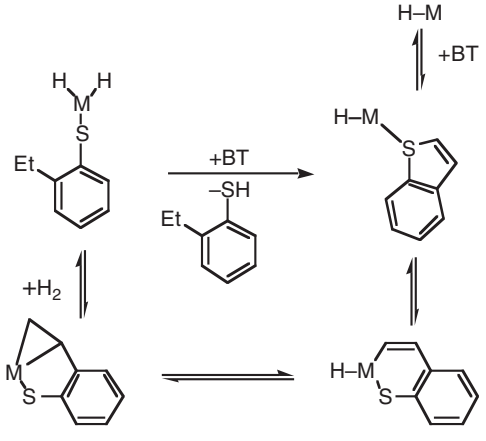

Scheme 12 The mechanism of homogeneous catalytic hydrogenolysis of benzothiophene.

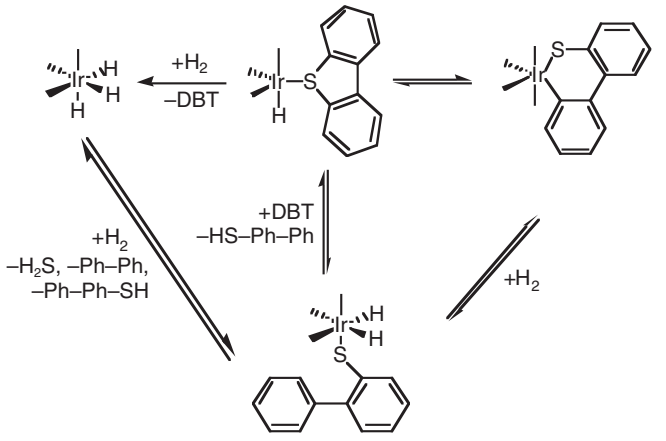

Scheme 13 Homogeneous catalytic HDS and hydrogenolysis of dibenzothiophene on Ir-triphos complexes.

The most active catalysts for the homogeneous HDS of a series of substituted thiophenes (2-MeOT, 3-MeOT, 3-AcT) to the corresponding hydrocarbons make use of thiaplatinacycles derived from the reactions of $[Pt(PEt_3)_3]$ with the corresponding thiophene; up to 81 turnovers were achieved at 100 °C and ca. 20 atm of H_2 in THF in the presence of mercury as a "sulfur trap".[105] In addition, the first Ni-based homogeneous HDS catalysts have been recently discovered; $[(dippe)NiH]_2$ and $Ni(PEt_3)_4$ promote the desulfurization of DBT, 4-MeDBT, and 4,6-Me_2DBT under mild conditions (refluxing toluene), by means of a cross-coupling reaction with Grignard reagents, according to the mechanism depicted in Scheme 14. For instance, DBT is converted mainly into Me–Ph–Ph–Me when MeMgBr is used in conjunction with the Ni complexes; curiously, when Pr^iMgCl is used instead, the major product is Ph–Ph, implying that the alkyl group attacks the Ni center and undergoes a β-H elimination to generate a transient Ni hydride, which is the species actually performing a straightforward HDS reaction. These results are extremely interesting, since they involve one of the commonly used metals in industrial

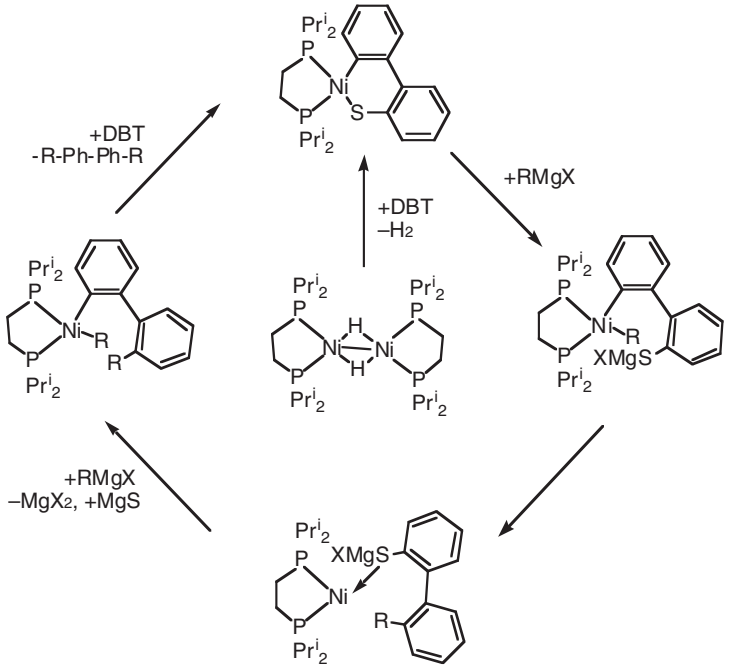

Scheme 14 Homogeneous catalytic desulfurization of dibenzothiophene on Ni complexes.

HDS and some of the most difficult substrates that remain in the heavier fractions during hydrocracking. Further work on these and related systems is expected to follow.

1.27.2.3.3 Conclusion

A variety of metal complexes activate the C–S bonds of thiophenic substrates, including the highly refractory Me_2DBT. Although a good proportion of this chemistry has been performed with metals known to be active in HDS as sulfides but not used in practice (Ru, Rh, Ir), examples involving typical components of commercial heterogeneous catalysts (Mo, W, Co, Ni) are now available and further examples of such chemistry will probably emerge. Electron-rich metal fragments are particularly adapted for η^1-S-bonding to thiophenes, and this seems to be the best form of activation toward C–S bond activation. Organometallic modeling suggests that in real catalysts, electron-rich surface metal centers of strained geometry with one coordinative unsaturation are the most likely active sites. In contrast, electron-poorer centers are better suited for hydrogenation reactions of C═C bonds of S-heterocycles, for example, benzothiophenes. Subtle electronic changes without major geometrical rearrangements can lead to drastic differences in reactivity, and it is interesting to extrapolate this idea to metal sulfide surfaces, where redox processes are facile and electron mobility is high. In contrast to heterogeneous systems, breaking the C–S bonds of thiols or thiolates is more difficult than breaking the first C–S bond of a thiophenic molecule in metal complexes, and complete desulfurization involves sulfido-bridged dinuclear species or clusters, or external "sulfur traps" like Hg or Mg. Efficient catalysts for the hydrogenolysis and hydrodesulfurization of thiophenes, including 4,6-Me_2DBT, continue to be discovered, and immobilization of homogeneous systems on solid supports offers much promise for practical developments. Further exciting results in the area of multimetallic complexes in HDS modeling as well as on new catalytic systems are to be expected.

1.27.2.4 HDS-relevant H_2 and H_2S Reactions with Metal Complexes

A key feature in HDS is the ability of metal sulfides to activate H_2. Experimental and theoretical evidence indicate that on Co–Mo–S catalysts hydrogen activation may occur on the metal or on any one of the various forms of surface sulfur atoms (M═S, M–S–M, M(S_2), $M_2(\mu\text{-}S_2)$). Hydrogen atoms activated on a metal–sulfide surface can behave as protons (in –SH sites) or as hydrides (on the metal centers, M–H); also, bridging H atoms in M–H–S, M–H–M, or S–H–S groups display intermediate acidity. Adsorbed H atoms are highly mobile and migrate throughout the catalyst surface via low-energy pathways, notably redox processes that easily interconvert H^+ and H^- units, as well as M–S, S–S, and S–H bond breaking and forming. In addition, the adsorption and reactions of H_2S at the surface of a catalyst are of great importance in connection with the formation and deactivation of active sites, and with the actual desulfurization processes.[1–3]

The chemistry of metal complexes with sulfur ligands[129,129a] provides interesting models for the interaction of H_2 with metal sulfide surfaces, but the relation of such chemistry to HDS catalysis has been little addressed in organometallic modeling studies. An interesting option is the heterolytic activation of H_2 with an S-donor ligand acting as the base required to remove the proton. Well-defined metal complexes of sulfide or disulfide ligands are relatively scarce but a number of reactions of H_2 with metal complexes of simple sulfur ligands are available and they may be related to H_2 activation on metal sulfide catalysts. In addition, the chemistry of metal complexes containing H_2S and –SH ligands provides information relevant to HDS.[4,4a,4b] Such compounds are rather uncommon and usually unstable; important examples of metal–sulfur derivatives and their reactions are described in this section.

1.27.2.4.1 Hydrogen activation on complexes containing sulfido or disulfido ligands

The reactions of hydrogen with dinuclear cyclopentadienyl Mo and Re complexes containing bridging sulfido and disulfido ligands have been extensively studied.[130,130a–130e] In a clear parallel to MoS_2 surfaces, $[(Cp'Mo)_2(\mu\text{-}S_2)(\mu\text{-}S)_2]$ (Cp′ = methylated cyclopentadienyls) take up H_2 at room temperature and atmospheric pressure to yield the corresponding bis(hydrosulfido) derivatives $[(Cp'Mo)_2(\mu\text{-}SH)_2(\mu\text{-}S)_2]$ (Equation (15)). Hydrogen addition takes place exclusively at the S_2^{2-} site; it is not reversible and it does not proceed further to yield H_2S, as is the case on solid catalysts. The bis(hydrosulfido) complex catalyzes H/D exchange under H_2/D_2 at room temperature and the homogeneous hydrogenation of elemental sulfur to H_2S at 75 °C and 1–3 atm H_2. Thiols exchange readily with the –SH ligands of the Mo dimer to liberate H_2S and form the corresponding thiolato derivatives (Equation (16)); this is a good molecular analog of a reaction commonly thought to intervene in HDS over solid sulfide catalysts.

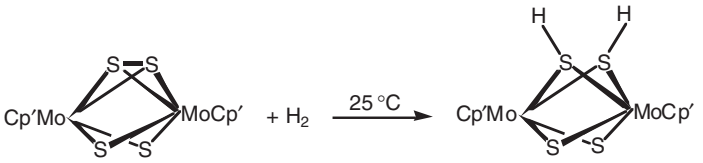

(15)

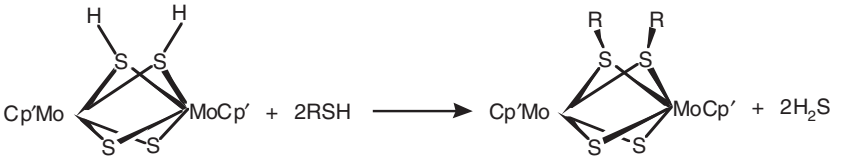

(16)

Only the bridging disulfido ligand reacts homolytically with hydrogen, in agreement with some heterogeneous mechanisms that invoke the dissociation of H_2 on surface S_2^{2-} groups. Nevertheless, in the related complex $[(CpMo)_2(\mu\text{-}SR)(\mu\text{-}S)(\mu\text{-}S_2CH_2)]$, a bridging S^{2-} group heterolytically activates H_2 assisted by an external base. A related rhenium complex $[Cp'Re(\mu\text{-}S_2)_2]_2Cl_2$ containing two bridging S_2^{2-} units also reacts with H_2 under mild conditions to yield H_2S and a trinuclear rhenium cluster $[(Cp'Re)_3S_4H_x]^{n+}$.[131] This hydrogenolysis of bridging sulfides is an important mechanistic model for the well-accepted pathway in the formation of anionic vacancies on metal sulfides. Hydrogen activation also takes place on $[(triphos)Rh(\mu\text{-}S)_2Rh(triphos)]^{2+}$ (triphos = $MeC(CH_2PPh_2)_3$) by heterolytic splitting mediated by the metal and the sulfido ligand to yield $[(triphos)Rh(H)(\mu\text{-}SH)_2Rh(H)(triphos)]^{2+}$. In this case, η^2-H_2 bonding precedes heterolytic activation with the bridging sulfide acting as the base required to capture the proton.[132,132a] This reaction is reminiscent of a proposal frequently encountered in the heterogeneous literature, which has been supported by solid-state NMR studies of hydrogenated RuS_2. Similarly, $Ir_2S_2(PPh_3)_4$ reacts with hydrogen by sequential homolytic and heterolytic H_2 splitting to yield $Ir_2H_2(\mu\text{-}H)(\mu\text{-}SH)(\mu\text{-}S)(PPh_3)_4$.[133]

In summary, the reactions of dimeric complexes containing μ-S^{2-} and μ-S_2^{2-} ligands with H_2 are interesting models for some key steps believed to happen on MoS_2 and related catalysts. Both homolytic and heterolytic activation pathways have been authenticated in these complexes and it is easy to extrapolate such mechanisms to surfaces. Hopefully, this chemistry will continue to be developed, thus providing further insight into the role of surface sulfur species in HDS mechanisms.

Besides hydrogen activation on bridging S_2^{2-} groups, mechanistic proposals for HDS on metal sulfides contemplate either the homolytic splitting of H_2 on a monometallic $M(S_2^{2-})$ site to yield $M(SH)_2$, or the heterolytic activation by a terminal M=S group leading to M(H)(SH) species. These possibilities are nicely modeled by reaction of $Cp^*_2Ti(\eta^2\text{-}C_2H_4)$ with sulfur to yield $Cp^*_2(py)Ti{=}S$, which further reacts with sulfur or with ethylene sulfide to produce $Cp^*_2Ti(\eta^2\text{-}S_2)$.[134,134a] The sulfido derivative reversibly reacts with H_2 at atmospheric pressure to produce the corresponding hydrido–hydrosulfido species $Cp^*_2Ti(H)(SH)$, through heterolytic splitting of a coordinated dihydrogen molecule with the S atom acting as the base. In turn, $Cp^*_2Ti(SH)_2$ is gradually produced upon interaction of $Cp^*_2Ti(S_2)$ with H_2 at 70 °C. Both products were characterized by NMR spectroscopy, but $Cp^*_2Ti(H)(SH)$ was unstable under those reaction conditions, readily eliminating H_2 and reverting back to $Cp^*_2(py)Ti{=}S$. An alternative route to $Cp^*_2Ti(H)(SH)$ involves treatment of $Cp^*_2Ti(\eta^2S_2)$ with H_2 in the presence of PPh_3 or PMe_3 as a sulfur scavenger. This remarkable set of reactions represents another excellent model for H_2 activation on metal sulfides; hopefully, other examples will become available in the future.

1.27.2.4.2 Reactions of H_2S with metal complexes

A limited number of complexes containing coordinated H_2S have been prepared, and very few have been structurally characterized.[4,4a,4b,129,129a] The synthetic methods used involve addition to coordinatively unsaturated compounds, displacement of labile ligands, or protonation of hydrosulfido ligands. Group 6 derivatives[129,129a,135,135a,135b] such as $(CO)_5M(SH_2)$ (M = Cr, W) or $Cp(CO)_3M(SH_2)$ (M = Mo, W) are good models for H_2S adsorption on MoS_2 or WS_2 surfaces although in the complexes the oxidation state of the metal is lower than in metal sulfides. For group 7, $Cp(CO)_2Mn(SH_2)$, $(PPh_3)(CO)_4Mn(SH_2)$, $[(CO)_5Re(SH_2)]BF_4$, and $[(triphos)(CO)_2Re(SH_2)]OTf$ are

known.[129,129a,136,136a,136b] Ru derivatives are the most numerous and stable, including $[(NH_3)_5Ru(SH_2)](BF_4)_2$, $[(NH_3)_4(ISN)Ru(SH_2)](BF_4)_2$ (ISN = isonicotinamide), $[(LS_4)(PPh_3)Ru(SH_2)]$ ($LS_4 = {}^{-}SC_6H_4S(CH_2CH_2SC_6\text{-}H_4S^{-}$), $[(P–N)(PR_3)RuX_2(SH_2)]$ (P–N = $Ph_2PC_6H_4NMe_2$; R = Ph, p-tol; X = Cl, Br); $[Cp'(PPh_3)_2Ru(SH_2)]OTf$ (Cp′ = Cp, $C_5H_3S–CH_2–C_5H_4^{-}$); $[Ru_2(CO)_5(\mu\text{-etipdp})_2(SH_2)](SbF_6)_2$ (etipdp = *N*-ethyl(tetraisoppropoxy)diphosphazane); and $[Ru(\eta^3,\eta^3\text{-}C_{10}H_{16})Cl_2(SH_2)]$.[4,4a,129,129a,137,137a–137f] For the heavier metals, $[IrH_2(SH_2)_2(PPh_3)_2]$ BF_4[138] and $[Pt(PPh_3)_2(SH_2)]$[139] are worth mentioning.

H_2S complexes are easily oxidized and their stabilization is usually accomplished by use of electron-rich metal centers in combination with bulky ligands. Other Lewis bases readily displace H_2S, which is also activated toward deprotonation by strong bases. Examples of oxidative addition of H_2S to give hydrido–hydrosulfido species are known; in some cases the oxidative addition proceeds further with elimination of dihydrogen and the consequent formation of a stable sulfido complex. For instance, $Cp^*_2Zr(CO)_2$ reacts with 2 equiv. H_2S to yield $Cp^*Zr(SH)_2$, but if H_2S is the limiting reagent, the product of the reaction is $[Cp^*Zr(SH)]_2(\mu\text{-S})$. Also, the reaction of $Cp^*_2Zr(CO)_2$ with elemental sulfur in the presence of pyridine yields the terminal sulfido complex $Cp^*_2Zr(S)(py)$, which undergoes oxidative addition of H_2S to produce the bis(hydrosulfido) complex.[129,129a] Reaction of $Cp^*_2TaH_3$ with excess sulfur yields $[Cp^*_2Ta(H)(\eta^2S_2)]$, and with H_2S produces $[Cp^*_2Ta(H)(S)]$.[140,140a]

Mo and W complexes of formula $M(PMe_3)_4(\eta^2\text{-}CH_2PMe_2)H$ (M = Mo, W) readily react with H_2S to yield *trans*-$M(PMe_3)_4(S)_2$; in the case of tungsten, a bis(hydrido)bis(hydrosulfido) intermediate can be isolated, which readily dehydrogenates in solution to yield $W(PMe_3)_4(S)_2$.[141,141a] The most numerous and thoroughly studied metal hydrosulfide complexes are those of Mo and they have often been used as models for HDS-related reactions and intermediates.[129,129a] For instance, the tris(dithiocarbamate) derivative **56** containing a hydrosulfido ligand on an Mo(IV) center in a "sulfur-only" environment is prepared by S-atom transfer from $[Cp_4Fe_4S_6]$ to $[(CO)_2Mo(S_2CNEt_2)_2]$. The structure of **56** closely resembles some of the geometries proposed for the active sites in MoS_2 or WS_2 catalysts.[142]

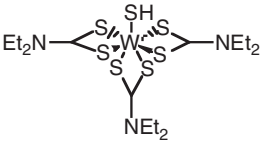

56

ReS_4^{-} reacts with H_2S in the presence of PMe_3 to yield $ReH(SH_2)(PMe_3)_4$, according to Equation (17). As suggested by the stoichiometry of this reaction, the Re(H)(H_2S) complex is a catalyst for the reaction of H_2S with PMe_3 to yield $H_2 + SPMe_3$, and also for H–D exchange between H_2 and D_2 and between H_2S and D_2.[143]

$$ReS_4^{-} + 3H_2S + 8PMe_3 \longrightarrow ReH(SH)_2(PMe_3)_4 + H_2 + 4S{=}PMe_3 \qquad (17)$$

The complex $[(PP_3)Fe(SH)]BPh_4$, where $PP_3 = P(CH_2CH_2PPh_2)_3$, was obtained by bubbling H_2S through an ethanolic solution of $[Fe(OH_2)_6][BF_4]_2$ in the presence of the PP_3 ligand.[144] Alternatively, this compound can be prepared from $[(PP_3)Fe(H)(H_2)](BPh_4)$ or $[(PP_3)Fe(H)(N_2)](BPh_4)$ by interaction with H_2S.[129,129a] Several examples of oxidative addition of H_2S to Ru complexes, leading to hydrosulfido derivatives, are known. They include the formation of $Ru(SH)_2(CO)_2(PPh_3)_2$ from $Ru(CO)_2(PPh_3)_3$ and the transformation of *cis/trans*-$Ru(H)_2(dpm)_2$ (dpm = $Ph_2PCH_2PPh_2$) into *trans*-$RuH(SH)(dpm)_2$ and *cis/trans*-$Ru(SH)_2(dpm)_2$ by reaction with H_2S.[129,129a,145] Dimeric Pd complexes $[(X)Pd(\mu\text{-dppm})_2Pd(X)]$ (X = Cl, Br) promote the decomposition of H_2S into H_2 + coordinated S. Kinetic and spectroscopic data led to the mechanism depicted in Scheme 15. H_2S adds reversibly across the Pd–Pd bond to yield $[(X)(H)Pd(\mu\text{-dppm})_2Pd(X)(SH)]$, which then undergoes elimination of H_2 by a concerted deprotonation of the –SH group and protonation of the Pd–H bond to produce the bridging sulfido derivative $[(X)Pd(\mu\text{-S})(\mu\text{-dppm})_2Pd(X)]$. Removal of the bridging S atom from through oxidation by H_2O_2 or *m*-chloroperbenzoic acid yields $[(X)Pd(\mu\text{-}SO_2)(\mu\text{-dppm})_2Pd(X)]$, which reversibly loses SO_2 to regenerate the starting complex. In this way, the process becomes catalytic for the conversion of H_2S into $H_2 + SO_2$. In a variation of this H_2S decomposition catalysis, an excess of the diphosphine can be used to abstract the bridging sulfide as dppm(S).[145]

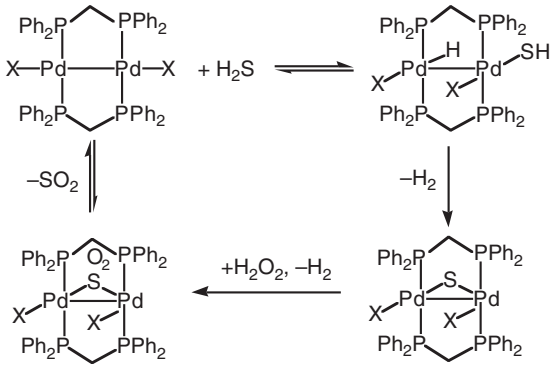

Scheme 15 Homogeneous catalytic conversion of H_2S into $H_2 + SO_2$ on Pd complexes.

1.27.3 Organometallic Models of the Hydrodenitrogenation Reaction

As mentioned in Section 1, HDN model studies using organometallic complexes are not as numerous as for HDS.[4,4a,4b,7,7a] The substrates most commonly used in HDN modeling (see Figure 1) may be divided into two main classes: the less basic pyrrole (Pyr) and indoles (In), in which the nitrogen lone pair is not available for interaction with electrophiles; and the strongly basic pyridine (py) and quinoline (Q), in which the N atom is accessible for bonding to metal ions. In both cases, it is also important to consider their higher homologs, their alkyl-substituted derivatives, and their partially or completely hydrogenated products. HDN modeling includes the structural characterization and bonding features of metal complexes of such N-donor ligands, as well as the hydrogenation N-heteroaromatics and the metal-mediated C–N bond activation.

1.27.3.1 Binding Modes of N-Heterocycles in Transition Metal Complexes

Both the basicity of the nitrogen atom and the presence of carbocyclic rings in addition to the N-containing ring are important in determining the binding modes of N-heterocycles to single or multiple metal sites. In addition, the steric and the electronic effects induced by substituents in the vicinity of the N atom play a key role in the stability and the chemistry of each type of complex. The most important possible bonding modes of HDN-related organonitrogen molecules are summarized in Figure 3. Table 2 contains a representative list of metal complexes of interest in connection with HDN; details for compounds reported previous to 1995 can be found in earlier reviews,[4,4a,4b,7,7a,146,147] and the more recently synthesized relevant derivatives will be referred to in the following sections.

1.27.3.1.1 Complexes of pyrrole, indole, carbazole, and related ligands

No examples of complexes containing η^1-N-bonded pyrrole or carbazole (Cbz) as ligands are known in accord with the low basicity of the N atom in these molecules. On the other hand, some examples of η^1-N-bonded indole species have been reported, but they are better described as η^1-N–3H–indolenine species, for example, $PdCl_2[\eta^1(N)–3H–In']_2$ ($In' = 2$-MeIn and 2,5-Me_2In), $Ir(CO)(PPh_3)_2[\eta^1(N)$-3H–$Me_2$In], $CpRe(NO)(PPh_3)[\eta^1(N)–3H–In']_2$. In addition, an osmium carbonyl cluster containing an orthometallated form of this tautomer of indole is known.[4,4a,4b,7,7a]

Metal derivatives containing olefin-like ligands, in either one of the tautomeric forms, η^2(C═C)–1H–Pyr or η^2(C═C)–2H–Pyr, have been characterized for $[Os(NH_3)_5(L)]^{2+}$ complexes.[66] The η^4-mode has only been observed in $Cp^*Ir[\eta^4$-1–Bu^t–2,3,4,5-$(CO_2Me)_4$Pyr], whose structure displays the pyrrole ligand bonded through the two C═C bonds, while the nitrogen atom is bent away from the ring to a non-bonding distance from Ir, analogous to η^4-thiophene structures. η^5-Bonded metal complexes of pyrroles are known for Cr, Mn, Fe, Co, Ru, Rh, Re, and Ir (see Table 2).[4,4a,4b,7,7a,146,147]

Pyrrolyl ligands are more frequent throughout the periodic table, and depending on the degree of electronic unsaturation of the metal fragment, binding through the N atom only, or through the entire π-ring is observed.

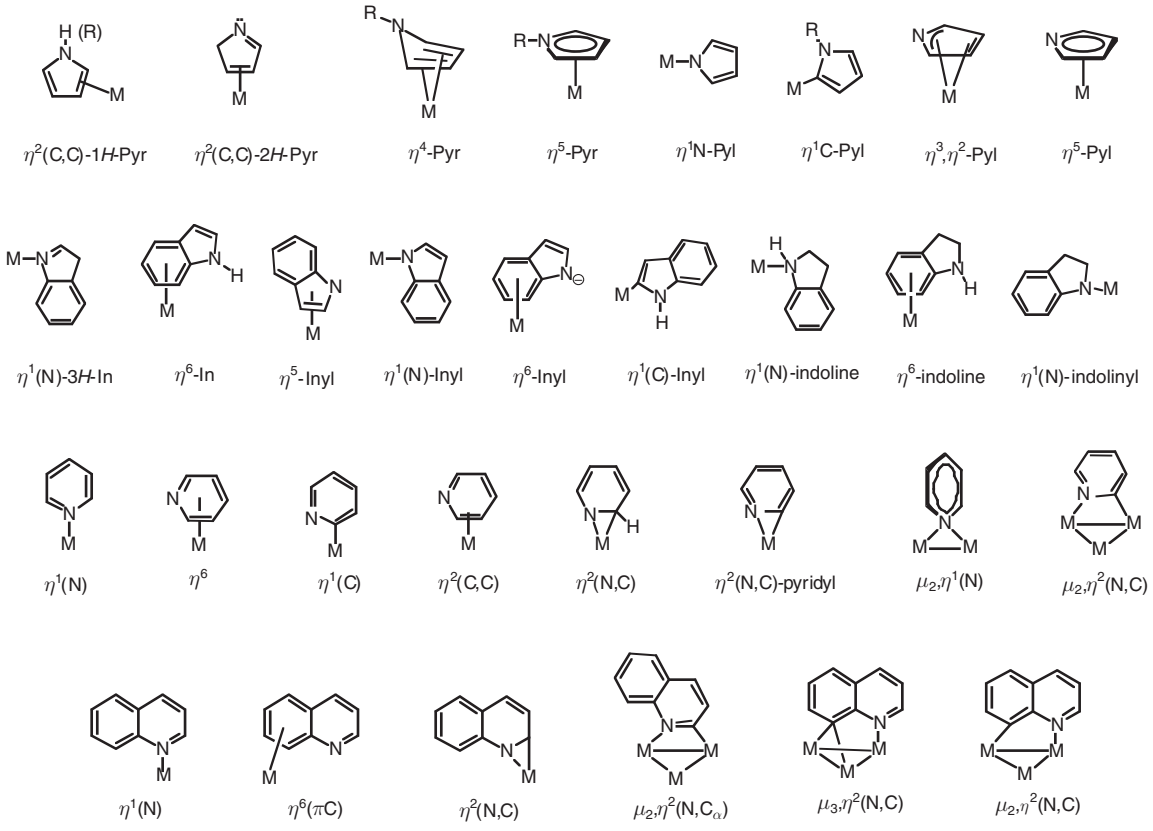

Figure 3 Bonding modes of N-heterocycles in metal complexes.

The η^5-bonded pyrrolyl complexes transform to η^1-bonded species by addition of extra ligands, as in the case of CpFe(η^5-Pyl), which reacts with CO or RNC to yield CpFe(η^1-Pyl)L_2. Oxidative addition of C–H bonds leading to η^1(C)pyrrolyl(hydride) metal complexes has also been described.[4,4a,4b,7,7a] The indolyl anion can bind to mononuclear complexes using the nitrogen atom only η^1-N, the entire heterocyclic ring η^5 or the entire carbocyclic ring η^6, thus making it a very versatile ligand; the dominant coordination mode for indoles is η^6, analogous to what is observed for BT, whereas for indolyl-type ligands η^5 is preferred. It does not seem that such bonding is directly related to HDN mechanisms on solid catalysts, but some of these species easily interconvert as, for instance, in the base-assisted η^6-In → η^5-indolyl shift that takes place on Cp^*M (M = Rh, Ir) or the acid-promoted η^1(N)–indolyl → η^1(N)–indolenine conversion on $CpRh(PPh_3)(NO)$.

Electron-rich metal fragments react with pyrroles or indoles yielding either the kinetic C–H or the thermodynamic N–H insertion products. C–N bond activation, on the other hand, is not observed in contrast with C–S bond breaking, which is readily promoted by electron-rich metal centers, as described above. Despite the fact that carbazole is a very good model compound of the most highly refractory HDN substrates, its coordination chemistry has not been investigated in detail, and to our knowledge, there are no examples of metal complexes containing an intact carbazole ligand. Thus, N–H activation leading to metal hydrido derivatives containing the carbazoyl ligand bound through the nitrogen atom is observed in the reaction of $Cp^*Rh(PMe)_3(H)(Ph)$ with carbazole to yield $Cp^*Rh(PMe)_3(H)(\eta^1$N-carbazoyl) together with the kinetic C–H activation isomer.[148] $Mo(PMe_3)_6$ reacts with pyrrole to yield $MoH(PMe_3)_3(\eta^5$-Pyl), the only Mo–pyrrolyl complex known, and with indole to give $MoH(PMe_3)_4(\eta^1$N–Inyl) **57**; the latter rearranges with loss of a phosphine as in Equation (18) into $MoH(PMe_3)_3(\eta^5$-Inyl) **58**, which can revert back to the η^1-N form by phosphine addition, or thermally convert into $MoH(PMe_3)_3(\eta^6$-Inyl) **59**, a rare example of an η^6-bonded indolyl anion. The latter complex may be regarded as zwitterionic with a formal positive charge on the Mo and a formal negative charge on the N. **59** does not convert back to **58** thermally, but this reverse reaction is brought

Table 2 HDN-relevant metal complexes of N-donor ligands

Pyrrole complexes

$[Os(NH_3)5(\eta^2(C{=}C)\text{-Pyr}')][OTf]_2$ (Pyr′ = Pyr, 1-MePyr, 2,5-Me_2Pyr, 1,2,5-Me_3Pyr, 5-EtPyr, 1,4-Me_2Pyr)

$Cp^*Ir[\eta^4\text{-}1^t\text{Bu-}2,3,4,5(CO_2Me)_4Pyr]$

$Cr(CO)_3(\eta^5\text{-1-MePyr})$

$[Mn(CO)_3(\eta^5\text{-Pyr})]^+$

$[CpFe(\eta^5\text{-1-MePyr}')]^+$ (Pyr′ = 1,2,5-Me_3Pyr, 2,3,4,5-Me_4Pyr, Me_5Pyr)

$[Fe(\eta^5\text{-1-MePyr})_2]^{2+}$

$[CpCo(\eta^5\text{-}Me_5Pyr')]^{2+}$

$[(p\text{-cymene})Ru(\eta^5\text{-Pyr}')][OTf]_2$

Pyr′ = 2,3,4,5-Me_4Pyr, Me_5Pyr

$[(p\text{-cymene})Ru(\eta^5\text{-}Me_5Pyr)][OTf]_2$

$(PPh_3)_2Re(H)_2(\eta^5\text{-}Me_5Pyr)$

$[Cp^*Rh(\eta^5\text{-}Me_5Pyr')]^{2+}$

$(PPh_3)_2Re(H)_2(\eta^5\text{-}Me_5Pyr)$

$[Cp^*Ir(\eta^5\text{-2,3,4,5-}Me_4Pyr')]^{2+}$

Pyrrolyl complexes

$MoH(PMe_3)_4(\eta^5\text{-Pyl})$

$CpFe(\eta^1\text{-Pyl})L_2$ (L = CO, RNC, R_2NPF_2)

$Fe(dmpe)_2H(\eta^1\text{-Pyl})$

$Ru(dmpe)_2H(\eta^1\text{-Pyl})$

$Ni(R)(PMe_3)_2(\eta^1\text{-Pyl}')$ (R = alkyl; Pyl′ = Pyl, 2,5-Me_2Pyl)

$IrHCl(PMe_3)_3(\eta^1\text{-Pyl})$

$Mn(CO)_3(\eta^5\text{-Pyl})$

$[CpFe(\eta^5\text{-Pyl}')]^+$ Pyl′ = Pyl, 2,3,4,5-Me_4Pyl, 2,5-^{t}Bu$_2$Pyl

(Carborane)$Co(\eta^5\text{-Pyl}')$ (Pyl′ = 2,5-Me_2Pyl, 2,3,4,5-Me_4Pyl)

$Cp^*Ru(\eta^5\text{-Pyl})$

$Ru(\eta^5\text{-Pyl})_2$

$(PR_3)_2RuCl_2(\eta^5\text{-Pyl})$

$[(p\text{-cymene})Ru(\eta^5\text{-2,3,4,5-}Me_4Pyl)][OTf]$

$[(p\text{-cymene})Os(\eta^5\text{-2,3,4,5-}Me_4Pyr)][OTf]$

$Cp^*Rh(H)(Pyl)$

$MH(PEt_3)_2(\eta^1\text{N-Pyl})$ (M = Ni, Pd, Pt)

Indole complexes

$PdCl_2[\eta^1\text{(N)-3H-In}']_2$ (In′ = 2-MeIn and 2,5-Me_2In)

$\{Ir(CO)(PPh_3)_2[\eta^1\text{(N)-3H–}Me_2In]\}^+$

$CpRe(NO)(PPh_3)[\eta^1\text{(N)-3X–In}']_2$ (X = H, Me; In′ = In, 3-MeIn, 3-EtIn)

$Cr(CO)_3(\eta^6\text{-In})$

$[Mn(CO)_3(\eta^6\text{-In})]^+$

$[Cp'Ru(\eta^6\text{-X-In}]^+$

$[(p\text{-cymene})Ru(\eta^6\text{-In}')][OTf]_2$ In′ = In, 1-MeIn, 2MeIn, 2,3-Me_2In

$[Cp^*M(\eta^6\text{-In})]^{2+}$ (M = Rh, Ir)

Indolyl complexes

$[(p\text{-cymene})Ru(\eta^1\text{-Inyl})(NCMe)_2][OTf]_2$

$CpRe(NO)(PPh_3)(\eta^1\text{-Inyl}')$ (L = CO, RNC, R_2NPF_2)

$Ir(CO)(PPh_3)_2[\eta^1\text{(N)-2,3-}Me_2Inyl]$

$Mn(CO)_3(\eta^5\text{-2-MeInyl})$

$[Cp^*M(\eta^5\text{-Inyl})]^+$ (M = Rh, Ir)

$[(p\text{-cymene})Ru(\eta^6\text{-In}')][OTf]$ (In′ = In, 1-MeIn, 2MeIn, 2,3-Me_2In)

$MH(PEt_3)_2(\eta^1\text{N–Inyl})$ (M = Ni, Pd, Pt)

Indoline complexes

$MoH(PMe_3)_4(\eta^1\text{-indoline})$

$MoH(PMe_3)(\eta^5\text{-indoline})$

$MoH(PMe_3)(\eta^6\text{-indoline})$

$[(cymene)Ru(\eta^1\text{-Indoline})(NCMe)_2][OTf]_2$

$PdCl_2(PPh_3)(\eta^1\text{-indoline})$

$Cr(CO)_3(\eta^6\text{-1-MeIndoline})$

$[(p\text{-cymene})Ru(\eta^6\text{-indoline})][OTf]_2$ (In′ = In, 1-MeIn, 2MeIn, 2,3-Me_2In)

Unusual pyridine and quinoline complexes

$\mu^2,\eta^1(N)$-complexes

$Mo_2O_2[S_2P(OPr^i)_2]_2(\mu\text{-O})(\mu\text{-S})[\mu,\eta^1\text{(N)–Py}]$

$\eta^2(C,C)$-complexes

TpRe(CO)(MeIm)(η^2(C,C)-2,6-lutidine)

$[Os(NH_3)_5(\eta^2\text{(C,C)-2,6-}Me_2Py)][OTf]_2$

$\eta^2(C,N)$-pyridine and pyridyl complexes

$[\eta^2\text{(C,N)-Py}]Nb(silox)_3$

$[\eta^2\text{(C,N)-Py}]Ta(silox)_3$

$[\eta^2\text{(C,N)-2,4.6-}t\text{-Bu}_3Py]Ta(OAr)_2Cl$ (Ar = 2,6-^{i}PrPh)

$[\eta^2\text{(C,N)-Q}']Ta(OAr)_nCl_m$ (Q′ = Q, 6-MeQ; Ar = 2,6-^{i}PrPh; n = 2, 3; m = 1, 0)

$Cp^*Lu(\eta^2\text{(N,C)–}NC_5H_4)$

$Cp^*Sc(\eta^2\text{(N,C)–}NC_5H_4)$.

$MoH(PMe_3)_4(\eta_2\text{(C,N)Py})$

η^6-complexes

$Mo(PMe_3)_3(\eta^6\text{N–Q})$

$Mo(PMe_3)_3(\eta^6\text{C–Q})$

$[(Cp^*Ru(\eta^6\text{-Py})][OTf]$

$Cp^*Rh(\eta^6\text{-2,4,6-}Me_3Py)$

about photochemically. Acridine produces only the η^6-bonded species.[149] Reaction of $RuH_2(H_2)_2(PCy_3)_2$ with pyrrole leads to $RuH(PCy_3)_2(\eta^5\text{-Pyr})$, which can be subsequently protonated with HBF_4 to yield $[RuH_2(PCy_3)_2(\eta^5\text{-Pyr})]BF_4$.[150] Zerovalent $M(PEt_3)_3$ (M = Ni, Pd, Pt) complexes that are very active for C–S bond-breaking reactions activate the N–H bond of pyrrole exclusively to produce the N-bonded derivative $M(PEt_3)_2(H)(\eta^1\text{N-Pyl})$; indole and carbazole react in the same way.[151]

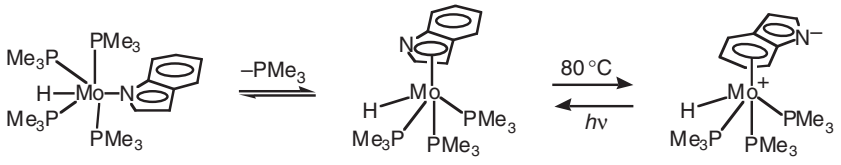

(18)

The interactions of dinuclear and polynuclear complexes with pyrroles and indoles have attracted attention as analogs of surface interactions. Clusters containing intact pyrrole or indole ligands are not known, as the reactions invariably involve N–H and/or C–H bond activation to yield derivatives containing bridging pyrrolyl or indolyl ligands. Nucleophilic attack of Pyr at the disulfide bond of $[Cp'Mo(\mu\text{-}S)_2(S_2CH_2)]_2^{2+}$ yields $[(Cp'Mo)_2(S_2CH_2)(\mu\text{-}S)(\mu\text{-}S\text{-pyrrolyl})]^+$ through heterolytic scission of the S–S bond by the heterocycle to give μ-pyrrolylthiolate and μ-SH dimeric products (Equation (19)). 1-MePyr, 1,2,5-Me_3Pyr, and 1-MeIn behave similarly, although the regiochemistry of electrophilic addition may vary depending on the number and on the position of the substituent.[152] This reaction is interesting in that it shows the interaction of pyrrole with a framework resembling a catalytic MoS_2 surface.

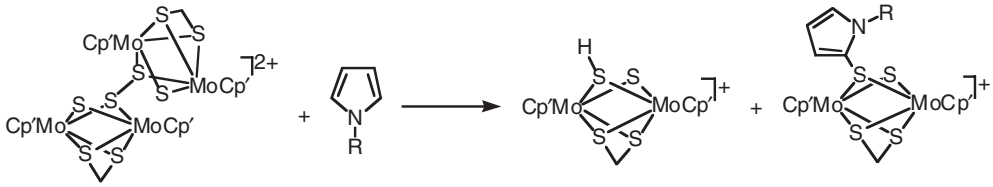

(19)

$[Cp^*Ir(H_2)(\mu\text{-}H)]_2$, which cleaves C–S bonds of thiophenes, also promotes the selective C–H bond cleavage of N-methylpyrrole under comparable experimental conditions, leading to $Cp^*Ir(H)\{\mu_2,\eta^1C,\eta^2(C,C)Pyr\}(\mu\text{-}H)_2IrCp^*$.[153] This is consistent with the higher energy barrier to C–N insertion as compared to C–S or C–H activation. Other examples of metal clusters containing pyrrole-derived ligands include the zwitterionic $Ru_3(\mu\text{-}H)(\mu^3,\eta^3\text{-}C_4H_3NMe)(CO)_9$ **60**, $Ru_3(\mu\text{-}H)_2(\mu^3,\eta^3\text{-}C_4H_2NMe)(CO)_9$ **61**, $Os_3(\mu\text{-}H)_2(\mu^3,\eta^3\text{-}C_4H_2NMe)(CO)_9$ **62**, $Os_3(\mu\text{-}H)(\mu,\eta^1\text{-}C_4H_2NMe)(CO)_9$ **63**.[154]

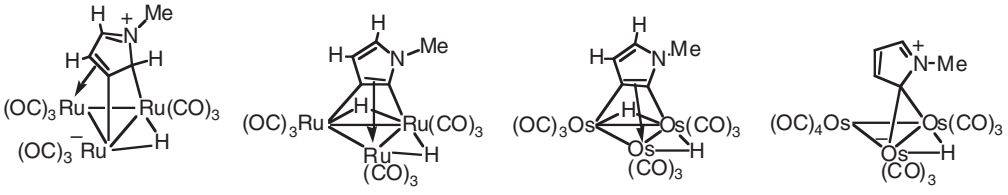

Both the η^6 and η^1(N) coordination modes of indoline, as well as their interconversion, have been reported for Re, Ru, and Pd complexes.[4,4a,4b,7,7a] This type of ligand is of particular relevance since N-aromatics need to be hydrogenated before nitrogen removal can take place in HDN catalysis. As an example, $[(p\text{-cymene})Ru(\eta^1\text{-indoline})(CH_3CN)_2)](OTf)_2$ converts into $[(p\text{-cymene})Ru(\eta^6\text{-indoline})](OTf)_2$ upon gentle heating in CH_2Cl_2, and can be deprotonated by use of, for example, triethylamine to give the corresponding (η^1-indolinyl) complex.[155]

1.27.3.1.2 Complexes with pyridine, quinoline, and related ligands

The pyridines and quinolines and their higher homologs are more basic ligands than five-membered heterocycles, and although the coordination chemistry of such molecules is considerably more developed, comparatively little organometallic chemistry is available. The most common coordination mode for py is by far through the nitrogen atom, which uses its lone pair for interaction with Lewis acceptors. Unlike thiophene, which binds to metals in a bent fashion, the lone pair in the nitrogen atom of py is located in the ring plane, and thus the M–N vector in η^1(N)–py complexes is also in the ring plane. Indeed, pyridine is one of the most frequently encountered classical ligands in coordination chemistry, and there are examples of η^1-N–py complexes for virtually every transition metal in more than one oxidation state;[156] therefore, no attempt will be made to include such numerous compounds in Table 2, where only some unusual coordination modes are exemplified, which may be of relevance in connection

with HDN.[4,4a,4b,7,7a] The η^6-mode of py is fairly common, and therefore, many studies directed at modeling HDN reactions have centered on the η^1(N)- and η^6-modes and the factors controlling their interconversion and/or prevalence. η^1(C)–Py derivatives are obtained by replacement of a proton by a metal fragment, usually via C–H bond activation by electron-rich metal fragments. The organometallic chemistry of quinoline (Q) does not differ significantly from that of Py except that the presence of the carbocyclic ring allows a further bonding mode η^6-C through the arene moeity.

Extensive studies on Cp–Ru(II) and –Rh(III) complexes of N-heterocycles show that in the absence of any steric constraints, the η^1(N) mode prevails over the η^6, particularly with the more electrophilic Rh(III) center. For example, $[Cp^*Rh(CH_3CN)_3]^{2+}$ reacts with 2-Mepy and 2,6-Me_2py yielding $[Cp^*Rh(\eta^1\text{(N)-py}')(CH_3CN)_2]^{2+}$, while the trisubstituted 2,4,6-Me_3py prefers to form the η^6-adduct $[Cp^*Rh(\eta^6\text{-py}')]^{2+}$. In the case of $[CpRu(CH_3CN)_3]^+$, in which the Ru center is more electron rich than Rh(III), a greater propensity of Ru(II) to stabilize the η^6-mode is observed and the $\eta^1(N) \rightarrow \eta^6$ interconversion of 2-methylpyridine and 2,4-dimethylpyridine was followed by NMR spectroscopy. With unsubstituted py, $[CpRu(\eta^1\text{(N)-Py})_3]^+$ is obtained; however, when Cp^* is employed, $[Cp^*Ru(\eta^1\text{(N)–Py})_3]^+$ is the kinetic product that thermally converts into the corresponding η^6-derivative.[4,4a,4b,7,7a] As for py, the most common coordination mode of Q in mononuclear complexes is the η^1(N), often in equilibrium with the η^6-arene form, as in the $\eta^1(N) \rightarrow \eta^6$ rearrangement detected by NMR in the reaction of Q with $[CpRu(CH_3CN)_3]^+$ (Equation (20)). If Cp^* is used instead of Cp, the η^6-complex is rapidly formed, while the corresponding η^1(N) adduct is not observed. Reaction of $RuH_2(H_2)_2(PCy_3)_2$ with py leads to $RuH_2(H_2)(\eta^1\text{-py})(PCy_3)_2$ with an extremely labile py ligand; in an analogous reaction, acridine binds in the rare η^4-mode to two C=C bonds in the product $RuH_2(\eta^4\text{-acridine})(PCy_3)_2$.[150] The complexes $[IrH_2(PPh_3)_2(\eta^1\text{-N–L})_2]PF_6$ (L = py, iQ, and pip, piperidine) were synthesized by hydrogenation of $[Ir(COD)(PPh_3)_2]PF_6$ in the presence of the appropriate N-donor ligand. These complexes undergo reactions with small molecules leading to, for example, the carbonyl derivative $[IrH_2(PPh_3)_2(CO)(\eta^1\text{-N–pip})]PF_6$ characterized by X-ray diffraction;[157] examples of metal–piperidine complexes and their crystal structures are very rare, and they are of particular relevance since piperidine is the initial product of the reaction of pyridine with hydrogen over heterogeneous HDN catalysts. These complexes serve as models of the simultaneous activation of H_2 and organonitrogen compounds on a single metal atom.

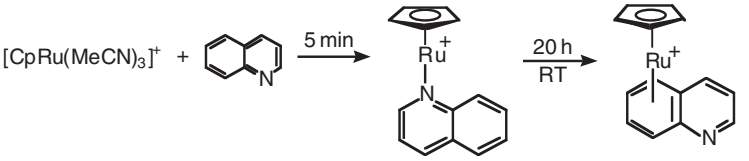

(20)

The complex $Mo(PMe_3)_6$ provides a remarkable set of reactions with six-membered N-heterocycles in relation to HDN on heterogeneous Mo-based catalysts. Reaction with pyridine proceeds by activation of the C–H bond α to the N atom to yield the side-bonded pyridyl derivative $[MoH(PMe_3)_4(\eta^2\text{-}C_5H_4N)]$; acridine affords the commonly encountered arene-bonded $[Mo(PMe_3)_3(\eta^6\text{-C–acridine})]$ and more interesting, quinoline gives the only known complex η^6-bonded to the heterocyclic ring, viz, $[Mo(PMe_3)_3(\eta^6\text{N-Q})]$, which isomerizes thermally to the more stable $[Mo(PMe_3)_3(\eta^6\text{-C–Q})]$ (Equation (21)). The η^6-N-derivative reacts further with H_2 to yield 1,2,3,4-tetrahydroquinoline (THQ), while the η^6-C isomer does not react with hydrogen under similar conditions, demonstrating the importance of binding the heterocycle to the metal in order to reduce it.[149]

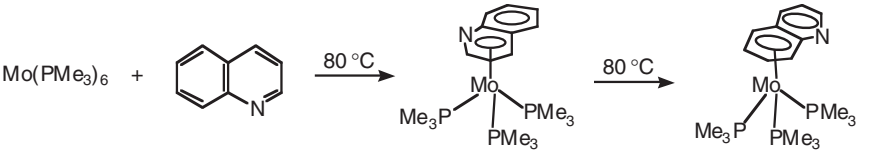

(21)

A rather rare coordination mode of pyridines is the η^2(C=C) mode, which is exclusively stabilized by the electron-rich $[Os(NH_3)_5]^{2+}$ fragment, for example, 2,6-lutidine. The olefin-like complex easily rearranges to the η^1(N) mode by a one-electron oxidation. Interestingly, the η^2(C=C) mode of lutidine rearranges with time to give an Os(II) lutidinium ylide. In contrast, the η^2(C,C) mode is maintained when $[Os(NH_3)_5(\eta^2\text{-lutidine})]^{2+}$ is protonated to give a lutidinium derivative.[66,66a,66b]

The bonding modes of pyridines described so far represent reasonable models for the adsorption and activation of pyridines, quinolines, and acridines on HDN catalysts, but none of them promotes C–N bond activation, which ultimately leads to nitrogen removal. In contrast, a curious η^2(N,C) coordination mode has been discovered, which

effectively activates the py ring toward C–N bond scission.[4,4a,4b,7,7a,159,159a,159b] The complex $(silox)_3Ta[\eta^2(N,C)py]$ **64** ($silox = Bu^t_3SiO^-$) was prepared by reaction of $Ta(silox)_3$ with pyridine, as illustrated in Equation (22). The structure of **64** is best viewed as a Ta(v) metallaaziridine, where the aromaticity of py has been substantially perturbed; analogous reactions with 2-picoline and lutidine give similar $\eta^2(N,C)$ products. Similar derivatives of other pyridines have been synthesized. Reduction of $(silox)_3NbCl_2$ with Na/Hg in py affords a kinetic $\eta^2(N,C)$–py product which thermally undergoes C–N insertion (*vide infra*).

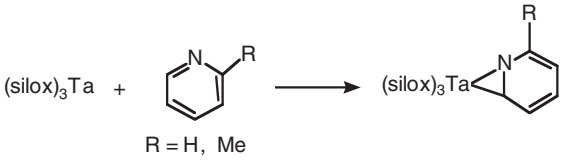

(22)

A related Ta compound containing $(dipp)_2ClTa(\eta^2(N,C)–2,4,6\text{-}NC_5H_2Bu^t_3)$ ($dipp = 2,6\text{-}OC_6H_3Pr^i_2$) was obtained through an indirect route involving insertion of a nitrile into a tantallacyclopentadiene complex. The $\eta^2(N,C)$ quinoline analog $(dipp)_3Ta(\eta^2(N,C)–Q)$ ($dipp = 2,6\text{-}OC_6H_3Pr^i_2$) is obtained in an analogous manner to the py derivative, via an η^1H-bonded intermediate.[146] Besides being precursors to C_α–N bond scission, intermediates containing $\eta^2(N,C)$ py ligands intervene in C–H-activation reactions leading to complexes containing $\eta^2(N,C)$–$NC_5H_4^-$ ligands like $Cp^*Lu(\eta^2(N,C)–NC_5H_4)$ and $Cp^*Sc(\eta^2(N,C)\text{-}NC_5H_4)$. Similar Ti derivatives with 2-substituted pyridines have been described. The reaction of py with a triosmium cluster results in a trinuclear compound $[Os_3(\mu\text{-}H)(\mu\text{-}NC_5H_4)(CO)_{10}]$, in which py uses the N atom and the C_α atom for coordination to two metal centers.[158]

Transition metal complexes of other relevant organonitrogen compounds such as isoquinoline, 5,6-benzoquinoline, 7,8-benzoquinoline, acridine, and phenanthridine are known, and they contain the ligand coordinated in the $\eta^1(N)$ or the η^6-arene fashion. The triosmium cluster $Os_3(CO)_{10}(CH_3CN)_2$ reacts with polyaromatic N-heterocycles such as 5,6-benzoquinoline and phenanthridine in an analogous manner to py and Q, yielding $\mu_3,\eta^2(N,C,C)$ complexes.[4,4a,4b,7,7a]

1.27.3.2 Reactions of N-heterocycles in Transition Metal Complexes Related to HDN

When N-heterocycles bind to a transition metal complex, their reactivity may be enhanced with respect to the free molecules. The reactions depend on the electronic and geometric characteristics of the metal-containing fragment, as well as on the nature of the organonitrogen substrate; however, no general trends relevant for HDN can be extracted from the accumulated literature. Nevertheless, two types of reactions merit further discussion, namely N-hetero-aromatic ring hydrogenation and the rare activation of C–N bonds by metal complexes.

1.27.3.2.1 Hydrogenation of N-heteroaromatic compounds

The hydrogenation of N-heteroaromatic compounds is of interest in relation to HDN, since selective hydrogenation of the nitrogen-containing rings always takes place prior to C–N bond breaking (see Scheme 2).[4,4a,4b,7,7a,160] Few examples are available of metal complex-catalyzed hydrogenation of pyridines, which is not easy due to their high aromatic character. $Rh_6(CO)_{16}$ under water-gas shift conditions ($CO + H_2O$) reduces pyridine but with low efficiency, and the reaction mechanism is not known. Early reports on the activity of $RhCl_3(py)_3/NaBH_4$ for pyridine reduction were not followed up. On the other hand, detailed work was carried out on the hydrogenation of 2-methylpyridine to 2-methylpiperidine by use of $[Cp^*Rh(NCMe)_3]^{2+}$ as the catalyst precursor. Mechanistic studies, based on NMR spectroscopy, deuteration experiments, and isolation of reaction intermediates, suggest that hydrogen addition to both C═N and C═C bonds is reversible, and that initial C═N bond reduction is the key step of the cycle by breaking the aromaticity of the ring. Partially hydrogenated pyridines are readily dehydrogenated back under the reaction conditions, confirming that re-aromatization is thermodynamically favored over C–N bond breaking during HDN.[161]

Much more success has been achieved in the hydrogenation of polynuclear N-heterocycles; the regioselective reduction of the N-containing ring in quinoline, isoquinoline, indole, benzoquinolines, acridine, and other related molecules can be achieved with relative ease under moderate conditions. Simple metal carbonyls of Mn, Cr, Mo, W, Fe, Ru, Rh display some hydrogenation activity for a variety of polynuclear N-heterocycles under H_2, H_2/CO, or CO/H_2O but conditions are harsh and turnovers low; metallic particles, rather than molecular species, may be involved. This makes them unattractive for practical use or for mechanistic studies. Cp and phosphine complexes

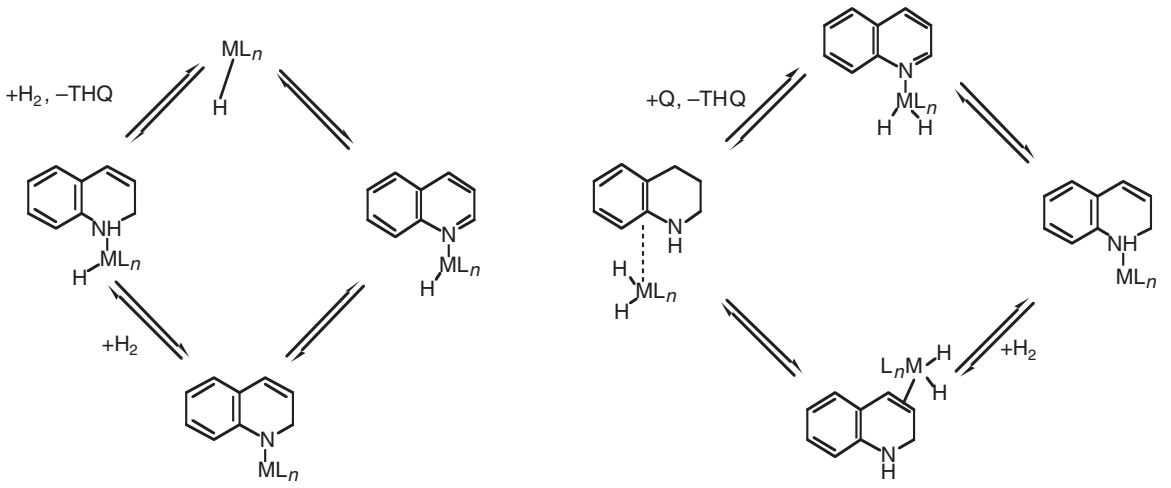

Scheme 16 General mechanisms of the homogeneous hydrogenation of quinoline.

of Ru and Rh are more efficient for N-heterocycle hydrogenation under moderate conditions, and some of them have been extensively investigated, particularly, $[CpRh(NCMe)_3]^+$, $RhCl(PPh_3)_3$, $[Rh(COD)(PPh_3)_2]^+$, $RuCl_2(PPh_3)_3$, $RuHCl(PPh_3)_3$, $MHCl(CO)(PPh_3)_3$ (M = Ru, Os), $[MH(CO)(NCMe)_2(PPh_3)_2]^+$ (M = Ru, Os). Scheme 16 summarizes the most important catalytic cycles for quinoline reduction deduced for monohydride and dihydride systems on the basis of kinetic measurements, *in situ* spectroscopic studies, isolation of intermediates, and theoretical calculations; further details may be found in previous reviews.[4,4a,4b,7,7a,160,161] The most interesting features of these mechanisms are: (i) the importance of η^1-N binding of Q to initiate the cycle, in line with heterogeneous proposals involving vertical adsorption of the heterocycle onto catalytic surfaces; (ii) the possibility of η^2(C═N)-bonded intermediates being involved in the hydrogenation step; (iii) the reversible hydrogenation of the C═N bond, followed by migration of the metal fragment to the C(3)═C(4) bond, which is also reversibly hydrogenated; and (iv) binding of the product THQ through either the N atom or the carbocyclic ring. The mechanisms of Scheme 16 are easily adapted to explain the hydrogenation of pyridine and of other polynuclear N-heterocycles, the rates of which follow a trend that decreases with increasing basicity and steric hindrance at the nitrogen atom: phenanthridine > acridine > quinoline > 5,6-benzoquinoline > 7,8-benzoquinoline > indole > 2-Me–quinoline > 2-Me–pyridine. Isoquinoline is only reduced with difficulty, and this has been associated with its high basicity; indole is also difficult to hydrogenate, and very few catalysts have been reported for this reaction, maybe due to the fact that indole tends to bind to metals through the C(2)═C(3) bond, rather than η^1-N, and thus the activation of the C═N bond is not very marked.

Water-soluble catalysts composed of $RuCl_3{\cdot}3H_2O$, *m*-monosulfonated, or trisulfonated triphenylphosphine (TPPMS, TPPTS), and a basic co-catalyst such as aniline or quinoline, which are active for the biphasic reduction of sulfur-containing heterocycles, can also be employed for the hydrogenation of N-heterocycles. The active species is thought to be $[RuHCl(PR_3)_2(L)_2]$ (PR_3 = TPPMS, TPPTS; L = Q, THQ, aniline), and the mechanism is the typical one for monohydride catalysts.[84,84a,84b] Other water-soluble complexes containing sulfonated ligands, viz, $[(DPPDS)Rh(H_2O)_2]Na$ (Na_2–PPPDS = $[\{NaO_3S(C_6H_4)CH_2\}_2C(CH_2PPh_2)_2]$), [(sulphos)Rh(COD)], and $[(sulphos)Ru(NCMe)_3]$–SO_3CF_3 (sulphos = $[NaO_3S(C_6H_4)CH_2C(CH_2PPh_2)_3]$) are also very efficient in catalyzing the regioselective hydrogenation of Q under reasonable reaction conditions in liquid biphasic media, or when supported on silica or on polymers, and in both cases high catalytic activities for the hydrogenation of quinoline have been found.[7] No reports are available on the homogeneous hydrogenation of carbazoles, which would be interesting substrates analogous to dibenzothiophenes.

Regioselectivity for the reduction of the heterocycle has been the norm in all cases with the catalysts described above. However, the complex $RuH_2(H_2)_2(PCy_3)_2$ hydrogenates quinoline, isoquinoline, and acridine selectively at the carbocyclic ring; it was suggested that this remarkable shift in selectivity may be due to η^4-arene coordination being involved in the hydrogenation mechanism. Indeed the complex $RuH_2(\eta^4$C–acridine$)(PCy_3)_2$ was isolated and shown to function as a catalyst precursor, thereby strongly indicating that it is an intermediate in the cycle.[150]

1.27.3.2.2 Metal-mediated C–N bond-activation reactions relevant to HDN

A crucial step in HDN is the scission of C–N bonds of amines and N-heteroaromatics, but few examples are available of metal complexes that can model such reactions. One interesting case is the activation of py when coordinated to metals in the unusual η^2(N,C) metallaaziridine mode, which has indeed resulted in C–N bond cleavage. The complex $(ArO)_2ClTa(\eta^2(N,C)\text{-}2,4,6\text{-}NC_5H_2Bu^t_3)$ ($ArO = 2,6\text{-}Pr^i_2PhO$) reacts with 1 equiv. of $LiHBEt_3$ in THF at low temperature to cleanly afford the corresponding C–N insertion product $(ArO)_2Ta[{=}NC^tBu{=}CHC^tBu{=}CHCH^tBu]$, characterized by X-ray diffraction. Additional experiments with other carbon nucleophiles (RMgCl, MeLi) in place of $LiHBEt_3$ have confirmed that the reaction occurs via initial addition of the hydride to the Ta atom, followed by an intramolecular *endo*-attack of the metal hydride onto the Py Cα atom, as depicted in Equation (23).[146]

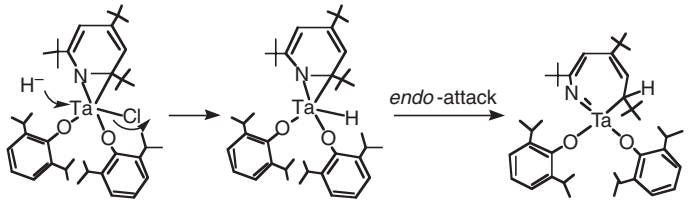

(23)

The most interesting conclusion that may be derived from this chemistry is that η^2(N,C) bonding produces a perturbation of the formally sp^2-Cα atom of py toward sp^3-hybridization, rendering it susceptible to nucleophilic attack by the hydride. However, this is not a general reaction, as the presence of the Bu^t groups on py is crucial for C–N bond cleavage. Neither the related Ta complex $(silox)_3Ta(\eta^2(N,C)\text{–}N\text{–}py)$ ($silox = OSiBu^t_3$) nor the quinoline derivative $(ArO)_2TaCl(\eta^2(N,C)\text{-}Q)$ undergoes C–N insertion upon nucleophilic addition. On the other hand, the η^2(N,C)-bonded Q ligand can be stoichiometrically hydrogenated to THQ under mild conditions, but free Q is not reduced. Another interesting related case of metal-assisted ring opening of py makes use of Nb complexes, as shown in Equation (24). The low-valent $(silox)_3Nb$ fragment coordinates py in the η^2(N,C) mode to yield $(silox)_3Nb(\eta^2(N,C)\text{–}NC_5H_5)$, which readily undergoes C–N insertion by thermolysis in benzene at 70 °C [56]. The stoichiometry of the reaction yields 0.5 equiv. of py and 0.5 equiv. of $(silox)_3Nb{=}CHCH{=}CHCH{=}CH\text{-}N{=}Nb(silox)_3$ as a thermodynamic mixture of *cis*,*cis*-, *trans*,*cis*-, *trans*,*trans*-, and *cis*,*trans*-isomers.

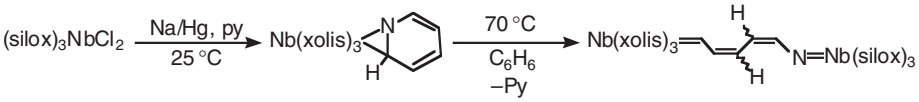

(24)

Within its own limitations, these reactions represent the only examples of ring-opening reactions of pyridines by metal complexes that can be related to HDN catalysis. The fact that in these cases C–N scission occurs without prior hydrogenation of the heterocycle is in contrast with the heterogeneous catalysis literature, which points to a dominant mechanism via prehydrogenation, but it has also been argued that C–N bond activation of the unsaturated molecule could be envisaged as a less H_2-consuming route for nitrogen extrusion.[146]

On the other hand, C–N bond hydrogenolysis of piperidine to various bis(piperidinyl)alkanes is promoted by $Rh_6(CO)_{16}$ in solution under water-gas shift conditions, but the real nature of this process is not clearly defined, and the harsh experimental conditions (150 °C, 60 atm CO) and the proven capability of heterogeneous catalysts to promote similar reactions of pyridines and piperidines have raised doubts on the homogeneous nature of the process. In addition, ring-substituted anilines $H_2N\text{–}Ph\text{–}X$ react with $(silox)_3Ta$ by oxidative addition of the N–H and/or the C–N bond, depending on the substituents present on the ring (Equation (25)):

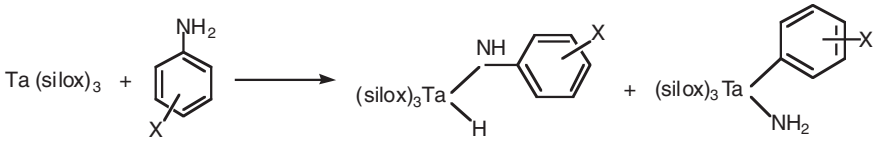

(25)

The propensity for C–N versus N–H activation correlates well with substituent Hammet parameters; groups that increase the basicity of aniline increase the relative rate of N–H activation, suggesting that nucleophilic attack by the amine at an empty d_{xz}/d_{yz} orbital of $Ta(silox)_3$ precedes oxidative addition. On the other hand, electron-withdrawing substituents decrease the rate of N–H activation and increase the rate of C–N activation, similarly to the effects observed on electrophilic aromatic substitution. Arylamine N–H versus C–N activation is therefore a consequence of

energetically similar pathways; electrophilic attack on the nitrogen lone pair is dominant in N–H scission, whereas nucleophilic attack on the arene ring is most important to C–N bond cleavage. This is a very interesting organometallic model of the last step in the heterogeneous HDN of quinoline, which involves the C–N bond cleavage of 2-Pr^n–aniline. Considering the composition of classical HDN catalysts (e.g., Ni–Mo–S or Ni–W–S), it is intriguing that this reaction takes place on an early transition metal complex. Related examples include the intramolecular oxidative addition of a C–N bond in the unstable intermediate "$[PhC(NSiMe_3)_2]_2Zr$" to yield $\{[PhC(NSiMe_3)_2]Zr(\eta^2\text{-}PhCNSiMe_3)(\mu\text{-}NSiMe_3)\}_2$[162] and the C–N bond cleavage of neutral and anionic amides by dinuclear Nb complexes.[163]

Late metals also cleave C–N bonds. For instance, $RuHCl(CO)(PPh_3)_3$ reacts with primary and secondary allylamines to yield the corresponding insertion products $Ru(CH_2CH_2CH_2NHR)Cl(CO)(PPh_3)_3$ (R = H, alkyl), but for tertiary amines (e.g., N,N-dimethylallylamine) the C–N bond is cleaved instead of inserting the olefinic moiety into the M–H bond, and the only metal-containing product is the stable π-allyl complex $Ru(\eta^3\text{-}C_3H_5)Cl(CO)(PPh_3)_2$; the nitrogen atom is eliminated with the hydride in the form of dimethylamine.[164] *N*,*N*,*N*′,*N*′-tetraethylethylenediamine undergoes single or double intramolecular dealkylation reactions in the presence of $[RuCl_2(diene)]_x$ under moderate conditions, according to Equation (26).[165]

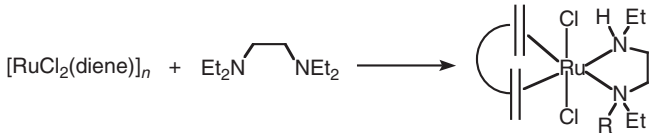

(26)

R = Et for NBD
R = H for COD

Alkyl–ammonium or –imminium tetraphenylborate salts readily undergo oxidative addition to $(Cy_3P)_2Ni(\eta^2\text{-}CO_2)$ or $(Cy_3P)_2Ni(\mu\text{-}N_2)Ni(PCy_3)_2$ at or below room temperature to yield the corresponding Ni(II) derivatives containing coordinated NH_3 or imine, besides the hydrocarbon moiety that remains bound to the metal in the form of a η^3-allyl ligand. This chemistry illustrates reaction pathways related to those taking part in HDN processes using Ni-based heterogeneous catalysts, where the organonitrogen substrates may be protonated by surface –OH or –SH groups prior to denitrogenation. The reaction on Ni phosphine compounds, however, does not seem to be general, since changing the substituent on the imminium cation from $-C_3H_5$ to $-CH_2Ph$ causes a switch from C–N to N–H activation. An extensive theoretical study of the mechanism of the Ni-induced C–N bond activation indicates that the active catalyst is the (bis)phosphine Ni complex; for allylammonium salts, the reaction proceeds by an associative rather than a dissociate mechanism involving coordination of the allylammonium cation to the metal center followed by oxidative addition of the C–N bond to Ni(0). The resulting NH_3 remains coordinated to Ni(II) in a pentacoordinated intermediate, and finally a phosphine is lost to generate the final product. The reaction of the imminium salts, on the other hand, follows a dissociative mechanism.[166–168]

1.27.3.3 Conclusion

Metal complexes are reasonable models for mimicking some of the steps involved in heterogeneous HDN. The η^1-N and η^6-coordination modes of aromatic N-heterocycles are involved in their hydrogenation, whereas η^2(N,C) binding can be related to C–N bond breaking and hydrogenolysis. While the hydrogenation of the heterocyclic rings is effectively accomplished by late transition metals, C–N bond cleavage of heteroaromatic rings is best accomplished with early transition metals. The fact that Nb complexes are capable of oxidatively adding the C–N bond of anilines takes the organometallic modeling a step closer to the more conventional HDN mechanisms. For non-aromatic amines, electron-rich late metals (Ru, Ni) are better suited for cleaving C–N bonds, more in line with the components of real HDN catalysts, particularly in the case of nickel. The mechanisms reported so far in these cases imply either an intramolecular nucleophilic attack by a metal hydride, or protonation of the N atom, followed by elimination of ammonia or an amine, similarly to the accepted denitrogenation mechanisms. Analogous reactions on primary aliphatic amines would be most welcome. Considering the complexity of the HDN mechanisms, the homogeneous modeling studies must taken with the necessary caution. Nonetheless, many reactions described involving transition metal complexes with N-heterocycles or other N-ligands show some striking analogies with related reactions occurring on the surface of heterogeneous catalysts. Organometallic HDN modeling is far behind HDS modeling, but the research described in this section opens the way for further work on this field of molecular analogs of surface

species and interactions. The development of this area is to be encouraged as an additional contribution to the understanding of the complex issues involved, and to the design of novel catalysts of better performance in practical applications.

1.27.4 Concluding Remarks

A number of exciting concepts have emerged over the last two decades connecting organometallic with surface chemistry and homogeneous with heterogeneous catalysis, in relation to the important HDS and HDN reactions. Organometallic modeling has become a powerful method to study many aspects of the complex HDS and HDN mechanisms, which is best used in conjunction with the modern analytical arsenal of solid-state and surface chemistry. As with any modeling, intrinsic limitations must always be kept in mind and extrapolations must be made with great caution. Solution chemistry of well-defined complexes necessarily ignores the influence of supports and other surface cooperative effects that are very important in heterogeneous catalysis. At the same time, solvent effects that have no relevance in reactions on solid catalysts are introduced when dealing with homogeneous solutions. Some molecular geometries and rearrangements that appear very reasonable in metal complexes, and particularly in clusters, may not be available in more rigid extended solids, and vice versa. Thus, the best possible chemical sense must be employed when trying to use organometallic models in order to explain surface phenomena. Still, this is a fascinating example of how two traditionally separated fields can come together in an effort to solve a complex fundamental chemical problem related to important environmental and industrial issues.

References

1. Topsøe, H; Clausen, B. S.; Masoth, F. E. Hydrotreating Catalysis. In *Catalysis Science and Technology*; Anderson, J. R., Boudart, M., Eds.; Springer: New York, 1996; Vol. 11.
2. Weber, T, Prins, R, van Santen, R. A., Eds.; *Transition Metal Sulphides, Chemistry and Catalysis*, NATO ASI Series; Kluwer: Dordrecht, 1998.
3. Kabe, T.; Ishihara, A; Qian, W. *Hydrodesulfurization and Hydrodenitrogenation;* Wiley: Tokyo, 1999.
4. Sánchez-Delgado, R. A.; Organometallic Modeling of the Hydrodesulfurization and Hydrodenitrogenation Reactions. In *Catalysis by Metal Complexes*; James, B. R., van Leeuwen, P. W. N. M., Eds.; Kluwer: Dordrecht, 2002; Vol. 24.

4a. Sánchez-Delgado, R. A. In *Encyclopedia of Catalysis*; Horvath, I. T., Ed., Wiley: New York, 2002.

4b. Sánchez-Delgado, R. A. *J. Mol. Catal.* **1994**, *86*, 287.

5. Angelici, R. J. *Coord. Chem. Rev.* **1990**, *105*, 61.

5a. Angelici, R. J. In *Encyclopedia of Inorganic Chemistry*; King, R. B., Ed.; Wiley: New York, 2002.

5b. Angelici, R. J. *Bull. Soc. Chim. Belg.* **1995**, *104*, 265.

5c. Angelici, R. J. *Polyhedron* **1997**, *16*, 3073.

5d. Angelici, R. J. *Organometallics* **2001**, *20*, 1259.

6. Bianchini, C.; Meli, A. *J. Chem. Soc., Dalton Trans.* **1996**, 801.

6a. Bianchini, C.; Meli, A. *Acc. Chem. Res.* **1998**, *31*, 109.

6b. Bianchini, C.; Meli, A. In *Transition Metal Sulfides, Chemistry and Catalysis*; Weber, Th., Prins, R., van Santen, R. A., Eds.; NATO ASI Series; Kluwer: Dordrecht, 1998.

7. Bianchini, C.; Meli, A.; Vizza, F. *Eur. J. Inorg. Chem.* **2001**, 43.

7a. Fish, R. H.; Bianchini, C. In *Encyclopedia of Catalysis*; Horvath, I. T., Ed.; Wiley: New York, 2002.

8. Reynolds, M. A.; Guzei, I. A.; Logsdon, B. C.; Thomas, L. M.; Jacobson, R. A.; Angelici, R. J. *Organometallics* **1999**, *18*, 4075.
9. Alvarez, M.; Lugan, N.; Donnadieu, B.; Mathieu, R. *Organometallics* **1995**, *14*, 365.
10. Churchill, D. G.; Bridgewater, B. M.; Parkin, G. *J. Am. Chem. Soc.* **2000**, *122*, 178.
11. Choi, M.-G.; Angelici, R. J. *Organometallics* **1991**, *10*, 2436.
12. Choi, M.-G.; Angelici, R. J. *Organometallics* **1992**, *11*, 3328.
13. White, C. J.; Angelici, R. J. *Organometallics* **1994**, *13*, 5132.

13a. Robertson, M. J.; White, C. J.; Angelici, R. J. *J. Am. Chem. Soc.* **1994**, *116*, 5190.

14. Reynolds, M. A.; Guzei, I. A.; Angelici, R. J. *J. Am. Chem. Soc.* **2002**, *124*, 1689.
15. Goodrich, J. D.; Nickias, P. N.; Selegue, J. P. *Inorg. Chem.* **1987**, *26*, 3424.
16. Catheline, D.; Astruc, D. *J. Organomet. Chem.* **1983**, *248*, C9.
17. Draganjac, M.; Rauchfuss, T. B.; Ruffin, C. J. *Organometallics* **1985**, *4*, 1909.
18. Bucknor, S. M.; Draganjac, M.; Rauchfuss, T. B.; Ruffin, C. J.; Fultz, W. C.; Rheingold, A. L. *J. Am. Chem. Soc.* **1984**, *106*, 5379.
19. Borowski, A. F.; Sabo-Etienne, S.; Donnadieu, B.; Chaudret, B. *Organometallics* **2003**, *22*, 4803.
20. Benson, J. W.; Angelici, R. J. *Organometallics* **1992**, *11*, 922.

20a. Vecchi, P. A.; Ellern, A.; Angelici, R. J. *J. Am. Chem. Soc.* **2003**, *125*, 2064.

20b. Vecchi, P. A.; Ellern, A.; Angelici, R. J. *Organometallics* **2005**, *24*, 2168.

21. Sánchez-Delgado, R. A.; Herrera, V.; Bianchini, C.; Masi, D.; Mealli, C. *Inorg. Chem.* **1993**, *32*, 3766.
22. Rao, K. M.; Day, C. L.; Jacobson, R. A.; Angelici, R. J. *Inorg. Chem.* **1991**, *30*, 5046.
23. Delafuente, D. A.; Myers, W. H.; Sabat, M.; Harman, W. D. *Organometallics* **2005**, *24*, 1876.
24. Spera, M. L.; Harman, W. D. *Organometallics* **1995**, *14*, 1559.

24a. Cordonne, R.; Harman, W. D.; Taube, H. *J. Am. Chem. Soc.* **1989**, *111*, 5969.
25. Bianchini, C.; Meli, A.; Peruzzini, M.; Vizza, F.; Moneti, S.; Herrera, V.; Sánchez-Delgado, R. A. *J. Am. Chem. Soc.* **1994**, *116*, 4370.
26. Chen, J.; Daniels, L. M.; Angelici, R. J. *Organometallics* **1989**, *8*, 2277.
27. Chen, J.; Angelici, R. J. *J. Am. Chem. Soc.* **1990**, *112*, 199.
28. Chen, J.; Angelici, R. J. *Coord. Chem. Rev.* **2000**, *206–207*, 63.
29. Luo, S.; Ogilvy, A. E.; Rauchfuss, T. B.; Rheingold, A. L.; Wilson, S. R. *Organometallics* **1991**, *10*, 1002.
30. Skaugset, A. E.; Rauchfuss, T. B.; Stern, C. L. *J. Am. Chem. Soc.* **1990**, *112*, 2432.
31. Luo, S.; Rauchfuss, T. B.; Wilson, S. R. *J. Am. Chem. Soc.* **1992**, *114*, 8515.
32. Luo, S.; Rauchfuss, T. B.; Wilson, S. R. *Organometallics* **1992**, *11*, 3497.
33. Fischer, E. O.; Öfele, K. *Chem. Ber.* **1958**, *91*, 2395.
34. Bailey, M. F.; Dahl, L. F. *Inorg. Chem.* **1965**, *4*, 1306.
35. Rauchfuss, T. B. *Prog. Inorg. Chem.* **1991**, *39*, 259.
36. Öfele, K. *Chem. Ber.* **1966**, *99*, 1732.
37. Sanger, M. J.; Angelici, R. J. *Organometallics* **1994**, *13*, 1821.
38. Janak, K. E.; Tanski, J. M.; Churchill, D. G.; Parkin, G. *J. Am. Chem. Soc.* **2002**, *124*, 4182.
39. Singer, H. *J. Organomet. Chem.* **1967**, *9*, 135.
40. Huckett, S. C.; Sauer, N. N.; Angelici, R. J. *Organometallics* **1987**, *6*, 591.
40a. Lesch, D. A.; Richardson, J. W., Jr.; Jacobson, R. A.; Angelici, R. J. *J. Am. Chem. Soc.* **1984**, *106*, 2901.
41. Guerchais, V; Astruc, D. *J. Organomet. Chem.* **1986**, *316*, 335.
42. Bachmann, P.; Singer, H. *Z. Naturforsch.* **1976**, *31b*, 525.
43. Lee, C. C.; Iqbal, M.; Gill, U. S.; Sutherland, R. G. *J. Organomet. Chem.* **1985**, *288*, 89.
44. Braitsch, D. M.; Kumarappan, R. *J. Organomet. Chem.* **1975**, *84*, C37.
45. Spies, G. H.; Angelici, R. J. *J. Am. Chem. Soc.* **1985**, *107*, 5569.
46. Sauer, N. N.; Angelici, R. J. *Organometallics* **1987**, *6*, 1146.
47. Hachgenei, J. W.; Angelici, R. J. *Organometallics* **1989**, *8*, 14.
48. Chaudret, B.; Jalón, F.; Pérez-Manrique, M.; Lahoz, F.; Plou, F. J.; Sánchez-Delgado, R. A. *Nouv. J. Chim.* **1990**, *14*, 331.
49. Lockemeyer, J. R.; Rauchfuss, T. B. A.; Rheingold, L.; Wilson, S. R. *J. Am. Chem. Soc.* **1989**, *111*, 8828.
50. Ganja, E. A.; Rauchfuss, T. B.; Wilson, S. R. *Organometallics* **1991**, *10*, 270.
51. Russell, M. J. H.; White, C.; Yates, A.; Maitlis, P. M. *J. Chem. Soc., Dalton Trans.* **1978**, 857.
52. Sánchez-Delgado, R. A.; Márquez-Silva, R.-L.; Puga, J.; Tiripicchio, A.; Tiripicchio-Camellini, M. *J. Organomet. Chem.* **1986**, *316*, C35.
53. Hucket, S. C.; Miller, L. L.; Jacobson, R. A.; Angelici, R. J. *Organometallics* **1988**, *7*, 686.
54. Dullagham, C. A.; Zhang, X.; Greene, D. L.; Carpenter, G. B.; Sweigart, D. A.; Camiletti, C.; Ralaseelan, E. *Organometallics* **1998**, *17*, 3316.
54a. Zhang, X.; Dullaghan, C. A.; Watson, E. J.; Carpenter, G. B.; Sweigart, G. B. *Organometallics* **1998**, *17*, 2067.
54b. Sun, S.; Dullaghan, C. A.; Sweigart, D. A. *J. Chem. Soc., Dalton Trans.* **1996**, 4493.
55. Lee, C. C.; Steele, B. R.; Sutherland, R. G. *J. Organomet. Chem.* **1980**, *186*, 265.
56. Hucket, S. C.; Angelici, R. J. *Organometallics* **1988**, *7*, 1491.
57. Wang, C.-M.; Angelici, R. J. *Organometallics* **1990**, *9*, 1770.
58. Chen, J.; Angelici, R. J. *Organometallics* **1999**, *18*, 5721.
59. Vecchi, P. A.; Ellern, A.; Angelici, R. J. *Organometallics* **2005**, *24*, 3725.
60. Reynolds, M. A.; Ovchinnikov, M. V.; Angelici, R. J.; Stinner, C.; Weber, T.; Prins, R. *J. Phys. Chem. A* **2001**, *105*, 4418.
61. Harris, S. *Organometallics* **1994**, *13*, 2628.
61a. Harris, S. *Polyhedron* **1997**, *16*, 3219.
62. Choi, M.-G.; Angelici, R. J. *J. Am. Chem. Soc.* **1989**, *111*, 8753.
63. Dong, L.; Duckett, S. B.; Ohman, K. F.; Jones, W. D. *J. Am. Chem. Soc.* **1989**, *114*, 151.
63a. Sargent, A. L.; Titus, E. *Organometallics* **1998**, *17*, 65.
64. Ruette, F.; Valencia, N.; Sánchez-Delgado, R. A. *J. Am. Chem. Soc.* **1989**, *111*, 40.
65. Schultz, R. H. *Organometallics* **2004**, *23*, 4349.
66. Harman, W. D. *Chem. Rev.* **1997**, *97*, 1953.
66a. Spera, M. L.; Harman, W. D. *Organometallics* **1999**, *18*, 2988.
66b. Brooks, B. C.; Gunnoe, T. B.; Harman, W. D. *Coord. Chem. Rev.* **2000**, *206–207*, 3.
67. Diez y Riega, H.; Rincón, L.; Almeida, R. *THEOCHEM* **1999**, *493*, 259.
68. Chen, J.; Angelici, R. J. *Inorg. Chim. Acta* **2002**, *334*, 204.
69. Skaugset, A. E.; Rauchfuss, T. B.; Stern, C. L. *J. Am. Chem. Soc.* **1990**, *112*, 2432.
70. Spies, G. H.; Angelici, R. J. *Organometallics* **1987**, *6*, 1897.
71. Watts, W. E. In *Comprehensive Organometallic Chemistry I*; Wilkinson, G., Stone, F. G. A., Abel, E. W., Eds.; Pergamon: Oxford, 1982; Vol. 8, p 1013.
71a. Semmelhack, M. F. In *Comprehensive Organometallic Chemistry II*; Abel, E. W., Stone, F. G. A., Wilkinson, G., Eds.; Elsevier: Oxford, 1995; Vol. 9, Chapters 9.1–9.3.
72. Hucket, S. C.; Angelici, R. J. *Organometallics* **1988**, *7*, 1491.
72a. Wang, C.-M.; Angelici, R. J. *Organometallics* **1990**, *9*, 1770.
73. Mc Kinley, S. G.; Angelici, R. J. *Energy Fuels* **2003**, *17*, 1480.
73a. Mc Kinley, S. G.; Vecchi, P. A.; Ellern, A.; Angelici, R. J. *Dalton Trans.* **2004**, 788.
74. Dyson, P. J. *Dalton Trans.* **2003**, 2964.
75. Widegreen, J. A.; Finke, R. G. *J. Mol. Catal. A: Chem.* **2003**, *191*, 187.
76. Fish, R. H. *Ann. N. Y. Acad. Sci.* **1983**, *415*, 292.
77. Grey, R. A.; Pez, G. P.; Wallo, A. *J. Am. Chem. Soc.* **1980**, *102*, 5949.
77a. Linn, D. E.; Halpern, J. *J. Am. Chem. Soc.* **1987**, *109*, 2969.
78. Bennet, M. A.; Huang, T.-N.; Turney, T. W. *J. Chem. Soc., Chem. Commun.* **1979**, 312.
79. Landis, C. R.; Halpern, J. *Organometallics* **1983**, *2*, 840.
80. Bianchini, C.; Meli, A. In *Aqueous-Phase Organometallic Catalysis – Concepts and Applications*; Cornils, B., Herrmann, W. A., Eds.; VCH: Weinheim, 1998, p 477.

80a. Bianchini, C.; Meli, A.; Vizza, F. In *Applied Homogenous Catalysis with Organometallic Compounds*; Wiley: New York, **2002**; Vol. 3, p 1099.
80b. Bianchini, C.; Meli, A.; Vizza, F. *J. Organomet. Chem.* **2004**, *689*, 4277.
81. Greenfield, H.; Metlin, S.; Orchin, M.; Wender, I. *J. Org. Chem.* **1958**, *23*, 1054.
82. Bianchini, C.; Meli, A.; Peruzzini, M.; Vizza, F.; Herrera, V.; Sánchez-Delgado, R. A. *Organometallics* **1994**, *13*, 721.
83. Sánchez-Delgado, R. A.; González, E. *Polyhedron* **1989**, *8*, 1431.
84. Paez, D. E.; Andriollo, A.; Sánchez-Delgado, R. A.; Valencia, N.; Lopez-Linares, F.; Galiasso, R. *(INTEVEP). U.S. Patent 5,753,584 5*, May 19 1998.
84a. Paez, D. E.; Andriollo, A.; Sánchez-Delgado, R. A.; Valencia, N.; Lopez-Linares, F.; Galiasso, R. *(INTEVEP). U.S. Patent 5,958,223*, September 28 1999.
84b. Paez, D. E.; Andriollo, A.; Sánchez-Delgado, R. A.; Valencia, N.; Lopez-Linares, F.; Galiasso, R. *(INTEVEP). U.S. Patent 5,981,421*, November 1999.
85. Bianchini, C.; Meli, A.; Moneti, S.; Oberhauser, W.; Vizza, F.; Herrera, V.; Fuentes, A.; Sánchez-Delgado, R. A. *J. Am. Chem. Soc.* **1999**, *121*, 7071.
86. Fish, R. H.; Baralt, E.; Smith, S. J. *Organometallics* **1991**, *10*, 54.
87. Sánchez-Delgado, R. A.; Herrera, V.; Rincón, L.; Andriollo, A.; Martín, G. *Organometallics* **1994**, *13*, 553.
88. Herrera, V.; Fuentes, A.; Rosales, M.; Sánchez-Delgado, R. A.; Bianchini, C.; Meli, A.; Vizza, F. *Organometallics* **1997**, *16*, 2465.
89. Bianchini, C.; Meli, A.; Patinec, V.; Sernau, V.; Vizza, F. *J. Am. Chem. Soc.* **1997**, *119*, 4945.
89a. Bianchini, C.; Meli, A. *Acc. Chem. Res.* **1998**, *31*, 109.
90. Baralt, E.; Smith, S. J.; Hurwitz, I.; Horváth, I. T.; Fish, R. H. *J. Am. Chem. Soc.* **1992**, *114*, 5187.
91. Hinchliffe, A.; Soscún-Machado, H. J. *THEOCHEM* **1995**, *334*, 235.
92. Gao, H.; Angelici, R. J. *J. Mol. Catal. A: Chem.* **1999**, *149*, 63.
92a. Gao, H.; Angelici, R. J. *Organometallics* **1999**, *18*, 989.
92b. Yang, H; Gao, H.; Angelici, R. J. *Organometallics* **2000**, *19*, 622.
92c. Stanger, K. J.; Tang, Y.; Anderegg, J.; Angelici, R. J. *J. Mol. Catal. A: Chem.* **2003**, *202*, 147.
93. Myers, A. W.; Jones, W. D. *Organometallics* **1996**, *15*, 2905.
94. Selnau, H. E.; Merola, J. S. *Organometallics* **1993**, *12*, 1583.
95. Paneque, M; Taboada, S.; Carmona, E. **1996**, *15*, 2678.
96. Jones, W. D.; Chin, R. M. *Organometallics* **1992**, *11*, 2698.
96a. Jones, W. D.; Chin, R. M. *J. Organomet. Chem.* **1994**, *472*, 311.
97. Paz-Sandoval, M. A.; Cervantes-Vasquez, M.; Young, V. M., Jr.; Guzei, I. A.; Angelici, R. J. *Organometallics* **2004**, *23*, 1274.
98. Mills, R. C.; Abboud, K. A.; Boncella, J. M. *J. Chem. Soc., Chem. Commun.* **2001**, 1506.
99. Bianchini, C.; Meli, A.; Peruzzini, M.; Vizza, F.; Frediani, P; Herrera, V.; Sánchez-Delgado, R. A. *J. Am. Chem. Soc.* **1993**, *115*, 2731.
100. Bianchini, C.; Jimenez, V.; Meli, A.; Vizza, F.; Herrera, V.; Sánchez-Delgado, R. A. *Organometallics* **1995**, *14*, 2342.
101. Bianchini, C.; Meli, A.; Moneti, S.; Vizza, F. *J. Organomet. Chem.* **1998**, *17*, 2636.
102. Rosini, G. P.; Jones, W. D. *J. Am. Chem. Soc.* **1992**, *114*, 10767.
103. García, J.; Maitlis, P. M. *J. Am. Chem. Soc.* **1993**, *115*, 12200.
103a. García, J.; Mann, B. E.; Adams, H.; Bailey, N. A.; Maitlis, P. M. *J. Am. Chem. Soc.* **1995**, *117*, 2179.
103b. García, J.; Arévalo, A.; Montiel, F.; del Rio, F.; Quiroz, B.; Adams, H.; Maitlis, P. M. *Organometallics* **1997**, *16*, 3216.
103c. García, J.; Arévalo, A.; Capella, S.; Chehata, A.; Hernández, M.; Montiel, F.; Picazo, G.; del Rio, F.; Toscano, A., Adams, H., *et al. Polyhedron* **1997**, *16*, 3185.
103d. Iretskii, A.; Adams, H.; García, J. J.; Picazo, G.; Maitlis, P. M. *J. Chem. Soc., Chem. Commun.* **1999**, 61.
103e. Iretskii, A.; García, J. J.; Picazo, G.; Maitlis, P. M. *Catal. Lett.* **1998**, *51*, 129.
103f. Arévalo, A.; Bernès, S.; García, J. J.; Picazo, G.; Maitlis, P. M. *Organometallics* **1999**, *18*, 1680.
104. Picazo, G.; Arévalo, A.; Bernès, S.; García, J. J. *Organometallics* **2003**, *22*, 4734.
105. Hernández, M.; Miralrio, G.; Arévalo, A.; Bernès, S.; García, J. J.; López, C.; Maitlis, P. M.; del Rio, F. *Organometallics* **2001**, *20*, 4061.
106. Chantson, J.; Görls, H.; Lotz, S. *J. Organomet. Chem.* **2003**, *687*, 39.
107. Vicic, D. A.; Jones, W. D. *J. Am. Chem. Soc.* **1997**, *119*, 10855.
107a. Vicic, D. A.; Jones, W. D. *Organometallics* **1998**, *17*, 3411.
107b. Vicic, D. A.; Jones, W. D. *J. Am. Chem. Soc.* **1999**, *121*, 4070.
107c. Jones, W. D. *J. Am. Chem. Soc.* **1999**, *121*, 7606.
108. Oster, S. S.; Lachicotte, R. J.; Jones, W. D. *Inorg. Chim. Acta* **2002**, *330*, 118.
109. Brorson, M.; King, J. D.; Kiriakidou, K.; Prestopino, F.; Nordlander, E. In *Metal Clusters in Chemistry*; Braunstein, P., Oro, L. A., Raithby, P. R., Eds.; Wiley: Weinheim, 1999; Vol. 2, p 741.
110. Kaesz, H. D.; King, R. B.; Manuel, T. A.; Nichols, L. D.; Stone, F. G. A. *J. Am. Chem. Soc.* **1960**, *82*, 4749.
110a. Hubener, P.; Weiss, E. *J. Organomet. Chem.* **1977**, *129*, 105.
110b. Ogilvy, A. E.; Draganjac, M.; Rauchfuss, T. B.; Wilson, S. R. *Organometallics* **1988**, 7, 1171.
111. Arce, A. J.; Arrojo, P.; Deeming, A. J.; De Sanctis, Y. *J. Chem. Soc., Dalton Trans.* **1992**, 2423.
111a. Arce, A. J.; De Sanctis, Y.; Karam, A.; Deeming, A. J. *Angew. Chem., Int. Ed. Engl.* **1994**, *33*, 1381.
112. Chehata, A.; Oviedo, A.; Arévalo, A.; Bernès, S.; García, J. J. *Organometallics* **2003**, *22*, 1585.
113. Matsubara, K.; Okamura, R.; Tanaka, M.; Suzuki, H. *J. Am. Chem. Soc.* **1998**, *120*, 1108.
114. Adams, R. D.; Kwon, O.-S.; Perrin, J. L. *J. Organomet. Chem.* **1999**, *584*, 223.
115. Reynolds, M. A.; Guzei, I. A.; Angelici, R. J. *Organometallics* **2001**, *20*, 1071.
115a. Reynolds, M. A.; Guzei, I. A.; Angelici, R. J. *J. Am. Chem. Soc.* **2002**, *124*, 1689.
115b. Reynolds, M. A.; Guzei, I. A.; Angelici, R. J. *Inorg. Chem.* **2003**, *42*, 2191.
116. Jones, W. D.; Chin, R. M. *J. Am. Chem. Soc.* **1994**, *116*, 198.
116a. Vicic, D. A.; Jones, W. D. *Organometallics* **1999**, *18*, 134.
116b. Vicic, D. A.; Jones, W. D. *Organometallics* **1997**, *16*, 1912.
117. Boorman, P. M.; Gao, X.; Fait, J. F.; Parvez, M. *Inorg. Chem.* **1991**, *30*, 3886.
118. Bianchini, C.; Jimenez, M. V.; Meli, A.; Moneti, S.; Patinec, V.; Vizza, F. *Organometallics* **1997**, *16*, 5696.
119. Dullagham, C. A.; Carpenter, G. B.; Sweigart, D. A.; Choi, S. S.; Lee, S. S.; Chung, Y. K. *Organometallics* **1997**, *16*, 5688.

120. Chen, J.; Angelici, R. J. *Inorg. Chim. Acta* **2002**, *334*, 204.
120a. Chen, J.; Young, V. G., Jr.; Angelici, R. J. *Organometallics* **2002**, *21*, 5951.
121. Chen, J.; Young, V. G., Jr.; Angelici, R. J. *Inorg. Chim. Acta* **2005**, *358*, 1623.
122. Li, H.; Yu, K.; Watson, E. J.; Virkaitis, K. L.; D'Acchiolo, J. S.; Carpenter, G. B.; Sweigart, D. A.; Czech, P. T.; Overly, K. R.; Coughlin, F. *Organometallics* **2002**, *21*, 1262.
123. Palmer, M. S.; Harris, S. *Organometallics* **2000**, *19*, 2114.
124. Riaz, U.; Curnow, O. J.; Curtis, M. D. *J. Am. Chem. Soc.* **1994**, *116*, 4357.
125. Curtis, M. D.; Drucker, S. H. *J. Am. Chem. Soc.* **1997**, *119*, 1027.
126. Herbst, K.; Monari, M.; Brorson, M. *Inorg. Chem.* **2002**, *41*, 1336.
127. Bianchini, C.; Casares, J. A.; Meli, A.; Sernau, V.; Vizza, F.; Sánchez-Delgado, R. A. *Polyhedron* **1997**, *16*, 3099.
128. Torres-Nieto, J.; Arévalo, A.; García-Gutierrez, P.; Acosta-Ramírez, A.; García, J. J. *Organometallics* **2004**, *23*, 4534.
129. Parkin, G. *Prog. Inorg. Chem.* **1998**, *47*, 1.
129a. Peruzzini, M.; De los Rios, I.; Romerosa, A. *Prog. Inorg. Chem.* **2001**, *49*, 169.
130. Rakowski DuBois, M. *Chem. Rev.* **1989**, *89*, 1.
130a. Rakowski DuBois, M.; Jagirdar, B.; Noll, B.; Dietz, S. In *Transition Metal Sulfur Chemistry: Biological and Industrial Significance*; Stiefel, E. I., Matsumoto, K., Eds.; American Chemical Society: Washington, DC, 1996; p 269.
130b. Rakowski DuBois, M. *Polyhedron* **1997**, *16*, 3089.
130c. Rakowski DuBois, M. In *Catalysis by Di- and Polynuclear Metal Cluster Complexes*; Adams, R. D., Cotton, F. A., Eds.; VCH: New York, 1998; p 127.
130d. Rakowski DuBois, M.; Van Derveer, M. C.; DuBois, D. L.; Haltiwanger, R. C.; Miller, W. K. *J. Am. Chem. Soc.* **1980**, *102*, 7456.
130e. Gabay, J.; Dietz, S.; Bernatis, P.; Rakowski DuBois, M. *Organometallics* **1993**, *12*, 3630.
131. Rakowski DuBois, M.; Jagirdar, B. R.; Dietz, S.; Noll, B. C. *Organometallics* **1997**, *16*, 294.
132. Bianchini, C.; Mealli, C.; Meli, A.; Sabat, M. *Inorg. Chem.* **1986**, *25*, 4618.
132a. Ienco, A.; Calhorda, M. J.; Reinhold, J.; Reineri, F.; Bianchini, C.; Peruzzini, M.; Vizza, F.; Mealli, C. *J. Am. Chem. Soc.* **2004**, *126*, 11954.
133. Linck, R. C.; Pafford, R. J.; Rauchfuss, T. B. *Inorg. Chem.* **2004**, *43*, 4314.
134. Sweeney, Z. K.; Polse, J. L.; Bergman, R. G.; Andersen, R. A. *J. Am. Chem. Soc.* **1997**, *119*, 4543.
134a. Sweeney, Z. K.; Polse, J. L.; Andersen, R. A.; Bergman, R. G. *Organometallics* **1999**, *18*, 5502.
135. Herberhold, M.; Süss, G. *Angew. Chem., Int. Ed. Engl.* **1976**, *15*, 366.
135a. Urban, G.; Sünkel, K. H.; Beck, W. *J. Organomet. Chem.* **1985**, *290*, 329.
135b. Herberhold, M.; Süss, G. *J. Chem. Res. Synop* **1977**, 246.
136. Strohmeier, W.; Guttenberger, J. F. *Chem. Ber.* **1964**, *97*, 1871.
136a. Harris, P. J.; Knox, S. A. R.; McKinney, R. J.; Stone, F. G. A. *J. Chem. Soc., Dalton Trans.* **1978**, 1009.
136b. Raab, K.; Beck, W. *Chem. Ber.* **1985**, *118*, 3830.
137. Kuehn, C. G.; Taube, H. *J. Am. Chem. Soc.* **1976**, *98*, 689.
137a. Sellman, D.; Lechner, P.; Knoch, F.; Moll, M. *J. Am. Chem. Soc.* **1992**, *114*, 922.
137b. Mudalige, D. C.; Ma, E. S.; Rettig, S. J.; James, B. R.; Cullen, W. R. *Inorg. Chem.* **1997**, *36*, 1809.
137c. Ma, E. S.; Rettig, S. J.; James, B. R. *J. Chem. Soc., Chem. Commun.* **1999**, 2463.
137d. Amarasekera, J.; Rauchfuss, T. B. *Inorg. Chem.* **1989**, *28*, 3875.
137e. Field, J. S.; Haines, R. J.; Sundermeyer, J.; Woolam, S. F. *J. Chem. Soc., Dalton Trans.* **1993**, 2735.
137f. Belchem, G.; Steed, J. W.; Tacher, D. A. *J. Chem. Soc., Dalton Trans.* **1997**, 1949.
138. Crabtree, R. H.; Davis, M. W.; Mellea, M. F.; Mihelcic, J. M. *Inorg. Chim. Acta* **1983**, *72*, 223.
139. Ugo, R.; La Monica, G.; Cenini, S.; Segre, A.; Conti, F. *J. Chem. Soc. A* **1971**, 522.
140. Bach, H.-J.; Brunner, H.; Wachter, J.; Tsunoda, M.; Leblanc, J.-C.; Moïse, C. *Inorg. Chem. B* **1973**, *29*, 584.
140a. Nelson, J. E.; Parkin, G.; Bercaw, J. E. *Organometallics* **1992**, *11*, 2181.
141. Murphy, V. J.; Parkin, G. *J. Am. Chem. Soc.* **1995**, *117*, 3522.
141a. Rabinovich, D.; Parkin, G. *Inorg. Chem.* **1996**, *34*, 6341.
142. Dupré, N.; Hendricks, H. M. J.; Jordanov, J. *J. Chem. Soc., Dalton Trans.* **1984**, 1463.
143. Schwartz, D. E.; Dopke, J. A.; Rauchfuss, T. B.; Wilson, S. R. *Angew. Chem., Int. Ed. Engl.* **2001**, *40*, 2351.
144. Di Vaira, M.; Midollini, S.; Sacconi, L. *Inorg. Chem.* **1977**, *16*, 1518.
145. James, B. R. *Pure Appl. Chem.* **1997**, *69*, 2213.
146. Weller, K. J.; Fox, P. A.; Gray, S. D.; Wigley, D. E. *Polyhedron* **1997**, *16*, 3139.
147. Rakowski DuBois, M. *Coord. Chem. Rev.* **1998**, *174*, 191.
148. Jones, W. D.; Dong, L; Myers, A. W. *Organometallics* **1995**, *14*, 855.
149. Zhu, G.; Tanski, J. M.; Churchill, D. G.; Janak, K. E.; Parkin, G. *J. Am. Chem. Soc.* **2002**, *124*, 13658.
150. Borowski, A. F.; Sabo-Etienne, S.; Donnadieu, B.; Chaudret, B. *Organometallics* **2003**, *22*, 1630.
151. López, C.; Barón, G.; Arévalo, A.; Muñoz-Hernández, M. A.; García, J. J. *J. Organomet. Chem.* **2002**, *664*, 170.
152. Rakowski DuBois, M.; Vasquez, L. D.; Ciancianelli, R. F.; Noll, B. C. *Organometallics* **2000**, *19*, 3507.
153. Vicic, D. A.; Jones, W. D. *Organometallics* **1999**, *18*, 134.
154. Arce, A. J.; Machado, R.; De Sanctis, Y.; Capparelli, M. V.; Atencio, R.; Manzur, J.; Deeming, A. J. *Organometallics* **1997**, *16*, 1735.
155. Vasquez, L. D.; Noll, B. C.; Rakowski DuBois, M. *Organometallics* **1998**, *17*, 976.
155a. Chen, S.; Vasquez, L. D.; Noll, B. C.; Rakowski DuBois, M. *Organometallics* **1997**, *16*, 1757.
156. Reedijk, J. In *Comprehensive Coordination Chemistry*; Wilkinson, G., Gillard, R. D., McCleverty, J., Eds.; Pergamon: Oxford, 1987; Vol. 2.
157. Rosales, M.; González, T.; Atencio, R.; Sánchez-Delgado, R. A. *Dalton Trans.* **2004**, 2952.
158. Deeming, A. J.; Stchedroff, M. J.; Whitaker, C.; Arce, A. J.; De Sanctis, Y.; Steed, J. W. *J. Chem. Soc., Dalton Trans.* **1999**, 3289.
159. Neithamer, D. R.; Parkanyi, L.; Mitchell, J. F.; Wolczanski, P. T. *J. Am. Chem. Soc.* **1988**, *110*, 4421.
159a. Covert, K. J.; Neithamer, D. R.; Zonnevylle, M. C.; LaPointe, R. E.; Schaller, C.; Wolczanski, P. T. *Inorg. Chem.* **1991**, *30*, 2494.
159b. Kleckley, T. S.; Bennett, J. L.; Wolczanski, P. T.; Lobkowsky, E. B. *J. Am. Chem. Soc.* **1997**, *119*, 247.
160. Sanchez-Delgado, R. A.; Rosales, M. *Coord. Chem. Rev.* **2000**, *196*, 249.
161. Baralt, E.; Smith, S. J.; Hurwitz, I.; Horváth, I. T.; Fish, R. H. *J. Am. Chem. Soc.* **1992**, *114*, 5187.
162. Hagadorn, J. R.; Arnold, J. *Organometallics* **1994**, *13*, 4670.

163. Tayebani, M.; Gambarotta, S.; Yap, G. P. A. *Angew. Chem., Int. Ed. Engl.* **1998**, *37*, 3002.
164. Hiraki, K.; Matsunaga, T.; Kawano, H. *Organometallics* **1994**, *13*, 1878.
165. Morilla, M. E.; Morfes, G.; Nicasio, M. C.; Belderrain, T. R.; Díaz-Requejo, M. M.; Tiripicchio, A.; Sánchez-Delgado, R.; Pérez, P. J. *Chem. Commun.* **2002**, 1848.
166. Aresta, M.; Quaranta, E.; Dibenedetto, A.; Giannocaro, P.; Tomassi, I.; Lanfranchi, M.; Tiripicchio, A. *Organometallics* **1997**, *16*, 834.
167. Kurosawa, H. *Inorg. Chem.* **1976**, *15*, 120.
168. Torrent, M.; Musaev, D. G.; Morokuma, K. *Organometallics* **2000**, *19*, 4402.

1.28
Organometallic Chemistry in the Gas Phase

D E Richardson, University of Florida, Gainesville, FL, USA
D A Plattner, Albert-Ludwigs-Universität, Freiburg, Germany

1.28.1 Introduction to Gas-Phase Organometallic Ion Chemistry

1.28.1.1 Overview

The chemistry of organometallic ions in the gas phase has been intensely studied by a large number of research groups over the past three decades. This chapter considers the ion chemistry of species with metal–carbon bonds in general and focuses in particular on relatively recent developments in the field. There have been many reviews on various aspects of organometallic gas-phase ion chemistry, and a major goal of this chapter is to provide an entry into the literature via these reviews. No attempt is made to be complete in coverage as there have been thousands of publications in the field since the release of COMC (1982). A particularly comprehensive review of the field was published in 1991 by Eller and Schwarz,[1] and that review may be consulted for coverage roughly up to the publication of COMC (1995). The general field of organometallic ion chemistry was not summarized by

way of a chapter in COMC (1982) and COMC (1995), but aspects of the field were covered in the various element-specific chapters. This chapter provides an introductory overview of the gas-phase chemistry methodologies with an emphasis on the rapidly expanding application of electrospray ionization mass spectrometry (ESI-MS) to organometallic molecules and ions.

Ion chemistry is an especially fruitful area of research on gas-phase species, since ions can be manipulated, trapped, and energized by use of electromagnetic fields, in contrast to neutral compounds, which are not as readily controlled in time and space. By far, the most common methods used involve techniques of MS for the production and analysis of ions and the products of their reactions with neutrals. This chapter briefly describes the various mass spectrometric techniques that can be used to produce organometallic ions and to explore their reactivity and thermochemistry. Many of the organometallic ion production and analysis techniques used today were developed prior to 1995 and are described in great detail in many articles cited in the Eller and Schwarz review[1] as well as some more recent reviews.[2–16] The widespread application of electrospray methods[17] in organometallic ion chemistry has occurred within the last 10 years and therefore gets significant coverage here. Studies focusing on the structural analysis of unknown organometallic compounds by mass spectrometric techniques are beyond the scope of this chapter.

The enormous published body of work in the field can be divided into several general areas for purposes of this chapter, as follows:

(i) the reactivity of bare metal ions (usually M^+) with hydrocarbons and other substrates,
(ii) the reactivity of metal complex ions with ancillary ligands bound (either coordinatively saturated or unsaturated complex ions),
(iii) determination of bond energies and related quantities, and
(iv) determination of ionization energies and electron-attachment energies.

These four topics will be introduced in this chapter. Theoretical investigations of gas-phase organometallic chemistry (such as bond-energy calculations) will not be covered, but references to theoretical studies can be found in many of the review articles cited.

1.28.1.2 Mass Spectrometric Methods—General

It is beyond the scope of this chapter to describe in detail the major mass spectrometric methods that are used to analyze and quantify ions, in particular, mass analyzers for determination of ion mass/charge (m/z) ratios. Later sections will mention various ionization sources that can be used to produce the ions for manipulation, study of ion–molecule reactions, and detection. Commonly used MS techniques are described in introductory books,[18,19] and extensive coverage of the field can be found in the 2003 set *Encyclopedia of Mass Spectrometry*.[20] Brief descriptions of the most common mass analyzers are given below.

In magnetic sector MS, ions are accelerated from the ion source by an electrostatic potential. The ion beam is subjected to a magnetic field, which accelerates the ions into a curved path, and the extent of bending of the path of each ion in the beam is proportional to its m/z value. By sweeping the magnetic field strength (or by holding the field constant and varying the ion velocity) and refocusing the ion beam, each m/z value can be directed into a detector, and a mass spectrum with high resolution can be produced.

In quadrupole MS, ions are accelerated into a chamber lined by four metal rods. By a combination of RF and DC potentials, specific m/z values can be selected to pass through the quadrupole chamber and are subsequently detected. Although only capable of relatively low resolution, the technique is amenable to multiple mass filters in series allowing for collisions in the space between the filters and fragment analysis.

Time-of-flight mass analyzers are most useful for pulsed ion sources, such as matrix-assisted laser desorption ionization (MALDI). The ions depart the source at the same time but arrive at the detector at different times depending on mass. These instruments have exceptionally high sensitivity and a high practical mass range.

Ion-trap methods include Fourier transform ion cyclotron resonance MS (FTICR-MS) and quadrupole ion traps (QIT or Paul traps). In these methods, ions are produced in or transferred into a region with appropriate geometry walls and some combination of magnetic fields, DC potentials, and RF potentials that confine the ions on the timescale of seconds to days. FTICR-MS[21] has been particularly popular for the study of organometallic ions in the gas phase. In FTICR-MS, the ions are confined by a magnetic field that constrains the ions to the center of the cell,

and by DC voltages applied to the ends of the cell to prevent drift along the magnetic axis. For detection, RF frequencies are applied at the natural cyclotron frequency of each m/z value (usually by a frequency sweep) to increase the radius of the ion motions so that an image current can be detected by receiver plates. The time domain signal is then converted by Fourier analysis into the frequency domain, thereby producing the mass spectrum. FTICR-MS has become a favored method for studying the post-ionization reactivity of ions with neutral molecules because of its high resolution and versatile ion manipulation methods. In addition, the high resolution makes it ideal to study ions produced by ESI (see below), which can produce ions with high charge (z values). In QIT MS, which is a lower-resolution ion-trap technique, a combination of RF and DC potentials is used to trap the ions in an appropriately shaped chamber, and a sweep of the RF field can be used to eject the ions from the trap for detection.

There is always the caveat that m/z ratios determined by MS are not highly informative about the chemical structure, and isomeric descriptions for the observed molecular ion formulas always have to be considered. Structures of product ions from ion–molecule reactions can sometimes be interrogated by collision-induced dissociation (CID) to confirm structures, but many product structures remain hypothetical and are assigned based on a combination of chemical intuition and analogies to the condensed phase. In recent years, various structural assignments have been investigated by high-quality quantum mechanical models, and this approach has proved to be increasingly useful.

1.28.1.3 Insights into Condensed-phase Chemistry from Gas-phase Studies

What might one hope to learn from gas-phase ion studies of organometallic compounds? After all, it is extremely unlikely that any chemistry in a gas-phase ion system will translate into a commercial reaction or catalyst operating in the gas phase. Condensed-phase chemistry dominates organometallic studies and processes, but it is possible to refine the understanding of such reactivity through the study of analogous gas-phase chemistry. Justifications for such work have routinely been offered in many review articles on the subject cited in this chapter. The next several paragraphs summarize some of the main issues that can be addressed, in principle, through the study of gas-phase ion chemistry.

Solvent effects and intrinsic reactivity. In the case of ions, in particular, the role of solvation in determining the chemical properties of molecules cannot be overlooked, and gas-phase studies offer the promise of eliminating such effects and revealing the underlying intrinsic reactivity of organometallic molecules. Often chemists tabulate and rationalize chemical reactivity based on the molecular and electronic structures of the species, ignoring the contributions of solvation to thermochemical trends, rates of reactions, etc. The impact of removing solvent on basic chemical properties, as investigated in gas-phase chemistry, has led to some reevaluations of this "molecule-centered" view of chemistry. For example, one of the major revolutions of understanding in acid–base chemistry arose from classic gas-phase ion studies done over 35 years ago. It was shown that the order of gas-phase acidity and basicity for series of acids and bases can be quite different in the gas phase, revealing that the strength of an acid or base in solution is strongly influenced by solvation, even to the point of reversing trends due to changes in substituents.[22–29] More recently, it was shown that alkyl substituent effects in the electrode potentials of nickelocenes and transition metal β-diketonate complexes could be reversed when going from polar solvents to the gas phase.[30,31] In addition to thermochemical changes, solvation has profound kinetic consequences. For example, approximately 20 years ago, it was shown that polar solvents reduced the rate constants of organometallic ion–molecule electron-transfer reactions (e.g., $MCp_2^{+/0}$ self exchange) from the gas-phase rate constants by a factor of $\sim 10^4$, in general, agreement with theories that had been accepted but not directly tested until then.[32–35]

Ancillary ligand effects. The extraordinary reactivity of bare metal ions (M^+) compared to their ligated counterparts (ML_x^+) shows how dramatically bound ligands can alter the reactivity of metal ions. Such observations clearly demonstrate the role of electronic structure in determining reactivity. For example, the cobaltocenium ion ($CoCp_2^+$) is a rather unreactive 18-electron gas-phase ion,[36] but Co^+(g) reacts rapidly with strong C–H bonds in alkanes.[1,7] Gas-phase ion–molecule studies can also reveal more subtle effects of ancillary ligand changes on reactivity, again without the potentially confusing interference of solvent. For example, variations in the ligand (L) environment of $L_2ZrCH_3^+$(g) will alter the intrinsic electrophilicity of the metal center as revealed by the kinetics of reactions with a variety of substrates such as H_2 and C_2H_4,[37–39] and such results are useful in interpreting experimental and computational data for condensed-phase Zr polymerization catalysts.[40]

Aggregation and ion pairing. In the study of ionic condensed-phase organometallic catalysts and reagents, it is often found that ion-pairing and/or aggregation phenomena can greatly complicate mechanistic understanding of their reactions. One clear advantage of gas-phase studies is that ions can be readily isolated from other ions and neutrals, thereby allowing one to observe intrinsic reactivity of the ion. Any pairing or aggregation that does occur is generally easy to quantify, since exact mass spectrometric methods are used. For example, the $L_2ZrCH_3^+$(g) species reacts in

an ion trap as the cation without the perturbing influence of ion pairing, which controls the solution reactivity to a large degree.[40–47]

The transition from metal clusters to surface chemistry. The study of metal cluster ions (e.g., M_n^+) can lead to insights concerning the properties of bulk solids and surfaces, particularly in the area of catalysis.[48] Of particular interest has been the point at which the chemistry of a gas-phase cluster begins to approach that of a solid.[49–52]

Thermochemical determinations. The use of various gas-phase methods for determining reaction energies is clearly an advantage of moving out of the condensed phase. Specific thermochemical quantities, such as bond energies, can be obtained using a variety of spectroscopic and collisional methods. The amount of thermochemical data for M–C bond-dissociation energies and related quantities from gas-phase experiments is truly impressive.[4,8,11–13] There has also been a reasonable amount of data produced on ionization energies and electron affinities for gas-phase organometallic compounds using mass spectrometric techniques.[53–57] The role of so-called thermochemical "ladders" based on ion–molecule reactions has been significant in much of this work.[58]

Direct observation of key reactive intermediates. Transient, metal-centered intermediates variously appear and disappear via the typical elementary steps of organometallic chemistry, such as oxidative addition, insertion, metallocyclization. However, due to their highly reactive nature, which is invariably linked to their role in catalytic cycles, organometallic intermediates are rarely observed. They usually exist only in infinitesimal concentration in steady-state and catalytic sequences. In solution, coordinatively unsaturated species interact significantly with virtually all solvents, even with alkane C–H bonds. Consequently, a detailed study of these intermediates and their reactivity toward solvent or substrates is beyond the reach of even the fastest spectroscopic methods. Gas-phase approaches to the problem of chemical transients do not suffer from this limitation. Hence, direct transfer of the relevant solution-phase intermediates or of suitable precursors circumvents all the problems related to solution-phase sensitivities. Thus, it does not come as surprise that applications of ESI-MS for the study of organometallic species have become increasingly popular. It is possible to analyze highly diluted solutions when using electrospray as an ionization method, and the mild conditions for the ionization process and for the transfer of charged species from solution to the gas phase. Neutralization–reionization MS is very useful for the characterization of transient neutral species in ion–molecule reactions.[15,16]

Identification of solution species (*speciation*). The precise identities and structures of organometallic catalysts and reactive ions are often unknown, since traditional methods such as NMR or X-ray crystallography may be less than informative or even impossible to use. There have been many attempts to do speciation analysis by MS, especially using the soft ionization methods such as ESI.[59–64] The relationship of the observed ions to the true solution composition is sometimes tenuous, but in favorable cases, there is certainly a strong confirmed relationship. Thus, techniques such as ESI-MS have many potential analytical applications in organometallic chemistry. Using this and other appropriate methods, even very large organometallic clusters can be characterized.[65]

Assessing the adequacy of quantum theoretical models. Experimental work in gas-phase ion chemistry produces data that are amenable to theoretical modeling, especially in recent years as computational power has increased and density functional theory (DFT) methods have developed into quantitative tools for handling large, metal-containing systems.[66–70] The attractiveness of experimental gas-phase data for theoreticians arises from the absence of solvent, which remains an extremely difficult challenge to thermochemically accurate quantum theory. In this way, the underlying competency of theoretical models for many-electron, metal-containing systems can be assessed for a variety of reaction types. Once calibrated for accuracy, the modeling of condensed-phase systems becomes more believable, although still computationally difficult.

Spectroscopic investigations of gas-phase organometallics. It is possible to obtain high-resolution spectroscopic data on gas-phase organometallic ions, as well as investigate photodissociation pathways[3,71–91] and photoelectron spectra of ions.[74,92,93] Recently, infrared spectra have been measured for metal ions complexed to organic molecules using a tunable free-electron laser coupled to FTICR-MS.[94–96] Moore *et al*. and Duncan and co-workers have reported the infrared spectroscopy of Ni^+, V^+, Cr^+, and Fe^+ adducts.[79,80,94,97] Duncan and co-workers also studied the formation and photochemistry of Ti^+, V^+, Ni^+, and U^+ benzene complexes,[78,81,98] and Metz reported work on photofragment spectroscopy of covalently bound metal complexes.[3]

1.28.2 Reactions of Bare Metal Ions (M_n^+ and M_n^-)

1.28.2.1 Experimental Methods—Ion Production

Production of unligated (bare) transition metal ions for gas-phase investigations has been accomplished primarily by well-established methods: electron impact on volatile precursors such as metal carbonyls, laser desorption from pure

metal targets, surface ionization at a hot filament, or glow discharge.[7] Special care must be taken in selecting a technique to establish the distribution of electronic states in the reactant metal ions, since their chemistry is state dependent.[99–101] Cluster ions M_n^+ can be produced by laser desorption from pure metal followed by entrainment in a high-pressure helium flow tube to cool and condense atoms and ions prior to experiments.[52,102,103]

1.28.2.2 Survey of Reviews and Recent Publications

Since the comprehensive review by Eller and Schwarz,[1] many reviews have been published on various aspects of bare metal ion chemistry.[2–10] In general, work in the field has continued vigorously, although there has been an increasing focus on clusters of metal atoms to probe the transition from heterogeneous catalysts to gas-phase clusters and atoms.[48]

In recent years, studies of the organometallic chemistry of bare metal ions, metal–heteroatom ions (e.g., MO^+ and MH^+), and metal clusters continue to focus on the themes of reactivity and thermochemistry. The following survey of the literature since the more recent reviews shows that studies of transition metal ions continue to dominate.

Schwarz and co-workers have published a significant amount of work in the organometallic area as well as in other related topics. They have contributed notable papers on the issues of spin-forbidden gas-phase reactions[104] and relativistic effects.[105] They have also considered diastereo- and enantioselective bond activation of alkanols by gaseous metal ions.[106,107]

Methane and small hydrocarbons continue to be favorite substrates, especially since the reactions can be modeled at high accuracy by quantum methods. Liu *et al.* studied the activation of CH_4 by Ni^+ and determined bond energies.[108] Zhang *et al.* investigated the activation of methane by FeH^+, CoH^+, and NiH^+.[109] Goncharov looked at the reactions of Tc^+ and Tc^{2+} with hydrocarbons.[110] Armentrout and co-workers have studied Zr^+ and Nb^+ reactions with small hydrocarbons.[111–113] Manard *et al.* have reported on Ag^+ reactions with small alkenes.[114,115]

Reactions with halocarbons have been common, for example, reactions of Cr^+ with organofluorines[116,117] and Cu^+, Au^+ with small halocarbons.[118,119] There have been several studies on Cr^+, Fe^+, Nb^+, and Ta^+ reactions with pyrenes.[120–123] Boutreau *et al.* studied the reactions of Cu^+ with glycerol and glycolic acid,[124,125] while Fordham *et al.* studied Cu^+ with ketones.[126] The reaction of Ni^+ with urea has been studied.[127] Reactions of first-row transition metal ions with propargyl alcohol in the gas phase have been reported with an emphasis on periodic trends.[128]

Lanthanide reactivity is certainly of interest in view of the rich nuclear chemistry of such elements. The reactions of lanthanide ions with alcohols have been investigated,[129] as have lanthanides and actinides reactions with Cp^*.[130] The theme of molecular recognition was explored in work on transition metal M^+ ions with paracyclophanes to investigate the role of cavity size on binding.[131]

MO^+ ions represent the smallest metal oxides, and there have been many studies of their reactivity, exemplified recently by the reactions of M^+ and MO^+ (M = V, Nb, Ta) with methanol,[132] studies of the mechanisms of hydrocarbon oxidation by MO^+,[133,134] and MO^+ reactions with methane.[135]

1.28.3 Reactions of Ligated Metal Ions

1.28.3.1 Experimental Methods for Production of Ions from Ligated Complexes

1.28.3.1.1 Electron ionization and chemical ionization of neutral organometallics

The methods described in this section are useful for volatile organometallic compounds. Given the higher molecular weights often encountered, it is not always possible to introduce the neutral compounds into the source at room temperature, and heating must be used. Typically, neutral organometallics must be vaporized from a heated solid probe inserted into the source region. Often, however, the vapor pressure is insufficient or the compound will decompose with heating, so softer ionization methods that do not require heating, such as electrospray, must be used.

Electron ionization (EI) is the traditional method for ionizing a neutral gas-phase compounds. A high-energy electron beam (often 70 eV) is allowed to pass through the sample vapor at relatively low pressure, leading to the general ionization equation

$$Y + e^- \rightarrow Y^+ + 2e^-$$

where Y^+ is the parent ion (traditionally abbreviated M^+, but altered here to avoid confusion with bare metal ions). In almost all cases, the high-energy beam produces fragment ions of lower mass than Y that are observed in high

abundance ($[Y–N_1]^+$, $[Y–N_2]^+$, etc., where N_i are neutral fragments lost from the original molecule). Of course, in traditional analytical MS, it is the fragment ions that provide crucial structural information, and the same type of data can be obtained for organometallic compounds. If one is interested in the reactivity of intact organometallic parent ions (e.g., $FeCp_2^+$(g) from ferrocene), then the electron beam energy can be reduced and the formation of the parent ion is enhanced. High-pressure sources, in which ions pass through a relatively high pressure (often 1 atm) of background gas prior to mass analysis, are particularly useful for producing ions that have been thermalized by many collisions while undergoing reactions.[53,136]

In chemical ionization (CI), various other ions are used to produce charged versions of the parent compound by ion-neutral attachment. For example, reaction of CH_5^+(g) (produced from EI on CH_4(g)) with a neutral molecule can lead to charged ion at a higher *m*/*z* value ($[Y + H]^+$), and the mass of Y is readily deduced. This is a softer ionization method driven by the binding energy of the proton or other ion (e.g., Na^+) to the neutral compound. With respect to studies of ion–molecule reactivity for organometallic ions, CI is less useful than low-potential EI since the parent ion is not produced, unless of course it is the protonated form that is of interest.

Electron attachment ionization should also be mentioned here. In this case, the goal is to deposit an electron on the neutral Y to produce the anion Y^-. When compounds have appreciable electron affinity, this can be accomplished easily by using an electron beam set at a very low potential (a few volts), allowing electron capture by the neutral molecule in the source. The flowing afterglow method can be applied to study the dynamics for organometallic ion–molecule reactions, particularly for anions.[14]

1.28.3.1.2 ESI—basic concepts

Methods such as EI and CI are suitable for ionization of volatile neutral compounds, but they are not useful in the case of involatile salts. Before the development of ESI-MS, methods for analyses of charged molecules in solution were specialized and not particularly general, but ESI-MS made analyses of salts and highly charged ions routine.[17] The method was first applied to MS by Fenn and co-workers, who used the method for the MS of biomolecules and polyethers.[137] Its value, especially to biological chemistry, was acknowledged with the Nobel prize for John B. Fenn in 2002.[138] Applications to organometallic salts have increased dramatically since the publication of COMC (1995), and details of the technique and recent organometallic applications will be covered below.

An electrospray source transfers molecules from a dilute solution directly to the gas phase by a complicated process involving charged droplet formation, fission, and field desorption. The method usually transfers existing ions from solution to the gas phase. Only neutral compounds with very low ionization energies ($\leq$7 eV), for example, *N*,*N*,*N*′,*N*′-tetramethyl-1,4-phenylenediamine or 2,3-benzanthracene,[139] metalloporphyrins,[140] or ferrocenes,[141] can be oxidized during the electrospray process. Preformed ions exist either because the molecule or complex is inherently charged, the normal case in organometallic chemistry, or, as in biomolecules and polymers, the molecule coordinates ions from solution to heteroatoms, for example, H^+, Na^+, or K^+. In large molecules, this leads to multi-charged species, much more readily than by previous methods,[142] and the spectra can be deconvoluted to obtain the mass of a hypothetical single-charged species. The major benefit of ESI is its gentleness. It allows transfer of large ions or even non-convalent receptor–ligand complexes without decomposition into the gas phase.

The mechanism of the electrospray process starts with formation of a thin jet when a stream of a conducting volatile liquid is passed through a small-bore needle maintained at a high potential relative to an opposing counter electrode.[17,143,144] The interaction between viscosity and surface tension produces so-called varicose waves on the surface of such a liquid jet. These waves grow in amplitude until they truncate the jet into a series of uniform droplets. In the electrospray case, the droplets all have charges of the same sign: excess cations or anions, depending on the polarity of the applied field. Coulomb repulsion thus results in a divergence of their trajectories to form a conical "electrospray cone" of charged droplets. In the original explanation offered by Dole and co-workers,[145] the assumption was made that these offspring droplets would continue to evaporate until they would reach the Rayleigh limit, that is, the point at which Coulomb repulsion would overcome surface tension, and break up into still smaller droplets. If the original solution were sufficiently dilute, a sequence of such evaporation–disruption episodes would ultimately produce droplets so small that each would contain only one solute molecule. As the last of the solvent evaporated from the ultimate droplet, the remaining solute molecule would retain some of the droplet charge, and thus become a free gas-phase ion. This mechanism is sometimes referred to as the "charged-residue model" (CRM). A later model proposed by Iribarne and Thomson, the so-called "ion-evaporation model" (IEM),[146] argues that before ultimate droplets containing only one solute molecule are formed, the field at a droplet's surface becomes sufficiently intense to lift a solute ion from the droplet surface into the ambient gas.

In a typical experiment, a 10^{-4} to 10^{-5} M solution of the analyte in a (normally polar) organic solvent is passed through a capillary at a flow rate of 3–15 μl min^{-1} and electrosprayed on the air (1 atm = 760 torr) at a potential of 3–5 kV. By adjusting the electrospray voltage, the concentration of the dissolved compound, the flow, and by the use of sheath gas the stability of the electrospray signal can be optimized. The ion beam thus produced enters a heated capillary (typically at 150–200 °C) where the ions are declustered and the remaining solvent molecules are evaporated. After that the ions enter the first stage of the mass spectrometer that is already at somewhat reduced pressure (0.5–1.0 torr) prior to mass analysis. It is now well known, following the work of Posey and others,[147–153] that metal complex ions can also be resolvated by solvent vapor introduced into the capillary flow, producing partially solvated ions with one or more outer-sphere solvent molecules bound.

Because an electrospray source transfers ions continuously to the gas phase, it is most easily coupled to a continuous mass analyzer. From the time of the first successful applications of this technique, linear quadrupoles proved to be of great practical use.[138] In triple-quadrupole mass spectrometers, a linear multipole guides the ions to a first quadrupole mass filter, followed by a second ion guide leading to a second quadrupole mass filter. Finally, an ion multiplier detects the ions. Differential pumping reduces the pressure from atmospheric pressure (API region, ESI source) to 10^{-6} mbar in the mass analyzer.

Recently, the coupling of ESI sources to quadrupole ion traps has been achieved.[154] Again, multipoles guide the ions from the API region to the low-pressure region of the ion trap. These instruments provide easy handling, good signal intensities, and high mass resolution in combination with low costs compared to linear instruments. Furthermore, ESI-MS instruments are easily coupled to liquid chromatographic techniques. However, the use of ion traps for the study of gas-phase organometallic chemistry is limited for a number of reasons. First, in an ion trap, ions are stored under collisional conditions before being scanned; thus, labile species decompose before analysis. Second, due to the complexity of the electronics and the packed assembly of commercial ion traps, modifications of the setup are difficult to accomplish, for example, introduction of a device to allow the use of collision gases other than He. Third, an ion trap works only in the low-pressure regime ($<7 \times 10^{-7}$ mbar) with a very limited range of damping gases.

ESI sources have been coupled to FTICR-MS.[155–157] In this method, the ions are accumulated in an external region (usually a multipole) before being inserted into the ion trap for reactions and analysis.

1.28.3.1.3 ESI—advantages for organometallic ion chemistry

Only during the last 10 years has the potential of ESI-MS for organometallic research been fully recognized.[158,159] Published studies of ESI applied to inorganic and organometallic molecules have been reviewed through 1995.[160,161] A few major traits of organometallic reactions and catalysis are challenging for conventional analytical techniques. Reactions at a transition metal center include a vast number of reaction channels that a substrate may undergo. This means a great number of intermediates, transition states, and reaction steps are involved in each possible reaction coordinate. In addition, these steps sometimes proceed on a millisecond timescale. The development of new reactions or the improvement of known reactions strongly depends on the knowledge of these factors. ESI-MS is a tool for mechanistic research with widespread but not unlimited possibilities. The ESI process does not always transfer intact sample ions to the gas phase, and each experimental result must be interpreted with caution if one is to draw conclusions about solution chemistry.

Some advantages of ESI-MS for studying organometallic species are as follows: (i) Convenient analysis of the m/z of all the species present in solution to get an idea of the type of products that are formed in a reaction or to get information about the elemental composition and mass of a certain compound (speciation). (ii) Being able to work directly from a dilute solution is a major advantage for studies of organometallic catalysis, in that the active species often are unstable or difficult to produce as concentrated solutions. (iii) Due to the gentle nature of the ESI process, even metal-containing compounds with weakly bound ligands will remain intact upon transfer to the gas phase. (iv) For the determination of supramolecular structures of, for example, coordination polymers and multinuclear metal clusters, ESI-MS has proved to be very useful.[162–167] (v) Fragmentation behavior observed in ESI tandem MS can provide useful information on decomposition pathways of compounds in solution.[168–171] (vi) Gas-phase ion–molecule reactions can also be used to obtain more insight in the mechanisms of reactions in solution (see below). (vii) ESI-MS/MS has also found its use in high-throughput screening of homogeneous catalysts.[172]

ESI works well in the concentration range 0.001–10 mM, which also corresponds to the concentration of many catalysts under realistic conditions. Therefore, by direct sampling from a running catalysis, a number of intermediates that are present in solution in small concentrations and with short life times can be isolated and identified. Isolated, intact catalyst ions or ions of any other species present in solution in the gas phase provide the opportunity to

investigate these compounds in the absence of unwanted ligand-exchange reactions or solvent influence. Ion–molecule reactions can be performed by addition of a reagent gas in the ion-guide regions of the mass spectrometer to determine, for instance, the intrinsic reactivity toward different substrates, or the relative stabilities of the metal–ligand bonds. If successive reactions are performed in the gas phase, intramolecular reactions can be investigated by the analysis of the products of the second reaction, often collision-induced dissociation (CID).

1.28.3.1.4 ESI—practical issues for organometallic compounds

One of the usual requirements for the use of ESI-MS is that the compounds that are transferred to the gas phase are charged. Stable neutral molecules can be detected as well, provided they have a high proton affinity[173] or form stable complexes with ions (the so-called "coordination ion-spray MS," CIS-MS).[174–179] Formation of cationic adducts with Lewis acids like Na^+, K^+, Ag^+, or protonation at basic sites of the molecule enables the analysis of otherwise undetected neutral species. Also, oxidation of neutral complexes resulting in monocationic species can occur in solution at the capillary tip before droplet formation takes place.

The electrochemical reactions that take place in the ESI source may influence the gas-phase ions formed and ultimately analyzed by MS, especially in the case of transition metal coordination compounds and organometallics. In the literature, one can find quite a few reports concerning such redox reactions: ferrocene derivatives,[141] metalloporphyrins,[179] metal complexes of L-histidine,[180] etc. Van Berkel has studied redox reactions taking place when using ESI-MS.[181–184] He found that oxidation reactions in the positive ion mode and reduction reactions in the negative ion mode dominate at the emitter electrode (the tip of the capillary where the solution is sprayed), whereas reduction reactions in positive ion mode and oxidation reactions in negative ion mode can dominate at the counter electrode (the entrance of the heated capillary). A number of factors determine which reactions can occur at the emitter electrode, their rates, and their extent. Some examples are: the magnitude of the electrospray current, the redox character and concentrations of all species in the system, the solution flow rate, solvent polarity, the spraying voltage, temperature, solvent dielectric constant, the electrode material,[185] geometry, area, and any other parameters that affect the flux of reactive species to the electrode surface.[17,186] As a result, such reactions (e.g., electrochemical ionization) can be exploited to ionize neutral electroactive analytes that would otherwise go undetected in ESI-MS. On the other hand, electrochemical reactions may modify the mass, structure, or charge of the analyte[187] or remove analytes from solution.[188] At the present stage, it is not possible to predict or control the extent of any or all of these analyte electrochemical reactions, which can render a direct translation of mass spectrometric detection into solution-phase composition difficult.

During the electrospray process, droplets shrink to the point where repulsive Coulombic forces approach the level of droplet cohesive forces. These droplets undergo a cascade of fission processes yielding smaller and smaller droplets until the electric field at the droplet surface is sufficient for ion desorption to take place. A high charge of the analytes that are being sprayed can also be disadvantageous. It makes the desorption process more difficult due to stronger interaction with the solvent. As a result, when an equimolar mixture of mono- and dicationic species is sprayed, the signals corresponding to the monocationic species will dominate in the mass spectra (the "dominant-ion" effect). For species having long aliphatic tails (e.g., oligomers), in polar solvents their solvophobicity increases with increasing tail length, thus decreasing the work needed to remove an ion from the liquid.[189] Also, due to their tail, such ions will have a higher concentration on the surface of the droplets. As a result, in an equimolar mixture of solvophobic and solvophilic compounds, the solvophobic ones will be over-represented in the mass spectra. Quaternary ammonium salts behave in the same manner. Another important factor is the surface tension: the higher it is, the higher the activation energy for the transfer of the ions to the gas phase, and thus the lower the efficiency of ion desorption.[173]

Using ESI-MS for analysis of extremely air-sensitive organometallic species can be problematic. In a dilute solution such compounds will often react rapidly with air, to which it is exposed to some extent during the nebulization process in the ESI source. This will result either in the observation of a number of unknown species (dicationic ones or species with one or several oxygen atoms built in) in the mass spectra, or simply in a decrease of signal intensity and stability. One way to circumvent this problem is the use of sheath gas, which would, to some degree, protect the complexes from a reaction with air during nebulization. Another way to try to prevent reactions with oxygen is going to higher flow rates. This will increase the droplet size[190] and decrease the surface-to-volume ratio. Provided the reaction with dioxygen only takes place at the droplet surface, increasing the flow reduces contact of the organometallic molecules with air and thus decomposition. On the other hand, the ready reaction with oxygen in the ESI source can be exploited to generate, for example, peroxometal complexes from suitable four-coordinate Rh(I) or Ir(I) precursors.[191]

1.28.3.2 Gas-phase Organometallic Reactions Investigated by ESI-MS

1.28.3.2.1 Overview of gas-phase reactions investigated by ESI-MS

By the introduction of soft ionization techniques such as electrospray, it has become possible for the first time to overcome the limitations of conventional ionization methods and address the gas-phase reactivity of organometallics with an array of ligand environments. The discussion of gas-phase organometallic chemistry presented in this chapter will be strictly limited to species that bear a close resemblance to solution-phase complexes and catalysts. When compared to gas-phase coordination chemistry,[10,192,193] examples for bona fide organometallics are still scarce, but it is safe to predict that with the growing awareness of the potential of mass spectrometric methods this gap will soon be closed.

1.28.3.2.2 C–H and C–C activation

The gas-phase reactions of Ir(III) complexes follow a previously unreported mechanism for their observed σ-bond metathesis reactions. Previous discussions of the solution-phase reaction had considered a two-step mechanism involving intermolecular oxidative addition of $[Cp^*Ir(PMe_3)(CH_3)]^+$ to the C–H bond of an alkane or arene producing an Ir(V) intermediate, followed by reductive elimination of methane, or a concerted σ-bond metathesis reaction similar to that seen in early transition metals. The Bergman system[194] proved to be particularly suitable for an ESI-MS study, since all the species of interest are already present as ions in solution. Electrospray ionizations of acetonitrile solutions of $[LIr(PMe_3)(CH_3)(CH_3CN)]^+ ClO_4^-$ (L = Cp or Cp^*) produced the molecular ion $[LIr(PMe_3)(CH_3)(CH_3CN)]^+$, with even the weakly bound solvent ligand still intact, as well as the bare, unsolvated 16-electron complex cation $[LIr(PMe_3)(CH_3)]^+$.[195] The gas-phase chemistry of the coordinatively unsaturated complex cations can be summarized as follows (Scheme 1).[196]

With some small differences, the reactions of the $[Cp^*Ir(PMe_3)(CH_3)]^+$ and $[CpIr(PMe_3)(CH_3)]^+$ complexes **1** and **3** were entirely parallel, with the Cp series of complexes showing qualitatively higher reactivity than their Cp^* analogs. None of the 16-electron complex cations displays any appreciable reactivity toward hydrocarbons in the gas phase. Collisional activation of $[Cp^*Ir(PMe_3)(CH_3)(CH_3CN)]^+$ or $[CpIr(PMe_3)(CH_3)(CH_3CN)]^+$ induces an intramolecular cyclometallation reaction, resulting in elimination of methane. Based on deuterium-labeling experiments, the structure of the resulting species was assigned as $[LIr(\eta^2\text{-}CH_2PMe_2)]^+$, the product of cyclometallation with one of the phosphine methyl groups and concomitant loss of methane. The cyclometallation products **2** and **4** react readily with benzene to yield the product of an overall σ-bond metathesis. Under gas-phase conditions, the addition to benzene is reversible, resulting in multiple additions/eliminations within the same encounter complex upon collisional activation. The three-membered ring intermediate not only reacts with benzene in the gas phase but also adds to less reactive hydrocarbons such as methane, pentane, or cyclohexane. However, these C–H activation products display a different reactivity pattern. The product of the addition to pentane, $[Cp^*Ir(PMe_3)(C_5H_{11})]^+$, undergoes β-hydride elimination to yield $[Cp^*Ir(PMe_3)(H)]^+$.

Generally, the differences in the gas-phase chemistry of the Cp^* complexes and the Cp analogs are confined to two areas. First, while the Cp-substituted complexes add to pentane, cyclohexane, or benzene, the Cp^*-substituted

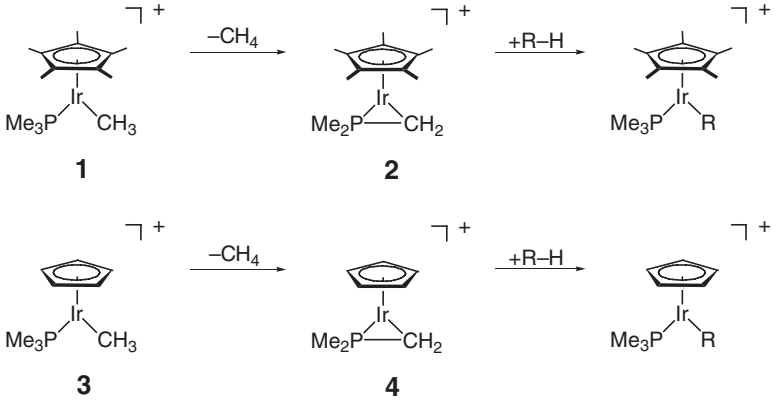

Scheme 1

analogs react with pentane or benzene only. Second, in the CID of the two phenyl-substituted complexes, there is complete deuterium scrambling in **4**, indicating reversibility of the cyclometallation reaction due to a more strongly bound ion–molecule complex, but only partial scrambling in the Cp^*-substituted analog (Scheme 2).

In summary, the electrospray mass spectra point to a gas-phase mechanism involving initial elimination of methane, followed by addition to an alkane or arene, in direct contrast to mechanistic conclusions drawn from solution-phase reactivites.[197,198]

C–H activation was also reported for Pt(II) complexes,[199] a system for which it was claimed that 2,2,2-trifluoroethanol (TFE) assists in the reaction.[200,201] The platinum(II) complexes **5** (L = H_2O or no ligand) (Scheme 3) were electrosprayed from TFE solutions containing up to 25% of water or acetonitrile.

Gas-phase reactions were performed in a triple-quadrupole mass spectrometer, housing two reaction multipoles and two mass analyzers. The reaction of **5a** with benzene in the gas phase gives rise to **6**, a reactivity that was confirmed by reaction with isotopically labeled benzene. Subsequent activation through collision yields **7**. When **6** was collided with either TFE or 1,1,1,2-tetrafluoroethane under identical conditions, no TFE- or 1,1,1,2-tetrafluoroethane-containing adducts or products could be detected, and the ratio of conversion of **6** to **7** in both cases was found to be identical within experimental error bounds. 1,1,1,2-tetrafluoroethane was used because it is similar to TFE in shape and polarity, but does not possess the same coordinative properties because it bears no oxygen atoms.

Rate coefficients were determined in an FTICR mass spectrometer for the formation of adduct ions in ion–molecule reactions between $M(bipy)_2^{2+}$ (M = Cr, Ru, Os; bipy = bipyridine) and several alkenes and molecular oxygen, respectively.[202] The complexes were generated by electrospray of solutions of tris(2,2′-bypiridine)metal(II) (M = Cr, Ru, Os) complexes in either methanol or acetonitrile, and reacted with an alkene or O_2 in an ICR chamber at around 10^{-8} mbar. Dioxygen leads to the formation of adducts of the general formula $M(bipy)_2(O_2)^{2+}$. Steady-state analysis was employed in order to determine if the adduct formation occurs by radiative or collisional activation. If collisional cooling were important in this process, the yield of adduct formation should increase with the pressure. Experiments showed that the adduct yield does not increase with pressure, so activation must be due to a radiative process. $Ru(bipy)_2^{2+}$ gains up to two molecules of ethene in gas-phase collisions. Upon collisional activation, both olefin units are lost stepwise, suggesting that they are bound as intact molecules. $Ru(bipy)_2(propene)^{2+}$, however, doesn't add a second molecule of propene, instead two other cations are formed: $Ru(bipy)_2(propene)(C_2H_3)^{2+}$ and $Ru(bipy)_2(propene)(C_3H_5)^{2+}$ (Scheme 4).

Upon collisional activation, these ions lose masses of 27 and 41, respectively, restoring the original propene complex. Mass selection of different ruthenium isotopes confirms these assignments. 1-Butene reacts with ruthenium

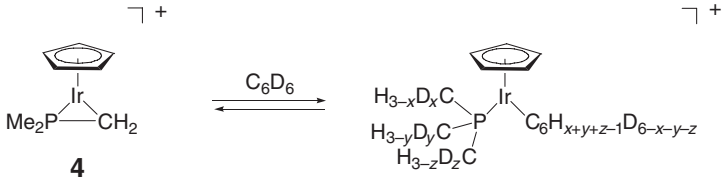

4

Scheme 2

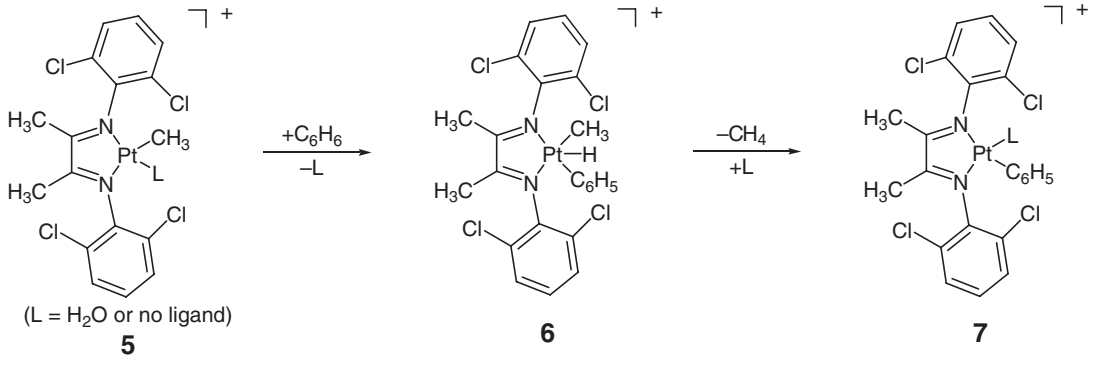

5 **6** **7**

Scheme 3

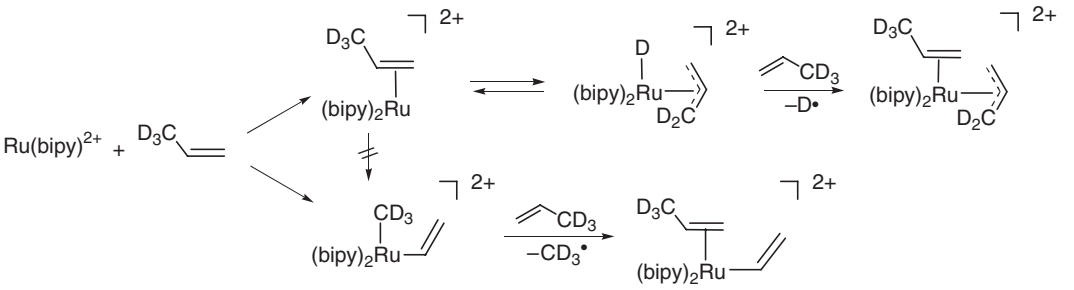

Scheme 4

complexes in a similar fashion, giving rise to $Ru(bipy)_2(butene)(C_2H_3)^{2+}$ and $Ru(bipy)_2(butene)(C_3H_5)^{2+}$. Based on experiments using propene-(3,3,3)-d_3 and $Ru(bipy)_2(propene)^{2+}$, a mechanism for the C–H and C–C insertion reactions was proposed (Scheme 4).

1.28.3.2.3 Ziegler–Natta-type olefin polymerization

On the technical scale, olefin polymerization is based on the activation of a suitable zirconocene precursor, typically Cp_2ZrMe_2 or Cp_2ZrCl_2, by a strong Lewis acid as co-catalyst. Mechanistic studies on Ziegler–Natta-like polymerization have long focused on the role of cationic alkylzirconocene species in the catalysis. There have been previous mass spectrometric studies of isolated metallocene ions in the gas phase, most notably by Richardson and coworkers.[38,203,204] The failure to observe olefin oligomerization in this study was attributed to incomplete thermalization of the intermediate ions formed by olefin insertion in the very low-pressure environment of an ICR mass spectrometer cell.

In a subsequent ESI-MS study by Feichtinger *et al.*,[205] stable solutions of the tetrakis(pentafluorophenyl)borate salt of the methylzirconocene cation $[Cp_2ZrCH_3]^+$ **8**, were prepared by treatment of $Cp_2Zr(CH_3)_2$ in acetonitrile with dimethylanilinium tetrakis(pentafluorophenyl)borate. Reaction of **8** with 1-butene under low-pressure conditions (1–5 mtorr) generated products analogous to those observed in the ICR experiments. Use of 1-butene for reaction and thermalization at a higher-pressure regime (up to 100 mtorr), however, produces a species **9** that corresponds to the product of insertion of the olefin into the Zr–C bond of the methylzirconocene cation (Scheme 5).

Collision of **9** with more 1-butene (at around 10 mtorr) displays a reactivity pattern as expected for a Ziegler–Natta-type reaction, that is, products corresponding to the addition of up to three units of the olefin are observed. Experiments with ethylene and propylene give similar results.

By and large, the gas-phase reaction resembles that for the condensed phase. The complete absence of elimination reactions from **10** indicates that the increased density of states associated with the growing alkyl side chain sufficiently slows the H_2-loss reaction, allowing collisional stabilization of the adduct or further addition reactions under conditions where higher pressures and shorter reaction times work against chemically activated reactions.

The most notable difference between the gas-phase results and the analogous reaction in solution is the large rate acceleration. A kinetic study of the Cp_2ZrCl_2/MAO system in solution-phase olefin polymerization found $k_p = 168$–$1670\,M^{-1}\,s^{-1}$ at 70 °C with an absolute upper-bound of $kp \leq 5{,}000\,M^{-1}\,s^{-1}$.[206] From the ESI-MS results, it was derived that the 1-butene addition to $[Cp_2ZrR]^+$ occurs with a second-order rate constant of $k \sim 10^8$–$10^9\,M^{-1}\,s^{-1}$ (at 70 °C).[205] The addition of 1-butene to the unsolvated cations occurs at a rate which is approximately 10^5 times faster than the corresponding solution-phase addition, for which the metallocene cation is part of an ion pair, often with one

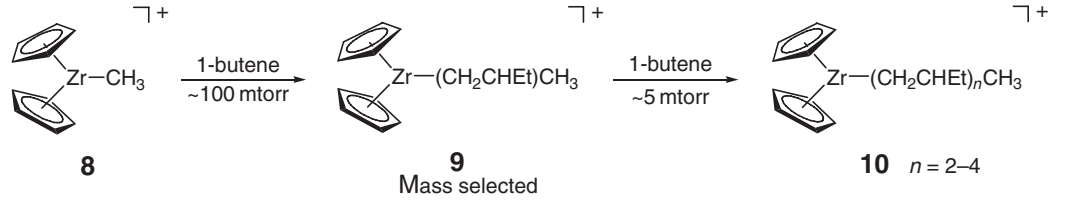

Scheme 5

or more additional coordinating ligands (e.g., solvent). This huge difference can be attributed to two factors: first, lacking a counterion or any charge donation by even a weakly coordinating solvent molecule, and furthermore lacking any pre-equilibria to form the active species, the isolated cations should be intrinsically more reactive; and second, the electrostatic interaction, either ion dipole or ion-induced dipole, which is screened out in solution, effectively lowers the activation energy of a bimolecular ion–molecule reaction by several kcal mol^{-1} relative to the same reaction in solution.

1.28.3.2.4 Olefin metathesis

Gas-phase studies on the mechanism of olefin metathesis have, for the most part, been confined to simple metal carbenes bearing little resemblance to solution-phase species, for example $[Mn{=}CH_2]^+$, $[Fe{=}CH_2]^+$, and $[Co{=}CH_2]^+$.[207–210] Most of the metatheses have been observed with deuterated ethylene.

The gas-phase reactivity of a typical homogeneous catalyst, described earlier by Grubbs and co-workers,[211] was the subject of an ESI-MS study.[212] Reacting the complex cation **11** with 1-butene at ca. 100 mtorr produces the propylidene complex **12**, indicating that an olefin metathesis reaction had occurred (Scheme 6).

This reactivity was confirmed by mass-selecting **11** in a first mass-selection stage and subsequent reaction with 1-butene. The only metathesis product observed was **12**. With cyclobutene or norbornene as substrates, the complexes **13** and **14** were formed predominantly as a result of ring-opening metathesis (ROM).

Many features that appear in solution-phase metathesis reactions also appear in the gas-phase reactions. Dissociation of one phosphine ligand is a prerequisite for metathesis reactions, as evidenced by the complete absence of products containing two phosphine ligands. The monocation **11** shows no metathesis reactivity with carbonyl compounds. In the reaction with 1-butene, only the propylidene complex is formed, while the alternative methylene complex is not detected. This kinetic preference becomes evident as a result of the non-equilibrating conditions in the gas-phase reaction. In ROM, the addition of the first cycloolefin unit is much faster than the subsequent addition steps, which resembles the observation in solution-phase studies that the rates of initiation are much larger than the rates of propagation.

In a subsequent ESI-MS study,[213] an experimental probe of reversibility in ring-opening metathesis polymerization (ROMP) was accomplished by using bifunctional substrates, which offer the product of an ROM reaction the chance to undergo a non-degenerate ring-closing metathesis (RCM) to a isotopically or otherwise substituted complex distinguishable from the original complex by mass. The ROMP substrate 4-[(*Z*)-2-pentenyl-3,4,4,5,5,5-d_6]-cyclopentene, for example, upon reaction with the ruthenium propylidene complex **15** leads to significant conversion of **15** to **15**-d_6, indicating that the ROM of cyclopentene occurs in a reversible fashion (Scheme 7).

Selected Grubbs-, Werner-, and Hofmann-type ruthenium catalysts were probed in the gas phase for their metathesis reactivity using ESI-MS techniques.[214] $[(RCy_2P)(Cl)_2Ru{=}CH{-}CH{=}CMe_2]^+$ (**16**, Cy = cyclohexyl, R = 2-(trimethylammonium)ethyl), $[(Cy_3P)_2(Cl)Ru{=}CH{-}CH{=}CMe_2]^+$ **17**, and $\{[(t\text{-}Bu)_2P(CH_2)P(t\text{-}Bu)_2](Cl)Ru{=}CH{-}CH{=}CMe_2\}^+$ **18** (Figure 1) were prepared by electrospray of their salts in CH_2Cl_2. Complexes **16**, **17**, and **18** were reacted with 1-butene in a multistage mass spectrometer. The relative reactivities were determined measuring the integrated peak intensities for reactants and products. It was found that Grubbs' catalyst reacts more than 40 times faster than the Hofmann catalyst in the gas phase. The Werner catalyst, on the other hand, appears to react too slowly for any product to be detected. It was assumed that the Werner catalyst had rearranged to its inactive

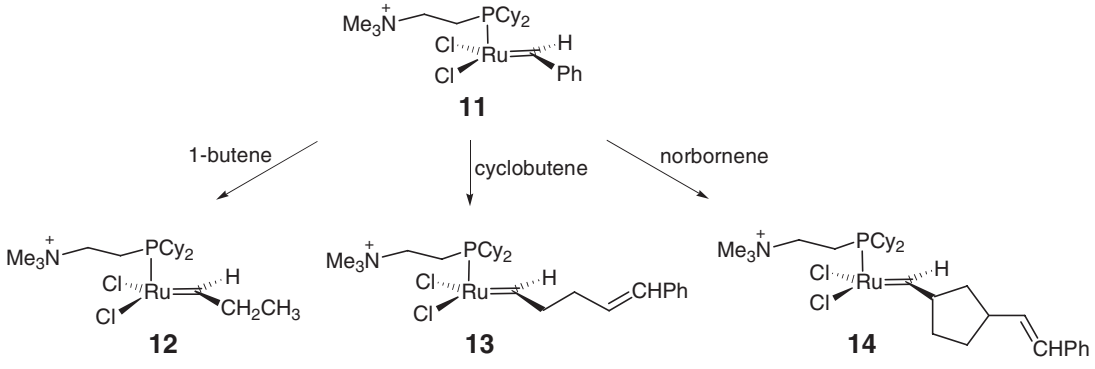

Scheme 6

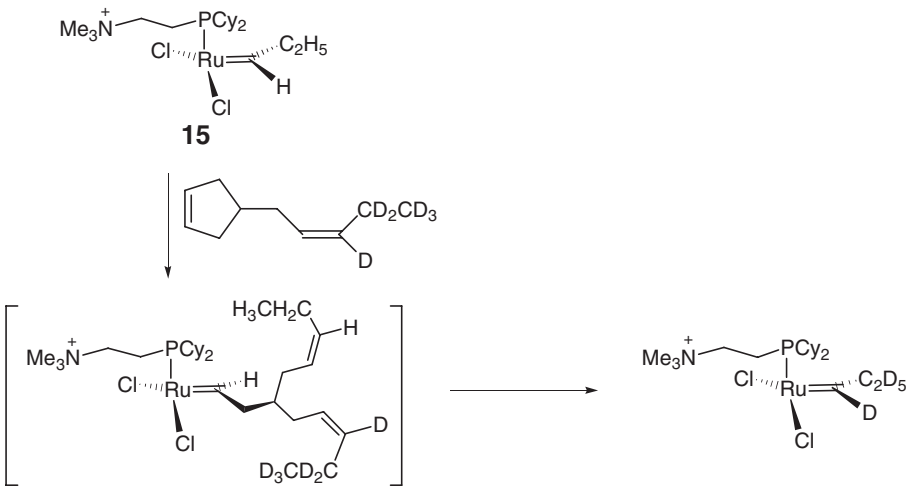

Scheme 7

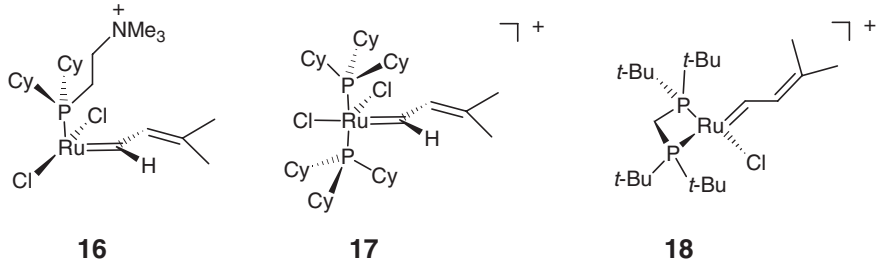

Figure 1 Ruthenium carbene complexes probed for metathesis activity in the gas phase.

carbyne form under electrospray conditions. The order of the gas-phase reactivity of complexes **16**, **17**, and **18** was completely reversed with regard to that in solution phase. Apparently, in solution, a pre-equilibrium step precedes metathesis and obviously determines the kinetics in condensed media, contrary to the reaction in gas phase, where only the intrinsic reactivity of the carbene complex matters.

ESI-MS was also employed for the study of the intrinsic reactivity of first- and second-generation Grubbs metathesis catalysts **19** $[(PCy_3)(Cl)_2Ru{=}CHR]^+$ (Cy = cyclohexyl, R = *p*-$Me_3NCH_2C_6H_4$) and **20** $[(NHC)(PCy_3)(Cl)_2Ru{=}CHR]^+$ (NHC = *N*-heterocyclic carbene).(Figure 2)[215] These complexes were mass selected and reacted with norbornene at ~5 mtorr. The second-generation catalyst reacted more than 100 times faster than the first-generation catalyst in the first ROM, but only 10 times faster in the subsequent ROMP steps.

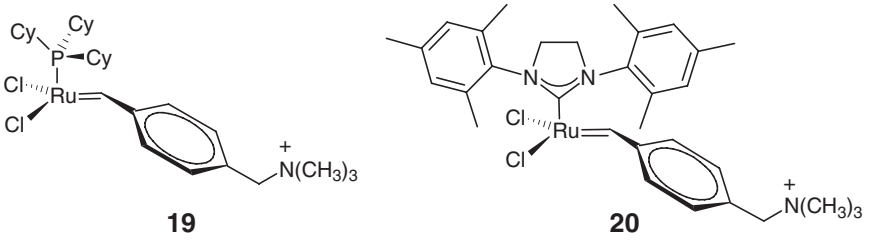

Figure 2 First generation (**19**) and second generation (**20**) Grubbs metathesis catalysts.

1.28.3.2.5 Carbene complexes

Fischer carbenes can be generated from diazomalonates in the gas phase, as reported by Beauchamp and co-workers.[216] Suitable cations for study were obtained by electrospray of solutions of Ag^+ or Cu^+ salts with the diazomalonate **21** in methanol : water : acetonitrile (80 : 20 : 0.1). The further reaction steps were conducted in a quadrupole ion trap spectrometer. Complexes formed via electrospray first undergo Fischer carbene formation and subsequently Wolff rearrangement upon collisional activation. Experiments with isotopically labeled diazomalonates suggest the underlying mechanism shown in Scheme 8.

Carbon atoms lost as CO molecules stem from the carbonyl groups in the starting material. Further experiments suggest that alkali metals do not promote this reaction. $[\mathbf{21} + M]^+$ ($M = Na^+$ or Rb^+) undergo simple fragmentation, giving rise to M^+ and (**21**). Experiments with divalent cations, like Ni^{2+}, do not produce any detectable carbenes, and afford only coordination compounds.

Rhenium carbenes can be generated in the gas phase from pentavalent diolate precursors.[217] Rhenium diolates were prepared by the addition of 1,2-propanediol and pyridine to $[ReOCl_3(SMe_2)(OPPh_3)]$ or $[(py)_4ReO_2]Cl$ in $CHCl_3$ or CH_2Cl_2, and were further diluted to 10^{-5} M before being electrosprayed in a tandem mass spectrometer. Complex **22** is formed in the electrospray process and affords **24** upon collision-induced dissociation with Xe (Scheme 9).

The mass-selected carbene complex **24a** was further reacted with *n*-propyl vinyl ether, yielding two products, **25** and **26**, presumably as a result of cyclopropanation and metathesis of the vinyl ether, respectively (Scheme 10).

In an extension of this work, several rhenium diolates were prepared starting from $ReOCl_3(SMe_2)(OPPh_3)$ or $[(py)_4ReO_2]Cl$ and a diol (1,2-propanediol, 1,2-butanediol, 1,2-pentanediol, 3,3-dimethyl-1,2-butanediol, 1,2-hexanediol) in $CHCl_3$ or CH_2Cl_2. The complexes thus formed were precipitated with hexane, and redissolved in polar

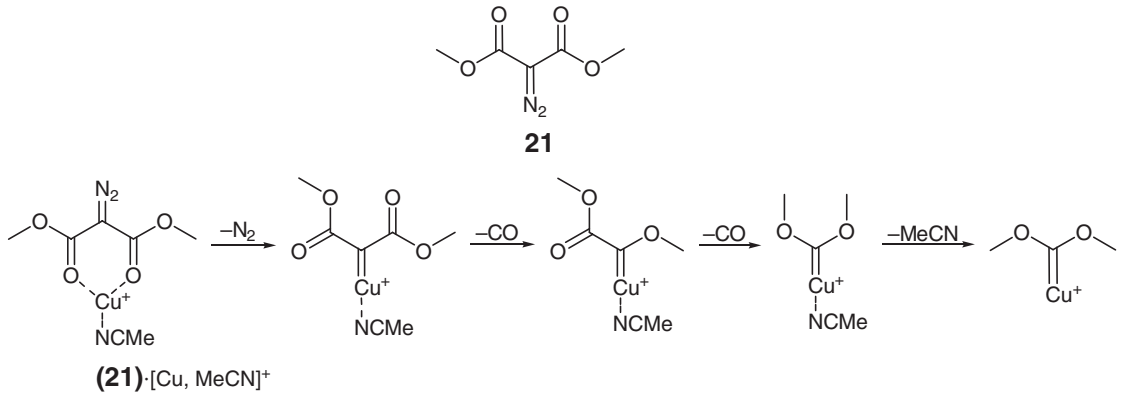

Scheme 8

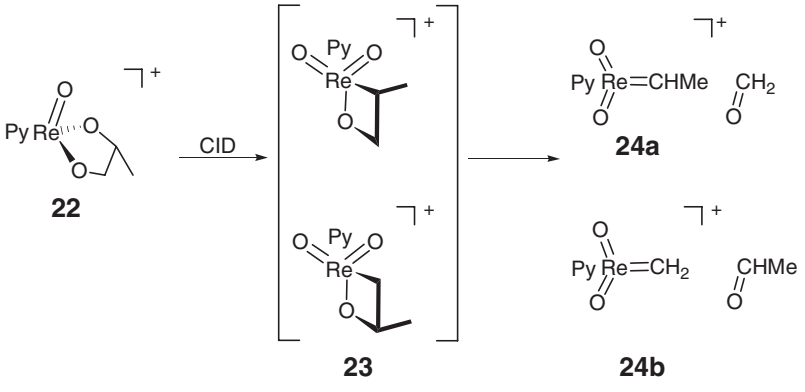

Scheme 9

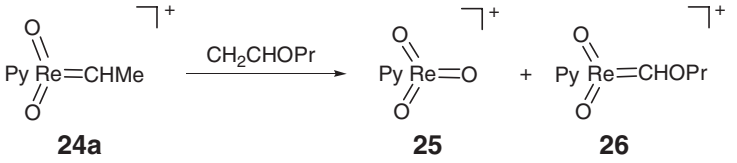

24a 25 26

Scheme 10

solvent before electrospray. Upon collisional activation, these diolates consistently produced monocationic species with a mass to charge ratio equal to that of the corresponding carbene. These products are believed to be formed via a metallaoxetane intermediate **23**, as supported by DFT calculations.[218]

1.28.3.2.6 Other examples

O'Hair and co-workers synthesized organomagnesates $[CH_3MgCl_2]^-$ and $[CH_3Mg(O_2CCH_3)_2]^-$ in the gas phase.[219] Solutions of $Mg(O_2CCH_3)_2$ and $MgCl_2$ in acetic acid were electrosprayed in negative ion mode, affording magnesium species of the composition $[Mg_n(O_2CCH_3)_{2n+1}]^-$ ($n = 1$–13) and $[Mg_nCl_x(O_2CCH_3)_y]^-$ ($n = 1$–3; $x + y = n + 1$), respectively. Upon mass selection in an ion trap, acetate complexes $[CH_3CO_2MgL_2]^-$ ($L = Cl^-$, $CH_3CO_2^-$) fragment upon collisional activation, yielding either organomagnesates of the general formula $[CH_3MgL_2]^-$ by loss of CO_2, or, by loss of neutral MgL_2, acetate (Scheme 11).

In order to further corroborate this mechanism, DFT calculations were performed. These calculations revealed that two different minimum energy structures exist for acetate- and chloride-ligated reactants, and that a four-centered transition state is involved, in which a methyl group is transferred from the carboxy moiety to the electrophilic MgL_2 center (Scheme 12).

These organomagnesates were reacted with protic neutral molecules like water, methanol, and ethanol, resulting in methane formation. Acetic acid is catalytically decarboxylated in the gas phase by a two-step mechanism. The first step involves addition of CH_3COOH to $[CH_3MgL_2]^-$ with concomitant elimination of CH_4 yielding $[CH_3CO_2MgL_2]^-$, followed by decarboxylation upon collisional activation to regenerate $[CH_3MgL_2]^-$.

Dietiker and Chen investigated the reaction of iridium complexes $[(PHOX)IrL]^+$ (PHOX = chiral phosphanyloxazoline, $L = H_2$, styrene) toward aromatic hydrocarbons.[220] $[(PHOX)IrH_2]^+$ was generated by electrospray and reacted with ethylbenzene, affording $[(PHOX)Ir(PhEt)]^+$ in the gas phase. This complex readily loses H_2 upon collision with Ar, and $[(PHOX)Ir(styrene)]^+$ is formed. In the "reverse" experiment, $[(PHOX)Ir(styrene)]^+$ was

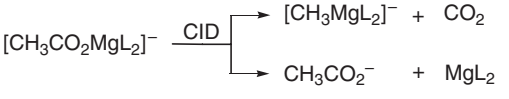

Scheme 11

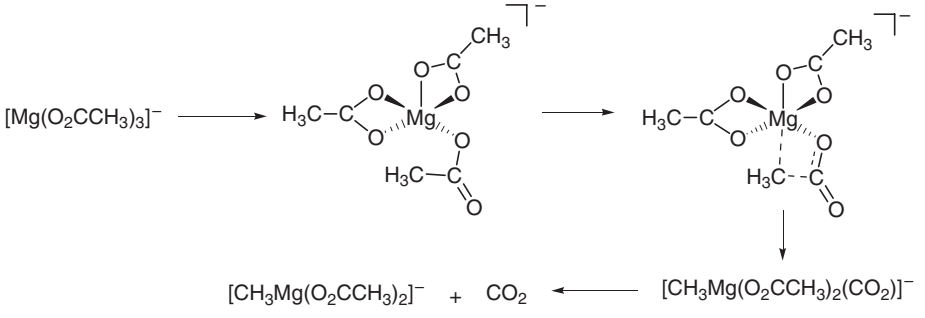

Scheme 12

reacted with D_2 in gas phase yielding products that bear one or two deuterium labels. According to these authors, these findings do not support the mechanism proposed by Anderson *et al.*[221]

1.28.4 Thermochemistry of Gas-Phase Organometallic Molecules

1.28.4.1 Thermochemical Methods

The multiplicity of competing mechanisms and energetically similar structural types in organometallic chemistry has often been blamed for the poor state of mechanistic understanding in this field. A notorious problem responsible for the lack of predictive models in organometallic chemistry (especially when compared to organic chemistry) is the paucity of reliable thermochemical data for the systems under investigation. Thermochemical methods, for example, calorimetry[222,223] or photoacoustic methods,[224–226] have been applied to organometallic species in condensed phases, but the number of studies is surprisingly small. Moreover, although such measurements can, in principle, provide thermochemical information on elementary reaction steps or metal–ligand bond energies, such data will always be unpredictably affected by side-reactions or solvent effects.

Again, gas-phase techniques provide the only means for an accurate determination of thermochemical parameters of well-defined molecular transformations. Principally, one has to distinguish between measurements of relative and absolute thermochemical values. For the former, a number of methods are available: equilibrium methods,[227,228] the kinetic method,[229–233] and CID method.[234] More relevant in the present context are measurements of absolute values. A variety of methods have been applied, from temperature-dependent equilibrium methods[235–240] and blackbody infrared radiative dissociation[241,242] to threshold CID.[12,13,243–247]

The number of studies on metal–ligand interactions employing the threshold CID technique has grown impressively during the last 15 years, mainly through the work of the Armentrout group. The available data are summarized in a number of review articles covering these studies.[245,248–250] As is the case with metal complex ion–molecule reactions, in general, the number of studies on coordination compounds by far exceeds those on bona fide organometallics. Moreover, the quantitative data available for organometallics confront the synthetic chemist in search of reliable metal–ligand bond energies with a twofold problem rather than with a clear-cut answer. First, while the binding of simple ligands, for example, alkyl or CO, in homoleptic complexes, has been addressed exhaustingly, reliable data for even marginally more complicated complexes are rare. Second, such data are available primarily for metal(I) compounds, which, for many main group and transition metals, is not a stable oxidation state in solution (and certainly not the only oxidation state).

1.28.4.2 Threshold Collision-induced Dissociation

The ability to determine accurate thermochemistry from CID data is a relatively recent development dating back to the early 1980s. The physical background, instrumentation, and data analysis in connection with this method have been thoroughly and expertly reviewed.[192,245] In order to measure the threshold for a CID reaction, the reactant ion must have a defined kinetic energy, undergo a collision (which leads to simple ligand fragmentation or a more complex chemical transformation), and have the resulting products analyzed. Such studies can be carried out in guided ion beam tandem, triple quadrupole, or ion cyclotron resonance mass spectrometers.

The number of quantitative threshold CID studies applied to organometallics that resemble solution-phase species is still very small. The main reason for this lack of studies is the so-called kinetic shift. Complete dissociation/reaction within the time the energized molecular ion resides in the collision chamber before entering the mass analyzer can only be expected for small polyatomic ions. Real-world molecules with many internal degrees of freedom will attain the required reaction rate only at internal energies that are somewhat higher than the threshold energy, that is, the kinetic shift produces threshold values that are too high. This effect becomes larger as the number of normal modes increases. For a transition metal complex ligated by a couple of medium-sized organic molecules, the kinetic shift can readily amount to values of the magnitude of the threshold itself, thus rendering a meaningful deconvolution problematic.

The quantitative CID threshold for the reaction $[CpIr(PMe_3)(CH_3)]^+ \rightarrow [CpIr(\eta^2\text{-}CH_2PMe_2)]^+ + CH_4$ (see Scheme 1) was determined this way.[196] The data were deconvoluted using Armentrout's "crunch" program. For the kinetic shift correction, using the Rice–Ramsperger–Kassel–Marcus (RRKM) formalism, a number of assumptions for the transition frequencies were made, yielding a deconvoluted threshold value for the endothermic cyclometallation of $E_0 = 13.6\,\text{kcal mol}^{-1}$.

In a typical example for obtaining absolute values for ligand-binding energies, the dissociation threshold in $[(bipy)Rh(PCH)]^+$ was determined. The phosphaethyne complex was prepared in the gas phase by sequential loss of methane from the precursor ion $[(bipy)Rh(PMe_3)_2(H)_2]^+$ by collisional activation. DFT calculations showed the side-on complex to be favored over the end-on coordination by ca. 25 kcal mol^{-1}. Using the data from these calculations, the threshold was deconvoluted to $E_0 = 46.6$ kcal mol^{-1}.[251]

A recent study of ligand bond energies in the Pt(II) complexes, **5** (L = H_2O, CF_3CH_2OH, or CH_3CN), competent in C–H activation (cf. Scheme 3), yielded values of 26.5 (trifluroethanol), 28.4 (water), and 35.1 kcal mol^{-1} (acetonitrile), respectively.[252]

1.28.5 Ionization Energies and Electron Affinities of Organometallics from Mass Spectrometric Methods

1.28.5.1 Overview of Electron-transfer Equilibrium (ETE) Method

Compared to the situation for atoms and organic molecules,[253–255] relatively few ionization potentials (IP) and electron affinities (EA) have been determined for organometallic compounds in the gas phase. These key physical quantities are important for understanding and predicting the oxidation–reduction properties of metal-containing molecules, and in addition, these values are useful for determination of fundamental quantities such as ion-solvation energies. Until the relatively recent application of mass spectrometric techniques to collect IP data, photoelectron spectroscopy of neutral molecules was the standard method for obtaining ionization energy data for organometallic compounds.[256,257] The methods described here complement and extend the photoelectron results, since they can be used to determine electron-attachment energies as well as ionization energies for neutrals. In addition, free energies for these quantities can be determined as opposed to the vertical energies measured in the photoelectron method.[55]

This section describes the techniques and results for determination of ionization and electron-attachment energetics for organometallic compounds and coordination complexes. The primary technique in this work is the electron-transfer equilibrium method (ETE),[53] which has been used to obtain gas-phase redox energetics for a variety of neutral complexes of the transition elements. The ETE method is a subset of the various ladder methods, in which a series of compounds are brought to equilibrium, and the equilibrium constants are then used to produce a scale of physical parameters.[58]

1.28.5.2 Free Energies for Ionization and Electron Attachment

MS is used in the ETE method to follow the equilibration of reactions of the type given in Equations (1) and (2).

$$Y(g) + R^+(g) = Y^+(g) + R(g) \quad (1)$$

$$Y(g) + R^-(g) = Y^-(g) + R(g) \quad (2)$$

Here, Y is the molecule of interest and R is the reference compound. The reactions are allowed to equilibrate at known pressures P_Y and P_R, and the relative ion populations (I) in the source or ion trap are determined by obtaining the mass spectrum. The standard free energy change for the reaction at temperature T as written can be obtained from the equilibrium constant as in Equation (3).

$$\Delta G_{et,T}^{\circ} = -RT\ln K_{eq} = -RT\ln[(I(Y^{\pm})P_R)/(I(R^{\pm})P_Y)] \quad (3)$$

The temperature dependence of the K_{eq} value can be used to obtain enthalpy and entropy changes in the vicinity of the experimental temperatures by using van't Hoff plots.

In one experimental method for studying ETE reactions, reactions can be followed in the ion trap of an FTICR-MS,[21] where the pressures of neutrals are in the 10^{-8} to 10^{-5} torr range. In a second common ETE technique, electron-transfer equilibrium constants have been determined by using pulsed high pressure MS (PHPMS).[53] In this method, the reaction comes to equilibrium quickly in a high pressure source (~1 torr total pressure including a background gas) following ion production by a pulsed high-energy electron beam. The ions exiting the source region are mass analyzed, and a time plot of ion currents can be used to extract the K_{eq} value at long reaction times.

To derive the free energy changes for Equations (1) and (2) from ETE results, the relevant thermodynamic quantities for the reference compounds R are used. If the free energy of ionization for the reference compound,

$\Delta G_{i,T}^{\circ}(R)$, is known (generally deduced from high resolution photoelectron spectroscopy coupled to statistical mechanics), then the corresponding energy for the new compound M can be obtained from Equation (4).

$$\Delta G_{i,T}^{\circ}(Y) = \Delta G_{i,T}^{\circ}(R) + G_{et,T}^{\circ} \quad (4)$$

In the same way, the free energy of electron attachment for a new compound, .$\Delta G_{a,T}^{\circ}(Y)$ Equation (2), can be obtained from the free energy change for the reaction in Equations (2) and (5).

$$\Delta G_{a,T}^{\circ}(Y) = \Delta G_{a,T}^{\circ}(R) + G_{et,T}^{\circ} \quad (5)$$

Once compounds are brought to equilibrium with primary reference compounds, an equilibrium ladder can be built with reactions involving secondary reference compounds. For example, the $SO_2^{0/-}$ couple is often used as an anchor for electron attachment ($G_{a,T=423}(SO_2) = -26.1$ kcal mol^{-1}).[258] In a similar manner, $(benzene)_2Cr^{0/+}$ can be used as a reference compound in the low ionization energy range (5–6 eV), while other metallocenes such as ferrocene can be used in higher ranges.[36]

Results from organometallic ETE and bracketing studies have been reviewed.[55,259] The prototype metallocene(0/+) and related MCp^*_2 couples have been investigated as a function of metal, and the trends are closely related to those observed for the vertical photoelectron ionization energies.[30,36,56] This similarity is not surprising given the relatively small structural and electronic reorganizations that occur between the neutral and cation (oxidized) states. Nickelocene is the only first-row metallocene that forms a stable negative ion, and substituent effects have been investigated for both metallocene(0/+), particularly ruthenocene couples, and nickelocene(0/−) couples.[30,260,261] The ETE method yields thermochemical quantities that can readily be incorporated into thermodynamic cycles for extracting fundamental solvation energetics and bond-disruption energies.[262,263] Free energies of ionization and electron attachment can be used to estimate differential solvation energies by combining the gas-phase data with solution electrochemical potentials. Rates of redox reactions for metallocene couples have been useful prototypes to compare solution- and gas-phase reactions.[35]

References

1. Eller, K.; Schwarz, H. *Chem. Rev.* **1991**, *91*(6), 1121–1177.
2. O'Hair, R. A. J.; Khairallah, G. N. *J. Cluster Sci.* **2004**, *15*(3), 331–363.
3. Metz, R. B. *Int. Rev. Phys. Chem.* **2004**, *23*(1), 79–108.
4. Operti, L.; Rabezzana, R. *Mass Spectrom. Rev.* **2003**, *22*(6), 407–428.
5. Uggerud, E. *Mass Spectrom. Rev.* **1999**, *18*(5), 285–308.
6. Kleiber, P. D.; Chen, J. *Int. Rev. Phys. Chem.* **1998**, *17*(1), 1–34.
7. Freiser, B. S. *J. Mass Spectrom.* **1996**, *31*(7), 703–715.
8. Freiser, B. S. *Organometallic Ion Chemistry*; Kluwer: Dordrecht, 1996.
9. Capron, L.; Mestdagh, H.; Rolando, C. *Coord. Chem. Rev.* **1998**, *180*, 269–330.
10. Fisher, K. J. In *Progress In Inorganic Chemistry*; Karlin, K. D., Ed.; Wiley-Interscience; 2001; Vol. 50, pp 343–432.
11. Simoes, J. A. M.; Beauchamp, J. L. *Chem. Rev.* **1990**, *90*(4), 629–688.
12. Armentrout, P. B. *Annu. Rev. Phys. Chem.* **2001**, *52*, 423–461.
13. Armentrout, P. B. *Int. J. Mass Spectrom.* **2003**, *227*(3), 289–302.
14. Damrauer, R. *Organometallics* **2004**, *23*(7), 1462–1479.
15. Zagorevskii, D. V.; Holmes, J. L. *Mass Spectrom. Rev.* **1999**, *18*(2), 87–118.
16. Schalley, C. A.; Hornung, G.; Schroder, D.; Schwarz, H. *Chem. Soc. Rev.* **1998**, *27*(2), 91–104.
17. Cole, R. B. *Electrospray Ionization Mass Spectrometry;* Wiley: New York, 1997.
18. Herbert, C.; Johnstone, R. In *Mass Spectrometry Basics*; CRC Press: Boca Raton, FL, 2002; p 496.
19. Watson, J. T. *Introduction to Mass Spectrometry*, 3rd ed.; Lippincott-Raven: Philadelphia, **1997**.
20. Gross, M. L.; Caprioli, R. M.; Armentrout, P. B., Eds. *Encyclopedia of Mass Spectrometry*; Elsevier: Oxford, 2003; *1*.
21. Marshall, A. G.; Hendrickson, C. L.; Jackson, G. S. *Mass Spectrom. Rev.* **1998**, *17*(1), 1–35.
22. Brauman, J. I.; Blair, L. K. *J. Am. Chem. Soc.* **1968**, *90*(23), 6561–6562.
23. Brauman, J. I.; Blair, L. K. *J. Am. Chem. Soc.* **1969**, *91*(8), 2126–2127.
24. Brauman, J. I.; Blair, L. K. *J. Am. Chem. Soc.* **1970**, *92*(20), 5986–5992.
25. Brauman, J. I.; Blair, L. K. *J. Am. Chem. Soc.* **1971**, *93*(16), 3911–3914.
26. Brauman, J. I.; Riveros, J. M.; Blair, L. K. *J. Am. Chem. Soc.* **1971**, *93*(16), 3914–3916.
27. Bowers, M. T.; Aue, D. H.; Webb, H. M.; McIver, R. T. *J. Am. Chem. Soc.* **1971**, *93*(17), 4314–4315.
28. Aue, D. H.; Bowers, M. T.; Webb, H. M. *J. Am. Chem. Soc.* **1972**, *94*(13), 4726–4728.
29. Aue, D. H.; Webb, H. M.; Bowers, M. T. *J. Am. Chem. Soc.* **1975**, *97*(14), 4137–4139.
30. Richardson, D. E.; Ryan, M. F.; Khan, M. N. I.; Maxwell, K. A. *J. Am. Chem. Soc.* **1992**, *114*(26), 10482–10485.
31. Sharpe, P.; Alameddin, N. G.; Richardson, D. E. *J. Am. Chem. Soc.* **1994**, *116*(24), 11098–11108.
32. Eyler, J. R.; Richardson, D. E. *J. Am. Chem. Soc.* **1985**, *107*(21), 6130–6131.
33. Richardson, D. E. *J. Phys. Chem.* **1986**, *90*(16), 3697–3700.

34. Richardson, D. E.; Christ, C. S.; Sharpe, P.; Eyler, J. R. *J. Am. Chem. Soc.* **1987**, *109*(13), 3894–3902.
35. Richardson, D. E.; Eyler, J. R. *Chem. Phys.* **1993**, *176*(2–3), 457–466.
36. Ryan, M. F.; Richardson, D. E.; Lichtenberger, D. L.; Gruhn, N. E. *Organometallics* **1994**, *13*(4), 1190–1199.
37. Alameddin, N. G.; Ryan, M. F.; Eyler, J. R.; Siedle, A. R.; Richardson, D. E. *Organometallics* **1995**, *14*(11), 5005–5007.
38. Richardson, D. E.; Alameddin, N. G.; Ryan, M. F.; Hayes, T.; Eyler, J. R.; Siedle, A. R. *J. Am. Chem. Soc.* **1996**, *118*(45), 11244–11253.
39. Richardson, D. E. In *Electron Transfer Reactions*; Advances in Chemistry Series; Isied, S. S., Ed.; American Chemical Society, 1997; Vol. 253, pp 79–90.
40. Zachmanoglou, C. E.; Docrat, A.; Bridgewater, B. M.; Parkin, G.; Brandow, C. G.; Bercaw, J. E.; Jardine, C. N.; Lyall, M.; Green, J. C.; Keister, J. B. *J. Am. Chem. Soc.* **2002**, *124*(32), 9525–9546.
41. Imanishi, Y.; Naga, N. *Prog. Polym. Sci.* **2001**, *26*(8), 1147–1198.
42. Pedeutour, J. N.; Radhakrishnan, K.; Cramail, H.; Deffieux, A. *Macromol. Rapid Commun.* **2001**, *22*(14), 1095–1123.
43. Hlatky, G. G. *Coord. Chem. Rev.* **1999**, *181*, 243–296.
44. Hlatky, G. G. *Coord. Chem. Rev.* **2000**, *199*, 235–329.
45. Chen, E. Y. X.; Marks, T. J. *Chem. Rev.* **2000**, *100*(4), 1391–1434.
46. Hamielec, A. E.; Soares, J. B. P. *Prog. Polym. Sci.* **1996**, *21*(4), 651–706.
47. Huang, J.; Rempel, G. L. *Prog. Polym. Sci.* **1995**, *20*(3), 459–526.
48. Bohme, D. K.; Schwarz, H. *Angew. Chem., Int. Ed.* **2005**, *44*(16), 2336–2354.
49. Armentrout, P. B. *Eur. J. Mass Spectrom.* **2003**, *9*(6), 531–538.
50. Liyanage, R.; Conceicao, J.; Armentrout, P. B. *J. Chem. Phys.* **2002**, *116*(3), 936–945.
51. Vardhan, D.; Liyanage, R.; Armentrout, P. B. *J. Chem. Phys.* **2003**, *119*(8), 4166–4178.
52. Liu, F. Y.; Zhang, X. G.; Liyanage, R.; Armentrout, P. B. *J. Chem. Phys.* **2004**, *121*(22), 10976–10990.
53. Kebarle, P.; Chowdhury, S. *Chem. Rev.* **1987**, *87*(3), 513–534.
54. Richardson, D. E.; Christ, C. S.; Sharpe, P.; Ryan, M. F.; Eyler, J. R. *ACS Symp. Ser.* **1990**, *428*, 70–83.
55. Richardson, D. E. In *Organometallic Ion Chemistry*; Freiser, B. S., Ed., Kluwer: Dordrecht, 1996.
56. Meotner, M. *J. Am. Chem. Soc.* **1989**, *111*(8), 2830–2834.
57. Sharpe, P.; Kebarle, P. *J. Am. Chem. Soc.* **1993**, *115*(2), 782–789.
58. McMahon, T. B. *Int. J. Mass Spectrom.* **2000**, *200*(1–3), 187–199.
59. Traeger, J. C. *Int. J. Mass Spectrom.* **2000**, *200*(1–3), 387–401.
60. Rosenberg, E. *J. Chromatogr. A* **2003**, *1000*(1–2), 841–889.
61. Stewart, I. I. *Spectrochim. Acta, Part B: At. Spectrosc.* **1999**, *54*(12), 1649–1695.
62. Schramel, O.; Michalke, B.; Kettrup, A. *J. Chromatogr. A* **1998**, *819*(1–2), 231–242.
63. Zoorob, G.; Brown, F. B.; Caruso, J. *J. Anal. At. Spectrom.* **1997**, *12*(5), 517–524.
64. Santos, L. S.; Knaack, L.; Metzger, J. O. *Int. J. Mass Spectrom.* **2005**, *246*(1–3), 84–104.
65. Johnson, B. F. G.; McIndoe, J. S. *Coord. Chem. Rev.* **2000**, *200*, 901–932.
66. Mori, S.; Nakamura, E. *J. Synth. Org. Chem. Jpn.* **2003**, *61*(2), 144–151.
67. Bernardi, F.; Bottoni, A.; Garavelli, M. *Quant. Struct.-Act. Relat.* **2002**, *21*(2), 128–148.
68. Fey, N. *J. Chem. Technol. Biotechnol.* **1999**, *74*(9), 852–862.
69. Mingos, D. M. P.; Lyne, P. D.; Pidun, U. *Pure Appl. Chem.* **1995**, *67*(2), 265–272.
70. Noodleman, L.; Lovell, T.; Han, W. G.; Li, J.; Himo, F. *Chem. Rev.* **2004**, *104*(2), 459–508.
71. Afzaal, S.; Freiser, B. S. *Chem. Phys. Lett.* **1994**, *218*(3), 254–260.
72. Buchanan, J. W.; Grieves, G. A.; Reddic, J. E.; Duncan, M. A. *Int. J. Mass Spectrom.* **1999**, *183*, 323–333.
73. Foster, N. R.; Grieves, G. A.; Buchanan, J. W.; Flynn, N. D.; Duncan, M. A. *J. Phys. Chem. A* **2000**, *104*(47), 11055–11062.
74. Duncan, M. A.; Knight, A. M.; Negishi, Y.; Nagao, S.; Judai, K.; Nakajima, A.; Kaya, K. *J. Phys. Chem. A* **2001**, *105*(44), 10093–10097.
75. Walker, N. R.; Grieves, G. A.; Walters, R. S.; Duncan, M. A. *Chem. Phys. Lett.* **2003**, *380*(1–2), 230–236.
76. Jaeger, T. D.; Duncan, M. A. *J. Phys. Chem. A* **2004**, *108*(51), 11296–11301.
77. Ayers, T. M.; Westlake, B. C.; Duncan, M. A. *J. Phys. Chem. A* **2004**, *108*(45), 9805–9813.
78. Jaeger, T. D.; van Heijnsbergen, D.; Klippenstein, S. J.; von Helden, G.; Meijer, G.; Duncan, M. A. *J. Am. Chem. Soc.* **2004**, *126*(35), 10981–10991.
79. Jaeger, T. D.; Pillai, E. D.; Duncan, M. A. *J. Phys. Chem. A* **2004**, *108*(32), 6605–6610.
80. Jaeger, T. D.; Duncan, M. A. *J. Phys. Chem. A* **2005**, *109*(15), 3311–3317.
81. Jaeger, T. D.; Duncan, M. A. *Int. J. Mass Spectrom.* **2005**, *241*(2–3), 165–171.
82. Vajda, S.; Rosendo-Francisco, P.; Kaposta, C.; Krenz, M.; Lupulescu, C.; Woste, L. *Eur. Phys. J. D* **2001**, *16*(1–3), 161–164.
83. Nanayakkara, V. K.; Freiser, B. S. *J. Mass Spectrom.* **1997**, *32*(5), 475–482.
84. Russon, L. M.; Heidecke, S. A.; Birke, M. K.; Conceicao, J.; Morse, M. D.; Armentrout, P. B. *J. Chem. Phys.* **1994**, *100*(7), 4747–4755.
85. Ranatunga, D. R. A.; Freiser, B. S. *Chem. Phys. Lett.* **1995**, *233*(3), 319–323.
86. Xu, Y. C.; Garcia, E.; Freiser, B. S.; Bauschlicher, C. W. *Int. J. Mass Spectrom. Ion Processes* **1996**, *158*, 249–263.
87. Surya, P. I.; Roth, L. M.; Ranatunga, D. R. A.; Freiser, B. S. *J. Am. Chem. Soc.* **1996**, *118*(5), 1118–1125.
88. Lin, C. Y.; Chen, Q.; Chen, H. P.; Freiser, B. S. *Int. J. Mass Spectrom.* **1997**, *167*, 713–722.
89. Hanratty, M. A.; Paulsen, C. M.; Beauchamp, J. L. *J. Am. Chem. Soc.* **1985**, *107*(18), 5074–5080.
90. Shin, S. K.; Beauchamp, J. L. *J. Am. Chem. Soc.* **1990**, *112*(6), 2066–2069.
91. Shin, S. K.; Beauchamp, J. L. *J. Mol. Struct.* **1991**, *249*(1), 1–9.
92. Yang, X.; Waters, T.; Wang, X. B.; O'Hair, R. A. J.; Wedd, A. G.; Li, J.; Dixon, D. A.; Wang, L. S. *J. Phys. Chem. A* **2004**, *108*(46), 10089–10093.
93. Waters, T.; Wang, X. B.; Yang, X.; Zhang, L. Y.; O'Hair, R. A. J.; Wang, L. S.; Wedd, A. G. *J. Am. Chem. Soc.* **2004**, *126*(16), 5119–5129.
94. Moore, D. T.; Oomens, J.; Eyler, J. R.; von Helden, G.; Meijer, G.; Dunbar, R. C. *J. Am. Chem. Soc.* **2005**, *127*(19), 7243–7254.
95. Valle, J. J.; Eyler, J. R.; Oomens, J.; Moore, D. T.; van der Meer, A. F. G.; von Helden, G.; Meijer, G.; Hendrickson, C. L.; Marshall, A. G.; Blakney, G. T. *Rev. Sci. Instrum.* **2005**, *76*(2).
96. Oomens, J.; Moore, D. T.; von Helden, G.; Meijer, G.; Dunbar, R. C. *J. Am. Chem. Soc.* **2004**, *126*(3), 724–725.
97. Moore, D. T.; Oomens, J.; Eyler, J. R.; Meijer, G.; von Helden, G.; Ridge, D. P. *J. Am. Chem. Soc.* **2004**, *126*(45), 14726–14727.
98. Pillai, E. D.; Molek, K. S.; Duncan, M. A. *Chem. Phys. Lett.* **2005**, *405*(4–6), 247–251.

99. Rue, C.; Armentrout, P. B.; Kretzschmar, I.; Schroder, D.; Schwarz, H. *Int. J. Mass Spectrom.* **2001**, *210*(1–3), 283–301.
100. Liyanage, R.; Armentrout, P. B. *Int. J. Mass Spectrom.* **2005**, *241*(2–3), 243–260.
101. Armentrout, P. B. *J. Anal. At. Spectrom.* **2004**, *19*(5), 571–580.
102. Liu, F. Y.; Li, F. X.; Armentrout, P. B. *J. Chem. Phys.* **2005**, *123*(6).
103. Liu, F. Y.; Armentrout, P. B. *J. Chem. Phys.* **2005**, *122*(19).
104. Schwarz, H. *Int. J. Mass Spectrom.* **2004**, *237*(1), 75–105.
105. Schwarz, H. *Angew. Chem., Int. Ed.* **2003**, *42*(37), 4442–4454.
106. Schroder, D.; Schwarz, H. *Top. Curr. Chem.* **2003**, *225*, 133–152.
107. Schroder, D.; Schwarz, H. *Int. J. Mass Spectrom.* **2004**, *231*(2–3), 139–146.
108. Liu, F.; Zhang, X. G.; Armentrout, P. B. *Phys. Chem. Chem. Phys.* **2005**, *7*(5), 1054–1064.
109. Zhang, Q.; Bowers, M. T. *J. Phys. Chem. A* **2004**, *108*(45), 9755–9761.
110. Goncharov, V. B. *Russ. J. Phys. Chem.* **2004**, *78*(6), 882–887.
111. Sievers, M. R.; Chen, Y. M.; Haynes, C. L.; Armentrout, P. B. *Int. J. Mass Spectrom.* **2000**, *196*, 149–170.
112. Sievers, M. R.; Armentrout, P. B. *Organometallics* **2003**, *22*(13), 2599–2611.
113. Armentrout, P. B.; Sievers, M. R. *J. Phys. Chem. A* **2003**, *107*(22), 4396–4406.
114. Manard, M. J.; Kemper, P. R.; Carpenter, C. J.; Bowers, M. T. *Int. J. Mass Spectrom.* **2005**, *241*(2–3), 99–108.
115. Manard, M. J.; Kemper, P. R.; Bowers, M. T. *Int. J. Mass Spectrom.* **2005**, *241*(2–3), 109–117.
116. Mazurek, U.; Koszinowski, K.; Schwarz, H. *Organometallics* **2003**, *22*(2), 218–225.
117. Koszinowski, K.; Schroder, D.; Schwarz, H. *Organometallics* **2005**, *24*(9), 2214–2223.
118. Taylor, W. S.; Matthews, C. C.; Parkhill, K. S. *J. Phys. Chem. A* **2005**, *109*(2), 356–365.
119. Taylor, W. S.; May, J. C.; Lasater, A. S. *J. Phys. Chem. A* **2003**, *107*(13), 2209–2215.
120. Srzic, D.; Kazazic, S.; Kralj, B.; Klasinc, L.; Marsel, J.; Gusten, H.; McGlynn, S. P. *Int. J. Mass Spectrom.* **2003**, *230*(2–3), 135–140.
121. Kazazic, S.; Klasinc, L.; Kovac, B.; Srzic, D. *Rapid Commun. Mass Spectrom.* **2003**, *17*(20), 2361–2363.
122. Kazazic, S.; Klasinc, L.; Rozman, M.; Srzic, D.; von Knop, J. *Croat. Chem. Acta* **2004**, *77*(1–2), 321–324.
123. Kazazic, S.; Kazazic, S. P.; Klasinc, L.; Rozman, M.; Srzic, D. *Croat. Chem. Acta* **2005**, *78*(2), 269–274.
124. Boutreau, L.; Leon, E.; Rodriguez-Santiago, L.; Toulhoat, P.; Mo, O.; Tortajada, J. *J. Phys. Chem. A* **2002**, *106*(44), 10563–10577.
125. Boutreau, L.; Toulhoat, P.; Tortajada, J.; Luna, A.; Mo, O.; Yanez, M. *J. Phys.Chem. A* **2002**, *106*(40), 9359–9368.
126. Fordham, P.; Deschasse, M.; Haldys, V.; Tortajada, J.; Morizur, J. P. *Eur. J. Mass Spectrom.* **2001**, *7*(4–5), 313–320.
127. Rodriguez-Santiago, L.; Noguera, M.; Sodupe, M.; Salpin, J. Y.; Tortajada, J. *J. Phys. Chem. A* **2003**, *107*(46), 9865–9874.
128. Zhao, X.; Xin, B.; Xing, X. P.; Zhang, X.; Wang, G. H.; Gao, Z. *Rapid Commun. Mass Spectrom.* **2001**, *15*(15), 1317–1321.
129. Carretas, J. A.; Marcalo, J.; de Matos, A. P. *Int. J. Mass Spectrom.* **2004**, *234*(1–3), 51–61.
130. Jackson, G. P.; Gibson, J. K.; Duckworth, D. C. *Int. J. Mass Spectrom.* **2002**, *220*(3), 419–441.
131. Grutzmacher, H. F.; Zoric, S.; Wellbrock, C. *Int. J. Mass Spectrom.* **2001**, *210*(1–3), 311–325.
132. Cao, Y. L.; Zhao, X. A.; Xin, B.; Xiong, S. X.; Tang, Z. C. *THEOCHEM* **2004**, *683*(1–3), 141–146.
133. Shiota, Y.; Yoshizawa, K. *J. Am. Chem. Soc.* **2000**, *122*(49), 12317–12326.
134. Shiota, Y.; Suzuki, K.; Yoshizawa, K. *Organometallics* **2005**, *24*(14), 3532–3538.
135. Goncharov, V. B. *Russ. J. Phys. Chem.* **2004**, *78*(10), 1560–1571.
136. Mautner, M. M. N.; Sieck, L. W. *Int. J. Mass Spectrom. Ion Processes* **1991**, *109*, 187–208.
137. Whitehouse, C. M.; Dreyer, R. N.; Yamashita, M.; Fenn, J. B. *Anal. Chem.* **1985**, *57*(3), 675–679.
138. Fenn, J. B. *Angew. Chem., Int. Ed.* **2003**, *42*(33), 3871–3894.
139. Vanberkel, G. J.; McLuckey, S. A.; Glish, G. L. *Anal. Chem.* **1991**, *63*(18), 2064–2068.
140. Vanberkel, G. J.; McLuckey, S. A.; Glish, G. L. *Anal. Chem.* **1991**, *63*(11), 1098–1109.
141. KaneMaguire, L. A. P.; Kanitz, R.; Sheil, M. M. *Inorg. Chim. Acta* **1996**, *245*(2), 209–214.
142. Roth, L. M.; Freiser, B. S. *Mass Spectrom. Rev.* **1991**, *10*(4), 303–328.
143. Kebarle, P. *J. Mass Spectrom.* **2000**, *35*(7), 804–817.
144. Kebarle, P.; Peschke, M. *Anal. Chim. Acta* **2000**, *406*(1), 11–35.
145. Dole, M.; Mack, L. L.; Hines, R. L.; Mobley, R. C.; Ferguson, L. D.; Alice, M. B. *J. Chem. Phys.* **1968**, *49*(5), 2240.
146. Iribarne, J. V.; Thomson, B. A. *J. Chem. Phys.* **1976**, *64*(6), 2287.
147. Stevens, S. M.; Dunbar, R. C.; Price, W. D.; Sena, M.; Watson, C. H.; Nichols, L. S.; Riveros, J. M.; Richardson, D. E.; Eyler, J. R. *J. Phys. Chem. A* **2002**, *106*(42), 9686–9694.
148. Stevens, S. M.; Dunbar, R. C.; Price, W. D.; Sena, M.; Watson, C. H.; Nichols, L. S.; Riveros, J. M.; Richardson, D. E.; Eyler, J. R. *J. Phys. Chem. A* **2004**, *108*(45), 9892–9900.
149. Burns, T. D.; Spence, T. G.; Mooney, M. A.; Posey, L. A. *Chem. Phys. Lett.* **1996**, *258*(5–6), 669–679.
150. Spence, T. G.; Burns, T. D.; Posey, L. A. *J. Phys. Chem. A* **1997**, *101*(2), 139–144.
151. Spence, T. G.; Burns, T. D.; Guckenberger, G. B.; Posey, L. A. *J. Phys. Chem. A* **1997**, *101*(6), 1081–1092.
152. Spence, T. G.; Trotter, B. T.; Posey, L. A. *J. Phys. Chem. A* **1998**, *102*(40), 7779–7786.
153. Spence, T. G.; Trotter, B. T.; Burns, T. D.; Posey, L. A. *J. Phys. Chem. A* **1998**, *102*(30), 6101–6106.
154. Stafford, J. G. *J. Am. Soc. Mass Spectrom.* **2002**, *13*(6), 589.
155. Hofstadler, S. A.; Laude, D. A., Jr., *J. Am. Soc. Mass Spectrom.* **1992**, *3*(6), 615–623.
156. Guan, Z.; Campbell, V. L.; Drader, J. J.; Hendrickson, C. L.; Laude, D. A., Jr., *Rev. Sci. Instrum.* **1995**, *66*(9), 4507–4515.
157. Laude, D. A.; Stevenson, E.; Robinson, J. M. In *Electrospray Ionization Mass Spectrometry*; Cole, R. B., Ed.; Wiley: New York, 1997; pp 291–319.
158. Plattner, D. A. *Int. J. Mass Spectrom.* **2001**, *207*(3), 125–144.
159. Plattner, D. A. *Top. Curr. Chem.* **2003**, *225*, 153–203.
160. Gatlin, C. L.; Turecek, F. In *Electrospray Ionization Mass Spectrometry*; Cole, R. B., Ed.; Wiley: New York, 1997; pp 527–570.
161. Colton, R.; DAgostino, A.; Traeger, J. C. *Mass Spectrom. Rev.* **1995**, *14*(2), 79–106.
162. Bussian, P.; Sobott, F.; Brutschy, B.; Schrader, W.; Schuth, F. *Angew. Chem., Int. Ed.* **2000**, *39*(21), 3901–3905.
163. Coronado, E.; Feliz, M.; Forment-Aliaga, A.; Gomez-Garcia, C. J.; Llusar, R.; Romero, F. M. *Inorg. Chem.* **2001**, *40*(24), 6084–6085.
164. Nierengarten, H.; Rojo, J.; Leize, E.; Lehn, J. M.; Van Dorsselaer, A. *Eur. J. Inorg. Chem.*573–579.
165. Nierengarten, H.; Leize, E.; Breuning, E.; Garcia, A.; Romero-Salguero, F.; Rojo, J.; Lehn, J. M.; Van Dorsselaer, A. *J. Mass Spectrom.* **2002**, *37*(1), 56–62.

166. Yim, H. W.; Lam, K. C.; Rheingold, A. L.; Rabinovich, D. *Polyhedron* **2000**, *19*(7), 849–853.
167. Pinkse, M. W. H.; Maier, C. S.; Kim, J. I.; Oh, B. H.; Heck, A. J. R. *J. Mass Spectrom.* **2003**, *38*(3), 315–320.
168. Dakternieks, D.; Lim, A. E. K.; Lim, K. F. *Chem. Commun.* **1999**, No. 15, 1425–1426.
169. de Bruin, B.; Verhagen, J. A. W.; Schouten, C. H. J.; Gal, A. W.; Feichtinger, D.; Plattner, D. A. *Chem. Eur. J.* **2001**, *7*(2), 416–422.
170. Schroeter, K.; Wesendrup, R.; Schwarz, H. *Eur. J. Org. Chem.* **1998**, No. 4, 565–571.
171. Schroder, D.; Loos, J.; Semialjac, M.; Weiske, T.; Schwarz, H.; Hohne, G.; Thissen, R.; Dutuit, O. *Int. J. Mass Spectrom.* **2002**, *214*(1), 155–170.
172. Chen, P. *Angew. Chem., Int. Ed.* **2003**, *42*(25), 2832–2847.
173. Ikonomou, M. G.; Blades, A. T.; Kebarle, P. *Anal. Chem.* **1991**, *63*(18), 1989–1998.
174. Yin, H. Y.; Hachey, D. L.; Porter, N. A. *J. Am. Soc. Mass Spectrom.* **2001**, *12*(4), 449–455.
175. Bayer, E.; Gfrorer, P.; Rentel, C. *Angew. Chem., Int. Ed.* **1999**, *38*(7), 992–995.
176. Hopfgartner, G.; Vilbois, F.; Piguet, C. *Rapid Commun. Mass Spectrom.* **1999**, *13*(5), 302–306.
177. Hayen, H.; Alvarez-Grima, M. M.; Debnath, S. C.; Hoordermeer, J. W. M.; Karst, U. *Anal. Chem.* **2004**, *76*(4), 1063–1068.
178. Timmerman, P.; Jolliffe, K. A.; Calama, M. C.; Weidmann, J. L.; Prins, L. J.; Cardullo, F.; Snellink-Ruel, B. H. M.; Fokkens, R. H.; Nibbering, N. M. M., Shinkai, S., *et al. Chem. Eur. J.* **2000**, *6*(22), 4104–4115.
179. Vandell, V. E.; Limbach, P. A. *J. Mass Spectrom.* **1998**, *33*(3), 212–220.
180. Lavanant, H.; Hecquet, E.; Hoppilliard, Y. *Int. J. Mass Spectrom.* **1999**, *187*, 11–23.
181. Van Berkel, G. J.; Asano, K. G.; Kertesz, V. *Anal. Chem.* **2002**, *74*(19), 5047–5056.
182. Van Berkel, G. J.; Asano, K. G.; Granger, M. C. *Anal. Chem.* **2004**, *76*(5), 1493–1499.
183. Van Berkel, G. J.; Asano, K. G.; Schnier, P. D. *J. Am. Soc. Mass Spectrom.* **2001**, *12*(7), 853–862.
184. Van Berkel, G. J.; Giles, G. E.; Bullock, J. S.; Gray, L. J. *Anal. Chem.* **1999**, *71*(23), 5288–5296.
185. Kertesz, V.; Van Berkel, G. J. *J. Mass Spectrom.* **2001**, *36*(2), 204–210.
186. Van Berkel, G. J. *J. Am. Soc. Mass Spectrom.* **2000**, *11*(11), 951–960.
187. Karancsi, T.; Slegel, P.; Novak, L.; Pirok, G.; Kovacs, P.; Vekey, K. *Rapid Commun. Mass Spectrom.* **1997**, *11*(1), 81–84.
188. Van Berkel, G. J. *J. Mass Spectrom.* **2000**, *35*(7), 773–783.
189. Fenn, J. B.; Rosell, J.; Meng, C. K. *J. Am. Soc. Mass Spectrom.* **1997**, *8*(11), 1147–1157.
190. Hoang, T. T.; May, S. W.; Browner, R. F. *J. Anal. At. Spectrom.* **2002**, *17*(12), 1575–1581.
191. Thewissen, S.; Plattner, D. A.; de Bruin, B. *Int. J. Mass Spectrom.* **2006**, *249/250*, 146–150.
192. Rodgers, M. T.; Armentrout, P. B. In *Comprehensive Coordination Chemistry II*; McCleverty, J. A., Meyer, T. J., Eds.; Elsevier: Amsterdam, 2003; Vol. 2, pp 141–158.
193. Henderson, W.; McIndoe, J. S. In *Comprehensive Coordination Chemistry II*; McCleverty, J. A., Meyer, T. J., Eds.; Elsevier: Amsterdam, 2003; Vol. 2, pp 387–391.
194. Arndtsen, B. A.; Bergman, R. G. *Science* **1995**, *270*(5244), 1970–1973.
195. Hinderling, C.; Plattner, D. A.; Chen, P. *Angew. Chem., Int. Ed. Engl.* **1997**, *36*(3), 243–244.
196. Hinderling, C.; Feichtinger, D.; Plattner, D. A.; Chen, P. *J. Am. Chem. Soc.* **1997**, *119*(44), 10793–10804.
197. Luecke, H. F.; Bergman, R. G. *J. Am. Chem. Soc.* **1997**, *119*(47), 11538–11539.
198. Alaimo, P. J.; Arndtsen, B. A.; Bergman, R. G. *Organometallics* **2000**, *19*(11), 2130–2143.
199. Gerdes, G.; Chen, P. *Organometallics* **2003**, *22*(11), 2217–2225.
200. Gerdes, G.; Chen, P. *Organometallics* **2004**, *23*(12), 3031–3036.
201. Johansson, L.; Tilset, M.; Labinger, J. A.; Bercaw, J. E. *J. Am. Chem. Soc.* **2000**, *122*(44), 10846–10855.
202. Nielsen, S. B.; Oiestad, A. M. L.; Bojesen, G.; Uggerud, E. *Int. J. Mass Spectrom.* **2005**, *243*(3), 231–239.
203. Christ, C. S.; Eyler, J. R.; Richardson, D. E. *J. Am. Chem. Soc.* **1988**, *110*(12), 4038–4039.
204. Christ, C. S.; Eyler, J. R.; Richardson, D. E. *J. Am. Chem. Soc.* **1990**, *112*(2), 596–607.
205. Feichtinger, D.; Plattner, D. A.; Chen, P. *J. Am. Chem. Soc.* **1998**, *120*(28), 7125–7126.
206. Chien, J. C. W.; Wang, B. P. *J. Polym. Sci., Part A: Polym. Chem.* **1990**, *28*(1), 15–38.
207. Stevens, A. E.; Beauchamp, J. L. *J. Am. Chem. Soc.* **1979**, *101*(21), 6449–6450.
208. Jacobson, D. B.; Freiser, B. S. *J. Am. Chem. Soc.* **1985**, *107*(1), 67–72.
209. Jacobson, D. B.; Freiser, B. S. *J. Am. Chem. Soc.* **1985**, *107*(9), 2605–2612.
210. Stockigt, D.; Schwarz, H. *Chem. Ber. Recl.* **1992**, *125*(12), 2817–2819.
211. Mohr, B.; Lynn, D. M.; Grubbs, R. H. *Organometallics* **1996**, *15*(20), 4317–4325.
212. Hinderling, C.; Adlhart, C.; Chen, P. *Angew. Chem., Int. Ed.* **1998**, *37*(19), 2685–2689.
213. Adlhart, C.; Hinderling, C.; Baumann, H.; Chen, P. *J. Am. Chem. Soc.* **2000**, *122*(34), 8204–8214.
214. Adlhart, C.; Volland, M. A. O.; Hofmann, P.; Chen, P. *Helv. Chim. Acta* **2000**, *83*(12), 3306–3311.
215. Adlhart, C.; Chen, P. *Helv. Chim. Acta* **2003**, *86*(4), 941–949.
216. Julian, R. R.; May, J. A.; Stoltz, B. M.; Beauchamp, J. L. *J. Am. Chem. Soc.* **2003**, *125*(15), 4478–4486.
217. Chen, X. Y.; Zhang, X. Y.; Chen, P. *Angew. Chem., Int. Ed.* **2003**, *42*(32), 3798–3801.
218. Zhang, X. Y.; Chen, X. Y.; Chen, P. *Organometallics* **2004**, *23*(14), 3437–3447.
219. O'Hair, R. A. J.; Vrkic, A. K.; James, P. F. *J. Am. Chem. Soc.* **2004**, *126*(38), 12173–12183.
220. Dietiker, R.; Chen, P. *Angew. Chem., Int. Ed.* **2004**, *43*(41), 5513–5516.
221. Brandt, P.; Hedberg, C.; Andersson, P. G. *Chem. Eur. J.* **2003**, *9*(1), 339–347.
222. Mortimer, C. T. *NATO ASI Ser., Ser. C: Math. Phys. Sci.* **1984**, *119*, 47–60 (Thermochem. Its Appl. Chem. Biochem. Syst.).
223. Burkinshaw, P. M.; Mortimer, C. T. *J. Chem. Soc., Dalton Trans.: Inorg. Chem. (1972–1999)* No. 1, 75–77.
224. Burkey, T. J. *NATO ASI Ser., Ser. C: Math. Phys. Sci.* **1992**, *367*, 75–94 (Energ. Organomet. Species).
225. Daffron, J. A.; Farrell, G. J.; Burkey, T. J. *Rev. Sci. Instrum.* **2000**, *71*(10), 3882–3885.
226. Jiao, T.; Leu, G.-L.; Farrell, G. J.; Burkey, T. J. *J. Am. Chem. Soc.* **2001**, *123*(21), 4960–4965.
227. Woodin, R. L.; Beauchamp, J. L. *J. Am. Chem. Soc.* **1978**, *100*(2), 501–508.
228. Taft, R. W.; Anvia, F.; Gal, J. F.; Walsh, S.; Capon, M.; Holmes, M. C.; Hosn, K.; Oloumi, G.; Vasanwala, R.; Yazdani, S. *Pure Appl. Chem.* **1990**, *62*(1), 17–23.
229. Cooks, R. G.; Wong, P. S. H. *Acc. Chem. Res.* **1998**, *31*(7), 379–386.
230. Cooks, R. G.; Koskinen, J. T.; Thomas, P. D. *J. Mass Spectrom.* **1999**, *34*(2), 85–92.

231. Cooks, R. G.; Patrick, J. S.; Kotiaho, T.; McLuckey, S. A. *Mass Spectrom. Rev.* **1994**, *13*(4), 287–339.
232. Armentrout, P. B. *J. Mass Spectrom.* **1999**, *34*(2), 74–78.
233. Armentrout, P. B. *J. Am. Soc. Mass Spectrom.* **2000**, *11*(5), 371–379.
234. Forbes, M. W.; Volmer, D. A.; Francis, G. J.; Bohme, D. K. *J. Am.Soc. Mass Spectrom.* **2005**, *16*(5), 779–791.
235. Peschke, M.; Blades, A. T.; Kebarle, P. *J. Phys. Chem. A* **1998**, *102*(48), 9978–9985.
236. Hoyau, S.; Norrman, K.; McMahon, T. B.; Ohanessian, G. *J. Am. Chem. Soc.* **1999**, *121*(38), 8864–8875.
237. Zhang, Q.; Kemper, P. R.; Bowers, M. T. *Int. J. Mass Spectrom.* **2001**, *210*(1–3), 265–281.
238. Bushnell, J. E.; Kemper, P. R.; Bowers, M. T. *J. Phys. Chem.* **1995**, *99*(42), 15602–15607.
239. Dzidic, I.; Kebarle, P. *J. Phys. Chem.* **1970**, *74*(7), 1466–1474.
240. Davidson, W. R.; Kebarle, P. *J. Am. Chem. Soc.* **1976**, *98*(20), 6133–6138.
241. Dunbar, R. C.; McMahon, T. B. *Science* **1998**, *279*(5348), 194–197.
242. Schnier, P. D.; Price, W. D.; Jockusch, R. A.; Williams, E. R. *J. Am. Chem. Soc.* **1996**, *118*(30), 7178–7189.
243. Armentrout, P. B. *Top. Curr. Chem.* **2003**, *225*, 233–262.
244. Armentrout, P. B. *Int. J. Mass Spectrom.* **2000**, *200*(1–3), 219–241.
245. Rodgers, M. T.; Armentrout, P. B. *Mass Spectrom. Rev.* **2000**, *19*(4), 215–247.
246. Rodgers, M. T.; Ervin, K. M.; Armentrout, P. B. *J. Chem. Phys.* **1997**, *106*(11), 4499–4508.
247. Armentrout, P. B. *Annu. Rev. Phys. Chem.* **1990**, *41*, 313–344.
248. Armentrout, P. B.; Beauchamp, J. L. *Acc. Chem. Res.* **1989**, *22*(9), 315–321.
249. Armentrout, P. B. *Acc. Chem. Res.* **1995**, *28*(10), 430–436.
250. Rodgers, M. T.; Armentrout, P. B. *Acc. Chem. Res.* **2004**, *37*(12), 989–998.
251. Kim, Y. M.; Chen, P. *Int. J. Mass Spectrom.* **2000**, *202*(1–3), 1–7.
252. Hammad, L. A.; Gerdes, G.; Chen, P. *Organometallics* **2005**, *24*(8), 1907–1913.
253. Franklin, J. L.; Dillard, J. G.; Rosenstock, H. M.; Herron, J. T.; Draxl, K.; Field, F. H. Ionization potentials, appearance potentials, and heats of formation of gaseous postive ions. *Nat. Bur. Stand.* (US) **1969**, *26*.
254. Rosenstock, H. M.; Draxl, K.; Steiner, B. W.; Herron, J. T. *J. Phys. Chem. Ref. Data* **1977**, *6* (suppl. 1).
255. Levin, R. D.; Lias, S. G. *Nat. Stand. Ref. Data Ser.* **1982**, 71.
256. Lichtenberger, D. L.; Kellogg, G. E.; Pang, L. S. K. *ACS Symp. Ser.* **1987**, *357*, 265–289.
257. Lichtenberger, D. L.; Kellogg, G. E. *Acc. Chem. Res.* **1987**, *20*(10), 379–387.
258. Chowdhury, S.; Heinis, T.; Grimsrud, E. P.; Kebarle, P. *J. Phys. Chem.* **1986**, *90*(12), 2747–2752.
259. Richardson, D. E. *NATO ASI Ser., Ser. C: Math. Phys. Sci.* **1992**, *367*, 233–251 (Energ. Organomet. Species).
260. Richardson, D. E.; Ryan, M. F.; Geiger, W. E.; Chin, T. T.; Hughes, R. P.; Curnow, O. J. *Organometallics* **1993**, *12*(3), 613–615.
261. Ryan, M. F.; Siedle, A. R.; Burk, M. J.; Richardson, D. E. *Organometallics* **1992**, *11*(12), 4231–4237.
262. Richardson, D. E. *Inorg. Chem.* **1990**, *29*(17), 3213–3217.
263. Ryan, M. F.; Eyler, J. R.; Richardson, D. E. *J. Am. Chem. Soc.* **1992**, *114*(22), 8611–8619.

1.29 Organometallic Chemistry in Aqueous and Biphasic Media

I T Horváth and D Lantos, Eötvös University, Budapest, Hungary

1.29.1 Biphasic Media and Organometallic Chemistry

The combination of organometallic and biphasic chemistry could lead to facile separation of organometallic reagents or catalysts from the products, a crucial issue for commercial applications. Theoretically, three types of separation methods can be used for chemical reactions performed in the liquid phase. If the reagent or catalyst is a gaseous molecule, it could dissolve in the liquid phase under pressure during reaction and simple depressurization could result in its complete removal from the product. A similar system could be imagined in which a soluble organometallic reagent or catalyst precursor is activated or turned on by a gaseous molecule under pressure and deactivated or turned off by depressurization after the product formed. The second and most popular approach involves the use of liquid–liquid biphasic systems, in which one of the phases contains the dissolved organometallic reagent or catalyst and the other the products (Figure 1). Since the formation of a liquid–liquid biphase system is due to the sufficiently different intermolecular forces of two liquids, the selection of a reagent or catalyst phase depends primarily on the solvent properties of the product phase at high conversion level. For example, if the product is apolar the reagent or catalyst phase should be polar, and vice versa, if the product is polar the reagent or catalyst phase should be apolar. The success of any biphasic system depends on whether the reagent or catalyst could be designed to dissolve preferentially in the reagent or catalyst phase. Perhaps the most important rule for such design is that the reagent or catalyst has to be reagent- or catalyst-phase like, since it has been known for centuries that "similia similibus solvuntur," or "like dissolves like." A biphasic reaction could proceed in either the reagent or catalyst phase or at the interface of the two phases, depending on the solubilities of the substrates in the reagent or catalyst phase. When the solubilities of the substrates are very low in the reagent or catalyst phase, the chemical reaction may still occur at the interface or appropriate phase transfer agents may be added to facilitate the reaction. It should be emphasized that a biphase system might become a one-phase system by increasing the temperature. Thus, a biphasic organometallic reagent or

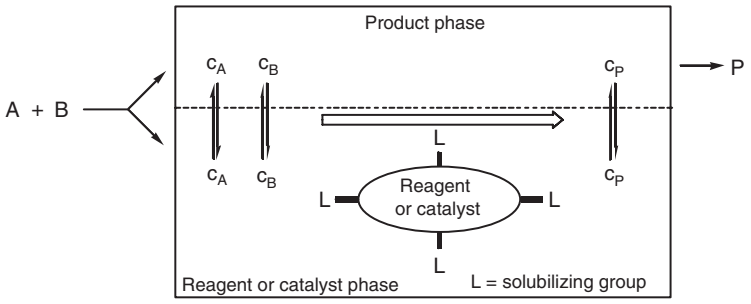

Figure 1 The liquid–liquid biphase concept for converting substrates A and B to product P. The attachment of appropriate solubilizing groups L to a reagent or catalyst ensures facile separation.

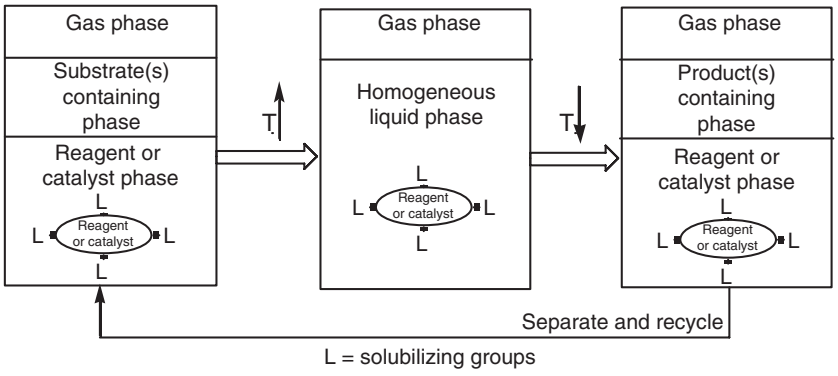

Figure 2 The temperature-dependent liquid–liquid/liquid biphase concept.

catalyst could combine the advantages of one-phase chemistry with biphasic product separation by running the reaction at higher temperatures and separating the products at lower temperatures (Figure 2). The third approach is based on solid–liquid separation. If the product has no or limited solubility in the liquid reaction mixture, it could be continuously removed by precipitation or crystallization. Alternatively, a solid organometallic reagent or catalyst can be dissolved in the reaction medium at higher temperature and later separated from the product by lowering the temperature again (Figure 3). It should be noted that the latter approach could also operate in the opposite manner,

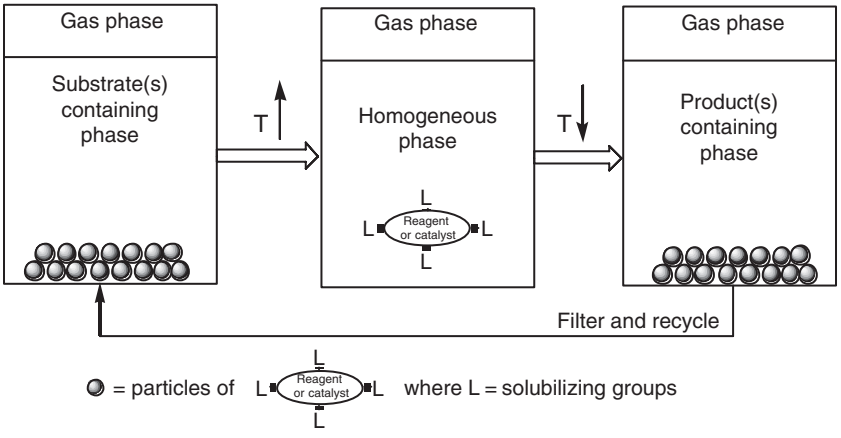

Figure 3 The temperature-dependent solid/liquid biphase concept.

when a solid organometallic reagent or catalyst precursor can be dissolved in the reaction medium at lower temperature and separated from the product by increasing the temperature.

1.29.2 Organometallic Chemistry in Aqueous Media

Although one of the first organometallic compounds was the Zeisse salt, $K[Pt(C_2H_4)Cl_3]$, the systematic investigations of organometallic compounds in water did not start until the late 1970s and was significantly accelerated after the commercialization of the first aqueous homogeneous catalytic process in the mid-1980s. The slow start is probably due to the fact that organometallic compounds are considered oxygen and water sensitive in general and therefore require special handling including the use of inert atmosphere techniques such as dry boxes or Schlenk tubes, anhydrous solvents. However, water is a very attractive medium for chemical reactions, because it is readily available, nonflammable, non-toxic, cheap, and easy to separate from many organics. Water could be an excellent medium for ionic reactions because it can readily solvate anions and cations and it could serve as a solvent and/or as a ligand. Water is a good σ-donor with very weak backdonation capability. The strong O–H bonds of water do not permit easy reactions with radicals and therefore could be excellent medium for radical reactions. Other important physical parameters (such as high heat capacity, high cohesive density, strong pressure dependence of the viscosity) make water a particular solvent, notwithstanding that it is indeed supporting everyday life quite well. Several aqua complexes have already been isolated, and some examples are shown in Figure 4.

Although the hydrolysis products of organometallic compounds are generally much more stable than that of the precursor organometallic compounds in water, the high activation energy for hydrolysis could provide reasonable protection at temperatures at which water remains a liquid under ambient pressure. Since the polarity of the M–C bonds could also influence the reactivity of the organometallic compounds, the rate of hydrolysis generally increases at higher polarity. Organometallic compounds having unoccupied molecular orbitals, electron-withdrawing ligands, and insufficient steric hindrance of the ligands around the metal center exhibit greater affinity to react with water. The η^5-cyclopentadienyl or η^6-arene complexes are generally much more stable than the corresponding η^1-alkyl or -aryl complexes. While ionic-metal hydrides such as NaH readily react with water, $HMn(CO)_5$ and $(\eta^5\text{-}C_5H_5)Fe(CO)_2H$ are not sensitive to water at all. Water can attack the M–C bond in nucleophilic or in electrophilic reactions (Figure 5).

Rare-earth organometallic complexes are typically very oxophilic and could readily react with water to form metal-hydroxy and metal-oxo species (Figure 6), some of which could have monomeric, dimeric, or oligomeric structures.[4] The tungsten containing alkylidyne complex reacts with water similarly to the rare-earth metals to form an air- and water-stable dimer with a liner oxo bridge and two terminal oxo groups.[5] In the oxo form the higher oxidation state of the transition metals helps to stabilize the M–C bond, because the greater electronegativity of the metal provides a higher covalence at the M–C bond, so the complex is more stable under hydrolitic conditions. The high oxidation state is often stabilized by π-donating and electron-withdrawing ligands, including oxo, imido, and sulfido ligands. The organometallic compounds generally act as Lewis bases; for example, the tungsten hydride turns into a water-soluble cationic trihydride after protonation (Figure 7).

Oxidative addition is the initial step of many important organometallic reactions. This can be the basis of the preparation of new products or can be the first step in the activation of small molecules such as H_2 or N_2. For example, the oxidative addition of HCl can be performed in aqueous environment and produces hydrides (Figure 8).

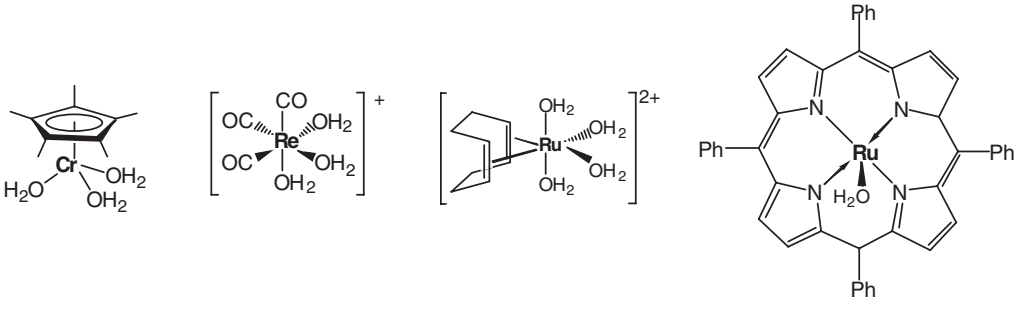

Figure 4 Aqua complexes.[1,2,3]

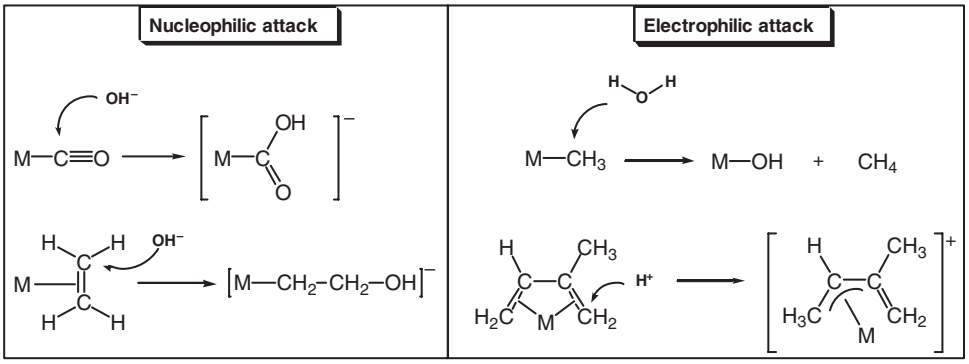

Figure 5 Typical reactions of the organometallic compounds with water.[4]

Figure 6

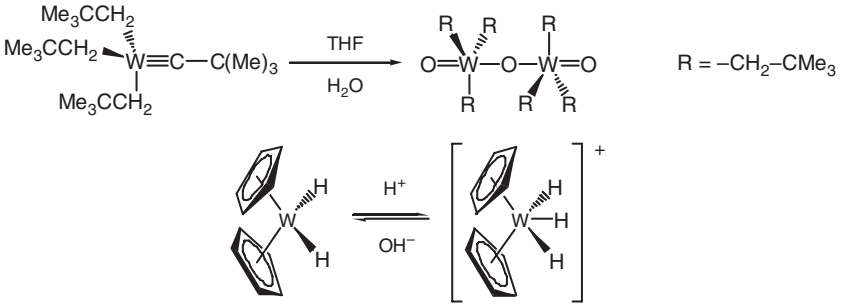

Figure 7

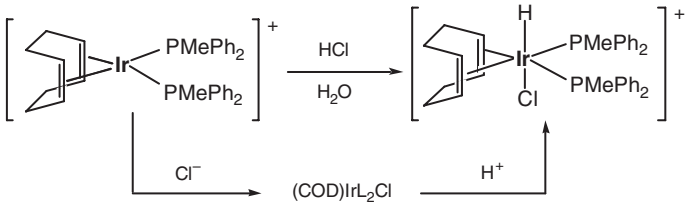

Figure 8 Oxidative addition to an iridium metal center.

In the case of cationic complexes, the reaction starts with the coordination of Cl^- followed by the protonation[6] and the intermediate can be isolated[7].

Water can enhance the rate of the oxidative addition; for example, the activation of H_2 by *trans*-[IrCl(CO)(TPPTS)$_2$] to yield *trans*-[H_2IrCl(CO)(TPPTS)$_2$] was increased by 50-fold by running the reaction in water in comparison to the reaction of *trans*-[IrCl(CO)(PPh_3)$_2$] in toluene.[8] It should be noted that 1, trisulfonated triphenylphosphine (TPPTS) is very similar electronically to PPh_3.

1.29.2.1 Ligands of the Organometallic Water-soluble Compounds

Organometallic compounds could be water soluble as they are, if they have appropriate hydrophilic ligands (H_2O, NH_3, SO_3H, etc.) or can be made water soluble by either reacting with water to form M–OH containing species or attaching polar solubilizing groups to the metal directly or to the ligands. Indeed, the previously mentioned organometallic aqua complexes are water soluble. Most of the organic ligands can be converted to water soluble by introducing hydrophilic substituents such as hydroxides, carboxylates, phosphonates, and ammonium, to the ligand structure. Alternatively, introducing polar groups that could involve in hydrogen bonding in the aqueous media[9] could also lead to high water solubility. The most frequently used ligands are phosphorus-, nitrogen- or sulfur-containing ligands.

1.29.2.1.1 Phosphorus-containing ligands

The most widely used approach is the functionalization of phosphines with polar or ionic substituents. The sulfonation of aryl phosphines is probably the most frequently used method. The aryl phosphines have strong affinity to the transition metal center, they are readily available, mostly air and water stable, and they dissolve very well in aqueous media over a wide range of pH.

The sulfonation of triphenyl phosphine with fuming sulfuric acid can give three possible products monosulfonated triphenylphosphine (TPPMS), disulfonated triphenylphosphine (TPPDS), and TPPTS **1**, depending on the reaction conditions[10,11] (Figure 9). Using this method many sulfonated aryl phophines have been prepared (**2b**,[12,12a] **2d**,[13] **3**,[14] **4**,[15] **5**[16]). The benzofuran-containing phosphine ligands **7** can be prepared under milder condition, only using sulfuric acid.[17]

Chiral phosphines can be made water soluble by using similar approaches and the two most important chiral diphosphines are sulfonated 2,2′-bis-(diphenylphosphinomethyl)-1,1′-binaphthyl (BINAS)-8 **15** and the BISBIS **16** (Figure 9). The preparation of these types of ligands involves sulfonation with fuming sulfuric acid, similarly to the other phosphines. The position of the sulfonate groups depends on the temperature and the SO_3 concentration.[18] The oxidation of the product can be hindered by the preparation of superacidic media from orthoboric acid and anhydrous sulfuric acid.[19]

Another method to solubilize organometallic compounds in water is the incorporation of quaternary ammonium salts (Figure 10). A characteristic member of this group is the AMPHOS ($[Ph_2P\text{-}(CH_2)_2\text{-}NMe_3]^+Cl^-$) **18**, which could be prepared from $Ph_2P\text{-}(CH_2)_2\text{-}NMe$ provided the phosphorus atom is protected by oxidation or coordination to a transition-metal center before forming the ammonium salt.[20,21]

The phosphine ligands can be solubilized with carboxylic groups. The alkali salt derivatives dissolve very well in water, but their free acids have lower solubility. The carboxyl group-containing phosphines (Figure 11) have been less investigated than the corresponding sulfonated analogs. There are different preparation methods of these ligands in the literature: standard alkylation or arylation in organic solvent or Pd-catalyzed P–C coupling reactions, etc.[22–25] The Ph_2PCH_2COOH **27** has already been used in the Shell Higher Olefin Process (SHOP), but not in aqueous, but in alcoholic liquid–liquid biphasic conditions. The cobalt and ruthenium complexes of AMPHOS **18** and 1,3,5-triaza-7-phospha-adamantane (PTA) **19** were used in hydrogenation and hydroformylation reactions.[20]

Polar and non-ionic substituent hydroxyl groups and polyethyleneglycol chains could also be used (Figure 12). Surprisingly, PTA dissolves in water either itself or after protonation. Phosphines attached to carbohydrates have been reported. Several free or protected hydroxyl groups attached to the cyclohexane skeleton ensure water solubility, which is lower than other polar phosphines such as **31** or **35**.

1.29.2.1.2 Nitrogen- and sulfur-containing ligands

The most well-known water-soluble nitrogen-containing complexing agent is EDTA (the sodium salt of ethylenediaminetetracetic acid). The transition metal complexes of EDTA have been used in carbonylation reactions, water–gas shift reaction, etc.[27] The triethanolamine (TEA), $N(CH_2CH_2OH)_3$ is very similar to EDTA, can form water-soluble compounds, and has limited compatibility with some organic solvents.[28] Other nitrogen-containing ligands include bipyridine functionalized with sulfonate or carboxylic groups (Figure 13). The development of the water-soluble sulfur-containing ligands was inspired by the investigations focusing on metal sulfide enzymes. The isolated and the biomimetic sulfur-containing complexes did not dissolve well in aqueous media only in organic solvents such as dimethyl sulfoxide (DMSO), dimethylformamide (DMF), tetrahydrofuran (THF), or CH_2Cl_2.[29] The iron-containing complexes could be solubilized by the carboxylation of the ligands (Figure 14).[30,31]

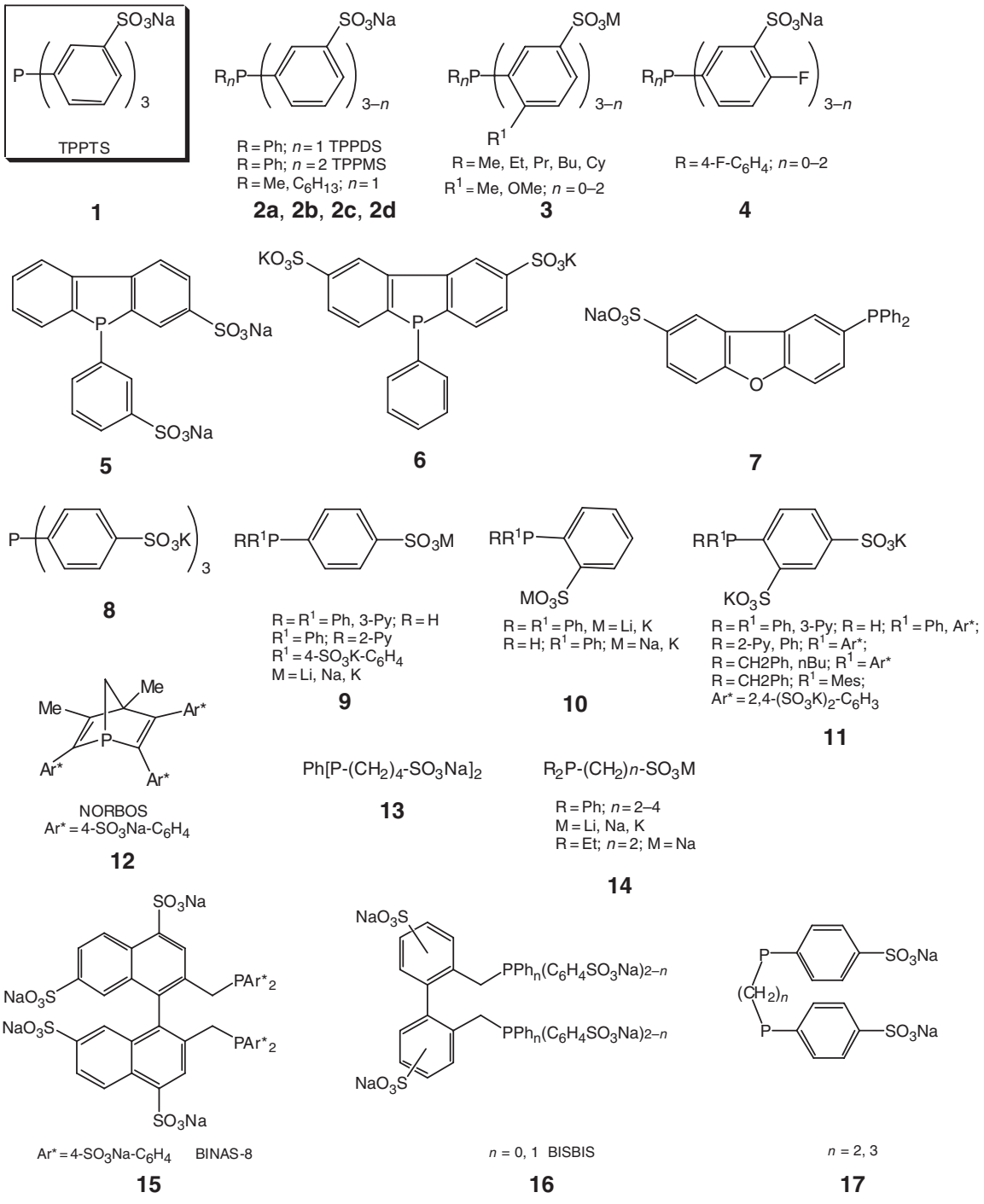

Figure 9 Water-soluble sulfonated phosphines. The most important phosphine is the TPPTS.[26]

1.29.2.2 Importance of the pH in Aqueous Media

Since water is an excellent medium for ionic reactions, the anions and the cations could play very important roles in aqueous organometallic chemistry and catalysis. The water-soluble complexes can have different structures depending on the pH. While aqua complexes are preferred at lower pH, metal–oxo-containing species could form at higher pH. If this pH dependence is irreversible, M═O compound can be converted into aqua species, which could

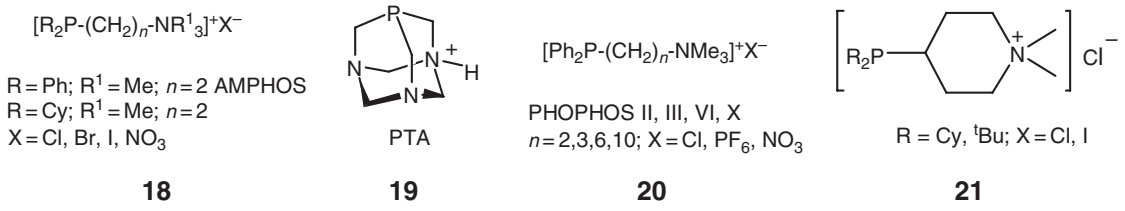

Figure 10 Water-soluble cationic phosphine ligands.

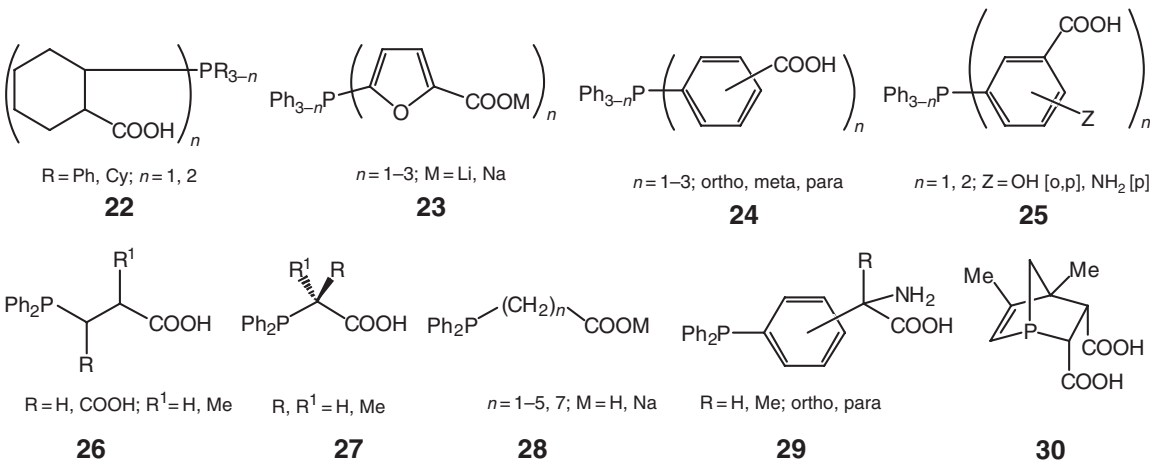

Figure 11 Water-soluble carboxylated phosphines.

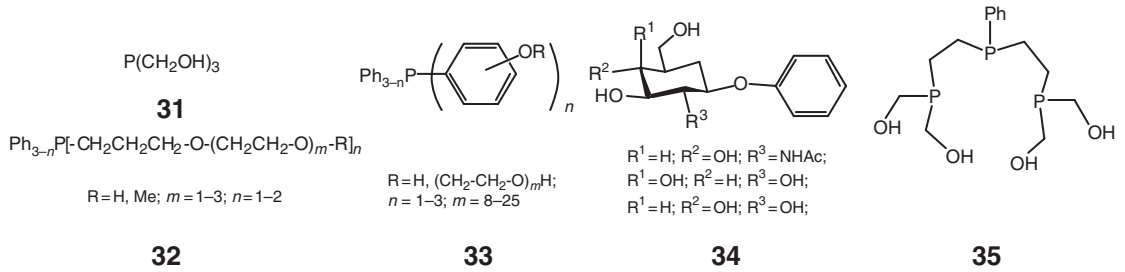

Figure 12 Some examples and variations to water-soluble polar, non-ionic phosphine ligands.

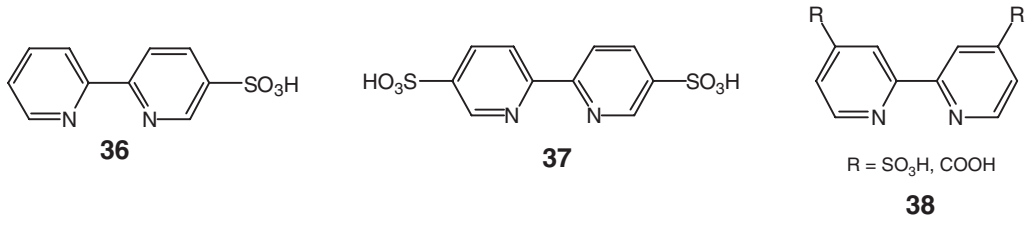

Figure 13 Nitrogen-containing water-soluble ligands.

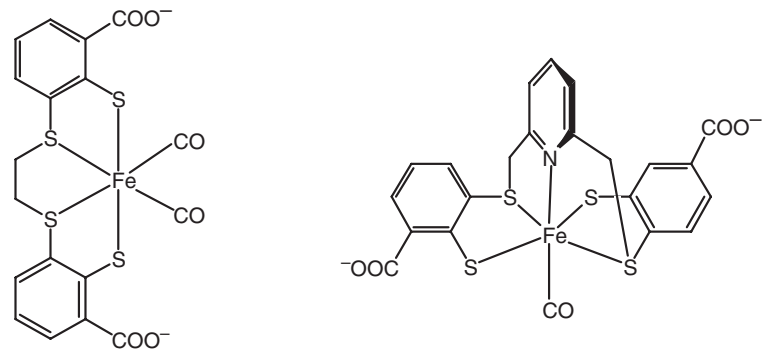

39 **40**

Figure 14 Water-soluble Fe complexes with S-containing ligands.

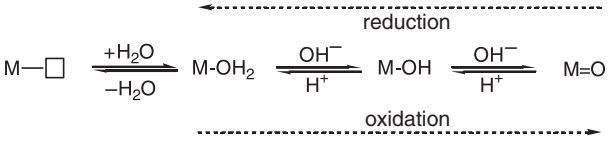

Figure 15 Transition metal complex in function of the pH (□ is the free coordination site).

generate an open coordination site by eliminating a coordinated water [9] (Figure 15). While at pH < 3 the aqua complex $[Mo(Cp^*)O_2(H_2O)_n]^+$ ($n = 0$ or 1) is the preferred species, the transient formation of $[Mo(Cp^*)O_2(OH)]$ complex could be observed between pH = 3–5, and only the anionic complex $[Mo(Cp^*)O_3]^-$ exists at pH > 5.[9] The Cp^*Rh aqua complexes is another good example of how the ligand sphere of the central atom changes at different pH. The Rh complex is monomeric at pH = 2–5, the dimer and the monomer structure are in a rapid exchange at pH = 5–7, and only the dimer is present at pH = 10 and above (Figure 16).

The transition metals can be reduced in basic aqueous solutions via other mechanism. For example, the metal carbonyls could be attacked by the hydroxide ions and the metal reduced to metal hydride species by the elimination of carbon dioxide to yield a hydride, which could then be deprotonated with the excess of hydroxide ions (Figure 17).[32] The reduction of the metal complexes by CO in aqueous phase is indeed a very important step in the "Reppe-type" catalysis and water–gas shift reactions.

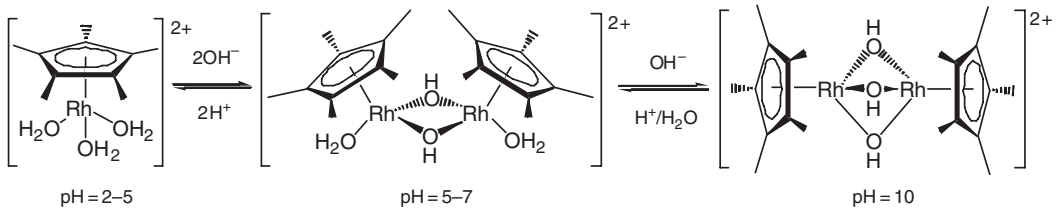

Figure 16

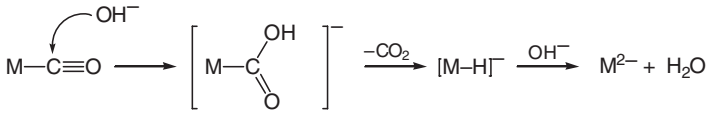

Figure 17

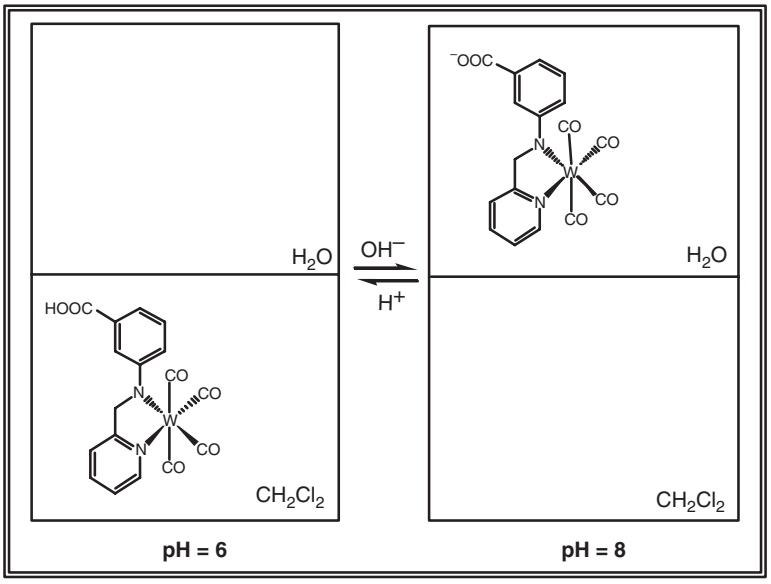

Figure 18 pH-dependent phase transfer of $W(CO_4)L$.

The changing pH can dramatically alter the solubility properties of the organometallic compounds, which could result in unexpected or desired transfer to the organic phase. This could be demonstrated by the pH-dependent behavior of $W(CO)_4L$ (where L = benzoic acid, 3-[(2-pyridinylmethylene)amino]). The W-complex could be moved from the aqueous to the organic and back to the aqueous phases by the subsequent addition of HCl and NaOH 20 times without decomposition (Figure 18),[33] because the protonated compound is soluble in aprotic polar solvents such as THF, DMF and the $[W(CO)_4L]^-Na^+$ is soluble in water.

1.29.2.3 Catalytic Reactions

Water is an attractive solvent for various chemical reactions and many catalytic reactions have been investigated in the last few years (Table 1).[4] While the majority of the studies have focused on hydrogenation, hydroformylation, carbonylation, hydrocyanation, and oxygenation, other types of reactions such as isomerization, alkylation, carbon–carbon coupling, oligomerization, and polymerization are receiving increased attention. Catalytic asymmetric synthesis in aqueous media has also been advanced by successful modification of known chiral ligands via functionalization by sulfonate or quaternary ammonium groups. The hydrophilic analogs of well-known enantioselective rhodium and ruthenium catalyst have been used in the reduction of unsaturated amino acid precursors, imines, and hydrogenolysis of epoxids. Very high enantioselectivities, close to the analogous hydrocarbon-soluble systems, have been achieved in several cases. However, as a general rule, enantioselectivity was found to be lower in aqueous systems than in organic solutions. Some selected reactions and their catalysts are collected in Table 1.

1.29.2.4 Hydroformylation

Rhône-Poulenc developed and Rurhchemie commercialized an aqueous biphasic process for the hydroformylation of propylene in the presence of $HRh(CO)[TPPTS]_3$.[59,60] The main product is *n*-butanal and the normal- and iso-butanal ratio is about 25, surprisingly high in comparison to the conventional PPh_3 modified rhodium catalyst. The overall reaction mechanism operating in the aqueous and organic phases is very similar (Figure 19). The reaction starts with the dissociation of a TPPTS ligand (a) followed by the coordination of the olefin (b). After the insertion of the olefin into the Rh–H bond (c) the coordinatively unsaturated alkyl species reacts with CO (d). The insertion reaction of a carbonyl ligand into the Rh–C bond results in an acyl derivative (e), which can react with hydrogen (f) to form the coordinatively saturated acyl derivative, which could reductively eliminate the product to regenerate the catalytically active species (g).

Table 1 Selected reactions catalyzed in aqueous media

Reaction catalyzed	*Substrates*	*Catalyst*	*References*
Oxidation	Fatty acids	$\{PO_4[WO(O_2)_2]_4\}^{3-}$	34
Oxidation	Alcohol	$Pd(OAc)_2$ or $PdCl_2$/(bpy)	35
Oxidation and epoxidation	Alkenes	$[Ru(napy)_2(H2O)_4Cl(OH)](ClO_4)_4$	36
Hydrogenation	Alkenes	$Na\{O_3S(C_6H_4)CH_2C(CH_2PPh_2)_3Ru\}_2(\mu\text{-}Cl)_3]$	37
Hydrogenation	CO_2	$[RuCl_3(NO)(TPPMS)_2]/[RuCl_3(NO)(TPPTS)_2]$	38
Hydrogenation	Olefins	$[RuCl_2(PTA)_4]$ $[RhCl(COD)(m\text{-}TPPMS)_3]$	39
Hydrogenation	Ketones	$[H_2Ru(TPPTS)_4]$	40
Hydrogenation	Acetonitrile	$[Os(CO)_3Cl_2]$	41
Hydroformylation	Alkenes	$Rh(acac)(CO)_2$/PNS	42
Hydroformylation	Alkenes	$RhCl(CO)(PPh_2\text{-PS-PEG-}PPh_2)$	43
Reduction	Carbonyl group	$Cp_2Mo(H)OTf$	44
Hydration	Alkyne	$cis\text{-}PtCl_2(TPPTS)_2$	45
Hydration	Alkyne	$[(Ph_3P)AuCH_3]/H_2SO_4$	46
Amination	Aromatic halides	$Pd(OAc)_2$ /BINAS	47
C–H activation	Allyles	$RuCl_2(PPh_3)_3$	48
Conjugated addition	Aldehydes	$Rh_2(COD)_2Cl_2$, $Rh_2(COD)_2BF_4$	48
Hydrocaboxylation	Styrenes	PdCl2/TPPTS	49
Isomerization	Allylic alcohols	$Ni(COD)_2/CF_3COOH/L^2$	50
Isomerization	Allylbenzene	$Trans\text{-}IrCl(CO)(TPPMS)_2$	51,51a
Synthesis of asymetric biaryls	Asymetric biaryls	Pd/C	48
Copolymerization	CO/olefins	$Pd(TTPTS)_3$	52
Metathesis	Olefins	$Ru(H_2O)(tos)_6$	53
Pauson–Khand-type		$[RhCl(COD)]_2$	54
Chiral Diels–Alder reaction		$Cu(NO_3)$/L-abrine	55
Heck reaction		$Pd(OAc)_2/m\text{-}TPPTC$	56
Suzuki-coupling		$Pd(TPPTMS)_3$	57
Karasch reaction		$PdCl_2(PhCN)_2$	58

L^1 = bis(hydroxymethyldihydroxyoxazolyl)pyridine; L^2 = 1,4-bis(diphenylphosphanyl)butane; L^3 = (*S*,*S*)-2,6-bis-(4-isopropyl-2-oxazolin-2yl)pyridine; PS-PEG = polystyrene-poly(ethyleneglycol); L-abrine = N-(a)-methyl-L-tryptophan; *m*-TPPTC = $P(m\text{-}C_6H_4CO_2Li)_3$.

The aqueous phase reaction is catalytically less active than its organic analogs, but more selective, the n/i ratio is higher in this case. It is believed that the coordination of the olefin to the coordinatively unsaturated $\{HRh(CO)(TPPTS)_2\}$ or $\{HRh(CO)_2(TPPTS)\}$ results in high or low normal- to iso-aldehyde ratio, respectively (Figure 20). Indeed, $HRh(CO)_2(TPPTS)$ was not detectable in water, which explains the higher selectivity in the aqueous biphasic system. The significantly higher activation energy of the dissociation of TPPTS from $HRh(CO)(TPPTS)_3$ compared with PPh_3 from $HRh(CO)(PPh_3)_3$, could be due to the intramolecular association of sulfonate substituents of the neighboring TPPTS ligands via hydrogen bonding in aqueous medium.[61]

One possible explanation for the lower catalytic activity of the aqueous biphasic system is the higher activation energy of the dissociation of TPPTS from coordinatively saturated rhodium intermediates to generate an active species.[61] Another theory suggests that in the three-phase system (gas–liquid–liquid) (Figure 21) the reaction rate depends on the solubility of the gases (CO and H_2) in the aqueous and the organic phase, the mass transfer between the phases, the droplet size in the dispersion, and the intrinsic kinetics of the reaction in the aqueous phase.[62] Mass transfer can be one of the bottlenecks in this reaction, as an emulsion is forming during the reaction, the catalyst is dissolved in the aqueous phase, and the reactant and the products are in the organic layer. One could overcome the mass transfer limits by using surfactants and micelle-forming reagents,[63] supported aqueous phase catalysts,[64] and catalyst-binding ligands (interfacial catalyst).[62]

1.29.2.5 Water–Gas Shift and Reppe Reaction

The water–gas shift reaction is a good example for the application of water and the utilization of the nucleophilic attack of the hydroxid anion on a metal–carbon bond (M–CO). The reaction starts with the nucleophilic attack of the OH^- on a carbonyl ligand resulting in a M–COOH species (a), which can decarboxylate to give a metal hydride (b),

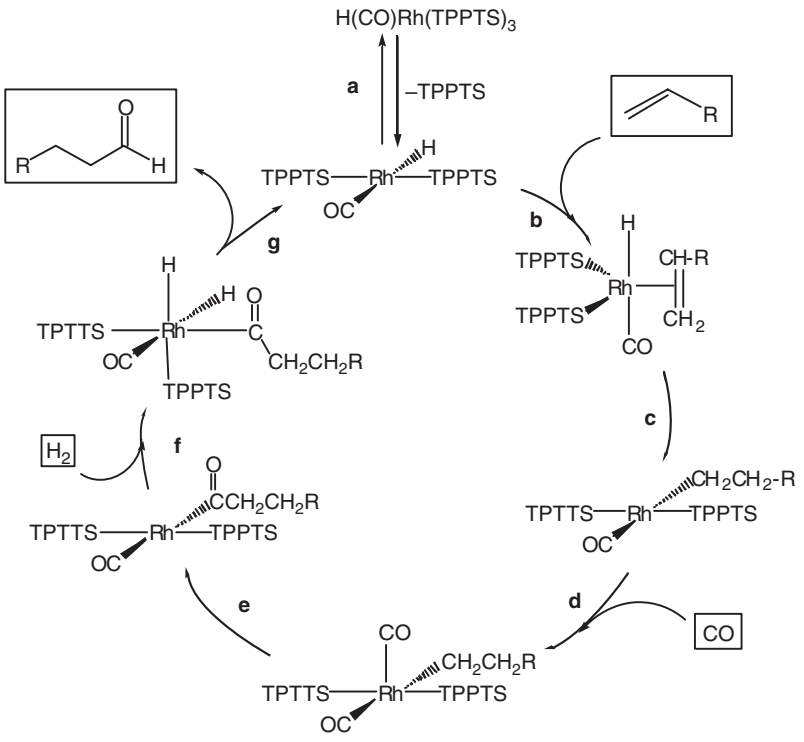

Figure 19 Hydroformylation with water-soluble ligands in aqueous media. TPPTS = trisulfonated triphenylphosphine.

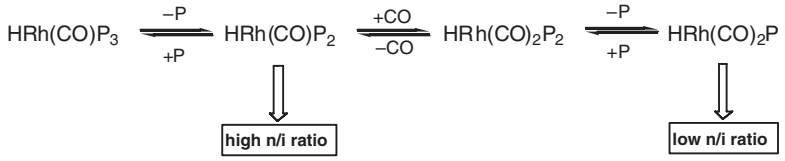

Figure 20 Initial equilibria forming the catalyst active species (P = PPh_3 or TPPTS).

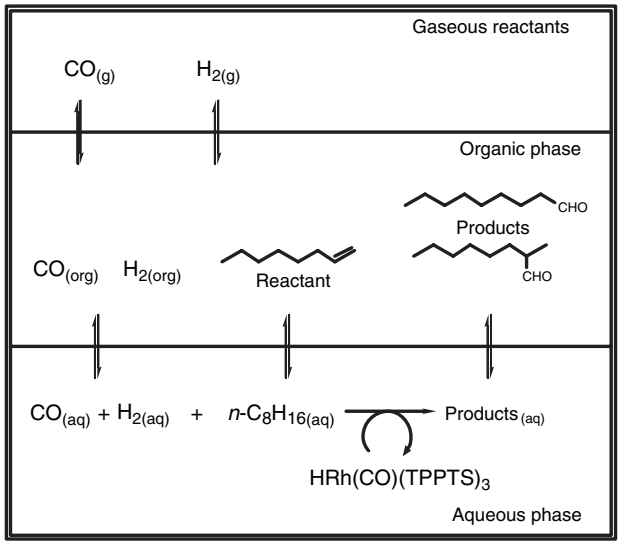

Figure 21 In biphasic systems the mass transfer between the immiscible phases is a very important factor.

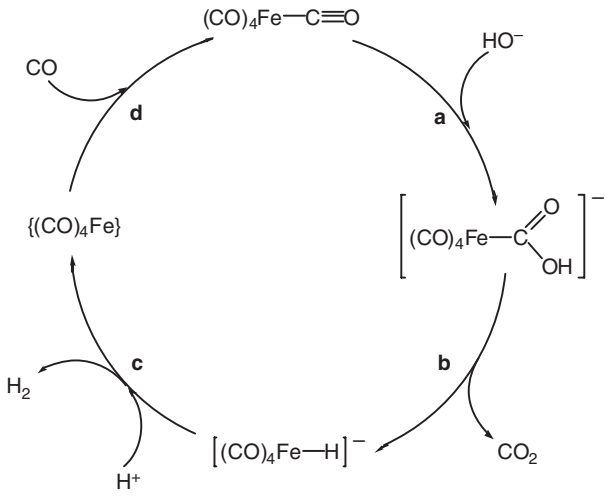

Figure 22 Water–gas shift reaction catalyzed by $Fe(CO)_5$.[65]

which can react with a proton followed by the elimination of hydrogen to regenerate the catalyst (Figure 22).[65,66] Similar mechanisms are operational when olefines or acetylenes are reacted with carbon monoxide and water resulting in saturated or unsaturated carboxylic acids. This reaction is called the Reppe reaction and is catalyzed by ruthenium and rhodium complexes.[67]

1.29.3 Wacker-type Oxidation

The Wacker-type oxidation of the olefins is one of the oldest homogeneous transition metal-catalyzed reactions. The mechanism of the oxidation of ethylene to acetaldehyde by a $PdCl_2/CuCl_2/O2$ system is shown in Figure 23.[68,68a] Interestingly, the selectivity of the oxidation of olefins with longer alkyl chains is dependent on their solubility in water. Furthermore, the production of chlorinated side-products and isomerized olefins has also occurred for olefins with low water solubility.[69,69a,70] In order to avoid the solubility issues, co-solvents such as DMSO, acetone, THF, dioxane, acetonitrile, DMF, and ethanol were used and DMF seemed to be the best.[69,69a]

1.29.3.1 Olefin Metathesis

The olefin metathesis is a useful tool to form new C–C carbon bonds by recombination of unsaturated hydrocarbons (Figure 24). While the early transition metal catalysts were air and moisture sensitive with low-functional-group tolerance, ruthenium-based catalysts are less sensitive and their heteroatom tolerance is increased (Figure 25).

ROMP and RCM are the two most frequently used methods in aqueous media. It was shown that the activity of the Ru catalyst is increased in the presence of small amount of water in the ROMP of 7-oxanorbornene derivatives. The most effective precursor was the aqua complex $[Ru(H_2O)_6](tos)_2$. After the polymerization was completed the aqueous catalyst phase could be reused and the catalytic activity increased in the subsequent reaction (Figure 26).[53] An aqua-ruthenium (II) olefin complex was isolated with higher catalytic activity than the adduct formed from the $[Ru(H_2O)_6](tos)_2$-complex and the 7-oxanorbornene derivative; it was suggested that the Ru-carbene complex was formed from this compound.[72]

Although the well-defined water-resistant metal–alkylidene complexes do not dissolve in water, they can be used in emulsion polymerizations.[73] Small size polymer particles and polymer latex can be prepared with this method in aqueous media in the presence of cationic surfactants (e.g., Dode cyltrimethylammonium bromide (DTAB)). Water-soluble, biologically active glycopolymers have been also synthesized with ruthenium–alkylidene complexes in ROMP.[74,74a,74b]

RCM is an important method in the preparation of medium-size macrocyclic compounds. Since the biologically active substrates are generally water soluble, the catalyst needs to have good solubility properties in water. The replacement of PPh_3 with $PhP(m\text{-}C_6H_4SO_3Na)_2$ could provide the required solubility in general. While this

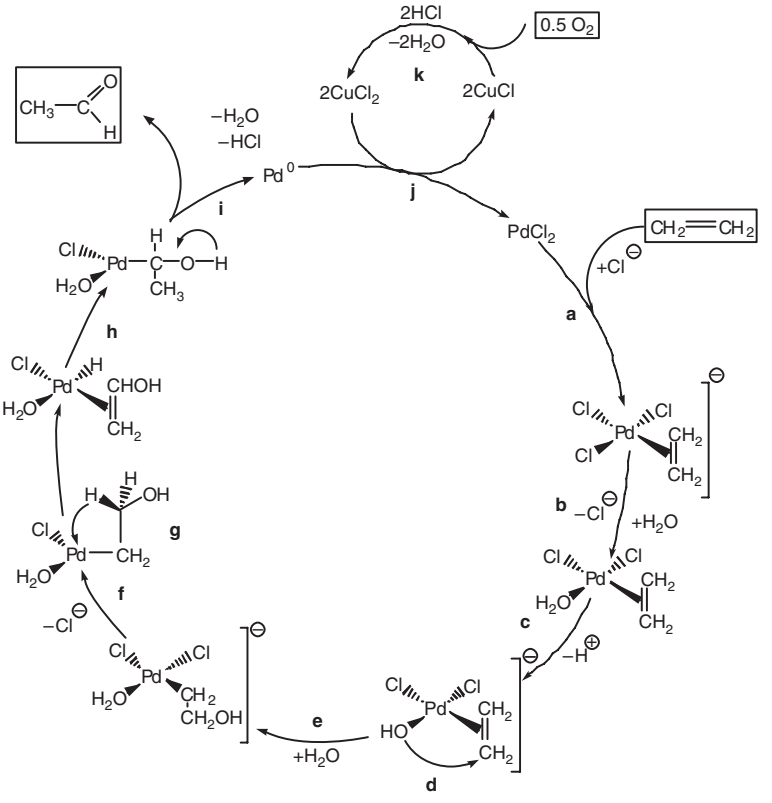

Figure 23 Wacker-type oxidation of ethylene.

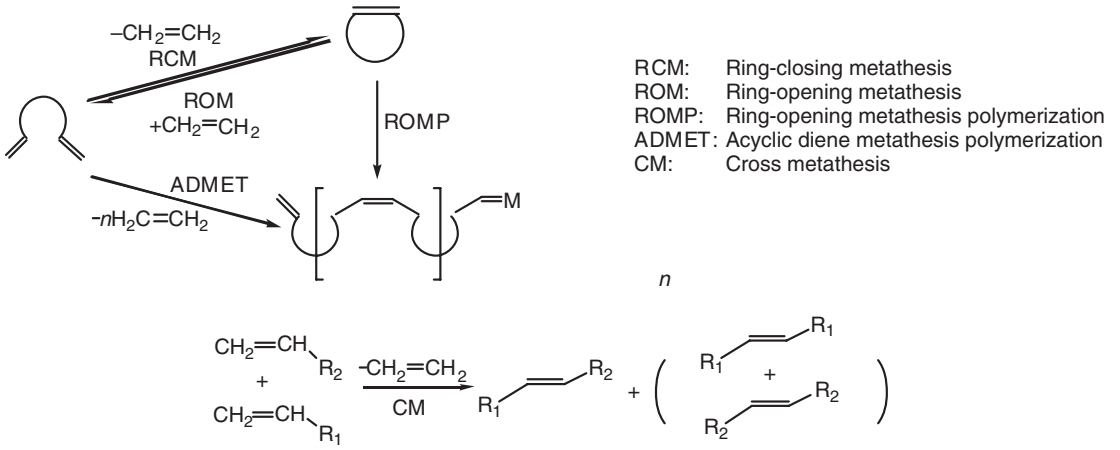

Figure 24 Type of metathesis reactions.

idea did work in many previous cases, it failed in this case since the phosphine ligand was too small and was an insufficient electron-donor leading to low catalytic activity.[75] When the phosphines were substituted with bulky and electron-rich analogs, the catalyst was soluble in water and its catalytic activity was high[76] (Figure 27).

The RCM of σ,ω-dienes was successfully catalyzed with a new-generation ionic ruthenium–alkylidene complex in water (Figure 28).[77]

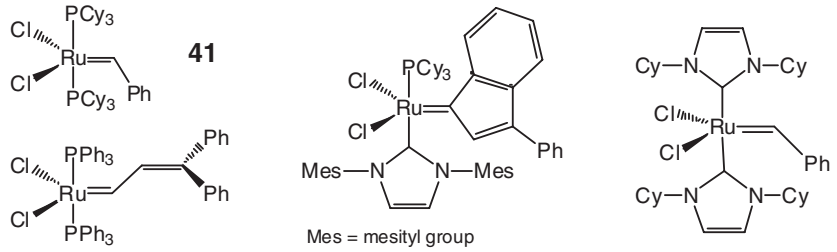

Figure 25 Some new-generation olefin metathesis catalyst.[71,71a,71b]

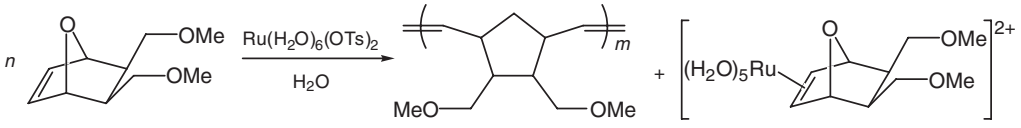

Figure 26 Reusable aqueous-phase ROMP.

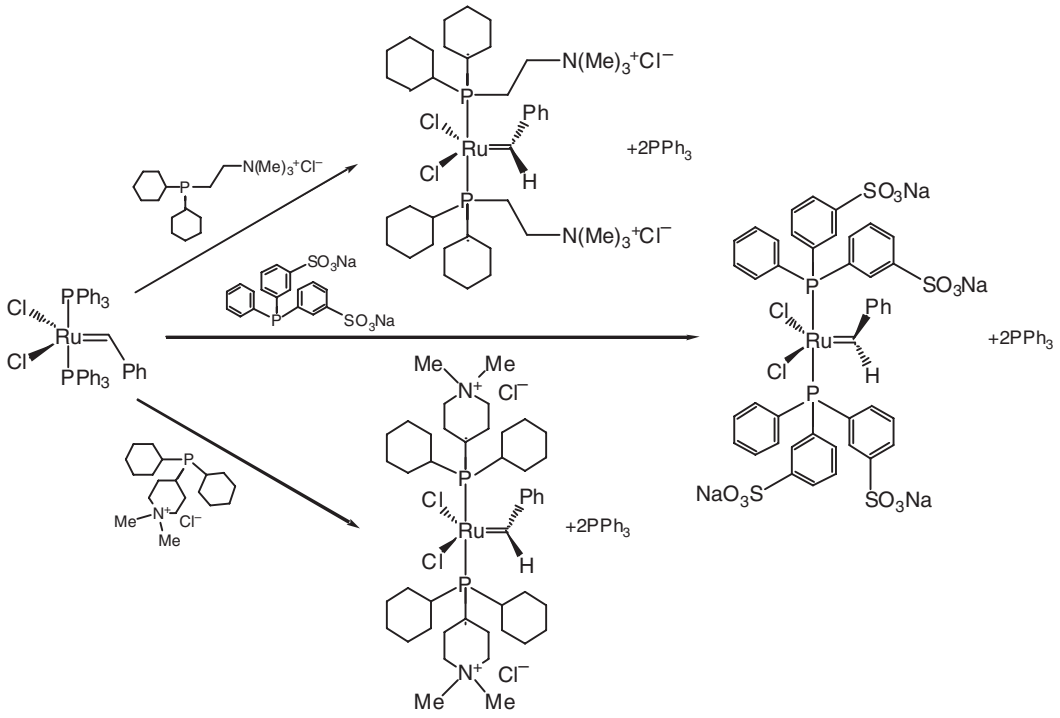

Figure 27 Preparation of ionic water-soluble alkylidene complexes.

1.29.4 Organometallic Chemistry in Alcohols

SHOP was the first industrial biphasic system in which the separation of the catalyst was successfully achieved. An Ni-based catalyst is used in 1,4-butanediol to catalyze the oligomerization of ethylene to liner olefins (Figure 29).[78,78a–78g] The catalytic reaction takes place in the alcoholic phase, and the products, the α-olefins, have limited solubility in the diol providing facile separation from the catalyst. The olefins are separated from each other by distillation in subsequent distillation towers. Although alcohols could be excellent solvents for various

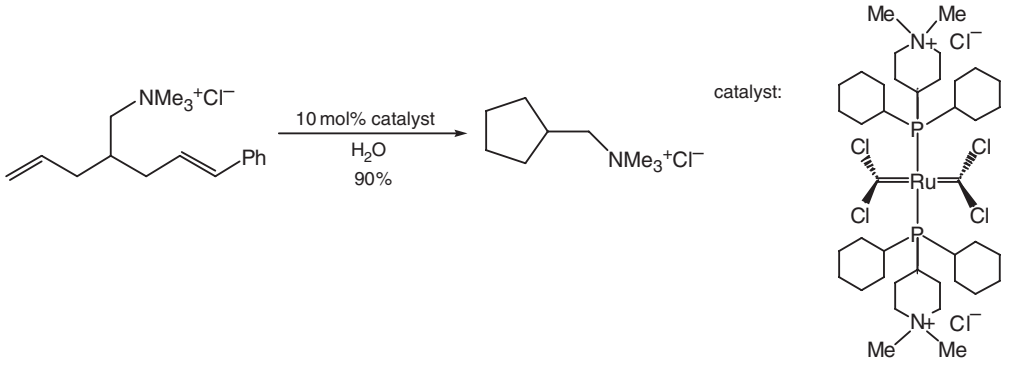

Figure 28 Metathesis reaction in aqueous media with ionic alkylidene complex.

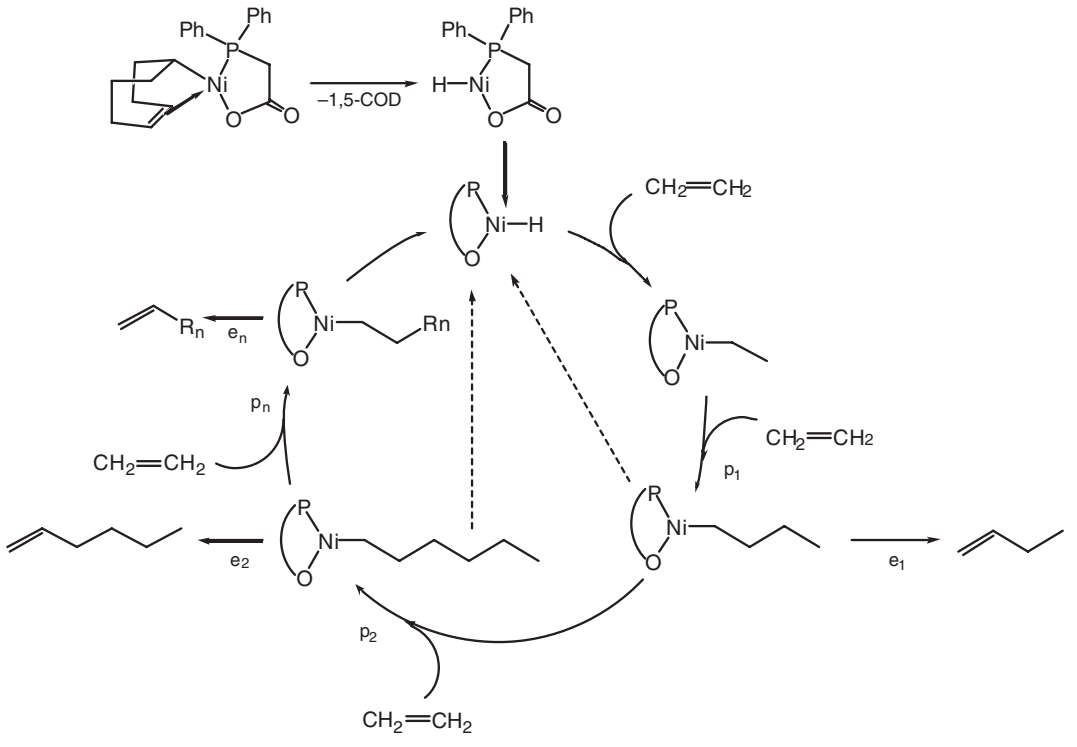

Figure 29 Ethylene oligomerization is catalyzed by a nickel-containing catalyst: p_1, p_2,...,p_n = propagation steps; e_1,e_2,...,e_n = elimination steps.[78–79]

homogeneous catalytic reactions, it has been used for only a few including hydrogenation, different coupling reactions, co-polymerization of ethylene and CO,[80a] because the solvent properties of alcohols and most products are too similar resulting in limited separation.

1.29.5 Organometallic Chemistry in Ionic Liquids

Ionic liquids are molten salts, which are liquids at or close to room temperature. While the cations are generally large organic compounds such as *N*,*N*′-dialkyl-imidazolium, *N*-alkyl-pyridinium, and *N*,*N*-alkylpyrolinium, the anions are smaller, usually $AlCl_4^-$, HF_2^-, BF_4^-, PF_6^-, SbF_6^-, $CF_3SO_3^-$, etc. (Figures 30 and 31)[81a–81d] and some of them are commercially available (Table 2).

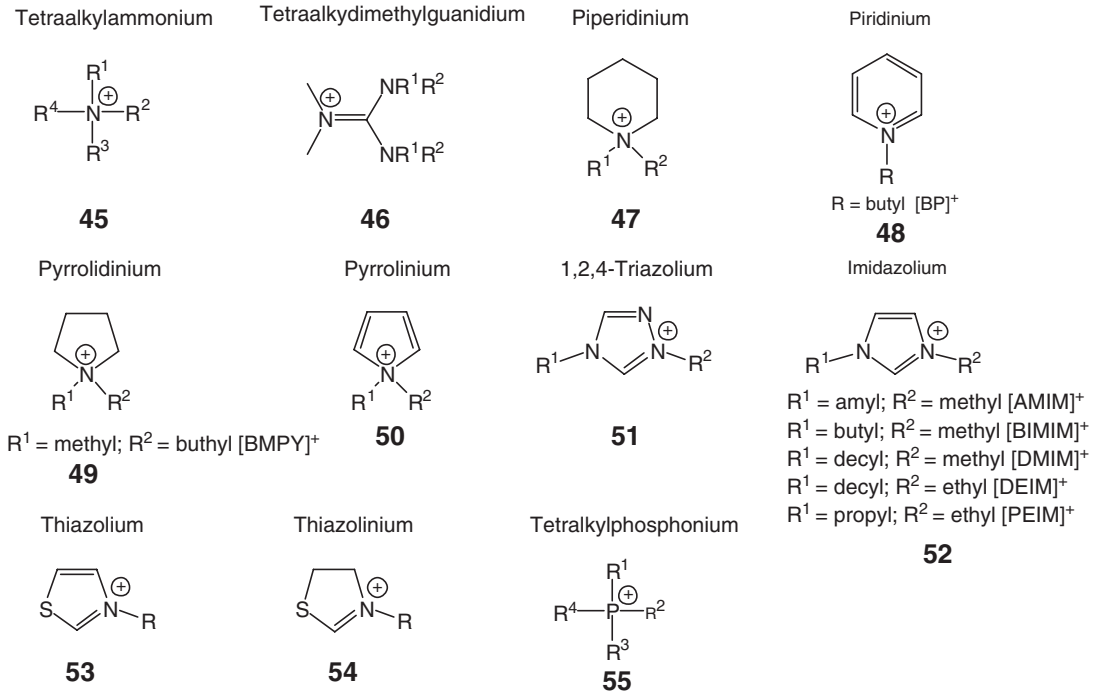

Figure 30 Typical cations of ionic liquids.

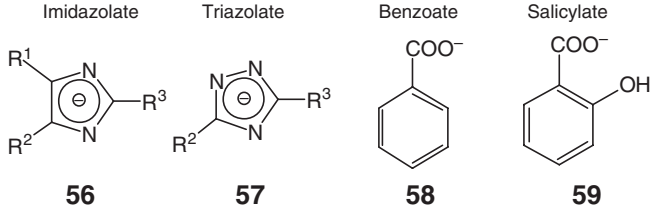

Figure 31 Typical organic anions of ionic liquids.

Table 2 Typical inorganic anions of ionic liquids

Halogenated anions	*Non-halogenated anions*	*Organometallic anions*
$[HF_2]^-$, $[Cl]^-$	$[N(CN)_2]^-$, $[N(SO_2CH_3)_2]^-$,	$[AlCl_4]^-$, $[Al_2Cl_7]^-$, $[Al_3Cl_{10}]^-$,
$[BF_4]^-$, $[PF_6]^-$, $[SbF_6]^-$, $[Sb_2F_{11}]^-$,	$[S(CN)]^-$,	$[FeCl_4]^-$, $[Fe_2Cl_7]^-$, $[SbF_6]^-$, $[Sb_2F_{11}]^-$,
$[CF_3SO_3]^-$, $[CF_3CO_2]^-$,	$[SO_4]^{2-}$, $[PO_4]^{3-}$, $[CH_3CO_2]^-$,	$[CoCO_4]^-$, $[AuCl_4]^-$,
$[N(SO_2CF_3)_2]^-$, $[N(CF_3)_2]^-$	$[RSO_3]^-$, $[RSO_4]^-$, $[R_2PO_4]^-$; (R = alkyl)	$[GaCl_4]^-$, $[SnCl_3]^-$, $[ZnCl_3]^-$, $[CuCl_3]^-$

The ionic liquids have been used as electrolytes in batteries, but many other interesting applications have been developed such as fuel and solar cells, inorganic and organic electrochemistry, and, most recently, a new medium for organic synthesis and catalysis (transition metal, enzymatic). One of the most attractive properties of ionic liquids is the very low vapor pressure. Furthermore, they are not flammable, easy to handle, they have reasonable thermal stability, and at large range of temperatures are liquids. They can behave as a Lewis acid and serve as a solvent at the same time or they can be a ligand and solvent simultaneously. Chiral ionic liquids can be prepared by functionalization with chiral substituents. Ionic liquids are excellent solvents for electrochemical reaction or reactions proceeding through ionic intermediates. They can be used as alternatives for aqueous systems, when the reagent or the catalyst is water sensitive and easily hydrolyzes. The disadvantages include high viscosity, low gas solubility, and the fact that polar nonvolatile

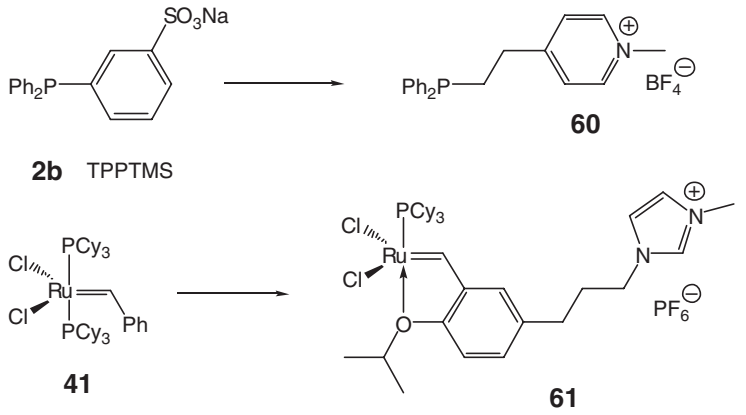

Figure 32 TPPTMS and Rh-alkylidene complex modified for ionic liquids.

products could be difficult to separate because of mutual miscibility. The fluorine-containing anions BF_4^- and PF_6^-, for example, are sensitive to water and the $CF_3CO_2^-$ anion is thermally instable. The purity of the ionic liquids is a very important issue, because traces of contaminants can modify significantly the physical parameters.

In order to achieve good solubility in ionic liquid, the incorporation of one or more ionic substituents in the organometallic species is required. One of the most trivial steps is the incorporation of an imidazolium moiety in the ligand of the transition metal complex (Figure 32) or the addition of functionalized ligands.[82–84a]

While the products can be separated by several methods, the best when the products are not miscible with or have limited solubility in the ionic liquids. If the products dissolve partially or totally in ionic liquids, they can be extracted with a non-polar, non-miscible solvent. Of course, when the products are volatile and the system is thermally stable, they can be distilled from the reaction mixture. In some special cases the ionic liquids are separated by crystallization. An alternative separation approach is the immobilization to solid supports.[85]

Supercritical carbon dioxide ($scCO_2$) can be combined with ionic liquids providing an efficient, simple, and environmentally friendly separation method. For example, methanol is miscible with the ionic liquids and forms one phase. When this phase is saturated with $scCO_2$, the formation of two phases could be observed and the upper phase contains most of the methanol.[86] It should be noted that $scCO_2$ reduces the viscosity of ionic liquids and could facilitate mass transfer. The $scCO_2$-philic, less polar products are easy to extract from reaction media.

Most of the reaction mechanisms in ionic liquids are similar to that of inorganic media. Contrary to polar organic solvents, ionic liquids offer limited solvation for organometallic species (Table 3). Therefore, the formation of coordinatively unsaturated intermediates could be much easier.[87,88]

1.29.6 Organometallic Chemistry in Supercritical Water

Supercritical fluid forms above the critical temperature and pressure (Figure 33). This value for water is $T_c = 647.3$ K and $p_c = 218.3$ atm.[102] At these conditions the water loses hydrogen bridges and many physical and chemical parameters are siginificantly different from liquid water. Since the dielectric constant drops from 78.5 to 6.0, scH_2O is very similar to the organic solvents and it is not a good solvent for ionic reactions.[103] The mechanism of organic reactions also changes at these conditions, the water can react at the same time as a solvent, a reactant, or a catalyst. The disadvantage of this method is the very high pressure combined with the high temperature. Generally it is used for organic syntheses, but a palladium-catalyzed Heck coupling reaction was reported in supercritical water. Transition metal oxides were applied for hydrogenation and dehydrogenation reactions of scH_2O.[104]

1.29.7 Organometallic Chemistry in Supercritical Carbon Dioxide

The critical point of carbon dioxide is near ambient conditions: $T_c = 304.2$ K, $p_c = 72.9$ atm.[102] The $scCO_2$ is the most commonly used supercritical fluid, because it is easier to use as compared to other substances: it is not corrosive as $scNH_3$, not flammable (the scN_2O has better solvent properties as $scCO_2$, but it is explosive), does not damage the

Table 3 Selected reactions performed in ionic liquids

Reaction	*Catalyst*	*Substrate*	*Ionic liquid*	*References*
Oligomerization	Ni(COD)(1,1,1,5,5,5-hexafluoro-pentane-2,4-dione)	1-Butene	[BMIM][Cl]/$AlCl_3$ = 0.43/0.53	89a
Oligomerization	$Cl_2W=NPh(PMe_3)_3$	Ethene	[BMIM][$AlCl_4$]	90
Polimerization	$(\eta^5\text{-Cp})_2TiCl_2$	Ethene	[EMIM][$AlCl_4$]	91
Polimerization	[$NbO(C_{16}H_{11}O_6)\text{-}(C_2O_4)$]	1,3-Butadiene	[BMIM][$AlCl_4$]	92
Hydrogenation	$RuCl_2(PPh_3)$	1-Hexene, butadiene	[BMIM][BF_4]	93
Hydrogenation	$[H_4Ru_4\text{-}(\eta^6\text{-}C_6H_6)_4][BF_4]_2$	Arenes	[BMIM][BF_4]	94
Diels–Alder	$Sc(CF_3SO_3)_3$		[BMIM][PF_6]	95
Hydroformylation	$[HRu_3(CO)_{11}]^-$, $[HRu_3(CO)_{11}(DIPHOS)]^-$	Olefines	[TBUP][Br] (tetrabutyl-phosphonium-bromide	96,96a
Hydroformylation	$Rh(CO)_2$(acac)/TPPTS	Olefines	[BMIM][PF_6]	84,84a
Oxidation	Bis(acetylacetonato)Ni(II)	Benzene	[*n*-Bu_4N] [BF_4]	97
Oxidation (Wacker-type)	$PdCl_2/H_2O$	Styrol	[BMIM][BF_4]	98
Heck-reaction	$PdCl_2(PPh_3)_2$	Bromoarenes	$[(C_{16}H_{34})(Bu)_3P][Br]$, $[(C_{16}H_{34})(Bu)_3P][Cl]$	99
Heck-reaction	$Pd(OAc)_2$/Dppp	*Butyl vinyl* ether and arylhalogenid	[BMIM][BF_4]	100
Suzuki cross-coupling	$Pd(PPh_3)_4$		[BMIM][BF_4]	101

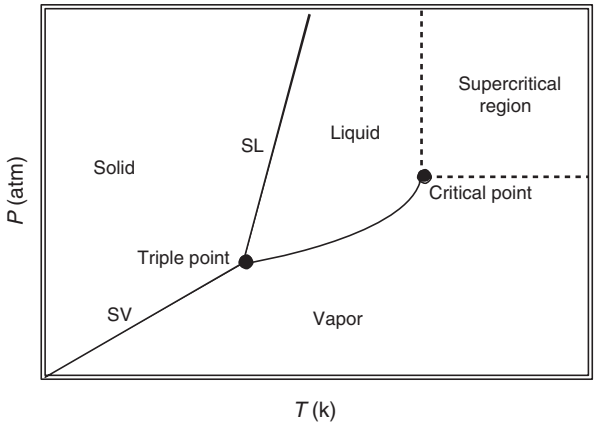

Figure 33 General *p–T* phase diagram for a non-defined pure substance.

ozone layer, and is relatively inexpensive. The dielectric constant of CO_2, which is an important property for chemical reactions, does not change so dramatically as in the case of water.

The oldest commercially used $scCO_2$ extraction process is the decaffeination of coffee beans. This is still the most profitable application of $scCO_2$, but supercritical fluids have been tested in the food industry, pharmaceutical industry, textile dyeing, impregnation, polymer synthesis and processing, dry cleaning, etc.[105]

The $scCO_2$ has other advantages for transition organometallic chemistry and catalysis. The gases are more miscible in supercritical fluid than in normal liquids, so mass transfer is not limited resulting in higher reaction rates—this is very useful in hydrogenation, oxidation, or carbonylation reactions. There is weak coordination, and changing the pressure in small amounts can change solubility properties and the selectivity properties of certain reactions. The $scCO_2$ can serve as a protecting group in the case of amines via the formation of carbamic acids. Since air and oxygen could be excluded, air-sensitive reactions can also be performed in $scCO_2$. However, some catalysts could be extremely air and moisture sensitive and they may decompose during recycling or can be attacked by the traces of water in $scCO_2$. It can be a solvent for many different reactions and used for catalyst recycling by different approaches (Figure 34):[106] (i) The reaction is

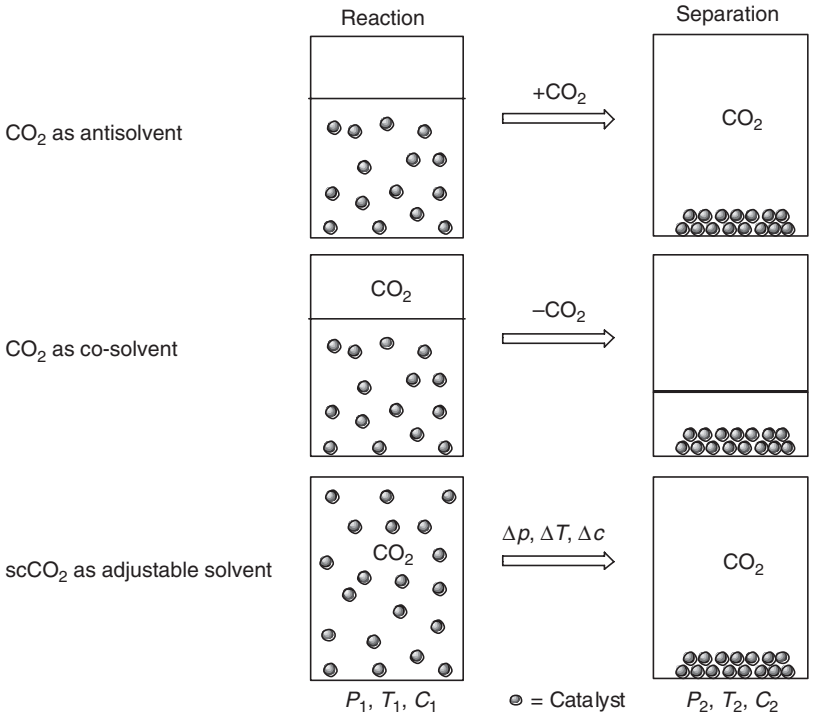

Figure 34 Some applications of CO_2 in homogeneous catalyses for catalyst recycling.

performed in a classical organic solvent with catalyst and after completion scCO$_2$ is added to decrease the polarity of the medium resulting in the rapid precipitation of the catalyst, (ii) The scCO$_2$ is used to solubilize the catalyst and after the reaction it is discharged to precipitate the catalyst, and (iii) CO_2 is used as an adjustable solvent. In this case the reaction and the separation take place only in CO_2 and there is no need for another solvent, organic or inorganic. In the beginning of the reaction the substrate(s) and the catalyst are in different phases, by reaching the supercritical state a single phase is formed and the reaction runs in a homogeneous phase. By changing the physical parameters (p, T, c), the catalyst could precipitate, or the more volatile compounds could remain in the CO_2 phase or the catalyst could be extracted from the reactor vessel.

Since few organic compounds are soluble in scCO$_2$, the solubilization of the catalyst is an important aspect of designing new catalysts. Since the solubility properties of scCO$_2$ are very similar to alkanes and perfluoroalkanes, compounds which are soluble in these solvents will readily dissolve in CO_2, too. The aliphatic compounds are more "scCO$_2$-philic" than the aromatic materials, and partial saturation can increase the solubility. Changing the methyl groups to trifluoromethyl groups is a good strategy; this can enhance the solubility of the compounds, but still the material is not fluorophilic. The classical Ru-containing metathesis catalyst was partially soluble in scCO$_2$, but the Mo-containing alkylidene complex with trifluoromethyl groups has higher solubility in scCO$_2$ (Figure 35).[107]

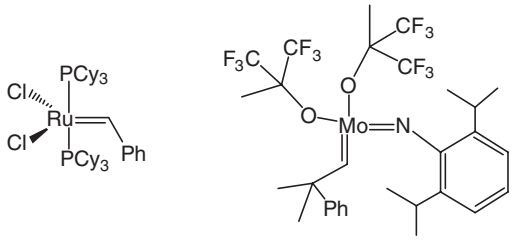

41 **62**

Figure 35 Alkylidene complexes tested in metathesis reactions in scCO$_2$.

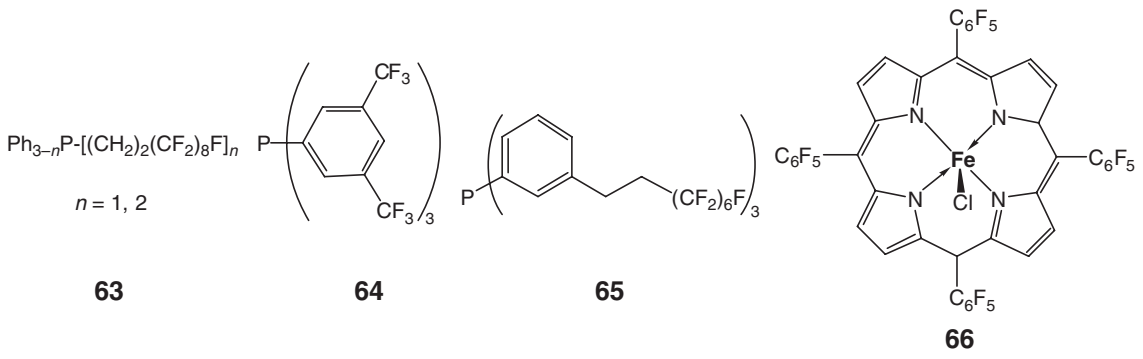

63 **64** **65** **66**

Figure 36 Some $scCO_2$-soluble fluorine containing ligands.

The carbonyl-containing transition metal catalysts are also good, and other classical ligands can be solubilized by the attachment of perfluoroalkyl groups. Therefore, fluorous-soluble compounds are suitable for homogeneous catalysis in $scCO_2$. By attaching perfluoroalkylated chains, as in fluorous biphasic chemistry, one could really increase the solubility of the compounds, partially as in the case of the other methods. However, the length of the perfluoroalkyl group does not have to be so long for $scCO_2$ as for fluorous biphasic systems.[108] These types of ligands have weak self-interactions and a specific F–CO_2 interaction.[109] Some examples are shown in Figure 36.

The $scCO_2$ is miscible with gases, so it is particularly suitable for reactions involving gases, such as, hydrogenation, hydroformylation, and hydrosilylation to CO_2. As a non-flammable substance, $scCO_2$, provides a safe environment for oxidation reactions. Some experiments carried out in $scCO_2$ are collected in Table 4.

1.29.8 Fluorous Organometallic Chemistry

Perfluorinated alkanes, dialkylethers, and trialkylamines are unusual because of their non-polar nature and low intermolecular forces. Their miscibility even with common organic solvents (such as toluene, THF, acetone, and alcohols) is low at room temperature; thus, these materials could form fluorous biphase systems.[119,120] The term fluorous was introduced,[121,122] as the analog to the term aqueous, to emphasize the fact that one of the phases of a biphase system is richer in fluorocarbons than the other. Fluorous biphase systems can be used in catalytic chemical transformations by immobilizing catalysts in the fluorous phase. A fluorous catalyst system consists of a fluorous phase containing a preferentially fluorous soluble catalyst and a second product phase, which may be any organic or non-organic solvent with limited solubility in the fluorous phase (Figure 1). Conventional homogeneous catalysts can be made fluorous soluble by incorporating fluorocarbon moieties to their structure in appropriate size and number. The most effective fluorocarbon moieties are linear or branched perfluoroalkyl chains with high carbon number that may contain other heteroatoms (the "fluorous ponytails"). It should be emphasized that perfluoroaryl groups do offer

Table 4 Selected reactions performed in $scCO_2$

Reaction catalyzed	*Catalyst*	*Ligands*	*References*
Isomerization	$Fe_3(CO)_{12}$		110,110a
Hydrogenation	MnH(CO)5		111
Hydroformylation	$Co_2(CO)_8$		112
Hydrosilylation of CO_2	RuH2-$[P(CH_3)_3]_4$		113
Pauson–Khand reaction	$Co_2(CO)_8$		114
Heck reaction	$Pd_2(dba)_3$	$P[3,5\text{-}(CF_3)_2C_6H_3]_3$	115
Heck, Suzuki, Sonogashira	$Pd(OAc)_2$	$Ph_{3\text{-}n}(CH_2CH_2C_6F_{13})_n$ ($n = 1$ or 2)	116
Oxidation	FeCl [5,10,15,20-tetrakis (pentafluorophenyl)porphyrin)]		117
Epoxidation	$Mo(CO)_6$		118

Table 5 Selected reactions performed in fluorous medium

Reaction catalyzed	*Catalyst*	*Ligands*	*References*
Hydroformylation	$Rh(CO)_2(acac)$	$P(C_2H_4C_6F_{13})_3$	121 122
Hydroformylation	$Rh(CO)_2(acac)$	$P(p\text{-}C_6H_4\text{-}C_6F_{13})_3$	125, 125a
Hydrogenation	$PhCl[P(C_2H_4C_6F_{13})_3]_3$		126
Oxydation	$CuBr.Me_2S$	4,4′-bis-(perfluorooctylbutyl)-[2,2′]bipyridinyl □	127
Heck reaction	$Pd_2(dba)_3$, $Pd(OAc)_2$	$P(p\text{-}C_6H_4\text{-}C_6F_{13})_3$, $P(p\text{-}C_6H_4\text{-}OCH_2C_7F_{15})_3$	128
Negishi reaction	$Pd_2(dba)_3$	$P(p\text{-}C_6H_4\text{-}C_6F_{13})_3$	129, 129a
Allylic substituion	$Pd_2(dba)_3$	$P(p\text{-}C_6H_4\text{-}C_6F_{13})_3$	130

dipole–dipole interactions,[123] making perfluoroaryl containing catalysts soluble in common organic solvents and therefore less compatible with fluorous biphase systems.

The most effective fluorous solvents are perfluorinated alkanes, perfluorinated dialkyl ethers, and perfluorinated trialkyl amines. Their remarkable chemical inertness, thermal stability, and nonflammability coupled with their unusual physical properties make them particularly attractive for catalyst immobilization. Furthermore, these materials are practically nontoxic by oral ingestion, inhalation, or intraperitoneal injection.[124] Although their thermal degradation can produce toxic decomposition products, such decomposition generally begins only at very high temperatures well above the thermal stability limits of most organometallic compounds.

A fluorous biphase reaction could proceed either in the fluorous phase or at the interface of the two phases, depending on the solubilities of the substrates in the fluorous phase. When the solubilities of the substrates are very low in the fluorous phase, the chemical reaction may still occur at the interface or appropriate phase-transfer agents may be added to facilitate the reaction. It should be emphasized that a fluorous biphase system might become a one-phase system by increasing the temperature. Thus, a fluorous catalyst could combine the advantages of one-phase catalysis with biphasic product separation by running the reaction at higher temperatures and separating the products at lower temperatures (Figure 3). Some fluorous reactions are listed in Table 5.

References

1. Koelle, U. *Coord. Chem. Rev.* **1994**, 135–136, 623.
2. Horváth, I. T.; Joó, F. *Aqueous Organometallic Chemistry and Catalysis*; Eds.; Kluwer: Dordrecht, 1995.
3. Lazarova, N.; James, S.; Babich, J.; Zubieta, J. *Inorg. Chem. Commun.* **2004**, 7, 1023.
4. Kühn, F. E.; Herrmann, W. A. In *Multiphase Homogeneous Catalysis*; Cornils, B., Herrmann, W. A., Horváth, I. T., Leitner, W., Mecking, S., Olivier-Bourbigou, H., Vogt, D., Eds.; Wiley-VCH: Weinheim, 2005; Vol. 46.
5. Feinstein-Jaffe, I.; Gibson, D.; Lippard, S. J.; Schrock, R. R.; Spool, A. *J. Am. Chem. Soc.* **1984**, *106*, 6305.
6. Ashworth, T. V.; Singleton, J. E.; de Waal, D. J. A.; Louw, W. J.; Singleton, E.; van der Stok, E. J. *J. Chem. Soc., Dalton Trans.* **1978**, 340.
7. Crabtree, R. H.; Quirk, J. M.; Fillebeen-Khan, T.; Morris, G. E. *J. Organomet. Chem.* **1979**, *181*, 203.
8. Paterniti, D. P.; Roman, P. J., Jr.; Atwood, J. D. *J. Chem. Soc., Chem. Commun.* **1996**, 2659.
9. Poli, R. *Chem. Eur. J.* **2004**, *10*, 332.
10. Kuntz, E. (Rhône-Poulenc Recherche). FR 2.314.910 1975.
11. Bartik, T.; Bartik, B.; Hanson, B. E.; Glass, T.; Bebout, W. *Inorg. Chem.* **1992**, *31*, 2667.
12. Bahrmann, H.; Cornils, B.; Lipps, W.; Lappe, P.; Springer, H. (Ruhrchemie AG) CA 1.247.642 1988 (*Chem. Abstr.* 111, 97 503).

12a. Bexten, L.; Cornils, B.; Kupies D. (Ruhrchemie AG). DE 3.431.643 1986.

13. Tóth, I.; Guo, I.; Hanson, B. E. *J. Mol. Catal. A: Chem.* **1997**, *116*, 217.
14. Albanese, G.; Manetsberger, R.; Herrmann W. A. (Hoechst AG). EP 704.450 1996.
15. Fell, B.; Papadogiannakis, G. *J. Prakt. Chem.* **1994**, *336*, 591.
16. Albanese, G.; Manetsberger, R.; Herrmann, W. A.; Schid R. (Hoechst AG). EP 704.452 1996.
17. Gelpe, A. E. S.; Veerman, J. J. N.; Goedheijt, M. S.; Kamer, P. C.; von Leeuwen, P. W. N. M.; Hiemstra, H. *Tetrahedron* **1999**, *55*, 6657.
18. Bahrmann, H.; Lappe, P.; Herrmann, W. A.; Manetsberger, R.; Albanese, G.: (Hoechst AG). DE 4.321.512 1993.
19. Herrmann, W. A.; Albanese, G.; Manetsberger, R.; Lappe, P.; Bahrmann, H. *Angew. Chem., Int. Ed. Engl.* **1995**, *34*, 811.
20. Smith, R. T.; Ungar, R. K.; Sanderson, L. J.; Baird, M. C. *Organometallics* **1983**, *2*, 1138.
21. Smith, R. T.; Baird, M. C. *Transition Met. Chem.* **1981**, *6*, 197.
22. Hoots, J. E.; Rauchfuss, T. B.; Wrobleski, D. A. *Inorg. Synth.* **1982**, *21*, 75.
23. Hingst, M.; Tepper, M.; Stelzer, O. *Eur. J. Inorg. Chem.* **1998**, 73.
24. Herd, O.; Hessler, A.; Hingst, M.; Machnitzki, P.; Tepper, M. *Catal. Today* **1998**, *42*, 413.

24a. Herd, O.; Hessler, A.; Hingst, M.; Tepper, M.; Stelzer, O. *J. Organomet. Chem.* **1996**, *522*, 69.

24b. Machnitzki, P.; Tepper, M.; Wenz, K.; Stelzer, O.; Häusler, T.; Sheldrick, W. S. *J. Organomet. Chem.* **2000**, *602*, 158.

25. Tepper, M.; Stelzer, O.; Häusler, T.; Sheldrick, W. S. *Tetrahedron Lett.* **1997**, *38*, 2257.

26. Bartik, T.; Bunn, B.; Bartik, B.; Hanson, B. E. *Inorg. Chem.* **1994**, *33*, 164.
27. Taqui Khan, M. M. *Platinum Met. Rev.* **1991**, *35*, 70.
28. Szalontai, S.; Kiss, G.; Bartha, L. *Spectrochim. Acta, Part A* **2003**, *59*, 195.
29. Rauchfuss, T. B. *Inorg. Chem.* **2004**, *43*, 14.
30. Sellmann, D.; Soglowek, W.; Knoch, F.; Ritter, G.; Dengler, J. *Inorg. Chem.* **1992**, *31*, 3711.
31. Sellmann, D.; Peters, K. P.; Heinemann, F. W. *Eur. J. Inorg. Chem.* **2004**, *3*, 581.
32. Ungermann, C.; Ladis, V.; Moya, S. A.; Cohen, H.; Walker, H.; Peaarson, R. G.; Rinker, R. G.; Ford, P. C. *J. Am. Chem. Soc.* **1979**, *101*, 5922.
33. Buffin, B. P.; Squattrito, P. J.; Ojewole, A. O. *Inorg. Chem. Commun.* **2004**, 7, 14.
34. Kozhenikov, I. V.; Mulder, G. P.; Steverink-de Zoete, M. C.; Oostwald, M. G. *J. Mol. Catal. A* **1998**, *134*, 223.
35. ten Brink, G. J.; Arends, I. W. C. E.; Hoogenraad, M.; Verspui, G.; Sheldon, R. A. *Adv. Synth. Catal.* **2003**, *345*, 497.
36. Boelrijk, A. E. M.; van Velzen, M. M.; Neenan, T. X.; Reedijk, J.; Kooijman, H.; Spek, A. L. *J. Chem. Soc., Chem. Commun.* **1995**, 2465.
37. Rojas, I.; Linares, F. K.; Valencia, N.; Bianchini, C. *J. Mol. Catal. A* **1999**, *144*, 1.
38. Kathó, A.; Opre, Z.; Laurenczy, G.; Joó, F. *J. Mol. Catal. A* **2003**, *204*, 143.
39. Joó, F. *Acc. Chem. Res.* **2002**, *35*, 738.
40. Darensbourg, D. J.; Joó, F.; Kannisto, M.; Kathó, Á.; Reibenspies, J. H.; Daigle, D. J. *Inorg. Chem.* **1994**, *33*, 200.
41. Cariati, E.; Dragonetti, C.; Manassero, L.; Roberto, D.; Tessore, F.; Lucenti, E. *J. Mol. Catal. A* **2003**, *204*, 279.
42. Trzeciak, A. M.; Ziólkowski, J. J. *Coord. Chem. Rev.* **1999**, 190–192, 883.
43. Uozumi, Y.; Nakazono, M. *Adv. Synth. Catal.* **2002**, *344*, 274.
44. Kuo, L. Y.; Weakley, T. J. R.; Awana, K.; Hsia, C. *Organometallics* **2001**, *20*, 4969.
45. Francisco, L. W.; Moreno, D. A.; Atwood, J. D. *Organometallics* **2001**, *20*, 4237.
46. Mizushima, E.; Sato, K.; Hayashi, T.; Tanaka, M. *Angew. Chem., Int. Ed.* **2002**, *41*, 4563.
47. Wullner, G.; Jansch, H.; Kannanberg, S.; Schubert, F.; Boche, G. *Chem. Commun.* **1998**, 1509.
48. Li, C.-J. *Acc. Chem. Res.* **2002**, *35*, 533.
49. Bertoux, F.; Tilloy, S.; Monflier, E.; Castanet, Y.; Mortreux, A. *J. Mol. Catal. A* **1999**, *138*, 53.
50. Bricout, H.; Monflier, E.; Carpentier, J. F.; Mortreux, A. *Eur. J. Inorg. Chem.* **1998**, *11*, 1739.
51. Bényei, A.; Joó, F. *J. Mol. Catal. A* **1990**, *58*, 15.

51a. Shertchook, H.; Avnir, D.; Blum, J.; Joó, F.; Kathó, Á.; Schumann, H.; Weimann, R.; Wernik, S. *J. Mol. Catal. A* **1996**, *108*, 153.

52. Verspui, G.; Feiken, J.; Papadogianakis, G.; Sheldon, R. A. *J. Mol. Catal. A* **1999**, *146*, 299.
53. Novak, B. M.; Grubbs, R. H. *J. Am. Chem. Soc.* **1988**, *110*, 960.
54. Fuji, K.; Morimoto, T.; Tsutsumi, K.; Kakiuchi, K. *Angew. Chem., Int. Ed.* **2003**, *42*, 2409.
55. Otto, S.; Boccaletti, G.; Engberts, J. B. F. *J. Am. Chem. Soc.* **1998**, *120*, 4238.
56. Armengual, R.; Genin, E.; Michelet, V.; Savignac, M.; Genet, J. P. *Adv. Synth. Catal.* **2002**, *344*, 393.
57. Casalnuvo, A. L.; Calabrese, J. C. *J. Am. Chem. Soc.* **1990**, *112*, 4324.
58. Motoda, D.; Kinoshita, H.; Shinokubo, H.; Oshima, K. *Adv. Synth. Catal.* **2002**, *344*, 261.
59. Kuntz, E. G. *Chem. Tech.* **1987**, *17*, 570.
60. Cornils, B.; Herrmann, W. A.; Eckl, R. W. *J. Mol. Catal. A* **1997**, *116*, 27.
61. Horváth, I. T.; Kastrup, R.; Oswald, A.; Mozeleski, E. *Catal. Lett.* **1989**, *2*, 85.
62. Chaudhari, R. V.; Bhanage, B. M.; Deshpande, R. M.; Delmas, H. *Nature (London)* **1995**, *373*, 501.
63. Chen, H.; Li, Y.; Chen, J.; Cheng, P.; He, Y.; Li, X. *J. Mol. Catal. A* **1999**, *149*, 1.
64. Arhancet, J. P.; Davies, M. E.; Merola, J. S.; Hanson, B. E. *Nature (London)* **1988**, *339*, 454.
65. Herrmann, W. A. In *Aqueous-Phase Organometallic Catalysis*; Cornils, B., Herrmann, W. A., Eds.; Wiley-VCH: Weinheim, 1998; Vol. 35.
66. Sweet, J. R.; Graham, W. A. G. *Organometallics* **1982**, *1*, 982.
67. Barborak, J. C.; Cann, K. *Organometallics* **1982**, *1*, 1726.
68. Herrmann, W. A.; Kühn, F. E. *Acc. Chem. Res.* **1997**, *30*, 169.

68a. Romão, C. C.; Kühn, F. E.; Herrmann, W. A. *Chem. Rev.* **1997**, *97*, 3197.

69. Clement, W. A.; Selwitz, C. M. *J. Org. Chem.* **1964**, *29*, 241.

69a. Tsuji, J.; Nagashima, H.; Nemoto, H. *Org. Synth.* **1984**, *62*, 9.

70. Henry, P. M. *J. Am. Chem. Soc.* **1966**, *88*, 1595.
71. Schrock, R. R. *Tetrahedron* **1999**, *55*, 8141.

71a. Trnka, T. M.; Grubbs, R. H. *Acc. Chem. Res.* **2001**, *34*, 18.

71b. Herrmann, W. A., *et al. Angew. Chem., Int. Ed.* **1999**, *38*, 262.

72. Grubbs, R. H. In *Aqueous Organometallic Chemistry and Catalysis*; Horváth, I. T., Joó, F., Eds.; Kluwer: Dordrecht, 1995.
73. Lynn, D. M.; Kanaoka, S.; Grubbs, R. H. *J. Am. Chem. Soc.* **1996**, *118*, 784.
74. Mortell, K. H.; Weatherman, R. V.; Kiessling, L. L. *J. Am. Chem. Soc.* **1996**, *118*, 2297.

74a. Kanai, M.; Mortell, K. H.; Kiessling, L. L. *J. Am. Chem. Soc.* **1997**, *119*, 9931.

74b. Manning, D. D.; Hu, X.; Beck, P.; Kiessling, L. L. *J. Am. Chem. Soc.* **1997**, *119*, 3161.

75. Mohr, B.; Lynn, D. M.; Grubbs, R. H. *Organometallics* **1996**, *15*, 4317.
76. Lynn, D. M.; Mohr, B.; Grubbs, R. H. *J. Am. Chem. Soc.* **1998**, *120*, 1627.
77. Kirkland, T. A.; Lynn, D. M.; Grubbs, R. H. *J. Org. Chem.* **1998**, *63*, 9904.
78. Keim, W.; Kowaldt, F. H.; Goddard, R.; Krüger, C. *Angew. Chem., Int. Ed.* **1978**, *17*, 466.

78a. Keim, W.; Behr, A.; Kimbäker, B.; Krüger, C. *Angew. Chem., Int. Ed.* **1983**, *22*, 503.

78b. Keim, W.; Behr, A.; Gruber, B.; Hoffmann, B.; Kowaldt, F. H.; Kürschner, U.; Limbäcker, B.; Sistig, F. P. *Organometallics* **1986**, *5*, 2356.

78c. Keim, W. *New J. Chem.* **1987**, *11*, 531.

78d. Keim, W. *J. Mol. Catal.* **1989**, *52*, 19.

78e. Müller, U.; Keim, W.; Krüger, C.; Betz, P. *Angew. Chem., Int. Ed.* **1989**, *28*, 1011.

78f. Keim, W. *Angew. Chem., Int. Ed.* **1990**, *29*, 235.

78g. Keim, W.; Schulz, R. P. *J. Mol. Catal.* **1994**, *92*, 21.

79. Vogt, D. In *Multiphase Homogeneous Catalysis*; Cornils, B., Herrmann, W. A., Horváth, I. T., Leitner, W., Mecking, S., Olivier-Bourbigou, H., Vogt, D., Eds.; Wiley-VCH: Weinheim, 2005.
80. Drent, E. (Shell). EP Appl. 121.965 1984. (*Chem. Abstr.* **1985**, *102*, 46423).

80a. Drent, E.; Broekhoven, J. A. M.; Doyle, M. J. *J. Organomet. Chem.* **1991**, *417*, 235.
81. Welton, T. *Chem. Rev.* **1999**, *99*, 2071.
81a. Gordon, C. M. *Appl. Catal A* **2001**, *222*, 101.
81b. Sheldon, R. A. *Chem. Commun.* **2001**, *23*, 2399.
81c. Olivier-Bourbigou, H.; Magna, L. *J. Mol. Catal. A* **2002**, 182–183, 409.
81d. Dupont, J.; Souza, R. F.; Suarez, P. A. Z. *Chem. Rev.* **2002**, *102*, 3667.
82. Sirieix, J.; Ossberger, M.; Betzemeier, B.; Knochel, P. *Synlett* **2000**, 1613.
83. Audic, N.; Clavier, H.; Mauduit, M.; Guillemin, J. C. *J. Am. Chem. Soc.* **2003**, *125*, 9248.
84. Dupont, J.; Silva, S. M.; de Souza, R. F. *Catal. Lett.* **2001**, *77*, 131.
84a. Wasserscheid, P.; Waffenschmidt, H.; Machnitzki,; Kottsieper, K. W.; Stelzer, O. *Chem. Commun.* **2001**, 451.
85. Mehnert, C. P.; Cook, R. A.; Dispenziere, N. C.; Afeworki, M. *J. Am. Chem. Soc.* **2002**, *124*, 12932.
86. Scurto, A. M.; Aki, S. N. V. K.; Brennecke, J. F. *J. Am. Chem. Soc.* **2002**, *124*, 10276.
87. Dupont, J.; de Souza, R. F.; Suarez, P. A. Z. *Chem. Rev.* **2002**, *102*, 3667.
88. Hussey, C. L. *Pure Appl. Chem.* **1988**, *60*, 1763.
89. Wassercheid, P.; Eichmann, M. *Catal. Today* **2001**, *66*, 309.
89a. Ellis, B.; Keim, W.; Wasserscheid, P. *J. Chem. Soc., Chem. Commun.* **1999**, 337.
90. Olivier, H.; Laurent-Gérot, P. *J. Mol. Catal. A: Chem.* **1999**, *148*, 43.
91. Carlin, R. T.; Wilkes, J. S. J. *J. Mol. Catal. A: Chem.* **1990**, *63*, 125.
92. Suarez, P. A. Z.; Rosa, N. T.; Einloft, S.; de Souza, R. F.; Dick, Y. P. *Polym. Bull.* **1998**, *41*, 175.
93. Suarez, P. A. Z.; Dullius, J. E. L.; Einloft, S.; de Souza, R. F.; Dupont, J. *Inorg. Chim. Acta* **1997**, *255*, 207–209.
94. Dyson, P. J.; Ellis, D. J.; Parker, D. G.; Welton, T. *Chem. Commun.* **1999**, 25–26.
95. Song, C. E.; Shim, W. H.; Roh, E. J.; Lee, S.; Choi, J. H. *Chem. Commun.* **2001**, 1122.
96. Knifton, J. F. *J. Mol. Catal.* **1987**, *43*, 65.
96a. Knifton, J. F. *J. Mol. Catal.* **1988**, *47*, 99.
97. Alcántara, R.; Canoira, L.; Guilhermo-Joao, P.; Santos, J.-M.; Vazquez, I. *Appl. Catal., A* **2000**, *203*, 259.
98. Varma, R. S.; Sahle-Demessie, E.; Pillai, U. R. *Green Chem.* **2002**, 170.
99. Kaufmann, D. E.; Nouroozian, M.; Henze, H. *Synlett* **1996**, 1091.
100. Xu, L. J.; Chen, W. R.; Ross, J.; Xiao, J. L. *Org. Lett.* **2001**, *3*, 295.
101. Mathews, C. J.; Smith, P. J.; Welton, T. *Chem. Commun.* **2000**, 1249.
102. Darr, J. A.; Poliakoff, M. *Chem. Rev.* **1999**, *99*, 495.
103. Siskin, M.; Katritzky, A. R. *Chem. Rev.* **2001**, *101*, 825.
104. Savage, P. E. *Chem. Rev.* **1999**, *99*, 603.
105. Scurto, A. M. In *Multiphase Homogeneous Catalysis*; Cornils, B., Herrmann, W. A., Horváth, I. T., Leitner, W., Mecking, S., Olivier-Bourbigou, H., Vogt, D., Eds.; Wiley-VCH: Weinheim, 2005.
106. Gordon, C. M.; Leitner, W. In *Multiphase Homogeneous Catalysis*; Cornils, B., Herrmann, W. A., Horváth, I. T., Leitner, W., Mecking, S., Olivier-Bourbigou, H., Vogt, D., Eds.; Wiley-VCH: Weinheim, 2005.
107. Fürstner, A.; Ackermann, L.; Beck, K.; Hori, H.; Koch, D.; Langemann, K.; Liebl, M.; Six, C.; Leitner, W. *J. Am. Chem. Soc.* **2001**, *123*, 9000.
108. Beckman, E. J. *J. Chem. Soc., Chem. Commun.* **2004**, 1885.
109. Dardin, A.; DeSimone, J. M.; Samulski, E. T. *J. Phys. Chem.* **1998**, *102*, 1775.
110. Manuel, T. A. *J. Org. Chem.* **1962**, *27*, 3941–3945.
110a. Bingham, D.; Webster, D. E.; Wells, P. B. *J. Chem. Soc., Dalton Trans.* **1974**, 1521.
111. Jessop, P. G.; Ikariya, T.; Noyori, R. *Organometallics* **1995**, *14*, 1510.
112. Rathke, J. W.; Klingler, R. J.; Krause, T. R. *Organometallics* **1991**, *10*, 1350.
113. Jessop, P. G. *Top. Catal.* **1998**, *5*, 95–103.
114. Jeong, N.; Hwang, S. H.; Lee, Y. W.; Lim, J. S. *J. Am. Chem. Soc.* **1997**, *119*, 10549.
115. Morita, D. K.; Pesiri, D. R.; David, S. A.; Glaze, W. H.; Tumas, W. *J. Chem. Soc., Chem. Commun.* **1998**, 1397.
116. Carroll, M. A.; Holmes, A. B. *Chem. Commun.* **1998**, 1395.
117. Wu, X.-W.; Oshima, Y.; Koda, S. *Chem. Lett.* **1997**, 1045.
118. Kreher, U.; Schebesta, S.; Walther, D. *Z. Z. Anorg. Allg. Chem.* **1998**, *624*, 602.
119. Hildebrand, J. H.; Praunitz, J. M.; Scott, R. L. *Regular and Related Solutions*; Van Nostrand-Reinhold: New York, 1970; Chapter 10.
120. Reichardt, C. *Solvents and Solvent Effects in Organic Chemistry*, 2nd ed.; VCH: Weinheim, 1990.
121. Horváth, I. T.; Rábai, J. *Science* **1994**, *266*, 72.
122. Horváth, I. T.; Rábai J. Exxon Research and Engineering Co. U.S. Patent 5,463,082 1995.
123. Filler, R. In *Fluorine Containing Molecules*; Liebman, J. F., Greenberg, A., Dolbier, W. R., Jr., Eds.; VCH: Weinheim, 1988; Chapter 2.
124. Clayton, J. W., Jr. *Fluorine Chem. Rev.* **1967**, *1*, 197.
125. Foster, D. F.; Adams, D. J.; Gudmunsen, D.; Stuart, A. M.; Hope, E. G.; Cole-Hamilton, D. J. *Chem. Commun.* **2002**, 722.
125a. Foster, D. F.; Gudmunsen, D.; Adams, D. J.; Stuart, A. M.; Hope, E. G.; Cole-Hamilton, D. J.; Schwarz, G. P.; Pogorzelec, P. *Tetrahedron* **2002**, *58*, 3901.
126. Rutherford, D.; Juliette, J. J. J.; Rokaboy, C.; Horváth, I. T.; Gladysz, J. A. *Catal. Today* **1998**, *42*, 381.
127. Betzemeier, B.; Cavazzini, M.; Quici, S.; Knochel, P. *Tetrahedron* **2002**, *58*, 3985.
128. Moineau, J.; Pozzi, G.; Quici, S.; Sinou, D. *Tetrahedron Lett.* **1999**, *40*, 7683.
129. Betzemeier, B.; Knochel, P. *Angew. Chem.* **1997**, *109*, 2736.
129a. Betzemeier, B.; Knochel, P. *Angew. Chem. Int. Ed. Engl.* **1997**, *36*, 2623.
130. Kling, R.; Sinou, D.; Pozzi, G.; Choplin, A.; Quignard, F.; Busch, S.; Kainz, S.; Koch, D.; Leitner, W. *Tetrahedron Lett.* **1998**, *39*, 9439.

1.30 Organometallic Chemistry in Ionic Liquids

J Dupont and F R Flores, Federal University of Rio Grande do Sul, Porto Alegre, Brazil

1.30.1 Introduction

The vast majority of chemical reactions involving organometallic compounds are performed in solution and therefore solvents play a major role on the outcome of these processes. It is obvious that the properties and nature of the solvent, such as its dielectric constant and coordination ability, can direct certain key intermediates or transition states and thus improve the rate and selectivity of a determined reaction. For example, polar and weakly coordinating solvents can promote reactions that involve charge-separated intermediates or transition states. The choice of solvent is not only crucial at the molecular level but also in the engineering of processes, since depending upon the differences between the solvent and the substrates/products, it is possible to build up multi-phase systems. In these multi-phase processes, it is possible to extract the primary products during the reaction and thus modulate the product selectivity (capitalizing on the different solubilities of the reaction products in a consecutive process). Moreover, multi-phase systems offer the possibility of facile separation of the products and recycling of the other reaction constituents when compared with processes performed under homogeneous conditions. A classical example of these processes is aqueous-phase chemistry, in particular, aqueous-phase organometallic catalysis.[1] More recently, other fluids have attracted attention such as perfluorinated solvents,[2] supercritical carbon dioxide ($scCO_2$),[3,4] and ionic liquids (ILs) and have been used as fluids for organometallic process. The elementary reactions typical of

organometallic compounds (ligand substitutions, oxidative additions, reductive eliminations, β-eliminations, insertions, oxidative couplings, etc.), when performed in these fluids, can be improved, accelerated, suppressed, or can generate different selectivities to those performed in classical organic solvents.

ILs are a special class of molten salts that are liquid at temperatures below 100 °C, such as tetrabutylphosphonium chloride (m.p. 80 °C) or a 1/1 mixture of triethylammonium chloride/copper chloride (m.p. 25 °C).[5–12] This type of molten salt has been known since the end of the nineteenth century, but it was only at the beginning of the 1990s that this class of fluids entered the organometallic chemistry scene with the use of water- and air-sensitive organoaluminate molten salts as "solvents" for the biphasic oligomerization of alkenes catalyzed by nickel compounds.[13] Since then, and in particular with the advent of more air- and water-compatible room-temperature ILs,[14,15] the renaissance of rich IL organometallic chemistry has begun and continues to flourish.

In this chapter, the main applications of these materials as fluids for organometallic chemistry achieved in the last 10 years will be disclosed.

1.30.2 General Aspects

1.30.2.1 ILs and Molten Salts: Overview

ILs can be arbitrarily defined as non-corrosive molten salts that are fluid at temperatures below 100 °C. The vast majority of these compounds are based in cations of tetraalkyl ammonium and phosphonium salts and heteroaromatics (Figure 1), typically associated with inorganic and organic anions such as BF_4, PF_6, $N(CF_3SO_2)_2$, CF_3SO_3, RCO_2, NO_3, ClO_4, amino-acids, MX_n.

The vast majority of these salts are effectively non-volatile (most of them exhibit negligible vapor pressure), non-flammable, and are liquid over a wide range of temperatures with relatively lower viscosity and higher densities than most classical organic solvents; possess usually higher thermal, electrochemical, and chemical stabilities compared to those of classical organic solvents; dissolve a very broad spectrum of organic, inorganic, biological, and organometallic compounds, and polymeric materials.[16] Moreover, their miscibility with these substances can be finely tuned by changing the nature of the cation and/or anion; the hydrophobicity can also be modulated by the judicious choice of the cation and/or anion or by changing the temperature of the process;[17] finally, they are easily prepared from commercially available reagents through classical synthetic procedures and several of these liquids are now commercially available.

1.30.2.2 Preparation and Purity

The vast majority of ILs are usually prepared by simple *N*- or *P*-alkylation of amines, heteroaromatics, and phosphines, often employing alkyl halides or alkyl sulfonates as alkylating agents, followed by association with metal halides or anion metathesis (Scheme 1).

Derivatives of 1,3-dialkylimidazolium cation associated with various anions are among the most popular and investigated class of ILs. This is most probably due to their ease of synthesis, stability, and the possibility of fine-tuning their physical–chemical properties by the simple choice of the *N*-alkyl substituents and/or anions. The 1,3-dialkylimidazolium and pyridinium cations will be abbreviated throughout this chapter as $[C_xC_yC_z\text{Im}]$ and $[C_x\text{Pyr}]$, respectively, where Im stands for imidazolium, Pyr for pyridinium, x and y are the number of the carbons of the *N*-alkyl chains, and z is the number of the carbons of other alkyl side chains present in the carbons of imidazolium or pyridinium nucleus (Figure 2).

The procedure involving the combination of metal halides such as $AlCl_3$, CuCl, CuBr, $ZnBr_2$, and $InCl_3$ with the 1,3-dialkylimidazolium halides (Cl or Br) or *N*-alkylpyridinium halides is simple, and can generate a variety of ILs with different Lewis acidities depending on the ratio organic salt/metal halide. The anion metathesis procedures

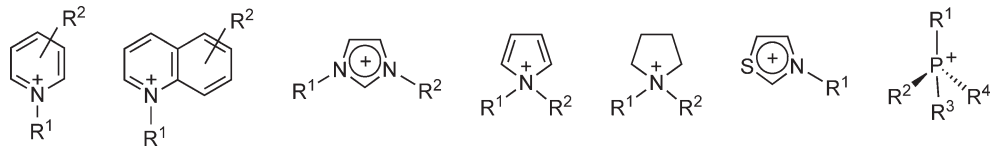

Figure 1 Examples of ILs.

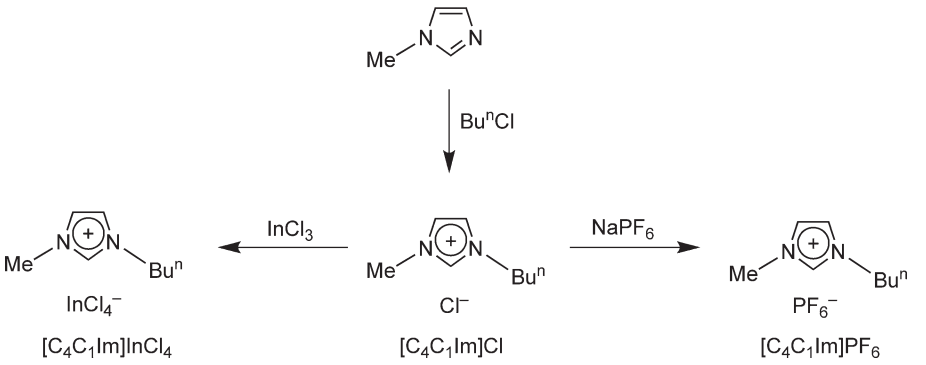

Scheme 1 Two different routes for the preparation of 1-*n*-butyl–3-methylimidazoilum ILs.

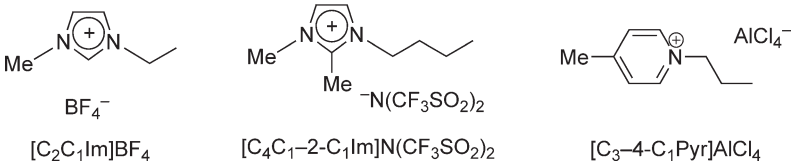

Figure 2 Examples of the abbreviations for the imidazolium and pyridinium ILs.

generate a large variety of 1,3-dialkylimidazolium-based ILs of good quality. The main contaminant is usually residual chloride that can be detected by an $AgNO_3$ test (limit of 1.4 mg l^{-1}), ion chromatography (below 8 ppm),[18] or, more conveniently, by cyclic voltammetry (ppb).[19,20] The water content can be determined by Karl Fischer titration or by cyclic voltammetry.[21] The presence and quantification of these impurities is essential in many applications, since the physical chemical properties of the ILs can vary significantly depending on their water and halide contents.[22]

Alternatively, halide-free 1,3-dialkylimidazolium ILs can be prepared from the five-component reaction (glyoxal, formaldehyde, two different amines and acids, Scheme 2),[23] and those containing alkyl sulfate or trifluoromethane sulfonate anions by simple alkylation of 1-alkylimidazole with the corresponding dialkylsulfate or alkyltrifluoromethane sulfonate ester, respectively.[24]

There are mainly two approaches to describe and rationalize the properties of ILs when used in chemical reactions: they behave as a solvent or as a liquid support. Although different and sometimes contradictory solvent properties have been derived from several studies, such as polarity (mainly using solvatochromic dyes), linear free relationships, and partitioning investigations, it is almost a consensus that ILs, in particular those based on 1,3-dialkylimidazolium cation, have polarities comparable to DMF, acetonitrile, and short-chain alcohols, and coordination ability similar to that of dichloromethane.[25–30] This approach is usually helpful for the rationalization of the physical and chemical process occurring in ILs, but in various cases this approach is not sufficient. However, ILs may also be regarded as liquid supports in which the introduction of other molecules occurs with formation of inclusion-type compounds.[16] This model is based on the fact that particularly imidazolium-based ILs possess a pronounced self-organization in the solid, liquid, and even in the gas phase. Indeed, simple analysis of the physical–chemical properties of solid salts can yield important information about the structural features of the same material in the liquid phase. This approach has been historically used in classical molten salt chemistry even if significant randomness in organization is necessary to describe the structure of a liquid. However, in most of the cases, there is only 10–15% volume expansion on going

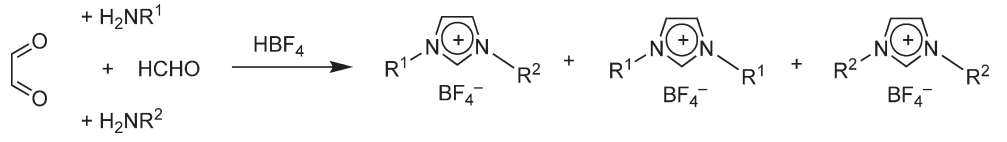

Scheme 2 One-pot five-component synthesis of 1,3-dialkylimidazolium tetrafluoroborate ILs.

from the crystalline to the liquid state, and the ion–ion or atom–atom distances are similar in both the solid and liquid states. For example, various X-ray and neutron-scattering studies of solid and liquid NaCl suggest that the structural organization observed in the crystal exists in the liquid phase.[31,32] Furthermore, while long-range order is lost on going from the crystal to the liquid, similarities remain as a consequence of the Coulombic forces between cations and anions of the ILs.[33] It is also clear that the long-range Coulomb interactions in ionic organic liquids can lead to longer spatial correlations than those in comparable classic van der Waals organic liquids.[34] This approach has been used also in the case of contemporary ILs, in particular, for imidazolium salts. In this respect, several physical studies—IR,[35–37] Raman,[38,39] XRD,[31,32,40] NMR,[41–43] ESI-MS,[44,45] and optical heterodyne-detected Kerr effect experiments—indicate that indeed 1,3-dialkylimidazoliums possess analogous structural patterns in both the solid and liquid phase.[33]

1.30.2.3 Physical–Chemical Properties

The physical–chemical properties of most of the ILs can, in principle, be finely tuned by, for example, varying the *N*-alkylimidazolium, *N*-alkylpyridinium, or *P*-alky/arylphosphonium substituents and/or the anion. For example, in the series containing the 1,3-dialkylimidzolium cation (Table 1), $[C_4C_1Im]PF_6$ melts at ca. 10 °C, whereas the $[C_4C_1Im]BF_4$ analog is liquid down to ca. 82 °C. Most of the imidazolium ILs start to decompose at temperatures above 400 °C.

ILs possess large electrochemical windows that can attain 7.0 V,[50] depending on the type of electrode, in the case of $[C_4C_1Im]PF_6$, that renders them interesting media for the investigation of oxidation–reduction processes of organometallic compounds. For example, self-focusing of intense microwave radiation at the tip of a 25 mm diameter platinum disk microelectrode immersed into $[C_4C_1Im]PF_6$ containing 1 mM ferrocene causes dramatically (two orders of magnitude) enhanced voltammetric current signals and temperatures in excess of 600 K (at the electrode surface).[51] ILs also provide interesting media for cyclic voltammetry studies for the detection of multiple organometallic reaction pathways that are not observable in organic solvents. For example, solid ferrocene derivatives and their one-electron-oxidized forms adhered to an electrode surface in contact with $[C_4C_1Im]PF_6$ revealed that the nature of the cyclic voltammetric response detected under these conditions is critically dependent on the solubility and the kinetics of dissolution and reprecipitation of the adhered solid in both the oxidized and reduced forms.[52]

1.30.2.4 The IL Effect

It is expected that due to the inherent ionic patterns of ILs, reaction paths that involve charge-separated intermediates or transition states will be accelerated—by lowering the activation barrier—in the presence of ILs compared with those performed in classical organic solvents. Indeed, this type of acceleration was observed in several catalytic reactions, such as in the biphasic hydrogenation of alkenes by the Osborn complex $[Rh(nbd)(PPh_3)_2]PF_6$ (nbd = norbornadiene) in $[C_4C_1Im]X$ (X = PF_6 and SbF_6),[15] oligomerization of ethene to higher linear olefins

Table 1 Selected physical chemical data of some 1-alkyl–3-methylimidazolium-based ionic liquids

R	*X*	T_g[a] (°C)	T_m[b] (°C)	T_d[c] (°C)	η (mPa s)[d]	d (g cm^{-3})[e]	σ (mS cm^{-1})[f]	*References*
Et	BF_4	−92	13	447	37	1.28	14	46
^{n}Pr	BF_4	−88	−17	435	103	1.24	5.9	46
^{n}Bu	BF_4	−85	None	435	180 (233)	1.21	3.5 (8.6)	35,46
^{n}Bu	PF_6	−61	10		219 (312)	1.37	1.6 (6.5)	35,47
^{n}Bu	$AlCl_4$	−88	None		(294)	1.23	(24.1)	42
^{n}Bu	CF_3SO_3		16		90	1.22	3.7	48
^{n}Bu	$N(Tf)_2$		−4	>400	69	1.43	3.9	48,49
^{n}Bu	CF_3CO_2	−30	None		73	1.21	3.2	48

[a]Glass transition temperature.
[b]Melting point.
[c]Decomposition temperature.
[d]Viscosity at 25 °C and in parentheses at 30 °C.
[e]Density at 25 °C.
[f]Conductivity at 25 °C and in parentheses at 60 °C.
Adapted from ref. 16.

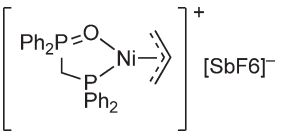

Figure 3 Cationic nickel complex.

catalyzed by a cationic nickel complex (Figure 3) in $[C_xC_1Im]PF_6$ ILs ($x = 4$, 6, 8, and 10),[53] alternating copolymerization of styrene and carbon monoxide by cationic palladium compounds in $[C_6Pyr]N(CF_3SO_3)_2$ or $[C_4C_1Im]N(CF_3SO_3)_2$,[54] and the dimerization of methylacrylate, also by cationic palladium compounds in $[C_4C_1Im]BF_4$.[55]

However, clear evidence of the IL effect was found for the regioselective arylation of olefins. It is generally accepted that the Heck reaction may proceed via two pathways, a neutral pathway leading to the preferential formation of linear olefins and an ionic counterpart more likely to give rise to branched olefins. Thus, $Pd(OAc)_2$ and 1,3-bis(diphenylphosphino)propane (DPPP) immobilized in $[C_4C_1Im]BF_4$ promote the exclusive α-arylation of several classes of electron-rich olefins with a wide range of aryl iodides and bromides in the absence of halide scavengers (Scheme 3).[56]

This exceptional regioselectivity (opposite to that observed in classical organic solvents) was attributed to the preferential cationic pathway induced by the IL (Scheme 4).

More strong evidence for the IL effect was provided in the displacement of anionic ligands by neutral molecules leading preferentially to a charge-separated species. Thus, $[C_6Pyr]N(CF_3SO_3)_2$ or $[C_4C_1Im]PF_6$ ILs promote the preferential formation of the ligand-substitution product in the reaction of 2-fluoropyridine (F–2-Py) with *trans*-$[Rh(NO_3)CO(PPh_3)_2]$, compared with the reaction performed in dichloromethane (Scheme 5).[57]

This effect was nicely put in evidence in the enantioselective hydrogenation of *N*-(1-phenylethylidene)aniline by cationic iridium complexes with chiral phosphinooxazoline ligands in ILs such as $[C_4C_1Im]BF_4$, $[C_4C_1Im]PF_6$, and $[C_2C_1Im]N(CF_3SO_2)_2$. In particular, it was demonstrated that the precursor is activated in the IL by anion exchange allowing the use of *in situ* catalysts and that the anion of the IL greatly influences the selectivity of the catalyst (Scheme 6).[58]

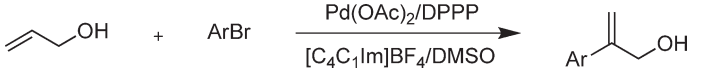

Scheme 3

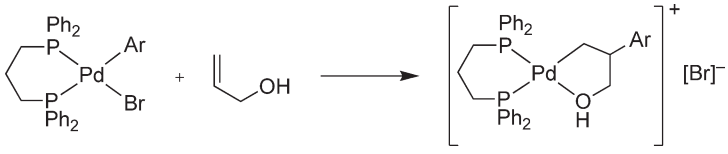

Scheme 4

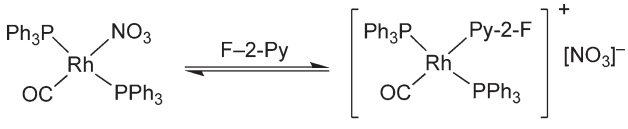

Scheme 5

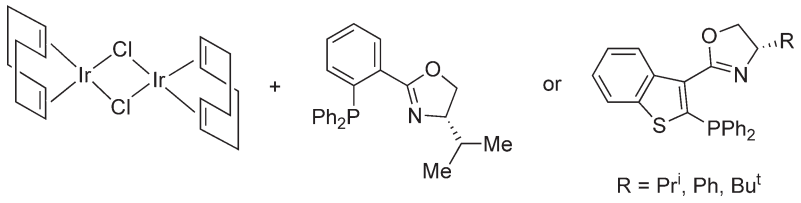

Scheme 6

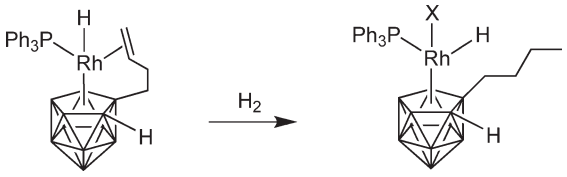

Scheme 7

This result is in sharp contrast with earlier assumptions that due to the inherently weak interactions between the chloride anion and the 1-butyl–3-methylimidazolium cation (ca. 15 kJ mol^{-1}), chloride dissociation from a transition metal complex can be thermodynamically disfavored in ILs.[59]

Interestingly, a bimolecular rate constant was observed in the solvent displacement in [Cr(η^6-C_6H_6)$(CO)_2$(solvent)].[60] The spectroscopic evidences showed the following order of Cr–solvent interaction strength: $C_6H_{12} < [C_4C_1Im]PF_6 < C_2H_4Cl_2$. It was also found that k_2 values for solvent displacement from [Cr(η^6-C_6H_6)$(CO)_2$(solvent)] by acetonitrile follow the trend: $C_6H_{12} > [C_4C_1Im]PF_6 > C_2H_4Cl_2$, and the displacement of PF_6^- by acetonitrile is up to two orders of magnitude greater than that of $C_2H_4Cl_2$. However, no displacement of $[C_4C_1Im]N(CF_3SO_3)_2$ from [Cr(η^6-C_6H_6)$(CO)_2$(solvent)] at an acetonitrile concentration of 5 mol dm^{-3} occurs. The $[C_4C_1Im]PF_6$ may be displaced more easily from a "vacant" transition metal-binding site of an organometallic complex than even a "low-polarity" solvent such as $C_2H_4Cl_2$, and, furthermore, the ease of displacement can be tuned by variation of the IL anion. These results do not correlate with ligand basicity as measured by β-values of these solvents in a simple manner.

It is well known that when H_2 is passed through a solution of $[RhCl(PPh_3)_3]$ in a classical organic solvent, oxidative addition occurs and the Rh(III) compound, $[RhCl(H)_2(PPh_3)_3]$, is formed.[61] However, the monohydride–rhodium compound *trans*-$[Rh(H)X(PPh_3)_2]$ ($X = AlCl_4^-$), formally resulting from a heterolytic H–H bond cleavage, is formed by reaction of hydrogen with *cis*-$[RhClX(PPh_3)_2]$ dissolved in $[C_4C_1Im]AlCl_4$ (0.67 molar fraction).[62] Hydrogen metathesis, which regenerates rhodium hydride species, was also observed in the hydrogenation of ketones by a rhodacarborane catalyst (Scheme 7) in $[C_4C_1Im]PF_6$, $[C_8C_1Im]BF_4$, and [C_4Pyr](*closo*-$CB_{11}H_{12}$) ILs.[63]

1.30.3 Metalloorganic Ionic Liquids

1.30.3.1 Organoaluminate ILs

Organoaluminate melts are the most investigated class of molten salts. These compounds are easily prepared by mixing quaternary ammonium salts, especially *N*-alkylpyridinium and 1,3-dialkylimidazolium halides with $AlCl_3$. *N*-ethylpyridinium halides/aluminum halides[64] were among the first ambient-temperature ILs, prepared in 1951.[65] The physical–chemical properties and the structure of these molten salts have been investigated in detail. Although these compounds are reactive toward air and water and difficult to handle, they are particularly suitable for Ziegler–Natta-type catalyst precursors, particularly the melts based on the 1,3-dialkylimidazolium cation. The combination of $[C_2C_1Im]Cl$ or $[C_4C_1Im]Cl$ with aluminum chloride produces ILs whose physical–chemical properties depend mainly upon the molar fraction of the aluminum compound.[66,67]

In particular, ILs with the liquid phase ranging down to −80 °C can be prepared with a relatively low viscosity. The Lewis acidity of these salts can be modulated by the relative amount of the aluminum compound and is usually expressed by the molar fraction (x) of the aluminum compound.[43] Conventionally, when $x = 0.5$ the mixture is called

$$[C_4C_1Im]Cl + AlCl_3 \rightleftharpoons [C_4C_1Im]AlCl_4$$
$$[C_4C_1Im]AlCl_4 + AlCl_3 \rightleftharpoons [C_4C_1Im]Al_2Cl_7$$
$$[C_4C_1Im]Al_2Cl_7 + AlCl_3 \rightleftharpoons [C_4C_1Im]Al_3Cl_{10}$$

Scheme 8

neutral, when $x > 0.5$ acidic, and when $x < 0.5$ basic. The advantage of these controlled Lewis acid molten salts is their use in Ziegler–Natta type catalytic reactions.[68] Depending on the relative proportion of $AlCl_3$, several equilibria were evidenced (Scheme 8); however, only two anions co-exist, and above 3 equiv. $AlCl_3$, the excess can be removed by sublimation.

The acidity of these organoaluminate molten salts has been investigated in detail by Osteryoung and Wilkes, and reviews on this subject are available.[69–71] However, since these melts are extremely air and water sensitive, and several organic substrates and organometallic compounds are not chemically inert in these media, their application as fluids for organometallic chemistry is limited.

1.30.3.2 Metalloorganic ILs

Metalloorganic ILs[72] that possess similar or complementary physical–chemical properties to those of organoaluminate melts without being reactive toward air, water, and organic molecules can be generated by the combination of 1-*n*-butyl–3-methylimidazolium chloride with other metal halides such as zinc, copper, iron, tin, gold, and indium chlorides, which affords air-stable room-temperature ILs that can be used as an alternative to organoaluminate melts. Interestingly, only in the case of $FeCl_3$, $ZnCl_2$, and $SnCl_2$ was the formation of polynuclear anions reported. In the case of $FeCl_3$, Raman scattering indicated the presence of $[FeCl_4]^-$ leading to the formation of $[Fe_2Cl_7]^-$ in the presence of an excess of $FeCl_3$. In opposition, only $[FeCl_4]^{2-}$-containing species were observed with $FeCl_2$. In the mixed melts containing both $FeCl_3$ and $FeCl_2$, only the mononuclear anions $[FeCl_4]^-$ and $[FeCl_4]^{2-}$ were formed (Scheme 9).[73,74]

With $SnCl_2$ and $ZnCl_2$, for a ratio of 2 : 1 relative to the cation, $[SnCl_3]^-$ and $[Sn_2Cl_5]^-$, and $[ZnCl_3]^-$, $[Zn_2Cl_5]^-$, $[Zn_3Cl_7]^-$, respectively, were identified.[75–82] The X-ray structure of $[C_1C_1Im]_2ZnBr_2Cl_2$ shows that the two imidazolium cations are paired with the tetrahalide anion.[82] The Lewis acidity of the tin-containing ILs can be easily accessed by Sn NMR[83] and the imidazolium zincates by IR.[84,85] In contrast, CuCl, $InCl_3$, $AuCl_3$, and $TeCl_4$ with imidazolium chloride formed only the monometal chloride anions, $[CuCl_2]^-$, $[InCl_4]^-$, $[AuCl_4]^-$, and $[TeCl_6]^{2-}$.[86–88]

The preparation of ILs using zinc chloride with pyridinium,[89] and quaternary ammonium salts, has also been reported.[76,77,90] Generally, ILs containing zinc chloride as the anion improved the catalytic performance, and this has been attributed at least in part to the co-catalyst behavior of the zinc chloride anion.[91]

There is only one example of an ambient-temperature IL containing an organometallic transition metal anion. This IL has been prepared by a metathesis reaction between $[C_4C_1Im]Cl$ and $Na[Co(CO)_4]$, and this IL catalyzes the debromination of 2-bromoketones.[92] Of note is the 1,3-dipentynylimidazolium bis(hexacarbonyldicobalt) tetrafluoroborate (Figure 4) salt, which melts at 100 °C.[93]

$$4\,[C_4C_1C_1Im]Cl + 2FeCl_3 + FeCl_2 \longrightarrow [C_4C_1C_1Im]_4[FeCl_4]_2[FeCl_4]$$

Scheme 9

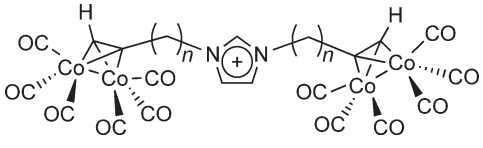

Figure 4 1,3-Dipentynylimidazolium bis(hexacarbonyldicobalt) tetrafluoroborate salt.

1.30.4 Fluorinated Ionic Liquids

ILs can act as both hydrogen bond acceptors (anions) and donors (cations), and as expected, they interact with substances with both acceptor and donor sites. In particular, 1,3-dialkylimidazolium ILs can dissolve a plethora of classical polar and non-polar compounds. All 1,3-dialkylimidazolium ILs reported to date are hygroscopic, and their miscibility with water is largely controlled by the nature of the anion. While salts containing nitrate, chloride, and perchlorate anions are usually miscible with water in all compositions, those associated with hexafluorophosphate and bis(trifluoromethane) sulfonylamidate anions are almost completely immiscible with water.[94] It is also known that an increase in the *N*-alkyl chain length increases the hydrophobicity for a series of 1-alkyl–3-methylimidazolium hexafluorophosphate ILs.[47] The miscibility of water in ILs can be increased by the addition of short-chain alcohols[95] or lowered by the addition of salts (salting-out effect).[96]

The solubility of 1,3-dialkylimidazolium hexafluorophosphate ILs decreases with an increase in molecular weight of alcohols, and is higher in secondary than in primary alcohols.[97–100] In these cases, alcohols most probably stabilize the hydrogen-donor sites, since they form hydrogen-bonded structures with both high enthalpies and constants of association. The solubility of saturated hydrocarbons is usually very low in 1,3-dialkylimidazolium ILs and increases with the augmentation of the length of the alkyl substituents at the imidazole ring, being in the order of 0.05 molar fraction for hexane and cyclohexane in $[C_4C_1Im]PF_6$ at room temperature.[101] Unsaturated hydrocarbons are, however, more soluble, and within this class of hydrocarbons, dienes are more soluble than alkenes. For example, the solubility of butadiene in $[C_4C_1Im]BF_4$ and $[C_4C_1Im]PF_6$ is 0.16 and 0.11 molar fraction, respectively, whereas this drops to 0.05 molar fraction for 1-butene in both ILs.[102] This is probably related to the relatively higher hydrogen-bond-accepting properties of the diene that can interact with the imidazolium cation,[103] compared to the monoene. Aromatic hydrocarbons are usually highly soluble in perfluorinated ILs, and can attain 0.35 molar fraction for benzene in $[C_4C_1Im]PF_6$ at room temperature. The solubility in ILs of aromatic hydrocarbons decreases with an increase of the molecular weight of the hydrocarbon, and the differences of solubilities of *o*-, *m*-, and *p*-xylenes are not significant.[104]

The solubility of various gases such as carbon dioxide, ethylene, ethane, methane, argon, oxygen, carbon monoxide, hydrogen, and nitrogen in $[C_4C_1Im]PF_6$ has been determined.[105] Carbon dioxide has the highest solubility and the strongest interactions with the IL, followed by ethylene and ethane. The solubility of carbon dioxide in $[C_4C_1Im]PF_6$ can reach 0.6 molar fraction at 8 MPa.[106] Argon and oxygen have very low solubilities and immeasurably weak interactions. Carbon monoxide, hydrogen, and nitrogen all have very low solubilities, but it was estimated that hydrogen is at least four times more soluble in $[C_4C_1Im]BF_4$ than in $[C_4C_1Im]PF_6$ at the same pressure and temperature.[107,108]

1.30.5 Task-Specific Ionic Liquids

The covalent tethering of a functional group to one or both of the ions of an otherwise ordinary IL can imbue the resulting salt with a capacity to interact with dissolved catalysts, substrates, and products in specific ways. These ILs are called task-specific ILs (TSILs), and such low melting salts are finding an increasing number of applications in synthesis, separations, catalysis, and electrochemistry.[109] In the case of organometallic catalysis, TSILs containing *N*-functionalities such as *N*-butylimidazole and nitrile attached to the imidazolium or pyridinium cation have been prepared and possess dual roles in the reaction acting as both "solvent" and ligand (Figure 5).[110–112]

1.30.6 Properties of Organometallic Compounds in Ionic Liquids

ILs are usually entirely innocent and non-coordinating solvents, but in some cases innocuous behavior is not always observed, in particular those based on the imidazolium cation.[113] Although most of the 1,3-dialkylimidazolium ILs are stable toward organic and inorganic substances, under determined reaction conditions, both the cation and anion

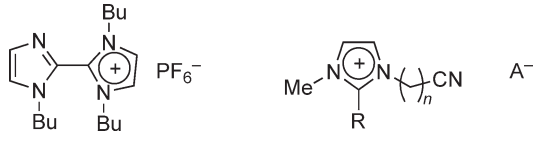

Figure 5 Examples of task-specific ILs.

can undergo "undesirable" transformations. The anions of imidazolium ILs can easily undergo hydrolysis, particularly those containing $AlCl_4^-$ and PF_6^- anions. In the case of the hexafluorophosphate anion, phosphate and HF are formed and 1,3-dialkylimidazolium phosphates and fluoride have been isolated during reactions or purification procedures.[114] The hydrolysis of the PF_6 anion may be more pronounced in reactions involving metals, which can catalyze this decomposition.[115,116] Cation metathesis was also observed with highly negatively charged complexes such as $Na_3Co(CN)_5$[117] and $Na_2[\{(UO_2)(NO_3)_2\}_2(\mu^4\text{-}C_2O_4)]$[118] dissolved in ILs with the precipitation of the respective coordination complexes associated with the imidazolium cation. Moreover, anion exchange through ion pairs plays an important role in the mechanism of metal ions transfer process.[119]

The reactivity of the imidazolium cation mainly stems from the relatively higher acidity ($pK_a = 21$–23) of the H2 hydrogen of the imidazolium nucleus, which has been found to be roughly intermediate between the acidities of acetone ($pK_a = 19.3$) and ethyl acetate ($pK_a = 25.6$).[120] In fact, it is well known that deprotonation at the C2 position of the imidazolium salt generates *N*-heterocyclic carbene ligands.[121] Not surprisingly, the formation of metal–carbene complexes has been observed in Pd-catalyzed Heck-type reactions performed in ILs (Scheme 10). In these cases, the side-reaction has a beneficial effect since the carbenes are most probably stabilizing the catalytically active species.[122] In the same line, under drastic conditions (200 °C/50 atm C_2H_4) reaction of the basic IL $[C_1C_2Im]Cl/AlCl_3$ (1.3 : 1) with $PtCl_2/PtCl_4$ led to [$PtCl_2$-*cis*-(C_2H_4)(1-ethyl–3-methyl]imidazol–2-ylidene)].[123] This clearly indicates that when employing ILs under basic conditions, there is a likelihood of carbene formation in the mixture with a detrimental or beneficial result.

Moreover, under even "less" basic conditions, the C2–H bond of the imidazolium nucleus bond can oxidatively add to electron-rich Ni(0) or Pd(0) complexes to generate stable carbene–metal–hydride compounds (Scheme 11).[124]

The 1,3-dimethylimidazolium cation also oxidatively adds to $[Pt(PPh_3)_4]$ as observed by ^{31}P NMR, although yields of the product *cis*-[PtH(1,3-dimethylimidazolin-2-ylidene)$(PPh_3)_2$]BF_4 were rather poor.[125] Interestingly, both the H2 and H5 in imidazolium salts can be activated under neutral conditions, as observed in the reaction of an imidazolium salt upon reaction with a Pd(II) derivative under base-free conditions where the carbene was formed through the activation of H5 of the imidazolium ring (Scheme 12).[126]

It is known that tetraalkylammonium salts can undergo dealkylation processes that are either thermally or chemically induced. The dealkylation of the imidazolium nucleus ("Hoffman elimination") was also observed in the catalytic hydrodimerization of butadiene by Pd(II) compounds immobilized in ILs (Scheme 13).[17]

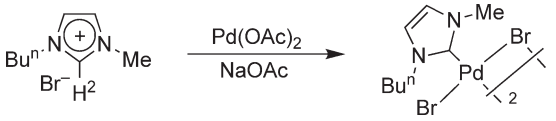

Scheme 10

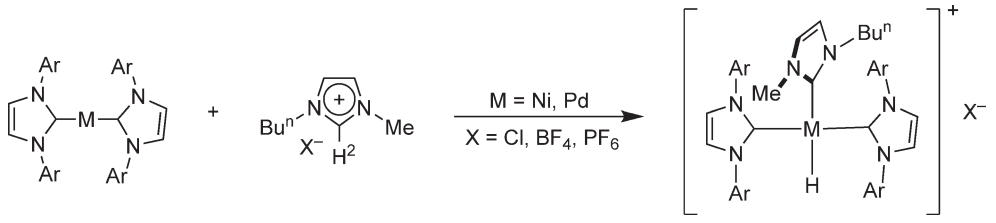

Scheme 11

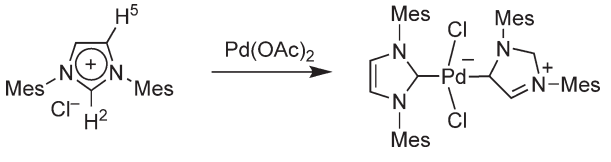

Scheme 12

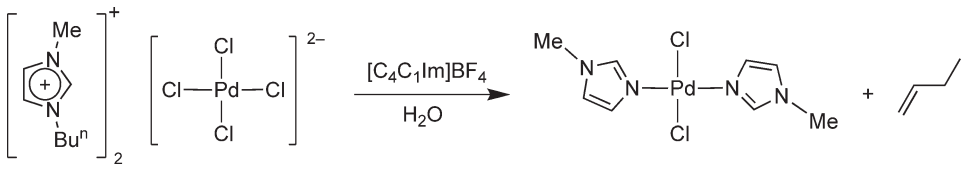

Scheme 13 Reactions of the imidazolium cation under ''neutral'' conditions.

1.30.7 Organometallic Catalysis in Ionic Liquids

1.30.7.1 Organometallic ILs as Catalysts

ILs can combine both "solvent" and catalyst properties; changing solvent leads to a faster reaction and the new fluid can be regarded as being a catalyst. Such effects have been observed in various reactions conducted in metalloorganic ILs, in particular, those performed in chloroaluminate ILs. Classical examples are the electrophilic substitutions in acidic $[C_2C_1Im]AlCl_4$[127–131] and $[C_2Pyr]BrAlCl_3$[132] ILs used in alkylation and acylation reactions of aromatic compounds with haloalkanes and the use of $[C_2C_1Im]AlCl_4$ for the alkylation of *iso*-butane.[133] In some cases, the IL induces the formation or stabilizes carbonium ions, implying that the alkylation and acylation occur, to some extent, via the dissociated carbonium ions. This was demonstrated in a moderately acidic IL; dissolution of chlorotriphenylmethane leads to the formation of the triphenylmethyl carbonium ion.[134]

A large variety of Lewis acid-promoted condensation reactions have been performed in chloroaluminate ILs. However, these reactions generate water as a principle byproduct, which reacts with the chloroaluminate anion reducing its acidity and eventually destroying the salt.[135–143]

1.30.7.2 Homogeneous/multi-phase Catalysis

Multi-phase organometallic catalysis, in particular, liquid–liquid biphasic catalysis involving two immiscible phases, may offer the possibility of circumventing the problems associated with the homogeneous process such as product separation, catalyst recycling, and the use of organic solvents. The concept of this system implies that the catalyst is soluble in only one phase whereas the substrates/products remain in the other phase. The reaction can take place in one (or both) of the phases or at the interface. In most cases, the catalyst phase can be reused and the products/substrates are simply removed from the reaction mixture by decantation.

Multi-phase catalysis performed in ILs can lead to various phase systems where the catalyst should reside in the IL. Prior to the reaction, and in cases where there are no gaseous reactants, two systems can usually be formed: a monophase, that is, the substrates are soluble in the IL; and biphasic systems where one or all the substrates reside preferentially in an organic phase. If a gas reactant is involved, biphasic and triphasic systems can be formed. At the end of the reaction, three systems can be formed: a monophasic system; a biphasic system where the residual substrates are soluble in the ionic catalytic solution and the products reside preferentially in the organic phase; and triphasic systems, formed, for example, by ionic catalytic solutions, with an organic phase containing the desired product and a third phase containing the byproducts. In most cases, catalysis performed in ILs involves two-phase systems (before and after catalysis).

Various catalytic processes can be "directly" transposed to ILs such as those based on homogeneous transition metal catalyst precursors[5–8,10,11] and colloids,[17] with significant advantages over those performed in organic solvents or in water. In particular, classical transition metal catalyst precursors are, in most cases, "soluble" in imidazolium Ils, and are not removed from the ionic solution by a great deal of organic compounds. Thus, a legion of transition metal-catalyzed reactions such as hydrogenations, oxidations, carbonylations, C–C coupling have been performed in ILs, and excellent reviews on the subject are available.[5–8,10,11] This is probably one of the great advantages of ILs in organometallic catalysis, that is, it allows the direct transposition of a well-known homogeneous process for liquid–liquid biphasic conditions without the use of specially designed ligands/complexes that are necessary for catalytic processes in aqueous, perfluorinated,[2] or supercritical fluids.[4,144] Moreover, in these IL multi-phase processes, it is possible to extract the primary products during the reaction and thus modulate the product selectivity (modifying the solubility of the different substrates and reaction products with the catalyst-containing phase). This approach can constitute a suitable method for avoiding consecutive reactions of primary products, and it has been exploited to some extent in IL catalytic process for the selective hydrogenation of dienes to monoenes[100] and benzene to

cyclohexene.[145] In cases where the catalyst is removed from the IL-containing catalytic solution by the products, catalyst leaching can be avoided by the use of modified ligands containing anionic or cationic groups such as sulfonic and quaternary ammonium and phosphonium.[146–148]

The separation of the products from the IL catalytic mixture can be performed in various cases by simple decanting and phase separation or by product distillation. In this respect, a continuous-flow process using toluene as extractant has been applied for the selective Pd-catalyzed dimerization of methyl acrylate in ILs.[149] However, in cases where the products are retained in the IL phase, extraction with $scCO_2$ can be used instead of classical liquid–liquid extraction, which necessitates the use of organic solvents that may result in cross-contamination products.

1.30.7.2.1 Hydrogenation

1.30.7.2.1.(i) Alkenes, dienes, aromatics, and polymers

The hydrogenation of simple alkenes catalyzed by classical transition metal catalysts such as $RhCl(PPh_3)_3$, $RuCl_2(PPh_3)_4$, and $NaCo(CN)_5$ can be performed in ILs in typical biphasic systems.[14,15,117] In the vast majority of cases, the classical $[C_4C_1Im]$ cation is associated with BF_4, PF_6, and $N(CF_3SO_3)_2$ anions. The hydrogenation of arenes[150] can also be performed with classical ruthenium clusters such as $[Ru_4H_4(\eta^6\text{-}C_6H_6)_4][BF_4]_2$ dissolved in $[C_4C_1Im]BF_4$.[151,152] The advantage of this biphasic system is the effective recycling and extra stabilization of the noble metal catalysts immobilized in these fluids. Recycling is very easy since alkanes are only marginally soluble in ILs and, therefore, form a two-phase system after the reaction, and the ionic phase can be recovered by simple decantation. At the same time, alkenes and arenes are sufficiently miscible with the ionic phase in order to maintain reasonable reaction rates that are usually higher than those performed with the same catalysts in aqueous-phase regimes or even in homogeneous conditions (acetone). Moreover, the IL provides an effective protective layer around the metal center toward oxidation, since the solubility of oxygen in these fluids is very low. For example, the addition of water enhanced catalytic activities significantly—probably due to the creation of a well-mixed "emulsion-like" system—in the hydrogenation of methyl–2-acetamidoacrylate with $[Rh(COD)(EtDuPhos)]CF_3SO_3$ (COD = 1,5-cyclooctadiene) and the C=C bond of 2-cyclohexen-1-one with Wilkinson's catalyst in $[C_4C_1Im]PF_6$. In these cases, the complexes were easily recycled, and $[Rh(COD)(EtDuPhos)]CF_3SO_3$ was even no longer air sensitive.[153]

$[RuCl_2(TPPMS)_3(DMSO)]$ is very soluble in $[C_4C_1Im]PF_6$, and catalyzes 1-hexene hydrogenation (500 psi H_2 and 100 °C) in a two-phase system, with 80% conversion in 24 h, with little substrate isomerization.[154]

Imidazolium salts with a nitrile functional group attached to the alkyl side chain, such as $[C_3CNC_1Im]BF_4$ (where C_3CNC_1Im is the 1-propylnitrile–3-methylimidazolium cation) and $[C_3CNC_1C_1Im]BF_4$ (where $C_3CNC_1C_1Im$ is the 1-propylnitrile–2,3-dimethylimidazolium cation), act as both solvent and ligand for the palladium-catalyzed hydrogenation of cyclohexadiene to cyclohexene.[155]

The hydrogenation of styrene by the anionic $[Ru_6C(CO)_{16}]^{2-}$ cluster, when immobilized in $[C_4C_1Im]BF_4$, is up to 3.6-fold faster than that observed in organic solvents such as methanol and octane. High-pressure NMR studies indicated that the improvement in activity is due to the increased stability of the anionic cluster species in the IL.[156]

ILs also provide effective media for the selective hydrogenation of dienes to monoenes and alkynes to alkenes. This selectivity is mainly due to the lower solubility of the alkene primary hydrogenation product compared to the diene substrate.[102,157,158] $[Rh(\eta^4\text{-}C_7H_8)(PPh_3)_2][BF_4]$ dissolved in $[C_8C_1Im]BF_4$ is a selective catalytic system for the hydrogenation of 2-butyne–1,4-diol dissolved in water.[159] Other examples involve the selective hydrogenation of aromatic rings attached to C=C[107] or C=O bonds.[160]

The hydrogenation of polymers such as NBR (acrylonitrile-butadiene rubber), SBR (styrene-butadiene rubber), and PBD (polybutadiene) has been also performed by Ru(II) compounds associated with phosphine ligands immobilized in classical imidazolium ILs or polyether-modified ammonium salts.[23,161–164]

There has been no study published to date that reveals why the ILs often lead to an improvement in the hydrogenation reaction rates. However, in one report, the identity of the species involved in the catalytic cycle of a hydrogenation reaction was investigated. A similar selectivity was observed for the hydrogenation of alkynes by $[Ir(H)_2(NCCH_3)_3(P\text{-}i\text{-}Pr_3)]BF_4$ using organic/IL biphasic conditions with toluene/$[C_4C_1Im]BF_4$, suggesting reaction mechanisms similar to those operating in organic solvents under homogeneous conditions. Moreover, the same alkenyl hydride intermediates were observed in the reactions performed in $CDCl_3$ or in $[C_4C_1Im]BF_4$.[165]

Supported liquid-phase catalysis[166] that combines the advantages of an IL phase with heterogeneous support materials has also been been employed in the Rh-catalyzed hydrogenation of olefins. Supported IL catalysis involves dissolving a homogeneous catalyst, an Rh(I) compound in this case, in a multiple layer of an IL, which is confined on the surface of a solid support (Figure 6). Although the resulting material is a solid, the active species is dissolved in

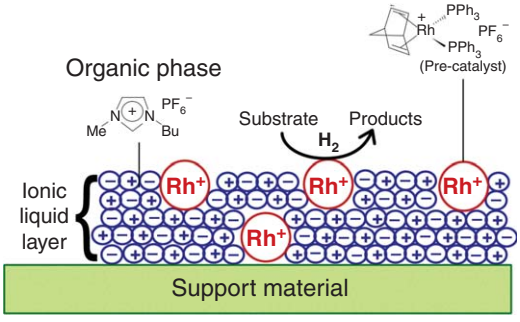

Figure 6 Schematic representation of supported liquid-phase catalysis involving ILs. Adapted from ref. 167.

the IL and performs like a homogeneous catalyst. The advantages of using the supported IL system are that it requires significantly reduced amounts of the ionic media, which is desirable from an economic and toxicological point of view.[167]

1.30.7.2.1.(ii) Asymmetric hydrogenation

The compatibility of some ILs with water has allowed the development of a highly efficient multi-phase system for the Rh-catalyzed hydrogenation of enamides (turnover numbers of >10,000). In many cases, such IL/water combinations are superior to conventional organic solvents and biphasic ILs/organic co-solvents media with respect to catalytic performance as well as to catalyst separation and recycling. The best results were obtained with Rh–ferrocenyl–diphosphine catalysts (>99% ee) in $[C_8C_1Im]BF_4$/water.[168]

The asymmetric hydrogenation of functionalized substrates such as enamides, aryl acrylic, and tiglic acids has also been successfully performed using [Rh(COD){(−)-DIOP}][PF_6] in $[C_xC_yIm]PF_6$[15] and [Rh(COD)-(RDuPhos)][CF_3SO_3] (R = Me, Et) in $[C_xC_yIm]$,[108] [$RuCl_2$–(*S*)-BINAP]$_2$·NEt_3, [Ru{(*R*)-Tol–BINAP}$(CH_3CO_2)_2$] in $[C_xC_yIm]$[169] supported in ILs. The hydrogenation products that are soluble in the ILs can be extracted with $scCO_2$.[170–172] Interestingly, the enantioselectivity is hydrogen-pressure dependent, or more precisely dependent on the hydrogen concentration in the IL phase as observed in the organic solvents.[107,108] However, in these cases, catalyst leaching into the product phase is quite a common process, and this has been overcome by using functionalized ligands containing ionic groups such as phosphonic anions or imidazolium cations, or using a transition metal complex with other ionic ligands, to improve the fixation of the catalyst in the IL phase. For example, the Rh-complex of a 1,4-bisphosphine bearing two imidazolium salt moieties (Figure 7) immobilized in $[C_4C_1Im]SbF_6$ has been used and reused several times for the hydrogenation of an enamide without significant loss of catalytic efficiency.[173]

A series of Ru(II) compounds associated with modified BINAP ligands (Scheme 14) dissolved in $[C_8C_1Im]BF_4$/methanol have been used as recyclable biphasic catalytic systems for the asymmetric hydrogenation of β-aryl ketoesters.[174]

The rhodacarborane complex (Scheme 15) in [C_4Pyr](*closo*-$CB_{11}H_{12}$) IL is an efficient catalytic system for the asymmetric hydrogenation of unsymmetrical aryl ketones. The extraordinary performance of this catalyst system is probably related to the stabilization of ionic organometallic species induced by the IL.[175]

Cationic iridium complexes with chiral phosphinooxazoline ligands in ILs such as $[C_4C_1Im]BF_4$ catalyze the biphasic enantioselective hydrogenation of *N*-(1-phenylethylidene)aniline. The products were readily isolated from

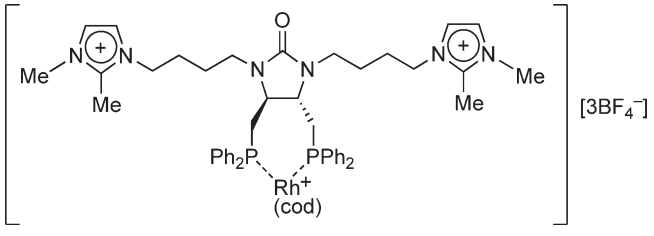

Figure 7 Imidazolium-modified 1,4-bisphosphine.

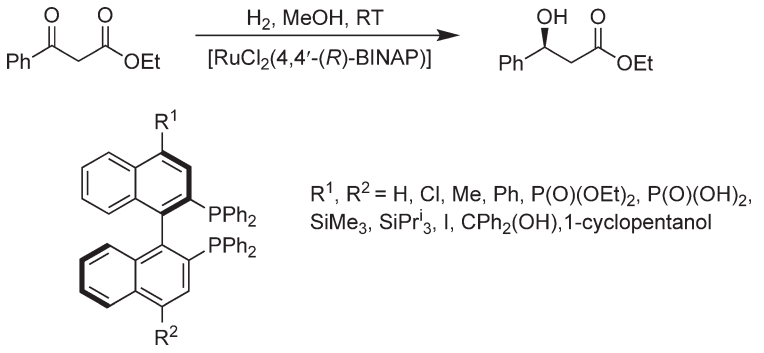

Scheme 14

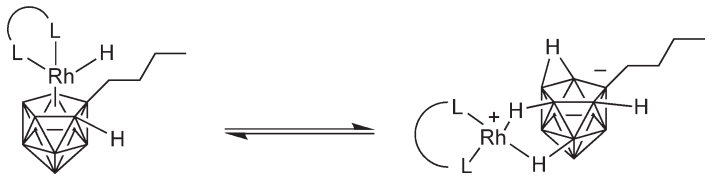

Scheme 15

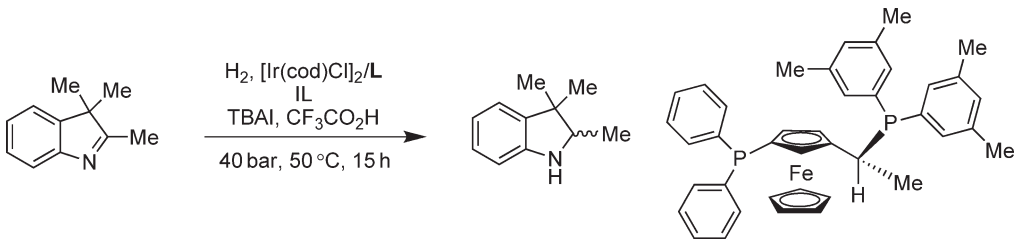

Scheme 16

the catalyst solution by CO_2 extraction without cross-contamination of the IL or catalyst, and the presence of CO_2 can be beneficial or even mandatory for efficient hydrogenation in the IL.[58] A similar system is used in the enantioselective hydrogenation of imines.[176] More interestingly, the enantioselective hydrogenation of imines can be carried out with Ir(I) compounds in $[C_{10}C_1Im]BF_4$ or in $[C_{10}$–4-$C_1Pyr]N(CF_3SO_2)_2$ ILs (Scheme 16).[177]

Ruthenium complexes associated with bis-ammonium-substituted BINAP ligands catalyze the asymmetric hydrogenation of ethylacetoacetate in imidazolium, pyridinium, and phosphonium room-temperature ILs.[178,179]

1.30.7.2.1.(iii) Hydrogen-transfer reductions

A benzene imidazolium-tagged ruthenium complex immobilized in $[C_4C_1C_1Im]PF_6$ is a highly enantioselective IL biphasic transfer hydrogenation catalyst (isopropanol/KOH) of acetophenone as compared with conventional (untagged) complexes (Figure 8).[180] Along the same lines, a diimide–imidazolium salt moiety associated with $[RuCl_2(C_6H_6)]_2$ is an efficient, recyclable catalyst for the asymmetric transfer hydrogenation of acetophenone derivatives with a formic acid–triethylamine azeotropic mixture in $[C_4C_1Im]PF_6$ (Figure 8).[181]

Polar bis(phosphonic acid)-derived Ru pre-catalysts (Figure 9) immobilized in room-temperature ILs were also successful for asymmetric transfer hydrogenation of ketones with ee values of up to 98%. Excellent catalytic performance and catalyst recycle were observed with 2-methyl–imidazolium-based ILs such as $[C_4C_1$–4-$C_1Im]BF_4$.[182]

These polar phosphonic acid-derived Ru–BINAP systems were also used to catalyze the asymmetric hydrogenation of β-keto esters in ILs with complete conversions and ee values higher than those obtained from homogeneous

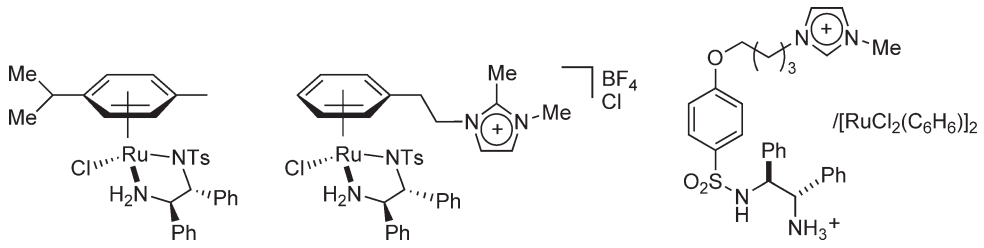

Figure 8 Ruthenium(II) complexes employed in hydrogen-transfer reductions.

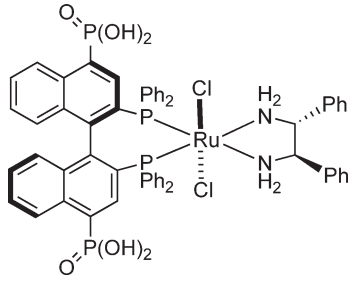

Figure 9 Polar bis(phosphonic acid)-derived Ru pre-catalyst.

reactions in MeOH (up to 99.3%).[183] Rhodium-catalyzed transfer hydrogenation reactions have also been performed in tetraalkyl/aryl phosphonium tosylates that are liquid at the reaction temperature and solid at room temperature, thereby facilitating catalyst recovery.[184]

1.30.7.2.2 Carbonylation

Carbonylation reactions have been extensively studied in ILs, in particular, the hydroformylation of higher alkenes. The intense academic and industrial interest is mainly due to the limitations of the current aqueous phase process to short-chain (≤5C) alkenes, due to the very low solubility of heavier olefins in water for an effective and reasonable reaction rate to occur. Note that 1-octene possesses a much higher solubility in $[C_xC_yIm]PF_6$ (~2 w/w%) than in water under the same conditions.

1.30.7.2.2.(i) Hydroformylation of alkenes

Classical Rh catalyst precursors immobilized in various ILs—in particular imidazolium—have been extensively investigated in the hydroformylation of 1-hexene, 1-octene, and other heavier alkenes. The observed reaction rates are quite superior to those performed in aqueous-phase regimes, and the selectivities are similar to those obtained in homogeneous conditions.

There are also some reports on the use of Pt, Co, and Ru complexes immobilized in ILs for the hydroformylation of olefins. The platinum-catalyzed hydroformylation of ethylene in a tetraethylammoniumchlorostannate molten salt was described as early as 1972. The relatively high melting point of the chlorostannate salt (m.p. 78 °C) causes some experimental problems for reaction parameters and processing conditions, since a syngas pressure of 400 bar should be used.[185] However, the complex $[PtCl_2(PPh_3)_2]$ dissolved in a slightly acidic chlorostannate IL—prepared by mixing different amounts of $SnCl_2$ with $[C_4C_1Im]Cl$ or $[C_4$–4-MePyr]Cl—is an active catalyst for the regioselective hydroformylation of methyl—3-pentenoate and 1-octene.[83,186]

The hydroformylation of olefins by Ru catalyst precursors (RuO_2 hydrate, $Ru(acac)_2$, $Ru_3(CO)_{12}$ cluster) dispersed in tetrabutylphosphonium bromide (m.p. 100–103 °C) was one of the first organometallic reactions to be performed in ILs. Spectroscopic investigation of these process indicated that the major species in solution is the $[H(Ru_3(CO)_{11}]^-$ polynuclear anion.[187,188] The modification of the catalytic system by combination of bidentate ligands such as 2,2′-bipyridine and 1,2-bis(diphenylphosphino)ethane allows the regioselective hydroformylation of internal olefins to yield linear alcohols and aldehydes with selectivities greater than 99%. The mechanism suggested for this process is similar to the proposed for homogeneous conditions.[189]

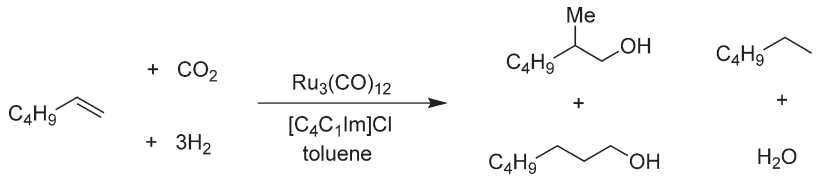

Scheme 17

The biphasic hydroformylation of 1-hexene with carbon dioxide (4 MPa)/hydrogen (4 MPa) can also be catalyzed by $Ru_3(CO)_{12}$ in ILs/toluene giving high yields and good chemoselectivity in heptanols with relatively low amounts of hexane (11%) (Scheme 17).[190]

There is a single report on the use of $Co_2(CO)_8$ immobilized in $[C_4C_1Im]N(CF_3SO_2)_2$ as a catalyst for the hydroformylation of 1-hexene.[191]

The first application of room-temperature ILs in Rh-catalyzed hydroformylation was reported by Chauvin. In this case, the biphasic hydroformylation of 1-pentene was performed with $[Rh(CO)_2acac]$ associated with phosphines and sulfonated phosphines in $[C_4C_1Im]PF_6$.[15] The biphasic hydroformylation of 1-octene was also performed using an Rh(I) complex associated with 1,1′-bis(diphenylphosphino)–cobaltocenium hexafluorophosphate, and 1,1′-bis[1-methyl(1-diphenylphosphino)ethyl]cobaltocenium hexafluorophosphate ligands immobilized in $[C_4C_1Im]PF_6$.[147] The same reaction using $[Rh_2(OAc)_4]/PPh_3$ as catalyst precursors can be performed in high-melting phosphonium tosylate salts, such as *n*-butyltriphenylphosphonium tosylate (m.p. 116–117 °C).[192] Polyether attached to ammonium melts can also be used as a polar phase for the biphasic hydroformylation of 1-tetradecene catalyzed by classical Rh complex catalyst in a two-phase medium.[193]

The hydroformylation of methyl–3-pentenoate by $[Rh(acac)(CO)_2]$ associated with PPh_3 and 2,2′-bis(((2,2′-bis(4-methoxy–6-*tert*-butyl)phenoxy)phosphino)–oxy)–1,1′-binaphthyl in $[C_4C_1Im]PF_6$ is a homogenous process, and catalyst recycling was achieved by reactive distillation where the IL acts as stabilizer.[194]

Detailed *in situ* spectroscopic investigations on the rhodium sulfoxantphos-catalyzed hydroformylation of 1-octene in $[C_4C_1Im]PF_6$ showed that the $[RhH(CO)_2(diphosphine)]$ catalytic species, observed in organic solvents, are formed in the IL with similar ee (bis-equatorial) and ea (equatorial-apical ratio). The ratio of the ee and ea isomers is influenced by both the temperature and syngas pressure. An increase in hydrogen partial pressure has no effect on the activity of the system during the reaction performed in $[C_4C_1Im]PF_6$, while some hydroformylation systems using xanthene backbone ligands in conventional organic solvents can be sensitive to hydrogen partial pressure.[195]

A high-pressure NMR study revealed that the solution structure of $[RhH(^{13}CO)(TPPTS)_3]$ (TPPTS = triphenylphosphine trisulfonate) in $[C_4C_1Im]BF_4$ is similar to that of $[RhH(^{13}CO)(PPh_3)_3]$ in toluene-d_8 at elevated syngas pressures.[196]

It has also been shown from high-pressure ^{13}C NMR spectroscopy that the rate of the hydroformylation of 5-hexen-2-one does not correlate with the CO solubility in ILs, as expected from the detailed relative solubility of CO compared to H_2.[197]

In the cases where the catalyst is removed from the IL catalytic solution by the products, catalyst leaching can be avoided by the use of modified ligands containing anionic or cationic groups such as sulfonic, quaternary ammonium, and phosphonium (Figure 10).

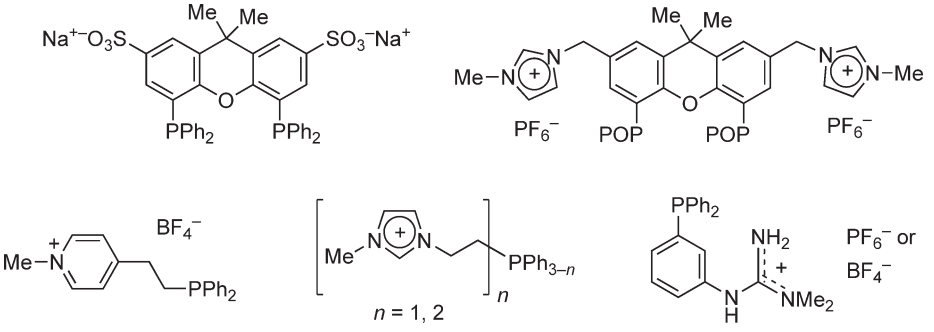

Figure 10 Examples of functionalized *P*-ligands employed in hydroformylation reactions.

For example, a highly active and regioselective catalyst for the hydroformylation of 1-hexene and 1-octene in ILs was obtained from the combination of the dicationic 2,7-di[5-(3-methylimidazolium)pentyl]–9,9-dimethyl–4,5-di(2,8-dimethyl–10-phenoxaphosphino)xanthene hexafluorophosphate and $[Rh(CO)_2(acac)]$. No catalyst leaching or losses in catalytic performance were observed during 1-octene hydroformylation recycle experiments in $[C_4C_1Im]PF_6$. At low catalyst loadings, the activity and regioselectivity were competitive with a one-phase catalysis in conventional solvents.[148,198]

Guanidinium-modified diphosphine ligands modified with a xanthene backbone or quaternized imidazolium-substituted phosphines with associated $[Rh(acac)(CO)_2]$ show high overall catalytic activity and high regioselectivity in the biphasic hydroformylation of oct-1-ene using hexafluorophosphate imidazolium ILs.[199,200] Similarly, a wide range of ILs based on imidazolium and pyrrolidinium cations and weakly coordinating anions are efficient liquid supports for the biphasic rhodium-catalyzed hydroformylation of 1-hexene; the reaction rate and regioselectivity, and the retention of the rhodium, can be modulated by fitting the nature of the anions and cations of the IL and the modified phosphite or phosphine ligands.[146]

The hydroformylation of 1-hexene was also performed using a combination of $[Rh(acac)(CO)_2]$ with specially designed diphenyl–2-*N*-methylpyridinium bis(trifluoromethanesulfonyl)amide ligand immobilized in triquaternary imidazolium or monoquaternary imidazolium salts (Figure 11).[201]

Moreover, an MCM-41 mesoporous silicas-supported water-sol TPPTS–Rh complex in the IL can also be used for the catalyst recycling without reducing the activity and selectivity in the hydroformylation of 1-hexene.[202]

The treatment of an IL covalently bound to a silica surface (Figure 12) with a classical imidazolium IL ($[C_4C_1Im]PF_6$ and $[C_4C_1Im]BF_4$) results in the formation of a multiple layer of free IL on the support. Rhodium complexes such as $[RhH(CO)(TPPTS)_3]$ immobilized in these systems generate a robust and recyclable catalytic system for the hydroformylation of 1-hexene.[203]

However, in various cases, the hydroformylation products are retained in the IL phase, and extraction with $scCO_2$ can be used instead of classical liquid–liquid extraction, which necessitates the use of organic solvents that may result in cross-contamination products.[204] This process was successfully used in catalyst recycling and product separation for the hydroformylation of 1-hexene, 1-dodecene, and other olefins catalyzed by $[Rh_2(OAc)_4]/[C_4C_1Im][Ph_2PC_6H_4–3-SO_3]$ employing a continuous-flow process in $scCO_2$–imidazolium ILs, such as $[C_4C_1Im]PF_6$, $[C_{10}C_1Im]N(SO_2CF_3)_2$ mixtures.[205–207] This system also reduces the mass-transfer constraints, because the $scCO_2$ usually increases the alkene solubility in the IL phase and reduces the ionic fluid viscosity. The fixed-bed reactor system was also used for the continuous-flow gas-phase hydroformylation of propene and 1-octene by $[Rh(acac)(CO)_2]$(sulfoxantphos)] in $[C_4C_1Im]n–C_8H_{17}OSO_3$ phase on a silica gel support.[208,209]

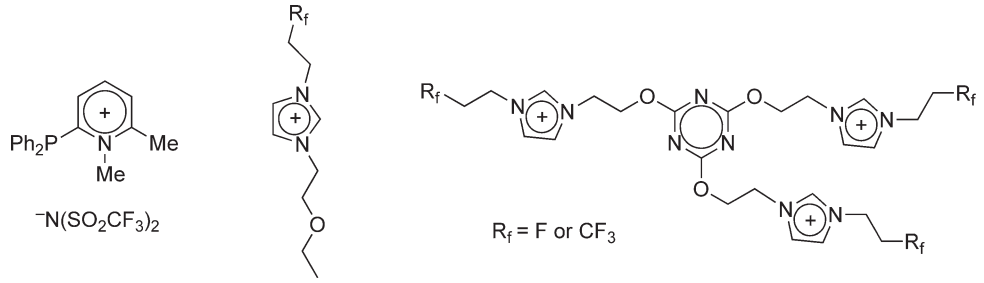

Figure 11 Diphenyl–2-*N*-methylpyridinium bis(trifluoromethanesulfonyl)amide ligand and monoquaternary and triquaternary imidazolium salts.

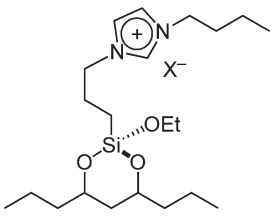

Figure 12 Imidazolium covalently bounded to a silica surface.

1.30.7.2.2.(ii) Alkoxy–hydro and amino carbonylation

$PdCl_2(PhCN)_2$ associated with phosphines such as (+)-neomenthyldiphenylphosphine (NMDPP) and *p*-toluenesulfonic acid (TsOH) dissolved in $[C_4C_1Im]BF_4$ catalyzes the hydroesterification of styrene derivatives to produce 2-arylpropionic esters in very good yields and regioselectivities (Scheme 18). The simple separation of the products and the use of lower CO pressures are the major advantages of the use of ILs in the hydroesterification of styrene derivatives as compared with the reactions performed under homogeneous conditions.[210]

The carbonylation of aryl halides was performed with [diiodobis(3-methyl–2(3H)-benzothiazolylidene)palladium] immobilized in tetrabutylammonium bromide (melt), $[C_4C_1Im]BF_4$, $[C_4C_1Im]Cl$, $[C_4C_1Im]Br$, and tricaprylmethylammonium chloride (aliquat).[211] Palladium acetate associated with phosphines immobilized in $[C_4C_1Im][PF_6]$ or $[C_4C_1Im]BF_4$ catalyze hydroxycarbonylation of aryl halides and benzyl chloride derivatives (Scheme 19), and the acids are separated by extraction with water.[212]

The same catalytic system in the presence of alcohols or diethylamine generates esters and amides and, depending on the reaction conditions, α-keto esters or α-keto amides (Scheme 20).[213]

Carbamates and ureas are easily prepared and separated from the oxidative carbonylation of amines catalyzed by $[PdCl_2(phenanthroline)]$ dissolved in $[C_4C_1Im]BF_4$.[214] The carbonylation of terminal 3-alkyn-1-ols and 1-alkyn-4-ols by palladium acetate/2-(diphenylphosphino)pyridine dissolved in $[C_4C_1Im]PF_6$ or $[C_4C_1Im]BF_4$ affords quantitatively and selectively *exo*-α-methylene (Scheme 21) and γ- and δ-lactones, respectively.[215]

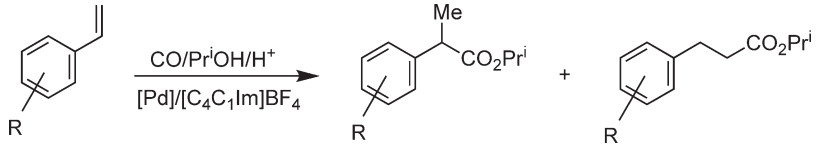

Scheme 18

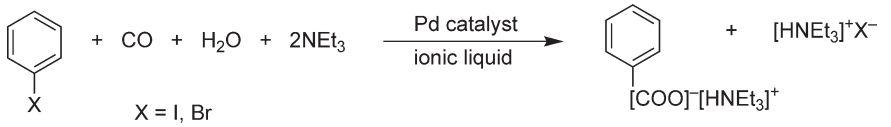

Scheme 19

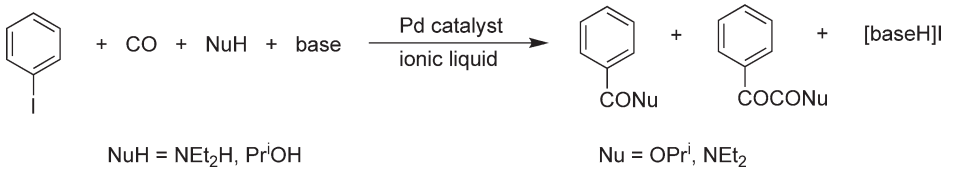

Scheme 20

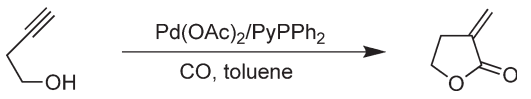

Scheme 21

1.30.7.2.3 Oxidation

Classical molten salts have been used as media and catalysts for oxidation reactions since the 1950s.[216] It has been reported that the *bis*(acetylacetonate)nickel(II)/tetra-*n*-butylammonium tetrafluoroborate salt system can be used in the liquid-phase oxidation of ethylbenzene in air yielding ethylbenzene hydroperoxide at atmospheric pressure.[217] The oxidation of cycloalkanes has been achieved by electron-deficient Mn(II) porphyrin in $[C_4C_1Im]PF_6$ in the presence of $PhI(OAc)_2$ as the oxidant (Scheme 22).[218,219]

Low-melting imidazolium and pyrimidinium ILs are stable toward strong chemical oxidizing agents, such as fuming sulfuric acid, and have a large stable electrochemical window (up to 7 V)[50,220] and are, therefore, suitable media for oxidation reactions.

1.30.7.2.3.(i) Oxidation of alcohols, thiols, and alkenes

Various aromatic aldehydes can be oxidized to the corresponding carboxylic acids using, for example, bis(acetylacetonate)nickel(II) in $[C_4C_1Im]PF_6$ and dioxygen at atmospheric pressure as the oxidant,[221] benzylic and aliphatic alcohols by tetrapropylammonium perruthenate,[222] $[RuCl_2(PPh_3)_2]$ and $RuCl_3{\cdot}xH_2O$ in conjunction with either *N*-methylmorpholine *N*-oxide or oxygen as oxidants dissolved in substituted imidazolium or other ammonium salts,[223] benzylic alcohols by Pd in imidazolium ILs,[224] benzylic and secondary alcohols with hydrogen peroxide catalyzed by 1-methyl–3-butylimidazolium decatungstate in $[C_4C_1Im]BF_4$[225] or $[C_4C_1Im]_3[(W(O)(O_2)_2)_4PO_4]$ in $[C_4C_1Im]BF_4$,[226] and various alcohols by CuCl associated with modified 2,2′-bipyridine in $[C_4C_1Im]PF_6$ (Scheme 23).[227]

Water-soluble iron(III) porphyrins and phosphotungstic acid in $[C_4C_1Im]BF_4$ are effective catalysts for the H_2O_2-mediated oxidation of the C═NOH bond in *N*-hydroxyarginine and other oximes (Scheme 24).[228]

The oxidation of alkenes by palladium complexes (Wacker reaction) has also been successfully performed in ILs such as the hydrogen peroxide oxidation of styrene to acetophenone by $PdCl_2$ in $[C_4C_1Im]PF_6$ or $[C_4C_1Im]BF_4$ (Scheme 25).[229]

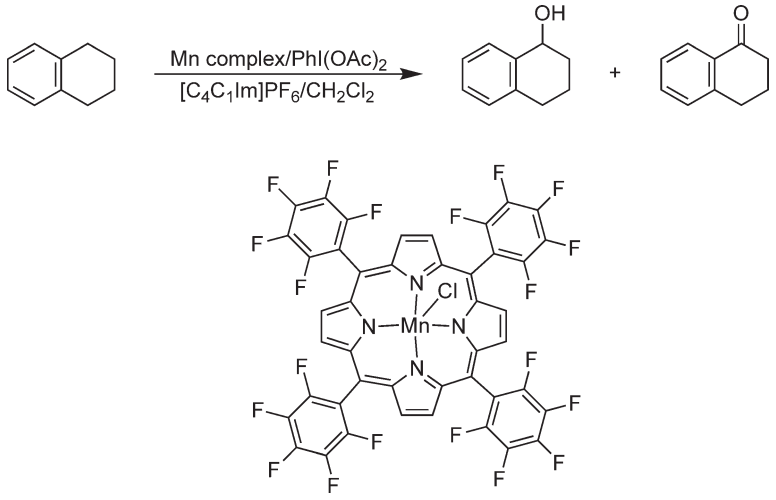

Scheme 22

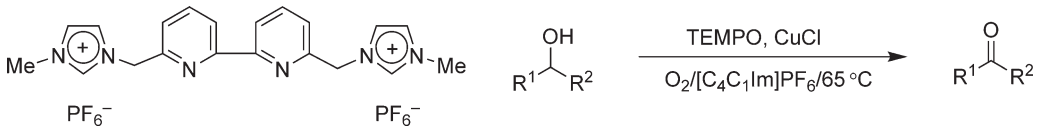

Scheme 23

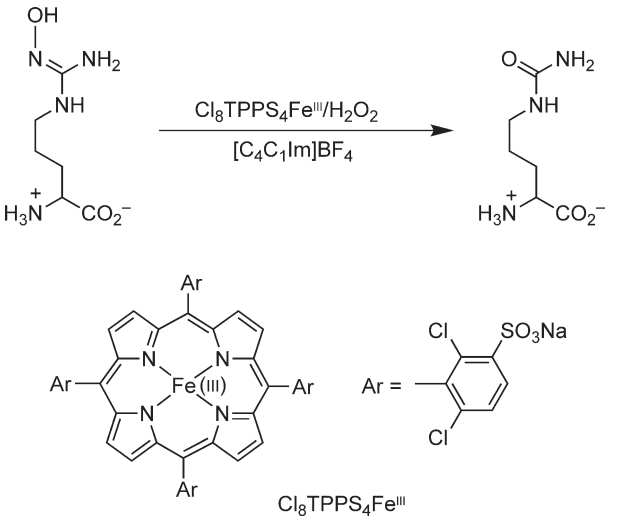

Scheme 24

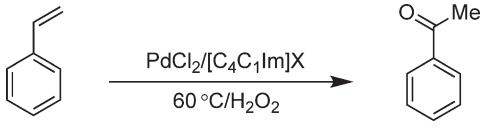

Scheme 25

The oxidation of thiols to disulfides with molecular oxygen has been achieved by Co(II)–phthalocyanine complexes in $[C_4C_1Im]BF_4$.[230] Hydrogen peroxide/methyltrioxorhenium in $[C_4C_1Im]PF_6$ or $[C_4C_1Im]BF_4$ promotes the oxidation of hydroxylated and methoxylated benzaldehydes and acetophenones to the corresponding phenols (Scheme 26)[231] or the Baeyer–Villiger reaction.[232]

The $[C_4C_1Im]Cl$ and $CuCl_2$ mixture catalyzes the selective oxidation of 2,3,6-trimethylphenol to trimethyl–1,4-benzoquinone (Scheme 27), which is an important precursor to vitamin E.[233]

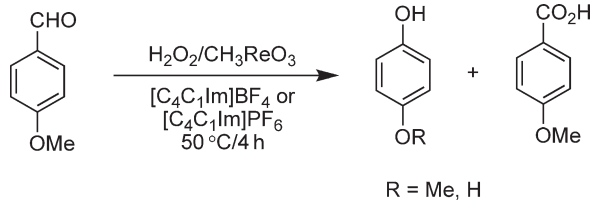

Scheme 26

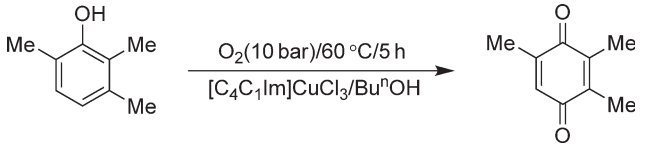

Scheme 27

1.30.7.2.3.(ii) Epoxidation and dihydroxylation of alkenes

Alkenes and allylic alcohols can be epoxidized using various transition metal complexes immobilized in ILs using different oxidants. In general, the conversion falls with decreasing alkene solubility in the IL, and the epoxidation reaction rates are comparable to those obtained in classical solvents. Moreover, these transition metal compounds immobilized in ILs constitute one of the most efficient and recyclable catalytic systems for the epoxidation of alkenes. Alkenes and allylic alcohols are epoxidized by methyltrioxorhenium (MTO) in $[C_2C_1Im]BF_4$ and urea hydrogen peroxide as the oxidizing agent,[234,235] by iron(III) porphyrins in $[C_4C_1Im]Br$ employing hydrogen peroxide as oxidizing agent,[236] Mn(II)–porphyrin (Figure 13) in $[C_4C_1Im]PF_6/CH_2Cl_2$ using $PhI(OAc)_2$ as oxidant,[237,238] dioxomolybdenum(VI) or $[Mo(\eta^5\text{-}C_5R_5)X(CO)_3]$ (X = Me, Cl; R = H, Me) complexes in $[C_4C_1Im]N(CF_3SO_2)_2$ and $[C_4C_1Im]PF_6$, or mixtures of these ILs using *tert*-butyl hydroperoxide as the monooxygen source[239,240]

The epoxidation of lipophilic alkenes can be accomplished by a simple manganese sulfate/bicarbonate catalytic system in $[C_4C_1Im]BF_4$ with hydrogen peroxide as the oxidant (Scheme 28).[241]

The asymmetric epoxidation of alkenes has been performed by the Jacobsen's (Mn(III)–salen chloride) catalyst in $[C_4C_1Im]PF_6$ using aqueous NaOCl as the oxidizing agent and CH_2Cl_2 as the co-solvent[242] or in pure $[C_4C_1Im]PF_6$ using molecular oxygen electroactivated[243]and by the Katsuki Mn(III)–salen catalyst in $[C_4C_1Im]PF_6$ or $[C_4C_1Im]BF_4$ using aqueous NaOCl as the oxidant.[244]

The classical and asymmetric catalytic dihydroxylation of alkenes by osmium compounds (Scheme 29) can be efficiently carried out in ILs such as $[C_4C_1Im]PF_6$ and tetraalkyldimethylguanidinium salts.[245–248] The leaching of osmium to the organic phase can be avoided using $scCO_2$ as the product extractant.[249]

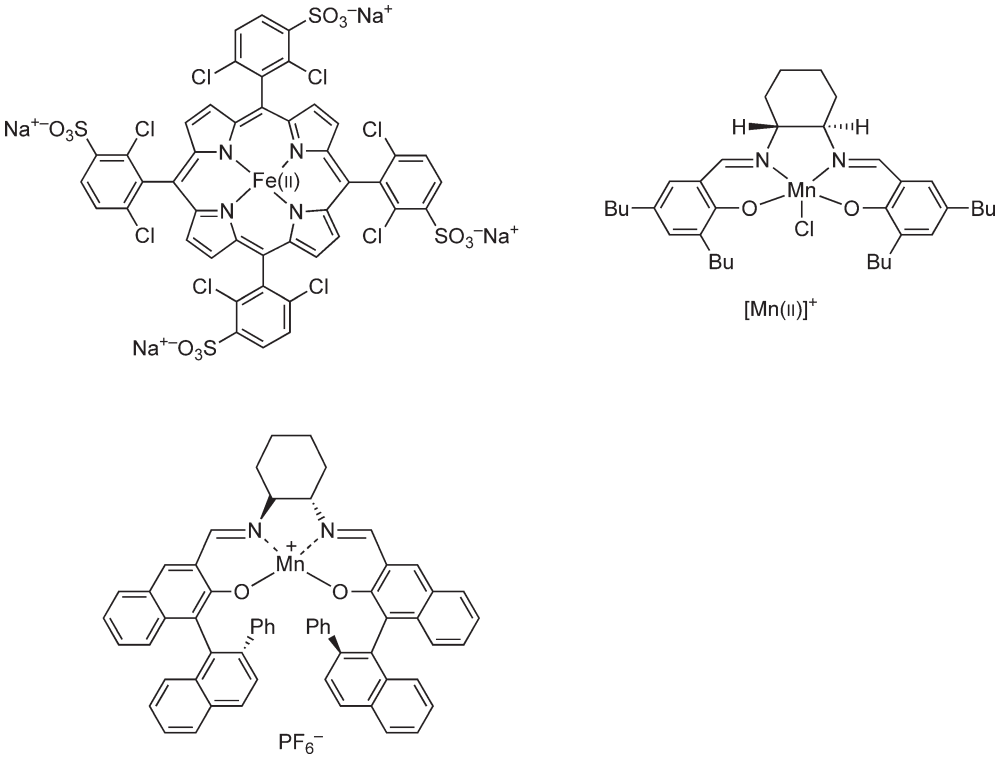

Figure 13 Fe(II) and Mn(II) porphyrins.

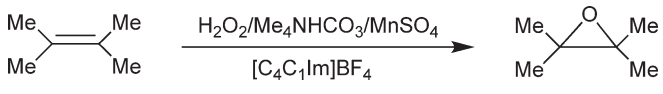

Scheme 28

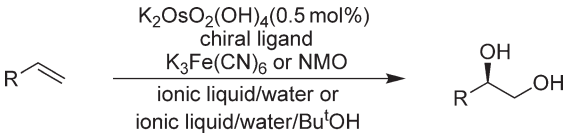

Scheme 29

1.30.7.2.4 Oligomerization and polymerization

1.30.7.2.4.(i) Oligomerization

Linear 1-olefins are oligomerized to dimers, trimers, and tetramers by the Lewis-acidic $[C_4C_1Im]AlCl_4$ (excess of 0.1 mol. equiv. $AlCl_3$) IL, without the presence of transition metal catalyst precursor.[250] Notwithstanding, classical nickel complexes such as [η^3-allylnickel bromide] are soluble in organoaluminate ILs, whereas alkenes possess only limited solubility. These properties have been used to develop a two-phase propene catalytic dimerization process.[13,68,251] The catalytic system was prepared by dissolution of the nickel catalyst precursor in the molten salt composed of $[C_4C_1Im]AlCl_4$ with different acidities, which were controlled by the addition of $AlEtCl_2$. The addition of ethylaluminum dichloride is essential to avoid cationic side-reactions since $AlEtCl_2$ acts as a proton scavenger in these media. In contrast to what was observed in the acidic melts, the catalytic system is not active in basic melts. This behavior is attributed to the displacement of most of the ligands on nickel by the chloride anions present in the medium, forming $[NiCl_4]^{2-}$ and $[NiCl_3L]^-$ anionic species (detected by UV spectroscopy), without alkylation of the nickel center.

The selectivity in 2,3-dimethylbutene, under homogeneous conditions, is well known to increase with the increasing steric hindrance of the ligands, and this was also the case in the two-phase reactions. This result demonstrates the effectiveness of the phosphine effect in ILs. In fact, there is no displacement of trialkyl phosphine coordinated to the nickel center by the anionic species present in the molten salt.

$[Ni(MeCN)_6][BF_4]_2$ dissolved in the $[C_4C_1Im]AlCl_4/AlEtCl_2$ IL (0.54 Al molar fraction) buffered with aromatic co-solvents catalyzes the selective dimerization of ethene to butenes,[252] and associated with 1 equiv. of PCy_3CS_2 promotes the oligomerization of butenes under mild reaction conditions.[253,254] The activities observed in the biphasic system are higher than those usually obtained using homogeneous catalytic systems.[253]

Linear 1-butene dimers can be selectively obtained from an [Ni(COD)(hfacac)] catalyst precursor (Figure 14) immobilized in $[C_4\text{–}4\text{-}C_1Pyr]AlCl_4$ salt buffered by the addition of weak organic bases (such as *N*-methylpyrrole, quinoline, or pyridines).[255]

Nickel(II)–diiminophosphorane complexes combined with alkylaluminum co-catalysts and dissolved in $[C_4C_1Im]$-$AlCl_4AlEtCl_2$ are active for the oligomerization of ethylene under biphasic reaction conditions. As observed in the homogeneous phase, the selectivity (dimers vs. higher oligomers) is related to the nature of the diiminophosphorane ligands (Figure 15). In $[C_4C_1Im]AlCl_4$, an enhancement of the catalytic activity and convergence of the selectivity are observed upon repeating cycles, indicating that organoaluminate anions replace the diiminophosphorane ligands in the coordination sphere of the active nickel species.[256]

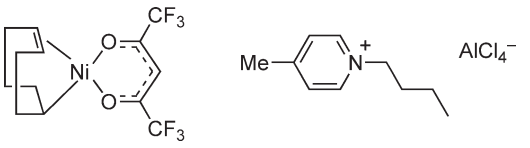

Figure 14 [Ni(COD)(hfacac)] catalyst precursor.

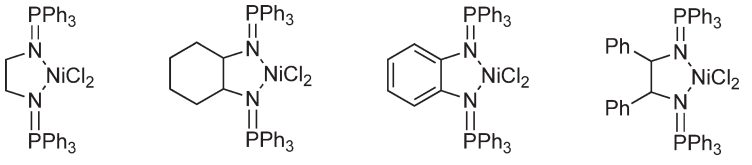

Figure 15 Nickel(II)–diiminophosphorane complexes.

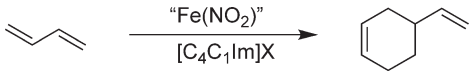

Scheme 30

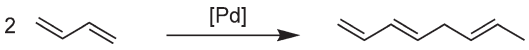

Scheme 31

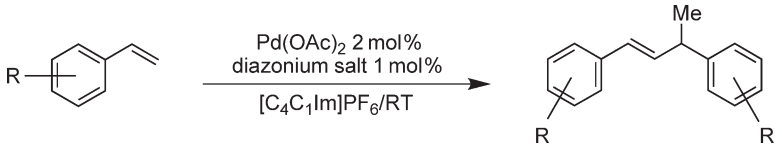

Scheme 32

The catalytically active species involved in the oligomerization reactions are probably nickel–hydride complexes, as indicated by their activity in carbon–carbon bond formations (oligomerization) and carbon–carbon double bond shifts (isomerization). The proposed mechanism of these biphasic reactions is analogous to the reactions occurring under one-phase conditions.[253]

The tungsten complex $[W{=}NPh(Cl_2)(PMe_3)_3]$ dissolved in $[C_4C_1Im]AlCl_4$ was described as being able to catalyze ethene oligomerization without using any co-catalyst.[257] An active Ni catalyst can also be formed, without aluminum activators, by reaction of $[Ni(COD)_2]$ with a Brönsted acid in non-chloroaluminate ILs. These solvents stabilize and activate nickel catalysts, even without ligand, and greatly enhance the reaction activity.[258] The biphasic oligomerization of olefins can also be performed in non-acidic ILs such as $[C_4C_1Im]PF_6$ using [(η^3-methallyl)[bis(diphenylphosphino)methane–monoxide-κ^2-*P*,*O*]nickel(II)] hexafluoroantimonate.[53,259]

The potential of ILs in oligomerization processes[260] has become a reality with the announcement of a commercial process for the dimerization of butenes to isooctenes (Difasol process) by IFP (France) based on nickel complexes immobilized in organoaluminate imidazolium ILs.[261]

The 1,3-butadiene cyclo-dimerization reaction can be performed by iron complexes, prepared *in situ* by the reduction of $[Fe_2(NO)_4Cl_2]$ with metallic zinc, dissolved in $[C_4C_1Im][BF_4]$ or $[C_4C_1Im][PF_6]$ ILs (Scheme 30).[262]

The linear dimerization of 1,3-butadiene can also be performed with Pd(II) salts (chloride or acetate)/PPh_3 catalyst precursor dissolved in $[C_4C_1Im]BF_4$ or $[C_4C_1Im]PF_6$ to produce 1,3,6-octatriene (Scheme 31).[263]

Palladium and diazonium salts in $[C_4C_1Im]PF_6$ promote a styrene dimerization reaction (Scheme 32).[264]

1.30.7.2.4.(ii) Polymerization

Ziegler–Natta-type polymerizations can also be carried out in dialkylimidazolium halides/aluminum halide molten salts using $AlCl_{3-x}R_x$ as co-catalysts. Ethylene was polymerized using $(\eta^5Cp)_2MCl_2$ (M = Ti, Zr, Hf), dissolved in $[C_2C_1Im]AlCl_4$, and using $AlCl_{3-x}R_x$ (R = Me, Et) as co-catalysts.[265]

The polymerization of ethene by titanium tetrachloride, dissolved in $[C_4C_1Im]AlCl_4$, generates branched, atactic polymers with narrow monomodal polydispersities as waxy or oily compounds. In contrast, the polymerization of ethene by titanium tetrachloride in toluene affords mainly linear polyethene with a broader polydispersity and a higher molar mass.[250]

It is known that the complex $[NbO(C_{16}H_{11}O6)(C_2O_4)]$ is able to polymerize 1,3-butadiene to a polybutadiene with a high 1,4-*cis*-units content under homogeneous conditions using $AlClEt_2$ as co-catalyst. When this reaction was carried out in $[C_4C_1Im]AlCl_4$, an unusual inversion of the selectivity was observed, that is, polybutadiene with a high 1,4-*trans*-units content was obtained.[266]

Polyethylenes with a bimodal molecular weight distribution have been obtained from the polymerization of ethylene by 1,4-bis(2,6-diisopropylphenyl)acenaphthene diiminedichloronickel(II) dissolved in $[C_4C_1Im]AlCl_4$ under mild reaction conditions.[267]

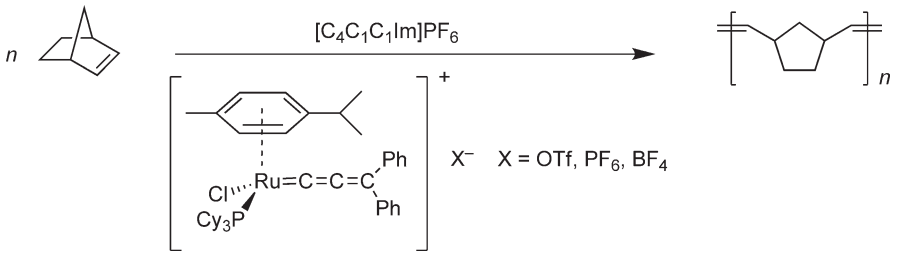

Scheme 33

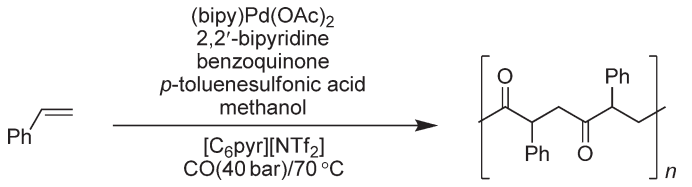

Scheme 34

The polyethylenes obtained present a typical bimodal molecular weight distribution indicating the formation of non-uniform nickel catalytic active centers in the IL phase. In opposition, the polyethylenes obtained under homogeneous conditions present only a slightly bimodal molecular weight distribution.[268]

Various Rh(I) compounds such as [RhTp(COD)] (Tp = tris(pyrazolylborate))[269] and [Rh(acac)COD], which are almost inactive in CH_2Cl_2, became active catalysts for phenylacetylene polymerization in chloride-free ILs such as $[C_4C_1Im]BF_4$ and $[C_4Pyr]BF_4$.[270–272]

Ring-opening metathesis polymerization (ROMP) of norbornene by a cationic ruthenium allenylidene pre-catalyst was carried out in a biphasic medium employing $[C_4C_1C_1Im]PF_6$ (Scheme 33).[273]

Alternating co-polymerization of styrene and carbon monoxide by cationic palladium compounds in $[C_6Pyr]N(CF_3SO_3)_2$ or $[C_4C_1Im]N(CF_3SO_3)_2$ gave improved yields and increased molecular weights when compared to polymerizations run in methanol (Scheme 34).[54]

Free-radical polymerizations, living cationic polymerizations, and group-transfer polymerization of methyl methacrylate and styrene using conventional organic initiators and transition metal complexes in room-temperature ILs have been reported several times.[274–278]

1.30.7.2.5 Olefin metathesis

Homogeneous transition metal-catalyzed olefin metathesis—encompassing reactions such as ROMP, acyclic diene metathesis (ADMET), ring-closing metathesis (RCM), and metathesis of acyclic olefins—is a focal issue in both organic synthesis and polymer chemistry, and such reactions have been performed in ILs.

Olefin disproportionation can be performed by transition metal metathesis catalysts based on W(VI) and Mo(V) compounds immobilized in $[C_4C_1Im]AlCl_4$ IL. For example, 2-pentene can be converted into the thermodynamic 50/25/25 mixture of 2-pentene/2-butene/3-hexene at room temperature in the presence of $[WCl_4(2,6\text{-}Ph_2C_3H_3O)_2]$ dissolved in $[C_4C_1Im]AlCl_4$ activated by $AlCl_2Et$.[279] The association of WCl_6 with $[C_4C_1Im]BF_4$ leads to a stable homogeneous solution, which catalyzed the metathesis of 1-hexene. The metathesis is preceded by isomerization of 1-hexene to 2-hexene, from which the main reaction product 4-octene is formed.[280,281]

Grubbs-type ruthenium alkylidenes have been shown to be catalytically active for ring-closing olefin metathesis in ILs such as $[C_4C_1Im]PF_6$ and $[C_4C_1Im]CF_3SO_3$, but their catalytic reactivity rapidly vanished in subsequent recycling runs and reuse.[273,282–285]

However, anchoring an imidazolium ring pattern to the catalyst prevents its leaching from the IL phase (Figure 16). These IL catalysts in $[C_4C_1Im]PF_6$ are remarkably stable and can be recovered and reused up to 10 consecutive cycles in RCM reactions of several dienes with excellent conversions.[286–290]

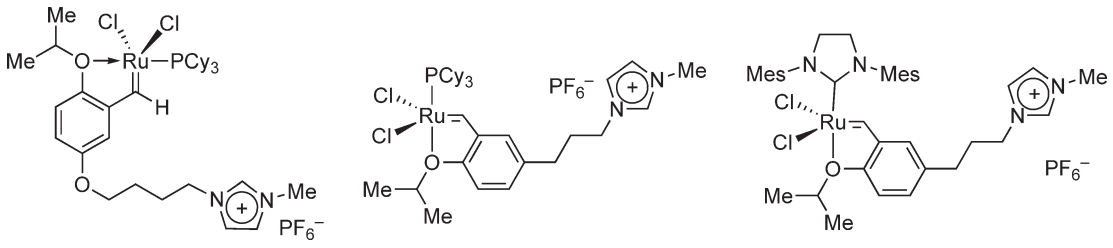

Figure 16 Imidazolium-modified Ru–carbene catalyst precursors.

$[Ru(=C=C=CPh_2)(p\text{-cymene})(PCy_3)Cl]CF_3SO_3$, dissolved in protic imidazolium ILs such as $[C_4HIm]CF_3SO_3$, is an efficient recyclable catalytic system for the RCM of *N*,*N*-diallyltosylamide.[291] Microwave heating is an efficient method for the acceleration of the RCM reactions using ruthenium-based catalysts in ILs.[285]

1.30.7.2.6 Telomerization of dienes

The telomerization of 1,3-dienes with water, methanol, and amines can be effectively catalyzed by palladium compounds in imidazolium and pyridinium ILs. Palladium catalyst precursors such as $[C_4C_1Im]_2[PdCl_4]$ dissolved in $[C_4C_1Im]BF_4$ promote the hydrodimerization of 1,3-butadiene (Scheme 35).[17]

These reactions were performed under homogeneous conditions at 70 °C. However, at temperatures below 5 °C, a two-phase system is formed, and the products are easily removed from the reaction mixture by simple decanting. Palladium(II) acetate in $[C_4C_1C_1Im]N(CF_3SO_2)_2$ with either triphenylphosphine or sodium diphenylphosphinobenzene–3-sulfonate promote the telomerization of butadiene and methanol at 85 °C. The reaction was also performed in $[C_4C_1Im]N(CF_3SO_2)_2$ and pyridinium ILs, but the catalytic system is not active in the imidazolium IL or not stable in the pyridinium salts.[292]

1-Octadienyl amines with high *E*/*Z* ratios have been prepared from the catalytic telomerization of 1,3-butadiene with diethylamine using palladium/sulfonated-phosphine complexes immobilized in $[C_4C_1Im]BF_4$.[293]

1.30.7.2.7 Heck, Suzuki, allylation, and other C–C coupling reactions

1.30.7.2.7.(i) Heck coupling

The coupling of alkenes with aryl halides can be accomplished by a plethora of palladium catalyst precursors under various reaction conditions. Inasmuch as the Heck reaction is usually performed in polar solvents and that salt additives such as $N(n\text{-}Bu)_4Br$ that can activate and stabilize the catalytically active palladium species, molten salts appear to be the ideal immobilizing agents.[294,295] Indeed, Kaufmann has demonstrated that the vinylation of aryl halides can be performed by simple palladium catalyst precursors such as palladium chloride, palladium acetate, and $[PdCl_2(PPh_3)_2]$ dissolved in hexadecyltributylphosphonium bromide and tetrabutylammonium chloride molten salts, without the addition of phosphine ligands.[296] After that, a legion of different palladium catalyst precursors dissolved in tetrabutylammonium bromide molten salt, phosphonium, pyridinium in imidazolium-based ILs have been tested in the coupling of aryl halides with alkenes: phospha–palladacycle catalyst precursor,[297,298] Pd–benzothiazole carbene ligands,[299,300] Pd(0)–monocarbene[301] immobilized in tetrabutylammonium bromide, $PdCl_2$, $Pd(OAc)_2$ in $[C_4C_1Im]PF_6$ or $[C_6Pyr]PF_6$,[302–304] $Pd(OAc)_2$ in 3-butyl–5-hydroxymethyl–1-methyl–3H-imidazol-1-ium salt,[305,306] Pd(II)–bisimidazole in $[C_4C_1Im]PF_6$,[307] *N*-containing palladacycle in $[C_4C_1Im]BF_4$,[308] $PdCl_2$ in pyrrolidinium and piperidinium tetrafluoroborates,[309] $[Pd_2(dba)_3]$ in trihexyl(tetradecyl)phosphonium chloride,[310,311] $[PdCl_2(NH_3)_4]$/silica[312] or $Pd(OAc)_2$/silica,[313] and a modified oxime–palladacycle[314] in $[C_4C_1Im]PF_6$ (Figure 17). The coupling of arenediazonium salts with alkenes can be catalyzed by $Pd(OAc)_2$ in $[C_4C_1Im]PF_6$.[264] A continuous microflow system was developed with efficient catalyst recycling for a Heck reaction of iodobenzene with *n*-butylacrylate, using a Pd(II)–carbene complex immobilized in $[C_4C_1Im]N(CF_3SO_3)_2$.[315,316]

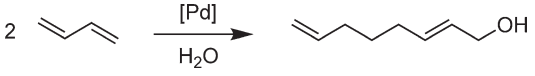

Scheme 35

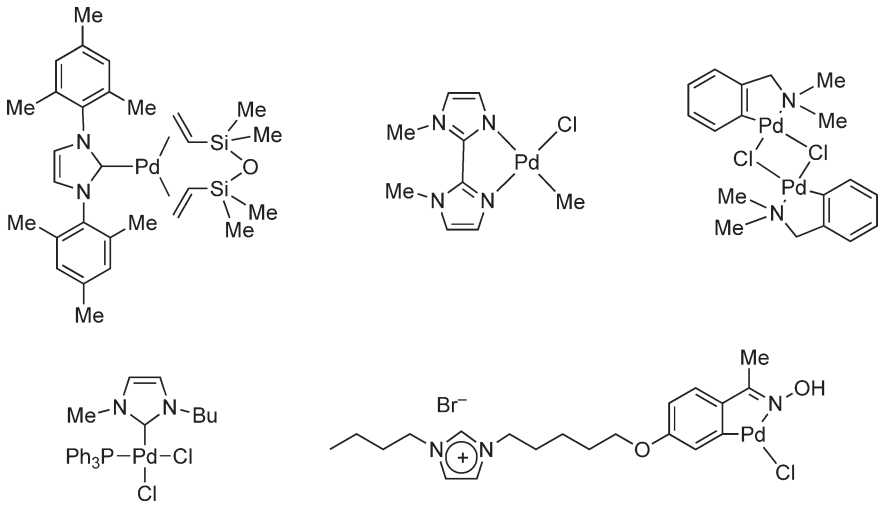

Figure 17 Examples of Pd(0) and Pd(II) catalyst precursors employed in Heck coupling reactions.

The IL derived from the monoquaternization of 2,2′-biimidazole with iodobutane acts as both the solvent and ligand for the $PdCl_2$ and catalyzes the coupling of chlorobenzene with alkenes (Figure 18).[317]

The synthesis (±)-pterocarpan was achieved by the Heck coupling of 7-benzyloxy–2H-chromene with 2-iodophenol in $[C_4C_1Im]PF_6$ and in the presence of the $[PdCl_2(PhCN)_2]/Ph_3P/Ag_2CO_3$.[318,319]

A series of benzofurans have been prepared from the intramolecular Heck coupling catalyzed by $PdCl_2$ in $[C_4C_1Im]BF_4$ (Scheme 36).[320]

Palladium acetate associated with DPPP (diphenylphosphinopropane) $[C_4C_1Im]BF_4$ catalyze the regioselective Heck arylation of electron-rich olefins–vinyl ethers, enamides, and allyltrimethylsilanes (Scheme 37).[321]

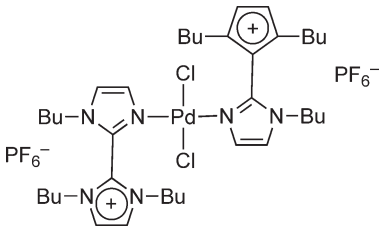

Figure 18 A Pd(II) complex containing the 2,2′-biimidazole-modified IL.

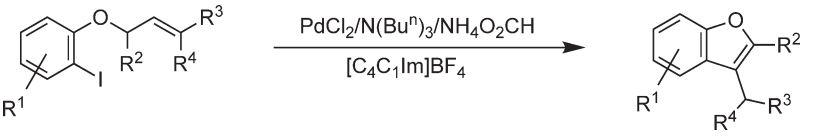

Scheme 36

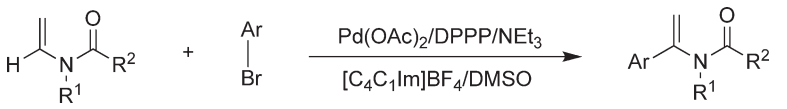

Scheme 37

The Heck reaction performed in ILs has various advantages compared with all previously described molecular solvents, such as catalytic efficiency for the vinylation of chloroarenes, improved thermal catalyst stability and lifetime during the reaction. In the reactions performed in 1,3-dialkylimidazolium ILs, *N*-heterocyclic carbene complexes of palladium can be formed *in situ*. These palladium–carbene complexes are formed from the deprotonation of the imidazolium cation in the presence of the catalyst precursor.[322]

Moreover, in various cases, it was observed that the palladium complexes decompose forming nanoparticles that are in fact the catalyst precursors for the Heck coupling reactions.[323–327]

1.30.7.2.7.(ii) Suzuki coupling

Palladium-catalyzed Suzuki cross-coupling reactions of aryl halides with arylboronic acids have been conducted in various ILs, usually exhibiting unprecedented reactivities (compared to the reactions performed in classical polar organic solvents) in addition to easy product isolation and catalyst recycling. In the majority of the cases, classical Pd catalyst precursors have been used in the coupling of aryl iodides and bromides, such as $[Pd(PPh_3)_4]$ (Scheme 38) and $[PdCl_2(PPh_3)_2]$ and various Pd imidazole complexes in $[C_4C_1Im]BF_4$,[328–330] Pd–carbene complexes in $[C_4C_1Im]N(CF_3SO_3)_2$,[316] modified oxime–palladacycle in $[C_4C_1Im]PF_6$,[314] Pd(II) compounds in nitrile-functionalized pyridinium ILs (such as $[C_3CNPyr]N(CF_3SO_3)_2$),[331] $PdCl_2$ in 2,2′-biimidazolium-based ILs,[332] $[Pd_2(dba)_3]$ in tetradecyltrihexylphosphonium chloride,[333] and $PdCl_2$ in pyrrolidinium and piperidinium tetrafluoroborates.[309]

Pd–biscarbene complexes (Figure 19) catalyzed Suzuki cross-coupling reactions of halobenzenes including chlorobenzenes with phenylboronic acid were achieved at room temperature in $[C_4C_4Im]BF_4$ with MeOH as co-solvent under ultrasonic irradiation.[334]

$[PdCl_2(PPh_3)_2]$ immobilized in $[C_2C_1Im]BF_4$ has been used for the coupling of reaction of 1-chloroquinoline with 1-naphthalene boronic acid.[335] The promoting effect of ILs usually observed on various transition metal-catalyzed reactions in solution was also demonstrated to be translatable to solid-phase synthesis, namely, in the Suzuki cross-coupling of 4-iodophenol immobilized on polystyrene–Wang resin with various arylboronic acids that is significantly accelerated by the use of $[C_4C_4Im]BF_4$ as a co-solvent (Scheme 39).[336]

As observed in Heck reactions, in the reactions performed in 1,3-dialkylimidazolium ILs, the formation of carbenes that may be involved in the stabilization of catalytically active species is not uncommon. The *in situ* formation of a mixed phosphine–imidazolylidene palladium complex, in $[C_4C_1Im]BF_4$, has been observed under conditions employed in many palladium-catalyzed coupling reactions (Scheme 40).[337]

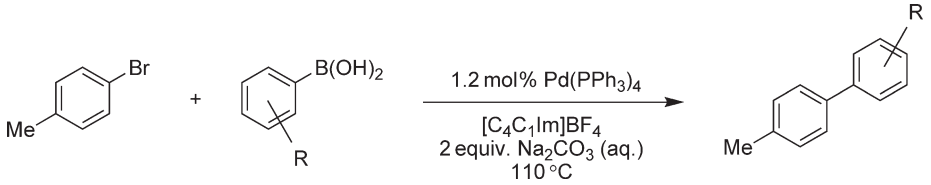

Scheme 38

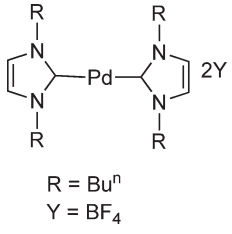

Figure 19 Pd–biscarbene complex.

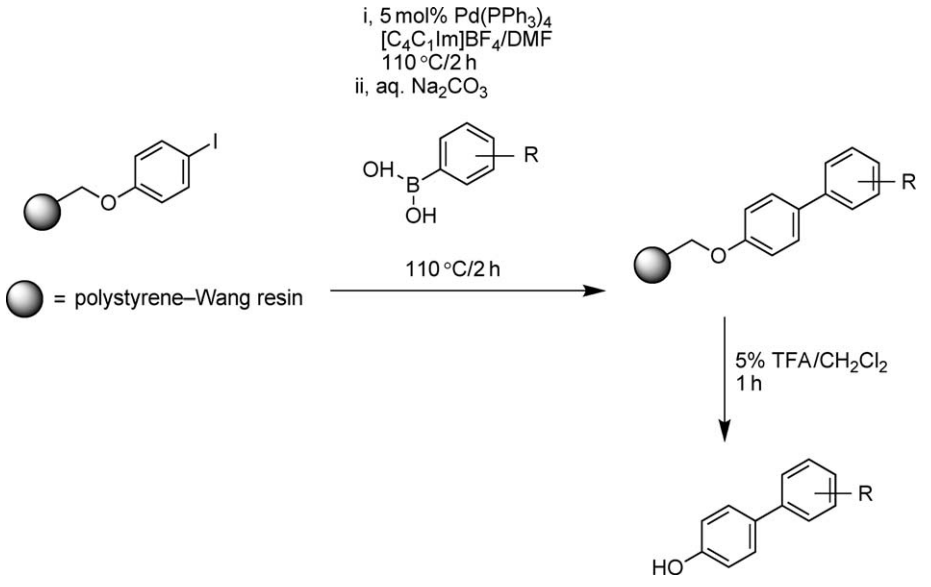

Scheme 39

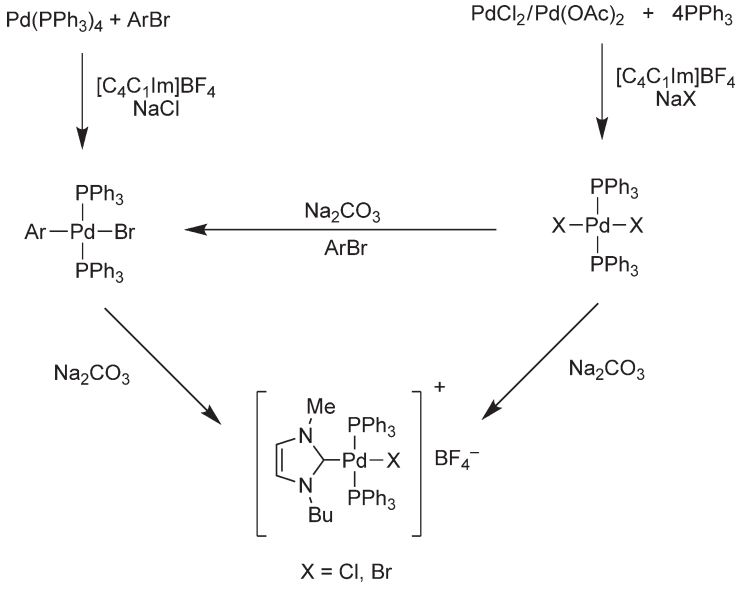

Scheme 40

1.30.7.2.7.(iii) Allylation reactions

The allylation of carbonyl compounds via allylboration,[338] allylstannation,[339] and $Sc(CF_3SO_3)_3$-[340] or $InCl_3$-[341,342] mediated process for the generation of a variety of homoallylic alcohols has been performed in various imidazolium ILs. The enantioselective allylation of aldehydes has been performed by In(III) complexes associated by PYBOX ligands in $[C_4C_1Im]PF_6$ (Scheme 41).[343]

Palladium acetate with PPh_3 dissolved in $[C_4C_1Im]BF_4$ catalyze the alkylation of 3-acetoxy–1,3-diphenylprop-1-ene by dimethylmalonate and other active methylene compounds (Scheme 42).[344]

When using PPh_3, separation or solvent extraction of the products from the ionic phase is not feasible. However, when the hydrophilic phosphine P(*m*-$C_6H_4SO_3Na)_3$ was used, the IL could be recovered and recycled three times without losing activity in the alkylation by dimethyl malonate.

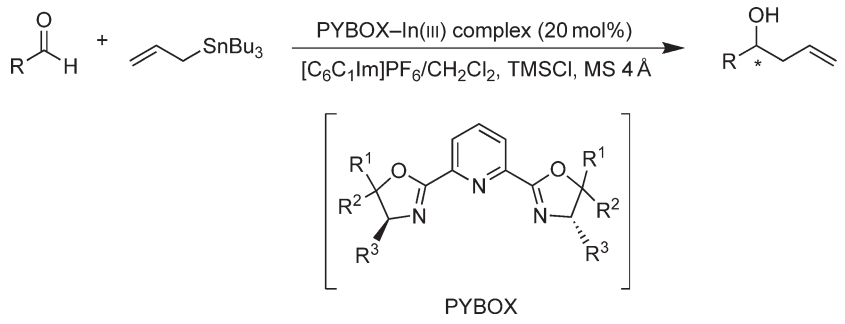

Scheme 41

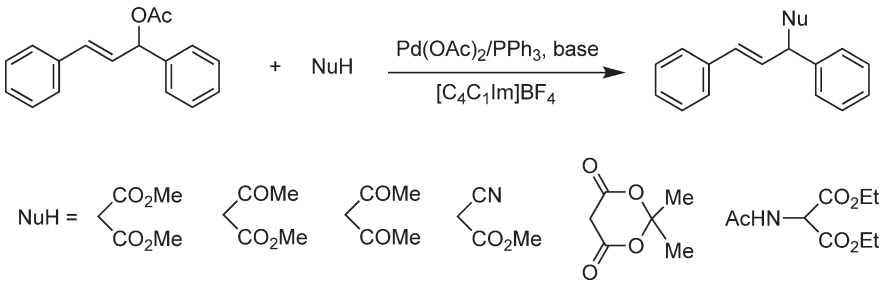

Scheme 42

The asymmetric version of this reaction is also feasible using palladium complexes associated with non-racemic ferrocenyl phosphine[345] and BINAP[346] ligands immobilized in $[C_4C_1Im]PF_6$. The palladium-catalyzed allylic alkylation is slower in THF than in $[C_4C_1Im]BF_4$, and these observations were rationalized in terms of different allylpalladium intermediates arising from the oxidative addition of the acetato substrates to active Pd(0) species.[347] These allylpalladium intermediates may exist as free cations in the IL but contact ion pairs in the organic solvent (Scheme 43). In these reactions, the phosphine ligands exert a profound effect on the catalytically active species, with more electron-donating phosphines affording faster reaction rates. It is worth noting that neutral allylic alkylation reactions, in which a base is generated *in situ* and which hence require no external bases, are significantly retarded when carried out in $[C_4C_1Im]BF_4$.[348]

The catalytic activity, selectivity, and catalyst stability is improved for Trost–Tsuji C–C coupling of cinnamyl carbonate and ethyl acetoacetate with a water-soluble Pd/TPPTS catalyst (sodium salt) when performed in $[C_4C_1Im]Cl$.[349] These Pd-catalyzed allylation reactions can also be performed under microwave conditions employing mixtures of $[C_2C_1Im]BF_4$/water.[350]

The direct coupling of aryl- and vinylboronic acids has been achieved by simple Rh(I) and Rh(III) compounds in $[C_4C_1Im]PF_6$ (Scheme 44), giving higher yields than the reactions performed in toluene of dichloromethane.[351]

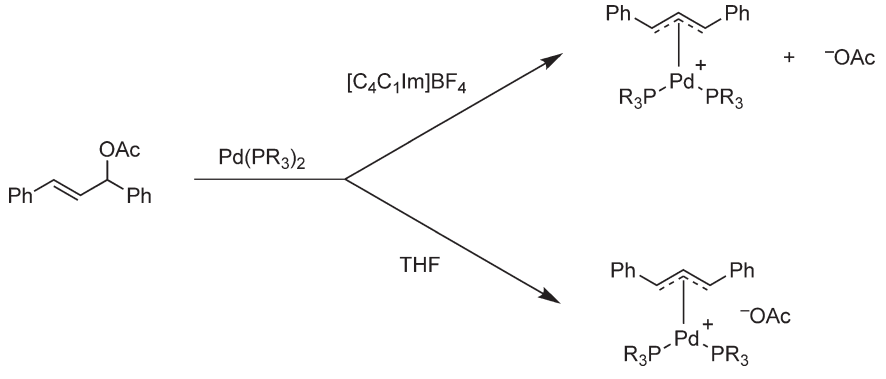

Scheme 43

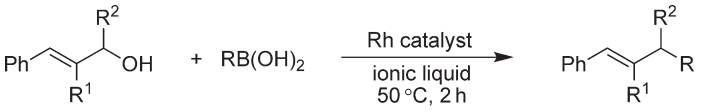

R = aryl, alkenyl, heteroaryl
R^1 = H, Me
R^2 = H, Ph

Scheme 44

1.30.7.2.7.(iv) Other C–C coupling reactions

Other C–C coupling reactions have been performed in ILs, and the selectivities and yields are similar to those obtained in classical organic solvents. The $NiCl_2(PPh_3)_2/Zn/PPh_3$-catalyzed homocoupling of various aryl halides have been conducted in $[C_4C_1Im]PF_6$.[221] Stille couplings using ligandless palladium catalyst precursors[352] and other palladium complexes in $[C_4C_1Im]BF_4$[353] or nitrile-functionalized pyridinium ILs (such as $[C_3CNPyr]N(CF_3SO_3)_2$) have also been reported.[112] The Sonogashira coupling between aryl iodides and terminal alkynes was reported to occur in $[C_4C_1Im]PF_6$,[354] and the hydroarylation of alkynes by [((*E,E,E*)-1,6,11-tris(*p*-toluenesulfonyl)–1,6,11-triazacyclopentadeca-3,8,13-triene)Pd(0)] in $[C_4C_1Im]BF_4$.[355]

1.30.7.2.8 Miscellaneous

Silylstannanes ($Bu_3SnSiMe_3$, for example) can be regioselectively added across terminal alkynes in the presence of Pd(0) catalyst precursors immobilized in $[C_4C_1Im]PF_6$[356] or $[C_4C_1Im]BF_4$,[357] which can usually be recycled without loss of activity. [Rh(COD)][BPh_4], immobilized in the same IL, is also an efficient recyclable catalytic system for the silylformylation of terminal alkynes.[358] The biphasic inter- and intramolecular hydroamination of alkynes $Zn(SO_3CF_3)_2$ immobilized in $[C_2C_1Im]CF_3SO_3$ have been performed in a continuous process (Scheme 45).[359]

The enantioselective alkyne–imine addition has been achieved using a copper(I)–bis(oxazoline) compound in $[C_4C_1Im]N(CF_3SO_2)_2$ (Scheme 46).[360]

Three-component synthesis of propargyl amines can be performed with copper(I) complexes[361,362] or AgI[363] in $[C_4C_1Im]PF_6$ (Scheme 47).

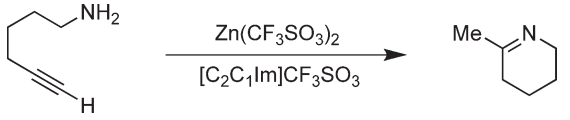

Scheme 45

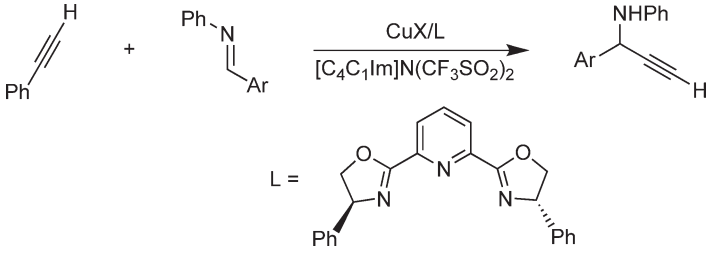

Scheme 46

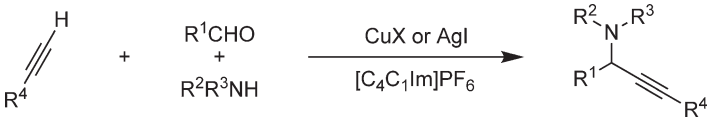

Scheme 47

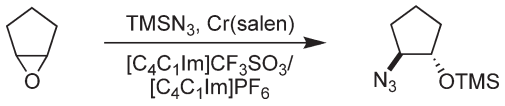

Scheme 48

Terminal alkynes undergo oxidative coupling in the presence of the CuCl–TMEDA catalytic system in $[C_4C_1Im]PF_6$ under aerobic conditions to produce 1,3-diynes.[364] Intermolecular Pauson–Khand reactions of strained alkenes with alkynes and $Co_2(CO)_8$ were performed in $[C_4C_1Im]PF_6$ either thermally or in the presence of NMO.[365]

Ring opening (fluorination, chlorination, or amination) of epoxides are usually facilitated when performed in ILs such as $[C_4C_1Im]PF_6$ without the addition of any other catalyst.[366–368] The reaction of trimethylsilyl azide with *meso*-epoxides is catalyzed by [*N*,*N*′(-bis(3,5-di-*tert*-butylsalicylidene)–1,2-cyclohexanediamine)chromium(III) chloride] dissolved in 1-*n*-butyl–3-methylimidazolium ILs (Scheme 48). The yield and enantioselectivity are strongly dependent upon the nature of counteranion; while the reaction performed in hydrophobic $[C_4C_1Im]PF_6$ IL gave high yields and degrees of enantioselectivity (similar to those obtained in organic solvents), the system is almost inactive when performed in hydrophilic $[C_4C_1Im]BF_4$. The best recyclable catalytic system was obtained by immobilizing the catalyst precursor in a mixture (5 : 1 v/v) of hydrophobic $[C_4C_1Im]PF_6$ and the hydrophilic $[C_4C_1Im]CF_3SO_3$ ILs.[369]

1.30.8 Conclusions and Trends

Although the exploration of ILs in organometallic chemistry is in its early days, these fluids have already been shown to be the immobilizing agents of choice for various classical transition metal catalyst precursors. The achieved catalytic performance in this medium is similar and in some cases superior to reactions performed in organic solvents or aqueous systems. However, the understanding of how the nature of ILs can affect the chemical reactions that occur in them remains to be achieved. There is no doubt that these fluids—in particular those based on the imidazolium cation—can induce, accelerate, or redirect reaction paths that involve ionic intermediates or transition states, thus opening new possibilities for selectivity and activity control in organometallic chemistry. It is clear that the design of specific ILs will lead to more effective fluids with dual behavior (solvent–ligand) for organometallic catalysis with "ligandless" transition metal precursors. Moreover, due to the absence of measurable vapor pressure of some of the ILs, it is possible to investigate the interactions and behavior of transition metal complexes in solution using physical and chemical methods that require special conditions such as high vacuum, and have been traditionally used only in solid-state chemistry.

References

1. Cornils, B., Herrmann, W. A., Eds.; *Aqueous-phase Organometallic Catalysis*, VCH Weinheim; 2nd ed. 2004; p 750.
2. Horvath, I. T. *Acc. Chem. Res.* **1998**, *31*, 641–650.
3. Jessop, P. G.; Ikariya, T.; Noyori, R. *Chem. Rev.* **1999**, *99*, 475–493.
4. Leitner, W. *Acc. Chem. Res.* **2002**, *35*, 746–756.
5. Dupont, J.; de Souza, R. F.; Suarez, P. A. Z. *Chem. Rev.* **2002**, *102*, 3667–3691.
6. Welton, T. *Chem. Rev.* **1999**, *99*, 2071–2083.
7. Wasserscheid, P.; Keim, W. *Angew. Chem., Int. Ed.* **2000**, *39*, 3773–3789.
8. Olivier-Bourbigou, H.; Magna, L. *J. Mol. Catal. A: Chem.* **2002**, *182*, 419–437.
9. Olivier, H. *J. Mol. Catal. A: Chem.* **1999**, *146*, 285–289.
10. Sheldon, R. *Chem. Commun.* **2001**, 2399–2407.
11. Gordon, C. M. *Appl. Catal., A: Gen.* **2001**, *222*, 101–117.
12. Welton, T. *Coord. Chem. Rev.* **2004**, *248*, 2459–2477.
13. Chauvin, Y.; Gilbert, B.; Guibard, I. *J. Chem. Soc., Chem. Commun.* **1990**, 1715–1716.
14. Suarez, P. A. Z.; Dullius, J. E. L.; Einloft, S.; DeSouza, R. F.; Dupont, J. *Polyhedron* **1996**, *15*, 1217–1219.
15. Chauvin, Y.; Mussmann, L.; Olivier, H. *Angew. Chem., Int. Ed. Engl.* **1996**, *34*, 2698–2700.
16. Dupont, J. *J. Brazil. Chem. Soc.* **2004**, *15*, 341–350.
17. Dullius, J. E. L.; Suarez, P. A. Z.; Einloft, S.; de Souza, R. F.; Dupont, J.; Fischer, J.; De Cian, A. *Organometallics* **1998**, *17*, 815–819.
18. Villagran, C.; Deetlefs, M.; Pitner, W. R.; Hardacre, C. *Anal. Chem.* **2004**, *76*, 2118–2123.
19. Villagran, C.; Banks, C. E.; Hardacre, C.; Compton, R. G. *Anal. Chem.* **2004**, *76*, 1998–2003.
20. Sweeny, B. K.; Peters, D. G. *Electrochem. Commun.* **2001**, *3*, 712–715.
21. Gallo, V.; Mastrorilli, P.; Nobile, C. F.; Romanazzi, G.; Suranna, G. P. *J. Chem. Soc., Dalton Trans.* **2002**, 4339–4342.
22. Seddon, K. R.; Stark, A.; Torres, M. J. *Pure Appl. Chem.* **2000**, *72*, 2275–2287.

23. de Souza, R. F.; Rech, V.; Dupont, J. *Adv. Synth. Catal.* **2002**, *344*, 153–155.
24. Holbrey, J. D.; Reichert, W. M.; Swatloski, R. P.; Broker, G. A.; Pitner, W. R.; Seddon, K. R.; Rogers, R. D. *Green Chem.* **2002**, *4*, 407–413.
25. Fredlake, C. P.; Muldoon, M. J.; Aki, S.; Welton, T.; Brennecke, J. F. *Phys. Chem. Chem. Phys.* **2004**, *6*, 3280–3285.
26. Crowhurst, L.; Mawdsley, P. R.; Perez-Arlandis, J. M.; Salter, P. A.; Welton, T. *Phys. Chem. Chem. Phys.* **2003**, *5*, 2790–2794.
27. Cammarata, L.; Kazarian, S. G.; Salter, P. A.; Welton, T. *Phys. Chem. Chem. Phys.* **2001**, *3*, 5192–5200.
28. Anderson, J. L.; Ding, J.; Welton, T.; Armstrong, D. W. *J. Am. Chem. Soc.* **2002**, *124*, 14247–14254.
29. Carmichael, A. J.; Seddon, K. R. *J. Phys. Org. Chem.* **2000**, *13*, 591–595.
30. Ali, Z.; Poole, C. F. *J. Chromatogr. A* **2004**, *1052*, 199–204.
31. Rovere, M.; Tosi, M. P. *Rep. Prog. Phys.* **1986**, *49*, 1001–1081.
32. Biggin, S.; Enderby, J. E. *J. Phys. C: Solid State Phys.* **1982**, *15*, L305–L309.
33. Martin, J. D. *ACS Symp. Ser.* **2002**, *818*, 413–427.
34. Cang, H.; Li, J.; Fayer, M. D. *J. Chem. Phys.* **2003**, *119*, 13017–13023.
35. Suarez, P. A. Z.; Einloft, S.; Dullius, J. E. L.; de Souza, R. F.; Dupont, J. *J. Chim. Phys. Phys.-Chim. Biol.* **1998**, *95*, 1626–1639.
36. Dieter, K. M.; Dymek, C. J.; Heimer, N. E.; Rovang, J. W.; Wilkes, J. S. *J. Am. Chem. Soc.* **1988**, *110*, 2722–2726.
37. Tait, S.; Osteryoung, R. A. *Inorg. Chem.* **1984**, *23*, 4352–4360.
38. Ozawa, R.; Hayashi, S.; Saha, S.; Kobayashi, A.; Hamaguchi, H. *Chem. Lett.* **2003**, *32*, 948–949.
39. Hayashi, S.; Ozawa, R.; Hamaguchi, H. *Chem. Lett.* **2003**, *32*, 498–499.
40. Hardacre, C.; Holbrey, J. D.; McMath, S. E. J.; Bowron, D. T.; Soper, A. K. *J. Chem. Phys.* **2003**, *118*, 273–278.
41. Heimer, N. E.; Del Sesto, R. E.; Carper, W. R. *Magn. Reson. Chem.* **2004**, *42*, 71–75.
42. Fannin, A. A.; King, L. A.; Levisky, J. A.; Wilkes, J. S. *J. Phys. Chem.* **1984**, *88*, 2609–2614.
43. Wilkes, J. S.; Frye, J. S.; Reynolds, G. F. *Inorg. Chem.* **1983**, *22*, 3870–3872.
44. Gozzo, F. C.; Santos, L. S.; Augusti, R.; Consorti, C. S.; Dupont, J.; Eberlin, M. N. *Chem. Eur. J.* **2004**, *10*, 6187–6193.
45. Dyson, P. J.; Khalaila, I.; Luettgen, S.; McIndoe, J. S.; Zhao, D. B. *Chem. Commun.* **2004**, 2204–2205.
46. Nishida, T.; Tashiro, Y.; Yamamoto, M. *J. Fluorine Chem.* **2003**, *120*, 135.
47. Huddleston, J. G.; Visser, A. E.; Reichert, W. M.; Willauer, H. D.; Broker, G. A.; Rogers, R. D. *Green Chem.* **2001**, *3*, 156–164.
48. Bonhote, P.; Dias, A. P.; Papageorgiou, N.; Kalyanasundaram, K.; Gratzel, M. *Inorg. Chem.* **1996**, *35*, 1168–1178.
49. Dyson Paul, J.; Laurenczy, G.; Ohlin, C. A.; Vallance, J.; Welton, T. *Chem. Commun.* **2003**, 2418–2419.
50. Suarez, P. A. Z.; Selbach, V. M.; Dullius, J. E. L.; Einloft, S.; Piatnicki, C. M. S.; Azambuja, D. S.; deSouza, R. F.; Dupont, J. *Electrochim. Acta* **1997**, *42*, 2533–2535.
51. Sur, U. K.; Marken, F.; Coles, B. A.; Compton, R. G.; Dupont, J. *Chem. Commun.* **2004**, 2816–2817.
52. Zhang, J.; Bond, A. M.; Schumann, H.; Suhring, K. *Organometallics* **2005**, *24*, 2188–2196.
53. Wasserscheid, P.; Gordon, C. M.; Hilgers, C.; Muldoon, M. J.; Dunkin, I. R. *Chem. Commun.* **2001**, 1186–1187.
54. Klingshirn, M. A.; Broker, G. A.; Holbrey, J. D.; Shaughnessy, K. H.; Rogers, R. D. *Chem. Commun.* **2002**, 1394–1395.
55. Zimmermann, J.; Wasserscheid, P.; Tkatchenko, I.; Stutzmann, S. *Chem. Commun.* **2002**, 760–761.
56. Mo, J.; Xu, L. J.; Xiao, J. L. *J. Am. Chem. Soc.* **2005**, *127*, 751–760.
57. Sliger, M. D.; P'Pool, S. J.; Traylor, R. K.; McNeil, J., III; Young, S. H.; Hoffman, N. W.; Klingshirn, M. A.; Rogers, R. D.; Shaughnessy, K. H. *J. Organomet. Chem.* **2005**, *690*, 3540–3545.
58. Solinas, M.; Pfaltz, A.; Cozzi, P. G.; Leitner, W. *J. Am. Chem. Soc.* **2004**, *126*, 16142–16147.
59. Daguenet, C.; Dyson, P. J. *Organometallics* **2004**, *23*, 6080–6083.
60. Swiderski, K.; McLean, A.; Gordon, C. M.; Vaughan, D. H. *Chem. Commun.* **2004**, 590–591.
61. Sacco, A.; Ugo, R.; Moles, A. *J. Chem. Soc. A* **1966**, 1670.
62. Mann, B. E.; Guzman, M. H. *Inorg. Chim. Acta* **2002**, *330*, 143–148.
63. Zhu, Y. H.; Carpenter, K.; Bun, C. C.; Bahnmueller, S.; Ke, C. P.; Srid, V. S.; Kee, L. W.; Hawthorne, M. F. *Angew. Chem., Int. Ed.* **2003**, *42*, 3792–3795.
64. Osteryoung, R. A. *NATO ASI Ser., Ser. C* **1987**, *202*, 329–364.
65. Hurley, F. H.; Wier, T. P. *J. Electrochem. Soc.* **1951**, *98*, 203–206.
66. Fuller, J.; Carlin, R. T.; Osteryoung, R. A. *J. Electrochem. Soc.* **1997**, *144*, 3881–3886.
67. Osteryoung, R. A.; Gale, R. J.; Robinson, J.; Linga, H.; Cheek, G. *J. Electrochem. Soc.* **1981**, *128*, C79.
68. Chauvin, Y.; Einloft, S.; Olivier, H. *Ind. Eng. Chem. Res.* **1995**, *34*, 1149–1155.
69. Robinson, J.; Osteryoung, R. A. *J. Am. Chem. Soc.* **1979**, *101*, 323–327.
70. Carlin, R. T.; Osteryoung, R. A.; Wilkes, J. S.; Rovang, J. *Inorg. Chem.* **1990**, *29*, 3003–3009.
71. Gilbert, B.; Chauvin, Y.; Guibard, I. *Vib. Spectrosc.* **1991**, *1*, 299–304.
72. Lin, I. J. B.; Vasam, C. S. *J. Organomet. Chem.* **2005**, *690*, 3498–3512.
73. Sitze, M. S.; Schreiter, E. R.; Patterson, E. V.; Freeman, R. G. *Inorg. Chem.* **2001**, *40*, 2298–2304.
74. Kolle, P.; Dronskowski, R. *Inorg. Chem.* **2004**, *43*, 2803–2809.
75. Dupont, J.; Suarez, P. A. Z.; Umpierre, A. P.; de Souza, R. F. *Catal. Lett.* **2001**, *73*, 211–213.
76. Abbott, A. P.; Capper, G.; Davies, D. L.; Rasheed, R. *Inorg. Chem.* **2004**, *43*, 3447–3452.
77. Abbott, A. P.; Capper, G.; Davies, D. L.; Munro, H. L.; Rasheed, R. K.; Tambyrajah, V. *Chem. Commun.* **2001**, 2010–2011.
78. Abbott, A. P.; Capper, G.; Davies, D. L.; Rasheed, R. H.; Tambyrajah, V. *Green Chem.* **2002**, *4*, 24–26.
79. Lin, Y. F.; Sun, I. W. *Electrochim. Acta* **1999**, *44*, 2771–2777.
80. Chen, P. Y.; Sun, I. W. *Electrochim. Acta* **1999**, *45*, 441–450.
81. Chen, P. Y.; Sun, I. W. *Electrochim. Acta* **2000**, *45*, 3163–3170.
82. Palgunadi, J.; Kwon, O. S.; Lee, H.; Bae, J. Y.; Ahn, B. S.; Min, N. Y.; Kim, H. S. *Catal. Today* **2004**, *98*, 511–514.
83. Wasserscheid, P.; Waffenschmidt, H. *J. Mol. Catal. A: Chem.* **2000**, *164*, 61–67.
84. Yang, Y. L.; Kou, Y. *Chem. Commun.* **2004**, 226–227.
85. Lecocq, V.; Graille, A.; Santini, C. C.; Baudouin, A.; Chauvin, Y.; Basset, J. M.; Arzel, L.; Bouchu, D.; Fenet, B. *New J. Chem.* **2005**, *29*, 700–706.
86. Neto, B. A. D.; Ebeling, G.; Goncalves, R. S.; Gozzo, F. C.; Eberlin, M. N.; Dupont, J. *Synthesis-Stuttgart* **2004**, 1155–1158.
87. Hasan, M.; Kozhevnikov, I. V.; Siddiqui, M. R. H.; Steiner, A.; Winterton, N. *Inorg. Chem.* **1999**, *38*, 5637–5641.
88. Yang, J. Z.; Tian, P.; Xu, W. G.; Xu, B.; Liu, S. Z. *Thermochim. Acta* **2004**, *412*, 1–5.

89. Koura, N.; Endo, T.; Idemoto, Y. *J. Non-Cryst. Solids* **1996**, *207*, 650–655.
90. Simanavicius, L.; Stakenas, A.; Sarkis, A. *Electrochim. Acta* **1997**, *42*, 1581–1586.
91. Vallee, C.; Valerio, C.; Chauvin, Y.; Niccolai, G. P.; Basset, J. M.; Santini, C. C.; Galland, J. C.; Didillon, B. *J. Mol. Catal. A: Chem.* **2004**, *214*, 71–81.
92. Brown, R. J. C.; Dyson, P. J.; Ellis, D. J.; Welton, T. *Chem. Commun.* **2001**, 1862–1863.
93. Fei, Z.; Zhao, D.; Scopelliti, R.; Dyson, P. J. *Organometallics* **2004**, *23*, 1622–1628.
94. Marken, F.; Blythe, A. N.; Wadhawan, J. D.; Compton, R. G.; Bull, S. D.; Aplin, R. T.; Davies, S. G. *J. Solid State Electrochem.* **2001**, *5*, 17–22.
95. Swatloski, R. P.; Visser, A. E.; Reichert, W. M.; Broker, G. A.; Farina, L. M.; Holbrey, J. D.; Rogers, R. D. *Green Chem.* **2002**, *4*, 81–87.
96. Gutowski, K. E.; Broker, G. A.; Willauer, H. D.; Huddleston, J. G.; Swatloski, R. P.; Holbrey, J. D.; Rogers, R. D. *J. Am. Chem. Soc.* **2003**, *125*, 6632–6633.
97. Domanska, U.; Marciniak, A. *J. Phys. Chem. B* **2004**, *108*, 2376–2382.
98. Domanska, U.; Bogel-Lukasik, E. *Ind. Eng. Chem. Res.* **2003**, *42*, 6986–6992.
99. Domanska, U.; Bogel-Lukasik, E.; Bogel-Lukasik, R. *Chem. Eur. J.* **2003**, *9*, 3033–3041.
100. Domanska, U.; Bogel-Lukasik, E.; Bogel-Lukasik, R. *J. Phys. Chem. B* **2003**, *107*, 1858–1863.
101. Domanska, U.; Marciniak, A. *J. Chem. Eng. Data* **2003**, *48*, 451–456.
102. Consorti, C. S.; Umpierre, A. P.; de Souza, R. F.; Dupont, J.; Suarez, P. A. Z. *J. Brazil. Chem. Soc.* **2003**, *14*, 401–405.
103. Aggarwal, A.; Lancaster, N. L.; Sethi, A. R.; Welton, T. *Green Chem.* **2002**, *4*, 517–520.
104. Huddleston, J. G.; Willauer, H. D.; Swatloski, R. P.; Visser, A. E.; Rogers, R. D. *Chem. Commun.* **1998**, 1765–1766.
105. Anthony, J. L.; Maginn, E. J.; Brennecke, J. F. *J. Phys. Chem. B* **2002**, *106*, 7315–7320.
106. Blanchard, L. A.; Hancu, D.; Beckman, E. J.; Brennecke, J. F. *Nature* **1999**, *399*, 28–29.
107. Dyson, P. J.; Laurenczy, G.; Ohlin, C. A.; Vallance, J.; Welton, T. *Chem. Commun.* **2003**, 2418–2419.
108. Berger, A.; de Souza, R. F.; Delgado, M. R.; Dupont, J. *Tetrahedron: Asymmetry* **2001**, *12*, 1825–1828.
109. Davis, J. H. *Chem. Lett.* **2004**, *33*, 1072–1077.
110. Xiao, J.-C.; Twamley, B.; Shreeve, J. n. M. *Org. Lett.* **2004**, *6*, 3845–3847.
111. Zhao, D.; Fei, Z.; Scopelliti, R.; Dyson, P. J. *Inorg. Chem.* **2004**, *43*, 2197–2205.
112. Zhao, D.; Fei, Z.; Geldbach, T. J.; Scopelliti, R.; Dyson, P. J. *J. Am. Chem. Soc.* **2004**, *126*, 15876–15882.
113. Dupont, J.; Spencer, J. *Angew. Chem., Int. Ed.* **2004**, *43*, 5296–5297.
114. Franks, F. *Chem. unserer Zeit* **1986**, *20*, 146–155.
115. Fonseca, G. S.; Umpierre, A. P.; Fichtner, P. F. P.; Teixeira, S. R.; Dupont, J. *Chem., Eur. J.* **2003**, *9*, 3263–3269.
116. Swatloski, R. P.; Holbrey, J. D.; Rogers, R. D. *Green Chem.* **2003**, *5*, 361–363.
117. Suarez, P. A. Z.; Dullius, J. E. L.; Einloft, S.; deSouza, R. F.; Dupont, J. *Inorg. Chim. Acta* **1997**, *255*, 207–209.
118. Bradley, A. E.; Hatter, J. E.; Nieuwenhuyzen, M.; Pitner, W. R.; Seddon, K. R.; Thied, R. C. *Inorg. Chem.* **2002**, *41*, 1692–1694.
119. Jensen, M. P.; Neuefeind, J.; Beitz, J. V.; Skanthakumar, S.; Soderholm, L. *J. Am. Chem. Soc.* **2003**, *125*, 15466–15473.
120. Amyes, T. L.; Diver, S. T.; Richard, J. P.; Rivas, F. M.; Toth, K. *J. Am. Chem. Soc.* **2004**, *126*, 4366–4374.
121. Arduengo, A. J. *Acc. Chem. Res.* **1999**, *32*, 913–921.
122. Xu, L. J.; Chen, W. P.; Xiao, J. L. *Organometallics* **2000**, *19*, 1123–1127.
123. Hasan, M.; Kozhevnikov, I. V.; Siddiqui, M. R. H.; Femoni, C.; Steiner, A.; Winterton, N. *Inorg. Chem.* **2001**, *40*, 795–800.
124. Clement, N. D.; Cavell, K. J.; Jones, C.; Elsevier, C. J. *Angew. Chem., Int. Ed.* **2004**, *43*, 1277–1279.
125. McGuinness, D. S.; Cavell, K. J.; Yates, B. F. *Chem. Commun.* **2001**, 355–356.
126. Lebel, H.; Janes, M. K.; Charette, A. B.; Nolan, S. P. *J. Am. Chem. Soc.* **2004**, *126*, 5046–5047.
127. Adams, C. J.; Earle, M. J.; Roberts, G.; Seddon, K. R. *Chem. Commun.* **1998**, 2097–2098.
128. Csihony, S.; Mehdi, H.; Homonnay, Z.; Vertes, A.; Farkas, O.; Horvath, I. T. *J. Chem. Soc., Dalton Trans.* **2002**, 680.
129. Boon, J. A.; Levisky, J. A.; Pflug, J. L.; Wilkes, J. S. *J. Org. Chem.* **1986**, *51*, 480–483.
130. Kim, D. S.; Ahn, W. S. *Kor. J. Chem. Eng.* **2003**, *20*, 39–43.
131. Yeung, K. S.; Farkas, M. E.; Qiu, Z. L.; Yang, Z. *Tetrahedron Lett.* **2002**, *43*, 5793–5795.
132. Koch, V. R.; Miller, L. L.; Osteryoung, R. A. *J. Am. Chem. Soc.* **1976**, *98*, 5277–5284.
133. Chauvin, Y.; Hirschauer, A.; Olivier, H. *J. Mol. Catal.* **1994**, *92*, 155–165.
134. Luer, G. D.; Bartak, D. E. *J. Org. Chem.* **1982**, *47*, 1238–1243.
135. Kemperman, G. J.; Roeters, T. A.; Hilberink, P. W. *Eur. J. Org. Chem.* **2003**, 1681.
136. Green, L.; Hemeon, I.; Singer, R. D. *Tetrahedron Lett.* **2000**, *41*, 1343–1346.
137. Potdar, M. K.; Mohile, S. S.; Salunkhe, M. M. *Tetrahedron Lett.* **2001**, *42*, 9285–9287.
138. Harjani, J. R.; Nara, S. J.; Salunkhe, M. M. *Tetrahedron Lett.* **2002**, *43*, 1127–1130.
139. Rebeiro, G. L.; Khadilkar, B. M. *Synthesis* **2001**, 370–372.
140. Paul, A. M.; Khandekar, A. C.; Khadilkar, B. M. *J. Chem. Res., Synop.* **2003**, 168–169.
141. Deng, Y. Q.; Shi, F.; Beng, J. J.; Qiao, K. *J. Mol. Catal. A: Chem.* **2001**, *165*, 33–36.
142. Lee, C. W. *Tetrahedron Lett.* **1999**, *40*, 2461–2464.
143. Yadav, J. S.; Reddy, B. V. S.; Reddy, M. S.; Niranjan, N.; Prasad, A. R. *Eur. J. Org. Chem.* **2003**, 1779–1783.
144. Yanes, E. G.; Gratz, S. R.; Baldwin, M. J.; Robison, S. E.; Stalcup, A. M. *Anal. Chem.* **2001**, *73*, 3838–3844.
145. Silveira, E. T.; Umpierre, A. P.; Rossi, L. M.; Machado, G.; Morais, J.; Soares, G. V.; Baumvol, I. L. R.; Teixeira, S. R.; Fichtner, P. F. P.; Dupont, J. *Chem. Eur. J.* **2004**, *10*, 3734–3740.
146. Favre, F.; Olivier-Bourbigou, H.; Commereuc, D.; Saussine, L. *Chem. Commun.* **2001**, 1360–1361.
147. Brasse, C. C.; Englert, U.; Salzer, A.; Waffenschmidt, H.; Wasserscheid, P. *Organometallics* **2000**, *19*, 3818–3823.
148. Bronger, R. P. J.; Silva, S. M.; Kamer, P. C. J.; van Leeuwen, P. *Chem. Commun.* **2002**, 3044–3045.
149. Picquet, M.; Stutzmann, S.; Tkatchenko, I.; Tommasi, I.; Zimmermann, J.; Wasserscheid, P. *Green Chem.* **2003**, *5*, 153–162.
150. Geldbach, T. J.; Dyson, P. J. *J. Organomet. Chem.* **2005**, *690*, 3552–3557.
151. Dyson, P. J.; Ellis, D. J.; Parker, D. G.; Welton, T. *Chem. Commun.* **1999**, 25–26.
152. Dyson, P. J.; Ellis, D. J.; Henderson, W.; Laurenczy, G. *Adv. Synth. Catal.* **2003**, *345*, 216–221.
153. Wolfson, A.; Vankelecom, I. F. J.; Jacobs, P. A. *Tetrahedron Lett.* **2005**, *46*, 2513–2516.
154. Suarez, T.; Fontal, B.; Reyes, M.; Bellandi, F.; Contreras, R. R.; Ortega, J. M.; Leon, G.; Cancines, P.; Castillo, B. *React. Kinet. Catal. Lett.* **2004**, *82*, 325–331.

155. Zhao, D. B.; Fei, Z. F.; Scopelliti, R.; Dyson, P. J. *Inorg. Chem.* **2004**, *43*, 2197–2205.
156. Zhao, D. B.; Dyson, P. J.; Laurenczy, G.; McIndoe, S. *J. Mol. Catal. A: Chem.* **2004**, *214*, 19–25.
157. Dupont, J.; Suarez, P. A. Z.; Umpierre, A. P.; de Souza, R. F. *J. Brazil. Chem. Soc.* **2000**, *11*, 293–297.
158. Steines, S.; Wasserscheid, P.; Drieben-Holscher, B. *J. Prakt. Chem.* **2000**, *342*, 348–354.
159. Dyson, P. J.; Ellis, D. J.; Welton, T. *Can. J. Chem.* **2001**, *79*, 705–708.
160. Fonseca, G. S.; Scholten, J. D.; Dupont, J. *Synlett* **2004**, 1525–1528.
161. Muller, L. A.; Dupont, J.; de Souza, R. F. *Macromol. Rapid Commun.* **1998**, *19*, 409–411.
162. Wei, L.; Jiang, J. Y.; Wang, Y. H.; Jin, Z. L. *Chin. Chem. Lett.* **2005**, *16*, 338–340.
163. Wei, L.; Jiang, J. Y.; Wang, Y. H.; Jin, Z. L. *J. Mol. Catal. A: Chem.* **2004**, *221*, 47–50.
164. MacLeod, S.; Rosso, R. J. *Adv. Synth. Catal.* **2003**, *345*, 568–571.
165. Navarro, J.; Sagi, M.; Sola, E.; Lahoz, F. J.; Dobrinovitch, I. T.; Katho, A.; Joo, F.; Oro, L. A. *Adv. Synth. Catal.* **2003**, *345*, 280–288.
166. Arhancet, J. P.; Davis, M. E.; Merola, J. S.; Hanson, B. E. *Nature* **1989**, *339*, 454–455.
167. Mehnert, C. P.; Mozeleski, E. J.; Cook, R. A. *Chem. Commun.* **2002**, 3010–3011.
168. Pugin, B.; Studer, M.; Kuesters, E.; Sedelmeier, G.; Feng, X. *Adv. Synth. Catal.* **2004**, *346*, 1481–1486.
169. Monteiro, A. L.; Zinn, F. K.; DeSouza, R. F.; Dupont, J. *Tetrahedron: Asymmetry* **1997**, *8*, 177–179.
170. Jessop, P. G.; Stanley, R. R.; Brown, R. A.; Eckert, C. A.; Liotta, C. L.; Ngo, T. T.; Pollet, P. *Green Chem.* **2003**, *5*, 123–128.
171. Liu, F. C.; Abrams, M. B.; Baker, R. T.; Tumas, W. *Chem. Commun.* **2001**, 433–434.
172. Brown, R. A.; Pollet, P.; McKoon, E.; Eckert, C. A.; Liotta, C. L.; Jessop, P. G. *J. Am. Chem. Soc.* **2001**, *123*, 1254–1255.
173. Lee, S. G.; Zhang, Y. J.; Piao, J. Y.; Yoon, H.; Song, C. E.; Choi, J. H.; Hong, J. *Chem. Commun.* **2003**, 2624–2625.
174. Hu, A. G.; Ngo, H. L.; Lin, W. B. *Angew. Chem., Int. Ed.* **2004**, *43*, 2501–2504.
175. Zhu, Y.; Carpenter, K.; Bun, C. C.; Bahnmueller, S.; Ke, C. P.; Srid, V. S.; Kee, L. W.; Hawthorne, M. F. *Angew. Chem., Int. Ed.* **2003**, *42*, 3792–3795.
176. Solinas, M.; Wasserscheid, P.; Leitner, W.; Pfaltz, A. *Chem. Ing. Tech.* **2003**, *75*, 1153.
177. Giernoth, R.; Krumm, M. S. *Adv. Synth. Catal.* **2004**, *346*, 989–992.
178. Berthod, M.; Joerger, J. M.; Mignani, G.; Vaultier, M.; Lemaire, M. *Tetrahedron: Asymmetry* **2004**, *15*, 2219–2221.
179. Berthod, M.; Saluzzo, C.; Mignani, G.; Lemaire, M. *Tetrahedron: Asymmetry* **2004**, *15*, 639–645.
180. Geldbach, T. J.; Dyson, P. J. *J. Am. Chem. Soc.* **2004**, *126*, 8114–8115.
181. Kawasaki, I.; Tsunoda, K.; Tsuji, T.; Yamaguchi, T.; Shibuta, H.; Uchida, N.; Yamashita, M.; Ohta, S. *Chem. Commun.* **2005**, 2134–2136.
182. Ngo, H. L.; Hu, A. G.; Lin, W. B. *Tetrahedron Lett.* **2005**, *46*, 595–597.
183. Ngo, H. L.; Hu, A. G.; Lin, W. B. *Chem. Commun.* **2003**, 1912–1913.
184. Comyns, C.; Karodia, N.; Zeler, S.; Andersen, J. A. *Catal. Lett.* **2000**, *67*, 113–115.
185. Parshall, G. W. *J. Am. Chem. Soc.* **1972**, *94*, 8716–8719.
186. Illner, P.; Zahl, A.; Puchta, R.; van Eikema, H. N.; Wasserscheid, P.; van Eldik, R. *J. Organomet. Chem.* **2005**, *690*, 3567–3576.
187. Knifton, J. F. *J. Mol. Catal.* **1987**, *43*, 65–78.
188. Knifton, J. F. *J. Mol. Catal.* **1988**, *47*, 99–116.
189. Mitsudo, T.; Suzuki, N.; Kondo, T.; Watanabe, Y. *J. Mol. Catal. A: Chem.* **1996**, *109*, 219–225.
190. Tominaga, K.; Sasaki, Y. *Chem. Lett.* **2004**, *33*, 14–15.
191. Magna, L.; Olivier, B. H.; Saussine, L.; Kruger-Tissot, V. Hydroformylation process using a cobalt catalyst in a non-aqueous ionic liquid with catalyst recycle. 2003-290842. EP 1352889 to IFP.
192. Karodia, N.; Guise, S.; Newlands, C.; Andersen, J. A. *Chem. Commun.* **1998**, 2341–2342.
193. Kong, F. Z.; Jiang, J. Y.; Jin, Z. L. *Catal. Lett.* **2004**, *96*, 63–65.
194. Keim, W.; Vogt, D.; Waffenschmidt, H.; Wasserscheid, P. *J. Catal.* **1999**, *186*, 481–484.
195. Silva, S. M.; Bronger, R. P. J.; Freixa, Z.; Dupont, J.; van Leeuwen, P. *New J. Chem.* **2003**, *27*, 1294–1296.
196. Mehnert, C. P.; Cook, R. A.; Dispenziere, N. C.; Mozeleski, E. J. *Polyhedron* **2004**, *23*, 2679–2688.
197. Ohlin, C. A.; Dyson, P. J.; Laurenczy, G. *Chem. Commun.* **2004**, 1070–1071.
198. Bronger, R. P. J.; Silva, S. M.; Kamer, P. C. J.; van Leeuwen, P. *Dalton Trans.* **2004**, 1590–1596.
199. Wasserscheid, P.; Waffenschmidt, H.; Machnitzki, P.; Kottsieper, K. W.; Stelzer, O. *Chem. Commun.* **2001**, 451–452.
200. Kottsieper, K. W.; Stelzer, O.; Wasserscheid, P. *J. Mol. Catal. A: Chem.* **2001**, *175*, 285–288.
201. Omotowa, B. A.; Shreeve, J. M. *Organometallics* **2004**, *23*, 783–791.
202. Yang, Y.; Lin, H. Q.; Deng, C. X.; She, J. R.; Yuan, Y. Z. *Chem. Lett.* **2005**, *34*, 220–221.
203. Mehnert, C. P.; Cook, R. A.; Dispenziere, N. C.; Afeworki, M. *J. Am. Chem. Soc.* **2002**, *124*, 12932–12933.
204. Leitner, W. *Pure Appl. Chem.* **2004**, *76*, 635–644.
205. Sellin, M. F.; Webb, P. B.; Cole-Hamilton, D. J. *Chem. Commun.* **2001**, 781–782.
206. Riisager, A.; Wasserscheid, P.; van Hal, R.; Fehrmann, R. *J. Catal.* **2003**, *219*, 452–455.
207. Webb, P. B.; Sellin, M. F.; Kunene, T. E.; Williamson, S.; Slawin, A. M. Z.; Cole-Hamilton, D. J. *J. Am. Chem. Soc.* **2003**, *125*, 15577–15588.
208. Riisager, A.; Fehrmann, R.; Flicker, S.; van Hal, R.; Haumann, M.; Wasserscheid, P. *Angew. Chem., Int. Edit.* **2005**, *44*, 815–819.
209. Riisager, A.; Eriksen, K. M.; Wasserscheid, P.; Fehrmann, R. *Catal. Lett.* **2003**, *90*, 149–153.
210. Monteiro, A. L.; Seferin, M.; Dupont, J.; deSouza, R. F. *Tetrahedron Lett.* **1996**, *37*, 1157–1160.
211. Calo, V.; Giannoccaro, P.; Nacci, A.; Monopoli, A. *J. Organomet. Chem.* **2002**, *645*, 152–157.
212. Mizushima, E.; Hayashi, T.; Tanaka, M. *Top. Catal.* **2004**, *29*, 163–166.
213. Mizushima, E.; Hayashi, T.; Tanaka, M. *Green Chem.* **2001**, *3*, 76–79.
214. Shi, F.; Peng, J.; Deng, Y. *J. Catal.* **2003**, *219*, 372–375.
215. Consorti, C. S.; Ebeling, G.; Dupont, J. *Tetrahedron Lett.* **2002**, *43*, 753–755.
216. Sunderme, W. *Angew. Chem., Int. Ed.* **1965**, *4*, 222–238.
217. Alcantara, R.; Canoira, L.; Joao, P. G.; Santos, J. M.; Vazquez, I. *Appl. Catal. A: Gen.* **2000**, *203*, 259–268.
218. Li, Z.; Xia, C.-G.; Xu, C.-Z. *Tetrahedron Lett.* **2003**, *44*, 9229–9232.
219. Li, Z.; Xia, C. G. *J. Mol. Catal. A: Chem.* **2004**, *214*, 95–101.
220. Nanjundiah, C.; Osteryoung, R. A. *J. Electrochem. Soc.* **1983**, *130*, 1312.
221. Howarth, J. *Tetrahedron Lett.* **2000**, *41*, 6627–6629.
222. Farmer, V.; Welton, T. *Green Chem.* **2002**, *4*, 97–102.

223. Wolfson, A.; Wuyts, S.; De Vos, D. E.; Vankelecom, I. F. J.; Jacobs, P. A. *Tetrahedron Lett.* **2002**, *43*, 8107–8110.
224. Seddon, K. R.; Stark, A. *Green Chem.* **2002**, *4*, 119–123.
225. Chhikara, B. S.; Tehlan, S.; Kumar, A. *Synlett* **2005**, 63–66.
226. Chhikara, B. S.; Chandra, R.; Tandon, V. *J. Catal.* **2005**, *230*, 436–439.
227. Wu, X. E.; Ma, L.; Ding, M. X.; Gao, L. X. *Chem. Lett.* **2005**, *34*, 312–313.
228. Jain, N.; Kumar, A.; Chauhan, S. M. S. *Tetrahedron Lett.* **2005**, *46*, 2599–2602.
229. Namboodiri, V. V.; Varma, R. S.; Sahle-Demessie, E.; Pillai, U. R. *Green Chem.* **2002**, *4*, 170–173.
230. Chauhan, S. M. S.; Kumar, A.; Srinivas, K. A. *Chem. Commun.* **2003**, 2348–2349.
231. Bernini, R.; Coratti, A.; Provenzano, G.; Fabrizi, G.; Tofani, D. *Tetrahedron* **2005**, *61*, 1821–1825.
232. Bernini, R.; Coratti, A.; Fabrizi, G.; Goggiamani, A. *Tetrahedron Lett.* **2003**, *44*, 8991–8994.
233. Sun, H.; Harms, K.; Sundermeyer, J. *J. Am. Chem. Soc.* **2004**, *126*, 9550–9551.
234. Owens, G. S.; Abu-Omar, M. M. *Chem. Commun.* **2000**, 1165–1166.
235. Owens, G. S.; Durazo, A.; Abu-Omar, M. M. *Chem. Eur. J.* **2002**, *8*, 3053–3059.
236. Srinivas, K. A.; Kumar, A.; Chauhan, S. M. S. *Chem. Commun.* **2002**, 2456–2457.
237. Li, Z.; Xia, C.-G. *Tetrahedron Lett.* **2003**, *44*, 2069–2071.
238. Li, Z.; Xia, C. G.; Ji, M. *Appl. Catal. A: Gen.* **2003**, *252*, 17–21.
239. Valente, A. A.; Petrovski, Z.; Branco, L. C.; Afonso, C. A. M.; Pillinger, M.; Lopes, A. D.; Romao, C. C.; Nunes, C. D.; Goncalves, I. S. *J. Mol. Catal. A: Chem.* **2004**, *218*, 5–11.
240. Kuehn, F. E.; Zhao, J.; Abrantes, M.; Sun, W.; Afonso, C. A. M.; Branco, L. C.; Goncalves, I. S.; Pillinger, M.; Romao, C. C. *Tetrahedron Lett.* **2004**, *46*, 47–52.
241. Tong, K.-H.; Wong, K.-Y.; Chan, T. H. *Org. Lett.* **2003**, *5*, 3423–3425.
242. Song, C. E.; Roh, E. J. *Chem. Commun.* **2000**, 837–838.
243. Gaillon, L.; Bedioui, F. *Chem. Commun.* **2001**, 1458–1459.
244. Smith, K.; Liu, S.; El-Hiti, G. A. *Catal. Lett.* **2004**, *98*, 95–101.
245. Liu, Q.; Zhang, Z.; van Rantwijk, F.; Sheldon, R. A. *J. Mol. Catal. A: Chem.* **2004**, *224*, 213–216.
246. Branco, L. C.; Afonso, C. A. M. *J. Org. Chem.* **2004**, *69*, 4381–4389.
247. Song, C. E.; Jung, D.-u.; Roh, E. J.; Lee, S.-g.; Chi, D. Y. *Chem. Commun.* **2002**, 3038–3039.
248. Yanada, R.; Takemoto, Y. *Tetrahedron Lett.* **2002**, *43*, 6849–6851.
249. Branco, L. C.; Serbanovic, A.; Nunes da Ponte, M.; Afonso, C. A. M. *Chem. Commun.* **2005**, 107–109.
250. Stenzel, O.; Brull, R.; Wahner, U. M.; Sanderson, R. D.; Raubenheimer, H. G. *J. Mol. Catal. A: Chem.* **2003**, *192*, 217–222.
251. Chauvin, Y.; Olivierbourbigou, H. *Chem. Tech.* **1995**, *25*, 26–30.
252. Einloft, S.; Dietrich, F. K.; DeSouza, R. F.; Dupont, J. *Polyhedron* **1996**, *15*, 3257–3259.
253. Chauvin, Y.; Olivier, H.; Wyrvalski, C. N.; Simon, L. C.; de Souza, R. F. *J. Catal.* **1997**, *165*, 275–278.
254. Simon, L. C.; Dupont, J.; de Souza, R. F. *Appl. Catal. A: Gen.* **1998**, *175*, 215–220.
255. Ellis, B.; Keim, W.; Wasserscheid, P. *Chem. Commun.* **1999**, 337–338.
256. Bernardo-Gusmao, K.; Queiroz, L. F. T.; de Souza, R. F.; Leca, F.; Loup, C.; Reau, R. *J. Catal.* **2003**, *219*, 59–62.
257. Olivier, H.; Laurent-Gerot, P. *J. Mol. Catal. A: Chem.* **1999**, *148*, 43–48.
258. Olivier-Bourbigou, H.; Lecocq, V. *Stud. Surf. Sci. Catal.* **2003**, *145*, 55–60.
259. Wasserscheid, P.; Hilgers, C.; Keim, W. *J. Mol. Catal. A: Chem.* **2004**, *214*, 83–90.
260. Ranwell, A.; Tshamano, M. A. *ACS Symp. Ser.* **2002**, *818*, 147–160.
261. Olivier-Bourbigou, H.; Travers, P.; Chadorge, J. A. *Petr. Tech. Quat.* **1999**, 141–149.
262. Ligabue, R. A.; Dupont, J.; de Souza, R. F. *J. Mol. Catal. A: Chem.* **2001**, *169*, 11–17.
263. Silva, S. M.; Suarez, P. A. Z.; de Souza, R. F.; Dupont, J. *Polym. Bull.* **1998**, *40*, 401–405.
264. Kabalka, G. W.; Dong, G.; Venkataiah, B. *Tetrahedron Lett.* **2004**, *45*, 2775–2777.
265. Carlin, R. T.; Wilkes, J. S. *J. Mol. Catal.* **1990**, *63*, 125–129.
266. Suarez, P. A. Z.; Rosa, N. T.; Einloft, S.; de Souza, R. F.; Dick, Y. P. *Polym. Bull.* **1998**, *41*, 175–182.
267. Pinheiro, M. F.; Mauler, R. S.; de Souza, R. F. *Macromol. Rapid Commun.* **2001**, *22*, 425–428.
268. Escher, F. F. N.; Mauler, R. S.; de Souza, R. F. *J. Braz. Chem. Soc.* **2001**, *12*, 47–51.
269. Trzeciak, A. M.; Ziolkowski, J. J. *Appl. Organomet. Chem.* **2004**, *18*, 124–129.
270. Mastrorilli, P.; Nobile, C. F.; Gallo, V.; Suranna, G. P.; Farinola, G. *J. Mol. Catal. A: Chem.* **2002**, *184*, 73–78.
271. Mastrorilli, P.; Nobile, C. F.; Gallo, V.; Suranna, G. P.; Giannandrea, R. *Stud. Surf. Sci. Catal.* **2003**, *145*, 535–536.
272. Mastrorilli, P.; Nobile, C. F.; Gallo, V.; Suranna, G. P.; Giannandrea, R. Rhodium (I) Catalysed Polymerization of Phenylacetylene in Ionic Liquids. *Studies in Surface Science and Catalysis* **2003**, *145*, 535–536.
273. Csihony, S.; Fischmeister, C.; Bruneau, C.; Horvath, I. T.; Dixneuf, P. H. *New J. Chem.* **2002**, *26*, 1667–1670.
274. Carmichael, A. J.; Haddleton, D. M.; Bon, S. A. F.; Seddon, K. R. *Chem. Commun.* **2000**, 1237–1238.
275. Hong, H. L.; Zhang, H. W.; Mays, J. W.; Visser, A. E.; Brazel, C. S.; Holbrey, J. D.; Reichert, W. M.; Rogers, R. D. *Chem. Commun.* **2002**, 1368–1369.
276. Biedron, T.; Kubisa, P. *J. Polym. Sci., Part A: Polym. Chem.* **2004**, *42*, 3230–3235.
277. Vijayaraghavan, R.; MacFarlane, D. R. *Chem. Commun.* **2004**, 700–701.
278. Vijayaraghavan, R.; MacFarlane, D. R. *Chem. Commun.* **2005**, 1149–1151.
279. Chauvin, Y.; Di Marco Van Tiggelen, F.; Di Marco-Van Tiggelen, F. 400041 10 Jan 1995. EP 665057 to IFP.
280. Vasnev, A. V.; Greish, A. A.; Kustov, L. M. *Rus. Chem. Bull.* **2004**, *53*, 2187–2191.
281. Vasnev, A. V.; Greish, A. A.; Kustov, L. M. *Mendeleev Commun.* **2004**, 59–61.
282. Martinez, V.; Blais, J.-C.; Astruc, D. *Org. Lett.* **2002**, *4*, 651–653.
283. Buijsman, R. C.; van Vuuren, E.; Sterrenburg, J. G. *Org. Lett.* **2001**, *3*, 3785–3787.
284. Semeril, D.; Olivier-Bourbigou, H.; Bruneau, C.; Dixneuf, P. H. *Chem. Commun.* **2002**, 146–147.
285. Mayo, K. G.; Nearhoof, E. H.; Kiddle, J. J. *Org. Lett.* **2002**, *4*, 1567–1570.
286. Audic, N.; Clavier, H.; Mauduit, M.; Guillemin, J. C. *J. Am. Chem. Soc.* **2003**, *125*, 9248–9249.
287. Yao, Q.; Zhang, Y. *Angew. Chem., Int. Ed.* **2003**, *42*, 3395–3398.
288. Clavier, H.; Audic, N.; Mauduit, M.; Guillemin, J.-C. *Chem. Commun.* **2004**, 2282–2283.

289. Yao, Q.; Sheets, M. *J. Organomet. Chem.* **2005**, *690*, 3577–3584.
290. Clavier, H.; Audic, N.; Guillemin, J. C.; Mauduit, M. *J. Organomet. Chem.* **2005**, *690*, 3585–3599.
291. Picquet, M.; Tkatchenko, I.; Tommasi, I.; Wasserscheid, P.; Zimmermann, J. *Adv. Synth. Catal.* **2003**, *345*, 959–962.
292. Magna, L.; Chauvin, Y.; Niccolai, G. P.; Basset, J.-M. *Organometallics* **2003**, *22*, 4418–4425.
293. Fonseca, G. S.; de Souza, R. F.; Dupont, J. *Catal. Commun.* **2002**, *3*, 377–380.
294. Jeffery, T. *Tetrahedron Lett.* **1985**, *26*, 2667–2670.
295. Jeffery, T. *J. Chem. Soc., Chem. Commun.* **1984**, 1287–1289.
296. Kaufmann, D. E.; Nouroozian, M.; Henze, H. *Synlett* **1996**, 1091–1092.
297. Bohm, V. P. W.; Herrmann, W. A. *Chem. Eur. J.* **2000**, *6*, 1017–1025.
298. Herrmann, W. A.; Bohm, V. P. W. *J. Organomet. Chem.* **1999**, *572*, 141–145.
299. Calo, V.; Nacci, A.; Lopez, L.; Mannarini, N. *Tetrahedron Lett.* **2000**, *41*, 8973–8976.
300. Calo, V.; Nacci, A.; Monopoli, A.; Lopez, L.; di Cosmo, A. *Tetrahedron* **2001**, *57*, 6071–6077.
301. Selvakumar, K.; Zapf, A.; Beller, M. *Org. Lett.* **2002**, *4*, 3031–3033.
302. Carmichael, A. J.; Earle, M. J.; Holbrey, J. D.; McCormac, P. B.; Seddon, K. R. *Org. Lett.* **1999**, *1*, 997–1000.
303. Howarth, J.; Dallas, A. *Molecules* **2000**, *5*, 851–855.
304. Vallin, K. S. A.; Emilsson, P.; Larhed, M.; Hallberg, A. *J. Org. Chem.* **2002**, *67*, 6243–6246.
305. Handy, S. T.; Okello, M.; Dickenson, G. *Org. Lett.* **2003**, *5*, 2513–2515.
306. Handy, S. T.; Okello, M. *Tetrahedron Lett.* **2003**, *44*, 8395–8397.
307. Park, S. B.; Alper, H. *Org. Lett.* **2003**, *5*, 3209–3212.
308. Zheng, R.; Yang, F.; Zou, G.; Tang, J.; He, M.-Y. *Chin. J. Chem.* **2003**, *21*, 1111–1113.
309. Zou, G.; Wang, Z.; Zhu, J.; Tang, J.; He, M. Y. *J. Mol. Catal. A: Chem.* **2003**, *206*, 193–198.
310. Gerritsma, D. A.; Robertson, A.; McNulty, J.; Capretta, A. *Tetrahedron Lett.* **2004**, *45*, 7629–7631.
311. McNulty, J.; Capretta, A.; Cheekoori, S.; Clyburne, J. A. C.; Robertson, A. J. *Chim. Oggi* **2004**, *22*, 13–16.
312. Okubo, K.; Shirai, M.; Yokoyama, C. *Tetrahedron Lett.* **2002**, *43*, 7115–7118.
313. Hagiwara, H.; Sugawara, Y.; Isobe, K.; Hoshi, T.; Suzuki, T. *Org. Lett.* **2004**, *6*, 2325–2328.
314. Corma, A.; Garcia, H.; Leyva, A. *Tetrahedron* **2004**, *60*, 8553–8560.
315. Liu, S.; Fukuyama, T.; Sato, M.; Ryu, I. *Org. Proc. Res. Dev.* **2004**, *8*, 477–481.
316. Liu, S.; Fukuyama, T.; Sato, M.; Ryu, I. *Synlett* **2004**, 1814–1816.
317. Xiao, J. C.; Twamley, B.; Shreeve, J. M. *Org. Lett.* **2004**, *6*, 3845–3847.
318. Kiss, L.; Papp, G.; Joo, F.; Antus, S. *Heterocycl. Commun.* **2001**, *7*, 417–420.
319. Kiss, L.; Kurtan, T.; Antus, S.; Brunner, H. *ARKIVOC* **2003**, 69–76.
320. Xie, X.; Chen, B.; Lu, J.; Han, J.; She, X.; Pan, X. *Tetrahedron Lett.* **2004**, *45*, 6235–6237.
321. Mo, J.; Xu, L.; Xiao, J. *J. Am. Chem. Soc.* **2005**, *127*, 751–760.
322. Xu, L.; Chen, W.; Xiao, J. *Organometallics* **2000**, *19*, 1123–1127.
323. Cassol, C. C.; Umpierre, A. P.; Machado, G.; Wolke, S. I.; Dupont, J. *J. Am. Chem. Soc.* **2005**, *127*, 3298–3299.
324. Calo, V.; Nacci, A.; Monopoli, A.; Fornaro, A.; Sabbatini, L.; Cioffi, N.; Ditaranto, N. *Organometallics* **2004**, *23*, 5154–5158.
325. Calo, V.; Nacci, A.; Monopoli, A.; Detomaso, A.; Iliade, P. *Organometallics* **2003**, *22*, 4193–4197.
326. Hamill, N. A.; Hardacre, C.; McMath, S. E. J. *Green Chem.* **2002**, *4*, 139–142.
327. Deshmukh, R. R.; Rajagopal, R.; Srinivasan, K. V. *Chem. Commun.* **2001**, 1544–1545.
328. Mathews, C. J.; Smith, P. J.; Welton, T. *Chem. Commun.* **2000**, 1249–1250.
329. McLachlan, F.; Mathews, C. J.; Smith, P. J.; Welton, T. *Organometallics* **2003**, *22*, 5350–5357.
330. Mathews, C. J.; Smith, P. J.; Welton, T. *J. Mol. Catal. A: Chem.* **2004**, *214*, 27–32.
331. Zhao, D. B.; Fei, Z. F.; Geldbach, T. J.; Scopelliti, R.; Dyson, P. J. *J. Am. Chem. Soc.* **2004**, *126*, 15876–15882.
332. Xiao, J.-C.; Shreeve, J. n. M. *J. Org. Chem.* **2005**, *70*, 3072–3078.
333. McNulty, J.; Capretta, A.; Wilson, J.; Dyck, J.; Adjabeng, G.; Robertson, A. *Chem. Commun.* **2002**, 1986–1987.
334. Rajagopal, R.; Jarikote, D. V.; Srinivasan, K. V. *Chem. Commun.* **2002**, 616–617.
335. Yang, C. H.; Tai, C. C.; Huang, Y. T.; Sun, I. W. *Tetrahedron* **2005**, *61*, 4857–4861.
336. Revell, J. D.; Ganesan, A. *Org. Lett.* **2002**, *4*, 3071–3073.
337. Mathews, C. J.; Smith, P. J.; Welton, T.; White, A. J. P.; Williams, D. J. *Organometallics* **2001**, *20*, 3848–3850.
338. Kabalka, G. W.; Venkataiah, B.; Das, B. C. *Green Chem.* **2002**, *4*, 472–473.
339. Gordon, C. M.; McCluskey, A. *Chem. Commun.* **1999**, 1431–1432.
340. Gordon, C. M.; Ritchie, C. *Green Chem.* **2002**, *4*, 124–128.
341. Lu, J.; Ji, S.-J.; Qian, R.; Chen, J.-P.; Liu, Y.; Loh, T.-P. *Synlett* **2004**, 534–536.
342. Howarth, J.; James, P.; Dai, J. *J. Mol. Catal. A: Chem.* **2004**, *214*, 143–146.
343. Lu, J.; Ji, S.-J.; Loh, T.-P. *Chem. Commun.* **2005**, 2345–2347.
344. Chen, W.; Xu, L.; Chatterton, C.; Xiao, J. *Chem. Commun.* **1999**, 1247–1248.
345. Toma, S.; Gotov, B.; Kmentova, I.; Solcaniova, E. *Green Chem.* **2000**, *2*, 149–151.
346. Kmentova, I.; Gotov, B.; Solcaniova, E.; Toma, S. *Green Chem.* **2002**, *4*, 103–106.
347. Ross, J.; Chen, W.; Xu, L.; Xiao, J. *Organometallics* **2001**, *20*, 138–142.
348. Ross, J.; Xiao, J. *Chem. Eur. J.* **2003**, *9*, 4900–4906.
349. De Bellefon, C.; Pollet, E.; Grenouillet, P. *J. Mol. Catal. A: Chem.* **1999**, *145*, 121–126.
350. Liao, M.-C.; Duan, X.-H.; Liang, Y.-M. *Tetrahedron Lett.* **2005**, *46*, 3469–3472.
351. Kabalka, G. W.; Dong, G.; Venkataiah, B. *Org. Lett.* **2003**, *5*, 893–895.
352. Chiappe, C.; Imperato, G.; Napolitano, E.; Pieraccini, D. *Green Chem.* **2004**, *6*, 33–36.
353. Handy, S. T.; Zhang, X. *Org. Lett.* **2001**, *3*, 233–236.
354. Kmentova, I.; Gotov, B.; Gajda, V.; Toma, S. *Monatsh. Chem.* **2003**, *134*, 545–549.
355. Cacchi, S.; Fabrizi, G.; Goggiamani, A.; Moreno-Manas, M.; Vallribera, A. *Tetrahedron Lett.* **2002**, *43*, 5537–5540.
356. Hemeon, I.; Singer, R. D. *Chem. Commun.* **2002**, 1884–1885.
357. Hemeon, I.; Singer, R. D. *J. Mol. Catal. A: Chem.* **2004**, *214*, 33–44.
358. Okazaki, H.; Kawanami, Y.; Yamamoto, K. *Chem. Lett.* **2001**, 650–651.

359. Neff, V.; Mueller, T. E.; Lercher, J. A. *Chem. Commun.* **2002**, 906–907.
360. Rosa, J. N.; Santos, A. G.; Afonso, C. A. M. *J. Mol. Catal. A: Chem.* **2004**, *214*, 161–165.
361. Park, S. B.; Alper, H. *Chem. Commun.* **2005**, 1315–1317.
362. Yadav, J. S.; Reddy, B. V. S.; Naveenkumar, V.; Rao, R. S.; Nagaiah, K. *New J. Chem.* **2004**, *28*, 335–337.
363. Li, Z.; Wei, C.; Chen, L.; Varma, R. S.; Li, C.-J. *Tetrahedron Lett.* **2004**, *45*, 2443–2446.
364. Yadav, J. S.; Reddy, B. V. S.; Reddy, K. B.; Gayathri, K. U.; Prasad, A. R. *Tetrahedron Lett.* **2003**, *44*, 6493–6496.
365. Becheanu, A.; Laschat, S. *Synlett* **2002**, 1865–1867.
366. Yoshino, H.; Nomura, K.; Matsubara, S.; Oshima, K.; Matsumoto, K.; Hagiwara, R.; Ito, Y. *J. Fluorine Chem.* **2004**, *125*, 1127–1129.
367. Xu, L.-W.; Li, L.; Xia, C.-G.; Zhao, P.-Q. *Tetrahedron Lett.* **2004**, *45*, 2435–2438.
368. Yadav, J. S.; Reddy, B. V. S.; Basak, A. K.; Venkat Narsaiah, A. *Tetrahedron Lett.* **2003**, *44*, 1047–1050.
369. Song, C. E.; Oh, C. R.; Roh, E. J.; Choo, D. J. *Chem. Commun.* **2000**, 1743–1744.

1.31
Bioorganometallic Chemistry

N Metzler-Nolte, Ruhr-Universitaet Bochum, Bochum, Germany

1.31.1 Introduction

In a recent contribution to COMC (1995), Riordan pointed out that 'the phrase "bioorganometallic chemistry" is rather nebulous, conjuring different visions to various communities of scientists.' In one attempt to capture this breadth, bioorganometallic chemistry has been defined as "... the study of organometallic complexes with bioligands..., and the use of these derived complexes in a variety of applications and basic research studies...." It is rather a pleasure to see so many different fields combined under one conceptual roof. Bioorganometallic chemistry is certainly a hot and exciting development, given that for many years organometallic compounds were, by the great majority of researchers, believed to be highly sensitive and unstable to air and moisture. Today, we see that this notion was premature. There are many exciting uses of organometallic compounds in medicine, medicinal diagnostics

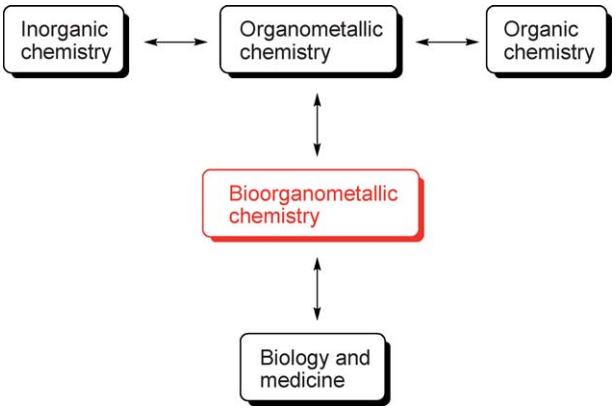

Figure 1

and bio-related analytics, molecular recognition of biomolecules, and bioprobes—to name just several important categories. On top of that, there is a growing number of organometallic compounds in nature. The most famous one, vitamin B_{12}, has been isolated in pure form about 60 years ago. Being a vital cofactor for a number of enzymatic transformations, it was long thought to be the only organometallic compound in nature. There is now well-founded evidence for organometallic intermediates and reactivity in over one dozen cases, and it is safe to forecast that this number will grow. Figure 1 tries to visualize the place of "bioorganometallic chemistry."

Recently, the first book entitled "*Bioorganometallic Chemistry*" was published.[1] It is obviously impossible to condense this book, which has over 440 pages, into this one single chapter. The author has chosen to give an overview of different aspects of what "bioorganometallics" means to him Several chapters in Volume 12 of this series cover selected aspects in more detail ("medicinal organometallic chemistry," "organometallic receptors," "organometallic compounds in biosensing," and "environmental and biological aspects of organometallic compounds"). An introductory chapter for students can be found in another book.[2] There are a number of reviews on the various subsections of this chapter, which are cited in the appropriate subsections. We have recently reviewed the bioorganometallic chemistry of ferrocene.[3] Volume 8 of *Comprehensive Coordination Chemistry II* (2003) has a number of excellent chapters on the model chemistry related to organometallic enzymes.

1.31.2 Naturally Occuring Organometallics

Organometallic compounds serve as cofactors, active sites, or intermediates in a number of biomolecules and biomolecular transformations. Compounds as yet identified are the cobalamins (vitamin B_{12} and derivatives), the hydrogenase enzyme family (H_2ases), acetyl coenzyme A synthase (ACS) and carbon monoxide dehydrogenase (COdH), and the Ni-containing reaction center in methyl coenzyme M reductase (F_{430}). These four classes are treated in more detail in the following sections. The discussion is, however, limited to the biological (organometallic) chemistry involved, and model complexes are not covered in any depth. Not treated are the other enzyme centers which exhibit reactivity that would typically be classified as "organometallic," such as the nitrogenase enzymes which convert atmospheric dinitrogen into ammonia under ambient conditions.[4] Iron carbene complexes may be involved in reductive dehalogenation reactions of cytochromes P_{450}.[5] Gaseous ethylene is an important signaling molecule for many plants.[6] It is effective at nanomolar concentrations, suggesting the presence of high-affinity receptors. It has been proposed that a Cu(I) center is involved in ethylene binding in *Arabidopsis* plants.[7] This is another beautiful example of bioorganometallic chemistry in nature, for which a model complex has been presented.[8]

1.31.2.1 Cobalamins

Cobalamins are a family of cobalt-containing cofactors, also known as the vitamin B_{12} family (Scheme 1). It was observed in the early 1900s that raw liver extracts could cure an otherwise fatal disease, pernicious anemia. In 1948, a red crystalline compound was isolated from liver extracts (cyanocobalamin), which was structurally characterized by Dorothy Hodgkin in 1956. These discoveries were honored by Nobel prizes in 1934 (to Whipple, Minot, and

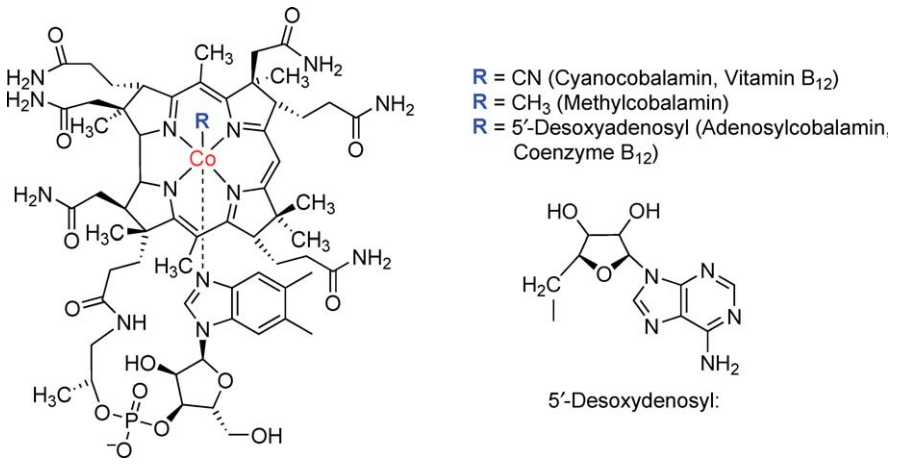

Scheme 1

Murphy) and 1964 (to Hodgkin). Methylcobalamin and adenosylcobalamin are the two biologically active cofactors. They are transformed into the stable cyanocobalamin during the isolation process. Cyanocobalamin or aquocobalamin is the active ingredient in vitamin B_{12}-containing medicines, both are converted into the physiologically active forms in the body. The cobalamins constitute the first, and for a long time the only, well-characterized examples of genuine organometallics in nature. There is an immense literature on cobalamins, including books and reviews on all the aspects of the enzymology, chemistry, and model compounds.[9–12] Therefore, only a few details are discussed here.

Cobalamins are unique cofactors from a synthetic point of view, which make use of the special properties of the metal–carbon bond.[13] They can provide carbanions ("nature's Grignard reagents"), carbocations, or carbon radicals. In the latter group, an adenosyl radical is released from coenzyme B_{12} which is used to initiate a 1,2-rearrangement. A classification has been proposed depending on the nature of the migrating and receiving groups (Scheme 2).[14,15] Class I enzymes are carbon-skeleton mutases (initial C–C bond breakage) and include glutamate mutase (GluM), 2-methyleneglutamate mutase (MGM), isobutyryl CoA mutase, and methylmalonyl CoA mutase (MMCM) (CoA = coenzyme A). The rearrangement of (*R*)-methylmalonyl CoA to succinyl CoA catalyzed by MMCM, which is probably the best-studied enzyme in this field, is shown in Scheme 3. Different crystal structures of MMCM from *Propionibacterium shermanii* have been solved by Mancia and co-workers. The first was reconstituted with desulfo-CoA,[16] while three structures were solved with adenosylcobalamin cofactor and the substrate as well as two inhibitors similar to substrate and products.[17] In these crystals, no adenosyl group could be detected bound to Co, as it was

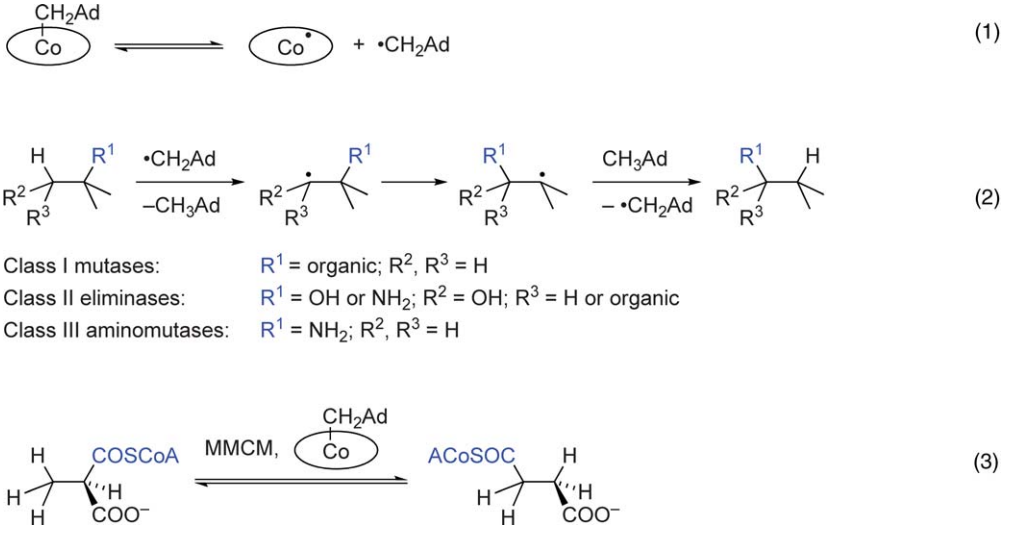

Scheme 2

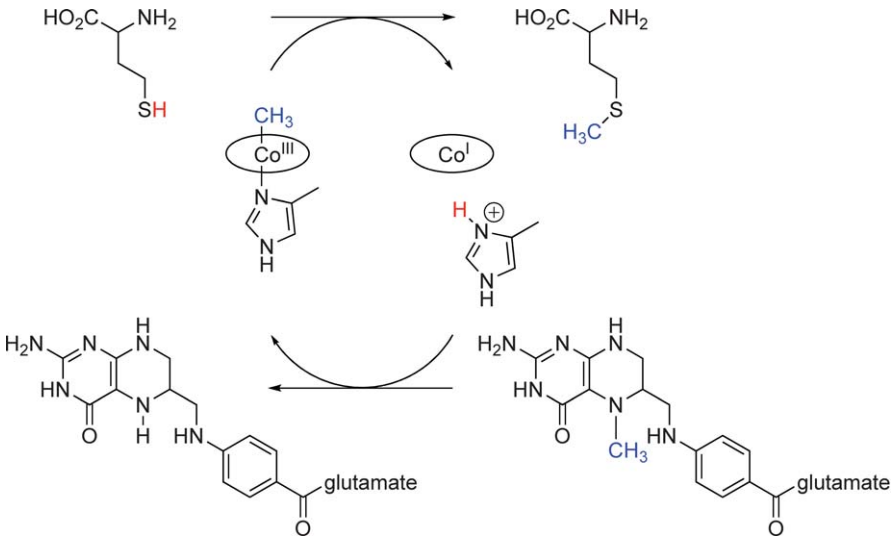

Scheme 3

apparently lost during crystallization. A previous structure with cofactor bound, but no substrate, had the adenosyl group attached to cobalt.[18] All structures were quite similar, suggesting that activation and substrate rearrangement take place without major conformational changes. It is interesting to note that MMCM is the only coenzyme B_{12}-dependent enzyme which occurs in both mammals and bacteria. It is a necessary enzyme in the metabolism of fatty acids with an odd number of carbon atoms. Lack of a functional enzyme is the origin for the human metabolic disease called methylmalonic acidemia.

Class II eliminases catalyze the migration of a hydroxyl or amino group to a carbon atom which already carries one hydroxyl group (initial C–O or C–N bond breakage), followed by an elimination step. Examples are propanediol dehydratase (DD) and glycerol dehydratase (GD). Ribonucleotide triphosphate reductase (RTPR) is also commonly counted into this class of B_{12}-dependent enzymes.[19] RTPR catalyzes the reduction of ribonucleoside triphosphates to 2′-deoxyribonucleoside triphosphates, but without a rearrangement reaction. Finally, class III aminomutase enzymes catalyze the migration of an amino group (initial C–N bond breakage). Examples include *β*-lysine-5,6-aminomutase and D-ornithine-4,5-aminomutase, both of which require pyridoxal phosphate as an additional cofactor.

The above three groups differ in a number of aspects, in addition to the migrating groups involved. Class I and III bind the adenosylcobalamin cofactor in a "base-off/His-on" mode. The cobalamin nucleotide loop is buried in a hydrophobic pocket of the enzyme, which in turn provides a histidine group from the active site to occupy the axial ligand position on the cobalt atom. Class II, in contrast, has the nucleotide loop remaining coordinated to the metal in all structures known so far. Class I and II also differ in their reactivity and EPR spectroscopic patterns. Class I EPR spectra show a relatively strong hyperfine coupling between a Co(II) center and the organic radical. Class II enzymes exhibit only weak coupling so that the two features are well resolved. Chemically, class I enzymes do not generally tolerate any alterations in the cofactor structure, while class II enzymes are rather promiscuous toward structural variations in the coenzyme. Taking all these considerations together, it may well be that the primary step in catalysis, homolysis of the metal–carbon bond, is initiated by more than one mechanism, which is quite an intriguing thought for an organometallic chemist and should spur more research in the area in the future.

Methylation reactions are the second major class of reactions that require methylcobalamin as a cofactor.[9,13,15] In fact, corrinoid-dependent methyl transferases are ubiquitous and occur in all organisms except plants. More than a dozen methyl transferases from different species have been isolated and characterized. Results in conjunction with the ACS/COdH system are described below for the synthesis of acetyl CoA. By far, the best studied example is methionine synthase (MetS).[9] MetS catalyzes a methyl group transfer from N^5-methyl tetrahydrofolate to homocysteine to form methionine via a methyl-cob(III)alamin intermediate (Scheme 3). The cobalamin thus serves as a shuttle for the methyl group transfer, shifting between Co(I) and Co(III) redox states. Formally, the methyl group is transferred as a carbocation. The highly reactive Co(I) intermediate gets occasionally inactivated as Co(II). Reactivation involves electron transfer from a ferridoxin and methylation. Numerous studies were carried out on MetS from various species. The MetS (650–896) cobalamine-binding domain from *Escherichia coli* was the first cobalamin-dependent enzyme to be structurally

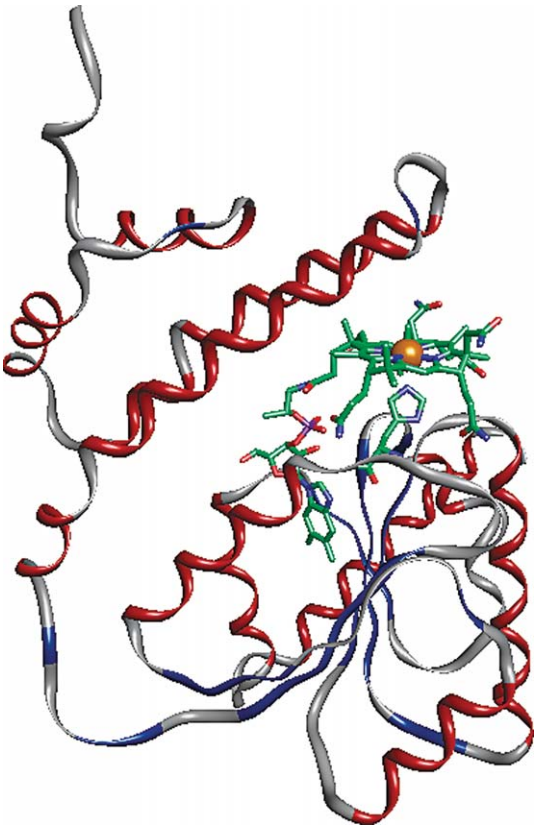

Scheme 4

characterized.[20,21] It showed the "base-off/His-on" binding motif already discussed above. Scheme 4 shows a schematic drawing of this enzyme fragment. More recently, a Co-corrinoid-dependent methyl transfer reaction that does not require methyl tetrahydrofolate was discovered.[22] Rather, these enzymes can use *O*-methyl compounds such as methanol and methyl ethers as a source of the methyl group by cleavage of the O–C bond.

Methylcobalamin is also involved in other biomethylation reactions. Examples include the methylation of inorganic As salts to volatile methyl arsines, as well as the biomethylation of Hg^{2+} salts to yield the highly toxic methyl–mercury cation $[CH_3–Hg]^+$ (see also Section 1.31.3.5). In this reaction, methylcobalamin serves as a Grignard-type reagent and the methyl group is transferred as a carbanion.

1.31.2.2 Hydrogenases (H_2ases)

H_2ases are a family of enzymes which catalyze the reversible conversion of dihydrogen into protons and electrons. They are found in archaebacteria and bacteria, as well as in green algae. These organisms use dihydrogen gas as their energy source; they are now often found in anaerobic environments.[23] In the H_2ase enzyme clusters, electrons are passed along a chain of FeS clusters to finally generate chemical reductants like NADH.

H_2ases are commonly classified by their active site (Scheme 5).[24,25] NiFe-H_2ase contains a bimetallic Ni–Fe center. In the NiFeSe subclass, the rare amino acid selenocysteine replaces one cysteine coordinated to Ni. The FeFe (also called Fe-only) class contains two Fe atoms that are held in place by a sulfur atom from a nearby FeS cluster. Finally, an H_2ase exists that was long thought to be metal free. It has recently been shown that even this H_2ase contains one Fe atom in an $Fe(CO)_2$ group, which is most probably functional.[26–28] It does not, however, contain any FeS clusters.[28,29] According to its biological function, this iron–sulfur cluster-free hydrogenase from methanogenic archaea is termed H_2-forming methylenetetrahydromethanopterin dehydrogenase (Hmd).

In all H_2ases, the Fe center is coordinated to carbonyl and cyanide ligands. Both ligands are ubiquitous in inorganic chemistry. Equally well, they are highly toxic and in fact strong enzyme inhibitors, for example, for Fe-containing

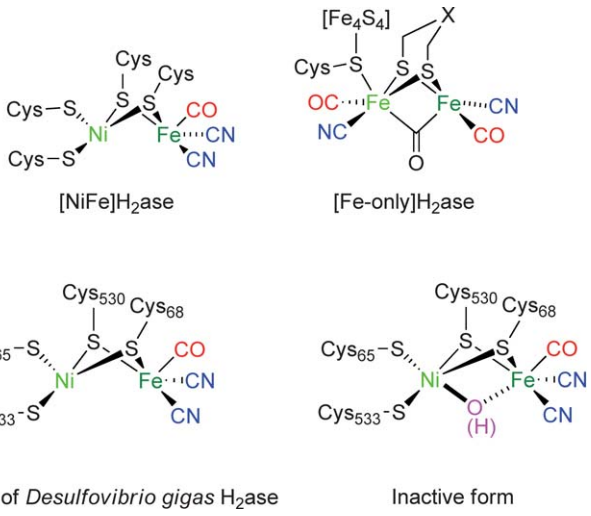

Scheme 5

$$H_2 \xrightleftharpoons{H_2ase} 2H^+ + 2e^- \quad (1)$$

$$H_2 + D_2O \xrightleftharpoons{H_2ase} HD + HOD \quad (2)$$

Scheme 6

heme oxygenases. Although we now understand the origin of these ligands in the H_2ase enzymes, it is still a miracle why nature uses the $Fe(CO)_x(CN)_y$ fragment. One characteristic of H_2ases is the ability to split dihydrogen heterolytically, that is, there must be a hydride intermediate. This was shown as early as 1954 by isotopic exchange between D_2O and H_2, to yield HOD and HD, being catalyzed by H_2ase enzymes (Scheme 6).

The most common enzymes for the H_2 uptake are the NiFe H_2ases.[25] They were also the first to be structurally characterized.[30,31] The organometallic $Fe(CO)(CN)_2$ core, which has a low-spin Fe(II) center, is linked to the Ni atom by two bridging cysteine residues (Scheme 5). The Ni center is furthermore coordinated by two more cysteine residues. One of them may be substituted by selenocysteine in the NiFeSe enzymes. Bridging and terminal cysteine residues are linked pairwise by a Cys–X–X–Cys motif. In the inactive form, the two metal centers are furthermore bridged by an oxide or hydroxide ion (Scheme 5). In addition to the atomic coordinates, the crystal structures reveal exit channels for protons (via hydrogen donor–acceptor groups such as carboxyl, amino hydroxyl, etc.) and electrons (a line of FeS clusters characteristically spaced by about 12 Å) from the bimetallic core in opposite directions. Furthermore, a hydrophobic channel filled with Xe atoms in one crystal structure looks like a plausible H_2 access route.[32] A similar channel is identified in all other H_2ases.

Obviously, the dihydrogen splitting reaction is reversible, and this is the case in fermentative bacteria that generate dihydrogen. It should be noted that although isolated enzymes catalyze reaction (1) in Scheme 6 completely reversibly, it will be typically committed to only one direction in any given organism or metabolic path. Thus, the Fe-only H_2ases are often used for H_2 production.[33,34] They are more efficient than the NiFe class, but also far more sensitive to dioxygen.[25] The active site is shown in Scheme 5 with two Fe(CO)(CN) centers, bridged by a dithiol with three light atoms in the chain.[35–37] Although the ambiguity (X = CH_2, NH, or O) could not be resolved by X-ray crystallography, the bridge is now generally assumed to be bis(methylthiol)amine (X = NH).[25,38] The bimetallic site is linked to the protein via a cysteine residue of an adjacent Fe_4S_4 cluster in addition to the hydrogen bonds to the cyanide ligands.

The activation of dihydrogen is a major topic in organometallic chemistry, and numerous structural as well as functional model systems for the H_2ase enzymes were proposed, which have been the topic of many books and reviews. A detailed discussion of all those is found in a recent book chapter.[25] The thoughts particularly intriguing to an organometallic chemist are as follows.

(i) H_2ases constitute a very old class of enzymes. Likewise, mixed $Fe(CO)_x(CN)_y$ compounds have been known for over a century. There is now a renewed interest in this class of compounds. Compounds like $[Fe(CN)_5(CO)]^{3-}$

and *trans*-$[Fe(CN)_4(CO)_2]^{2-}$ were recently studied in great detail, in particular, with respect to their spectroscopic properties by Koch and co-workers.[39,40] Hieber and co-workers prepared the first iron carbonyl sulfide complex $Fe_2S_2(CO)_6$ and the iron hydride $FeH_2(CO)_4$ in the 1930s. Seyferth and co-workers examined iron carbonyl sulfides in more detail in 1980,[41] but the field really took off following the structural characterization of an Fe-only H_2ase.[42–44]

(ii) Several different redox states have been characterized for the H_2ase enzymes, including activated forms in the presence of H_2 or CO-inhibited forms. IR spectroscopy of the CO and CN ligands is a great help in identifying and characterizing these different states, as well as to distinguish between terminal and bridging carbonyls. It is not at all surprising for the organometallic chemist (but indeed, an uncommon experiment for a biologist) that the exact nature of the CO and CN ligands in the first crystal structure of NiFe H_2ase from *Desulfovibrio gigas* could only be resolved by subsequent IR spectroscopic investigations![45–47] Another long-known and simple compound serves as an excellent spectroscopic model for the $Fe(CO)(CN)_2$ core in NiFe H_2ases, namely, $[CpFe(CO)(CN)_2]^-$.[48,49]

(iii) It is surprising that the exact mechanism of dihydrogen activation in H_2ases still remains unclear. In fact, even the site of activation is not identified beyond doubt in the NiFe family. Dihydrogen complexes were first isolated and fully characterized by Kubas in 1984,[50,51] and their bonding situation is now well understood.[52] Stable Fe(II) dihydrogen complexes were later synthesized by Morris and co-workers.[53] This, together with the fact that the above-mentioned hydrophobic access channel points toward the Fe atom in NiFe H_2ase, seems to favor the Fe center as the primary point of H_2 binding. Prior to the structural results, well-founded spectrosocpic and chemical evidence led Lindahl to suggest Ni(Cys)–hydride intermediates.[54] A number of theoretical calculations have tackled the problem, invoking also bridging hydrides.

1.31.2.3 Carbon Monoxide Dehydrogenase (COdH) and Acetyl Coenzyme A Synthase (ACS)

The interconversion of CO and CO_2 is carried out by carbon monoxide dehydrogenases (COdH's). These enzymes are major components in the global carbon cycle. They are often, but not exclusively, found in bifunctional enzymes together with ACS, which synthesizes acetyl coenzyme A from CO, a methyl group, and the thiol coenzyme A. Scheme 7 demonstrates the relevance of COdH and ACS in the early stages of carbon assimilation of anaerobic organisms.[55]

Monofunctional COdH includes two distinct classes, namely, an aerobic protein with a molybdopterin cofactor, and anaerobic phototrophs. Only the second class is relevant to this review, and all known anaerobic COdHs contain an NiFeS active site (called the C cluster), at which the CO-to-CO_2 transformation takes place. Spectroscopic and structural studies from different species reveal some diversity in the C cluster. The two most extensively studied proteins are from *Rhodospirillum rubrum* (monofunctional COdH) and *Moorella thermoacetica* (formerly *Clostridium thermoaceticum*, bifunctional COdH and ACS).[10] X-ray structural results are available for *R. rubrum*,[56] and another monofunctional COdH from *Carboxydothermus hydrogenoformans* (Scheme 8).[57] Both consist of a cuboidal $NiFe_3S_4$ cluster with an additional *exo*-Fe atom. All mechanistic proposals so far involve bimetallic pathways, but despite some effort, the exact nature of the catalytic species remains in question. One suggestion is the attack of an Fe–OH to the Ni-bound CO, followed by CO_2 liberation from the metallocarboxylic acid.[58] A very similar proposal reverses the two metals, that is, Ni–OH and Fe–CO

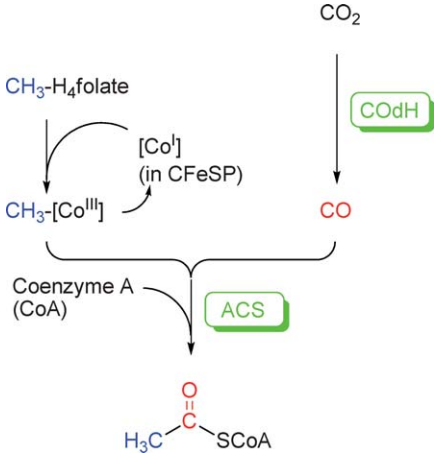

Scheme 7

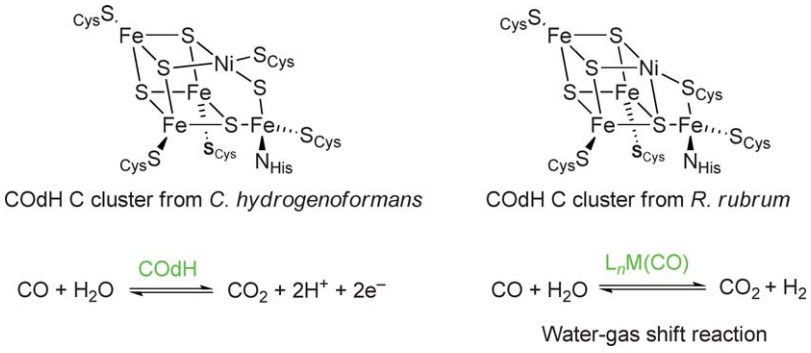

Scheme 8

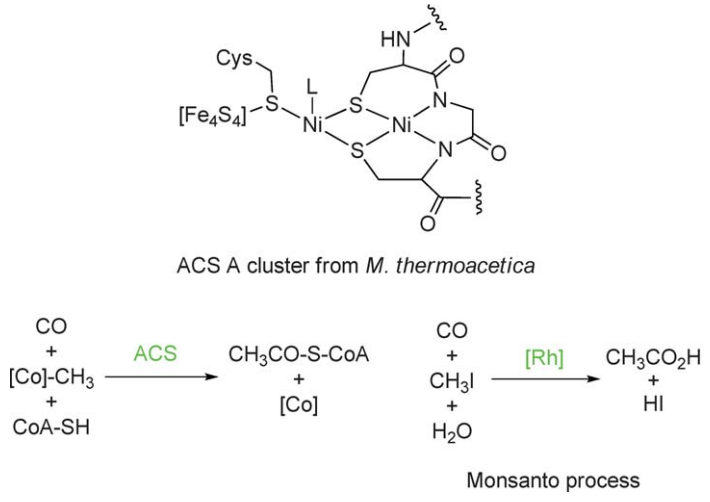

Scheme 9

form the intermediates.[59] Finally, Ludden an co-workers suggested a different pathway with Ni hydride intermediates.[60,61] From an organometallic point of view, there is a striking similarity to the industrial water-gas shift reaction. A notable difference is that the latter generates dihydrogen, rather than protons and electrons (Scheme 8, bottom).

All known ACS enzymes are bifunctional in that they possess a C cluster with COdH activity in addition to an A cluster (the ACS active site, Scheme 9). In the enzymes, a "CO tunnel" is described through which CO can pass directly from the C cluster, where it is generated from CO_2, to the A cluster, where acetyl CoA synthesis takes place.[62–64] Again, two mechanisms were proposed that differ in the order of binding events and redox states involved. In essence, however, CO binds to an Ni–CH_3 species, followed by insertion and generation of an Ni–acetyl species, which upon reaction with CoA liberates the acetyl CoA product. It is interesting to note that methylation of Ni occurs by reaction with methyl cobalamin (Scheme 7). In *M. thermoacetica*, the cobalamin is the cofactor for a rather unique protein called the corrinoid iron sulfur protein (CFeSP). The above process, even if mechanistic details still remain in question, resembles the industrial Monsanto acetic acid synthesis process (Scheme 9, bottom). In this case, however, the reaction is catalyzed by a low-valent Rh catalyst.

Numerous structural and functional models for both COdH and ACS were published, many of these results were recently reviewed.[10,65]

1.31.2.4 Methyl coenzyme M reductase (F_{430})

It is worth noting that the toxicity of one of the simplest organometallic Ni compounds, $Ni(CO)_4$, was discovered almost as soon as the compound itself. Consequently, nickel was long considered a toxic metal with no function in biology. Therefore, it came as a big surprise when Thauer discovered that nickel was absolutely required for the growth of

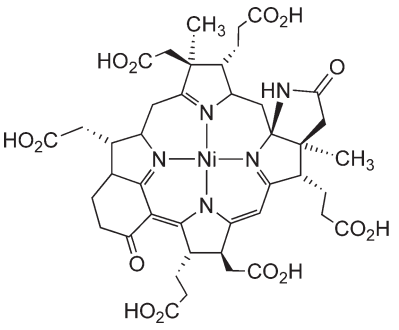

Scheme 10

methane-producing archaebacteria. These bacteria are strict anaerobes, they die quickly when exposed to dioxygen.[66] Several C_1 donors are used by the rather diverse class of methanogens, in particular, acetate and CO_2. Dihydrogen or formate serve as reducing equivalents. As a unifying theme for all different pathways, a methyl equivalent is reduced to methane in the final, energy-conserving step of the catalytic cycle.[67,68] This observation led to the isolation of Ni-containing enzymes from these bacteria and to their characterization as Ni-containing macrocycles with a reduced porphyrinoid ring, which is known as cofactor F_{430} (Scheme 10).[69,70] In the activated state, the enzyme is believed to contain Ni(I), to which methyl groups can be oxidatively added. Methane is finally released upon addition of a proton and reductive elimination, and the Ni(I) state is regenerated.[10] Although this is certainly an intriguing and convincing mechanism for an organometallic chemist, it is not without question. Based on density functional theory (DFT) studies, Sigbahn and Crabtree have suggested a mechanism for methane production that does not involve any Ni–methyl intermediates.[71]

1.31.3 Medicinal Organometallic Chemistry

Medicinal aspects have always played a major role in the development of bioorganometallic chemistry. In fact, Salvarsan, the first cure for syphilis developed by Ehrlich in the early 1900s, is an organometallic compound. Today, we have a more detailed understanding of the molecular basis of diseases, and refined synthetic methods as well as structure–activity relationships (SAR). Given the thermodynamic as well as kinetic stability of organometallic compounds, the multitude of structural possibilities, and the additional properties of metal complexes such as redox activity, it is likely that the importance of medicinal organometallic chemistry is going to grow.[72] In this introductory chapter, only a few examples are highlighted. A more comprehensive chapter on "medicinal organometallic chemistry" follows in Volume 12 of this series.

1.31.3.1 Anticancer Agents

Anticancer agents have been a focus for the drug development for many years. Following the success of Cisplatin, $Pt(NH_3)_2Cl_2$, which is one of the three most prescribed anticancer drugs, numerous other metal compounds have been tested, among them many organometallics. To the present day, however, none of these compounds has successfully passed clinical trials.

An anti-proliferative effect has been demonstrated for metallocenes by Köpf and Köpf-Maier. Even simple ferrocenium salts were shown to have an anti-proliferative effect on certain types of cancer cells. The mechanism of action has not yet been elucidated and several targets including nuclear DNA, the cell wall, and the enzyme topoisomerase were proposed. Osella *et al.* showed that ferrocenium salts may generate hydroxyl radicals in physiological solutions.[73,74] Whether these radicals damage the DNA or other targets, as for example, the cell wall, is unclear. In addition, there are conflicting reports on whether or not the redox state of the iron atoms is crucial for cytotoxicity. Neuse and co-workers found significantly enhanced cytotoxicity when ferrocenes were bound to polymeric supports.[75–77]

For the bent metallocene dihalides, structure–activity relationships were established for the halides and substitution of the Cp rings.[78–81] Also, hydrolysis reactions were studied in detail with a view on aqueous stability. Model studies with amino acids, nucleic acids, proteins, and blood plasma provided more insight into the mechanism of action.[82] Titanium compounds were most active, and titanocene dichloride has entered clinical trials.[83] Although very promising

in animal models, the clinical response was not encouraging enough to justify continuing trials, which were recently abandoned for titanocene dichloride. Due to its decomposition and low solubility in water, there were also problems with the formulation of the drug. Mainly because titanocene dichloride seems superficially similar to Cisplatin with two halide ligands in a *cis*-position, a related mode of action was assumed, that is, binding to DNA and eventually apoptosis of the cancer cell.[84–86] Despite much effort, at no point was clear evidence for such a mode of action obtained. Instead, Ti binding to transferrin following hydrolysis was proposed,[87] and even a stimulatory effect of aqueous Ti species on hormone-dependent breast cancer cells was observed.[88] To circumvent some of these problems, modifications have recently been proposed. Titanocenes with amino groups were synthesized to increase aqueous solubility, and *ansa*-titanocenes exhibit much greater hydrolytic stability.[89–91] Both groups of compounds show promising biological activity.

Research has also concentrated on molybdocene derivatives. Several X-ray structures with the Cp_2Mo fragment coordinated to nucleobases were obtained.[92–94] In addition, extensive spectroscopic studies, mainly by ^{1}H and ^{31}P NMR, were carried out in solution.[93,95–97] Although Cp_2MoCl_2 was originally less active than Cp_2TiCl_2, it may in the long run be a more successful lead structure.[97] Harding and co-workers investigated cellular uptake and intracellular localization of different bent metallocene dihalides by X-ray fluorescence.[98,99] Only low levels of Ti and V were detected inside cells, and only Mo seemed to accumulate in significant amounts in the cellular nuclei (Figure 2). These findings agree well with the notion that all metallocenes have a different biological profile. Interestingly, molybdocene dichloride was also shown to hydrolyze phosphate esters and is thus a rare case of an organometallic nuclease.[100,101]

Ruthenium arenes are another interesting class of organometallics with proven anticancer activity.[102] The most active complex [(η^6-biphenyl)Ru(ethylene–diamine)Cl]$^+$ **1** (Scheme 11) had an activity comparable to Carboplatin against a human ovarian cancer cell line.[103,104] The interaction of this compound with different biomolecules has been studied, and again, DNA has been suggested as the primary target.[105,106] It is, however, unclear at present which events following the initial binding of the drug lead to the cell death. Sadler and co-workers solved the co-crystal structure of [(cymene)$RuCl_2$] with lysozyme in order to shed more light on the possible interactions of this class of organometallics with proteins.[107] As can be seen in Scheme 12, the organometallic compound occupies a pocket of the protein, but both chloride ions remain coordinated to Ru under the conditions of crystallization and one imidazole ring from a histidine binds to the Ru atom.

More recently, another approach to organometallic anticancer agents was proposed. Organometallic fragments were mainly seen as large lipophilic groups that can replace phenyl rings in drugs. This approach has led to a ferrocene derivative ("ferrocifen," **2**) of tamoxifen **3** (Scheme 13).[108,109] Tamoxifen, a so-called selective estrogen receptor modulator (SERM), is the first-line drug for patients with hormone-dependent breast cancer. It works by competitive binding to the estrogen receptor (ERα), thus repressing estradiol-mediated DNA transcription in the tumor tissue.[110] Although tamoxifen is a highly active drug, it does not work on hormone-independent cancers, which constitute about one-third of all patients. In addition, expression of the ERα may become down-regulated under tamoxifen treatment, turning the drug ineffective.

Ferrocifen is a tamoxifen derivative, in which one of the phenyl rings has been replaced by a ferrocenyl group (Scheme 13). It is as active as tamoxifen on hormone-dependent cancer cell lines. Surprisingly, it is also active against hormone-independent cancer cell lines.[109] Other organometallic fragments in place of the ferrocenyl group were also

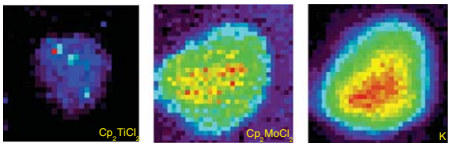

Figure 2 Distribution of metal compounds inside a single cell as studied by X-ray fluorescence: (a) Cp_2TiCl_2 is barely found inside the cell, (b) Cp_2MoCl_2 is well taken up and partly accumulated in the nucleus, and (c) K serves as a reference.

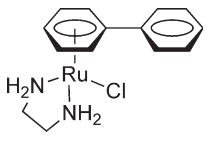

1

Scheme 11

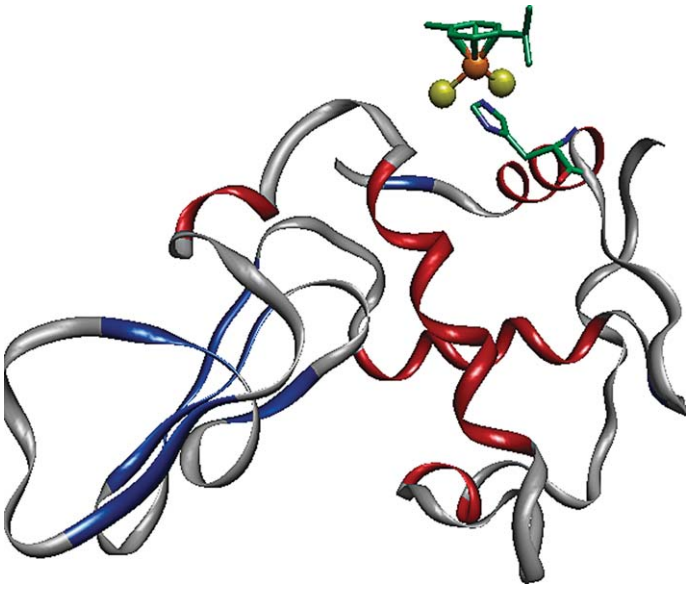

Scheme 12

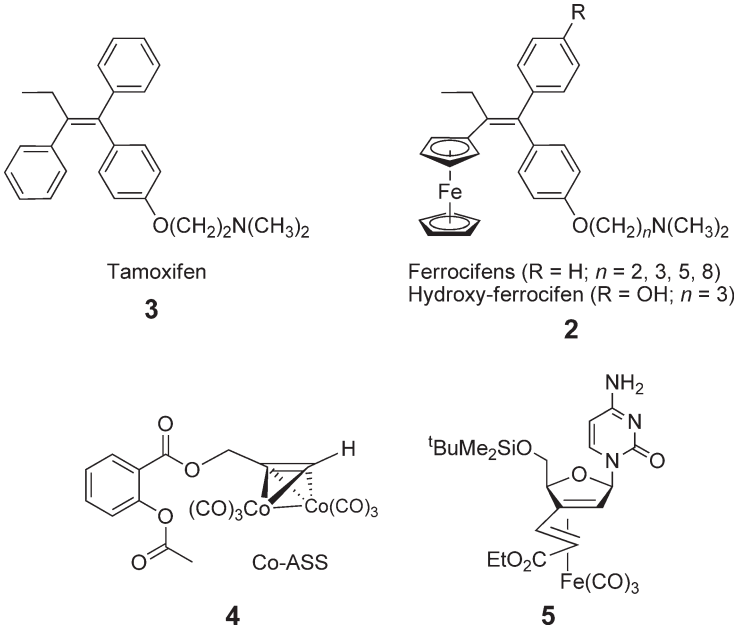

Scheme 13

tested, but found to be inactive in the later test.[88,109,111] This suggests two different modes of action for ferrocifen. In addition to tamoxifen-like binding to the ERα receptor, which was independently shown,[109] a second pathway must exist which is critically dependent on the metal. In an elegant study, redox activation has been proposed as the second mode of action.[112] The active metabolite hydroxyferrocifen is readily oxidized yielding a chinone methide intermediate which is activated for nucleophilic attack by nucleophiles. Extensive structure–activity relationship studies in correlation with electrochemical properties support this hypothesis. It is particularly noteworthy, and highly encouraging for the organometallic chemist, that redox activity of the metallocene is the key for additional biological activity that exceeds that of a purely organic analog. This idea, which is related to the concept of "oxidative stress" in connection with reactive oxygen species (ROS), has in fact been suggested previously[113] and is gaining new popularity recently.[72]

$Co_2(CO)_6$(alkyne) complexes represent another class of molecules with anti-proliferative properties in cancer cells. Derivatives of well-known inhibitors of cyclooxygenase (COX) enzymes were particularly active.[114–117] Many analgetics and anti-inflammatory drugs are COX inhibitors. This class is commonly known as non-steroidal anti-inflammatory drugs (NSAID). The link between inflammation and cancer has been pointed out[118] and organic irreversible COX-2 inhibitors were published.[119] The most active metal derivative today is the dicobalt hexacarbonyl complex of (2-propyn-1-yl)acetylsalicylate (Co-ASS, **4**; Scheme 13). which is derived from the drug acetylsalicylic acid (Aspirin®).[120] This compound is a potent inhibitor of COX. Its anti-proliferative effect is greater than that of Cisplatin, and Co complexes were generally more active than the metal-free derivatives. Other cellular targets were also evaluated, and the cellular uptake of Co was quantified by atomic absorption spectroscopy (AAS).[117,120] As for ferrocifen, an additional, metal-specific mode of action seems to be involved. In this context, but seemingly unrelated, reactive intermediates derived from $Co_2(CO)_6$(alkynes) have been investigated computationally.[121]

Finally, yet another class of metal carbonyls with anti-neoplastic properties was discovered recently by Schmalz and co-workers.[122] They tested iron carbonyl derivatives of nucleosides, such as **5** (Scheme 13). For this series of compounds, a clear structure–activity relationship emerges.[123] The most active derivatives have IC_{90} values in the low μM range against BJAB cell lines. In addition, selected derivatives of this class of compounds showed good *in vitro* activity against leukemia cells from patients with acquired resistance against common anticancer drugs. The mechanism of cell death was also investigated. Although the BJAB cells were finally apoptotic, apoptosis did not seem to be initiated by the regular signaling cascades.[122,123] Further investigation is in progress,[124] and it is certainly interesting to note that organometallic compounds may invoke a new mechanism of action.

1.31.3.2 Antimicrobial Agents

1.31.3.2.1 Antibacterial

The first drug which was discovered by systematic screening was, in fact, an organometallic one. Compound number 606 in Paul Ehrlich's laboratory proved to be particularly effective against syphilis. It was marketed as Salvarsan® in Europe (arsphenamine in the USA, **6**, Scheme 14) and its structure was originally thought to be an analog of azobenzene with an As═As double bond. Later studies made an oligomeric structure more likely, and arsenobenzene is a cyclic hexamer. In the absence of a crystal structure for Salvarsan, a recent mass spectrometric study provides the best structural data today.[125] Interestingly, the hydrochloride of Salvarsan is too toxic for humans, so the compound had to be administered in basic solution, in which it is only poorly soluble. The more soluble NeoSalvarsan **7** was later introduced to the market for the same disease. Both compounds are easily oxidized in air and in the body, and indeed the phenarsine oxide is the active metabolite. This compound, Mapharsen, which probably also has an oligomeric structure, was also marketed in the 1920s. The As-containing antibiotics were later gradually replaced by penicillins and sulfonamides. There is, however, renewed interest due to the growing resistance in bacteria to many of the common antibiotics. Also, organic mercury compounds have been in use as mild antiseptics until recently. Concerns have been raised[126] (and subsequently debated)[127] that some cases of autism and Asperger's syndrome in children might be related to mercury poisoning.

The design concept for the anticancer-active ferrocifen mentioned above is replacement of a phenyl ring by a ferrocene substituent. The very same principle has previously been applied to a number of antimicrobial agents. The first ferrocene derivatives of penicillins and cephalosporins have been synthesized by Edwards and co-workers.[128–130] Further derivatives were later investigated.[131–136] Unlike the anti-malarials discussed below, there has been no real breakthrough for organometallic antibacterials.

Small peptides are a promising class of antibacterial compounds. They are mostly comprised of cationic and lipophilic amino acids, and minimal motifs containing only Arg and Trp have been suggested. Presumably, interaction of these peptides with the bacterial cell membrane contributes to their activity. Assuming that metallocenes are bulky, lipophilic groups, which may (cobaltocenium) or may not (ferrocene) possess additional charges, we have

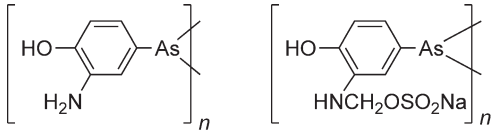

Salvarsan NeoSalvarsan

6 **7**

Scheme 14

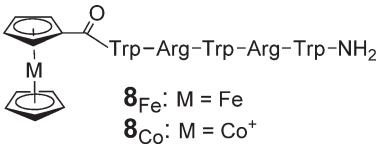

Scheme 15

prepared a number of metallocene peptide conjugates and tested their antibacterial activity on different Gram-positive and Gram-negative bacteria (Scheme 15).[137] In these compounds, the metal complex did not increase the overall activity, but could switch selectivity. For example, the ferrocene–peptide conjugate 8_{Fe} is about 5 times more active against the Gram-positive *Staphylococcus aureus* than against Gram-negative *E. coli*, whereas the activity is reversed for the cobaltocenium–peptide conjugate 8_{Co}.[138] For both compounds, the minimum inhibitory concentration (MIC) is comparable to the natural antibiotic peptide Pilosulin 2, which is also more active against *E. coli*.

1.31.3.2.2 Antimalarial

Antimalarial drugs is another area of medicinal chemistry which is successfully investigated. The malaria parasite *Plasmodium falciparum* is increasingly developing strains which are resistant against common antimalarial drugs such as chloroquine. Brocard and co-workers have synthesized a ferrocene analog of chloroquine,[139] which is active even against chloroquine-resistant *Plasmodium* strains with IC_{50} values in the low nM range.[140–142] Ferroquine **9** was able to protect mice from infection and is now in clinical phase I trials (Scheme 16). Trapping of the compound in the food vacuole of the parasite and inhibition of hemozoin formation is the primary mechanism of action.[141,143,144] In this respect, ferroquine is similar to chloroquine **10**, but clearly, the lipophilic metallocene is needed for enhanced bioactivity. Structure–activity relationships have been established.[145] At present, it appears that subtle changes such as increased lipophilicity and differences in geometric and electronic structure suffice to account for the activity even against chloroquine-resistant strains.[144,146] It remains to be established, however, whether there is an additional, as yet undiscovered, mode of action, similar to the case of ferrocifen.

It is worth noting that the two optical isomers of ferroquine exist due to the planar chirality of the unsymmetrically 1,2-substituted ferrocene moiety. Both enantiomers were prepared by enzymatic resolution of an ester intermediate in >98% optical purity. Both isomers display similar activity *in vitro*.[147] Although both enantiomers are less active than the racemate *in vivo*, the (+)-enantiomer displays better curative effects than the optical antipode. This different behavior indicates different pharmacokinetics of the two enantiomers. Ferrocene derivatives of other antimalarial drugs like artemisinine, quinine, and mefloquine have also been tested,[141,148,149] as well as various other chloroquine-derived organometallics.[150] Moss and co-workers synthesized and tested chloroquine and ferroquine derivatives with other organometallic groups.[151–153]

1.31.3.3 NO/CO Drugs

Carbon monoxide, although toxic in higher concentrations, appears to be an important signaling molecule in the body, particularly with relation to the cardiovascular system. Metal carbonyls are among the oldest and best investigated classes of organometallic compounds. However, it has only recently been discovered that many simple metal carbonyls like $Fe(CO)_5$, $Mn_2(CO)_{10}$, and $[RuCl_2(CO)_3]_2$ may release CO under physiological conditions (possibly with irradiation) and will thus effect vasodilation and reduce acute hypertension *in vivo*.[154] More compounds were tested, and $[RuCl(CO)_3(glycinate)]$ **11** appears to be the most promising candidate so far. The compound had remarkable protective effects in animal experiments. A condition of induced ischemia was survived with no damage

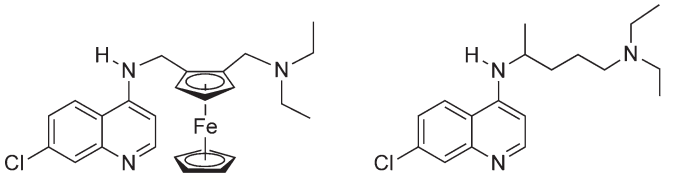

Ferroquine **9**

Chloroquine **10**

Scheme 16

in isolated rat hearts when 50% of the tissue was damaged without addition of **11**. Correspondingly, survival rates of mice with a heart transplant were much higher when **11** was given during the transplant. These effects may partly be attributed to the inhibition of blood platelet aggregation of the compound.[155] As yet, the exact mechanism of action is unclear. Inhibition of heme enzymes has been suggested as well as CO acting as a reductant. There may be some relation to the ACS/COdH reactivity discussed above. Although it is still early in the investigation of metal carbonyls as CO-releasing drugs, there seems to be much promise in the area.[154]

Actually, neither the notion of CO being an important signaling molecule, nor the fact that CO-containing metal complexes have potential as drugs comes as a surprise. Carbon monoxide is isoelectronic with NO^+. NO, on the other hand, has been known to be a major second messenger with a variety of functions. This discovery was awarded a Nobel prize recently, and *Science* magazine declared NO the molecule of the year in 1992. Nitroprusside sodium $Na[Fe(CN)_5NO]$, which is an organometallic compound by definition (although this volume deliberately excludes cyanide ligands), has been an important drug for over a century.

1.31.3.4 Radiopharmaceuticals

Metal carbonyls and the isoelectronic isonitriles do also play an important role as radiopharmaceuticals. ^{99m}Tc is probably the most frequently used metal isotope for radioimaging. ^{99m}Tc ($t_{1/2} = 6$ h) is by far the most widely used metal isotope in radiopharmaceuticals. This pre-eminent position is due to its very favorable physical properties that allow chemical synthesis and radioimaging on a reasonable timescale without extended exposition of the patient. The low-valent Tc isonitrile complex $[Tc(CN–CH_2–C(CH_3)_2–OCH_3)]^+$ (Sestamibi, **12**) was reported by Davison in 1983,[156] and has found widespread use in radioimaging of the heart (Cardiolite® by DuPont). The d^6-low-spin configuration makes this compound particularly stable, even under physiological conditions. Its selectivity for cardiac tissue has been attributed to its size, lipophilicity, and positive charge.

^{99m}Tc radiopharmaceuticals must be prepared and used "on the spot." Ideally a "kit" formulation without the need for subsequent purification should be provided for maximum ease and safety of use by the technical staff in hospitals. Alberto, Schubiger and co-workers have made a significant step forward towards this goal by the preparation of the $[^{99m}Tc(CO)_3(H_2O)_3]^+$ cation **13**.[157,158] This compound can be readily synthesized in one step from TcO_4^- by BH_4^- reduction in the presence of CO. It has been used, *inter alia*, for the labeling of serotonergic receptors in the brain and His-tagged antibodies.[159,160] A more recent and also more convenient preparation for **13** uses the long-known boranocarbonate $[BH_3CO_2H]^-$ (Scheme 17).[161] A "kit" preparation using this chemistry is marketed by the Mallinkrodt company (Isolink®). The $Tc(CO)_3$ fragment has quickly found widespread use, for instance, for the labeling of peptides by various groups,[162–168] vitamin B_{12},[167] and a number of other biomolecules.[169] A simple route has been proposed for the synthesis of $CpTc(CO)_3$ compounds with an acetyl-substituted Cp ring.[170] The labeling of biomolecules with $CpTc(CO)_3$ by double ligand transfer (DLT) reactions from ferrocene derivatives was used by Katzenellenbogen and co-workers.[163,171,172] DLT is, in fact, quite an old technique that was originally explored by Wenzel and co-workers in the 1960s.[173]

1.31.3.5 Toxicology and Environment

Environmental issues related to the toxicology of organometallic compounds have played an immense role in the past, and they may likely continue to do so. Two books have been published on the subject.[174,175] Volume 12 of this series has a full chapter on "environmental and biological aspects of organometallic compounds." Therefore, this section only superficially touches a few examples involving As, Hg, Sn, and Pb. While the term "bioorganometallic" is certainly appropriate to describe CO- or CN-inhibited forms (and thus poisoning) of heme proteins, such species will not be discussed here. On the other hand, the toxicology of organometallic compounds is inevitably related to their reactions with biomolecules, especially proteins.[176]

Organoarsenic compounds have a history not just for good (see Salvarsan above), but also for use as poison gas in World War I. Lewisite ($ClCH{=}CHAsCl_2$) was tested but luckily never used. Research into possible antidotes led to the development of 2,3-dimercaptopropanol, known as mercaprol or British anti-Lewisite (BAL). This compound to

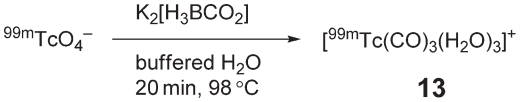

Scheme 17

date is a potent and rather versatile antidote against metal poisoning. It works best for those soft heavy metal ions which form strong metal–sulfur bonds (Hg, Pb, As, etc.). The water-soluble complex is then excreted. Of historical interest is the fact that wallpapers in the nineteenth century were frequently painted with metal salts, for instance, the so-called Scheele's green (cupric arsenite). In the damp and ill-ventilated rooms at the time, these wallpapers gave off volatile As compounds, mainly consisting of trimethylarsine. Methylcobalamin is evidently a vital cofactor for the molds that produce these arsines.[177] They were, for a long time, thought to be responsible for illnesses and deaths among people living in these rooms. The famous Napoleon Bonaparte was long thought to be a victim. However, this rather compelling story has little scientific credibility as trimethylarsine lacks the toxicity to be a poison gas.[178] Arsine, AsH_3, on the other hand, is acutely hemotoxic, resulting in almost certain death if inhaled in larger quantities.[179] It has therefore nowadays mostly been banned from undergraduate teaching laboratories, where it had long been used in a famous (and reliable) analytical test for As (Marsh's Test).

Another fateful event involving organomercury compounds makes methylmercury chloride one of the most intensely studied of all organometallics. In the coastal town of Minamata, Japan, thousand of victims died from mercury poisoning in 1953.[180] It turned out that the mercury originated from a factory preparing acetaldehyde, from which contaminated waste water was released into the ocean. Mercury was then accumulated in shellfish, bio-toxified by methylation, so that the highly toxic methylmercury–methylthioether $CH_3Hg–SCH_3$ was ingested by consumption of the shellfish by the local population. Organic mercury compounds, and in particular methylated mercury species, are potent neurotoxins.[181] The tragic case of a colleague is well documented. She spilled a few drops of dimethylmercury on her hands when preparing an NMR sample, went home untreated (because the spill seemed minor and she was wearing vinyl gloves), and died almost one year later, after months of agony, from incurable mercury poisoning.

The use of tetraethyl lead ($PbEt_4$), which was first prepared by Löwig as early as 1853, as a fuel additive has raised major environmental concerns to the effect that it is banned in most countries today.[182] Diethyltin iodide was widely distributed in 1954 in France as a cure for staphylococcal infections. The sample, which was contaminated with the much more toxic triethyltin iodide, caused over 100 deaths. Tributyl- or even trioctyltin compounds, which are far more lipophilic, have been used as preservants in plastics, clothes, and as antifouling paintings on ships. They are, however, seen with increasing skepticism and have been mostly replaced by hopefully less toxic compounds. Nonetheless, these examples underscore the necessity for constant and critical evaluation of all the chemicals in common usage.

1.31.4 Organometallic Compounds For Biological Studies

A large number of organometallic compounds have been covalently attached to biomolecules like amino acids, proteins, sugars, nucleobases and nucleotides, lipids, hormones, and others. Inclusion of these conjugates into the definition "bioorganometallics" certainly constitutes a very large subgroup. To even try to cover the field comprehensively is beyond the scope of this chapter. The discussion is hence limited to such conjugates that were used in biological studies. An excellent review, published by Severin *et al.* in 1998, covers organometallic amino acid and peptide derivatives.[183] A Russian review deals with the ferrocene conjugates of DNA and its constituents.[184] All these are also contained in our more extensive review on the bioorganometallic chemistry of ferrocene.[3] Two recent book chapters cover organometallic peptide and peptide nucleic acid (PNA) conjugates[185] and the labeling of proteins[186] in detail.

1.31.4.1 Amino Acid, Peptide, and Protein Derivatives

In 1957, Schlögl reported the synthesis and characterization of several ferrocene amino acids, including ferrocenylalanine (Fer, **14**; Scheme 18).[187] Other organometallic amino acids include alanine, phenylalanine (Phe), glycine derivatives, as well as further ferrocene-based amino acids, which are discussed below. The Schlögl paper also describes the reaction of ferrocene carboxylic acid and ferrocene carbaldehyde with amino acids. The chemistry was later picked up in numerous publications, and ferrocene carboxylic acid amides or ferrocene imines with basically all amino acids and many dipeptides were reported.[3,185] Such conjugates may serve as ligands for other transition metal ions.[188–194] Kraatz has prepared ferrocene carboxylic acid conjugates with short peptides that serve as enzyme inhibitors.[195–197]

Improved syntheses for **14** were reported, also for enantiomerically pure derivatives.[198–201] Asymmetric hydrogenation was used for this purpose, as well as Pd-catalyzed coupling of iodoferrocene with a serine-derived organozinc reagent. In the 1980s, this amino acid was incorporated into small peptides, including biologically relevant peptides in which Fer replaces Phe. Examples are the neuropeptide [Fer^4]-enkephalin[202–204] and the peptide hormones Substance P ([Fer^7]-SP, [Fer^8]-SP),[205] bradykinin ([Fer^5]-BK, [Fer^8]-BK),[205] and sarcosine derivatives of angiotensin II

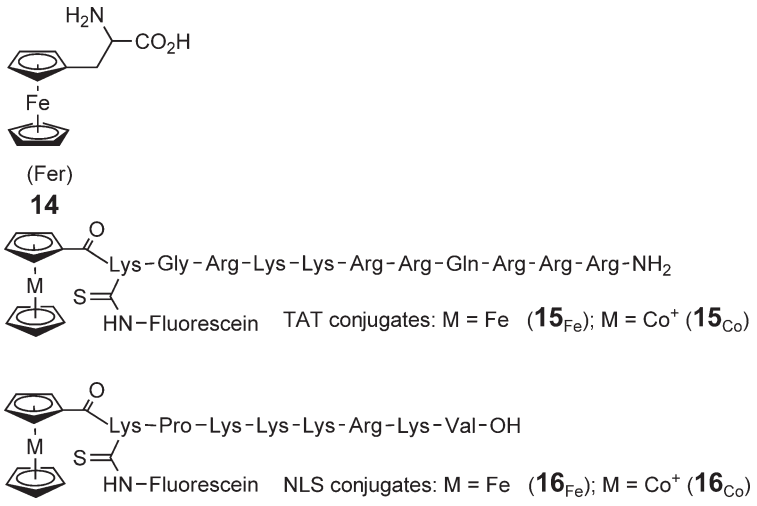

Scheme 18

([Sar[1],Fer[8]]-AT).[206,207] Other organometallic peptide conjugates were based on enkephalin,[204] Substance P,[208] neurokinin A,[209] angiotensin II,[206,207] gonadotropin-releasing hormone,[210] secretin,[211,212] and glutathion.[213,214] Some of these peptide conjugates were tested for their biological activity, for instance, receptor-binding affinity. The syntheses of these conjugates were carried out by the traditional Merrifield solid-phase peptide synthesis (SPPS) technique. The harsh conditions for deprotection and cleavage caused at least partial decomposition of the conjugates. Characterization of these early conjugates is indeed scarce. Therefore, the biological results have to be treated with caution.

We have recently studied cellular uptake and subcellular localization of the metallocene peptide conjugates with ferrocenoyl or cobaltocenium groups (Scheme 18).[215,216] The conjugates were prepared by SPPS, purified, and comprehensively characterized. To enable visualization inside living cells, an additional fluorescence tag was added on an orthogonally protected lysine residue. TAT–metallocene conjugates **15** were prepared to study how the lipophilic metallocene will influence cellular uptake.[216] Nuclear localization was studied by binding the metallocene to the simian virus SV40 nuclear localization sequence (NLS, **16**).[215] Representative results are shown in Figure 3. The ferrocene–TAT conjugate $\mathbf{15}_{Fe}$ is readily taken up by HepG2 cells. It is mainly localized in the cytoplasm. Both the ferrocene-NLS and cobaltocenium-NLS conjugates **16**, on the other hand, are readily taken up and also localized in the nucleus of the cells. Radioactive ($^{99m}Tc(CO)_3$-labeled) NLS conjugates were later used by Alberto and co-workers to induce radiation damage to nuclear DNA in B16F1 mouse melanoma cells.[217]

Our group has initiated a project to search for milder methods for the preparation of organometallic peptide conjugates by SPPS. By using a base-labile linker to the resin and suitable side-chain protecting groups, we were able to prepare acid-sensitive organometallics amendable to SPPS techniques. As an example, enkephalin derivatives with the covalently bound Mo(allyl)$(CO)_2$ moiety such as **17** were successfully prepared (Scheme 19).[218–221] An attractive alternative is the "two-step labeling procedure." In this case, a robust anchoring group is placed in the peptide at the

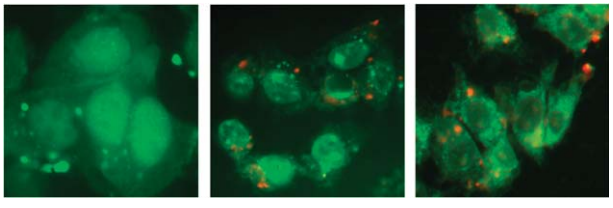

Figure 3 Cellular uptake and intracellular distribution of metallocene–peptide conjugates (see text): (a) cobaltocenium-NLS ($\mathbf{16}_{Co}$), (b) ferrocene-NLS ($\mathbf{16}_{Fe}$) and (c) ferrocene-TAT ($\mathbf{15}_{Fe}$). Nuclear localization is seen for the two NLS conjugates, while the ferrocene–TAT conjugate accumulates almost exclusively in the cytoplasm and does not enter the nucleus.

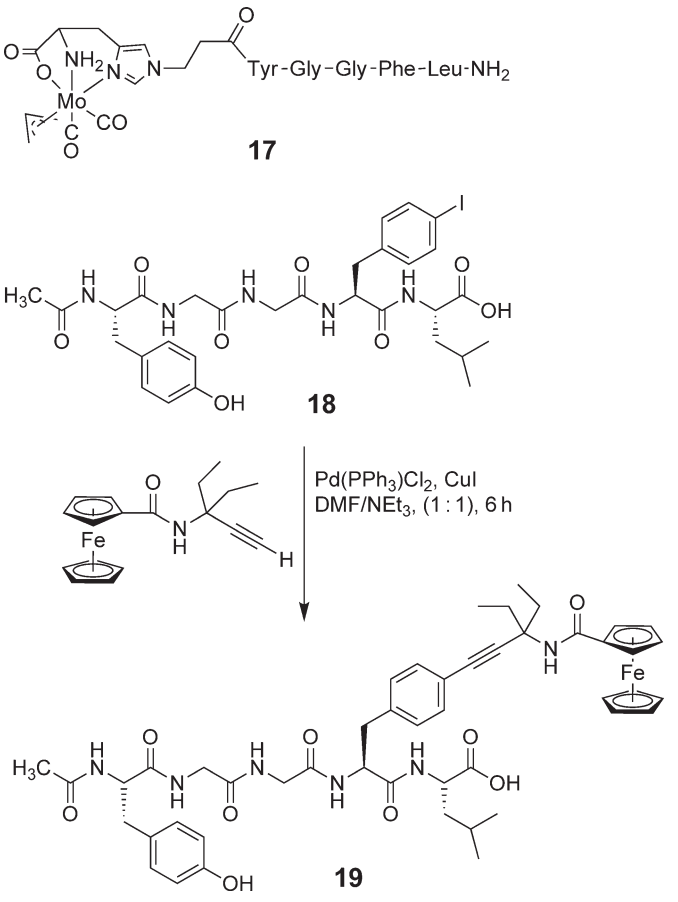

Scheme 19

desired position. In a second step, the organometallic group is bound to this anchoring group after cleavage from the resin and purification of the anchor peptide. Labeling reagents for cysteine and lysine residues are well established for this purpose in bioorganic chemistry. We have used Sonogashira coupling to link organometallics selectively to peptides in such a two-step procedure (Scheme 19). [222–224] For this purpose, *p*-iodo-phenylalanine (Phe^{I}) serves as the anchoring group and replaces Phe. Following studies on the model dipeptides, a modified enkephalin (H-Tyr-Gly-Gly-Phe^{I}-Leu-OH) **18** was prepared by SPPS, purified, and reacted in solution with ferrocene alkynes to yield structurally novel organometallic peptide bioconjugates **19** (Scheme 19).[224]

Metallocenes, in particular ferrocene, may also serve as peptide mimetics. Herrick and co-workers were the first to recognize that 1,1′-disubstituted ferrocene may serve as a peptide turn mimetic, since it holds the two peptide strands in a geometry similar to turn structures found in proteins.[225,226] Further work by several groups unraveled the rules which govern those structures.[196,227–241] In addition to X-ray crystallography, variable-temperature NMR, IR, and CD spectroscopy were employed to provide structural insights in solution. Very stable structures result if at least two interstrand hydrogen bonds form and it appears that out of many possibilities, only very few types of structures are actually realized. It is interesting to note that helical chirality of the metallocene is possible. Due to the low energy of rotation about the metal–Cp bonds (in the order of a few kJ mol^{-1}), *M* and *P* isomers interconvert readily in solution. They can, however, be "locked" by hydrogen bonds between peptide substituents on the two rings, as indicated in Scheme 20. The structural results have recently been summarized and a systematic nomenclature has been proposed.[242] Depending on the metallocene backbone, three different peptide orientations are conceivable (Scheme 21). Ferrocene 1,1′-dicarboxylic acid (class-I) has been predominantly studied, but examples of ferrocene-1,1′-diamine (class-III) have recently been published. Both ferrocene derivatives will orient the peptides in a parallel fashion. Peptide derivatives of 1′-aminoferrocene-1-carboxylic acid (ferrocene amino acid, Fca, class-II) are most similar to natural turn structures as they orient the pendant peptide strands in an antiparallel fashion. Fca was

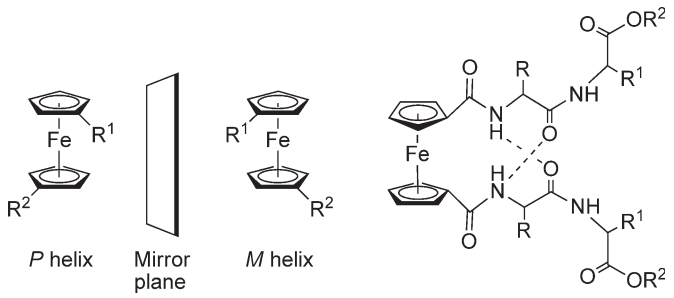

Scheme 20

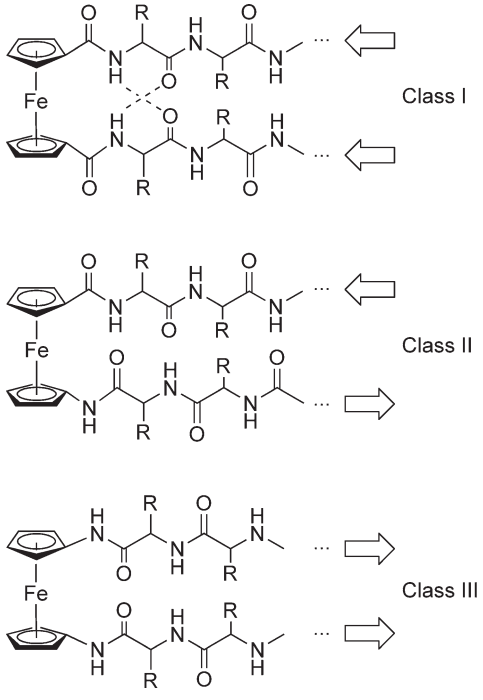

Scheme 21

prepared independently by two groups in 1998.[243,244] Rapic and co-workers reported several differently protected Fca derivatives.[245] An improved synthesis was reported by Heinze and co-workers,[246] who used Fca dimers as electrochemical anion sensors. This group also contributed computational studies for structural dynamics of Fca–peptide conjugates in solution. In collaboration with Rapic's group, we have prepared the first Fca peptide conjugates by SPPS [247] and reported the X-ray single crystal structure of the tetrapeptide Boc–Ala–Fca–Ala–Ala–OMe.[248] A comprehensive paper investigates the solution and solid-state properties of Fca peptides.[249] Very recently, Kraatz's group has shown that Fca-containing peptides may serve as collagen mimics.[250] The same group has also structurally characterized the first synthetic model for β-barrel structures, which also incorporates Fca.[251] It is highly interesting that 1,1′-disubstituted ferrocenes were used as haptens to generate antibodies for the stereoselective Diels–Alder reaction.[252,253] In this context, the idea of helical chirality (and the ease of interconversion between the two enantiomers) was implicitly mentioned and used by Janda and co-workers. They also reported the first synthesis of Fca derivatives (similar to the Rapic route) and the X-ray single crystal structure of an antibody, which was co-crystallized with a ferrocene derivative.[254] Scheme 22 shows the helical chirality of this protein-embedded ferrocene derivative, which is only held in place by non-covalent interactions and hydrogen bonds.

A number of other ferrocene-based amino acids were reported, for example, 1,2-ferrocenylbisalanine,[255] ferrocenyl-β-alanine and 1,1′-ferrocenylbis-β-alanine,[256] 1,1′-ferrocenylbisglycine,[257] and ferrocenylenebisvaline.[258]

Scheme 22

1,1′-Ferrocenylbisalanine **20** has been prepared in an enantiomerically pure form. Via a sophisticated synthetic route, Frejd and co-workers prepared an enantiomerically pure derivative of 1,1′-ferrocenylbisalanine with orthogonal protecting groups (**21**, Scheme 23).[259–262] After lactamization, the resulting 1,1′-ferrocenophane was incorporated into several peptides as a substitute for two aromatic amino acids (Phe or Tyr).[260,261]

Many proteins have been labeled with organometallic complexes, mostly for analytical purposes. Some of those are mentioned in Section 1.31.5 of this chapter, and the topic has been comprehensively reviewed by Salmain.[186] Ryabov published an earlier review on the topic.[176] The labeling techniques are mostly the same as for organic derivatives, that is, cysteine-selective reactions (maleiimides, acetic acid halogenides), activated acids, aldehydes, or thiocyanates that react with lysines, biotin-(strept)avidine labeling, and others.

The use of alkoxycarbene complexes is probably most interesting for an organometallic chemist. Reaction of the tungsten methoxycarbene **22** with primary amino groups in peptides (such as lysine side chains or the amino terminus) gives the aminocarbene **23** (Scheme 24). In a reaction with the protein bovine serum albumin (BSA), four out of six lysine residues were shown to be available for reaction with the tungsten complex.[263] Tungsten

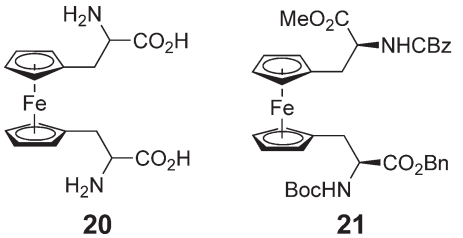

20 **21**

Scheme 23

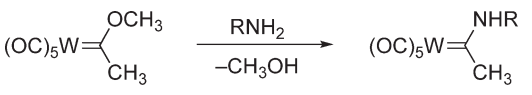

22 **23**

Scheme 24

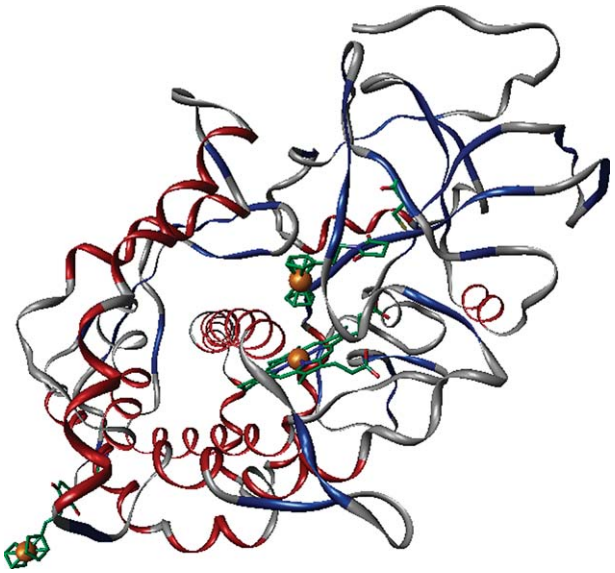

Scheme 25

aminocarbene adducts of lysozyme were also investigated.[264] Similar results were obtained with organometallic pyrylium salts of $(Cr(CO)_3$(arene) and ruthenocene.[265,266]

In two papers, Hill *et al.* studied ferrocenyl derivatives of the enzyme cytochrome $P450_{cam}$ ($CyP450_{cam}$).[267,268] This enzyme catalyzes the regioselective oxidation of camphor to 5-*exo*-hydroxycamphor. Like all cytochromes, $CyP450_{cam}$ has a heme group in its active center. The highlight of these papers is the X-ray single crystal structure at 2.2 Å resolution of a $CyP450_{cam}$(C334A) mutant with the two ferrocenyl maleimides covalently bound to the enzyme (Scheme 25).[268] While the Cys136 is on the periphery of the enzyme, the Cys85-bound ferrocenyl moiety is very close to the active center, and indeed, camphor is displaced by the ferrocenyl maleimide which is an irreversible inhibitor of the enzyme.

1.31.4.2 DNA, RNA, and PNA Derivatives

In contrast to the amino acid, peptide, and protein conjugates, where a number of different organometallic complexes were used for labeling, DNA derivatives are by and large limited to ferrocene. This is very likely due to the attractive electrochemical properties of ferrocene. Indeed, electrochemical DNA sensors are covered in more detail in Section 1.31.5.2. Two recent reviews cover the ferrocene conjugates with nucleobases, nucleosides and nucleotides, DNA and RNA, as well as their applications.[3,184]

In most of the work on oligo-deoxynucleotides (ODNs) to date, very similar chemistry has been used for covalent binding of organometallics to the ODNs (Schiff base, activated acids, metal-catalyzed couplings). Anne *et al.* reported an interesting enzymatic reaction to extend the 3′terminus of an ODN.[269] They use a ferrocenylated di-deoxynucleotide uridine triphosphate (Fc-ddUTP) as the substrate, which is accepted as an enzyme substrate and terminates the oligomer. Other Fc-dUTP derivatives were also tested as substrates for common DNA polymerases.[270] This approach was later extended to ferrocene-labeled RNA, and electrochemical RNA detection on Au-DNA electrodes could be achieved.[271]

It is interesting to note that early work on ferrocene derivatives of nucleosides uses Sonogashira coupling of ethynylferrocene to 5-iodouridine or 8-bromoadenosine.[272] This reaction was later used to synthesize ferrocenylated ODNs by solid-phase synthesis techniques. Depending on the conditions, a cyclization reaction occurs with uracil derivatives.[273–275] Instead of ethynylferrocene, Grinstaff *et al.* used ferrocene carboxylic acid propargyl amide.[276–278] The same compound was used by our group before in peptide chemistry and a crystal structure has been reported.[223] The stability of metallated ODNs with complementary DNA or RNA has been investigated by UV melting studies.[3]

PNAs are a class of DNA analogs with very promising properties for applications in molecular biotechnology or medicine. Compared to DNA, the ribose phosphate ester backbone is replaced by a pseudo-peptide backbone in

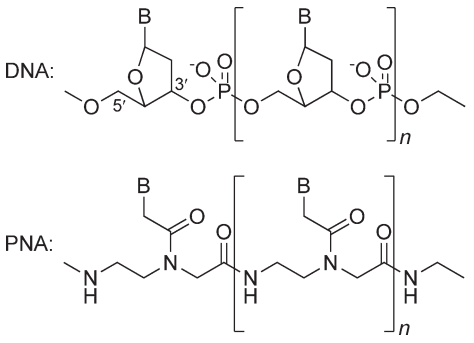

Scheme 26

PNA (Scheme 26). The nucleobases are linked to this backbone via a carboxymethylene linker.[279,280] PNA binds to complementary DNA or RNA oligomers according to Watson–Crick rules with high stability.[281–284] An increase in stability, as measured by the melting temperature (UV T_m), between 1 and 3 °C per base pair in a PNA·DNA duplex has been observed compared to a homologous ds-DNA. In addition, PNA shows a higher mismatch sensitivity toward non-complementary DNA than is commonly observed in ds-DNA.[285,286] These favorable properties led to numerous applications for PNA oligomers in biotechnology and as anti-sense agents.[287–291] Furthermore, a large number of structural variations of the original PNA have been published.[292]

Our group published the first organometallic derivatives of PNA monomers.[293] Ferrocene carboxylic acid and benzoic acid chromium tricarbonyl were coupled to the amino group of PNA monomers with different nucleobases in solution using HBTU as the coupling agent to give compounds **24** and **25**, respectively (Scheme 27). *C*-terminally labeled organometallic PNA monomers and dimers were also obtained.[185] Maiorana's group have used the Ugi four-component reaction (Ugi-4CR, for **26**)[294,295] and olefin metathesis (for **27**)[296] for the preparation of other metal–PNA derivatives (Scheme 28, the different colors indicate individual components in the respective reactions).[297]

PNA oligomers with covalently linked organometallics were also first reported by our group. Originally, ferrocene carboxylic acid and chromium tricarbonyl benzoic acid were incorporated into PNA heptamers with the sequence H-tgg atc g-Gly by solid-phase peptide synthesis techniques.[298] (According to common convention, the same four-letter code is used for PNA as for DNA; small letters, however, indicate PNA oligomers. The PNA sequence is written in peptide convention from *N*- to *C*-terminus.) Whereas the conjugate Fc-CO-tgg atc g-Gly-NH_2 was purified by preparative high-performance liquid chromatography (HPLC) and shown to have the correct mass by mass spectrometry (MS), the chromium tricarbonyl derivative could not be obtained in a pure form. In order to increase stability and solubility in water, we have incorporated cobaltocenium carboxylic acid into PNA oligomers by solid-phase synthesis.[299] Following initial studies on smaller oligomers to optimize coupling and deprotection conditions, the decamer $CpCo^+C_5H_4$-CO-acc ctg tta t-Lys-OH **28** was synthesized by solid-phase synthesis techniques, purified by preparative HPLC, characterized by MALDI-TOF mass spectrometry. A square wave voltammogram was clearly indicative for the presence of the cobaltocenium group. This conjugate was also studied in the interaction with complementary DNA. Compared to acetylated PNA of the same length and sequence, a slight stabilization of about

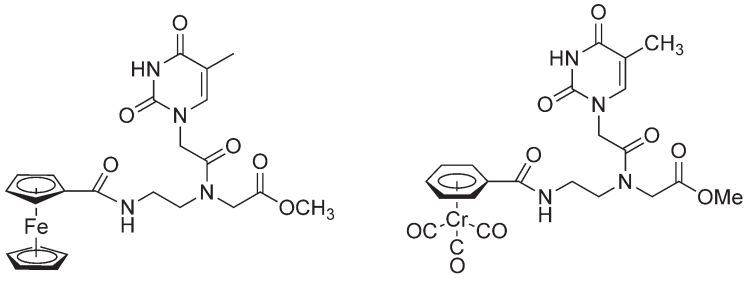

24 **25**

Scheme 27

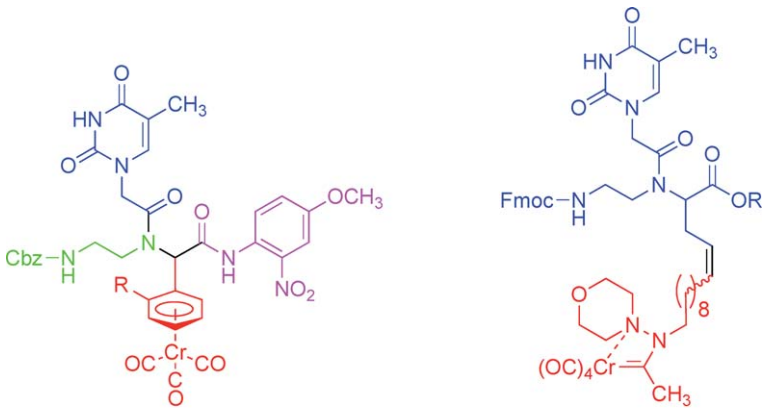

26 27

Scheme 28

1 °C is observed for the cobaltocenium conjugate **28**, which might be attributed to an attractive force between the positively charged cobaltocenium group and the negatively charged DNA strand.[299] Metallocene PNA oligomers were deposited on Au microelectrodes, and their electrochemical properties were found to be very attractive for electrochemical DNA sensors.[299,300] Also, novel $Re(CO)_3$ conjugates with PNA decamers were reported by our group.[301] These conjugates have interesting spectroscopic properties.

1.31.4.3 Others

Numerous other organometallic conjugates with all kinds of biomolecules were prepared. There is obviously a tremendous potential in the use of chiral biomolecules as synthons or ligands in organometallic catalysis. Furthermore, modern natural product synthesis almost inevitably involves organometallic reactions. None of these topics is touched in here, although undoubtedly bioorganometallic intermediates are involved which may even be isolable. In the following, the focus is on the sugar derivatives, lipids, receptor ligands, and the use of organometallics in peptide synthesis.

1.31.4.3.1 Sugar derivatives

Starting in 1961, a large number of ferrocene sugar conjugates were prepared. Originally, the interest was mostly in synthesis and characterization, and ester, thioester, or amide derivatives of ferrocene carboxylic acid were the main objectives. Scheme 29 summarizes many of the 1,1′-ferrocene dicarboxylic acid compounds that are known. The X-ray single crystal structure of **29** was reported by Keppler's group.[302] This compound had poor cytotoxic activity. All other compounds in Scheme 29 had similar EC_{50} values around 20 μM against a mouse mammary tumor cell line. The same compounds had far lower antimalarial activity than quinine as shown by Itoh's group.[303]

Metal carbene derivatives of sugars were extensively investigated by Dötz and co-workers.[304,305] These compounds can be prepared by nucleophilic addition to the metal-coordinated carbene atom, by conjugate addition to the vinylogous position in alkenyl or alkynyl carbene ligands, or by stoichiometric olefin metathesis.[306] Highly complex molecules with several chiral centers form in cycloaddition reactions with sugar-derived metal carbenes in excellent diastereoselectivity, as exemplified in Scheme 30. While the fully protected sugar metal carbenes are lipophilic organometallics that are soluble in organic solvents, *O*-deprotection will increase aqueous solubility as a result of the free hydroxy groups. Upon addition of the long alkyl chains to such molecules, organometallic gelators with interesting properties form.[307]

1.31.4.3.2 Lipids

Compared to many other classes of biomolecules, organometallic derivatives of lipids are a largely under-developed area of research. An early paper reports the use of ferrocene conjugates for the electrochemical HPLC detection of

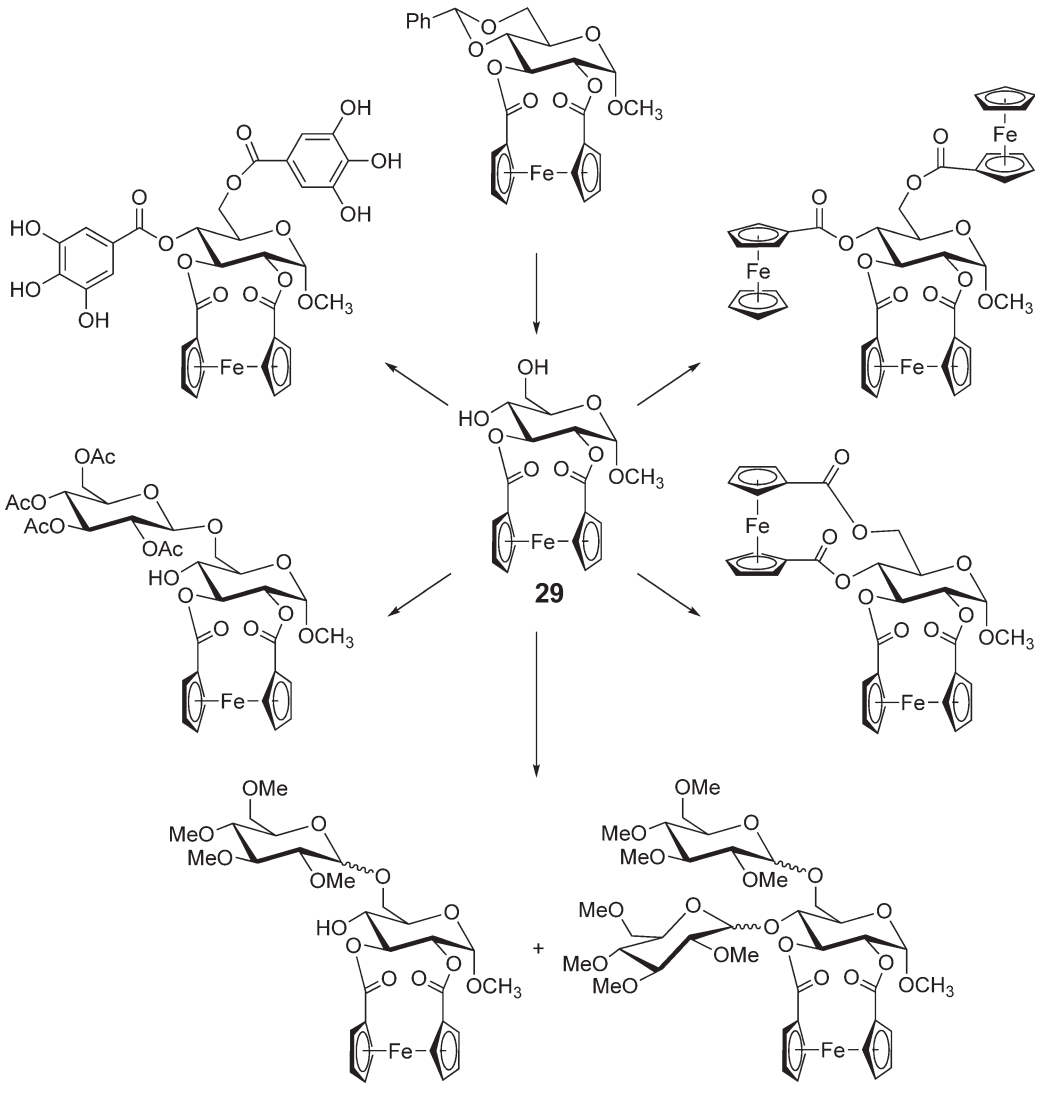

Scheme 29

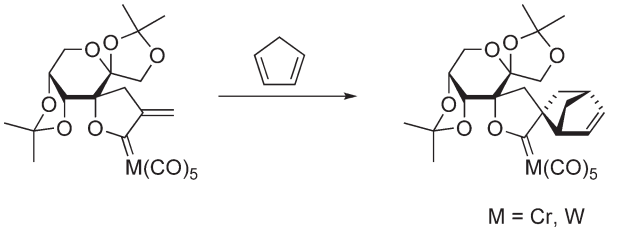

Scheme 30

fatty acids.[308] Conjugates with glycerol and cholin were also prepared.[309] A ferrocenyl cholin conjugate was shown to be a competitive inhibitor of the enzyme butyrylcholinesterase with a K_i value in the μM range.[310]

Very recently, a significant influence of the redox state of the metallocene in ferrocene-containing cationic lipids was demonstrated.[311] In the neutral ferrocene state, high levels of transfection with DNA coding for enhanced green fluorescent protein (EGFP) were observed similar to standard transfection reagents. In the cationic ferrocenium state,

however, transfection was almost completely shut down and only very little green fluorescence was observed. Clearly, the difference in charge and concomitantly different lipophilicity directly influenced transfection efficiency of the system.

1.31.4.3.3 Receptor ligands

Organometallic derivatives of steroid hormones have been used to study ligand–receptor interactions for quite some time. SERMs with anti-tumor activity have already been discussed in Section 1.31.3.1. Other applications were developed for metallo-immuno assays and are discussed in Section 1.31.5.3. For such applications, binding of the organometallic compound to a receptor is necessarily implied but not always proved or quantified.

The steroid hormone estradiol **30** has been the subject of labeling with a number of different organometallic compounds. The structure of **30** (R = H) and its derivatives is shown in Scheme 31, Table 1 summarizes the relative binding affinities of organometallic estradiol derivatives to the ERα. Most derivatives so far are 17α-substituted estradiols, that is, the organometallic group R is pointing backward on C17. Top and co-workers carried out molecular modeling studies to understand binding affinities of organometallic selective estrogen receptor modulators (SERMs) to the ERα based on its crystal structure.[312]

Very recently, Gmeiner and co-workers prepared metallocene-derived receptor ligands for G-protein-coupled receptors (GPCRs) such as dopamine and serotonin receptor subtypes. They used ruthenocene and ferrocene derivatives, in which the metallocenes replaced cyclophanes as so-called "fancy bioisosters."[319] In particular, compound **31** (Scheme 32) showed sub-nanomolar affinity and high specificity for the dopamine D_4 and serotonin HT_{1A} receptor subtypes, and may thus be a suitable lead structure for the further development of selective organometallic GPCR ligands.

In the above example, as in the ferrocifen series and many others above, the organometallic group (e.g., ferrocene) simply serves as an inert, bulky, lipophilic residue. Indeed, it often replaces benzene in an organic structure. In a slightly different approach, Meggers' group has developed organometallic compounds in which the metal's role is to correctly place other (organic) groups in three-dimensional (3-D) space. Their target was to design analogs of protein kinase (PK) inhibitors based on the structure of the purely organic inhibitor (+)-staurosporin.[320–322] Scheme 33 shows

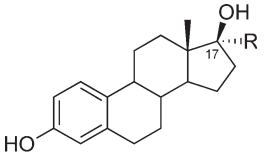

30

Scheme 31

Table 1 Relative binding affinity (RBA) of some mononuclear organometallic estradiol derivatives to the ERα[a,b,c]

R	*RBA*[a]	*References*[b]
Fc	8	313[d]
(η-C_5H_4)Ru(Cp)	2	313[d]
-≡-Fc	28, 37[e]	314[d]
(η-C_6H_5)Cr(CO)$_3$	11	315
-≡-(η-C_6H_5)Cr(CO)$_3$	24	315
-≡-(η-C_5H_4)Mn(CO)$_3$	15	316
-≡-(η-C_5H_4)Re(CO)$_3$	16	316
CH_2-(η-C_5H_4)Mn(CO)$_3$	2.5	316
CH_2-(η-C_5H_4)Re(CO)$_3$	0.8	316
[(η-C_5H_4)Ru(Cp^*)]OTf	0	315

[a]RBA values determined in a competitive radioreceptor binding assay at 0 °C.
[b]For examples of estradiol conjugates with dinuclear organometallic complexes, see Refs: 317, 318.
[c]See also Scheme 31.
[d]X-ray crystal structure reported.
[e]RBA to the ERβ.

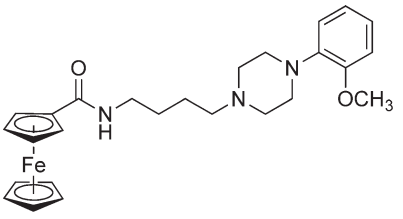

31

Scheme 32

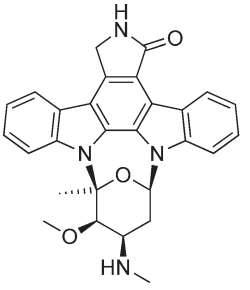

32

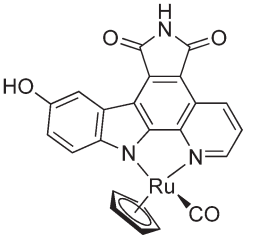

33

Scheme 33

the structure of (+)-staurosporin **32** and a CpRu analog thereof. In addition to a similar molecular shape and surface, Scheme 34 also shows that the electrostatic potential surfaces of staurosporin and its organometallic analog **33** are very comparable.[72] On the basis of a co-crystal structure of enantiomerically pure (*S*)-**33** and the PK Pim-1, it has been suggested that electrostatic interactions indeed play a crucial role to explain the very high affinity of **33** to Pim-1.[72,322] Indeed, the affinity of (*S*)-**33** to Pim-1 is far higher than that of (+)-staurosporin. As expected, the affinity of the enantiomer (*R*)-**33** to Pim-1 is also several orders of magnitude smaller. More than 60 PKs are known today, which are all quite similar. This makes the design of specific inhibitors for one single PK a very difficult task. It is thus remarkable that **33** is highly selective for Pim-1. Pim-1 is especially interesting since it is overexpressed in human prostate cancer cells. (*S*)-**33** or derivatives might therefore find application as novel chemotherapeutic agents against prostate cancer.

PKs in general are key players in the modulation of enzyme activity by transfer of the γ-phosphate group of the adenosinetriphosphate (ATP) co-substrate to hydroxy groups of either serine, threonine, or tyrosine in the target protein. This phosphorylation is especially important in the control of cellular signal transduction pathways, and disregulated kinase activity is a frequent cause of diseases. Organometallic compounds similar to **33** are stable *in vitro* and *in vivo*. One such derivative (which specifically inhibited glykogen synthase kinase 3)[320] was utilized as a tool to switch on the signal transduction pathways in *Xenopus* frog embryos, which could even be visualized by changes in the phenotype.[321] This results from the ATP-binding site being blocked by the organoruthenium compound.

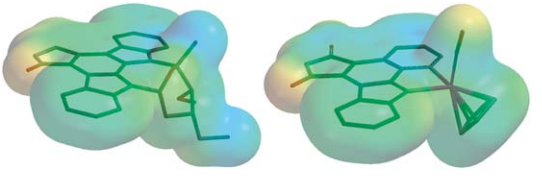

32 33

Scheme 34

1.31.4.3.4 Peptide synthesis

Many interesting applications of organometallic compounds for amino acid or peptide synthesis were published, for example, to obtain unnatural amino acids. In here, mention is made only of some of those in which distinct organometallic peptide intermediates were isolated and characterized. Weiß and Fischer have used aminocarbenes of chromium or tungsten as *N*-terminal protecting groups in conventional solution-phase peptide synthesis up to tetrapeptides.[323,324] The metal carbene group is finally removed by trifluoroacetic acid (TFA) under mild conditions. Similarly, the ferrocenylmethyl (Fem) group may serve as a tag to the amino groups in peptides which enhances lipophilicity[325,326] and enable electrochemical detection of the peptides.[327,328] The Fem group is also removed by dilute acid. The $[Fe(CO)_3(C_6H_7)]^+$ cation (Fed) is an alternative to the Fem group.[329–331] Compound **34** is a potent chiral auxiliary in Ugi four-component reactions (Ugi-4CR) for the synthesis of tripeptides (Scheme 35).[332] Using **34** and related ferrocenylamines, numerous peptides were prepared.[333–336] The ferrocenylamine can be readily regenerated for further usage.[337,338] Stoichiometric olefin metathesis can be used to introduce metal carbonyl markers into peptides. Both Ugi-4CR and olefin metathesis have also been used to introduce organometallic markers into PNA, as mentioned in Section 1.31.4.2. The ruthenium-mediated coupling of aryl ethers is another attractive route to linear peptoids[339] and cyclic peptides.[340–343]

Hegedus and co-workers developed the metal carbene chemistry mentioned in the previous paragraph into a unique route to unnatural amino acids, as shown in Scheme 36.[344] Photolysis of the $Cr(CO)_5$ amino carbene **35** produces a metal-complexed amino ketene, which can be trapped with amino acid esters to yield a dipeptide **36**. Use of an appropriate chiral auxiliary on the carbene amino atom generally gives high enantiomeric purity of the newly formed stereocenter. Although the chemistry can be performed on the resin as part of an SPPS scheme, it is most successfully carried out in solution as part of a fragment condensation scheme for peptide synthesis.[344] The octapeptide Boc-Gly-Ala-***D*-homoPhe-*D*-Ala-Phe**-Val-Leu-Gly-OMe (homoPhe: homo-phenylalanine) was successfully prepared by this method.[345] In this peptide, the central tripeptide *D*-homoPhe-*D*-Ala-Phe (marked boldface) was synthesized in solution by chromium carbene photochemistry. The tripeptide fragment was added to the tripeptide Val-Leu-Gly on the resin, and the synthesis was completed by addition of the two *N*-terminal amino acids by SPPS. The crude product was obtained in 72% yield based on the chromium carbene tripeptide and could be readily purified and characterized.

An alternative approach to metal-catalyzed peptide synthesis was proposed by Beck and co-workers. Their method uses half-sandwich complexes of Rh, Ir, or Ru.[346–351] In this reaction, *N*,*N*′-coordinated peptides are elongated at the *N*-terminus by condensation with amino acid esters. Scheme 37 shows the postulated reaction sequence.[348] It is worth noting that formation of the peptide bond does not require activating reagents or protecting groups. The key step is nucleophilic attack of the deprotonated terminal amino group at the ester carbonyl group. Repeated addition of amino acid esters yields a growing peptide in the coordination sphere of the metal complex. All reactions proceed under relatively mild conditions in the coordination sphere of the chiral metal half-sandwich fragment and no racemization has been observed. The peptide is finally released from the metal template by methanolic HCl.

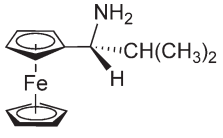

34

Scheme 35

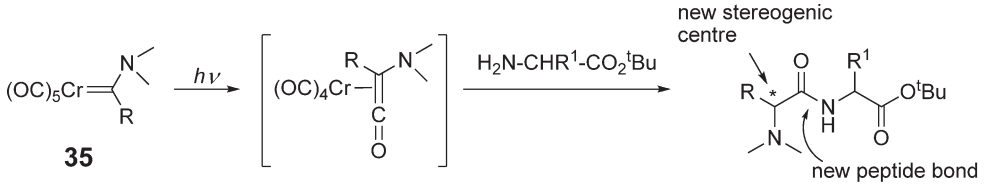

35 **36**

Scheme 36

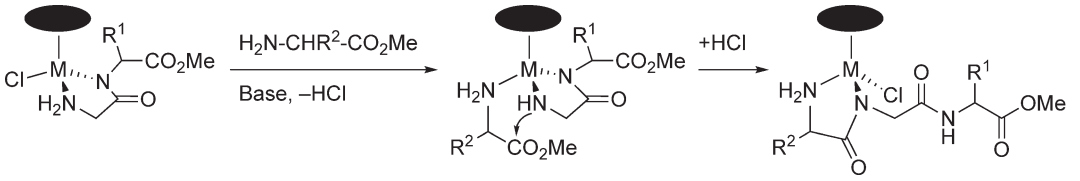

Scheme 37

Several intermediates have been isolated and characterized spectroscopically as well as by X-ray crystallography.[347,348] In one paper, the catalytic formation of up to a nonapeptide H-(Gly)$_9$-OMe on a {(*p*-cymene)RuCl} fragment is described.[349] The formation of cyclic tetrapeptides on a metal template is also reported.[350]

1.31.5 Biosensors Based on Organometallics

In a very general sense, Stephenson has defined the term "bioprobes" as "... functional molecules or devices that provide information about biological systems...." The high kinetic and thermodynamic stability of many organometallic complexes, in addition to their electronic and spectroscopic properties, have spurred their use in numerous sensor applications. Among those are sensors which involve biomolecules, or which detect biomolecules. In this chapter, only a few selected examples are presented as an introduction to the field. Organometallic biosensors are comprehensively summarized in four chapters in a recent book on bioorganometallic chemistry.[186,352–354] A more detailed treatment is also found in a chapter in Volume 12 of this series.

1.31.5.1 Protein-based Redox Probes

Most work related to the covalent labeling of proteins with organometallic is related to the development of enzyme or antibody amperometric biosensors.[186] For the majority of redox enzymes, the active center (or redox-active cofactors) are buried inside the protein and are therefore electrically inaccessible for direct electron transfer to the electrode surface of an amperometric biosensor. This problem has been resolved by (i) addition of a diffusional redox-active mediator, (ii) covalent tethering of the mediator to the protein, or (iii) immobilization of the protein in a redox-active polymer.[355] Ferrocenyl derivatives have frequently been used in all three formats as mediators because of their almost ideal electrochemical properties.

The redox enzyme glucose oxidase (GOD) has been a primary target of investigation. It forms the basis of amperometric glucose biosensors which are used to monitor the level of glucose in patients suffering from diabetes. In the first marketed hand-held device for patient's use (the ExacTECH^{TM} pen), the 1,1′-dimethylferrocene/1,1′-dimethylferrocenium couple served as a diffusional redox mediator.[356,357] Subsequently, many covalent modifications of GOD were explored and more advanced devices have reached the market. Methods of ferrocene derivatization of GOD were tabulated in two recent reviews.[3,186] Ferrocene labeling of all kinds of proteins and enzymes (both redox-active and non-redox-active) is comprehensively treated in one of those articles.[3]

1.31.5.2 DNA Sensors

Similar to the labeling of enzymes with redox mediators, genosensors were developed for sequence-specific DNA detection by making use of the electrochemical properties of organometallic compounds, mainly ferrocene and its derivatives.[354] Electrochemical genosensors are particularly attractive because they are highly sensitive and robust, cheap compared to other detection modes such as fluorescence, and they can be easily miniaturized.[358] The potential in this technique has attracted commercial interest.[359,360]

DNA oligomers can be labeled with ferrocene derivatives in a number of ways (see also Section 1.31.4.2). Upon binding to complementary DNA or RNA (target) strands, an electrochemical signal can be detected, for example, after separation by HPLC[361,362] or capillary gel electrophoresis (CGE).[363,364] Electrochemical detection is also possible after triplex formation with a ferrocenylated ODN.[365,366] The sensitivity of the system may be enhanced after DNA amplification by PCR,[367] or through amplification of the current by coupling to an enzymatic reaction, for example, the oxidation of glucose by GOD.[368] Ferrocene can be readily modified chemically. Depending on the

substituents of both rings, a different redox potential of the Fe(II)/Fe(III) couple results. The four differently substituted ferrocenes **37–40** (Scheme 38) were used as covalent labels on the 5′ end of four PCR primers which differ in one base only. Thus, each redox potential "codes" for one specific nucleobase in the position of interest.[363] Using sinusoidal voltammetry, the different potentials could be reliably differentiated, and a novel system for single nucleotide polymorphism was established.[364] This strategy is, in principle, analogous to the so-called "four-color DNA sequencing."

Ferrocenylated ODNs were first immobilized in a self-assembled redox-active monolayer on Au electrodes by Letsinger and co-workers.[369] Upon hybridization of a complementary strand, the electrochemical potential of the ferrocene changes. In addition to applications as electrochemical DNA sensors, such self-assembled DNA monolayers with electro-active groups may provide information on the mechanism of electron transfer through DNA, and indirectly also on molecular mobility within short stretches of DNA.[370–374] We have recently extended this idea by the use of immobilized metallocene-labeled PNA on Au electrodes.[299,300] Because PNA is an uncharged molecule, a surface with improved properties forms, and electrochemical detection, also of single mismatches, is facilitated.

A slightly different approach is used in a so-called "sandwich assay."[375,376] First, a capture probe is immobilized on an Au electrode. The target DNA binds to this capture probe if a complementary sequence is present. In addition, the target DNA carries a binding sequence (for example poly-A). The ferrocenylated poly-T signaling probe hybridizes with the poly-A sequence of the target ODN. If the target also binds to the capture probe, the ferrocene comes close to the electrode surface and a signal is measured. The system has later been characterized in detail[377] and was refined.[359,378]

Finally, attempts have been made to perform electrochemical DNA detection without having to use metal-modified ODNs.[354,376] This can be achieved by immobilizing the capture ODN on an electrode, allowing it to hybridize with the target DNA, and then adding an electro-active compound that will interact only with ds-DNA. Quite a number of compounds have been used for detection, including Co complexes, ethidium bromide, and

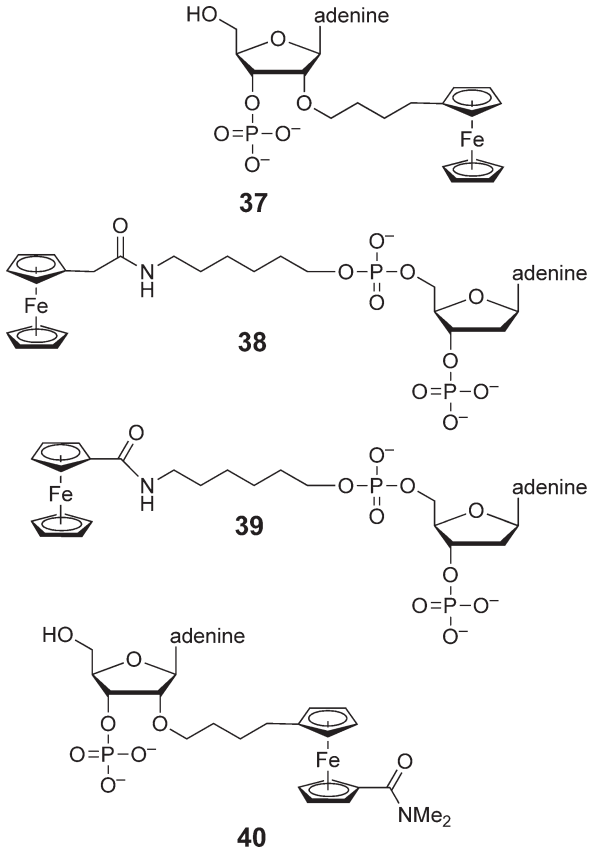

Scheme 38

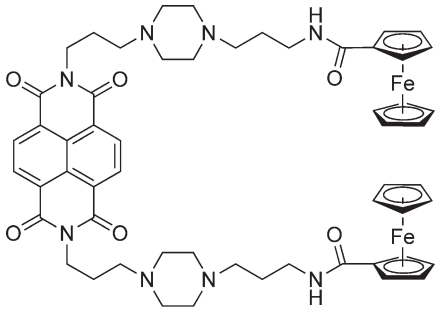

41

Scheme 39

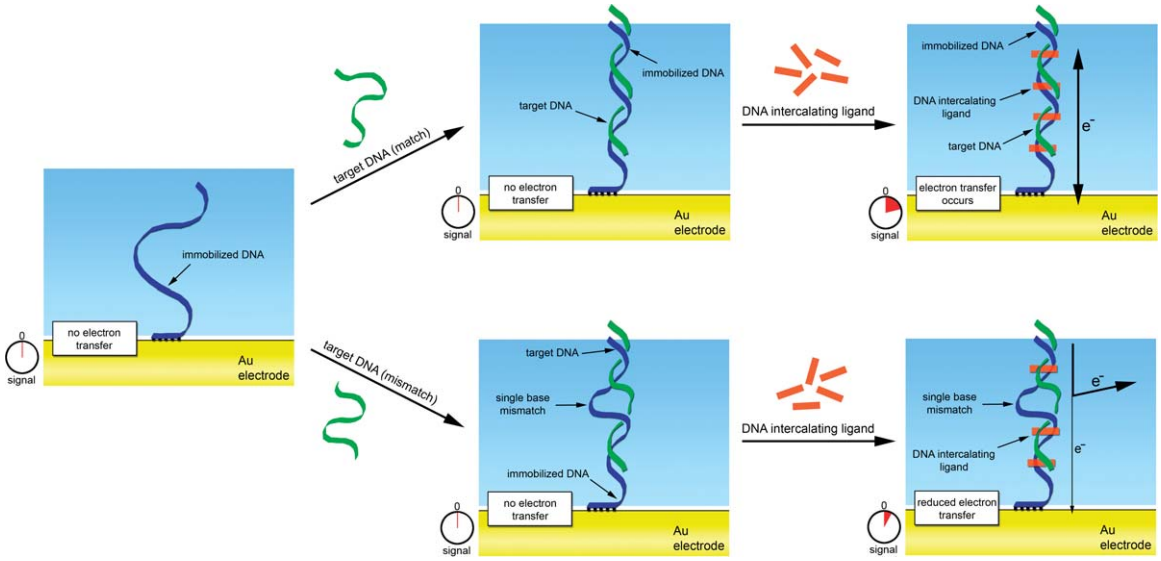

Scheme 40

intercalating drugs such as daunorubicin. Takenaka's group has successfully used the ferrocene-modified naphthalenediimide **41** as threading intercalator (Scheme 39).[368,379,380] This system is chemically very robust and highly sensitive, reaching a detection limit of 10 zmol DNA under favorable conditions.[380] The sensitivity of the system could be enhanced by coupling it to an enzymatic reaction like the glucose oxidation using GOD.[368] Furthermore, the system has the potential of direct mismatch detection by determining the number of intercalated molecules or the rate of electron transfer.[379] Scheme 40 compares a perfect match situation with a case where the target strand has a single mismatch. It is assumed that less electrons will be transferred less fast if the local geometry is perturbed by a single base mismatch. Evidently, this system needs careful calibration and probably optimization for every single application. On the other hand, it is versatile in the sense that one and the same simple electro-active probe **41** is used for every ODN sequence to be investigated. An application that enables the rapid analysis of heterozygous deficiency of the human lipoprotein lipase gene has been reported.[381]

1.31.5.3 Metallo-immuno Assays

One prominent use of organometallic complexes is in metallo-immuno assays. The traditional radio-linked immuno assay (RIA) is highly sensitive but has obvious disadvantages related to the use of radioactivity. Modern alternatives use colorimetric, fluorescence, or enzyme-linked detection schemes (ELISA). The idea of using non-radioactive metals for specific, highly sensitive detection in immuno assays was first mentioned by Cais, who used steroid

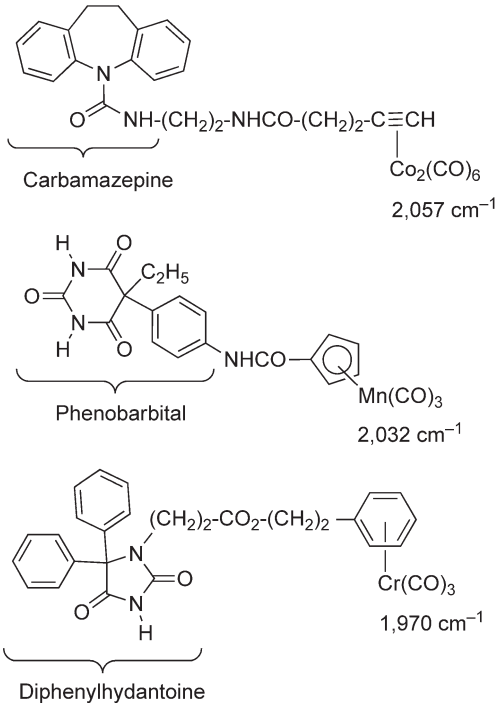

Scheme 41

hormones as haptens and atomic absorption spectroscopy (AAS) for detection.[382,383] The idea was later modified by Jaouen's group, who used infrared spectroscopy of metal carbonyl compounds for detection. The metal C–O stretching vibrations around 2,000 cm^{-1} are generally quite strong. In addition, few organic molecules have absorptions in this region, which is thus rather blank and well suited for detection. A first use of this technique was published in 1985,[384] and the method was described as carbonyl metallo immuno assay (CMIA) in 1992.[385] Several reviews have been published.[158,352,386,387] Initial work has concentrated on steroid hormones and their receptor interaction.[388–390] More recently, the method was extended as an analytical tool for the quantification of anti-epileptic drugs in patients. By careful choice of the organometallic complex, it has been possible to quantify two[391] or even three different drugs simultaneously and independently.[392] Scheme 41 shows three such organometallic conjugates of different anti-epileptic drugs as an example. The IR bands used for detection are indicated. Also, interesting applications for environmental analytics such as pesticide analysis were reported mainly by Salmain and co-workers.

1.31.5.4 Colorimetric Assays and Luminescent Probes

Colorimetric, fluorescence, and luminescent assays are arguably by far the most important detection methods in bioanalytics. In relation, the importance of metal-based complexes in this field is negligible. Nevertheless, some metal complexes have very favorable properties, for example, long fluorescence or luminescence lifetimes and emission at very long wavelengths. It is probably fair to say that the potential of organometallic complexes in this area is greater than the number of workers advocating their use.

There are, however, some unique uses of organometallic complexes in bioanalytics. Since the mid-1960s, lithium salts are among the most frequently used drugs for patients suffering from bipolar disorder. Severin and co-workers could show that organometallic receptors are an interesting alternative to the commonly used organic ionophores for the selective sequestering and sensing of lithium ions. A trinuclear metallamacrocycle was obtained from a dihydroxypyridine derivative and a commercially available ruthenium complex in buffered aqueous solution (Scheme 42). The macrocycle acts as a potent and selective receptor for lithium ions.[393] With the help of a subsequent redox reaction, the binding event can be transduced into a color change, which allows to detect lithium ions in the pharmacologically relevant concentration range of ~1 mM by the "naked eye."

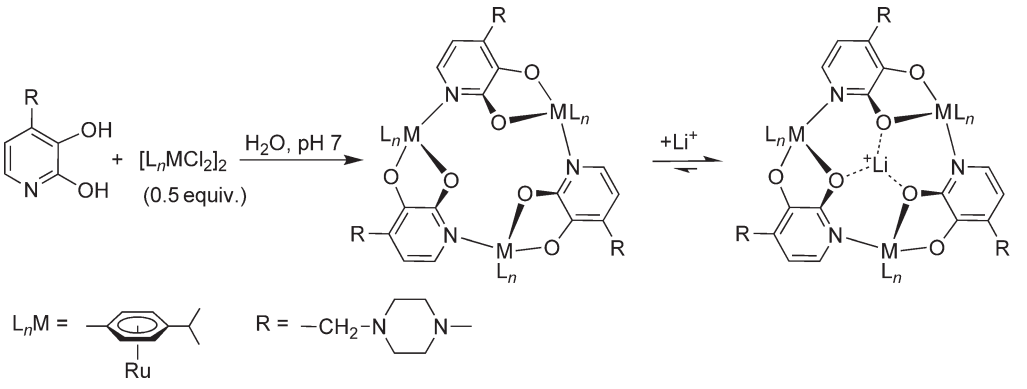

Scheme 42

A synthetic receptor, which is bound via non-covalent interactions to a dye, is able to function as a chemosensor. The basic requirement is that the displacement of the dye by an analyte results in a change of its optical properties.[394] Recently, it was shown that the combination of an organometallic Cp^*Rh^{III} complex with the dye azophloxine allows to selectively detect histidine- and methionine-containing peptides in water at neutral pH.[395] Due to the high binding constants of the organometallic Rh complex, peptides could be detected at concentrations as low as 300 nM. In direct extension of this work, it was shown that the selectivity of such bioorganometallic assays can be increased significantly when they are performed in an array format.[396] Thus, it was possible to identify all the 20 natural amino acids with a fidelity of 97% using UV–VIS spectroscopy in combination with a multivariate analysis. Closely related analytes such as leucine and isoleucine were clearly distinguishable, a result which would be very difficult to achieve with a classical "one sensor–one analyte" approach.

1.31.5.5 Heavy Metal Probes for Crystallography and Electron Microscopy

Heavy atoms are often essential for solving the "phase problem" in the X-ray crystallography of biomacromolecules. In many cases, crystals are soaked with a solution of the compound, and it is hoped that the heavy atoms will occupy well-defined sites in the crystal with a high occupancy factor. Organomercury compounds are frequently used for this purpose.

The ideal reagent will react efficiently with one single, well-defined site of the biomolecule, for example, a protein. It should not disturb the crystallization process, better even facilitate crystallization. Electron-dense transition metal complexes could serve such a purpose in principle. $[Pt(CN)_4]^{2-}$ and $[Au(CN)_4]^-$ have been suggested, but are rather unselective, possibly reacting with multiple sites of the protein.[397,398] Polynuclear Ir, Ru, or Os carbonyl clusters have been proposed for this purpose, and they can be monofunctionalized with activated esters or maleiimide groups, as exemplified for the first such monofunctional cluster **42** prepared by Jahn (Scheme 43).[399] Other kinetically inert half-sandwich complexes (W, Re, Ir) might also be suitable, and in principle many of the ideas and compounds discussed in Section 1.31.4.1 are directly applicable.[400–403] For instance, tungsten alkoxycarbene complexes have been used for the labeling of the enzyme lysozyme in an analogous manner to the one depicted in Scheme 24.[264] However, multiple adducts were found, and it has not been shown that there was a benefit for crystallization.[186] The tetrairidium cluster **42** has been instrumental in the structure elucidation of a ribosomal particle.[399,404,405]

There is even more potential for the site-specific covalent labeling with heavy atom derivatives in cryo-electron microscopy.[186] Very large particles, such as viruses or protein aggregates, can be visualized. Because the

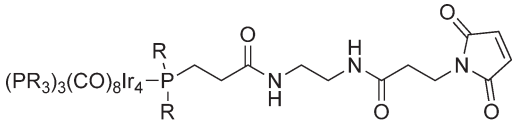

42

Scheme 43

electron-dense metals could be "seen" directly over the mostly carbon-containing protein background, site-selective labeling would be enormously helpful for the construction of images with molecular resolution. Clearly, this is an area with a lot of potential. To develop the right molecules, reagents and conditions will require a close collaboration of synthetic organometallic chemists with molecular and structural biologists.

Acknowledgments

The author is most grateful to all the co-workers who have contributed to the success of this chapter. Special thanks go to Bernie Kraatz for an excellent collaboration and many stimulating discussions and to Karin Weiß for her equally excellent and ever-friendly support of the group in the Heidelberg years. Margaret Harding provided the pictures for Figure 2, the Milan group (Maiorana, Licandro, and Baldoli) freely shared its enthusiasm for organometallic PNAs, Karl Heinz Dötz provided valuable literature, and Dr. Fozia Noor made valuable suggestions on the final draft of the chapter.

References

1. Jaouen, G. *Bioorganometallics*; Wiley-VCH: Weinheim, 2006.
2. Kraatz, H.-B.; Metzler-Nolte, N. *Concepts and Models in Bioinorganic Chemistry*; Wiley-VCH: Weinheim, 2006.
3. van Staveren, D. R.; Metzler-Nolte, N. *Chem. Rev.* **2004**, *104*, 5931–5985.
4. Holland, P. L. Nitrogen Fixation. In *Comprehensive Coordination Chemistry II*; Que, L. J., Tolman, W. B., Eds.; Elsevier: Amsterdam, 2003; Vol. 8, pp 569–599.
5. Li, S.; Wackett, L. P. *Biochemistry* **1993**, *32*, 9355–9361.
6. Bleeker, A. B.; Kende, H. *Ann. Rev. Cell Biol.* **2000**, *16*, 1–18.
7. Rodríguez, F. I.; Esch, J. J.; Hall, A. E.; Binder, B. M.; Schaller, G. E.; Bleeker, A. B. *Science* **1999**, *283*, 996–998.
8. Hirsch, J.; George, S. D.; Solomon, E. I.; Hedman, B.; Hodgson, K. O.; Burstyn, J. N. *Inorg. Chem.* **2001**, *40*, 2439–2441.
9. Brown, K. L. *Chem. Rev.* **2005**, *105*, 2075–2149.
10. Riordan, C. G. Bioorganometallic Chemistry of Cobalt and Nickel. In *Comprehensive Coordination Chemistry II*; Que, L. J., Tolman, W. B., Eds.; Elsevier: Amsterdam, 2003; Vol. 8, pp 677–714.
11. Banerjee, R. *Chemistry and Biochemistry of B_{12}*; Wiley: New York, 1999.
12. Kräutler, B.; Arigoni, D.; Golding, B. T. *Vitamin B_{12} and B_{12} Proteins*; Wiley-VCH: Weinheim, 1998.
13. Golding, B. T.; Anderson, R. J.; Ashwell, S.; Edwards, C. H.; Garnett, I.; Kroll, F.; Buckel, W. A. Mechanistic Overview of B_{12} Dependent Processes. In *Vitamin B_{12} and B_{12} Proteins*; Kräutler, B., Arigoni, D., Golding, B. T., Eds.; Wiley-VCH: Weinheim, 1998; pp 201–216.
14. Golding, B. T.; Buckel, W. In *Comprehensive Biochemical Catalysis*; Sinnott, M. L., Ed.; Academic Press: London, 1997; Vol. 3, pp 239–259.
15. Buckel, W.; Golding, B. T. *Chem. Soc. Rev.* **1996**, 329.
16. Mancia, F.; Keep, N. H.; Nakagaw, A.; Leadlay, P. F.; McSweeney, S.; Rasmussen, B.; Bösecke, P.; Diat, O.; Evans, P. R. *Structure* **1996**, *4*, 339.
17. Mancia, F.; Smith, G. A.; Evans, P. R. *Biochemistry* **1999**, *38*, 7999.
18. Mancia, F.; Evans, P. R. *Structure* **1998**, *6*, 711.
19. Stubbe, J.; Licht, S.; Gerfen, G.; Silva, D.; Booker, S. Adenosylcobalamin-dependent Ribonucleotide Reductases: Still Amazing but no Longer Confusing. In *Vitamin B_{12} and B_{12} Proteins*; Kräutler, B., Arigoni, D., Golding, B. T., Eds.; Wiley-VCH: Weinheim, 1998; pp 321–331.
20. Drennan, C. L.; Huang, S.; Drummond, J. T.; Matthews, R. G.; Ludwig, M. L. *Science* **1994**, *266*, 1669.
21. Drennan, C. L.; Dixon, M. M.; Hoover, D. M.; Jarrett, J. T.; Goulding, C. W.; Matthews, R. G.; Ludwig, M. L. Cobalamin-dependent Methyionine Synthase from *E. coli*: Structure and Reactivity. In *Vitamin B_{12} and B_{12} Proteins*; Kräutler, B., Arigoni, D., Golding, B. T., Eds.; Wiley-VCH: Weinheim, 1998; pp 133–155.
22. Stupperich, E.; Konle, R.; Lehle, M. Corrinoid-dependent Methyl Transfer Reactions in *Sporomusa ovata*. In *Vitamin B_{12} and B_{12} Proteins*; Kräutler, B., Arigoni, D., Golding, B. T., Eds.; Wiley-VCH: Weinheim, 1998; pp 179–187.
23. Happe, R. P.; Roseboom, W.; Pierik, A. J.; Albracht, S. P. J.; Bagley, K. A. *Nature* **1997**, *385*, 126–126.
24. Adams, M. W. W.; Stiefel, E. I. *Curr. Opin. Chem. Biol.* **2000**, *4*, 214–220.
25. Georgakaki, I. P.; Darensbourg, M. Y. Hydrogen Activation. In *Comprehensive Coordination Chemistry II*; Que, L. J., Tolman, W. B., Eds.; Elsevier: Amsterdam, 2003; Vol. 8, pp 549–568.
26. Shima, S.; Lyon, E. J.; Sordel-Klippert, M.; Kauss, M.; Kahnt, J.; Thauer, R. K.; Steinbach, K.; Xie, X.; Verdier, L.; Griesinger, C. *Angew. Chem., Int. Ed.* **2004**, *43*, 2547–2551.
27. Lyon, E. J.; Shima, S.; Boecher, R.; Thauer, R. K.; Grevels, F.-W.; Bill, E.; Roseboom, W.; Albracht, S. P. J. *J. Am. Chem. Soc.* **2004**, *126*, 14239–14248.
28. Lyon, E. J.; Shima, S.; Buurman, G.; Chowdhuri, S.; Batschauer, A.; Steinbach, K.; Thauer, R. K. *Eur. J. Biochem.* **2004**, *271*, 195–204.
29. Shima, S.; Lyon, E. J.; Thauer, R. K.; Mienert, B.; Bill, E. *J. Am. Chem. Soc.* **2005**, *127*, 10430–10435.
30. Volbeda, A.; Charon, M. H.; Piras, C.; Hatchikian, E. C.; Frey, M.; Fontecilla-Camps, J. C. *Nature* **1995**, *373*, 580–587.
31. Fontecilla-Camps, J. C. *J. Biol. Inorg. Chem.* **1996**, *1*, 91–98.
32. Montet, Y.; Amara, P.; Volbela, A.; Vernède, X.; Hatchikian, E. C.; Field, M. J.; Frey, M.; Fontecilla-Camps, J. C. *Nature Struct. Biol.* **1997**, *4*.
33. Nicolet, Y.; Lemon, B. J.; Fontecilla-Camps, J. C.; Peters, J. W. *Trends Biochem. Sci.* **2000**, *25*, 138–143.
34. Nicolet, Y.; Cavazza, C.; Fontecilla-Camps, J. C. *J. Inorg. Biochem.* **2002**, *91*, 1–8.
35. Peters, J. W.; Lanzilotta, W. N.; Lemon, B. J.; Seefeldt, L. C. *Science* **1998**, *282*, 1853–1858.
36. Nicolet, Y.; Piras, C.; Legrand, P.; Hatchikian, E. C.; Fontecilla-Camps, J. C. *Structure* **1999**, *7*, 13–23.
37. Nicolet, Y.; de Lacey, A. L.; Vernede, X.; Fernandez, V. M.; Hatchikian, E. C.; Fontecilla-Camps, J. C. *J. Am. Chem. Soc.* **2001**, *123*, 1596–1601.
38. Fan, H.-J.; Hall, M. B. *J. Am. Chem. Soc.* **2001**, *123*, 3828–3829.

39. Jiang, J.; Acunzo, A.; Koch, S. A. *J. Am. Chem. Soc.* **2001**, *123*, 12109–12110.
40. Jiang, J.; Koch, S. A. *Angew. Chem., Int. Ed.* **2001**, *40*, 2629–2631.
41. Seyferth, D.; Womack, G. B.; Gallagher, M. K.; Cowle, M.; Hames, B. W.; Fackler, J. P., Jr.; Mazany, A. M. *Organometallics* **1987**, *6*, 283–294.
42. Gloaguen, F.; Lawrence, J. D.; Schmidt, M.; Wilson, S. R.; Rauchfuss, T. B. *J. Am. Chem. Soc.* **2001**, *123*, 12518–12527.
43. Gloaguen, F.; Lawrence, J. D.; Rauchfuss, T. B. *J. Am. Chem. Soc.* **2001**, *123*, 9476–9477.
44. Rauchfuss, T. B. *Inorg. Chem.* **2004**, *43*, 14–26.
45. Bagley, K. A.; Duin, E. C.; Roseboom, W.; Albracht, S. P. J.; Woodruff, W. H. *Biochemistry* **1995**, *34*, 5527–5535.
46. Volbeda, A.; Garcia, E.; Piras, C.; de Lacey, A. L.; Fernandez, V. M.; Hatchikian, E. C.; Frey, M.; Fontecilla-Camps, J. C. *J. Am. Chem. Soc.* **1996**, *118*, 12989–12996.
47. de Lacey, A. L.; Hatchikian, E. C.; Volbeda, A.; Frey, M.; Fontecilla-Camps, J. C.; Fernandez, V. M. *J. Am. Chem. Soc.* **1997**, *119*, 7181–7189.
48. Darensbourg, D. J.; Reibenspies, J. H.; Lai, C.-H.; Lee, W.-Z.; Darensbourg, M. Y. *J. Am. Chem. Soc.* **1997**, *119*, 7903--7904.
49. Lai, C.-H.; Lee, W.-Z.; Miller, M. L.; Reibenspies, J. H.; Darensbourg, D. J.; Darensbourg, M. Y. *J. Am. Chem. Soc.* **1998**, *120*, 10103–10114.
50. Kubas, G. J.; Ryan, R. R.; Swnason, B. I.; Vergamini, P. J.; Wasserman, H. J. *J. Am. Chem. Soc.* **1984**, *106*, 451–452.
51. Kubas, G. J. *Acc. Chem. Res.* **1988**, *21*, 120–128.
52. Heinekey, D. M.; Oldham, W. J., Jr. *Chem. Rev.* **1993**, *93*, 913–926.
53. Forde, C. E.; Landau, S. E.; Morris, R. H. *J. Chem. Soc., Dalton Trans.* **1997**, 1663–1664.
54. Roberts, L. M.; Lindahl, P. A. *Biochemistry* **1994**, *33*, 14339–14350.
55. Hegg, E. L. *Acc. Chem. Res.* **2004**, *37*, 775–783.
56. Drennan, C. L.; Heo, J. Y.; Sintchak, M. D.; Schreiter, E.; Ludden, P. W. *Proc. Natl. Acad. Sci. USA* **2001**, *98*, 11973--11978.
57. Dobbek, H.; Svetlitchnyi, V.; Gremer, L.; Huber, R.; Meyer, O. *Science* **2001**, *293*, 1281–1285.
58. DeRose, V. J.; Telser, J.; Anderson, M. E.; Lindahl, P. A.; Hoffmann, B. M. *J. Am. Chem. Soc.* **1998**, *120*, 8767–8776.
59. Qiu, D.; Kumar, M.; Ragsdale, S. W.; Spiro, T. G. *Science* **1994**, *264*, 817–819.
60. Staples, C. R.; Heo, J. Y.; Spangler, N. J.; Kerby, R. L.; Robert, G. P.; Ludden, P. W. *J. Am. Chem. Soc.* **1999**, *121*, 11034–11044.
61. Heo, J.; Staples, C. R.; Telser, J.; Ludden, P. W. *J. Am. Chem. Soc.* **1999**, *121*, 11045–11057.
62. Maynard, E. L.; Lindahl, P. A. *J. Am. Chem. Soc.* **1999**, *121*, 9221–9222.
63. Maynard, E. L.; Lindahl, P. A. *Biochemistry* **2001**, *40*, 13262–13267.
64. Seravalli, J.; Ragsdale, S. W. *Biochemistry* **2000**, *39*, 1274–1277.
65. Riordan, C. G. *J. Biol. Inorg. Chem.* **2004**, *9*, 509–510.
66. Thauer, R. K.; Diekert, G.; Schonheit, P. *Trends Biochem. Sci.* **1980**, *5*, 304–306.
67. Ermler, U.; Grabarse, W.; Shima, S.; Goubeaud, M.; Thauer, R. K. *Curr. Opin. Struct. Biol.* **1998**, *8*, 749–758.
68. Thauer, R. K. *J. Inorg. Biochem.* **1999**, *74*, 54–54.
69. Diekert, G.; Jaenchen, R.; Thauer, R. K. *FEBS Lett.* **1980**, *119*, 118–120.
70. Ermler, U.; Grabarse, W.; Shima, S.; Goubeaud, M.; Thauer, R. K. *Science* **1997**, *278*, 1457–1462.
71. Pelmenschikov, V.; Blomberg, M. R. A.; Siegbahn, P. E. M.; Crabtree, R. H. *J. Am. Chem. Soc.* **2002**, *124*, 4039–4049.
72. Schatzschneider, U.; Metzler-Nolte, N. *Angew. Chem., Int. Ed.* **2006**, *45*, 1504–1507.
73. Osella, D.; Ferrali, M.; Zanello, P.; Laschi, F.; Fontani, M.; Nervi, C.; Cavigiolio, G. *Inorg. Chim. Acta* **2000**, *306*, 42–48.
74. Tabbi, G.; Cassino, C.; Cavigiolio, G.; Colangelo, D.; Ghiglia, A.; Viano, I.; Osella, D. *J. Med. Chem.* **2002**, *45*, 5786–5796.
75. Caldwell, G.; Meirim, M. G.; Neuse, E. W.; van Rensburg, C. E. J. *Appl. Organomet. Chem.* **1998**, *12*, 793–799.
76. Shen, W.-C.; Beloussow, K.; Meirim, M. G.; Neuse, E. W.; Caldwell, G. *J. Inorg. Organomet. Polym.* **2000**, *10*, 51–60.
77. Neuse, E. W. *Macromol. Symp.* **2001**, *172*, 127–138.
78. Köpf-Maier, P.; Hesse, B.; Voigtländer, R.; Köpf, H. *J. Cancer Res. Clin. Oncol.* **1980**, *97*, 31–39.
79. Köpf-Maier, P.; Köpf, H. *Chem. Rev.* **1987**, *89*, 1137–1152.
80. Köpf-Maier, P.; Köpf, H. *Struct. Bond.* **1988**, *70*, 105–185.
81. Murray, J. H.; Harding, M. M. *J. Med. Chem.* **1994**, *37*, 1936–1941.
82. Harding, M. M.; Mokdsi, G. *Curr. Med. Chem.* **2000**, *7*, 1289–1303.
83. Mross, K.; Robben-Bathe, P.; Edler, L.; Baumgart, J.; Berdel, W. E.; Fiebig, H.; Unger, C. *Onkologie* **2000**, *23*, 576–579.
84. Jamieson, E. R.; Lippard, S. J. *Chem. Rev.* **1999**, *99*, 2467–2498.
85. Wang, D.; Lippard, S. J. *Nature Rev. Drug Discov.* **2005**, *4*, 307–320.
86. Lippert, B. *Cisplatin*; Verlag Helvetica Chimica Acta: Zürich, 1999.
87. Sun, H.; Li, H.; Weir, R. A.; Sadler, P. J. *Angew. Chem.* **1998**, *110*, 1622–1625.
88. Top, S.; Kaloun, E. B.; Vessières, A.; Laios, I.; Leclercq, G.; Jaouen, G. *J. Organomet. Chem.* **2002**, *643–644*, 350–356.
89. Allen, O. R.; Croll, L.; Gott, A. L.; Knox, R. J.; C., M. P. *Organometallics* **2004**, *23*, 288–292.
90. Tacke, M.; Allen, L. T.; Cuffe, L.; Gallagher, W. M.; Lou, Y.; Mendoza, O.; Müller-Bunz, H.; Rehmann, F. J. K.; Sweeney, N. *J. Organomet. Chem.* **2004**, *689*, 2242–2249.
91. Tacke, M.; Cuffe, L.; Gallagher, M. K.; Lou, Y.; Mendoza, O.; Müller-Bunz, H.; Rehmann, F. J. K.; Sweeney, N. *J. Inorg. Biochem.* **2004**, *98*, 1987–1994.
92. Kuo, L. Y.; G., K. M.; Marks, T. J. *J. Am. Chem. Soc.* **1987**, *109*, 7207–7209.
93. Kuo, L. Y.; Kanatzidis, M. G.; Sabat, M.; Tipton, A. L.; Marks, T. J. *J. Am. Chem. Soc.* **1991**, *113*, 9027–9045.
94. Kuo, L. Y.; Liu, A. H.; Marks, T. J. Metallocene Interactions with DNA and DNA-processing Enzymes. In *Metal Ions in Biological Systems*; Sigel, H., Ed.; Decker: New York, 1996; pp 53–85.
95. Harding, M. M.; Prodigalidad, M.; Lynch, M. J. *J. Med. Chem.* **1996**, *39*, 5012–5016.
96. Harding, M. M.; Harden, G. J.; Field, L. D. *FEBS Lett.* **1993**, *322*, 291–294.
97. Waern, J. B.; Harding, M. *J. Organomet. Chem.* **2004**, *689*, 4655–4668.
98. Waern, J. B.; Dillon, C. T.; Harding, M. M. *J. Med. Chem.* **2005**, *48*, 2093–2099.
99. Waern, J. B.; Harris, H. H.; Lai, B.; Cai, Z.; Harding, L. M.; Dillon, C. T. *J. Biol. Inorg. Chem.* **2005**, *10*, 443–452.
100. Kuo, L. Y.; Kuhn, S.; Ly, D. *Inorg. Chem.* **1995**, *34*, 5341–5345.
101. Kuo, L. Y.; Barnes, L. A. *Inorg. Chem.* **1999**, *38*, 814–817.
102. Melchart, M.; Sadler, P. J. Ruthenium Arene Anticancer Complexes. In *Bioorganometallics*; Jaouen, G., Ed.; Wiley-VCH: Weinheim, 2006; pp 39–64.

103. Morris, R. E.; Aird, R. E.; del Socorro Murdoch, P.; Chen, H.; Cummings, J.; Hughes, N. D.; Parsons, S.; Parkin, A.; Boyd, G.; Jodrell, D. I.; Sadler, P. J. *J. Med. Chem.* **2001**, *44*, 3616–3621.
104. Aird, R. E.; Cummings, J.; Ritchie, A. A.; Muir, M.; Morris, R. E.; Chen, H.; Sadler, P. J.; Jodrell, D. I. *Br. J. Cancer* **2002**, *86*, 1652–1657.
105. Chen, H.; Parkinson, J. A.; Morris, R. E.; Sadler, P. J. *J. Am. Chem. Soc.* **2003**, *125*, 173–186.
106. Novakova, O.; Chen, H.; Vrana, O.; Rodger, A.; Sadler, P. J.; Brabec, V. *Biochemistry* **2003**, *42*, 11544–11554.
107. McNae, I. W.; Fishburne, K.; Habtemariam, A.; Hunter, T. M.; Melchart, M.; Wang, F.; Walkinshaw, M. D.; Sadler, P. J. *Chem. Commun.* **2004**, 1786–1787.
108. Jaouen, G.; Top, S.; Vessières, A.; Leclercq, G.; Quivy, J.; Jin, L.; Croisy, A. *C. R. Acad. Sci. Paris Série IIc* **2000**, 89–93.
109. Jaouen, G.; Top, S.; Vessières, A.; Leclercq, G.; McGlinchey, M. J. *Curr. Med. Chem.* **2004**, *11*, 2505–2517.
110. Shiau, A. K.; Barstad, D.; Lorisa, P. M.; Cheng, L.; Kushner, P. J.; Agard, D. A.; Greene, G. L. *Cell* **1998**, *95*, 927–937.
111. Pigeon, P.; Top, S.; Vessières, A.; Huché, M.; Hillard, E.; Salomon, E.; Jaouen, G. *J. Med. Chem.* **2005**, *48*, 2814–2821.
112. Hillard, E.; Vessières, A.; Thouin, L.; Jaouen, G.; Amatore, C. *Angew. Chem., Int. Ed.* **2006**, *45*, 285–290.
113. Kovavic, P.; Popp, W. J.; Ames, J. R.; Ryan, M. D. *Anti-cancer Drug Des.* **1988**, *3*, 205–216.
114. Jung, M.; Kerr, D. E.; Senter, P. D. *Arch. Pharm.* **1997**, *330*, 173–176.
115. Schmidt, K.; Jung, M.; Keilitz, R.; Schnurr, B.; Gust, R. *Inorg. Chim. Acta* **2000**, *306*, 6–16.
116. Roth, T.; Eckert, C.; Fiebig, H.-H.; Jung, M. *Anticancer Res.* **2002**, *22*, 2281–2284.
117. Ott, I.; Kircher, B.; Gust, R. *J. Inorg. Biochem.* **2004**, *98*, 485–489.
118. Coussens, L. M.; Werb, Z. *Nature* **2002**, *420*, 860–867.
119. Kalgutkar, A. S.; Crews, B. C.; Rowlinson, S. W.; Garner, C.; Seibert, K.; Marnett, L. J. *Science* **1998**, *280*, 1268–1270.
120. Ott, I.; Schmidt, K.; Kircher, B.; Schumacher, P.; Wiglenda, T.; Gust, R. *J. Med. Chem.* **2005**, *48*, 622–629.
121. Pfletschinger, A.; Koch, W.; Schmalz, H.-G. *Chem. Eur. J.* **2001**, 7, 5325–5332.
122. Schlawe, D.; Majdalani, A.; Velcicky, J.; Heßler, E.; Wieder, T.; Prokop, A.; Schmalz, H.-G. *Angew. Chem., Int. Ed.* **2004**, *43*, 1731–1734.
123. Velcicky, J.; Lanver, A.; Lex, J.; Prokop, A.; Wieder, T.; Schmalz, H.-G. *Chem. Eur. J.* **2004**, *10*, 5087.
124. Lanver, A.; Schmalz, H.-G. *Eur. J. Org. Chem.* **2005**, *16*, 1444–1458.
125. Lloyd, N. C.; Morgan, H. W.; Nicholson, B. K.; Ronimus, R. S. *Angew. Chem., Int. Ed.* **2005**, *44*, 941–944.
126. Bernard, S.; Enayati, A.; Redwood, L.; Roger, H.; Binstock, T. *Med. Hypoth.* **2001**, *56*, 462–471.
127. Henderson, D. C. *Lancet* **2002**, *360*, 1711–1712.
128. Edwards, E. I.; Epton, R.; Marr, G. *J. Organomet. Chem.* **1976**, *107*, 351–357.
129. Edwards, E. I.; Epton, R.; Marr, G. *J. Organomet. Chem.* **1976**, *122*, C49–C53.
130. Edwards, E. I.; Epton, R.; Marr, G. *J. Organomet. Chem.* **1979**, *168*, 259–272.
131. Simionescu, C.; Lixandru, T.; Tataru, L.; Mazilu, I.; Vata, M.; Luca, S. *J. Organomet. Chem.* **1983**, *252*, C43–C46.
132. Simionescu, C.; Lixandru, T.; Scutaru, D.; Vata, M. *J. Organomet. Chem.* **1985**, *292*, 269–273.
133. Scutaru, D.; Mazilu, I.; Tataru, L.; Vata, M.; Lixandru, T. *J. Organomet. Chem.* **1990**, *406*, 183–187.
134. Scutaru, D.; Tataru, L.; Mazilu, I.; Diaconu, E.; Lixandru, T.; Simionescu, C. *J. Organomet. Chem.* **1991**, *401*, 81–85.
135. Scutaru, D.; Mazilu, I.; Vata, M.; Tataru, L.; Vlase, A.; Lixandru, T.; Simionescu, C. *J. Organomet. Chem.* **1991**, *401*, 87–90.
136. Scutaru, D.; Tataru, L.; Mazilu, I.; Vata, M.; Lixandru, T.; Simionescu, C. *Appl. Organomet. Chem.* **1993**, *7*, 225–231.
137. Chantson, J.; Varga Falzacappa, M. V.; Crovella, S.; Metzler-Nolte, N. *J. Organomet. Chem.* **2005**, *690*, 4564–4572.
138. Chantson, J.; Varga Falzacappa, M. V.; Crovella, S.; Metzler-Nolte, N. *Bioconjugate Chem.* **2006**.
139. Biot, C.; Glorian, G.; Maciejewski, L. A.; Brocard, J. S.; Domarle, O.; Blampain, G.; Millet, P.; Georges, A. J.; Abessolo, H. Dive, D., *et al. J. Med. Chem.* **1997**, *40*, 3715–3718.
140. Domarle, O.; Blampain, G.; Agnaniet, H.; Nzadiyabi, T.; Lebibi, J.; Brocard, J. S.; Maciejewski, L. A.; Biot, C.; Georges, A. J.; Millet, P. *Antimicrob. Agents Chemother.* **1998**, *42*, 540–544.
141. Biot, C.; Delhaes, L.; N'Diaye, C. M.; Maciejewski, L. A.; Camus, D.; Dive, D.; Brocard, J. S. *Bioorg. Med. Chem.* **1999**, *7*, 2843–2847.
142. Delhaes, L.; Abessolo, H.; Biot, C.; Berry, L.; Delcourt, P.; Maciejewski, L. A.; Brocard, J. S.; Camus, D.; Dive, D. *Parasitol. Res.* **2001**, *87*, 239–244.
143. Biot, C.; Delhaes, L.; Abessolo, H.; Domarle, O.; Maciejewski, L. A.; Mortuaire, M.; Delcourt, P.; Deloron, P.; Camus, D. Dive, D., *et al. J. Organomet. Chem.* **1999**, *589*, 59–65.
144. Biot, C.; Taramelli, D.; Forfar-Bares, I.; Maciejewski, L. A.; Boyce, M.; Nowogrocki, G.; Brocard, J. S.; Basilico, N.; Olliaro, P.; Egan, T. J. *Mol. Pharmaceutics* **2005**, *2*, 185–193.
145. Chibale, K.; Moss, J. R.; Blackie, M.; van Schalkwyk, D.; Smith, P. J. *Tetrahedron Lett.* **2000**, *41*, 6231–6235.
146. Biot, C. *Curr. Med. Chem., Anti-infective Agents* **2004**, *3*, 135–147.
147. Delhaes, L.; Biot, C.; Berry, L.; Delcourt, P.; Maciejewski, L. A.; Camus, D.; Brocard, J. S.; Dive, D. *ChemBioChem* **2002**, *3*, 418–423.
148. Delhaes, L.; Biot, C.; Berry, L.; Maciejewski, L. A.; Camus, D.; Brocard, J. S.; Dive, D. *Bioorg. Med. Chem.* **2000**, *8*, 2739–2745.
149. Biot, C.; Delhaes, L.; Maciejewski, L. A.; Mortuaire, M.; Camus, D.; Dive, D.; Brocard, J. S. *Eur. J. Med. Chem.* **2000**, *35*, 707–714.
150. Sanchez-Delgado, R. A.; Navarro, M.; Pérez, H.; Urbina, J. A. *J. Med. Chem.* **1996**, *39*, 1095–1099.
151. Beagley, P.; Blackie, M. A. L.; Chibale, K.; Clarkson, C.; Moss, J. R.; Smith, P. J. *J. Chem. Soc., Dalton Trans.* **2002**, 4426–4433.
152. Blackie, M. A. L.; Beagley, P.; Chibale, K.; Clarkson, C.; Moss, J. R.; Smith, P. J. *J. Organomet. Chem.* **2003**, *688*, 144–152.
153. Beagley, P.; Blackie, M. A. L.; Chibale, K.; Clarkson, C.; Meijboom, R.; Moss, J. R.; Smith, P. J.; Su, H. *Dalton Trans.* **2003**, 3046–3051.
154. Johnson, T. R.; Mann, B. E.; Clark, J. E.; Foresti, R.; Green, C. J.; Motterlini, R. *Angew. Chem., Int. Ed.* **2003**, *42*, 3722–3729.
155. Motterlini, R.; Clark, J. E.; Foresti, R.; Sarathchandra, P.; Mann, B. E.; Green, C. J. *Circ. Res.* **2002**, *90*, e17–e24.
156. Abrams, M. J.; Davison, A.; Jones, A. G.; Costello, C. E.; Pang, H. *Inorg. Chem.* **1983**, *22*, 2798–2800.
157. Alberto, R.; Schibli, R.; Egli, A.; Schubiger, A. P.; Abram, U.; Kaden, T. A. *J. Am. Chem. Soc.* **1998**, *120*, 7987–7988.
158. Metzler-Nolte, N. *Angew. Chem., Int. Ed.* **2001**, *40*, 1040–1044.
159. Alberto, R.; Schibli, R.; Schubiger, A. P.; Abram, U.; Pietzsch, H. J.; Johannsen, B. *J. Am. Chem. Soc.* **1999**, *121*, 6076–6077.
160. Waibel, R.; Alberto, R.; Willuda, J.; Finnern, R.; Schibli, R.; Stichelberger, A.; Egli, A.; Abram, U.; Mach, J. P., Pluckthun, A., *et al. Nature Biotechnol.* **1999**, *17*, 897–901.
161. Alberto, R.; Ortner, K.; Wheatley, N.; Schibli, R.; Schubiger, P. A. *J. Am. Chem. Soc.* **2001**, *123*, 3135–3136.
162. Egli, A.; Alberto, R.; Tannahill, L.; Schibli, R.; Abram, U.; Schaffland, A.; Waibel, R.; Tourwe, D.; Jeannin, L., Iterbeke, K., *et al. J. Nucl. Med.* **1999**, *40*, 1913–1917.
163. Spradau, T. W.; Edwards, W. B.; Anderson, C. J.; Welch, M. J.; Katzenellenbogen, J. A. *Nucl. Med. Biol.* **1999**, *26*, 1–7.

164. Langer, M.; La Bella, R.; Garcia-Garayoa, E.; Beck-Sickinger, A. G. *Bioconjugate Chem.* **2001**, *12*, 1028–1034.
165. Bullok, K. E.; Dyszlewski, M.; Prior, J. L.; Pica, C. M.; Sharma, V.; Piwnica-Worms, D. *Bioconjugate Chem.* **2002**, *13*, 1226–1237.
166. Garcia-Garayoa, E.; Bläuenstein, P.; Bruehlmeier, M.; Blanc, A.; Iterbeke, K.; Conrath, P.; Tourwé, D.; Schubiger, P. A. *J. Nucl. Med.* **2002**, *43*, 374–383.
167. van Staveren, D. R.; Mundwiler, S.; Hoffmanns, U.; Kyoung Pak, J.; Spingler, B.; Metzler-Nolte, N.; Alberto, R. *Org. Biomol. Chem.* **2004**, *2*, 2593–2603.
168. Lin, K.-S.; Luu, A.; Baidoo, K. E.; Hashemzadeh-Gargari, H.; Chen, M.-K.; Brenneman, K.; Pili, R.; Pomper, M.; Carducci, M. A.; Wagner, H. N., Jr., *Bioconjugate Chem.* **2005**, *16*, 43–50.
169. Alberto, R. Radiopharmaceuticals. In *Bioorganometallics*; Jaouen, G., Ed.; Wiley-VCH: Weinheim, 2006; pp 97–124.
170. Wald, J.; Alberto, R.; Ortner, K.; Candreia, L. *Angew. Chem., Int. Ed.* **2001**, *40*, 3062–3066.
171. Cesati, R. R.; Tamagnan, G.; Baldwin, R. M.; Zoghbi, S. S.; Innis, R. B.; Kula, N. S.; Baldessarini, R. J.; Katzenellenbogen, J. A. *Bioconjugate Chem.* **2002**, *13*, 29–39.
172. Muli, E. S.; Sattigeri, V. J.; Rodriguez, A. L.; Katzenellenbogen, J. A. *Bioorg. Med. Chem.* **2002**, *10*, 1381–1398.
173. Wenzel, M.; Klinge, C. *J. Labelled Compd. Radiopharm.* **1994**, *34*, 981–987.
174. Thayer, J. S. *Organometallic Compounds and Living Organisms*; Academic Press: Orlando, 1984.
175. Craig, P. J. *Organometallic Compounds in the Environment*, 2nd ed.; Wiley: Chichester, 2003.
176. Ryabov, A. D. *Angew. Chem., Int. Ed. Engl.* **1991**, *30*, 931–941.
177. Bentley, R.; Chasteen, T. G. *Microbiol. Mol. Biol. Rev.* **2002**, *66*, 250–271.
178. Cullen, W. R.; Bentley, R. *J. Environ. Monit.* **2005**, *7*, 11–15.
179. Winski, S. L.; Barber, D. S.; Rael, L. T.; Carter, D. E. *Fund. Appl. Toxicol.* **1997**, *38*, 123–128.
180. Tsubaki, T.; Irukayama, K. *Minamata Disease: Methylmercury Poisoning in Minamata and Niigata Japan*; Kodansha: Tokyo, 1977.
181. D'Itric, P. A.; D'Itric, F. M. *Mercury Contamination: A Human Tragedy*; Wiley: New York, 1997.
182. Hall, S. K. *Environ. Sci. Technol.* **1972**, *6*, 30–35.
183. Severin, K.; Bergs, R.; Beck, W. *Angew. Chem., Int. Ed.* **1998**, *37*, 1634–1654.
184. Zatsepin, T. S.; Andreev, S. Y.; Hianik, T.; Oretskaya, T. S. *Russ. Chem. Rev.* **2003**, *72*, 537–554.
185. Metzler-Nolte, N. Conjugates of Peptides and PNA with Organometallic Complexes: Syntheses and Applications. In *Bioorganometallics*; Jaouen, G., Ed.; Wiley-VCH: Weinheim, 2006; pp 125–179.
186. Salmain, M. Labeling of Proteins with Organometallic Complexes: Strategies and Applications. In *Bioorganometallics*; Jaouen, G., Ed.; Wiley-VCH: Weinheim, 2006; pp 181–213.
187. Schlögl, K. *Monatsh. Chem.* **1957**, *88*, 601–621.
188. Freiesleben, D.; Polborn, K.; Robl, C.; Sünkel, K.; Beck, W. *Can. J. Chem.* **1995**, *73*, 1164–1174.
189. Fehn, A.; Briel, O.; Beck, W. *Chem. Ber.* **1997**, *130*, 1467–1473.
190. Böhm, A.; Schreiner, B.; Steiner, N.; Urban, R.; Sünkel, K.; Polborn, K.; Beck, W. *Z. Naturforsch. B* **1998**, *53*, 191–205.
191. Kayser, B.; Altman, J.; Nöth, H.; Knizek, J.; Beck, W. *Eur. J. Inorg. Chem.* **1998**, 1791–1798.
192. Bauer, W.; Polborn, K.; Beck, W. *J. Organomet. Chem.* **1999**, *579*, 269–279.
193. Moriuchi, T.; Yoshida, K.; Hirao, T. *J. Organomet. Chem.* **2001**, *637–639*, 75–79.
194. Moriuchi, T.; Yoshida, K.; Hirao, T. *Organometallics* **2001**, *20*, 3101–3105.
195. Kraatz, H.-B.; Galka, M. *Metal Ions Biol. Syst.* **2001**, *38*, 385–409.
196. Xu, Y.; Saweczko, P.; Kraatz, H.-B. *J. Organomet. Chem.* **2001**, *637–639*, 335–342.
197. Plumb, K.; Kraatz, H.-B. *Bioconjugate Chem.* **2003**, *14*, 601–606.
198. Pospisek, J.; Toma, S.; Fric, I.; Bláha, K. *Coll. Czech. Chem. Commun.* **1980**, *45*, 435–441.
199. Kira, M.; Matsubara, T.; Shinohara, H.; Sisido, M. *Chem. Lett.* **1997**, 89–90.
200. Brunner, H.; König, W.; Nuber, B. *Tetrahedron Asymmetry* **1993**, *4*, 699–707.
201. Jackson, R. F. W.; Turner, D.; Block, M. H. *Synlett* **1996**, 862–864.
202. Cuignet, E.; Sergheraert, C.; Tartar, A.; Dautrevaux, M. *J. Organomet. Chem.* **1980**, *195*, 325–329.
203. Epton, R.; Marr, G.; Willmore, G. A.; Hudson, D.; Snell, P. H.; Snell, C. R. *Int. J. Biol. Macromol.* **1981**, *3*, 395–396.
204. Cuignet, E.; Dautrevaux, M.; Sergheraert, C.; Tartar, A.; Attali, B.; Cros, J. *Eur. J. Med. Chem.* **1982**, *17*, 203–206.
205. Brunet, J. C.; Cuignet, E.; Dautrevaux, M.; Demarly, A.; Gras, H.; Marcincal, P.; Sergheraert, C.; Tartar, A.; Vanvoorde, J. C.; Vanpoucke, M. Use of Organometallic Amino Acids as a Tool for Studying Interactions in Phenylalanine-containing Peptides. In *Peptides 1980*; Proceedings of the Sixteenth European Peptide Symposium; Brunfeldt, K., Ed.; Scriptor: Copenhagen, 1981; pp 603–607.
206. Tartar, A.; Demarly, A.; Sergheraert, C.; Escher, E. Structural and Conformational Considerations: Angiotensin. In *Proceedings of the 8th American Peptide Symposium*; Hruby, V. J., Rich, D. H., Eds.; Pierce Chemical: Rockford, 1983; pp 377–380.
207. Maes, P.; Ricouart, A.; Escher, E.; Tartar, A.; Sergheraert, C. *Coll. Czech. Chem. Commun.* **1988**, *53*, 2914–2919.
208. Hublau, P.; Sergheraert, C.; Ballester, L.; Dautrevaux, M. *Eur. J. Med. Chem.* **1983**, *18*, 131–133.
209. Le Borgne, F.; Beaucourt, J. P. *Tetrahedron Lett.* **1988**, *29*, 5649–5652.
210. Ricouart, A.; Maes, P.; Battmann, T.; Kerdelhue, B.; Tartar, A.; Sergheraert, C. *Int. J. Pept. Protein Res.* **1988**, *32*, 56–63.
211. Grotjahn, D. B.; Joubran, C.; Combs, D.; Brune, D. C. *J. Am. Chem. Soc.* **1998**, *120*, 11814–11815.
212. Grotjahn, D. B. *Coord. Chem. Rev.* **1999**, *192*, 1125–1141.
213. Rudolf, B.; Zakrzewski, J.; Salmain, M.; Jaouen, G. *New J. Chem.* **1998**, 813–818.
214. Salmain, M.; Jaouen, G.; Rudolf, B.; Zakrzewski, J. *J. Organomet. Chem.* **1999**, *589*, 98–102.
215. Noor, F.; Wüstholz, A.; Kinscherf, R.; Metzler-Nolte, N. *Angew. Chem., Int. Ed.* **2005**, *44*, 2429–2432.
216. Noor, F.; Metzler-Nolte, N. Unpublished results.
217. Haefliger, P.; Agorastos, N.; Renard, A.; Giambonini-Brugnoli, G.; Marty, C.; Alberto, R. *Bioconjugate Chem.* **2005**, *16*, 582–587.
218. van Staveren, D. R.; Weyhermüller, T.; Metzler-Nolte, N. *Organometallics* **2000**, *19*, 3730–3735.
219. van Staveren, D. R.; Bill, E.; Bothe, E.; Bühl, M.; Weyhermüller, T.; Metzler-Nolte, N. *Chem. Eur. J.* **2002**, *8*, 1649–1662.
220. van Staveren, D. R.; Metzler-Nolte, N. *J. Chem. Soc., Chem. Commun.* **2002**, 1406–1407.
221. Metzler-Nolte, N. *Special. Chem. Mag.* **2002**, 34–36.
222. Brosch, O.; Weyhermüller, T.; Metzler-Nolte, N. *Inorg. Chem.* **1999**, *38*, 5308–5313.
223. Brosch, O.; Weyhermüller, T.; Metzler-Nolte, N. *Eur. J. Inorg. Chem.* **2000**, 323–330.
224. Hoffmanns, U.; Metzler-Nolte, N. *Bioconjugate Chem.* **2006**, *17*, 204–213.

225. Herrick, R. S.; Jarret, R. M.; Curran, T. P.; Dragoli, D. R.; Flaherty, M. B.; Lindyberg, S. E.; Slate, R. A.; Thornton, L. C. *Tetrahedron Lett.* **1996**, *37*, 5289–5292.
226. Moriuchi, T.; Hirao, T. *Chem. Soc. Rev.* **2004**, 294–301.
227. Nomoto, A.; Moriuchi, T.; Yamazaki, S.; Ogawa, A.; Hirao, T. *J. Chem. Soc., Chem. Commun.* **1998**, 1963–1964.
228. Moriuchi, T.; Nomoto, A.; Yoshida, K.; Hirao, T. *J. Organomet. Chem.* **1999**, *589*, 50–58.
229. Moriuchi, T.; Nomoto, A.; Yoshida, K.; Ogawa, A.; Hirao, T. *J. Am. Chem. Soc.* **2001**, *123*, 68–75.
230. Moriuchi, T.; Nomoto, A.; Yoshida, K.; Hirao, T. *Organometallics* **2001**, *20*, 1008–1013.
231. Moriuchi, T.; Hirao, T. *J. Synth. Org. Chem. Jpn.* **2001**, *59*, 1195–1203.
232. Moriuchi, T.; Yoshida, K.; Hirao, T. *J. Organomet. Chem.* **2003**, *668*, 31–34.
233. Moriuchi, T.; Nagai, T.; Hirao, T. *Org. Lett.* **2005**, *7*, 5265–5268.
234. Moriuchi, T.; Nagai, T.; Hirao, T. *Org. Lett.* **2006**, *8*, 31–34.
235. Xu, Y.; Kraatz, H.-B. *Tetrahedron Lett.* **2001**, *42*, 2601–2603.
236. Appoh, F. E.; Sutherland, T. C.; Kraatz, H.-B. *J. Organomet. Chem.* **2004**, *689*, 4669–4677.
237. van Staveren, D. R.; Weyhermüller, T.; Metzler-Nolte, N. *J. Chem. Soc., Dalton Trans.* **2003**, 210–220.
238. de Hatten, X.; Weyhermüller, T.; Metzler-Nolte, N. *J. Organomet. Chem.* **2004**, *689*, 4856–4867.
239. Kirin, S. I.; Wissenbach, D.; Metzler-Nolte, N. *New J. Chem.* **2005**, 1168–1173.
240. Sheehy, M. J.; Gallagher, J. F.; Yamashita, M.; Ida, Y.; White-Colangelo, J.; Johnson, J.; Orlando, R.; Kenny, P. T. M. *J. Organomet. Chem.* **2004**, *689*, 1511–1520.
241. Savage, D.; Malone, G.; Gallagher, J. F.; Ida, Y.; Kenny, P. T. M. *J. Organomet. Chem.* **2005**, *690*, 383–393.
242. Kirin, S. I.; Kraatz, H.-B.; Metzler-Nolte, N. *Chem. Soc. Rev.* **2006**, *35*, 348–354.
243. Okamura, T.; Sakauye, K.; Ueyama, N.; Nakamura, A. *Inorg. Chem.* **1998**, *37*, 6731–6736.
244. Butler, I. R.; Quayle, S. C. *J. Organomet. Chem.* **1998**, *552*, 63–68.
245. Barisic, L.; Rapic, V.; Kovac, V. *Croat. Chem. Acta* **2002**, *75*, 199–210.
246. Heinze, K.; Schlenker, M. *Eur. J. Inorg. Chem.* **2004**, 2974–2988.
247. Barisic, L.; Rapic, V.; Metzler-Nolte, N. *Eur. J. Inorg. Chem.* **2006** (accepted).
248. Barisic, L.; Dropucic, M.; Rapic, V.; Pritzkow, H.; Kirin, S. I.; Metzler-Nolte, N. *J. Chem. Soc., Chem. Commun.* **2004**, 2004–2005.
249. Barisic, L.; Cakic, M.; Mahmoud, K. A.; Liu, Y.-N.; Kraatz, H.-B.; Pritzkow, H.; Kirin, S. I.; Metzler-Nolte, N.; Rapic, V. *Chem. Eur. J.* **2006**, *12*, 4965–4980.
250. Dey, S. K.; Kraatz, H.-B. *Bioconjugate Chem.* **2006**, *17*, 84–89.
251. Chowdhury, S.; Sanders, D. A. R.; Schatte, G.; Kraatz, H.-B. *Angew. Chem., Int. Ed.* **2006**, *45*, 751–754.
252. Yli-Kauhaluoma, J. T.; Ashley, J. A.; Lo, C.-H.; Tucker, L.; Wolfe, M. M.; Janda, K. D. *J. Am. Chem. Soc.* **1995**, *117*, 7041–7047.
253. Cannizzaro, C. E.; Ashley, J. A.; Janda, K. D.; Houk, K. N. *J. Am. Chem. Soc.* **2003**, *125*, 2489–2506.
254. Heine, A.; Stura, E. A.; Yli-Kauhaluoma, J. T.; Gao, C.; Deng, Q.; Beno, B. R.; Houk, K. N.; Janda, K. D.; Wilson, I. A. *Science* **1998**, *279*, 1934–1940.
255. Kaluz, S.; Toma, S. *Coll. Czech. Chem. Commun.* **1988**, *53*, 638–642.
256. Adamczyk, M.; Reddy, R. E.; Rege, S. D. *Synth. Commun.* **2000**, *30*, 1389–1400.
257. Dialer, H.; Steglich, W.; Beck, W. *Tetrahedron* **2001**, *57*, 4855–4861.
258. Dialer, H.; Polborn, K.; Ponikwar, W.; Sünkel, K.; Beck, W. *Chem. Eur. J.* **2002**, *8*, 691–699.
259. Basu, B.; Chattopadhyay, S. K.; Ritzen, A.; Frejd, T. *Tetrahedron Asymmetry* **1997**, *8*, 1841–1846.
260. Maricic, S.; Ritzen, A.; Berg, U.; Frejd, T. *Tetrahedron* **2001**, *57*, 6523–6529.
261. Maricic, S.; Berg, U.; Frejd, T. *Tetrahedron* **2002**, *58*, 3085–3093.
262. Maricic, S.; Frejd, T. *J. Org. Chem.* **2002**, *67*, 7600–7606.
263. Salmain, M.; Licandro, E.; Maiorana, S.; Tran-Huy, H.; Jaouen, G. *J. Organomet. Chem.* **2001**, *617–618*, 376–382.
264. Salmain, M.; Blais, J. C.; Tran-Huy, H.; Compain, C.; Jaouen, G. *Eur. J. Biochem.* **2001**, *268*, 5479–5487.
265. Egan, D. P.; Salmain, M.; McArdle, P.; Jaouen, G.; Caro, B. *Spectrochim. Acta A* **2002**, *58*, 941–951.
266. Salmain, M.; Caro, B.; Le Guen-Robin, F.; Blais, J. C.; Jaouen, G. *ChemBioChem* **2004**, *5*, 99–109.
267. Di Gleria, K.; Hill, H. A. O.; Wong, L. L. *FEBS Lett.* **1996**, *390*, 142–144.
268. Di Gleria, K.; Nickerson, D.; Hill, H. A. O.; Wong, L.-L.; Fülöp, V. *J. Am. Chem. Soc.* **1998**, *120*, 46–52.
269. Anne, A.; Blanc, B.; Moiroux, J. *Bioconjugate Chem.* **2001**, *12*, 396–405.
270. Wlassoff, W. A.; King, G. C. *Nucleic Acids Res.* **2002**, *30*, e58.
271. Di Giusto, D. A.; Wlassoff, W. A.; Giesebrecht, S.; Gooding, J. J.; King, G. C. *Angew. Chem.* **2004**, *116*, 2869–2872.
272. Meunier, P.; Ouattara, I.; Gautheron, B.; Tirouflet, J.; Camboli, D.; Besançon, J. *Eur. J. Med. Chem.* **1991**, *26*, 351–362.
273. Yu, C. J.; Yowanto, H.; Wan, Y.; Meade, T. J.; Chong, Y.; Strong, M.; Donilon, L. H.; Kayyem, J. F.; Gozin, M.; Blackburn, G. F. *J. Am. Chem. Soc.* **2000**, *122*, 6767–6768.
274. Coutouli-Argyropoulou, E.; Tsitabani, M.; Petrantonakis, G.; Terzis, A.; Raptopoulou, C. *Org. Biomol. Chem.* **2003**, *1*, 1382–1388.
275. Pike, A. R.; Ryder, L. C.; Horrocks, B. R.; Clegg, W.; Elsegood, M. R. J.; Connolly, B. A.; Houlton, A. *Chem. Eur. J.* **2002**, *8*, 2891–2899.
276. Beilstein, A. E.; Tierney, M. T.; Grinstaff, M. W. *Comments Inorg. Chem.* **2000**, *22*, 105–127.
277. Beilstein, A.; Grinstaff, M. W. *J. Organomet. Chem.* **2001**, *637–639*, 398–406.
278. Beilstein, A. E.; Grinstaff, M. W. *Chem. Commun.* **2000**, 509–510.
279. Nielsen, P. E.; Egholm, M.; Berg, R. H.; Buchardt, O. *Science* **1991**, *254*, 1497–1500.
280. Dueholm, K. L.; Engholm, M.; Behrens, C.; Christensen, L.; Hansen, H. F.; Vulpius, T.; Petersen, K. H.; Berg, R. H.; Nielsen, P. E.; Buchardt, O. *J. Org. Chem.* **1994**, *59*, 5767–5773.
281. Egholm, M.; Buchardt, O.; Christensen, L.; Behrens, C.; Freier, S. M.; Driver, D. A.; Berg, R. H.; Kim, S. K.; Norden, B.; Nielsen, P. E. *Nature* **1993**, *365*, 566–568.
282. Leijon, M.; Gräslund, A.; Nielsen, P. E.; Buchardt, O.; Nordén, B.; Kristensen, S. M.; Eriksson, M. *Biochemistry* **1994**, *33*, 9820–9825.
283. Eriksson, M.; Nielsen, P. E. *Nature Struct. Biol.* **1996**, *3*, 410–413.
284. Menchise, V.; Simone, G. D.; Tedeschi, T.; Corradini, R.; Sforza, S.; Marchelli, R.; Capasso, D.; Saviano, M.; Pedone, C. *Proc. Natl. Acad. Sci. USA* **2003**, *100*, 12021–12026.
285. Ratilainen, T.; Holmén, A.; Tuite, E.; Haaima, G.; Christensen, L.; Nielsen, P. E.; Nordén, B. *Biochemistry* **1998**, *37*, 12331–12342.
286. Ratilainen, T.; Holmén, A.; Tuite, E.; Nielsen, P. E.; Nordén, B. *Biochemistry* **2000**, *39*, 7781–7791.

287. Nielsen, P. E. *Perspect. Drug Discovery Des.* **1996**, *4*, 76–84.
288. Good, L.; Nielsen, P. E. *Antisense Nucl. Acid Drug Dev.* **1997**, *7*, 431–437.
289. Knudsen, H.; Nielsen, P. E. *Anti-cancer Drugs* **1997**, *8*, 113–118.
290. Larsen, H. J.; Bentin, T.; Nielsen, P. E. *Biochim. Biophys. Acta* **1999**, *1489*, 159–166.
291. Nielsen, P. E. *Curr. Opin. Biotechnol.* **1999**, *10*, 71–75.
292. Uhlmann, E.; Peyman, A.; Breipohl, G.; Will, D. W. *Angew. Chem.* **1998**, *110*, 2954–2983.
293. Hess, A.; Metzler-Nolte, N. *J. Chem. Soc., Chem. Commun.* **1999**, 885–886.
294. Baldoli, C.; Maiorana, S.; Licandro, E.; Zinzalla, G.; Perdicchia, D. *Org. Lett.* **2002**, *4*, 4341–4344.
295. Baldoli, C.; Giannini, C.; Licandro, E.; Maiorana, S.; Zinzalla, G. *Synlett* **2004**, 1044–1048.
296. Maiorana, S.; Licandro, E.; Perdicchia, D.; Baldoli, C.; Vandoni, B.; Giannini, C.; Salmain, M. *J. Mol. Catal. A* **2003**, *204–205*, 165–175.
297. Baldoli, C.; Falciola, L.; Licandro, E.; Maiorana, S.; Mussini, P.; Ramani, P.; Rigamonti, C.; Zinzalla, G. *J. Organomet. Chem.* **2004**, *689*, 4791–4802.
298. Verheijen, J. C.; van der Marel, G. A.; van Boom, J. H.; Metzler-Nolte, N. *Bioconjugate Chem.* **2000**, *11*, 741–743.
299. Maurer, A.; Kraatz, H.-B.; Metzler-Nolte, N. *Eur. J. Inorg. Chem.* **2005**, 3207–3210.
300. Maurer, A.; Kraatz, H.-B.; Metzler-Nolte, N. **2006**. Unpublished results.
301. Hamzavi, R.; Happ, T.; Weitershaus, K.; Metzler-Nolte, N. *J. Organomet. Chem.* **2004**, *689*, 4745–4750.
302. Hartinger, C. G.; Nazarov, A. A.; Arion, V. B.; Giester, G.; Jakupec, M.; Galanski, M.; Keppler, B. K. *New J. Chem.* **2002**, *26*, 671–673.
303. Itoh, T.; Shirakami, S.; Ishida, N.; Yamashita, Y.; Yoshida, T.; Kim, H.-S.; Wataya, Y. *Bioorg. Med. Chem. Lett.* **2000**, *10*, 1657–1659.
304. Dötz, K. H. *Angew. Chem., Int. Ed. Engl.* **1984**, *23*, 587–606.
305. Dötz, K. H.; Jäkel, C.; Haase, W.-C. *J. Organomet. Chem.* **2001**, *617–618*, 119–132.
306. Dötz, K. H.; Koch, A.; Werner, M. Polyfunctional Metal Carbenes for Organic Synthesis. In *Handbook of Functionalized Organometallics: Applications in Synthesis*; Knochel, P., Ed. Wiley-VCH: Weinheim, 2005; Vol. 2, pp 451–502.
307. Bühler, G.; Feiters, M. C.; Nolte, R. J. M.; Dötz, K. H. *Angew. Chem., Int. Ed.* **2003**, *42*, 2494–2497.
308. Shimada, K.; Sakayori, C.; Nambara, T. *J. Liq. Chromatogr.* **1987**, *10*, 2177–2187.
309. Troitskaya, L. L.; Sokolov, V. I. *J. Organomet. Chem.* **1985**, *285*, 389–393.
310. Kim, W. H. *Diss. Abstr. Int. B* **1978**, *39*, 1774.
311. Abbott, N. L.; Jewell, C. M.; Hays, M. E.; Kondo, Y.; Lynn, D. M. *J. Am. Chem. Soc.* **2005**, *127*, 11576–11577.
312. Top, S.; Vessières, A.; Leclercq, G.; Quivy, J.; Tang, J.; Vaissermann, J.; Huché, M.; Jaouen, G. *Chem. Eur. J.* **2003**, *9*, 5223–5236.
313. Tang, J.; Top, S.; Vessières, A.; Sellier, N.; Vaissermann, J.; Jaouen, G. *Appl. Organomet. Chem.* **1997**, *11*, 771–781.
314. Osella, D.; Nervi, C.; Galeotti, F.; Cavigiolio, G.; Vessières, A.; Jaouen, G. *Helv. Chim. Acta* **2001**, *84*, 3289–3298.
315. El Amouri, H.; Vessières, A.; Vichard, D.; Top, S.; Gruselle, M.; Jaouen, G. *J. Med. Chem.* **1992**, *35*, 3130–3135.
316. Top, S.; Elhafa, H.; Vessieres, A.; Quivy, J.; Vaissermann, J.; Hughes, D. W.; McGlinchey, M. J.; Mornon, J. P.; Thoreau, E.; Jaouen, G. *J. Am. Chem. Soc.* **1995**, *117*, 8372–8380.
317. Vessières, A.; Jaouen, G.; Gruselle, M.; Rossignol, J. L.; Savignac, M.; Top, S.; Greenfield, S. *J. Steroid Biochem.* **1988**, *30*, 301–305.
318. Vessières, A.; Vaillant, C.; Salmain, M.; Jaouen, G. *J. Steroid Biochem. Mol. Biol.* **1989**, *34*, 301–305.
319. Schlotter, K.; Boeckler, F.; Hübner, H.; Gmeiner, P. *J. Med. Chem.* **2005**, *48*, 3696–3699.
320. Bregman, H.; Williams, D. S.; Atilla, G. E.; Caroll, P. J.; Meggers, E. *J. Am. Chem. Soc.* **2004**, *126*, 13594–13595.
321. Williams, D. S.; Atilla, G. E.; Bregman, H.; Arzoumanian, A.; Klein, P. S.; Meggers, E. *Angew. Chem., Int. Ed.* **2005**, *44*, 1984–1987.
322. Meggers, E. *Angew. Chem., Int. Ed.* **2006**, *45*, 1580–1585.
323. Weiß, K.; Fischer, E. O. *Chem. Ber.* **1973**, *106*, 1277–1284.
324. Weiß, K.; Fischer, E. O. *Chem. Ber.* **1976**, *109*, 1868–1886.
325. Eckert, H.; Seidel, C. *Angew. Chem.* **1986**, *98*, 168–170.
326. Eckert, H.; Forster, B.; Seidel, C. *Z. Naturforsch. B* **1991**, *46*, 339–352.
327. Eckert, H.; Koller, M. *Z. Naturforsch. B* **1990**, *45*, 1709–1714.
328. Eckert, H.; Koller, M. *J. Liq. Chromatogr.* **1990**, *13*, 3399–3414.
329. Kane-Maguire, L. A. P.; Kanitz, R. *J. Organomet. Chem.* **1988**, *353*, C33–C34.
330. Carver, J. A.; Fates, B.; Kane-Maguire, L. A. P. *J. Chem. Soc., Chem. Commun.* **1993**, 928–929.
331. Kane-Maguire, L. A. P.; Kanitz, R.; Jones, P.; Williams, P. A. *J. Organomet. Chem.* **1994**, *464*, 203–213.
332. Urban, R.; Ugi, I. *Angew. Chem.* **1975**, *87*, 67–69.
333. Urban, R.; Eberle, G.; Marquarding, D.; Rehn, D.; Rehn, H.; Ugi, I. *Angew. Chem.* **1976**, *88*, 644–646.
334. Urban, R.; Marquarding, D.; Ugi, I. *Hoppe-Seyler's Z. Physiol. Chem.* **1978**, *359*, 1541–1552.
335. Ugi, I.; Marquarding, D.; Urban, R. Synthesis of Peptides by Four-component Condensation. In *Chemistry and Biochemistry of Amino Acids, Peptides and Proteins*; Weinstein, B., Ed.; Dekker: New York, 1982; Vol. 6, pp 245–289.
336. Urban, R. *Tetrahedron* **1979**, *35*, 1841–1843.
337. Ratajczak, A.; Misterkiewicz, B. *J. Organomet. Chem.* **1975**, *91*, 73–79.
338. Eberle, G.; Ugi, I. *Angew. Chem.* **1976**, *88*, 509–510.
339. Schmid, A.; Lindel, T. *Angew. Chem., Int. Ed.* **2004**, *43*, 1581–1583.
340. Pearson, A. J.; Lee, K. *J. Org. Chem.* **1994**, *59*, 2304–2313.
341. Pearson, A. J.; Zhang, P.; Lee, K. *J. Org. Chem.* **1996**, *61*, 6581–6586.
342. Janetka, J. W.; Rich, D. H. *J. Am. Chem. Soc.* **1995**, *117*, 10585–10586.
343. Janetka, J. W.; Rich, D. H. *J. Am. Chem. Soc.* **1997**, *119*, 6488–6495.
344. Hegedus, L. S. *Acc. Chem. Res.* **1995**, *28*, 299–305.
345. Pulley, S. R.; Hegedus, L. S. *J. Am. Chem. Soc.* **1993**, *115*, 9037–9047.
346. Beck, W.; Krämer, R. *Angew. Chem., Int. Ed. Engl.* **1991**, *30*, 1467–1468.
347. Krämer, R.; Maurus, M.; Bergs, R.; Polborn, K.; Sünkel, K.; Wagner, B.; Beck, W. *Chem. Ber.* **1993**, *126*, 1969–1980.
348. Krämer, R.; Maurus, M.; Polborn, K.; Sünkel, K.; Robl, C.; Beck, W. *Chem. Eur. J.* **1996**, *2*, 1518–1526.
349. Hoffmüller, W.; Maurus, M.; Severin, K.; Beck, W. *Eur. J. Inorg. Chem.* **1998**, 729–731.
350. Haas, K.; Ponikwar, W.; Nöth, H.; Beck, W. *Angew. Chem., Int. Ed.* **1998**, *37*, 1086–1089.
351. Haas, K.; Ehrenstorfer-Schafers, E. M.; Polborn, K.; Beck, W. *Eur. J. Inorg. Chem.* **1999**, 465–469.

352. Salmain, M.; Vessières, A. Organometallic Complexes as Tracers in Non-isotopic Immunoassay. In *Bioorganometallics*; Jaouen, G., Ed.; Wiley-VCH: Weinheim, 2006; pp 263–302.
353. Stephenson, G. R. Organometallic Bioprobes. In *Bioorganometallics*; Jaouen, G., Ed.; Wiley-VCH: Weinheim, 2006; pp 215–262.
354. Takenaka, S. Genosensors Based on Metal Complexes. In *Bioorganometallics*; Jaouen, G., Ed.; Wiley-VCH: Weinheim, 2006; pp 303–319.
355. Willner, I.; Katz, E. *Angew. Chem., Int. Ed.* **2000**, *39*, 1180–1218.
356. Cass, A. E. G.; Davis, G.; Francis, G. D.; Hill, H. A. O.; Aston, W. J.; Higgins, I. J.; Plotkin, E. V.; Scott, L. D. L.; Turner, A. P. F.; *Anal. Chem.* **1984**, *56*, 667–671.
357. Wang, J. *Electroanalysis* **2001**, *13*, 983–988.
358. Wilson, E. K. *Chem. Eng. News* **1998**, 47–49.
359. Umek, R. M.; Lin, S. W.; Vielmetter, J.; Terbrueggen, R. H.; Irvine, B.; Yu, C. J.; Kayyem, J. F.; Yowanto, H.; Blackburn, G. F.; Farkas, D. H., *et al. J. Mol. Diag.* **2001**, *3*, 74–84.
360. Farkas, D. H. *Clin. Chem.* **2001**, *47*, 1871–1872.
361. Ihara, T.; Maruo, Y.; Takenaka, S.; Takagi, M. *Nucleic Acids Res.* **1996**, *24*, 4273–4280.
362. Takenaka, S.; Uto, Y.; Kondo, H.; Ihara, T.; Takagi, M. *Anal. Biochem.* **1994**, *218*, 436–443.
363. Brazill, S. A.; Kim, P. H.; Kuhr, W. G. *Anal. Chem.* **2001**, *73*, 4882–4890.
364. Brazill, S. A.; Kuhr, W. G. *Anal. Chem.* **2002**, *74*, 3421–3428.
365. Bucci, E.; De Napoli, L.; Di Fabio, G.; Messere, A.; Montesarchio, D.; Romanelli, A.; Picciallia, G.; Varra, M. *Tetrahedron* **1999**, *55*, 14435–14450.
366. Petraccone, L.; Erra, E.; Messere, A.; Montesarchio, D.; Piccialli, G.; Barone, G.; Giancola, C. *Biophys. Chem.* **2003**, *104*, 259–270.
367. Uto, Y.; Kondo, H.; Abe, M.; Suzuki, T.; Takenaka, S. *Anal. Biochem.* **1997**, *250*, 122–124.
368. Takenaka, S.; Uto, Y.; Takagi, M.; Kondo, H. *Chem. Lett.* **1998**, 989–990.
369. Mucic, R. C.; Herrlein, M. K.; Mirkin, C. A.; Letsinger, R. L. *Chem. Commun.* **1996**, 555–557.
370. Long, Y.-T.; Li, C.-Z.; Sutherland, T. C.; Chahma, M.; Lee, J. S.; Kraatz, H.-B. *J. Am. Chem. Soc.* **2003**, *125*, 8724–8725.
371. Chahma, M.; Lee, J. S.; Kraatz, H.-B. *J. Electroanal. Chem.* **2004**, *567*, 283–287.
372. Anne, A.; Bouchardon, A.; Moiroux, J. *J. Am. Chem. Soc.* **2003**, *125*, 1112–1113.
373. Fan, C.; Plaxco, K. W.; Heeger, A. J. *Proc. Natl. Acad. Sci. USA* **2003**, *100*, 9134–9137.
374. Kim, K.; Yang, H.; Park, S. H.; Lee, D.-S.; Kim, S.-J.; Lim, Y. T.; Kim, Y. T. *Chem. Commun.* **2004**, 1466–1467.
375. Ihara, T.; Nakayama, M.; Murata, M.; Nakano, K.; Maeda, M. *J. Chem. Soc., Chem. Commun.* **1997**, 1609–1610.
376. Takenaka, S. *Bull. Chem. Soc. Jpn.* **2001**, *74*, 217–224.
377. Nakayama, M.; Ihara, T.; Nakano, K.; Maeda, M. *Talanta* **2002**, *56*, 857–866.
378. Yu, C. J.; Wang, H.; Wan, Y.; Yowanto, H.; Kim, J. C.; Donilon, L. H.; Tao, C.; Strong, M.; Cong, Y. *J. Org. Chem.* **2001**, *66*, 2937–2942.
379. Yamashita, K.; Takagi, M.; Kondo, H.; Takenaka, S. *Chem. Lett.* **2000**, 1038–1039.
380. Takenaka, S.; Yamashita, K.; Takagi, M.; Uto, Y.; Kondo, H. *Anal. Chem.* **2000**, *72*, 1334–1341.
381. Yamashita, K.; Takagi, A.; Takagi, M.; Kondo, H.; Ikeda, K.; Takenaka, S. *Bioconjugate Chem.* **2002**, *13*, 1193–1199.
382. Cais, M.; Dani, S.; Eden, Y.; Gandolfi, O.; Horn, M.; Isaacs, E. E.; Josephy, Y.; Saar, Y.; Slovin, E.; Snarsky, L. *Nature* **1977**, *270*, 535–536.
383. Cais, M.; Slovin, E.; Snarsky, L. *J. Organomet. Chem.* **1978**, *160*, 223–230.
384. Jaouen, G.; Vessières, A.; Top, S. *J. Am. Chem. Soc.* **1985**, *107*, 4778–4780.
385. Salmain, M.; Vessières, A.; Brossier, P.; Butler, I. S.; Jaouen, G. *J. Immun. Meth.* **1992**, *148*, 65–75.
386. Jaouen, G.; Vessières, A.; Butler, I. S. *Acc. Chem. Res.* **1993**, *26*, 361–369.
387. Vessières, A.; Salmain, M.; Brossier, P.; Jaouen, G. *J. Pharm. Biomed. Anal.* **1999**, *21*, 625–633.
388. Vessières, A.; Top, S.; Ismail, A. A.; Butler, I. S.; Louer, M.; Jaouen, G. *Biochemistry* **1988**, *27*, 6659–6666.
389. Vessières, A.; Top, S.; Vaillant, C.; Osella, D.; Mornon, J.-P.; Jaouen, G. *Angew. Chem.* **1992**, *104*, 790–792.
390. Philomin, V.; Vessiéres, A.; Gruselle, M.; Jaouen, G. *Bioconjugate Chem.* **1993**, *4*, 419–424.
391. Varenne, A.; Vessières, A. M. S.; Durand, S.; Brossier, P.; Jaouen, G. *Anal. Biochem.* **1996**, *242*, 172–179.
392. Salmain, M.; Vessières, A.; Varenne, A.; Brossier, P.; Jaouen, G. *J. Organomet. Chem.* **1999**, *589*, 92–97.
393. Grote, Z.; Scopelliti, R.; Severin, K. *J. Am. Chem. Soc.* **2004**, *126*, 16959–16972.
394. Wiskur, S. L.; Ait-Haddou, H.; Lavigne, J. J.; Anslyn, E. V. *Acc. Chem. Res.* **2001**, *34*, 963–972.
395. Buryak, A.; Severin, K. *Angew. Chem., Int. Ed.* **2004**, *43*, 4771–4774.
396. Buryak, A.; Severin, K. *J. Am. Chem. Soc.* **2005**, *127*, 3700–3701.
397. Petsko, G. A. *Methods Enzymol.* **1985**, *114*, 147–156.
398. Sawyer, L.; Green, D. W. *Biochim. Biophys. Acta* **1979**, *579*, 234–239.
399. Jahn, W. *Z. Naturforsch.* **1989**, *44b*, 79–82.
400. Gorfti, A.; Salmain, M.; Jaouen, G.; McGlinchey, M. J.; Bennouna, A.; Mousser, A. *Organometallics* **1996**, *15*, 142–151.
401. Salmain, M.; Gorfti, A.; Jaouen, G. *Eur. J. Biochem.* **1998**, *258*, 192–199.
402. Osella, D.; Ravera, M.; Vincenti, M.; Salmain, M.; Jaouen, G. *Organometallics* **1996**, *15*, 3037–3041.
403. Osella, D.; Pollone, P.; Ravera, M.; Salmain, M.; Jaouen, G. *Bioconjugate Chem.* **1999**, *10*, 607–612.
404. Weinstein, S.; Jahn, W.; Hansen, H.; Wittmann, H. G.; Yonath, A. *J. Biol. Chem.* **1989**, *264*, 19138–19142.
405. Weinstein, S.; Jahn, W.; Glotz, C.; Schlunzen, F.; Levin, I.; Janell, D.; Harms, J.; Kolln, I.; Hansen, H.; Gluhmann, M., *et al. J. Struct. Biol.* **1999**, *127*, 141–151.